Copyright **© ECMS2013**

Printed: ISBN: 978-0-9564944-6-7 **European Council for Modelling**

CD: ISBN: 978-0-9564944-7-4 **and Simulation**

Cover picture **© Norwegian Maritime Competence Center**

Printed by **Digitaldruck Pirrot GmbH**
66125 Sbr.-Dudweiler, Germany

PROCEEDINGS

27th European Conference on Modelling and Simulation ECMS 2013

May 27th – May 30th, 2013
Ålesund, Norway

Edited by:
Webjørn Rekdalsbakken
Robin T. Bye
Houxiang Zhang

Organized by:
ECMS - European Council for Modelling and Simulation

Hosted by:
Aalesund University College, Norway

Sponsored by:
Aalesund University College, Norway
The Research Council of Norway
Møre and Romsdal County Municipality
Rolls-Royce Marine
Offshore Simulator Centre AS
Farstad Shipping
Sparebanken Møre
Tekna
Norwegian Maritime Competence Center

International Co-Societies:

IEEE - Institute of Electrical and Electronics Engineers

ASIM - German Speaking Simulation Society

EUROSIM - Federation of European Simulation Societies

PTSK - Polish Society of Computer Simulation

LSS - Latvian Simulation Society

ECMS 2013 ORGANIZATION

Conference Chair

Webjørn Rekdalsbakken

Aalesund University College

Norway

Conference Co-Chair

Robin T. Bye

Aalesund University College

Norway

Programme Chair

Robin T. Bye

Aalesund University College

Norway

Programme Co-Chair

Houxiang Zhang

Aalesund University College

Norway

President of European Council for Modelling and Simulation

Evtim Peytchev

Nottingham Trent University

United Kingdom

Managing Editor

Martina-Maria Seidel

St. Ingbert

Germany

INTERNATIONAL PROGRAMME COMMITTEE

Agent-Based Simulation

Track Chair: **Michael Möhring**
University of Koblenz-Landau, Germany

Co-Chair: **Ulf Lotzmann**
University of Koblenz-Landau, Germany

Simulation in Industry, Business and Services

Track Chair: **Alessandra Orsoni**
University of Kingston, United Kingdom

Co-Chair: **Serhiy Kovela**
University of Kingston, United Kingdom

Co-Chair: **Arne Petermann**
Berlin University for Professional Studies, Germany

Simulation of Intelligent Systems

Track Chair: **Zuzana Kominková Oplatková**
Tomas Bata University of Zlín, Czech Republic

Co-Chair: **Roman Senkerik**
Tomas Bata University of Zlín, Czech Republic

Finance, Economics and Social Science

Track Chair: **Javier Otamendi**
University of Rey Juan Carlos Madrid, Spain

Co-Chair: **Barbara Dömötör**
Corvinius University of Budapest, Hungary

Simulation of Complex Systems & Methodologies

Track Chair: **Krzysztof Amborski**
Warsaw University of Technology, Poland

Co-Chair: **Jaroslav Sklenar**
University of Malta, Malta

Simulation, Experimental Science and Engineering in Maritime Operations

Track Chair: **Hans Petter Hildre**
Aalesund University College, Norway

Co-Chair: **Sashidharan Komandur**
Aalesund University College, Norway

Simulation and Visualization for Training and Education

Track Chair: **Vilmar Æsøy**
Aalesund University College, Norway

Co-Chair: **Eilif Pedersen**
Norwegian University of Science and Technology, Norway

Modelling, Simulation and Control of Technological Processes

Track Chair: **Jiři Vojtěšek**
Tomas Bata University in Zlín, Czech Republic

Co-Chair: **Petr Dostál**
Tomas Bata University in Zlín, Czech Republic

Co-Chair: **František Gazdoš**
Tomas Bata University in Zlín, Czech Republic

Discrete Event Modelling and Simulation in Logistics, Transport and Supply Chain Management

Track Chair: **Gaby Neumann**
Technical University of Applied Sciences Wildau, Germany

Co-Chair: **Edward J. Williams**
University of Michigan-Dearborn, USA

High Performance Modelling and Simulation

Track Chair: **Joanna Kolodziej**
Institute of Computer Science Cracow University of Technology, Poland

Co-Chair: **Horacio-Gonzalez-Velez**
National College of Ireland Dublin, Ireland

Co-Chair: **Ewa Niewiadomska-Szynkiewicz**
NASK, Warsaw, Poland

Policy Modelling

Track Chair: **Maria Wimmer**
University of Koblenz-Landau, Germany

Programme Chair: **Scott Moss**
University of Koblenz-Landau, Germany
Visiting Professor

Modelling and Simulation in Computer Vision for Image Understanding

Track Chair: **Stephen Chen**
Zhejiang University of Technology, China

Co-Chair: **Mai Xu**
Tsinghua University, China

Simulation and Optimization

Track Chair: **Frank Herrmann**
University of Applied Sciences Regensburg, Germany

Co-Chair: **Erik Krobat**
University of Bundeswehr in Munich, Germany

Co-Chair: **Thorsten Claus**
International Graduate School (IHI) Zittau, Germany

Modeling and Simulation in Robotic Applications

Track Chair: **Wei Wang**
Beijing University of Aeronautics and Astronautics, China

Co-Chair: **Sigal Berman**
Ben-Gurion University of the Negev, Israel

Simulation and Computational Neuroscience

Track Chair: **Yasser Roudi**
Kavli Institute for Systems Neuroscience and Centre for the Biology of Memory, Norwegian University of Science and Technology, Norway

Co-Chair: **Gaute Einevoll**
Norwegian University of Life Science (UMB), Norway

Simulation of Social Interaction

Track Chair: **Bruce Edmonds**
Manchester Metropolitan University Business School, United Kingdom

Co-Chair: **Flaminio Squazzoni**
University of Brescia, Italy

IPC Members in Alphabetical Order

Pavel O. Abaev, Peoples' Friendship University of Russia, Russia

Petra Ahrweiler, University College Dublin, Ireland

Athena Akrami, SISSA, Italy

Marco Aldinucci, University of Turin, Italy

Frédéric Amblard, University of Toulouse, France

Piotr Arabas, Warsaw University of Technology, NASK, Poland

Hans-Peter Barbey, University of Applied Sciences in Bielefeld, Germany

Shusheng Bi, Robotics Institute BeiHang University in Beijing, China

Kashif Bilal, North Dakota State University, USA

Ove Bjørneset, STX-OSV, Norway

Frøy Birthe Bjørneset, Rolls-Royce Marine, Norway

Giangiacomo Bravo, University of Turin, Italy

Øyvind Bunes, Rolls-Royce Marine, Norway

Aleksander Byrski, AGH Univ. of Science and Technology, Poland

Piers Campbell, The University of Newcastle, Callaghan, Australia

Steve Capes, Cambridge Shire County Council, United Kingdom

Ester Camiña Centeno, University Complutense Madrid, Spain

Krzysztof Cetnarowicz, AGH Univ. of Science and Technology, Poland

Petr Chalupa, Tomas Bata University in Zlín, Czech Republic

Edmund Chattoe-Brown, University of Leicester, United Kingdom

Dan Chen, China University of Geosciences, Wuhan, China

Catherine Cleophas, FU-Berlin, Germany

Péter Csóka, Corvinus University of Budapest, Hungary

Mate J. Csorba, Marine Cybernetics, Norway

Peter De Smedt, Research Center of the Flemish Government, Belgium

Ciprian Dobre, Politechnical University of Bucharest, Romania

Sanja Dogramadzi, University of the West of England, United Kingdom

Luis Miguel Doncel Pedrera, University Rey Juan Carlos Madrid, Spain

Bernabé Dorronsoro, University of Lille, France

František Dušek, University of Pardubice, Czech Republic

Andrzej Dzielinski, Warsaw University of Technology, Poland

Yael Edan, Ben-Gurion University, Israel

Atis Elsts, EDI, Latvia

Cain Evans, Birmingham City University, United Kingdom
Doron Friedman, Interdisciplinary Center, Israel
Pilar Grau-Carles, University Rey Juan Carlos Madrid, Spain
Dag. Sverre Gronmyr, Rolls Royce Marine, Norway
Antoni Guasch, UPC, Barcelona Tech, Spain
Weidong Guo, Robotics Institute BeiHang University in Beijing, China
David Hales, Open University, United Kingdom
Dániel Havran, Corvinius University of Budapest, Hungary
Poul Heegaard, Norwegian Univ. of Science and Technology, Trondheim, Norway
Thomas Hellström, Umea University, Sweden
Karl Henning Halse, Aalesund University College, Norway
Gerald Holowicki, University of Michigan-Dearborn, USA
Daniel Honc, University of Pardubice, Czech Republic
Mark Hoogendorn, VU University of Amsterdam, The Netherlands
Thomas Hußlein, OptWare GmbH in Regensburg, Germany
Martin Ihrig, University of Pennsylvania, United States
Teruaki Ito, University of Tokushima, Japan
Yumi Iwashita, Kyushu University, Japan
Luis Izquierdo, University of Burgos, Spain
Wander Jager, University of Groningen, The Netherlands
Mo Jamshidi, The University of Texas at San Antonio, USA
Marijn Janssen, TU Delft, The Netherlands
Marco Janssen, Arizona State University, United States
Cara H. Kahl, TU Hamburg-Harburg, Germany
Osman Khalid, North Dakota State University, Fargo, USA
Zaheer Abbas Khan, CERN, Switzerland
Natalie Kliewer, FU Berlin, Germany
Frank Klingert, TU Hamburg-Harburg, Germany
Petia Koprinkova-Hristova, Bulgarian Academy of Sciences, Bulgaria
Victor Y. Korolev, Lomonosov Moscow State University, Russia
Igor Kotenko, St. Petersburg Institute, Russia
Martina Kotyrba, University of Ostrava, Czech Republic
Marek Kubalcik, Tomas Bata University in Zlín, Czech Republic
Jane Labadin, University Malaysia Sarawak, Malaysia

Jiting Li, Robotics Institute BeiHang University in Beijing, China
Dario G. Liebermann, Tel-Aviv University, Israel
Henrik Lindén, KTH, Sweden
Sheng Liu, Zhejiang University of Technology, China
Rong Liu, Robotics Institute BeiHang University in Beijing, China
Arne Løkketangen, Molde University College, Norway
Ahmad Lotfi, Nottingham Trent University, United Kingdom
Euripidis Loukis, Aegean-Research Unit, Greece
David Ludlow, University of West England, United Kingdom
Susan Lysecky, University of Arizona, United States
Przemyslaw Majewski, Fido Intelligence, Poland
Saif U. R. Malik, North Dakota State University, Fargo, USA
Michael Manitz, University Duisburg-Essen, Germany
Michal Marks, NASK Warsaw, Poland
Katarina Matějíčková, VUCHT, Slovakia
Radek Matušů, Tomas Bata University in Zlín, Czech Republic
Artis Mednis, EDI, Latvia
Weiliang Meng, NLPR, China
Nicolas Meseth, University of Osnabruck, Germany
Hermann Meuth, University of Applied Science, Germany
Michela Milano, University of Bologna, Italy
Yuri Misnikov, University of Leeds, United Kingdom
Christian Müller, TH Wildau, Germany
Nazmun Nahar, University of Jyvaskyla, Finland
Pavel Nahodil, Czech Technical University of Prague, Czech Republic
Libero Nigro, University of Calabria, Italy
Yifeng Niu, University of Hamburg, Germany
Jakub Novák, Tomas Bata University in Zlín, Czech Republic
Felix Obschonka, FU Berlin, Germany
Adegboyega Ojo, DERI, Ireland
Dominik Olszewski, Warsaw University of Technology, Poland
Johan Oppen, Molde University College, Norway
Paul Ormerod, Volterra, United Kingdom
Ottar L. Osen, Aalesund University College, Norway

Nazmiye Ozkan, Univ. of Westminster, United Kingdom
Mario Paolucci, ISTC/CNR, Italy
Paweł Pawlewski, Poznan University of Technology, Poland
Johnatan E. Pecero, University of Luxembourg, Luxembourg
Alexander V. Pechinkin, Russian Academy of Sciences and Peoples', Russia
Anna Plichta, Cracow University of Technology, Poland
Gary Polhill, James Hutton Institute Aberdeen Scotland, United Kingdom
Dmitriy Ponkratov, Aalesund University College, Norway
Matthijs Pontier, VU University Amsterdam, The Netherlands
Florian Pop, Polithechnical University of Bucharest, Romania
Ioan Popa, University of Craiova, Romania
Roberto Protil, Federal University of Viçosa, Brazil
Rostislav V. Razumchik, Russian Academy of Sciences and Peoples', Russia
Karl-Johan Reite, SINTEF Fisheries & Agriculture, Norway
Napoleon H. Reyes, Massey University, New Zealand
Young Ro, University of Michigan-Dearborn, United States
Boris Rohal-Ilkiv, Technical University of Bratislava, Slovakia
Juliette Rouchier, GREQAM/CNRS, France
Toni Ruohonen, University of Jyväskylä, Finland
Konstantin E. Samoylov, Peoples' Friendship University of Russia, Russia
Hans Georg Schaathun, Aalesund University College, Norway
Sabrina Scherer, University of Koblenz-Landau, Germany
Thomas Schulze, Otto-von-Guericke University Magdeburg, Germany
Weiguo Sheng, Zhejiang University of Technology, China
Zvi Shiller, Ariel University Center, Israel
Peer-Olaf Siebers, University of Nottingham, United Kingdom
Anders Skoogh, Chalmers University of Technology, Goteborg, Sweden
Andrzej Sluzek, Technical University of Singapore, Singapore
Katarzyna Smelcerz, Cracow University of Technology, Poland
Roman Smierzchalski, Gdansk University of Technology, Poland
Trygve Solstad, NTNU, Norway
Mojca Indihar Stemberg, University of Ljubljana, Slovenia
Girts Strazdins, Aalesund University College, Norway
Yipeng Sun, Tsinghua University, China

Magdalena Szmajduch, CDN-Partner Cracow, Poland
Károly Takács, Corvinius University of Budapest, Hungary
Themis Tambouris, University of Macedonia, Greece
Tom Tetzlaff, FZ Juelich, Germany
Peter Trkman, University of Ljubljana, Slovakia
Klaus G. Troitzsch, University Koblenz-Landau, Germany
Christopher Tubb, University of Wales Newport, United Kingdom
Kata Váradi, Corvinus University of Budapest, Hungary
Harko Verhagen, Stockholm University, Sweden
Alexey A. Voinov, University of Twente, The Netherlands
Eva Volna, University of Ostrava, Czech Republic
Dangxiao Wang, Robotics Institute BeiHang University in Beijing, China
Roland Wertz, Fraunhofer IPA Stuttgart, Germany
Tomasz Wiktor Wlodarczyk, University of Stavanger, Norway
Aree Witoelar, NTNU, Norway
Daniel Wójcik, Nencki Institute, Poland
Weili Xiong, Jiangnan University, China
Pan Yushan, Aalesund University College, Norway
Michael Zaggl, TU Hamburg-Harburg, Germany
Jianhua Zhang, University of Hamburg, Germany
Yuru Zhang, Robotics Institute BeiHang University in Beijing, China
Marcello Zottolo, Lee Memorial Health System, United States

PREFACE

We at the Aalesund University College (AAUC) are grateful for having the honour of hosting the 27th European Conference on Modelling and Simulation, or ECMS 2013. Located in the Art Nouveau town of Ålesund, AAUC lies at the heart of the maritime industry cluster on the west coast of Norway. With five faculties and more than 2000 students and 200 staff, the university college offers a wide range of study programmes in engineering, maritime operations, biotechnology, international business, and health science, including a newly accredited master programme in simulation and visualisation. Rooted in our strategy plan is a strong focus on applied maritime technology and operations, which manifests itself through some of the world's most advanced offshore simulators and our close ties to the maritime industry in both training, education, and research. As a result, modelling and simulation permeate almost everything we do at AAUC, from basic engineering courses, through training of offshore personnel, to novel research.

Across all tracks, this year's conference has received excellent contributions from some of the world's most highly regarded researchers in their fields. In particular, with the human brain as a common denominator, keynote speakers Stephen Grossberg and May-Britt Moser present their respective work on grid cells, place cells, and brain maps for space; Peter and Megan Neilson introduce their adaptive model theory and human movement control systems; and Sigal Berman talks about telerobotics and hand gestures for remote control. Having secured these keynote speakers has also spawned the creation of new tracks in robotic applications and computational neuroscience, the latter of which include specially invited talks by Peter Latham and Matteo Marsili.

We are very proud that six brand new tracks are introduced at ECMS 2013, dealing with modelling, simulation and visualisation in training and education; maritime technology and operations; robotic applications; computational neuroscience; optimization; computer vision; and social interaction. In addition, ten traditional tracks are offered in topics such as agent-based simulation; complex systems; finance, economics and social science; high performance modelling and simulation; industry, business, and services; intelligent systems; logistics, transport, and management; process control; and policy modelling. In total, some 141 accepted papers and oral talks are presented, with more than 170 participants from all over the world attending the sessions.

For 27 years, ECMS has set the stage for an independent, highly interdisciplinary scientific forum for researchers and practitioners from all over the world to present and discuss the latest findings, challenges, and future directions of their work. We, the organisers of ECMS 2013, hope that the high quality of accepted papers and participants as well as our exciting scientific, social, and cultural programme all ensure the success of this year's conference and we look forward in excitement to which directions the conference will take in the future.

Webjørn Rekdalsbakken	Robin T. Bye	Houxiang Zhang
Conference Chair	Conference Co-Chair Programme Chair	Programme Co-Chair

TABLE OF CONTENTS

Plenary Talks

Invited Talks for Computational Neuroscience

Agent-Based Simulation

Simulation of Complex Systems and Methodologies

Simulation, Experimental Science and Engineering in Maritime Operations

Simulation and Visualization for Training and Education

Finance, Economics and Social Science

Simulation in Industry, Business and Services

Simulation of Intelligent Systems

Modelling, Simulation and Control of Technological Processes

High Performance Modelling and Simulation

Discrete Event Modelling and Simulation in Logistics, Transport and Supply Chain Management

Policy Modelling

Modelling and Simulation in Robotic Applications

Simulation and Optimization

Modelling and Simulation in Computer Vision for Image Understanding

Simulation and Computational Neuroscience

ECMS 2013
SCIENTIFIC PROGRAM

Plenary Talks

Coordinated learning of grid cell and place cell spatial and temporal properties: Multiple scales, attention, and oscillations

Stephen Grossberg
Center for Adaptive Systems, Graduate Program in Cognitive and Neural Systems,
Center for Computational Neuroscience and Neural Engineering,
Department of Mathematics, Boston University, Boston, MA 02215
steve@bu.edu, http://cns.bu.edu/~steve

How do grid cells and place cells arise through development and learning? Medial entorhinal grid cells and hippocampal place cells provide neural correlates of spatial representation in the brain. A place cell typically fires whenever an animal is present in one or more spatial regions, or places, of an environment. A grid cell typically fires in multiple spatial regions that form a regular hexagonal grid structure extending throughout the environment. Different grid and place cells prefer spatially offset regions, with their firing fields increasing in size along the dorsoventral axes of the medial entorhinal cortex and hippocampus. The spacing between neighboring fields for a grid cell also increases along the dorsoventral axis.

The GridPlaceMap neural model shows how grid cells and place cells may develop in a hierarchy of self-organizing maps. In this conception, grid cells and place cells are learned spatial categories in these maps. The model responds to realistic rat navigational trajectories by learning grid cells with hexagonal grid firing fields of multiple spatial scales, and place cells with one or more firing fields that match neurophysiological data about these cells and their development in juvenile rats. The place cells represent much larger spaces than the grid cells, which enable them to support navigational behaviors.

Homologous self-organizing map laws for grid cell and place cell learning. The grid cell and place cell self-organizing maps both obey the same laws, and both amplify and learn to categorize the most frequent and energetic co-occurrences of their inputs. The different receptive field properties emerge because they experience different input sources. The place cells learn from the developing grid cells of multiple scales that input to them. The grid cells learn from stripe cells of multiple scales that input to them, each with a different directional selectivity. The name “stripe cell” acknowledges that the spatial firing pattern of each such cell exhibits parallel stripes as the environment is navigated. Burgess and his colleagues introduced an analogous concept of “band cells”, but they are formed by the mechanism of oscillatory interference.

Grid and place cell learning occurs in models that are built up from either rate-based or spiking neurons. The results using spiking neurons build upon a previous rate-based model of grid and place cell learning, and thus illustrate a general method for converting rate-based adaptive neural models into models whose cells obey spiking dynamics. Remarkably, the spiking model continues to exhibit key analog properties of the data. New properties also arise in the spiking model, including the appearance of theta band modulation. The spiking model also opens a path for implementation in brain-emulating nanochips comprised of networks of noisy spiking neurons with multiple-level adaptive weights for controlling autonomous adaptive robots capable of spatial navigation.

Learning the dorsoventral gradient of receptive field sizes and oscillation frequencies. Both the spatial and temporal properties of grid cells vary along the dorsoventral axis of the medial entorhinal cortex. *In vitro* recordings of medial entorhinal layer II stellate cells have revealed subthreshold membrane potential oscillations (MPOs) whose temporal periods, and time constants of excitatory postsynaptic potentials (EPSPs), both increase along

Proceedings 27th European Conference on Modelling and Simulation ©ECMS Webjørn Rekdalsbakken, Robin T. Bye, Houxiang Zhang (Editors)
ISBN: 978-0-9564944-6-7 / ISBN: 978-0-9564944-7-4 (CD)

this axis. Slower (faster) subthreshold MPOs and slower (faster) EPSPs correlate with larger (smaller) grid spacings and field widths. The self-organizing map model simulates how the anatomical gradient of grid spatial scales can be learned by cells that respond more slowly along the gradient to their inputs from stripe cells of multiple scales. The model cells also exhibit MPO frequencies that covary with their response rates, and exhibit some properties of modular organization of the different spatial scales. The gradient in intrinsic rhythmicity is thus not compelling evidence for oscillatory interference as a mechanism of grid cell firing.

Homologous spatial and temporal mechanisms: Neural relativity. This spatial gradient mechanism is homologous to a gradient mechanism for temporal learning in the lateral entorhinal cortex and its hippocampal projections that was proposed in the 1980s. Such adaptively timed learning has simulated data about the role of hippocampus in supporting learning that bridges temporal gaps, such as occurs during trace conditioning and delayed matching-to-sample. This type of "spectrally timed learning" has Weber Law properties that have been confirmed by recent experiments that have discovered "time cells" in the hippocampus. Spatial and temporal representations may hereby arise from homologous mechanisms, thereby embodying a mechanistic “neural relativity” that may clarify how episodic memories are learned.

Homologous processing of angular and linear velocity path integration inputs. The inputs that drive the initial development of grid cells and place cells are angular and linear velocity signals that are activated by an animal's navigational movements. The model proposes that both angular and linear velocity signals are processed by ring attractor neural circuits. Angular velocity signals are proposed to be processed by ring attractors that are composed of head direction cells, whereas linear velocity signals are proposed to be processed by ring attractors that are composed of stripe cells. The outputs of head direction cells modulate the linear velocity signals to multiple directionally-selective stripe cell ring attractor circuits. This modulation is sensitive to the cosine of the difference between the current heading direction of movement and the ring attractor’s directional preference. Each stripe cell ring attractor is sensitive to a different direction and spatial scale. Stripe cells are the individual cells within each such ring attractor circuit and are activated at different spatial phases as the activity bump moves across their ring locations. They may be activated periodically as the activity bump moves around the ring attractor more than once in response to the navigational movements of the animal.

The model’s assumption that both head direction cells and stripe cells are computed by ring attractors that drive grid and place cell development is consistent with data showing that adultlike head direction cells already exist in parahippocampal regions of rat pups when they actively move out of their nests for the first time at around two weeks of age.

Stable learning, attention, realignment, and remapping. Place cell selectivity can develop within seconds to minutes, and can remain stable for months. The hippocampus needs additional mechanisms to ensure this long-term stability. This combination of fast learning and stable memory is often called the *stability-plasticity dilemma*. Self-organizing maps are themselves insufficient to solve the stability-plasticity dilemma in environments whose input patterns are dense and are non-stationary through time, as occurs regularly during real-world navigation. However, self-organizing maps augmented by learned top-down expectations that focus attention upon expected combinations of features can do so.

Adaptive Resonance Theory, or ART, proposes how to dynamically stabilize the learned categorical memories of self-organizing maps. Experimental data about the hippocampus from several labs are compatible with the predicted role of top-down expectations and attentional matching in memory stabilization. These experiments clarify

how cognitive processes like attention may play a role in entorhinal-hippocampal spatial learning and memory stability. The proposed mechanism of top-down attentional matching may also help to clarify data about grid and place cell remapping and alignment of grid orientations.

Beta, gamma, and theta oscillations. Within ART, a sufficiently good match can trigger fast gamma oscillations that enable spike-timing dependent plasticity to occur, whereas a big enough mismatch can trigger slow beta oscillations that do not. Such beta oscillations occur in hippocampus during the learning of novel place cells, and have the properties expected when mismatches occur and receptive field refinements are learned. Beta oscillations also occur at the expected times in visual cortex and in the frontal eye fields during shifts in spatial attention. Thus, the match/mismatch dynamics leading to gamma/beta oscillations seem to occur in multiple brain systems.

The theta rhythm has been associated with properties of spatial navigation, as has firing of entorhinal grid cells. Recent experiments have reduced the theta rhythm by inactivating the medial septum (MS) and demonstrated a correlated reduction in the hexagonal spatial firing patterns of grid cells. These results, along with properties of intrinsic membrane potential oscillations in slice preparations of entorhinal cells, have been proposed to support an oscillatory interference model of grid cells. Our self-organizing map model of grid cells can explain these data without invoking oscillatory interference. In particular, the adverse effects of MS inactivation on grid cells can be understood from how the concomitant reduction in cholinergic inputs may increase conductances of leak potassium and slow and medium after-hyperpolarization channels.

Model parsimony. Our emerging neural theory of spatial and temporal processing in the entorhinal-hippocampal system exhibits a remarkable parsimony and unity in at least three ways: It proposes that similar ring attractor mechanisms compute the linear and angular path integration inputs that drive map learning; that the same self-organizing map mechanisms can learn grid cell and place cell receptive fields, despite their dramatically different appearances; and that that the dorsoventral gradient of multiple scales and modules of spatial learning through the medial entorhinal cortex to hippocampus may use mechanisms that are homologous to mechanisms earlier proposed for temporal learning through the lateral entorhinal cortex to hippocampus ("neural relativity"), as reflected by data about trace conditioning, delayed matching-to-sample, and "time cells". This mechanistic homolog clarifies why both spatial and temporal processing occur in the entorhinal-hippocampal system and why episodic learning may be supported by this system. No less striking is the fact that both grid cells and place cells can develop by detecting, learning, and remembering the most frequent and energetic co-occurrences of their inputs, properly understood. This co-occurrence property is naturally computed in response to data, such as navigational signals, that take on contextual meaning through time.

Supported in part by the SyNAPSE program of DARPA (HR0011-09-C-0001).

Modeling References (see http://cns.bu.edu/~steve)

Fortenberry, B., Gorchetchnikov, A. and Grossberg, S. (2012). Learned integration of visual, vestibular, and motor cues in multiple brain regions computes head direction during visually-guided navigation. *Hippocampus*, **22**, 2219-2237.

Gorchetchnikov, A., and Grossberg, S. (2007). Space, time, and learning in the hippocampus: How fine spatial and temporal scales are expanded into population codes for behavioral control. *Neural Networks*, **20**, 182-193.

Grossberg, S. (2009). Beta oscillations and hippocampal place cell learning during exploration of novel environments. *Hippocampus*, **19**, 881-885.

Grossberg, S. (2012). Adaptive Resonance Theory: How a brain learns to consciously attend, learn, and recognize a changing world. Neural *Networks,* **37**, 1-47.

Grossberg, S. and Merrill, J.W.L. (1992). A neural network model of adaptively timed reinforcement learning and hippocampal dynamics. *Cognitive Brain Research*, **1**, 3-38.

Grossberg, S. and Merrill, J.W.L. (l996). The hippocampus and cerebellum in adaptively timed learning, recognition, and movement. *Journal of Cognitive Neuroscience,* **8**, 257-277.

Grossberg, S., and Pilly, P.K. (2012). How entorhinal grid cells may learn multiple spatial scales from a dorsoventral gradient of cell response rates in a self-organizing map. *PLoS Computational Biology,* **8(10)**: 31002648. Doi:10.1371/journal.pcbi.1002648.

Grossberg, S. and Versace, M. (2008). Spikes, synchrony, and attentive learning by laminar thalamocortical circuits. *Brain Research*, **1218**, 278-312.

Grossberg, S. and Schmajuk, N.A. (1989). Neural dynamics of adaptive timing and temporal discrimination during associative learning. *Neural Networks*, **2** , 79-102.

Mhatre, H., Gorchetchnikov, A., and Grossberg, S. (2012). Grid cell hexagonal patterns formed by fast self-organized learning within entorhinal cortex. *Hippocampus*, **22**, 320-334.

Pilly, P.K., and Grossberg, S. (2013). How do spatial learning and memory occur in the brain? Coordinated learning of entorhinal grid cells and hippocampal place cells. *Journal of Cognitive Neuroscience*, **24**, 1031-1054.

Pilly, P.K., and Grossberg, S. (2012). How reduction of theta rhythm by medium septum inactivation may disrupt periodic spatial responses of entorhinal grid cells by reduced cholinergic transmission. Submitted for publication.

Pilly, P.K., and Grossberg, S. (2013). Spiking neurons in a hierarchical self-organizing map model can learn to develop spatial and temporal properties of entorhinal grid cells and hippocampal place cells. *PLoS ONE*, in press.

Brain maps for space

May-Britt Moser,
Norwegian University of Science and Technology
Kavli Institute for Systems Neuroscience and
Centre for Neural Computation,
Trondheim
Norway

27th European Conference on Modelling and Simulation (ECMS) Ålesund, May 27 to 30th, 2013

The brain controls spatial navigation in mammals by activating functionally specialized cell types in the medial temporal lobe. A key component of the spatial mapping system is the place cell, located in the hippocampus. These cells – discovered by O´Keefe and Dostrovsky in 1971 - are active only when the animal is entering a specific location in the environment. I will describe the discovery of another component of the mammalian spatial mapping system – the grid cell – which we found upstream of the hippocampus, in the medial entorhinal cortex, in 2005. Grid cells are activated whenever an animal enters locations that are distributed in a spatially periodic pattern across the environment. The repeating unit of the grid pattern much is an equilateral triangle. Grid cells are co-localized with head direction cells and border cells, which contain information about the direction in which the animal is moving and the boundaries of the environment. Despite the discovery of several elements of the mammalian spatial map, the interaction between the components is poorly understood. We addressed this question first by using optogenetics together with electrophysiologal recordings of cells in the entorhinal cortex. Hippocampal neurons were infected with an adenoassociated virus carrying genes for a peptide tag that can be visualized by fluroescent antibodies as well as the light-sensitive cation channel channelrhodopsin-2 (ChR2). The virus was engineered to enable retrograde transport through axons of cells with projections into the hippocampus. Infected entorhinal cells were detected by local flashes of light. Channelrhodopsin-expressing cells responded with a short and constant latency to the light. All cell types in the entorhinal cortex were found to respond to the light, suggesting that place signals may be generated in the hippocampus by convergence of signals from all these entorhinal cell types. In addition to discussing the transformation of entorhinal to hippocampal spatial signals, I will devote a part of my talk to asking how the grid-cell network is intrinsically organized. To adress this question we used multi-channel recording from a much larger number of cells than recorded ever before in individual animals. Grid cells were found to cluster into a small number of modules with distinct grid scales, grid orientations and grid asymmetries, as well as distinct patterns of temporal organization. The different modules responded independently to changes in the geometry of the environment.

The existence of distinct and independent modules or grid maps makes entorhinal maps different from the many other sensory cortices where functions tend to be more graded and continous. This is in agreement with the suggestion that the grid map is a product of self-organizing network dynamics rather than specificity in the input. Because the crystal-like structure of the grid pattern is generated within the brain, not depending on specific sensory inputs, we are confronted with an unique situation in which we, by trying to understand how the grid pattern is formed, may obtain insights into how patterns are formed in the mammalian cortex.

Proceedings 27th European Conference on Modelling and Simulation ©ECMS Webjørn Rekdalsbakken, Robin T. Bye, Houxiang Zhang (Editors)
ISBN: 978-0-9564944-6-7 / ISBN: 978-0-9564944-7-4 (CD)

Adaptive Model Theory: A History

Megan D. Neilson & Peter D. Neilson

Our accompanying presentation overviews the constructs of Adaptive Model Theory, a computational account of human movement control that has evolved over a research lifetime that began in the 1950s. Its origins are in the fascination of two young people with the prospect of applying their training in physics, mathematics, and engineering principles to the modelling of biological systems. Unlike today, it was an era in which such interdisciplinary work was rare and the path to undertaking it was essentially of one's own making. In this presentation we explore some of the history of that journey. There was the getting of technical jobs in UNSW's newly established medical school to provide a gateway to the biological world; the finding of labs where "way-out" ideas were tolerated, if not entirely understood; and the support for part-time graduate research. Not to mention the finding of unmeetable mentors accessible only via the literature.

Experimental work began with studies (without benefit of automated A-D conversion) into investigating the human tonic stretch reflex, not during rest as was usually done, but by modelling the input-output characteristics during voluntary contraction. From these followed a string of experimental investigations to investigate movement disorders, cerebral palsy in particular, but also Parkinson's disease, stroke, cerebellar disorder, and stuttering. At the time the latter was still widely believed to be psychological in origin. The voluntary movement tracking experiments carried out to model the input-output characteristics of the auditory-motor loop in stuttering and non-stuttering subjects gave strong credence to the now-accepted neurological basis of the disorder. Likewise, following on from the studies of reflexes in cerebral palsied subjects, experimental use of tracking paradigms to separate voluntary and involuntary activity in the purposive movements of this group showed a clear result which is now well accepted clinically. Quite apart from unwanted reflex activity, cerebral palsied subjects lack the ability to generate appropriate movements for a voluntary task, despite a cognitive understanding of what is required. In each of the neurological disorders we studied the experimental evidence pointed to deficits in the formation, maintenance and/or selection of the adaptive sensory-motor models underlying the forward control of voluntary movement.

Hence enter Adaptive Model Theory and the quest for a more general understanding of how the brain achieves control of the inherently nonlinear, nonstationary, uncertain, redundant, unstable system that implements human movement. In parallel with the theoretical development came more experiment, now mostly with normal subjects. This included examination of control-display compatibility in tracking, acquisition of tracking skill with practice, tracking with differing degrees of freedom, tracking with unusual systems that variously involved gain change, cross-coupling and instability, as well as investigations of predictability in tracking and the response planning strategies that apply. And of course there were the simulations that necessarily accompany the experimental findings and so guide the theoretical evolution. This ultimately has encompassed an account of motor development from the foetus to the mature system. So where now? It's a long way today from recognising that we can learn about biological systems by modelling their inputs and outputs. A great deal has been done, and not least in understanding the principles of sensory-motor control. But it's far from done yet. The mathematics of Riemannian geometry currently offers a new window into the planning of responses of complex systems. Therein lies a future understanding of human movement and its disorders.

Proceedings 27th European Conference on Modelling and Simulation ©ECMS Webjørn Rekdalsbakken, Robin T. Bye, Houxiang Zhang (Editors)
ISBN: 978-0-9564944-6-7 / ISBN: 978-0-9564944-7-4 (CD)

Selected publications:

Lance, J. W., De Gail, P., & Neilson, P. D. (1966). Tonic and phasic spinal cord mechanisms in man. *Journal of Neurology, Neurosurgery, and Psychiatry*, *29,* 535-544.

Neilson, P. D. (1972). Frequency-response characteristics of the tonic stretch reflexes of biceps brachii muscle in intact man. *Medical and Biological Engineering*, *10,* 460-472.

Neilson, P. D. (1972). Interaction between voluntary contraction and tonic stretch reflex transmission in normal and spastic patients. *Journal of Neurology, Neurosurgery, and Psychiatry*, *35,* 853-860.

Andrews, C. J., Neilson, P. D., & Lance, J. W. (1973). Comparison of stretch reflexes and shortening reactions in activated normal subjects with those in Parkinson's disease. *Journal of Neurology, Neurosurgery, and Psychiatry*, *36,* 329-333.

Neilson, P. D. (1974). Measurement of involuntary arm movement in athetotic patients. *Journal of Neurology, Neurosurgery, and Psychiatry*, *37,* 171-177.

Neilson, M. D., Neilson, P. D., & Quinn, P. T. (1976). A cybernetic approach to control of speech. *Australian Journal of Human Communication Disorders*, *4,* 79-84.

Neilson, P. D., & Lance, J. W. (1978). Reflex transmission characteristics during voluntary activity in normal man and in patients with movement disorders. In J. E. Desmedt (Ed.), *Cerebral Motor Control in Man: Long Loop Mechanisms.* (pp. 263-299). Basel: Karger.

Neilson, P. D., Andrews, G., Guitar, B. E., & Quinn, P. T. (1979). Tonic stretch reflexes in lip, tongue and jaw muscles. *Brain Research*, *178,* 311-327.

Neilson, P. D., & Neilson, M. D. (1980). Influence of control-display compatibility on tracking behaviour. *Quarterly Journal of Experimental Psychology*, *32,* 125-135.

Neilson, P. D., & O'Dwyer, N. J. (1981). Pathophysiology of dysarthria in cerebral palsy. *Journal of Neurology, Neurosurgery, and Psychiatry*, *44,* 1013-1019.

Neilson, P. D., & O'Dwyer, N. J. (1984). Reproducibility and variability of speech muscle activity in athetoid dysarthria of cerebral palsy. *Journal of Speech and Hearing Research*, *27,* 502-517.

Neilson, M. D., & Neilson, P. D. (1985). Speech motor control and stuttering. In D. G. Russell & B. Abernethy (Eds.), *Motor Memory & Control: The Otago Symposium, Dunedin, New Zealand, 1982* (pp. 69-83). Dunedin, NZ: Human Performance Associates.

Neilson, M. D., & Neilson, P. D. (1987). Speech motor control and stuttering: A computational model of adaptive sensory-motor processing. *Speech Communication*, *6,* 325-333.

Neilson, P. D., O'Dwyer, N. J., & Neilson, M. D. (1988). Stochastic prediction in pursuit tracking: an experimental test of adaptive model theory. *Biological Cybernetics*, *58,* 113-122.

Neilson, P. D., Neilson, M. D., & O'Dwyer, N. J. (1995). Adaptive optimal control of human tracking. In D. J. Glencross & J. P. Piek (Eds.), *Motor control and sensory-motor integration: Issues and directions* (pp. 97-140). Amsterdam: Elsevier.

Neilson, M. D., & Neilson, P. D. (1999). A computational theory of motor development. Part 1: Development in utero. In P. Treffner & S. Morrison (Eds.), *Abstracts of the 5th Biennial Motor Control & Human Skill Research Workshop* (Surfers Paradise, QLD, January, 2000) (p. 36). Gold Coast, QLD: School of Physiotherapy & Exercise Science, Griffith University.

Neilson, P. D., & Neilson, M. D. (1999). A computational theory of motor development. Part 2: Development after birth. In P. Treffner & S. Morrison (Eds.), *Abstracts of the 5th Biennial Motor Control & Human Skill Research Workshop* (Surfers Paradise, QLD, January, 2000) (p. 37). Gold Coast, QLD: School of Physiotherapy & Exercise Science, Griffith University.

Neilson, P. D., & Neilson, M. D. (1999). A neuroengineering solution to the optimal tracking problem. *Human Movement Science*, *18,* 155-183.

Neilson, P. D., & Neilson, M. D. (2002). Anisotropic tracking: Evidence for automatic synergy formation in a bimanual task. *Human Movement Science*, *21,* 723-748.

Neilson, P. D., & Neilson, M. D. (2004). A new view on visuomotor channels: The case of the disappearing dynamics. *Human Movement Science*, *23,* 257-283.

Neilson, P. D., & Neilson, M. D. (2005). Motor maps and synergies. *Human Movement Science, 24,* 774-797.

Adaptive Model Theory: Modelling the Modeller

Peter D. Neilson & Megan D. Neilson

The human brain is an analogical modelling device. It forms adaptive models of the environment and of the body in interaction with the environment and it uses these models in the planning and control of purposive movement. The movement system includes the entire musculoskeletal system in interaction with the environment. There are some 700 functional muscles (groups of muscle fibres with the same mechanical action that are controlled independently by the nervous system) controlling about 110 elemental movements. From the perspective of the brain, the system to be controlled consists of three multiple input–multiple output nonlinear dynamical systems connected in cascade (i) muscle control systems (muscles and their reflex systems), (ii) biomechanical system (biomechanical loads on muscles), and (iii) external systems (external world). Sensory systems continuously monitor the input and output signals of all three of these subsystems and form adaptive models of the nonlinear dynamical relations within and between the various sensory modalities involved. The brain compares model predictions with actual sensory signals (afference) and takes discrepancies very seriously. Discrepancies lead to an increase in brain activity as the brain analyses errors and attempts to update its models. It also defends against perturbations by slowing movements and stiffening.

While it can be demonstrated behaviourally that the nervous system forms these adaptive models, many technical issues stand in the way of understanding computationally how it does so. Not least of these technical issues is the large amount of redundancy in afferent signals. Tens of thousands of receptors are involved in detecting, for example, muscle tensions and elemental movements. It is not possible to form accurate models of multiple input–multiple output systems when the inputs are strongly interrelated, and it is not possible to form accurate inverse models when the number of outputs is less than the number of inputs or when the outputs are contaminated with large amounts of noise. Because of this the nervous system has to remove redundancy from afferent signals and extract well-conditioned signals suitable for adaptive modelling.

It does this in two stages involving (i) slow adaptation and (ii) fast adaptation, respectively. (i) Slow adaptation involves correlational-based mechanisms of synaptic plasticity in networks of neurons connecting sensory receptors to the cerebral cortex (sensory pathways). Over several weeks to months, correlational-based mechanisms of synaptic plasticity lead to the adaptive formation of sensory maps in the cortex. In the somatosensory cortex, for example, maps of elemental movements and of the lengths and tensions of functional muscles are formed. Similar sensory maps for all other sensory modalities are formed in other cortical areas of the brain.

(ii) According to Adaptive Model Theory, fast adaptation depends on the existence of networks of neural adaptive filters within every sensory modality. The tuneable input-output transfer characteristic of each neural adaptive filter is preset in anticipation of a planned

Proceedings 27th European Conference on Modelling and Simulation ©ECMS Webjørn Rekdalsbakken, Robin T. Bye, Houxiang Zhang (Editors)
ISBN: 978-0-9564944-6-7 / ISBN: 978-0-9564944-7-4 (CD)

movement by patterns of neural activity held on-line in working memory. This activity modulates the synaptic gains of neurons in the adaptive filters. The modulating activity can be transferred from working memory into intermediate and long-term memory and, given an appropriate memory selection code, can be retrieved from intermediate or long-term memory and reinstated as a pattern of neural activity in working memory. This enables the tuning of neural adaptive filters to be switched quickly and smoothly between a library of settings acquired through previous sensory-motor experience and stored in memory.

The network of neural adaptive filters within each sensory modality extracts a small number of independently varying feature signals (determined by the movement being performed) from the large number of covarying signals within the sensory map for that modality. It does this by performing a type of Gramm-Schmidt orthogonalization (or QR factorization) but, instead of algebraic regression coefficients as used in these algorithms, it employs neural adaptive filters with nonlinear dynamical transfer characteristics. For example, when turning the steering wheel of a car some 20 elemental movements at the shoulders, elbows, forearms and wrists have to be coordinated to vary together in a nonlinear dynamically coupled way in order to generate a single movement feature signal corresponding to rotation of the steering wheel. The network of neural adaptive filters "learns" this coordination by adaptively modelling the nonlinear dynamical relationships between the covarying elemental movement signals in the somatosensory cortical sensory map and by extracting a single independently varying movement feature signal, the controlled degree of freedom of the task. Higher level planning and control of the movement can then be carried out within this low-dimensional subspace thereby greatly reducing demand on central processing resources. Slave copies of the same neural adaptive filters can be employed in the inverse direction to transform low-dimensional required feature signals planned centrally back into a large number of covarying elemental movements.

Similar feature extraction takes place simultaneously in every sensory modality. The resulting feature signals in each modality are then well-conditioned for forming adaptive models of the nonlinear dynamical forward and inverse relationships between them. These between-modality models are used in the planning and control of movement. For example, in steering a car, the required visual response associated with steering the car can be transformed into the elemental movements required to turn the steering wheel, thence into the muscle tensions that must be generated to produce those movements, and finally into the descending motor commands required to generate those tensions.

In this presentation we explore circuitry in cortico-cerebellar-cortical pathways in the brain capable of functioning as neural adaptive filters with third-order nonlinear dynamical transfer characteristics. We hold that Adaptive Model Theory demonstrates a means by which such circuitry can model the relationships between the incoming sensory signals despite these typically being non-Gaussian, non-white and non-stationary. In so doing the theory delineates a neurally realistic account of how the adaptive models necessary for movement control can be achieved. In that sense Adaptive Model Theory seeks to model the supreme modeller that is the human brain.

Selected publications:

Neilson, P. D., Neilson, M. D., & O'Dwyer, N. J. (1985). Acquisition of motor skills in tracking tasks: Learning internal models. In D. G. Russell & B. Abernethy (Eds.), *Motor Memory & Control: The Otago Symposium, Dunedin, New Zealand, 1982* (pp. 25-36). Dunedin, NZ: Human Performance Associates.

Neilson, P. D., Neilson, M. D., & O'Dwyer, N. J. (1988). Internal models and intermittency: A theoretical account of human tracking behavior. *Biological Cybernetics*, *58,* 101-112.

Neilson, P. D., Neilson, M. D., & O'Dwyer, N. J. (1992). Adaptive model theory: application to disorders of motor control. In J. J. Summers (Ed.), *Approaches to the Study of Motor Control and Learning* (pp. 495-548). Amsterdam: North Holland.

Neilson, P. D. (1993). The problem of redundancy in movement control: The adaptive model theory approach. *Psychological Research*, *55,* 99-106.

Neilson, P. D., Neilson, M. D., & O'Dwyer, N. J. (1997). Adaptive model theory: Central processing in acquisition of skill. In K. Connolly & H. Forssberg (Eds.), *Neurophysiology & Neuropsychology of Motor Development* (pp. 346-370). London: Mac Keith Press.

Neilson, P. D., & Neilson, M. D. (2005). An overview of adaptive model theory: solving the problems of redundancy, resources, and nonlinear interactions in human movement control. *Journal of Neural Engineering*, *2,* S279-S312.

Bye, R. T., & Neilson, P. D. (2008). The BUMP model of response planning: Variable horizon predictive control accounts for the speed–accuracy tradeoffs and velocity profiles of aimed movement. *Human Movement Scienc*e, *27*, 771-798.

Neilson, P. D., & Neilson, M. D. (2010). On theory of motor synergies. *Human Movement Science, 29,* 655-683.

Neilson, P. D., & Neilson, M. D. (2013). A Riemannian geometry model of human movement: The geodesic synergy hypothesis. *Forthcoming.*

HAND GESTURES FOR REMOTE CONTROL

Sigal Berman
Department of Industrial Engineering and Management
Ben-Gurion University of the Negev
Beer-Sheva 84105, Israel
E-mail:sigalbe@bgu.ac.il

KEYWORDS
Gesture recognition, Remote control, Human computer interaction

ABSTRACT

Gestures can be used as an alternative to traditional human computer interaction devices such as the keyboard and mouse. Gesture interaction can be flexible, natural, and intuitive. They can increase user immersion in virtual environments and reduce the need for learning systems specific interaction methods. In the talk, the general structure and main building blocks of gesture recognition systems will be discussed. The concepts discussed will be demonstrated as part of two applications employing hand gestures for remote control: control of the TV menu and control of a robotic manipulator.

INTRODUCTION

People use gestures as part of their daily interaction for communication of directives, thoughts, and feelings, enhancing or replacing spoken words. Use of gestures for human-computer interaction (HCI) can replace traditional interface devices such as mouse, keyboard or hand-held remote control. Gestures offer a natural, intuitive, and flexible HCI modality.

For computer-based simulation training, gestures can offer several advantages over traditional interfaces. Gestures can improve user immersion in virtual environment, they can reduce or even eliminated the need for learning simulation specific interaction methods, and gestures can enhance training to include actual interaction required in the physical scenario.

Previously gesture-based HCI was limited by the requirement for expensive and/or cumbersome sensing equipment such as magnetic trackers, sensor gloves, high-end image sensors, and touch screens. In recent years a plethora of low cost sensors suitable for gesture-based HCI has entered the market. For unencumbered gestures sensors such as the Kinect™ vision sensor suitable for remote hand and full body gesturing (0.5-5 meter) or the newly introduced Leep Motion™ controller for near hand and finger gestures (up to 1 meter) are now available at very low costs. For encumbered gestures various technologies are readily available and touch screens are now fully integrated within Windows 7™ operating system.

In order to utilize the benefits of gesture-based HCI it is important to gain understanding of gesture recognition technology. Gesture recognition systems (GRS) integrate both hardware and software components which should suit the task, environment, and user capabilities. In the current talk GRS architecture and main building blocks will be presented along with two examples of GRS for remote control: a GRS for television menu control and a GRS for tele-operation of a robotic manipulator.

GESTURE RECOGNITION SYSTEMS

The GRS operation cycle (Figure 1) includes the gesture executed by the user, which is sensed using a capture device and recognized using various algorithms (segmentation, tracking, feature extraction, classification). The recognized gesture is reported to the controlled application, which changes its state accordingly, and displays the outcome to the user. Due to the high interest in GRS, there are many reviews of their operation from various perspectives (e.g., (Aggarwal and Park 2004; Berman and Stern 2012; Garg and Aggarwal 2009; Mitra and Acharya 2007; Rautaray and Agrawal 2012; Wachs et al. 2011; Yilmaz et al. 2006).

There are many different types of gestures. Gestures may be performed using different body parts such as hands, head, legs, full body etc. Currently most GRS are based on hand gestures. Manipulative gestures are gestures where the executed motion directly influences the trajectory of the controlled object, similar to the relationship between the motion of the computer mouse and the curser on the screen. Semantic gestures encode commands by gesture features similar to the operation of keyboard keys. In dynamic gestures meaning is encoded by motion and in static gestures the meaning is encoded by the static hand or arm pose. Hybrid gestures encode meaning by both pose and motion. A gesture vocabulary is the set of gestures used within the application context.

The required building blocks of GRS are greatly influenced by the context of use, that is, by the gesture vocabulary and by the environment in which the system operates. For instance when manipulation gestures are

Proceedings 27th European Conference on Modelling and Simulation ©ECMS Webjørn Rekdalsbakken, Robin T. Bye, Houxiang Zhang (Editors)
ISBN: 978-0-9564944-6-7 / ISBN: 978-0-9564944-7-4 (CD)

used, the system does not require a classification module, or when the environment has very poor illumination RGB cameras cannot be used for gesture capture.

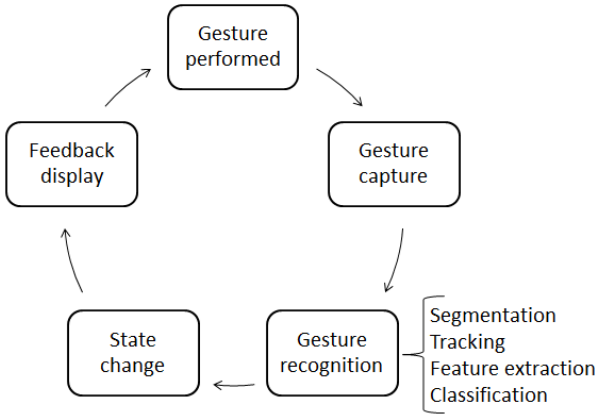

Figure 1: Gesture Recognition Cycle

Gesture capture devices can be divided by gesture stimuli into five groups (Berman and Stern, 2011): electric, optic, acoustic, magnetic, and mechanic. While optic based gesture capture facilitates unencumbered (free-hand) gestures, other stimuli require some assistive device either worn or in contact with the hand/body for gesture capture. For unencumbered GRS 2D vision sensors are still in use, but the low cost of currently available vision based distance sensors makes them the popular choice for GRS implementation.

Motion tracking is required when using manipulative or dynamic gestures. In vision-based GRS motion tracking requires hand segmentation from the background image. Segmentation difficulty is greatly alleviated when using distance information available from 3D vision sensors. Color cue is often used for hand tracking as people have a distinctive Hue range (Stern et al. 2010).

Classification is required when using symbolic gestures. With dynamic symbolic gestures, tracking provides a stream of segmented hand positions, and the classification algorithm must also determine gesture start and end. An additional challenge stems from motion variability within and between users. Hidden Markov Models (HMM), Dynamic Time Warping (DTW), and Longest Common Sub-sequence (LCS) are among the successfully applied classification methods (Frolova et al. 2012; Stern et al. 2013).

GRS FOR TELEVISION OPERATION

A vision-based GRS was developed for remote control of an Internet Protocol TV (IPTV) in a living-room environment (Stern et al, 2010). The living-room environment dictates a recognition range of up to a few meters and robustness to low and changing lighting conditions. Two additional constraints were imposed for the developed system: use of low-cost hardware components facilitating suitability to the consumer market, and adhering to the existing TV set-top box interface.

The gesture vocabulary was based on dynamic symbolic hand gestures. Dynamic unencumbered hand-gestures were used since their recognition is robust even with low quality sensing equipment, due to the distance requirements, and to facilitate “come-as-you-are” operation. Symbolic gestures were used for interfacing to the existing displays. Two system prototypes were developed based on 2D and 3D vision sensors. The vision sensors were located above or below the TV screen so several users sitting in the room could use the system together. For the 2D sensor a modified CAMShift algorithm was implemented based on motion and color cues with face detection and handling. For the 3D camera the OpenNI (http://www.openni.org/) tracking functionality was used. Two gesture classification algorithms were implemented: a tree-based classifier ensemble based on gesture trajectory features, and a modified Longest Common Subsequence (LCS) classifier. The system was implemented using a standard home theater streamer.

While system feasibility was clearly demonstrated the requirement of adhering to the existing interface was very limiting. The displays were originally developed for hand-held remote operation. Using the same displays for gesture-based control prevented full exploitation of the usability facilitated by gesture-based interfaces.

GRS FOR TELE-OPERATION

A sensor-glove based system was developed for tele-operation of a robotic manipulator (Berman et al. 2008). Maintaining a spatial resemblance between human and robotic motion is problematic when the structure of the robotic system is considerably different from that of the human. In order to harness the high level task understanding capabilities of the human while alleviate the burden of translating the required actions to those feasible for the robotic system an object-action abstraction was implemented. Such an abstraction is in-line with current finding on manipulation task representations in the central nerves system (CNS). Human actions in a virtual environment were recognized based on hand and arm motion and the object on which they were performed. A robotic grasp suitable for the object and recognized action was selected from a set of a-priori programed grasps. The object motion trajectory was formed based on the demonstrated trajectory.

The approach feasibility was demonstrated for control of a five degree of freedom serial manipulator. The tasks performed included building a block tower, pouring from a jar and screwing/unscrewing jar lids. Users unfamiliar with robotic operation succeeded in performing the missions, yet their performance improved over time as they gained understanding of

system operation. That is the users did learn interface specific knowhow that aided them in attaining improved operation.

SUMMARY AND FUTURE RESEARCH

Gesture-based interfaces offer a highly natural modality for HCI. Available low-cost sensors today facilitate fast development of GRS for various applications. GRS have both hardware and software component with a multitude of different implementation options. Understating GRS operation and the different alternatives is important for implementing a high quality interface.

ACKNOWLEDGEMENTS

This work was supported in part by Deutsche Telekom AG and by the Paul Ivanier Center for Robotics Research.

REFERENCES

Aggarwal J.K. and Park, S. 2004. "Human motion: Modeling and recognition of actions and interactions". *in Proc. 2nd Int. Symp. 3D Data Process., Vis., Transmiss*., 640–647.

Berman, S. Friedman, J., Bakır, G. and Flash, T. 2008. Action Identification for Teleoperation Based on Object - Action Abstraction, *IEEE SMC International Conference on Distributed Human-Machine Systems (DHMS)*.

Berman, S. and Stern, H. 2012. "Sensors for Gesture Recognition Systems", *IEEE Transactions on Systems, Man, and Cybernetics-Part C* 42(3), 277-290.

Garg, P. Aggarwal, N. and Sofat, S. 2009. "Vision based hand gesture recognition*". in Proc. World Acad. Sci., Eng. Technol*. 49, 972–977.

Frolova, D., Stern, H. and Berman, S. 2012. "Most Probable Longest Common Subsequence for Recognition of Gesture Character Input". *IEEE Systems Man and Cybernetics, part B, September (in press)*.

Mitra S. and Acharya, T. 2007. "Gesture recognition: A survey". *IEEE Trans. Syst., Man, Cybern*. 37(3), 311–324.

Rautaray, S.S. and Agrawal, A. 2012. "Vision based hand gesture recognition for human computer interaction: a survey". *Artificial Intelligence Review*, 1-54.

Stern, H., Frolova, D. and Berman S., 2010. Hand Gesture Recognition for TV Remote Control using Tree-Based Ensemble and LCS Classifiers, *WORLDCOMP'10 The 2010 World Congress in Computer Science, Computer Engineering, and Applied Computing*.

Stern, H., Shmueli, M. and Berman, S. 2013. "Most Discriminating Segment - Longest Common Subsequence (MDSLCS) Algorithm for Dynamic Hand Gesture Classification". *Pattern Recognition Letters* (Special issue on 'Smart Approaches for Human Action Recognition'), (in press).

Wachs, J., Kolsch, M., Stern, H. and Edan, Y. 2011. "Vision-based hand gesture applications: Challenges and innovations". *Commun. ACM* 54(2), 60–71.

Yilmaz, A. Javed, O. and Shah, M. 2006. "Object Tracking: A Survey". *ACM Comput. Survey* 38(4), 1–45, 2006.

AUTHOR BIOGRAPHIES

SIGAL BERMAN is a lecturer and head of the intelligent system M.Sc. track in the Department of Industrial Engineering and Management at the Ben-Gurion University of the Negev, Beer-Sheva. She received a M.Sc. in Electrical and Computer Engineering, and a Ph.D. in Industrial Engineering, both from Ben-Gurion University of the Negev, and a B.Sc. in Electrical and Computer Engineering, from the Technion, Haifa; Dr. Berman was the primary investigator of the gesture recognition for remote control user interface project for Deutsche Telekom laboratories at BGU. Her research interests include: robotics and motor control, computer integrated manufacturing, and human machine interfaces. Her e-mail address: sigalbe@bgu.ac.il and her Web-page can be found at http://www.bgu.ac.il/~sigalbe.

Invited Talks
for
Computational Neuroscience

On modeling and sampling complex systems

Matteo Marsili

The study of complex systems is limited by the fact that only few relevant variables are accessible for modeling and sampling. In addition, empirical data most often undersample the space of possible states. We discuss the consequences of this in a simple framework inspired by maximum entropy considerations. Our arguments suggest that models can be predictable only when the number of relevant variables is less than a critical threshold. Within our framework, the undersampling regime can be distinguished from the regime where the sample becomes informative of system's behavior. In the undersampling regime, the most informative frequency size distributions have power law behavior and Zipf's law emerges at the crossover between the undersampled regime and the regime where the sample contains enough statistics to make inference on the behavior of the system. These ideas are illustrated in some applications, showing that they can be used to identify relevant variables or to select most informative representations of data, e.g. in data clustering.

Proceedings 27th European Conference on Modelling and Simulation ©ECMS Webjørn Rekdalsbakken, Robin T. Bye, Houxiang Zhang (Editors)
ISBN: 978-0-9564944-6-7 / ISBN: 978-0-9564944-7-4 (CD)

Olfaction as probabilistic inference

Peter Latham

Inferring what odors are in the air is a hard problem, for at least two reasons: the number of odorant receptor neurons (the first neurons in the olfactory pathway) is smaller than the number of possible odors, and multiple odors can be present at once. Consequently, even if there is a simple mapping from odors to odorant receptor neurons that mapping cannot be uniquely inverted. Presumably, the brain solves this problem by computing the probability that any particular odor is present. We present an inference algorithm that does this, discuss how it maps onto olfactory circuitry, and comment on what we learn about sensory processing in general.

Proceedings 27th European Conference on Modelling and Simulation ©ECMS Webjørn Rekdalsbakken, Robin T. Bye, Houxiang Zhang (Editors)
ISBN: 978-0-9564944-6-7 / ISBN: 978-0-9564944-7-4 (CD)

Agent-Based Simulation

Personality Simulation in Interactive Agents Through Emotional Biases

José Serra
Instituto de Telecomunições – Porto
Rua Dr. Roberto Frias
4200-465 Porto, Portugal
jserra@dcc.fc.up.pt

Pedro Nogueira
Artificial Intelligence and Computer Science Laboratory – Porto
Rua Dr. Roberto Frias
4200-465 Porto, Portugal
pedro.alves.nogueira@fe.up.pt

KEYWORDS
Emotions, personality simulation, BDI, cognitive simulation, framework.

ABSTRACT

Personality simulation has been for the past decades a recurrent topic, as it is a non-trival problem where a multitude of equally valid approaches can (and have) been taken. However, no general consensus has emerged from this discussion, which further difficults novel contributions. Being a multidisciplinary research topic between computer science and psychology further complicates the aforementioned issue, as a large number of models for emotion definition currently exist. Thus, methods capable of simulating the variations that occur at an emotional level due to personality and at the same time provide an easy way to define behavior are still lacking. In this paper, we propose the usage of emotions as the prime factor in the personality definition process, which is done using a height-map that represents a gravity field to define the emotional biases that each individual's personality encompasses. The use of this model eases the definition of how the emotional variations occur. We propose a novel architecture, which is capable of receiving and produce any kind of stimuli and reaction. The method was implemented as a proof-of-concept and initial tests show it is effective, behaving as expected.

INTRODUCTION

Emotions play a crucial role on peoples lives, influencing their social interactions reactions to external stimuli both consciously and unconsciously. This phenomenon occurs due to emotions' nature as complex psychophysiological experiences of an individual, which influenced by a state of mind, arise as the result of interacting biochemical reactions and environmental interactions. As they occur at a deep and sometimes instinctual or subconscious level, emotions influence humans in a very meaningful and critical way, often overriding even rational thought. In fact, emotions influence many aspects of the mental process, such as decision-making, planning, memory and attention (Berkowitz 2000), thus being crucial for human intelligence (Bower and Cohen 1982) and largely guiding how people adapt their behaviour to the world around them. Damasio has shown that people which lack emotional responses to stimuli, make poor decisions that can affect their integration in society (Damasio 1994]. As a result, when simulating human-like interactions with an environment it is necessary to take into account the influence of emotions when choosing adequate courses of action.

An agent is an entity that receives inputs, usually from a sensor or set of sensors, analyses them and chooses an action according to some model or ruleset. In the case of humanoid agents, if the chosen action is always determined by a non-stochastic mechanism i.e. reacting in a nil entropic manner, the simulation will not be realistic. This is extremely important in areas such as crowd-simulation or video-games, where the chosen behaviours should be as realistic, coherent and believable as possible. If the behaviour selection mechanism does not take this into account, the simulation will, at some point, inevitably fail. This breakes the illusion of a realistic system and ultimately leads to an awkward and unengaging interaction with the player. Thus, it is crucial to model the emotional component when simulating human behaviours.

In this paper we propose a method for simulating a personality based on emotional biases as a means for simulating a believable emotional component in an agent's behavior. In our model, each agent's state is defined by its current mood, i.e. the emotion it has at a specific step in the simulation. This mood is modified by the occurrence/perception of external stimulus. Each stimulus has an associated emotional weight that determines how each one influences the current mood. However, the main feature of our model is that the aforementioned stimuli do not act in a linear fashion, as their effect on each agent depends on the agent's personality. This personality represents the agent's emotional biases, i.e. if an agent has a tendency towards positive emotional states and a negative emotional stimulus is given, the stimulus's impact on the mood will be reduced. Conversely, an agent with a negative bias would interpret the stimuli in the opposite manner. Thus the agents' mood converges to a specific range of emotional states depending on his personality. The suggested approach is based on a novel methodology to define personalities through the use of height-maps, where the height value of each mood is directly correlated to its influence on the provided stimuli. Based

Proceedings 27th European Conference on Modelling and Simulation ©ECMS Webjørn Rekdalsbakken, Robin T. Bye, Houxiang Zhang (Editors)
ISBN: 978-0-9564944-6-7 / ISBN: 978-0-9564944-7-4 (CD)

on the similarity to the current mood and its own predefined mood, the agent reacts to the stimuli by choosing an action. The created method is completely focused on the emotion selection and calculus based on the influence of the personality and the emotional weight of the perceived stimuli. In sum, the method is capable of automatically - and without the common necessity to define all possible emotion-stimulus combinations - model the emotions and behaviours of an agent by taking into account the influence of the current emotion and given stimulus.

This paper's remaining sections are organized as follows: the state of the art describes the current research in emotional-based behaviour and some of the currently accepted emotional models, on which we base our system's internal emotion representation. The method description specifies how the agent is configured and the calculus of the emotional state after an external stimulus occurs. The proof of concept section describes the model's prototypical implementation and discusses the results obtained so far. Finally, the last section presents our conclusions and future work plans.

STATE OF THE ART

Emotion modelling significantly influences the believability of an agent. As result this is an active research topic in the field of artificial intelligence (Guojiang et al. 2010, Hu et al. 2010). Most emotional models are based on the psychological understanding of emotions, being important to note that, so far, there is no universally accepted theory. Hu et al. states that, from a psychological perspective, emotions are evaluations of the relation between oneself and his surrounding environment. The emotional reaction is generated by external stimuli and affected by the demands and requirements of each individual. From an agents' perspective, emotions are the evaluations and reactions that are based on its internal state and the relation of its desires and plans towards an exterior environment (Hu et al. 2007]. Thus, the model sees emotions as the result of the cognitive process. An example, of such a theory, is the OCC model (Ortony 1988, Steunebrink et al. 2009), which admits the existence of 22 separate emotions and categorises them according to the agent's circumstances and situations. This division is performed based on the positive and negative factor (valence) of emotions that result from specific events and the interactions with other agents and objects. In our model, we concentrate on the agent's emotional state as a means of altering its analysis and judgment of each possible action, the process through which it selects the most appropriate one to suit its desires or goals.

For a broader understanding of our model, consider the classic Belief-Desire-Intention (Rao1 and Georgeff 1995) model extended with the OCC model of emotion, presented in Figure 1 from (Parunak and Bisson 2006).

The agent's Analysis of its current state is fed by its Beliefs, which are inferred from the environment by its sensors (Perception), and its Desires, which may or may not change over time. In turn, this analysis leads the agent to an Intention, through which it interacts with the environment. In the extended BDI model, Beliefs also feed an Appraisal process that alters the agent's current emotional state. This emotional state may then influence the agent's Perception of the observed environmental stimuli, his analysis of it, or both. In our work, we deviate from the OCC model, using Russel's model instead to continuously model emotion and allow the agent's emotional state to affect its Perception of the environment. In turn, this re-interpretation of the environment affects the agent's Beliefs and ultimately, its Analysis of the current situation. Parallel to this, we also allow the agent's Emotion to directly affect its Analysis. In our experiments this is done by imposing an emotional stress tolerance that the agents may not exceed when choosing how to interact with the environment. For a more comprehensive description, we refer the reader to the proof of concept section, where we detail the created environment and the agent's perception and interaction with it.

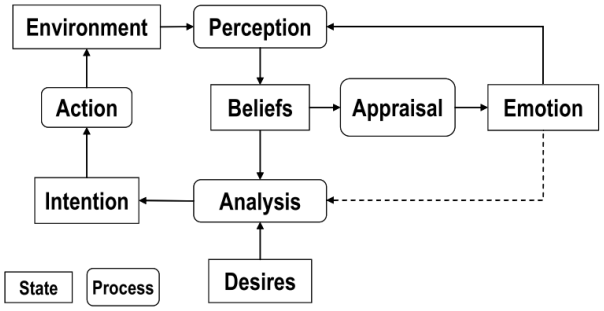

Fig. 1. BDI enhanced with OCC, adapted from (Parunak and Bisson 2006).

Computational Models of Emotion

It is also important to note that emotions are classified according to two (Guojiang et al. 2010) categories, which are associated with different theories: the basic emotions theory, such as described by OCC and Ekman (Ekman and Friesen 1971) and the dimensional theory, where emotions are classified according to a coordinate system. An example of the latter is presented by Russel (Russel 1991). In this model, emotions are represented in a two dimensional referential, where the abscissa represents arousal and the ordinate is associated to valence (the hedonic component) (Russel 1991). An illustrative diagram, extracted from (Guojiang et al. 2010) is shown in Figure 2. Another example of the dimensional theory is Plutchik's emotion wheel (Plutchik 1980), also shown in Figure 2. In this model, the vertical axis represents each emotions' intensity and the circular component represents the similitude between them. Due to the familiarity and ease of computation presented by Russell's model cartesian plane, it has been widely accepted by computer

scientists, being one of the most popular computational models of emotion.

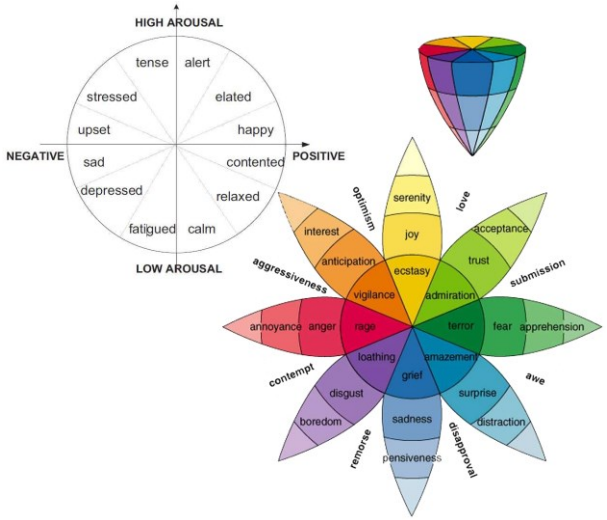

Fig. 2. Two dimensional emotional classification models. On the left is the Russel model (Russel 1991). only with two dimensions. On the right is the Plutchik three dimensional model (Plutchik 1980).

Emotion Simulation Mechanisms

Traditionally, the creation of artificial agents relies mostly on the definition of a rule-set that guides the agent's behaviour and its action decision mechanism(s). In fact, this is still the most common and accepted approach in various applied/industrial research applications and multimedia industry, where the virtual characters are controlled using scripting, finite-state machines and/or visual logic representations, such as graphs. However, this approach usually leads to stiff behaviours, i.e. always following the same patterns, which inflicts a negative impact on the player experience. As a result, suspension of disbelief is broken by inadvertently gaining insight to the agent's logic mechanism(s). This leads to lessened enjoyment and believability factors and ultimately shallower immersion levels (Nacke and Lindley 2010), all of which are essential aspects of the gaming/multimedia experience, thus presenting a critical issue. Consequently, work has been done with models capable of realistic behaviour in view.

A recently popular method of solving the behaviour repetitiveness is to add a fuzzy layer, thus introducing a certain degree of entropy to the behaviour selection process. However this may lead to behavioural incoherences if the entropy levels are not kept in check. In order to avoid this issue, formal rule verification mechanisms must be employed, resulting in an overly-complex and costly development cycle. An also popular alternative is to add emotion-simulation to the action-selection mechanism. Hu. et al attempted this by adding emotions to the BDI model (Hu et al. 2007). Their goal was achieving time-coherent action choices, where the choices were based on previous ones.

Chown et al. proposed a cognitive architecture (Chown et al. 2002) that used emotions to influence the decision making process. However the emotion representation was not quantified, thus making it difficult to create a real-world applicable application. In (Hu et al. 2010), the authors also used emotions to influence the action selection process. In their case, emotions were divided into: cognitive (based on the OCC model), expected and reflex. Gratch addressed the problem of simulating the emotional appraisal (Gratch 2000), which refers to the emotion that results not only from an external stimuli but that also takes into account the agents plans and goals. Guojiang et al. proposed a method that defines the emotions with the Russel model and combines them with motivations and behaviour decisions based on the Markov Decision Process (Guojiang et al. 2010). Finally, Bryson and Tanguy defined a framework for creating behaviour (Bryson and Tanguy 2010) specifically thought for the easy definition of virtual intelligent actors. In this work the emotions have onsets, sustains and decays, which is extremely important when simulating lasting emotions. They also added moods that reflect a general state of mind over a longer period of time than that exhibited by emotions.

The main problem with the current models is the difficulty associated with controlling the way the emotions are influenced by external stimuli, usually requiring the user to define a set of parameters that directly control the weights of each one. The proposed work is based on a bi-dimensional emotion model used to define agents' personalities, which control the emotional variations that an external stimulus induces in the current emotional state. Besides presenting a simple method for defining emotional behaviour, our method also offers a seamless integration with existing architectures (e.g. BDI), such that its integration in novel work and subsequent comparison is straightforward.

METHOD

The presented method has the main goal of simulating the changes that occur in the emotional component of the human behaviour when an external stimuli occurs. The method relies on Russel's bi-dimensional representation of emotions (Russel 1991) to define and control the agent's personality and current emotion, which are associated to the given stimuli and current mood. The feature space is circular to maintain all points comparable based on their distance to the origin. Thus, each emotion is defined as a two coordinate set in this Cartesian plane. The architecture is divided in three layers: the input abstraction layer, responsible for the mapping between the stimuli and their emotional weights, the stimuli evaluation layer (SEL), that keeps track of the agent's emotion and alters it according to the observed stimuli and personality, and the output

abstraction layer, in charge of the action decision process. The described architecture can be seen in the Figure 3.

The input abstraction layer defines the mapping between the external stimuli and their emotional weight. Like emotions, the weight is defined by two coordinates in the emotional feature space. A stimulus is an abstract entity and can thus represent anything from social interactions to abstract sensory stimuli, such as an image or sound, as long as it has the two coordinates associated. It is also necessary to take into account that in the real-world stimuli do not usually occur in an isolated manner. Therefore, in the case of multiple concurrent stimuli there are (at least) two possible approaches. The first one is to simply consider the event as a sequence and sequentially feed them to the emotional response layer. The second alternative is to combine them according to their weights and create a new emotional weight. However, these two approaches are not equivalent, as in the former each stimuli would be analysed differently taking into account the result of the previous ones. On the other hand, the latter approach equates to applying only one stimuli. More formally, the emotional weight of a linear combination of stimuli is not necessarily equal to the individual sum of their weights. As such, caution is advised when selecting an alternative. Since the proposed method only takes an emotional weight it is up to the user to define how they are obtained and pre-processed.

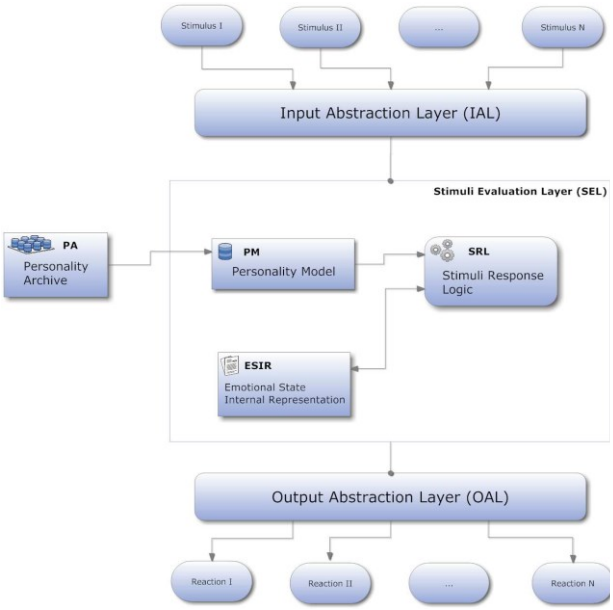

Figure 3: Architecture of the proposed system divided in three layers: on top, the input abstraction layer (IAL), with the mapping between the stimuli and emotional weights, the stimuli evaluation layer (SEL) that has the agent's emotion and alters it according to the observed stimuli and personality, and the output abstraction layer (OAL) that decides the action.

The agent's emotional response is the Stimuli Evaluation Layer's (SEL) responsibility. This layer contains the Emotional State Internal Representation (ESIR), describing the agent's current mood, i.e. its current emotion and personality model (PM). In fact, the way the personality is defined and how it affects the mood is the core component of the layer, also being the main contribution of the present article. An agent's personality is defined through an height-map, such as shown in Figure 4. The concept of height-map is usually associated with computer graphics, where it is used to represent the height of a terrain or texture, based on the brightness of each pixel. In the presented method, these brightness values represent the force that each vally in the height-map exerts on the perceived stimuli. A simple metaphor would equate this force to a gravitational pull towards a gravity well (the aforementioned valley). This gravitational pull influences the perception the agent has of the stimuli by simulating his emotional bias towards a specific emotion or group of emotions. In reference to Figure 4, the darker an area is for a corresponding area of the emotional space, the more it pulls the stimulus emotional vector towards it. As a result, if a stimulus tries to move the agent's current mood away from a gravity well, the stimulus's strength will be reduced, representing the countering gravitational vector. On the other hand, if the stimulus is in the same direction as the gravity well, the stimulus strength will be increased. Several personalities can be defined in the Personality Archive (PA) and each agent has only one associated with it, at each given time. An example can be seen in Figure 4.

A personality valley (or gravitational well, if using the gravitation analogy) is defined by its center coordinates, height, radius and by the definition of how the height at each point varies. There are multiple ways to define such height variation, it is possible to simply obtain the height based on a linear variation obtained from the distance to the center, or based on a gaussian distribution. It is up to the user to define how the height is obtained based on the previous parameters. In Figure 4 the variation from the valley's center follows a Gaussian distribution.

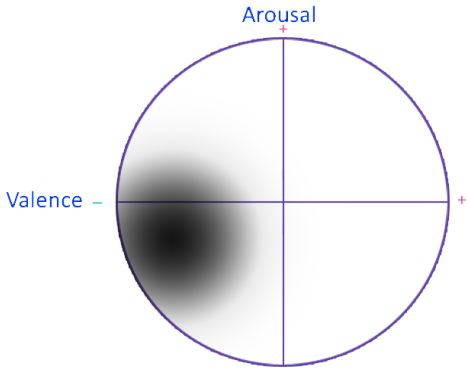

Figure 4: An example of a personality height-maps of a typical depressive person that after becoming sad it is hard to change to another emotional state.

The change of the current mood is done within the Stimuli Response Logic, SRL and is based on formula (1), where the m_c represents the current mood's value, defined by its two coordinates. This value is summed to the influence of the nearest personality valley, obtained from the multiplication of the v_d, i.e. the vector from the current mood to the center of the valley, and the height h_c of the current mood, given by the distribution function. In the case of the m_c being exactly in the middle of two or more personality valleys, the vd is the cross product of all the vectors that originate from the mc to each valley. It is important to note that the closer the current mood is from the valley center, the smaller the vd is and the higher is hc, thus influencing it more. Finally, it is also necessary to add the influence of the stimulus emotional weight s_w, which is multiplied by the inverse of the current h_c. With this formula, the current mood is changed based on the stimulus and the personality.

$$m_n = m_c + v_d * h_c + s_w * (1 - h_c) \quad (1)$$

SEL outputs the new current mood each time a stimulus is received, which is then passed to the Output Abstraction Layer (OAL). This layer is responsible for the choice of the agent's behaviour, as a reaction to the provided stimulus. There are multiple ways to choose an action based on the current emotional state; however they usually have a common dictionary that translates a space coordinate to the desired action. Usually, action decision mechanisms rely on the creation of an emotion-to-action dictionary. Some examples in this domain are: choose the action based on the distance from the current mood to the emotional coordinates of the actions defined in the dictionary since, like the stimuli, actions have to be defined with 2 dimensional coordinates. It is then just a matter of calculating the euclidean distance to all the actions and choosing the one that is nearest. Another option is to define areas for each action in the feature space and choosing the one that has the current mood inside it. A third option is the obtain the action directly from the current emotion through a parameter interpolation technique, which is useful e.g. when generating a 3D character expression from the current mood.

PROOF OF CONCEPT

The proposed architecture was implemented in C++ and validated by analysing the variations produced in the agent's emotional state by a stimuli set. The tests were performed on 2 personality models and for a series of 500 and 1000 random stimuli chosen from the game event dictionary. The emotional variations associated with the depressive personality are presented in the form of a scatter graphic shown in Figure 5.

Discussion

The graphics show that the current emotion tends to converge to the personality valleys previously defined. However, this does not prevent the current emotion from moving outside each valley's influence radius, thus converging to the personality valleys. It is then possible to conclude that the personality model successfully influences the agent's emotional states in the intended way. However, as seen in Figure 4, these initial tests revealed an interesting issue with the proposed model: the high concentration on the limits of the circumference. This phenomena is easily attributed to two causes: one of human error and a second central to the model itself. The first of these, was that the manually created stimuli were too high (in the range of 0.3 and 0.6 Arousal or Valence units), which means that if a current emotion is already near the limit, it will attempt to exceed it and thus clipping occurs. The other problem is a consequence of not simulating the emotional decay that occurs over time, i.e. as time passes after even a strong stimuli, its effect will degrade and thus becomes less effective in influencing the current emotion, resulting in the current emotion decaying either to a neutral emotional state or to the personality's main tendency. As this is not simulated the current emotion always stays at the limit until an opposite stimuli is perceived. It is also important to note that in our tests generated stimuli's distribution is completely random. However, this may not be the case in reality, as most experiences have a limited range of emotional states which they eleicit (their emotional spectrum, so to speak). For example, when watching a horror movie, it is unlikely that positively valenced stimuli arise. Therefore, this must also be taken into account when interpreting these results or trying out new personalities for specific case studies.

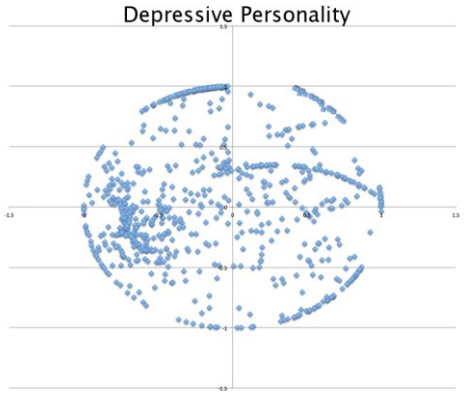

Figure 5: Personality model for a depressible person and scatter graphic after 1000 randomly chosen stimuli from the dictionary. The scatter graphic shows the distribution of the emotional variations, based on the personality model, that occur after all the stimuli were applied.

CONCLUSION & FUTURE WORK

Throughout this paper three main contributions were presented. The first one was PERSONA, which proposes a novel architecture for personality-based emo tional response simulation. Secondly, the input and output abstraction layers provide a transparent and powerful abstraction of stimuli and their elicited reactions. Finally, and at the core of these three contributions, a simple personality-definition method through the use of height-maps, was invented.

The variations induced by this approach were tested at section 4, validating it as a proof of concept, however further tests are needed. The mood distribution tests showed that the given a random distribution of stimuli, the agent did tend to interpret them according to his personality model, while the trajectory tests proved that our influence model adequately influenced the given stimuli. Thus, it was proven that the proposed method is capable of describing the psychological tendencies that compose a personality, therefore being able to adequately simulate it's responses. Some examples of uses of the abstraction layer were given as a way to point into practical uses of the proposed approach, thus we believe that in synchrony with an agent they are a versatile and powerful tool that has real-time in further applications.

The validation tests did however point-out that since the agent has no notion of time, he remains on the elicited emotional state until elicited otherwise, which means he will easily reach the maximum emotional charge allowed. Performing a further analogy to the real world, this is as if all the stimuli were given almost instantaneously to someone, all the while not letting them process the information and emotionally straining them. This issue will be addressed in the future work through the implementation of a stimuli timestamp and an emotional decay function over a time axis. Other aspects that need consideration include: a GUI for increased interaction ease, as defining a personality solely on parameters is time-consuming and error-prone, and the increased versatility of an height-map definition through a mesh instead of Gaussian mixtures. As a final statement, the authors would like to point out that although the proposed approach does not consider all the possibly available information in a real-world scenario (nor does it strive to), both the proposed architecture and imbued agent logic have shown themselves capable of modelling individuals' personalities through emotional responses.

ACKNOWLEDGEMENTS

The authors would like to thank Instituto de Telecomunições – Porto and Artificial Intelligence and Computer Science Laboratory for hosting and supporting their respective PhDs research. They also acknowledge the Portuguese Foundation for Science and Technology (FCT) for fully funding the aforementioned PhD research under the scholarships: SFRH/BD/79905/2011 and SFRH/BD/77688/2011.

REFERENCES

Berkowitz, L. 2000. *"Causes and consequences of feelings."* Cambridge Univ Pr. 2000.

Bower, G. and Cohen, P. 1982. *"Emotional Influences in Memory and Thinking: Data and Theory"*. Affect and Cognition. M. Clark and S. Fiske. London, Eds.: Lawrence Erlbaum Associated Publishers.

Bryson, J. and Tanguy, E. 2010. *"Simplifying the design of human-like behaviour: Emotions as durative dynamic state for action selection"*. International Journal of Synthetic Emotions.

Chown, E.; Jones, M. and Henninger, A. 2002 *"An architecture for emotional decision-making agents,"* Proceedings of the first international joint conference on autonomous agents and multi-agent systems.

Damasio, A. 1994 *"Descartes error: emotion, reason and the human brain"*. Avon Books.

Ekman, P. and Friesen, W. 1971 *"Constants across cultures in the face and emotion"*. J. Personality and Social Psychology.

Gratch, J. 2000. *"Smile: marshalling passions in training and education"*. In proceedings of the Fourth International Conference on Intelligent Agents.

Guojiang, W.; Xiaoxiao, W. and Kechang, F. 2010. *"Behavior Decision Model of Intelligent Agent Based on Artificial Emotion"*. Advanced Computer Control (ICACC).

Hu, J.; Chen, Y. and Guan, C. 2007. *"Emotional Agent Based on Rough Set"*. Computational Intelligence and Security Workshop.

Hu, J.; Yin, Q.; Feng, L. and Deng, H. 2010 *"A Computational Architecture for Modeling Emotional Behavior in Synthetic Agent"*. Computer Modeling and Simulation, (ICCMS)

Nacke, L. and Lindley, C 2010 "*Affective Ludology, Flow and Immersion in a First- Person Shooter: Measurement of Player Experience"*. Loading...: The Journal of the Canadian Game Studies Association.

Ortony, A.; Clore, G. and Collins, A. 1988 *"The Cognitive Structure of Emotions"*. Cambridge University Press, Cambridge, UK.

Parunak, H. and Bisson, R. 2006. "A Model of Emotions for Situated Agents". AAMAS '06, Proceedings of the fifth international joint conference on Autonomous Agents and MultiAgent Systems, pp: 993-995.

Plutchik, R. 1980. *"A General Psychoevolutionary Theory of Emotion"*. Emotion: Theory, research, and experience. New York Academic.

Rao, A. and Georgeff, M. 1995 "*BDI-agents: From Theory to Practice*", In Proceedings of the First International Conference on Multiagent Systems (ICMAS'95),

Russel, J. 1991. *"Culture and the Categorization of Emotions"*. In Psychological bulletin.

Steunebrink, B.; Dastani, M., and Meyer, J. 2009 "*The OCC Model Revisited".* In Proceedings of the 4th Workshop on Emotion and Computing: Current Research and Future Impact.

AUTHOR BIOGRAPHIES

JOSÉ SERRA José Serra, born in 1988, is a Ph.D. student in MAP-i Doctoral programme. He is currently being advised by Verónica Orvalho from University of Porto and Miguel Sales Dias from Microsoft (MLDC). His work deals with combining procedural facial animation with artificial intelligence to create a fully automatic facial animation system based on external stimuli. He has previously worked on the NECO (NEtwork COding) simulator, which was integrated in the N-Crave project and is available online for download. He has also worked on the issue of automatically animating a speech based on an audio input as part of his MSc thesis, within the scope of the LIFEisGAME project. Other interests include human computer interaction, artificial intelligence, physics and security. His e-mail address is : `jserra@dcc.fc.up.pt` and his web-page can at `http://www.dcc.fc.up.pt/~jserra`.

PEDRO NOGUEIRA is a Ph.D. student at the

Artificial Intelligence and Computer Science Lab in Portugal and the HCI and Game Studies Group in the University of Ontario's Institute of Technology. He is co-supervised by Prof. Eugénio Oliveira and Prof. Rui Rodrigues at the University of Porto, Prof. Lennart Ncake at the University of Ontario. Before starting his Ph.D. studies, Pedro has worked in various European research projects. His work has ranged from conceptualizing and prototyping usable biometric monitoring systems for high-risk emergency scenarios, to developing intelligent biomedical image annotation algorithms for drug research. His current work focuses on the study of how user's gameplay experience is affected by emotional state variations and how these can be enforced to produce more immersive and enjoyable experiences. To this end he is working on methods to determine players' reactions to specific game events, which can be collated into time-evolving, self-adapting affective reaction profiles. His final goal is to use these user-independent profiles to provide a biofeedback loop with the necessary information on how it should plan future interactions, effectively implementing an automatic, data-driven regulation of the user's affective experience. His current institutional e-mail address is: `pedro.alves.nogueira@fe.up.pt`.

SIMULATION OF INCENTIVE MECHANISMS FOR RENEWABLE ENERGY POLICIES

Andrea Borghesi and Michela Milano
DISI University of Bologna, Italy
michela.milano@unibo.it
Marco Gavanelli
ENDIF University of Ferrara, Italy
marco.gavanelli@unife.it
and Tony Woods
PPA Energy, UK
tony.woods@ppaenergy.co.uk

KEYWORDS

Policy modeling; Social simulation.

ABSTRACT

Designing sustainable energy policies has a strong impact on economy, society and environment. Beside a planning activity, policy makers are called to design a number of implementation instruments to enforce their plans. They encompass subsidies, fiscal incentives, feed in tariffs to name a few. Understanding the impact of these instruments on the energy market is essential to select the most efficient one. We propose in this paper a multi-agent simulator that mimics the adoption of photovoltaic as a consequence of a number of implementation instruments. The simulator mainly considers economic evaluations in the agent decision-making procedure, but we are aware also social aspects play an important role and they are subject of current research.

INTRODUCTION

Following the strategy outlined in [Europe, 2020], the EU growth strategy for the coming decade - the EU is strongly committed to reducing its greenhouse gas emissions by at least 20% by 2020, relative to 1990 levels, increasing the share of renewable energy sources in final energy consumption to 20% and increasing energy efficiency in Europe by 20%. To drive progress and set the EU on a pathway towards meeting these targets, every country and every region should be committed to providing its own contribution to these objectives.

Therefore, national and regional energy policies need to take account of these guidelines and be designed to meet these ambitious objectives. With a view to achieve the 20% renewable energy target in the EU by 2020, the Renewable Energy Directive establishes legally binding individual targets for the share of renewable energy in final energy consumption for each Member State. E.g., Italy is supposed to reach a 17% renewable energy share, UK 15% and Austria 30%.

To achieve these objectives, each country and, in some cases, regions are implementing a number of actions focused on the promotion and wide adoption of energy production from renewable energy sources. An important class of such energy policy instruments are incentives. There are a number of incentive mechanisms used in various EU member countries and some of these will be outlined in next Section. Examples of such incentives include investment grants (incentives to construct energy plants), feed-in tariffs (money given to produce and/or self-consume renewable energy), and fiscal incentives (low interest loans and many others). However, the effectiveness of these mechanisms is not clear. By analysing past data one conclusion that has emerged is that there is some evidence that a greater effect at lower cost may be achieved by a stable feed-in tariff regime that is sustained over a significant period. As a result of this, many countries have adopted feed-in tariffs as the basic incentive mechanism. In addition, certain regions have implemented other incentive mechanisms to further support renewable energy adoption. In this paper we focus on the Italian context, by considering national mechanisms and comparing different regional instruments implemented in the Emilia-Romagna region of Italy.

This paper has a particular emphasis on renewable energy sources and, specifically on photovoltaic (referred to as PV) power generation. We have analysed a number of incentive mechanisms for promoting the adoption of PV in Emilia-Romagna and simulated them from an economic perspective in order to understand their efficiency. We have utilised agent-based simulation [Troitzsch et al., 1999], [Matthews et al., 2007], [Gilbert, 2010], where agents represent the key players involved in the decision-making process. The hypothesis is that for modelling complex systems, agent-based simulation is a suitable approach to understand such systems in a more natural way. We are aware that not only economic aspects should be considered. We have analysed two social aspects, but recognise that the one

Proceedings 27th European Conference on Modelling and Simulation ©ECMS Webjørn Rekdalsbakken, Robin T. Bye, Houxiang Zhang (Editors)
ISBN: 978-0-9564944-6-7 / ISBN: 978-0-9564944-7-4 (CD)

we propose is far from being a social simulator.

We have developed an agent-based simulator in Netlogo [Sklar, 2011] implementing both national and regional incentives and have compared the efficacy of regional incentives regarding PV adoption. We have considered feed-in tariffs as national incentives (Italian incentives derived from the *Quarto Conto Energia*, Fourth Feed-In-Scheme [Ministerial Decree, 2011]. In addition to these national incentives, we have considered four alternative regional incentives, namely investment grants, fiscal incentives, interest funds and guarantee funds. We will explain these incentives in detail and will show the results of the economic simulator.

From an economic perspective, it could be concluded from this study that the interest fund is the most efficient, followed by fiscal incentives and guarantee fund which appear to have a similar impact. The least effective instrument is the investment grant, the only mechanism so far implemented by the Emilia-Romagna region to foster PV adoption.

INCENTIVES TO RENEWABLES

We have surveyed the types of incentives utilised to promote renewable energy in the EU and around the world. A number of categories have been identified:

Feed-in tariffs A feed-in tariff is a fixed and guaranteed price paid to the eligible producers of electricity from renewable sources, for the power they feed into the grid.

Premium In a feed-in premium system, a guaranteed premium is paid in addition to the income producers receive for the electricity from renewable sources that is being sold on the electricity market.

Quota obligation Quota obligations create a market in the provision of renewable electricity. The government creates a demand through imposing an obligation on consumers or suppliers to source a certain percentage of their electricity from renewable sources.

Investment Grant grants for renewable generation are often devised to stimulate the take-up of less mature technologies such as PV.

Tax exemptions Some countries provide tax incentives related to investments (including income tax deductions or credits for some fraction of the capital investment made in renewable energy projects, or accelerated depreciation). Other approaches are production tax incentives that provide income tax deduction or credits at a set rate per unit of produced renewable electricity, thereby reducing operational costs.

Fiscal Incentives This category includes soft loans, i.e., loans with a rate below the market rate of interest. Soft loans may also provide other concessions to borrowers, including longer repayment periods or interest holidays.

Compulsion A more radical approach would involve compulsion. Whilst no examples have been identified in the renewable generation market, similar situations have been noted: in some urban parts of Scandinavia it is a legal obligation for newly constructed homes to be connected to the local heat network.

Green Power marketing Under this arrangement, electricity customers can choose to buy electricity which is sourced partially or wholly from renewable sources. Typically they pay a premium compared to other available tariffs. Sometimes standards need to be set to ensure that sufficient and appropriate renewable generation is supporting the product.

The various categories listed above are not necessarily mutually exclusive so that more than one policy instrument may be in use at the same time.

These various incentive schemes can also generally be characterised as either

- **Production-based incentives** where the benefit of the scheme is related to the amount of energy generated. This includes feed-in tariffs and quota obligations. The features of such arrangements may include:

  Technological differentiation as different renewable technologies are at varying levels of development and cost levels in relation to existing market prices there is a risk of "free riding" (i.e., a potential ongoing windfall benefit) for technologies that are close to being economic in the absence of subsidy if only one support level is provided to all technologies. Thus increasingly technological differentiation has been introduced into the support mechanisms used.

  Inflation adjustment the level of support (i.e. feed-in tariff price) may vary in line with inflation.

  Digression the level and availability of support may be varied according to take-up. Thus if such take-up is large then the support may be curtailed. Whilst this sometimes happens by unexpected Government decisions, arrangements are increasingly being established during the design of the incentive mechanism.

  Own-use arrangements for feed-in tariffs there may be differences in the rate paid for electricity used on the premises where the electricity is generated rather than that feed into the distribution network. This also raises questions in regard to metering or the assumptions made about the proportion of the electricity generated used for each purpose.
- **Investment-based incentives** these schemes tend to provide support for the initial investment irrespective of the amount of electricity that is actually generated. Examples of such arrangements include:-

  loans (interest free or at rates below the market level)

  loan guarantees (where the repayment of the loan may be guaranteed by a national or regional government) which has the effect of facilitating both the availability of loan finance and reducing its cost

  tax benefits such as VAT exemption or reduction or reduced corporate taxation via accelerated depreciation or improved capital allowances, although this will only provide advantages to profit making companies.

In Italy a national feed-in tariff for PV is in place and this paper considers the following mechanisms that could be implemented in the Emilia-Romagna region to provide a further incentive for the installation of PV:

1. Investment Grants: incentives are given as a grant, and no money is returned to the Region. The grants that are provided represent a proportion of the total plant cost. The financial requirement on the Region would be front-loaded as funds would need to be pro-

vided in advance of equipment installation.
2. Fiscal Incentives: incentives are given as soft loans, including longer repayment periods or interest holidays. Again the financial requirement on the Region would be front-loaded as funds would need to be provided in advance of equipment installation. In this case the loan would usually, eventually be paid back to the Region.
3. Interest funds: incentives are given as a grant to pay all or part of the interest on bank loans taken out in order to purchase PV equipment. Again no money is returned to the Region. In this case the financial burden on the Region would be spread over the lifetime of the loans which are likely to be a number of years.
4. Guarantee fund: the Region provides a guarantee to the bank providing the loan to the investor who is purchasing PV equipment, that the loan will be repaid. This provides security to the bank which is therefore more likely to approve the loan request and to charge a lower interest rate than would otherwise be the case. There would be little or no immediate financial burden on the Region and the overall cost over the longer term would depend on the level of default of the investors which in turn would depend on the credit worthiness of the investors that the Region chooses to support.

The approach so far used by the Emilia-Romagna Region to provide a further incentive for the installation of PV has been by means of investments grants.

ECONOMIC SIMULATOR

In order to establish a relationship between the subsidies of the Region and the total installed MW of electrical power from photovoltaic, we developed an agent-based simulation model. This simulator mainly takes into consideration economic aspects, and only marginally recognises potential other ones. This results from the fact that these economic aspects are better understood, and that for many people installing a PV plant is primarily a type of investment, as advertised and reported in major economic newspapers in Italy.

The simulator considers two types of agents: the Region, and House owners.

The Region provides incentives to house owners, and each year there is a certain amount of money that is available to the Region to fund such incentives. At the start of the period there are some initial funds and each year the Region receives a further constant budget to foster installation of PV plants. Moreover, depending on the adopted funding scheme, the Region may receive the repayment of loans or other charges from house owners which can be recirculated to other house owners.

House owner agents may install PV panels on top of their roof, depending on a number of parameters, including

- *Surface of the roof* A^r, in square meters
- *Budget* B
- *Energy consumption*, in kWh per year
- *Objective*: the percentage of energy consumption that the agent wants to be covered by PV
- *Increase of Energy Requirements*: on average the energy consumption of a family increases with time; this parameter represents the percentage increase in energy requirements in a year.
- *Obstinacy*: a parameter indicating the inclination toward green economy of the agent.

As previously menioned, most of these parameters are economic, reflecting the fact that for many people the installation of PV panels is mainly an economic issue. The only non-economic parameter is the *obstinacy* in pursuing the installation of the PV plant: in case for some reason the PV installation is not advisable (from a strictly economic viewpoint), the agent could still want to install it for other reasons, not detailed in this simulator, and roughly accounted for by this parameter.

As a first step, the house owner agent performs a feasibility study (that in real life is usually done by an installer of PV panels). The agent considers various global parameters like:

- Price of electricity. Depends also on the (yearly) energy consumption of the agent.
- Yearly increase of energy prices
- Average cost of a PV plant, in €/kWp (cost per peak power producible by the plant)
- Subsidies
- Interest rate of treasury bills (as a comparison)
- Energy minimal buying price for the grid manager.

Once these parameters are given as input by the user, the simulator determines the local parameters of a set of agents, either selecting randomly their values, or by using historical data (when available).

Once all the parameters are known to the model, it can compute the feasibility of the plant, in particular its size A^{pv} (m^2) and its cost C^{pv} (€). These values are compared with the available surface of the roof A^r and the agent's budget B; four cases can occur:

	$A^{pv} \leq A^r$	$A^{pv} > A^r$
$C^{pv} \leq B$	Consider Increase	Consider Decrease
$C^{pv} > B$	Consider Loan	Forgo

If none of the two feasibility conditions is satisfied, the agent decides against purchasing PV (Forgo) and terminates. Otherwise, resizing the plant, or asking for a loan is considered. If only one of the conditions is satisfied, the agent behaves according to its obstinacy: the parameter *Obstinacy* is utilised as a probability that the agent insists in pursuing the installation of the plant, notwithstanding adverse circumstances. The *Obstinacy* is compared to a randomly generated number, and if the test succeeds the agent considers asking for a loan (if the budget is not enough) or installing a smaller plant (if the available area is not enough).

In the case where both feasibility conditions are satisfied, the agent definitely installs the plant, and, moreover, considers increasing the size of the plant. In the fourth feed-in scheme, if in a year the total produced energy is higher than the energy that the household consumes, the difference is paid at a much lower rate, so again the agent will consider upgrading the plant with a probability given by its *Obstinacy*.

Finally, the simulator adopts a very preliminary model to account for social aspects. In human societies, the behaviour of a person is influenced by the per-

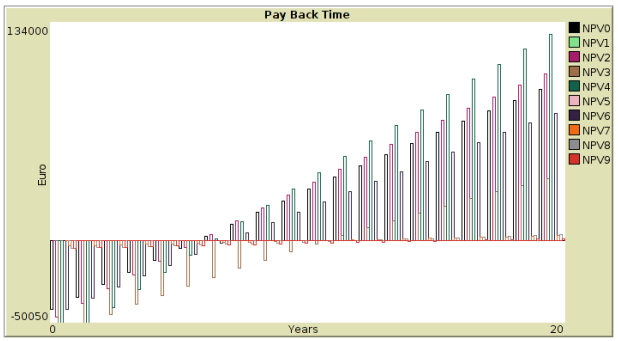

Fig. 1: Screenshot of the simulator, showing PBT and NPV of investments in the course of time, based on when the plant was built, ranging from first term of 2012 (NPV0) to second term of 2016 (NPV9).

sons near to him/her: neighbours, relatives, colleagues, friends, etc. In this simulator, each agent lives in a bi-dimensional world, and it is influenced by the agents that live within a predefined range. In particular, the *Obstinacy* of an agent is increased proportionally to the number of agents in its influence range that have installed PV panels.

The output of the simulator provides several data items including economic data for the agents (such as the Payback Time (PBT), the Return On Equity and the Net Present Value (NPV) of the investment, plotted in Figure 1), the total cost of subsidies provided by the Region, and the total power of installed PV plants.

EXPERIMENTAL EVALUATION

Our goal has been to understand the relationship between the capacity of PV that is installed and the budget available for regional incentives. We have treated all regional incentives as if they were independent from each other, i.e., we run simulations using one type of regional incentive at a time (on top of the national ones).

A large number of simulations have been undertaken (300) for each value of the regional budget from zero to €40 million, in steps of €1 million, and for each type of incentive, resulting in a total of 48,000 simulations. For each simulation the total installed power in kW of photovoltaic plants was recorded.

Of course, an individual simulation does not, of itself, provide much useful information and some statistics should be extracted from a significant number of such simulations to obtain a better insight. In order to derive a model of the relationship between the installed power and the available budget, we averaged the results of all the simulations with the same amount of budget, obtaining a point for each value in the range from 0M€ to 40M€ (Figures 2, 3, 4 and 5).

Using these results, machine learning was utilised to learn functions establishing the relationship between the available budget and the installed power. One function was determined for each incentive type. Various regression algorithms were used: linear models [Rousseeuw and Leroy, 1987], polynomial models [Stigler, 1974], [Gergonne, 1815] and local regression [Cleveland, 1981] (LOESS).

For each type of incentive we chose the best regression model using statistical analysis to evaluate which fitted best our data - when two or more models offered similar results, we used the simplest one.

The statistical analysis was carried out using *R* [Ihaka and Gentleman, 1996]. We evaluated the goodness of fit of regression models through numerical analysis, e.g. computing the coefficient of determination, evaluating the statistical significance (F-test) [Fisher, 1925], [Box, 1953], and graphical analysis, e.g. residuals scatter plots or normal probability plots.

The coefficient of determination R^2 is a number between 0 and 1, used to describe how well a regression line fits a set of data; the higher R^2, the better the data fit [Steel and Torrie, 1960], [Draper and Smith, 1998].

The graphical analysis was made taking into account that if the model fit to the data were correct, the residuals would approximate the random errors that make the relationship between the explanatory variables and the response variable a statistical relationship. Therefore, if the residuals appear to behave randomly, it suggests that the model fits the data well. On the other hand, if non-random structure is evident in the residuals, it is a clear sign that the model fits the data poorly [NIST/SEMATECH, 2012].

We can examine now the behaviour of the four types of incentives, namely the investment grant, the interest fund, the fiscal incentive and the guarantee fund.

Investment Grants

With an investment grant the installed power rises according to the budget increase, exhibiting an almost linear relation for budget smaller than 30M€ and a ratio decrease for bigger values. This is probably caused by the fact that once we meet the requests from most of the agents in the simulation with a budget big enough, further increases are less and less effective.

In Fig. 2 the linear, quadratic, 10th degree polynomial and LOESS models are compared with the points obtained through our simulations. Except the linear one, the other models fit the data quite well, without great differences.

In Table I we can see the numerical results used to evaluate the goodness of fit of our regression models. We reported the values for linear, quadratic, cubic and tenth degree polynomial model; since the LOESS model is not parametrical, we cannot compute those values for this model and rely on a graphical evaluation of the goodness of fit. DF stands for Degrees of Freedom (numerator and denominator).

Regression	R^2	*F-Test*	*p-value*
Linear	0.7601	186.9 on 1 and 39 DF	$< 2.2 \cdot 10^{-16}$
Quadratic	0.907	282.7 on 2 and 38 DF	$< 2.2 \cdot 10^{-16}$
Cubic	0.9074	186.3 on 3 and 37 DF	$< 2.2 \cdot 10^{-16}$
10^{th} Poly	0.9429	82.51 on 10 and 30 DF	$< 2.2 \cdot 10^{-16}$

TABLE I: Investment Grant, Regression results

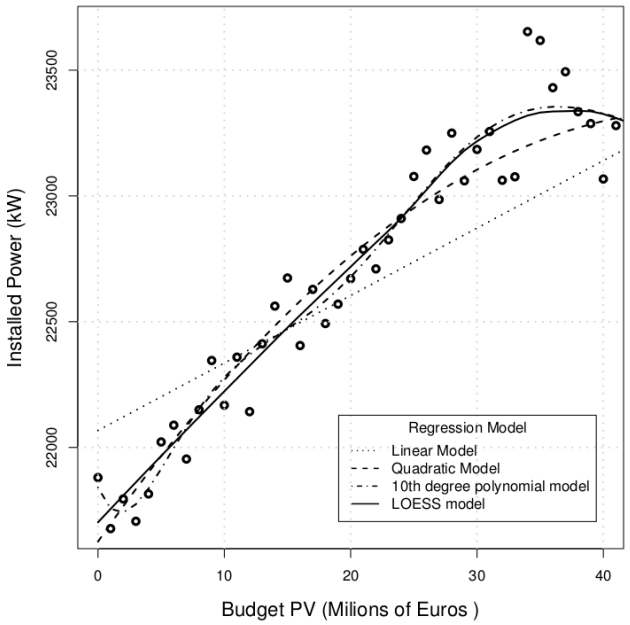

Fig. 2: Regression Models, Investment Grant

Interest Fund

With interest fund incentives, the function relating budget and installed power shows a surge in the installed power for low budget values (up to about 3M€) but after that new budget increases do not translate into further increases in the amount of PV installed; this behaviour is probably due to the fact that this kind of incentive is by far the one requiring the least amount of money, so it is relatively easier to fulfill all simulated agents who would like to benefit from it.

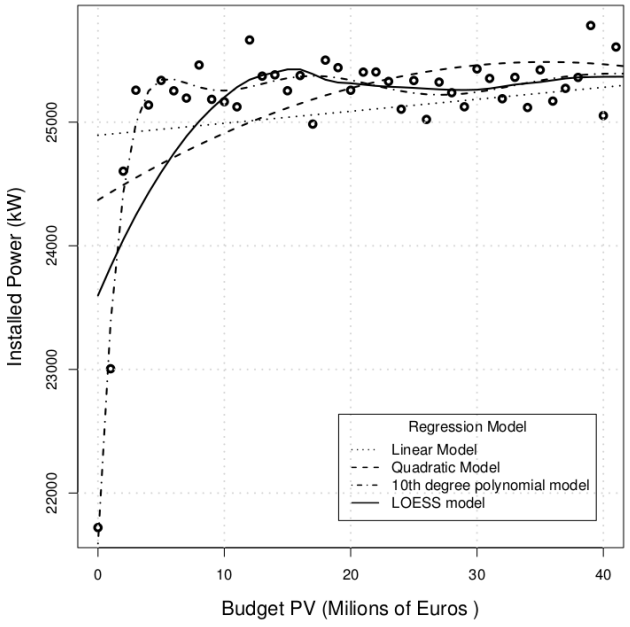

Fig. 3: Regression Models, Interest Fund

Fig. 3 shows that the tenth degree polynomial regression provides the best fit to our data. Table II shows the numerical results used to evaluate the goodness of fit.

Regression	R^2	*F-Test*	*p-value*
Linear	0.09055	5.874 on 1 and 39 DF	0.01845
Quadratic	0.2789	11.22 on 2 and 38 DF	$7.621 \cdot 10^{-5}$
Cubic	0.412	13.31 on 3 and 37 DF	$1.074 \cdot 10^{-6}$
10^{th} Poly	0.9012	45.61 on 10 and 30 DF	$< 2.2 \cdot 10^{-16}$

TABLE II: Interest Fund, Regression results

Fiscal Incentives

For fiscal incentives the function learned is similar to that for investment funds (Fig. 2), but with this incentive, compared to the previous one, the rise of the installed power for lower budgets is faster and the curve's slope declines more slowly.

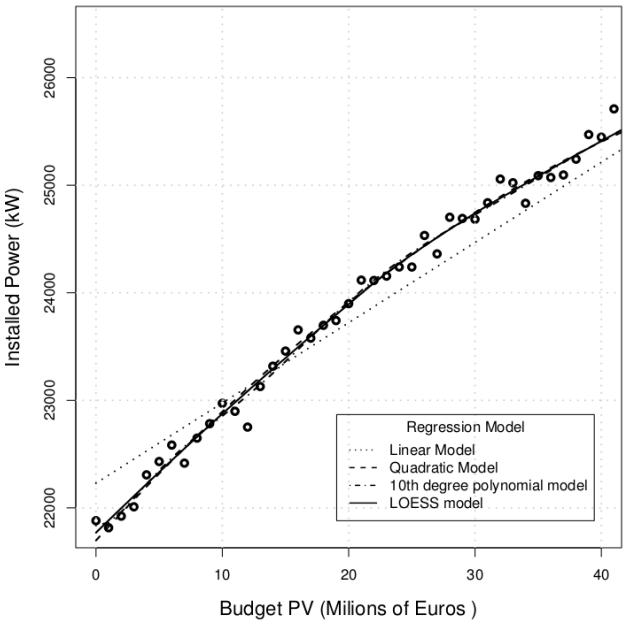

Fig. 4: Regression Models, Fiscal Incentives

The regression models used, except for the linear one, fit the data very well (Fig. 4). Again we preferred a quadratic model for the regression, for its simplicity and at the same time goodness of fit and statistical significance. Table III displays the results of the numerical analysis.

Regression	R^2	*F-Test*	*p-value*
Linear	0.9486	1089 on 1 and 39 DF	$< 2.2 \cdot 10^{-16}$
Quadratic	0.9831	1683 on 2 and 38 DF	$< 2.2 \cdot 10^{-16}$
Cubic	0.9838	1155 on 3 and 37 DF	$< 2.2 \cdot 10^{-16}$
10^{th} Poly	0.9849	327.1 on 10 and 30 DF	$< 2.2 \cdot 10^{-16}$

TABLE III: Fiscal Incentives, Regression results

Guarantee Fund

Finally, the last type of regional incentives is considered, the guarantee fund. From Figure 5, we can again note a trend characterized by an initial increase in installed power in response to the rise of available

budget, represented by an almost linear curve up to about 15M€. Then the installed power stabilises after a certain budget level (about 20M€), probably because also in this case – as with the interest fund – it is possible to satisfy a large fraction of the requests made by simulated agents with budgets smaller than the investment grant and fiscal incentives. The stabilization appears here for higher levels of budget with respect to the interest fund. This could be explained by the fact that the interest fund needs less money than guarantee fund to satisfy the same number of agents.

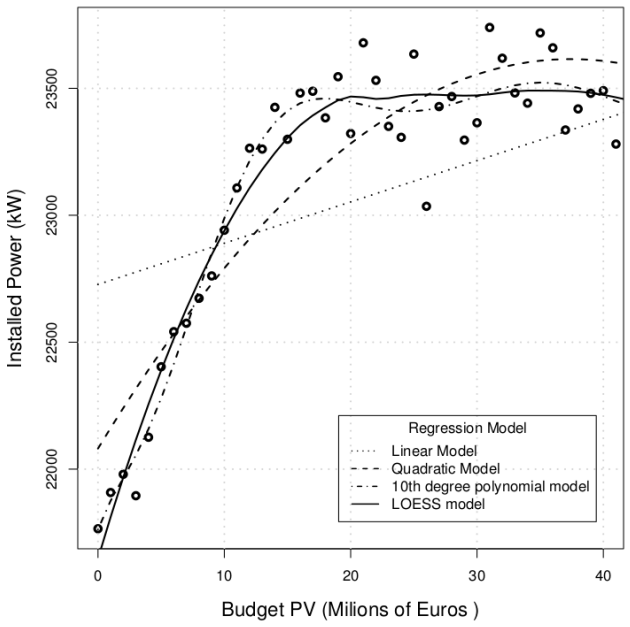

Fig. 5: Regression Models, Guarantee Fund

In Fig. 5 we can see that the linear and quadratic models do not perform very well, while the tenth degree polynomial and LOESS model offer better results, with the latter having a slightly better fit.

The numerical analysis reveals that both these models have a good statistical significance, but eventually we opted for a local regression model because it was less sensitive to outliers - at least with guarantee fund incentives.

Again, in Table IV the numerical values used to evaluate the goodness of fit are shown.

Regression	R^2	*F-Test*	*p-value*
Linear	0.3737	35.21 on 1 and 39 DF	$1.667 \cdot 10^{-07}$
Quadratic	0.7941	111.9 on 2 and 38 DF	$< 2.2 \cdot 10^{-16}$
Cubic	0.9059	183 on 3 and 37 DF	$< 2.2 \cdot 10^{-16}$
10^{th} Poly	0.937	74.39 on 10 and 30 DF	$< 2.2 \cdot 10^{-16}$

TABLE IV: Guarantee Fund, Regression results

Comparison

In Figure 6 all the four incentives are compared. It can be noted that the interest fund is the best type of incentive for almost the whole budget range that has been considered (this range is consistent with the

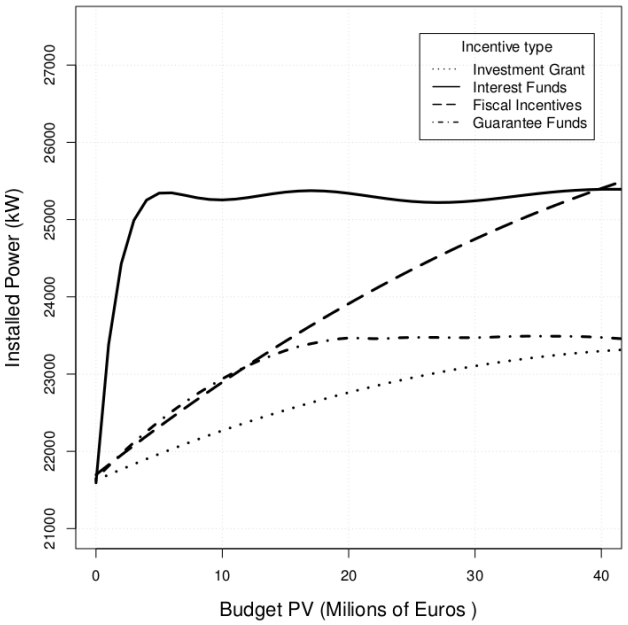

Fig. 6: Comparison among incentives

funds provided by the region in reality), with a slight advantage for fiscal incentives for budgets larger than 40M€. The guarantee fund and fiscal incentives present a similar behaviour for lower levels of funding, but with higher budget values fiscal incentives behave clearly better; overall, the investment fund (the only one implemented so far by the Emilia-Romagna region) turned out to be the least effective type of incentive in enhancing the installation of photovoltaic plants.

DISCUSSION AND FUTURE WORK

This paper represents a first step toward the understanding of the efficiency of different incentive mechanisms adopted as energy policies implementation instruments.

A number of research avenues are still open that we try to describe below.

Simulator extensions. The simulator has been developed in such a way that it simulates a single incentive mechanism and observes the results. We could in principle simulate combinations of instruments instead of single mechanisms. This extension would possibly highlight their interactions. Second, we could include auction mechanisms for the distribution of the regional budget taking into account fairness and truthfulness. Third, other agent types beside house owners should be considered.

The social aspect of the simulator is extremely important. All the social drivers that affect the decision making of an agent should be incorporated, even if it is extremely difficult to "measure" them. Up to now the simulator takes into account the environmental sensitivity that is basically randomly set and the network structure linking agents enables us to simulate emulation behaviours. Therefore the probability that an agent installs a PV plant is higher if its neighbors have already installed it. More complex social interactions

could be considered as well.

Simulator validation. We are currently validating the simulator on a set of real data taken from the GSE web site [GSE, 2012]. Basically the data are about existing PV plants divided by region of Italy and time of installation. This is an extremely interesting set of data to validate the results of the simulator.

Concerning the validation, an important aspect concerns scalability. It is clear that we cannot have a simulation with 4.5M agents (that is equivalent to the population of the Emilia-Romagna region) nor 1.8M agents representing families in the Emilia-Romagna region. We therefore have to understand if results that we obtain for thousands of agents, that is the maximum number we can simulate can be "linearly" scaled for larger numbers. In addition, we are looking for a kind of asymptotic behaviour that could establish a minimum number of agents that can be projected to the Emilia-Romagna population in a realistic way.

Feedback on policy modeling These results are interesting if they could provide a feedback to the policy maker who could adjust the implementation strategy of his/her policies. We have defined a number of potential interactions mechanisms, described in [Gavanelli et al., 2012], between the optimization component [Gavanelli et al., 2013] and a simulator. We are now integrating the functions derived by this work linking the budget with the installed power into the optimization model for defining a regional plan. In this way, beside the regional plan, we are able to provide the best possible implementation schema to achieve it as described in [Milano, 2013].

Acknowledgements

The research leading to these results has received funding from the European Union Seventh Framework Programme (FP7/2007-2013) under grant agreement n. 288147.

References

[Box, 1953] Box, G. (1953). Non-normality and tests on variances. *Biometrika*, 40(3/4):318–335.

[Cleveland, 1981] Cleveland, W. S. (1981). LOWESS: A Program for Smoothing Scatterplots by Robust Locally Weighted Regression. *The American Statistician*, 35:54.

[Draper and Smith, 1998] Draper, N. and Smith, H. (1998). *Applied Regression Analysis*. Wiley-Interscience.

[Europe, 2020] Europe (2020). `http://ec.europa.eu/europe2020/`.

[Fisher, 1925] Fisher, R. (1925). *Statistical methods for research workers*. Oliver and Boyd.

[Gavanelli et al., 2012] Gavanelli, M., Milano, M., Holland, A., and O'Sullivan, B. (2012). What-if analysis through simulation-optimization hybrids. In *Proceedings of the European Conference on Modeling and Simulation*, ECMS2012.

[Gavanelli et al., 2013] Gavanelli, M., Riguzzi, F., Milano, M., and Cagnoli, P. (2013). Constraint and optimization techniques for supporting policy making. In Yu, T., Chawla, N., and Simoff, S., editors, *Computational Intelligent Data Analysis for Sustainable Development*, Data Mining and Knowledge Discovery Series, chapter 12. Taylor & Francis.

[Gergonne, 1815] Gergonne, J. (1974 [1815]). The application of the method of least squares to the interpolation of sequences. *Historia Mathematica*, 1(4):439 – 447.

[Gilbert, 2010] Gilbert, N. (2010). *Computational Social Science*. SAGE.

[GSE, 2012] GSE (2012). Feed-in scheme results. `http://www.gse.it/en/feedintariff/Supportmechanismsoutcomes/`.

[Ihaka and Gentleman, 1996] Ihaka, R. and Gentleman, R. (1996). R: A language for data analysis and graphics. *Journal of Computational and Graphical Statistics*, 5(3):299–314.

[Matthews et al., 2007] Matthews, R., Gilbert, N., Roach, A., Polhill, G., and Gotts, N. (2007). Agent-based land-use models: a review of applications. *Landscape Ecology*, 22(10).

[Milano, 2013] Milano, M. (2013). Sustainable energy policies: Challenges and opportunities. In *Proceedings of Design and Automation Europe*, DATE2013.

[Ministerial Decree, 2011] Ministerial Decree (5 May 2011). Incentivazione della produzione di energia elettrica da impianti solari fotovoltaici. See `http://www.gse.it/en/feedintariff/Photovoltaic/Fourth%20feed-in%20tariff/`.

[NIST/SEMATECH, 2012] NIST/SEMATECH (2012). *e-Handbook of Statistical Methods*. www.itl.nist.gov/div898/handbook.

[Rousseeuw and Leroy, 1987] Rousseeuw, P. J. and Leroy, A. M. (1987). *Robust regression and outlier detection*.

[Sklar, 2011] Sklar, E. (2011). NetLogo, a multi-agent simulation environment. *Artificial Life*, 13(3):303–311.

[Steel and Torrie, 1960] Steel, R. G. D. and Torrie, J. H. (1960). *Principles and Procedures of Statistics*. McGraw-Hill.

[Stigler, 1974] Stigler, S. M. (1974). Gergonne's 1815 paper on the design and analysis of polynomial regression experiments. *Historia Mathematica*, 1(4):431 – 439.

[Troitzsch et al., 1999] Troitzsch, K. G., Mueller, U., Gilbert, G. N., and Doran, J. (1999). Social science microsimulation. *J. Artificial Societies and Social Simulation*, 2(1).

AUTHOR BIOGRAPHIES

ANDREA BORGHESI is postgraduate student at the Department of Computer Science and Engineering, University of Bologna, Italy. His research interests are on Artificial Intelligence techniques, with particular emphasis on multi-agent systems and optimization.

MICHELA MILANO is Associate Professor in Intelligent Systems at the Department of Computer Science and Engineering, University of Bologna, Italy. Her research interests span from Artificial Intelligence to Operations Research to build hybrid optimization techniques. Her personal web page is at `http://ai.unibo.it/people/MichelaMilano`.

MARCO GAVANELLI is Ricercatore (Assistant Professor) in Computer Science at the Department of Engineering, University of Ferrara, Italy. His research interests are on Logic Programming and Constraint Programming and their applications. His personal web page is at `http://www.ing.unife.it/docenti/MarcoGavanelli/`.

TONY WOODS has been Chief Financial Officer and a director of PPA Energy, a UK based energy and management consultancy company since 2008. In recent years he has undertaken a wide variety of consultancy projects both in the UK and for overseas clients including in Ireland, Uganda, Bangladesh, Guyana, West Africa and South Africa. Tony is a visiting professor at Imperial College.

EFFECT OF DECLARATION ON EMERGENCE OF COOPERATION IN DEMOGRAPHIC DONOR-RECIPIENT GAME

Tsuneyuki Namekata
Department of Information and Management Science
Otaru University of Commerce
Midori 3-5-21, Otaru, Hokkaido, 047-8501
E-mail: namekata@res.otaru-uc.ac.jp

Yoko Namekata
E-mail: PallaYoko@namekata.org

KEYWORDS
Demographic Model, Donor-Recipient Game, Emergence of Cooperation, Indirect Reciprocity, Agent-Based Simulation.

ABSTRACT

We consider effect of declaration on emergence of cooperation in demographic Donor-Recipient game. Players are initially randomly distributed in square lattice of cells. In each period, players move locally to random cell in neighbors or globally to random unoccupied cell in the whole lattice, and play multiple games against local neighbors or against randomly selected global players. We restrict patters of move (play) to local or global; local (global) means with high probability the player moves (plays) locally (globally). If wealth (accumulated payoff) of player becomes negative or his age becomes greater than his lifetime, he dies. If his wealth becomes greater than some amount and there is unoccupied cell in neighbors, he has an offspring. In Donor-Recipient game, one player is selected at random as Donor and the other as Recipient. Donor has two moves Cooperate or Defect; Cooperate means Donor pays cost for Recipient to receive benefit. Defect means Donor does nothing. We introduce one option for Recipient; Recipient can declare that he is cooperative before Donor's move. We show, by Agent-Based Simulation, declaration promotes emergence of cooperation, but some players need to distinguish true declaration from false one if Donor can punish suspicious declaration.

INTRODUCTION

This paper investigates the effect of declaration on the emergence of cooperation and the distribution of strategies in demographic Donor-Recipient game (DR). We introduce one option for Recipient into usual DR game. Recipient can declare that he is cooperative before Donor's move.

Epstein (2006) introduces demographic model. He shows the emergence of cooperation where AllC and AllD are initially randomly distributed in a square lattice of cells. Here AllC always Cooperate and AllD always Defect. In each period, players move locally (that is, to random cell within the neighboring 4 cells, that is, north, west, south, and east cells; von Neumann neighbors, if unoccupied) and play Prisoner's Dilemma (PD) game against local (neighboring) player(s). If wealth (accumulated payoff) of a player becomes negative or his age becomes greater than his lifetime, he dies. If his wealth becomes greater than some amount and there is an unoccupied cell in von Neumann neighbors, he has an offspring and gives the offspring some amount from his wealth. Namekata and Namekata (2011) extend Epstein's original model discussed above by introducing global move, global play, Reluctant players, who delay replying to changes and use extended forms of TFT, into demographic PD game and consider the effect of Reluctant players on the emergence of cooperation, and show cases where the reluctance promotes the emergence of cooperation. Here TFT Cooperates at first period and at later periods uses the same move as the opponent did in the previous period. Namekata and Namekata (2012) examine the effect of move-play pattern on the emergence of cooperation and the distribution of strategies. They restrict patters of move and play of a player to simple structure; local or global, where local or global means that with high probability the player moves (plays) locally or globally, respectively. For example, a player with global move and local play (abbreviated as gl) moves globally with high probability and plays DR games against (possibly different) local opponents with high probability at each period. They show that cooperative strategies evolutionarily tend to move and play locally, defective do not, and AllC and AllD are abundant unless all strategies initially play locally.

Nowak and Sigmund (1998) consider the emergence of cooperation in different non-demographic setting where two players are randomly matched, and play DR game at each period. Rate of a strategy at the next period is proportional to the payoff of the strategy earned at the current period, which is also different from that in our demographic model. The chance that the same two players meet again over periods is very small. Every player has his own image score that takes on some range, is initially zero, and increases or decreases by one if he cooperates or defects, respectively. Donor decides his move (Cooperate or Defect) depending on the opponent's image score. Riolo et al. (2001) deal with similar repeated DR game setting where, instead of image score, every player has his own tag and tolerance and Donor cooperates only if the difference between his tag and the opponent's is smaller than his tolerance.

In general, reciprocity explains the emergence of cooperation in several situations (Nowak and Sigmund

Proceedings 27th European Conference on Modelling and Simulation ©ECMS Webjørn Rekdalsbakken, Robin T. Bye, Houxiang Zhang (Editors)
ISBN: 978-0-9564944-6-7 / ISBN: 978-0-9564944-7-4 (CD)

2005): Direct reciprocity assumes that a player plays games with the same opponent repeatedly and he determines his move depending on moves of the same opponent. If a player plays games repeatedly and the opponents may not be the same one, indirect (downstream) reciprocity assumes that the player determines his move to the current opponent depending on the previous moves of this current opponent, or indirect upstream reciprocity, or generalized reciprocity, assumes that the player determines his move to the current opponent depending on the previous experience of his own. Since a player in Namekata and Namekata (2011, 2012) determines his move depending on his own previous experience, they deal with generalized reciprocity. Nowak and Sigmund (1998) deal with indirect (downstream) reciprocity because Donor determines his move to his opponent Recipient depending on the image score of the Recipient that relates to the previous moves of the Recipient. There is no reciprocity, either direct or indirect in the model of Riolo et al. (2001) because Donor's move does not depend on the opponent's previous moves as well as his own previous experience.

This paper examines the effect of declaration on the emergence of cooperation and the distribution of strategies. In real life cooperative player is willing to cooperate if the opponent is expected also to be cooperative. In our Donor-Recipient game setting, the cooperative Donor is willing to cooperate if Recipient is expected also to be cooperative. Therefore the Recipient has an incentive to make the Donor believe the Recipient to be cooperative. We introduce a costless option for Recipient; Recipient can declare that he is cooperative before Donor's move. Donor tries to distinguish true declaration from false one by his ability and make his move based on his distinction. Some do not have any ability to distinguish but believe the declaration as it is with high probability or with low probability. Some do distinguish true declaration from false one with high probability. Further we introduce Donor's punishment for suspicious declaration, which means Donor defects if he judges Recipient's declaration to be suspicious. We show, by Agent-Based Simulation, that declaration promotes the emergence of cooperation, but some players need to have ability to distinguish true declaration from false one if Donor's punishment for suspicious declaration is allowed.

MODEL

We start with extending TFT as follows in order to introduce reluctant strategy: Let m=0,1,2; t=0,…,m+1; s=0,…,m. Strategy (m,t;s) is illustrated in Figure 1. It has m+1 inner states. The inner states are numbered 0,1,…,m; thus m is the largest state number. State i is labeled D_i if $i<t$ or C_i if not. If current state is labeled C or D, then the strategy prescribes using C or D, respectively. In other words, the strategy prescribes using D if the current state $i<t$ and using C if not; thus the value t is the threshold which determines the move of a player. Initial state in period 0 is state s; its label is D_s if $s<t$ or C_s if not. If current state is i, then the next state is $\min\{i+1,m\}$ or $\max\{i-1,0\}$ given that the opponent uses C or D, respectively, in this period. If $m>1$, then the strategy may delay replying to its opponent's change. Note that TFT is expressed as (1,1;1) in this notation. Thus strategy (m,t;s) is an extended form of TFT. To sum up, our strategies are expressed as (m,t;s); m is the largest state number, t is the threshold, and s is the initial state number. We omit the initial state like (m,t;*) if it is determined randomly. We also omit the initial state like (m,t) if we have no need to specify it. Note that reluctant strategy (m,t;s) by itself decides its move to the current opponent depending on the previous experience of its own, meaning indirect upstream reciprocity. Also that AllC is denoted by (m,0) and AllD by (m,m+1).

We deal with Donor-Recipient (DR) game as a stage game. DR game is a two-person game where one player is randomly selected as Donor and the other as Recipient. Donor has two moves, Cooperate (C) and Defect (D). C means Donor pays cost c in order for Recipient to receive benefit b ($b>c>0$). Defect means Donor does nothing. Since it is common in demographic dilemma game that the sum of payoffs of a player, in two successive games once as Donor and once as Recipient, to be positive if the opponent uses C and negative if D and the worst sum of a player is equal to the best sum in absolute value, we transform the original payoffs to new ones by subtracting constant x. Constant

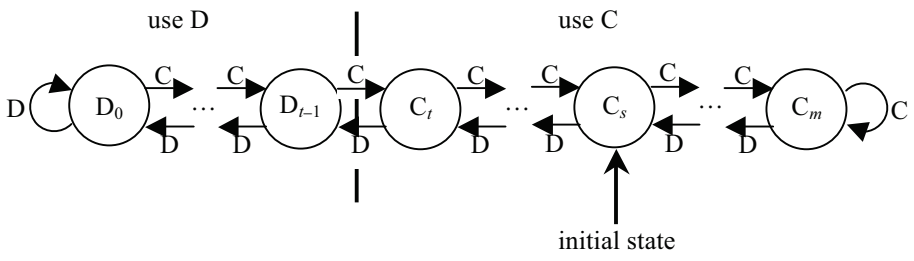

Figure 1: Strategy (m,t;s) in Case of $t<s<m$
Circles denote inner states. Initial state is the state pointed by arrow labeled "initial state". Threshold divides states into two subclasses; one prescribes using D and the other using C. The transition between states occurs along the arrow labeled C or D if the opponent uses C or D, respectively.

x is given by $x = \frac{b-c}{4}$. We set b=4 and c=1 in this paper. Table 1 shows the transformed payoff matrix of DR game. We assume that each player plays 8 games against (possibly different) players at each period.

Table 1: Payoff Matrix of DR Game

		Recipient
Donor	C	$-c-x$, $b-x$
	D	$-x$, $-x$

In this paper, we introduce two costless moves for Recipient, Declare or not, one of which is made before Donor's move. Declare means that Recipient declares he is cooperative. Not declare means that Recipient does nothing. In case of Recipient's declaration, Donor (except AllC or AllD) tries to distinguish true declaration from false one by the Donor's ability. Donor uses C if he judges the Recipient's declaration to be reliable. We assume three types of Donor in this ability; High (H) has no ability to distinguish them but believes the declaration to be reliable with high 80% probability, Low (L) also has no ability to distinguish them but believes the declaration to be reliable with low 20% probability, and Good (G) has ability to distinguish true declaration from false one with about high 80% probability. We explain the ability of Good in more detail. The probability $\Pr_{Re|G}(r)$ with which Good Donor judges Recipient's declaration to be reliable given that the Recipient has cooperation rate r, the number of move C used by the Recipient divided by the number of games played by the Recipient as a Donor until now, is given by

$$\Pr_{RelG}(r) = \begin{cases} 1.2r + 0.2 & (r \le 0.5) \\ 0.8 & (r > 0.5) \end{cases}$$

If r=0 (the Recipient is AllD), then Donor judges the declaration to be suspicious with high probability 0.8. If $r > 0.5$ (including AllC), then Donor judges the declaration to be reliable with high probability 0.8. Thus Good Donor has ability to distinguish true declaration from false one with about 80%. In the same notation we have $\Pr_{RelH}(r) = 0.8$ and $\Pr_{RelL}(r) = 0.2$. Our model also deals with indirect downstream reciprocity because Good Donor decides his move by partial information about Recipient. Our way to introduce indirect downstream reciprocity is different from that of the second incomplete information model in Nowak and Sigmund (1998), where the result of one DR game is observable only a randomly selected subset of all players and thus every player may have different incomplete image score of the same player. Thus our results discussed later about the promotion of emergence of cooperation is the effect of our way of indirect downstream reciprocity in addition to our indirect upstream reciprocity in the form of reluctant strategy in the Demographic DR game.

We further introduce the possibility for Donor to punish suspicious declaration, which means Donor defect in case that the Donor judges the declaration of Recipient to be suspicious.

A player has the following properties that are inherited from parents to offspring; rateOfDeclaration (rDec), distinction, punishment, strategy, rateOfGlobalMove (rGM), and rateOfGlobalPlay (rGP); whose initial distributions are summarized in Table 2. Recipient declares with probability rDec. Donor (except AllC and AllD) distinguishes Recipient's declaration by his distinction if the Recipient declares. Donor uses his strategy if the Recipient does not declare or does declare but the Donor judges the declaration to be suspicious in case of non-punisher.

In period 0, N (=100) players (agents) are randomly located in 30-by-30 lattice of cells. The left and right borders of the lattice are connected. If a player moves outside, for example, from the right border, then he comes inside from the left border. So are the upper and lower borders. Players use strategies of (m,t;s) form. Initial wealth of every player is 6. Their initial (integer valued) age is randomly distributed between 0 and deathAge (=50).

In each period, each player (1st) moves, and (2nd) plays DR games given by Table 1 against other players. Positive payoff needs opponent's C. (The detailed description of (1st) move and (2nd) play is given in Table 3.) The payoff of the game is added to his wealth. If the resultant wealth is greater than fissionWealth (=10) and there is an unoccupied cell in von Neumann neighbors, the player has an offspring and gives the offspring 6 units from his wealth. His age is increased by one. If the resultant wealth becomes negative or his age is greater than deathAge (=50), then he dies. Then next period starts.

In our simulation we use synchronous updating, that is, in each period, all players move, then all players play, then all players have an offspring if possible. We remark that the strategy and its initial state of the offspring are set to the current strategy and its current state of the parent. There is a small mutationRate (=0.05) with which inheriting properties are not inherited. Initial distributions of inheriting properties given in Table 2 are also used when mutation occurs. We assume that with errorRate (=0.05) a player makes mistake when he makes his move. Thus AllC may defect sometime. Especially note that Recipient declares with low (L) or high (H) probability and Donor (except AllC and AllD) has no ability to distinguish Recipient's declaration (L or H) or partial ability to distinguish true declaration from false one (G), from Table 2. And that the initial distribution of strategy is 2ASYM (including AllC, (2,1), (2,2), and AllD) or AllCAllD. Also that the initial distribution of (rGM, rGP) has simple structures; with high probability a player moves and plays locally or globally, thus there are 4 move-play patters such as ll, lg, gl, and gg.

Table 2: Initial Distribution of Inheriting Properties

property	initial distribution
rDec	We deal with distribution {(1/2)L, (1/2)H}, which means rDec is uniformly distributed in interval L or H with equal probability 1/2. L:=(0.05,0.2) and H :=(0.8,0.95). In other words, a player declares with low probability (L) or high probability (H).
distinction	We deal with 12 distributions, Ig, LIg, HIg, GIg, HL, GL, GH, HLIg, GLIg, GHIg, GHL, and GHLIg, of Donor's distinction. For example, GHL:={(1/3)G, (1/3)H, (1/3)L}, which means the ability of a player to distinguish is determined randomly to be G, H, or L. L has no ability and believes the declaration to be suspicious with 80%. H has no ability and believes the declaration to be reliable with 80%. G has ability to distinguish true declaration from false one with about 80%. Ig ignores Recipient's declaration and uses his strategy as if the Recipient does not declare.
punishment	Donor (except AllC and AllD) can be punisher or non-punisher. He is punisher with probability rateOfPunisher (rP). rP takes 0, 0.5, or 1. rP=0 means there is no punishing Donor. rP=1 means every Donor (except AllC and AllD) punishes suspicious declaration. rP=0.5 means Donor (except AllC and AllD) is determined randomly to be punisher or non-punisher.
strategy	We deal with two populations, 2ASYM and AllCAllD as follows: 2ASYM:= {(1/4)(2,0), (1/4)(2,1;*), (1/4)(2,2;*), (1/4)(2,3)}, and AllCAllD:= {(1/2)(0,0), (1/2)(0,1)}. The notation, for example, of 2ASYM, means that with probability 1/4 strategy (2,0) (AllC) is selected, with probability 1/4 strategy (2,1;*) is selected, and so on, where * indicates that initial state is selected randomly. Note that initially 50% of players use C on the average since both AllC and AllD are included with the same probability and so are both (m,t;*) and (m,$m-t$+1;*).
(rGM,rGP)	We deal with distribution {(1/4)ll, (1/4)lg, (1/4)gl, (1/4)gg}. For example, gl means rGM is distributed in interval g and rGP in interval l, where l:=(0.05,0.2) and g:=(0.8,0.95). {(1/4)ll, (1/4)lg, (1/4)gl, (1/4)gg} means rGM and rGP are selected randomly among ll, lg, gl, and gg.

Table 3: Detailed Description of Move and Play
(1) describes move and (2) describes play in detail

(1)	With probability rateOfGlobalMove (abbreviated as rGM), a player moves to random unoccupied cell in the whole lattice. If there is no such cell, he stays at the current cell. Or with probability 1− rGM, a player moves to random cell in von Neumann neighbors if it is unoccupied. If there is no such cell, he stays at the current cell.
(2)	With probability rateOfGlobalPlay (abbreviated as rGP), the opponent against whom a player plays dilemma game is selected at random from all players (except himself) in the whole lattice. Or with probability 1− rGP, the opponent is selected at random from von Neumann neighbors (no interaction if none in the neighbors). This process is repeated 8 times. (Opponents are possibly different.)

If population of strategy is AllCAllD, rGM=0, and rGP=0, then our model is similar to that of Epstein (2006). His model uses asynchronous updating while our model uses synchronous updating.

We comment on the difference among Donor's distinctions (L, H and G) and Ig. Let us denote, for example, a strategy ((2,1) or (2,2)) with distinction L who is punisher by LP, and with distinction L who is not punisher by LN, respectively. We have the following basic relations among Donor's distinctions:

- LN=(20%-AllC, 80%-Ig; Ig), which means LN is equal to AllC with probability 20% and to Ig with probability 80% in case of Recipient's declaration; and LN is equal to Ig in case of no Recipient's declaration.
- LP=(20%-AllC, 80%-AllD; Ig).
- HN=(80%-AllC, 20%-Ig; Ig).
- HP=(80%-AllC, 20%-AllD; Ig).
- Ig<LN<HN, LP<LN, Ig<HN, LP<HP<HN, and GP<GN, where, for example, Ig<LN means that LN prescribes using C more frequently than Ig on the average.
- LN is similar to Ig with more than 80% probability but different from LP.
- HN is similar to HP with more than 80% probability but different from Ig.

Thus we expect that H promotes cooperation more often than L even if H and L have no ability to distinguish Recipient's declaration. Also that G promotes cooperation more often than L and H because G has some ability to distinguish true declaration from false one.

SIMULATION AND RESULT

Our purpose to simulate our model is to examine the effect of declaration and punishment for suspicious

declaration on the emergence of cooperation and the distribution of strategies. We use Ascape (http://sourceforge.net/projects/ascape/) to simulate our model.

We execute 300 runs of simulations in each different setting. We judge that the cooperation emerges in a run if there are more than 100 players and the average C rate is greater than 0.2 at period 500, where the average C rate at a period is the average of the player's average C rate at the period over all players and the player's average C rate at the period is defined as the number of move C used by the player divided by the number of games played as Donor at the period. (We interpret 0/0 as 0.) This average C rate is the rate at which we see cooperative move C as an outside observer. Since negative wealth of a player means his death in our model and he has a lifetime, it is necessary for many players to use C in order that the population is not extinct. We are interested in the emergence rate of cooperation that is the rate at which the cooperation emerges.

We summarize the emergence rate of cooperation, Ce, in Table 4. The second (rP=0), third (rP=0.5), and fourth (rP=1) columns contain Ce for the corresponding initial distribution (distinction in case of 2ASYM) such as AllCAllD, LIg or GHLIg of 2ASYM if all Donors do not punish, about half of Donors do punish, and all Donors do punish, respectively, for Recipient's suspicious declaration.

Table 4: Emergence Rate of Cooperation, Ce

population distinction	rP=0	rP=0.5	rP=1
AllCAllD	0.283	---	---
2ASYM			
Ig	0.407	---	---
LIg	0.517	0.356	0.273
HIg	0.647	0.520	0.497
GIg	0.807	0.797	0.820
HL	0.643	0.453	0.323
GL	0.763	0.677	0.567
GH	0.870	0.903	0.843
HLIg	0.600	0.433	0.407
GLIg	0.713	0.617	0.547
GHL	0.840	0.657	0.587
GHLIg	0.710	0.687	0.563

First we examine whether Recipient's declaration promote the emergence rate of cooperation or not in case of no punishment for suspicious declaration. The second (rP=0) column shows that the cooperation emerges 28.3% in AllCAllD population and 40.7% in Ig. Since Ig of 2ASYM ignores Recipient's declaration whose emergence rate of cooperation is 40.7%, the cooperation emerges 51.7% in LIg, and more than or equal to 60% in other distinctions, the increases of Ce from 40.7% by declaration are due to our way of indirect downstream reciprocity different from the second incomplete information model in Nowak and Sigmund (1998). We conclude the following observation:

1. Declaration promotes the emergence of cooperation. Furthermore, if initial distinctions contain G or contain H except G or contain L except H and G, then the emergence rate of cooperation is larger than 70% or 59.9% or 50%, respectively. Thus L, H, and G promote the emergence of cooperation roughly in this order.

Now we examine the effect of declaration on the emergence of cooperation if punishment for suspicious declaration is allowed. Let us judge declaration to promote the emergence of cooperation if the emergence rate of cooperation is larger than 50%. As the third (rP=0.5) and fourth (rP=1) columns of Table 4 show, we conclude the following observation:

2. Initial distinctions needs to contain G (except one case, HIg, rP=0.5) for declaration to promote the emergence of cooperation if punishment for suspicious declaration is allowed. Furthermore, the emergence rate of cooperation decrease as the rate of punisher increases except GIg and GH.

Next we examine the rate of players who declare with High probability (H). Table 5 shows them at period 500 if the emergence rate of cooperation is larger than 50% and the table concludes the following observation:

3. The rates of players who declare with H at period 500 are larger than the initial rate 50%. They decrease as the rate of punisher increases. Distinctions L, H, and G make these rates larger roughly in this order.

Table 5: Rate of Players to Declare with High Probability at period 500

population distinction	rP=0	rP=0.5	rP=1
2ASYM			
Ig	---	---	---
LIg	0.631	---	---
HIg	0.864	0.814	---
GIg	0.947	0.832	0.734
HL	0.909	---	---
GL	0.965	0.815	0.672
GH	0.988	0.855	0.834
HLIg	0.858	---	---
GLIg	0.916	0.798	0.627
GHL	0.952	0.840	0.782
GHLIg	0.929	0.831	0.685

Next we investigate the effect of declaration on the distribution of strategies, distinctions, and declarations with Low probability or with High probability by focusing on 2ASYM, GHLIg, and rP=0.5 case. Figure 2-1 is scatter diagram of (rate of distinction G, number of population) at period 500 of successful runs. Figure 2-2 is scatter diagram of (rate of distinction H, number of population) at period 500 for the runs with rate of distinction G < 0.15. For convenience sake, let us divide all successful runs into three cases, A, B and C;

A for rate of distinction G, rG >= 0.15, B for rG < 0.15 (found that rate of distinction L, rL is also small) and rate of distinction H, rH < 0.3, and C for the others.

Figure 3-1, 3-2, and 3-3 show piled distribution (2,1)G, (2,2)L, and AllD of one run (circled in Figure 2-1; rG=0.42, rH=0.0014, rL=0.36) in case A over periods, respectively. The other strategies (distinctions) such as AllC, HP and HL almost vanish. Note that although there exist GP, GN, LP and LN, LP is fairly small. They declare with High probability (not shown here). AllD, who tends to declare with Low probability because of punishment by GP, diminishes as time goes.

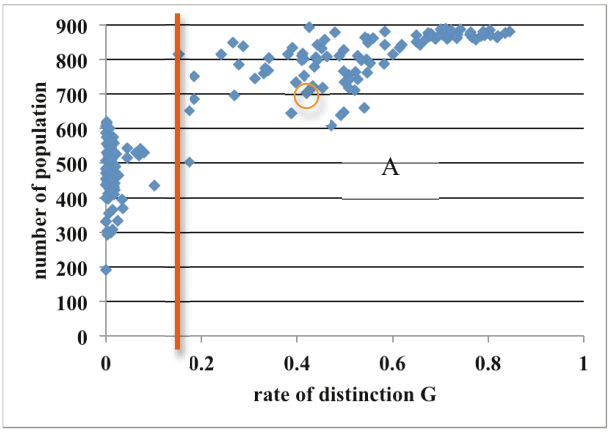

Figure 2-1: Scatter Diagram (rG,p) at Period 500

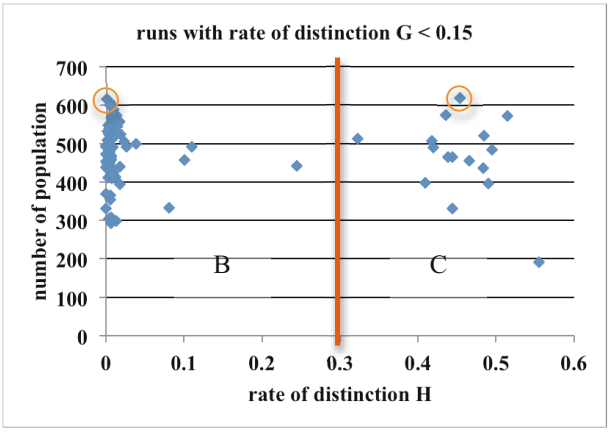

Figure 2-2: Scatter Diagram (rH,p) at Period 500

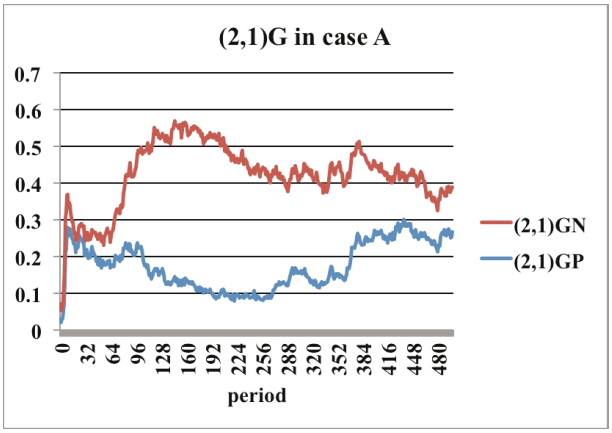

Figure 3-1: Distribution (2,1)G of One Run in Case A

Figure 4-1 and 4-2 are related to one run (circled in Figure 2-2; rG=0.0016, rH=0, rL=0.003) in case B. There exist AllC and AllD, who declare roughly with High probability. The other strategies (distinctions) such as (2,1) and (2,2) almost vanish.

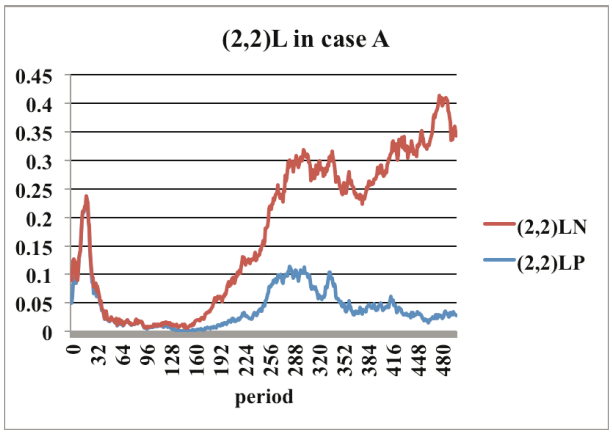

Figure 3-2: Distribution (2,2)L of One Run in Case A

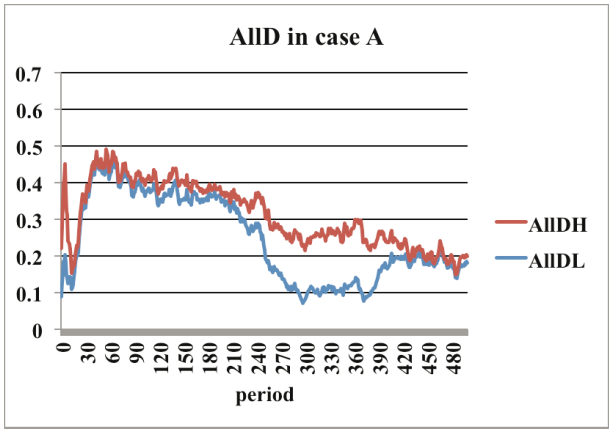

Figure 3-3: Distribution AllD of One Run in Case A

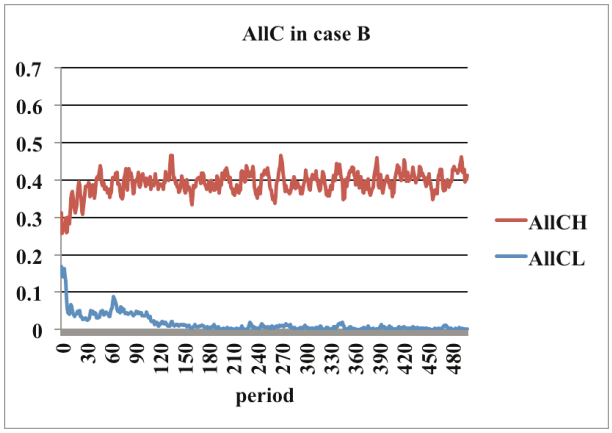

Figure 4-1: Distribution AllC of One Run in Case B

Figure 5 shows piled distribution (2,2)H of one run (circled in Figure 2-2; rG=0.0016, rH=0.45, rL=0.011) in case C over periods. HP (punisher) vanishes. The rest of the population consists almost of AllD. (2,2)HN and AllD declare with High probability because of almost no punisher (not shown graphically here).

Figure 6 shows the average distributions of strategies at period 500 for case A, B, and C, respectively. Large G (>0.15) makes (2,2) or (2,1) bar high and AllD bar low because of his ability to distunguish in case A. There is almost no effect of declaration and AllC and AllD bars are high in case B, which corresponds with Namekata and Namekata (2012). Large H (>0.3) makes (2,2) or (2,1) bar high but AllD bar is still high because of no ability of H's to distinguish in case C.

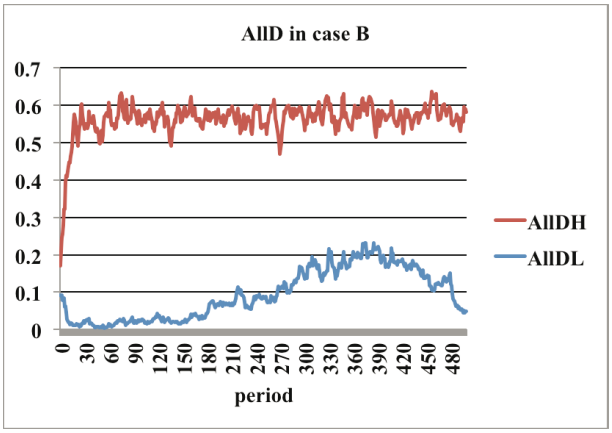

Figure 4-2: Distribution AllD of One Run in Case B

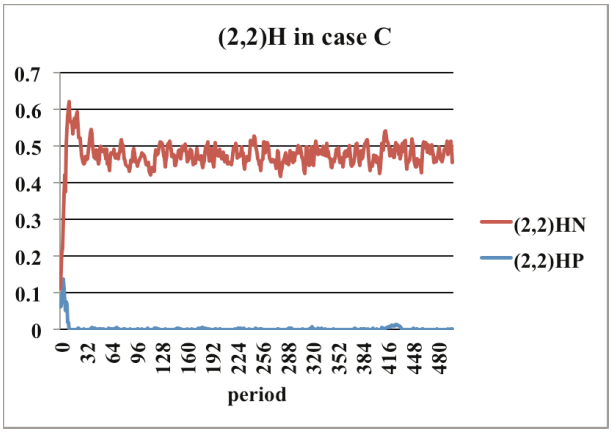

Figure 5: Distribution (2,2)H of One Run in Case C

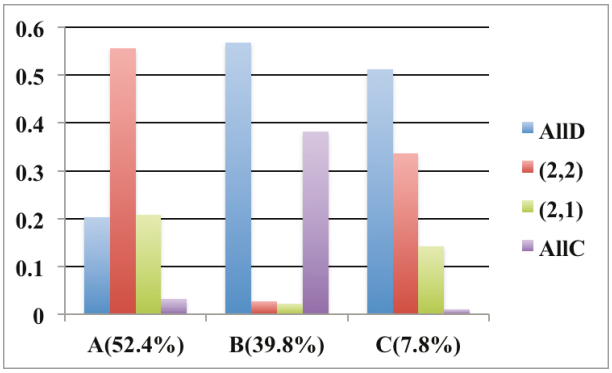

Figure 6: Average Distribution of Strategies at period 500

CONCLUSION

We investigate the effect of declaration on the emergence of cooperation and the distribution of strategies in Demographic Donor-Recipient game. We show, by Agent-Based Simulation, that Recipient's declaration promotes emergence of cooperation even if Donor has no ability to distinguish true declaration from false one in case of no punishment, but some Donors need to have some ability if punishment is allowed. We also show three types of distributions of strategies.

Suppose that you and another person come to the only one seat available, while you are a bit ahead of the person. You are Donor and the person is Recipient. Defect means you take the seat. The person may say "After you" to impress you that he is cooperative. Our results suggest that in order to promote cooperation it is effective for you to declare yourself cooperative, to trust declaration of others, and not to punish suspicious declaration if you cannot appreciate the declaration correctly.

Our future research is to find some feature of a player other than declaration or reluctance, which is oriented toward cooperation, and to investigate its effect on the emergence of cooperation.

REFERENCES

Epstein, J. M. 2006. "Zones of Cooperation in Demographic Prisoner's Dilemma." In: *Generative Social Science*. Princeton University Press, 199-221.

Namekata, T. and Namekata, Y. 2011. "Effect of Reluctant Players in Demographic Prisoner's Dilemma Game." In: R. Bartak (ed.): *Proceedings of the 14th Czech-Japan Seminar on Data Analysis and Decision Making under Uncertainty* (held in September 18-21, 2011, Hejnice, Czech Republic), 102-109.

Namekata, T. and Namekata, Y. 2012. "Emergence of cooperation and patterns of move-play in Demographic Donor-Recipient Game." In: Masahiro Inuiguchi, Yoshifumi Kusunoki and Hirosaki Seki (eds.): *Proceedings of the 15th Czech-Japan Seminar on Data Analysis and Decision Making under Uncertainty* (held in September 24-27, 2012 Osaka, Japan), 51-58.

Nowak, M. A. and Sigmund, K. 1998. "Evolution of indirect reciprocity by image scoring." *Nature*, No 393, 573-577.

Nowak, M. A. and Sigmund, K. 2005. "Evolution of indirect reciprocity." *Nature*, No. 437, 1291-1298.

Riolo, R. L., Cohen, M. D. and Axelrod, R. 2001. "Evolution of cooperation without reciprocity." *Nature*, No. 414, 441-443.

AUTHOR BIOGRAPHIES

TSUNEYUKI NAMEKATA is a Professor in Department of Management Science at Otaru University of Commerce. He holds a PhD in the field of Dynamic Programming and Cooperative Game Theory from Osaka University (Japan). He is currently interested in the emergence of cooperation in dilemma game through Agent-Based Simulation.

YOKO NAMEKATA co-authored two books about Game Theory and Fair Allocation and several papers about Dilemma Games. Her current research interest is to incorporate Japanese typical feature emphasizing on relation into player to promote cooperation in dilemma situation.

AN AGENT-BASED MODEL TO SIMULATE PATHOGEN TRANSMISSION BETWEEN AQUACULTURE SITES IN THE ROMSDALSFJORD

Saleh Alaliyat, Ottar L. Osen
Faculty of Engineering and Natural Sciences
Aalesund University College
N-6025, Aalesund, Norway
Emails: saal@hials.no, oo@hials.no

Kristina Øie Kvile
Centre of Ecological and Evolutionary Synthesis
University of Oslo
N-0316, Oslo, Norway
Email: k.o.kvile@ibv.uio.no

KEYWORDS
Agent-based modeling, aqua farms, NetLogo, pathogen transmission, diseases in aquaculture.

ABSTRACT

Fish farming is an important industry along the Norwegian west coast. This industry provides labor opportunities and financial income in areas that are often thinly populated. Fish are subject to diseases carried by pathogens. The value of the fish that are lost due to disease is worrisome, and emergent diseases continue to pose a severe challenge to the aquaculture industry. We have built an agent-based model to simulate the emergence of a hypothetical fish pathogen in an aquaculture facility in the Romsdalsfjord[1] to observe how this pathogen possibly spreads to multiple facilities within the fjord. This model enables us to observe how key parameters such as current speed, current direction, pathogen life span, contagiousness and fish density affect the disease dynamics. The model is implemented in NetLogo, and we have included three aquafarms at the Romsdalsfjord in the experiment.

INTRODUCTION

Aquaculture is about to revolutionize the way we consume fish and other marine food products as agriculture already did on land. During the past few decades world capture fisheries have stabilized or decreased, whereas aquaculture production has increased massively (FAO 2012). In 2010, aquaculture stood for 47% of global food fish production, and in Norway the export value of farmed seafood now exceeds that of wild caught species (FKD 2013). Today, fish is the third most important export product after oil/gas and metal, and accounts for 5.7 per cent of the total Norwegian export value according to Statistics Norway (SSB 2013). Norway is the largest exporter of aquaculture products in Europe, and number six globally, after Asian nations such as China, India and Indonesia (FAO 2012). It is thus clearly of high importance for Norwegian economy to ensure a sustainable aquaculture industry.

However, emergent diseases continue to be a serious challenge to the aquaculture industry and set constraints to its expansion (Murray & Peeler 2005). Diseases both induce large economic costs to the industry (Werkman *et al.* 2011) and might threaten wild populations (Murray & Peeler, 2005). A major problem in many areas has been the uncontrolled use of antibiotics leading to resistant bacteria strains (Defoirdt et al. 2011). Although the antibiotics use in Norway today is restricted, and some important pathogens have been reduced through vaccination programs, new and/or resistant pathogens still emerge (Olsen & Hellberg 2011). Combatting these diseases is therefore an important research field (Johansen *et al.* 2011) and a hot topic in public debates (e.g. NTB 2011).

Atlantic salmon is by far the most important species in Norwegian aquaculture. The most troublesome diseases for the salmon aquaculture are caused by viruses (Olsen & Hellberg 2011). All major viruses affecting Norwegian aquaculture are thought to spread between fish through sea water (Johansen *et al.* 2011), as infected fish shed pathogens to the surrounding waters. To keep fish farms at appropriate distances is therefore a potential measure to combat this horizontal transmission.

This model aims to simulate the pathogen transmission between aquaculture sites in a Norwegian fjord and observe how this pathogen possibly spreads to multiple facilities within the fjord. This model uses many key parameters such as current speed, direction, pathogen life span, contagiousness and fish density to find possible pathogen transmission patterns. Before describing the model in detail; a more complete background on the dynamics of fish disease transmission and previous studies on this issue will be given in the next section.

Diseases in aquaculture

Knowledge of pathogens in wild fish stocks is generally poor, and it is therefore difficult to predict which diseases might occur once an aquaculture facility is established in an area (Bergh 2007). A wide range of pathogens exists, from viruses and bacteria to crustacean parasites (Olsen & Hellberg 2011). These might be introduced to an aquaculture system through various pathways: movement of infected stocks, equipment or fish products from other areas; or by exposition to wild fish pathogens (Murray & Peeler 2005). Once introduced, pathogens can benefit from the aquaculture environment and pose a graver risk to farmed fish than wild stocks. This is both because of factors such as poor environment, stress and pollution that might reduce individual fish resistance (Murray &

[1] Romsdalsfjorden is 88 km Long and located in the Romsdal district of Møre og Romsdal county.

Proceedings 27th European Conference on Modelling and Simulation ©ECMS Webjørn Rekdalsbakken, Robin T. Bye, Houxiang Zhang (Editors)
ISBN: 978-0-9564944-6-7 / ISBN: 978-0-9564944-7-4 (CD)

Peeler 2005), but moreover because the artificial high density of fish, and thus potential hosts for the pathogen, in a fish farm can induce outbreaks (Bergh 2007; Rimstad 2011). Pathogens that benefit from higher host densities follow so-called *density-dependent transmission* (Murray 2009). The rate of transmission is the product of the densities of susceptible and infected individuals.

As previously mentioned, disease transmission can happen with currents, depending on the survival time of the pathogen in water masses, but also through vectors such as wild fish or escaped farmed fish (Murray & Peeler 2005). Hydrodynamic spreading will usually be a local-scale problem, whereas wild fish can become infected nearby a farm and transmit the pathogen over larger distances (Werkman *et al.* 2011). An example of a waterborne virus is the Salmonid alphavirus causing Pancreas disease (PD), an increasing problem in Norwegian aquaculture (Kristoffersen *et al.* 2009). Stochastic models have emphasized the importance of the distance between farms for disease transmission of both this and other diseases affecting farmed salmon, such as heart and skeletal muscle inflammation (HSMI) and infectious salmon anaemia (ISA) (Aldrin *et al.* 2010).

Using an Agent-based model (ABM) to simulate disease transmission in aquaculture

Previous modeling studies on the transmission of pathogens within and between farmed fish populations have either used classical SIR disease transmission models (Susceptible, Infected, Recovered) that focus on the population as a whole (e.g. Murray 2009; Green 2010), or such population models coupled with simple hydrodynamic models or distance measures of transmission between separate populations (Viljugrein *et al.* 2009; Aldrin *et al.* 2010; Werkman *et al.* 2011; Salama & Murray 2011). To our knowledge no studies have previous applied ABMs to assess the transmission of diseases within and/or between aquaculture fish populations. On the other hand, ABMs have been applied to simulate transmission of human viral diseases such as influenza (e.g. Ciofi degli Atti *et al.* 2008; Milne *et al.* 2008). ABMs can be valuable for analyses focusing on individual interactions, and also to incorporate the spatial aspect of the system. Whereas classical SIR-models used in disease transmission modeling represent total populations, we here apply an ABM to simulate individual fish becoming infected, and how pathogens spreads spatially by also representing these as agents. By applying an ABM instead of e.g. differential equations more complexity can be added and analysed through simulations. Another reason for applying an ABM is that empirical data regarding fish pathogens are often lacking. It is therefore difficult to predict the threshold for density-dependent outbreaks of diseases in classical disease transmission models (Krkosek 2010). In an ABM, the parameters regarding disease transmission can easily be varied.

Modelling a real system

Since there are presently research activities regarding aqua farms in the Romsdalsfjord, we decided to look for both inspiration for research problems and potential parameter values that have emerged from these studies. From these studies we pursued the effect of the fact that pathogens may survive in water for days without a host. Furthermore, since there are many aqua farms in the Romsdalsfjord (DF 2013), about 35 (*see figure 1*), the close proximity between the farms becomes an important factor in disease transmission. It is a relevant issue in current research efforts to study under which conditions one infected aqua farm may spread disease to other farms by pathogens "jumping" from one aqua farm to the next, creating a domino effect.

Figure 1: Map, which shows the aqua farms in Romsdalsfjorden.

THE MODEL

This section describes how our model works. The model is implemented in NetLogo (*Figure 2*).The idea behind the model is to simulate three aquafarms which reside in the same fjord area, and that we can suspect are subject to cross contamination between each other. All parameters used in the model are listed in *Table 1*.

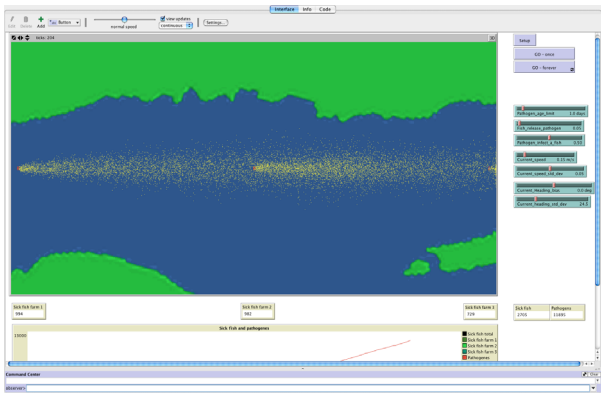

Figure 2: NetLogo model

We do not specifically model the background of introduction of a disease, and assume that the pathogen

is a new variant for which no vaccination is yet in place. The model presented is a general model, which can be adjusted to various pathogens and environmental scenarios. Salmon aquaculture is the most common form of aquaculture in Norway, and since the most important mode of transmission of salmon disease is by water currents we chose to model this process.

Table 1: Parameters used in the model

Parameter	*Description*	*Estimate*	*Source*
Current speed	Current speed in m/s	0.02 – 0.2	4,6,7
Current direction	Current direction in degrees		6,7
Transmission parameter [+]	Probability that a fish is infected by a pathogen in its surrounding water	$5.416^{x}10^{-4}$ – $8.912^{x}10^{-4}$/hour (minimum values)	3
Shedding parameter [+]	Number of pathogens shed by infected fish	High*	1,2,5
Pathogen lifespan [+]	Lifespan of pathogen in seawater in days	8.33 – 62.5 hours Depends on pathogen and environment	3

[+]Pathogen values for Infectious salmon anaemia virus (ISAV), Infectious pancreatic necrosis virus (IPNV) and Salmonid alphavirus (SAV).
* Different sources use different units and values are ranging from $10^{6.5}$ PFU/fish/h (PFU= plaque forming units) (1), 10^{5}—10^{8} CFU/fish/h (CFU=colony forming units) (2) and 6.8 *10^{3} $TCID_{50}$ /ml/ kg fish/ h/ (maximum rates) ($TCID_{50}$ =the amount of virus required to kill 50% of infected hosts) (5). The units are not single pathogens but units that are measureable in the lab. Since the numbers are very high, and computationally difficult to implement in the model we set a probability between 0-1 (adjustable) that an infected fish sheds a pathogen, but this pathogen represents a large number. The probability value is likely to be high (close to 1) as observed shedding rates are on these ranges.

References:

1. Gregory, A. (2008) A Qualitative Assessment of the Risk of Introduction of a Qualitative Assessment of the Risk of Introduction of Viral Haemorrhagic Septicaemia Virus into the Rainbow Trout Industry Scotland. Aberdeen, UK.
2. Rose, A.S., Ellis, A.E. & Munro, A.L.S. (1989) The infectivity by different routes of exposure and shedding rates of Aeromonas salmonicida subsp. salmonicida in Atlantic salmon, Salmo salar L., held in sea water. Journal of Fish Disease, 12, 573–578.
3. Salama, N. & Murray, A. (2011) Farm size as a factor in hydrodynamic transmission of pathogens in aquaculture fish production. Aquaculture Environment Interactions, 2, 61–74.
4. Urke, H.A., Kristensen, T., Daae, K.L., Bergan, M.A., Ulvund, J.B. & Alfredsen, J.A. (2011) Konsekvenser Av Sjødeponi i Repparfjorden for Anadrom Laksefisk. Delutredning i KU Program for Planlagt Gruvedrift i Nussir Og Ulveryggen i Kvalsund Kommune.
5. Urquhart, K., Murray, a G., Gregory, a, O'Dea, M., Munro, L. a, Smail, D. a, Shanks, a M. & Raynard, R.S. (2008) Estimation of infectious dose and viral shedding rates for infectious pancreatic necrosis virus in Atlantic salmon, Salmo salar L., post-smolts. Journal of fish diseases, 31, 879–87.
6. MODS Strømmodellering og smitte-spredning, http://mods.sinmod.no/
7. Stene, A., Hansen, G.A., Yttredal, E.R. and Solevåg, S.E. (2009), Integrert Akvakultur - Effektiv utnyttelse av kystsonen – Effekt på arealbinding og interessekonflikter, Ålesund, 03 2009.

Scaling the model in space and time

As a real-world basis for our model we use the aqua farms at Midsund (*Figure 3*), in the Romsdalsfjord. This part of the fjord currently hosts three aqua farms, with a distance of about 8 km between each site. The farms have a size of around 10,000 square meters and host around a million fish each (DF 2013). The total area of interest is about 16 km wide. We constructed the model in a rectangular space of 16 x 8 km. In our model all three aqua farms have the same size, 80 m x 120 m. The farm sizes are thus close to some of the real fish farms in the Romsdalsfjord (DF 2013). Each fish farm is populated with 1000 fish, while in reality you would expect to see about 1000 times more fish in an actual fish farm at this size. This simplification was made in order to save computer resources while running the model.

Figure 3: Midsund

According to MODS (2012) the average current speed in the Romsdalsfjord is typically 0.2 m/s. This equals 12 m/min or 120 m/tick. Tick is the time step in the model and its representing 10 minutes. The model enables the current speed to be varied around the default value of 0.2 m/s, and in order to move the pathogens at the correct speed in the simulations the conversion factor was incorporated.

The fish agents

The fish are created during the setup procedure of the model. In each of the three farms; 1000 fish are distributed across the farm's area. When the simulation starts all fish are healthy, i.e. belonging to the susceptible group. The exception is one infected fish in Farm 1. Healthy fish may become infected if there is a pathogen present at the same place as the fish. Once a fish is infected they start to produce pathogens at a rate given by a certain parameter (*Fish_release_pathogen*). This parameter represents the probability that one fish produces one pathogen in one time step. The probability that a healthy fish gets infected while being on same place as a pathogen during one time step is given by the parameter *pathogen_infect_a_fish*. The two probabilities for pathogen production and infection are flexible (between 0 and 1).

Pathogen agents and current simulations

Pathogens are also represented as agents. It is important to note that one pathogen agent does not represent one pathogen, but a batch of a high number of pathogens. Each pathogen is moved by the currents, with the current speed and direction given by the place the pathogen is at by the start of the time step.

In order to create a model that incorporates some of the variation present in nature we used normally distributed random numbers for both the current speed and current direction. By introducing this randomness we avoid to some extent to end up with a very specific case scenario that would be less valuable for generalizations. In theory, the model can be built with very complex current patterns (*see Figure 4*): pathogens inherit the current direction of the place they are presently on, and by moving to a new place they change the direction to the direction inherited from that place. In our Nelogo model, current angle was set directly inwards in the fjord. During each time step a random deviance is added to this current angle. This randomness is given by two parameters: A current standard deviation (*Current_heading_std_dev*) which can be set from 0 to 90 degrees and a bias term (*Current_heading_bias*) used to offset the direction given by the patch[2], which can be set between -5 and 5 degrees. When moving the pathogen might hit dry land. In this case the pathogen is removed from the model (dies).

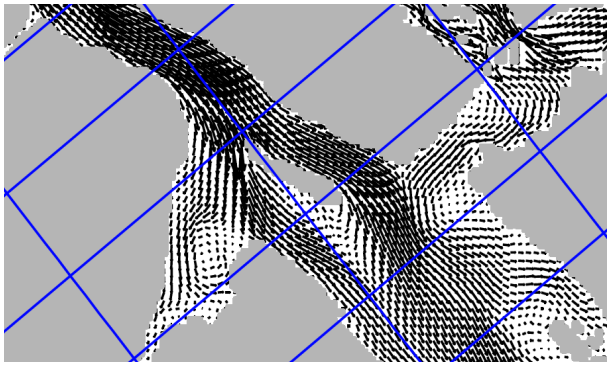

Figure 4: Currents direction in Romsdalsfjorden, MODS (2012).

The current speed is decided by the parameter *Current_speed*, and can be set from 0 to 2 m/s, with a default of 0.2 m/s. The current speed it is also accompanied by a random variation term, given by the parameter *Current_std_dev,* which can be set between 0 - 0.1 m/s. As we expect that current speed is not constant through time and space, this random term is used to make the model more realistic. Likewise the current speed can also depend on the individual patch. This is useful in order to model how current speed varies with the geometry of the fjord (e.g. changes in the width of the fjord, the presence of islands and peninsulas etc.). This aspect is incorporated by adding a constant to each patch, *the relative speed*. Relative speed is a number by which the global current speed is multiplied for each patch. Hence, a relative speed below one indicates a speed below the average in that particular patch. Likewise, a relative speed greater than one indicates a speed higher than the average.

The pathogens are given a fixed life span in the range of the values we found in literature. In the model this parameter can be set between one and ten days, with a resolution of 0.1 day. At each tick all individual pathogens' ages are updated by adding 10 minutes (corresponding to 10/24/ 6 = 0.069 days) to their cumulative age. When a pathogen's age exceeds the value given by the age limit it dies.

RESULTS OF THE EXPERIMENT

A simulation experiment was set up for the model. The model was run for 400 time steps, and three of the model parameters were varied in the following manner:

- Current speed: 0.05 to 0.25 m/s, at steps of 0.5 (5 values)
- Infection rate (Pathogen infect a fish): 0.1 – 1, at steps of 0.1 (10 values)
- Pathogen age: 0.2 – 3, at steps of 0.2 (15 values)

The simulation experiment output was the number of infected fish in each of the three fish farms (Farm 1, Farm 2 and Farm 3) at each time step. Running the experiment by using normal machine took around 15 hours, but to run it by using super-computer with 6 processers took around 5 hours. *Figure 5* (a,b,c,d and e) shows the number of infected fish in Farm 2 after 400 time steps. The interpretations of the figures follow in the next section.

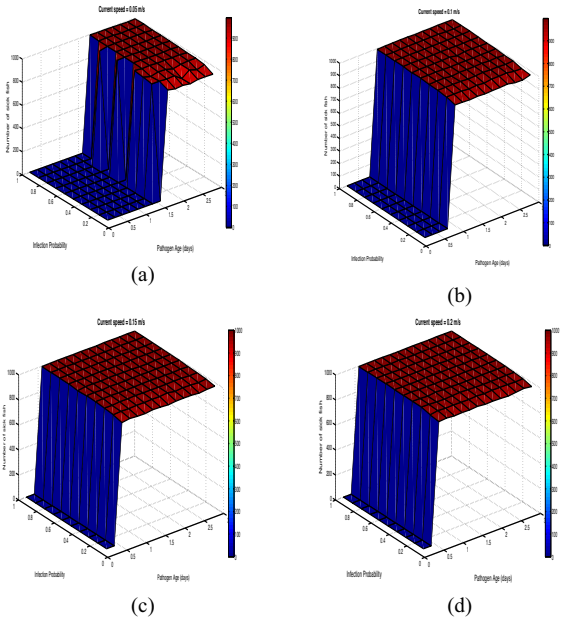

(a) (b) (c) (d)

[2] Patchs represent the grids in the landscape in NetLogo.

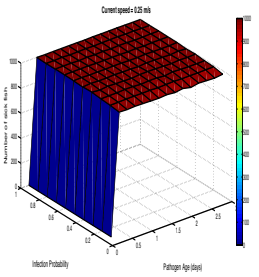

(e)

Figure 5: Number of sick fish (z-axis) in Farm 2 after 400 time steps, with current speed set at five different values (0.05, 0.1, 0.15, 0.2 and 0.25 m/s), and infection probability (x-axis) and pathogen (y-axis) varied.

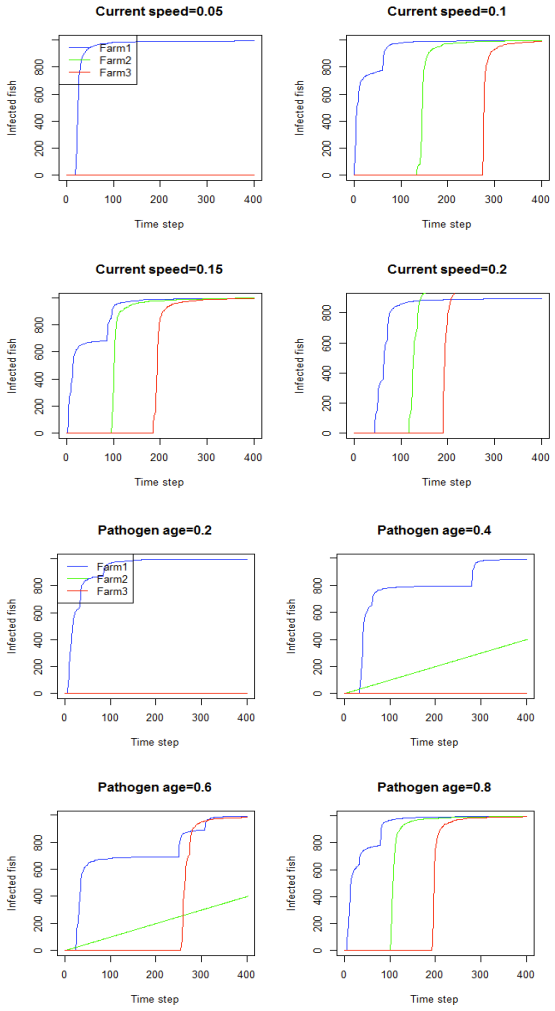

Figure 6: Number of infected fish per time step in the three fish farms (blue line=Farm 1, green line=Farm 2, red line= Farm 3). For the four graphs on the top infection rate and pathogen life span were held constant at 0.5 and 2, respectively and current speed was varied at four different levels. For the four graphs down pathogen age was varied, while infection rate was set at 0.5 and current speed=0.15 m/s.

DISCUSSION

As described above, the aquaculture industry is increasingly important for both the Norwegian economy and people's marine food availability worldwide. A major challenge for aquaculture development is the emergence of diseases, which can be due to a large variety of pathogens. It is therefore highly relevant to study how pathogen transmission between aquaculture sites can vary due to factors such as currents and pathogen virulence. Using an ABM we were able to simulate both fish and pathogens as individual agents and specifically study the movement of pathogens in a simplified fjord system. ABMs have to our knowledge never been employed in this type of study before. Although the model is simplified, we believe that it provides some insight into the transmission of pathogens between fish farm sites.

The simulation output

Current speed was the most important parameter controlling the number of infected fish in the aquaculture sites. The age limit of the pathogens was also important for the number of sick fish in Farm 2 and Farm 3. In fact, as long as the pathogen age was above a certain threshold, all fish in the fish farms would ultimately become infected. When current speed was held constant, the infection rate also had a significant impact on the number of sick fish in Farm 2 and 3, and for Farm 1 for low current speeds (<0.2).

The minimum pathogen age required to get infection in Farm 2 within 400 time steps, and at the lowest current speed we tested (0.05 m/s), was from 1.4 to 1.6 days, depending on infection probability. For Farm 3, the minimum current speed needed in order to get infection within 400 time steps was 0.1 m/s. At this current speed, the minimum pathogen age limit was 0.8 days. With this combination of current speed and pathogen life span the infection process occurs in Farm 2, which is subsequently sending new pathogens to Farm 3. If the current speed maximized to 0.25 m/s, only a lifespan of 0.2 days is needed in order to get infection in Farm 2, and subsequently in Farm 3. I.e., at current speeds above 0.1 m/s the dynamics of Farm 2 and 3 are similar, as Farm 2 acts as a new source of pathogens for Farm 3, and the distances are the same.

Scaling the model

If we were going to represent a realistic number of agents (fish and pathogens) the model simulation would be very computationally demanding. In Norway today, aqua farms can host fish in the order of millions (DF 2013) and for pathogens the numbers would be uncountable, in the order of trillions or higher, depending if we are studying bacteria or virus. In order to be able to run the model we therefore had to scale it down significantly. Even so, the relative magnitude between the number of fish and pathogens is likely

incorrect, with the number of pathogens underestimated. To compensate for this, the probabilities of infection and pathogen release should be adjusted accordingly, meaning that they should be set higher than what might be expected. A challenge in this approach is that these parameters are largely unknown. Another issue arising from scaling down the model is that the pathogens might less easily "hit" the aqua farms, since there are likely fewer pathogens in the system than what would be realistic. It is harder to compensate for this issue by adjusting the probability of infection, since infection requires the actual presence of the pathogen. Increasing the probability of pathogen release would, on the other hand, compensate for this issue by creating more pathogens in the system. Another solution could be to make the aqua farms bigger (scaling up their size) in order to increase the probability of an encounter between the pathogens and the sites.

The matter of scaling thus leads to many challenges for creating a model that represents the real world. We still lack good solutions to many of these challenges, but we are aware of their existence and the results of the model simulations should accordingly be interpreted with this in mind. In essence, our simplified model of the Romsdalsfjord is aimed at studying effects that may occur, but it is not appropriate to make any numerical predictions.

Simulating pathogen transmission and infection

The most challenging part of the modeling process was to simulate the pathogen transmission process, due to lacking empirical data on these issues in the literature. There are several uncertain factors regarding the process of transferring illness between fishes. To create a realistic model for the infection process is therefore difficult, and our approach was to model a simplified scenario that can later be tuned to reproduce results observed in fish farms. Moreover, the few studies that have quantified the rates by which pathogens are shed by infected fish use different units which are not single pathogens, but units that are measureable in the lab or practical for disease monitoring (Salama & Murray, 2011). It was not straightforward to convert these values into probabilities, and we therefore had to experiment to find appropriate values. The probability of pathogen infection was varied during the simulations, while the shedding rate (Fish release pathogen probability) was kept constant (0.05). This was done in order to facilitate the interpretation of the results, and because we lacked any references as to what would be realistic values for the latter parameter.

CONCLUSIONS AND FUTURE WORK

In this ABM, we have simulated three fish farms in the Romsdalsfjord. The number of infected fish in each farm is predicted by factors such as current speed and pathogen life span. The results provide a good base for exploring the relationship between these variables and others (infection rate, pathogen release rate current bias etc.), and platform on which more complexity can be added to the model at a later stage. Such possible complexities are described hereunder.

Pathogen transmission

In reality, the proliferation of a pathogen can be highly dependent on environmental conditions such as temperature, and thus vary with seasonal and inter-annual environmental changes (Krkosek 2010). Also, the virulence of the pathogen and the conditions of the host (health, age, stress etc.) will affect the likelihood of an outbreak (Rimstad 2011). At this stage, we have only modeled a short disease proliferation period, and therefore assumed temperature to be constant. A next step could be to incorporate a dynamic temperature variable in our modeled fjord which would affect infection probability and pathogen release.

In this model, we focused on the distance between aquaculture sites, but not their individual sizes. But water-transmitted pathogens can also benefit from the size of the aquaculture site. A next step for our model could be to vary both distances and sizes of the fish farms. This could be interesting for managers deciding upon which areas would be appropriate in order to avoid disease transmission between fish farms.

Currents modeling

In our model, we have assumed the currents speed and direction act according to MODS (2012), and depend on what is written in the literature. We have assumed that current direction is inwards in the fjord and changes between 0.05 to 0.25 m/s in our experiment (at Midsund, *see figure 3*). We have selected these values by analyzing the geographic of the fjord (at Midsund) and results from MODS (2012). But in the reality, the current speed and direction are more variable and depend on many other factors, as season, snow melting rate, and the geographic of the fjord. The model would become more realistic if it was connected to a current model of the fjord.

Fish movement

Although the transmission through water is the most important route for marine pathogens, a further step could be to incorporate the movement of the farmed fish, with a certain probability of escaping (and which could be infected or not). Fish escapees can in fact pose a risk to the wild population through spreading of diseases (Naylor *et al.* 2005), a risk that increases when farmed fish are in the vicinity of wild populations of the same species and the farmed population contributes a large quantity compared to the wild fish.

Another interesting, but challenging, possibility would be to include wild fish agents. A study on the distribution of saithe within a fjord with salmon aquaculture showed aggregations around aquaculture facilities and a high proportion of fish moving between different farms, indicating that the wild fish might constitute an important connection between fish farms (Uglem et al. 2009). The fish might aggregate around the farms to feed on waste pellets under or around the nets. A range of pathogens is thought to be common to salmon and saithe, but the likelihood of transmission between caged and wild fish is unknown.

Altogether, the model presented here offers an interesting first step towards more complex models of disease transmission between aquaculture sites, an important research issue for the aquaculture industry.

REFERENCES

Aldrin, M., Storvik, B., Frigessi, A., Viljugrein, H. & Jansen, P. a. (2010) A stochastic model for the assessment of the transmission pathways of heart and skeleton muscle inflammation, pancreas disease and infectious salmon anaemia in marine fish farms in Norway. *Preventive veterinary medicine*, 93, 51–61.

Bergh, O. (2007) The dual myths of the healthy wild fish and the unhealthy farmed fish. *Diseases of aquatic organisms*, 75, 159–64.

Ciofi degli Atti, M.L., Merler, S., Rizzo, C., Ajelli, M., Massari, M., Manfredi, P., Furlanello, C., Scalia Tomba, G. & Iannelli, M. (2008) Mitigation measures for pandemic influenza in Italy: an individual based model considering different scenarios. *PloS one*, 3, e1790.

Defoirdt, T., Sorgeloos, P. & Bossier, P. (2011) Alternatives to antibiotics for the control of bacterial disease in aquaculture. *Current opinion in microbiology*, 14, 251–8.

DF (2013), Directorate of Fisheries, http://www.fiskeridir.no/ (accessed 18.01.2013).

FAO (ed). (2012) *The State of World Fisheries and Aquaculture*. Rome, Italy.

FKD (2013), The Norwegian Ministry of Fisheries and Coastal Affairs, www.fisheries.no (accessed 18.01.2013).

Green, D.M. (2010) A strategic model for epidemic control in aquaculture. *Preventive Veterinary Medicine*, 94, 119–27.

Johansen, L.-H., Jensen, I., Mikkelsen, H., Bjørn, P.-A., Jansen, P.A. & Bergh, Ø. (2011) Disease interaction and pathogens exchange between wild and farmed fish populations with special reference to Norway. *Aquaculture*, 315, 167–186.

Kristoffersen, A.B., Viljugrein, H., Kongtorp, R.T., Brun, E. & Jansen, P.A. (2009) Risk factors for pancreas disease (PD) outbreaks in farmed Atlantic salmon and rainbow trout in Norway during 2003-2007. *Preventive veterinary medicine*, 90, 127–36.

Krkosek, M. (2010) Host density thresholds and disease control for fisheries and aquaculture. *Aquaculture Environment Interactions*, 1, 21–32.

Milne, G.J., Kelso, J.K., Kelly, H.A., Huband, S.T. & McVernon, J. (2008) A small community model for the transmission of infectious diseases: comparison of school closure as an intervention in individual-based models of an influenza pandemic. *PloS one*, 3, e4005.

MODS (2012), Strømmodellering og smitte-spredning, http://mods.sinmod.no/

Murray, A.G. (2009) Using simple models to review the application and implications of different approaches used to simulate transmission of pathogens among aquatic animals. *Preventive Veterinary Medicine*, 88, 167–77.

Murray, A.G. & Peeler, E.J. (2005) A framework for understanding the potential for emerging diseases in aquaculture. *Preventive veterinary medicine*, 67, 223–35.

Naylor, R., Hindar, K., Fleming, I.A.N.A., Goldburg, R., Williams, S., Volpe, J., Whoriskey, F., Eagle, J. & Kelso, D. (2005) Fugitive Salmon : Assessing the Risks of Escaped Fish from Net-Pen Aquaculture. *BioScience*, 5, 427–437.

NTB. (2011) Advarer mot økt fiskeoppdrett i nord. URL http://nrk.no/nyheter/distrikt/troms_og_finnmark/1.7448985 [accessed 4 December 2012]

Olsen, A.B. & Hellberg, H. (eds). (2011) The Health Situation in Norwegian Aquaculture 2011. p. 39. Norwegian Veterinary Institute.

Rimstad, E. (2011) Examples of emerging virus diseases in salmonid aquaculture. *Aquaculture Research*, 42, 86–89.

Salama, N. & Murray, A. (2011) Farm size as a factor in hydrodynamic transmission of pathogens in aquaculture fish production. *Aquaculture Environment Interactions*, 2, 61–74.

SSB (2013), Statistics Norway, Fishing and fish farming, http://www.ssb.no/fiskeri_havbruk_en/ (accessed 01.02.2013).

Stene, A., Hansen, G.A., Yttredal, E.R. and Solevåg, S.E. (2009), Integrert Akvakultur - Effektiv utnyttelse av kystsonen – Effekt på arealbinding og interessekonflikter, Ålesund, 03 2009.

Uglem, I., Dempster, T., Bjørn, P., Sanchez-Jerez, P. & Økland, F. (2009) High connectivity of salmon farms revealed by aggregation, residence and repeated movements of wild fish among farms. *Marine Ecology Progress Series*, 384, 251–260.

Viljugrein, H., Staalstrøm, a, Molvaelr, J., Urke, H. a & Jansen, P. a. (2009) Integration of hydrodynamics into a statistical model on the spread of pancreas disease (PD) in salmon farming. *Diseases of aquatic organisms*, 88, 35–44.

Werkman, M., Green, D.M., Murray, a G. & Turnbull, J.F. (2011) The effectiveness of fallowing strategies in disease control in salmon aquaculture assessed with an SIS model. *Preventive Veterinary Medicine*, 98, 64–73.

AUTHOR BIOGRAPHIES

SALEH ALALIYAT was born in Jenin, Palestine. He is currently working as a PhD candidate at Aalesund University College, Norway. He received his Master's degree in Media Technology from Gjøvik University College in Norway.

Ottar L. Osen was born in Aalesund, Norway. He has a M.Sc. in cybernetics from NTNU and is currently teaching at Aalesund University College, Norway (ass. Professor) and hold the position of Head of R&D at ICD Software AS.

Kristina Øie Kvile was born in Aalesund, Norway. She is currently working as a PhD candidate at the Centre of Ecological and Evolutionary Synthesis at the Unviersity of Oslo, Norway. She has a M.Sc. in marine biodiversity and conservation through the EU-programme Erasmus Mundus.

BEHAVIOURAL QUEUING WITH INTERACTING CUSTOMERS AND SERVICE PROVIDERS: A SIMULATION BASED APPROACH

Carlos Arturo Delgado-Alvarez
Department of Industrial Engineering
ICESI University
Calle 18 No. 122-135, Cali, Colombia
E-mail: cadelgado@icesi.edu.co

Ann van Ackere
HEC, School of Business and Economics
University of Lausanne
Dorigny, 1015, Lausanne, Switzerland
E-mail: ann.vanackere@unil.ch

Erik R. Larsen
Institute of Management
University of Lugano
6904, Lugano, Switzerland
E-mail: erik.larsen@usi.ch

KEYWORDS
Queuing problems, endogenous service and arrival rates, cellular automata (CA), adaptive expectations.

ABSTRACT

We address a service facility problem with captive interacting customers and service providers. This problem is modelled as a deterministic queuing system. Customers must routinely decide which facility to join for service, whereas service providers must decide how much to adjust the service capacity of their facilities. Both service providers and customers base their decisions on their perceptions about the system. Customers use their previous experience and that of their neighbours to update their perceptions about the average sojourn time, while service providers form their perceptions based on the queue length. We use cellular automata (CA) to model the interaction between customers and service providers. We perform a simulation to assess the way the customers' and service providers' decisions evolve and affect the system behaviour. Our results show that the more conservative the service providers, the larger the market share they achieve and the lower probability that their facility closes down.

INTRODUCTION

Most queuing problems are modelled assuming static conditions, and exogenous arrival and service rates. They are analysed in steady-state, despite the fact that they are dynamic and that agents' decisions depend on the state of the system. The analysis of queuing problems could be aimed either at optimising performance measures to improve the operating characteristics of the system without accounting for customer behaviour or at understanding the agents' behaviour through the analysis of their decisions.

Over the last decades, some researchers have attempted to move away from these predominant assumptions of traditional queuing theory towards a more dynamic context in which agents' decisions are increasingly considered. The present paper goes in this direction. We will focus on studying the behavioural aspects of queuing problems by using deterministic simulation.

A very broad range of studies has addressed the behaviour of customers and service providers in queuing problems. Nevertheless, this literature is scattered and not well-organised. The literature related to customer behaviour has been broadly discussed by Delgado (2012). The research on customer behaviour in queuing systems has been mainly tackled by marketing researchers, who study the relationships among waiting times, customer satisfaction and service quality in service facilities (Davis and Heineke 1998; Hui and Tse 1996; Taylor 1994). These studies attempt to understand the influence of waiting time on customer satisfaction, customer loyalty and service quality (Bielen and Demoulin 2007; Law, et al. 2004). Their aim is to endow service providers with information about customers' attitudes to enable them to redesign their service facility accordingly. For a review of the literature, see in Bielen and Demoulin (2007) and Gallay (2010).

As service providers (throughout the remaining of the paper we will use the term "managers" instead of service providers) value their customers because they increase the value of the firm, customers value their time (Delgado et al. 2011a). "Time is money", such as the adage says. Whatever the service customers require, waiting for service represents a waste of time for them which affects their utility. This impact is even stronger when customers repeatedly patronise a facility for service. When customers perceive that their utility is being affected, they look for another manager who maximises their utility. Some examples of this kind of systems include car owners who annually or biannually (depending on the country) must choose a garage for the emission, students or workers who daily has to choose an hour and/or a restaurant for lunch, a person who goes monthly to the bank to pay her bills, and a person who goes weekly to the supermarket, and so forth. In all these examples, customers take into account their previous experience to decide which facility to use for service. This experience enables them to choose the time and/or place that they consider less crowded. There are also situations in which customers are not necessarily humans. For instance, customers could be a stack of files waiting at an office to be dealt with, jobs at a factory waiting to be performed or dispatched, and vehicles waiting at a garage to be repaired, among

Proceedings 27th European Conference on Modelling and Simulation ©ECMS Webjørn Rekdalsbakken, Robin T. Bye, Houxiang Zhang (Editors)
ISBN: 978-0-9564944-6-7 / ISBN: 978-0-9564944-7-4 (CD)

others. Still, note that behind each of these objects is a human being waiting (e.g. the final customer of the garage is the car owner).

The complexity of the relationship between managers and customers increases in real life when many service facilities compete to render a same service. In this case, the managers' actions will affect their future decisions, those of the customers as well as those of the rival managers.

Concerning the managers' decisions, the literature have focused on analysing policies of optimal pricing and capacity decisions to control problems associated with congestion in service facility systems. P. Naor (1969) is the seminal paper on this subject. He formalised the insight originally formulated by W. A. Leeman (1964) and then discussed by T. L. Saaty (1965) and W. A. Leeman (1965). These authors suggest using pricing to help reduce queues in many service systems. Naor's model was subsequently generalised by Yechiali (1971), Edelson (1971), Edelson and Hilderbrand (1975), Stidham Jr. (1985, 1992), Mendelson and Whang (1990), Dewan and Mendelson (1990), among others. More recently, Sinha, et al. (2010) applied an optimal pricing scheme of surplus capacity to control the joint problem of existing and potential customers who are differentiated according to a pre-specified service quality level.

Although some managers' strategies effectively consider either the demand or the supply perspective when adjusting their service capacity, optimal strategies should incorporate the perspective of the two conflicting parts of the system (Pullman and Thompson 2002). Our research is motivated by the logic behind this assertion and the complexity of the interaction between the decisions of customers and managers in service facility systems. Consequently, our modelling approach considers a service facility system where competing facilities render a service which customers require routinely. Each facility has its own queue and manager. Queues are assumed to be invisible to the customers. We assume that customer interact with their neighbours and share information about their most recent experience. They use their experience and that of their best performing neighbour to update their expectations of their previously chosen queue and the one used by their quickest neighbour. Then, based on their expectations, customers choose a facility for the next time. Managers take their decision to adjust service capacity on the basis of their desired service capacity which they determine based on their perception of the queue length at their facility and a market reference sojourn time. This market reference is a benchmark whereby managers compete with each other to attract more customers to their facilities. In other words how managers perform compared to this benchmark is a competitiveness index of the facilities.

In order to study this complex problem we propose an idealised queuing model with reactive and adaptive customers and managers in which the decisions of both types of agents are interdependent. This model is built using a cellular automata-based framework. The interaction between customers is portrayed in a one-dimensional cell lattice. The main structure of the cellular automata (CA) model is similar to that of the model proposed by Delgado et al. (2011a and 2011b). However, the factors which determine the average sojourn time customer experience at the facilities are different. While in those papers this experience depended only on customers' decisions because the service capacity remained constant (i.e. exogenous service rates), now this experience is also influenced by the managers' decisions (i.e. endogenous service capacity).

Our results show that the more conservative a manager is, the larger his market share. Additionally, his facility is less likely to close down. Similarly, the facilities of reactive managers are less likely to remain in operation in the long term.

This paper is organised as follows. The next section describes the one-dimensional CA model we use to study the agents' behaviour in a multichannel service facility system. We deal in turn with the managers' and the customers' decision rules. Then, we describe the managers' and customers' profile depending on the model parameters. The next section presents the simulation results. We perform an experiment in which we analyse the influence which the different managers' parameters have on the performance of the facilities. Finally, we present the conclusion and contributions of the paper.

MODEL DESCRIPTION

Consider the queuing system and the CA model explained in Delgado et al. (2011a and 2011b). This model represents a fixed population of N reactive and adaptive customers arriving periodically at a service facility system. Each period, they must choose one between m facilities for service. Delgado et al. (2011a and 2011b) consider endogenous arrival rates (λ_{jt}) and exogenous service rates (μ). We deviate from these papers by assuming both arrival and service rates as endogenously determined. We endow managers with the ability to adjust the facilities' service capacity. In this sense, we model a system in which customers are free to choose a facility for service and the managers adjust their capacity depending on the customers' behaviour. The managers' actions can either encourage or discourage customers to use a certain facility (Delgado 2012). Consequently, the average sojourn time (i.e. customer's experience) depends on both the customers' and managers' decisions. In other words, the ability of a facility (state) to be more attractive for customers (cells) than the others depends on the behaviour of all agents in the system. For the remaining

of the paper we will use the term "agents" when referring to both the managers and the customers.

Customers' Decisions

We model the service facility's customers as a social network of colleagues, friends, or neighbours who interact in a one-dimensional *K*-neighbourhood (*K* is the number of neighbours each customer interacts with on each side). When customers patronise a facility for service, they experience an average sojourn time (W_{jt}) which depends on the arrival rate (λ_{jt}) and the service rate (μ_{jt}) of that facility. This average sojourn time represents a congestion measure of the facilities and is given by Equation (1). This equation is proposed and explained by Delgado et al. (2011b) and considers that arriving customers can temporarily surpass the service rate in a transient period, but it also satisfies the behavioural characteristics of steady-state.

$$W_{jt} = \frac{\lambda_{jt}}{\mu_{jt}^2} + \frac{1}{\mu_{jt}} \quad (1)$$

Customers use their most recent experience to form expectations of the average sojourn time for their most recently chosen facility. Customers also share their experiences with their neighbours and use this information to update their expectations regarding the average sojourn time for the previously facility chosen by their quickest neighbour. Then, we endow customers with computational memory which enables them to update their expectations for their previously patronised facility and that chosen by their best performing neighbour.

We follow Delgado et al. (2011a) and assume that customers can apply different weights to update their memory depending on the source of information. In this sense, we denote by α the weight that customers give to their own information and by β the weight for the information provided by their best performing neighbour. We apply adaptive expectations (Nerlove 1958) to model the updating process of the customer's memory (M_{ijt+1}). The adaptive expectations concept, also known as exponential smoothing (Theil and Wage, 1964), is based on the weighted average of two sources of evidence: the latest evidence (the most recent observation, W_{ijt}), and the value computed one period before (M_{ijt}). (Theil and Wage 1964). Then M_{ijt+1} is given by:

$$M_{ijt+1} = \theta * M_{ijt} + (1 - \theta) * W_{ijt} \quad (2)$$

$$s.t. \quad \theta = \begin{cases} \alpha & when\ using\ own\ information \\ \beta & when\ using\ neighbours'\ infomation \end{cases}$$

where θ denotes the coefficient of expectations and takes two different values depending on the source of information, as explained above. The logic behind this coefficient is explained in Delgado et al. (2011a) and W_{ijt} is computed using Equation (1). We label "conservative" those customers who give more weight to their memory than to the new information, i.e. α and β greater than 0.5. In contrast, when they give more weight to new information, we call them "reactive".

Once customers update their memories, they will decide to patronise the facility with the lowest expectation of sojourn time. Longer (shorter) queues bring about higher (lower) sojourn times and increase (decrease) customers' perceptions. When customers' perception about a certain facility exceeds the expectations they have regarding some other, they decide to switch facility. Otherwise they remain at the same facility

Managers' Decisions

We endow managers with similar abilities as the customers. In this sense, we assume that managers have a memory and react to customer behaviour by adjusting the service capacity of their facility. Although customers cannot observe the queues before choosing a facility, managers have information about the number of customers arriving at their facilities. They thus use this information to form their perceptions about the future arrival rate, $\hat{\lambda}_{jt}$. The managers' memory also enables them to update their perceptions each period using an adaptive expectation model, as follows:

$$\hat{\lambda}_{jt+1} = \delta * \hat{\lambda}_{jt} + (1 - \delta) * \lambda_{jt} \quad (3)$$

where hats indicate the expected queue length, and δ the coefficient of expectations (Nerlove, 1958). δ can be interpreted as the speed at which managers adjust their perceptions. This parameter follows the same logic as explained above for the customers' parameters (α and β).

Managers use their estimate about the future demand (i.e. arrival rate) to determine the service capacity required to meet their customers' expectations of sojourn time. Managers do not have accurate information regarding these expectations, but they know a reference average sojourn time, τ_{MR}, which is considered by the market to be acceptable to the customers. This market reference can be interpreted as a benchmark the managers use to evaluate the competitiveness of their firms. This benchmark is assumed to be exogenous and fixed. Given $\hat{\lambda}_{jt}$ and τ_{MR}, managers can determine their desired service capacity, $\dot{\mu}_{jt}$, by using Equation 1. Rewriting this equation in terms of these three variables we have:

$$\tau_{MR} = \frac{\hat{\lambda}_{jt}}{\dot{\mu}_{jt}^2} + \frac{1}{\dot{\mu}_{jt}} \quad (4)$$

Note that this is a second order equation for which there are two possible solutions. Nevertheless, due to the

nature of the problem it is impossible to have negative arrival and service rates. Hence, we only consider the positive solution of Equation 4. This solution is given by:

$$\dot{\mu}_{jt} = \begin{cases} 0 & if\ \hat{\lambda}_{jt} = 0 \\ \dfrac{1 + \sqrt{1 + 4 * \tau_{MR} * \hat{\lambda}_{jt}}}{2 * \tau_{MR}} & if\ \hat{\lambda}_{jt} > 0 \end{cases} \quad (5)$$

We assume $\dot{\mu}_{jt}$ to be the service capacity which managers consider as sufficient to satisfy the customers' needs regarding expected sojourn times. Then, the aim of managers is to adapt their available service capacity (μ_{jt}) to their desired service capacity. They must therefore decide when and how much capacity to add or remove. Nonetheless, once the adjustment decision has been made, its implementation process does not materialise immediately. In fact, when managers decide how much capacity they wish either to add or remove, there is usually a lag between the moment they take their decision and it is implemented. Examples of this kind of delays include the delivery delay entailed when purchasing new machines; the time required to build new infrastructure; the period for training new employees; and the legal notice period to lay off staff.

When managers decide how much capacity to add (x_t), these orders accumulate as capacity on order (μ^{+}_{jt}) until they are available for delivery. Once the delivery time (d^{+}) expires the ordered capacity is available for service. That is, order x_t is fulfilled in period $t + d^{+}$. Assuming that there is no capacity on order at the beginning of the simulation, i.e. $\mu^{+}_{jt} = 0$ for $t \leq 1$ and $x_t = 0$ for $t < 1$, the cumulative orders are given by:

$$\mu^{+}_{jt} = \sum_{k=t-d^{+}+1}^{t-1} x_k \qquad t > 1 \quad (6)$$

Similarly, when the capacity adjustment implies removing capacity, the capacity managers decide to withdraw (y_t) is designated as capacity to be retired (μ^{-}_{jt}). This capacity remains available for customers until the dismantling time (d^{-}) expires, i.e. y_t is removed from the service capacity in period $t + d^{-}$. Assuming that there are no previous retirement decisions at the start of the simulation, i.e. $y_t = 0$ for $t < 1$ and hence $\mu^{-}_{jt} = 0$ for $t \leq 1$, the capacity retirements accumulate as follows for $t > 1$:

$$\mu^{-}_{jt} = \sum_{k=t-d^{-}+1}^{t-1} y_k \quad (7)$$

The capacity decisions that have not yet been implemented ($\mu^{\pm}_{jt}$) are given by:

$$\mu^{\pm}_{jt} = (\mu^{+}_{jt} - \mu^{-}_{jt}) \quad (8)$$

We propose a heuristic which enables managers to know how much capacity either to add (x_t) or remove (y_t) and when to do so. The required capacity adjustment depends on the gap managers observe between their desired capacity ($\dot{\mu}_{jt}$) and the service capacity, which they perceive to have currently. When this gap is positive, new capacity orders will be placed, whereas new capacity retirements will be carried out when the gap is negative.

The current available service capacity (μ_{jt}) and the managers' previous decisions, which are still in the process of implementation ($\mu^{\pm}_{jt}$), make up the capacity that managers are expecting to have in service if no further changes are decided. Nevertheless, managers do not necessarily keep in mind all their previous decisions, which have not been yet implemented. Denoting by ψ the proportion of the not yet implemented capacity adjustment, which managers remember, we obtain that the service capacity they perceive to have at time t, is given by:

$$\bar{\mu}_{jt} = \mu_{jt} + \psi * \mu^{\pm}_{jt} \quad (9)$$

where ψ is nonnegative and less than or equal to 1. We call ψ the "coherence factor" of managers. If managers are rational when making capacity decisions they should take into account their previous decisions, which are still in process of execution. In this case, $\psi = 1$. Otherwise, if they only account for part of these past decisions, $\psi < 1$.

By computing the difference between the service capacity, which managers consider they currently have, and their desired capacity, we obtain the required capacity adjustment ($\Delta\mu_{jt}$):

$$\Delta\mu_{jt} = \dot{\mu}_{jt} - \bar{\mu}_{jt} \quad (10)$$

Managers may make this adjustment as fast or as slow as they wish. That is, we assume that managers can be prudent when taking their decisions. The second element of the heuristic tackles this issue. Let ζ be the speed at which managers decide to adjust capacity, i.e. how fast they decide to either add or remove capacity. Then, when the desired capacity exceeds the current capacity, which managers perceive to have, they decide to add capacity and the ordered capacity (x_{jt}) will be:

$$x_{jt} = \zeta * (\dot{\mu}_{jt} - \bar{\mu}_{jt}) \quad if\ \dot{\mu}_{jt} > \bar{\mu}_{jt} \quad \forall \quad 0 \leq \zeta \leq 1 \quad (11)$$

while if this decision implies to withdraw capacity, the capacity to be retired is:

$$y_{jt} = \zeta * (\bar{\mu}_{jt} - \dot{\mu}_{jt}) \quad if\ \dot{\mu}_{jt} < \bar{\mu}_{jt} \quad \forall \quad 0 \leq \zeta \leq 1 \quad (12)$$

ζ is small when managers take their decisions slowly, i.e. they are prudent decision makers. On the contrary, a high ζ implies that managers take actions quickly, i.e. they are aggressive decision makers.

To summarise the managers' dynamics: The more customers patronise a facility, the higher its manager's perception of the arrival rate is. High (low) manager's expectations increase (decrease) his desired service capacity. The higher (lower) the desired service capacity the more capacity the managers order (remove). With a delay, the capacity orders will increase the service capacity, while the capacity retirements will decrease it. This will affect the number of customer arriving at that facility.

CUSTOMERS' AND MANAGERS' PROFILE

Both customers and managers can be characterised according to their attitude towards new information when updating their perceptions (α, β, and δ). Managers are additionally described according to their coherence when taking decisions (ψ) and the speed at which they implement these decisions (ζ). Considering their attitude towards new information, customers and managers can be defined as conservative, hesitant or reactive. We say they are conservative or reluctant regarding new information when they have more confidence in their memory than in recent experiences (i.e. α or β high for customers and δ high for managers). When the contrary occurs, we call customers reactive (i.e. α or β low for customers and δ low for managers). When a roughly equal weight is given to memory and to the new information, we call hesitant customers (i.e. α or β intermediate).

SIMULATION RESULTS AND DISCUSSION

Due to the number of parameters the model has, we limit our simulation analysis to evaluating the dynamics of a system which is configured with 3 facilities and 120 customers (i.e. a one dimensional lattice of 120 cells, where each cell can take exactly one of three states). Each facility is initially provided with a service capacity of 5 customers per time unit, a manager and its own queue. Agents are endowed with an initial memory (i.e. expected average sojourn times for customers and expected arrival rates for managers). This initial memory is randomly allocated to the agents using a uniform distribution, whose maximum and minimum values are respectively 10% above and below the sojourn time of the Nash equilibrium. Given that all facilities have the same service capacity at the beginning, the Nash equilibrium occurs when customers are split equally among the three facilities, i.e. 40 customers patronising each. This distribution yields an average sojourn time of 1.8 time units.

We assume the implementation and dismantling delays involved in the managers' decisions to be fixed and equal to 4 and 2 periods, respectively. That is, once managers decide to increase capacity, this order will be delivered 4 periods later. Similarly, when they decide to reduce capacity, the capacity to be retired will still be available for service during the next 2 periods.

We develop and simulate the model using the numerical computing environment MATLAB and use STATA to test statistical hypotheses related to the performance of the facilities.

In this paper we focus on analysing the impact of the managers' profile on the system behaviour. To do this, we simulate 1,000 iterations (i.e. 1,000 different random seeds) of the model for a number of different combinations of the managers' parameters ($\delta 1$, $\delta 2$, $\delta 3$, ψ, ζ) for the case where $\alpha = 0.3$ and $\beta = 0.7$. In order to validate if 1,000 iterations are enough to draw conclusions about the different scenarios the system exhibits in steady state, we have run 10,000 iterations of the model and extended the simulated time to 10,000 time periods for several parameter combinations. The steady-state period was computed for the last 100 time period. We found that there were no significant differences in the number of facilities closing compared to 1,000 iterations over 500 periods. We therefore assume that 1,000 simulations of the model over 500 time periods are appropriate for our analysis. The results are discussed in terms of the possible scenarios (regarding the number of facilities remaining open at the end of the simulation period) which we can obtain when simulating the model. Table 1 contains the eight possible scenarios according to the number of facilities considered in the model.

Table 1: Possible scenarios generated by simulating the model.

Numerical Code	Scenario
0	All facilities close
1	Facility 1 is the only one open
2	Facility 2 is the only one open
3	Facility 3 is the only one open
12	Facilities 1 and 2 remain open, while facility 3 closes
13	Facilities 1 and 3 remain open, while facility 3 closes
23	Facilities 2 and 3 remain open, while facility 3 closes
123	All facilities remain open

Figure 1 shows the relative frequency of each scenario described in Table 1 for the nine possible combinations of parameters (ψ, ζ) using the three values {0.2, 0.5, 0.8}. The coefficients of expectations of managers and customers are: {$\delta 1 = 0.2$, $\delta 2 = 0.5$, $\delta 3 = 0.8$, $\alpha = 0.3$ and $\beta = 0.7$}. The nine combinations of parameters (ψ, ζ) are

on the horizontal axis. The first three combinations (i.e. I, II, and III) illustrate the cases where the managers are slow decision makers (ζ = 0.2) and have different degrees of rationality when accounting for their not-yet implemented decisions (ψ). The next three combinations (i.e. IV, V, VI) represent those cases where managers are moderate decision makers and the last three (i.e. VII, VIII, IX) those where managers are fast decision makers.

Figure 1 indicates that the scenario where the three facilities remaining open (see the line labelled as "Facilities 123") is the most likely when managers take their decisions slowly (see cases I, II and III). This probability decreases as the decision making process is faster and it is close to zero when managers are faster decision makers (ζ = 0.8) and almost rational when accounting for their not-yet implemented decisions (ψ = 0.8) (case IX). When one facility closes, this is mostly facility 1 (see line "Facilities 23"), whose manager is the most reactive ($\delta 1$ = 0.2). This scenario is the most likely in all the cases in which managers are moderate decision makers (cases IV, V and VI) and in those cases where they are fast decision makers and either slightly irrational or almost rational when considering their not-yet implemented decisions (cases VIII and IX).

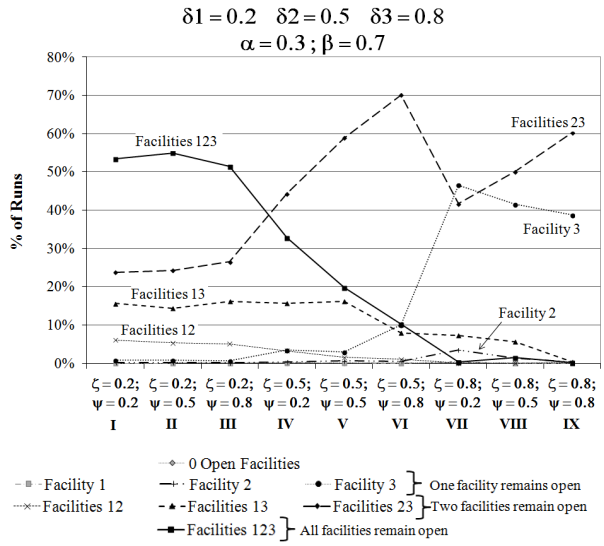

Figure 1: Percentage of runs which yield each possible scenario depending on the consistency factor (ψ) and the speed factor (ζ).

The faster the decision making process, the lower the probability of the most conservative manager (i.e. manager 3, $\delta 3$ = 0.8) being the only one who closes his facility (Facilities 12). The probability of the hesitant manager (i.e. manager 2, $\delta 2$ = 0.5) being the only one to close his facility (Facilities 13) is higher when the decision making process is slow (cases I, II and III) and lower when such a process is fast (cases VII, VIII and IX). When the most conservative manager (i.e. manager 3) decides quickly he is more likely to achieve a monopoly position (See line labelled as Facility 3 in cases VII, VIII and IX). In the case where managers are almost rational and take decisions fast, the probability of the most conservative manager closing his facility is negligible (less than 0.1%) (case IX). Finally, it is worth mentioning that the scenario in which the three facilities shut down is very unlikely (less than 0.2%) for this case.

Concerning the market share of the facilities in each scenario, we hypothesise that the most conservative managers' facilities capture a larger market share than the others. We use the Mann-Whitney-Wilcoxon test (MWW) (Newbold 1988), a non-parametric statistical test also called the Mann-Whitney U-test, to assess the null hypothesis that the median of the average arrival rates of two facilities during steady-state are the same. The alternative hypothesis assumes that the median of the average number of customers arriving at the most conservative manager's facility in steady-state is greater than that at the other facility. We have applied a non-parametric test because we do not know the distribution of the data and for some scenarios we have very little data. Parametric tests are not appropriate in these cases. Instead, the MWW-test is appropriate because the distributions have enough symmetry to assume that the median and the average are similar.

Table 2 provides the test-statistics of the MWW-test to assess the difference between the medians of the distributions of average arrival rates at each facility in steady-state for the scenarios where at least two facilities remain open, as monopolistic situations are irrelevant in this context. This table contains the median of the number of customers arriving at each facility for the same nine cases of Figure 1.

Table 2: The values of the median for the number of customers arriving at each facility during steady-state for 1,000 simulations of the model as a function of ψ and ζ

	2 FACILITIES OPEN						3 FACILITIES OPEN					
Case	**Facilities 12**		**Facilities 13**		**Facilities 23**		**Facilities 123**			**F1-F2**	**F1-F3**	**F2-F3**
	F1	**F2**	**F1**	**F3**	**F2**	**F3**	**F1**	**F2**	**F3**			
I	48	72 a	48	72 a	60	60	30	40	50	a	a	a
II	49	71 a	46	74 a	57	63 a	26	40	52	a	a	a
III	51	69 a	44	76 a	54	66 a	27	39	53	a	a	a
IV	35	86 a	39	81 a	50	70 a	27	45	48	a	a	a
V	37	83 a	27	93 a	47	73 a	25	39	56	a	a	a
VI	38	82 a	34	86 a	38	82 a	20	43	52	a	a	a
VII	66	54 a	60	60	66	54 c	43	30	20		b	
VIII	-	-	6	114 a	50	70 a	49	33	40			a
IX	15	106 d	6	114 a	36	85 a	14	61	45	d	d	d

The letters (i.e. "a", "b", "c", and "d") next to the median value of the second facility of each scenario indicate the results of the MWW-test for the null

hypothesis that the median arrival rate is the same for the assessed facilities. The letters "a" and "b" indicate that this hypothesis is rejected at a significance level of 0.01 and 0.1, respectively, against the alternative hypothesis that the median arrival rate of the most conservative manager's facility is significantly greater than that of the other facility. The letter "c" indicates that the null-hypothesis is rejected at a significance level of 0.01, against the alternative hypothesis that the median arrival rate of the most conservative manager's facility is significantly lower than that of the other facility. The letter "d" indicates that the null hypothesis cannot be tested because of lack of data. For instance, the letter "a" in case I when facility 1 ($\delta 1$ = 0.2) and 3 ($\delta 3$ = 0.8) remain open (medium green scenario) indicates that according to the MWW-test the median number of customers using facility 3 (i.e. with the most conservative manager) is significantly greater than that using facility 1 at a significance level of 0.01. In the scenario where the three facilities remain open, this test is assessed by pairs of facilities and the significance of the test is indicated in the last three columns for each pair of facilities. For instance, in case I, the MWW-test indicates that at a significance level of 0.01, the median of facility 3 ($\delta 3$ = 0.8) is significantly greater than that of facility 2 ($\delta 2$ = 0.5) and facility 1 ($\delta 1$ = 0.2) and that the median of facility 2 ($\delta 2$ = 0.5) is significantly greater than that of facility 1 ($\delta 1$ = 0.2).

In most cases, the p-values computed by MWW-test suggest rejecting the null hypotheses at the 1% level of significance. This enables us to conclude that the facility of the most conservative manager (i.e. manager 3, $\delta 3$ = 0.8) usually attracts more customers than the other facilities. Most of the exceptions are due to lack of data. For instance, the yellow scenario (i.e. the three facilities remain open) in case IX (ψ = 0.8 and ζ = 0.8), which is unlikely (0.1% of iterations barely visible in Figure 1).

In case VII, where managers are moderately irrational (ψ = 0.2) and fast decision makers (ζ = 0.8), the scenario in which the most reactive manager (i.e. manager 1, $\delta 1$ = 0.2), shuts down his facility (i.e. light green scenario) contrasts with the expected behaviour. That is, the less conservative manager of the two still active managers, who is manager 2 (i.e. $\delta 2$ = 0.5), usually captures the largest market share.

We repeated the experiment with the same combinations of the managers' coefficient of expectations for another combination of the customers' parameters. We have tested all the extreme and intermediate cases regarding the customers' attitudes toward the new information. Again, the main insights, about that the most conservative managers' facility captures a larger market share than the others, remain valid. One significant observation is that the scenario in which the three facilities are still open at time 500 is much more frequent when customers are either hesitant or very conservative regarding new information, no matter its provenance. Conversely, the scenario where the conservative managers achieve a monopoly position is more likely when customers are more reactive with respect to their own information and more conservative regarding that of their neighbours.

CONCLUSIONS

In this paper we have extended the CA model proposed by Delgado et al. (2011a) by incorporating the service rate as an endogenous variable. We have endowed the managers with the ability to adjust the service capacity of their facility. Managers are provided with a memory which enables them to update their expectations regarding the number of customers arriving at their facilities each period. Other attributes, which characterise the managers' profile, are the extent to which they account for their previous decisions when deciding by how much to adjust capacity and the speed at which they take decisions. The former indicates the level of irrationality of managers when the decision making involves delays (i.e. coherence factor).

We have performed some experiments to analyse the sensitivity of the model to the managers' profiles. We conclude that the facility of the most conservative manager usually achieves the highest market share. Additionally this facility is the most likely to remain open until the end of the simulation period (i.e. it is less likely that this facility shuts down).

This work can be extended by analysing the sensitivity of the model to the customers' parameters and the delays involved in the implementation of the managers' decisions. Further work in this field includes adding uncertainty parameters to the customers and managers' decision rules (as was done in the previous paper for the customers) and assessing the influence of other service factors in the customers and managers' decisions, such as price and quality.

REFERENCES

Bielen, F., and N. Demoulin. 2007. "Waiting Time Influence on the Satisfaction-Loyalty Relationship in Services". *Managing Service Quality* 17, No. 2, 174-193.

Davis, M. M. and J. Heineke. 1998. "How Disconfirmation, Perception and Actual Waiting Times Impact Customer Satisfaction". *International Journal of Service Industry Management* 9, No. 1, 64-73.

Delgado, C. A.; A. van Ackere; E. R. Larsen; and K. Sankaranarayanan. 2011a. "Collective Behavioral Patterns in a Multichannel Service Facilities System: a Cellular Automata Approach". In *Operations Research, Computing, and Homeland Defense: Proceedings of the 12th INFORMS Computing Society Conference* (Monterey CA, 9-11). INFORMS, Hanover, MD, 16-27.

Delgado, C. A.; A. van Ackere; E. R. Larsen; and K. Sankaranarayanan. 2011b. "Modelling Decisions under Uncertainty in a Behavioural Queuing System". In *Proceedings of the 25th European Conference on*

Modelling and Simulation (Krakow, Poland, Jun. 7-10), ECMS, Dudweiler, Germany, 34-40.

Delgado, C.A. 2012. "Behavioural Queueing: Cellular Automata and a Laboratory Experiment". *PhD Diss*., Université de Lausanne.

Dewan, S. and H. Mendelson. 1990. "User Delay Costs and Internal Pricing for a Service Facility". *Management Science* 36, No. 12 (Dec), 1502-1517.

Edelson, N. M. 1971. "Congestion Tolls under Monopoly". *The American Economic Review* 61, No. 5 (Dec), 873-882.

Edelson, N. M. and Hildebrand, D. K. 1975. "Congestion Tolls for Poisson Queuing Processes". *Econometrica* 43, No. 1 (Jan), 81-92.

Gallay, O. "Agent-Based Routing in Queueing Systems". *PhD Diss.*, Ecole Polytechnique Fédérale de Lausanne, 2010

Hui, M. K. and D. K. Tse. 1996. "What to Tell Consumers in Waits of Different Lengths:an Integrative Model of Service Evaluation". *The Journal of Marketing* 60, No. 2 (Apr), 81-90.

Law, A. K. Y.; Y. V. Hui; and X. Zhao. 2004. "Modeling Repurchase Frequency and Customer Satisfaction for Fast Food Outlets". *International Journal of Quality & Reliability Management* 21, No. 5, 545-563

Leeman, W. A. 1964. "The Reduction of Queues Through the Use of Price". *Operations Research* 12, No. 5 (Sep-Oct): 783-785.

Leeman, W. A. 1965. "'Comments' on Saaty's 'The Burdens of Queuing Charges'". *Operations Research* 13, No. 4 (Jul-Aug), 680-681.

Mendelson, H. and S. Whang. 1990. "Optimal Incentive-Compatible Priority Pricing for the M/M/1 Queue". *Operations Research* 38, No. 5 (Sep-Oct), 870-883.

Naor, P. 1969. "The Regulation of Queue Size by Levying Tolls". *Econometrica* 37, No. 1 (Jan), 15-24.

Nerlove, M. 1958. "Adaptive Expectations and cobweb phenomena". *The Quarterly Journal of Economics* 72, No. 2 (May), 227-240.

Newbold, P. 1998. *Statistics for business and economics*. (2nd ed.). Prentice Hall, Englewood Cliffs, NJ.

Pullman, M. E. and G. M. Thompson. 2002. "Evaluating capacity- and demand- management decisions at sky resort". *Cornell Hotel and Restaurant Administration Quarterly* 43, No. 6 (Dec), 25-36.

Saaty, T. L. 1965. "The Burdens of Queuing Charges-Comments on a Letter by Leeman." *Operations Research* 13, No. 4 (Jul-Aug), 679-680.

Sinha, S. K.; N. Rangaraj; and N. Hemachandra. 2010. "Pricing surplus server capacity for mean waiting time sensitive customers". *European Journal of Operational Research* 205, No. 1(Aug), 159-171

Stidham, S. Jr. 1985. "Optimal Control of Admission to a Queueing System". *IEEE Transaction on Automatic Control* 30, No. 8 (Aug), 705-713.

Stidham, S. Jr. 1992. "Pricing and Capacity Decisions for a Service Facility: Stability and Multiple Local Optima". *Management Science* 38, No. 8 (Aug): 1121-1139.

Taylor S. 1994. "Waiting for Service: the Relationship Between Delays and Evaluations Of Service". *The Journal of Marketing* 58, No. 2 (Apr), 56-69.

Theil, H. and S. Wage. 1964. "Some observations on adaptive forecasting". *Management Science* 10, No.2 (Jan), 198-206.

van Ackere, A. and E. R Larsen. 2004. "Self-Organising Behaviour in the Presence of Negative Externalities: a Conceptual Model of Commuter Choice". *European Journal of Operational Research* 157, No. 2 (Sep), 501-513.

van Ackere, A.; C. Haxholdt; and E. R Larsen. 2013. "Dynamic Capacity Adjustments with Reactive Customers". *Omega* 41, No. 4 (Aug), 689-705.

Yechiali, U. 1971. "On Optimal Balking Rules and Toll Charges in the Gi/M/1 Queuing Process". *Operations Research* 19, No. 2 (Mar-Apr), 349-370.

AUTHOR BIOGRAPHIES

CARLOS A. DELGADO-ALVAREZ is Professor of Operations Research and Modeling and Simulation at the Department of Industrial Engineering of the ICESI University, Cali, Colombia since 2012. He obtained his PhD in Information Systems from the School of Business and Economics, University of Lausanne, Switzerland. He received his M.Sc. in Systems Engineering and a B.Eng. in Industrial Engineering from the Faculty of Mines, National University of Colombia, where he also worked for three years as a research engineer and teaching assistant for bachelor courses in systems simulation and Algorithms and Programming. He is a member of INFORMS society. His research interests include operations management, system simulations, social complex systems and experimental economics.

ANN VAN ACKERE is Professor of Decision Sciences at HEC Lausanne, the School of Business and Economics of the University of Lausanne, Switzerland since 1999. She obtained her PhD from the Stanford Graduate School of Business and joined the faculty of London Business School, UK, upon graduation.

ERIK R. LARSEN is Professor at the Institute of Management and vice dean of the Faculty of Economics at the University of Lugano, Switzerland. Previously he held appointments at Cass Business School (London), London Business School, and Copenhagen Business School. During the period 1996-1998, he was an EU Marie Curie Fellow at the University of Bologna, Italy. He obtained his PhD from the Institute of Economics, Copenhagen Business School and his M.Sc. from the Technical University of Denmark.

EXPERIMENTS WITH SIMULATION OF BOTNETS AND DEFENSE AGENT TEAMS

Igor Kotenko
Laboratory of Computer Security Problems
St. Petersburg Institute for Informatics and Automation
39, 14th Liniya, St. Petersburg, 199178, Russia
E-mail: ivkote@comsec.spb.ru

KEYWORDS
Agent-based Simulation, Network Simulation, Network attacks and defense, Botnets, DDoS.

ABSTRACT

Botnets allow malefactors manage millions of infected computers simultaneously and provide large-scale successful attacks. The paper suggests an approach for multi-agent simulation of botnets and botnet protection mechanisms. The main contribution of the paper is an improved simulation environment for agent based simulation of botnets and experimentation with this environment for analysis of different botnets and protection mechanisms. Experiments demonstrate the capabilities of the simulation environment for investigating various stages of the botnet lifecycle and the efficiency of different protection mechanisms.

1. INTRODUCTION

Botnets allow malefactors manage millions of infected computers simultaneously and provide large-scale successful attacks. One of the promising approaches for investigation of botnets and protection mechanisms is agent-based simulation.

The paper is devoted to the study of botnets propagating using network computer worms and used to execute Distributed Denial of Service (DDoS) attacks. The paper is based on earlier publications of the authors on agent-based simulation (Kotenko and Ulanov 2007; Kotenko 2009; Kotenko 2010; Kotenko et al. 2012-1; Kotenko et al. 2012-2). In the paper we try to elaborate the agent-oriented approach suggested in these works for simulation of botnets and botnet protection mechanisms in the Internet. The used agent-oriented approach supposes that the network counteraction is represented as the interaction of different teams of software agents (Kotenko and Ulanov 2007; Kotenko 2009; Taveter et al. 2010), and the aggregated system behavior appears by means of the local interactions of particular agents in a dynamic environment that is defined by the model of the Internet.

In distinction from those papers, the main contribution of the paper is the improved simulation environment for agent based simulation of botnets and experimentation with this environment for analysis of different botnets and protection mechanisms. Many new experiments were added, their representation and analysis methods were improved. This enabled us to compare the capabilities of the defense methods against botnets in the course of their life cycle. The rest of the paper is organized as follows. Section 2 discusses the related work. Section 3 presents the simulation framework and the architecture of the simulation environment developed. Section 4 describes a set of experiments fulfilled. Concluding remarks are given in Section 5.

2. RELATED WORK

Research on agent-based simulation is based on a variety of methods and approaches. The classical frameworks and architectures for multi-agent simulation of distributed complex systems are shared plans theory (Grosz and Kraus 1996), joint intentions theory (Cohen and Levesque 1991) and hybrid approach (Tambe 1997). The techniques based on belief-desire-intention, distributed constraint optimization, distributed Partially observable Markov decision process, and game-theoretic (Tambe et al. 2005) are emphasized. Different mechanisms for collaborative agent team maintenance are used (Kaminka et al. 2007; Stone et al. 2010; Agmon et al. 2011).

In the studies on the analysis of botnets, the definition of their lifecycle is given (Govil and Jivika 2007; Feily et al. 2009; Naseem et al. 2010). It consists of the phases (or stages) of primary infection, propagation, management and control, and attack. The roles of the participants of botnets are considered (Feily et al. 2009), features of the botnets with centralized (Govil and Jivika 2007; Naseem et al. 2010) and decentralized (Bailey et al. 2009; Grizzard et al. 2007; Feily et al. 2009; Wang et al. 2007) architecture are analyzed, and various types of attack executed using botnets are described. In (Dagon et al. 2007) the efficiency criteria of botnet operation are discussed.

Studies on simulation for investigation of botnets and computer networks mainly rely on methods of discrete-event simulation of processes being executed in network structures (Simmonds et al. 2000; Wehrle et al. 2010), as well as on trace-driven models initiated by trace data taken from actual networks (Owezarski and

Proceedings 27th European Conference on Modelling and Simulation ©ECMS Webjørn Rekdalsbakken, Robin T. Bye, Houxiang Zhang (Editors)
ISBN: 978-0-9564944-6-7 / ISBN: 978-0-9564944-7-4 (CD)

Larrieu 2004). G.Riley et al. (Riley et al. 2004) implement a network worm propagation model. A.Suvatne (Suvatne 2010) suggests a model of "Slammer" worm propagation by using "Wormulator" (Krishnaswamy 2009) simulation environment. M.Schuchard (Schuchard et al. 2010) presents simulation tool which allows to simulate a large scale botnet. Gamer and Mayer (Gamer and Mayer 2009) consider a DDoS simulation tool, called Distack using OMNeT++. Li et al. (Li at al. 2002) propose own simulation environment to estimate the quality of implementation of botnet protection mechanisms.

This paper describes the approach which combines agent-based and discrete-event packet-level simulation of network protocols. Initially this approach was suggested for DDoS attack and defense simulation (Kotenko and Ulanov 2007). In the present paper, as against other works of authors, the various methods of botnet attacks and counteraction against botnets are explored by implementing comprehensive libraries of attack and defense components.

3. SIMULATION FRAMEWORK AND ENVIRONMENT

The proposed simulation environment realizes simulation models which implement the processes for operation of botnet agent teams and defense agent teams. Main components of the simulation framework which is implemented in the simulation environment are as follows:

- Ontology of application domain containing application notions and relations between them;
- Protocols of teamwork and taskwork maintenance for the agents of different teams;
- Models of scenario behavior of agents for team, group and individual levels;
- Libraries of agent basic functions;
- Communication platform and components for agent message exchange;
- Models of functioning environment, including topological, functional and other components;
- Models that provide the interaction of teams (antagonistic and non-antagonistic competing, cooperation, adaptation).

We distinguish at least three types of agent teams: the botnet teams, the defense teams, and the teams of usual users and servers.

Botnet teams include the following types of agents: (bot)master, command centre (C&C), zombies (bots). Botmaster, by sending different commands, sets goals for the botnet and controls the behaviour of the network at the highest level. C&C carries out the delivery of commands received from the botmaster to bots. Bots, receiving the commands from the C&C, immediately carry out actions under the orders of the botmaster.

According to the types of communication channels between the agents, four kinds of structures of teams are used (Figure 1-3): (1) centralized; (2) simple distributed; (3) multilevel distributed; (4) peer to peer (P2P). In P2P team (Figure 3) each node can be represented as (bot)master, C&C or zombies (bots).

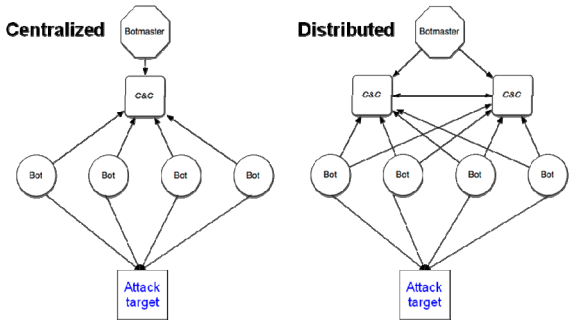

Figure 1: Centralized and simple distributed Botnet Teams

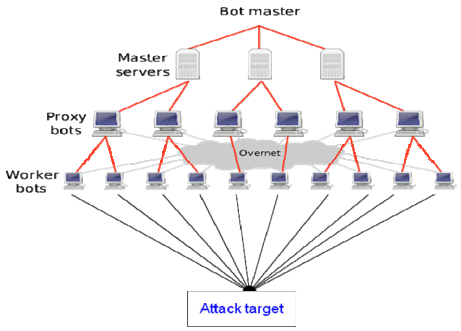

Figure 2: Multilevel distributed Botnet Team

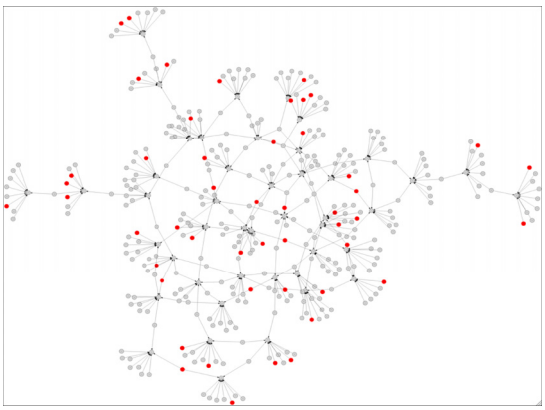

Figure 3: Peer to peer (P2P) Botnet Team

Defense teams are represented by the following common classes of agents (Figure 4): information processing (sampler); attack detection (detector); filtering (filter); investigation (investigator); rate limitation (limiter). Samplers collect and process network data for anomaly and misuse detection. Detector coordinates the team, correlates data from samplers, and detects attacks. Filters are responsible for traffic filtering using the rules provided by detector.

Investigator tries to defeat attack agents. Limiter is for implementation of cooperative defence. Its local goal is to limit the traffic according to the team goal. It lowers the traffic to the attack target and allows other agents to counteract the attack more efficiently.

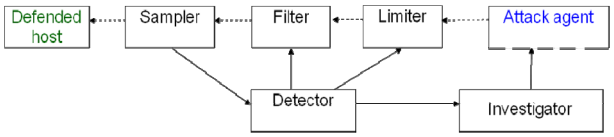

Figure 4: Defense team

To generate a *legitimate traffic*, "user" and "server" agents are determined. These agents generate the traffic statistically similar to traffic of standard user computers and web servers.

These models are implemented in the simulation environment as a sequence of internal abstraction layers (Figure 5): (1) discrete event simulation on network structures, (2) computational network with packet switching, (3) network services, (4) botnet and defense agent teams. Specification of every subsequent layer is an extended specification of the previous one.

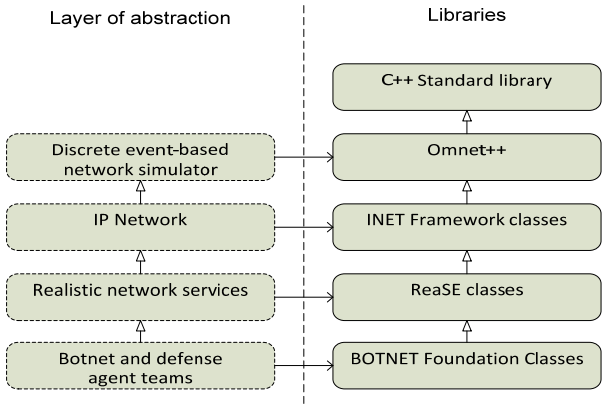

Figure 5: Simulation environment (tool) architecture

The simulation environment relies on the implemented libraries and the third party libraries. Functional purpose of each library matches to the appropriate layer of abstraction. All components of the simulation environment are implemented in C++ programming language with standard runtime libraries. Each particular library provides a set of modules and components which are implementations of entities of appropriate semantic layer. Any given library can rely on the components exported by the libraries of the previous layer and can be used as a provider of components needed for the subsequent layer implementation. The first layer of abstraction is implemented by use of the discrete event simulation environment OMNET++ (Varga 2010). The OMNET++ provides the tools for simulation of network structures of different kinds and processes of message propagation in them. The library INET Framework (INET Framework 2013) is used for simulation of packet-switching networks. This library provides components implemented as OMNET++ modules and contains large variety of models of network devices and network protocols. Simulation of realistic computer networks is carried out by using the library ReaSE (ReaSE 2013).

An example of the user interface of the simulation environment is shown in Figure 6. In the upper left corner you can see the main window that displays the components included in the model and control elements that allow users to interact with them. In the lower left corner the network configuration window is outlined. The main window also includes controls for managing the model time (e.g., one can perform the simulation step-by-step or express mode). There are also controls for searching the entity of interest for editing its state. The structure of a network node is in the lower right corner. In the upper right corner (Figure 6) the window of parameters is depicted. There are the following specification elements to define the investigated network models, attack and defence mechanisms:

- Network topology: quantity and types of hosts, channels between them and their types.
- Botnet team: quantity of bots; botmaster's address and port used for interactions; bot's ports used to send attack packets; victim's address and port; time of attack; attack intensity; address spoofing technique.
- Attack: victim type (application, host or network); type of attack (brute force (UDP/ICMP flood, smurf/fraggle, etc.); attack rate dynamics (can be constant or variable); etc.
- Defense team: address of defended host; detector's address and port for interactions; server's reply size and delay time; adaptation scheme depending on attack severity, etc.
- Defense: deployment location; the stages the defence method can implement (attack prevention, attack detection, tracing the attack source, attack counteraction); attack detection technique (misuse and anomaly detection; etc.
- User team: quantity of users; server's address and port; time to start; quantity of requests to server, interval between them and their size; interval between connections.
- Simulation: simulation duration; quantity of experiments; initialization of random number generator.

4. EXPERIMENTS

On the top level the network topology is simulated on the level of the autonomous systems (AS) where the technique of positive-feedback preference (PFP) (Zhou et al. 2006) is used to model the network topology.

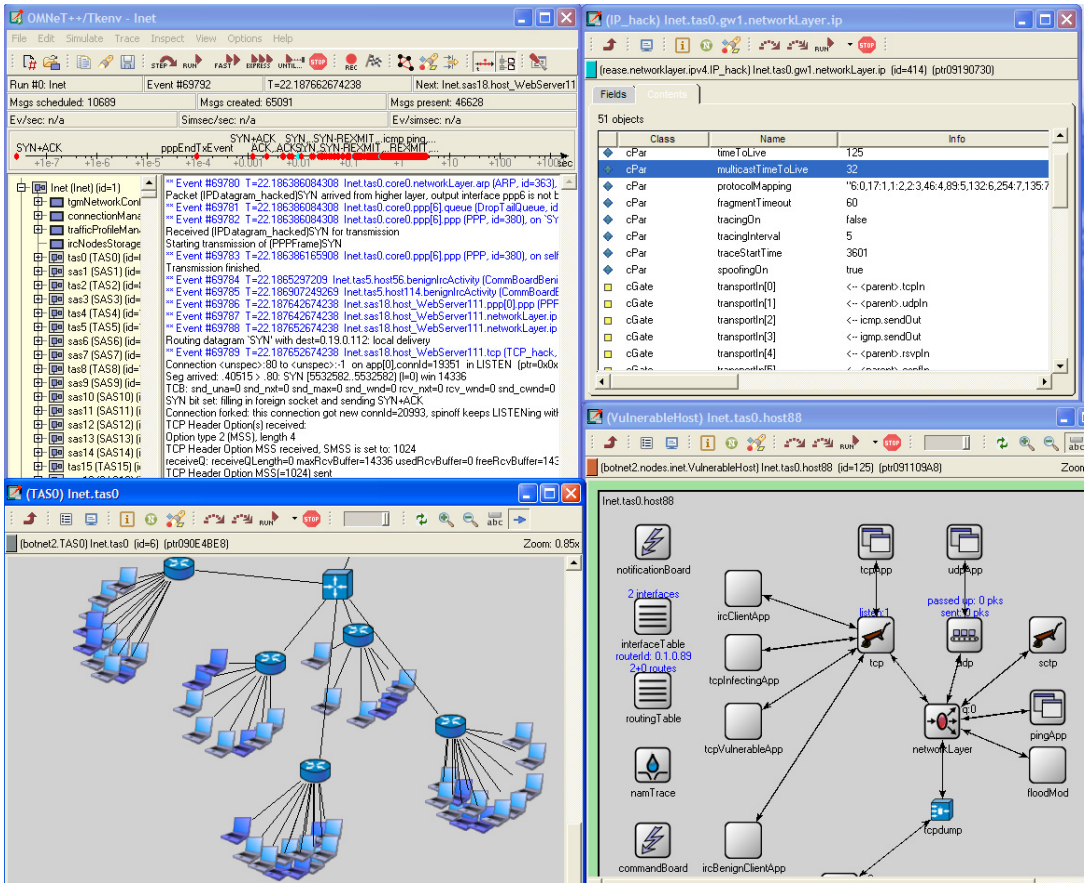

Figure 6: User interface of the simulation environment

On the lower level for each AS the router-level topology is simulated by using the HOT-model (Heuristically Optimal Topology) (Li et al. 2004).

The experiments with the agent-based simulation environment demonstrated the operability of the developed simulation environment and main characteristics of botnets and defense mechanisms investigated. Experiments investigated botnet actions and defense mechanisms on stages of botnet propagation, botnet management and control (reconfiguration and preparation to attacks), and attack execution.

We analysed several techniques, including Virus Throttling (Williamson 2002) and Failed Connection (Chen and Tang 2004), to protect from botnet on the propagation stage. Botnet propagation was performed via network worm spreading. We researched techniques of IRC-oriented botnet detection to counteract botnets on the management and control stage. We also analyzed techniques which work on the different stages of defense against DDoS attacks. These techniques include SAVE (Source Address Validity Enforcement Protocol) (Li et al. 2002), SIM (Source IP Address Monitoring) (Peng et al. 2004) and Hop-count filtering (Jin et al. 2003).

Let us consider only examples of experiments on the stage of botnet management and protection against botnet on this stage. The example of the user interface of the simulation environment during these experiments is shown in Figure 7 which depicts different fragments of the network, and bots are darker.

Let us describe the usage only one of the protection technique which was proposed by M. Akiyama et al. (Akiyama et al. 2007). This technique involves monitoring of IRC-traffic, passing through the observer node, and subsequent calculation of the metrics “Relationship”, “Response” and “Synchronization”, based on the content of network packets. The metric “Relationship” characterizes the distribution of clients in IRC-channel. Too high value of this metric is considered as abnormal. The metric “Response” is calculated as the distribution of response time to the broadcasting request. The metric “Synchronization” characterizes the synchronism in the behaviour of IRC clients.

The IRC traffic was monitored by using sampler agents, installed on the core routers of large network segments. Information about IRC channel and its clients is defined by analysis of IRC packets. Then, based on data obtained, the relationship metrics of observed channels were calculated in real time. It is assumed that the data,

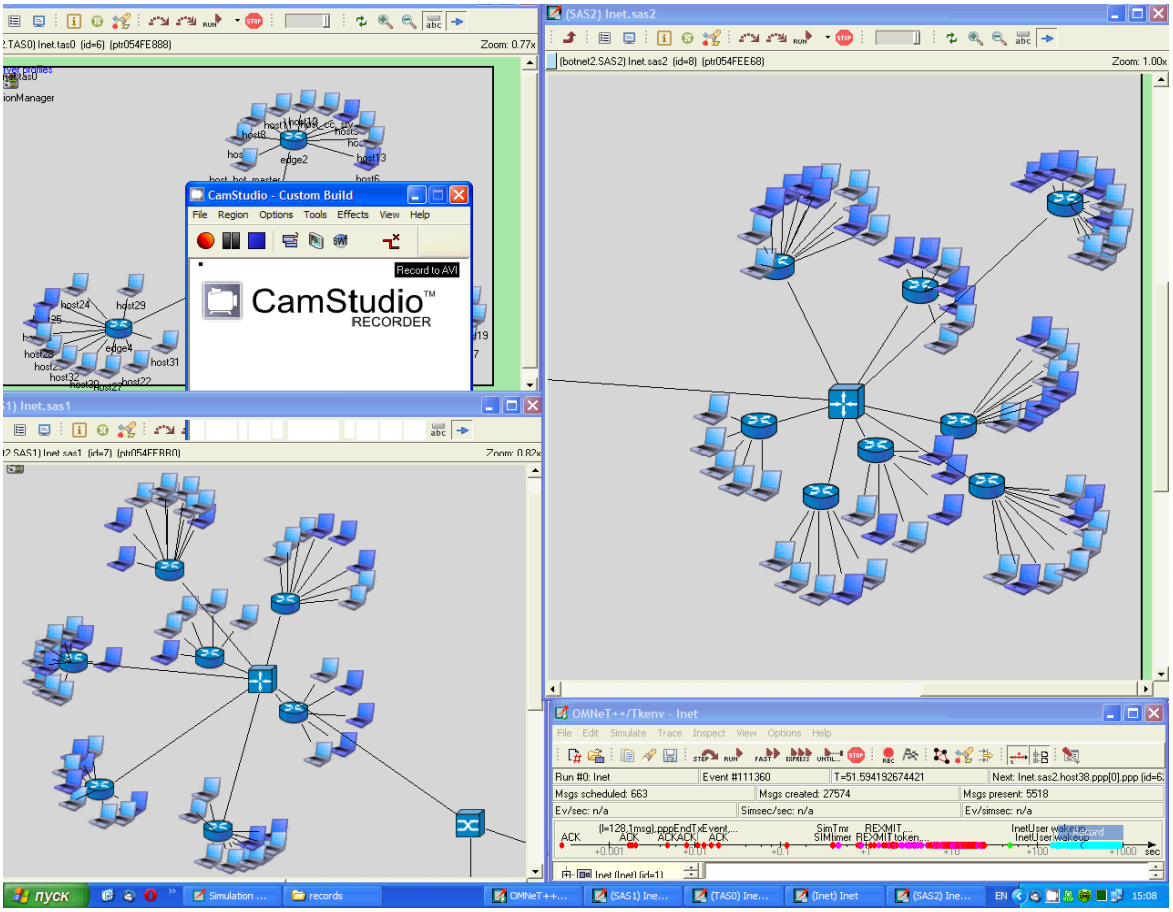

Figure 7: User interface of the simulation environment experiments on the stage of botnet management

obtained from sampler agents, will strongly depend on the location of sampler agents in relation to main IRC flows, merging near the network segment that contains the IRC server.

Table 1 shows a part of observed relationship metrics for IRC channels in various network locations. There are data for the botnet control channel (Irc-bot) and the channel for legitimate IRC communication (Irc-1). The number of clients in the Irc-1 channel is ten. For the legitimate channels, either all the participants are detected or none of the participants are detected. This is because the legitimate IRC communication is performed by exchanging broadcast messages; therefore, if an observer resides on the way of the IRC traffic, it detects all the clients of the corresponding channel. For the control channel Irc-bot, there is significant differentiation of the observed metric depending on the location of sampler agents. This is due to the features of botnet client communication in the IRC channels. Rather than broadcasting messages to all the channel participants, the botnet nodes exchange information only with a small number of nodes belonging to the set of botmaster nodes. It is seen from Table 1 that there are two routers on which the botnet control channel was detected almost completely. The analysis of the network topology showed that the IRC server was located in the segment sas17, while the segment tas0, which was in the close vicinity of sas17, operates as a transit segment between the IRC server and the greater part of the bot clients.

Table 1: Relationship Metrics of IRC Channels

#Sensor	#Irc-bot	#Irc-1
sensor_sas17	97,91%	100,00%
sensor_tas0	95,82%	100,00%
sensor_tas4	26,82%	100,00%
sensor_sas18	7,27%	0,00%
sensor_sas26	5,45%	100,00%
sensor_sas11	5,45%	0,00%
sensor_tas5	5,27%	0,00%
sensor_sas20	5,09%	100,00%
sensor_sas13	5,00%	0,00%

Analysis of the topology of the simulated network shows that the segment sas17 (sensor_sas17) has an IRC server node. The segment tas0, located in proximity to the segment sas17, is a transit for the traffic between the IRC server and the most of IRC bots.

Thus, we can suppose that a defense agent, located on a small number of routers which are transit for the main IRC traffic, can be as effective as the defense agent installed in more number of routers. We can also assume that a defense agent, having a small covering of the protected network, generally will not be efficient,

because only a small part of the IRC control traffic passes the vast majority of routers.

In the experiments the IRC traffic was monitored in different network locations. Based on monitoring results, the synchronization metrics were calculated. Let us consider the synchronization metrics determined by monitoring the traffic on the core router of network segment tas0 (Figure 8).

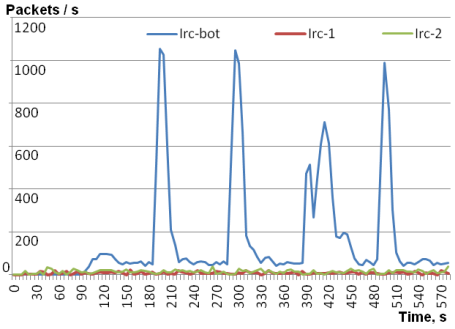

Figure 8: Synchronization Metrics for tas0

From 200 seconds of simulation time, every 100 seconds we can observe sharp spikes of traffic volume related to the botnet control IRC channel. These bursts are caused by response messages from bots on a request from the botmaster.

The network segment tas0 is located in proximity from the network segment which includes the IRC server. Thus, a significant part of the IRC control traffic is transmitted through the router of the network segment tas0. For this reason, the bursts of control channel traffic are expressed against the traffic of legitimate communication.

The traffic on the network segment router sas13 was measured (Figure 9) to evaluate the impact of the proximity of the sampler agent from the IRC server on the severity of bursts of control traffic (and thus on the discernibility of synchronization metric). Traffic measurements show a general decrease of traffic level in the observation point sas13, as well as a good visibility of traffic spikes on the core router of this network segment. Thus, the results of experiments demonstrate the applicability of synchronization metric to detect the IRC control traffic.

The filtering method, based on the relationship metric, used in agents-filters, uses an assumption that the IRC channels with a very large number of clients are anomalous. We carried out a series of experiments where the relationship metric was used for different configurations of filtering components and different critical levels of relationship. It was shown that the efficiency of the IRC traffic detection and filtering, based on the relationship metric, increases sharply when the routers, which are transit for the IRC control traffic, are fully covered by filters.

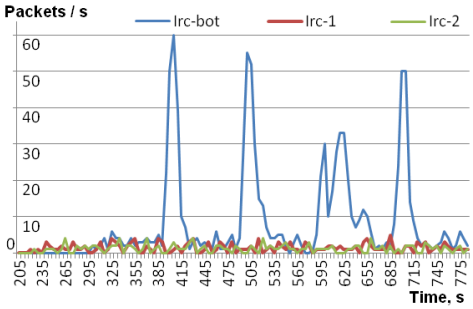

Figure 9: Synchronization Metric for sas13

The filtering method, based on the synchronization metric, uses an assumption that the short synchronous messaging in a single IRC channel is anomalous. The observed synchronization metric is calculated as the number of IRC packets, passing through the samplers for a fixed period of time. In the experiments fulfilled, the filtering criterion is a fivefold increase in traffic for 20 seconds followed by a return to its original value. The results of experiments allow concluding about low quality of the method in the current configuration, since false positive rate has a rather high value.

5. CONCLUSION

In the paper, an agent-based simulation approach for investigating botnets and defense mechanisms against them was proposed. The general architecture of the agent-based environment for the simulation of botnets and defense mechanisms against them was presented. This architecture was implemented on the basis of the discrete events simulation system OMNeT++, and several specialized libraries implementing the models of botnets and defense agent teams. Experiments were performed that demonstrate the behavior of botnets and defense agent teams at the phases of propagation, management and control, and attack. The paper describes only the experiments at the phases of management and control. The experiments confirmed the practical usefulness of the proposed approach for the simulation of complex botnets and the analysis of security of network segments. In future research we are planning to fulfill a comprehensive analysis of effectiveness of botnets and defense agent teams operation, and futher improvement of the implemented simulation environment.

ACKNOWLEDGEMENT

This research is being supported by grant # 13-01-00843 of the Russian Foundation of Basic Research, Program of fundamental research of the Department for Nanotechnologies and Informational Technologies of the Russian Academy of Sciences (contract #2.2), State contract #11.519.11.4008 and the EU as part of the SecFutur and MASSIF projects.

REFERENCES

Agmon, N.; S. Kraus; and G. A. Kaminka. 2011. "Multi-Robot Patrol in Strong Adversarial Environments." *Journal of Artificial Intelligence Research*, 42.

Akiyama, M.; T. Kawamoto; M. Shimamura; T. Yokoyama; Y. Kadobayashi; S. Yamaguchi. 2007. "A proposal of metrics for botnet detection based on its cooperative behavior." In *Proceedings of SAINT Workshop.*

Bailey, M.; E. Cooke; F. Jahanian; et al. 2009. "A Survey of Botnet Technology and Defenses," In *Proceedings of the Cybersecurity Applications Technology Conf. for Homeland Security*.

Chen, S. and Tang Y. 2004. "Slowing Down Internet Worms." In *Proceedings of the 24th International Conference on Distributed Computing Systems*.

Cohen, P. and H.J. Levesque. 1991. "Teamwork." *Nous*, 35.

Dagon, D.; G. Gu; C.P. Lee; et al. 2007. "A Taxonomy of Botnet Structures." In *Proceedings of ACSAC'07*.

Feily, M.; A. Shahrestani; S. Ramadass. 2009. "A Survey of Botnet and Botnet Detection". In *Proceedings of Third Int. Conf. on Emerging Security Information Systems and Technologies*.

Gamer, T. and C. Mayer. 2009. "Large-scale Evaluation of Distributed Attack Detection." In *Proceedings of the 2nd International Workshop on OMNeT++*.

Govil, J. and G. Jivika. 2007. "Criminology of Botnets and Their Detection and Defense Methods," In *Proceedings of of IEEE Int. Conf. on Electro-Information Technology*.

Grizzard, J.B.; V. Sharma; C. Nunnery; et al. 2007. "Peer-to-Peer Botnets: Overview and Case Study." In *Proceedings of the Workshop on Hot Topics in Understanding Botnets*.

Grosz, B. and S. Kraus. 1996. "Collaborative Plans for Complex Group Actions." *Artificial Intelligence*. 86, 2.

INET Framework. 2013. http://inet.omnetpp.org/

Kaminka, G.A.; A. Yakir; D. Erusalimchik; and N. Cohen. 2007. "Towards Collaborative Task and Team Maintenance." In *Proceedings of AAMAS-07*.

Jin, C.; H. Wang; K.G. Shin. 2003."Hop-count filtering: An effective defence against spoofed DDoS traffic." In *Proceedings of ACM Conference on Computer and Communications Security*.

Kotenko, I. and A. Ulanov. 2007. "Agent-based Simulation Environment and Experiments for Investigation of Internet Attacks and Defense Mechanisms." In *Proceedings of ECMS 2007*.

Kotenko, I. 2009. "Simulation of Agent Teams: the Application of Domain-Independent Framework to Computer Network Security." In *Proceedings of* ECMS 2009.

Kotenko, I. 2010. "Agent-Based Modelling and Simulation of Network Cyber-Attacks and Cooperative Defence Mechanisms." *Discrete Event Simulations*. InTech.

Kotenko I.; A. Konovalov; A. Shorov. 2012-1. "Agent-based simulation of cooperative defence against botnets." *Concurrency and Computation: Practice and Experience*, Vol. 24, Issue 6.

Kotenko I.; A. Konovalov; A. Shorov. 2012-2. "Discrete-Event Simulation of Botnet Protection Mechanisms." *Discrete Event Simulations - Development and Applications*. InTech.

Krishnaswamy, J. 2009. *Wormulator: Simulator for Rapidly Spreading Malware*, Master's Projects.

Li, J.; J. Mirkovic; M. Wang; P. Reither; L. Zhang. 2002. "Save: Source address validity enforcement protocol." In *Proceedings of IEEE INFOCOM.*

Li, L.; D. Alderson; W. Willinger; J. Doyle. 2004. "A first-principles approach to understanding the internet router-level topology." *ACM SIGCOMM Computer Communication Review*.

Owezarski, P. and N. Larrieu. 2004. "A trace based method for realistic simulation." In *Proceedings of 2004 IEEE International Conference on Communications*.

Naseem, F.; M. Shafqat; U. Sabir; et al. 2010. "A Survey of Botnet Technology and Detection." *Intern. Journal of Video & Image Processing and Network Security*, 10, 1.

Peng, T.; C. Leckie; K. Ramamohanarao. 2004. "Proactively Detecting Distributed Denial of Service Attacks Using Source IP Address Monitoring." *Lecture Notes in Computer Science*, 3042.

ReaSE. 2013. https://i72projekte.tm.uka.de/trac/ReaSE

Riley, G.; M. Sharif; W. Lee. 2004. "Simulating internet worms." In *Proceedings of the 12th International Workshop on Modeling, Analysis, and Simulation of Computer and Telecommunication Systems.*

Schuchard, M.; A. Mohaisen, D. Kune; N. Hopper; Y. Kim, E. Vasserman. 2010. "Losing control of the internet: using the data plane to attack the control plane." In *Proceedings of the 17th ACM Conference on Computer and communications security*.

Simmonds, R.; R. Bradford; B. Unger. 2000. "Applying parallel discrete event simulation to network emulation." In *Proceedings of the fourteenth workshop on Parallel and distributed simulation.*

Stone, P.; G. A. Kaminka; S. Kraus; and J. S. Rosenschein. 2010. "Ad hoc autonomous agent teams: Collaboration without pre-coordination." In *Proceedings of the* AAAI'10.

Suvatne, A. 2010. *Improved Worm Simulator and Simulations*. Master's Projects.

Tambe, M.; E. Bowring; H. Jung; et al. 2005. "Conflicts in teamwork: Hybrids to the rescue." In *Proceedings of AAMAS-05*.

Taveter, K.; M. Parmak; and M. Meriste. 2010. "Agent-oriented modelling for simulation of complex environments." In *Proceedings of IMCSIT 2010.*

Varga, A. 2010. "OMNeT++." Chapter in the book *Modeling and Tools for Network Simulation*. Springer Verlag.

Wang, P.; S. Sparks; C.C. Zou. 2007. "An Advanced Hybrid Peer-to-Peer Botnet." In *Proceedings of the First Workshop on Hot Topics in Understanding Botnets*.

Wehrle, K.; M. Gunes; J. Gross; 2010. *Modeling and Tools for Network Simulation*. Springer-Verlag.

Williamson, M. 2002. "Throttling Viruses: Restricting propagation to defeat malicious mobile code." In *Proceedings of ACSAC Security Conference*.

Zhou, S.; G. Zhang; G. Zhang; Z. Zhuge. 2006. "Towards a Precise and Complete Internet Topology Generator." In *Proceedings of Intern. Conference on Communications.*

AUTHOR BIOGRAPHY

IGOR KOTENKO is Professor of computer science and a head of the Laboratory of Computer Security Problems in St. Petersburg Institute for Informatics and Automation of the Russian Academy of Science. His research interests include simulation, multi-agent systems and computer network security.

AGENT METHODOLOGICAL LAYERS IN REPAST SIMPHONY

Franco Cicirelli, Angelo Furfaro, Libero Nigro, Francesco Pupo
Laboratorio di Ingegneria del Software
Dipartimento di Elettronica Informatica e Sistemistica
Università della Calabria
87036 Rende (CS) – Italy
Email: {f.cicirelli,a.furfaro}@deis.unical.it, {l.nigro,f.pupo}@unical.it

KEYWORDS
Agent-based modeling and simulation, Repast Simphony, Java, actors, P–DEVS, Petri nets.

ABSTRACT

Repast Simphony (RS) is a popular toolbox for agent-based modeling and simulation (ABMS) of complex systems. It can be used from within the Eclipse IDE with Java being the main implementation language. Moreover, visual modeling is supported by agent flowcharts. Powerful features of RS include contexts and projections which allow the modeler to build e.g. situated multi-agent systems (MAS) which can easily be configured and visualized in the RS runtime system. RS lacks of a reference agent methodology. Rather the modeler is free to define and follow her/his own methodology with RS: procedurally, declaratively or visual-based. This openness was exploited in this work for supporting different notions of agents, thus addressing the modeling needs of various application domains. In particular this paper proposes an embed in RS of an actor model which provides a lightweight notion of agents. The actor model is then used as a kernel for supporting more abstract but rigorous modeling languages like Parallel DEVS (P–DEVS) and time-extended Petri nets. A P–DEVS modeling example is reported to demonstrate the usefulness of supporting multiple agent methodological layers in RS.

INTRODUCTION

Agent-based modeling and simulation (ABMS) is currently recognized (North & Macal, 2007)(Macal & North, 2011) as a fundamental tool for predicting the behavior of complex systems in such diverse fields as financial, social, biological and engineering domains. The strength of ABMS stems from its ability to mimics a reality by means of domain specific components/agents interacting and coordinating to one another and to organize agents on the basis of their behaviors. Nowadays ABMS can be practiced by using several modeling languages and tools. Repast Simphony (RS) is a leading free and open-source ABMS toolkit which is integrated with Eclipse IDE. It is the latest member of the REcursive Porous Agent Simulation Toolkit family which is mainly based on Java. RS (North *et al*., 2005a-b), though, adds visual point-and-click tools for designing agents, specifying agent behaviors, and for executing, collecting and inspecting simulation results using a variety of external analysis tools. Contexts and projections are a key for organizing agents over spatial structures (e.g. toroidal grids and networks) which have a connection to display and visualization means of the RS runtime system. A basic feature of RS is the absence of a reference agent methodology. For instance, the modeler can introduce agents as plain-old-java-objects (POJO) whose methods can be annotated with declarative scheduling (scheduled methods or watch annotations). In the general case, method scheduling has to be explicitly achieved by submitting actions e.g. to the default scheduler, at an arbitrary dense time.

In the work described in this paper, RS openness is exploited to experiment with different agent based modeling methodologies, tailored to the needs of specific problem domains. In particular, as a basic agent kernel, a lightweight actor model (Cicirelli *et al*, 2009) was adapted to work with RS. Actors encapsulate a data status and interact to one another by asynchronous message-passing. Actor behaviors are realized as finite state machines, possibly patterned as distilled statecharts (Cicirelli *et al*., 2011a). The actor model has proved to be very flexible and suitable for scalable complex agent-based simulations (Cicirelli *et al*., 2009). It was also used as the execution platform for distributing RepastJ models over HLA for high-performance conservative parallel simulations (Cicirelli *et al*., 2011b).

The original contribution of authors current work is to use RS enriched by actors so as to provide a clean agent methodology integrated with agent spaces and visualization means of RS. A benefit of the actor framework is its ability to support higher agent layers e.g. enabling more abstract but rigorous agent modeling. In particular a Parallel DEVS (Zeigler *et al*., 2000)(Zeigler & Sarjoughian, 2005) layer was achieved and on top of it a Time Petri Net layer (Merlin & Farber, 1976) and a Time Stream Petri Net layer (Diaz & Senac, 1994)(Cicirelli *et al*., 2013) enabling real-time, multimedia and workflow modeling and analysis. Other layers can be added.

This paper is structured as follows. First the basic actor model is proposed and embedded in Repast Simphony, which is suited for general ABMS of large and scalable systems. Then a P–DEVS modeling layer is described which was achieved on top of actors. After that a modeling example is presented and simulated using

Proceedings 27th European Conference on Modelling and Simulation ©ECMS Webjørn Rekdalsbakken, Robin T. Bye, Houxiang Zhang (Editors)
ISBN: 978-0-9564944-6-7 / ISBN: 978-0-9564944-7-4 (CD)

P–DEVS, exploiting features provided by Repast Simphony. The possibility of customizing P–DEVS modeling to cope with conflict management e.g. in time-extended Petri nets, is then discussed. Finally, conclusions are drawn with an indication of on-going work.

ACTORS - A BASIC AGENT LAYER FOR REPAST SIMPHONY

Actors are lightweight agents which *encapsulate* a *data status* and have a *behavior* for responding to messages belonging to a given *message interface*. The communication model is based on *asynchronous message-passing*. Actor behavior is modeled by a finite state machine. An actor is a *reactive object* which responds to an incoming message on the basis of its current state and message contents. Message reception is implicit. An actor is at rest until a message arrives. Message processing triggers a state transition and the execution of a not pre-emptable atomic action. Messages can be unexpected in the current state. Unexpected messages can be discarded or their processing postponed by remembering them in local data or in states of the life cycle. Basic operations on actors are:

- *new*, for creating a new actor
- *become*, for changing the actor state
- (non blocking) *send* for transmitting messages to *acquaintance* actors (including itself for proactive behavior). The send operation carries a message and an absolute timestamp at which the message has to be heard. When absent, the timestamp evaluates to current time (now)
- *now*, which returns the time notion to actors. The now operation is actually provided by a control machine (see below).

The evolution of a subsystem of actors running on a single processor is regulated by a *control machine* component, which is in charge of (transparently) scheduling sent messages, applying to them an application dependent control structure (e.g. based on discrete-event simulation) and dispatching them to actors e.g. according to time. Actors are thread-less. Only one thread exists in the control machine which supports the interleaved execution of actors. The control machine repeats a basic loop where at each iteration one message is selected in the set of pending messages, and delivered to its target actor by invoking on it the *handler* method with the message as an argument. Messages are the unit of scheduling.

The above picture of the actor model corresponds to a single execution node of the more general Theatre distributed architecture (Cicirelli *et al*., 2009) which is beyond the scope of this paper.

The actor framework is implemented in Java through the services of a few base abstract classes (see also Fig. 2): Actor, Message and ControlMachine. Programmer defined actor classes must derive, directly or indirectly, from Actor. Application message classes must inherit from Message. The Message class includes such fields (and related get/set methods) as *receiver*, *timestamp*, and *removed* flag. The time model is assumed to be dense. The removed flag is used to invalidate a scheduled message so that it will no longer be dispatched. It is worth noting that the flag avoids physically dropping the message from the message queue used by the control machine.

Mapping actors onto Repast Simphony (RS) was achieved by developing a RepastS_Simulation class which is a specialization of ControlMachine (see Fig. 2) and by adopting the Java based modeling style enabled by RS. RepastS_Simulation rests on the RS default scheduler and customizes basic schedule/unscheduled methods of the ControlMachine by interfacing with the RS scheduler. An actor message is wrapped into an RS action. Action scheduling specifies (i) the message receiver as the target agent, (ii) the message timestamp as the action occurrence tick, and (iii) the handler method on the receiver actor which has to be invoked, at action dispatch time, with the message as an argument.

To complete preparation of a Java based ABMS model based on actors and RS, a context builder class (see pseudo code in Fig. 1) has to be prepared equipped of *build*, *initialize* and *finalize* methods. The build method is responsible of instantiating the RepastS_Simulation control machine, getting any simulation parameters (including the simulation time limit) entered by the user through the RS runtime system, and to create actors and adding them to the root main context of RS. The actual initialization of actors is realized in the initialize method, whose execution at time 0 is scheduled in the build method. The initialize method also schedules the execution of the finalize method at the end time of the simulation.

```
public class ModelCxtBuilder extends
    ContexBuilder<Object>{
    common model data declaration
    public Context<Object>
        build( Context<Object> context ){
        //to properly enable the use of projections
        set the id of (root) context
        achieve default scheduler of Repast Simphony
        get simulation parameters, if there are any, from the
            runtime system
        create a RepastS_Simulation instance with the
            simulation time limit as an argument
        create actor instances and add them to context
        add actors to context
        schedule execution of the initialize method at time 0
        return context
    }//build
    void initialize(){
        initialize actors by sending first messages
        schedule execution of the finalize method at the time
            limit of simulation
    }//initialize
    void finalize(){
        execute model finalization actions
    }//finalize
}//ModelCxtBuilder
```

Figure 1 – Schema of a model context builder based on actors

The resultant actor framework is effective and provides to the RS modeler the ability to follow a simple yet powerful and general agent methodology for building complex and scalable ABMS models which can exploit contexts and projections (spaces) and the services exposed by the RS runtime system, i.e. parameter setting, simulation batches with parameter sweep, collection of simulation results and their graphical rendering for analysis and so forth. Besides modeling at the actor/agent layer, more abstract methodological layers can be built and used for ABMS.

A PARALLEL DEVS METHODOLOGICAL LAYER

A Parallel DEVS (P–DEVS) (Zeigler *et al*., 2000)(Zeigler & Sarjoughian, 2005)(Cicirelli *et al*., 2007)(Cicirelli *et al*., 2013) implementation based on actors was achieved, which enables Repast Simphony to be used also according to formal P–DEVS modeling.

An overview to Parallel DEVS

A model is a coupled component which consists of an interconnection of atomic (or behavioral) and coupled (or structural) components, and so forth recursively. As a consequence, a P–DEVS model has a natural hierarchically structure. An atomic component is a structure M defined as $M=<X,S,Y,\delta_{int},\delta_{ext},\delta_{con},\lambda,ta>$ where

- X is the set of input values
- S is a set of states
- Y is the set of output values
- $\delta_{int}:S\rightarrow S$ is the *internal transition* function
- $\delta_{ext}:Q\times X^b\rightarrow S$ is the *external transition* function, where $Q=\{(s,e)|s\in S,\ 0\leq e\leq ta(s)\}$ is the set of *total states* and e is the *elapsed time* since last transition
- X^b denotes the collection of *bags* over X (in a bag some elements may occur more than once)
- $\delta_{con}:Q\times X^b\rightarrow S$ is the *confluent transition* function
- $\lambda:S\rightarrow Y^b$ is the *output function*
- $ta:S\rightarrow R^+_{0,\infty}$ is the time *advance function.*

Sets X, S and Y are typically products of other sets. S, in particular, is normally the product of a set of *control states* (or *phases*) and other sets built over the values of a certain number of variables used to describe the system at hand.

Meaning of the elements of M can be stated as follows. At any time the system is in some state $s\in S$. The system can stay in s for the time duration (dwell-time) $ta(s)$. ta(s) can be 0, in which case s is said a *transitory state*, or it can be ∞, in which case it is said a *passive state* because the system can remain forever in s if no external event interrupts. Provided no external event arrives, at the end of (supposed finite) time value $ta(s)$, the system moves to its next state $s'=\delta_{int}(s)$ established by the internal transition function δ_{int}. Moreover, just *before* making the internal transition, the system produces the output computed by the output function $\lambda(s)$. During its remaining in s, the system can receive an external event x which can cause s to be exited earlier than $ta(s)$. Let $e\leq ta(s)$ be the elapsed time since the entering time in s (or, equivalently, the time of last transition). The system then exits the state s moving to the next state $s'=\delta_{ext}(s,e,x)$ determined by the external transition function δ_{ext}. As a particular case, the external event x can arrive when $e=ta(s)$. In this case two events occur simultaneously: the internal transition event and the external transition event. The next state s', in this *collision* situation, is determined by the confluent transition function δ_{con}. Default behavior of δ_{con} consists of executing the output function and then the external transition function on the phase determined by application of the internal transition (see Fig. 3). This behavior can be redefined to comply with the application needs. After entering state s', the new time advance value $ta(s')$ is computed and the same story continues. Following a self-loop external transition, i.e. where $s'=s$, there is no need to stop time advancement in current state.

It is worth noting that there is no way to generate an output directly from an external transition. An output can only occur just before an internal transition. To have an external transition cause an output without a delay, a transitory state can be entered from which the exiting internal transition is preceded by the generation of the output value.

Parallel DEVS emphasizes that a *bag* of simultaneous inputs can be received by an atomic component which in general can have a specific reaction to the combination of inputs which is different from the effect of sequential reactions to the separately received inputs.

In practice, an atomic component receives its inputs from *typed input ports* and generates outputs through *typed output ports*. Ports are architectural elements which favor a modular system design. A component refers only to its interface ports. It has no knowledge about the identity of cooperating partners. A coupled component (subnet) is a port interconnection of existing atomic or coupled (hierarchical) components.

Each component can be equipped with its own simulator. In this work, though, a single simulation structure is used which serves an entire P–DEVS flattened model where it is minimized the number of exchanged messages.

Mapping P–DEVS onto RS actors

In the following, an original implementation of P–DEVS which builds on previous authors work, e.g. (Cicirelli *et al*., 2007), and complies specifically with Repast Simphony, is presented. The organization is portrayed in the UML class diagram of Fig. 2.

AtomicDEVS abstract class, derived from Actor, is the base for achieving, through inheritance, the concrete atomic components required by an application.

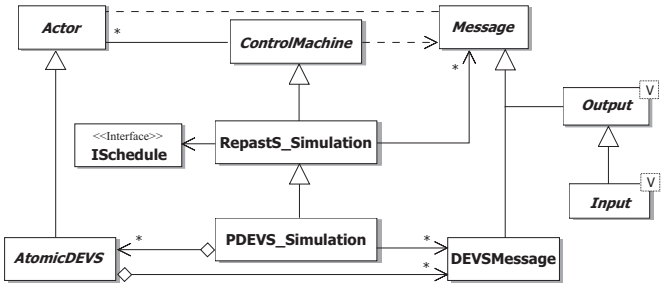

Figure 2 – UML class diagram supporting P–DEVS on top of actors in Repast Simphony

```
public abstract int delta_int( int phase );
public abstract int delta_ext( int phase,
                        double e, Iterable<Message> x );
public int delta_con( int phase, double e,
                        Iterable<Message> x ){
    //default behavior
    lambda( phase );
    return delta_ext( delta_int( phase ), 0, x );
}//delta_con
public abstract double ta( int phase );
public abstract void lambda( int phase );
public void handler( Message m );
public void handler( Iterable<DEVSMessage> bag );
public void initialPhase( int phase ); //sets the initial phase of
                                       //the component
```

Figure 3 - AtomicDEVS method interface

Component internal phases are coded as integers. Method signatures in AtomicDEVS are shown in Fig. 3. Typed input/output ports of components are directly mapped on to messages. In particular the Output<V> and Input<V> derived classes of Message are introduced which are generic in the type V of the carried data. In particular, Input<V> is derived from Output<V>. Services get()/set() permit respectively to achieve/modify the data component of an Output<V> message. The method linkTo(receiver) of DEVSMessage allows an output message to be bound to a given receiver actor.

PDEVS_Simulation specializes RepastS_Simulation by taking into account the specific semantics of P–DEVS models and constraints introduced by RS. An evolution of a P–DEVS model can be viewed as a sequence of *epochs* where all the actions (simultaneous events) to be accomplished at a same time are carried out in due order. Toward this timed and untimed messages are handled.

Timed messages, scheduled by RS, correspond to internal events of atomic components which have exhausted their dwell-time in current phase. Untimed messages are managed by PDEVS_Simulation and are grouped into bags to be received as external messages in the current epoch. As required by P–DEVS, all instantaneous messages created at current time must be collected into bags so as for them to be processed by relevant recipients before starting the next epoch.

Therefore, it is the responsibility of PDEVS_Simulation to ensure first all contemporary timed messages (and corresponding internal transitions) are processed and, finally, all the collected bags of messages are sent to target components. When all bags existing in current time have been processed, the next epoch is entered.

Since contemporary timed messages and bags have the same occurrence time (i.e. they are simultaneous events), it is mandatory to order messages in such a way that timed message processing precedes bags processing. More precisely, PDESV_Simulation maintains the collection of the atomic devs components which have bags at current time. Dispatch of bags to these components is accomplished by a dispatchBags method of PDEVS_Simulation. A single action for executing dispatchBags is scheduled at current time to occur at the *end* of present epoch. To achieve the required ordering, the priority field of RS actions is exploited. The scheduled action for dispatchBags gets a lower priority than that used for scheduling timed messages.

Moreover, the AtomicDEVS introduces two versions of the handler method (see Fig. 3). The first one overrides the handler method of the Actor base class. It receives a Message as an argument and executes the output and internal transition functions of the component. The second version of handler has a bag as parameter, modeled as an Iterable<DEVSMessage> object. This version of the handler method executes actions of the external transition of the component. The basic version of handler is also capable of discovering a collision situation which occurs when the timed message finds a non empty bag destined to the component. In these cases the confluent function of the component is invoked instead of output and internal transition functions.

From the above discussion it follows that the modeler has to concentrate only to the specification of the basic functions of atomic components, namely the time advance, lambda (output), the delta_int (internal transition), delta_ext (external transition) and delta_con (confluence transition) functions. All of this delivers a declarative modeling style, with all the scheduling burden being insulated in the PDEVS_Simulation and the AtomicDEVS classes.

A Modelling Example based on Parallel DEVS

Fig. 4 shows a coupled model inspired by (Zeigler & Sarjoughian, 2002). The example concerns a simple neural network where components (neurons) are interconnected by input/output ports. The network models a direct graph e.g. of cities, with assigned distances between adjacent cities. The problem is to find the shortest path between a Start and a Dest pair of cities.

Nodes of the graph are instances of the FireOnceNeuron (FON) and PulseGenerator atomic components. The PulseGenerator is in charge of generating pulses which are then simultaneously broadcast to A, B, I and C components.

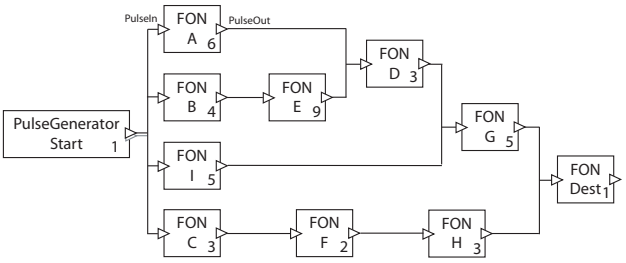

Figure 4 – A P–DEVS neural network for computing the shortest path in a direct graph

In Fig. 4 the firing delay of neurons (shown in the component box) expresses the weight (e.g. travelling time) of the arcs. Each atomic component is supposed to be equipped by a single input and a single output port carrying pulses. The final component Dest has its output port unconnected. The PulseGenerator atomic component has an array of output ports.

The FireOnceNeuron model (see Fig. 5) remains in the RECEPTIVE phase until one or a bag of pulse external events arrive. The external transition function moves it to the FIRE state where the component remains for a duration given by firingDelay>0, after which it emits a pulse and enters the REFRACT state. The time advance of REFRACT is infinity. Therefore, the neuron after firing moves and remains in REFRACT forever, never being able to fire again. Further pulses received when staying in FIRE or REFRACT are simply ignored. In this example a bag of input pulses has the effect corresponding to any single pulse of the bag.

In Fig. 5, thick arrows denote external transitions, thin arrows internal transitions, dashed arrows output generation. The FireOnceNeuron Java class directly corresponds to the P–DEVS formal definition of the component. The only extra code added is related to placing the component over the adopted grid space. The model *linkto* relationships are also established explicitly as network links.

Table 1 depicts the formal P–DEVS definition of the FireOnceNeuron. The output function has been explicitly defined only for states with a finite time advance value. For RECEPTIVE and REFRACT states the output function implicitly associates the null output.

From the property of FireOnceNeuron to propagate only the first received pulse, which necessarily is the faster one, derives the ability of the overall network to naturally computing the shortest path. It is worth noting that the model of Fig. 5 adopts the default confluent transition function.

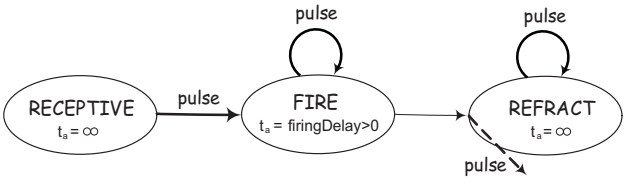

Figure 5 - Control states and transitions of the FireOnceNeuron atomic component

Table 1. P–DEVS specification of FireOnceNeuron

X={pulse}
S={RECEPTIVE, FIRE, REFRACT}
Y={pulse}
δ_{int}(FIRE)=REFRACT
δ_{ext}(RECEPTIVE,e, pulse^b)=FIRE
δ_{ext}(FIRE,e, pulse^b)=FIRE
δ_{ext}(REFRACT,e, pulse^b)=REFRACT
λ(FIRE)={pulse}
ta(RECEPTIVE)=∞
ta(FIRE)=firingDelay
ta(REFRACT)=∞

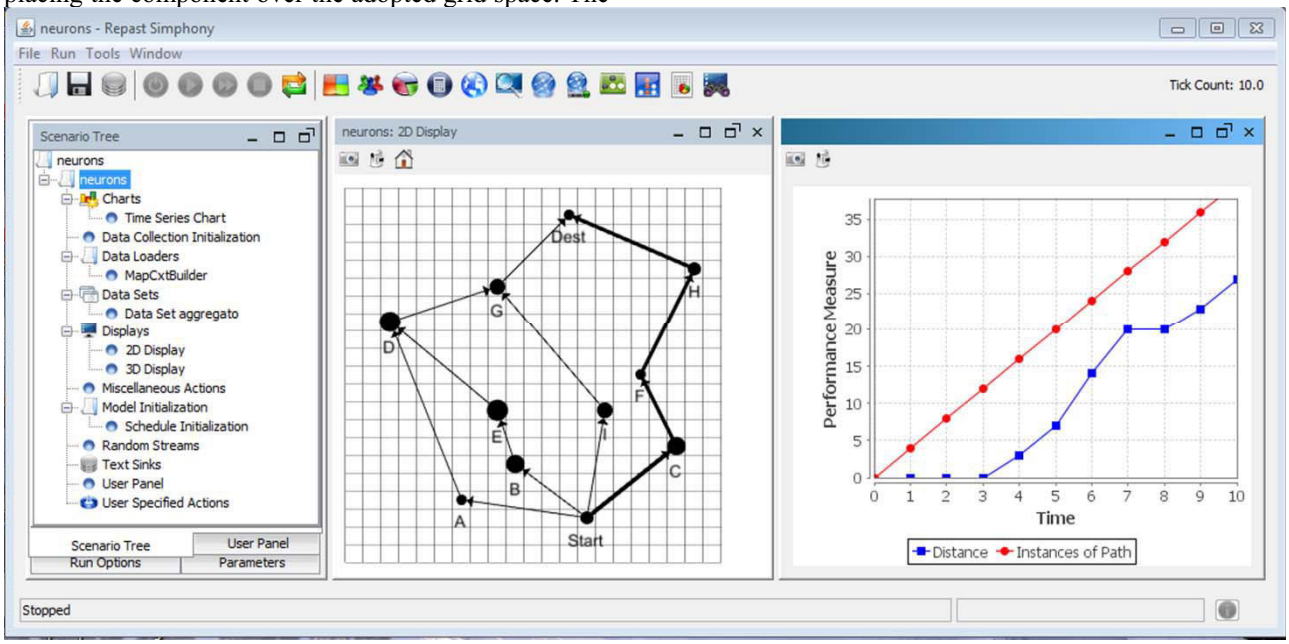

Figure 6 – A screenshot of the RS runtime environment relevant to the execution of the neurons model

The neural network model was configured in a MapCxtBuilder class which creates the component instances and links them according to the topology portrayed in Fig. 4. Components are situated on a grid projection and their inter-relationships expressed by a network projection.
Four instances of a class Path are injected, periodically, by the PulseGenerator as values on to its output ports and flow through the network. A Path object collects the id of crossed component nodes along the current travelled distance. As a consequence the path object which arrives to the Dest component will contain the shortest path.
Fig. 6 shows model display in the RS runtime environment. As one can see the shortest path gets highlighted in the 2D display panel. For demonstration purposes, a time series chart was also generated which reports the number of path objects injected, from time to time, in the network by the pulse generated and the cumulative distance, i.e. the sum of distances travelled by path objects at each time. The latter can be viewed as a sort of cost tied to the algorithm. It worth noting that generation of the chart time series is an orthogonal aspect of the model, i.e. no information has been put in the modeled system about the chart. The simulation stops as soon as the faster path object reaches the Dest node. As a consequence, the last time point in the x axes of the chart also mirrors the length of the found shortest path.

Time Extended Petri Nets Layers

The P–DEVS framework described in the previous section was successfully used as a starting point for supporting Time Petri Nets (TPN) (Merlin & Farber, 1976) and Time Stream Petri Nets (TSPN)(Diaz & Senac, 1994) which are useful for modeling and analysis of time-dependent systems, e.g. embedded real-time systems with time-constraints, multimedia/ hypermedia systems, workflow systems (Cicirelli *et al*., 2013). TSPNs associate a dense time interval to input arcs only, whereas TPNs specify a dense time interval to transitions only, which constrains transition firing. In a TSPN model one out of ten firing or synchronization rules can be attached to a transition. Depending on the firing rule, the transition is then able to determine, at each time it becomes enabled, a dynamic time interval (possibly empty) which affects its firing. In common with TPN transitions, a *strong firing model* is ensured: a TSPN transition can only fire at any time of its time interval, provided it remains continually enabled.
Every TPN/TSPN transition is modeled as a distinct P–DEVS atomic model.
Proper TPN/TSPN modelling requires the handling of a problem not covered by standard P–DEVS: that of *conflicts* arising, in a component, at the last time of stay in its current phase (Cicirelli *et al*., 2007). Whereas P–DEVS normally relies on the *maximal parallelism* hypothesis which implies that all timed messages occurring at a same epoch are always committed and there is no way for an internal event to forbid the processing of a different timed message of the same epoch, in TPN/TSPN and similar models, the firing of a transition, although occurring at the last time point of its dynamic time interval, can be disabled by the firing of a conflicting transition.
Conflict management can be achieved, in these models, through a redefinition of the confluent function so as to coincide with the external transition function, thus permitting the removal of some pending timed messages of current epoch, and the discard of the corresponding lambda/output function which would send messages to partner components. The mentioned redefinition allows a transition to be informed at any time of the firing of a conflicting transition so as to adjust its state accordingly.

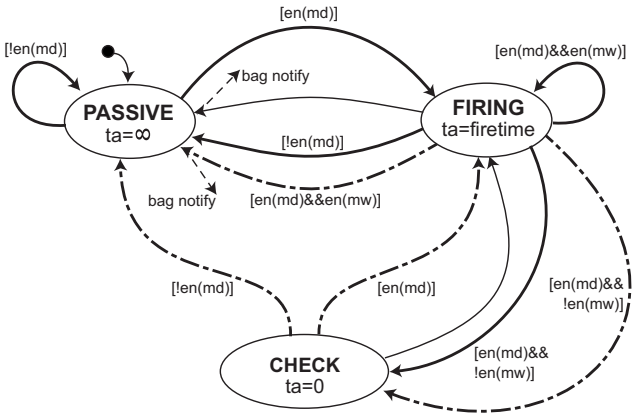

Figure 7 – P–DEVS model of a TSPN transition

Fig. 7 portrays the dynamic behaviour of a TSPN transition (a similar model exists for a TPN transition). Thick arrows represent external transitions triggered by a bag of Notify() messages. Arrows which are both tick and dashed denote confluent transitions. Before accomplishing an internal transition (thin arrow), the lambda() function (thin dashed arrows in Fig. 7) is executed which generates output events to partner components. More in particular, the lambda() function of a fired transition creates a bag of Notify() messages as a consequence of changing the marking of places during its firing process. When coming back from CHECK to FIRING due to the elapsed time internal event, the lambda() function is simply void.
A bag of messages is received by the external/confluent function of a Transition component, as an Iterable object. The en() predicate returns true if the transition is logically enabled, i.e., a sufficient number of tokens is available in the preset. As part of the en() service, the dynamic firing interval of the transition is calculated, on the basis of the enabledness and temporal interval of the input arcs and the synchronization rule selected for the transition.
The atomic firing process of a transition *t* occurs in two steps: first tokens are withdrawn from the preset of *t*, then tokens are deposited in the postset of *t*. A critical point is concerned with the detection of under firing

transitions which lose their enabling during the first withdrawl step of the firing process of *t*, but are anyway enabled at the end of the firing process. Such transitions must correctly be handled as newly enabled transitions.
In order to realize the firing process, different notify messages are employed to separately carry out a withdraw marking and a deposit marking relevant to a given transition.
In Fig. 7, the arrival of a bag of Notify() messages in the FIRING phase, causes a self-loop external transition in the case the transition is persistent to current firing, i.e. it is enabled both during and at the end of the firing. As soos as a transition detects it loses its enabling in a withdrawal step, but it is enabled in the deposit phase, it switches from FIRING to the CHECK transitory phase. From CHECK the transition can re-enter the FIRING phase if the transition finds itself ultimately enabled in the deposit step, otherwise it reaches the PASSIVE phase. It should be noted that due to interleaving of concurrent actions occurring at a same time, it is perfectly possible that an under CHECK transition can lose its enabling for the firing process of another conflicting transition.
As a final remark, it is worthy of note that a time violated TSPN transition, i.e. one which has no valid dynamic firing interval, remains in the FIRING phase until it gets disabled, without the possibility of completing its firing.
A TSPN model is configured by first creating the (passive) place objects and the transition components. For each transition the synchronization rule is furnished. Places are then added to the preset/postset of transitions. After that input arc connections among places and transitions and vice versa are established. Model bootstrap is finally ensured by defining the initial marking of each place which in turn generates the initial bags for transitions.
The TSPN modeling layer was exploited, in a significant case, in the modeling and simulation of complex workflow systems (Cicirelli *et al*., 2013).

CONCLUSIONS

The Repast Simphony agent methodological layers described in this paper are a key for promoting agent modeling eclecticism, that is the possibility of choosing the agent modeling layer most apt to a given problem domain. The realizations are founded on a lightweight actor model which provides asynchronous message passing and control specific strategies of message scheduling/dispatching.

On-going work is geared at

- improving and optimizing the realizations by applying them to ABMS of large systems
- exploring visual modeling with some agent layer, e.g. P–DEVS which is almost declarative in character, in the sense that an atomic component rests only on local variables and the specification of basic internal transition, external transition, confluent transition, time advance and lambda/output functions
- experimenting with time-extended Petri nets layers in the modeling and analysis of real-time tasking sets
- extending the approach by addressing other agent layers as well.

REFERENCES

Cicirelli, F., A. Furfaro, L. Nigro (2007). Conflict management in PDEVS: An experience in modeling and simulation of time Petri nets. In *Proc. of Summer Computer Simulation Conference (SCSC'07)*.

Cicirelli, F., A. Furfaro, L. Nigro (2009). An Agent Infrastructure over HLA for distributed simulation of reconfigurable systems and its application to UAV coordination. *Simulation Trans. of The Society for Modelling and Simulation International*, **85**(1):17-32.

Cicirelli, F., A. Furfaro, L. Nigro (2011a). Modelling and simulation of complex manufacturing systems using statechart-based actors. *Simulation Modelling Practice and Theory*, **19**(2):685-703.

Cicirelli, F., A. Furfaro, A. Giordano, L. Nigro (2011b). HLA_ACTOR_REPAST: An approach to distributing Repast models for high-performance simulations. *Simulation Modelling Practice and Theory*, **19**(1):283-300.

Cicirelli, F., A. Furfaro, L. Nigro (2013). Using time stream Petri nets for workflow modeling analysis and enactment. *Simulation Trans. of The Society for Modelling and Simulation International*, **89**(1): 68-86.

Diaz, M., P. Senac (1994). Time stream Petri nets: A model for timed multimedia information. In *Proc. of the 15th Int. Conf. on Application and Theory of Petri Nets*, London, UK, pp. 219–238.

Macal, C.M., M.J. North (2011). Introductory tutorial: agent-based modeling and simulation. In *Proc. of Winter Simulation Conference*, pp. 1456-1469.

Merlin, P., D. Farber (1976). Recoverability of communication protocols–implications of a theoretical study. *IEEE Trans. on Comm*. **24**: 1036–1043.

North, M.J., T.R. Howe, N.T. Collier, J.R. Vos (2005a). Repast Simphony development environment. In *Proc. of the Agent 2005 Conf. on Generative Social Processes, Models and Mechanisms*, ANL/DIS-06-01, Oct.

North, M.J., T.R. Howe, N.T. Collier, J.R. Vos (2005b). Repast Simphony runtime system. In *Proc. of the Agent 2005 Conf. on Generative Social Processes, Models and Mechanisms*, ANL/DIS-06-01, Oct.

North, M.J. & C.M. Macal (2007). *Managing business complexity – Discovering solutions with Agent-Based Modeling and Simulation*, Oxford University Press.

Repast, on-line, http://repast.sourceforge.net

Zeigler, B.P., H. Praehofer, T.G. Kim (2000). *Theory of modeling and simulation*. Second Edition, Academic Press.

Zeigler, B.P. and H.S. Sarjoughian (2002). DEVS component-based M&S framework: an introduction. *http://www.acims.arizona/EDUCATION/ECE575Fall03/ECE575Fall03.html.*

Zeigler, B.P. and H.S. Sarjoughian (2005). Introduction to DEVS modeling and simulation with Java: developing component-based simulation models. *http://www.acims.arizona.edu.*

INTERACTIVE, GPU-BASED URBAN GROWTH SIMULATION FOR AGILE URBAN POLICY MODELLING

Michel Krämer and Andreas Kehlenbach
Fraunhofer Institute for Computer Graphics Research IGD
Competence Center for Spatial Information Management
Fraunhoferstr. 5, 64283 Darmstadt, Germany
Email: michel.kraemer@igd.fraunhofer.de
Email: andreas.kehlenbach@cs.uni-frankfurt.de

KEYWORDS

GPU computing, Agent-based modelling (ABM), Urban simulation, Urban policy modelling, Urban planning, Geographic information systems (GIS)

ABSTRACT

In this paper we present a novel approach of simulating urban growth by utilising the computation power of modern GPUs. The simulation results can be used in urban policy modelling to reduce turnaround times in the policy cycle. We use a state-of-the-art agent-based simulation model that consists of rules to describe human behaviour. The simulation incorporates geospatial information such as land-use, current population density and road network data. In order to simulate the phenomena of urbanisation, in our model citizens more likely settle near roads or existing settlements/cities. In this paper we present our implementation that is based on the FLAME GPU framework. Each agent on the GPU represents a group of citizens at a specific location. In order to evaluate our approach we present a practical use case. We measure the performance of our implementation and compare it with a Java-based solution. Finally, we discuss our approach and show opportunities for agile and interactive urban policy modelling.

INTRODUCTION AND MOTIVATION

The term "urban sprawl" describes the problem of modern cities growing quickly resulting in wide-spread developments with a very low density. This often has negative effects on environment and therefore on people's health: more land is covered with buildings or streets; public transport in suburbs is often not sufficiently developed and so citizens have to use the car to get to their job or to the city centre which effectively leads to a higher air pollution. Besides, urban sprawl may also affect the cultural life and family life. People living in suburbs sometimes participate less in cultural events than people living near the city centre. Long travels to work and back to home reduce the time an employee can spend with his or her family.

Urban planning and policy modelling therefore aim for creating more compact but at the same time sustainable and healthy cities. This development requires infrastructure changes that have to be well thought out. So, urban planners more and more involve citizens in the discussion about urban development plans in order to create a city that is well received by everyone. They make use of simulations based on geospatial information. Innovative techniques such as 3D visualisation help urban planners to present the simulation results to decision makers and to the public.

Modern urban policy modelling deploys a so-called policy cycle (see Krämer et al., 2013). Simulations and 3D visualisations are used to gain feedback from decision makers and citizens. This feedback can then be incorporated in new simulations which are presented to the public again. This loop repeats until a general agreement on the planning has been found. The shorter the feedback cycle is, the faster a final decision can be made.

Creating such simulations is currently a time-consuming task that may take several hours or even days with existing solutions (see section "Performance" below). Urban planners often make use of modern satellite imagery to improve their calculations. For example, satellite images or LIDAR data spanning several years allow urban planners to calculate urban growth and hence to estimate future trends. The ongoing development of sensor technology leads to more accurate data sets which may be exploited to achieve better simulation results. However, at the same time the volume of data to process becomes larger and larger which makes them harder to process with standard geospatial information systems (GIS). Nonetheless, quickly creating simulations based on such data sets is a crucial part for the urban policy feedback cycle.

Modern computer architectures with multi-core CPUs and GPUs allow for creating high performance applications (cf. Owens et al., 2007). However, current GIS solutions do not fully take advantage of this yet. In practice, urban planners process raster data or point clouds such as satellite images or LIDAR data respectively with software tailored to simple workstations. In recent years these workstations have evolved and already include sophisticated graphics hardware. With this hardware it now becomes possible to not only create high performance 3D visualisations but also to make use of the thousands

Proceedings 27th European Conference on Modelling and Simulation ©ECMS Webjørn Rekdalsbakken, Robin T. Bye, Houxiang Zhang (Editors)
ISBN: 978-0-9564944-6-7 / ISBN: 978-0-9564944-7-4 (CD)

and millions of cores offered by a modern GPU to create geospatial simulations.

Modelling the behaviour of citizens in an urban environment can be rather complex in that it is non-linear and possibly chaotic. A lot of individual factors have to be taken into account that make the model large and hard to comprehend. Agent-based modelling (ABM) attempts to simplify such problems. Agents are autonomous units that act on their own, just like citizens. Modelling urban life becomes a lot easier by considering only one citizen or a group of similar citizens and by representing them as individual agents. Modern graphics hardware allows agent-based simulations to run on the GPU. So, it is possible to create high-performance simulations modelling urban life on the graphics card.

To summarise, in order to create sustainable, compact cities, urban planners deploy a feedback cycle that is based on geospatial simulations. The shorter this cycle is, the faster decisions can be made. However, geospatial data—which provides the basis for such simulations—becomes larger and larger and so simulations take more and more time with current GIS technology. In this paper we therefore present a new approach of interactively simulating urban development with modern GPU hardware. We use agents to model real urban life. We describe our implementation and evaluate its performance compared to a pure Java application. We conclude with a final discussion on the applicability of our approach to a practical use case, and we show opportunities for agile urban policy modelling.

RELATED WORK

Agent-based simulation has already been applied in the area of geographical information systems (GIS). For example, Gimblett proposes to model social and ecological phenomena such as population dynamics, disease epidemics or urban growth with agents (Gimblett, 2002). Gilbert and Troitzsch explain how to use the multi-agent approach to perform social simulation including population changes or business forecasting (Gilbert and Troitzsch, 2005). Gebetsroither presents the MASGISmo platform (Multi-paradigm Agent-based System Dynamics GIS modelling platform) that he uses to simulate social behaviour, natural resources, land use change, or environmental changes (Gebetsroither, 2010). He claims agents to be more appropriate to describe human behaviour than differential equations that try to model complex system dynamics. On the other hand, strategic problems and long-term policy development also have an influence on urban development. Gebetsroither therefore combines multi-agent simulation with elements from the area of system dynamics. He also includes stochastic variation to increase realism. This multi-paradigm approach is based on an idea by Scholl (Scholl, 2001).

The MASGISmo platform uses the RepastJ framework which is a Java library that is able to perform agent-based simulation using multiple CPU cores. RepastJ does not exploit the possibilities of modern graphics hardware. Although geographical information systems (GIS)—such as MASGISmo and others—could make great use of the performance gain offered by GPUs, this possibility has not been fully exploited yet. However, since the advantages of performing parallel computations on the GPU have already been described (Owens et al., 2007; Lupton and Thulin, 2008; Nickolls and Dally, 2010) there is some work trying to apply this approach to GIS. Balz and Haala, for example, use GPUs to perform SAR (Synthetic-Aperture Radar) image interpretation in realtime (Balz and Haala, 2006). They implement algorithms such as SAR rasterisation or LIDAR point triangulation on the GPU. They state that their solution is able to "simulate and visualise huge amounts of 3D data" and that it is therefore "the best choice for simulating city models" (Balz and Haala, 2006).

Combining the multi-agent approach with the advantages of GPU-based calculation offers a great opportunity for geospatial simulation. For example, Strippgen and Nagel use GPUs to simulate urban aspects—in their case traffic (Strippgen and Nagel, 2009). They use agents to model human behaviour. In their algorithm each agent has a certain plan for the whole day consisting of activities and routes. An agent participates in the traffic simulation when it moves from one activity to another. Strippgen and Nagel are able to achieve a high performance gain by using the GPU compared to a pure Java solution.

There are a number of frameworks available that support agent-based simulation as well as GIS operations. AnyLogic, for example, is a commercial solution developed by XJ Technologies (http://www.anylogic.de). MASON (http://cs.gmu.edu/∼eclab/projects/mason) and NetLogo (http://ccl.northwestern.edu/netlogo) are open source products written in Java and Scala respectively. Another open source solution is Repast (http://repast.sourceforge.net) which is available for Java, .NET and Python. Apart from that, there are libraries that support spatial operations on the graphics card. CudaGIS (Zhang and You, 2012), for example, offers the possibility to model geospatial primitives on the GPU but it does not support agent-based simulations. There is currently only one framework that supports both, agent-based simulation as well as GIS operations on the GPU. Its name is FLAME GPU (http://www.flamegpu.com). It is an extension to the FLAME framework which was written in C. FLAME GPU uses the same XML-based approach to describe agents as FLAME, but runs the simulation on the graphics card. In this work we hence use FLAME GPU.

EXAMPLE USE CASE AND REQUIREMENTS

In this section we describe a simple, yet realistic use case that we will utilise later to evaluate our approach. The use case is about simulating the development of population density in a certain area. Our test data set consists of

three rectangular grids in the ESRI ASCII grid file format. Each of them covers an area of 4300×2200 cells with a precision of 100 meters per cell in both directions. The first grid provides information on current land use. Each cell contains a number that means a certain type of land use—e.g. 1 for forest, 2 for river, 3 for building land, etc. The second grid contains information about population density. Each cell in this grid contains the number of citizens living there. The third grid represents the road network. A cell denoted with 1 contains a road whereas a cell with a 0 does not.

While testing this data with pure Java applications such as MASGISmo (see above) we observed the following:

- Since performing an urban growth simulation with existing tools takes a long time (often more than several hours up to a few days) it cannot be used well for agile and interactive policy modelling as it is described above.
- Existing tools using agent-based modelling are only able to manage a certain number of agents (depending on the system environment). Up to this number the performance typically increases, but beyond this break-even point the simulation will actually become slower.
- If the used data sets are large—even though the number of agents is low—a single computation step takes a noticeable amount of time.

These issues lead us to the following requirements:

- The user should be able to control parameters to interactively affect the simulation results.
- Our implementation should be able to manage much more agents as traditional implementations.
- It should significantly decrease the amount of time needed for one simulation step.

SIMULATION MODEL

In order to let our simulation create realistic results, based on the results from Gebetsroither we defined the following rules (cf. Gebetsroither, 2010):

- At the beginning the population grows.
- If the population reaches a specific density, we assume that from then on the population growth stagnates.
- We assume that citizens more likely settle near roads and existing cities or settlements. So, the population grows faster in these areas.

We use the information from the land use grid to let citizens settle down on grid cells which are denoted as building land whereas we do not allow citizens to settle down on cells which are denoted as forest, river, etc. At the beginning, we initialise our simulation with the contents of the population density grid. Later this grid is used to store population density changes—i.e. the simulation results. The third grid containing the roads is used for the last rule, namely that the population grows faster near roads as well as existing cities and settlements. Information on the latter is gained from the other two grids.

At the beginning we associate one agent to each population grid cell. This agent represents the group of citizens in this cell but not one particular citizen. This works, because the population density grid only contains abstract numbers about how many citizens live in each cell. An agent is able to let the population density grow or decline in its cell. Therefore it uses information from neighbouring cells. We use the Moore neighbourhood here, which means we only take direct neighbours into account.

We first start with a randomly generated number of citizens who want to settle down in the area. We let the agents decide where these citizens settle down. They do so with decreasing probability near roads and already settled citizens. If a citizen settles down, the population density in the respective cell will be increased.

In each simulation step a certain number of new citizens are born. To simulate negative growth or stagnation we introduce a mortality rate. If the birth rate is higher than the mortality rate the overall population will grow. Otherwise the overall population will decline. We dynamically alter both rates so that the population first grows and then stagnates.

The chosen model leads to a population growth in two dimensions. On the one hand, if agents settle on new cells the populated area will grow and new cities or settlements will be founded. On the other hand, a growing population density in a few single cells will lead to high-rise buildings.

In our use case we want to simulate urbanisation and so we do not model the aspect of citizens moving away from the cities.

IMPLEMENTATION

In this section we present our simulation tool and how we implemented it based on the FLAME GPU framework.

In order to load the input data into our tool we enhanced FLAME GPU to support ESRI ASCII grids in addition to the standard XMML format containing the simulation model. An ERSI ASCII grid consists of a small header containing the grid's size or resolution, a so-called NODATA value and the geospatial location of the covered area's lower-left corner. The NODATA value is used for all empty grid cells that do not contain a valid value. It is typically negative whereas all other values can be integers or floating point numbers. The values are separated by a whitespace character. For our use case we prefer ESRI ASCII grids over the XMML format already supported by FLAME GPU because our input data

is quite large and XMML is not designed for such an amount of data. ESRI ASCII grids store values in a much more compact way. Besides, the input data is already available as ESRI ASCII grid files so we don't have to convert them.

In order to be able load the large grid files into memory we split them into smaller chunks. The chunk size is defined by the FLAME GPU memory model which relies on a fixed number of agents that must be a power of two. As described above, we use one agent per cell, so our chunk size also has to be a power of two. FLAME GPU requires the developer to define this number at compile time. Splitting the grids into chunks allows us to use a fixed number at compile time as well as to load grids of arbitrary size.

In FLAME GPU agents are implemented as special functions that are executed on the GPU. Such functions are also known as *CUDA kernels*. Each simulation step consists of two kernels that are called consecutively. In the first kernel all agents send out a message containing their state—i.e. the population density in their respective grid cells. In the second kernel the agents decide whether to let population grow or not and then update their internal state. To build up communication between agents we use a Communicating X-Machine (COMX), a computation model provided by the FLAME GPU framework. A COMX consists of several X-Machines—a model that is similar to Finite State Machines (FSM)—that run in parallel. These machines communicate by sending messages over communication channels called *ports*. COMX are superior to pure Finite State Machines, because they are able to cover dynamic and static aspects of a system. In FLAME GPU messages sent by agents are saved to a global message list that resides in the graphics card's global memory.

Listing 1 outlines the first kernel and listing 2 the second one.

```
1  __FLAME_GPU_FUNC__ int ↩
       output_state(xmachine_memory_cell* xmemory, ↩
       xmachine_message_state_list* state_messages, ↩
       RNG_rand48* rand48)
2  {
3      // Add cell state to the global message list
4      add_state_message<DISCRETE_2D>( ↩
           state_messages, xmemory->color, ↩
           xmemory->population, xmemory->state, ↩
           xmemory->x, xmemory->y);
5      return 0;
6  }
```

Listing 1: The first CUDA kernel. Each agent sends its state as a message to the global message list.

In listing 2 we first iterate through the global message list. As described above, our simulation model requires citizens to more likely settle down near neighbouring roads and other citizens. So, we skip messages that are not from our direct neighbours. Based on the information received we then check if the current agent will increase population in its cell or not. The agent finally updates its internal state.

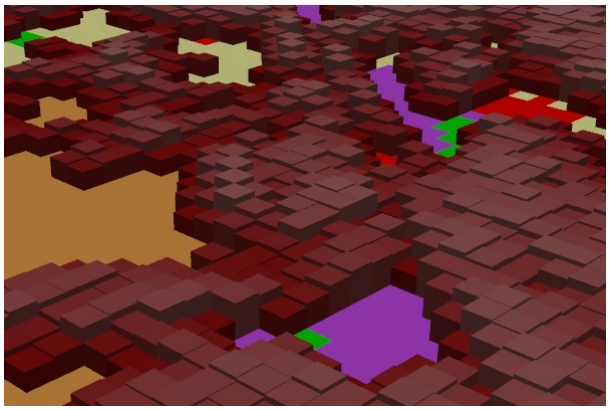

Figure 1: 3D visualisation of simulation results in our tool.

```
1  __FLAME_GPU_FUNC__ int ↩
       update_state(xmachine_memory_cell* xmemory, ↩
       xmachine_message_state_list* state_messages, ↩
       int* color_table, RNG_rand48* rand48)
2  {
3      // Initialize
4
5      // Iterate through global message list
6      xmachine_message_state* state_message = ↩
           get_first_state_message<DISCRETE_2D>( ↩
           state_messages, xmemory->x, xmemory->y);
7      while(state_message)
8      {
9          // Messages sent by neighbours are treated ↩
               separately.
10         // Get next message
11         state_message = ↩
               get_next_state_message<DISCRETE_2D>( ↩
               state_message, state_messages);
12     }
13
14     // Is settling allowed on this cell?
15     // Increase or decrease population in this cell.
16     // Save new state.
17
18     return 0;
19 }
```

Listing 2: The second kernel. The agent first evaluates all messages received from its direct neighbours. Then it decides whether to increase population or not and finally updates its internal state.

Our tool allows the user to interactively affect the simulation results. The user can change the population maximum for a single cell. That means if one cell reaches a maximum number of citizens new ones that want to settle there as well are redirected to neighbouring cells. The user can also interactively alter the land use grid. For example, he or she might declare a certain area as building land where citizens can settle down. The interaction possibilities help urban planners in the aforementioned policy modelling feedback cycle. By letting the user interactively change the simulation the feedback cycle's turnaround time can be reduced significantly.

Our tool contains a 3D visualisation of the simulation results. The calculated population density is displayed with blocks of different heights. The greater a cell's population density is, the higher the respective block will be. The cell's colour depends on the actual land use—e.g.

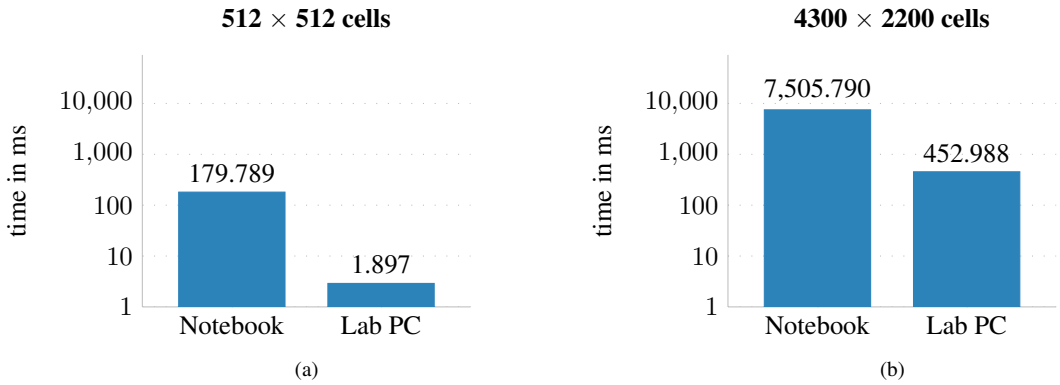

Figure 2: Subfigure (a) shows the number of milliseconds needed to perform a single simulation step on a grid chunk with 512×512 cells; (b) shows measurements for the complete grid with 4300×2200 cells.

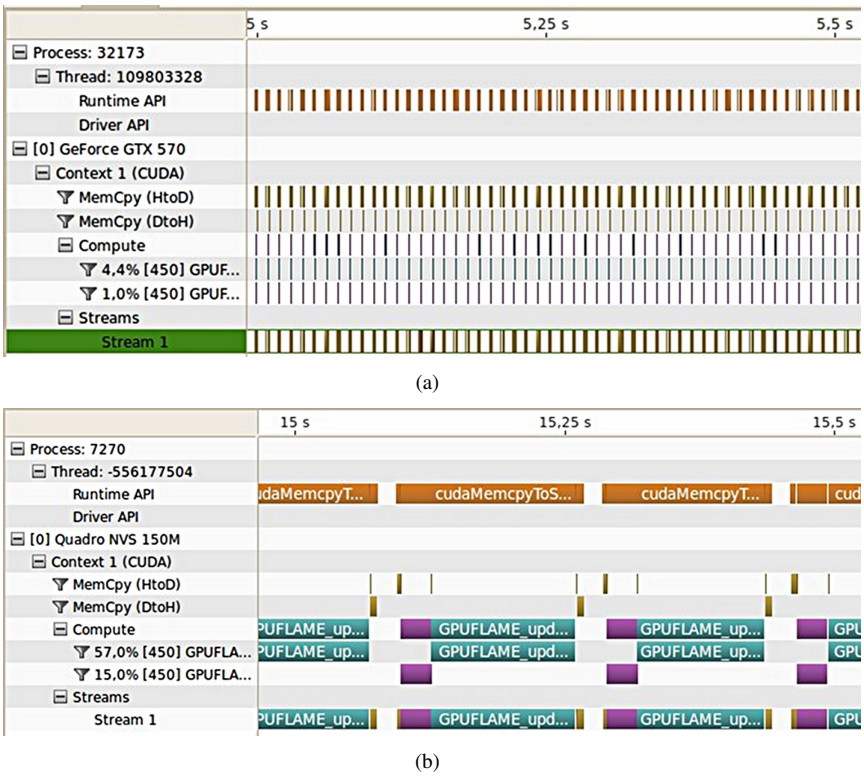

Figure 3: Comparison of the executed CUDA kernels per second between the lab PC (a) and the notebook (b).

settlements are displayed in red, forest in green, etc. If there is no population at all in a cell, it will be visualised as a flat plane. Figure 1 shows a screenshot of our tool. Scrolling over the grid, zooming in and out and freely rotating the grid allows the user to inspect and analyse the simulation results.

PERFORMANCE

In this section we present the results from evaluating our tool's performance based on time measurements and deep profiling with the NVIDIA Visual Profiler. The performance evaluation was executed on two computers:

- a lab PC equipped with an Intel Core i7 CPU, a NVIDIA GeForce GTX 750 (1,280 MiB RAM), and a NVIDIA Tesla C2075 GPU (5,375 MiB RAM);
- a notebook with an Intel Core 2 Duo CPU and a NVIDIA Quadro NVS 150M GPU (255 MiB RAM).

We evaluated two data sets: a single grid chunk with 512×512 cells and a complete grid with 4300×2200 cells. Figure 2 shows that only the simulation of the whole grid on the notebook is not very fast (almost 7 seconds per simulation step). The notebook's GPU simply has not enough computation power. But in comparison to

the plain Java application MASGISmo the results of both computers are fine. On our notebook the Java application was able to simulate about 100 agents in about 1 second. It therefore needed more than 2,600 seconds to compute a chunk with 512×512 cells. The GPU-based solution only needs a tiny fraction of this, even on the notebook.

Figure 3 depicts the results of profiling our implementation with the NVIDIA Visual Profiler. It shows that on the lab PC the GPU is not fully used to its capacity. It very often has to wait for more data to be transferred from the computer's main memory to the graphics card's memory. Performance can be improved by putting data transfer and simulation into separate streams that run in parallel. Nevertheless, this approach would not lead to much benefit on the notebook. In order to gain comparable results on both computers we did not implement this. An approach which dynamically splits up a grid depending on the size of the graphics card's memory could help to achieve optimal and scalable results on a given PC.

CONCLUSION

In this paper we described a novel approach of simulating urban growth using modern GPU hardware. We presented our simulation model which is based on rules that mimic the properties of urbanisation. In this paper we also presented a practical use case for our approach. We were able to show that it works well with the given data set. Also, we evaluated our implementation's performance and compared it to the existing Java application MASGISmo. Although the Java solution also uses agent-based modelling, our implementation is a lot faster. This has two reasons: a GPU is able to process a lot more agents within a single computation step than a CPU; and due to a GPU's superior computational power a simulation step takes much less time.

As a first step towards agile and interactive policy modelling our implementation allows the user to change the maximum number of citizens per cell and to alter current land use. These interaction possibilities are based on realistic procedures in urban planning. Restricting the number of citizens per cell corresponds to limiting the maximum number of stories for a building. Altering the land use grid corresponds to reassigning area usage types—for example, from agricultural land to building land.

Current GIS systems are not able to fully exploit the possibilities of modern computer hardware yet. Our GPU-based approach can be used to significantly speed up processing geospatial data. In particular, urban growth simulations can be performed in much less time. As shown above, our simulation only needs a tiny fraction of the time needed by MASGISmo. This opens up the possibility for real agile urban policy modelling that includes urban planners as well as stakeholders such as decision makers and even the public into the discussion. The fast turnaround time allows urban planners to deploy a feedback cycle that consists of planning, simulating, presenting the plan and the simulation results to the audience, and finally gaining feedback. This cycle repeats until a sustainable solution is found that is well received by every stakeholder. Moreover, the interaction possibilities in our implementation allow stakeholders to simulate different urban planning scenarios and to directly discuss about them.

In this paper we only presented a single use case for urban growth. We also tested only one raster data set. However, geospatial applications typically have to deal with many heterogeneous use cases and requirements as well as with lots of different data exchange formats. Apart from that, our simulation model only uses one modelling technique (agent-based modelling). MASGISmo on the other hand uses a multi-paradigm approach to increase realism—which by the way contributes only a little to the bad performance of this pure Java solution. Nevertheless, the results presented in this paper show that there's a lot of potential to make use of GPUs and agent-based modelling in geospatial applications. In particular, we think that our approach can be applied to other urban planning scenarios as well—for example, traffic simulation (Promnoi et al., 2009; Strippgen and Nagel, 2009; Caceres, 2012) or pedestrian and crowd simulation (Richmond and Romano, 2008; Passos et al., 2008).

ACKNOWLEDGEMENT

Research presented here is partly carried out within the project "urbanAPI" (Interactive Analysis, Simulation and Visualisation Tools for Urban Agile Policy Implementation), funded from the 7th Framework Program of the European Commission, call identifier: FP7-ICT-2011-7, under the grant agreement no: 288577, started in October 2011.

REFERENCES

Balz, T. and Haala, N. (2006). Improved real-time sar simulation in urban areas. In *International Geoscience and Remote Sensing Symposium (IGARSS)*, pages 3631–3634.

Caceres, N. (2012). Traffic Flow Estimation Models Using Cellular Phone Data. *IEEE Transactions on Intelligent Transportation Systems*, pages 1–12.

Gebetsroither, E. (2010). Combining Multi Agent System modeling and System Dynamics modeling. In Trappl, R., editor, *Proceedings of the 20th European Meeting on Cybernetics and Systems Research (EMCSR)*, volume 2, Vienna, Austria.

Gilbert, G. N. and Troitzsch, K. G. (2005). *Simulation for the Social Scientist*. Open University Press, 2nd ed. edition.

Gimblett, H. (2002). *Integrating geographic information systems and agent-based modeling techniques for simulating social and ecological processes*. Oxford University Press, USA.

Krämer, M., Ludlow, D., and Khan, Z. (2013). Domain-specific languages for agile urban policy modelling. In *Proceedings of the 27th European Conference on Modelling and Simulation (ECMS)*.

Lupton, G. and Thulin, D. (2008). Accelerating HPC Using GPUs. Technical report, Hewlett-Packard Company.

Nickolls, J. and Dally, W. J. (2010). The GPU Computing Era.

Owens, J. D., Luebke, D., Govindaraju, N., Harris, M., Krüger, J., Lefohn, A. E., and Purcell, T. J. (2007). A Survey of General-Purpose Computation on Graphics Hardware. *Computer Graphics Forum*, 26(1):80–113.

Passos, E., Joselli, M., Zamith, M., Rocha, J., Montenegro, A., Clua, E., Conci, A., and Feijó, B. (2008). Supermassive crowd simulation on gpu based on emergent behavior. In *Proceedings of the VII Brazilian Symposium on Computer Games and Digital Entertainment*, pages 81–86.

Promnoi, S., Tangamchit, P., and Pattara-Atikom, W. (2009). Road traffic estimation with signal matching in mobile phone using large-size database. *12th International IEEE Conference on Intelligent Transportation Systems*, pages 1–6.

Richmond, P. and Romano, D. (2008). A high performance framework for agent based pedestrian dynamics on gpu hardware. In *Proceedings of EUROSIS ESM*.

Scholl, H. J. (2001). Agent Based and System Dynamics Modeling: A Call for Cross Study and Joint Research. In *Hawaii International Conference on System Sciences*.

Strippgen, D. and Nagel, K. (2009). Multi-agent traffic simulation with CUDA. *2009 International Conference on High Performance Computing Simulation*, pages 106–114.

Zhang, J. and You, S. (2012). CudaGIS: Report on the Design and Realization of a Massive Data Parallel GIS on GPUs. In *ACM SIGSPATIAL IWGS Workshop*.

AUTHOR BIOGRAPHIES

MICHEL KRÄMER is deputy department head of the Spatial Information Management competence center of the Fraunhofer Institute for Computer Graphics Research IGD in Darmstadt, Germany. His research interests are in Compiler Construction, Language Recognition and Artificial Intelligence as well as Big Data and Cloud Computing. He's development lead of the 3D GIS area and has contributed to various open source products. Michel Krämer holds a master's degree in computer science from the THM University of Applied Sciences, Gießen, Germany where he's now also a lecturer. His email address is `michel.kraemer@igd.fraunhofer.de`.

ANDREAS KEHLENBACH holds the master's degree of Science in Computer Science from the Goethe University Frankfurt a.M., Germany. His master thesis was about interactive urban planning simulation on the GPU, which was discussed in this paper. His email address is `andreas.kehlenbach@cs.uni-frankfurt.de`.

Simulation of Complex Systems and Methodologies

PSEUDO-CODE SIMULATION OF DESIGNER ACTIVITY IN CONCEPTUAL DESIGNING OF SOFTWARE INTENSIVE SYSTEMS

Petr Sosnin
Computer Department
Ulyanovsk State Technical University
Ulyanovsk, 432027, Russia
E-mail: sosnin@ulstu.ru

KEYWORDS

Conceptual designing, pseudo-code, simulation.

ABSTRACT

The paper presents an experiential approach to a real time activity of designers at a conceptual stage of their work. The offered approach is based on a pseudo-code simulation of such activity. The simulation are being implemented by the designer who investigate own actions aimed at the conceptual solution of the project task.

INTRODUCTION

An important feature of designing the Software Intensive Systems (SIS) is a collaborative activity of designers in conditions of a high complexity. Negative influence of human factors in such a kind of the activity is an essential reason of an extremely low degree of a success (about 35%) in designing the SIS (El Emam and Koru 2008).

In general sense the complexity (or simplicity) of SIS reflects the degree of a difficulty for designers in their interactions with definite models of SIS (or its components) in solving the definite tasks.

The system or its any component is complex, if the designer (interacting with the system) does not have sufficient resources for the achievement of the necessary level of understanding or achieving the other planned aims.

Often enough various interpretations of Kolmogorov measure (Li and Vitanui 2008) are applied for estimations of a degree of the system complexity. This measure is connected with the minimal length of program P providing the construction of system S from its initial description D. Distinctions in interpretations are caused usually by features of system S and formal descriptions to be used for objects P and D.

In accordance with their destinations the programs of P-type it is more preferable to build as programmable systems (P-systems) of designers' activity with using the certain metaprogramming M.

Explicit and/or implicit means for managing the designers' activity are used in any technology of designing the SIS. An actuality of such managing demonstrates that the complexity of P-program is no less than the complexity of SIS in its any used state. Moreover, any M-program providing the construction of P-program should be built on the base of the same initial description D as the system S.It can be presented by the following chain $D \rightarrow M \rightarrow P \rightarrow S$.

Named relations between D, M, P can be used by designers for disuniting the process of designing on stages $[D(t_0) \rightarrow M_1 \rightarrow P_1 \rightarrow S(t_1)]$, $[D(t_1) \rightarrow M_1 \rightarrow P_1 \rightarrow \rightarrow S(t_2)]$,…, $D(t_i) \rightarrow M_1 \rightarrow P_1 \rightarrow S(t_{i+1})]$, …., $[D(t_{n-1}) \rightarrow \rightarrow M_1 \rightarrow P_1 \rightarrow S(t_n)]$ where a set $\{S(t_i)\}$ collects the states of creating SIS.

Division of designing on stages is a base of any modern technology providing the creation of SIS. In technologies such manner is used in different forms for different aims. This manner helps to decrease the complexity of interactions with SIS in its any state $S(t_i)$. But till now the viewpoint of programming on the designer activity is not being supported instrumentally in early stages of designing.

It is necessary to note that a creation of instrumental means for the explicit work with artifacts of M- and P-types essentially depends on their understanding. This paper presents the empirical approach to such artifacts which are like experimental setups helping to find the solutions of project tasks and opening the possibility for their confirmatory reuse. The offered approach is based on the use of a specialized toolkit WIQA (Working In Questions and Answers) providing the pseudo-code simulation of the designer activity (Sosnin 2012).

PRELIMINARY STATEMENTS

The offered approach focuses on the designer activity at the conceptual stage of designing the SIS when any project task should be conceptually solved and registered in the form which is suitable for the reuse in the computerized medium (because collaborative designing in life cycle of SIS).

We consider that any task solution should give an opportunity to any member of designers' team for repeating the activity of the designer who has solved this task in the conceptual form.

One of possible such forms is a protocol of designer actions registered in a natural language L^A in its algorithmic usage. Creating of protocols and their using in repeatable solutions of tasks can be implemented similarly creations and executions of programs. In this case a function of the language L^A can be fulfilled by the executable pseudo-code language L^P helping to create pseudo-code programs for corresponding protocols.

Any protocol in any its form and in the program form also is a model of the designer activity. The value of models of such a type is being defined by activity units registering in protocols. As minimum the registered

Proceedings 27th European Conference on Modelling and Simulation ©ECMS Webjørn Rekdalsbakken, Robin T. Bye, Houxiang Zhang (Editors)
ISBN: 978-0-9564944-6-7 / ISBN: 978-0-9564944-7-4 (CD)

units should provide understanding of the conceptual solution and checking its conformity to requirements.
In the offered approach an achievement of indicated goals is being provided by experiments of the designer researching a certain task situation. The designer creates the necessary experimental setup the use of which demonstrates the conceptual solution of the project task. The experimental setup is created as a pseudo-code program (model) of the designer activity for its researching. Any model of such type consists of program operators each of which registers the corresponding action of the designer.
Thus experiment steps as program operators are being registered by the designer in the solution protocol for the corresponding project task. Hence any protocol is a plan (program, model) which should be accessible for interested designers in a rational and suitable form. It should open for designers an opportunity for step by step performing the programmed plans in order to understand and check their conceptual solutions for corresponding tasks. In such actions any designer will actively interact with personal and collective experience and also with models of useful experience units (or shortly with the accessible experience). Any operator of indicated programs registers a certain "trace" of designer interactions with the accessible experience.
Certainly, it is possible to create many other models of the designer activity. Even in the offered approach the described model of the program type is a part of integrated model of a precedent type underlining the behavioral nature of the designer activity. In accordance with Cambridge dictionary "precedents are actions or decisions that have already happened in the past and which can be referred to and justified as an example that can be followed when the similar situation arises" (http: //dictionary.cambridge.org/dictionary/british/precedent). Thus any action corresponding to the certain program operator can be also interpreted as the precedent.
Models of precedents are used in the offered approach as structural units of the accessible experience in any its forms. Moreover any task solved by designers is being included to the SIS project and/or to processes of designing as the model of the corresponding precedent. Therefore interactions with the accessible experience in the context of the use of precedents occupy an essential place in our version of programming the designer activity.
Interactions of a human with personal experience reflect their own existence in the dialog forms (question-answer forms) in consciousness. A question is a natural phenomenon which appears when a human should use or wants to use the experience. If the phenomenon of such type is revealed by the human the revealed question can be described in the natural language. Any of such description is no more than a linguistic (symbolic) model of the question. Interactions with the symbolic model of the question can renew the phenomenon of this question in brain structures of designers for its reuse.
The adequacy of any model of any question should be carefully tested because such a model is used for creating the necessary answer. The definite question and corresponding answer are bound as "cause and effect". They supplement each other. The answer form depends on the use of the answer.
Questions have different types. A very important class of questions is tasks. Any statement of any task is its symbolic model also. There are several useful forms of the answer for the tasks, for example, "method of task solving", "solution idea", "conceptual solution" and "programmed solution".
Thus questions and answer are used not only for interactions with the experience. They can be used, for example, for the access to the appropriate unit of experience or for modeling the unit of experience or for reasoning in different cases. Any human has the rich experience of using the questions and answers and their models.
It is necessary note that presented statements and their described understanding have been used in a programmable simulation of the designer activity described below.

RELATED WORKS

Registering the human activity in program forms has been offered and specified constructively for Human Model Processor (MH-processor) in the paper (Karray et al. 2008). The EPIC version of MH-processor is oriented on programs written in the specialized command language Keystroke Level Model (KLM). A set of basic KLM actions includes the following operators: K – key press and release (keyboard), P – point the mouse to an object on screen, B – button press or release (mouse), H – hand from keyboard to mouse or vice versa and others commands. Operators of KLM-language and their values help to estimate temporal characteristics of human interactions for alternative schemes of interfaces. KLM-programs are far from the sense of used reasoning and therefore they do not reflect interactions with the accessible experience.
Explicit programmable forms of the designer activity are not used in modern technologies of SIS designing. For example in technologies based on Rational Unified Process (Borges et al. 2012) the conformity to requirements and understandability are being reached with the help of "block and line" diagrams expressed in the Unified Modeling Language (UML). The content of diagrams built by designers is being clarified by necessary textual descriptions. But UML is not the language of the executable type and therefore diagrams are not suitable for experimenting with them as with programs of P-type.
For collaborative solving the tasks in coordination the RUP suggests the means of normative workflows the relations between which are being regulated by a set of rules. For any task of the definite normative workflow the RUP has its interactive diagrammatic model with a set of components the use of which can help in solving the task. Forms of programming are not used also in all of these means. The similar state of affairs with conceptual designing exists in other known technologies supporting the development of SIS.
In the offered approach its scientific point of view correlates with two faces of the software engineering described in (Cares et al. 2006) where functional

paradigms and scientific paradigms are discussed. In the context of this paper the approach means are oriented on scientific paradigms used by software engineers.
An empirical line of the approach inherits understanding the place and role empirical methods in software engineering generally presented in (Sjoberg 2007). It is necessary to mark numerous papers of V. Basili (especially papers (Basili et al. 2001) and (Basili 2012).
The important group of related works concern means of Question-Answering, for example, papers (Webber and Webb 2010) and (Xu and Rajlich 2005). In this group the nearest work presents experience-based methodology "BORE" (Henninger 2003) where question-answering is applied also but for the other aims and this methodology does not support programming of the intense designer activity.

QUESTION-ANSWER INTERACTIONS WITH ACCESIBLE EXPERIENCE

In the suggested approach the designers interact with all tasks being solved in the WIQA environment in accordance with the scheme presented in figure 1.

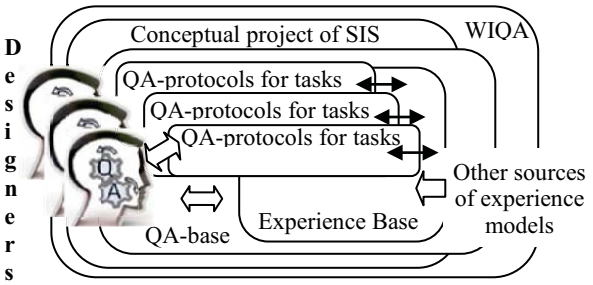

Figure 1: Experiential interactions with tasks

Solving any appointed task, the designer registers the used question-answer reasoning (QA-reasoning) in a specialized protocol (QA-protocol) so that this QA-protocol can be used as the task model (QA-model).

Models of such a type can be used by designers for experimenting in the real time with tasks being solved. Units of the experiential behavior extracted from solution processes are being modeled on the base of QA-models of tasks. Created behavioral models are being loaded in the question-answer database (QA-base) and Experience Base of WIQA. After that they can be used by designers as units of the accessible experience. Experience models from the other sources can be uploaded in the Experience Base also.
If designers of SIS use the toolkit WIQA they have the opportunity for conceptual modeling the tasks of different types. In this case the current state of tasks being solved collaboratively is being registered in QA-base of the toolkit and this state is visually accessible in forms of a tree of tasks and QA-models for corresponding tasks. The named opportunity is presented figuratively in figure 2 where QA-base is interpreted as a specialized QA-memory the cells of which are visualized by inquiries of designers. First of all, the cells are used for storing the registered units of QA-reasoning.
Any cell has the following basic features:

1. Cell is specified by a set of normative attributes reflecting, for example, the textual description of the stored interactive object, its type and unique name, the name of its creator, the time of last modification and the others characteristics.

2. Designer has the possibility to appoint to the cell a number of additional attributes if it will be useful for the work with the object stored in the cell.

Having chosen necessary attributes the designer can adjust the cell for storing any question or any answer in a form of an interactive object which is accessible by inquiries as designers so programs. Thus any question and its answer are stored in QA- memory as a pair of related interactive objects named below as QA-unit.

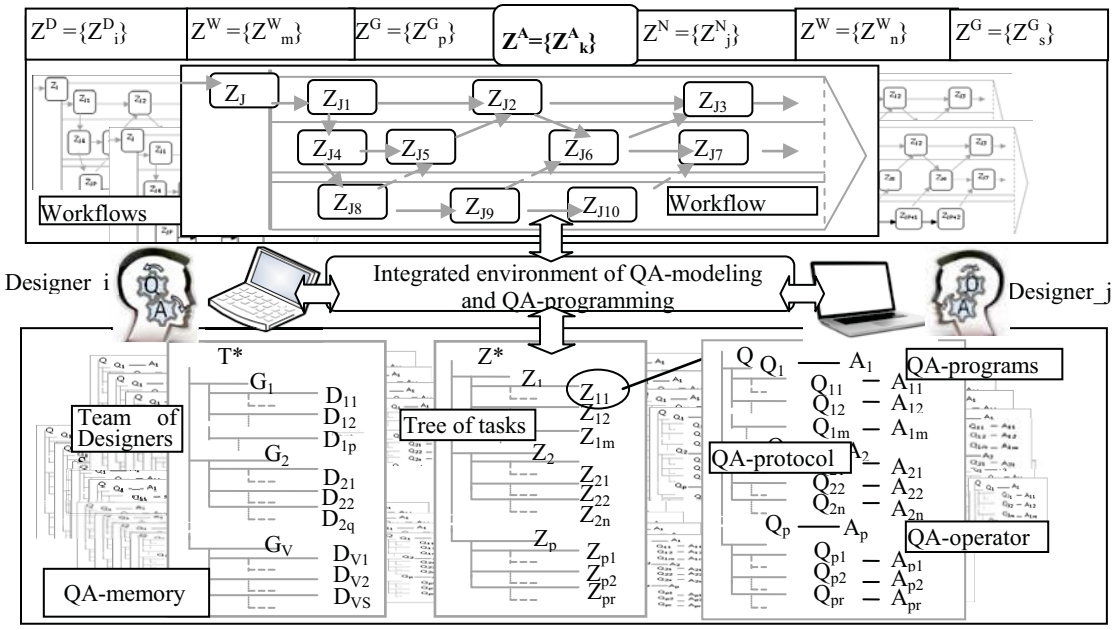

Figure 2: Sinking of tasks in WIQA-environment

QA-units are stored in QA-memory as data the abstract type of which will be named as QA-data. The use of this type helps to emulate other data types, including descriptions of operators. First of all it is necessary for the use of QA-memory in pseudo-code programming. Thus cells of QA-memory destined for storing QA-units can be adjusted for storing the units of the other nature, for example, units used in solving the tasks.

In figure 2 the scheme of QA-memory demonstrates the store of presentations for "Team of designers", "Tree of tasks" and a pseudo-code program with its operators and data. The program, its operators and used data are designated as QA-program, QA-operators and QA-data to underline that they inherit the features of QA-memory cells.

The responsibility for tasks being solved is being distributed among designers in accordance with the competence of each of them. The team competence should be sufficient for the real time work with following sets of tasks: subject tasks $Z^S = \{Z^S_i\}$ of SIS subject area; normative tasks $Z^N = \{Z^N_j\}$ of technology used by designers; adaptation tasks $Z^A = \{Z^A_j\}$ providing an adjustment of tasks $\{Z^N_j\}$ for solving the tasks $\{Z^S_i\}$; workflow tasks $\{Z^W_m\}$ providing the works with tasks of Z^S-type in workflows $\{W_m\}$ in SIS; workflow tasks $\{Z^W_n\}$ providing the works with tasks of Z^N-type in corresponding workflows $\{W_n\}$ in the used technology; workflow tasks $\{Z^G_p\}$ and $\{Z^G_r\}$ any of which corresponds to the definite group of workflows in SIS or in technology.

The indicated diversity of tasks emphasizes that designers should be very qualified specialists in the technology domain but that is not sufficient for successful designing. Normative tasks are invariant to the SIS domain and therefore designers should gain certain experience needed for solving the definite tasks of the SIS subject area. The most part of the additional experience is being acquired by designers in experiential learning when tasks of Z^S-type are being solved. Solving of any task Z^S_i is similar to its expanding into a series on the base of normative tasks.

Objects uploaded to QA-memory are bound in hierarchical structures. In their real time work the designers interact with such objects. They process them with the help of appropriate operations helping to find and test the solution of tasks.

One way for conceptual solving any task indicated types is based on creating its QA-model as a system of questions and answers which have accompanied the solution process. The generalized scheme of such models is presented in figure 3.

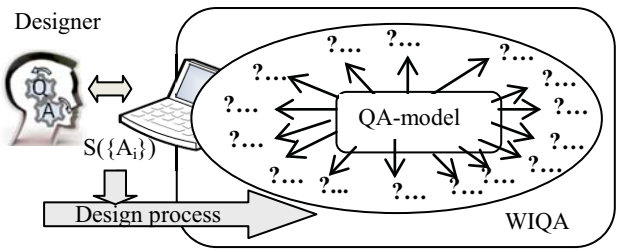

Figure 3: Interactions with QA-model of Task

Question-answer models, as well as any other models, are created for an extraction of answers to the questions enclosed in the model. Moreover, the model is a very important form of the representation of questions, answers on which are being generated during visual interactions of designers with this model.

The description of any behavioral unit composed of designer interactions with QA-model in accordance with the definite scenario can fulfill the role of a model of such designer activity. In order to distinguish this type of models from other types of models they can be named "QA-models of the designer activity". Any such scenario as a specific program reflects designer interactions (actions) aimed at understanding the corresponding task and its solution.

The other way of coding the designer activity is bound with its programming in the context of the scientific research of the task. All tasks indicated above are being uploaded to QA-memory with the rich system of operations with interactive objects of Z-, Q- and A-types. Designers have the possibility to program the interactions with necessary objects. Such programs are similar to the plans of the experimental activity in conceptual designing of SIS. Operators of programs are placed in Q-objects. Corresponding A-objects are used for registering the facts or features of executed operations.

Thus, experimenting with units of the own behavior the designer has a flexible means for specifying the QA-programs, QA-operators and QA-data used in simulating of such behavior's units. Experimenting is being fulfilled in forms of QA-modeling aimed at solving tasks in conceptual designing.

PSEUDO-CODE LANGUAGE L^{WIQA}

QA-reasoning can be used by designers when they create different conceptual models of tasks, for example, in formulating the task statement or in cognitive analyzing of the formulated statement or in (pseudo-code) programming the solution plan of the task. The toolkit WIQA supports the creative work of designers with all indicated conceptual modes and conceptual models of the other types.

So the specialized pseudo-code language L^{WIQA} has been developed for the use of QA-reasoning in programming the solution plans. This language is oriented on its use in experiential interactions of designers with the accessible experience when they create programs of the own activity and investigate them. Step by step L^{WIQA} has been evolved till the state included following components:

1. **Traditional types of data** such as scalars, lists, records, sets, stacks, queues and the other data types.

2. **Data model** of the relational type describing the structure of database.

3. **Basic operators** including traditional pseudo-code operators, for example, Appoint, Input, Output, If-

Then-Else, GOTO, Call, Interrupt, Finish and the others operators.

4. **SQL-operators** in their simplified subset including Create Database, Create Table, Drop Table, Select, Delete From, Insert Into, Update.

5. **Operators for managing the workflows** oriented on collaborative designing (Seize, Interrupt, Wait, Cancel and Queue).

6. **Operators for visualization** developed for the creation of dynamic view of cards presenting QA-units in the direct access of the designer to objects of QA-memory.

The important type of basic operators is an explicit or implicit command aimed at the execution by the designer the definite action. Explicit commands are being written as imperative sentences in the natural language in its algorithmic usage. When designer interactions with descriptions of questions or answers are used as causes for designer actions then such descriptions can be interpreted as implicit commands written in L^{WIQA}. For example, questions are a very important class of implicit commands.
In general case QA-program can include data and operators from different enumerated subsets. But traditional meaning of such data and operators is only the one side of their content. The other side is bound with attributes of QA-units in which data and operators are uploaded. As told above QA-data and QA-operators inherit the attributes of corresponding cells of QA-memory. They inherit not only attributes of QA-units but their understanding as "questions" and "answers" also.

SIMULATING THE DESIGNER'S BEHAVIOR

The principal feature of the offered approach is an experimental investigation by the designer the programmed own behavior which has led to the conceptual solution of the appointed task. Any solution of such a type should demonstrate that its reuse meets necessary requirements when any designer of the team will act in accordance with QA-program of the investigated behavior.
In order to achieve it the designer should work similarly to the scientist who prepare and conduct experiments with behavior units of M- or P-types. In the discussed case the designer will experiment in the environment of the toolkit WIQA. In this environment to prove achieving the aims of any experiment the designer has possibilities of experimenting with any QA-operator of investigated QA-program and/or with any group of such QA-operators or with QA-program as a whole. Describing the experiment for the reuse the designer should register it in an understandable form for other members of the team.
To begin the definite experiment the initial text of QA-program should be built. In general case such work includes the following steps:

1. Formulation of the initial statement of the task.

2. Cognitive analysis of the initial statement with the use of QA-reasoning and its registering in QA-memory

3. Logical description of "cause-effect relation" reflected in the task.

4. Diagrammatic presentation of the analysis results (if it is necessary or useful).

5. Creation of the initial version of QA-program.

Indicated steps are being fulfilled by the designer with the use of the accessible experience including the personal experience and useful units from Experience Base of WIQA.
Only after that the designer can conduct the experiment, interacting with QA-program in the context of the accessible experience. The specificity of interactions can be clarified on examples of QA-operators of any QA-program or its fragment, for example, the fragment of QA-program coding the well-known method of SWOT-analysis (Strengths, Weaknesses, Opportunities, and Threats):

```
Q 2.5 PROCEDURE &SWOT main&
   Q 2.5.1 &t_str& :=
QA_GetQAText(&history_branch_qaid&)
   Q 2.5.2 SETHISTORYENTRIES(&t_str&)
   Q 2.5.3 CALL &ShowHistory&
   Q 2.5.4 IF &LastHistoryFormResult& == -1 THEN
RETURN
   Q 2.5.5 IF &LastHistoryFormResult& == 0 THEN
&current_action_qaid& :=
QA_CreateNode(&current_project&,
&history_branch_qaid&, 3, "") ELSE
&current_action_qaid& := &LastHistoryFormResult&
   Q 2.5.6 &t_str& :=
QA_GetQAText(&current_action_qaid&)
   Q 2.5.7 SWOT_DESERIALIZE(&t_str&)
   Q 2.5.8 &t_int& := SWOT_SHOWMAINFORM()
   Q 2.5.9 &t_str& := SWOT_GETSERIALIZED()
   Q 2.5.10 IF &t_int& == 0 THEN
QA_UpdateNode(&current_project&,
&current_action_qaid&, &t_str&)
   Q 2.5.11 IF &t_int& != 0 RETURN
   ……..
Q 2.5.14 FINISH
```

This source code demonstrates a habitual syntax but features of the code are being opened in interactions of the designer with it. Conditions and means of experimenting are shown in figure 4, where one of operators (with address name *Q2.5.2*) is shown in the context of previous and subsequent operators. Any QA-program is being executed by the designer step by step any of which is aimed at the corresponding QA-operator. In this work the designer uses the plug-in "Interpreter" embedded to the toolkit.

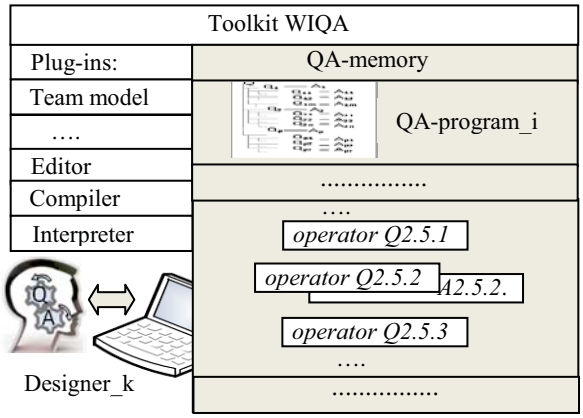

Figure 4: Experimenting of designer with QA-program

Interpreting the current operator (for example, *Q2.5.2*), the designer can fulfill any actions till its activation (for example, to test existing circumstances) and after its execution (for example, to estimate the results), using any means of the toolkit WIQA. When the designer decides to start the work with QA-operator this work can include different interactive actions with it as with corresponding QA-units or with their elements. The designer can analyze values of their attributes and makes useful decisions

Moreover, the designer can appoint the necessary attributes for any QA-operator and for any unit of QA-data in any time. In accordance with appointments the designer can include changing in the source code of QA-program being executed (investigated). Such work can be fulfilled as in QA-memory so with the help of the plug-in "Editor".

The current QA-program or its fragment can be executed or step by step by the designer or automatically as a whole with the help of the plug-in "Compiler". Therefore all aforesaid about the work with QA-operator can be used for any their group and for any QA-program as a whole. That is why the execution of QA-operator by the designer is similarly experimenting. Thus the designer has a flexible possibility for the experimental research of any task being solved conceptually. This is the principal feature which distinguishes pseudo-code QA-programs from programs written in pseudo-code languages of different types including the class of Domain Specific Languages (Karsai G. et al).

The specificity of the described kind of the designer activity is the work controlled by QA-program executed by the designer interacting with the accessible experience. To underline this specificity the specialized role named "intellectual processor" (I-processor) was defined and supported in the use of WIQA (Sosnin 2012). This role is additional for other kinds of roles used in conceptual designing (Borges et al. 2012).

As told above any fulfilled experiment should be presented by the designer in the understandable and reusable form. In the offered version of experimenting the function of such form is being fulfilled by the typical integrated model of the precedent shown in figure 5.

The scheme, fulfilling the function of framework F(P) for models of precedents, allows integrating the very useful information accompanying the experiment process in its actions indicated above.

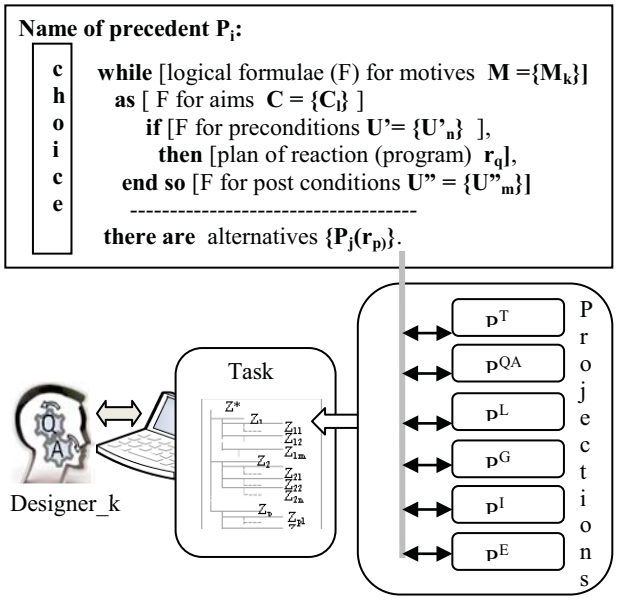

Figure 5: Interactions of designer with precedent

The central place in this model is occupied the logical scheme of the precedent. The scheme explicitly formulates "cause-effect regularity" of the simulated behavior of the designer Framework F(P) includes following components: textual model P^T of the solved task, its model P^{QA} in the form of registered QA-reasoning, logical formulae P^L of modeled regularity, graphical (diagram) representation P^G of precedent, pseudo-code model P^I in QA-program form and executable code P^E. Any component or any their group can be interpreted as projections of F(P), the use of which allow to build the precedent model in accordance with the precedent specificity. But in any case the precedent model should be understandable for its users.

All built models of precedents are divided in two classes one of which includes models embedded in Experience base of WIQA used by the team not only in a current project. The second class includes models only for the current project.

INTELLECTUAL PROCESSOR

Any designer playing the role of intellectual processor uses question-answer reasoning and its models for the access to the experience.

The essence of I-processor is being defined by features enumerated below.

1. First of all I-processor is a role being played by any designer solving the appointed tasks in conceptual designing of the SIS. In life cycle of any SIS its conceptual stage is an area of intensive modeling the tasks being solved.

2. I-processors are intended for experimenting with tasks the solving of which are problematically without the explicit real time access to the personal

experience and/or collective experience and/or models of useful experience.

3. In its activity any I-processor interprets tasks as precedents and interacts with experience units as with models of precedents.

4. The real time work of any I-processor is being accompanied by QA-reasoning and its models being registered in QA-memory of the toolkit WIQA.

5. QA-reasoning is used by I-processor for creating QA-models of tasks in different forms including their versions as QA-programs.

6. The use of QA-reasoning in interactions of I-processor with QA-programs is being implemented in the pseudo-code language L^{WIQA}. Knowing and effective using of this language by I-processor is a very important its feature.

7. In general case the activity of I-processor is similar to the experimental activity of the designer who creates QA-model of the task for experimenting with the prototype of its solution. In such experimenting with tasks I-processor can use as means of QA-modeling so and means of QA-programming.

As told above the use of QA-programs by I-processor for experimenting with tasks is the very essential its feature. That was a cause to create the library of the specialized QA-programs providing some versions of such experimenting. This library includes a number of QA-techniques for cognitive tasks analysis, decision-making and typical procedures of estimations.
It is necessary to note that our materialization of I-processor implements by means of WIQA but it is our solution. In principle requirements to I-processor can be implemented on the base of instrumental means distinct from the toolkit WIQA.

COLLABORATIVE ACTIVITY OF DESIGNERS

Conceptual designing of SIS is the collaborative activity of designers working in coordination. Typical units of such activity are workflows any of which can be simulated with the empirical approach also. In this case experiments will be fulfilled collaboratively by the group of designers playing the roles of I-processors. For QA-programming of workflows the specialized subset of operators has been included to the language L^{WIQA}.
A number of plug-ins is embedded to the toolkit WIQA for supporting the collaborative activity of I-processors. For example, plug-in "Organizational structure" supports the real time appointing of tasks to members of the designer team. The copy of the team model $(T^*,\{G_v\}, \{D_{vs}\})$ can be uploaded in QA-memory in the form presented in figure 2. This plug-in is used not only to appoint tasks. For example, the toolkit supports relations among I-processors through solving of a number of communication tasks in their collaborative experimenting with project tasks. And as told above the toolkit provides the real time management of workflows the tasks of which are being executed by groups of I-processors.

Means of "Organizational structure" support the real time appointments of tasks embedded in workflows to their executors (designers) from the certain group G_v of the team T*. The group manager uses the subsystem "Controlling of assignments" for binding any assignment with planned time of its fulfillment by the designer who is responsible for the assigned task. Subsystem "Kanban" (Wang 2010) automatically reflects the steps of the workflows execution with the help of visualizing the current state of queues of tasks. It helps to control by the process of designing.

Pseudo-code programming of workflows is based on using the library of workflow patterns (Van der Aalst and Hofstede 2004). Coding the units of this library illustrates the example of the workflow pattern "Simple Merge". This pattern is described by the statement: *The convergence of two or more branches into a single subsequent branch such that each enablement of an incoming branch results in the thread of control being passed to the subsequent branch).*

For three tasks Z_1, Z_2 and Z_3 this pattern has the following view:

```
Q.3.5 PROCEDURE &Simple_Merge&// index name
are inherited also but from library of pattern
Q 3.5.1SET &out&, 4; &ins[0]&, 1; &ins[1]&, 2;
&outgroup[0]&, 1; &outgroup[1]&, 2; &cnt&, 0
Q 3.5.2 LABEL &L1&
Q 3.5.3 SEIZE &outs[&cnt&]&,
&outgroup[&cnt&]&
Q 3.5.4 INC &cnt&
Q 3.5.5 TEST L, &cnt&, &ins&.length &L1&
Q 3.5.6 LABEL &L2_1&
Q 3.5.7 SET &cnt&, 0;
Q 3.5.8 LABEL &L2&
Q 3.5.9 TEST E, &ins[&cnt&]&,
&ins[&cnt&]&.state, DONE &L3&
Q 3.5.10 INC &cnt&
Q 3.5.11 TEST L, &cnt&, &ins&.length &L2_1&
Q 3.5.12 TRANSFER &L2&
Q 3.5.13 LABEL &L3&
Q 3.5.14 QUEUE &out&, TRUE
Q 3.5.15 SET &ins[&cnt&]&.state, WAITING
Q 3.5.16 TRANSFER &L2_1&
Q 3.5.17 ENDPROC &Edit_Assignment&
```

Execution results of similar programs are being placed in Kanban queues which are visualized in WIQA. Any designers interacts with the own queue with the help of "Subsystem of interruption".
The pattern source code also as previous QA-program is presented only for the demonstration of syntax and therefore without explanations. But used specimens of QA-programs are not so difficult for their understanding.

It is necessary to note that programming of workflows leads to QA-programs of M-type presenting the activity of designers on the level of their collaboration. Programs of this type simulate parallel work of designers in workflows. They simulate also pseudo-parallel work of any designer with several appointed tasks.

CONCLUSION

The approach described in this paper has led to the system of means simplifying the complexity arising in the use of the experiential behavior in conceptual designing the SIS. Simplifying is being achieved due to programming of behavior units in the form supposing its reuse in any time by any designer working in the team.

In the centre of the suggested approach is the additional new role named "intellectual processor" the responsibility of which is focused on constructive interactions of the designer with the accessible experience. The activity of I-processor is being supported by the toolkit WIQA providing the opportunity for QA-modeling and QA-programming of the experiential behavior of designers. The language L^{WIQA} embedded to the toolkit allows creating pseudo-code programs of QA-type for tasks corresponding to M- and P-programs to be used in programmed workflows.

There is a possibility for the separate execution of any operator of QA-program by the designer playing the role of I-processor. Before and after execution of the operator the designer can check or investigate its preconditions and post-conditions. In such actions the designer can interact with the accessible experience. Thus there is an opportunity for experimenting with any programmed task of any workflow being executed in conceptual designing of SIS.

Pseudo-code programs of behavior units have very useful features. Debugged QA-programs are the source of resources of the M- and P-types which are not only simplifying the complexity in their reuse. For example, the language L^{WIQA} was used in creating the system of the living project documentation. Suggested means are used in the professional activity of one project organization developing the family of SIS.

The offered approach and its instrumental means can be used not only for conceptual designing. They can fulfill the function of a shell for creating a number of other applications. For example, they have been used in the creation of "Multi-agent system for simulation of surrounding the sea vessel".

REFERENCES

Basili V. R., Lindvall M. and P. Costa. 2001. "Implementing the experience factory concepts as a set of experience bases." In *Proceedings of the 20011 International Conference on Software Engineering & Knowledge Engineering*, 102-109.

Basili V. R. 2013. "Learning through Application, SEMAT position." http://semat.org/wp-content/uploads/2012/03/

Borges P., Machado R.J. and P. Ribeiro. 2012. Mapping RUP Roles to Small Software Development Teams. In *Proceedings of the* 2012 *International Conference on Software and System Process*, 190-199.

Cares C., Franch X. and Mayol E. 2006. "Perspectives about paradigms in software engineering." In *Proceedings of the 2006 2nd International workshop on Philosophical Foundations on Information Systems Engineering* (PHISE'06), 737-744.

Cho Y. 2010. "The state of the art of action learning research," *Advances in Developing Human Resources,* 2 No.12, 163-180.

El Emam K. and A.G. Koru. 2008. "A Replicated Survey of IT Software Project Failures." *IEEE Software* 25 No. 5, 84-90.

Henninger S. 2003. "Tool Support for Experience-based Software Development Methodologies." *Advances in Computers* 59, 29-82.

Karray F., Alemzadeh M., Saleh J. A. and M. N. Arab. 2008. "Human-Computer Interaction: Overview on State of the Art", *Smart sensing and intelligent systems* 1 No. 1, 138-159.

Karsai G, Krahn H., Pinkernell C., Rumpe B., Schindler M. and S. Völkel. 2009. "Design Guidelines for Domain Specific Language," I*n Proceedings of the 9th OOPSLA Workshop on Domain-Specific Modeling*, 7-13.

Li M. and P. Vitanui 2008. "An Introduction to Kolmogorov Complexity and Its Applications." *Series: Text in Computer Science*, 3rd ed., Springer.

Sjoberg D.I. K., Dyba T. and M. Jorgensen. 2007. "The Future of Empirical Methods in Software Engineering Research." In *Proceedings of the* 2007 *workshop Future of Software Engineering,* 358-378.

Sosnin P. 2012. "Experiential Human-Computer Interaction in Collaborative Designing of Software Intensive Systems," *In Proceedings of the 11th International conference on Software Methodology and Techniques*, 180-197

Van der Aalst W.M.P. and A.H.M. Hofstede. 2004. "Workflow Patterns Put Into Context." *Software and Systems Modeling* 11 No.3, 319-323.

Wang J. X. 2010. "Kanban: Align Manufacturing Flow with Demand Pull." Chapter in the book: Lean Manufacturing Business Bottom-Line Based, CRC Press, 185-204.

Webber, B. and N. Webb. 2010. "Question Answering." In *Clark, Fox and Lappin (eds.): Handbook of Computational Linguistics and Natural Language Processing*. Blackwells.

Xu, S. and V. Rajlich. 2005. "Dialog-Based Protocol: An Empirical Research Method for Cognitive Activity in Software Engineering." *In Proceedings of the 2005 ACM/IEEE International Symposium on Empirical Software Engineering*, 397-406.

PETR SOSNIN was born in Ulyanovsk in the USSR, on July 12, 1945. He graduated from the Ulyanovsk Polytechnic Institute (1968).

His employment experience included the Ulyanovsk Polytechnic Institute and Ulyanovsk State Technical University. His special field of interests includes AI applications for computer aided design. P. Sosnin defended doctor degree in Moscow Aviation Institute (1994). He is an author of eight books and more two hundred articles.

Modeling and Simulation Semantics for Building Large-Scale Multi-Domain Embedded Systems

Joshua D. Carl, Zsolt Lattmann, and Gautam Biswas
Institute for Software Integrated Systems, Vanderbilt University
Nashville, TN 37235
{carljd1, lattmann, biswas}@isis.vanderbilt.edu

Keywords

Multi-domain models, hybrid systems, hybrid bond graphs

Abstract

This paper discusses a set of semantic constraints that have to be applied for multi-domain modeling of complex, embedded systems. In particular, using the Hybrid Bond Graph (HBG) modeling language, we analyze issues that deal with consistent causality assignments across model reconfigurations using hybrid switching junctions, and the complementarity of the electrical and mechanical domains by imposing additional constraints in the modeling environment. A case study of a Reverse Osmosis system developed at NASA JSC illustrates the effectiveness of our approach.

Acknowledgments

This work was partially funded by DARPA META contract FA8650-10-C-7082.

I. Introduction

Today's embedded and cyber physical systems incorporate complex hybrid behaviors. Hybrid models of these systems capture the continuous behavior of physical processes interspersed with discrete changes that may be attributed to controller actions and abstractions of complex nonlinear behaviors. It is important to model these behaviors accurately to support design, control, monitoring, and safety analysis.

Bond graphs are an intuitive graphical energy-based multi-domain paradigm for modeling physical processes for modeling large complex systems. However, the core bond graph paradigm does not support the modeling of hybrid behaviors. In our research [6], we have developed hybrid bond graphs (HBGs) to support hybrid system modeling by incorporating switched junctions that accommodate dynamic mode switching and model updates during simulation. We have successfully applied this approach to develop modeling, simulation and analysis environments [7] [9]. However, to generate correct models, the modeler has to consider a number of modeling constraints, which were not explicitly defined in the earlier HBG paradigms, to ensure that a correct model is constructed. In this paper, we detail these additional modeling constraints. The constraints specifically relate to (1) ensuring causally feasible models in all modes of operation, and (2) taking into account domain differences between the electrical, hydraulic, and mechanical physical domains.

II. Hybrid Bond Graph Review

Bond graphs [5], and hybrid bond graph extensions, provide a modeling paradigm for modeling and simulating of hybrid cyber-physical systems. Bond Graphs model power and energy flow through multi-domain systems using generalized effort and flow variables to support domain independence. Generic Bond graph elements include: dissipaters (resistors, R), storage elements (capacitors, C, and inertias, I), transformers (transformers, TF, and gyrators, GY), sources and sinks (source of effort, Se, and source of flow, Sf), and idealized distribution elements(1-junctions, 1, and 0-junctions) [5]. Each element has its set of constitutive equations governing its behavior, and are connected to the rest of the system using bonds. Each bond is associated with an effort and a flow variable (effort $\times$ flow = power). Causality assignment in the graph identifies the dependent and independent variables for individual elements, and facilitates simulation of system behavior.

Hybrid Modeling Schemes

A number of researchers have proposed schemes for modeling hybrid behavior with bond graphs. [4] and [8] proposed a new switch element that exhibited different behavior depending on the junction it is connected to. A switch connected to a 1-junction forces zero effort when on, and zero flow when off. Similarly, when connected to a 0-junction the switch forces zero flow when on and zero effort when off. The behavior generated by this scheme is equivalent to HBGs [6] but it is not as intuitive because the switch element changes behavior depending on the junction it is connected to. [3] suggested similar functionality but did not use the switched bond graph element. [2] proposed a method of switching using a modulated transformer and a constant resistor. The transformer parameter changes between 1 and 0 to represent the switch being on or off and the connected resistor has a constant value representing the on conductance or the off resistance depending on the causality assigned to the resistor. The

Proceedings 27th European Conference on Modelling and Simulation ©ECMS Webjørn Rekdalsbakken, Robin T. Bye, Houxiang Zhang (Editors)
ISBN: 978-0-9564944-6-7 / ISBN: 978-0-9564944-7-4 (CD)

TABLE I: Primitive bond graph elements

Element Name	Causality	Equations
Source of effort, (Se)	Se:$u(t)$ ⟶	$e = u(t)$
Source of flow, (Sf)	Sf:$u(t)$ ⟼	$f = u(t)$
Resistor, (R)	⟶ R:R ⟼ R:R	$f = e/R$ $e = Rf$
Inertia, (I)	⟶ I:I	$f = \frac{1}{I}\int e dt$
Capacitor, (C)	⟼ C:C	$e = \frac{1}{C}\int f dt$
Transformer, (TF)	1 ⟼ TF:n ⟼ 2 1 ⟶ TF:n ⟶ 2	$e_1 = n * e_2$ $f_2 = n * f_1$ $e_2 = e_1/n$ $f_1 = f_2/n$
Gyrator, (GY)	1 ⟼ GY:r ⟶ 2 1 ⟶ GY:r ⟼ 2	$e_1 = r * f_2$ $e_2 = r * f_1$ $f_2 = e_1/r$ $f_1 = e_2/r$
1-junction, (1)	1 ⟼ 1 ⟼ 2 3	$f_1 = f_2 = f_3$ $e_1 = e_2 + e_3$
0-junction, (0)	1 ⟶ 0 ⟶ 2 3	$e_1 = e_2 = e_3$ $f_1 = f_2 + f_3$

method also proposed a simpler approach where only a resistance with a variable parameter value was used as the switch. Both of these approaches have the advantage of modeling non-ideal switches and the causality assignment is the same for both states of the switch. However, this method does not allow models where the switch physically disconnects, and, therefore, no power flows through the switch.

[10] introduced the concept of switched power junctions (SPJ). The SPJ generalized the traditional bond graph junction causality laws to allow for multiple determining bonds for each junction, but only one of the determining bonds could be active (transferring power) at a time. SPJs preserve causality for all switch modes, but the bond graph models can quickly become complicated with the extra bonds increasing the complexity of the system structure in each operating mode.

Hybrid Bond Graphs

Hybrid Bond Graphs, introduced in [6], proposed the idea of idealized switches in the form of switching junctions that can be turned on and off to represent different system modes. When on, a switched junction behaves as a normal 1- or 0-junction. When off, a switched 1-junction forces zero flow on its connected bonds, and an off 0-junction forces zero effort on its connected bonds.

Two different ways have been proposed to implement hybrid junctions. The original definition, shown in Fig 1 replaces the "off" state of the 1- (0-)junction with a corresponding zero flow (effort) source [6]. Later, [7] and [9], implemented the "off" state of a junction by removing the bonds incident on the junction (Fig 2) assuming that these bonds transferred no power, therefore, they had no effect on system behavior and could be safely removed. However, this is not always true, as demonstrated in Fig 3. The circuit behavior is relatively simple. The switch starts closed and the capacitor charges from an uncharged state. At some point the switch is opened, which, in the ideal case, blocks the current flow through the system and causes the capacitor to maintain its charge. The unsimplified bond graph for the circuit is also shown in Fig 3. When the hybrid behavior is implemented by removing the bonds connected to the hybrid junction, the remaining bonds on the adjacent 1-junction allows the capacitor, C to discharge through the resistance, R. This is counter to the behavior expected from the circuit diagram. Therefore, the hybrid junction implementation shown in Fig 1 is not valid in general.

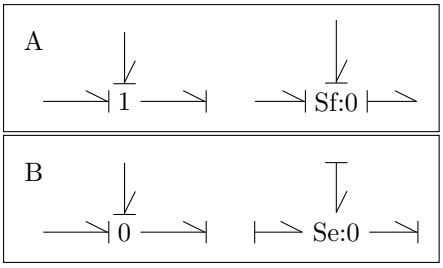

Fig. 1. Method of Implementing Hybrid Bond Graphs by Forcing Zero Effort/Flow in the Off Hybrid Junction

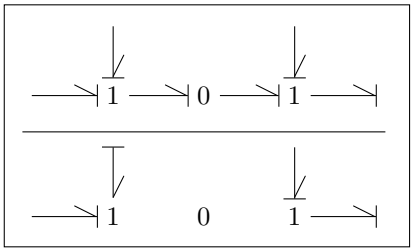

Fig. 2. Method of Implementing Hybrid Bond Graphs by Removing Bonds Attached to the Off Hybrid Junction

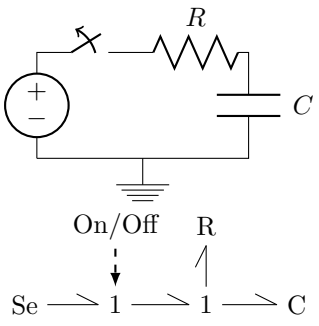

Fig. 3. Circuit Example and Unsimplified Bond Graph

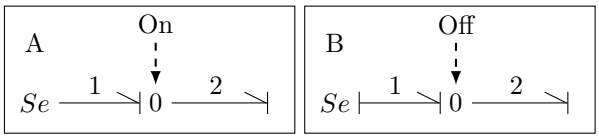

Fig. 4. Part A: Bond Graph with 0-Junction On and Part B: Causal Conflict on Bond 1

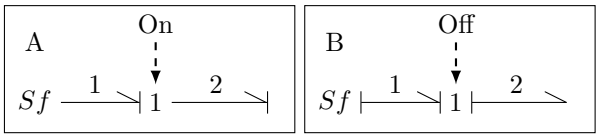

Fig. 5. Part A: Bond Graph with 1-Junction On and Part B: Causal Conflict on Bond 1

III. **Hybrid-Bond Graph Modeling Constraints**

When creating HBG models a set of constraints have to be applied to ensure the generated models are correct by: (1) avoiding structures that produce causality conflicts, and (2) being cognizant of the duality between mechanical versus electrical and fluid domains when constructing the hybrid junction structures for a system.

Modeling Constraint 1: Prohibited Structures

Assuming our models represent physical processes, the causality of the elements should not be violated in any mode of operation. Situations that violate causality may appear legitimate, but when the junction turns off there can be no causality assigned to the system. Such situations occur when a Se (Sf) element is directly connected to switching a 0-junction (1-junction). Turning the junction off creates a causality violation because there are two active sources of the same type incident on the 0- or 1-junction, respectively. This is illustrated in Figs. 4 and 5, respectively.

A related situation occurs when a capacitor (inertia) in integral causality is connected to a hybrid 0-junction (1-junction). When on, the capacitor (inertia) determines the junction effort (flow) value. When the junction turns off, keeping the capacitor (inertia) element in integral causality, (i.e., the determiner of the state variable effort (flow) value) creates a causality conflict with the zero effort (zero flow) source introduced to model the "off" state of the junction. Since a source element has fixed causality, the capacitor (inertia) is changed to derivative causality to accommodate the conflict. This implies that the derivative of effort (flow) immediately goes to zero, causing an instant discharge of all of its stored energy. This may not represent the correct behavior of the capacitor, i.e., it should retain its charge when it is isolated. (A similar statement can be made about the flux value on the inductor).

The situations described above are caused by the forced change in the determining bond (i.e., the bond that determines the effort value of a 0-junction and the flow value of a 1-junction) when the junction switches from on to off. In the examples in Figs. 4 and 5, causally correct structures across switching states can be retained by pairing a source of effort with a hybrid 1-junction, and a source of flow with a hybrid 0-junction. We introduce this as a formal constraint into our embedded systems modeling paradigm.

Modeling Constraint 2: Handling Complimentary Domains

Bond graph represent power flow through a system in a domain independent way. However, with HBGs, additional constraints may have to be added to created correct models.

The basis for this domain duality is based on fundamental differences between the physical domains. Each domain has a variable that represents a relative quantity, and a variable that represents an absolute quantity. That is, in the electrical domain (the hydraulic domain has similar behavior) the voltage (effort) at a point can only be measured relative to another point, while the current (flow) can be measured at any point in the system and does not need a reference. The opposite is true for the mechanical domains, where the velocity (flow) can only be measured relative to another point, while measuring the force (effort) does not require a reference point. The relative and absolute variables in the electrical and mechanical domains are represented by complementary bond graph variables. This difference translates to how configuration switching is modeled in each domain. Regardless of domain, each switch operates at a specific point in a system, not across or in reference to another point. This means that an electrical switching junction turned off will result in zero current (flow) through that node, while a mechanical switch turned off will result is zero force or torque (effort) being transmitted between objects. Given that switches in the different domains have dual semantics, they need to be represented as different junctions. In the electrical and hydraulic domains, the primary switches are modeled as 1-junctions to impose the constraint that flow (current and mass flow) is zero when the switch is off. In the mechanical domain, the primary switches are modeled as 0-junctions, because the effort (force and torque) are not transferred across the open switch. The other junction can be included in bond graph models as a secondary switch, but the physical implementation of the secondary switch is more complicated than the primary switch. This will be illustrated in the following section.

Similar logic can be used to determine the behavior for the reference point in each domain. The reference point in each domain provides the base reference for measuring the relative variables in that domain. The reference point is used in relation to other points in the model, therefore, the reference point forces a zero value on the relative quantity in that domain, which is the opposite quantity affected by a switch. For example, in the electrical domain an ideal ground forces zero voltage (effort) and supports infinite current (flow), and in the rotational domain an ideal fixed point forces zero velocity (flow) and supports infinite force (effort). (See Table II.)

TABLE II: Switches and their Reference Points across Domains

Domain	Primary Switch Forces Zero	Implemented As	Fixed Forces Zero
Electrical	Current	1-Junction	Voltage
Mechanical Translation	Force	0-Junction	Velocity
Mechanical Rotation	Torque	0-Junction	Angular Velocity
Hydraulic	Mass Flow	1-Junction	Pressure

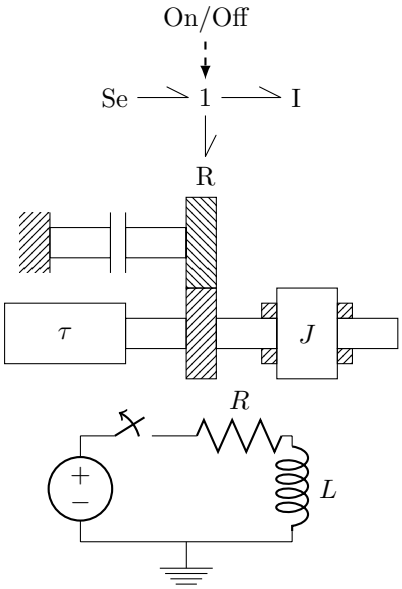

Fig. 6. Domain Duality Example 1

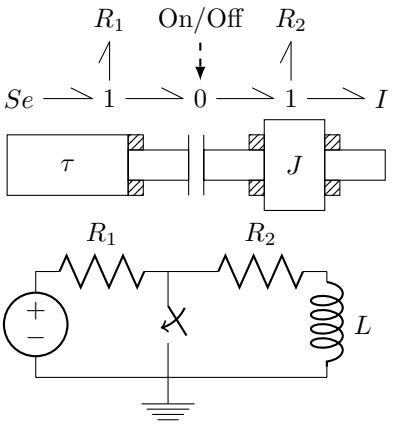

Fig. 7. Domain Duality Example 2

Complimentary Domains Example

To understand how the domain duality affects bond graph design, it helps to take a reverse modeling approach where the bond graph is the starting point instead of the end point. Figs 6 and 7 show an example of a simple bond graph implemented in two different domains.

In Fig 6 the hybrid 1-junction starts on, the flow in the system is dictated by the inertia element, and the sum of the efforts on each element sum to 0:

$$p = f * I = \int edt \tag{1}$$

$$e_I = e_{Se} - e_R. \tag{2}$$

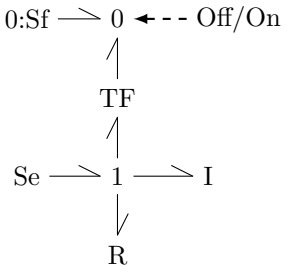

Fig. 8. Bond Graph of Rotational System in Fig 6

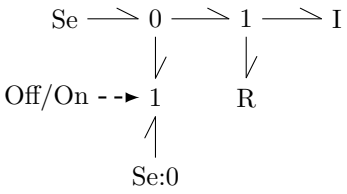

Fig. 9. Bond Graph Version of Electrical System in Fig 7

The variable p represents the momentum in the system and describes the system's state. At some point the 1-junction turns off, which will force the flow in the system to zero and will cause the inertia element to discharge instantly (that is, the momentum, p, in the system immediately drops to 0). The effort values also no longer need to sum to 0 because there is no more power flowing to each element:

$$p = f * I = \int edt = 0. \tag{3}$$

It is easy to see how the electrical circuit is an implementation of the bond graph. There is only a single flow path through the bond graph, and that is reflected in a single current through the electrical system. However, the corresponding mechanical rotation implementation is difficult to construct due to the switched 1-junction in the bond graph. A hybrid 1-junction is not easy to represent in the mechanical rotational domain because, in the rotational domain, only a fixed reference point can force the zero flow (velocity) required by the hybrid 1-junction. Implementing the hybrid 1-junction requires that the clutch be connected to a fixed point through a set of gears. The clutch operates opposite the switch in the bond graph so that when the hybrid junction is on (behaving as a normal junction) the clutch is open (off) to let the shaft spin freely. When the hybrid junction turns off to force zero flow, the clutch closes (turns on) so that the zero velocity forced by the fixed point transfers to the load. The mechanical rotation implementation in Fig 6 is better represented by the

bond graph in Fig. 8, where the hybrid 1-junction is replaced by a hybrid 0-junction, a transformer, and a source of flow representing the fixed point.

The situation is similar for the bond graph referenced in Fig. 7. The hybrid 0-junction starts on, which forces a single effort across both sides of the clutch, and the velocities on both sides of the clutch must sum to 0 (since there are only two bonds the velocities are going to be equal in magnitude but opposite in direction): $e_1 = e_2$ and $v_1 = -v_2$; where e_1 and v_1 are associated with the bond to the left of the 0-junction and e_2 and v_2 are associated with the bond on the right. At some point the hybrid junction turns off, which means the 0-junction now forces zero effort on its bonds: $e_1 = e_2 = 0$. The mechanical rotation implementation of the bond graph is simple, because the open clutch forces zero torque (effort) across it when open as required by the hybrid 0-junction. The electrical implementation is complex because it requires positioning the switch such that it creates a short to ground; which is the only way to force zero voltage (effort) as required by the off 0-junction. The electrical circuit in Fig 7 is better represented by the bond graph in Fig. 9. In this case the hybrid 0-junction is replaced by a regular 0-junction, a hybrid 1-junction, and a source of effort representing ground.

The extra structures needed to implement the secondary switch in each domain are actually the primary switch, a fixed point, and, potentially, extra elements to force the desired behavior. Using the secondary switching junction in each domain is possible, but it is impractical because the underlying physical structure of the system will simply use the primary switching junction.

IV. Case Study

As a case study to demonstrate the effectiveness of the definition of switching junctions and the role of the two constraints in the modeling task, we consider the Reverse Osmosis (RO) system, previously modeled in [1] and [9]. Both presentations of the RO system do not follow the definition of hybrid junctions, and instead implement hybrid behavior by assuming the bonds connecting an off junction are removed from the system.

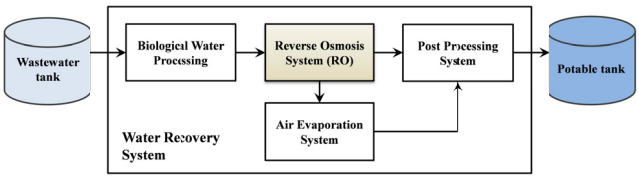

Fig. 10. NASA Water Recovery System.

Reverse Osmosis Overview

The RO system is part of the Advanced Water Recovery System (AWRS) (Fig 10), which is a subsystem of the NASA Advanced Life Support System (ALS). The ALS was designed as a way to support life for extended duration space missions by reclaiming waste water. The RO subsystem uses a membrane to remove inorganic matter and particles from water (Fig 11). The different modes of operation are controlled with a three-way valve, where each position of the valve specifies a different mode of operation. During the first two modes of operation, identified as M1 and M2, clean water leaves the system through the membrane, but dirty water, brine, is recirculated in a feedback loop to be filtered again. As a result of the feedback, the concentration of impurities in the water increases with time until it must be purged from the system, during mode P, to be processed by a different subsystem.

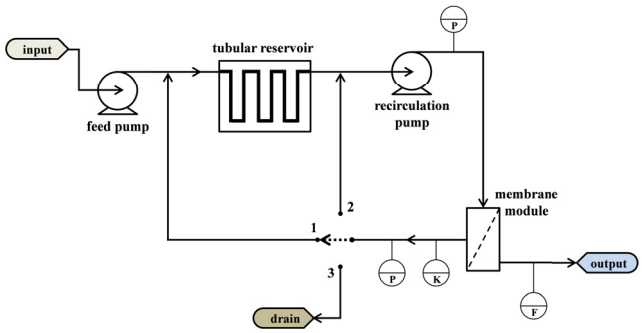

Fig. 11. RO Subsystem Schematic

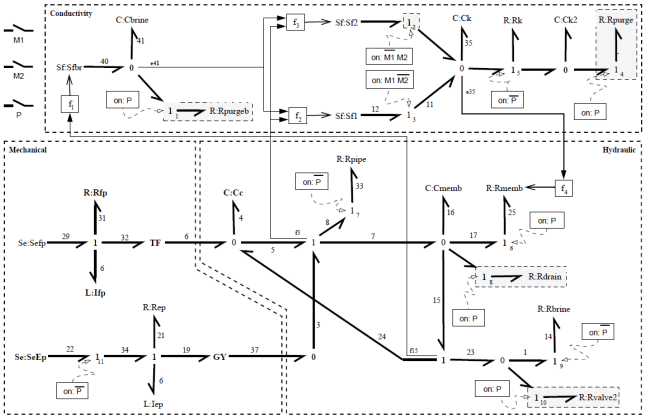

Fig. 12. RO System Bond Graph Version 1

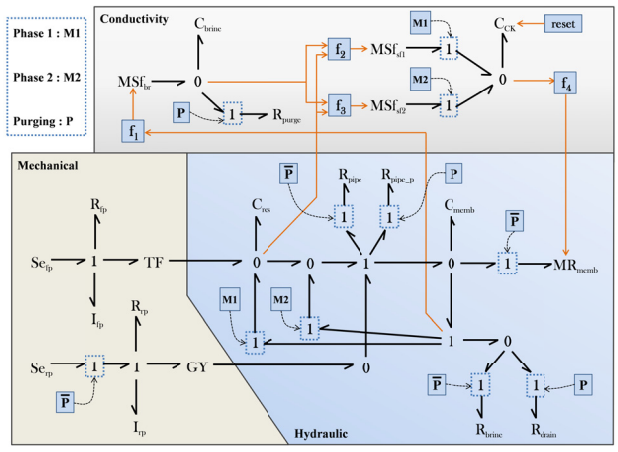

Fig. 13. RO System Bond Graph Version 2

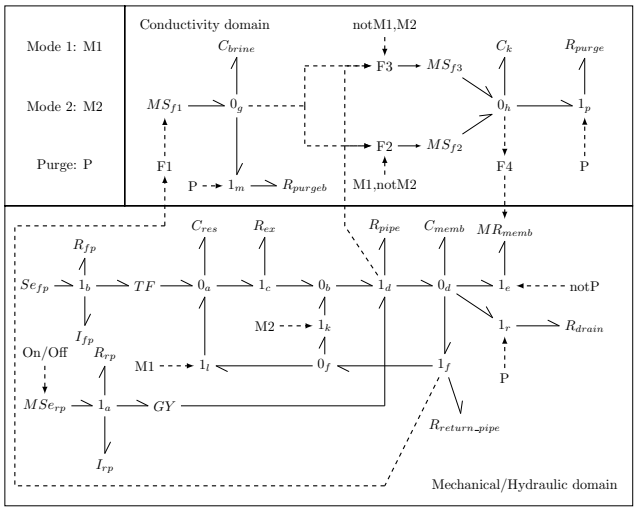

Fig. 14. Corrected Version of the RO System

Design Problems

The RO system has been modeled before, and the implementation from [1] is shown in Fig. 12 and the implementation from [9] is shown in Fig. 13. The hybrid junction implementations in these examples are based on the method presented in Fig. 2, where the only bonds removed from the system are the bonds directly connected to the hybrid junction. In both models, there are several places where multiple 1-junctions are connected together and one of the junctions is a hybrid junction. In Fig. 12 junction 7 (connected to *Rpipe* at the top of the mechanical domain) is a hybrid 1-junction connected through bond 8 to another 1-junction. The other situation in that figure is junction 11 (connected to source of effort *SeFp*), where a hybrid 1-junction is connected through bond 34 to a non-hybrid 1-junction. Fig. 13 has three situations where a non-hybrid 1-junction is connected to at least one hybrid 1-junction. The first case is the same as junction 11 in Fig. 12. The other two cases have a non-hybrid 1-junction connected to two hybrid 1-junctions, and the hybrid junctions are configured so that only one of the hybrid junctions is on at a time. The first instance is the two 1-junctions connected to the resistors R_{pipe} and R_{pipe_p}. The second instance is the 1-junction below the C_{memb} component that is connected to the two hybrid 1-junctions that switch on M1 and M2.

In both models, the intended behavior of these multiple junction structures is that there will be flow through the non-hybrid 1-junction when the connected hybrid junctions are off. However, when the proper definition of hybrid junctions is applied to these structures, the off 1-junction will stop the flow of fluid through the connected non-hybrid 1-junctions. This effectively makes the system inoperable as there will never be flow through the non-hybrid 1-junctions.

Another problem with Fig. 13 is that there are two 0-junctions next to each other near the middle of the figure (one 0-junction is connected to the capacitor C_{res}). The second 0-junction is supposed to represent the fluid path for mode M2 that avoids the reservoir, C_{res}, and forces fluid more quickly through the membrane. However, because the two 0-junctions function as a single junction, the fluid path for mode M2 is the same as for mode M1.

A final problem with both models is in the conductivity domain. There are two modulated flow sources, $Sf1$ and $Sf2$ that are connected to hybrid 1-junctions. When the hybrid junctions turn off there will be a causality conflict on the bond connecting the flow source and the junction because both will be trying to force a different value for the flow on that bond.

The simulation results for Fig. 13 are presented in Figs. 15 and 16. These results conflict with the results presented in [9] because they were generated using different definitions for the hybrid junctions. The results presented in [9] were created by removing the bonds connected to an off junction, while the results presented here were generated by forcing zero flow on the off hybrid 1-junctions. In Fig. 16 the system never transitions out of the purge mode because there is a check in the system that enables that transition based on the amount of brine in the system. As seen in Fig 15 the brine concentration is static, so the system is never able to complete the check, and, therefore, the system will stay in the purge mode indefinitely. The transitions out of modes M1 and M2 are strictly based on time, and are, therefore, not affected by the behavior of the system.

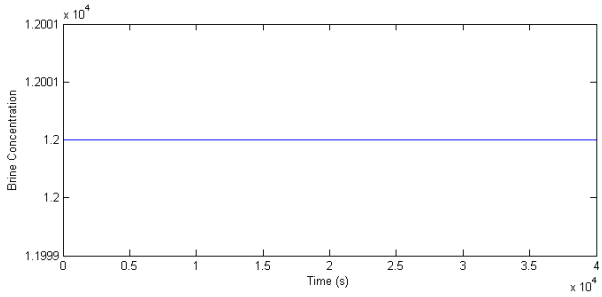

Fig. 15. Brine Concentration for the RO System Presented in Fig 13

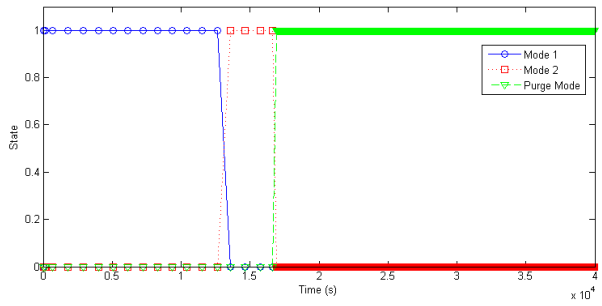

Fig. 16. Mode Transitions for the RO System Presented in Fig 13

Corrected Reverse Osmosis Model

To overcome the problems discussed above, a corrected bond graph of the RO system is shown in Fig. 14.

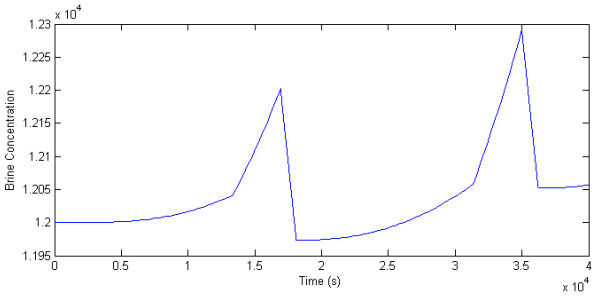

Fig. 17. Brine Concentration for the Corrected RO System

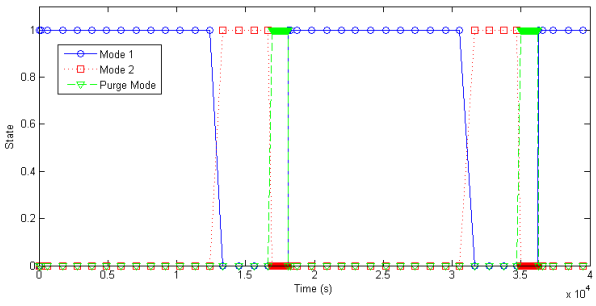

Fig. 18. Mode Transitions for the Corrected RO System

The hybrid 1-junctions at the top of the hydraulic domain have been removed and replaced with a single resistor element. This better models the fluid flow as it must pass through the pipe represented by junction 1_d in all modes. There is a 0-junction (junction 0_f) separating the M1 and M2 triggered 1-junctions. This 0-junction functions as a flow dividing junction and allows the hybrid 1-junctions to be turned on and off independently. In purge mode both junctions are off, which will force zero flow through junction 1_f, effectively turning it off even though it is not explicitly declared as a hybrid junction. The recirculation pump, MSe_{rp}, is now a modulated source of effort that replaces the hybrid 1-junction. Also, there is a new 1-junction (junction 1_c) with a connected resistor that separates the two series 0-junctions. This 1-junction allows there to be two different fluid flows for modes M1 and M2. Finally, the hybrid 1-junctions connected to the sources of flow in the conductivity domain have been removed and the hybrid functionality moved into the functions that define the values for the modulated sources of flow. The updated simulation results are presented in Figs. 17 and 18.

V. Conclusion

Hybrid bond graphs are an excellent cross domain method of representing the behavior of hybrid systems that capture the energy domain constraints and configuration switching constraints imposed on physical processes to ensure that models remain consistent before and after mode changes. The semantics of hybrid bond graphs produce valid behavior across multiple physical domains, provided the proper definition of a hybrid junction is followed, and the associated constraints are not violated. We have shown that only one type of primary switched junction makes sense physically in each domain, and even though the complementary junction can be used in each domain the physical system is better represented by using the ideal junction plus a few added elements. When the semantic constraints are applied, the HBG modeling paradigm is able to accurately represent the behavior of hybrid systems.

References

[1] Gautam Biswas, Eric-J. Manders, John Ramirez, Nagabhusan Mahadevan, and Sherif Abdelwahed. Online model-based diagnosis to support autonomous operation of an advanced life support system. *Habitation - International Journal for Human Support Research*, 10(1):21–38, 2004.

[2] G. Dauphin-Tanguy and C. Rombaut. Why a unique causality in the elementary commutation cell bond graph model of a power electronics converter. In *Systems, Man and Cybernetics, 1993. 'Systems Engineering in the Service of Humans', Conference Proceedings., International Conference on*, volume 1, pages 257–263, Oct 1993.

[3] Yakup Demir, Mustafa Poyraz, and Muhammet Köksal. Derivation of state and output equations for systems containing switches and a novel definition of a switch using the bond graph model. *Journal of the Franklin Institute*, 334(2):191 – 197, 1997.

[4] Krister Edström. *Switched Bond Graphs Simulation and Analysis*. PhD thesis, Linköping University, 1999.

[5] Dean C. Karnopp, Donald L. Margolis, and Ronald C. Rosenberg. *System Dynamics*. John Wiley & Sons, Inc., Hoboken, New Jersey, 4 edition, 2006.

[6] Pieter J. Mosterman and Gautam Biswas. A theory of discontinuities in physical system models. *Journal of the Franklin Institute: Engineering and Applied Mathematics*, 335B(3):401–439, January 1998.

[7] Indranil Roychoudhury, Matthew J. Daigle, Gautam Biswas, and Xenofon Koutsoukos. Efficient simulation of hybrid systems: A hybrid bond graph approach. *Simulation: Transactions of the Society for Modeling and Simulation International*, 87(6):467–498, 2010.

[8] Jan-Erik Strömberg, Jan Top, and Ulf Söderman. Variable causality in bond graphs caused by discrete effects. 1993.

[9] Tamas Szarka. Structural, behavioral and functional modeling of cyber-physical systems, August 2011.

[10] Amod C. Umarikar and L. Umanand. Modelling of switching systems in bond graphs using the concept of switched power junctions. *Journal of the Franklin Institute*, 342(2):131 – 147, 2005.

Author Biographies

JOSHUA D. CARL is currently a graduate student at Vanderbilt University and is a member of the Institute for Software Integrated Systems (ISIS). His research interests include cross domain modeling of embedded and cyber physical systems. His email address is: carljd1@isis.vanderbilt.edu.

ZSOLT LATTMANN received his MSc. in Electrical Engineering from Vanderbilt University in 2010. He has been working at ISIS as a Staff Engineer since 2010 and develops complex cyber-physical tool chains. His email address is: lattmann@isis.vanderbilt.edu.

GAUTAM BISWAS is a Professor in the EECS Department and a Senior Research Scientist at ISIS at Vanderbilt University. His primary research interests are modeling and simulation of complex systems and applying these models for diagnosis and fault adaptive control. His email address is: biswas@isis.vanderbilt.edu.

THE DISCRETE EVENT SIMULATION FRAMEWORK DESMO-J: REVIEW, COMPARISION TO OTHER FRAMEWORKS AND LATEST DEVELOPMENT

Johannes Göbel, Philip Joschko, Arne Koors, Bernd Page
Department of Informatics
University of Hamburg
Vogt-Kölln-Str. 30, 22527 Hamburg, Germany
E-mail: {goebel, joschko, koors, page}@informatik.uni-hamburg.de

KEYWORDS
Discrete Event Simulation, Simulation Software, Simulation Framework, Open Source, Java, .NET, Visualization.

ABSTRACT

This review paper focusses on DESMO-J, a comprehensive and stable Java-based open-source simulation library. DESMO-J is recommended in numerous academic publications for implementing discrete event simulation models for various applications. The library was integrated into several commercial software products. DESMO-J's functional range and usability is continuously improved by the Department of Informatics of the University of Hamburg (Germany). The paper summarizes DESMO-J's core functionality and important design decisions. It also compares DESMO-J to other discrete event simulation frameworks. Furthermore, latest developments and new opportunities are addressed in more detail. These include a) improvements relating to the quality and applicability of the software itself, e.g. a port to .NET, b) optional extension packages like visualization libraries and c) new components facilitating a more powerful and flexible simulation logic, like adaption to real time or a compact representation of production chains and similar queuing systems. Finally, the paper exemplarily describes how to apply DESMO-J to harbor logistics and business process modeling, thus providing insights into DESMO-J practice.

INTRODUCTION

A practitioner aiming to conduct a simulation study has the choice between two types of simulation software to base his or her model on:

- *Integrated simulation development environments*, typically commercial software, often support the simulation study as whole, including data collection, model design, experimentation and evaluation. Model design often is done by *assembling* ready-to-use components on drag and drop basis in a graphical user interface. Plant Simulation (Siemens PLM Software, www.plm.automation.siemens.com) or FlexSim (FlexSim Software, www.flexsim.com) are well-known examples.
- *Simulation libraries* have a narrower focus, typically concentrating on model implementation and experimentation. They require models are *coded* in a general-purpose or special programming language, sacrificing comfort for flexibility. Though their modeling capabilities are often similar to commercial development environments, most of such libraries are open source software: apart from being available for free, advantages include source code analysis, debugging, modification, and the permission to re-distribute extended versions according to the relevant license. Examples include DESMO-J (Page 2013) and others, as compared later in this paper.

The purpose of this paper is easing the difficulty of this choice by clarifying the state of the art for the second type of software: This paper presents DESMO-J as example of a modern open source library for Java-based discrete event simulation. The subsequent section describes DESMO-J's functional range and important design decisions and provides a comparison to other open source simulation libraries. For examples of how DESMO-J is applied in different real-world scenarios consider the next section, namely extensions for harbor logistics and business process modeling. The following section can be understood as an update to previous publications like Page and Neufeld (2003) and Göbel, Krzesinski and Page (2009), as the latest extensions to DESMO-J are described, namely real time capability, 2D and 3D visualization, a .NET port, efficient simulation of processes based on coroutines and continuations, generic components for production chains and other queuing systems, recording and logging of simulation objects, as well as advanced simulation dynamics analysis on basis of quantitative finance risk metrics. This permits the conclusion in the final section that libraries like DESMO-J should be recognized as alternatives to commercial development environments.

DESMO-J

DESMO-J (Discrete-Event Simulation and Modelling in Java) is a comprehensive framework for developing discrete event simulation models, see Banks et al. (2010) or Page and Kreutzer (2005), in the object-

Proceedings 27th European Conference on Modelling and Simulation ©ECMS Webjørn Rekdalsbakken, Robin T. Bye, Houxiang Zhang (Editors)
ISBN: 978-0-9564944-6-7 / ISBN: 978-0-9564944-7-4 (CD)

oriented programming language Java. The first subsection discusses the reasons for choosing Java, followed by a short primer about modeling in DESMO-J. Afterwards, the most important design decisions and a comparison to other simulation libraries are addressed.

Implementation Language

Simulation modeling in DESMO-J actually means implementing models in *Java*. Particularly, the model structure including properties and behavior of all components has to be coded in appropriate Java classes. In contrast, the simulation infrastructure, e.g. simulation clock, event list, random number distributions and experiment conduction including reporting is readily available.

In comparison to the other main approach of providing simulation functionality to a user, namely graphically assembling models on "drag and drop" basis, simulation programming may be less intuitive to learn (especially for beginners) and slower to apply; this at least holds for standard cases like production lines which are covered by the building blocks included in GUI-based modeling environments like Plant Simulation or FlexSim. However, the most important advantage of simulation programming based on a library like DESMO-J is flexibility, as any model logic can be described in a general purpose programming language like Java; no constrains are imposed by a restricted simulator API or a product-specific script language. Therefore, DESMO-J is particularly well-suited for complex models for which graphical modeling cannot be done adequately and efficiently.

Furthermore, choosing Java as simulation programming language means addressing a large community of programmers. It ensures all features of a modern object-oriented language are available. Java's pervasiveness is unmatched: so-called Java virtual machines are provided for almost every modern operating system. Java programs can not only be executed on desktops, but also as Web Service or as Applets on web sites. Just-in-time compilation including optimization of Hot Spot execution and garbage collection has helped to achieve run time performance similar to languages that compile sources to binary code.

DESMO-J in a Nutshell

We refer to DESMO-J as a simulation *framework* as it provides a coherent software architecture of components exhibiting a well-defined cooperative behavior designed to effectively and conveniently serve the task of model building and experiment conduction: as much implementation effort as possible is removed from the user. Wherever feasible, DESMO-J makes available so-called *black-box* components, which are classes that are ready-to-use. Such classes are parameterized by the user; usually, their code needs not be touched. Figure 1 shows the most important classes from DESMO-J's core functionality. Black-box components include the `Experiment` class responsible for conducting discrete event simulation runs. Following the *façade* design pattern, `Experiment` hides the infrastructure it requires, like the scheduler and the event list it operates on, the simulation clock, and the generation of experiment reports. Additional black-box components offer generic model components like queues with finite or infinite space, random number generators based on a variety of random number distributions and different means of collecting statistical data. Important functionality of the statistics classes includes counting, uniform or time-weighted aggregation of samples, determining confidence intervals and generating histograms. The last-mentioned black-box components are subclasses of `Reportable`, automatically generating statistical data available in the experiment report.

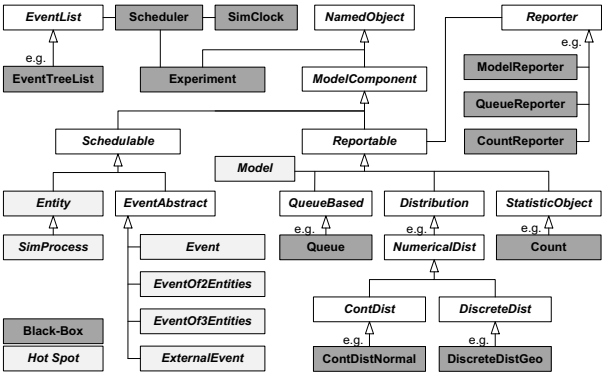

Figure 1: Important DESMO-J Classes

With this set of black-box components at hand, the modeler is able to focus on implementing the logic of the system to simulate by using additional objects referred to as `Schedulable`s. Such `Schedulable` objects can be put onto the event list; they are typical examples of DESMO-J's white-box components or *hot spots*: the unknown structure and behavior of a user's model require more flexibility than parameterized black-boxes can provide. Consequently, hot spots are abstract Java classes whose methods have to be completed by the user.

To implement a model, the DESMO-J user may choose between the event-oriented and the process-oriented view:

The *event-oriented perspective*, also referred to as "bird's eye view", requires the user to describe the model behavior in terms of event routines which are assumed executed as an atomic transaction without interruption and without simulated time passing. Model dynamics arise from sequentially executing events. Entities are represented by classes inheriting from `Entity`. The events implemented by the user have to be derived from one of the four subclasses of `EventAbstract`; which subclass to base a modeled event on depends on the number of entities associated to the event, namely one (`Event`), two (`EventOfTwoEntities`), three (`EventOfThreeEntities`) or none (`ExternalEvent`). For example, a service end event of an item leaving a machine in a

production line typically is modeled as an `EventOfTwoEntities`, as two entities are affected: one item proceeding to the next machine and one machine processing the next item, if available. In contrast, an event referring to no specific entity, but to the system as whole, e.g. a power failure, could be implemented as `ExternalEvent`. An event's behavior is defined in its `eventRoutine()` method; typically, event routines include entities being created and destroyed, entities entering or leaving queues, statistical data collectors being updated and further events scheduled or cancelled.

In contrast, *process modeling* describes model logic in terms of processes that persist as simulation time passes. Model dynamics arise from process interaction and transfer of program control among each other. For each process, the user has to subclass `SimProcess`, providing a *life cycle* containing the behavior of the process over time, yielding a "worm's eye view" of the model. In their user-defined `lifeCycle()` methods, processes may create other processes (which are special entities), modify queues or update statistic objects. Furthermore, simulation processes are able to wait for a certain period of simulated time ("hold") or for an indeterminate period ("passivate") until activation by another process ("activate"). A process may interrupt another process on hold, causing the interrupted process to resume its life cycle execution at a time instant prior to its original schedule.

With true *coroutines* not being available in Java, process execution internally is based on event scheduling: each process runs in its own Java thread; process threads are suspendable and are resumed by events implicitly scheduled when processes are held or activated/interrupted. Note that the section describing latest developments presents an alternative approach of implementing processes which is less resource-consuming.

DESMO-J does not enforce an exclusive decision for either event or process modeling; the user is free to combine both modeling styles in a single model (e.g. an event activating a process which in turn schedules another event), so that the modeling perspective best suited for each specific aspect of a model can be applied.

Comparison to other Tools

When conducting a simulation study using a Java-based simulation framework like DESMO-J, the model developer may choose out of a number of different tools. An of course non-exhaustive list of open source discrete event simulation libraries in Java includes

- DESMO-J (Page 2013),
- DSOL (Verbraeck 2009),
- J-Sim (Kačer 2006),
- JavaDEMOS (Computer Science Group 2009),
- JSL (Rossetti 2013),
- PtolemyII (Lee 2011),
- SimKit (Buss 2012) and
- SSJ (L'Ecuyer 2012).

For URLs of these libraries including API documentation and examples see the corresponding Reference entries. Table 1 compares some key features of DESMO-J and its competitors.

Table 1: DESMO-J compared to other Java Discrete Event Simulation libraries

Package name	Events / Processes	Visualization	Random distributions	Tutorial / Examples	License **	Commercial use	Last version
DESMO-J	E/P	2D/3D	25	Yes	ASL2.0	Yes	2013
DSOL	E/P	2D	21	Yes	Special	–	2009
J-Sim	E/P	–	5	Yes	AFL2.1	–	2006
J'DEMOS	E/P	–	15	Yes	Special	–	2009
JSL	E	–	9	Yes	GPL	–	2013
PtolemyII	E/P*	2D	23	Yes	Special	Yes	2011
SimKit	E	2D	25	Yes	LGPL	Yes	2012
SSJ	E/P	–	64	Yes	GPL	–	2012

* Processes based on an Actor approach
** ASL = Apache Software License, AFL = Academic Free License, GPL = GNU General Public License, LGPL = GNU Lesser General Public License

These key features include support of event and process modeling and availability of 2D or 3D visualization of model behavior; different means of 2D visualization are available, e.g. schematic representation of the spatial model structure similar to Plant Simulation, where entities are drawn using icons, or important statistics as displayable in DESMO-J, or dynamically annotated event graphs as in DSOL. The number of random distributions has not much intrinsic value on its own, as generators for additional distributions can be implemented quickly. Nevertheless, it is included in the table as an exemplary indicator for each framework's extent, which is difficult to measure. E.g. number of classes or download size might be misleading measurements, as they depend on various design decisions, e.g. few monolithic or many specialized classes, data collection separated from the source generation of the data or not, functionality partially delegated to sub-libraries… Furthermore, the table addresses the availability of tutorials or example models, the licenses under which the libraries are available to the public and whether commercial use is permitted. For commercial application, we particularly require permission for usage in closed-source, proprietary software and inclusion in releases of such software without endorsement from the libraries' authors. The table concludes with the date of the most recent version as of February 2013.

Observe that the combination of features DESMO-J offers is unmatched among the other Java-based simulation frameworks: as already explained, DESMO-J allows event and process modeling and offers both 2D and 3D visualization of the model behavior as will be described below. The DESMO-J website (Page 2013) contains an extensive tutorial not only describing how a container logistics example model is implemented using either events or processes and how experiments are conducted. A variety of advanced topics is also ad-

dressed, e.g. different data collectors and higher modeling features like conditional waiting or implicit process synchronization.
Another unique feature is the availability of a companion book: *The Java Simulation Handbook* (Page and Kreutzer 2005), available as printed version and as eBook, covers discrete event simulation fundamentals and simulation modeling based on UML and DESMO-J as well as simulation statistics, model validation and verification, multi-agent simulation, simulation optimization, simulation projects in practice and various other topics.

EXTENDING DESMO-J AND APPLICATION SCENARIOS

General Expandability

Every time a model is implemented with DESMO-J by deriving entities and processes/events from DESMO-J classes, a kind of 'domain-specific extension' is written. Classes designed with the intention of general reusability within diverse models are called DESMO-J *extensions*. These might be general, more technical extensions like multi-agent-based simulation entities (Knaak, Kruse and Page 2006) or domain-specific extensions, containing reusable entities for easier composition of models in that particular domain, see next sections or Joschko, Page and Wohlgemuth (2009).
Furthermore, DESMO-J can be integrated into other software products, such as extensive modeling suites with own graphical user front-end and model editors, allowing modeling without writing Java code. Due to the flexibility of ASL 2.0 under which DESMO-J is licensed, it is possible to implement individual solutions without using an open-source license – an important issue in non-public, commercial projects.
Since expandability is a very important aspect in using DESMO-J, we sum up some domain-specific solutions in the following sections.

Harbor and Container Terminals

Simulation is an established method for optimizing strategies and resource allocation in logistic contexts. Since Hamburg accommodates one of the ten largest container ports worldwide, we had the opportunity to gain substantial experience in simulating container terminals in a number of cooperation projects. We presented our first DESMO-J harbor extension in Page and Neufeld (2003). This class library extension is still available in DESMO-J, offering three types of objects: dynamic, mobile, temporary objects like ships, trucks and trains; dynamic, mobile, permanent objects like cranes and van carriers; and stationary, permanent objects like holding areas, gates, jetties and yards (Joschko, Brandt and Page 2009).
Worldwide, many other working groups use DESMO-J in logistic investigations in harbor context, see e.g. Asperen et al. (2004) and Henesey, Aslam and Khurum (2006).

The traditional aim in executing logistic simulation experiments is to compare different handling strategies in order to determine terminal layout or optimize usage of transport vehicles (Bornhöft, Page and Schütt 2010). These strategic simulation approaches take place in the design and implementation phase of container terminals. In the operation phases of container terminals, tactical simulation can be used to support decision-making in resource allocation, finding good storage positions and accepting orders.
A completely different approach in this phase is to use simulation for integration tests on terminal operating systems. Together with the Hamburger Hafen und Logistik AG (HHLA), we implemented a DESMO-J extension for a broad range of applications in the context of container terminals, called COCoS, see Brandt (2008) or Joschko, Brandt and Page (2009). Entities in COCoS (van carriers, quay cranes etc.) are assembled from different exchangeable layers and sub-components that manipulate model state by scheduling DESMO-J events. The granularity depends on the level of detail needed for the object of investigation. Whereas in logistic experiments an abstract, stochastic representation of transport device behavior is needed, a high level of detail is required when connecting the model to a real terminal operating system. The exact kinematic characteristics of transport devices have to be mapped. A TCP-based communication layer enables message exchange between the simulation model and the container terminal operating system. Last but not least, deceleration of simulation adjusts the model to real time (see next chapter). A graphical user interface comprises visualization of the model's state and buttons permitting user interaction with the job list or a device. Fulfilling these conditions with DESMO-J and COCoS, a simulated terminal system can be controlled by a real terminal operating system. In this way, a "terminal operating system can be tested with help of a terminal model" (Joschko, Brandt and Page 2009).

Business Process Modeling

In Business Process Analysis, a graphical modeling notation (BPMN, EPC, UML, Petri-Nets etc.) is used to visualize production processes and information flows. Apart from other purposes, such a graphical representation facilitates communicating existing procedures and discussing improvements. Augmenting such methodology with simulation capabilities enables empirically founded comparison of alternatives, e.g. resource allocation or strategy optimization. Regardless of the chosen modeling notation, a business process model can be transformed into a simulation model if it is enhanced with simulation properties. Particularly, stochastic parameters affect the duration of activities and the inter-arrival time of events. Once again, resource allocation is one of the most interesting issues. The total cost of activities, the number of concurrently running processes, the duration of (sub-)processes, the length of waiting queues and the occurring frequency of specified events are also relevant performance indicators.

Several commercial business process modeling tools use DESMO-J as simulation engine in order to support such analysis. To our knowledge, DESMO-J is a part of *Tibco Business Studio*, *Borland Together*, *eClarus Business Process Modeler for SOA Architects* and *Intellivate IYOPRO*, the latter being our favorite in user friendliness. This list may be incomplete as not all DESMO-J software integrators necessarily get in touch with us.

In cooperation with Intellivate GmbH, the developer of IYOPRO, our working group has developed a DESMO-J extension for simulating business processes notated in Business Process Model and Notation 2.0 (BPMN). Since IYOPRO is a Silverlight web application, we used a .NET port of DESMO-J (see below) in order to implement a BPMN extension for DESMO-J. This software now contains a special BPMN-process derived from DESMO-J's `SimProcess` class as well as implementations of most BPMN flow elements, like activities, several event types and sequence flows. Furthermore, it includes message flows, pools, swim lanes and data-objects derived from DESMO-J's `Entity` class. Integrated into the graphical model editor of IYOPRO, model parameters can be set using a property editor. Additionally, process variables for data-objects and expressions for splitting gateways can be declared. Therefore, the choice of path can depend on the state of a process instance. The simulation report is enhanced with pie charts and histograms, linked to the corresponding model elements. See Joschko et al (2012) for more details about business process simulation, enhancing models for simulation purposes and deploying simulation experiments using BPMN 2.0 and IYOPRO.

LATEST DEVELOPMENT

Leaving the application level, we now describe some recent features of DESMO-J itself, thus giving an insight into the library's continuous development process.

Real-time Capability

The handling of simulation time has been completely re-engineered as of DESMO-J version 2.2.0, see Klückmann (2009): typically, a simulation experiment is executed as fast as possible; simulation time advance depends on CPU speed only. Special cases, however, may require intentionally decelerating an experiment: examples include concurrent animation or real-word systems in which the behavior of some components is emulated by a simulator. DESMO-J now offers the feature to link simulation time advance to real time, subject to a user-defined time lapse factor. If this factor is set to 1, the simulation experiment will execute synchronously to real time.

Re-engineering time handling also introduced some minor improvements: for the modeler's convenience, references to time can alternatively be based on time instants or durations, thanks to parameter overloading: for example, either an absolute point in time (`TimeInstant`, "hold until") or a duration (`TimeSpan`, "hold for") can be passed to a process' `hold()` method.

Additional improvements include the support of `java.util.Calendar` and `java.util.Date` for reading and writing time statements, multiple time zones in a single model, a class for shift schedules, as well as time-weighted data collection (`Accumulate`) being switched on and off, e.g. in order to ignore a night's downtime.

2D Visualization

Modern simulation tools support model state and behavior visualization; reasons include communication with model users and decision makers as well as detection of erroneous model logic and – though no replacement for a statistically well-founded analysis – basic means of evaluation, e.g. identification of potential bottlenecks. DESMO-J supports two different means of visualization, presented in this and the next subsection.

The 2D visualization component – a contribution of Prof. Dr. Christian Müller and his research group at the Technical University of Applied Sciences Wildau, Germany – provides a means of schematically representing the model logic on a 2D plane: every entity (including processes, compare Figure 1) can be shown in the visualization, after an icon and location in terms of x/y-coordinates have been assigned. Visualization supports uniform entity motion from an origin to a destination during a certain time span on a pre-defined path. Entities can also be shown inside a waiting area of queues while enqueued. Furthermore, data collectors can be included in the visualization, featuring their current or last values as well as mean and standard deviation values. Figure 2 shows an example screenshot from a bungee tower model; see the DESMO-J webpage (Page 2013) for a Java Applet version of this animation running directly inside the web browser.

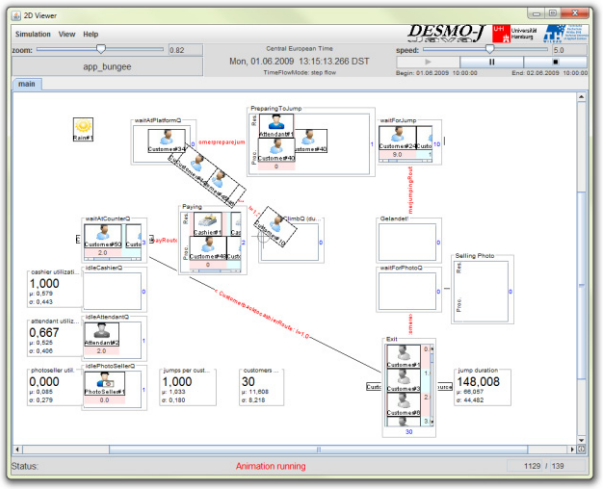

Figure 2: Screenshot of the 2D Visualization of a bungee tower model

To create a 2D visualization, a developer just has to replace the DESMO-J core classes like `Model`, `Entity`, `SimProcess`, `Queue` or `Count` with their appropriate subclasses `ModelAnimation`, `EntityAnimation`,

`SimProcessAnimation`, `QueueAnimation` or `CountAnimation` from the 2D visualization package. Constructors and methods are identical to the core classes except for additional means for defining a position or exchanging an entity's icon reflecting a state modification, e.g. job completion or change of order priority.
As 2D visualization works *offline*, a simulation experiment has to finish before visualization starts: rather than providing a "live" view of the experiment, opposed to the 3D framework described below, a simulation run generates an XML-script describing all updates to appear in the visualization, e.g. entity motion or data collector values adjusted. After completion of a simulation run, a viewer is launched in which the script can be played back. Basic features include zooming and adjusting animation speed (time lapse, stepwise execution). Additional examples, a 2D visualization tutorial and documentation are available at a dedicated web site (Müller 2011).

3D Framework

Alternatively, we provide a 3D framework which includes several libraries for three-dimensional modeling and visualizing. First, there is a DESMO-J extension which provides a basic spatial concept, see Sun (2010): the interfaces `SpatialObject` and `MovableSpatialObject` enhance the DESMO-J classes `Entity`, `SimProcess` or `Queue` with coordinates, orientation and movement behavior. The class `SpatialData` encapsulates coordinates and orientation in a 4 × 4 transformation matrix, thus movements are represented as matrix multiplications. The environment's layout contains navigation points and routes between them. It can be defined in an XML file.
Second, there is an optional kinematic library for calculating the arrival time of entities, requiring acceleration, deceleration and maximum speed of a `MovableSpatialObject` being given. While position and orientation are calculated when a movement is finished, the class `SpatialMovementManager` interpolates speed, position and orientation of objects on demand. Instead of the kinematic calculation, arrival time can also be scheduled conventionally by stochastic distributions.
Third, the visualization framework animates the position, orientation and movement of objects with help of OpenGL and Java 3D. 3D shape files are linked to logical model elements by an XML file, thus the visual appearance of objects is determined. Input and output ports enable 3D modeling of entities like queues. In order to get messages about movement events, the visualization framework signs itself up at the spatial classes. Between start and termination of a movement, the actual position is updated regularly by the `SpatialMovementManager`. The parallel deployment of spatial concept, kinematic library and visualization framework enables three-dimensional, concurrent animation *during* a simulation run. Figure 3 shows a 3D visualization of a simple logistics model.

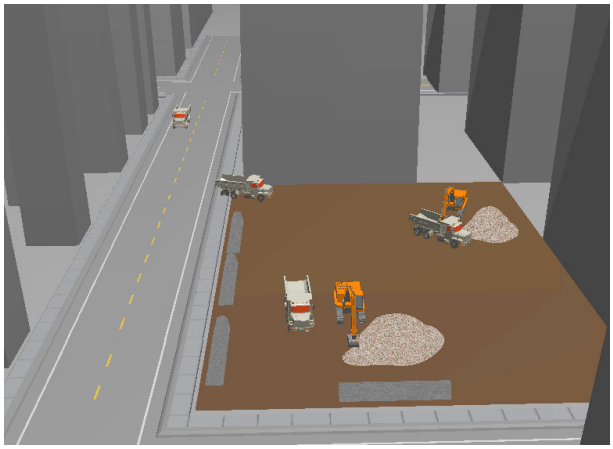

Figure 3: Screenshot of the 3D Visualization of a truck loading model

.NET-Versions of DESMO-J

This far, integration of DESMO-J into existing software suites is limited to Java. A platform similarly widespread is .NET from Microsoft. Like Java, .NET is based on a virtual machine, yet it allows programming in diverse languages, e.g. C# or Visual Basic. Since DESMO-J is constantly improved and enhanced, maintaining two branches of DESMO, one in Java and one in C#, would have been too costly. Nevertheless, a .NET version of DESMO-J always aligned with the maturity level of the Java version was desirable. We successfully explored two approaches of automatically porting DESMO-J into .NET's Intermediate Language code or into C# source code, respectively.
IKVM is an implementation of the Java Virtual Machine for .NET and Mono, see Frijters (2012). It provides an implementation of the Java standard libraries and some tools which enable interoperability of Java and .NET respectively Mono classes. The command '`ikvmc`' is able to compile a .NET DLL file out of a Java JAR file. The resulting DLL file has dependencies to several IKVM libraries. These files can be included in a .NET based software application and used as if they were ordinary compiled .NET classes. Since differences between Java and .NET do exist, we examined the feasibility of this solution in practice. We tested whether the behavior of a 'DESMO.NET' library produced by IKVM is identical to that of the original DESMO-J library. Therefore, we compared simulation results of several simulation runs with several models, and could not find any deviations.
As a consequence, we developed a sophisticated ERP simulation model in C#, interfacing with a Microsoft Windows-based ERP system in a .NET environment, while employing broad simulation functionality of DESMO-J converted to .NET by IKVM (Kühnlenz 2011, Schäfer 2011). Though the model was quite complex and extensively used simulation functionality, we

did not encounter any problems introduced by the conversion process of IKVM.
Another approach is to directly transform the Java high-level language code into C# code. The syntax of Java and C# is quite similar. However, method calls to classes in the Java core libraries have to be mapped to equivalent method calls in the .NET framework.
Among the tools supporting such transformations, we gathered experience with the open-source software Sharpen (2013). As the transformation process is incomplete, additional work is required. First, converting multi-dimensional arrays and changing the parameter order of class library methods is not fully supported. Second, the tool does not adequately resolve some particular differences between Java and C#. E.g. in C# it is not possible to reference raw types of generic classes, a technique used in DESMO-J.
We developed an Ant script that prepares the Java code before transformation into C# (e.g. removing raw type references), and adjusts the result in order to eliminate remaining errors. In consequence, we are now able to generate C# source code, which is nearly equivalent to our Java-based DESMO-J.
We argue that IKVM offers a fast, easy and reliable way to generate .NET versions out of DESMO-J. If a more lightweight solution is desired that does not require integration of IKVM libraries into the target simulation application, transforming Java sources into C# sources is feasible, with an additional manual effort.

Alternative Process Implementation

The class `SimProcess` (see DESMO-J introduction) internally relies on an instance of `java.lang.Thread` for life cycle execution. This permits halting a simulation process whenever needed, persisting its method pointer and process state, and reactivating it at a later time. A disadvantage of using `java.lang.Thread` is the upper limit of concurrent existing threads in Java – independent of whether they are actually working in parallel or not. For a typical JVM, the maximum number of concurrently existing simulation processes is approximately 2500 plus a few thousand additional processes obtainable by increasing heap space. However, if millions of concurrent processes are needed, the model had to be implemented in an event-oriented manner, until recently.
Now, we present an alternative `SimProcess` implementation that allows simulating huge numbers of concurrent processes in the process-oriented world view (e.g. simulation of telecommunication compatibilities). It is based on the concept of continuations and coroutines, which are not included in the Java standard libraries so far. However, the Apache library JavaFlow fills this gap by providing the concept of continuations. This library is licensed under ASL 2.0. The continuation class permits the implementation of custom coroutines that run mutually exclusively in a single thread. Testing this implementation, we aborted the simulation run manually, after reaching 2.5 million concurrently existing simulation processes.
Unfortunately, this solution requires byte code re-engineering, not only of the simulation model, but of all classes that may appear on the method stack of a coroutine. Although this can be automated based on e.g. an Ant task, we do not provide this functionality in our standard deployment since compiling becomes unnecessarily complicated for learners and most users. However, all necessary classes, libraries and a build script including byte-code re-engineering are obtainable from our SVN repository for those interested in the alternative simulation process implementation delineated above.

Processing Chains

Model logic frequently consists of repetitive tasks to be executed by multiple model components in a similar way. For example, consider work stations in a typical production line processing items and forwarding them to the next stations. Stations may e.g. differ in processing and setup time distributions. Efficient modeling of such systems may be conducted by providing complex, integrated components specifically designed for the relevant application domain, as e.g. described above for the example of harbor logistics. For application areas, however, in which such solutions do not (yet) exist, a level of abstraction between basic event/process modeling and domain-specific components is desirable, facilitating a compact and redundance-free representation of models containing similar or repetitive tasks.
To address this need, the DESMO-J core contains a set of *higher-level modeling components* since its earliest versions, e.g. finite resource pools or buffers: if a pool or buffer contains fewer resources than requested by a consuming simulation process, the process is implicitly passivated until its demand is met. The user needs not explicitly activate the process at the right instant of time; instead, s/he may proceed in process description, assuming the resource has been acquired successfully.
The *chaining* components (package `desmoj.extensions.chaining`) are higher-level modeling components no longer necessarily requiring an event or process description of the model behavior at all: such components – representing sources, work stations, sinks, mergers and splitters in a queuing system – offer comprehensive means of parameterization (e.g. a workstation: buffer size, number of parallel processors and distributions of setup time, processing time, recovery time, transport time) and, most importantly, they can be chained to each other: e.g. the output of a source is assumed forwarded to a work station. This permits describing basic production or queueing systems with very few lines of code. At the same time, the implementation remains flexible, as more complex work station behavior can be introduced based on subclassing. Flexibility also includes interaction with non-chaining components: all entities whose types do match can be fed into a work station, not only those created by the chaining source. On the other side, the description of what happens with the output of a station is encapsulated as event, which defaults to a forward to the next station; an alternative

event provided by the user may for example divert some entities to another station or cause a re-entry to the current station with a certain probability.

Recording and Logging

In various application areas, it may be of interest to examine particular experiment phases in detail, e.g. transition from a warm-up phase to a steady state phase or disruptions of steady state phases.
Although DESMO-J's simulation trace output may be turned on and off at any time during an experiment, the resulting file by default only contains the most important data, like model, time, the acting entity, process or event and the action itself, e.g. scheduling entities or activating/passivating processes, queue manipulation, random number access or statistical updates.
If certain constellations of simulation objects have to be explored in detail, the output trace files are a) too coarse, b) safely accessible only after an experiment has finished and c) not in an easily machine-readable format.
To address these shortcomings, the concept of *recording*s was introduced. A recording contains a sequence of observations of any type of simulation object, e.g. `double` or `long` values, `String`s, entire `Entity` objects or even the whole state of a waiting `Queue`, over consecutive simulation time instants.
A recording may be paused or resumed at any time during a simulation experiment. Its contained sequence of copies of original simulation objects is ready for analysis by further algorithms at any point of simulation time.
Recordings are typed, and for clarity we recommend to employ one recording per individual observation variable. Hence, examining the interdependencies of *n* simulation objects leads to *n* recordings. For ease of use, any number of recordings may be linked to a *recorder*. A recorder controls the recordings that registered with it. Pausing and resuming a recorder is passed on to all of its assigned recordings, enabling the experimenter to centrally handle whole groups of recordings. Thus, entire interconnected segments of a model may be recorded, e.g. when observing critical model behavior.
Recordings are created volatilely in memory, with no default mechanism of persistence. As it may be of interest to study recordings after simulation has finished or to visualize recordings during simulation execution, *loggers* may register at recordings. Whenever a recording is updated with an observation, it forwards a copy of the observation together with the current simulation time stamp to all registered loggers. A concrete logger (derived from the abstract class `Logger`) may implement any desirable behavior in order to process the observed data on-line during an experiment run. Applications include – but are not limited to – writing observation objects to files (Text, XML, CSV etc.), storing observations in databases, conducting model-dependent computations on observation streams, representing observation object states in specially tailored online GUIs or simply printing observations on the console, for tracing und debugging purposes.
In all of these scenarios, the simulation framework does not need to contain methods or knowledge of how to process observations in the context of files, databases, GUIs etc., this is left to the registered corresponding loggers. This IOC approach ("inversion of control") has only been used internally in DESMO-J to date, e.g. in reporting and statistics, but so far had not been offered as an interface to arbitrary downstream functionality or external applications.
Now, a comfortable mechanism for easier unidirectional integration with external software components or functional extensions is available.

Risk Metrics

Until recently, simulation dynamics could only be captured in DESMO-J standard statistics, regarding observation state variables of interest. These statistics typically accomplish counting of (arriving or leaving) entities, tallies or histograms of waiting times, or time weighted accumulation of queue length or resource utilization.
Most standard statistics comprise mean, minimum, maximum and standard deviation values; histograms additionally offer a visual impression of state distribution of observation variables.
Nevertheless, none of these statistics gives an idea of e.g. how fast the state of an observation variable shifts from the median observed state to an extreme state or how typical pathways of fluctuations in steady state phases can be characterized.
In order to give better insight into the potential and risk of model dynamics, the four most accepted risk metrics from the application field of Quantitative Finance have been generalized and transferred to discrete event simulation (Koors and Page 2012). Namely, these metrics are Semi-Variance, Value at Risk, Expected Shortfall and Drawdown.
Semi-Variance measures state deviation, accounting only for positive resp. negative deviation from the mean state. If positive and negative Semi-Variance differ significantly from each other, model dynamics towards higher or lower observation variable states is distributed asymmetrically and should be examined carefully.
Value at Risk was generalized to the metric Delta at Risk (DaR). DaR quantifies the maximum extent of state change expected (i.e. risk, in terms of quantitative finance) with regard to a chosen confidence level α, after a certain time interval, and according to four well-defined reference states of an observation variable (minimum, median, maximum and most frequent observed states). A typical conclusion based on the simulation report could be "Starting with an empty queue and given a confidence level of 99%, the queue length will not exceed *z* entities after 1 hour of simulated wall clock time".
Expected Shortfall was generalized to the metric Conditional Delta at Risk (CDaR). CDaR expresses the expected mean state for the α fraction of cases where DaR is exceeded. A typical finding based on the simulation report could be "If, starting with an empty queue and

given a confidence level of 99%, the queue length exceeds the Delta at Risk value of z entities after 1 hour of simulated wall clock time, then an average queue length of $z + c$ entities can be expected". Hence, CDaR is a metric for estimating the extent of state movement in unlikely cases of extreme events (in terms of the choice of α).

In steady state phases, Drawdowns and RunUps describe the magnitude and time structure of interim downward or upward phases in observation variable state, until the median or most frequent state is reached again. This metric and its various self-elaborated derivatives and analysis options give a good insight into distribution, characteristics and individual pathways of both usual and extraordinary model dynamics.

The set of four risk metrics described above depends on the same data basis, and especially Delta at Risk and Conditional Delta at Risk share the same basic time series. As an alternative type of statistics implementation, none of these metrics saves its own internal data, like DESMO-J standard statistics do. Instead, all four metrics refer to commonly shared recordings (see section above) set by the modeller. Thus, a noticeable amount of memory space and processing time is saved by avoiding redundant collection of basic statistic state observations.

All in all, the newly introduced risk metrics facilitate a better assessment of risky or desirable model dynamics than the DESMO-J standard statistics could provide to the experimenter before.

SUMMARY

This paper's aim was to clarify the state of the art in open source simulation libraries by exemplarily presenting functional range and usability of DESMO-J, including a comparison to other Java based simulation libraries. We have pointed out technical improvements like real time capability, recording and logging functionality, which is useful for coupling simulation models to external systems. An alternative process implementation allows concurrent existence of millions of process entities. We have presented two alternatives of automatically generating a "DESMO.NET" out of DESMO-J Java sources. Moreover, enhancements in modeling like processing chains and further analysis functionality like generalized risk metrics have been delineated.

We also have introduced two visualization extensions. While the 2D visualization package can easily be adapted to existing models, the 3D visualization package needs more implementation effort, as 3D shapes for entities are required.

Describing container terminal simulation and business process modeling, we gave two examples how domain-specific simulation applications can build upon DESMO-J. Useful features include implementation of graphical editors, customizing simulation reports as desired and embedding DESMO-J models into external systems.

Despite a variety of new features being introduced, an important design criterion is the backward compatibility of DESMO-J, ensuring models built upon older versions of DESMO-J will also work with the newest version.

Finally, we emphasize that DESMO-J is a powerful, flexible and easily usable simulation framework, recommending it to the reader as a tool to consider for the next simulation study.

ACKNOWLEDGEMENT

We would like to thank Sönke Claasen, Nicolas Denz, Johannes Haan, Tim Janz, Gunnar Kiesel, Felix Klückmann, Sven Kruse, Tim Lechler, Christian Mentz, Ruth Meyer, Christian Müller, Olaf Neidhard, Eugenia Neufeld, Thorsten Planeth, Thomas Schniewind, Fred Sun, Malte Unkrig and Jörg Willig for providing their work to the DESMO-J community.

REFERENCES

Asperen, E. van; R. Dekker; M. Polman; and H. de Swaan Arons. 2004. "Arrival processes in port modeling: insights from a case study". Available at http://publishing.eur.nl/ir/repub/asset/1275. Accessed 2013-02-13.

Banks, J.; J.S. Carson II; B.L. Nelson; and D.M. Nicol. 2010. *Discrete-event system simulation.* Pearson, Upper Saddle River NJ.

Bornhöft, K.; B. Page; and H. Schütt. 2010. "Modelling of innovative Technologies for Container Terminal Yard Stacking Systems using an Object-Oriented Simulation Framework". In *The International Workshop on Applied Modelling and Simulation.* Rio de Janeiro.

Brandt, C. 2008. "Entwurf und Implementierung eines Frameworks zur Entwicklung von Containerterminal-Gesamtmodellen mit DESMO-J". Master's thesis, University of Hamburg, Hamburg, Germany.

Buss, A. 2012. Simulation software *SimKit*. Naval Postgraduate School, Monterey. Available at http://diana.nps.edu/Simkit. Accessed 2013-02-13.

Computer Science Group. 2009. Simulation software *JavaDEMOS*. University of Duisburg-Essen. Available at http://sysmod.icb.uni-due.de/index.php?id=52. Accessed 2013-02-13.

Frijters, J. 2012. Java implementation *IKVM*. Available at http://www.ikvm.net/. Accessed 2013-02-13.

Göbel, J.; A.E. Krzesinski; and B. Page. 2009. "The Discrete Event Simulation Framework DESMO-J and its Application to the Java-based Simulation of Mobile Ad Hoc Networks". In *Proceedings of the 21st European Modeling and Simulation Symposium, Vol. I,* R.M. Aguilar, A.G. Bruzzone; and M.A. Piera (Eds.). La Laguna, Spain (Sep).

Henesey, L.; K. Aslam; and M. Khurum. 2006. "Coordination of Automated Guided Vehicle in a Container Terminal". In *Proceedings of 5th International Conference on Computer Applications and Information Technology in the Maritime Industries.* Oud Poelgeest, Netherlands.

Joschko, P.; J. Haan; T. Janz; and B. Page. 2012. "Business Process Simulation with IYOPRO und DESMO-J". In *Proceedings of the International Workshop on Applied Modelling and Simulation,* Bruzzone, Buck, Cayirci, Longo (Eds.). Rome, Italy (Sep).

Joschko, P.; C. Brandt; and B. Page. 2009. "Combining Logistic Container Terminal Simulation and Device Emulation using an Open-Source Java Framework". In *Proceedings of the International Conference on Harbor, Maritime & Multimodal Logistic Modelling and Simula-*

tion, Number c, A.G. Bruzzone, Cunha, Martínez; and Merkuryev (Eds.). La Laguna, Spain.
Joschko, P.; B. Page; and V. Wohlgemuth. 2009. "Combination of job oriented simulation with ecological material flow analysis as integrated analysis tool for business production processes". In *Proceedings of the 2009 Winter Simulation Conference,* A.G. Bruzzone et al. (Ed.). Austin, Texas (May).
Kačer, J. 2006. Simulation software *J-Sim*. University of West Bohemia. Available at http://www.j-sim.zcu.cz/. Accessed 2013-02-13.
Klückmann, F. 2009. "Realzeitsynchrone Simulation – Begriffe, Anwendungen und exemplarische Umsetzung anhand des Simulationsframework DESMO-J". Master's thesis, University of Hamburg, Hamburg, Germany.
Knaak, N.; S. Kruse; and B. Page. 2006. "An agent-based simulation tool for modelling sustainable logistics systems". In *Proceedings of the iEMSs Third Biennial Meeting: Summit on Environmental Modelling and Software. International Environmental Modelling and Software Society.* Burlington, Vermont.
Koors, A. and B. Page. 2012. "Transfer and Generalisation of Financial Risk Metrics to Discrete Event Simulation". In *Proceedings of the International Workshop on Applied Modelling and Simulation,* Bruzzone, Buck, Cayirci, Longo (Eds.). Rome, Italy (Sep).
Kühnlenz, C.-M. 2011. "Interaktion von Simulationswerkzeugen mit ERP-Systemen – Konzeption und Realisierung von Interaktionsworkflows am Beispiel von DESMO-J und Infor ERP COM". Master's thesis, University of Hamburg, Hamburg, Germany.
L'Ecuyer, P. 2012. Simulation software *SSJ*. Université de Montréal. Available at http://www.iro.umontreal.ca/~simardr/ssj/indexe.html. Accessed 2013-02-13.
Lee, E.A. 2011. Simulation software *PtolemyII*. University of Berkeley. Available at http://ptolemy.berkeley.edu/. Accessed 2013-02-13.
Müller, C. 2011. Additional DESMO-J 2D Animation resources. Technical University of Applied Sciences, Wildau, Germany. Available at http://www.wi-bw.tfh-wildau.de/~cmueller/SimulationAnimation/. Accessed 2013-02-13.
Page, B. and E. Neufeld. 2003. "Extending an object-oriented discrete event simulation framework in Java for harbour logistics". In *International Workshop on Harbour, Maritime and Multimodal Logistics Modelling and Simulation.* Riga, Latvia.
Page, B. and W. Kreutzer. 2005. *The Java Simulation Handbook – Simulating Discrete Event Systems with UML and Java.* Shaker, Aachen, Germany.
Page, B. 2013. Simulation software *DESMO-J*. University of Hamburg. Available at http://desmo-j.de. Accessed 2013-02-13.
Rossetti, M.D. 2013. Simulation software *JSL*. University of Arkansas. Available at http://www.uark.edu/~rossetti/research/research_interests/simulation/java_simulation_library_jsl/. Accessed 2013-02-13.
Schäfer, F. 2011. "Interaktion von Simulationswerkzeugen mit ERP-Systemen – Konzeption und Realisierung von Datenanalysen sowie technischen Schnittstellen am Beispiel von DESMO-J und Infor ERP COM". Master's thesis, University of Hamburg, Hamburg, Germany.
Sharpen. 2013. Eclipse plug-in for multi-platform development. Available at http://community.versant.com/Projects/html/projectspaces/db4o_product_design/sharpen.html. Accessed 2013-02-13.
Sun, F. 2010. "Raumkonzept und 3D-Visualisierung für die ereignis-diskrete Simulationsengine DESMO-J". Master's thesis, University of Hamburg, Hamburg, Germany.
Verbraeck, A. 2009. Simulation software *DSOL*. Delft University of Technology. Available at http://sk-3.tbm.tudelft.nl/simulation. Accessed 2013-02-13.

AUTHOR BIOGRAPHIES

JOHANNES GÖBEL holds a master in Information Systems from the University of Hamburg, at whose Modeling & Simulation research group he is scientific assistant and PhD candidate now; his research interests focus on discrete simulation and network optimization.

PHILIP JOSCHKO studied Computer Science at the University of Hamburg. He works as a scientific assistant and PhD candidate within the Modeling & Simulation workgroup of Prof. Dr. Page. Research interests are business process simulation, simulation software development and offshore wind parks. Since 2005 he takes part in improving DESMO-J. He applied DESMO-J in several simulation projects.

ARNE KOORS obtained his master degree in Computer Science from University of Hamburg, Germany. Since then he has been working as a software developer and management consultant in the manufacturing industry, primarily in the field of demand forecasting and planning. Furthermore, he works as a research associate and on his PhD thesis on financial strategy simulation in the Modeling & Simulation research group led by Prof. Dr. Page.

BERND PAGE holds degrees in Applied Computer Science from the Technical University of Berlin, Germany and from Stanford University, USA. As professor for Modeling & Simulation at the University of Hamburg he researches and teaches in Computer Simulation and Environmental Informatics. He is the head of the workgroup which developed DESMO-J and the author of several simulation books.

TOOL FOR DISCRETE EVENT SIMULATION IN MATLAB

Jaroslav Sklenar
Department of Statistics and Operations Research
University of Malta
Msida MSD 2080, Malta
E-mail: jaroslav.sklenar@um.edu.mt

ABSTRACT

The paper introduces a new tool for programmed discrete event simulation in Matlab. As Matlab's language became one of the most frequently taught languages for computations in mathematics, statistics, and operations research, we need a simple to use and fast to learn tool for creation of simple and medium-scale simulation models. Moreover we need a tool where the code is clearly visible and where all functions like generation of random numbers are directly under user's control. This is caused by the need to incorporate simulation models into various outer algorithms for repetitive experiments, variance reduction techniques, and simulation-based optimization. We believe that the tool satisfies the requirements. Basic ideas of its implementation are presented together with an example simulation of a queuing network and an optimization by simulation example.

KEY WORDS

Simulation Tools, Discrete Event Simulation, Queuing Systems, Matlab.

INTRODUCTION

One of the first decisions before starting building a simulation model is the nature of the simulation tool to be used. Or simply, will the simulation model be programmed (in a simulation language or a simulation library based on a general language), or will it be drawn by mouse by using a visual interactive tool? With respect to this fundamental decision we may identify two trends. For classical simulation applications like manufacturing, transportation, or similar described typically as queuing systems, programming is used less and less. For these systems the classical GPSS view of the world as represented by interactive tools like Arena, Simul8, Witness, etc. is satisfactory and programming simulation models of such systems is often considered as a waste of time and money. On the other hand there are areas where simulation techniques are becoming more and more important and where the classical view of entities passing through a block diagram does not work. It is for example stochastic programming, finance, stochastic integration, reinforcement learning to mention just a few. Also systems with dynamically changing behavior and topology fall into this category. In our situation there are two more arguments in favor of programmed simulation models where the user has full control over the model. In Statistics and OR courses we have recently introduced a study-unit called "Computational Methods in Statistics and OR" for students who are not supposed to be advanced programmers. In fact they know only basics of programming in Matlab. For the simulation part of this unit the obvious choice was an interactive simulation tool, in our case Arena (Kelton et al. 2006). Problems started with teaching Variance Reduction Techniques (L'Ecuyer 2007). Though some of these techniques are included in Arena and similar packages, we need to show their implementation. Another area where full control over the model is required is simulation-based optimization. There are optimization tools included in interactive simulation tools like OptQuest of Arena (Bradley 2007), but there is no feasible possibility to apply other than the built-in optimization algorithm and control over its working is very limited, leaving alone techniques like for example infeasibility detected by simulation. So to summarize, we need a simple to use and a simple to learn tool for creating discrete event simulation models in Matlab. Simulation models should take a form of a function that given model specification and run control arguments provides the required results as outputs. Such function can then be incorporated into other algorithms, in our case algorithms used in variance reduction and simulation-based optimization.

SIMULATION IN MATLAB

Support is needed for simulation models with continuous time and discrete behavior. Simulation of discrete time or timeless models typical in finance and stochastic programming (often called Monte Carlo Simulation) is from the time control point of view relatively easy and no special support in Matlab is needed. We are aware of two Matlab based discrete event simulation tools. SimEvents (Gray 2007) is a commercial interactive tool based on Simulink of Matlab. It belongs to the category of interactive tools with limited control over the model. MatlabDEVS2 (Deatcu 2003) is a tool created primarily as a support for research and education of abstract Zigler's DEVS theory, so its use is not practical in our case either. That's why it has been decided to create a new tool with simplicity and transparency being the main objectives. The tool is not supposed to be used for large-scale computationally demanding simulation studies.

Proceedings 27th European Conference on Modelling and Simulation ©ECMS Webjørn Rekdalsbakken, Robin T. Bye, Houxiang Zhang (Editors)
ISBN: 978-0-9564944-6-7 / ISBN: 978-0-9564944-7-4 (CD)

IMPLEMENTATION OF THE TOOL

These are the main facilities available in simulation languages and libraries:

- Time control (scheduling and canceling of future activities).
- Synchronization and communication of processes.
- Generation of random numbers from theoretical and empirical distributions.
- Automatic or user-friendly collection and evaluation of statistical data.
- Report generation.
- Control over the dynamically allocated memory.
- Facilities for user-friendly work with data structures used typically in discrete simulation models (queues).
- Diagnostics and facilities for observing model behavior.

The first and the most important decision is the time control paradigm. Though process oriented simulation has become a standard, we have decided to implement simpler "atomic" event oriented approach. It is much simpler to implement and the new tool is not supposed to be used for large-scale simulation studies that would benefit from more natural and advanced process view of the world. So processes are represented by sequences of events with no synchronization and communication support.

Matlab has many functions for generation of random numbers, so only few functions were written for missing theoretical distributions (Erlang, triangular) and for empirical table distribution.

For statistics two typical objects (accumulator and tally) were implemented together with supporting functions computing elementary descriptive statistics.

For reporting there are Matlab functions for presentation graphics and advanced statistics. Also memory control was left up to the Matlab engine.

So far three basic types of queues were implemented – FIFO, LIFO, and priority queue.

No support for model debugging is available; again we assume that the tool will not be used for large-scale or complex models.

To simplify use of the tool as much as possible, all models are created as separate functions with most of the code same for all models. The user just adds code at given places, mostly just few lines. All is clearly explained by comments, so the best way of creating models is by modifying available typical examples. Next chapters provide more details.

Time Control

We assume that the reader is familiar with the classical event-oriented paradigm based on the sequencing set made of event notices. In our case the event notices are made of the event time, unique event notice identification, user event number, and user event notice data. The sequencing set is made of four arrays whose *i*-th items represent the event notice *i*. The set is not ordered, scheduling places the new items at the end, next event to be activated is found by the *min* function of Matlab in the array of event times. Removing notices is done in usual Matlab way by storing empty values [ ] in the four items. This approach is certainly not very fast, but it is simple and it works satisfactorily. Current time is available in the system variable `s_time`. From the user's point of view 4 functions are available:

`function id = s_chedule(t,e,d)` schedules the event *e* at time *t* with user data *d*. It returns the event notice identification *id* assigned by the engine.

`function s_cancel(id)` removes the notice *id* from the sequencing set.

`function s_imulation` starts the simulation run. It is assumed that at least one event has been scheduled.

`function s_terminate` ends the simulation run by clearing the sequencing set.

In addition to the above functions, the user has to write the common user event function:

`function event(e,d,id)` that starts the event *e* with data *d* and identification *id*. It typically tests the event number *e* and activates the particular event functions. In addition to user events, there may be system events with negative numbers used by application-oriented additions to the basic tool – see later.

The simulation engine is the function `s_imulation` that repeatedly removes the next event notice from the sequencing set and activates either the user function `event` or a hidden system event function. The run ends when the empty sequencing set is detected.

Statistics

With respect to time there are two types of statistics. Time dependent statistics (using Arena terminology *time-persistent statistics*) is based on time integrals. We call such statistical objects accumulators, typical example is the statistics on a queue length. The other type is statistics based only on a collection of assigned values (using Arena terminology *counter statistics*). We call such statistical objects tallies, typical example is the statistics on waiting time in a queue. The following functions are available:

`function s_tupdate(t,x)` updates the tally *t* by the value *x*. The function keeps the minimum and the maximum values, the sum of assigned values, the sum of squared assigned values needed to compute the variance and the number of updates.

`function [mean,min,max,variance,updates] = s_tallystat(t)` returns the descriptive statistics on tally *t*.

`function s_aupdateto(a,x)` updates accumulator *a* to the value *x*. Call to this function replaces the assignment $a = x$.

`function s_aupdateby(a,x)` updates accumulator *a* by the value *x*. Call to this function replaces the assignment $a = a+x$. Both functions keep the minimum and the maximum values, the time integral and the time integral of squared assigned values needed to compute the variance. Both integrals are exact because they are made of sums of rectangular areas.

`function [mean,min,max,variance,lastvalue] = s_accumstat(a)` returns the descriptive statistics on accumulator *a*.

All statistical activities except assignment of accumulator values start after a user-defined warming

up delay, for accumulators the user has to specify the initial values, mostly zeros.

Queues

Three usual types of queues (FIFO, LIFO, priority) with possibly limited capacity are implemented. Queues are represented by data structures with various fields used for statistics. Stored items are represented by the arrays of items structures, entry times, and priorities for priority queues. The following functions are available:

`function r = s_enqueue(q,i)` inserts the item *i* into the queue *q*. The output *r* specifies whether the insertion was successful (1) or not (0). Treatment of rejected arrivals is application dependent. Item data structure is specified by the user, the only compulsory field is *service* – the service duration when entering a queue. The implementation is very simple, for all types of queues the item is placed at the end of an array.

`function [i,wt] = s_remove(q)` removes the next item from the queue *q*. The outputs are the item *i* and its waiting time *wt*. For priority queue the item is found by the Matlab function *min* in the array that contains the priorities. For all queues the item is physically removed by storing the empty values in the arrays.

`function s_nowait(q)` is used for statistics to record not waiting items in the queue *q*.

`function [...] = s_questat(q)` returns the statistics on queue *q*. The outputs are: mean queue length, mean waiting time, mean waiting of those who waited and left, maximum queue length, maximum waiting time, attempted arrival rate, effective arrival rate, rate of rejections, probability that the queue is full, number of attempted arrivals, number of rejected arrivals, number of not waiting arrivals and duration of statistics collection.

Model Function Structure

Simulation models are written as functions with a fixed structure. The input and output arguments are defined by the user. These are the parts of the model that have to be included in the given order:

- System functions
- User model initialization
- System model initialization
- User model functionality

The two system parts are the same for all models and of course though not protected, they should not be modified. The two user parts can be any mixture of commands and local functions and of course any external functions can be called, typically functions for generation of random numbers. Anyway a very simple structure is suggested.

User Model Initialization

This part first tests the validity of model input arguments and initializes user model variables, if any. This optional code is of course totally application dependent. It is supposed to test the arguments of random number generators, array sizes, integrality, etc.

Next some system variables have to be initialized by the user. This is in fact a part of the model specification. Currently the following 8 system variables must be defined:

- Types of queues array. The items are 0/1/2 for FIFO, LIFO, and priority queues respectively.
- Maximum lengths of queues array. The items are non-negative integers or Inf for unlimited queues. Zero for pure overflow models is accepted.
- Numbers of parallel channels array. It is assumed that each queue is served by several identical parallel channels. These three arrays must have the same length, but they can be empty.
- Data structure that represents entities (customers) stored in queues. In addition to already mentioned compulsory field *service*, there must be also the field *priority* if priority queues are part of the model. Other fields are user-defined, like for example attributes representing the history of the entity, types of entities, etc.
- Data structure that represents the user part of event notices. If stations are used (see later), the compulsory fields are *station* and *channel* used by the system event *end of service*.
- Warming-up delay for statistics collection.
- Number of tallies used in the model.
- Initial values of accumulators used in the model.

User code of the model is split into two parts because the values of the above system variables are needed for the system model initialization that prepares the sequencing set, the queues, and all statistics for the simulation run.

User Model Functionality

This part of user code follows the classical event-oriented paradigm. After scheduling at least one event, typically first arrival(s), breakdowns, etc., the simulation run is started by calling the function `s_imulation` followed by the run evaluation, preferably implemented by another function. This function collects the statistics and assigns values to the model outputs.

As already mentioned the simulation engine repeatedly activates the user function `event` that tests the event notice data and activates appropriate event functions that represent the model behavior. So lexicographically this part of code is made of few lines followed by user functions.

Support for Queuing Systems

The tool is general; the only requirement is the possibility to express the model behavior in terms of events. Though the definition of the above 8 system variables has to be present, the values can be all empty, so there can be no queues in the models, no standard statistics, etc. Nevertheless typical application of discrete simulation is analysis and optimization of queuing systems, which is also our case. That's why we included a simple support that makes simulation of queuing networks simple and straightforward. We associate queues with a number of parallel channels

serving the entities from the queue. This makes the so called stations supported by the following functions:

`function r = s_arrival(q,c)` is an arrival of the customer *c* to the station (queue) *q*. The result *r* specifies the outcome (0 = lost (rejected), 1 = enqueued, 2 = served without waiting). The user has to decide what to do in case of rejection due the limited capacity.

`function s_eos(ed)` is a system function activated by the engine `s_imulation` that is transparent to the user. It is an end of service specified by the data part *ed* of the corresponding event notice. For this purpose, if stations are used in the model, there are the two compulsory fields *station* and *channel* in the event notice data. After all necessary updates and statistics collection the following function is activated.

`function customer_leaving(s,c)` is the user's activity associated with the end of service to customer *c* in station *s*. Typically there is some decision about the next service, a call to `s_arrival`, or leaving the network.

`function r = s_stop(s,c)` stops the channel *c* in station *s*. The result *r* specifies the channel status (0 = idle, 1 = busy (the operation is completed), 2 = was already suspended).

`function r = s_resume(s,c)` re-activates the channel *c* in station *s*. The result *r* specifies the channel status (0 = idle, 1 = busy, 2 = suspended). Warning is given for the first two cases.

Additional statistics provided for stations by the function `s_questat` is the mean number of working channels and their utilization. Due to possible suspensions (failures) there is no simple relationship between these two figures.

The above mentioned functionality of stations is enabled by using the system events, so far only end of service was implemented. System events have negative numbers, are activated by the engine and for the user they are transparent. Also note that the functions `s_arrival` and `customer_leaving` offer a sort of process-oriented view of the system dynamics. Call to `s_arrival` starts an internal process made of possible waiting in the queue and the service that ends when the customer appears as the argument in `customer_leaving`.

EXAMPLE SIMULATION

Figure 1 depicts the abstraction of a workshop where machines are adjusted by two operations that may be repeated. The service times are triangular, the intervals are uniform, branching probabilities and parameters of the distributions are given in the figure. All times are given in minutes. We assume that the numbers of machines waiting for the two operations are not limited. Moreover the facilities for both operations may break down. The mean times between failures are exponentially distributed with means 180 and 120 respectively. After breakdown the facilities are repaired in uniformly distributed times in [5,25] and [7,20] respectively. We need a simple statistics on the number *L* of machines in the workshop and the time *W* a machine spends in the workshop (for both mean, minimum, maximum, variance), and other usual performance parameters of the two stations.

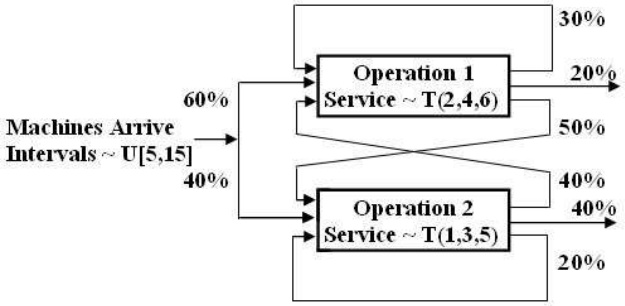

Figure 1. Workshop abstraction by a queuing network

The simulation model is implemented by the `function [W L Wmin Wmax Wvar Lmin Lmax Lvar] = exnet(duration,warming)` with self-explaining arguments and outputs. The function performs one simulation run and for simplicity the model parameters are directly included in the code. Next we give details on the two user parts of the model.

User initialization part

After a simple test of the two arguments, the following initialization of the 8 system variables is written:

```
s_types = [0 0];
s_maxq = [Inf Inf];
s_channels = [1 1];
s_item = struct('service',0,'arrival',0);
s_edata =
struct('station',0,'channel',0);
s_warming = warming;
s_tallies = 1;
s_accums = [0];
```

Referring to the text above we note that the model is made of two stations. Both queues are FIFO, unlimited, and served by single channels. Machines are represented by data structures that in addition to the compulsory *service* used to store the service time, contain the field *arrival* where the arrival time to the workshop is stored. Next data structure is the user part of event notices. Only the two compulsory fields are used. Warming up delay for statistics collection is given by the model argument; there is one tally for statistics on total network (sojourn) time and one accumulator initialized to zero for statistics on total number of machines in the workshop.

User Model Behavior Part

The following commands schedule the first arrival, the end of simulation run, and the first failures of the two stations. First arguments are the times of these events, the second arguments are their numbers. Then the engine is activated and the run is evaluated.

```
s_chedule(5 + 10*rand,1,s_edata);
s_chedule(duration,2,s_edata);
s_chedule(exprnd(180),3,s_edata);
s_chedule(exprnd(120),4,s_edata);
```

```
s_imulation;
evaluation;
```

Above commands are followed by user functions. The following one is activated by engine for each user event:

```
function event(enumber,data,id)
switch enumber
 case 1            % arrival to network
   nextarrival;
 case 2            % end of run
   s_terminate;
 case 3          % breakdown of station 1
   s_stop(1,1);
   s_chedule(s_time+5+25*rand,5,s_edata);
                   % end of repair at 1
 case 4          % breakdown of station 2
   s_stop(2,1);
   s_chedule(s_time+7+20*rand,6,s_edata);
                   % end of repair at 2
 case 5      % end of repair at station 1
   s_resume(1,1);

s_chedule(s_time+exprnd(180),3,s_edata);
         % next breakdown of station 1
 case 6      % end of repair at station 2
   s_resume(2,1);
 s_chedule(s_time+exprnd(120),4,s_edata);
         % next breakdown of station 2
 otherwise
 error(['Unknown event'...
         num2str(enumber)]);
end
end
```

We note that all events are so simple that only arrival (event number 1) is written as a separate function. End of run (2) terminates the run by clearing the sequencing set. Breakdowns (3, 4) stop the operation of the particular channel and schedule the end of repair. Ends of repairs (5, 6) resume the operation of the channel and schedule the next breakdown. The next function is the activity associated with arrivals:

```
function nextarrival
 s_aupdateby(1,1);
   % accumulator 1 = total # in network
 s_chedule(s_time+5+10*rand,1,s_edata);
   % next arrival after U[5,15]
 itm = s_item;     % machine created
 itm.arrival = s_time;
 if rand < 0.6
  itm.service = triangular(2,4,6,rand);
  s_arrival(1,itm);% arrival to station 1
 else
  itm.service = triangular(1,3,5,rand);
  s_arrival(2,itm);% arrival to station 2
 end
end
```

The first command increments the accumulator that collects the statistics on the total number of machines in the network. Then after scheduling the next arrival, the item/machine data structure is created and arrival time is recorded in it. After random branching, see Figure 1, the particular service time is generated and the actual arrival is done by calling the function `s_arrival` whose first argument is the station number. The next function is the activity associated with customers leaving the stations:

```
function customer_leaving(qn,itm)
r = rand;
switch qn
 case 1
  if r<0.3            % branching after 1
    itm.service = triangular(2,4,6,rand);
    s_arrival(1,itm); % arrival back to 1
  elseif r<0.5
    s_tupdate(1,s_time - itm.arrival);
      % departure, tally 1 = sojourn time
    s_aupdateby(1,-1);
      % accumulator 1 = total # in net
  else
    itm.service = triangular(1,3,5,rand);
    s_arrival(2,itm); % arrival to 2
  end
 case 2
  if r<0.2            % branching after 2
    itm.service = triangular(1,3,5,rand);
    s_arrival(2,itm); % arrival back to 2
  elseif r<0.6
    s_tupdate(1,s_time - itm.arrival);
      % departure, tally 1 = sojourn time
    s_aupdateby(1,-1);
      % accumulator 1 = total # in net
  else
    itm.service = triangular(2,4,6,rand);
    s_arrival(1,itm); % arrival to 1
  end
 otherwise
  error(['Wrong station number '...
    num2str(qn) ' in customer_leaving']);
 end
end
```

For both stations the branching decides whether the item proceeds to a station or leaves the network. If another service follows, the particular service time is generated followed by the arrival. If the item leaves the network, the tally for sojourn time is updated by the total time spent in the network and the accumulator for the total number of items in the network is decremented.

User run evaluation by the following function is very simple:

```
function evaluation
 [...] = s_questat(1)
 [...] = s_questat(2)
 [W,Wmin,Wmax,Wvar] = s_tallystat(1);
 [L,Lmin,Lmax,Lvar] = s_accumstat(1);
 LL = LQ1+LQ2+reff1+reff2;%L in other way
end
```

The first two commands get and display all available statistics on the two stations as explained above. The required model outputs are obtained from the tally and the accumulator. The last command is a check that computes the total number of items in the network from the two mean queue lengths and the two mean numbers of working channels that is the mean number of items being served.

The following is a formatted extract from outputs provided by a run of the length 100,000 minutes with

warming up delay 100 minutes (and 'twister' generator initialized to default initial state). Note that the two ways of obtaining L provide equal values. The run took about 16s (Pentium 4 CPU 3.2 GHz, 2GB RAM).

```
>>[W,L,Wmin,Wmax,Wvar,Lmin,Lmax,Lvar]=...
    exnet(100000,100)

LQ1=1.5111   WQ1=8.4847 ... util1=0.7125
LQ2=0.5123   WQ2=3.1998 ... util2=0.4802

LL = 3.2162

W = 32.1639          Wmin = 1.0890
Wmax = 472.9047      Wvar = 1.5051e+003

L = 3.2162           Lmin = 0
Lmax = 20            Lvar = 6.2687
>>
```

OPTIMIZATION BY SIMULATION EXAMPLE

Let's consider a hypothetical single queue single channel system with uniform distribution of inter-arrival intervals in [0, x] and uniform distribution of service duration in [0, y]. The values x and y are under our control. Arrival rate can be decreased, the service rate can be increased with associated costs $c_A x$ and c_B/y respectively. Then we consider waiting cost $c_W L_Q$ where L_Q is the average length of the queue. The constants c_A and c_W are costs per appropriate time unit, c_B is the cost per unit service rate. We want to find such values of x and y that would minimize the total cost, so we solve the problem:

$$\min\{c_W L_Q(x,y) + c_A x + c_B / y \mid x > y, x > 0, y > 0\}$$

The first constraint guarantees stability (traffic rate $\rho <$ 1). Moreover we assume an unconstrained ("not at a boundary") minimum because otherwise there would be no solution due to the open feasible set. The function $L_Q(x,y)$ can only be evaluated by simulation because we have a G/G/1 system with continuous distributions.

Creating a simulation model whose purpose is just obtaining the mean queue length is very easy. There is one station with one service channel, from user's point of view there is only one event type – customer arrival. The arrival function only schedules the next arrival and calls the system function `s_arrival` that moves the arriving customer to the station. The end of service is the system function, no user reaction is needed, so the function `customer_leaving` is left empty. The code is in fact a very simplified version of what has been described in the previous chapter. The results provided by the model are the standard quantitative parameters of single queue systems provided by the system function `s_questat`, but here only the mean queue length over time is used.

For optimization a supporting function was written whose arguments are the parameters of the system being optimized together with the length of each simulation run expressed as the number of simulated arrivals and the number of repeated runs. The function returns the total cost for given optimization variables x and y. Figure 2 depicts the objective function that is the total cost for c_W = 10, c_A = 1, and c_B = 30. The second figure is a horizontal view showing the very flat minimum that is unfortunately typical for similar optimization problems. The mesh in Figure 2 was created with the step 0.05 for x in [6,8] and y in [3,5]. So there are 1600 points, each of them was evaluated by 100 repetitions, each made of 20,000 simulated arrivals.

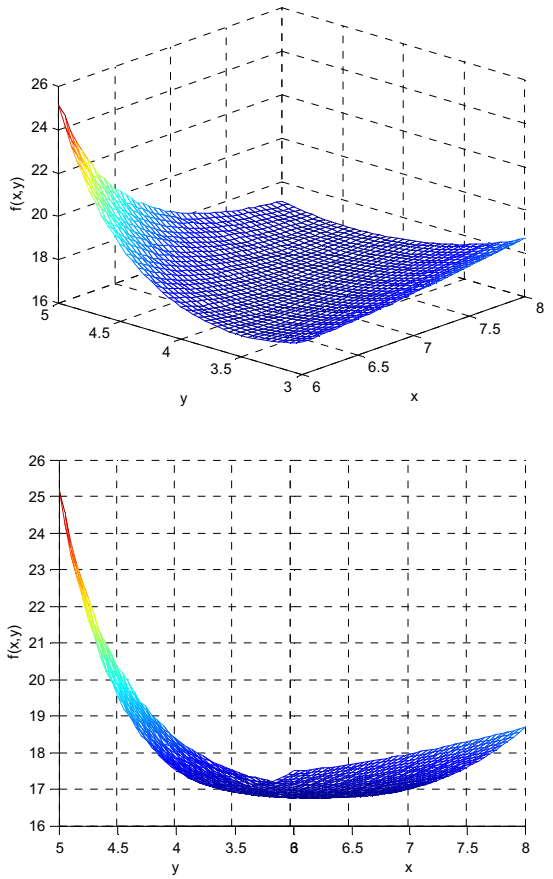

Figure 2. Objective function visualization

For optimization we used the standard Matlab function `fminsearch` that uses the robust moving simplex algorithm based only on function evaluations without making use of gradients. We believe that gradient evaluation by simulation would cause problems due to a very flat minimum and the well-known fact that at the optimum the gradient converges to zero. By the way the minimum was found at x = 7.22, y = 4.10 with total cost equal to 16.75 in our abstract currency units. Even for the very robust moving simplex algorithm it was necessary to decrease the argument and the objective function tolerance to 0.01. This is due to the fact, that simulation based evaluation of the objective function is never accurate and so the objective function evaluation is strictly speaking inconsistent with the obvious optimization algorithm assumption that for given x and y the objective is known exactly. So the result would be a chaotic movement of small simplexes (triangles in our case) close to the minimum.

CONCLUSION

After creating several simulation models, we believe that the objective has been met. The user parts of the

simulation models are very short, lucid, and very similar. The differences are of cause given by the specific behavior of particular models. Due to the choice of the event-oriented paradigm, the code resembles very much programs in simulation languages of this type, for example Simscript II. In fact the author has implemented the Simscript language for the Czechoslovak mainframes T200 in early seventies. Similar to these languages the user is relieved from "background" functionality like time control, queues management, statistics, etc. and can concentrate on the model behavior. All this is achieved without a need to learn a special-purpose simulation language, in fact intermediate Matlab programming skills are enough to create simulation models of medium size and complexity. As already mentioned, the whole model code is a single function with local functions, so though not recommended, it is possible to modify the system functions in any way. Having all under control and directly visible was in fact the main objective. There is no hidden random number generation, so implementation of various variance reduction techniques is not restricted. Single function simulation models can be incorporated in programs for various repetitive experiments, optimization algorithms, etc.
So far the tool exists in the first version intended for testing and evaluation. Of course there is a lot of room for its further improvement. Both sequencing set and the queues are implemented in a very simple inefficient way. Also security might become an issue; so far there are no restrictions. Though we believe that these drawbacks are not serious because the tool is not supposed to be applied in large simulation studies, its further development will address these issues.

REFERENCES

Bradley, A. 2007. "OptQuest for Arena - user's guide". Rockwell Automation Technologies, Inc.

Deatcu, C. "An object-oriented solution to ARGESIM comparison C6 - Emergency Department" with MATLAB-DEVS2". 2003, *Simulation News Europe,* 38/39, 56.

Gray, M.A. "Discrete event simulation: a review of SimEvents". 2007. *Computing in Science and Engineering*, 9(6), 62-66.

Kelton, W.D.; R.P. Sadowski; and D.A. Sadowski, 2006. *Simulation with Arena.* McGraw-Hill.

L'Ecuyer, P. "Variance reduction greatest hits". 2007. In *Proceedings of European Simulation and Modelling Conference ESM'2007*, Malta, 5-12.

Sklenar, J. "Discrete Simulation Language SIMSCRIPT T200". 1981. *Automatizace*, 4, 108-110.

The MathWorks, Inc. 2005. *SimEvents user's guide*.

The MathWorks, Inc. 2005. *Simulink: a program for simulating dynamic systems, user guide*.

AUTHOR BIOGRAPHY

JAROSLAV SKLENAR was born in Brno, now Czech Republic where he received his PhD degree from the Brno University of Technology. He worked there at the Department of Telecommunications where he specialized in simulation of various telecommunication systems. He implemented the Simscript language for the then Czechoslovak mainframes T200/300. He is also a user of the Simula language and the member of the ASU (Association of Simula Users) Council. From 1989 he teaches Operations Research at the Department of Statistics and OR of the Faculty of Science of the University of Malta, currently at the post of an Associated Professor. Apart from Simulation, his research is also oriented to Dynamic Programming and Stochastic Optimization in general. His web page can be found at http://staff.um.edu.mt/jskl1/. Visit it to find various on-line simulators and solvers.

MODELLING OF MIST REACTOR : EFFECT OF PACKING FRACTION AND FILM THICKNESS ON THE GROWTH OF HAIRY ROOTS

Manish Vashishtha* and Kumar Saurabh
Department of Chemical Engineering
Malaviya National Institute of Technology,
J.L.N Marg, Jaipur, India
*Corresponding E-mail: mvche.mnit@gmail.com

KEYWORDS

Nutrient Mist Reactor (NMR),differential equation, Hairy roots, Mist ON-OFF cycle, MATLAB.

ABSTRACT

Hairy roots have been successfully cultivated in a variety of reactor configurations. Nutrient mist reactors have been found specially suited to grow these roots because of its easy operation, high oxygen concentration, lack of shear, low pressure, ease in manipulating the gas composition, effective gas exchange in a densely growing biomass and ease of scaling up. In present work, a mathematical model has been developed to study the effect of variation of packing fraction and liquid film thickness on growth rate, liquid hold up and held up liquid concentration of nutrients. The simulation of developed model equations for the nutrient mist reactor is done with the help of MATLAB software.

INTRODUCTION

Higher plants are the source of varieties of biochemicals, which are produced from both primary and secondary metabolism. The metabolites produced from secondary metabolism are of immense importance because of their various important biological activities like antibiotic, insecticidal, hormonal properties, and valuable pharmacological and pharmaceutical activities [1]. In addition many of the secondary metabolites are also used as flavours, fragrances and agrochemicals. Various culture systems have been
adopted for the production of important secondary metabolites from the plants. Although there are some commercialized, industrial scale plant cell cultures [2], the biggest challenge of producing secondary metabolites from plant cell cultures is that secondary metabolites are generally produced by specialized cells and/or distinct developmental
stages [3]. Also, many products of interest are synthesized in organized tissues (roots), but not formed in suspension or callus culture (shoots, leaves). Due to this, a great deal of attention has been focussed on the root culture for the production of secondary metabolites.

HAIRY ROOT CULTURES

Hairy roots can be induced in susceptible plants by transformation with *Agrobacterium rhizogenes,* resulting in so called hairy root disease. These roots can be grown indefinitely with rapid growth rate and are less prone to genetic variation than callus or suspended cells. Therefore, hairy roots can offer a valuable root derived secondary metabolites that are useful in pharmaceuticals, cosmetics and food additives.

The cultivation of hairy roots in the bioreactors faces several challenges. When bioreactors are designed for mass cultivation of hairy roots at production scales, the physiology and morphology of hairy roots and their unusual rheological properties should be taken into consideration. One of them is to ensure sufficient mass transfer in the culture. Non-uniform distribution of biomass in the medium (and culture vessel) causes different technological problems. In addition to the hairy root growth restriction, the densely packed mass of roots causes nutrient and especially oxygen limitations, this leads to the reduction in secondary metabolite production or even to cell necrosis and autolysis.

Bioreactor's Design For Hairy Root Cultivation

For cultivation of hairy roots, variety of reactor configurations has been used by different workers [4, 5, 6]. Based on the continuous phase, reactors used to culture hairy roots can be roughly divided into three types: liquid phase, gas phase and hybrid reactors.

In the liquid phase reactors (e.g. Stirred tank reactors, bubble column reactor, airlift reactor and submerged convective flow reactors) roots are submerged in the medium in liquid phase reactors so the term 'submerged reactors' are also used for this type of reactors. The main drawbacks in cultivation of hairy roots using liquid phase reactors were damaging of roots resulting in callus formation and ultimately poor biomass production [7]. Also the oxygen deficiency due to mass transport limitation is a growth limiting factor in these liquid phase reactors.

In gas phase reactors (e.g. Trickle bed reactor, droplet phase and nutrient mist reactors (NMR)), the roots are exposed to air or other gas mixtures. Nutrients (medium)

Proceedings 27th European Conference on Modelling and Simulation ©ECMS Webjørn Rekdalsbakken, Robin T. Bye, Houxiang Zhang (Editors)
ISBN: 978-0-9564944-6-7 / ISBN: 978-0-9564944-7-4 (CD)

are usually delivered to roots as droplets. However, there is considerable variation in size of droplets used in different gas phase bioreactors. For NMR, using ultrasonic transducers, the droplet size is usually micron scale (0.5- 30 μm) [8]. For trickle bed or other gas phase reactors, using spray nozzles, the size of droplets may be much larger [9]. Since the continuous phase is gas, the roots must be immobilized in the reactors. The disadvantage of gas phase reactors is that there is no way to uniformly distribute the roots in the growth chamber without manual loading.

The problems associated with gas phase reactors can be overcome by using hybrid reactors. Here, the reactors are firstly run as a bubble column reactor in order to suspend, distribute and attach roots to the packing rings in the reactors. After two weeks of growth, root's clumps were dense and the reactor was switched to a trickle bed operation, thus exposing roots to a gas environment [10].

Nutrient Mist Reactor

Nutrient mist reactors (NMR) are basically a gas phase reactor. It consists of a mist generating system, a culture medium reservoir, a peristaltic liquid pump, a filtered air supply, a gas flow meter, a timer to regulate the misting time and a culture chamber. Some supporting means are also required by many of the NMR to support the suspended roots in the growth chamber. The successful use of various design of mist reactors have been reported by many scientists [8, 11]. In NMR, the hairy root culture is dispersed in an air phase by immobilizing on the mesh support and the liquid medium is introduced in the reactor in the form of mist of very small droplet size (0.5-30 μm). The very small size mist droplets are generated by an ultrasonic transducer and these mist droplets are carried to the bed by air as opposed to being dropped onto the bed. Because of such arrangement, there is an even distribution of liquid media (nutrients) throughout the root bed and there is less liquid hold up. However there is considerable variation in the size of droplets.

While comparing the performance and operation of NMR (for the cultivation of hairy roots) with other possible reactor's designs, it was found that they offer definite advantage over other reactor configurations such as ease of operation, high dissolved oxygen tension present in the mist and ease of scale up.

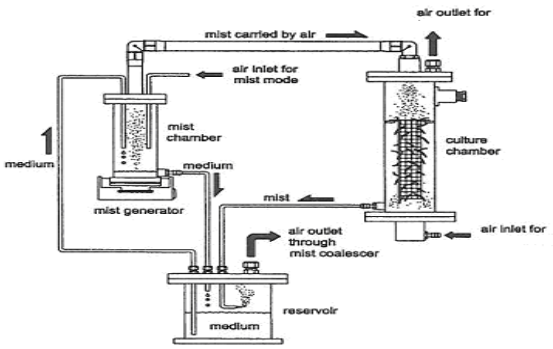

Figure 1: Flow Diagram Of Mist Reactor [11]

The comparison between NMR with various bioreactors for the cultivation of hairy roots was initially done by P. J. Whitney [12]. The tissue in NMR is continuously bathed in nutrient mist, providing an environment for rapid replenishment of nutrients as well as removal of toxic by-products. Also the nutrient mist can be dispersed homogeneously within the culture chamber, eliminating the need of mechanical agitation and thereby reducing the shear stress. Also the carrier gas for nutrient mist can consist of any gas mixture, enabling physiological studies of gaseous environments to be performed.

MATHEMATICAL MODEL

The various factors affecting the performance of NMR were firstly described by Wyslouzil et al. [13]. The inherent assumptions of filter models were valid in the bioreactors for the description of particle capture efficiency (η) by the root bed. The particle capture efficiency (η), which is the ratio of the liquid volume captured by the hairy root bed to the total volume of mist fed per unit time, represents the overall effect of the following three contributions (i) diffusion (capture due to the random motion of the droplets), (ii) interception (capture due to the particle's size), and (iii) impaction (capture due to the particle's inertia). The capture efficiency of root bed generally increases with an increase in droplet diameter.

THEORY AND CONCEPTS

An important controlling parameter for the operation of NMR is drainage rate. The effect of drainage rate using logarithmic and linear drainage models have been studied by Ranjan et al. [14]. In the linear model, the drainage rate is proportional to the difference between the specific liquid holdup at any time and the liquid holdup at saturation ($Y - Y_{sat}$). In the logarithmic model, it is proportional to the logarithmic difference between the liquid holdup at any time and the liquid accumulated at saturation [$\ln(Y) - \ln(Y_{sat})$]. The proportionality constant in either case has to be determined by fitting the model to data gathered from actual drainage experiments performed on similar beds. Another important parameter that affects the NMR performance is packing fraction (P_f) of root bed. Roots in NMR are often too sparsely packed to capture mist particles efficiently and therefore, cannot meet the nutrient demands required to maintain high growth rates. With increase in initial packing fraction, growth rates of A. annua hairy roots increased significantly [15] as shown in **Figure 2**.

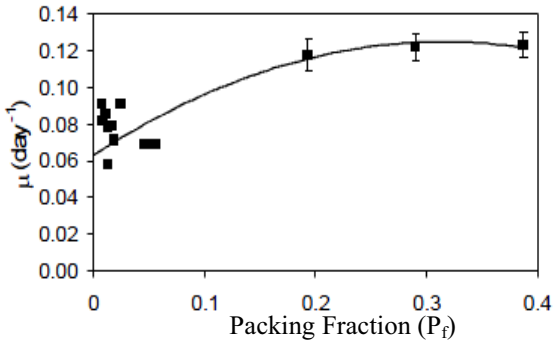

Figure 2: Effect Of Initial Packing Fraction On The Growth Rate Of Transformed Roots Of A. Annua Grown In The Small Mist Reactor [15].

Assumptions

The following assumptions have been made for the development of model equations used in present analysis of NMR.

1. There is complete mixing in the held up liquid.
2. The distribution of liquid over the root surface is uniform.
3. The structure of hairy root is assumed as cylinder and the whole root bed is also treated as cylinder.
4. The nutrient consumption by the growing roots can be taken to be proportional to dry mass of the root.
5. There is a constant capture efficiency of nutrients by the roots.
6. Linear drainage rate characteristics.
7. The combined effect of nutrient mass transfer and resistance provided by the growing film thickness with increased feed flow rate is taken to be negligible.

Development Of Mathematical Model

Model equations for a NMR can be developed by applying the mass and component balance across the root bed for mist-ON and mist-OFF cycles. Also the equation for the growth rate of roots can also be developed by considering Monad equation. Mist deposition is controlled by the capture of the liquid droplets by the root bed and determined by the capture efficiency. The capture efficiency (η) can be defined as the volume of the liquid captured by the root bed to the total volume of the mist per unit time.

Various data from different researches suggest that there should be an optimum misting cycle to achieve maximum growth of roots in NMR. Mist is deposited during the ON cycle of the reactor and the deposited liquid is then drained during the OFF cycle. During ON cycle, the liquid holdup will be distributed as layers of liquid over the roots. The nutrients in this liquid layer, such as sugar, are never depleted in the liquid phase, due to continuous fresh supply from the incoming mist. Thus, in the ON cycle, growth is most likely to be arrested by the mass transfer limitations of the gas phase nutrients through the liquid layer. During OFF cycle, the liquid layer gets continuously thinner (due to drainage) and depleted (due to uptake of nutrients by the roots). The ON and OFF cycles are schematically shown in **Figure 3 and 4** respectively.

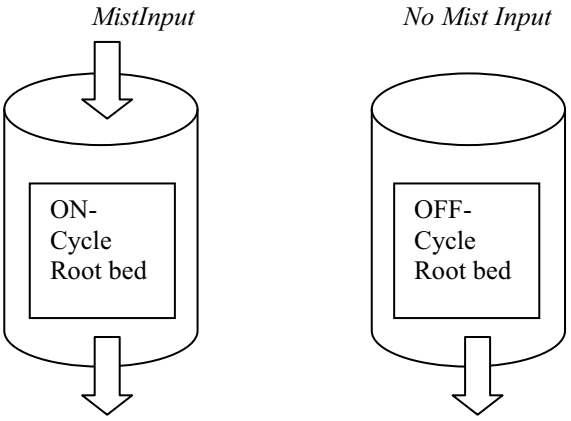

Figure 3 Figure 4

Figure 3 And 4: Schematic Diagram For The Mass Balance Across The Root Bed During ON Cycle And OFF Cycle Respectively.

The input and output terms for the mist in an NMR can be mathematically expressed as

Specific flow rate of mist into root bed

$$= \eta Q_0 \left(\frac{m_t}{m_0} \right)^{\alpha} \quad \text{..... (1)}$$

The linear drainage rate of mist

$= K_2 (Y - Y_{sat})$ ..... (2)

The value of exponent α for cylindrical root bed for the two extremes cases of size of liquid droplets i.e. for small droplets and large droplets are calculated and found to be **0** and **-1/2** respectively.

The rate of nutrient consumption by the roots can be derived by developing the equation for diffusion of mist per unit time per unit mass of the roots. Thus,

Rate of nutrient consumption by the roots

$$= \left(\frac{4D}{L_f d\rho} \right) (C - C_m) z \,.. \quad \text{.... (3)}$$

The equation for growth rate of roots growing inside the NMR is based on Monad model and can be represented by first order kinetics,

Growth rate of roots

$$\frac{dm_t}{dt} = \mu m_t \quad \text{..... (4)}$$

Growth rate of roots per unit mass of the roots:

$$\mu = \frac{1}{m_t}\frac{dm_t}{dt} \quad \text{..... (5)}$$

There is only a partial intake of nutrients by roots. Let this fraction of diffused nutrients be K_1. Therefore, combining equations 3-5 yield

$$\frac{dm_t}{dt} = \left(\frac{4DK_1}{L_f d\rho}\right)(C - C_m)m_t \quad \text{.....(6)}$$

It is clear from Eq. 6 that the specific growth rate is dependent on diffusivity and concentration of nutrients and root bed parameters.

From the experimental findings of Towler et al. (2007), it was clear that the growth rate of hairy roots in the NMR is a strong function of packing fraction (P_f) of root bed. The experimental data showing variation of growth rate with varying packing fraction of root bed is tabulated below.

Table 1: Experimental Data Showing Variation Of Growth Rate With Packing Fraction [15]

Packing fraction (P_f)	0.01	0.12	0.2	0.3	0.39
Growth rate (μ)	0.07	0.098	0.108	0.12	0.119

The derivation of mathematical equation showing relation between P_f and μ is done by method of best fitting of curve. The following two equations were obtained. One is logarithmic and other is linear equation.

Logarithmic Equation

$\mu = 0.0137(\ln P_f) + 0.1318$ **.....**(7)

Linear Equation

$\mu = 0.128P_f + 0.0767$ **.....**(8)

The mathematical relation between growth rate of roots and liquid film thickness (L_f) can be obtained by suitable manipulation of equation 4 and 6, which gives

$$\mu \propto \frac{4DC}{Lf\rho d} \quad \text{..... (9)}$$

From the above equation, it is clear that the growth rate of roots varies with varying thickness of liquid film.

The equation for the ON cycle in an NMR can be derived by consideringoverall liquid balance per unit mass of the root bed which can be written as

Rate of mist retained in the reactor = Input – Drainage

Putting values from Equation 1 and 2 in above equation gives

$$\frac{dY}{dt} = \eta Q_0\left(\frac{m_t}{m_0}\right)^{\alpha} - K_2(Y - Y_{sat}) \quad \text{.....(10)}$$

The component balance when applied for the unit mass of root yields

$$\frac{d(YC)}{dt} = \eta Q_0\left(\frac{m_t}{m_0}\right)^{\alpha} C_0 - K_2(Y - Y_{sat})C - \left(\frac{4D}{L_f d\rho}\right)(C - C_m) \quad \text{.....(11)}$$

Further solving the above equation and putting the value from Eq. 10 gives

$$\frac{dC}{dt} = \frac{\eta Q_0\left(\frac{m_t}{m_0}\right)^{\alpha}}{Y}(C_0 - C) - \frac{1}{Y}\left(\frac{4D}{L_f d\rho}\right)(C - C_m) \quad \text{.....(12)}$$

Eq. 10 and Eq. 12 represents the specific liquid hold up profile and concentration profile at time t for mist-ON cycle respectively.

Similarly for the OFF cycle the equation can be derived, since the flow rate of feed during the OFF cycle becomes zero as the feed supply is stopped, hence Eq. 10 and Eq. 12 becomes;

$$\frac{dY}{dt} = -K_2(Y - Y_{sat}) \quad \text{.....(13)}$$

$$\frac{dC}{dt} = -\frac{1}{Y}\left(\frac{4D}{L_f d\rho}\right)(C - C_m) \quad \text{.....(14)}$$

Eq. 13 and Eq. 14 represents the specific liquid hold up profile and concentration profile at time t for mist-OFF cycle respectively.

Numerical Simulation And Values Of Parameters

Solutions for mist ON - OFF cycles were obtained by integrating the set of coupled ordinary differential equations (ODEs) by ODE45 (an inbuilt ode solver) using MATLAB (version 7.12, Release name R2011a). The ode45 solver uses a variable step Runge-Kutta procedure. The numerical solver ODE45 combines a fourth order method and fifth order method, both of which are similar to the classical fourth order Runge-Kutta (RK) method. The modified RK method varies the step size, choosing the step size at each step in an attempt to achieve the desired accuracy.For the evaluation of the performance of NMR, numerical values for model parameters were taken from the literature [13, 15, 16]. Numerical values were chosen within a practical range for the root culture system. The chosen parameter values are Q_0 = 2.11 ml/day-mg, C_0 = 50 mg/ml, m_0 = 600 mg, μ = 0.2 per day, K_2 = 4 per day, Y_{Sat} = 0.01ml/mg, C_m = 10 mg/ml, D = 0.72 mm^2/day, η = 0.1, α = -0.5, ρ = 1000 mg/ml, d = 1 mm and L_f = 0.1 mm.

DISCUSSION OF RESULTS

The numerical results of the modelled equation for growth rate of roots inside the NMR is presented in **Figure 5** which shows the growth rate of roots with time. It was found that there is an exponential growth of roots with time.

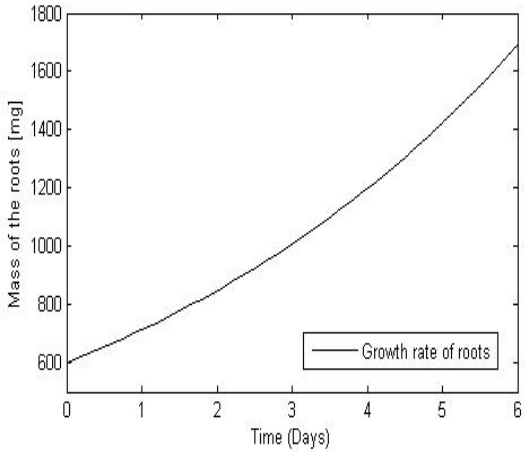

Figure 5: Variation Of Mass Of Root With Time In Mist Reactor

The experimental findings from the published literature of Towler et al. have been shown in **Figure 6**. By comparing figure 5 and 6, it can be seen that there is a close resemblance of the present model with the experimental data of *A. Annua* rootgrowth in the NMR (Towler et al.). This resemblance confirms the practical applicability of the present model.

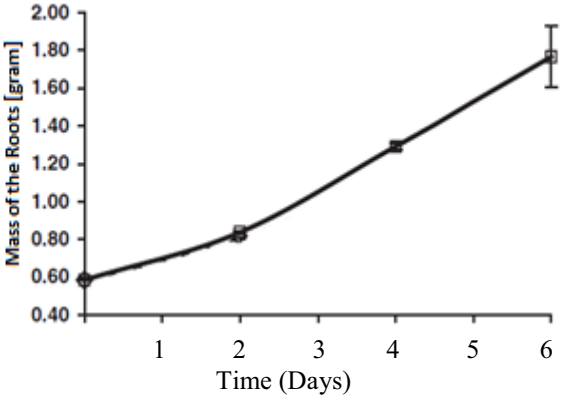

Figure 6: Experimental Finding For Growth Rate Of A. Annua In NMR From Literature [15].

Study Of Effect Of Packing Fraction (P_f) On Nmr Performance

The effect of P_f on growth rate is shown in **Figure 7** which presents the linear variation of mass of roots (growth of roots) with time for different packing fraction of root bed. Here, top to bottom lines correspond to P_f = 0.71, 0.60, 0.45 and 0.25 respectively. The value of other parameters are Q_0 = 2.11 ml/day-mg, C_0 = 50 mg/mldensity =1000mg/ml, m_0 = 600 mg, μ = 0.2 per day, K_1 = 0.3 per day, C_m = 10 mg/ml, D= 0.72 mm^2/day,L_f = 0.2 mm and d = 1mm. From this figure it is clear that with increasing value of packing fraction of root bed, the growth rate increases.

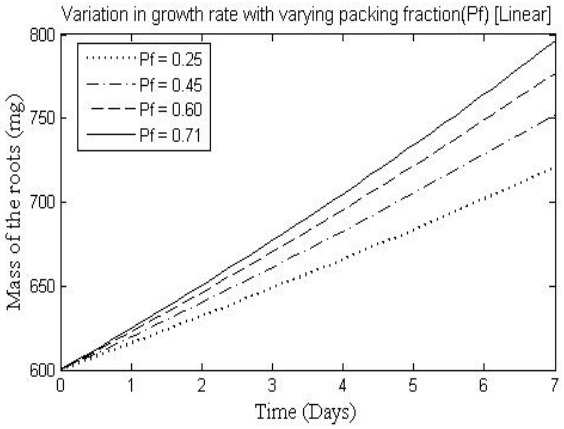

Figure 7: Variation Of Mass Of Roots With Time For Different Packing Fraction (P_f) .Top To Bottom Line Correspond To P_f = 0.71, 0.60, 0.45 And 0.25 Respectively.

This is due to the fact that the particle capture efficiency of root bed increases with increasing packing fraction of bed. Due to this, the availability of nutrients for the growing roots gets increased. This manifest itself in an increased growth rate at higher packing fractions. This result also supports the experimental findings of Towler et al. and thereby providing further support to the validity of present model.

The effect of P_f on liquid holdup is shown in **Figure 8.** The variation of liquid holdup with time for different packing fractions of root bed is shown. Here, top to bottom lines correspond to P_f = 0.25, 0.45, 0.60 and 0.71respectively. The other parameters remain same. It can be seen that liquid holdup decreases with higher packing fraction. This can be attributed to the fact that a higher packing fraction implies for higher growth rate which occurs at the expense of a greater consumption of nutrients, thereby leading to a lower liquid hold up.

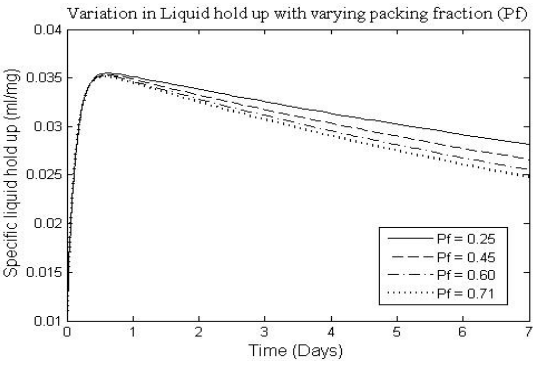

Figure 8: Variation Of Liquid Holdup With Time For Different Packing Fraction Of Bed (P_f). Top To Bottom Line Corresponds To P_f= 0.25, 0.45, 0.60 And 0.71 Respectively.

Figure 9 represents the variation of held up liquid concentration with time for different packing fractions. Following the same trend of above figure 8, the top to bottom lines correspond to P_f = 0.25, 0.45, 0.60 and 0.71respectively. The value of other parameters remains

same. It can be observed from the figure that the decrease in concentration of nutrients is faster for more densely packed beds. The faster decrease in concentration is due to the fact that higher growth rate is observed at higher packing fraction and so more nutrient is consumed.

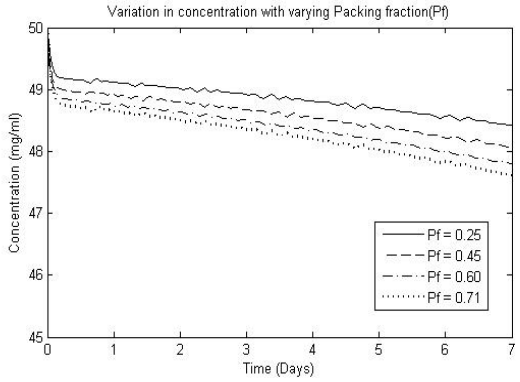

Figure 9: Variation Of Held Up Liquid Concentration With Time For Different Packing Fraction (P_f). Top To Bottom Line Corresponds To P_f = 0.25, 0.45, 0.60 And 0.71 Respectively.

Study Of Effect Of Liquid Film Thickness (L_f) On Nmr Performance

Figure 10 presents the variation of mass of roots with time at different liquid film thickness. In this figure, top to bottom line correspond to L_f = 0.1 mm, 0.2 mm and 0.3 mm respectively. The value of other parameters are Q_0 = 2.11 ml/day-mg, C_0 = 50 mg/ml,density =1000mg/ml, m_0 = 600 mg, μ = 0.2 per day, K_1 = 0.3 per day, C_m = 10 mg/ml, D= 0.72 mm^2/day and d = 1mm. An increase in the film thickness leads to a decrease in growth rate. This increase in film thickness engenders higher mass transfer resistance for the transfer of nutrient from mist to root bed resulting in a decreased growth of roots.

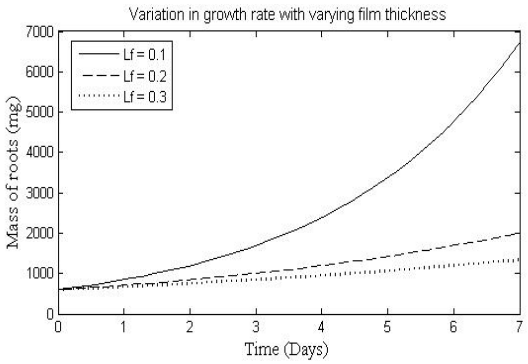

Figure 10: Variation Of Mass Of Roots With Time At Different Liquid Film Thickness (L_f). Top To Bottom Line Correspond To L_f = 0.1mm, 0.2 Mm And 0.3 Mm Respectively.

The variation of liquid holdup with time for different liquid film thicknessis shown in **Figure 11** where top to bottom lines correspond to L_f = 0.4 mm, 0.3 mm and 0.2 mmrespectively. The other parameters remain same. It is observed that liquid holdup increases with increasing liquid film thickness. These results are in accordance with theoretical expectation because the mass transfer resistance increases with increasing liquid film thickness and this will lead to a higher amount of liquid holdup inside the mist reactor.

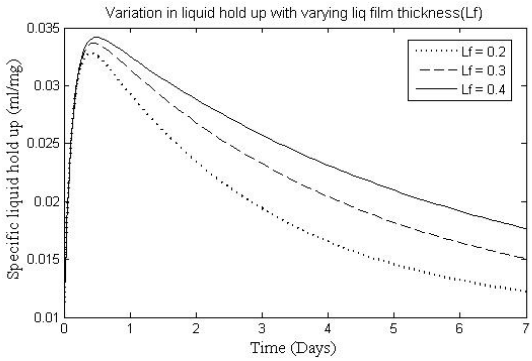

Figure 11: Variation Of Liquid Holdup With Time At Different Liquid Film Thickness (L_f).Top to bottom line corresponds to L_f = 0.4, 0.3 and 0.2 respectively.

Figure 12 represents the variation of held up liquid concentration with time for varying liquid film thickness and top to bottom lines correspond to L_f = 0.3 mm, 0.2 mm and 0.1 mmrespectively. The value of other parameters is kept same. These results are in tune with theoretical concept because the decrease in concentration is faster with thinner liquid films since with increased thinning of films, more nutrients will be transferred to the bed and get consumed.

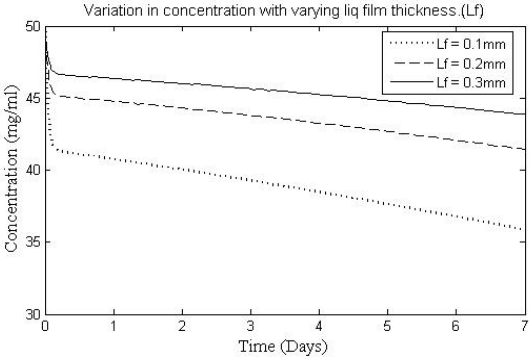

Figure 12: Variation Of Held Up Liquid Concentration With Time For Different Liquid Film Thickness (L_f). Top To Bottom Line Corresponds To L_f = 0.30mm, 0.20mm And 0.1mm Respectively.

CONCLUSION

For enhanced production of various useful secondary metabolites by plant culture system, different design and configurations of reactors have been studied for the production of secondary metabolites and it was found that NMR clearly offer some significant benefits for culturing hairy roots, including lack of oxygen stress, rapid growth, and production of high yields. The effect of packing fraction of root bed and liquid film thickness on growth of roots, liquid hold up and also on held up liquid concentration is studied with simulation of a simplified mathematical model for a cylindrical root bed.

In the present work, it is found that the growth rate of root increases while liquid holdup and held up liquid concentration decreases with increasing values of packing

fraction of root bed. On the other hand, the growth rate of root decreases while liquid holdup and held up liquid concentration increases with increasing liquid film thickness. However, optimization of packing fraction and thickness of liquid film over the roots is still under ambit of active research on NMR performance analysis.

NOMENCLATURE

C : Nutrient concentration in the feed [mg/ml]
C_m : Minimum concentration of the nutrients at the root surface [mg/ml]
C_0 : Initial concentration of the nutrient in the feed [mg/ml]
D : Diffusivity coefficient of liquid nutrient [mm^2/day]
d : Root fibre diameter [mm]
K_1 : Proportionality constant for growth equation [day^{-1}]
K_2 : Proportionality constant for drainage equation [day^{-1}]
L_f : Liquid film thickness [mm].
m_0 : Mass of the root at time t = 0[mg].
m_t : Mass of the root at time 't'[mg].
P_f : Packing fraction of root bed.
Q_0 : Feed (Mist) flow rate at the start (t = 0) [ml/day]
Q_t : Feed (Mist) flow rate at any given time 't' [ml/day]
t : Time [day]
Y : Current specific liquid hold up [ml/mg]
Y_{Sat}: Specific liquid hold up at saturation [ml/mg]

GREEK LETTERS

α : Dimensionless exponent for effective flow rate
μ : Specific growth rate of the roots [per day]
ρ : Density of liquid [mg/ml]
η : Particle capture efficiency

REFERENCES

1. H. E. Flores and P. Filner., *in Primary and secondary metabolism of plant cell cultures*. K.H. Newmann, W. Barz and E. Reinhard Eds. Springer-Verlag, Berlin, (1985).
2. W. R. Curtis, S.A. McKelvey, J. A. Gehrig and K. A. Hollar, *Biotechnol. Prog*., **9**, 317 (1993).
3. M. F. Balandrin, J. Klocke, E. S. Wurtele and W. H. Bollinger, *Science*. **228**, 1154 (1985).
4. M. G. Hilton and M. J. C. Rhodes, *Appl. Microbial. Biotechnol*., **33**, 132 (1990).
5. J. M. Sharp and P. M. Doran, *J. Biotechnol*., **16**, 171 (1990).
6. H. E. Flores and W. R. Curtis, *Ann. NY Acad. Sci*., **665**, 188 (1992).
7. M. D. Chilton, D. Tepfer, A. Petit, C. David and J. Tempe, *Nature,* **295**, 432 (1982).
8. P. D. G. Wilson, M. G. Hilton, R. J. Robins, and M. J. C. Rhodes, *In Bioreactors and Biotransformations,* Eds G. W. Moody & P. B. Baker. Elsevier, New York (1987).
9. P. J. Weathers, B.E. Wyslouzil, K. K. Wobbe, Y. J. Kim, and E. Yigit, *In Vitro Cell Develop Biol Plant*. **35**, 286 (1999).
10. D. G. Wilson, *in Hairy Roots: culture and applications*, PM Doran, Ed, Gordon and Breach/Harwood Academic, UK, (1997)
11. M. J. Towler, Y. Kim, B. E. Wyslouzil, M. J. Correll and P. J. Weathers, *in Plant Tissue Culture Engineering,* S. D. Gupta and Y. Ibaraki, Eds, Springer, The Netherlands, 119, (2006).
12. P. Whitney, *Enz Microbiol Technol,* **14**, 13 (1992).
13. B. E. Wyslouzil, M. Whipple, C. Chatterjee, D. B. Walcerz, P. J. Weathers, and D. P. Hart, *Biotechnol. Prog.* **13**, 185, (1997).
14. R. Ranjan, N. Ahmed, R. Khanna, and B. N. Mishra, *Biotechnology and Bioprocess Engineering,* **14**, 38 (2009).
15. M. J. Towler, B. E. Wyslouzil, and P. J. Weathers, *Biotechnol. Bioeng*., **96**, 881, (2007)
16. M. Watt, W. E. Silk, and J. B. Passioura, *Oxford journal*, **97**, 839, (2006).

AUTHOR'S BIOGRAPHY

Manish Vashishthawas born in Karauli (Rajasthan, India) and obtained his Bachelor of Engineering (with Honours) in Chemical Engineering, from Malaviya National Institute of Technology (MNIT), Jaipur (India) and Master of Technology (M.Tech.) and Doctor of Philosophy (Ph.D) degrees in Chemical Engineering, from Indian Institute of Technology (IIT), Delhi, New Delhi (India). He is working as Assistant Professor in Department of Chemical Engineering, at MNIT, Jaipur. His areas of research include Interfacial Engineering, Thin liquid films, Modelling and Simulation, , Particle Science and Thermodynamics. He has published around 40 research papers in various Journals and conferences including some in high impact factor journals like Physical review E, Physical Chemistry Chemical Physics, Journal of Physical Chemistry B, Particuology etc. . He is life member of Institution of Engineers (India), Indian society for Technical Education and Indian Institute of Chemical Engineers.
His e-mail address is *mvche.mnit@gmail.com*

SIMULATING PUBLIC PRIVATE NETWORKS as EVOLVING SYSTEMS

Ameneh Deljoo, Marijn Janssen and Bram Klievink
Department of Technology, Policy and Management
Delft University of Technology
2628 BX, Delft, the Netherlands
E-mail: a.deljoo@tudelft.nl

KEYWORDS

Agent-based modeling, agent-based simulation, complex adaptive system, public-private service network, operations, social network

ABSTRACT

Public-private service networks (PPSN) consist of social and technology components. Development of PPSN is ill-understood as these are dependent on a complex mix of interactions among stakeholders and their technologies and is influenced by contemporary developments. The aim of this paper is to advance our understanding of PPSN by modeling its evolution. Agent-based modeling (ABM) is used to understand and analyses self-organization and emergent aspects. In a case study of the vehicle administration we show the evolution of PPSN including changes in the structure of network.

INTRODUCTION

The most difficult challenge in understanding social phenomena and also PPSN is their intractably complex nature (Peltoniemi 2005). For much of the 20th century social researchers attempted to unravel the complexities of the social scope by simulating the methodologies of the natural sciences (Jacobson 2011). Although these approaches enhanced social science research, they have fallen short of capturing emergent behavior and self-organization. Nowadays, new approaches to the study of Complex Adaptive Systems (CASs) have offered researchers in both the physical and social sciences an important new theoretical and methodological framework for helping to understand a variety of nonlinear, dynamic systems. CAS is characterized often by ‘‘agents’’ interacting or capable of interacting with each other in a dynamic environment and in nonlinear ways (Furneaux 2009).
Complex systems are systems with multiple interacting components whose behavior cannot be simply inferred from the behavior of the components. In a similar vein, Public-private service networks (PPSN) consist of interacting organizations and persons supported by technology. Coleman (1994) proposes to explain “the behavior of social systems by means of three components: the effects of properties of the system on the constraints or orientations of actors; the actions of actors who are within the system; and the combination or interaction of those actions, bringing about the systemic behavior” (p. 27). Social system can be considered as network which PPSN is part of this network. In PPSNs are actors are self-interested and interact with each other and environment. These interactions make up the structure of network. Agent-based modeling can be used to model social interaction, structure and technology (Bradshaw 2008), and will be used to model the system in this research.
The aim of this paper is to advance our insight in the evolution of PPSN. We investigate the case of the PPSN of the vehicle administration and use ABM to model its evolution. The paper is organized as following. In the following section we give an overview of PPSN. Thereafter we present a case study and conceptualize the case by using agents, actors and taking technology components in account. This is followed by the specification of the model with empirical data. We run the model in which it evolves from the old to the new situation. Finally, conclusions are drawn and further research steps are discussed.

PPSN

Organizations can be viewed as a shifting multiple-goal political coalition (March 1989). Network organizations can be defined by elements of structure, process, and purpose (Podolny and Page 1998). Structurally, a network consists of self-interested organizations. Procedurally, a network organization constrains participating agents' actions via their roles and positions within the network while allowing agents' influence to emerge or fade with the (Baker 1992).
A network organization is usually considered as an organization that is quick and flexible in adapting to changes in its environment. But changes in the structure of the organization can also be detrimental in the medium run, since it is partly the knowledge of the organizations structure that mediates (Podolny and Page 1998). This is what is called evolving phenomenon which is the subject of this research.
PPSN is a specific type of organizational network in which public and private organizations collaborate. PPSN *can be defined as a network consisting of (at least three) autonomous public, private and non-profit organizations which aim to provide a service to individual citizens or businesses (Deljoo 2013).* PPSN consists of many organizations having their own goals, requirements and installed base of systems that determine the network evolvement. The behavior of PPSN is made up by interacting organizations.

Proceedings 27th European Conference on Modelling and Simulation ©ECMS Webjørn Rekdalsbakken, Robin T. Bye, Houxiang Zhang (Editors)
ISBN: 978-0-9564944-6-7 / ISBN: 978-0-9564944-7-4 (CD)

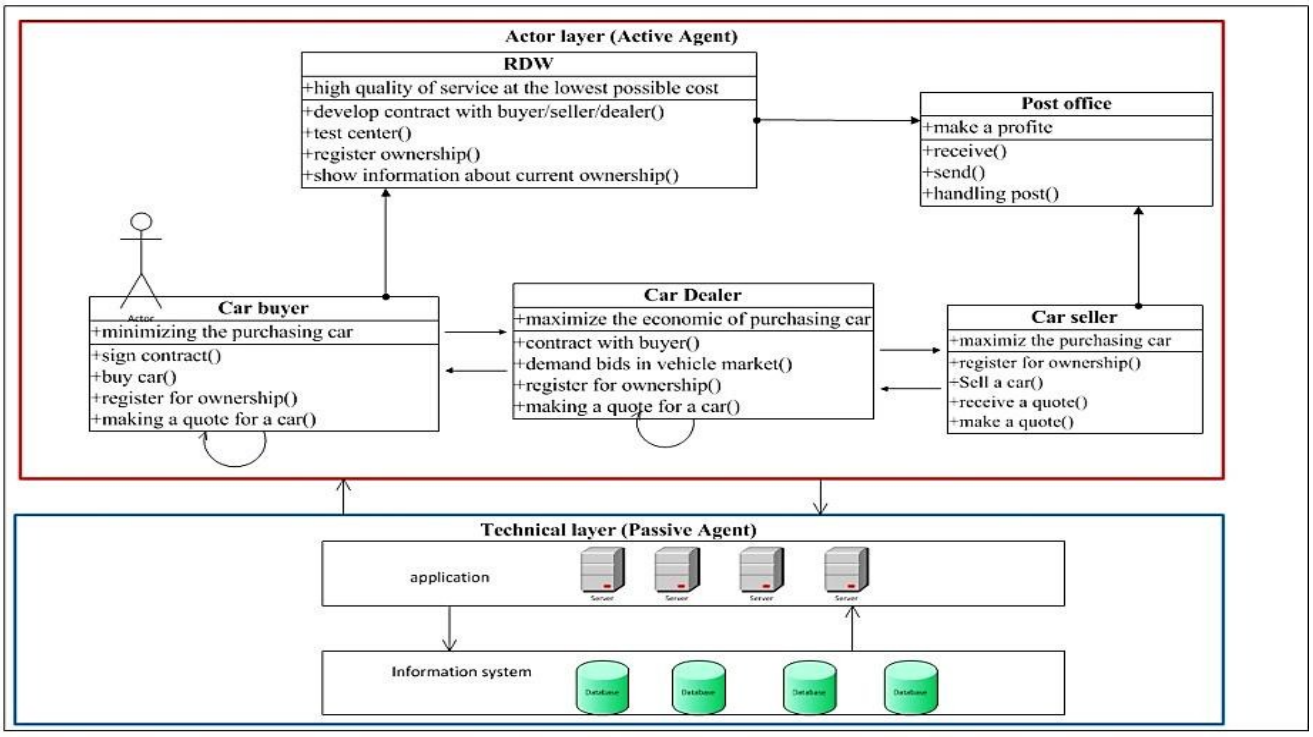

Figure 1: Structure of Agent and Interaction in Vehicle Organization (blue color: passive layer, red color: active layer)

CASE STUDY: VEHICLE ADMINISTRATION

Our aim is to investigate the evolvement of the PPSN surrounding the vehicle administration. We focused on the Dutch organizations as data concerning its evolvement was available. This allowed for conceptualizing and specifying a model with empirical data. In principle, the same conceptualization can be used to simulate many other countries, simply by using different data sets and different network.

The RDW is an executive agency under the responsibility of the Ministry of Infrastructure and Environment. The RDW is the Dutch admission authority for vehicles: passenger cars, vans, trucks, motorcycles, mopeds, scooters, etc. The RDW is aimed at ensuring that vehicles meet the required safety and environmental aspects. The RDW is also the manager of the basic registration vehicles in the Netherlands based on information stewardship. These are vehicle registration data and the data of the owner / keeper. Many government organizations and in some cases companies like insurance companies make use of this register. For this paper we consider the organizations: Car buyers, Sellers, Car dealers, Post office, RDW.

MODEL CONCEPTUALIZATION

The conceptualization is aimed at modeling the evolvement of the organizational network which is determined by technology adoption. Therefore we both model the organizations and the technology components. The organizations interacting with each other are the Car buyers, Sellers, Car dealers, Post office, RDW. The organizations utilized technologies to communicate with each other. Actor layer (model as active agent as actors are purposeful) and technical layer (passive agent as they can only be manipulated by actors) as a whole is depicted in figure 1. We distinguished two layers with two different colors, blue color for passive layer, and red color for active layer. The actors are modeled by their goals and by their interactions with each other. The technical layers consist of information systems and applications supporting organizational processes and interactions with other organizations. The entities in both layers have interactions with each other. As shown in figure 1 car buyers, and dealers are connected with each other and car sellers reconnected to dealers, which in turn are connected to the RDW and post office. Each agent in the actor layer has a relationship with themself for transfer their experience about the other agents (car buyer/dealer, seller) and organizations. In the technical layer there are a variety of information systems and applications for establishing the communication between the agents in the up layers (actor layer) and also, for storing data, searching, and generated report. This layer is used for facilitating and supporting the interactions among the active agent. Each layer has an impact on another layer.

The actors in the active layer are represented as *active agents* in the model. *Car buyer* takes the actual decisions about which car to buy from which car seller or dealer. The car price is determined by the negotiation between the car buyer and dealer.

A buyer, in this case, is the representation of somebody who wants to buy a car and to which the ownership of the car should be transferred. Buyer choice is contracted by a variety of factors such as (color, model, guaranty, second/first hand). Finally, the government sets the rules of the game (regulative author): it implements policies and acts on them, for instance by collecting taxes, asking for information such as the total distance covered by the car (to avoid fraud) and the requirement to register ownership.

Table 1: Structuring of The Agent and Interactions

Actors	Objective	Behavior and interaction
Car Buyer	Minimizing the purchasing cost Minimizing administrative costs	(1) Behaviors: sign contract with car dealer, pay tax and insurance bill to RDW, sign contract with insurance company (2) Interactions with internal /external agents
Car Dealer	Maximize the economic benefit of purchasing car Minimizing administrative costs	(1) Behaviors: Develop contracts with buyer and the RDW, make demand bids in vehicle market (2) Interactions with external agents
RDW	high quality of service at the lowest possible cost Ensure safety and security of Vehicles Minimizing administrative costs	(1) Behaviors: Test Centre, register, license, sign contract with car dealer, buyers, tax organizations, insurance organizations

In addition to the organizations, which are represented by active agents, there are technological components, representing by passive agents. We do not model the actual cars that are traded, instead we focus on the information and communication components that support the information exchange, as these determine how the network evolves. The following list comprises the main components in the physical subsystem:

- applications
- Information systems

Interactions. Interactions take place between the actors and their applications and information systems. We define social interactions to be between social components, technical interactions to be between technical components, and socio-technical interactions to be between social and technical components.
Social Interactions are communications and negotiations between social elements or agents. A main type of social interaction is contact between buyers, car sellers, car dealers and insurance companies, and tax administration and RDW through their social network. Buyer may discuss about car and experiences with others or observe others. Government interacts with RDW by providing information through information and awareness campaigns. Furthermore, governments can implement policies, such as bans on products (i.e. cars with a lot of pollution), taxation schemes and subsidies. RDW interact with car dealers by signing a contract and collecting information about their purchase and sales. Car dealers, seller and buyers interact with each other to buy and sell products and determine the price.

Performance indicators. We wanted to have insight in the resulting network to compare the performance differential between the initial and the evolved situation. For this purpose we used social network parameters *and* operational indicators. We used operational parameters information quality (IQ), lead time and social network metric betweenness centrality and closeness centrality for measuring the functionality of the network which they are SNA indicator (Otte and Rousseau 2002). Betweenness centrality is a measure of the centrality of a node in a network, and is normally calculated as the fraction of shortest paths between node pairs that pass through the node of interest. In our work the interest node is RDW and node pairs are car buyer, dealer and seller and post office. Closeness centrality is an important concept in social network analysis. In a graph representing a social network, closeness centrality measures how close a vertex is to all other vertices in the graph we measured the distance of RDW to the other vertex (L.Breiger 2004). Hence, by figure out the closeness centrality we can investigate the lead time and IQ. The first are focused on the operational (day-to-day) behavior of the system, whereas the latter provides insight in the evolution from the traditional situation in which car buyers and sellers provide information to the RDW to the situation in which care dealers provide this information to the RDW.

MODEL SPECIFICATION

We implemented the model in network analyzer Gephi (Bastian et al. 2009). An agent-based model of the vehicle organization is developed, which include car buyer agent as a customer, a car dealer as retailer agent, and a portfolio of database and software (portal) as technology the car buyer, seller and car dealer agents are at the core of the model: it makes the decision to purchase/buy car. In deciding which insurance company chose, a buyer will need information on the different existing alternatives and this process applies for when car buyers are searching for sellers. Agents use their individual preferences to compare the alternatives and make a choice. In addition, the agents interact with the other agents like: insurance company, technology, RDW and environment. This is schematically shown in figure 2. In these figures we have different groups of agent and organization and their connections with different view we will discuss about it in the next section. We have a different group in this network for example group b_i (***b***uyer i, i=1 till n), group c_j (***c***ar dealer j, j=1 till m), and group INS_k (***I***nsurance company k, k=1 till[1]), and RDW, post office and tax company. For the model used n= 50, m= 30 and o= 20. In figure 2(a) the network is enhance than

[1] o= 20

the network in figure 2(b) because of the number of agent which is added to the network during time. Structure of the network is changed during time. In this paper for make and analysis sociometric of PPSN we chose Gephi analyzer (Bastian et al. 2009).
When evolving the number of players (n buyers, m car dealers and k insurance companies) can change, as new players enter the market and old players may disappear.

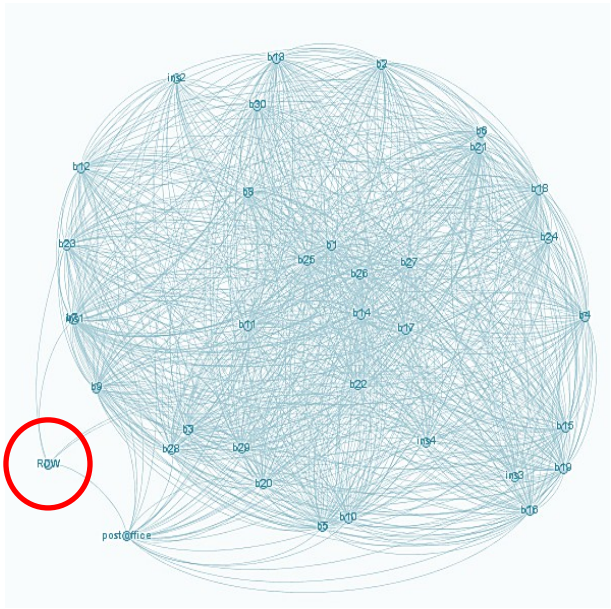

(a) Initial Situation

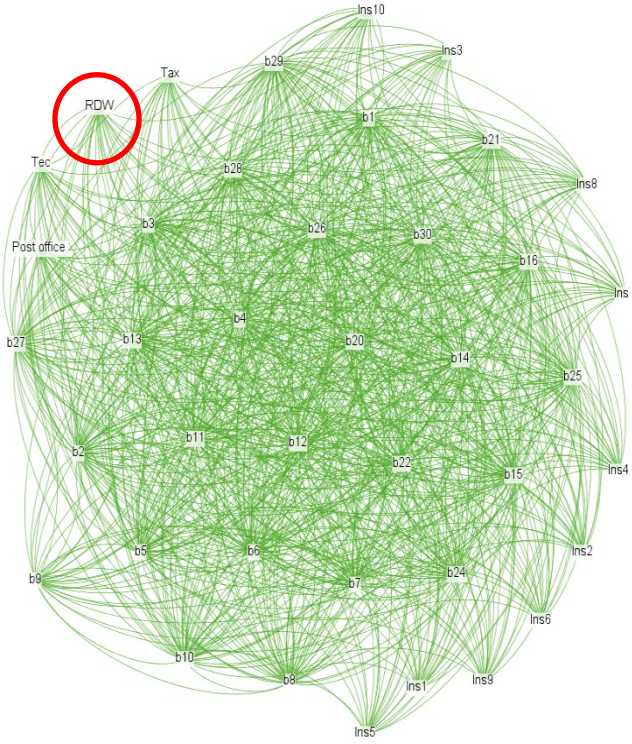

(b) Situation after Evolving

Figure 2: (a) Social Structure of New Network as the start (b) and after the network has evolved

RESULTS

In this section we discuss the result of the simulation and investigated the functionality of RDW after having evolved to the new situation.
As we shown in the figure 2 (a, b) we model our system. In the initial situation, the system has limited in the physical layer and functionality (figure 2(a)). In this model, car buyer for registration his/her vehicle is used to refer to the post office and in the post office they are asking an owner to fill in the form. After that, they check the information and when they confirm that the information is correct so, they send the information to the RDW. In this perspective, customer and RDW have no contact with each other and a customer take a lot of time to register his/her vehicle in the system.
Due to the technology changes, new types of interactions become available resulting in the evolvement of the network. In new situation of network, structure and the policy of network is changed. In this form, because of the number of car buyer, car dealer is raised network structure is changed as we shown in figure 2(b). This new form of network, RDW is the center of network and plays an intermediate role between other agents with government. In spite of the other network each agent can access to the post office and RDW simultaneously.
In the traditional situation the post office is the center of the relationship in the system in addition in this view customer must be waiting very long to register in this system. In the evolved situation the number of car buyers because of bid for vehicles are increased and in the network we have a numerous interactions between the stakeholders and other organizations, which is combination the network for example: tax organization, insurance company, and RDW. As we shown in the figure 1, car buyers have social interaction with each other car buyers and with car seller, car dealer and post office and RDW. In the second situation, each car buyer directly makes a relationship with the RDW and registers his/her vehicle in the vehicle organizations without asking the post office for permission. In this network, cycle of registration or change information in the network takes a less time than the older one.
The purpose of this paper is to understand how a PPSN evolves. Deep insight into the evolving phenomenon shows that is the PPSN gradually changing over time. New interactions are introduced and more and more car dealers connect directly to the RDW instead of using the post office. For this purpose new information systems are adopted. For this concept, systems (organization) are changed and expand their domain while these developments are occurred during the life of system (organization). System will grow gradually (i.e. develop the scope, more employee, more facilities, more sub-domain, etc.) without changing in the mission of this system (Stebbings and Braganza 2009).

The model is changed, by increasing the number of information system and applications. As we shown in figure 2 by red circles in the initial state RDW organization have 5 connections to the other organizations such as post office, insurance company, car dealer/ car seller and technologies. On the other hand, in figure 2(b) after evolving in the network, RDW has a more connections to the other agents (e.g. car buyer/dealer/ seller) and insurance company and post office and technologies. Therefore, the structure of network is changed.

Previous studies have identified that evolving changing in the system without changing or modifying in the structure (Capra 2002) but in this paper the structure of the network is changing. In this regards, both organizations (public or private organizations) during time added to the PPSN. Figure 2 (b) shows that the network is adapted to the new form.

CAS acknowledge that the system is changing this has impact to the other agents and environment (Dooley 1997; Eidelson 1997). In our situation new technology is introduced to enable new interactions between the parties which results in changes in the interactions among participants. Over time the post office is bypassed and more and more direct communication between car dealers and RDW takes place. The car dealer functions as a trusted party for the RDW ensuring the quality and correctness of the ownership transfer.

In table 2 the results on the performance indicators show the performance differential between the initial and new situation of the network. In the new form of network closeness centrality is less than in the initial network. The indicators show that density of network is increased and network is grown and that the network adapted to the modifications. Also the lead time decreased; as a result customer satisfaction is higher because the process of registration or transformation is quickly.

Less missing data and an increased leading time is realized due to the system evolvement. In the old situation processing of data was done by hand resulting in data entering mistakes and difficult to read forms. From another standpoint, customer satisfaction and IQ in the new form of network is higher. Instead, betweenness centrality decreases as decrease in Lead time and seeks to describe cycle of information in the both networks, and in table 2 we show that the new system has rapid movement for data.

Table 2 : Performance of the old and adapted network

Quality measurement	**Old situation**	**situation after evolving**
Lead time	2days	days
IQ	Low	High
Betweenness centrality	3.056	2.667
Closeness centrality	1.971	1.650

CONCLUSION

The conceptualization of PPSN of the RDW helps to understand the evolvement, as it shows the emergent effects of new technology and organizations in the network. Both the organizations as well as the technology components are conceptualized. The visualization helped to understand the changes in interactions among parties, whereas the performance indicators provide insight into the overall performance of the systems. The introduction of new technology results in the bypassing of the post office and car dealers acting as trusted parties communicating the transfer of the ownership to the vehicle administration. We demonstrated the new face of evolving when the mission and the structure of the network changed. In the RDW case study we demonstrated the evolvement and investigated the effect of the evolvement on various criteria. Qualitative criteria include: IQ, lead time, customer satisfaction, betweenness centrality, and closeness centrality. In this paper, we are modeling both organizational and technology aspect of PPSN.

The concept of evolving in complex adaptive systems provides a useful construct to understand the dynamics of public-private network, particularly when changes are occurred in the structure of network. Our conceptualization of the situation was initialing held at a high level of abstraction. Our further empirical work is aimed at eliciting additional changes to rules, agent to increase the depth and breadth of analysis.

REFERENCES

Baker, W.E. 1992. "The network organization in theory and practice." Networks and organizations: Structure, form and action 397:429.

Bastian, M., S. Heymann and M. Jacomy. 2009. "Gephi: An open source software for exploring and manipulating networks."

Bradshaw, D. 2008. Introduction: Wiley Online Library.

Capra, Fritjof 2002. The Hidden Connections: A Science for Sustainable Living. NewYork: Anchor Books.

Coleman, J.S. 1994. Foundations of social theory: Belknap Press.

Deljoo, A., Janssen 2013. "Conceptualization of Public Service Networks as Complex Adaptive Sys-tems." In ECEG'13 Como, Italy.

Dooley, Kevin J. 1997. "A Complex Adaptive Systems Model of Organization Change." Nonlinear Dynamics, Psychology, and Life Sciences Vol. 1(No. 1):pp. 69-97.

Eidelson, Roy J. . 1997. "Complex Adaptive Systems in the Behavioral and Social Sciences." the Educational Publishing Foundation, Vol. 1(No. 1):pp. 42-71.

Furneaux, C.W., Brown, K.A. and Gudmundsson, A. 2009. "Managing infrastructure transitions: A complex

adaptive systems perspective." In IRSPM 2009. Copenhagen, Panel track.
Jacobson, Michael J., Kapur, Manu So, Hyo-Jeong Lee, June. 2011. "The Ontologies of Complexity and Learning about Complex Systems." Instructional Science: An International Journal of the Learning Sciences 39(5):763-783.
L.Breiger, Ronald ed. 2004. The Anaalysis of social network.
March, J.G. 1989. Decisions and organizations: Blackwell Oxford.
Otte, Evelien and Ronald Rousseau. 2002. "Social network analysis: a powerful strategy, also for the information sciences." Journal of Information Science 28(6):441-453.
Peltoniemi, M.; Vuori, E. 2005. "Business ecosystem as the new approach to complex adaptive business environments." In Frontiers of e-Business Research 2004.
Podolny, J.M. and K.L. Page. 1998. "Network forms of organization." Annual Review of Sociology:57-76.
Stebbings, H. and A. Braganza. 2009. "Exploring continuous organizational transformation: Morphing through network interdependence." Journal of Change Management Vol. 9(No. 1):pp. 27-48.

AUTHOR BIOGRAPHIES

AMENEH DELJOO was born in Shiraz, Iran and went to the Shiraz University, where she studied information technology and obtained her master degree in 2012. She is moving in 2012 to the Netherlands and started her PhD research in Delft University of technology under Prof. Marijn Janssen supervision in faculty of technology, policy and management. She is interested in complex adaptive system, agent based modeling and public-private network. Her e-mail address is: a.deljoo@tudelft.nl or you can follow her in the LinkedIn with this address http://www.linkedin.com/in/amenedeljoo and her Web-page can be found at https://sites.google.com/site/amenedeljoo/.

Dr. Marijn Janssen is professor and chair in ICT and governance, Director of the interdisciplinary Systems Engineering, Policy Analyses and Management (SEPAM) and of the Compliance Management Master programmes of the Technology, Policy and Management Faculty of Delft University of Technology. His research interests are in the field of infrastructures; public-private networks and focuses on orchestration, shared services, brokers, intermediaries, open data and open government. He has been a consultant for the Ministry of Justice and received a Ph.D. in information systems (2001). He is associate Editor of Government Information Quarterly (GIQ), serves on several editorial boards and is involved in the organization of a number of conferences, including IFIP EGOV. He has published over 240 refereed publications. For more information: www.tbm.tudelft.nl/marijnj.

Dr. Bram Klievink is assistant professor at the Information and Communication Technology section of the Faculty of Technology, Policy and Management at Delft University of Technology. He holds a PhD degree in technology and public management, an MSc degree inpolitical science, and a degree in business information systems. His PhD dissertation is on coordination mechanisms for public-private service networks. Furthermore, he participated in research projects on integrated, demand-driven e-government and on multi-channel management in government. Bram was aboard member of the Dutch Alliance for Vital Governance, a strategic research alliance for collaboration and knowledge transfer between government organizations and research institutes in the Netherlands. Currently, he is involved in multiple Dutch and European research projects and teaches in courses at both Bachelor and Master level.

BIFURCATION EFFECTS IN DEGENERATE DIFFERENTIAL MODELS OF SUBPOPULATION DYNAMICS

Serge V. Chernyshenko
Olexandr O. Kuzenkov
Department of Applied Mathematics and Social Informatics
Khmelnitsky National University
29000, Khmelnitsky, Ukraine
E-mail: svc@a-teleport.com, kuzenkov1986@mail.ru

KEYWORDS
Bifurcation, cross-coefficient, mathematical model, Lotka-Volterra model, phase portrait.

ABSTRACT
The model of subpopulation dynamic of the Lotka-Volterra type has been investigated. Stability of stationary points and hyper-planes of the system was in the focus of the article; appearance conditions are found. Bifurcation analysis of system has been realized also.

MATHEMATICAL MODEL

The majority of existing models of population dynamics describe dynamics of whole populations, their interaction and influence of environment for them. The phenomenon of subpopulation dynamics is considered with much less attention. One of reasons is the fact that in most cases subpopulations aren't isolated from each other and exchange by individuals.
For taking into account the subpopulation effects, let's consider the general model of subpopulation dynamics in the form:

$$\dot{x}_i = \sum_{j=1}^{n} A_{ij} \cdot f_j(x_1,...,x_n), i = \overline{1,n}, A_{ji} \in [0;1],$$

where x_i is a biomass of i-th subpopulation. In the right hand part of each equation, the "base functions" $f_i(x_1,..,x_n)$ are combined linearly; each of them is "distributed" between all equations in accordance with some coefficients A_{ij} ("cross coefficient").

In [3] the model of subpopulation dynamics was investigated for the case of the logistic base functions. It was also supposed that the total size of the population (the total sum of sizes of all the subpopulations) was limited by some fixed niche capacity. In the current article, individual niche capacities for each subpopulations is considered. Correspondingly, the initial model of subpopulation dynamics can be represented in the following form:

$$\frac{dx_i}{dt} = \sum_{j=1}^{n} A_{ij} \cdot \left(a_j - c_j \cdot \sum_{k=1}^{n} x_k \right) \cdot x_j, i = \overline{1,n}, \quad (1)$$

Here the coefficients A_{ij} describe exchange by specimens between the subpopulations, a_i is a birth rate of i-th subpopulation, c_i is a level of sensitivity of i-th subpopulation to inter-subpopulation competition, n - amount of subpopulations (a_i/c_i - niche capacity for i-th subpopulation). It can be easily shown, that the model can find applications not only in ecology, but also in economy, sociology, etc.
Under a condition

$$\sum_{i=1}^{n} A_{ij} = 1, 0 \le A_{ij} \le 1, \quad (2)$$

the system can be considered as "closed" [5]. The condition (2) reflects the assumption that all population as a whole is closed, i.e. there are no migratory processes both to population and from it.
In the case $n = 2$ the system (1) takes a form:

$$\begin{cases} \frac{dx_1}{dt} = \lambda_1 a_1 \left(1 - \frac{x_1 + x_2}{a_1/c_1}\right) x_1 + (1-\lambda_2) a_2 \left(1 - \frac{x_1 + x_2}{a_2/c_2}\right) x_2 \\ \frac{dx_2}{dt} = (1-\lambda_1) a_1 \left(1 - \frac{x_1 + x_2}{a_1/c_1}\right) x_1 + \lambda_2 a_2 \left(1 - \frac{x_1 + x_2}{a_2/c_2}\right) x_2 \end{cases} \quad (3)$$

For investigation of system critical points, the Lyapunov's method [4] was used. There are three critical points: $(0;0)$, $(a_1/c_1;0)$, $(0;a_2/c_2)$ and a stationary straight line:

$$x_1 = a_1/c_1 - x_2, \quad (4)$$

which exists under a condition

$$a_1/c_1 = a_2/c_2. \quad (5)$$

BIFURCATION ANALYSIS OF THE MODEL

Theorem 1: Points of the stationary regular hyper-plane (4) of the system (3), exist under an additional condition (5), are degenerate, i.e. the Jacobi matrix is equal to zero in them.

Proof:
An ij-th element of the Jacobi matrix of the system (3) has a form:

$$J_{ij} = \sum_{j=1}^{2} \left[a_j A_{ij} \left(1 - \frac{(x_1 + x_2)}{a_j/c_j}\right) - c_j x_j \right]. \quad (6)$$

Taking into account the condition (5),

Proceedings 27th European Conference on Modelling and Simulation ©ECMS Webjørn Rekdalsbakken, Robin T. Bye, Houxiang Zhang (Editors)
ISBN: 978-0-9564944-6-7 / ISBN: 978-0-9564944-7-4 (CD)

$$J_{ij} = \sum_{j=1}^{n} \left(- c_j \cdot x_j\right).$$

As J_{ij} doesn't depend directly from i, $J_{pi} = J_{hi}$, $p,h = \overline{1,n}$. So, the column vectors of the Jacobi matrix are linearly dependent, and $\det(J) = 0$.

The theorem is proved.

All stationary sets of the system can be easily explained. The stationary point in the origins or with one zero coordinate reflects the situation when both subpopulations are absent at all or one population has zero size and the other one totally fill the niche. In the conditions of lack of resources the subpopulations divide the ecological niche. In the case of equality of niche sizes for all the subpopulations, they can coexist with different size ratio among themselves. The equilibrium ratio will depend on initial conditions.

Elements of the Jacobi matrix of system (3) look like:

$$J_{11} = \lambda_1\left(a_1 - c_1\left(2x_1 + x_2\right)\right) + c_2 x_2\left(\lambda_2 - 1\right),$$
$$J_{12} = \left(1 - \lambda_2\right)\left(a_2 - c_2\left(2x_2 + x_1\right)\right) - \lambda_1 c_1 x_1,$$
$$J_{21} = \left(1 - \lambda_1\right)\left(a_1 - c_1\left(2x_1 + x_2\right)\right) - \lambda_2 c_2 x_2,$$
$$J_{22} = \lambda_2\left(a_2 - c_2\left(2x_2 + x_1\right)\right) + c_1 x_1\left(\lambda_1 - 1\right).$$

In the origin of coordinates the matrix is:

$$J\big|_{(0;0)} = \begin{pmatrix} \lambda_1 \cdot a_1 & \left(1 - \lambda_2\right) \cdot a_2 \\ \left(1 - \lambda_1\right) \cdot a_1 & \lambda_2 \cdot a_2 \end{pmatrix}, \quad (7)$$

and in nonzero critical points $\left(a_1/c_1;0\right)$ and $\left(0;a_2/c_2\right)$ it has the forms:

$$J\big|_{(a_1/c_1;0)} = \begin{pmatrix} -\lambda_1 a_1 & \left(1-\lambda_2\right)\left(a_2 - \dfrac{a_1 c_2}{c_1}\right) - \lambda_1 a_1 \\ \left(\lambda_1 - 1\right)a_1 & \lambda_2\left(a_2 - \dfrac{a_1 c_2}{c_1}\right) + a_1\left(\lambda_1 - 1\right) \end{pmatrix}, \quad (8)$$

and

$$J\big|_{(0;a_2/c_2)} = \begin{pmatrix} \lambda_1\left(a_1 - \dfrac{a_2 c_1}{c_2}\right) + a_2\left(\lambda_2 - 1\right) & \left(\lambda_2 - 1\right)a_2 \\ \left(1-\lambda_1\right)\left(a_1 - \dfrac{a_2 c_1}{c_2}\right) - \lambda_2 a_2 & -\lambda_2 a_2 \end{pmatrix}. \quad (9)$$

respectively.

In the Table 1 coefficients of the characteristic equation of system (3) (for each critical point) are presented.

Table 1: Factors of the characteristic equation of system (3) in special points

Stationary point	$b = -Tr(J)$	$c = Det(J)$
$(0;0)$	$-\left(\lambda_1 a_1 + \lambda_2 a_2\right);$	$a_1 a_2\left(\lambda_1 + \lambda_2 - 1\right)$
$\left(\dfrac{a_1}{c_1};0\right)$	$a_1 - \lambda_2\left(a_2 - \dfrac{c_2 a_1}{c_1}\right)$	$a_1\left(1 - \lambda_1 - \lambda_2\right)\times$ $\times\left(a_2 - \dfrac{c_2 a_1}{c_1}\right)$
$\left(0;\dfrac{a_2}{c_2}\right)$	$a_2 - \lambda_1\left(a_1 - \dfrac{c_1 a_2}{c_2}\right)$	$a_2\left(1 - \lambda_1 - \lambda_2\right)\times$ $\times\left(a_1 - \dfrac{c_1 a_2}{c_2}\right)$

Theorem 2: The system (3), under the conditions

$$\begin{cases} a_1 = 0 \\ a_2 = 0 \\ \lambda_1 + \lambda_2 = 1 \\ \begin{cases} a_1 a_2\left(\lambda_1 + \lambda_2 - 1\right) > 0 \\ \lambda_1 a_1 + \lambda_2 a_2 = 0 \end{cases} \end{cases}$$

is degenerate in a vicinity of the origin.

Proof: the origin is a critical point of the system (3). The Jacobi matrix has in it the form (7). The determinant of a characteristic matrix $Det(J) = a_1 a_2\left(\lambda_1 + \lambda_2 - 1\right)$ under theorem conditions it is equal to zero.

Roots of the characteristic equation are complex under the condition $Tr^2(J) - 4Det(J) < 0$, and the condition of equality to zero of their real part is $Tr(J) = \lambda_1 a_1 + \lambda_2 a_2 = 0$. So, a general condition of zero real part for the case of complex roots is

$$\begin{cases} a_1 a_2\left(\lambda_1 + \lambda_2 - 1\right) > 0 \\ \lambda_1 a_1 + \lambda_2 a_2 = 0 \end{cases}.$$

The theorem is proved.

Theorem 3: The origin is the saddle stationary point of the system (3) under the condition:

$a_1 a_2\left(\lambda_1 + \lambda_2 - 1\right) < 0$.

If

$0 < a_1 a_2\left(\lambda_1 + \lambda_2 - 1\right) < 0{,}25\left(\lambda_1 a_1 + \lambda_2 a_2\right)^2$,

the point is a knot, and under the condition

$a_1 a_2\left(\lambda_1 + \lambda_2 - 1\right) > 0{,}25\left(\lambda_1 a_1 + \lambda_2 a_2\right)^2$

it is a focus.

In the last two cases the point is stable if $\lambda_1 a_1 + \lambda_2 a_2 < 0$,

and unstable if

$\lambda_1 a_1 + \lambda_2 a_2 > 0$.

Proof: The Jacobi matrix of the system (3) has in the origin the form (7), and its characteristic equation is

$t^2 - \left(\lambda_1 a_1 + \lambda_2 a_2\right)t + a_1 a_2\left(\lambda_1 + \lambda_2 - 1\right) = 0$.

Under the condition

$Det(J) = a_1 a_2\left(\lambda_1 + \lambda_2 - 1\right) < 0$

determinant of the characteristic equation
$D(J) = Tr(J)^2 - 4Det(J)$.
Is positive, and the product of the equation roots (according to the Vieta theorem) is less than a zero. The critical point, by definition, has the saddle type.
Let's assume that $Det(J) > 0$. The determinant $D(J)$ of the characteristic equation has the form:
$D(J) = (\lambda_1 a_1 + \lambda_2 a_2)^2 - 4a_1 a_2 (\lambda_1 + \lambda_2 - 1)$.
Under the condition:
$a_1 a_2 (\lambda_1 + \lambda_2 - 1) > 0{,}25(\lambda_1 a_1 + \lambda_2 a_2)^2$,
The stationary point is elliptic; the real part of the complex roots is $\lambda_1 a_1 + \lambda_2 a_2$. Under the condition $\lambda_1 a_1 + \lambda_2 a_2 < 0$, the origin has the "stable focus" type; and under the condition $\lambda_1 a_1 + \lambda_2 a_2 > 0$ it is "unstable focus". If
$$a_1 a_2 (\lambda_1 + \lambda_2 - 1) < \frac{(\lambda_1 a_1 + \lambda_2 a_2)^2}{4},$$
the stationary point is hyperbolic. According to the assumption $Det(J) > 0$, the roots of the characteristic equation have an identical sign, therefore under a condition $\lambda_1 a_1 + \lambda_2 a_2 < 0$ the point has type "steady knot", and under a condition $\lambda_1 a_1 + \lambda_2 a_2 > 0$ it is "unstable knot".
The theorem is proved.

Similarly to the proof of the theorem 2 and 3, one can prove the following statements:

Theorem 4: The system (3), under the condition
$$\begin{cases} a_1 = 0 \\ (1 - \lambda_1 - \lambda_2) = 0 \\ (a_2 - c_2 a_1 / c_1) = 0 \\ \begin{cases} a_1 (1 - \lambda_1 - \lambda_2)(a_2 - c_2 a_1 / c_1) > 0 \\ \lambda_2 (a_2 - c_2 a_1 / c_1) - a_1 = 0 \end{cases} \end{cases}$$
is degenerate in a vicinity of $(a_1 / c_1; 0)$.

Theorem 5: The point $(a_1 / c_1; 0)$ has the saddle type has systems (3) under the condition $a_1 (1 - \lambda_1 - \lambda_2)(a_2 - c_2 a_1 / c_1) < 0$. If
$0 < a_1 (1 - \lambda_1 - \lambda_2)(a_2 - c_2 a_1 / c_1) <$
$< (\lambda_2 (a_2 - c_2 a_1 / c_1) - a_1)^2 / 4$
th point has the hub type; and if
$a_1 (1 - \lambda_1 - \lambda_2)(a_2 - c_2 a_1 / c_1) >$
$> (\lambda_2 (a_2 - c_2 a_1 / c_1) - a_1)^2 / 4$
It is "focus". In the last two cases the point is steady under a condition
$\lambda_2 (a_2 - c_2 a_1 / c_1) - a_1 < 0$,
It is unstable if $\lambda_2 (a_2 - c_2 a_1 / c_1) - a_1 > 0$.

Theorem 6: The system (3) under the condition
$$\begin{cases} a_2 = 0 \\ (1 - \lambda_1 - \lambda_2) = 0 \\ (a_1 - c_1 a_2 / c_2) = 0 \\ \begin{cases} a_2 (1 - \lambda_1 - \lambda_2)(a_1 - c_1 a_2 / c_2) > 0 \\ \lambda_1 (a_1 - c_1 a_2 / c_2) - a_2 = 0 \end{cases} \end{cases}$$
is degenerate in a vicinity of the critical point $(0; a_2 / c_2)$.

Theorem 7: The critical point $(0; a_2 / c_2)$ of the system (3) is a saddle under the condition $a_2 (1 - \lambda_1 - \lambda_2)(a_1 - c_1 a_2 / c_2) < 0$. If
$0 < a_2 (1 - \lambda_1 - \lambda_2)(a_1 - c_1 a_2 / c_2) <$
$< (\lambda_1 (a_1 - c_1 a_2 / c_2) - a_2)^2 / 4$
the point has the hub type; and if
$a_2 (1 - \lambda_1 - \lambda_2)(a_1 - c_1 a_2 / c_2) >$
$> (\lambda_1 (a_1 - c_1 a_2 / c_2) - a_2)^2 / 4$,
it is "focus". In the last two cases the point is steady under the condition $\lambda_1 (a_1 - c_1 a_2 / c_2) - a_2 < 0$, and it is unstable if $\lambda_1 (a_1 - c_1 a_2 / c_2) - a_2 > 0$.

All possible cases of the system topology are represented in the Table 2 and Fig. 1-9.

Table 2: Different topology of the system (3) phase portrait

Design-ations	Type of point $(0;0)$	Type of point $(a_1 / c_1; 0)$	Type of point $(0; a_2 / c_2)$
1	Stable	Stable	Saddle
2	Stable	Saddle	Stable
3	Stable	Saddle	Saddle
4	Stable	Saddle	Unstable
5	Stable	Unstable	Saddle
6	Saddle	Stable	Stable
7	Saddle	Stable	Saddle
8	Saddle	Stable	Unstable
9	Saddle	Saddle	Stable
10	Saddle	Saddle	Unstable
11	Saddle	Unstable	Stable
12	Saddle	Unstable	Saddle
13	Saddle	Unstable	Unstable
14	Unstable	Stable	Saddle
15	Unstable	Saddle	Stable
16	Unstable	Saddle	Saddle
17	Unstable	Saddle	Unstable
18	Unstable	Unstable	Saddle

In Fig. 1-9 one can see bifurcation charts of system (3) in different parametrical spaces of dimension 2 with fixed values of other parameters. It is important to note, that the bifurcation charts are presented in two variants (with different signs of $(\lambda_1 + \lambda_2 - 1)$).

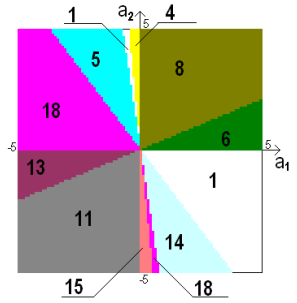

Figure.1.The bifurcation diagram of system (3) with parameters $\lambda_1 = 0.7;\ \lambda_2 = 0.2;\ c_1/c_2 = -0.1;$

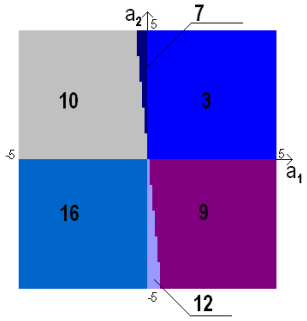

Figure.2. The bifurcation diagram of system (3) with parameters $\lambda_1 = 0.7;\ \lambda_2 = 0.8;\ c_1/c_2 = -0.1;$

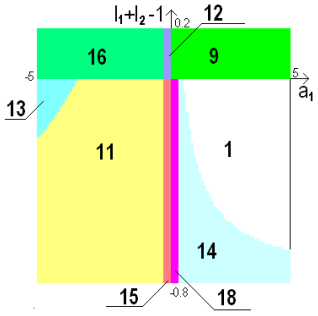

Figure.3. The bifurcation diagram of system (3) with parameters $a_2 = -3;\ c_1/c_2 = -0.1;$

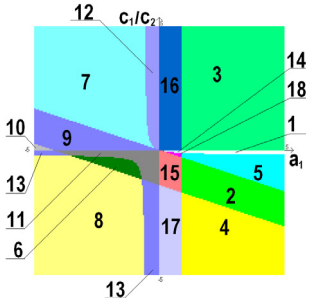

Figure.4. The bifurcation diagram of system (3) with parameters $a_2 = -3;\ \lambda_1 = 0.7;\ \lambda_2 = 0.2;$

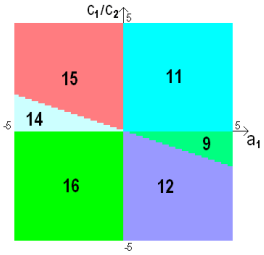

Figure.5. The bifurcation diagram of system (3) with parameters $a_2 = -3;\ \lambda_1 = 0.7;\ \lambda_2 = 0.8;$

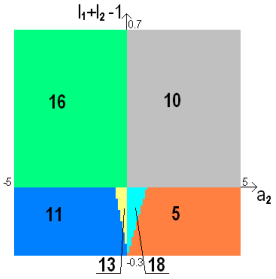

Figure.6. The bifurcation diagram of system (3) with parameters $a_1 = 1; c_1/c_2 = -0.1;$

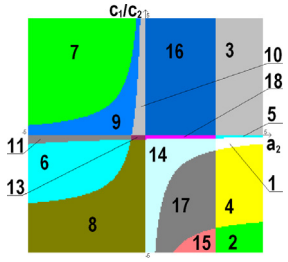

Figure.7. The bifurcation diagram of system (3) with parameters $a_1 = 1;\ \lambda_1 = 0.7;\ \lambda_2 = 0.2;$

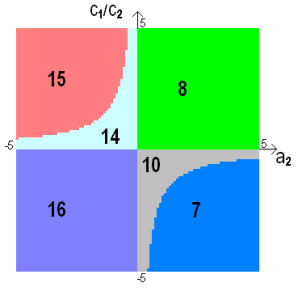

Figure.8. The bifurcation diagram of system (3) with parameters $a_1 = -2;\ \lambda_1 = 0.7;\ \lambda_2 = 0.8;$

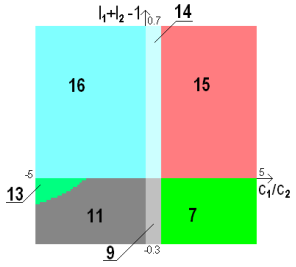

Figure.9. The bifurcation diagram of system (3) with parameters $a_1 = 1;\ a_2 = -3;$

Invariant analysis of the system shows that topology of the system is determined by values of four parameters: a_1, a_2, $(\lambda_1 + \lambda_2 - 1)$ и c_1 / c_2. It is important: are positive or negative values of parameters a_1, a_2, $(\lambda_1 + \lambda_2 - 1)$; is value of c_1 / c_2 less than zero, belongs to the interval [0; 1], or more than zero. Maximal quantity of different phase portrait topologies is equal to $3 \times 3 \times 3 = 27$. More precise analysis shows that there are only 18 topologies; 9 cases (tab. 3) are theoretically impossible.

Table 3: Impossible topologies of the system phase portraits

№	Type of point $(0;0)$	Type of point $(a_1/c_1;0)$	Type of point $(0;a_2/c_2)$
1	Stable	Stable	Stable
2	Stable	Stable	Unstable
3	Stable	Unstable	Stable
4	Stable	Unstable	Unstable
5	Saddle	Saddle	Saddle
6	Unstable	Stable	Stable
7	Unstable	Stable	Unstable
8	Unstable	Unstable	Stable
9	Unstable	Unstable	Unstable

Excluding x_1 / x_2 symmetrical cases, the system (3) is characterised by 11 types of non-equivalent phase portraits (Tab. 4) only.

Table 4: Non-equivalent phase portraits of system (3)

№	Type of point $(0;0)$	Type of point $(a_1/c_1;0)$	Type of point $(0;a_2/c_2)$
1	Stable	Stable	Saddle
2	Stable	Saddle	Unstable
3	Stable	Saddle	Saddle
4	Saddle	Stable	Stable
5	Saddle	Stable	Saddle
6	Saddle	Stable	Unstable
7	Saddle	Saddle	Unstable
8	Saddle	Unstable	Unstable
9	Unstable	Stable	Saddle
10	Unstable	Saddle	Saddle
11	Unstable	Saddle	Unstable

As an illustration, typical bifurcation, based on change of value of the birth rate of the first subpopulation, through the zero value is represented in the Fig.1.

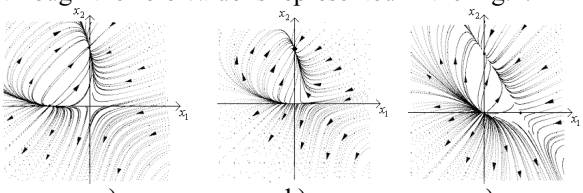

a) b) c)

Figure.10. The phase portrait of the system (3) with parameters $a_2 = 1{,}5;\ \lambda_1 = 0{,}8;\ \lambda_2 = 0{,}75;$ $c_1 = c_2 = 0{,}01;$ and a) $a_1 = -1$;b) $a_1 = 0$;c) $a_1 = 1$.

CONCLUSION:

A new degenerate model of subpopulations dynamics has been proposed. It can be used, particularly, for description of dynamics of genetically not isolated populations. It is assumed, that some specimens, born within one subpopulation, has probability to join another subpopulation by its genotype. Such probability is defined by many factors, including present and past isolation of the subsystems, character of genetic variance within the subpopulations and so on.

The model is a sketch model, similarly to Lotka-Volterra one, which is, on one hand, rather simple for its analytical research, but is quite adequate qualitatively, with possibility to use results of analytic investigation in practice.

For the analysed system, three possible equilibrium states and one stationary hyper-plane exist. Its potential bifurcations are determined by signs of special characteristic indexes of the system.

Adequacy of the model is confirmed by number of phase portraits and charts, which illustrate conditions of qualitative changes in behaviour of the system.

Bifurcation properties of the model were in the focus of the research. The bifurcations have obtained rather natural applied interpretations; and it was possible to estimate qualitatively factors, which influence on dynamics of the system. As usual, bifurcation analysis gives opportunity to find critical values of parameters, a tend to which can point for danger of essential reordering the system or even its destroying. Such analysis for ecological models, particularly, models of population dynamics, can give a tool for preventing unexpected ecological catastrophes.

BIBLIOGRAPHY:

Andronov A.A. The theory of bifurcation of dynamic systems on plane / A.A. Andronov, E.A.Leontovich, I.I.Gordon, etc. - M: Science, 1967. - 487 pages.

Bautin N. N. Methods and technique of qualitative analysis of dynamic systems on plane: / N. N. Bautin, E.A.Leontovich. – M: Science,1990.–488p.

Kuzenkov O. O. Numerical analysis of heterogeneous population dynamics / O.O.Kuzenkov, V.S. Chernyshenko//Pitannya prikladnoy mathematiki i matematichnogo modeluvanya – Dnepropetrovsk: 2007. - Page 337-346.

Lyapunov A.M. A general problem of stability of movement / A.M.Lyapunov. - L.: Publishing house of Academy of Sciences of the USSR, 1956. - T. 2. – 264 pages.

Magnitsky N. New methods of chaotic dynamics: / N.A.Magnitsky, S.V.Sidorov. - M.: Editorial, 2004. - 320 pages.

AUTHOR BIOGRAPHY

SERGE V. CHERNYSHENKO was born in Dnipropetrovsk, Ukraine and graduated from the Dnipropetrovsk State University. After obtaining PhD degree on computing in 1986, was, successively, head of Laboratory of Mathematical Modelin in Biology, head of Computer Science Department, dean of Applied Mathematics Faculty at Dnipropetrovsk National University; head of Department of Applied Mathematics and Social Informatics in Khmelnitsky National University. He was a supervisor of several Ukrainian national projects on mathematical modelling. From 2009 he is a visiting professor of Koblenz-Landau University, Faculty of Informatics. His e-mail address is svc@a-teleport.com and his website can be found at www.uni-koblenz.de/~svc

OLEXANDR O. KUZENKOV was born in Dnepropetrovsk, Ukraine and graduated from the Dnepropetrovsk National University. From 2011 he is postgraduate student of Khmelnitsky National University, Department of Applied Mathematics and Social Informatics. His e-mail address is kuzenkov1986@mail.ru.

METHODS USED TO DEVELOP HYDROGEOLOGICAL MODEL OF LATVIA

Aivars Spalvins, Janis Slangens, Inta Lace, Kaspars Krauklis, Olgerts Aleksans
Environment Modelling Centre
Riga Technical University
¼ Meza str., Riga, LV-1007, Latvia
E-mail: emc@cs.rtu.lv

KEYWORDS
Regional hydrogeological model, MODFLOW, boundary conditions, finite difference approximation.

ABSTRACT

In 2010-2012, the hydrogeological model (HM) of Latvia LAMO was established by scientists of Riga Technical University. The model will be applied for management of water resources of Latvia. The commercial program Groundwater Vistas (GV) is used for running LAMO. GV includes the MODFLOW program that is worldwide applied for development of HM. Original methods were used to develop LAMO. They took part in performing the following tasks: creating geometry of HM; arrangement of various boundary conditions (digital terrain map, hydrographical network, infiltration flow, conditions on the HM shell surface); calibration process of HM. The methods have been proposed and developed by the RTU team. Because their appliance considerably improves quality of HM they may be of interest for modelers worldwide.

INTRODUCTION

This publication is focused on methods (Spalvins et al. 2011a) used to develop LAMO. For this reason, there only scarce data are presented about applications and construction of LAMO (Spalvins et al. 2012a; Spalvins et al. 2012d). LAMO simulates steady state average hydrogeological situation of Latvia. LAMO covers the 475km×300km area (Figure 1). For the current LAMO version, the land territory of Latvia and the area of the Gulf of Riga constitute the HM active area (Figure 2). The passive area represents border territories of the neighbouring countries. The active and passive areas are separated by the 4km wide border zone that is used for fixing boundary conditions for the active area. However, LAMO is open for transboundary modeling projects. The neighbouring country must provide data for activating the HM area involved. To describe methods used for establishing LAMO, the basic mathematics of 3D-steady state models must be considered. By applying 3D-finite difference approximation, the *x, y, z* – grid of HM is built using (*h*×*h*×*m*) sized bocks (*h* is block plane size, *m* is the variable thickness of a geological layer).

The model constitutes a rectangular *p*–tiered *xy*–layer system where p is the number of geological layers. For LAMO, *p*=25, *h*=500 metres.

Figure 1: Location of LAMO

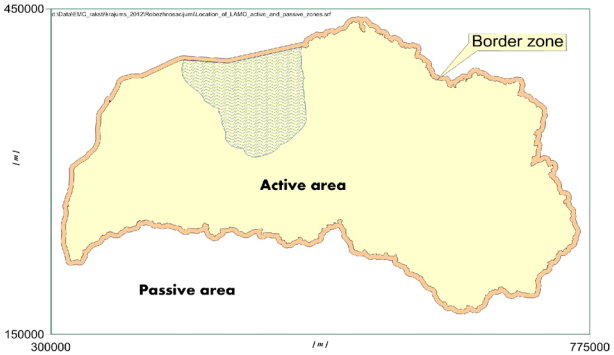

Figure 2: Location of LAMO active and passive areas

The modelling program controls the whole area of HM that contains also the passive area that takes no part in simulation. The active HM volume is enveloped by the border zone. Its outer vertical surface represents an impermeable shell that blocks transboundary groundwater flow. The relief (ground surface) and the

Proceedings 27th European Conference on Modelling and Simulation ©ECMS Webjørn Rekdalsbakken, Robin T. Bye, Houxiang Zhang (Editors)
ISBN: 978-0-9564944-6-7 / ISBN: 978-0-9564944-7-4 (CD)

lower side of the model are its geometrical top and bottom, accordingly.

Vector φ of the piezometric head is the numerical solution of the boundary field problem which is approximated in nodes of the HM *xyz*–grid by the following algebraic expression:

$$A\varphi=\beta\text{-}G\psi, \qquad A=A_{xy}+A_z \tag{1}$$

where A is the symmetric sparse matrix of the geological environment which is presented by the *xy*-layer system containing horizontal (A_{xy} - transmissivity) and vertical (A_z – vertical hydraulic conductivity) elements of the HM grid; ψ - the boundary head vector: ψ_{rel}, ψ_{bot}, ψ_{out} ψ_{riv} - subvectors of ψ that represent boundary conditions of the HM top, bottom, border zone and rivers, accordingly; G – the diagonal matrix (part of A) assembled by elements, linking the nodes where φ must be found with the points where ψ is given (for ψ_{top}, ψ_{bot}, ψ_{out} these points are nodes of the HM grid); β - the boundary flow vector. The elements a_{xy}, a_z of A_{xy}, A_z (or g_{xy}, g_z of G) are computed as follows:

$$a_{xy} = k\,m, \quad a_z = (h^2\,k)/m,\ m_i=z_{i-1}-z_i\,, \quad i=1, 2, \ \ldots, p \tag{2}$$

where z_{i-1}, z_i are elevations, accordingly, of the top and bottom surfaces of the i-th geological layer; z_0 represents the ground surface elevation ψ_{rel}-map with the hydrographical network included; k, m are, respectively, elements of digital *m, k*-maps of the computed layer thickness and permeability.

If in some areas m_i=0, then the i-th layer is discontinuous. To prevent the "division by zero", in the a_z calculation of (2), m_i=0 must be replaced by a small $\varepsilon > 0$ (for LAMO, ε=0.02 metres).

The set of z–maps represents the geometry of LAMO. Creating of these maps is the most burdensome task, because geometry of the geological environment of Latvia is very complex (Paskevicus 1997).

For the GV system (Environmental Simulations 2011), only z-maps serve as the initial ones and m-maps (thicknesses of layers) are obtained by GV itself.

In LAMO, the β–vector of flows is represented only by the withdrawal rates β_w of well fields. It is not applied for usual simulation of recharge and evaporation flows on the HM top and the flows for other boundary surfaces.

For LAMO, the ψ –conditions were applied, instead of the β–flows due to the two main reasons:

- the ψ–conditions shortened the time needed for solving of (1), because they increased impact of the matrix G as the diagonal dominance factor of A (Strang 1976; Spalvins and Slangens 2007a);
- numerical values of the ψ–conditions were known much better than the ones of the β–flows.

For LAMO, the most important are boundary conditions ψ_{rel}, ψ_{out} ψ_{riv}.

ARRANGEMENT OF BOUNDARY CONDITIONS

The digital relief map and the head distribution of the D2pr aquifer

Appliance of piezometric boundary condition ψ_{rel}, on the HM top, instead of the conventional recharge and discharge (evaporation) flows (β_{inf} –conditions for infiltration flow) has considerably reduced the effort of developing HM, especially, of the large regional models where the groundwater infiltration distribution is very complex. It must account for numerous recharge and discharge areas. No modeller is able to guesswork the right β_{inf} distribution for a large 3D HM (see Figure 6).

The ψ_{rel}-map was obtained by using the data of the Geospatial Information Agency of Latvia. Methods used to create the map are described in (Slangens and Krauklis 2011).

If the ψ_{rel} – map is used, the flow $q_{inf}=q_{aer}$ passes through the aeration (vadose) zone:

$$q_{aer}=G_{aer}(\psi_{rel}-\varphi_{Q2}) \tag{3}$$

where φ_{Q2} is the computed head (subvector of φ) for the aquifer Q_2; G_{aer} (diagonal submatrix of G) contains the vertical links g_{aer} of the aeration zone connecting the fixed ψ_{rel} with the computed φ_{Q2}. The expression (3) gives the ordinary result of HM, when a ψ-condition is applied. As a rule, even the first run of HM provides feasible results for q_{inf}.

The vertical links g_{aer} of the diagonal matrix G_{aer} are controlling the q_{aer} distribution. Values g_{aer} depend on h^2, k_{aer} and m_{aer} (formula (2)) where h=500, k_{aer} and m_{aer} are, accordingly, the permeability and the thickness of the aeration zone. Initially, k_{aer} and m_{aer} are unknown. In nature, $m_{aer}=\psi_{rel}-\varphi_{Q2}$ if $q_{aer}>0$. If $q_{aer}<0$ then, in LAMO, m_{aer}=0.02. The negative infiltration flow is caused mainly by lowlands, rivers and lakes. First, the following values of the aeration zone were tried: m_{aer}=0.02 [m], $k_{aer}=10^{-6}$ [m/day] (for recharge areas); $k_{aer}=10^{-4}$ [m/day] (for areas of lakes and sea); $k_{aer}=10^{-8}$ [m/day] (for areas of swamps).

To avoid iterative changes of the HM geometry, during calibration of HM, m_{aer}=0.02 was kept constant, until the calibrated q_{aer}–flow was obtained (Figure 6) by adjusting the k_{aer}–distribution.

The piezometric head distribution ψ_{D2pr} of the D2pr aquifer is applied as the boundary condition on the LAMO bottom surface (z=25). The ψ_{D2pr}-map was obtained by using information of (Dzilna 1970). Influence of ψ_{D2pr} is small, because it is separated from the HM body by the thick regional D2nr aquitard.

There are two reasons for application of this boundary condition: it may be useful if a modeller carries out research regarding the role of tectonic faults of the D2nr aquitard; the D2pr aquifer contains drinking water at the North-East part of Latvia.

Design of Boundary Conditions for the Border Zone

Due to the presence of the HM passive area, the outer vertical surface of the boundary zone (shell) is impermeable for the transboundary groundwater flow. This factor distorts the natural groundwater regime in the close vicinity of the shell. Because the border zone width is 4km, the distortion is smaller on the inner surface of the zone. There exists the flow q_{out} passing through this surface. One must try to recover the natural groundwater regime on this border surface. It can be done by fixing auxiliary boundary conditions ψ_{out} on the middle line of the border zone. As the initial data for obtaining ψ_{out} of aquifers, three data sources were used that provided linewise information: the ψ_{rel} −map; ψ_{out} for the D2ar aquifer; data extracted from the head distribution map of the prequaternary surface $\varphi_{preQ.}$ The φ_{preQ} −surface can provide only fragments of ψ_{out} that can be observed from the bird's eye view. Special software was developed for extracting these data and for providing information that was necessary to design the interpolation tool that provided ψ_{out} for aquifers of HM. Principles used to create the tool were reported in (Spalvins 2002). The design of the interpolation tool is based on the fact that a set of vertical links a_z exists along the middle line of the border zone, which join the neighbouring aquifers. These links account both for the k and m parameters of the aquitards (formula (2)). If values of these links are considerably enlarged (at least, 1000 times), then this set of transformed vertical links behaves like a spatial interpolation device. It provides the unknown components of ψ_{out} for aquifers. The above mentioned software detected these locations of the aquitards where they existed (m≠0). For the m=0 areas, no transformation of the a_z −values was done.

Therefore, the ψ_{out} boundary condition is obtained by HM itself, as follows: the components originated from the ψ_{rel}, φ_{D2ar}, φ_{preQ}−maps are fixed as the initial ones; the other components of ψ_{out} are supported by the spatial interpolation tool that contains transformed a_z−links. The interpolator is not a part of the LAMO active volume and it can be used permanently. This feature is very useful during the HM calibration when the a_z −set gets changed and the ψ_{out} conditions follow these changes.

Rivers as boundary conditions

The conditions ψ_{rel} , ψ_{D2pr} , ψ_{out} are fixed on the outer surfaces of HM and they exist in the nodes of the HM grid. The condition ψ_{riv} that represents water levels of rivers is attached to inner nodes of the HM grid via the set of the river bed conductance matrix $G_{riv.}$ The flow q_{riv} caused by rivers is given by the expression:

$$q_{riv} = G_{riv} (\varphi_{riv} - \psi_{riv}) \qquad (4)$$

where the diagonal matrix G_{riv} is a part of G; ψ_{riv} is subvector of ψ, φ_{riv} represents these nodes where the corresponding components of ψ_{riv} are attached via the links belonging to G_{riv}. Components of ψ_{riv} belong to a set of points located outside the HM grid. The value of a single element g_{riv} of G_{riv} is presented by the formula:

$$g_{riv} = h\, w_{riv}\, k_{riv} / m_{riv} \qquad (5)$$

where h=500 (plane step); w_{riv} − the river width; k_{riv}, m_{riv}−permeability and thickness of the river bed layer, accordingly; these parametres are unknown. Value m_{riv}=1 was fixed and k_{riv}=0.008 was found experimentally. Therefore, as the initial try, the formula (5) gives g_{riv}=4w_{riv}. For LAMO, rivers are presented by their middle lines. The only exception is three artificial lakes of the Daugava river that have been formed by the Riga, Kegums, Plavinas hydro electrical power plants.

To obtain the ψ_{rel} −conditions (formulas (4) and (5)), the following items were prepared: the xy −location of a river line; the long line profile (water levels ψ_{riv} of a river along its line); the width w_{riv} of a river along its line; the z−attachment g_{riv} of a river line.

The last item accounts for the fact that a river, on its run, may be joined with different geological layers. For example, the river Gauja runs through the Quaternary, the lower and upper Devonian layers. As about 200 rivers of Latvia are included in LAMO, no modeller is able to join them properly with a model. It was necessary to develop special software for preparing all data files that are needed for creating the ψ_{riv}−conditions.

The program also performed the search for the river z −attachment. Presently, the empirical value k_{riv} =0.008 is applied for all rivers. In nature, k_{riv} may be different not only for each river, but also for their fragments. The elements g_{riv} can be controlled also by changing the value of m_{riv} for formula (5). The task of finding more realistic k_{riv} distributions is very complex, because observed in nature river flows of (4) must be used. Knowledge of these flows provides more exact estimates of the interaction between groundwater and rivers.

CREATING OF Z-MAPS

The most time consuming part of developing LAMO was preparation of the digital z-maps that served as initial data for the GV system. For LAMO, most of the layers are outcropping (Figure 3). They are not continuous, and for this reason, they are not existing everywhere in the area of HM.

The geometry of LAMO is based on the geological information accumulated by the Latvian Environment, Geology and Meteorology Centre (LEGMC). The information includes stratigraphical data of boreholes, geological maps and descriptions regarding geology of Latvia. The LAMO geometry results in the set of z−maps. It includes 26 surfaces for 25 geological layers presented in HM. The top surface of HM (z=0) is the digital hydrogeological relief of Latvia. It includes the

hydrographical network (rivers, lakes, sea). The z=1 surface is the digital geological relief. It represents the ground surface elevations. For LAMO, this map accounts for depth of the sea and of three artificial lakes of hydro electrical power plants of the Daugava river. These two maps were created by using data provided by the Geospatial Information Agency of Latvia (Slangens and Krauklis 2011).

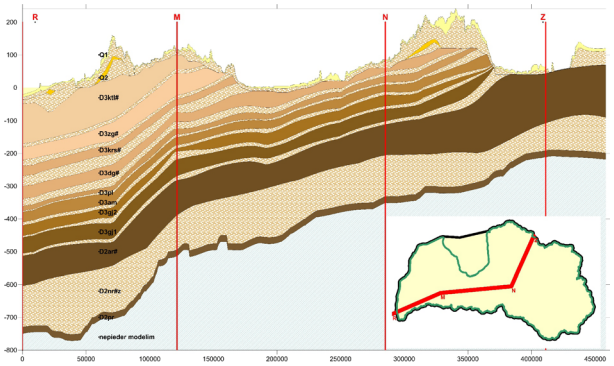

Figure 3: Geological cross section

The LEGMC specialists have prepared two important geological maps: the prequaternary surface preQ (z=6), the D2pr surface (z=24). They are presented in Figure 4 and Figure 5, accordingly. The volumes of the Quaternary and primary geological layers are included between the z=0, z=6 and z=24 surfaces, correspondingly.

The most time consuming and difficult task (Spalvins et al. 2012b) was creating of z–maps for the primary geological layers (z=7, 8, …, 23). The basic stratigraphical information is carried by the boreholes and elevations of geological borderlines located on the preQ surface (Figure 4). The number of borehole data provided by LEGMC was large (about 20×10^3). However, very often data of boreholes were contradictory and it was not always possible to mend them. To reduce laborious work of checking the quality of all available borehole data, the set of representing geological cross sections was used where the chosen boreholes with trustworthy data were located. Deep boreholes were used, which provided stratigraphical data for all geological layers of the HM. As a rule, data gaps occurred along a section laterally and vertically (along a borehole axis). These gaps were filled by complementary data that were concordant with the existing borehole data. The z–maps must always give positive thicknesses m. For this reason, the data of the sections must match this condition for layers of HM.

The m=0 areas of discontinuous layers also must be accounted for. It is done by using $m=\varepsilon$=0.02 instead of the zero thickness. There are three main reasons why the value of ε must be small for the m=0 areas: geometrical distortions are minimal even if the number of overlaying m=0 areas is large (northern part of Latvia); transmissivity $T=\varepsilon k$ of aquifers is small even if their permeability k is considerable; vertical conductivity g_v of aquitards $g_v=h^2k/\varepsilon$ is large even if their permeability k is small.

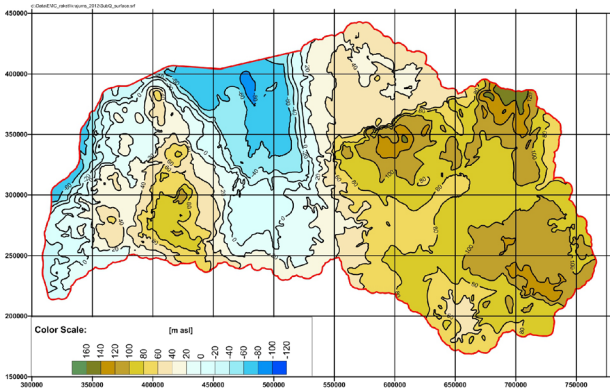

Figure 4: The prequaternary preQ surface (z=6)

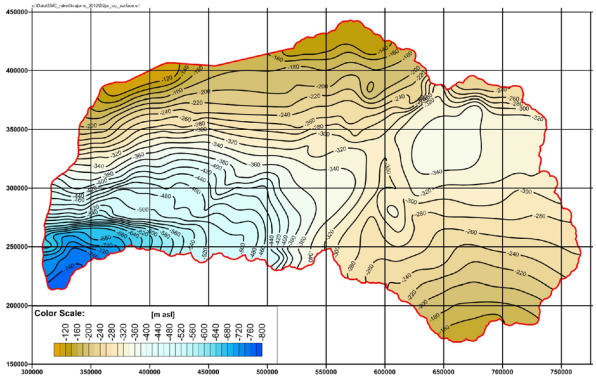

Figure 5: The D2pr top surface (z=24)

If ε=0.02 then LAMO in its m=0 areas behave normally without special control measures for outcropping strata. This first stage of preparing data for z–maps was performed by using the EXCEL system (Walkenbach 2009).

During the second stage of preparing z–maps, the SURFER system (Golden Software 2010) was applied for obtaining a preliminarily version of the maps. The pointwise data prepared by EXCEL and spaced out pointwise data carried by the geological borderlines were used by SURFER.

Unfortunately, the SURFER system cannot provide good z–maps, because of the following reasons: only pointwise data can be processed and their number is limited; the maximum – minimum principle is not insured for output data; the condition m>0 is often violated; for the m=0 areas, the requirement ε=0.02 is neglected. However, results obtained by SURFER provided valuable information for correcting possible errors of initial data.

The final version of z–maps was obtained by the Geological Data Interpolation (GDI) system (Spalvins and Slangens 2007b). GDI uses points, lines and

surfaces as data carriers. By interpolating pointwise data along lines of cross sections, much more informative concordant linewise data are obtained. GDI applies data of the cross sections, of the geological borderlines and of surfaces that are extracted from the preQ surface map (Figure 4).

For example, GDI reproduces the whole top surface of the D3ktl aquifer (z=6). For other deeper layers, GDI uses fragments of surfaces that are enclosed between neighbouring borderlines on the preQ map.

Geometry of buried valleys and cuts of rivers in the body of primary geological layers were not simulated by LAMO. Accounting for the buried valleys is difficult and the data about the material that fills them are uncertain. The cuts of rivers were taken into account indirectly when rivers were input into LAMO (Spalvins et al. 2012c; Spalvins et al. 2011b)

CALIBRATION PROCESS

After all the necessary digital maps have been uploaded into the GV system, the model starts functioning and its calibration has to be accomplished.

Due to unavoidable limitations in the initial data, HM has no unique solution of (1). Calibration of HM is a controlled iterative process involving the addition of complementary data, until HM of a required quality is obtained. The quality is checked and maintained by tracing calibration targets. The following targets are usually set:

- original data should not be contradicted by data generated by HM; for example, the ψ and φ distributions of (1) must reproduce observed head values, the matrix A must incorporate observed permeability and geometrical features of k and z−maps, etc.;
- within the HM body, groundwater flows should not reach unnaturally large values (infiltration flow, flows regarding the hydrological network, etc.);
- results of HM must confirm the real hydrogeological situation, because formal agreement between computed and observed target data does not assure correct simulation; unfortunately, automatic calibration tools can sometimes provide almost worthless results.

The first and second targets are formal components of HM, but the third target always requires subjective evaluation.

The calibration will never succeed if serious HM errors are present. Problems can include faults in data coordinates or values, mistakes in geological layer identification, mismatched reference data, unreliable boundary conditions or inadequate software.

The main subjects controlled during LAMO calibration were the k-maps of aquitards, because their filtration parameters were unknown.

A valuable instrument of searching for the right k-maps was distributions of vertical flows passing between neighbouring layers. The flows were computed by the SURFER program, as follows:

$$q_{i,i+1}= 0.73\times10^{6}(\varphi_i-\varphi_{i+1}) / (m_i / k_i+ m_{i+1} / k_{i+1}) \qquad (6)$$

where $q_{i,i+1}$ was the vertical flow [mm/year] passing between the i-th and i+1-th layers. The formula holds even if both m_i and m_{i+1} are representing the "zero" m=0.02 areas.

The k-maps have the following structure:

$$k=k_c\, k_{out} \qquad (7)$$

where k_c and k_{out} are, accordingly, the core and outer diagonal k-matrixes. The k_c matrix has no dimension and its basic value is 1.0. In the course of calibration, some areas of k_c must be changed to values that are larger or smaller than the base value 1. The matrix k_{out} serve as the general factor for controlling the k-map for all nodes of an HM grid plane.

The most important is calibration of the k_{aer} –map for the aeration zone aer. Initially, its core matrix k_c values are 100.0 and 0.01 for areas of lakes and swamp areas, respectively. The following formula was used for correcting the initial k_c matrix

$$k_c = k_c\, c, \quad c=1, \text{ if } \Delta\le M \quad \text{or} \quad c=(M/\Delta)^n \text{ if } \Delta>M, \quad \Delta= \psi_{rel} -\varphi_{Q2} \qquad (8)$$

where c is the correction matrix; the parameter M accounts for limitedness of the flow if $\Delta>M$ [metres].

For the areas where $\Delta>M$, the flow q_{aer} gets limited, as follows:

$$q_{aer}=k_{aer}\, M^n\, \Delta^{1-n} /0.02. \qquad (9)$$

If n=1, q_{aer} does not depend on Δ. Then q_{aer} is controlled by the parameters k_{aer} and M. For LAMO, the empirical values M=4 and n=0.75were used.

By using the formula (9), a rather smooth limitation of the infiltration flow q_{aer} was achieved for highland areas (Figure 6). Formula (9) was used also for other aquitards of HM.

During the calibration process, the thickness m_{aer} =0.02 of the aer-zone is kept unchanged. As the final step, the real thickness m_{aer} of must be obtained:

$$m_{aer} =0.02 \text{ if } \Delta\le0.02 \quad \text{or} \quad m_{aer} =\Delta \text{ if } \Delta>0.02$$
$$\Delta= \psi_{rel} -\varphi_{Q2}, \quad k_{aer} = (k_{aer})_c\, c, \quad c = m_{aer} / 0.02 \qquad (10)$$

where $(k_{aer})_c$ is the calibrated value and c is the correction matrix where its elements have values 1 and m_{aer} / 0.02 if m_{aer}=0.02 and Δ, correspondingly.

If for the *aer* zone, its real thickness m_{aer} is obtained, then the thickness $(m_{Q2})_c$ decreases: $m_{Q2}=(m_{Q2})_c - m_{aer}$.

It happens that m_{Q2} <0. It means that the Q2 aquifer there is drained of.

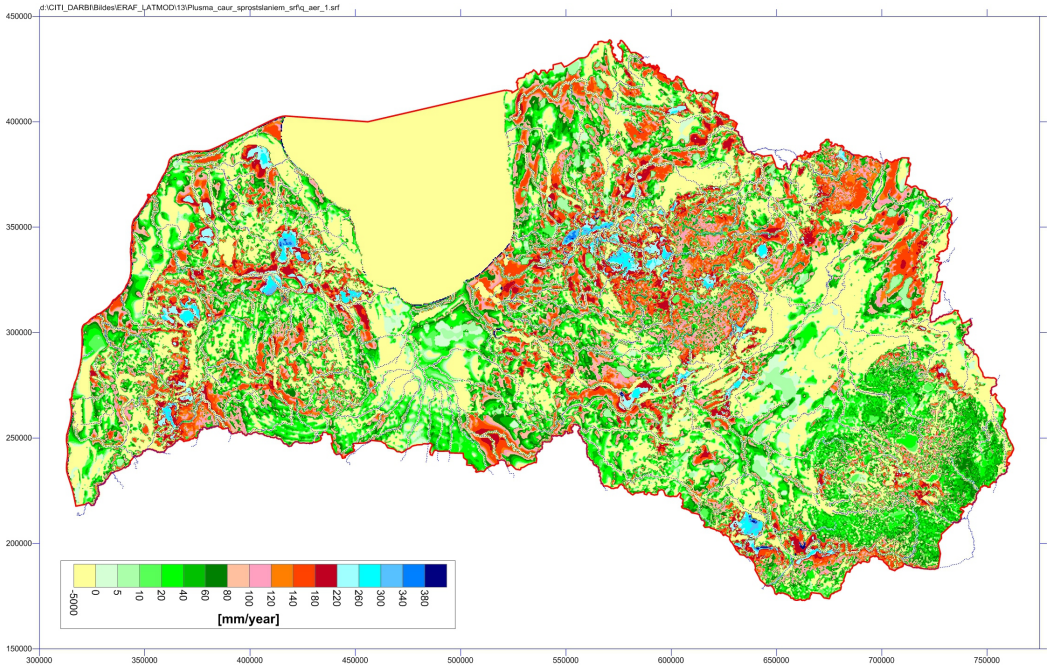

Figure 6: Calibrated q_{aer} distribution [mm/year]

To avoid considerable changes of the HM geometry, the assumption was made that, at least 0.2m of the Q2 aquifer remained saturated. This assumption is hold if m_{aer} is changed, as follows:

$$(m_{aer})_c = m_{aer} \text{ if } m_{Q2} > 0.2 \text{ or } (m_{aer})_c = c\, m_{aer} \text{ if } m_{Q2} \le 0.2, \quad c = (1 + (m_{Q2} - 0.2)/m_{aer}); \quad (11)$$
$$\text{when } c\, m_{aer} < 0.02 \text{ then } (m_{aer})_c = 0.02$$

where $(m_{aer})_c$ is the changed value of m_{aer}; $c \le 1$ is the correction factor.

Table 1: Groundwater flow [thous.m^3/day] distribution

Code of aquifer	Top flow q_{top}	Bottom flow q_{bot}	Inflow (2+3) q_{in}	Rivers flow q_{riv}	Boundary flow q_{out}	Withdrawal flow β_w	Balance (4+5+6+7)
1	2	3	4	5	6	7	8
Q2	6782	-3392	3390	-3233	-100	-57	0
Q1	3392	-3368	24	-2	-22	0	0
D3ktl	3368	-3171	197	-193	-3	-1	0
D3zg	3171	-3102	69	-42	-22	-5	0
D3krs	3102	-3078	24	-12	-8	-4	0
D3dg	3078	-2465	613	-592	-16	-5	0
D3pl	2465	-1965	500	-413	-70	-17	0
D3am	1965	-1822	143	-97	-45	-1	0
D3gj2	1822	-1437	385	-271	-89	-25	0
D3gj1	1437	-959	478	-349	-103	-26	0
D2ar	959	-103	856	-466	-360	-30	0
Model	6782	-103	6679	-5670	-838	-171	0
Q1+Q2	6782	-3368	3414	-3235	-122	-57	0
Primary aquifers	3368	-103	3265	-2435	-716	-114	0

After dewatering of the Q2 aquifer, it was necessary to continue the calibration process.

Presently, the residual (difference between monitored and computed φ values) does not exceed 1.7 metres (quadratic error) and 2% (relative error).

The preliminarily version of flow distribution for LAMO aquifers is presented by Table 1. There the total flow of rivers q_{riv} was the calibration target. Its rough value was obtained from the book (Dzilna 1970). It follows from Table 1 that the mean infiltration is 6782×0.365/64.5=38 mm/year (64.5 thous.km^2 is land area of Latvia).

However, the calibration process of LAMO is not completed, because the links of the hydrographical network with the HM body are yet not adjusted properly.

CONCLUSIONS

The hydrogeological model of Latvia has been developed. To create the model, original methods were used to obtain maps representing complex geometry of the geological environmental of Latvia and to arrange various types of boundary conditions (digital relief map, conditions regarding hydrographical network, etc.). Effective methods were used to calibrate HM.

LAMO was developed in framework of the Project "Creating of hydrogeological model of Latvia to be used for management of groundwater resources and for evaluation of their recovery measures". The Project was co-financed by the European Regional Development Fund.

REFERENCES

Dzilna, I. 1970. Resources, composition and dynamics of groundwater for the middle part of the Baltic area. Zinatne, Riga, p. 197 (in Russian)

Environmental Simulations, 2011. Inc. Groundwater Vistas. Version 6, Guide to using.

Golden Software. 2010. SURFER-9 for Windows. Users Manual.

Paskevicus, J. 1997. The geology of the Baltic republics. Vilnius university, Vilnius, p. 387, ISBN 9986-623-20-0

Slangens, J. and K. Krauklis. 2011. "Creating of digital relief map for regional hydrogeological model of Latvia". *Scientific Journal of Riga Technical University in series "Computer Science". Boundary Field Problems and Computer Simulation,* vol. 5, 49. (53)–th issue, Riga, RTU, 21-25

Spalvins, A.; J. Slangens; O. Aleksans; K. Krauklis; and I. Lace. 2012a. „Regional hydrogeological model of Latvia for management of its groundwater resources". *In Proceedings 5-th International scientific conference Applied information and communication technologies,* 24.-26. april 2012, Jelgava, Latvia, 135-155 (CD)

Spalvins, A.; J. Slangens; I. Lace; K. Krauklis; O. Aleksans; and N. Levina. 2012b. "Methods and software tools used to designate geometry for regional hydrogeological model of Latvia". *Scientific Journal of Riga Technical University Boundary Field Problems and Computer Simulation*, 51-th issue, Riga, RTU, 13-19, ISSN 1407 – 7493

Spalvins, A.; J. Slangens; I. Lace; and K. Krauklis. 2012c. "Arrangement of boundary conditions for hydrogeological model of Latvia". *Scientific Journal of Riga Technical University Boundary Field Problems and Computer Simulation,* 51-th issue, Riga, RTU, 20-24, ISSN 1407 – 7493

Spalvins, A.; J. Slangens; I. Lace; K. Krauklis; V. Skibelis; O. Aleksans; and N. Levina. 2012d. "Hydrogeological model of Latvia, first results". *Scientific Journal of Riga Technical University Boundary Field Problems and Computer Simulation,* 51-th issue, Riga, RTU, 4-13, ISSN 1407 – 7493

Spalvins, A.; J. Slangens; K. Krauklis; and I. Lace. 2011a. "Methods and tools to be applied for creating of regional hydrogeological model of Latvia". *In Proceedings 25th European Conference on Modelling and Simulation*, June 7-10, 2011, Krakow, Poland, 132-141, (ISBN: 978-0-9564944-2-9)

Spalvins, A.; J. Slangens; K. Krauklis; I. Lace; and V. Skibelis. 2011b. "Creating of initial data maps for regional hydrogeological model of Latvia". *Scientific Journal of Riga Technical University in series "Computer Science". Boundary Field Problems and Computer Simulation*, vol. 5, 50–th issue. Riga: RTU, 14-22

Spalvins, A. and J. Slangens. 2007a. "Impact of boundary conditions on quality of hydrogeological models". *Proceeding of Riga Technical University in series Computer Science. Boundary Field Problems and Computer Simulation* , vol. 5, 33(49)–th issue. Riga: RTU, 108-116

Spalvins, A., and J. Slangens, 2007b. "Reliable data interpolation method for a hydrogeological model conductivity matrix". *In Proceedings Sixth International Conference on "Calibration and Reliability in Groundwater Modeling. Credibility in Modelling"*. Vol.2, 9-13 September 2007, Copenhagen, Denmark, 137-142

Spalvins, A. 2002. "Modelling as a powerful tool for predicting hydrogeological change in urban and industrial areas". *K.W.F. Howard and R.G. Israfilov (eds.) Current problems of Hydrology in Urban Areas. Urban Agglomerates and Industrial Centres*. Kluwer Academic Publishers. Printed in Netherlands, 57-75.

Strang, G. 1976. Linear algebra and its applications. Academic Press, New York, 373 INC.

Walkenbach, J. 2007. Excel 2007 Bible. Wiley Publishing, Inc., Indianapolis, Indiana, p. 808

AUTHOR BIOGRAPHIES

AIVARS SPALVINS was born in Latvia. In 1963, he graduated from Riga Polytechnic Institute (since 1990, Riga Technical University) as a computer science engineer. In 1967, A. Spalvins received the degree of Cand.Sc. (Dr.sc.). A. Spalvins has been with the university since 1958 (as a student) until now. His present scientific interests are computer modeling of groundwater flows and migration of contaminants. He is Director of the Environment Modelling Centre of the University. His e=mail address is: emc@cs.rtu.lv
and the Centre Web-page is http://www.emc.rtu.lv

JANIS SLANGENS was born in Latvia. In 1969, he graduated from Riga Polytechnic Institute (since 1990, Riga Technical University) as a computer science engineer. In 1985, J. Slangens received the degree of Cand. Sc (Dr.sc.). Since 1969, he was with the the University. He is a senior researcher of the Environment Modelling Centre. His present scientific interests are computer modeling of groundwater flows. E-mail: emc@cs.rtu.lv

INTA LACE was born in Latvia. In 1971, she graduated from Riga Polytechnic Institute (since 1990, Riga Technical University) as a computer science engineer. In 1995, I. Lace received the degree of M.sc. (applied computer science). Since 1991, she is a researcher of the Environment Modelling Centre, Faculty of Computer Science and Information Technology. E-mail: emc@cs.rtu.lv

OLGERTS ALEKSANS was born in Latvia. In 1979, he graduated from Vilnius State University (since 1988, The University of Vilnius) as a hydro geologist & engineering geologist. In 2011, O. Aleksans received the Doctoral Degree in Geology at the University of Latvia. In the time period from 1997 till 2011 he was one of the company's VentEko Ltd founders and its Scientific Director. From 2011 he works as the researcher in the Environment Modeling Centre of Riga Technical University. E-mail: olgerts.aleksans@gmail.com

KASPARS KRAUKLIS holds M.Sc. degree of engineering science in computer systems from Riga Technical University (2007) and the certificate in Teaching of Engineering Sciences from RTU Institute of Humanities (2005). Currently he works as a researcher in the Environment Modelling Centre of Riga Technical University. E-mail: emc@cs.rtu.lv

STRUCTURE ADAPTATION OF MODELS DESCRIBING SCHEDULING PROCESSES IN COMPLEX TECHNICAL-ORGANIZATIONAL SYSTEMS (CTOS)

Dmitry Ivanov
Berlin School of Economics and Law,
Chair of International Supply Chain Management,
10825 Berlin, Germany
E-Mail: divanov@hwr-berlin.de

Boris V. Sokolov, Semyon A. Potryasaev,
Vjasheslav A. Zelentsov, Olga V. Brovkina
Russian Academy of Science,
Saint Petersburg Institute of Informatics and Automation
(SPIIRAS)
39, 14 Linia, VO
St.Petersburg, 199178, Russia
E-mail: sokol@iias.spb.su, semp@mail.ru

KEYWORDS

Complex technical systems, planning and scheduling, structure adaptation of models.

ABSTRACT

In this paper, a dynamical multiple criteria model of integrated adaptive planning and scheduling for complex technical – organizational system (CTOS) is presented. Various types of CTOS are used nowadays, for example: virtual enterprises, supply chains, telecommunication systems, etc. Hereafter, we mostly interpret CTOS as the systems of the above-mentioned types. The above-mentioned CTOS peculiarities do not let produce an adequate description of control processes in existing and designed CTOS on a basis of single-class models. That is why the concept of integrated modeling and simulation that was proposed by the authors can be useful here. Possible directions of its realization were considered in their papers and books (Okhtilev et al.,2006, Ivanov et al., 2010).
Here we consider two general actual problems of the CTOS structure-dynamics investigation: the problem of selection of optimal CTOS structure-dynamics control programs at different states of the environment; the problem of structural adaptation of models describing CTOS structure-dynamics control programs.

INTRODUCTION

In practice the processes of CTOS operation are non-stationary and nonlinear. The perturbation impacts initiate the CTOS structure-dynamics and predetermine a sequence of control inputs compensating the perturbation. In other words we always come across the CTOS structure dynamics in practice. There are many possible variants of CTOS structure dynamics control (Ohtilev et al., 2006).
In this paper we propose new approach to the problem of structure adaptation of models describing CTOS structure-dynamics program control. Existence of various alternative descriptions for CTOS elements and control subsystems gives an opportunity of adaptive models selection (synthesis) for program control under changing environment.
Mathematical research of control processes in CTOS can be divided into three primary approaches: optimization, simulation, and heuristics. Optimization is an analysis method that determines the best possible method of designing a particular complex system. Earlier literature presents several optimization-based approaches to CTOS operation planning and scheduling. For instance, (Ivanov et al., 2010) have applied integer programming in supporting partner selection. (Ip et al., 2004) presented a branch and bound algorithm for subcontractor selection in agile manufacturing environment.
Simulation is imitating the behaviour of one system with another. By making changes to the simulated adaptive supply chains (ASC), one expects to gain understanding of the ASC dynamics. Simulation is an ideal tool for further analyzing the performance of a proposed design derived from an optimization model. Regarding the ASC complex adaptive systems (CAS) and multi agent systems (MAS) are one of the most popular simulation techniques (Swaminanthan et al. 1998; Rabelo et al., 2002). The past research on utilization of the MAS to the ASC have been mostly dealing with agent based frameworks and software architectures. It is mostly underestimated that these paradigms offer a valuable theoretical perspective on decentralized network management. (Nillson and Darley, 2006) proposed to combine CAS and MAS and to use the CAS as theoretical approach and MAS the implementation method. (Kuehnle, 2007) considers agents as a part of the complex of interrelated models for ASC planning.
Heuristics are intelligent rules that often lead to good, but not necessarily the best solutions. Heuristic approaches typically are easier to implement and require less data. However, the quality of the solution is usually unknown. Unless there is a reason that optimization cannot be used, heuristics are an inferior approach. In the ASC settings the nature based heuristics such as genetic algorithms (Huang et al., 2005) and Ant Colony Optimization (ACO) (Teich, 2003) are usually used. For instance, (Fischer et al., 2004) elaborated an approach for optimizing the selection of partners in production networks based on an ACO-algorithm.
In this paper we present a new integrated approach to planning control process in CTOS. It accumulates three above-mentioned approaches.

Proceedings 27th European Conference on Modelling and Simulation ©ECMS Webjørn Rekdalsbakken, Robin T. Bye, Houxiang Zhang (Editors)
ISBN: 978-0-9564944-6-7 / ISBN: 978-0-9564944-7-4 (CD)

Our investigations are based on results of the CTOS adaptive control theory which is being developed now by Professor Skurihin V.I in Ukraine (Skurihin et al., 1989). The analysis of known investigations on the subject (Skurihin et al., 1989, Rastrigin, 1981, Bellman, 1972, Fleming, 1975, Nillson and Darley, 2006), confirms that the traditional tasks of CTOS control should be supplemented with procedures of structural and parametric adaptation of special control software (SCS). Here the adaptive control should include the following main phases:

− parametric and structural adaptation of structure-dynamics control (SDC) models and algorithms to previous and current states of objects-in-service (SO), of control subsystems (CS), and of the environment;
− integrated planning and scheduling of CTOS operation (construction of SDC programs);
− simulation of CTOS operation, according to the schedules, for different variants of control decisions in real situations and analysis of planning and scheduling simulation;
− structural and parametric adaptation of the schedule, control inputs, models, algorithms, and SDC programs to possible (predicted by simulation) states of SO, CS, and of the environment,
− realization of CTOS structure-dynamics control processes.

To implement the proposed concept of adaptive control let us consider two groups of parameters (Skurihin et al., 1989, Rastrigin, 1980, 1981) for CTOS SDC models and algorithms: parameters that can be evaluated on the basis of real data available in CTOS; parameters that can be evaluated via simulation models for different scenarios of future events.

The adaptation procedures can be organized in two blocks (models) (Ohtilev, 2006, Skurihin et al., 1989, Ivanov et al., 2010, 2012): external adapter of planning and scheduling models; internal adapter of planning and scheduling models.

When the parametric adaptation of SCS does not provide simulation adequacy then the structural transformations can be needed. Two main approaches to structural model adaptation are usually distinguished (Bellman, 1972, Rastrigin, 1980, 1981). The first approach lies in the selection of a model from a given set. The model must be the most adequate to SO and CS. The second approach stands for CTOS SDC model construction of elementary models (modules) in compliance with given requirements. The second approach provides more flexible adjustment of SO and CS for particular functioning conditions. However, the first one is faster and can be effective if the application knowledge base is sufficiently large.

Both approaches need active participation of system analysts and decision-makers who interact with special control software of simulation system (SIS) and consider hard-formalizing factors and dependences within the general procedure of CTOS SDC program selection.

Let us consider formal statement of structural and parametric adaptation problems for CTOS SDC models and after that we are going to investigate the problem of parametric adaptation for models describing CTOS structure-dynamics control. Adaptation of algorithms and control software does not belong to the scope of this paper.

We have implemented the conceptual model and technology of parametric and structural adaptation of models describing CTOS SDC processes via original simulation system (SIS). This simulation system consists of the following elements (Moiseev, 1974, Sowa, 2002): a) simulation models (the hierarchy of models); b) analytical models (the hierarchy of models) for a simplified (aggregated) description of objects being studied; c) informational subsystem that is a system of data bases (knowledge bases); d) control-and-coordination system for interrelation and joint use of the previous elements and interaction with the user (decision-maker).

In this paper we want to describe and to investigate concrete algorithm of structure models adaptation via integrated modeling and simulation procedures that are realized in the SIS.

PROBLEM STATEMENT

We assume that there are several variants of CTOS SDC models inscribed in the set

$$\overline{\overline{M}} = \{M_1, M_2, \ldots, M_W\} = \{M_\Theta, \Theta \in I\}, I = \{1, \ldots W\},$$

moreover the vector $\vec{\beta}$ of CTOS parameters includes the subvector $\vec{\beta}_0$ of fixed CTOS characteristics and besides of it the subvector $\vec{w} = \left\| \vec{w}^{(1)\mathrm{T}}, \vec{w}^{(2)\mathrm{T}}, \vec{w}^{(3)\mathrm{T}} \right\|^{\mathrm{T}}$ of parameters being adjusted through SS external/internal adapter or defined within structural adaptation. According to (Skurihin et al., 1989), these parameters can be divided into the following groups: $\vec{w}^{(1)}$ is a vector of parameters being adjusted through the internal adapter; $\vec{w}^{(2)}$ is a vector of parameters being adjusted through the external adapter; $\vec{w}^{(3)}$ is a vector of parameters being adjusted within structural adaptation of CTOS SDC models.

Now we can present the modified multiple-model multi-criteria description of CTOS SDC problems:

$$\vec{J}_\Theta\left(\vec{x}(t), \vec{u}(t), \vec{\beta}, \vec{\xi}(t), t\right) \to \underset{\vec{u}(t) \in \Delta_\Theta}{extr}, \quad (1)$$

$$\Delta_\Theta = \left\{ \vec{u}(t) \middle| \vec{x}(t) = \vec{\phi}_\Theta\left(T_0, \vec{x}(T_0), \vec{x}(t), \vec{u}(t), \vec{\xi}(t), \vec{\beta}_\Theta, t\right) \right\}, \quad (2)$$

$$\vec{y}(t) = \vec{\psi}_\Theta\left(\vec{x}(t), \vec{u}(t), \vec{\xi}(t), \vec{\beta}_\Theta, t\right), \quad (3)$$

$$\vec{x}(T_0) \in X_0\left(\vec{\beta}_\Theta\right), \vec{x}(T_f) \in X_f\left(\vec{\beta}_\Theta\right), \quad (4)$$

$$\vec{u}(t) = \left\| \vec{u}_{pl}^{\mathrm{T}}(t), \vec{v}^{\mathrm{T}}\left(\vec{x}(t), t\right) \right\|^{\mathrm{T}};$$

$$\vec{u}_{pl}(t) \in Q_\Theta\left(\vec{x}(t), t\right);$$

$$\vec{v}\left(\vec{x}(t),t\right)\in V_{\Theta}\left(\vec{x}(t),t\right);$$
$$\vec{\xi}(t)\in \Xi_{\Theta}\left(\vec{x}(t),t\right);\vec{\beta}_{\Theta}\in B;\vec{x}(t)\in X\left(\vec{\xi}(t),t\right);$$
$$\vec{\beta}_{\Theta}=\left\|\vec{\beta}_0^{\mathrm{T}}\vec{w}^{\mathrm{T}}\right\|^{\mathrm{T}};\ \vec{w}=\left\|\vec{w}^{(1)\mathrm{T}},\vec{w}^{(2)\mathrm{T}},\vec{w}^{(3)\mathrm{T}}\right\|^{\mathrm{T}}. \quad (5)$$

The formulas define a dynamic system describing CTOS structure-dynamics control processes. Here $\vec{x}(t)$ is a general state vector of the system, $\vec{y}(t)$ is a general vector of output characteristics. Then, $\vec{u}(t)$ and $\vec{v}\left(\vec{x}(t),t\right)$ are control vectors. Here $\vec{u}(t)$ represents CTOS control programs (plans of CTOS functioning), $\vec{v}\left(\vec{x}(t),t\right)$ is a vector of control inputs compensating perturbation impacts $\vec{\xi}(t)$). The vector $\vec{\beta}_{\Theta}$ is a general vector of CTOS parameters. The vector of CTOS effectiveness measures is described as (6).

$$\vec{J}_{\Theta}\left(\vec{x}(t),\vec{u}(t),\vec{\beta},\vec{\xi}(t),t\right)=$$
$$\left\|\vec{J}^{(g)\mathrm{T}},\vec{J}^{(o)\mathrm{T}},\vec{J}^{(k)\mathrm{T}},\vec{J}^{(p)\mathrm{T}},\vec{J}^{(n)\mathrm{T}},\vec{J}^{(e)\mathrm{T}},\vec{J}^{(c)\mathrm{T}},\vec{J}^{(v)\mathrm{T}}\right\| \quad (6)$$

Its components state control effectiveness for motion, interaction operations, channels, resources, flows, operation parameters, structures, and auxiliary operations (Okhtilev et al., 2010, Ivanov et al., 2010, 2012). The indices «*g*», «*o*», «*k*», «*p*», «*n*», «*e*», «*c*», «*n*» correspond to the following models: models of order progress control ($M_{<g,Q>}$); models of operations control ($M_{<o,Q>}$); models of technological chains control ($M_{<k,Q>}$); models of resources control ($M_{<p,Q>}$); models of flows control ($M_{<n,Q>}$); models of operations parameters control ($M_{<e,Q>}$); models of structures control ($M_{<c,Q>}$); models of auxiliary operations control ($M_{<n,Q>}$). In (5) the transition function $\vec{\phi}_{\Theta}\left(T_0,\vec{x}(T_0),\vec{x}(t),\vec{u}(t),\vec{\xi}(t),\vec{\beta}_{\Theta},t\right)$ and the output function $\vec{\psi}_{\Theta}\left(\vec{x}(t),\vec{u}(t),\vec{\xi}(t),\vec{\beta}_{\Theta},t\right)$ can be defined in analytical or algorithmic form within the proposed simulation system; $Q_{\Theta}\left(\vec{x}(t),t\right)$, $V_{\Theta}\left(\vec{x}(t),t\right)$, $\Xi_{\Theta}\left(\vec{x}(t),t\right)$ are correspondingly allowable areas for program control, real-time regulation control inputs, perturbation inputs; B is a area of allowable parameters; $X\left(\vec{\xi}(t),t\right)$ is an area of allowable states of CTOS structure-dynamics. Expression (4) determines end conditions for the CTOS state vector $\vec{x}(t)$ at time $t = T_0$ and $t = T_f$ (T_0 is the initial time of a time interval the CTOS is being investigated at, and T_f is the final time of the interval).

General formal statements for structure adaptation of CTOS SDC modules can be written as problems of two subclasses (Skurihin et al., 1989).

Problem C1

$$AD\left(M_{\Theta}^{(l)},\bar{P}_{cs}\right)\rightarrow \min, \quad (7)$$

$$t_{st}\left(\vec{w}^{(3)},M_{\Theta}^{(l)}\right)\le \bar{t}_{st}, \quad (8)$$
$$M_{\Theta}^{(l)}\in\overline{\overline{M}},\vec{w}^{(3)}\in W^{(3)},$$
$$M_{\Theta}^{(l)}=\overline{\overline{\Phi}}\left(M_{\Theta}^{(l-1)},\vec{w}^{(3)},\bar{P}_{cs}\right),l=1,2,\ldots, \quad (9)$$

where $AD\left(M_{\Theta}^{(l)},\bar{P}_{cs}\right)$ is a functional characterizing the adequacy of the model $M_{\Theta}^{(l)}$ for CTOS. The latter is described, in its turn, with a set $\bar{P}_{cs}(t)=\left\{\bar{P}_{\bar{g}}^{(cs)},\bar{g}=1,\ldots,\bar{G}\right\}$ of characteristics; t_{st} is a total time of CTOS SDC models structure adaptation; $\bar{t}_{st}$ is a maximal allowable time of structural adaptation; $\overline{\overline{\Theta}}$ is an operator of iterative construction (selection) of the model $M_{\Theta}^{(l)}$, l is the current iteration number; $W^{(3)}$ is a set of allowable values for the vectors of structure-adaptation parameters.

Problem C2

$$t_{st}\left(\vec{w}^{(3)},M_{\Theta}^{(l)}\right)\rightarrow \min, \quad (10)$$
$$AD\left(M_{\Theta}^{(l)},\bar{P}_{cs}\right)\le \varepsilon_2, \quad (11)$$
$$M_{\Theta}^{(l)}\in\overline{\overline{M}},\vec{w}^{(3)}\in W^{(3)}, \quad (12)$$
$$M_{\Theta}^{(l)}=\overline{\overline{\Phi}}\left(M_{\Theta}^{(l-1)},\vec{w}^{(3)},\bar{P}_{cs}\right),$$

where ε_2 is a given constant establishing an allowable level of the CTOS SDC model $M_{\Theta}^{(l)}$ adequacy, $\overline{\overline{M}}$ is a set of CTOS SDC models.

The analysis of expressions (7)-(9) shows that the structural adaptation starts and stops according to a criterion characterizing the similarity of a real object and an object described via models (a condition of models adequacy is applied) (Sokolov et al., 2012). The adequacy of CTOS models does not mean description of all "details". It means that simulation results meet the changes and relations observed in reality.

The main purpose of quantitative estimation of the model M_{Θ} adequacy at time t is to raise decision-maker's confidence in conclusions made on real situation. Therefore, the utility and correctness of CTOS SDC simulation results can be measured via adequacy degree of models and objects.

The adequacy functional should meet the following requirements (Sokolov, 2012).

$AD\left(M_{\Theta}^{(l)},\bar{P}_{cs}\right)>0,\forall M_{\Theta}^{(l)}\in\overline{\overline{M}},\bar{P}_{cs}\in\overline{\overline{P}}_{cs}$, where $\overline{\overline{M}}$ is a set of CTOS models; $\overline{\overline{P}}_{cs}$ is a set of possible values of CTOS characteristics.

$AD\left(M_{\Theta}^{(l)},\bar{P}_{cs}^{(1)}\right) > AD\left(M_{\Theta}^{(l)},\bar{P}_{cs}^{(2)}\right)$, where the model $M_{\Theta}^{(l)}$ is more adequate to CTOS with the characteristics set $\bar{P}_{cs}^{(2)}$ than to CTOS with the characteristics set $\bar{P}_{cs}^{(1)}$.

$AD\left(M_{\Theta_1}^{(l)},\bar{P}_{cs}^{(1)}\right) > AD\left(M_{\Theta_2}^{(l)},\bar{P}_{cs}^{(1)}\right)$, where the model $M_{\Theta_2}^{(l)}$ is more adequate than the model $M_{\Theta_1}^{(l)}$ to CTOS with the characteristics set $\bar{P}_{cs}^{(1)}$.

It is assumed that parameters of the models are adjusted for particular CTOS.

It is important that the changes of CTOS characteristics should be observed and forecasted so that corrections of models structure and of parameters can be done in time.

The time of corrections can be determined as a compromise between an aspiration for receiving proper values of $\bar{P}_{cs}$ and necessity of a new model construction, adjustment, and preparation for use (Ivanov et al., 2010).

ALGORITHM OF STRUCTURE ADAPTATION OF MODELS DESCRIBING SCHEDULING PROCESSES IN CTOS

The proposed algorithms for structural adaptation of CTOS SDC models are based on the evolutionary (genetic) approach. As before in PROBLEM STATEMENT, let us exemplify these algorithms in the structural adaptation of a model describing structure dynamics of one CTOS output characteristic [of one element of the vector $\vec{y}\left(t_{\langle k\rangle}\right)$].

The residual of its estimation via the model M_{θ}, as compared with the observed value of the characteristic, can be expressed like this:

$$Q_{\langle k\rangle}^{\langle\theta\rangle} = \left[\psi_{\langle\theta,k\rangle}\left(\vec{x}\left(t_{\langle k\rangle}-1\right),\vec{u}\left(t_{\langle k\rangle}\right),\vec{\xi}\left(t_{\langle k\rangle}\right),\vec{\beta}_{\theta},t_{\langle k\rangle}\right)-\tilde{y}\left(t_{\langle k\rangle}\right)\right] \quad (13)$$

To simplify formulas, we assume that the perturbation impacts $\vec{\xi}(t)$ are described via stochastic models. Thus, the following quality measure can be introduced for the model M_{Θ}:

$$\bar{Q}_{\langle K\rangle}^{\langle\theta\rangle} = \sum_{k=1}^{K} g^{(K-k)}\bar{Q}_{\langle k\rangle}^{\langle\theta\rangle}, \quad (14)$$

where $0 \le g \le 1$ is a "forgetting" coefficient that "depreciate" the information received at the previous steps (control cycles) (Ivanov et al., 2010). If $g = 0$ then $\bar{Q}_{\langle K\rangle}^{\langle\theta\rangle} = Q_{\langle K\rangle}^{\langle\theta\rangle}$, i.e., the weighted residual is equal to one received at the last step, as the prehistory have been "forgotten". An extension of formula (13) was proposed in (Sokolov et al., 2012). The coefficient $g^{(K-k)}$ was substituted for the function $f(K)$:

$$\bar{Q}_{\langle K\rangle}^{\langle\theta\rangle} = \sum_{k=1}^{K} f\left(K-k\right)Q_{\langle K\rangle}^{\langle\theta\rangle}, \theta = 1,\ldots,\Theta \quad (15)$$

Here $f(\cdot)$ is a monotone decreasing function of "forgetting". It has the following properties:

$$\begin{aligned} &f(\alpha) > 0, f(0) = 1, \lim_{\alpha\to?} f(\alpha) = 0, \\ &f(\alpha) \ge f(\alpha+1), \alpha = 0,1,\ldots. \end{aligned} \quad (16)$$

Now the structural-adaptation algorithm is reduced to a search for the structure M_{Θ}, such that

$$\bar{Q}_{\langle K\rangle}^{\langle\theta'\rangle} = \min_{\theta=1,\ldots\Theta} \bar{Q}_{\langle K\rangle}^{\langle\theta\rangle} \quad (17)$$

Thus, it is necessary to calculate the quality measures (13) for all competitive structures M_{Θ}, $q = 1,\ldots,Q$ of CTOS SDC models at each control cycle $k = 1,\ldots,K$. All quality measures should be compared, and the structure M_{Θ} with the best measure (minimal residual) should be chosen.

Another way to choose model $M_{\Theta}^{(l)}$ is probabilistic approach. In this case the following formula is used

$$p_1\left(M_{\Theta}^{l}\right) = \frac{\sum_{\rho=k-d}^{k-1} J_i\left(M_i^{\langle\rho,L\rangle}\right)}{\sum_{\Theta=1}^{\Theta^{(k-1)}}\sum_{\rho=k-d}^{k-1} J_i\left(M_{\Theta}^{\langle\rho,L\rangle}\right)} \quad (18)$$

where $J_i\left(M_i^{\langle\rho,L\rangle}\right)$ – generalized quality measure value of model $M_i^{\langle\rho,L\rangle}$ functioning on previous time intervals, d – is a "forgetting" coefficient. It should be emphasized that the calculation of the quality measure is expected to carry out each time on the basis of a solution of the problem of multi-type selection. Thus, despite the random choice of the next model (multiple-model complex) greater opportunity to be chosen gets the model, which had the best value of the generalized quality measure in the previous cycle control.

The parametric adaptation of the model M_{Θ} (Ivanov et al., 2010, 2012) should follow the structural one.

It is important to determine a proper "forgetting" function under the perturbation impacts $\vec{\xi}(t)$. The higher is the noise level in CTOS, the slower decrease of the function should be implemented. However, if CTOS highly changes its structure then the function $f(\alpha)$ should be rapidly decreasing in order to "forget" the results of the previous steps (Ivanov et al., 2012). It can be show that the structural-adaptation algorithms based on model construction (synthesis) of atomic models (modules) are rather similar to the algorithms of the CTOS structure-functional synthesis (Okhtilev et al., 2006). These algorithms only differ in the interpretation of results.

EXAMPLE

Example demonstrates a structural adaptation of CTOS containing the plurality of realization and multifunctional character.

CTOS is presented as an original software for the remote sensing (RS) data treatment for the forest cuts identification. CTOS consists of three main blocks: input RS data (block 1), automatic RS data processing (block 2) and results (block 3). The perturbation influences are presented by the control model parameters, $\vec{w}^{(3)}$, that can be evaluated on the real data

available in CTOS (block 1) and parameters that can be evaluated via simulation models for different scenarios of future events (block 2).

The problem consists of the structure adaptation of CTOS models to perturbation influences. According to mentioned in the paper algorithm it is necessary to choose the model for sceduling of CTOS functioning under perturbation influences.

Evaluated model parameters from block 1 include:

− type of the satellite system, above all spectral and spatial resolutions;

− square of the processing area of the space image.

Evaluated model parameters from block 2 include:

− threshold of the Normalized Differentiated Vegetation Index;

− method of the classification, furthermore number of classes, distance function;

− method of the reclassification;

− threshold of the entropy;

− minimum forest cut dimension;

− spectral radiance value from Database.

Evaluated model parameter from block 3 includes forest cuts outlines.

The following global optimization problem is considered: $AD\left(w_1^{(3)}, w_2^{(3)}, \ldots w_n^{(3)}\right) \to \min$, (see formula (7)) where the arguments $w_1^{(3)}, w_2^{(3)}, \ldots w_n^{(3)}$ are model parameters from blocks 1-3 to be varied in order to receive the minimal (the best) value of function *AD*. It is possible to recognize clearly forest cuts due to the vector of program control based on the evaluated model parameters.

The general algorithm is suggested:

Step 1: *Input RS data.* The spectral and spatial resolutions are marked. The part of the space image area for processing is indicates.

Step 2: *Processing RS data. The first phase.* The feature space of the image splits up two classes by means *NDVI (Normalized Vegetation Differencial Index)* values – the vegetation and the rest. *NDVI* values can vary between 0,2 to 0,9.

Step 3: *Processing RS data. The second phase.* The feature space of the vegetation class splits up *k*-classes by means of the *m*-method of classification (m=1..δ) for the forest cuts extraction. Simultaneously the reclassification and texture are computed. The polygons agglomeration is carried out according to minimum desired value of the forest cut. In current program implementation δ=5.

Step 4: *Processing RS data. The third phase.*The feature space of each polygon on the image is created per *NDVI* and *NIR/RE* values. The classification of the polygons to identify the range of the forest cuts resumption is accomplished. These result is automatically transmitted to geoinformation system.

Step 5: *Processing RS data. The fourth phase.* The model forest cuts outlines are compared with the reference outlines of the digital map. Function *AD* should be taken the best value, otherwise decision about new control model parameters, $\vec{w}^{(3)}$ is make.

Consequently, the probability of the model parameters choice based on the task solution is determined (expression (18), where *J* is the forest cut square).

Examples of the various results of the forest cuts identification conditionally of the subvector of model parameters are being illustrated on the website of the ESTLATRUS projects 1.2./ELRI-121/2011/13.

ACKNOWLEDGMENTS

The research described in this paper is supported by the Russian Foundation for Basic Research (grants 13-07-00279, 13-08-00702, 13-08-01250, 12-07-13119-ofi-i-RGD, 11-08-01016, 11-08-00767, 12-06-00276, 12-07-00302), Department of nanotechnologies and information technologies of the RAS (project 2.11), by ESTLATRUS projects 1.2./ELRI-121/2011/13 «Baltic ICT Platform» and 2.1/ELRI-184/2011/14 «Integrated Intelligent Platform for Monitoring the Cross-Border Natural-Technological Systems» as a part of the Estonia-Latvia-Russia cross border cooperation Program within European Neighborhood and Partnership instrument 2007-2013.

REFERENCES

Ohtilev, M.Yu., Sokolov, B.V., Yusupov, R.M. 2006. Intellectual Technologies for Monitoring and Control of Structure-Dynamics of Complex Technical Objects. Moscow, Nauka, 410 p. (in Russian)

Ivanov, D., Sokolov, B. (2010), Adaptive Supply Chain Management, Springer, London et al.

Ivanov, D., Sokolov, B., Kaeschel, J. (2010). A multi-structural framework for adaptive supply chain planning and operations with structure dynamics considerations. European Journal of Operational Research, 200(2), P. 409-420.

Ivanov D., Sokolov B. (2012) Dynamic supply chain scheduling / Journal of Scheduling, 15(2). London: Elsevier.

Ivanov D., Sokolov B. (2012): Control and system-theoretic identification of the supply chain dynamics domain for planning, analysis and adaptation of performance under uncertainty. European Journal of Operational Research. Volum 224, Issue 2. London: Elsevier. P.313-323.

Sokolov B, Zelentsov V., Yusupov R., Merkuryev Y. Information Fusion Multiple-Models Quality Definition And Estimation. // Proceedings of the Int. Conf. on Harbor Maritime and Multimodal Logistics M&S, Vienna, Austria, September, 19-2l, 2012. - P. 102-111.

Skurihin V.I., Zabrodsky V.A., Kopeychenko Yu.V. Adaptive control systems in machine-building industry. – M.: Mashinostroenie, 1989 (in Russian).

Rastrigin L.A. Modern principles of control for complicated objects. – M.: Sovetscoe Radio, 1980 (in Russian).

Bellmann R., 1972. Adaptive Control Processes: A Guided Tour. Princeton Univ. Press, Princeton, New Jersey.

Rastrigin L.A. Adaptation of complex systems. – Riga: Zinatne, 1981 (in Russian).

Fleming, W.H., Richel R.W., 1975. Deterministic and stochastic optimal control. Springer-verlag, Berlin, New York.

Moiseev, N.N. Element of the Optimal Systems Theory. – M.: Nauka, 1974 (in Russian).

Sowa, J. Architecture for intelligent system. IBM System Journal,.Vol.41. N 3, 2002.

Zypkin Ya. Z. Adaptation and teachning in automatic systems. – M.: Nauka, 1969 (in Russian).

Bryson, A.E., and Yo-Chi Ho., 1969. Applied optimal control: Optimization, Estimation and Control. Waltham Massachusetts, Toronto, London.

Chernousko, F.L., Zak, V.L. On Differential Games of Evasion from Many Pursuers J. Optimiz. Theory and Appl. 1985. Vol.46, N 4, pp.461-470.

Singh, M., and A. Titli, 1978. Systems: Decomposition, Optimization and Control, Pergamon Press, Oxford.
Petrosjan, L.A., and N.A. Zenkevich, 1996. Game Theory. World Scientific Publ., Singapure, London.
Roy, B., 1996. Multi-criteria Methodology for Decision Aiding. Kluwer Academic Pulisher, Dordreeht.
Fischer M, Jaehn H, Teich T. Optimizing the selection of partners in production networks. Robotics and Computer-Integrated Manufacturing 2004; Vol. 20, pp. 593–601.
Huang G, Zhang Y, Liang L. Towards integrated optimal configuration of platform products, manufacturing processes, and supply chains. Journal of Operations Management 2005, Vol. 23, pp. 267-290.
Kuehnle H. A system of models contribution to production network (PN) theory. Journal of Intelligent Manufacturing 2007, pp. 157-162.
Nilsson F, Darley V. On complex adaptive systems and agent-based modeling for improving decision-making in manufacturing and logistics settings. Int. Journal of Operations and Production Management, 2006, Vol. 26(12), pp. 1351-1373.
Rabelo RJ, Klen AAP, Klen ER 2002. Multi-agent system for smart coordination of dynamic supply chains. In: Proceedings of the 3rd International Conference on Virtual Enterprises, PRO-VE'2002. pp. 379–387.
Teich T. Extended Value Chain Management (EVCM). GUC-Verlag: Chemnitz; 2003.
Wu N, Mao N, Qian Y. An approach to partner selection in agile manufacturing. Journal of Intelligent Manufacturing 1999, Vol. 10(6), pp. 519–529.
Wu N, Su P. Selection of partners in virtual enterprise paradigm. Robotics and Computer-Integrated Manufacturing, 2005, Vol. 21, pp. 119–31.

AUTHOR BIOGRAPHIES

DMITRY IVANOV is a professor at Department of Business and Economics at the Berlin School of Economics and Law and Chair of the German-Russian Coordination Office for Logistic. He studied production management and engineering (2000). In 2002, he graduated in Saint Petersburg as a Ph.D. in Economics on the topic of operative supply chain planning and control in virtual enterprises. In 2006, he received the Dr.rer.pol. degree at the Chemnitz University of Technology. He is an author of six scientific books and more than 70 papers published in international and national journals, books and conference proceedings. Since 2001, he has been involved in research and industry projects on supply chain management and virtual enterprises. Dr. Ivanov received a German Chancellor Scholarship Award in 2005. His e-mail address is: idm@hrz.tu-chemnitz.de.

BORIS V. SOKOLOV obtained his main degrees in Mozhaisky Space Engineering Academy, Leningrad. MS in Automation Control Systems of Space Vehicles in 1974. Candidate of Technical Sciences subject the area of planning automation and decision making in 1982. Doctor of Technical Sciences subject the area of military cybernetics, mathematical modeling and methods in military research. Professional Interests: Basic and applied research in mathematical modeling and mathematical methods in scientific research, optimal control theory, mathematical models and methods of support and decision making in complex organization-technical systems under uncertainties and multi- criteria. At present he is a deputy director of SPIIRAS. His e-mail address is: sokol@iias.spb.su and his Web-page can be found at http://litsam.ru

VIACHESLAV A. ZELENTSOV was born in Gorky in 1955**.** He obtained his main degrees in Mozhaisky Space Engineering Academy, Leningrad (1977). Ph.D Eng, Dr. Sc. Eng. and Prof., Leading researcher, Laboratory for Information Technologies in Systems Analysis and Modeling, Head of Research Consulting Center for Space Information Technologies and Systems at SPIIRAS, professor and Director of Research and Education Center "AeroSpaceInfo" in St Petersburg State University of Aerospace Instrumentation. **Author of** more than 180 scientific paper, more over 50 research and engineering projects, 5 teaching books.

SEMYON A. POTRYASAEV is PhD research fellow at the Russian Academy of Science, Saint Petersburg Institute of Informatics and Automation. He graduated from the Baltic State Technical University "VOENMEH" with a degree of control systems engineer and Moscow Institute of International Economic Relations as an economist in finance and credit. Research interests: applied research in mathematical modeling, optimal control theory, mathematical models and methods of support and decision making in complex organization-technical systems under uncertainties and multicriteria.

OLGA V. BROVKINA is PhD at the Herzen State Pedagogical University of Russia, St. Petersburg. She graduated from the St.Petersburg State University of Aerospase Instrumentation with a degree of control systems engineer and Institution of Russian Academy of Sciences Saint-Petersburg Scientific-Research Centre for Ecological Safety RAS (SRCES RAS) in the speciality of Aerospace research of the Earth and Photogrammetry. Professional Interests: treatment of the RS data, ecological monitoring and state value of the ecosystem, applying the results of the RS data processing to the Forestry.

Robust Control of Air-Flow in Air-Heating Set

Marek Dlapa
Department of Automation and Control Engineering
Faculty of Applied Informatics
Tomas Bata University in Zlin
nám. T. G. Masaryka 5555, 760 01 Zlín, Czech Republic
E-mail: dlapa@fai.utb.cz

KEYWORDS

Algebraic approach, controller design, PID control, structured singular value, Differential Migration, evolutionary algorithms.

ABSTRACT

The paper deals with the robust control of air-flow in air-heating set. The identification is perrfomred using step responses and approximation via second order system. The controller is designed using the structured singular value (SSV or μ) and algebraic approach. Since the cost function is nonconvex the optimization cannot be done using standard tools. Hence an evolutionary algorithm - Differential Migration (DM) is employed yielding good results in this case. The functionality of the comtroller is verified though experiments on the real plant.

INTRODUCTION

This contribution is another article documenting the power of the robust control in practical design. The robust control treats both parametric and dynamic structured uncertainties. The most advanced methods in the field are derived from Zames' small gain theorem (Zames 1981) and consequent structured singular value theory denoted SSV or μ yielding the tools for both the robust stability and performance evaluation taking into account the parametric and dynamic structured uncertainties (Doyle 1982). There are two well known methods for derivation of the controller: the *D-K* iteration (Doyle 1985) and μ-*K* iteration (Lin et al. 1993). In these two methods, the state-space formulae for the $\mathbf{H}_\infty$ suboptimal controller (Doyle et al. 1989, Gahinet and Apkarian 1994) imply the necessity of the open-loop to be stable. This requirement is a limiting factor for achieving the asymptotic tracking. The cure is the algebraic approach (Dlapa et al. 2009, Dlapa and Prokop 2010, Dlapa 2011) solving the issue and yielding simple controllers with no degradation consequent upon the simplification of the controller.

In this paper, the algebraic approach and *D-K* iteration are applied to control of the air flow in an air-heating set with nonlinear behaviour and the results are compared with other standard methods. The controllers are verified through experiments on the real plant.

CONTROL OF AIR-HEATING TUNNEL

The laboratory plant has three control signals and seven measured quantities (see Table 1 and Figure 1 and 2). The control signals are the voltage on the bulb and the main and secondary fan. The control signals are generated by the CTRL unit connected to a standard IBM PC computer via serial port. The CTRL unit generates analogue signals to the transformation and unification unit giving the right voltage for the actuators. Similarly the analogue signals from sensors are transformed to the unified voltage 0 - 10 V.

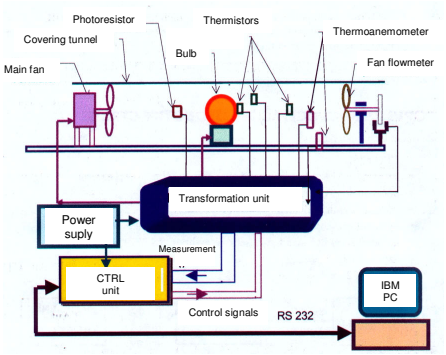

Figure 1. The scheme of air-heating tunnel

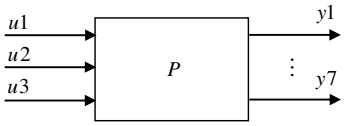

Figure 2. Inputs and outputs of the plant

Table 1: Inputs and outputs to the CTRL unit

Input channel	Sensor	Output channel	Actuator
$y1$	bulb brightness sensor	$u1$	voltage on the bulb
$y2$	temperature sensor close to the bulb T_2	$u2$	voltage on the main fan
$y3$	temperature of the bulb sensor T_3	$u3$	voltage on the adjacent fan
$y4$	temperature at the output of the tunnel sensor T_4		
$y6$	thermometer TA_6		
$y7$	fan airflow sensor		

Proceedings 27th European Conference on Modelling and Simulation ©ECMS Webjørn Rekdalsbakken, Robin T. Bye, Houxiang Zhang (Editors)
ISBN: 978-0-9564944-6-7 / ISBN: 978-0-9564944-7-4 (CD)

IDENTIFICATION

The response to stepwise changes of the voltage on the main fan is in Figure 3 and 4. Via approximation of these characteristics second order transfer functions were obtained with a dead zone, which was omitted in the final model. These transfer functions make the set

$$\mathbf{P}_{27} \equiv \left\{ \frac{k}{(T_1 s+1)(T_2 s+1)} : \begin{matrix} k \in (0.58; 0.84), \\ T_1 \in (0.96; 1.86), \\ T_2 \in (1.80; 3.38) \end{matrix} \right\} \qquad (1)$$

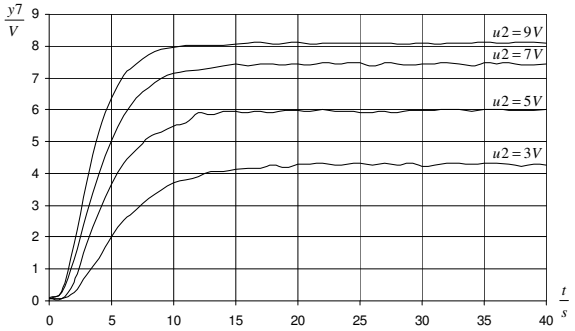

Figure 3. Responses of the measured quantity *y*7 to stepwise changes of *u*2 in the range 3-9V with other control signals at 0V

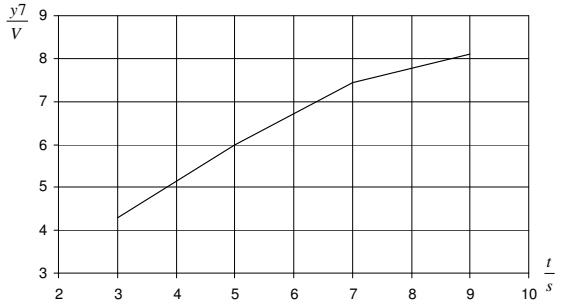

Figure 4. Static characteristics of the measured quantity *y*7 to stepwise changes of *u*2 in the range 3-9V with other control signals at 0V

μ-SYNTHESIS

The nominal plant has its parameters equal to mid values:

$$P_{27}(s) = \frac{0.71}{(1.41 s+1)(2.59 s+1)} \qquad (2)$$

Parameter uncertainty is treated by additive and two quotient uncertainties connected in serial interconnection (see Figure 5).

The set $\mathbf{P}_{27}$ can be treated via LFT as follows

$$\tilde{P}_{27}(s,\Delta) = \frac{0.71+0.13\delta_2}{(1.41 s+1)(2.59 s+1)} \frac{1}{\left(1+\frac{0.45\delta_3 s}{1.41 s+1}\right)\left(1+\frac{0.79\delta_4 s}{2.59 s+1}\right)}, \qquad (3)$$

$$\Delta = \begin{bmatrix} \delta_2 & 0 & 0 \\ 0 & \delta_3 & 0 \\ 0 & 0 & \delta_4 \end{bmatrix}, \ \delta_2, \delta_3, \delta_4 \in (-1; +1)$$

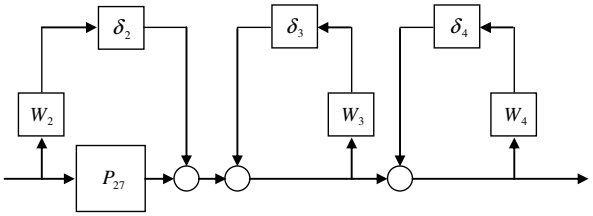

Figure 5. LFT interconnection for the family of plants $\mathbf{P}_{27}$

Denote

$$W_2(s) = \frac{0.13}{(1.41 s+1)(2.59 s+1)}, \ W_3(s) = \frac{0.45 s}{1.41 s+1},$$
$$W_4(s) = \frac{0.79 s}{2.59 s+1} \qquad (4)$$

then

$$\tilde{P}_{27}(s,\Delta) = [P_{27}(s) + \delta_2 W_2(s)] \frac{1}{1+\delta_3 W_3(s)} \frac{1}{1+\delta_4 W_4(s)} \qquad (5)$$

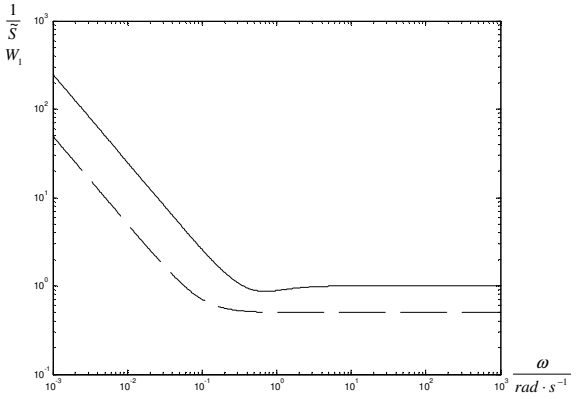

Figure 6. Bode plot of $1/\tilde{S}$ and W_1

The desired complementary sensitivity function has the form

$$\tilde{T}(s) = \frac{1}{(2 s+1)^2} \qquad (6)$$

which for performance condition $\|W_1 S\|_\infty < 1$ gives the weight (see Figure 6)

$$W_1(s) = \frac{10 s+1}{20 s+0.0001} \text{ and } \frac{10 s+1}{20 s} \qquad (7)$$

for the *D-K* iteration and algebraic approach, respectively. The noise weight has a similar form as in previous cases

$$W_n(s) = \frac{s/0.001+1}{s/0.5+1}0.0005 \tag{8}$$

The algebraic μ-synthesis is performed for the interconnection in Figure 7 and the perturbation matrix in the form:

$$\mathbf{\Delta} \equiv \{\mathrm{diag}[\delta_1, \delta_2, \delta_3, \delta_4, \delta_n]: |\delta_{i,n}| < 1, \\ \delta_{2,3,4} \in \mathbf{R}, \delta_{1,n} \in \mathbf{C}\} \tag{9}$$

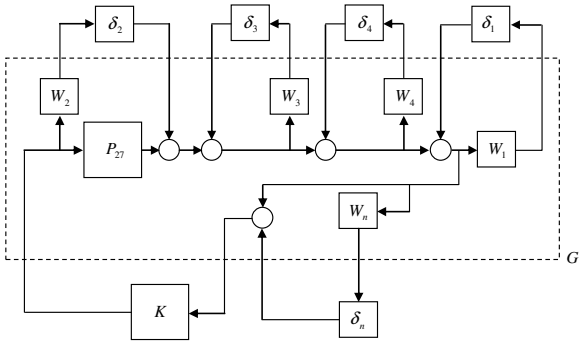

Figure 7. Interconnection for the μ-synthesis

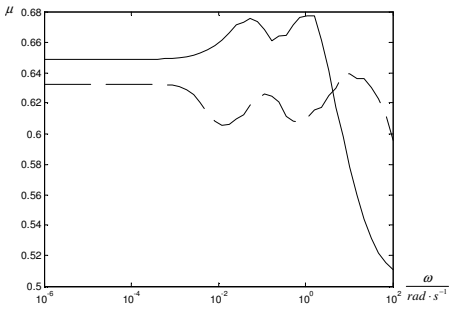

Figure 8. μ-plots for the algebraic approach (full) and the *D-K* iteration (dashed)

Stabilizing controller *K* satisfies the robust performance and stability condition if and only if for each frequency $\omega \in \mathbf{R}$ the structured singular value

$$\mu_{\Delta}[\mathbf{F}_l(\mathbf{G}, K)(j\omega)] < 1 \tag{10}$$

The aim of synthesis is to design a controller which satisfies the condition:

$$\sup_{\substack{\omega \\ K \text{ stabilizing } \mathbf{G}}} \mu_{\mathbf{\Delta}}\{\mathbf{F}_L[\mathbf{G}(\omega), K(\omega, \alpha_1, \ldots, \alpha_4)]\} \le 1, \\ \omega \in (-\infty; +\infty) \tag{11}$$

where are the nominal closed loop poles in and $\mu_{\mathbf{\Delta}}$ denotes the structured singular value of LFT on generalized plant **G** and controller *K* with **Δ** defined in (11).

The controller $K = N_K/D_K$ is obtained by solving the Diophantine equation

$$AD_K + BN_K = 1 \tag{12}$$

with $A, B, D_K, N_K \in \mathbf{R}_{\mathrm{ps}}$. All feedback controllers N_K/D_K are given by

$$K = \frac{N_K}{D_K} = \frac{N_{K_0} - AT}{D_{K_0} + BT}, \; N_{K_0}, D_{K_0} \in \mathbf{R}_{\mathrm{PS}} \tag{13}$$

where N_{K_0}, $D_{K_0} \in \mathbf{R}_{\mathrm{PS}}$ are particular solutions of (12) and *T* is an arbitrary element of $\mathbf{R}_{\mathrm{PS}}$.

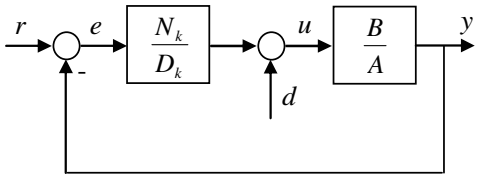

Figure 9. Nominal feedback loop

The controller *K* satisfying equation (12) guarantees the BIBO (bounded input bounded output) stability of the feedback loop in Figure 9. This is a crucial point for the theorems regarding the structured singular value. If the BIBO stability is held, then the nominal model is internally stable and theorems related to robust stability and performance can be used. The BIBO stability also guarantees stability of $\mathbf{F}_L(\mathbf{G}, K)$ making possible usage of performance weights with integration property implying nonexistence of state-space solutions using DGKF formulae (Doyle *et al.*, 1989) due to zero eigenvalues of appropriate Hamiltonian matrices. Such procedure results in zero steady-state error in the feedback loop with the controller obtained as a solution to equation (12). This technique is neither possible in the scope of the standard μ-synthesis using DGKF formulae, nor using LMI approach (Gahinet and Apkarian 1994) leading to numerical problems in most of real-world applications.

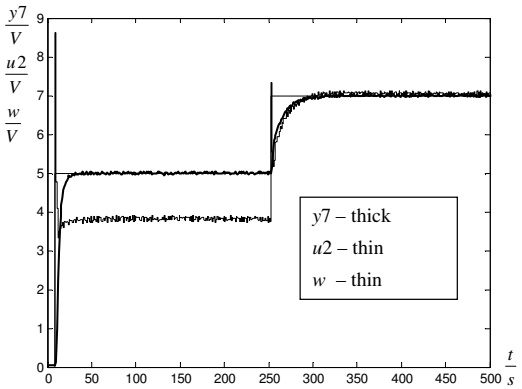

Figure 10. Control of the real plant for the algebraic μ-synthesis

In order to overcame the multimodality of the cost function (10) evolutionary algorithm Differential Migration is used (Dlapa 2009) giving the poles

$$\alpha_1 = 18.676;\ \alpha_2 = 0.787;\ \alpha_3 = 0.401;\ \alpha_4 = 0.094 \quad (14)$$

giving the proper PID controller

$$K_A(s) = \frac{17.69\,s^2 + 14.65\,s + 2.86}{s^2 + 18.86\,s} \quad (15)$$

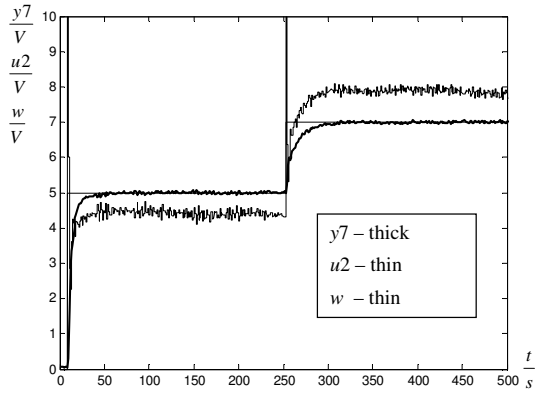

Figure 11. Control of the real plant for the *D-K* iteration

The controller obtained via the *D-K* iteration is approximated by a 5th order system

$$K_{D-K}(s) = \frac{0.017\,s^5 + 1.408\,s^4 + 3.896\,s^3 + 2.061\,s^2 + 0.311\,s + 0.001}{0.00001\,s^5 + 0.0015\,s^4 + 0.1443\,s^3 + 1.7942\,s^2 + 0.0071\,s} \quad (16)$$

The μ-plot and control of the real plant is in Figure 8 and 10. It is apparent that the frequency properties of the controller obtained via the algebraic approach are almost the same as for the *D-K* iteration. However, it must be considered that the *D-K* iteration uses the weight without the unstable pole on the imaginary axis. For the weight with unstable pole the $\mu \to \infty$ for $\omega \to 0$. The real plant control for both controllers are similar, however, the algebraic approach yields lower control signal at the beginning and faster tracking.

SYNTHESIS IN Rps WITH THE POLES IN ONE POINT

Synthesis in $\mathbf{R}_{ps}$ with the poles in one point is applied to the nominal plant (2) and the perturbed plant

$$P'_{27}(s) = \frac{0.84}{(1.86\,s + 1)(3.38\,s + 1)} \quad (17)$$

The minimum of $\eta(\alpha)$ occurs for $\alpha = 0.4$. The control law for this value has the transfer function

$$K_{RPS}(s) = \frac{0.686\,s^2 + 0.606\,s + 0.132}{s^2 + 0.505\,s} \quad (18)$$

The controller has a high overshoot for step from 0 to 5 V, for the step from 5 to 7 V there is no overshoot. No oscillation of the measured quantity is present (see Figure 12).

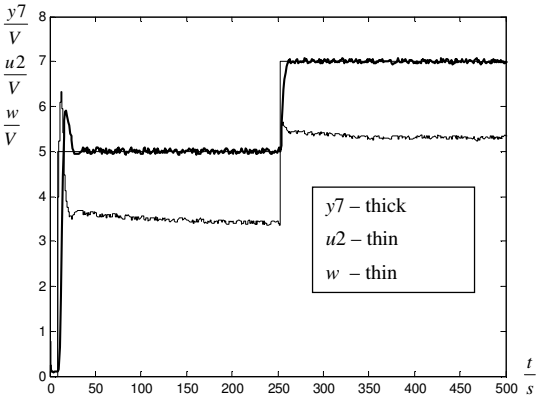

Figure 12. Control of the real plant for the design in $\mathbf{R}_{ps}$ with poles in one point

NASLIN METHOD

The Naslin method for the nominal plant P_{27} and the desired overshoot 1% (α = 2.4) yields the PI controller

$$Q_N(s) = \frac{1.18\,s + 0.50}{s} \quad (19)$$

Control of the real plant exhibits a high overshoot for low temperatures and oscillations (see Figure 13).

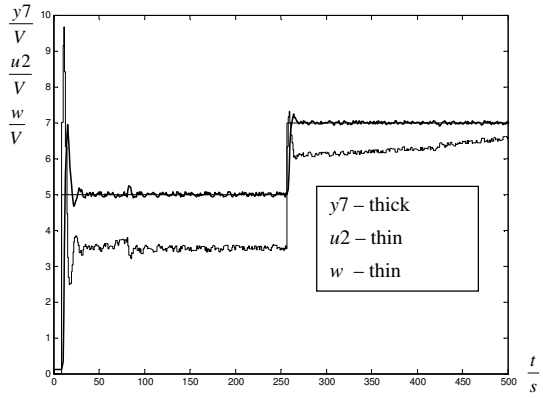

Figure 13. Control of the real plant for the Naslin method

The Naslin method has 40% overshoot for the step from 0 to 5 V (Figure 13). For the step from 5 to 7 V the overshoot decreases to 10%, which is due to different set point in the upper part of the static characteristic. Both the algebraic μ-synthesis and the *D-K* iteration yield no overshoot for both steps of the reference (Figure 10 and 11) due to considering parameter uncertainties of the controlled plant. Moreover, the measured quantity has only small oscillations from the set point. Compared to the *D-K* iteration algebraic approach has smaller control effort at the beginning and faster tracking of the reference signal.

ACKNOWLEDGEMENTS

This work was supported by the European Regional Development Fund under the Project CEBIA-Tech No. CZ.1.05/2.1.00/03.0089.

REFERENCES

Dlapa, M. 2009. "Differential Migration: Sensitivity Analysis and Comparison Study," *Proceedings of 2009 IEEE Congress on Evolutionary Computation (IEEE CEC 2009)*, pp. 1729-1736, ISBN 978-1-4244-2959-2.

Dlapa, M.; R. Prokop and M. Bakošová. 2009. "Robust Control of a Two Tank System Using Algebraic Approach," *Proceedings of EUROCAST 2009*, pp. 603-609, ISBN 978-84-691-8502-5.

Dlapa, M. and R., Prokop. 2010. Algebraic approach to controller design using structured singular value, *Control Engineering Practice*, Vol. 18, No. 4, pp. 358–382, ISSN 0967-0661.

Dlapa, M. 2011. Controller Design for a Two Tank System Using Structured Singular Value and Direct Search Methods, *18th World Congress of the International Federation of Automatic Control (IFAC)*, Milan, Italy, pp. 7511-7516, ISSN: 1474-6670.

Doyle J.C. 1982. "Analysis of feedback systems with structured uncertainties," *Proceedings of IEE, Part-D*, 129, pp. 242-250.

Doyle J.C. 1985. "Structure uncertainty in control system design," *Proceedings of 24th IEEE Conference on decision and control*, pp. 260-265.

Doyle J.C.; P.P. Khargonekar and B.A. Francis. 1989. State-space solutions to standard H_2 and H_∞ control problems, *IEEE Transactions on Automatic Control*, Vol. 34, No. 8, pp. 831-847.

Gahinet, P. and P., Apkarian 1994. A linear matrix inequality approach to H_∞ control, *International Journal of Robust and Nonlinear Control*, Vol. 4, pp. 421-449.

Lin J. L.; I. Postlethwaite and D. W. Gu. 1993. "μ-K iteration: a new algorithm for μ synthesis," *Automatica*, **29**, 219-224.

Zames G. 1981. "Feedback and optimal sensitivity: model reference transformations, multiplicative seminorms, and approximate inverse," *IEEE Trans. Auto. Control*, **26**, pp. 301-320.

AUTHOR BIOGRAPHIES

MAREK DLAPA was born in Zlín, Czech Rep. and went to the Tomas Bata University in Zlín, where he studied chemical technology and obtained his degree in 2000. After a couple of years he was given Ph.D. degree at TBU in Zlín in 2004. Now he works as a research worker at TBU in Zlín. His web page can be found at http://dlapa.cz.

Simulation, Experimental Science and Engineering in Maritime Operations

USING AN HLA SIMULATION ENVIRONMENT FOR SAFETY CONCEPT VERIFICATION OF OFFSHORE OPERATIONS

Christoph Läsche
OFFIS – Institute for Information Technology
Escherweg 2
D-26131, Oldenburg, Germany
E-Mail: laesche@offis.de

Volker Gollücke and Axel Hahn
Carl von Ossietzky Universität Oldenburg
Ammerländer Heerstr. 114-118
D-26129, Oldenburg, Germany
E-Mail: {golluecke,hahn}@wi-ol.de

KEYWORDS

Distributed Simulation; Risk Observer; Hazards; Hazard Analysis; HLA; Failures; Physical World Simulator; Offshore; Risk Assessment; Safety Concept; Simulation;

ABSTRACT

One of the effects of the radically changing energy market is the construction of more and more offshore wind turbines. Many new companies with different levels of experience are entering the market to meet the demand of renewable energy. To this end, we introduce a distributed simulative approach for verifying a safety concept for offshore missions to support the involved companies. In this paper, we present our vision of the emerging simulation environment and introduce the components that we currently work on. More precisely, we introduce a Physical World Simulator (PWS) that allows the simulation of the environment, persons, and resources of offshore operations. The simulator can be interconnected to other simulators and to a Failure and Hazard Observer (FHO) which we also present in the paper. The observer tracks the occurrence of hazards and thus checks if they have been considered while creating a safety concept for an offshore mission. We use the High Level Architecture (HLA) as the simulator communication interface for which we developed a helper library which also extends its features while maintaining compatibility with the standard. The simulation framework enables us to automatically verify the safety concept by performing simulation runs and injecting identified failures.

I. INTRODUCTION

With merely twelve years of experience in the commercial installation of offshore wind farms, the industry is still in an early development stage. A huge change towards renewable energy in a short time can only be realized by a large amount of companies constructing multiple facilities concurrently. The development and implementation of the necessary practices and processes is a highly complex task for the new companies entering the market. Recent events have shown that profound assessments of risks are essential to protect personnel as well as the environment.This is why we aim to support the planing and the execution of safe offshore operations for construction and maintenance of offshore wind turbines.

In this paper, we will describe how we plan to verify the completeness of identified hazards in a safety concept using a simulative approach. This is a novel approach as a safety concept is normally manually verified and thus might have not considered all possible failures that lead to a hazard. Our approach is still a work in process, nevertheless we will introduce our vision of the simulation environment which is used to perform the verification. Afterward, we describe the components that have already been developed or are currently under development. We especially describe our *HLA Helper Library*, the used *Physical World Simulator* (PWS), and the *Failure and Hazard observer* (FHO). We conclude with the next steps that are to be performed to realize our vision.

II. RELATED WORK

Numerous works deal with co-simulation and distributed simulation. For example, [Alexander, 2007] addresses a similar problem in his thesis. He wants to analyze hazards when simulating systems of systems. However his approach is focused on machine learning and he does not use distributed simulation. [Vinnem, 2007] addresses the methods of risk assessment currently performed for oil and gas offshore platforms. However, all analyses are performed in a non-model-based manner in the described approaches. [Lemessi et al., 2010] and [Raab et al., 2011] introduce a similar approach for distributed simulation which also includes observers. The observers are not used for safety analysis as in our approach, but for controlling the simulation and for quality measurement.

III. VISION

Our goal is to improve the safety of offshore operations. We want to achieve this by creating a safety concept similar to HSE (Health Safety Environment) plans (cf. [Sobiech et al., 2012] for HSE plans). However, these concepts are planned to contain more information than the HSE plans. In order to make the safety concept verifiable, we want to use a model-based approach that allows to execute and analyze the processes under investigation using simulation.

A. *SCENARIO AND SAFETY CONCEPT CREATION*

A scenario that will be analyzed has to be modeled in beforehand. For this, we want to provide an easy modeling

Proceedings 27th European Conference on Modelling and Simulation ©ECMS Webjørn Rekdalsbakken, Robin T. Bye, Houxiang Zhang (Editors)
ISBN: 978-0-9564944-6-7 / ISBN: 978-0-9564944-7-4 (CD)

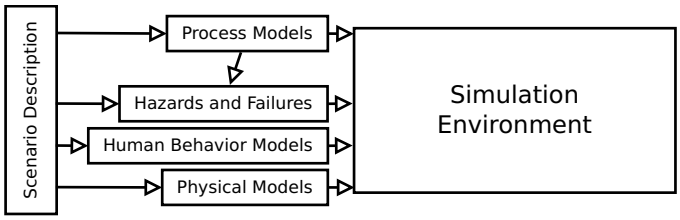

Fig. 1: Inputs for the simulation environment

tool that can be used by maritime experts without extended modeling background. The tool is also intended to be able to assist in creating a safety concept for the scenario.

The safety concept consists, following ISO 26262[ISO, 2011] and IEC 61508[IEC, 2010], of all identified potential hazards and the failures that might lead to these hazards. A hazard is defined by the IEC 61508 as "potential source of harm", a failure as the "termination of the ability of a functional unit to provide a required function or operation of a functional unit in any way other than as required". It has to be ensured that no single failure might lead to a hazard and that the hazards and their impacts are sufficiently considered. This is done by assessing the frequency, consequence, and controllability as described in previous papers ([Droste et al., 2012] and [Läsche et al., 2012].

The novelty in our approach is that we support the verification of the safety concept by using a distributed simulation. This allows, to a certain confidence level, to verify if all failures leading to a hazard have been considered. Formerly, this verification had to take place in a manual manner which is more time-consuming and also prone for oversights.

B. *SIMULATION ENVIRONMENT*

To ensure that all failures for a hazard are considered correctly and no hazard occurs unexpectedly, we want to use a distributed simulation to verify the safety concept. We use several kinds of models that can be found in figure 1. All of them originate from the *Scenario Description* of the offshore operation and are used as inputs for the various simulation participants. The proposed structure of the simulation environment is depicted in figure 2. The central component of

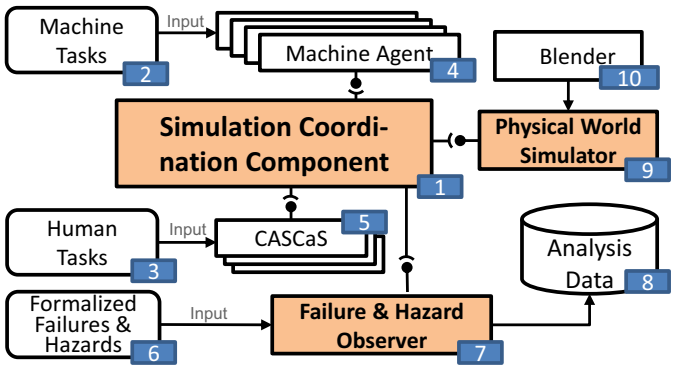

Fig. 2: Structure of our proposed simulation environment

the simulation is the *Simulation Coordination Component* **(1)** which manages the communication between the simulators and the time synchronization among them.

The simulation is controlled by agents. Those are differentiated in *Machine Agents* **(4)** that reflect the behavior of machines and *Human Agents*. Human agents are implemented using the *CASCaS* framework **(5)** (cf. [Lüdtke et al., 2009]) that allows to simulate the non-deterministic behavior of humans. Both execute *Tasks*, the *Machine Agents* execute the *Machine Tasks* **(2)** and *CASCaS* those that are performed by human actors **(3)**. The PWS **(9)** is used to represent the environment and its physics. Further simulators for physics for a special component might be added to the simulation environment if the PWS is not adequate enough for displaying its behavior. A certain kind of this is the *CASCaS* framework **(5)** (cf. [Lüdtke et al., 2009]) that allows to simulate the non-deterministic behavior of humans. The *Blender* tool **(10)** is used to model simulated *Objects* and to design the rough scenario environment.

To determine if the safety concept is correct, the *Failure and Hazard Observer* **(7)** is used. It uses *Formalized Failures and Hazards* **(6)** that originate from the identified failures and hazards of the safety concept. The output of the observer **(8)** is used as a verification of the concept and also as a source for further concept input, e.g. if there is a failure that has not been considered.

C. *CASE STUDY*

We want to use our approach in a scenario in which a *Cargo* is transported on a *Ship Deck* and followed by a *Cargo Supervisor*. It is designed to cover a test case for all components of the simulation environment. It addresses human and environmental behavior, the execution of an operation plan, and hazards and failures that occur during the execution.

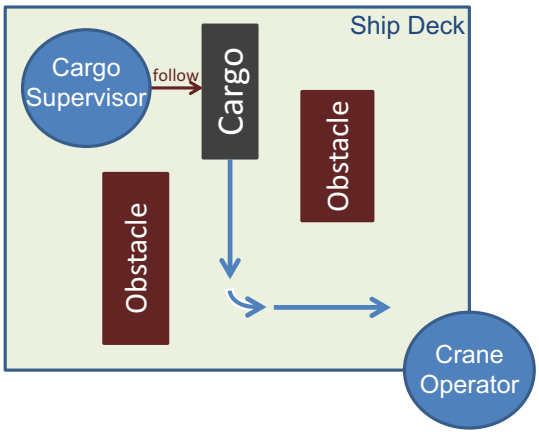

Fig. 3: Overview of the Case Study

Figure 3 outlines the scenario. The *Cargo* is transported along the path marked by arrows whereas the *Cargo Supervisor* follows the *Cargo* to be able to observe it, keeping a distance of at least two meters. The obstacles on the ship deck might cut off the line of sight between the *Cargo Supervisor* and the *Crane Operator*. Further, they might hinder the *Cargo Supervisor* to maintain sufficient distance to the *Cargo*. A failure that has to be detected is a distance lower than two

meters between the *Cargo Supervisor* to the *Cargo*. As the distance drops, the failure has to be detected and indicated.

The case study is a first approach of evaluating our concept and will be extended to a larger one in the future.

IV. IMPLEMENTATION STATUS

This section gives an overview of the current concepts and implementation status of our simulation environment. We already have developed a way to identify potential failures and hazards of a scenario using a Generic Hazard List as described in our previous works ([Droste et al., 2012] and [Läsche et al., 2012]). By the means of this list, we are able to create a preliminary safety concept which contains all potential hazards and the failures that might lead to the hazards. It is created by an offshore safety expert and contains a quantitative rating for each hazard. We also have introduced an approach for modeling scenarios in a previous paper [Sobiech et al., 2012].

The safety concept is verified using the proposed simulation framework. In the following, we want to introduce which of its components have already been developed.

A. *SIMULATION FRAMEWORK*

In order to exchange objects and messages between the various simulators, a communication interface had to be realized. There exist numerous communication frameworks, like *ZeroC IceStorm*[1], but many of these frameworks do not support clock synchronization. Therefore, we chose to use the *High Level Architecture* (HLA) which besides communication using objects and messages also supports timed synchronization of a simulation. Other standards for this purpose are, for example, DIS or TENA (cf. [Henninger et al., 2008]). However, DIS is a limited and superseded standard. TENA offers much of the same capability as HLA but is not as widely spread and supported. We choose to use HLA because of its wide distribution as well as of our previous good experience using it.

1) ***HIGH LEVEL ARCHITECTURE****:* HLA is a standard for implementing a simulation framework that allows the exchange of object instances and interaction messages. The communication takes place over a central component, the *Run-Time Infrastructure* (RTI). All simulators, called *Federates* in HLA vocabulary, register to the RTI. They communicate which objects and interactions they want to update and for which they want to be notified about updates. To support this, a common definition of all object classes and interactions exists.The base for this is called *Object Model Template* (OMT) and is used as *Federation Object Model* (FOM) by the RTI and as *Simulation Object Model* (SOM) by all Federates.

A simulation environment consisting of multiple Federates and an RTI is called *Federation* in the HLA terms. Every Federate in the Federation has an own SOM. The SOM specifies the entities relevant for the single Federate. By this, the Federate can indicate for which instance changes it wants to receive notifications and for which it provides attribute updates itself. The RTI has an aggregated version of all SOMs, the FOM. By this, the RTI knows about all communicated entities and thus can coordinate the communication by providing unambiguous handles for each of them and their instances.

As HLA is just a specification, no reference implementation exists. There are several implementations, both commercial and non-commercial ones. We chose the open source implementation *CERTI*[2] as we already had some experience with it and we found in previous works that its performance is similar to that of a commercial RTI implementation (cf. [Puch et al., 2012]). Thus, there is no significant speed or reliability impact when using the open source implementation.

2) ***COMMUNICATING VIA HLA****:* Communication in the HLA takes place via instances of *Objects* and *Interactions*. *Object Instances* can be used to update the representation of actors or resources within the simulation, i.e. they are used for persistent entities. In contrast, *Interactions* are used for communicating temporary information, like for example an instruction for a simulator.

The reception of data takes place using callback functions. If a Federate wants to be informed about *Object Instance* updates, it subscribes to the *Object Class*. From now on, all changes of *Object Instances* of the *Object Class* performed by any Federate result in a function call at the subscribing Federate. The update might include the time stamp of the update. Similar applies to *Interactions*. If a Federate has updated an *Object Instance* in its simulation, the new attributes have to be manually communicated by invoking a function of the HLA library and thus transmitting the new attributes to the RTI which manages the callback invocations of all subscribing Federates. After all *Object Instances* are transmitted and the simulator proceeds to the next time step, the new simulation time has to be requested using HLA. The moment all other Federates have reached the time, the step is granted and the simulator may continue with the simulation.

3) ***HLA HELPER LIBRARY****:* As mentioned before HLA does not have a reference implementation, it is just a definition that describes how the simulation framework has to be implemented. Three versions of the definition are used (1.3, cf. [U.S. Department of Defense, 1998], 1516-2000, cf. [IEEE, 2000], 1516-2010, cf. [IEEE, 2010]), which are not fully compatible among each other. Actually, even the version 1516-2000 is incompatible among different implementations, as the standard is faulty and two different interpretations of it exist (cf. [Granowetter, 2004]).

This is one of the reasons why we choose to implement a helper library for the HLA implementation. It allows to switch the internally used HLA implementation without a change of the interface to the simulators. Just the library itself has to be adjusted, as well as it might support several implementations that can be exchanged in an easy way. A possible solution for this problem is SimArch (cf. [Gianni et al., 2008]). However, SimArch provides a further abstraction to also use other frameworks than HLA and cannot be used in our software because it is licensed under the terms of the GPL. TrickHLA (cf. [NASA, 2011]) also provides an abstraction from the used HLA implementation but is not freely available and thus could not be used by us.

[1] http://www.zeroc.com/

[2] http://savannah.nongnu.org/projects/certi/

Another reason is the missing representation of relations between *Objects Instances* in the HLA framework. We want to be able to define and update relations between *Object Instances*, for example the distance. Therefore, we added this feature to the library. Internally, we wrapped those relations in special *Object Classes* and let the library interpret them. This allows to maintain full compatibility to Federates that do not use our library. The library is implemented in C++, as the PWS and the FHO are. We also provide a "wrapper for the wrapper" using SWIG[3] to support Java and other programming languages. The concept of callback functions is preserved, although we tried to minimize the amount of different functions performing the same action.

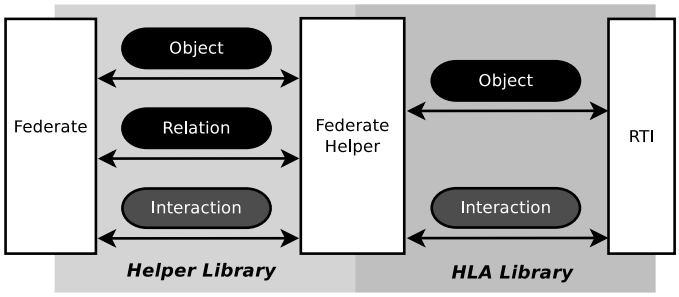

Fig. 4: Interaction between HLA helper library and the specific HLA implementation

Figure 4 depicts the structure of our HLA helper library. Only the library is linked to the Federate, not the specific HLA implementation that is used. Thus, replacing the HLA implementation is easily possible. Further, the library maps the relations to HLA *Objects* which allows the Federate to use relations without having to extend HLA to support them. We also outsourced the time request and grant calls to the library to make the usage of HLA easier. Thus, Federates just have to request a time step. The size of the time step is constant during the simulation and configured in beforehand. Federates are informed as soon as the time is granted.

B. *PHYSICAL WORLD SIMULATOR*

The PWS is used to provide a 3D model of the scenario and of the physical and environmental conditions. Physical effects are, for example, the collision of objects, the buoyancy of the simulated ship or soft body effects which are used to simulate the swinging of a crane rope. Environmental conditions are, in our case, particle effects like rain or snow, blinding by the sun or lamps, or the appearance of fog. This simulator is based on the *GameKit*[4] game engine which contains *Ogre*[5] as visualization and *Bullet*[6] as physics engine. Both components have a huge range of functions and a large, active community. Enhancements can easily be added because of the good documentation and the strongly pronounced object orientated approach. The engine itself is open source software, thus freely customizable. It can load models and scenarios created using Blender[7], an open source 3D content creation

[3]http://www.swig.org/
[4]http://code.google.com/p/gamekit/
[5]http://www.ogre3d.org/
[6]http://bulletphysics.org/wordpress/
[7]http://www.blender.com/

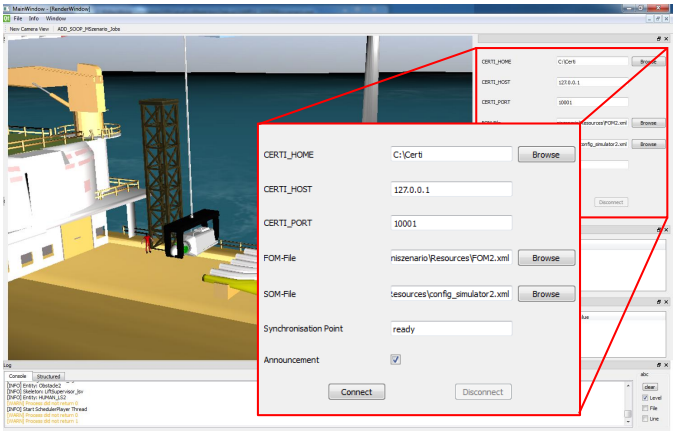

Fig. 5: PWS GUI with marked HLA connection interface

suite, which is another huge advantage, as Blender models of some of the used ships already exist. The PWS has an integrated visualization which is handy for testing purposes, manual observations, or to demonstrate the simulation. But the PWS can also be executed without graphical output to achieve a simulation speed up. A detailed description of the PWS and its components can be found in [Schweigert et al., 2012].

On the basis of the scenario model, our PWS creates the initial configuration for the simulation runs. This includes the initial poses of the used objects, i.e. their position and orientation, as well as the initial environment conditions. There are three general tasks the PWS has to take care of:

- Informing the other simulation participants about object and environmental changes,
- Giving the possibility to control simulation objects and environmental conditions, and
- Injecting failures throughout a simulation run.

For the PWS, the HLA helper library as described in section IV-A3 was fully integrated and was targeted to be an easy usable tool. Thus, the triggering of the attribute updates and the next step calls are performed by the PWS. This was achieved by connecting the PWS scheduler to the HLA helper library update mechanism. The PWS can be connected to any HLA Federation from the simulator interface by entering host, port, and the path to the SOM file (cf. figure 5). We also allow to use a local RTI to test components without requiring the complete simulation environment to be configured and running.

*1) **UPDATING ATTRIBUTES**:* So called *HLASIMElements* are used to update attributes in the PWS. These elements connect HLA Attributes with simulation objects like the mentioned Cargo Supervisor or environmental conditions like wind strength. *HLASIMElements* consist of *single elements* and *related elements*. *Single elements* are used to describe attributes (*HLASIMAttribute*) of a single simulation object or environmental condition. *Single elements* can also be automatically created for every simulation object in the used scenario, in which standard attributes like position, orientation, and the scale factor are observed and updated. *Related elements* are

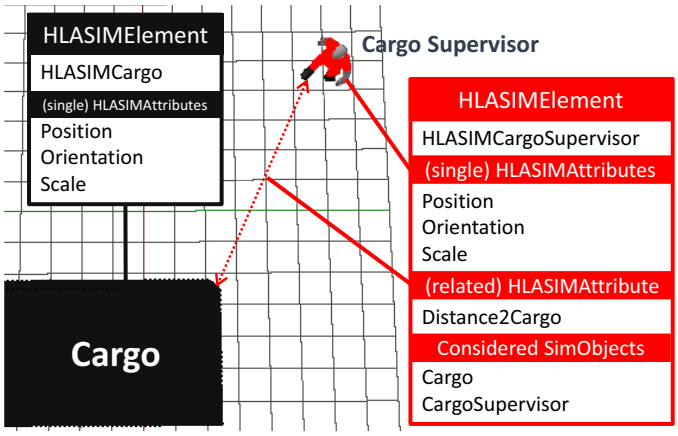

Fig. 6: Example for HLASIMElements with single and related HLASIMAttributes

updated attributes which display relations between two or more simulation objects. An example for this is the distance between two objects in the PWS. In this case, the *related element* observes the two objects and triggers an update of the connected HLA Attribute when one or both objects change their position, orientation, or scale.

An example for *HLASIMElements* as well as single and related *HLASIMAttributes* is shown in figure 6. The Cargo and the Cargo Supervisor have single attributes like the position while the Cargo Supervisor has an additional related attribute which represents the distance to the Cargo. Furthermore, the created *HLASIMElements* are automatically registered at the *RTI* when the simulation starts.

2) ***CONTROLLING THE PHYSICAL WORLD SIMULATOR****:* To control objects within the PWS, like moving to a given position, the *Interaction* concept of the HLA architecture is used. The PWS provides *HLASIMInteractions* which consist of *standard interactions* and *own interactions*. *Standard interactions* are already present in the simulator and comprise the possibilities to translate, rotate, and scale every controllable simulation object. *Own interactions* can be extended *standard interactions*, like moving to a waypoint, or completely new integrated operations. The *HLASIMInteractions* are implemented as PWS jobs which can be started at any given simulation time and have to return a `done` statement when the *Interaction* has been processed. In the case of a *Move to waypoint Interaction*, the pose of the object is interpolated between the start and target pose while looking at the speed or duration parameters of the *Interaction*.

The controlling of environmental conditions, like the maximum wave height, the fog density, or the sun position, is done by listening for *Interaction* calls which change the simulation properties to the received parameters from the responsible simulation participant.

The PWS uses an extension of the controlling solution to give the possibility to inject manual or automatic failures into a simulation run. The difference to the `normal` controlling is that *Failure Injection Components* are attributes connected to hazards or failures which can be defined in beforehand. This can for example be the appearance of fog to disturb the vision or an obstacle at a given position to block an usually used path of the Cargo Supervisor.

The *Failure Injection Components* are visible as special GUI parts of the PWS for a manual injection as well as properties which can be set by a separated control unit to allow automatic injections in the later implementation phase. Failure Injection Components are also memorized to optimize the running times of a simulation while omitting already tested scenarios.

C. FAILURE AND HAZARD OBSERVER

The simulation has to be observed to determine if a hazard occurs during the simulation of the scenario. We are also interested in all occurring failures, as we want to verify the dependencies of the hazards. This information is used for the verification of the safety concept.

We use an FHO framework which joins the Federation and subscribes to the relevant *Objects* and *Interactions*. To be able to observe hazards and failures, the ones identified in the safety concept have to be formalized. Possible ways of formalization include LTL (Linear Temporal Logic) with past operators (cf. [Latvala et al., 2005] for details on PLTL). The challenge is to create executable FHO clients from the hazards and failures that are described in LTL. For now, the FHO clients are manually coded based on the hazard specification. Another aspect regarding the simulation framework is, that it has to be determined which *Objects*, *Interactions*, and *Relations* are necessary to be observed and thus have to be subscribed to. A quite simple approach is to create one FHO for all FHO clients and to subscribe to all *Objects*, *Interactions*, and *Relations* that are mentioned in the LTL formalizations of the failures and hazards. However, this might render into poor performance. One could think of distributing FHO clients among multiple FHOs in order to minimize the amount of subscribed data for each FHO and thus optimizing the performance. This is a further optimization challenge.

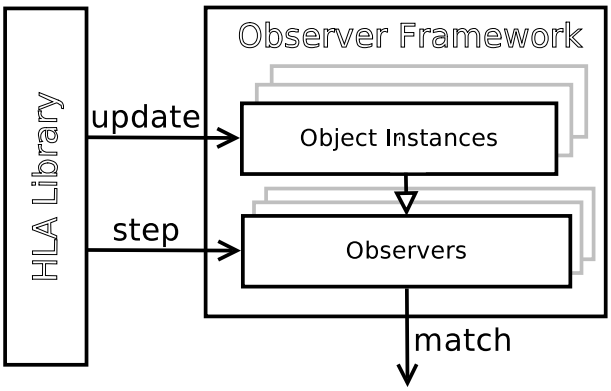

Fig. 7: Outline of the functionality of the Failure and Hazard Observer

Figure 7 outlines the functionality of a possible FHO. It receives updates whenever a simulator updates the simulation *Objects* and stores the relevant *Objects* as well as their history, if this is required. In every simulation step, the FHO clients are evaluated, regarding the *Objects* received in this time step and possibly saved *Objects* from previous steps. If a match is detected, it is indicated by writing to a file, including the trace of all received *Objects* and *Interactions* that lead to the match.

Using the output of the FHO, it is possible to assess if all failures have been correctly assigned to the hazards when creating the safety concept. The safety concept is faulty if a hazard occurs without all of its identified depending failures having occurred. It has to be corrected in this case. To check the safety concept for all identified hazards, all failures have to be injected in all possible combinations during all possible time steps of the simulation. However, there has to be an abstraction of this method because of the feasibility. Again, this is a step that currently is performed manually. But in the future, failures might be automatically injected by taking them from the formalized hazards. The analysis if a hazard has occurred without the required preconditions is also a step manually performed for now. We will try to automate this using the formalized hazards as well.

D. FURTHER SIMULATION COMPONENTS

As described in section III, we also want to include the CASCaS framework for representing human behavior. The Component itself already exists (cf. [Lüdtke et al., 2009]) and will adjusted to be used within the simulation environment. Further information can be found in a previous work [Lenk et al., 2012].

A second component that already exists in a preliminary version is a framework to execute the Machine Agents. Those agents are modeled using the *Business Process Model and Notation* (BPMN2)[8] and define the steps that have to be performed during an operation. The agents will be addressed in a future paper.

V. CONCLUSION AND NEXT STEPS

We have introduced our simulation environment for the verification of a safety concept for offshore operations in this paper. It interconnects several simulators using the standardized HLA for which we added a helper library that allows us to depict relations among actors and resources. The physical simulation is performed in a Physical World Simulator (PWS) which we extended to be usable with HLA. The Failure and Hazards Observer (FHO) allows to determine if a failure or a hazard has occurred.

We successfully implemented the case study as described in section III-C using our simulation concept using the Machine Agents, the PWS, and the FHO. The communication took place over the HLA interface. The Machine Agent sends a commands to the PWS and the PWS executes actions. When an action has been performed, the Machine Agent the next command, and so on. Figure 8 shows the output of the PWS while executing the study. The FHO correctly determined that the distance between Lift Supervisor and Cargo dropped below two meters at the end of the scenario and indicated this. This meas that the case study has been executed as planned and all its components worked as intended. The scenario will be extended by the missing simulators and the already used components will be extended, e.g. by further failures and hazards.

[8] http://www.bpmn.org/

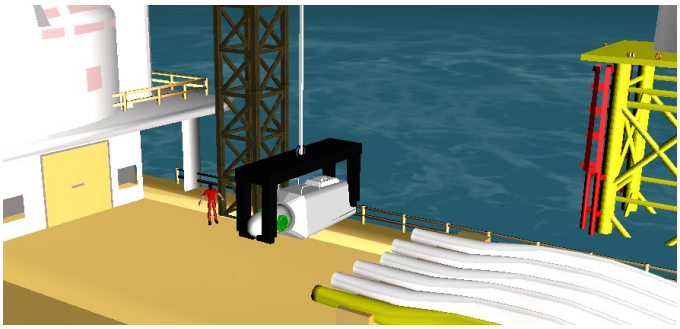

Fig. 8: 3D Output of the Case Study

A next step is to add the CASCaS framework to the simulation environment in order to add human behavior. Further, a common meta model will be developed to create a common understanding of communicated objects between all simulators. A preliminary version already exists.

The next step regarding the observers is to allow the automatic generation of observers. We want to propose a hazard specification language that allows to formalize hazards and failures and automatically generate code out of the formalizations which can be used within the observer framework.

Considerations regarding the automatic injection of possible failures at suitable time steps have to be taken to allow a more systematic and automated investigation of the system. Preparations for this have been taken as described in section IV-B2. A simple, abstracted approach is to randomly inject failures and perform a lot of simulation runs. Of course, this can be further optimized and thus further concepts will be developed.

In the future, we might also use the observers to determine the frequency of occurring hazards. This can for example be done by extending the models by a probability for failures and by performing a lot of simulation runs to gain a confident frequency value.

ACKNOWLEDGMENTS

This work was partially supported by the European Regional Development Fund (ERDF) within the project *S*afe *O*ffshore *OP*erations (SOOP), http://soop.offis.de/.

REFERENCES

[IEEE, 2000] (2000). *IEEE Standard for Modeling and Simulation (M&S) High Level Architecture (HLA) – Framework and Rules*. The Institute of Electrical and Electronics Engineers, Inc., 345 East 47th Street, New York, NY 10017, USA.

[IEEE, 2010] (2010). *IEEE Standard for Modeling and Simulation (M&S) High Level Architecture (HLA) – Framework and Rules*. The Institute of Electrical and Electronics Engineers, Inc., 345 East 47th Street, New York, NY 10017, USA.

[Alexander, 2007] Alexander, R. D. (2007). *Using simulation for systems of systems hazard analysis*. PhD thesis, University of York.

[Droste et al., 2012] Droste, R., Lässche, C., Sobiech, C., Böde, E., and Hahn, A. (2012). Model-Based Risk Assessment Supporting Development of HSE Plans for Safe Offshore Operations. In Stoelinga, M. and Pinger, R., editors, *Formal Methods for Industrial Critical Systems*, volume 7437 of *Lecture Notes in Computer Science*, pages 146–161. Springer.

[Gianni et al., 2008] Gianni, D., D'Ambrogio, A., and Iazeolla, G. (2008). A layered architecture for the model-driven development of distributed simulators. In *Proceedings of the 1st international conference on Simulation tools and techniques for communications, networks and systems & workshops*, page 61. ICST (Institute for Computer Sciences, Social-Informatics and Telecommunications Engineering).

[Granowetter, 2004] Granowetter, L. (2004). IEEE 1516 Compliance – Will the Real C++ API Please Stand Up? *MÄK Technologies*.

[Henninger et al., 2008] Henninger, A. E., Cutts, D., Loper, M., Lutz, R., Richbourg, R., Saunders, R., and Swenson, S. (2008). Live virtual constructive architecture roadmap (lvcar) final report. Technical report, Institute for Defense Analyses.

[IEC, 2010] IEC (2010). *IEC 61508*. International Electrotechnical Commission .

[ISO, 2011] ISO (2011). *ISO/DIS 26262 - Road vehicles - Functional safety*. International Organization for Standardization.

[Lässche et al., 2012] Lässche, C., Böde, E., and Peikenkamp, T. (2012). A Method for Guided Hazard Identification and Risk Mitigation for Offshore Operations. volume 7612 of *Lecture Notes in Computer Science*, pages 37–48. Springer.

[Latvala et al., 2005] Latvala, T., Biere, A., Heljanko, K., and Junttila, T. (2005). Simple is better: Efficient bounded model checking for past LTL. In *VMCAI. Volume 3385 of LNCS*, pages 380–395. Springer.

[Lemessi et al., 2010] Lemessi, M., Rehn, G., Raab, M., and Schulze, T. (2010). Unterstützungssystem zur Verteilten Simulation. In Zülch, G. and Stock, P., editors, *Integrationsaspekte der Simulation: Technik, Organisation und Personal*, number 14 in Fachtagung der Arbeitsgemeinschaft Simulation; ASIM-Fachtagung "Simulation in Produktion und Logistik", pages 485–492. KIT Scientific Publishing.

[Lenk et al., 2012] Lenk, J. C., Droste, R., Sobiech, C., Lüdtke, A., and Hahn, A. (2012). Towards Cooperative Cognitive Models in Multi-Agent Systems. In *COGNITIVE 2012, The Fourth International Conference on Advanced Cognitive Technologies and Applications*, pages 67–70. ISBN: 978-1-61208-218-9.

[Lüdtke et al., 2009] Lüdtke, A., Weber, L., Osterloh, J.-P., and Wortelen, B. (2009). Modeling Pilot and Driver Behavior for Human Error Simulation. In Duffy, V. G., editor, *Digital Human Modeling. Second International Conference, ICDHM 2009, Held as Part of HCI International 2009*, volume 5620/2009 of *Lecture Notes in Computer Science*, pages 403–412. Springer.

[NASA, 2011] NASA (2011). TrickHLA Framework Facilitates IEEE 1516 Simulation Integration. *http://www.nasa.gov/centers/johnson/techtransfer/technology/MSC-24544-11-trickhla.html*. Last visit: 24. January 2013.

[Puch et al., 2012] Puch, S., Osterloh, J.-P., Fränzle, M., and Lässche, C. (2012). Rapid Virtual–Human–in–the–Loop Simulation with the High Level Architecture. In *Proceedings of Summer Computer Simulation Conference 2012 (SCSC 2012)*, number 10 in Simulation Series Vol, pages 44–50. Bruzzone, A., Curran Associates, Inc.

[Raab et al., 2011] Raab, M., Masik, S., and Schulze, T. (2011). Support System for Distributed HLA Simulations in Industrial Applications. In *Principles of Advanced and Distributed Simulation (PADS), 2011 IEEE Workshop on*, pages 1 –7.

[Schweigert et al., 2012] Schweigert, S., Droste, R., and Hahn, A. (2012). Multi-Agenten basierte 3D Simulation für die Evaluierung von Offshore Operationen. In *Go-3D*.

[Sobiech et al., 2012] Sobiech, C., Droste, R., Hahn, A., and Korte, H. (2012). Model based Development of Health, Safety, and Environment Plans and Risk Assessment for Offshore Operations. In *MCMC - 9th IFAC Conference on Manoeuvring and Control of Marine Craft*. in print.

[U.S. Department of Defense, 1998] U.S. Department of Defense (1998). *High-Level Architecture Rules, Version 1.3*. The Institute of Electrical and Electronics Engineers, Inc., 345 East 47th Street, New York, NY 10017, USA.

[Vinnem, 2007] Vinnem, J. E. (2007). *Offshore Risk Assessment : Principles, Modelling and Applications of QRA Studies*. Springer, London, 2nd edition.

AUTHOR BIOGRAPHIES

Christoph Lässche received his M.Sc. in Computer Science (focus: Embedded Systems and Microrobotics) in 2011 at the University of Oldenburg and started to work at OFFIS in the research group SAV (Safety Analysis and Verification) afterwards. Currently, he is working within the project SOOP (Safe Offshore OPerations), which focuses on risk assessment in the offshore wind sector. is E-Mail address is *laesche@offis.de* and his group can be found at http://www.offis.de/en/start.html.

Volker Gollücke received his M.Sc. in Computer Science in 2012 at the University of Oldenburg and started to work at the University of Oldenburg in the Business Engineering Group afterwards. Currently, he is working within the project SOOP (Safe Offshore OPerations), which focuses on risk assessment in the offshore wind sector. His E-Mail address is: *golluecke@wi-ol.de* and the homepage of his group is http://be.wi-ol.de/.

Axel Hahn is full professor at the University of Oldenburg and leads the working group Business Engineering and board member of the division Transportation at the research institute OFFIS. His research topics are safety and efficiency in marine transportation systems. His E-Mail address is: *hahn@wi-ol.de* and the homepage of his group is http://be.wi-ol.de/.

VIRTUAL OBEYA: COLLABORATIVE TOOLS AND APPROACHES TO BOOST THE USE OF SIMULATORS IN CONCEPT DESIGN

Detlef Blankenburg, Kjetil Kristensen, Knut Einar Aasland, Ole Ivar Sivertsen

Norwegian University of Science and Technology
Department of Engineering Design and Materials
N-7491 Trondheim, Norway
E-mail: {detlef.blankenburg,kjetil.kristensen,knut.e.aasland,ois}@ntnu.no

KEYWORDS
Collaborative engineering, Collaborative tools, Virtual Obeya, Knowledge acquisition

ABSTRACT

This paper presents research results from a study on user requirements for in-context lean engineering collaboration. The study forms an integral part of multidisciplinary research on collaborative tools and approaches addressing sources of waste in lean engineering in the European large-scale integrating project LinkedDesign.

The results are guiding the research and technology development work on a Virtual Obeya; a digital, improved version of the Obeya collaborative arena concept pioneered by Toyota and later adopted in a range of companies and industries using lean engineering principles. Topics of particular interest include geographically distributed project teams collaborating closely on concept and product development, and also sharing of models, tools and techniques in collaborative team environments - including simulators and their use within such teams. The paper summarizes project objectives for the Virtual Obeya, results from an analysis of frequently observed sources of waste in collaboration and finally selected approaches for improving collaborative performance in engineering teams.

INTRODUCTION

Teams involved in the development of new products, technologies and concepts, face numerous challenges. A number of technologies, engineering approaches and collaborative work patterns add to these challenges, but they also represent new opportunities and potential sources of competitive advantage for companies willing to explore new approaches and new ways of executing projects. Among these, the tendency towards executing split location projects with global teams spanning multiple geographic sites, is important. Another key trend is the use of advanced modelling and simulation tools to reduce of the need for physical models in the early stages of the engineering process, thereby making large savings both in cost and in time consumption.

One of the challenges of geographically distributed project teams is that certain new and productive work methods are difficult to implement, as some aspects of these methods, in their proven, original form, are closely tied to the team being collocated. The use of the Obeya is one of these areas, as this concept was originally developed to support collocated rather than split location engineering teams.

Obeya is a term used for a ”large room” originally connected to project work in the automotive industry. Its origin is in the G21 project at Toyota in the 1990s, a project which led up to the first generation Prius. At the onset of this project, the Chief Engineer felt that he lacked the necessary authority to make the optimal decisions, and thought he could be overrun by experienced discipline leaders in a way that was not optimal for the project as such. He therefore needed the support of the other discipline leaders whenever he had a decisive discussion with one of them. In order to achieve this, he instituted the “large room” – Obeya in Japanese – as an arena for all his discussions with the discipline leaders. In this room, the other discipline leaders would be present, and documents and data would be available to all [Aasland and Blankenburg, 2012; see e.g. Liker, 2003; Morgan & Liker, 2006; Osono, Shimizu & Takeuchi, 2008 for an overview of collaboration and management principles in Toyota, the company that pioneered the Obeya concept].

LinkedDesign (Linked Knowledge in Manufacturing, Engineering and Design for Next-Generation Production) is a European large-scale integrating project with 13 partners from 7 countries. The main output of the LinkedDesign project is the technology platform LEAP (**L**inked **E**ngineering and m**A**nufacturing **P**latform), currently under development. This platform will provide an integrated, holistic view on data, persons and processes across the full product lifecycle.

An integral element of the technology platform LEAP is the Virtual Obeya being developed in one of the Research and Technology Development work packages of the project (“WP5: Collaborative Environments and UI Concepts for Context-driven Engineering”),

Proceedings 27th European Conference on Modelling and Simulation ©ECMS Webjørn Rekdalsbakken, Robin T. Bye, Houxiang Zhang (Editors)
ISBN: 978-0-9564944-6-7 / ISBN: 978-0-9564944-7-4 (CD)

exploring more effective and efficient engineering collaboration. The research supporting the development of the Virtual Obeya combines semantic UI principles, Active Knowledge Modeling [AKM; Lillehagen and Krogstie, 2008] and a context based approach to enable context-driven, activity-centric, dynamic and interactive visualization of engineering knowledge, information and data with high relevance to and between multiple engineering roles, including simulation [Kristensen et. al., 2012].

The LEAP Virtual Obeya is a front-end concept in the LinkedDesign project; the user interface and navigation that enables and supports the close contact and process-oriented knowledge exchange between experts of different working domains. The LinkedDesign front-end provides context-driven data access and collaboration support for teams involved in engineering and simulation tasks, as indicated in the upper part of the figure below.

LEAP is designed to be user centric rather than information centric. To foster collaboration between users across different disciplines, LEAP will use and extend lean engineering principles and implement a collaboration workbench enabling effective internal and external collaboration.

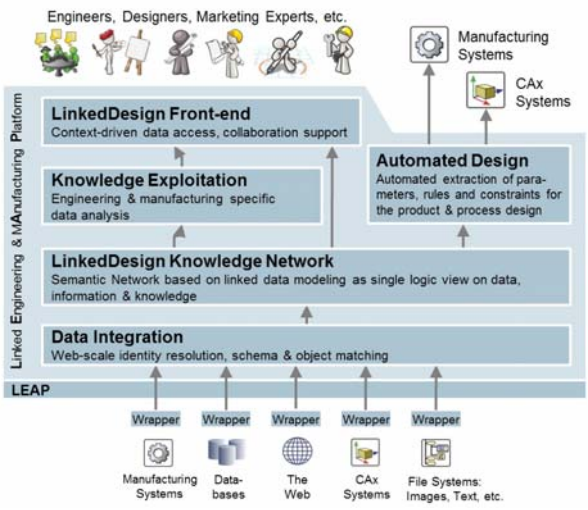

Figure 1: LEAP Overview

The Virtual Obeya is a new concept addressing certain limitations in a traditional Obeya, as piloted by Toyota and later adopted by many other companies and industries. The main objective is to accelerate value creation by applying new visual project management approaches to develop purposeful, powerful and simple tools for improving engineering team collaboration and communication:

The LinkedDesign Virtual Obeya offers a rich, relevant and context-specific front end supporting user collaboration across multiple tasks in a product lifecycle.

Specifically, the Virtual Obeya will be developed as a collaborative, context-driven user interface that enables user friendly access to all required engineering data and information sources.

With the Virtual Obeya, it is possible to alleviate some of the disadvantages of development projects involving engineering and simulation across multiple geographic sites. Models are very often a necessity in efficient development, and although physical models cannot be shared across sites, computer models and the tools and processes using them can easily be shared in real time. A particularly interesting case is the use of simulators, because they are highly beneficial, they are large, complex and expensive installations, and their application depends on expertise. Sharing models, simulations and simulator across the sites of a project opens new possibilities regarding efficient and effective product development and engineering design.

Thus, the Virtual Obeya has the potential to boost the real time use of advanced tools like simulators in split location engineering teams. Some of the key characteristics of the context-specific front end, that the LEAP Virtual Obeya represents, are:

- The focus is on value creation. This is achieved by providing high usability and in-context, easy and rapid access to aggregated knowledge level. Relevance, purposefulness and transparency are guiding principles.
- LinkedDesign has conducted research exploring rich interaction possibilities – suggesting an in-context feature set that is comprehensive within the scope of what is needed in any single situation, based on lean engineering principles. This includes – but is not limited to – simulators and their application as well as Knowledge Based Engineering; KBE [La Rocca, 2012; Sivertsen et. al., 2012].
- Furthermore, the LinkedDesign project has explored drivers for relevance, purposefulness and transparency across multiple tasks in a product lifecycle. This research is on-going and targeting provisioning of key insights, knowledge and information through visual project management – specifically interactive electronic task boards and integrated workflow environments.
- A Virtual Obeya for engineering collaboration and visual project management will be piloted, implemented and demonstrated through subsequent tasks in the LinkedDesign work package on Collaborative Environments and UI Concepts for Context-driven Engineering. The LEAP Virtual Obeya will support different levels of work coupling [Neale et. al., 2004].

The goal of this task is to collect and analyse integrated product development and concurrent engineering requirements (design and production data), and analyse lean product development principles based on semantics and front end value drivers.

EXISTING THEORIES AND WORK

Peter F. Drucker stated that task identification is the most important driver of knowledge worker productivity [Drucker, 1999]. This is highly relevant for discussions related to improving collaboration, as successful task identification in today's complex projects usually requires active involvement from several disciplines and roles. The inherent multidisciplinarity of today's complex products, services, projects and processes implies that collaboration is a cornerstone of knowledge work. In order to avoid poor decisions and quality problems that must be revisited, the most knowledge intensive processes require that all stakeholders with the power to veto a solution is directly involved in the design process.

Collaborative work environments can, if combined with today's state of the art technologies provide an immersive, context-driven experience that systematically removes filters that get between the people working together and the task at hand. Through this, LEAP aims to enable a level of shared understanding where engineers and other knowledge workers can devote their full attention to what they are doing right now [Kristensen et. al., 2012]. While task execution is the primary vehicle or carrier of efficiency, user collaboration plays a central role in making sure multiple task execution activities are coordinated and purposeful in the context of overall project objectives. User collaboration can thus be regarded as a primary vehicle or carrier of effectiveness. As described above, Drucker [1999] ranked task identification as the number one factor determining knowledge worker productivity. Task identification precedes task execution, and more often than not involves user collaboration, particularly in a highly complex, multidisciplinary engineering setting.

Frequently Observed Sources of Waste in Collaboration

As described in the introduction, the Obeya room is an arena for rich interaction typically taking place between the Chief Engineer and the respective discipline leaders. In this room, typically all relevant discipline leaders would be present, and documents and data would be available to all. The team can discuss and work shoulder to shoulder whilst "co-navigating" complex, interlinked issues of a multidisciplinary character. How to mimic and preferably improve similar processes in distributed / split location engineering teams is of special interest.

The LinkedDesign consortium will explore processes similar to these later in the project to address commonly occurring waste in collaboration [Manyika et. al. 2009], when suitable concepts are ready for piloting.

Based on Manyika et. al. (2009) the following sources of waste have been identified in order of priority (based on input from all LinkedDesign project partners):

- Searching (highest priority)
- Misunderstanding
- Under-communicating
- Extra processing
- Waiting
- Misapplication
- Interpreting (lowest priority)
- Divergence (not a priority source of waste)
- Motion (not a priority source of waste)
- Translation (not a priority source of waste)

Approaches for Improving Collaborative Performance in Engineering Teams

Engineering collaboration is dynamic; it constitutes a mix of planned and ad hoc interactions as well as involving structured / formalized and unstructured / informal knowledge sources. Moreover, it evolves over time and co-exists in a large and growing number of different forms. Effectively supporting high-performance collaborative work patterns across a variety of different engineering contexts requires competencies for both individual knowledge workers and process owners. Moreover, performance is typically linked to collaboration on both a strategic and an operational level, both for work and reflection on work for learning and process improvement.

While technology is an important enabler of new collaborative work forms with attractive characteristics, technology alone is not sufficient to enable new, high-performance lean engineering practices. Broader change initiatives including smart combinations of people resources, technology, work processes, business culture and organizational models, are needed to fully exploit the value of collaboration. This is further complicated by the current lack of well-known, industrial frameworks for A) evaluating the impact of and B) systematically improving collaboration. There are however a number of tools and diagnostic frameworks that can be applied as decision support tools to make informed decisions that reduce risk and manage success factors for collaboration, e.g. Hansen [2009, 2004], Rosen [2007] and Mattesich et. al. [2001]. Succeeding with collaboration is a complex undertaking, and few companies succeed in exploiting the full potential of deep collaboration.

One of the main reasons for this is that collaboration is suffering from major coherency disconnects:

First, improvement efforts often fail because strategic initiatives and decisions are not followed up by operational measures – instating a policy that collaboration constitutes a main element in running the business does not lead to change unless it is followed by specific, clearly defined work practices that spells out how to use collaboration operationally to achieve business objectives. Collaborative engineering must not remain a loosely defined, ambiguous term – it must be given a clearly defined content.

Second, improvement efforts often fail because collaboration is seen and treated as something that is domain-specific rather than an enterprise-wide concept. This happens in part because the provision side has a strong position, and is able to influence terminology and shape managers' thinking on collaboration.

Collaboration does not equal a single collaboration tool or platform, or even a set of tools or platforms; indeed most activities in engineering companies today include some collaborative aspect(s). Unless these misconceptions are cleared and a proper understanding of how to facilitate and manage collaboration as a broad set of business activities is in place, it will be difficult to reap the full benefits of collaboration – and equally avoid misapplications of collaboration (that can reduce performance).

FINDINGS

Multidisciplinary engineering collaboration involving simulation activities is a very complex set of interactions and activities, and a comprehensive body of research suggests that this should be optimized on a system level [Kristensen and Kijl, 2010]. Current Obeyas commonly shared a set of limitations as indicated below [Kristensen et. al, 2012].

- Lack of distributed collaboration support
- Manual knowledge aggregation only
- No in-context adaptive GUI provision
- Only passive; no or limited opportunities to interact directly with underlying information architecture
- No information persistence between task boards / knowledge briefs
- Fragmented records; development typically documented across multiple sources and formats
- No simple import / export functions between physical (often paper-based) and virtual media formats

Characteristics of Traditional Obeyas

- Static, cluttered, no filtering
- «Low threshold» solution (high usability)
- Inefficient separation of computer-based «work» formats and physical «decision» formats
- No split location collaboration support

Characteristics of the LEAP Virtual Obeya (under Development)

- Semantics, dynamic filtering based on relevance criteria; context- and role-based knowledge aggregation
- Allows direct interaction with underlying information architecture – softer or no separation of «work» and «decision» formats
- Enables user collaboration over distance – with symmetrical or asymmetrical views, depending on role and context

The Virtual Obeya will consist of one or several "rooms", spaces or dashboards; each demonstrating a contextualized, purpose-driven aggregated representation of engineering information presented in a manner that aids effective and efficient processing of knowledge and development of insights.

Knowledge Acquisition for Knowledge Based Engineering (KBE)

According to Stokes [2001], tasks that have to be done on a rotational basis (routine tasks) cover nearly 80% of the overall design work. In consequence, to enable a quality increase while decreasing lead-time in product development means changing this ratio substantially. This leads to the field of Knowledge Based Engineering and respective research by La Rocca [2012]. According to La Rocca an extended definition of KBE is:

"Knowledge based engineering (KBE) is a technology based on the use of dedicated software tools called KBE systems, which are able to capture and systematically reuse product and process engineering knowledge, with the final goal of reducing time and costs of product development by means of the following:

- *Automation of repetitive and non-creative design tasks*
- *Support of multidisciplinary design optimization in all the phases of the design process"*

Structuring information and knowledge for easy reuse is the basis for any KBE system. Still, the knowledge and information that is entered into a knowledge system has to come from somewhere, and the Knowledge engineer is rarely experts in the field they are building a system for. For this reason, it is vital to have good communication with the domain experts.

One of the industrial partners in the LinkedDesign project, Aker Solutions, is systematically exploring new collaboration technologies and collaborative work practices based on lean thinking, as illustrated in the figure below.

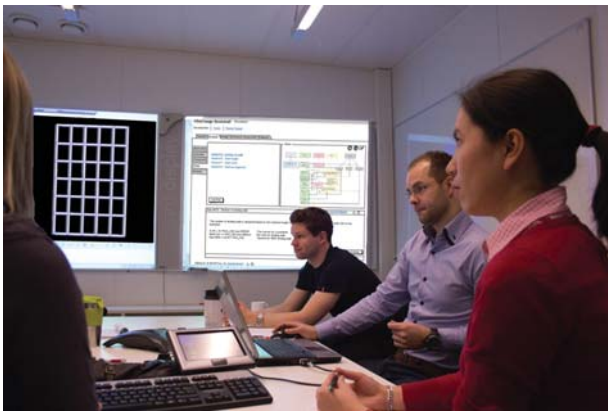

Figure 2: Aker Solutions Engineering Team (Image: Aker Solutions)

Today's procedure for the acquisition of knowledge is slow and old fashioned. It is based on one to one interviews, and hardcoding of engineering rules into rigid systems (or frameworks). The next generation of knowledge acquisition systems promises to radically change this. Collaboration tools will not only make it easier for the knowledge engineer to understand the knowledge the domain experts have, but the domain experts will also be able to collaborate effectively with each other, ensuring that the system gets the best information available. This will ensure that the LEAP platform has an excellent tool for lean, user friendly and collaborative knowledge acquisition.

In the context of LinkedDesign, one special topic of interest is the rather complex interface between typical automated design tasks, refer Sivertsen et. al. [2012] and typical user collaboration tasks, refer Kristensen et. al. [2012]. Consultations with the industry partner indicate that this interface is poorly understood, despite the fact that many frequently occurring tasks of significant importance can be described as taking place in this interface, as when engineers are shifting back and forth between automated design tasks and consultations with other stakeholders (user collaboration). In addition, classification can be difficult because tasks often involve elements of both categories. The following aspects are explored:

- **Automated design / knowledge acquisition as a consultative process with / between several stakeholders**: Today's engineering operations are largely multi-disciplinary. Discussions, clarifications, negotiations and decisions that occur in the interfaces between different phases and disciplines is an interdisciplinary value creation process, thus constitutes a large portion of typical engineering projects.
- **Automated design process as an iterative cycle between core automated design tasks and consultations**: In order to optimize productivity in current engineering companies, there is a need to integrate 1) typical formal engineering processes that are documented in accordance with formal rules in dedicated systems (here as in KBE), with 2) informal processes, which are documented more or less in a random fashion. The latter category is largely unmanaged, but nevertheless represents a large portion of the total interaction taking place, and hence represents a potentially valuable source of information if managed better. It is believed that there is considerable potential for productivity increases in coordinating these two categories closely. A rationale for these consultations should be provided, focusing on explicit value creation. Consultations could then be explored more systematically by using Nonaka & Takeuchi's knowledge cycle model (knowledge development as a cyclic spiral and interchange between tacit and explicit knowledge).
- **Waste reduction in collaborative KBE**: In accordance with lean principles, LinkedDesign targets waste reduction in user collaboration (also related to knowledge acquisition). Consultations with the industry partner indicate that effective and efficient user collaboration has the potential of acting as a catalyst in KBE – by simultaneously improving the quality of the process (reducing the risk of misunderstandings) and through acting as a process accelerator by reducing other forms of waste. This is discussed in further detail in Kristensen et. al. [2012].

DISCUSSION

Given the sources of waste identified and prioritized by the project partners, observations indicate that LEAP could add value by supporting a continuum from informal, ad hoc collaboration (low-threshold mechanisms for capturing knowledge created as a result of ad hoc creativity in teams) to more formalized engineering processes. A combination of pull- (search) and push-based knowledge provision mechanisms could represent added value in complex, multidisciplinary and collaborative situations such as "knowledge assists" where the person(s) in need of knowledge may or may not exactly know what to look for, how to retrieve it or what knowledge objects that could, semantically, be of interest or relevance. Selected benefits from the Virtual Obeya, based on initial investigations and industry partner consultations:

- **High usability** will be achieved by making the Virtual Obeya work on many levels. The simplest level will be to use it as a conference room with some added features, and this will make the threshold for using it low. Then – as experience is gained – more advanced functionality (shared walls, shared programs, shared data access, etc.) can be taken up, thereby turning the room into a functional Virtual Obeya.

- **In-context, easy and rapid access to aggregated knowledge** is a key to an efficient Obeya. During a project, loads of data are collected and generated, and it is easy for the project members to "drown" in them, so that they don't find what is needed without a lot of work. By structuring the data so that they can be retrieved based on context, this problem will be alleviated.
- **Rich interaction possibilities** will be explored during the project. We know that multitude of interaction modes is a characteristic of traditional Obeyas, and the virtual variety will have a challenge replicating these, but will also offer new possibilities compared to traditional Obeyas. Among the possibilities that must be explored is the use of shared virtual reality worlds. This would mean simulators that span the participating locations, with separate roles allocated to the participants.
- **Multi-role, multi-context interfaces** will extend the Virtual Obeya functionality to external collaborators that have access to the team space(s) using a regular PC, a tablet or even a smartphone. Graceful degradation and mobile first approaches will be explored to ensure access to the right knowledge in any context.

CONCLUSION

This paper presents research results from a study on user requirements for in-context lean engineering collaboration, as a part of multidisciplinary research on collaborative tools and approaches addressing sources of waste in lean engineering.

The results are guiding the research and technology development work for a Virtual Obeya, a digital, improved version of the Obeya collaborative arena concept pioneered by Toyota and later adopted in a range of companies and industries using lean engineering principles. Knowledge acquisition is the bottleneck for efficient KBE implementation and initial investigations indicate that collaboration techniques combined with the LinkedDesign "Virtual Obeya" concept looks very promising as an efficient tool for significantly enhancing the KBE knowledge acquisition process. This will be further explored in the later stages of the project, together with further integration with work processes in the demonstrator work packages.

A generic format for knowledge codification, as mentioned above, will also enhance the acquisition process as a common knowledge interface between domain experts, knowledge experts and the software engineers implementing a KBE system.

ACKNOWLEDGEMENT

This work has been partly funded by the European Commission through the Large-scale Integrating Project *LinkedDesign: Linked Knowledge in Manufacturing, Engineering and Design for Next-Generation Production* (FoF-ICT-2011.7.4, Project No: 284613). The authors wish to acknowledge the Commission for their support. We also wish to acknowledge our gratitude and appreciation to all the LinkedDesign project partners for their contribution during the development of various ideas and concepts presented in this paper.

REFERENCES

Aasland K. E., Blankenburg, D.: An analysis of the uses and properties of the Obeya. The 18th International Conference on Concurrent Enterprising ICE 2012, Munich, Germany, 2012.

Drucker, Peter: Knowledge-Worker Productivity: The Biggest Challenge, California Management Review, Vol. 41, No. 2, 1999.

Hansen, Morten T.: The Collaboration Toolkit. Harvard Business Press, 2009

Hansen, Morten T.: Nohria, N.: How to Build Collaborative Advantage. MIT Sloan Management Review, Vol 46, No 1, 2004, pp. 22-30.

Kristensen Kjetil: Collaborare non humanum est: Collaboration et environnements hybrids (French translation byFrançoise et Loukhoum Bronner). Office et Culture Magazine, June 2010, pp. 32-39.

Kristensen Kjetil, Aasland Knut E., Blankenburg Detlef, Marthinusen Ivar, Sivertsen Ole Ivar, Krogstie John, Ivanov Petko, Perales Fernando: D5.1 Next generation collaborative design methodology report. LinkedDesign project report, LinkedDesign, FoF-ICT-2011.7.4 Project No: 284613, 2012.

Kristensen Kjetil, Fanguy Darrel: Future Perspectives on Collaboration in the Oil and Gas Industry. 71st EAGE Conference & Exhibition incorporating SPE EUROPEC 2009 in Amsterdam, the Netherlands, 2009.

Kristensen Kjetil, Kijl Björn: Collaborative Performance: Addressing the ROI of Collaboration. International Journal of eCollaboration. Vol 6, No. 1, 2010.

La Rocca, G, "Knowledge based engineering: Between AI and CAD. Review of a language based technology to support engineering design", Journal of Advanced Engineering Informatics, 2012

Liker, J: The Toyota Way – 14 management principles from the world's greatest manufacturer. McGraw-Hill Professional Publishing, Blacklick OH, 2003.

Lillehagen, Frank, Krogstie, John: Active Knowledge Modeling of Enterprises, Springer, 2008.

Manyika J., Sprague K., Yee L. (2009). Using technology to improve workforce collaboration. What Matters. McKinsey Digital, October 2009.

Mattesich Paul W, Murray-Close M, & Monsey B. R.: Collaboration: What Makes It Work, 2nd Ed. Fieldstone Alliance, 2001.

Morgan, J, Liker, J: The Toyota Product Development System – Integrating people, process and technology. Productivity Press, New York, 2006.

Neale Dennis C, Carroll John M, Rosson Mary Beth: Evaluating Computer-Supported Cooperative Work: Models and Frameworks. Proceedings of the CSCW'04, Chicago, IL, 2004.

Osono, E, Shimizu, N, Takeuchi, H: Extreme Toyota: Radical Contradictions That Drive Success at the World's Best Manufacturer. John Wiley & Sons, New York, 2008.

Rosen Evan: The Culture of Collaboration. Red Ape Publishing, San Francisco, 2007.

Sivertsen Ole Ivar, Lützenberger Johannes, Marthinusen Ivar, Kristensen Kjetil, Iversen Geir, Klein Patrick, Rutkowska Gabriela: D6.1 Methods for KBE related knowledge acquisition and codification report. LinkedDesign project report, LinkedDesign, FoF-ICT-2011.7.4 Project No: 284613, 2012.

Stokes, M., "Managing engineering knowledge: MOKA: methodology for knowledge based engineering applications", Professional Engineering Publishing, 2001

Toyota Driver's Seat: New Product Quality System Turns Data into Visuals That Drive Decisions. WWW page. http://toyotadriverseat.com/pr/tds/new-product-quality-system-turns-216494.aspx, accessed 10.2.2013.

AUTHOR BIOGRAPHIES

DR. DETLEF BLANKENBURG is Associate Professor at NTNU. His field of experience is Engineering design in practice and engineering design methodology, Lean Product Development and Concurrent Engineering. He studied Mechanical Engineering at RWTH Aachen in Germany and got his PhD at NTH in Trondheim in 1994. After a period as research scientist at SINTEF (The Foundation for Scientific and Industrial Research at the Norwegian Institute of Technology), he was appointed as associate professor of Engineering Design at NTNU, first at the dep. of Product Design, later at the dep. of Engineering Design and Materials - IPM. Head of department at IPM from 2002 to 2005 and assistant head of department since 2012. His e-mail address is: detlef.blankenburg@ntnu.no and his web page is: http://www.ntnu.edu/employees/detlef.blankenburg

DR. KJETIL KRISTENSEN is an Adjunct Associate Professor at NTNU. He has extensive experience from research and management consulting in the research areas collaborative strategies, new work concepts, knowledge work productivity and collaborative innovation. He obtained his PhD in the research program Productivity 2005 at NTNU, developing collaborative working environments supporting high-performance split location engineering design and collaborative innovation. He has been actively involved in the EU projects ECOSPACE (IP; FP6/IST, through ESoCE-NET) and LinkedDesign. His e-mail address is kjetil.kristensen@ntnu.no, his Twitter address is @DrKristensen and his blog can be found at http://www.collaborationperspectives.com.

DR. KNUT E. AASLAND grew up in Oslo, Norway and studied Mechanical Engineering at NTH in Trondheim. He got his MSc degree in 1980, and did a PhD at the same university in 1995. He has worked for the research institute SINTEF as scientist, senior scientist and research manager. His focus was first CAD, later design methodology. Since 2004 he has been teaching engineering design at NTNU, Norway's leading technical university. His e-mail address is: knut.e.aasland@ntnu.no and his web page is: http://www.ntnu.edu/employees/knut.e.aasland

PROF. OLE IVAR SIVERTSEN is currently heading the study program Engineering Science and ICT at NTNU. He has a 20+ year long track record of managing international and national research projects. He also has experience from commercialization of results from earlier EU projects in the area of CAE / simulation. Professor Sivertsen is the author of the book Virtual testing of Mechanical Systems, Theories and Techniques, 2002. His research interests are industrial ICT, Knowledge Based Engineering (KBE), automated design, virtual testing, CAE, collaborative engineering, collaborative innovation and new learning approaches. Over the last 6-7 years he has been working closely together with the large industry partner Aker Solutions within the field of industrial ICT and KBE. His e-mail address is: ois@ntnu.no and his web page is: http://www.ntnu.edu/employees/ole.ivar.sivertsen

EMERGING TOOLS FOR CONCEPTUAL DESIGN: THE USE OF GAME ENGINES TO DESIGN FUTURE USER SCENARIOS IN THE FUZZY FRONT END OF MARITIME INNOVATION

Snorre Hjelseth
Faculty of Technology and Maritime Sciences
The Oslo School of Architecture and Design, Vestfold University College
Raveien 197, Borre, 3184, Norway
E-mail: snorre.hjelseth@hive.no

KEYWORDS

Design, Conceptualization, Simulation, Maritime innovation.

ABSTRACT

This paper discusses and describes how simulated user scenarios can be created and used in the front end of maritime innovation processes. The paper introduces the use of game engines as design tool to create dynamic scenario environments that are used as means to facilitate interdisciplinary collaboration between users and actors in a design process. The goal of the research was to see if it is possible to integrate realistic real-time simulations with user input in the conceptualization phases of innovation. The paper describes a micro case from the maritime industry that shows some of the complexity levels regarding the understanding of user scenarios in interdisciplinary design groups. The second case study reports on an ongoing development project where simulation has been used to explore crisis scenarios in the Oslo fjord. The results show that the use of design thinking and user involvement in combination with simulation tools can create a platform for an iterative process to develop complex user scenarios that drive conceptual innovation.

INTRODUCTION

Conducting user centered design in the Fuzzy Front End (Koen, 2004) of maritime innovation is a challenge. The fuzzy front end refers to the process and activities that comes before the more structured new product development process with traditional stage gates (Cooper 2001). If designing is about "changing existing situations into preferred ones" (Simon, 1981), understanding situations or scenarios is a key element. Problems concerning users are often 'wicked' (Rittel et al, 1973) or ill-defined because factors and solutions are often unknown (Lawson, 2005; Lawson and Dorst, 2009). Dealing with these types of problems often requires a more radical approach in contrast to incremental development where the goals are often increased product performance.

In order to explore and understand such unknown factors, designers need approaches other than what is currently the practise in the maritime industry. In addition, one of the bottlenecks for implementing new types of conceptualisation processes in the industry is the complex nature of maritime innovation on multiple levels. These include:

- Design and development are often dependent on collaboration between multiple companies within a maritime cluster
- The maritime contexts at sea are often not available for experience by the designer
- Products and systems often contain a range of different technology
- Carrying out task analysis is often a challenge because of the complexity of operations
- Testing new concepts is often not possible because of matters of safety and risk.

Emma Linder (2008) and Jan Inge Jenssen (2003) describe some of these innovation challenges.

The first part of this paper explores some of these challenges when effecting user centred design through a case study where a new seismic simulator was designed. Through participatory action research and qualitative interviews we explored answers to the following question: How is it possible to understand and analyse complex user scenarios via simulation in the maritime and offshore industry?

Based on results from this study we proposed a game engine tool to simulate scenarios that can be created in the design conceptualisation phases of the activity. The porous character of this tool lay in the ability to create and visualize complexity in a way that more easily allows designers to obtain a holistic overview and enable fast design modifications.

Existing research about the use of simulators and VR tools in early product development phases shows that user scenario simulation improves information quality and quantity from end-user feedback that can identify usability issues (Thalen, 2011). However these areas tend to focus on creating life-like interface experiences for user evaluation and not on the potential as an iterative design tool.

Proceedings 27th European Conference on Modelling and Simulation ©ECMS Webjørn Rekdalsbakken, Robin T. Bye, Houxiang Zhang (Editors)
ISBN: 978-0-9564944-6-7 / ISBN: 978-0-9564944-7-4 (CD)

When these types of tools have been used for conceptualisation in design processes they often only utilize the real-time rendering engine to walk through static 3D models. The *Lumion* simulation software is an example of this. This application of the tool might cover the needs of architects designing buildings to develop an more immersed experience of a design concept, but it offers little flexibility when designing for complex maritime tasks or operations where a more dynamic approach to behaviours is needed. The central question this paper tackles is how game engines might be used as a design tool to visualize and simulate user scenarios for conceptualisation in maritime innovation.

MARITIME INNOVATION AND INDUSTRIAL DESIGN

The maritime industries often have a conservative approach to innovation strategy that is lodged in decades of experience. This industry typically uses engineering methods to design and solve most of its problems. These problems are mainly technical or systems oriented where human input is a sub-factor of the overall innovation strategy.

Innovation and operation in the maritime sector have seen increased interest in human safety and operation performance. If a human focus is needed in design, it is often referred to as human factors or ergonomics (Meister, 1999). The problem with human factors in the maritime sector is that its not implemented in the core design activities in the innovation processes that are undertaken. The reason for this is that engineers are not trained in designing for user experience or with human factors orientation. Human factors are then often seen more as requirements than innovation possibilities. This gap in competence in the maritime innovation process has opened up possibilities for industrial and interaction designers with special competencies in design thinking, engagement and user centered design.

Recently, some projects in the maritime sector have included industrial designers as part of their core innovation strategy. The K-Master operator chair (Figure 1) project carried out by industrial designer Magne Høyby in Hareide Design is a good example not only of how design thinking and human factors can be part of an innovation strategy, but also how the design process itself can manage the conceptualisation phases in collaboration with technical engineers.

Figure 1. K-Master operator chair designed for Kongsberg Maritime by Hareide Design

SIMULATION

Simulation tools are often used in late stages of innovation where tests are made to evaluate a finished design. When human factors are simulated, tests are often performed in simulators that are costumed designed for training purposes. Simulators might be very useful in user evaluation and in usability testing, but they are often not used until later stages in the development process where changes of the design are costly.

One challenge with simulation software is that it is not designed to be used as a tools in conceptualisation processes. Creating simulations can be time consuming where considerable programing must be implemented even to do simple task such as importing 3D models. Often these types of programing tasks are preformed in low-cast representations.

3D CAD tools have eventually become crucial in product development, but the tools are not basically designed for creative cross-professional design processes, where “changing existing situations into preferred ones” (Simon, 1981) is at stake. Laurel (2003) describes how visualisations and models are created to simulate future scenarios that are often used in the final presentation of concepts and not as creative tools in the conceptualisation phases when designing.

The idea of using 3D game engines as a tool in the design process is to improve the ability to understand existing and develop future user scenarios much earlier in the design process (Tideman 2008; Thalen 2011; Manninen 2000). There are several types of game engines on the market and the most popular is *Unity*, *Unreal engine*, and *CryENGINE*.

A game engine is a software framework that is used to create games for platforms like *Xbox*, *PlayStation* or personal computers. Typical functionalities are 2D or 3D graphics-rendering engine, object collision detection, physics engine, animation integration, artificial intellegance, sound integration, scripting and network extensions. All these functionalities can be

simulated simultaneously to create realistic game experiences. Such tools can be used to simulate existing and future user scenarios in development of products, systems and services.

Simulation needs immersion and immersion allows the user to experience the simulation in a way that stimulates possibilities that otherwise would have been impossible (Turkle 2009). Squyres (2006) describe such simulation cases that have been designed on screen, like structuring molecules in virtual space, nuclear explotions and controlig a romotly operated vihicle on Mars. At the same time as immersion is beneficial it makes one also vulnerable if the model and outcome are not seen with critical eyes (Turkle 2009). Immersion has seductive capabilities that overshadow the real implications of simulation.

In the case described in this paper there are two levels of immersion. One is the software visual simulation it self that aims to create realistic representation of the scenarios, and two the screen system that displays the simulation. Both are important in order to create the overall immersive experience of the simulation.

Design places like the *Envisionment and Discovery Collaboratory* have been made in relation to dealing with human computer interaction and simulation systems in collective design process (Arias 2000). The idea is to create a system where an interdisciplinary team will more easily address implications based on their background from a shared visual perspective.

This can be realised by drawing on the notion of co-design (Sanders and Stappers 2008) and participatory design (Ehn and Löwgren 1997). In these approaches where externalisations of ideas and knowledge are made to create shared understanding and facilitate collective creativity (Sanders and Rim 2001) between interdisciplinary actors.

Figure 2. Jernbaneverket shows different alternatives for new railroad tracks using visual simulations in the SimSam-lab at Vestfold University College.

In this research we have been using a visual immersive system *SimSam* (Figure 2) that allows a team of actors and users to experience the simulation simultaneously in a design place (Jan & Hjelseth 2012). The wide angle of the screen covers more of the view angle of the actors and gives stronger sense experiences that raise the level of immersion. This can sometimes have negative effect where the actor feels seasick. The CAVE [Cruz-Neira et al., 1992], is another example of an visual immersive system designed to explore and interact with virtual environments.

The most common argument for why these tools are used in product design processes is that the software itself is oriented towards software engineers and that the game engine editors require a great deal of programing code. The trend in the development of game engines is to create editors with interfaces that do not require a lot of programing and that it is possible to create simple games and simulations with a minimum knowledge about codes (Kraus 2012). With the introduction of touch interface devices like the iPad and the iPhone there has been an increasing interest among designers to use 3D game engines to create tangible applications. The Oslo School of Architecture and Design has now integrated game engine tools as part of their master courses in interaction design in order to explore the use of such tools in design practice.

RESEARCH METHODS

An explorative research methods was used in case studies to develop and explore the simulation and simulation tools in relation to design processes. This was based on existing methods and knowledge about the use of scenarios in design conseptualisation phases, co-design and 3D software expertise. In the cases presented here this author researcher has been actively involved in the design activities that have been placed within a methodology drawn from participatory action research (PAR) (Hult and Lennung, 1980; Denzin and Lincoln, 2000). Through the use of PAR it was possible for the researcher to get an holistic experience of the process when designing the simulations and its relevance when used in a co-design workshop with multiple actors.

Empirical data based on observations during design workshops was produced through the case studies in real-life situations (Yin, 2009). The obervations focused on the way the simulation and the simulation tool was used by the designer and particepaticipants during these workshops. It was observed how actors established a shared scenario understanding, created analogies to other scenarios, and how ideas or suggestions to change were stimulated.

The engineers, project maneger and customers in the PGS case study were interviewed using a qualitative interview method (Kvale and Rygge, 2009). This interview method allowed for a subjective and personal insight in the actors' own experience of design tools used in the design process.

DESIGNING THROUGH SCENARIOS

Referring back to our qualitative interviews with Kongsberg Simulation, one of the leading simulation companies in the maritime market, we have seen been increasing interest in the maritime and offshore market to simulate future scenarios. One of the goal with this type of simulation is to get a full overview of the scenarios so unknown factors can be discovered and solved.

Implications of carrying out user studies in the maritime domain have been researched through a micro case study in a design process of a seismic streamer recovery simulator at Kongsberg Simulation. The starting point for the design team was a technical system oriented approach to understand the recovery operation. The problem with this approach was that the user's perspective was not addressed at this early stage and was supposed to be implemented later on in the process. The design team found it hard to understand the user scenarios based on written description from users with pictures and small video clips. This "task oriented" method is being applied in their more incremental processes where small changes are done to existing products. The problem of obtaining a shared understanding between the engineers delayed the whole project for six months. To understand the scenarios from a user's perspective, a new approach was needed. In order to obtain a better overview of the whole process we placed five action cameras on different positions and two of them where mounted on the heads of the winch-operators. Through this multiple angle view (Figure 3) it was possible to link the users' tasks to the overall recovery operation scenario.

Figure 3. Video of the seismic recovery operation with multiple view angles showing overall operation view, and tasks performed by crew and winch operators.

This design process showd that it is difficult to understand complex scenarios in the maritime industry. The interviews from this case study showed that the ability to have multiple view angles gave a much better understanding of the scenarios complex user scenarios. One interviewee, for example, mentioned that the video material was very important to help everyone to understand what was happening and that having good video material is not to be underestimated when trying to understand this type of operations. A more detailed description and analysis of the interviews will be published in a future article.

Findings

A number of findings were drawn from this study. These were that:

- User tasks in maritime and offshore operations are often complex
- Existing float diagrams are sometimes to complex to get a holistic overview of the user task
- The float diagram has a problem of creating a shared understanding within the design team.
- Collecting user information trough probes did not give a satisfied overview, and tacit user knowledge was not implemented
- A combination of video and user involvement improve understanding of the user tasks
- Multiple view angle cameras provided the means to understand simultaneous operation in a holistic view.

ONGOING CASE STUDY: SIMULATING CRISIS SCENARIOS IN THE OSLO FIORD

The background for this case is is the development of a new ferry concession between Horten and Moss in the Oslo fiord. In the new concession it is proposed that number of departures be increased in response to increased vehicle traffic. The ferry line is already the most profitable in Norway. Yet, the Norwegian Coastal Administration has reported that the Oslo fiord is the most hazardous coastline in Norway. The development group Maritime Competence Oslofjord (MKO) is a combination of different companies that have started a project to look at different risk factors in the Oslo fiord that opens for new product, services or business opportunities. The project has been developed and facilitated through workshop meetings with interdisciplinary participants.

The first workshop was about finding existing risk scenarios and possible future risks with the increased ship and ferry traffic. Part of this workshop included participation by former captains, vessel traffic central (VTS), ship pilots, Norwegian Maritime Education (NMU) and the Norwegian Coastal Administration. To facilitate discussion we used acrylic ship models on a Microsoft Surface screen where we displayed different types of maps and AIS information (Figure 4). The participants used the models as boundary objects to explain different risk scenarios (Figure 5). These typically include tangible objects that can be transformed or arranged in order to communicate ideas or knowledge. Examples are: clay models, foam models,

drawings, paper mockups, CAD models, rapid prototypes or pictures.

Figure 4. Actors interacting with ship models on a multi-touch screen.

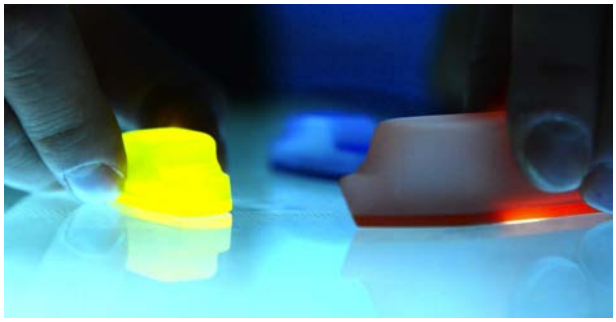

Figure 5. Acrylic ship models.

After the workshop different risk scenarios were simulated in the game engine. The surrounding landscape was auto-generated in 3D using data from *NorgeDigitalt* and also textured using pictures. The boat 3D models were downloaded from Google Warehouse and imported into the game engine with existing boat-vehicle scripts that allow for AI behaviour, collision detection, physics and hydrodynamic properties.

In the second workshop (Figure 6) the goal was to explore the risk scenarios and discuss possible ideas and solutions. Different local companies, organisations and ship captains represented the assembled and key actors.

Figure 6. Interdisciplinary actors discussing possible VTS applications when using the simulation as means to stimulate discussion in the second workshop.

Figure 7. Crisis scenario in which a cruise ship has hit a containership in the Oslo fjord.

By using the simulated scenario (Figure 7) the captain explained the different risk scenarios to the other actors. The scenario took place before, during and after ship accidents. Through the game function it was possible to play different crisis roles that were part of the scenario. The game function enabled better user participation where participants could play an avatar role to share their knowledge end experience.

When a scenario is created it is possible to include multiple user inputs in combination with artificial intelligence and avatars. Consequently, design workshop participants play roles as captain, passenger (Figure 8), ship, crew, rescue boat or rescue helicopter (Figure 9) in the same scenario. This allows for a better understanding across disciplines and experiences, and offers a means to visualize and interact with the complex nature and processes of the crisis.

Figure 8. Avatar view from passenger who has jumped into the water.

Figure 9. The avatar view from rescue helicopter when approaching the sinking ship.

Based on the simulation, the design actors then created ideas and new concepts on VTS systems, crisis management plans, new training courses and automated ship docking systems. The aim of this move in the process was to create a collective understanding of the different user roles and to see how they influenced the overall crisis. This enabled new approaches to understand the crisis scenario from different user perspectives and inspire new ideas for innovation.

DISCUSSION

The results of the first workshops show that it is possible to use the game engine as an iterative design tool for design conceptualisation. One of the most important functions to the tools used to create concepts is the ability to utlise a fast workflow. The use of ready-made 3D models makes this workflow easier, but if the design project requires a lot of custom modelling it might create a bottleneck in the work pipeline.

The fuzzy front end of innovation is never predictable and the use of design tools changes according to problems, actors and context. To use game engines to simulate scenarios in a design workshop is relatively more complicated than working with low-fidelity boundary objects like physical mock-ups, cardboard models and rapid prototypes. Tim Brown (2008) argues that:

Prototypes should command only as much time, effort, and investment as are needed to generate useful feedback and evolve an idea. The more "finished" a prototype seems, the less likely its creators will be to pay attention to and profit from feedback. The goal of prototyping isn't to finish. It is to learn about the strengths and weaknesses of the idea and to identify new directions that further prototypes might take.

The initial phase of using the game engine to create the scenarios is more time consuming in relation to more traditional methods, but the iterative process is very fast because of the layered based structure of working with 3D models in real time environments. Adding new items and modifying the scenario is much faster when the initial phase of creating basic elements are in place.
The rendering technology used in the game engines creates automatic hi-fidelity realistic images that might give the feeling of more finished result; it has not shown any negative effects when ideas to concepts are created. However if the simulations have behavior error or digital artifacts it might draw attention.

On a more negative note, the use of game engines might not be suitable as a design tool in all contexts in the fuzzy front end, however, more optimostically, it has shown to be valuable in the conceptualization phase in maritime innovation.

CONCLUSION

Maritime innovation processes are complex and may require different and untraditional approaches when designing for diverse users who face different degrees of complexity and situations of ease and risk. However, the industry often lacks competence in how to fulfill user centered design, and human factors are often seen more as requirements than innovation opportunities. As an early counterweight to such perspectives, this paper describes some of the complexity levels regarding user centered design in maritime innovation.

The use of game engines to visualize and simulate existing end future user scenarios in the design conceptualisation phases were introduced. The results from what is still an ongoing case study show that it is possible to implement this tool and that it allows an iterative conceptual approach within the front end of innovation. The actual tested scenarios and simulations provided experiential settings and contexts of collaborative engagement and dialogue that offer alternatives to building richer understanding of the complexity of contextual activities on the sea.

Using simulated behaviours and artificial intelligence in combination with realistic visualizations enabled our small experimental group of interdisciplinary design participants to develop fuller and more holistic overviews of complex scenarios. In addtion - and importantly for design in the martime sector - the usability friendly interface of the game engine enabled the designer to modify and add the simulated scenarios during the design workshop. The tool also allows expert users to share their knowledge and experience through the role of an avatar in the scenarios that improves feedback information quality and quantity.

Taken together these design rich aspects of involving simulated uses in critical settings in the maritime sector may help enhance our perception and responses to fiend critical experiences and emergent an given needs. There would appear to be further room to investigate the role of design in the fuzzy front end of wider innovation processes in the sector so as to improve consistency and clarity in safety, operations and shared activities that unfold in contexts of use.

REFERENCES

Arias, E., Eden, H. 2000. "Transcending the individual human mind and creating shared understanding through collaborative design." *ACM Trans. Comput.-Hum. Interact.*, *7*(1): 84-113.

Cooper, R. G. 2001. *Winning at New Products*, 3rd edition, Perseus Publishing, Cambridge, MA.

Cruz-Neira, C., Sandin, D. J 1992. "The CAVE: audio visual experience automatic virtual environment." *Communications of the ACM*, *35*(6), 64-72.

Brown, T. 2008. "Design Thinking". *Harvard Business Review, The Magazine,* June, 84-96.

Denzin, N., Lincoln, Y. 2000. *Handbook of Qualitative Research.* Thousand Oaks, Calif., Sage.

Ehn, P., Löwgren, J. 1997. "Design for Quality-in-Use: Human-Computer Interaction Meets Information System Development," In M. G. Helander, T. K. Landauer, & P. V. Prabhu (eds.), Handbook of Human-Computer Interaction, Elsevier Science B. V., Amsterdam, pp. 299-313.

Hult, M., Lennung, S. 1980. "Towards a definition of action research: A note and bibliography". *Journal of Management Studies*, *17*(2), 241-450.

Jenssen, J. (2003). Innovation, capabilities and competitive advantage in Norwegian shipping. *Maritime Policy & Management , 30* (2), 93-106.

Koen, P. 2004. "The Fuzzy Front End for Incremental, Platform, and Breakthrough Products". *The PDMA Handbook of New Product Development,* John Wiley & Sons, New York: pp. 81–91.

Kraus, M. 2012. *User-Centered Design of GPU-Based Shader Programs.* In Richard, R., & Braz, J. (Eds.), *Proceedings of the International Conference on Computer Graphics Theory and Applications: GRAPP 2012*. (pp. 248-253). Portugal: Institute for Systems and Technologies of Information, Control and Communication.

Kvale, S., Rygge, J. 2009. *Det kvalitative forskningsintervju. (The Qualitative Research Interview).* Oslo, Gyldendal akademisk.

Rhea, D. 2003. "Bringing Clarity to the 'Fuzzy Front End'. A predictable process for innovation," *in: B. Laurel; Design Research. Methods and Perspectives.* Cambridge, Mass.: MIT Press, pp. 145-154.

Lawson, B. 2005. *How Designers Think: The design process demystified.* 4th edition. Oxford, Elsevier.

Lawson, B., Dorst K. 2009. *Design Expertise.* Oxford, Elsevier.

Linder, E. 2008. "Industrial designers in the offshore ship design industry". *Paradoxes within Design Research – Mechanisms and Contradictions, 7th Nordcode Seminar & Workshop.* Lund. Division of Industrial Design at Lund University 2008.

Manninen, T. 2000. "Multimedia Game Engine as Distributed Conceptualisation and Prototyping Tool - Contextual Virtual Prototyping". In *Proceedings of IMSA2000 Conference*, November 19-23, Las Vegas, Nevada, USA, IASTED/ACTA Press.

Meister, D. 1999. *The History of Human Factors and Ergonomics*. Mahwah, NJ, Lawrence Erlbaum Associates.

Rittel, H., Webber, M. 1973. "Dilemmas in a General Theory of Planning,". *Policy Sciences*, *4*, 155–169.

Sanders, E., Rim, L. 2001. Collective Creativity, *LOOP: AIGA Journal of Interaction Design Education*, *3*, 1-6.

Sanders, E., Stappers, P. 2008. "Co-creation and the new landscapes of design." *CoDesign, 4*(1), 5-18.

Simon, H. 1981. *The Sciences of the Artificial.* Cambridge, Mass., MIT Press. 2nd edition.

Squyres, S. 2006. *Roving Mars: Spirit, Opportunity, and the Exploration of the Red Planet*. The University of Michigan: Hyperion Books.

.

Thalen, J., Voort, M. 2011. "Turning VR into something useful. A case study on electing requirements for virtual reality design tools". *Diversity and Unity: Proceedings of IASDR2011, 4th World Conference on Design Research*. Delft: TU Delft 2011, p. 738..

Tideman, M.. Voort, M. Houten, F. 2008. "A new product design method based on virtual reality, gaming and scenarios." *International Journal on Interactive Design and Manufacturing (IJIDeM*), ***2***(4), 195-205.

Turkle, S. 2009. *Simulation and its Discontents.* Cambridge, Mass, The MIT Press.

Yin, R. 2009. *Case Study Research: design and methods*. Los Angeles, Sage.

AUTHOR BIOGRAPHY

Snorre Hjelseth in as industrial designer with special interest in design thinking in the maritime and offshore innovation sector. His PhD research focuses on visualization and simulation as means in interdisciplinary design processes. Snorre is part of the SimSam-lab development project at Vestfold University College (HiVe) where an immersive system has been developed to help facilitate design workshops. He received a Master's in Industrial Design from the Oslo School of Architecture and Design (AHO), and the Indian Institute of Technology Bombay (IIT). He is now a PhD-fellow at AHO with a position at HiVe.

TACTILE CUES FOR SHIP BRIDGE OPERATIONS

Yushan Pan, Sathiya Kumar Renganayagalu and Sashidharan Komandur
Maritime Human Factors Laboratory
Aalesund University College
N-6009, Aalesund, Norway
E-mail: yupa@hials.no, sathiya.renga@gmail.com, sash.kom@hials.no

KEYWORDS

Tactile, auditory, visual, maritime operations, dynamic position, response time, survey.

ABSTRACT

Current modes of conveying operational information on ship bridges are mainly in the form of visual and auditory sensory inputs. During safety critical situations, such as dynamic positioning (DP) operation, reliance on these two senses may be insufficient. In a DP operation the role of the DP operator is critical and most incidents happen due to lack of operator´s situational awareness. Therefore exploitation of other sensory inputs in addition to visual and auditory must be investigated. This paper surveys recent research on response times of vibro-tactile, visual and auditory cues. The survey concludes that tactile cue always has shorter response time compared to other stimuli. And its combination with other cues such as visual and auditory can enhance the effectiveness of response time. Therefore new ship bridge developers should take this knowledge into account to increase design efficiency.

BACKGROUND

Visual, auditory and tactile are the most used cues for evaluating reaction/response speed in different areas, from everyday life to maritime domain. Several research areas, such as medical technologies, physical education, neuroscience, transportation, aviation, robotics, information systems and maritime operations, are focusing on these cues to measure human reaction.

The ship bridge is a room or station from where ship is controlled and navigated. A typical ship bridge consists of voyage system, radar, GPS, control console, communication, alarm center, helm and chart table. In addition, offshore vessels also have dynamic positioning system. It is normal to see clusters of consoles and screens on a ship bridge and attention from bridge watch (the person who is incharge of watch duty on ship bridge) is required time to time. Currently these screens attract attention by flashing or raising sounds, such as buzzer or alarms. As most alarm sounds in current ship bridges are similar, bridge watch find it difficult to distinguish. Earlier research in this field mentioned that high number of irrelevant alarms may lead the bridge watch to ignore important alarms (Hudson 2007). This problem can be mitigated either by suppressing alarms or delegating alarm information to relevant people. However, alarm suppression has disadvantages, as critical alarms can be unintentionally suppressed by human operators (Hudson 2007). Delegating alarm to only the relevant person seems to be promising solution for the above problem and tactile cue is a method for alarm delegation.

Dynamic positioning can be defined as: a computer controlled system to automatically maintain ship's position and heading by using her own propellers and thrusters (Bray 2003). The role of DP operator is passive monitoring, where the situational awareness of the operator is often low (A. Tjallema 2007). This is known as the 'out-of-the-loop' performance problem, as the operator is not an active part of the process (Endsley 1996). The human visual and auditory modalities can only reliably differentiate 6-7 stimuli each at any time (Miller 1956). Presenting certain types of information using other sensory modalities, such as audio, tactile versus visual can result in performance gains (L. R. Elliott 2009). We hypothesize that tactile actuators on DP operators in addition to critical information changes in displays may help the operator respond faster and stay 'in-the-loop'. The specific aim of this paper is to compare reaction/response time between different sensory inputs namely visual, auditory and tactile.

METHODS

In order to find the effectiveness of auditory, visual and tactile cues and their impact on human reactions in various real life environments, several recent empirical studies were analyzed. Comparison of individual cues and their combinations, for example auditory, visual and tactile cues and their combinations in several fields has been analyzed. Articles were searched in databases, such as Science Direct, Association for Computing Machinery (ACM) Digital Library, Human Factors and Ergonomic Society and BIBSYS, using the following keywords: tactile, auditory, visual, maritime DP operations and survey. 25 papers were selected published between 1994 and 2012.

Evaluation of auditory, visual and tactile cues is based on response time and its impact on human response behavior, see tables 1-3. All systems are classified is two non-intersecting classes – complex systems and simple systems. Complex system is defined as a system

Proceedings 27th European Conference on Modelling and Simulation ©ECMS Webjørn Rekdalsbakken, Robin T. Bye, Houxiang Zhang (Editors)
ISBN: 978-0-9564944-6-7 / ISBN: 978-0-9564944-7-4 (CD)

composed of interconnected parts that as a whole exhibit one or more properties not obvious from the properties of the individual parts (Joslyn 2002). A system is considered as simple system if it is not complex.

RESULTS

A survey of neuroscience and medicine concludes that auditory response time is faster than the visual response time, and that male athletes have faster response time when compared to females for both auditory as well as visual stimuli (Shelton 2010). Human response time can help researchers detect which modality stimuli is faster perceived by participants, however the factors of age, gender and education can have influence on stimuli response time (Annie W. Y. Ng 2012). In 1995, Motoyuko Akamatsu et al (Motoyuki Akamatsu 1995) compared tactile, auditory, and visual feedback in a research study. Participants were pointed in specific areas on a screen and asked to use a mouse-type device to finish a task. The study concluded that response time for tactile cue is shorter than combination of tactile, auditory and visual. Other studies have shown that participant response is faster for vibro-tactile alerts, compared to visual and auditory alert messages in simulated driving and aircraft scenes (Jan B. F van Erp 2001, Cristy Ho 2005b, J.J. Scott 2008, Cristy Ho 2005c, Kirby Gilliland 1994, Cristy Ho 2005a, Jan B.F. Van Erp 2004).

Different neural processing is needed for tactile and visual cues. Response time may vary for different tasks and participants. Processing time of tactile information differs depending on the distance between the brain and the stimulated body surface area. Visual information reaches the brain at a constant time, regardless of the distance to perceived object (Vanessa Harrar 2005). Therefore, in particular situations combination of visual and tactile stimuli can reduce response time (Bettina Forster 2002, Tan 2002).

Tactile cue was also used in a study where participants were asked to detect changes in information displays(Alberto Gallace and Hong Z. Tan 2005). The US army performed an example task where they combined the audio and tactile stimuli together to enhance soldier performance in human-robot interaction (Ellen Haas 2007).

Vibro-tactile alert can help people to avoid dangerous behaviors in interaction with control systems, such as robotic systems and driving scenes. In addition, combination of auditory and visual stimuli can also significantly improve machine operator performance. Visual stimuli have longer response time compared to auditory stimuli due to various kinds of reasons, including mistakenly perceived symbols, poor eyesight or a dark environment. However, audio stimuli alone can lead operators to incorrect decisions. For instance, drivers may make mistakes if sound from the following car is perceived without any observation. Hence, only meaningful auditory warning signals can provide effective means of capturing attention and enhance the operator performance(Motoyuki Akamatsu 1995, Cristy Ho 2005b, Liu 2010, Ellen C. Haas 2005, R. Parasuraman 1997).

Table 1 illustrates the comparison of visual, tactile and their combination in research survey. Table 2 presents the comparison of visual, auditory, tactile and combination of visual and auditory cues. Table 3 shows comparison of visual, auditory, tactile and combination of the three cues in recent research. Figure 1 shows how many recent research articles suggest which stimuli having the shortest response time.

Our survey was based on comparison of each individual stimuli and their combination. Through analyzing and comparing recent research articles, we have summarized the P-value (Goodman 1999) in Table 4. It shows that there is significant difference between each stimuli ($p<.05$). To the best of our knowledge, there is no study comparing different pairs of stimuli see Table 2. There is also little research of the effectiveness of auditory and tactile cue combination. The results displayed in Table 1, Table 2, Table 3 and Figure 1 show that tactile sensory cue has the most rapid response time. However, there is significant difference between each individual stimuli and their combination (Table 1, 2 and 3).

DISCUSSION

Human response time for different stimuli, visual, auditory, tactile cues and their combination with conventional modalities can also improve the situational awareness in the maritime domain. As known in Table 1-3 and Figure 1, recent research concludes that tactile cue has the most rapid response time from the fields of vehicle navigation, automobile/transports, neuroscience, medical technology and information technology. But very little research has been done in the impact of tactile cues on ship bridge alarms. In ships, alarms are installed all over the environment to warn the crew during dangerous situations. Currently the alarm systems provide visual and audible indications of alarms. However, earlier research shows that the above indications alone are insufficient in particular situations. Müller et al (Demuth 2010) mention that nautical staff do not have the ability to distinguish the acoustically and visually cognition of alerts due to the lack of classified or graduated critical information appearances (Demuth 2010).

Table 1: Comparison of Response Time (milliseconds) for Individual Visual and Tactile Cues, and Their Combinations, Results from Analyzed Recent Research Studies

Authors	Field	System Type	Visual(V)	Tactile(T)	V+T	Response
Jan B.F. Van Erp et al (Jan B.F. Van Erp 2004)	Vehicle navigation system	Complex system	660	680	665	The response time in the tactile condition was in between the visual and multimodal conditional, but did not significantly differ from both. But there is difference between the visual and tactile conditions.
Vaness Harrar et al*(Vanessa Harrar 2005)	Neural processing	Complex system	Light on hand : 170	Tactile on foot: 60		There is a linear relationship between distance and response time, e.g. visual on hand and foot, and tactile on hand and foot. When both stimuli were on the foot, subjects perceived them simultaneously when the light came significantly earlier than the touch, despite similar processing times for these stimuli. When the stimuli were both on hand, there is a significant processing time difference between the light and touch.
			Light on foot : 210	Tactile on hand: 90		
			Light on hands: 220	Tactile on feet:100		
			Light on feet : 270	Tactile on hands:120		
Jan B. F. van Erp et al(Jan B. F van Erp 2001)	Automobiles	Complex system	980	940	950	Driver reacts faster to the tactile messages than to the visual message.
Bettina Forster et al(Bettina Forster 2002)	Visual Science	Simple system	292.8	271.2	252.8	There is significant difference between visual and tactile stimuli. Tactile is faster than visual. The combination of visual and tactile is significantly faster than single stimuli of visual and tactile.
Rob Gray et al**(Tan 2002)	Information Technology	Simple systems	CloserW :480, 490, 520	Miss Left: 610		There is significant difference between tactile on shoulder and wrist. Also there is a significant difference between vision directions.
			Same: 470, 450, 490			
			CloserS: 510, 480, 440	Hit: 570		
			CloserW : 490, 460, 450			
			Same: 450, 440, 480	Miss Right: 620		
			CloserS: 470, 480, 520			

*The experiment had two constraint conditions –"light" and "touch" on hand or foot.

**The experiment was performed by different conditions. "CloserW" - stimuli is used for wrist. "CloserS" - stimuli is used for shoulder. "Same" - visual stimuli is used in the same direction.

Table 2: Comparison of Response Time (milliseconds) for Individual Visual, Auditory and Tactile Cues and Their Combination, Results from Analyzed Recent Research Studies

Authors	Fields	System Type	Visual(V)	Auditory(A)	Tactile	V+A	Response
Yung Ching Liu(Liu 2010)	Information systems, Ergonomics	Simple System	3255	2678		2607	There is significant difference between auditory and visual stimuli during driving performance with simple and complex warning signals. The combined stimuli response time is faster during the driving scenes.
		Complex system	5081	3247		2792	
G.B. Taware et al* (G. B. Taware 2012)	Medical Technology	Simple System	Red: 126.8, 142,97, 148.63, 179.83		Eyes open: 126.13, 137.14, 144.9, 182.43		The difference was found to be statistically significant for both green as well as red light for four age groups. The auditory response time in response to click showed an increase from group 1 to group 4. There is a significant increase in tactile response time. Young person has shortest response time than old person.
			Green: 127.6, 144.13, 146.67, 182.3		Eyes closed: 128.8, 146.87, 145.93, 189		
Cristy Ho et al(Cristy Ho 2005a)	Applied psychology/ Automobile	Complex system	34076	2519		3977	There is significant difference between visual and auditory. Spatial auditory warning signals were shown to facilitate visual information detection (subsequent reactions) in a simulated driving set-up.
Jose Shelton et al**(Shelton 2010)	Neuroscience and medicine	Simple system	Male: 331 Female: 350	Male: 284 Female: 310			Auditory response time is faster than the visual response time. Men are faster than women in stimuli testing.
Ellen C. Hanna et al***(Ellen C. Haas 2005)	Robotics	Complex system	Visual signals at 0 degrees absolute azimuth: no position info: 3460. With position info: 4900	Visual signals at 0 degrees absolute azimuth: no positional info: 4200. With positional info: 2600			There is a significant difference between audio with visual and degree only and audio without visual information and degree. Participants' response time is faster when they know the position information with audio signal.

*There are two conditions in the experiment, visual was divided into red and green light with eyes open and closed. The participant was grouped by their age.

** The participants in the experiment were grouped by gender.

*** The experiment has 2 conditions. There were visual signals with absolute azimuth degree and without absolute azimuth degree vs. auditory.

Table 3: Comparison of Response Time (milliseconds) for Individual Visual, Auditory and Tactile Cues and Their Combination, Results from Analyzed Recent Research Studies

Authors	Field	System Type	Visual(V)	Auditory(A)	Tactile(T)	A+T	V+A+T	Response
Alberto Gallace et al*(Alberto Gallace and Hong Z. Tan 2005)	Information Technology	Simple system			4000 2500			Participants made significantly slower reactions in change condition than in no change condition. Change condition is tactile stimuli in different area of human body.
Cristy Ho et al(Cristy Ho 2005b)	Information Technology	Simple system	791	831	762			Participants responded more rapidly to vibro-tactile targets than to visual targets, Auditory targets imposed the slowest response.
MotoyukiAkamatsu et al(Motoyuki Akamatsu 1995)	Information Technology	Simple system	265	262	237		246	Participants responded rapidly to tactile cues, slightly slower to combination of all three cues. Auditory response had even slower response, and visual – the slowest.
J.J Scott et al(J.J. Scott 2008)	Transportation/Automobile	Simple system	900	800	650			With a short warning time, driver response time is more rapid to visual and the slowest to visual.
Ellen Haas et al*(Ellen Haas 2007)	Information Technology	Complex System		20s: 2800 30s: 3700 40s: 4000	20s: 4000 30s: 3900 40s: 3900	20s: 4000 30s: 4000 40s: 6500		Audio, tactile or combined audio and tactile display modalities have been shown to provide shorter response time.
Kirby Gilliland et al**(Kirby Gilliland 1994)	Information Display	Simple system			6 sites: 1028 8 sites: 1520 10 sites: 1564 12 sites: 1838			Tactile stimulation of the human head for information display gives different response times depending on stimuli spot count: 6 spots impose substantially shorter response time compared to stimuli in 8, 10, or 12 spots.

*The participants in the experiment were grouped as 4 groups based on their age.

** The participant head was treated by the same tactile stimuli in 6, 8, 10 and 12 spots.

The above argument is further supported by the investigation report of the grounding of Royal majesty, a Panamanian passenger ship. The report states that both auditory and visual alarms of GPS were left completely unnoticed (Lützhöft 2002). Potential explanation: repeated sound and visual alarms induce sensorial and psychological stress and fatigue (Muntean 2010). Barsen et al(Muntean 2010) also mentioned that during their study many participants muted the alarm sounds or were preoccupied by canceling the alarm sound rather than reading the important information shown on the displays. Therefore it is evident that in maritime settings, sound alarms are often distracting and visual alarms are ignored. There are projects that are now looking to address this issue. iCAS (Intelligent Central Alarm System) from Kongsberg maritime suppresses the superfluous alarms (Konsberg). AS (Bridge Alarm System) from Ulstein, investigates novel approach, including 'dead man' system (Ulstein) and transferring alarms to specific locations outside the bridge to alert and call the master. However, these new alarms focus only on centralizing and integrating the alarms and very little study has been done in terms of graduating the sensory input by type and intensity. Advantages of these alarms over tactile and visual cues still have to be investigated.

Miscellaneous stimuli are also widely used for high technology products, such as intelligent gloves(Galambos 2012) and vest (Veen 2003) used for telemanipulation, 3D hand tracking and recognition. Using remote grasping, the operator can receive vibro-tactile feedback from the glove to feel the weight of an object (Galambos 2012). This feedback is, especially important in micro-gravity or non-gravity environment, such as outer space where a specific tactile vest for astronauts is always used for collecting information (Veen 2003).

Table 4: P-value from recent research results

	Visual	Auditory	Tactile	V+A	V+T	A+T	V+A+T
Visual(V)		P<.001	P<.01	-	P<.05	-	P<.005
Auditory(A)	P<.005	P=.001	P<.01	P=.0013	-	P<.05	P<.005
Tactile(T)	P<.05	P<.005	Onset*: p<.05 Offset*: p =0.07	-	P<.01	P=0.0002	P=0.005
V+A	P <.001	P=.0013		-	-	-	-
V+T	P<.01		P<.01	-	-	-	-
A+T		P<.005	-	-	-	-	-
V+A+T	P<.005	P<.005	P<.005	-	-	-	-

*Two experiment conditions in Alberto Gallance et al (2005). Participants attempted to detect changes to tactile patterns presented sequentially on the body surface. The types of tactile patterns are onset and offset.

CONCLUSIONS AND FUTURE WORK

Tactile stimuli in combination with visual and auditory stimuli may enhance awareness, especially in safety critical operations such as a DP operation. In future work, we will start with the above statement as a hypothesis to investigate the effectiveness of tactile stimuli in ship bridges to enhance situational awareness.

ACKNOWLEDGEMENT

This work has been supported by Aalesund University College (AAUC), through a PhD scholarship to one of the authors. We would like to thank Professor Hans Petter Hildre for his generous support to our research laboratory at AAUC. We would like to thanks Girts Strazdins for his inputs to improve this paper

REFERENCE

A. Tjallema, H. Grimmelius, C. va der Nat and D. Staperma. 2007. The Road to Elimniating Operator Related Dynamic Positioning Incidents. Paper read at MTS Dynamic Positioning at Houston.

Alberto Gallace and Hong Z. Tan, Charles Spence. 2005. Tactile Change Detection. Paper read at The First Joint Euroaptics Conference And Symposium on Haptic Interfaces for Virtual Environment and Teleoperator System(Whc'05).

Annie W. Y. Ng, Alan H. S. Chan. 2012. Finger Response Times to Visual, Auditory and Tactile Modality Stimuli. In *The International MultiConference of Engineering and Computer Scientists*. HONG KONG.

Bettina Forster, Cristiana Cavina-Pratesi, Salvatore M. Aglioti, Giovanni Berlucchi. 2002. "Redundant Target Effect and Intercessory Facilitation from Visual-Tactile Interactions in Simple Reaction Time." *Exp. Brain Res* no. 143:480-487.

Bray, D. 2003. *Dynamic Positioning - 2nd Edition*: Oilfield Publications Ltd, London, UK.

Cristy Ho, Charles Spence. 2005a. "Assessing the effectiveness of Various Auditory Cues in Capturing a Driver's Visual Attention." *Experiment Psychology: Applied* no. 11 (3):157-174.

Cristy Ho, Charles Spence, Hong Z. Tan. 2005b. Warning Signals Go Multisensory. In *HCI International*. Erlbaum.

Cristy Ho, Hong Z. Tan, Charles Spence. 2005c. "Using Spatial Vibro-tactile Cues to Direct Visual Attention in Driving Scenes." *Transportation Research Part F: Psychology and Behavior* no. 8 (6):397-412.

Demuth, Müller and. 2010. Knowledge based Information Evaluation for Integrated Ship Bridge Systems. Paper read at Informatik 2010: Service Science -

NeuePerspektivenfür die Informatik, Beiträge der 40. Jahrestagung der GesellschaftfürInformatike.V. (GI), Band 2, at Leipzig.

Ellen C. Haas, Ramakrishna S. Pillalamarri, Christopher C. Stachowiak, Michael A. Lattin. 2005. Audio Cues to Assist Visual Search in Robotic Systems Operator Control Unit Displays. edited by Army Research Laboratory.

Ellen Haas, Christopher C. Stachowiak. 2007. Multimodal Displays to Enhance Human Robot Interaction On-The-Move. In *PerMIS'07*, edited by ACM 978-1-59593. Washington, D.C.

Endsley, M. R. 1996. "Automation and Situational Awareness." *R. Parasuraman & M. Mouloua : Automation and Human Performance - Theory and Applications*:163-181.

G. B. Taware, M. V. Bhutkar, P.M. Bhutkar, V. P. Doijad and A. D. Surdi. 2012. "Effect of Age on Audio-Visual and Whole Body Reaction Time." *Al Ame en JMedSci* no. 5 (1):90-94.

Galambos, Peter. 2012. "Vibro-tactile Feedback for Haptics and Telemanipulation: Survey, Concept and Experiment." *Act a Polytechnica Hungarica* no. 9 (1).

Goodman, Steven N. 1999. "Toward Evidence-based Medical Statistics. 1: The P – value fallacy." *Annals of internal medicine* no. 130:995-1004.

Hudson, P. Traub and R. 2007. Alarm Management Strategies on Ships Bridges and Railway Control Rooms: A Comparison of Approaches and Solutions. Paper read at RINA Event, at London.

J.J. Scott, Robert Gray. 2008. "A Comparison of Tactile, Visual, and Auditory Warnings for Rear-Eng Collision Prevention in Simulated Driving." *The Journal of the Human Factors and Ergonomics Society* (50):246.

Jan B. F van Erp, Hendrik A. H. C. van Veen. 2001. Vibro-Tactile Information Presentation in Automobiles. University of Birmingham.

Jan B.F. Van Erp, Hendrik A.H.C.Van Veen. 2004. "Vibro-tactile in-vehicle navigation system." *Transportation Research Part F: Traffic Psychology and Behavior* doi: 10.1016/j.trf.2004.09.003.

Joslyn, Cliff, and Luis M. Rocha. 2002. Towards Semiotic agent-based models of socio-technical organizations. Paper read at AI, Simulation and Planning in High Autonomy Systems, at Tucson, Arizona. .

Kirby Gilliland, Robert E. Schlegel. 1994. "Tactile Stimulation of the Human Head for Information Display." *Human Factors and Ergonomics Society* no. 36 (700).

L. R. Elliott, M. D. Coovert. 2009. A review of Meta-Analysis of Vibro-tactile and Visual Information Displays. In *ARL-TR-4955*.

Liu, Yung-Ching. 2010. "Comparative Study of the Effects of Auditory, Visual and Multimodality Displays on Driver's Performance in Advanced Traveler Information Systems " *Ergonomics* no. 44 (4):425-442.

Miller, G. A. 1956. "The magical number seven, plus or minus two: Some limits on our capacity for processing information." *Psychologi- cal Review* no. 63:81-97.

Motoyuki Akamatsu, Scott I. Mackenzie, Thierry Hasbrouc. 1995. "A Comparison of Tactile, Auditory, and Visual Feedback in a Pointing Task Using a Mouse-Type Device." *Ergonomics* no. 38:816-827.

R. Parasuraman, P. A. Hancock and O. Olofinboba. 1997. "Alarm Effectiveness in Driver-Centred Collision-Warning Systems." *Ergonomics* no. 40 (3):390-399.

Shelton, Jose; Kumar, Gideon Praveen. 2010. "Comparison between Auditory and Visual Simple Reaction Times." *Neuroscience & Medicine* no. 1 (1):30.

Tan, Rob Gray and Hong Z. 2002. "Dynamic and Predictive Links between Touch and Vision." *Exp. Brain Res* no. 145 (1:50-5).

Vanessa Harrar, Laurence R. Harris. 2005. "Simultaneity Constancy: Detecting Events with Touch and Vision." *Exp. Brain Res(2005)* no. 166:465-473.

Veen, Jan B. F. van Erp and Hendrik A.H.C van. 2003. "A Multi-purpose Tactile Vest for Astronauts in the international Space System." *Euro-Haptics*.

AUTHOR BIOGRAPHIES

YUSHAN PAN obtained his master's degree in Information Systems Engineering from the Department of Computer and Information Science at Norwegian University of Science and Technology (NTNU) in Trondheim, 2012. Then he moved to Aalesund and joined Maritime Human Factors Lab at Aalesund University College (AAUC) as a research assistant. He is currently working in research related to usability and user experience for complex computer-supported systems, such as ship bridges, oil and gas platforms.

SATHIYA KUMAR RENGANAYAGALU obtained his bachelor's degree in automobile engineering from Anna University, India. He is currently a master student in product and system design at AAUC. He is also a research assistant at Maritime Human Factors Lab.

SASHIDHARAN KOMANDUR obtained his Ph.D. in industrial engineering from the University of Washington-Seattle. He also has a master's degree in ocean engineering from University of California-Berkeley. He is leading a research group in the field of human factors in maritime operations at AAUC. He is also the Global Maritime Knowledge Hub (GMKH-Norway) chair for human factors in maritime operations.

Hierarchical task analysis, situation-awareness and support software

Hans Georg Schaathun[1] ⟨hasc@hials.no⟩ Magne Aarset[2] ⟨maaa@hials.no⟩ Runar Ostnes[2] ⟨ro@hials.no⟩ Robert Rylander[2] ⟨rory@hials.no⟩

[1]Faculty of Engineering and Physical Sciences / [2]Faculty of Maritime Technology and Operations
Aalesund University College
N-6025 Ålesund, Norway

Keywords

Hierarchical task analysis, state machine, situation awareness, demanding marine operations, human factor

Abstract

Offshore activity is developing and resulting in new demanding high-risk operations. Operation complexity increases with factors like heavier loads, subsea installations, and arctic waters; operational planning requirements increase as well. Demanding offshore operations are usually planned in detail, where plans may fill several binders, leading to information overload for the ship crews. Extracting critical information becomes a challenge. In some cases, only a basic plan exists, and aborted operations are quite frequent, also where a contingency plan could have enabled recovery. This results in substantial extra costs for the operating company.

The industry is facing two key challenges concerning operational planning. One is to develop good planning frameworks, to enable plans with robust risk management and control. This calls for modelling techniques for operational plans. Another is optimal presentation of the plan for each individual crew member, both in the briefing and in the execution phase of the operation. It is important that every individual has easy access to the most relevant and safety critical information for his given role and the current situation, in an easily accessible and comprehensible format. This calls for operational software to support situation-awareness. A fundamental necessity to achieve this is modelling techniques which support a joint understanding of the operation between operational planners, ship crew, software engineers, and ultimately the support software. In this paper we show how to translate hierarchical task analysis (HTA) models into software models and then into situation-aware software prototypes.

I. Background

Offshore activity, dominated by oil production but but also including other installations like wind mills, require a range of demanding operations to operate. Examples include anchor handling for oil rigs and deployment of subsea equipment. Careful planning is required, and this is conducted partially by contractors, partially by clients, and some joint work. Both general and specific procedures may be in force, and both ship owner, rig owner, and project owner may have their own rules and procedures. Complex plans are typically developed by onshore engineering teams in charge of the overall operation. The result is an extensive procedural framework, which is increasingly difficult to digest and utilise in an effective way for the operational crew on-board an offshore vessel.

Fig. 1. Status quo. Plans and procedures on paper.

Current planwork and procedures are mainly based on paper (as in Figure 1) or possibly PDF-documents. Available software is mainly standard office packages, with Microsoft Word as the dominant player. Diagrams and figures may be produced by CAD tools or project management software, with no method of integrating information from different tools in electronic form.

Operational crew may have very limited time to review the complete planwork and it is very difficult to extract the safety critical aspects of the plan before decisions have to be made. To reach Earth's remaining petroleum resources the offshore activity is extending into deeper waters and more hostile environments, such as the arctic region. The technological development is often the limiting factor, and both operations and vessels become increasingly complex as technology advances. Obviously more complex operations lead to higher risk and an increasing number of issues for the operational crew to relate to. Decision makers on board will have to relate to increasingly complex systems, and often several different systems and subsystems to extract the required information to execute a safe operation [8], [12]. In order to deal with the increasing

Proceedings 27th European Conference on Modelling and Simulation ©ECMS Webjørn Rekdalsbakken, Robin T. Bye, Houxiang Zhang (Editors)
ISBN: 978-0-9564944-6-7 / ISBN: 978-0-9564944-7-4 (CD)

amount of information, better methods of structuring and presentation are required.

An increased focus on bridge system integration has been observed the last years [11]. With improved data protocols [10], [14] it is possible to accumulate any dynamic information into an intelligent software system. The challenge is to present the crew with necessary, and only necessary, information to conduct a safe operation. Necessary information is defined by the situation, and will change throughout the operation. Situation awareness is an important concept in human factor research, in the sense that the human operator requires an accurate understanding of the current state of affairs. We put to you that situation awareness is also a desired feature in the on-board software systems. In order to present the operator with the most relevant information, the software must be able to track the current situation, with respect to both external environment and the operational plan.

Existing research on related support software is sparse in the literature. Decision support systems were studied by Glässer *et al.* [6], [7], but they focused on using sensor data from the ship and did not incorporate operational plans in the software. In fact, their focus was on search and rescue operations, which cannot be planned ahead of time with the same level of detail. Embrey *et al.* [3] studied techniques for workload assessment for on-board crew, and considered a number of modelling and task analysis techniques for this purpose. There are also two notable initiatives considering risk assessment [5] and risk management [9]. Unfortunately, the underlying models and software architecture have not been published.

In terms of linking modelling frameworks from different disciplines, the human-computer interaction (HCI) community has done some interesting work, with several examples linking task models to software architecture models. E.g, Bastide [2] integrates task models and use-case models on the metamodel level. However, the task models used in HCI will be different from ours, as they focus on interaction with the software system and the software is an integral part of the operation. In our case, the software serves purely as a source of information and has no active part in the operation. Thus our models do not consider software interaction.

The purpose of the paper is to outline model transformations between operational and software models, and further to demonstrate how the resulting models enable situation-awareness in software. The aim is a proof of concept rather than a complete formalisation, and further research will be outlined in the conclusion. To limit the scope, a single-ship operation is considered at this stage. Our main contribution is to link the different disciplines involved, including software engineering, operational modelling, and offshore vessel crew. In the conclusion we are able propose specific research questions within each discipline, and their answers will lead to formalisation at a later stage.

II. Modelling

A *model* is a difficult term because it is used for widely different concepts in so many areas of science and engineering, Bran Selic [13] uses the following definition for an *engineering model* in many of his speeches:

«A selective representation *of some system that captures* accurately and concisely *all of its essential properties of interest* for a given set of concerns.*»*

This definition highlights a number of features which will be critical for modelling in most domains, and it explains why models are used. First of all, the model is a representation of a system, so that we can understand the system by studying the model. Essentially, this representation is selective, i.e. a copy is not a model, and the selection is made in view of a given set of concerns. Thus, different kinds of analysis will require different kinds of models, capturing the properties relevant for the analysis. The level of accuracy may depend on the domain, depending, probably, more on feasibility than on requirement.

Clearly, this definition says little about what the model will look like. It may be diagrams, text, mathematical equations, pictures, scale models, etc. It does, however, give us a hint about *why* we need modelling. Models aid the understanding of complex systems.

A. Literature overview

Several modelling frameworks and languages exist for the domains of software engineering, risk management, business administration and so on. Modelling does not necessarily require formalised languages. Blackboard diagrams go a long way. However, for our purpose, we need to match models between the operational domain and the software domain, and then some formalism is required to guarantee accurate correspondence.

Hierarchical task analysis is well-known in operational communities, and we discuss that one below. Other, more complex and formal modelling frameworks exist, such as the classic Structured Analysis and Design Technique (SADT) [1] and the more current IDEF0 standard building thereon. Tasks are modelled as activity boxes, with arrows representing information flow between activities or decisions to proceed to a subsequent activity. The system is hierarchical, so that a coarse description can be made with a few, complex activities, and each activity (recursively) analysed in further detail using layers of SADT diagrams.

Software engineering has a rich literature on modelling techniques and languages. Most well known is the Unified Modeling Language (UML), which is not just one language but rather a family of languages aiming to model different aspects of the system. As a standard, UML has developed a very complex syntax to allow detailed representation of models, but most of the modelling *techniques* promoted by UML are well-known in other contexts and fully usable with a much simpler syntax.

Software engineering also studies model transforms, that is automatic translation between models. In this

respect, source code is viewed as a model of the software, so code generation is a special case of model transform. Metamodels are used to formalise the structure of models, and thus to enable formal definition of modelling transforms. This area is known as model-driven engineering in academia and as model-driven development in industry.

Models can fundamentally be categorised as either descriptive or prescriptive. Descriptive models are made after the original, in order to describe something already existing. In contrast, prescriptive models are made before the 'original' in order to explain how to build the system. In this paper we are interested in models which can *describe* the operation (or operational plan) and *prescribe* the operation support software.

B. Hierarchical Task Analysis

Candidate modelling techniques for the operational plan can be drawn from a range of related domains, such as risk management, human performance, or organisational processes. We will focus on Hierarchical task analysis (HTA) which emerged from psychology and human performance research around 1970, and it is still popular. It lends itself very well to modelling demanding (marine) operations. A good introduction is given by Stanton [15].

HTA is an iterative technique. At the first level, the operation is viewed as a single task, with a clearly described goal. Tasks are repeatedly broken down into subtasks with an increasing level of detail. Three key principles should be observed throughout the process:

1. The process is goal-driven, and every task must be clearly defined by an objective statement of the planned outcome.
2. Tasks can iteratively be broken down into subtasks, each subtask in turn being treated as a task with an objective definition of its goal as above.
3. The important relationship between task and subtasks is one of inclusion; in a hierarchical (tree-like) structure. The subtasks may or may not be proceduralised with an instruction that they be executed in sequence. We will discuss different execution patterns below.

Example 1: As a running example, we will consider a *non*-demanding marine operation as an example: a fishing trip by rowboat. An HTA analysis is shown in Table I. The operation consists of four first-level tasks, preparing the boat, going to the site, fishing, and returning. Each phase is divided into a number of subtasks.

There is no limit to the number of levels in the HTA tree; it is merely a question of the desired level of detail. A trivial task should not be subdivided just for the sake of it. Some branches may require more levels than others.

Our fishing example illustrates how subtasks sometimes should be executed in order, as in Phases 1 and 4, and sometimes not. The tasks of Phases 2 and 3 must be executed in parallel. In general, every task requires an execution instruction, and where there are subtasks,

0. Get enough fish for dinner
Do in sequence:
1 Prepare boat
Do in sequence:
1.1 Take life jacket on
1.2 Load fishing gear
1.3 Untie moorings
2 Row to your favourite fishing site
Do in parallel:
3.1 Go to fishing site
3.2 Watch for other vessels
3 Catch enough fish
Do in parallel:
3.1 Fish until bucket is full
3.2 Monitor distance to cliffs
4 Return to quay
Do in sequence:
4.1 Go to the quay
4.2 Moor the boat
4.3 Unload the boat

TABLE I: HTA tree for a fishing trip.

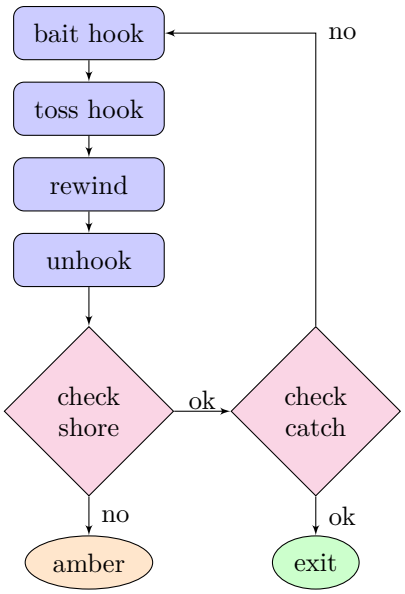

Fig. 2. A flow chart with subtasks for the fishing task.

this instruction explains how to use them. This description is often verbal, but Stanton [15] gives examples both using verbal descriptions and flowcharts.

An example flowchart is shown in Figure 2, breaking Task 3.1 in Table I into subtasks. The rectangular nodes represent operational tasks, to bait the hook, to toss the hook into the sea, to rewind the line, and to unhook and slaughter fish if any is caught. The diamond shaped nodes represent test or observation tasks, where we need to check if certain conditions are true: checking the distance to shore, in case we need to move further away, and checking if we have sufficient catch to return home. Finally the oval nodes represent transitions into new tasks, either because the task is complete (green

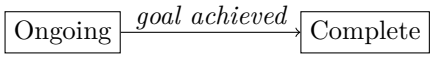

Fig. 3. Simple state machine of an operation (HTA level 1).

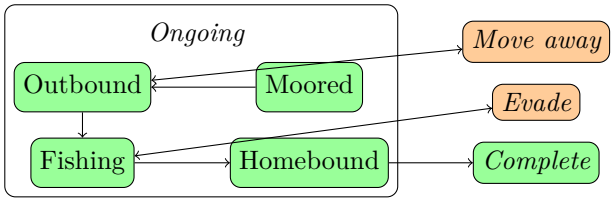

Fig. 4. Example of a hierarchical state machine.

'exit' node) or because it is suspended for the purpose of error recovery (amber node). This will be discussed further in Section II-D.

C. State Machines

One of the most fundamental modelling techniques in computer and software engineering is that of a state machine.

Definition 1: A state machine is a directed graph, with nodes called *states* and edges called *transitions*. Each transition is labelled with a Boolean condition.

The states can be thought of as mutually exclusive situations, and the transitions represent the event where the system is brought from one state to another, which happens when the label of the transition is true. As a very simple example of a state machine, consider an operation in Figure 3. This model corresponds to the first level of HTA, with only one task defined. The two states correspond to the operation being ongoing or complete respectively. A single transition is included, from ongoing to complete, corresponding to the event that the operation goal be achieved.

Using additional levels from the hierarchical task analysis, we will break states into smaller ones. To follow the pattern from HTA, it is useful to use hierarchical state machine, as known for instance from UML. Using the fishing example, we can break the *Ongoing* state into substates as shown in Figure 4. The original state *Ongoing* represents the union of the substates *Moored*, *Outbound*, *Fishing*, and *Homebound*.

Each state in the state machine correspond to a task in the HTA, which defines the plan to be executed in the given state. The converse is not true. In Tasks 2 and 3, the two subtasks are executed concurrently, and we cannot subdivide the corresponding states, *Rowing* and *Fishing*, based on the HTA. In contrast, the *Moored* and *Homebound* states should be subdivided, with substates corresponding to subtasks of Phases 1 and 4.

From a practical viewpoint, it is very important *not* to break the operation down into too small states. The states should be small enough to allow a clear and concise description of what needs to be done, reducing cognitive stress. However, if the states are too small, cognitive stress is caused by rapid transitions. Parallel tasks, like row and keep watch, will be commonplace, and they must be parallel, and therefore they must be associated with one and the same state.

When flowcharts are used in HTA, these can easily be mapped into state machines. In essence, the rectangular blocks in the flowchart can be viewed as substates in the state machine, while the diamond nodes are pseudostates existing purely to handle multiple outgoing transitions. However, care must be taken to avoid overmodelling. Even if we are able to model a certain task using flowcharts and state machines, we should only do it if it makes it easier for the crew to understand than an instruction using natural language and figures.

D. Modelling undesirable situations

So far, we have only discussed linear state diagrams, with a single path from a unique start to a unique end state. Likewise, the HTA tree has assumed that everything goes according to plan. For real operations, contingency planning is a critical part. Each contingency plan consist of a set of conditions defining when it comes into effect, and a task with the goal of returning to a safe state, either by recovering to continue the operation or aborting.

Contingency planning is very easy to model in the state machine. For each contingency plan, we add a state corresponding to the situation(s) where the plan come into effect. Transitions into this state are labelled with the appropriate conditions. A contingency plan constitutes itself a task, which can be analysed using HTA and mapped into a hierarchical state machine as explained above. There will be transitions into the new states corresponding to the conditions associated with the contingency plan. It may be useful to colour code the states, green for planned states, amber for states where the contingency plan aim to recover, and red for states where we abort.

The contingency plan is itself a task which can be analysed in depth using HTA and consequently mapped into a states and state transitions. Some contingency plans may be complex, and require a large HTA tree to elaborate. In the state machine, that will mean a long path through multiple amber states before we recover in a green state.

In the HTA tree, the contingency plans will be associated with some testing or monitoring task which is used to identify the conditions for the plan to take effect. The HTA easily becomes cluttered if all the contingency plans are elaborated within the same tree, but it is not a problem for the model to elaborate them as separate trees and cross-reference.

Example 2: As an example, we can return to the fishing trip. In the *Outbound* state we keep watch for other vessels. This is an example of monitoring a safety condition. If a vessel is spotted on a collision course, we transition into an amber state aiming to escape the collision. If the evasive manoeuvre is successful, we transition back to the *Outbound* green state. Similarly, in the *Fishing* state we keep watch to avoid getting too close to the shore. If we do get too close, we enter an *amber* state to move away.

E. Some features of a state

Every task in HTA implies some instruction about how to execute the task, and this information must be carried over to the state machine model. We have identified three commonplace task categories which can, and should, be modelled:
1. Subtasks executed in sequence (Tasks 1 and 4).
2. Subtasks executed in any order.
3. Continuous monitoring in parallel with other tasks (as in Tasks 2 and 3).

The first case is handled by elaborating the state machine, with one substate per subtask. In each substate there is only one task eligible for execution and we proceed to the next subtask/substate when it is complete.

The second case could in theory be modelled in a state machine with 2^n substates for n tasks, corresponding to every combination of complete and incomplete tasks. This leads to unnecessary complexity. A simpler solution is to introduce a *task list* (list of subtasks) associated with the state. Think of the task list as a check list to be completed by the captain. There are no substates, and transition to the next state occurs when all tasks are checked.

Case 3 commonly occurs in combination with other cases, where some numbers, known as *key indicators* (KI) must be monitored. These KI numbers may be performance parameters or safety parameters. Any on-board support software should obviously offer a user friendly display of all KI-s defined in the plan. The set of relevant KI-s may vary from state to state.

Example 3: Typical KI-s for the *Fishing* state of the example would be distance to land (safety parameter) and amount of fish in the boat (performance parameter).

Another fundamental concept in operational plans are *stop criteria*, i.e. conditions where the operation must be aborted. In the state machine model, this specifies a transition into a red state. We can formalise the definition as follows.

Definition 2: A stop criterion is defined as the label of a transition from an amber or green state into a red one.

Since not every detail can be formally modelled, we expect every state to be accompanied by an *instruction sheet* using natural language and figures.

F. Caveats

We have introduced the state machine as if we want to complete the operational planning using HTA and then transform it into a state machine. In practice, it is probably a better idea to use both HTA and state machines together in planning, as two different views on the same model. An HTA model designed without concern of the state machine approach may be very hard to translate, as HTA is very permissive, and subtask instructions may be both complex and informal.

Two distinct model views is a potential strength for planning. HTA emphasises what has to be done, while the state machine emphasises the different circumstances of different situations. An important part of operational planning should be the priorities, requirements, and provisions in each situation, and state machine thinking should support a focus on this. If the HTA analyst keeps states and state transitions in mind, it will give a better transformation into a state machine, without diminishing the quality of the HTA model.

The framework discussed offers the flexibility of choosing between very detailed, formalised models and coarser models supported by long instructions in natural language. A major challenge will be to find the right balance, and use detailed, formal models when it aids understanding and not when it obstructs it.

We have not decided on who should be the final arbiter on when a state transition occurs. By suggesting automatic reading of key indicators from other on-board systems, combined with well-defined state transition criteria, we have enabled automatic state transitions. Traditional thinking (for good reasons) dictates that it is the captain who orders the execution of a contingency plan, corresponding to the transition into a red or amber state. Automating this decision may be a radical choice which should be made lightly. Undoubtedly, the system should monitor the conditions related to transitions into red and amber states to alert the crew, but the state transition decision may be left to the captain. Transition into green states is indirectly under manual control, since most of the tasks must be checked off manually. Still it could be useful to have a final transition approval from the captain.

III. Software

The state machine model of the operational plans is the foundation for creating situation-aware software for operational support. We propose a simple software architecture, and a prototype to demonstrate that the core concepts work. The emphasis here is on a support system to be used during the execution of the operation. A presentation system for use in briefing and debriefing would be similar, and so would an educational tool for use with simulator training. A planning tool, to prepare operational plans, could also be built on the same core, but we have not at this stage considered editing interfaces.

To get a clean and comprehensible architecture, we have sought to limit dependencies on existing on-board systems. This is known as *low coupling* in software engineering. For maximum functionality, it is clear that an on-board, situation-aware planning tool should receive data from other on-board systems. Most obvious is integration with alarm systems (IAS). In fact, one could envision the situation-aware tool with intelligent algorithms interpreting alarms in context. This is left for later stages of development.

A. Architecture

The proposed software architecture is depicted in Figure 5, using a typical three-tier framework. The Static Model Layer handles the operational plan as described prior to the operation, using a state ma-

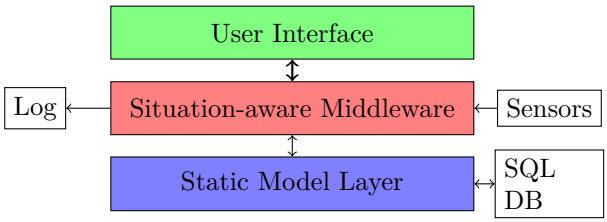

Fig. 5. Software architecture

chine model as discussed before. The middle layer is situation-aware, or state aware, keeping track of what state is applicable at any point in time, as well as the status of any tasks and task lists, stop criteria, transition conditions, as well as key indicators. The top layer is the user interface. Different user interfaces may be created for different purposes. We may want to provide each crew member with his own view, tailor made for his or her needs.

We have indicated communication with some external systems. Key indicators must be read from other on-board systems, but it should be noted that this interaction is read only; so interference is limited. The log is a suggested feature; the idea is that task completion and state transitions be logged. This could be a dedicated service for this system, or it could feed logging data back to existing on-board systems. The SQL database is purely an implementational convenience, and does not add functionality; it is merely a simple way to store the model.

A model-view-controller (MVC) architecture should be used, to allow multiple and different views with consistent data about the current state of the operation. The model is in the State-Aware Layer and the view in the User Interface Layer. Controllers may appear both in the User Interface Layer, taking input from the user, and in the State-Aware Layer, taking input from sensors and other on-board systems. Thus state transitions may be either manual or automatic.

The State-Aware Layer includes objects representing each of the conditions associated with state transitions, recording the current truth value. Design patterns [4] provide a structured and standardised approach to supporting certain key features in the architecture. The condition objects should implement the Observer pattern so that the state-aware logic can observe them and decide when the state changes. The Specification design pattern can be used to allow composition of conditions using Boolean arithmetic, in which case compound condition objects can observe their constituent conditions to change their truth value as appropriate. Tasks and task lists can be viewed as a special case of conditions, which are true when the user has checked them as complete.

B. Prototype

We have created a prototype demonstrating the core ideas in the work. Figure 6 shows the prototype view, intended for the captain. The operational plan as a state machine is defined in a simple XML file which is loaded into an SQL database by the Static Model Layer.

The current view comprises four panes, from left to right: a task list, a list of risks, key indicators, and an info pane. The task list shows the name of the current state and a list of tasks to be executed in any order to achieve the goal of the state. Each task is represented by one object in the GUI and a model object in the State-Aware Layer, according to the MVC architecture. The GUI object is a view, coloured green if the task is complete and white otherwise, using the Observer pattern to know when to change colour. It is also a controller, telling the model to check the task when clicked.

When all the tasks in the current state are completed, the State-Aware Layer will notice a state transition. Again, this will be detected by the view using the Observer pattern, and the pane will change to show the new state.

The key indicators are shown as a bar chart, representing readings from ship sensors. In the prototype, these sensors are simply mimicked by random processes for illustration. Each state in the model defines a separate set of key indicators which should be monitored manually in that state. Thus the key indicator pane will change accordingly upon a state transition.

The risks correspond to adjacent amber and red states in the state machine, giving an impression of conditions that must be avoided in the current state. This also changes automatically, when a state transition happens in the State-Aware Layer. Finally, the info pane is used to display details about a state or task when the associated ‘info’ button is pressed. Currently, only a dummy descriptive text is displayed, but it is anticipated that a one-page procedure, say in PDF, may be provided at a later stage.

There is one major caveat, namely the handling of misclicks in the user interface. A completed task cannot be uncompleted, which is logical in the model, but does not consider misclicks. This may trigger immature state transitions. The problem may be handled in two different ways, either at the model or the implementation level. At the model level, we could introduce error correction transitions in the state machine, with or without intermediate amber states. At the implementation level we could add extra prompts and safety mechanisms to correct misclicks immediately. The problem is clearly soluble, but further research is needed to choose the approach.

IV. Conclusions and open problems

We have given a proof of concept, showing how an operational plan can be modelled in a software compatible way, and how software can be designed to structure and visualise key elements from the plan. The significance of this work is in the linking of operational modelling and software modelling, establishing a common foundation of understanding for operational planners, ship officers, and software engineers. This helps us define key open problems for further research, both of theo-

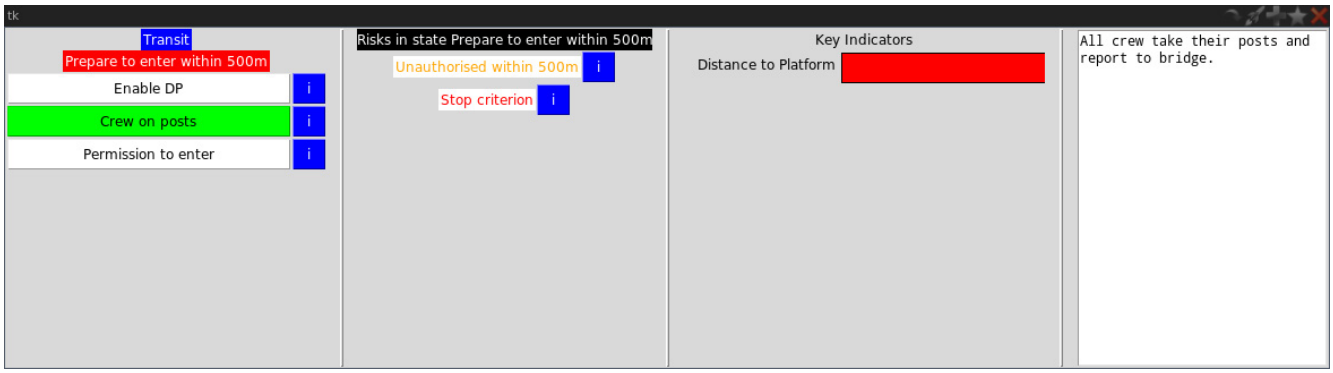

Fig. 6. Prototype screen shot.

retical and of practical interest.

Armed with the proposed modelling techniques, we can continue the study of operational plans, providing structure and identifying common patterns and key parameters. It is an acknowledged problem that highly complex, textual plans are extremely hard to validate, read, or use. More structured plans will be a great tool for training and for briefing, as well as a guide for software implementation.

The underlying modelling framework of the system also requires further research. The HTA and state machines discussed in the paper provide only a coarse structure for the plan. We need a careful review of real operational plans, both to assess the suitability of the current framework, and to identify any critical aspects which require additional modelling features. Other modelling frameworks for operations should be explored, e.g. SADT and IDEF0, assessing if they can be wholly or partially integrated in our framework, with transformation into software models.

In particular, the modelling framework must be extended to define multiple roles corresponding to different crew members. It is known that this can be done in HTA, and there are also software modelling techniques which support it. Further research is needed to formalise it and to elaborate the transformation. Ultimately, a hierarchy is required, with multiple teams (e.g. ships) taking part in a project, and multiple roles (crew members) within each team. The need to for a two-level hierarchy, headed by a project leader and a number of team leaders (e.g. captains) is obvious. It may or may not be necessary to generalise for an arbitrary number of levels.

With respect to the software tool, a better understanding is needed of the work situation of the ship's crew. Two questions are obviously crucial. What information is required in each conceivable situation? And how should the required information be presented?

On the theoretical side, it would be useful to formalise the modelling framework, with well-defined metamodels. This could further lead to a useful amalgamation with modelling techniques from other domains, such as HCI, UI design, or business process modelling.

References

[1] Magne V. Aarset. *Kriseledelse*. Fagbokforlaget, 2010.

[2] Rémi Bastide. An integration of task and use-case metamodels. In Julie A. Jacko, editor, *HCI (1)*, volume 5610 of *Lecture Notes in Computer Science*, pages 579–586. Springer, 2009.

[3] David Embrey, Claire Blackett, Philip Marsden, and Jim Peachey. Development of a human cognitive workload assessment tool. Technical report, Human Reliability Associates Ltd., July 2006. MCA Final Report.

[4] Erich Gamma, Richard Helm, Ralph Johnson, and John Vlissides. *Design Patterns*. Addison-Wesley, Boston, MA, January 1995.

[5] B Gauss, M Rötting, and D Kersandt. Naridas – evaluation of a risk assessment system for the ship's bridge. In *Human Factors in Shop Design, Safety and Operation. RINA - The Royal Institution of Naval Architects. International Conference.*, March 2007. London, UK.

[6] Uwe Glässer, Piper Jackson, Ali Khalili Araghi, and Hamed Yaghoubi Shahir. Intelligent decision support for marine safety and security operations. In *Intelligence and Security Informatics (ISI), 2010 IEEE International Conference on*, pages 101 –107, May 2010.

[7] Uwe Glässer, Piper Jackson, Ali Khalili Araghi, Hans Wehn, and Hamed Yaghoubi Shahir. A collaborative decision support model for marine safety and security operations. In Mike Hinchey, Bernd Kleinjohann, Lisa Kleinjohann, Peter A. Lindsay, Franz J. Rammig, Jon Timmis, and Marilyn Wolf, editors, *Distributed, Parallel and Biologically Inspired Systems*, volume 329 of *IFIP Advances in Information and Communication Technology*, pages 266–277. Springer Berlin Heidelberg, 2010.

[8] Michelle Rita Grech, Tim John Horberry, and Thomas Koester. *Human Factors in the Maritime Domain*. CRC Press, 2008.

[9] Hans Hederström, Diethard Kersandt, and Burkhard Müller. Task-oriented structure of the navigation process and quality control of its properties by a nautical task management monitor (ntmm). *European Journal of Navigation*, 10(3), December 2012.

[10] Lee A. Luft, Larry Anderson, and Frank Cassidy. Nmea 2000 a digital interface for the 21st century. In *Institute of Navigation Technical Meeting*, January 2002.

[11] Margareta Lützhöft. *The technology is great when it works*. PhD thesis, 2004.

[12] Jonathan M. Ross. *Human Factors for Naval Marine Vehicle Design and Operation*. Ashgate, 2009.

[13] Bran Selić. Abstraction patterns in model-based engineering, February 2011. Keynote slides from ModProd 2011 at `http://www.modprod.liu.se/MODPROD2011?l=en`.

[14] Steve Spitzer, Lee A. Luft, and David Morchhauser. Nmea 2000, past, present and future. In *RTCM Annual Assembly Meeting and Conference*, May 2009.

[15] Neville A. Stanton. Hierarchical task analysis: Developments, applications, and extensions. *Applied Ergonomics*, 37(1):55 – 79, 2006. Special Issue: Fundamental Reviews.

PROPULSION MACHINERY OPERATING IN ICE – A MODELLING AND SIMULATION APPROACH

Dražen Polić
Dept. of Marine Technology
HIÅ and NTNU
E-mail: podr@hials.no

Sören Ehlers
Dept. of Marine Technology
NTNU and HIÅ
E-mail: soren.ehlers@ntnu.no

Vilmar Æsøy
Dept. of Marine Technology
HIÅ
E-mail: ve@hials.no

Eilif Pedersen
Dept. of Marine Technology
NTNU
E-mail: eilif.pedersen@ntnu.no

KEYWORDS
Ice-propeller interaction, propulsion machinery response, 20-sim, bond graph, ice strengthened vessel.

ABSTRACT

Shipping activity and offshore operations in Arctic areas are increasing as a result of more effective transportation routes and oil/gas exploration. Vessels navigating in ice covered areas are exposed to additional loads from different ice conditions. In this paper the dynamic loads on propellers are investigated to better understand the impact on propeller, power transmission elements and engine. An ice-propeller interaction model is implemented with a full propulsion machinery to simulate the systems response to ice loads. The ice load models are developed based on the DNV and IACS rules for ice-propellers. Modelling and simulation of interactive multi body systems is a rather complex task, involving hydrodynamics, mechanics, electronics and control systems. This paper describes an approach to link the different models to simulate the overall system response and the interactions between the sub-systems. Therein, the rule-based ice loads are implemented in two ways for comparison: a) a coupled and b) an uncoupled treatment of the ice load and system response. The simulation results show that the dynamic peak loads are 10-20% lower than the maximum peaks predicted by the uncoupled simulation, i.e. conventional rule-based. Simulations also show that the peak loads are damped through the transmission elements, and therefore reducing the load on critical machinery components.

INTRODUCTION

As the amount of vessels capable of navigation in ice-covered waters increases, further understanding of ice-related loads acting on the propeller become important for safe and efficient design and operations of the ice going vessels. Therefore, a simple model of the propulsion machinery is developed to investigate the influence of ice loads on propulsion machinery response. Therefore, DNV and IACS rules for ice strengthened vessels are adopted here to identify the ice loads acting on the propeller. Furthermore, the simulations to be carried out in this paper will focus on merchant vessels with ice class 1A, because this ice class is typically found to be most economic for arctic operations, see Erikstad and Ehlers (2012). Hence, in order to compare IACS and DNV the class notation PC-7 and DNV ICE-1A is utilized, respectively. Further the ice influence described by DNV and IACS rules is extended by relating the ice related loads as a function of angular velocity of the propulsion machinery, i.e. a coupled treatment of the ice loads and system response will be presented.

Propulsion machinery in ice

The propulsion machinery is a coupled system connecting the main engine through a shaft with the propeller to create a directional thrust, see Figure 1. This directional thrust allows the vessel to maneuver and sail in open and ice-covered waters. The latter typically involves the breaking of ice pieces and their submergence in the direction of the water flow around the hull. Consequently, this influences on the hydrodynamic performance of the propeller, because the water inflow to the propeller, i.e. wake field, is disturbed. Furthermore, if a submerged ice piece proceeds further towards the advancing propeller, contact between the ice pieces and the propeller will occur, resulting in an ice-induced contact load. This process is called ice-propeller interaction.

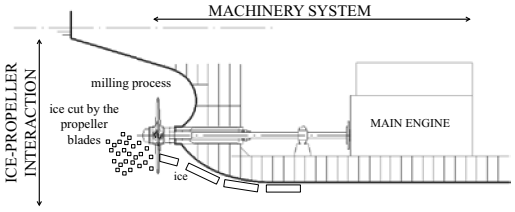

Figure 1: Propulsion machinery in ice

The propeller, being one element of the propulsion machinery, transmits this ice-related contact load together with the hydrodynamic load, being a result of the surrounding water, to the other elements of the propulsion machinery, such as the shaft, flexible and shaft couplings, clutches and gears. In turn, the main

Proceedings 27th European Conference on Modelling and Simulation ©ECMS Webjørn Rekdalsbakken, Robin T. Bye, Houxiang Zhang (Editors)
ISBN: 978-0-9564944-6-7 / ISBN: 978-0-9564944-7-4 (CD)

engine transmits the machinery power to the propeller, which clearly represents a coupled relationship.

Ice-propeller interaction

Veitch (1995) describes the ice-propeller interaction process qualitatively in terms of three stages: approach, blockage and contact. During the approach and blockage stage at least one ice piece is in the path of the advancing propeller. In those conditions, the relative motions between the water and the ice piece as well as the disturbance around the ice piece will increase. This influence is called ice piece wake and it affects only the hydrodynamic performance of the propeller. As the ice moves closer to the propeller the ice piece wake will grow. This growth reaches its maximum just before the ice piece impacts the propeller on the upstream side. Consequently, in the next instance physical contact between the propeller and the ice piece occurs. This contact stage currently defines the strength requirements of the propeller blades and the design load of the propulsion machinery.

The Classification Societies DNV (2012) and IACS (2011) are describing the design load, as a sum of the ice-related contact and hydrodynamic load. The hydrodynamic load is based on open water design parameters. In rules, the torque component of ice-related contact load is defined based on propeller geometrical parameters, angular velocity (rps), and ice thickness and strength. For higher ice class of vessel the ice thickness and strength will grow in the way that thicker ice will have higher strength. The DNV calculation is neglecting the increase in strength by assuming constant strength index of unit value. Except for this the propeller blade thickness is neglected in the ice torque load calculation of the DNV rules. These differences in calculations are presented in equations (1, 2, 3 and 4) in Appendix A. The maximal value of torque is obtained at the maximal allowable rps in ice-covered waters.

The excitation of the torque due to ice-propeller interaction is described with different excitation conditions presented in Table 1. Using the C_q and α_i parameters with maximum torque, equation (1), a single blade impact is described as a half sine shape with function of the propeller rotational advancement:

$$Q(\varphi) = C_q \cdot Q_{\max} \cdot \sin(\pi(\frac{\varphi}{\pi})) \text{ for } \varphi = [0, \alpha_i] \quad (1)$$

$$Q(\varphi) = 0 \text{ for } \varphi = [\alpha_i, 2\pi] \quad (2)$$

where:
Q_{max} – maximum torque [Nm]
φ – propeller rotational position [rad]

Further, number of ice impact is defined as:

$$N = 2 \cdot Z \cdot H_{ice} \quad (3)$$

where:
Z – number of propeller blades
H_{ice} – design thickness of ice [m]

Table 1: Torque excitation factors for different ice cases

Torque excitation	Ice-propeller interaction	C_q	α_i
Case 1	Single ice block	0.5	45°
Case 2	Single ice block	0.75	90°
Case 3	Single ice block	1	135°
Case 4	Two ice blocks	0.5	45°

In Figure 2 the summarized torque component of ice-induced contact load from all blades and with N-numbers of ice impact is presented for case 1, 2 and 3.

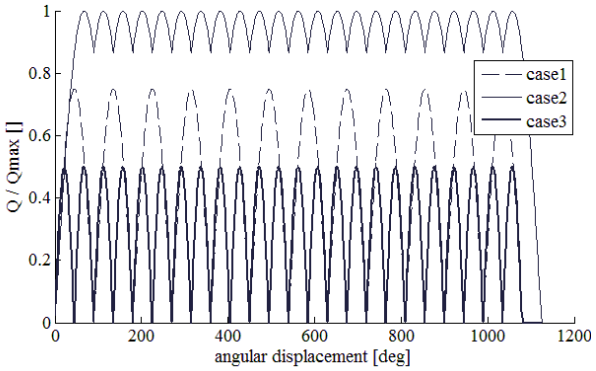

Figure 2: A typical response of the propulsion machinery during ice-propeller interaction for a four-bladed propeller in 1.5 m thick ice (IACS)

Furthermore, in this paper only case 2 and 3 are analysed, because the influence of the ice related load is most dominant here. Additionally, case 4 for is essentially equal to case 1, however, having twice the amount of ice block impacts following two ice blocks impacting the propeller. Further, DNV neglects case 1 entirely due to its low significance and generally utilizes a linear ramp function for 270° of propeller advancement at beginning and at the end of the ice-propeller interaction (see also Figure 7 and 8 for comparison of DNV and IACS). This makes the first two impacts of ice, in the case of propeller with four blades, less impulsive than for the IACS rules, which increase the load with the first impact to the full load level. Common for both rules, is that the torque excitation is given as a function of maximum allowable propeller angular velocity. This assumes a constant propeller angular velocity and thus the coupled relationship between the propeller and the engine is neglected. On the top of this the hydrodynamic torque needs to be added as well as the dynamic response of the propulsion machinery.

Therefore, a dynamic simulation model is developed using the same parameters and equations as described by the rules above, but with a propeller torque as function of the propulsion machinery response. Using this approach the angular velocity and angular position of the propeller are considered in calculation of the torque excitation. The influence of the torque excitation

in the coupled simulation due the propeller angular velocity drop from ω_1 to ω_3 during a single ice impact is illustrated in Figure 3. Further, the growth at the end of a single ice impact will depend on the dynamics of the main engine.

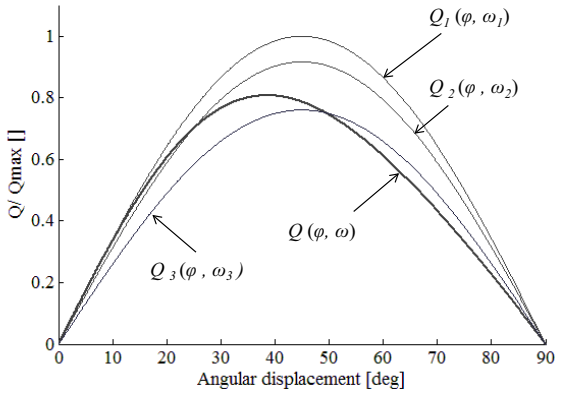

Figure 3: Simplified comparison of uncoupled $Q(\varphi,\omega_{1..3})$ and coupled $Q(\varphi,\omega)$ simulation for a single ice impact

Power transmission system

The most common and most efficient transmission systems are mechanical connections between the propeller and engine shaft. Mechanical transmissions are modelled as a multi-body system, consisting of a series of rigid bodies connected through various types of flexible joints. For long shaft lines a modal model is applied to include the higher order oscillations. Typical constraints to these flexible elements are: dynamic stress causing fatigue problems and maximum allowable angular deformations of shaft 0.2 – 0.4 deg/m and flexible couplings up to 30 deg/m.

To protect critical components from the dynamic stress and fatigue, the overall system must be analysed and designed in a holistic fashion. Dynamic overload can be avoided through shock absorbing elements such as flexible coupling, or even by introducing a weak link which is easy to repair in case of overload.

Main engine

The engine layout analysed in this paper is the most common solution for merchant ships. Typical constraints to the diesel engine are: 1) only one source of propulsion power; 2) engine designed for open water steady state operations; 3) engine dynamic is dependent on the ice-propeller interaction; 4) engine is directly exposed to the dynamical loads from ice-propeller interaction, causing irregularities in working operation and possible torsion vibrations which can damage the mechanical parts and cause thermal stress and fatigue; 5) rapid load variations also cause combustion problems resulting in thermal stress, soot formation, and unwanted exhaust gas emissions; 6) engine torque and speed limitations may cause stop and start problems caused by blocking ice.

MODELING

The developed mathematical model, which will be used for the simulation of the dynamic response of the propulsion machinery, consists of the following: a fixed pitch propeller (FPP) in direct connection to a low-speed engine through a shaft and a flexible coupling, see Figure 4. This arrangement is energy efficient, robust and hence the most common solution for merchant vessels. All elements of the propulsion machinery are modelled in the 20-sim-software Version 4.3 and presented as sub-models in Figure 4. The bond graph method is used to describe the power transfer and energy flow between the corresponding sub-elements and within the components of the sub elements as the product of effort (e) and flow (f). In bond graph terminology these two variables are called power variables. Additionally, the generalised momentum (p) and displacement (q) are called energy variables. Consequently, the energy supply is presented as effort (S_e) or flow (S_f), while the energy storage as momentum (I) and displacement (C), see Figure 5. The energy dissipation is presented as a resistor (R). Furthermore, to enable interaction between these system components we need to introduce power element *TF* and junction elements 1 and 0. A transformer is an element which transforms an effort on one port into an effort on the other port with some magnitude m, while a junction element is an ideal power transmitter, which transmits power instantly between ports without storing or dissipating energy. Further, the *0*-junction represents geometric compatibility, while the *1*-junction represents a dynamic force balance. For further details please see, for example, Karnopp et al. (2005) and Pedersen and Engja (2010).

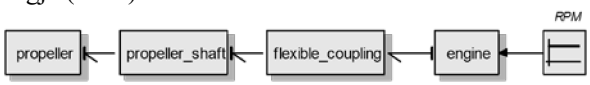

Figure 4: FP propeller directly coupled with engine

In the present model effort, flow, momentum and displacement are representing torque, angular velocity, angular momentum and angular displacement (angle), respectively. Further, the S_e-, *I*-, *C*- and *R*-elements present respectively the main engine as a source of torque, the moment of inertia, a torsional stiffness and the propeller as energy consumers. Additionally, the connections between these elements are represented with a *1*-junction if the velocity is equal otherwise with a *0*-junction. Additionally, the relationship for the energy transfer between and within these system elements of the bond graph representation needs to be derived. The latter is presented in the following sub-chapters.

Propeller

The propeller is described through its moment of inertia and its resistance. In bond graph terminology, this relates to the *I*- and *R*- element, respectively. The constant propeller moment of inertia is calculated based on its geometrical parameters, while the propeller

resistance is obtained based on the angular velocity. The latter is equal for both elements and thus allows their connection with a *1*-junction. Together, these three elements are used to describe the propeller torque in ice as follows: 1) the *1*-junction element transmits the effort (*e*), i.e. torque, from the propulsion machinery to the propeller; 2) under the assumption of linear dependency, between the propeller and the remainder of the propulsion machinery, this effort is distributed between the *I*- and *R*- elements; and 3) a flow response is derived as a function of effort and the propeller inertia.

Transmission system model

Power transmission between the FPP and the low-speed engine is realized with a so-called directly coupled system using a shaft and a flexible coupling. Therein, the shaft is modelled as a system of finite lumps or modes deduced from a modal decomposition of the continuous representation of the shaft. Following the bond graph concept a combination of the latter is possible (see Margoli et al. 1977, Karnopp et al. 2000) which also allows a reduction of the model extent without simulation accuracy loss. In order to do so, the natural frequencies and modes of the system must be maintained (see Margoli et al. 1977, Karnopp et al. 2000, Valland 1999). Considering the latter the mode shapes of the shaft were evaluated at the location of the torque and added inside *TF* element as a magnitude m = 1. The only exception is a *TF6* element, where m = -1 due to shape of the mode 2 and torque location $x = L$. Further, for each mode the modal shaft stiffness (*C*), mass (*I*) and damping (*R*) is calculated using the initial propeller position as a shaft origin.

Since the present flexible coupling is a short element, only few modes and natural frequencies exist. However, its dynamic properties must be approximated with sufficient accuracy, i.e. the stiffness of the rubber material or the hydrodynamic damping arising from the oil inside the flexible coupling. Using *C*- and *R*-elements those dynamic properties are included and connected to a *0*-junction. The reason for the latter arises from the change in flow and angular velocity over the shaft length, while the amount of effort, i.e. torque, is constant over the entire cross-section.

Engine model

A simplified model of the diesel engine is applied in this study Figure 5. The combustion process is modelled as a torque source (*MTF*) supplying power from the engine speed controller signal to the crank shaft, represented by a single inertia element (*I*). Mechanical friction is modelled as a resistor (*R*). The PID angular velocity governor, proportional-integral-derivative controller, is controlling the fuel injection limited by the engine operational constraints. As a result, the response angular velocity output from this simplified engine system is derived and compared with the angular velocity reference input. The torque input are controlled within a range of 10% to 110% of its maximum value, which is given as a function of angular velocity.

Propulsion machinery model

In Figure 3 the combined bond graph of each sub system is shown representing the entire propulsion machinery model.

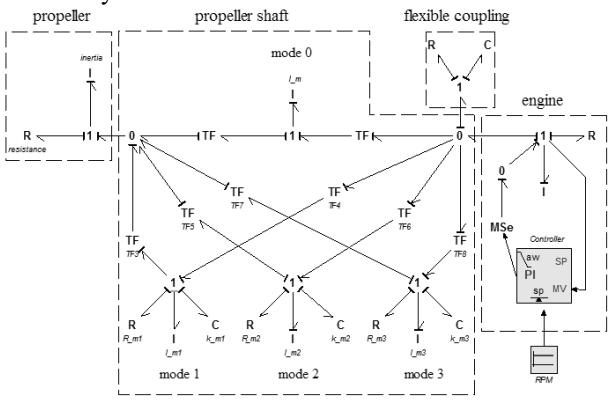

Figure 5: Overall bond graph model of the propulsion machinery system

RESULTS

Using the propulsion machinery model described in the previous chapter uncoupled and coupled response simulations for ice-propeller interaction are carried out. Coupled simulations includes the dynamic response of the entire machinery, while uncoupled is the load when propeller is assumed to run at constant speed without dynamic response. In order to do so, the required propeller geometry and efficiency diagram as well as the resistance in ice is selected from Lee (2008) for the case study vessel. Therefrom, the four-bladed propeller rpm are obtained for a selected sailing speed of 5 knots in 1.5m thick ice as well as the related hydrodynamic load acting on the propeller in open water at this rpm rating. Furthermore, based on the required rpm for maximum open water speed we selected an appropriate engine that delivers the required power for navigation in ice. Additionally, the damping and stiffness of the flexible coupling, see Figure 5, as well as the shaft diameter is defined based on the design load defined in the ice-propeller interaction chapter. The details are given in appendix A/B. Therein also the engine controller parameters, used in this study, are presented.

The results of the simulation are presented in Figure 6, 7 and 8, and they describe the distribution of the torque load for case 2 and 3 of the ice-propeller interaction simulations. In Figure 2 a coupled simulation of the propulsion machinery is presented for case 2 and 3 with normalized values of torque load and the propeller angular velocity, presented as revolutions per minute (rpm). Therein, it can be seen that both cases show comparatively small differences, even though 75% of the maximum ice related load is applied in case 2; see parameter Cq in Table 1; while 100% of the maximum ice-related contact load are applied in case 3. The reason

for this similarity in torque in spite of the ice related load difference arises from the increase of the hydrodynamic load in case 2. Therein, the hydrodynamic load is a function of the propeller rpm's being a function of the system response in turn. The relationship between this hydrodynamic load and the propeller rpm's is given in appendix A/B of this paper.

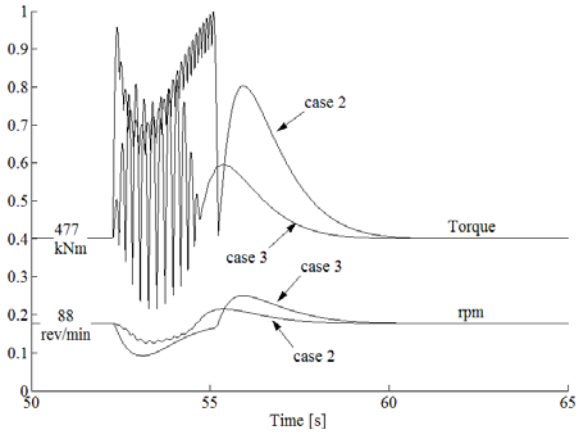

Figure 6: A typical response of the propulsion machinery during the milling of a single ice block

The largest influence of the ice on the propeller load is found in case 3, which is therefore presented in Figure 7 and 8 for DNV and IACS, respectively. These figures include, besides the load for the coupled and uncoupled simulation, the hydrodynamic and ice-related contact load for comparison. Thereby it can be seen that the ice-related contact load is nearly constant during the ice-propeller interaction while the deviation of the coupled load is caused by the change in hydrodynamic load. Furthermore, a difference between the ice-related coupled and uncoupled contact load can be identified.
Most importantly however, it can be seen in Figure 7 and 8 that the load in a coupled simulation is lower, except last two ice impacts with the linear ramp function described by DNV, than the load in an uncoupled simulation. The reason for this is the dependency of the coupled load, consisting of the hydrodynamic and ice-related contact load, on the propeller rotational speed. The latter decreases once ice impacts the propeller, which consequently causes a reduction in coupled load. However, after this initial impact and speed reduction the machinery system accelerates and thus increases the coupled torque, in the current example above the initial ice-impact load level. The latter however depends on the engine capabilities, since only an engine with additional power reserve is capable to compensate and accelerate further, in case this reserve is not available, the propeller will be blocked by the ice and the rps's drop to zero.

To present the influence of the coupled or uncoupled simulation further, Table 2 compares case 2, triangular shaped ice-related contact load, with case 3, which has a cumulatively increasing ice-related load as shown in Figure 2. The resulting difference between these cases is shown by means of maximum torque value for the uncoupled and coupled simulations, respectively. The uncoupled simulation results in higher torque values since the load is independent from propeller angular velocity.

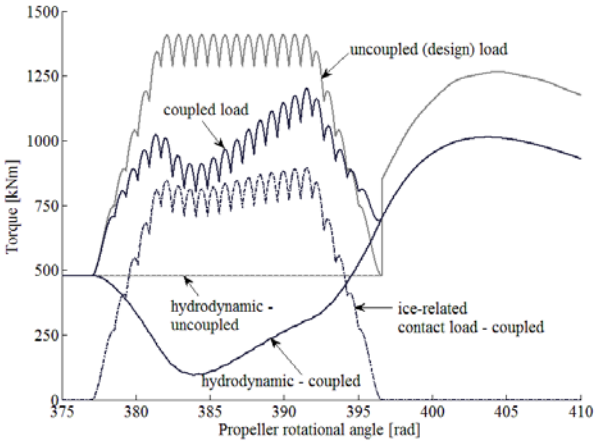

Figure 7: Comparison of the propeller response for the uncoupled and coupled DNV torque for case 3

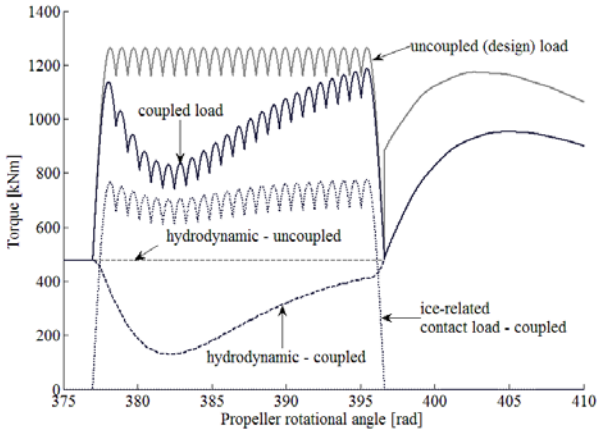

Figure 8: Comparison of the propeller response for the uncoupled and coupled IACS torque for case 3

Table 2: Comparison of uncoupled and coupled (*) design torque of the ice-propeller interaction for case 2 and case 3.

	Case 2	Case3
	max Q [kNm]	max Q [kNm]
DNV (100%)	1180	1410
DNV*	83%	85%
IACS	91%	90%
IACS*	85%	84%

In addition to the presented differences for the coupled and uncoupled simulations, the presented model can be used to analyse the load acting on different components of the machinery system. Hence, we can identify the deformation of shaft and a flexible coupling element caused by the excitations of the design load. Therein, the deformation magnitude is defined by the amplitude and shape of the loading, which was found to be higher for case 3, see Figure 9. In case 2, where the steep initial slope of the design load applied causes the deformations

grow rapidly. This growth of deformation $\Delta\dot{\theta}$ per single ice block impact is presented in Table 3 and 4 for an interval of 0.1s. Therein, the results are given relative to the base case set by the DNV loading and a simple multiplication of the deformation growth with the duration Δt will result in the maximum deformation per ice impact. Furthermore, it can be stated that the steep initial slope at the beginning and at the end of the milling sequence, described by IACS, causes a higher deformation growth. In all cases, the deformation and deformation growth are 10 to 20% lower in the coupled simulation compared to the uncoupled simulation.

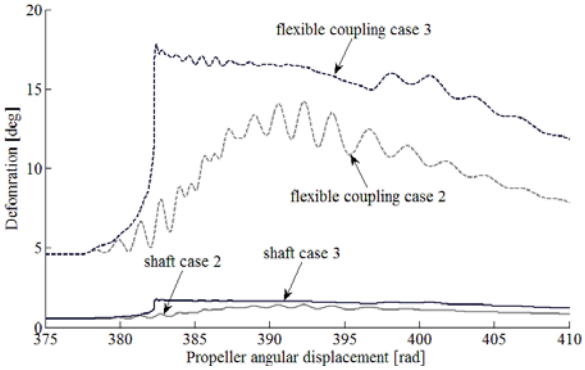

Figure 9: Comparison of the twist angle in shaft and flexible coupling for uncoupled DNV case 2 and 3

Table 3: CASE 2 - Influence of the uncoupled and coupled (*) simulations on the deformations of the shaft, θ1, and the flexible element, θ2.

	max θ_1 [deg]	max $\Delta\dot{\theta}_1$ [deg/s]	Δt_1 [s]	max θ_2 [deg]	max $\Delta\dot{\theta}_2$ [deg/s]	Δt_2 [s]
DNV (100%)	1.42	0.25	0.11	14.22	2.69	0.11
DNV*	73%	111%	97%	71%	112%	96%
IACS	93%	101%	101%	92%	101%	102%
IACS*	75%	120%	86%	72%	118%	88%

Table 4: CASE 3 - Influence of the uncoupled and coupled (*) simulations on the deformations of the shaft, θ_1, and the flexible element, θ_2.

	max θ_1 [deg]	max $\Delta\dot{\theta}_1$ [deg/s]	Δt_1 [s]	max θ_2 [deg]	max $\Delta\dot{\theta}_2$ [deg/s]	Δt_2 [s]
DNV (100%)	1.75	0.05	0.10	17.80	0.54	0.10
DNV*	81%	123%	140%	80%	115%	164%
IACS	96%	225%	144%	96%	218%	149%
IACS*	76%	216%	127%	75%	209%	132%

Further, the torque in the shaft and flexible coupling element is analysed and compared with propeller load. The largest influence is found in uncoupled simulation of DNV case 2 and case 3, which is therefore presented in Figure 10. Thereby it can be seen that the torque difference in shaft and flexible coupling is insignificant and the reason is in the small angular velocity of propulsion machinery and shaft inertia. However the most important is to see a delay in the torque between the propeller and power transmission elements caused by propeller inertia. Particularly in this case, propeller has ten times higher moment of inertia than the power transmission elements. Furthermore, in all cases the torque maximum value is higher inside power transmission elements than the torque experienced by the propeller.

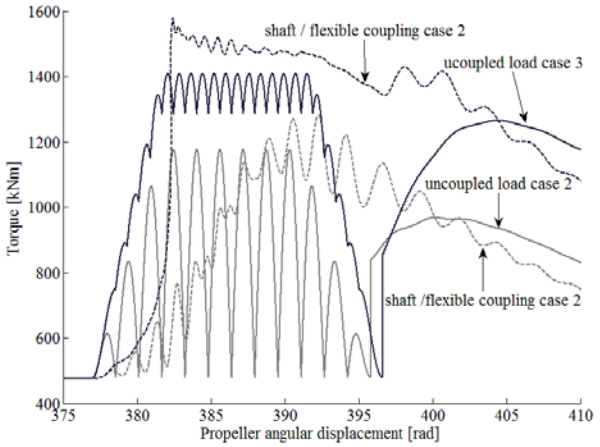

Figure 10: Comparison of the torque in shaft and flexible coupling with propeller load for uncoupled DNV case 2 and 3

SUMMARY AND DISCUSSION

This paper presents dynamic response of the propulsion machinery in ice. A simple model was developed to identify the influence of ice-propeller interaction also introducing an uncoupled and coupled simulation. DNV and IACS rules where used to calculate the propeller torque load, and angular velocity. As a result, maximum values of torque and angular deformation indicate that the uncoupled simulation is more conservative and thus may lead to over dimensioning of the machinery system. Furthermore, the coupled simulation highlights the necessity to consider the dependency between the propeller design load and angular velocity of propulsion machinery. However, this coupled simulation needs to be extended further to identify the validity of the rule-based ice-related loads and the accuracy of the engine response. In other words, the dependency of the propulsion machinery, especially power transmission system, on the hydrodynamic and ice-related contact load must be investigated further. Furthermore, the ice-propeller loads need to be related to actual ice properties, while the main engine acceleration and power with the actual combustion process. Additionally, the simulation approach shall be extended to include medium-speed engines coupled to the propeller shaft by a reduction gear, or electric motor(s) driving the propeller using power from the diesel generators. In conclusion, the present study forms a basis for the evaluation of the current design load and propulsion machinery scantling determination for ice going vessels.

ACKNOWLEDGEMENTS

This research is funded through the Norwegian Research Council project.no.194529

REFERENCE

DNV rules. 2012. “Ships for Navigation in Ice.”

Erikstad, S.O.; Ehlers, S. 2012. “Decision Support Framework for Exploiting Northern Sea Route Transport Opportunities”, Journal for Reserch in Ship Technology, Vol. 59, No. 3. 34 – 43.

IACS rules. 2011. “Requirements Concerning Polar Class.”

Karnopp, D.C.; Margolis, D.L. and R.C. Rosenberg. 2005. “ System Dynamics - Modelling and Simulation of Mechatronic Systems.” John Wiley & Sons Inc., Fourth edition.

Lee, S.K. 2008. “Combining Ice Class Rules with Direct Calculations for Design of Arctice LNG Vessel Propulsion.” Gastech conference proceedings 2008.

Margolis, D.L.; Young, G.E. 1977. “Reduction of Models of Large Scale Lumped Structures Using Normal Modes and Bond Graphs.” Journal of the Franklin Institute, Vol. 304, No.1.

Pedersen, E.; Engja, H. 2010. “ Lecture Notes in TMR4275 Modelling, Simulation and Analysis of Dynamic Systems.” NTNU.

Valland, H. 1999. “Analysis of Torsional Vibration in Branched Shafting Systems.” The TORSIO system, Computational Methods. NTNU, Dept. of marine engineering, Trondheim.

Wilson, C.E. 1997. “Computer Integrated Machine Design”, Prentice-Hall International.

Veitch, B. 1995. “Prediction of Ice Contact Forces on a Marine Screw Propeller During the Propeller-Ice Cutting Process.” PhD thesis, Acta Polytechnica Scandinavica, Finland.

APPENDIX A

DNV and IACS equations for propeller torque calculation. Maximal torque on a propeller due to ice influence is equal to:
$Q_{\max}$ is the maximum ice-related torque on a propeller.
For $D < D_{limit}$

$$Q_{max\_DNV} = 7.7 \cdot (1 - \frac{d}{D}) \cdot \left(\frac{P_{0.7}}{D}\right)^{0.16} \cdot (nD)^{0.17} \cdot D^3 \quad (1)$$

$$Q_{max\_IACS} = 105 \cdot (1 - \frac{d}{D}) \cdot S_{qice} \cdot \left(\frac{P_{0.7}}{D}\right)^{0.16} \cdot (\frac{t_{0.7}}{D})^{0.6} \cdot (nD)^{0.17} \cdot D^3 \quad (2)$$

For $D \geq D_{limit}$

$$Q_{max\_DNV} = 14.6 \cdot (1 - \frac{d}{D}) \cdot \left(\frac{P_{0.7}}{D}\right)^{0.16} \cdot (nD)^{0.17} \cdot D^{1.9} \cdot H_{ice}^{1.1} \quad (3)$$

$$Q_{max\_IACS} = 202 \cdot (1 - \frac{d}{D}) \cdot S_{qice} \cdot \left(\frac{P_{0.7}}{D}\right)^{0.16} \cdot (\frac{t_{0.7}}{D})^{0.6} \cdot (nD)^{0.17} \cdot D^{1.9} \cdot H_{ice}^{1.1} \quad (4)$$

with:

$$D_{limit} = 1.8 \cdot H_{ice} \quad (5)$$

d – external diameter of propeller hub [m]
D – propeller diameter [m]
S_{qice} – ice strength index for blade ice torque
$P_{0.7}$ – propeller pitch at 0.7 radius at MCR in free running conditions [m]
$t_{0.7}$ – maximal thickness at 0.7 radius [m]
n – propeller rotational speed [rev/s]
H_{ice} – maximum ice block thickness [m]

APPENDIX B

LNG vessel DNV ICE 1A with twin screw
L = 200 m // length
B = 28 m // breadth at water line
T = 9 m // maximal draft
V = 40 000m^3 // cargo capacity
w = 0.143 // wake factor
v_{ow} = 17 kn// vessel open water speed
v_{ice} = 5 kn // vessel speed in ice
R_{ow} = 1192.5 kNm // vessel total resistance at v_{ow}
R_{ice} = 2 157.8 kNm // vessel total resistance at v_{ice}

Ice class parameters
H_{ice} = 1.5m // ice thickness
S_{qice} = 1 // ice strength index for torque

Propeller parameters
D = 6m // propeller diameter
d = 1.8m // external diameter of propeller hub
$P_{0.7}$ = 4.2m// propeller pitch at 0.7R
$t_{0.7}$ = 0.1016m // maximal blade thickness at 0.7R
EAR = 0.55 // expended area ratio
J_p = 46000 kgm^2 // propeller inertia
RPM = 88 // propeller rpm’s needed at v_{ice}
RPM_ow = 102 // propeller rpm’s needed at v_{ow}
Q_{ow} = 640.36 kNm // propeller torque required at open water conditions at v_{ow}
Relationship between propeller rpm and hydrodynamic torque:

$$Q_{ow} = L_{ow} \cdot abs\left(RPM_{ow}\right) \cdot RPM_{ow} \quad (1)$$

L_{ow} = 5618.43 kNm/s^2 // propeller loading coefficient

Shaft parameters
L_{shaft} = 10 m // shaft length
G = 78 GPa // shear modulus for steel
ρ = 7800 kg/m^3 // steel density
T = 1410 kNm // max torque
N_{sf} = 3.5 // factor of safety
S_{yd} = 655 MPa // steel yield stress
d_{shaft} = 0 m // shaft inner diameter
Using Von Misses Stress criteria and safety parameters, given in (Wilson 1997), shaft diameter is calculated using equation:

$$D_{shaft} = \left(\frac{32 \cdot \sqrt{3} \cdot T \cdot N_{sf}}{\pi \cdot (1 - \frac{d_{shaft}}{D_{shaft}}) \cdot S_{YP}}\right)^{\frac{1}{3}} \quad (2)$$

D_{shaft} = 0.5 m // shaft diameter

Flexible coupling
C_{Tstat} = 4.78 MNm/rad // static stiffness
ω = 46 rad/s // phase velocity of vibration
ω_0 = 690 rad/s // characteristic coupling frequency

$$\kappa = 0.02 + 1.1\frac{\omega}{\omega_0} \quad (3)$$

κ = 0.09 // undimensioned damping factor

$$k = \frac{\kappa \cdot C_{Tstat}}{\omega} \quad (4)$$

k = 9.711 kNms/rad // linear viscous damping

Engine (2 - stroke)
Type 2 – stroke
J_e = 5060 kgm^2// Engine (crank shaft) inertia
RPM*= 105 // engine rated rpm
P = 11.3 MW // engine power in ice
P* = 13.3 MW // engine rated power
η_m = 0.8 // mechanical efficiency

Engine controller
Type PI – controller (20-sim reference PI_sp_aw)
κ = 0.005 // proportional gain
T_i = 0.1 s // Integral time constant
b = 0 // proportional set point weighting parameter
T_a = 1 s // tracking time constant
$minimum$ = 0.1 // minimum controller output
$maximum$ = 1.1 // maximum controller output

Simulation parameters
n_{b_ice} = 60 // number of blade revolutions before ice contact
t_{simu} = 0.1 ms // time step of simulation
Method BDF // backward differential formula

CONTROL DESIGN FOR SLOW SPEED POSITIONING

Anna Witkowska
Gdansk University of Technology,
Electrical and Control Engineering Department,
Gdansk, Poland
E-mail: awitkowska@ely.pg.gda.pl

KEYWORDS
Backstepping, state estimation, wave filtering, dynamic positioning

ABSTRACT

The problem under study is a synthesis of position and heading control system for low frequency model of surface vessel described by 3 DOF mathematical model. The recursive vectorial backstepping control design was used to keep fixed position and heading in presence of wave disturbances. The controller has been simulated on computer model of scaled supply vessel. It has been assumed that the actuators produce generalized forces in all 3 degrees of freedom. The backstepping controller proposed in this paper in configuration with passive observer and wave filtering make a good quality to keep fixed position and heading at low forward speed in comparison with PD controller.

INTRODUCTION

For many years, scientists have been conducting research which aim to study integrated systems of the vessel's motion management. Despite the increase in the level of automation, steering the ship is still in the area of intensive research, especially at the entrances to ports and narrow waterways corridors. In view of the manoeuvre difficulties caused by the weight of ships, it is not as easy task to improve the quality of navigation, especially for ships moving at slow speeds - (e.q. slow speed positioning - called dynamic positioning).

Dynamic positioning system for marine vehicles is a challenging practical problem. It includes station keeping, position mooring and slow speed references tracking. Of that three, the main purpose of the DP system is to maintain a certain accurate position and course, regardless of the interference such as waves and wind. This task should only be achieved under its own propulsion and using navigation systems. Application of the appropriate method of adjustment for DP vessel is directly related to the adopted model, its purpose, structure and number of the installed actuators. A significant number of vessels have a single propeller and rudder. In such device configuration large ships must be put into port by auxiliary ships. Currently, most of ships have installed an additional tunnel thruster at the bow of the vessel. It gives the possibility to fully actuate the ship for maneuvering at low speeds with mild entering the ports and narrow waterways corridors. Unfortunately, such system loses its properties at high speeds. Today a future of DP systems are azipod propulsion systems, which produces full nominal torque, available in either direction over the entire speed range.
The Diesel - Electric drivers are currently used on polyvalent ships of AHTS and PSV type. They have an aim to transport large cargo for drilling platform and anchor. Equipped with DP2 positioning system, are designed for use in all sea areas, regardless of weather conditions.
The station keeping for DP system can be achieved using only three control inputs when it is considered a fully actuated ship operating in the horizontal plane. Hence, the dynamic positioning system can be designed by using feedback from position and heading angle (Fossen 2002). These state variables are in some cases available through satellite navigation systems as GPS / DGPS, supported by the gyros and accelerometers. But in general more signals like for example velocities accelerations and stationary varying disturbances due to wind, ocean current and nonlinear wave effects, are necessary in the control law. In the process of steering the ship, direct measurement of longitudinal and transverse velocity is not available when they attain low speed values. However, it is possible to calculate the estimated value of velocity on the basis of the measurements of the position and direction by the state observer. In most cases, an accurate measurement of the position and direction is disturbed by the wind, waves and sea currents, as well as by the interference of the measuring sensors. Therefore the estimates should be filtered by using so-called wave filtering (WF) techniques. Oscillatory disruptions of a WF motion component are filtered before feedback is applied. However, the remaining LF motion components which are associated with the deviation from the given position and direction are compensated by the steering system

The examples of several solutions mentioned above to solve these problems have been recently obtained. Most of them base on signal filtering, state estimation and appropriate selection of the steering method. The first DP systems were designed using conventional PID controllers in cascade with low-pass and notch filters. There, the wave disturbances are filtered before feedback is applied in order to avoid unnecessary control action. Model-based controls for positioning of ships includes also LQG, sliding mode control (Tomera

Proceedings 27th European Conference on Modelling and Simulation ©ECMS Webjørn Rekdalsbakken, Robin T. Bye, Houxiang Zhang (Editors)
ISBN: 978-0-9564944-6-7 / ISBN: 978-0-9564944-7-4 (CD)

2010), robust H∞ control (Grimble et al. 1993; Messer, and Grimble 1993), non-linear backstepping (Krstic et al. 1995; Fossen and Strand 1999) method and another state - space techniques (Fossen 2002). A number of works were carried out within the scope of application of the dynamic positioning of artificial intelligence (Xu et al. 2011), fuzzy logic (Cao et al. 2001) and neural nets (Cao et al. 2000). In the DP systems, filtering the wave and state estimation are resolved using an extended Kalman filter (EKF) (Grimble and Fung. 1983) or Luenberger observer. Unavailable, meaning immeasurable size measurement, is estimated on the basis of the mathematical model which binds both estimated and measured size. In contradiction to linear systems, no general theoretical guarantee can be given for nonlinear systems for a stable observer-controller combination, as for nonlinear systems no general separation principle exist. Another method is the linearization of nonlinear systems and multi-controller synthesis (Banka et al. 2010). There is no guarantee for global stability of the total system. In addition, controlling the total system by a set of linearized systems will decrease the performance of the total system.

Unfortunately, if the extended Kalman filter and Luenberger observer are combined with a state feedback controller, using the estimates of the states global expotential stability cannot be quaranteed. This is the most important drawback of EKF. Alternative solution for the state feedback controllers is observer backstepping (Fossen and Grovlen 1998), passive observer and wave filtering (Fossen and Strand 1999). This methods were used by Lyapunov stability theorem and Kalman Yakubovich - Popov theorem during designing GES observer. Passive observer in comparison to the backstepping observer has less tuning parameters so it is easier to apply.

In the DP systems, specific steering algorithms calculate required forces and moments which compensate for the deviation, on the basis of the estimated size of the input including the measurement of the location and direction compared with setpoints. Modern methods of steering use nonlinear control methods which let to take into account the complex dynamics of the vessel, its purpose, structure and number of the installed devices, in the process of designing the control law. One of them is a Backstepping method (Krstic et al. 1995, Witkowska and Smierzchalski 2012). The backstepping controller proposed in this paper in configuration with passive wave filtering make possibility to keep fixed position and heading at low forward speed. The observer-controller system has been simulated on computer model of scaled supply vessel. It has been assumed that the actuators produce generalized forces in all 3 degrees of freedom.

LOW SPEED MODEL FOR DYNAMICALLY POSITIONED SHIP

During dynamically positioning (DP) it is a common assumption to consider the low speed, low frequency model omitting the centrifugal/coriolis forces, moments and nonlinear damping effects. Consequently for DP, the 6 DOF is reduced to a simpler 3 DOF model that is linear in kinetic part. Since we only consider the 3 horizontal DOF's, the kinematical equations for surface ships which describe the relationship between the earth-centred and the geographical reference frames are given by:

$$\eta' = R(\psi)\nu. \tag{1}$$

The state vector $\eta=[x,y,\psi]^T$ where (x,y) is the position of ship in an earth-centred inertial frame and $0<\psi<2\pi$ is the heading angle of the ship relative to geographic North. The vector $\nu=[u,v,r]^T$ contains linear body fixed velocities in surge, sway and angular in yaw. Rotation matrix R with the property $R^T= R^{-1}$ is defined by

$$R(\psi) = \begin{bmatrix} cos\psi & -sin\psi & 0 \\ sin\psi & cos\psi & 0 \\ 0 & 0 & 1 \end{bmatrix} \tag{2}$$

For DP (station keeping), the linear dynamical models for surface ship denote the control forces in surge, sway and moment in yaw by τ.

$$M\nu' + D\nu = \tau + \tau_w \tag{3}$$

where $M \in \mathbf{R}^{3x3}$ is the matrix of inertia, $D \in \mathbf{R}^{3x3}$ is the damping matrix, $\tau_w = R(\psi)^T b$ is a vector of slowly varying forces and moments that act on the hull due to environmental disturbances such as wind, currents and waves or unmodelled dynamics. The vector $\tau \in \mathbf{R}^3$, $\tau=[\tau_x, \tau_y, \tau_n]^T$ of forces and moments acting on the ship's hull refers to the forces generated by the propellers and rudders, can be written as.

$$\tau = Bu. \tag{4}$$

The matrix B is the control matrix described the thruster configuration and u is the control input.

DP CONTROLLERS

Vectorial backstepping

When designing the control law with backstepping method, we assumed that we have precise information about an object, i.e. we considered the model parameters as known in the ship model. Then the DP controller could be derived using the classical vectorial backstepping method, as it was discussed in detail (Krstic et al. 1995).

The dynamic positioning problem, considered in this paper is to find a feedback control law, which provides asymptotic convergence $\eta \rightarrow \eta_d$, at $\nu \approx 0$. The reference

signals needed for control are the desired state vector $\eta_d=[x_d,y_d,\psi_d]^T$ and its first and second order derivatives. All reference signals the heading angle ψ_d and the desired position (x_d,y_d) are assumed to be bounded. The vectorial backstepping design for ship mathematical model (1)- (4) was performed in two steps.
The first step of backstepping is to define new error variables $z_1 \in \mathbf{R}^3$ and $z_2 \in \mathbf{R}^3$ as:

$$z_1=[z_{11}, z_{12}, z_{13}]=\eta-\eta_d, \quad (5)$$
$$z_2=\eta'-\alpha, \quad (6)$$

The vector of functions $\alpha=[\alpha_1,\alpha_2,\alpha_3]^T$ stabilizes the system with respect to control Lyapunov functions (clf) candidate. The following DP controller is proposed

$$\tau=Dv-MR^T(C_2z_2+z_1+R'v+C_1z_1'-\eta_d'')-R(\psi)^Tb,$$

using the error definitions (5)-(6); control Lyapunov functions candidate $V_1=0.5z_1^Tz_1$ and $V_2=V_1+0.5z_2^Tz_2$ and the vector of stabilizing functions $\alpha=-C_1z_1+\eta_d'$.
Now, the error dynamics can be written as:

$$z_1'=-C_1z_1+z_2,$$
$$z_2'=-z_1-C_2z_2.$$

While all reference signals η_d are constant and assuming that the state variables are available measurably, the equilibrium point $(z_1, z_2)=(0,0)$ is GAS. Stability is established by using LaSalle's theorem, since $V_2>0$ and $V_2'\leq 0$. Among other things it is satisfied where designed parameter matrices $C_1=C_1^T>0$ and $C_2=C_2^T>0$ are chosen in a diagonal form.

PD

Nowadays, autopilots which are part of equipment on vessels, use the algorithm of PD controller to adjust the position and heading angle of a ship. The operation of a classic, conventional PD controller for DP is defined by the following formula:

$$\tau=K_p(\eta-\eta_d)+T_d(\eta'-\eta_d')$$

where K_p, T_d - are vectors of coefficients illustrating the influence of individual components of a proportional and differentiation in three degrees of freedom.
When the state variables are not available measurably, then it is necessary to estimate them. Next, on the basis of the estimated values, derivatives of state variables required in the controller are calculated. It is assumed that only position and heading measurements are availble. The observer was used to produce the velocity estimates for feedback control. The position and heading should not containing a WF part of the motion.

DP MODEL-BASED OBSERVER

The model-based observer described in detailed in (Fossen and Strand 1999) was used to reconstruct the system's non-measured states. The chosen observer was designed on the basis of the Lyapunov Stability Theory. The idea of the state observer is to reproduce in the mathematical model (virtually) a state that accurately reflects the reality. There are some differences between the real output and the model output. This error is fed back into the mathematical model to correct the difference and bring the mathematical model closer to the reality. The technique of the state observer consists in developing a model for the system under analysis and comparing the estimated outputs with the measured ones. It is assumed that only position and heading measurements are availble. The following ship model (1)-(4) was considered. The measured position and heading, y_m can be seen as a superposition of the LF motions and WF motions.

$$y_m=\eta+\eta_w$$

The zero mean Gaussian measurement noise is assumed to be negligible with respect to the first-order-wave disturbance η_w. The idea of passive observer is to reconstruct η, η_w from y based on output y and vector forces τ.
The following WF model approximation was used for simplified DP model of the ship dynamics.

$$h_i(s)=\frac{2\zeta_i\varpi_{0i}\sigma_i}{s^2+2\zeta_i\varpi_{0i}s+\varpi_{0i}^2}, \quad (7)$$

where: ζ_i - relative damping ratio, ω_{0i} - dominating wave frequency, σ_i-wave intensity parameter
Wave model is generated for each degree of freedom (i=1,2,3). The wave forces were added to the positions and heading measurements. A state space realization of wave frequency (WF) model (7) can be expressed as

$$\chi'=\Omega\chi, \quad (8)$$
$$\eta_w=\Gamma\chi, \quad (9)$$

Here $\chi \in R^6$ is a state vector, $\Omega \in R^{6x6}$ is a constant matrix results directly from transformation of the transmittance (7) to the state space model, $\Gamma \in R^{3x6}$ is a constant matrix converts the vector χ to space R^3 as the vector dimension η_w.
The bias state b can be used to represent slowly-varying environmental forces and moments due to second-order wave drift, ocean currents, wind and unmodelled dynamics. The bias state is modelled by a first-order Markov process

$$b'=-T^{-1}b \quad (10)$$

where $T \in R^{3x3}$ is a diagonal matrix representing positive bias time constants.

On the basis of a complete model of the system ship-environment which consists of a ship model (1) - (4), bias model (10) and WF model (8) - (9), proposed in (Fossen and Strand 1999) resulting observer is composed of the following equations described state estimators:

$$\dot{\hat{\eta}} = \mathrm{J}(\mathrm{y_m})\hat{v} + K_2\tilde{y}$$
$$\dot{\hat{v}} = -\mathrm{M}^{-1}\mathrm{D}\hat{v} + \mathrm{M}^{-1}\mathrm{J}(\mathrm{y_m})^{\mathrm{T}}\hat{b} + \mathrm{M}^{-1}\tau + \mathrm{J}(\mathrm{y})^{\mathrm{T}}K_4\tilde{y}$$

measurements estimator:

$$\hat{y} = \hat{\eta} + \Gamma\hat{\chi}$$

If a state observer is applied estimates of the bias and WF motion components can also be computed.
bias estimator:

$$\dot{\hat{b}} = -\mathrm{T}^{-1}\hat{b} + K_3\tilde{y}$$

wave estimator:

$$\dot{\hat{\chi}} = \Omega\hat{\chi} + K_1\tilde{y}$$

Here $\tilde{y} = y_m - \hat{y}$ is the estimation error and $K_1 \in R^{6x3}$, $K_2 \in R^{3x3}$, $K_3 \in R^{3x3}$ and $K_4 \in R^{3x3}$ are observer gain matrices. More details can be found in the literature (Fossen and Strand, 1999) and (Fossen, 2002). Both the GES and passivity for the observer were proven.

CONTROL SYSTEM STRUCTURE

Simulation studies were carried out in the system shown in Figure 1. Ship control structure consists of a block "Set point" which sets selected turn point position and direction with which they should be achieved. According to the assumption of DP steering, control takes place at low speeds of the ship. Therefore, turn points and parameters do not have to be determined automatically. They are usually defined by the operator. Wave interference influence on the state variables. Waves were modeled on the basis of the transmittance (7). In the considered system occurs block "DP controller", in which the set points of the position and course are compared with estimated values. In the "Observer" block, status variables are estimated based on the measured input and output signals of the model. In the simulation studies, a linear mathematical model of the ship CyberShip 2 was used as the object.

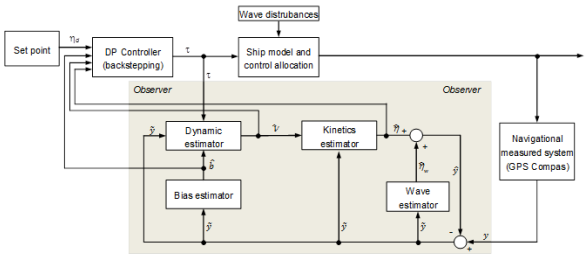

Figure 1: Simplified diagram of the DP system with an observer

The tested control systems were modeled in the computing environment called Matlab/Simulink. Simulations were carried out in the time domain. Numerical integration was done using Runge-Kutta method in fourth-order integration with a period equal to 0.1s.

SIMULATION RESULTS

Simulation model

The mathematical model of Cybership 2 was used during simulation. The model is 1:70 scaled of supply ship. The length is 1.255m. and the weight is 23.8kg. The CG is located about 4.25cm. of midship. Cybership 2 is modeled by the linear dynamic positioning model (1) - (4) with following mass and damping matrix coefficients:

$$M = \begin{bmatrix} 25.8 & 0 & 0 \\ 0 & 33.8 & 1.0115 \\ 0 & 1.0115 & 2.76 \end{bmatrix}$$

$$D = \begin{bmatrix} 2 & 0 & 0 \\ 0 & 7 & 0.1 \\ 0 & 0.1 & 0.5 \end{bmatrix}$$

The maximum surge force is 2N, the maximum sway force is 1.5N and the maximum yaw moment is about 1.5N.

The ship model selected for designing and testing the control system with the backstepping method, was developed at the Department of Engineering Cybernetics, Norwegian University of Science and Technology (NTNU), Trondheim, Norway. The physical model of this ship sails in the Marine Cybernetics Laboratory (MCLab), NTNU.
Five actuators actuate the ship. In the bow, there is a small two-bladed rpm controlled tunnel thruster which produces a sway force. At the stern, there are two rpm controlled main propellers with rudders which produce a surge and sway force.

Reference (Skjetne 2005, Tomera 2010) give more information about model structure and his dimensional hydrodynamic coefficients, also thrust allocation.

Case study

Consider the Cybership 2 DP model in combination with observer and backstepping controller, the results of the simulations are shown in Figures 2-3.

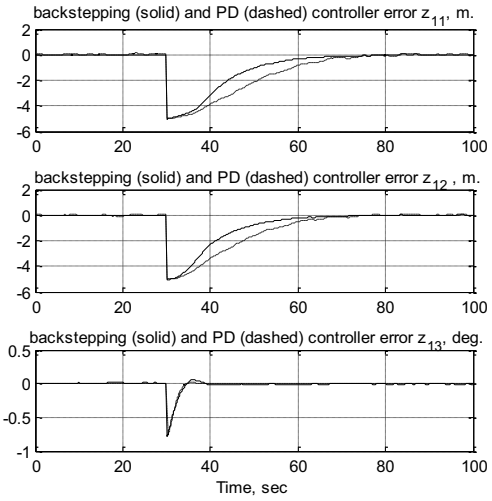

Figure 2:Position and heading observer-controller errors of the DP model.

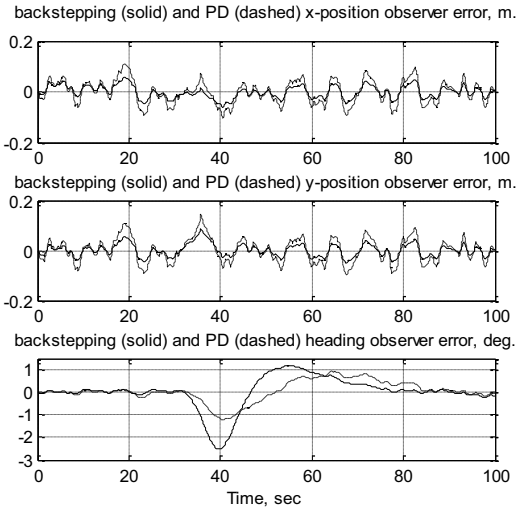

Figure 3:Position and heading observer errors of the DP model

The vessel starts with u_0=0.01m/s., v_0=0m., $\psi'_0=0^0$, x_0=0m. y_0=0m., $\psi_0=0^0$ while the initial values of the estimates are set as zero. After 30s. the designed states was generated by x_d=5m., y_d=5m. and $\psi_d=45^0$.

The simulation studies of the vectorial backstepping controller with observer were carried in the presence of the wave disturbances (7). The set parameters of the first order wave induced motion model were set as ζ_i =0.1, ω_{0i}= 0.8rad/s, σ_i=0.5m. The amplitudes of the wave - induced motion were limited to 1.0m., 1.0m., 2^0 respectively for surge, sway and yaw.

The observer - wave gains were chosen for the same order as the gains used in (Fossen and Strand 1999):

$$\Omega = \begin{bmatrix} 0 & I \\ \Omega_{21} & \Omega_{22} \end{bmatrix},$$

$$\Omega_{21} = -\mathrm{diag}(\varpi_{01}^2, \varpi_{02}^2, \varpi_{03}^2),$$

$$\Omega_{21} = -\mathrm{diag}(2\zeta_1\varpi_{01}, 2\zeta_2\varpi_{02}, 2\zeta_3\varpi_{03}),$$

$$\Gamma = [0 \quad I],$$

Filter gains are set as K_1=[diag(1.1,1.1,1.1), diag (0.8,0.8,0.8)]^T and K_2=1.1*diag(0.8, 0.8, 0.8), bias gains: K_3=diag(0.1, 0.1, 0.01), velocity observer gains: K_4=diag(0.1, 0.1, 0.01), bias time constants T=diag (100,100,100). For the PD controller, two vector parameters were to be selected as K_p=[0.3, 0.18, 2]^T, T_d=[3, 3, 3]^T. At the same time for the backstepping control law, designed parameter matrices are chosen in a diagonal form: C_1=diag (0.01,0.01,0.01) and C_2=diag (10,10,10).

The simulation tests aim at checking the operation correctness of the vectorial backstepping controller with passive observer and wave filtering for DP model. First the computer simulation is performed to show the convergence of the position and heading to their desired value. The time-histories shown in Fig. 2 confirm the good ability of the backstepping and PD control system to keep fixed position and heading in presence of wave disturbances. In comparison with PD, the backstepping method gives better time quality coefficients such as rise time, maximum overshoot, time control. The new state vector components z_1 = [z_{11}, z_{12}, z_{13}] tend to zero after about 30s. for both position and after about 10s. for heading. The surge, sway velocity and yaw angle were estaimated from observer. To compare the simulation results shown in Figs. 3 - 6 it is seen that all the observer errors tend to zero for velocity, position and heading. Velocity estimation errors does not exceed 2% of the steady-state. The time-histories in Figs. 5 and 6 show additionaly measured and estimated LF position and heading of the DP model with backstepping and PD controller.

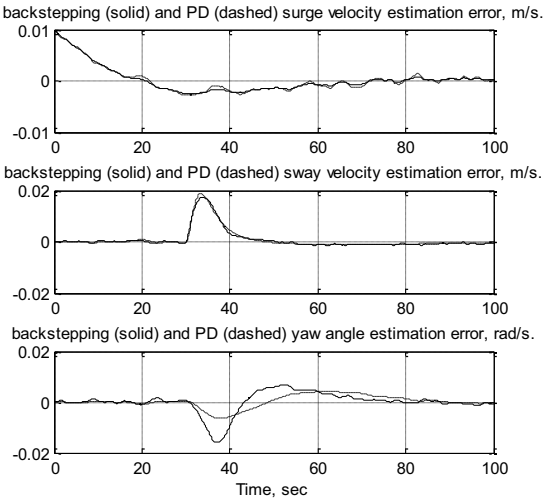

Figure 4:Estimation error of surge, sway velocity and yaw angle of the DP model.

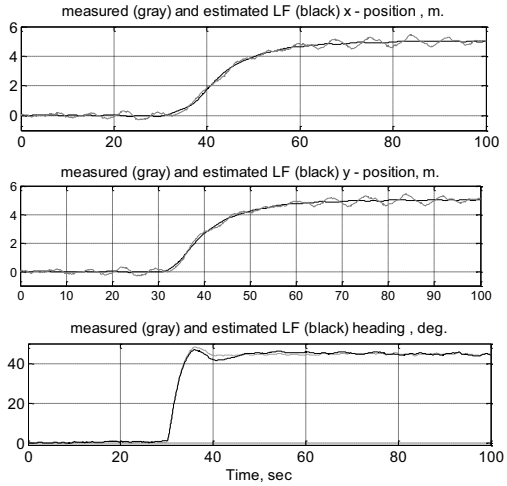

Figure 5: Measured and estimated LF position and heading of the DP model with backstepping controller.

CONCLUSIONS

Ships with DP system are used to perform operations on the sea, especially in the output of crude oil. Functions, that these vessels implement, are able to eliminate the tugs work and are able to quickly respond to changes in weather or operating parameters. This gives the versatility of using this type of vessels. In this paper the station keeping for DP system was achieved using only three control inputs when it is considered a fully actuated ship operating in the horizontal plane.

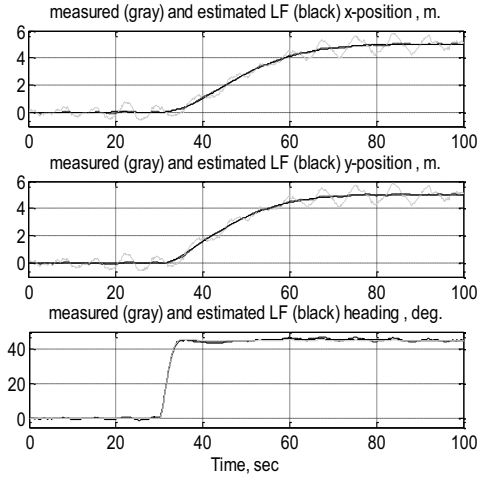

Figure 6:Measured and estimated LF position and heading of the DP model with PD controller.

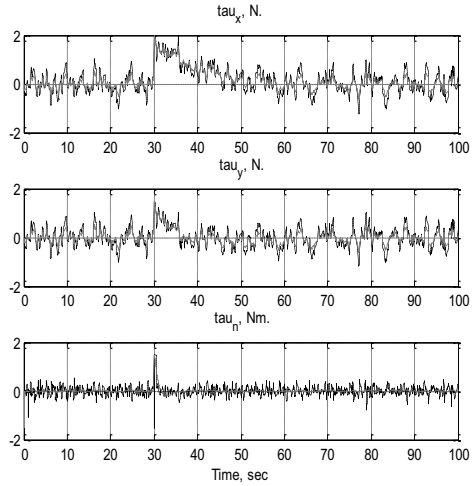

Figure 7: Control inputs in surge, sway and yaw (PD - gray line, backstepping - black line).

In this paper output feedback controller for DP was derived using vectorial backstepping method. The backstepping requires that state variables position, headings and velocities are available measurably for feedback control. For velocity estimates and wave filtering the controller was developed with observer. This combination of controller-observer confirm the good ability of the control system to keep fixed position and heading in presence of wave disturbances. It is known (Fossen and Strand) that in the case where disturbances were neglected the system was GAS. Basis on simulation results in presence of wave disturbances only the input-to state stability property is maintained. The system can be an alternative to using the method of control systems with PID or switching systems.

In simulation results was assumed precise knowledge of ship model parameters. But in practical solution the model has an parametric uncertainties. So the adaptive backstepping DP control law is necessary to consider. It will be disscused in the next part of research.

REFERENCES

Banka, S. and P. Dworak and M. Braasel. 2010. "On control of nonlinear dynamic mimo plants using a switchable structure of linear modal controllers. *Measurement Automation and Monitoring.* Vol. 56, No.5, 385–391.

Cao, Y. and T. Lee, D. Garrett and Chappell. 2001. "Dynamic Positioning of Drilling Vessels with A Fuzzy Logic Controller ". *Dynamic Positionig Conference*. Houston

Cao, Y. and Z. Zhou and W. Vorus. 2000. "Application of a Neural Network Predictor/Controller to Dynamic Positioning of Offshore Structures". *Dynamic Positionig Conference*. Houston.

Fossen, T.I. 2002. Marine Control Systems: Guidance, Navigation, and Control of Ships, Rigs and Underwater Vehicles. Marine Cybernetics, Trondheim.

Fossen, T.I and A. Grovlen. 1998. Nonlinear output feedback control of dynamically positioned ships using vectorial observer backstepping. *Transaction on Control System Technology,* IEEE.Vol. TCST -6, 121-128.

Fossen,T.I and J.P. Strand. 1999. "Passive Nonlinear Observer Design for ships Using Lyapunov Methods: Experimental Results with a Supply vessel". *Automatica.* Vol. 35, No.1 (Jan), 3-16.

Grimble M. and P. Fung. 1983. "Dynamic Ship Positioning Using a Self-tuning Kalman Filter". *Transaction on Automatic Control*. IEEE. Vol. AC-28, No. 3.

Grimble, M. and Y. Zhang, and M.R. Katebi. 1993. "H∞-based ship autopilot design". *Ship Control Symposium, Ottawa*, Canada, 678–683.

Krstic, M. and I. Kanellakopulos, and P.V. Kokotovic. 1995. *Nonlinear and Adaptive Control Design*. John Wiley and Sons Ltd., New York, NY.

Lindegaard, K.-P. and Fossen T.I. 2002. "Fuel efficient rudder and propeller control allocation for marine craft: Experiments with model ship". *Transactions on Control Systems Technology*. IEEE .Vol.11, No.6, 850–862.

Messer, A. and M. Grimble. 1993. "Introduction to robust shiptrack-keeping control design". *Transactions of the Institute of Measurement and Control.* Vol.15, No.3, 104–110.

Skjetne, R. 2005. The Maneuvering Problem, Ph.D. thesis, Norwegian University of Science and Technology, Trondheim.

Tomera, M. 2010. "Nonlinear controller design of a ship autopilot". *International Journal of Applied Mathematics and Computer Science.* Vol.20, No.2, 271–280.

Witkowska, A. and R. Śmierzchalski. 2012. "Designing a ship course controller by applying the adaptive backstepping method". *Int. J. Appl. Math. Comput. Sci.*, 2012, Vol. 22, No. 4, 985–997.

Xu, R.and Q.Wang and Y. Song and R. Zheng and M. Chen. 2011 "Study on Ship Dynamic Positioning System's Thruster Allocation Based on Genetic Algorithm". *International Conference on Information Science and Technology*. Nanjing, Jiangsu, China

AUTHOR BIOGRAPHIES

ANNA WITKOWSKA holds an M.Sc. in mathematics and computer science from the University of Gdansk, Poland (2001) and a Ph.D. in automatic control and robotics (2011) from the Technical University of Warsaw. Her research interests include automation, especially control of nonlinear systems such as ocean vehicles. Her e-mail address is : awitkowska@ely.pg.gda.pl

KINECT-BASED SYSTEMS FOR MARITIME OPERATION SIMULATORS?

Girts Strazdins[1], Sashidharan Komandur[1], and Arne Styve[2]
[1] Maritime Human Factors Lab, Aalesund University College, Larsgardsvegen 2, 6009 Aalesund, Norway, Email: gist@hials.no, sash.kom@hials.no
[2] Offshore Simulator Centre AS, Borgundvegen 340, 6009 Aalesund, Norway, Email: asty@offsim.no

KEYWORDS

Kinect, Natural User Interface, Maritime Operations, Simulator

ABSTRACT

Maritime operations involve complex tasks that must be taught through practical training. Using modern technologies offshore simulators can serve as realistic environment for training. The degree of immersiveness can be increased by replacing conventional input devices (keyboards, joysticks) with natural user interface (NUI) devices. This paper surveys different NUI technologies and advocates that vision-based systems, such as Microsoft Kinect, can provide gesture recognition with high fidelity. The unobtrusiveness of vision-based technologies is highly important to avoid user resistance and preserve realism of the simulation.

INTRODUCTION

Maritime field is an important part of industry, providing global supply of fish and oil. To increase safety and efficiency in offshore operations it is critical to provide training for the personnel. Modern technology offers wide range of interactive training options, and simulators are an important part of it. A significant objective of simulator designers is to create truly immersive simulation environment and realistic experience for the users, that must threat the simulation as real work instead of a simple game. One direction of realism improvement is to replace conventional keyboards and joysticks with natural user input (NUI) technologies, such as natural gesture, posture and movement recognition.

On the other hand, maritime personnel is a rather skeptic professional community, preferring well-proven methods, and criticizes new technologies thoroughly. Therefore it is important to select NUI technologies that offer advanced features while not disturbing natural environment and not requiring users to learn completely new concepts. New technology introduction in maritime field is an incremental process, an evolution, not revolution.

This paper reviews NUI technologies for offshore operation simulators intended for maritime personnel training. The main stress is on actual applicability of technologies: availability - existence of commercial hardware and software components (instead of pilot stage research studies); and unobtrusiveness - to ensure acceptance among personnel.

NUI TECHNOLOGY OVERVIEW

Natural user interface is a term used to describe technologies for human-machine interaction that are:

- fully invisible
- based on natural and widely used gestures and notions, not requiring users to learn new paradigms and concepts

Invisibility is the ideal goal of NUI, that is pursued incrementally by technological advancement. Integration of natural postures, gestures, movements and concepts into user interface assures faster technology adaptation and less resistance of the users. It allows control of machines to user groups that are neither experts in IT nor willing to become ones.

In the maritime simulator context NUI technological solutions can be divided into three classes: vision based, wearable and tangible systems.

Vision based NUI systems

Vision based NUI use external camera for graphical scene record and analysis. The camera may capture light in different spectra, including visible and infrared range. Active systems may be used, where specific patterns of light (or other type of electromagnetic waves) are transmitted into the scene and then the reflected waves are analyzed. A system is called passive, if it only records image without transmitting any waves into the scene.

Vision based NUI system advantages:

- The solution is completely unobtrusive for the users. No need to wear or hold any items, no wires, clear space of interaction.
- Users can perform the gestures exactly as they would in real life, not requiring to mimic scaled gestures (for example, performing a hand gesture with a finger). From the perspective of motion, this approach is the most "natural".
- Installation is a one time activity, if the simulation space is static. Some calibration may be required for each user, yet it can be automated.
- It is easy to switch between users interacting with the system. No need to change clothes or change on-body equipment, to test sensor alignment.
- The acquired data stream contains a lot of information - usually consisting of color and depth images, sometimes also sound.
- The intelligence of processing is offloaded to a computer, that can perform complex image processing and storage operations.
- Large existing library, framework and example code base

Proceedings 27th European Conference on Modelling and Simulation ©ECMS Webjørn Rekdalsbakken, Robin T. Bye, Houxiang Zhang (Editors)
ISBN: 978-0-9564944-6-7 / ISBN: 978-0-9564944-7-4 (CD)

can be reused and adapted for the solution. Many processing, simulation and analysis tools can be used.

Vision based NUI system drawbacks:

- There is no tactile feedback for the user, no feeling of boundaries. Visual feedback must be present for the user to understand, what part of the human body can be seen by the cameras, what is recognized, and what are the boundaries of gestures.
- Vision based systems have higher price, compared to inertial or tangible systems, as there are higher requirements for sensor quality and the included know-how has high cost. However, there are consumer level vision based NUI devices, such as Microsoft Kinect [Microsoft, 2013] or PlayStation Move [Sony, 2013] with price less than $300.
- There are lighting and clothing constraints for the systems to detect persons in the scene correctly. Mirrors or other light sources may interfere with NUI systems, and people may not be detected correctly, when they wear clothes hiding natural human silhouette.
- The interaction space is limited, depending on camera resolution. There are higher-end systems with interaction space up to 50x50 meters [WorldViz, 2013], yet consumer-grade devices have distance of interaction less than 5 meters.
- The system may not be able to detect face and body in some strange positions, for example, a person crouching.
- Image processing requires high performance computer, it is not suited for energy-efficient embedded systems.
- If acquired data is recorded for offline processing, it requires large amounts of storage space, compared to other raw signals, such as accelerometer or gyroscope data used in inertial wearable systems.

The main advantage of vision based systems is complete unobtrusiveness of the system. It allows the persons to act, as if there was no system installed. The users can move freely in the simulation space, and are not frightened by wearable devices. This aspect makes vision based systems superior compared to wearable and tangible technologies. Tangible interfaces might be a good addition to vision based and in some simulation contexts they might be preferred, for example realistic simulation of box lifting or door opening. But for gesture recognition in offshore simulators vision based systems are recommended due to their higher acceptance among simulator users. None of the vision based system constraints is critical for maritime simulator environment.

Wearable NUI systems

NUI systems are called wearable if some of the components are attached to human body. Usually wearable systems consist of multiple nodes with inertial measurement unit (IMU). These are attached to various parts of human body and sense relative movement and orientation in space of these points. More sophisticated wearable nodes may contain video capture and processing. In addition to sensing, wearable nodes can have actuators that give tactile or audio feedback to the wearer.

Examples of wearable systems include:

- Xsens MVN [Xsens, 2013] - full body, camera-less inertial motion capture solution. Consists of 17 inertial sensors, with 6 degrees of freedom, attached to users body by a lycra suit or straps. Sensors have wired connection to a central hub node that transmits data to computer wirelessly. Solution contains software toolchain for body position capture in 3D and export to popular 3D animation software, such as 3DSMax and Maya.
- CyberGlove products [CyberGlove Systems, 2013] for hand, finger and arm tracking and interaction with virtual reality. Bending, rotation and force sensors are used. CyberForce products also provide tactile feedback.

In addition to commercially available products, pilot research results have been shown, including hand tracking wristband by Microsoft research [Kim et al., 2012], that uses infrared laser, camera and IMU. Gloves and other forms of wearable devices, such as Peregrine wired glove [Peregrine, 2010] and Genius Ring mouse [Genius, 2011] are also popular as replacements for conventional keyboard and mouse (not actually NUI devices).

Wearable NUI system advantages:

- Wearable systems usually have lower price, compared to vision based systems, as the hardware is simpler, including sensors. However, if multiple nodes are required to track the whole human body, the price may increase.
- Inertial sensors may achieve higher accuracy, compared to vision based systems, especially for hand and finger tracking.
- Sensor nodes can be implemented, using low-power microcontrollers and sensors, therefore no large batteries or mains power is required.
- The installation requirements are transferred from environment to users - wearable systems can function in virtually any environment without re-installation.
- No strict requirements for the environment: indoors, outdoors, virtually any environment is acceptable. An exception: magnetometer sensors may not function correctly in presence of large metallic objects or strong magnetic fields. No strict requirement for user clothing and accessories.
- In addition to sensing, feedback can be given to users, including tactile signals.

Wearable NUI system drawbacks:

- More complex and time consuming to change system users.
- May disturb the activities of users and introduce psychological resistance against the technology.
- Nodes use either wires that are cumbersome, or wireless transmission that limits data transmission bandwidth.
- In most cases only a part of the body is tracked, for example, human hands.
- Devices that must be moved and changed from person to person tend to brake more often and have a shorter life cycle.
- Wearable devices may have problems with wide variance of user height, weight and girt.

Tangible NUI systems

NUI system is called tangible if users interact with digital environment using physical objects.

One tangible NUI examples is Nintento Wii Remote (Wiimote) - the controller for Nintendo Wii gaming console [Nintendo, 2013]. It has a 3-axis accelerometer and an optical sensor, used to detect device location relative to the consoles Sensor Bar, which is places above or below TV

and transmits infrared light in predefined pattern. Wii Remote can be used as pointing device as well as a tool for hand gesture detection (without finger separation). An additional module, called Wii MotionPlus, can be plugged in the Wii Remote to increase tracking accuracy by adding gyroscope sensors.

Tangible NUI system advantages:

- Physical objects are not worn or attached to human body, rather simply touched, grasped and carried. This leads to simpler setup and switching between users.
- Interaction between objects is more natural and intuitive.
- More realistic sensory feedback, compared to vision based systems.

The main drawback of tangible NUI systems: basically interaction with hands only, no ability to capture position of the whole skeleton.

Hybrid systems

Vision can be merged with wearable or tangible approaches to increase accuracy. Examples:

- PlayStation Eye Move [Sony, 2013] mixes vision technology by PlayStation Eye camera and wand with inertial sensors (3-axis accelerometer, 3-axis angular rate sensor, magnetometer) and a sphere illuminated with visible light of specific spectra acting as a marker tracked by PlayStation Eye camera.
- Microsoft wearable hand tracking wristband [Kim et al., 2012], that uses infrared laser and camera, worn around persons wrist to detect finger gestures.
- A prototype glove, uses specific color segmentation and video processing for hand tracking [Wang and Popović, 2009].
- WorldViz PPT - long range, high quality cameras, used to recognize and track specific markers, attached to objects [WorldViz, 2013].

Hybrid systems may combine the advantages of multiple technologies. However, hybrid approach may also have a mixture of constraints imposed by all the used technologies. For example, wearable and vision based approach combination may increase accuracy, while requiring users to wear some objects and setting limitations on room lighting and person clothing.

MICROSOFT KINECT

Kinect is a motion sensing device by Microsoft, that was released on November 2010 for the XBox 360 video game console. It is a vision-based motion and gesture recognition system that uses infrared active scanning technology to detect distance to players and objects in the field of view. The technology was widely accepted in the gamer community and Kinect sensor holds the Guiness World Record of being the "fastest selling gaming peripheral" - 8 million units sold in the first 60 days [Guinness World Records, 2011]. Shortly after the release of Kinect for XBox, open source community created a Linux driver for the device, and *hacking Kinect* became popular [Xia et al., 2011], [Frati and Prattichizzo, 2011] . Microsoft realized the potential of the technology beyond gaming and released official development kit in February 2011, containing a software development kit (SDK) and also a sensor device, called "Kinect for Windows", optimized to be used with PC computers and Windows 7 environment. Numerous interesting Kinect applications have been demonstrated, including virtual dressing room [Zhou et al., 2012], room scanner [Manctl, 2013] and virtual furniture fitting [NCONNEX, 2012].

Technolgy and hardware

Kinect sensor provides the following raw data:

- Depth image stream, resolution 640x480 pixels, 30 frames/sec. Distances from 1.2m up to 3.5m are suggested, while theoretically distances from 0.8m to 4.0m are available. Near mode tracking is also available, where person tracking in distances from 0.4m is available (different tracking technology is used, with lower accuracy). Depth map is calculated using active infrared scanning. Infrared light is transmitted in a predefined pattern in the space and time of flight of light waves is calculated by infrared camera.
- Color image stream, resolution 680x480 at 30 frames/sec or 1280x960 pixel resolution at 12 frames/sec. Different image formats are available: RGB, YUV or Bayer. Color camera sensor is used to capture image stream.
- Audio stream, captured by a four-element linear microphone array.
- Sensor orientation relative to the ground, captured from 3D accelerometer sensor.

In addition, Kinect tilt can be detected and adjusted in 54 degree range by sending commands to the built-in motor.

Software and preprocessed data

Microsoft Kinect is not only accurately selected hardware components. The true power lies in the SDK containing data preprocessing algorithms that incorporate knowledge and results of extensive research work [Shotton et al., 2013].

The official Kinect SDK by Microsoft allows development of Kinect-enabled applications for Windows, using Visual Studio and .Net environment, in either C#, C++ or Visual Basic. The SDK contains simple yet rich API. In addition, Microsoft provides well organized documentation and developer toolkit, containing extensible application examples. Drivers for the Kinect sensor are also included.

The Kinect SDK can detect up to 6 people from the depth images, and skeleton joint positions can be tracked for up to 2 from them. All the image processing is done by the Kinect SDK. Joint positions in 3D space relative to Kinect sensor position are exposed.

The SDK can record audio signal from the microphone array. In addition, it can detect direction of the audio source and filter background noise.

Each new version of the SDK adds new feature support, such as relative bone rotations, seated mode (only upper part of human body visible), improved image quality and performance.

Additional features can be used by bridging Kinect with other Microsoft SDKs:

- Speech recognition by using Microsoft SDK and Kinect for Windows Language packs. A total of 12 languages are supported at the moment (Language pack v11.0).
- Face recognition and tracking by using Microsoft Face Tracking SDK (included in Kinect SDK since v1.5)

Third party drivers and SDKs

In addition to official Microsoft SDK, third party drivers and software libraries have been developed by open source communities:

- OpenKinect [OpenKinect, 2012] - open source Kinect libraries, C language. Provides only basic access to raw data streams, no player detection or skeleton tracking available. Its usability for gesture recognition is limited, as player joint tracking implementation is a rather complex task. OpenKinect can be used in computer vision research projects, where custom detection and tracking algorithms must be evaluated.
- OpenNI framework - an open source SDK used for the development of 3D sensing middleware libraries and applications [PrimeSense, 2013c], originally in C++ language, yet wrappers to other languages are available, including Java and Python. The community promotes interoperability between different NUI devices by creating multi-layer framework, that abstracts hardware and provides unified interface for higher level middleware, such as PrimeSense NITE [PrimeSense, 2013b] - a computer vision framework, implementing skeleton tracking, hand tracking and gesture detection algorithms.

In contrast to Microsoft SDK, these open source solutions are designed to be platform independent: Windows, Linux, MacOS. OpenNI is even device-independent. OpenKinect and OpenNI have open source (NITE middleware is not), however, the generality of OpenNI framework in first versions (v1.x) makes its source code and documentation hard to understand. New version of OpenNI (v2.x) has been recently released (December 18th, 2012). It has been rewritten from scratch, with simplified API. While it lacks some of the later features (no Java and Python wrappers are available at the moment), the OpenNI seems to be a promising alternative in future.

Both open source solutions support Kinect for XBox and are having issues with support of Kinect for Windows device. There are bridging solutions available which use official Microsoft Kinect drivers and SDK, and implementing a hardware abstraction layer for OpenNI [Washio, 2012].

Author experience shows, that the existing versions of open source solutions are unstable for Kinect for Windows device. The situation may change in coming years, if the communities put enough effort to develop the OpenNI framework, yet at the moment official Microsoft SDK is significantly more stable, easier to use and understand and should be preferred for NUI applications.

Kinect in Java

One of the most popular programming languages is Java. However, official SDK supports only .Net environment and development in Microsoft Visual Studio. The most convenient approach for Kinect programming in Microsoft SDK is to use C# language, as it has a high-level API with simple workflow. However, wrapping C# to Java is not directly possible.

Multiple alternatives do exist to provide access to Kinect for Java programmers:

- Manually create a two-layer C# to Java wrapper, using procedural C as an intermediate layer. Java Native Access (JNA) [JNA, 2013] or Java Native Interface (JNI) [Oracle, 2011] can be used for wrapping. Official SDK also provides C++ interface. Wrapping is a bit easier in this case, yet it adds complexity of handling garbage collection manually.
- Use automated C# to Java wrapping solutions, such as JNBridge Pro [JNBridge LLC, 2013]. Java interface is created from a .Net DLL automatically. Yet some specifics of data passing between .Net and Java have to be considered to get maximum performance. And some of the tools may require purchase of a license.
- Create your own forwarder of Kinect data streams, approach used in JNect - an Eclipse plugin for Kinect [Aumann, 2012].
- Java bindings are supported in OpenNI v1.x framework, and can be used, if the OpenNI framework is suitable for a particular application. OpenNI version 2.0 does not have Java bindings, yet the implementation should come in near future.

Advantages

There are several advantages of using Kinect as NUI technology in maritime operation simulators:

- Unobtrusiveness. This is the most important advantage: the technology is fully unobtrusive from user perspective - no additional devices, joysticks, sensors, or markers are required to be held or worn by the users to be recognized.
- Accuracy. Research studies show, Kinect provides accuracy with error below 4cm [Khoshelham and Elberink, 2012]. While there may be difficulties of distinguishing finger gestures in larger distances, this accuracy is more than satisfactory for skeleton tracking needs. In addition, Kinect does not have error accumulation effect that is present for inertial systems.
- High value know-how. Extensive image processing research work has been done to create raw data preprocessing in the SDK and provide high level skeleton tracking API [Kohli and Shotton, 2013].
- Simplicity. Easy to use API is provided, supplemented by rich example set and documentation.
- Rich sensor set. The device contains sensors and provides data streams that can be useful in a variety of scenarios: depth map, color video stream, audio capture, gravity and tilt sensing.
- Integration. Kinect SDK integrates with speech recognition and face detection SDKs by Microsoft.

Constraints

To use Kinect technology, developers must take the following constraints into account:

- Clear space is required, where players are distinguishable from the room.
- While Kinect is able to work in full darkness, direct sunlight or other bright lightning conditions are not desired.
- Player clothing should not be reflective or hiding the human silhouette. Specialized costumes, such as used by clowns or cheerleaders may interfere with skeleton tracking.
- The range or operation is limited to a small room - distance range 0.4-3.5 meters, and only a couple of meters in horizontal and vertical directions, depending on the distance to Kinect.

• Kinect may have problems in environments, where other infrared light sources are present. The same applies to using multiple Kinect devices simultaneously.
• The official Microsoft SDK supports Visual Studio and .Net on Windows only. Open source alternatives, with their advantages and drawbacks, were mentioned above.

Unintended gesture avoidance

One issue to solve for Kinect application in maritime operation simulators is false gesture rejection. The operator performs series of other actions during training in addition to hand signals. In his book David Catuhe suggests to use the following methods to separate between hand signal and ambient motion contexts [Catuhe, 2012]:

• The user is ready to give hand signals when the body is in a stable position. It can be detected by comparing recent positions of one or several joints of the skeleton, for example, hip center.
• The user should be facing the sensor. It can be detected by comparing distance of both shoulders to Kinect or detecting orientation of the head, using Microsoft Face Tracking SDK (included in Kinect SDK since v1.5)

KINECT EXTENSIONS

Kinect technology can be extended to get improved accuracy, additional features or better user experience. Examples of extensions include:

• Using multiple Kinect sensors to track human body in full 360 degree range. While a single Kinect is only able to analyze the surface in front of the sensor, multiple devices can be places in different angles and may capture the whole body, even when the person has turned back or side to the first Kinect. Examples include iPi Soft[iPi Soft, 2013] - a software to capture 3D video, using two Microsoft Kinect, Sony PlayStation Eye [Sony, 2013] or Asus Xtion Pro [ASUS, 2013] camera sensors.
• Omni direction treadmill floor - to allow movement of the character while keeping the person in place [Inition, 2013].
• Microsoft Kinect official SDK provides skeleton tracking, without hand and finger separation. Hand tracking can be added by using third party software, such as NITE middleware [PrimeSense, 2013b] or SigmaNIL framework [SigmaNIL, 2012]. In short range interfacing, devices, such as Leap Motion [Leap Motion, 2013], can be used for finger separation in gestures.

KINECT ALTERNATIVES

Kinect is only one of 3D user tracking devices. It includes hardware developed by PrimeSense company. The same hardware is included in Asus Xtion Pro Live [ASUS, 2013] and PrimeSense Carmine [PrimeSense, 2013a] 3D depth sensors. All the devices with PrimeSense hardware are supported by OpenNI open-source NUI framework [PrimeSense, 2013c] and NITE middleware [PrimeSense, 2013b]. On one hand, OpenNI offers platform-independency and source open for extension. On the other hand, as experience of our research group shows, OpenNI is unstable for *Kinect for Windows* sensor device. Unstable operation was encountered on Windows 7, as well as on Mac OSX 10.7 Lion operating systems. Although it may change in near future, the existing version of official Microsoft SDK (v1.6, October 2012) is more stable compared to current OpenNI framework versions (v2.0 and v1.5.4.0).

A 3D user tracking device, without PrimeSense hardware, is provided by Panasonic: D-Imager (EKL3105) [Panasonic, 2012]. Panasonic promises ranges up to 9m, 4cm accuracy, and provides software for depth map extraction only, no skeletal tracking. Theoretically it can be used with OpenNI, a third party developer driver with unknown state is available [danielpq, 2012].

Assuming the stability of drivers and skeleton tracking routines, authors suggest to choose Kinect for Windows device with official Microsoft SDK. Microsoft Research team at Cambridge has made a great effort to incorporate accurate and fast state-of-art pose detection algorithms in the Kinect sensor [Shotton et al., 2013]. Alternative solutions may become more rich and stable in the future, but are incomplete at the moment.

DISCUSSION

Maritime operation training is a simulator use case, that poses specific requirements on the technology and environment. The trainees are adults from the maritime field. As opposed to teenage or preschool children, these are mature people that prefer training atmosphere to maintain a certain level of seriousness. While some entertainment and gaming aspects may seem attractive in public demonstrations, is not particularly welcome in real training sessions. Advanced technologies, that might increase engagement in youth and video game fans in particular, may interfere with trainee experience and decrease the degree of immersiveness. Thus, the technologies must be selected carefully to ensure maximum realism, that lets the users perceive the simulation as a reality and feel the same level of responsibility while performing the operations.

In 2005, Offshore Simulator Centre was performing pilot studies on using a virtual reality helmet (head-mounted display) in the training simulation. The technology was discarded for two basic reasons: the quality of visuals was too low to provide realistic interface; and the users did not accept devices that interfere with their natural movements.

While the former argument might be outdated today, the latter still applies: adult simulator users, and maritime operation experts in particular, are resistant to wearable technologies. Traditional tools are preferred as much as possible, and any *high-tech* device makes the maritime experts feel as fictional movie characters, and it certainly is against the basic principle of simulators - to provide realistic experience.

Existing offshore operation simulator confirm the preference of using vision based NUI technologies:

• Kongsberg Offshore Vessel Simulator for Seismic Streamer Operations Training - uses Kinect for avatar movement control [Kongsberg Maritime, 2012].
• Maersk Offshore Helicopter Landing Officer (HLO) training simulator incorporates experimental use of Kinect for item selection in the graphical user interface and gesture recognition for helicopter landing operations as part of offshore operations [Maersk Training, 2011].

To conclude the discussion - the unobtrusiveness of NUI technologies is very important to provide realistic simulation environment that is treated as a serious real-life experience by the users in operation.

FUTURE WORK

Our existing research is focused on incorporating NUI technologies for more natural and immersive user experience in maritime operation simulators. A gesture recognition framework is being developed, targeted primarily for crane operator training. Objective gesture recognition accuracy evaluation and subjective training experience improvement assessment is planned as part of future work.

CONCLUSION

This paper analyzes natural user interface technology applicability to maritime operation simulators. The Microsoft Kinect vision-based 3D user skeleton tracking system is suggested as optimal commercial solution currently available. The preference is substantiated by providing arguments from maritime training experts who advocate on the superiority of fully unobtrusive technologies that are required to maintain the realism of immersive simulations.

ACKNOWLEDGMENT

The authors would like to thank Qi Xu for contribution to NUI device survey, Robert Rylander and Hans Petter Hildre for providing feedback and access to expert knowledge in maritime operation training.

This study is supported by Norwegian Research Council (NFR) Grant in Marine Technology, Nr. 210797.(2011-2013).

REFERENCES

[ASUS, 2013] ASUS (2013). Xtion PRO LIVE. Available from: http://www.asus.com/Multimedia/Xtion_PRO_LIVE [cited 2013-04-05].

[Aumann, 2012] Aumann, A. (2012). jnect: An Eclipse Plug-In providing a Java Adapter for the Microsoft Kinect SDK. Available from: http://code.google.com/a/eclipselabs.org/p/jnect/ [cited 2013-04-05].

[Catuhe, 2012] Catuhe, D. (2012). *Programming with the Kinect for Windows Software Development Kit*. Microsoft Press.

[CyberGlove Systems, 2013] CyberGlove Systems (2013). CyberGlove III. Available from: http://www.cyberglovesystems.com/products/cyberglove-III/overview [cited 2013-04-05].

[danielpq, 2012] danielpq (2012). OpenNI Module to TOF Panasonic DImager camera. Available from: http://opennidimagermodule.codeplex.com/ [cited 2013-04-05].

[Frati and Prattichizzo, 2011] Frati, V. and Prattichizzo, D. (2011). Using kinect for hand tracking and rendering in wearable haptics. In *IEEE World Haptics Conference (WHC)*, pages 317–321. IEEE.

[Genius, 2011] Genius (2011). Ring mouse 2. Available from: http://www.geniusnet.com/wSite/ct?xItem=56975ctNode=3619mp=1 [cited 2013-04-05].

[Guinness World Records, 2011] Guinness World Records (2011). Kinect for XBox 360: Fastest-Selling Gaming Peripheral. Available from: http://www.guinnessworldrecords.com/world-records/9000/fastest-selling-gaming-peripheral [cited 2013-04-05].

[Inition, 2013] Inition (2013). MSE Omni-directional Floor. Available from: http://inition.com/3D-Technologies/mse-omni-directional-floor [cited 2013-04-05].

[iPi Soft, 2013] iPi Soft (2013). Motion Capture for The Masses. Available from: http://www.ipisoft.com/ [cited 2013-04-05].

[JNA, 2013] JNA (2013). Java Native Access (JNA). Available from: https://github.com/twall/jna [cited 2013-04-05].

[JNBridge LLC, 2013] JNBridge LLC (2013). JNBridge Pro. Available from: http://www.jnbridge.com/ [cited 2013-04-05].

[Khoshelham and Elberink, 2012] Khoshelham, K. and Elberink, S. O. (2012). Accuracy and resolution of kinect depth data for indoor mapping applications. *Sensors*, 12(2):1437–1454. Available from: http://www.mdpi.com/1424-8220/12/2/1437 [cited 2013-04-05].

[Kim et al., 2012] Kim, D., Hilliges, O., Izadi, S., Butler, A., Chen, J., Oikonomidis, I., and Olivier, P. (2012). Digits: freehand 3D interactions anywhere using a wrist-worn gloveless sensor. In *Proceedings of the 25th annual ACM symposium on User interface software and technology*, pages 167–176. ACM.

[Kohli and Shotton, 2013] Kohli, P. and Shotton, J. (2013). Key developments in human pose estimation for kinect. In Fossati, A., Gall, J., Grabner, H., Ren, X., and Konolige, K., editors, *Consumer Depth Cameras for Computer Vision*, Advances in Computer Vision and Pattern Recognition, pages 63–70. Springer London.

[Kongsberg Maritime, 2012] Kongsberg Maritime (2012). Kinect for Windows integrated with KONGSBERG Offshore Vessel Simulator for Seismic Streamer Operations Training. Available from: http://goo.gl/bjYdp [cited 2013-04-05].

[Leap Motion, 2013] Leap Motion (2013). Individual Hand And Finger Gesture Detection Device. Available from: https://www.leapmotion.com [cited 2013-04-05].

[Maersk Training, 2011] Maersk Training (2011). User Guide HLO Simulator. Available from: http://offshoresimulator.com/hlo_guide.pdf [cited 2013-04-05].

[Manctl, 2013] Manctl (2013). Skanect: 3D Scaning Made Easy. Available from: http://skanect.manctl.com/ [cited 2013-04-05].

[Microsoft, 2013] Microsoft (2013). Kinect for Windows. Available from: http://www.microsoft.com/en-us/kinectforwindows/ [cited 2013-04-05].

[NCONNEX, 2012] NCONNEX (2012). Room Designer. Available from: http://nconnex.com/portfolio/room-designer/ [cited 2013-04-05].

[Nintendo, 2013] Nintendo (2013). Wii gaming console. Available from: http://www.nintendo.com/wii [cited 2013-04-05].

[OpenKinect, 2012] OpenKinect (2012). OpenKinect Project. Available from: http://openkinect.org [cited 2013-04-05].

[Oracle, 2011] Oracle (2011). Java Native Interface (JNI). Available from: http://docs.oracle.com/javase/6/docs/technotes/guides/jni/ [cited 2013-04-05].

[Panasonic, 2012] Panasonic (2012). D-Imager EKL 3105. Available from: http://www2.panasonic.biz/es/densetsu/device/3DImageSensor/en/ [cited 2013-04-05].

[Peregrine, 2010] Peregrine (2010). Gaming glove. Available from: http://www.theperegrine.com/ [cited 2013-04-05].

[PrimeSense, 2013a] PrimeSense (2013a). Carmine 3d sensor. Available from: http://www.primesense.com/solutions/sensor/ [cited 2013-04-05].

[PrimeSense, 2013b] PrimeSense (2013b). NITE Middleware. Available from: http://www.primesense.com/solutions/nite-middleware/ [cited 2013-04-05].

[PrimeSense, 2013c] PrimeSense (2013c). OpenNI: The standard framework for 3D sensing. Available from: http://www.openni.org/ [cited 2013-04-05].

[Shotton et al., 2013] Shotton, J., Sharp, T., Kipman, A., Fitzgibbon, A., Finocchio, M., Blake, A., Cook, M., and Moore, R. (2013). Real-time human pose recognition in parts from single depth images. *Commun. ACM*, 56(1):116–124. Available from: http://doi.acm.org/10.1145/2398356.2398381 [cited 2013-04-05].

[SigmaNIL, 2012] SigmaNIL (2012). Vision Framework for Natural User Interfaces. Available from: http://www.sigmanil.com/ [cited 2013-04-05].

[Sony, 2013] Sony (2013). PlayStation Move. Available from: http://us.playstation.com/ps3/playstation-move/ [cited 2013-04-05].

[Wang and Popović, 2009] Wang, R. and Popović, J. (2009). Real-time hand-tracking with a color glove. In *ACM Transactions on Graphics (TOG)*, volume 28, page 63. ACM.

[Washio, 2012] Washio, T. (2012). kinect-mssdk-openni-bridge. Available from: http://code.google.com/p/kinect-mssdk-openni-bridge/ [cited 2013-04-05].

[WorldViz, 2013] WorldViz (2013). PPT - Precision Position Tracker. Available from: http://www.worldviz.com/products/ppt [cited 2013-04-05].

[Xia et al., 2011] Xia, L., Chen, C., and Aggarwal, J. (2011). Human detection using depth information by kinect. In *Computer Vision and Pattern Recognition Workshops (CVPRW), 2011 IEEE Computer Society Conference on*, pages 15–22. IEEE.

[Xsens, 2013] Xsens (2013). MVN - Inertial Motion Capture. Available from: http://www.xsens.com/en/general/mvn [cited 2013-04-05].

[Zhou et al., 2012] Zhou, Z., Shu, B., Zhuo, S., Deng, X., Tan, P., and Lin, S. (2012). Image-based clothes animation for virtual fitting. In *SIGGRAPH Asia 2012 Technical Briefs*, page 33. ACM.

AUTHOR BIOGRAPHIES

GIRTS STRAZDINS obtained his masters degree in computer science from University of Latvia in 2008. He worked as a wireless sensor network researcher at the Institute of Electronics and Computer Science (EDI), Riga, Latvia, from 2010 to 2012, when he moved to Aalesund and joined Maritime Human Factors Lab at the Aalesund University College. He is currently working in research related to natural user interface and gesture incorporation in offshore simulators.

SASHIDHARAN KOMANDUR was born in India, obtained his bachelor's degree in naval architecture & ocean engineering from IIT-Madras, masters degree in ocean engineering from University of California Berkeley and Ph.D. in industrial engineering from the University of Washington-Seattle. He is leading a research group in field of human factors in marine operations at Aalesund University College. He is also the Global maritime knowledge hub (GMKH-Norway) chair for Human factors in marine operations. His main work revolves around understanding human factor issues that exist in the ship bridge environment of modern ships.

ARNE STYVE was born in Bergen, Norway and went to the University of Newcastle upon Tyne where he studied Microelectronics and Software Engineering and obtained his B.Eng w/Hons degree in 1991. He worked for a few years in Siemens Defense Industries (later Thales) in Oslo, where he was project manager and principal engineer developing solutions for the Norwegian Army. In 1999 he moved to Aalesund and worked as an Assistant Professor at Aalesund University College teaching Object Oriented SW Development. In 2005 he joined the project that later became the Offshore Simulator Centre AS (OSC AS), a company developing advanced offshore simulators for team based training of critical offshore operations. He is currently the manager of the R&D department.

TOWARDS A DESIGN SIMULATOR FOR OFFSHORE SHIP BRIDGES

Helge T. Kristiansen
Faculty of Engineering and Natural Sciences
Aalesund University College
N-6025, Aalesund, Norway
E-mail: hkr@hials.no

Kjetil Nordby
Institute of Design
The Oslo School of Architecture and Design
N-0130, Oslo, Norway

KEYWORDS

Conceptual design, Simulation, Simulators, Prototyping, Design simulator, Fuzzy front-end.

ABSTRACT

The development of new design concepts for ship bridges on modern offshore vessels is a considerable challenge for engineering and design professions. Such ships perform advanced missions in extreme environmental conditions that are very different to those in which most design processes take place. Although site visits can help narrow this gap, such opportunities are limited by both funding and access constraints. We suggest the use of design simulators as tools for conceptual design, mediating collaboration between various disciplines and users. This paper reports on work in progress, in which we analyse and explore possibilities and challenges regarding the use of a simulator for the design of ship bridges, comparing the nature of conceptual design with the current use and capabilities of existing maritime simulators. Through this analysis, we suggest there is potential for combining training simulators with tools and techniques from conceptual design processes in ship bridge design. We also discuss some challenges regarding the effective use of simulators as a design tool.

INTRODUCTION

The maritime industry of Sunnmøre, Norway, has a long tradition of building specialized vessels for operations such as platform supply, anchor handling, and sub- sea field-interventions. The region has a cluster of companies that develop solutions for the demanding needs of the oil industry. Due to continuous introduction of new technologies on offshore ship bridges, these working environments are increasing in complexity. This imposes additional mental burden—and requires greater competence—among crew members (Petersen and Lützhöft 2009).

Recent attention to the complexity of work environments has led to greater use of industrial- and interaction designers in bridge design processes. These fields focus on the design of user-centred products and systems by applying tools and techniques to explore and resolve complex design problems (Lawson 2006). These fields place great emphasis on the early stages of the design phase, during which major changes are made.

A ship bridge is a complex workplace that is both very different from the context of design processes and difficult to access. This is a challenge within conceptually-oriented design processes that require access to user context while also maintaining rapid development of new design concepts. In this article, we present work in progress that investigates how simulators can better support early-phase design of modern ship bridges. The work draws on experiences in managing a conceptual design process within the on-going research project Ulstein Bridge Concept (UBC). UBC is oriented towards developing next-generation ship bridges, and is a collaboration between The Oslo School of Architecture and Design (AHO), Aalesund University College, Ulstein Power & Control (UPC), and Kwant Controls.

The project currently employs two design labs at AHO and UPC. The UPC lab at Aalesund has installed a simulator from Offshore Simulator Centre AS (OSC, www.offsim.no), while the Oslo lab connects remotely to the simulator. The project has also used simpler, game-based simulators (Ship Simulator Extremes 2010, Shipsim.com) as part of the process.

In the following sections, we outline some basic characteristics of traditional ship simulators before describing conceptual design with an emphasis on goals, methods, and tools. Further, we compare conceptual design and the capabilities of existing simulators. Based on the comparison, we suggest future developments that might enhance the use of simulators as tools in early-phase conceptual design.

SHIP BRIDGE SIMULATORS IN DESIGN

Conceptual design is an important but challenging part of design processes, which is oriented towards driving innovation in the maritime sector. This is particularly important, since it is difficult to envision proposed ideas in the context of the full complexity of an operational ship bridge. We suggest this problem might be approached through increasing use of ship simulators in early-phase conceptual design.

Currently, most simulators are used for educational purposes, performance evaluation, and research in various domains. Applications range from training simulators in aviation (Page 2000), medical (Rosen

Proceedings 27th European Conference on Modelling and Simulation ©ECMS Webjørn Rekdalsbakken, Robin T. Bye, Houxiang Zhang (Editors)
ISBN: 978-0-9564944-6-7 / ISBN: 978-0-9564944-7-4 (CD)

2008), and maritime (Saus et al. 2012) domains, to studying human factors in the nuclear industry (Skjerve and Bye 2011). In recent years, advances in the computer-gaming industry have also initiated the concept of "serious games" for training in areas such as military, government, or education (Susi et al. 2007).

Although widely used in industry and research, the use of simulators in conceptual processes has only been partly explored. Most car manufactures use vehicle simulators as part of product conception (Kallmann et al. 2003), but there is limited published research literature on such work. Vestfold University College explored how 3D visualization in an immersive visualization theatre may engage users as co-designers in the fuzzy front-end of product development (Hjelseth 2011). Others are investigating virtual reality, gaming, and scenarios to express lifelike interaction with a computer model, such as during product design (Tideman et al. 2008).

Ship simulators, such as those in Aalesund (Figure 1) are used to train both individuals and teams of maritime personnel. Their core function is to mirror something real, like the offshore bridge, or the crane on an oilrig. The developers of the simulator attempt to provide a next-to-real experience of this maritime domain, and strive to bring context to the user experience. They construct realistic scenarios together with domain specialists, which give the simulation natural behaviours.

Figure 1 – The bridge in an offshore simulator, source: Offshore Simulator Centre AS (OSC)

The simulators in Aalesund also target complex and challenging offshore operations like anchor handling or subsea lifting operations. This is achieved via three main components 1. A simulator model representing the dynamic properties of, e.g., a ship and its attaching systems; 2. A visual system that provides the contextual experience; and 3. The physical space, within which appropriate input and output devices are available. Several such stations are interconnected in order to provide team training among various operators.

Recent advances in technology and 3D capabilities have made high quality synthetic environments inexpensive, and simulators can today convey immersive experiences (Kincaid and Westerlund 2009).

When training crew members, it is essential to provide the participants with a realistic experience. These immersive capabilities and realistic behaviours are central to how the simulator becomes a natural arena for the participants to act out their normal (work) behaviours.

The following summarizes the characteristics of the Aalesund simulators:

- A realistic work setting.
- Simulator models of various artefacts (e.g., a ship, a cable, or a crane) and their associated systems and surroundings.
- Visual systems that can provide an immersive experience.
- A physical space in which appropriate input and output devices are available for real-time interaction with the simulator models.
- Scenarios of complex maritime operations.
- Networking capability for team training in complex offshore operations.
- Video recording equipment for work analysis.

Although such a system can be used to present finalised designs, it is not necessarily the best setup in which to evaluate conceptual designs. To understand the gap between design and simulators, we need to unpack conceptual design.

CONCEPTUAL DESIGN IN SHORT

Conceptual design is a crucial part of design processes for most professions; however, in this article, we address the conceptual processes of industrial and interaction design. These design disciplines have a long tradition focusing on creative development oriented towards cultural and functional needs (Lawson 2006; Lawson and Dorst 2009).

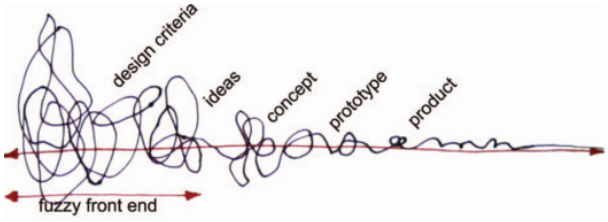

Figure 2 - A simple representation of the present-day design process, Source: Sanders and Stappers (2008)

Conceptual design is an iterative approach used in the early phases of the design process, when the problem is difficult to grasp due to its complexity and conflicting goals. This is also referred to as ill-structured or wicked problems (Rittel and Webber 1973). This is the fuzzy front-end of innovation (Figure 2)—a phase where many activities take place in order to inform and inspire discussions around open-ended questions that serve the ambiguous and chaotic nature of the design problem (Sanders and Stappers 2008). Ulrich (2011) states that exploration of design ideas and concepts is a fundamental activity during this phase. As he sees it,

good designers tend to build, test, and refine artefacts during this process, rather than refining a perfect theoretical plan.

Designers, as those trained in the traditions of industrial design or interaction design, are often said to apply "design thinking" (Rowe 1987), and to have a reasoning of design that is more disorderly compared to their counterparts in design engineering (Rittel 1987). Here, design engineering is understood as design with particular emphasis on the technical aspects of a product (Robinson 2012).

Rittel claims that "learning what the problem 'is' IS the problem" (Rittel 1987: p 2). He suggests that there is no clear separation between the activities of problem definition, synthesis, and evaluation (Rittel 1987). Further, he argues that this reasoning can be seen as a process of argumentation with the designer himself or with others; and in this process, Schön argues, the designer externalizes design ideas via tools such as sketching, mock-ups or prototyping (Schön 1991).

In the next section, we will investigate this difference further by examining the goals of conceptual design processes.

CHALLENGES IN CONCEPTUAL DESIGNING OF SHIP BRIDGES

The messy process of conceptual design is very different to the present applications of maritime simulators. Traditional simulators represent stable bridge designs that can be used by the crew memebers. However, in conceptual processes, the main focus would be to change any aspect of the ship bridge, as necessary, and in response to user feedback. The difference between the two approaches to simulator technologies are here summarized via the two main goals of conceptual design processes that can be supported by simulator technology.

Understanding current and future user needs and desires

The fundamental aspect of design is domain understanding, which has led to the need to connect with users, observing and interviewing them (Ulrich 2011). In recent decades, designers have increasingly moved closer to potential users in order to better understand what they need or desire (Sanders and Stappers 2008; Nelson and Stolterman 2012). This approach aims to involve stakeholders in the development of design concepts in order to improve the quality of future design solutions. This overall trend is termed human-centred design; it incorporates the area of participatory design that originated in Scandinavia during the 1970s (Bødker et al. 2000), and which involves bringing the user closer to the design process as a co-designer or co-creator early in the design process (Sanders and Stappers 2008).

Undertaking a human-centred design process of ship bridges is challenging, due to the complex nature of the bridge environment. An offshore bridge consists of numerous technical systems that are developed by different sub-suppliers to support the mariners' work in challenging operations. However, for a user, the bridge is a single, integrated unit in which all the designed artefacts are just part of a total work environment. It is difficult to adopt this holistic view when designing ship bridges because the target environment is very different to the context of the design team on land.

Experience of the target environment is important in order to provide an interdisciplinary design team with mutual understanding and first-hand appreciation of existing and future conditions (Buchenau and Suri 2000); "the experience of even simple artifacts does not exist in a vacuum but, rather, in dynamic relationship with other people, places and objects" (Buchenau and Suri 2000: p 424).

Figure 3 - The design lab in Oslo connected to a ship simulator, source: Ulstein Bridge Concept

A simulator may help overcome these challenges by making a dynamic representation of a ship bridge available to the land-based design office. As an early test, we have made this connection between the physical design lab in Oslo and a ship simulator (Figure 3).

Address complexity by exploring design ideas

As stated by Ulrich (2011), design requires exploration, and exploration inevitably involves recourse to develop and evaluate alternatives that will eventually be abandoned. This exploration, he argues, almost never results in a single plan, but rather exposes several alternatives that merit serious consideration. During design synthesis, designers make explicit this normally implicit process of understanding and framing (Kolko 2010). Kolko explains this as a process of manipulation, organizing, pruning, and filtering of data in an effort to produce information and knowledge of the design problem.

Externalization of design ideas is crucial in this process in order to reflect on and evaluate their potential possibilities and limitations (Schön 1991). The goal is to investigate many ideas and very different ideas, that are generated by externalizing potential solutions to form different views of the understood problem (Ulrich 2011).

Early testing and evaluation of design ideas then becomes central to conceptual design in order to handle the design complexity in the fuzzy front-end. A connection between conceptual design tools and simulator permits these early design ideas to be easily explored and evaluated in-context. This requires a means of easily connecting input/output signals between the simulator and different externalized versions of design concepts (ranging from low-fi mock-ups to more refined prototypes of physical devices), or interaction design.

Given this connection between the simulator and design artefacts, physical mock-ups, prototypes, and screen layouts can be investigated in-context on a simulated ship bridge without actually being there. Technical advances now permit this design exploration to take place at the premises of the ship simulator itself (the offshore simulator in Aalesund), in the design lab (UBC lab in Oslo), or even at the design office where the individual designers do their everyday work.

DESIGN METHODS IN SIMULATORS

Conceptual design processes may also be characterised by the methods and tools used. Tools and techniques such as sketches, mock-ups, and prototypes are indispensable in generating a wide array of ideas for further selection.

Sketching and mock-ups

Schön describes the use of design tools as the way in which the designer has a “conversation” or dialog with a sketch. When the design ideas are externalized, the world can “speak back” to us (Schön 1991). Learning from these tools of externalization is also based on their ambiguous nature of representation, encouraging various interpretations without specifying everything; inviting suggestions, criticisms, and changes (Buxton 2007).

Here, sketching is the archetypal activity and skill for design. Sketches have the typical attributes that they are quick and inexpensive to make, can be provided when needed, are disposable, and tend to be plentiful (Buxton 2007). Mock-ups are often made of simple materials like paper and cardboard, as described by Ehn and Kyng (1991). Such mock-ups may be used in collaborative design sessions where designers and users can explore different application scenarios in what they call design-by-doing. These paper and cardboard mock-ups give hands-on experience, are cheap and fast to make, make it possible for everybody to make changes with scissors and pens, and mean that changes are immediately visible.

Gaver and Martin (2000) argue that design ideas should be presented with a concreteness that is balanced with openness, and with functionality that is not necessarily fully resolved. This will allow for design proposals to remain more open to imaginary extensions, developments, and modifications in a way that is difficult with more finished examples.

The ability to sketch for communication and reflection is fundamental to conceptual design processes. This raises the question of whether—or how—sketching can be done within—or connected to—a simulated environment. Simulators are not currently equipped to handle the speed, versatility, or openness of traditional pen and paper sketches.

Prototyping

The term prototype has different meanings in different fields. Various prototypes can be produced with differing levels of fidelity, including rapid prototyping (RP), CAD-based simulation, high-fidelity renderings, and real-time graphics (Lim et al. 2008; Capjon 2004). Here, we employ prototype to describe a design externalisation that is, to some extent, testable by users or designers.

Prototypes are widely recognized as a core means of exploring and expressing designs (Houde and Hill 1997). However, as discussed by Lim et al. (2008), prototypes in the conceptual design phase are not like the requirement-oriented ones used in, e.g., software engineering, which focus on usability issues. They describe prototypes as representative and manifested forms of design ideas, while prototyping is the activity of making and utilizing prototypes in design. In this understanding, prototypes have a form wherein designers may organically and evolutionary learn, discover, generate, and refine designs.

Klemmer and Hartmann (2006) propose the notion of thinking through prototyping as a perspective to a design challenge. This is based on Schön's (1991) view that physical action and cognition is interconnected, suggesting a framing and evaluation of a design challenge by working it through, rather than just thinking it through. Successful designs result from a series of conversations with materials (Schön and Bennett 1996).

Simulators do, in many respects, support the notion of prototyping. However, there are multiple barriers to producing such prototypes efficiently during a design process. Today, every use of the simulator has to be facilitated by the simulator developers, who are mainly software developers with advanced knowledge of computer programming. To designers that do not have programming skills, this represents a barrier to using the simulator as an effective design tool to mediate a conceptual design phase with mock-ups and prototyping tools used in interdisciplinary collaboration, preferably on-the-fly.

Collaboration

In the conceptual design of ship bridges, there is a need to integrate expertise from several professions in design collaboration (Cutler 2010), which should also involve the end-users of the future design (Sanders and Stappers 2008). In this respect, the members of such interdisciplinary design teams have to communicate their specialised knowledge. The difference in communication and understanding between disciplines is what Lave and Wenger (1991) explained as different professions having a community of practice, with a shared understanding of notion.

The strength of a ship simulator is its ability to simulate reality—using visualization to provide a maritime context. When the simulator offers context and possibilities for design exploration, it can also be used as a tool for design collaboration. In this respect, the simulator can facilitate collaborative design exploration of conceptual design ideas through active feedback of design changes on-the-fly.

The simulator, with connected tools for conceptual design, will in this understanding act as a boundary object—an arena for mediating communication and understanding between individuals from different disciplines or professions (Star and Griesemer 1989). A boundary object is here understood as having the characteristics that it establishes a shared language for individuals to represent their knowledge; to specify and learn about their differences and similarities across a given semantic boundary; and facilitates a process where individuals can collaboratively understand, communicate, and transform their knowledge (Huybrechts et al. 2009).

The interdisciplinary design team and users are stakeholders in the conceptual design work, and need to use the aforementioned tools to rapidly generate new externalizations of design ideas in collaboration. This might be facilitated using the idea of a design collaboratorium (Bødker and Buur 2002), which is both a process and a physical place mediating active collaboration between participants. In this understanding, the design team can collectively communicate, explore, and test their design ideas using conceptual design tools that substantiate a perspective of prototyping as 'sketching in hardware' (Moussette and Dore 2010). The UBC design lab in Oslo is an example of such a collaboratorium. However, in the Oslo collaboratorium, a simulator is directly integrated with other design tools such as spaces for building mock-ups, drawing equipment, workstations, display areas; and close proximity to metal, plastic, RP, and wood workshops. The simulator therefore becomes one of many tools in the design lab.

Such design collaboration in the design collaboratorium even has the potential for mediating participatory design sessions: a design collaboration where domain users participate as co-designers or co-creators in the conceptual design phase (Sanders and Stappers 2008), actively exploring design ideas the same way that Ehn and Kyng (1991) used their cardboard computers. In addition, the offshore simulator can facilitate complex offshore operations, allowing new design concepts and ideas to be tested in different operational scenarios. This type of functionality is impossible to achieve in real operation.

Currently, training simulators provide insufficient support for collaborative design processes, as they do not offer the speed or the tools that allow a team of designers and other stakeholders to collaborate freely on ship bridge design within the context of a simulation. Significant technical advances will be necessary before the full potential of simulation can be realised in collaborative design processes.

DISCUSSION

In the previous sections we have elaborated simulators in the context of collaborative conceptual design processes; and looked into using simulators for understanding user needs and handling design complexity. In addition, we have taken up sketching, mock-ups, prototyping, and collaboration within the context of a design simulator. It is clear that current simulators require significant development in order to meet the needs of conceptual design processes. However, our experiences of using simulators in the UBC project have shown that, although there are significant challenges to using simulators in design processes, there are also great opportunities. Most of the barriers we encounter can be separated into two categories.

First, there is a lack of tools allowing efficient transformation of the physical and virtual components of a simulated ship bridge. Consoles, virtual elements, and physical and virtual interfaces need to be as open as

possible to opportunities for transformation. This places emphasis on the technological flexibility of software and hardware architecture, where 3D models, simulations, physical interfaces, and physical components in general should have a low threshold for transformation.

Second, there is a lack of simulator-centric design methods. It is to be expected that simulator technologies would not be appropriate for all stages of conceptual design. The question is, rather: which design methods can be improved by using simulators? For instance, a design process uses different types of sketches and prototypes of different quality throughout the process. Sometimes a realistic setup is needed, whereas others require the equivalent of a wire-frame interface. The design simulator also needs to work alongside many additional design tools; maybe as part of a design collaboratorium; integrated into participatory design processes; or used by a single designer in a standard desktop computer.

These two perspectives of technical flexibility and design methods for simulators are mutually interdependent. Thus, we suggest a design simulator can best be achieved by working with technical and methodological development in tandem. We are pursuing this strategy in the UBC project through the development of new simulator-based tools to support our on-going conceptual design process.

The core nature of ship simulators is their ability to bring the maritime context into the designer's daily work situation. This does not in any way compensate for the very important fieldwork where designers and researchers observe real work in real contexts. However, simulator will, in its simplest form, bring context or "the ocean" into the design office, and give designers access to the ship bridge whenever needed. We believe, in time, this will become a powerful tool in helping design teams to maintain their understanding of the domain and context for which they are designing.

Technological advances have given designers the opportunity to use more sophisticated tools for conceptual design exploration and evaluation, such as rapid prototyping (RP), CAD-based simulations, high-fidelity renderings, and real-time graphics that are useful in the conceptual design phase. Using such tools, a more refined version of a design can be product quickly and inexpensively. We believe simulators might be one such tool in the future. However, in order for that to happen, simulators need to be better adapted to the messiness of actual design processes.

In the UBC project, we will further investigate several of the aforementioned issues through greater integration and adaption between the simulators and the UBC lab. We will investigate the idea of a design collaboratorium, conduct design sessions in various settings, and collate case material for further evaluation and suggestions on how to develop the design simulator for offshore ship bridges.

ACKNOWLEDGEMENT

We wish to express our gratitude for the contributions made by all the participants in the UBC project; also, special thanks to Ulstein Power & Control for their contribution to this article. The UBC project is funded by The Research Council of Norway and by Ulstein Power & Control.

REFERENCES

Buchenau, M. and Suri, J.F., 2000. Experience prototyping D. Boyarski and W. A. Kellogg, eds. *Proceedings of the conference on Designing interactive systems processes practices methods and techniques DIS 00*, pp.424–433.

Buxton, B., 2007. *Sketching User Experiences: Getting the Design Right and the Right Design*, Morgan Kaufmann.

Bødker, S. et al., 2000. Co-operative Design — perspectives on 20 years with "the Scandinavian IT Design Model". In *NordiCHI*. Stockholm, Sweden: KTH, Royal Institute of Technology, pp. 1–9.

Bødker, S. and Buur, J., 2002. The Design Collaboratorium — a Place for Usability Design. *ACM Transactions on Computer-Human Interaction*, 9(2), pp.152–169.

Capjon, J., 2004. *Trial-and-Error-based innovation: Catalysing Shared Engagement in Design Conceptualisation*. The Oslo School of Architecture and Design (AHO).

Cutler, T., 2010. *Designing Solutions to Wicked Problems: A Manifesto for Research and Design*, Melbourne, Australia: Design Research Institute, RMIT University.

Ehn, P. and Kyng, M., 1991. Cardboard Computers: Mocking-it-up or Hands-on the Future. In J. Greenbaum and M. Kyng, eds. *Design at work: Cooperative design of computer systems*. Hillsdale, NJ, USA: Laurence Erlbaum Associates Inc., pp. 169–195.

Gaver, B. and Martin, H., 2000. Alternatives: exploring information appliances through conceptual design proposals. In *Proceedings of the SIGCHI conference on Human factors in computing systems*. ACM, pp. 209–216.

Hjelseth, S., 2011. 3D-Visualizations as a means for engaging users and actors as co-designers in the fuzzy front-end of product development. In *Diversity and unity: Proceedings of IASDR2011, the 4th World Conference on Design Research*. Delft, the Netherlands, pp. 1–9.

Houde, S.H.C. and Hill, C., 1997. What do Prototypes Prototype? In M. Helander, T. Landauer, and P. Prabhu, eds. *Handbook of Human-Computer Interaction*. Elsevier Science B.V.

Huybrechts, L. et al., 2009. Living Spaces: A Participatory Design Process Model Drawing on the Use of Boundary Objects. *International reports on socio-informatics*, 6(2), pp.6–21.

Kallmann, M. et al., 2003. Immersive Vehicle Simulators for Prototyping, Training and Ergonomics. In *Computer Graphics International (CGI)*. Tokyo, Japan, pp. 90–95.

Kincaid, J. and Westerlund, K., 2009. Simulation in education and training. In *Proceedings of the 2009 Winter Simulation Conference (WSC)*. Austin, TX, pp. 273–280.

Klemmer, S. and Hartmann, B., 2006. How bodies matter: five themes for interaction design. In *Proceedings of the 6th conference on Designing Interactive systems*. University Park, PA, USA: ACM, pp. 140–149.

Kolko, J., 2010. Sensemaking and Framing: A Theoretical Reflection on Perspective in Design Synthesis. In *Proceedings of the 2010 DRS Montreal Conference*. Montréeal: Design Research Society.

Lave, J. and Wenger, E., 1991. *Situated Learning - Legitimate Peripheral Participation*, Cambridge: Cambridge University Press.

Lawson, B., 2006. *How Designers Think: The design process demystified* 4th ed., Architectural Press.

Lawson, B. and Dorst, K., 2009. *Design Expertise*, Oxford, UK: Architectural Press.

Lim, Y.-K., Stolterman, E. and Tenenberg, J., 2008. The anatomy of prototypes: Prototypes as filters, prototypes as manifestations of design ideas. *ACM Transactions on Computer-Human Interaction*, 15(2), pp.1–27.

Moussette, C. and Dore, F., 2010. Sketching in Hardware and Building Interaction Design: tools, toolkits and an attitude for Interaction Designers. In *Proceedings of Design Research Society*. Montreal, Canada.

Nelson, H.G. and Stolterman, E., 2012. *The Design Way: Intentional Change in an Unpredictable World* second edi., MIT Press.

Page, R.L., 2000. Brief history of flight simulation. In *Proceedings of SimTecT 2000*. Sydney, Australia, pp. 1–11.

Petersen, E. and Lützhöft, M., 2009. A Human Factors Approach to the Design of Maritime Software Applications. In *RINA Human Factors in Ship Design and Operation*. London, UK.

Rittel, H.W.J., 1987. The Reasoning of Design. In *Arbeitspapier zum International Congress on Planning and Design Theory*. Boston, pp. 1–9.

Rittel, H.W.J. and Webber, M.M., 1973. Dilemmas in a General Theory of Planning. *Policy Sciences*, 4(2), pp.155–169.

Robinson, M.A., 2012. How design engineers spend their time: Job content and task satisfaction. *Design Studies*, 33(4), pp.391–425.

Rosen, K.R., 2008. The history of medical simulation. *Journal of critical care*, 23(2), pp.157–66.

Rowe, P., 1987. *Design thinking*, Cambridge, MA: MIT Press.

Sanders, E. and Stappers, P.J., 2008. Co-creation and the new landscapes of design. *CoDesign*, 4(1), pp.5–18.

Saus, E.-R. et al., 2012. Who benefits from simulator training: Personality and heart rate variability in relation to situation awareness during navigation training. *Computers in Human Behavior*, 28(4), pp.1262–1268.

Schön, D.A., 1991. *The reflective practitioner: how professionals think in action*, Aldershot: Avebury.

Schön, D.A. and Bennett, J., 1996. Reflective Conversation with Materials. In T. Winograd, ed. *Bringing Design to Software*. New York, NY, USA: Addison Wesley.

Skjerve, A.B. and Bye, A. eds., 2011. *Simulator-based Human Factors Studies Across 25 Years: The History of the Halden Man-Machine Laboratory*, London: Springer.

Star, S.L. and Griesemer, J.R., 1989. Institutional Ecology, "Translations" and Boundary Objects: Amateurs and Professionals in Berkeley's Museum of Vertebrate Zoology, 1907-39. *Social Studies of Science*, 19(3), pp.387–420.

Susi, T., Johannesson, M. and Backlund, P., 2007. *Serious games: An overview*, University of Skovde, Sweden.

Tideman, M., Voort, M.C. and Houten, F.J. a. M., 2008. A new product design method based on virtual reality, gaming and scenarios. *International Journal on Interactive Design and Manufacturing (IJIDeM)*, 2(4), pp.195–205.

Ulrich, K.T., 2011. *Design: Creation of Artifacts in Society*, University of Pennsylvania.

AUTHOR BIOGRAPHIES

HELGE T. KRISTIANSEN is an assistant professor at Aalesund University College. He has masters degrees in Electrical Engineering from the Norwegian University of Science and Technology (NTNU); and in Information Technology from Aalborg University. He has presented lectures on a wide range of subjects, including interaction design and human–computer interaction.

Helge is presently a PhD fellow at The Oslo School of Architecture and Design, participating in the research project Ulstein Bridge Concept (UBC).

E-mail address: hkr@hials.no and web page http://www.designresearch.no/

KJETIL NORDBY is an industrial designer with a master's degree in Interaction Design from Umeå Design School and a PhD from The Oslo School of Architecture and Design (AHO).

Kjetil has been part of several start-up ventures and has worked as an industrial- and interaction designer for leading Norwegian companies. He has also tutored AHO students at undergraduate and graduate level and hosted graduate courses at Oslo University Institute of Informatics. Kjetil currently leads the Ulstein Bridge Concept (UBC) research project.

Simulation and Visualization for Training and Education

PRELIMINARY EXPERIMENTS WITH EVA - SERIOUS GAMES VIRTUAL FIRE DRILL SIMULATOR

José Fernando M. Silva[1], João Emílio Almeida[1†], António Pereira[1†], Rosaldo J. F. Rossetti[1†], António Leça Coelho[2]
[1]Department of Informatics Engineering
[†]LIACC – Laboratory of Artificial Intelligence and Computer Science
Faculty of Engineering, University of Porto
Rua Roberto Frias, S/N, 4200-465, Porto, Portugal
{ei06123, joao.emilio.almeida, amcp, rossetti}@fe.up.pt

[2]LNEC – National Laboratory of Civil Engineering
Av. Brasil, 101, 1700-066, Lisboa, Portugal
alcoelho@lnec.pt

KEYWORDS
Evacuation simulation, fire drill, serious games.

ABSTRACT

Fire keeps claiming a large number of victims in building fires. Although there are ways to minimize such events, fire drills are used to train the building occupants for emergency situations. However, organizing and implement these exercises is a complex task, and sometimes not sucessfull. Furthermore, fire drills require the mobilization of some finantial resources and time, and affect the normal functioning of the site where they occur. To overcome the aforementioned issues, computer games have a set of features that might overcome this problem. They offer engagement to their players, keeping them focused, and providing training to real life situations. The game evaluate users, providing them some feedback, making possible for the players to improve their performance. The proposed methodology aims to study the viability of using a game that recreates a fire drill in a 3D environment using Serious Games. The information acquired through the player's performance is very valuable and will be later used to implement an artificial population. A sample of 20 subjects was selected to test the application. Preliminary results are promising, showing that the exercise had a positive impact on users. Moreover, the data acquired is of great important and will be later used to demonstrate the possibility of creating an artificial population based on human behaviour.

INTRODUCTION

Statistics related to building fires reveals a high loss of lifes as result of them. In addition to the goods destroyed during a fire, there is still a high number of victims, some dead, others with severe injuries. Events such as the recent fire in the Brazilian discotheque "Kiss", this past January, where more than 230 young lives were lost, happen more frequently than they should. Some authors allege that failures during the evacuation process are one of the causes that mainly contributes for the building fires victims. Although there are ways to reduce the impact of this tragic events, fire keeps claiming a considerable number of victims. Emergency plans are poorly designed, and even worse implemented. In Madrid, during the Halloween party, an overcrowded concert led to the death of five young women when spectators crushed in one of the tunnels (illustrated in Figure 1).

Figure 1 - Stampede in Madrid Arena, 2012[1]

Fire drills are used to train the building occupants for emergency situations. However, the participants some times have prior knowledge of their realization and, as result of this, they are not focused as they should. Moreover, fire drills require the mobilization of some resources, with the correspondent finantial costs: facilities must stop their normal activities, businesses are affected, educational activities in schools are compromised, surgeries and medical appointments must be rescheduled. Performing a fire drill will always affect the normal functioning of the place where they take place; for this reason, sometimes they are not performed at all. In some special locations, like hospitals, fire drills are unsuitable.

To overcome the aforementioned issues, computer games have a set of features that enable them to address

[1] http://www.20minutos.es/noticia/1641576/0/cronologia/tragedia/madrid-arena/

Proceedings 27th European Conference on Modelling and Simulation ©ECMS Webjørn Rekdalsbakken, Robin T. Bye, Houxiang Zhang (Editors)
ISBN: 978-0-9564944-6-7 / ISBN: 978-0-9564944-7-4 (CD)

this problem. In fact they provide engagement to their players, keeping them concentrated; besides they allow players to become experts in the resolution of challenges. The game allows evaluating the users' performance, providing also to them some feedback, and making possible for the players to improve their skills.

Some work has been done in this domain, proposing the use of Serious Games (SG) as a means to overcome such drawbacks, since immersion into the emergency scenario artificially created using computer videogames is easier to accomplish. The availability of game engines such as Unity3D provide a rapid way for prototyping 3D scenarios thus enabling to recreate the environment needed for a virtual fire drill simulator.

Another important issue is concerned with the acquisition of human behaviour in such emergency situations. By using the SG concept, it is possible to record some metrics regarding the players' decisions.

In this paper a test bed is presented, including the results obtained from a sample of 20 players. The metrics, and some data that were recorded, was later used to drive the artificial agents trying to recreate the players' decisions, based on their previous selections and the selected category of behaviour.

The remaining part of this paper is organised as follows. We start by briefly presenting some related concepts that concern this project, such as pedestrian evacuation simulators and serious games. We then discuss on applying serious games to evacuation training, following the presentation and formalisation of our problem. We propose the approach implemented in this paper and suggest a preliminary experiment using our prototype. Some results are also discussed, after which we finally draw some conclusions and give clues of some further steps in this research.

BACKGROUND AND RELATED WORK

Pedestrian evacuation simulators

Pedestrian evacuation simulators, a subset of pedestrian computer simulations, are developed mainly to test scientific theories and hypotheses, to assess design strategies, and to recreate the phenomena about which to theorize (Pan et al., 2007). Applications range from the entertainment to more serious uses like pedestrian behaviour in the real world or in panic situations (Almeida et al, 2011). Another important domain of application consists in the evaluation of the level of life safety provided by buildings (Kuligowski et al., 2010). When engineers use performance-based design approach to assess buildings' life safety, sometimes they use hand calculations, based on the equations provided by the Society of Fire Protection Engineers Handbook (SFPE, 2002), to provide them approximate egress times. However, these calculations are far from being accurate and other methodologies should be used instead (Coelho, 1997).

To correctly represent pedestrian flow, both the collective and the individual issues should be addressed (Hoogendoorn et al., 2004). Timmermans et al. (2009) states that the pedestrian decision-making process, as well as its movement, is of critical importance in the development of pedestrian models that aim to reproduce the reality. Teknomo divided pedestrian studies in two phases, namely data collection and data analysis (Teknomo, 2002). Whilst data collection focuses on characteristics such as speed, movement and path-planning, the latter is more focused in the pedestrians' behaviour.

Models can be classified according the level of depth: macroscopic or microscopic. Predicting the movement of crowds fall in the first category whilst individual pedestrian actions are in the second. The latter (microscopic level) is where most of pedestrian simulators are focused. Models of crowd based on the hydraulic or gas metaphor are used for the macroscopic level (Santos and Aguirre, 2004). In the microscopic models each person is described individually, thus allowing individual behaviours to be taken into account. According to (Castle, 2007), one possible classification of pedestrian evacuation simulators uses the occupants or enclosure perspective: i) coarse network models provide a macroscopic approach; ii) cellular automata models (Neumann, 1966, Beyer et al., 1985) and iii) continuous space models present a microscopic view (see Figure 2).

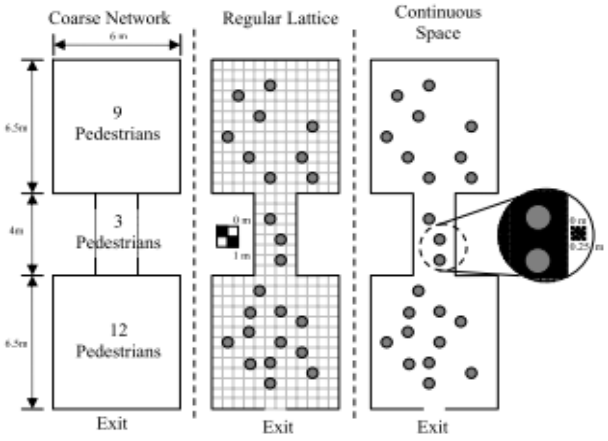

Figure 2 - Examples of pedestrian models (Castle, 2007)

Two of the various possible ways to model the pedestrian movement and interactions between persons, obstacles and the environment, are the magnetic forces model (Okazaki & Matsushita, 1993) and the social forces model (Helbing et al., 1995; Helbing et al., 2001; Helbing et al., 2002).

The validation and verification of pedestrian models relies on data collected by means of direct observations, photographs, time-lapse films (Coelho, 1997; Qingge et al., 2007) and also by stated preferences questionnaires (Cordeiro et al, 2011).

The emergent behaviour of groups of animals was addressed by Reynolds, who proposed a model to simulate the aggregate motion in a realistic way (Reynolds, 1987). Kuligowski had indeed studied human behaviour under emergency situations and she had also brought some insights on this matter regarding human

behavioural process during evacuation from buildings (Kuligowski, 2008, 2011).

Serious Games

Video games were the leitmotif for advent of Serious Games (SG) with multiple applications other than entertainment, using appealing software with high-definition graphics and state-of-the-art gaming technology, for purposes that go beyond the traditional ones, such as educational as well as training. The variety of applications includes a wide range of domains, being social simulation one of them (Frey et al., 2007; McGonigal, 2011; Ribeiro et al., 2012).

SG purpose varies accordingly with the domain of application, such as education, training, health, advertising or social change (Hays, 2005).

Benefits of combining SG with other training activities include: the learners' motivation is higher; completion rates are higher; possibility of accepting new learners; possibility of creating collaborative activities; learn through doing and acquiring experience (Freitas, 2006).

The aforementioned aspects are a subset of the characteristics of SG-based frameworks that makes them so appealing to use for social simulations.

EVA: A SG EVACUATION SIMULATOR

Based on the Unity3D game engine, some research has been carried out at LIACC concerning the development of a SG-based Evacuation Simulator (Ribeiro et al, 2012). The version presented in this paper was coined EVA from the three initial letters of EVAcuation. It also relates to the first woman known, Eve (that is Eva in Latin languages, such as in Portuguese). Unity3D is a successful platform used worldwide for the development of video games, with appealing graphics, in which we can use the First Person Shooters (FPSs) game genre.

Unity3D was selected due to its characteristics among others: i) availability and free use; ii) powerful graphical interface; iii) ability to import models from other sources, such as Revit from Autodesk; iv) capability to develop code in JavaScript, C# or Boo. Detailed characteristics of the implemented environment are presented hereafter.

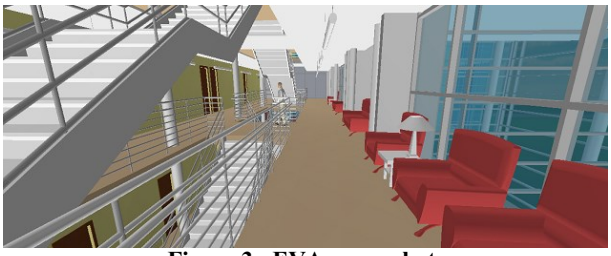

Figure 3 - EVA screenshot

The game genre – First Person Shooter

First Person Shooters (FPS) are used widely in video games. FPS are characterised by placing players in a 3D virtual world which is seen through the eyes of an avatar. Aim is to give the feeling of immersion in the virtual environment (illustrated in Figure 3).

The controls for this game use the FPS common standards, combination of keyboard and mouse to move the player around the environment. The complete action mapping is as follows:

- **Mouse movement** - camera control, i.e. where the player is looking at;
- **W** - move forward;
- **S** - move backwards;
- **A** - move to the left;
- **D** - move to the right;
- **F** – to open or close doors.

Game scenario

The game scenario used, a large three-floor building, was imported from Autodesk's Revit and its external view is represented in Figure 4.

Figure 4 - Exterior view of the building used

The 3D model was converted into the Unity3D framework, and some furniture was added to increase the realms and give a more realistic, almost photo-quality, ambience. A character using the FPS-game genre was created. Mr. Adam is another character in a wheelchair, a patient in a clinic hospital (shown in Figure 5).

Figure 5 - Inside view of Mr. Adam's Ward

Game description

The game starts with the player at location "E" (see Figure 6), leaving the lift and pushing Mr. Adam's wheelchair towards his ward at "F". Suddenly, the fire alarm bells start ringing. The player is asked then what should be done (Figure 7). Possible answers include: a) nothing; probably it is a false alarm; b) wait for security personnel instructions; c) try to understand what is going on; d) leave the building as quickly as possible. The option selected is saved for later analysis.

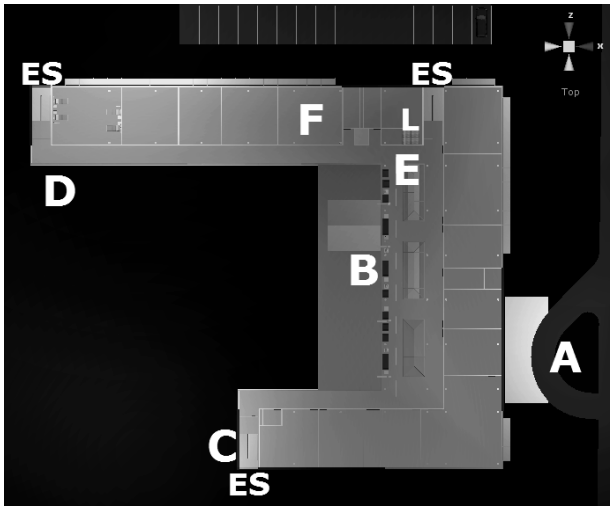

Figure 6 - Building layout: A-main entrance; B-back entrance; C-south wing exit; D-northwest exit; E-starting point; F-ward; L-lift; ES-emergency exit

Then, the player is instructed to leave the building due to a real fire alarm. Meanwhile, another important decision has to be made: will the player bring Mr. Adam or not? This is another option that will be recorded. If the player chooses to steer Mr. Adam in his wheelchair towards the exit reaching a safe zone, such as a different fire compartment or protected emergency stairs, the total time since the beginning of the fire alarm until that point is registered, and the player is greeted for that achievement, that is, for having rescued Mr. Adam to a safe zone.

Finally, the player is urged to go as quickly as possible to the outside to find a route to exit the building. The game will end as soon as the player reaches a valid exit. Total evacuation time is recorded. The valid exits are shown in Figure 4: A is building main entrance; B is back entrance or access to back yard; C is the exit of south wing emergency stair; D is the exit of northwest emergency stair.

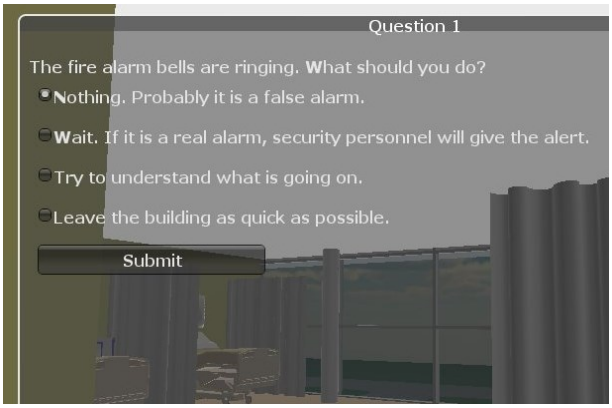

Figure 7 - Questionnaire presented to the player after the fire alarm sounds

EXPERIMENTAL SETUP

The EVA prototype was run under a Windows 7 typical commodity computer with no special specifications. All subjects were tutored in the game controls usage, keyboard and mouse, and were given a small time to adapt on controlling the FPS character. Data acquired during the game was recorded in a text file. The players had no previous knowledge of the building or scenario and, to keep them the same chances, each player had only one run, to capture first reactions to the game experience and its controls, to avoid biased the data. This aspect is important to be noticed because one goal was to acquire genuine surprise with the fire alarm situation and to record the behaviour. For that reason, only one run was allowed for each player, because the next time he would be already expecting the alarm and what was expected to do.

Population Sample

A total of 20 subjects were selected as sample to test the developed prototype. These testers can be classified according to the parameters presented in Table 1. This data was collected in a questionnaire presented to the players at the end of the game.

Table 1 - Population sample

	YES	NO
Regular video game player	13	7
Previous training in fire safety	9	11
Previous fire drill's experience	12	8
Been into a real fire	1	19
Followed emergency signage to find exit route	16	4

Description

As stated before, each subject could play only once. Some time was given to the user to get acquainted with the keyboard and mouse controls. No explanation on the game purpose, other than having to steer Mr. Adam in his wheelchair to the ward, was given. After hearing the alarm siren, the player had to answer the questionnaire shown in Figure 7. Finally, the player was advised to go as quickly as possible to the outside of the building. The game ends as soon as the player passes one of the building's exit.

Data Collected

The results of answers to the initial questionnaire (Figure 7) are presented in Table 2. From the possible answers, the option c) or d) should be the ones to be chosen. If the subject, in a real situation, is confronted with a fire alarm, if he/she does not decided to leave immediately the building, at least should go and seek for information regarding the origin of such alarm. From the data collected, most players choosed options c) or d), equally, but two players choose the other options, one each.

Table 2 - Answers to initial question

	Answers
a) nothing; probably it is a false alarm	1
b) wait for security personnel instructions	1
c) try to understand what is going on	8
d) leave the building as quickly as possible	9

Ignoring the alarm is a bad option and waiting for instructions from security personnel or some responsible person, is a risky option, because in a fire or emergency situation, things can go wrong and emergency plans might fail. Also the exit chosen by each player was registered, and the results are displayed in Table 3. Half of players opted for the back entrance, while only one opted for the south wing exit.

Table 3 - Exits used by the players

	Number of players
A-main entrance	4
B-back entrance	10
C-south wing exit	1
D-northwest exit	5

Preliminary results analysis

The immersion provided by the game scenario was one of the positive remarks that most players made. The setup of the experiment was also referred to be a realistic one, concerning the goal of evaluating the reaction of users when faced with an unexpected fire alarm. Many of the players said that in a real situation their behaviour would be the same, thus proving a valuable feed back. For fire scientists and researchers, the issue of the pre-evacuation time, corresponding to the amount of time between the fire alarm until a decision is made, is of great importance. Not much data is available regarding this issue. Furthermore, this phase of the evacuation process is of crucial significance, because it can determine the success of the evacuation process.

It was noticed that some players did not choose the best or fastest route towards the outside of the building. Although the safest route and preferable one, from the starting point, was the northwest exit (D), only 5 of the subjects (25%) choose this exit. To this matter, the fact that many of the players confessed not to have followed the emergency signage, pointing towards the nearest and safest exit, must empahsized.

The evacuation times, although recorded, are not significant as absolute values, since the movement speed of the game character is set to 1.5 m/s and some aspects related with the cinematic movement of pedestrians, such as variable speed, walking versus running, and the steering of the characters, could bias the results. On the other hand, for validation and verification, experiments in the real building should be performed to compare results, but this is outside the scope of this experiment.

CONCLUSION AND FUTURE WORK

Since the population sample is reduced, results must be analysed with caution. However, the validity of the tool for training and to provide some education on how a building occupant should behave when confronted with a fire alarm, is promising.

Another aspect to be noticed is the possibility of using EVA and SG for human behaviour data collection. This data is of great importance to feed pedestrian simulators of evacuation scenarios. Particularly when this data can be divided

The very next steps in this research include the improvement of the prototype for rapidly setting up different simulation environments from Revit models of buildings. We also intend to include other performance measures to study individual and social behaviour in circumstances other than hazardous scenarios. Ultimately, this framework is also expected to be used as an imperative decision support tool, providing necessary and additional insights into evacuation plans, building layouts, and other design criteria to enhance places where people usually gather and interact rather socially.

ACKNOWLEDGMENT

This project has been partially supported by FCT (Fundação para a Ciência e a Tecnologia), the Portuguese Agency for R&D, under grant SFRH/BD/72946/2010.

REFERENCES

Almeida, J. E., Rosseti, R., and Coelho, A. L. 2011. “Crowd Simulation Modeling Applied to Emergency and Evacuation Simulations using Multi-Agent Systems”. In *Proceedings of the 6th Doctoral Symposium on Informatics Engineering*, DSIE’11, Porto.

Almeida, João Emílio, Zafeiris Kokkinogenis, and Rosaldo J. F. Rossetti. 2012. “NetLogo Implementation of an Evacuation Scenario.” In *WISA’2012 (Fourth Workshop on Intelligent Systems and Applications)*. Madrid, Spain. http://ieeexplore.ieee.org/xpls/abs_all.jsp?arnumber=6263226.

Beyer, W.; Sellers, P.; Waterman, M. 1985. “Stalinslaw m. Ulam’s contributions to theoretical theory”. Letter in *Mathematical Physics* 10:231-242.

Castle, Christian J. E. 2007. *Guidelines for Assessing Pedestrian Evacuation Software Applications*. Centre for Advanced Spatial Analysis - UCL University College London. http://eprints.ucl.ac.uk/3471/1/3471.pdf.

Coelho, L. 1997. *Modelação de Evacuação de Edifícios Sujeitos à Acção de um Incêndio* (in Portuguese), Ph.D. Dissertation, FEUP-LNEC, Lisboa.

Cordeiro, E., Coelho, A. L., Rossetti, R. J. F., and Almeida, J. a. E. 2011. “Human Behavior under Fire Situations – A case–study in the Portuguese Society”. In the Proceedings of *Advanced Research Workshop: Evacuation and Human Behavior in Emergency Situations*, pages 63–80, Santander, Spain. GIDAI. Universidad de Cantabria.

Epstein, Joshua M. 1999. “Agent-based Computational Models and Generative Social Science.” *Complexity* 4 (5) (May): 41–60.

Freitas, S. (2006). *Using Games and Simulations for Supporting Learning*. Learning, Media and Technology, 31(4):343– 358.

Frey, A., Hartig, J., Ketzel, A., Zinkernagel, A., and Moosbrugger, H. 2007. “The Use of Virtual Environments Based on a Modification of the Computer Game Quake III ArenaR in Psychological Experimenting”. *Computers in Human Behavior*, 23(4):2026–2039.

Hays, R. 2005. “The Effectiveness of Instructional Games: a Literature Review and Discussion”. Technical report, Naval Air Warfare Center Training Systems Division Orlando, FL.

Helbing, Dirk, and P Molnar. 1995. “Social Force Model for Pedestrian Dynamics.” *Physical Review E*.

Helbing, Dirk, Péter Molnár, Illés J Farkas, and Kai Bolay. 2001. “Self-organizing Pedestrian Movement.” *Environment and Planning B: Planning and Design* 28 (3): 361–383. doi:10.1068/b2697.

Helbing, Dirk, I.J. Farkas, Péter Molnár, and Tamás Vicsek. 2002. “Simulation of Pedestrian Crowds in Normal and Evacuation Situations.” *In Pedestrian and Evacuation Dynamics*, ed. M. Schreckenberg and S.D. Sharma, 21:21–58. Berlin: Springer.

Hoogendoorn, S.P., and P.H.L. Bovy. 2004. “Pedestrian route-choice and activity scheduling theory and models”. *Transportation Research Part B: Methodological 38* (2) (February): 169-190.

Kuligowski, E. D. 2008 “Modeling Human Behavior during Building Fires”. NIST Technical Note 1619.

Kuligowski, E. D., Peacock, R., and Hoskins, B. L. 2010. “A Review of Building Evacuation Models, 2nd Edition”. NIST Technical Note 1680.

Kuligowski, E. D. 2011. “Predicting Human Behavior During Fires.” Fire Technology (November 13). http://www.springerlink.com/index/10.1007/s10694-011-0245-6

McGonigal, J. 2011. *Reality Is Broken: Why Games Make Us Better and How They Can Change the World*, volume 22. The Penguin Press HC.

Neumann, V. 1966. *Theory of self-reproducing automata*. Champaign IL: University of Illinois Press.

Okazaki, Shigeyuki, and Satoshi Matsushita. 1993. “A Study of Simulation Model for Pedestrian Movement.” In *First International Conference on Engineering for Crowd Safety*, 271–280. London, England: Elsevier.

Pan, X., Han, C. S., Dauber, K., & Law, K. H. 2007. “A multi-agent based framework for the simulation of human and social behaviors during emergency evacuations”. *Ai & Society* 22 (2) (June 29) , 113-132.

Qingge, J., Can G. 2007. “Simulating Crowd Evacuation with a Leader-Follower Model”. *IJCSES International Journal of Computer Sciences and Engineering Systems*, Vol.1, No.4, October 2007.

Reynolds, C. 1987. “Flocks, Herds and Schools: A Distributed Behavioral Model”. *ACM SIGGRAPH Computer Graphics*, 21(4):25–34.

Ribeiro, João, João Emílio Almeida, Rosaldo J F Rossetti, António Coelho, and António Leça Coelho. 2012. “Towards a Serious Games Evacuation Simulator.” In *26th European Conference on Modelling and Simulation ECMS 2012*, ed. Klaus G. Troitzch, Michael Möhring, and Ulf Lotzmann, 697–702. Koblenz, Germany: ECMS2012.

Teknomo, K. 2002. *Microscopic Pedestrian Flow Characteristics: Development of an Image Processing Data Collection and Simulation Model*. Ph.D. Thesis. Tohoku University, Japan.

Timmermans, H. 2009. *Pedestrian Behavior: Models, Data Collection and Applications*. Emerald Group Publishing Limited.

SFPE. 2002. *SFPE Handbook of Fire Protection Engineering*. Society of Fire Protection Engineers, NFPA, Quincy, MA.

Wooldridge, Michael. 2002. *An Introduction to Multiagent Systems*. John Wiley & Sons, Ltd.

AUTHOR BIOGRAPHIES

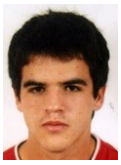

JOSÉ FERNANDO MOREIRA DA SILVA is a undergraduated student, will conclude his MSc in Informatics and Computing Engineering in 2013, from Faculty of Engineering, University of Porto, Portugal. He specialised in Digital Games development and Artificial Intelligence, combining the concepts of multi-agent systems and serious games. He can be reached by e-mail at: ei06123@fe.up.pt.

JOAO EMILIO ALMEIDA holds a BSc in Informatics (1988), and MSc in Fire Safety Engineering (2008). He is currently reading for a PhD in Informatics Engineering at the Faculty of Engineering, University of Porto, Portugal, and a researcher at LIACC. He has co-authored many fire safety projects for complex buildings such as schools, hospitals and commercial centres. His areas of interest include Serious Games, Artificial Intelligence, and multi-agent systems; more specifically he is interested in validation methodologies for pedestrian and social simulation models. His e-mail is joao.emilio.almeida@fe.up.pt.

ANTONIO PEREIRA was born in Porto, Portugal, and has a PhD in Informatics Engineering from University of Porto. Since 2003 he is dedicated to research in the field of Agent-Based Simulation, Distributed Artificial Intelligence, Intelligent Systems, and Optimization of Complex Systems. His e-mail is amcp@fe.up.pt and his personal webpage can be found at http://www.fe.up.pt/~amcp.

ROSALDO ROSSETTI is an Assistant Professor with the Department of Informatics Engineering at the University of Porto, Portugal. He is also a Research Fellow in the Laboratory of Artificial Intelligence and Computer Science (LIACC) at the same University. Dr. Rossetti is a member of the Board of Governors of IEEE Intelligent Transportation Systems Society (IEEE ITSS) and a co-chair of the Technical Activities sub-committee on Artificial Transportation Systems and Simulation of IEEE ITSS. His areas of interest include Artificial Intelligence and agent-based modelling and simulation for the analysis and engineering of complex systems and optimisation. His e-mail is rossetti@fe.up.pt and his Web page can be found at http://www.fe.up.pt.com/~rossetti/.

A. LEÇA COELHO holds both the Electrotechnical and Civil Engineering degrees, as well as a Master's and PhD in Civil Engineering. He is currently a Principal Researcher with Habilitation at LNEC. His areas of interest include fire safety and risk analysis. He can be reached by e-mail at alcoelho@lnec.pt.

A DESIGN SPACE EXPLORATION FRAMEWORK FOR AUTOMOTIVE EMBEDDED SYSTEMS AND THEIR POWER MANAGEMENT

Gregor Walla
Walter Stechele
Andreas Herkersdorf
Institute for Integrated Systems
Technische Universitaet Muenchen
Munich, Germany
Email: gregor.walla@tum.de

Zaur Molotnikov
Andreas Barthels
Institute for Informatics
Technische Universitaet Muenchen
Munich, Germany

Hans-Ulrich Michel
BMW Group
Research and Technology
Munich, Germany

KEYWORDS

Automotive, E/E architecture, embedded, modeling, simulation, design space exploration, power consumption

ABSTRACT

The E/E (electric/electronic) architecture of a modern vehicle is a complex distributed system, where up to 80 electronic control units (ECUs), interconnected by several communication buses, need to collaborate with each other in order to implement the various comfort and safety features.

The presented E/E design space exploration framework supports engineers during the development process of new E/E architectures by providing a graphical modeling and simulation environment with an interactive visualization of simulation-based results. Furthermore, it contains an advanced business logic which administrates the modeling, storing, retrieving and cloning of evaluation sessions consisting of complex experiments. Due to a high-level modeling approach, future architectures can be evaluated in respect to power consumption and performance values already in an early stage of the design process and design alternatives can be easily compared with each other.

INTRODUCTION

The E/E (electric/electronic) architecture of a modern vehicle consists of a large number of electronic control units (ECUs) forming a complex distributed embedded system. Sensors detect the surrounding environment, computational units process the obtained information and actuators control the behavior of the vehicle.

With every vehicle generation the demand for safety and comfort features is increasing, resulting in an ever-increasing complexity of the overall system. Various subsystems need to collaborate with each other, which makes the design of the E/E architecture a major challenge. Furthermore, the power consumption of the electric and electronic components is also becoming a subject of consideration. It negatively affects the fuel consumption of vehicles with combustion engines or the maximum range for electric vehicles.

In order to address this situation, tool support for modeling and simulation in an early phase of the development process is necessary. The engineer needs to evaluate design alternatives and check whether all design goals will be achieved, e.g. functional requirements, performance constraints or power budgets.

The commercially available tool PREEvision allows model-based E/E development (Vector Informatik GmbH, 2013). It provides several abstraction layers for modeling a system from different architectural viewpoints, e.g. requirements, logical architecture, hardware component architecture. Through the usage of different metrics, it is possible to evaluate static properties of the system, such as communication dependencies. However, it is not possible to simulate the models and gain information about the dynamic behavior.

Another CASE tool for the model-based development of embedded systems is AutoFOCUS 3 which is specialized for reactive and embedded systems (Hölzl and Feilkas, 2011). It supports different layers of models and allows for timing simulation and verification of the modeled application.

The tool box UPPAAL is used for modeling, simulation and verification of real-time systems. It focuses on model checking of applications that can be modeled as networks of timed automata extended with integer variables, structured data types, user defined functions, and channel synchronization (Behrmann et al., 2004).

The performance and timing analysis tool SymTA/S uses formal scheduling analysis techniques and symbolic simulation in order to determine system-level performance data such as end-to-end latencies, bus and processor utilization, and worst-case scheduling scenarios (Henia et al., 2005). It can be used for design space exploration and verification of heterogeneous architectures.

In this paper, we propose E/E-MaSiF (E/E Modeling and Simulation Framework), a domain specific framework, specialized for the evaluation of E/E architectures. The novelty is the focus on the design space exploration with respect to power consumption in an early phase of the development process. The framework provides a visual modeling environment and supports the engineer through basic consistency checks and automated genera-

Proceedings 27th European Conference on Modelling and Simulation ©ECMS Webjørn Rekdalsbakken, Robin T. Bye, Houxiang Zhang (Editors)
ISBN: 978-0-9564944-6-7 / ISBN: 978-0-9564944-7-4 (CD)

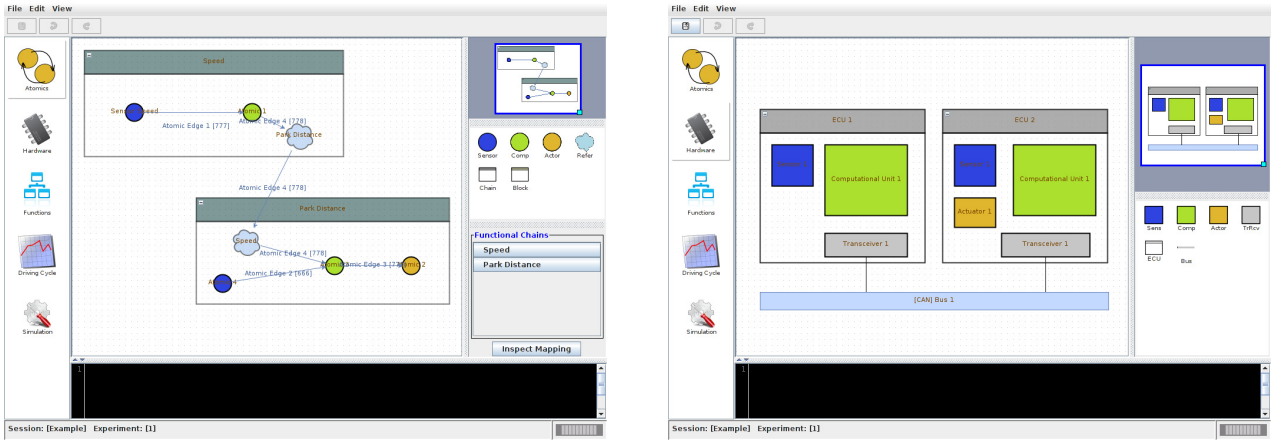

(a) Functional Network Consisting of Two Functional Chains and 5 Functional Blocks

(b) Technical Architecture Consisting of Two ECUs Interconnected by a Communication Bus

Figure 1: Screenshots of the Visual Modeling Environment (*VME*)

tion of parts of the model.

Once an E/E architecture is fully specified, the framework can simulate it with respect to power consumption and performance values and provide a graphical representation of the results. Due to the high-level modeling approach, the simulation results are only approximated values, but it makes it possible to compare design alternatives already in an early stage of the development process. The engineer can clone and reuse existing E/E models, modify them, and evaluate the behavior of the changed system.

The rest of this paper is structured as follows: the next section introduces the modeling framework and the overall UI concept. Later on, the system architecture is described. As one building block of the architecture the business logic is highlighted and described in more detail. Afterwards, an example of the visualization of the simulation-based results is presented. Finally, the last section concludes the paper and gives an outlook on future work.

DESIGN SPACE EXPLORATION

The presented framework is built around the ITE-Sim simulator (Walla et al., 2012b) and is used to evaluate design alternatives in an early stage of the E/E architecture development process. The framework automatically generates the necessary input files for the simulator and provides a visual representation of the simulation results to the user.

In order to cope with the overall complexity, model-based development has to be applied. Figure 1 shows two screenshots of the modeling environment. The user can switch between the different views of the application by using the navigation bar on the left-hand side.

As can be seen in figure 1a the different functions of a vehicle can be modeled as directed graphs called functional chains, where the nodes represent functional blocks and the edges indicate the communication flow (Hillenbrand and Muller-Glaser, 2009). This abstraction indicates the logical architecture of the application, since the actual implementation is not yet available during that design phase. However, the internal behavior of each functional block is further specified through a separate trace primitive description. This concept was introduced in (Walla et al., 2012b). It allows an annotation of each functional block with it's computation and communication properties, i.e. data to be processed when a block is executed or the amount of data to be transmitted when a block is communicating with other blocks. Through this abstraction of the real implementation, the modeling of the functions of a vehicle is independent from the underlying hardware.

Figure 1b shows the modeling view of the technical architecture of the vehicle, where the hardware layout of the distributed system can be specified. The user can drag and drop new ECUs into the view and connect them via communication buses. Furthermore, each ECU is described in more detail by defining sub-components inside it, i.e. computational units, communication transceivers, sensor interfaces, or actuators. The sub-components are assumed to be operated in various power states with different power and performance properties.

Having modeled the functional chains and the technical architecture, the designer needs to decide which functional block will be executed on which hardware component. This mapping is restricted by various functional constraints, e.g. location of sensor/actuators or available hardware resources, but is mainly based on the knowledge of previous vehicle generations.

However, since power consumption is becoming increasingly important, the partitioning needs to be done also with energy-efficiency considerations in mind, e.g. power savings due to temporarily switching off unused functions or ECUs is highly dependent on the deployment of the various vehicle functions (Walla et al., 2012a).

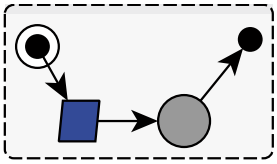

Figure 2: Exemplary Power Management Plan, Starting up the Hardware, then Running Functional Block

In order to evaluate the power consumption of the system, the power management strategy needs to be defined. This is done by modeling a set of power management plans (PMP) for each ECU. A PMP is a directed graph over power states of the sub-components of an ECU and functional blocks mapped on the ECU together with timing conditions (Barthels et al., 2011). On the one hand, this graph indicates the scheduling of the functional blocks, and on the other hand, it describes the change of the operating points of the sub-components, e.g. switching to an idle-mode when all required functional blocks have been executed.

An example of a PMP is shown in figure 2. The concept of PMPs enables the evaluation of various power management strategies, like Partial Networking (Fuchs et al., 2010) or Pretended Networking (Schmutzler et al., 2010).

With this information it is possible to evaluate the modeled E/E architecture with respect to power consumption. The user defines a specific driving scenario (Samuel et al., 2002), which corresponds to the input for the sensors over time, and can simulate the execution of the vehicle functions.

In order to be able to perform a design space exploration, it is possible to clone a modeled E/E architecture, perform modifications to them, for example, change the mapping of functional blocks or the power management strategy, and repeat the simulation. This enables the designer to compare the power related consequences of different experiment configurations in a short period of time.

SYSTEM ARCHITECTURE

The overall system architecture is shown in figure 3 in form of components. The components are arranged in tiers. They have data flow between them, user and simulator interaction, and a database for persistency. The rectangular components encapsulated in the tiers together represent a standalone system, a visual modeling environment (VME). The VME supports the user on the way towards the full experiment configuration, needed to perform simulation, serving as an intermediary between the simulator and the user.

On the presentation tier the user interacts with a graphical user interface, built with Swing and JGraphX technologies. The graphical user interface invokes processing functions of the business logic (BL) component in the logic tier. The business logic contains the data model of

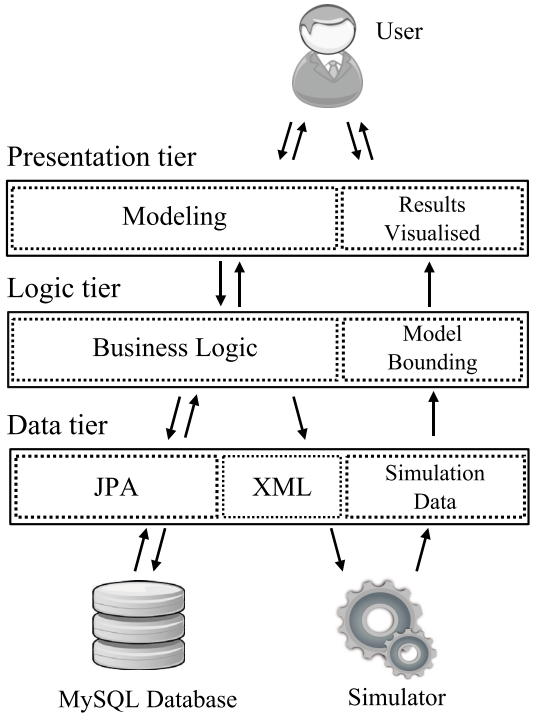

Figure 3: Schematical System Architecture Diagram

the experiment as well as domain relevant functionality, which is discussed separately in the following section.

Persistence for the configuration is supported in the data tier via Java Persistence API (JPA), which interfaces a MySQL database.

When the modeling is finished, the business logic component performs post configuration checks and calls an XML generator, to transform the configuration data into XML input to the simulator. The external simulator component is described well in (Walla et al., 2012b). After getting the input from the VME, the simulator communicates back to the VME via standard output and a specialized communication protocol based on sockets. The simulation data component is responsible to receive the simulator output and pass it one level up, where the data is associated back again with the model in the BL component, from which the simulator input generation has been performed.

Later on, the result visualization component presents to the user the simulation data in a graspable and analyzable form. All components of the VME are clearly separated, which allows for reuse and ease of modifications.

BUSINESS LOGIC

As described in the section on the system architecture, the business logic component is a central component for the system, meaning that all other modules communicate to it and use functions provided by it. Among the BL component functionality most of the domain oriented functions are concentrated. These domain oriented functions are discussed next.

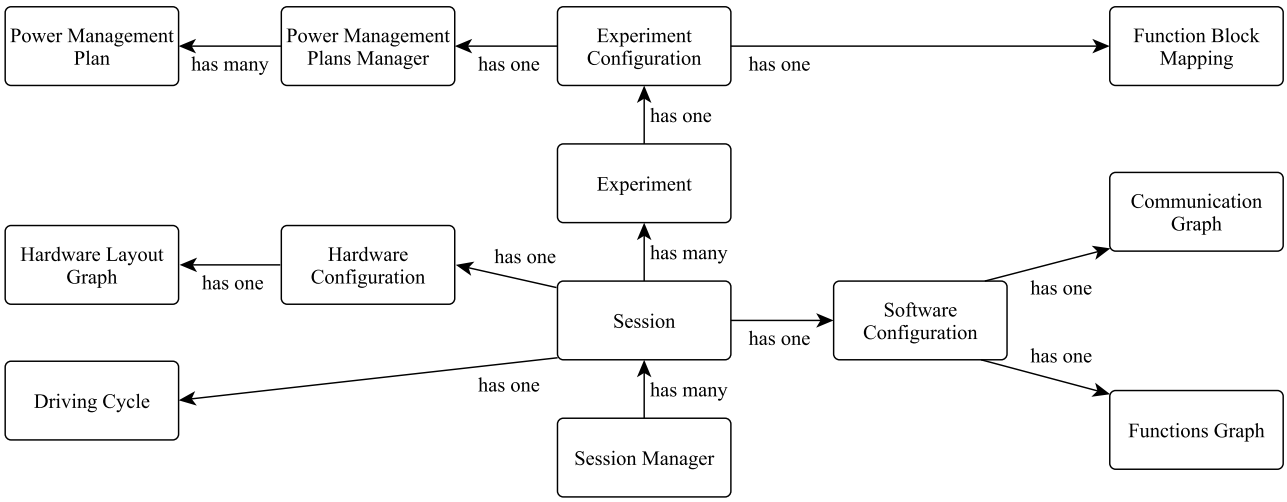

Figure 4: The Data Structure of the Business Logic Component

Experiment Cloning

To support the reuse of configuration parts, some of the parts are stored in the Session object, and only the parts specific for one particular experiment are stored in the Experiment object.

When experimenting with different power management strategies, and different functional block mappings, it is handy to be able to reuse the pure hardware and software configuration parts. This is performed by placing exactly this information into the Experiment objects, which can be many in one session.

In order to practically benefit from the information sharing in the Session object among several Experiment objects, one should create several experiments, which differ. The difference, however, between two experiments, can be "minor", e.g. one functional block remapped, and the power management plans (PMPs) modified accordingly.

After the first experiment has been configured, the second and further experiments, can be created as a clone of the existing one. Starting from the Experiment object in the structure shown in figure 4, all objects allow to create a clone of themselves.

The task of cloning starts to be less trivial, when it comes to cloning a PMP, which is a BL object containing a graph together with the JGraphX visual model of it. Cloning of such a structure must preserve the coherence of the new graph clone (BL model) and its JGraphX model newly acquired clone. The corresponding isomorphism is computed during the cloning.

Correct by Construction Principle

Manipulating on the BL objects, the user has to maintain the configuration in a correct state. Correctness here is taken in a most general, or weak, sense, which does not include the configuration completeness, and rather means mechanical consistency of the model.

The BL component takes care, that after each operation starting from a correct state, the user ends up in a new state which is also correct (in a sense as above). The system architecture is designed in such a way, that more complex routines to support correctness (in a stronger sense) can be integrated.

All operations on the data model within the BL component provide information on their success or failure, and automations are performed to keep the correct state.

As an example here we can consider a deletion of a functional block. It should not be possible to delete a functional block and to keep all edges leading to it in the visual representation. Furthermore, the deleted functional block has to be removed from the software-to-hardware mapping, and all other parts referencing it. The BL component takes care of the deletion, performing routine clean-up operations.

After the deletion of a functional block from the configuration, one of the PMPs, as a graph, can turn to be disjoint, which is logically incorrect (unreachable nodes appear). Post configuration checks are implemented in the BL component to filter out this and similar situations.

Post-Configuration Checks Infrastructure

The weakness of the correct by construction approach gives birth to a need for the post-configuration checks. Trivial examples of a not valid configuration would be a not complete configuration, where the user does not specify some vital configuration details, e.g. newly added functional blocks not mapped on the hardware components or PMPs. The post-configuration checks are implemented in each of the configuration objects and allow to test the object by itself, as well as the valid state of its descendants as on figure 4.

In the area of configuration validation and verification, the current system can be significantly improved, running checks dynamically (in the time of modeling) as well as making the checks more complete and complex. A good example of a useful checks could be PMP timing checks, as a check for schedulability, with all timing properties preservation.

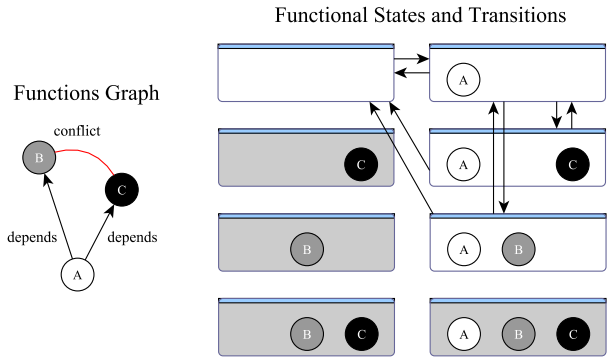

Figure 5: Functional State Modeling

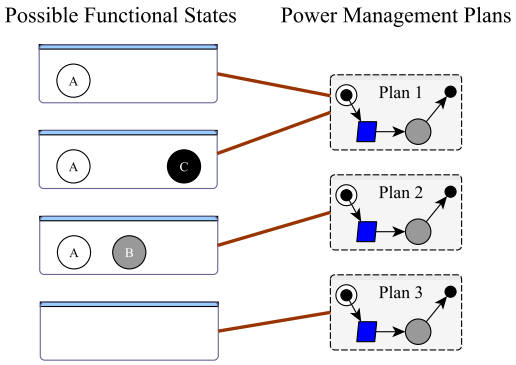

Figure 6: Power Management Plan Matching

Functional States Generation, Power Management Plans Matching

Here the term *function* means a feature of the system being modeled. Applying to the automotive domain examples could be: ignition ready, engine running, parking sensor working, wind screen wipers cleaning and similar. A function is defined as a set of functional blocks, supporting its operation. In the related work, common concepts are also denoted as feature (Metzger, 2004), or service interaction (Broy, 2005).

The interrelation of functions is shown figure 5. On the left, a so-called functions graph (FG) is shown. Nodes in the graph correspond to system functions. A function *B* can have a dependency on another function *A* (an edge from *A* to *B*), which means that *B* can only be activated (at a run time) after *A* has already been activated. Two functions can be denoted as conflicting, when they can not be active together at the same time.

The modeled system (vehicle) can have different states of operation. A set of functions, activated together at some point of time, we name here a functional state (FS). Figure 5 shows 8 functional states in the right part as rectangles. If there are N functions in the system, the amount of the FSs, in general, can be 2^N. The amount of transitions can have then the order of $2^N * (2^N - 1)$. Later in this work we call FSs and their transitions Functional State Graph (FSG).

Of the 8 functional states depicted in figure 5, only 4 stay to be valid (rectangles with the white background) due to the conflicts and dependencies defined by the FG on the left-hand side. Among the valid FSs, 8 transitions exist, which corresponds to switching particular functions on or off.

A full experiment configuration must include all possible FSs. For every FS the configuration has to specify transition conditions (under which circumstances the system reaches the FS) as well as a PMP for each of the ECUs. These procedures are automated in E/E-MaSiF.

For the user of E/E-MaSiF, the task to model the FSs and match them to corresponding PMPs is simplified to providing the functions graph, as in figure 5.

The FSG generation starts from the empty FS. Then all the functions are activated one by one, respecting dependencies and conflicts. New FSs are acquired, and the transitions to them are collected. Each of the FSs then participates again in the process of adding new functions. Set equivalent FSs are merged, combining the respective transition sets. When no more functions are available to extend the FSs, one by one the functions are switched back off from each FS, generating new transitions. The FSs merging stage is repeated after each FS generation step.

After the FSs and transitions are generated, the matching of the PMPs is performed (figure 6) for each ECU. The aim of this procedure is to identify, which PMP an ECU has to run, when the system enters a given FS.

For each of the ECUs a set of user-composed PMPs is specified together with the generated FSG. For each FS a set of supporting PMPs are defined, as PMPs containing all the FS required by the functional blocks. The *minimal* PMP of all matching PMPs is assigned to be the PMP to activate, when the system enters a given FS.

The minimality criteria can vary, depending on the user preferences. Currently, it means simply the lowest number of functional blocks present in each PMP.

The user of the system is verbosely informed, if the matching can not be performed due to lack compatible artifacts for specific FS.

SIMULATION VISUALIZATION

Once the user has modeled a concrete instance which passes all checks of the business layer, the model is translated to a simulation specification using XML. This specification contains all generated model properties like concrete functional states and matched power management plans. The simulator runs this specification and yields power and performance values for the architecture at hand.

Concrete model instances can be analyzed and visualized with the tool. Different specifications can be compared and visualized in a standardized way. Figure 7 depicts the aggregated consumptions per ECU and per ECU Component Type for an exemplary system specification. It shows on the left hand-side, that within the current experiment, a quarter of the total system's consumption is

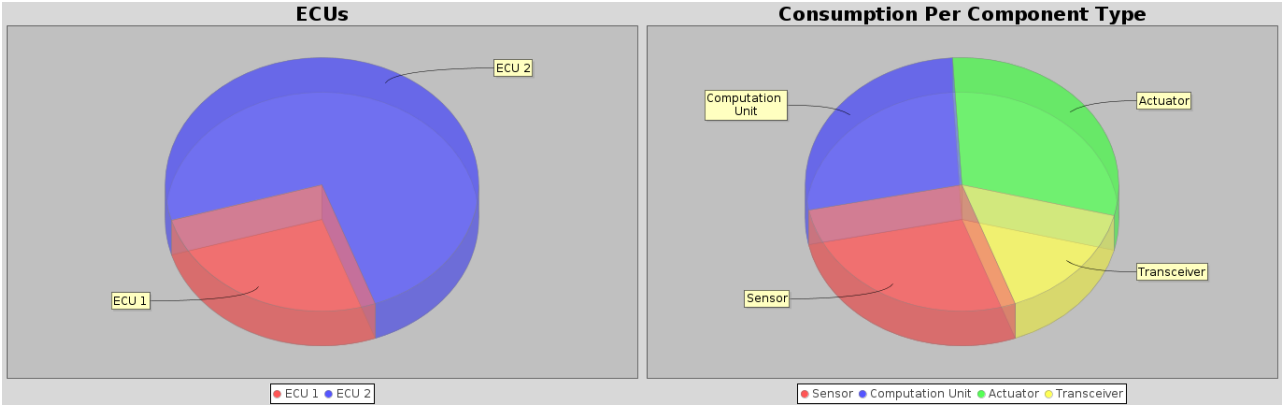

Figure 7: Overall Power Consumption per ECU and per ECU Component Type for one Experiment

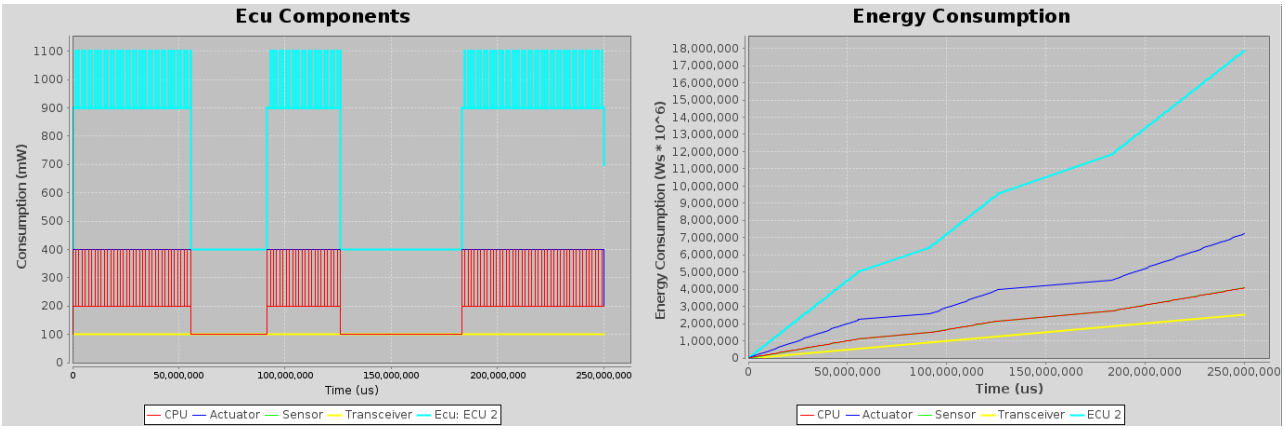

Figure 8: Instantaneous Power Consumption and Accumulated Energy Consumption per ECU Component of an ECU

amounted to ECU 1 while three quarters are amounted to ECU 2. On the right side, the total consumption during the experiment is amounted to the type of components. It is visible that in the example at hand, all component types except the Transceivers roughly amount for an equal share of the total consumption.

Selecting a specific ECU, the user can visualize detailed consumptions. This type of chart is depicted in figure 8. The charts are showing the dynamics of the system. On the left hand-side, the instantaneous power consumption of the selected ECU are given, while on the right hand-side, the accumulated energy consumption can be analyzed.

The possibility to open, maintain, and visualize different experiments at the same time enables the user to explore the design space and to evaluate different specifications of complex automotive systems.

CONCLUSION

This paper presented a new modeling and simulation framework for the evaluation of automotive embedded systems. It supports engineers in an early phase of the development by providing simulation-based information about the power consumption and performance of future E/E architectures.

The business logic of the framework provides basic consistency checks and assists the user through automated generation of some parts of the model. Furthermore, it administrates the storing, retrieving and cloning of evaluation sessions.

Simulating different variants in an early stage can help the developer understand the interplay of different vehicle functions and their power management and energy consumption.

Future work includes an OpenGL extension to the visualization of the simulation-based results. The user will be able to understand and to analyze the behavior of the vehicle in respect to a certain power management strategy, e.g. temporary switching of unused ECUs, in a 3D environment.

ACKNOWLEDGMENT

This work is part of an interdisciplinary research project of the Technische Universitaet Muenchen and BMW Group Research and Technology. It is organized under the CAR@TUM initiative, where the decades longstanding cooperation between the Technische Universitaet Muenchen and the BMW Group is intensified and restructured.

REFERENCES

Barthels, A., Ruf, F., Walla, G., Fröschl, J., Michel, H., and Baumgarten, U. (2011). A model for sequence based power management in cyber physical systems. *Information and Communication on Technology for the Fight against Global Warming*, pages 87–101.

Behrmann, G., David, A., and Larsen, K. (2004). A tutorial on uppaal. *Formal methods for the design of real-time systems*, pages 33–35.

Broy, M. (2005). Service-oriented systems engineering: Specification and design of services and layered architectures. *Engineering Theories of Software Intensive Systems*.

Fuchs, M., Scheer, P., and Grzemba, A. (2010). Selektiver teilnetzbetrieb im fahrzeug: Eine realisierung für den can-bus und adaption auf andere bussysteme. *GMM-Fachbericht-AmE 2010-Automotive meets Electronics*.

Henia, R., Hamann, A., Jersak, M., Racu, R., Richter, K., and Ernst, R. (2005). System level performance analysis-the symta/s approach. In *Computers and Digital Techniques, IEE Proceedings-*, volume 152, pages 148–166. IET.

Hillenbrand, M. and Muller-Glaser, K. (2009). An approach to supply simulations of the functional environment of ecus for hardware-in-the-loop test systems based on ee-architectures conform to autosar. In *Rapid System Prototyping, 2009. RSP'09. IEEE/IFIP International Symposium on*, pages 188–195. IEEE.

Hölzl, F. and Feilkas, M. (2011). Autofocus 3-a scientific tool prototype for model-based development of component-based, reactive, distributed systems. *Model-Based Engineering of Embedded Real-Time Systems*, pages 317–322.

Metzger, A. (2004). Feature interactions in embedded control systems. *Computer Networks*, 45(5):625–644.

Samuel, S., Austin, L., and Morrey, D. (2002). Automotive test drive cycles for emission measurement and real-world emission levels-a review. *Proceedings of the Institution of Mechanical Engineers, Part D: Journal of Automobile Engineering*, 216(7):555–564.

Schmutzler, C., Kruger, A., Schuster, F., and Simons, M. (2010). Energy efficiency in automotive networks: Assessment and concepts. In *High Performance Computing and Simulation (HPCS), 2010 International Conference on*, pages 232–240. IEEE.

Vector Informatik GmbH (2013). Preevision: Model-based electric/electronic development from architecture design to series-production readiness. *http://www.vector.com*.

Walla, G., Barthels, A., Ruf, F., Dörfel, R., Michel, H., Fröschl, J., Baumgarten, U., Herzog, H., Stechele, W., and Herkersdorf, A. (2012a). Aspects of function partitioning in respect to power management. *2nd International Energy Efficient Vehicles Conference (EEVC), Dresden, Germany*.

Walla, G., Gabriel, D., Barthels, A., Ruf, F., Michel, H., and Herkersdorf, A. (2012b). Ite-sim: A simulator and power evaluation framework for electric/electronic architectures. *The 8th IEEE Vehicle Power and Propulsion Conference, Seoul, Korea,*.

AUTHOR BIOGRAPHIES

GREGOR WALLA is a research staff member at the Institute for Integrated Systems at the Technische Universitaet Muenchen. He received the Dipl.-Ing. degree in Systems of Information and Multimedia Technology from the Friedrich-Alexander-Universitaet Erlangen-Nuernberg, Germany, in 2010.

ZAUR MOLOTNIKOV is a graduate student of the faculty of Informatics at the Technische Universitaet Muenchen, Master of Science Informatics program. He received a Univ. Dipl. in Applied Mathematics and Informatics at Southern Federal University, Rostov-on-Don, Russia, in 2009.

ANDREAS BARTHELS is a research staff member at the Institute for Informatics at the Technische Universitaet Muenchen, where he also received a Master's degree in 2009. Previously he received a Bachelor's degree in Informatics and Mathematics from Heinrich-Heine-Universität Düsseldorf in 2006.

HANS-ULRICH MICHEL received a Dipl.-Phys. degree in Physics from the Technical University in Darmstadt, Germany. After joining the BMW Group he has been responsible for the development of aftersales E/E subsystem products. After changing to BMW Group Research and Technology, he represented BMW in standardisation activities like the OSGi consortium, where he was a board member and chair of the vehicle expert group. Currently he is working on various research projects in the area of advanced telematic concepts with a special focus on the in-vehicle architecture.

WALTER STECHELE is an Academic Director at the Institute for Integrated Systems at the Technische Universitaet Muenchen. He received the Dipl.-Ing. and Dr.-Ing. degrees in Electrical Engineering from the Technische Universitaet Muenchen, Germany, in 1983 and 1988, respectively. In 1990 he joined the Kontron Elektronik GmbH in Germany, where he was responsible for the ASIC and PCB design department.

ANDREAS HERKERSDORF is a Full Professor and Chair of the Institute for Integrated Systems at the Technische Universitaet Muenchen. He joined the IBM Zurich Research Laboratory as a PhD student in 1988. In 1991, he became a Research Staff Member in the Communications Systems department of the IBM Zurich and in 2000 manager of the network processor hardware group. He received the Dipl.-Ing. degree from the Technische Universitaet Muenchen in 1987 and the Dr. techn. degree from the ETH Zurich (Swiss Federal Institute of Technology), Switzerland, in 1991, both in Electrical Engineering.

FLEXIBLE MODELING AND SIMULATION ARCHITECTURE FOR HAPTIC CONTROL OF MARITIME CRANES AND ROBOTIC ARMS

F. Sanfilippo, H. P. Hildre, V. Æsøy and H.X. Zhang
Department of Maritime Technology and Operation
Norwegian University of Science and Technology
Postboks 1517, 6025 Aalesund, Norway

E. Pedersen

KEYWORDS

Bond Graph modeling, haptic control, maritime cranes.

ABSTRACT

This paper introduces a modular prototyping system architecture that allows for the modeling, simulation and control of different maritime cranes or robotic arms with different kinematic structures and degrees of freedom using the *Bond Graph Method*. The resulting models are simulated in a virtual environment and controlled using the same input haptic device, which also provides the user with a valuable force feedback. The arm joint angles can be calculated at runtime according to the specific model of the robot to be controlled.

The idea is to develop a library of crane beams, joints and actuator models that can be used as modules for simulating different cranes. The base module of this architecture is the crane beam model. Using different joint modules to connect several such models, different crane prototypes can be easily built. The library also includes a simplified model of a vessel to which the crane models can be connected in order to get a complete model.

Related simulations were carried out using the so-called *20-sim* simulator to validate efficiency and flexibility of the proposed architecture. In particular, a two-beam crane model connected to a simplified vessel model was implemented. To control the arm, an *omega.7* from Force Dimension was used as an input haptic device.

I. INTRODUCTION

In the maritime industry, the last few decades have seen a growing interest in developing new technologies for controlling modern vessels and related maritime equipment to perform increasingly demanding marine operations. One of the biggest challenges concerns the operation of maritime cranes. Cranes are widely used to handle and transfer objects from large container ships to smaller lighters or to the quays of the harbours. The control of robotic maritime cranes is always a challenging task, which involves many problems such as load sway, positioning accuracy (Yi et al. 2003), wave motion compensation (Johnson 1985), collision avoidance (McKenna & Leithead 2007) and manipulation security (Hellrand et al. 1990). Moreover, traditional on-board maritime cranes, which are relatively big, heavy and stiff, rely on complex kinematic models of their system as well as an equally complex model of the environment with which they interact. However, in this paper, the main focus is on building a flexible modeling and simulation architecture for controlling the end effector of maritime cranes. The crane cable and all problems related to rope pendulations or wave impacts on the payload are not considered in this preliminary work but they can be included in the model at a later stage.

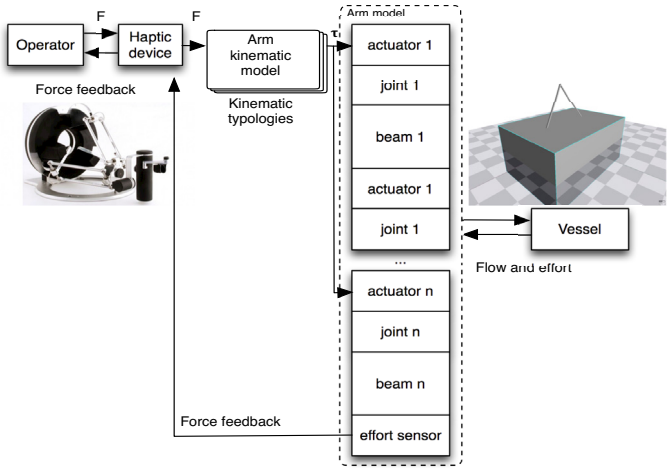

Fig. 1. The modular idea: a library of crane beam, joint and actuator models that can be used as modules to simulate different cranes or robotic arms. The arm joint angles can be calculated at runtime according to the specific kinematic model of the robot which can be selected among a set of different kinematic typologies.

Currently, it is still quite common to use simple joysticks to control maritime crane operations. Most of the control approaches are based on the concept of tele-operation, and usually each input device can control only one specific robotic crane. When considering working efficiency and safety, this kind of control is extremely difficult to manage and extensive experience with high control skill levels is required of the operators (Nielsen 2007). Therefore, low control flexibility and non-standardisation are indeed two crucial points of the current crane control architecture that need to be overcome.

To improve safety and efficiency on board, it could be useful to employ some kind of common controller that would be much more intuitive for the crane operators. Such interfaces could also provide the machinist with force feedback so that he would be able to feel the lifted loads and better manage the operations. Such types of devices are known as haptic interfaces. Haptics is a particular area of study within

Proceedings 27th European Conference on Modelling and Simulation ©ECMS Webjørn Rekdalsbakken, Robin T. Bye, Houxiang Zhang (Editors)
ISBN: 978-0-9564944-6-7 / ISBN: 978-0-9564944-7-4 (CD)

the Human Machine Interface (HMI) field concerning tactile (touch) feedback through forces, vibrations, and/or motions to the user (Amerongen 2000). The use of these devices can reduce the cognitive load of the operator and make the work more efficient and safe.

Since 2012, our research group started to work on designing and developing a more flexible and safe control system for maritime cranes. This work is supported by the programme for maritime activities and offshore operations (also named MAROFF) which is promoted by the Research Council of Norway. In our opinion, virtual prototyping is a crucial step during the design process and includes several benefits (Lumia et al. 1997) (de Melo & Mangili 2009). Development time can be significantly reduced. Building a proof of concept virtual prototype takes much less time than building a physical prototype. Therefore, simulations and virtual prototyping are indeed necessary steps to validate the design before committing to making a physical prototype.

In this paper, the authors present a modular prototyping system architecture, shown in Figure 1, that allows for modeling, simulating and controlling different robotic arms and cranes regardless of their kinematic structure, degrees of freedom, body morphology, constraints, affordances and so on. The resulting models are simulated in a virtual environment and controlled by using the same input haptic device which provides the user for a valuable force feedback. The idea is to develop a library of rigid bodies, joints, actuators and kinematic models that can be used as modules to simulate different cranes or robotic arms. The base module of this architecture is the crane beam model. Using different joint modules to connect several such models, different crane models can be easily built. The arm joint angles can be calculated at runtime according to the specific kinematic model of the robot which can be selected among a set of different kinematic typologies. The library also includes a simplified model of a vessel to which the arm models can be connected to get a complete model.

The paper is organised as follows. In Section II, justifications for the chosen modeling technique and a review of the related research work are given. In Section III, we focus on the description of the system model. In Section IV, a simplified vessel model with a crane consisting of two beams connected together is presented as an example. The related simulations and the obtained results are also shown. In Section V, conclusions and future works are outlined.

II. Related Research Work

Several aspects were considered in choosing a modeling technique to develop the prototyping system.

- Energy based approach. An important aspect in the design of this system is the interaction with human beings that have to be intrinsically safe. Robust stability is needed and such a level of stability can be obtained if controllers and controlled systems behave like physical passive systems, as stated by Hogan (Hogan 1984) with the principle of physical equivalence. This postulate motivates the energy-based approach followed in this paper.
- Multi-domain and complex systems. Since the idea is to develop a common haptic control system for cranes and robots that operate on ship decks, a mathematical model - which also includes the vessel dynamics - is needed. Such a model can be complicated in the sense that we have to deal with multi-domain systems where a large number of degrees of freedom and a large number of rigidly connected parts are involved.
- Modular approach. Since the aim of this work is to control different robotic arms using the same haptic device, the mathematical model have to be flexible enough to easily modify the kinematics and dynamics of the controlled device. The modular approach used in this work is a possible way to obtain such flexibility.
- Physical interaction. The Newton-Euler technique and Lagrange's technique are two of the classic methods used for the modeling of the dynamics of mechatronic systems (Craig 2004). These techniques however, tend to hide the physical interaction between elements involved and do not facilitate the implementation and integration of other subsystems at a later stage.

For all these reasons, the so-called Bond Graph Method (BGM) (Karnopp et al. 2006) was chosen by the authors as a natural way to model the system. In fact, the BGM is a highly modular energy-based approach for modeling and simulation of multi-domain dynamic systems.

One of the biggest advantages of using the BGM is that once the BG model of the system is ready, the system state equations can be algorithmically derived from it in a systematic manner. This process is usually automated using appropriate software, which can also derive equations in symbolic form. The so-called *20-sim* simulator (Amerongen 2000) was used in this work.

In recent years, the benefits of the BGM have been increasingly recognised by the scientific community. In (Vaz et al. 2003), Vaz et al. discussed certain issues involved in modeling robotic manipulators using BGs and presented a new approach for symbolic derivation of Jacobian matrices. However, this algorithm is not easy to adapt to different robotic arms or cranes.

Another problem that arises when modeling is that dynamic systems involving rigidly coupled inertia elements often result in derivative causality problems when represented in BG form. This means that explicit state equations can only be obtained after algebraic manipulation. In (Karnopp 1992), Karnopp presented a practical solution that consists of trying to eliminate the derivative causality by defining an I-field or an IC-field using generalised momentum and (if necessary) generalised coordinates, as is done when applying Lagrange's or Hamilton's equations. Later, in (Pedersen 2009), this same approach has been used by Pedersen for an efficient implementation of rotordynamic models in bond graphs. Eventually, the author, also proposed a derivation of the same concept for Marine Vehicle Dynamics (Pedersen 2012).

In (Allen 1979), Allen presented a technique based on multi-dimensional BG or Vector BG which produces explicit Lagrange or Hamilton equations for dynamic mechanisms suitable for computer solutions. Using a similar approach, Filippini et al. in (Filippini et al. 2004) applied the multibody theory through the Vector BG technique with the purpose of designing a multibond graph library for such systems. This

represents one of the first attempts to build a model that can be used to model different mechatronic systems. In (Fagereng 2011), Fagereng proposed an implementation in Vector BG of the general rigid body equations of motion for a marine vehicle in 6 DOF. The main advantage of this approach is that it supports the modeling process and setup of different marine mechatronic systems. However, no force feedback was considered in the previous literature.

In our work, rigid body dynamics are used in combination with vector BGs so that the model of the systems can be created in a easier way and incorporated with the vessel dynamic equations as discussed in (Fagereng 2011). Moreover, valuable force feedback is integrated in the control loop and provided to the crane operator.

III. System architecture

The idea is to develop a library of rigid bodies, joints and actuators models that can be used as modules to simulate different cranes or robotic arms. The base module of this architecture is the crane beam model. Using different joint modules to connect several such models, different crane models can be easily built. The library also includes a simplified model of a vessel to which the arm models can be connected to get a complete model.

In this section all the modules of the library are presented. One possible way to realise this architecture consists of combining rigid body dynamics and multi-dimensional power bonds (Pedersen 2009) (Pedersen 2012). Lagrange's method has proven to be particularly useful for such situations and it can be included in Hamiltonian form in the BGs by way of a modified version of an I-field or by using a special type of element known as an IC-field, which is a multiport generalisation and a combination of an I element and a C element. (Karnopp et al. 2012).

A. Crane beams and rigid body modeling

In order to implement a crane beam model, which will be the base model for our modular system, the motion of a rigid body in space has to be studied. Let us consider a rigid body in space with density ρ, mass m and velocity v. Let x, y, z be a coordinate frame with origin o, fixed in the rigid body and moving with it, and let X, Y, Z be the corresponding inertial coordinate frame with origin O from where the body is generally observed. The general motion equations in 6 DOF can be found and put in matrix form as:

$$M\dot{\vec{v}} + C(\vec{v})\vec{v} = \vec{\tau}, \tag{1}$$

where $\vec{\tau} = [\vec{F}_x, \vec{F}_y, \vec{F}_z, \vec{M}_x, \vec{M}_y, \vec{M}_z]^\top$ is the external force/momentum vector, M is the mass matrix and $C(\vec{v})$ is the Coriolis-centrifugal matrix. In order to implement this equation in the BG the kinetic energy of the rigid body has to be considered. It can be expressed as:

$$T = \frac{1}{2}\iiint \rho(\vec{v} + \vec{\omega} \times \vec{r})^\top (\vec{v} + \vec{\omega} \times \vec{r}) dV, \tag{2}$$

where, in this case, $\vec{v} = [\vec{v}_x, \vec{v}_y, \vec{v}_z]^\top$ and $\vec{\omega} = [\vec{\omega}_x, \vec{\omega}_y, \vec{\omega}_z]^\top$ are the linear and angular velocities of the local reference frame, respectively; while $\vec{r}$ is the radius vector of a point within the body from the axis. Thus, the kinetic energy can be rewritten as:

$$\begin{aligned} T &= \frac{1}{2} m\vec{v_O} \cdot \vec{v_O} + \vec{v_O}(\vec{\omega} \times \int \rho \vec{r} dV) + \frac{1}{2}\int \rho(\vec{\omega} \times \vec{r})(\vec{\omega} \times \vec{r}) dV \\ &= \frac{1}{2} m\vec{v_O} \cdot \vec{v_O} + \vec{v_O} \cdot (\vec{\omega} \times m\vec{r_c}) + \frac{1}{2}\vec{\omega}^\top \{I\}\vec{\omega}, \end{aligned} \tag{3}$$

where $\vec{r_c}$ is the centre of mass and $\{I\}$ is the inertia tensor. Now that we have the kinetic energy, the motion equations can be written in a quasi-Lagrangian formulation as:

$$\frac{d}{dt}\left(\frac{dT}{d\vec{v}}\right) + \vec{\omega} \times \frac{dT}{d\vec{v}} = \vec{\tau}_v, \tag{4}$$

$$\frac{d}{dt}\left(\frac{dT}{d\vec{\omega}}\right) + \vec{\omega} \times \frac{dT}{d\vec{\omega}} + \vec{v} \times \frac{dT}{d\vec{v}} = \vec{\tau}_\omega. \tag{5}$$

Using the Lagrange formulation, the equations for the generalised momentum can be written as:

$$\vec{p}_v = \frac{dT}{d\vec{v}}, \tag{6}$$

$$\vec{p_\omega} = \frac{dT}{d\vec{\omega}}. \tag{7}$$

Consequently, the motion equation can be rewritten in the momentum form:

$$\frac{\vec{p}_v}{dt} + \vec{\omega} \times \frac{dT}{d\vec{v}} = \vec{\tau}_v, \tag{8}$$

$$\frac{\vec{p_\omega}}{dt} + \vec{\omega} \times \frac{dT}{d\vec{\omega}} + v \times \frac{dT}{d\vec{v}} = \vec{\tau}_\omega. \tag{9}$$

Considering that the expression of the generalised momentum always assumes the same special form when the actual differentiations are carried out, the equation for the generalised momentum can be written in matrix form as:

$$\vec{p} = \mathbf{M}(\vec{q},t)\vec{v} + \mathbf{a}(\vec{q},t), \tag{10}$$

where $\mathbf{M}(\vec{q},t)$ is a $N \times N$ symmetric matrix of elements each possibly functions of the displacement $\vec{q}$ and the time t, and $\mathbf{a}(\vec{q},t)$ a vector of elements which only occurs if the system includes time-varying velocity sources. Solving for $\dot{\vec{q}}$ and ignoring the time-varying component gives an expression for the rate of change of the generalised displacement as:

$$\dot{\vec{q}} = \mathbf{M}^{-1}(\vec{q},t)\vec{p}. \tag{11}$$

In this way, the rigid body equation can be programmed in a modified I-field connected to only one one-junction representing the motion in 6 DOF as shown in Figure 2. The

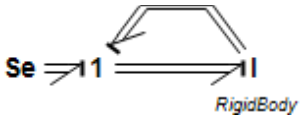

Fig. 2. Rigid body bond graph.

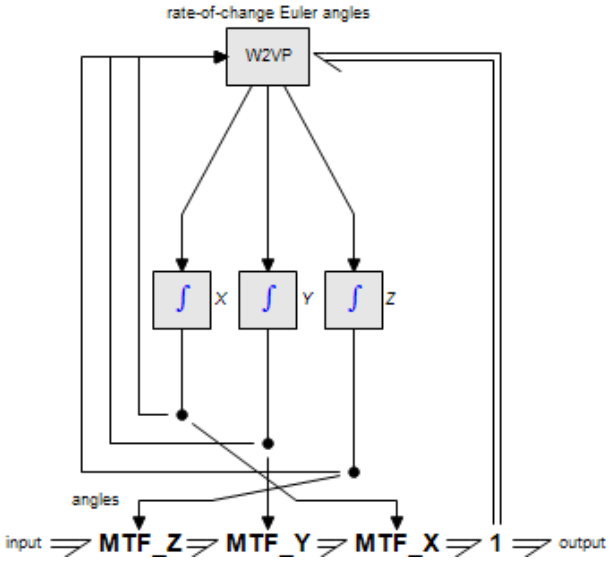

Fig. 3. Euler angle XYZ transformation.

constitutive relation for the I-field is:

$$f = \mathbf{M}^{-1}\vec{p}, \tag{12}$$

$$e = \mathbf{C}(\vec{v})\vec{v}. \tag{13}$$

In order to have a complete BG of the crane beam, the relation between the local coordinate frame and the global reference from which all motion is observed has to be derived. These transformations can be expressed using the Euler angles (Karnopp et al. 2006). In this paper, the so-called XYZ convention was adopted to generate the set of rotation matrices. To find the values of the Euler angles, the relation between the body-fixed rotational velocities and the rate of change of the Euler angles must be considered. Thus, the time rate of change of the Euler angles can be obtained as follows:

$$\dot{\theta} = cos(\phi)\omega_y - sin(\phi)\omega_z, \tag{14}$$

$$\dot{\psi} = \frac{sin(\phi)}{cos(\theta)}\omega_y + \frac{sin(\phi)}{cos(\theta)}\omega_z, \tag{15}$$

$$\dot{\phi} = \omega_x + sin(\phi)tan(\theta)\omega_y + cos(\phi)tan(\theta)\omega_z. \tag{16}$$

The resulting transformations can be implemented in modulated transformer elements, MTF-elements, one for each sub-transformation as shown in Figure 3. The rotational velocities are collected and sent to a box containing the rate-of-change Euler angles. The solved rate-of-change Euler angles are then integrated to obtain the angles and sent to their respective transformation element.

By connecting the whole transformation element to our I-field model we can describe motion and forces in our rigid body system. In Figure 4, all the transformations are incorporated in one sub-model called $MTF_{to-global}$. This is the base module of our system and represents a crane beam. By connecting together several of such modules, different crane models can be implemented.

However, when two rigid bodies are connected rigidly, the three linear and three angular velocities cannot all be implemented, meaning that not all the I-elements are able

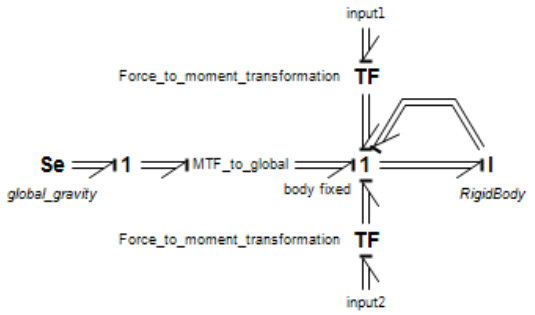

Fig. 4. Complete rigid body bond graph of a crane beam. The TF-elements represent the beam tips where the joint modules can be connected.

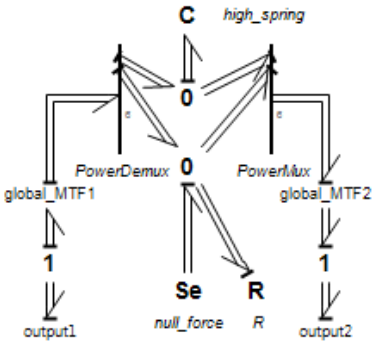

Fig. 5. Spherical joint bond graph.

to have integral causality (Karnopp et al. 2006). Since it is known that the source of derivative causality in such elements is the rigid connection, a possible solution consists of realising flexible connections. An imaginary infinite spring is used to connect two rigid bodies. Whenever forces acting on the two bodies try to pull them apart, a proportional large spring force will oppose separation. Such an imaginary spring can be modelled in BGs using a 6 DOF C-element that behaves almost like a rigid connection.

B. Joints

Joints are used to make connections between two bodies and to impose constraints on their relative movement. The spring connection is the basis for the modeling of joints (Filippini et al. 2004). Using spring elements the three basic representations of joints (spherical, revolute and prismatic) can be implemented in BGs.

Spherical joints: a spherical joint allows the three main axis rotations between the joined bodies while translation is prohibited. The BG model of this element is shown in Figure 5. In this model, the *PowerDemux* element separates the linear and angular efforts and flows coming from the 6 DOF input power bond and sends out two power bonds: the top one represents the linear component and the bottom one represents the angular contribution. The linear velocities are then constrained with a C-element that has a sufficiently high spring constant, which means that translation is forbidden. The Se-element that is attached to the unconstrained angular velocities is a zero-torque element, which means that the effort value is set to zero, thus representing total freedom to rotate. The *PowerMux* element collects the angular and linear velocities and merges them into one power bond. Moreover, at each end of the model

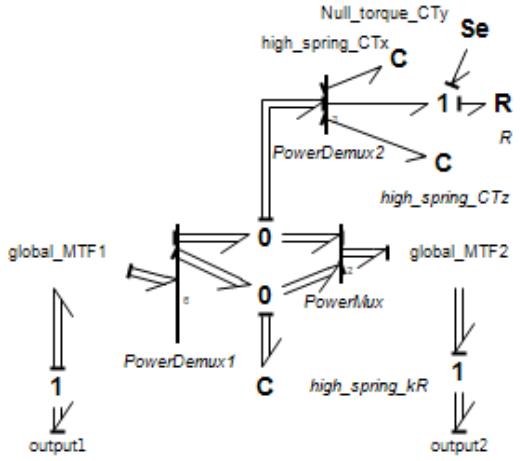

Fig. 6. Prismatic joint bond graph.

there is a coordinate transformation block. This element is similar to the one used when transforming between global and local coordinates but this time it is tuned to only account for the transformation of linear velocities and forces. Finally, in order to model the energy dissipation in the joint, R-elements can be added to the BG just as the Se-elements.

Revolute joints: A revolute joint is similar to a spherical joint but only allows for rotation in one angular direction, meaning that the other two are constrained in addition to the translational degree of freedom.

Prismatic joints: a prismatic joint allows for translation in one direction while the other two translational degrees of freedom as well as the all three rotational movements are constrained. The unconstrained power bond has a zero effort source meaning total freedom to translate as shown in Figure 6.

C. Actuators

The joint elements can be used to model elongation and rotation of crane beams and robots links. To control the joint movements, actuators imposing force or torques in the unconstrained directions can be used. Typical actuators are electric motors and hydraulic cylinders, as is often the case with cranes. In this work, the focus is on hydraulic actuators.

Rotary actuators: When modeling hydraulic rotary actuators, the joint motion can be controlled by applying a counter torque whose centre of application is somewhere along the beam. Applying a counter torque actually requires almost no modifications to the joint BG models. In fact, the effort value can simply be applied to the joint Se-elements, which previously represented zero efforts.

Linear actuators: Hydraulic linear actuator forces acting on the beam can be added in different ways. A possible approach involves using the existing Se-element that models the gravity force or adding a new Se-element to the global one-junction, thus representing a force in the positive global z direction for instance. This solution is quite close to representing the physical actuator since the torque in the global x direction will decrease as the beam is elevated.

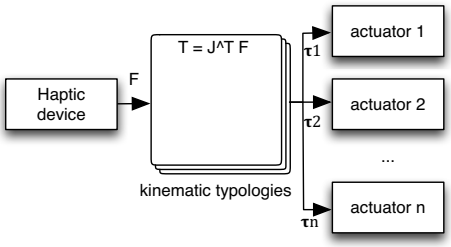

Fig. 7. Joint actuation.

D. Control

Thanks to the modularity of the discussed architecture, several beam models can be connected using different joint models and various cranes or robotic structures can be implemented. However the control of the system is still missing. To implement the control part, instead of using simple effort sources as inputs for the actuator models, the actual actuator forces can be calculated according to the dynamic model of the arm that has to be controlled. In particular, the force that the user applies on the haptic device can be used to calculate the actual actuator efforts. To do this the principle of virtual works (Zhang & Song 1993) can be applied:

$$\vec{T} = J^T \vec{F}, \tag{17}$$

where $\vec{F}$ is the vector of the forces and torques that have to be realised, J is the Jacobian matrix of the controlled crane and $\vec{T}$ is the vector containing the actuator efforts. The idea is shown in Figure 7. A set of different Jacobian matrices which correspond to a set of different kinematic typologies was included in the proposed library. The parameters of each generic Jacobian matrix, such as for instance the length of the links, have to be set according to the specific crane to be controlled.

E. Force feedback

In order to provide the user with valuable force feedback, a BG effort sensor can be used to measure forces and torques exerted on the end effector of the controlled arm. These efforts can be scaled and sent to the haptic device that will actuate them.

F. Vessel model

The vessel model may take into account radiation-induced forces (added mass, hydrodynamic damping and restoring forces), environmental forces (ocean currents, wind and waves) and propulsion forces (propeller/thruster forces and control surface/rudder forces). The general motion equation can be extended to include all of these contributions:

$$\begin{aligned}[M_{RB}+M_A]\,\dot{\vec{v}} + [C_{RB}(\vec{v})+C_A(\vec{v})]\,\vec{v} + D(\vec{v})\vec{v} + G(\vec{\eta}) \\ = \vec{\tau} + \vec{\tau}_H,\end{aligned} \tag{18}$$

where $M_{RB}\dot{\vec{v}}$ represents the rigid body forces and momentum, $M_A v$ indicates the hydrodynamic added mass forces and moments, $C_{RB}(\vec{v})v$ denotes the rigid body Coriolis and centripetal forces and moments, $C_A(\vec{v})$ is the hydrodynamic Coriolis and centripetal forces and moments, $D(\vec{v})\vec{v}$ is the combined expression for the hydrodynamic forces and moments which

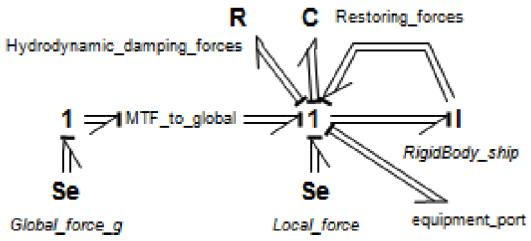

Fig. 8. Vessel bond graph.

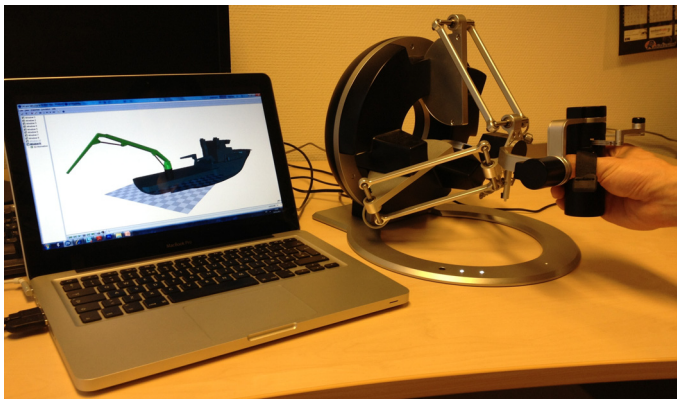

Fig. 9. The two beam crane model that was implemented and tested.

may include radiation-induced potential damping, linear skin friction damping, wave drift damping and vortex shedding damping, $G(\vec{\eta})$ is the restoring forces and moments, $\vec{\tau}$ represents the propulsion forces and moments, $\vec{\tau_H}$ represents the environmental forces and moments.

As shown by Pedersen in (Pedersen 2012) and Fossen in (Fossen 1994), the vessel can be also modelled as a rigid body with the addition of a C-element representing the restoring forces and an R-element representing the hydrodynamic damping. The model is shown in Figure 8. To fully complete the vessel model, an effort source is connected to the one-junction for the earth-fixed coordinate system representing gravity. There is also another effort source connected to the local one-junction, which can be used to simulate local forces on the vessel. Finally there is a port that can be used to attach some equipment to the model - it will be used to attach the crane.

IV. Simulations and Experimental Results

In order to validate efficiency and flexibility of the proposed system architecture, a two beam crane model connected to a simplified vessel model was implemented and tested as shown in Figure 9 .

In this preliminary study, a commercial haptic device, the *omega.7* from *Force Dimension*, was used as universal input for the system. The *omega.7* is a 7 DOF haptic interface with high precision active grasping capabilities and orientation sensing. Finely tuned to display perfect gravity compensation, its force-feedback gripper offers extraordinary haptic capabilities, enabling instinctive interaction with complex haptic applications. Thanks to the modularity of the proposed system, the same input device can be also used to control several different models.

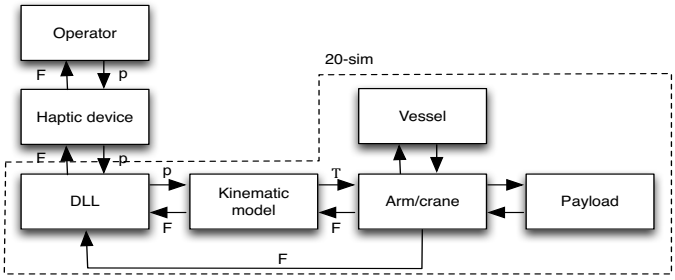

Fig. 10. The static-link library invocation that allows for connecting the haptic device to the simulator environment.

The system was implemented by means of a BG and simulated in *20-sim* (Broenink 1999). *20-sim* is a modeling and simulation package that provides a large library containing all standard BG elements. Next to standard elements *20-sim* supports custom user made BG models. This functionality was utilised in this work to develop the proposed library of rigid bodies, joints and actuators models that can be used as modules to simulate different cranes or robotic arms.

A *static-link DLL* library was implemented in order to connect the *omega.7* haptic device to the simulator environment as shown in Figure 10. At each simulation time-step the static dll sub-model calls a specific function to read the position of the input device's end effector and to write down the efforts that are used to give force feedback to the operator.

In order to simulate the vessel model, the added mass matrix and the Coriolis matrices were simplified because, in practice, deriving all of their coefficients can be an extensive process. The simplified version of the added mass matrix only has diagonal terms and the coefficients are simplified to only one parameter. These simplifications can be justified by the fact that the off diagonal terms in the added mass matrix tend to be much smaller the diagonal, having less impact on the model behavior. These approximations are actually valid assuming small velocities and that the vehicle has three planes of symmetry (Fossen 1994). The simplified versions of the matrices are

$$M_A = -diag\{X_{\dot{\vec{u}}}, Y_{\dot{\vec{v}}}, Z_{\dot{\vec{w}}}, K_{\dot{\vec{p}}}, M_{\dot{\vec{q}}}, N_{\dot{\vec{r}}}\}, \tag{19}$$

$$C_A(\vec{v}) = \begin{bmatrix} 0 & 0 & 0 & 0 & -Z_{\dot{\vec{w}}}\vec{w} & Y_{\dot{\vec{v}}}\vec{v} \\ 0 & 0 & 0 & Z_{\dot{\vec{w}}}\vec{w} & 0 & -X_{\dot{\vec{u}}}\vec{u} \\ 0 & 0 & 0 & -Y_{\dot{\vec{v}}}\vec{v} & X_{\dot{\vec{u}}}\vec{u} & 0 \\ 0 & -Z_{\dot{\vec{w}}}\vec{w} & Y_{\dot{\vec{v}}}\vec{v} & 0 & -N_{\dot{\vec{r}}}\vec{r} & M_{\dot{\vec{q}}}\vec{q} \\ Z_{\dot{\vec{w}}}\vec{w} & 0 & -X_{\dot{\vec{u}}}\vec{u} & N_{\dot{\vec{r}}}\vec{r} & 0 & -K_{\dot{\vec{p}}}\vec{p} \\ -Y_{\dot{\vec{v}}}\vec{v} & X_{\dot{\vec{u}}}\vec{u} & 0 & -M_{\dot{\vec{q}}}\vec{q} & K_{\dot{\vec{p}}}\vec{p} & 0 \end{bmatrix}, \tag{20}$$

The complete model of the crane connected to the vessel was simulated and tested. The plot in Figure 11 shows the motion of the crane end-effector along the z axis as a result of the haptic input device's movements which is operated by the user. In this particular case, the operator manoeuvres the crane model to lift the end effector up at first, then down and up again. Similar results were obtained for the x axis showing that the system is quite responsive to the user's inputs. The operator also perceives a force feedback that is proportional to the end effector's elevation as shown in Figure 12.

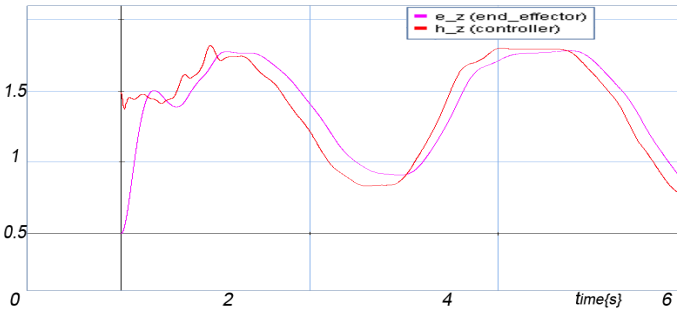

Fig. 11. Motion of the crane end-effector (in m) along the z axis as a result of the haptic input device's movements which is operated by the user.

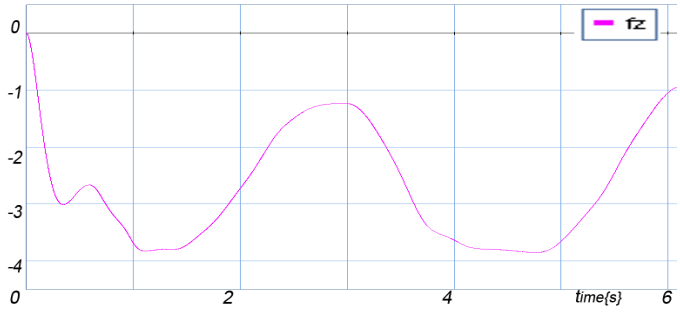

Fig. 12. Force feedback (in Newton) perceived by the crane operator.

All the simulations were performed using damping elements in the joints in order to reduce high frequencies and thus shorten the simulation time. The damping parameters were set to values that ensured that the system would be critically damped in all our simulations.

V. Conclusion and Future Work

In this paper, the so-called Bond Graph Method was used to introduce a modular system architecture that allows for modeling and simulating different maritime cranes or robotic arms. The base module of this architecture is the crane beam model. Using different joint modules to connect several such models, different crane models can be easily built. The resulting models can be simulated and controlled by using the same input haptic device which provides the user for a valuable force feedback. The arm joint angles are calculated at runtime according to the specific dynamic model of the robot to be controlled. Using the proposed approach, each arm model can be connected to a simplified model of a vessel, providing a complete model.

Related simulations were carried out to validate the efficiency and flexibility of the proposed architecture. In this preliminary study, the results show a general trend and a qualitative idea of the system behaviour. However the proposed approach can be used to get more accurate results using proper parameter tuning and deriving a more realistic set of coefficients according to the specific case of study.

As future work, it will be useful to model, simulate and compare different crane configurations to prove the flexibility of the proposed architecture. A comparison with traditional modeling methods will also be necessary to prove the advantage of using Bond Graphs over other modeling techniques.

Another issue that has to be better investigated in the next future concerns the effectiveness of using such a haptic device on board of a vessel from a human factor point of view.

In the future, the proposed system architecture could be used for finding dynamic responses in complex marine operations or for controlling a real crane on a vessel. However, for such applications, the level of accuracy in the model must be raised and a more accurate tuning of all the involved parameters has to be carried out.

References

Allen, R. (1979), 'Multiport representation of inertia properties of kinematic mechanisms', *Journal of the Franklin Institute* **308**(3), 235–253.

Amerongen, J. (2000), Modeling, simulation and controller design for mechatronic systems with 20-sim 3.0, *in* '1st IFAC conference on Mechatronic Systems, Darmstadt, Germany'.

Broenink, J. (1999), '20-sim software for hierarchical bond-graph/block-diagram models', *Simulation Practice and Theory* **7**(5), 481–492.

Craig, J. (2004), Introduction to robotics: mechanics and control, Prentice Hall.

de Melo, L. & Mangili, J. (2009), Virtual simulator with mobile robot rapid prototyping for navigation systems, *in* 'ICIA International Conference on Information and Automation', IEEE, pp. 899–904.

Fagereng, C. (2011), Mathematical Modeling for Marine Crane Operations, PhD thesis, Norwegian University of Science and Technology.

Filippini, G., Delarmelina, D., Pagano, J., Alianak, J., Junco, S. & Nigro, N. (2004), 'Dynamics of multibody systems with bond graphs', *Mecánica Computacional* **26**, 2943–2958.

Fossen, T. (1994), 'Guidance and control of ocean vehicles', *New York* .

Hellrand, A., Moen, L. & Faanes, T. (1990), Crane control system with active heave compensation and constant tension modes onboard the vessel stena wel/servicer, *in* 'Offshore Technology Conference'.

Hogan, N. (1984), Impedance control: An approach to manipulation, *in* 'American Control Conference', IEEE, pp. 304–313.

Johnson, P. (1985), Offshore crane wave motion compensation apparatus, Technical report.

Karnopp, D. (1992), 'An approach to derivative causality in bond graph models of mechanical systems', *Journal of the Franklin Institute* **329**(1), 65–75.

Karnopp, D., Margolis, D. & Rosenberg, R. (2006), *System dynamics: modeling and simulation of mechatronic systems*, Vol. 3, John Wiley & Sons New Jersey.

Karnopp, D., Margolis, D. & Rosenberg, R. (2012), *System Dynamics: Modeling, Simulation, and Control of Mechatronic Systems*, Wiley.

Lumia, R., Starr, G., Wood, J., Jones, B., Shohet, I. & Ledman, E. (1997), An approach to minimize robotics system development and integration time, *in* 'Proceedings., International Conference on Robotics and Automation', Vol. 4, IEEE, pp. 3220–3225.

McKenna, P. & Leithead, W. (2007), Semi-autonomous control of offshore cranes, *in* 'Institution of Engineering and Technology Conference on Autonomous Systems', IET, pp. 1–6.

Nielsen, F. (2007), 'Lecture notes in marine operations', *Department of Marine Structures, Norwegian University of Science and Technology, Trondheim, Norway* .

Pedersen, E. (2009), Rotordynamics and bond graphs: basic models, *in* 'Journal of Mathematical and Computer Modeling of Dynamical Systems', Vol. 15, No.4, pp. 337–352.

Pedersen, E. (2012), Bond graph modeling of marine vehicle dynamics, *in* 'Bond Graph Modeling: Theory and Practice Symposium at the 7th Vienna International Conference on Mathematical Modeling'.

Vaz, A., Kansal, H. & Singla, A. (2003), Some aspects in the bond graph modeling of robotic manipulators: angular velocities from symbolic manipulation of rotation matrices, *in* 'TENCON Conference on Convergent Technologies for Asia-Pacific Region', Vol. 1, IEEE, pp. 294–299.

Yi, J., Yubazaki, N. & Hirota, K. (2003), 'Anti-swing and positioning control of overhead traveling crane', *Information Sciences* **155**(1), 19–42.

Zhang, C. & Song, S. (1993), 'An efficient method for inverse dynamics of manipulators based on the virtual work principle', *Journal of Robotic Systems* **10**(5), 605–627.

AUTHOR BIOGRAPHIES

FILIPPO SANFILIPPO is a PhD candidate in Engineering Cybernetics at the Norwegian University of Science and Technology, and research assistant at the faculty of Maritime Technology and Operation, Aalesund University College, Norway. He obtained his Masters Degree in Computer Engineering at University of Siena, Italy.
Email: fisa@hials.no

HANS PETTER HILDRE is a Professor on Product and System Design at the Department of Maritime Technology and Operation, Aalesund University College, Norway.
Email: hh@hials.no.

VILMAR ÆSØY received his PhD in Mechanical Engineering in 1996 at the Norwegian University of Science and Technology, Department of Marine Technology. From 1997-2002 he worked in the maritime industry as researcher in Aker Maritime and R&D manager in Rolls-Royce Marine. Since 2002 as Assistant Professor in Mechanical and Marine Systems Engineer at Aalesund University College, Department of Maritime Technology and Operation.
Email: ve@hials.no.

HOUXIANG ZHANG received Ph.D. degree in Mechanical and Electronic Engineering in 2003. From 2004, he worked as Postdoctoral Fellow at the Institute of Technical Aspects of Multimodal Systems (TAMS), Department of Informatics, Faculty of Mathematics, Informatics and Natural Sciences, University of Hamburg, Germany. Dr. Zhang joined the Department of Maritime Technology and Operation, Aalesund University College, Norway in April 2011 where he is a Professor on Robotics and Cybernetics.
Email: hozh@hials.no.

EILIF PEDERSEN is a Associate Professor on Modeling and simulation of machinery systems at the Department of Marine Technology, Norwegian University of Science and Technology, Norway.
Email: eilif.pedersen@ntnu.no.

Methodology of tolerance synthesis using bond graph

Van Hoa NGUYEN[+], Damien EBERARD[+], Wilfrid MARQUIS-FAVRE[+], Laurent KRAHENBUHL[*]
[+]Université de Lyon, INSA de Lyon, Laboratoire Ampère (CNRS UMR5005),
Address: 20 Avenue Albert Einstein 69621 Villeurbanne cedex - France,
Email: surname.name@insa-lyon.fr
[*]Université de Lyon, École Centrale de Lyon, Laboratoire Ampère (CNRS UMR5005)
Address: 36 avenue Guy de Collongue - 69134 Ecully Cedex - France,
Email: laurent.krahenbuhl@ec-lyon.fr

KEYWORDS

Tolerance synthesis, Bond graph, Inverse model, Aleatory uncertainty, Probability theory

ABSTRACT

This paper presents a methodology of parametric tolerance synthesis with respect to output aleatory uncertainty specifications. It relies on density function propagation through the inverse model. The resulting parameter density function is then used to synthesize a confidence interval suitable for sizing purpose. As an illustration, parametric tolerance synthesis on a DC motor rotating a load is processed.

INTRODUCTION

Nowadays, mechatronics touches a wide range of applications, in daily life as well as in industry. Following technologies improvements, design process has to balance time development and manufacturing cost while systems requirements become increasingly sharp. Part of this process is concerned with parametric tolerance intended for manufacturers towards minimal cost components design with respect to requirements.

In the framework of this paper, we are interested in the problem of **parametric tolerance synthesis with respect to specifications including output aleatory uncertainties**. The aim is to obtain the tolerance of the design parameter to keep satisfying the requirement. We adopt the bond graph language (for system modelling, structural analysis and inverse model generation) and probability tools (for aleatory uncertainties representation and propagation).

Classically represented by its transfer function, or state equations, mechatronic system are often treated as a whole, without consideration to local physical phenomena. We propose, in this paper, to use the **bond graph language** [1] to represent the mechatronic system, in order to better adapt the modelling to physical phenomena and causalities. Bond graph is a multi-discipline language, which facilitates the representation of multi-domain mechatronic system. It is popularly used in engineering applications [2, 3], especially multi-domain physical systems [4,5]. A mathematical foundation of bond graph is established in [6].

The bond graph framework provides users with model inversion algorithms [7, 8]. Based on the concept of bi-causality [9], the bond graph model serves for design purposes while keeping the same structure as that of the direct model. Inverse model approach reduces the calculus time and the number of simulating iterations, while, at the same time, takes a good view on physical phenomena and effects. The structural invertibility of a bond graph model is easily checked thanks to existing procedures based on power lines [8] and causal paths [10].

Uncertainty in a mechatronic system is categorized into three distinct classes: *variability, uncertainty, and error* [11]. Different approaches for uncertainty characterizing and managing are required for the different classes. In this paper we focus on aleatory uncertainty. A similar procedure to deal with epistemic uncertainty in mechatronic system tolerance synthesis has been treated in [12].

Aleatory uncertainty in a mechatronic system refers to the inherent variation associated with the physical system or the environment. In the simplest form, aleatory uncertainty is often quantified with interval arithmetic [13, 14]. However, it is proven to be expensive in computation time and the propagation result is often over-estimated. Therefore, aleatory uncertainty is usually represented by probability theory in the form of probability density function (PDF).

Having the inverse model and uncertainties on output specifications, one has to propagate them to the design parameters. In order to propagate aleatory uncertainty through a mechatronic model, there are several popular approaches: the classical Monte-Carlo and Polynomial Chaos. Monte-Carlo is a computational sampling and simulation methods. A general overview of this method is given in [15]. Polynomial Chaos is based on the solution of stochastic differential equations. Firstly developed in [16], this method was continuously refined and applied into structural analysis problems [17–20]. The cost of polynomial chaos method is much cheaper than Monte-Carlo, yet is still significantly high.

Based on the principle of conservation of probability, a stochastic formulation of physical system was proposed in [21]. That formulation was applied to the inverse model to propagate the PDFs [22] and to form the probabilistic bond graph. This method takes into account the dynamics of stochastic systems and can be applied to an inverse model. However, it requires to determine firstly the joint PDF of the energy variables and their derivatives, which is

Proceedings 27th European Conference on Modelling and Simulation ©ECMS Webjørn Rekdalsbakken, Robin T. Bye, Houxiang Zhang (Editors)
ISBN: 978-0-9564944-6-7 / ISBN: 978-0-9564944-7-4 (CD)

sometimes hard to obtain.

In this paper, we shall use the probability density function to represent output uncertainties specifications. Moreover, uncertainty propagation through inverse model is processed using an analytical way.

The paper is organized as follows. In the next section, the problem of tolerance synthesis is briefly formulated. In the third section, a methodology of tolerance synthesis is presented. The methodology is illustrated in the fourth part by an example of tolerance synthesis on a DC motor where both cases of output mono-uncertainty and output multi-uncertainty are considered.

FORMULATION OF THE PROBLEM

Our goal is to determine the tolerances of design parameters given the probabilistic representation of aleatory output uncertainties.

System's specifications contain the deterministic behaviour that characterizes the (ideal) scenario to be followed. The associated set of desired output trajectories is then considered to be subject to aleatory uncertainties. Output uncertainties are translated into a family of trajectories living in the neighbourhood of the desired ones. The model gives us the relation between the output behaviours and the design parameters, which sets a base of knowledge for tolerance synthesis.

Let us consider a given mechatronic system. We shall use probability density functions to quantify the output aleatory uncertainties included in the specifications. It describes the relative likelihood for the output to behave in a given way. Once the aleatory output behaviour is quantified with PDFs, the aim is to link it with the design parameters. The inverse model gives us this link with an explicit relation between outputs and design parameters. The PDF of the output uncertainty is then propagated through the inverse model using theorem 1 [22]:

Theorem 1: Let Θ_1 be an aleatory variable with marginal PDF $\phi_{\Theta_1}(\theta_1)$, and Θ_2 another aleatory variable such that $\Theta_2 = g(\Theta_1)$ where g is a diffeomorphism. Then the associated PDF $\phi_{\Theta_2}(\theta_2)$ is given by

$$\phi_{\Theta_2}(\theta_2) = \frac{\phi_{\Theta_1}(g^{-1}(\theta_2))}{|g'(g^{-1}(\theta_2))|},$$

where g^{-1} is the inverse function of g and g' its differential.

The latter remains true for a vector of aleatory variables.

Moreover, notice that when g is not a global differomorphism (a popular scenario) but satisfies some smoothness condition, the θ_1-space can be partitioned in such a way that g restricted to any subpart is a local diffeomophism denoted g_i. In that case, the marginal PDF of Θ_2 is given by

$$\phi_{\Theta_2}(\theta_2) = \sum_{i=1}^{k} \frac{\phi_{\Theta_1}(g_i^{-1}(\theta_2))}{|g'(g_i^{-1}(\theta_2))|}.$$

In practice, one not only consider a single variable but rather a vector of aleatory variables. In that case, the aleatory uncertainties are represented by the joint PDFs of those vectors and the propagation is actualized on those joint PDFs.

The above theorem assumes that the vectors of aleatory variables Θ_1 and Θ_2 have the same dimension. If it is not the case, fictive variables have to be added in order to complete the dimension.

Propagating the uncertainty in output behaviours yields the probability density functions of the design parameters, which allow the determination of tolerances of design parameters with respect to the specifications.

METHODOLOGY OF TOLERANCE SYNTHESIS IN THE PRESENCE OF ALEATORY UNCERTAINTY

We propose the next procedure to solve our problem of tolerance synthesis:

A **Modelling:** Construct the bond graph of the system, model the aleatory uncertainties included in the output specifications with probability density function, determine the set of design parameters and outputs.

B **Adequacy:** Check the adequacy between the system structure and the input/output specifications [22].

C **Inversion:** Test the structural invertibility [8, 10] and construct the inverse model [22, 23]

D **Propagation:** Deduce the PDF associated with the design parameters by propagating the output uncertainties through the inverse model.

E **Tolerance synthesis:** Synthesize the tolerance of the design parameters from their computed uncertainties.

F **Validation:** Verify the chosen tolerance in simulation in direct model.

A. *Modelling*

The bond graph model is constructed based on the physical phenomena of the deterministic mechatronic system. Because we focus on the problem of tolerance synthesis, the structure of the model is assumed to be known and fixed (which means that there is no black-box, models commutation, discontinuity). The parameters of system are then classified into two sets: the set of known parameters and the set of design parameters (those of interest for tolerance synthesis).

Output uncertainties are modelled with their probability density functions.

B. *Adequacy verification*

Depending on its nature, some types of specifications are not compatible with certain types of dynamic systems or model workspace, etc.... A verification of adequacy between the system's structure and the input/output specifications is therefore essential. In the case of linear system, an adequacy verification procedure based on the order of system is given in [22]. This step means to avoid unnecessary further advancement, if the structure of system is not adequate with the demanded specifications. It gives also hints to redefine a proper set of requirements in that case.

C. *Inversion*

We shall deduce an explicit relation between the outputs and the design parameters via the inverse bond graph model. The direct model outputs will be the inputs of the inverse model and the design parameters will be the outputs of the inverse model. A structural analysis of causal paths and

power lines [22,23] has to be done to verify the invertibility. The inverse model of minimum order can be found from the bicausal bond graph with the procedure detailed in [22]. It is necessary to find the model of minimum order, because it decides the order of derivatives of outputs in the inverse model, hence, in the calculation cost.

D. Propagation

There are two ways to propagate the uncertainties throughout the inverse bond graph model: global approach and local approach. In global approach, the system is considered as a whole and the output (or vector of outputs) is directly connected to the parameter(s) by a global relation (or a set of relations); the uncertainties on output (or vector of outputs) is propagated to the parameter(s) under interest by applying the theorem 1 to that global relation (or a set of relations). Another approach is the local propagation: PDFs from outputs (or vector of outputs) are transferred from element to element in the (inverse) bond graph model, until it reaches the design parameters. This approach offers a closer look to the effects of uncertainty to local physical phenomena.

In case of output multi-uncertainty, the obtained PDF is the joint PDF of design parameters (including "fictive" parameters, if they were added to balance the vector dimension). In order to determine the marginal PDF of one design parameter, we need to integrate the joint PDF on all the domains of definition of the other parameters (including the "fictive" variables) following theorem 2 below.

Theorem 2: Given the joint PDF $\phi_{(\Theta_1,\Theta_2,\ldots,\Theta_n)}$, the marginal PDF of an element θ_1 is calculated:

$$\phi_{\Theta_1}(\theta_1) = \int_{\Theta_2} \ldots \int_{\Theta_n} \phi_{(\Theta_1,\Theta_2,\ldots,\Theta_n)}(\theta_1,\theta_2,\ldots,\theta_n) d\theta_2 \ldots d\theta_n$$

E. Tolerance synthesis

The final PDF obtained for the design parameter provides us with information on its distribution law. Different from interval analysis, where we obtain only the "worst case solution", with the PDF, we obtain more information about the distributing interval of the design parameters. This PDF is, however, not necessarily Gaussian nor symmetric, which is required in most manufacturing processes. An adaptation step is therefore necessary. In the frame of our research, the tolerances of the design parameters are defined as a Gaussian laws with the same mean and variance as the computed PDF.

F. Validation

From the obtained tolerance, we generate a number of samples, following the synthesized PDF of the parameter, and re-inject them into the direct bond graph model. Simulation is made with the generated values to verify the specifications on system's performance. The simulated results are checked with the set of requirements. Since the initial specifications are given in the form of PDFs, on may have to compare the PDF obtained from simulation's results and initial PDFs.

This can be done visually if the PDF obtained from simulations stays totally inside the interval of the initial PDF. However, in some case, the comparison is hard to be done visually, a numeric criterion is therefore needed. We adopt here the criterion of quantiles:

Definition 1: The quantile function Q_X at level u is defined by $Q_X(u) = \inf\{x/F_X(x) \geq u\}$ where F_X is the distribution function of the aleatory variable X.

The two PDFs are considered similar enough if the error between them is less than 15%:

Criterion 1: The criterion of quantiles gives the mean average error (MAE) as follows

$$MAE = \Sigma \frac{|Q_i^1 - Q_i^2|}{\sigma^1} \leq 15\%$$

with $i = \{1, 5, 25, 50, 75, 95, 99\}\%$, σ^1 is the variance of the first PDF.

In the next part, we illustrate our proposed procedure on the example of a DC motor rotating a load.

EXAMPLE

Consider a DC motor rotating a load (Figure 1). As an illustration of our methodology, we process the tolerance synthesis of the internal resistance of the DC motor. We shall study a simple output mono-uncertainty case and an output multi-uncertainty case.

Modelling assumptions: The electrical part contains a voltage source u, an internal resistance R and an inductance L. The (ideal) electromechanical coupling is characterized by a torque constant k_c. The mechanical part takes into account the motor axis inertia J_m and the load inertia J_c, a reduction gear ratio $1/N$ and the viscous friction coefficient b_c on the load axis.

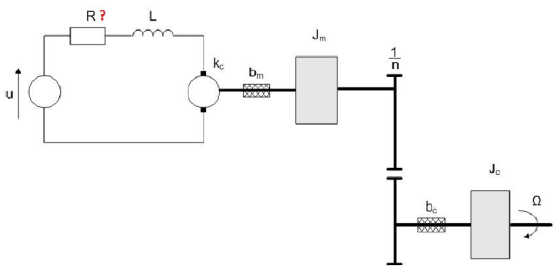

Fig. 1: Scheme of a DC motor rotating a load

Data specifications.

L	Motor internal self inductance	$0.001[H]$
k_c	Electromechanical coupling	$0.031[N.m/A]$
J_m	Motor axis inertia	$1.8 \times 10^{-6}[kg.m^2]$
N	Gear ratio	$1/20$
J_c	Load inertia	$2 \times 10^{-4}[kg.m^2]$
b_c	Viscous friction coefficient	$0.0001[N.m/rad.s^{-1}]$
u	Input voltage	$20[V]$

Performance specifications. The output angular velocity Ω is desired to follow a second order step response with an amplitude $K = 32$, a damping ratio $\xi = 24$ and an undamped frequency $\omega_n = 650$ rad.s^{-1}.

Uncertainty specifications. The stationary output velocity may vary in the interval $\delta K = \pm 1$. For the other two parameters, one specifies $\delta\xi = \pm 3$ and $\delta\omega_n = \pm 30\ s^{-1}$.

These variations form an envelop that the output trajectory is expected to lie within.

We shall first study the mono-uncertainty case where only uncertainty on the amplitude K is taken into account. Then, we study the multi-uncertainty case where variations on K, ξ and ω_n are considered.

Mono-uncertainty

Modelling. The bond graph model of the system is given in Fig. 2. The internal motor resistance R is the design

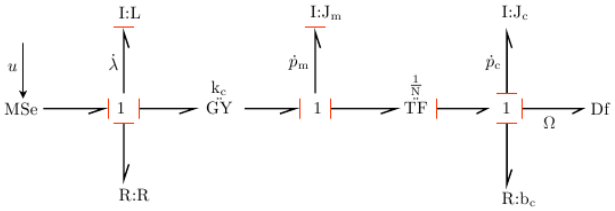

Fig. 2: Causal bond graph representation of a DC motor rotating a load

parameter and the output is the angular velocity Ω.

We model the uncertainty on K as a Gaussian distribution with density probability function ϕ_K, which has as expectation the nominal deterministic value $\mu_K = 32$ and variance $\sigma_K = 1/3$.

$$\phi_K = \mathcal{N}(\mu_K, \sigma_K)\,.$$

Adequacy. We note $J = \frac{J_m}{n} + nJ_c$ and $b = \frac{b_m}{n} + nb_c$. The dynamic response writes

$$\left(\frac{k_c}{n} + \frac{Rb}{k_c}\right)\Omega + \left(\frac{RJ + Lb}{k_c}\right)\dot{\Omega} + \frac{LJ}{k_c}\ddot{\Omega} = u \qquad (1)$$

The considered model is therefore a second order. As a result, its structure is in adequacy with the specification.

Inverse model. The structure of system verifies the criterion of invertibility [23] from the output Ω to the design parameter R. The bicausal bond graph model is given in Fig. 3.

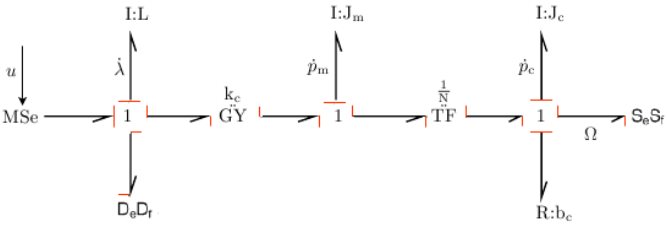

Fig. 3: Bicausal bond graph representation of inverse model

The minimum order inverse model, obtained from [22] applied to the model depicted in Figure 3, is given by

$$\begin{aligned} R &= \frac{u - L\left[\frac{1}{k_c}\left(\frac{J_m}{n} + nJ_c\right)\ddot{\Omega} - \frac{1}{k_c}\left(\frac{b_m}{n} + nb_c\right)\dot{\Omega}\right] - \frac{k_c}{n}\Omega}{\frac{1}{k_c}\left(\frac{J_m}{n} + nJ_c\right)\dot{\Omega} + \frac{1}{k_c}\left(\frac{b_m}{n} + nb_c\right)\Omega} \\ &= g(u, \Omega, \dot{\Omega}, \ddot{\Omega}) \\ &= h(u, K, \xi, \omega_n)\,. \end{aligned} \qquad (2)$$

Propagation. Uncertainty on the amplitude K is propagated to the internal resistance R through the inverse model h given by (2). This results in the PDF ϕ_R which represents the uncertainty on the design parameter R evolving in time (Fig. 4).

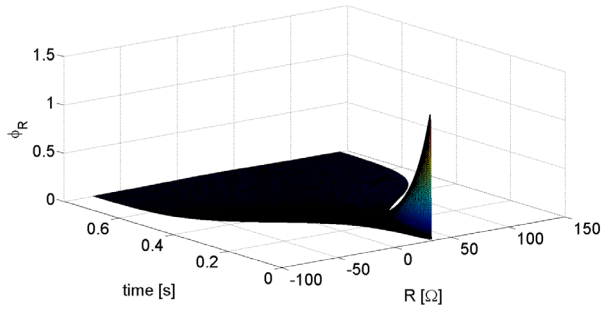

Fig. 4: ϕ_R evolving in time

Tolerance synthesis. Projecting the obtained PDF set onto (R, t), we obtain the set of values of r with $\phi_R(r) > 0$ and the curve of modal value of R (Fig. 5). We want the

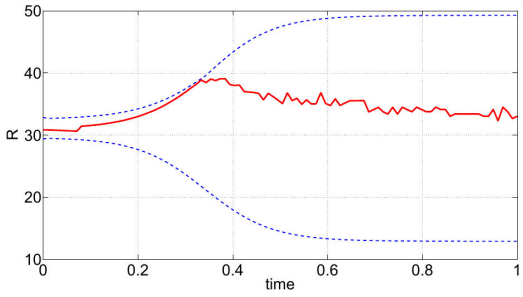

Fig. 5: Set of values of r with $\phi_R(r) > 0$ and modal value of R

output trajectories to be bounded by the specified envelop (blue dotted curve). The value of R is therefore supposed to stay inside the interval defined by the minimum of the upper curve and the maximum of lower curve in Fig. 5. However, since the amplitude uncertainty mainly acts on the steady-state values of the response and little on the transient response, we shall determine the tolerance of R from the PDF at an *ad hoc* time. In this example, we have arbitrary chosen 0.1 second. The output trajectory is therefore expected to stay inside our envelop from 0.1 second. This PDF is however, not necessarily Gaussian, we choose therefore the PDF of the tolerance as an Gaussian with same mean and variance.

Validation. We generate random samples of R according to the PDF tolerance and re-inject into our direct model.

The simulations give us the corresponding gains and trajectories (Fig. 6). As predicted, the trajectories go out of the

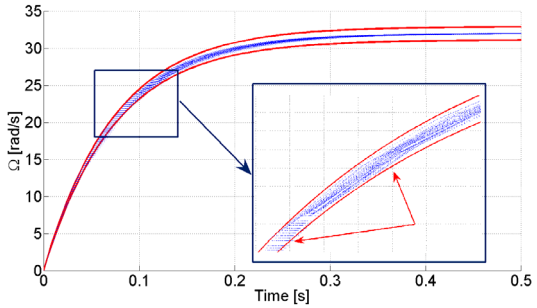

Fig. 6: Simulations with the synthesized tolerance

envelop for a short time, but they do lie inside the envelop from 0.1s (Fig. 6). The PDFs of K are synthesized from the obtained samples. We notice also that the PDF of K obtained from simulated samples is much more concentrated to the nominal value than the desired PDF (Fig. 7). The specifications on K is met. We can therefore validate our choice of tolerance on R

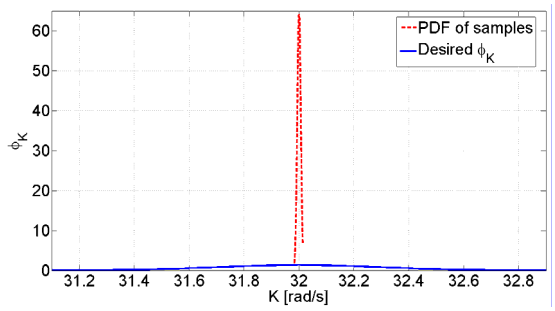

Fig. 7: Desired PDF of K and obtained PDF from samples

Output multi-uncertainty

Modelling. The modelling assumptions are identical to the previous case. We thus deal with the same bond graph model given in Fig. 2. The only difference resides in the fact that we now add the damping ratio ξ and the undamped frequency ω_n uncertainties in order to take into account transient response uncertainties. Similarly, the uncertainties on the undamped natural frequency ω_n and on the damping ratio ξ are represented by their PDFs (assumed to be Gaussian)

$$\phi_K = \mathcal{N}(32, 0.33), \quad \phi_\xi = \mathcal{N}(24, 1), \quad \phi_{\omega_n} = \mathcal{N}(650, 10).$$

The steps of **adequacy verification** and **inversion** are identical to the previous case.

Propagation. The uncertainty is given on a vector $\begin{bmatrix} K \\ \omega_n \\ \xi \end{bmatrix}$. In order to propagate, we need to add, for instance, K and ω_n (as fictive variables) to R to form a vector. The uncertainty vector is then $\begin{bmatrix} R \\ K \\ \omega_n \end{bmatrix}$ and we have the relation

$$\begin{bmatrix} R \\ K \\ \omega_n \end{bmatrix} = G \begin{bmatrix} K \\ \omega_n \\ \xi \end{bmatrix}$$

where the linear map is given by $G = (g, id_K, id_{\omega_n})$. We assume that K, ω_n and ξ are independent variables. From independency, the joint PDF of (K, ω_n, ξ) is the product of marginal PDFs and is calculated as

$$\phi_{(K,\omega_n,\xi)} = \phi_K . \phi_{\omega_n} . \phi_\xi$$

Thefore, the Jacobian of G, denoted $|J_G|$ is

$$|J_G| = \det \begin{bmatrix} \frac{\partial g(K,\omega_n,\xi)}{\partial K} & \frac{\partial g(K,\omega_n,\xi)}{\partial \omega_n} & \frac{\partial g(K,\omega_n,\xi)}{\partial \xi} \\ \frac{\partial K}{\partial K} & 0 & 0 \\ 0 & \frac{\partial \omega_n}{\partial \omega_n} & 0 \end{bmatrix}$$

The joint PDF of (R, K, ω_n) is then computed as (following Theorem 1) as

$$\phi_{(R,K,\omega_n)} = |J_G|^{-1} . \phi_{(K,\omega_n,\xi)}$$

The PDF of R is deduced from the joint PDF of (R, K) while integrating along K and ω_n (see Theorem 2). The obtained PDF, depicted in Figure 8, represents the variability of R evolving in time.

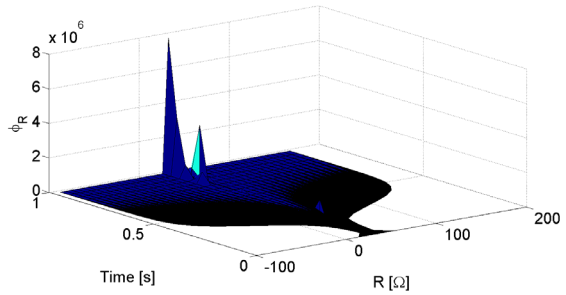

Fig. 8: ϕ_R evolving in time

Tolerance synthesis. Projecting this PDF set to (R, t), we obtain the set of values of r with $\phi_R(r) > 0$ and the curve of modal value of R (Fig. 9) The tolerance of R is therefore synthesized as PDF that gives the smallest interval of R with $\phi_R(r) > 0$ in t.

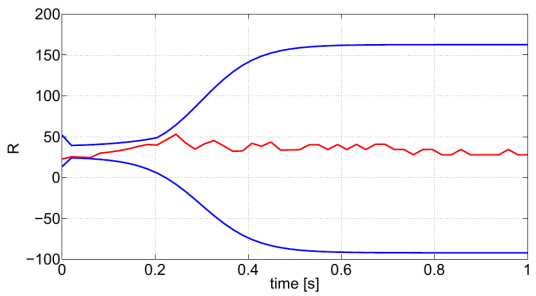

Fig. 9: Set of values of r with $\phi_R(r) > 0$ and modal value of R

Validation We generate random samples of R according to the PDF tolerance and re-inject into our direct model. The

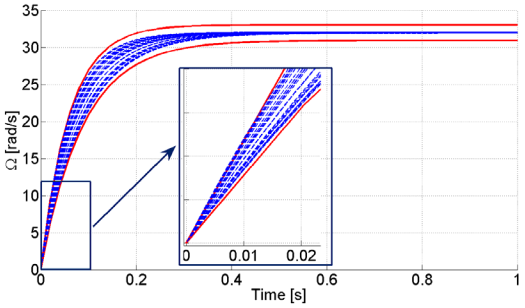

Fig. 10: Simulations with the synthesized tolerance

simulation gives us the corresponding gains and trajectories (Fig. 10). A tiny part of the trajectories goes out of the envelop before 0.01 sec. However, it is numerical error due to the fact that we began the simulation at 0.01 sec, and can be eliminated by setting the start point of simulation closer to 0. We verify also the PDFs of K, ω_n, ξ computed from the simulated samples. They are all much more concentrated to the nominal value than the demanded PDF, therefore verified. We present here only the PDF of K (Fig. 11). The

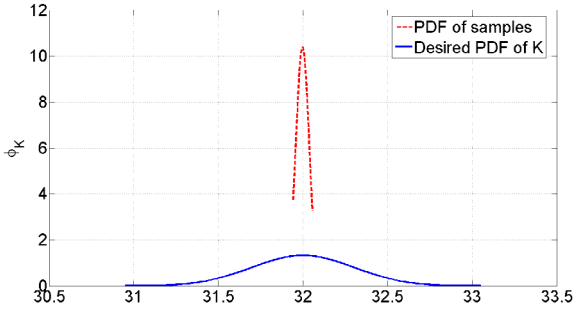

Fig. 11: Simulations with the synthesized tolerance

specifications are met. We can therefore validate our choice of tolerance on R

Conclusion and Outlook

In this paper, a methodology to address the problem of parametric tolerance synthesis in the presence of aleatory uncertainties has been presented.

Bond graph was chosen as the modelling tool, because of its multi-disciplinary and acausality. The inverse approach was adopted. That methodology proves its interest over the direct approach in term of calculation cost. However, it requires the structure of system to be invertible.

The proposed methodology provides users with the probability density function of the design parameter, evolving in time, which offers a complete view on the parameter's distribution. The methodology was illustrated on a simple example of tolerance synthesis on a DC motor.

As we mentioned above, three types of uncertainties coexist in mechatronic systems, which, in general, can not be treated separately. A combined representation and resolution should be investigated. Another perspective concerns stochastic uncertain systems which demand to handle much more complex specifications.

References

[1] H. Paynter, *Analysis and Design of Engineering Systems*, ISBN.0262160048 ed. Cambridge, USA: The M.I.T Press, 1961.

[2] P. C. Breedveld, "Modeling and simulation of dynamic systems using bond graphs," *In Control Systems, Robotics and Automation, from Encyclopedia of Life Support Systems (EOLSS), Developed under the Auspices of the UNESCO. EOLSS Publishers*, p. 1–36, 2008.

[3] D. Karnopp, D. Margolis, and R. Rosenberg, *System Dynamics. Modeling and Simulation of Mechatronic systems*, 4th ed. Hoboken, New Jersey: John Wiley & sons, Inc, 2012.

[4] P. Breedveld, "Port-based modelling of multidomain physical systems in terms of bond graphs," *Simulation Techniques for Applied Dynamics*, p. 141–190, 2009.

[5] D. Karnopp, "Bond graph models for electrochemical energy storage : electrical, chemical and thermal effects," *Journal of the Franklin Institute*, vol. 327, no. 6, pp. 983–992, 1990.

[6] S. Birkett and P. Roe, "The mathematical foundations of bond graphs—I. algebraic theory," *Journal of the Franklin Institute*, vol. 326, no. 3, pp. 329–350, 1989.

[7] S. Scavarda, M. Amara, and E. Richard, "Determination of the output power in terms of output variables using bond graph," *IMACS-IFAC Symposium MCTS 91 Modelling and Control of Technological systems*, p. 15, 1991.

[8] R. F. Ngwompo, S. Scavarda, and D. Thomasset, "Inversion of linear time-invariant SISO systems modelled by bond graph," *Journal of the Franklin Institute*, vol. 333, no. 2, pp. 157–174, Mar. 1996.

[9] P. Gawthrop, "Bicausal bond graphs," *SOCIETY FOR COMPUTER SIMULATION*, vol. 27, pp. 83—88, 1995.

[10] A. Jardin, W. Marquis-Favre, and D. Thomasset, "Bond graph sizing of mechatronic systems: Coupling of inverse modelling with dynamic optimization," in *Proceedings MATHMOD 09 Vienna - Full Papers CD Volume*, F. B. I. Troch, Ed., Vienne, Autriche, Feb. 2009, pp. 1929–1938, ISBN 978-3-901608-35-3.

[11] W. L. Oberkampf, S. M. DeLand, B. M. Rutherford, K. V. Diegert, and K. F. Alvin, "Error and uncertainty in modeling and simulation," *Reliability Engineering & System Safety*, vol. 75, no. 3, p. 333–357, 2002.

[12] V. H. Nguyen, D. Eberard, W. Marquis-Favre, and L. Krahenbuhl, "Tolerance synthesis using bond graph inversion and fuzzy logic," *IEEE International Conference on Mechatronics - ICM2013*, Feb. 2013.

[13] J. C. Helton, J. D. Johnson, W. L. Oberkampf, and C. J. Sallaberry, "Representation of analysis results involving aleatory and epistemic uncertainty," *International Journal of General Systems*, vol. 39, no. 6, p. 605–646, 2010.

[14] J. Helton, J. Johnson, and W. Oberkampf, "An exploration of alternative approaches to the representation of uncertainty in model predictions," *Reliability Engineering & System Safety*, vol. 85, no. 1–3, pp. 39–71, Jul. 2004.

[15] R. E. Melchers, *Structural Reliability Analysis and Prediction*, 2nd ed. Wiley, Apr. 1999.

[16] N. Wiener, "The homogeneous chaos," *American Journal of Mathematics*, vol. 60, no. 4, p. 897, Oct. 1938.

[17] R. Ghanem, "Ingredients for a general purpose stochastic finite elements implementation," *Comput. Methods Appl. Mech. Engrg*, vol. 168, p. pp., 1999.

[18] R. Ghanem and J. Red-Horse, "Propagation of probabilistic uncertainty in complex physical systems using a stochastic finite element approach," *Physica D: Nonlinear Phenomena*, vol. 133, no. 1–4, pp. 137–144, Sep. 1999.

[19] O. P. Le Maitre, O. M. Knio, H. N. Najm, and R. G. Ghanem, "A stochastic projection method for fluid flow," *Journal of Computational Physics*, vol. 173, no. 2, pp. 481–511, Nov. 2001.

[20] C. Dinescu, S. Smirnov, C. Hirsch, and C. Lacor, "Assessment of intrusive and non-intrusive non-deterministic CFD methodologies based on polynomial chaos expansions," *International Journal of Engineering Systems Modelling and Simulation*, vol. 2, no. 1/2, p. 87, 2010.

[21] J. Li and J. Chen, "The principle of preservation of probability and the generalized density evolution equation," *Structural Safety*, vol. 30, no. 1, pp. 65–77, Jan. 2008.

[22] M. E. Feki, "Analyse et synthèse de tolérance pour la conception et le dimensionnement des systèmes mécatroniques," Ph.D. dissertation, Ecole Centrale de Lyon, Jul. 2011.

[23] A. Jardin, "Contribution à une méthodologie de dimensionnement des systèmes mécatroniques : analyse structurelle et couplage à l'optimisation dynamique," Ph.D. dissertation, Jan. 2010.

A NOVEL APPROACH TO ANTI-SWAY CONTROL FOR MARINE SHIPBOARD CRANES

Siebe B. van Albada[1], G. Dick van Albada[2], Hans Petter Hildre[3] and Houxiang Zhang[3]
[1]Faculty of Engineering and Natural Sciences
[3]Faculty of Maritime Technology and Operation
Aalesund University College
Postboks 1517, N-6025 Aalesund, Norway

[2]Section Computational Science, Informatics Institute, Faculty of Science
Universiteit van Amsterdam
Sciencepark 904, 1098 XH Amsterdam, The Netherlands

KEYWORDS
Anti-sway, Maritime cranes, integrated method.

ABSTRACT

This paper addresses the development of a novel anti-sway control approach for marine shipboard cranes, offering stability, safety, and efficiency during lifting, handling, transportation, and other manipulation. The proposed idea consists of the development of an integrated system with control strategies to both reduce the effect of three-dimensional payload pendulation and to minimize wave impact during shipboard crane manipulation. We propose to use a control mechanism based on energy dissipation. The simulation results confirm the principle and effectiveness of the proposed methods for damping out pendulation. In future work, we aim to minimize wave impact on the payload by reducing the dynamic forces through controlling the length of the hoist cable while adapting to the lateral wave velocity. During the final phase of this project, the proposed control strategy will be implemented as a real physical prototype for controlling different kinds of shipboard cranes.

I. INTRODUCTION

Shipboard cranes are widely used to handle and transfer objects from large container ships to smaller lighters or to the quays of the harbours. The control of cranes is always a challenging task which involves many problems such as load sway, positioning accuracy, suppression, collision avoidance, and manipulation security. Generally, shipboard cranes are relatively big, heavy, stiff, and rely on complex kinematic models of their system as well as an equally complex model of the environment with which they interact. Typical shipboard crane operations are shown in Figure 1. There are two big challenges during crane operation. First, unlike cranes mounted on solid bases, load sway is affected by the ship's motion when the load is hoisted by a shipboard crane. This motion produces large pendulations of the hoisted cargo and causes operations to be suspended. Second, when the payload is hit by waves on the surface of the sea, it is subject to an impulsive hydrodynamic slamming force, which, in harsh sea conditions, can damage the payload.

The pendulation caused by the payload and the sway caused by the waves not only limits the functionality of marine facilities in adverse weather conditions, but also poses a threat to the safety of personnel and equipment during off-shore operations. The pendulation is often induced by a combination of the vessel's motions and the crane operator's normal actions. In general, the payload acts as a spherical pendulum whose attachment point is manoeuvred using the crane's degrees of freedom. As the operator commands the various axes of the crane to affect rigid body payload translation and rotation, the payload's sway degrees of freedom can be excited. This payload pendulation problem becomes much more complicated if the crane is mounted to a moving vessel. An experienced operator can often generate crane inputs correctly, in such a way that the payload is sway-free at the end of the manoeuvre. However, training an operator to use a crane requires significant resources and poses potential hazards. Imagine the challenge of installing a 200 ton sub-sea module at 2000 meters sea depth with an accuracy of centimetres! When considering both working efficiency and safety, quality control is impossible to achieve.

Figure 1 Typical shipboard Crane operation.

We propose a combined control strategy that both reduces the effects of payload pendulations and minimizes wave impact on shipboard crane manipulation. The new control approach will improve the safety of demanding marine operations. In this paper, we only present the first phase and current work of this project. The research result will be integrated with the current "crane/winch simulator" developed by

Proceedings 27th European Conference on Modelling and Simulation ©ECMS Webjørn Rekdalsbakken, Robin T. Bye, Houxiang Zhang (Editors)
ISBN: 978-0-9564944-6-7 / ISBN: 978-0-9564944-7-4 (CD)

the Offshore Simulator Centre. Finally, a real prototype will be built and tested at the Rolls-Royce marine AS.

II. RELATED WORK

There are two challenging problems of handling shipboard cranes. To date, cargo loading operations at sea are often paused in case of unfavourable weather conditions. Without an efficient control mechanism, a modest movement of the ship can result in a large sway motion of the cargo. This can lead to dangerous situations. As a consequence, time and money are often wasted on waiting for better weather conditions, or worse, the risk may be taken to load the cargo in dangerous conditions. Once sea conditions build to a low sea state 3 (as defined by the Piersion-Moskowitz Sea Spectrum, with significant wave heights in the range of 1.0 - 1.6 m), hoisted payload pendulations on crane ships become dangerously large and operations must be suspended [1]. An analysis of worldwide weather and sea-condition data show that more than 35% of all potential joint logistics over the shore operations (JLOTS) sites have sea conditions of sea state 3 or higher 50% of the time during which operations would be suspended [1], [2]. Nojiri and Sasaki [3] calculated that payload pendulations due to excitation frequencies near the resonance frequency of the cable-payload assembly also have a pronounced effect on the rolling and pitching motion of the crane vessel under the influence of both regular and irregular waves.

The other problem during the lifting and transportation of shipboard cranes with long hoist cables is wave impact. When the payload is hit by the waves on the surface of the sea, it is subject to an impulsive hydrodynamic slamming force which, in harsh sea conditions, can damage the payload. Also in this case, if the sea conditions become prohibitive, the operations have to be suspended.

Regarding the load pendulation, many researchers investigated the problem for fixed-base cranes. As the rolling motion of a ship is dominating, and the cranes usually work from the sides of the ship, the swaying of the payload is mainly confined to two dimensions. Some controllers were originally designed for boom cranes, while others were modifications of earlier work on gantry cranes. Two main approaches can be identified among this research: one targets pendulation suppression throughout the whole transport manoeuvre, while the other is more concerned with end-of-manoeuvre pendulation suppression, the so-called "elimination of residual pendulation". In both approaches, limited research included the operator as a part of the model plan. Lewis et al. [4] and Parker et al. [5] presented a three-dimensional linear model of a boom crane. A controller applies quasi-static filters to the operator's input commands to avoid exciting the natural frequency of the cable-payload assembly. Experimental results showed a significant reduction in both the in-plane and out-of-plane payload pendulations.

Balachandran et al. [6, 7] modified the common boom-crane configuration in order to suspend the payload from a pivot that in turn was suspended under the boom. The pivot acted as a non-linear vibration absorber, a mechanical filter, to absorb the cargo oscillations. They derived two-dimensional and three-dimensional models of this new configuration. Their simulations showed that the absorber can suppress sub-critical bifurcations and shift the bifurcation points arising from the non-linear dynamics of the cable-payload assembly. Current ship cranes use a Rider Block Tagline System (RBTS). In this method, the intention is to change the natural frequency of the pendulum. The current RBTS has many deficiencies. As a result, Hunt et al. [8] proposed a new crane structure to suppress the pendulation using adjustable damping to dissipate the pendulation energy. In 1999, Kimiaghalam et al. [9] studied a crane with an additional tagline connecting the rope and the boom. They used the length of the tagline as the single control parameter, and designed a fuzzy controller in order to keep the load in place. However, they found that load oscillations were decreased by only about 50 %. In 2000, Kimiaghalam et al.[10] considered a crane with a rope suspended from two points on the boom, with the cargo hanging from a pulley in the middle. They showed that it is possible to almost eliminate sway motion by applying a combination of feedback and feed-forward control to the rope length and luffing angle of the boom. Thus, an implementation of this system seems to solve the problem of in-plane payload-pendulation. In their approach, Kimiaghalam et al. focused on keeping the equilibrium position of the pulley in place, which they approached by using feedback and feed-forward control on the angle of the boom with the horizon. Although this approach has proven to lead to good results for small rolling angles, we expect it to quickly break down under more extreme conditions. We state that real-time tracking of the load position is essential in order to cope with heavy weather conditions. The main reason for this is that the distance from the suspension point to the actual cargo can be very large, and as such, a tiny movement of the suspension point can lead to large oscillations of the cargo. In addition, not only the angle of the boom is of importance, but also the position and velocity of the payload should be considered at the same time. This becomes more important at larger rolling amplitudes of the ship.

In the rest of the paper, we will present our anti-sway approach. Firstly, in Section III, we outline the main control methods, which includes three important cases. In addition, we show simulation results for the different control algorithms. A series of simulation will be introduced to confirm the strategy. Finally, in section IV, we discuss the results and draw our conclusions as well as describe our ideas for future work.

III. INTEGRATED ANTI-SWAY APPROACH : METHODS AND RESULTS

We model the crane/winch system as a frictionless, non-elastic spherical pendulum. The motion of the pendulum is fully determined by algorithms steering the position of the support point and the length L of the cable via the winch, and external noise acting upon the position of the support point. Both the support and the wire are modelled as massless objects. The mass m of the load is in this approximation irrelevant for the motion of the pendulum. First, consider the simple pendulum moving in a plane, as shown in Figure 2, consisting of a mass m attached to a cable of lenght L.

A load is connected to a massless cable that is suspended from a support point. The position of the pendulum is determined by its angle θ with its rest position (green) or the distance s from the rest position along its circular trajectory. The forces acting upon the load are the gravitational force F_g (pointing vertically down, not shown in the figure) and the centrifugal force F_{cf} (pointing outward along the cable). F_g and F_{cf} are given by (1),

$$F_g = mg, F_{cf} = m\omega^2 L \tag{1}$$

where g is the gravitational acceleration and ω is the angular velocity of the load. If the lateral dispacement d of the support point is in the direction of the load, as shown in Figure 2, the work done is negative, such that energy is taken out of the system.

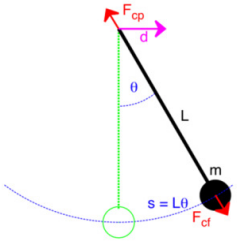

Figure 2 Simple Pendulum

At a given time t, the cable is under an angle θ with the vertical axis. We describe the position of the payload by the arc length s measured from the rest point along the trajectory of the payload. The equation of motion follows from Newton's second law in the direction of the payload motion (2),

$$g \sin\theta = \frac{\mathrm{F}}{\mathrm{m}} = a = \frac{d^2 s}{dt^2} = \frac{d^2(L\theta)}{dt^2} = L\frac{d^2\theta}{dt^2} \tag{2}$$

where F and a are the force on the payload and its acceleration, both in the direction of motion. We find the well-known differential equation (3), which is most easily solved by numerical methods.

$$\frac{d^2\theta}{dt^2} = \frac{g}{L}\sin\theta \tag{3}$$

In the present work, we propagate the motion of the pendulum in three dimensions, while we in addition freely move the support position which determines the motion of the pendulum. We derive the equations of motion from the Lagrangian $L = K–V$, in which K is the kinetic energy, as given in (4),

$$\frac{K}{m} = \frac{1}{2}[(\dot{x} + \dot{x_0})^2 + (\dot{y} + \dot{y_0})^2 + (\dot{z} + \dot{z_0})^2] \tag{4}$$

where $\boldsymbol{r}=(x, y, z)$ is the relative position of the load with respect to the support position $r_0 = (x_0, y_0, z_0)$, and V is the potential energy (5),

$$\frac{V}{m} = g(z + z_0) \tag{5}$$

We use spherical coordinates to find the equations of motion as shown in (6).

$$\left.\begin{aligned} r = |r|, \theta = atan\left(\frac{\sqrt{x^2+y^2}}{z}\right), \phi = atan2\left(\frac{y}{x}\right) \\ \Phi = \dot{\phi} \\ \Theta = \dot{\theta} \\ \dot{\Phi} = \frac{-2L\Theta\Phi\cos\theta + \ddot{x_0}\sin\phi - \ddot{y_0}\cos\phi}{L\sin\theta} \\ \dot{\Theta} = \frac{1}{L}(-\ddot{x_0}\cos\phi\cos\theta\sin\phi - \ddot{y_0}\sin\phi\cos\theta \\ -\ddot{z_0}\sin\theta - g\sin\theta + L\Phi^2\sin\theta\cos\theta) \end{aligned}\right\} \tag{6}$$

These equations have been implemented in a C program that propagates the system in time using Runge Kutta 4. The input of the system is given by the acceleration of the support point as a function of time. These equations are valid as long as the hoist cable is fully stretched, which was verified by testing for positive tension on the wire.

In addition, the length L of the wire is controlled via the winch. Although the results presented in this paper are in 2 dimensions, all simulations were done in 3 dimensions, and the methods presented here also are valid for 3-dimensional motion.

In order to control the motion of the pendulum, we will subsequently consider the following cases:
1. Damping out a large non-driven in-plane swaying motion.
2. Transport of the load from one position to another.
3. Damping out a driven planar oscillation.

III.I DAMPING A NON-DRIVEN OSCILLATION

We will start with the first case, damping out a non-driven planar swaying motion. This is the main method that we propose to use in order to damp out swaying motion. The approach is based on reducing the energy of the system. In the current section, we use the method to damp out a non-driven oscillation. We will show that the method also works to damp out driven oscillations. In addition, we have tested the method in three dimensions, both for driven and non-driven oscillations, with similar results. Most importantly, we expect similar methods to work in combination with operator-driven actions.

When the amplitude of the pendulum is large, our approach is to dissipate the energy from the swaying motion as quickly as possible. We can do this by making the work performed by the support on the pendulum maximally negative. This, in turn is done by moving the support point into the direction of the displacement of the pendulum, as shown in Figure 2.

The work performed by the support point on the pendulum can be obtained by (7):

$$dW = \boldsymbol{F}_{\text{sup}} \cdot d\boldsymbol{r}_0 \tag{7}$$

where $\boldsymbol{F}_{\text{sup}}$ is the force applied by the support point on the cable. The displacement $\boldsymbol{r}_0$ is in the horizontal direction whereas the force applied by the support point is directed along the direction of the hoist cable. The force applied by the support on the pendulum consists of three parts: a gravitational component $F_g \cos\theta = mg\cos\theta$, a centrifugal component $F_{cp} = m\omega^2 L$ and, if the support point in addition moves horizontally, a component depending on its acceleration:

$$F_{sup} = F_{cp} + F_g \cos\theta - m\ddot{x}_0 \sin\theta \tag{8}$$

First assume that the support point remains at its initial position. As the displacement is zero, we see from (7) that no work is performed by the support. In addition, we see from (8) that the applied force vanishes if the acceleration of the support is given by (9)

$$a = \frac{d^2x_0}{dt^2} = \frac{(\omega^2 L + g\cos\theta)}{\sin\theta} \tag{9}$$

This may happen for large accelerations of the support of the order of the gravitational constant, and large angles θ near 45 degrees. In this case, the hoist cable is no longer stretched. Also in this case the support point does not perform any work (8), this time because the applied force is zero, rather than the displacement. We see that the larger the instantaneous acceleration of the support is, the less negative is the work dW. As we wish to make the applied work as negative as possible, it might seem beneficial to apply a low acceleration. However, it is not only the instantaneous work that determines the energy dissipation from the pendulum, but its integrated value over time. Since the applied work is proportional to the displacement of the support point, it is beneficial to initially accelerate the support point maximally in the lateral direction towards the load until the maximal velocity has been reached. This is the method we apply in order to quickly dissipate energy from the pendulum at large swaying amplitudes. The results can be seen in Figure 3. The figure shows that whenever the x position of the load crosses the x position of the support point, the latter starts accelerating at maximum acceleration $a_{\max}$ into the new direction of the load, until its maximum velocity $v_{\max}$ has been reached. This method effectively dissipates energy from the pendulum, and eventually results in a situation where the support and load move together at a final velocity smaller than $v_{\max}$ (see Figure 3).

We also propose a general method for dissipating energy from the system: While applying the Lagrange method to integrate the equations of motion, we choose a trial step for the acceleration of the support point during the next time step. We then compute and record the total kinetic plus potential energy $K+V$ after this trial step. We repeat this for all possible accelerations $\frac{d^2 r_0}{dt^2}$ in all directions of the support point at the current position, and then choose the direction that leads to the state of minimal total energy. We then proceed to the next time step. In this way, energy is removed from the system as quickly as possible at all moments in time.

However, as we have mentioned before, minimizing the instantaneous work at all time does not lead to the desired result of minimizing the integrated work over time. On the other hand, when we instead minimize the kinetic energy of the system at all moments in time, rather than the kinetic plus potential energy, the system does exactly what we want: The support point moves at its maximal velocity into the direction of the load, such that the latter loses its kinetic energy as quickly as possible. This is the algorithm we use to dissipate energy from the system and in this way damp out large swaying motions. The results can be seen in Figure 3. The methods have been verified to work for three-dimensional oscillations as well (results not shown).

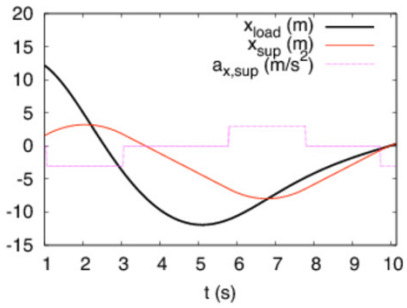

Figure 3 Basic control method: Damping by crane motion only. Positions of the load (black line) and support point (red line) as well as the acceleration of the support point (pink line) are shown as a function of time.

In Figure 3, the length of the hoist cable is 20 meter, the maximum speed of the crane $v_{\max}$ is 3 m/s and its maximum acceleration $a_{max} = 3\, m/s^2$. The initial displacement of the load is 45 degrees. The support point always moves at maximum speed towards the load position. The support point starts decelerating in advance when it approaches the lateral position of the load, in order to prevent an overshoot. When the maximum velocity of the support $v_{\max}$ has been reached, the acceleration is set to zero. In the final situation, the support point and the load move together at constant velocity.

In order to assure that the load is not accelerated into the wrong direction, the time of the next crossing between the x positions of the support and the load is calculated by extrapolation, in order to let the acceleration vanish exactly at this point in time. The lateral distance

between the position of the load and the support at which the support point has to start its acceleration into the new direction is given by (10):

$$\Delta x = x_{load} - x_{sup} = \left(\frac{1}{2} v_{sup} - v_{load}\right) \Delta t \qquad (10)$$

where $\Delta t = \left|\frac{v_{sup}}{a_{max}}\right|$ is the time it takes to decelerate the support point to a standstill. In this way, motion of the the load and the support is always in opposite directions. Since the positions of the support point and the load are close, we neglect the acceleration of the load in the above computation.

Another method to dissipate energy from the pendulum in order to damp out a large swaying motion is by using the winch to vary the length of the hoist cable over time. We can study how the length of the cable should be varied in order to minimize the work performed by the winch. As before, the force applied by the load is always directed downward, along the direction of the cable, as long as there is tension on the wire. In this case, that means that the downward acceleration of the winch should not be larger than the component of the gravitational acceleration of the load along the cable, plus the acceleration caused by the centripetal force $\frac{F_{cp}}{m}$. We see that the force applied by the winch at the position of the support point is directed along the direction of the cable, i.e. pointing away from the direction of the load, under all normal circumstances. As a consequence, in order to minimize the instantaneous work performed by the winch on the pendulum, the cable should at all times be extended, and the acceleration should at the same time be small enough to keep a positive tension on the cable. To indefinitely extend the length of the cable is, of course, undesirable, although it is possible to damp out the swaying motion in this way. Instead, it is preferable to reduce the cable length at times when the force on the cable is minimal, and extend it when the force is largest. In this way, the applied work is smaller than zero. We can achieve this by using the winch to lift the load when it is at its highest points (with maximum potential energy; the force on the cable is minimal), and lowering it when it is at its lowest point (with maximum kinetic energy; the force on the cable is maximal). In effect, this means shortening the wire at constant speed when the load moves away from the support and lengthening it at constant speed when the load moves towards the support.

Figure 4 and Figure 5 show the simulation results for this method. It can be seen that this method uses a long time to dissipate energy from the pendulum, especially for longer cable lengths.

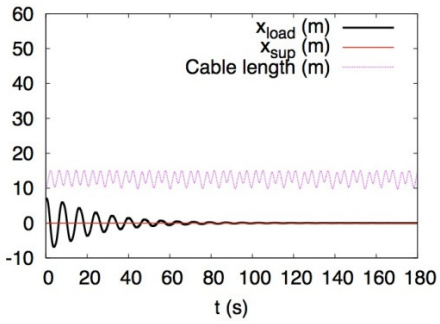

Figure 4 Winch damping.

In Figure 4, an initial displacement of 45° of the pendulum is damped out by adjusting the length of the cable by operating the winch. The maximum acceleration and velocity of the winch are 5 m/s^2 and 3 m/s, respectively, the cable length is varied between 10 and 15 meters.

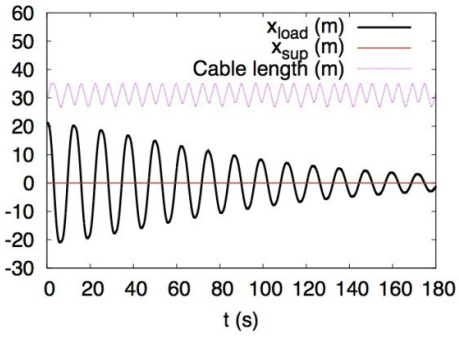

Figure 5 Winch damping for a long cable.

Figure 5 shows the same simulation results as those in Figure 4, the only difference being that the length L of the cable now equals 30 meters and is varied between 25 and 35 meters. It is seen that the damping process takes very much longer in this case.

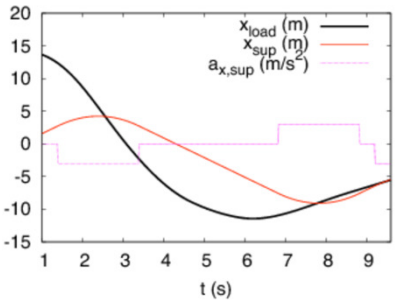

Figure 6 Damping by the combined effect of crane and winch.

In Figure 6, an initial displacement of the pendulum is damped out by a combination of the above methods for energy dissipation by crane motion and winch control. The positions of the load (black line) and support point (red line) as well as the acceleration of the support point (pink line) are shown as a function of time. Parameters are the same as in Figure 3; in addition the maximum velocity of the winch is set to 3 m/s, its maximum

acceleration is set to 5 ms^{-2}. As can be seen by comparison to Figure 3, the additional effect of damping by using the winch is small: a steady state is reached about 10 % earlier than by only crane motion.

III.II TRANSLATION

Besides damping out oscillatory motion (section III.I), another important method is to transport the load from one position to another, in the absence of external noise. This is a typical operation which a crane operator is trained at. Nevertheless, we implemented and tested the method for two reasons. Firstly, the method is ideal to damp out any lateral motion that is left after having damped out a motion by means of the methods in the previous section. Secondly, the method is an ideal test case for our simulations as a virtual operation which one can perform without needing an operator. Namely, the operation is able to perfectly move the load from one position to another, without any final oscillation. In the presence of noise, we can combine the translational motion with the methods for damping out oscillations of section III.I and III.III.

The method is exact when the load is initially hanging still, and there are no perturbations. Importantly, the method can also be combined with the above-mentioned method for energy dissipation to damp out sway motion, both initially, and during the phase where the crane moves at constant velocity.

In order to explain the method, it is easiest to first consider how the load can be accelerated from a standstill to a final velocity v_f without causing it to sway. This is what is done during the first 5 seconds in Figure 7. In the second half of the translation in Figure 7 (5 s < t < 10 s), the reverse process is applied, in which the load is decelerated back to a standstill.

In order to first accelerate the support and load from standstill to a simultaneous movement at a velocity v_f (at t=5 sec in Figure 5) we first accelerate the support to $\frac{v_f}{2}$ by a constant acceleration a_{const} during a time t_{acc} (although the method works as well for irregular accelerations over time). This is done during the first t_{acc} ≈ 0.5 seconds in Figure 7. Next, the support point keeps this exact velocity during a time $t_{1/2}$, until the payload has exactly the same velocity ½ v_f (slightly after 2 secconds in Figure 7). Note that the position of the load at that moment in time still lags behind the support position, although the velocities v_{sup} and v_{load} are exactly equal. From here on, we let the support point keep the same velocity $\frac{v_f}{2}$ for another time $t_{1/2}$ (until the start of the second acceleration pulse, shortly after 4 seconds in Figure 7), and finally we accelerate it to v_f using the same constant acceleration a_{const} during a time t_{acc} (until the end of the second acceleration pulse, shortly after 4 seconds). At the end (t=t_{end}, shortly after 4 seconds in Figure 7), the support and the payload move together at a speed v_f, without any sway. We can see this by using the fact that the system is time-reversible, and by applying the following Galilean transformation (11),

$$\boldsymbol{v}_{\mathrm{sup}}(\boldsymbol{t}) = \boldsymbol{v}_{\mathbf{sup}}(\boldsymbol{t}_{\mathbf{end}}) - \boldsymbol{v}_{\mathrm{sup}}(\boldsymbol{t}_{\mathbf{end}} - \boldsymbol{t}) \quad (11)$$

where the subscript "end" indicates the place and time directly after the second acceleration pulse (shortly after 4 seconds in Figure 7). Since both velocities at $\frac{1}{2}t_{end} = t_{acc} + t_{1/2}$ are invariant under the above transformation, the transformation has to apply also for the rest of the trajectory:

$$v_{\mathrm{load}}(t) = v_{\mathrm{sup}}(t_{\mathrm{end}}) - v_{\mathrm{load}}(t_{\mathrm{end}} - t) \quad (12)$$

But then, it follows from symmetry that

$$x_{load}(t_{end}) = \int v_{load}\,dt = x_{sup}(t_{end}) = \frac{1}{2}t_{end}v_{sup}(t_{end}) \quad (13)$$

In conclusion, at t = t_{end} the support and load move together at the same x position and velocity, such that we are able to accelerate the system to any desired velocity, starting from the system at rest. In the same fashion, we can decelerate suspension and payload from any given initial velocity to its rest position (see section III.II). This process is shown in the second half in Figure 7 (5 s < t < 10 s), where the payload is decelerated from a velocity of 3 m/s towards a standstill.

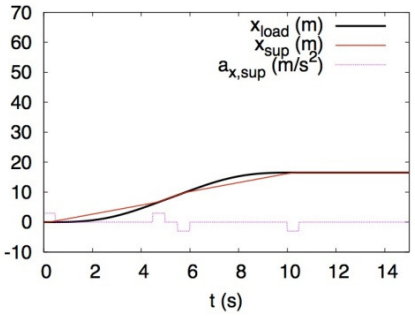

Figure 7 Translational motion by the double pulse method.

In Figure 7, the length L of the wire is 20 meters; the load is translated from a standstill at an intial position x = 0 m to a final position x = 16.5 m in 10 seconds. Maximum lateral acceleration and velocity of the support are 3 ms^{-2} and 3 ms^{-1}, respectively.

III.III DRIVEN OSCILLATION

We here consider the response of the pendulum to a lateral periodic disturbance. A cosine signal is fed to the x position of the support point. Without the presence of damping, the system is unstable. If the feeding frequency is similar to the natural frequency of the system, the oscillations grow significantly in amplitude already after few oscillation periods.

In order to damp out the oscillations, we apply the same methods as in section III.I. As shown in Figure 8, an initial displacement of the load of 45° and a driven lateral oscillation of the support are quickly damped out

by the method considered under section III.I, in which the support at all times moves at its maximum speed into the lateral direction of the load. The used maximum acceleration and velocity of the support are 9 ms^{-2} and 3 ms^{-1}, respectively. The lateral oscillation of the support position in Figure 8 is given by $f(t) = 5m\cos(\frac{2\pi t}{10s})$ while the wire length L is 20 meters. The pendulum's resonance frequency is therefore (for moderate displacements) $\frac{1}{2\pi}\sqrt{\frac{g}{L}} = 0.11s^{-1}$, close to the driving frequency of 0.1 s^{-1}. Without a control algorithm, the oscillation would therefore quickly gain amplitude. The amplitude of the periodic wave is as large as 5 meter, but still the algorithm is able to fully damp out the oscillations, resulting in a linear motion that simply can be compensated for by the method discussed under section III.II.

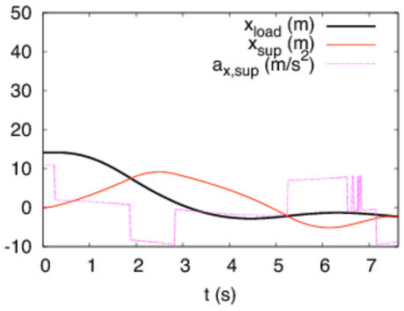

Figure 8 Damping out a periodic input signal.

IV. DISCUSSION AND CONCLUSION

Our proposed idea consists of developing an integrated system with control strategies that reduce the effect of payload pendulation and that minimize wave impact on shipboard crane manipulation. We here present simulation results confirming the principle and effectiveness of the methods for damping out pendulation.

An important advantage of the proposed methods for dissipating energy is that they are expected to be relatively easily combined with operator-induced actions. When a human operator is involved, it is unwanted and dangerous if the control algorithm without a warning performs actions opposite to those of the crane operator. With our proposed method, we expect to be able to effectively damp out oscillations by using values of a_{max} and v_{max} that are small as compared to the accelerations and velocities used by the crane operator. In addition, the values of a_{max} and v_{max} can easily be adapted to the the current sea state: Without the presence of external noise both values may be set to zero, at intermediate sea states the values are set to fractions of the maximum velocity and acceleration of the crane, while at extreme sea states they may be set to their maximal values.

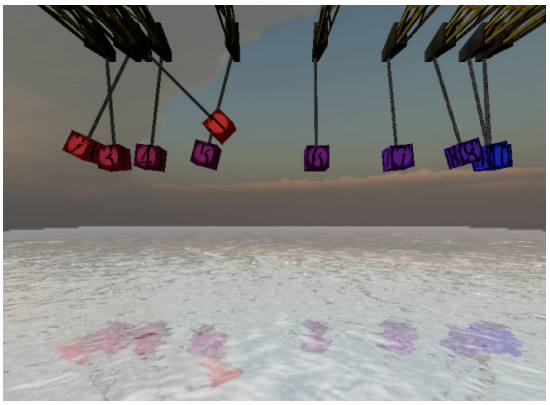

Figure 9 Combined crane-winch simulation.

A simulation of a combined crane-winch operation is shown in Figure 9. An initial 45° displacement (position 1 (pos. 1)) is damped out (pos. 1-3) by the combined crane and winch methods described under section III.I. Directly after this, the payload is translated over a (very) large distance of 62 meters. In order to do so, the support point is first accelerated (pos. 4-5) until it moves at fixed speed (pos. 6) and finally decelerated (pos. 7-9) until the prescribed position has been reached (pos. 10). The wire length is 20 meters and the total duration of the operation is 23 seconds. The simulation shows some of the working capabilities and efficiency of our integrated anti-sway approach. The simulation results were visualized by using Unity3D game engine. Although not shown in the figure, the same methods also apply when the system is under the influence of a driven planar perturbation during the operation, as well as a three-dimensional perturbation.

There is still a great amount of work left for future research. Considering the difficulties of integrating features of hydraulic cranes into the control method, we are currently focusing on investigating the nonlinear dynamic models of all related hydraulic components in the crane system. The work will be integrated with the "crane/winch simulator" developed by the Offshore Simulator Centre. Finally, a real prototype will be built and tested at Rolls-Royce Marine AS.

ACKNOWLEDGEMENTS

This work is supported by the Research Council of Norway with project no. 217769, "A Novel Integrated Anti-sway System for Rolls-royce Marine Shipboard Cranes", within the Maritime operations and offshore operations (MAROFF) program. The authors want to thank Yingguang Chu from the Mechatronics Lab at AAUC for formatting and proofing the paper.

REFERENCES

[1]. Vaughers, T.G. 1994. "Joint logistics over the shore operations." *Naval Engineers Journal* 106, No.3, 256-263.

[2]. Vaughers, T.G. and M.F. Mardiros. 1997. "Joint logistics over the shore operations in rough seas." *Naval Engineers Journal* 109, No.3, 385-393.

[3]. Nojiri, N. and T. Sasaki. 1983. “Motion characteristics of crane vessels in lifting operation.” *15th Annual Offshore Technology Conference* (Houston, TX, May 2-5) 4603-MS.
[4]. Lewis, D. et al. 1998. “Command shaping control of an operator in the loop boom crane.” *Proceedings of the American Control Conference* 5 (Philadelphia, PA, Jun.24). 2643-2647.
[5]. Parker, G.G. et al. 1999. “Experimental verification of a command shaping boom crane control system.” *Proceedings of the American Control Conference* 1 (San Diego, CA, Jun.2-4). 86-90.
[6]. Balachandran, B. and Y. Li. 1997. “A mechanical filter concept to suppress crane load oscillations.” In *DETC'97 Proceedings of the ASME Design Engineering Technical Conferences* (Sacramento, CA, Sep.14-17). DETC97/VIB-4091, ASME, New York, 1997.
[7]. Balachandran, B., Li, Y. and C. Fang. 1999. “A mechanical filter concept for control of non-linear crane-load oscillations.” *Journal of Sound and Vibration* 228, 651-682.
[8]. Baptista, M.S. et al. 2001. “Control of shipboard cranes.” *A Course in Mathematical and Statistical Ecology*, Kluwer Academic Publishers, 75.
[9]. Kimiaghalam, B., Homaifar, A. and M.U. Bikdash. 1999. “Pendulation suppression of a shipboard crane using fuzzy controller.” Proceedings of the *American Control Conference* 1 (San Diego, CA, Jun.2-4). IEEE, 586-590.
[10]. Kimiaghalam, B., Homaifar, A. and M.U. Bikdash. 2000. “Feedback and feedforward control law for a ship crane with Maryland rigging system.” Proceedings of the *American Control Conference* 2 (Chicago, IL, Jun.28-30). IEEE, 1047-1051.
[11]. Sagatun, S.I. 2002. “Active control of underwater installation.” *Control Systems Technology* 10, IEEE, 743-748.
[12]. Johansen, T.A. et al. 2003. “Wave synchronizing crane control during water entry in offshore moonpool operations-experimental results.” *Journal of Oceanic Engineering* 28. IEEE, 720-728.
[13]. Faltinsen, O.M. and R. Zhao. 1997. “Water entry of ship sections and axisymmetric bodies.” *AGARD FDP and Ukraine Institute of Hydromechanics workshop on high-speed body motion in water*. Report 827, Paper no. 24. 1-11
[14]. Skaare, B. 2004. “Control of loads through the wave zone in marine operations.” Ph.D. thesis, NTNU, Trondheim, Norway.
[15]. Messineo, S., Celani, F. and O. Egeland. 2008. “Crane feedback control in offshore moonpool operations.” *Control Engineering Practice,* Elsevier, Vol. 16, 356-364. 3.
[16]. Moon, M.S., VanLandingham, H.F. and Y.J. Beliveau. 1996. “Fuzzy time optimal control of crane load.” *Decision and Control* 2. IEEE, 1127-1132.
[17]. Zhang, H. et al. 2006. “Sky cleaner 3: a real pneumatic climbing robot for glass-wall cleaning.” *Robotics and Automation Magazine* 13. IEEE, 32-41.
[18]. Ernst-B. Johansen A.S. 2011. Cranemaster.no. [Online], http://cranemaster.no.
[19]. SmartCrane. 2011. Smartcrane.com. [Online] LLC, http://www.smartcrane.com/SmartCrane/Welcome.html

AUTHOR BIOGRAPHIES

SIEBE VAN ALBADA works as a researcher and Associate Professor at Aalesund University College, Norway at the Faculty of Engineering and Natural Sciences and the Faculty of Maritime Technology and Operations. Email: siva@hials.no.

DICK VAN ALBADA is as an Assistant Professor and works at the Informatics Institute, Faculty of Science, Universiteit van Amsterdam, The Netherlands. Email: G.D.vanAlbada@uva.nl

HANS PETTER HILDRE is a Professor on product and system design at the Department of Technology and Nautical Sciences, Aalesund University College, Norway. Email: hh@hials.no.

HOUXIANG ZHANG is a Professor on product and system design at the Department of Technology and Nautical Sciences, Aalesund University College, Norway. Email: hozh@hials.no.

Finance, Economics and Social Science

GENDER DIFFERENCES IN CAPACITY AUCTIONS: A SIMULATION EXPERIMENT WITH *econport*

F. Javier Otamendi[1]
Luis Miguel Doncel[1]
Universidad Rey Juan Carlos
[1]Departamento Economía Aplicada I
Paseo Artilleros s/n
28032 Madrid, Spain
E-mail: franciscojavier.otamendi@urjc.es

KEYWORDS
Auctions, On-line simulation, gender studies

ABSTRACT

A simulation environment has been used to study the behaviour of buyers when participating in capacity auctions. Gender differences have been found among buyers, which are university students, according to auction types. Males are more active in auctioning, they are also willing to take more risks and therefore they get more products than they should, but paying more than females for them.

INTRODUCTION

Auction simulators have been extensively used in research and teaching in computational and experimental economics (Kagel and Roth 2011), showing that these simulators might be particularized ad-hoc to study the behaviour of the real world.

We focus in this case on the gender aspect and the different behaviour between men and women in auction processes (Shehryar, 2008; Yeh, Hsiao and Yang, 2012).

We employ, for the first time to our knowledge, an auction simulator which has been particularized to study capacity auctions in general and in the energy market in particular (Otamendi et al. 2012, Otamendi and Doncel 2013).

Out of the available options, we select *econport* due to its wide use and its functional interface (Chen et al. 2003; Cox et al. 2005), as well as its enormous parameterisation potential that favours its particularisation to capacity auctions and facilitates experimentation.

Section 2 is used to define the process to offload liquefied natural gas and the auctioning of related capacity rights while Section 3 is devoted to introduce *econport* and the simulation environment. Section 4 describes the experiment that has been carried out and Section 5 shows the results. Section 6 includes a discussion of the results considering gender aspects while Section 7 is used to conclude and to define new lines of research.

CAPACITY AUCTIONS: THE CASE OF LNG

Companies that wish to offload liquefied natural gas (LNG) at the harbour tanks have to reserve or buy capacity, since the resources are very much limited. The usage of the harbour facilities have been addressed in the literature using simulation (Bruzzone et al. 1998; or more recently, Gyoungwoo et al. 2009), including the problem when unloading ships that carry coal (Otamendi 2008) or the loads on LNG terminals (Rezende et al. 2007).

The procedures to reserve capacity are currently known by the players, but may be rapidly changed, according to the Spanish regulation set back in December of 2007. There is a trend to liberalize the markets by installing auctions at any of the supply chain stages. In addition to those available for the price of gas and LNG, markets will be also set for capacities, that is, for allocation of capacity slots at the harbours for offloading, at the plants for regasification, at the network for transportation or at the underground buffers for storage. In Spain, the auctions started in 2009 with the underground storage capacity auction (Comisión 2012). It looks like the appropriate time for the companies to understand the new system and rules and develop platforms which will help in the new auction era.

Let's further define the offloading system. A company buys LNG that is transported by ship and must be offloaded at a harbour. Ships or tankers are usually large. The investments in LNG are therefore high and the price to pay for not offloading at the proper time is ever increasing with the delays. The size of the tankers will also force the company to buy just a few offloading rights over a long period of time. So timing is very important and bidding for the proper slots in critical.

Therefore, the companies that are going to participate in the auction and buy offloading rights must learn how to proceed in this new situation and design strategies that will allow them to maximize their profit while maintaining the reliability of service. If a simulator

Proceedings 27th European Conference on Modelling and Simulation ©ECMS Webjørn Rekdalsbakken, Robin T. Bye, Houxiang Zhang (Editors)
ISBN: 978-0-9564944-6-7 / ISBN: 978-0-9564944-7-4 (CD)

existed that resembled the capacity auctions… The simulator has been developed in *econport* with the help of Enagás, the owner of the pipelines and responsible for the transportation in Spain.

Other examples of capacity auctions are: slots at airports or the assignment of radio frequencies in public auctions.

econport and CAPACITY AUCTIONS

econport was designed by the Experimental Economics Center of Georgia State University back in 2006 as an experimental tool to research in economics. It has one module that allows for simulating auctions. In particular, it has one routine that resembles one market in which one seller offers several goods to different bidders. This module could be used as the basis for simulating capacity auctions.

To create an experiment, the auctioneer sets the following parameters:

- Number of goods or consecutive periods in which one good is auctioned at a time.
- Value of the goods, which might be individually set by hand or randomly assigned according to a uniform distribution
- Type of auction among four possibilities:
  a) Sealed-bid auctions: all the bidders submit simultaneously a single bid within the allotted time.
     1. First price: the good is awarded to the bidder who has submitted the highest bid.
     2. Vickrey or second highest price: the good is awarded to the bidder who has submitted the highest bid, but at the second highest price.
  b) Dynamic: the bids keep on varying along time, which is limited by design.
     3. English or ascending: the bids keep on rising until time is over. The good is awarded to the bidder who has submitted the last bid.
     4. Dutch or descending: The price keeps decreasing following a pre-set clocked pattern until one bidder stops the proceedings by accepting and paying the current price.

The auctioneer posts then the experiment on the web and sends instructions to the bidders, including a password. Each bidder might then join the experiment and send a message to the auctioneer with the username.

After a good is sold, each bidder knows the selling price, but not the name of the awarding bidder. He also gets information about his performance in terms of profit, calculated as the difference between value and bid. The profit accumulates after each good is sold.

EXPERIMENT DESCRIPTION

Each session lasts about 3 hours, with the following program:

- Theoretical explanation of the four auction types
- Access to the web simulator by the participants
- One experiment with 4 periods, so that the participants get acquainted with the simulator. The experiment is repeated for each of the four auction types. The values were sampled from a distribution of values (V dist) that follows a Uniform distribution that ranges between 0 and 20, U(0,20).
- One experiment with 6 periods, repeated for each auction type. The values were sampled from a distribution of values (V dist) that follows a Uniform distribution that ranges between 5 and 15, U(5,15).
- One experiment with 20 periods, repeated for each auction type. The values were sampled from a distribution of values (V dist) that follows a Uniform distribution that ranges between 0 and 20, U(0,20).

To account for gender, the participants were told to include a username that starts with an H for male ("hombre" in Spanish) and an M for female ("mujer" in Spanish).

To avoid buyer's curse (Kagel and Levin, 1986), a prize was given to the overall winner of the session. The winner was the participant with the highest profit after adding the profits of the last two experiments over the four auction types.

EXPERIMENT RESULTS

One of *econport* miscues is the difficulty to upload the experimental results into a database for further analysis. The output of the program is in *.xlm format and must be converted into MsExcel (in our case).

After tedious coding, the results of all the experiments are included in the same worksheet with the following columns:

- Register Number
- Date: in which the auction took place
- Group: a name for the group of participants
- V dist: random variable for values
- Auction Type
- Incremental Units Bid: the number of decimals allowed for the bids
- Period Length (secs): allotted time to place a bid
- Starting Price: at which to start the auction in clock auctions

- Tick Length: intervals between changes in bids in descending auctions
- Period: identification of the good that it is being auctioned
- Player: internal identification number assigned by the simulator
- Name: participant username
- Value: the random value assigned to the participant
- Bid: the bid placed by a participant
- Buyer: a dummy variable indicating with a 1 that the participant has bought the good
- Awarded Price/Pay: the price that has to be paid by the buyer
- Theoretical Buyer: a dummy variable indicating with a 1 that the participant should have bought the good since its value was the largest among all the bidders
- Efficiency: a dummy variable indicating with a 1 that the participant that should have bought the good had indeed bought it, and with a -1 if it had not bought it
- Value-Bid: absolute risk taken by the participant
- Profit: profit obtained by a participant
- -(Value - Bid)/Value (%): relative risk taken by the participant
- Gender: a binary variable, with H indicating male and M indicating female.

EXPERIMENT ANALYSIS

Two identical sessions were carried out:

- On Nov 16th, 2012, with 24 undergraduates students in Economics, 17 male and 7 female
- On Nov 30th, 2012, with 26 undergraduates students in Business Administration, 9 male and 17 female

Therefore, the participants account for a total of 26 males and 24 females. Each of them might bid a maximum of 104 times, that is, 4 auction types and 26 periods (or an experiment of 6 periods and another of 20 periods). There was however a mishap in the second session in one experiment and only 12 periods were run for the English auction in the Business Administration group, so only 96 registers are available for them. Overall, the total number of registers in the output database was 4992.

Figure 1 shows the analysis by gender according to auction type. The rows of the table show minimum, average, maximum and standard deviation values for each of the following output variables:

- The values, in order to verify the random assignment done by the simulator
- The bids
- The absolute risk, measured as Value-Bid
- The pay or awarded price
- The profit, calculated as Value-Pay

At the bottom of the table, there is also a summary of the awarding process, indicating:

- The number of goods that have been bought
- The number of goods that should have been bought
- The efficiency, calculated as an average between correct assignments of goods to highest value participants and incorrect assignments

The last row of the table includes the bidding strategy of the participants calculated as the number of bids that have been submitted out of the total number of products that have been auctioned.

A series of hypothesis tests on averages and proportion have been performed to study gender differences. The left-hand side columns in Figure 1 include the corresponding z-values. Those values that are black coloured with white figures are those in which the average for males is significantly higher than for females. Those values with a grey background correspond to significantly higher averages for females.

Considering gender differences, it looks like on average terms:

- The values are randomly assigned, not showing differences across gender or auction type.
- The bids are higher for male students, especially during Vickrey auctions, showing a will to take higher risks since the awarded price will be that of the second highest bid.
- There are no differences in absolute risk, although the z-values are all positive, indicating a slightly higher underbid for females
- The amount of money paid is higher in general terms for males. However, by auction type, males pay more during Vickrey and Dutch auctions and females during First and English auction. Once again, the riskier types call for males to get the capacity right.
- There are again no differences in profits, although the z-values are all positive, indicating higher values for female participants.
- Females have a lower efficiency rate, except for Vickrey auctions. They lose some auctions that they should have won.
- Females tend to place more bids except for the Dutch auction, in which they are not as anxious as males.

Figure 1. Analysis of bids, pays and profits

Group	(Todas)
Valid	(Todas)

Significance Level 0.05
-1.9600

z-values							GenderFinal	Auction Type									
	FEMALE-MALE						FEMALE				Total FEMALE	MALE				Total MALE	Total general
	Dutch	English	First	Vickrey	TOTAL	Variables	Dutch	English	First	Vickrey		Dutch	English	First	Vickrey		
						Count Value	624	488	624	624	2360	676	604	676	676	2632	4992
						Mín. Value	0.05	0.07	0.04	0.02	0.02	0.01	0.01	0.04	0.02	0.01	0.01
	-0.10	1.40	0.72	-1.22	0.31	Average Value	10.23	10.33	10.18	9.37	10.01	10.26	9.89	9.97	9.72	9.96	9.98
						Máx. Value	19.95	19.98	19.95	19.99	19.99	19.96	19.99	19.99	19.99	19.99	19.99
						StdevValue	5.25	5.04	5.19	5.17	5.19	5.36	5.17	5.17	5.27	5.25	5.22
						Count Bid	21	129	606	584	1340	30	97	571	539	1237	2577
						Mín. Bid	14.23	2.00	0.01	0.01	0.01	14.18	1.00	0.01	0.01	0.01	0.01
	-1.03	-0.51	-0.94	-2.89	-2.72	Average Bid	17.72	13.39	10.10	9.70	10.36	18.29	13.73	10.38	10.60	10.93	10.63
						Máx. Bid	20.50	19.60	20.50	21.00	21.00	20.50	19.80	23.00	25.00	25.00	25.00
						StdevBid	2.13	4.45	5.14	5.21	5.26	1.71	5.13	5.08	5.14	5.26	5.27
						Count Value-Bid	624	488	624	624	2360	676	604	676	676	2632	4992
						Mín. Value-Bid	-1.07	-0.52	-1.54	-20.11	-20.11	-3.58	-8.55	-11.57	-12.48	-12.48	-20.11
	1.52	0.99	0.89	0.07	1.16	Average Value-Bid	0.15	1.04	0.25	-0.07	0.18	0.09	0.89	0.20	-0.08	0.13	0.16
						Máx. Value-Bid	0.95	16.92	11.06	11.46	16.92	1.20	15.13	7.83	18.75	18.75	18.75
						Desvestp de Value-Bid	0.47	2.37	0.56	1.75	1.45	0.85	2.72	1.32	2.13	1.86	1.66
						Count Pay	624	488	624	624	2360	676	604	676	676	2632	4992
						Mín. Pay	14.23	13.50	14.05	12.19	12.19	14.18	13.25	14.00	14.00	13.25	12.19
	-5.31	2.50	3.47	-11.24	-5.35	Average Pay	17.73	17.77	18.58	16.53	17.64	18.29	17.46	18.20	17.86	17.96	17.81
						Máx. Pay	20.50	19.40	20.50	19.51	20.50	20.50	19.80	23.00	20.00	23.00	23.00
						Desvestp de Pay	2.08	1.99	1.83	2.34	2.22	1.71	2.14	2.18	1.87	2.00	2.11
						Count Profit	624	488	624	624	2360	676	604	676	676	2632	4992
						Mín. Profit	-1.07	0.00	-1.54	-1.47	-1.54	-3.58	-6.99	-6.83	-1.60	-6.99	-6.99
	0.13	0.91	1.52	0.92	1.90	Average Profit	0.00	0.01	0.00	0.03	0.01	0.00	0.00	-0.02	0.02	0.00	0.01
						Máx. Profit	0.95	1.29	0.55	3.53	3.53	1.20	2.15	0.76	3.20	3.20	3.53
						StdevProfit	0.09	0.09	0.08	0.25	0.15	0.18	0.40	0.40	0.21	0.31	0.25
						Sum Buyer	22	17	26	26	91	30	27	26	26	109	200
						Sum Theoretical Buyer	24	18	24	30	96	28	26	28	22	104	200
						Average Efficiency	-0.0016	-0.0020	0.0048	-0.0064	-0.0013	0.0044	0.0033	-0.0030	0.0059	0.0027	0.0008
	-4.93	7.61	2.50	2.86	6.59	Bid Percentage	3.37%	26.43%	97.12%	93.59%	56.78%	4.44%	16.06%	84.47%	79.73%	47.00%	51.62%

CONCLUSIONS

The experiment has shown gender differences among the participants during the simulation games in which capacity rights are auctioned. It looks like males are more aggressive than females although they bid less often. They steal more products to women with the highest value than vice-versa, and buy more during Dutch auctions, where there is no information at all about the values.

Females bid almost always but without any risk, so they pay usually less when they buy a product in Vickrey and Dutch auctions, whereas they buy more in traditional English and First Price auctions.

The simulator has proven to be a reliable tool to perform the experiments, so more games will be carried out to back the preliminary conclusions of this paper up. Moreover, the simulation environment will be used in the future as a test-bench for other behavioural economics experiments.

ACKNOWLEDGEMENTS

This research has been partly funded by the Universidad Rey Juan Carlos by an Educational Innovation Project.

REFERENCES

Bruzzone A.G.; R. Musca; P.D. Esposti; S. Vacante and A. Carbone. 1998. "Distributed development of simulation models for harbour processes." *Computational methods in water resources* 5, 145-154.

Chen H.; D. Zeng; R. Kalla; H. Zan; J.C. Cox and J.T. Swarthout. 2003. "EconPort: a digital library for Microeconomics education." In *Proceedings Joint Conference on Digital Libraries*.

Comisión Nacional de la Energía (CNE). 2012. *Analysis of Cross Border Transmission Gas Tariffs between Portugal and Spain*. Ocassional working paper.

Cox J.C. and J.T. Swarthout. 2005. *EconPort: Creating and Maintaining a Knowledge Commons*. Andrew Young School of Policy Studies Research Paper No. 06-38 (Dec).

Gyoungwoo L.; S Svendran; and K. Sang-Hyun. 2009. "Algorithms to control the moving ship during harbor entry." *Applied Mathematical Modelling* 33, No 5, 2474-2490.

Kagel J.H. and D. Levin. 1986. "The winner's curse and public information in common value auctions." *American Economic Review*76, 894-920.

Kagel, J.H, and A. E. Roth. 2011. *The Handbook of Experimental Economics* (Eds.). Princenton University Press.

Otamendi, F.J. (2008). "Visualization and Scheduling Of Jetty Operations In Harbours". In *Proceedings of the Sixth International Conference on Simulation in Industry and Services*. Public University of Navarre, 31-52.

Otamendi, F.J., L.M. Doncel, P. Grau and J. Ramos de Castro (2012). "Simulating capacity auctions with *econport*". In *Proceedings of the 24th European Conference on Modeling and Simulation*, University of Erlangen.

Otamendi J., L.M. Doncel. 2013. "Integration and implementation of web simulators in experimental e-learning: an application for capacity auctions". *The Turkish Online Journal of Educational Technology* 12 (1), 88-101.

Rezende F.; L. Xin and C. Xiao-Bo. 2007. "Second order loads on LNG terminals in multi-directional sea in water of finite depth." In *Proceedings of the 26th International Conference on Offshore Mechanics and Artic Engineering* 1, 259-266.

Shehryar, O. (2008). The effect of buyer's gender, risk-proneness, and time remaining in an internet auction on the decision to bid or buy-it-now. *Journal of Product & Brand Management*, *17*(5), 356-365.

Yeh, J.C.; K.L. Hsiao and W.N. Yang. 2012. "A study of purchasing behavior in Taiwan's online auction websites in Taiwan: Effects of uncertainty and gender differences". *Internet Research*, *22*(1), 5-5.

AUTHOR BIOGRAPHIES

F. JAVIER OTAMENDI received the B.S. and M.S. degrees in Industrial Engineering at Oklahoma State University, where he developed his interests in Simulation and Total Quality Management. Back in his home country of Spain, he received a B.S. in Business Administration and a Ph.D. in Industrial Engineering. He is currently a simulation and statistics consultant and university professor at the Rey Juan Carlos University in Madrid.

LUIS MIGUEL DONCEL obtained a BS in Economics, from University Complutense of Madrid. Later he attended University of York achieving a Master in Economics and Finance. Back to Spain he got a Ph.D. in Economics from the Rey Juan Carlos University with a research about foreign exchange rates and simulation. Currently he is a lecturer at Rey Juan Carlos University. He has been an external consultant for monetary affairs for the EU in Bulgaria and Dominican Republic. His research focuses on financial markets and Simulation. His e-mail address is: luismiguel.doncel@urjc.es

TOWARDS A JAVA SIMULATION EXPERIMENT WITH AGENT-BASED TRADING PROCESSES

Roman Šperka
Dominik Vymětal
Marek Spišák
Department of Informatics
Silesian University in Opava, School of Business Administration
733 40, Univerzitní nám. 1934/3a, Karviná, Czech Republic
E-mail: sperka@opf.slu.cz, vymetal@opf.slu.cz, spisak@opf.slu.cz

KEYWORDS
Business process, agents, modeling and simulation, framework, virtual company, trading, verification.

ABSTRACT

The motivation of the paper is to introduce an agent-based business process model in the Java simulation experiment. A virtual company trading processes are simulated in order to use proposed methods as a part of a decision support tool. As in other cases, such simulation needs sufficient input parameters. However, in the case of business systems, real business parameters are not always available. Therefore, multi-agent system as a simulation framework, often operates with randomly (resp. pseudo randomly) generated data. Some of the business process simulation inputs are randomly generated in this paper. This method can also represent unpredictable phenomena. The core of the paper is to introduce the business process simulation implementation (simulation framework) and the simulation results. Finally, obtained results after the validation show that using business process model and the implementation proposed can lead to the correct output data and therefore can be used to simulate real business processes.

INTRODUCTION

Simulations used in the experiments in the paper could be described as agent-based simulations (Macal and North 2005) of Business Process Management (BPM). Business process is an activity adding the value to the company. Usual business process simulation approaches are based on the statistical calculation (e.g. Scheer and Nuttgens 2000). But only a few problems can be identified while using the statistical methods. There are a lot of other influences which are not able to be captured by using any business process model (e.g. the effects of the collaboration of business process participants or their communication, experience level, cultural or social factors). This method has only limited capabilities of visual presentation while running the simulation. Finally, an observer does not actually see the participants of business process dealing with each other.

Agent-based simulations dealing with a company simulation can bring several crucial advantages (De Snoo 2005), (Jennings et al. 2000). They can overcome some of the problems identified herein above. It is possible to involve unpredictable disturbance of the environment into the simulation with the agents. All of the mentioned issues are the characteristics of a multi-agent system (MAS).

One of the problems the simulations of business processes tackle with is the lack of real business data. Many researchers (Hillston 2003), (Yuan and Madsen 2010) use randomly generated data instead. On the basis of our previous research, we use a normal distribution in our simulation experiments. We reported on more issues dealing with the business process and financial market simulations (Sperka and Spisak 2011), (Vymetal and Sperka 2011). The simulation approach described in this paper uses a generic structure model of a company (Vymetal and Sperka 2011), (Barnett 2003) as a core principle. The influence of randomly generated parameters on the simulation outputs while using different kinds of distributions is presented in (Vymetal et al. 2012).

The novel methodology and the workflow described in this paper are implemented in the form of MAS (Wooldridge 2009). JADE (Bellifemine et al. 2010) development platform was chosen for the realization. JADE provides robust running and simulation environment allowing the distribution of thousands of software agents. Multi-agent system is used as a BPM framework in this paper. When finished, it shall cover the whole company structure from the supply of the material, through the production process, up to the selling and shipment. The overall idea of the proposed methodology is to simulate real business processes and to provide predictive results concerning the management impact. This should lead to the improved and effective business process realization. For the validation of simulation results real business data are used.

This paper is structured as follows. Section 2 briefly informs about the simulation framework. Multi-agent system implementation and the description of the production function are presented in Section 3. In Section 4 the simulation parameters and the results are introduced. In Section 5 the validation of the simulation

Proceedings 27th European Conference on Modelling and Simulation ©ECMS Webjørn Rekdalsbakken, Robin T. Bye, Houxiang Zhang (Editors)
ISBN: 978-0-9564944-6-7 / ISBN: 978-0-9564944-7-4 (CD)

results is presented. At the end, the conclusion and future research steps find their places.

SIMULATION FRAMEWORK

To ensure the outputs of the simulations a simulation framework was implemented and used to trigger the simulation experiments. The framework covers business processes supporting the selling of goods by company sales representatives to the customers (Fig. 1). It consists of the following types of agents: sales representative agents (representing sellers, sales reps), customer agents, an informative agent (provides information about the company market share, and company volume), and manager agent (manages the communication between seller and customer). All the agent types are developed according to the multi-agent approach. The interaction between agents is based on the FIPA contract-net protocol (FIPA 2002).

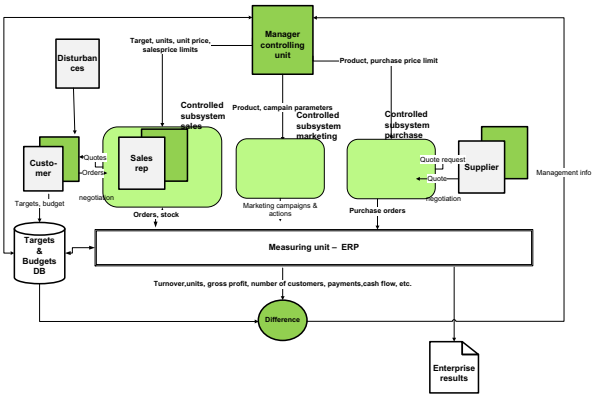

Figure 1: Generic model of a business company (Source: adapted from Šperka et al. 2013).

The number of customer agents is significantly higher than the number of sales representative agents in the model because the reality on the market is the same. The behavior of agents is influenced by two randomly generated parameters using the normal distribution (an amount of requested goods and a sellers' ability to sell the goods). In the lack of real information about the business company, there is a possibility to randomly generate different parameters (e.g. company market share for the product, market volume for the product in local currency, or a quality parameter of the seller). The influence of randomly generated parameters on the simulation outputs while using different types of distributions was presented in (Vymetal et al. 2012).

PRODUCTION FUNCTION DESCRIPTION

In this section, the mathematical definition of a production function is proposed. Production function is used during the contracting phase of agents' interaction. It serves to set up the limit price of the customer agent as an internal private parameter.

Only one part of the company's generic structure, defined earlier, was implemented. This part consists of the sales reps and the customers trading with stock items (e.g. tables, chairs). One stock item simplification is used in the implementation. Participants of the contracting business process in our system are represented by the software agents - the seller and customer agents interacting in course of the quotation, negotiation and contracting. There is an interaction between them. The behavior of the customer agent is characterized in our case by proposed customer production function (Equation 1).

Each period turn (here we assume a week), the customer agent decides whether to buy something. His decision is defined randomly. If the customer agent decides not to buy anything, his turn is over; otherwise he creates a sales request and sends it to his seller agent. The seller agent answers with a proposal message (a certain quote starting with his maximal price - limit price * 1.25). This quote can be accepted by the customer agent or not. The customer agents evaluate the quotes according to the production function. The production function was proposed to reflect the enterprise market share for the product quoted (a market share parameter), sales reps' ability to negotiate, total market volume for the product quoted etc. (in e.g. Vymetal and Sperka 2011). If the price quoted is lower than the customer's price obtained as a result of the production function, the quote is accepted. In the opposite case, the customer rejects the quote and a negotiation is started. The seller agent decreases the price to the average of the minimal limit price and the current price (in every iteration is getting effectively closer and closer to the minimal limit price), and resends the quote back to the customer. The message exchange repeats until there is an agreement or a reserved time passes.

The sales production function for the *m*-th sales representative pertaining to the *i*-th customer determines the price that the *i*-th customer accepts (adjusted according to Vymetal et al. 2012).

$$c_n^m = \frac{\tau_n T_n \gamma \rho_m}{Ov} \qquad (1)$$

Where:

c_n^m - a price of the *n-th* product quoted by the *m-th* sales representative,

τ_n - a company market share for the *n-th* product $0 < \tau_n < 1$,

T_n - a market volume for the *n-th* product in local currency,

γ - a competition coefficient lowering the sales success $0 < \gamma \leq 1$,

ρ_m - a quality parameter of the *m-th* sales representative, $0.5 \leq \rho_m \leq 2$,

Z - a number of customers,

I - a number of iterations,

P - a mean probability for the request in 1 iteration,
O - a number of orders ($O=ZIP$),
ν - a requested number of the n-th product by the i-th customer at the m-th sales rep.

Customer agents are organized in groups and each group is being served by concrete seller agent. Their relationship is given; none of them can change the counterpart. Seller agent is responsible to the manager agent. Each turn, the manager agent gathers data from all seller agents and stores key performance indicators (KPIs) of the company. The data is the result of the simulation and serves to understand the company behavior in a time – depending on the agents' decisions and behavior. The customer agents need to know some information about the market. This information is given by the informative agent. This agent is also responsible for the turn management and represents outside or controllable phenomena from the agents' perspective.

SIMULATION PARAMETERS AND RESULTS

The parameterization of the model and the obtained simulation results are analyzed in this section. Production function (Equation 1) is the engine of the simulation. Based on it, the customer agents decide to buy or not to do so. One year of sales and purchasing processes was simulated. Each turn represents one week. Five simulation experiments were done. Each purchase of the product type was registered. In order to include randomly generated inputs, two important agents' attributes were chosen to be generated by pseudo random generator. Firstly, the seller agent's ability, and secondly the customer agent's decision about the quantity for the purchase.
For the generating of random numbers from a normal distribution (Gaussian) the Java library called Uncommon Maths written by (Dan Dyer 2010) was used. For the values generation random MerseneTwisterRNG class was implemented. The class is a pure Java port of Makoto Matsumoto and Takuji Nishimura's proven and ultra-fast Mersenne Twister Pseudo Random Number Generator for C.
The parameterization of the MAS is listed in Table 1. The table represents the parameters listed by the name and the value for each type of an agent (customer, sales representative). It also shows the number of agent type instances (how many of a particular agent types is present in the system).

Table 1: List of agents' parameters

AGENT TYPE	AGENT COUNT	PARAMETER NAME	PARAMETER VALUE
Customer Agent	500	Maximum Discussion Turns	10
		Mean Quantity	5m
		Quantity Standard Deviation	4
Seller Agent	25	Mean Ability	0.7
		Ability Standard Deviation	0.03
		Minimal Price	EUR 0.3
Manager Agent	1	Purchase Price	EUR 0.17
Market Info	1	Item Market Share	0.25
		Item Market Volume	EUR 1 950 000
		Competition coefficient	0.8

The results of the simulation are the number of product units sold (amount, pieces), income (amount x item price, EUR), costs (EUR), and revenues (EUR) obtained for the selling these products. We name these results categories as the KPIs. The parameters of the simulation were set up according to the real company trading with the UTP cable. Therefore, the units traded are the meters (m).

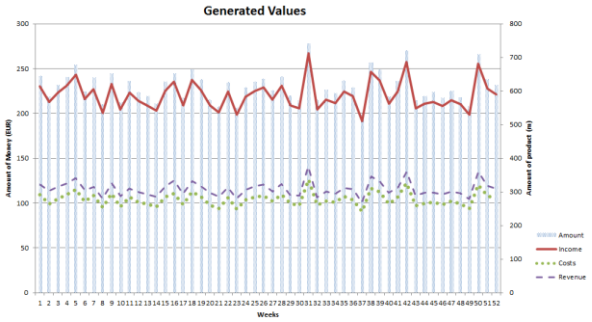

Figure 2: The generation values graph – weekly (source: own)

In Figure 2 the generated KPIs per week are depicted. The volatility of the curves shows a stable position of the company on the UTP cable market. The trends of KPIs point to the balanced selling during the whole year.

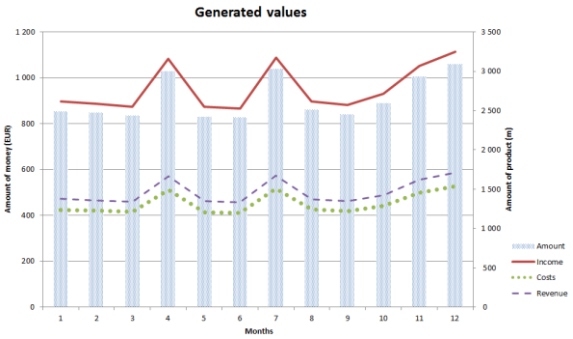

Figure 3: The generation values graph – monthly (source: own)

In Figure 3 the monthly KPIs are presented. The difference between the Figure 2 and 3 is the time step. The values resulted from the 53 weeks of the company

trading. Implemented MAS provides necessary results in the form of KPIs every week (or months) during one year of trading. Obtained KPIs could be compared from one simulation experiment to the another. This could be used to analyze different simulation parameterizations and the impact on the company performance.
In the next section, real data will be used to validate the proposed model. If the validation confirms correct simulation results, the used model generates correct results.

VALIDATION OF SIMULATION RESULTS

Simulation results were compared with the real data from an anonymous computer selling company with 30 employees (from Slovakia). The real data were taken from the company's accounting information system. For the comparison of simulated and real data, monthly averages were used.
The results of the simulation are represented by the item price (Fig. 4). The graph shows monthly averages of simulated and real price. The real price trend is stabile – not growing and not falling. Generated price is quite constant. However, when we depict on the axis with generated data the values with 3 decimal places, slightly falling trend is visible. Nevertheless, the real and the generated time series have similar development in the time. All curves are located in the range from EUR 0.355 up to EUR 0.38. This evidently shows that the simulation model is valid and we are able to simulate real business processes properly.

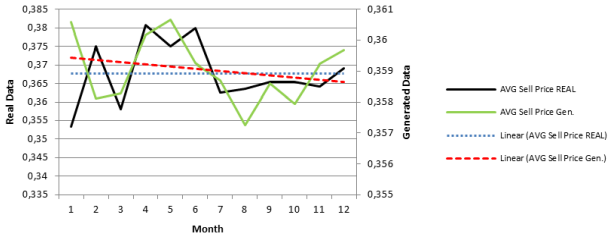

Figure 4: Prices – month averages (Source: Own).

From the statistical data listed in the following table is obvious that the dispersion and the standard deviation are higher in the real data time series. Real data are more distributed in opposite to the generated values. These points to our idea to use the disturbance agent in our simulation framework in order to bring more of the unpredictable impacts to the model. The generated values tend to be smoother with lower dispersion. We could bring more randomness into the time series development with the disturbances.

Table 2: Statistical data (Source: Own).

	value	average	dispersion	std. dev.
GENER.	Price	0,359	0,000	0,002
REAL	Price	0,367	0,003	0,055

To sum up, the results presented herein above visualise the real possibilities of the method proposed to be used for the real business processes simulation.

CONCLUSION AND FUTURE RESEARCH

The BPM simulation experiment in the form of MAS was introduced in this paper. Proposed simulation model was implemented in order to simulate the business process participants in a virtual company. Overall methodology is based on the company's generic structure. The simulation provides useful information about the core business processes. The comparison of the generated results with real data proofs the validity of the simulation model.
The next steps of our research concentrate on the statistical test of the validation, and the formal definition of the algorithm implemented. To conclude, using of a MAS implemented as a decision support tool for the management of a company will be the leading idea in the future.

ACKNOWLEDGEMENT

This work was supported by the grant "Innovation of Study Programmes at Silesian University in Opava, School of Business Administration in Karvina, Reg. no. CZ.1.07/2.2.00/28.0017".

REFERENCES

Barnett, M. 2003. "*Modeling & Simulation in Business Process Management*". Gensym Corporation, pp. 6-7, http://news.bptrends.com/publicationfiles/1103%20WP%20Mod%20Simulation%20of%20BPM%20-%20Barnett-1.pdf. Accessed 16 January 2012.

Bellifemine, F.; G. Caire; and T. Trucco. 2010. "*Jade Programmer's Guide*". Java Agent Development Framework. http://jade.tilab.com/doc/programmersguide.pdf. Accessed 16 January 2012.

De Snoo, D. 2005. "*Modelling planning processes with TALMOD*". Master's thesis, University of Groningen.

Dyer, D.W. 2010. "*Uncommons Maths - Random number generators*". Probability distributions, combinatorics and statistics for Java. http://maths.uncommons.org. Accessed 16 January 2012.

Foundation for Intelligent Physical Agents, FIPA. 2002. "*FIPA Contract Net Interaction Protocol*". In Specification [online], http://www.fipa.org/specs/fipa00029/SC00029H.pdf. Accessed 13 June 2011.

Hillston, J. 2003. "*Random Variables and Simulation*". http://www.inf.ed.ac.uk/teaching/courses/ms/notes/note13.pdf. Accessed 16 January 2012.

Jennings, N.R.; P. Faratin; T.J. Norman; P. O'Brien; and B. Odgers. 2000. "Autonomous agents for business process management". *Int. Journal of Applied Artificial Intelligence* 14, pp. 145–189.

Liu, Y. and K.S. Trivedi. 2011. "*Survivability Quantification: The Analytical Modeling Approach*". Department of Electrical and Computer Engineering, Duke University, Durham, NC, U.S.A. http://people.ee.duke.edu/~kst/surv/IoJP.pdf. Accessed 16 January 2012.

Macal, C.M. and J.N. North. 2005. "Tutorial on Agent-based Modeling and Simulation". In Proceedings: *2005 Winter Simulation Conference*.

Scheer, A.W. and M. Nuttgens. 2000. "ARIS architecture and reference models for business process management". Bus. In: van der Aalst WMP, Desel J, Oberweis A (eds.) *Business Process Management*. LNCS, vol. 1806, pp. 376–389. Springer, Heidelberg

Spisak, M. and R. Sperka. 2001. "Financial Market Simulation Based on Intelligent Agents - Case Study". *Journal of Applied Economic Sciences*, Volume VI, Issue 3(17), Romania, Print-ISSN 1843-6110, pp. 249-256.

Šperka, R.; D. Vymětal; and M. Spišák. 2013. " Validation of Agent-based BPM Simulation". In proceedings: *Agent and Multi-Agent Systems: Technology and Applications* 2013. Hue City, Vietnam. (to be published)

Vymetal, D. and R. Sperka. 2011. "Agent-based Simulation in Decision Support Systems". In proceedings: *Distance learning, simulation and communication* 2011. ISBN 978-80-7231-695-3.

Vymetal, D.; M. Spisak; and R. Sperka. 2012. "An Influence of Random Number Generation Function to Multiagent Systems: In proceedings: *Agent and Multi-Agent Systems: Technology and Applications* 2012. Dubrovnik, Croatia.

Wooldridge, M. 2009. "*MultiAgent Systems: An Introduction to*". 2nd edition, John Wiley & Sons Ltd, Chichester.

Yuan, J. and O.S. Madsen. 2010. "On the choice of random wave simulation in the surf zone processes". *Coastal eingeneering*. http://censam.mit.edu/publications/ole3.pdf. Accessed 16 January 2012.

AUTHOR BIOGRAPHIES

ROMAN ŠPERKA is an assistant and Ph.D. candidate at the Silesian University in Opava, School of Business Administration in Karvina, Department of Informatics, Czech Republic, European Union. He completed his master degrees in System engineering and Informatics in 2010 at Silesian University in Czech Republic, and in Information systems in 2011 at University of Ostrava in Czech Republic, Faculty of Sciences. His research interests include multi-agent systems in the field of economics, business and management. He is also interested in BPM, business process modeling and simulation. His e-mail address is: sperka@opf.slu.cz and his web-page can be found at http://www.roman-sperka.com.

DOMINIK VYMĚTAL was appointed to a chair in Information Technologies Silesian University, School of Business Administration in Karvina, Czech Republic in fall 2006. His previous appointments were at Konica Minolta Business Solutions Austria and Czech Republic where he was responsible for Strategy, Operations and Support of Company Information Systems for the last 16 years. Formerly he spent 22 years in Iron and Steel Works Trinec, Czech Republic in Research and IT Operations. He received his CSc degree at Institute of Steel in Moscow, Russia in 1975 on modeling metallurgical processes and DrSc degree at the same institution in 1985 on Methodology of Information Systems Development. He lives in the Czech Republic. His main topics of research are Information Systems Design, value based business modeling, agent-based simulations and their formal description and also juridical questions of e-commerce. His e-mail address is: vymetal@opf.slu.cz.

MAREK SPIŠÁK is an assistant and Ph.D. student at the Silesian University in Opava, School of Business Administration in Karvina, Department of Informatics, Czech Republic, European Union. He has graduated in System Engineering and Informatics in 2001 at Silesian University in Czech Republic. In research he focuses on multiagent simulations, especially on economical field – business process or financial market modeling, process optimization. His e-mail address is: spisak@opf.slu.cz and his web-page can be found on http://www.spisak.cz.

ASSESSING THE SEVERITY OF RECREATIONAL BOATING ACCIDENTS

F. Javier Otamendi[1]
José Ramón González de Vega[2]
Universidad Rey Juan Carlos
[1]Departamento Economía Aplicada I
Paseo Artilleros s/n
28032 Madrid, Spain
E-mail: franciscojavier.otamendi@urjc.es
[1]Comisariado Español Marítimo
Pintor Juan Gris 4
28020 Madrid, Spain
jrgonzalez@comismar.es

KEYWORDS
Recreational crafts, marine surveyor, incident costs, location profile, policy factors

ABSTRACT

The severity of the incidents of recreational boats in Spain during 2011 is analyzed in terms of the region in which the crafts were registered. The data was obtained and coded from the damage reports of one of the main Spanish marine surveyors, source that has been used for the first time to our knowledge in the academic literature. About 1400 incidents are statistically compared in terms of location, craft characteristics and skipper accreditations. Multiple hypothesis tests of averages are used to determine which categories of the study variables by location are different than the country average.

INTRODUCTION

Iberia is a peninsula with very good weather, so recreational boating might be practiced year round. In Spain alone, the number of registered crafts was more than 200,000 in 2011. Recreational crafts are defined as “those of all kinds, irrespective of the means of propulsion, having a hull length of between 2.5 and 24 meters, designed and intended for recreational and sports purposes, and carrying not more than 12 passengers" (Spanish Royal Decree 1434 / 1999).

In the scientific literature, only one reference has been found relative to recreational boating practices (Virk and Pikora, 2011) although some others might be lately found relative to marine accidents (O’Connor and O’Connor, 2005; Warner et al., 2000; Mullai and Paulson, 2011; LeBlanc et al., 2001; Psarros et al., 2010).

With regards to location, these studies are country specific: Australia, New Zealand, Norway, Sweden or the Mississippi river. They use different types of data sources: coroner’s data, the administration (Marine Safety Based Units, Swedish Maritime Department, Lloyd’s Register FairPlay or the Norwegian Maritime Directorate) or even telephone interviews. The main aim of these studies is the classification of the causes of the incidents, which are usually divided into human, environmental or craft/equipment related. Another primary aim is to identify the types of those incidents, classified as collision between crafts, rammings with objects or grounding.

The objective of this research is to study the costs of incidents related to recreational boating in Spain so as to determine location profiles for future insurance studies, framing the analysis within the current literature, but using an additional data source that might be of help: data from damage reports elaborated by the marine surveyors. There are more than 1600 reports dated in 2011 and signed by the Comisariado Español Marítimo (COMISMAR), one of the main marine surveying companies in Spain that covers about 25% of the incidents. These reports include information relative to the incidents, the crafts and the skippers.

Section 2 includes an explanation of the sources of data and the methods that have been used, which include descriptive analysis, multiple hypothesis testing and linear regression analysis. Sections 3, 4 and 5 are devoted to introduce the severity results by region while section 6 is used to conclude and show future lines of research.

DATA AND METHODS

Concerning the incidents, the marine surveyor produces expert reports that are kept in text format. For its records, COMISMAR also keeps some key information in a computerized database, although it does not include all the necessary data fields to perform a full analysis of recreational boating practices. Manual coding of the damage reports is therefore necessary.

The basic MsAccess database, with 1646 registers for 2011, includes the following incident fields: a code to

Proceedings 27th European Conference on Modelling and Simulation ©ECMS Webjørn Rekdalsbakken, Robin T. Bye, Houxiang Zhang (Editors)
ISBN: 978-0-9564944-6-7 / ISBN: 978-0-9564944-7-4 (CD)

uniquely identify the incident, the name of the craft, the date of the incident, the type of the incident, **the severity of the incident in monetary value**, the date of the requirement for expert evaluation and the closest harbor to the incident. As a first step, the harbor location is further coded into country and region.

In order to deepen the study, the database was updated with information included in the text damage reports. Some variables were related to the craft (brand, length, power, propulsion, manufacturing year, list and registry number, navigation certificate) and some to the skipper (education certificate, gender, age, validity of certificate, telephone, ID number, name).

After the tedious coding process of the reports, carried out by just one experienced researcher in data coding to avoid inter-coder reliability (Dietz et al.2000), an additional cleaning task was performed. Duplicated registers (same craft, amount and date) were eliminated to get a first set of 1525 registers. Then those registers with a missing data on width, power or registry number were also eliminated. Locations outside Spain were maintained. The full coded database for 2011 of 1368 complete incidents from the marine surveyor was therefore ready for analysis.

First, a descriptive analysis is performed by region, based on the variable called "**Monetary Value**", which defines the repair cost determined by the marine surveyor. The variable is crossed with each of the coded variables.

Second, an inferential method is performed to determine which categories of the variables by region are statistically different than the grand country average. Multiple hypothesis tests of averages are performed following statistical quality control principles (Grant and Leavenworth, 1988), in which each category is individually compared against a grand total. In this case, average values are studied using the so-called $\bar{x}$-charts which adjust for different sample sizes. These tools have already been applied in the social sciences with success to establish location profiles (Cañibano et al., 2011).

Third, linear regression techniques are used to identify the skipper and boat characteristics that jointly affect the severity of the incidents.

Throughout the analysis, a word of caution is however necessary. COMISMAR's average of analyzed incidents is considered to be 25% of the total number in Spain, so there might be slight deviations in the conclusions, but without losing their generality.

DESCRIPTIVE ANALYSIS OF INCIDENTS

Table 1 includes the relative frequency of the categorical variables that were fully answered and therefore were liable to serve as the basis for the sound study of 1368 incidents that required expert analysis by COMISMAR.

Table 1. Incident frequency univariate distributions

Type	Rammings (31.07%); Collision (20.25%); Grounding (17.25%); Other (10.89%); Environment (7.46%); Theft (7.38%); Capsize (3.87%); Craft (1.02%); Fire (.8%)
Location	Balearic Islands (25.%); Andalusia (18.64%); Galicia (11.77%); Valencia (10.31%); Catalonia (9.58%); Murcia (7.6%); Cantabria (4.97%); Basque Country (4.31%); Canary Islands (2.63%); Asturias (2.19%); Castilla-LaMancha (.58%); Madrid (.51%); Ceuta (.44%); Melilla (.37%); Extremadura (.29%); Aragon (.22%); France (.22%); Sardinia (.15%); Castilla-Leon (.07%); Gibraltar (.07%); Greece (.07%)
Registry Code	Balearic Islands (20.61%); Catalonia (18.86%); Andalusia (17.69%); Valencia (13.67%); Galicia (8.99%); Murcia (7.02%); Basque Country (4.17%); Cantabria (4.09%); Canary Islands (2.49%); Asturias (1.9%); Ceuta (.29%); Melilla (.22%)
Length	00-08 (61.62%); 08-12 (28.95%); 12-15 (6.14%); 15-18 (1.9%); 18-24 (1.39%);
Power	001-065 (28.58%); 125-250 (22.88%); 250-500 (18.79%); 065-125 (16.15%); 500+ (13.6%)
Propulsion	Motor (80.63%); Sail (19.37%)
Navigation certificate	Yes (81.14%); Not given (14.25%); No (4.61%)
Degree	PER – Recr. Boat Skipper (55.41%); Not provided (16.3%); PY – Yacht Skipper(14.04%); PNB – Basic Skipper (5.85%); Not necessary (3.51%); CY – Yacht Captain (2.92%); Association (1.75%); PMN – Jet ski Skipper (.15%); out-dated PER (.07%)
Gender	Male (96.35%); Female (3.65%)

The majority of incidents occurred in the Balearic Islands. Of course, it is the region with the highest number of registered crafts. Small boats are involved in more accidents, which is again consistent with the fleet categorization and other studies (dinghies – O'Connor and O'Connor, 2005). Power patterns are not so obvious, especially if the ratio between power and length is to be maintained for all the classes. This ratio appears to be a possible significant factor of incidents (O'Connor and O'Connor, 2005). More incidents are related to motor-propelled crafts with correct certification, although not in the proportion of motor-propelled boats in the fleet.

Concerning the skippers, almost all of them males, they had obtained different accreditation degrees, with PER being the most frequent. PER means "Patrón de Embarcación de Recreo", or Recreational Boat Skipper, which allows the skipper to practice within 12 miles of the shore. It is also worth mentioning that skippers with at least a PER-level education (which include yacht skippers and captains) are 72.37%.

DESCRIPTIVE ANALYSIS OF SEVERITY

The selected measure for the study of severity is the average of the damage included in the marine surveyor reports. This measure is included in the main MsExcel spreadsheet kept by COMISMAR. The analysis by region is included in Table 2. The inferential analysis by boat and skipper characteristics is left for the next section.

Valencia shows a large total due to a single accident that involves a large yacht. The rest of the regions do not show large differences.

Table 2. Severity per region

AVERAGE OF COSTS	
Region	Total
Andalusia	3686.0
Asturias	5297.0
Balearic Islands	5901.3
Valencia	21905.0
Canary Islands	4957.9
Cantabria	2468.7
Catalonia	4420.8
Ceuta	2555.1
Galicia	4162.9
Melilla	1690.3
Murcia	5611.9
Basque Country	4813.3
Total general	**6976.3**

INFERENTIAL ANALYSIS OF SEVERITY

Hypothesis testing

The selected tool to compare among regions is the $\bar{x}$-chart, which performs a series of hypothesis tests on the averages, adjusting for different sample sizes.

This chart belongs to the set of tools used in Total Quality Management (TQM) in general, and Statistical Process Control (SPC) in particular (Grant and Leavenworth, 1988). First, the average population behavior is estimated using the whole sample, receiving the name of grand average. Second, the average of each sample is compared against the grand average using traditional tests of hypothesis.

This exercise is performed in this case both for the whole population, comparing across regions or by craft or skipper characteristics.

Figure 1 shows the results after comparing each region against the Spanish grand average of 6976.3 €. The only significantly different behavior is that of Melilla (1690.0 €), well below the overall average. Valencia is not significantly different since the variability within this region is very high.

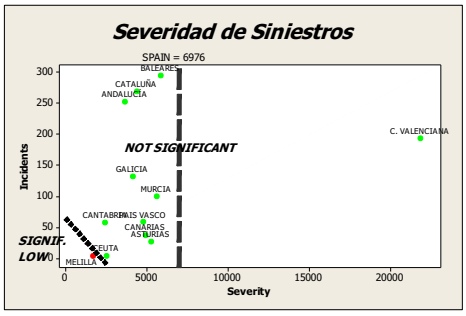

Figure 1. Severity by region

It seems appropriate though to perform the study by categories of craft and skipper, looking for further significant factors that affect the severity of the incidents.

In terms of boat characteristics, Table 3, incidents involving short crafts of less than 8 meters (3680.5 €) are significantly less severe in Cantabria (2066.9 €). Ceuta (2526.5 €), Melilla (272.0 €) and the Basque Country (1900.1 €) show a lower cost than the grand average (5480.8 €) regarding boats between 8 and 12 meters. Andalusia (3299.4 €), Asturias (3037.4 €), the Canary Islands (2840.9 €), Cantabria (903.9 €) and the Basque Country (2316.0 €) are below the grand average of 5741.3 € for boats between 12 and 15 meters. Finally, for large boats between 15 and 18 meters (7292.1 €), Andalusia (2790.5 €) and the Balearic Islands (2204.1 €) show a low average whereas the Basque Country (32230.5 €) shows a very high average cost.

Regarding power, for the low-powered crafts with less than 65 HP (3729.7 €), Galicia show very high costs (5844.9 €) and Asturias (1653.6 €) and Cantabria (2477.6 €) very low totals. For boats between 65 and 125 HP, Andalusia (1892.7 €), the Canary Islands (2079.8 €) and Ceuta (290.0 €) are below country average (3590.7 €). For the medium-powered boats between 125 and 250 HP (4162.5), only Cantabria shows a low average (1403.2 €). Finally, for high-powered boats between 250 and 500 HP, four regions – Asturias (933.4 €), Valencia (3085.3 €), Galicia (3176.9 €) and the Basque Country (1012.2 €) – incur in a significantly lower severity than the grand average of the category (4862.9 €).

There are no differences found in motor boats across regions. Sail boats (4379.1 €) incur in less severe incidents in Asturias (712.6 €), Cantabria (2456.6 €), Melilla (272.0 €) and the Basque Country (1956.1 €).

One interesting category is that of the certificate of navigability. Those incidents with a valid certificate do not show differences across regions, although the average is as high as 7643.4 €. If the certificate is not provided, Asturias (1849.1 €), Ceuta (1237.6 €) and the Basque Country (1247.8 €) incur in less severe accidents than the grand country average of (4005.6 €). The Balearic Islands (1957.9), Galicia (1865.2 €) and Melilla (710.0 €) show a low total compared to Spain (5251.8).

In terms of the skipper characteristics (Table 4), and the degree of the diploma, those that are yacht captains (7585.1 €) are involved in very severe accidents in Murcia (14986.1 €) and low-cost incidents in Asturias (2567.2) and the Canary Islands (4563.1 €). For skippers with just an association permit (3682.2), the severity is lower in the Canary Islands (514.5 €), Catalonia (1198.3 €) and the Basque Country (240.3 €).

Interestingly enough, for the practitioners certified with the more common education diploma (PER - 55%), there are no severity differences whereas the incidents in which a degree was not necessary showed lower totals across the regions.

Lastly, males (7080.4 €) are less costly in Melilla (1690.3 €) and females (4234.5 €) incur in less severe accidents in Andalusia (1021.6 €), Cantabria (1290.8 €) and the Basque Country (1412.0 €).

Table 3. Regions with significant incident frequencies compared with the country average by craft characteristics (++, larger at 0.01; +, larger at 0.05; -, lower at 0.05; lower at 0.01).

	LENGTH					POWER					PROP.		CERTIFICATE of NAVIGABILITY		
	00-08	08-12	12-15	15-18	18+	001-065	065-125	125-250	250-500	500+	Sail	Motor	No	Not Given	Yes
ANDALUSIA			-	-			-								
ASTURIAS			-			-			-		-			-	
BALEARIC ISLANDS				-									-		
VALENCIA									-						
CANARY ISLANDS			-				-								
CANTABRIA	-		-			-		-			-				
CATALONIA															
CEUTA		-					-							-	
GALICIA						+			-				-		
MELILLA		-									-		-		
MURCIA															
BASQUE COUNTRY		-	-	+					-		-			-	
SPAIN	**3680.5**	**5480.8**	**5741.3**	**7292.1**	**163097.6**	**3729.7**	**3590.7**	**4162.5**	**4862.9**	**25500.2**	**4379.1**	**7605.1**	**5251.8**	**4005.6**	**7643.4**

Table 4. Regions with significant incident frequencies compared with the country average by user characteristics (++, larger at 0.01; +, larger at 0.05; -, lower at 0.05; lower at 0.01).

	DEGREE									GENDER	
	Yacht captain	Association	Not provided	Not necessary	PER – Recreational boat skipper	Out-dated PER	Jet ski skipper	Basic skipper	Yacht skipper	Female	Male
ANDALUSIA										-	
ASTURIAS	-			-							
BALEARIC ISLANDS											
VALENCIA											
CANARY ISLANDS	-	-		-							
CANTABRIA				-						-	
CATALONIA		-		-							
CEUTA											
GALICIA				-							
MELILLA											-
MURCIA	+			-							
BASQUE COUNTRY		-								-	
SPAIN	**7585.1**	**3682.2**	**18309.8**	**4409.8**	**4248.7**	**18089.4**	**679.6**	**3500.1**	**5926.1**	**4234.5**	**7080.4**

Location patterns

Starting at the Northwest, Galicia incur in severe accidents with small boats and in mild incidents with large crafts. Going East, Asturias and Cantabria are less severe with medium-size, low-powered vessels, and also with sail boats. The Basque Country shows a similar pattern, but it also has a significant high severity with long crafts.

Andalusia, in the South, shows low severity with medium-size, medium-power boats.

At the Mediterranean Sea, Catalonia and Murcia do not show any differences with the country average, whereas Valencia show a low severity with high-powered boats.

Concerning the islands, the Balearic Islands show low severity of long vessels and the Canary Islands' pattern is similar to that of Andalusia.

Ceuta and Melilla are significantly below the average in boats with a length between 8 and 12 meters.

REGRESSION ANALYSIS

The location patterns are not concerned with absolute monetary values, but with relative differences within a category. To assess severity quantitatively, as a prior step before converting it to insurance premiums, a linear regression analysis is to be performed.

The model is to include all the variables that cover the craft or the skipper characteristics and that are liable to identify factors that might be controlled when setting insurance policies.

The dependent variable for each recreational boat is the severity or average cost and the independent variables are the craft and skipper variables that have been used throughout the paper, but coded to have numerical values.

Regarding the craft, both length and power are already continuous, whereas propulsion is coded as a binary variable (0 = sail; 1 = motor). The navigation certificate is coded as follows: 1 = yes, 0.5 = not given, and 0 = no.

The skipper variables are studied as follows. For gender, males are assigned a value of 1 and females a value of 0. The accreditation degree is coded with a discrete variable: 3 (CY - Captain of yacht), 2 (PY – Yacht Skipper), 1 (PER) and 0 otherwise.

After running the linear regression model, the craft characteristics that are significant are the length and the power, which are directly proportional to the severity. Regarding the skipper, there are no significant factors as shown by the low absolute t-values. The model is significant even if the r^2 value is not high.

Table 5. Significant factors affecting severity

α=0.05		**SEVERITY is LOWER if:**					
		SHORTER	**LESS**	**NO**	**NO**	**NO**	**NO**
	Constant	**Length**	**Power**	**Propulsion**	**Certificate**	**Degree**	**Gender**
Coefficient	-38484.65	3.0829	0.0199	6636.120356	5678.4491	-2077.9023	5953.1282
Error	16538.66	0.7979	0.0090	7036.6705	6313.2846	5169.8452	12711.2260
t		3.8640	2.2177	0.9431	0.8994	-0.4019	0.4683
r^2	3.4%						
F	8.3505	2.1050		**Significant Model**			
df	1414						
k	6						

CONCLUSIONS

The marine surveyor reports have proven to be a very good source to quantify the severity of the incidents of recreational boats.

Location profiles indicate the regions of Spain that incur in milder incidents. There are clear differences among the seas and coasts of Spain.

The obvious direct relationship between severity and the length and the power of the boats has been established, so it can be used to set insurance premiums. In order to do so, this first analysis is going to be coupled with the analysis of the frequency of incidents in future studies.

ACKNOWLEDGEMENTS

This research has been funded by Fundación MAPFRE, Madrid, Spain.

REFERENCES

Cañibano C., Otamendi F.J., Solís, F., 2011. International temporary mobility of researchers: a cross-discipline study. Scientometrics 89, 653-675.

Dietz, J., Chompalov, I., Bozeman, B., O'Neil E., Park J., 2000. Using curriculum vita to study the career paths of scientists and engineers: an exploratory assessment. Scientometrics 49, 419-442.

Grant, E. L., Leavenworth, R. S., 1988. Statistical Quality Control. McGraw-Hill, New York.

Le Blanc L.A., Hashemi, R.R., Rucks, C.T., 2001. Pattern development for craft accidents: a comparison of statistical and neural computing techniques. Expert Systems with Applications 20, 163-171.

Mullai A., Paulsson U., 2011. A grounded theory model for analysis of marine accidents. Accident Analysis and Prevention 43, 1590-1603.

O'Connor P.J., O'Connor N., 2005. Causes and prevention of boating fatalities. Accident Analysis and Prevention 30, 689-698.

Psarros G., Skjong R., Eide M.S. 2010. Under-reporting of maritime accidents. Accident Analysis and Prevention 42, 619-625.

Virk A., Pikora T.J., 2011. Developing a tool to measure safe recreational boating practice. Accident Analysis and Prevention 43, 447-450.

Warner N., Smith, G.S., Langley, J.D., 2000. Drowning and alcohol in New Zealand: what do the coroner's files tell us. Aust. N.Z. J. public Health 24 (4), 387-390.

AUTHOR BIOGRAPHIES

F. JAVIER OTAMENDI received the B.S. and M.S. degrees in Industrial Engineering at Oklahoma State University, where he developed his interests in Simulation and Total Quality Management. Back in his home country of Spain, he received a B.S. in Business Administration and a Ph.D. in Industrial Engineering. He is currently a simulation and statistics consultant and university professor at the Rey Juan Carlos University in Madrid.

JOSÉ RAMÓN GONZÁLEZ DE VEGA is a Naval Architect by the "Universidad Politécnica de Madrid". He is the Technical Manager of COMISARIADO ESPAÑOL MARITIMO, in charge of all the technical net of the company that carry out more than 2.000 pleasure craft damage inspection per year. His work involves the investigation of the main cause of the damages, environmental conditions and human behaviour. He has a large experience in ship casualties investigation. He is a member of the Spanish Naval Architect Association, Class surveyor on behalf International Naval ship Bureau (INSB), Panama flag surveyor and RINAVE surveyor. He is a certified ISM auditor by BV, and a ISPS auditor by STET. He has the pleasure craft license PER (Patrón de Embarcaciones de Recreo).

COST SIMULATION OF AN INFLATION-LINKED AND A FLOATER BOND WITH BACKTESTING

Kata Váradi, Ph.D.
Ágnes Vidovics-Dancs
Department of Finance
Corvinus University of Budapest
H-1093, Fővám tér 8, Budapest, Hungary
E-mail: agnes.dancs@uni-corvinus.hu

KEYWORDS
Inflation-linked bond, interest rate models, financial simulation

ABSTRACT

In this paper we focus on simulating and backtesting the costs of two special government securities, from the point of view of the issuer. Our research has two main goals. The first one is to assess the costliness of an inflation-linked bond in comparison with a floater one. The second one is to backtest the simulation results on real market data. We carry out the cost simulations with Monte Carlo simulation. The basis of the calculations is the Cox-Ingersoll-Ross interest rate model for the floater bond; and a first order autoregressive model for the inflation-linked bond. Our findings are: (i) the inflation-linked bond appears to be more expensive than the floater one and this relationship holds true for ex-ante (simulated) and ex-post (actually realised) costs as well; and (ii) the simulations predict the total present value of the costs adequately for both instruments, but the individual cash flows of the floater bond are significantly under- or overestimated in the different years. This shortcoming is in line with our expectations, since the model is calibrated on a tranquil period but applied on a very volatile one.

INTRODUCTION

A wide range of financial models, intending to describe the behaviour of different market processes and to predict the future movements in the market have a great and general problem. Namely, the model parameters are estimated from historical databases, but then the models are applied to capture future market movements when the circumstances are not necessarily the same. The events of the last decade or so provide great examples of rapidly changing market environments. Built upon this observation, one of our motivations in this paper is to examine what happens when we calibrate a model on a tranquil period but apply it to predict financial market movements in a more volatile environment.

This phenomenon will appear in this paper when we estimate the future cash flows of two hypothetic bonds as if they were issued in Hungary in 2006. The model calibrations are carried out on a database of a tranquil period (1999-2006), while the backtesting of the estimations is based on a very volatile period (2006-2011). We expect that discrete estimations might have only modest predicting power but since we simulate more (four or five) cash flows of the bonds chosen, we give a chance that on the long run the models approximate the average costliness of the instruments acceptably.

The examined bonds are an inflation-linked and a floater bond. The core motivation was to measure the costliness of the indexed bond because the issuance of such a Hungarian government security was a relevant and current topic in 2006. As benchmark instrument we chose a floater bond since these two types of bonds have a very important common feature: their future nominal cash flows are not known in advance, i.e. have to be estimated. Since we analyse bonds with five years maturity, we already know the ex-post, realised values of the relevant risk factors (especially interbank interest rate and inflation), hence we can perform a comprehensive backtest as well.

The rest of the paper is organised as follows. First we introduce the basic features of traditional (fixed or floater) and inflation-linked bonds. Afterwards, we shed some light on the evolution of the indexed bonds' market, highlighting also the scarce experiences that Hungary has with this bond type. Then, we present the theoretical background and the outputs of the cost simulations. Finally, we analyse and backtest the results and conclude our findings.

TRADITIONAL BONDS

A traditional bond is a debt instrument that obligates the issuer to make specified payments on predetermined dates for the bondholder. The most important features of a bond are its *face value* (it is also called *principal* or *notional amount*) which is the debt that has to be paid back; and its *coupon rate* which determines the interest payment that has to be paid after the outstanding notional amount (Bodie et al., 2008).

There are two basic types of bonds, the *fixed rate* and the *floating rate* (or *floater*) bond. In case of the first type the coupon rate is a fixed percentage of the face value, while in case of a floater it is varying according

Proceedings 27th European Conference on Modelling and Simulation ©ECMS Webjørn Rekdalsbakken, Robin T. Bye, Houxiang Zhang (Editors)
ISBN: 978-0-9564944-6-7 / ISBN: 978-0-9564944-7-4 (CD)

to a current market rate called *fixing* or *benchmark rate*. In practice, the interest payment of a floater is usually the chosen market rate plus a spread. Since the market rate is changing continuously, the cash flow of a floater bond will change from one payment date to the other as well. It is important to mention that the payment is determined always one period in advance, according to the current value of the fixing rate. The benchmark is usually an interbank rate, i.e. the interest rate that banks use for lending to each other, like for example the London Interbank Offered Rate (*Libor*).

Besides these two types of bonds, there are numerous innovations in the bond markets (e. g. the inverse floater or the asset-backed bonds) out of which we introduce one special type, the inflation-linked bond in more detail, since this is in the focus of our research.

INFLATION-LINKED BONDS

Inflation-linked bonds (*IL-bond*s) belong to the class of indexed bonds. The speciality of these instruments is that their payments are tied to a general price index (Bodie et al., 2008). An IL-bond, contrary to a fixed rate bond where the coupon rate is expressed in nominal terms, has a *real coupon* which is a fix percentage of the *real value* of the principal. More precisely, when the consecutive cash flow of the IL-bond falls due, the face value is multiplied with an *index factor* that represents the inflation of the time period passed since the last payment. The cash flow is determined then as the product of the real coupon and this modified face value.

Calculating the future cash flows of an IL-bond is not as evident as in case of a traditional fixed bond, hence the pricing of the bond poses some problems as well. The first difficulty is that in most of the cases we do not know what the exact rate of the inflation in the last time period was. These data are available only with a few months delay, which means that we have to have a certain delay in the indexation as well. The second problem is the definition of the inflation. It is not clear which indicator should be used. There are several possibilities, like the GDP deflator or the consumer price index. It is one of the most important questions at the issuance of an IL-bond, which indicator to be used.

An important characteristic of an IL-bond is the payment method of the principal's inflation increments. These increments could be redeemed at the time of the corresponding coupon payment, but in practice it is more widespread that they are paid in one sum at maturity. At this point it is worth to mention that since economies might face not only inflation but deflation as well, being indexed to a price level does not necessary mean increasing payments in nominal terms.

From the point of view of our analysis, it is important to emphasise that future cash flows involve uncertainty either for floater, or for IL-bonds. With other words, both instruments have cash flow risk. An essential difference is that the following payment of a floater is always known in advance. In Table 1 we listed those parameters that define the cash flows of a fixed rate, an inflation-linked and a floater bond.

Table 1: Factors defining the cash flows of bonds

Fixed rate	**Inflation- linked**	**Floating rate**
Face value	Face value	Face value
Maturity	Maturity	Maturity
Frequency of coupon payment	Frequency of coupon payment	Frequency of coupon payment
Principal payment method	Principal and inflation increment payment method	Principal payment method
Coupon	Real coupon	Spread
	Price index	Fixing curve

Index Calculation and Pricing

The central question in determining the cash flow and the price of an IL-bond is the calculation of the index factor. For the purposes mentioned it is indispensable to use a method that enables us to determine the price index at any time. Given that inflation statistics are available only monthly, this might be difficult, but there are several ways to handle this problem. In practice the prevailing method is the Canadian model, for this reason we introduce it briefly.

The Canadian model was elaborated in 1991. The essence of this model is that we do not need the nominal value of the next coupon payment for determining the price; we only need the value of the price index. The price index at any day is calculated as the linear interpolation of two preceding index values. Since the inflation data are published at least with a two months delay and usually only monthly, this means that these indices will be the two and three month earlier price index values. Equation (1) shows the price index calculation on an arbitrary day t_0.

$$\mathrm{PI}_{t_0} = \mathrm{PI}_{M-3} + \frac{t_0 - 1}{D}\left(\mathrm{PI}_{M-2} - \mathrm{PI}_{M-3}\right) \tag{1}$$

where PI is the price index, M stands for the month of t_0, and D is the number of days in month M.

The index factor of Equation (2) – which is used to modify the principal – is the ratio of the price index on the examined day (PI_{t0}) and on the basis day (PI_B).

$$\mathrm{IF}_{t_0} = \frac{\mathrm{PI}_{t_0}}{\mathrm{PI}_B} \tag{2}$$

For more information about inflation-linked securities in general see Deacon et al. (2004).

International Markets

IL-bonds have been issued in a bigger amount after the Second World War in countries like Brazil, Argentina, or Finland. That time the main reason for the issuance in these countries was the two-digit inflation rate. With the issuance the government wanted to show its commitment to decrease inflation in the following years. (Pecchia and Piga, 1995). The global market for IL-bonds started to grow notably in 1981, when the British government has started to issue IL bonds, called IL-Gilts. The reason for the issuance was that the inflation expectation of the government was lower than that of the market. The government hoped that it could save on interest expenses in this way (Farkas et al., 2005). The market experienced another significant increase when several countries introduced inflation targeting monetary policy, like Canada, Sweden, Australia, etc.

Nowadays, the total outstanding amount of the IL-bonds on the three biggest markets are $500 billion TIPS (Treasury Inflation-Protected Securities) in the USA, $300 billion IL-Gilts in the UK, and $200 billion OATi/OAT€i IL-bonds in France[1].

Since the basic of our simulations and backtesting is a Hungarian IL-bond, we summarise the experiences of this country with indexed government bonds.

Hungarian Market

The Hungarian Government Debt Management Agency (*GDMA*) started the issuance of the first (and only one so far) inflation-linked government security in 1998. As a consequence of the lack of interest from investors, the IL-bond was auctioned only four times, with continuously decreasing demand.

After the maturity of the IL-bond, Farkas et al. (2005) analysed the cost efficiency of the instrument from the viewpoint of the GDMA. The authors used two methods, cost analysis with future value calculation, and break-even inflation calculation. Their main result was that the ex-post cost efficiency of the IL-bond is rather questionable.

After the maturity of the first IL-bond, it has been suggested that GDMA might have tried to issue a new one. It seemed to be possible that the market of Hungarian government bonds became more mature and that the issuance of a new IL-bond could be successful. This was the main reason why Dancs (2006) made an analysis and simulated the future costs of a hypothetic five year maturity IL-bond assuming an issuance in 2006. In what follows we reproduce these simulations with slight modifications and extend the analysis with backtests[2].

[1] Data sources: US Department of the Treasury, UK Debt Management Office, Agence France Tresor.

[2] We have to complete the story by adding that in 2006 GDMA decided on not issuing new IL-bond. It did not launch such instrument for institutional investors in the following years either. However, from 2009 there exists a similar retail security for small investors.

EX-ANTE COST-ESTIMATION

In this part we are simulating the expected costs of two hypothetic government bonds issued by the GDMA on the 1st of March 2006. The next part will backtest the results. The characteristics of the two hypothetic bonds are summarised in Table 2.

Table 2: Characteristics of the bonds

Type	**Inflation-linked**	**Floater**
Currency	EUR	EUR
Face value	10,000	10,000
Issue date (d/m/y)	1/3/2006	1/3/2006
Maturity (d/m/y)	1/3/2011	1/3/2011
Interest payment period	annual	annual
Principal payment method	at maturity with inflation increments	at maturity
Real coupon / Spread	1.9%	0.01%
Price index / Fixing curve	HICP[3] euro area (ex tobacco)	Libor 12M

When determining the characteristics of the bonds, our main goal was to ensure comparability. Not only the two bonds have the same issue and payment dates, both are also denominated in the same currency (euro), hence we do not have to estimate future FX rates. The most decisive point was choosing the real coupon of the IL-bond and the spread of the floater. We intended to examine bonds that have the same issue price which for the sake of simplicity equals the face value. In this way, the initial revenue of the issuer is identical for the two bonds. Market circumstances (i.e. comparable data of relevant Hungarian and European sovereign bonds) and experts' estimations were considered to determine the real coupon and the spread that matches this criterion. However, we have to keep in mind that possible under- or overestimation of these parameters may influence which bond turns out to be more expensive.

For both bonds, we give ex-ante estimations on their future cash flows. The methodology used is Monte Carlo simulation, so the first step is identifying the stochastic processes that determine the cash flows. In case of the floater bond we model future Libor path with the Cox-Ingersoll-Ross interest rate model, while in case of the IL-bond we estimate the index-factor with the help of an autoregressive model. Parameter calibrations are based on historical data.

[3] Harmonised Index of Consumer Prices, a comparable indicator of inflation in the EU states. HICP for the euro area is the weighted average of the price indices in the member countries.

Modelling the Libor

The Cox-Ingersoll-Ross model (*CIR-model*) is a continuous, one factor stochastic interest rate model, first proposed by Cox et al. (1985). In this model the instantaneous interest rate dynamics are given by the following stochastic differential equation:

$$dr_t = \alpha(\beta - r_t)dt + \sigma\sqrt{r_t}\,dW_t \qquad (3)$$

where α, β and σ are positive constants, r_t is the interest rate, t is time. W_t denotes the standard Wiener process, a continuous-time stochastic process used very frequently in quantitative finance.

The most important characteristics of the Wiener process are as follows: (i) the trajectories are continuous, (ii) the increments on disjunctive time intervals are independent, (iii) the increments are stationary i.e. increments on time intervals with the same length have the same probability distribution, and (iv) the increment W_t-W_s is distributed normally with zero expected value and (t-s) variance. For further information on Wiener process and generally on the mathematical background of quantitative finance see Medvegyev (2007), while Cairns (2004) gives a comprehensive discussion specifically about interest rate models.

As one may observe, the interest rate in the CIR-model follows a mean-reverting process with long-term average β: when $r_t<\beta$, the drift term in Equation (3) becomes positive so the interest rate will increase and vice versa. The speed of adjustment to the long run mean is measured by α. The volatility term is proportional to the square root of the interest rate level. Cox et al. (1985) also showed that the future interest rate in their model (conditional on its current value) has a non-central chi-squared distribution.

When using the CIR-model for simulation purposes, we have to find the values of the model's three parameters. Here we present a possible method developed by Chan et al. (1992). This approach is based on the econometric estimation procedure called Generalised Method of Moments (*GMM*). For more information about GMM in general see Hansen (1982). Another application of the method for interest rate models can be found in Li (2000).

Chan et al. (1992) developed their procedure to estimate the parameters of the following general interest rate model:

$$dr_t = \alpha(\beta - r_t)dt + \sigma r_t^{\gamma} dW_t \qquad (4)$$

It is easy to see, that Equation (4) gives the CIR-model if we substitute γ=0.5.

In Equation (5) we discretise (4) with the Euler approximation.

$$r_t = \alpha\beta\delta_t + (1-\alpha\delta_t)r_{t-1} + \sigma r_{t-1}^{\gamma}\sqrt{\delta_t}\,e_t \qquad (5)$$

where δ_t is the length of time between two observations of r_t, and e_t are independent, standard normal random variables.

Let us rewrite Equation (5) in the following form:

$$r_t - r_{t-1} = \alpha\beta\delta_t - \alpha\delta_t r_{t-1} + \varepsilon_t \qquad (6)$$

The first two moments (expected value and variance) of the variable ε_t can be determined quickly by comparing Equation (5) and (6):

$$E(\varepsilon_t) = 0 \qquad (7)$$

$$E(\varepsilon_t^2) = \sigma^2\delta_t r_{t-1}^{2\gamma} \qquad (8)$$

where *E()* denotes expected value. The parameters are estimated with the null hypotheses of Equations (6), (7) and (8).

For estimating the future cash flows of the floater bond we model the future Libor rates with the CIR-model defined in Equation (3). Model calibration is based on a historical database which contains daily Libor rates from 1st December 2000 to 1st March 2006, all in all a sample of 1,340 observations. We use the above described GMM method and substitute δ_t=1/250=0.004 in Equation (6). (We have observations for trading days, hence one calendar year contains 250 Libor rates.) Table 3 shows the results of the parameter estimations.

Table 3: Calibration of the CIR-model

Parameter	Estimated value	t-statistic	p-value
α	0.937	2.990	0.003
β	0.025	10.885	0.000
σ	0.001	26.780	0.000

Once the parameter values of the CIR-model are determined, then we can estimate the future cash flows of the floater bond. As it has been pointed out, the next cash flow and the principal payment at maturity of a floater bond are always known. Therefore, from all cash flows of the bond there remain only four unknown interest payments to be estimated. Table 4 illustrates in details which cash flows are subjects of our simulations and which are fixed at issuance. Afterwards, Figure 1 shows relative frequencies of the four estimated payments generated from 10,000 simulations.

Table 4: Cash flows of the floater bond
(*italic* expressions are to be estimated)

Date	Cash flow	Payment type
1/3/2006	+10,000	Issue price
1/3/2007	-309	Interest
1/3/2008	-10,000*$Libor_{1/3/2007}$	*Interest*
1/3/2009	-10,000*$Libor_{1/3/2008}$	*Interest*
1/3/2010	-10,000*$Libor_{1/3/2009}$	*Interest*
1/3/2011	-10,000*$Libor_{1/3/2010}$	*Interest*
1/3/2011	-10,000	Principal

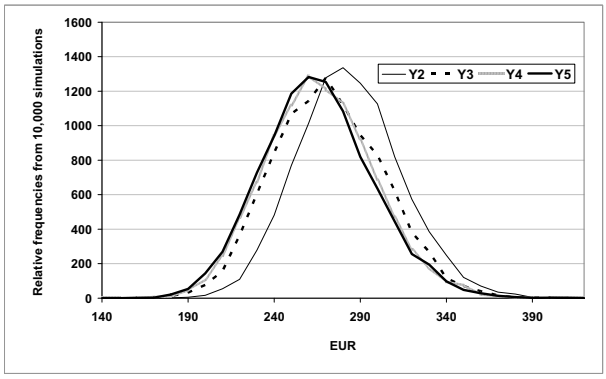

Figure 1: Relative frequencies of the floater bond's estimated cash flows

We will analyse the results in comparison with the cash flows of the IL-bond.

Modelling the Index Factor

For estimating the future costs of the IL-bond we have to predict future index factors. Our goal is capturing the main characteristics of the price index chosen without building a complicated model about the whole economy and making assumptions on wide range of macroeconomic aggregates.

We will model the inflation with the following first order autoregressive process:

$$\Delta \mathrm{HICP}_{\mathrm{M}} = \mathrm{a}\Delta \mathrm{HICP}_{\mathrm{M-1}} + \mathrm{b}\overline{\mathrm{Libor}}_{\mathrm{M}} + \eta \quad (9)$$

where $\Delta \mathrm{HICP}_{\mathrm{M}}$ is the month-on-month inflation measured by the annual rate of change of the price index given in Table 2, $\overline{\mathrm{Libor}}_{\mathrm{M}}$ is the average level of the Libor rate in month M and η is normally distributed residual term. The autoregressive feature of the model defined in Equation (9) is easily justifiable: sequential month-on-month statistics measure the inflation of highly overlapping periods.

We estimate regression of Equation (9) with Ordinary Least Squares method. We use historical data of HICP in the euro area from mid-1999 to mid-2005. Since data are available on a monthly basis, we have 74 observations. Table 5 shows the results of the parameter estimations.

Table 5: Estimation of the autoregressive model

Parameter	Estimated value	t-statistic	p-value
a	0.904	24.219	0.000
b	0.060	2.725	0.008

The adjusted R-square of the autoregressive model is 72 percent. From the following simulations' point of view, it is important to test the normality of the residuals. We performed Jarque-Bera test and received a p-value of 68 percent. It means that rejecting the null hypothesis of normality would be a wrong decision with probability of 68 percent.

In case of the IL-bond, we have to estimate five cash flows. The initial revenue of the issuer is known (under our assumption the real coupon is set so that the issue price is the face value), but all the other payments, including the principal redemption at maturity, depend on future inflation. Similarly to the floater bond, we summarise in a table the cash flows indicating the factors that should be estimated (Table 6). Relative frequencies of the five estimated interest payments generated from 10,000 simulations are depicted in Figure 2.

Table 6: Cash flows of the IL bond
(*italic* expressions are to be estimated)

Date	Cash flow	Payment type
1/3/2006	+10,000	Issue price
1/3/2007	-10,000*$IF_{1/3/2007}$*1.9%	*Interest*
1/3/2008	-10,000*$IF_{1/3/2008}$*1.9%	*Interest*
1/3/2009	-10,000*$IF_{1/3/2009}$*1.9%	*Interest*
1/3/2010	-10,000*$IF_{1/3/2010}$*1.9%	*Interest*
1/3/2011	-10,000*$IF_{1/3/2011}$*1.9%	*Interest*
1/3/2011	-10,000*$IF_{1/3/2011}$	*Principal*

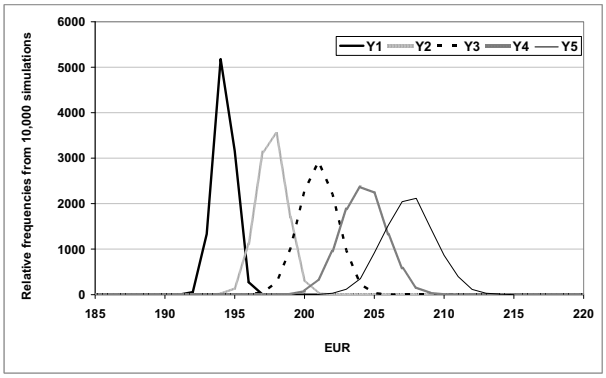

Figure 2: Relative frequencies of the IL-bond's estimated cash flows

Interpreting the Results

In Figure 1 and Figure 2 it is worth to observe that the cash flows' distribution is flatter in each year for the floater bond. This means higher variance which is in line with the construction of the bonds. In case of the IL-bond the magnitude of the costs is predetermined by the real coupon and 'only' the modifying index factor is unknown, while in case of the floater bond it is the coupon itself that we estimate. The latter means higher uncertainty especially for initial years where the index factor represents the inflation of shorter periods.

Another observation is that both the mean and the variance (the flatness) of the IL-bond cash flows are increasing significantly in time. This is due to fact that later cash flows have to compensate the investor for the inflation of a longer period. This feature results in higher and more volatile nominal cash flows as time passes. In the next section we will compare the estimated cash flows of the two bonds and will also backtest the results.

ANALYSIS AND BACKTEST OF THE RESULTS

In Table 7 and Table 8 we summarise the results of our estimations and also inform the reader about what cash flows would have actually realised ex-post. From the estimations we present the mean and the 95th percentile (pctl. in the Tables) of the 10,000 simulations. Since we are talking about the issuer, from our point of view the main risk is having higher costs than expected or estimated. This is why we included in the Tables an upper percentile. Furthermore, we also calculated the present values of the annual cash flows (PV in the Tables), which is important because of comparability. We would like to know which bond is cheaper on the whole, so we have to add all the future costs of the bonds, and since it is not fair to sum up cash flows due at different times, we discounted all the payments to the date of the issuance. For discounting we used a flat 3% yield curve. The choice of the fair discount curve is of course influencing the results, but from our points of view (comparing the two bonds and testing the simulations) this impact is so small that we decided on not going into the very depth of this financial problem.

Table 7: Actual and estimated cash flows of the floater bond

Date	Cash flow		
	actual (ex post)	estimated (ex-ante)	
		mean	95% pctl.
1/3/2007	309.14		
1/3/2008	417.71	278.55	330.37
1/3/2009	448.00	266.64	320.69
1/3/2010	212.94	261.87	314.75
1/3/2011	10,129.75	10,260.31	10,315.26
PV	**10,031.06**	**9,890.01**	**10,082.70**

Table 8: Actual and estimated cash flows of the inflation-linked bond

Date	Cash flow		
	actual (ex post)	estimated (ex-ante)	
		mean	95% pctl.
1/3/2007	193.42	193.73	194.82
1/3/2008	199.80	197.16	198.85
1/3/2009	202.00	200.46	202.64
1/3/2010	203.41	203.73	206.34
1/3/2011	11,171.28	11,101.95	11,267.80
PV	**10,378.15**	**10,315.03**	**10,465.06**

The first purpose of our calculations was comparing the costs of the two bonds. Our results show that the IL-bond turns out to be more expensive, the present value of all the future payments is higher for this instrument. This statement holds true for the ex-ante, estimated costs and for the ex-post, actually realised cash flows as well.

At this point we have to come back to the problem of setting the real coupon and the spread of the bonds. The calibration of these parameters is of course influencing the final conclusion. If the bonds with these parameters could not have been issued at face value, we should have included the issue price in the calculations as well. Because of this uncertainty it is useful to mention that if the real coupon is unchanged, the spread of the floater bond should be increased to 80-90 basis points so that the actual present values of the two instruments were approximately equal. All in all, our opinion is that the assumptions do not involve so much uncertainty that the relative costliness of the bonds would change.

Our second goal was backtesting the simulation results. As we expected, Libor showed much higher volatility between 2006 and 2011 than it was estimated according to the previous, much tranquil period. The actual cash flows are significantly underestimated in the first two years and then significantly overestimated in the second two years. However, for that very reason the total cash flow (in present value) is estimated quite well. For the IL-bond, the payment estimations are generally acceptable separately and in present value as well – the exception is the second cash flow which is higher than the estimated 95th percentile.

We have to remark that the main uncertainties in our assumptions, namely the value of the real coupon and the spread of the floater bond are not affecting the accuracy of the estimations. If these parameters were different, that would change the actual and the estimated cash flows in the same way.

CONCLUSION

In this paper we presented the main features of the inflation-linked bonds. Since it was a case at issue for Hungary in 2006, we examined a hypothetic IL-bond launched in that year by GDMA. We analysed this bond from the point of view of costliness, the benchmark instrument was a floater bond. We made ex-ante (as we were in 2006) cost-simulations for both bonds and also backtested the results. The base of the Monte Carlo simulations was the CIR-model for the floater and an autoregression for the IL-bond. Our simulations suggest that the IL-bond would have been more expensive and this result is confirmed by the ex-post data as well. Backtests also showed that the CIR-model failed to capture the individual annual costs of the floater bond. This was an anticipated shortcoming since we calibrated the model according to a period prior to 2006, i.e. not taking into account the financial crises which brought high volatility and unexpected movements in the financial markets. Nevertheless, the simulations predicted the total present values of the cash flows adequately for both bonds.

REFERENCES

Bodie, Z., Kane, A., and Marcus A. J. 2008. *Essential of Investments*. McGarw-Hill Irwin, New York. 7th edition.

Cairns, A. 2004. *Interest Rate Models: An Introduction*. Princeton University Press. Princeton-Oxford.

Chan, K., Karolyi, A., Longstaff, A., and Sanders, A. 1992. "An Empirical Comparison of Alternative Models of the Short-Term Interest Rate". *The Journal of Finance*, No. 3, 1209-1227.

Cox, J., Ingersoll, E., and Ross, A. 1985. "A Theory of the Term-Structure of Interest Rates". *Econometrica*, No. 53, 385-407.

Dancs, Á. 2006. "Tőkeindexált államkötvények". Thesis work, Corvinus University of Budapest, Budapest.

Deacon, M., Derry, A. and Mirfendereski, D. 2004. *Inflation-Indexed Securities: Bonds, Swaps and Other Derivatives*. John Wiley & Sons, Chicester. 2nd edition.

Farkas, R., Mosolygó, Zs. and Páles, J. 2005 "A tőkeindexált állmkötvény jellemzői, nemzetközi helyzete és hazai tapasztalatai". *Hitelintézeti szemle*, Vol. 4, No. 5-6, 84-107.

Hansen, L. 1982. "Large Sample Properties of Generalized Method of Moment Estimators". *Econometrica*, No. 4, 1029-1054.

Li, S. 2000. "An Empirical Study of Australian Short-Term Interest Rate: A Comparison of Single Factor Models". Working Paper Series, School of Finance and Business Economics, August.

Medvegyev, P. 2007. *Stochastic Integration Theory*. Oxford University Press, Oxford-New York.

Pecchi, L. and Piga, G. 1997. "Who's Afraid of Index-Linked Bonds?". In *Managing Public Debt: Index-Linked Bonds in Theory and Practice 1997,* De Cecco, M., Pecchi, L. and Piga, G (Eds.). Edward Elgar Publishing, Cheltenham-Brookfield, 173-194.

AUTHOR BIOGRAPHIES

KATA VÁRADI is currently a lecturer at the Corvinus University of Budapest (CUB), at the Department of Finance. She graduated also at the CUB in 2009, and after it obtained a PhD in 2012. Her main research area is market liquidity – the topic of her PhD dissertation was the liquidity of the stock markets –, but she also does researches related to the bonds markets and capital structure of companies. She also worked as a risk analyst at a multinational bank in 2008-2009. Her e-mail address is: kata.varadi@uni-corvinus.hu

ÁGNES VIDOVICS-DANCS is an assistant professor of the Department of Finance at Corvinus University of Budapest. Her main research areas are government debt management in general and especially sovereign crises and defaults. She worked as a junior risk manager in the Hungarian Government Debt Management Agency in 2005-2006. Her e-mail address is: agnes.dancs@uni-corvinus.hu

MODELLING OPTIMAL HEDGE RATIO IN THE PRESENCE OF FUNDING RISK

Barbara Dömötör
Department of Finance
Corvinus University of Budapest
1093, Budapest, Hungary
E-mail: barbara.domotor@uni-corvinus.hu

KEYWORDS[1]

Corporate risk management, Optimal hedge ratio, Funding liquidity

ABSTRACT[2]

In the broad literature of corporate risk management classic models of optimal hedging assume a one-period hedging decision, and therefore no financing need arises to maintain the hedge position. The multi-period models are usually based on the assumption of no liquidity constraints, and accordingly the eventual financing need can always be met from the market. As a consequence of the recent crisis even interbank deals need to be collateralized, so the funding need of any financial transactions can be disregarded. Another usual assumption of the financial models refers to a zero expected value of the hedging position, which contradicts the also the practice. This study investigates the optimal hedge position as a function of 3 factors that determine the corporate utility function: the risk aversion ratio of the company, the expected value of the hedge position and the financing costs deriving from the hedging itself.

INTRODUCTION

The relevance of corporate risk management is shown from different aspects in the financial theories. The main reason for corporate hedging in all of the theories is some imperfectness of the markets: the presence of taxes (Smith and Stulz, 1985); transaction costs (Dufey és Srinivasulu, 1984); the asymmetric information among market participants (Myers and Majluf, 1984 and Tirole, 2006), or the consequences of unavailable financing can cause financial distresses (Smith and Stulz, 1985; Froot et al. 1993). The latest explanation, the lack of financing, is modeled usually in a two-periods model, in which the hedging itself is concluded in the first, and settled in the second period, and so it has no additional cash-flow consequences (except for the potential upfront fees). The availability of financing is however critical from the aspect of the hedging deal as well, than in contrast to the theory, during the lifetime of the deal it may need to meet financing requirements. These can derive from upfront paying obligations, maturity mismatches, mark-to-market settlements of derivative positions, or cash-collaterals. In case of infinite access to liquidity (in the absence of transaction costs) these issues can be ignored. In reality however meeting these requirements is costly, or even impossible, therefore neglecting liquidity considerations lead to incorrect hedging solutions.

Two different approaches of modelling the liquidity consequences of hedge positions are offered by Deep (2002) and Korn (2003). Deep considers the daily settlement need of the mark-to-market value of futures. On the other hand the model of Korn assumes, that the unrealized loss of forward agreement is to be collateralized. Both models use a concave corporate utility function, the expected value of which is to be maximized.

This paper develops a model based on the concept of Korn, and investigates the effect of the financing cost on the corporate hedging.

The next session describes the applied model, then presents an analytical solution for the lower and upper bound of the optimal hedge ratio. The following part includes the results of the simulation: the optimal hedge ratio is modeled as a function of the affecting factors. The last part concludes and shows some further research possibilities.

THE MODEL

The model assumes a company being exposed to the change of the market price of its product, so its revenue and profit bears market risk. We assume furthermore that hedging of this open position in form of forward agreements is available at the market. The spot price (S) follows geometrical Brownian motion with an expected drift of μ and volatility of σ. According to the stochastic calculus the change of the forward price (F) also follows a geometrical Brownian motion as it can be seen in Equation (1):

$$dF = (\mu - r)Fdt + \sigma Fdw \tag{1}$$

[1] The paper is based on the 4. chapter of the thesis proposal The effect of funding liquidity on hedging of market risk. (Dömötör, 2012)

[2] The paper was supported by the European Union and co-financed by the European Social Fund in the framework of TÁMOP-4.2.2/B-10/1-2010-0023 project.

Proceedings 27th European Conference on Modelling and Simulation ©ECMS Webjørn Rekdalsbakken, Robin T. Bye, Houxiang Zhang (Editors)
ISBN: 978-0-9564944-6-7 / ISBN: 978-0-9564944-7-4 (CD)

where r stands for the riskless return and dw - the change of the Wiener-process- is a standard normal distributed random variable.

In contrast to the model of Deep and Korn I do not suppose Equation (1) to be a martingale, so the drift rate can differ from zero in either direction, depending on the relation between μ and r[3].

The model is built up as follows: the company decides at time 0 about its production quantity (Q) and the hedging amount (h), in our case the amount sold on forward. Maturity of the forward agreement and realization of the production are at time 2, and during the lifetime of the derivative position the unrealized loss is to be collateralized at time 1, according to Figure 1.

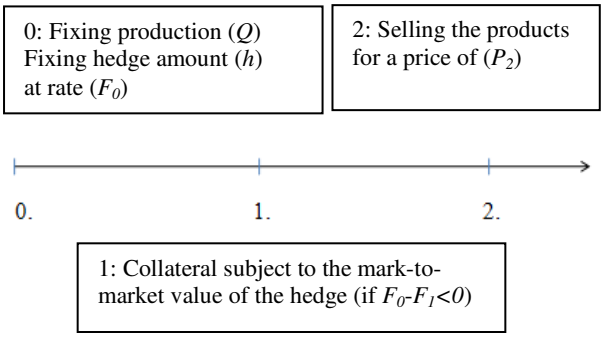

Figure 1: The process of corporate operation

The corporate profit (Π) is realized at time 2:

$$\Pi = S_2 Q - c(Q) + h(F_0 - S_2) + k \min\left[h\frac{(F_0 - F_1)}{1+r};0\right] \quad (2)$$

The indices refer to the time, the new parameter, k stands for the credit spread to be paid by the hedger company, k is considered to be constant.

The differences between this model and the model of Korn are the non-zero expected value of the forward agreement, the exogenous production amount and lack of adjustment of the hedged amount in time 1.

Although the aim of the company is the maximization of the shareholders' value, and the corporate utility function is meaningless, the corporate decision making is to be modelled in a risk-return framework, which is described by the maximization of the expected utility. The corporate utility function is supposed to be increasing and concave, reflecting a decreasing marginal utility (risk aversion). Based on the literature the model applies a CRRA (constant relative risk aversion) type utility function according to Equation (3):

$$U(\Pi) = \frac{\Pi^{1-\gamma}}{1-\gamma} \quad (3)$$

where γ is a measure of the risk aversion.

The optimal hedge amount (h), which maximizes the expected utility, meets the following requirement:

$$E\left[U'(\Pi) * (F_0 - S_2 + k \min[0;\frac{F_0 - F_1}{1+r}])\right] = 0 \quad (4)$$

Equation (4) can be written in the next form:

$$E[U'(\Pi)] * E\left[F_0 - S_2 + k \min[0;\frac{F_0 - F_1}{1+r}]\right] = - \operatorname{cov}(U'(\Pi); F_0 - S_2 + k \min[0;\frac{F_0 - F_1}{1+r}]) \quad (5)$$

where the $U'(\Pi)$ is the first derivative according to h, as described in Equation (6)

$$U'(\Pi) = \left[S_2 Q - c(Q) + h(F_0 - S_2) + kh \min[0;\frac{F_0 - F_1}{1+r}]\right]^{-\gamma} \quad (6)$$

The sign of the left hand side of Equation (5) is equal to the sign of the expected value of the short forward position, as the utility function is increasing. If the expected value is positive ($\mu<r$) equality holds only if the covariance term on the right hand side is negative. As the second variable in the covariance is affected negatively by S_2 and F_1, independently from the hedged amount, the negativity of the covariance requires the first part ($U'(\Pi)$) to be a positive function of the stochastic variables. In the absence of financing costs (k=0), this requires h (the hedging amount) to exceed the quantity of the production (Q). From this follows, that it is optimal to overhedge, similarly to the model of Holthausen (1979).

However funding liquidity risk (in the form of financing cost) reduces the optimal hedge ratio, as the effect of F_1 (being positively correlated with S_2) is positive for any positive value of h. The reduction of the optimal hedging depends on the level of the financing costs (k). It can be similarly shown, that the negative expected value of the hedge position causes a lower than 1 optimal hedge ratio, that is further reduced by the eventual financing costs.

In sum this means, that the hedging affects the corporate utility, since the financing cost and the expected value of the hedge position influence the expected value of the profit. The effect of the financing cost to the utility is always negative; the expected value can have both

[3] In case S refers to a foreign-exchange rate, this means that interest rate parity does not hold, which is a stylized fact of FX-markets, investigated by Darvas (2009).

negative and positive impact; while utility increases through variance-reduction.

The result of this threefold effect is a function of the determining parameters: the corporate credit spread, the expected value of the hedge position and the corporate risk aversion factor.

The optimal hedge ratio of the above presented model differs from that of the model of Korn, since risk cannot be eliminated here perfectly, just at a given significance level, as the profit is the function of two not perfectly correlated risk factors (F_1 and S_2).

Despite of the positive correlation of the risk factors, under extreme circumstances the corporate profit can become negative at any hedging level. The worst outcome occurs if the short hedge position is to be financed because of the growing market price of the first period, but this higher market price is not used to complete the hedge position, and the falling market price causes an operating loss on the unhedged part of the firm's production.

THE THEORETICAL BOUNDS OF THE OPTIMAL HEDGE RATIO

The exact value of the optimal hedge ratio is to be calculated in the function of the parameters of Equation (5) numerically. The bounds of the optimum can be however determined analytically.

The optimal solution has to ensure a positive profit at any price evolution. The theoretically lowest value of S_2 equals to zero. By substituting S_2=0, Equation (2) takes the following form in Equation (7):

$$\Pi = -c(Q) + h(F_0) + k \min\left[h\frac{(F_0 - F_1)}{1+r}; 0 \right] > 0 \tag{7}$$

In the absence of financing cost the lower bound of the hedge ratio (h/Q) is the same as in the Korn-model, as it is shown in Equation (8), based on (Korn, 2003):

$$\frac{h}{Q} > \frac{\bar{c}}{F_0} \tag{8}$$

This means that the hedge ratio has to exceed the ratio of average cost to the initial forward price.

The minimal hedge amount has to cover not only the operating costs, but the financing cost of the position as well. As the financing cost is an unlimited stochastic variable[4], this coverage can be ensured only at a given significance level. Supposing a maximum of the price change ($\Delta F_{1max\alpha}$) and substituting into Equation (2), the result will be the following:

$$\Pi = -c(Q) + h(F_0) + kh\frac{(\Delta F_{1\max\alpha})}{1+r} > 0 \tag{9}$$

After the rearrangement of Equation (9), the hedge ratio can be seen in Equation (10):

$$\frac{h}{Q} > \frac{\bar{c}}{F_0 - \frac{\Delta F_{1\max\alpha}}{1+r}k} \tag{10}$$

The minimal hedge ratio in this case is given by the ratio of the average cost and the initial forward price reduced by the maximum of the financing costs at a certain (α) level. This ratio ensures a positive end of period profit at any low level of the market price at maturity, even if the hedge position caused financing costs.

The maximum of the hedge ratio is the level, where the financing cost and the negative value of the hedged position are counterbalanced by the realized higher operating income. Denoting the maximum of the price at maturity by $S_{2max} = F_0 + \Delta F_{2max\alpha,}$ and substituting it and the maximum of F_1 into Equation (2) we will get Equation (11):

$$\Pi = F_0 + \Delta F_{2\max\alpha} - c(Q) + h(F_0 - F_0 + \Delta F_{2\max\alpha}) + \\ + kh\frac{(F_0 - (F_0 + \Delta F_{1\max\alpha}))}{1+r} > 0 \tag{11}$$

After rearrangement and simplification we receive the upper bound of the hedge ratio in Equation (12):

$$\frac{h}{Q} < \frac{F_0 + \Delta F_{2\max\alpha} - \bar{c}}{\Delta F_{2\max\alpha} + \frac{\Delta F_{1\max\alpha}}{1+r}k} \tag{12}$$

As shown above, the level of the financing costs (k) moderates the measure of over- and underhedge also. If k goes up, the lower bound increases, while the upper bound decreases.

The optimal hedge ratio is determined through Monte Carlo Simulation, using corporate specific parameters (cost function, credit spread, risk aversion) and the chosen parameters of the forward price movement process (drift and volatility).

RESULTS OF THE SIMULATIONS

I run Monte Carlo simulation in MS Excel, based on the generation of 2000 normally distributed random variable for the price change. The initial forward rate was given, F_0=1. In order to catch the fat tail phenomena in Finance - namely the higher probability of the extreme values, than predicted by the normal

[4] As the price movement has no upper limit, the financing cost can be theoretically even infinitive.

distribution, - I set two extremes into the sample manually: F_1=2 and F_2=4, then F_1=2 and F_2=0. These extreme outcomes has no significant effect on the expected value, as their probability is very low (the probability of a 100% increase in the price is $1{,}3*10^{-11}$, based on a normal distribution with 15% standard deviation). The appearance of the extremes however excludes those hedging solutions that would cause negative corporate profit under extreme market circumstances.

The utility of the end of profit was calculated for each outcomes. The aim of the optimization was to find the hedge ratio, where their average, considered to be the expected utility, was maximized.

This paper focuses on the effect of financing costs, so the credit spread is a changing variable on all of the following charts. Table 1 summarizes the investigated set of the parameters.

The cost function is assumed to be linear, the average cost is expressed as a percentage of the initial forward rate.

Table 1: The investigated set of the parameters

Parameter		Notation	Figure 2	Figure 3	Figure 4	Figure 5
Corporate specific	Average cost	c^*	10%	50%	10%	10%
	Credit spread	k	changing variable	changing variable	changing variable	changing variable
	Risk aversion	γ	changing variable	changing variable	2	0,5
Forward price process	Drift	μ	0	0	changing variable	changing variable
	Volatility	σ	15%	15%	15%	15%
	Initial forward rate	F_0	1	1	1	1
	Riskless return	r	5%	5%	5%	5%

Figure 2 depicts the optimal hedge ratio, by choosing similar fix parameters, than Deep and Korn: the drift of the forward price is supposed to be zero, volatility of 15% and average operating cost of 10%. Because of the zero expected value of the forward position this factor has no impact to the utility function.

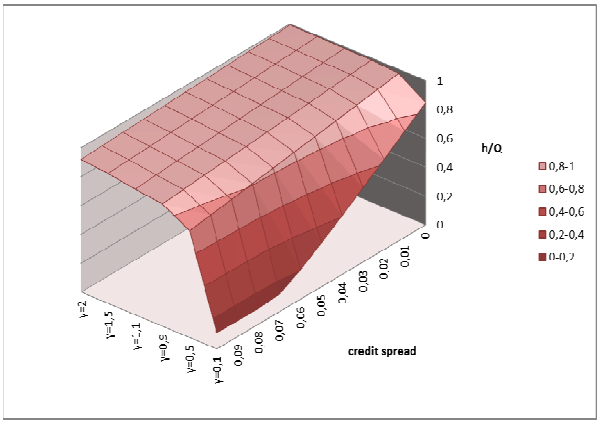

Figure 2: Optimal hedge ratio as a function of the credit spread and risk aversion (forward drift: 0%, volatility: 15%, average cost 10%)

The results are very close to the conclusion of the Korn-model: the operating margin is high enough (90%), so that for a risk averse firm (gamma above 0,5), the utility enhancement deriving from the reduced volatility, exceeds the utility reduction of the potential financing costs of the hedge. As a consequence, 1 percentage point rise of the credit spread reduces the optimal hedging ratio by only 2,5%-point for a firm with 0,5 risk aversion coefficient.

With the fall of the sensitivity towards risks (decreasing gamma) the marginal utility of the hedge offsets less and less the effect of the financing costs. For a firm with a risk aversion factor of 0,1, the optimal hedge ratio drops to the minimum hedging level shown in Equation (10), which ensures the positivity of the profit, if the credit spread hits 7%.

Figure 3 illustrates the optimal hedge ratio taking the same parameters than the former simulation except for the average cost, which is constant 50% here. The increase of the average cost causes a slight enhancement of the hedging ratio in each case, but through its effect on the minimal hedge ratio, the optimum is affected significantly for the less risk averse hedgers.

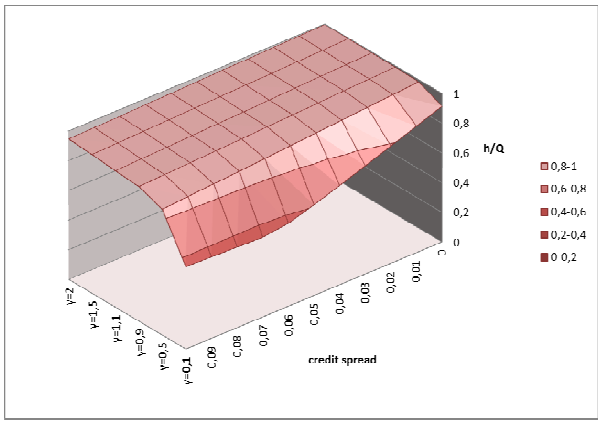

Figure 3: Optimal hedge ratio as a function of the credit spread and risk aversion (forward drift: 0%, volatility: 15%, average cost 50%)

The following simulations show the effect of the non-zero drift of the forward position, namely the drift of Equation (1) differs from zero. Although in case of currencies, according to the uncovered interest rate parity, the expected value of the forward position is zero, it can be shown that carry trade has a significant role in financial markets.

The expected value of the hedge position takes a more significant effect on the optimal hedge ratio, than financing costs. The positive drift (μ) of the forwad price causes an expected loss for a hedger in short position, that leads to a substantial reduction of the hedge ratio even for a more risk averse (γ=2) firm.

The optimal hedge ratio is modelled as a function of the financing costs and the expected value of the hedge in the following figures. The volatility and the average cost are the initial constant rates (15% and 10% respectively), the risk aversion coefficient (γ) is set to 2 in Figure 4. As the chart shows, 1 %-point increase of the forward drift causes some 20%-point lower optimal hedge ratio. In case of negative drift – which causes the positivity of the expected value of the position – the optimal hedge ratio exceeds 100%.

A minor difference from zero drift leads to significant under- or overhedging in the optimum. Moreover the bounds of the optimal hedge ratio are reached at a 5% drift of the forward price, in our case the upper bound of 130% and the lower bound of 11% (credit spread=11%).

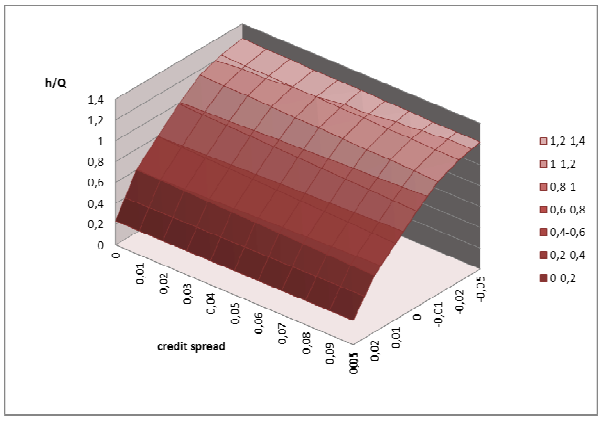

Figure 4: Optimal hedge ratio as a function of the financing cost and forward drift (γ=2, volatility: 15%, average cost 10%)

With the fall of the risk aversion and so the marginal utility of variance reduction, the optimal hedge ratio converges faster to the upper or lower bound. As Figure 5 shows, 1% positive (negative) drift of the forward price is enough to shift the optimal hedging level to the minimum (maximum) quantity, if the risk aversion factor is 0,5.

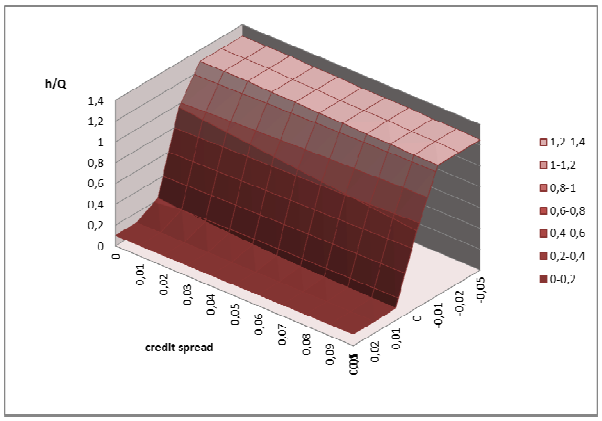

Figure 5: Optimal hedge ratio as a function of the credit spread and forward drift (γ=0,5, volatility: 15%, average cost 10%)

If the expected value of the forward hedge exceeds 1%, the financing cost affects the optimal hedging only by its effect on the minimum/maximum hedging ratio.

CONCLUSION

The paper investigates the corporate hedging decision, by considering funding liquidity risk and expected value of the hedge position itself. Funding cost is quantified through the financing cost of the collateral to be placed for the mark-to market loss of the hedging position. The bounds of the optimal hedge ratio are

presented and the optimum is modelled as a function of the corporate credit spread (financing cost) and expected drift of the forward price. The analysis shows, that 1 percentage point increase of the credit spread causes some (2-3) percentage point decrease in the optimal hedging ratio. The effect of the expected value of the forward position proved to be more significant in the simulations, 1 percentage-point (+/-) change of the expected value leads to a dramatic (20-30%-point) change of the optimal hedging ratio. It seems that this later effect can better explain the empirical fact of corporate under- or overhedge. The above analysis assumes static credit spread, at which financing is always available. Releasing this assumption is the topic of further research.

REFERENCES

Darvas, Zs 2009. "Leveraged Carry Trade Portfolios." *Journal of Banking & Finance*, 33, No. 5, 944–957.

Deep, A. 2002. "*Optimal Dynamic Hedging Using Futures under a Borrowing Constraint"*. Working Paper, Bank for International Settlements, Basle, 1629-1658.

Dömötör, B. 2012. "*The effect of funding liquidity on market risk hedging"*. PhD thesis proposal, Corvinus University of Budapest, Budapest

Dufey, G., Srinivasulu, S. L. 1984. The Case for Corporate Management of Foreign Exchange Risk. *Financial Review* 19, No. 3, 39-47.

Froot, K. A., Scharfstein, D. S., Stein, J. C. 1993. "Risk Management: Coordinating Corporate Investment and Financing Policies." *The Journal of Finance* 48, No. 5, 1629-1658.

Holthausen, D. M. 1979. "Hedging and the Competitive Firm under price Uncertainty." *The American Economic Review* 69, No 5, 989-995.

Korn, O. 2003. "*Liquidity Risk and Hedging Decisions."* Working Paper, University of Mannheim, Mannheim

Myers, S. C., Majluf, N. S. 1984. "Corporate Financing and Investment Decisions when Firms have Information that Investors do not have." *Journal of Financial Economics* 13, No. 2, 187-221.

Stulz, R. M., Smith, C. W. 1985. "The Determinants of Firms' Hedging Policies." *Journal of Financial and Quantitative Analysis,* 20, No.4, 391-405.

Tirole, J. 2006. *The Theory of Corporate Finance.* Princeton University Press, Princeton and Oxford

AUTHOR BIOGRAPHIES

BARBARA DÖMÖTÖR is an Assistant Professor of the Department of Finance at Corvinus University of Budapest. Before starting her PhD studies in 2008, she worked for several multinational banks. She is now working on her doctoral thesis about corporate hedging. She is lecturing Corporate Finance, Financial Risk Management and Investment Analysis, her main research areas are financial markets, financial risk management and corporate hedging. Her e-mail address is: barbara.domotor@uni-corvinus.hu

THE MODIFIED EMPIRICAL MODE DECOMPOSITION METHOD FOR ANALYSING THE CYCLICAL BEHAVIOR OF TIME SERIES

Vladimir Sebesta, Roman Marsalek and Jitka Pomenkova,
Department of Radio Electronics
Brno University of Technology
BRNO, Czech Republic
Email: marsaler@feec.vutbr.cz

KEYWORDS

empirical mode decomposition; instantaneous frequency; cyclical behavior

ABSTRACT

This paper is devoted to the analysis of time series using the Empirical Mode Decomposition (EMD) method. This method decomposes the analyzed time series into a small set of narrow-band components (modes) that fully represent the original time series. The modified EMD method that eliminates excessive changes of individual mode periods is proposed and evaluated on one example application of industrial production data. In contrast to other decomposition methods, like the singular value decomposition, the empirical mode decomposition can describe the time-variation of the period of individual components.

INTRODUCTION

The Empirical Mode Decomposition (EMD) method followed by the Hilbert spectrum estimation represents an important tool for time-frequency analysis of nonstationary and nonlinear random processes (Huang N.E. et al., 1998). Its advantage is the ability to analyze the local behavior of estimated parameters and thus to quantify the time evolution of the process. EMD has been first proposed for earthquake/wind data analysis (Huang N.E. et al., 1998), the application to time series in economy can be found in (Huang N.E. et al., 2003). Some improvements such as using the beating phenomena of waves (Chen, Y. and M.Q. Feng, 2003) have been researched in the past.

The results of EMD are obtained in the form of so-called Intrinsic Mode Functions (IMF) and the Hilbert spectrum. The Modified EMD (MEMD) method described in this paper is based on the decomposition of the time series to several modes described by IMF. The first step is decomposition using classic EMD followed by the determination of mode boundaries, local periods and local significances. Whenever the local period of the IMF significantly differs from the average mode period, the corresponding segment of the IMF is considered as the different mode. This is an improvement over the existing EMD described in (Huang N.E. et al., 1998, 2003), in which some modes can contain parts with strongly different values of period.

Several other methods can be used for the time-frequency analysis as the Short Time Fourier Transform or Singular Value Decomposition (SVD) (Carvalho, M. et al., 2012) . The first mentioned method requires the time series to be de-trended (e.g. using high-pass filters). Due to non-ideal filter approximation, the de-trending operation influence the analysis results. The SVD does not require de-trending prior to its application similarly to EMD, but it has other disadvantages that will be discussed later.

EMD ALGORITHMS

Original EMD

The EMD method is based on the decomposition of analyzed time series $s(n)$ into IMFs obtained through the sifting process (Huang N.E. et al., 1998). Sifting makes use of two signal envelopes - the one defined by the local minima and the second by the local maxima of the time series. These extremes are connected with cubic splines. From the signal processing theory, the IMFs correspond to narrow-band signals with amplitude and phase modulation and randomly varying parameters (Haykin, S. and B. Van Veen, 2003). The algorithm can be described as:

Sifting:

$$h_{j,k}(n) = h_{j,(k-1)}(n) - m_{j,k}(n), \tag{1}$$

IMF definition:

$$c_j(n) = h_{j,\hat{k}}(n), \tag{2}$$

Remainder calculation:

$$r_j(n) = r_{j-1}(n) - c_j(n), \tag{3}$$

Proceedings 27th European Conference on Modelling and Simulation ©ECMS Webjørn Rekdalsbakken, Robin T. Bye, Houxiang Zhang (Editors)
ISBN: 978-0-9564944-6-7 / ISBN: 978-0-9564944-7-4 (CD)

where n is discrete-time step , j is the index of the j-th IMF $c_j(n) = h_{j,\hat{k}}(n)$, $h_{j,\hat{k}}(n)$ is sifted time series after k iterations, $m_{j,k}(n)$ is the mean between the two signal envelopes, $r_j(n)$ is the $j-$th remainder and $r_0(n) = s(n)$. The sum of all IMFs and the residue is the original time series $s(n)$.

Modified EMD

The application of the EMD method can result in a situation where the instantaneous period of the IMF locally significantly exceeds its mean value and corresponds to the period of another mode. This is evident from the results in (Huang N.E. et al., 2003) and figure 2 below. This effect will be suppressed by the MEMD method described below.

In MEMD, each $j-$th IMF $c_j(n)$ from eq. 2 is analyzed prior to its subtraction from the previous remainder $r_{j-1}(n)$ in eq. 3 as follows:

- $c_j(n)$ is partitioned into L_j segments $c_{j,l}(n)$, where $l = 1 \dots L_j$ with approximately constant instantaneous period per segment
- the instantaneous frequency (equivalently its reciprocal quantity - instantaneous period $T_{j,l}(n)$) and amplitude $a_{j,l}(n)$ of each segment is computed with the use of the Hilbert transform (Haykin, S. and B. Van Veen, 2003), (Huang N.E. et al., 1998). Due to the use of EMD, the instantaneous frequency and amplitude are estimated very locally, practically from three successive samples of data.
- the weighted means $\bar{T}_{j,l}$ of instantaneous period in each segment $c_{j,l}(n)$ are computed as

$$\bar{T}_{j,l} = \frac{\sum_{n=1}^{N_{j,l}} a_{j,l}(n) T_{j,l}(n)}{\sum_{n=1}^{N_{j,l}} a_{j,l}(n)}, \qquad (4)$$

  where $N_{j,l}$ is the length of the l-th segment. The instantaneous amplitude $a_{j,l}(n)$, corresponding to the period significance is used for weighting.
- if the period $\bar{T}_{j,l_i}$ of any l_i-th segment significantly differs from the other $\bar{T}_{j,l}, \forall l$, the segment $c_{j,l_i}(n)$ is excluded from $c_j(n)$ and its corresponding part remains in the remainder $r_j(n)$.

The principle and usefulness of the proposed modification will be further illustrated on a real time series. Another modification of the original EMD was aimed at improving the performance on a short time series with a small number of maxima and minima. In order not to shorten the analyzed time series in each sifting, both the first local maxima and minima are copied to the beginning of the signal as two new fictive local extremes. A similar arrangement holds also for the end of the sifted time series.

EXPERIMENT AND RESULTS

Analyzed data

The MEMD method has been evaluated and compared with EMD on the industrial production index data of EU15 countries (transformed by natural logarithm) gathered from Eurostat. The period of the analyzed data is 1991/M1-2011/M3 resulting in a total number of 243 samples (months). Note that in all figures, the time axis description corresponds to the month index (discrete time n) with 1 equal to January 2001. For simple notation, n is sometimes omitted in the following text.

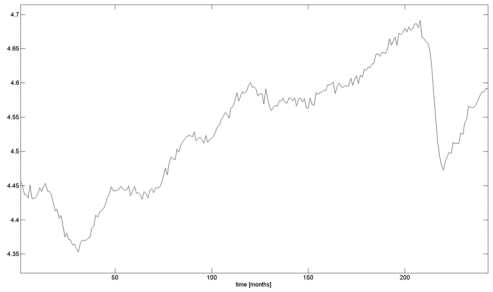

Figure 1: Analysed data

Original EMD results

As the first step, EMD is performed according to (Huang N.E. et al., 1998). The results: IMFs $c_1 - c_5$ are shown in Fig. 2. Apparently the frequency (period) of modes changes. In some cases, e.g. the mode c_1 between month 211 and 221 (marked by an arrow), the instantaneous frequency is much lower and corresponds rather to the instantaneous frequency of mode c_2. This is the motivation for the MEMD method.

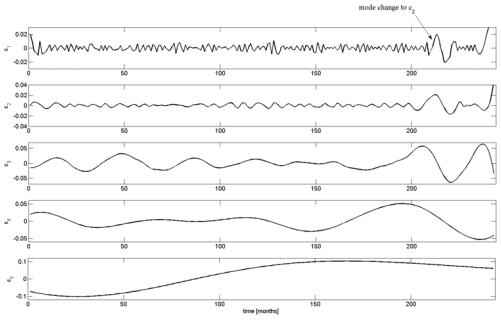

Figure 2: EMD results

Results of modified algorithm

The MEMD analysis will be explained in the example of the first IMF c_1. This IMF has been partitioned into $L_1 = 4$ segments according to the instantaneous frequency.

Analysis of c_1 - 1^{st} segment

The time plot of segment $c_{1,1}$, instantaneous period $T_{1,1}$ and instantaneous amplitude $a_{1,1}$ further denoted as significance are shown in Fig. 3. The mean period $\bar{T}_{1,1}$ in this segment is 0.292 years (1,168 quarters). The instantaneous values of period exceeding the value 1 are considered to be incorrectly estimated and have been excluded from the mean calculation. The reason for their incorrect estimation is that the sampling frequency is too close to the Nyquist theorem (Haykin, S. and B. Van Veen, 2003) limit. As the presence of the aliasing effect is not foreclosed, the real period of $c_{1,1}$ could possibly be equal to $1/\left(0.292 + 12 \cdot N\right) = 0.0648$, 0.0365, 0.0254, 0.0194 ... years, where N is integer and 12 corresponds to monthly sampling frequency. It is worth noting that the period of 0.0194 corresponds to the length of one week. The interpretation and possible application of this phenomena is out of the scope of this paper.

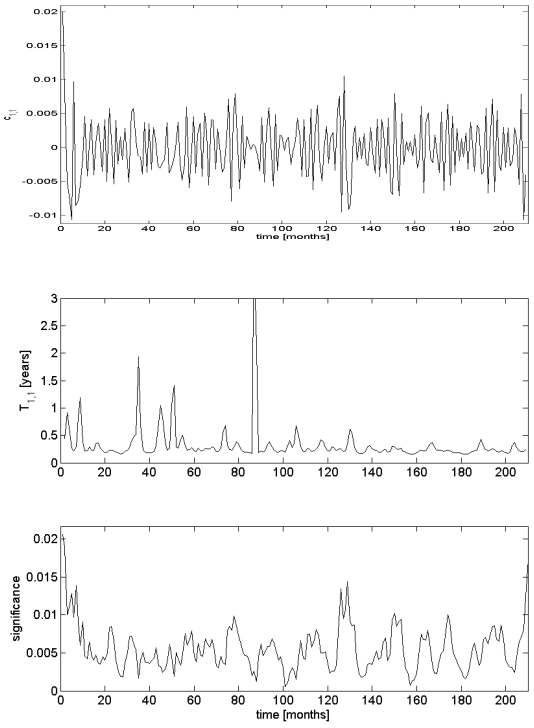

Figure 3: First segment $c_{1,1}$ of the first IMF: time domain plot (top), instantaneous period (middle) and significance (bottom)

Analysis of c_1 - 2^{nd} segment

The time plot of segment $c_{1,2}$, instantaneous period $T_{1,2}$ and amplitude $a_{1,2}$ (significance) are shown in Fig. 4. The mean period $\bar{T}_{1,2}$ in this segment is 0.783 years (3,132 quarters). This period significantly differs from the period in the previous segment $T_{1,1}$. We thus claim that the second segment of the first IMF does not correspond to mode c_1 but rather to a mode with lower instantaneous frequency. The segment $c_{1,2}$ will thus be excluded from c_1 and replaced by zeros. This is also evident from Fig. 7.

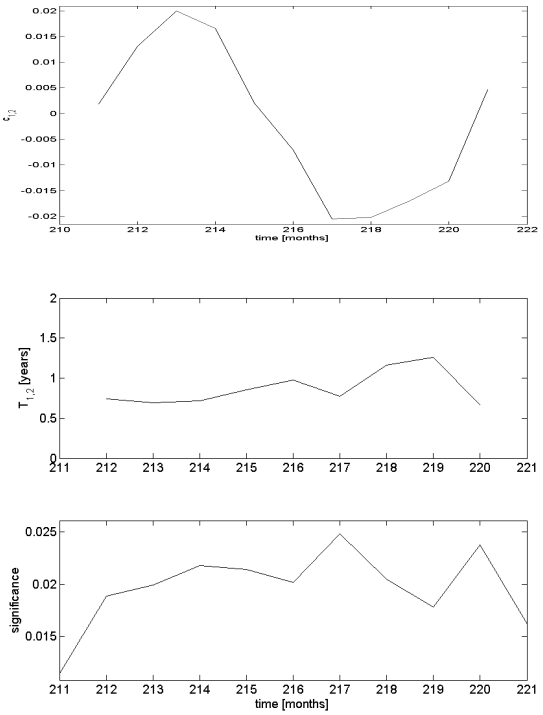

Figure 4: Second segment $c_{1,2}$ of the first IMF: time domain plot (top), instantaneous period (middle) and significance (bottom)

Analysis of c_1 - 3^{rd} segment

In the third segment of c_1 with the analysis results in Fig. 5, the weighted period $\bar{T}_{1,3}$ is similar to the first segment: 0.219 years (0.876 quarters). The mode c_1 is thus present in this segment. The Hilbert transform estimation accuracy suffers from both the short data length and sampling frequency close to the Shannon limit.

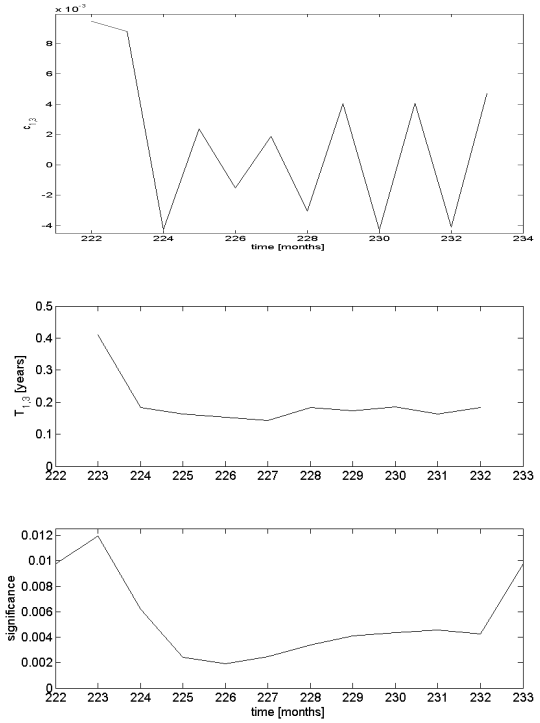

Figure 5: Analysis of third segment $c_{1,3}$ of the first IMF: time domain plot (top), instantaneous period (middle) and significance (bottom)

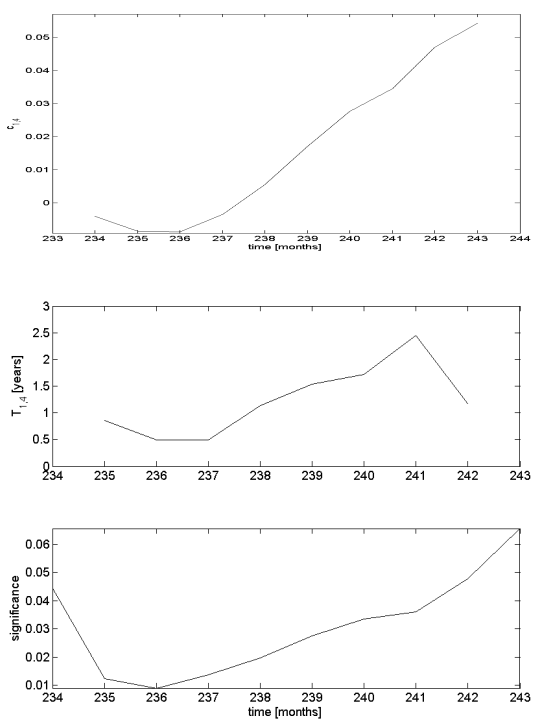

Figure 6: Fourth segment $c_{1,4}$ of the first IMF: time domain plot (top), instantaneous period (middle) and significance (bottom)

Analysis of c_1 - 4^{th} segment

The period in the fourth segment is similar to the period in the second segment - thus it does not correspond to mode c_1 and is excluded. The fourth segment of c_1 is thus replaced by zeros. The $\bar{T}_{1,4}$ is equal to 0.7386 years (2.95 quarters).

Analysis of $c_2 \ldots c_5$

Because of space limitations, the results of the segment-by-segment analysis of modes in $c_2 - c_5$ are not presented in detail. The identified weighted mean periods for all segments of IMFs c_1 - c_5 are summarized in Table 1. The segments with the values in italic have been excluded from the corresponding IMFs. It can be concluded, that only the modes c_3 and c_4 lie in the business cycle frequency range (6 to 32 quarters). Mode c_3 is present during the whole observed time range, while c_4 does not exist before month 120.

Time plots of all IMFs of MEMD are shown in Fig. 7.

$\bar{T}_{\text{column,row}}$	1	2	3	4
1	1.168	*3.132*	0.876	*2.956*
2	2.812	*13.124*	3.864	-
3	13.324	-	-	-
4	*112*	30.88	-	-
5	104	-	-	-

Table 1: Estimated weighted mean periods (in quarters) in segments of modes $c_1 - c_5$

COMPARISON WITH SVD

The application of SVD for band-pass filtering of US business cycles has been demonstrated in (Carvalho, M. et al., 2012). The number of SVD components into which the time series is decomposed depends on the observation window length. Having a small number of components (e.g. 6) results in the superposition of several inseparable narrowband signals in each of them - see Fig. 8 left. On the contrary, a high number of decomposed components (and thus large window length) makes the interpretation of the results unfeasible - it is not possible to distinguish between two adjacent components as the result of their very close period (Fig. 8 right).

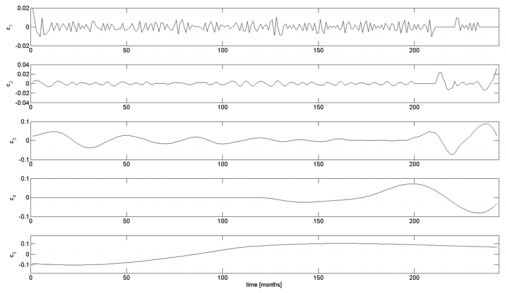

Figure 7: MEMD results

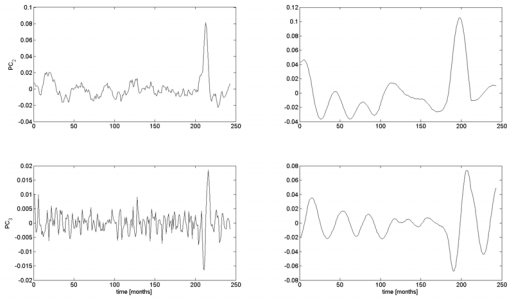

Figure 8: SVD as reference method: 2nd (PC_2) and 3rd (PC_3) components for observation window lengths 6 (left) and 32 (right)

CONCLUSIONS

In this paper, the Modified Empirical Mode Decomposition method has been proposed and evaluated. The proposed modification eliminates the excessive local changes of an instantaneous period of decomposed components. Although the proposed method represents only one possibility among various decomposition techniques, it is advantageous in a small number of resulting components and easier interpretation in comparison with the above mentioned alternatives. Due to using the instantaneous frequency estimation by applying the Hilbert transform, the temporal variation of the components can be easily observed.

From among the wide range of prospective applications ranging from the geophysical or biomedical signal analysis, electrical engineering to economy, the evaluation of described method on the data representing the industrial production index of EU15 is presented. The MEMD method identified two important cycles corresponding to the business cycle frequency range (6-32 quarters) in the analyzed data. The first is the component with a period of 13.3 quarters present in the whole data set, the second is the component with a period of 30.9 quarters present in the period December 1998-March 2011.

Acknowledgements

This research was performed in the laboratories of the SIX research center, reg. no. CZ.1.05/2.1.00/03.0072. It was partially supported by the Czech Science Foundation grant No. P402/11/0570 and by the projects CZ.1.07/2.3.00/20.0007 WICOMT and internal project FEKT-S-11-12 (MOBYS).

References

Huang N.E. et al. 1998. "The empirical mode decomposition and Hilbert spectrum for non-linear and non-stationary time series analysis", *Proc. Roy. Soc London A*,Vol. 454, 1998, 903–995.

Huang N.E. et al. 2003. "Applications of Hilbert-Huang transform to non-stationary financial time series analysis", *Applied stochastic models in business and industry*,2003; 19, 245-268.

Chen, Y. and M.Q. Feng. 2003. "A technique to improve the empirical mode decomposition in the Hilbert-Huang transform", *Earthquake engineering and engineering vibration*, Vol. 2, No. 1, June 2003, 75–85.

Carvalho, M. et al. 2013. "Tracking the US business cycle with a singular spectrum analysis", *Economics Letters*, 114 (2012), 32 - 35.

Haykin, S. and B. Van Veen. 2003. *Signals and Systems*, John Wiley, 2003

AUTHOR BIOGRAPHIES

VLADIMIR SEBESTA is the emeritus professor at the Department of Radio Electronics, head of the Signal processing laboratory of Institute of Radio electronics, Brno University of Technology until 2006. His research interests include digital signal processing and analysis, communication theory and wireless communications. His email adress is `sebesta@feec.vutbr.cz`.

ROMAN MARSALEK received his Master degree in control and measurements in 1999 from the Brno University of Technology and the Ph.D. in electronics and signal processing from Universite de Marne la Vallee, France in 2003. His email adress is `marsaler@feec.vutbr.cz`.

JITKA POMENKOVA received the Ph.D. degree in applied mathematics at Ostrava University in 2005, the habilitation degree in Econometric and operational research at Mendelu in Brno in 2010. From 2011 she is the Senior researcher at Department of Radio electronics, Brno University of Technology. Her email adress is `pomenkaj@feec.vutbr.cz`.

Simulation in Industry, Business and Services

A SMARTPHONE APPLICATION FOR THE MONITORING OF DOMESTIC CONSUMPTION OF ELECTRICITY

Franco Cicirelli, Emmanuele Neri, Libero Nigro, Francesco Pupo
Laboratorio di Ingegneria del Software
Dipartimento di Elettronica Informatica e Sistemistica
Università della Calabria
87036 Rende (CS) – Italy
Email: f.cicirelli@deis.unical.it, emmanuele.neri@gmail.com, {l.nigro,f.pupo}@unical.it

KEYWORDS
Smartphone distributed applications, advanced metering, energy use, simulation in industry, business and services.

ABSTRACT

The work presented in this paper concerns the development of a smartphone application for the monitoring of energy consumption relative to a domestic electricity grid. An algorithm has been integrated in the smartphone application allowing Enel (the main Italian Electrical Company) customers to have, on their mobile phone, clear and transparent information about the energy consumption of their houses in real time.

INTRODUCTION

Nowadays, producing and consuming energy constitutes the fundamental requirement for the political, economic and sociological development of humanity. So far, we have followed a model linked to a continuous increase in consumption, which has led us to a misuse of exhaustible fossil resources (European Commission, 2011).
The scarcity of such resources, together with the increasing environmental pollution, linked to the production and consumption of energy, represent the reasons why we can regard such a model as inadequate and inefficient. Global phenomena such as population growth, modernization of developing countries and technological development, contribute to increasing the demand for electrical energy (Energy Authority, 2009).
Therefore, the optimization of their use becomes extremely important, minimizing the waste of resources considerably. Several studies (Kamal, 2012), (Energy Authority, 2009) on the subject suggest how to update users on their actual consumption and relative costs in real time (Enel, 2010), (Enel, 2012).
Starting from the display of the consumption of energy in kWh, the transformation of the quantity of kWh into its equivalent in monetary terms (EUROs) does not turn out to be simple. This is mainly due to the non-linearity of the function that allows the calculation of energy consumption in terms of costs. The non-linearity is owing to the retroactivity of the cost of energy and represents a big obstacle. In this work it is highlighted a detailed analysis of the elements that constitute the energy costs (Darby, 2006) in order to analyze the algorithms, which have been processed to obviate the retroactivity, seeking a cost estimation that is as reliable as possible.
We argue, therefore, that this work represents an experimental step towards the future, since its purpose is to make people familiar with the world of energy, providing them with clear information concerning the consumption and production both in terms of energy (kWh) and in terms of costs (EUROs) (European Commission, 2011), not only for what regards a private use, but also for what involves business activities, making users more aware of a more intelligent, practical use of energy (Faruqui, 2009).
Information and communication technology (ICT) can help in many ways to conserve energy. On the one hand it does so by optimizing various industrial processes (and thus increasing their energy efficiency); on the other hand it can increase transparency, create energy awareness, and support individuals to make informed decisions that contribute to a more efficient energy use (Weiss et al., 2010).
With the rise of ubiquitous computing, data about real-world events is being captured at an increasingly detailed level. Together with the rapid growth of the mobile phone market and mobile internet access, this has led to a large number of mobile applications which aim to support users' daily life in a wide range of areas. To name a few, this ranges from insurance claims assistance (Baecker, 2009) over shopping assistance (Adelmann, 2007) to emergency response (Landgren & Nulden, 2007).
The main contribution of this paper is the development of a mobile phone application for residential energy monitoring based on consumption data acquired by the domestic electronic meter. The resulting prototype on *Android* and *iOs* devices shows how mobile phones can

Proceedings 27th European Conference on Modelling and Simulation ©ECMS Webjørn Rekdalsbakken, Robin T. Bye, Houxiang Zhang (Editors)
ISBN: 978-0-9564944-6-7 / ISBN: 978-0-9564944-7-4 (CD)

help users to monitor and control their energy consumption.
This article is organized as follows: the following section describes a technical analysis of energy cost. In this section we describe the components of energy price, the Italian AEEG (Energy Authority, 2013) and its role in the market. The third section summarizes the way how the energy bill is composed and invoiced, giving an exhaustive explanation of the algorithm being behind the calculation to invoice a determined quantity of energy. The fourth section describes the planning of cost functionality, presenting the definition of the problem of retroactive costs, the choice of the input for the simulation and an analysis of the results and management relative to retroactive costs. Finally, the fifth section refers to the system architecture that allows to obtain and to present the consumption data.

THE COMPONENTS OF PRICE

The price of electrical energy for final users is calculated in order to cover all the expense items linked to the electrical energy supply. It is, thus, the result of the sum of numerous components, each of which is present in a different percentage (Energy Authority, 2013b), as you can see from Figure 1.

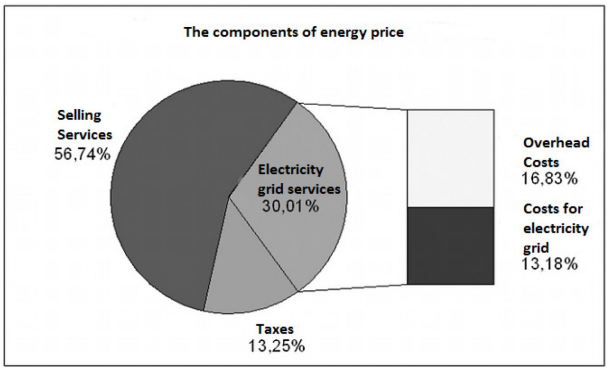

Figure 1, Percentage composition of the price of electricity in Italy

More than half of the total is characterized by the selling costs of electrical energy, fixed either by the "*Free Market"* for the so-called "suited" customers, or by the "*Service for Maximum Protection",* for those bound by one of the companies dealing with electrical energy. Such selling costs, together with the general ones and the costs for the electricity grid, are fixed by AEEG and updated every three months.

Now, let us see more carefully what every single component of cost refers to:

A) COSTS FOR SELLING SERVICES: they are the different activities set by the provider to purchase and sell electrical energy to the final user.
B) COSTS FOR ELECTRICITY GRID SERVICES: they are the activities that allow providers (both operating in the "*Free Market"* and in the "*Service for Maximum Protection"*) to transport electrical energy to national and local grids as far as the electricity meter.
C) OVERHEAD COSTS: they are fixed by AEEG and are bound to pay taxes introduced by laws ministerial decrees.
D) TAXES: a percentage of the payment of the electricity bill is intended to cover some taxes such as ACCISA and IVA.

CALCULATION OF THE ELECTRICITY BILL

The price of the components of the electricity bill is calculated through some unit costs per kWh, taking cognizance of the quantity of energy, consumed and recorded during a specific period (Energy Authority, 2013a), (Energy Authority, 2013b).

Summary readings and withdrawals

Reference period January-March 2011

	Active Energy Previous 31/12/2010	Active Energy Actual 31/03/2011	Consumption Active Energy (kWh)
F1	2.057	2.196	139
F2	1.869	2.086	217
F3	18.750	18.985	235
Total			591

Figure 2, Part of bill in which actual consumption of energy is stated.

To understand the algorithm that is behind the calculation of the quantity of energy invoiced, which is obtained either by reading the electricity meters or by estimating users' historical consumption, we need to describe in what its distribution of annual consumption consists.

Let us establish what the annual tiers of cost, which determine the final tariff, are:

I° Tier 0-900 [kWh]
II° Tier 900-1800 [kWh]
III° Tier 1800-2640 [kWh]
IV° Tier 2640-3540 [kWh]
V° Tier 3540-4440 [kWh]
VI° Tier over 4440 [kWh]

The calculation of the retroactive cost is drawn from the organization of consumption through tiers of annual estimation.
All information about consumption can be divided into more than a temporal sub-interval, because rates are updated every three months and, consequently, the consumption of a month's time can refer to rates of a

term of three months, which is different from that concerning the following month.

Example:
Let us suppose that we consume *333 kWh* from September 5 to 30, *26 days (b)*. These 333 *kWh (a)* can be either the result of updated meter readings or the outcome of estimations, based on the user's historical consumption. To reach the annual estimation *(SA),* composed of 365 days, supposing we have consumed 333 kWh in 26 days, we make a proportion (1):

$$333:26 = X:365 \rightarrow \frac{333}{26} \times 365 = 4675\ kWh \quad (1)$$

4675 kWh would be the annual estimation if the consumption remained constant.

Let divide the 333 kWh into tiers, applying the daily rate to 4675 kWh:

$$I°\ Tier \rightarrow \left(\frac{(900\ kWh - 0\ kWh)}{365\ gg}\right) \times 26gg = 64\ kWh$$

$$4675\ kWh - 900\ kWh = 3775\ kWh$$

$$II°\ Tier \rightarrow \left(\frac{(1800\ kWh - 900\ kWh)}{365\ gg}\right) \times 26gg = 64\ kWh$$

$$3775\ kWh - 900\ kWh = 2875\ kWh$$

$$III°\ Tier \rightarrow \left(\frac{(2640\ kWh - 1800\ kWh)}{365\ gg}\right) \times 26gg = 60\ kWh$$

$$4875\ kWh - 840\ kWh = 2035\ kWh$$

$$IV°\ Tier \rightarrow \left(\frac{(3540\ kWh - 2640\ kWh)}{365\ gg}\right) \times 26gg = 64\ kWh$$

$$2035\ kWh - 900\ kWh = 1135\ kWh$$

$$V°\ Tier \rightarrow \left(\frac{(4440\ kWh - 3540\ kWh)}{365\ gg}\right) \times 26gg = 64\ kWh$$

$$1135\ kWh - 900\ kWh = 235\ kWh$$

$$the\ remainder\ (333 - 64 - 64 - 60 - 64 - 64)\ kWh = 17\ kWh$$
$$goes\ to\ the\ last\ tier.$$

The variable quota regarding electricity grid costs and overhead costs is retroactive.
In Figure 3 the computational process of retroactive costs is summed up.
To give coherence to the costs that users can view, we have chosen as *input* the average of consumption of a determined period, that is to say the invoicing period.

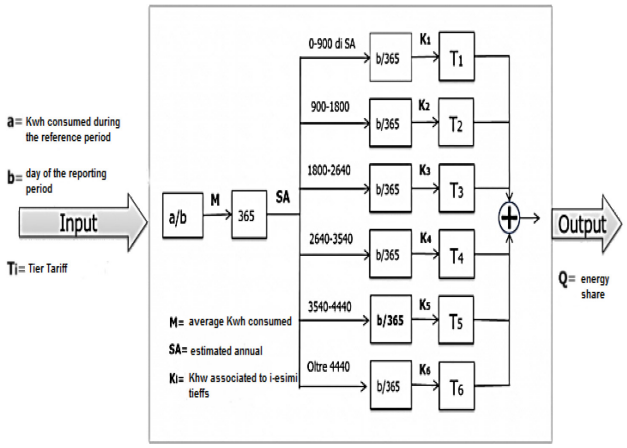

Figure 3, Computational process of retroactive costs.

COST FUNCTIONALITY

This simulation results from the necessity to study how the energy bill works as time passes by (Energy@home, 2011), (Darby, 2006), in order to show costumers, more transparently, the costs they have to bear (Kamal, 2012), (Darby, 2006). The complexity of the model is mainly due to the retroactivity of the price of consumed energy (Energy Authority, 2013b). Every company providing electrical energy usually sends electricity bill to its clients every two months, taking into consideration the actual quantity of energy used in this time. This determines an estimation of annual consumption, on which the application of prices is based. As a result, if we calculate how much we have spent in a week, the cost may be subject to changes in the future, as the average and the annual estimation tend to vary as time goes on (Kamal, 2012). This basically means that if we visualized a time span of the cost of used energy (Faruqui, 2009), different from the period of two months, there would be incoherence with the total cost of energy consumed at the end of the period of two months. It is therefore impossible to have coherent information on the cost, which may undergo sharp changes.

Selection of *input* for the simulation
We have chosen to display on the device two profiles linked to energy cost: one linked to the "*Service for Maximum Protection*" and the other bound by the fixed price decided by the "*Free Market*" of electrical energy.
In the analysis of results we have decided to focus on the *Service for Maximum Protection* since the price is totally determined by the staggered costs (Energy Authority, 2013b), bringing to light all problems connected with them.

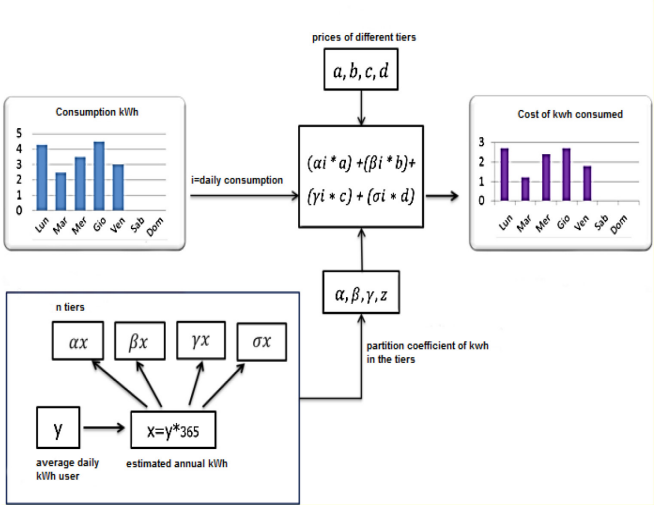

Figure 4, Algorithm for the calculation of models of energy consumption.

For both profiles we have analyzed the progress through different time intervals. All this has been possible by linking a quantity of energy used in two months and distributing it to sub-intervals, taking a *Gaussian* mean of usual consumption into account.

Analysis of results and management of retroactive costs

The energy cost of a determined time span is established according to the daily average of consumption; nonetheless it is not useful to consider the daily average to calculate the energy cost relating to time intervals displayed on our device (U. E. Administration , 2011). In order to maintain coherence in the period of two months in question, with regard to all time intervals that users can view on our device, the displayed cost, for example, in the first month, must correspond to the sum of the displayed costs of every week (Enel, 2012).
In order that this can be possible, the calculation has been managed in two ways:

1. **Management of costs pertinent to the period of two months:**
   Every time users view an interval of cost (week or month), the algorithm, at heart of computation, will calculate consumption in Kwh from the beginning of the period of two months to this moment, as well as the daily average and, through this, the cost of the whole period. Once the cost of such a period has been obtained, some measures for the relative consumption will be linked to the models of the chart (Energy Authority, 2013b); for example, if we wanted to view the costs relating to a week, what would most interest us would be to know the measures connected with single days. Such measures will allow us to divide the total cost, previously calculated, among all models, which, then, will be displayed by bars on the chart of costs relative to the time span selected.
   If the daily average does not undergo sudden changes, for this type of computation, the calculation of costs, on a time span of two months, should adopt a linear course.

2. **Management of costs pertinent to the historical average of consumption:**
   The situation would be different if we did not have any date of invoicing. Presuming that the daily average of consumption has a constant trend, as it reflects user's habits, we should take into consideration the daily average of the historical consumption of a recent period.
   After we have done this, determining the percentages of energy, linked to the tiers, through the relative estimation of annual consumption, for every quantity of energy model shown in the charts below, we can calculate the cost by multiplying the energy percentages relative to the *i-th* day by the prices that correspond to the tiers. In this case, we will obtain the opposite process to the previous one that provided for the calculation of cost and its division. According to such an algorithm, on the other hand, it is the energy that is divided among tiers of price, in order to determine the cost of the period in which we are interest.

As we can see from Figure 5 and 6, although the incoherence of costs among the different time sub-intervals has been worked out, the incoherence relative to the possibility of observing, for a similar interval of visualization, different costs in different instants, still remains. This happens because of the calculation of the average; in fact, if it changes as time goes by, the values, in terms of cost, of a time span of a determined period change too.

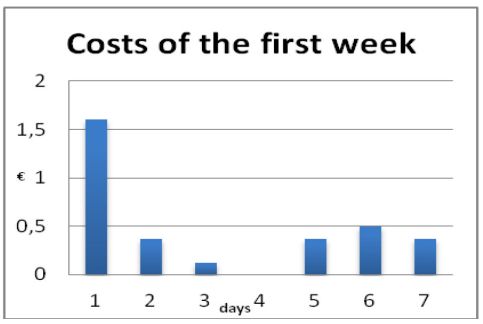

Figure 5, Calculation of daily consumption costs relative to the first week of a period of two months.

In consequence of a recalculation, relative to the first or second algorithm of a period previously consulted, if the daily average turns out to be modified, there will be an incoherence among the values viewed.

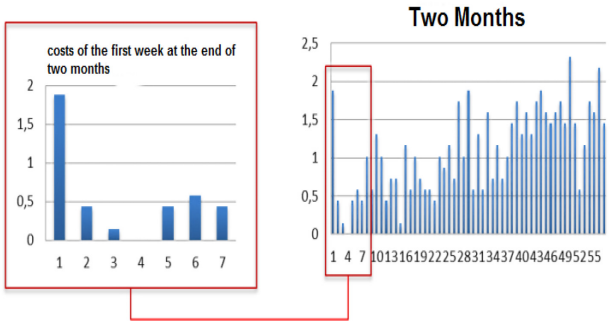

Figure 6, Calculation of daily consumption costs relative to the first week of a period of two months at the end of this.

The statistic nature of information determines the possibility of providing users with information that diverges from reality, just for this reason, users should be aware of this anomaly. In case there were changes in user's consumption habits, they should be informed, by notification, for example, that what they view is temporary cost information and that, as time goes by, it may be updated by more accurate estimations.

Figure 7, Conversion kWh-Euro display.

SYSTEM ARCHITECTURE

The designed distributed system is composed of three elements that interact with each other through Internet.

More in detail there is a part of the system installed at home, with the purpose of acquiring the data, composed of a hardware device in communication with the counter (the SmartInfo) and a PC application that transmits the device data on the web.

Another part of the system consists of a web application that interacts with a database, on the one hand making persistent and aggregating the data received from home, the other transmitting this data to the end user client.

Finally, there is the client application on the user's mobile device, that allows it to access, wherever it is, the aggregated data from the web application.

In case you want to handle even the energy production data instead, the system is more articulated. In fact, in these cases are typically installed in the user house two counters: the first connected to the mains and the second to the production plant.

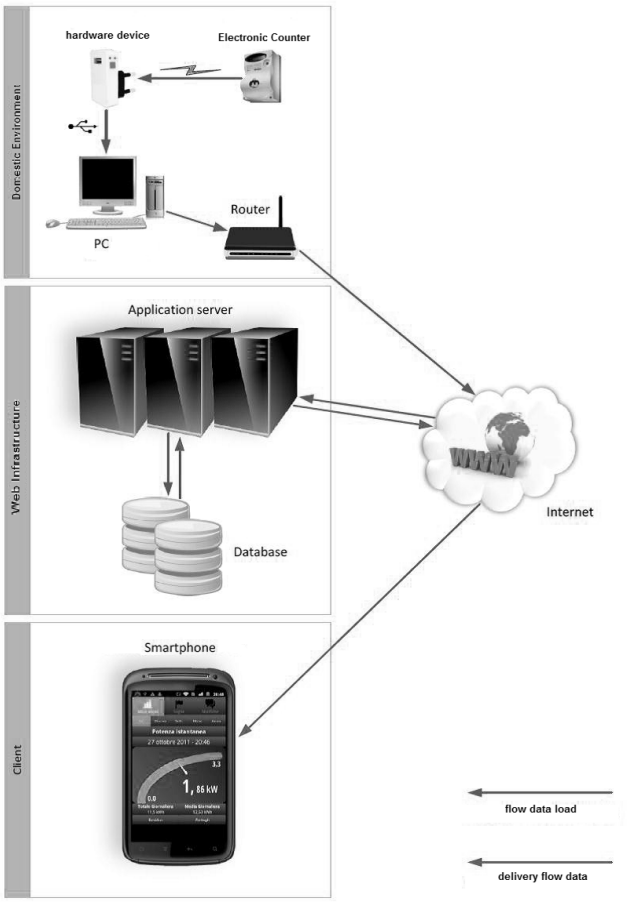

Figure 8, The overall distributed system.

CONCLUSIONS

The goal of the work described in this paper was to analyze the energy market and the actors being part of it (Energy Authority, 2010), (Energy Authority, 2013); studying what the processes being behind the calculation of energy bills, which often appear little transparent to us, are and analyzing the variety of tariffs

determining the range of offers, now present in the *Free Market* (U. E. Administration, 2011), (Energy Authority, 2009), to which every customer can access. All this has led us to integrate new applications with the device, thanks to the development of an algorithm that can show users the costs linked to their own consumption, that surely represent, for users, useful information and more direct feedback (Faruqui, 2009) for the final aim of the "mission" concerning the project itself: saving electrical energy.

REFERENCES

Adelmann R., 2007. Mobile Phone Based Interaction with Everyday Products on the Go*. In: Proc. NGMAST 2007*.

Baecker O., Ippisch T., Michahelles F., Roth S., Fleisch E., 2009. Mobile claims assistance. In: Proc. MUM 2009.

Council Directive, 2006. Directive 2006/32/Ec of the European Parlament and of the Council on energy end-use efficiency and energy services and repealing. Council Directive 93/76/EEC (April, 5). *http://eur-lex.europa.eu/LexUriServ/LexUriServ.do?uri=OJ:L:2006:114:0064:0064:en:pdf*

Darby, S. (2006). The effectiveness of feedback on energy consumption.*http://www.eci.ox.ac.uk/research/energy/downloads/smart-metering-report.pdf*

Enel (2010). How to use the single-phase electronic meter and discover all the advantages. http://www.enel.it/it-IT/ doc/reti/enel_distribuzione/Contatore_Monofase_v1.pdf

Enel (2012). The electronic meter*. http://www.enel.it/it-IT/reti/enel_distribuzione/qualita/progetti_contatore_elettronico/*

Energy Authority (2009). Actions in the management and control of the application and promotion of efficient energy. *http://www.autorita.energia.it/it/docs/09/056-09arg.htm*

Energy Authority (2010). *Deliberation 25 March 2010-ARG/elt39/10*.http://www.autorita.energia.it/allegati/docs/10/039-10arg.pdf.

Energy Authority (2013a). Authority for Electrical Energy and Gas: http://www.autorita.energia.it/it/index.htm

Energy Authority (2013b). Percentage composition of the price of electricity for a domestic consumer type. *http://www.autorita.energia.it/it/dati/ees5.htm*

Energy@home (2011). *Energy@home: a "User-Centric" Energy Management System.* http://www.energy-home.it/Documents/110518Energy@Home_Whitepaper.pdf

European Commission (2011). Climate Action - EU action against climate change. http://ec.europa.eu/climateaction/eu_action/index_it.htm

Faruqui, A. S. , 2009. The impact of informational feedback on energy consumption. *http://www.smartgridnews.com/artman/uploads/1/The_Impact_of_Informational_Feedback__05-20-09_.pdf.*

Kamal, D. (2012). *Mobile Computing. Oxford University Press*, Sept.

Landgren J., Nulden U.A, 2007. A study of emergency response work: patterns of mobile phone interaction*. In: Proc. CHI 2007.*

Patel, S. R., 2007. A flick of a switch. *http://abstract.cs.washington.edu/~shwetak/papers/ubicomp2007_flick.pdf.*

U. E. Administration (2011). International energy outlook 2011.*http://205.254.135.24/forecasts/ieo/pdf/0484(2011).pdf.*

Weiss M., Loock C.-M, Staake T., Mattern F., Fleisch E., 2012. Evaluating Mobile Phones as Energy Consumption Feedback Devices*. P. Senac, M. Ott, A Seneviratne (Eds): MobiQuitous 2010, LNICST, vol 73, pp. 63-77*.

AUTHOR BIOGRAPHIES

FRANCO CICIRELLI, PhD, is a computer science post doctoral fellow at University of Calabria (Unical), DEIS - department of electronics informatics and systems science, making research on agent and service paradigms for the development of distributed systems, parallel simulation, Petri nets, distributed measurement systems. He is a member of ACM.

EMMANUELE NERI, has obtained the bachelor degree (2009) and the master degree (2012) in computer engineering at the University of Calabria – DEIS. He worked as a junior analist for Enel and ELIS Consulting in Rome. He is currently working for the Open Reply company in Milan, on projects of mobile applications.

FRANCESCO PUPO, PhD, is a computer science associate professor at Unical, DEIS, teaching distributed systems and mobile devices programming. His research interests include: multi-agent systems, Petri nets, parallel simulation, verification of time-dependent systems, service oriented computing, distributed systems. He is a member of ACM and IEEE.

LIBERO NIGRO is a full professor of computer science at Unical, DEIS, where he teaches object-oriented programming and real-time systems courses. He is the responsible of Software Engineering Laboratory (www.lis.deis.unical.it). His current research interests include: software engineering of time-dependent and distributed systems, real-time systems, Petri nets, modeling and parallel simulation of complex systems, multi-agent systems, service oriented computing. Prof. Nigro is a member of ACM and IEEE.

INVESTIGATING THE USE OF SEMANTIC TECHNOLOGIES IN SPATIAL MAPPING APPLICATIONS

Taha Osman, Luke Shires
School of Science and Technology,
Nottingham Trent University,
Nottingham NG11 8NS
{taha.osman, luke.shires}@ntu.ac.uk

Tope Omitola, Nigel Shadbolt
School of Electronics and Computer Science
University of Southampton
Southampton SO17 1BJ
Email: {t.omitola, nrs }@ecs.soton.ac.uk

Jeremy Hague
Business Innovation Team,
Nottingham Trent University,
Nottingham NG1 4BU
jeremy.hague@ntu.ac.uk

KEYWORDS
Semantic Web, Spatial Mapping, Context Awareness, Linked Data, Information Retrieval, Semantic Knowledgebase.

ABSTRACT

Semantic Web Technologies are ideally suited to build context-aware information retrieval applications. However, the geospatial aspect of context awareness presents unique challenges such as the semantic modelling of geographical references for efficient handling of spatial queries, the reconciliation of the heterogeneity at the semantic and geo-representation levels, maintaining the quality of service and scalability of communicating, and the efficient rendering of the spatial queries' results. In this paper, we describe the modelling decisions taken to solve these challenges by analysing our implementation of an intelligent planning and recommendation tool that provides location-aware advice for a specific application domain. This paper contributes to the methodology of integrating heterogeneous geo-referenced data into semantic knowledgebases, and also proposes mechanisms for efficient spatial interrogation of the semantic knowledgebase and optimising the rendering of the dynamically retrieved context-relevant information on a web frontend.

INTRODUCTION AND MOTIVATION

Ubiquitous and affordable access to interactive mapping solutions such as Google Maps and OpenStreetMap has encouraged their use beyond simple navigation to develop powerful tools that are useful in a multiplicity of applications from reporting and monitoring local crime to tourism.

The research reported in this paper was inspired by work on a multidisciplinary project at Nottingham Trent University that aimed to develop an interactive mapping tool that can visually map a multidimensional (social, economic, recreational, etc.) sense of real places and communities. The tool should, for instance, visually aid local authorities in planning for public services provisioning in specific geographic regions by correlating petty crime statistics to economic affluence and to the residents' sense of belonging to the place.

The specification of the proposed interactive mapping tool lends itself naturally to context-aware modelling, as it has to analyse the situational condition associated with a geographical space and map them in accordance to the user needs. We argue that Semantic Web technologies are best placed to implement the proposed tool because of the following:

- Semantic Web technologies allow the modelling of the contexts using formal, machine comprehensible representations that can be interpreted by software agents in accordance with the user query parameters.
- Formal semantic modelling also allows leveraging the increasingly rich amount of relevant datasets available in the Linked Open Data (LOD) cloud; of particular interest are the large volumes of semantically-annotated data released by the UK government (on health, crime, housing, etc.) as part of the open government project (data.gov.uk).
- Semantic models are inherently extensible. New domains of interest and respective datasets can seamlessly be added and integrated into existing models using object and data properties (Alemang and Hendler 2011). The semantic knowledgebase developed for this project was adapted in another project (Brown et al. 2010), quite seamlessly, to power location-aware assistive technology aiding people with disabilities.

Nevertheless, there are a number of challenges associated with the geospatial representation and of the semantic knowledge and the efficient utilisation of Semantic Web technology to deliver good quality of service to the interactive mapping application users. In particular, in this paper we present a host of design decisions and development solutions to aid in the uniform interrogation of heterogeneous geo-tagged

Proceedings 27th European Conference on Modelling and Simulation ©ECMS Webjørn Rekdalsbakken, Robin T. Bye, Houxiang Zhang (Editors)
ISBN: 978-0-9564944-6-7 / ISBN: 978-0-9564944-7-4 (CD)

datasets, optimise the utilisation of semantic repository in context-aware processing of geospatial queries, and render the retrieved information on web-based interactive maps.

The remainder of the paper is organised as follows: section 2 surveys related work, section 3 introduces the specification of the semantic interactive mapping tool, section 4 discusses the construction of the semantic knowledgebase, section 5 discusses the challenges of managing the geospatial aspects in semantic technologies, and section 6 concludes the paper and presents our plans for further work.

RELATED WORK

While the use of Semantic Web technologies in driving mapping applications is becoming increasingly popular, a large body of the reported work, while valuable in its domain of interest, either focuses on the usability of the semantic of geo-spatial applications (Cloug et al. 2011)(Becker and Bizer 2009), or predominantly focuses on geo-spatial problem solving aspects (Miron et al. 2007)(Brodaric 2007). Research that is more related to our work investigates more explicitly the processes of exploiting the Semantic Web technology.

There is a large body of work that endeavours to contribute to the middleware supporting semantic geo-spatial indexing. For instance, the effort in (Brodt et al. 2010) reports on the implementation of a triple store that natively integrates spatial query processing (deep integration). In their implementation, spatial query predicates of the OpenGIS specification are supported via SPARQL filtering. Another important contribution at the same middleware level is the work in (Cantador et al. 2008), which reports on the experience of integrating Geographic Information Systems (GIS) and Semantic Web technologies. They integrated geospatial features as a plugin to the LarKC platform for building web-scale semantic computing. A mapping tool was used to convert the GIS data into SPARQL-accessible virtual RDF format, resulting in the loss of the geospatial features, which were partially restored by populating the street and intersection coordinates into the AllegroGraph triplestore. A pathfinder workflow is also developed that implements a reasoner level plugin to find the shortest path in a semantic graph.

In our investigation, we focus on the utilisation of the geo-spatially enabled semantic technologies rather than their implementation. We adopted OWLIM (Geo-Spatial 2013) to host our semantic knowledgebase as it offers non-restricted and well-supported version for academic use. OWLIM also scored very well in terms of response-time and recall in a benchmarking investigation we performed in partnership with the Press Association (Thakker et al. 2010).

The focus of the LinkedGeoData project ()Auer et al. 2009) is on the transformation and publication of the OpenStreetMap (OSM) data as semantically tagged spatial information. They adopt a mixed approach for storing part of the OSM data to reduce the amount of data and increase performance. The reported work details the huge effort put into dynamic interlinking with other spatial datasets by using the Triplify approach (Auer et al. 2009b) to publish linked data from relational databases, and learning algorithms for mapping semantic datasets at the Description Logic level.
The class of applications that our use-case represents focuses on consuming (localising) external datasets rather than integration with and republication as Linked Open Data, assuming black-box use of geo-enabled semantic technology.

REQUIREMENT SPECIFICATION OF THE SEMANTIC INTERACTIVE MAPPING TOOL

Figure 1 below shows a screenshot of the PLace Market mapping tool interface; the tool's name originates from the Lace Market, a historic area in Nottingham, which was the centre of the world's lace industry during the days of the British Empire. The inspiration behind the project was to produce a mapping tool that can aid the multidimensional regeneration of the Lace Market area in the centre of Nottingham by promoting business investment, tourism, and increasing local awareness of the area's heritage. The demonstrated use-case in Figure 1 aids entrepreneurs in selecting a business startup location by visually mapping relevant information about competitors, suppliers, product outlets, local talent, population demographics, as well as multimedia of cultural aspects of the area.

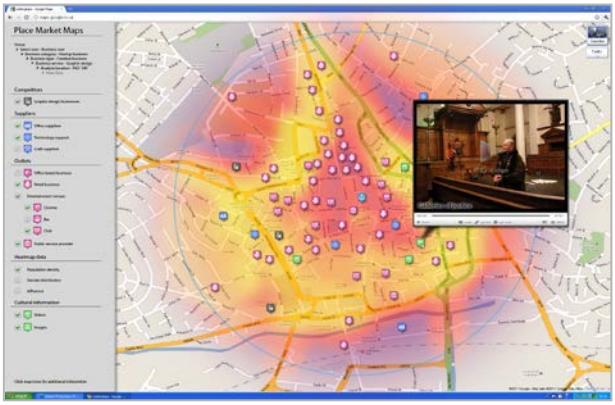

Figure 1: The PLace Market interactive mapping tool

The tool is intended for public use; hence, naturally, a web interface is required. Several web-based mapping applications are available including Google Maps, Bing Maps and OpenStreetMap. We required a mapping application that provided a programming API, allowing developers to create an application using the mapping service as a base, which alleviates the complex task of generating the required set of map tiles and also the requirement of setting up a hosting server for the map tiles that provides a real-time streaming service for map tiles. We adopted Google Maps to build our user

interface as it provides a convenient and well-documented JavaScript API to support mapping application development.

Given the requirement to maintain cross-device and cross-platform deployment, the user interface was built using HTML5 as it supports advanced JavaScript functionality allowing applications to be developed entirely within a web page.

The application interface provides the user with a facet-based hierarchical menu that can be navigated to compile a profile that can be used to generate semantic queries tailored to the individual user's needs; for instance, a business user, looking to startup a new venture specialising in Graphic Design, may be interested in competitor and outlet information in the area around the NG1 3AY postcode.

In passive mode, the semantic repository is then queried to retrieve sets of relevant geo-tagged information to be visualised on the map, which the user can toggle off or on. The retrieved information is displayed as marker icons or multimedia HTML elements. The tool can also display data that is continuous across regions using heatmapping. Specifically, heatmaps were used to illustrate information about population density and demography.

POPULATING THE MAPPING TOOL'S SEMANTIC KNOWLEDGEBASE

The mapping tool ontology is primarily focused around the concepts of a place, user, spatial and temporal descriptors, and a service (public or private). It also contains hierarchical classifications and interrelationships between these entities, such as built spaces, businesses, employees, user opinions, media, outlets, and suppliers.

The Business Innovation Team at NTU provided the base data for our use-case. It provided information about the creative industries in the area such as location, turnover, number of employees, etc., and the tool needed to respond to complex queries with regard to business start-up, supply-outlet chain, local skills, market potential, etc.

We further enriched the base data with two public datasets, data.gov.uk's population statistics and OpenStreetMap/LinkedGeoData (LinkedGeoData 2013) along with geo-referenced information about available services (retail, health, food, tourism, etc.). The interactivity requirement of the mapping tool necessitates minimizing the query response time, hence the taxonomy of the public datasets was mapped into our ontology and they were locally cached to optimise their use.

Despite the 'openness' promise of linked data, such data is not always available in RDF, which would have significantly encouraged their reusability and/or localisation for internal consumption. With respect to data.gov.uk datasets, Prof Shadbolt and Sir Tim Berners Lee were instrumental in the process of opening-up government data (Omitola et al. 2010). However, only a small percentage of the data is accessible as semantic datasets. In our use-case, we demonstrated the benefit of utilising geo-referenced population data to aid the decision-making process in business setup and relocation. Unfortunately, at the time of implementing the tool, the population data was available only in CSV format, necessitating a cumbersome process of manual extraction of data and geo-tagging its elements before mapping it into our semantic ontology.

Similarly, to localise the OpenStreetMap (Haklay and Weber 2008) dataset, we initially converted a MySQL dump of the dataset into N3 format using the D2RQ server (Casanave 2013), and then mapped it into our sematic ontology using SPARQL CONSTRUCT queries as illustrated below.

```
CONSTRUCT {
?inst a services:GPSCordinate.
?gpsid a services:label.
?inst services:label ?gpsid.
?lat a services:hasLatitude.
?inst services:hasLatitude ?lat.
?lon a services:hasLongitude.
?inst services:hasLongitude ?lon.
?created a services:created.
?inst services:created ?created .
}
WHERE {
?inst a vocab:gpsName.
?inst vocab:gpsid ?gpsid.
?inst vocab:lat ?lat .
?inst vocab:lon ?lon .
?inst vocab:created ?created .
};
```

Once the semantic knowledgebase was modelled, the challenge was to utilise and adapt the appropriate Semantic Web technologies to deliver the required QoS by the interactive mapping tool.

MANAGING THE GEOSPATIAL FACTORS OF SEMANTIC TECHNOLOGIES

Reconciling the Coordinate Systems

The semantic repository was populated with data from two main sources. The creative industry dataset provided rich information detailing many attributes of creative businesses including data such as turnover, employment and services provided. Data from OpenStreetMap was used to provide crowd-sourced information regarding relevant points-of-interest such as restaurants, hospitals, museums, etc. The third dataset was sourced from Data.Gov.UK to provide demographic information about the UK population. The OpenStreetMap data is gathered with the intention of mapping and provides accurate GPS based location.

The data used in our use-case was provided by a survey about describing creative businesses in the UK midlands area and referred only to UK postcodes. The postcode geographic representation was obtained from the Ordnance Survey (OS), which provides the coordinates in the OSGB36 coordinate reference system (Ordnance Survey 2013). However, the underlying spatial indexing system used by the semantic repository (OWLIM) and the mapping API (Google Maps) uses the World Geodetic System WGS84 (World Geodetic 2013). Therefore, we first deployed a third party library (Convert Coordinates 2013) to perform the complex conversion of the postcode polygon points from OSGB32 to WGS84 in order to reconcile the drastically different geo-referencing systems. Then we computed the centre location of the postcode area to use it as an approximate position for the creative businesses within that postcode.

A further challenge is that the postcode geo-reference is not accurate, so when two creative businesses lay in the same postcode, the marker position on the map is identical. The results in one marker being completely occluded by the other, and the problem increases as the number of creative businesses in a postcode increases. More precise GPS location of individual postal addresses can be commercially obtained, but this was not considered a cost-effective solution.

This inconsistency in location resolution between different businesses in the repository caused problems when trying to implement geospatial queries to find nearby businesses. The businesses gathered from OpenStreetMap have a direct link to their GPS location, while to resolve the creative industry locations the applications must traverse the relationship to the attached postcode, then to the postcode's centre point geo position. To allow both types of location specification to be queried simultaneously, the non geospatial part of a query was separated and two versions of the query were produced, one that uses the postcode location resolution and the other that looks for direct GPS location. These are then joined into a single SPARQL query using the UNION keyword.

```
SELECT ?x ?y ?bus {
  {
    ?bus rdf:type place:Business .
    ?bus place:hasLocation ?loc .
    ?loc ontoGeo:nearby(lat long dist) .
    ?loc place:hasLongitude ?x .
    ?loc place:hasLatitude ?y .
  }
  UNION {
    ?bus rdf:type place:Business .
    ?bus place:hasPostalCode ?pcode .
    ?pcode place:hasCenterPoint ?loc .
    ?loc ontoGeo:nearby(lat long dist) .
    ?loc place:hasLongitude ?x .
    ?loc place:hasLatitude ?y .
  }
```

Efficient Retrieval of Geo-Tagged Semantic Information

By and large, data for mapping applications is gathered for a large geographic area or region even though the user is typically interested in viewing data from a smaller geographic area of interest. Hence, the interactive mapping tool requires a scalable solution that can cope with the linear increase in the size of retrieved data with the size of the queried geographic region while maintaining a good user experience.

Semantic Spatial Indexing to Improve Query Performance

The interaction requirement of the mapping tool's visual interface imposes real-time constraints on the spatial information retrieval process from the underlying semantic knowledgebase.

Due to the geospatial nature of the application, the data was tagged with geo positioning information. Therefore, it was straightforward to determine if the data is in the user's area of interest by examining the longitude and latitude of its geo points. Using SPARQL, the standard FILTER operation can be used to select geo point results based on longitude and latitude values.

```
...
?place NtuSpatial:hasLat ?lat.
?place NtuSpatail:hasLng ?lng.
FILTER (?lat>40.0 && ?lat<42.1 &&
?lng>20.34 && ?lng<23.7)
}
```

This code segment shows how to limit the ?place geo point to geo points that are within the defined longitude and latitude points. This filter creates a bounding box aligned to longitude and latitude lines around the earth. More complex filter operations using more mathematical operations could provide different shaped areas of interest.

However, using this filtering method requires locating every geo point, retrieving its longitude and latitude positions, and then evaluating them against the filter condition. This means that every geo position stored in the repository must be evaluated to determine if it is in the area of interest. Therefore, adding more geo places to the repository would negatively impact on the query response time regardless of their spatial proximity to the query area of interest. This presents problems for a typical mapping application as it could contain a large number of geo points but only be interested in a small subset of these when looking at a specific geographic region.

The OWLIM semantic repository provides a solution by providing SPARQL extensions to allow for indexing of URIs based on longitude and latitude values. It divides the globe into a finite set of bounding boxes along the global longitude and latitude lines. The extension creates an index based on the longitude and latitude position of geographic points classified as the RDF type SpatialThing, which was provided through an

ontology that was integrated into the OWLIM repository. Our implementation of the geospatial semantic repository uses SpatialThing as the base-type for all other spatial types in our geo-spatial ontology, thus allowing all geospatial information to benefit from OWLIM's scalable indexing method. Using the base SpatialType as the root spatial property, several abstract basic spatial types were identified that could be used and combined to represent real spatial geographic information. GeoPoints were created as a simple node with latitude and longitude decimal literal properties with direct mapping to the underlying SpatialThing. Axis-aligned BoundingBoxes were a collection of two GeoPoints marking the upper left and the lower right coordinates. Concave polygons were created as an ordered list of GeoPoints.

Queries can then make use of the geospatial SPARQL extensions to filter results based on bounding box, radius from a geo point, or a polygon define by geo points. These extensions are able to determine what indexing regions are close to the user's geographic area of interest, thus resulting in more efficient geospatial information retrieval. This can significantly reduce the number of geo points that need to be evaluated, and as a result dramatically speed up query times.

Using a subset of the OpenStreetMap dataset containing the locations of businesses relevant to this application, two benchmarks were performed to evaluate the spatial query response time based on standard SPARQL filter methods in comparison to OWLIM's spatial indexing technology.

The first benchmark limited the OpenStreetMap dataset to business locations within Nottingham (1275 places), as it was geared to evaluate the technology's performance with respect to the use-case and its class of applications. The second benchmark used the OpenStreetMap data for all business locations (world-wide available data – 760,706 places) to examine scalability.

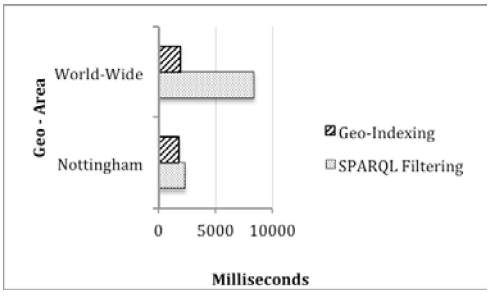

Figure 2: Query response time for the filtering and geo-indexing spatial query mechanisms

The test results in Figure 2 above showed little difference in the query response time between the two mechanisms when used to retrieve data from the Nottingham locality. However, for the large volume of geo-positions evaluated in the second test, the test results show that the OWLIM spatial indexing is clearly outperforming the standard SPARQL filtering methods. Another important remark is that, for the size of evaluated geo-positions, spatial indexing does not seem to be significantly affected by the increase in data size. However, the SPARQL filtering method is clearly not scalable and could only be applied in scenarios with small datasets.

Optimising the Utilisation Of the Geo-Enabled Semantic Repository

OWLIM supports SPARQL query extensions that allow the retrieval of points positioned within a user-specified concave polygon. Therefore, it would be beneficial if our spatial data representation allowed querying over polygons stored in the semantic repository. However, this proved challenging as a limitation in the OWLIM polygon querying method is that the number of points within the polygon must be specified at the time of composing the query; consequently, any polygons used to geo-reference data in the semantic repository must have the same number of points as specified in the SPARQL spatial query.

In order to avoid utilising an inefficient multistage query workaround, a solution was to model all polygons with a fixed number of points. The polygon datasets acquired from the Ordnance Survey were found to be highly detailed, with some containing over a thousand points. To accommodate this, the vast majority of polygons that were smaller would have to contain hundreds of duplicated points. This was clearly a wasteful solution and would enforce an upper limit on the number of points any polygon could contain. A waypoint structure similar to the polygon was considered, but the use-case data provided did not require it and was omitted from the prototype system.

Deciding that it was not feasible to perform queries on polygons directly inside the repository, we developed a comma separated values structure that stored the list of polygon points as a single string literal. This significantly reduced the number of relationships that repository had to manage. For situations where the exact polygon area was not required for spatial computation, each polygon was preprocessed to provide its own bounding box giving a rough indication of the polygon area that could potentially be used for early escape intersection tests.

The aforementioned basic spatial types were used to represent real world spatial information such as postcode and Super Output Areas (SOA), which is a set of geographical areas developed following the UK 2001 census to facilitate the calculation of the Indices of deprivation, crime, employability, etc. The postcode and SOA data were compiled from data gathered from the Ordnance Survey and the Office for National Statistics, respectively. When the repository was populated with basic spatial representations, additional data could be added and mapped to the repository using these spatial

instances to provide a relationship to a geographic position that could be used to position the data on a map. This use-case described in this paper involved mapping geo-referenced data about creative businesses, public and entertainment services, and the local population/demography.

OWLIM's spatial indexing method breaks the world down into finite spatial regions based on longitude and latitude. Each SpatialThing is assigned to one spatial region based on where their longitude and latitude attributes lie, which allows fast retrieval of all SpatialThings that belong to a given region. The built in OWLIM SPARQL spatial query extensions can take advantage of this fact and ignore triples not associated with relevant spatial indexes, allowing a significant number of triples to be ignored during the query process. This is a clear advantage over non spatially-enabled semantic repositories as the alternative involves discarding results outside of the area of interest through the SPARQL FILTER method. This method must evaluate every possible query match then discard results during the filtering stage. For instance, when querying results in a small geographic region, all SpatialThings in the repository must be considered and then filtered out. Hence, this method does not scale well as the entire repository must be considered during a query. The spatial indexing technology provides a scalable solution as it limits the data that must be evaluated to that which is geographically close to the target area, allowing most data to be safely ignored.

To benchmark the scalability of OWLIM's geospatial indexing, a query to find all business in a Nottingham area that provided a food service was run over a repository created by extracting all businesses from the OpenStreetMap dataset. In the small dataset, only businesses from within the Greater Nottingham area were included. In the larger set, the entire UK area was used.

The smaller set contained 1135 total businesses, of which 170 were known to provide food service. The large set contained 286,236 total businesses, of which 39,567 provided a food service. For both datasets, the query looked for food services within 2.1km of the latitude longitude point of 52.9647027748771 -1.1715030670066016 (Nottingham city centre).

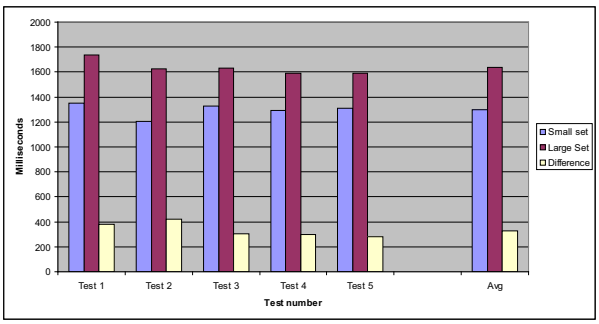

Figure 3: Evaluating the scalability of semantic geo-indexing

As Figure 3 shows the difference in query time between the two data sets is around 300 milliseconds longer for the larger data set. However, the large set is over 250 times larger then the small set. Although the query time has increased, it is sub-liner and is still within an acceptable query time for an interactive application.

Coping with Demanding Visualisation Eements - Heatmaps

Our mapping tool uses heatmaps to display data that is continuous across regions, specifically to illustrate information about population density and demography, which can be useful, for instance, to assess customer-base. A heatmap is usually shown as an overlay layer to the map the uses colour to represent the changing values of space. In most mapping applications, heatmaps can be preprocessed to display a specific dataset that is already determined before the application is run, but owing to the dynamic nature of our context-aware application, the data that needs to be conveyed to the user is context-specific and cannot be pre-computed. To overcome this problem, we leveraged the facility of the HTML5 canvas element that allows real time rendering of image inside a web page, thus allowing heatmaps to be generated at runtime and dynamically overlaid in accordance with the user context. The client-side processing of the heatmap allows the map user interface to react instantly to any changes in the user context without the need for server-side reprocessing to rebuild large heatmap tile sets.

The disadvantage of real-time processing of heatmaps is that it can incur considerable overhead on the response time of mapping applications, which is exacerbated by longer retrieval times because of the processing of the semantic metadata. We developed a technique to optimise the heatmap rendering to bring response times to within a few seconds of the users request.

The HTML5 canvas element provides a virtual image to the web application. Since heatmapping images are generally low resolution, we purposely utilised a small canvas element of 200x200 pixels to render the heatmap image while still capturing most of the important image detail. Once rendered, the heatmap can then be stretched to fit the user's display. Stretching the heatmap by several factors adds significant blur to the image, which is actually desirable as continuous spatial data rarely conforms to statistical boundaries and allowing this blurring shows a more realistic view of the statistics.

In contrast to low-resolution heatmaps, the high accuracy geo polygons captured by the Ordnance Survey contained sub-pixel resolution data. Rendering polygons with a large number of points (often around 800 per polygon) took significant time with the low-resolution heatmap unable to show this level of detail. A simple polygon reduction algorithm was used to greatly reduce

the number of points within the polygon while maintaining its general shape. Although the heatmap generation now involved an additional polygon reduction stage, the reduced rendering time was shortened significantly to bring the overall generation time to within a second.

We tested the performance gain from the polygon-reduction mechanism on a variety of HTML5-enabled web browsers. The tests were carried out on 8GB RAM Intel Core 2 Quad CPU at 3 GHz running Windows XP. JavaScript does not allow multi threading so there is no advantage from the multiple CPU cores. The browsers were Chrome version 12.0, FireFox version 3.6.13 and Safari version 5.0.5.

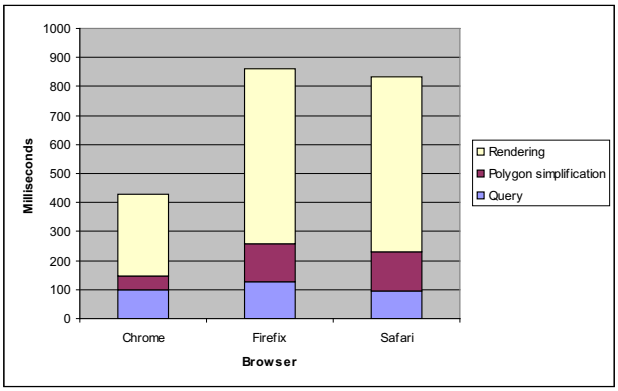

Figure 4: Evaluating the performance of the heatmapping mechanism

CONCLUSIONS AND FURTHER WORK

This paper draws on our experience in developing an interactive mapping tool in order to contribute to the efforts in tackling the challenges associated with using Semantic Web technologies in the development of context-sensitive geospatial applications. The first challenge was developing a method for the reconciliation and uniform interrogation of heterogeneous geo-tagged datasets. The next challenge was the efficient retrieval of context-specific information from the semantic knowledgebase, where we deployed a semantic repository with geospatial reasoning capabilities and optimised its utilisation by readapting its polygon query technology and introduced an efficient query transfer method with the web front-end before evaluating the scalability of the semantic repository in processing geospatial datasets. The paper also presents an efficient mechanism for real-time rendering of heatmaps, which is important for maintaining an acceptable response time in dynamic context-aware applications.

Our plans for further work include investigating the deployment of clustering algorithms for improved visualisation of highly condensed interactive maps while retaining user specific accessibility to the semantically tagged data. We also intend to experiment with the utilisation of specialised semantic geographic data representations such as GeoRDF (GeoRDF 2013) and evaluate the use of Linked Data mapping applications such as map4rdf (map4rdf 2013) to streamline the consumption and support dynamic integration of Linked Geo Data.

REFERENCES

Allemang, D. and Hendler, J. 2011. “Semantic Web for the Working Ontologist: Effective Modeling in RDFS and OWL.” Morgan Kaufmann- 2nd edition.

Auer, S., Dietzold, S., Lehmann, J., Hellmann, S., Aumueller, D. 2009b “Triplify - lightweight linked data publication from relational databases.” In Proceedings of the 17th International Conference on World Wide Web, WWW 2009, pages 621–630, Madrid, Spain.

Auer, S., Lehmann, J., Hellmann, S.2009. “LinkedGeoData: Adding a spatial dimension to the Web of data.” In Proceedings of Eighth International Semantic Web Conference (ISWC 2009), pp. 731-746, Chantilly, Virginia.

Becker, B. and Bizer, C. 2009. “Exploring the Geospatial Semantitc Web with DBpedia Mobile.” Published in: Journal Web Semantics: Science, Services and Agents on the World Wide Web archive. Volume 7 Issue 4, December, 2009.

Brodaric, B. 2007. “Geo-Pragmatics for the Geospatial Semantic Web.” Transactions in GISVol-ume 11, Issue 3, pages 453–477, June 2007.

Brodt, A., Nicklas, D., Ossietzky, C., Mitschang, B. 2010. “Deep integration of spatial query pro-cessing into native RDF triple stores.” In: Proceedings of the 18th SIGSPATIAL Interna-tional Conference on Advances in Geographic Information Systems (GIS '10), pp. 33-42 , San Jose, California.

Brown, D.; Standen, P., Evett, L., Battersby, S., Shopland, N. 2010. “Designing Serious Games for People with Dual Diagnosis: Learning Disabilities and Sensory Impairments.” In P. Zemliansky, & D. Wilcox (Eds.), Design and Implementation of Educational Games: The-oretical and Practical Perspectives, pp. 424-439.

Cantador, I., Bellogín, A., Castells, A. 2008. “News@hand: A Semantic Web Approach to Rec-ommending News.” ADAPTIVE HYPERMEDIA AND ADAPTIVE WEB-BASED SYSTEMS. Lecture Notes in Computer Science, 2008, Volume 5149/2008, pp. 279-283.

Clough, P., Tang, J., Hall, M., Warne, A. 2011 “Linking archival data to location: a case study at the UK National Archives.” Aslib Proceedings: New Information Perspectives, 2011, Vol.63(2/3), p.127-14.

Convert Coordinates between WGS-84 and OSGB36. 2013 (last accessed Feb 2013). http://www.movable-type.co.uk/scripts/latlong-convert-coords.html.

Cory Casanave, C. 2013 (last accessed Feb 2013). “Designing a semantic repository.” http://www.w3.org/2007/06/eGov-dc/papers/SemanticRepository.pdf

Geo-Spatial Indexing in Owlim. 2013 (last accessed Feb 2013). http://www.ontotext.com/owlim/geo-spatial

GeoRDF - An RDF compatible profile for geo information. 2013. (last accessed Feb 2013) http://www.w3.org/wiki/GeoRDF

Haklay, M. and Weber, P. 2008. “OpenStreetMap: User-Generated Street Maps.” IEEE Pervasive Computing Magazine, Volume: 7 , Issue: 4, pp. 12-18 Oct.-Dec. 2008.

LinkedGeoData. 2013 (last accessed Feb 2013). http://linkedgeodata.org

map4rdf - Map viewer of RDF with Geometrical Information. 2013 (last accessed Feb 2013). http://oegdev.dia.fi.upm.es/map4rdf/.

Miron, A., Gensel, J., Villanova-Oliver, M., Martin, H. 2007. "Towards the Geo-spatial Querying of the Semantic Web with ONTOAST." Web and Wireless Geographical Information Sys-tems. Lecture Notes in Computer Science Volume 4857, 2007, pp. 121-136.

Omitola, T., Koumenides, T., Popov, I., Yang, Y., Salvadores, M., Szomszor, M., Berners-Lee, T., Gibbins, N., Hall, W., Schraefel, M., and Shadbolt, N. 2010. "Put in Your Postcode, Out Comes the Data: A Case Study". In: ESWC. Ed. by L. Aroyo, G. Antoniou, E. Hyvönen, A. ten Teije, H.Stuckenschmidt, L. Cabral, and T. Tudorache. Lecture Notes in Computer Science 6088. Springer, June 2010, pp. 318–332.

Ordnance Survey osgb36 coordinate system. 2013 (last accessed Feb 2013) http://www.ordnancesurvey.co.uk/oswebsite/gps/information/coordinatesystemsinfo/guidecontents/guide5.html. Last accessed.

Thakker, D., Osman, T., Gohil, S., Lakin, P. 2010. "A Pragmatic Approach To Semantic Repos-itories Benchmarking". ESWC'10 Proceedings of the 7th international conference on The Semantic Web: research and Applications - Volume Part I. pp 379-393.

World Geodetic System 1984. 2013 (last accessed Feb 2013). http://earth-info.nga.mil/GandG/publications/tr8350.2/tr8350_2.html.

AUTHOR BIOGRAPHIES

Taha Osman is a principle Lecturer at the College of Science and Technology, Nottingham Trent University. He gained his PhD in Fault-Tolerance of Distributed Computing Systems from the same University in 1998 and immediately joined its academic staff. Dr Osman leads the Semantic Web research network at the department of computing and informatics and his research interests include Semantic Web, Knowledge Engineering and Intelligent Information Retrieval, Intelligent Agent Systems.

Luke Shires studied at Nottingham Trent University for a BSc in Computer Science graduating in 2011. He also received the Vice Chancellors award for his involvement in founding and maintaining the Nottingham Trent Developers Society, which creates work and placement opportunities for students by enabling them to learn skills in game development. He is primarily interested researching how games and game technologies can be applied to solve real world problems. Luke is currently working towards a Ph.D. looking at the application of markerless tracking technologies to improve games for upper extremity rehabilitation following stroke. Prior to beginning his Ph.D. he has worked on several projects including the use of applying sematic knowledge bases to enable intelligent mapping solutions for helping cognitively impaired users during route learning and using games technologies to create a real time simulation of visual impairments.

Tope Omitola is a Research Fellow at the Web and Internet Science Group in electronics and computer science at the University of Southampton. His research interests include the Linked Data and Semantic Web, Web science, and knowledge technologies. Omitola is a graduate of King's College London and Jesus College Cambridge.

Nigel Shadbolt is a professor of artificial intelligence and head of the Web and Internet Science Group in electronics and computer science at the University of Southampton, and is the co-director of the Open Data Institute in London. He is also an adviser to the UK government on open data and a member of the UK Public Sector Transparency Board.
His research interests include the Semantic Web, Web science, and knowledge technologies. Shadbolt has a PhD in AI from the University of Edinburgh.

Following a degree in clothing and textile management, **Dr. Jeremy Hague** worked for nine years within a multi-disciplinary action research team at Nottingham Trent University. Funded solely through consultancy and research income, the team specialised in promoting innovation through employee involvement and new forms of working; particularly team-based manufacturing. During this time Jeremy pioneered the use of forum theatre in business settings, which stimulated creative development across all levels of an organisation. Jeremy currently leads the Business Innovation Team within NTU's Commercial Directorate. The team supports the development of commercial products, relationships and income through company networks and funded programmes. Jeremy also represents the University in the Officers Group of D2N2, the Local Enterprise Partnership for Derbyshire and Nottinghamshire

A STUDY OF COST EFFECTIVE SCHEDULING OF NURSES BASED ON THE DOMAIN TRANSFORMATION METHOD

Geetha Baskaran
University of Nottingham, Malaysia Campus
Jalan Broga , 43500 Semenyih, Selangor
E-mail: Geetha.Baskaran@nottingham.edu.my

Andrzej Bargiela
University of Nottingham, Nottingham, UK &
Krakow Technical University. Krakow, Poland.
E-mail: abb@cs.nott.ac.uk

Rong Qu
School of Computer Science
University of Nottingham, Jubilee Campus
Nottingham NG8 1BB, UK.
E-mail: rxq@cs.nott.ac.uk

KEYWORDS

Domain Transformation, Demands, Nurse Scheduling, Granulation, Simulation.

ABSTRACT

This paper discusses and analyses the tradeoff between the flexibility afforded with greater number of staff and the implied cost of employing extra staff in the context of the nurse-scheduling problem. If the number of staff is constant, our study allows quantification of the degree of pressure put on the staff resulting from the schedules that do not satisfy their preferences for shift allocation. We present a practical approach, based on our domain transformation methodology that achieves good quality schedules without high computational requirements.

INTRODUCTION

A common problem in healthcare systems worldwide is the shortage of nursing staff [Ulrich, 2002]. This is partially due to the demanding nature of the nursing profession that requires availability for shift work. In this context the task of producing work schedules that not only satisfy the clinical cover demands but also take into account specific requests and preferences of nurses, becomes a key to staff satisfaction and retention. A failure to deal with this issue inevitably leads to not having enough skilled nurses in clinical settings and a significant negative impact on patient outcomes, including mortality [Aiken, 2002].

From the perspective of hospital management there is an inseparable link between the scheduling activity and the decision about the total numbers of staff. In their publications [Costa, 1996] and [Knauth, 1996] have provided some guidelines in this respect. However, employing more nurses than is needed to meet the required clinical care standards, is an expense that hospitals are keen to avoid. One way of ensuring that the hospitals strike this delicate balance is to deploy computationally efficient software tools enabling construction of work schedules not only in the long- and medium-term planning mode but also in response to immediate requests from staff.

Independent studies have supported the view that the investment in the advanced scheduling of nursing staff translate into significant enhancement of job satisfaction, and savings in labor costs due to reduced nurse turnover [Bester, 2007, Blythe, 2005]. However, producing schedules that meet hospital requirements and satisfy individual preferences and ad-hoc requests is an extremely complex task [Gino et. Al., 2012].

In this study, we have approached the problem of cost-effective scheduling of nurses using the domain transformation method introduced in [Baskaran et al. 2009, 2012] as a practical illustration of the information granulation methodology [Bargiela et al. 2002, 2008]. Based on this solution we investigate the optimum balance between the staffing levels of the ward and the ability to achieve good quality schedules.

NURSE SCHEDULING PROBLEM

The nurse-scheduling problem can be defined as a problem of assigning to each nurse a specific shift within a pre-defined scheduling horizon. Such an assignment is subject to hard constraints that originate from contractual agreements, legal requirements and local good practice. Any schedule that satisfies these constraints is referred to as a feasible schedule. However, satisfying hard constraints is only a starting point for the construction of a good quality schedule. The degree of satisfaction of additional constraints reflecting staff preferences for allocation of specific shifts provides a measure of the quality of the schedule.

Without the loss of generality we consider here a nurse scheduling scenario based on the operation of an intensive care units in Dutch hospitals [Baskaran et al. 2009, 2012]. In order to appreciate the computational complexity of the scheduling problem, we consider a specific case of a ward with 16 nurses employed on a 36-hours/week contracts and a scheduling period of 5 weeks (35 days). There are five shift types; as itemized in Table 1, that are allocated to the nurses. The Early (e), Day (d) and Late (l) shifts are of 9-hours duration;

Proceedings 27th European Conference on Modelling and Simulation ©ECMS Webjørn Rekdalsbakken, Robin T. Bye, Houxiang Zhang (Editors)
ISBN: 978-0-9564944-6-7 / ISBN: 978-0-9564944-7-4 (CD)

the Night (N) shift is of 8-hours duration; and the Rest (R) shift lasts a minimum of 2 days.

Table 1: Shift Types and the required numbers of nurses on specific shifts

Shift Type	Start Time	End Time	Number of nurses on shifts						
			M	T	W	T	F	S	S
Early	07.00	16.00	3	3	3	3	3	2	2
Day	08.00	17.00	3	3	3	3	3	2	2
Late	14.00	23.00	3	3	3	3	3	2	2
Night	23.00	07.00	1	1	1	1	1	1	1
Rest	Notional shift that last minimum of 2 days								

Night = N Early = e Day = d Late = l Rest=R

The scheduling problem in the above scenario represents a combinatorial optimisation in a space of $\mathbf{16*5^{35}=4.6*10^{25}}$ possible schedules. Figure 1 illustrates the challenge of the schedulling problem by providing an example of two possible sequences of shifts allocated to Nurse 1 in Week 1. A simple change of one shift implies a non-monotonic change in the cost associated with the violation of constraints.

.

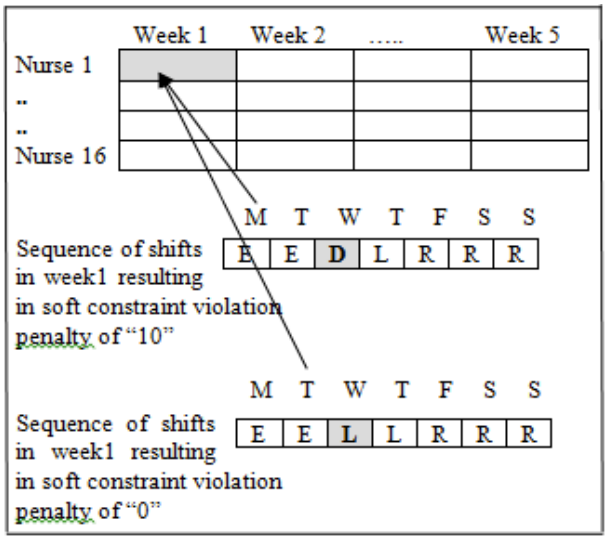

Figure1: Example of a single shift change in a schedule

Because of the large number of possible schedules and the non-monotonic change of the cost with different combinations of shifts, the optimisation of the overall schedule by the modification of individual shifts and/or various groups of shifts is considered as an NP-hard problem [Celia et. al., 2010]. However, this classification is predicated on the assumption of the deployment of scheduling algorithms that explore directly the solution space. An overview of such algorithms is given in [Burke et al., 2004, Lim et al., 2010].

METHODOLOGY

The domain transformation approach introduced in [Baskaran et al. 2012] departs from the orthodoxy of direct exploration of the space of schedules, as described in the preceeding section. We observe that the three 9-hour shifts (e, d, l) are subject to identical soft constraints. Consequently, the first simplification of the scheduling problem is afforded by considering the e-, d- and l-shifts as being of the same type. We denote this combined shift as D-shift and will refer to this transformation as transformation from the edlNR domain to the DNR domain.

In the DNR domain the requirement for staff cover during the corresponding shifts is summarised in Table 2. This in itself does not have any adverse effect on the computational complexity of the scheduling process. However, the important gain is that the reduction of the number of shifts from 5 to 3 makes the number of possible schedules in the DNR domain reduce to $\mathbf{16*3^{35}=8*10^{17}}$. This represents a reduction by a factor of 10^8. But although the application of the traditional scheduling methods would be much more efficient in this reduced space we do not advocate the use of these methods as we notice a potential for additional domain transformation and the associated computational gain.

Table 2: Shift Types and the required numbers of nurses on specific shifts in the DNR domain

Shift type	Number of nurses on specific shifts						
	M	T	W	T	F	S	S
d	9	9	9	9	9	6	6
N	1	1	1	1	1	1	1
R	Notional shift that last minimum of 2 days						

We note that the soft constraints are expressed in therms of penalties associated with specific shift sequences during one week. We can therefore produce sequences of shifts of one-week duration that do not have any penalties associated with them and sequencies that have some arbitrary penalties. We will call those sequencies "patterns" and we will use them as basic building blocks for the schedules. Figure 2 provides examples of such zero-cost patterns and Figure 3 provides examples of non-zero-cost patterns.

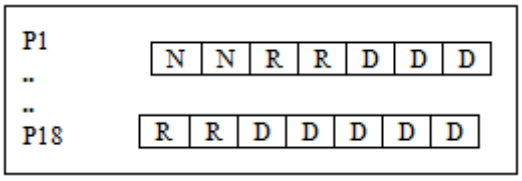

Figure2: No violation of Soft constraints (called as zero cost patterns)

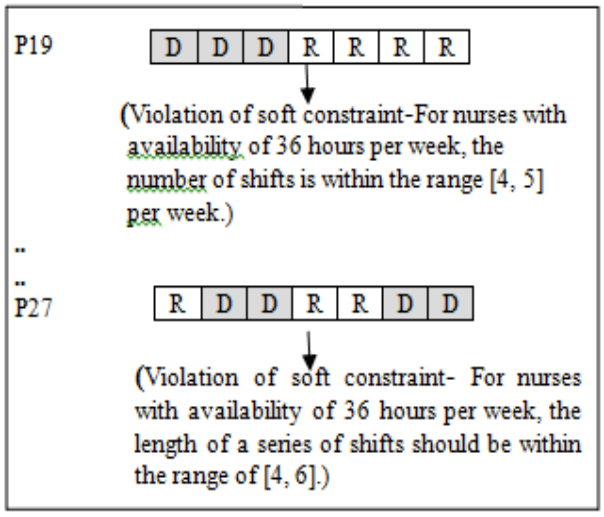

Figure3: Violation of Soft constraints with Cost 10 (called as non-zero cost patterns)

The problem of scheduling shifts is therefore transformed into the problem of scheduling patterns. The computational gain that can be attained from this domain transformation depends on the number of patterns that need to be considered. It turns out that the number of zero-cost patterns and patterns with other pre-specified cost is relatively small. In the scenario considered above there are only 18 zero-cost patterns. This means that there are only $\mathbf{16*18^5=3*10^7}$ 5-week schedules that can be constructed from 18 patterns for 16 nurses. This is a number of schedules that can be completely enumerated within seconds on an average PC.

It is worth highlighting that the combined two domain transformations have achieved an enormous reduction of the space of possible schedules by a factor 10^{18}. In other words, one second of computations in the domain of patterns is equivalent to 100,000,000,000 years of computations in the edlNR domain. Of course, the solution of the scheduling problem in the domain of patterns needs to be converted back into the original edlNR domain. This involves small computational effort primarily concerned with the consideration of the specific requirements with regard to the precedence of e-, d- and l-shifts as summarised in Table 2.

Table 2: Penalties of violation for the conversion of ***D***NR domain to edlNR domain.

		Succeeding shifts			
		N	E	D	L
Preceding Shift	N	ok	n/f	n/f	n/f
	E	ok	ok	ok	ok
	D	ok	5	ok	ok
	L	ok	n/f	n/f	ok

Our *domain transformation* approach can be summarised as a 3-stage process:

I) conversion of the problem from the original edlNR domain into a problem in the ***D***NR domain;
II) solution of the problem in the ***D***NR domain
III) conversion of the ***D***NR solution into a solution in the original edlNR domain

In practice we are able to achieve further gains in performance by considering the patterns with N-shifts first and, by doing so, reducing the number of nurses that need to be allocated patterns with D-shifts.

BALANCING THE COST OF SOFT CONSTRAINTS AND THE STAFF COST

Nurse scheduling is inextricably linked with determining total number of nurses. Most of healthcare systems are under pressure to control costs while trying to provide high levels of service. This is a difficult balance to strike. Having a small number of nurses may impact quality of care while employing a large number of nurses and not utilizing their contractual hours is clearly wasteful. In our approach, we are balancing these concerns by combining the cost for the under-utilization of nurses with the costs of violation of soft constraints into a single performance index.

The expectation is that with the decreasing number of nurses we will find a progressively higher cost of violation of constraints up to the point when hard constraints would have to be broken – thus no feasible solution could be found. On the other hand, with the increasing number of nurses we expect that although it becomes easier to find schedules that don't violate soft constraints (i.e. one may find low- or zero- cost schedules) the pro-rata cost of unused contractual hours of extra nurses dominates the balance.

For the sake of clarity we demonstrate our balancing approach only in the context of full time nurses employed on 36 hours/week contracts. The under-utilisation of nurses (U) is measured as:

$$U = TC - TW \qquad (1)$$

where:

TC is the Total Number of contractual hours per week
TW is the Total Number of hours worked by all nurses in one week (as defined by the shift-cover requirement)

Process of checking the demands

It is important to appreciate that the number of hours defined by the shift-cover requirement (TW) does not determine, on its own, the required staff numbers. A simple division of TW by the number of hours per week stipulated by the employment contract provides only a lower bound on the number of the required staff but it does not provide a good estimate of the actual staffing

requirement. This is because the varying (hard and soft) constraints, may imply the need for extra staff despite identical shift-covers and nurse contracts.

For the purpose of balancing the nurse schedules and staff numbers we consider only positive values of U in equation (1). This is because the negative numbers represent the requirement that a nurse works longer hours then implied through the contract and this is already penalizes through the hard/soft constraints. The comparison of the cost associated with violation of constraints with the monetary cost of employing extra staff requires adoption of some convention that would make these costs comparable. Here we assume that the following represent s well the notional cost of under-employment of staff:

$$CU = U * 10 \qquad (2)$$

where:
CU = Cost of under- utilization

NUMERICAL RESULTS

Numerical experiments described in this section provide a representative sample of the simulation studies conducted to balance the degree of satisfaction of soft constraints vs. the decisions on employing additional nursing staff. We have varied the required cover on individual shifts to simulate the decision support functionality that may be required by the hospital management. As discussed in the previous section, the total number of schedules in the re-defined problem domain of patterns is of the order of $\mathbf{3*10^7}$ and the solution can therefore be found by enumeration of schedules and the selection of the lowest cost solution.

In order to understand the behaviour of our model, multiple demand vs. number of nurses scenarios were generated. For each scenario, the solution time is also calculated in seconds using a Workstation with Intel ® Core ™ Dual Quad CPU Q8200 @ 2.33Ghz 4Core running Windows 7 Ultimate with 4GB.

Test Data on Original Demand
Based on the original problem, we have changed few sample runs of different number of nurses Table 3 presents the results of the best set of nurses which satisfies the demand of the original problem with a very reasonable cost for a month. While Table 4 and 5 represents the alternative demands with the number of nurses and however this is concluded in the Graph 1, Graph 2 and Graph 3 which shows clearly the representation of the various cost.

The results tables use the following notation:
TN = Total number of nurses
TC = Total number of contractual hours
U(h/w) = Under Utilization of Nurses (hours/week)
CSC = Cost of violating Soft constraint
CU = Cost of under- utilization
T(s) = Time (in seconds) to execute the software

Case 1:

Table 3: The balance of violation of soft constraints and the underutilisation of nurses for the "9999966" D-shift and the "1111111" N-shift cover (57*9+7*8=569 hours)

TN	TC	U (h/w)	CSC	CU	Ctot	T(s)
14	504	0	1250	0	1250	706
15	540	0	375	0	375	503
16	576	7	**210**	**70**	**280**	139
17	612	43	185	430	615	31
18	648	79	180	790	970	22

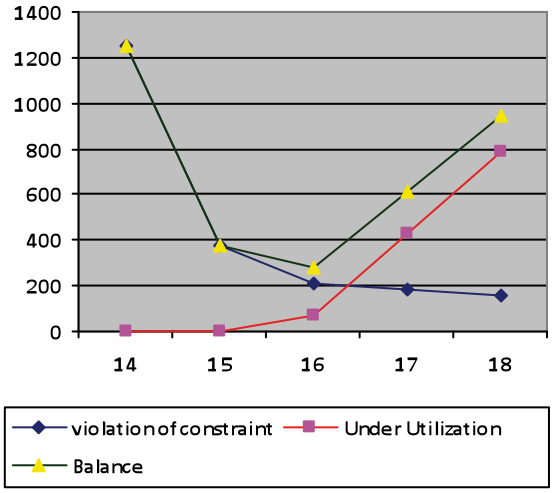

Graph 1: Balance between the constraint cost and the Under Utilization cost for the cover "9999966"

Case 2:

Table 4: The balance of violation of soft constraints and the underutilisation of nurses for the "8888855" D-shift and the "1111111" N-shift cover (50*9+7*8=506 hours)

TN	TC	U (h/w)	CSC	CU	Ctot	T(s)
14	504	0	2854	0	2854	761
15	540	34	**345**	**340**	**685**	501
16	576	70	290	700	990	204
17	612	106	190	1060	1250	71
18	648	142	160	1420	1580	73

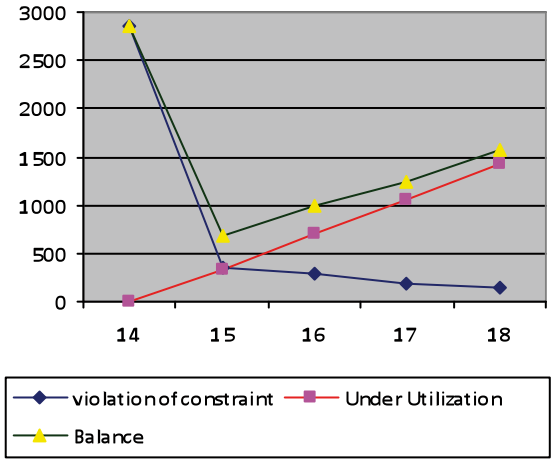

Graph 2: Balance between the constraint cost and the Under Utilization cost for the cover "8888855"

Case 3:

Table 5: The balance of violation of soft constraints and the underutilisation of nurses for the "101010101077" D-shift and the "1111111" N-shift cover (64*9+7*8=632 hours)

TN	TC	U (h/w)	CSC	CU	Ctot	T(s)
14	504	0	7175	0	7175	863
15	540	0	4350	0	4350	809
16	576	0	3900	0	3900	790
17	612	0	2550	0	2550	779
18	648	16	**300**	**160**	**460**	504
19	684	52	355	520	875	515
20	720	88	430	880	1310	641

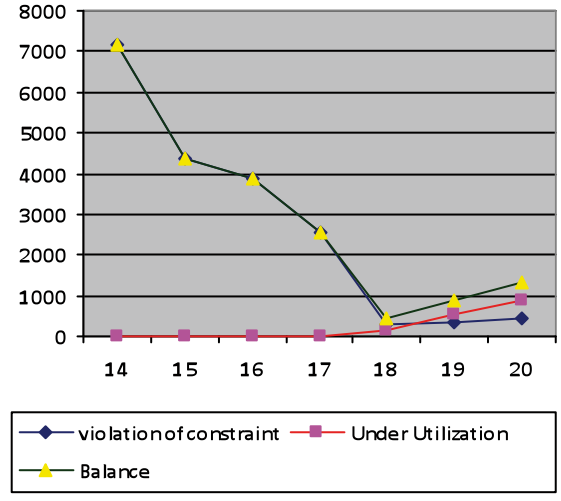

Graph 3: Balance between the constraint cost and the Under Utilization cost for the cover "101010101077"

Discussion

This study illustrates our investigation of the combined nurse schedulling and the management decision support concerning the staffing levels. The study quantifies how the constraints associated with the scheduling problem influence the cost-effectiveness of employing additional staff. We have shown this using a representative set of 3 different scenarios with different number of nursing staff considered in each scenario.

The result indicates that for the original problem demand of "999966" D-shift, the exact balance is 16 nurses, as indicated in the graph 1. With fewer then 16 nurses we can't satisfy the clinical cover requirement and having larger numbers of nurses implies unnecessarily high employment cost.

The balance for the alternative clinical cover requirements (demands) of "8888855" is 15 nurses; and for the "10 10 10 10 10 7 7" the required numbrt of nurses is 18.

CONCLUSION

Nurse rostering problem, considered at the level of detailed time constraints and different types of day-shifts, represents a very significant computational challenge. In this paper we evaluate the effectiveness of our domain transformation approach to achieving a good balance between staffing and the satisfactory work schedules. By automating the nurse rostering process we have reduced the scheduling effort and have ensured that specific scheduling requirements of staff are taken into consideration more easily.
The proposed domain-transformation approach to nurse rostering represents a significant departure from the heuristic/metaheuristic approaches that rely on the randomisation of the search procedure in the vast search space. By contrast, out approach offers deterministic reproducibility of solutions since the domain of patterns allows for full enumeration of solutions. However, it must be noted, that although our proposed method provides competitive and transparent results, it does not guarantee the global optimum. This is because the selection of non-zero cost patterns that are used in a specific scheduling process is guided only by a (rational) notion of making use of cheaper patterns first.

REFERENCES

Aiken, L.H, Clarke, S.P, Sloane, D.M, Sochalski, J and Silber, J.H. 2002. "Hospital nurse staffing and patient mortality, nurse burnout, and job dissatisfaction," The Journal of American Medical Association. vol. 288. no. 16. pp. 1987-1993.

Bard J. and Purnomo H.W. 2005. "Preference Scheduling for Nurses using Column Generation". *EJOR*. 164: 510-534.

Bargiela A., 1985. "An algorithm for observability determination in water-system state estimation", IEEE Proceedings Part D. 132. 245-249.

Bargiela, A., and Pedrycz, W. 2002. “Granular Computing – An Introduction”, Kluwer Academic Publishers. 2002. http://dx.doi.org/10.1007/978-1-4615-1033-8

Bargiela, A. and Pedrycz, W. 2008. “Toward a theory of Granular Computing for human-centred information processing”, IEEE Trans. On Fuzzy Systems. 16(2): 320-330. http: //dx.doi.org/10.1109/TFUZZ.2007.905 912

Baskaran Geetha, Bargiela Andrzej, Qu Rong. 2009. “Hierarchical method for nurse rostering based on granular pre-processing of constraints”, *Proc. 23rd European Conference on Modelling and Simulation, ECMS*, Madrid, Spain, pp.855-861, June 2009, (doi: 10.7148/2009-0855-0861).

Baskaran, G., Bargiela, A., Qu, R. 2012. “From Simplified to Detailed Solutions to the Nurse Scheduling Problem”, *25th European Conference on Operational Research, EURO, Session TC-14*, p.134-135, Vilnius, Latvia, July 2012.

Bester, M, Nieuwoudt, I. and Vuuren, J.H.V. 2007. "Finding good nurse duty schedules: a case study", Journal of Scheduling. vol. 10. no. 6. pp. 387-405,

Blythe, J, Baumann, A, Zeytinoglu, I, Denton, M. and Higgins, A. 2005. "Full-Time or Part-Time Work in Nursing: Preferences, Tradeoffs and Choices", Healthcare Quarterly. vol. 8. no. 3. pp. 69-77.

Burke E., De Causmaecker P., Vanden Berghe G. and Van Landeghem H.2004. “The State of the Art of Nurse Rostering”. *Journal of Scheduling.* 7(6). 441-499.

Chase, M. and Kohlweiss, M. 2011. “ A Domain Transformation for Structure-Preserving Signatures on Group Elements”, IACR Cryptology ePrint Archive 2011: 342 .

Celia, A.G. and Roger, A.K. 2010. “ The nurse rostering problem: A critical appraisal of the problem structure”, Europeran Journal of Operational research 202(2010) :379-389. (doi:10.1016/j.ejor.2009.05.046)

Cheung, G., Ishida, J., Kim, W., Kubota, A., Ortega, A. 2011. “Transform Domain Sparsification of Depth Maps using Iterative Quadratic Programming," IEEE International Conference on Image Processing, Brussels, Belgium, September 2011.

Cheung, G., Kim, W., Ortega, A., Ishida, J., Kubota, A. 2011."Depth Map Coding using Graph Based Transform and Transform Domain Sparsification", IEEE International Workshop on Multimedia Signal Processing, Hangzhou, China, October 2011

Costa, G. 1996. “ The Impact of Shift and Night Work on Health”, Appl. Ergonomics. 27. 9-16.

Gino J.L. , Mobasher, A., Murray J.C., 2012. “Multi-objective Nurse Scheduling Models with Patient Workload and Nurse”, Preferences Management 2012. 2(5): 149-160 DOI: 10.5923/j.mm.20120205.03.

Isken, M.W. and Hancock, W.M. 1998. “Tactical staff scheduling analysis for hospital ancillary units”. J Soc Health Syst 5:11.

Knauth, P. 1996. “ Design Better Shift System”, Appl. Ergonomics. 27. 39-44.

Kim, J., Jones, K. and Horowitz, M. 2007. “Variable domain transformation for linear PAC analysis of mixed-signal systems”, Paper presented at the International Conference on Computer-Aided Design. ICCAD , 05 - 08 Nov 2007. San Jose, California, USA.

Lim, H.T., and Ramli, R. 2010. “Recent Advancements of Nurse Scheduling Models and A Potential Path”, Proceedings of the 6th IMT-GT Conference on Mathematics, Statistics and its Applications (ICMSA2010). Universiti Tunku Abdul Rahman, Kuala Lumpur, Malaysia

Payne, J.F, Bruce, B.B, Lee, L.B, and Yeh, S. “ Logarithmic transformation of spectral-domain optical coherence tomography data in uveitis-associated macular edema. Investigative Ophthalmology & Visual Science, November 2011, Vol. 52, No. 12: 8939–8943.

Pedrycz W, Smith M.H., Bargiela A. 2000. “Granular signature of data”, Proc. 19th Int. (IEEE) Conf.NAFIPS'2000, Atlanta. July 2000; 69-73. http://dx.doi.org/10.1109/NAFIPS.2000.877387

Stanley, L. 2001. “Optimal Shape Design Using Domain Transformations and Continuous Sensitivity Equation Methods”, System Modelling and Optimization. Volume 258 of IFIP Conference Proceedings. page 301-316. Kluwer.

Ulrich, C. et al. 2002. "The nursing shortage and the quality of care,", The New England Journal of Medicine. vol. 347. no. 14. pp. 1118-1119.

AUTHOR BIOGRAPHIES

GEETHA BASKARAN was born in Melaka, Malaysia. She is an Assistant Professor at the University of Nottingham, Malaysia Campus. She is a member of the Automated Scheduling and Planning research group in the School of Computer Science at the University of Nottingham. She is currently pursuing her PhD studies here focussing on Nurse Scheduling. Her main research area include nurse scheduling, domain transformation, information granulation, heuristic, IP.ILP, matrix exploration.

ANDRZEJ BARGIELA is Professor in the School of Computer Science at the University of Nottingham. He served as President of the European Council for Modelling and Simulation (ECMS) during 2002-2006 and 2010-2012. He is Associate Editor of the IEEE Transactions on Systems Man and Cybernetics and Associate Editor of the Information Sciences. His research involves investigation into Granular Computing, human-centred information processing as a methodological approach to solving large-scale data mining and system complexity problems.

DR RONG QU is a Lecturer in the School of Computer Science at the University of Nottingham. She gained her PhD in Computer Science from the University of Nottingham in 2002. Her main research areas include meta-heuristics, constraint programming, IP/ILP, case based reasoning methodologies and knowledge discovery techniques on scheduling, especially educational timetabling, healthcare personnel scheduling, network routing problems and graph colouring. In total she has more than 30 papers published or to appear at international journals and peer-reviewed international conferences. Dr Qu is also a guest editor for special issues at the journal of Memetic Computing and the Journal of Scheduling, and the program chair of several workshops and an IEEE symposium.

A TUTORIAL ON MODELLING CALL CENTRES USING DISCRETE EVENT SIMULATION

Benny Mathew
Innovation Lab – Performance Engineering
Tata Consultancy Services
Quadra-II, Hadapsar, Pune, India 411028
Email: benny1.m@tcs.com

Manoj K. Nambiar
Innovation Lab – Performance Engineering
Tata Consultancy Services
Gateway-Park, Andheri, Mumbai, India 400093
Email: m.nambiar@tcs.com

KEYWORDS
Discrete Event Simulation, Workforce Planning, Call Centre Modelling, Manpower Planning, Skill-Based Routing, Multi-Skill Call Centre

ABSTRACT

Arriving at an optimal schedule for the staff and determining their required skills in a call centre is imperative to balance the conflicting requirements of delightful customer experience, high employee satisfaction and low cost. Due to the complex nature of modern call centres, simulation modelling is increasingly being used to predict their performance. We have modelled a call centre using our in-house discrete event simulation tool called DESiDE.

This paper describes how every component of call centres were modelled as simulation resources. This paper also describes the changes that had to be made to DESiDE in order to handle the special requirements of call centre modelling and also the metrics used by call centres.

1. INTRODUCTION

Companies have realized the importance of service in order to attract and to retain customers. Over the years, call centres have become the preferred channel in providing service to customers. At a call centre, arriving at optimal level of staffing, their schedule and skills is essential for achieving high level of customer satisfaction and at the same time it is necessary to keep costs low. In current practice, most call centres use analytical models developed by Erlang and Palm to arrive at staffing requirements. These models are ideal during initial operations of a call centre when there is little information available and it is necessary to make assumptions. However, as more and more information of the call centre gets available, use of simulation will yield more accurate results. Using simulation one can remove assumptions made in analytical models and one can also factor in more complex behaviour of call centres. In this paper we describe how this complexity was handled while modelling each resource of a call centre. For simulation we are using an in-house discrete event simulation tool called DESiDE. This paper also describes some of the changes/additional components that were required to make DESiDE handle modelling and simulation of call centre and also report the call centre metrics.

2. CALL CENTRE TERMINOLOGY

A *Call Centre* is a centralized office used for the purpose of receiving and transmitting a large volume of requests by telephone. A call centre is operated by a company to administer incoming product support or information inquiries from consumers. Outgoing calls for telemarketing, clientele, product services, and debt collection are also made. In addition to a call centre, collective handling of letters, faxes, live chat, and e-mails at one location is known as a *Contact Centre*.

2.1 Call Centre Components

Figure 1 shows the components of a typical call centre. Inbound calls are those initiated by customers calling in to the centre (Gans et al. 2003). If all trunk lines are busy, the call will be *blocked*, else the call is first answered by an Interactive Voice Response (IVR) unit. IVR is a technology that allows a computer to interact with humans through the use of voice and keypad inputs. Customers may be able to complete the service interaction at the IVR. If this case, the calls are passed from the IVR to an Automatic Call Distributor (ACD). An ACD is a specialized switch designed to route each call to an individual agent; if no qualified agent is available, then the call is placed in a queue. A queued customer may *abandon* without receiving service.

In a multi-skill call Centre, we distinguish various call types, and we distinguish agents by their skill-set. Skill-set is the set of call types which an agent can handle. Skill-Based Routing (SBR), or simply routing, refers to rules (programmed in the ACD) that control the agent-to-call and call-to-agent assignments in real time.

If more than one agent with requisite skill is available, agent selection criteria comes into picture. The selection criteria can be programmed in the ACD. These methods are described in detail in section 4.1.6.

2.2 Call Centre Metrics

Though there are many Call Centre metrics, only those influencing number of staff and skills required are listed below:

Proceedings 27th European Conference on Modelling and Simulation ©ECMS Webjørn Rekdalsbakken, Robin T. Bye, Houxiang Zhang (Editors)
ISBN: 978-0-9564944-6-7 / ISBN: 978-0-9564944-7-4 (CD)

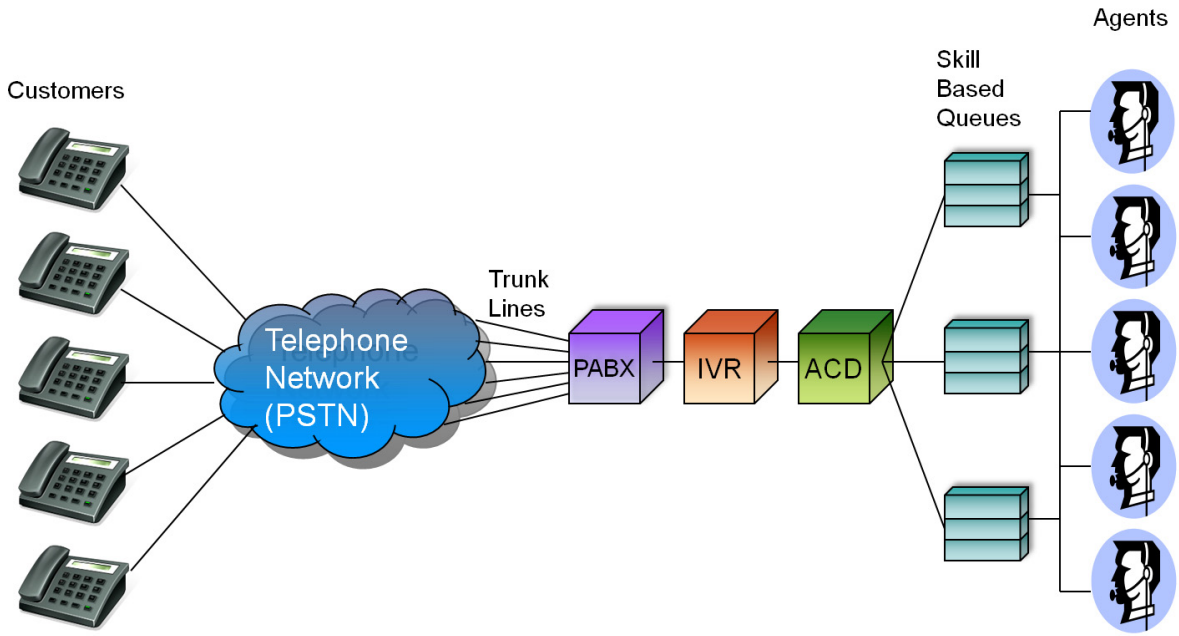

Figure 1: Call Centre Terminology

Blockage: Indicates what percentage of customers will not be able to access the centre at a given time due to insufficient network facilities in place. Most centres measure blockage by time of day or by occurrences of "all trunks busy" situations (Reynolds 2003).

Abandon Rate: Percentage of calls abandoned while waiting to be answered. Abandon rate is not typically a measure associated with e-mail communications, as e-mail does not abandon the "queue" once it has been sent, but it does apply to web-chat interactions.

Average Speed of Answer(SOA): Average time (usually in seconds) it takes for a call to be answered by the service desk. This is one of the most important metrics as far as customer satisfaction is concerned. The percentile value of SOA is called as *Time Service Factor (TSF)*. 80/20 TSF means that 80 percent of the customers have to wait for less than 20 seconds to speak to an agent.

Service Level: Percentage of calls answered within a defined timeframe. TSF is a hence a service level metric.

Agent Occupancy/Utilization: Agent occupancy is the measure of actual time an agent is busy on customer related work as compared with available time. This is calculated by dividing workload hours by staff hours.

Staff Shrinkage: The amount of time staff is unavailable for handling calls due to training, time off, breaks, etc.

Average Call Handle Time: Average time taken by agent to complete a call.

Cost Per Call: This is usually the cost of staff cost per call. However, some call centres may also include other costs like cost of telecom infrastructure, power and other rents.

3. ANALYTICAL AND SIMULATION MODELLING

Analytical models of call centres developed by Erlang (Angus 2001) and Palm (Mandelbaum and Zeltyn 2005) have served the telecommunications industry since the publication of Erlang's paper in 1917. Several enhancements of these models have also been made in order to address the complexities of a modern call centre (Garnett and Mandelbaum 2000, Garnett et al. 2000 and Jouini et al. 2006). These models are used for planning number of agents required, their skills and the schedules they should be following to meet acceptable service levels for projected call volumes.

Simulation is then used to validate the analytical model. Simulation is also used to conduct what-if analysis so as to manage and improve the call centre operations and to plan ahead, in the face of potential scenarios (Anton et al. 2002). The reasons for using simulation is effectively summarised in Bouzada's (2009) paper. In this paper he concludes with the following reasons for using simulation: (i) it is possible to include more details of the operation, to use statistical distributions more compatible with the input data and to have the model closer to reality, assuring the collection of more accurate results; (ii) the service level computed by Erlang formulas is usually underestimated, mainly because these formulas ignore the calls abandonment; (iii) other performance indicators (not available while using analytical approaches, as the abandonment rate) can be evaluated, presented and analyzed; (iv) minimum and maximum values of each important indicator can be obtained, the analyst not being restricted to the average values as when using the Queue Theory; (v) a better understanding of the operation is achieved with the adoption of the

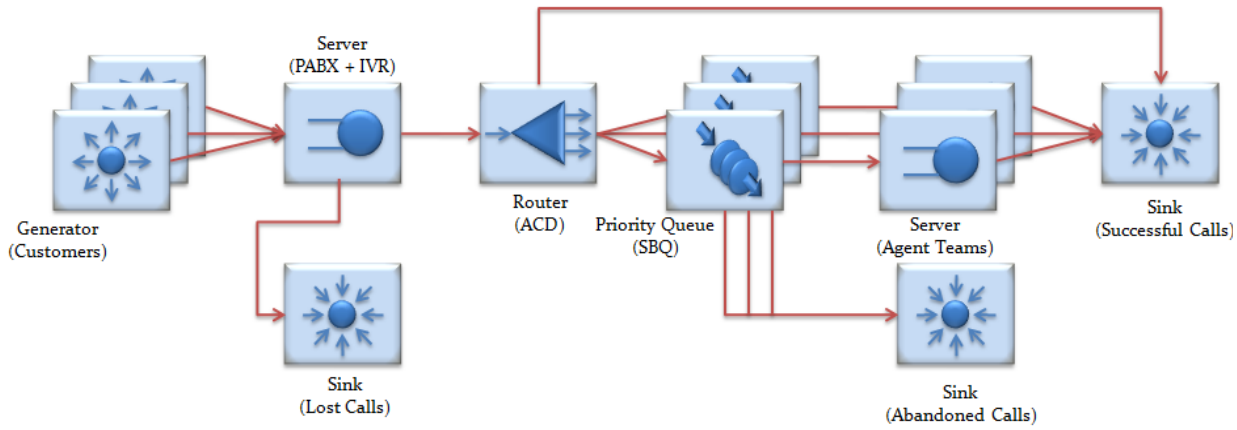

Figure 2: Queuing Network Diagram of Call Centre

experimental approach, which provides the possibility to dynamically follow up the system behaviour and its performance indicators behaviour and, therefore, understand why the queues are being formed and the reason why the waiting time is high, for example, while throughout the Erlang methodology it is possible to see only the generated outputs (numeric indicators) in relation to the provided inputs, making more difficult the complete comprehension of the operation; (vi) the communication can become easier via the use of graphic animations.

4. SIMULATION MODELLING OF CALL CENTRES

While there is sufficient literature on how simulation modelling has helped in improving accuracy of call centre performance predictions (Brigandi et al. 1994, Akhtar and Latif 2010, Mehrotra and Fama 2003), there is very little or no material on how the complexities of a call centre have been tackled in the modelling environment. Also, not all factors that affect performance of a call centre have been covered. For example, there is little or no literature that deals with modelling of misdirected calls.

We at TCS are using DESiDE to model and predict various call centre metrics. Though DESiDE is a generic discrete event simulation tool, a customized version has been built to carry out call centre simulation.

4.1 Call Centre Resource Models

A queuing network representation of a call centre is shown in Figure 2. Each component shown in the figure is modelled as discrete event resource in DESiDE. During simulation the attributes of these resources can be changed. The attributes (also called parameters in certain simulation tools) of each resource influence the resource's behaviour. This enables creating different scenarios and carrying out what-if analysis. On completion of the simulation, a report is generated that comprises the various metrics of a call centre. The various resources modelled in DESiDE and their attributes are listed below:-

4.1.1 Customer

The Customer resource generates the entities that represent incoming calls to a Call Centre. A Call Centre simulation will have several resources of Customer type. Each one generates entities that demand one particular skill on the part of the agent. This is represented by class of entity. The Customer resource also has the following attributes:

Inter-arrival Time[#]*:* Represents time between arrival of calls and is expressed as random distribution. In case number of arrivals is specified for 15/30 minute durations, then the inter-arrival distribution is limited to options of Deterministic or Exponential. Note that in simulation, the end state of one period automatically becomes the starting state of the subsequent period.

Percent High Priority: Represents percentage of calls made by high priority customers.

Retrial Percent: Percentage of customers that will retry calls in case previous attempt did not get through because all lines were busy

Retrial Time[#]*:* The time between retrials expressed as a random distribution.

[#] These attributes are used to generate time required to generate events or time required for completion of service. They can be selected from a rich set of distributions in DESiDE like Normal, Exponential, Lognormal. Weibull, Gamma, Uniform, Erlang. The distributions in DESiDE also supports transformations like bound, translate and scale.

In case data has not been fit to any distribution, the measured data can be provided to DESiDE in textual format. DESiDE will generate numbers that match distribution of data in the file.

Patience Time[#]*:* The time that a customer will spend on hold before abandoning the call expressed as random distribution.

4.1.2 PABX

This resource standing for Private Automatic Branch Exchange (PABX) keeps track of total number of live calls in the exchange. The attribute of PABX is the *number of trunk lines*. In case all trunk lines are busy, subsequent calls will get blocked till at least one of the lines is freed.

4.1.3 IVR

This resource emulates time spent by the customer at the IVR. The IVR has a single attribute, namely *IVR Time*[#]. This is distribution of service time or time spent by customer before being forwarded to agent. In certain cases calls may be completed at the IVR itself. Based on the user interactions with IVR the skill required on the part of the agent is decided and this interaction time will be different for different skill requirements.

4.1.4 ACD

One attribute of ACD is the *routing matrix* based on which the calls are routed to the correct Skill Based Queues (SBQ). This matrix maps class (skill) and priority of call to a particular team. The ACD does not directly route the call to team but to its associated queue. In case there is no mapping for incoming task, it is assumed to have been completed at the IVR itself.

Another attribute of ACD is *percentage of misdirected calls*. A certain percentage of incoming calls may get directed to an agent who does not have the requisite skill. This can happen due to wrong option selected by the caller or due to wrong interpretation by the speech recognition software in the IVR.

4.1.5 SBQ

The ACD forwarded calls wait at the Skill Based Queues (SBQ) till an agent with requisite skill is available. The check for free agent is triggered whenever a new call is queued at SBQ or when an agent arrives either at time his/her shift starts or after a break and also when an agent is freed after completing a call. An SBQ does not have any user settable attributes.

4.1.6 Team

The attributes for team are of two types, one applicable for all the entire team and another set that has to be provided individually for each agent.

The attributes for the entire team are *agent handle time*[#]*, redirection time*[#] and *agent selection criteria*. The handle time will be different for each class of call. If more than one agent is available then the agent selection criteria comes into picture.

DESiDE supports the following options for agent selection criteria.

Uniform Call Distribution (UCD): An incoming call is routed to the agent has been idle for the longest time.

Expert Agent Distribution (EAD): An incoming call is routed to the agent who is best qualified to handle the call.

Least Occupied Agent (LOA): An incoming call is routed to the agent whose utilization is the least.

Least Skills: An incoming call is routed to the agent who has the least number of skills. Calls are allocated preferably to single skilled agent so as to preserve availability of agents who can handle more than one skill

Least Cost: Calls are allocated to available agent costing the least in terms of wages drawn.

Mix of agent selection methods is also possible based on how busy the call centre is. For example at low loads (say less than 60% of agents are busy), UCD can be used and when the call centre load increases, we could use a more advanced strategy like EAD. Note that only few of the above options are usually available in standard call centre hardware.

The attributes that need to be provided for individual agents are:

Schedule: Each agent can follow different schedule in terms of arriving and leaving from work as well as having breaks.

Skillset: An agent can be specialised or cross-trained. A specialised agent will take only one type of call (corresponding to one SBQ). A cross-trained agent can handle more than one type of call and hence answer calls coming to more than one SBQ. Skillset for an agent is defined as the subset of call types that the agent can handle.

Expertise: To account for variation in the level of expertise of agents, one can set an expertise factor for each agent. For arriving at service time distribution, one can take data of average performing agents. These agents are then given expertise factor of 1. Better performing agents are given expertise factor greater than 1 and lower performing or trainee agents are given expertise factor lower than 1. This is particularly useful when a batch of inexperience agents join (expertise factor less than 1) or a batch of agents undergo special training (expertise factor greater than 1).

Hourly Wages: The hourly salary that the agent receives.

4.2 Call Centre Simulation

Before the simulation can begin, values need to be assigned to the attributes of all the call centre resources. Apart from all the attributes, the simulator also requires the number of repetitions.

Since DES depends upon the generation of pseudo-random numbers, the longer the simulation runs more confident we have on the simulation results. The solution takes input data of one week and carries out the simulation. This simulation is repeated multiple times in order to improve the confidence in the simulation results. At the end of the simulation, the various metrics of call centre like time to answer, agent utilization, total cost, and number of blocked and abandoned calls are reported. In the report, the confidence level of each metric is also mentioned. The confidence level is calculated using method of batch means (Law 1977). In case the desired confidence level is not met, the simulation is rerun after increasing the number of repetitions.

Simulation can be used to carry out complex what-if analysis. The attributes of the resources can be changed in order to generate many scenarios. For example one can examine the impact on cost and customer service level if the schedule is modified (through change in shift timing or staggering of breaks), if a few agents are cross-training, if agents efficiency changes (through training or as result of new agents joining), if agent selection criteria is changed and also if there is a dedicated team to handle high-priority customers.

Using the simulator, a study (Mathew and Nambiar 2012) was conducted to find how call centres performance metrics are affected by agent efficiency, handle time distribution and call-to-agent allocation criteria on the call centres performance and some interesting findings were reported.

5. DESiDE CUSTOMIZATION

Given that DESiDE is a generic DES tool, and call centres have very different metrics requirements, there were many changes required to make modelling and reporting easier. Mainly the changes required were related to metric and calculations. Other changes were made to enable data entry and reuse and libraries were added to support the complex call to agent allocation logic. Some of these customizations are listed below.

5.1 Excel Based Input and Reporting

Section 4 describes the various resource models and their attributes. Given that the attribute set is so large, it is difficult to enter such a large volume of data every time through a graphical interface (GUI). Hence, instead of developing a GUI, an excel spreadsheet serves to provide input data for simulation. To begin with, workforce managers/analysts are already familiar in using Excel spreadsheets with built-in Erlang calculators and hence it is easy for them to adapt. Using Visual Basic for Applications (VBA) scripts makes it possible to validate user entered data. When reporting time, work duration, breaks, meetings and skills available of each agent is provided, VBA scripts automatically display how many agents and with what skills are available at 30 minute intervals. This aids the user in arriving at the initial roster for agents.

Once the simulation is completed, the copy of excel input file is created and new tabs are inserted into this excel file. This new file serves as the report file with the results available in the newly inserted tabs. As a result, both inputs of simulation as well as results of the simulation are available in the same file making it easier to refer later.

5.2 Quantile Reporting

One important metric that represents performance of a call centre is the percentile value of speed of answer (SOA). Unlike mean and standard deviation that requires only single pass of data, calculations of quantiles like percentiles require several passes of the data. Hence individual observations are required to be stored till the simulation ends. Since we require to report quantiles every 30 minute for each skill, this not only/ would have resulted in large memory overhead, but also lot of CPU time for calculation at the end of the simulation.

This problem has been addressed using the P^2 algorithm (Jain and Chlamtac 1985). This algorithm has been used when 30 minute quantiles are required. For weekly quantile calculations, DESiDE provides choice of using either fixed-bin or variable-bin histogram approaches.

5.3 Call to Agent Routing

Since incoming calls from a customer and agents both have certain set of attributes to match, the complexity of code that allocates calls to the right agent in DES is on the higher side. Calls have priority and also require certain skill on the part of the agent. The agent side is even more complex since agents can have one or more skills, they work in shifts, and they can be on leave or take breaks

To handle calls waiting in SBQ, priority queues are used [Figure 3]. Separate queues are used for each skill. The calls are ordered first on priority and then by time of entry to the SBQ. These queues are in a wrapper class which provides means to insert and retrieve waiting calls. The wrapper call provides APIs to insert calls into corresponding skill queue and retrieve the first/head call from all the queues. The retrieved calls are in sorted order of priority and SBQ arrival time

Priority queues are used to handle free agents too. Free agents are agents who are currently available to take incoming calls. Here too, like with incoming calls, separate queues are used to keep information of free agents available for each skill. Since an agent can have multiple skills, an agent can be present in multiple skill queues. Within each queue, the order in which the agents are maintained depends upon the call allocation strategy. If the strategy is UCD, the agent who has been idle for the longest will have highest priority, while if the strategy is EAD, the priority will be based on the agent's efficiency. The different ordering of queues based on call

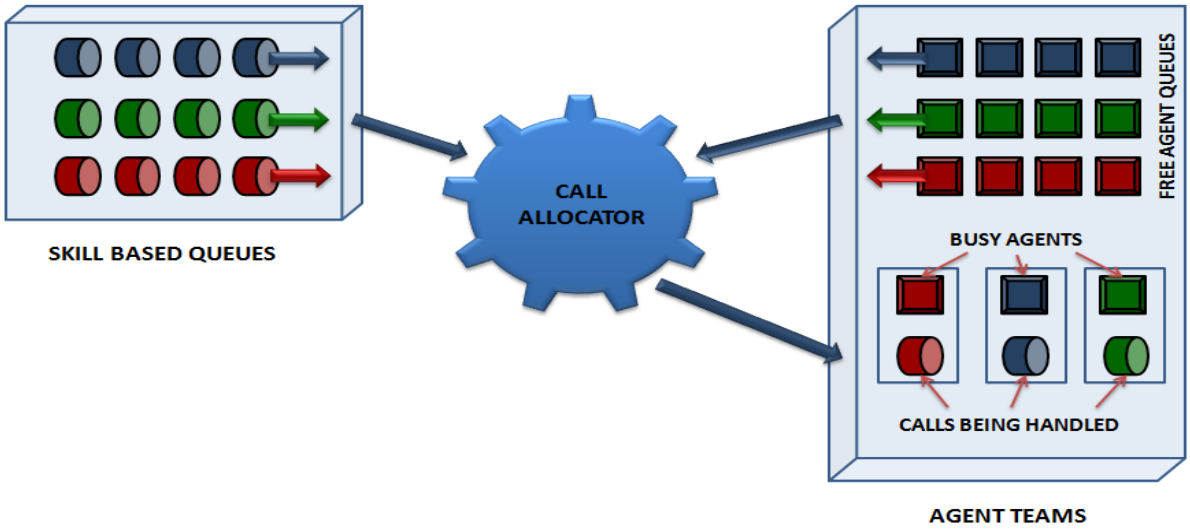

Figure 3: Call Routing

allocation strategy is achieved by using the *compareTo* (Naftalin and Wadler 2006) function available in Java. The priority queues with information of the free agents are maintained by a wrapper class. This wrapper class provides APIs to set allocation strategy, insert/remove the agent information from the priority queue. The wrapper class ensures that agent's information is available in all queues corresponding to the agent's skill. When an agent is not longer available to take new incoming calls, either because the agent is already attending a call or because it is time for break or meeting or end of shift, the wrapper class ensures that the agent is removed all skill queues

The call allocator [Figure 3] is responsible to allocate calls to free agents. The call allocator retrieves the calls in head of queue of each skill and checks corresponding free agent queues. In case there is a match, the call gets allocated. The call allocator carries out its function whenever there is a trigger. These triggers are new call insertions into wait queue and agent insertions into free agent queue. An agent will enter a free agent queue at the start of the days shift, after each break and on the completion of a call.

Note that Figure 3 is for representation purpose only. If there are agents in free list with a particular skill, there will not be any waiting calls requiring that particular skill.

6. CONCLUSION AND FUTURE WORK

This paper explains the reason why simulation modelling is increasingly being used to predict call centre performance. While there are many papers on theory behind modelling of call centres, the focus of this paper is more on implementation of the same in a DES environment. The complexities of modelling call centre resources in DES and the handling of call centre metrics are explained in detail in this paper.

While we have developed the solution using our own DES tool, the same can be implemented in any tool that allows flexibility in adding custom resource models and metrics.

Our call centre model supports a large set of attributes and some of these were covered in a sensitivity analysis study (Mathew and Nambiar 2012). We would like to extend this study to cover the remaining attributes. Such an extensive study will help in arriving at a guide which will list the most influential attributes in resolving a given call centre problem scenario.

REFERENCES

Akhtar, S. and M. Latif. 2010. "Exploiting Simulation for Call Centre Optimization". *Proceedings of the World Congress of Engineering, Vol III*, 2963 – 2970

Angus, I. 2001. "An Introduction to Erlang B and Erlang C". *Telemanagement #187*, 6-8

Anton J.; V. Bapat and B. Hall. 2002 "Call Centre Performance Enhancement Using Simulation and Modelling". ISBN-13: 978-1557531827, 32-35

Bouzada, M. A. C. 2009. "Dimensioning a Call Centre: Simulation or Queue Theory?". *The Flagship Research Journal of International Conference of the Production and Operations Management Society, Vol. 2 No. 2*, 34-46

Brigandi, A.; D. Dargon; M. Sheehan and T. Spencer. 1994. "AT&T's call processing simulator (CAPS): Operational design for inbound call centres". *Interfaces 24,* 6-28

Gans, N.; G. Koole and A. Mandelbaum. 2003. "A. Telephone Call Centres: A Tutorial and Literature Review". *Manufacturing and Service Operations Management,* vol. 5, 79–141

Garnett, O. and A. Mandelbaum. 2000. "An Introduction to Skills-Based Routing and its Operational Complexities". *Technion*, Israel.

Garnett, O.; A. Mandelbaum and M. Reiman. 2000. "Designing a call centre with impatient customers". *Bell Laboratories*, Murray Hill, N. J, 208-227

Jain, R. and I. Chlamtac. 1985. "The P^2 algorithm for dynamic calculation of quantiles and histograms without storing observations". *Communications of the ACM, Vol. 28 No. 10*, 1076-1085

Jouini, O.; A. Pot; G. Koole and Y. Dallery. 2006. "Real-Time Scheduling Policies for Multiclass Call Centres with Impatient Customers". *International Conference on Service Systems and Service Management*, 971-976

Law, A. M. 1977. "Confidence intervals in discrete event simulation: A comparison of replication and batch means". *Naval Research Logistics Quarterly, Volume 24, Issue 4*, 667-678

Mandelbaum, A. and S. Zeltyn. 2005. "Service Engineering in Action: The Palm/Erlang-A Queue with Applications to Call Centres". *Advances in Services Innovations,* Springer-Verlag, 17-48

Mathew, B. and M. K. Nambiar. 2012. "Cross Training - Is it a Panacea for all Call Centre Ills?". *Proceedings of the International MultiConference of Engineers and Computer Scientists, Vol II, IMECS*, 1543-1548

Mehrotra, V. and J. Fama. 2003. "Call Centre Simulation Modelling: Modelling, Challenges, and Opportunities". *Proceedings of 2003 winter Simulation Conference*, 135-143

Naftalin, N. and P. Wadler. 2006. "Java Generics and Collections". *O'Reilly Media*, ISBN-13: 978-0596527754, 31-36

Reynolds, P. 2003. "Call Centre Staffing: The Complete, Practical Guide to Workforce Management". ISBN-13: 978-0974417905, 180-196

AUTHOR BIOGRAPHIES

BENNY MATHEW is a Senior Scientist with the TCS Innovation Lab – Performance Engineering. Benny Mathew holds a Masters Degree in Reliability Engineering from Indian Institute of Technology Bombay, Mumbai. He has worked for 5 years in Symantec Software and 11 years in TCS in the area of Software Performance Engineering. His expertise lies in discrete event simulation of computer systems, call centres and business processes. He has also worked in the areas of performance measurement, testing and file systems performance, databases and middleware. His email address is benny1.m@tcs.com

MANOJ K. NAMBIAR is Chief Scientist with TCS Innovation Lab – Performance Engineering. Manoj holds a Bachelors Degree in Computer Engineering from the University of Mumbai. At TCS, he worked from 1994 for seven years in the design, implementation and support of ISDN BRI products of NORTEL Networks. Later he started work in the area of Performance Engineering of enterprise systems as a consultant before moving in 2006 to the Corporate Technology Office - R&D Unit where he is now serving as a council member in the Systems Research area and leading a research group in the field of Performance Engineering - monitoring, analysis & modelling. His e-mail address is: m.nambiar@tcs.com and his Web-page can be found at http://www.tcs.com/about/research/researchers/Pages/Nambiar-Manoj.aspx

The Influence of Management for breaking organizational paths - A Simulation Study

Felix Obschonka
Department of Management
Free University of Berlin
Garystrasse 21, 14195 Berlin, Germany
E-Mail: felix.obschonka@fu-berlin.de

Arne Petermann
Department of Management
Berlin University for Professional Studies
Katharinenstraße 17-18, 10711 Berlin, Germany
E-Mail: arne.petermann@duw-berlin.de

KEYWORDS

social simulation, agent based modelling, path dependence, path breaking, organization studies

ABSTRACT

We examine how means of management affect the breaking of organizational paths. Prior studies on the interplay between management and organizational path dependence explored the self-assertion of increasing returns in hierarchies, path dependence in management teams, influence of rigid cognitive maps on organizational change or the short-term thinking in strategic planning (Petermann, 2010; Beckman & Burton, 2008; Tripsas & Gavetti, 2000; Holtmann, 2008). But up to now there is only little known about how management affects breaking of organizational paths. As the strategic inflexibility of path dependence may result in inefficiencies for an organization, means for breaking paths are of interest not only for the theoretical concept of path dependence but also for practicioners. We contribute to close this research gap by developing an intraorganizational learning model of path constitution in a narrow sense and then examine the influence of integration, restructuring and turnover on their ability to break paths. In doing so we focus on an information and balance rule on micro level and observe emerging properties on system level.

Our findings indicate that the proposed means could potentially break paths with the probability of path break depending on the micro behaviour of actors. We further found that turnover on management level is the most effective approach and hint to difficulties in breaking paths.

INTRODUCTION

The notion of path dependence recently gained momentum in the field of management studies and especially in organization science (Sydow, 2009). Defined as a process where an initial contingent decision leads to a potentially inefficient lock-in situation due to increasing returns, path dependence emerges in organizations from interactions between actors.

Prior literature highlights the influence of management on organizational path dependencies. Recently by taking an institutional view on organizations it was shown that self-reinforcing complementary effects could prevail against hierarchies (Petermann et al., 2012). In a similar direction the case on the Bertelsmann Book Club underlined that short-term profit targets set by the top management undermined the search for new opportunities (Holtmann, 2008: 211). Lock-in because of cognitive rigidity on the top management team impeded Polaroid to adapt, although knowledge for coping with environmental change locally existed in the organization (Tripsas & Gavetti, 2000).

While we already have knowledge about the constitution of path dependence in organizations and the influence of management on organizational paths, the literature is inconclusive regarding the process of breaking paths. As most organizations ground on the principle of command and control it could be argued that escaping a lock-in is possible simply by the top management team setting a new strategy and aligning subunits or individuals in the organization through incentive systems. But as control over processes in an organization is limited by ambiguities, uncertainties or cognitive capabilities of actors, an effective alignment might prove difficult (Simon & March, 1954, Sydow et al., 2009). This ambiguity is reflected in empirical research: Whereas some studies suggest that the top level of an organization may restore the external fit of an organization (Siggelkow, 2001) others emphasize the difficulties inherent in breaking path dependencies through interventions from the management (Holtmann, 2008; Tripsas & Gavetti, 2000). Although the concept of path dependence includes the notion of deliberately breaking paths or unintentionally dissolving paths, studies of breaking path dependencies are still scarce (Sydow et al., 2009; Castaldi & Dosi, 2006; Tolbert, 1988; Siggelkow, 2001). Because of severe consequences stemming from path dependence it is a

Proceedings 27th European Conference on Modelling and Simulation ©ECMS Webjørn Rekdalsbakken, Robin T. Bye, Houxiang Zhang (Editors)
ISBN: 978-0-9564944-6-7 / ISBN: 978-0-9564944-7-4 (CD)

worthwhile endeavor to take a closer look at the interplay between path dependence and approaches the management could pursue to break organizational paths.

LITERATURE REVIEW AND RESEARCH QUESTION

Originally the concept of path dependence stems from a market perspective. Brian Arthur (1989) proved with a polya-urn model that if increasing return technologies compete for adoption in a market, chance may lead to a situation where a technology corners this same market and locks-out other alternatives. Thus, even under rational choice, sub-optimal technologies could dominate the market when there are increasing returns at play, due for example to external economies of scale or learning effects. This however is in sharp contrast to the view of neoclassical theory of markets stating that market forces will under certain conditions select the most efficient solution. David's (1990) historical analysis of the typewriter market is a vivid empirical example of such path dependence. A small event was responsible for the QWERTY keyboard design prevailing against other designs, although with the DVORAK keyboard a more efficient alternative was known. Other examples include the market penetration of the video home system, modern gasoline engines or light-weight nuclear reactors (Cusumano, Mylonadis, & Rosenbloom, 1992; Cowan, 1990). Despite its critics, path dependence is nowadays a widely acknolwedged phenomenon in the market penetration of technologies and the evolution of technologies (Liebowitz & Margolis, 1995; Dosi, 2006; Kauffmann, 1993; Arthur et al., 1987; Arthur, 2009; Rosenberg, 1994).

Apart from path dependencies in technologies Nelson & Winter (1982), March (1991), Levinthal (1997), Carrol & Harrison (1994), Cohen & Levinthal (1990) and Kogut & Zander (1992) highlight the occurence of path dependence in organizations. But deviating from the original definition the notion of path dependence in current organization research is mostly a broad label that merely emphasizes that "*history matters"*. Defining mechanisms proposed by Arthur (1989) for a process to be called path dependent like contingency, increasing returns or lock-in are mostly not reflected in current research on path dependence in organizations (Mahoney, 2000; Sydow et al., 2009). But as using the term path dependence to state that history matters will bring us close to a truism, a more narrow definition is appropriate when we want path dependence to be more than an ubiquitous history matters argument (Sydow et al., 2005; Teece et al. 1997; Antonelli, 1999). Sydow et al. (2009) therefore suggested a more distinct framework for organizational path dependence left ajar on Arthur's definition of technological path dependence.

A framework for organizational path dependence

To account for the peculiarities of social systems, the market model has to be adjusted towards an organizational context. One implication is that history always matters in organizations and social systems don´t exhibit the same characteristics as a lock-in on markets because of the ongoing variation in behaviours. Development phases are hence deviating from path dependence of technology adoption and are less strict. Sydow et al. (2009) developed a model of organizational paths describing organizational path dependence as a process consisting of three development phases. The *first phase* is characterized by a relative open situation where a range of choices are possible. Nevertheless because of imprinting effects, history matters from the beginning on and therefore is already limiting the scope of action. Instead of looking for new distant solutions, search is carried out locally in the proximity of the organizations domain. This is also in line with the notion of bounded rationality, which states that cognitive limitations of actors impede rational choice decisions and may therefore lead to suboptimal outcomes (Simon & March, 1963). Transition to the next phase is caused by an initially contingent choice serving as a triggering event or bifurcation (Kauffmann, 1993). One can refer to this bifurcation as a critical juncture because from there on it becomes more difficult to go back to prior alternatives. In *phase two* self-reinforcing effects lead to the emergence of a dominant solution in the organization. Repetition of choices with increasing returns crowd out other choices hence progressively restricting the capacity to act. Still, different choices are possible. Eventually in the *third phase* the self-reinforcing dynamics further reduce the scope of choice and lock the organization into a single potentially inefficient state. Even when the external environment changes, the pattern is reproduced and the organization is unable to adapt. One can think of this lock-in as an "underlying core pattern with some variation of practicing it" (Sydow et al., 2009: 695). Figure 1 aggregates the remarks on path constitution in a narrow sense:

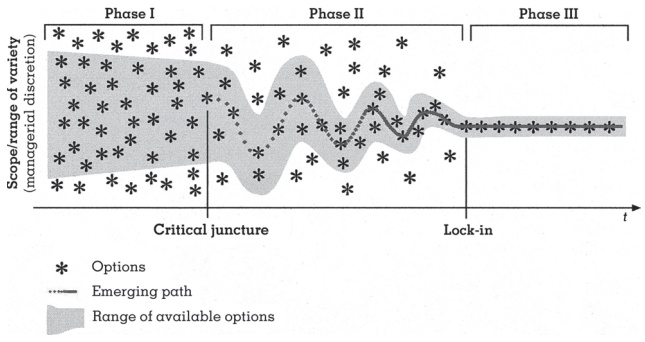

FIGURE 1: Constitution process of an organizational path in the Berlin Model (Sydow et al., 2009)

Breaking organizational paths

In contrast to physical or biological systems, in social systems individuals may recognise and act strategically to counter emergent processes (Gilbert, 1995). If path

dependence results in an inefficient system state an organization needs to recognize this and change in order to survive. This is easier said than done since self-reinforcing patterns on the micro level are still at work and make adaptation difficult.

In general one can think of two possibilities to overcome path dependence: unintentional dissolution of a path or intentional breaking a path. A well-known example for path dissolution is Intels switch from the memory business towards microprocessors (Burgelman, 1991). Although the top management team of Intel favored the memory business, consisting routines allowed the middle management to redirect ressources towards microprocessor manufacturing. While the dissolution of a path happens accidentialy path breaking requires awareness and purpose. As a path can be fatal waiting for path dissolution may not be appropriate.

Specfic means to break paths are conceiveable. For example, Sydow et al. (2005) propose discursive, behavioral and systemic approaches to break organizational paths but also highlight, *"that none of these approaches deals explicitly with issues of path dependencies, not to mention provides a theory of unlocking paths that builds upon a theory of path constitution and specifies the conditions under which a once chosen path may be unlocked*" (Sydow et al., 2005: 22). While they explicitly name approaches to break paths, they also admit that these approaches, although carefully derived from the literature, can only serve as a suggestion and need further research. Adopting an evolutionary economics point of view, Castaldi & Dosi (2006) propose the (purposeful) loss of organizational memory, restructuring of the organization, increasing cognitive dissonance between beliefs held in the organization and labour respectively management turnover as means to overcome the lock-in. But evidence on the effectiveness of these approaches is missing. To close this gap, we here pick means derived from literature of organizational change namely integration, restructuring and turnover. To give evidence of the effectiveness we later test these approaches with a computer simulation.

Integration

Partitioning of organzations in different subunits according to different tasks can locally maintain diversity and may break organizational paths through the integration of beliefs from formerly isolated subunits (March, 2004). For example, Fang et al. (2010) argue that semi-isolation of subunits enables an organization to achieve ambidextry and examine the optimal degree to which the subunits need to be interconnected. In their model selected actors serve as boundary spanners searching for new ideas in other subunits, when no satisfying solution can be found in the local neighborhood. Through this process new ideas spread through the organization, questioning the status-quo in the organization. This diffusion of beliefs among subunits could also break path dependencies. In practice, managers of organizations achieve semi-isolation of a subunits by setting up a skunkwork group, corporate venturing programs or working in a network organization (Fosfuri & Ronde, 2009; Block & MacMillan, 1995; Phelps, 2010). One empirical example of sucessfully breaking an organizational path in a broader sense through integration of ideas from a corporate venturing subgroup is the development of bioterials at DSM (Vanhaverbeke & Peeters, 2005). To what extent integration can be used to escape lock-ins arising from path dependence in a narrow sense still has to be answered.

Restructuring

In literature on organizational renewal restructuring is seen as a mean to overcome inertia, which is related to the concept of path dependence (Zajac & Kraatz, 2007; Carley & Svoboda, 1996; Burgleman, 1991; Bowman & Singh, 2007). For example, research on moving organizational members across subunits suggests that member rotation can be an instrument for stimulating the formation of new beliefs in groups if they share some common practices (Kane et al., 2005). While this may hint to a potential candidate for breaking a path, one has to bear in mind the differences between the formal and informal structure of an organization. Managers have the ability to set a formal structure in organizations by assigning actors to certain tasks. More precise, the formal structure is defined through job roles, responsibilities and communication structures between actors in an organization. Managers may change this composition in their role as organizational architects (Jacobides, 2006). Resulting recombinations facilitate flow of information and may stop disfunctional routines hence allowing the formation of new beliefs (Simon, 1962; Jacobides, 2006). But affected by the formal structure an informal structure is emerging through unintended patterns of interactions between actors. While managers could rapidly alter the formal organization, the informal organization may not be affected by the same extent (Miller and Friesen 1984, Nickerson and Zenger 2002). Interactions within an organization may perpetuate informally although the formal structure has been changed. This is in line with the argument brought forward by Sydow et al. (2009) that a path is developing behind the backs of actors and is goverened by hidden rules. To examine the possibility to break path dependence by restructuring through the moving of members we focus on informal interaction processes in the organization.

Turnover

A considerable amount of organizational knowledge exists in the beliefs of individual members. Labour turnover can therefore hamper the retention of knowledge in an organization (Hollenbeck, Ilgen, Sego, Hedlund, Major & Philips, 1995). If knowledge rests solely in individuals, organizational lock-in could be

overcome by selecting individuals with obsolete knowledge and replace them with individuals bringing in new beliefs. However knowledge is not only embedded in individuals but also in the interactions between them. Knowledge embedded in interactions is less likely to depreciate as knowledge embedded in individuals (Cohen & Bacdayan, 1994; Argote, Beckman & Epple, 1990; Argote, 1999). Retention of knowledge embedded in interactions is hence more likely to survive turnover. Nevertheless labour turnover may provide a reframing of current views in the organization eventually leading to change.

Besides initiating labour turnover changes of the composition in the management team are likely to result in modifications of the cognitive structure. As in a hierarchy the interpretation of the environment is influenced by management, bringing in new members could break paths. An empirical study on Liz Claiborne, a retailer and manufacturer of apparel, revealed that changes in the composition of the management team lead to the breaking of an organizational path in a broader sense (Siggelkow, 2001).

Research questions

Derived from the three approaches described above we want to contribute to the literature on organizational path dependence by answering the following research questions:

RQ1: Does the integration of isolated subunits affect an organizational path?

RQ2: Does restructuring of the organization affect an organizational path?

RQ3: Does (1) labour turnover or (2) turnover of management affect an organizational path?

In the subsequent section we present a model to answer the research questions at hand.

METHOD

Empirically examining path dependent processes is afflicted with methodological difficulties (Dobusch, 2012; Dosi & Castaldi, 2006). Vergne and Durand (2010) stress that evidence on the contingency condition inherent in the concept of path dependence is impossible to produce using field studies and that long run suboptimaility is hard to show because outcomes are sensitive to the choice of time frames. Along the same line Pentland et al. (2012) argue that it is not possible to reconstruct the development of a path if not being involved as an insider to the group and even then the memory of participants could be faulty and conclusions drawn may be wrong. To overcome these methodological problems, Vergne and Durand (2010) recommend the application of controlled laboratory experiments or computer simulations. We follow this argument by conducting computer simulation experiments to answer the research questions at hand. First we create a formal intraorganizational learning model of path dependence, second the model is extended by the three approaches mentioned above and third experiments are conducted by transferring the model into a numeric computer simulation.

An intra-organizational learning model

In general we regard organizations as complex adaptive systems where local interactions between individuals take place in order to achieve individual or organizational goals. In particular, individuals posses beliefs about an exogenous environment and may adopt beliefs of other individuals through interacting with them. Such change of beliefs presupposes besides the existence of multiple individuals the presence of different beliefs. Referring to this representation of an organization, the question arises *how* an individual selects another individual to interact with and *how* the updating of beliefs takes place.

Selection

Economic and behavioural models highlight the utility maximizing behaviour of individuals, where selection of information sources takes place according to an expected benefit. Organizational learning models take for example the performance, defined as the match between the environment and the individual set of beliefs, as the decision criteria for whom to learn from and update their beliefs according to the beliefs of superior organizational actors (Siggelkow, 2002; Levinthal, 1998; Lazer & Friedman, 2007; Miller, 2006; March, 1991). Reasons for individuals to update their beliefs according to a performance measure are that actors want to achieve their ends through superior beliefs (Katz and Kahn, 1978), reduce uncertainty (Radner, 1986), conserve or attaine power (Pfeffer & Salancik, 1978; Burns and Stalker, 1961) or just out of pure curiosity (Freedman, 1965).

Differently to a performance maximizing view a stream of literature in social psychology argues that individuals are maximizing their utility by learning from individuals simliar to them (Byrne, 1971; Friedkin, 1994; McPherson, Smith-Lovin and Cook, 2002). Actors actively seek for information endorsing their decisions and avoid contradicting information sources. Choosing individuals who are similar is preferred as it is reducing cognitive dissonance (Festinger, 1950, 1957, 1967). Literature on absorptive capacity gives as further explanation that learning is facilitated if individiuals posess similiar knowledge bases (Cohen & Levinthal, 1990). Another emphasize that growing cognitive distance between individuals impedes learning hence individuals prefer to update their beliefs from individuals with a small cognitive distance (Nooteboom et al., 2007).

In our intra-organizational model we integrate both views in one selection rule. Systems where actors update their beliefs in accordance with these competing processes are defined as balance and information systems (Frank & Fahrbach, 1999). Equation 1 describes such a simple selection rule:

$$\boldsymbol{selection} = \boldsymbol{inf}\left\{\begin{pmatrix}\boldsymbol{m}_{1,I_N}\\ \vdots \\ \boldsymbol{m}_{m,I_N}\end{pmatrix} \times \begin{pmatrix}\boldsymbol{m}_{1,E}\\ \vdots \\ \boldsymbol{m}_{m,E}\end{pmatrix}\right\} + \boldsymbol{sim}\left\{\begin{pmatrix}\boldsymbol{m}_{1,I_0}\\ \vdots \\ \boldsymbol{m}_{m,I_0}\end{pmatrix} \times \begin{pmatrix}\boldsymbol{m}_{1,I_N}\\ \vdots \\ \boldsymbol{m}_{m,I_N}\end{pmatrix}\right\} \quad (1)$$

The parameter *inf* describes the weight actors put on gathering new *information* and the parameter *sim* describes the weight actors put on updating beliefs from *similar* individuals. To account for organizational distance and local search processes individuals can only select direct neighbours to update their beliefs (Nooteboom, 2007; Lazer & Friedman, 2007).

Updating

After selection the updating of beliefs takes place. Updating describes the process of adopting beliefs of other actors. Commonly behavioural learning models set learning rates to characterize the speed with which beliefs are updated (March, 1991; Miller, 2006). We follow this notion, but instead of setting the rate as exogenous parameter we adjust the learning rate with regard to the similarity of actors. The more beliefs are shared among actors the easier learning takes place, emphasizing the importance of similarity for the acquintance of beliefs (Cohen & Levinthal, 1990). Equation 2 delinates the updating rule:

$$\boldsymbol{updating} = \left\{\begin{pmatrix}\boldsymbol{m}_{1,I_0}\\ \vdots \\ \boldsymbol{m}_{m,I_0}\end{pmatrix} \times \begin{pmatrix}\boldsymbol{m}_{1,I_N}\\ \vdots \\ \boldsymbol{m}_{m,I_N}\end{pmatrix}\right\} \quad (2)$$

Basic simulation model of path constitution

Following a building-block approach we base our model on an intra-organizational learning model of Miller et al. (2006). Basicall the model of Miller is extending March`s (1991) organizational learning model by allowing for direct interactions instead of exchanging beliefs through an organizational code. As in the original model our basic model consists of an *environment* and *individuals* interacting within an *organization*.

Environment: Organizations operate in a broader environment and need to adapt to changes in order to survive in the long term. It is assumed, that the environment is external and is not influenced through actions of the organization. In particular, actors are not enacting their beliefs on the environment (Weick, 1979). Similar to March (1991) the environment consists of *m* independent dimensions where a random value of 1 or -1 is assigned to each dimension with equal probability. We fix the number of dimensions to *m=75*.

Individuals: Individuals hold beliefs about the environment by assigning a value of -1 or 1 to a particular dimension. If an individual is not sure or does not know about a specific attribute of the environment a value of 0 is assigned.

Organization: An organization consists of n individuals with initially random beliefs of the environment. Individuals are positioned on a square grid and are locally interconnected giving them the possibility to directly interact with each other. Interaction happens according to the selection and updating mechanisms described above. Through interaction actors might develop new sets of beliefs that no actor possessed before (Argote, Gruenfeld & Naquin, 2001). We set the length and height of the grid to ten, hence *n=100* individuals in an organization.

With this model at hand all three phases of a path dependent process are reprodcued. *Phase 1* delinates a relatively open situation for an organization. Although each actor is carrier of its own history acquired through prior experiences when entering the organization on an organizational level the scope of choice is fairly open. The model captures this condition by assigning random actors to the organization, each with its own history, but without a socially shared history among the actors in the organization. Beliefs held by the actors in the beginning are conceived as prior experiences of the actors, as for example education or previous working experiences. During the course of time interactions between actors shape individual beliefs and contribute to the emergence of repetitive patterns. Based on the selection criteria actors in the model choose who to update from. When positive feedback effects through the updating of beliefs are occuring, the system will switch to a regime goverend by increasing returns. This commences in *phase 2* where self-reinforcing effects narrow the scope of action through a crowding out of possible choices in the system. Favorable interactions between actors are repeated more often and performed with higher reliability. The model takes this into account by an endogenous learning rate which is increasing according to the updating mechanism. In *phase 3* the self-reinforcing effects narrow the scope of choice to a small corridor, the lock-in. In the model interactions between actors can become locked-in when the updating of beliefs is fixed because self-reinforcing learning effects crowd out alternatives. These stable interaction patterns result in an equilbrium maintained indefinitley if no interventions are conducted.

The computer simulation is building on the JAVA programming language and uses the Eclipse IDE. If not stated differently, we pursue the Monte Carlo Method and iterate 150 simulation runs over a time frame of 300 steps.

Basic Model

As a basic model we take the intra-organizational learning model derived above as a starting point and keep the selection mechanism fixed with *inf=0.9* and *sim=0.1*. We then subsequently add environmental change, employee rotation as a representation of restructuring, a hierarchy directing orders on individuals and turnover of individuals on two different hierarchical levels.

Basic model with environmental change

Figure 2 reflects the results of the basic model and the model extended with environmental change. In the basic model an equilbrium is achieved in step t=75 with a performance[1] of 85 percent. We include in our model a shock in the environment, where the environment vector is randomly renewed. We expect a serious drop in performance for a path dependent organization. Figure 2 confirms this statement: Performance drops to 1% and remains at this level until the run ends.

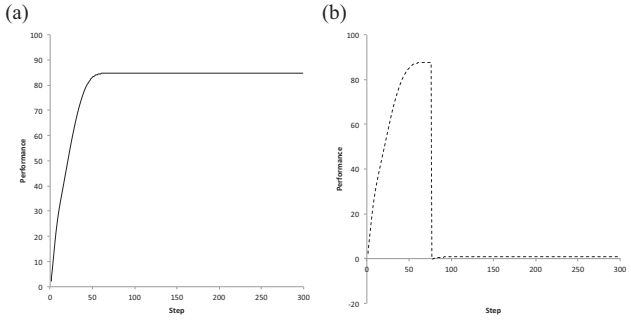

FIGURE 2: (a) Basic Model with inf=0.9 & sim=0.1 and (b) Model with environmental shock at t=75 for inf=0.9 & sim=0.1

Referring to the concept of aspiration levels, the management initiates interventions when performance falls below a historic aspiration level (Greve, 2003). Approaches to break an organizational path therefore will be conducted after the environmental shock takes place. We now compare the three different approaches with our basic model to draw conclusions about the ability to break organizational paths.

RQ1: Integration

By tuning the weights of the selection rule we can simulate the emergence of different organizational subunit structures. In our model, we define a subunit as an organizational entity where individuals share the same beliefs about the environment. Figure 3 shows the outcome for different values of *inf* on performance and on the emergence of subunits. The higher an individual puts the weight on *similarity* (*sim)*, the more groups emerge. Similarity hence causes a seggregation effect in the organization, leading to homogenous beliefs within a subunit and heterogenous beliefs across subunits.

[1] Performance is here defined as the mean sum of the product of individual beliefs and the according environmental dimension.

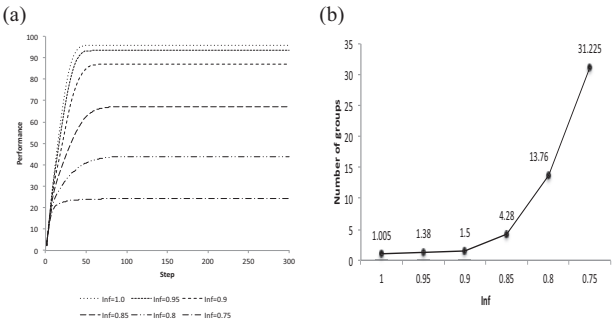

FIGURE 3: (a) Performance and (b) number of subunits for different values of inf

When performance suffers because of an environmental shock, the management may decide to formally integrate subunits. For example, it could integrate a business development or R&D subunit to promote the diffusion of beliefs in the organization (Fang, 2010; Tripsas & Gavetti, 2000). The informal structure of the organization, in our model represented as interactions between the actors, may impede integration because beliefs of other subunits are too dissimilar. Figure 4 shows the results of integration for performance and number of units in the organization.

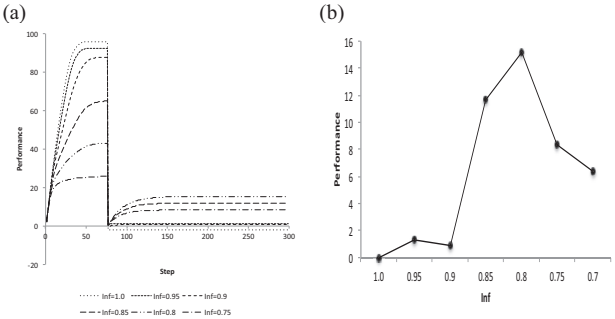

FIGURE 4: (a) Performance before & after environmental shock (b) optimal value of inf for integration

For *inf* =0.2 we found a maximum in performance and for *inf*=0 a minimum. At the maximum the number of groups decreased from 4.28 to 1.98 exhibiting an integration rate of 216%. We consider a path to be broken when the performance after the intervention exceeds a designated threshold value. We then calculate the probability of breaking a path by counting the number of runs exceeding the threshold and divide it by the number of runs. Figure 5 provides an overview of the probability with regard to different threshold levels.

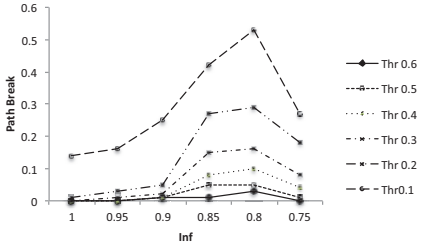

FIGURE 5: Comparsion of different performance thresholds for considering an organizational path break

While the trajectories are similiar from a qualitative perspective, the probability of breaking a path is decreasing significantly with an increase in threshold. As the concept of path dependence states that at least one superior alternative has to be found in order to consider a path to be broken we here assume that this is the case when the performance value exceeds 10%. In case of integration, we conclude that integration of subunits can break in 5% of the simulation runs an organizational path for *inf=0.1* confirming RQ1. As management can surpress variety and prevent integration these results may only hold if integration of subunits is supported (Rivkin & Siggelkow, 2006; Greve, 2006).

RQ2: Restructuring

We model restructuring by randomly rotating an actor with another actor of the organization and define a rotation probability of 0.1 as low and a value of 0.9 as high. Figure 7 exhibit the results for different values of *inf.*

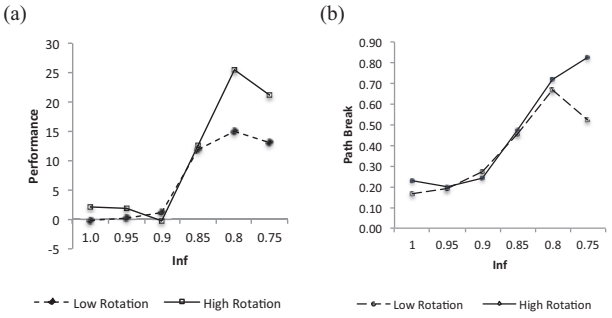

FIGURE 6: (a) Performance of the organization after restructuring and (b) probability of breaking paths for low and high rotation rates.

In general high rotation leads to higher performance values than low rotation. Particularly for *inf<0.85* the difference in performance becomes apparent. While the average performance is higher for a rotation rate of 0.9 the result for *inf=0.8* mirrors that it is not necessarily more appropriate to break paths. Performance values are more dispersed implying riskiness for high rotation rates. This may suggest that high efforts made in restructuring do not pay out. Nevertheless it does affect the probability of un-locking paths positively therefore confirming RQ2.

RQ3: Turnover

Turnover describes the process of replacing individuals in the organization with individuals from outside of the organization. We distinguish between labour turnover and turnover on the management level. In the case of labour turnover we randomly replace individuals with a probability of 0.01 (low) or 0.1 (high). For management turnover we choose 0.2 (low) and 1 (high) reflecting partial turnover and full turnover of management.

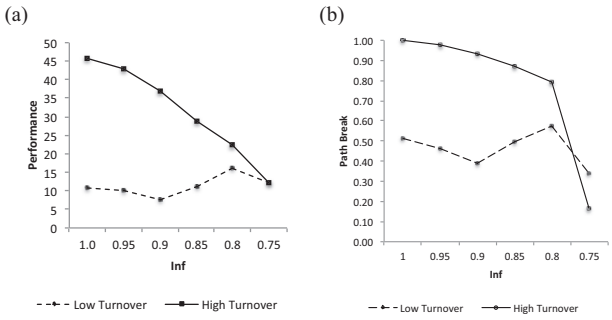

FIGURE 7: (a) Performance for high & low turnover values (b) Probability of breaking a path

High turnover of labour increases performance and the probability of path break for all *inf>0.75.* Performance is then decreasing with an increase in weight on *similarity.* This was expected as *similarity* ensures heterogenous beliefs among different groups and impedes proper integration of new beliefs. For low turnover the picture is different. The local maximum for *inf=1* reflects the positive effects of turnover in an organization due to the possibility that superior beliefs can more easily propagate through the organization. This effect is decerasing until the local minima at *inf=0.9* as it gets more difficult for beliefs to propagate through the organization. From 0.8<*inf<0.9* low turnover supports the integration of subunits while the performance drop for *inf=0.75* stems from the property that individuals are not able to integrate new beliefs because of high weight on similarity. We therefore confirm RQ3.1.

To test the effects of turnover on management level, we integrate a hierarchical management according to the dominant coalition in Miller`s (2006) model by assigning at the beginning the best performing 5% of the organization the status of a management member. The members of the management bargain a strategy according to a simple majority rule. Each individual in the organization updates beliefs on every dimension according to this strategy with a probability of 0.01 for low influence and 0.1 for high influence of the management. Aligning individuals to a strategy coordinates actors in the organization and improves performance as shown in Figure 6. Coming at the cost of lower belief variety in the organization this can hamper the possibility of endogenously breaking paths.

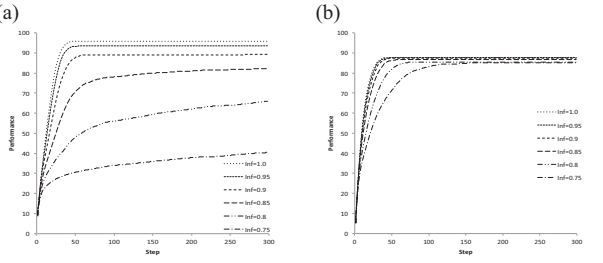

FIGURE 8: (a) Performance for low influence of management and (b) performance for high influence of management

We test if management turnover can break paths by conducting simulation runs for high turnover (all management members are replaced) and low turnover (20% are replaced) for each high and low influence of management. Actors in the organization start learning from the management after the shock occured. Figure 9 shows that high turnover is beneficial for performance and breaking paths irrespective the degree of influence.

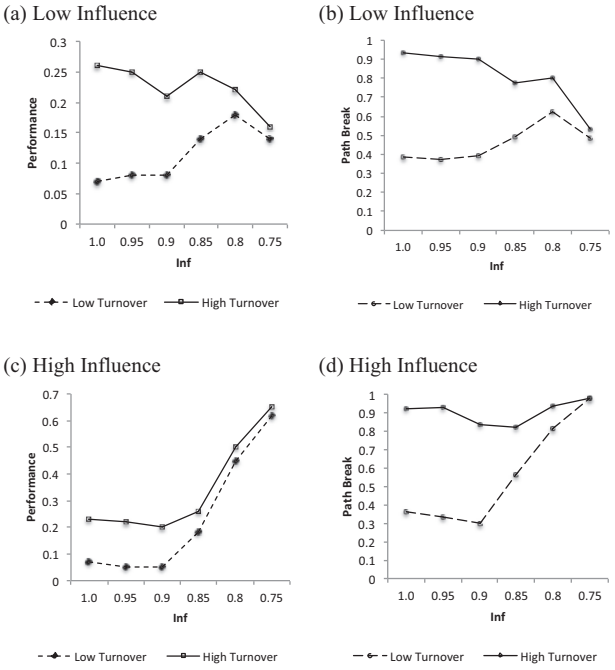

FIGURE 9: (a) performance for different degress of turnover and low influence of management and (b) probability of a path break (c) performance for different degress of turnover and high influence of management and (d) probability of a path break

The gap between high and low turnover becomes smaller for decreasing values of *inf*. As beliefs of management captured by the strategy are normative for actors in the organization the likelihood of overlapping beliefs is increasing with the influence of management. Moreover this overlap in beliefs increases the similarity between actors hence making it more likely for actors to learn from each other when the weight on *sim*>0. This can be comprehended as the coordination effect of strategy because the alignment allows actors to integrate superior beliefs from other subunits. Especially for low values of *inf* coordination is important to obtain high performance. Furthermore, as for high turnover the whole management is replaced with new members holding random beliefs the resulting strategy may not reflect the reality accurately. Hence the mere presence of shared beliefs, even if wrong, may achieve high performance because increasing similarity facilitates learning. High turnover and high influence of management make it more likely to break a path for low *inf* values compared to low turnover and low influence. When there is only little management succession and the influence of the management is low it is more likely that the path will persist. The findings indicate that turnover on management level affects the probability of breaking a path hence confirming RQ 3.2.

CONCLUSION

On the basis of a simulation model we demonstrated that each of the three approaches could potentially break organizational paths depending on the weights of similarity (*sim)* and information *(inf)*. Probability of path breaking for integration and restructuring are on average lower as for turnover. The main reason we discovered is that while turnover induces new beliefs hence increasing the variety in the organization, integration and restructuring draw on existing beliefs. Nevertheless we could show that paths can be broken endogenously through integration and restructuring. This confirms the argument of Pentland et al. (2012) that the same micro rules that caused path dependence may under certain conditions break paths. The results also emphasize the difficulties inherent in breaking paths by exhibiting constellations where the probability of breaking a path approaches zero. Table 1 summarizes the approaches according to their effectiveness of breaking path dependencies.

Approach	Integration	Restructure	Labour Turnover	Management Turnover
Probability	low	moderate	high	very high

TABLE 1: Probability of path break for different approaches

FURTHER RESEARCH

As computer simulations can only contribute but not substitute empirical research we propose to examine our findings empirically to overcome some of the limitations of the method applied. For example, one could explore the approaches in ongoing change processes qualitatively or conduct experiments with managers. Also one can think of more approaches to break path dependence as for example induced errors in communication (Walsh & Unger, 1981; March, 2006). We considered that a path is broken when the performance value exceeds 10%. Altering the level will yield different results about the impact of different interventions. Taking a higher value will decrease the chance of path break. Furthermore we used a very simple selection rule in the model. A complex rule could capture the behaviour of individuals in organizations more acurate. One can also think of different rule guided micro behavior besides the balance-information rule as for example conformity, opportunism or creativity and examine how these rules alter the outcome of the simulation. For the time being we work at further extensions of the simulation to test such approaches.

REFERENCES

Antonelli, C. (1999): "The economics of path dependence in industrial organization", International journal of Industrial Organization, 15. 643-675.

Arthur, WB. (1994): "Increasing Returns and Path Dependence in the Economy", Ann Arbor: University of Michigan Press.

Arthur, WB. (2009): "The Nature of Technology: What it is and how it evolves". The Free Press (Simon & Schuster).

Augsdorfer, P. (2005): "Bootlegging and path dependency". Research Policy, 34(1). 1-11.

Axelrod, R. (1997): "The Complexity of Cooperation" Princeton University Press, Princeton, NJ.

Becker, K. (2005): "Individual and organisational unlearning: directions for future research". International Journal of Organisational Behaviour, 9 (7). 659-670.

Beckman, CM; Burton, MD. (2008): "Founding the future: Path dependence in the evolution of top management teams from founding to IPO", Organization Science, 19. 3–24.

Block, Z.; MacMillan, IC. (1995): "Corporate venturing: creating new businesses within the firm". Harvad Business School Press, Cambrudge/MA.

Bowman, EH.; Singh, H. (2007): "Corporate restructuring: Reconfiguring the firm". Strategic Management Journal, 14 (1). 5-14.

Burgelman, RA. (1991): "Intraorganizational ecology of strategy making and organizational adaptation: Theory and field research". Organization Science, 2 (3). 239-262.

Burns, T.; & Stalker, GM. (1961): "The management of innovation". London: Tavistock.

Byrne, D. (1971): "The Attraction Paradigm". Academic Press, New York.

Carley, KM.; Svoboda, DM. (1996): "Modelling organizational adaptation as a simulated annealing process". Sociological Methods & Research, 25 (1). 138-168.

Carroll, GR.; Harrison, RJ. (1994): "On the Historical Efficiency of Competition between Organizational Populations." American Journal of Sociology, 100: 720-749.

Castaldi, C., Dosi, G. (2006): "The Grip of History and the Scope for Novelty. Some Results and Open Questions on Path Dependence" in A. Wimmer and R. Koessler, eds., Understanding Change, Palgrave.

Cohen, MD.; Bacdayan, P. (1994): "Organizational routines are stored as procedural memory: Evidence from a laboratory study" Organization Science 5(4). 554-568.

Cohen, WD.; Levinthal, DA. (1990): "Absorptive capacity: A new perspective on learning and innovation", Administrative Science Quarterly, 35 (1). 128-152.

Coleman, J. (1990): "Foundations of Social Theory". Cambridge, MA, and London: The Belknap Press of Harvard University Press.

Collins, D. (1998): "Organizational Change: Sociological Perspectives". London, UK: Routledge.

Cowan, R. (1990): "Nuclear Power Reactors: A Study in Technological Lock-in". The Journal of Economic History, 50 (3). 541-567.

Cusumano, MA; Mylonadis, Y.; Rosenbloom, RS. (1992): "Strategic Maneuvering and Mass Market Dynamics The Triumph of VHS over Beta". Business History Review, 66. 51-94.

Cyert, RM., March, JG. (1963): "A Behavioral Theory of the Firm". Prentice Hall, Englewood Cliffs, NJ.

David, PA. (1985): "Clio and the Economics of QWERTY". American Economic Review, 75. 332-337.

Dosi, G.; Marengo, L.; Fagiolo, G. (2003): "Learning in Evolutionary Environments," LEM Papers Series2003/20, Laboratory of Economics and Management (LEM), Sant'Anna School of Advanced Studies, Pisa, Italy.

Dosi, G.; Marengo, L.; Paraskevopoulou, E.;Valente, M. (2011): "The value and dangers of remembrance in changing worlds: a model of cognitive and operational memory of organizations". LEM Working Paper, in progress.

Egidi, M.; Narduzzi, A. (1997): "The emergence of path dependent behaviors in cooperative contexts". International Journal of Industrial Organization, 15. 677-709.

Fang, C.; Lee, J.; Schilling, MA. (2010): "Balancing exploration and exploitation through structural design: The isolation of subgroups and organizational learning. Organization Science, 21 (3). 625-642.

Festinger, L. (1950): "Informal social communication". Psych. Rev. 57, 271–282.

Festinger, L. (1957): "A Theory of Cognitive Dissonance". Stanford, CA: Stanford University Press.

Festinger, L. (1964). "Conflict, Decision, and Dissonance". Stanford, CA: Stanford University Press.

Freedman, J. (1965): "Preference for dissonant information" J. Personality and Soc. Psych., 2. 195–202.

Friedkin, NE.; Marsden, P. (1994): "Network studies of social influence". S. Wasserman, J. Galaskiewicz, eds. Advances in Social Network Analysis Thousand Oaks, CA. Sage, 1–25.

Fosfuri, A.; Ronde, T. (2009): "Leveraging resistance to change and the skunk works innovation". Jorunal of economic behavior & organization, 72(1). 274-289.

Giddens, A. (1984): "The constitution of society: Outline of the theory of structuration". Cambridge: Polity Press.

Gilbert, N. (1995): "Emergence in social simulation" in Artificial Societies: the computer simulation of social life, edited by N. Gilbert and R. Conte. London: UCL Press. 144-156.

Greve, HR. (2003): "Organizational learning from performance feedback: A behavioral perspective on innovation and change". Cambridge University Press.

Harrison, GA. (1988): "Human Biology: An Introduction to Human Evolution, Variation, Growth, and Adaptability". Oxford University Press: Oxford, U.K

Holtmann, JP. (2008): "Pfadabhängigkeit strategischer Entscheidungen. Eine Fallstudie am Beispiel des Bertelsmann Buchclubs Deutschland.". Gabler Verlag, Wiesbaden.

Kane, AA; Argote, L; Levine, LM (2005): "Knowledge transfer between groups via personnel rotation: Effects of social identity and knowledge quality". Organizational Behavior and Human Decision Processes, 96. 56–71.

Kauffman, SA. (1993): "Origins of order: Self-organization and selection in evolution". Oxford: Oxford University Press.

Katz, D.; Kahn, R. (1978): "The Social Psychology of Organizations". Wiley, New York.

Kenneth, KF.; Fahrbach, K. (1999): Organization culture as a complex system: Balance and information in models of influence and selection. Organization Science, 10(3). 253-277.

Kogut, B.; Zander, U. (1992): "Knowledge of the Firm, Combinative Capabilities, and the Replication of Technology," Organization Science 3(3): 383-397.

Lazer, D.; Friedman, A. (2007): "The network structure of exploration and exploitation". Administrative Science Quarterly, 52 (4): 667-694.

Levinthal, DA. (1997): "Adaptation on rugged landscapes". Management Science, 43 (7). 934-950.

Liebowitz, SJ.; Margolis, SE. (1995): "Path Dependence, Lock-in, and History". Journal of Law, Economics and Organization, Oxford University Press, 11(1). 205-226.

Mahoney, J. (2000): "Path dependence in historical sociology". Theory and Society, 29 (4). 507-548.

March, J.; Simon, HA. (1958): "Organizations". Wiley, New York.

March, JG. (1991): "Exploration and exploitation in organizational learning" Organization Science, 2 (1). 71-87.

March, JG. (2006): "Rationality, foolishness, and adaptive intelligence". Stratgeic Management Journal, 27: 201-214.

Miller, KD.; Zhao, M.; Calantone, RJ. (2006): "Adding interpersonal learning and tacit knowledge to March`s exploration-exploitation model". The Academy of Management Journal, 49(4). 709-722.

Miller, KD.; Lin, S. (2010): "Different truths in different worlds". Organization Science, 21(1). 97-114.

Monteiro, FL.; Arvidsson, L.; Birkinshwa, J. (2007): "Knowledge Flows Within Multinational Corporations: Explaining Subsidiary Isolation and Its Performance Implications". Organization Science, 19 (1). 90-107.

Nelson, RR.; Winter, SG. (1982): "An Evolutionary Theory of Economic Change". Belknap Press/Harvard University Press: Cambridge.

Nooteboom, B. (2007): "Cognitive distance in and between communities and firms: Where do exploitation and exploration take place, and how are they Connected?". Discussion Paper 2007 (4), Tilburg University, Center for Economic Research.

Ocasio, W. (1997): "Towards an attention-based view of the firm". Strategic Management Journal, 18. 187-206.

Pentland, BT.; Feldman, MS.; Becker, MC.; Liu, P. (2012): "Dynamics of organizational routines: A generative model". Journal of Management Studies, 49(8). 1484-1508.

Petermann, A. (2010): "Pfadabhängigkeit und Hierarchie: Zur Durchsetzungskraft von selbstverstärkenden Effekten in hierarchischen Organisationen". Berlin.

Petermann, A.; Klaußner, S.; Senf, N. (2012):

Organizational Path Dependence: The Prevalence of Positive Feedback Economics in Hierarchical Organizations. In: Troitzsch KG, Möhring M and Lotzmann U (eds.): In Proceedings 26th European Conference on Modelling and Simulation, Koblenz, p.721-730.

Pfeffer, J.; Salancik, J. (1978): "The external control of organizations" New York: Harper and Row.

Phelps, CC. (2010): "A longitudinal study of the influence of alliance network structure and composition on firm exploratiry innovation". Academy of management journal, 53 (4). 890-913.

Radner, R. (1986): Preface based on “Radner on Marschak” (1984). C. McGuire, R. Radner, eds. Decision and Organization; A Volume in Honor of Jacob Marschak University of Minnesota Press, Minneapolis. xxi.

Rosenberg, N. (1994): "Exploring the Black Box: Technology, Economics and History". Cambridge: Cambridge University Press.

Siggelkow, N. (2001): "Change in the presence of fit: The rise, the fall, and the renaissance of Liz Claiborne". Acad. Management Journal, (44). 838–857.

Siggelkow, N. (2002): "Evolution toward fit." Administrative Science Quarterly, 47. 125–159.

Siggelkow, N.; Levinthal, D. (2003): "Temporarily divide to conquer: Centralized, decentralized, and reintegrated organizational approaches to exploration and adaptation". Organization Science, 14. 650–669.

Suarez, FF.; Oliva, R. (2005): "Environmental change and organizational transformation". Industrial and Corporate Change, 14 (6). 1017-1041.

Sydow, J.; Schreyögg, G.; Koch, J. (2009): "Organizational path dependence: Opening the black box". Academy of Management Review, 34(4). 689-709.

Sydow, J.; Schreyögg, G.; Koch, J. (2005): "Organizational Paths: Path dependency and beyond". 21st EGOS Colloquium, June 30 – July 2, 2005, Berlin, Germany.

Tolbert, PS. (1988): "Institutional sources of organizational culture in major law firms". In L. G. Zucker (Ed.), Institutional patterns and organizations: 101–113. Cambridge, MA: Ballinger.

Tripsas, M.; Gavetti, G. (2000): " Capabilities, cognition, and inertia: evidence from digital imaging". Strategic Management Journal, 21 (10). 1147-1161.

Vanhaverbeke, W.; Peeters, N. (2005): " Embracing Innovation as Strategy: Corporate Venturing, Competence Building and Corporate Strategy Making". Creativity and Innovation Management, 14 (3).

Vergne, JP.; Durand, R. (2010): "The Missing Link Between the Theory and Empirics of Path Dependence: Conceptual Clarification, Testability Issue, and Methodological Implications". Journal of Management Studies, 47(4). 736-759.

Weick, KE. (1979): The Social Psychology of Organizing, 2nd ed. Random House, New York.

Zajac, EJ.; Kraatz, MS. (2007): "A diametric forces model of strategic change: Assessing the antecedents and consequences of restructuring in the higher education industry". Strategic Management Journal, 14 (1). 83-102.

AUTHOR BIOGRAPHIES

Felix Obschonka was born in Filderstadt, Germany and went to the Technical University of Berlin, where he studied Electrical Engineering & Business. He obtained his Diploma in Engineering in 2010. Before starting his doctoral studies he was working in multi-national companies, as a consultant and founded a leading VoIP-company. His research focuses on path dependencies in organizations and approaches to break or dissolve organizational paths. His e-mail adress is felix.obschonka@fu-berlin.de.

Arne Petermann is Professor of Management at the Berlin University for Professional Studies. In his research he focuses on organization, leadership, entrepreneurship and social simulation. His research results have been presented at the leading conferences in his field, have been recognized with a best paper award and are published in peer-reviewed Journals and books. He is also founder and CEO of Linara GmbH, a international HR agency for the European home care sector.

Agent-based simulation as a support for price-setting in passenger transport

Norman Kellermann
Freie Universität Berlin
Department of Business & Economics
Garystr. 21, 14195 Berlin, Germany
Email: norman.kellermann@fu-berlin.de

KEYWORDS

Agent-based Modelling, Pricing, Revenue Management, Passenger Transport, Prospect Theory, Path Dependence

ABSTRACT

Companies operating in passenger transport face the challenge that they cannot easily assess the effects of pricing decisions they take. Particularly, many incumbent European Railways are revisiting their traditional pricing structures based on static distance-based fares and develop new ways for pricing their services. Building on insights of behavioural pricing and Revenue Management, I investigate on alternative, more revenue-efficient pricing structures for a focal railway company given individual passenger price reaction behaviour and intramodal competition. First experiments with the model suggest that a limited quota for permanent special offers is counterproductive, while an increase in fuel price gets relatively quickly absorbed by the market.

MOTIVATION

Pricing is a public transport operator's key parameter for stimulating demand by – for instance – allowing lower fares in exchange for higher utilisation of capacity in off-peak periods. Within their long-standing history, European railways have developed a specific pattern for pricing their services: the standard railway tariff relying basically on the kilometre travelled. Liberalisation in the European railway sector was partly introduced to overcome "dissatisfaction with the price and quality of rail transport" (European Commission 1996: 3), hoping for similar effects as those observed in the airline and telecommunications branches. But up to the present, a large number of contemporary rail operators' pricing strategy remains quite far away from dynamic forms of pricing, even including newly-founded companies. On the other hand, many airlines are struggling with revenue management practices as competition leads them to a downward drive of their prices. Is there a more efficient way of pricing for railways beyond copying airlines and keeping the static tariff?

THEORETICAL BACKGROUND

Definitions

Belobaba (2009: 73) defines pricing in passenger transport as "the process of determining the fare levels, combined with various service amenities and restrictions […]". Tariffs in the railway sector are fares and conditions of carriage set by train operating companies. A tariff structure in this paper is seen as the conceptual framework for the collective fares of an operator. In the following, railway tariffing is examined within the framework of general pricing theory including revenue management approaches and the concept of path dependence.

Pricing: from production cost to revenue management

In management literature, explicit theoretical assumptions of how and when prices are set or changed are not always easily found. Primarily, problems of pricing are addressed in marketing science, where pricing is seen as the most prominent element of the marketing-mix.

While the price of a good was commonly perceived as the value of its production cost in the classic era of economic thought, neoclassical scholars introduced the concept of a market price fitting utility-based demand and cost-based supply. Before the equilibrium price is attained, a Walrasian auctioneer excludes any transaction. Otherwise, multiple equilibria differing from the theoretical optimum are possible (cf. Jaffé 1967; Bridel & Huck 2002).

Using insights from psychology, behavioural pricing theorists focus on understanding and explaining the complex individual processes triggered by price stimuli. Based on the theory of reference prices (Helson 1964; Monroe 1973), Kahneman & Tversky (1979) find evidence for irrational behaviour that stands in contrast to neoclassical assumptions on utility; and thus present an alternative utility concept with their Prospect Theory. Thaler (1985) further develops these insights to a theory on mental accounting. This way of accounting does not follow rational rules, but is deeply shaped by individual coding. As an example, see biased flat-rate and pay-per-use decisions observed by Lambrecht & Skiera (2006).

Revenue (or yield) management can certainly be seen as one of the most famous pricing practices in the last

Proceedings 27th European Conference on Modelling and Simulation ©ECMS Webjørn Rekdalsbakken, Robin T. Bye, Houxiang Zhang (Editors)
ISBN: 978-0-9564944-6-7 / ISBN: 978-0-9564944-7-4 (CD)

decades, as managing supply and demand through manipulation of product availability in time has spread to a variety of industries. Belobaba (2009) lists three "economic principles" (p. 76) for determining prices: cost-based, demand-based (i. e. pure price discrimination), and service-based (i. e. product differentiation) pricing. For Talluri & van Ryzin (2004), the innovation of revenue management consists in providing "technologically sophisticated, detailed, and intensely operational" (p. 4) methods of decision-making dedicated for increasing revenue.

Explaining rigidity: organisational path dependence

The concept of path dependence is a widely used approach in the social sciences. Building on the pioneering work of David (1985) and Arthur (1989), Sydow et al. (2009) define the phenomenon of path dependence for organisations "as rigidified, potentially inefficient action pattern built up by the unintended consequences of former decisions and positive feedback processes" (p. 696). Generally, a path-dependent process is characterised by a set of properties comprising contingency, a (limited) multiplicity of potential outcomes, self-reinforcing mechanisms, and lock-in. Sydow et al. (ibid) substantiate self-reinforcing mechanisms as coordination effects, complementarity effects, learning effects, and adaptive expectation effects. Being locked-in means for agents in the affected area that their scope of action is limited in a way that their agency can just reproduce the status quo. This stadium can be considered as at least potentially inefficient if it comes to a change in the environmental situation.

RESEARCH OBJECTIVES

Inertia and potential inefficiency of pricing is a topic that has so far been avoided by many scholars. Dutta et al. (2003) describe pricing as a "strategic capability" rarely addressed by researchers "because [they] assume that the processes by which prices are set or changed are relatively costless or simple […]" (p. 616). Miller & Page (2007) recommend research effort on the question how markets generally equilibrate: "Is there a coherent, plausible model that can help us understand the mechanism by which prices form in decentrali[s]ed markets?" (p. 243). The real-world process of price formation is obviously not the Walrasian one, nor can middle-range theories on individual price reaction fully explain it. Particularly, other than the concept of path dependence, conventional pricing theory lacks to explain the emergence of a persistent suboptimal pricing pattern. In contrast to the airline industry, revenue management problems have rarely been studied on passenger train operating companies (cf. Sato & Sawaki 2012). From their survey on railway revenue management literature, Armstrong & Meissner (2010) recommend to "bring passenger rail pricing to the same level that is [] seen in more mature areas of revenue management" (p. 19). This work is aimed at answering the question what price parameters would constitute a – ceteris paribus – superior tariff structure to the predominant distance-based, static portfolio for a contemporary passenger train operator. As a starting point for research on alternative options of pricing, the path formation process of the railway tariffing standard in Europe has been reconstructed using the path constitution analysis method outlined by Sydow et al. (2012). It can be shown that the described typical railway tariff remained a prevalent pricing pattern of European railways for decades despite of deteriorating economic situation of European railways since the late 1960s. The following research question results:

What railway tariff structure(s) produce(s) a more efficient outcome in terms of revenue than the static distance-based tariff?

METHOD

In order to explore on a more revenue-efficient set of price parameters for railways, pricing policy of suppliers under competition and behavioural individual reactions to the price stimulus on the demand side are observed with the help of an agent-based simulation model (cf. Gilbert & Troitzsch 2010; Gilbert 2008). Within the framework of the model, parameters can be manipulated under ceteris paribus conditions. Through running the model repeatedly, outcomes of these manipulations can be analysed statistically.

Computational modelling in general and agent-based objects in specific have gained broader acceptance among social scientists in recent years (Miller & Page 2007; Harrison et al. 2007; Davis et al. 2007). Simulation models have been introduced in operations research for capturing the dynamics of pricing measures and demand reactions after a number of time periods (cf. Cleophas 2012; Bitran & Caldentey 2003). Agent-based models are specifically suitable for revenue simulations because they "support the creation [of] autonomous agents that flexibly learn about and interact with their environment and with each other" (Cleophas 2012: 241). This allows for exploring revenue effects of price measures introduced at different points of time.

A revenue-inefficient or suboptimal tariff structure in this context can be perceived as a less elevated plateau or summit on a NK performance landscape (Porter & Siggelkow 2008; Rivkin & Siggelkow 2002; Siggelkow 2001).

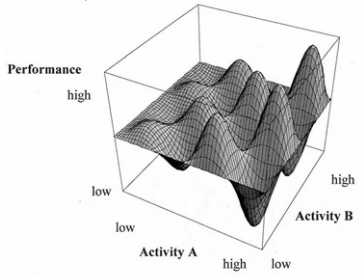

Figure 1: A generic performance landscape
(Source: Porter & Siggelkow 2008: 39)

In the realm of tariff strategy, different dimensions (e. g., fixed vs. flexible pricing and non-restricted vs. perfectly restricted) can be tested on local optima. Described graphically, some combinations of elements of a tariff structure may form a "revenue summit.

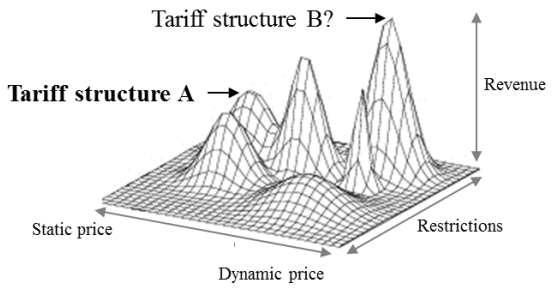

Figure 2: Local revenue optima within two dimensions (Source: own figure based on Verel 2012)

All possible measures of pricing are supposed to trigger a certain market reaction as proposed by Prospect Theory (Kahneman/Tversky 1979). In order to enable individuals to "calculate" their utility for a given fare, the theory is operationalised according to Nitzsch 1998 (p. 630):

- let *U(p)* the utility in function of the price
- let *la* the individual loss aversion factor
- let c=2 ln $\left(\frac{1}{r}-1\right)$
- let *r* a sensitivity parameter 0.5<r<1. The higher it is, the faster sensitivity decreases
- let *norm* a parameter that allows to align the utility values to U(reference price ./. norm) = 1 (however, *norm* can be set to any other value except 0, too).

For p <= reference price

$$(1)\quad U(p) = \frac{1-e^{-c\left(\frac{reference\ price-p}{norm}\right)}}{1-e^{-c}}$$

For p > reference price:

$$(2)\quad U(p) = -la\left(\frac{1-e^{-c\left(\frac{p-reference\ price}{norm}\right)}}{1-e^{-c}}\right)$$

The choice function involves a reference price that further develops with any (memorised) transaction made as well as some product-specific features. For calibrating the model, the set-up of the simulator is closely aligned with the revenue management branch of a train operator. Market research data for precisely shaping customer preferences as well as booking data for the line under investigation are provided by this source.

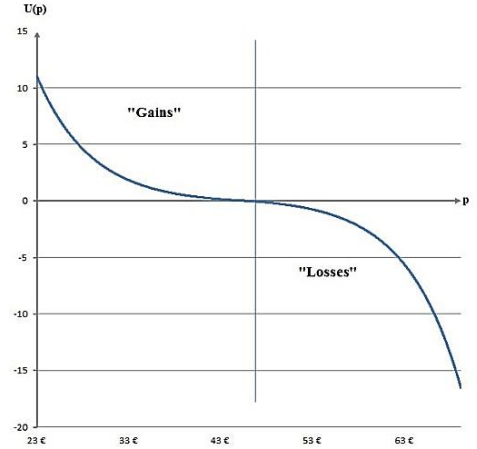

Figure 3: Utility as a function of the reference price (Source: own figure)

THE MODEL

The simulation environment is used as a setting for artificial experiments. It has been set up on the Netlogo platform, which is a fully programmable open source environment developed at Northwestern University. The model is programmed in a building block principle (Harrison et al. 2007), thus, by starting with a simple market transaction model which is subsequently elaborated with more complexity (e. g., rules of supplier behaviour in case of intramodal competition; mutual monitoring of passengers; fuzzy memory of passengers).

In its formal structure, the model contains a limited number of agents on the supply side (train, bus, air operators) and a multitude of individual agents on the demand side. A part of this population is provided with an individual car. Therefore, car transit acts as a passive transport operator. Every period of time (tick), a mobility demand is injected to a random part of the demand side. Then, individuals seek to fulfil their demand by searching a transport offer that rewards them with maximal utility calculated out of the operationalised price reaction function derived from Prospect Theory. For computational performance reasons, it is not possible to model the entire network of an incumbent train operator. Therefore, two highly frequented long-distance lines have been selected for being modelled.

In more detail, the supply side can be set to one, two, or three public transport operators with an own tariff structure involving a base fare, rebates and optional application of quantity-based revenue management. The agentset of passengers receives a monthly mobility budget and, besides individual features like age or links with others, is grouped into six sociological fractions representing their propensity to use public transport. The population of passengers is 5'000 individuals who are randomly interlinked to each other; half of them own a car. A part of the population is additionally equipped with a railcard. All passengers have a randomly set loss aversion factor between 1 and 2.

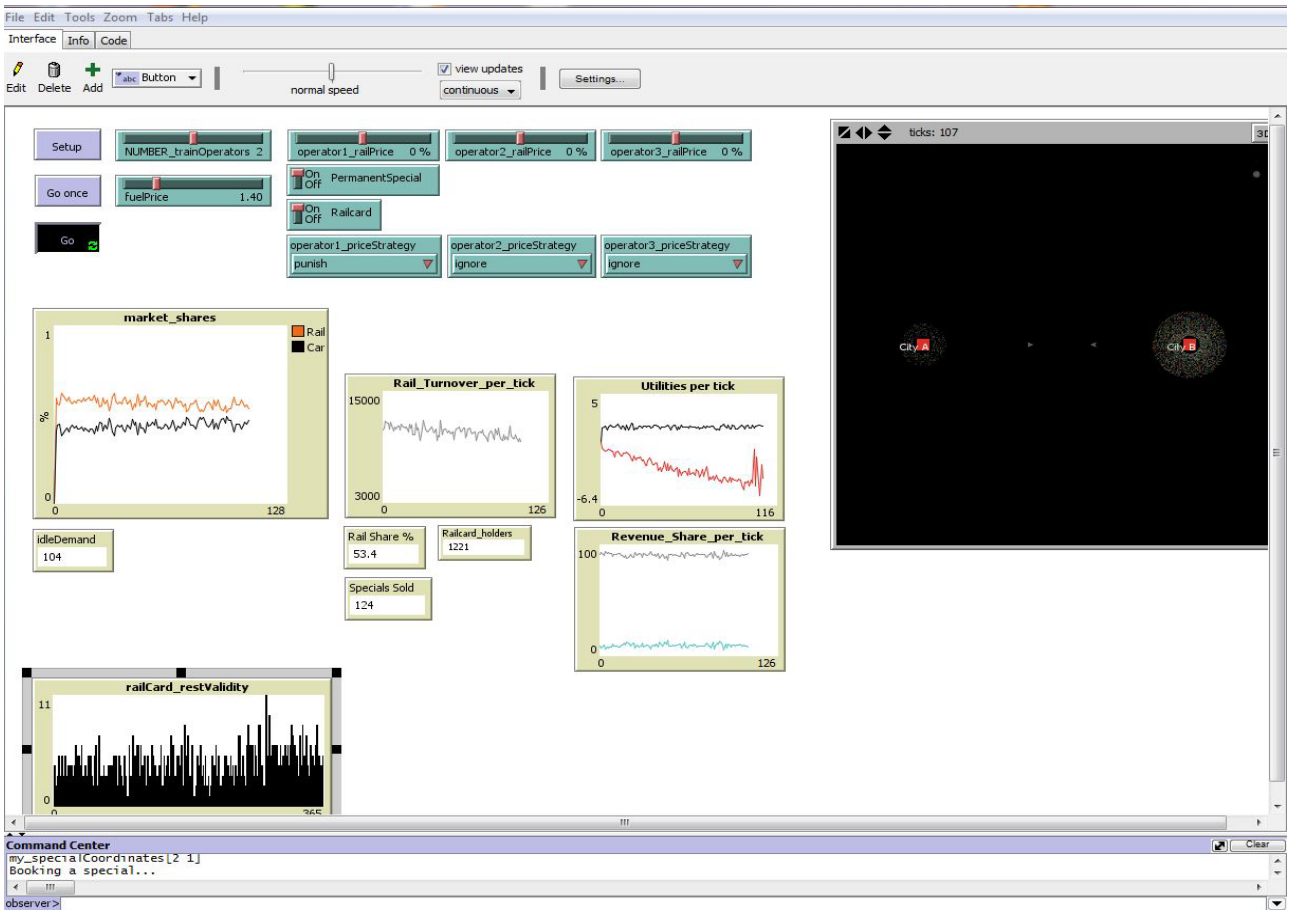

Figure 4: Screenshot of the Netlogo model for one origin-destination

After an initial learning phase, transport operators who use revenue management approaches create special offers and allocate a seat quota at different price levels. Passengers are always offered the cheapest fare fitting their demand. From their transactions, passengers memorise the price they have paid until they forget. There are several possible experiments within the current version of the model:

- Does the sheer application of Revenue management increase overall revenue, regardless what quota is allocated for the specials?
- Can permanent specials be a replacement for a railcard in case the latter is set off from the market?
- What is the long-term effect of a fuel price change?
- What is a more revenue-efficient quota of permanent special prices than a given one?
- Using the Behavior Search extension of Netlogo, what setting parameters is needed for obtaining a certain revenue target?
- Is there an optimal range of occupancy?

Relating to Prospect Theory, fuzziness of price memory can be tested against a "perfect" memory including a number of *n* last transactions. What is more, revenue effects related to marginal change of the loss aversion factor can easily be assessed. Later extensions of the model will involve competitive pricing between operators and a more active search for lower prices made by a part of the passengers.

PRELIMINARY RESULTS OF FIRST EXPERIMENTS

The base case scenario of the experiments made so far is as follows: agents could choose between individual car transport and a half-hourly frequency of trains operated by operator 1 as well as an hourly service of operator 2. Operator 2 doesn't accept any railcards. Operator 1 grants a 50% discount for railcard holders. Revenue generated by selling railcards is neutral. The operators ignore each other's pricing. Every tick, 500 agents receive a random mobility demand. For representing the features of the railway line, a time advantage of 20% in favour for rail was implemented; according to their sociological group, individuals accord a fix utility bonus to car transport.

The model in its basic features was run 50 times for 200 ticks each, which corresponds to a time of approximately six months. Within this framework, experiments for investigating on the revenue effects of the following scenarios have been conducted:

Scenario	Description
0	Base case (see description above)
1 “high specials quota”	After an initial learning phase of 100 ticks, operator 1 creates special prices for the 20% most under-utilised trains. There was a quota for a best-buy and a more expensive special. Operator 2 continues to use a fixed base fare only.
2 “low specials quota”	In this second experiment, the setting of experiment 1 was unchanged, except that the quota for permanent specials was reduced by 50%.
3 “Fuel price 10% up”	In this simple third experiment, the manipulation of the base case scenario consisted in computing a one-time 10% increase of the fuel price at tick 100.
4 “Railcard removal”	In the fourth experiment, the manipulation consisted in deactivating the railcard applicability after 100 ticks, with no regard to the rest validity of the cards. At the same time, operator 1’s base fare is reduced by 25%.

Table 1: First experiments with the model

Congruently to the base case, all manipulated models have been run 50 times for 200 ticks each. In all scenarios, the simulation is stopped after 200 ticks, thus, creating a total revenue out of 200 ticks.

Statistical results

After having conducted the experiments, data was collected and analysed by means of descriptive statistics. The following table shows revenue generated after 200 ticks for each operator as well as the total revenue generated by both rail operators across the base case (0) and scenarios 1 to 4.

		N	Mean	Std. Deviation
Operator1_Revenue	0	50	1.810.477	110.562
	1	50	1.779.026	87.668
	2	50	1.763.170	90.738
	3	50	1.856.922	102.566
	4	50	1.731.440	68.904
Operator2_Revenue	0	50	179.757	60.133
	1	50	181.546	53.172
	2	50	188.621	55.268
	3	50	183.951	56.536
	4	50	179.845	42.685
Total_Revenue	0	50	1.990.233	63.872
	1	50	1.960.572	46.213
	2	50	1.951.791	46.200
	3	50	2.040.873	80.810
	4	50	1.911.285	47.431

Table 2: Descriptives of experiments

The number of passenger agents getting a mobility demand was set arbitrarily due to performance constraints of the computer hardware. Hence, a robustness check for the base case was performed to elicit if the model produces similar results with 250 and 1,000 instead of 500 passenger agents. The model behaviour was the same across those numbers. Due to the still limited number of simulation runs, significance tests have not been performed.

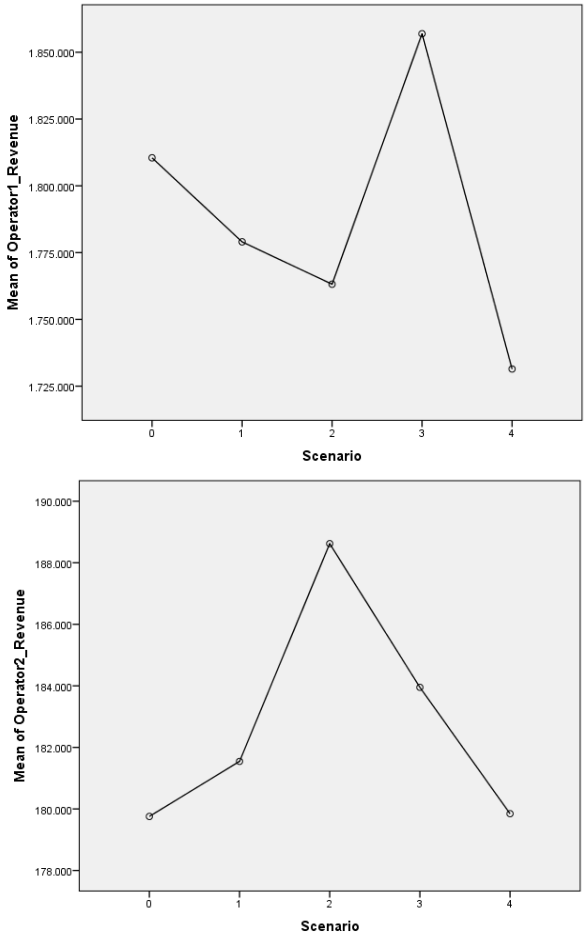

Figure 5: Effects of manipulations on each operator’s revenue

Interpretation

As suggested by Prospect Theory, individuals react sharply to prices higher than their individual reference price. For that reason, the positive utility effects of a special offer are easily foiled if no similar offer is found by the individual at a later occasion. The simulation model at its present state involves a strong dissatisfaction with a cheaper base fare of one of the operators because individuals aggregate a general “operatorless” rail reference price for themselves. It is interesting that a lower quota for special offers seems to reinforce that tendency, leading to a weaker revenue base for the operator who offers those specials and producing higher revenue for its competitor. However, further experiments need to be performed to find out if there is a coherent relation between the specials quota

and the revenue generated by an operator who doesn't apply any specials.

In this context, functions of price competition strategies different from autonomous pricing (such as a price follower strategy) are currently being implemented in the model. A follower strategy may produce a significantly higher level of revenue for all suppliers.

Even though a higher fuel price causes frustration of the agents at first sight, it gets accepted on a longer run as the new reference price gets more and more memorised by the agents.

A removal of operator 1's railcard has literally no effect to operator 2, but seems to be unfavourable for operator 1. In this area, decision rules and search behaviour for passengers with railcards have to be refined to calibrate the impact of this rather eminent change in the tariff structure.

CONCLUSION & CONTRIBUTIONS

An agent-based simulation model can be used as a tool for assessing possible impacts of one or more pricing measures. Within the limitations of the model, a first indication on the effects of single price measures or consequences of the adoption of a radically new pricing strategy can be given. The processual character of the simulation is likely to reveal possible negative long-term effects of pricing measures that seem to be successful on a short run. The model continues to be calibrated and refined with more empirical data and more individual behaviour in choosing means of transport. Netlogo's Behavior Search extension permits to search for parameters needed to obtain a defined revenue target.

Bridging individual behaviour and aggregated market outcome through agent-based modelling contributes to marketing research as well as Revenue Management. The behavioural pricing aspect is susceptible for enriching operations research in Revenue Management, as recent research is more focused on individual strategic buying decisions of customers. For marketing, a ceteris-paribus analysis of changes in a tariff structure allows learning about large-scale effects of individual price reaction. Behavioural pricing inspired by Prospect Theory can be enriched through a very detailed parameterisation of the individual price-reaction-function.

On a general level, the potential of inertia (or an eventual lock-in), and inefficiency in the field of price-setting may form an impetus to re-think the way how prices are set and changed. This may provide insights for managers of transport operating companies, but also for policy-makers, e. g., in the European Commission, and management research in other industries.

REFERENCES

Armstrong, A. & Meissner, J. (2010). Railway Revenue Management: Overview and Models: Working Paper. Retrieved from http://www.meiss.com

Arthur, W. B. (1989). Competing Technologies, Increasing Returns, and Lock-In by Historical Events. The Economic Journal, (99), 116–131.

Belobaba, P. (2009). Fundamentals of Pricing and Revenue Management. In P. Belobaba, A. Odoni, & C. Barnhart (Eds.), The Global Airline Industry (pp. 73–111). J. Wiley & Sons.

Bitran, G., & Caldentey, R. (2003). An Overview of Pricing Models for Revenue Management. Manufacturing & Service Operations Management, 5(3), 203–229.

Bridel, P., & Huck, E. (2002). Yet another look at Léon Walras's theory of tâtonnement. European Journal of the History of Economic Thought, 9(4), 513–540.

Cleophas, C. (2012). Multi-agent modelling for revenue management. Journal of Revenue & Pricing Management, 11(2), 240–242.

David, P. A. (1985). CLIO and the Economics of QUERTY. American Economic Review, 75(2), 332–337.

Davis, J. P., Eisenhardt, K., & Bingham, C. B. (2007). Developing Theory Through Simulation Methods. Academy of Management Review, 32(2), 480–499.

Dutta, S., Zbaracki, M., & Bergen, M. (2003). Pricing Process as a Capability: A Resource-Based Perspective. Strategic Management Journal, (24), 615–630.

European Commission. (1996). White Paper: A Strategy for Revitalising the Community's Railways (No. COM(96)421). Brussels.

Gilbert, G. N. (2008). Agent-based models. Los Angeles: Sage Publications.

Gilbert, G. N., & Troitzsch, K. G. (2010). Simulation for the social scientist (2nd ed.). Maidenhead: Open University Press.

Harrison, R. J., Zhiang, L., Carroll, G. R., & Carley, K. M. (2007). Simulation Modeling in Organizational and Management Research. Academy of Management Review, 32(4), 1229–1245.

Helson, H. (1964). Adaption-Level Theory. New York.

Jaffé, W. (1967). Walras' Theory of Tatonnement: A Critique of Recent Interpretations. Journal of Political Economy, 75(1), 1–19.

Kahneman, D., & Tversky, A. (1979). Prospect Theory: An Analysis of Decision under Risk. Econometrica, 47(2), 263–291.

Lambrecht, A., & Skiera, B. (2006). Paying Too Much and Being Happy about It: Existence, Causes, and Consequences of Tariff-Choice Biases. Journal of Marketing Research, 43(2), 212–223.

Miller, J. H., & Page, S. E. (2007). Complex adaptive systems: An introduction to computational models of social life. Princeton, N.J: Princeton University Press.

Monroe, K. B. (1973). Buyers' Subjective Perceptions of Price. Journal of Marketing Research, 10(1), 70–80.

Nitzsch, R. v. (1998). Prospect Theory und Käuferverhalten [Prospect Theory and Consumer Behaviour]. DBW Die Betriebswirtschaft 58(5), 622-634

Porter, M., & Siggelkow, N. (2008). Contextuality Within Activity Systems and Sustainability of Competitive Advantage. Academy of Management Perspectives, 22(2), 34–56.

Rivkin, J. W., & Siggelkow, N. (2002). Organizational sticking points on NK Landscapes. Complexity, 7(5), 31–43.

Sato, K., & Sawaki, K. (2012). Dynamic pricing of high-speed rail with transport competition. Journal of Revenue & Pricing Management, 11(5), 548–559.
Siggelkow, N. (2001). Change in the Presence of Fit: The Rise, the Fall, and the Renaissance of Liz Claiborne. The Academy of Management Journal, 44(4), 838–857.
Sydow, J., Schreyögg, G., & Koch, J. (2009). Organizational Path Dependence: Opening the Black Box. Academy of Management Review, 34(4), 689–709.
Sydow, J., Windeler, A., Müller-Seitz, G., & Lange, K. (2012). Path Constitution Analysis: A Methodology for Understanding Path Dependence and Path Creation. BuR Business Research Journal, 5(2), 1–22.
Talluri, K. T., & van Ryzin, G. (2005). The theory and practice of revenue management (1st ed.). International series in operations research & management science: Vol. 68. New York: Springer.
Thaler, R. (1985). Mental Accounting and Consumer Choice. Marketing Science, 4(3), 199–214.
Verel, S. (2012). Fitness Landscapes and Graphs: Multimodularity, Ruggedness and Neutrality: Tutorial, Nice.

AUTHOR BIOGRAPHY

NORMAN KELLERMANN is a member of the research group on organisational paths funded by Deutsche Forschungsgemeinschaft (DFG). Born in Magdeburg, Germany, he studied Business Administration at Freie Universität Berlin, where he obtained his diploma degree in 2007. Following this, he worked as a business analyst for Germany's leading railway operator Deutsche Bahn AG. He specialised in intermodal mobility, regional passenger transport and sales.

AGENT-BASED SIMULATION ANALYSIS OF PATH DEPENDENCE IN CORPORATE IS NETWORKS FOR STRATEGIC IT MANAGEMENT

Daniel Fürstenau
Freie Universität Berlin
School of Business & Economics
Garystr. 21, 14195 Berlin, Germany
E-mail: daniel.fuerstenau@fu-berlin.de

KEYWORDS
Agent-based simulation, path dependence, strategic IT management, business information systems, IS networks

ABSTRACT

This study extends Arthur's model of path dependence for strategic IT management by introducing a more complex organizational structure with topology-adjusted network externalities and complementarities. A partial lock-in measure is developed to distinguish partial and global lock-ins. The study finds that complementarities can result in partial rather than global lock-ins. These findings suggest that, contrary to classical path dependence theory, strategic IT managers can contain global lock-ins by partitioning organizational structures. Results from an agent-based simulation study are presented and discussed.

1. INTRODUCTION

What are the features of path dependence in strongly coupled information system (IS) networks in organizations as opposed to technology markets? Previous simulation research tremendously improved our knowledge on path dependence (e.g. Arthur 1989; Leydesdorff and van den Besselaar 1997; Frenken et al. 2012), but focused mostly on technology markets. Generative mechanisms of path dependence inside complex business organizations are not yet sufficiently understood.

Applying simulation research in the field of complex business organizations is important, as will be illustrated at the example of the airline industry. In particular, interviews with airline managers suggest inertia to overcome rigidities in the pricing domain (Isler and D'Souza 2009). Pricing, distribution and other airline capabilities co-evolved and mutually adjusted for decades based on common standards, such as booking classes. This created and escalated a positive feedback loop; lock-in of the pricing capability resulted.

This extreme case carries several interrelated implications. One is that although existing models of path dependence enable a good understanding of market-based technology adoption, the airline case points directly to the appealing theoretical possibility that technological standards go on to diffuse into many interrelated domains *inside* an organization. Over time, this builds additional barriers to change. Thereby, managerial choice is a function of the value that agents assign to information systems and standards in a restricted neighborhood of complementaries rather than to the entire organization or market. Another implication is that agents' repeated choices to exploit a technology may appear beneficial in the short run but produce sticky local optima over time. I believe that an agent-based simulation model should figure centrally the effects of local complementarities and positive feedback to adaptation in a portrayal of path dependence in business organizations.

In this contribution, I propose an extension of Arthur's path dependence model using an agent-based simulation within the field of strategic IT management (refer to Ward and Peppard 2009 for general background). My primarily theoretical aim is to gain a better understanding of path dependence in corporate IS networks. The paper proceeds as follows. Section 2 introduces theoretical antecedents. Section 3 describes the model based on deviations from Arthur's efforts. Section 4 presents the experimental setup and results. The contribution ends with a conclusion and discussion of future research opportunities.

2. THEORETICAL BACKGROUND

2.1 Strategic Planning for Corporate IS Networks

The airline case illustrates the role of complementarities in creating IT value. This section briefly introduces a related technique from strategic IS planning. As shown in Figure 1, *master plans* conceptualize an organization as a two-dimensional matrix (a grid) where the x-axis represents business processes (or value chain elements) and the y-axis represents organizational units, e.g. divisions, departments or regions (Lankhorst et al. 2009).

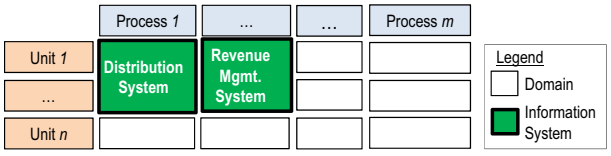

Figure 1: Master plan as *m x n* grid (processes and units)

The *m* x *n* grid positions, called domains, depict current and envisioned IS support. Master plans are used to identify complementarities: For instance, the airline IT manager from section 1 may propose to standardize

Proceedings 27th European Conference on Modelling and Simulation ©ECMS Webjørn Rekdalsbakken, Robin T. Bye, Houxiang Zhang (Editors)
ISBN: 978-0-9564944-6-7 / ISBN: 978-0-9564944-7-4 (CD)

information systems in neighboring domains, e.g. in sales/distribution ($process_1$) and pricing/managing revenues ($process_2$). Problems of path dependence in business organizations can ensue when IT managers overstress short-term opportunities from complementarities while overlooking potential long-term downsides.

2.2 Problems of Path Dependence in IS Networks

The field of strategic IT management offers numerous anecdotal examples of inert IT systems resulting in organizational "capability lock-ins" (Ross et al. 2006, p. 50) or "rigidity traps" (Bharadwaj 2000, p. 187). From these predecessors follows that the managerial scope of action rises and falls with contingent decisions on capabilities to develop by providing advanced IT systems. Scholarly work has, however, rarely explicitly modeled the conditions when and where in turn possible negative consequences of such capability-building processes will occur. Antecedents for this can be found in the literature on path dependence.

The Arthur model of *technological path dependence* (Arthur 1989), which is explained in the next section, shows when standards in markets of adopters can lock-in. Lock-ins occur when one technology gains momentum under positive network externalities and becomes dominant. Previous studies illustrate that path dependence related to network effects also impacts corporate IS networks (Weitzel et al. 2006) and that technical standards are incorporated in components forming "artifacts" (Widjaja 2011, p. 35). Network effect theory assumes that it gets more and more attractive for adopters to choose a blooming technology. Recent studies (Weitzel et al. 2006), considered in the model conception, found that the outcome is thereby influenced by the topology.

Building on the Arthur model, the *Berliner Modell* of organizational path dependence (Sydow et al. 2009) highlights several positive feedback mechanisms to explain lock-ins of social processes in organizations. Complementarities, defined as two or more activities that interact in mutually stimulating ways, are one key mechanism (Sydow et al. 2009). Organizational path dependence theory assumes that complementary processes show super-additive payoffs. In turn, deviations from this set of processes can become unattractive due to prior mutual adaptations.

These two streams of literature allow to distill two key feedback mechanisms expected to produce path dependence in organizational IS networks:

- Topology-adjusted network externalities and
- Complementarities

Consistent with this view, the following sections develop an agent-based simulation model of path dependence in organizations to address the following question: *When and where will topology-adjusted network externalities and complementarities in IS networks result in lock-ins?*

3. DESCRIPTION OF THE MODEL

Building on the airline case and the theoretical antecedents, this section formally models path dependence in corporate IS network. Starting with the Arthur model to account for general properties of path dependent processes, topology-adjusted network externalities and complementarities are examined regarding their influence on lock-ins.

3.1 Baseline Model

The Arthur model has long been used to illustrate problems of path dependence in technological markets, where the main ingredients are network effects *r* and *s* (see Table 1). These lead to lock-in when the parameters are positive (Arthur 1989). Arthur also informed models of innovation dynamics (e.g. Leydesdorff and van den Besselaar 1997; Frenken et al. 2012), standard diffusion in technological networks (e.g. Weitzel et al. 2006; Beck et al., 2008), and institutional rule adoption (e.g. Petermann 2010). The model functions as a starting point here as it aptly captures the path dependent features of technological standard diffusion processes resulting from individual agents' decisions. More specifically, the model assumes that two types of agents (*R* and *S* agents) enter a market sequentially and adopt a technology as described in Table 1.

Table 1: Utilities in Arthur's model of path dependence

	Technology A	Technology B
R-agent	$a_R + r*n_A$	$b_R + r*n_B$
S-agent	$a_S + s*n_A$	$b_S + s*n_B$

When applied to situations with two technologies, the model thus involves the following straightforward steps: each tick, the model creates a new agent of a certain type with corresponding base preferences (a_R or a_S) and network preferences (*r* and *s*), sums up the previous adopters for each technology (n_A and n_B), determines the winning technology (*A* or *B*), and increases the adoption counter (n_A or n_B) by one for the winner. The Arthur model captures the positive feedback from network influences and therefore serves as a constructive baseline for modeling standard diffusion in IS networks.

3.2 IS Network Structure

To implement the mechanisms described in section 2 in the model, the organizational IS network of a firm is conceptualized as shown in Figure 2.

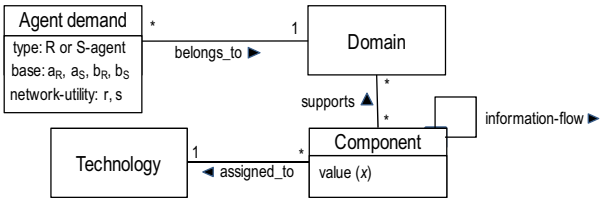

Figure 2: Meta model of IS network structure

The extension accounts for the organizational and the IS network dimension. The organizational dimension is expressed as a two-dimensional matrix (a grid), where each matrix cell represents a particular *domain* (see Figure 2). For instance, distribution is an exemplary airline domain. *Demands* of agents are assigned to exactly one domain. Agents evaluate a *set of components* available in their domain to fulfill the demand. Components are assigned to strictly one of two *technologies* (see Figure 2) and support one or more domains. Thus, domains are resource slots, housing multiple components with different qualities. Components are active or inactive, depending on agents' prior decisions. More specifically, components become active only after an agent decides to implement his or her demand using them. When activating a component, the agent's base utility is decreased by fixed setup costs. When agents adapt a component, its value increases and a special link type, called information-flow, is created (Figure 2). This works as follows: If the component is not active yet, increase the value by 1 and set its state to *active*; otherwise just increase the value. Consistent with predecessors in the field (e.g. Widjaja 2011), the network utility is conceptualized as the sum of the value of the components. In a network of components, the value of a component thus influences later decisions to choose other components based on the same technological platform.

Based on these descriptions, the agents' decision making can be defined in more detail. In Arthur's model, agents calculate the utility to choose technology A or B by summing up the base utility of these technologies (a_R, b_S) with the network effect strength (r, s) multiplied by the adoption count (n_A, n_B). Used by itself, however, the Arthur model has limitations. When applied to a given organizational IS network, it considers complete connectedness, making no allowance for the varying benefits flowing in from components with different positions in the IS networks. Although complete connectedness may accurately describe some IS structures, it is likely to mischaracterize most networks of interest to IT managers (Weitzel et al. 2006). Consequently, to build in more complex network influences into the model, I turn to topology-adjusted *network externalities* and *complementarities*. Their mechanics are now explained as the backcloth of the approach.

Topology-adjusted network externalities. Based on Arthur's utility function (see Table 1), the network terms are adapted to account for varying influences of the network structure. Table 2 shows the modified utility functions for R-agents and S-agents.

Table 2: Modified agents' utility functions

	Technology A	Technology B
R-agent	$a_R + r^* \sum_{i \in N(j)} x_{A,i}$	$b_R + r^* \sum_{i \in N(j)} x_{B,i}$
S-agent	$a_S + s^* \sum_{i \in N(j)} x_{A,i}$	$b_S + s^* \sum_{i \in N(j)} x_{B,i}$

Essentially, the only difference to Arthur's model is that not all adopters are connected. The departure from Arthur's model lies in the network influences (n_A and n_B), considered when choosing a component. The factors n_A and n_B for a given component i are replaced by the summed value of all neighboring components j based on the same technology A or B, where N again denotes the number of all active components. The important classification becomes that of neighborhood. More specially, two types of neighbors are distinguished: First order neighbors j_1 are components based on the same technology, and are connected to i by a flow of information. Second order neighbors j_2 are components based on the same technology, but are not (yet) connected to i by a flow of information. If we consider a hypothetical relational matrix X, where $\boldsymbol{X} = [x_{ij}]$, $x_{ii} = 0$ denotes the inflow of value between component i (self) and component j (neighbor) based on the same technology, then we can model each agents' decisions to invest in component i by extending the calculus of Table 2 as follows:

$$\sum_{i \in N(j)} x_{P,i} = w_1 \sum_{i \in N(j1)} x_{P,i} + w_2 \sum_{i \in N(j2)} x_{P,i} \text{ with } P\{A,B\} \quad (1)$$

Where w_1 and w_2 denote weighting terms that agents put on first order and second order neighbors. When applied to IS networks represented by a relational matrix $\boldsymbol{X}$, Equation (1) thus involves the following steps: Collect the first order neighbors j_1 of i, sum up their inflowing value x, and then collect the second order neighbors j_2 of i and sum up their inflowing value. If w_1 and w_2 are 0, i is completely autonomous. If, by contrast, the number of neighbors (j_1 and j_2) increases, then i will be more strongly influenced by other components. Again, the winning component is activated, the base utility is decreased by fixed setup costs, if necessary, and the function counter is incremented by 1.

Complementarities. To bring in complementary-based decision making, the factors n_A and n_B are adjusted.

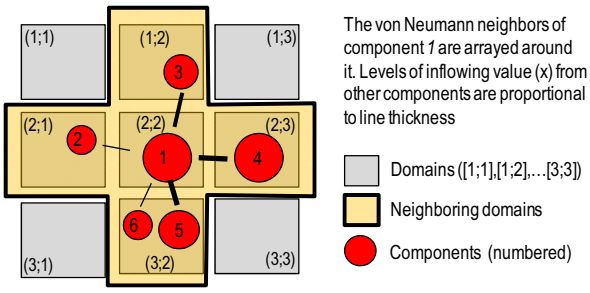

Figure 3: The von Neumann neighborhood

This time, the core idea is that agents only benefit from the value of components in neighboring domains. As illustrated in Figure 3, the agents' inflowing value from other components is restricted to von Neumann neighbors (Gilbert and Troitzsch 2005, p. 134). In a nutshell, the proposed model is best understood as a set of small-scale Arthur models. The calculation of the value $x_{P,i}$ for

a component is described in Equation (2), which extends the agents' utility functions of Table 2 as follows:

$$\sum_{i \in N(j)} x_{P,i} = \sum_{i \in N(j,vonNeumann)} x_{P,i} \quad \text{with } P\{A,B\} \quad (2)$$

This involves the following steps: Collect all components on the same technological platform (*A* or *B*) assigned to the von Neumann neighborhood domains. Sum up their value, determine the winning component, and set it active. As it is theorized that complementarities are often "mutually reinforcing" (Porter and Siggelkow 2009, p. 50; Sydow et al. 2009), the value of the chosen component *and* the value of all (technologically equal) components assigned to neighboring domains is incremented by 1. Focusing on the von Neumann neighbors thus limits the network effects. Consistent with the airline example (see section 1), agents will now strive for complementary IS support in neighboring domains.

Lock-In. In what follows, a measure for *partial lock-ins* is developed to separate partial from global lock-ins. Arthur (1989, p. 120) outlines an absorbing barrier, which is described as a situation where, for example, S-agents must switch to technology *A* despite their opposing preference for technology *B*, because the difference in adoption pushed technology *A* too far ahead. He shows that if $n_A - n_B > ((b_S - a_S)/s)$ holds, all further S-agents must choose *A* (and vice versa). It follows from the Arthur model that individual misfits boost lock-ins on the global level. It is thus a useful proxy for the expected number of global lock-ins (Draisbach et al. 2012). However, Arthur's absorbing barrier assumes complete connectedness. Consequently, to build in the network structure, replace n_A and n_B by the summed value of components relying on technology A ($x_{A,k}$) minus those on B ($x_{B,k}$) in a particular domain *k*. Agents in other domains rely on inflowing value from that domain. The restriction to domains accounts for the fact that agents are dragged to the leading technology of neighboring domains. For instance, a domain *distribution* (refer to coordinates [2;2] in Figure 3) might be locked-in, because it is strongly dominated by a global distribution system on GDS technology. Other domains, e.g. the *pricing* domain [2;1], might in turn become increasingly forced to adopt GDS technology as *distribution*. An agent in the *pricing* domain might thus decide to choose a system based on GDS technology, although he or she prefers another technology. Thus, if Equation (3) holds a *partial lock-in* in domain *k* for technology *A* is indicated:

$$\sum x_{A,k} - \sum x_{B,k} > \frac{b_s - a_s}{s} \quad (3)$$

Where $n_{k,A}$ ($n_{k,B}$) is a component in domain *k* on technology *A (B)* and *x* is the value of that component. Similarly, to pass the barrier of technology *B* in domain *k* the equation $sum(x_{A,k})$ - $sum(x_{B,k}) < (b_R - a_R)/r$ must hold. Note that partial lock-in is a binary variable that switches to 1 if the barrier is passed. It thus indicates when S-agents in neighboring domains are forced to choose *A* despite preferring *B*. Consequently, *global lock-in* occurres if the sum over the lock-ins of all domains divided by the number of domains is *1*. Note that the partial lock-in measure equals Arthur's absorbing barrier for settings with one domain, because if *k=1* then the value x_A (x_B) in domain *k* equals the value n_A (n_B) over the entire network.

3.3 Simulation Procedure

The next section presents simulation experiments to examine the effect of IS network structures on the likelihood of partial and global lock-ins (see Figure 4).

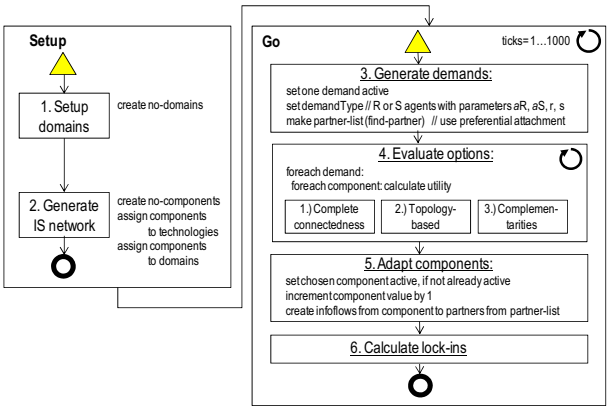

Figure 4: Simulation Procedure

At the start of the simulation (*step 1*), domains are set. The domains are modeled as a nested list that is a sublist of the list [1 1], [1 2], […], [m n]. Thereby, each domain is a two-dimensional vector with an x and y position. In model 1 and model 2 the number of domains is restricted to one domain. In model 3, the number of domains is varied iteratively (*i.e. 2, 5, 10, 15, 20, 25*). Afterwards, the following IS networks are created (*step 2*): (1.) In the baseline model, *two* components are created and assigned to exactly *two* technologies. As the components in the model are not linked and the model ensures that both technologies are available, the situation in model 1 is equal to the Arthur model. (2.) In model 2, *n* components (with *n = 5, 10, 25, 100)* are created and randomly assigned to strictly one of two technologies. Thereof, a random number of components is activated and linked using Erdös and Renyi's random network algorithm as presented by Jackson (2008) with a link probability of 0.1. (3.) In model 3, each domain is equipped with one active component based on technology A and B. Thus, the component number is double the domain number. Subsequently, the simulation is executed so that in step 3 of each round one agent (demand) of a particular type (R-agent or S-agent) is created (both types are equally probable) and assigned to strictly one domain. The agents' demand is set *active* and a list of potential link partners is created. Partners are found via the preferential attachment algorithm as described by Jackson (2008, p. 130 et seq.). The *find-partners* proce-

dure is repeated five times; duplicates are removed. In what follows (step 4), the agents evaluate options based on the decision logic described in the previous section: *(a)* complete connectedness as in the Arthur model, *(b)* topology-adjusted network externalities or *(c)* complementarities. After strictly one option is chosen in step 5, the component is activated, links are created, and value is incremented. Finally, step 6 calculates the lock-in measures.

4. SIMULATION RESULTS

4.1 Research Overview

This study uses an agent-based simulation approach (Gilbert and Troitzsch 2005). The concept was implemented with NetLogo 4.1.3. The work is currently in a prototypical stage.

4.2 Experimental Setup

The experiments were designed around three distinct models (see Table 3 for parameter descriptions).

Table 3: Parameter description for the experiments

	baseline model 1	model 2 (topology)	model 3 (compl.)
# ticks	1,000		
# demands	1,000 (per tick 1 demand is created)		
# techs.	2 (technologies A and B)		
# domains	1	1	2, 5, 10, 15, 20, 25
# components	2	5, 10, 25, 100	*2 * # domains*
link-prob	n.a.	0.1	
w_1, w_2	n.a.	(1 1), (1.0 0.5),(1.0 0.0)	n.a.
$r = s$	0.1		
a_R, a_S	R-agent: [0.8 0.2], S-agent: [0.2 0.8]		
setupCosts	0.0	2.0	0.0
# runs	100	3 * w_2 * 4 * #comp = 1,200	6*# domains* 100 = 600

Model 1, the baseline model, aims to confirm Arthur's findings and thus to increase the validity of the model and the lock-in measure. For model 2 and model 3, which extend the base model, a full-factorial design (Law and Kelton 1991, p. 656 et seq.) was chosen to develop an understanding of the solution space for experimental factors not yet analysed. In model 2, which examines the effect of *topology-adjusted network externalities* on lock-ins, the experimenter manipulates the factor *weighting term* (w_2) in 3 levels, controlling for the factor *number of components*. In model 3, under complementary-based decision making, the factor *number of domains* was varied in 6 levels.

4.3 Results

Model 1. Model 1 is intended to reproduce Arthur's findings. The plot **A** on the left in Figure 5, which shows the fraction of value of components on technological platform *A* vs. *B* against time, offers a portrayal of typical diffusion patterns in model 1. As suggested by Arthur's model, in model 1 initially one technology gains momentum and new agents are pulled towards the leading technology. As observable from the right-hand plot (**B**) in Figure 5, the misfit rate initially increases and then plateaus around 50% (*mean of misfit rate 0.48, std.dev. 0.023, N=100).* Model 1 integrates previous efforts from Arthur's model as both the measure for partial lock-ins (see section 3.2) and the absorbing barrier from Arthur (1989, p. 120) equally produce global lock-ins over all simulation runs.

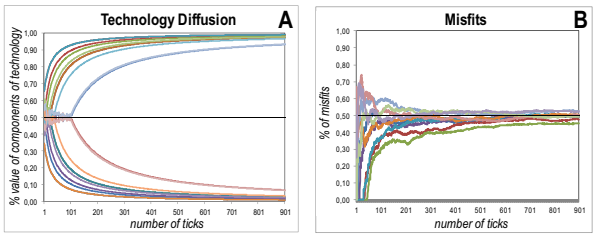

Figure 5: Typical diffusion patterns for model 1

Model 2 (Topology-adjusted network externalities). Here, the inflowing value x_i for component i is constrained to first and (less important) second order neighbors. Diffusion patterns as illustrated in Figure 6 were observed. In contrast to Figure 5, plot **A** and **B** of Figure 6 suggest that model 2 requires more ticks until lock-ins occur. It can be observed that agents, on average, were able to choose their preferred technology for more ticks.

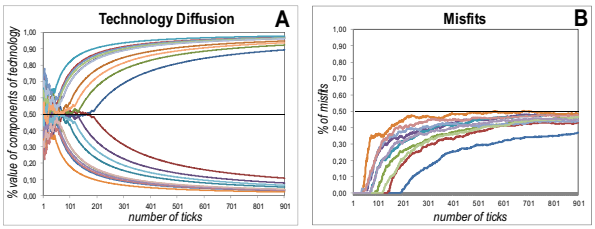

Figure 6: Diffusion pattern for model 2 (25 components)

Descriptive statistics derived from model 2 with three different weighting term factors w_1 and w_2 for 25 components appear in Table 4. Differing misfit rates across different weighting terms indicate the intensity of lock-ins to depend on the strength of the weighting factors *(F-stat.= 14.522, $p < 0.001$; Levene-stat.= 3.128; $p = 0.045$).* Given the nature of the model, it is reasonable to assume that the decreasing strength of the network effects for lower factor levels of w_2 resulted in longer average time intervals until lock-ins occur.

Table 4: Descriptives for misfit rate in model 2

w_1,w_2	N	Mean	Std.dev.	Std.err.	Min	Max
1.0/0.0	100	0.4685	0.02205	0.00221	0.40	0.52
1.0/0.5	100	0.4706	0.02636	0.00264	0.38	0.51
1.0/1.0	100	0.4844	0.01887	0.00189	0.43	0.53
Total	300	0.4745	0.02364	0.00136	0.38	0.53

Model 3 (Complementarities). Two characteristic diffusion patterns were observed. Consider in this connection the three-by-three plot series (Figure 8), where the upper figures show diffusion and misfit plots for a setting with a global lock-in (**A-C**), and the bottom plots (**D-F**) illustrate runs with partial lock-ins. The outstanding feature of the bottom plots is the convergence to a fractional level for both technologies.

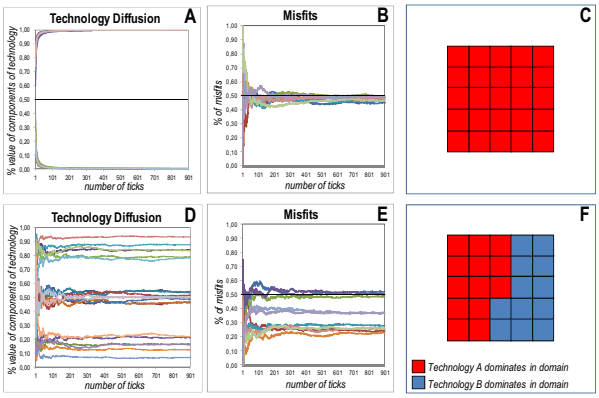

Figure 7: Typical diffusion patterns for model 3 (*illustrated for 25 domains, r = s = 0.1*)

Table 5: Global lock-in * no domains cross tabulation

Count (for IS networks with 25 components)							
Global Lock-In?	no. domains						Total
	2	5	10	15	20	25	
No	0	11	14	19	32	44	120
Yes	100	89	86	81	68	56	480
Total	100	100	100	100	100	100	100

Global lock-in was found in 56-100% of the cases in model 3 depending on the number of domains (see Table 5, ^{2}*-stat. = 77,375, p < 0.001)*. The most important observation from Table 5 is the decreasing number of global lock-ins for larger number of domains. An analysis of the underlying decision patterns, as illustrated by plot **F** in Figure 8, revealed that convergence occurred despite different technologies dominating in the different domains. Plot F of Figure 8 illustrates a grid where 13 domains are dominated by technology *A* and 12 domains by technology *B*. Unlike model 2, where strong theoretical expectations about the expected outcome were available from the studies of Weitzel et al. (2006), there was less guidance available in the literature for anticipating the effect of increasing complexity on partial and global lock-ins. Yet, it is possible to sketch informal reasons for the decreasing number of global lock-ins based on the nature of the model. As larger grids have less overlaps – that is, as units are more dispersed in more complex organisations – initially unconnected areas on the grid come into existence and evolve separately. Additionally, as agents decide sequentially in different domains, more complex organizations will have more time to grow local clusters. It is thus possible that two distinct areas initially thrive and eventually sustain.

Robustness checks. To explore the robustness of the findings, I increased and decreased the strength of the network effects (r = s). For higher levels, the results might be weaker as increasing dynamics might boost global lock-ins. Interestingly, an increase of r = s by factor 10 (r = s = 1.0) instead produced a decreasing number of global lock-ins. The level dropped from 81% to 72% against a defined baseline (*15 domains, model 3, r = s = 0.1*), but no conclusive evidence for a significant deviation was observed (*t – stat. = 1.502, p = 0.135 > 0.05, Levene-stat. = 9.176, p < 0.003*). When decreasing the network effects by factor 10 (*r = s = 0.01*) the model was more prone to change - that is domains changed their orientation more often. The level of global lock-ins dropped significantly from 81% to 67% (*t – stat. = 2.275, p < 0.024, lev. stat. = 21.108, p < 0.001*).

5. CONCLUSION

This contribution aimed to advance our understanding of lock-ins in corporate IT infrastructures. The approach is framed on the backdrop of prior analysis of path dependence in technological markets. I extended prior models due to the importance of coupling among the nodes that compromise organizational IS networks. Combining approaches from strategic IT management literature with the Arthur model of path dependence, I developed a model that is attentive to the position components hold in the IS network. Using an agent-based simulation approach, initially replicating Arthur's findings and subsequently bringing in more complex structures as anticipated in the airline case, I illustrated the importance of organizational structures for the likelihood of global lock-ins.

By using an agent-based simulation approach, the (verbal) theory from Sydow et al. (2009) on complementarities was formalized. The proposed model confirmed the effect of complementarities on lock-ins. This highlighted an association that IT managers have to incorporate into their strategic thinking. My primary contribution is, however, to illustrate that *global lock-ins* become less likely in more complex organizational settings (see Table 5) and rather *partial* lock-ins occur in an increasing number of cases. This points to the theoretical possibility that lock-ins can be contained to particular domains to prevent their global spreading.

In the introduction, an example from the airline industry illustrated problems of path dependence inside complex business organizations. The model increases our understanding on the case in two directions. First, it turns attention to the importance of neighborhood in settings where complementarities exist. The model illustrates how local neighbors mutually adjust to each other and how interacting dynamics produce a positive feedback loop, which in turn often results in lock-ins of connected domains (see Figure 8). The model suggests that IT managers should use their knowledge on complementarities to group connected areas as pricing and distribution to profit from positive feedback, while they might

disconnect other areas deliberately, e.g. by dispensing the use of booking classes in bonus miling, to minimize lock-in risks. Secondly, the model also shows that sequence matters, as early decisions in different parts of the organization become reinforced by further adaption decisions and build up additional barriers to change over time. In this context, the model illustrated that global lock-ins might become less likely in more complex organizations (see Table 5), due to sequential decisions enabling different areas of the organization to gain enough momentum to resist a global standard. The model thus suggests that it might be possible to grow an alternative standard, e.g. a new distribution capability, in an independent "incubator".

I emphazise three conditions that limit the generalizability of the model. First, the partial lock-in measure from Equation (3) is preliminary. The measure is a first approach based on the difference in adoption for both technologies. With one domain, it follows directly from the agents' utility functions. For the *n* domain case, however, network effects from further domains might still perturbate the system. Second, the conclusion drawn from Table 5 that global lock-ins become less likely in complex organizational settings might be misleading when other structural conditions exist. The model only accounts for local complementarities and other models, e.g. with connections across *n* domains, could produce different results. Third, the model would benefit from a comparison with data, which is beyond the scope of this paper.

Ongoing work includes gathering exemplary IS network data from two airline companies' IT records to calibrate and validate the proposed model. In this, I employ a history-friendly validation approach (Windrum et al. 2005) for the problem instance of airline revenue management and distribution. Further research should model strategic agent behavior to test the effect of strategic IS planning procedures (Ward and Peppard 2009; Ross et al. 2006) on the likelihood of partial and global lock-ins. Instead of using a "shopping-list" approach (Ward and Peppard 2009, p. 121), where agents' demands are fulfilled sequentially, this should include balancing present and future needs as well as prioritizing agents' demands.

REFERENCES

Arthur, W.B. 1989. "Competing technologies, increasing returns, and lock-in by historical events", *The economic journal*, Vol. 99 No. 394, 116–131.

Beck, R., Beimborn, D., Weitzel, T. and König, W. 2008. "Network effects as drivers of individual technology adoption", *IS Frontiers*, Vol. 10 No. 4, 415–429.

Bharadwaj, A. 2000. "A resource-based perspective on information technology capability and firm performance: An empirical investigation", *MIS Q*, Vol. 24, 169–196.

Draisbach, T., Widjaja, T. and Buxmann, P. 2012. "Lock-Ins auf Netzeffektmärkten - Ergebnisse einer Simulationsstudie", in *MKWI 2012 Conf. Proc.*, 691–704.

Frenken, K., Izquierdo, L.R. and Zeppini, P. 2012. "Branching innovation, recombinant innovation, and endogenous technological transitions", *Environmental Innovation and Societal Transitions*.

Gilbert, G.N. and Troitzsch, K.G. 2005. *Simulation for the social scientist,* 2nd., Open Univ. Press, Maidenhead.

Isler, K. and D'Souza, E. 2009. "GDS capabilities, OD control and dynamic pricing", *Journal of Revenue and Pricing Management*, Vol. 8 2-3, 255–266.

Jackson, M.O. 2008. *Social and economic networks*, Princeton Univ. Press, Princeton, NJ.

Lankhorst, M. 2009. *Enterprise architecture at work: Modelling, communiation and analysis,* 2nd, Springer, NY.

Law, A.M. and Kelton, W.D. 1991. *Simulation modeling and analysis, McGraw Hill series in industrial engineering and management science,* 2nd ed., McGraw Hill, NY.

Leydesdorff, L. and van den Besselaar, P. 1997. "Competing technologies: Lock-ins and lock-outs", in *AIP Conf. Proc.* 437, pp. 309-323

Petermann, A. 2010. *Pfadabhängigkeit und Hierarchie*. Diss., Freie Univ, Berlin.

Ross, J.W., Robertson, D.C. and Weill, P. 2006. *Enterprise architecture as strategy: Creating a foundation for business execution*, HBS Press, Boston, Mass.

Sydow, J., Schreyögg, G. and Koch, J. 2009. "Organizational path dependence: Opening the black box", *Academy of Management Review*, Vol. 34 No. 4, 689–709.

Ward, J. and Peppard, J. 2009. *Strategic planning for information systems, Wiley series in information systems,* 3rd ed., Wiley, Chichester.

Weitzel, T., Beimborn, D. and König, W. 2006. "A Unified Economic Model of Standard Diffusion: The Impact of Standardization Cost, Network Effects, and Network Topology", *MIS Quarterly*, Vol. 30, 489-514.

Widjaja, T. 2011. "Standardisierungsentscheidungen in mehrschichtigen Systemen", Diss., Techn. Univ, Darmstadt.

Windrum, P., Fagiolo, G. and Moneta, A. 2007. "Empirical Validation of Agent-Based Models: Alternatives and Prospects", *JASSS,* Vol. 10 No. 2, p. 8.

DANIEL FUERSTENAU was born in Riesa, Germany, and went to the Universities of Potsdam, Germany, and Âbo, Finland, where he studied business administration and information systems. He worked as an IT consultant before moving to Freie Universität Berlin in 2011 where he is now working on his PhD in the field of simulation and path dependence. Correspondence may be directed to daniel.fuerstenau@fu-berlin.de. His web page is http://www.pfadkolleg.de/fuerstenau.

Simulation of Intelligent Systems

METHODOLOGY FOR ELLIOTT WAVES PATTERN RECOGNITION

Martin Kotyrba
Eva Volna
Michal Janosek
Hashim Habiballa
David Brazina
Department of Informatics and Computers
University of Ostrava
70103, Ostrava, Czech Republic
E-mail: martin.kotyrba@osu.cz
E-mail: eva.volna@osu.cz
E-mail: michal.janosek@osu.cz
E-mail: hashim.habiballa@osu.cz
E-mail: david.brazina@osu.cz

KEYWORDS

Elliott waves, Fibonacci analysis, neural networks, pattern recognition, prediction.

ABSTRACT

The article is focused on an analysis and pattern recognition in time series, which are fractal in nature. The proposal methodology is based on an interdisciplinary approach that combines artificial neural networks, analytic programming, Elliott wave theory and knowledge modelling. The heart of the methodology are a methods, which is able to recognize Elliott waves structures including their deformation in the charts and helps to more efficient prediction of its trend. The functionality of the proposed methodology was validated in experimental simulations, for whose implementation was designed and created an application environment. Experimental simulations have shown that the method is usable to a wider class of problems than the theory itself allows only Elliott waves.This paper introduces a methodology that allows analysis of Elliot wave's patterns in time series for the purpose of a trend prediction.

INTRODUCTION - ELLIOTT WAVE PERSONALITY AND CHARACTERISTICS

Elliott wave analysts hold that each individual wave has its own signature or characteristic, which typically reflects the psychology of the moment (Poser2003). Understanding those personalities is a key to the application of the Wave Principle; they are defined as follows (Frost and Prechter 2001):

Five wave pattern - dominant trend (see Fig. 1)

- **Wave 1:** Wave one is rarely obvious at its inception. When the first wave of a new bull market begins, the fundamental news is almost universally negative. The previous trend is considered still strongly in force. Fundamental analyses continue to revise their earnings estimates lower; the economy probably does not look strong. Sentiment surveys are decidedly bearish, put options are in vogue, and implied volatility in the options market is high. Volume might increase a bit as prices rise, but not by enough to alert many technical analysts.

- **Wave 2:** Wave two corrects wave one, but can never extend beyond the starting point of wave one. Typically, the news is still bad. As prices retest the prior low, bearish sentiment quickly builds, and "the crowd" haughtily reminds all that the bear market is still deeply ensconced. Still, some positive signs appear for those who are looking: volume should be lower during wave two than during wave one, prices usually do not retrace more than 61.8% (see Fibonacci relationship) of the wave one gains, and prices should fall in a three wave pattern.

- **Wave 3:** Wave three is usually the largest and most powerful wave in a trend (although some research suggests that in commodity markets, wave five is the largest). The news is now positive and fundamental analysts start to raise earnings estimates. Prices rise quickly, corrections are short-lived and shallow. Anyone looking to "get in on a pullback" will likely miss the boat. As wave three starts, the news is probably still bearish, and most market players remain negative; but by wave three's midpoint, "the crowd" will often join the new bullish trend. Wave three often extends wave one by a ratio of 1.618:1.

- **Wave 4:** Wave four is typically clearly corrective. Prices may meander sideways for an extended period, and wave four typically retraces less than 38.2% of wave three (see Fibonacci relationships). Volume is well below than that of wave three. This is a good place to buy a pull back if you

Proceedings 27th European Conference on Modelling and Simulation ©ECMS Webjørn Rekdalsbakken, Robin T. Bye, Houxiang Zhang (Editors)
ISBN: 978-0-9564944-6-7 / ISBN: 978-0-9564944-7-4 (CD)

understand the potential ahead for wave 5. Still, fourth waves are often frustrating because of their lack of progress in the larger trend.

- **Wave 5:** Wave five is the final leg in the direction of the dominant trend. The news is almost universally positive and everyone is bullish. Unfortunately, this is when many average investors finally buy in, right before the top. Volume is often lower in wave five than in wave three, and many momentum indicators start to show divergences (prices reach a new high but the indicators do not reach a new peak). At the end of a major bull market, bears may very well be ridiculed (recall how forecasts for a top in the stock market during 2000 were received).

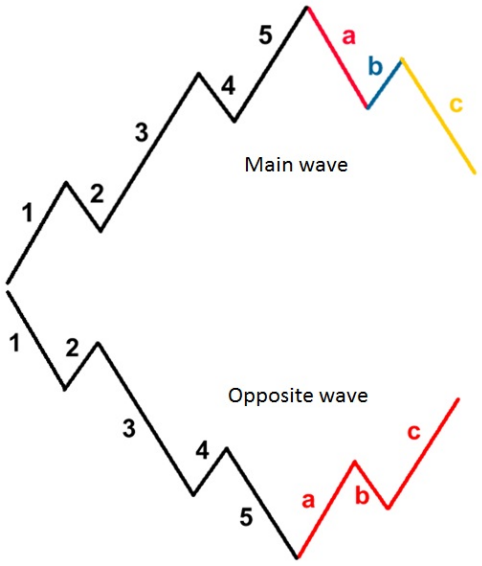

Figure 1: The basic pattern of Elliott wave

Three wave pattern - corrective trend (see Fig. 1)

- **Wave A:** Corrections are typically harder to identify than impulse moves. In wave A of a bear market, the fundamental news is usually still positive. Most analysts see the drop as a correction in a still-active bull market. Some technical indicators that accompany wave A include increased volume, rising implied volatility in the options markets and possibly a turn higher in open interest in related futures markets.

- **Wave B:** Prices reverse higher, which many see as a resumption of the now long-gone bull market. Those familiar with classical technical analysis may see the peak as the right shoulder of a head and shoulders reversal pattern. The volume during wave B should be lower than in wave A. By this point, fundamentals are probably no longer improving, but they most likely have not yet turned negative.

- **Wave C:** Prices move impulsively lower in five waves. Volume picks up, and by the third leg of wave C, almost everyone realizes that a bear market is firmly entrenched. Wave C is typically at least as large as wave A and often extends to 1.618 times wave A or beyond (Frost and Prechter 2001).

FIBONACCI ANALYSIS AND ELLIOTT WAVE THEORY

Fibonacci numbers provide the mathematical foundation for the Elliott Wave Theory. While the Fibonacci ratios have been adapted to various technical indicators, their utmost use in technical analysis remains the measurement of correction waves (Frost and Prechter 2001).
The Fibonacci number sequence 1, 1, 2, 3, 5, 8, 13, 21, 34, 55, 89,...is made by simply starting at 1 and adding the previous number to arrive at the new number:

0+1=1, 1+1=2, 2+1=3, 3+2=5, 5+3=8, 8+5=13, 13+8=21, 21+13=34, 34+21=55, 55+34=89,…

This series has very numerous interesting properties:

- The ratio of any number to the next number in the series approaches 0.618 or 61.8% (the golden ratio) after the first 4 numbers. For example: 34/55 = 0.618

- The ratio of any number to the number that is found two places to the right approaches 0.382 or 38.2%. For example: 34/89 = 0.382

- The ratio of any number to the number that is found three places to the right approaches 0.236 or 23.6%. For example: 21/89 = 0.236

These relationships between every number in the series are the foundation of the common ratios used to determine price retracements and price extensions during a trend (see Fig. 2).

Figure 2: Fibonacci price retracements and price extensions (adapted fromhttp://www.markets.com/education/technical-analysis/fibonacci-elliot-wave.html)

A retracement is a move in price that "retraces" a portion of the previous move. Usually a stock will retrace at one of 3 common Fibonacci levels- 38.2%, 50%, and 61.8%. Fibonacci price retracements are determined from a prior low-to high swing to identify possible support levels as the market pulls back from a high.Retracements are also run from a prior high-to-low swing using the same ratios, looking for possible resistance levels as the market bounces from a low (Frost and Prechter 2001).
Fibonacci price extensions are used by traders to determine areas where they will wish to take profits in the next leg of an up-or downtrend. Percentage extension levels are plotted as horizontal lines above/below the previous trend move. The most popular extension levels are 61.8%, 100.0%, 138.2% and 161.8%.
In reality it is not always so easy to spot the correct Elliott wave pattern, nor do prices always behave exactly according to this pattern. Therefore it is advisable for a trader not to rely solely on Fibonacci ratios, but rather to use them in conjunction with other technical tools.

ELLIOT WAVES DETECTION

Elliott waves are characterized by wide and numerous descriptions of their distinctive phases, thus they are difficult to detect in time series.

Detection according to the rules

The first eventuality is the classification which gradually runs from smallest to largest parts of Elliott waves. This method is described in (Dostál and Sojka 2008). The process starts with finding a scale and separate mono-waves marking. There are completed patterns according to particular ratios. These patterns are a base for other patterns. This approach is often used for manual evaluation with their subsequent processing. The method uses seven rules, which classify waves into groups depending on a ratio of heights of neighbouring waves. The rules use Fibonacci ratios with a deviation of 5%. The only possibility of searching is to check each mono-wave through the conditions and some experience of a researcher is expected as well. Here, the aim is not to deal with the evaluated segment, but to respect single figures as complex units. This method is accurate, but it is computationally very time consuming and it is limited to the detection of mono-waves according to the predetermined number of specific rules.

Detection units and their progressive separation

The second eventuality is classification of big parts of Elliott waves and their subsequent decomposition into smaller parts. Patterns of impulsive character can be detected clearly thanks to more accurate conditions than patterns of correction phase. Therefore it is possible to detect patterns proposed in input data. Here, the aim is to find a figure and then to classify its smaller units. A disadvantage is that impulse phases are only detected directly, while correction phases must be derived. Another disadvantage during detection of large parts is that their internal structure is unknown as long as other pulses are not found in these parts.

Detection according to characteristic figures

The third eventuality is to restrict detection to some significant figures, which are significant with respect to parts of patterns according to the Elliott theory. Therefore, the method does not restrict to detecting mono-waves. Found figures can be processed further, while found figures generate additional parameters for further processing. A disadvantage is that we are able to find a lot of characteristic patters in input data, which is time consuming. Here, we have to choose patterns correctly for detection and to have sufficient amount of test data to disposal. However, this approach is very effective and, therefore, it was chosen as a detection method in the article.

DETECTION SYSTEM FOR ELLIOT WAVES PATTERN RECOGNITION BASED ON NEURAL NETWORKS

The core of detection system is the multi-classifier, which consists of the for the pattern recognition of structures with fractal dynamics. The multi-classifier (Fig. 3) is based on neural networks which are adapted by backpropagation (Volna, Kotyrba and Jarusek 2013).

- The first neural network is designed to recognize selected Elliott wave's patterns. Emphasis is placed on the ability of a network to evaluate the found patterns with a degree of consensus of similarity with the defined pattern from training set. It is also necessary to network guarantee information about a quality of the found pattern.

- The second neural network evaluated prediction of trend component on the basis of the recognized pattern. The whole prediction is based on the IF-THEN rules from which the training set is composed for the second neural network. In essence, the neural network represents a rule-based of knowledge system that is able to decide whether a time series respects corrective or impulse direction.

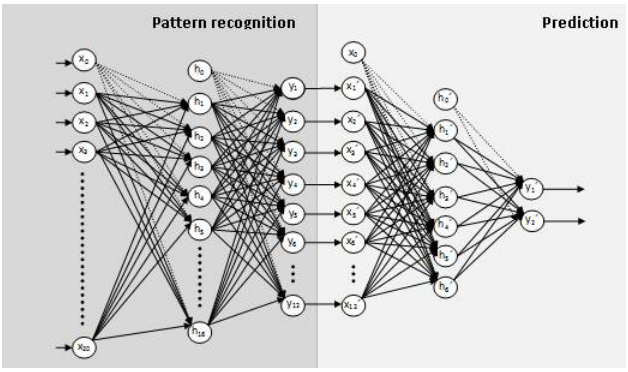

Figure 3: The multi-classifier proposal for the purpose of pattern recognition with consecutive prediction

Preparation of the training set of the first neural network using Fibonacci sequence

All patterns of training set were defined in order to represent the characteristics of Elliott wave to be identified in dependently of the time scale or the nature of the monitored data. When creating patterns, we used the properties of the Fibonacci sequence, which we used as a time filter so we could estimate when the impulse or correction would terminate. Time incorrections:

A wave = X units of time
B wave = 1.681 × X or B=< 0.618 × X
C wave = 0.618 × A (B) or
C=> 1.618 × A (B) or C= A+B

In the impulsive waves were taken into consideration waves where the first, third and fifth wave extended. These are patterns P6, P8, P10 in Fig. 4.

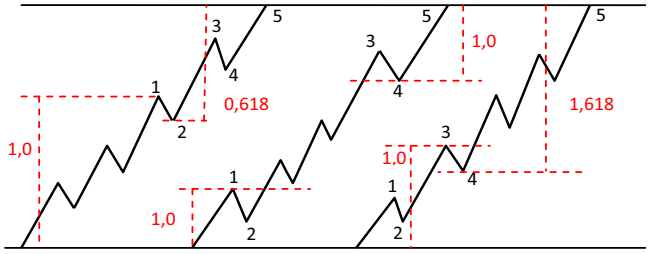

Figure 4: Extended phase of the impulse character

For example, when wave 3 is extended, waves 1 and 5 tend towards equality or a 0.618 relationship, as illustrated in Fig. 4. Actually, all three impulsive waves tend to be related by Fibonacci mathematics, whether by equality, 1.618 or 2.618 (whose inverses are 0.618 and 0.382). These impulse wave relationships usually occur in percentage terms. Wave 5's length is sometimes related by the Fibonacci ratio to the length of wave 1 through wave 3, as illustrated in Fig. 4. In those rare cases when wave 1 is extended, it is wave 2 that often subdivides the entire impulse wave into the wave, as shown in Fig. 4. In such cases, the latter portion is 0.382 of the total distance when wave 5 is not extended. This guideline explains why a retracement following the fifth wave often has double resistance at the same level: the end of the preceding fourth wave and the 0.382 retracement point (Frost and Prechter 2001).
We used the backpropagation method for the adaptation with the following parameters: first 5000 iterations havethe learning rate value 0.5, and for the next 2000 iterations the learning rate value is 0.1, momentum is 0. The conducted experimental studies also showed that in each cycle of adaptation is to present an adequate network of training patterns mixed randomly to ensure their greater diversity, but also acts as a measure of system stability. Uniform system in a crisis usually collapses entirely, while in the diversion system through a crisis of its individual parts, but the whole remains functional. The condition of end of the adaptation algorithm specified thelimit value of the overall network error, E <0.07. It concernsthe perfectthetraining set adaptation.
The second neural network of the proposed multi classifier simulates the knowledge system. Knowledge modelling is the concept of representing information and the logic of putting it to use in a digitally reusable format for purpose of capturing, sharing and processing knowledge to simulate intelligence. A knowledge base is designed in the form of rules. Each rule consists of a conditional and a consequential part. All rules are expressed in the following form: *IF a THEN b.* The left side of each rule represents a conditional part of the rule whereas its right side represents consequential part of the rule. For our purposes, it was essential to create suitable form of rules which should include all important features of the designed knowledge system. The rules in our system were presented in the following form:

IF *found pattern* & *fulfilment of consensus of similarity* THEN *trend direction*

There are two basic variables in the antecedent. It means fulfilment of consensus of similarity and found patterns which we gained as results (outputs) from the first part of classifier. After prediction of trend direction the consequent is composed like thisupward trend or downward trend. Consensus of similarity was set at 90% or more. In summary, the topology of neural network contains 12 input, 6 hidden and 2 output neurons. In the active phase, outputs of the first of neural networks are entering, which represent the degree of consensus of recognized Elliott wave pattern. The parameters of the backropagation algorithm (Fausett1994, Hertz et al. 1991) are the following: first 1000 iterations have learning rate value 0.5, and for the next 3000 iterations the learning rate value is 0.1, momentum is 0. These learning rates were set according to the experimental study. Calculation is halted after every 1000 cycles and the coefficient of the learning rate is set to a smaller value, resulting in subsequent weight gain soft. The Condition of the end of the adaptation algorithm specified the limit value of the overall network error, E < 0.07. It concerns the perfect the training set adaptation. Error function history (E) of both parts of multiclassifier during adaptation is shown in figure 5 (Kotyrba et al. 2012).

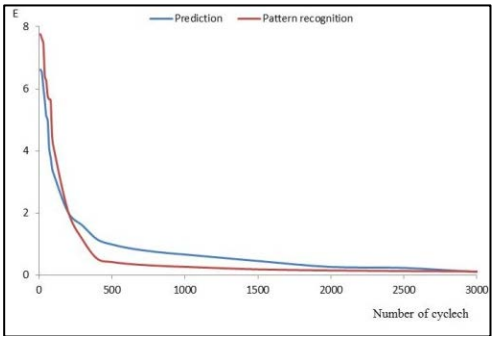

Figure 5: Error function history

METHODOLOGY OF RECOGNITION OF STRUCTURES WITH FRACTAL DYNAMICS

Aim of the proposed methodology is to propose a procedure for automatic pattern recognition in the systems with fractal dynamics in order to predict the trend. Using the proposed methodology, in the context of this articleis limited tothe stock market, but the area of application is much wider character, such as the prediction of sunspots or volume wave forms etc. The proposed methodology represents a sequence of actions whose implementation will help in the recommended sequence recognition of individual parts of structures Elliott waves, which can be used to predict the trend of the analyzed time series. The sequence of these activities is shown in Table 1.

Table 1: Steps of methodology

	Name of activity methodology	Character activities within publications	Selection tool
1	Obtaining data- time series with fractal dynamics.	It is essential to have appropriate data representing the solved problem.	World Wide Web.
2	Selection of structures for the purpose of detection and analyzing their characteristics.	Elliott wave analysis for identification of characteristic structures.	Elliott's theory.
3	Choice of classification methods and setting its parameters.	Settings of the first neural network topology, type of transfer function and adaptation parameters.	Neural network.
4	Preparing data for the first part of multiclassifier which realizes pattern recognition.	Preparation of standard training set patterns which represent individual parts Elliott waves.	Neural network, Elliott´s theory.
5	Application of methods.	Adaptation of the first neural network.	Neural network.
6	Proposal of knowledge system, preparing the base rules. Implementation of knowledge system in a form of the second part multiclassifier.	Preparation of normalized patterns for the training set for the second neural network that represents a rules-based knowledge system, designed to predict the trend line. Settings of the second neural network topology, type of transfer functionand adaptation parameters.	Neural network, Knowledge modeling.
7	Analysis and data processing and their preparation for further use.	Selection of test data series and its standardization. Adapted neural network recognizes patterns in test data with different degrees of compliance. Real outputs of the first neural network, also represents the inputs to the second neural network.	Neural network.
8	Evaluation of the solution results.	Validation of the results and their comparison with existing methods for overall evaluation.	Analytic Programming, Box-Jenkins methodology, Refined Elliott Trader, etc. Fuzzy logic toolbox etc.

ANALYSIS AND EVALUATION OF THE RESULTS

During our experimental study we applied a database from the area of financial forecasting [8] that is a set of data that reflects the situation on the market. Data shows volume behavior of Ebay corp.

In the first phase, a set of values with the found degree of consensus that is assigned to each recognized pattern from training set in test set is the output from the first neural network. It is important to realize what can be considered as an effective criterion. Whether there is about 90% agreement with the original pattern or is sufficient 70% for us? The proposed boundaries of the degree of consensus, comes from results of the performed experimental studies and it was set to at least 90%. The neural network is able to find dependences which are unobservable for humans. Therefore it may be a situation where the degree of consensus marked with neural networks is more than 90% and the visual evaluation of the expert is much less. Figure 6 shows the degree of consensus more than 78% even if expert could not determine such a real similarity with the original pattern. The performed experimental study shows success of the proposed methodology.

We examined a total of 10 data sets. Each of them contains 300 values. A propose methodology allows to recognize 5421 patterns with consensus of similarity greater than 70%, next 4852 patterns with consensus of similarity greater than 80% and 1752 patterns with consensus of similarity greater than 90% (Kotyrba et al. 2012).

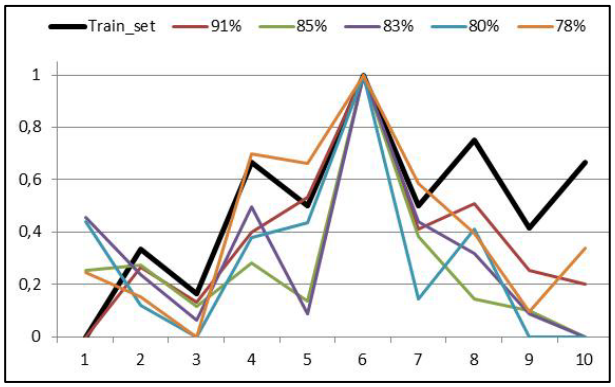

Figure 6: Similarities with degree of consensus more than 78%

Trend prediction was verified only for patterns with consensus of similarity greater than 90% and their number is 1189, what is 67.8 % successful prediction in total. In this case, the proposed multi-classifier is justifiable because the prediction percentage greater than 50% means success in the case of predictive exchange software.

CONCLUSION

In this paper, a short introduction into the field of time series pattern recognition using our methodology based on neural network has been given. According to the results of experimental studies, it can be stated that Elliot wave's patterns were successfully extracted in given time series and recognized using the suggested method as can be seen from the figures in the result section. The proposed methodology is based on an interdisciplinary approach that combines various methods of artificial intelligence. Experimental results show that the methodology can also be used on a wider class of problems than just detection of Elliott waves in the price charts and achieving successful prediction.

ACKNOWLEDGMENT

The research described here has been financially supported by University of Ostrava grant SGS23/ PřF/2013.

REFERENCES

Dostál, P., Sojka, Z. "Elliottovy vlny" *Tribuns.r.o*., Brno 2008, ISBN 978-80-7399-630-7.

Fausett, L., 1994, "Fundamentals of Neural Network". *1st ed. Prentice Hall*, ISBN: 0-13-334186-0.

Hertz, J. and Kogh, A. and Palmer, R G, 1991: "Introduction to the Theory of Neural Computation", *Addison – Wesley*.

Frost, A.J. and Prechter, R.2001. "Elliott Wave Principle: Key to Market Behavior", ISBN 0471988499, *John Wiley & Sons*.

Poser, S. 2003. "Applying Elliott Wave Theory Profitably". *Publisher*: Wiley. ISBN-10: 0471420077.

Volna, E. Kotyrba, M. and Jarusek, R. 2013 "Multiclassifier based on Elliott wave's recognition" *Computers and Mathemacics with Applications*, doi: 10.1016/j.camwa.2013.01.012

Kotyrba, M., Volná, E., Bražina, D., Jarušek, R. „Elliott waves recognition via neural networks", In Troitzsch, K.G., Möhring, M., Lotzmann, U. (eds.): *Proceedings 26th European Conference on Modellingand Simulation*, ECMS 2012, Koblenz, Germany, 2012, pp. 361-366. ISBN: 978-0-9564944-4-3. doi: 10.7148/2012

A database from the area of financial forecasting *[online, Accessed 10 January 2013*], http://www.forexrate.co.uk and http://www.fxhistoricaldata.com

MARTIN KOTYRBA is a doctor at the Department of Computer Science at University of Ostrava, Czech Republic. His interests include artificial intelligence, formal logic, soft computing methods and fractals. He is an author of more than 30 papers in proceedings of conferences.

EVA VOLNA is an associate professor at the Department of Computer Science at University of Ostrava, Czech Republic. Her interests include artificial intelligence, artificial neural networks, evolutionary algorithms, and cognitive science. She is an author of more than 50 papers in technical journals and proceedings of conferences.

MICHAL JANOSEK is a doctor at the Department of Computer Science at University of Ostrava, Czech Republic. His interests include artificial intelligence, multi-agent systems, modeling and simulations. He is an author of more than 20 papers in proceedings of conferences.

HASHIM HABIBALLA is an associate Professor at University of Ostrava, Dept. of Informatics and Computers and researcher of Centre of Excelence IT4Innovations - Institute for Research and Application of Fuzzy Modeling. Holds MSc. (1999) and Ph.D. (2007) in Information Systems, holds also PhD. and EdD. in CS Education (2004). He focuses to artificial intelligence, logic, formal languages and is author of 100 publications.

DAVID BRAZINA is an doctor at the Department of Computer Science at University of Ostrava, Czech Republic. His interests include computer graphics, neural networks. He is an author of more than 10 papers in technical journals and proceedings of conferences.

IRIS DATA CLASSIFICATION BY MEANS OF PSEUDO NEURAL NETWORKS BASED ON EVOLUTIONARY SYMBOLIC REGRESSION

Zuzana Kominkova Oplatkova, Roman Senkerik

Tomas Bata University in Zlin, Faculty of Applied Informatics
Nam T.G. Masaryka 5555, 760 01 Zlin, Czech Republic
{oplatkova, senkerik}@fai.utb.cz

KEYWORDS
Iris data, Pseudo Neural Network, Analytic programming, Differential Evolution.

ABSTRACT

This research deals with a novel approach to classification. Iris data was used for the experiments. Classical artificial neural networks, where a relation between inputs and outputs is based on the mathematical transfer functions and optimized numerical weights, was an inspiration for this work. Artificial neural networks need to optimize weights, but the structure and transfer functions are usually set up before the training. The proposed method utilizes the symbolic regression for synthesis of a whole structure, i.e. the relation between inputs and output(s) and tested on iris data in this case. For experimentation, Differential Evolution (DE) for the main procedure and also for meta-evolution version of analytic programming (AP) was used.

INTRODUCTION

The interest about classification by means of some automatic process has been enlarged with the development of artificial neural networks (ANN). They can be used also for a lot of other possible applications like pattern recognition, prediction, control, signal filtering, approximation, etc. All artificial neural networks are based on some relation between inputs and output(s), which utilizes mathematical transfer functions and optimized weights from training process. The setting-up of layers, number of neurons in layers, estimating of suitable values of weights is a demanding procedure. On account of this fact, pseudo neural networks, which represent the novelty approach using symbolic regression with evolutionary computation, is proposed in this paper.

Symbolic regression in the context of evolutionary computation means to build a complex formula from basic operators defined by users. The basic case represents a process in which the measured data is fitted and a suitable mathematical formula is obtained in an analytical way. This process is widely known for mathematicians. They use this process when a need arises for mathematical model of unknown data, i.e. relation between input and output values. The symbolic regression can be used also for design of electronic circuits or optimal trajectory for robots and within other applications (Back et al., 1997), (Koza, 1998), (Koza, 1999), (O'Neill et al., 2003), (Zelinka et al., 2011), (Oplatkova, 2009), (Varacha et al., 2006). Everything depends on the user-defined set of operators. The proposed technique is similar to synthesis of analytical form of mathematical model between input and output(s) in training set used in neural networks. Therefore it is called Pseudo Neural Networks.

Initially, John Koza proposed the idea of symbolic regression done by means of a computer in Genetic Programming (GP) (Back et al., 1997), (Koza, 1998), (Koza, 1999). The other approaches are e.g. Grammatical Evolution (GE) developed by Conor Ryan (O'Neill et al., 2003) and here described Analytic Programming (Zelinka et al., 2011), (Oplatkova, 2009), (Varacha et al., 2006).

The above-described tools were recently commonly used for synthesis of artificial neural networks but in a different manner than is presented here. One possibility is the usage of evolutionary algorithms for optimization of weights to obtain the ANN training process with a small or no training error result. Some other approaches represent the special ways of encoding the structure of the ANN either into the individuals of evolutionary algorithms or into the tools like Genetic Programming. But all of these methods are still working with the classical terminology and separation of ANN to neurons and their transfer functions (Fekiac, 2011). In this paper, the proposed technique synthesizes the structure without a prior knowledge of transfer functions and inner potentials. It synthesizes the relation between inputs and output of training set items used in neural networks so that the items of each group are correctly classified according the rules for cost function value. The data set used for training is Iris data set (Machine Learning Repository, Fisher 1936). It is a very known benchmark data set for classification problem, which was introduced by Fisher for the first time.

Firstly, Analytic Programming used as a symbolic regression tool is described. Subsequently Differential Evolution used for main optimization procedure within Analytic Programming and also as a second algorithm within metaevolution purposes is mentioned. After that a brief description of artificial neural network (ANN) follows. Afterwards, the proposed experiment with differences compared to classical ANN is explained. The result section and conclusion finish the paper.

Proceedings 27th European Conference on Modelling and Simulation ©ECMS Webjørn Rekdalsbakken, Robin T. Bye, Houxiang Zhang (Editors)
ISBN: 978-0-9564944-6-7 / ISBN: 978-0-9564944-7-4 (CD)

ANALYTIC PROGRAMMING

Basic principles of the AP were developed in 2001 (Zelinka et al., 2005), (Zelinka et al., 2008), (Oplatkova, 2009), (Zelinka et al., 2011). Until that time only genetic programming (GP) and grammatical evolution (GE) had existed. GP uses genetic algorithms while AP can be used with any evolutionary algorithm, independently on individual representation. To avoid any confusion, based on use of names according to the used algorithm, the name - Analytic Programming was chosen, since AP represents synthesis of analytical solution by means of evolutionary algorithms.

The core of AP is based on a special set of mathematical objects and operations. The set of mathematical objects is set of functions, operators and so-called terminals (as well as in GP), which are usually constants or independent variables. This set of variables is usually mixed together and consists of functions with different number of arguments. Because of a variability of the content of this set, it is called here "general functional set" – GFS. The structure of GFS is created by subsets of functions according to the number of their arguments. For example GFS_{all} is a set of all functions, operators and terminals, GFS_{3arg} is a subset containing functions with only three arguments, GFS_{0arg} represents only terminals, etc. The subset structure presence in GFS is vitally important for AP. It is used to avoid synthesis of pathological programs, i.e. programs containing functions without arguments, etc. The content of GFS is dependent only on the user. Various functions and terminals can be mixed together (Zelinka et al., 2005), (Zelinka et al., 2008), (Oplatkova, 2009).

The second part of the AP core is a sequence of mathematical operations, which are used for the program synthesis. These operations are used to transform an individual of a population into a suitable program. Mathematically stated, it is a mapping from an individual domain into a program domain. This mapping consists of two main parts. The first part is called discrete set handling (DSH) (See Figure 1) (Zelinka et al., 2005), (Lampinen and Zelinka, 1999) and the second one stands for security procedures which do not allow synthesizing pathological programs. The method of DSH, when used, allows handling arbitrary objects including nonnumeric objects like linguistic terms {hot, cold, dark…}, logic terms (True, False) or other user defined functions. In the AP DSH is used to map an individual into GFS and together with security procedures creates the above mentioned mapping which transforms arbitrary individual into a program.

AP needs some evolutionary algorithm (Zelinka, 2004) that consists of population of individuals for its run. Individuals in the population consist of integer parameters, i.e. an individual is an integer index pointing into GFS. The creation of the program can be schematically observed in Fig. 2. The individual contains numbers which are indices into GFS. The detailed description is represented in (Zelinka et al., 2005), (Zelinka et al., 2008), (Oplatkova et al., 2009).

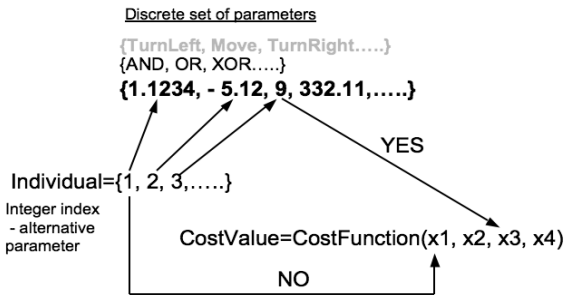

Figure 1: Discrete set handling

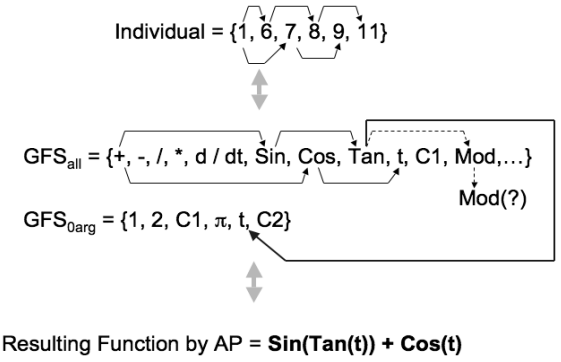

Figure 2: Main principles of AP

AP exists in 3 versions – basic without constant estimation, AP_{nf} – estimation by means of nonlinear fitting package in Mathematica environment and AP_{meta} – constant estimation by means of another evolutionary algorithms; meta means metaevolution.

ARTIFICIAL NEURAL NETWORKS

Artificial neural networks are inspired in the biological neural nets and are used for complex and difficult tasks (Hertz et al., 1991), (Wasserman, 1980), (Gurney, 1997), (Fausset, 2003). The most often usage is classification of objects as also in this case. ANNs are capable of generalization and hence the classification is natural for them. Some other possibilities are in pattern recognition, control, filtering of signals and also data approximation and others.

There are several kinds of ANN. Simulations were based on similarity with feedforward net with supervision. ANN needs a training set of known solutions to be learned on them. Supervised ANN has to have input and also required output.

The neural network works so that suitable inputs in numbers have to be given on the input vector. These inputs are multiplied by weights which are adjusted during the training. In the neuron the sum of inputs multiplied by weights are transferred through mathematical function like sigmoid, linear, hyperbolic tangent etc. Therefore ANN can be used for data approximation (Hertz et al., 1991) – a regression model on measured data, relation between input and required (measured data) output.

These single neuron units (Fig. 3) are connected to different structures to obtain different structures of ANN (e.g. Fig. 4 and Fig. 5), where $\sum \delta = TF[\sum (w_i x_i + b w_b)]$ and $\sum = TF[\sum (w_i x_i + b w_b)]$; TF is logistic sigmoid function in this case.

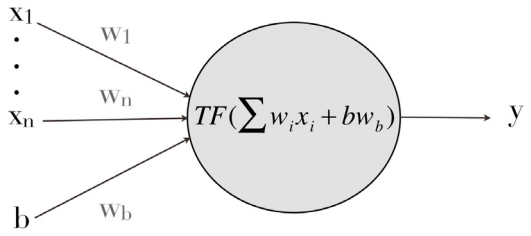

Figure 3: Neuron model, where TF (transfer function like sigmoid), x_1 - x_n (inputs to neural network), b – bias (usually equal to 1), w_1 – w_n, w_b – weights, y – output

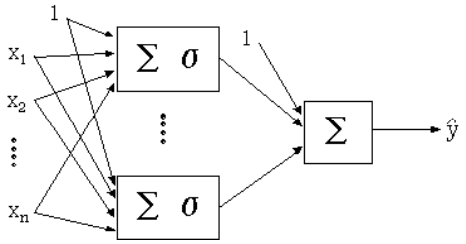

Figure 4: ANN models with one hidden layer

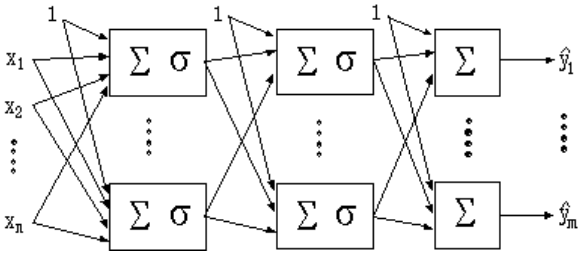

Figure 5: ANN models with two hidden layers and more outputs

The example of relation between inputs and output can be shown as a mathematical form (1). It represents the case of only one neuron and logistic sigmoid function as a transfer function.

$$y = \frac{1}{1 + e^{-(x_1 w_1 + x_2 w_2)}}, \qquad (1)$$

where y – output
x_1, x_2 – inputs
w_1, w_2 – weights.

The aim of the proposed technique is to find similar relation to (1). This relation is completely synthesized by evolutionary symbolic regression – Analytic Programming.

USED EVOLUTIONARY ALGORITHMS

This research used one evolutionary algorithm Differential Evolution (Price, 2005) for both parts – main procedure and metaevolutionary part of the analytic programming. Future simulations expect a usage of soft computing GAHC algorithm (modification of HC12) (Matousek, 2007) and a CUDA implementation of HC12 algorithm (Matousek, 2010).

Differential evolution

DE is a population-based optimization method that works on real-number-coded individuals (Price, 2005). For each individual $\vec{x}_{i,G}$ in the current generation G, DE generates a new trial individual $\vec{x}'_{i,G}$ by adding the weighted difference between two randomly selected individuals $\vec{x}_{r1,G}$ and $\vec{x}_{r2,G}$ to a randomly selected third individual $\vec{x}_{r3,G}$. The resulting individual $\vec{x}'_{i,G}$ is crossed-over with the original individual $\vec{x}_{i,G}$. The fitness of the resulting individual, referred to as a perturbed vector $\vec{u}_{i,G+1}$, is then compared with the fitness of $\vec{x}_{i,G}$. If the fitness of $\vec{u}_{i,G+1}$ is greater than the fitness of $\vec{x}_{i,G}$, then $\vec{x}_{i,G}$ is replaced with $\vec{u}_{i,G+1}$; otherwise, $\vec{x}_{i,G}$ remains in the population as $\vec{x}_{i,G+1}$. DE is quite robust, fast, and effective, with global optimization ability. It does not require the objective function to be differentiable, and it works well even with noisy and time-dependent objective functions. Description of used DERand1Bin strategy is presented in (2). Please refer to (Price and Storn 2001, Price 2005) for the description of all other strategies.

$$u_{i,G+1} = x_{r1,G} + F \bullet \left(x_{r2,G} - x_{r3,G}\right) \qquad (2)$$

PROBLEM DESIGN – IRIS PLANT DATA SET DEFINITION

For this classification problem, iris data set was used (Machine Learning Repository, Fisher 1936). This set contains 150 instances. Half amount was used as training data and the second half was used as testing data. The data set contains 3 classes of 50 instances each, where each class refers to a type of iris plant. One class is linearly separable from the other 2; the latter are NOT linearly separable from each other. Each instance has 4 attributes (sepal length, sepal width, petal length and petal width) and type of class – iris virginica (Fig. 6), iris versicolor (Fig. 7) and iris sentosa (Fig. 8). The attributes were of real values. Usually, the class is defined by 3 output neurons in classical artificial neural net and binary code. In this paper, AP was able to create pseudo neural net structure between inputs and one output. Therefore, three classes were designed as continues value of the output, i.e. iris setosa was -1 for output less than -1, iris virginica has value 1 for output

greater than 1, and iris versicolor was 0 for outputs between -1 and 1.
The cost function value is given in eq. (3), i.e. if the cv is equal to zero, all training patterns are classified correctly.

$$cv = \sum_{i=1}^{n} \left| requiredOutput - currentOutput \right| \qquad (3)$$

Figure 6**:** Iris virginica

Figure 7: Iris versicolor

Figure 8: Iris setosa

RESULTS

As described in section about Analytic Programming, AP requires some EA for its run. In this paper AP_{meta} version was used. Meta-evolutionary approach means usage of one main evolutionary algorithm for AP process and second algorithm for coefficient estimation, thus to find optimal values of constants in the structure of pseudo neural networks.
In this paper, DE was used for main AP process and also in the second evolutionary process. Settings of EA parameters for both processes were based on performed numerous experiments with chaotic systems and simulations with AP_{meta} (Table 1 and Table 2).

Table 1: DE settings for main process

PopSize	20
F	0.8
CR	0.8
Generations	50
Max. CF Evaluations (CFE)	1000

Table 2: DE settings for meta-evolution

PopSize	40
F	0.8
CR	0.8
Generations	150
Max. CF Evaluations (CFE)	6000

The set of elementary functions for AP was inspired in the items used in classical artificial neural nets. The components of input vector x contain values of each attribute (x_1, x_2, x_3, x_4).

Basic set of elementary functions for AP:
GFS2arg= +, -, /, *, ^, exp
GFS0arg= x_1, x_2, x_3, x_4, K

Total number of cost function evaluations for AP was 1000, for the second EA it was 6000, together 6 millions per each simulation.

From carried simulations, several notations of input dependency were obtained, e.g. (4) and (5). The case (4) had a training error equal to 2 misclassified items (it means 2.66% error, 97.34% success from all 75 training patterns) and testing error equal to 3 misclassified items (4% error, 96% success). The case (5) was worse, during training phase the error equal to 3 misclassified patterns was reached and testing error was equal to 5.

Following numbers (6) are the outputs from the pseudo neural network for the training set, which has been then saturated to 3 numbers -1, 0 and 1 according to the class type interval (7). The (8) and (9) is the same way obtained numbers for the testing set.

$$y = \left(-\frac{7.57336\, e^{-x_3}\, x_2}{x_4} - x_3 + x_4\right)\exp\left(-6.91605\times 10^{117^{344.416^{e^{-x_2^{x_4}}\left(x_1+1.0796\times10^{-233x_1}-e^{x_2}\right)}-e^{-x_4-e^{x_2}}}}\right) \quad (4)$$

$$y = \left(e^{-0.0066007\,(x_4+693.44)}\right)^{-0.00311885\,(x_3+e^{x_3}-144.991)} - 953.535\, e^{x_3\,(-x_4-637.961)}\left(-x_2 - x_4 + \frac{6.11200456962\times10^{625}}{(x_2\, x_4)^{223.656}}\right) \quad (5)$$

classical output = {-2.32401, -1.82401, -2.02399, -1.92404, -2.42401, -2.51714, -2.1247, -2.22404, -1.72401, -2.01559, -2.52404, -2.22406, -1.91558, -1.91555, -2.82397, -3.01703, -2.51692, -2.2247, -2.52481, -2.52474, -2.22408, -2.31703, -2.42392, -1.80036, -2.22413, -0.100247, 0.162017, 0.259989, 0.561469, 0.56151, 0.0595996, 0.344323, -0.153875, -0.0407742, 0.403247, 0.245674, 0.36354, 0.0445453, 0.199753, -0.037034, 0.00106313, 0.362017, -0.45568, 1.16202, -0.0659825, 1.08403, 0.0614693, 0.859989, -0.163289, -0.0396526, 4.23024, 1.94265, 2.4494, 1.37783, 2.90987, 2.44134, 1.45294, 1.37241, 1.77628, 3.92834, 1.8341, 1.94088, 2.45401, 2.53511, 4.15996, 3.21541, 1.27861, 2.0981, 3.79167, 1.15948, 3.20947, 2.23613, 2.21791, 1.58326, 2.15171} (6)

saturated output to class type = {-1, -1, -1, -1, -1, -1, -1, -1, -1, -1, -1, -1, -1, -1, -1, -1, -1, -1, -1, -1, -1, -1, -1, -1, -1, 0, 0, 0, 0, 0, 0, 0, 0, 0, 0, 0, 0, 0, 0, 0, 0, 0, 1., 0, 1., 0, 0, 0, 0, 1., 1., 1., 1., 1., 1., 1., 1., 1., 1., 1., 1., 1., 1., 1., 1., 1., 1., 1., 1., 1., 1., 1., 1., 1., 1.} (7)

testing classical output = {-1.82406, -2.01709, -2.32404, -2.22401, -2.02406, -1.92406, -2.01703, -3.01559, -3.02401, -2.01559, -2.02397, -2.32399, -2.01559, -1.82399, -2.22404, -2.22466, -1.02466, -2.02399, -1.87359, -2.41725, -1.7247, -2.62406, -2.02401, -2.52404, -2.12401, 0.101063, 0.299317, 0.949556, 0.462017, -0.354326, 0.0342867, -0.154778, -0.0607432, 0.941977, 0.362017, 0.245497, 0.261003, 0.559973, -0.138905, 0.361469, 0.0376652, 0.10019, 0.0389384, -0.053875, 0.160721, -0.361698, -0.0392787, -0.0396526, -0.063559, 0.0610953, 1.07473, 1.48403, 1.28326, 2.65286, 0.637876, 1.83378, 1.22094, 3.11249, 0.558975, 0.495828, 3.40353, 3.55155, 1.17861, 1.28403, 2.35517, 3.85155, 3.31839, 1.94265, 3.2065, 4.23593, 3.4169, 2.14354, 2.03309, 3.01393, 1.28171} (8)

testing saturated output to class type = {-1, -1, -1, -1, -1, -1, -1, -1, -1, -1, -1, -1, -1, -1, -1, -1, -1, -1, -1, -1, -1, -1, -1, -1, -1, 0, 0, 0, 0, 0, 0, 0, 0, 0, 0, 0, 0, 0, 0, 0, 0, 0, 0, 0, 0, 0, 0, 0, 0, 0, 1., 1., 1., 1., 0, 1., 1., 1., 0, 0, 1., 1., 1., 1., 1., 1., 1., 1., 1., 1., 1., 1., 1., 1., 1.} (9)

From the above values, it can be visible which items were classified in a wrong group. During training iris versicolor was misclassified twice as iris sentosa, in the testing phase it was viceversa – iris sentosa as iris versicolor.

CONCLUSION

This paper deals with a novel approach – pseudo neural networks. Within this approach, classical optimization of the structure or weights was not performed. The proposed technique is based on symbolic regression with evolutionary computation. It synthesizes a whole structure in symbolic form without a prior knowledge of the ANN structure or transfer functions. It means that the relation between inputs and output(s) is synthesized. As can be seen from the result section, such approach is promising. For further tests some observed critical points have to be taken into consideration. Future plans will be focused on further tests and comparisons with classical neural nets.

ACKNOWLEDGEMENT

This work was supported by the European Regional Development Fund under the project CEBIA-Tech No. CZ.1.05/2.1.00/03.0089.

REFERENCES

Back T., Fogel D. B., Michalewicz Z., *Handbook of evolutionary algorithms*, Oxford University Press, 1997, ISBN 0750303921

Fausett L. V.: Fundamentals of Neural Networks: Architectures, Algorithms and Applications, Prentice Hall, 1993, ISBN: 9780133341867

Fekiac J., Zelinka I., Burguillo J. C.: A review of methods for encoding neural network topologies in evolutionary computation, ECMS 2011, Krakow, Poland, ISBN: 978-0-9564944-3-6

Fisher R. A. (1936). "The use of multiple measurements in taxonomic problems". Annals of Eugenics 7 (2): 179–188. doi:10.1111/j.1469-1809.1936.tb02137.x

Gurney K.: An Introduction to Neural Networks, CRC Press, 1997, ISBN: 1857285034

Hertz J., Kogh A. and Palmer R. G.: Introduction to the Theory of Neural Computation, Addison – Wesley 1991

Koza J. R. et al., *Genetic Programming III; Darwinian Invention and problem Solving*, Morgan Kaufmann Publisher, 1999, ISBN 1-55860-543-6

Koza J. R., *Genetic Programming,* MIT Press, 1998, ISBN 0-262-11189-6

Lampinen J., Zelinka I., 1999, "New Ideas in Optimization – Mechanical Engineering Design Optimization by

Differential Evolution", Volume 1, London: McGraw-hill, 1999, 20 p., ISBN 007-709506-5.

Machine learning repository with Iris data set http://archive.ics.uci.edu/ml/datasets/Iris

Matousek R., 2010, „HC12: The Principle of CUDA Implementation". In MENDEL 2010, Mendel Journal series, pp. 303-308. ISBN: 978-80-214-4120- 0. ISSN: 1803- 3814.

Matousek R., 2007, „GAHC: Improved GA with HC station", In WCECS 2007, San Francisco, pp. 915-920. ISBN: 978-988-98671-6-4.

O'Neill M., Ryan C., *Grammatical Evolution. Evolutionary Automatic Programming in an Arbitrary Language*, Kluwer Academic Publishers, 2003, ISBN 1402074441

Oplatkova Z.: Metaevolution: Synthesis of Optimization Algorithms by means of Symbolic Regression and Evolutionary Algorithms, Lambert Academic Publishing Saarbrücken, 2009, ISBN: 978-3-8383-1808-0

Price K., Storn R. M., Lampinen J. A., 2005, "Differential Evolution : A Practical Approach to Global Optimization", (Natural Computing Series), Springer; 1 edition.

Price, K. and Storn, R. (2001), *Differential evolution homepage*, [Online]: http://www.icsi.berkeley.edu/~storn/code.html, [Accessed 29/02/2012].

Wasserman P. D.: Neural Computing: Theory and Practice, Coriolis Group, 1980, ISBN: 0442207433

Zelinka et al.: Analytical Programming - a Novel Approach for Evolutionary Synthesis of Symbolic Structures, in Kita E.: Evolutionary Algorithms, InTech 2011, ISBN: 978-953-307-171-8

Zelinka I., Varacha P., Oplatkova Z., *Evolutionary Synthesis of Neural Network*, Mendel 2006 – 12th International Conference on Softcomputing, Brno, Czech Republic, 31 May – 2 June 2006, pages 25 – 31, ISBN 80-214-3195-4

Zelinka I.,Oplatkova Z, Nolle L., 2005. *Boolean Symmetry Function Synthesis by Means of Arbitrary Evolutionary Algorithms-Comparative Study*, International Journal of Simulation Systems, Science and Technology, Volume 6, Number 9, August 2005, pages 44 - 56, ISSN: 1473-8031.

MODELLING AND REASONING WITH FUZZY LOGIC REDUNDANT KNOWLEDGE BASES

Hashim Habiballa
Eva Volná
Michal Janošek
Martin Kotyrba
Department of Computer Science
Faculty of Science, University of Ostrava
30. dubna 22, Ostrava, Czech republic
Email: hashim.habiballa@osu.cz

KEYWORDS

Fuzzy logic; Knowledge base; Resolution reasoning

ABSTRACT

Fuzzy Predicate Logic with evaluated syntax together with resolution principle is presented. The paper focuses mainly on modelling and treating redudancy in knowledge bases. It presents original resolution rule together with algorithm DCF - Detection of Consequent Formulas developed especially for fuzzy logic with evaluated syntax.

REASONING IN FUZZY PREDICATE LOGIC WITH EVALUATED SYNTAX

The problem of effective modelling and reasoning on knowledge bases rises especially when dealing with many-valued logics. We would like to recall previously devised notions and methods of fuzzy resolution principle and then show original efficient methods making such a reasoning tractable.

Fuzzy Predicate Logic with Evaluated Syntax (FPL) [Novák, V., Perfilieva, I., Močkoř, J., 1999] is a well-studied and wide-used logic capable of expressing vagueness. It has a lot of applications based on robust theoretical background. It also requires an efficient formal proof theory. However the most widely applied resolution principle [Dukić, N., Avdagić, Z., 2005] brings syntactically several obstacles mainly arising from normal form transformation. There are also recent attempts of similarity based resolution [Mondal, B., Raha, S., 2012], but our approach is based on classical proof theory of FPL. FPL is associating with even harder problems when trying to use the resolution principle. Solutions to these obstacles based on the non-clausal resolution [Bachmair, L., Ganzinger, H., 1997] were already proposed in [Habiballa, H., 2006].

In this article it would be presented a natural integration of these two formal logical systems into fully functioning inference system with effective proof search strategies. It leads to the refutational resolution theorem prover for FPL ($RRTP_{FPL}$). Another issue addressed in the paper concerns to the efficiency of presented inference strategies developed originally for the proving system. It is showed their perspectives in combination with standard proof-search strategies. The main problem for the fuzzy logic theorem proving lies in the large amount of possible proofs with different degrees and there is presented an algorithm (Detection of Consequent Formulas - DCF) solving this problem. The algorithm is based on detection of such redundant formulas (proofs) with different degrees.

The article presents the method which is the main point of the work on any automated prover. There is a lot of strategies which make proofs more efficient when we use refutational proving. We consider well-known strategies - orderings, filtration strategy, set of support etc. One of the most effective strategies is the elimination of consequent formulas. It means the check if a resolvent is not a logical consequence of a formula in set of axioms or a previous resolvent. If such a condition holds it is reasonable to not include the resolvent into the set of resolvents, because if the refutation can be deduced from it, then so it can be deduced from the original resolvent, which it implies of.

Resolution and Fuzzy Predicate Logic

The fuzzy predicate logic with evaluated syntax is a flexible and fully complete formalism, which will be used for the below presented extension [Novák, V., Perfilieva, I., Močkoř, J., 1999]. In order to use an efficient form of the resolution principle we have to extend the standard notion of a proof (provability value and degree) with the notion of refutational proof (refutation degree). Propositonal version of the fuzzy resolution principle has been already presented in [Habiballa, H., 2002]. We suppose that set of truth values is Łukasiewicz algebra. Therefore we assume standard notions of conjunction, disjunction etc. to be bound with Łukasiewicz operators.

We will assume Łukasewicz algebra to be

$$\mathcal{L}_{\text{Ł}} = \langle [0,1], \wedge, \vee, \otimes, \rightarrow, 0, 1 \rangle$$

Proceedings 27th European Conference on Modelling and Simulation ©ECMS Webjørn Rekdalsbakken, Robin T. Bye, Houxiang Zhang (Editors)
ISBN: 978-0-9564944-6-7 / ISBN: 978-0-9564944-7-4 (CD)

where [0, 1] is the interval of reals between 0 and 1, which are the smallest and greatest elements respectively. Basic and additional operations are defined as follows:

$$a \otimes b = 0 \vee (a + b - 1) \quad a \to b = 1 \wedge (1 - a + b)$$

$$a \oplus b = 1 \wedge (a + b) \quad \neg a = 1 - a$$

The biresiduation operation $\leftrightarrow$ could be defined $a \leftrightarrow b =_{df} (a \to b) \wedge (b \to a)$, where $\wedge$ is infimum operation. The following properties of $\mathcal{L}_{\mathrm{L}}$ will be used in the sequel:
$a \otimes 1 = a$, $a \otimes 0 = 0$, $a \oplus 1 = 1$, $a \oplus 0 = a$, $a \to 1 = 1$, $a \to 0 = \neg a$, $1 \to a = a$, $0 \to a = 1$
The syntax and semantics of fuzzy predicate logic is following:
- terms $t_1, ..., t_n$ are defined as in FOL
- predicates with $p_1, ..., p_m$ are syntactically equivalent to FOL ones. Instead of 0 we write $\bot$ and instead of 1 we write $\top$, connectives - **&** (Łukasiewicz conjunction), ∇ (Łukasiewicz disjunction), $\Rightarrow$ (implication), $\neg$ (negation), $\forall X$ (universal quantifier),$\exists X$ (existential quantifier) and furthermore by F_J we denote set of all formulas of fuzzy logic in language J
- FPL formulas have the following semantic interpretations (D is the universe): Interpretation of terms is equivalent to FOL, $\mathcal{D}(p_i(t_{i_1}, ..., t_{i_n})) = P_i(\mathcal{D}(t_{i_1}), ..., \mathcal{D}(t_{i_n}))$ where P_i is a fuzzy relation assigned to p_i, $\mathcal{D}(\mathbf{a}) = a$ for $a \in [0, 1]$, $\mathcal{D}(A \,\&\, B) = \mathcal{D}(A) \otimes \mathcal{D}(B)$, $\mathcal{D}(A \,\nabla\, B) = \mathcal{D}(A) \oplus \mathcal{D}(B)$, $\mathcal{D}(A \Rightarrow B) = \mathcal{D}(A) \to \mathcal{D}(B)$, $\mathcal{D}(\neg A) = \neg \mathcal{D}(\mathbf{A})$,
$\mathcal{D}(\forall X(A)) = \bigwedge \mathcal{D}(A[x/d] | d \in D)$, $\mathcal{D}(\exists X(A)) = \bigvee \mathcal{D}(A[x/d] | d \in D)$

Graded fuzzy predicate calculus assigns grade to every axiom, in which the formula is valid. It will be written as a/A where A is a formula and a is a syntactic evaluation. We use several standard notions defined in [Novák, V., Perfilieva, I., Močkoř, J., 1999] namely: inference rule, formal fuzzy theory with set of logical and special axioms, evaluated formal proof.

Definition 1: Inference rule
An n-ary inference rule r in the graded logical system is a scheme

$$r : \frac{a_1/A_1, ..., \; a_n/A_n}{r^{evl}(a_1, ..., a_n)/r^{syn}(A_1, ..., A_n)} \qquad (1)$$

using which the evaluated formulas $a_1/A_1, ..., \; a_n/A_n$ are assigned the evaluated formula $r^{evl}(a_1, ..., a_n)/r^{syn}(A_1, ..., A_n)$. The syntactic operation r^{syn} is a partial n-ary operation on F_J and the evaluation operation r^{evl} is an n-ary lower semicontinous operation on L (i.e. it preserves arbitrary suprema in all variables).

Definition 2: Formal fuzzy theory
A formal fuzzy theory T in the language J is a triple

$$T = \langle \mathrm{LAx}, \mathrm{SAx}, R \rangle$$

where $\mathrm{LAx} \subsetneq F_J$ is a fuzzy set of logical axioms, $\mathrm{SAx} \subsetneq F_J$ is a fuzzy set of special axioms, and R is a set of sound inference rules.

Definition 3: **Evaluated proof, refutational proof and refutation degree**
An evaluated formal proof of a formula A from the fuzzy set $X \subsetneq F_J$ is a finite sequence of evaluated formulas $w := \; a_0/A_0, \; a_1/A_1, ..., \; a_n/A_n$ such that $A_n := A$ and for each $i \leq n$, either there exists an m-ary inference rule r such that
$a_i/A_i := \; r^{evl}(a_{i_1}, ..., a_{i_m})/r^{syn}(A_{i_1}, ..., A_{i_m})$,
$i_1, ..., i_m < n$ or $a_i/A_i := \; X(A_i)/A_i$.
We will denote the value of the evaluated proof by $Val(w) = a_n$.
An evaluated refutational formal proof of a formula A from X is w, where additionally $a_0/A_0 := \; 1/\neg A$ and $A_n := \bot$. $Val(w) = a_n$ is called refutation degree of A.

Definition 4: **Provability and truth**
Let T be a fuzzy theory and $A \in F_J$ a formula. We write $T \vdash_a A$ and say that the formula A is a theorem in the degree a, or provable in the degree a in the fuzzy theory T.

$$T \vdash_a A \text{ iff}$$
$$a = \bigvee \{Val(w) | \text{ w is a proof of A from } \mathrm{LAx} \cup \mathrm{SAx}\}$$

We write $T \models_a A$ and say that the formula A is true in the degree a in the fuzzy theory T.

$$\mathcal{D} \models T \text{ if } \forall A \in \mathrm{LAx} :$$
$$\mathrm{LAx}(A) \leq \mathcal{D}(A), \; A \in \mathrm{SAx} : \; \mathrm{SAx}(A) \leq \mathcal{D}(A)$$

$$T \models_a A \text{ iff } a = \bigwedge \{\mathcal{D}(A) \,|\, \mathcal{D} \models T\}$$

The fuzzy modus ponens rule could be formulated (we use special notion of most general unifier as defined in [Habiballa, H., 2012]):

Definition 5: Fuzzy modus ponens

$$r_{MP} : \frac{a/A, \; b/A \Rightarrow B}{a \otimes b/B} \qquad (2)$$

where from premise A holding in the degree a and premise $A \Rightarrow B$ holding in the degree b we infer B holding in the degree $a \otimes b$.

In classical logic r_{MP} could be viewed as a special case of the resolution. The fuzzy resolution rule presented below is also able to simulate fuzzy r_{MP}. From this fact the completeness of a system based on resolution can be deduced. It will only remain to prove the soundness. It is possible to introduce following notion of resolution w.r.t. the modus ponens.

Definition 6: **General resolution for fuzzy predicate logic** (GR_{FPL})

$$r_{GR} : \frac{a/F[G_1, , ..., G_k], \; b/F'[G'_1, ..., G'_n]}{a \otimes b/F\sigma[G/\bot] \,\nabla\, F'\sigma[G/\top]} \qquad (3)$$

where $\sigma = MGU(A)$ is the most general unifier (MGU) of the set of the atoms
$A = \{G_1, \ldots, G_k, G'_1, \ldots, G'_n\}$, $G = G_1\sigma$. For every variable α in F or F', $(Sbt(\gamma) = \alpha) \cap \sigma = \emptyset \Rightarrow$
F is called positive and F' is called negative premise, G represents an occurrence of an atom. The expression $F\sigma[G/\bot] \vee F'\sigma[G/\top]$ is the resolvent of the premises on G.

Lemma 1: **Soundness of r_{GR}**
The inference rule r_{GR} for FPL based on $\mathcal{L}_{\mathrm{L}}$ is sound i.e. for every truth valuation $\mathcal{D}$,

$$\mathcal{D}(r^{syn}(A_1, ..., A_n)) \geq r^{evl}(\mathcal{D}(A_1), ..., \mathcal{D}(A_n)) \qquad (4)$$

holds true.

Definition 7: **Refutational resolution theorem prover for FPL**
Refutational non-clausal resolution theorem prover for FPL ($RRTP_{FPL}$) is the inference system with the inference rule GR_{FPL} and sound simplification rules for $\bot$, $\top$ (standard equivalencies for logical constants). A refutational proof by definition 3 represents a proof of a formula G (goal) from the set of special axioms N.

Definition 8: **Simplification rules for $\nabla, \Rightarrow$**

$$r_{s\nabla} : \frac{a/\bot \nabla A}{a/A} \quad and \quad r_{s\Rightarrow} : \frac{a/\top \Rightarrow A}{a/A}$$

Lemma 2: **Provability and refutation degree for GR_{FPL}**
$T \vdash_a A$ iff $a =$
$\bigvee\{Val(w)|$ w is a refutational proof of A from LAx$\cup$ SAx$\}$

Theorem 1: **Completeness for fuzzy logic with r_{GR}, $r_{s\nabla}$, $r_{s\Rightarrow}$ instead of r_{MP}**
Formal fuzzy theory, where r_{MP} is replaced with r_{GR}, $r_{s\nabla}$, $r_{s\Rightarrow}$, is complete i.e. for every A from the set of formulas $T \vdash_a A$ iff $T \models_a A$.

MODELLING OF REDUNDANCY

The author also currently implements the non-clausal theorem prover into fuzzy logic as an extension of previous prover for FOL (GEneralized Resolution Deductive System - GERDS) [Habiballa, H., 2006]. Experiments concerning prospective inference strategies can be performed with this extension. The prover called Fuzzy Predicate Logic GEneralized Resolution Deductive System (Fig. 1) - FPLGERDS provides standard interface for input (knowledge base and goals) and output (proof sequence and results of fuzzy inference, statistics).

There are already several efficient strategies proposed by author (mainly Detection of Consequent Formulas (DCF) adopted for the usage also in FPL). With these strategies the proving engine can be implemented in real-life applications since the complexity of theorem proving in FPL is dimensionally harder than in FOL (the need to search for all possible proofs - we try to find the best refutation degree). The DCF idea is to forbid the addition of a resolvent which is a logical consequence of any previously added resolvent. For refutational theorem proving it is a sound and complete strategy and it is emiprically very effective. Completeness of such a strategy is also straight-forward in FOL:

$$(R_{old} \vdash R_{new}) \wedge (U, R_{new} \vdash \bot) \Rightarrow (U, R_{old} \vdash \bot)$$

Example: $R_{new} = p(a)$, $R_{old} = \forall x(p(x))$, $R_{old} \vdash R_{new}$.

DCF could be implemented by the same procedures like General Resolution (we may utilize self-resolution). Self-resolution has the same positive and

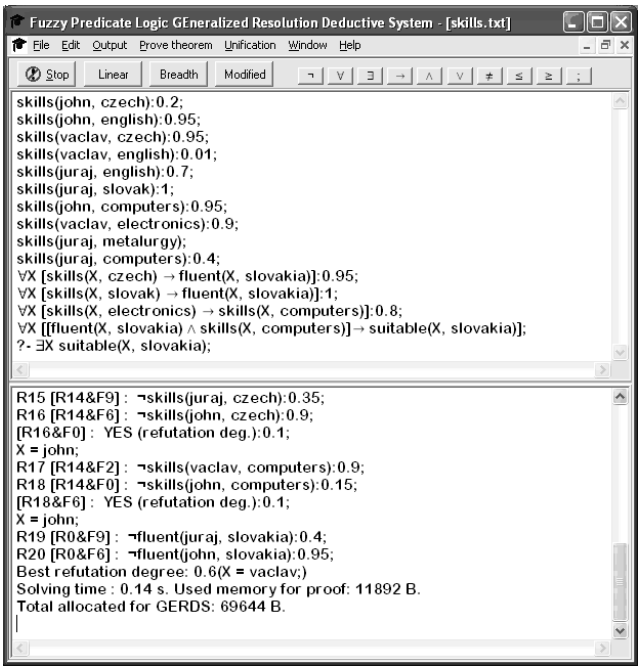

Fig. 1. Fuzzy Predicate Logic GEneralized Resolution Deductive System

negative premise and needs to resolve all possible combinations of an atom. It uses the following scheme:

$$R_{old} \vdash R_{new} \Leftrightarrow \neg(R_{old} \rightarrow R_{new}) \vdash \bot$$

Even the usage of this teachnique is a semidecidable problem, we can use time or step limitation of the algorithm and it will not affect the completeness of the $RRTP_{FOL}$.
Example: $R_{new} = p(a)$, $R_{old} = \forall x(p(x))$, $\neg(\forall x(p(x)) \rightarrow p(a))$
MGU: $Sbt(x) = a$, $Res = \neg(\bot \rightarrow \bot) \vee \neg(\top \rightarrow \top) \Rightarrow \bot$
We have proved that R_{new} is a logical consequence of R_{old}.

In FPL we have to enrich the DCF procedure by the limitation on the provability degree. if $U \vdash_a R_{old} \wedge U \vdash_b R_{new} \wedge b \leq a$ then we can apply DCF. DCF Trivial check performs a symbolic comparison of R_{old} and R_{new} we use the same provability degree condition. In other cases we have to add R_{new} into the set of resolvents and we can apply DCF Kill procedure. DCF Kill searches for every R_{old} being a logical consequence of R_{new} and if $U \vdash_a R_{old} \wedge U \vdash_b R_{new} \wedge b \geq a$ then Kill R_{old} (resolvent is removed).

We will now show some efficiency results concerning many-valued logic both for Fuzzy Predicate Logic. We have used the above mentioned application FPLGERDS and originally developed DCF strategy for FPL. It is clear that inference in $RRTP_{FPL}$ and $RRTP_{FDL}$ on general knowledge bases is a problem solved in exponential time. Nevertheless as we would like to demonstrate the need to search for every possible proof (in contrast to the two-valued logic) will not necessarily in particular cases lead to the inefficient theory. We have devised knowledge bases (KB) on the following typical problems related to the use of fuzzy logic.

We have performed experimental measurements concerning efficiency of the presented non-clausal resolution principle and also DCF technique. These measurements were done using the FPLGERDS application [Habiballa, H., 2006a]. Special testing knowledge bases were prepared and several types of inference were tested on a PC with standard Intel Pentium 4 processor as described below.

FUZZY PREDICATE LOGIC REDUNDANCY-BASED INEFFICIENT KNOWLEDGE BASES

As it was shown above in the theorem proving example the problem of proof search is quite different in FPL and FDL in comparison with the two-valued logic. We have to search for the best refutation degree using refutational theorem proving in order to make sensible conclusions from the inference process. It means we cannot accept the **first successful** proof, but we have to check **"all possible proofs"** or we have to be sure that every omitted proof is **worse** that some another one. The presented DCF and DCF Kill technique belong to the third sort of proof search strategies, i.e. they omit proofs that are really worse than some another (see the explication above). Proofs and formulas causing this could be called redundant proofs and redundant formulas. Fuzzy logic makes this redundancy dimensionally harder since we could produce not only equivalent formulas but also equivalent formulas of different evaluation degree.

Example 1: **Redundant knowledge base**
Consider the following knowledge base (fragment):

...,
$0.51/a \wedge b_1 \Rightarrow z$,
$0.61/a \wedge b_1 \wedge b_1 \Rightarrow z$,
$0.71/a \wedge b_1 \wedge b_1 \wedge b_1 \Rightarrow z$,
$0.81/a \wedge b_1 \wedge b_1 \wedge b_1 \wedge b_1 \Rightarrow z$,
$0.91/a \wedge b_1 \wedge b_1 \wedge b_1 \wedge b_1 \wedge b_1 \Rightarrow z$, $1/b_1$,
...,
$0.52/a \wedge b_2 \Rightarrow z$,
$0.62/a \wedge b_2 \wedge b_2 \Rightarrow z$,
$0.72/a \wedge b_2 \wedge b_2 \wedge b_2 \Rightarrow z$,
$0.82/a \wedge b_2 \wedge b_2 \wedge b_2 \wedge b_2 \Rightarrow z$,
$0.92/a \wedge b_2 \wedge b_2 \wedge b_2 \wedge b_2 \wedge b_2 \Rightarrow z$, $1/b_2$,
...,
Goal: $? - a \Rightarrow z$

Searching for the best proof of a goal will produce a lot of logically equivalent formulas with different degrees. These resolvents make the inference process inefficient and one of the essential demands to the presented refutational theorem prover is a reasonable inference strategy with acceptable time complexity.

We have compared efficiency of the standard **breadth-first search**, **linear search** and **modified linear search** (starting from every formula in knowledge base) and also combinations with DCF and DCF-kill technique [Habiballa, H., 2006a]. We have prepared knowledge bases of the size 120, 240, 360, 480 and 600 formulas. It has been compared the time and space efficiency on the criterion of 2 redundancy levels. This level represents the number of redundant formulas to which the formula is equivalent (including the original formula). For example the level 5 means the knowledge base contain 5 equivalent redundant formulas for every formula (including the formula itself). The basic possible state space search techniques and DCF heuristics and their combinations are presented in the following tables.

Search		**Description**
Breadth	B	Level order generation
Linear	L	Resolvent $\Rightarrow$ premise
Mod-Linear	M	Resolvent $\Rightarrow$ premise, goal+SAx

Table 1. Proof search algorithms

We use standard state space search algorithms in the FPLGERDS application - Breadth-first and Linear search. Breadth-first method searches for every possible resolvent from the formulas of the level 0 (goal and special axioms). These resolvents form formulas of the level 1 and we try to combine them with all formulas of the same and lower level and continue by the same procedure until no other non-redundant resolvent could be found. Linear search performs depth-first search procedure, where every produced resolvent is used as one of the premises in succeeding step of inference. The first produced resolvents arises from the goal formula. Modified linear search method posses the same procedure as linear one, but it starts from goal and also from all the special axioms.

DCF type		**Description**
Trivial	T	Exact symbolic comparison
DCF	DC	New consequent resol. dispose
DCF Kill	DK	DCF + all old consequent res.

Table 2. DCF heuristics

DCF methods for reduction of resolvent space are basically three. The simplest is trivial DCF method, which detects redundant resolvent only by its exact symbolic comparison, i.e. formulas are equivalent only if the are syntactically the same. Even it is a very rough method, it is computationally very simple and forms necessary essential restriction for possibly infinite inference process. The next method of DCF technique enables do detect the equivalency of a formula (potential new resolvent) by the means described above. DCF Kill technique additionally tries to remove every redundant resolvent from the set of resolvents. The important aspect of the theorem DCF lies in its simple implementation into an automated theorem prover based on general resolution. The prover handles formulas in the form of syntactical tree. It is programmed a procedure performing general resolution with two formulas on an atom. This procedure is also used for the implementation of the theorem. A "virtual tree" is created from candidate and former resolvent (axiom) connected by negated implication. Then it remains to perform self-resolution on such formula until a logical value is obtained. Let us compare the efficiency of standard strategies and the above-defined one.

Search	**DCF**	Code	**Description**
Breadth	Trivial	BT	Complete
Breadth	DCF	BDC	Complete
Breadth	DCF Kill	BDK	Complete
Mod. Linear	Trivial	MT	Incomplete (+)
Mod. Linear	DCF	MDC	Incomplete (+)
Mod. Linear	DCF Kill	MDK	Incomplete (+)
Linear	Trivial	LT	Incomplete
Linear	DCF	LDC	Incomplete
Linear	DCF Kill	LDK	Incomplete

Table 3. Inference strategies

We have built-up 9 combinations of inference strategies from the mentioned proof search and DCF heuristics. They have different computational strength, i.e. their completeness is different for various classes of formulas. Fully complete (as described above) for general formulas of FPL and FDL are only breadth-first search combinations. Linear search strategies are not complete even for two-valued logic and horn clauses. Modified linear search has generally bad completeness results when an infinite loop is present in proofs, but for guarded knowledge bases it can assure completeness preserving better space efficiency than breadth-first search.

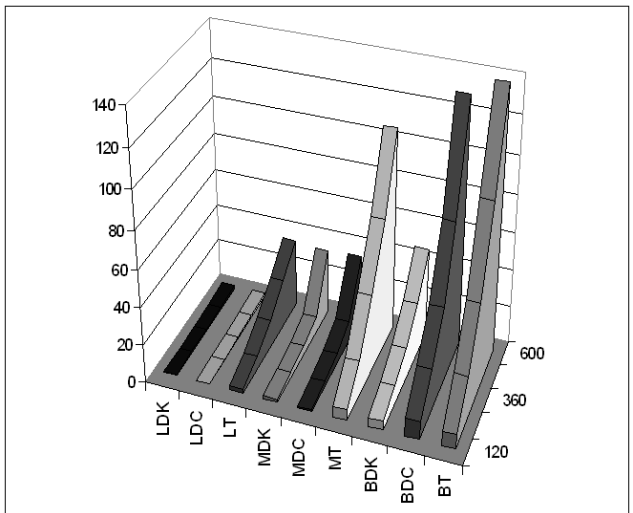

	120	240	360	480	600
BT	7,44	25,09	50,55	90,91	138,67
BDC	9,52	23,73	43,76	76,63	129,94
BDK	4,68	10,1	17,64	29,54	47,31
MT	5,86	18,85	41,46	70,01	106,68
MDC	0,93	3,09	5,14	10,54	35,14
MDK	1,45	3,2	5,03	8,84	34,32
LT	2,17	7,24	14,76	24,98	35,77
LDC	0,26	0,52	0,57	0,8	1,96
LDK	0,28	0,5	0,57	0,78	1,99

Fig. 2. Time complexity for redundancy level 5 (seconds)

We tested presented inference strategies on sample knowledge bases with redundancy level 5 with 20, 40, 60, 80 and 100 groups of mutually redundant formulas (total number of formulas in knowledge base is 120, 240, 360, 480 and 600). At first we have tested their time efficiency for inference process. As it could be observed from figure 2, the best results have **LDK and LDC** strategies. For simple guarded knowledge bases (not leading to an infinite loop in proof search and where the goal itself assures the best refutation degree) these two methods are **very efficient**. DCF strategies significantly reduces the proof search even in comparison with LT strategy (standard), therefore the usage of any non-trivial DCF heuristics is significant. Next important result concludes from the comparison of BDK and MDK, MDC strategies. We can conclude that MDK and MDC strategies are relatively comparable to BDK and moreover BDK preserves completeness for general knowledge bases.

Space complexity is even more significantly affected by the DCF heuristics. There is an interesting comparison of trivial and non-trivial DCF heuristics in figure 3. Even BDK strategy brings significant reduction of resolvents amount, while LDK, LDC, MDK, MDC strategies have minimal necessary amount of kept resolvents during inference process.

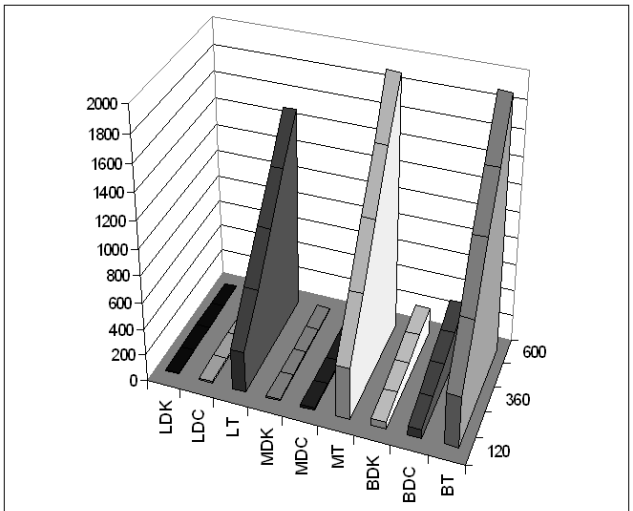

	120	240	360	480	600
BT	385	765	1185	1525	1905
BDC	65	125	185	245	306
BDK	46	86	126	166	205
MT	385	765	1145	1525	1905
MDC	14	14	14	14	12
MDK	14	14	14	14	12
LT	304	604	904	1204	1504
LDC	12	12	12	12	10
LDK	12	12	12	12	10

Fig. 3. Space complexity for redundancy level 5 (resolvents)

Performed experiments shows the significance of originally developed DCF strategies in combination with standard breadth-first search (important for general knowledge bases - **BDK**). We also outlined high efficiency for linear search based strategies (mainly **LDK**). Even this strategy is not fully complete and could be used only for guarded fragment of FDL, this problem is already known in classical (two-valued) logic programming and automated theorem proving. We also use

these highly efficient linear search strategies, even they are not complete.

CONCLUSIONS

The *Non-clausal Refutational Resolution Theorem Prover* forms a powerful inference system for automated theorem proving in fuzzy predicate logic. The main advantage in contrast with other inference systems lies in the possibility to utilize various inference strategies for effective reasoning. Therefore it is essential for practically successful theorem proving.

The Detection of Consequent Formulas algorithms family brings significant improvements in time and space efficiency for the best proof search. It has been shown results indicating specific behavior of some combinations of the DCF and standard proof search (breadth-first and linear search). DCF strategies (BDC, BDK) have interesting results even for fully general fuzzy predicate logic with evaluated syntax, where the strategy makes the inference process practically manageable (in contrast to unrestricted blind proof-search). However it seems to be more promising for practical applications to utilize incomplete strategies with high time efficiency like LDK (even for large knowledge bases it has very short solving times). It conforms to another successful practical applications in two-valued logic like logic programming or deductive databases where there are also used efficient incomplete strategies for fragments of fully general logics.

It has been briefly presented some efficiency results for the presented automated theorem prover and inference strategies. They show the significant reduction of time and space complexity for the DCF technique. Experimental application FPLGERDS can be obtained from URL:
http://irafm.osu.cz/en/c104_fplgerds/
The package contains current version of the application, source codes, examples and documentation.

ACKNOWLEDGEMENT

This work was supported by the European Regional Development Fund in the IT4Innovations Centre of Excellence project (CZ.1.05/1.1.00/02.0070) and also by University of Ostrava grant SGS/PŘF/2013.

REFERENCES

[Bachmair, L., Ganzinger, H., 1997] Bachmair, L., Ganzinger, H. (1997). A theory of resolution. Technical report: Max-Planck-Institut, 1997.

[Bachmair, L., Ganzinger, H., 2001] Bachmair, L., Ganzinger, H. (2001). Resolution theorem proving. In Handbook of Automated Reasoning, MIT Press, 2001.

[Dukić, N., Avdagić, Z., 2005] Dukić, N., Avdagić, Z. (2005). Fuzzy Functional Dependency and the Resolution Principle. In Informatica, Vilnius: Lith. Acad. Sci. (IOSPRESS), 2005, Vol.16, No. 1, pp. 45 - 60, 2005.

[Habiballa, H., 2002] Habiballa, H., Novák, V. (2002). Fuzzy General Resolution. In Proc. of Intl. Conf. Aplimat 2002. Bratislava, Slovak Technical University, 2002. pp. 199-206.

[Habiballa, H., 2006] Habiballa, H. (2006). Resolution Based Reasoning in Description Logic. In Proc. of Intl. Conf. ZNALOSTI 2006, Univ. of Hradec Kralove, 2006.

[Habiballa, H., 2006a] Habiballa, H.(2006a). Fuzzy Predicate Logic Generalized Resolution Deductive System. Technical Report, Institute for Research and Application of Fuzzy Modeling, University of Ostrava, 2006.

[Habiballa, H., 2012] Habiballa, H.(2012).Resolution principle and fuzzy logic. In Fuzzy Logic algorithms, techniques and implementations. InTech:Rijeka, 2012. ISBN 978-953-51-0393-6.

[Hájek, P., 2000] Hájek, P. (2000). Metamathematics of fuzzy logic. Kluwer Academic Publishers - Dordrecht, 2000.

[Hájek, P., 2005] Hájek, P. (2005). Making fuzzy description logic more general. Fuzzy Sets and Systems 154(2005),pp. 1-15.

[Mondal, B., Raha, S., 2012] Mondal, B., Raha, S., Approximate reasoning in fuzzy resolution. Fuzzy Information Processing Society (NAFIPS), 2012 Annual Meeting of the North American, pp.1-6, 6-8 Aug. 2012. ISBN 978-1-4673-2336-9.

[Novák, V., Perfilieva, I., Močkoř, J., 1999] Novák, V., Perfilieva, I., Močkoř, J. (1999). Mathematical principles of fuzzy logic. Kluwer, 1999.

HASHIM HABIBALLA
(*1976) Associate Professor at University of Ostrava, Dept. of Informatics and Computers and researcher of Centre of Excelence IT4Innovations - Institute for Research and Application of Fuzzy Modeling. Holds MSc.(1999) and Ph.D.(2007) in Information Systems, holds also PhD. and EdD. in CS Education (2004). He focuses to artificial intelligence, logic, formal languages and is author of 100 publications.

EVA VOLNÁ
Associate professor at the Department of Computer Science at University of Ostrava, Czech Republic. Her interests include artificial intelligence, artificial neural networks, evolutionary algorithms, and cognitive science. She is an author of more than 50 papers in technical journals and proceedings of conferences.

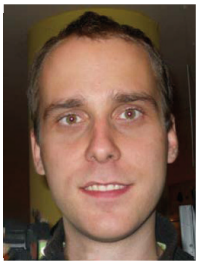

MICHAL JANOŠEK
He is a doctor at the Department of Computer Science at University of Ostrava, Czech Republic. His interests include artificial intelligence, multi-agent systems, modelingand simulations. He is an author of more than 20 papers in proceedings of conferences.

MARTIN KOTYRBA
He is a doctor at the Department of Computer Science at University of Ostrava, Czech Republic. His interests include artificial intelligence, formal logic, soft computing methods and fractals. He is an author of more than 30 papers in proceedings of conferences.

PREDATOR-PREY SIMULATION'S PARAMETERS AND LEVERAGE POINTS

Michal Janošek
Václav Kocian
Eva Volná
Martin Kotyrba
Hashim Habiballa
Department of Informatics and Computers, University of Ostrava
30. dubna 22, Ostrava, 702 00, Czech Republic
michal.janosek@osu.cz
vaclav.kocian@osu.cz
eva.volna@osu.cz
martin.kotyrba@osu.cz
hashim.habiballa@osu.cz

KEYWORDS
Simulation, self-organisation, parameter, mediator. leverage point

ABSTRACT

For many natural systems there is an advantage in their simulating on a computer. In this article, a way how to determine the influence of the predator-prey simulation's parameters on the model's behaviour based on the leverage points is examined. An investigation whether it is possible to sort the parameters according to the importance and if it is possible to automate the process to a certain degree is performed.

INTRODUCTION

Many natural systems are complex. They consist of a lot of interacting entities and, moreover, their interactions are random. There are two ways how to look at and how to simulate a complex system, *top-down* and *bottom-up*. *System dynamics* is a typical *top-down* modelling approach. System's status is expressed using summary variables; the behaviour of the system is expressed using equations. Feedback loops are expressed explicitly in the model. On the contrary, modelling with agents is typical for the *bottom-up* approach. Agents (basic elements) and their behaviour are defined. Mutual interactions among agents (and positive and negative feedback loops as well) result from agents' behaviour. This article is focused on the *bottom-up* approach. The behaviour of the system as a whole is not directly encoded in the rules governing individual elements nor there is an external source of order. Order in the system is the result of self-organisation. In biological systems, self-organisation is a process in which a pattern at the global level of a system emerges solely from numerous interactions between the lower-level components of the system. Moreover, the rules specifying interactions between the system's components are executed using only local information, without reference to the global pattern (Camazine et al. 2003). Self-organisation is closely related to the phenomenon called emergence. Emergence is a spontaneous creation of macroscopic properties and structures of the complex system that are not easy to be derived from the properties of their elements (Fromm 2004). An example of emergence in biology is the view of biological organisation of life from the subatomic level to the entire biosphere.

Leverage points are places in a complex system where a small change in one part of the system can result in a great change in all of its parts (Pelánek 2011). Lever (in the system concept) is the ratio of the output change to the input change. Then the leverage point is a place in a system where the system can be effectively controlled (Harich 2010). The leverage points' concept is used in various fields, such as biology, ecology, sustainability, managements, economics, and others. The study *Managing the Ecosystem by Leverage Points: A Model for a Multispecies Fishery* is the result of five years research of the south-eastern Australian continental shelf fishery ecosystem. It shows how leverage points can be found in this particular system (Bax et al. 1999). In the study *Environmental and Societal Factors Affect Food Choice and Physical Activity: Rationale, Influences, and Leverage Points*, the leverage points are used in the field of nutrition and dietetics (Booth et al. 2001). The concept of leverage points was developed and generalised by Donella H. Meadows in her article *Leverage points: Places to intervene in a system* (Medows 1999). She also introduced a sort of hierarchy of leverage points which is not limited to specific applications and has general use. The concept of leverage points is still being developed, e.g. in the article *Change Resistance as the Crux of the Environmental Sustainability Problem*, where the author deals with environmental sustainability (Harich 2010).

PARAMETERS AND LEVERAGE POINTS

In this article, we are going to use a *bottom-up* simulation approach. When the model's parameters during simulation phase are set, we would like to know what influence different parameters would have on the

Proceedings 27th European Conference on Modelling and Simulation ©ECMS Webjørn Rekdalsbakken, Robin T. Bye, Houxiang Zhang (Editors)
ISBN: 978-0-9564944-6-7 / ISBN: 978-0-9564944-7-4 (CD)

model's behaviour. But how is it possible to know which parameters are more and which less important? As a tool to know which parameters are more and less important, it is possible to follow the hierarchy of leverage points (Fig. 1, Meadows 1999). Even though the hierarchy is built from the perspective of system dynamics (top-down), useful points for agent modelling (bottom-up) can be found.

Places to intervene in a system in increasing order of effectiveness

12. Constants, parameters, numbers

11. The sizes of buffers and other stabilizing stocks, relative to their flows

10. The structure of material stocks and flows (such as transport networks)

9. The lengths of delays, relative to the rate of system change

8. The strength of negative feedback loops

7. The gain around driving positive feedback loops.

6. The structure of information flows

5. The rules of the system

4. The power to add, change, evolve, or self-organize system structure

3. The goals of the system

2. The mindset or paradigm out of which the system (its goals, structure, rules, etc.) arises

1. The power to transcend paradigms

Figure 1: Leverage points' hierarchy (Meadows 1999, in descending order as in the original paper)

As can be seen, the parameters themselves are on the least important place in the hierarchy (Figure 1). Yet, not all parameters are unimportant; some of them correspond with the more important leverage points. All that must be done is to match every parameter with the corresponding leverage point. Then it is possible to sort these parameters according to their influence on the system's behaviour.

EXPERIMENT

For our experiment, Wolf Sheep Predation simulation (Wilensky 1997, Figure 2) is used which is available at (http://ccl.northwestern.edu/netlogo/models/WolfSheep Predation). This classical but still current model explores the stability of predator-prey ecosystems. Wolves and sheep wander randomly around the landscape while the wolves look for sheep to prey on. Each step costs the wolves energy and they must eat sheep in order to replenish their energy - when they run out of energy they die. The sheep must eat grass in order to maintain their energy as well. The simulation runs for each discrete step in which individual agents perform their actions.

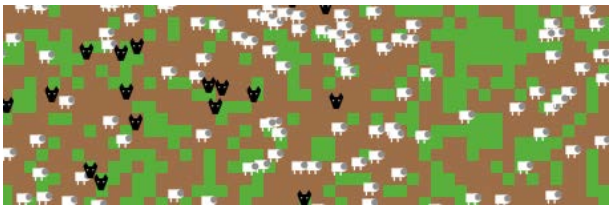

Figure 2: Wolf Sheep Predation simulation environment

First of all, it is necessary to verify that the parameters of this simulation are related to the concept of leverage points. The Wolf Sheep Predation simulation has seven parameters (Table 1): *grass-regrowth-time*, *initial-number-sheep*, *initial-number-wolves*, *sheep-gain-from-food*, *wolf-gain-from-food*, *sheep-reproduce* and *wolf-reproduce*.

Table 1: Wolf Sheep Predation simulation's parameters

Parameter	Description	default	Range
grass-regrowth-time	how long it takes for grass to regrow	30	0-100
initial-number-sheep	initial size of sheep population	100	0-250
initial-number-wolves	initial size of wolf population	50	0-250
sheep-gain-from-food	amount of energy sheep get for every grass patch eaten	4	1-50
wolf-gain-from-food	amount of energy wolves get for every sheep eaten	20	1-100
sheep-reproduce	probability of a sheep reproducing at each time step	4	1-20
wolf-reproduce	probability of a wolf reproducing at each time step	5	0-20

To be able to evaluate the impact of these seven input parameters on the behaviour of the simulation model, we must also specify the output indicator to reflect this behaviour. As there are several input parameters, it is possible to have several output indicators as well. In this case, only one output indicator is chosen – *total population*. *Total population* indicator reflects the total population of wolves and sheep in every step of the simulation. So let's assign leverage points to each input parameters according to (Figure 1).

Parameters *initial-number-wolves* and *initial-number-sheep* are associated with the leverage point 12 because they are just numbers or constants. They are the least important parameters with regard to the output indicator which influences the size of the *total population*. Parameters *sheep-reproduce* and *sheep-gain-from-food* are associated with the leverage point 7 because they affect the positive feedback loop. The more food the sheep gets from the grass, the longer it is able to survive and the more offspring it can have. Analogously, the larger the value of *sheep-reproduce* is, the more sheep

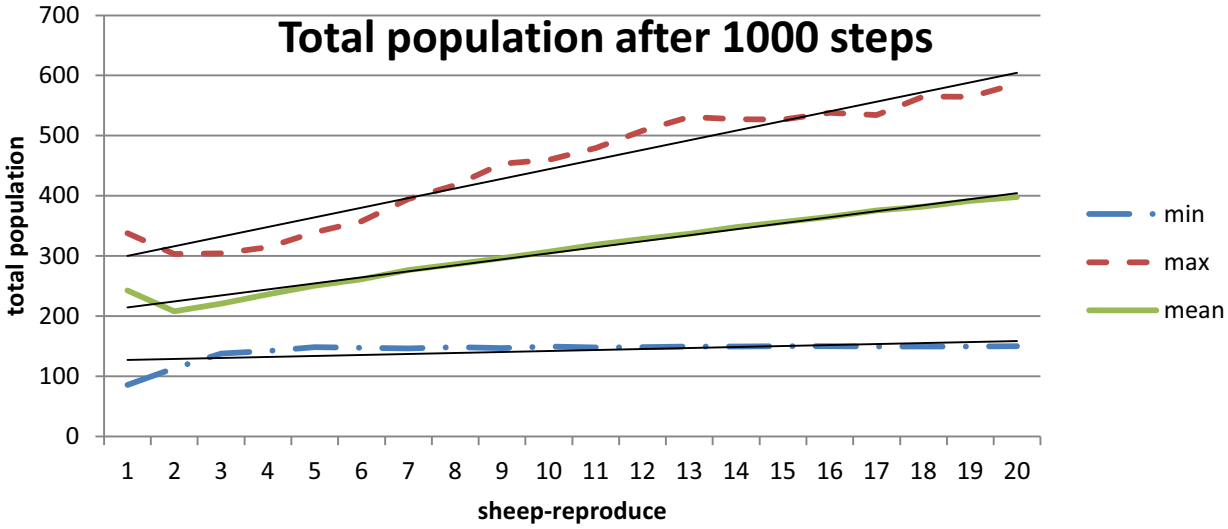

Figure 2: Total population after 1000 steps

are born in each step, etc. Parameter *grass-regrowth-time* corresponds with the leverage point 8, as it affects the negative feedback loop. Increasing the values of this parameter extends the interval between the time it takes the grass to regrow, which increases the effect of negative feedback loop to the sheep and then to the wolves' population. The last two parameters, *wolf-gain-from-food* and *wolf-reproduce* affect both positive and negative feedback loop (leverage point 8 and 7). A higher value of *wolf-reproduce* and *wolf-gain-from-food* parameter increases the wolf population and thus the overall population as well. But more wolves eat more sheep, thus reducing the population of sheep, which on the contrary negatively affects the overall population of both species. Because these parameters affect both negative and positive feedback loops, their effects should cancel out.

AUTOMATIC PARAMETERS' INFLUENCE SORTING

The aim of this chapter is to confirm the leverage points' concept for this scenario and also to find a procedure according to which it would be possible to automatically sort the input parameters according to their influence on the output indicator. This procedure consists of two steps. First of all, it is necessary to test all input parameters of simulation in their pre-defined range and then to determine the influence of these parameters on the desired output indicator from the results of the testing.

The aim of testing the input parameters is to obtain the necessary data to evaluate the influence of input parameters on the output indicator. A prerequisite for this step is an already working simulation with default values of all input parameters (Table 1). Input parameters are tested progressively, one after another. Each parameter's value is always tested in its entire range, leaving other parameters at their default value.

In (Figure 2), it can be seen what influence the input parameter sheep-reproduce (value 1-20) has on the output indicator total population. For each input parameter value the simulation was run 5 times so the results were averaged. Each simulation run lasted for 1000 steps. In the graph there is minimum, maximum and average value of the total population output indicator.

Table 2: Slope of a regression line for each input parameter

parameter	slope of a regression line (mean)	leverage point
grass-regrowth-time	-7.25	8
wolf-gain-from-food	-0.63	7/8
initial-number-wolves	0.00	12
initial-number-sheep	0.01	12
wolf-reproduce	0.01	7/8
sheep-reproduce	9.98	7
sheep-gain-from-food	40.57	7

In (Table 2) there are results of testing of all input parameters. One way how to compare the effects of input parameters is to interleave the result values from the simulation with the regression line (mean line). The slope of the line (its absolute value) determines the influence of the input parameter on the output indicator. A positive or negative value of the slope determines positive or negative influence of the input parameter to the output indicator. In the third column (Table 2) there are leverage points assigned previously to each input parameter in contrast to the slope of a regression line. As we can see, the test results (slope of a line value) as well as the original associated leverage points match in the influence magnitude they have on output indicator.

Parameters *initial-number-wolves* and *initial-number-sheep* have almost no effect on the output indicator. Even the parameters *wolf-gain-from-food* and *wolf-reproduce* have almost no effect on the output indicator, as they have impact on both the negative and the positive feedback loop. On the other hand, the last three parameters (*grass-regrowth-time*, *sheep-reproduce* and *sheep-gain-from-food*) do have some influence.

By sorting these parameters according to the standardised absolute value of the slope of a line, we get some sort of hierarchy of the simulation parameters with growing influence on the output indicator. The more the

slope is close to zero, the smaller the influence of the input parameter on the output indicator is and vice versa. A positive or negative value of a slope corresponds to the positive or negative effect on the output indicator.
Let's choose parameters *grass-regrowth-time*, *sheep-reproduce* and *sheep-gain-from-food* as the parameters that have the biggest influence on the output indicator *total population.* To verify that we have chosen these parameters correctly, let's do multivariate regression (Table 3).

Table 3: Multivariate regression results

	Sheep-gain-from-food	Sheep-reproduce	Grass-regrowth-time
Coefficient	48.32921	1.425784	-1.75775
standard error	0.629046	0.36318	0.028245
t-statistics	76.82936	3.925834	-62.2321
T(0.05;941)	1.962488		
R^2	0.912318		
Df	941		

The R^2 tells us that these three parameters have given us approximately 91% of the information and explained the variation of our model by 91%. The degrees of freedom have been used to determine what the critical t-value is and we have compared it to our t-statistics. The benchmark t-value is approximately 1.96, so any number above this number is significant variable. We can state that all of these three chosen variables are significant variables then.

CONCLUSION

Based on the experiments we can say that in order to assess the influence of input parameters on the predator-prey simulation, we can use the concept of leverage points. A similar interpretive value also has a regression line, obtained by testing all input parameters. Input parameters sorted by their influence according to the leverage points and input parameters sorted by their influence according to regression lines of the tested parameters match. Even though we use univariate regression, results are fast and reliable enough as it was confirmed in the experiment. On the other hand, multivariate regression is very time consuming to calculate, taking into consideration all the parameters of the simulation. Calculating the regression line and thus determining the influence of parameters can also be automated. Reliable and fast sorting of parameters according to their influence is one of the important steps to adaptation of the system's behaviour (Janošek et al. 2011).

ACKNOWLEDGEMENT

The research described here has been financially supported by University of Ostrava grant SGS23/PřF/2013. Any opinions, findings and conclusions or recommendations expressed in this material are those of the authors and do not necessarily reflect the views of the sponsors.

REFERENCES

Bax N. J., Williams A., Davenport S., Bulman C. Ecosystem Approaches for Fisheries Management. 1999. Managing the ecosystem by leverage points: a model for a multispecies fishery; p. 283-303. Alaska Sea Grant College Progam. ISBN: 1-56612-061-6

Booth, S. L., Sallis, J. F., Ritenbaugh, C., Hill, J. O., Birch, L. L., Frank, L. D., Glanz, K., Himmelgreen, D. A., Mudd, M., Popkin, B. M., Rickard, K. A., Jeor, S. St. and Hays, N. P. (2001), Environmental and Societal Factors Affect Food Choice and Physical Activity: Rationale, Influences, and Leverage Points. Nutrition Reviews, 59: S21–S36. ISSN: 0029-6643.

Camazine, Deneubourg, Franks, Sneyd, Theraulaz, Bonabeau, Self-Organization in Biological Systems, Princeton University Press, 2003. ISBN 0-691-11624-5 --ISBN 0-691-01211-3 (pbk.) p. 8

Fromm, Jochen (2004), The Emergence of Complexity, Kassel University Press, ISBN 3-89958-069-9

Harich, J. (2010), Change resistance as the crux of the environmental sustainability problem. Syst. Dyn. Rev., 26: 35–72. doi: 10.1002/sdr.431

Janošek M., Kocian V., Kotyrba M. Volná E. Pattern recognition and system adaptation. Aplimat - Journal of Applied Mathematics, volume 4 (2011), number 1, pp. 261-270. ISSN: 1337-6365

Meadows, D. H.: Leverage points: Places to intervene in a system. www.sustainer.org/pubs/Leverage_Points.pdf. The Sustainability Institute. 1999.

Pelánek, R.: Modelování a simulace komplexních systémů, Masaryk University, 236 p., 2011. ISBN: 978-80-210-5318-2.

Wilensky, U. (1997). NetLogo Wolf Sheep Predation model. Center for Connected Learning and Computer-Based Modeling, Northwestern University, Evanston, IL

AUTHOR BIOGRAPHIES

MICHAL JANOŠEK is a doctor at the Department of Informatics and Computers at the University of Ostrava, Czech Republic. His interests include artificial intelligence, multi-agent systems, modeling and simulations. He is an author of more than 20 papers in proceedings of conferences.

VÁCLAV KOCIAN is a Ph.D. student at the Department of Informatics and Computers at the University of Ostrava, Czech Republic. His interests include artificial intelligence, artificial neural networks, and soft computing methods. He is an author of more than 15 papers in proceedings of conferences.

EVA VOLNA is an associate professor at the Department of Informatics and Computers at the University of Ostrava, Czech Republic. Her interests include artificial

intelligence, artificial neural networks, evolutionary algorithms, and cognitive science. She is an author of more than 50 papers in technical journals and proceedings of conferences

MARTIN KOTYRBA is a doctor at the Department of Informatics and Computers at the University of Ostrava, Czech Republic. His interests include artificial intelligence, formal logic, soft computing methods and fractals. He is an author of more than 30 papers in proceedings of conferences.

HASHIM HABIBALLA is an associate Professor at University of Ostrava, Dept. of Informatics and Computers and researcher of Centre of Excelence IT4Innovations - Institute for Research and Application of Fuzzy Modeling. Holds MSc. (1999) and Ph.D.(2007) in Information Systems, holds also PhD. and EdD. in CS Education (2004). He focuses on artificial intelligence, logic, formal languages and is an author of 100 publications.

Collaborative Data Dissemination Methods in VANETs for Identifying Road Conditions Zone boundaries

Emadeddin A. Gamati, Richard Germon, Evtim Peytchev
{emadeddin.gamati, richard.germon, evtim.peytchev }@ntu.ac.uk
Nottingham Trent University - School of Science and Technology - Computing and Informatics Building, Clifton Lane, Nottingham, NG11 8NS, UK.

Abstract: Vehicle to vehicle communication (V2VC) is a modern approach to exchanging and generating traffic information with (yet to be realised) potential to improve road safety, driving comfort and traffic control. In this paper, we present a novel algorithm which is based on V2V communication, uses in-vehicle sensor information and, in collaboration with other vehicles' sensor information, can detect road conditions and determine the geographical area where these road conditions exist e.g. an area where there is traffic density, unusual traffic behaviour, a range of weather conditions (raining), etc. The built-in automatic geographical restriction of the data collection, aggregation and dissemination mechanisms allows warning messages to be received by other cars not necessarily sharing the identified road conditions, which may then be used to inform them of the optimum route to take (to avoid bottlenecks or dangerous areas including accidents or congestion on their current routes).

We propose two approaches in this paper that are simple, flexible and fast and do not rely on any kind of roadside infrastructure equipment. They will offer live road condition information channels at – almost – no cost to drivers and public/private traffic agencies and have the potential to become an indispensable part of any future intelligent traffic system (ITS).

Keywords: Networking, VANET, Protocols, Routing, Dissemination, Broadcasting,

1 Introduction

Currently used traffic information systems are centralised vehicular applications using technologies like Traffic Message Channel (TMC), which provides information about road traffic conditions. However, it (i) lacks short delay times (due to the centralised approach), (ii) averages information for large geographical areas (due to cost-sensitiveness of detailed sensor networks and limited radio resources) and (iii) does not have the opportunity to provide services for locally interesting and time-critical applications [1]. Moreover, as discussed in [2], implementation for complete coverage would require new infrastructure that is cost-sensitive, as shown in [3] through a case study. Such systems would, for example, not meet the requirements of an accident avoidance application, because they have long delays and would require large capacity due to the large geographical area of service. In contrast, VANET-based systems can have short delays and the capacity can be reused more efficiently. Moreover, the structure o f VANET can be distributed, which improves the level of independence, scalability and stability.

The vehicular application can be classified based on the improvement of safety and the time-critical nature of the service. Examples of application categories are safety applications (e.g. avoidance of collision, information about loss of control of the vehicle), which can improve road safety significantly (a new level of road safety assistance), but are highly time-critical. In comparison, a service about traffic condition information is less time-critical, as discussed in [4], due to the low level of variation of traffic conditions in a short time (traffic jams have to build up) and it has a lower impact on improvement of road safety than, for example, traffic accident assistance applications. This categorisation can be extended with expected improvement of safety or comfort level e.g. (example for safety) intersection collision avoidance; (for comfort) dissemination of free parking places in large parking lots [5].

This important to note the importance of understanding the requirements of vehicular applications. Different applications might have significantly different needs for information-spreading properties (e.g. delay, distance). Therefore different dissemination strategies (including technology employed) need to be employed for various vehicular applications. We aim to find model to study the effect of these diverse dissemination strategies on information spreading and how we can employ those strategies to identify the boundaries of sensed road conditions.

Proceedings 27th European Conference on Modelling and Simulation ©ECMS Webjørn Rekdalsbakken, Robin T. Bye, Houxiang Zhang (Editors)
ISBN: 978-0-9564944-6-7 / ISBN: 978-0-9564944-7-4 (CD)

2 Dissemination strategies

Most VANET-based systems assume *a priori* knowledge about the underlying road network, which is usually interpreted as a weighted graph [6]. A common approach is to divide the roads into sections with different weights, but certainly not with the same length. The weights are given according to a certain property, which can be physical like a message traversal delay [7] or stochastic probability based on the distance between vehicles [8].

Vehicles are assumed to be equipped with sensors that provide data about the status of the vehicle e.g. speed, geographical position, temperature or even sensors to detect bumps, acceleration [9] or honking [10]. This status represents local information about a geographical area at a certain moment. Distribution of local information needs to be detailed within closer vicinity, and coarser with the increase of distance, as proposed in [11]. For example, a driver would be interested in the average speed of vehicles way ahead, but the exact speed of a vehicle 100 metres ahead to be able to avoid a collision.

Based on the ***type of communication*** three main categories can be introduced. First are vehicles sending their messages via a cellular system – and/or Road-Side Unit (RSU) – to a central server or to another peer as described in [12]. The disadvantage of such systems is the high cost of construction and maintenance of the infrastructure.

Second is the group of systems that do not use cellular systems, but another dedicated system like Urban Multi-hop Broadcast Protocol, as suggested in [13], or more general communication technologies for VANET (e.g. Wi-Fi) [14]. Last, a hybrid solution, a combination of both systems, seems to be the most powerful but most complex approach.
The fundamental idea of information dissemination for VANET is to have ***periodic broadcast*** messages for routine information, and event-driven messages for causes of emergency situations. Most of the time vehicles send messages about their current status (velocity, heading) and/or knowledge about the network performance (e.g. delay of certain links, density of cars at a road section). Data from multiple inputs are processed and a new message calculated and transmitted if the routing protocol requests it. The aforementioned information should be aggregated to fulfil scalability requirements.

Flooding, as a distribution method (where each message is sent to all) however, is not scalable, consumes large amount of energy, bandwidth and memory space while being inefficient. Therefore, techniques to reduce network load are required. The main goal is to provide less information with a higher distance to keep the system scalable, as shown in [15]. Atomic information (e.g. velocity) is aggregated with information from other nodes [1] or about road sections [7] to have aggregated messages. The message has to be aggregated with new information from the current node before another broadcast takes place.

For ***aggregation***, geographically hierarchical approaches are being introduced. The level of hierarchy can, for example, be represented in different resolutions of the road network between landmarks, as suggested in [13]. Another approach is to form grids of different sizes based on various sizes of geographical area, as shown in [16]. In both cases the amount of information about a faraway geographical area is reduced, therefore data needs to be maintained as well. Dynamic store and forward approaches are used to maximise the probability that two messages are going to be present at the same time at the current node and it will have a chance to aggregate them into a single message and transmit it.

We have also identified an evolution in flooding and directed broadcast transmission to the target area to a distributed (Content Addressable Network (CAN)-based) subscriber/publisher approach [17]. The nodes subscribe to certain groups of information (for example, information about certain road sections on the route ahead) and push out messages in a distributed fashion (dissemination is distribution as well as the location of the stored data). Vehicles send (push into the network) information about their observations and abrupt events.
Data is preferably stored in a distributed fashion like CAN, which has a *d* dimensional key space that is used to give the address of a certain area based on its geographical position. It allows the possibility of reaching nodes that are responsible for storing data about a certain area without knowing their address

3 Dissemination characteristics

3.1 Keeping information alive

Information must migrate and be kept alive. This is achieved by retransmission. A message that is received and retransmitted gains two things. It survives a period in time, and it might migrate to new receivers. A retransmission can be done in two ways: either it retransmits to specific addresses, or it retransmits to everyone.

Transmission to specific addresses is most effective if the environment and receivers are static or motionless. Once the discovery and determination of neighbours is finished, each message needs to be sent only once, which saves capacity and time. This solution might demand special hardware such as directive antenna and controllers.

Flooding is like opening a door with a sledgehammer instead of a key. It is big, noisy and brutal, but it gets the job done. The biggest problem with flooding is the sheer number of messages that are received, when each node transmits all new messages to any receiver within reach.

If there are *n* receivers within reach (Figure 1), this will cause the sender to receive nine messages that are of no value. If all the other receivers can reach nine nodes, 90 messages are wasted. This will unfortunately introduce interference, and possible loss of each other's messages; the message will be received n*(n-1) times.

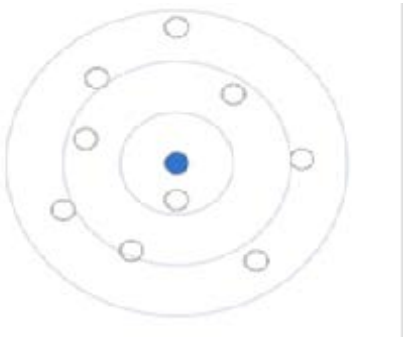

Figure 1: Flooding to nearby nodes (n=10)

The problem that presents itself is that we do not have a master in the network. Then who is going to be responsible for updating the information in the system? With no master the responsibility lies within each vehicle. An approach to this is presented in this paper.

3.2 Keeping the information consistent

The mechanisms used to keep messages alive might cause problems with keeping the information consistent and updated. Retransmissions and replication might produce duplicate messages. This introduces the need for telling the messages apart.

The information in the system depicts the real environment as truthfully as possible. As time passes, the conditions – once observed in the environment – might have changed, moved or disappeared.

A major issue is that there might be many different interpretations about what the 'truth' is. Each vehicle, or node, in the system might have a slightly different perception of what is the overall status in the network.

A bigger problem is the arrival of new vehicles. How can they get an impression about what the status is?

The vehicles most likely to have the most complete picture of what the status is in the network are probably those that are closest to the centre of the network. These vehicles have the highest probability of having received all messages that have migrated through the network.

A new vehicle will have difficulties discovering these centrally located vehicles, so an easier solution might be to rely on the nearest vehicle instead. Due to the many interpretations about status, it is not enough to ask just one neighbour. A majority vote between any vehicles within reach would provide a fairly good estimate about what the status is at this part of the network. This is definitely a 'best-effort' task.

3.3 Infrastructure

The goal is to produce a robust, self-configuring and autonomous network. If the network is reliant on infrastructure the network might be limited to operations in areas where the infrastructure is in place.

It is better for the network to be independent of existing infrastructure, but use whatever resources are available. A lamppost equipped with the same communications equipment as the vehicles might be regarded as a very slow-moving vehicle (as seen from the network). This permanent equipment can be used to supply the network with important information from 'the outside' (i.e. traffic information or congestion warnings) and might gather information for some centralised services (statistical information about troublesome areas).

Permanent infrastructure might be helpful to cover 'black holes' or difficult positions (i.e. can cover both sides of a difficult corner). The directivity and mounting height of the antenna plays a major part in the connectivity [9]. On a vehicle the most natural choice is an omni-directional antenna. The mounting height of this is limited by the vehicle and aesthetic concerns. On a permanent structure it is possible to use very different equipment depending on the location, and needs, of the area.

There is another type of infrastructure that might be useful. Buses and trams use a predictable route at predictable times. The bus or tram might work as a buffer, they get information from a source, and they can release this information when they get to new areas. A moving infrastructure comes in handy for gathering statistical information, as it covers a large area at regular intervals.

3.4 Applications built on Inter-Vehicle Communication (IVC)

The vast class of IVC applications can make driving safer and more comfortable for vehicle occupants [18][19]. IVC services can be achieved through different methods by exchanging data between vehicles and sometimes through roadside infrastructure units. Figure 2 shows the classification of vehicular communication applications. It helps us to focus on specific equipment to fulfil services and solve diverse problems.

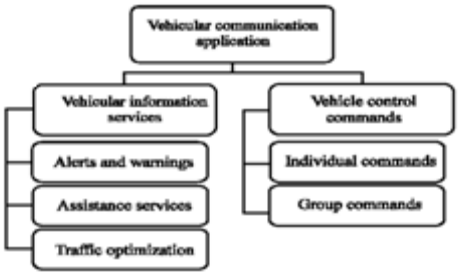

Figure 2: Classification of vehicular communication applications

To clarify the exchange approaches we propose in this paper, it will be useful to present some examples of the possible road situations (conclusions) we can come up with based on sharing individual car sensor data (the numbers quoted in (table 1) are representative rather than conclusive for the condition and represent a matter for future investigation in real-life experiments).

	Individual Car sensors data	Optimum Num example/case	Possible Conclusion
1	Windscreen Wipers	30% of cars = ON	Rainy
2	ABS Control.	5 cars = ON	Slippery (snow)
3	Slippery Oil Spot.	2 cars	Slippery spot
4	Fog light.	50% of cars ON	Foggy
5	Traffic flow Speed.	(60%) Slow/Stop	Traffic Jam
6	Reduce Speed.	5 cars within 1sec	Hazard Ahead

Table 1:Examples of some situations

We can consider that column two contains, in effect, Search Condition Limitation numbers. Assuming that this Search Condition Limitation is reached then a zone with the condition (third column) is identified and the information system can tell other nearby cars to be aware of the situation within that zone if they plan to pass through it.

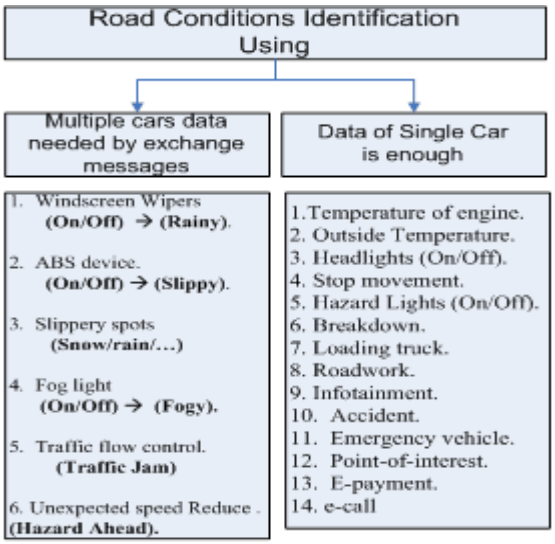

Figure 3: Aggregate data

Each message needs to be in a format that is small in size and rich in content. Two methods of collaboratively collecting data by exchanging messages based on vehicle-to-vehicle communication have been identified.

Figure 3 classifies the recognisable road conditions based on the number of cars needed for it. The examples are of discoverable road situations that need just a single car to identify the road condition/problem to generate a warning message and broadcast it to all nearby cars, and of road conditions that need multiple cars' information by exchanging messages (their data) to identify the conditions of the road they are on. So, two stages are needed: first, exchange of messages to discover whether the road has a certain condition or not; and second, generation of a warning message to inform all nearby cars of the discovered condition, if any.

4 Schemes for road condition zone boundary identification

In both proposed approaches we consider a scenario in which multiple cars' data is needed to identify a road situation. So, exchange information between nodes (cars) is needed in a way that each node requests/sends information from/to the other vehicles to collectively identify the conditions of the road. This is gathering information about how many vehicles have sensed the same specific conditions. It can be something like 'How many cars have their fog light ON?', 'Are there any queues in front of me?'. The answers to such questions should be extracted from the conclusion of the aggregated data for the cars in the zone. In the following section the mechanism for the proposed approaches to data collection from nearby nodes is given.

4.1 Blind Zone Scan Scheme (BZS)

This is two phases approach. First phase is to scan the region for any detected traffic conditions (using discovery message generated by nodes who sensed that situation) to identify the boundaries of the situation zone. The second phase is to issue warning message broadcasts to inform all nearby nodes for the situation and its boundaries. By using this approach, we investigate and identify the optimum value for two parameters: 1 The number of hops used by the discovery message (How large the scanned area is), and 2 the best possible delay time used in each node before rebroadcasting (to reduce the noise in the network) This mechanism involves the following steps:

1) If *a node detects or senses any identifiable road conditions* it becomes an *active node* (AN).

a. If it has not received other nodes' SDMs (*Situation Discovery Message*) with the same condition discovery requests within a certain past time-out period, it generates an SDM and broadcasts it to all nodes in its range as a first wave (called first hop) to inform all nodes of its current situation (Figure 4a) and to enquire if other nodes have the same condition.

b. Periodic regeneration and rebroadcasting of SDM after the time-out expires will be performed, until either the situation disappears (becomes a Non-Active Node (NAN)), or a new, different, SDM is received which shows another node has sensed the same situation (become AN) and it recognizes the current one as AN.

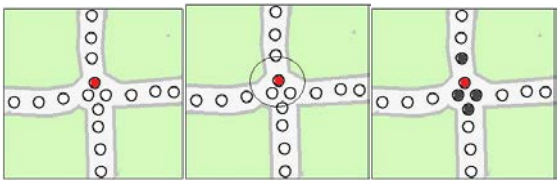

Figure 4a: Crossroad scenario – first hops

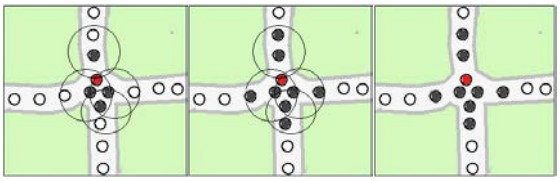

Figure 4b: Crossroad scenario – second hops

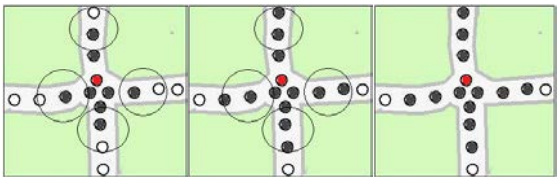

Figure 4c: Crossroad scenario – third hops and so on …

2) *In each node that receives the SDM,*

a. If the maximum hops number is not reached (an SDM reaches the maximum number of hops if the pre-set number of hops are transmitted by nodes) and if none of the nodes have the same situation, they forward the same SDM to the next neighbour nodes as a second wave (second hop) to inform the others of the current situation (Figure 4b).

b. However, if one of its neighbours has a new situation at the same time as receiving the message, it will generate a new SDM that contains its current condition and also all the information it has previously identified about the nearby nodes.

c. Again, all nodes forward the same SDM to the next neighbour as a third hop (Figure 4c) after they have updated the message on the current situation. These steps are repeated until the Conditions Search Limitations (CSL) become true or the maximum number of hops is reached.

3) *Each node is capable* of:

a. Keeping track of all seen messages, which allows it to discard all redundant messages. Also each node keeps all the information it has about all 'seen' nodes – all nodes contained in the messages received in the node – in two different lists: the first for ANs and the second for NANs.

b. If any node – at any hops – has the same/new situation, a new SDM will be generated containing additional information as well as the information it holds about the other surrounding nodes and broadcasts it to all nearby nodes. Previous steps will be repeated until – again – the CSL becomes true.

4) *After a short period* of exchanging SDMs:

a. Nodes will have got all about the surrounding nodes' information. Each node should hold three lists: a seen messages list (to reduce redundancy), an active node seen list and a non-active node seen list.

b. Each time a node receives a message it updates its lists and checks whether the optimum number for each detectable situation is achieved or not. If it is not, it will forward an SDM to the next hops.

5) In the case of an optimum number being achieved, the car which got this information will *calculate the boundary of the situation zone* based on the information it already has about the surrounded cars (Figure 5). Then, a new Situation Warning Message (SWM) will be generated and sent to warn all nearby cars by the situation and its position. Also, a new CSL will be set up for an SWM to determine the lifetime.

Figure 5: Situation Zones has been identifier

4.2 Cloud Zone Scan Scheme (CZS)

Based on real life, road conditions occur in certain places that will affect groups of nearby cars inside that zone. For instance, usually if a car discovers foggy weather (fog light goes ON), mostly, all nearby cars have the same condition. Or, if a car senses rain (windscreen wipers go ON), often, all nearby cars have the same situation or – at least – will sense the same very soon.

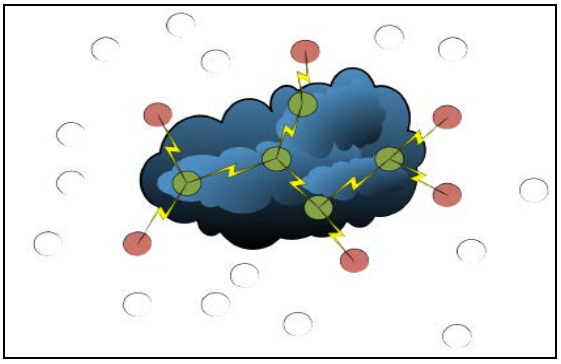

Figure 6: Raincloud

CZS scheme is based on this assumptions and *the cars which sense a situation (AN) will trigger SDM*:

1) This SDM will travel from car to car, until reaching the first node that does not have (sensed) the same situation, which will not retransmit the SDM (stopping the forwarding of the SDM).
2) It will reply toward the source node of the SDM message with its geographic position to inform all nearby cars that the boundary of the situation is here (its position), meaning, that this approach looks for the nodes (cars) located on the borders of a situation zone (e.g. raincloud).

Figure 6 illustrates five vehicles inside a raincloud. These vehicles communicate with each other, and with the vehicles just outside the cloud. The vehicles on the outside of the cloud respond by returning their positions, and information that they don't sense rain, to the vehicles inside the cloud. The vehicles inside the cloud update their information tables, and pass this information to the other vehicles inside the cloud. Based on the data in the information tables the vehicles can calculate the area that the cloud covers, generate SWM and broadcast it to the cars in the region.

5. Results & Conclusion

We propose in this paper schemes that are using 'intelligent flooding' instead of blind flooding broadcasting (selected nodes will retransmit the messages). These were tested using an NS2 simulator, these experiments showed that 'intelligent flooding' was faster and less resource consuming than 'pure flooding', thereby confirming our hypothesis. The results of the simulator were as expected, and the simulation proved that 'intelligent flooding' produced far fewer messages, and is significantly faster than 'pure flooding'. It also showed that 'intelligent flooding' is vulnerable to interference, and because of that important packets could be lost. Resolving these issues the focus of further research..

As aforementioned, The BZS scheme attempts to identify the optimum value for two parameters: *the number of hops* and *the delay time* needed to scan the area and identify the boundary of the situation zone. The assumption is that different situations are detected by different numbers of recognised ANs/NANs (e.g. the situation is rainy if 33% of nodes are AN, while, a slippery spot can be detected by three ANs regardless the number of NANs).

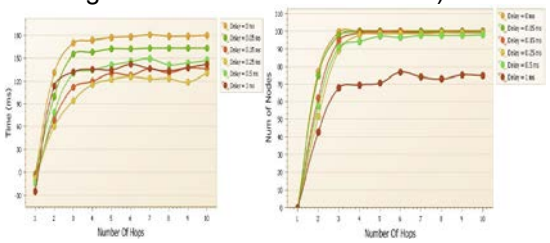

Figure 7: Message Exchange Time

And # of Nodes Saw more than 50% of AN

Analysis of the graphs' trends (the results simulate this scheme–Figure 7) indicates that:

a. There is no fixed optimum number either for delay time or number of hops. Consequently a range of numbers for these two parameters must be considered dependent on the detection cases. Based on these assumptions, we are looking for the best results that can recognise from 50% up to 100% active nodes (ANs), which will be enough to cover all cases.

b. Also, the graphs present the point of saturation i.e. where an increase in the value of the investigated parameter gives relatively small improvement in the quantity of sent/received/discarded messages. The results show clearly that using from three up to five hops is optimum to detect any traffic condition if we consider the abovementioned indicators.

c. The results show that the greatest delay time will reduce the number of exchanged messages, but will increase the total time needed to recognise the biggest possible number of ANs/NANs. This is a difficult compromise between time and noise, though a figure between 0.01 and 0.1 seconds seems to be indicated.

There is much work to be done in calculating the specific details based on the information gathered from 'intelligent flooding'. The migration of the common status is also an interesting aspect that would benefit from further study. A study of behaviour with different technologies could provide useful information.

References

[1] Wischoff, L., Ebner, A., Rohling, H., Lott, M. and Halfmann, R.(2003) 'Sotis, a selforganizing traffic information system' in *IEEE Vehicular Technology Conference,*pp. 2442-2446.

[2] Valerio, D., D'Alconzo, A., Ricciato, F. and Wiedermann, W. (2009) 'Exploiting cellular networks for road traffic estimation: a survey and a research roadmap' in *IEEE Vehicular Technology Conference (VTC)*, pp. 1-5.

[3] Yoon, J., Noble, B. and Liu, M. (2007) 'Surface street traffic estimation' in *ACM international conference on Mobile Systems, Applications and Services*, pp. 220-232.

[4] Yu, B., Gong, J. and Xu, C. (2008) 'Catch-up: a data aggregation scheme for vanets' in *ACM international workshop on Vehicular Internetworking*, pp. 49-57.

[5] Lu, R., Lin, X., Zhu, H. and Shen, X. (2009) 'Spark: a new vanet-based smart parking scheme for large parking lots' in *IEEE INFOCOM*, pp. 1413-1421.

[6] Dashtinezhad, S., Nadeem, T., Dorohonceanu, B., Borcea, C., Kang, P. and Iftode, L. (2004) 'TrafficView: a driver assistant device for traffic monitoring based on car-to-car communication' in *IEEE, Vehicular Technology Conference (VTC)*.

[7] Thiagarajan, A., Ravindranath, L., LaCurts, K., Madden, S., Balakrishnan, H., Toledo, S. and Eriksson, J. (2009) 'VTrack: accurate, energy-aware road traffic delay estimation using mobile phones' in *ACM Conference on Embedded Networked Sensor Systems*, pp. 85-98.

[8] Zhuang, Y., Pan, J. and Cai, L. (2010) 'A probabilistic model for message propagation in two-dimensional vehicular ad-hoc networks' in *ACM international workshop on Vehicular Internetworking*, pp. 31-40.

[9] Mohan, P., Padmanabhan, V. and Ramjee, R. (2008) 'Nericell: rich monitoring of road and traffic conditions using mobile smartphones' in *ACM conference on Embedded Network Sensor Systems*, pp. 323-336.

[10] Sen, R., Raman, B. and Sharma, P. (2010) 'Horn-ok-please' in *ACM international conference on Mobile Systems, Applications, and Services*, pp. 137-150.

[11] Lochert, C., Scheuermann, B. and Mauve, M. (2007) 'Probabilistic aggregation for data dissemination in VANETs' in *ACM international workshop on Vehicular Ad Hoc Networks (VANET)*, pp. 1-8.

[12] Lochert, C., Scheuermannm B., Wewetzer, C., Luebke, A. and Mauve, M. (2008) 'Data aggregation and roadside unit placement for a vanet traffic information system' in *ACM international workshop on Vehicular Internetworking*, pp. 58-65.

[13] Korkmaz, G., Ekici, E., Özgüner, F. and Özgüner, U. (2004) 'Urban multi-hop broadcast protocol for inter-vehicle communication systems' in *ACM international workshop on Vehicular Ad Hoc Networks (VANET)*, pp.76-85.

[14] ElBatt, T., Goel, S., Holland, G., Krishnan, H. and Parikh, J. (2006) 'Cooperative collision warning using dedicated short range wireless communications' in *ACM international workshop on Vehicular Ad Hoc Networks.*pp1-9.

[15] Scheuermann, B., Lochert, C., Rybicki, J. and Mauve, M. (2009) 'A fundamental scalability criterion for data aggregation in VANETs' in *ACM international conference on Mobile Computing and Networking*,pp.285-296.

[16] Caliskan, M., Graupner, D. and Mauve, M. (2010) 'Decentralized discovery of free parking places' in *ACM international workshop on Vehicular Ad Hoc Networks (VANET)*,pp. 30-39.

[17] Rybicki, J., Scheuermann, B., Kiess, W., Lochert, C., Fallahi, P. and Mauve, M. (2007) 'Challenge: peers on wheels – a road to new traffic information systems' in *ACM international conference on Mobile Computing and Networking*, pp. 215-221.

[18] Popescu-Zeletin, R., Radusch, I. and Rigani, M. A. (2010) 'Vehicular-2-X Communication: State-of-the-Art and Research in Mobile Vehicular Ad Hoc Networks. USA: Springer, pp. 5-38.

[19] Palazzi, C. E., Pezzoni, F. and Ruiz, P. M. (2012) 'Delay-bounded data gathering in urban vehicular sensor networks', *Pervasive and Mobile Computing*, 8, pp. 180-193.

Autonomous Design of Modular Intelligent Systems

Pavel Nahodil, Jaroslav Vítků
Czech Technical University in Prague
Faculty of Electrical Engineering
Department of Cybernetics
Technicka 2, 16627, Prague 6, Czech Rep.
Email: nahodil@fel.cvut.cz, vitkujar@fel.cvut.cz

KEYWORDS

Agent, Architecture, Artificial Life, Creature, Behaviour, Hybrid, Neural Networks, Evolution.

ABSTRACT

We propose our original system capable of autonomous design of general-purpose complex modular hybrid systems. The resulting hybrid systems will be able to employ various techniques of learning, decision-making, prediction etc. Presented topic is from Artificial Life domain, but contributes also to fields such as Artificial Intelligence, Biology, Computational Neuroscience, Ethology, Cybernetics and potentially into many other aspects of research. The autonomous design is implemented as an optimization of system topology with respect to given problem. The principle of design is based on modified neuro-evolution and can be compared to modular neural networks. One of the main requirements is standardization of communication between very different subsystems. Here, each subsystem - module implements arbitrary algorithm and is treated as a Multiple-Input Multiple-Output subsystem. First, the design of simulator used is described, then the basic principle of hybrid networks is explained with it benefits and drawbacks. Finally, simple example is mentioned.

INTRODUCTION

The main research focus of this paper lies in design of modular hybrid agent architectures. Until now, there is no superior architecture solving all possible tasks. Rather, agents are designed specifically for solving a particular problem in a given domain. Such agents are usually composed of some set of sub-systems. The selection of these subsystems and their interconnection is chosen by a human designer based on his knowledge and experience.

But the correct selection of particular modules and their connectivity is more and more complicated. Now, the research is composed from more and more isolated and specialized fields. It is very hard to track latest changes in more than one field and to maintain some general picture. Even though, it is obvious that there is some redundancy in particular approaches. For example there are the same problems solved by more abstract (e.g. Markov chains for sequence recognition (Fink 2003)) or more biologically-plausible (e.g. neural-based sequence recognition (Wang and Arbib 1990; Nguyen et al. 2012; Wang and Tsai 1998; Murre et al. 1989)) approaches. There is also redundancy how to solve the same problem between various research fields.

In many tasks, there is available some metric which says how good is a behaviour generated by the agent. Based on this metric (fitness), there is possible to design agent architectures by means of some optimization technique. There are many potential benefits of automatic design of modular systems.

THEORETICAL BACKGROUND

Design methods can be generally divided into the following three primary groups:

- **Knowledge based architecture (top down)**: Knowledge based architectures use knowledge to guide agent behaviour. Much of the debate regarding the role of knowledge within an agent aims on how it is represented within the context of the control system. Knowledge representations involve "physical structures which have correlations with aspects of the environment representation (relationship with the external world) and thus a predictive power (ability to predict from actual knowledge) for the system". Agent modules are functional blocks like planning, learning or perception blocks and the behaviours (avoid obstacles, identify object, explore the environment) emerge from the interaction of the modules.
- **Behaviour based architecture (bottom up)**: behaviour based architectures build up the system of behaviour producing modules instead of functional, as is the case in knowledge based architectures. Agent modules are behaviours such as avoid obstacles, identify object, and explore the environment. The functions of the system (planning, learning and others) emerge from the interaction of these modules and the environment. The most important phenomenon of behaviour based architectures is emergent behaviour. Emergent behaviour implies a holistic capability where the sum is considerably greater than its parts. Emergence is the appearance of novel properties in whole system. Intelligence emerges of the components of the system (Kadleček and Nahodil 2001).

Proceedings 27th European Conference on Modelling and Simulation ©ECMS Webjørn Rekdalsbakken, Robin T. Bye, Houxiang Zhang (Editors)
ISBN: 978-0-9564944-6-7 / ISBN: 978-0-9564944-7-4 (CD)

• **Hybrid approach (combined)**: Hybrid architectures integrate a knowledge based component for planning and problem solving with behavioural components that produce robust performance in complex and dynamic domains. Strong evidence exists, that hybrid systems are found in biology, implying that they are compatible, symbiotic, and potentially suitable for use in agent control. The focus of research in this area lies in defining an interface between deliberation and reactivity, which is poorly understood so far. Hybrid models include hierarchical integration and coupled planning and reacting.

Artificial Neural Networks

Differences between Artificial Neural Networks and classical computation executed by computers are mentioned in various literature. We will only mention that von-Neumann type of computer implements from its principle deterministic computation based on exact data. The bottleneck of this architecture poses constraints to the maximum speed of computation. The fact that individual information have to be distinguished without errors causes consumption of considerable amount of energy. Also the second characteristic makes the architecture unfeasible for processing the real-world data. Compared to this, brain is computational system designed by evolution with the following requirements:

- highly power-efficient
- highly robust against errors in hardware
- works well with real world noisy data

These requirements probably determined that the brain implements highly parallel type of computation, that the computation as well as memory is decentralized. We can see that these features are often direct opposite to von-Neumann architecture, so as to many computation models based on it.

There are several reasons why the Artificial Neural Networks are not used more widely, one of them is that neural networks often work as a black-boxes and we do not have methods to design networks of appropriate size. This is addressed in our work too.

Hybrid Networks

Hybrid networks combine top-down and bottom-up approaches in one network with heterogeneous nodes. Various classification schemes of hybrid systems have been proposed so far. According to (Wermter and Sun 2000), there are three main types of hybrid systems. These are divided according to ways how the integration of symbolic and sub-symbolic systems are done. These are:

• **Unified neural architectures** - these systems rely solely on connectionist representations, but symbolic interpretations of nodes or links are possible. Often, a specific knowledge of the task is built into a unified neural architecture.

• **Hybrid transformation architectures** - transform symbolic representations into neural representations or vice versa. The main processing is performed by neural representations but there are automatic procedures for transferring neural representations to symbolic representations or vice versa.

• **Hybrid modular architectures** - contain both symbolic and neural modules appropriate to the task. Here, symbolic representations are not just initial or final representations as in a transformation architecture.

This paper proposes approach which designs naturally the third one - *Hybrid modular architectures*. Based on modules used, the resulting modular systems can be also of another type (e.g. network of only subsymbolic systems).

Evolutionary Design of Hybrid Networks

One of the most challenging goals of our research still remains to propose efficient Evolutionary Algorithm (EA) for design of networks composed of MIMO systems. In case of design networks with no constraints on topology, the space of possible solutions grows extremely fast. Nowadays, there are many solutions how to pose constraints on the topology, so the problem becomes feasible for EAs (Fekiac et al. 2011). As a good example can be mentioned Cartesian Genetic Programming (CGP) (Fišer et al. 2010) used for automatical design of logic circuits. Other useful method for design of hybrid networks is called Multi-Layered Iterative Algorithm of Group Method Data Handling (MIA-GMDH), a modification of original GMDH (Ivakhnenko 1970). In (Kordík 2006), the modification of MIA GMDG, called Group of Adaptive Models Evolution (GAME) is used for evolutionary design of feed-forward hybrid neural networks. However, all these methods employ only Multiple-Input Single-Output (MISO) neurons (subsystems).

OUR APPROACH

There are many benefits provided our approach to hybridization of Artificial Neural Networks. These range from comparison of performance between various subsystems, better general overview of available approaches and potentially autonomous research in the future. Also, there are many requirements posed by our approach, these main requirements will be described in the following sub-sections.

Reusable Modules

It is very time-consuming to re-implement outcomes of a particular research. It would be easier to test and publish resulting algorithms or systems in a reusable manner. In situation when researchers will share actual working prototypes of their work, the speed of research can be highly increased. Requirements for system which allows us to reuse work are mainly:

- Standardized communication
- Programming language independence
- Simple to use
- Decentralized - modular design.

In such a system, particular modules published by various researchers can be interconnected together in one working system. In the field of robotics, these

requirements are already addressed by system called Robotic Operating System (ROS) (Quigley et al. 2009). We do not see the reason why this system should not be used more broadly, at least also in AI or ALife research.

Unified Communication

Despite the unification of communication on some level, different modules of very different complexity typically use very different types of communications. However, our autonomous design of modular systems poses even more challenging requirement: to use one type of communication in the entire system.

Since it is known that an arbitrary function can be approximated by feed-forward neural network with only one hidden layer (Cybenko 1989; Hornik et al. 1989), it can be assumed that any behaviour of arbitrary complexity can be build by means of neural networks with more complex topologies and/or more complex models of neurons.

Therefore the neural networks can be seen as theoretical way how to build an arbitrary system. Based on this fact, we adopt neural-based communication in our design of systems. The resulting modular networks can be compared to modular neural networks (Auda and Kamel 1999), where each subsystem (module) is represented by Multiple-Input Multiple-Output (MIMO) system.

HYBRID MODULAR SYSTEMS

We define a hybrid modular system as a network of interconnected modules in a given topology. These modules communicate by means of defined connections. As mentioned earlier, there is no common communication language for all types of subsystems. Therefore the "language" used by ANNs was used in the entire system. Because of similarities with neurons, these subsystems are called *neural modules*. Typical neural module is implemented as a black-box with m inputs and m outputs, this can be seen in 1.

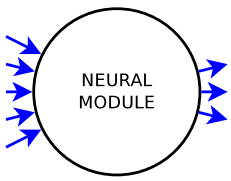

Fig. 1. Concept of neural module - black box with general number of independent inputs and outputs

In order to reuse many current implementations of systems, the ROS nodes are used here. The Fig.2 depicts how messages from ROS node are translated in modem into "language of ANNs". In current implementation, each connection represents one value of primitive type float, ideally in range $val = \langle -1; 1 \rangle$. Modem is used for modulating and demodulating this signal from/into ROS messages.

The drawback of this encoding is in the fact that encoding of more complex data types requires many

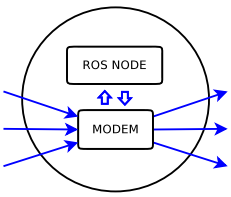

Fig. 2. Neural Module which encapsulates one ROS node. Blue lines represent neural communication (real-valued data) and blue arrows denote ROS messages. ROS node is launched as an external process by the simulator. Modem translates ROS messages into neural communication and back

neural connections. There are many techniques for autonomous design of ANN topologies. Many of them also try to deal with many connections in the networks. So this problem will be dealt with in the future by finding the appropriate encoding for these networks. The main requirements are:

- Ability to efficiently represent large numbers of connections
- Ability to represent connections of MIMO nodes.

The main advantage of such hybrid approach is in combining top-down and bottom-up approaches tightly together. It deals with one of the biggest drawbacks of ANNs: by adding (top-down designed) a subsystem of known structure, the resulting network becomes a grey-box. On the other hand, the top-down systems empowers with the main benefits of ANNs, such is robustness.

Moreover: the user can choose how much top-down and how much bottom-up architecture wants to design. This is done simply by providing more or less complex neural modules to the algorithm.

THE SIMULATOR NENGOROS

The simulator of complex modular hybrid systems has to be able to simulate systems of various complexities and levels of abstraction, ranging from Artificial Neural Networks (ANNs) to pure symbolic approaches. For these purposes we decided to combine two current software tools into one simulator, called NengoRos.

Nengo

The first component is large-scale neural networks simulator called Nengo (available at `nengo.ca`). This simulator supports various types of neurons, both of second and third generation (Maass 1996), even in one simulation. Also modularity in networks is well supported. Design of networks in this simulator is based on Neural Engineering Framework (NEF) (Eliasmith and Anderson 2003), but standard design of ANNs can be used too. The Fig.3 shows an example neural-circuit implemented in Nengo simulator.

Robotic Operating System

In order to be able to integrate ANN simulation with more abstract subsystems contained in modules, the Robotic Operating System was selected (available at `ros.org`). ROS is a decentralized software tool to simulate modular systems, mainly for purposes of robotic

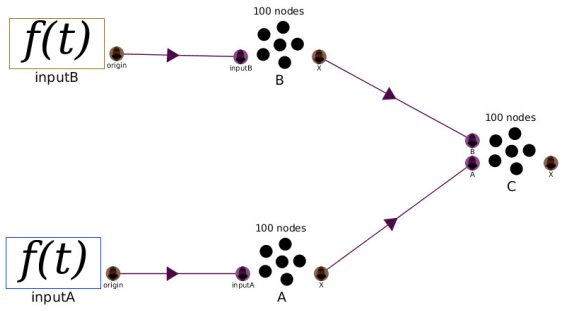

Fig. 3. Example of neural-based system in Nengo. The system contains three neural ensembles, 10, Example of neural-based system in Nengo. The system contains three neural ensembles, two represent input value and the third one computes the sum

research. Modules (nodes) run in own processes and communicate by means of messages over peer-to-peer network. Each module can publish/subscribe to arbitrary type of predefined messages, see Fig.4.

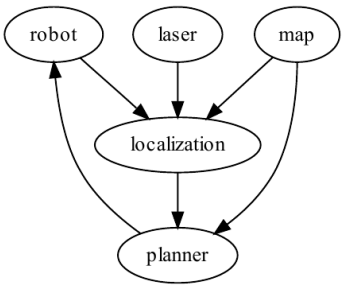

Fig. 4. Example of simple network of ROS nodes

ROS modules communicate by means of predefined messages. These messages are composed of arrays of primitive data types often.

MODIFICATION OF WEIGHT MATRIX ENCODING

For the rudimentary testing of new simulator of hybrid systems, it was decided to show one of the advantages of hybrid networks. It is a smaller number of connections between modules, compared to classical ANN.

Weight Matrix Encoding

The simplest encoding, based on a matrix containing the connection weights, was chosen. The form of matrix is depicted in the Fig.5.

The matrix contains weights between neurons represented by real-values in a given range. This matrix can be encoded in a linear chromosome by concatenating particular lines. Standard EA can be then used to modify this chromosome - to search through the space of possible connections.

Modified Encoding for a Hybrid System

We need to modify this encoding in order to be able to use it for systems with MIMO nodes. While neural

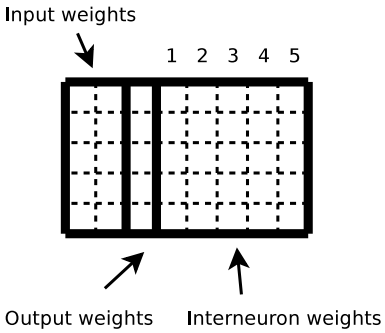

Fig. 5. Example of weight-matrix encoding ANN with two-dimensional input, one-dimensional output and 5 neurons

module have m inputs and n outputs in general. In the simplest case, it is possible to represent each input/output of module as one neuron and use standard encoding described earlier. As can be seen in the Fig.7, it is necessary to hold only upper triangle matrix. Decoding then has three parts:

- Make undirected connections according to matrix
- Change connection directions so they match inputs/outputs
- Discard invalid edges.

In this encoding, and invalid edge connects input with input or output with output, see Fig.7.

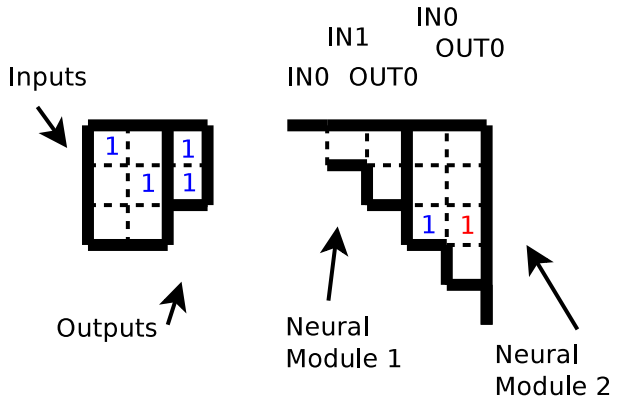

Fig. 6. Modified Weight Matrix Encoding for Network of MIMO nodes

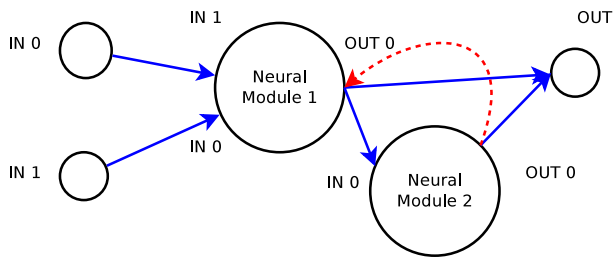

Fig. 7. Topology of a hybrid network encoded by a modified weight-matrix encoding (depicted in the previous Figure)

The obvious benefit is that we do not need so big matrix when connecting MIMO systems. The length of chromosome which encodes the topology with N modules is:

$$l = \frac{\alpha^2 - \alpha}{2} + IN \sum_k in_k + OUT \sum_k out_k, \quad (1)$$

and:

$$\alpha = \sum_k in_k + \sum_k out_k, \quad (2)$$

where k is number of nodes in the network, IN is number of inputs, OUT is number of outputs and $\sum_k OUT_k$ is sum of all outputs for all neural modules.

The drawback is that (in order to get unambiguous encoding) each single neuron has to be represented by its separate input and output in the matrix. This means that in case of encoding only simple ANN (where $m = 1$ and $n = 1$ for all modules), the chromosome will be twice long as in normal, matrix based encoding.

EXPERIMENTS

In order to gain some proof of our concept, a simple experiment was concluded. In this experiment, we compare performance of evolutionary algorithm designing standard (homogenous) ANN with EA designing hybrid modular network. Complexity of both networks (number of connections between nodes) will be similar, but the hybrid network will include a priory knowledge inside one neural module. This experiment should show that complexity of a modular system can be partially encapsulated by neural modules, therefore a design of these hybrid systems is simpler, compared to ANN.

Here, as depicted in the Fig.8, the EA optimizes parameters of a network in order to approximate behavior of a plant. Fitness function of network is computed as inverse of Means Squared Error (MSE) from one simulation. Topology of both networks was set to fully recurrent, so the EA searches just for optimal weights between nodes in the network (inside the NN-based model - Fig.8). Presented results are concluded from 10 runs of EA. In this case, the plant implements simple Fuzzy OR function, which is described by the equation:

$$y = max(\mu(a), \mu(b)). \quad (3)$$

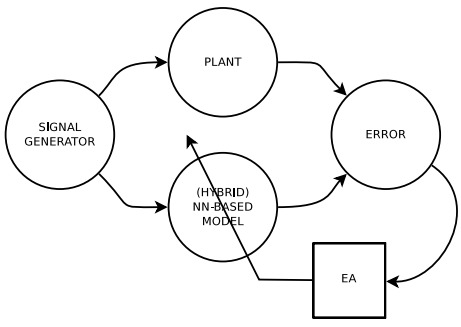

Fig. 8. Scheme of optimization of (hybrid) neural network topology. The goal is to build the model of plant (Fuzzy OR module here)

Evolution of ANN-based Model

The first part is in finding the weights in classical ANN. This model of network of 3rd generation uses Leaky Integrate-and-Fire (LIF) models of neurons (which is often used in emerging new HW platforms (Galluppi et al. 2010)). Neurons of third generation communicate with series of spikes between them. Input signal to the network is converted into spikes and output of the network is converted from spikes to real-valued variable. ANN is composed of $N = 4$ hidden neurons, two input neurons and one output neuron. Since the EA uses matrix-based encoding, this results of vector of real-valued numbers of length $l = 28$.

In the Fig.9 we can see the final setup of the experiment in the NengoRos simulator: signal generator feeds random, two-dimensional signal into the plant and a sub-network. In the sub-network (on the bottom), the particular dimensions are separated, converted into spikes and connected to the population of spiking neurons. Weighted signal from hidden neurons is fed into output neuron, where is converted into real-valued output signal.

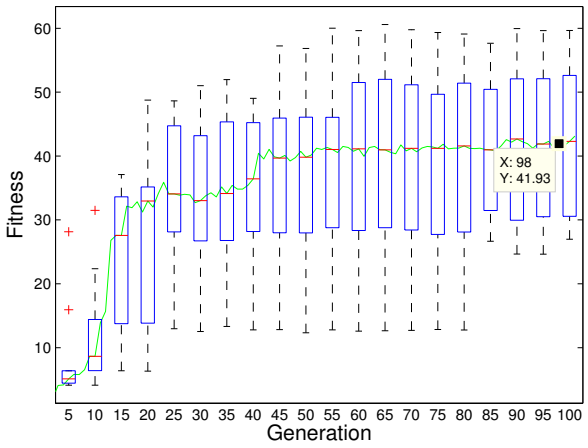

Fig. 10. Fitness of the best artificial neural network during the neuro-evolution

The graph in the Fig.10 shows a course of fitness value of the best network in the population.

Evolution of Hybrid ANN Model

Here, the model is composed according to our framework of hybrid modular networks. These networks can include selected MIMO modules. Obviously it is important which modules we use in order to solve some task. This model should prove that correct choice of modules can speed up the design of architecture and improve its results.

We are introducing neural module which implements "Fuzzy OR", this means that our hybrid network is able to use model of the plant directly. This hybrid network uses our modified weight-based encoding. In order to acquire similar complexity of model parameters, the number of neurons is selected to $N = 2$. According to

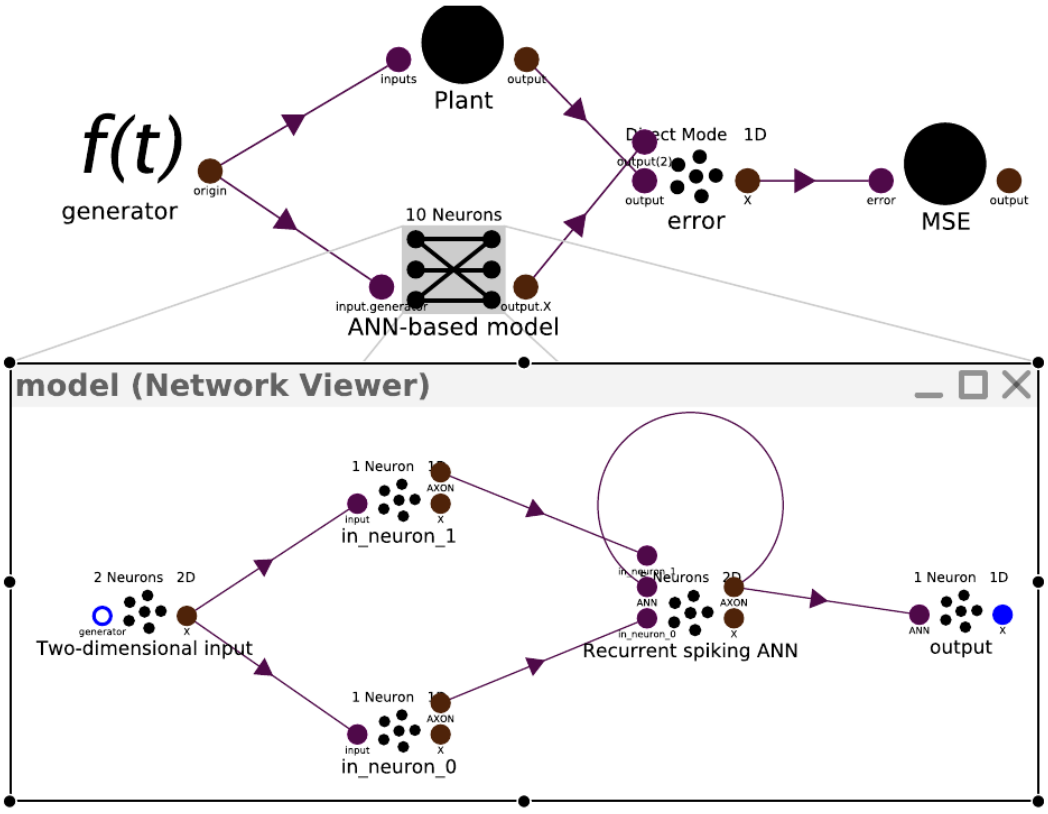

Fig. 9. Example of hybrid modular system - recurrent ANN of third generation tries to approximate plant

the eq.1, the length of genome is slightly higher than in case of classical ANN: $l = 32$. The rest of experiment setup is identical to the previous simulation, our neural module can be also connected in this fully recurrent architecture.

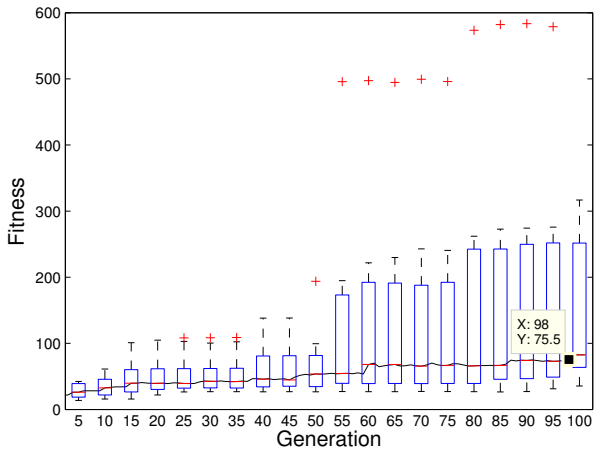

Fig. 11. Fitness of the best hybrid modular network during the neuro-evolution

The graph in the Fig.11 shows that evolution of the hybrid model was able to produce significantly better approximation of plant than classical ANN-based model.

CONCLUSIONS

In this paper we presented our approach to designing agent architectures based on hybrid modular systems. First, we defined requirements for such a system. Then we built simulator of these systems, so we are now able to test new methods of neuro-evolution. These methods will have to be able to compactly represent topologies with general MIMO subsystems. First version of such encoding was tested on small example network. We hope that our approach will enable us to automatically design modular architectures specially for on a given task. Also, such designer could combine current subsystems (neural modules) into new, so far unexplored combinations which exhibit interesting and potentially useful behavior.

The main challenge for the future work stays in finding the suitable representation of network topology. The main benefits of our approach are in combining top-down and bottom-up approaches while designing modular architectures. Now, the user can choose how robust and parallel, and how synoptical and efficient system to design. This can be done by providing specific neural modules.

ACKNOWLEDGEMENT

This research has been funded by the Dept. of Cybernetics, Faculty of Electrical Engineering, Czech Technical University in Prague under SGS Project SGS12/146/OHK3/2T/13.

REFERENCES

Auda, G. and Kamel, M. (1999). Modular neural networks: a survey. *Int J Neural Syst*, 9(2):129–151.

Cybenko, G. (1989). Approximation by superpositions of a sigmoidal function. *Mathematics of Control, Signals, and Systems (MCSS)*, 2:303–314.

Eliasmith, C. and Anderson, C. H. (2003). *Neural Engineering: Computation, Representation, and Dynamics in Neurobiological Systems*. The MIT press, Cambridge, ISBN: 0-262-05071-4.

Fekiac, J., Zelinka, I., and Burguillo, J. C. (2011). A review of methods for encoding neural network topologies in evolutionary computation. In *Proceedings 25th European Conference on Modelling and Simulation ECMS*, pages 410–416. ISBN: 978-0-9564944-2-9.

Fink, G. A. (2003). *Markov Models for Pattern Recognition*. Springer. ISBN 978-3-540-71766-9.

Fišer, P., Schmidt, J., Vašíček, Z., and Sekanina, L. (2010). On logic synthesis of conventionally hard to synthesize circuits using genetic programming. In *IEEE 13th International Symposium on Design and Diagnostics of Electronic Circuits and Systems (DDECS)*, pages 346–351.

Galluppi, F., Jin, X., and Furber, S. (2010). The leaky integrate-and-fire neuron: A platform for synaptic model exploration on the spinnaker chip. In *The 2010 International Joint Conference on Neural Networks (IJCNN)*, pages 1–8.

Hornik, K., Stinchcombe, M., and White, H. (1989). Approximation capabilities of multilayer feedforward networks. *Journal Neural Networks*, 2:359–366.

Ivakhnenko, A., G. (1970). Heuristic self-organization in problems of engineering cybernetics. *Automatica*, 6:207–219.

Kadleček, D. and Nahodil, P. (2001). *New Hybrid Architecture in Artificial Life Simulation*, volume 2159 of *Advances in Artificial Life*. Springer Verlag, LNCS edition. ISBN: 978-3-540-42567-0.

Kordík, P. (2006). *Fully automated knowledge extraction using group of adaptive models evolution*. PhD thesis, Czech Technical University in Prague, FEE, Dep. of Comp. Sci. and Computers.

Maass, W. (1996). Networks of spiking neurons: The third generation of neural network models. *In Journal Neural Networks*, 10:1659–1671.

Murre, J. M. J., Phaf, R. H., and Wolters, G. (1989). Calm networks: a modular approach to supervised and unsupervised learning. In *Proc. Int Neural Networks IJCNN. Joint Conf*, pages 649–656.

Nguyen, V., Starzyk, J., Goh, W.-B., and Jachyra, D. (2012). Neural network structure for spatio-temporal long-term memory. In *IEEE Transactions on Neural Networks and Learning Systems*, volume 23, pages 971–983.

Quigley, M., Conley, K., Gerkey, B., Faust, J., Foote, T., Leibs, J., Wheeler, R., and Ng, A. (2009). Ros: an open-source robot operating system. In *ICRA Workshop on Open Source Software*.

Wang, D. and Arbib, M. A. (1990). Complex temporal sequence learning based on short-term memory. 78(9):1536–1543.

Wang, J.-H. and Tsai, M.-C. (1998). Learning recognition of temporal sequences by coding temporal distance in neural networks. In *In Proceedings of IEEE International Joint Conference on Neural Networks*, volume 2, pages 1422–1427.

Wermter, S. and Sun, R. (2000). *Hybrid Neural Systems*. Springer, Heidelberg, New York.

AUTHOR BIOGRAPHIES

PAVEL NAHODIL was born in Prague, Czech Republic. He obtained EE degree (Dipl. Ing) in Technical Cybernetics at the Faculty of Electrical Engineering at the CTU in Prague in 1970 and Ph.D. degree in the same branch in 1980. He has been working at the Department of Cybernetics at the Faculty of Electrical Engineering, Czech Technical University in Prague, where he was also appointed the Professor in Technical Cybernetics. He has led and consulted more than 110 diploma thesis here so far. He was also supervisor of about 30 PhD students till now. His present professional interest includes artificial intelligence, multi-agent systems, on behavior based intelligence robotics (control systems of artificial creatures) and the artificial life design in general. He is (co-)author of several books, university lecture notes, hundreds of scientific papers and large collection of scientific studies. He is also the organizer of some international conferences + reviewer (IPC Member) and a member of many Editorial Boards. His e-mail address is: `nahodil@fel.cvut.cz`.

JAROSLAV VÍTKŮ was born in Prague, Czech Republic. He graduated in 2011 in Czech Technical University in Prague, Faculty of Electrical Engineering in Artificial Intelligence. His diploma thesis "An Artificial Creature Capable of Learning from Experience in Order to Fulfill More Complex Tasks" was awarded by Price of Dean. Currently, he is a PhD student at the Department of Cybernetics, CTU in Prague, still under the guidance of his supervisor Pavel Nahodil. Here elaborates the results of his thesis as an automated design of complex modular systems inspired by Nature. His research interest includes hybrid neural networks, cognitive science, biologically inspired algorithms, behavioral robotics and Artificial Life in common. His e-mail address is: `vitkujar@fel.cvut.cz`.

SCHEDULING THE FLOW SHOP WITH BLOCKING PROBLEM WITH THE CHAOS-INDUCED DISCRETE SELF ORGANISING MIGRATING ALGORITHM

Donald Davendra
Department of Computer Science
Faculty of Electrical Engineering and Computer Science
VSB-Technical University of Ostrava
17. listopadu 15, 708 33 Ostrava-Poruba
Czech Republic.
Email: donald.davendra@vsb.cz

Magdalena Bialic-Davendra,
Tomas Bata University in Zlin,
Faculty of Management and Economics,
Nam T.G. Masaryka 5555, 760 01 Zlin,
Czech Republic.
Email: bialic@fame.utb.cz

Roman Senkerik and Michal Pluhacek,
Tomas Bata University in Zlin,
Faculty of Applied Informatics,
Nam T.G. Masaryka 5555, 760 01 Zlin,
Czech Republic.
Email: {senkerik,pluhacek}@fai.utb.cz

KEYWORDS

Discrete Self Organising Migrating algorithm, flow shop with blocking, chaos Lozi map

ABSTRACT

The dissipative Lozi chaotic map is embedded in the Discrete Self Organising Migrating Algorithm (DSOMA) algorithm, as a pseudorandom number generator (PRNG). This novel chaotic based algorithm is applied to the flow shop with blocking scheduling problem. The algorithm is tested on the Taillard problem sets and compared favourably with published heuristics.

INTRODUCTION

One of the core premises of EA's is their reliance on *stochasticity*, the ability to generate a random event, which in turn, hopefully, provides the spark of perturbation towards the desired goal. The task of generating these stochasticity is generally in the realm of *pseudorandom number generators* (PRNG); a structured sequence of mathematical formulation which tries to yield a generally optimal range of distributed numbers between a specified range.

A wide variety of such PRNG's exist, however the most common in usage is the *Mersenne Twister* (Matsumoto and Nishimura, 1998). A number of its variants has been designed; for a full listing please see Matsumoto (2012). Some other common PRNG's are the *Mother Of All*, *CryptoAPI*, *Indirection, Shift, Accumulate, Add, and Count* (ISAAC), *Keep it Simple Stupid* (KISS) and *Mutiply-With-Carry* (MWC).

The first aspect of the research work presents a novel approach to generating such pseudorandom numbers, one with a lineage in chaos theory. The term *chaos* describes the complex behaviour of simple, well behaved systems. When casually observed, this behaviour can seem erratic and somewhat random, however, these systems are deterministic, whose precise knowledge of future behaviour is well known. The question is then to reconcile the notion of nonlinearity of these systems.

Sudden and dramatic changes in some nonlinear systems may give rise to a complex behaviour called chaos. The noun *chaos* and the adjective *chaotic* are used to describe the time behaviour of a system when that behaviour is aperiodic (it *never* exactly repeats) and appears apparently random or noisy (Hilborn, 2000).

This aperiodic non-repeating behaviour of chaotic systems is the core foundation of this research. The objective is then to use a valid chaotic system, and embed it in the EA's as a PRNG. Four general branches of chaotic systems exist, which are the dissipative systems, fractals, dissipative and high-dimensional systems and conservative systems. The chaos system used for this research is the *discrete* dissipative system of the Lozi map. This system is relatively simple, in terms of period density, and therefore easier to obtain data through sectional cropping.

Many chaotic maps in the literature have shown to possess certainty, ergodicity and the stochastic property. Recently, chaotic sequences have been adopted instead of random sequences with improved results. They have been used to improve the performance of EA's (Alatas et al. (2009)) and Caponetto et al. (2003)). They have also been used together with some heuristic optimisation algorithms (Davendra et al. (2010) and Zuo and Fan (2006)) to express optimisation variables. The choice of chaotic sequences is justified theoretically by their unpredictability, i.e., by their spread-spectrum characteristic, non-periodic, complex temporal behaviour, and ergodic properties (Ozer, 2010).

Davendra et al. (2010) has applied the canonical Dif-

Proceedings 27th European Conference on Modelling and Simulation ©ECMS Webjørn Rekdalsbakken, Robin T. Bye, Houxiang Zhang (Editors)
ISBN: 978-0-9564944-6-7 / ISBN: 978-0-9564944-7-4 (CD)

ferential Evolution (DE) to solve the PID optimisation problem, whereas Ozer (2010) applied a sequence of chaotic maps to optimise a range of benchmark problems, with the conclusion that the Sinus map and Circle map have somewhat increased the solution quality, with the ability to escape the local optima. The economic dispatch problem was solved by Lu et al. (2011), where the *Tent Map* was utilised as a chaotic local search in order to bypass the local optima. It should also be noted that Yuan et al. (2008) has developed a chaotic hybrid DE, where the parameter selection and operation is handled by chaotic sequences to solve combinatorial optimisation problem.

This research looks at modifying the DSOMA with the Lozi map as the RPNG and using it to solve the Flow shop with blocking problem. The paper is organised as follows; The first section introduces the Lozi map followed by the flow shop with blocking problem. Thereafter, SOMA and DSOMA algorithms are introduced. Subsequently the experimentation results are presented followed by the conclusion.

LOZI MAP

The *Lozi map* is a two-dimensional piecewise linear map whose dynamics are similar to those of the better known Henon map and it admits strange attractors. This system belongs to the *discrete dissipative* systems.

The advantage of the Lozi map is that one can compute every relevant parameter exactly, due to the linearity of the map, and the successful control can be demonstrated rigorously.

The Lozi map equations are given in equations (1) and (2).

$$X_{n+1} = 1 - a \cdot |X_n| + b \cdot Y_n \tag{1}$$

$$Y_{n+1} = X_n \tag{2}$$

The parameters used in this work are $a = 1.7$ and $b = 0.5$ as suggested in Caponetto et al. (2003) and the initial conditions are X_0 = -0.1 and Y_0 = 0.1. The Lozi map is given in Figure 1.

FLOW SHOP WITH BLOCKING

Consider *m* machines in series with *zero* intermediate storage between successive machines, which have to process *n* jobs. If a given machine finishes the processing of any given job, the job cannot proceed to the next machine while that machine is busy, but must remain on that machine, which therefore remains *idle*. This phenomenon is refereed to as *blocking* (Pinedo, 1995).

In this paper, only flow shops with zero intermediate storage are considered (FSSB), since any flow shop with positive (but finite) intermediate storage between machines can be modelled as a flow shop with zero intermediate storage. This is due to the fact that the storage space capable of containing one job may be regarded as

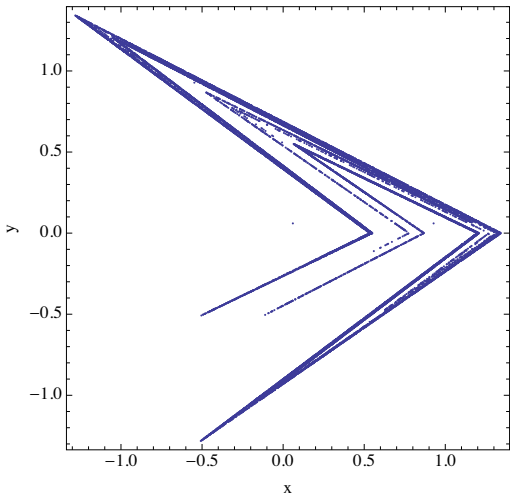

Figure 1: Lozi map

a machine on which the processing time of all machines is equal to zero.

Pinedo (1995) has defined the problem of minimising the makespan in a flow shop with zero intermediate storages is referred to in what follows as:

$$Fm\,|block\,|C_{\max}$$

Let $D_{i,j}$ denote the time that job *j* actually departs machine *i*. Clearly $D_{i,j} \geq C_{i,j}$. Equality holds that job *j* is not blocked. The time job *j* starts its processing at the first machine is denoted by $D_{0,j}$. The following recursive relationship hold under the job sequence $j_1, \ldots, j_n$:

$$D_{i,j_1} = \sum_{l=1}^{i} p_{l,j_1} \quad i = 1, \ldots, m \tag{3}$$

$$D_{i,j_k} = \max\left(D_{i-1,j_k} + p_{i,j_k}, D_{i+1,j_{k-1}}\right) \quad i = 2, \ldots, m \;\; k = 2, \ldots, n \tag{4}$$

$$D_{m,j_k} = D_{m-1,j_k} + p_{m,j_k} \tag{5}$$

DISCRETE SELF ORGANISING MIGRATING ALGORITHM

DSOMA (Davendra, 2009) is the discrete version of SOMA (Zelinka, 2004), developed to solve permutation based combinatorial optimisation problem. The same ideology of the sampling of the space between two individuals of SOMA is retained. Assume that there are two individuals in a search space, where the objective for DSOMA is to transverse from one individual to another, while mapping each discrete space between these two individuals.

The major input of this algorithm is the sampling of the jump sequence between the individuals in the populations, and the procedure of constructing new trial individuals from these sampled jump sequence elements. The overall outline for DSOMA can be given as:

Table 1: DSOMA parameters.

Name	Range	Type	Description
J_{min}	(1+)	Control	Min number of jumps
Population	10+	Control	Num. of individuals
Migrations	10+	Termination	Number of iterations

1. **Initial Phase**
   (a) *Population Generation*: An initial number of permutative trial individuals is generated for the initial population.
   (b) *Fitness Evaluation*: Each individual is evaluated for its fitness.
2. **DSOMA**
   (a) *Creating Jump Sequences*: Taking two individuals, a number of possible jump positions is calculated between each corresponding element.
   (b) *Constructing Trial Individuals*: Using the jump positions; a number of trial individuals is generated. Each element is selected from a jump element between the two individuals.
   (c) *Repairment*: The trial individuals are checked for feasibility and those, which contain an incomplete schedule, are repaired.
3. **Selection**
   (a) *New Individual Selection*: The new individuals are evaluated for their fitness and the best new fitness based individual replaces the old individual, if it improves upon its fitness.
4. **Generations**
   (a) *Iteration*: Iterate the population till a specified migration.

DSOMA requires a number of parameters as given in Table 1. The major addition is the parameter J_{min}, which gives the minimum number of jumps (sampling) between two individuals. The SOMA variables PathLength, StepSize and PRT Vector are not initialised as they are dynamically calculated by DSOMA using the adjacent elements between the individuals.

Initialisation
The population is initialised as a permutative schedule representative of the size of the problem at hand (6). As this is the initial population, the superscript of *x* its set to 0.

$$x_{i,j}^{0} = \begin{cases} 1 + INT\left(rand\left()\cdot(N-1)\right)\right. \\ \text{if } x_{i,j}^{0} \notin \left\{x_{i,1}^{0}, \ldots, x_{i,j-1}^{0}\right\} \\ i = 1, \ldots, \beta;\ j = 1, \ldots, N \end{cases} \tag{6}$$

Each individual is vetted for its fitness (7), and the best individual, whose index in the population can be assigned as *L* (leader) and it is designated the leader as X_L^0 with its best fitness given as C_L^0.

$$C_i^0 = \Im\left(X_i^0\right), \quad i = 1, \ldots, \beta \tag{7}$$

After the generation of the initial population, the migration counter *t* is set to 1 where $t = 1, \ldots, M$ and the individual index *i* is initialised to 1, where $i = 1, \ldots, \beta$. Using these values, the following sections are recursively applied.

Creating Jump Sequences
DSOMA operates by calculating the number of discrete jump steps that each individual has to circumnavigate. In DSOMA, the parameter of minimum jumps ($J_{\min}$) is used in lieu of PathLength, which states the minimum number of individuals or sampling between the two individuals.

Taking two individuals in the population, one as the incumbent (X_i^t) and the other as the leader (X_L^t), the possible number of jump individuals $J_{\max}$ is the mode of the difference between the adjacent values of the elements in the individual (8). A vector *J* of size *N* is created to store the difference between the adjacent elements in the individuals. The *mode ()* function obtains the most common number in *J* and designates it as J_{max}.

$$\begin{aligned} J_j &= \left| x_{i,j}^{t-1} - x_{L,j}^{t-1} \right|, \quad j = 1, \ldots, N \\ J_{\max} &= \begin{cases} mode\left(J\right) & if \ \ mode\left(J\right) > 0 \\ 1 & otherwise \end{cases} \end{aligned} \tag{8}$$

The step size (*s*), can now be calculated as the integer fraction between the required jumps and possible jumps (9).

$$s = \begin{cases} \left\lfloor \frac{J_{\max}}{J_{\min}} \right\rfloor & \text{if } \ J_{\max} \geq J_{\min} \\ 1 \ \text{otherwise} \end{cases} \tag{9}$$

Create a jump matrix $\mathbf{G}$, which contains all the possible jump positions, that can be calculated as:

$$\mathbf{G}_{l,j} = \begin{cases} x_{i,j}^{t-1} + s \cdot l & \text{if } x_{i,j}^{t-1} + s \cdot l < x_{L,j}^{t-1} \\ & \text{and } x_{i,j}^{t-1} < x_{L,j}^{t-1} \\ x_{i,j}^{t-1} - s \cdot l & \text{if } x_{i,j}^{t-1} + s \cdot l < x_{L,j}^{t-1} \\ & \text{and } x_{i,j}^{t-1} > x_{L,j}^{t-1} \\ 0 \quad \text{otherwise} \\ j = 1, \ldots, N;\ l = 1, \ldots, J_{\min} \end{cases} \tag{10}$$

Constructing Trial Individuals
For each jump sequence of two individuals, a total of $J_{\min}$ new individuals can now be constructed from the jump positions. Taking a new temporary population *H* ($H = \{Y_1, \ldots, Y_{J_{\min}}\}$), in which each new individual Y_w ($w = 1, \ldots, J_{\min}$), is

constructed piecewise from $\mathbf{G}$. Each element $y_{w,j}$ ($Y_w = \{y_{w,j}, \ldots, y_{w,N}\},\ j = 1, 2, \ldots, N$) in the individual, indexes its values from the corresponding j^{th} column in $\mathbf{G}$. Each l^{th} ($l = 1, \ldots, J_{\min}$) position for a specific element is sequentially checked in $\mathbf{G}_{l,j}$ to ascertain if it already exists in the current individual Y_w. If this is a new element, it is then accepted in the individual, and the corresponding l^{th} value is set to zero as $\mathbf{G}_{l,j} = 0$. This iterative procedure can be given as in equation (11).

$$y_{w,j} = \begin{cases} \mathbf{G}_{l,j} \begin{cases} \text{if} \quad \mathbf{G}_{l,j} \notin \{y_{w,1}, \ldots, y_{w,j-1}\} \\ \qquad \text{and } \mathbf{G}_{l,j} \neq 0; \\ \text{then } \mathbf{G}_{l,j} = 0; \end{cases} \\ 0 \quad \text{otherwise} \end{cases}$$
$$l = 1, \ldots, J_{\min};\ j = 1, \ldots, N;\ w = 1, \ldots, J_{\min} \tag{11}$$

Repairing Trial Individuals

Some individuals may exist, which may not contain a permutative schedule. The jump individuals Y_w ($w = 1, 2, \ldots, J_{min}$), are constructed in such a way, that each infeasible element $y_{w,j}$ is indexed by 0.

Taking each jump individual Y_w iteratively from *H*, the following set of procedures can be applied recursively.

Take *A* and *B*, where *A* is initialised to the permutative schedule $A = \{1, 2, \ldots, N\}$ and *B* is the complement of individual Y_w relative to *A* as given in equation (12).

$$B = A \backslash Y_w \tag{12}$$

If after the complement operation, *B* is an empty set without any elements; $B = \{\}$, then the individual is correct with a proper permutative schedule and does not require any repairment.

However, if *B* contains values, then these values are the missing elements in individual Y_w. The repairment procedure is now outlined. The first process is to randomise the positions of the elements in set *B*. Then, iterating through the elements $y_{w,j}$ ($j = 1, \ldots, N$) in the individual Y_w, each position, where the element $y_{w,j} = 0$ is replaced by the value in *B*. Assigning B_{size} as the total number of elements present in *B* (and hence missing from the individual Y_w), the repairment procedure can be given as in equation (13).

$$y_{w,j} = \begin{cases} B_h & \text{if } \ y_{w,j} = 0 \\ y_{w,j} & \text{otherwise} \end{cases} \\ h = 1, \ldots, B_{size};\ j = 1, \ldots, N \tag{13}$$

After each individual is repaired in *H*, it is then evaluated for its fitness value as in equation (14) and stored in γ, the fitness array of size J_{min}.

$$\gamma_w = \Im\left(Y_w\right), \quad w = 1, \ldots, J_{\min} \tag{14}$$

Population update

2 Opt local search is applied to the best individual Y_{best} obtained with the minimum fitness value ($\min(\gamma_w)$). After the local search routine, the new individual is compared with the fitness of the incumbent individual X_i^{t-1}, and if it improves on the fitness, then the new individual is accepted in the population (15).

$$X_i^t = \begin{cases} Y_{best} & \text{if } \Im\left(Y_{best}\right) < C_i^{t-1} \\ X_i^{t-1} & \text{otherwise} \end{cases} \tag{15}$$

If this individual improves on the overall best individual in the population, it then replaces the best individual in the population (16).

$$X_{best}^t = \begin{cases} Y_{best} & \text{if } \Im\left(Y_{best}\right) < C_{best}^t \\ X_{best}^{t-1} & \text{otherwise} \end{cases} \tag{16}$$

Table 2: Operating parameters for DSOMA$_C$ for FSSB.

Parameter	Value
Individuals	100
Migrations	20
Sampling (J_{min})	20
Local Search	2 Opt

Iteration

Sequentially, incrementing *i*, the population counter by 1, another individual X_{i+1}^{t-1} is selected from the population, and it begins its own sampling towards the designated leader X_L^{t-1}. It should be noted that the leader does not change during the evaluation of one migration.

Migrations

Once all the individuals have executed their sampling towards the designated leader, the migration counter *t* is incremented by 1. The individual iterator *i* is reset to 1 (the beginning of the population) and the migration loop is re-initiated.

2 Opt local search

The local search utilised in DSOMA is the 2 Opt local search algorithm (Lin and Kernighan, 1973). The reason as to why the 2 Opt local search was chosen, is that it is the simplest in the *k*-opt class of routines. As the DSOMA sampling occurs between two individuals in *k*-dimension, the local search refines the individual. This in turn provides a better probability to find a new leader after each jump sequence. The placement of the local search was refined heuristically during experimentation.

The complexity of this local search is $O\left(n^2\right)$. As local search makes up the majority of the complexity time of DSOMA, the overall computational complexity of DSOMA for a single migration is $O\left(n^3\right)$.

CHAOS DRIVEN DISCRETE SELF ORGANISING MIGRATING ALGORITHM

The Lozi map is embedded in the DSOMA algorithm in place of the PRNG, and the new algorithm (DSOMA$_C$) is used to solve the FSSB problem. The operational parameters of DSOMA$_C$ are given in Table 2.

DSOMA$_C$ experiment on FSSB problem

The Taillard benchmark problems used for the experiments is referenced from Taillard (1993). These benchmarks comprise of 12 different sets of problems ranging from 20 jobs and 5 machines to 500 jobs and 20 machines. Each set contains 10 unique instances, hence a total of 120 instances Beasley (2009).

Each instance has 10 independent replications and in each replication, the percentage relative difference *(PRD)* is computed as follows:

$$PRD = \frac{100 \times \left(C^{Ron} - C^{DSOMA_C}\right)}{C^{Ron}} \quad (17)$$

where C^{Ron} is the referenced makespan provided by Ronconi (2005), and C^{DSOMA_C} is the makespan found by the DSOMA$_C$ algorithm. Furthermore, average percentage relative difference *(APRD)*, maximum percentage relative difference *(MaxPRD*), minimum percentage relative difference *(MinPRD)* and the standard deviation (SD) of *PRD* are calculated. The average execution time for each set (T(s)) is also displayed.

Termination and Starting Criteria

Comparison of DSOMA$_C$ is done with a number of published algorithms. The first comparison is with the DE variant and its hybrid equivalent (HDE) of Qian et al. (2009). The HDE algorithm was modified by Ling et al. (2010) for the blocking flow shop scheduling problem. The second variant of DE is the discrete DE (DDE) and the hybrid discrete DE (HDDE) of Ling et al. (2010). The third algorithm is the GA of Caraffa et al. (2001), and finally the TS and its multimoves (TS+M) variant of Grabowski and Pempera (2007).

The principle termination criteria for DSOMA$_C$ is set at 20 migrations (see Table 2). This is against the termination criteria of other recent algorithms of HDDE, DDE, HDE and DE, which have a termination criteria based on computational time set as $5\,(m \cdot n)\; ms$. This however is in line with TS, TS+M and GA who have the termination set for the number of generation of which the minimum is 100.

Another important aspect is the starting population of the different algorithms. DSOMA$_C$ has a random population, whereas the DDE, HDDE, DE, HDE, TS and TS+M have a population based on a constructed seed individual utilising the NEH (Nawaz et al., 1983) algorithm, which is one of the well known and better performing heuristics that guarantees an initial solution with a certain quality and diversity. In order to bring parity to the algorithms, the experiment for the Taillard sets is redesigned with a seed individual created using the NEH (Nawaz et al., 1983) algorithm included in the initial population.

Comparison of DSOMA$_C$ with DE/HDE algorithms

A very good analytical presentation is given in Ling et al. (2010), where the authors compared their own discrete DDE and hybrid HDDE algorithms with the HDE algorithm of Qian et al. (2009).

The comparison of DSOMA$_C$ is done with the HDE algorithm of Qian et al. (2009) and the DE (without local search) variant of HDE given in Table 3.

DSOMA$_C$ has better performance indices for all the specifications compared to HDE and DE. It has better ARPD values for all the 12 different sets and on average has a better APRD, MinPRD and MaxPRD.

Comparison of DSOMA$_C$ with DDE/HDDE algorithms

Table 4 compares the results for DSOMA$_C$ with the DDE and its hybrid variant HDDE of Ling et al. (2010). The hybrid component of HDDE is a novel insert-neighbourhood-based speed-up method.

From the results obtained, DSOMA$_C$ performs better than both DDE and HDDE in two of the five performance specifications. In ten out of the 12 sets, it obtains better APRD values as well as higher MaxPRD values. Overall DSOMA$_C$ has on average a superior APRD, which is the key measure of performance, and MaxPRD.

Comparison of DSOMA$_C$ with GA algorithm

This comparison of the result of DSOMA$_C$ with that of GA algorithm of Caraffa et al. (2001) is given in Table 5. For all the problem instances, DSOMA$_C$ produces better results for the PRD.

Comparison of DSOMA$_C$ with TS and TS+M

Table 6 compares the results of DSOMA$_C$ with the TS and its hybrid variant TS+M algorithms of Grabowski and Pempera (2007). TS is considered one of the best constructive heuristics, and it has successfully been applied to a number of complex optimisation tasks (Grabowski and Pempera, 2007).

The comparison of results are given are Table 6. Based on the results DSOMA$_C$ is the better performing heuristic in all 12 problem sets. Overall, it obtains four times better results in the APRD than the TS+M algorithm (4.03 - 0.81). As the termination criteria of TS and TS+M are set to 100 generations, the average execution time of DSOMA$_C$ is significantly lower.

T-test of DSOMA$_C$ with HDDE, TS+M and RON

To test the performances of DSOMA$_C$ with that of HDDE, TS+M and RON, a series of paired *t*-test at the 95% significance level was carried out. The point of interest in the paired *t*-test is in the difference in two observations within the pairs. The paired results of DSOMA$_C$ with HDDE, TS+M and RON are given in Table 7.

In all three two paired *t*-tests, the null hypothesis is rejected and the alternate hypothesis is accepted, stating that there is significant differences between the two compared heuristics in terms of the average relative percent deviations generated. What this implies is that DSOMA$_C$ is significantly better performing than HDDE, TS+M and RON algorithms, given the better results obtained by DSOMA$_C$.

Table 3: Computation comparison of $DSOMA_C$ with DE and HDE of Qian et al. (2009)

J x M	$DSOMA_C$ [1]					DE [2]					HDE [2]				
	APRD	MinPRD	MaxPRD	SD	T(s)	APRD	MinPRD	MaxPRD	SD	T(s)	APRD	MinPRD	MaxPRD	SD	T(s)
20 x 5	0.46	0.00	1.83	0.60	0.25	-0.78	-1.32	-0.05	0.4	0.5	0.26	0	0.44	0.16	0.5
20 x 10	2.40	0.57	5.36	1.48	0.6	1.73	1.29	2.14	0.3	1	2.3	2.13	2.39	0.1	1
20 x 20	3.30	2.13	4.48	0.72	1.08	2.86	2.49	3.18	0.22	2	3.25	3.14	3.3	0.06	2
50 x 5	4.81	0.97	7.45	1.77	2.31	-4.32	-5.2	-3.33	0.61	1.25	3.09	2.59	3.62	0.36	1.25
50 x 10	6.23	4.86	7.36	0.89	3.54	-0.3	-0.89	0.43	0.44	2.5	4.57	4.1	5.06	0.31	2.5
50 x 20	6.62	4.48	8.40	1.42	4.63	1.99	1.47	2.51	0.33	5	5	4.58	5.51	0.3	5
100 x 5	2.24	1.00	3.74	0.95	8.31	-13.99	-14.62	-13.06	0.48	2.5	-0.32	-0.84	0.31	0.36	2.5
100 x 10	5.90	4.67	7.94	0.93	17.08	-5.7	-6.25	-5.11	0.35	5	3.4	2.88	3.99	0.35	5
100 x 20	5.14	4.00	6.01	0.62	28.42	-2.42	-2.8	-1.93	0.29	10	3.05	2.69	3.47	0.26	10
200 x 10	4.03	2.56	5.49	1.09	195.33	-11.12	-11.46	-10.63	0.26	10	0.33	-0.14	0.88	0.34	10
200 x 20	3.99	2.82	4.81	0.66	243.33	-5.82	-6.1	-5.46	0.2	20	1.36	1	1.82	0.26	20
500 x 20	3.23	2.53	4.03	0.46	435.34	-8.2	-8.33	-8.02	0.1	50	0.25	-0.06	0.59	0.2	50
Mean	4.03	2.55	5.57	0.97	78.35	-3.84	-4.31	-3.28	0.33	9.15	2.21	1.84	2.62	0.26	9.15

[1] MacBook Pro, 2.3GHz Intel Core i7 (2nd gen), 8 GB RAM
[2] Pentium P-IV, 3.0 GHz, 512 MB

Table 4: Computation comparison of $DSOMA_C$ with DDE and HDDE of Ling et al. (2010)

J x M	$DSOMA_C$ [1]					DDE [2]					HDDE [2]				
	APRD	MinPRD	MaxPRD	SD	T(s)	APRD	MinPRD	MaxPRD	SD	T(s)	APRD	MinPRD	MaxPRD	SD	T(s)
20 x 5	0.46	0.00	1.83	0.60	0.25	0.34	0.18	0.45	0.1	0.5	0.43	0.33	0.46	0.05	0.5
20 x 10	2.40	0.57	5.36	1.48	0.6	2.34	2.16	2.39	0.08	1	2.38	2.36	2.4	0.02	1
20 x 20	3.30	2.13	4.48	0.72	1.08	3.25	3.15	3.3	0.06	2	3.29	3.24	3.3	0.02	2
50 x 5	4.81	0.97	7.45	1.77	2.31	4.15	3.73	4.61	0.28	1.25	4.24	3.88	4.67	0.25	1.25
50 x 10	6.23	4.86	7.36	0.89	3.54	5.36	4.94	5.83	0.28	2.5	5.75	5.43	6.12	0.23	2.5
50 x 20	6.62	4.48	8.40	1.42	4.63	5.55	5.25	5.87	0.2	5	6.03	5.74	6.34	0.2	5
100 x 5	2.24	1.00	3.74	0.95	8.31	0.37	0.03	0.79	0.24	2.5	1.42	1.04	1.86	0.26	2.5
100 x 10	5.90	4.67	7.94	0.93	17.08	3.9	3.59	4.25	0.21	5	5.17	4.92	5.56	0.21	5
100 x 20	5.14	4.00	6.01	0.62	28.42	3.62	3.36	3.88	0.16	10	4.68	4.39	5.01	0.19	10
200 x 10	4.03	2.56	5.49	1.09	195.33	1.29	1.04	1.58	0.17	10	3.09	2.8	3.47	0.2	10
200 x 20	3.99	2.82	4.81	0.66	243.33	2.17	1.99	2.35	0.11	20	3.57	3.31	3.86	0.17	20
500 x 20	3.23	2.53	4.03	0.46	435.34	1.19	1.08	1.34	0.08	50	2.47	2.16	2.78	0.2	50
Mean	4.03	2.55	5.57	0.97	78.35	2.79	2.54	3.05	0.16	9.15	3.54	3.3	3.82	0.17	9.15

[1] MacBook Pro, 2.3GHz Intel Core i7 (2nd gen), 8 GB RAM
[2] Pentium P-IV, 3.0 GHz, 512 MB

Table 5: Computation comparison of $DSOMA_C$ with GA of Caraffa et al. (2001).

J x M	$DSOMA_C$ [1]					GA [2]	
	APRD	MinPRD	MaxPRD	SD	T(s)	PRD	T(s)
20 x 5	0.46	0	1.83	0.6	0.25	-6.36	0.1
20 x 10	2.4	0.57	5.36	1.48	0.6	-4.35	0.2
20 x 20	3.3	2.13	4.48	0.72	1.08	-1.26	0.4
50 x 5	4.81	0.97	7.45	1.77	2.31	-8.53	0.3
50 x 10	6.23	4.86	7.36	0.89	3.54	-5.97	0.5
50 x 20	6.62	4.48	8.4	1.42	4.63	-4.33	1.1
100 x 5	2.24	1	3.74	0.95	8.31	-14.4	0.5
100 x 10	5.9	4.67	7.94	0.93	17.08	-7.89	1.1
100 x 20	5.14	4	6.01	0.62	28.42	-5.64	2.1
200 x 10	4.03	2.56	5.49	1.09	195.33	-11.04	2.2
200 x 20	3.99	2.82	4.81	0.66	243.33	-7	4.3
500 x 20	3.23	2.53	4.03	0.46	435.34	-8.08	10.8
Mean	4.03	2.55	5.57	0.97	78.35	-7.07	1.97

[1] MacBook Pro, 2.3GHz Intel Core i7 (2nd gen), 8 GB RAM
[2] Pentium P-IV 1000MHz

Table 6: Computation comparison of $DSOMA_C$ with TS and TS+M of Grabowski and Pempera (2007).

J x M	$DSOMA_C$ [1]					TS [2]		TS+M [2]	
	APRD	MinPRD	MaxPRD	SD	T(s)	PRD	T(s)	PRD	T(s)
20 x 5	0.46	0	1.83	0.6	0.25	-1.64	2.4	-0.34	2.7
20 x 10	2.4	0.57	5.36	1.48	0.6	1.45	4.1	1.76	4.6
20 x 20	3.3	2.13	4.48	0.72	1.08	2.88	7.1	2.94	7.6
50 x 5	4.81	0.97	7.45	1.77	2.31	-0.55	6	0.55	6.2
50 x 10	6.23	4.86	7.36	0.89	3.54	1.98	10.6	3.52	10.8
50 x 20	6.62	4.48	8.4	1.42	4.63	3.68	19	4.26	19.3
100 x 5	2.24	1	3.74	0.95	8.31	-3.03	12.2	-2.62	12.4
100 x 10	5.9	4.67	7.94	0.93	17.08	1.71	21.9	2.66	22.1
100 x 20	5.14	4	6.01	0.62	28.42	2.01	39.2	3.03	39.4
200 x 10	4.03	2.56	5.49	1.09	195.33	-0.6	44.1	0.58	44.3
200 x 20	3.99	2.82	4.81	0.66	243.33	1.24	79.2	2.31	79.4
500 x 20	3.23	2.53	4.03	0.46	435.34	0.63	207	1.47	209
Mean	4.03	2.55	5.57	0.97	78.35	0.81	37.73	1.68	38.15

[1] MacBook Pro, 2.3GHz Intel Core i7 (2nd gen), 8 GB RAM
[2] Pentium P-IV, 1000 MHz

Table 7: Paired t-test for $DSOMA_C$ against HDDE, TS+M and RON.

$DSOMA_C$ vs	t-value	p-value	$p < 0.05$	Better
$HDDE$	3.8813	0.0001	Yes	$DSOMA_C$
$TS + M$	11.4269	0.0001	Yes	$DSOMA_C$
RON	11.4052	0.0001	Yes	$DSOMA_C$

CONCLUSION

In this research, the DSOMA algorithm is embedded with the Lozi chaotic map and applied to the FSSB problem and compared with a number of current best performing algorithms for this problem. The initial population was modified with a NEH heuristic, in order to provide a decent seed individual. The termination criteria were modified from the problem sized based to one of migration based. The reasoning is that with evolving hardware specifications, and the extensive usage of greedy search based techniques, using the problem size as the benchmark is illogical. While this topic remains open to debate, based on the experimentation results, $DSOMA_C$ was better performing than all other compared heuristics of DE, HDDE, TS, TS+M and GA, based on the APRD. In terms of operational time, however, it was more expensive especially for the large sized problems. Based on the t-test comparison $DSOMA_C$ was significantly better than the compared heuristics.

ACKNOWLEDGEMENT

This work was supported by the Technology Agency of the Czech Republic under the Project TE01020197 and the Internal Grant Agency of Tomas Bata University under the project No. IGA/FAI/2013/012.

REFERENCES

Alatas, B., Akin, E., and Ozer, A. (2009). Chaos embedded particle swarm optimization algorithms. *Chaos, Solitons and Fractals*, 40(4):1715–1734.

Beasley, J. (2009). Operations research library. http://people.brunel.ac.uk/ mastjjb/jeb/info.htm.

Caponetto, R., Fortuna, L., Fazzino, S., and Xibilia, M. (2003). Chaotic sequences to improve the performance of evolutionary algorithms. *IEEE Transactions on Evolutionary Computation*, 7(3):289–304.

Caraffa, V., Ianes, S., Tapan, P., and Sriskandarajah, C. (2001). Minimizing makespan in a blocking flowshop using genetic algorithms. *International Journal of Production Economics*, 70(2):101 – 115.

Davendra, D. (2009). *Chaotic Attributes and Permutative Optimization*. PhD thesis, Tomas Bata University in Zlin.

Davendra, D., Zelinka, I., and Senkerik, R. (2010). Chaos driven evolutionary algorithms for the task of pid control. *Computers amp; Mathematics with Applications*, 60(4):1088 – 1104.

Grabowski, J. and Pempera, J. (2007). The permutation flow shop problem with blocking. a tabu search approach. *Omega*, 35(3):302 – 311.

Hilborn, R. (2000). *Chaos and Nonlinear Dynamics: An Introduction for Scientists and Engineers*. OUP Oxford, UK.

Lin, S. and Kernighan, B. (1973). An effective heuristic algorithm for the traveling-salesman problem. *Operations Research*, 21(2):498–516.

Ling, W., Quan-Ke, P., Suganthan, P., Wen-Hong, W., and Ya-Min, W. (2010). A novel hybrid discrete differential evolution algorithm for blocking flow shop scheduling problems. *Computers & Operations Research*, 37(3):509 – 520.

Lu, Y., Zhou, J., Qin, H., Wang, Y., and Zhang, Y. (2011). Chaotic differential evolution methods for dynamic economic dispatch with valve-point effects. *Engineering Applications of Artificial Intelligence*, 24(2):378 – 387.

Matsumoto, M. (2012). Mersenne twister webpage. http://www.math.sci.hiroshima-u.ac.jp/ m-mat/MT/ARTICLES/earticles.html.

Matsumoto, M. and Nishimura, T. (1998). Mersenne twister: A 623-dimensionally equidistributed uniform pseudorandom number generator. *ACM Transaction on Modeling and Computer Simulation*, 8(1):3–30.

Nawaz, M., Enscore, E., and Ham, I. (1983). A heuristic algorithm for the m- machine, n-job flowshop sequencing problem. *OMEGA The International Journal of Management Science*, 11:91–95.

Ozer, A. (2010). Cide: Chaotically initialized differential evolution. *Expert Systems with Applications*, 37(6):4632 – 4641.

Pinedo, M. (1995). *Scheduling: theory, algorithms and systems*. Prentice Hall, Inc., New Jersey.

Qian, B., Wang, L., Huang, D., and Wang, X. (2009). An effective hybrid de-based algorithm for flow shop scheduling with limited buffers. *International Journal of Production Research*, 47.

Ronconi, D. (2005). A branch-and-bound algorithm to minimize the makespan in a flowshop with blocking. *Annals OR*, 138(1):53–65.

Taillard, E. (1993). Benchmarks for basic scheduling problems. *European Journal of Operations Research*, 64:278–285.

Yuan, X., Cao, B., Yang, B., and Yuan, Y. (2008). Hydrothermal scheduling using chaotic hybrid differential evolution. *Energy Conversion and Management*, 49(12):3627 – 3633.

Zelinka, I. (2004). Soma - self organizing migrating algorithm. In G., O. and B., B., editors, *New Optimization Techniques in Engineering*. Springer-Verlag, Germany.

Zuo, X. and Fan, Y. (2006). A chaos search immune algorithm with its application to neuro-fuzzy controller design. *Chaos, Solitons and Fractals*, 30(1):94–109.

AUTHOR BIOGRAPHIES

DONALD DAVENDRA is an Assistant Professor of Computer Science at VSB - Technical University of Ostrava, Czech Republic. His email is donald.davendra@vsb.cz

MAGDALENA BIALIC-DAVENDRA is a Post-Doctoral researcher in the Centre of Applied Economic Research, at Tomas Bata University in Zlin. Her email is bialic@fame.utb.cz

ROMAN SENKERIK is an Assistant Professor of Informatics at Tomas Bata University in Zlin, Czech Republic. His email is senkerik@fai.utb.cz

Michal Pluhacek is a doctoral student at Tomas Bata University in Zlin, Czech Republic. His email is pluhacek@fai.utb.cz

MULTIPLE CHOICE STRATEGY FOR PSO ALGORITHM – PERFORMANCE ANALYSIS ON SHIFTED TEST FUNCTIONS

[1]Michal Pluhacek, [1]Roman Senkerik, [1]Ivan Zelinka and [2]Donald Davendra

[1]Tomas Bata University in Zlin , Faculty of Applied Informatics
Nam T.G. Masaryka 5555, 760 01 Zlin, Czech Republic
{pluhacek,senkerik,zelinka}@fai.utb.cz

[2]Department of Computer Science, Faculty of Electrical Engineering and Computer Science
VB-TUO, 17. listopadu 15, 708 33 Ostrava-Poruba, Czech Republic
donald.davendra@vsb.cz

KEYWORDS
PSO, Optimization, Evolutionary Algorithms, Swarm intelligence, Shifted test functions

ABSTRACT

A new promising strategy for the PSO (Particle swarm optimization) algorithm is proposed and described in this paper. This new strategy presents alternative way of assigning new velocity to each individual in particle swarm (population). This new multiple choice particle swarm optimization (MC-PSO) algorithm is tested on two different shifted test functions to show the performance on problems that are not constant in time. The promising results of this alternative strategy are compared with the not modified PSO version.

INTRODUCTION

Optimization started to play a crucial part for almost every engineering and informatics tasks during recent years. Optimization problems often represent very complex tasks and non-heuristic methods are very limited in finding of the proper solutions. As the complexity of optimization problems increases, the non-heuristic methods may not be able to solve them even in very distant future, whereas the new heuristic methods can solve such tasks. Among these so called "soft-computing" methods belong evolutionary algorithms, which are inspired by evolution theory and natural behavior, and have helped to achieve very impressive results in solving various problems.

PSO ALGORITHM

Particle swarm optimization algorithm is the evolutionary optimization algorithm based on the natural behavior of bird and fish swarms and was firstly introduced by R. Eberhart and J. Kennedy in 1995 (Kennedy, Eberhart 1995, Eberhart, Kennedy 2001). As an alternative to genetic algorithms (Goldbeg, David, 1989) and differential evolution (Storn, Price, 1997), Given its unique principle and good performance, PSO is often used to solve different difficult optimization problems and in general, this algorithm is widely modified (Arani et al., 2012, Keshavarz, Zamani, 2013, Pluhacek et al., 2013).

Term "swarm intelligence" (Eberhart, Kennedy, 2001) can be explained as an capability of particle swarms to exhibit surprising intelligent behavior assuming that some form of communication (even very primitive) can occur among the swarm particles (individuals).
In each generation, a new location of a particle is calculated based on its previous location and velocity, where by velocity is understood "velocity vector" i.e. velocity for each dimension of the problem.
Known disadvantages of basic PSO algorithm are the rapid acceleration of particles which causes them to abandon the defined area of interest and poor local search capability. For these reasons, several modifications of PSO were introduced to handle these problems. (Shi, Eberhart 1998)
Within this research, PSO strategy with linear decreasing inertia weight (Shi, Eberhart 1998) was used. Default values of all PSO parameters were chosen according to the recommendations given in (Kennedy, Eberhart 1995, Eberhart, Kennedy 2001). Inertia weight is designed to influence the velocity of each particle differently over the time (Nickabadi et al., 2011). In the beginning of the optimization process, the influence of inertia weight factor w is minimal. As the optimization continues, the value of w is decreasing, thus the velocity of each particle is decreasing, since w is the number < 1 and it multiplies previous velocity of particle in the process of new velocity value calculation. Inertia weight modification PSO strategy has two control parameters w_{start} and w_{end}. New w for each generation is then given by Eq. 1, where i stands for current generation number and n for total number of generations.

$$w = w_{start} - \frac{\left(\left(w_{start} - w_{end}\right) \cdot i\right)}{n} \tag{1}$$

$$v(t+1) = w \cdot v(t) + c_1 \cdot Rand \cdot (pBest - x(t)) + c_2 \cdot Rand \cdot (gBest - x(t)) \tag{2}$$

Where:

$v(t+1)$ – New velocity of particle.
$v(t)$ – Current velocity of particle.
c_1, c_2 – Priority factors.

Proceedings 27th European Conference on Modelling and Simulation ©ECMS Webjørn Rekdalsbakken, Robin T. Bye, Houxiang Zhang (Editors)
ISBN: 978-0-9564944-6-7 / ISBN: 978-0-9564944-7-4 (CD)

pBest – Best solution found by particle.
gBest – Best solution found in population.
$x(t)$ – Current position of particle.
Rand – Random number, interval <0,1>

New position of particle is then given by Eq. 3, where $x(t+1)$ represents the new position:

$$x(t+1) = x(t) + v(t+1) \quad (3)$$

MULTIPLE CHOICE PARTICLE SWARM OPTIMIZATION ALGORITHM (MC-PSO)

A new strategy, which is proposed in this research, alters the original way (Eq. 2) of calculating the particle velocity for the next generation. At first, three numbers b_1, b_2 and b_3 are defined at the start of algorithm. These numbers represent limit values for different rules, so they should follow the pattern: $b_1 < b_2 < b_3$. In this study following values were used:

$b_1 = 0.2$, $b_2 = 0.4$, $b_3 = 0.7$.

Afterwards during the calculation of new velocity of each particle a random number r is generated from the interval <0, 1>. Finally the new velocity is calculated based on following four rules:

If $r \leq b_1$ a new velocity of particle is given by Eq. 4:

$$v(t+1) = 0 \quad (4)$$

If $b_1 < r \leq b_2$ a new velocity of particle is given by Eq. 5:

$$v(t+1) = w \cdot v(t) + c \cdot Rand \cdot (x_r(t) - x(t)) \quad (5)$$

Where $x_r(t)$ is the position of randomly chosen particle.

If $b_2 < r \leq b_3$ a new velocity of particle is given by Eq. 6:

$$v(t+1) = w \cdot v(t) + c \cdot Rand \cdot (pBest - x(t)) \quad (6)$$

If $b_3 < r$ a new velocity of particle is given by Eq. 7:

$$v(t+1) = w \cdot v(t) + c \cdot Rand \cdot (gBest - x(t)) \quad (7)$$

The priority factors c_1 and c_2 from original equation (Eq. 2) are replaced within this novel approach with a new parameter c. In this novel strategy parameter c defines not the priority (which is naturally given by b_1, b_2 and b_3 setting) but the overstep value. In other words how far past the target (*pBest*, *gBest* or random particle) can the active particle go. Within this initial research, parameter c was set to 2.

TEST FUNCTIONS

In order to investigate on the performance of a new multiple choice strategy for PSO algorithm on functions closer to real problems than static test functions, two shifted test functions were chosen. The position of shifted function global optimum moves with each start of the algorithm but keeps the basic function characteristic thus simulates the time-variant real problems.
Following shifted test functions were used in this study:

Shifted 1st De Jong`s function is given by Eq. 8.

$$f(x) = \sum_{i=1}^{\dim} (x_i - shift_i)^2 \quad (8)$$

Function minimum:
Position for E_n: $(x_1, x_2 \ldots x_n) =$ ***shift***
Value for E_n: $y = 0$

Shifted Rastrigin`s function is given by Eq. 9.

$$f(x) = 10\dim + \sum_{i=1}^{\dim} (x_i - shift_i)^2 - 10\cos(2\pi x_i - shift_i) \quad (9)$$

Function minimum:
Position for E_n: $(x_1, x_2 \ldots x_n) =$ ***shift***
Value for E_n: $y = 0$

$Shift_i$ is a random number from interval <-5.11, 5.11>. Where <-5.11, 5.11> are the low and high bounds for the population individuals. ***Shift*** vector is randomly generated on each start of the optimization process.

ESPERIMENT SETUP

The control parameters of PSO algorithm were set up in the following way:

Population size: 100
Generations: 500
w_{start}: 0.9
w_{end}: 0.4
Dimension: 40, 100, 1000

Within all performance testing two PSO versions were used. The first one was the classic not modified PSO with linear decreasing inertia weight, noted PSO Weight. The second one was the new multiple choice strategy PSO version (noted MC-PSO).

From the statistical reasons, optimization for each setting was repeated 100 times. Tables 1 and 2 contain statistical evaluation of the results obtained for Shifted 1st De Jong`s function and Shifted Rastrigin`s function. Furthermore the history of the best found solution was tracked for each run along with the mean history of global best value (see Figures 1-6). The best obtained results are highlighted by the bold number.

Table 1: Results – Shifted 1st De Jong´s function

Dimension:	40		100		1000	
PSO Version:	PSO Weight	MC-PSO	PSO Weight	MC-PSO	PSO Weight	MC-PSO
Mean CF Value:	76.7202	**13.069**	443.34	**180.526**	8394.55	**7098.29**
Std. Dev.:	20.3527	6.37184	51.2814	40.5187	249.932	271.386
CF Value Median:	76.2736	12.6879	444.301	181.723	8412.06	7086.47
Max. CF Value:	130.102	29.1458	579.137	293.427	8929.99	7786
Min. CF Value:	36.802	**3.08677**	330.788	**99.3495**	7772.37	**6502.95**

Table 2: Results – Shifted Rastrigin´s function

Dimension:	40		100		1000	
PSO Version:	PSO Weight	MC-PSO	PSO Weight	MC-PSO	PSO Weight	MC-PSO
Mean CF Value:	291.148	**270.97**	1160.78	**1077.85**	17416	**16795.4**
Std. Dev.:	44.7661	44.7673	89.1601	98.8159	316.087	359.76
CF Value Median:	283.37	267.804	1164.03	1083.69	17410.8	16752
Max. CF Value:	416.366	424.118	1353.92	1334.8	18248.6	17773.6
Min. CF Value:	195.101	**170.359**	941.013	**778.611**	16487.7	**16125.3**

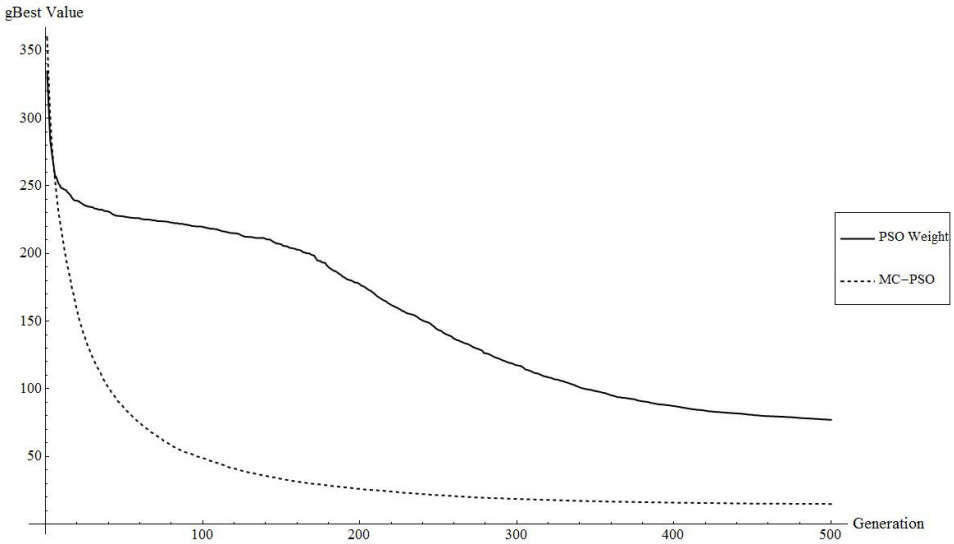

Figure 1: Mean *gBest* history for 100 runs – shifted 1st De Jong`s function – dimension = 40

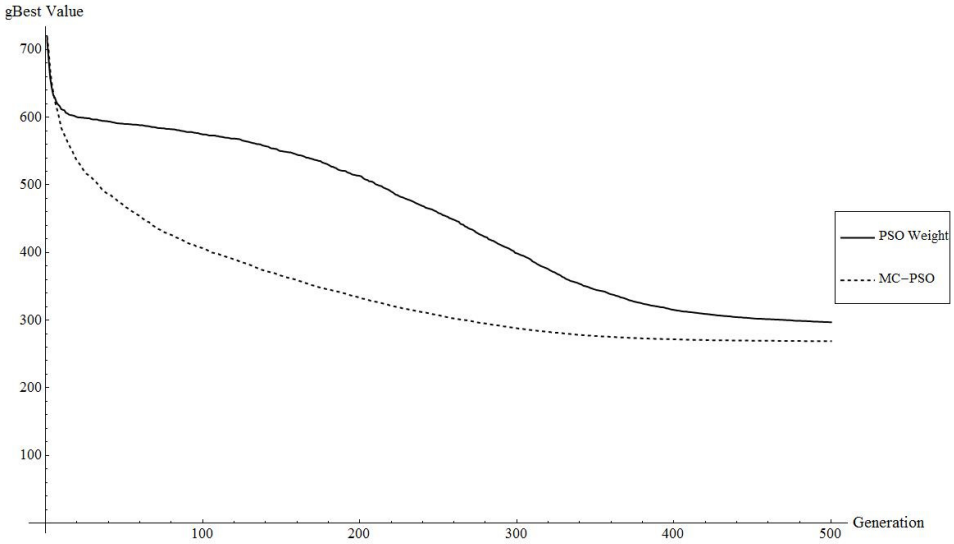

Figure 2: Mean *gBest* history for 100 runs – shifted Rastrigin`s function – dimension = 40

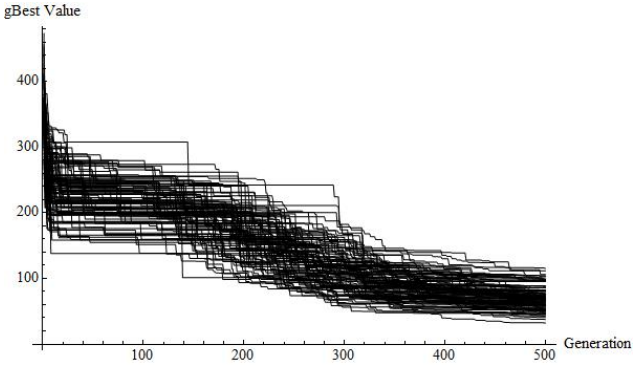

Figure 3: PSO Weight - *gBest* history – shifted 1st De Jong`s function – dimension = 40

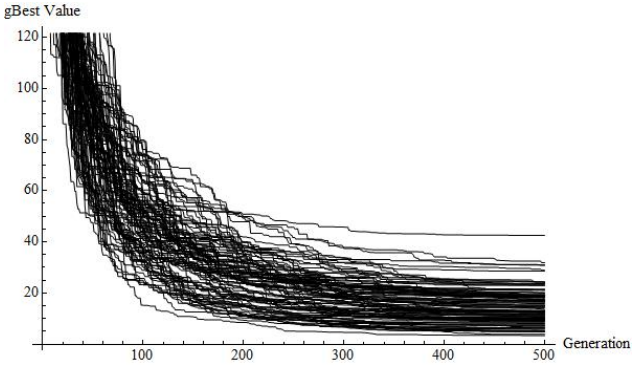

Figure 4: MC-PSO - *gBest* history – shifted 1st De Jong`s function – dimension = 40

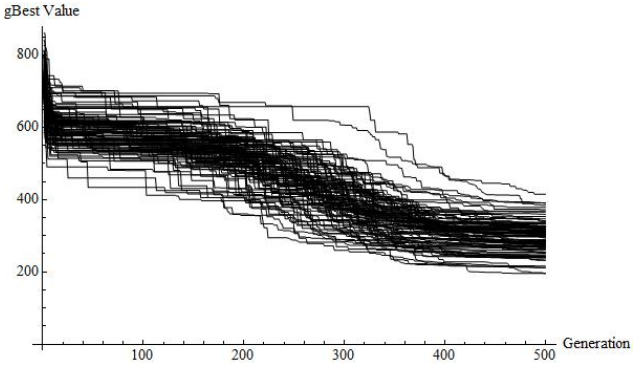

Figure 5: PSO Weight - *gBest* history – shifted Rastrigin`s function – dimension = 40

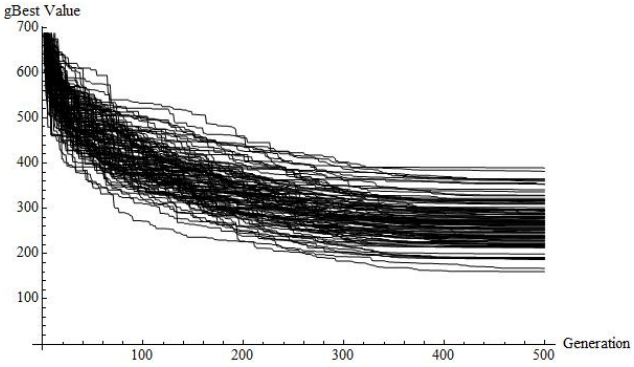

Figure 6: MC-PSO - *gBest* history – shifted Rastrigin`s function – dimension = 40

BRIEF ANALYSIS OF THE RESULTS

The presented data in Tables 1 and 2 support the claim that presented strategy seems to have positive impact on the performance of PSO algorithm. Furthermore, based on the history of *gBest* presented on Figures 1-6 the multiple choice strategy seems to have very positive impact on the convergence speed of optimization and overall performance of the algorithm.

CONCLUSION

Novel multiple choice strategy for PSO algorithm was introduced in this paper. The algorithm was tested on two different shifted test functions and results compared with the original version of PSO algorithm with linear decreasing inertia weight. Statistical evaluation was presented in tables and history of the global best value was depicted on figures. This paper brought promising results that motivate the future research focused on this novel strategy.

AKNOWLEDGMENT

This work was supported by Grant Agency of the Czech Republic—GACR P103/13/08195S, by the project Development of human resources in research and development of latest soft computing methods and their application in practice, reg. no. CZ.1.07/2.3.00/20.0072 funded by Operational Programme Education for Competitiveness, co-financed by ESF and state budget of the Czech Republic; European Regional Development Fund under the project CEBIA-Tech No. CZ.1.05/2.1.00/03.0089; by the Technology Agency of the Czech Republic under the Project TE01020197; and by Internal Grant Agency of Tomas Bata University under the project No. IGA/FAI/2013/012.

REFERENCES

Arani B. O., Mirzabeygi P., Panahi M. S., An improved PSO algorithm with a territorial diversity-preserving scheme and enhanced exploration–exploitation balance, Swarm and Evolutionary Computation, Available online 9 January 2013, ISSN 2210-6502

Dorigo, M., Ant Colony Optimization and Swarm Intelligence, Springer, 2006.

Eberhart, R., Kennedy, J., Swarm Intelligence, The Morgan Kaufmann Series in Artificial Intelligence, Morgan Kaufmann, 2001.

Goldberg, David E. (1989). Genetic Algorithms in Search Optimization and Machine Learning. Addison Wesley. p. 41.ISBN 0201157675.

Kennedy, J.; Eberhart, R. (1995). "Particle Swarm Optimization".Proceedings of IEEE International Conference on Neural Networks. IV. pp. 1942–1948

Keshavarz A., Zamani N., Optimization of optical absorption coefficient in asymmetric double rectangular quantum wells by PSO algorithm, Optics Communications, Available online 8 January 2013, ISSN 0030-4018

Nickabadi A., Mohammad Mehdi Ebadzadeh, Reza Safabakhsh, A novel particle swarm optimization algorithm with adaptive inertia weight, Applied Soft Computing, Volume 11, Issue 4, June 2011, Pages 3658-3670, ISSN 1568-4946

Pluhacek M., Senkerik, R., Davendra, D., Kominkova Oplatkova, Z., Zelinka, I., 2013, On the behavior and performance of chaos driven PSO algorithm with inertia weight, Computers and Mathematics with Applications, (article in press), ISSN 0898-1221, DOI 10.1016/j.camwa.2013.01.016.

Shi Y.H., Eberhart R.C., A modified particle swarm optimizer, IEEE International Conference on Evolutionary Computation, Anchorage Alaska, 1998, pp. 69–73

Storn R., Price K., Differential evolution—a simple and efficient heuristic for global optimization over continuous spaces, Journal of Global Optimization 11 (1997) 341–359

.

AUTHOR BIOGRAPHIES

MICHAL PLUHACEK was born in the Czech Republic, and went to the Tomas Bata University in Zlin, where he studied Information Technologies and obtained his MSc degree in 2011. He is now a doctoral student at the same university. His email address is: pluhacek@fai.utb.cz

ROMAN SENKERIK was born in the Czech Republic, and went to the Tomas Bata University in Zlin, where he studied Technical Cybernetics and obtained his MSc degree in 2004 and Ph.D. degree in Technical Cybernetics in 2008. He is now a lecturer at the same university (Applied Informatics, Cryptology, Artificial Intelligence, Mathematical Informatics). His email address is: senkerik@fai.utb.cz

IVAN ZELINKA was born in the Czech Republic, and went to the Technical University of Brno, where he studied Technical Cybernetics and obtained his degree in 1995. He obtained Ph.D. degree in Technical Cybernetics in 2001 at Tomas Bata University in Zlin. Now he is a professor (Artificial Intelligence, Theory of Information). Email address: ivan.zelinka@vsb.cz .

ANALYTIC PROGRAMMING IN THE TASK OF EVOLUTIONARY SYNTHESIS OF THE ROBUST CONTROLLER FOR SELECTED DISCRETE CHAOTIC SYSTEMS

[1]Roman Senkerik, [1]Zuzana Kominkova Oplatkova, [2]Ivan Zelinka, [1]Michal Pluhacek

[1]Tomas Bata University in Zlin , Faculty of Applied Informatics
Nam T.G. Masaryka 5555, 760 01 Zlin, Czech Republic
{senkerik , oplatkova , pluhacek}@fai.utb.cz

[2]Department of Computer Science, Faculty of Electrical Engineering and Computer Science
VB-TUO, 17. listopadu 15, 708 33 Ostrava-Poruba, Czech Republic
ivan.zelinka@vsb.cz

KEYWORDS
Deterministic chaos, Control, Discrete chaotic maps, Evolutionary computation, Symbolic regression, Analytic programming, SOMA, Differential Evolution

ABSTRACT

This research deals with a utilization of a tool for symbolic regression, which is analytic programming, for the purpose of the synthesis of a new robust control law. This universal synthesized robust chaotic controller secures the fully stabilization of selected set of discrete chaotic systems. The paper consists of the descriptions of analytic programming as well as selected chaotic systems, used heuristic and cost function. For experimentation, Self-Organizing Migrating Algorithm (SOMA) and Differential evolution (DE) were used.

INTRODUCTION

During the recent years, usage of new intelligent systems in engineering, technology, modeling, computing and simulations has attracted the attention of researchers worldwide. The most current methods are mostly based on soft computing, which is a discipline tightly bound to computers, representing a set of methods of special algorithms, belonging to the artificial intelligence paradigm. The most popular of these methods are neural networks, evolutionary algorithms, fuzzy logic and tools for symbolic regression like genetic programming. Currently, evolutionary algorithms are known as a powerful set of tools for almost any difficult and complex optimization problem.
The interest about the interconnection between evolutionary techniques and control of chaotic systems is spread daily. First steps were done in (Liu et al., 2007) representing the utilization of differential evolution algorithm for the synchronization and control of chaotic systems. The papers (Senkerik et al., 2010), (Zelinka et al., 2009) were concerned to tune several parameters inside the original control technique for discrete chaotic systems. The evolutionary tuned control technique was based on Pyragas method: Extended delay feedback control – ETDAS (Pyragas, 1995). Another example of interconnection between deterministic chaos and evolutionary algorithms represents the research focused on the embedding of chaotic dynamics into the evolutionary algorithms (Aydin et al., 2010), (Davendra et al., 2010), (Pluhacek et al., 2013).
This paper shows a possibility how to generate the whole robust control law by means of analytic programming (AP) (not only to optimize several parameters) for the purpose of stabilization of a set of chaotic systems. The synthesis of control is inspired by the Pyragas's delayed feedback control technique (Just, 1999), (Pyragas, 1992).
AP is a superstructure of EAs and is used for synthesis of analytic solution according to the required behaviour. Control law from the proposed system can be viewed as a symbolic structure, which can be synthesized according to the requirements for the stabilization of the chaotic system.
Firstly, AP is explained, and then a problem design is proposed. The next sections are focused on the description of used softcomputing tools and the design of cost function. Results and conclusion follow afterwards.

MOTIVATION

This work is focused on the expansion of AP application for synthesis of a whole robust control law instead of parameters tuning for existing and commonly used control technique to stabilize desired Unstable Periodic Orbits (UPO) of set of selected discrete chaotic systems.
This work represents an extension of previous research (Kominkova Oplatkova et al., 2013), (Senkerik et al., 2013), where the new control laws were evolutionary synthesized only individually for the particular chaotic systems.
In general, this research is concerned to stabilize set of chaotic systems at p-1 UPO, which is a stable state, utilizing the only one universal robust synthesized control law.

Proceedings 27th European Conference on Modelling and Simulation ©ECMS Webjørn Rekdalsbakken, Robin T. Bye, Houxiang Zhang (Editors)
ISBN: 978-0-9564944-6-7 / ISBN: 978-0-9564944-7-4 (CD)

SELECTED DISCRETE CHAOTIC SYSTEMS

This section contains the brief description of selected and used discrete chaotic systems within this research.

Logistic Equation

The first described example of discrete chaotic systems is the one-dimensional Logistic equation in form (1):

$$x_{n+1} = r x_n (1 - x_n). \tag{1}$$

The Logistic equation (logistic map) is a one-dimensional discrete-time example of how complex chaotic behaviour can arise from very simple non-linear dynamical equation (Hilborn 2000). This chaotic system was introduced and popularized by the biologist Robert May (May, 2001). It was originally introduced as a demographic model as a typical predator – prey relationship. The chaotic behaviour can be observed by varying the parameter r. At $r = 3.57$ is the beginning of chaos, at the end of the period-doubling behaviour. At $r > 3.57$ the system exhibits chaotic behaviour. The example of this behaviour can be clearly seen from bifurcation diagram (Figure. 1).

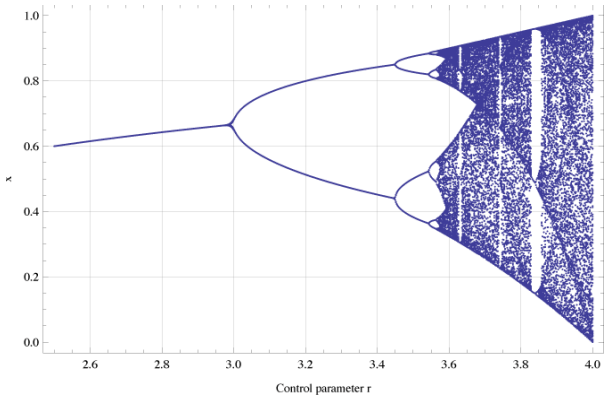

Figure 1: Bifurcation diagram of Logistic Equation

Hénon map

The second chosen example of chaotic system was the two dimensional Hénon map in form (2):

$$\begin{aligned} x_{n+1} &= a - x_n^2 + b y_n \\ y_{n+1} &= x_n \end{aligned} \tag{2}$$

This is a model invented with a mathematical motivation to investigate chaos. The Hénon map is a discrete-time dynamical system, which was introduced as a simplified model of the Poincaré map for the Lorenz system. It is one of the most studied examples of dynamical systems that exhibit chaotic behavior. The map depends on two parameters, a and b, which for the canonical Hénon map have values of $a = 1.4$ and $b = 0.3$. For these canonical values the Hénon map is chaotic (Hilborn 2000). The example of this chaotic behavior can be clearly seen from bifurcation diagram – Figure 2.

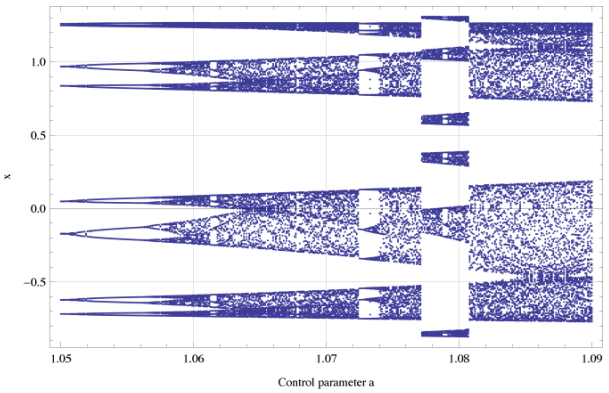

Figure 2: Bifurcation diagram of Hénon Map

Figure 2 shows the bifurcation diagram for the Hénon map created by plotting of a variable x as a function of the one control parameter for the fixed second parameter.

Lozi Map

The last example of discrete chaotic systems is the Lozi map, which represents the simple discrete two-dimensional chaotic map. The x, y plot of the Lozi map is depicted in Figure 3. The map equations are given in Eq. 3. The parameters are: $a = 1.7$ and $b = 0.5$ as suggested in (Sprott, 2003).

$$\begin{aligned} X_{n+1} &= 1 - a|X_n| + bY_n \\ Y_{n+1} &= X_n \end{aligned} \tag{3}$$

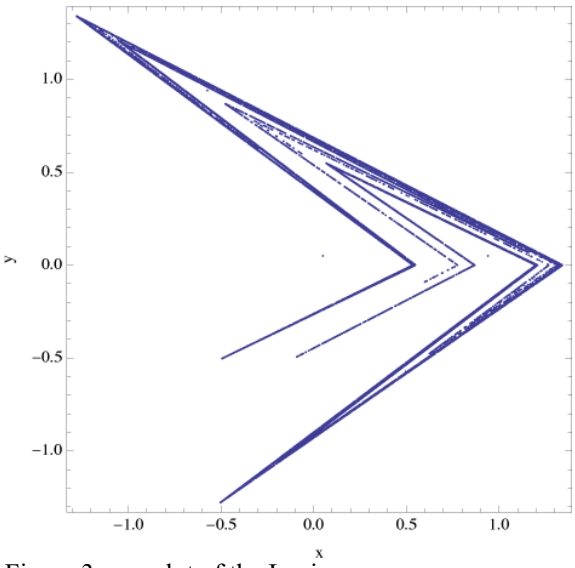

Figure 3: x, y plot of the Lozi map

ORIGINAL TDAS CHAOS CONTROL METHOD

This work is focused on explanation of application of AP for synthesis of a whole control law instead of demanding tuning of any original method control law to stabilize desired Unstable Periodic Orbits (UPO). In this research desired UPO is only p-1 (the fixed point, which represents the stable state). Original TDAS delayed feedback control method was used in this research as an

inspiration for synthesizing a new feedback control law by means of evolutionary techniques and for preparation of sets of basic functions and operators for AP.
The original control method – TDAS has form (4) and its discrete form is given in (5).

$$F(t) = K\left[x(t-\tau) - x(t)\right] \tag{4}$$

$$F_n = K\left(x_{n-m} - x_n\right) \tag{5}$$

Where: K is adjustable constant, F is the perturbation, τ_d is a time delay; and m is the period of m-periodic orbit to be stabilized. The perturbation F_n in equation (5) may have arbitrarily large value, which can cause diverging of the system. Therefore, F_n should have a value between $-F_{\max}$, $F_{\max}$. In this work a suitable $F_{\max}$ value was taken from the previous research.

USED SOFTCOMPUTING TOOLS

This section gives the brief overview and the description of used softcomputing tools. This research utilized the symbolic regression tool, which is analytic programming and two evolutionary algorithms: Self-Organizing Migrating Algorithm (Zelinka, 2004); and Differential Evolution (Price, 2005).
Future simulations expect a usage of soft computing GAHC algorithm (modification of HC12) (Matousek and Zampachova, 2011) and a CUDA implementation of HC12 algorithm (Matousek, 2010).

Analytic Programming

Basic principles of the AP were developed in 2001. Until that time only genetic programming (GP) and grammatical evolution (GE) had existed. GP uses genetic algorithms while AP can be used with any evolutionary algorithm, independently on individual representation. AP represents synthesis of analytical solution by means of evolutionary algorithms. Various applications of AP are described in (Zelinka et al., 2008), (Oplatkova et al., 2009), (Zelinka et al., 2011), (Chramcov and Varacha, 2013).
The core of AP is based on a special set of mathematical objects and operations. The set of mathematical objects is set of functions, operators and so-called terminals (as well as in GP), which are usually constants or independent variables. This set of variables is usually mixed together and consists of functions with different number of arguments. Because of a variability of the content of this set, it is called here "general functional set" – GFS. The structure of GFS is created by subsets of functions according to the number of their arguments. For example GFS_{all} is a set of all functions, operators and terminals, GFS_{3arg} is a subset containing functions with only three arguments, GFS_{0arg} represents only terminals, etc. The subset structure presence in GFS is vitally important for AP. It is used to avoid synthesis of pathological programs, i.e. programs containing functions without arguments, etc. The content of GFS is dependent only on the user. Various functions and terminals can be mixed together (Zelinka et al., 2005), (Oplatkova et al., 2009).
The second part of the AP core is a sequence of mathematical operations, which are used for the program synthesis. These operations are used to transform an individual of a population into a suitable program. Mathematically stated, it is a mapping from an individual domain into a program domain. This mapping consists of two main parts. The first part is called discrete set handling (DSH) (Zelinka et al. 2005) and the second one stands for security procedures which do not allow synthesizing pathological programs. The method of DSH, when used, allows handling arbitrary objects including nonnumeric objects like linguistic terms {hot, cold, dark…}, logic terms (True, False) or other user defined functions. In the AP DSH is used to map an individual into GFS and together with security procedures creates the above mentioned mapping which transforms arbitrary individual into a program.
AP needs some evolutionary algorithm that consists of population of individuals for its run. Individuals in the population consist of integer parameters, i.e. an individual is an integer index pointing into GFS. The individual contains numbers which are indices into GFS. The detailed description is represented in (Zelinka et al., 2011).
AP exists in 3 versions – basic without constant estimation, AP_{nf} – estimation by means of nonlinear fitting package in Mathematica environment and AP_{meta} – constant estimation by means of another evolutionary algorithms; meta means metaevolution.

Self Organizing Migrating Algorithm - SOMA

Self Organizing Migrating Algorithm (SOMA) is a stochastic optimization algorithm that is modelled on the social behaviour of cooperating individuals (Zelinka, 2004). It was chosen because it has been proven that the algorithm has the ability to converge towards the global optimum (Zelinka, 2004). SOMA works on a population of candidate solutions in loops called *migration loops*. The population is initialized randomly distributed over the search space at the beginning of the search. In each loop, the population is evaluated and the solution with the highest fitness becomes the leader L. Apart from the leader, in one migration loop, all individuals will traverse the input space in the direction of the leader. Mutation, the random perturbation of individuals, is an important operation for evolutionary strategies (ES). It ensures the diversity amongst the individuals and it also provides the means to restore lost information in a population. Mutation is different in SOMA compared with other ES strategies. SOMA uses a parameter called PRT to achieve perturbation. This parameter has the same effect for SOMA as mutation has for genetic algorithms.
The novelty of this approach is that the PRT Vector is created before an individual starts its journey over the search space. The PRT Vector defines the final movement of an active individual in search space.

The randomly generated binary perturbation vector controls the allowed dimensions for an individual. If an element of the perturbation vector is set to zero, then the individual is not allowed to change its position in the corresponding dimension.
An individual will travel a certain distance (called the PathLength) towards the leader in *n* steps of defined length. If the PathLength is chosen to be greater than one, then the individual will overshoot the leader. This path is perturbed randomly. The main principle is depicted in Figures 4 and 5.

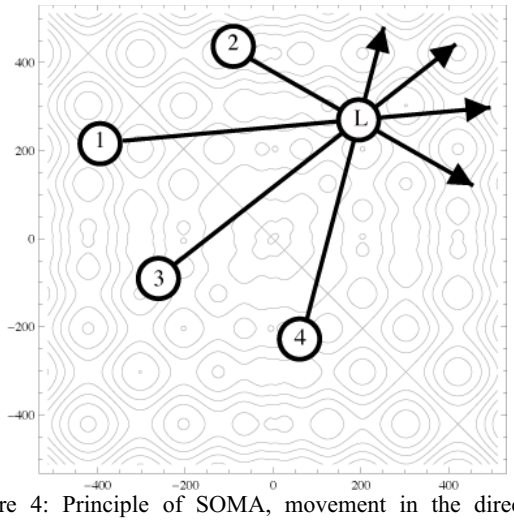

Figure 4: Principle of SOMA, movement in the direction towards the Leader

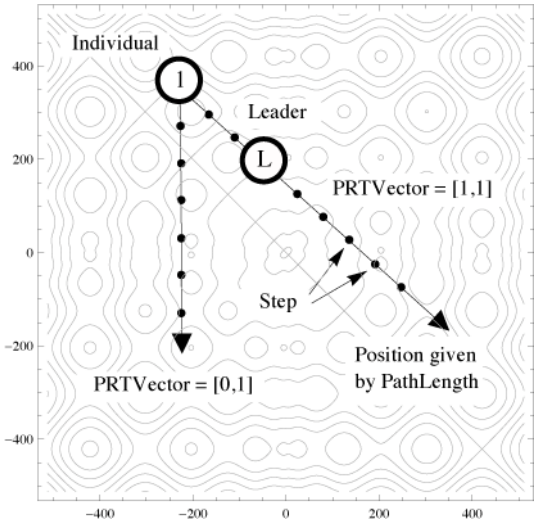

Figure 5: Basic principle of crossover in SOMA

Differential evolution

DE is a population-based optimization method that works on real-number-coded individuals (Lampinen and Zelinka, 1999), (Price, 2005). DE is quite robust, fast, and effective, with global optimization ability. It does not require the objective function to be differentiable, and it works well even with noisy and time-dependent objective functions. Description of used DERand1Bin strategy is presented in (6). Please refer to (Price and Storn 2001, Price 2005) for the description of all other strategies.

$$u_{i,G+1} = x_{r1,G} + F \cdot \left(x_{r2,G} - x_{r3,G}\right) \tag{6}$$

COST FUNCTION DESIGN

The proposal of the basic cost function (CF) is in general based on the simplest CF, which could be used problem-free only for the stabilization of p-1 orbit. The idea was to minimize the area created by the difference between the required state and the real system output on the whole simulation interval – τ_i. This CF design is very convenient for the evolutionary searching process due to the relatively favorable CF surface. Nevertheless, this simple approach has one big disadvantage, which is the including of initial chaotic transient behavior of not stabilized system into the cost function value. As a result of this, the very tiny change of control method setting for extremely sensitive chaotic system causing very small change of CF value, can be suppressed by the above-mentioned including of initial chaotic transient behavior
But another universal cost function had to be used for stabilizing of extremely sensitive chaotic system and having the possibility of adding penalization rules. It was synthesized from the simple CF and other terms were added.
This CF is in general based on searching for desired stabilized periodic orbit and thereafter calculation of the difference between desired and found actual periodic orbit on the short time interval - τ_s (40 iterations for higher order UPO) from the point, where the first minimal value of difference between desired and actual system output is found (i.e. floating window for minimization – see Figure 6.).

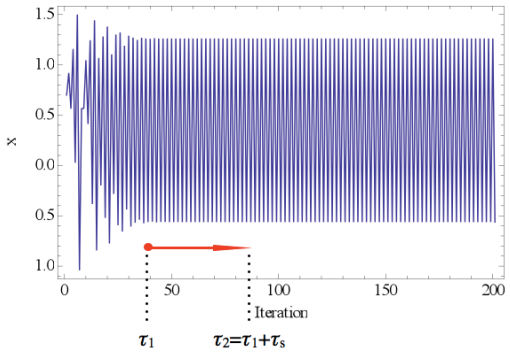

Figure 6: "Floating window" for minimization

Such a design of universal CF should secure the successful stabilization of either p-1 orbit (stable state) or higher periodic orbits anywise phase shifted. Furthermore, due to CF values converging towards zero, this CF also allows the using of decision rules, avoiding very time demanding simulations. This rule stops EA immediately, when the first individual with good parameter structure is reached, thus the value of CF is lower then the acceptable (CF_{acc}) one. Based on the

numerous experiments, typically CF_{acc} = 0.001 at time interval τ_s = 20 iterations, thus the difference between desired and actual output has the value of 0.0005 per iteration – i.e. successful stabilization for the used control technique. The CF_{Basic} has the form (7):

$$CF_{Basic} = pen_1 + \sum_{t=\tau 1}^{\tau 2} \left| TS_t - AS_t \right|, \quad (7)$$

where:
TS - target state, AS - actual state
τ_1 - the first min value of difference between TS and AS
τ_2 – the end of optimization interval ($\tau_1 + \tau_s$)
$pen_1 = 0$ if $\tau_i - \tau_2 \geq \tau_s$;
$pen_1 = 10*(\tau_i - \tau_2)$ if $\tau_i - \tau_2 < \tau_s$ (i.e. late stabilization).

Finally, the CF used within the evolutionary synthesis of a new robust control law is given in (8). It was evaluated as a sum of the three partial cost functions values each for one of the selected chaotic system.

$$CF_{Final} = CF_{Basic\_Logistic} + CF_{Basic\_Hénon} + CF_{Basic\_Lozi} \quad (8)$$

RESULTS

As described in the section about Analytic Programming, AP requires some EA for its run. In this paper AP_{meta} version was used. Meta-evolutionary approach means usage of one main evolutionary algorithm for AP process and the second algorithm for coefficient estimation, thus to find optimal values of constants in the evolutionary synthesized control law.
SOMA algorithm was used for the main AP process and DE was used in the second evolutionary process. Settings of EA parameters for both processes given in Table 1 and Table 2 were based on performed numerous experiments with chaotic systems and simulations with AP_{meta}.

Table 1: SOMA settings for AP

SOMA Parameter	Value
PathLength	3
Step	0.11
PRT	0.1
PopSize	50
Migrations	4
Max. CF Evaluations (CFE)	5345

Table 2: DE settings for meta-evolution

DE Parameter	Value
PopSize	40
F	0.8
CR	0.8
Generations	150
Max. CF Evaluations (CFE)	6000

The data set for AP required only constants, operators like plus, minus, power and output values x_n and x_{n-1}.

Basic set of elementary functions for AP:
GFS2arg= +, -, /, *, ^
GFS0arg= $data_{n-1}$ to $data_n$, K

Total number of cost function evaluations for AP was 5345, for the second EA it was 6000, together 32.07 millions per each simulation. See Table 3 for simple final CF values statistic.

Table 3: Cost Function values

Statistical parameter	Value
Min	$4.2186 \cdot 10^{-15}$
Max	$7.3693 \cdot 10^{-7}$
Average	$8.1544 \cdot 10^{-8}$
Median	$2.0881 \cdot 10^{-10}$
Std. Deviation	$1.8478 \cdot 10^{-7}$

Following description of the two selected experiments results contains illustrative examples of direct output from AP – synthesized control law without coefficients estimated (9) and (11); further the notation with simplification after estimation by means of second algorithm DE (10) and (12), Tables 4 and 5 with corresponding CF statistics and the average error value between actual and required system output, and finally Figures 7 – 12 with simulation results.

Experiment result 1

$$F_n = \left(x_n - x_{n-1}\right)\left(K_1 x_{n-1} + \frac{1}{K_2\left(K_3 + 2x_n\right)}\right) \quad (9)$$

$$F_n = \left(x_n - x_{n-1}\right)\left(1.12677 x_{n-1} + \frac{0.0667783}{2x_n - 1.25027}\right) \quad (10)$$

Table 4: Experiment 1 results attributes

Results attributes	Value
Final CF value	$4.2186 \cdot 10^{-15}$
$CF_{Logistic}$ value	$1.3323 \cdot 10^{-15}$
$CF_{Hénon}$ value	$1.7764 \cdot 10^{-15}$
CF_{Lozi} value	$1.1102 \cdot 10^{-15}$
Average error per iteration	$8.44 \cdot 10^{-17}$

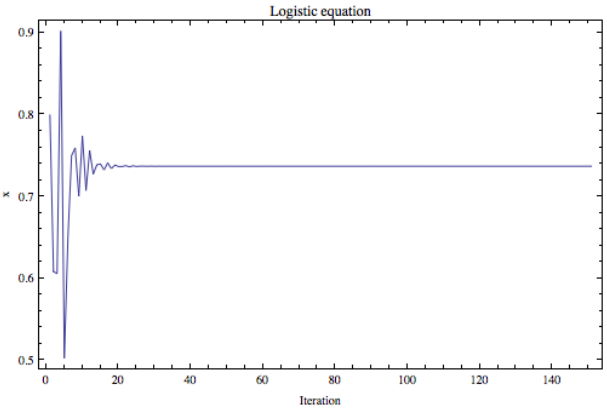

Figure 7: Experiment 1 – Simulation for Logistic equation

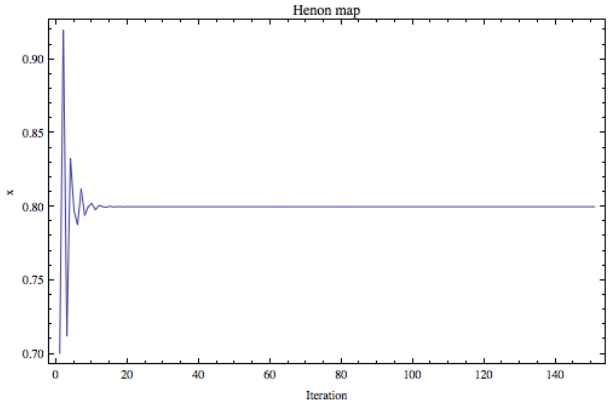

Figure 8: Experiment 1 – Simulation for Hénon map

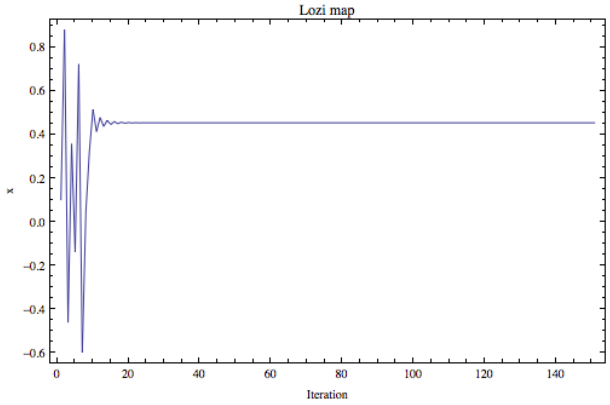

Figure 9: Experiment 1 – Simulation for Lozi map

Experiment result 2

$$F_n = \frac{K_1 x_{n-1} x_n (x_n - x_{n-1})}{2x_{n-1} + x_n - 1} \tag{11}$$

$$F_n = \frac{1.30511 x_{n-1} x_n (x_n - x_{n-1})}{2x_{n-1} + x_n - 1} \tag{12}$$

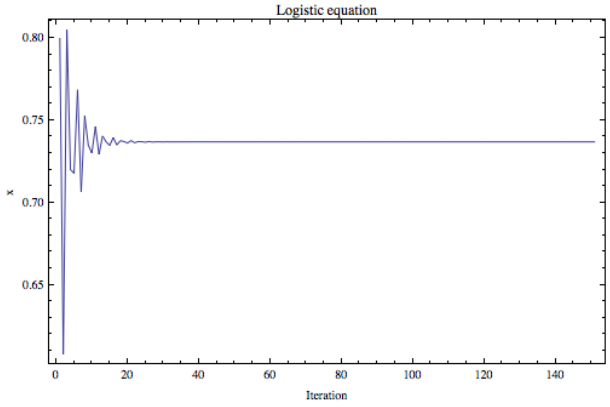

Figure 10: Experiment 2 – Simulation for Logistic equation

Table 5: Experiment 2 results attributes

Results attributes	Value
Final CF value	$4.6629 \cdot 10^{-15}$
$CF_{Logistic}$ value	$6.6613 \cdot 10^{-16}$
$CF_{Hénon}$ value	$2.9976 \cdot 10^{-15}$
CF_{Lozi} value	$9.9920 \cdot 10^{-16}$
Average error per iteration	$9.33 \cdot 10^{-17}$

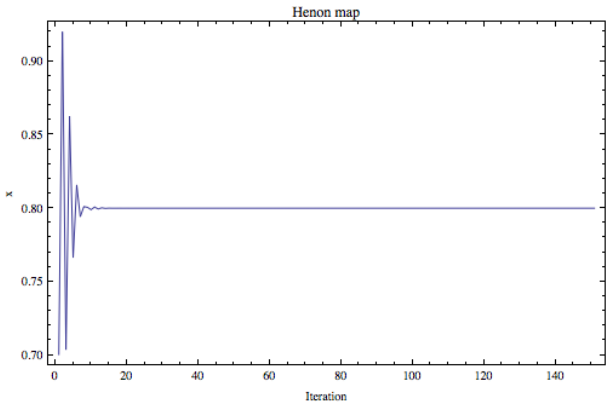

Figure 11: Experiment 2 – Simulation for Hénon map

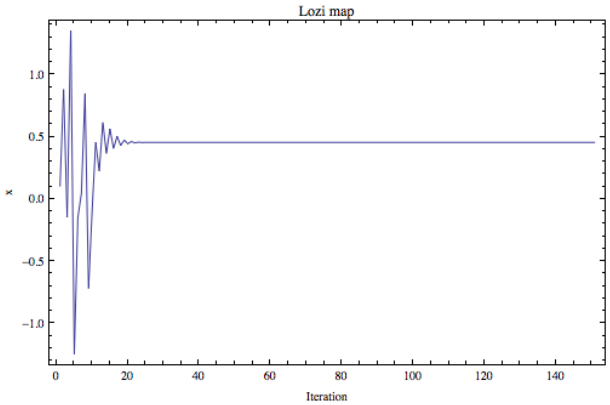

Figure 12: Experiment 2 – Simulation for Lozi map

CONCLUSION

This paper deals with a synthesis of a new universal robust control law by means of AP for stabilization of selected discrete chaotic systems at fixed point. One-dimensional Logistic equation, Hénon map and Lozi map as the examples of two-dimensional discrete chaotic systems were used in this research.

Obtained results reinforce the argument that AP is able to solve this kind of difficult problems and to produce a new robust synthesized control law in a symbolic way securing desired behaviour and precise stabilization of the selected set of chaotic systems.

The future research will include the development of better cost functions, testing of different AP data sets, and performing of numerous simulations to obtain more results and produce better statistics, thus to confirm the robustness of this approach.

ACKNOWLEDGEMENT

This work was supported by Grant Agency of the Czech Republic GACR P103/13/08195S; by the project Development of human resources in research and development of latest soft computing methods and their application in practice, reg. no. CZ.1.07/2.3.00/20.0072 funded by Operational Program Education for Competitiveness, co-financed by ESF and state budget of the Czech Republic; by European Regional Development Fund under the project CEBIA-Tech No. CZ.1.05/2.1.00/03.0089 and by Internal Grant Agency of Tomas Bata University under the project No. IGA/FAI/2013/012.

REFERENCES

Aydin I., Karakose M., Akin E. 2010, "Chaotic-based hybrid negative selection algorithm and its applications in fault and anomaly detection", *Expert Systems with Applications*, Vol. 37, No. 7, pp. 5285–5294.

Davendra, D., Zelinka, I., Senkerik, R. 2010, "Chaos driven evolutionary algorithms for the task of PID control", *Computers & Mathematics with Applications*, Vol. 60, No. 4, pp. 1088-1104, ISSN 0898-1221.

Hilborn R.C., 2000. Chaos and Nonlinear Dynamics: An Introduction for Scientists and Engineers, Oxford University Press, ISBN: 0-19-850723-2.

Just W., 1999, "Principles of Time Delayed Feedback Control", In: Schuster H.G., Handbook of Chaos Control, Wiley-Vch, ISBN 3-527-29436-8.

Kominkova Oplatkova Z., Senkerik R., Zelinka I., Pluhacek M., 2013, "Analytic programming in the task of evolutionary synthesis of a controller for high order oscillations stabilization of discrete chaotic systems", *Computers & Mathematics with Applications*, ISSN 0898-1221, DOI 10.1016/j.camwa.2013.02.008. (article in press)

Lampinen J., Zelinka I., 1999, "New Ideas in Optimization – Mechanical Engineering Design Optimization by Differential Evolution", Volume 1, London: McGraw-hill, 20 p., ISBN 007-709506-5.

Liu B., Wang L., Jin Y.H., Huang D.X., Tang F., 2007, "Control and synchronization of chaotic systems by differential evolution algorithm", *Chaos, Solitons & Fractals*, Volume 34, Issue 2, pp. 412-419, ISSN 0960-0779

Matousek R. and Zampachova E., 2011, „Promising GAHC and HC12 algorithms in global optimization tasks", *Optimization Methods & Software*, Vol. 26, No. 3, pp. 405-419. ISSN 1055-6788.

Matousek R., 2010, „HC12: The Principle of CUDA Implementation". *In Proceedings of 16th International Conference On Soft Computing Mendel 2010*, pp. 303-308. ISBN 978-80-214-4120- 0.

May R.M., 2001, *Stability and Complexity in Model Ecosystems*, Princeton University Press, ISBN: 0-691-08861-6.

Oplatková, Z., Zelinka, I.: 2009. Investigation on Evolutionary Synthesis of Movement Commands, Modelling and Simulation in Engineering, Volume 2009 (2009), Article ID 845080, 12 pages, Hindawi Publishing Corporation, ISSN: 1687-559.

Pluhacek M., Senkerik, R., Davendra, D., Kominkova Oplatkova, Z., Zelinka, I., 2013, On the behavior and performance of chaos driven PSO algorithm with inertia weight, *Computers & Mathematics with Applications*, ISSN 0898-1221, DOI 10.1016/j.camwa.2013.01.016, (article in press).

Price, K. and Storn, R. (2001), *Differential evolution homepage*, [Accessed 28/02/2013]: http://www.icsi.berkeley.edu/~storn/code.html

Price K., Storn R. M., Lampinen J. A., 2005, "Differential Evolution: A Practical Approach to Global Optimization", (Natural Computing Series), Springer.

Pyragas K., 1992, "Continuous control of chaos by self-controlling feedback", *Physics Letters A*, 170, 421-428.

Pyragas K., 1995. "Control of chaos via extended delay feedback", *Physics Letters A*, vol. 206, pp. 323-330.

Senkerik R., Zelinka I., Davendra D., Oplatkova Z., 2010, "Utilization of SOMA and differential evolution for robust stabilization of chaotic Logistic equation", *Computers & Mathematics with Applications*, Volume 60, Issue 4, pp. 1026-1037.

Senkerik, R., Oplatkova, Z., Zelinka, I., Davendra, D. 2013, "Synthesis of feedback controller for three selected chaotic systems by means of evolutionary techniques: Analytic programming", *Mathematical and Computer Modelling*, Vol. 57, No. 1 - 2, pp. 57 – 67, ISSN 0895-7177.

Sprott J.C., 2003, *Chaos and Time-Series Analysis*, Oxford University Press.

Chramcov B., Varacha, P., 2013, Usage of the Evolutionary Designed Neural Network for Heat Demand Forecast. *In:Proceedings of Nostradamus 2012: Modern Methods of Prediction, Modeling and Analysis of Nonlinear Systems*, p. 103-122. ISBN 978-3-642-33226-5.

Zelinka I., 2004. "SOMA – Self Organizing Migrating Algorithm", In: *New Optimization Techniques in Engineering*, (B.V. Babu, G. Onwubolu (eds)), chapter 7, 33, Springer-Verlag, 2004, ISBN 3-540-20167X.

Zelinka I.,Oplatkova Z, Nolle L., 2005. *Boolean Symmetry Function Synthesis by Means of Arbitrary Evolutionary Algorithms-Comparative Study*, International Journal of Simulation Systems, Science and Technology, Volume 6, Number 9, August 2005, pages 44 - 56, ISSN: 1473-8031.

Zelinka, I., Guanrong Ch., Celikovsky S., 2008. Chaos Synthesis by Means of Evolutionary algorithms, *International Journal of Bifurcation and Chaos*, Vol. 18, No. 4, pp. 911–942.

Zelinka I., Senkerik R., Navratil E., 2009, "Investigation on evolutionary optimization of chaos control", *Chaos, Solitons & Fractals*, Volume 40, Issue 1, pp. 111-129.

Zelinka, I., Davendra, D., Senkerik, R., Jasek, R., Oplatkova, Z., 2011, "Analytical Programming - a Novel Approach for Evolutionary Synthesis of Symbolic Structures", In: *Evolutionary Algorithms*, Eisuke Kita (Ed.), InTech.

Modelling, Simulation and Control of Technological Processes

DESIGN AND SIMULATION OF SELF-TUNING PREDICTIVE CONTROL OF TIME-DELAY PROCESSES

Vladimír Bobál[1,2], Marek Kubalčík[2] and Petr Dostál[1,2]
Tomas Bata University in Zlín
[1]Centre of Polymer Systems, University Institute
[2]Department of Process Control, Faculty of Applied Informatics
T. G. Masaryka 5555
760 01 Zlín
Czech Republic
E-mail: bobal@fai.utb.cz

KEYWORDS
Time-delay systems, Model Predictive Control, CARIMA model, Quadratic criterion, Simulation

ABSTRACT

Majority industrial processes such as thermal, chemical biological, metallurgical, plastic etc., have time-delays. Therefore, the problem of the identification and optimal control of such systems is of great importance. These time-delay processes can be effectively handled by the Model-based Predictive Control method. The paper deals with design of an algorithm for self-tuning predictive control of such processes. The self-tuning principle is one of possible approaches to control of nonlinear systems or systems with uncertainties. Three types of processes were chosen for simulation verification of the designed self-tuning predictive controller. The program system MATLAB/SIMULINK was used for testing and verification of this predictive controller.

INTRODUCTION

Time delay is very often encountered in various technical systems, such as electric, pneumatic and hydraulic networks, chemical processes, long transmission lines, robotics, etc. The existence of pure time lag, regardless if it is present in the control or/and the state, may cause undesirable system transient response, or even instability. Consequently, the problem of controllability, observability, robustness, optimization, adaptive control, pole placement and particularly stability and robustness stabilization for this class of systems, has been one of the main interests for many scientists and researchers during the last five decades.

For control engineering, such processes can often be approximated by the FOTD (First-Order-Time-Delay) model. Time-delay in a process increases the difficulty of controlling it. However the approximation of higher-order process by lower-order model with time-delay provides simplification of the control algorithms. When high performance of the control process is desired or the relative time-delay is very large, the predictive control strategy is one of possible approaches. The predictive control strategy includes a model of the process in the structure of the controller. The first time-delay compensation algorithm was proposed by (Smith 1957). This control algorithm known as the Smith Predictor (SP) contained a dynamic model of the time-delay process and it can be considered as the first model predictive algorithm. First versions of Smith Predictors were designed in the continuous-time modifications, see e.g (Normey-Rico and Camacho 2007). Because most of modern controllers are implemented on digital platforms, the discrete versions of the time-delay controllers are more suitable for time-delay compensation in industrial practice. Most of authors designed the digital time-delay compensators with fixed parameters. However, the time-delay compensators are more sensitive to process parameter variations and therefore require an auto-tuning or adaptive (self-tuning) approach in many practical applications. Two adaptive modifications of the digital Smith Predictors are designed in (Hang et al. 1989; Bobál et al. 2011) and implemented into MATLAB/SIMULINK Toolbox (Bobál et al. 2012a; Bobál et al. 2012b).

Model predictive control (MPC) is becoming increasable popular method in industrial process control where time-delays are component parts of the system. However, an accurate appropriate model of the process is required to ensure the benefits of MPC. Furthermore, perturbations of a time-delay and parameters of an external linear model may induce complex behaviours (oscillations and instabilities) of the closed-loop system. Problems with time-variant model parameters can be solved using adaptive (self-tuning) approach.

MODEL PREDICTIVE CONTROL

Model Predictive Control, also known as Receding Horizon Control (RHC), attracts considerable research attention because of its unparalleled advantages.
These include (Lu 2008):

- Applicability to a broad class of systems and industrial applications.
- Computational feasibility.

Proceedings 27th European Conference on Modelling and Simulation ©ECMS Webjørn Rekdalsbakken, Robin T. Bye, Houxiang Zhang (Editors)
ISBN: 978-0-9564944-6-7 / ISBN: 978-0-9564944-7-4 (CD)

- Systematic approach to obtain a closed-loop control and guaranteed stability.
- Ability to handle hard constraints on the control as well as the system states.
- Good tracking performance.
- Robustness with respect to system modeling uncertainty as well as external disturbances.

The MPC strategy performs the optimization of a performance index with respect to some future control sequence, using predictions of the output signal based on a process model, coping with amplitude constraints on inputs, outputs and states. For a quick comparison of MPC and traditional control scheme, such as PID control, Fig. 1 shows the difference between the MPC and PID control schemes in which "anticipating the future" is desirable while a PID controller only has capacity of reacting to the past behaviours. The MPC algorithm is very similar to the control strategy used in driving a car (Lu 2008).

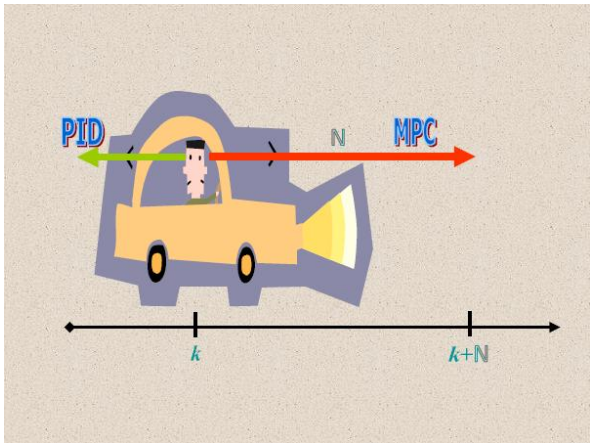

Figure 1: Difference between the MPC and PID control

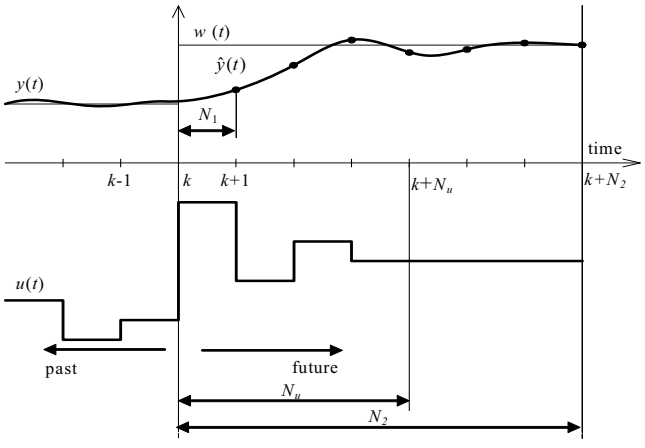

Figure 2: Principle of MPC

At current time k, the driver knows the desired reference trajectory for a finite control horizon, say (k, k + N), and by the taking into account the car characteristics to decide which control actions (accelerator, brakes, and steering) to take in order to follow the desired trajectory. Only the first control action is adopted as the current control law, and the procedure is then repeated over the next time horizon, say (k + 1, k + 1+ N). The term "*receding horizon*" is introduced, since the horizon recedes as time proceeds. The basic MPC strategy is shown in Fig. 2, where $u(t)$ is the manipulated variable, $y(t)$ is the process output and $w(t)$ is the reference signal, N_1, N_2 and N_u are called minimum, maximum and control horizons, respectively. The block diagram is shown in Fig. 3.

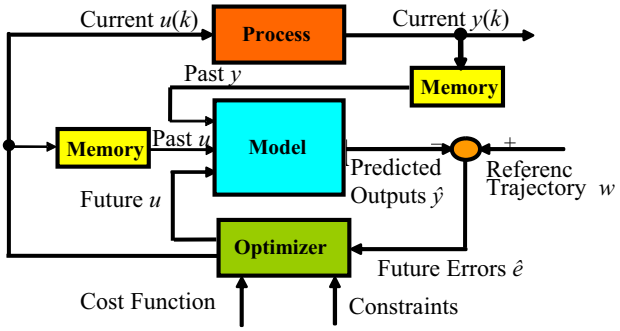

Figure 3: Block diagram of MPC

Calculation of Optimal Control

The designed control algorithm is based on the Generalised Predictive Control (GPC) method (Clarke et al. 1987a,b). The standard cost function used in GPC contains quadratic terms of control error and control increments on a finite horizon into the future (Camacho and Bordons 2004; Mikleš and Fikar 2008)

$$J = \sum_{i=N_1}^{N_2} \left[\hat{y}(k+i) - w(k+i)\right]^2 + \sum_{i=1}^{N_u} \left[\lambda(i)\Delta u(k+i-1)\right]^2 \tag{1}$$

where $\hat{y}(k+i)$ is the process output of i steps in the future predicted on the base of information available upon the time k, $w(k+i)$ is the sequence of the reference signal and $\Delta u(k+i-1)$ is the sequence of the future control increments that have to be calculated. Parameters N_1, N_2 and N_u are called minimum, maximum and control horizons. The parameter $\lambda(i)$ can be generally a sequence which affects future behaviour of the controlled process. The output of the model (prediction) is computed as the sum of the forced response $\boldsymbol{y}_n$ and the free response $\boldsymbol{y}_0$

$$\hat{\boldsymbol{y}} = \boldsymbol{y}_n + \boldsymbol{y}_0 \tag{2}$$

The free response is that part of the prediction which is determined by past values of the manipulated variable and past values of the systems output. The forced response is determined by future increments of the

manipulated variable. The forced response is computed as the multiplication of the matrix $\boldsymbol{G}$ (Jacobian Matrix of the model) and the vector of future control increments $\Delta\boldsymbol{u}$, which is generally a priori unknown

$$\boldsymbol{y}_n = \boldsymbol{G}\Delta\boldsymbol{u} \tag{3}$$

where

$$\boldsymbol{G} = \begin{bmatrix} g_1 & 0 & 0 & \cdots & 0 \\ g_2 & g_1 & 0 & \cdots & 0 \\ g_3 & g_2 & g_1 & \cdots & 0 \\ \vdots & \vdots & \vdots & \ddots & \vdots \\ g_{N_2} & g_{N_2-1} & g_{N_2-2} & \cdots & g_{N_2-N_u+1} \end{bmatrix} \tag{4}$$

is matrix containing values of the step sequence.
It follows from (2) and (3) that the predictor in a vector form is given by

$$\hat{\boldsymbol{y}} = \boldsymbol{G}\Delta\boldsymbol{u} + \boldsymbol{y}_0 \tag{5}$$

By assumption that λ is scalar, the cost function (1) can be modified to the form

$$\begin{aligned} J &= \left(\hat{\boldsymbol{y}} - \boldsymbol{w}\right)^T \left(\hat{\boldsymbol{y}} - \boldsymbol{w}\right) + \lambda\Delta\boldsymbol{u}^T\Delta\boldsymbol{u} = \\ &= \left(\boldsymbol{G}\Delta\boldsymbol{u} + \boldsymbol{y}_0 - \boldsymbol{w}\right)^T \left(\boldsymbol{G}\Delta\boldsymbol{u} + \boldsymbol{y}_0 - \boldsymbol{w}\right) + \lambda\Delta\boldsymbol{u}^T\Delta\boldsymbol{u} \end{aligned} \tag{6}$$

Minimisation of the cost function (6) now becomes a direct problem of linear algebra. The solution in an unconstrained case can be found by setting partial derivative of J with respect to $\Delta\boldsymbol{u}$ as zero and yields

$$\Delta\boldsymbol{u} = \left(\boldsymbol{G}^T\boldsymbol{G} + \lambda\boldsymbol{I}\right)^{-1}\boldsymbol{G}^T\left(\boldsymbol{w} - \boldsymbol{y}_0\right) \tag{7}$$

Equation (7) gives the whole trajectory of the future control increments and such is an open-loop strategy. To close the loop, only the first element is applied to the system and the whole algorithm is recomputed at time k+1. If we denote the first row of the matrix $\left(\boldsymbol{G}^T\boldsymbol{G} + \lambda\boldsymbol{I}\right)^{-1}\boldsymbol{G}^T$ as $\boldsymbol{K}$ then the actual control increment can be calculated as

$$\Delta u(k) = \boldsymbol{K}\left(\boldsymbol{w} - \boldsymbol{y}_0\right) \tag{8}$$

DERIVATION OF PREDICTOR

An important task is computation of predictions for arbitrary prediction and control horizons. Dynamics of most of processes requires horizons of length where it is not possible to compute predictions in a simple straightforward way. Recursive expressions for computation of the free response and the matrix $\boldsymbol{G}$ in each sampling period had to be derived. There are several different ways of deriving the prediction equations for transfer function models. Some papers make use of Diophantine equations to form the prediction equations (Kwon et al. 2002) In (Rossiter 2003) matrix methods are used to compute predictions. We derived a method for recursive computation of both the free response and the matrix of the dynamics (Kubalčík and Bobál 2011; Bobá1 et al. 2010).

Computation of the predictor for the time-delay system can be obtained by modification of the predictor for the corresponding system without a time-delay. At first we will consider the second order system without time-delay and then we will modify the computation of predictions for the time-delay system.

Second Order System without Time Delay

The deterministic model is described by the discrete transfer function

$$G\left(z^{-1}\right) = \frac{B\left(z^{-1}\right)}{A\left(z^{-1}\right)} = \frac{b_1 z^{-1} + b_2 z^{-2}}{1 + a_1 z^{-1} + a_2 z^{-2}} \tag{9}$$

Model (9) can be also written in the form

$$A\left(z^{-1}\right)y(k) = B\left(z^{-1}\right)u(k) \tag{10}$$

A widely used model in GPC is the CARIMA model which can be obtained from the nominal model (10) by adding a disturbance model

$$A\left(z^{-1}\right)y(k) = B\left(z^{-1}\right)u(k) + \frac{C\left(z^{-1}\right)}{\Delta}n_c(k) \tag{11}$$

where $n_c(k)$ is a non-measurable random disturbance that is assumed to have zero mean value and constant covariance and $\Delta = 1 - z^{-1}$. Inverted Δ is then an integrator. The difference equation of the second order CARIMA model without the unknown term $n_c(k)$ can be expressed as

$$\begin{aligned} y(k) = {} & (1 - a_1)\,y(k-1) + (a_{1'} - a_2)\,y(k-2) \\ & + a_2 y(k-3) + b_1\Delta u(k-1) + b_2\Delta u(k-2) \end{aligned} \tag{12}$$

It was necessary to compute three step-ahead predictions in a straightforward way by establishing of lower predictions to higher predictions. The model order defines that computation of one step-ahead prediction is based on three past values of the system output. The three step-ahead predictions after modifications can be written in a matrix form

$$\begin{aligned} \begin{bmatrix} \hat{y}(k+1) \\ \hat{y}(k+2) \\ \hat{y}(k+3) \end{bmatrix} = {} & \begin{bmatrix} g_1 & 0 \\ g_2 & g_1 \\ g_3 & g_2 \end{bmatrix} \begin{bmatrix} \Delta u(k) \\ \Delta u(k+1) \end{bmatrix} \\ & + \begin{bmatrix} p_{11} & p_{12} & p_{13} & p_{14} \\ p_{21} & p_{22} & p_{23} & p_{24} \\ p_{31} & p_{32} & p_{33} & p_{34} \end{bmatrix} \begin{bmatrix} y(k) \\ y(k-1) \\ y(k-2) \\ \Delta u(k-1) \end{bmatrix} \end{aligned} \tag{13}$$

where the individual matrix elements in (13) are

$$g_1 = b_1; \quad g_2 = b_1(1 - a_1) + b_2;$$
$$g_3 = (a_1 - a_2)b_1 + (1 - a_1)^2 b_1 + (1 - a_1)b_2$$

$$p_{11}=(1-a_1);\quad p_{12}=(a_1-a_2);$$
$$p_{13}=a_2;\quad p_{14}=b_2;$$
$$p_{21}=(1-a_1)^2+(a_1-a_2);\quad p_{22}=(1-a_1)(a_1-a_2)+a_2;$$
$$p_{23}=a_2(1-a_1);\quad p_{24}=b_2(1-a_1);$$
$$p_{31}=(1-a_1)^3+2(1-a_1)(a_1-a_2)+a_2;$$
$$p_{32}=(1-a_1)^2(a_1-a_2)+a_2(1-a_1)+(a_1-a_2)^2;$$
$$p_{33}=a_2(1-a_1)^2+(a_1-a_2)a_2;\quad p_{34}=b_2(1-a_1)^2+(a_1-a_2)b_2.$$

It is possible to divide computation of the predictions to recursion of the free response and recursion of the matrix of the dynamics. Based on the three previous predictions it is repeatedly computed the next row of the free response matrix in the following way:

$$\begin{aligned}
p_{41}&=(1-a_1)p_{31}+(a_1-a_2)p_{21}+a_2p_{11}\\
p_{42}&=(1-a_1)p_{32}+(a_1-a_2)p_{22}+a_2p_{12}\\
p_{43}&=(1-a_1)p_{33}+(a_1-a_2)p_{23}+a_2p_{13}\\
p_{44}&=(1-a_1)p_{34}+(a_1-a_2)p_{24}+a_2p_{14}
\end{aligned} \tag{14}$$

The first row of the matrix is omitted in the next step and further prediction is computed based on the three last rows including the one computed in the previous step. This procedure is cyclically repeated. It is possible to compute an arbitrary number of rows of the matrix.

The recursion of the dynamics matrix is similar. The next element of the first column is repeatedly computed in the same way as in the previous case and the remaining columns are shifted to form a lower triangular matrix in the way which is obvious from the equation (13). This procedure is performed repeatedly until the prediction horizon is achieved. If the control horizon is lower than the prediction horizon a number of columns in the matrix is reduced. Computation of the new element is performed as follows:

$$g_4=(1-a_1)g_3+(a_1-a_2)g_2+a_2g_1 \tag{15}$$

Second Order System with Time-Delay

The nominal second order model with d steps of time-delay is considered as

$$G(z^{-1})=\frac{B(z^{-1})}{A(z^{-1})}z^{-d}=\frac{b_1z^{-1}+b_2z^{-2}}{1+a_1z^{-1}+a_2z^{-2}}z^{-d} \tag{16}$$

where d is a number of time-delay steps.

The CARIMA model for time-delay system without the unknown term $n_c(k)$ takes the form

$$\Delta A(z^{-1})y(k)=z^{-d}B(z^{-1})\Delta u(k) \tag{17}$$

In order to compute the control action it is necessary to determine the predictions from d+1 to d+N_2. The predictor (14) is then modified for an arbitrary number of time delay steps to

$$\begin{bmatrix}\hat{y}(k+3)\\ \hat{y}(k+4)\\ \hat{y}(k+5)\end{bmatrix}=\begin{bmatrix}p_{(1+d)1} & p_{(1+d)2} & p_{(1+d)3}\\ p_{(2+d)1} & p_{(2+d)2} & p_{(2+d)3}\\ p_{(3+d)1} & p_{(3+d)2} & p_{(3+d)3}\end{bmatrix}\begin{bmatrix}y(k)\\ y(k-1)\\ y(k-2)\end{bmatrix}+\begin{bmatrix}g_1 & 0\\ g_2 & g_1\\ g_3 & g_2\end{bmatrix}\begin{bmatrix}\Delta u(k)\\ \Delta u(k+1)\end{bmatrix}$$
$$+\begin{bmatrix}g_{1+d-1} & g_{2+d-1} & p_{(1+d)4}\\ g_{2+d-1} & g_{3+d-1} & p_{(2+d)4}\\ g_{3+d-1} & g_{4+d-1} & p_{(3+d)4}\end{bmatrix}\begin{bmatrix}\Delta u(k-1)\\ \Delta u(k-2)\\ \Delta u(k-3)\end{bmatrix} \tag{18}$$

Recursive computation of the matrices is analogical to the recursive computation described for the second order system without time-delay.

RECURSIVE IDENTIFICATION PROCEDURE

The regression (ARX) model of the following form

$$y(k)=\boldsymbol{\Theta}^T(k)\boldsymbol{\Phi}(k)+n_c(k) \tag{19}$$

is used in the identification part of the designed controller predictive algorithm, where

$$\boldsymbol{\Theta}^T(k)=\begin{bmatrix}a_1 & a_2 & b_1 & b_2\end{bmatrix} \tag{20}$$

is the vector of the parameters estimates and

$$\boldsymbol{\Phi}^T(k-1)=\begin{bmatrix}-y(k-1) & -y(k-2) & u(k-d-1) & u(k-d-2)\end{bmatrix} \tag{21}$$

is the regression vector. For calculating of the parameter estimates $\hat{\boldsymbol{\Theta}}(k)$ is utilized the recursive least squares method, its numerical stability is improved by means of LD decomposition and adaptation is supported by directional forgetting (Kulhavý 1987; Bobál et al. 2005).

SIMULATION VERIFICATION OF SELF-TUNING MPC

A simulation verification of the designed predictive algorithm was performed in MATLAB/SIMULINK environment. A typical control scheme, which was used, is depicted in Fig. 4. This scheme is used for systems with time-delay of two sample steps. Individual blocks of the Simulink scheme correspond to blocks of the general control scheme presented in Fig. 3. The controller block represents the controlled system. This block consists of the recursive identification, predictive and optimization parts. This block has two inputs (process output *y_s* and initial condition *y_in*) and three outputs (controller output *u*, generating of reference signal *w* and model parameter estimates $\hat{a}_1, \hat{a}_2, \hat{b}_1, \hat{b}_2$). It is possible to influence the output of the process by non-measurable variables – the white noise n_c and the step v disturbances.

The above mentioned predictive controller is not suitable for control of unstable processes. Therefore, three types of processes were chosen for simulation verification of digital self-tuning predictive controller algorithms. Consider the following continuous-time transfer functions:

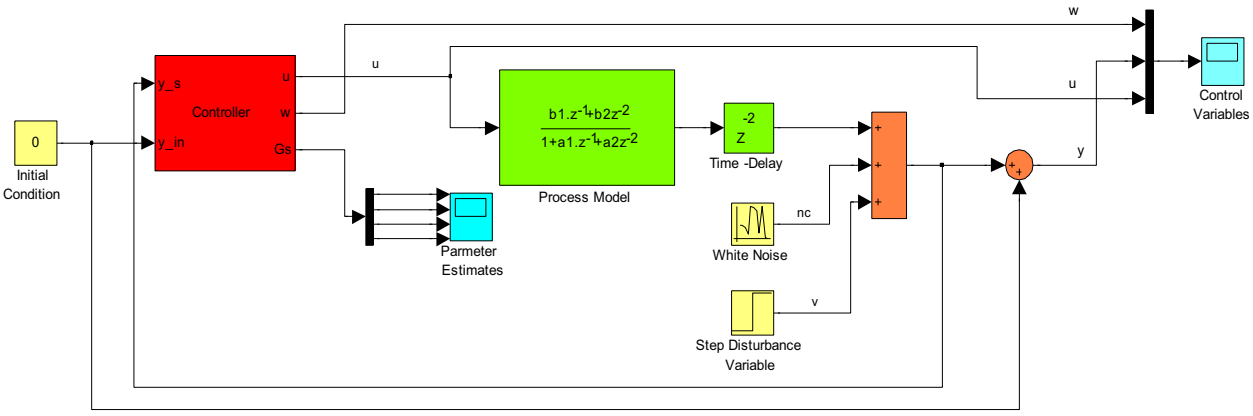

Figure 4: Simulink control scheme

1) Stable non-oscillatory $G_1(s) = \dfrac{2}{(s+1)(4s+1)} e^{-4s}$

2) Stable oscillatory $G_2(s) = \dfrac{2}{4s^2+2s+1} e^{-4s}$

3) Non-minimum phase $G_3(s) = \dfrac{2(1-5s)}{(s+1)(4s+1)} e^{-4s}$

Let us now discretize them with a sampling period $T_0 = 2$ s . The discrete forms of these transfer functions

$$G_1(z^{-1}) = \frac{0.4728z^{-1} + 0.2076z^{-2}}{1 - 0.7419z^{-1} + 0.0821z^{-2}} z^{-2}$$

$$G_2(z^{-1}) = \frac{0.6806z^{-1} + 0.4834z^{-2}}{1 - 0.7859z^{-1} + 0.3679z^{-2}} z^{-2}$$

$$G_3(z^{-1}) = \frac{-1.0978z^{-1} + 1.7783z^{-2}}{1 - 0.7419z^{-1} + 0.0821z^{-2}} z^{-2}$$

were used in the Simulink control scheme for the verification of the dynamical behavior of individual closed control loops.

Simulation control of model $G_1(z^{-1})$

This model was chosen for the complex verification of self-tuning MPC properties for time-delay systems. The most important parameters in terms of quality process control are sampling period, penalization factor λ, initial parameter estimates $\hat{\boldsymbol{\Theta}}(0)$ (*a priori information*) and initial diagonal elements of the covariance matrix $\boldsymbol{C}_{ii}(0)$. The control performance is dependent also on the variance of the non-measurable noise σ^2.

At first, the model parameter estimates were chosen without *a priori* information

$$\hat{\boldsymbol{\Theta}}^T(0) = [0.5 \quad 0.5 \quad 0.5 \quad 0.5]$$

$C_{ii}(0) = 1000$, $\sigma^2 = 0.01$, in time t = 150-300 s a step disturbance $v(t) = 5$ affected the systems output. Figs. 5 and 6 illustrate an influence of the penalization factor λ on the control performance.

The individual horizons were chosen for all experiments: $N_1 = 3$, $N_2 = 30$, $N_u = 28$.

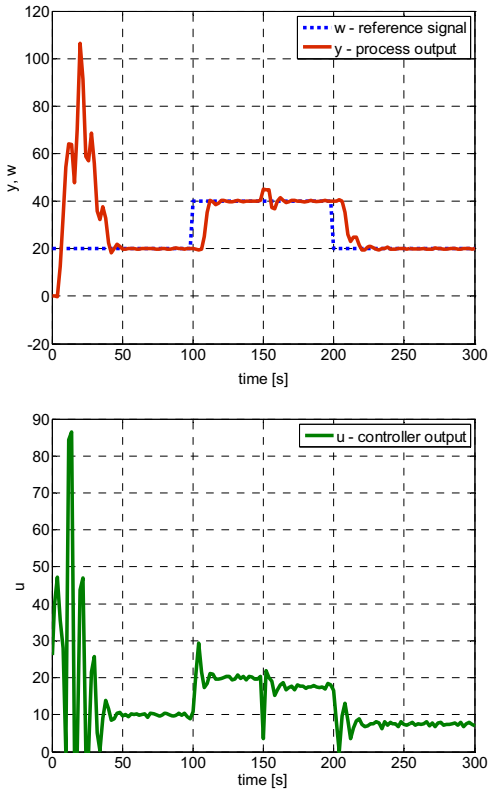

Figure 5: Control of the model $G_1(z^{-1})$, $\lambda = 0.1$

The courses of the control variables oscillate in the initial control interval. When model parameter estimates are converged, the quality of the control process is very good. It is obvious that by increasing λ oscillations of the controller's output $u(k)$ are eliminated which has a positive influence on the course of the process output $y(k)$. In the subsequent

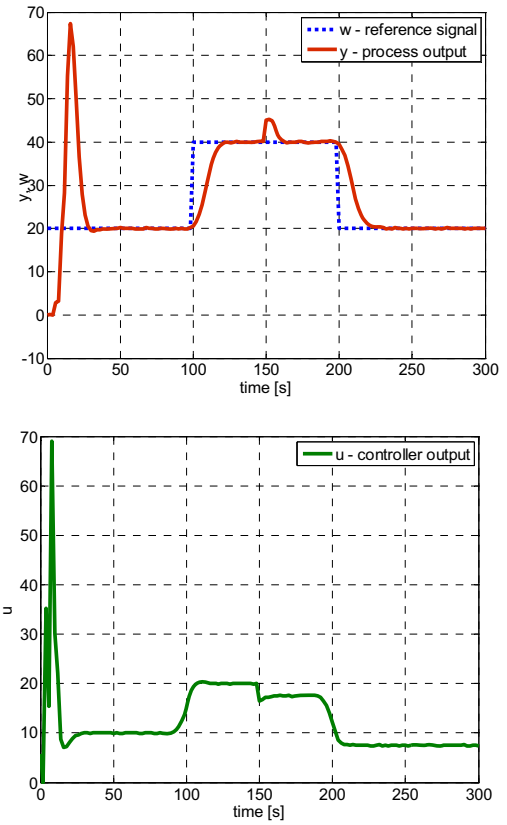

Figure 6: Control of the model $G_1(z^{-1})$, $\lambda = 10$

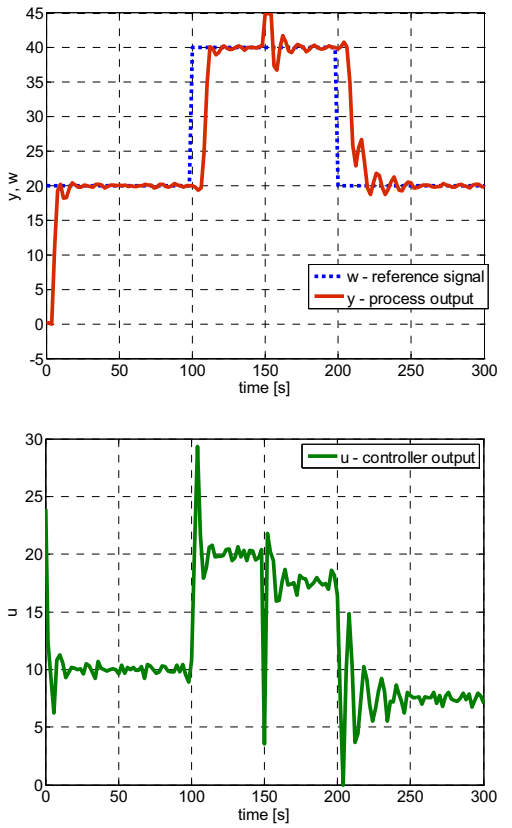

Figure 7: Control of the model $G_1(z^{-1})$, $\lambda = 0.1$

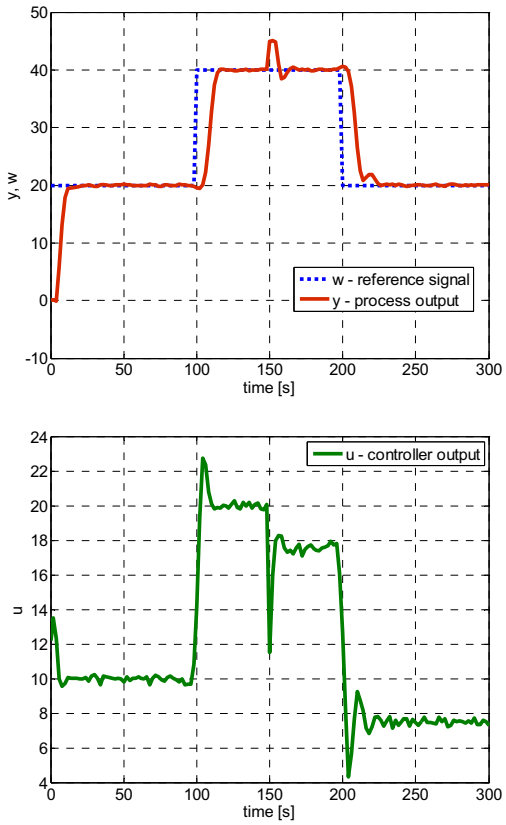

Figure 8: Control of the model $G_1(z^{-1})$, $\lambda = 1$

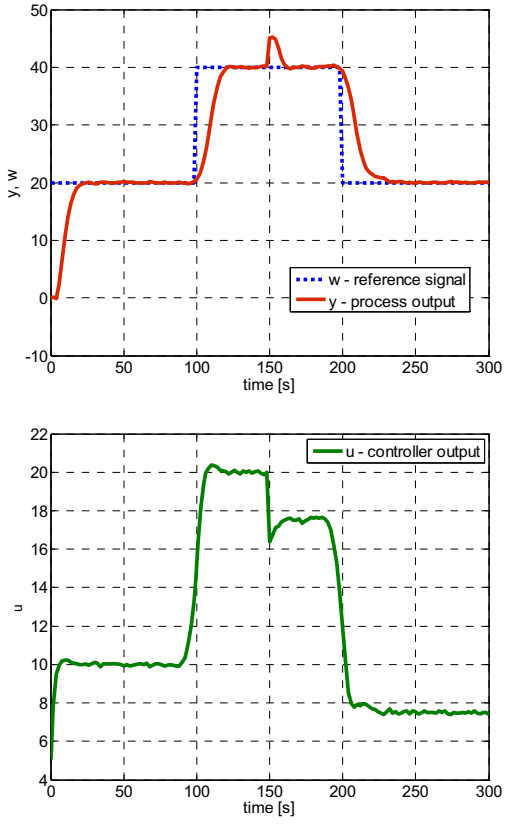

Figure 9: Control of the model $G_1(z^{-1})$, $\lambda = 10$

experiment the model parameter estimates were chosen using *a priori* information

$$\hat{\boldsymbol{\Theta}}^T(0) = [-0.75 \quad 0.08 \quad 0.5 \quad 0.2]$$

$C_{ii}(0) = 10^{-3}$ (an assumption of the parameter estimates dispersion in a narrow interval). The other initial parameters were chosen to be the same as in the previous simulations – see Figs. 7 - 9. The courses of the control variables are satisfactory including the initial interval of control. The influence of the penalization factor λ is also evident on the control courses.

Simulation control of model $G_2(z^{-1})$

Simulation control of the model $G_2(z^{-1})$ (a stable oscillatory model) was realized upon similar conditions as in the previous case using *a priori* information. The initial vector of parameter estimates has the form

$$\hat{\boldsymbol{\Theta}}^T(0) = [-0.8 \quad 0.4 \quad 0.7 \quad 0.5]$$

The control courses are shown in Fig. 10, the quality of control is very good.

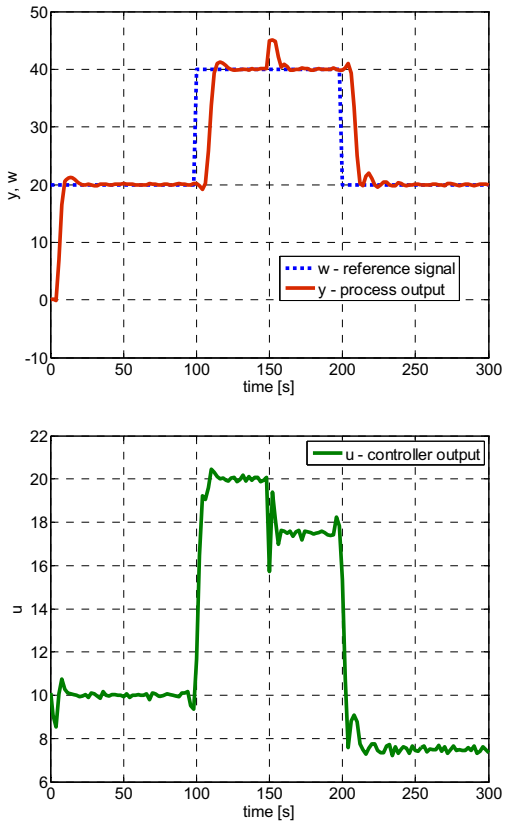

Figure 10: Control of the model $G_2(z^{-1})$, $\lambda = 1$

Simulation control of model $G_3(z^{-1})$

Simulation control of the model $G_3(z^{-1})$ (the non-minimum phase model) was realized upon similar conditions as in the previous cases using *a priori* information. The initial vector of parameter estimates has the form

$$\hat{\boldsymbol{\Theta}}^T(0) = [-0.75 \quad 0.08 \quad -1 \quad 1.8]$$

The control courses are shown in Fig. 11, the quality of control is very good.

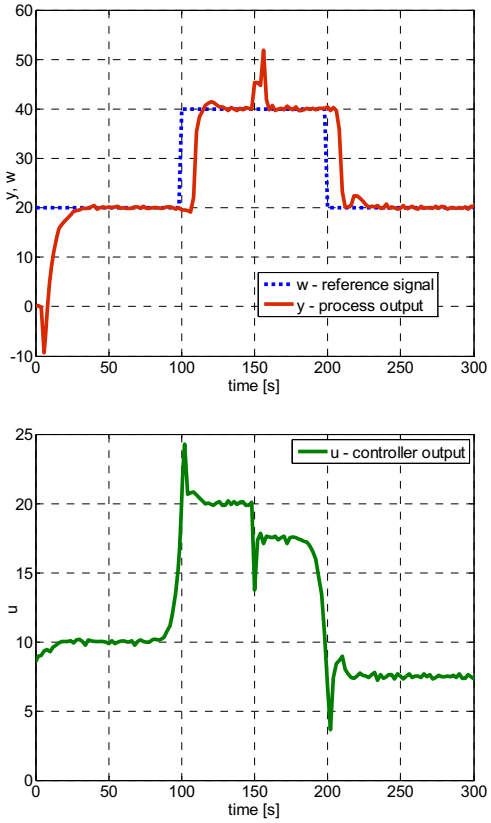

Figure 11: Control of the model $G_3(z^{-1})$, $\lambda = 1$

CONCLUSION

The contribution presents the self-tuning predictive control applied to time-delay processes. The predictive controller is based on the recursive computation of predictions by direct use of the CARIMA model. The computation of predictions was extended for time-delay systems. A linear model with constant coefficients used in pure model predictive control can not describe the control system in all its modes. Therefore, a self-tuning approach was applied. It consists of the recursive identification and the predictive controller. The model parameter estimates obtained from the identification procedure are used in the self-tuning predictive controller. MPC based on minimization of the quadratic criterion was derived and tested. Three models of control processes were used for simulation verification (the stable non-oscillatory, the

stable oscillatory and the non-minimum phase). The designed predictive controller was successfully verified not only by simulation but also in real-time laboratory conditions for control of a heat exchanger.

ACKNOWLEDGMENT

This article was created with support of Operational Programme Research and Development for Innovations co-funded by the European Regional Development Fund (ERDF), national budget of Czech Republic within the framework of the Centre of Polymer Systems project (reg. number: CZ.1.05/2.1.00/03.0111).

REFERENCES

Bobál, V., Böhm, J., Fessl, J. and J. Macháček. 2005. *Digital Self-tuning Controllers: Algorithms, Implementation and Applications.* Springer-Verlag, London, 2005.

Bobál, V., Chalupa, P., Kubalčík, M. and P. Dostál. 2010. "Self-tuning predictive control of non-linear servomotor." *Journal of Electrical Engineering* 61, 265-372.

Bobál, V., Chalupa, P., Dostál, P. and M. Kubalčík. 2011. "Design and simulation verification of self-tuning Smith predictors." *International Journal of Mathematics and Computers in Simulation* 5, 342-351.

Bobál, V., Chalupa, P., Novák, J. and P. Dostál. 2012a. "MATLAB Toolbox for CAD of self-tuning of time-delay processes." In *Proc. of the International Workshop on Applied Modelling and Simulation*, Roma, 44 – 49.

Bobál, V., Chalupa, P. and J. Novák. 2012b. Toolbox for CAD and Verfication of Digital Adaptive Control Time-Delay Systems. Available from http://nod32.fai.utb.cz/promotion/Software_OBD/Time_Delay_Tool.zip.

Camacho, E. F. and C. Bordons. 2004. *Model Predictive Control.* Springer-Verlag, London.

Clarke, D. W., Mohtadi, C. and P. S. Tuffs. 1987a. "Generalized predictive control, part I: the basic algorithm." *Automatica* 23, 137-148.

Clarke, D. W., Mohtadi, C. and P. S. Tuffs. 1987b. "Generalized predictive control, part II: extensions and interpretations." *Automatica* 23, 149-160.

Hang, C. C., Lim, K. W. and B. W. Chong. 1989. "A dual-rate digital Smith predictor."*Automatica* 20, 1-16.

Kubalčík, M., and V. Bobál. 2011. "Techniques for predictor design in multivariable predictive control." *WSEAS Transactions on Systems and Control* 6, 349-360.

Kulhavý, R. 1987. "Restricted exponential forgetting in real time identification."*Automatica* 23, 586-600.

Kwon, W. H., Choj, H., Byun, D. G. S. Noh. 1992. "Recursive solution of generalized predictive control and its equivalence to receding horizon tracking control." *Automatica*, 28(6), 1235–1238.

Li, M. Ch. 2008. *Delay Identification and Model Predictive Control of Time Delayed Systems.* Ph.D. Thesis, Mc Gill University, Montreal, Canada.

Mikleš, J. and M. Fikar. 2008. *Process Modelling, Optimisation and Control.* Springer-Verlag, Berlin.

Normey-Rico, J. E. and E. F. Camacho. 2007. *Control of Dead-time Processes*, Springer-Verlag, London.

Rossiter, J. A. 2003. *Model Based Predictive Control: a Practical Approach.* CRC Press.

Smith, O.J. 1957. "Closed control of loops."*Chem. Eng. Progress*, 53, 217-219.

AUTHOR BIOGRAPHIES

VLADIMÍR BOBÁL graduated in 1966 from the Brno University of Technology, Czech Republic. He received his Ph.D. degree in Technical Cybernetics at Institute of Technical Cybernetics, Slovak Academy of Sciences, Bratislava, Slovak Republic. He is now Professor at the Department of Process Control, Faculty of Applied Informatics of the Tomas Bata University in Zlín, Czech Republic. His research interests are adaptive and predictive control, system identification and CAD for automatic control systems. You can contact him on email address bobal@fai.utb.cz.

MAREK KUBALČÍK graduated in 1993 from the Brno University of Technology in Automation and Process Control. He received his Ph.D. degree in Technical Cybernetics at Brno University of Technology in 2000. From 1993 to 2007 he worked as senior lecturer at the Faculty of Technology, Brno University of Technology. From 2007 he has been working as an associate professor at the Department of Process Control, Faculty of Applied Informatics of the Tomas Bata University in Zlín, Czech Republic. Current work cover following areas: control of multivariable systems, self-tuning controllers, predictive control. His e-mail address is: kubalcik@fai.utb.cz.

PETR DOSTÁL studied at the Technical University of Pardubice, Czech Republic, where he obtained his master degree in 1968 and PhD. degree in Technical Cybernetics in 1979. In the year 2000 he became professor in Process Control. He is now head of the Department of Process Control, Faculty of Applied Informatics of the Tomas Bata University in Zlín. His research interests are modelling and simulation of continuous-time chemical processes, polynomial methods, optimal and adaptive control. You can contact him on email address dostalp@fai.utb.cz.

MODELING OF ALCOHOL FERMENTATION IN BREWING – COMPARATIVE ASSESSMENT OF FLAVOR PROFILE OF BEERS PRODUCED WITH FREE AND IMMOBILIZED CELLS

Stoyan Vassilev, Vessela Naydenova, Mariana Badova, Vasil Iliev, Maria Kaneva, Georgi Kostov
Department "Technology of wine and brewing"
University of Food Technologies
4002, 26 Maritza boulvd., Plovdiv, Bulgaria
E-mail: george_kostov2@abv.bg; vesi_nevelinova@abv.bg; m_kaneva@abv.bg; stoyanvassilev5@gmail.com; mariqna_badova@abv.bg; vasil_iliev_1988@abv.bg;

Silviya Popova
Institute of System Engineering and Robotics
Bulgarian Academy of Sciences
Acad. G. Bonchev str. bl.2, Sofia-1113, Bulgaria
E-mail: popova_silvia2000@yahoo.com

KEYWORDS

modeling, kinetics, flavor profile, esters, aldehydes, higher alcohols, metabolism

ABSTRACT

A detailed investigation of bioengineering constants for the accumulation of major yeast metabolites in beer produced by free and immobilized cells was carried out. The kinetic constants were used to determine the effect of immobilization on yeast metabolism. The esters synthesis dynamics was similar for the free and the immobilized cell which was confirmed by the kinetic model. The dynamics of the higher alcohol synthesis was comparable for the free and immobilized cell, but there were some differences. The dynamics of the higher alcohols accumulation for the free and immobilized cells was similar, but there were some differences between the two used strains. These differences were due to the influence of mass transfer between the liquid and the capsules, which reflected mostly in the metabolism of some amino acids. There were significant differences in the aldehyde synthesis and reduction by immobilized and free cells. The free cells of both yeast strains showed distinct maximum of aldehydes, where after the aldehydes reduction started. On the other hand, the aldehyde peaks were not so distinct for the immobilized cells and the aldehydes concentration was relatively constant during fermentation. The explanation for this difference can be found in the kinetic parameters. The model described with high accuracy the beer fermentations with immobilized and free cells and confirmed the experimental data. The obtained data would be used for developing of control strategy fermentation process to obtain beverages with different organoleptic profile.

INTRODUCTION

The main stages in the brewing process are: wort production; alcoholic fermentation and maturation; processing and stabilization of the beer (Kunze 2003; Handbook of brewing: Processes, Technology, Markets 2009). The wort transforms into beer during alcoholic fermentation and maturation. The ethanol fermentation occurs as a result of enzymatic activity of the yeast at Embden-Meyerhof Parnas pathway, which leads to glucose conversion to pyruvate. Under anaerobic conditions the yeasts convert pyruvate to ethanol and CO_2. In aerobic conditions, yeasts consume sugars, mainly for biomass accumulation and CO_2 production (Boulton and Quain, 2001).

Yeast metabolism during fermentation and maturation affects significantly on beer flavor. Ethanol, CO_2, esters and fusel alcohols have positive contributions to beer flavor. Dimethyl sulphide and hydrogen sulphide, diacetyl, and aldehydes contribute to flavor defects of beer (Meilgaard, 1975). Therefore, the synthesis and reduction of yeast metabolites on the microbiological and bioengineering levels have to be studied for the purpose of yeast by-products optimization in certain limits. Fermentation and maturation are the longest processes in brewing. The primary fermentation lasts between 3-6 days and the maturation - up to 2 weeks depending on the fermentation type and the used equipment. In such a competitive market, the potential time savings, proposed by immobilized cell technology (ICT) have to be taken into account. Immobilized yeast cell technology allows the production of beer to be accomplished in as little as 2-3 days (Branyik et al, 2005). Immobilized cell systems are heterogeneous systems in which considerable mass transfer limitations can occur, resulting in a changed yeast metabolism (Willaert, 2007). Consequently, the main challenge for ICT is to reproduce the traditional beer flavor.

Proceedings 27th European Conference on Modelling and Simulation ©ECMS Webjørn Rekdalsbakken, Robin T. Bye, Houxiang Zhang (Editors)
ISBN: 978-0-9564944-6-7 / ISBN: 978-0-9564944-7-4 (CD)

The aim of this work is to determine the influence of immobilization on the yeast metabolism using mathematical models. The dynamics of the main yeast metabolites - ethanol and CO_2, the biomass concentration and some of secondary yeast metabolites - esters, aldehydes and higher alcohols were studied. The differences between fermentations with immobilized and free cells were determined by the developed mathematical models for yeast metabolites.

MICROORGANISMS AND FERMENTATION CONDITIONS

The fermentations were carried out with top-fermenting yeast strain *Saccharomyces cerevisiae* S-33 and bottom-fermenting yeast strain *Saccharomyces pastorianus* S-23. Wort with 3 different original extracts – 9, 11 and 13% was used for fermentations. All media were sterilized at 121 °C for 20 min before fermentations.
Immobilization procedure and fermentation conditions were previously reported in (Parcunev et.al. 2012). In this study the fermentations with free and immobilized cells were investigated for the same intervals of time (10 days) to determine the impact of immobilization on the yeast metabolism. Although the fermentation with immobilized cells was faster than the one with free cells, the metabolites accumulation in the fermenting medium was influenced by diffusion limitations.
Biomass concentration of immobilized cells was determined according to mathematical model proposed in (Parcunev et.al. 2012). The concentrations of yeast metabolites – aldehydes, esters and higher alcohols were measured according to (Marinov, 2010). Because of the limited volume of wort, the analyzes were performed on the 1st, 3rd, 5th, 7th and 9th day for the fermentation with top-fermenting yeast and on the 2nd, 4th, 6th, 8th and 10th day for the fermentation with bottom fermenting yeast.

MATHEMATICAL MODELS AND THEIR EXPLANATION

Equation of fermentation

The fermentation with immobilized cells can be described with the equations for batch fermentation with free cells as previously reported (Parcunev et.al. 2012):

$$\begin{cases} \dfrac{dX}{dt} = \mu(t)X(t) \\ \dfrac{dP}{dt} = q(t)X(t) \\ \dfrac{dS}{dt} = -\dfrac{1}{Y_{x/s}}\dfrac{dX}{dt} - \dfrac{1}{Y_{p/s}}\dfrac{dP}{dt} \end{cases} \quad (1)$$

The values of parameters have to be corrected with efficiency coefficients:

$$\eta_\mu = \frac{\mu_{\max}^{imm}}{\mu_{\max}^{free}};\ \eta_q = \frac{q_{\max}^{imm}}{q_{\max}^{free}} \quad (2)$$

In our previous study (Parcunev et.al. 2012) three fermentation models were investigated, but the Monod model showed highest accuracy for description of fermentation with immobilized and free cells. Therefore, it was chosen for further modeling of the fermentation processes:

$$\mu = \mu_{\max}\frac{S}{K_{sx}+S};\ q = q_{p\max}\frac{S}{K_{sp}+S} \quad (3)$$

The Monod equation provides a good basis for the management of the fermentation. However, it gives no information about the concentration of yeast by-products in beer and the influence of immobilization on the beer flavor profile.

Models of beer flavor profile

Beer flavor profile is formed from a large number of compounds. It is impossible to be made a mathematical model which includes the all flavor-active compounds. Therefore, three important groups of them will be used for the model of our work - higher alcohols, esters, and aldehydes. The other important flavor-active group of compounds – vicinal diketones will be discussed in next papers because of their specific synthesis and reduction. The basis of our mathematical model will be the microbiological aspects of yeast by-products synthesis and the work of (Ramirez and Maciejowski, 2007). In their paper, an algorithm for the fermentation control was made. It was based on the various substrates uptake and the synthesis of different groups of metabolites. The application of their model for the purpose of our work requires certain simplifications in the model. On the other hand, the model has to take into account the knowledge of biochemical and microbiological characteristics of processes.

Higher alcohols synthesis

More than 40 higher alcohols have been identified in beers (Engan, 1981). The flavor impressions reach from flowery to solvent-like and alcoholic. Higher alcohols are the precursors for more flavor active esters (Briggs et al., 2004). Higher alcohols can be synthesized via two routes: "*de novo*" from wort carbohydrates (the anabolic route) or as by-products of amino acid assimilation (the catabolic route) (Rusell, 2006). At the ends of primary fermentation over 90% of the higher alcohols have been built, the rest arise during the maturation process (Handbook of brewing: Processes, Technology, Markets 2009). Therefore, the higher alcohols synthesis may be associated with the biomass growth and can be described by equation (4):

$$\frac{dFA}{dt} = Y_{FA}.\mu.X(t) \quad (4)$$

Ester synthesis

Esters comprise possibly the most important set of flavor-active beer components which arise as a result of yeast metabolism. In the region of 100 distinct esters have been identified in beers (Boulton and Quain, 2001). They are formed by the intracellular reaction between a fatty acyl-coenzyme A and an alcohol (Willaert and Nedovic, 2006). Esters are produced by yeast cells during the exponential phase (60%) and the stationary phase (40%). Ethyl esters are present in the highest quantity presumably because ethanol is present in large amounts (Rusell, 2006). As mentioned above,

most of the higher alcohols are formed during primary fermentation and, since these compounds are required for ester synthesis, ester synthesis is delayed. Therefore, a significant amount of esters is built when yeast growth declines (Handbook of brewing: Processes, Technology, Markets 2009). This means that the esters synthesis may be associated with cell growth and their change can be described by equation (5):

$$\frac{dE}{dt} = Y_E.\mu.X(t) \quad (5)$$

Carbonyls (aldehydes) synthesis and reduction

Some 200 carbonyl compounds have been detected in beers of importance to beer flavor and aroma and influenced by yeast metabolism are acetaldehyde and several other aldehydes and vicinal diketones (Boulton and Quain, 2001). Several aldehydes arise during wort production, others are formed as intermediates in the biosynthesis of higher alcohols from oxo-acids by yeasts. Acetaldehyde is of special interest as an immediate precursor of ethanol (Briggs et al., 2004). Acetaldehyde synthesis is linked to yeast growth. Its concentration is maximal at the end of the growth phase, and is reduced at the end of the primary fermentation and during maturation by the yeast cells (Willaert, 2007). Removal of acetaldehyde is favored by increased yeast content during maturation (Rusell, 2006). Therefore, it must be highlighted that the aldehyde synthesis is associated with yeast growth, and their reduction - with the biomass concentration in the bioreactor and the aldehydes concentration in fermenting beer (6):

$$\frac{dA}{dt} = Y_A.\mu.X(t) - k_A.A.X \quad (6)$$

Vicinal diketones are very important for beer flavor. Their synthesis is also linked to yeast growth. Unlike aldehydes, their reduction has both chemical and biochemical stages and therefore they will not be discussed in this paper. However, they will be mentioned in the analysis of the results.

As shown in the equations (4), (5) and (6) the synthesis of key metabolites is linked to yeast growth and can be determined by yield coefficients - Y_{FA}, Y_E, and Y_A. The aldehydes reduction can be described by k_A and the current concentrations of yeast and aldehydes in beer.

Therefore, the obtained mathematical model includes equations (1), (3), (4), (5) and (6) for the fermentation with free cells and equations (1), (2), (3), (4), (5) and (6) for the fermentation with immobilized cells

RESULTS OF FERMENTATIONS. BASIC KINETIC PARAMETERS.

The results for the yeast metabolites accumulation of yeast strain *Saccharomyces cerevisiae S-23* are shown in Figure 1. Figure 2 presented the results for yeast by-product accumulation of yeast strain *Saccharomyces pastorianus S-33.* The results are the average of three independent fermentation processes. The fermentation process kinetics was described with the ordinary differential equation (1 to 6). The identification of parameters was made by software programs in MatLab Environment (Kostov et. al. 2012; Mitev and Popova, 1995; Popova 1997). The software minimized the sum of squared errors of the model outputs with respect to the experimental data:

$$E(r) = (X(k_1,k_2,...,k_n) - X^e)^2 + (S(k_1,k_2,...,k_n) - S^e)^2 + (P(k_1,k_2,...,k_n) - P^e)^2 +$$
$$+ (E(k_1,k_2,...,k_n) - E^e)^2 + (FA(k_1,k_2,..,k_n) - FA^e)^2 + (A(k_1,k_2,...,k_n) - A^e)^2$$

For that purpose the function "fmincon" was applied. Here k_i, i=1÷n was vector of model parameters to be determined as output of minimization procedure. For that purpose the following complimentary differential equation:

$$dk_i / dt = 0$$

were added to the ordinary differential equations model because ki, i=1÷n were constant. For solving the overall differential equations system based on the explicit Runge-Kutta of 4-5 order formula using MATLAB function "ode45". All parameters are shown on tables 1. Table 2 presents the efficiency coefficients, which indicate the influence of the immobilization on the kinetic parameters. Efficiency coefficients are the ratio of parameters of fermentation with the immobilized cells to the same parameter of fermentation with free cells.

Table 1

Kinetic parameters of metabolites accumulation in beer during fermentations with free and immobilized cells

Original extract	Y_E	Y_{FA}	Y_A	K_A	Error
	mg/(g.d)				-
***Saccharomyces pastorianus* S-23**					
9% F	12.23	12.55	7.63	0.023	**0.259**
9% IMM	13.03	4.68	16.06	0.0205	**0.345**
11% F	116.4	20.47	29.42	0.01	**0.429**
11% IMM	144.2	33.6	45.94	0.035	**0.573**
13% F	61.05	13.61	21.19	0.025	**0.129**
13% IMM	31.72	8.15	11.36	0.0513	**0.234**
***Saccharomyces cerevisiae* S-33**					
9% F	31.99	18.8	120.1	0.0345	**0.462**
9% IMM	41.75	17.36	79.81	0.046	**0.346**
11% F	34.45	11.31	15.45	0.045	**0.547**
11% IMM	21.68	3.64	6.52	0.0678	**0.247**
13% F	184.36	19.52	51.01	0.0456	**0.101**
13% IMM	152.43	23.44	59.82	0.081	**0.246**

It was found in (Parcunev et.al. 2012) that the fermentation with immobilized cells was characterized with higher specific rates. They resulted in reduced primary fermentation time, but not in reduced total fermentation time. The total fermentation time was depended on the time for aldehydes and vicinal diketones reduction (maturation time). Therefore, the changes in the metabolism after primary fermentation were essential for the formation of a product with high quality. In terms of the mathematical model this feature should be considered. Therefore, the secondary metabolites accumulation by immobilized cells should be considered under the similar conditions with free cells for the complete evaluation of the advantages and disadvantages of the immobilized cells systems.

The modeling data (Figure 1, Table 1 and Table 2) showed no significant differences in the metabolism of free and immobilized cells of yeast strain *Saccharomyces pastorianus S-23*. The developed mathematical model describes with high accuracy the experimental data. It indicates the typical process dynamics to a large degree. However, there are also some problematic areas in the model which need to be taken into account when the model is used.

The modeling data (Figure 1, Table 1 and Table 2) showed no significant differences in the metabolism of free and immobilized cells of yeast strain *Saccharomyces cerevisiae S-33*. Similarly, the proposed model described with high accuracy the experimental data, but the similar problems as with yeast strain S-23 were observed.

These problems are connected with the microbiological aspects of fermentation and some physicochemical processes during the fermentation which have to be taken into account in the modeling. The problems will be discussed in groups, because the mathematical model was created in the same way.

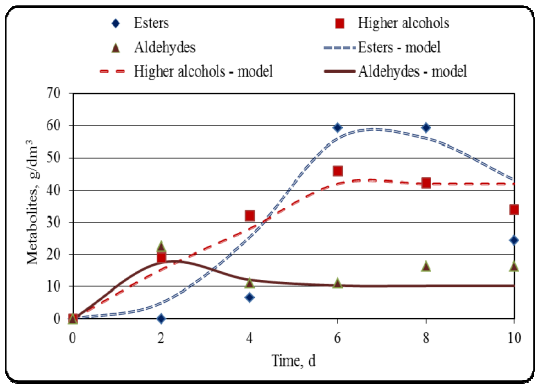

a) free cells; original extract 9%

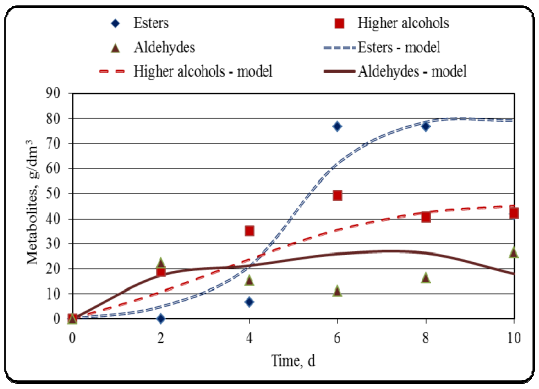

b) immobilized cells; original extract 9%

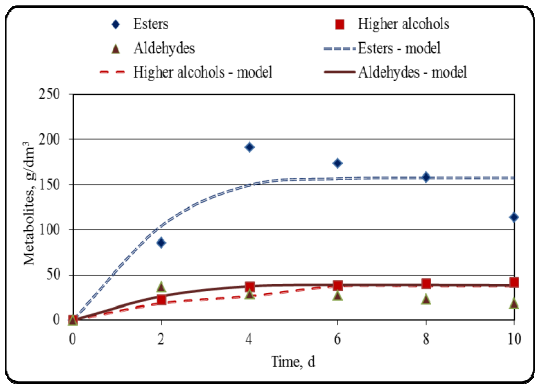

c) free cells; original extract 11%

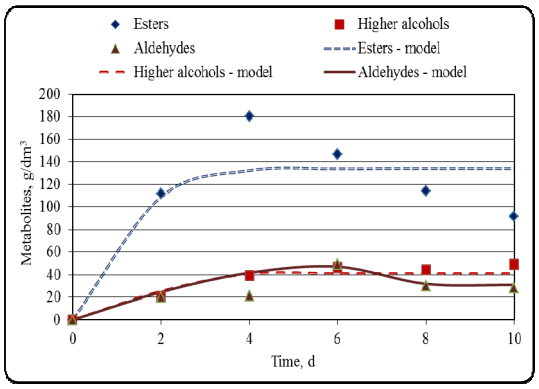

d) immobilized cells; original extract 11%

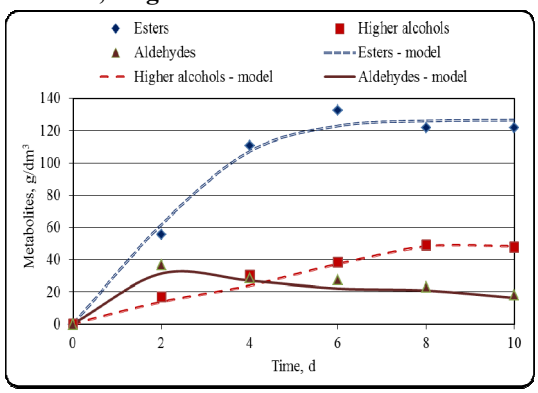

e) free cells; original extract 13%

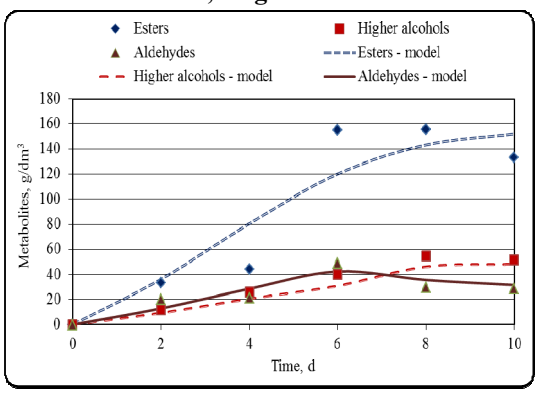

f) immobilized cells; original extract 13%

Figure 1 Experimental data and mathematical models for esters, higher alcohols and aldehydes during beer fermentation with free and immobilized cells of yeast strain Saccharomyces pastorianus S-23

Esters

The esters synthesis dynamics was similar for the free and the immobilized cells of yeast strain *S. cerevisiae S-33*. It should be mentioned that the immobilized cells accumulated more esters than free cells at low original wort extracts - 9% and 11%. The increase in original wort extract resulted in increased ester concentration for free cells than immobilized ones. The immobilized cells of yeast strain *S. pastorianus S-23* produced more esters than free cells. The amount of esters increased with the

increase of original wort extract. The mathematical models for both strains confirmed the experimental data. It should be highlighted that the immobilized cells accumulated a little more esters at lower original wort extracts. It can be explained that immobilization induces the inhibition of fatty acid synthesis, resulting in an accumulation of acyl-CoA that together with high levels of ethanol in immobilized cell systems enhance ethyl acetate formation (Shen et al., 2003). Furthermore, higher original wort extract limits oxygen solubility in wort, which also leads to increased ester synthesis (Dufour et al., 2003).

The major disadvantage of the mathematical model is that it does not take into account the chemical reduction (hydrolysis) of esters due to some physicochemical processes.

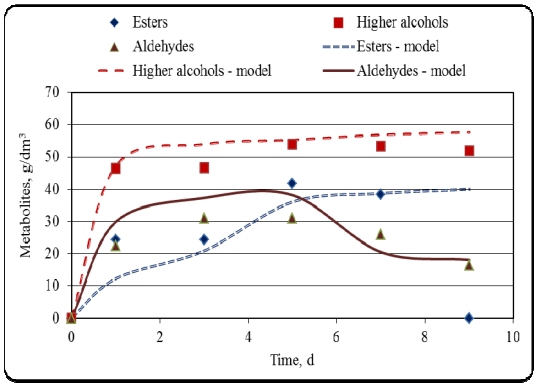

a) free cells; original extract 9%

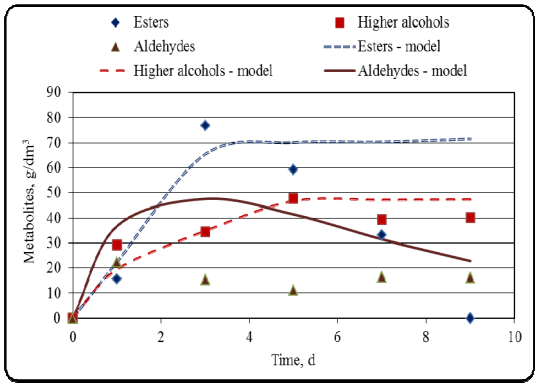

b) immobilized cells; original extract 9%

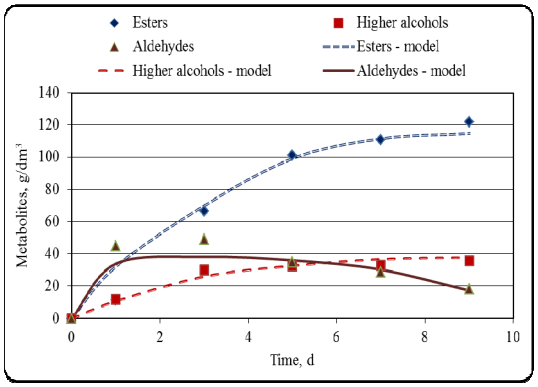

c) free cells; original extract 11%

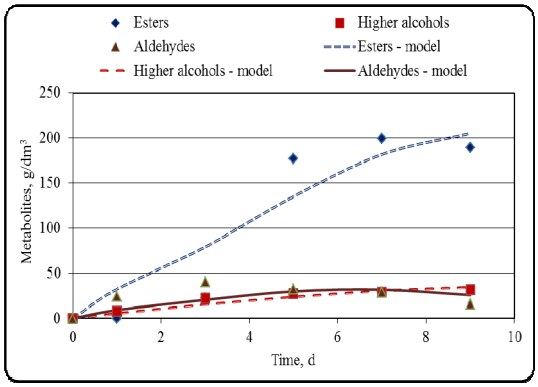

d) immobilized cells; original extract 11%

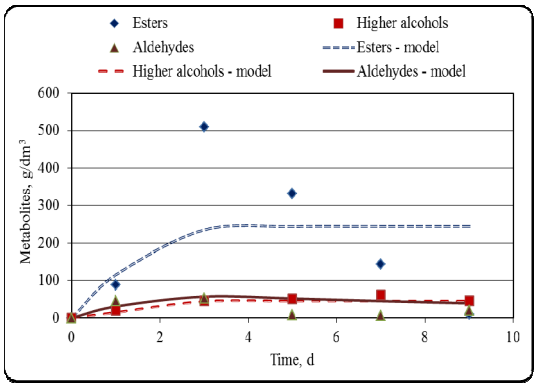

e) free cells; original extract 13%

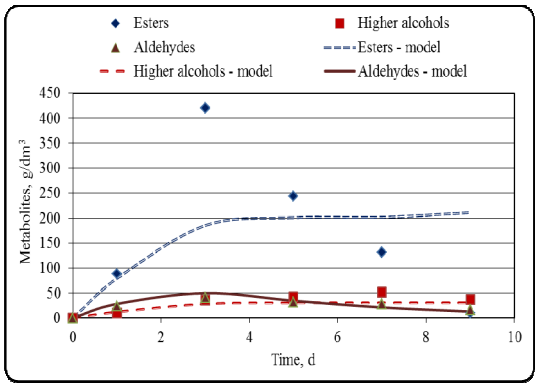

f) immobilized cells; original extract 13%

Figure 2 Experimental data and mathematical models for esters, higher alcohols and aldehydes during beer fermentation with free and immobilized cells of yeast strain Saccharomyces cerevisiae S-33

Higher alcohols

The immobilized cells produced more fusel alcohols than the free ones of yeast strain *S. pastorianus S-23.* The value of η_μ (Table 2) confirms the suggestion that rapid yeast growth of immobilized cells leads to enhanced anabolic production of amino acid precursors with concomitant synthesis of higher alcohols (Willaert and Nedovic, 2006). Decreased higher alcohol production by immobilized cells as opposed to free cell fermentation was shown in Figure 2. Mass (i.e. amino acids) transfer limitations results in decreased higher alcohol synthesis (Willaert and Nedovic, 2006). Table 2 shows that reduced synthesis of higher alcohols was observed for the majority of the studied variants with immobilized cells. The reduction varied between 8 and 68%. However, two of studied variants showed

enhanced synthesis of higher alcohols. It can be attributed to the diffusion resistances and the local changes in the diffusion coefficients of metabolites. The proposed mathematical model describes the experimental data with high accuracy and takes into account all the specificities of the fermentation process.

Aldehydes

There were significant differences in the aldehyde synthesis and reduction by immobilized and free cells. The free cells of both yeast strains showed distinct maximum of aldehydes, whereafter the aldehydes reduction started. On the other hand, the aldehyde peaks were not so distinct for the immobilized cells and the aldehydes concentration was relatively constant during fermentation. The explanation for this difference can be found in the kinetic parameters (Table 1 and Table 2). The specific rate of aldehydes synthesis of almost all immobilized cells of yeast strain *S. pastorianus* S-23 was higher than the one of free cells. It decreased with the increase of original wort extract. The specific rate of aldehydes synthesis of immobilized cells of yeast strain *S. cerevisiae* S-33 varied with different original wort extracts. The differences can be determined by the diffusion resistance, which are different in each case of fermentation.

Table 2

Efficiency coefficients for the description of fermentation with immobilized cells

Original extract	η_{μ} *	η_{q} *	η_{e}	η_{fa}	η_{a}	η_{ka}
	mg/(g.d)				-	
***Saccharomyces pastorianus* S-23**						
9%	0.708	1.350	1.065	0.373	2.105	0.891
11%	2.564	2.724	1.239	1.641	1.562	3.500
13%	1.339	1.276	0.520	0.599	0.536	2.052
***Saccharomyces cerevisiae* S-33**						
9%	1.248	0.914	1.305	0.923	0.665	1.333
11%	0.918	0.695	0.629	0.322	0.422	1.507
13%	0.559	0.879	0.827	1.201	1.173	1.776

*** according to Parcunev et. al., 2012**

The specific rate of aldehydes reduction depends on the current aldehydes concentration in beer and the biomass concentration in the working volume of the reactor. Table 2 shows that almost all specific rates of aldehydes reduction of immobilized cells were between 1.3 and 3.5 times higher than the ones of free cells. There was an exception with similar values of specific rates of aldehydes reduction between free and immobilized cells. It can be concluded that leads to the observed differences in this fermentation. Rapid reduction of aldehydes resulted in the retention of almost constant concentration of these compounds in beer produced with immobilized cells. At the end of fermentation the aldehyde concentration in all beers varied between 20 and 40 mg/dm^3.

The specific rate of aldehydes reduction can be increased by the increase of the temperature at the end of the fermentation process (maturation).

As it was previously mentioned, another group of compounds - vicinal diketones affects the beer flavor profile. Their synthesis is associated with yeast growth and their reduction has two stages - chemical and biochemical. The biochemical synthesis and reduction of vicinal diketones can be described with a similar model as equation (6). The chemical reduction depends on fermentation and maturation temperature, the mass transfer, the ethanol concentration in the beer, and etc. The modeling of synthesis and reduction of vicinal diketones will be the subject of further investigations.

The results of experimental and model data showed that the immobilization had no significant effect on the yeast metabolism. The flavor profile of beers produced with immobilized and free cells was comparable because the concentrations of the main groups of yeast by-products were similar. The observed differences in the synthesis and reduction of the main groups of metabolites had no effect on the beer quality. It can be suggested that the chosen carrier for immobilization was proper for implementation in beer technology because it did not affect the fermentation.

CONCLUSION

A mathematical model for the description of the synthesis and reduction of main flavor-active yeast by-products - esters, aldehydes and higher alcohols was developed and validated. The model described with high accuracy the beer fermentations with immobilized and free cells and confirmed the experimental data. Moreover, the results were in accordance to the previous study (Parcunev et al, 2012) and showed the impact of immobilization on the fermentation activity and metabolism of the yeast. The model did not take into account some biochemical and physicochemical processes during fermentation, but they are not essential for its accuracy.

ACKNOWLEDGEMENTS

This work was partially supported by the National Science Fund under the Project No DTK 02/27 “Increasing the efficiency of bio-fuel purpose ethanol production”. Our team expresses our sincere thanks to the brewery "Kamenitza" - Plovdiv for the supply of wort.

LIST OF SYMBOLS

X(t) – biomass concentration, g/dm^3; P(t) – ethanol concentration, g/dm^3; S(t) – substrate (extract) concentration, g/dm^3; μ - biomass specific growth rate, h^{-1}; μ_{max} – maximal biomass specific growth rate, h^{-1}; q_p – ethanol specific accumulation rate, g/(g.h); q_{pmax} – ethanol specific accumulation rate, g/(g.h); K_{SX} – Monod constant for the substrate, g/dm^3; K_{SP} – Monod constant for the product,

g/dm^3; FA – fusel (higher) alcohol concentration, g/dm^3; E – esters concentration, g/dm^3; A – aldehydes concentration, g/dm^3; $Y_{X/S}$ – yield coefficient biomass from glucose; $Y_{P/S}$ - yield coefficient ethanol from glucose; Y_{FA} – yield coefficient for fusel alcohols, mg/(g.d); Y_E – yield coefficient for esters, mg/(g.d); Y_A – yield coefficient for aldehyds, mg/(g.d); k_A – reduction coefficient for aldehydes, mg/(g.d); η – efficiency coefficient; ($_{\mu,\ q,\ FA,\ E,\ Al,\ KAL}$ denotes the experimental parameters) E(r) – error between the experimental and model data; free – free cells fermentation; imm – immobilized cells fermentation;

REFERENCES

Branyik, T.; A. Vicente; P. Dostalek; and J.A. Teixeira. 2005 "Continuous beer fermentation using immobilized yeast cell bioreactor systems", *Biotechnol. Prog.*, 21, 653-663

Briggs, D.; C. Boulton; P. Brookes; and R. Stevens. 2004. *Brewing science and practice*, Woodhead publishing in food and science, CRC Press

Boulton C. and D. Quain 2001. "Brewing yeast and fermentation." *Blackwell Science*, ISBN 0-632-05475-1

Engan, S., 1981."Beer composition: volatile substances", In: Pollock, J.R.A (editor) Brewing Science,., *Academic Press*, vol. 2, p.98-105.

Dufour, J.-P. , Malcorps, Ph., Silcock, P., 2003 "Control of ester synthesis during brewery fermentation, In: Brewing yeast and fermentation performance", Smart, K. (Editor), *Blackwell Science*, 213-234

Handbook of brewing: Processes, Technology, Markets. 2009. Hans Michael Esslinger (ed.), ISBN 978-3-527-31674-8, *WILEY-VCH Verlag GmbH & Co. KGaA,* Weinheim

Kostov G.; S. Popova; V. Gochev; P. Kpoprinkova-Hristova; M. Angelov. 2012. "Modeling of batch alcohol fermentation with free and immobilized yeasts Saccharomyces cerevisiae 46 EVD." *Biotechnology and Biotechnological equipment*, ISSN 1310-2818, Vol. 26, 3, doi: 10.5504/bbeq.2012.0025

Kunze W. 2003. "Technology of brewing and malting, 3rd edition", ISBN 3-921690-49-8, *VLB-Berlin*

Marinov M. 2010. "Practice for analysis and control of alcohol beverages and ethanol", *Academic Publisher of UFT*, ISBN 987-954-24-0150-6, p. 196 (in bulgarian)

Meilgaard, M. 1975. "Flavour chemistry of beer. Part 2: Flavour and threshold of 239 aroma volatiles", *Technical Quarterly of the Master Brewers Association of the Americas,* 12, 151-168.

Mitev S.V.; S. B. Popova. 1995. "A model of yeast cultivation based on morphophysiological parameters." *J. Chemical and Biochemical Engineering Quarterly*, 3, Zagreb, 119-121.

Parcunev, I, V. Naydenova; G. Kostov; Y. Yanakiev, Zh. Popova; M Kaneva; I. Ignatov, 2012. "Modelling of alcoholic fermentation in brewing – some practical approaches". In: Troitzsch, K. G, Möhring., M. and Lotzmann, U. (Editors), Proceedings 26th European Conference on Modelling and Simulation, ISBN: 978-0-9564944-4-3, pp. 434-440

Popova S. 1997. "Parameter identification of a model of yeast cultivation process with neural network", Bioprocess and Biosystems Engineering, 16(4), 243-245, DOI: 10.1007/s004490050315

Ramirez W.F., Maciejowski, J. 2007. "Optimal beer fermentation" J. Inst. Brew. 113(3), 325–333

Rusell I., 2006, "Yeast", In: Priest F.G. and Stewart G.G (Editors) Handbook of brewing, *Taylor & Francis Group*, LLC, 281-333

Shen H.-Y., Moonjai N., Verstrepen K., Delvaux F., 2003. "Impact of attachment immobilization on yeast physiology and fermentation performance". *J. Am. Soc. Brew. Chem*., 61(2), 79-87

Willaert R., 2007." The beer brewing process: wort production and beer fermentation". In: Y.H. Hui (Editor) Handbook of food products manufacturing, *John Wiley & Sons, Inc*., Hoboken, New Jersey, 443-507

Willaert R., Nedovic, V. 2006. "Primary beer fermentation by immobilised yeast – a review on flavour formation and control strategies". *J Chem Technol Biotechnol*, 81, 1353–136

AUTHOR BIOGRAPHIES

GEORGI KOSTOV is associated professor at the department "Technology of wine and brewery" at University of Food Technologies, Plovdiv. He received his MSc in "Mechanical engineering" in 2007 and PhD on "Mechanical engineering in food and flavor industry. His research interests are in the area of bioreactors' construction, biotechnology, microbial population's investigation and modeling, hydrodynamics and mass transfer problems, fermentation kinetics.

SILVIA POPOVA. Associate Professor Dr. Silviya Popova received her MSc in mathematics from University of Sofia, Bulgaria (1977) and PhD on "New methods for automatization of videomicroscopy microbiological investigation" from the Bulgarian Academy of Sciences (2001). Her research interests are in modeling and identification of biotechnological processes, estimation and control of biotechnological processes, adaptive control, neural networks and image processing.

VESSELA NAYDENOVA is a PhD student at the department "Technology of wine and brewery" at University of Food Technologies, Plovdiv. Her research interests are in the area of beer fermentation with free and immobilized cells; yeast specification and fermentation activity. The PhD thesis is named "Possibilities for beer production with immobilized yeast cells"

VASIL ILIEV is a PhD student at the department "Technology of wine and brewery" at University of Food Technologies, Plovdiv. His research interests are in the area immobilized cells reactors modeling and application. The PhD thesis is named "Intensification of the processes in column bioreactor with immobilized cells"

MARIA KANEVA is assistant professor at the department "Technology of wine and brewery" at University of Food Technologies, Plovdiv. Her research interests are in the area on non-alcoholic beverages, herbal extracts for beverages, modeling of extraction processes.

STOYAN VASSILEV is a student at the department "Technology of wine and brewery". His bachelor degree thesis is on the subject of "Investigation on alcoholic fermentation for obtaining beer with free and immobilized top fermented yeast"

MARIANA BADOVA is a student at the department "Technology of wine and brewery" at University of Food Technologies, Plovdiv. Her bachelor degree thesis is on the subject of "Investigation on alcoholic fermentation for obtaining beer with free and immobilized bottom fermented yeast"

DATABASE OF UNSTABLE SYSTEMS: A NEW SITE FOR MODELS OF UNSTABLE PROCESSES

František Gazdoš and Jaroslav Kolařík
Faculty of Applied Informatics
Tomas Bata University in Zlin
Nam. T. G. Masaryka 5555, 760 01 Zlin, Czech Republic
E-mail: gazdos@fai.utb.cz

KEYWORDS
Unstable systems, Modelling, Simulation, Web, Database.

ABSTRACT

The paper presents a new site for unstable systems which can be used as an information database about unstable processes and stability. It is an open, easily extensible system in the bilingual version (ENG/CZ) containing mathematical models of real unstable processes together with their simulation models in e.g. MATLAB/Simulink environment. Basic information about stability of dynamical systems is also included. This contribution outlines motivation for development of this site, presents its basic structure and suggests areas of prospective use. Several models of unstable processes from the site are also presented and discussed briefly.

INTRODUCTION

Many industrial processes, such as various types of reactors, combustion systems, distillation columns, etc. possess unstable behaviour (Chidambaram 1997; Padma Sree and Chidambaram 2006). Besides industrial, aviation and military areas, there are also many systems and processes in the environmental and social fields that are naturally unstable. Experiments with such systems without proper knowledge can be hazardous (Stein 2003). Designers and control engineers have to understand basic limitations that stem from the process instability (Middleton 1991; Skogestad et al. 2002). Therefore, modelling and simulation tools play an important role in this area. Before a decision is made and implemented on a real unstable process, a proper simulation analysis has to be done in order to ensure safe implementation.

The presented site has been developed to enable students, teachers, scientist, control engineers and many others interested in unstable processes easy access to mathematical models of such systems. All these people can easily use presented models for their own simulation experiments, testing control algorithms, etc. This will broaden awareness about unstable processes and problems they cause. Due to the fact that the database is easily accessible via the Internet (located at http://www.unstable-systems.cz) it can be used by wide range of users for various purposes, e.g. pedagogical, scientific and others.

This paper is structured as follows: after a brief introduction into the stability of dynamical systems the contribution continues by examples of unstable processes including their simplified mathematical models. Further, a basic structure of the developed site is outlined and explained and the paper concludes suggesting possible extensions of the project.

STABILITY OF DYNAMICAL SYSTEMS

Stability is the fundamental required property of control systems. Therefore a great deal of effort has been focused towards proper definition, testing and attainment of system stability.

Defining Stability

Although all people naturally understand the concept of stability and are able to describe what stable behaviour is and what is not, as outlined in e.g. Fig. 1, a proper mathematical definition is not so straightforward. Generally, stability can be formulated as ability to recover from perturbations – short-time disturbances or non-zero initial conditions.

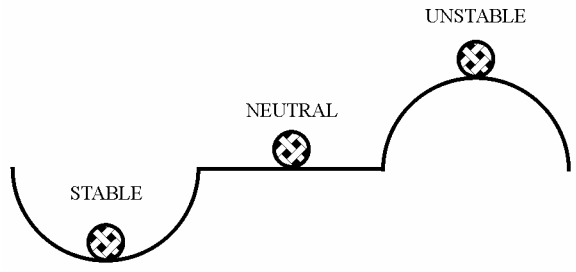

Figure 1: Basic Understanding of Stability – Ball in the Gravitational Field

One of the definitions says that a system is stable if bounded input into the system produces a bounded output from the system. This is so called *BIBO* (Bounded Input – Bounded Output) *stability*, e.g. (Willems 1970; Skogestad and Postlethwaite 2005), illustrated in Fig. 2-3 where examples of some typical step-responses of stable and unstable systems are presented.

Proceedings 27th European Conference on Modelling and Simulation ©ECMS Webjørn Rekdalsbakken, Robin T. Bye, Houxiang Zhang (Editors)
ISBN: 978-0-9564944-6-7 / ISBN: 978-0-9564944-7-4 (CD)

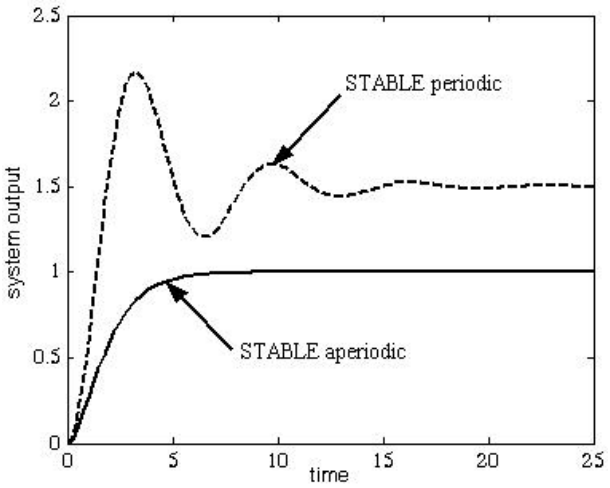

Figure 2: Stable Systems Responses

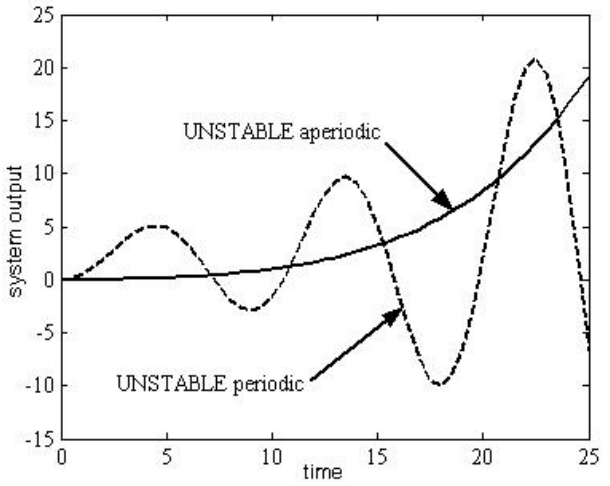

Figure 3: Unstable Systems Responses

Another recognized and more general definition is the *Lyapunov stability*, e.g. (Willems 1970; Parks 1992; Skogestad and Postlethwaite 2005; Åström and Murray 2008). It states, simply speaking, that a system is Lyapunov stable if its output and all states are bounded and converge asymptotically to zero from a sufficiently small initial conditions. Its concept in the state-space (for two states) is graphically illustrated in Fig. 4.

Testing Stability

During the decades many methods of stability testing have been developed. Usage of a particular method depends on the properties of the system to be tested – e.g. if it is linear or nonlinear, continuous-time or discrete-time, time-variant or time-invariant, etc. The methods can be both numerical and graphical. An interested reader can found details in books focused on systems theory or control engineering, e.g. (Willems 1970; Skogestad and Postlethwaite 2005; Åström and Murray 2008; Doyle et al. 2009).

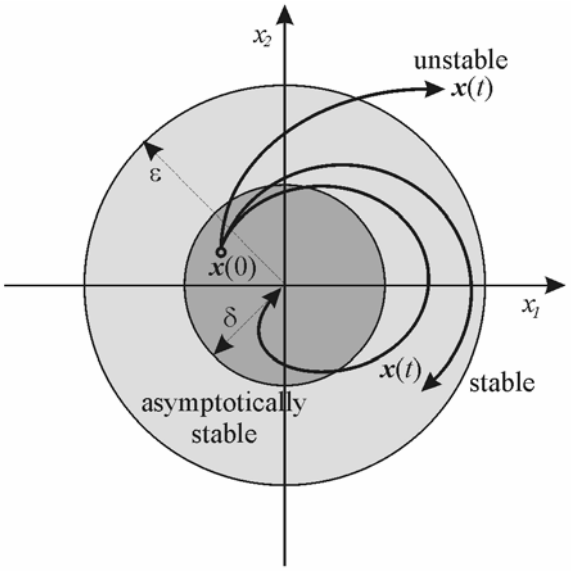

Figure 4: Lyapunov Stability

Attainment of Stability

An unstable system can be stabilized by feedback. There many sources focused on the control system design for unstable processes, e.g. (Chidambaram 1997; Park et al. 1998; Marchetti et al. 2001; Lozano et al. 2004; Padma Sree and Chidambaram 2006; García et al. 2006; Dostál et al. 2008). Many of these works solve the control system design problem connected also with delayed and non-minimum-phase systems which are also problematic to control.

Besides testing and attainment of stability it is often important to test and ensure certain measure of stability, i.e. *relative stability* which gives answer to the question how far the system is from instability. For control systems design, so called *gain* and *phase margins* are frequently used, for details see e.g. (Skogestad and Postlethwaite 2005; Åström and Murray 2008; Doyle et al. 2009).

The so-called *robust stability* is next important term in control engineering. It is used for the case we want to test/achieve stability not only for one system but for a certain class of systems, typically a nominal system and some neighbourhood, which is useful in the case of uncertain models. An interested reader is referred to books devoted to the robust systems design, e.g. (Barmish 1994; Bhattacharyya et al. 1995).

EXAMPLES OF UNSTABLE SYSTEMS

As explained in the introduction section unstable processes are common in many areas of our daily lives. Several such systems are briefly described in this section. Mathematical models together with simulation files and original sources are also available online from the developed site (Gazdoš and Kolařík 2012).

Nonideal CSTR

This process is represented by a continuous stirred-tank reactor (CSTR) with nonideal mixing decribed by the Cholette's model. The process can be sketched as illustrated in Fig. 5.

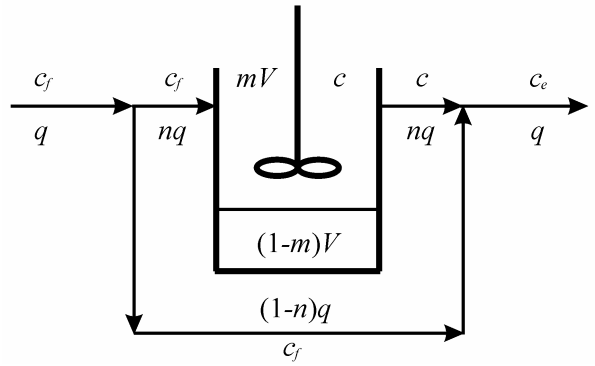

Figure 5: Schematic Representation of a Nonideal CSTR

A simplified mathematical model of the process dynamics can be expressed by these formulas (Liou and Chien 1991; Padma Sree and Chidambaram 2006):

$$\frac{dc(t)}{dt} = \frac{nq}{mV}\left[c_f(t) - c(t)\right] - \frac{k_1 c(t)}{\left[1 + k_2 c(t)\right]^2}. \qquad (1)$$
$$nc(t) + (1-n)c_f(t) = c_e(t)$$

In the picture and equations, $c(t)$ is the concentration of the reactant in the well mixed zone, $c_e(t)$ is the concentration in the exit stream (controlled variable) and $c_f(t)$ is the feed concentration (manipulated variable). Further, n is the fraction of the reactant feed that enters the zone of perfect mixing and m is the fraction of the reactor total volume V where the reaction occurs. Constants k_1, k_2 describe the reaction rate and q is the inlet flow rate. Parameters of the model are presented in the first part of Table 1 below; its second part describes values of the input, output and state variables in a nominal operating point.

Table 1: Parameters of the Nonideal CSTR

Symbol	Value [unit]
n	0.75 [-]
m	0.75 [-]
V	1 [l]
q	0.033 [l/s]
k_1	10 [s^{-1}]
k_2	10 [l/mol]
c_f	6.484 [mol/l]
c_e	1.8 [mol/l]
c	0.2387 [mol/l]

Linearization of the model (1) around the given nominal operating point gives the transfer function model as:

$$\frac{\Delta c_e(s)}{\Delta c_f(s)} = \frac{0.7725s - 0.1727}{3.1s - 1}. \qquad (2)$$

A state-space representation of the linearized model in the general form:

$$\begin{aligned} \boldsymbol{x}'(t) &= \boldsymbol{A}\boldsymbol{x}(t) + \boldsymbol{B}\boldsymbol{u}(t) \\ \boldsymbol{y}(t) &= \boldsymbol{C}\boldsymbol{x}(t) + \boldsymbol{D}\boldsymbol{u}(t) \end{aligned}, \qquad (3)$$

where $\boldsymbol{x}(t)$ defines a vector of state variables, $\boldsymbol{y}(t)$ a vector of output variables and $\boldsymbol{u}(t)$ a vector of input variables can be obtained e.g. in this form (using the MATLAB function *ssdata*):

$$\begin{aligned} &\boldsymbol{A} = [0.3226],\ \boldsymbol{B} = [0.1250], \\ &\boldsymbol{C} = [0.1974],\ \boldsymbol{D} = [0.2492]. \end{aligned} \qquad (4)$$

In the case of the presented reactor the variables $\boldsymbol{x}(t)$, $\boldsymbol{y}(t)$ and $\boldsymbol{u}(t)$ are only scalar and correspond to the reactor variables $c(t)$, $c_e(t)$ and $c_f(t)$ respectively (consequently $\boldsymbol{A}, \boldsymbol{B}, \boldsymbol{C}, \boldsymbol{D}$ are also only scalars).
From the control theory point of view, the models (2)-(4) represent a first-order proper system which is unstable (one positive *pole*, i.e. denominator root, located at $p_1 = 0.3226$) with non-minimum-phase behaviour (one positive *zero*, i.e. numerator root, located at $z_1 = 0.2236$), and with gain $k = 0.1727$ [-]. Such systems which are both unstable and non-minimum-phase are not so easy to control. The step-response of the model recorded in Fig. 6 clearly demonstrates instability of the system.

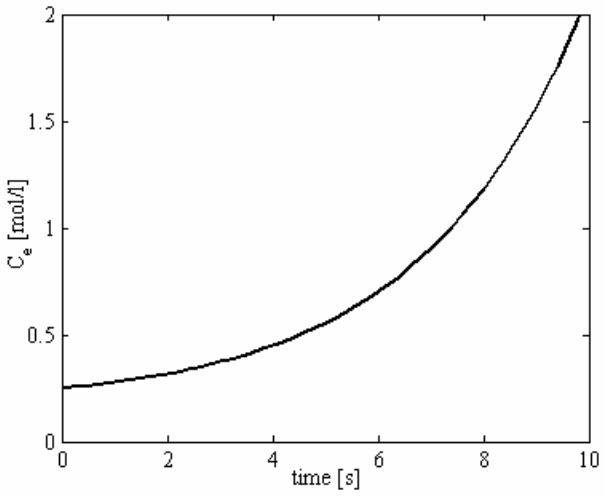

Figure 6: Nonideal CSTR Step-Response

Ballistic Missile

A ballistic missile sketched simply in Fig. 7 can represent another unstable system from the military industry. Although it is completely different from the previous one, it shares the property of instability and consequently problematic control.

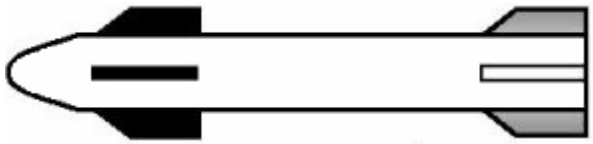

Figure 7: Ballistic Missile

When controlling altitude of the ballistic missile, the transfer function relating the altitude $y(t)$ to the thrust chamber deflection $\delta(t)$ has the following form (Blakelock 1991; Padma Sree and Chidambaram 2006):

$$\frac{\Delta y(s)}{\Delta \delta(s)} = \frac{7.21(s+0.0526)}{(s+1.6)(s-1.48)(s-0.023)}. \qquad (5)$$

Its state-space representation in the general form (3) can be obtained e.g. as (MATLAB function *ssdata*):

$$\boldsymbol{A} = \begin{bmatrix} -0.0970 & 1.1854 & -0.0545 \\ 2 & 0 & 0 \\ 0 & 0.5 & 0 \end{bmatrix}, \boldsymbol{B} = \begin{bmatrix} 2 \\ 0 \\ 0 \end{bmatrix}, \qquad (6)$$
$$\boldsymbol{C} = [0 \quad 1.8025 \quad 0.1896], \boldsymbol{D} = [0].$$

From the control theory point of view the missile represents a strictly proper unstable system of 3rd order. The instability is given by the two poles (denominator roots) located in the right half of the complex plane ($p_1 = 0.023$, $p_2 = 1.48$), as illustrated in Fig. 8 where the *Pole-Zero Map* is presented. The system also has relatively fast dynamics with time-constants in seconds.

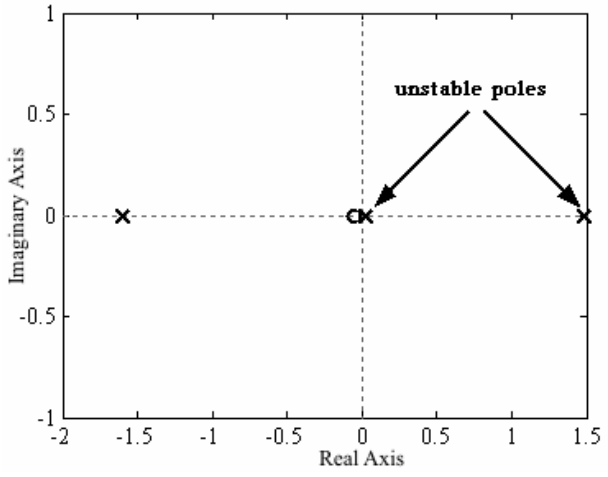

Figure 8: Pole-Zero Map of the Ballistic Missile

X-29 Aircraft

The X-29 sketched in Fig. 9 was an experimental aircraft that tested forward-swept wing, canard control surfaces, and other novel aircraft technologies. It was deliberately designed with static instability to increase its maneuverability and speeds of command response. However, as a consequence, it was impossible to pilot this airplane conventionally by manual flight controls and it required the use of so-called fly-by-wire (computerized) control system. In addition special hardware (sensors, control processors and actuators) had to be used in order to stabilize the system over all flight regimes and all loading conditions. Considerable effort has been devoted to the design of flight control system for this airplane, e.g. (Rogers and Collins 1992; Clarke et al. 1994; Stein 2003).

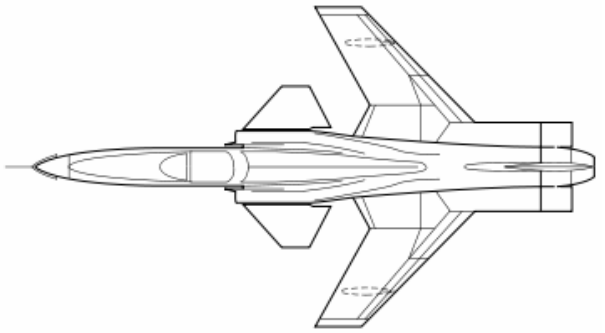

Figure 9: X-29 Aircraft

The benefits of instability (better maneuverability and faster reaction) were desired in the transonic and supersonic flight regimes, so the airplane was designed to be modestly unstable in those regimes. However, due to a basic aerodynamic phenomenon the X-29's slight instability at supersonic speeds turned into a much more dramatic instability at subsonic speeds. A simplified linearized model at one such flight condition given by a transfer function has the following form:

$$G(s) = \frac{s-26}{s-6}. \qquad (7)$$

As can be clearly seen, the airplane's real pole (denominator root) is as large as +6 rad/s which makes this system nearly impossible to control manually – it can be compared, simply speaking, to balancing a 1-ft-long stick (Stein 2003). Besides the unstable pole the systems has also strong non-minimum-phase behaviour, i.e. inverse response (a *zero* – numerator root, located at $z_1 = 26$). These facts make this system very difficult to control. State-space realization in the general form (3) can be obtained e.g. as (MATLAB function *ssdata*):

$$\boldsymbol{A} = [6], \boldsymbol{B} = [4], \qquad (8)$$
$$\boldsymbol{C} = [-5], \boldsymbol{D} = [1].$$

Next figure (Fig. 10) shows sensitivity function $S(\omega)$ of a X29 prototype.

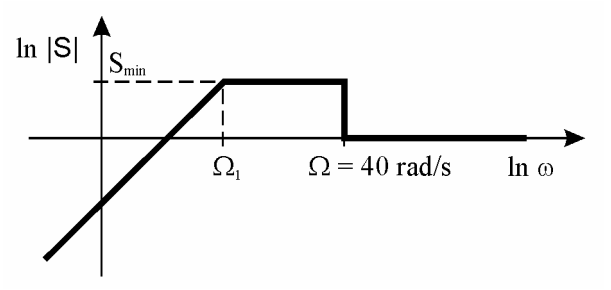

Figure 10: X-29 Sensitivity Function

From the plot it can be seen that the system has considerably limited bandwidth (up to 40 rad/s) which is given by the used HW components (sensors, control processors, actuators), airplane mechanical structure and aerodynamics conditions. Consequently it narrows possibilities of convenient control system design.

All here discussed models are available online at the presented site (Gazdoš and Kolařík 2012) with short description, downloadable model in the MATLAB/ Simulink environment and selected references related to modelling, simulation, control system analysis and design of the processes/systems. Next section briefly presents main structure of the site devoted to unstable systems and outlines main possibilities it offers.

SITE STRUCTURE AND POSSIBILITIES

The database of unstable system has been developed as an open, easily extensible system in the bilingual version (English/Czech). It is easily accessible on-line at the web-address http://www.unstable-systems.cz. A starting version of the site was implemented within the final work (Kolařík 2012) using a free and open source content management system Joomla! of the 2.5 version, available online at http://www.joomla.org and described in e.g. (Marriott and Waring 2013). This makes administration of the site very easy. Basic structure of the web is presented in Fig. 11. Apart from this there are also user-related services such as registration, profile editing and web administration.

HOME Bookmark

The *HOME* bookmark is the starting point of the site. It introduces a purpose of the site, enables registration, shows latest news and recent posts together with simple statistics and some useful links. Registered users have the following possibilities:

- access to files with simulation models of the systems
- access to latest news via a newsletter
- possibility of articles rating
- possibility to add comments to the systems models

It is also possible to search within the site and change language (ENG/CZ) here.

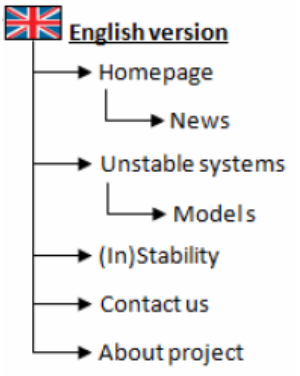

Figure 11: Basic Structure of the Website

UNSTABLE SYSTEMS Bookmark

This bookmark is the main part of the site which contains mathematical models of unstable processes. So far (March 2013) it contains following models:

- ballistic missile
- fluidized bed reactor
- inverted pendulum
- magnetic levitation system
- nonideal continuous stirred-tank reactor
- X-29 aircraft

Every model has the following information:

- brief description of the system
- scheme of the process or picture of the system
- simplified mathematical model
- definition of used variables and parameters
- downloadable model in e.g. MATLAB/Simulink environment
- sources of further information

It is also possible to generate a printable version of the models or send a link of a model by e-mail. Registered users can download the simulation models, add comments and rate them. Besides this it is also possible to search within the models and sort them.

(IN)STABILITY Bookmark

This part of the site explains basics about stability of systems – general understanding of the term, several definitions, such as *BIBO* (Bounded Input – Bounded Output) and *Lyapunov* stability. It also offers further reading on this subject.

Next bookmark *CONTACT US* enables to send questions, suggestions and remarks, etc. on the site and models to the authors. The final bookmark *ABOUT PROJECT* briefly introduces basic information about this project including main authors, brief description and terms of use.

CONCLUSIONS

Modelling and simulation tools play important roles in our lives nowadays. In the case of unstable systems analysis and control design, they role is crucial, however. Experiments with such systems without the proper knowledge about possible consequences can be very hazardous. The goal of this contribution is to present a starting project of the web-based database of unstable systems. This site can help students, teachers, designers, scientists and many others to understand basic properties of unstable systems. This is done via available models of the systems and suggested further readings. The developed web-site is an open, constantly developing system which is still "under construction". Therefore experiences of users, their remarks, suggestions and comments are welcome.

Further development of the site will be focused on the completing an extension of the given information concerning the systems stability, description of the models and suggested further readings. The number of available unstable systems models will of course grow as well as the number of simulation files (not necessarily limited to the MATLAB/Simulink environment). Another interesting extension can be seen in the possibility to implement simulation directly into the site, e.g. using the popular *Easy Java Simulations* open-source software tool. At the moment only the site administrator can add articles into the system. The possibility to do this by registered users is also being considered, which would help to develop the database.

REFERENCES

Åström, K.J. and R.M.Murray. 2008. *Feedback Systems: An Introduction for Scientist and Engineers*. Princeton University Press.

Barmish, B.R. 1994. *New Tools for Robustness of Linear Systems*. Macmillan.

Bhattacharyya, S.P.; H. Chapellat, and L.H. Keel. 1995. *Robust Control-The Parametric Approach*. Prentice-Hall.

Blakelock, J.H. 1991. *Automatic Control of Aircraft and Missiles*. John Wiley, New York.

Chidambaram, M. 1997. "Control of unstable systems: a review." *J. energy, heat and mass transfer*, No.19,49-57.

Clarke, R.; J.J. Burken; J.T. Bosworth and J.E. Bauer. 1994. "X-29 flight control system – lessons learned." *Int. J. Control* 59, No.1,199-219.

Dostál, P.; F. Gazdoš and V. Bobál. 2008. "Design of controllers for time delay systems - part II: integrating and unstable systems." *Journal of el. engineering*, No.59, 3-8.

Doyle, J.C.; B.A. Francis and A.R. Tannenbaum. 2009. *Feedback Control Theory*. Dover Publications.

García, P.; P. Albertos and T. Hägglund. 2006. "Control of unstable non-minimum-phase delayed systems." *Journal of Process Control*, No.16, 1099-1111.

Gazdoš, F. and J. Kolařík. 2012. *Database of unstable systems* [online]. Available at: http://www.unstable-systems.cz

Kolařík, J. 2012. Web-based Database of Unstable Systems. *Bachelor's thesis*. Tomas Bata University in Zlín, CZ.

Liou, C.T. and Y.S. Chien. 1991. "The effect of nonideal mixing on input multiplicities in a CSTR." *Chem. Eng. Sci.*46, 2113-2116.

Lozano, R.; P. Castillo; P. Garcia and A. Dzul. 2004. "Robust prediction-based control for unstable delay systems: application to the yaw control of a mini-helicopter." *Automatica*, No.40, 603-612.

Marchetti, G.; C. Scali and D.R. Lewin. 2001. "Identification and control of open-loop unstable processes by relay methods." *Automatica*, No.37, 2049-2055.

Marriott, J. and E. Waring. 2013. *The official Joomla! Book*. Addison-Wesley Professional.

Middleton, R.H. 1991. "Trade-offs in linear control system design." *Automatica*, No.27, 281-292.

Padma Sree, R. and M. Chidambaram. 2006. *Control of unstable systems*. Alpha science Int. Ltd., Oxford.

Park, Sung and Lee. 1998. "An enhanced PID control strategy for unstable processes." *Automatica*, No.34, 751-756.

Parks P.C. 1992. "A.M. Lyapunov's stability theory - 100 years on." *IMA Journal of Mathematical Control & Information* 9, No.4, 275-303.

Rogers and Collins. 1992. "X-29 H_∞ controller synthesis." *J. Guidance control and dynamics* 15, No.4, 962-967.

Skogestad, S.; K. Havre and T. Larsson. 2002. "Control limitations for unstable plants". In *Proc. 15th Triennial World Congress* (Barcelona, Jul.21-26). IFAC, 485-490.

Skogestad and Postlethwaite. 2005. *Multivariable Feedback Control: Analysis and Design*. Wiley, Chichester.

Stein, G. 2003. "Respect the unstable, IEEE Control system magazine." No. 23, 12-25.

Willems, J.L. 1970. *Stability Theory of Dynamical Systems*. Wiley, New York.

AUTHOR BIOGRAPHIES

FRANTIŠEK GAZDOŠ was born in Zlín, Czech Republic in 1976, and graduated from the Brno University of Technology in 1999 with MSc. degree in Automation. He then followed studies of Technical Cybernetics at Tomas Bata University in Zlín, obtaining Ph.D. degree in 2004. He became Associate Professor for Machine and Process Control in 2012 and now works in the Department of Process Control, Faculty of Applied Informatics of Tomas Bata University in Zlín, Czech Republic.

He is author or co-author of more than 70 journal contributions and conference papers giving lectures at foreign universities, such as Politecnico di Milano, University of Strathclyde Glasgow, Universidade Técnica de Lisboa and others. His research cover the area of process modelling, simulation and control. His e-mail address is: `gazdos@fai.utb.cz`.

JAROSLAV KOLAŘÍK was born in Zlín, Czech Republic in 1989, and graduated from the Tomas Bata University in Zlín in 2012 with Bachelor's degree in Information and Control Technologies. Now he continues his studies at the Faculty of Applied Informatics in the Master's degree programme Automatic Control and Informatics. His interests cover the area of web technologies and applications. His e-mail address is: `kolarikjarek@gmail.com`.

HYBRID ADAPTIVE LQ CONTROL OF CHEMICAL REACTOR

Jiri Vojtesek and Petr Dostal
Faculty of Applied Informatics
Tomas Bata University in Zlin
Nam. TGM 5555, 760 01 Zlin, Czech Republic
E-mail: {vojtesek,dostalp}@fai.utb.cz

KEYWORDS
Adaptive control, Polynomial approach, LQ approach, Recursive identification, spectral factorization, isothermal CSTR

ABSTRACT

The paper shows one approach to control of a nonlinear process represented by an isothermal continuous stirred-tank reactor. The hybrid adaptive controller designed with the use of a polynomial synthesis, Linear-Quadratic approach and spectral factorization was used for controlling of the product‘s concentration via change of the volumetric flow rate of the reactant. An adaptivity of the system is satisfied by the on-line recursive identification of a external linear delta model of the system. The proposed control method satisfies basic control requirements such as a stability, a disturbance attenuation and a reference signal tracking. All methods are tested by the simulation on the mathematical software MATLAB.

INTRODUCTION

A major group of systems in the nature not only in the industry has a nonlinear behavior. The chemical rector is a typical member of nonlinear processes widely used in the chemical or the biochemical industry. The behavior of such processes could be observed by experiments on the real system or its smaller real model (Vojtesek and Dostal 2008). This method produce more realistic results but it could be dangerous or time and money demanding. The other approach uses modeling techniques for creating of a mathematical model as an abstract representation of the system. The mathematical model in the form of the set of Ordinary Differential Equations (ODE) is then subjected to simulations which show the static and the dynamic behavior of the system. The role of the simulation grows nowadays with the increasing speed and the decreasing price of computers.
The control of these processes with the conventional controllers with fixed parameters could lead to the unstable, inaccurate or unwanted output response when the state of the system change or the disturbance occurs. The adaptive control (Åström and Wittenmark 1989) is one way how we can solve these problems. This control method uses idea from the nature where plants or animals “adapt” their behavior to the actual state or environmental conditions. The adaptive controller adapts parameters or the structure to parameters of the controlled plant according to he selected criterion (Bobal et al. 2005).
The adaptive approach here is based on the choice of the External Linear Model (ELM) as a linear approximation of the originally nonlinear system, parameters of which are identified recursively and parameters of the controller are recomputed according to identified ones. The choice and the order of the ELM come from the dynamic analysis. The δ-models (Middleton and Goodwin 2004) used here are special type of discrete-time (DT) models parameters of which are related to the sampling period. It was proofed, that parameters of the δ-model approach to parameters of the continuous-time (CT) model for the small sampling period (Stericker and Sinha 1993).
The polynomial synthesis (Kucera 1993) together with the spectral factorization and the Linear-Quadratic (LQ) approach were used for designing of the controller. The product of this synthesis is the continuous-time controller which satisfies basic control requirements such as the stability, the reference signal tracking and the disturbance attenuation. The resulted controller is called “hybrid” because it works in continuous-time but its parameters are recomputed in discrete time intervals together with the δ-ELM identification.
The control technique was tested on the mathematical model of the isothermal Continuous Stirred-Tank Reactor (CSTR) the mathematical model of which is described by the set of five ordinary differential equations (Ingham et al. 2000).
All results shown in this contribution come from the simulation on the mathematical model and they were done on the mathematical simulation software Matlab.

ISOTHERMAL CHEMICAL REACTOR

The nonlinear system under the consideration is an isothermal Continuous Stirred-Tank Reactor (CSTR). The schematic representation of this reactor is in Figure 1. The reactions inside the reactor could be described by the scheme:

$$\begin{aligned} A + B &\xrightarrow{k_1} X \\ B + X &\xrightarrow{k_2} Y \\ B + Y &\xrightarrow{k_3} Z \end{aligned} \qquad (1)$$

The must be introduced some simplifications to reduce the complexity of the system. First, as it is isothermal reactor, we expect that the temperature inside the reactor is constant during the reaction. We also assume

Proceedings 27th European Conference on Modelling and Simulation ©ECMS Webjørn Rekdalsbakken, Robin T. Bye, Houxiang Zhang (Editors)
ISBN: 978-0-9564944-6-7 / ISBN: 978-0-9564944-7-4 (CD)

constant volume of the reactor and perfect mixture of the reactant with the use the stirrer. The mathematical model of the system comes from the material balances inside the reactor together with all assumptions mentioned above.

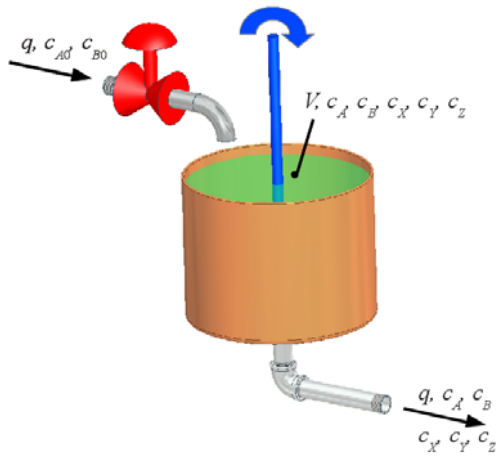

Figure 1: Isothermal Continuous Stirred-Tank Reactor

This model is then described by the set of Ordinary Differential Equations (ODEs) (Russell and Denn 1972):

$$\begin{aligned}
\frac{dc_A}{dt} &= \frac{q}{V}(c_{A0}-c_A)-k_1\cdot c_A\cdot c_B \\
\frac{dc_B}{dt} &= \frac{q}{V}(c_{B0}-c_B)-k_1\cdot c_A\cdot c_B- \\
&\quad -k_2\cdot c_B\cdot c_X-k_3\cdot c_B\cdot c_Y \\
\frac{dc_X}{dt} &= \frac{q}{V}(c_{X0}-c_X)+k_1\cdot c_A\cdot c_B-k_2\cdot c_B\cdot c_X \\
\frac{dc_Y}{dt} &= \frac{q}{V}(c_{Y0}-c_Y)+k_2\cdot c_B\cdot c_X-k_3\cdot c_B\cdot c_Y \\
\frac{dc_Z}{dt} &= \frac{q}{V}(c_{Z0}-c_Z)+k_3\cdot c_B\cdot c_Y
\end{aligned} \tag{2}$$

where q denotes volumetric flow rate, V is used for volume of the reactant, c_A, c_B, c_X, c_Y and c_Z are concentrations, $k_{1\text{-}3}$ are rate constants and t is time. The fixed parameters are in Table 1 (Russell and Denn 1972).

Table 1: Fixed parameters of the reactor

Rate constants	$k_1 = 5\times10^{-4}\ m^3.kmol^{-1}.s^{-1}$ $k_2 = 5\times10^{-2}\ m^3.kmol^{-1}.s^{-1}$ $k_3 = 2\times10^{-2}\ m^3.kmol^{-1}.s^{-1}$
Input concentrations	$c_{A0} = 0.4\ kmol.m^{-3}$ $c_{B0} = 0.6\ kmol.m^{-3}$ $c_{X0} = c_{Y0} = c_{Z0} = 0\ kmol.m^{-3}$
Volume of the reactant	$V = 1\ m^3$

ADAPTIVE CONTROL

The control strategy here is based on the adaptive approach where the adaptivity is satisfied by the recursive identification of the External Linear Model (ELM) of the controlled nonlinear system.

The ELM comes from the static and dynamic analyses of the system. These analyses were discussed in detail in (Zelinka et al. 2006). If we choose the working point defined by the volumetric flow rate of the reactant $q^s = 1\times10^{-4}\ m^3.s^{-1}$, the steady-state values of the state variables in (2) are:

$$\begin{aligned}
c_A^s &= 0.2407\ kmol.m^{-3} & c_B^s &= 0.1324\ kmol.m^{-3} \\
c_X^s &= 0.0024\ kmol.m^{-3} & c_Y^s &= 0.0057\ kmol.m^{-3} \\
c_Z^s &= 0.1513\ kmol.m^{-3}
\end{aligned} \tag{3}$$

Although there are six possible inputs to the system, such as a volumetric flow rate of the reactant q and input concentrations c_{A0}, c_{B0}, c_{X0}, c_{Y0} and c_{Z0}, from the control point of view only q could be used. Output concentrations of the product c_B was chosen as output variable. Variable y denote difference from their steady-state values, i.e.

$$y(t) = c_B(t) - c_B^s \tag{4}$$

It practically means that curves start from zero because these steady-state values are input conditions to the dynamic analysis. This helps better recognize of the gain of the system.

The results of six step changes ±100%, ±60% and ±30% of $q^s = 1\times10^{-4}\ m^3.s^{-1}$ are shown in following figure.

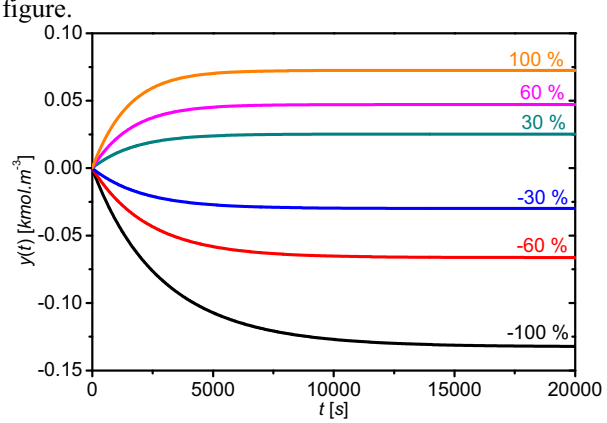

Figure 2: The course of the output concentration y_1 for the step changes of the volumetric flow rate q

External Linear Model (ELM)

Let us suppose, that the ELM of the controlled output displayed in Figure 2 could be described by the second order transfer function with relative order one in the s-plain, e.g.

$$G(s) = \frac{b(s)}{a(s)} = \frac{b_1 s + b_0}{a_2 s^2 + a_1 s + a_0} \tag{5}$$

where parameters of polynomials $a(s)$ and $b(s)$ are commensurable polynomials and the feasibility condition is fulfilled for $\deg a(s) \geq \deg b(s)$.

The transfer function is relation of the output from the system to the input which mathematically means that this continuous-time (CT) model (5) could be rewritten to:

$$a(\sigma)y(t) = b(\sigma)u(t) \tag{6}$$

where $a(\sigma)$ and $b(\sigma)$ are polynomials from (5) and σ is the differentiation operator. The identification of the CT model is not very simple. On the other hand, discrete-time(DT) identification could be inaccurate. Compromise between these two methods can be found in the use of so called Delta (δ-) models. This model uses a new complex variable γ defined generally as (Mukhopadhyay et al. 1992):

$$\gamma = \frac{z-1}{\beta \cdot T_v \cdot z + (1-\beta)\cdot T_v} \tag{7}$$

It is clear that we can obtain infinitely many models for the optional parameter β from the interval $0 \le \beta \le 1$ and a sampling period T_v. A forward δ-model was used in this work. The γ operator is then $\beta = 0 \rightarrow \gamma = (z-1)/T_v$ and the continuous model (6) could be then rewritten to

$$a^{\delta}(\delta)\, y(t') = b^{\delta}(\delta)\, u(t') \tag{8}$$

where polynomials $a^{\delta}(\delta)$ and $b^{\delta}(\delta)$ are discrete polynomials and their coefficients are different from those of the CT model $a(\sigma)$ and $b(\sigma)$. Time t' is the discrete time and with the new substitution $t' = k - n$ for $k \ge n$ the δ-model for this concrete transfer function would be:

$$\begin{aligned} \delta^2 y(k-n) = b_1^{\delta}\delta u(k-n) + b_0^{\delta} u(k-n) - \\ - a_1^{\delta}\delta y(k-n) - a_0^{\delta} y(k-n) \end{aligned} \tag{9}$$

The equation (9) produces both the regression vector $\boldsymbol{\varphi_\delta}$ and the vector of parameters

$$\begin{aligned} \boldsymbol{\varphi_\delta}(k-1) &= \left[-y_\delta(k-1), -y_\delta(k-2), u_\delta(k-1), u_\delta(k-2)\right]^T \\ \boldsymbol{\theta_\delta}(k) &= \left[a_1^{\delta}, a_0^{\delta}, b_1^{\delta}, b_0^{\delta}\right]^T \end{aligned} \tag{10}$$

where y_δ and u_δ denotes the recomputed output and input variables to the δ-model and

$$\begin{aligned} y_\delta(k) &= \frac{y(k) - 2y(k-1) + y(k-2)}{T_v^2} \\ y_\delta(k-1) &= \frac{y(k-1) - y(k-2)}{T_v} \\ y_\delta(k-2) &= y(k-2) \\ u_\delta(k-1) &= \frac{u(k-1) - u(k-2)}{T_v} \\ u_\delta(k-2) &= u(k-2) \end{aligned} \tag{11}$$

The differential equation (9) has then the vector form:

$$y_\delta(k) = \boldsymbol{\theta_\delta}^T(k)\cdot\boldsymbol{\varphi_\delta}(k-1) + e(k) \tag{12}$$

where $e(k)$ is a general random immeasurable error.

On-line Identification

It is clear, that the unknown parameter from the differential equation (12) is the vector of parameters $\boldsymbol{\theta_\delta}$. The regression vector $\boldsymbol{\varphi_\delta}$ is constructed from the previous values of the measured inputs u and outputs y. The Recursive Least-Squares (RLS) method is widely used for this on-line identification (Rao and Unbehauen 2005). This method is well-known and easily programmable. The RLS method with the changing exponential forgetting used here is described by the set of equations:

$$\begin{aligned} \varepsilon(k) &= y(k) - \boldsymbol{\varphi}_\delta^T(k)\cdot\hat{\boldsymbol{\theta}}_\delta(k-1) \\ \xi(k) &= \left[1 + \boldsymbol{\varphi}_\delta^T(k)\cdot\mathbf{P}(k-1)\cdot\boldsymbol{\varphi}_\delta(k)\right]^{-1} \\ \boldsymbol{L}(k) &= \xi(k)\cdot\mathbf{P}(k-1)\cdot\boldsymbol{\varphi}_\delta^T(k) \\ \mathbf{P}(k) &= \frac{1}{\lambda_1(k-1)}\Big[\mathbf{P}(k-1) - \dots \\ \dots &- \frac{\mathbf{P}(k-1)\cdot\boldsymbol{\varphi}_\delta(k)\cdot\boldsymbol{\varphi}_\delta^T(k)\cdot\mathbf{P}(k-1)}{\lambda_1(k-1) + \boldsymbol{\varphi}_\delta^T(k)\cdot\mathbf{P}(k-1)\cdot\boldsymbol{\varphi}_\delta(k)}\Big] \\ \hat{\boldsymbol{\theta}}_\delta(k) &= \hat{\boldsymbol{\theta}}_\delta(k-1) + \boldsymbol{L}(k)\varepsilon(k) \end{aligned} \tag{13}$$

where the changing forgetting factor λ_1 is computed from the equation

$$\lambda_1(k) = 1 - K\cdot\xi(k)\cdot\varepsilon^2(k) \tag{14}$$

and K is small number, in our case $K = 0.001$.

Design of Controller

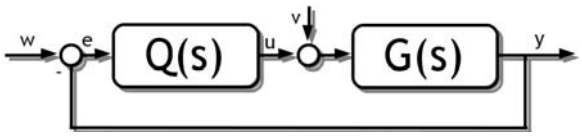

Figure 3: 1DOF control scheme

We can now introduce one simple feedback controller – see Figure 3, where $G(s)$ represents the transfer function (5) of the controlled output and $Q(s)$ denotes the transfer function of the controller in the continuous-time, generally:

$$Q(s) = \frac{q(s)}{p(s)} \tag{15}$$

where $q(s)$ and $p(s)$ are again commensurable polynomials with the properness condition $\deg p(s) \ge \deg q(s)$.

The Laplace transform of the transfer function $G(s)$ in (5) is

$$G(s) = \frac{Y(s)}{U(s)} \Rightarrow Y(s) = G(s)\cdot U(s) \tag{16}$$

where Laplace transform of the input signal u is from Figure 3

$$U(s) = Q(s)\cdot E(s) + V(s) = Q(s)\cdot\left[W(s) - Y(s)\right] + V(s) \tag{17}$$

If we put polynomials $a(s)$, $b(s)$, $p(s)$ and $q(s)$ into (17) instead of Laplace transforms $G(s)$ and $Q(s)$, the equation (16) has form

$$\begin{aligned} Y(s) &= \frac{b(s)q(s)}{a(s)p(s) + b(s)q(s)}\cdot W(s) + \dots \\ \dots &+ \frac{a(s)p(s)}{a(s)p(s) + b(s)q(s)}\cdot V(s) \end{aligned} \tag{18}$$

and as you can see, both fractions has the same denominators which are called a characteristic

polynomial of the closed loop and this polynomial can be rewritten to the form

$$a(s)\cdot p(s)+b(s)\cdot q(s)=d(s) \qquad (19)$$

where $d(s)$ is a stable optional polynomial and the whole equation (19) is called Diophantine equation (Kucera 1993). The stability of the control system is fulfilled for the stable polynomial $d(s)$ on the left side of the Diophantine equation (19). Asymptotic tracking of the reference signal and disturbance attenuation is attained if the polynomial $p(s)$ includes the least common divisor of denominators of transfer functions of the reference w and disturbance v:

$$p(s)=f(s)\cdot\tilde{p}(s) \qquad (20)$$

If we expect both these signals from the range of the step functions, the polynomial $f(s) = s$. The Diophantine equation (19) is then

$$a(s)\cdot s\cdot\tilde{p}(s)+b(s)\cdot q(s)=d(s) \qquad (21)$$

and the transfer function of the feedback controller is

$$\tilde{Q}(s)=\frac{q(s)}{s\cdot\tilde{p}(s)} \qquad (22)$$

As it is written above, the polynomial $d(s)$ on the right side of the Diophantine equation (21) is the stable optional polynomial. There are several ways how we can construct this polynomial. The simples one is the based on pole-placement method where $d(s)$ is divided into one or more parts with double, triple, etc. roots, e.g.

$$d(s)=(s+\alpha)^m;\ d(s)=(s+\alpha_1)^{m/2}\cdot(s+\alpha_2)^{m/2},\ldots \qquad (23)$$

where $\alpha > 0$. The disadvantage of this method can be found in the uncertainty. There is no general rule which can help us with the choice of roots which are, of course, different for different controlled processes. One way how we can overcome this unpleasant feature is to use spectral factorization. Big advantage of this method is that it can make stable roots from every polynomial, even if it is unstable. The polynomial $d(s)$ is in this case

$$d(s)=n(s)\cdot g(s) \qquad (24)$$

where parameters of the polynomial $n(s)$ are computed from the spectral factorization of the polynomial $a(s)$ in the denominator of (5), i.e.

$$n^*(s)\cdot n(s)=a^*(s)\cdot a(s) \qquad (25)$$

The second part, polynomial $g(s)$, is computed with the use of the Linear Quadratic (LQ) tracking (Hunt at al. 1992) which is based on the minimizing of the cost function in the complex domain

$$J_{LQ}=\int_0^\infty\left\{\mu_{LQ}\cdot e^2(t)+\varphi_{LQ}\cdot\dot{u}^2(t)\right\}dt \qquad (26)$$

where $\varphi_{LQ} > 0$ and $\mu_{LQ} \geq 0$ are weighting coefficients, $e(t)$ is the control error and $\dot{u}(t)$ denotes the difference of the input variable. It practically means, that parameters of the polynomial $g(s)$ are computed from the spectral factorization

$$\left(a(s)\cdot f(s)\right)^*\cdot\varphi_{LQ}\cdot a(s)\cdot f(s)+b^*(s)\cdot\mu_{LQ}\cdot b(s)=\ldots$$
$$\ldots=g^*(s)\cdot g(s) \qquad (27)$$

Degrees of unknown polynomials $\tilde{p}(s)$, $q(s)$ and $d(s)$ are for the fulfilled properness condition generally:

$$\begin{aligned}&\deg\tilde{p}(s)\geq\deg a(s)-1\\&\deg q(s)=\deg a(s)+\deg f(s)-1\\&\deg d(s)=2\deg a+1\\&\deg n(s)=\deg a(s)\\&\deg g(s)=\deg d(s)-\deg n(s)\end{aligned} \qquad (28)$$

and these degrees and polynomials are for our concrete second order transfer function in (5)

$$\begin{aligned}&\deg\tilde{p}(s)=2\Rightarrow\tilde{p}(s)=s^2+p_1s+p_0\\&\deg q(s)=2\Rightarrow q(s)=q_2s^2+q_1s+q_0\\&\deg d(s)=2\deg a+1=2\cdot2+1=5\\&\deg n(s)=2\Rightarrow n(s)=s^2+n_1s+n_0\\&\deg g(s)=3\Rightarrow g(s)=s^3+g_2s^2+g_1s+g_0\end{aligned} \qquad (29)$$

Polynomials $n(s)$ and $g(s)$ are computed as a results of spectral factorizations (25) and (27):

$$\begin{aligned}&g_0=\sqrt{\mu_{LQ}b_0^2},\ g_1=\sqrt{2g_0g_2+\varphi_{LQ}a_0^2+\mu b_1^2},\\&g_2=\sqrt{2g_1g_3+\varphi_{LQ}\left(a_1^2-2a_0\right)},g_3=\sqrt{\varphi_{LQ}},\\&n_0=\sqrt{a_0^2},n_1=\sqrt{2n_0+a_1^2-2a_0}\end{aligned} \qquad (30)$$

Polynomials $a(s)$ and $b(s)$ of the ELM are known from the recursive identification described in previous parts.

The goal of the control strategy is to find parameters of polynomials $\tilde{p}(s)$ and $q(s)$. The method of uncertain coefficients which compares coefficients of individual s-powers can be used for formulating of these coefficients. The transfer function of the controller (22) has than CT form:

$$\tilde{Q}(s)=\frac{q(s)}{s\cdot\tilde{p}(s)}=\frac{q_2s^2+q_1s+q_0}{s\cdot\left(s^2+p_1s+p_0\right)} \qquad (31)$$

This transfer function could be then transformed to the differential equation which is easily solvable with the use of numerical methods.

The final controller is called "hybrid" because the control input is computed in the continuous time but the identification of the ELM runs in the discrete time with the use of δ-models.

SIMULATION RESULTS

The proposed hybrid adaptive LQ controller was tested on the mathematical model of CSTR described above. Three simulation experiments were done. The first and the second compares influence of weighting factors φ_{LQ} and μ_{LQ} respectively and the third simulation observes impact of disturbances to the control of the system.

The controlled output was difference of the product's B concentration c_B from its steady-state value and the input variable was the change of the volumetric flow rate from it's steady-state value in percent for all simulations, i.e.

$$y(t) = c_B(t) - c_B^s \left[kmol.m^{-3} \right]$$
$$u(t) = \frac{q(t) - q^s}{q^s} \cdot 100 \left[\% \right] \tag{32}$$

The simulation time was set to 15 000 *s*, the sampling period was T_v = 10 *s*. The input variable $u(t)$ was limited inside the bounds <-100%; 100%>.

The first study sets factor μ_{LQ} = 0.5 and the second factor was set to φ_{LQ} = 4×10^{-5}; 8×10^{-4} and 5×10^{-3}. Six different step changes were done during the control and results are shown in Figure 4 and Figure 5.

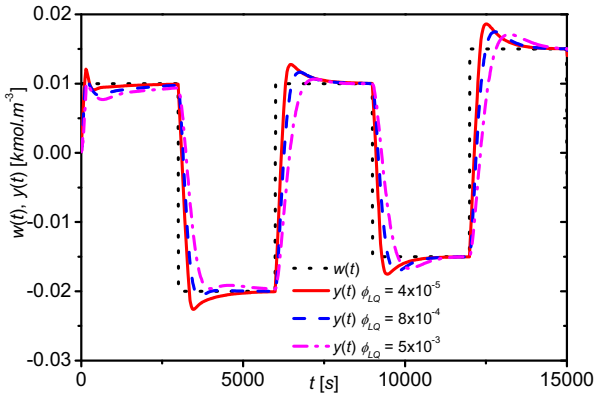

Figure 4: The course of the reference signal $w(t)$ and output responses $y(t)$ for different values of weighting factor φ_{LQ}

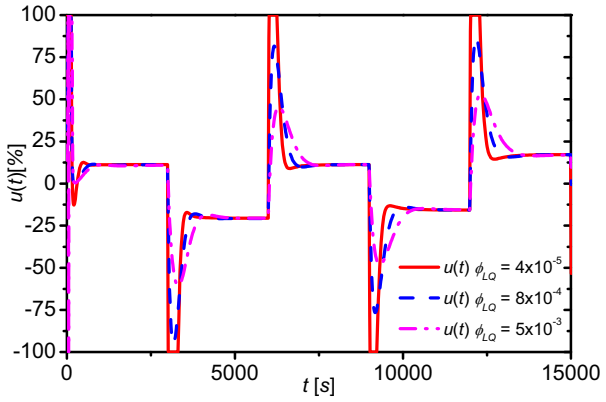

Figure 5: The course of the input signal $u(t)$ for different values of weighting factor φ_{LQ}

The results of the first study shows that the value of the weighting factor φ_{LQ} affects mainly the speed of the control. The increasing value of this factor produces slower course of the output variable $y(t)$ without overshoots – see Figure 4 and smoother course of the input variable $u(t)$ in Figure 5.

The second study was done for different values of the weighting factor μ_{LQ} = 0.5; 2 and 10 and a fixed value of the second weighting factor φ_{LQ} = 0.05. The same step changes as in the previous case were done and results are shown in Figure 6 and Figure 7.

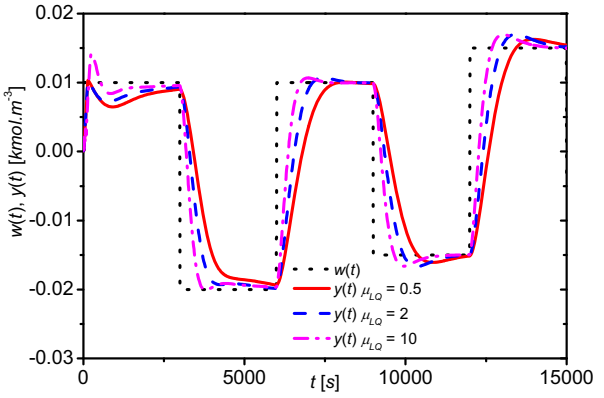

Figure 6: The course of the reference signal $w(t)$ and output responses $y(t)$ for different values of weighting factor μ_{LQ}

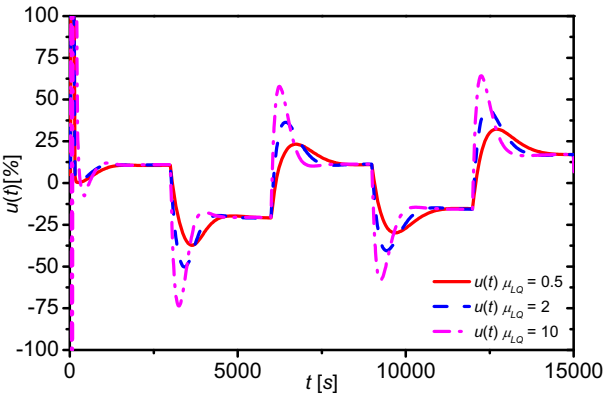

Figure 7: The course of the input signal $u(t)$ for different values of weighting factor μ_{LQ}

The affect of the weighting factor μ_{LQ} presented in previous graphs is opposite to the previous simulation study – increasing value of μ_{LQ} makes the course of the output variable $y(t)$ quicker but with small overshoots which depends on the change of the reference signal $w(t)$. Bigger change of $w(t)$ results in bigger overshoot and vice versa.

The only problem of both simulation studies can be found at the very beginning of the control where the course of the input variable and of course the output variable is very inaccurate. This is caused by the recursive identification which purposely starts from the general point $\boldsymbol{\theta}_{\delta}(0) = \left[0.1, 0.1, 0.1, 0.1\right]^T$ and it takes time 50-100 *s* to get the right vector of parameters.

The goal of the last simulation study is to show how this controller cope with the disturbances. Weighting factors were set to μ_{LQ} = 5; φ_{LQ} = 5×10^{-4} and two disturbances were injected into the system. The first disturbance was on the input concentration c_{B0}, $v_1(t)$ = -10% of c_{B0} for $t \in \langle 5000;15000 \rangle s$ and the second disturbance on the output concentration c_B, $v_2(t)$ = +20% of c_B, was injected for the time $t \in \langle 10000;15000 \rangle s$. The results are in the following figures.

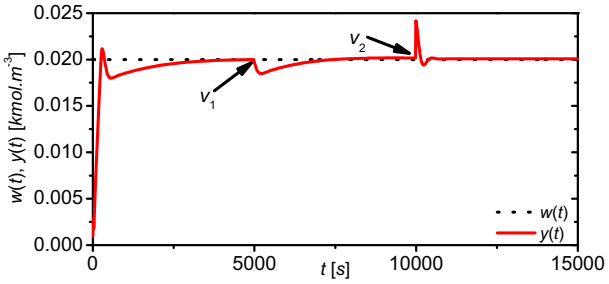

Figure 8: The influence of disturbances $v_1(t)$ and $v_2(t)$ to the output variable $y(t)$

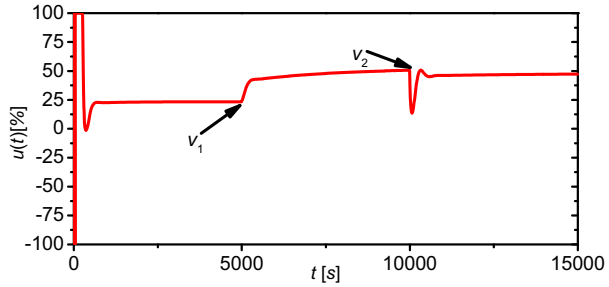

Figure 9: The influence of disturbances $v_1(t)$ and $v_2(t)$ to the input variable $y(t)$

Obtained results have shown, that proposed controller cope with both these disturbances without major problems even though both of these disturbences affects the system during simulation time $t \in \langle 10000;15000 \rangle s$.

CONCLUSION

The contribution shows one approach for controlling of the nonlinear process with lumped parameters represented by the isothermal CSTR. The hybrid controller was defined in the continuous-time but recursive identification uses discrete-time model based on the δ-model theory. The LQ approach together with the spectral factorization provides good control results although the system has nonlinear properties. The controller could be tuned with the choice of weighting factors φ_{LQ} or μ_{LQ}. Affect of both weighting factors was discussed in the practical simulation part. The value of these factors influence mainly the speed of the control and overshoots. This control strategy could be used also for similar types of nonlinear processes such as bath reactors, stirred reactor, tubular reactors, heat exchangers etc.

REFERENCES

Åström, K.J.; Wittenmark, B. 1989. *Adaptive Control*. Addison Wesley. Reading. MA, 1989, ISBN 0-201-09720-6.

Bobal, V.; Böhm, J.; Fessl, J.; Machacek, J. 2005 *Digital Self-tuning Controllers: Algorithms. Implementation and Applications*. Advanced Textbooks in Control and Signal Processing. Springer-Verlag London Limited. 2005, ISBN 1-85233-980-2.

Hunt, K. J.; Kucera, V.; Sebek, M. 1992. "Optimal regulation using measurement feedback. A polynomial approach". *IEEE Transactions on Automation Control*, 37, no. 5, pp. 682-685.

Ingham, J.; Dunn, I. J.; Heinzle, E.; Prenosil, J. E. 2000 *Chemical Engineering Dynamics. An Introduction to Modeling and Computer Simulation*. Second. Completely Revised Edition. VCH Verlagsgesellshaft. Weinheim, 2000. ISBN 3-527-29776-6

Kucera, V. 1993. "Diophantine equations in control – A survey". *Automatica*. 29, 1993, p. 1361-1375.

Middleton, H.; Goodwin, G. C. 2004. *Digital Control and Estimation - A Unified Approach*. Prentice Hall. Englewood Cliffs, 2004, ISBN 0-13-211798-3

Mukhopadhyay, S.; Patra, A. G.; Rao, G. P. 1992 "New class of discrete-time models for continuos-time systems". *International Journal of Control*, vol.55, 1992, 1161-1187

Rao, G. P.; Unbehauen, H. 2005 "Identification of continuous-time systems". *IEEE Process-Control Theory Application*, 152, 2005, p.185-220.

Russell, T.; Denn, M. M. 1972 "Introduction to chemical engineering analysis". New York: Wiley, 1972, xviii, 502 p. ISBN 04-717-4545-6.

Stericker, D. L.; Sinha, N. K. 1993 "Identification of continuous-time systems from samples of input-output data using the δ-operator". *Control-Theory and Advanced Technology*. vol. 9, 1993, 113-125.

Vojtesek, J.; Dostál, P. 2008. "Adaptive LQ Approach Used in Conductivity Control inside Continuous-Stirred Tank Reactor", In *Proceedings of the 17th IFAC World Congress*, Soul, 2008, p. 12929-12934, ISBN-ISSN 978-1-1234-7890-2.

Zelinka, I.; Vojtesek, J.; Oplatkova, Z. 2006. "Simulation Study of the CSTR Reactor for Control Purposes". In: *Proc. of 20th European Conference on Modelling and Simulation ESCM 2006*. Bonn, Germany, p. 479-482

AUTHOR BIOGRAPHIES

JIRI VOJTESEK was born in Zlin. Czech Republic and studied at the Tomas Bata University in Zlin. where he got his master degree in chemical and process engineering in 2002. He has finished his Ph.D. focused on Modern control methods for chemical reactors in 2007. His email contact is `vojtesek@fai.utb.cz`.

PETR DOSTAL studied at the Technical University of Pardubice. He obtained his PhD. degree in Technical Cybernetics in 1979 and he became professor in Process Control in 2000. His research interest are modeling and simulation of continuous-time chemical processes. polynomial methods. optimal. adaptive and robust control. You can contact him on email address `dostalp@fai.utb.cz`.

PREDICTIVE VERSUS VECTOR CONTROL OF THE INDUCTION MOTOR

Sergiu Ivanov
Virginia Ivanov

Vladimir Rasvan
Eugen Bobasu
Dan Popescu
Florin Stinga

University of Craiova
Faculty of Electrical Engineering
Faculty of Automation, Computer and Electronics
107 Decebal Blv., 200440, Craiova, Romania
E-mail: sivanov@em.ucv.ro, vivanov@elth.ucv.ro
E-mail: [vrasvan, ebobasu, dpopescu, florin]@automation.ucv.ro

KEYWORDS
Induction motor, vector control, predictive control.

ABSTRACT

The paper deals with the vector control and predictive control of the induction motor. For the vector control, the rotor flux oriented one is pointed out, with highlight on the voltage source inverter type. The influence of the most important parameter variations (e.g. stator resistance) is discussed. A simple (and practical) method for avoiding these influences is presented, based on proper simulation models. Following the basics of the predictive control, a simulation model for this type of command is presented, together with simulations results. Finally, the results are cross analysed and further actions are proposed the work continuation.

INTRODUCTION

On one hand, since the basic work concerning torque and field control due to Leonhard, Blaschke and their followers in the 1970s, the AC drives became a competitive technology with respect to the traditional one, based on DC drives. In rotating references, solidar with the rotor flux, stator flux or magnetizing flux respectively, there is an obvious decoupling between the two components of the stator current: while the direct component acts on the flux modulus only and produces the reactive component, the quadrature component generates the torque, being the active component. The two components of the stator current may be thus controlled independently and the flux and torque generation are thus decoupled, similarly to the DC motor. Due to results simplicity, the rotor flux orriented control has imposed almost as a standard. From here, two types of control were engineered. On one hand we have the direct control drives, where flux position and modulus are known while the reactive and active components of the stator current are computed in the proper reference frame using the set-point torque and flux. On the other hand we have the indirect control drives, where the slip frequency is computed and imposed without direct knowledge of the flux, while the reference system change from the flux-reference to stator-reference one is performed by integration of the sum of the motor speed and the speed corresponding to the computed slip (Casadei et al. 2002, Vas 1998). A very simple method for the toque control is also the Direct Torque Control (DTC), suited for electrical traction applications (Takahashi and Noguchi 1986, Baader et al. 1992, Ehsani et al. 1997, Faiz et al. 1999, Haddoun et al. 2007, Ivanov 2009, Ivanov 2010).
On the other hand, the increased computational capabilities of the existing DSP allow the implementation of the predictive control at the level of the converters which induce the hybrid character of the overall control system of the drive. We infer that predictive control has established itself in the last 5-7 years as a very proficient form of controlling highly nonlinear and uncertain systems; moreover the most recent results show its applicability to fast processes among which drives and their converters have a central position (Seo et al. 2009, Prieur and Tarbouriech 2011, Geyer et al. 2008, Mariethoz et al. 2010, Geyer et al. 2009, Trabelsi et al. 2008, Shi et al. 2007, Rodriguez et al. 2007, Larrinaga et al. 2007, Richter et al. 2010, Almer et al. 2010).
The paper will briefly present in the first section the basics of the vector control for the rotor flux oriented control for voltage source inverter, with highlight on the influence of the parameters variations on the drive performance. A simple method for reducing these influences will be discussed based on appropriated models. The basics of the predictive control will be presented in Section 2. Section 3 will analyse the predictive control applied to the induction motor, based also on a Simulink model. Finally, conclusions will be issued and ideas for continuation will be pointed out.

VECTOR CONTROL OF INDUCTION MOTOR

As stated above, the vector control strategy most often used is the rotor flux oriented one. The reasons reside in the simplicity of the expressions resulted from the *rotor* voltage equation which mainly gives the rotor flux speed and further, by integration, the rotor flux position, used

Proceedings 27th European Conference on Modelling and Simulation ©ECMS Webjørn Rekdalsbakken, Robin T. Bye, Houxiang Zhang (Editors)
ISBN: 978-0-9564944-6-7 / ISBN: 978-0-9564944-7-4 (CD)

at its turn for the transformation of the reference currents/voltages from the rotary frame to the stationary one.

For the squirrel cage induction motor, the rotor voltages equation in terms of phasors is

$$0 = R_r \underline{i}_{r\Psi r} + \frac{d\underline{\Psi}_{r\Psi r}}{dt} + j\left(\omega_{mr} - P\omega_r\right)\underline{\Psi}_{r\Psi r}, \qquad (1)$$

where R_r is the rotor resistance, $\underline{i}_{r\Psi r}$ is the rotor current, ω_m is the rotor flux speed, ω is the mechanical speed of the rotor and P is the number of pairs of poles. The Ψ subscript highlights that (1) is expressed in the rotary frame synchronous with the rotor flux $\underline{\Psi}_{r\Psi r}$.

By assuming unsaturated operation (realistic hypothesis when the stator currents are precisely controlled), the rotor flux expressed in terms of magnetizing inductance L_m and rotor magnetizing current $\left|\underline{i}_{mr}\right|$ is $\left|\underline{\Psi}_r\right| = L_m \cdot \left|\underline{i}_{mr}\right|$

Consequently, (1) becomes

$$0 = R_r \underline{i}_{r\Psi r} + L_m \frac{d\left|\underline{i}_{mr}\right|}{dt} + j\left(\omega_{mr} - P\omega_r\right)\cdot\left|\underline{i}_{mr}\right|\cdot L_m. \quad (2)$$

The rotor current $\underline{i}_{r\Psi r}$, being immeasurable for the squirrel cage motor, is expressed in terms of the stator current $\underline{i}_{s\Psi r}$ and the magnetizing one. By denoting the rotor time constant $T_r = L_r / R_r$, (2) becomes

$$T_r \frac{d\left|\underline{i}_{mr}\right|}{dt} + \left|\underline{i}_{mr}\right| = \underline{i}_{s\Psi r} - j\left(\omega_{mr} - P\omega_r\right)T_r\left|\underline{i}_{mr}\right|, \quad (3)$$

L_r being the total rotor inductance which includes the leakages ($L_r = L_m + L_{\sigma r}$). By identifying the terms on each of the axes *d*, *q*, the following two expressions result which are the simplest among all the vector control types

$$T_r \frac{d\left|\underline{i}_{mr}\right|}{dt} + \left|\underline{i}_{mr}\right| = i_{sd}, \qquad (4)$$

$$\omega_{mr} = P\omega_r + \frac{i_{sq}}{T_r\left|\underline{i}_{mr}\right|}. \qquad (5)$$

We notice from (4) that if the flux is kept constant ($\left|\underline{i}_{mr}\right| = \text{ct.}$), then $\left|\underline{i}_{mr}\right| = i_{sd} = \text{ct.}$ As the electromagnetic torque expressed in the rotor flux oriented frame is

$$t_e = \frac{3}{2} P \frac{L_m^2}{L_r} i_{sd} \cdot i_{sq}, \qquad (6)$$

from (5) and (6) results that the slip speed (term 2 in (5)) is proportional with the torque and further, the mechanical characteristic of the induction motor are straight lines, quite similar to the DC motor.

When the motor is supplied by a voltage source inverter, the necessary voltages are obtained by considering the *stator* voltages equation expressed in the same rotary frame synchronous with the rotor flux $\underline{\Psi}_{r\Psi r}$:

$$\underline{u}_{s\Psi r} = R_s \underline{i}_{s\Psi r} + L_s \frac{d\underline{i}_{s\Psi r}}{dt} + L_m \frac{d\underline{i}_{r\Psi r}}{dt} + \\ + j\omega_{mr} L_s \underline{i}_{s\Psi r} + j\omega_r L_m \underline{i}_{r\Psi r} \qquad (7)$$

where R_s is the stator resistance, $\underline{i}_{s\Psi r}$ is the stator current and L_s is the total stator inductance which includes the leakages ($L_s = L_m + L_{\sigma s}$).

By expressing the rotor current in terms of the stator current and the magnetizing one and denoting the stator time constant $T_s = L_s / R_s$, stator transient time constant $T_s' = L_s' / R_s$, with $L_s' = L_s - \frac{L_m^2}{L_r}$ stator transient inductance, it results from (7) the two necessary voltages

$$u_{sd} = R_s i_{sd} + L_s' \frac{di_{sd}}{dt} - \omega_{mr} L_s' i_{sq} + \left(L_s - L_s'\right)\cdot\frac{d\left|\underline{i}_{mr}\right|}{dt}, \quad (8)$$

$$u_{sq} = R_s i_{sq} + L_s' \frac{di_{sq}}{dt} + \omega_{mr} L_s' i_{sd} + \left(L_s - L_s'\right)\cdot\omega_{mr}\left|\underline{i}_{mr}\right|. \quad (9)$$

We notice from (8) and (9) that the two expressions are not independent. By assuming some hypothesis ($\left|\underline{i}_{mr}\right| = i_{sd} = \text{ct.}, i_{sq} = \text{ct.}$), result simplified expressions of the preset voltages in terms of the preset values of the two stator current components (reactive i_{sd}^* and active one i_{sq}^* respectively)

$$u_{sd}^* = R_s i_{sd}^* - \omega_{mr} L_s' i_{sq}^*, \qquad (10)$$

$$u_{sq}^* = R_s i_{sq}^* + \omega_{mr} L_s i_{sd}^*. \qquad (11)$$

The second term of each equation will determine the structure of the so called decoupling circuit (Fig. 1).

Results of the simulation of step start followed by a speed reversal are plotted in Fig. 2. Even there are some transients when the speed reference changes, the overall behaviour is good.

In simulation everything seems to be perfect. In practice, the decoupling circuit raises two problems. On one hand, by considering only the value of the stator resistance in (10) and (11), the "parasitic" voltage drops (on semiconductors, cables, DC circuit in high dynamics) are neglected. The consequences are evident on the final currents. Fig. 3.a plots the reactive and active currents obtained by experiment.

We notice that the both currents do not follow the preset values and consequently, the torque is about one half of the expected one.

Experimentally increasing the value of the resistance used in (10) and (11), the two currents reach the preset values (Fig. 3.b) and the developed torque attains the expected value. But these results are obtained with a value of the stator resistance double that in previous case.

This observation raises another question: what happens in practice when the real resistance of the motor changes (increases) during the operation due to the temperature.

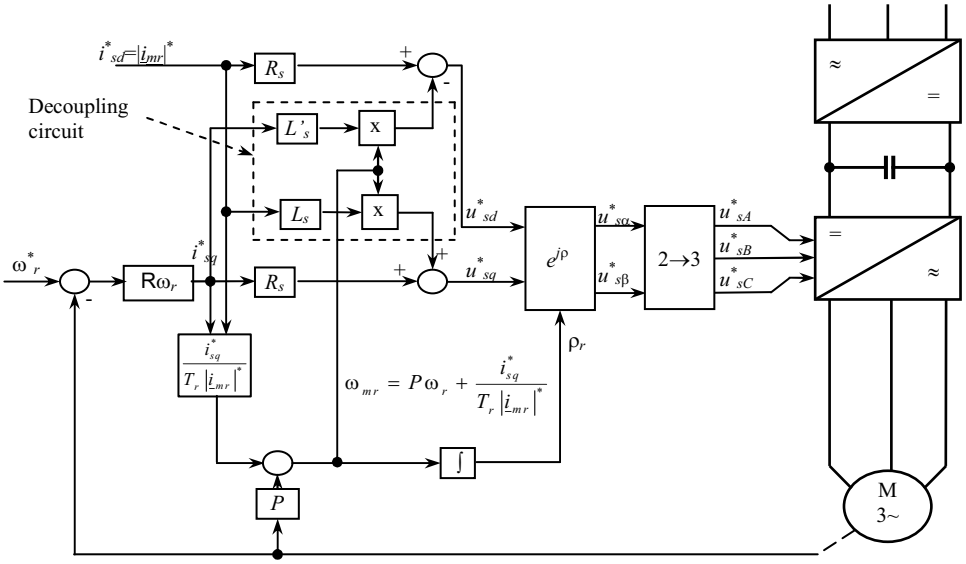

Figure 1: Rotor Flux Oriented Control of the Induction Motor Supplied by Voltage Source Inverter

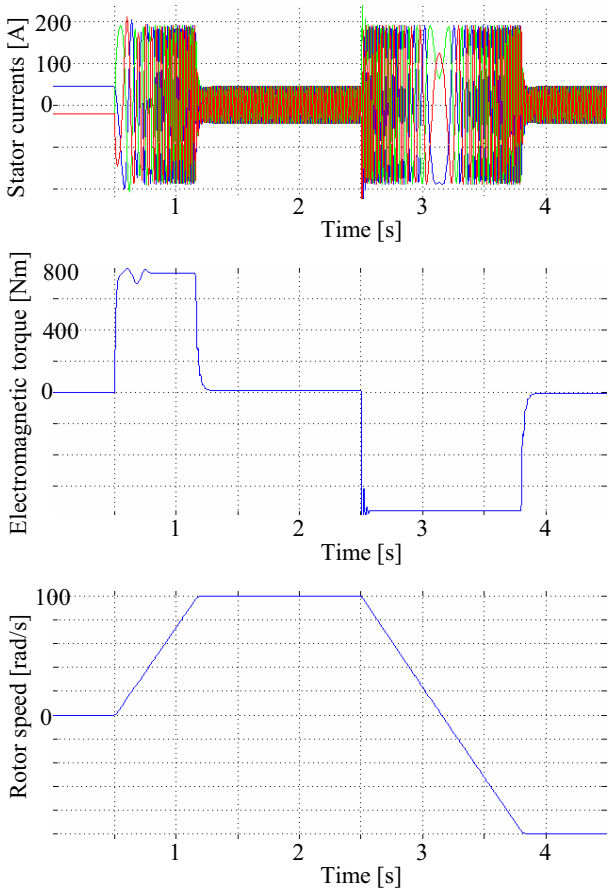

Figure 2: Simulation of the Classic Rotor Flux Oriented Control of the Induction Motor Supplied by Voltage Source Inverter

The expected results could be the same if the decoupling circuit does not adapt itself.
In practice, the decoupling circuit is replaced by two controllers, one for each component of the stator current, Fig. 4.

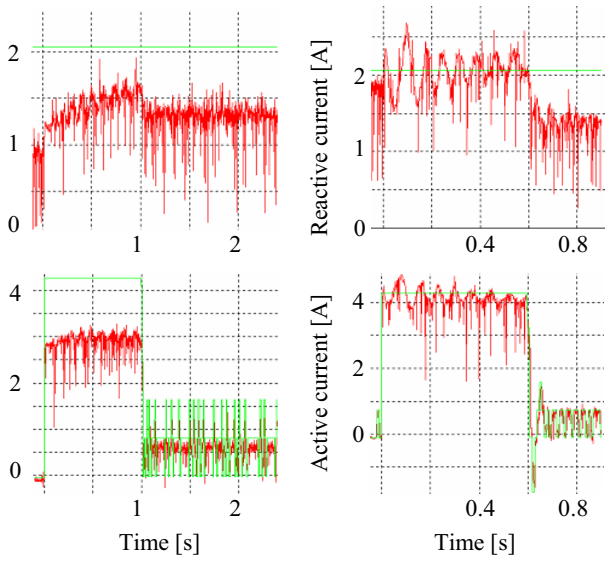

a) R_s b) $2R_s$

Figure 3: Experimental Results with Two Values of the Stator Resistance

In addition, the flux speed and position are computed based on the real values of the two components of the stator current, not the reference ones as in previous case. The results of the simulation, plotted in Fig. 5 look even better. There are not transients when the speed reference changes.
This is the type of control industrially implemented, for example in the dsPIC30F from Microchip.
By using in the motor model different values of the stator resistance (alteration due to the temperature for example), the results do not change almost at all. This observation leads to the conclusion that this type of control is much less sensitive to the parameters' variations.

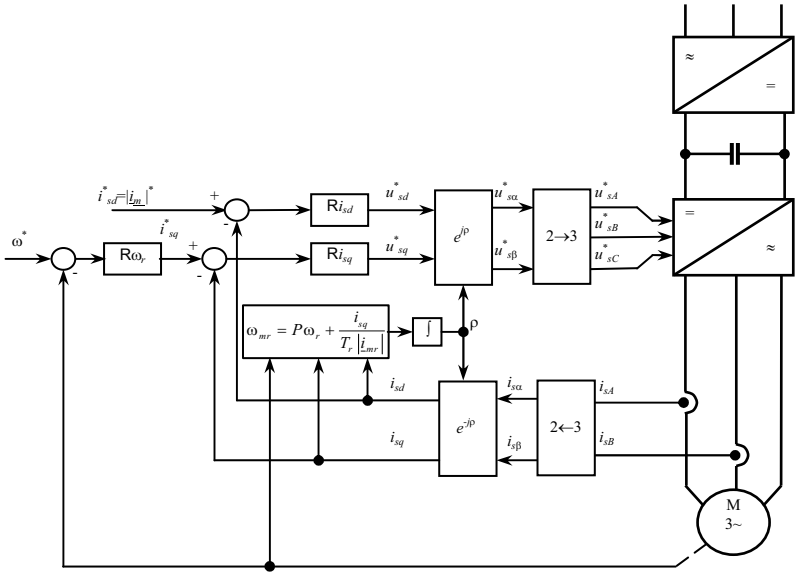

Figure 4: Decoupling Circuit Replaced by Current Controllers

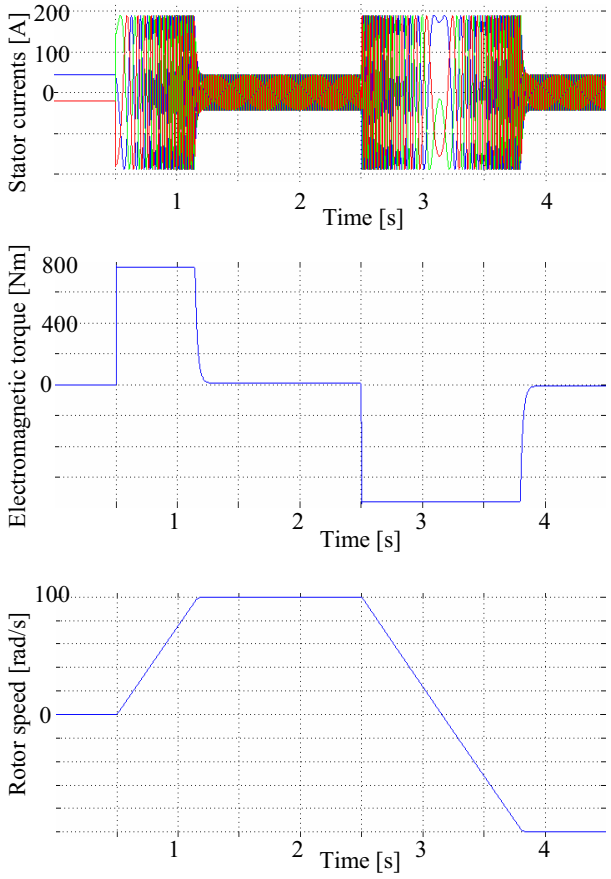

Figure 5: Simulation of the Rotor Flux Oriented Control with Current Controllers

BASICS OF PREDICTIVE CONTROL

The model predictive control is a control technique which has been successfully implemented in industry. The predictive control techniques were used to control both continuous as well as discrete systems (Camacho and Bordons 2004, Bemporad 2007, Lazăr 2006, Maciejowski 2000, Stinga 2012).

The predictive control is derived from optimal control, yet, in this case the optimal control problem involves additional constraints.

The predictive control techniques require solving an open loop optimal control problem, taking into account constraints on input, state and/or output variables. At every moment k, the measured variables and the model of the process are used to compute (to predict) the future behaviour of the system over a prediction horizon N (Fig. 6).

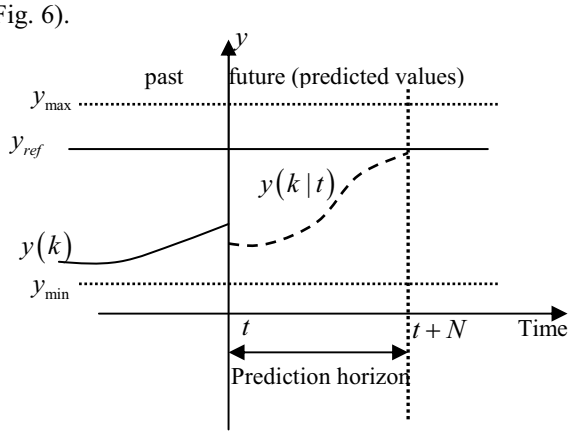

Figure 6: Evolution of System Output Using Predictive Control Strategy (Stinga 2012)

This task is accomplished by determining a set of future control inputs such that the objectives and the system constraints are satisfied. The control input is determined by minimization of a cost function over a time horizon N_c.

Generally, the cost function used in predictive control is defined as follows:

$$J(k) = \sum_{t=1}^{N} \left\| y(k|t) - y_{ref}(k) \right\|^2_{Q(t)} + \sum_{t=1}^{N_c} \left\| u(k|t) \right\|^2_{R(t)}, \quad (12)$$

subject to constraints specified on the inputs, outputs and input increments (Fig. 7):

$$u_{\min} \le u(k) \le u_{\max},$$
$$y_{\min} \le y(k) \le y_{\max},$$

where:
$Q(t)$ - positive definite error weighting matrix;
$R(t)$ - positive semi-definite control weighting matrix;
$y(k|t)$ - vector of predicted output signals;
$y_{ref}(k)$ - vector of future set points;
$u(k|t)$ - vector of future control inputs;
N - prediction horizon;
N_c - control horizon.

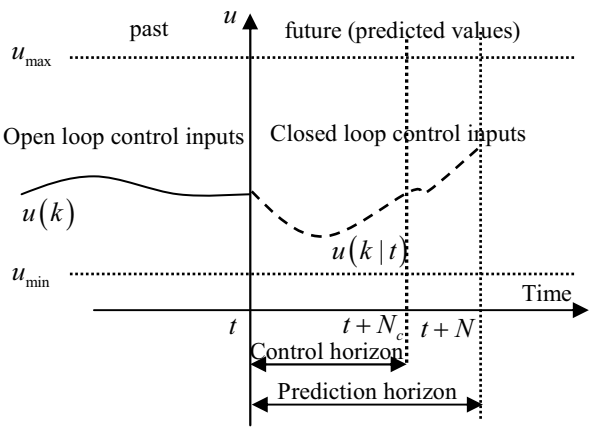

Figure 7: The Control Inputs Applied to the System Using the Predictive Control Strategy (Stinga 2012)

PREDICTIVE CONTROL OF THE INDUCTION MOTOR

The model is based on the ideas presented in Merabet 2012. The model of the motor is written in the stationary frame (α, β), in terms of stator currents and rotor flux. The outputs chosen to be controlled are the mechanical speed and the modulus of the rotor flux.
The control diagram uses a state observer based on the motor model, adjustable on basis of stator currents errors. It results the sensorless diagram depicted in Fig. 8.

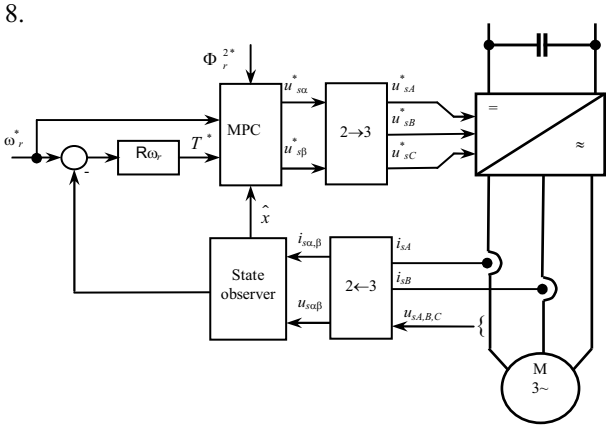

Figure 8: The Control Diagram of the Sensorless Predictive Control

The simulation of the control system for the same operation as in Fig. 2 and 5 determined the evolutions plotted in Fig. 9. This time, the currents plot displays the (α, β) components.

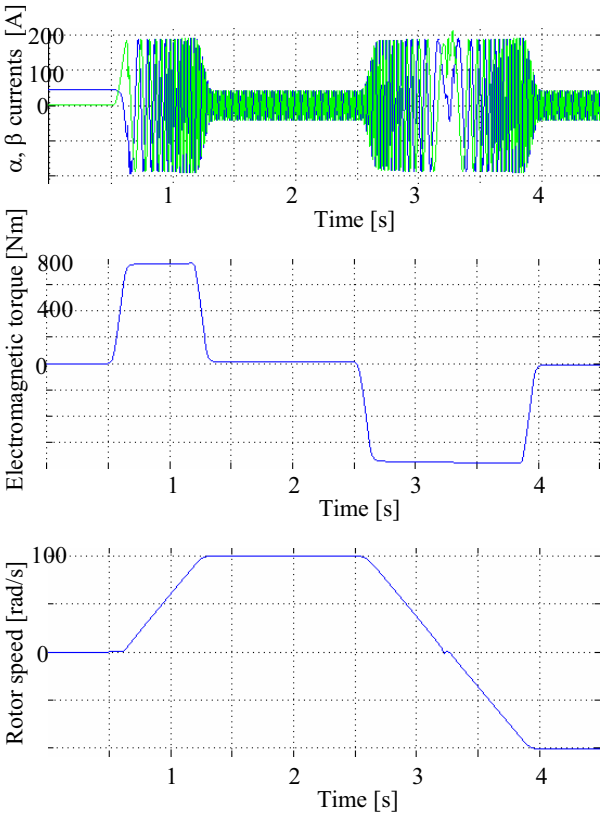

Figure 9: Simulation of the Sensorless Predictive Control of the Induction Motor

It is noticed that the general behaviour of the drive keeps good shapes for the plotted signals.

CONCLUSIONS

The paper describes some control possibilities for the induction motor. The rotor flux vector control is analysed and the influence of the stator resistance variance is discussed. A control diagram which avoids the effects of these variations is presented and simulated. The results plotted in Fig. 5 emphasis good dynamic behaviour. For the considered motor (55 kW), the acceleration time up to the rated speed is only 0.65 seconds. Further, the model predictive control of the induction motor is analysed. The goal of the research is to implement the predictive control for an industrial drive which will be offered on the market. The results of the simulation, presented in Fig. 9 highlight the behaviour of the drive. The dynamic performances are slightly reduced (acceleration time 0.8 seconds), but the advantages of the sensorless control must be underlined. Further research will be focused both on the improvement of the dynamic performances and on the stability study and immunity to the parameters variations.

ACKNOWLEDGMENTS

Authors whish to thank the UEFISCDI and their partners in the HYDICO project (PN-II-PT-PCCA-2011-3.2-1082), in the frame of which their study has been performed.

REFERENCES

Almer S. et al. 2010. "Piecewise Affine Modeling and Control of a Step-Up DC-DC Converter". *American Control Conference Paper* ThB05.3.

Baader U., Depenbrock M., Gierse G. 1992. "Direct self control (DSC) of inverter-fed induction machine: a basis for speed control without speed measurement". In *IEEE Transactions on Industrial Applications*, vol. 28, pp. 581–588.

Casadei D., Profumo F., Serra G., Tani A. 2002. "FOC and DTC: Two Viable Schemes for Induction Motors Torque Control", In *IEEE Trans. Power Electronics*, Vol. 17, nr.5.

Ehsani M. et al. 1997. "Propulsion system design of electric and hybrid vehicles". In *IEEE Trans. Industrial Electronics*, vol. 45, nr.1, pp 19-27.

Faiz J. et al. 1999. "Direct torque control of induction motor for electric propulsion systems," In *International Journal on Power Systems*, vol. 51, pp. 95–101.

Geyer T. et al. 2008. "Hybrid Model Predictive Control of the Step Down DC-DC Converter". In *IEEE Trans. Contr. Syst. Technol*. Vol. 16, no.6, pp. 1112-1124.

Geyer T. et al. 2009. "Model Predictive Direct Torque Control—Part I: Concept, Algorithm, and Analysis". In *IEEE Transactions on Industrial Electronics*. Vol. 56, no.6, pp. 1894-1905.

Haddoun A., Benbouzid M., Dialo D., Abdessemed R., Ghouili J., Srairi K. 2007. "A loss-minimization DTC Scheme for EV Induction Motor" In *IEEE Transactions on vehicle technology*, vol.56, nr.1, pp.81-88.

Ivanov, S. 2009. "The influence of the sampling period on the performance of the regulation by DTC of the induction motor". In *Proceedings of the 23rd European Conference on Modelling and Simulation*, Madrid, Spain, 776-780.

Ivanov, S., 2010. "Continuous DTC of the Induction Motor". In *Advances in Electrical and Computer Engineering*, vol. 10, no. 4, 149-154. (http://dx.doi.org/10.4316/AECE.2010.04024).

Larrinaga S.A. et al. 2007. "Predictive Control Strategy for DC/AC Converters Based on Direct Power Control". In *IEEE Trans. Ind. Electronics*. Vol. 54, no.3, pp. 1261-1270.

Mariethoz S. et al. 2010. "Comparison of Hybrid Control Techniques for Buck and Boost DC-DC Converters". In *IEEE Trans. Contr. Syst. Technol*. Vol. 18, no.5, pp. 1126-1145.

Merabet A. 2012. "*Nonlinear model predictive control for induction motor drive*" – chapter in "Frontiers of Model Predictive Control", edited by Zheng, T, Intechweb.org, pp. 109-130.

Prieur C. and Tarbouriech S. 2011. "New directions in hybrid control systems" (editorial). In *Int. Journal Robust Nonlin. Control*. Vol. 21, pp. 1063-1065.

Richter S. et al. 2010. "High-Speed Online MPC Based on a Fast Gradient Method Applied to Power Converter Control". *American Control Conference Paper* FrA01.6.

Rodriguez J. et al. 2007. "Predictive Current Control of a Voltage Source Inverter". In *IEEE Trans. Ind. Electronics*. Vol. 54, no.1, pp. 495-503.

Seo S. et al. 2009. "Hybrid Control System for Managing Voltage and Reactive Power". *In the JEJU Power System, Journal of Electrical Eng. and Technol*. Vol. 4, no.4 pp. 429-437.

Shi X.L. et al. 2007. "Implementation of Hybrid Control for Motor Drives". In *IEEE Trans. Ind. Electronics*. Vol. 54, no. 4, pp. 1946-1952.

Takahashi I. and Noguchi T. 1986. "A new quick-response and high efficiency control strategy of an induction motor". In *IEEE Transactions on Industrial Applications*. vol. IA-22, no.5, pp. 820-827.

Trabelsi M. et al. 2008. "Hybrid Control of a Three-Cell Converter Associated to an Inductive Load". *IEEE paper* 978-1-4244-1668-4/08.

Vas P. 1998. *Sensorless Vector and Direct Torque Control*. Clarendon Press, Oxford.

Camacho E.F. and Bordons C. 2004. *Model predictive control*. Springer-Verlag.

Bemporad A. 2007. *Model predictive control of hybrid systems*, 2nd HYCON PhD. School on Hybrid Systems, Siena.

Lazăr M. 2006. *Model Predictive Control of Hybrid Systems: Stability and Robustness*, Ph.D. Thesis, Eindhoven, Holland.

Maciejowski J.M. 2000. *Predictive control with constraints*, Prentince Hall.

Stinga F. 2012. *Control strategies for hybrid systems. Applications*, Ph.D. Thesis, Craiova, Romania.

AUTHOR BIOGRAPHIES

SERGIU IVANOV was born in Hunedoara, Romania and went to the University of Craiova, where he studied electrical engineering. He obtained his degree in 1986. He worked for the Institute for Research in Motors, Transformers and Electrical Equipment Craiova before moving in 1991 to the University of Craiova. He obtained his PhD in 1998 with a topic in the field of the control of the electric drives systems. He is involved in modelling of the electromechanical systems.

VLADIMIR RASVAN graduated from the Polytechnic Institute of Bucharest, Romania in 1967 (Automatic Control) and obtained his Ph.D. in System Theory in 1972. After a 10 years career in applied research for control in Power systems, he became an associate professor (1982) and eventually professor (1990) at the University of Craiova. His main scientific interests are in mathematical approaches for dynamics in engineering systems. He is author of 7 books and some 200 papers published in scientific journals and proceedings of scientific/technical conferences.

EUGEN BOBAŞU received the B.S. and M.Sc. degrees (1977), both in automatic control, and the Ph.D. degree in control

systems (1997) from the University of Craiova, Romania. Since 1981 he is with the University of Craiova, where he is currently Professor in the Department of Automatic Control.
He is involved in national and international research projects in the field of modelling, identification and hydraulics. His present research interests are on modelling of complex systems and identification of nonlinear systems. He has published more than 90 journal and conference papers, and he is author or co-author of 5 books.
Prof. Bobaşu is member of IEEE, SRAIT and of ARR.

DAN POPESCU received the B.S. and M.Sc. degrees (1977), both in automatic control, and the Ph.D. degree in control systems (1997) from the University of Craiova, Romania. Since 1981 he is with the University of Craiova, where he is currently Professor in the Department of Automation, Electronics and Mechatronics. His present research interests are on robust control, time delay systems and predictive control. Prof. POPESCU is member of IEEE and IFAC TC 2.5 "Robust Control".

FLORIN STINGA was born in Craiova, Romania. He received the B. Eng., M.S. and Ph.D. degrees in system engineering, all from University of Craiova, in 2000, 2003 and 2012. Currently, he is Assistant Professor in the Department of Automation, Electronics and Mechatronics at the Faculty of Automation, Computers and Electronics, Craiova. His researches interested are in hybrid dynamical systems and embedded systems.

VIRGINIA IVANOV was born in Vela, Dolj, Romania, 1963. She was graduated in Electrical Engineering at University of Craiova, Romania, in 1986 and Doctor in Electrical Engineering in 2004. From 1986 to 1998 she worked as researcher with the Researching Institute for Motors, Transformers and Electric Equipment Craiova. In 1998 she joined the Faculty for Electrical Engineering, Department of Electrical Equipment and technologies.

STATE-SPACE CONSTRAINED MODEL PREDICTIVE CONTROL

Daniel Honc and František Dušek
Department of Process Control
Faculty of Electrical Engineering and Informatics
University of Pardubice
nám. Čs. legií 565, 532 10 Pardubice, Czech Republic
E-mail: daniel.honc@upce.cz

KEYWORDS
State-space Model Predictive Control, Constrained MPC, Laboratory Hydraulic-Pneumatic System.

ABSTRACT

Constrained State-space Model Predictive Control is presented in the paper. Predictive controller based on incremental linear state-space process model and quadratic criterion is derived. Typical types of constraints are considered – limits on manipulated, state and controlled variables. Control experiments with nonlinear model of multivariable laboratory process are simulated first and real experiment is realized afterwards.

INTRODUCTION

Model Predictive Control is very popular control method treated in academic area and used in industry as well (Clarke et al. 1987a; Clarke et al. 1987b; Clarke and Mohtadi 1989; Camacho and Bordons 2007). It is very general, easy to understand and intuitive concept how to solve optimal control problem. Future control actions are calculated to minimize quadratic cost function - at least future control movements and control errors are penalized. Dynamic model of the process is used for future plant behaviour – to calculate vector of future controlled variable. Only actual control action (first element from the vector of calculated control actions) is applied to the process and whole procedure is repeated – this is called receding horizon concept and it introduces feedback in some way. Many process models exist and also cost function formulations which gives arise to wide range of different methods. Some of them are more practical and some are treated by academicians more frequently.

In the paper Constrained State-space Model Predictive Control is presented as very powerful approach. Calculations are straightforward and easy to program. Using of state-space model leads naturally to matrix formulation of prediction equations even for multivariable systems, terminal state can be easily penalized in the cost function and constrains on the state variables can be respected too. The last mentioned property is a key feature for the paper – because our controlled process has state variables with limits that should not be exceeded. Furthermore not all the state variables are measured so they must be estimated which is another elegant task for state-space models. Predictive controller is derived fist and applied to a laboratory process afterwards.

STATE-SPACE PREDICTIVE CONTROLLER

Following finite horizon quadratic criterion is considered

$$J = \sum_{j=N_1}^{N_2} \sum_{m=1}^{n_y} r_m \left[w_m(k+j) - \hat{y}_m(k+j) \right]^2 + \\ + \sum_{j=1}^{N_3} \sum_{n=1}^{n_u} q_n \Delta u_n(k+j-1)^2 \tag{1}$$

Where N_1 and N_2 are minimum and maximum prediction horizons, N_3 is control horizon - after first N_3 control moves the control signal is kept constant, n_y is number of the system outputs, n_u is number of the system inputs, $y_m(k+j)$ is an optimum j-step ahead prediction of the m-th system output, $w_m(k+j)$ is a future set-point or reference sequence for the m-th output. $\Delta u_n(k+j\text{-}1) = u_n(k+j\text{-}1) - u_n(k+j\text{-}2)$ is n-th control increment, r_m and q_n are positive weighting coefficients.

State-space model for multivariable process is expressed as

$$\begin{aligned} \bar{\mathbf{x}}(k+1) &= \overline{\mathbf{M}}\,\bar{\mathbf{x}}(k) + \overline{\mathbf{N}}\,\mathbf{u}(k) \\ \mathbf{y}(k) &= \overline{\mathbf{Q}}\,\bar{\mathbf{x}}(k) \end{aligned} \tag{2}$$

$$\mathbf{u}(k) = \begin{bmatrix} u_1(k) \\ u_2(k) \\ \vdots \\ u_{n_u}(k) \end{bmatrix}, \quad \bar{\mathbf{x}}(k) = \begin{bmatrix} x_1(k) \\ x_2(k) \\ \vdots \\ x_{n_x}(k) \end{bmatrix}, \quad \mathbf{y}(k) = \begin{bmatrix} y_1(k) \\ y_2(k) \\ \vdots \\ y_{n_y}(k) \end{bmatrix}$$

where $\bar{\mathbf{x}}(k)$ is the state vector composed from n_x state variables, $\mathbf{u}(k)$ is vector of inputs, $\mathbf{y}(k)$ is vector of outputs and $\overline{\mathbf{M}}$, $\overline{\mathbf{N}}$ and $\overline{\mathbf{Q}}$ are system matrices.

If we extend the state vector with the last control action $\mathbf{u}(k\text{-}1)$, we get the state-space system with control increments as inputs (incremental form)

Proceedings 27th European Conference on Modelling and Simulation ©ECMS Webjørn Rekdalsbakken, Robin T. Bye, Houxiang Zhang (Editors)
ISBN: 978-0-9564944-6-7 / ISBN: 978-0-9564944-7-4 (CD)

$$\underbrace{\begin{bmatrix}\bar{\mathbf{x}}(k+1)\\ \mathbf{u}(k)\end{bmatrix}}_{\mathbf{x}(k+1)}=\underbrace{\begin{bmatrix}\overline{\mathbf{M}} & \overline{\mathbf{N}}\\ \mathbf{0}_{n_u\times n_x} & \mathbf{I}_{n_u\times n_u}\end{bmatrix}}_{\mathbf{M}}\underbrace{\begin{bmatrix}\bar{\mathbf{x}}(k)\\ \mathbf{u}(k-1)\end{bmatrix}}_{\mathbf{x}(k)}+$$
$$+\underbrace{\begin{bmatrix}\overline{\mathbf{N}}\\ \mathbf{I}_{n_u\times n_u}\end{bmatrix}}_{\mathbf{N}}\Delta\mathbf{u}(k) \tag{3}$$
$$\mathbf{y}(k)=\underbrace{\begin{bmatrix}\overline{\mathbf{Q}} & \mathbf{0}_{n_y\times n_u}\end{bmatrix}}_{\mathbf{Q}}\underbrace{\begin{bmatrix}\bar{\mathbf{x}}(k)\\ \mathbf{u}(k-1)\end{bmatrix}}_{\mathbf{x}(k)}$$

The optimum one-step ahead prediction of the model output is

$$\begin{aligned}\hat{\mathbf{x}}(k+1)&=\mathbf{M}\,\mathbf{x}(k)+\mathbf{N}\,\Delta\mathbf{u}(k)\\ \hat{\mathbf{y}}(k+1)&=\mathbf{Q}\,\hat{\mathbf{x}}(k+1)=\mathbf{QM}\,\mathbf{x}(k)+\mathbf{QN}\,\Delta\mathbf{u}(k)\end{aligned} \tag{4}$$

The optimum two-step ahead prediction is

$$\begin{aligned}\hat{\mathbf{x}}(k+2)&=\mathbf{M}\,\hat{\mathbf{x}}(k+1)+\mathbf{N}\,\Delta\mathbf{u}(k+1)=\mathbf{M}^2\,\mathbf{x}(k)+\\ &+\mathbf{MN}\,\Delta\mathbf{u}(k)+\mathbf{N}\,\Delta\mathbf{u}(k+1)\\ \hat{\mathbf{y}}(k+2)&=\mathbf{Q}\,\hat{\mathbf{x}}(k+2)=\mathbf{QM}^2\,\mathbf{x}(k)+\mathbf{QMN}\,\Delta\mathbf{u}(k)+\\ &+\mathbf{QN}\,\Delta\mathbf{u}(k+1)\end{aligned} \tag{5}$$

Generally the optimum j-step ahead prediction is

$$\hat{\mathbf{y}}(k+j)=\mathbf{QM}^j\,\mathbf{x}(k)+\sum_{i=0}^{j-1}\mathbf{QM}^{j-i-1}\mathbf{N}\,\Delta\mathbf{u}(k+i) \tag{6}$$

Set of N_2 j-step ahead predictions starting from N_1 and with N_3 future control moves in matrix form can be expressed as

$$\mathbf{Y}=\mathbf{H}\Delta\mathbf{U}+\mathbf{F}\mathbf{x}(k) \tag{7}$$

where $\mathbf{Y}$, $\Delta\mathbf{U}$ and $\mathbf{F}$ are

$$\mathbf{Y}=\begin{bmatrix}\hat{\mathbf{y}}(k+N_1)\\ \hat{\mathbf{y}}(k+N_1+1)\\ \vdots\\ \hat{\mathbf{y}}(k+N_2)\end{bmatrix},\ \Delta\mathbf{U}=\begin{bmatrix}\Delta\mathbf{u}(k)\\ \Delta\mathbf{u}(k+1)\\ \vdots\\ \Delta\mathbf{u}(k+N_3-1)\end{bmatrix},$$
$$\mathbf{F}=\begin{bmatrix}\mathbf{QM}^{N_1}\\ \mathbf{QM}^{N_1+1}\\ \vdots\\ \mathbf{QM}^{N_2}\end{bmatrix}.$$

and $\mathbf{H}$ is block lower triangular matrix with its non-null i-row and j-column elements defined by $(\mathbf{H})_{ij}=\mathbf{QM}^{i-j}\mathbf{N}$. First term of (7) is called as forced response and second part as free response – response from actual state without changing the manipulated variables.

Criterion (1) can be rewritten in matrix form as

$$J=(\mathbf{W}-\mathbf{Y})^T\,\overline{\mathbf{R}}(\mathbf{W}-\mathbf{Y})+\Delta\mathbf{U}^T\,\overline{\mathbf{Q}}\Delta\mathbf{U} \tag{8}$$

where $\mathbf{W}$ is

$$\mathbf{W}=\begin{bmatrix}\mathbf{w}(k+N_1)\\ \mathbf{w}(k+N_1+1)\\ \vdots\\ \mathbf{w}(k+N_2)\end{bmatrix}$$

and $\overline{\mathbf{R}}$ and $\overline{\mathbf{Q}}$ are diagonal matrices filled with diagonal sub matrices of weighting coefficients.

If we substitute predictions from (7) into equation (8) we get

$$\begin{aligned}J&=(\mathbf{W}-\mathbf{H}\Delta\mathbf{U}-\mathbf{F}\mathbf{x}(k))^T\,\overline{\mathbf{R}}(\mathbf{W}-\mathbf{H}\Delta\mathbf{U}-\mathbf{F}\mathbf{x}(k))+\\ &+\Delta\mathbf{U}^T\,\overline{\mathbf{Q}}\Delta\mathbf{U}=\mathbf{U}^T\mathbf{S}\Delta\mathbf{U}+2\mathbf{s}^T\Delta\mathbf{U}+k\end{aligned} \tag{9}$$

where $\mathbf{S}$, $\mathbf{s}$ and k are

$$\mathbf{S}=\mathbf{H}^T\,\overline{\mathbf{R}}\mathbf{H}+\overline{\mathbf{Q}},\quad \mathbf{s}=-\mathbf{H}^T\,\overline{\mathbf{R}}(\mathbf{W}-\mathbf{F}\mathbf{x}(k)),$$
$$k=(\mathbf{W}-\mathbf{F}\mathbf{x}(k))^T\,\overline{\mathbf{R}}(\mathbf{W}-\mathbf{F}\mathbf{x}(k))$$

Without constraints explicit solution - minimization of (9) can be expressed as

$$\begin{aligned}\Delta\mathbf{U}_{N3}&=-\mathbf{S}^{-1}\cdot\mathbf{s}=\\ &=\underbrace{\left(\mathbf{H}^T\,\overline{\mathbf{R}}\mathbf{H}+\overline{\mathbf{Q}}\right)^{-1}\mathbf{H}^T\,\overline{\mathbf{R}}}_{\mathbf{L}}(\mathbf{W}-\mathbf{F}\mathbf{x}(k))\end{aligned} \tag{10}$$

Control law is a linear gain matrix $\mathbf{L}$ that multiplies predicted control error – difference between future reference and free response of the plant. Receding strategy means that only first element of the sequence $\Delta\mathbf{U}_{N3}$ is applied to process and next control action is calculated according to a new state of the process which must be measured or observed.

Numerical optimization method must be used if manipulated, state or controlled variables are constrained or other types of constrains occurs. Minimization of (9) with respect to linear inequalities

$$\mathbf{A}\cdot\Delta\mathbf{U}\le\mathbf{b} \tag{11}$$

is called Quadratic Programming (QP).

In the following text transformation to the form of equation (11) is shown for typical and often used constraints types.

a) Limits on the manipulated variables

$$\mathbf{u}_{\min} \le \mathbf{u}(i) \le \mathbf{u}_{\max}, \quad i \in \{k, k+N_3-1\} \tag{12}$$

$$\begin{bmatrix} \mathbf{I}_{n_u \times n_u} & \cdots & \mathbf{0}_{n_u \times n_u} \\ \vdots & \ddots & \vdots \\ \mathbf{I}_{n_u \times n_u} & \cdots & \mathbf{I}_{n_u \times n_u} \end{bmatrix} \Delta\mathbf{U} \le \begin{bmatrix} \mathbf{I}_{n_u \times n_u} \\ \vdots \\ \mathbf{I}_{n_u \times n_u} \end{bmatrix} (\mathbf{u}_{\max} - \mathbf{u}(k-1)) \tag{13}$$

$$\begin{bmatrix} -\mathbf{I}_{n_u \times n_u} & \cdots & \mathbf{0}_{n_u \times n_u} \\ \vdots & \ddots & \vdots \\ -\mathbf{I}_{n_u \times n_u} & \cdots & -\mathbf{I}_{n_u \times n_u} \end{bmatrix} \Delta\mathbf{U} \le \begin{bmatrix} -\mathbf{I}_{n_u \times n_u} \\ \vdots \\ -\mathbf{I}_{n_u \times n_u} \end{bmatrix} (\mathbf{u}_{\min} - \mathbf{u}(k-1)) \tag{14}$$

b) Limits on the state variables

$$\mathbf{x}_{\min} \le \mathbf{x}(i) \le \mathbf{x}_{\max}, \quad i \in \{k+1, k+N_2\} \tag{15}$$

$$\begin{bmatrix} \mathbf{N} & \mathbf{0} & \cdots & \mathbf{0} \\ \mathbf{MN} & \mathbf{N} & \cdots & \mathbf{0} \\ \vdots & \vdots & \ddots & \vdots \\ \mathbf{M}^{N_2-1}\mathbf{N} & \mathbf{M}^{N_2-2}\mathbf{N} & \cdots & \mathbf{N} \end{bmatrix} \Delta\mathbf{U} \le \begin{bmatrix} \mathbf{I}_{n_x \times n_x} \\ \mathbf{I}_{n_x \times n_x} \\ \vdots \\ \mathbf{I}_{n_x \times n_x} \end{bmatrix} \mathbf{x}_{\max} - \begin{bmatrix} \mathbf{M} \\ \mathbf{M}^2 \\ \vdots \\ \mathbf{M}^{N_2} \end{bmatrix} \mathbf{x}(k) \tag{16}$$

$$-\begin{bmatrix} \mathbf{N} & \mathbf{0} & \cdots & \mathbf{0} \\ \mathbf{MN} & \mathbf{N} & \cdots & \mathbf{0} \\ \vdots & \vdots & \ddots & \vdots \\ \mathbf{M}^{N_2-1}\mathbf{N} & \mathbf{M}^{N_2-2}\mathbf{N} & \cdots & \mathbf{N} \end{bmatrix} \Delta\mathbf{U} \le \begin{bmatrix} -\mathbf{I}_{n_x \times n_x} \\ -\mathbf{I}_{n_x \times n_x} \\ \vdots \\ -\mathbf{I}_{n_x \times n_x} \end{bmatrix} \mathbf{x}_{\min} + \begin{bmatrix} \mathbf{M} \\ \mathbf{M}^2 \\ \vdots \\ \mathbf{M}^{N_2} \end{bmatrix} \mathbf{x}(k) \tag{17}$$

b) Limits on the controlled variables

$$\mathbf{y}_{\min} \le \mathbf{y}(i) \le \mathbf{y}_{\max}, \quad i \in \{k+N_1, k+N_2\} \tag{18}$$

$$\mathbf{H}\Delta\mathbf{U} \le \begin{bmatrix} \mathbf{I}_{n_y \times n_y} \\ \vdots \\ \mathbf{I}_{n_y \times n_y} \end{bmatrix} \mathbf{y}_{\max} - \mathbf{F}\mathbf{x}(x) \tag{19}$$

$$-\mathbf{H} \cdot \Delta\mathbf{U} \le \begin{bmatrix} -\mathbf{I}_{n_y \times n_y} \\ \vdots \\ -\mathbf{I}_{n_y \times n_y} \end{bmatrix} \mathbf{y}_{\min} + \mathbf{F}\mathbf{x}(x) \tag{20}$$

Practically it means that we have to calculate Hess matrix **S** (as function of process model and penalizations only) and gradient **s** (except process model and penalization also function of future set-point and actual state – predicted control error), fill linear inequalities matrix **A** and vector **b** and use QP to find optimal future control actions. Again only first element is applied as control action to the process and whole procedure is repeated in next sample time – only gradient **s** is updated and QP is solved.

LABORATORY PROCESS

Laboratory Hydraulic-Pneumatic System (HPS) was designed and realized at Department of Process Control University of Pardubice (Klán et al. 2005; Honc and Dušek 2012) - see Fig. 1. It includes a combination of hydraulic and pneumatic components. The pneumatic circuits H and L create cross coupling between both classical double tank sections and form a multivariable system with non-typical feature – multivariable effect exists in transient state only. Water is pumped by two pumps into upper tanks LH and RH, flows into lower tanks LL and RL and from here back into the reservoir. Water flow rates are controlled by input signal of the pumps u_L, u_R. The levels in lower tanks are measured indirectly by difference pressure sensors with output signals y_L, y_R.

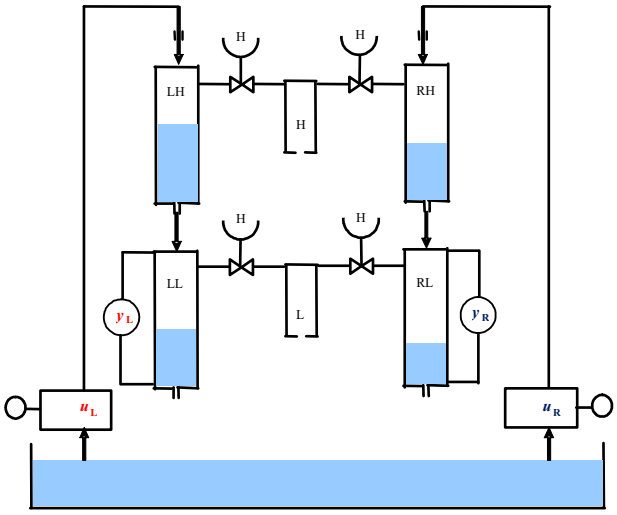

Figure 1: Scheme of HPS

CONTROL OBJECTIVE

Our task is to control water levels in lower tanks – to control multivariable system with two inputs and two outputs. Problem from the control point of view is easy overflow or underflow of higher tanks. Higher water

levels are not measured so no direct safety actions can be applied. For conventional controllers only ad-hoc solution for specific set-point shape, change size or working point is possible by tuning the controller, setting slew rate limits on the control signal or by set-point modification. If we have state-space model of the process and use state observer we have full information about the state variables (water levels in all tanks and pressure in pneumatic loop) and we can solve problem synergistically as "state variables constrained model predictive control". We will calculate optimal control actions without violation higher water tanks maximum or minimum levels and also with respect to the input and output process variables limits.

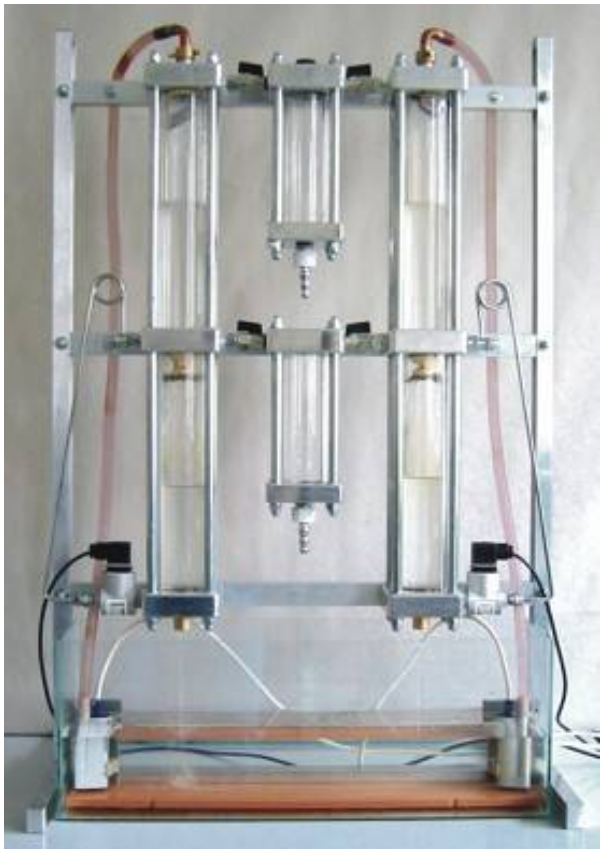

Figure 2: Hydraulic-Pneumatic System

CONTROL EXPERIMENTS

Control experiments are simulated with nonlinear process model first and real experiment is carried out afterwards. Nonlinear model together with its linearized form was presented in (Honc and Dušek 2012). Predictive controller is using state-space 5th order linear model with two inputs and two outputs. Parameters of predictive controller are listed in Table 1. Set-points are changed in time 10 and 20 minutes as step changes. Sample time of the controller is 10 s. Response of the simulated control experiment are plotted in Fig. 3 and Fig. 4. Real control experiment is in Fig. 5 and Fig. 6. Meaning of the used variables is in Table 2.

Table 1: MPC Parameters

Parameter	Value
N_1	1
N_2	18
N_3	18
r_1, r_2	1
q_1, q_2	5

Table 2: Variables Notation

Variable	Meaning
u_L, u_R	pump control voltages
y_L, y_R	pressure sensors signals
h_{LL}	water level in left lower tank
h_{RL}	water level in right lower tank
h_{LH}	water level in left higher tank
h_{RL}	water level in right higher tank

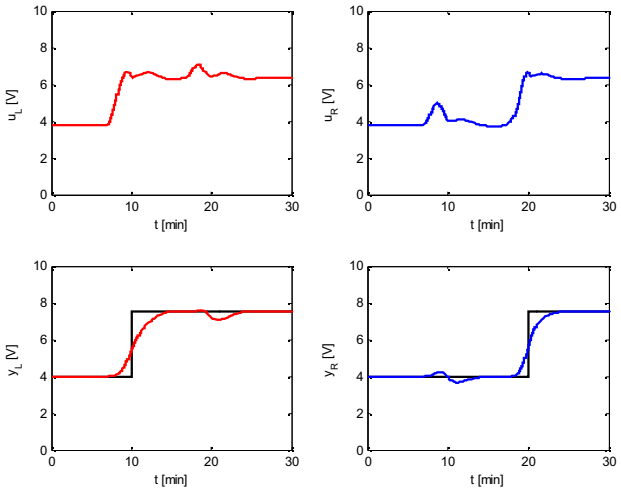

Figure 3: Simulated Control Experiment

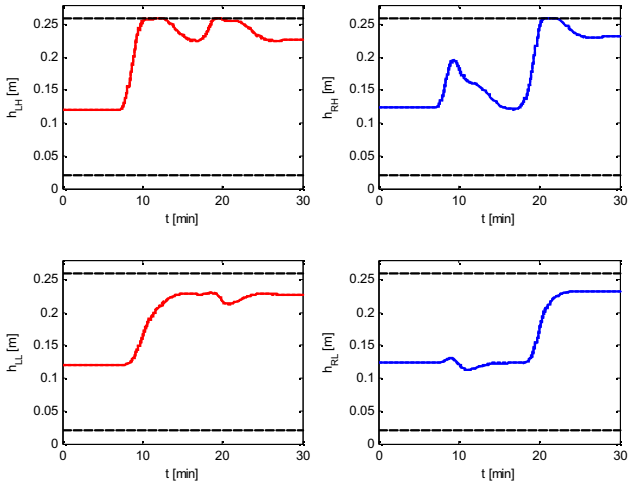

Figure 4: Water Levels by Simulated Experiment

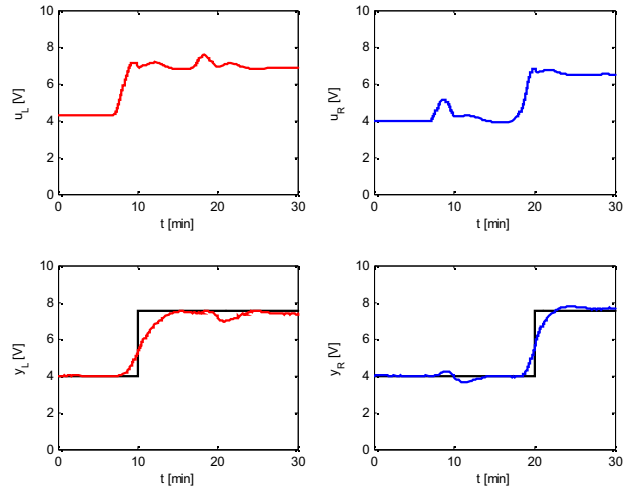

Figure 5: Real Control Experiment

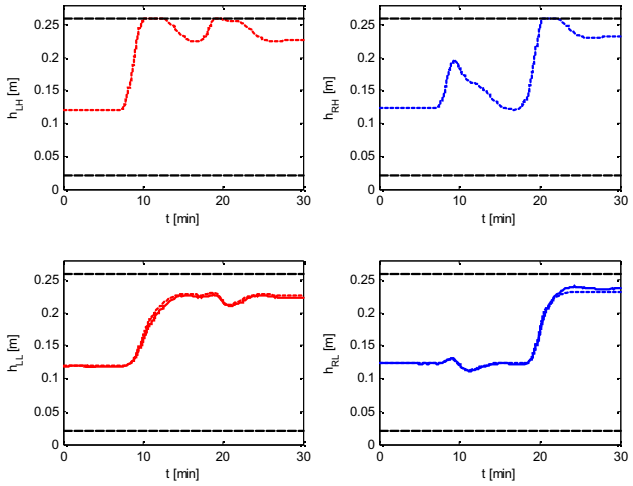

Figure 6: Water Levels by Real Experiment

CONCLUSIONS

State-space Constrained Model Predictive Control was presented and applied in the paper. The key feature for our laboratory application can be seen in Fig. 4 and Fig. 6 – water levels in higher tanks LH and RH do not exceed limits marked by horizontal dashed line – controller respects state variables constraints. There are two trends – solid line for simulated or measured variable and dotted line for its estimation. By real experiment we do not have information about water level in higher tanks – we can only estimate those variables. The other interesting feature is that the control actions starts even before the set-point step change. This is because the predictive controller knows future set-points on whole control horizon and can react in "predictive" way. This information together with multidimensionality of the controller significantly reduces cross effects – changes in other manipulated variables act as disturbances. Similarity of responses in Fig. 3 and Fig. 5 can be seen as a proof of model quality. Model Predictive Control with state-space process model is very elegant and straightforward example of modern control technique. Its application is enabled with increase of computational power and development of automation means. Existence of state-space model of the controlled system is the prerequisite. Derivation and programming of the prediction equations is easy compared to solving of Diophantine equations in case of multivariable input-output process model. Also criterion extension of terminal state or other requirements is possible as well as dealing with constraints on state variables. State estimation allows us to take into account also unmeasured or immeasurable information and it is from some point of view optimal way of filtering. Some disadvantage of using the state for the controller arises if measurement or estimation is not unbiased or model mismatches. Then the controller leaves steady-state control error – the controlled variable estimation follows the set-point but the real output has an offset.

This research was supported by Institutional support of The Ministry of Education, Youth and Sports of the Czech Republic.

REFERENCES

Camacho, E.F.; C. Bordons. 2007. *Model Predictive Control*. Springer-Verlag London Limited, Great Britain.

Clarke, D.W.; C. Mohtadi; P.S. Tuffs. 1987a. "Generalized Predictive Control – Part I. The Basic Algorithm", *Automatica*, Vol. 23, No. 2, 137-148.

Clarke, D.W.; C. Mohtadi; P.S. Tuffs. 1987b. "Generalized Predictive Control – Part II. Extensions and Interpretations", *Automatica*, Vol. 23, No. 2, 149-160.

Clarke, D.W., C. Mohtadi. 1989. "Properties of Generalized Predictive Control", *Automatica*, Vol. 25, No. 6, 859-875.

Honc, D.; F. Dušek. 2012. "Novel multivariable laboratory plant". In *26th European Conference on Modelling and Simulation*, (Koblenz, Germany, May 29 - June 1). ECMS, 468-473.

Klán, P.; M. Hofreiter; J. Macháček; O. Modrlák; L. Smutný and V. Vašek. 2005. "Process Models for a New Control Education Laboratory". In *16th World IFAC Congress*, (Prague, Czech Republic, July 4 - 8).

DANIEL HONC was born in Pardubice, Czech Republic and studied University of Pardubice field of Process Control and obtained his Ph.D. degree in 2002. He is head of the Department of Process Control at Faculty of Electrical Engineering and Informatics. His e-mail address is: daniel.honc@upce.cz.

FRANTIŠEK DUŠEK was born in Dačice, Czech Republic and studied Faculty of Chemical Technology Pardubice field of Automation and obtained his MSc. degree in 1980. He worked for pulp and paper research institute IRAPA. Now he is a vice dean of Faculty of Electrical Engineering and Informatics. In 2001 he became Ass. professor. His e-mail address is: frantisek.dusek@upce.cz.

SATURATION RELAY VS. RELAY TRANSIENT IDENTIFICATION TESTS FOR A TDS MODEL

Libor Pekař
Roman Prokop
Faculty of Applied Informatics, Tomas Bata University in Zlín
nám. T. G. Masaryka 5555, 76001, Czech Republic
E-mail: {pekar, prokop}@fai.utb.cz

KEYWORDS
Saturation relay, ATV+, Autotuning, Time delay system, Heating system.

ABSTRACT

The paper brings a comparison of two novel combinations of a relay identification test with a Time Delay System (TDS) model. Namely, the on/off plus saturation relay test and relay transient experiment are introduced. In the former case with more then two unknown model parameters, it is necessary to apply some technique for frequency response multiple-points identification; here, the Autotune Variation Plus (ATV+) procedure introducing an artificial delay is utilized. Limit cycles data are evaluated via an unordinary time-domain approach and using the Discrete Time Fourier Transform (DTFT), respectively. Both methodologies are verified and compared on a model of the circuit heating laboratory system with internal delays.

INTRODUCTION

By autotuning (i.e. automatic tuning), a set of methods which enable the controller to be tuned automatically on demand from an operator or an external signal is meant (Åström and Hägglund 1984; Hang et al. 2002). Industrial experience has clearly indicated that this is highly desirable and useful feature. The whole procedure usually consists of two basic steps: Process model parameters identification followed by controller tuning; however, some approaches do not require explicit model identification.

The relay feedback autotuning (identification) test performing limit cycle oscillations was successfully applied to the autotuning of PID controllers in (Åström and Hägglund 1984) and it is widely used and in practice as a well applicable technique. It is robust, easy to implement, timesaving, easy to use and close-loop control which keeps the process close to the setpoint. The classical relay-feedback loop scheme with a symmetrical relay is depicted in Figure 1.

If the process is stabilizable and has a phase lag of at least π radians, the process input $u(t)$ and output $y(t)$ are logged until the system reaches stationary oscillations, the amplitude A of error $e(t)$ equals the amplitude of $y(t)$ and the phase shift between $e(t)$ and $y(t)$ is $-\pi$.

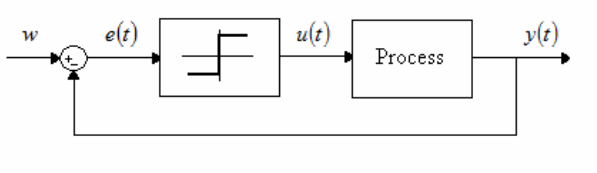

Figure 1: Relay-feedback Test Scheme

However, the original relay feedback test - sometimes called ATV (Autotune Variation) – see (Luyben 1987; Yu 2006) – has two basic drawbacks. First, due to an approximation, the estimation of the critical point is not accurate enough for some processes, such as those with large time delays (Wang et al. 1999). For example, there is an error of 23% for a first order unstable system with input-output delay. Second, the basic test enables to estimate only single point of the frequency characteristics. Hence, there have been investigated and developed many advanced techniques, which should eliminate the two mentioned deficiencies. Much research has been undertaken in identifying multiple points on the process frequency response, for instance, inserting of an integral or a delay element into the open loop (Scali et al. 1999; Tan et al. 1996).

In this paper, the basic on/off relay test is improved by the use of a saturation relay (Shen et al. 1996; Yu 2006) for more accurate model parameters estimation followed by the above mentioned artificial-delay test. This approach is confronted with a technique utilizing the relay transient with DTFT (Hang et al 1995; Wang et al. 1997). The advantage of the latter method is that arbitrarily many points on the Nyquist curve can be estimated by a single test.

The novel merit of this contribution is that the two methods are verified and benchmarked on a simulated identification relay experiment for a TDS model of a circuit heating laboratory plant (Dostálek et al. 2008; Pekař et al. 2009).

Proceedings 27th European Conference on Modelling and Simulation ©ECMS Webjørn Rekdalsbakken, Robin T. Bye, Houxiang Zhang (Editors)
ISBN: 978-0-9564944-6-7 / ISBN: 978-0-9564944-7-4 (CD)

RELAY-FEEDBACK TEST

Let us concisely describe model parameters estimation from the relay feedback test. Consider a simple feedback with and on/off relay as in Figure 1. If the process is stabilizable and has a phase lag of at least π radians, the process input $u(t)$ and output $y(t)$ are logged until the system reaches stationary oscillations, the amplitude A of error $e(t)$ equals the amplitude of $y(t)$ and the phase shift between $e(t)$ and $y(t)$ is $-\pi$. Hence, the *ultimate period* T_u is obtained from oscillations, which gives the information about the critical point, together with the *ultimate gain* which is approximately given by

$$k_u = \frac{4B}{\pi A} \qquad (1)$$

where B is the relay amplitude. The *ultimate* (critical) *frequency* is close to the value of $\omega_u = 2\pi / T_u$. Formula (1) comes from linearization of the relay output via Fourier series approximation when upper harmonic components of the signal are neglected, since a relay is a non-linear element and it can be linearized for linear theory approaches, details can be viewed e.g. in (Yu 2006).

An asymmetric (biased) relay, after removing stationary (dc) components, enables to estimate the static gain of the system according to

$$k = \frac{\int_t^{t+T_u} y(\theta)d\theta}{\int_t^{t+T_u} u(\theta)d\theta} \qquad (2)$$

see (Luyben 1987; Vyhlídal 2003). The static characteristic of a biased relay is displayed in Figure 2, where $B^+ \neq B^-$.

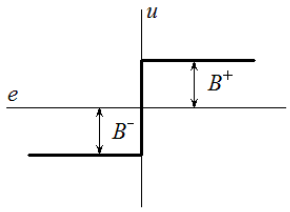

Figure 2: Asymmetric (Biased) Relay Static Characteristics

Nevertheless, this estimation of k can be inaccurate, due to e.g. model nonlinearities or a shift of the operation point.

Dominant input-output delay, say τ, can be estimated as a lag between the change of $u(t)$ and the maximum (minimum) value of $y(t)$ within the period (Yu 2006), which is clear from Figure 3.

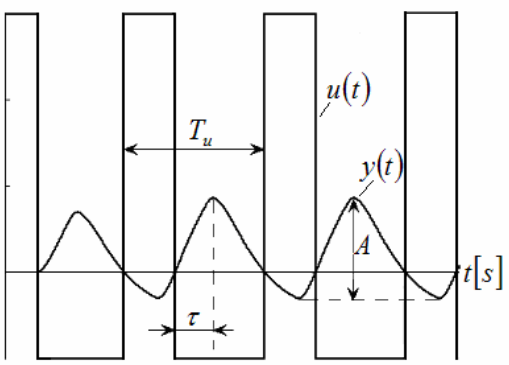

Figure 3: Dominant Input-Output Time Delay Estimation

Let $G(s)$ be the controlled system transfer function and $R(A)$ the describing (linearized) function of a relay (or a nonlinear element, in general), then for sustained oscillation holds $R(A)G(\mathrm{j}\omega_u) = -1 + 0\,\mathrm{j}$, or equivalently

$$\left|R(A)G(\mathrm{j}\omega_u)\right| = 1, \arg\left[R(A)G(\mathrm{j}\omega_u)\right] = -\pi \qquad (3)$$

which describes one point at the open-loop Nyquist plot giving rise to the estimation of two plant model parameters by the solution of it.

SATURATION RELAY

Model parameters estimation can be improved by a saturation relay (Shen et al. 1996; Yu 2006), the static characteristics of which is depicted in Figure 4.

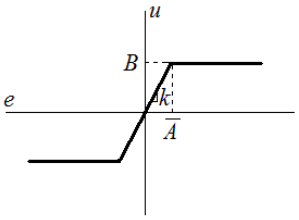

Figure 4: Saturation Relay Static Characteristics

Its advantage lies in the feature that relay output is not stepwise (i.e. with an abrupt slope change at the zero point), but it provides a smooth transient around the zero point. The relay input signal $e(t)$ is multiplied by k up to the limit value $B = k\bar{A}$ of $u(t)$, hence $u(t)$ is (ideally) in the form of a harmonic (sine) waves with an upper and lower limit. The output of the nonlinear element $u(t)$ looks like a truncated sinusoidal wave, see Figure 5. The meaning of $\bar{A}$ is clear from the figure.

Obviously, the ideal case is that when $u(t)$ has the shape of $e(t)$ while $\bar{A} = A$, where A is the amplitude of $e(t)$. In this case, the ultimate gain equals the value of k exactly. Another limit case arrives when $k \to \infty$, which agrees with the standard on-off relay.

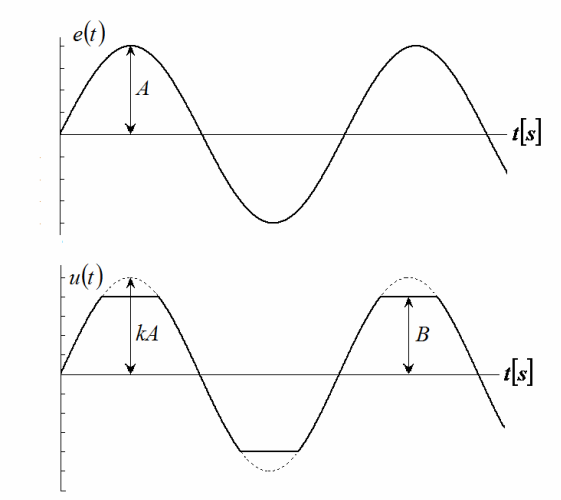

Figure 5: Relay Input and Output Signals for Saturation Relay

The describing function of the relay can be obtained from the Fourier series expansion of $u(t)$ and $e(t)$ as follows

$$R(A) = k_u = \frac{2B}{\pi \overline{A}} \left(\arcsin\left(\frac{\overline{A}}{A}\right) + \frac{\overline{A}}{A}\sqrt{1-\left(\frac{\overline{A}}{A}\right)^2} \right) \quad (4)$$

Hence, the aim is to find k (or $\overline{A}$) such that $\overline{A} = A$ for a given B, which provides the exact critical gain estimation. On the other hand, there is also a potential problem that can make the test fail. If the slope of the static characteristics k is too small, or equivalently, if $\overline{A} > A$, a limit cycle may not exist. To avoid this, there has been proposed a two-step procedure finding a rough estimate of the lower bound on k, say $k_{\min}$, followed by a saturation relay test (Shen et al. 1996; Yu 2006):

1) Select the height B of the relay (manipulated input).
2) Use an ideal relay (set the slope to a large value) to estimate k_u according to (1). Set $k_{\min} = k_u$.
3) Calculate the slope of the saturation relay $k = 1.4k_{\min}$.
4) Use the saturation relay with calculated *k*.
5) Find ω_u from the relay feedback test and compute the ultimate gain from (4).

A USE OF ARTIFICIAL DELAY

As mentioned above, the standard relay feedback test enables to identify only one point at the Nyquist curve, i.e. two unknown parameters of the model, and the estimation of other model parameters requires a special technique.

One of the possibilities is to use the ATV+ (Autotune Variation Plus) (Li et al. 1991; Scali et al. 1999; Marchetti and Scalli 2000). The first step of the ATV+ procedure is a standard relay test. The second step introduces an artificial delay τ^+ between the relay and the process.

The overall phase shift is $-\pi$, however only a part of this is attributed to the process, as τ^+ is characterized by the phase leg $\phi_D = \tilde{\omega}_u \tau^+$ where $\tilde{\omega}_u$ is a new ultimate frequency. The new amplitude $\tilde{A}$ of the output can be read as well. Every next setting of τ^+ determines one point of the Nyquist curve, hence, one needs to set the number $\lceil n/2 - 1 \rceil$ of various values of τ^+ where n is the number of unknown model parameters.

In (Li et al. 1991) the following setting was suggested

$$\tau^+ = \frac{5\pi}{12\omega_u} \quad (5)$$

where ω_u means the ultimate frequency with no artificial delay.

RELAY TRANSIENT

In (Hang et al. 1995), there was proposed a technique that could obtain multiple points on the process frequency response in a step test by removing stationary components followed by applying the Discrete Fourier Transform (DFT), Discrete-Time Fourier Transform (DTFT), or Fast Fourier Transform (FFT) to the remaining signals there. The procedure was improved in (Wang et al. 1997) where a method that can identify multiple points simultaneously under one relay test was proposed, the description of which follows.

Using a standard relay test, $u(t)$ and $y(t)$ are recorded from the initial time until the system reaches a stationary oscillation and they are subjected to exponential decaying as

$$\overline{u}(t) = u(t)\exp(-at), \overline{y}(t) = y(t)\exp(-at) \quad (6)$$

Obviously, $\overline{u}(t)$ and $\overline{y}(t)$ will decay to zero for $a > 0$ and $t \to \infty$.

The Fourier transform applied to (6) results in

$$\begin{aligned} \overline{U}(\mathrm{j}\omega) &= \int_0^\infty \overline{u}(t)\exp(-\mathrm{j}\omega t)\mathrm{d}t \\ &= \int_0^\infty u(t)\exp(-at)\exp(-\mathrm{j}\omega t)\mathrm{d}t = U(\mathrm{j}\omega + a) \\ \overline{Y}(\mathrm{j}\omega) &= \int_0^\infty \overline{y}(t)\exp(-\mathrm{j}\omega t)\mathrm{d}t \\ &= \int_0^\infty y(t)\exp(-at)\exp(-\mathrm{j}\omega t)\mathrm{d}t = Y(\mathrm{j}\omega + a) \end{aligned} \quad (7)$$

Hence

$$G(\mathrm{j}\omega+a)=\frac{\overline{Y}(\mathrm{j}\omega)}{\overline{U}(\mathrm{j}\omega)}=\frac{Y(\mathrm{j}\omega+a)}{U(\mathrm{j}\omega+a)} \qquad (8)$$

$\overline{U}(\mathrm{j}\omega)$ and $\overline{Y}(\mathrm{j}\omega)$ can be computed at discrete frequencies with DTFT as

$$\overline{U}(\mathrm{j}\omega)=\mathrm{DTFT}(\overline{u}(t))=T\sum_{k=0}^{N-1}\overline{u}(kT)\exp(-\mathrm{j}\omega_l kT),\ l=1,2,...,m$$
$$\overline{Y}(\mathrm{j}\omega)=\mathrm{DTFT}(\overline{y}(t))=T\sum_{k=0}^{N-1}\overline{y}(kT)\exp(-\mathrm{j}\omega_l kT),\ l=1,2,...,m \qquad (9)$$

where T is the sampling interval, N means the number of samples and $t_f=(N-1)T$ expresses the final time for which the value of $\overline{u}(t)$ (or $\overline{y}(t)$) is sufficiently small. Usually, $m=N/2$ and $\omega_l=2\pi l/(NT)$, see e.g. (Wang et al. 1999a). If, moreover, $N=2^n, n\in\mathrm{N}$, then the standard FFT can be used for faster computing.

TIME DELAY SYSTEMS

Time delay systems (TDS) have usually been assumed to contain delay elements in input-output relations only. All the system dynamics has been hence modeled by point accumulations in the form of a set of ordinary differential equations. The Laplace transform then results in a transfer function expressed by a serial combination of a delayless term and a delay. However, this conception is somewhat restrictive in effort to fit the real plant dynamics because inner feedbacks are often of time-distributed or delayed nature.

Anisochronic (or *hereditary*) TDS models, in the contrary, offer a more universal dynamics description applying both integrators and delay elements either in lumped or distributed form so that delays appear on the left side of a differential equation which is no longer *ordinary* (ODE) but rather *functional* (FDE) - this brings the concept of *internal* (or *state*) delays.

Theory, models, analyses and/or applications of these systems can be found e.g. in (Bellmann and Cooke 1963; Górecki et al. 1989; Hale and Verduyn Lunel 1993; Richard 2003; Michiels and Niculescu 2007) etc.

Loosely speaking, a linear time-invariant TDS can be characterized by a transfer function in the form of a ratio of so-called quasipolynomials, i.e.

$$G_S(s)=\frac{b(s)}{a(s)} \qquad (10)$$

where $a(s)$ is a quasipolynomial of degree *n* and the $b(s)$ can be factorized as $b(s)=b_0(s)\exp(-\tau s),\ \tau\geq 0$ where $b_0(s)$ is a (quasi)polynomial of degree $l\leq n$ of the general form $b_0(s)=s^l+\sum_{i=0}^{l}\sum_{j=1}^{h_i}b_{ij}s^i\exp(-\vartheta_{ij}s),\ \vartheta_{ij}\geq 0$.

Obviously, such a system (model) is infinite-dimensional due to its infinite spectrum which equals the set of denominator roots, in most cases.

In (Vyhlídal and Zítek 2001; Pekař 2008) the relay-feedback experiment was used to identify a stable time-delay model of the first order with one input-output and one internal delay, where an additional (artificial) delay was utilized. A sketch of the idea of a time-domain limit cycles evaluation introduced in the latter reference is briefly described below.

To name just one non-relay method for incessant (self-tuning) identification for systems with input-output delays, the reader is referred to (Bobál et al. 2012).

TIME-DOMAIN LIMIT CYCLES EVALUATION

The simple idea of the limit cycles evaluation in time domain from a relay test stems from the fact that rectangular waves on a plant input can be approximated by (or viewed as) sinus waves using linearization (1) or (4). Hence, using, for instance, an on-off relay, the approximating input sinus signal is

$$u(t)=\frac{4B}{\pi}\sin(t\omega_u) \qquad (11)$$

Since the ideal relay does not evoke a phase shift, a plant output has a phase shift $-\pi$, in other words, a plant output is given by

$$y(t)=-A\sin(t\omega_u) \qquad (12)$$

i.e. $y'(t)=-A\omega_u\cos(t\omega_u)$ etc. which is then inserted to the model differential equation. Subsequently, by placing the appropriate time values into the modified equation, relations for the unknown model parameters can be derived. A saturation relay test can be treated analogously with respect to (4).

The use of an additional delay element gives rise to the a phase lag ϕ_D, i.e. $y(t)=-A\sin(t\omega_u+\phi_D)$. Again, this is inserted to the appropriate FDE with a selected value of t. Note that only two distinct time values can be chosen for one test. For further details, the reader is referred e.g. to (Pekař 2008).

EXAMPLE

A simulation example comparing the two methodologies, i.e. the use of an on/off and saturation relay with additional delay, and the use of a relay transient, performed in Matlab/Simulink environment follows. In particular, relay-based parameters identification of the model of a laboratory circuit heating plant is introduced. The appliance was assembled at the Faculty of Applied Informatics, Tomas Bata University in Zlín, Czech Republic (Dostálek et al. 2008). A photo and a sketch of the scheme of it are displayed in Figure 6.

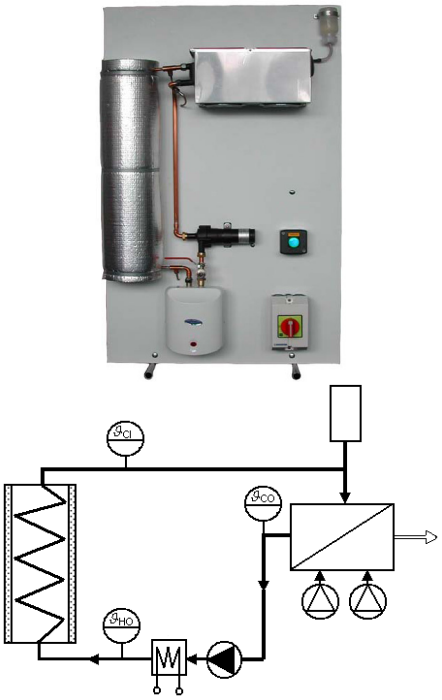

Figure 6: Circuit Heating Plant - Photo and a Scheme

The heat transferring fluid (namely distilled water) is transported using a continuously controllable DC pump {6} into a flow heater {1} with maximum power $P_H(t)$ of 750 W. The temperature of a fluid at the heater output is measured by a platinum thermometer giving value of $\vartheta_{HO}(t)$. Warmed liquid then goes through a 15 meters long insulated coiled pipeline {2} which causes the significant delay in the system. The air-water heat exchanger (cooler) {3} with two cooling fans {4, 5} represents a heat-consuming appliance. The speed of the first fan can be continuously adjusted, whereas the second one is of on/off type. Input and output temperatures of the cooler are measured again by platinum thermometers giving $\vartheta_{CI}(t)$ and $\vartheta_{CO}(t)$, respectively. The expansion tank {7} compensates for the expansion effect of the water.

A detailed mathematical model was presented in (Pekař et al. 2009). Although there are three continuous-time manipulated inputs ($P_H(t)$, voltage input to the pump, $u_P(t)$, and voltage input to the cooler, $u_C(t)$) and three measured outputs ($\vartheta_{HO}(t)$, $\vartheta_{CI}(t)$, $\vartheta_{CO}(t)$), the intention is to control $\vartheta_{CO}(t)$ only by means of $P_H(t)$. For this relation, it was derived the following transfer function

$$G(s)=\frac{\vartheta_{CO}(s)}{P_H(s)}=\frac{[b_{0D}\exp(-\tau_0 s)+b_0]\exp(-\tau s)}{s^3+a_2 s^2+a_1 s+a_0+a_{0D}\exp(-\vartheta s)} \quad (13)$$

It was determined that for the working point

$$\begin{aligned}&[u_p,u_c,P_H,\vartheta_{HO},\vartheta_{CI},\vartheta_{CO},\vartheta_A]\\&=[5\,\text{V},3\,\text{V},300\,\text{W},44.1\,^\circ\text{C},43.8\,^\circ\text{C},36.0\,^\circ\text{C},24.0^\circ\text{C}]\end{aligned} \quad (14)$$

it holds that

$$\begin{aligned}&b_{0D}=2.334\cdot10^{-6}, b_0=-2.146\cdot10^{-7},\\&a_2=0.1767, a_1=0.009, a_0=1.413\cdot10^{-4},\\&a_{0D}=-7.624\cdot10^{-5}, \tau_0=1.5, \tau=131, \vartheta=143\end{aligned} \quad (15)$$

Relay experiment follows. Consider model (13) as an "exact" system description and let us introduce the following simplified model

$$G_m(s)=\frac{b_0\exp(-\tau s)}{s+a_0+a_1\exp(-\vartheta s)} \quad (16)$$

The task is to find conditional equations for identification of model parameters by means of a relay feedback test with an on-off and saturation relay. There are five unknown real parameters in the model, i.e. $b_0, a_0, a_1, \tau, \vartheta$; however, two of them can be estimated not from the knowledge of the ultimate gain and frequency. Namely, the static gain $k=b_0/(a_1+a_0)$ can be calculated from (2) or from the step-response (as it has been performed herein), and the value of input-output delay τ can be estimated as in Figure 3.

Hence, in the first step, a biased on-off relay with hysteresis is used to estimate these two parameters. Then, a simple (symmetrical) on-off relay and a saturation relay can be utilized to calculate the remaining parameters from (3) and the use of an artificial delay τ^+. Four conditional equation can be obtained by doing this, therefore one may improve the estimation of k or τ.

Follow now the idea of the time-domain limit cycles evaluation. Model transfer function agrees with the FDE

$$y'(t)+a_0 y(t)+a_1 y(t-\vartheta)=b_0 u(t-\tau) \quad (17)$$

which implies

$$\begin{aligned}&-A_0(\omega_u\cos(t\omega_u)-a_0\sin(t\omega_u)-a_1\sin((t-\vartheta)\omega_u))\\&=b_0\frac{4B}{\pi}\sin((t-\tau)\omega_u)\end{aligned} \quad (18)$$

First, let $t=\omega_u^{-1}(2l\pi)$, $l\in Z_0^+$, and l be chosen so that $t>\max\{\tau,\vartheta\}$ and the limit cycle is stable (settled). Then

$$f_1:=A(-\omega_u+a_1\sin(\vartheta\omega_u))+b_0\frac{4B}{\pi}\sin(\tau\omega_u)=0 \quad (19)$$

As second, let $t=\omega_u^{-1}((0.5+2l)\pi)$, $l\in Z_0^+$, then

$$f_2:=-A(a_0+a_1\cos(\vartheta\omega_u))-b_0\frac{4B}{\pi}\cos(\tau\omega_u)=0 \quad (20)$$

Analogously, the use of an additional delay element gives rise to the following conditions

$$f_3 := \tilde{A}\left(-\tilde{\omega}_u + a_1 \sin\left(\vartheta\tilde{\omega}_u\right)\right) + b_0 \frac{4B}{\pi}\sin\left(\tau\tilde{\omega}_u + \phi_D\right) = 0$$
$$f_4 := -\tilde{A}\left(a_0 + a_1 \cos\left(\vartheta\tilde{\omega}_u\right)\right) - b_0 \frac{4B}{\pi}\cos\left(\tau\tilde{\omega}_u + \phi_D\right) = 0 \quad (21)$$

The application of the saturation relay leads analogously to the following conditions

$$f_5 := -\omega_u + a_1 \sin\left(\vartheta\omega_u\right) + b_0 \frac{2B}{\pi\overline{A}}\left(\arcsin\left(\frac{\overline{A}}{A}\right) + \frac{\overline{A}}{A}\sqrt{1-\left(\frac{\overline{A}}{A}\right)^2}\right)\sin\left(\tau\omega_u\right) = 0$$
$$f_6 := a_0 + a_1 \cos\left(\vartheta\omega_u\right) + b_0 \frac{2B}{\pi\overline{A}}\left(\arcsin\left(\frac{\overline{A}}{A}\right) + \frac{\overline{A}}{A}\sqrt{1-\left(\frac{\overline{A}}{A}\right)^2}\right)\cos\left(\tau\omega_u\right) = 0$$
$$f_7 := -\tilde{\omega}_u + a_1 \sin\left(\vartheta\tilde{\omega}_u\right) + b_0 \frac{2B}{\pi\overline{\tilde{A}}}\left(\arcsin\left(\frac{\overline{\tilde{A}}}{\tilde{A}}\right) + \frac{\overline{\tilde{A}}}{\tilde{A}}\sqrt{1-\left(\frac{\overline{\tilde{A}}}{\tilde{A}}\right)^2}\right)\sin\left(\tau\tilde{\omega}_u + \phi_D\right) = 0$$
$$f_8 := a_0 + a_1 \cos\left(\vartheta\tilde{\omega}_u\right) + b_0 \frac{2B}{\pi\overline{\tilde{A}}}\left(\arcsin\left(\frac{\overline{\tilde{A}}}{\tilde{A}}\right) + \frac{\overline{\tilde{A}}}{\tilde{A}}\sqrt{1-\left(\frac{\overline{\tilde{A}}}{\tilde{A}}\right)^2}\right)\cos\left(\tau\tilde{\omega}_u + \phi_D\right) = 0 \quad (22)$$

Due to the limited space, only final numerical results in table and graphical forms, respectively, are presented.

Table 1: Time-Domain Solution with Saturation Relay and Artificial Delay

	LM method	NM method	Excel Solver
a_0	$9.93016 \cdot 10^{-3}$	$9.93016 \cdot 10^{-3}$	$9.93016 \cdot 10^{-3}$
a_1	$-3.99513 \cdot 10^{-3}$	$-3.99513 \cdot 10^{-3}$	$-3.99513 \cdot 10^{-3}$
τ	159.83	159.83	159.83
ϑ	130.75	130.75	130.75
e	$1.82 \cdot 10^{-13}$	$3.38 \cdot 10^{-25}$	$2.11 \cdot 10^{-21}$

Table 2: Solution by the Use of the Relay Transient

	LM method	NM method	Excel Solver
a_0	$3.06598 \cdot 10^{-2}$	$3.06598 \cdot 10^{-2}$	$7.41042 \cdot 10^{-3}$
a_1	$-1.7488 \cdot 10^{-2}$	$-1.7488 \cdot 10^{-2}$	$-2.60727 \cdot 10^{-3}$
τ	143.42	143.42	136.7
ϑ	158.08	158.08	136.69
e	$3.19 \cdot 10^{-14}$	$1.59 \cdot 10^{-15}$	$1.29 \cdot 10^{-8}$

We utilized the well-known Levenberg-Marquardt (LM) (Madsen et al. 2004) and Nelder-Mead (NM) algorithms (Nelder and Mead 1965). Note that NM algorithm and the MS Excel Solver minimize the sum of squares of the left-hand sides of (21) and (22), which agrees with error e in the tables.

Graphical results are presented in Figure 7 where Result 1 agrees with that presented in Table 1, Result 2 means LM and NM methods in Table 2 and Result 3 is that obtained from the MS Solver in Table 2.

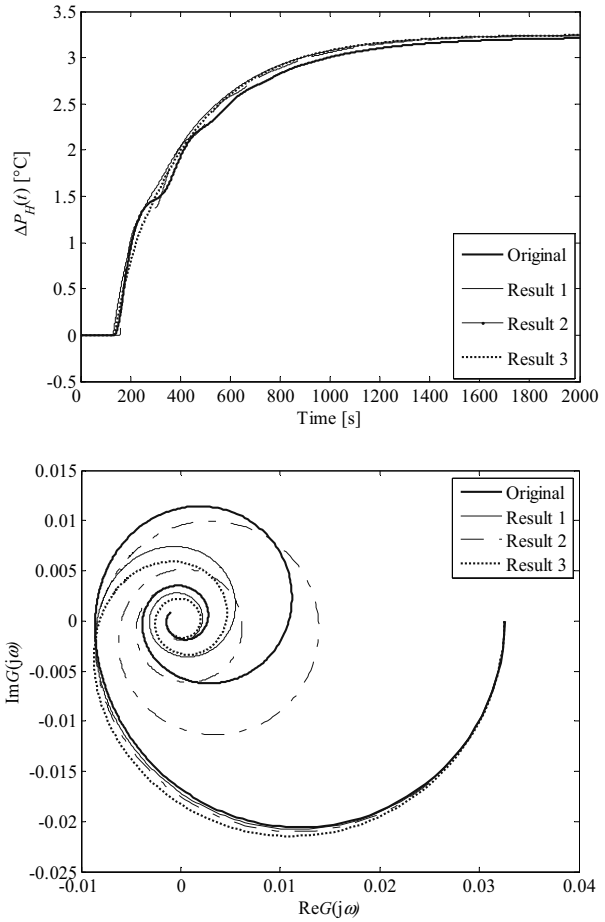

Figure 7: Step Responses and Nyquist Plots, Respectively, of the Original and Approximated Models via Relay Feedback Tests

The best theoretical (simulated) result is provided by the use of the relay transient with LM and NM methods (which can be verified numerically); nevertheless, all the presented procedures provide a very good outcome.

CONCLUSIONS

The proposed contribution has presented a concise description and a comparison study case of relay-feedback identification tests. Namely, it has covered two distinct methodologies – a combination of an on/off and biased relay with the use of an artificial delay, and the idea of a relay transient for multiple parameters estimation during a single test.

The consequent simulated example has demonstrated the usability of the proposed methods for model

parameters identification of a real (laboratory) system with delays. It has confirmed that both procedures provide us with very good results as well.

In the future, practical measurements are desirable to be performed and the eventual models can be used to real-time control of the laboratory appliance for verification of several control algorithms for time delay systems.

ACKNOWLEDGEMENTS

The authors kindly appreciate the financial support which was provided by the European Regional Development Fund under the project CEBIA-Tech No. CZ.1.05/2.1.00/03.0089.

REFERENCES

Åström, K.J. and T. Hägglund. 1984. "Automatic Tuning of Simple Controllers with Specification on Phase and Amplitude Margins." *Automatica*, Vol. 20, No.5, 645-651.

Bellman, R. and K.L. Cooke. 1963. *Differential-Difference Equations*. Academic Press, New York.

Bobál, V.; P. Chalupa; M. Kubalčík; and P. Dostál. 2012. "Identification and Self-tuning Control of Time-Delay Systems." *WSEAS Transactions on Systems*. Vol.11, No.10, 596-606.

Dostálek, P.; J. Dolinay; and V. Vašek. 2008. "Design and Implementation of Portable Data Acquisition Unit in Process Control and Supervision Applications. " *WSEAS Transactions on Systems and Control*, Vol.3, No.9, 779-788.

Górecki, H.; S. Fuksa; P. Grabowski; and A. Korytowski. 1989. *Analysis and Synthesis of Time Delay Systems*. PWN – Polish Scientific Publishers, Warszawa, co-editor John Wiley & Sons.

Hale, J.K. and S.M. Verduyn Lunel. 1993. *Introduction to Functional Differential Equations*. In *Applied Mathematical Sciences*, Vol.99. Springer, New York.

Hang, C.C., Q.G. Wang, L.S. Cao. 1995. "Self-tuning Smith Predictors for Processes with Long Dead Time." *International Journal of Adaptive Control and Signal Processing*, Vol.9., No.3, 255-270.

Hang, C.C.; K.J. Åström; and Q.G. Wang. 2002. "Relay Feedback Auto-tuning of Process Controllers – A Tutorial Review. " *Journal of Process Control*, Vol.12, No.1, 143-162.

Li, W.; E. Eskinat; and W.L. Luyben. 1991. "An Improved Autotune Identification Method." *Industrial & Engineering Chemistry Research*, Vol.30, No.7, 1530-1541.

Luyben, W.L. 1987. "Derivation of Transfer Functions for Highly Nonlinear Distillation Columns." *Industrial & Engineering Chemistry Research*, Vol.26, No.12, 2490-2495.

Madsen, K.; H.B. Nielsen; and O. Tingleff. 2004. *Methods for Non-linear Least Square Problems*. *Informatics and Mathematical Modelling*. Technical University of Denmark, Lyngby.

Marchetti, G. and C. Scali. 2000. "Use of Modified Relay Techniques for the Design of Model-based Controllers for Chemical Processes. *Industrial and Engineering Chemistry Research*, Vol.39, No.9, 3325-3334.

Michiels, W. and S.-I. Niculescu. 2007. *Stability and Stabilization of Time-Delay Systems. An Eigenvalue Based Approach*. SIAM Publications, Philadelphia.

Nelder, J.A. and R. Mead. 1965. "A Simplex Method for Function Minimization." *The Computer Journal*, Vol.7, No.4, 308–313.

Pekař, L.; R. Prokop; and P. Dostálek. 2009. "Circuit Heating Plant Model with Internal Delays." *WSEAS Transaction on Systems*, Vol.8, No.9, 1093-1104.

Richard, J. P. 2003. "Time-delay Systems: An Overview of Some Recent Advances and Open Problems." *Automatica*, Vol.39, No.10, 1667-1694.

Scali, C.; G. Marchetti; and D. Semino. 1999. "Relay and Additional Delay for Identification and Autotuning of Completely Unknown Processes." *Industrial and Engineering Chemistry Research*, Vol.38, No.5, 1987-1997.

Shen, S.-H.; H.-D. Yu; and Ch.-Ch. Yu. 1996. "Use of Saturation-Relay Feedback for Autotune Identification." *Chemical Engineering Science*, Vol.51, No.8, 1187-1198.

Tan, K.K.; T.H. Lee; and Q.G. Wang. 1996. "An Enhanced Automatic Tuning Procedure for PI/PID Controllers for Process Control." *AIChE Journal*, Vol.42, No.9, 2555-2562.

Vyhlídal, T. 2003. *Analysis and Synthesis of Time Delay System Spectrum*. Ph.D. Thesis. Faculty of Mechanical Engineering, Czech Technical University in Prague.

Vyhlídal, T. and P. Zítek. 2001. "Control System Design Based on a Universal First Order Model with Time Delays." *Acta Polytechnica*, Vol.44, No.4-5, 49-53.

Wang, Q.G.; C.C. Hang; and Q. Bi. 1997. "Process Frequency Response Estimation from Relay Feedback." *Control Engineering Practice*, Vol.5, No.9, 1293-1302

Wang, Q.G.; C.C. Hang; and Q. Bi. 1999. "A Technique for Frequency Response Identification from Relay Feedback." *IEEE Transactions on Control Systems Technology*, Vol.7, No.1, 122-128.

Yu, Ch.-Ch. 2006. *Autotuning of PID Controllers: A Relay Feedback Approach*. 2nd edition. Springer, London.

AUTHOR BIOGRAPHIES

LIBOR PEKAR was born in Zlín, Czech Republic, in 1979. He studied automation and control engineering at Tomas Bata University in Zlín where he obtained his MSc. degree in 2005. He has been working as an assistant at the same institute. Nowadays, he is finishing his Ph.D. degree in algebraic control of time delay systems. His e-mail address is: pekar@fai.utb.cz.

ROMAN PROKOP was born in Hodonín, Czech Republic, in 1952. He obtained his MSc. degree at Czech Technical University in Prague in 1976, then Ph.D. degree at Slovak Technical University in Bratislava in 1983, and he became a professor at Technical University of Brno in 2004. Now he has been a professor at Tomas Bata University in Zlín. His professional interests cover algebraic control methods, autotuning and robust control. His e-mail address is: prokop@fai.utb.cz.

SIMULATION MODEL OF THE MUNICIPAL HEAT DISTRIBUTION SYSTEMS

Lubomir Vasek
Viliam Dolinay
Faculty of Applied Informatics
Tomas Bata University in Zlin
Nad Stranemi 4511, 760 05 Zlin, Czech Republic
E-mail: lvasek@fai.utb.cz, vdolinay@fai.utb.cz

KEYWORDS

Heat consumption, heat distribution, identification, simulation model.

ABSTRACT

This paper deals with the topics of heat consumption in the municipal heat distribution systems and problems linked with modeling and simulation of systems providing heat supply. These systems will be called SHDC (System of Heat Distribution and Consumption). The significant problem in the controlling mechanism of such systems consists in transport delay of transferring heat media. As a result the control mechanism must operate in prediction kind of mode. Essential parameters, or control variables, are temperature of heat carrier and its flow rate. Their time behavior must be predicted for efficient control of the whole heat energy supply. Main focus will be placed on description of the proposed and implemented computer model of the heat distribution system in the selected agglomeration. This model is proposed as a discrete simulation model and implemented in the form of computer application. Model has been tested on real operational data.

INTRODUCTION

The requests of distribution and consumption of heat energy in the municipal location are very topical, especially in the context of finite worldwide classic energy resources and the constant increase in energy prices. There are also important ecological aspects, because obtaining and using of energy generally has mostly negative environmental impact. Especially the coal-fired power is considerable burden on nature. On the other side, nuclear power plants represent unacceptable risk for many countries. Therefore, it is necessary to seek all paths leading to energy production, distribution and consumption efficiency (Balate et al. 2007)

The effective management of distribution and subsequent management of production of the heat energy is one of the issues that can lead to savings of energy. Heat energy must be transported to the location of consumption in time when it is required and in the expected quantity and quality. Quality of supplied heat energy is expressed mostly in the temperature of heat transferring media. The correct delivery time, quantity and quality of heat energy must go hand in hand with minimal distribution costs (Navratil et al. 2012). It is noticeable that the heat distribution is inseparably linked to its consumption and can therefore be spoken about management of the heat distribution and consumption.

Specifically, the article deals with the issues of heat consumption in the urban agglomeration with centralized heat energy source – heating plant - and a large distribution network. Principal scheme is shown in Figure 1.

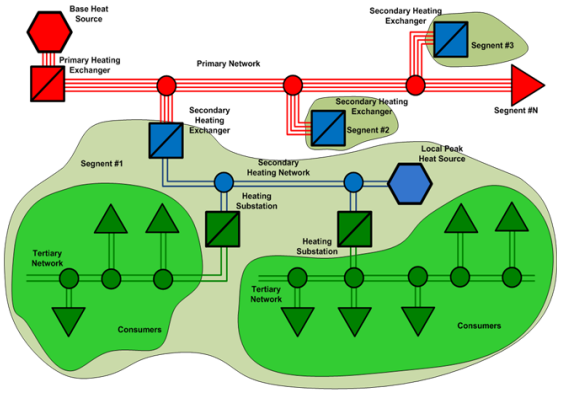

Figure 1: Schematic diagram of SHDC (Unis 2011)

All three areas - energy production, distribution and consumption - are closely related and are optimal when they work in mutual energy balance. However, it must be said that it is the energy balance in the time interval, not the energy balance at each time point. This means that the amount of thermal energy that is consumed for a certain time period Δt starting in time t, must be produced in time advance and transported from place of production to place of consumption, see example in Figure 2. The distribution system has a specific, and usually not small, ability to accumulate heat energy and it is able to compensate immediate differences between the amount of heat produced and consumed energy. The size of accumulation is determined by the amount of heat energy bound in heat transfer media - usually water in the distribution system and mass of the heated object.

Proceedings 27th European Conference on Modelling and Simulation ©ECMS Webjørn Rekdalsbakken, Robin T. Bye, Houxiang Zhang (Editors)
ISBN: 978-0-9564944-6-7 / ISBN: 978-0-9564944-7-4 (CD)

BASIC ASSUMPTIONS

For the simplification, the same length of the time interval Δt for produced and consumed heat is assumed. Denote the $\delta(t)$ as the time interval between heat production and consumption (transport delay), $P_p(t - \delta(t))$ as production heat power in time $(t - \delta)$, $P_c(t)$ consumption heat power in time t and considering the time interval Δt, the following equation for heat energy balance can be expressed:

$$\int_t^{t+\Delta t}(P_P(t-\delta(t))dt = \int_t^{t+\Delta t} P_C(t)dt + \int_t^{t+\Delta t} A(t)dt \quad (1)$$

It can be simplified as

$$Q_P = Q_C + \Delta A \quad (1a)$$

where:

Q_p is the heat produced during the time interval Δt, however started in time t-δ, prior to the consumption time.

Q_c is the heat consumed during the time interval Δt and

ΔA is the change of heat energy accumulation in the distribution network in the time interval Δt.

The effective procedure to manage such system, i.e. procedure which will lead to savings in heat energy, must respect the dependencies expressed in equation (1). The goal is to reach a situation where changes of accumulation, which results in changing the temperature of the heat transfer medium at the outlet of the distribution network, were minimal. Thus, the temperature of the returned water should fluctuate as little as possible.

It is obvious that the analytical solution satisfying equation (1) is very difficult, especially for the following reasons:

1) The time course of consumed heat Q_c is not possible to accurately predict because it is a stochastic variable depending on many factors, Highlights from the outdoor temperature and other climatic influences at the point of consumption, time of day and day type (weekday, weekend day or holiday). The prediction of the external temperature is itself also a stochastic variable with relatively high variance.
2) Determination of transport timing delay, which is also variable and stochastic variable, it is also very complicated. Its size generally depends on the sizes of Q_p and Q_c, which are active in different times. Moreover the Q_c, generally consists of partial consumptions Q_{ci} in different parts of the distribution network and the activity time is different for each Q_{ci}.

With regard to the above-mentioned, the discrete computer model of the SHDC (System of Heat Distribution and Consumption) was implemented. This discrete model is designed with a number of freely usable parameters (Vasek and Dolinay 2011).

There are many different approaches for simulation models and operational optimization of heating networks and heat-load modeling (Navratil et al. 2012). Proposed approach is to use data mining combined with simple model of heating network (Vasek et al. 2011). The adaptive parts of the model utilize real data measured in heat distribution systems to set up its internal structures for subsequent use in prediction and regulation.

For the model, the distribution network of chosen city was simplified and model was trained on the real measured data (Vasek and Dolinay 2010). The main purpose of all experiments faces the question: When and how much heat energy should be produced and what temperature is to set-up for hot water supply.

SIMULATION MODEL

The simulation is one of the few methods, which can be effectively used for the analysis of large and complex systems. For the simulation is characteristic to create a model of the system, usually an abstract model and today almost exclusively a computer model. With this model are performed experiments and their results are then applied to the original system (Vasek and Dolinay 2011).

The use of a simulation model in this case is fundamentally twofold:

1) *offline model using*
   It is possible to analyze the properties and behavior of simulated system as a wide dynamic system
2) *online model using*
   Simulation model can be integrated into the control system simulated system as an instrument to prediction of its behavior at a certain (limited) time in the future.

Proposed model of SHDC is, in contrast to the continuous models commonly-used in this area, discretized in time.

Model Description

The distribution network can be presented as a set of sources of heat energy (supply heating stations) and heat consumers, which are cross connected through piping. One simple example of one part of distribution network is presented in the Figure 2,

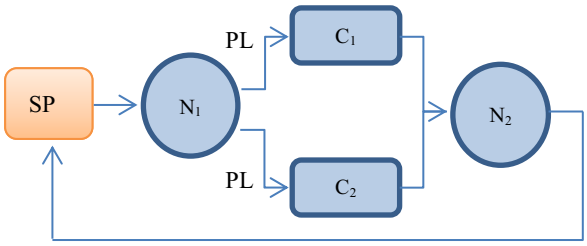

Figure2: Schematic example of the distribution network

where:

C consumer, PL pipe line, N node, SP supply

The pipes and heat consumers are concentrated for model in sections, which are connected in nodes. Section starts and ends in the node and can be divided in several elements of the distribution net (pipe lines and heat consumers). Each this element has its own constant characteristics from the point of view flow and heat transfer.

Simulation time is running in discrete time intervals constant length signed as Δt. Time interval Δt is identical to the sampling time interval and Δt_j determine the simulation step j.

As basic "moving" element ("transaction" in simulation terminology) consider "discrete flow quantum" DFQ of fluid (water). The DFQ flows through the network and gradually loses its energy, depending on the current position. The volume of the quanta is determined by the quantity of water entering into the distribution network for the time interval Δt in given step of simulation. Amount of heat energy in DFQ is based on water quantity and its temperature (Vasek and Dolinay 2010)

Proposed model is used for modeling of two closely connected processes: mass flow and heat transfer.

Flow Modeling

To monitor the flow quantum passing through the distribution network, it is necessary to respect the fundamental physical laws applicable to the fluid flow and heat energy transfer - conservation of mass and energy and the law of continuity. Based on these laws were defined the rules for describing the mass flow in network nodes and in interconnecting pipes.

According to these rules is then modeled the mass flow in the distribution network. In each simulation step, indexed j, the each flow quantum, indexed i and denoted ${}^{j}DFQ_i$ in the network is monitored. For illustration the ${}^{j}DFQ_i$ in pipe is shown in the Figure 3,

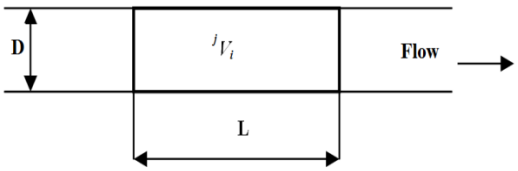

Figure 3: Discreet flow quantum ${}^{j}DFQ_i$

where:

- D is pipe diameter in current ${}^{j}DFQ_i$location,
- L is current ${}^{j}DFQ_i$ length,
- ${}^{j}V_i$ is volume of ${}^{j}DFQ_i$

Heat Transfer Modeling

For each flow quantum, which is at a given time in the distribution network, its heat balance is calculated in every simulation step. The heat balance is based on law of the preservation of the thermal energy. As mentioned above, the time interval Δt may have length of the few minutes, so it was considered appropriate to model the temperature T of DFQ according to the formulas for cooled object. For it is valid differential equation.

$$\frac{dT}{dt} = K * (T - T_{ext}) \qquad (2)$$

where

- K is the constant describing thermal characteristics for the particular element of the distribution network and heating medium (e.g. K for the pipe line depends on pipe wall material, its isolation, its diameter, velocity and specific capacity of the heating medium - hot water)
- T is the current temperature DFQ in the particular simulation step j,
- T_{ext} is the current outside temperature

Solving the equation (2), the (3) is obtained

$$T_1 = exp\ (-K*t) * (T_0 - T_{ext}) + T_{ext} \qquad (3)$$

where:

T_0 and T_1 are the water temperature at the beginning and end of the time interval Δt

The amount of the heat ΔQ, transferred in given time interval is then function of the heat capacity c_p, volume V, density ρ of heating water and temperature difference T_0 and T_{ext}, i.e.:

$$\Delta Q = c_p * V * (T_0 - T_{ext}) * (1 - exp\ (-K * \Delta t)) \qquad (4)$$

MODEL USE AND ITS APPLICABILITY

It is expected that the proposed simulation model will be used in the control system SHDC for the following purposes:

- Identification of model parameters for the selected time period
- Prediction of appropriate timing of the supplied amount of heat

Identification of Model Parameters for the Selected Time Period

Significant for the modeling approach to SHDC is to determine the function $s_r(...)$, which describes heat consumption for the consumer r. As the analysis of the real data show, the amount of heat consumed is mostly affected by the external temperature and time of the day. With using of (5), which describes the dependences on the T_{ext}, is possible for simplicity write

$$s_r(...) = \lambda_r * ({}^jT_i - T_{ext})*(1-exp(-K*\Delta t)) * k_h \quad (5)$$

where:

- ${}^jT_i$ is the current temperature of ${}^jDFQ_i$ for the particular simulation step j
- k_h is coefficient which corrects heat consumption oscillations during a day
- λ_r is the coefficient including other factors (e.g. another meteorological influences – sun intensity, wind etc.) which affect the consumption in r element of the distribution network

The coefficient k_h is considered as a function of time, specified for the discrete set of values (usually in one hour intervals). It is possible in the time between hours to use the value from the previous hour or use interpolated values, with application of the linear or other more complex interpolation.

To determine searched values k_h for 24 points of timeline is possible to use several methods based on principles allowing us to find a function(s) which should have the best course approximating analyzed variables. One option is, for example, to use genetic algorithms. In the presented solution was the method PSO (Particle Swarm Optimization) used - see (Kral et al. 2010). This method has been lately compared with other methods, such as SOMA, neural networks (Varacha and Jasek 2011), and Levenberg-Marquard algorithms for nonlinear methods of least squares. It was found that the results, achieved in terms of accuracy and speed of convergence are similar. PSO is therefore comparable for the determination of the correction factors and was used in the further work.

Designated coefficients k_h can be then used in the simulation model as the parameters for its further use.

Prediction of Appropriate Timing of the Supplied Amount of Heat

It should be noted that the idea of building a predictor in the project gradually evolved and changed. At the beginning of the project, the opinion prevailed that it will be enough to identify a model for a longer period and once identified, the model could be used for this period without any modifications. But it turned out that this approach does not lead to sufficiently accurate results, the characteristics of the system are not sufficiently "stable". It is probably due to both the details of the processed model and major stochastic nature of the whole system. Therefore, the idea was abandoned, and the work moved in the direction of the procedure described below. Given the fact, that the work on the project is not yet finished, described process reflects the present state of the solution and may not be definitive.

The proposed procedure is based on several fundamental ideas:

1) SHDC will behave similarly under similar conditions.
2) Predicted period is suitable to choose short and necessary calculations (including simulation) to perform for the shorter period repeatedly. This is depending, as already mentioned, on speed changes inside the SHDC and size of sampling period Δt. If this period is few minutes, it is easy to perform calculations repeatedly.
3) To control the production and distribution of heat, there are two control variables - temperature T_v and mass flow M. It will be necessary to find and use an appropriate cost function, which allows the required amount of supplied heat to optimally divide to the parts obtained mass flow M and the temperature T_v. Search for this objective function is the task for other parts of the project and is not in this article further discussed.

Simulation and control can be described in the following steps:

1) *obtain weather forecast for day to propose*,
   More frequent updates and increased accuracy for a particular location is an advantage
2) *seek and choose best matching day from the past*
   Looking for days of ancient history has no sense, e.g. previous years, heating season, because the system is constantly changing. Days from the surrounding area should be preferred. It is also advisable to monitor the previous days, because if it is such a day following a significant change in the weather, the behavior of consumers is considerably in an unstable state

3) *train the model*
Behavior of consumers is such nonlinear that find a general function describing its behavior is practically impossible. Better is to identify a particular period and model optimization for a given situation.

4) *predict behavior for proposing day*
System trained on a similar day can learn from any mistakes and optimize the management of individual variables to the optimal operation.

IMPLEMENTATION

Introduced model was implemented in the form of a software application. The program modules are written in Java, data – historical operational data, configuration and description data for distribution network, simulation results – are stored in database.
Application is able to run several tasks in parallel, each in their own thread. It gives higher performance for calculation, especially in case, when many simulation experiments must be provided.

EXPERIMENTS

One of the practical experiments for presented research was carried on the part of the secondary distribution system of the small town in Czech Republic. The model for circuit of selected heat exchangers was prepared. Selected circuit mainly consisted of housing estate or groups of family houses. Such systems deal with distribution between heat exchanger station and individual door stations. Later shown results present the data obtained in the simulation of single house.
However, the model can bind together individual parts of the heat exchanger circuit, or bind circuits with main city supply line and in this way cover most of the significant parts of the distribution systems.
With regard to proposed model requirements, the similar period were identified. Compliance between measured and output data after model identification is shown in Figure 4.

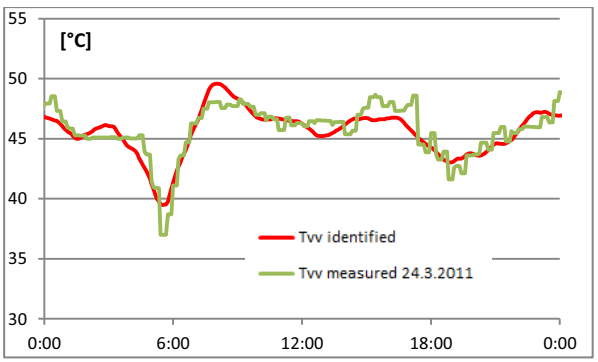

Figure 4: Identification results

Successfully identified model were after that used for system behavior prediction. The result from the model was compared with the real system responses. Obtained results are shown in following pictures, where red curves are predicted and green measured courses.

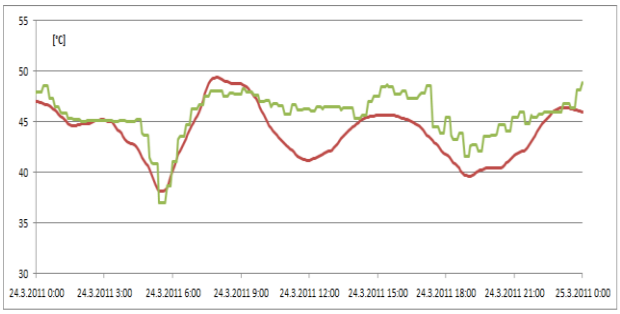

Figure 5: Predicted and measured values T_{vv} (returned water)

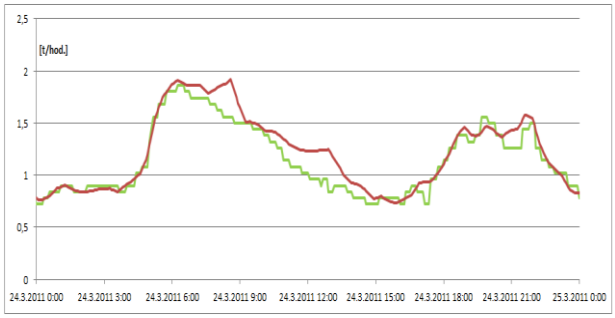

Figure 6: Predicted and measured values G (mass flow)

CONCLUSION

The results obtained during the experiments show, that the proposed simulation model can be useful tool for analyzing the properties and behavior of SHDC. It also appears that the prediction accuracy of the individual variables is strongly dependent on the accuracy of weather forecasts especially the outdoor air temperature is very essential.
Introduced simulation model can be used also in different manner. It can be incorporated into the control system to predict the behavior of SHDC at a certain (limited) time in the future, to streamline the management of SHDC.
Application of the presented simulation model will be especially interesting for large systems, where is the large distance between production and consumption of heat, which means that a long time is needed to transfer thermal energy from source to consumer.

ACKNOWLEDGMENT

The work was supported by the European Regional Development Fund under the Project CEBIA-Tech No. CZ.1.05/2.1.00/03.0089.

REFERENCES

Balate, J. “Automatic Control”, 2nd edition, BEN - technical literature, ISBN 80-7300-148-9, Prague, 2004.

Balate J., Chramcov B., Navratil P. ”Strategy evolution of control of extensive district heating systems”, Powereng 2007: International Conference on power engineering – energy and electrical drives proceedings, vols 1 & 2 Pages: 678-683 Published: 2007.

Chramcov B. ”Identification of time series model of heat demand using Mathematica environment”. In Recent Researches in Automatic Control: Proceedings of 13th WSEAS Int. Conference on Automatic Control, Modelling& Simulation. Lanzarote: WSEAS Press, 2011. pp. 346-351. ISBN 978-1-61804-004-6.

Incropera, F. P.; DeWitt, D. P. & Bergman, T. L. “Introduction to Heat Transfer”, Wiley, ISBN: 978-0471457275, London, 2006.

Kral E., Vasek L.,Dolinay V. & Varacha P. “Usage of PSO Algorithm for Parameter Identification of District Heating Network Simulation”, Proceedings of 14th WSEAS International Conference on Systems, Corfu Island, Greece, July 22-25, 2010, pp. 657-659.

Navratil P., Klapka, J., Balate J., Konecny, P. (2012). Optimization of load of heat source described by nonlinear mathematical model. In: Proceedings of the 18th International Conference on Soft Computing MENDEL 2012. Editor: Matousek, R., Published by Brno University of Technology, Brno, CR, p. 356-362. (ISBN 978-80-214-4540-6, ISSN 1803-3814) [June 27-29]

Navratil, P., Pekar, L. (2012). Possible Approach to Creation and Utilization of Linear Mathematical Model of Heat Source for Optimization of Combined Production of Heat and Electric Energy. International Journal of Mathematical Models and Methods in Applied Sciences. Vol. 6, No. 10, pp. 943-954, North Atlantic University Union NAUN (ISSN 1998-0140)

Saarinen, Linn. “Modelling and control of a district heating system”. Uppsala, 2008. 67 s. Uppsala University. ISSN 1650-8300.

UNIS Ltd. “Final report on project 2C06007” August 2011

Vasek L., Dolinay V. “Simulation Model of Heat Distribution and Consumption in Municipal Heating Network”. International journal of mathematical models in applied sciences, <http://www.naun.org/journals/m3as/>. ISSN 1998-0140, 2010.

Varacha P., Jasek R. ANN Synthesis for an Agglomeration Heating Power Consumption Approximation. In Recent Researches in Automatic Control. Montreux : WSEAS Press, 2011, s. 239-244. ISBN 978-1-61804-004-6.

Vasek L., Dolinay V. “Simulation Model of Heat Distribution and Consumption in Practical Use”. Proceedings of the 13th WSEAS International Conference on Automatic Control, Modeling and Simulation, Lanzarote, WSEAS Press 2011, pp. 321-324, ISBN 978-1-61804-004-6.

Vasek L., Dolinay V., Kral E. “Methods for Prediction of Heat Distribution Parameters”. Mathematical Methods and Techniques in Engineering and Environmental Science, Catania, Sicily, Italy, WSEAS Press 2011, pp. 335-340, ISBN 978-1-61804-046-6.

AUTHOR BIOGRAPHIES

LUBOMIR VASEK was born in Zlin, Czech Republic. He went to the Technical University Brno, where he studied mechanical engineering and obtained his degree in 1968. He worked all-time for this university and from year 1996 also for Tomas Bata University in Zlin. The main area of his work is simulation of technological processes, in discrete and continuous systems. His e-mail address is: lvasek@fai.utb.cz

VILIAM DOLINAY was born in Zlin, Czech Republic. He went to Tomas Bata University in Zlin, where he studied automation and control engineering and obtained his degree in 2003. Hi is working for this university as junior researcher, currently on projects focused on heating system. His e-mail address is: vdolinay@fai.utb.cz

MATHEMATICAL MODELING OF BACTERIAL CELLULOSE PRODUCTION BY *ACETOBACTER XYLINUM* USING ROTATING BIOLOGICAL FERMENTOR

D.M.S.C. Dissanayake and F. M. Ismail[1],
[1]Department of Chemical and Process Engineering,
University of Moratuwa, Sri Lanka
E-mail- susanthadmscd@gmail.com, marliya_i@uom.lk

KEYWORD

Mathematical model, Rotating Biological Fermentor, Bacterial Cellulose

ABSTRACT

Bacterial cellulose (BC) has a basic cellulose structure that gives high purity, high crystalline ability, high mechanical strength, and high water holding capacity. During the last few decades, BC has gained as an important biomaterial because of these unique physical and chemical characteristics. BC is synthesized by *Acetobacter xylinum* extracellularly in a suitable substrate media. Researchers have produced BC using a synthetic media or using coconut water and inoculating with *Acetobacter xylinum* in a static fermentation system. In order to eliminate shortcomings in static fermentation and to achieve increased cellulose production, agitated and aerated fermentation systems were experimented. Rotating Biological Fermentor (RBF) is an is aerated and agitated system, which gives continuous oxygen flux to the fermentation medium thereby increasing the yield of biomass and cellulose synthesized.

In this study, a mathematical model for the synthesis of BC in a RBF system was developed. The growth of cellulose is considered as a biofilm from a mono culture. Glucose depletion, cellulose production and microbial growth in the fermentation medium were explained using the developed models. It was shown that the simulated and experimental results were in close agreement. In addition, the model was successful in predicting yield of cellulose at different rotational speeds of the RBF unit.

INTRODUCTION

Cellulose is one of the most abundant polymers in nature. It is found as a structural component in the cell wall of plants. In addition, a few bacterial species, taxonomically related to the genus *Acetobacter xylinum* (acetic acid bacteria), extracellularly secrete bacterial cellulose (BC) as fibres. BC produced by *Acetobacter* species, displays unique properties, including high mechanical strength, high water absorption capacity, high crystallinity, and an ultra-fine and highly pure fibre network structure. It is expected to be a new commodity with diverse applications, if its mass production process could be improved. Presently BC is used as a fibre reinforcement material, as a wound dressing material, as a dietary fibre and as diaphragm of speakers (Lina et al. 2005 and Yoshinaga et al. 1997). Many researchers have produced BC using a synthetic media while most Asian researchers have produced BC using coconut water inoculated with *Acetobacter xylinum*. Coconut water can be recognized as a waste material in desiccated coconut industry with high BOD and COD values (Jayakody et al. 2011). Considering the level of natural sugar content in coconut water, it can be directly used to produce BC as a culture medium (Gamage 2012).

Due to the numerous importance of BC, researchers have focused on producing BC using different technologies (Bungay and Serafica 1999; Verschuren et al. 2000). Currently the technique of producing commercial scale BC has been limited to static fermentation system. However, research is in progress to use aerated and agitated continuous systems to produce BC in large scale (Yang et al. 1997 and Cheng et al. 2009). Rotating Biological Fermenter (RBF) that could be considered as an agitated and aerated fermentation system is one of the innovative techniques developed to produce BC (Patel et al. 2008). An RBF unit consists of a set of discs connected to a shaft and immersed in a container having a suitable substrate media. A similar study carried out by Dissanayake and Ismail (2013) showed that BC production in the RBF unit using coconut water as the substrate medium produced a maximum cellulose yield when the discs were rotating at 30 rpm. In addition, this study showed that the biomass was entrapped in the secreted BC matrix that was attached to the rotating discs. Cell growth and product formation are significantly influenced by mass –transport phenomena of nutrients and oxygen to the interface.

BC attached to a rotating disc can be considered as a biofilm. According to Wilderer and Characklis (1989), biofilm is a layer of prokaryotic and eukaryotic cells anchored to a substratum surface and embedded in an organic matrix of biological origin. One dimensional

Proceedings 27th European Conference on Modelling and Simulation ©ECMS Webjørn Rekdalsbakken, Robin T. Bye, Houxiang Zhang (Editors)
ISBN: 978-0-9564944-6-7 / ISBN: 978-0-9564944-7-4 (CD)

mixed culture biofilm model for flow of water was investigated by Lee and Park (2007). A similar experiment was conducted by Warner et al (2006) and different models were introduced to the analysis of biofilm growth. Erkmen and Albane, (2002) experimented the citric acid production using *Aspergillus Niger* and a mathematical model was developed to simulate the microbial growth and metabolic byproduct formation in an accurate manner. However prediction of growth of microbial culture for some bioprocess systems could be a complex task as it can be hindered by factors such as endogenous respiration, accumulation of toxic byproduct in the medium, decrease of oxygen penetration and spore formation in the medium (Novick 1955; Kenneth 2008).

The objective of this study is to develop a mathematical model which can describe the RBF system. For the convenience of developing the mathematical models and calculations, RBF unit was considered as a batch reactor and the cellulose growth was considered as a biofilm. In order to simplify the complex system, few assumptions were made. Later model was simulated using AQUASIM numerical software (Reichert P. 1998) and simulated results were compared with the experimented results.

ASSUMPTION

1. Bio film substratum is inert
2. Bacteria consume only dissolve oxygen as the source of oxygen
3. For a given microorganism, metabolic reaction rate is depends on one single rate limiting substrate.
4. Even though liquid is prominent in the system, solid biofilm is the main focus on modeling
5. System is a completely mixed system with batch type reactor
6. Density of the system is assumed to be constant.
7. Cellulose growth and microbial reaction decrease when turbulence flow occurs.

MODEL DISCRIPTION

RBF unit that is considered as a batch reactor, consist of coconut water inoculated with *Acetobacter xylinum* and operated for 8 days continuously.

Table 1: Model variables

Symbol	Notation	Values/ Units
$\mathbf{mass_{in}}$	Mass inflow	g day^{-1}
$\mathbf{mass_{out}}$	Mass outflow	g day^{-1}
$\mathbf{Biomass_{gene}}$	Growth of microorganism	g COD l^{-1} day^{-1}
$\mathbf{Biomass_{deca}}$	Decay of microorganism	g COD l^{-1} day^{-1}
$\mathbf{D_{decay}}$	Decaying rate	g COD l^{-1} day^{-1}
$\mathbf{m_G}$	Glucose weight	g
$\mathbf{m_X}$	Weight of microorganism	g
$\mathbf{m_C}$	Cellulose weight	g
$\mathbf{C_G}$	Concentration of Glucose	g l^{-1}
$\mathbf{C_{Gini}}$	Initial glucose concentration	32.567 g l^{-1} Jayakody et al. 2011
$\mathbf{C_X}$	Micro organism concentration	g COD l^{-1}
$\mathbf{C_{Xin}}$	Initial microorganism concentration	1500 g COD l^{-1} Grady et al. 1972
$\mathbf{C_C}$	Concentration of cellulose	g l^{-1}
$\mathbf{K_G}$	First-order rate	0.336 day^{-1} Alpkvist et al. 2006
$\mathbf{K_S}$	Concentration giving one half of the maximum rate	20 g l^{-1}
$\mathbf{K_D}$	Decay rate constant	0.1 day^{-1} Alpkvist et al. 2006
$\mathbf{K_{DO}}$	Flux of dissolve oxygen	rpm^{-1}
$\mathbf{K_{DO,\omega}}$	Rate of dissolve oxygen due to disc rotation	rpm^{-1}
$\mathbf{K_{DO,static}}$	Dissolve oxygen in very low rpm	rpm^{-1}
$\mathbf{K_{BF}}$	Proportional constant	$mm^4 l\ g^{-2}$
$\mathbf{\mu_{max,C}}$	Maximum specific cellulose growth rate	0.475 day^{-1}
$\mathbf{\mu_{max,X}}$	Maximum specific growth of microorganism	4.707 day^{-1} Alpkvist et al. 2006
$\mathbf{\omega}$	Rotational speed	rpm
$\mathbf{BF_L}$	Thickness of biofilm	mm
$\mathbf{BF_{L,\omega}}$	Thickness of biofilm with agitation	mm rpm^{-1}
$\mathbf{BF_A}$	Biofilm attachment	g l^{-1} day^{-1}
$\mathbf{BF_D}$	Biofilm detachment	g l^{-1} day^{-1}
$\mathbf{R}$	Rates	
$\mathbf{R_G}$	Rate of glucose depletion	g l^{-1} day^{-1}
$\mathbf{R_X}$	Rate of micro organism generation	g COD l^{-1} day^{-1}
$\mathbf{R_{X,\omega}}$	Rate of micro organism generation with agitation	g COD l^{-1} day^{-1} rpm^{-1}
$\mathbf{R_C}$	Rate of cellulose production	g l^{-1} day^{-1}
$\mathbf{R_{C,\omega}}$	Rate of cellulose production with agitation	g l^{-1} day^{-1} rpm^{-1}
$\mathbf{\rho_C}$	Density of cellulose	g l^{-1}
$\mathbf{a}$	Constant specific for RBF unit	0.009 rpm^{-3}
$\mathbf{b}$	Constant specific for RBF unit	1 rpm^{-2}
$\mathbf{c}$	Constant specific for RBF unit	0.36 rpm^{-1}

For this batch reactor, a general mass balance can be given as;

$$\frac{dm}{dt} = mass_{in} - mass_{out} + R \quad (1)$$

If the system density is assumed to be constant, then;

$$\frac{dm_G}{dt} = \frac{dC_G}{dt} = R_G \quad (2)$$

For a batch reactor, $mass_{in} - mass_{out}$ is equal to zero. In other words net flux is zero.
Similarly, the microbial growth in the system can be given as;

$$\frac{dm_X}{dt} = \frac{dC_X}{dt} = R_X \quad (3)$$

Therefore rate of biomass generation can be shown as

$$\frac{dC_X}{dt} = Biomass_{generation} - Biomass_{decay} \quad (4)$$

$Biomass_{decay}$ can be seen in microbial culture as due to endogenous respiration.

Cellulose growth in the system can also be represented by using a similar kind of equation

$$\frac{dm_C}{dt} = \frac{dC_C}{dt} = R_C \quad (5)$$

Rates of the three different reactions can be modeled for the system as given below.

BC production is affected by DO in the fermentation medium. Therefore, a new parameter K_{DO} that considers the variation in DO in the system due to the rotational speed of discs ω was defined.

Since, K_{DO} depends on ω ;

$$K_{DO} \propto \omega \quad (6)$$

At low rotational speeds, the flow streams in the substrate medium would behave in the laminar region. However, increase in rotational speeds will create turbulence that would disturb cellulose attachment to the discs while supplying excessive DO to the system. Therefore this explains that the rotational speed that changes the flow regimes would give the maximum cellulose production.
Then mathematically, function of K_{DO} for culture medium can be written as a quadratic equation which describes the influence of DO.

$$K_{DO} = -a\omega^2 + b\omega + C \quad (7)$$

$$K_{DO} = K_{DO,\omega} + K_{DO,static} \quad (8)$$

At very low rpm it can be assumed,

$$K_{DO,\omega} = 0 \quad (9)$$

Then,

$$K_{DO} = K_{DO,static} = C \quad (10)$$

Value of C can be experimentally obtained. Values of 'a' and 'b' were coefficients which describe the contribution from other factors such as disc and container characteristics in the system are given in Table 1.

Rate of glucose depletion in the system is considered as behaving as first order kinetics.

$$R_G = -K_G \times C_G \quad (11)$$

Negative sign is due to the depletion of glucose with time.

Increase in biomass and formation of cellulose depends largely on glucose and DO level. In addition to the major dependent factors pH, concentration of growth inhibitors and concentration of byproducts can have an effect on cellulose growth. However for the modeling purposes only major components were taken into account. Then as the initial step in the derivation, the rates of biomass and cellulose could be taken as proportional to glucose substrate utilization so that;

$$R_X \propto R_G \text{ and } R_C \propto R_G \quad (12)$$

Further, rate of biomass generation can be expressed using Monod equation (1949). However, Monod equation was modified to express heterotrophic micro organism growth with heterotrophic decay and the dependency of DO by including the term K_{DO}, as defined previously. Then, rate of biomass generation in dynamic system could be expressed as,

$$R_X = \left\{\left[\mu_{max,X}\left(\frac{C_G}{K_S + C_G}\right)C_X\right] - D_{decay}\right\} \quad (13)$$

$$R_{X,\omega} = \left\{\left[\mu_{max,X}\left(\frac{C_G}{K_S + C_G}\right)C_X\right] - D_{decay}\right\}K_{DO} \quad (14)$$

D_{decay} kinetics could be given by

$$D_{decay} = K_D \times C_X \quad (15)$$

An expression for the cellulose production can be derived similar to Eq. 12 -14. Development of model for cellulose production was taken as an ordinary concentration of culture which contains mix of both living and dead cells where heterotrophic decaying has been eliminated. Moreover, Monod equation can be used to describe a microbial system with byproduct formation. However rate of maximum production of

byproduct is obviously a lower value than the rate of maximum heterotrophic microorganism growth. Rate of maximum production of byproduct; cellulose, is represented by $\mu_{max,C}$. Then $\mu_{max,X}$ in general Monod equation (1949) could be replaced with $\mu_{max,C}$. Further, BC production too is affected by DO and glucose concentration in the fermentation medium. Then the growth of bacterial cellulose in the dynamic system could be given as;

$$R_C = \left[\mu_{max,C} \left(\frac{C_G}{K_S + C_G}\right) C_C\right] \quad (16)$$

$$R_{C,\omega} = \left[\mu_{max,C} \left(\frac{C_G}{K_S + C_G}\right) C_C\right] K_{DO} \quad (17)$$

In the RBF system, generated cellulose continuously attach to the discs. Attached cellulose can be considered as a biofilm. According to Wanner et al (2004) growth of biofilm is proportional to the biofilm attachment rate and detachment rate. Then;

$$R_{C,\omega} \propto BF_A - BF_D \quad (18)$$

Then;

$$\frac{dBF_L}{dt} = \rho_C \times K_{BF}(-BF_D + BF_A) \quad (19)$$

For a batch reactor, inflow and out flow net fluxes are equal to zero. Then BF_D can be neglected as produced cellulose that is retained on dices or sedimented inside the reactor liquid volume. Then;

$$BF_A = R_{C,\omega} \quad (20)$$

Then biofilm conversion can be written as;

$$\frac{dBF_{L,\omega}}{dt} = \rho_C \times K_{BF} \times R_{C,\omega} \quad (21)$$

The physical meaning of K_{BF} is mm of biofilm growth per unit concentration per unit density.

RESULTS AND DISCUSSION

Mathematical model that described the BC synthesis in a RBF system was solved to obtain solutions for glucose depletion, micro organism growth and for cellulose production. Simulated numerical solution that was obtained by solving equation 11, which describes glucose depletion in the system, is as shown in Figure 1. This result was compared with the experimented results of Yang et al (1997). According to Yang et al (1997), depletion of glucose starts after 10-15 hours of inoculation and then it begins to decrease drastically. At the end of the 3rd day of inoculation, glucose concentration becomes closer to a zero level. Similarly, simulated results were derived with an initial glucose concentration (C_{Gini}) of 32 g l^{-1} which is the case in coconut water. Then it shows the continuous depletion of glucose in the media until the 14th day where it becomes zero. The two conditions have given similar trends with a shift in time scale. This could be due to the difference in the systems, culture volume and the specific microbial culture strain used.

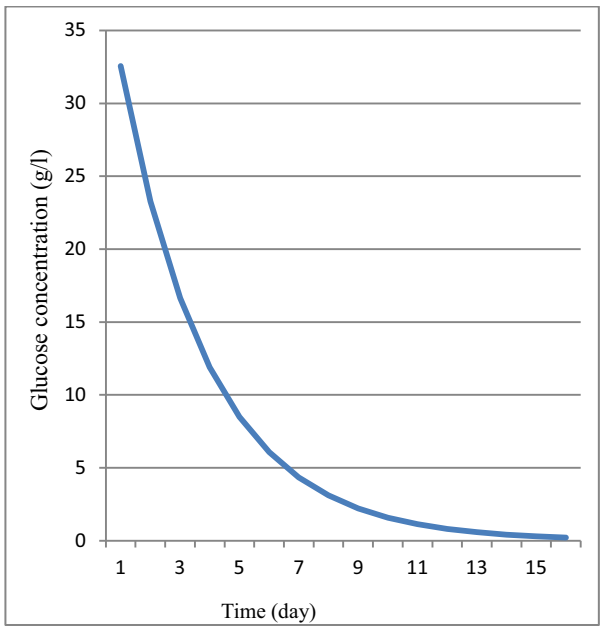

Figure 1: Simulated results of depletion of Glucose in the RBF unit

Figure 2 shows the simulated microbial growth with time which was obtained by solving equation 13. It shows an initial lag phase and an exponential growth phase which closely resembles Monod kinetics. A similar bacterial growth pattern was observed in the modeled results of Erkmen and Albane (2002). Moreover, Hammes et al (2007) investigated a monoculture micro organism and used a biofilm model to simulate the experimented results successfully. Even though growth rates and other parameters vary in different experiments (Erkmen and Albane. 2002; Hammes et al. 2006), a generalized growth curve was derived in this study and made it specific for the bioprocess under consideration. Further, Yang et al (1997) and Verschuren et al (2000) experimentally proved that microbial growth can be increased by increasing the dissolved oxygen in the media through aeration and agitation. In this study, this effect was proved through mathematical modeling of the microbial growth at different rotational speeds of the RBF system.

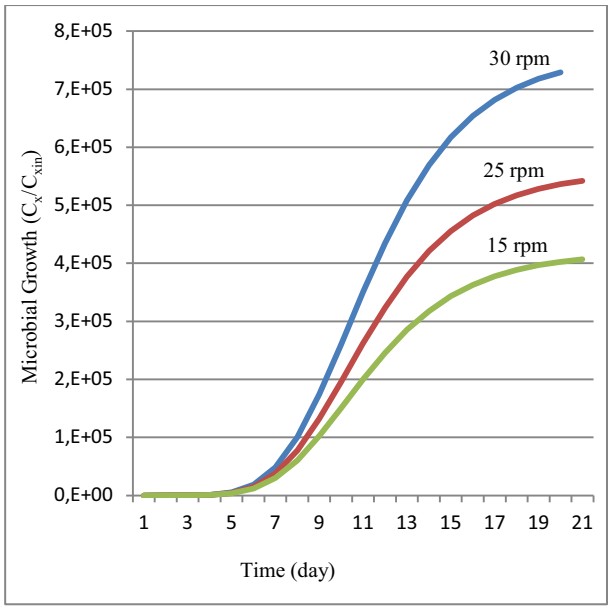

Figure 2: Microbial growth in RBF system for 30, 25, 15 rpm

Further, it is important to understand the yield of cellulose when the RBF system is operated at different rotational speeds. The simulated results obtained by solving equation 15 which gives the yield of cellulose when the rotational speeds are 30, 25, and 15 rpm for a batch volume of 2.75 liters are given in Figure 3. Initial cellulose concentration was considered as very small at the beginning of the experiments. Hornung et al (2009) did a similar study for static fermentation where they derived a model and verified with experimental results. They too showed that the yield of cellulose increase with time and reaches a maximum.

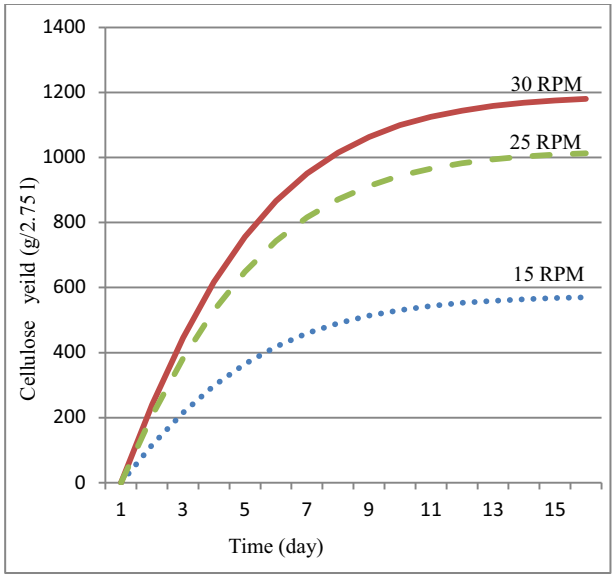

Figure 3: Simulated results of cellulose growth at three different rotational speeds in the RBF system

Moreover Figure 3 shows that the yield of cellulose could be increased when the rotational speed is increased. In a previous study, Dissanayake and Ismail (2013) experimented the yield of cellulose in a RBF system at the three different rotational speeds that are under consideration. These experimented results are in close agreement with simulated results at the 8th day of fermentation as shown in Table 2. Many researchers attempted to increase the cellulose production by increasing the oxygen content in the medium by aeration and agitation (Tantratian et al. 2005, Verschuren et al. 2000, Kauda et al. 1997). This is because the growth of *Acetobacter,* a typical aerobic BC producer, is dependent on oxygen and supply of oxygen is directly associated with BC productivity in an aerated and agitated culture system.

Therefore, the simulated and experimentally validated results support this argument. However, there is a significant percentage error when the rotational speed was 15 rpm. According to Dissanayake and Ismail (2013), at low rotational speeds, the experimental system behaves similar to a static medium. Hence it could be that the developed mathematical model does not take into account the limitations in diffusion of oxygen and glucose at low rpm values to the disc surface where the growth of cellulose occurs. This could also be the reason, for simulated results to show a maximum yield of cellulose on 10th – 11th day, although the experimental maximum and simulated values that are compared after 8 days are coherent.

Table 2: A comparison of simulated results of yield cellulose with experimented results of Dissanayake and Ismail (2013) at 8 days

rpm	Experimented results (g)	Simulated results (g)	Difference	Percentage error %
30	1098.25	1065	33.25	3.02
25	892	915.1	-23.1	(-2.58)
15	721	516.7	204.3	(-28.33)

Further, the derived model was tested to obtain the yield of cellulose at five different rotational speeds as given in Figure 4. Accordingly it shows that there is an optimum rotational speed 55- 65 rpm that would give a maximum yield of cellulose. Tantratian et al (2005) who studied the effect of dissolve oxygen on cellulose production by *Acetobacter Sp.* in an agitated system has also experienced similar results. They have obtained a maximum cellulose yield at an optimum rotational speed of 100 rpm and further increase in rotational speed have resulted in low yields of cellulose. According to Tantratian et al (2005), the excess oxygen that dissolves in the medium increases the accumulation of gluconic acid and adversely affects the cellulose production. On the other hand, too low an amount of dissolved oxygen content in the medium could not provide enough oxygen for the culture to grow and that caused the reduction of cellulose production. Further, Kauda et al (1997) mention that microbial cells could

oxidize due to excessive aeration. Thus these explanations are clearly in line with the simulated results.

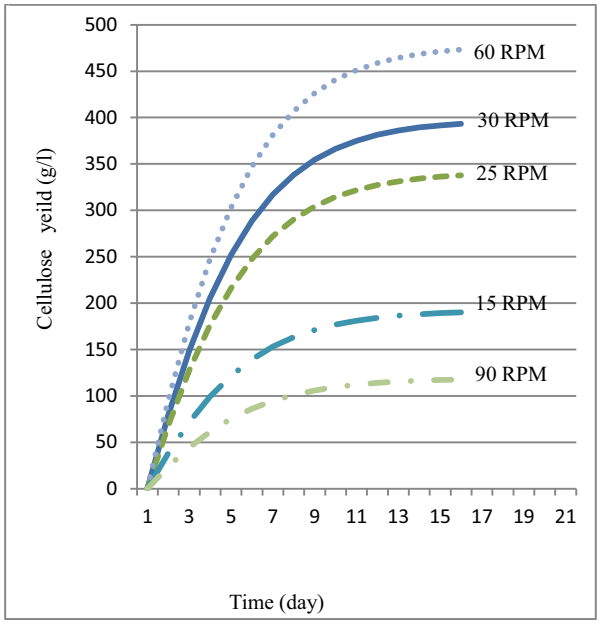

Figure 4: Simulated results of yield of cellulose at different rotational speeds

CONCLUSION

The mathematically derived model to explain the synthesis of BC in a RBF system is closely related to the experimented values. Developed models and constant could be used to describe depletion of glucose, AX growth and cellulose production in a coconut water based culture medium. This also means that the assumptions that were made in deriving the model are within acceptable limits. Model on the other hand could be used to predict the yield of cellulose, at any given rotational speed. However, there were limitations in using the model when the RBF unit closely resembles a static fermentation system.

RECOMMENDATION

Further analysis should be done in order to describe the BC synthesis in static fermentation.

AKNOWLEDGEMENT

I wish to convey my special thanks to the M.Sc. funds which was given by NOMA, Norway and for the collaboration of Telemark University College, Norway.

REFERENCES

Alpkvist, E.; C. Picioreanu; V.M.C.M. Loosdrecht; A. Heyden. 2006. "Three-dimensional biofilm model with individual cells and continuum EPS matrix". *Biotechnol. Bioeng* 94, (5), 961–979.

Bungay H.R. and G.C. Serafica. 1999, "Production of microbial cellulose using a rotating disc film bioreactor". *US Patent* 5,955-326.

Cheng C. K.; J. F. Catchmark; A. Demirci. 2009. "Enhanced production of bacterial cellulose by using a biofilm reactor and its material property analysis". *Journal of Biological Engineering* 3 – 12.

Dissanayake D.M.S.C and F.M. Ismail. 2013. "Comparison of bacterial cellulose growth in Rotating Biological Fermentation (RBF) and in Static Fermentation (SF)". *Proceeding of the 2nd Sri Lankan round table on sustainable consumption and production.* National Cleaner Production Center, Sri Lanka.

Erkmen O. and E. Alben. 2002. "Mathematical modeling of citric acid production and biomass formation by *Aspergillus niger* in undersized semolina". *Journal of Food Engineering* 52, 161–166.

Gamage N.S. 2012. "Developing a wound dressing from bacterial cellulose". *M.Sc. Thesis,* University of Moratuwa, Sri Lanka.

Grady, C.P.L. Jr.; L.J. Harlow; R.R. Riesing. 1972. "Effects of growth rate and influent substrate concentration on effluent quality from chemostats containing bacteria in pure and mixed culture" *Biotechnology and Bioengineering* 14, 3,391–410.

Hammes, F.; M. Vital; J. Rubulis; T Juhna. 2007. "Modeling planktonic and biofilm growth of a monoculture (P. *flurescens*) in drinking water". *Techneau.*6.

Hornung, M.; R. Biener; H.S. Peter. 2009. "Dynamic modeling of bacterial cellulose formation". *Eng. Life Sci.* 9, 4, 342–347.

Jayakody, J.R.U.C.; A.D.U.S. Amarasinghe; S.H.P. Gunawardena. 2011. "Effect of Evaporation on Sugar Content of Coconut Water in Desiccated Coconut Industry". *Annual Transactions* of IESL, 406-411.

Kenneth T. 2008. "The growth of bacterial population". *online textbook of Bacteriology*, 3. http://www.ukessays.com

Kouda, T.K.; Y.Y. Nagata; H.F.Y. Yano. 2000. "Method for cultivating apparatus for the production of bacterial cellulose in an aerated and agitated culture" *US Patent* 6,013,490.

Lina, F.; Z. Yue; Z. Jin; Y. Guang. 2005. "Bacterial Cellulose for Skin Repair Materials". *Biomedical Engineering*, Frontiers and Challenges, 249-274.

Lee W.M. and J.M. Park. 2007. "One-dimensional mixed-culture biofilm model considering different space occupancies of particulate components". *Water research* 41, 4317 – 4328.

Monod J. 1949. "The growth of Bacterial culture." *Ann. Rev.* Microb, 3, 371.

Novick A. 1955 "Growth of Bacteria". *Annual Review of Microbiology* 9, 97-110.

Patel U.D. and Suresh S. 2008, "Complete dechlorination of pentachlorophenol using palladized bacterial cellulose in a rotating catalyst contact reactor". *Journal of Colloid and Interface Science* 319, 462–469.

Reichert P. 1998. "Computer Program for the Identification and Simulation of Aquatic Systems". AQUASIM 2.0 user manual, ISBN: 3-906484-16-5.

Tantratian, S.; P. Tammarate; W. Krusong; P. Bhattarakoso; A. Phunsri. 2005. "Effect of Dissolved Oxygen on Cellulose Production by Acetobacter sp". *Journal of Science.* Chulankong University, 30, (2), 179-186.

Verschuren, P.G.; T.D. Cardona; Z.M.J.R. Nout; K.D.D. Gooijer; J.C.V.D. Heuvel. 2000. "Location and Limitation of Cellulose Production by *Acetobacter xylinum* Established

from Oxygen Profiles". *Journal of Bioscience and Bioengineering* 89, (5), 414-419.
Wanner, O.; J.E. Hermann; E. Morgenroth; R.N. Daniel; C. Picioreanu; B.E. Rittmann; C.M. Mark; V. Loosdrecht 2004. "Mathematical modeling of biofilm". *Water Science and Technology* 49, 11-12.
Wilderer P.A. and W.G. Characklis 1989. "Structure and function of biofilms". *In Structure and function of biofilms*(eds. W.G. Characklis and P.A. Wilderer), 5-17, John Wiley & Sons, New York, USA.
Yoshinaga, F.; N. Tonouchi; K. Watanabe. 1997. "Research progress in production of bacterial cellulose by aeration and agitation culture and its application as a new industrial material". *Biosci, biotech, biochem* 61C2D, 219-224
Yang, Y.K.; S.H. Park; Z.J.W. Hwang; Y.R. Pyun; Y.S. Kimit. 1998. "Cellulose Production by *Acetobacter xylinum* BRCS under Agitated Condition". *Journal of Fermentation and Bioengineering* 85, (3), 312-317.

AUTHORS BIOGRAPHY

SUSANTHA C. DISSANAYAKE, He was born in up country Sri Lanka and completed his degree in Food Science and Technology at University of Sri Jayewardenepura, Sri Lanka in 2009. Then he worked for an overseas company before moving to University of Moratuwa where he is studying for his Masters' in Sustainable Process Development which is being conducted in collaboration with Telemark University College Norway. His e-mail address is *susanthadmscd@gmail.com* and his mobile number is (+94) 712950703

MARLIYA ISMAIL, She did her first degree in Chemical Engineering at University of Moratuwa and her Graduateship in Chemistry at the Institute of Chemistry, Sri Lanka. Then she proceeded to University of Manchester, UK to do her doctorate in Cereal Process Engineering. Since completing her PhD, she is attached to the Department of Chemical and Process Engineering, University of Moratuwa, Sri Lanka as a Senior Lecturer specializing in food process engineering and biomaterial from wastes resources. Her e- mail address is *marliya_i@uom.lk* and her mobile number is (+94) 717223753

High Performance Modelling and Simulation

Lightweight Distributed Component-oriented Multi-agent Simulation Platform

Daniel Krzywicki, Łukasz Faber, Kamil Piętak,
Aleksander Byrski, Marek Kisiel-Dorohinicki
AGH University of Science and Technology, Al. Mickiewicza 30, 30-059 Krakow, Poland
e-mail: {krzywic,faber,kpietak,olekb,doroh}@agh.edu.pl

Abstract— **Existing solutions for agent-based systems turn out to be limited in some applications, like agent-based computing or simulations, where very large numbers of clearly defined agents interact heavily within a closed system. In those cases, fully-fledged, FIPA[1] compliant environment introduce unnecessary overhead, but simple tools fail to scale when confronted to bigger problems. In this paper, we introduce an alternative agent environment called *AgE*, targeted at medium-sized simulation and computational applications, which use multi-agent and computational intelligence paradigms, but does not need full FIPA compliancy, and would benefit from a component-based approach and distributed computing capabilities. After giving a short review of selected popular multi-agent platforms, the main features of AgE are presented. Next, some basic usability topics are addressed. Then the most interesting architectural aspects of the platform are discussed. Finally, AgE possibilities are demonstrated with two example applications.**

Keywords— **agent-based computing, component-based systems, agent-based simulation**

INTRODUCTION

Multi-agent systems (MAS), and more generally the concept of an intelligent agent, have found multiple applications, both as a mean to model complex systems and as a programming paradigm to implement them. Several established agent-based technological solutions exist, including FIPA compliant, fully-fledged environments like JADE or JADEX, where agents are a basic unit of software abstraction. As an example of another approach, there are also minimalistic and easy-to-use tools like NetLogo, where agents are only present at a domain level, as means of problem decomposition.

The first class of systems can be used to solve any problem that benefits from using an agent-oriented approach. However, in some particular classes of applications, this can be very inefficient. This happen especially in the case of simulation and computational applications, where agents and their behaviours are well defined. Such MAS might not need to be open to other systems, to require the possibility of code migration or to support FIPA-compliant communication.

In these cases, systems of the second class are more efficient and a much better choice. However, they suffer from other drawbacks, as they do not support component-oriented approach, which affects code reusability and make more complex problems hard to program. Also, these systems are usually not suited for running in distributed environments. In other words, they do not scale well with bigger problems or more complex systems.

In this paper, we introduce an alternative MAS environment called *AgE*, which aims to overcome the above issues. It is targeted at medium-sized simulation and computational applications, which use multi-agent and computational intelligence paradigms [1], but do not need full FIPA compliancy, and would benefit from a component-based approach and distributed computing capabilities. The presented work is a continuation of the platform presented in [2] and [3]. In this paper, however, we focus on component-orientation and distribution, as well as on the possibilities of the platform with regard to simulational and computational applications.

The AgE platform is designed with efficiency and usability in mind. We wanted to make it easy to experiment, prototype and tune simple MAS simulations or computations, then scale them to bigger problems and run in a distributed environment. In turn, the use of a component-based approach allows to create very flexible and reusable systems. It is important to stress that AgE is not meant as a replacement to existing agent-based technology, but rather as a convenient alternative dedicated to a specific class of applications.

The rest of this paper is structured as follows: First, a short review of some of the currently popular multi-agent systems is provided. Next, the main features of AgE from a multi-agent point of view are presented, including hierarchical environments, topologies and agent execution. After that, some basic usability topics are addressed, such as implementing custom agents or configuring applications using configuration mixins. Then, some of the more interesting architectural aspects of the platform are discussed, including agent execution, configuration and communication aspects. Finally, the advantages of using AgE are demonstrated with two example applications.

EXISTING SOLUTIONS FOR AGENT-BASED SYSTEMS

Agent-based software environments use agents as basic units of software abstraction. They focus on inter-agent relation and intra-agent intelligence [4], provide facilities for the discovery of agents, communication, life-cycle management etc. The FIPA standard allows to create such open, interoperable multi-agent systems, where fully-fledged autonomous software agents can express their needs or perceive the environment (and other agents) using specific languages, ontologies, etc. The most established solutions of this kind include JADE [5] and JADEX [6], the latter also using an active component approach.

A multi-agent system may also be implemented without any software structures corresponding to agents. This often happens in the case of simulations or computations, where

[1] Foundation for Intelligent Physical Agents

Proceedings 27th European Conference on Modelling and Simulation ©ECMS Webjørn Rekdalsbakken, Robin T. Bye, Houxiang Zhang (Editors)
ISBN: 978-0-9564944-6-7 / ISBN: 978-0-9564944-7-4 (CD)

the introduction of agents facilitates the modelling of complex phenomena, such as natural or social ones. In such cases, agents constitute building blocks of the *model*, which in turn may not at all be implemented with the use of agent technology. We describe briefly below some of the most popular tools of this kind, namely RePast [7], Mason [8], and MadKit [9].

MASON is an agent-oriented simulation framework developed at George Mason University. It is advertised as fast, portable, 100% Java based. The multi-layer architecture brings complete independence of the simulation logic from visualisation tools. The models are self-contained and may be included in other Java-based programs.

The programming model of MASON follows the basic principles of object-oriented design. An agent is instantiated as an object of a class, added to a scheduler and its `step` method is called during the simulation. There are no predefined communication nor organisation mechanism. There are neither ready-to-use distributed computing facilities nor component-oriented solutions.

RePast is a widely used agent-based modelling and simulation tool. It has multiple implementations in several languages and built-in adaptive features such as genetic algorithms and regression. The framework uses fully concurrent discrete event scheduling. Dynamic access to the models in the runtime (introspection) is possible using a graphical user interface.

In Repast Simphony, a new organisational concept called 'context' was introduced. It consists in a group of unorganised agents (they may be organised using so-called projections) and may create a hierarchical structure (context can have many sub-contexts and so on). This idea affects the perception of agents in such way, that an agent in the subcontext also exists in the parent context, but the reverse is usually not true.

MadKit is a modular and scalable multi-agent platform written in Java, aimed at modelling different agent organisations, groups and roles in artificial societies. It is built based on a so called Agent/Group/Role organisational model [10], using a plugin-based architecture. The architecture of MadKit is based on micro-kernels which provide only the basic facilities: local messaging, management of groups and roles, launching and killing of agents. Other features (remote messages, visualisation, monitoring and control of agents) are performed by agents. Both thread based and scheduled agents may be developed.

Simulations do not require any particular structure or model to run. However, it is possible to add an arbitrary scheduler or create complex agent communities and relationships. Agents can locate other agents having some specific role or belonging to some particular group. Agents can communicate with each other using these roles or group membership (i.e. using broadcast messages).

MAS FEATURES

The following section describes the main features of the AgE platform from a MAS point of view, as they are available to end users.

A. Agent Types

The AgE platform includes two types of agents: heavyweight agents and lightweight ones.

Heavy agents are realised as separate threads, as in the JADE platform. They communicate through asynchronous message passing. This is an effective model when the number of agents is small or agent interactions are sparse (i.e. each agents communicates only with a small number of other agents).

However, in simulation and computation scenarios where there is a large number of heavily communicating agents, experiments have shown that a fully concurrent approach does not perform efficiently. In fact, most of the execution time tends to be spend on handling message queues and switching threads context[11].

In order to overcome this issue, AgE introduces *lightweight agents*. Populations of such agents are thread-contained and execute pseudo-concurrently, one step each at a time. Some restrictions on how agents may change each other state, along with communication constraints, described further below, emulate concurrency effects and execution interleaving. From these agents perspective, they are effectively processed in parallel.

Thus, the platform API available to heavyweight and lightweight agents is very similar. The main difference is in efficiency and determinism, as needed in a particular case.

B. Agent Environments

Each agent in AgE belongs to some environment. Agents can communicate with each other within their environment or query it to acquire some information.

In the case of heavy agents, the environment simply consists of multiple distributed nodes. All heavy agents on all connected nodes belongs to it. For more information on this virtual execution environment, see Section -F.

B.1 Hierarchy of Environments

When it comes to lightweight agents, environments are treated as agents themselves. These *aggregate* lightweight agents also have properties, behaviour, and also execute in some higher level environment. Thus, following the Composite design pattern [12], lightweight agents form hierarchies, as shown in Fig. 1. The root agent is a heavy one and is called a *workspace*. A workspace encompasses all the hierarchy within its thread and initiates step based, pseudo-concurrent execution.

As an application of agents hierarchies, consider a flocking MAS where multiple flocks, composed of multiple agents, coexist. Particular agents can interact within a flock, but flocks as wholes can also interact. They can compete over limited resources or exchange information, reflected by the agents within them.

B.2 Topology of Environments

By default, all environments are assumed flat, i.e. all contained agents can see each other. It is however possible for users to restrict this visibility, by defining a custom topology.

As an example, consider a topology which takes into account the network latency between distributed computing

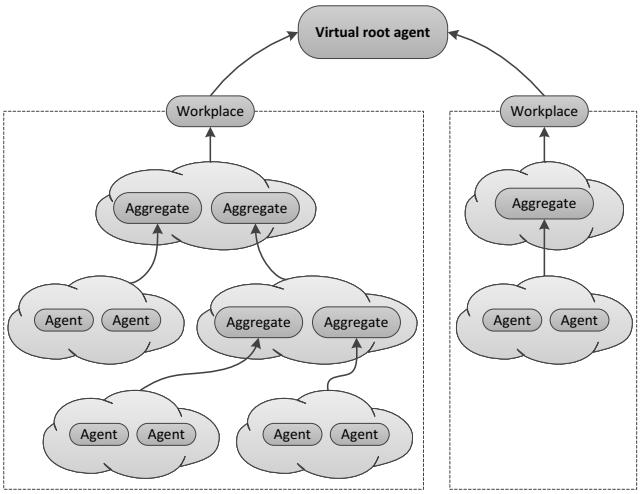

Fig. 1: Lightweight agents environments can form hierarchies. Each environment agent is called an aggregate. The root one is called a workspace and is implemented as a heavy agent. The whole hierarchy executes within the root's thread.

nodes. Limiting interactions to agents physically nearby can dramatically increase performance. Another example would be a topology which clusters agents based on their features, then restricts visibility to within a cluster.

Remark that introducing a topology is not the same as splitting an environment into multiple ones, as the induced relation can be arbitrary. In particular, it needs not be symmetric or transitive.

C. Agent Execution

As mentioned before, heavy agents execute concurrently in their own threads, usually spinning in a loop or waiting for incoming messages.

Lightweight agents in turn execute pseudo-concurrently, one step at a time. The order of execution in a given environment is by default arbitrary (though this policy can be customized). Child agents in the hierarchy execute their step before their parent, so that changes bubble up the tree from leaves to the root.

A consistent iteration order over the agent hierarchy needs to be preserved. To this end, any structural modifications of an environment (such as the addition, removal or migration of agents) is postponed until all the agents in that environment are done with their step. In consequence, any such modification will only be visible in the environment in the next step.

Beside executing custom logic, both heavyweight and lightweight agents can interact with each other through asynchronous *messages* or perform *queries* on their environment. Additionally, lightweight agents are free to interact synchronously within a given environment and to submit asynchronous *actions* to their environment for later execution.

C.1 Messages

Agent communication in AgE is mainly based on message-passing. Immutable messages consist in an target address and arbitrary payload.

All agents are provided with an unique address by a distributed addressing service. Messages can be targeted for unicast, multicast, anycast or broadcast transmission.

Agents do not send messages directly. Instead, they submit them to the environment, which handles delivery. Heavy agent messages are handled fully concurrently. In the case of lightweight agents, however, a message sent in one step will be received in the next step.

C.2 Queries

Queries offer agents the possibility to gather, analyse and process data from both local and remote environments. They allow to perform tasks like computing the average value of some agent property in the environment, select and inspect arbitrary objects in collections and much more. They can be applied to arbitrary properties using reflection or specialized for efficiency.

Queries are defined using a simple, declarative, yet extensible query language, following the Fluent Interface design pattern [12]. They are built without the knowledge of the target object, so a single query can be reused on multiple objects, yielding different results.

The platform also offers the possibility to cache query results for efficiency. Such a wrapping query is given some expiration time and will recompute the result only if that time has elapsed.

C.3 Actions

Sometimes step-based processing does not provide appropriate granularity. In particular, a single step may be composed of several distinct phases which should execute consecutively.

As an example, consider an algorithm where, in each step, agents first exchange energy, then reproduce and create new agents. Obviously, we would like that all agents first exchange energy, then all agents potentially reproduce. What we get instead, with simple step processing, is that the first agent exchanges energy and reproduces, then the second agent does the same, etc.

In order to achieve truly *interleaved execution* with lightweight agents, the AgE platform introduces asynchronous *actions*. Following the Command Object design pattern [12], instead of executing at once, parts of the algorithm are encapsulated into actions objects. These actions are then submitted to the environment for later execution.

When all agents in the environment have finished their step, the environment executes the submitted actions. They are first reordered so that actions of the same type are grouped together. Then, such groups are executed in a FIFO order (this policy can also be customized, by providing an explicit total order over action types).

Using this method, a single step can be decomposed into a sequence of actions, which are effectively interleaved.

As the actions to be executed can be injected into the agent from configuration, this lead to an interesting model: Agents types only define state, but behaviour is fully encapsulated into actions and composed at configuration time. In order to change the behaviour of an agent, only the configuration needs to be updated, without recompilation. Multi-

ple similar agents can also have slightly different behaviour. Moreover, it also becomes possible to change the behaviour at runtime.

USING THE PLATFORM

This section briefly describes MAS simulations and computations can be implemented and configured in AgE.

The platform has been intentionally designed to use standard Java technologies, concepts and patterns, so that it could be used just like other mainstream MAS or component platforms. Because of that, we believe it to have an efficient learning curve.

D. Creating Agents

Agents in AgE are implemented in Java or Scala with the use of a very simple API, reflecting the features described in Sec. . The platform then handles distribution and concurrency transparently to the user.

Just like in Jadex, agents are actually components managed by an IoC container. They can have properties and dependencies, the latter being wired and injected by the container.

Specific parts of the algorithm, such as a clustering method or a preselection technique in a genetic algorithm, can be extracted to dedicated components. These can be shared, as dependencies, by multiple agents, following the Strategy design pattern. The platform provides several such components out of the box, especially for evolutionary computations.

E. Configuring an Application

The configuration of an AgE application is decoupled from the implementation of agents and other components. The main way to describe an AgE application is to provide an XML configuration file with a syntax very similar to the one found in frameworks like Spring.

In such a file, the user can define all of the components, initialize their properties, specify explicit dependencies (optionally, as these will be autowired otherwise). This is all very similar to Spring configurations.

However, there are a few notable outstanding features when compared to Spring or similar solutions. These features are *nested definitions* and *configuration mixins*.

In AgE, component definitions can be nested in one another. This is different from inner beans found in Spring, as inner components will only be visible to the outer component and other components nested inside it. Such a solution allows to solve the so-called *robot-leg problem*.

E.1 Configuration mixins

The other novel feature is the possibility of configuration *mixins*. Most frameworks allow users to include configuration files one in another. AgE takes this one step further: it is possible to define named structural blocks in configuration files. When including some other file, the blocks it contains can then be extended or overridden.

In this way, one can achieve inheritance-like functionality, or more generally — mixins (as inclusion can happen in multiple places).

This greatly improves the reusability of configuration files, as it becomes possible to create complex, but general configurations. Custom computations need only define components specific to the problem being solved.

As an example, consider the configuration for an evolutionary algorithm, where operators such as selection or variation are given default implementations. Such a configuration can be reused as is — the user just needs to include it and provide some representation and fitness function. However, the user can also overwrite particular blocks in the original configuration, in order to supply custom operators.

IMPLEMENTATION ASPECTS

In this section we will briefly discuss the most important technical aspects of the platform.

F. Virtual Execution Environment

The platform introduces a *virtual execution environment* (Fig. 2). In distributed systems, it allows to perform operations involving workplaces located on different nodes, without their awareness of physical distribution. Such operations are executed by the core service according to the *Proxy* design pattern [12]. A core service uses the communication service to communicate with core services located on other nodes.

The global namespace of agents can be narrowed by introducing an *agent neighbourhood*, that defines the visibility of top level agents. An agent can only interact with agents in its neighbourhood. For heavy agents, the neighbourhood is realised and managed by a topology service. In the case of lightweight agents, this functionality is performed by the environment, which will usually delegate it to some dedicated component.

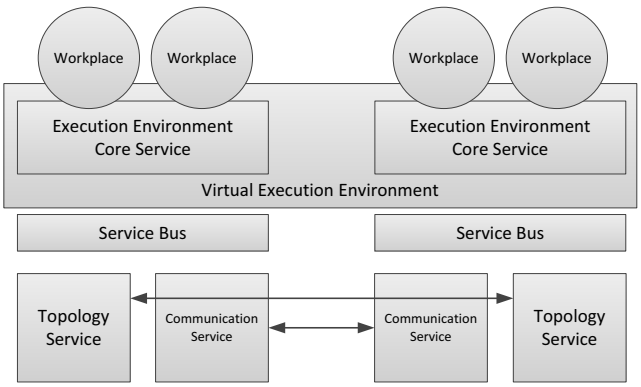

Fig. 2: Virtual execution environment. Workplaces see a unified, global namespace of agents and are not aware of physical distribution among many nodes. Communication is carried by the communication service. The topology service may introduce logical divisions of the namespace.

G. Agents Execution

Lightweight agents execute pseudo-concurrently, by repeatedly executing some step callback function. From their point of view, lightweight agents effectively execute in parallel. The platform emulates this parallelism by introducing

several constrains on message propagation and change visibility.

First, messages have a positive time of propagation. It means that a message send in one step will only be received at the earliest in the next step. Lightweight agents must thus assume latency just like heavy ones.

Secondly, within a given environment, lightweight agents can interact synchronously. Obviously, there is no need for synchronization, as they actually execute sequentially. However, there is no guarantee (from an agent point of view) over the order in which they do. Therefore, they must make assumptions similar to those they would need in a truly concurrent environment.

Thirdly, the platform enforces some strict semantics on the way changes propagate in the environments hierarchy. In particular, agents in a given environment are assumed parallel, but agents in separate environments are assumed independent.

This implicates that any agent in the hierarchy can only directly (synchronously) change a sibling or child agent (if it is itself an aggregate). However, all the agents above in the tree are available in "read only" mode. This which ensures that agents in two different subtrees can never make conflicting changes.

Of course, it may be necessary to modify the agent tree above, for example by adding a new agent to the environment. Some changes can be requested simply a sending a message to the target agents. Changes which need to be executed before the next step (such as adding a new agent to the environment) can be wrapped in asynchronous actions submitted to the environment.

An aggregate agent will first let its children carry out their tasks. Then, it will execute the actions which they submitted. Finally, it will execute its own tasks.

Therefore, from the point of view of the whole agent tree, actual execution is performed in a post-order way, from the leaves up to the root, level after level. With each level, the visibility restriction are softened, and eventually, all leaf environments are synchronized in the root.

G.1 Messages

Message passing (described in Sec. -C.1) is the basic communication mechanism offered by AgE, simple but flexible. Both agents and services use it. However, types of a sender and receivers cannot be mixed — there is no possibility for an agent to send a message to a service and vice versa. They can be easily extended to use more structured payloads and carry additional metadata in headers.

In the case of simple agents, message sending and delivery is performed by their parent aggregate. The sender adds a message event to its parent queue. The parent handles the message by locating all receivers and calling a handler on each of them. These messages are placed on a queue and can be received by the target agent during its next step.

Thread-based agents use a similar queue of messages but are not restricted by the execution semantics and can inspect it at any point of time.

As mentioned above, in order to emulate asynchronous messaging, a message sent by an lightweight agent in a given step will be available to the receiver in the next step.

H. Component Model and Framework

The platform defines *components* close to classes, i.e. a component is represented by a single class (called *component stub*) enhanced with additional description (called *component specification*). Such an approach gives a possibility to construct computational agent-based systems from relatively small parts and gain advantages from component-oriented programming. However classes are not a good unit of deployment [13, chap. 2]. Therefore the deployment model assumes that component classes are provisioned and deployed in bigger containers, such as jar files in the Java environment.

A component in the runtime environment is identified by a unique textual name, which is generated by default from a fully qualified name of the component stub. A component specifies its *capabilities*, *requirements* and *configurable properties*.

By default all interfaces implemented by the class are treated as component capabilities, but there is a possibility to narrow them by explicit specification using Java annotations.

Requirements specify conditions that must be fulfilled before a component can serve its capabilities. The presented model defines a requirement as the declaration of a dependency to some other interface. Dependencies can consist in annotated fields, methods or constructor parameters, following the JSR-330 specification. A dependency declaration can be enhanced with an additional qualifier which points to a concrete name of a component. Such dependencies are called *named dependencies*. Configurable properties are defined according to the Java Beans convention.

The model does not specify one concrete method of defining a component specification – particular implementations can use different methods.

The platform uses the dependency injection pattern and is built on top of the PicoContainer framework[2]. A container is used to instantiate and assembly component instances, based on a system configuration. A configuration can come in a variety of formats and syntaxes: it could be an architecture description language expressed in XML format or written in a dedicated Domain Specific Language, or be defined in some interactive console or GUI. All these must be interpreted in a consistent way by an appropriate configuration subsystem.

In order to express this diversity, the architecture of such a subsystem could become excessively complex. To avoid that, the representation of the configuration has been split into two layers: a user-specific format, and a Configuration Object Model.

As shown in Figure 3, multiple user format and tools are acceptable (the default, XML-based approach was discussed in Section -E). They are transformed into a common abstract representation, the Configuration Object Model, which can be used in turn by an IoC Container to instantiate a concrete graph of component instances.

This approach decouples the way the configuration is seen by the users from the way it is interpreted by the system. Adding a new configuration format is just a matter

[2]http://www.picocontainer.org

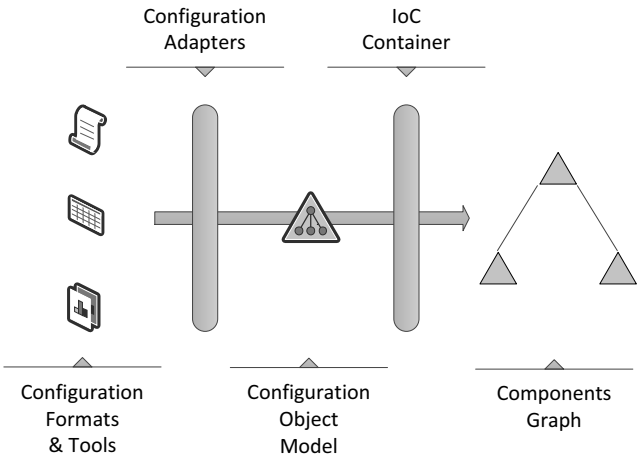

Fig. 3: Multiple configuration adapters may handle different configuration formats, translating them to a common Configuration Object Model. This common representation is in turn used by the container to instantiate a graph of components.

of creating a corresponding adapter, while the in-memory representation of the configuration can be kept as compact and simple as possible. Both can then evolve independently, making the system open for extensions.

H.1 Configuration Object Model

The *configuration object model* is an abstract way to describe a graph of components. It contains all information required to instantiate and initialise components and wire them up together.

The configuration object model is a collection of component definitions that represent component runtime configurations defined in the presented component model. These consist of a unique name, a type and a scope. The scope of a component definition can be either a *singleton* or a *prototype* one.

A definition's *singleton* scope indicates that there should exist at most one instance of the component it describes. If the definition has a *prototype* scope, it indicates that each dependency to this component should be resolved with a separate instance, following the Prototype pattern [12].

Definitions can be assigned constructor and property arguments, which are used to instantiate and initialise components. These arguments can be a reference to another definition (i.e. a dependency to other component expressed by a name of the target), or a value-type parsable from some string representation (i.e. a configurable property).

Component definitions can be nested and effectively form a tree. Inner definitions are only visible to their parent and its other descendants, which form together a *context*. When resolving dependencies, components from the same context take precedence over those from the outside one. This makes it possible to create hierarchical configurations, where inner definitions can hide outer ones by type or by name (this is the only exception for the name-uniqueness).

Together with *mixins* in XML files, this feature improves configuration reusability, as global configuration files can define components for global or mock services, but these can be hidden by local implementations.

H.2 Components Initialisation

A component can be instantiated when all of its requirements are met. An object of the component stub class is created, all dependencies are initialised with references to instances of other components (created if needed) and properties values are set to their defaults. After that, depending on component attributes, some additional initialisation operations can be performed. Components can be instantiated at system startup (eager loading) or on demand, before first use (lazy loading).

H.3 Relationship Between Components and Agents

Some agents may perform similar tasks, but work with different structures and mechanisms. Thus, from a software engineering perspective, it may be said that the system is decomposed into particular agents, but a single agent implementation is too complex to serve as an assembly unit.

Agents implementations may actually be further decomposed into functional parts (components), which are replaceable, as long as they are compatible to one another, even when used by different agents (this ensures agents interoperability at implementation level). This is a realization of the Strategy design pattern [12].

A particular application is thus decomposed into agents and strategies, which provide the implementation of some specific part of agent behaviour. Both agents and strategies are implemented as classes and they are provided to a runtime environment as components. But, in regard of their different characteristic, they are provided with two distinct scopes.

Agents are represented as objects with well-defined lifecycle and attributes which define their state. Many agents of the same type (i.e. the same class) can exist in one environment. Moreover some of them can be differently configured: have different values of named properties or various implementations of dependent strategies.

According to such assumptions, agents are provided as components with a *prototype* scope. This allow to create many instances of the same agent type with the same configuration. However, these instances are not identifiable. To solve this issue, agent addresses have been introduced. Agents of the same type, but configured differently, are provided as distinct components with different names, however pointing to the same class.

In turn, strategies are provided to the environment as components with a *singleton* scope. It is sufficient to hold only one instance of a strategy, as it provides only stateless action implementations. Therefore, strategies can be identified by components names and there is no need to introduce an additional address schema.

I. Distributed Computation

The platform assumes that a computation may be executed in a distributed environment, comprised of nodes connected via communication services. Each node is a separated process, possibly executed on a different physical machine. This means that two modes of distribution are distinguished: on the service level (opaque) and on the computation level (transparent). This simply means that services in a given node are aware of the existence of other nodes

and know that to communicate with them, they need to use a specialised facility. On the other hand, agents should not notice that their communication is carried over the network.

Services use the communication service by simple method calling. Usually, communication between remote services is limited to services of the same type and performed using a message passing with the platform-wide message types. However, messaging is not the only way for services to communicate. Currently, basic synchronisation primitives, like global (environment-wide) barriers, are also available.

The separation between the underlying deployment scenario and the computation itself gives us even more possibilities. An amount of work may differ a lot between workplaces. Moreover, workplaces can be moved between nodes. These two facts lead straightforwardly to implementing load balancing on a workplace level. Workplaces can be migrated from more loaded nodes to these that are free. This also makes it possible to add more nodes to an already running computation to speed it up.

Computations may also be run one after another, on the same node instances. After finishing one execution, another configuration file may be loaded and a new computation deployed.

APPLICATION EXAMPLES

J. Transport Simulation

We have successfully implemented and tested several transport simulation examples. We will briefly present one of them as a demonstration of how the concept of agent hierarchy can be used.

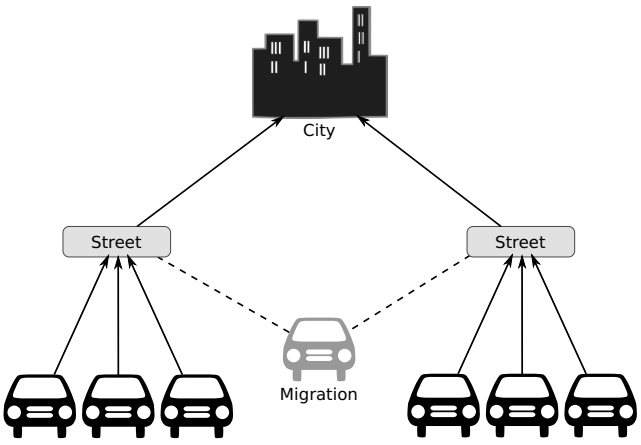

Fig. 4: Hierarchy of agents in a transport simulation example. The top-level aggregate represents a city. The next level consists in street aggregates. Simple agents on the lowest level represent individual cars.

This scenario consists of simulating road transport in a city with continuous space. We distinguish three main components interacting with each other: cars (or any other road vehicles), streets and an environment. All of their instances are represented as agents. This model is simple but general could easily be extended by introducing further types of objects into the simulation: pedestrians, bicycles, static obstacles, etc.

Cars are implemented as simple, lightweight agents, collected in streets which are represented as aggregates. Similarly, all streets are collected in the aggregate which represents the whole city (or a district if its large enough).

Each car can have a separate and unique driving strategy. Car movements within a street are efficiently computed within the aggregate, by executing agent actions such as braking, turning, etc. Cars movements between streets are represented as agents migrations. Collisions and illegal movements are easily detected by street aggregates.

K. Evolutionary Multi-agent Systems

Another area of application of lightweight agents and agent hierarchies is evolutionary optimization. Multi-agent systems can be combined with evolutionary algorithms, in order to solve optimization problems[14][15].

Individual agents are assigned with a solution to the problem and some coresponding fitness. They are also given some initial energy and then put to competition. Agents with a higher fitness take energy from those with lower fitness, inducing an emergent selective pressure.

Agents die if their energy drops to zero. In turn, if they gather enough energy, they can reproduce, yielding new agents. These are assigned with new solutions, obtained through standard evolutionary operators applied on the parents.

Competition can also happen on a higher level, by grouping agents into competing flocks[16], resulting in a more general version of the Island Model in Evolutionary Computation.

Arbitrarily nested flocks can easily be represented in AgE agent hierarchy. Individual agent interactions, such as fights and reproduction, can be represented as actions. Agent in different flocks can in turn have separate evolutionary operators, also allowing meta-optimization of the algorithm.

CONCLUSIONS

In this paper, we have presented an MAS computing environment called AgE, targeted at medium-sized simulation and computational applications, which use multi-agent and computational intelligence paradigms, but does not need full FIPA compliancy, and would benefit from a component-based approach and distributed computing capabilities.

Up till now, we have been able to successfully implement and test various simulation scenarios. We consider two of them as the most interesting: transport simulation [17] and evolutionary multi-agent systems [18]. The former extensively used both the hierarchy capabilities of AgE and its configuration and re-use facilities. The latter is an idea based on joining the classical evolutionary computation with agent-based paradigms and is an unusual approach e.g. to artificial life.

Through the concept of lightweight agents, AgE is optimized for a large numbers of heavily interacting agents, which corresponds to many agent-based simulation and computational applications. The platform can also be distributed over multiple nodes. A component-oriented approach allows to achieve high flexibility and reusability,

both at code and at configuration level because of configuration mixins. The use of technological standards results in low switching costs from other agent technology and an efficient learning curve. As such, we believe the AgE platform to be a convenient alternative, dedicated to a specific class of applications.

The work on the development of AgE continues. In particular, we consider the following improvements in the near future:

- stronger support for the Scala language, along with a functional agent paradigm and actor-based concurrency,
- visualization facilities, experiment scheduling and persistence of results,
- component migration, dynamic reconfiguration, acquisition of components from remote repositories,
- virtualised deployment in the cloud.

ACKNOWLEDGMENT

The research presented here was partially supported by the grant "Biologically inspired mechanisms in planning and management of dynamic environments" funded by the Polish National Science Centre, No. N N516 500039.

REFERENCES

[1] M. Kisiel-Dorohinicki, G. Dobrowolski, and E. Nawarecki, "Agent populations as computational intelligence," in *Neural Networks and Soft Computing*, ser. Advances in Soft Computing, L. Rutkowski and J. Kacprzyk, Eds. Physica-Verlag, 2003, pp. 608–613.

[2] A. Byrski and M. Kisiel-Dorohinicki, "Agent-based model and computing environment facilitating the development of distributed computational intelligence systems," in *Computational Science - ICCS 2009, 9th International Conference*, ser. LNCS, vol. 5544. Springer-Verlag, 2009.

[3] Ł. Faber, K. Pietak, A. Byrski, and M. Kisiel-Dorohinicki, "Agent-based simulation in AgE framework," in *Advances in Intelligent Modelling and Simulation*, ser. Studies in Computational Intelligence, A. Byrski, Z. Oplatková, M. Carvalho, and M. Kisiel-Dorohinicki, Eds. Springer Berlin Heidelberg, 2012, vol. 416, pp. 55–83.

[4] M. Wooldridge, *Reasoning About Rational Agents*. The MIT Press, 2000.

[5] B. Bellifemine, A. Poggi, and G. Rimassa, "Jade – a fipa-compliant agent framework," in *Proc. of PAAM'99, London*, 1999, pp. 97–108.

[6] A. Pokahr, L. Braubach, and W. Lamersdorf, "Jadex: Implementing a bdi-infrastructure for jade agents," *EXP - in search of innovation (Special Issue on JADE)*, vol. 3, no. 3, pp. 76–85, 9 2003.

[7] M. North, T. Howe, N. Collier, and J. Vos, "A declarative model assembly infrastructure for verification and validation," in *Advancing Social Simulation: The First World Congress, Springer, Heidelberg, FRG (2007)*, S. Takahashi, D. Sallach, and J. Rouchier, Eds., 2007.

[8] S. Luke, C. Cioffi-Revilla, L. Panait, K. Sullivan, and G. Balan, "MASON: A multi-agent simulation environment," *Simulation: Transactions of the society for Modeling and Simulation International*, vol. 82, no. 7, pp. 517–527, 2005.

[9] O. Gutknecht and J. Ferber, "The madkit agent platform architecture," in *In Agents Workshop on Infrastructure for Multi-Agent Systems*, 2000, pp. 48–55.

[10] J. Ferber and O. Gutknecht, "A meta-model for the analysis and design of organizations in multiagents systems," in *Proc. of ICMAS'98 Conference, Paris*, Y. Demaseau, Ed., 1998, pp. 128–135.

[11] M. Thompson, D. Farley, M. Barker, P. Gee, and A. Stewart, "Disruptor: High performance alternative to bounded queues for exchanging data between concurrent threads," http://disruptor.googlecode.com/files/Disruptor-1.0.pdf, 2011, [Online; last access 31-March-2013].

[12] E. Gamma, R. Helm, R. Johnson, and J. Vlissides, *Design Patterns: Elements of Reusable Object-Oriented Software*. Addison-Wesley, 1995.

[13] A. J. A. Wang and K. Qian, *Component-Oriented Programming*. Wiley-Interscience, 2005.

[14] K. Cetnarowicz, M. Kisiel-Dorohinicki, and E. Nawarecki, "The application of evolution process in multi-agent world to the prediction system," in *Proceedings of the Second International Conference on Multi-Agent Systems, ICMAS*, vol. 96, 1996, pp. 26–32.

[15] A. Byrski and M. Kisiel-Dorohinicki, "Agent-based evolutionary and immunological optimization," in *Computational Science–ICCS 2007*. Springer, 2007, pp. 928–935.

[16] M. Kisiel-Dorohinicki, "Flock-based architecture for distributed evolutionary algorithms," *Artificial Intelligence and Soft Computing-ICAISC 2004*, pp. 841–846, 2004.

[17] E. Nawarecki, J. Koźlak, G. Dobrowolski, and M. Kisiel-Dorohinicki, "Discovery of crises via agent-based simulation of a transportation system," in *Multi-Agent Systems and Applications IV*, ser. LNAI, M. Pěchouček, P. Petta, and L. Varga, Eds., vol. 3690. Springer-Verlag, 2005, pp. 132–141.

[18] M. Kisiel-Dorohinicki, "Agent-based models and platforms for parallel evolutionary algorithms," in *Computational Science – ICCS 2004. Part III*, ser. LNAI, M. Bubak, G. D. van Albada, P. M. A. Sloot, and J. Dongarra, Eds., vol. 3038. Springer-Verlag, 2004, pp. 225–236.

ABOUT THE AUTHORS

Daniel Krzywicki obtained his M.Sc. in 2012 at AGH University of Science and Technology in Cracow and is currently a Ph.D. student at the Department of Computer Science of AGH-UST. His research interests include agent-based computations, functional programming and distributed systems.

Łukasz Faber obtained his M.Sc. in 2012 at AGH University of Science and Technology in Cracow and is currently a Ph.D. student at the Department of Computer Science of AGH-UST. His research interests include agent-based modeling and distributed systems.

Kamil Piętak obtained M.Sc. in 2008 at AGH University of Science and Technology in Cracow and is currently a Ph.D. student at the Department of Computer Science of AGH-UST. His research interests include component-oriented programming and Eclipse RCP technologies.

Aleksander Byrski obtained his Ph.D. in 2007 at AGH University of Science and Technology in Cracow. He works as an assistant professor at the Department of Computer Science of AGH-UST. His research focuses on multi-agent systems, biologically-inspired computing and other soft computing methods.

Marek Kisiel-Dorohinicki obtained his Ph.D. in 2001 at AGH University of Science and Technology in Cracow. He works as an assistant professor at the Department of Computer Science of AGH-UST. His research focuses on intelligent software systems, particularly using agent technology and evolutionary algorithms, but also other soft computing techniques.

REAL LIFE DATA ACQUISITION IN WIRELESS SENSOR NETWORK LOCALIZATION SYSTEM

Michal Marks
Research and Academic Computer Network (NASK)
Wawozowa 18, 02-796 Warsaw, Poland
and
Institute of Control and Computation Engineering,
Warsaw University of Technology
Nowowiejska 15/19, 00-665 Warsaw, Poland
Email: mmarks@elka.pw.edu.pl

KEYWORDS

Wireless Sensor Network; real-life deployments; positioning; stochastic optimization; localization system; distributed computing; HPC;

ABSTRACT

The paper treats the problem of localization in Wireless Sensor Network (WSN). In our work, we present and evaluate *Wireless Sensor Network Localization System*, which supports sensor node localization from data gathering from real-life deployments through modelling and applying different localization methods up to distributed computing in HPC environment. The paper describes extension of *WSN Localization System* with modules supporting real-life sensor data acquisition. A provided case study demonstrates the localization accuracy obtained for a few example networks generated by simulation models and based on acquired sensor data.

INTRODUCTION TO WSN LOCALIZATION

The aim of localization is to assign geographic coordinates to each node in the sensor network in the deployment area. Wireless sensor network localization is a complex problem that can be solved in different ways, [Karl and Willig, 2005]. A number of research and commercial location systems for WSNs have been developed. They differ in their assumptions about the network configuration, distribution of calculation processes, mobility and finally the hardware's capabilities, [Mao et al., 2007], [Awad et al., 2007], [Zhang et al., 2010].

Recently proposed localization techniques consist in identification of approximate location of nodes based on merely partial information on the location of the set of nodes in a sensor network. An anchor is defined as a node that is aware of its own location, either through GPS or manual pre-programming during deployment. Identification of the location of other nodes is up to an algorithm locating non-anchors. Considering hardware's capabilities of network nodes we can distinguish two classes of methods: range based (distance-based) methods and range free (connectivity based) methods.

The former is defined by protocols that use absolute point to point distance estimates (ranges) or angle estimates in location calculation. The latter makes no assumption about the availability or validity of such information, and use only connectivity information to locate the entire sensor network. The popular range free solutions are hop-counting techniques. Distance-based methods require the additional equipment but through that much better resolution can be reached than in case of connectivity based ones. In our works we concentrate on range based methods.

The paper is structured as follows: at the beginning we shortly describe the distance-based localization problem. Next, we provide an overview of our software environment for WSN localization and an extension applied to our software in order to acquire data from real-life deployments. Finally, we provide a case study results and conclusions.

DISTANCE BASED LOCALIZATION

Let us consider a network formed by M sensor devices (anchor nodes) that are aware of their location, either through GPS or manual recording and entering position during deployment, and N sensor devices (non-anchor nodes) that are not aware of their location in a network system. The goal of a localization system is to estimate coordinate vectors of all N non-anchor nodes. In general, distance based localization schemes operate in two stages:

- *Inter-node distances estimation stage* – estimation of true inter-node distances based on inter-node transmissions and measurements.
- *Position calculation stage* – transformation of calculated distances into geographic coordinates of nodes forming the network.

Inter-node Distances Estimation Stage

In spite of the available hardware, distance based localization systems exploit the following techniques

Proceedings 27th European Conference on Modelling and Simulation ©ECMS Webjørn Rekdalsbakken, Robin T. Bye, Houxiang Zhang (Editors)
ISBN: 978-0-9564944-6-7 / ISBN: 978-0-9564944-7-4 (CD)

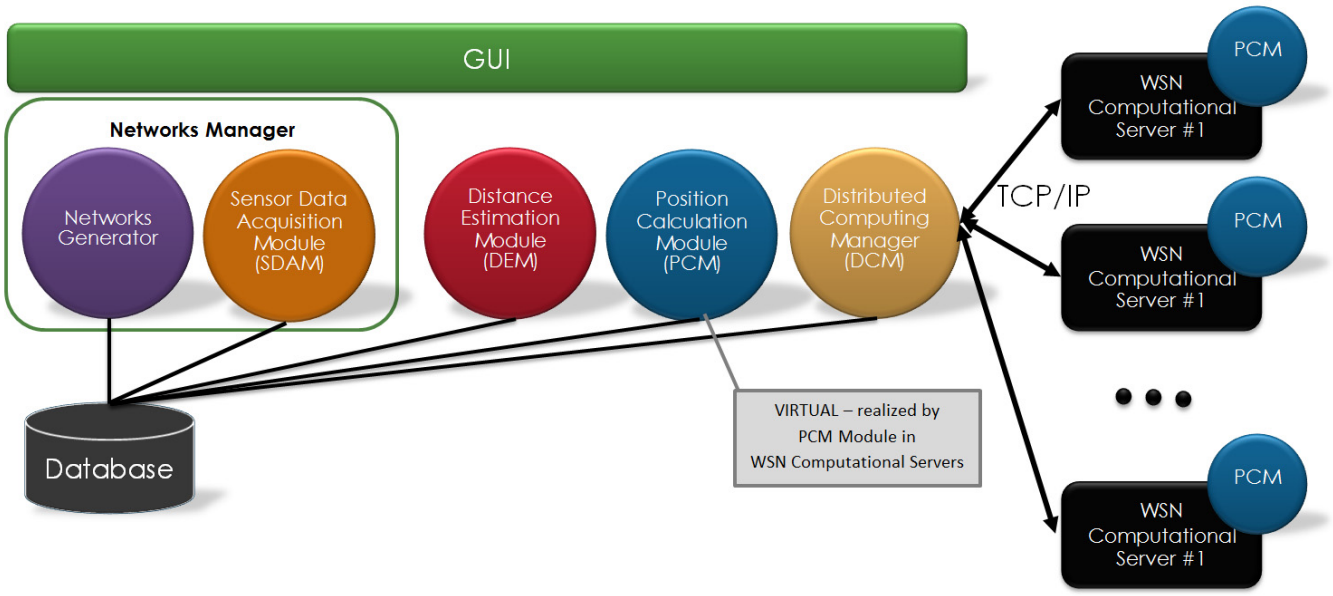

Fig. 1. The components of the WSNLS

widely described in literature [Benkic et al., 2008], [Karl and Willig, 2005], [Mao et al., 2007]:

- Angle of Arrival (AoA),
- Time of Arrival (ToA),
- Time Difference of Arrival (TDoA),
- Received Signal Strength Indicator (RSSI).

AoA, ToA and TDoA methods need an additional equipment such as antennas or accurately synchronized clocks. The most popular technique is the RSSI method because of easy configuration, deployment and no additional hardware needed (low cost). The disadvantage of this solution is low quality of measurement accuracy due to high variability of RSSI value [Benkic et al., 2008], [Ramadurai and Sichitiu, 2003]. Nevertheless some authors indicate that new radio transceivers can give RSSI measurements good enough to be a reasonable distance estimator [Barsocchi et al., 2009], [Srinivasan and Levis, 2006].

Position Calculation Stage

In the position calculation stage the computed internode distances are used to estimate the geographic coordinates of all non-anchor nodes in a considered network. Position estimation can be done by using different techniques. There are many widely used techniques such as: triangulation, trilateration, multitrilateration and multidimensional scaling. The common idea of other methods is formulating the localization problem as the linear, quadratic or nonconvex nonlinear optimization problem solved by linear, quadratic or nonlinear (often heuristic) solvers.

Recently, a popular group consists of *hybrid systems* that combines more than one technique to estimate location, i.e., results of initial localization are refined using another localization method. All mentioned methods are described and evaluated in literature, see [Akyildiz and Vuran, 2010], [Biswas and Ye, 2004], [Kannan et al., 2005], [Kannan et al., 2006], [Mao and Fidan, 2009], [Mao et al., 2007], [Niewiadomska-Szynkiewicz, 2012], [Niewiadomska-Szynkiewicz et al., 2011].

WIRELESS SENSOR NETWORK LOCALIZATION SYSTEM OVERVIEW

The Wireless Sensor Network Localization System (WSNLS) is an integrated software environment for testing various localization schemes on parallel computers or computer clusters. It provides not only a set of solvers for localization WSN nodes but supports the whole localization process from test network defining, radio signal modelling and processing, real-life data acquisition up to parallel execution of localization schemes.

An open architecture and object-oriented programming make the software easily extendable with implementations of new approaches for calculating locations of nodes in a network. WSNLS can be used to estimate the geographic coordinates of all devices forming the real life sensor network. Moreover, it can be used for tuning and performance evaluation of various localization solvers that are integrated with the framework before their practical application to a real life network.

Since its first realization, described in [Marks, 2012], WSNLS architecture has been improved in many aspects and extended by adding Sensor Data Acquisition Module (SDAM). The system is still composed of a runtime platform (formed by two components, i.e., *Distributed Computing Manager* and *Computational Server*) responsible for calculation management and interprocess communication. However in second version of the system, *Networks Manager* has been reorganized and contains *Networks Generator* – a component for modeling a network to be simulated and *Sensor Data*

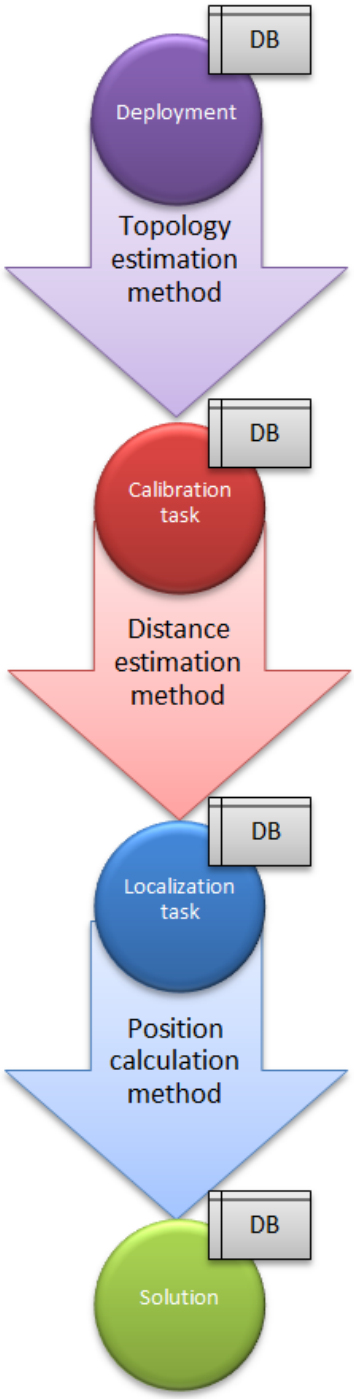

Fig. 2. Dataflow in WSNL system

Acquisition Module – component responsible for data gathering from real-life deployments. There are still two components responsible for location calculations, i.e., *Distance Estimation Module* and *Position Calculation Module*, database for recording data of all examined networks and results of calculations, and a set of tools to support the interaction with a user (GUI), but all the features of *Position Calculation Module* are realized by computational servers. The architecture of WSNLS is presented in Fig. 1.

DATA FLOW IN WSNLS

Since the aim of WSNLS is providing support for the whole localization process – from test network defining up to nodes location estimation – the data processing requires applying specialized methods on three stages as it is shown in Fig. 2. Computational method used on two stages i.e. distance estimation methods and position calculation methods are described in more details in [Marks, 2012], [Marks and Niewiadomska-Szynkiewicz, 2011]. However the first stage in presented dataflow relies on topology estimation methods, which were partially unavailable in first version of Wireless Sensor Network Localization System.

Topology estimation methods

Topology estimation methods provide a means for gathering information about network topology. This information can be obtained by using appropriate modelling or by data acquisition from real-life deployments. In general the proper modeling of low-power links is very difficult since the links characterization depends on radio chips (e.g., TR1000, CC1000, CC2420, etc), operational environments (indoor, outdoor) and many other parameters such as traffic load or radio channel – [Baccour et al., 2012]. In our software we decided to provide models based on *Link Layer Model for MATLAB* provided by [Zuniga and Krishnamachari, 2004], where we focus on wireless channel modeling and no radio modulation and encoding are considered. Much better solution, of course applicable only for institution which have at least laboratory WSN deployments, is to acquire data directly from real Wireless Sensor Networks. More information about real-life data acquisition is provided in section *Sensor Data Acquisition Module*.

Distance estimation methods

Distance estimation methods transform RSSI measurements into internode distances estimations. At present *Distance Estimation Module* has registered three approaches to distance estimation: Ordinary Least Square Method (OLS), Weighted Least Square Method (WLS) and Geometric Combined Least Square Method (GCLS). More information about distance estimation stage can be found in [Marks and Niewiadomska-Szynkiewicz, 2011].

Position calculation methods

Position calculation methods estimate the coordinates of non-anchor nodes in the network using internode distances. Position Calculation Module is realized in the object-oriented way and it can be easily extended with new localization algorithms. Currently Trilateration, SA (Simulated Annealing) and TSA (Trilateration & Simulated Annealing) methods are supported, in the near future TGA (Trilateration & Genetic Algorithm) method will be added. More information about position calculation methods can be found in [Niewiadomska-Szynkiewicz and Marks, 2009].

SENSOR DATA ACQUISITION MODULE

There are three types of information which are needed for distance based localization and localization quality verification in case of using RSSI readings:

- anchor nodes coordinates,
- RSSI readings between nodes in the network,
- all nodes coordinates (optional).

The anchor nodes coordinates and RSSI readings between nodes in the network are mandatory and there is no chance to localize nodes in global space without both this data. Coordinates of all the nodes in the network are optional and they are needed only for localization accuracy verification. In *WSN Localization System* we assumed two ways of providing the information.

The fist one is just the form where user is asked for providing data about number of nodes, number of anchor nodes and coordinates for anchor nodes. Filling the data about non-anchor nodes coordinates is not mandatory, but it can be done using the same form.

Second part of acquiring information is done automatically. After registration starting the *Sensor Data Acquisition Module* initiates data collection from the network through a sensor node playing a role of *Edge Router* which is connected to our system via USB connector and has the capability to communicate with other sensor nodes using IEEE 802.15.4 radio. The overview of data gathering process is depicted in Fig. 3. Of course it is possible to organize data collection only by using this automatic approach, but this approach implies then the necessity of equipping all anchor nodes with GPS modules or hardcoding information about their locations which is not the most convenient solution.

Data collection protocol is based on *BLIP 2.0* stack. BLIP 2.0 – Berkeley Low-power IP stack, is an reimplementation in *TinyOS* of a number of IP-based protocols including IPv6, RPL anc CoAP. More information can be found in [Silva et al., 2009], [Rodrigues and Neves, 2010]. Each sensor node in the network is responsible for exchanging packets with all the nodes in its neighbourhood and collection a vector of pairs *neighbour id* and *received signal strength*. After collection such vectors are transmitted using multi-hop unicast transmission to edge router and then registered in database by *Sensor Data Acquisition Module*.

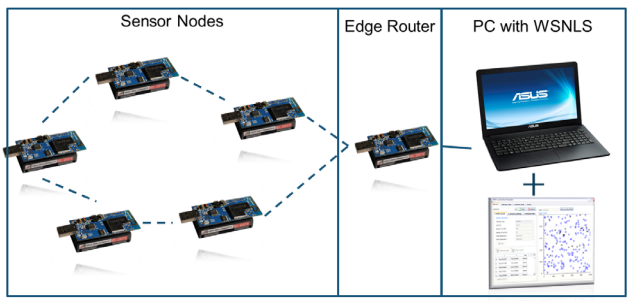

Fig. 3. Scheme of data acquisition system

EXPERIMENTAL RESULTS

Sensor platform

Wireless Sensor Network Laboratory organized in Institute of Control and Computation Engineering Warsaw University of Technology is equipped with over 130 sensors. Laboratory contain 28 MicaZ nodes produced by Memsic Company (former Crossbow) and over 100 Advantic Technology CM3000 and CM5000 sensors (clone of TelosB platform). All experiments described in this paper were realized using MicaZ sensor nodes based on ATmega128L low-power microcontrollers and Chipcon CC2420 radio transeivers (2.4GHz). One of the nodes is presented in Fig. 4.

Fig. 4. MicaZ node from ICCE WUT Laboratory

Localization technique

In this experiment a trilateration – the simplest method available in the Wireless Sensor Network Localization System was used. The *trilateration* technique requires the distance measurements between the node with unknown location and its neighbors (in 2-D space three neighbors with known locations are sufficient). The minimization problem with the performance function calculated as a difference between the measured and estimated distances is formulated and solved. Several variants of *multitrilateration* method are proposed in literature to reduce limitations of the typical trilateration scheme.

Atomic multitrilateration incorporates distance measurements from multiple neighbors. It is used to improve an accuracy of the location estimation if the distance measurements are noisy.

The idea of *iterative multitrilateration*, implemented in our software, is to repeat trilateration for increased number of anchor nodes (every iteration each node with estimated position changes its role to anchor).

Considered topologies

In this section preliminary results obtained for two real-life deployments are presented. In both cases sensor nodes where deployed in a square region. In the first scenario anchor nodes are located evenly in the whole

considered area, while the second scenario describes situation where all anchor nodes are located unevenly – they are grouped in one quarter of the deployment area. All experiments where done in the interior of Main Auditorium Warsaw University of Technology. The place of experiment realization had a big impact on quality of obtained location estimates because of a big problems with signal reflections of stone elements and a high radio waves density (multiple Wifi networks operating in this area).

TABLE I: Scenario 1: Localization error for anchor nodes deployed evenly

Method	Real-life network	Simulated network
dv-hop	62.72%	55.34%
trilateration	49.87%	16.67%

TABLE II: Scenario 1: Localization error for anchor nodes deployed unevenly (1/4 of deployment area)

Method	Real-life network	Simulated network
dv-hop	87.29%	70.49%
trilateration	86.13%	49.10%

In tables I and II localization errors for two considered scenarios are presented. To compare the performance of the tested algorithms we used the mean error between the computed and the actual unknown location of the nodes in the network, defined as follows

$$LE = \frac{1}{N} \cdot \frac{\sum_{i=1}^{N}((\tilde{x}_i - \hat{x}_i)^2 + (\tilde{y}_i - \hat{y}_i)^2)}{R^2} \cdot 100\% \quad (1)$$

where $(\tilde{x}_i, \tilde{y}_i)$ is true location of sensor node i, $(\hat{x}_i, \hat{y}_i)$ estimated location of sensor node i and R radio range. The location error LE is expressed as a percentage error. It is normalized with respect to the radio range to allow comparison of results obtained for different size and range networks.

Both tables contains the comparison of localization errors for two methods – described earlier *Trilateration* and a connectivity-based method *dv-hop* [Niculescu and Nath, 2003] which is treated as a reference point as it is commonly used in practical applications. The results obtained for simulated networks shows that trilateration is capable to provide much better results – three times smaller error for scenario 1 and almost two times smaller for scenario 2. However in case of data acquired from real-life deployments the difference is almost invisible for scenario 2 and less than two for scenario 1. Conducted experiments shows how important is verification of WSN algorithms in real-life deployments. Of course the main reason of the differences in localization quality is realization of experiment in a very difficult environment. The differences between localization accuracy for reference dv-hop method, where distance estimation is not necessary, are acceptable.

CONCLUSIONS AND FUTURE WORKS

We have presented the design and evaluation of our *WSN Localization System* extended with Sensor Data Acquisition Module. The software can be used for creation and solving different WSN localization problems using various methods from *Position Calculation Module* – such as trilateration, SA or TSA methods. The software can be easily extended with another methods utilizing the same software framework. Emphasis was placed on the distributed computation modules which allows us for maximizing the methods robustness for different tasks.

Conducted experiments shows how important is verification of WSN algorithms in real-life deployments. In our future research, we would like to conduct additional experiments with much bigger numer of sensor nodes and more sophisticated localization techniques (SA and TSA) which allows to obtain much more accurate localization results.

ACKNOWLEDGMENT

This work was supported by Ministry of Science and Higher Education under grant NN514 672940.

REFERENCES

[Akyildiz and Vuran, 2010] Akyildiz, I. and Vuran, M. (2010). *Wireless Sensor Networks*. John Wiley & Sons, Ltd, West Sussex, UK.

[Awad et al., 2007] Awad, A., Frunzke, T., and Dressler, F. (2007). Adaptive distance estimation and localization in wsn using rssi measures. In *Digital System Design Architectures, Methods and Tools, 2007. DSD 2007. 10th Euromicro Conference on*, pages 471 –478.

[Baccour et al., 2012] Baccour, N., Koubaa, A., Mottola, L., Zuniga, M., Youssef, H., Boano, C., and Alves, M. (2012). Radio link quality estimation in wireless sensor networks: a survey. *ACM Transactions on Sensor Networks*, 8(4).

[Barsocchi et al., 2009] Barsocchi, P., Lenzi, S., Chessa, S., and Giunta, G. (2009). Virtual calibration for rssi-based indoor localization with ieee 802.15.4. In *Communications, 2009. ICC '09. IEEE International Conference on*, pages 1 –5.

[Benkic et al., 2008] Benkic, K., Malajner, M., Planinsic, P., and Cucej, Z. (2008). Using rssi value for distance estimation in wireless sensor networks based on zigbee. In *Systems, Signals and Image Processing, 2008. IWSSIP 2008. 15th International Conference on*, pages 303 –306.

[Biswas and Ye, 2004] Biswas, P. and Ye, Y. (2004). Semidefinite programming for ad hoc wireless sensor network localization. In *IPSN '04: Proc. of the third international symposium on Information processing in sensor networks*, pages 46–54, New York, NY, USA. ACM Press.

[Kannan et al., 2006] Kannan, A., Mao, G., and Vucetic, B. (2006). Simulated annealing based wireless sensor network localization with flip ambiguity mitigation. In *63rd IEEE Vehicular Technology Conference*, pages 1022–1026.

[Kannan et al., 2005] Kannan, A. A., Mao, G., and Vucetic, B. (2005). Simulated annealing based localization in wireless sensor network. In *LCN '05: Proceedings of the The IEEE Conference on Local Computer Networks 30th Anniversary*, pages 513–514, Washington, USA. IEEE Computer Society.

[Karl and Willig, 2005] Karl, H. and Willig, A. (2005). *Protocols and Architectures for Wireless Sensor Networks*. Wiley.

[Mao and Fidan, 2009] Mao, G. and Fidan, B. (2009). *Localization Algorithms and Strategies for Wireless Sensor Networks*. Information Science Reference, Hershey, USA.

[Mao et al., 2007] Mao, G., Fidan, B., and Anderson, B. D. O. (2007). Wireless sensor network localization techniques. *Computer Networks: The International Journal of Computer and Telecommunications Networking*, 51(10):2529–2553.

[Marks, 2012] Marks, M. (2012). Enhancing wsn localization robustness utilizing hpc environment. In Troitzsch, K. G.,

Mhring, M., and Lotzmann, U., editors, *Proceedings 26th European Conference on Modelling and Simulation*, pages 167–170, Germany.

[Marks and Niewiadomska-Szynkiewicz, 2011] Marks, M. and Niewiadomska-Szynkiewicz, E. (2011). Self-adaptive localization using signal strength measurements. In *SENSORCOMM 2011, the Fifth International Conference on Sensor Technologies and Applications*, pages 73–78, Nice, France. IARIA.

[Niculescu and Nath, 2003] Niculescu, D. and Nath, B. (2003). Dv based positioning in ad hoc networks. *Telecommunication Systems*, 22(1):267–280.

[Niewiadomska-Szynkiewicz, 2012] Niewiadomska-Szynkiewicz, E. (2012). Localization in wireless sensor networks: Classification and evaluation of techniques. *Int. J. Appl. Math. Comput. Sci*, 22(2):281–297.

[Niewiadomska-Szynkiewicz and Marks, 2009] Niewiadomska-Szynkiewicz, E. and Marks, M. (2009). Optimization schemes for wireless sensor network localization. *International Journal of Applied Mathematics and Computer Science*, 19(2):291–302.

[Niewiadomska-Szynkiewicz et al., 2011] Niewiadomska-Szynkiewicz, E., Marks, M., and Kamola, M. (2011). Localization in wireless sensor networks using heuristic optimization techniques. *Journal of Telecommunications and Information Technology*, 4:55–64.

[Ramadurai and Sichitiu, 2003] Ramadurai, V. and Sichitiu, M. L. (2003). Localization in wireless sensor networks: A probabilistic approach. In *Proceedings of International Conference on Wireless Networks (ICWN 2003)*, pages 300–305, Las Vegas, USA.

[Rodrigues and Neves, 2010] Rodrigues, J. J. and Neves, P. A. (2010). A survey on ip-based wireless sensor network solutions. *International Journal of Communication Systems*, 23(8):963–981.

[Silva et al., 2009] Silva, R., Silva, J. S., and Boavida, F. (2009). Evaluating 6lowpan implementations in wsns. *Proceedings of 9th Conferncia sobre Redes de Computadores Oeiras, Portugal*, pages 1–5.

[Srinivasan and Levis, 2006] Srinivasan, K. and Levis, P. (2006). Rssi is under appreciated. In *In Proceedings of the Third Workshop on Embedded Networked Sensors (EmNets)*, Cambridge, USA.

[Zhang et al., 2010] Zhang, X., Wu, Y., and Wei, X. (2010). Localization algorithms in wireless sensor networks using non-metric multidimensional scaling with rssi for precision agriculture. In *Computer and Automation Engineering (ICCAE), 2010 The 2nd International Conference on*, volume 5, pages 556 –559.

[Zuniga and Krishnamachari, 2004] Zuniga, M. and Krishnamachari, B. (2004). Analyzing the transitional region in low power wireless links. In *In First IEEE International Conference on Sensor and Ad hoc Communications and Networks (SECON)*, pages 517–526, Santa Clara, USA.

MICHAŁ MARKS received his M.Sc. in computer science from the Warsaw University of Technology, Poland, in 2007. Currently he is a Ph.D. student in the Institute of Control and Computation Engineering at the Warsaw University of Technology. Since 2007 with Research and Academic Computer Network (NASK). His research area focuses on wireless sensor networks, global optimization, distributed computation in CPU and GPU clusters, decision support and machine learning. His e-mail is `mmarks@ia.pw.edu.pl`

SIMULATION OF ENERGY-AWARE BACKBONE NETWORKS

Ewa Niewiadomska-Szynkiewicz, Andrzej Sikora, Marcin Mincer, Piotr Arabas
Institute of Control and Computation Engineering
Warsaw University of Technology
Nowowiejska 15/19, 00-665 Warsaw, Poland
Research and Academic Computer Network (NASK)
Wawozowa 18, 02-796 Warsaw, Poland
Email: ens@ia.pw.edu.pl, A.Sikora@elka.pw.edu.pl, M.Mincer@stud.elka.pw.edu.pl, parabas@nask.pl

KEYWORDS

Network Simulation, Energy-Efficient Computer Network, Routing, Traffic Engineering, OMNet++

ABSTRACT

An optimization of the energy consumption in network systems has been recently an important research issue. The main challenge is to design, develop and test novel technologies, integrated control strategies and mechanisms for network equipment enabling energy saving by adapting network capacities and resources to current traffic loads and user requirements, while ensuring end-to-end Quality of Service. In general, the idea is to develop low power devices or nano-processors, concentrate network traffic on a minimal subset of network components, and modulate network devices using dynamic voltage and frequency scaling methods. Various power adapting technologies for network devices are described in literature. We developed a framework for a backbone network management which leads to the minimization of the energy consumption by this network. The concept is based on activity control of the network equipment. The framework is presented in (Niewiadomska-Szynkiewicz et al., 2012b). In this paper we describe the design, performance and potential applications of the software environment for energy efficient backbone network optimization and simulation. This system was used to illustrate the performance of our control framework for energy-aware IP networks.

INTRODUCTION

The problem of reducing power consumption in computer networks, while providing for adequate transmission quality has been a hot topic in the last years. It has been observed that information communication technology sector belongs to the group of the big power consumers. Therefore, enabling the reduction of energy requirements of telecommunication networks is the goal of many research groups, network equipment manufactures and Internet Service Providers (ISPs). New solutions both in hardware and software have been developed to achieve the desired trade-off between total power consumption and the network performance according to the network capacity, actual traffic and requirements of the users (Bianzino et al., 2012; Bolla et al., 2010; Chiaraviglio et al., 2009; Coiro et al., 2011; Goma et al., 2011). Approaches ranging from traffic engineering, to routing protocols, and novel architectures have been developed and investigated.

Computer simulation is a standard tool for understanding and predicting the behavior of network systems under the influence of various realistic and stochastic input scenarios. Although simulation has traditionally been viewed as an approach of last resort, recent advances in computer hardware and software have made it one of the most popular technique to attack many real-life problems. In order to efficiently perform simulation experiments, good software tools are needed hence, in recent years we can observe a rapid growth of network simulators. We have developed a software environment for green (in our research energy-aware) IP networks optimization and simulation. We used it to evaluate the performance of our control scheme for such type of networks.

BACKGROUND AND RELATED WORK

In general, power management methodologies in networks can be classified into static and dynamic technologies (Kołodziej et al., 2012). Recently various activities aimed at developing energy-efficient network devices have been undertaken and described in literature, see (Bianzino et al., 2012; Bolla et al., 2011; Niewiadomska-Szynkiewicz et al., 2012b) for an overview. These devices can operate in different states, which differ in the power usage, and implement dynamic power manage-

Proceedings 27th European Conference on Modelling and Simulation ©ECMS Webjørn Rekdalsbakken, Robin T. Bye, Houxiang Zhang (Editors)
ISBN: 978-0-9564944-6-7 / ISBN: 978-0-9564944-7-4 (CD)

ment techniques. Power scaling and smart standby capabilities are widely used to reduce power consumption. The power scaling capability assumes scaling the performance of the device to reduce the energy requirements. The smart standby is the capability of reducing the energy requirements by switching off the device or its component or putting it in very low energy mode.

In (Niewiadomska-Szynkiewicz et al., 2012b) we described a control framework for an energy-aware backbone network, and possible algorithms to exploit smart standby capabilities of nodes and links in such type of network, developed by the ECONET project (http://www.econet-project.eu). Our framework requires the presence of a central control unit. The decisions about activity and power status of devices in a whole network are calculated by the central operator. In our scheme we tackle the minimization of the power consumption by putting in low energy states selected network devices, such as routers, line cards and ports, (Niewiadomska-Szynkiewicz et al., 2012b; Arabas et al., 2012). Next, the respective routing tables for the MPLS protocol are computed due to suggested optimal states of these devices. The optimal network performance is calculated based on known network topology and expected demands (traffic matrix).

ALGORITHM FOR GREEN IP NETWORKS

It can be observed that the traffic is subject to strong fluctuations, especially when comparing incoming traffic during the day and night. Therefore, many network devices are underutilized when traffic is low (during off-peak hours). Hence, forcing a sleep state for selected network equipment and using the rest to transmit the whole traffic through the network can significantly reduce the power consumption. Thus, to reduce the energy requirements we have to calculate the optimal operational modes for all network devices based on current load, traffic and estimated demands. We consider a network formed by R routers ($r = 1, \ldots, R$), each equipped with C cards ($c = 1, \ldots, C$). Each card contains P ports ($p = 1, \ldots, P$). All pairs of ports from different routers and cards are connected by E direct links ($e = 1, 2, \ldots, E$). Routers, cards and links (both connected ports) can operate in one of K energy-aware states ($k = 1, \ldots, K$). These states are related to the application of power scaling and standby techniques, and are defined as power settings. We assume that both routers and cards can operate in only two states, i.e., active and sleeping, and each link can operate in several (at least two) states with different energy usage and at the same time different capacity. Hence, in our approach the power profile model is defined by a stepwise function describing power consumption due to a given throughput – the throughput of link e in state k is defined as M_{ek}. The power consumption in state k is defined as ξ_{ek}. Moreover, fixed power levels W_c and T_r are associated to cards and routers, respectively. We assume D demands transmitted by means of flows allocated to given MPLS paths under QoS requirements ($d = 1, \ldots, D$). The volume of demand d is equal to V_d, and is estimated by the central network operator. The demand d is associated with a link connecting two ports: the port of the source node (s_d) and the port of the destination node (t_d).

Given the presented notation, we can formulate the complete energy-aware network management problem assuming full routing calculation and energy state assignment to all links in a network, (Niewiadomska-Szynkiewicz et al., 2012a,b). In this formulation the total power used in the network system is assumed to be minimized. The constraints guarantee ensuring end-to-end Quality if Service.

$$\min_{x_c, y_{ek}, z_r, u_{ed}} \{F_{LN} = \sum_{e=1}^{E}\sum_{k=1}^{K} \xi_{ek} y_{ek} + \sum_{c=1}^{C} W_c x_c + \sum_{r=1}^{R} T_r z_r\}, \tag{1}$$

subject to the constraints:

$$\forall_{\substack{d=1,\ldots,D,\\ c=1,\ldots,C}} \quad \sum_{p=1}^{P} l_{cp} \sum_{e=1}^{E} a_{ep} u_{ed} \leq x_c, \tag{2}$$

$$\forall_{\substack{d=1,\ldots,D,\\ c=1,\ldots,C}} \quad \sum_{p=1}^{P} l_{cp} \sum_{e=1}^{E} b_{ep} u_{ed} \leq x_c, \tag{3}$$

$$\forall_{\substack{r=1,\ldots,R,\\ c=1,\ldots,C}} \quad g_{rc} x_c \leq z_r, \tag{4}$$

$$\forall_{e=1,\ldots,E} \quad \sum_{k=1}^{K} y_{ek} \leq 1, \tag{5}$$

$$\forall_{\substack{d=1,\ldots,D,\\ p=s_d}} \quad \sum_{e=1}^{E} a_{ep} u_{ed} - \sum_{e=1}^{E} b_{ep} u_{ed} = 1, \tag{6}$$

$$\forall_{\substack{d=1,\ldots,D,\\ p\neq t_d, p\neq s_d}} \quad \sum_{e=1}^{E} a_{ep} u_{ed} - \sum_{e=1}^{E} b_{ep} u_{ed} = 0, \tag{7}$$

$$\forall_{\substack{d=1,\ldots,D,\\ p=t_d}} \quad \sum_{e=1}^{E} a_{ep} u_{ed} - \sum_{e=1}^{E} b_{ep} u_{ed} = -1, \tag{8}$$

$$\forall_{e=1,\ldots,E} \quad \sum_{d=1}^{D} V_d u_{ed} \leq \sum_{k=1}^{K} M_{ek} y_{ek}, \tag{9}$$

where $g_{rc} = 1$ if the card c belongs to the router r (0 otherwise), $l_{cp} = 1$ if the port p belongs to the card c (0 otherwise), $a_{ep} = 1$ if the link e is outgoing from the

port p (0 otherwise), $b_{ep} = 1$ if the link e is incoming to the port p (0 otherwise), $z_r = 1$ if the router r is used for data transmission (0 otherwise), $x_c = 1$ if the card c is used for data transmission (0 otherwise), $u_{ed} = 1$ if the path d belongs to the link e (0 otherwise), $y_{ek} = 1$ if the link e is in the state k (0 otherwise).

The meaning of the above constraints is as follows. The constraints (2)-(4) determine the number of routers and cards that are used for data transmission. The conditions (5) assure that each link can be in one energy-aware state. The constrains (6)-(8) are formulated according to Kirchhoff's law applied for source, transit and destination nodes. The constraint (9) assures that the flow will not exceed the capacity of a given link.

SOFTWARE ENVIRONMENT FOR TESTING GREEN NETWORKS

Modeling and simulation are traditional methods used to evaluate network design. Therefore, we have developed an integrated software environment that can by used to support the design of energy-aware control strategies and algorithms. Our software provides tools for defining and implementing the problem of the optimal management of network devices w.r.t. the power consumption, optimization solver for solving the formulated problem and energy-aware network simulator for evaluating the calculated decision policy and checking the compliance of demands.

Components of the System

The software environment *Optimizer&GNS* to test energy-aware network applications consists of two components: optimizer and energy-aware networks simulator, Fig. 1. The *Optimizer-ASim* consists of an user interface responsible for user-system interaction and calculation results presentation, and an optimization solver. In the current version of the system the mixed integer programming (MIP) algorithm implementing branch-and-bound approach is provided. In our future work we plan to extend the optimizer component, and implement a library of solvers. The optimizer is built based on ASim/Java library – a software tool for discrete event systems simulation, (Sikora and Niewiadomska-Szynkiewicz, 2009; Niewiadomska-Szynkiewicz and Sikora, 2012). We used ASim/Java classes to model a network to be simulated and implement the optimization problem as described in the previous section. The user interface is graphical and built based on ASim/Java classes, too. GUI provides setting and display windows. Setting windows (see Fig. 2) are used to define a network topology and its attributes and

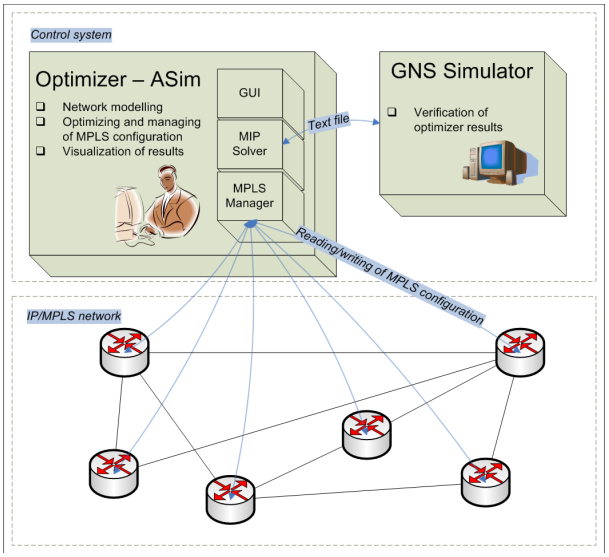

Figure 1: Software environment *Optimizer&GNS*.

introduce all configuration parameters. Display windows are used to present results of the optimization.

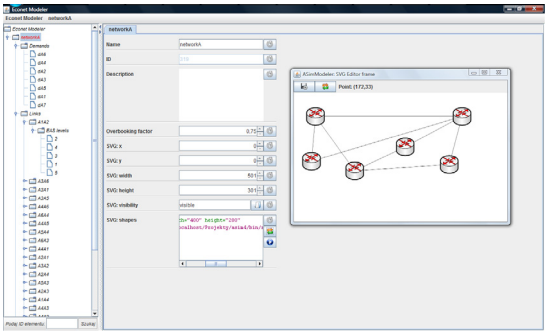

Figure 2: Graphical user interface of *Optimizer-ASim*.

The second component of our software environment named *GNS Simulator* allows to simulate the network systems utilizing energy-aware control strategies and algorithms for reducing of the power consumption. It is packet-level network simulator. *GNS* is completely based on OMNeT++ network simulation framework – free software for academic and non-profit use, and widely used platform in the global scientific and research community. OMNeT++ (http://www.omnetpp.org/) is an extensible, modular, component-based C++ simulation library and framework, primarily for building wired and wireless network simulators. It offers an Eclipse-based IDE, a graphical runtime environment as well as handy results browser. In our system we extensively use the open-source communication networks simulation pack-

age for OMNeT++ developed by the INET project. The INET framework (http://inet.omnetpp.org/) provides library of models for networking protocols including UDP, TCP, IP, IPv6, Ethernet, MPLS, OSPF, etc., and models of network hardware, i.e., routers, switches, network cards, etc. *GNS* provides green extensions to the models of devices offered in the INET library. The C++ implementations of routers and line cards were modified to enrich them with basic green abstraction layer functionalities (GAL) developed by the ECONET project and described in details in (Reforgiato et al., 2012). In general, GAL is the standard interface between control algorithms and hardware for exchanging data regarding the power status of the device and its components. The objective is to hide the implementation details of energy saving techniques, as well as to provide standard interfaces between control and monitoring layers and energy-aware technologies. Therefore, the simulators of network components provided in *GNS* introduce methods for setting energy-aware states, and allow for switching the devices to suggested states and measuring energy used by each device.

The *GNS* simulator provides the graphical user interface that was built based on OMNeT++ modules. GUI is organized in a set of nested windows. Setting and display windows can be distinguished. Setting windows are used to define a scenario of the experiment and introduce all configuration parameters. The other way is to load a network to be simulated from the disc file generated by the optimizer module. Display windows are used to present the simulation results, see Fig. 3.

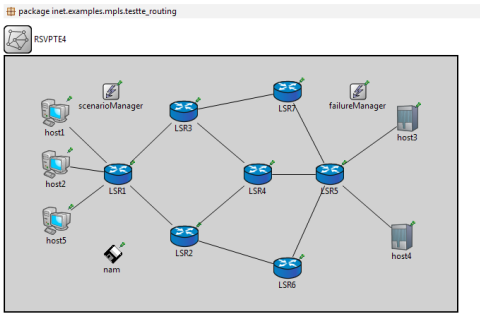

Figure 3: Simulation results presentation.

Both the *Optimizer-ASim* and the *GNS Simulator* can operate as a standalone tools. The optimizer can be used to calculate and compare various control strategies for energy-aware networks, and the simulator can be used to simulate various green networks applications.

User Application and Calculation Stages

Two calculation stages can be distinguish: a preparatory and decision calculation stage, and an experimental stage. At the first stage the model and the properties of the network system to be simulated are investigated and optimal configuration due to power consumption is calculated. The user's task is to define the model of the network. It can be implemented in the XML schema specification and saved in the XML file or created using GUI, Fig. 2. The optimization problem (1)-(9) is formulated and solved for a given network, taking into account its topology and expected demands. The MIP solver is used to solve the optimization task. The result of calculations is optimal power status of all network components (routers, cards and ports). Next, the routing tables for the MPLS protocol are computed for the optimal configuration of the network. Thus, the final outcome of the optimizer is a set of routing tables and optimal states of all devices that are saved to the disc file.

Next, the experimental stage begins. The network topology and the optimal routing tables are loaded from the disc files, the simulation time horizon is defined and the simulation experiment starts. The programs corresponding to all network devices are executed and the results of calculations are displayed in the on-line mode (states of devices, packages transmission, etc.), Fig. 3.

EXPERIMENTAL EVALUATION

Our software environment *Optimizer&GNS* has already proved to be very useful when performing the analysis of green solutions for network systems. We validated our control scheme based on optimization problem formulated in this paper and energy-aware traffic engineering using MPLS and RSVP-TE protocols through simulation. We solved the optimization problem (1)-(9) for several network configurations and evaluated calculated decisions using *GNS* simulator. In this paper we present the results obtained for two synthetic network topologies. The first network system N1 formed by 6 routers connected by 20 links is presented in Fig. 4. The second network system N2 formed by 12 routers connected by 28 links is presented in Fig. 5. The Table 1 reports the power used in different energy-aware states k and corresponding throughput.

We performed experiments both for N1 and N2 networks assuming various numbers of demands D and overbooking factor equal to 0.75. The routers in our tests were equipped with one or more cards. We assumed that each router and card could operate in two states – active and sleeping. Each link could operate in 5 energy-aware states ($k = 1, 2, 3, 4, 5$). $k = 0$ denotes that the link

Router	power = 1 900 W (active state)
Card	power = 90 W (active state)
k=1	throughput = 200 Mb/s, power = 16 W
k=2	throughput = 400 Mb/s, power = 32 W
k=3	throughput = 600 Mb/s, power = 48 W
k=4	throughput = 800 Mb/s, power = 64 W
k=5	throughput = 1000 Mb/s, power = 80 W

Table 1: Power costs and corresponding throughputs.

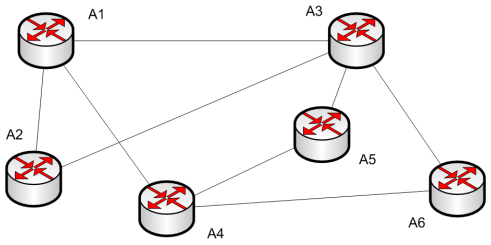

Figure 4: The synthetic network N1.

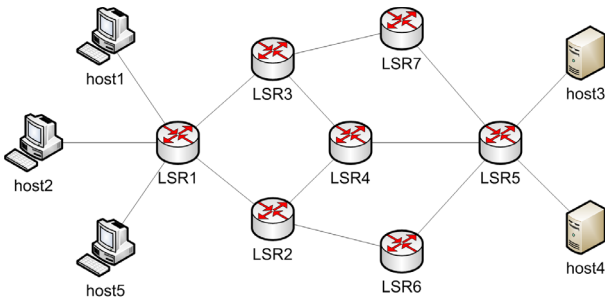

Figure 5: The synthetic network N2.

was not used for data transmission. Selected results of calculations, i.e., the outcome of the *Optimizer-ASim* for both networks – N1: $D = 3$, $D = 7$, $D = 13$ and N2: $D = 3$, $D = 6$, $D = 9$ are presented in tables 2 and 3. The total energy usage without any energy saving mechanisms for both networks are as follows: N1: 13 900 W, N2: 26 120 W. Three last rows in tables 2 and 3 give: numbers of routers, cards and links used for data transmission, total power consumption in a network, reduction in energy consumption relative to the case without any power management.

Next, we validated the results of optimization through simulation. The goal was to test how power saving strategy reduce total energy consumption and affects the end-to-end Quality of Service. We performed several simulation experiments for networks N1 and N2 taking into account routing tables and power status of devices calculated by the optimizer, and presented in tables 2 and 3. In our experiments we assumed energy costs of all devices

Link (router/card)	Optimal energy state (k)		
	$D = 3$	$D = 7$	$D = 13$
A1/2 → A2/2	1	1	1
A1/2 → A3/1	1	2	0
A1/2 → A4/1	0	0	2
A2/2 → A4/1	0	0	2
A2/2 → A3/1	0	1	0
A3/2 → A5/1	0	1	1
A3/2 → A6/1	1	2	0
A4/2 → A5/1	0	0	1
A4/2 → A6/1	0	0	3
A2/2 → A1/2	1	1	1
A3/1 → A1/2	1	2	0
A4/1 → A1/2	0	0	2
A4/1 → A2/2	0	0	2
A3/1 → A2/2	0	1	0
A5/1 → A3/2	0	1	1
A6/1 → A3/2	1	2	0
A5/1 → A4/2	0	0	1
A6/1 → A4/2	0	0	3
Routers/cards/links	4/5/6	5/6/10	6/7/12
Power consumption	8 146 W	10 264 W	12 350 W
Power reduction	5 754 W	3 636 W	1 550 W

Table 2: Routers and cards used for data transmission, and energy states of links (N1 network).

as presented in Table 1. The size of queue of each router was equal 100 packages (default value in OMNet++). We used simple traffic generator TCPSessionApp provided in OMNet++. It is single-connection TCP application (a connection is opened, the given number of bytes is sent, and the connection is closed). Sending may be one-off, or may be controlled by a "script" which is a series of (time, number of bytes) pairs. In tested networks the maximal throughput was equal to 1000 Mb/s.

Three series of experiments for different quality of forecasts of demands were performed: F1-good quality, F2-medium quality and F3-bad quality. The whole simulation horizon was equal to 25 seconds. In the case of F1 we assumed that the volumes of all demands (V_d, $d = 1, \ldots, 9$) were equal to those established during optimization. F2 and F3 denote cases in which the real demands V_d^* were greater than forecasted ones, respectively for F2 $V_d^* = 1.5V_d$, and for F3 $V_d^* = 2V_d$. The results of simulation of 40 ms of the network N2 operation are given in tables 4 and 5.

The simulation results indicate that in case of accurate forecasts of expected demands and adequate overbooking factor we can reduce the total power consumption while ensuring QoS (packet loss is very small). It is obvious that a problem appears for bad quality forecast of demands when application of routing tables generated by

Active link (router/card)	Optimal energy state of link (k)		
	$D = 3$	$D = 6$	$D = 9$
host1/1 → LSR1/1	2	2	2
LSR1/1 → host1/1	2	2	2
host2/1 → LSR1/1	2	2	2
LSR1/1 → host2/1	2	2	2
host5/1 → LSR1/1	2	2	2
LSR1/1 → host5/1	2	2	2
LSR2/1 → LSR1/1	0	5	0
LSR1/1 → LSR2/1	0	5	0
LSR3/1 → LSR1/1	5	0	5
LSR1/1 → LSR3/1	5	0	5
LSR3/1 → LSR7/1	5	0	0
LSR7/1 → LSR3/1	5	0	0
LSR3/1 → LSR4/1	0	0	5
LSR4/1 → LSR3/1	0	0	5
LSR2/1 → LSR4/1	0	5	0
LSR4/1 → LSR2/1	0	5	0
LSR5/1 → LSR4/1	0	5	5
LSR4/1 → LSR5/1	0	5	5
LSR5/1 → LSR7/1	5	0	0
LSR7/1 → LSR5/1	5	0	0
host3/1 → LSR5/1	5	5	5
LSR5/1 → host3/1	5	5	5
host4/1 → LSR5/1	0	0	1
LSR5/1 → host4/1	0	0	1
Routers/cards/links	8/8/14	8/8/14	9/9/16
Power consumption	16 752 W	16 752 W	18 774 W
Power reduction	9 368 W	9 368 W	7 346 W

Table 3: Hosts, routers and cards used for data transmission, and energy states of links (N2 network).

the optimizer can result in packets loss (see Table 4). To achieve the trade-off between power consumption and a network performance according to the traffic load a two-level decision scheme consisting of central and local decision mechanisms is proposed. In this approach the goal of the optimizer (the central unit) is to calculate the optimal status for each device, and send it to a local control mechanism of this device. Each device makes decisions about final status for its components based on current load, incoming traffic and expected demands, taking into account decisions from the central unit.

A few local control strategies (LC) have been developed by the ECONET project. In the current version of our simulator a very simple technique is implemented – every assumed time step (1 ms) the local control mechanism checks whether any packets were dropped from the queue. In the case of lost packets it switches the link state to the higher one. The reduction of packets loss due to our local control mechanism is presented in Table 4. The reduction in energy consumption by networks applying energy saving mechanism (1)-(9) relative to the

For. of D	Dem.	Lost pac. (without LC)	Lost pac. (with LC)	Total number of packages
F1	$D = 3$	31	4	52120
	$D = 6$	52	6	64754
	$D = 9$	70	16	67889
F2	$D = 3$	90	12	76586
	$D = 6$	163	18	91616
	$D = 9$	220	39	101545
F3	$D = 3$	137	84	100680
	$D = 6$	304	124	120011
	$D = 9$	437	241	131567

Table 4: Reduction in packets loss due to LC.

case without any power management (E_{N2}=1 044 800 J) is presented in Table 5.

Forecast of D	Demand	Energy consumption [J]	Energy reduction [J]
F1	$D = 3$	670 080	374 720
	$D = 6$	671 462	373 338
	$D = 9$	760 358	284 442
F2	$D = 3$	673 685	371 115
	$D = 6$	676 254	368 546
	$D = 9$	776 273	268 527
F3	$D = 3$	695 251	349 549
	$D = 6$	695 451	349 349
	$D = 9$	805 496	239 304

Table 5: Reduction of energy consumption (applied LC).

SUMMARY AND CONCLUSION

This paper presents the software environment *Optimizer&GNS* for designing, developing and testing control frameworks for energy-aware wired networks. We formulated the energy optimization as a mathematical programming problem, and solved it for sample small and medium size networks using our solver from *Optimizer&GNS* package. The designed green network applications were evaluated through simulation. In the nearest future we plan to use *Optimizer&GNS* to test and evaluate other energy-aware control mechanisms developed by the ECONET project and those described in literature. We will compare different solutions due to the energy saving, while providing for adequate transmission quality. Finally, we plan to provide an empirical evaluation of developed control algorithms on a testbed network.

Acknowledgment
This work was partially supported by 7 Framework Program UE grant ECONET, No: 258454.

REFERENCES

Arabas, P., Malinowski, K., and Sikora, A. (2012). On formulation of a network energy saving optimization problem. In *Proc. of 4th Inter. Conference on Communications and Electronics (ICCE 2012)*, pages 122–129.

Bianzino, A. P., Chaudet, C., Rossi, D., and Rougier, J.-L. (2012). A survey of green networking research. *IEEE Communication surveys and tutorials*, 2.

Bolla, R., Bruschi, R., Carrega, A., and Davoli, F. (2010). Theoretical and technological limitations of power scaling in network devices. In *Proc. 2010 Australasian Telecommunication Networks and Applications Conference (ATNAC)*, pages 37–42. IEEE.

Bolla, R., Bruschi, R., Davoli, F., and Cucchietti, F. (2011). Energy Efficiency in the Future Internet: A Survey of Existing Approaches and Trends in Energy-Aware Fixed Network Infrastructures. *IEEE Communications Surveys & Tutorials*, 13:223–244.

Chiaraviglio, L., Mellia, M., and Neri, F. (2009). Energy-aware backbone networks: a case study. In *Proc. 1st International Workshop on Green Communications, IEEE International Conference on Communications (ICC'09)*, pages 1–5. IEEE.

Coiro, A., Listani, M., and Valenti, A. (2011). Dynamic power-aware and wavelength assignment for green WDM optical networks. In *Proc. IEEE International Conference on Communications (ICC'11)*, pages 1–6. IEEE.

Goma, E., Canini, M., Toledo, A. L., Laoutaris, N., Kosti, D., Rodriguez, P., Stajonevi, R., and Valentin, P. Y. (2011). Insomnia in the access or how to curb access network related energy consumption. In *Proc. SIGCOMM'11*. ACM.

Kołodziej, J., Khan, S., Wang, L., and Zomaya, A. (2012). Energy efficient genetic-based schedulers in computational grids. *Concurrency and Computation: Practice and Experience*, DOI: 10.1002/cpe.2839.

Niewiadomska-Szynkiewicz, E. and Sikora, A. (2012). A Software Tool for Federated Simulation of Wireless Sensor Networks and Mobile Ad Hoc Networks. In *Lecture Notes in Computer Science (LNCS)*, volume 7133, pages 303–313. Springer-Verlag.

Niewiadomska-Szynkiewicz, E., Sikora, A., Arabas, P., and Kołodziej, J. (2012a). Control Framework for High Performance Energy Aware Backbone Network. In *Proc. of European Conference on Modelling and Simulation (ECMS 2012)*, pages 490–496.

Niewiadomska-Szynkiewicz, E., Sikora, A., Arabas, P., and Kołodziej, J. (2012b). Control system for reducing energy consumption in backbone computer network. *Concurrency and Computation: Practice and Experience*, DOI: 10.1002/cpe.2964.

Reforgiato, D., Lombardo, A., Davoli, F., Fialho, L., Collier, M., Donadio, P., Bolla, R., and Bruschi, R. (2012). Exporting Data-Plane Energy-Aware Capabilities from Network Devices toward the Control Plane:. In *Proc. 17th European Conference on Network and Optical Communication (NOC 2012)*, pages 1–5.

Sikora, A. and Niewiadomska-Szynkiewicz, E. (2009). A Parallel and Distributed Simulation of Ad Hoc Networks. *Journal of Telecommunications and Information Technology*, 3:76–84.

AUTHOR BIOGRAPHIES

EWA NIEWIADOMSKA-SZYNKIEWICZ DSc (2005), PhD (1995), professor of control and information engineering at the Warsaw University of Technology, head of the Complex Systems Group. She is also the Director for Research of Research and Academic Computer Network (NASK). The author and co-author of 3 books and over 130 papers. Her research interests focus on complex systems modeling, optimization, control and simulation, parallel computation and computer networks. Her email is `ens@ia.pw.edu.pl`.

ANDRZEJ SIKORA M.Sc. (2003) in computer science from the Warsaw University of Technology (WUT). Ph.D. student at the Institute of Control and Computation Engineering at WUT. Since 2005 with Research and Academic Computer Network (NASK). His research area focuses on parallel simulation, computer networks, ad hoc networks and database systems. His email is `A.Sikora@elka.pw.edu.pl`.

MARCIN MINCER B.Sc. (2011) in computer science from the Warsaw University of Technology (WUT). M.Sc. student at the Institute of Control and Computation Engineering at WUT. In the period 2011-2013 worked as a contractor for the ECONET project. A co-founder and CEO of IT company Blade Polska s.c. His research area focuses on energy-aware networks, social network analysis and software for simulation. His email is `M.Mincer@stud.elka.pw.edu.pl`.

PIOTR ARABAS PhD (2004) in computer science from the Warsaw University of Technology (WUT), assistant professor at the Institute of Control and Computation Engineering, WUT. Since 2002 with Research and Academic Computer Network (NASK). His research area focuses on computer networks, predictive and hierarchical control. His email is `parabas@nask.pl`.

BIO-INSPIRED RATE CONTROL FOR MULTI-PRIORITY DATA TRANSMISSION OVER WMSN

Xin-Wei Yao
College of Computer Science & Technology
Zhejiang University of Technology
Hangzhou, China 310023
Email:yxw_zjut@hotmail.com

Wan-Liang Wang
College of Computer Science & Technology
Zhejiang University of Technology
Hangzhou, China 310023
Email:wwl@zjut.edu.cn

Shuang-Hua Yang
Department of Computer Science
Loughborough University
Leicestershire, UK LE11-3TU
Email:S.H.Yang@lboro.ac.uk

KEYWORDS

Rate control, Multi-priority, LV model,WMSN

ABSTRACT

The irrational use of limited network resources in conjunction with the unpredictable nature of traffic load injection in wireless multimedia sensor networks (WMSN) may lead to congestion. Traditional transmission schemes were not designed for supporting prioritized QoS, especially not for guaranteeing strict QoS required by real-time services such as voice and video. To overcome these deficiencies, an optimized rate control approach is proposed for multi-priority data transmission based on the extended Lotka-Volterra competitive model. The key idea is, when some new traffic flows are initialized and injected into the WMSN due to unexpected events, a novel bio-inspired rate control (Bio-RC) approach is designed to consider their effects on the system stability according to the limited network resources and competitions with others traffic flows, ensuring that the system will rapidly converge to a global and stable equilibrium point (EP) and all traffic flows are of peaceful coexistence and differentiated with QoS and priorities. At the same time, the network resources can be utilized adequately and congestion can be brought down or avoided effectively. Extensive simulations reveal that the proposed approach achieves adaptability and scalability to dynamic network traffic load, and coexistence with service differentiation for data flows.

INTRODUCTION

The rapid development of low-cost hardware (e.g. smart phones and CMOS cameras) has fostered the implementation of Wireless Multimedia Sensor Networks (WMSN), i.e. networks of wirelessly interconnected devices that are able to ubiquitously retrieve multimedia content such as video and audio streams, still images, and scalar sensor data from the environment[1]. WMSN will not only enhance existing sensor network applications (e.g. localization, tracking, smart home, and environmental monitoring), but also enable several new applications such as multimedia surveillance sensor networks, traffic avoidance/enforcement and control systems, industrial process control, advanced health care delivery, etc.

However, in order to support most of the above applications, the traditional sensor network paradigm should be rethought in view of the need for protocols and mechanisms to transmit multimedia content with a certain level of QoS. The various applications envisaged on WMSN will have different QoS requirements. Therefore, service differentiation for multi-priority data flows initiated from numerous kinds of applications should be supported and guaranteed[2,3]. For example, the applications can be real-time and delay-tolerant applications, and loss-tolerant and loss-intolerant applications[1].

In this paper, a self-adaptive and decentralized bio-inspired priority-based rate control (Bio-RC) approach is proposed, which is based on the extended Lotka-Volterra (LV) competitive model. And the sending rate of each flow is regulated by the varying network conditions and data flow trends of a local network. It aims to provide efficient resource allocation and smooth rate control while maintaining service differentiation and coexistence for multi-priority data flows, and also providing graceful performance as some traffic load is injected or removed. Moreover, global system stability and convergence is investigated based on the model parameters selection as well as interactions among competing data flows.

The remainder of this paper is organized as follows: Section II analyzes the related work for multi-priority data transmission over WMSN. In Section III, we introduce the ecosystem in rate control for data transmission (i.e. the extended LV model). Section IV proposes the bio-inspired rate control approach for multi-priority data transmission. We presents the performance assessment of the proposed approach in Sections V. The paper is concluded in Section VI.

MULTI-PRIORITY DATA TRANSMISSION

With rapid development and miniaturization in hardware, a sensor node of a WMSN may have e-

Proceedings 27th European Conference on Modelling and Simulation ©ECMS Webjørn Rekdalsbakken, Robin T. Bye, Houxiang Zhang (Editors)
ISBN: 978-0-9564944-6-7 / ISBN: 978-0-9564944-7-4 (CD)

quipped with various types of sensors which gather different kinds of data. It is observed that the data collected may have different levels of importance and priority, so the WMSN should allocate more bandwidth in disseminating packets with a higher priority. For example, whenever an important event occurs in a safety system, some alarm messages (e.g. video streaming or still image) detected by the sensor node should be priorly sent to the monitor or user. And usually this kind of higher priority traffic is bursty and unpredictable, i.e. some high priority traffic is generated only within a short period of time while other low priority traffic usually exists in the network and produce large amount of packets periodically. However, most of current rate control schemes or algorithms[4,5,7,13,14] for WMSN assume that all the traffic flows are assigned with the same level of priority, and the network resources (e.g. bandwidth) are allocated to all of the existing flows fairly, which cannot provide service differentiation for multiple different classes of applications.

Differentiated QoS requirements have recently been considered for WMSN[6,8-11], and one important research question is how to estimate the maximum sending rate that can be allocated to a new injected flow while it will be contending with other existing flows, and estimate the decrease of the throughput and the increase of the delay of existing flows under the new arrival flow. There have been quite a few rate control approaches for priority-based data transmission proposed by academic and industry, which can be broadly classified into three categories based on the collected information: 1) parameter-based approaches [9,10] (e.g. contention window size); 2) performance-based approaches[8] (e.g. throughput, delay); 3) hybrid approaches[11]. Although these approaches have achieved success in their respective target applications, many of them are application specific.

ECOSYSTEM IN RATE-CONTROL FOR DATA TRANSMISSION

The nature of the world shows that the dynamics of many biological systems and laws governing them are based on a surprisingly small number of simple generic rules which yield collaborative and effective patterns for resource management, task allocation and social differentiation without the need for any externally controlling entity[12].

Since the population size of each species changes over time as a result of numerous interactions with other species and limited resources in their environment (i.e. food, water and territory), this process can be investigated by being modeled with a simple balance equation. The well-known Lotka-Volterra (LV) model originally focusing on ecological population dynamics, which is proposed by Lotka and Volterra, has been extensively investigated in the literatures [5,12-14]. The main idea of LV model is that when two or more species live in a ecosystem and share the limited environment resources, they usually compete each other to survive and may coexist with limited resources. This idea of LV competitive model is first borrowed to analyze the optimum sending rate of each data flow is first borrowed for single-priority data transmission in [5,13,14], in which a WMSN is considered as a simplified prototype of an ecosystem.

It is well-known that a general ecosystem comprises of multiple species, which live in proximity and interact with resources and competitors for the objective of survival and coexistence. Similarly, a traditional WMSN involves a number of wireless nodes. Each node is able to initiate a data flow with a different priority, but has a limited ability to access the shared wireless bandwidth. Then the data flows in a WMSN play the role of species in an ecosystem that compete with each other for limited network bandwidth, while passing through a set of intermediate nodes to the monitor or user. Then the sending rate of each flow can be seen as the population size of each species. According to the integrated competitions from other data flows [5,14], the sending rate evolution of each flow can be described as follows:

$$\frac{dx_i(t)}{dt} = x_i(t)\left(r_i - \frac{\beta_i r_i}{N_i}x_i(t) - \frac{r_i}{N_i}\left(\sum_{j=1,j\neq i}^{n} a_{ij}x_j(t)\right)\right) \quad (1)$$

where $x_i(t)$ is the sending rate of traffic flow i at time t ($x_i(t) > 0$). r_i indicates the growth rate intensity of data flow i. N_i is the total network bandwidth. The sending rate of each flow reproduces proportionally to the current sending rate of the same type flows, by the intra-specific competition coefficient β_i. N_i/β_i is the maximum sending rate of flow i that can be sustained in the WMSN under the absence of other flows competing for the limited bandwidth.

If the WMSN is a single-priority network (i.e. without considering the differentiated QoS requirement of multiple data flows), then the inter-specific competition coefficient of any two flows i and j are constant, $a_{ij} = a$, and the intra-specific competition coefficient equals to the inter-specific coefficient, $\beta = a$. This type of single priority network is widely-used in the current protocols of wireless nodes and routers. Therefore, the value of sending rate generated by each data flow converges to a global and stable state x_i^* [5,14] given by

$$x_i^* = \frac{N}{a\,(n-1)+a} \quad (2)$$

However, this rate control approach focuses on single-priority data transmission with a result of fairly sharing the wireless bandwidth, so it only can work on the networks without considering the differentiated QoS requirements. Therefore, it can not be satisfied by multi-priority data transmission in WMSN. To the authors' knowledge, there are not any works by using the extended LV model to deal with multi-priority data transmission, especially in WMSN.

BIO-INSPIRED RATE CONTROL APPROACH FOR MULTI-PRIORITY DATA TRANSMISSION INWMSN

In order to support multi-priority data transmission, a Bio-inspired rate control (Bio-RC) approach is proposed based on the extended LV model shown in Equation (1). It is found that the species of an ecosystem have different positions in its biological chain, i.e. some species are much stronger and more powerful than others, they will consume more resources from the surrounding environment. This phenomenon can also been seen in WMSN, that the data flows with a higher priority are much more important than ones with a lower priority, and bandwidth of the network will be priorly allocated to the data flows with the highest priority, which means that the packets of the flow with the highest priority have more opportunities to be transmitted. And in analogy with an ecosystem, the goal of a WMSN is expected to achieve service differentiation and coexistence of all data flows.

According to the above analysis, there are five correspondences between a WMSN and an ecosystem, i.e. a) the data flows n initiated by each node refer to competing species; b) the sending rate $x_i(t)$ of flow i corresponds to the population size of species i; c) the sending rate of each flow is influenced by inter-actions among competing flows as well as the available bandwidth, named inter-specific or intra-specific competition coefficient a_{ij}; d) the growth rate intensity r_i of each flow refers to the growth rate intensity of each species; e) the limited bandwidth N of a WMSN plays the role of the natural resource in the ecosystem, which is ignored by the original Lotka-Volter model.

As discussed in Section II, WMSN will need to support service differentiation for various applications with a certain level of QoS requirement, such as real-time or delay-tolerant applications, and loss-tolerant or loss-intolerant applications. We consider four categories of data flows from highest priority to lowest priority in this paper: real-time loss-intolerant traffic, real-time loss-tolerant traffic, delay-tolerant loss-intolerant traffic and delay-tolerant loss-tolerant traffic. Each traffic class is assigned with a different priority. To simplify the notations, we rename four categories of traffic as Prio_4, Prio_3, Prio_2 and Prio_1 from the highest priority to the lowest priority in the rest of this paper.

So this paper adopts the above idea in the design of rate control approach for competing flows of data in WMSN, specially for data flows with different levels of QoS requirements. The proposed Bio-RC approach is based on the extended LV competitive model, and describes competitions among data flows with objective of coexistence, where the sending rate of each flow is influenced by the presence of other data flows and allocation of available network bandwidth. Moreover, the Bio-RC approach is expected to meet differentiated QoS requirements for various applications based on their priorities, and quickly converge to a global stable equilibrium point (EP) under randomly changing network conditions.

To support the service differentiation between the above four categories of traffic, four assumptions are made as follows:

1. The effect of inter-specific coming from flow i to flow j is identical to the effect from flow j to flow i with the same value of i and j, i.e. the coefficient $a_{ij} = a_{ji}$.
2. The effect of intra-specific of all traffic flows is a constant, i.e. the coefficient $a_{ii} = \beta (i = 1, ..., n)$ where n is the number of all traffic flow.
3. The growth rate intensity of any data flow i is a constant, i.e. the coefficient $r_i = r$.
4. The maximum sending rate of each flow is equal to the limited bandwidth of a WMSN, i.e. the coefficient $N_i = N$.

Then the extended Lotka-Volterra model of WMSN as shown in Equation (1) can be rewritten in vector form:

$$dx/dt = X \cdot (B - Ax) \tag{3}$$

where $X = diag\,(x_1(t), x_2(t), \cdots, x_n(t))$, $B = (r, r, \cdots, r)^{\mathrm{T}}$ is an n-dimensional constant vector, and $x = (x_1(t), x_2(t), \cdots, x_n(t))^{\mathrm{T}}$ is also an n-dimensional state vector of all data flows in WMSN, and superscript $^{\mathrm{T}}$ denotes the transpose operation. $A = (a_{ij})_{n \times n}$ is an $n \times n$ real symmetrical matrix based on the assumption $a_{ij} = a_{ji}$, i.e.

$$A = \frac{r}{N} \begin{bmatrix} \beta & a_{12} & a_{13} & \cdots & a_{1n} \\ a_{12} & \beta & a_{23} & \cdots & a_{2n} \\ a_{13} & a_{23} & \beta & \cdots & a_{3n} \\ \vdots & \vdots & \vdots & \ddots & \vdots \\ a_{1n} & a_{2n} & a_{3n} & \cdots & \beta \end{bmatrix} \tag{4}$$

For data flow i, its sending rate $x_i(t)$ can be calculated as follows (see the Appendix):

$$x_i(t) = \frac{w(t) \cdot x_i(0) \cdot e^{\frac{w(t)r}{N}t}}{w(t) - \beta x_i\,(0) + \beta x_i(0) \cdot e^{\frac{w(t)r}{N}t}}, \tag{5}$$

$$w(t) = N - \sum_{j=1, j \neq i}^{n} a_{ij} x_j(t)$$

Then the sending rate of each flow is regulated on the basis of Equation (5) for $i = 1, 2, ..., n$. And the stable equilibrium point x^*, i.e. the desirable sending rate of each flow, can be obtained as follows

$$X^* \cdot (B - Ax^*) = 0 \tag{6}$$

In the presence of all data flows with different priorities, there will be three combinations of equilibrium points: all data flows coexist, all data flows extinct, and the combination of some data flows can be transmitted and some can not. From a network system point of view, the sending rates of all data flows must be non-negative. Therefore, Equation (6) can be simplified as

$$B - A \cdot x^* = 0$$

Parameter selection of the proposed multi-priority approach is discussed in detail in the next Section.

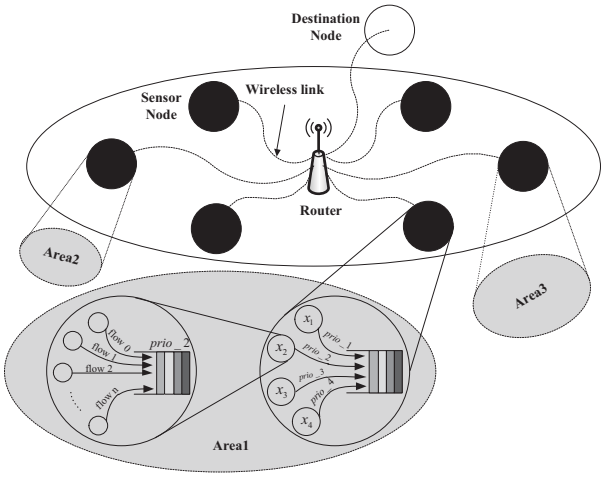

Fig. 1. Network topology

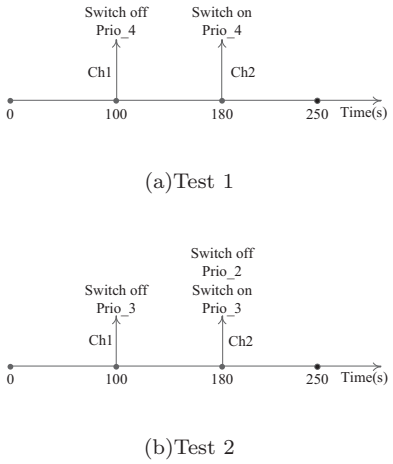

Fig. 2. Removing and/or injecting traffic flow

PERFORMANCE ASSESSMENT

A. Experiment environment and setting

In order to evaluate the performance of the proposed Bio-RC approach for WMSN, simulation studies are used to evaluate the performance in terms of graceful performance degradation, self-adaptivity, scalability and service differentiation. In addition, evaluation studies investigate how parameters affect the performance of the Bio-RC approach in terms of stability and convergence and provide effective parameter setting on the basis of congestion-oriented metrics. The simulation experiments are conducted in a wireless sensor network, the traffic flows are transmitted by wireless medium through a Router to the Destination Node (DN) as shown in Fig. 1. The time interval between two successive evaluations of sending rate of data flow initiated by Sensor Node (SN) is set to 1 second.

The parameters setting of the proposed Bio-RC model shown in Equation (4) are set up as follows: $A = \frac{r}{N} \cdot \begin{bmatrix} 3 & 1.7 & 1.4 & 1.2 \\ 1.7 & 3 & 1.3 & 1.1 \\ 1.4 & 1.3 & 3 & 1.1 \\ 1.2 & 1.1 & 1.1 & 3 \end{bmatrix}$, $r = 1$, $N = 1024$, where N means the maximum available bandwidth of the network, i.e. 1Mbps. As discussed above, the rate of each traffic flow converges to a global stable EP when all the eigenvalues of matrix A are positive.

B. Stability analysis under different traffic loads

Two random network scenarios (Test1 and Test2) with two changes, such as removing or injecting data flows, are used to evaluate the performance of the proposed approach, such as the stability, scalability and adaptivity. Each scenario with a random initial rate of traffic flows has two changing network states, change1 (Ch1) and change2 (Ch2), as shown in Fig.2 and three global stable states (stable, stable1 and stable2) as shown in Table I. In Test I, we switch off the flow Prio_4 at $t = 100s$, and then switch on it again at $t = 180s$. While in Test2, we switch off the flow Prio_3 at $t = 100s$, and then switch on it again and switch off the flow Prio_2 at $t = 180s$. Individual element in Table I is the data flow rate. Moreover, we assume that all data flows have the same characteristics of the growth rate r, the intra-specific competition coefficient β and the maximum capacity N of each data flow. However, the inter-specific competition coefficient between any two flows are various among them, such as the inter-specific competition coefficient of flows Prio_1 and Prio_2 is $a_{12} = 1.7$, while the inter-specific competition coefficient of flows Prio_1 and Prio_3 is $a_{13} = 1.4$.

TABLE I: The EP of the proposed mechanism under different network conditions

Test	Priority	Initial	Stable	Stable1	Stable2
		0s	100s	180s	250s
Test1	Prio_1	70.0	113.1	154.0	113.1
	Prio_2	50.0	139.7	169.1	139.7
	Prio_3	50.0	159.7	196.2	159.7
	Prio_4	150.0	186.3	0.0	186.3
Test2	Prio_1	20.0	113.1	157.1	173.0
	Prio_2	150.0	139.7	173.6	0.0
	Prio_3	150.0	159.7	0.0	185.8
	Prio_4	70.0	186.3	214.9	204.0

As observed in Table I, the experiments of Test1 and Test2 have the same values of stable EP, which illustrates the proposed approach having one stable EP under an arbitrary nonnegative initial value. The point (113.1,139.7,159.7,186.3) is the global stable EP for all flows co-existing in the bandwidth-limited WMSN. When the flow Prio_4 becomes extinct at $t = 100s$ for some unknown reasons in Test1, the other data flows will soon adaptively reach another new EP (154.0, 169.0, 196.2, 0.0). At the instant $t = 180s$, the flow Prio_4 is injected into the network again, then the system returns back to the original EP. Similarly, Test2 also shows the excellent performance of the Bio-RC approach in terms of adaptivity, scalability and stability. When the flow Prio_3 is switched off at $t = 100s$,

other categories of flows will reach a new stable EP (157.1, 173.6, 0.0, 214.9), and then the WMSN will reach another new stable EP (173.0, 0.0, 185.8, 204.0) after switching off the flow Prio_2 and switching on the flow Prio_3 at $t = 180s$ in Test2.

Fig. 3 takes a close look at the behavior of all traffic flows with differentiated priority under the changing network load. We aim to reveal the process of the system keeping stable after changes are introduced into the network. As can be seen, when the data flow is changed for some reasons (i.e., some flows are injected or removed), the system can re-converge to a new stable EP quickly for its characteristic of self-adaptivity. And the convergence time is very short (about twenty iterations) for each violation of the stable condition as shown in Fig. 3(b) at $t = 100s$ and $t = 180s$. Moreover, the proposed Bio-RC approach provides smooth transmission rates for all the traffic flows, which also assists in avoiding or reducing the possibility of buffer overflow and network congestion. When some high priority emergency data streams are injected into the network as shown in Fig. 3, the proposed mechanism can also achieve graceful performance degradation.

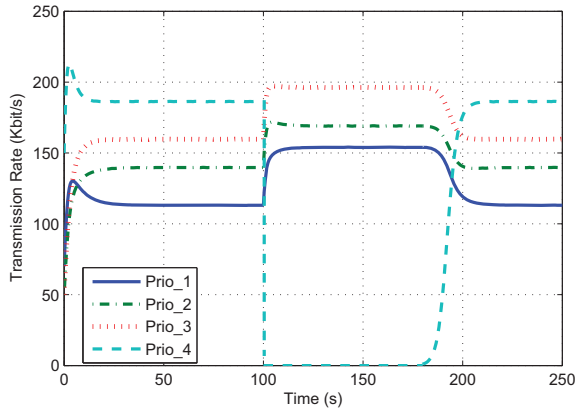

(a)Test 1

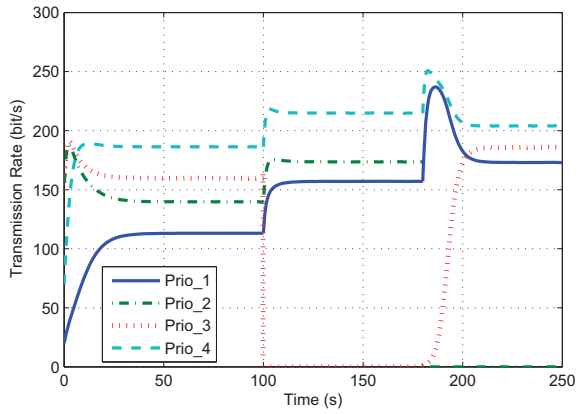

(b)Test 2

Fig. 3. Transmission rates

C. Parameter setting and analysis

In this section, the impact of parameters β, r on a realistic network environment is investigated. Each scenario, concerning different combinations of β, r values, is executed 10 times and the average values of metrics over all scenarios are presented below.

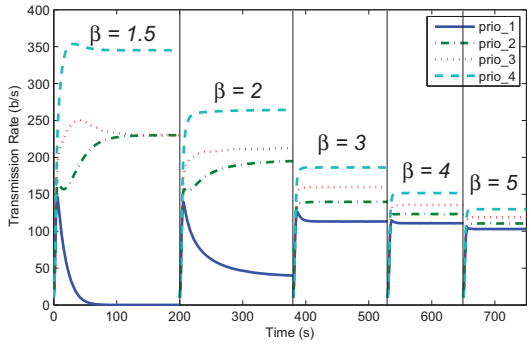

Fig. 4. The equilibrium point with different β values

When β increases from 1.5 to 5 as shown in Fig. 4, the sending rates of all data flows become less differentiated, and the remaining difference in data flow rate is mainly caused by the different inter-specific competition coefficients. With the increment of value β, i.e. the competitive effect of flow j on the sending rate of flow i is much less than that from the inside of flow i, the total sending rate of all data flow is found being decreased. Even though there is no upper bound for β value, it is worth pointing out that as β increases, the EP value decreases and the received data rate at the DN may be reduced.

The phase plane of the scenarios with different values of β as shown in Fig. 5 illustrates the stability, rapid convergence and differentiation of transmission rates of two data flows with all the combinations of priorities. As observed in Fig. 5(c) when $\beta = 3$, the sending rate of each flow can converge to the global stable point without any fluctuations. Moreover, with the increment of intra-specific competition coefficient β, the phase plane inclines to a small region (the EP), which means that there is less difference among four priorities. However, when the value of intra-specific competition coefficient is equal to 1.5 (i.e. the inequality $a_{ij} < \beta$ is not satisfied, for $a_{12} = 1.7$), the network system is not stable as shown in Fig.5(a), which can be effectively avoided from proper parameter settings.

In all the previous scenarios, the parameter r for each flow is set to 1. Further simulation studies are carried out to study the influence of r on stability. Results show that the stability of all traffic flows is independent on r, i.e. the stable EP (113.1, 139.7, 159.7, 186.3) is constant for any flow growth rate as shown in Fig. 6. This implies the stable equilibrium state x_i^* for flow i keeps its sending rate unchanged whatever its initial growth rate r_i increases to. Analytical evaluations from the comparisons in Fig. 6 suggest that high values of r can contribute to fast convergence to the stable equilibrium solution.

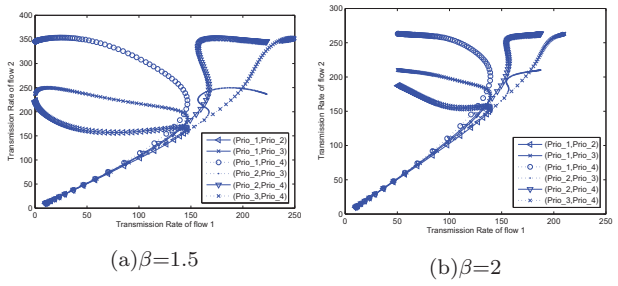

(a)β=1.5 (b)β=2

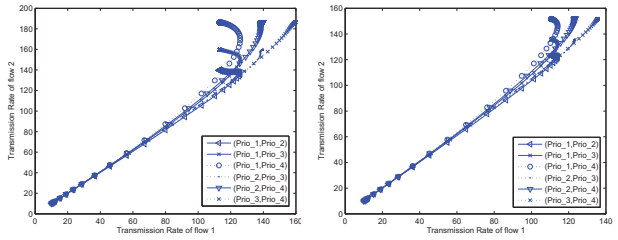

(c)β=3 (d)β=4

Fig. 5. Phase plane of two species

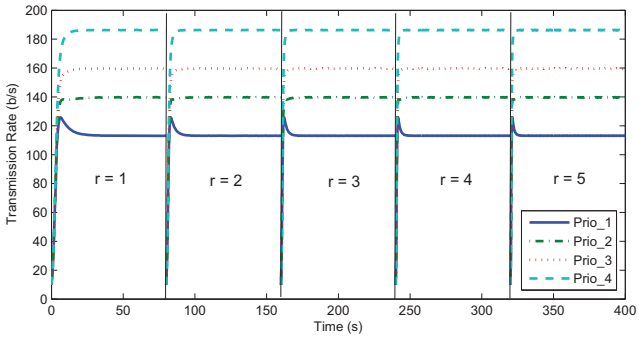

Fig. 6. Transmission rate under different r values

CONCLUSIONS

In this paper, we propose a novel bio-inspired rate control (Bio-RC) approach to meet the differentiated QoS requirements for various applications in WMSN. Based on the extended competitive LV model, the Bio-RC model considers the effect of injected bursty data flows on the system stability as well as the limited network resources and competitions from other data flows. It is proven that Bio-RC approach has a global stable EP and can fast re-converge to a new EP under changing network conditions, while keeping all data flows co-existing and serviced with differentiated QoS. The source traffic rates can be adjusted optimally according to the value of EP. From the analysis of simulation results, we illustrate how the variations of the approach's parameters influence stability, scalability and distinction of traffic flows. Performance evaluations suggest certain values for parameters a_{ij}, β_i and r that are able to achieve low packet loss probability and guarantee bandwidth for real time traffic with a higher priority .

Appendix

According to the ordinary differential equation, the Equation (4) can be rewritten for data flow i as:

$$\frac{dx_i(t)}{dt}\cdot\frac{1}{r\cdot x_i^2(t)}=\frac{N-\sum_{j=1,j\neq i}^{n}a_{ij}x_j(t)}{Nx_i(t)}-\frac{\beta}{N}$$

$$-\frac{1}{r}\cdot\frac{d\left(\frac{1}{x_i(t)}\right)}{dt}=\frac{w(t)}{Nx_i(t)}-\frac{\beta}{N},\quad w(t)=N-\sum_{j=1,j\neq i}^{n}\alpha_{ij}x_j(t)$$

We define: $y(t)=\frac{1}{x_i(t)}$, then the above equation can be written as:

$$\frac{dy(t)}{dt}+\frac{w(t)\cdot r}{N}\cdot y(t)=\frac{\beta\cdot r}{N}$$

$$y(t)=e^{-\frac{w(t)r}{N}\cdot t}\cdot\left(\int\frac{\beta r}{N}\cdot e^{\frac{w(t)r}{N}\cdot t}dt+C\right)$$

Define: $t=0$,then $C=\frac{1}{x_i(0)}$.

$$e^{-\frac{w(t)r}{N}\cdot t}\cdot\left[\frac{\beta}{w(t)}\cdot\left(e^{\frac{w(t)r}{N}\cdot t}-1\right)+\frac{1}{x_i(0)}\right]=\frac{1}{x_i\,(t)}$$

$$x_i\,(t)=\frac{w(t)\cdot x_i\,(0)}{\beta x_i\,(0)+[w(t)-\beta x_i\,(0)]\cdot e^{-\frac{w(t)r}{N}t}}$$

then we can obtain Equation (5).

REFERENCES

1I.F. Akyildiz, T. Melodia, K.R. Chowdhury. A survey on wireless multimedia sensor networks. Computer Networks, 2007. 51(4): p. 921-960.

I.T. Almalkawi, M.G. Zapata, J.N. Al-Karaki, J. Morillo-Pozo. Wireless Multimedia Sensor Networks: Current Trends and Future Directions. Sensors, 2010, 10(7): p. 6662-6717.

S. Misra, M. Reisslein, G. Xue. A Survey of Multimedia Streaming in Wireless Sensor Networks. IEEE Communications Surveys & Tutorials. 2008,10(4):p. 18-39.

M. Chen, A. Zakhor. Rate control for streaming video over wireless. IEEE INFOCOM 2004, Hong Kong, China: p.1181-1190.

P. Antoniou, A. Pitsillides. A bio-inspired approach for streaming applications in wireless sensor networks based on the Lotka-Volterra competition model. Computer Communications, 2010,33(17Sp. Iss. SI): p. 2039-2047.

K. Karenos, V. Kalogeraki, S.V. Krishnamurthy. A rate control framework for supporting multiple classes of traffic in sensor networks. Proceeding of 26th IEEE International Real-Time Systems Symposium, 2005.

C. Lee, T.W. Jeong, S. Lian. Tournament-based congestion control protocol for multimedia steaming in ubiquitous sensor networks. International Journal of Communication Systems. 2011,24(10):p. 1246-1260.

L.Q. Tao, F.Q. Yu. ECODA: Enhanced Congestion

Detection and Avoidance for Multiple Class of Traffic in Sensor Networks. 2010,56(3):p. 1387-1394.
X.W. Yao, W.L. Wang, S.H. Yang, S.Y. Chen. PABM-EDCF: parameter adaptive bi-directional mapping mechanism for video transmission over WSNs. Multimedia Tools and Applications. 2011. Doi:10.1007/s11042-011-0934-7.
M.H. Yaghmaee, D.A. Adjeroh. Priority-based rate control for service differentiation and congestion control in wireless multimedia sensor networks. Computer Networks. 2009,53(11):p. 1798-1811.
Y.L. Chen, H.P. Lai. Priority-based transmission rate control with a fuzzy logical controller in wireless multimedia sensor networks. Computers and Mathematics with Applications (2011). Doi:10.1016/j.camwa.2011.09.034.
F. Dressler, O.B. Akan. A survey on bio-inspired networking. Computer Networks, 2010,54(6):p. 881-900.
C. Zhu, G. Yin. On competitive Lotka-Volterra model in random environments. Journal of Mathematical Analysis and Applications, 2009,357(1): p. 154-170.
X.W. Yao, W.L. Wang, S.H. Yang, J.W. Zheng, Y.F. Cen, Y.W. Zhao. Bio-inspired rate control scheme for IEEE 802.11e WLANs. 2012 UKACC International Conference on Control, 2012: 674-679.

AUTHOR BIOGRAPHIES

XIN-WEI YAO received the B.S. degree in Mechanical Engineering from Zhejiang University of Technology, Hangzhou, China, in 2008. Since September 2008, he has been pursuing the Ph.D. degree in Institute of Intelligent Systems, College of Computer Science & Technology, Zhejiang University of Technology (ZJUT), Hangzhou, China.

From 2012 to 2013, he has been with Department of Computer Science as an academic visitor, Loughborough University, Leicestershire, UK. His current research interests include Multimedia transmission Modeling, MAC layer algorithms, modeling and optimization in wireless ad hoc networks, and wireless sensor networks. His e-mail address is: yxw_zjut@hotmail.com.

WAN-LIANG WANG received the Ph.D. degree from Tongji University, China, in 2001. He is currently a Professor in Zhejiang University of Technology, China. His research interests include computer control, computer network, CMIS, and production scheduling. In 2002, he visited University of Manchester Institute of Science and Technology (UMIST) and Loughborough University, UK. In 2007, he visited Georgia Institute of Technology and University of Michigan, USA.

Now, he is the nationally outstanding teacher and the dean of College of Computer Science & Technology, ZJUT. Prof. Wang is the council member of Chinese Association for Artificial Intelligence. His e-mail address is: wwl@zjut.edu.cn.

SHUANG-HUA YANG is currently a Professor of networks and control and the Director of the Networks and Control Research Group at Loughborough University, Leicestershire, UK. His current research interests include wireless sensor networks, networked control, safety critical systems, and real-time software maintenance. He is a member of the Editorial Advisory Board of the International Journal of Information and Computer Security, and an Associate Editor of the International Journal of Systems Science, International Journal of Automation and Computing, and Arabian Journal for Science and Technology. Prof. Yang is a Fellow of the Institute of Measurement and Control, a Senior Member of IEEE, and a Chartered Engineer in the UK. His e-mail address is: S.H.Yang@lboro.ac.uk.

A Toolchain for Profiling Virtual Machines

Jiaqi Zhao
School of Basic Sciences
Changchun University of Technology, China
scorpiozhao@yahoo.com.cn

Jie Tao
Steinbuch Center for Computing
Karlsruhe Institute of Technology, Germany
jie.tao@kit.edu

Lizhe Wang
Center for Earth Observation and Digital Earth
Chinese Academy of Sciences, China
lizhe.wang@gmail.com

Andreas Wirooks
Steinbuch Center for Computing
Karlsruhe Institute of Technology, Germany
andreas.wirooks@kit.edu

ABSTRACT

Performance tuning is a common topic in the research domain High Performance Computing. Currently, various tools have been developed to help programmers understand the runtime execution behavior of their applications. It is clear that such tools are also required for performance analysis on virtual machines, where applications, together with their execution environment, sit on top of a virtualization layer rather than running directly on the physical machines.

This work developed a toolchain (also called workflow system in the following), specifically for performance analysis on virtual machines. Starting with a profiling tool, the workflow system first collects the runtime performance data on both physical and virtual machines. The performance data are filtered, combined, transformed, and then delivered to a visualization tool, where graphical views are produced to demonstrate the performance difference between native executions and the execution on virtual machines. We tested the toolchain with standard benchmark applications running either sequentially or in parallel with multiple threads.

KEYWORDS

Performance Tools, Profiling, Virtual Machines, Performance Analysis

INTRODUCTION

Virtual machines have been increasingly used in different scientific domains for various purposes like provisioning customized computing environments, running legacy codes, fault-tolerance, and easy system management. However, virtualization causes a performance loss due to the fact that applications now run on top of a virtualization layer, the so-called hypervisor or Virtual Machine Monitor (VMM). A tool support for comparative study of the performance and the runtime execution behavior of applications on both physical and virtual machines can surely help programmers find reasons that cause the performance deficit on virtualized architectures and further optimize their applications towards a performance improvement.

Actually, performance tools have long been applied by programmers in performance analysis and tuning. Over the last years, a number of performance tools have been implemented. Vampire (Brunst et al., 2009), TAU (Shende et al., 2006), and Intel Vtune (Intel, 2013) are several well-known and widely used examples. These tools have significantly supported programmers in developing scientific codes (Ciorba et al., 2010; Malony et al., 2011; Hammond et al., 2012).

Existing tools are mostly developed for applications running directly on the host machines. For virtual machines, however, there are few implementation work that supports performance analysis. Observing available performance tools it can be seen that the role of a performance tool is to present the runtime behavior of events like memory access, cache access, inter-process communication, synchronization, and I/O operations. This role remains for virtual machines. However, an additional point has to be considered for virtual machine specific tools, i.e., the difference between physical and virtual machines for the same event. Programmers have to compare the performance of executions on virtual machines with the physical runs to detect bottlenecks, where physical machine outperform the virtual ones. This discovery is the base for any further optimization. Therefore, providing a comparative view of the performance events must be a major focus of tools specifically designed for virtual machines.

We implemented a toolchain, a workflow system, that builds an automatic process, from data acquisition up to visualization, to support programmers in the task of performance analysis on virtualized architectures. The runtime performance data are collected using the Linux profiling tool *perf*, which is delivered together with the Linux kernel. Performance data on both the physical machine and the virtual machine are then filtered, combined, and converted to a specific form that can be handled by BIRT (Eclipse, 2013), an Eclipse-based open source reporting system actually designed for Web applications. In this work we use BIRT as a visualization tool to illustrate the performance data with graphical presentations. We validated the developed toolchain with OpenMP applications from standard benchmark suites,

Proceedings 27th European Conference on Modelling and Simulation ©ECMS Webjørn Rekdalsbakken, Robin T. Bye, Houxiang Zhang (Editors)
ISBN: 978-0-9564944-6-7 / ISBN: 978-0-9564944-7-4 (CD)

running in both the sequential mode or parallel with multiple threads. Experimental results show some interesting behavior on the virtual machines.

The remainder of the paper is organized as follows: Section gives an overview of profiling on virtual machines, together with some related work. Section describes the developed workflow system in detail. Section shows sample experimental results. The paper concludes in Section with a short summary and several future directions.

PROFILING VIRTUAL MACHINES AND THE RELATED WORK

The runtime performance data are the basis for any performance analysis tools. Such data can be collected by different software approaches like simulation and code instrumentation. However, a more direct way to gather the runtime information about the applications memory access or execution behavior is to use the hardware counters provided by modern processor architectures in the form of a Performance Monitoring Unit (PMU). These counters can record the occurrence of various CPU or software events such as cache miss, TLB miss, I/O events, and specific instructions.

In the last years, different low-level libraries or high-level interfaces have been implemented for programmers to access the performance counters in the source codes. *perf* (de Melo, 2010) is a low level profiling tool delivered by the Linux kernel. It provides a simple commandline interface for uses to start profiling a running application for specific events. *perf* supports a number of measurable events including the software events, like context-switches and minor-faults, as well as the hardware events such as the number of CPU cycles and cache misses. *perf* aggregates the occurrences of the user-specified events and provides the profiling results as perf-reports at the end of applications execution. The results with the events are split into individual functions including the routines of system libraries.

PAPI (Browne et al., 2000) is a well-known and widely applied programming interface for accessing the hardware counters within an application's source code. PAPI provides both a simple, high level interface for the acquisition of simple measurements and a fully programmable, low level interface to the underlying counter hardware. The low level PAPI interface deals with hardware events in groups while the high level interface simply provides the ability to start, stop, and read specific events. A set of performance tools, including TAU and Vampire, use PAPI as the interface to performance counters. Besides PAPI, there are other well-known programming interfaces for hardware counters. *perfmon* (Sourceforge, 2013) and oProfile (OProfile, 2013) are two system-wide profilers for Linux systems.

On virtual machines, however, the hardware counters are invisible to the applications, i.e., they cannot be directly accessed within a virtual machine. The access to these registers can only be done via the hypervisor. Xenoprof (Menon et al., 2005) is an implementation that allows the performance profiling within a running virtual machine instance. It is a system-wide statistical profiling toolkit implemented for the Xen virtual machine environment. The Xenoprof toolkit supports coordinated profiling in a Xen environment to obtain the distribution of hardware events. Xenoprof allows the profiling of concurrently executing virtual machines, and provides profiling data at the fine granularity of individual processes and routines executing either within the virtual machine or on the physical host.

Researchers have applied the Xenoprof toolkit to study application performance on architectures virtualized with the Xen hypervisor. For example, work in (Youseff et al., 2008) studies memory hierarchy features of para-virtualized machines and memory intensive applications; work in (Tikotekar et al., 2008) studies the behavior of L2 cache, DTLB, ITLB, and the overall performance penalty of HPC applications.

Xen (Barham et al., 2003) is a well-known hypervisor and an open source development that has been widely used for system virtualization. It supports both para-virtualization and full virtualization, where the former uses hypercalls for the guest Operating System (OS) to communicate with the hypervisor with the necessarily of a slight OS modification, while the latter translates the sensitive instructions to a new sequence of instructions for the virtualized hardware without changing the OS running on a virtual machine.

Nevertheless, there is currently a trend of replacing Xen with KVM (Kernel-based Virtual Machine) (KVM, 2013). KVM is also an open source product. It adds the virtualization capacities directly in the Linux kernel, achieving the thinnest hypervisor of only a few hundred thousand lines of code. Therefore, KVM is being increasingly deployed, even though it requires the virtualization extensions in the hardware of modern microprocessors (e.g. Intel VT and AMD-V).

For KVM-virtualized machines, however, there exists no profiling tool, similar to Xenoprof, which supports system-wide profiling also within the virtual machines. Fortunately, KVM developed recently a virtualized performance monitoring unit (VPMU) that emulates the hardware counters and provides each virtual machine with a performance monitoring unit. The Linux system tool *perf* already supports VPMUs and can be used for system-wide profiling in KVM-based systems. Some high level interfaces, like PAPI, also supports now the VPMUs. However, they currently run only on Intel processors. AMD architectures have not been supported yet.

We aim at profiling KVM-virtualized machines, independent of the target architecture. Therefore, we use the low level Linux tool *perf* to collect initial performance data. For a better understanding of the counter events as well as a comparison between performance on the host and the virtual machines, we developed the workflow system of tools to visualize the runtime behavior of sys-

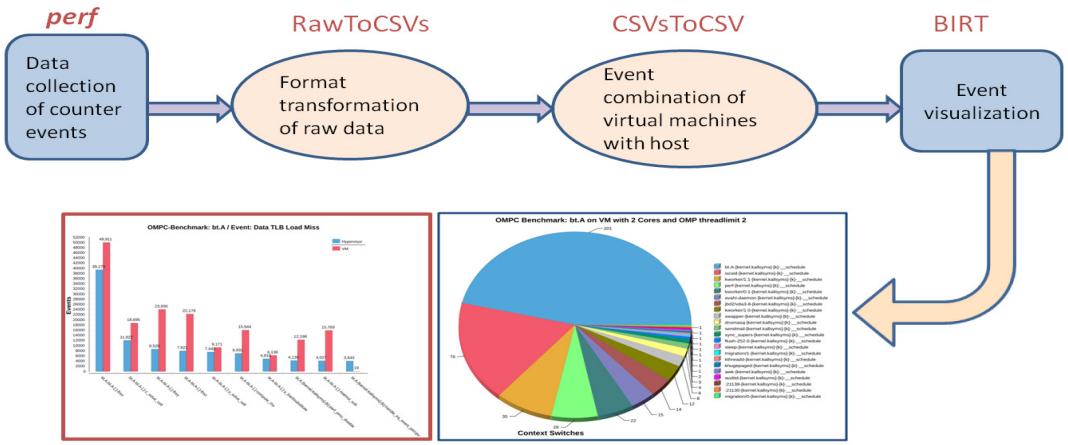

Figure 1: The toolchain for collecting, transforming, and visualizing event data.

tem hardware and software events.

THE WORKFLOW SYSTEM

The developed workflow system is illustrated in Figure 1. The whole toolset is based on the *perf* tool that can be used to collect initial performance data from hardware counters. *perf* offers a simple commandline interface for users to interact with the system. During the profiling period *perf* writes the events with their related memory addresses in a binary file, which can be transformed to a text report after the profiling.

perf can be run in several modes. Mode *stat* allows the users to profile an application as a whole, whereby only events that occur within the application are counted together without a detail insight into the individual methods of both the program and the system library. Mode *record* enables the system-wide profiling and is based on sampling. Hence, this mode is not accurate in contrast to *stat*. However, with this mode it is capable of acquiring a detailed report about the methods of a program as well as the libraries and kernel functions at either thread or CPU level. Mode *top* performs also system-wide profiling but shows the results directly on the terminals like the standard Unix command "top" rather than recording the events in a file. *kvm* is a special mode that works only for a KVM-virtualized machine, where the host and several virtual machines run in parallel. It functions similarly to *record* and works on both the host and a virtual machine. This mode is exactly what we need for building the toolchain.

However, the *perf* report, even in a text format, is a low-level presentation. Therefore, we follow the traditional solution to show the performance data graphically with a visualization tool, the Business Intelligence and Reporting Tool (BIRT). Before the data can be visualized with BIRT, they have to be processed because BIRT works with the CSV (Comma-separated values) data format. In addition, the profiling results on the host and on the virtual machine are stored in separate files. These files have to be combined into a single input for BIRT. Moreover, the *perf* reports contain both information that is not related to the events and data that are not interested to users. These data have to be moved out.

We developed three scripts to perform the data processing tasks. Their source codes are depicted in Listing 1, Listing 2, and Listing 3 individually. The script RawToCSVs first calls a self-coded program *perf2csv* to transform a *perf* report from its text (ASCII) format to CSV. It then calls the program *splitcsv*, again self-written, to split a CSV file into several individual ones, with each only containing the profiling results of a single event. This makes it easy to produce the required data for visualizing the behavior of a counter event. In case that the user has not used it correctly the script gives an error report.

Listing 1: Source code of the script RawToCSVs.

```
#! /bin/bash
if [ $# -eq 1 ] then
  if [ -f "$1" ] then
    perf2csv $1
    if [ $? -eq 0 ] then
      echo "The report was successfully converted."
      splitcsv $1.csv
      lastindex = $?
      if [ $? -eq -1 ] then
        echo "The report CSV cannot be split"
      else
        echo "The report CSV has been split by Index
              $lastindex."
      endif
    else echo "The report cannot be converted to CSV."
    endif
  else echo "The file does not exist."
  endif
else echo "This program requires a perf report file as
          parameter."
endif
```

For each event there are two CSV files, one for the host and the other for the virtual machines. The script CSVsToCSV combines the two files into a single one. As depicted in Listing 2, it first performs some sorting tasks with the two original CSV files and then calls the *primarykeyjoin* program to put the two files together with the

corresponding routines stored on the same line. The *primarykeyjoin* program is specifically written for this purpose. In the next step, it reduces the amount of lines in the combined CSV file to 10 entries for a better presentation of the event later in the graphical view. Actually, users are also only interested in the routines with a high value of an event.

The last script, as shown in Listing 3, is used to generate diagrams for demonstrating the profiling results in graphical views. The results of the same event for an application on both the host and the virtual machine are contained in a single diagram. The script takes the combined file, generated by CSVsToCSV in the previous step, as input and creates from this file a temporary file for BIRT. The BIRT file contains all information for creating a diagram, including the data, the caption, and the labels for the bars in the diagram. The resulted graphical files are in the form of vectorized SVG (Scalable Vector Graphics) and stored in the same directory as the input file of the script. Finally, the SVG file is processed to produce another two graphical files in the form of EPS and PNG separately.

Listing 2: Source code of the script CSVsToCSV.

```
#! /bin/bash
if [ $# -eq 2 ] then
  if [ -f "$1" -a -f "$2" ] then
    old = ${1//.?.csv/}
    new = ${2//.?.csv/}
    for file in $old.?.csv do
    cat $file | sed -e '1d' | sort -s -t, -k 3,3 |
      sort -s -t, -k 4,4 | sort -s -t, -k 6,6 >
          $file.sorted
    primarykeyjoin $file.sorted
    sort -s -t, -k 3,3 < $file.sorted.key > $file.sorted
    rm $file.sorted.key
    tmp1 = $(dirname $new)
    tmp2 = $(basename $file)
    cat $tmp1/$tmp2 | sed -e '1d' | sort -s -t, -k 3,3 |
      sort -s -t, -k 4,4 | sort -s -t, -k 6,6 >
          $tmp1/$tmp2.sorted
    primarykeyjoin $tmp1/$tmp2.sorted
    sort -s -t, -k 3,3 < $tmp1/$tmp2.sorted.key >
         $tmp1/$tmp2.sorted
    rm $tmp1/$tmp2.sorted.key
    join --check-orde -t, -j 3 $file.sorted $tmp1/$tmp2.
        sorted | sort -s -t, -k 3,3 -n | tail -n 10 >
        $file.combined
    rm $file.sorted
    rm $tmp1/$tmp2.sorted
    done
  else echo "One of the two files is not available."
  endif
else echo "This program needs a split CVS report and a"
     echo "second path to the first file of the report"
     echo "for comparison with the first one."
endif
```

Listing 3: Source code of the script BirtChart.

```
#! /bin/bash
actualdir = $PWD
scriptdir = $(dirname "$(readlink -e "$0") ")
givenfile = $(readlink -e "$1")
if [ $# -eq 4 ] then
  if [ -f "$1" ] then
    if [ -f "$1".svg ] then
       echo "The target file already exists."
    else
       cd "$scriptdir"
       cp birt-chart.rptdesign tmp.rptdesign
       sed -e "s#YYYYYYZZ#$givenfile#g" -i tmp.rptdesign
       sed -e "s#ABCDEFGH#$2#g" -i tmp.rptdesign
       sed -e "s#IJKLMNOP#$3#g" -i tmp.rptdesign
       sed -e "s#QRSTUVWX#$4#g" -i tmp.rptdesign
       export BIRT_HOME=/home/project/bin/birt-run
              time-4_2_0; /home/project/bin/birt-
              runtime-4_2_0/ReportEngine/genReport.
              tmp.rptdesign
       cp image/customl.svg $givenfile.svg
       rm image/customl.svg
       rmdir image
       rm tmp.rptdesign
       rm tmp.html
       cd "$actualdir$"
       inkscape -z -t -e $givenfile.svg.eps
                $givenfile.svg
       inkscape -z -t -e $givenfile.svg.png
                $givenfile.svg
    endif
  else
    echo "The files are not available."
  endif
else
  echo "This program requires an input file with four"
  echo "parameters. 1: the file name with an absolute;
  echo "path; 2: caption of the diagram; 3: name of"
  echo "the blue bar; 4: name of the red bar."
endif
```

In summary, we implemented a set of tools to achieve the goal of showing the applications runtime performance in graphical views with a comparative presentation of the behavior on the host and the virtual machine. The entire working process of the toolchain is demonstrated in Figure 2. It starts with the *perf* tool using its runtime mode of *kvm*. The applications are executed once on the host machine and once on a virtual machine. During the execution of the application *perf* produces a profiling report in the form of a binary file. Using its "report" tool, the binary file is transformed to a text report. The work of our self-developed tools starts with the text report. First, RawToCSVs converts the text report to a CSV form and splits the CSV file into several files with each for a single event. In the following, CSVsToCSV combines the two CSVs with the same event, one for the host and the other for the virtual machine, and reduces the number of items in the combined file in order to highlight the interesting behavior later in the visualization. Finally, BirtChart calls BIRT to creates graphical presentations in three different image formats.

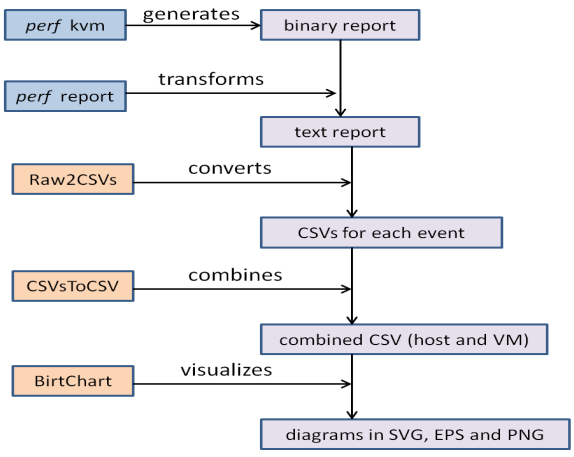

Figure 2: The data flow and functionality of the developed toolchain.

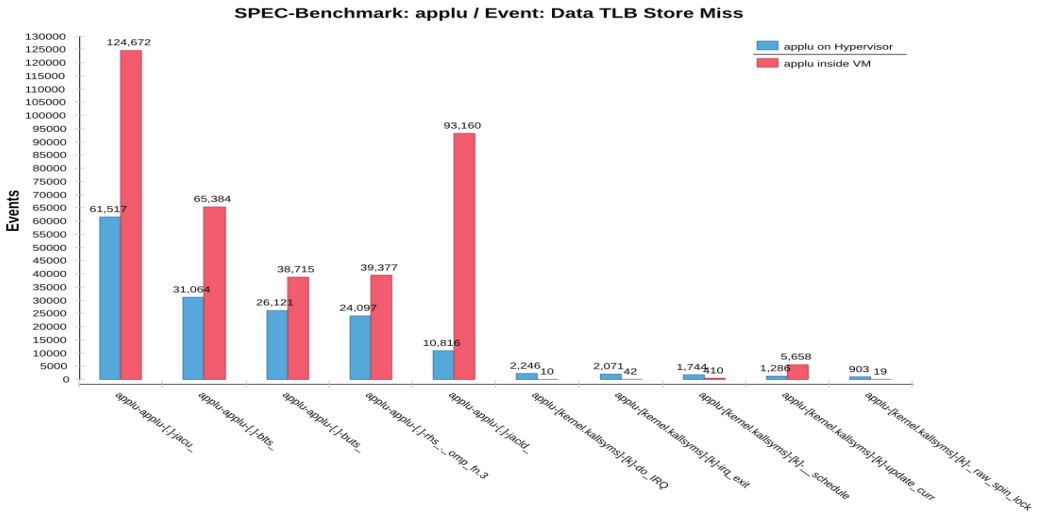

Figure 3: Data TLB Store Miss with the applu application.

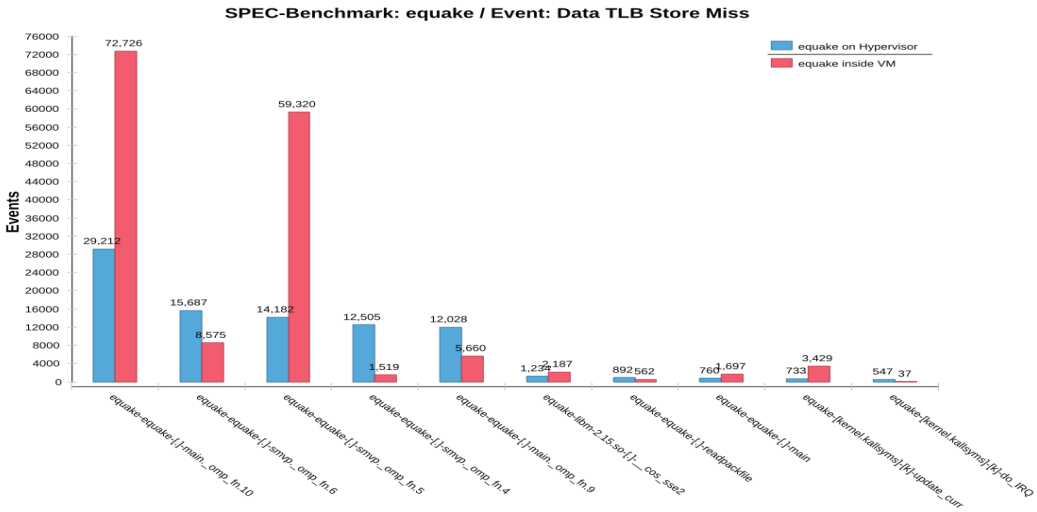

Figure 4: Data TLB Store Miss with the equake application.

SAMPLE RESULTS

We validated the developed toolchain with the NAS and the SPEC parallel benchmarks. We tested a set of applications from both suites. The physical machine used in the testing is an eight-core multiprocessor system equipped with two AMD processor 2356. The total size of RAM is 16GB. The virtual machine is configured with eight VCPUs and 2GB of memory. The applications were run either with a single thread or multiple threads. We measured different counter events, for example, cache miss, TLB miss, context switch and the application execution time.

Figure 3 to Figure 7 shows several sample experimental results. The two diagrams in Figure 3 and Figure 4 are the profiling results of event Data TLB Store Miss with the *applu* and the *equake* application in the SPEC benchmark suite. The profiling was perfromed as the application ran individually either directly on the hypervisor (i.e. host) or within a virtual machine. Each diagram shows the first 10 functions, either in the application code (marked with [.]) or the system libraries (marked with [kernel...]), which have a higher value of the monitored event. To each function there are two bars. The left bar corresponds to the execution on the host machine and the other one is for the virtual machine. It can be commonly seen that the virtual machine produces more TLB misses. For some routines, e.g. the *jacld* function of *applu* in the fifth bar-pair of the upper diagram, our toolchain reports a nine folds data TLB store miss on the virtual machine in contrast to the physical machine.

However, the behavior of this event changes when different applications run simultaneously on the target ma-

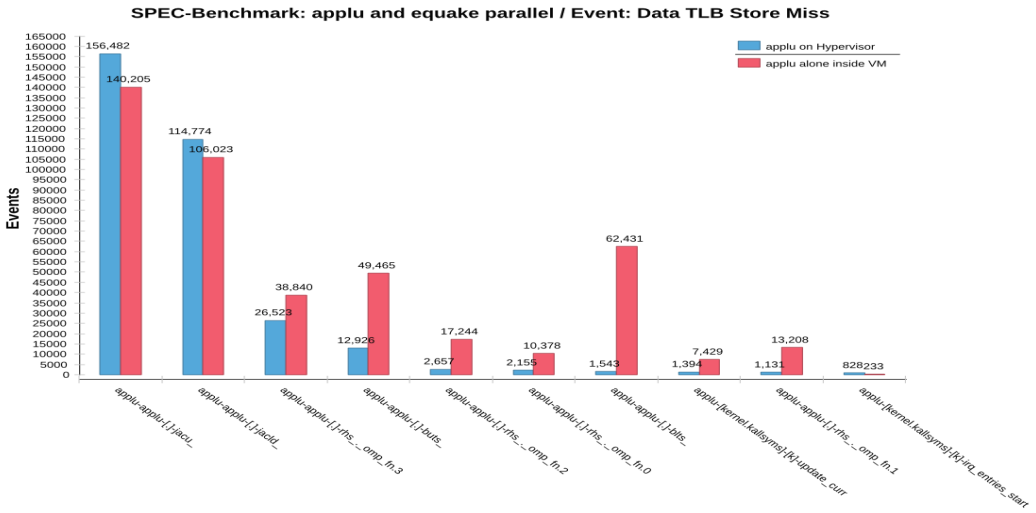

Figure 5: Data TLB Store Miss with parallel run of different applications: results of applu.

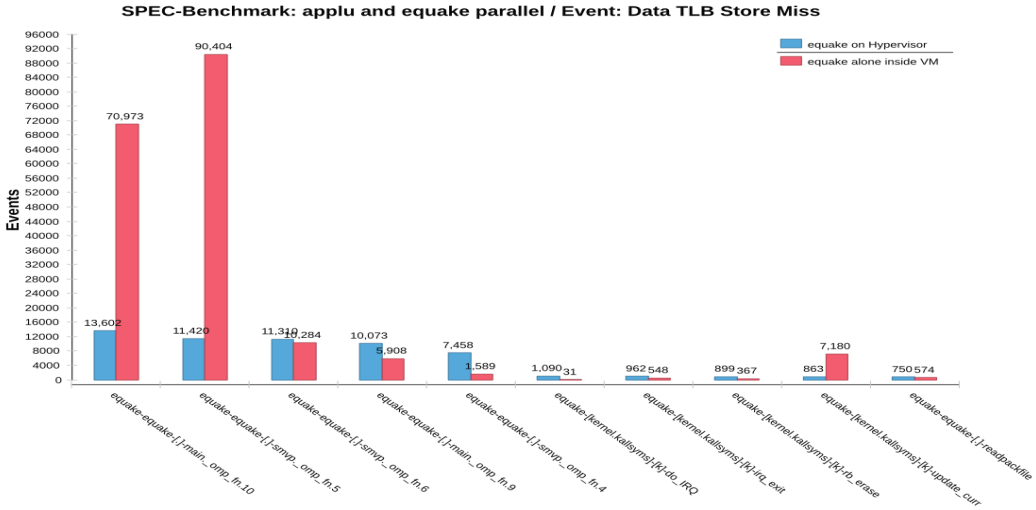

Figure 6: Data TLB Store Miss with parallel run of different applications: results of equake.

chine. Figure 5 and Figure 6 shows the result with the two SPEC applications. For the experiments we first ran both applications on the host in parallel and then ran them separately with each on a single virtual machine. We use again a bar-pair to present the event value with the left bar for running on the host and the right one for running on a single virtual machine. Observing the left two bar-pairs of *applu* in Figure 5, it can be seen that the virtual machine performs better with this event. Comparing the diagram with the one in Figure 3, the reason is clear. The reason is that the host machine produces double of the TLB misses with *applu* when it runs in parallel with *equake*, while the number of the TLB miss produced by the virtual machine remains similarly for the two scenarios. This means that *applu* profits from the parallel run in terms of data TLB miss. Nevertheless, the parallel run enlarged the number of TLB miss of several functions of the *equake* application on the virtual machines, for example, the second bar-pair of the right diagram. This also indicates that there is a large space for programmers to combine the applications for performance tuning.

Besides graphical views in the form of bar charts, our toolchain also provides views of other forms. Figure **??** demonstrates a circle presentation of the counter event "Context Switch". The data was collected by running the BT application from the NAS benchmark suite with two threads. The upper diagram is the result on the host and the lower one is on a virtual machine. Each function is presented with a colored area. The size of the area is related to the number of measured context switches with the corresponding function. A graphical view in such a form can hence highlight the hot functions that have a

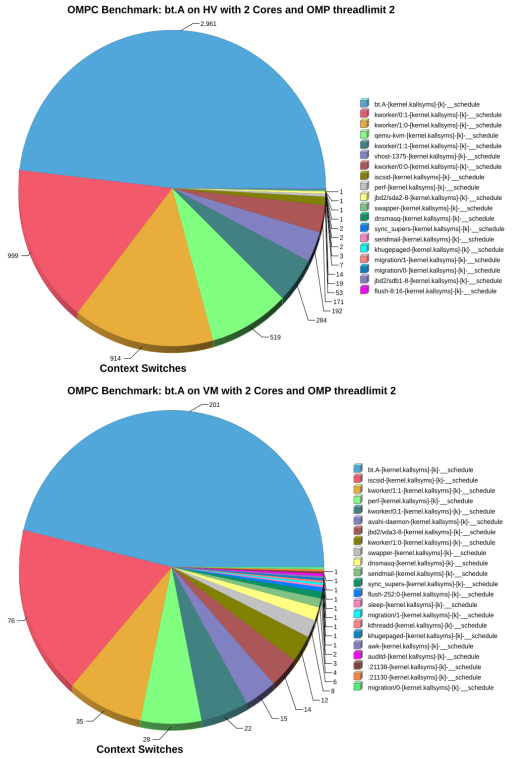

Figure 7: Behavior of event Context Switch with the BT application (upper: host machine, lower: virtual machine).

distinct behavior with a counter event.

CONCLUSIONS

This paper describes a toolchain that was developed to compare the runtime performance of applications on a virtual machine with the behavior on the physical machine. The toolset adopts a low-level Linux profiling tool to collect the raw performance data and then works with the data step by step towards a graphical presentation of the runtime behavior. The paper describes the functionality of the developed tools and shows some experimental results.

The goal of this work is to provide support for programmers to analyze their applications. Hence, for the initial phase we did not perform any optimization with the detected behavior. This can be a future work. Additionally, we plan to study realistic applications with the implemented toolchain.

REFERENCES

Barham, P., Dragovic, B., and Fraser, K. (2003). Xen and the Art of Virtualization. In *Proceedings of the nineteenth ACM Symposium on Operating Systems Principles*, pages 164–144.

Browne, S., Dongarra, J., Garner, N., Ho, G., and Mucci, P. (2000). Portable Programming Interface for Performance Evaluation on Modern Processors. *The International Journal of High Performance Computing Applications*, 14(3):189–204.

Brunst, H., Hackenberg, D., Juckeland, G., and Rohling, H. (2009). Comprehensive Performance Tracking with Vampir 7. In Mller, M., Resch, M., Schulz, A., and Nagel, W., editors, *Tools for High Performance Computing*, pages 17–29. Springer.

Ciorba, F. M., Groh, S., and Horstemeyer, M. F. (2010). Parallelizing discrete dislocation dynamics simulations on multicore systems. *Procedia CS, International Conference on Computational Science (ICCS 2010)*, 1(1):2135–2143.

de Melo, A. C. (2010). The New Linux 'perf' Tools. In *Proceedings of 17 International Linux System Technology Conference*.

Eclipse. BIRT Project - Business Intelligence and Reporting Tools. http://www.eclipse.org/birt/.

Tikotekar, A. T., et al. (2008). An Analysis of HPC Benchmarks in Virtual Machine Environments. In *Proceedings of Euro-Par 2008 Workshops - Parallel Processing*, volume LNCS 5415, pages 63–71.

Hammond, J. R., Krishnamoorthy, S., Shende, S., Romero, N. A., and Malony, A. D. (2012). Performance Characterization of Global Address Space Applications: A Case Study with NWChem. *Concurrency and Computation: Practice and Experience*, 24(2):135–154.

Intel. Intel VTune Amplifier XE 2013: Performance and Thread Profiler. http://software.intel.com/en-us/intel-vtune-amplifier-xe.

KVM. Kernel Based Virtual Machine. http://www.linux-kvm.org/.

Malony, A. D., Biersdorff, S., Shende, S., Jagode, H., Tomov, S., Juckeland, G., Dietrich, R., Poole, D., and Lamb, C. (2011). Parallel Performance Measurement of Heterogeneous Parallel Systems with GPUs. In *Proceedings of International Conference on Parallel Processing*, pages 176–185.

Menon, A., Santos, J. R., Turner, Y., Janakiraman, G., and Zwaenepoel, W. (2005). Diagnosing performance overheads in the xen virtual machine environment. In *The 1st ACM/USENIX international conference on Virtual execution environments*, pages 13–23.

OProfile. A System Profiler for Linux. http://oprofile.sourceforge.net/.

Shende, S. and Malony, A. D. (2006). The TAU Parallel Performance System. *International Journal of High Performance Computing Applications*, 20(2):287–311.

Sourceforge. perfmon2 - Improving Performance Monitoring on Linux. http://perfmon2.sourceforge.net/.

Youseff, L., Seymour, K., You, H., Dongarra, J., and Wolski, R. (2008). The impact of paravirtualized memory hierarchy on linear algebra computational kernels and software. In *Proceedings of the 17th international symposium on High performance distributed computing*, pages 141–152.

GENETIC-BASED SOLUTIONS FOR INDEPENDENT BATCH SCHEDULING IN DATA GRIDS

Joanna Kołodziej
Cracow University of Technology, Poland
Email: jokolodziej@pk.edu.pl

Magdalena Szmajduch
CDN Partner Cracow, Poland
E-mail: magdalena.szmajduch@cdnpartner.pl

Samee U. Khan
North Dakota State University
Fargo, USA
Email: samee.khan@ndsu.edu

Lizhe Wang
Center for Earth Observation and Digital Earth
Chinese Academy of Sciences
Beijing, China
Email: LZWang@ceode.ac.cn

Dan Chen
China University of Geosciences
Wuhan, China
E-mail:Danjj43@gmail.com

KEYWORDS

Data Grid, Scheduling, Data Center, Expected Time to Transmit, Data replication, Genetic Algorithm

ABSTRACT

Scheduling in traditional distributed systems has been mainly studied for system performance parameters without data transmission requirements. With the emergence of Data Grids (DGs) and Data Centers, data-aware scheduling has become a major research issue. In this work we present two implementations of classical genetic-based data-aware schedulers of independent tasks submitted to the grid environment. The results of a simple empirical analysis confirm the high effectiveness of the genetic algorithms in solving very complex data intensive combinatorial optimization problems.

INTRODUCTION

In today's modern heterogeneous computational systems with massive data processing, data-aware scheduling is one of the crucial problem, which has attracted considerable attention of researchers in data intensive computing. Much of the current efforts are focused on scheduling tasks workloads, data location reorganization [8] and energy-effective scheduling in large-scale data centers [4]. In many grid and cloud approaches, the scheduling problems are divided into two main classes: (i) those, which can be solved in computational systems, where usually it is assumed that data is delivered a priori and no data transfer times, data access rights, data availability (replication) and security issues are considered; and (ii) those, which can be solved just in Data Grids or data centers. However, efficient grid or cloud schedulers must take into account the features of both computing and data infrastructures to achieve desired performance of grid-enabled applications [7]. In such systems the data hosts are usually distributed in similar way as the computational nodes, which makes the general scheduling problem a real research challenge [3].

In this work, we address a general grid scheduling problem of data intensive applications submitted independently by the grid end users. Based on our previous work [6], we have integrated the data transmission and data nodes location criteria with the traditional scheduling objectives, namely makespan and flowtime. We provided a simple empirical analysis with genetic-based schedulers, that have been also tested in our previous works for similar class of problems, where data access and processing were ignored (see [5] for details). This analysis confirms a high effectiveness of genetic-based

Proceedings 27th European Conference on Modelling and Simulation ©ECMS Webjørn Rekdalsbakken, Robin T. Bye, Houxiang Zhang (Editors)
ISBN: 978-0-9564944-6-7 / ISBN: 978-0-9564944-7-4 (CD)

schedulers in solving complex data-intensive combinatorial optimization problems in the dynamic computational environments. All the experiments have been conducted by using *Data-Sim-G Batch* data-aware grid simulator developed by the authors.

The remainder of this paper is structured as follows. First we define a modified Expected Time to Compute matrix model for data-aware independent batch scheduling. A brief presentation of the genetic schedulers and main concept of *Data-Sim-G Batch* grid simulator is followed by a simple analysis of the experiments conducted for two variants of the genetic schedulers. The paper ends with simple conclusions and future research plan.

DATA-AWARE SCHEDULING IN THE GRID SYSTEM

Data-aware ETC Matrix model

We consider in this paper a general batch scheduling problem of tasks independently submitted to the system by the data-grid end users. This problem can be defined by the following four components (see also [6]):

- a batch of grid applications (tasks) $N_{batch} = \{t_1, \ldots, t_n\}$, where n - is the size of the batch (the number of tasks in the batch);
- a set of computational grid resources $M_{batch} = \{m_1, \ldots, m_k\}$, ($k$ - is the total number of machines available in the system for a given batch;
- a set of data-files $F_{batch} = \{f_1, \ldots, f_r\}$ needed for the completion of the tasks from N_{batch}; and
- a set of data-hosts $DH = \{dh_1, \ldots, dh_s\}$ with the necessary data service capabilities.

We assume that 'tasks' in our model can be complex data-intensive applications, and 'machines' can be single CPUs, parallel machines or even small local computing clusters. Those applications require multiple data files from data hosts, which can be also distributed in the grid system. It means that data files needed for completing the grid applications can be located (and/or replicated) at various grid nodes and their transfer to the computational nodes can be provided by the networks of varying capability.

For the characteristics of tasks in the batch, we introduce a *batch workload vector* $WLoad_{batch} = [wload_1, \ldots, wload_n]$, where $wload_j$ denotes an estimation of the computational load of a task t_j (in Millions of Instructions –MI). Each task t_j requires a set of files $F_j = \{f_{(1,j)}, \ldots, f_{(r,j)}\}$ ($F_j \subseteq F_{batch}$) that are distributed on a subset DH_j of the data nodes DH. We assume that each data host can serve multiple data files at a time and data replication is *a priori* defined as a separate replication process [6].

The computational nodes of the grid system can be characterized by a a *computing capacity vector* $CC_{batch} = [cc_1, \ldots, cc_m]$, where cc_i denotes the computing capacity of the node i. Each cc_i parameter ($i = 1, \ldots, m$) can be expressed by clock frequencies or by MIPS (Million Instructions Per Second) calculated for CPUs in the resources. The estimation of the prior load of each computational node from a given M_{batch} set is defined by a *ready times vector* $ready\_times_{(batch)} = [ready_1, \ldots, ready_m]$. The workload and computing capacity parameters for tasks and computing grid nodes can be generated by using the Gamma probability distributions for the expression of tasks and machines heterogeneities in the system (see [5] , chapter 2 , for details).

Data-aware task execution time model

We use the *Expected Time to Compute (ETC)* matrix model [1] for an estimation of times needed for the completion of the tasks assigned to the grid resources assuming also the data transmission times from the data nodes. A general concept of conventional ETC matrix model, used very often for solving the independent grid scheduling problems is based on the ETC array structure $ETC = [ETC[j][i]]_{n \times m}$, where $ETC[j][i]$ denotes an expected (estimated) time needed for the computing the task t_j at the resource m_i. The values of $ETC[i][j]$ parameters depend depend on the processing speed of the machines, to which they are assigned. However, in data-aware scheduling, the data transmissions times must be included into the model. Let us denote by $TT[i][j][f_{(p,j)}]$ a time needed for the transfer of the data file $f_{(p,j)}$ ($p \in \{1, \ldots, r\}$) from the data host $dh_{(p,j)} \in D_j$ to

the computational node m_i. This parameter can be calculated as follows [6]:

$$TT[i][j][f_{(p,j)}] = response_{time}(dh_{(p,j)}) + \\ + \frac{Size[f_{(p,j)}]}{B(dh_{(p,j)},i)} \quad (1)$$

where $response_{time}(dh_{(p,j)})$ denotes a time needed for receiving the first byte of the data file $f_{(p,j)}$ by the computational node m_i calculated from the moment of receiving data request by the data host $dh_{(p,j)}$, and $B(dh_{(p,j)}, i)$ denotes a bandwidth of the (logical) link between $dh_{(p,j)}$ and m_i.

The impact of the data transfer time on the task completion time depends on the mode, in which the data files are processed by the task. The are two main such scenarios which can be considered: (a) in the first scenario all data files needed for the execution of the task t_j are transferred *before* the computational process starts, and (b) the second scenario, where it is assumed that those data files which are not necessary for the initialization of the the execution of task t_j may be sent to the computational node later during the calculation process (the files are accessed as data streams during the calculations).

Let us denote by We denote by $completion[j][i]$ an estimated completion time for the task t_j on machine m_i, calculated from the task's submission till its completion in node m_i with the assumption of the access and transfer of all required data from the data hosts. In the first scenario this parameter can be calculated as follows:

$$completion[j][i] = \sum_{f_{(p,j)} \in F_j} TT[i][j][f_{(p,j)}] + ETC[j][i]. \quad (2)$$

where $\sum_{f_{(p,j)} \in F_j} TT[i][j][f_{(p,j)}]$ denotes the total time required for the 'sequential' transfer of all data files needed for the execution of task t_j.

In the second scenario (case(b)) the completion times for computational machines and tasks are calculated in the following way:

$$completion[j][i] = \max_{f_{(p,j)} \in \widehat{F_j}} TT[i][j][f_{(p,j)}] + \\ + \sum_{f_{(l,j)} \in [F_j \setminus \widehat{F_j}]} TT[i][j][f_{(l,j)}] ETC[j][i]. \quad (3)$$

where $\widehat{F_j}$ denotes a set of data files which are transferred prior the task execution. We will use the above $completion[i][j]$ parameters for the definition of the optimization criteria (schedulers' performance measures) in our simply empirical analysis presented in the next section.

For making the system easily adaptable to various scheduling scenarios, we consider the data hosts as the data storage centers separated from the computing resources. The scalability and effectiveness of the whole such system depends strongly on the replication mechanism and the resource data storage and computation capacities, which in some cases can be the main barrier in the schedulers' performance improvement. In our previous works [5,7] we assumed that each computing resource has its own data storage module. In such cases the internal data transfer times were low and we ignored them.

EMPIRICAL ANALYSIS

In this section we present the results of a simple empirical analysis of the performance of two implementations of GA-based energy-aware schedulers for static and dynamic versions of the data-aware independent batch scheduling problem in grid. We have developed a *Data-Sim-G Batch* simulator by a simple extension of our previously defined *Sim-G Batch* grid simulation toolkit (see [5]) by a data processing module The GA-based schedulers were evaluated on two benchmarks composed by a set of static and dynamic instances generated by the grid simulator.

Scheduling Objectives

Scheduling phases in the data-ware scheduling are similar to grid scheduling without data sets, and most of the conventional grid scheduling objectives, such as makespan and flowtime, can be easily adapted to the data-aware scheduling. For the scenario presented in in the following way:

- **Makespan:**

$$Makespan = \min_{Sched} \max_{m_i \in M_{batch}} completion[m_i] \quad (4)$$

where $completion[m_i]$ is computed as the sum of the completion times of tasks assigned to

machine m_i (see Eq. 3);

- **Flowtime:**
  - Flowtime for a machine i can be calculated as a workflow of the sequence of tasks on a given machine m_i, that is to say:

$$F[i] = ready_i + \sum_{j \in Sorted[i]} completion[j][i] \quad (5)$$

    where $Sorted[i]$ denotes a set tasks assigned to the machine m_i sorted in ascending order by the corresponding ETC values.
  - The cumulative flowtime in the whole system is defined as the sum of $F[i]$ parameters, that is:

$$F = \sum_{i \in M} F[i] \quad (6)$$

Both objectives are minimized. We consider hierarchical optimization process with makespan as the privileged (major) criterion. Flowtime is optimized with a constrain of not increasing the generated best makespan value. The wider list of the scheduling criteria in data grids can be found in [2].

Genetic-based data-aware schedulers

As a result of the wide assortment of constraints and different optimization criteria in the grid scheduling, meta-heuristic methods are the effective solutions for data intensive grid scheduling problems [10]. Genetic-based schedulers can easily explore the robustness of the search space and they can tackle various scheduling attributes.

For solving the data-aware independent batch scheduling problem, we have used in this paper two implementations of simple genetic grid schedulers, similar to the methodologies used in our previous works, where the big set of benchmarks and instances of the problem has been defined (see [5] for the summary of the results). These implementations, namely *GA* and *StGA* differ in the replacement mechanisms. The general frameworks of the schedulers are based on classical (μ+λ) evolutionary strategy (see e.g. [9]), adapted to the scheduling problem through the implementation of the following genetic operators:

- **Initialization method:** Randomly generated initial population;
- **Selection method:** Linear Ranking Selection;
- **Crossover operator:** Partially Mapped Crossover (PMX);
- **Mutation operator:** Rebalancing;
- **Replacement operators:** Elitist Generational (GA) and Struggle (StGA).

The detailed definition of these techniques can be found in [5].

Data-aware Batch grid Simulator - basic concept

The main concept of *Data Sim-G Batch* simulator is presented in Fig. 1.

Figure 1: General concept of *Data Sim-G Batch*

We have extended the *Sim-G Batch* grid toolkit defined in [5] by an implementation of additional data processing module responsible for generating (i) a set of data files, (ii) a set of data hosts, (iii) data transmission time matrix, (iv) response time vector, and (v) bandwith vector. All those data are considered

as basic characteristics of an instance of the problem and together with (vi) workload vector of tasks, (vii) computing capacity vector, (viii) prior load vector, and (ix) ETC matrix are passed on to the selected scheduler, which computes the schedule of the task assignments to the machines. Finally, the scheduler sends the schedules back to the simulator, which makes the allocation.

Key input parameters for simulator and schedulers

The performance of genetic-based schedulers analyzed in two types of grid environment: static and dynamic. In both cases four grid size scenarios: small (32 hosts/512 tasks), medium (64 hosts/1024 tasks), large (128 hosts/2048 tasks), and very large (256 hosts/4096 tasks). The schedulers' key parameters, including mutation and crossover probabilities, population size and stopping criteria (can be the maximal number of evolution steps or termination time criterion, are presented in Table 1.

Table 1: Shedulers' key parameters for static and dynamic benchmarks.

Parameter	GA	StGA
evolution steps	$20 * m$	
pop. size (pop_size)	$4 * (\log_2(m) - 1)$	
cross probab.	0.9	1.0
mutation probab.	0.2	
termin. time crit.	40 secs ($static$) / 75 secs ($dynamic$)	

The values of key parameters for the simulator for static and dynamic grid scenarios are presented in Table 2.

$N(*, **)$ denotes the Gaussian distribution. The detailed interpretation of all parameters is available in [5].

Each experiment was repeated 30 times under the same configuration of operators and parameters.

Results

The averaged makespan and flowtime values are presented in Tables 3 and 4.

It can be observed from the comparison of the result that the struggle replacement mechanism has rather crucial impact on the performance of the genetic scheduler. In all instances but three, calculated for both criteria in static and dynamic scenarios, *StGA* outperforms classical *GA* scheduler. The minimization of the flowtime, where *StGA* was the best in all instances, is in fact noticeable if we have into account that flowtime was considered a secondary (less important) objective in the optimization process. Both schedulers are rather stable in the optimization, which is confirmed by the low values of the $C.I.$ parameters. Finally, compare to the results achieved by similar implementations of the schedulers but in the case, where data transfer times are ignored (see [5], Chapter 4 for details), the values of makespan and flowtime have increased average by 10–25 %, which confirms the high importance of this criterion in data intensive scheduling.

CONCLUSIONS AND FUTURE WORK

In this paper we have addressed a general problem of data-aware scheduling problem of tasks submitted independently by the grid end-users. We assumed that for the completion of each task there are required some data files distributed also in the grid system and stored at heterogeneous data hosts. We have formalized the transmission time, in a way that it can be easily integrated into classical optimization objectives of grid scheduling, namely makespan and flowtime expressed in the terms of completion times of task on computational grid nodes, where data can be transferred *a priori* or immediately during the task computation. For the empirical analysis, we have implemented two versions of simple genetic-based grid scheduler for solving the considered scheduling problem aiming to minimize both makespan and flowtime scheduling objectives in the hierarchical mode, with makespan as major (privileged) objective. The empirical analysis has been performed by using the developed *Data-Sim-G Batch* grid simulator.

Table 2: Parameter setting for the grid simulator static instances

	Small	**Medium**	**Large**	**Very Large**
Static Instances				
Number of hosts	32	64	128	256
Resource capacities (in MIPS)	$N(1000, 175)$			
Total number of tasks	512	1024	2048	4096
Workload of tasks	$N(250000000, 43750000)$			
Dynamic Instances				
Init. hosts	32	64	128	256
Max. hosts	37	70	135	264
Min. hosts	27	58	121	248
Add host	$N(625000, 93750)$	$N(562500, 84375)$	$N(500000, 75000)$	$N(437500, 65625)$
Delete host	$N(625000, 93750)$			
Total tasks	512	1024	2048	4096
Init. tasks	384	768	1536	3072
Workload	$N(250000000, 43750000)$			

Table 3: Average Makespan and Flowtime values (± %C.I.) for static instances (C.I.: confidence interval)

Scheduler	**Small**	**Medium**	**Large**	**Very Large**
Makespan values (in arbitrary time units)				
GA	**4171630.27**	4286741.95	4306153.30	4338090.10
	(±)0.5714%	(±)0.7950%	(±)0.9351%	(±)1.1843%
StGA	4072614.96	**4179528.76**	**4286350.17**	**4299442.95**
	(±)0.6421%	(±)0.7714%	(±)1.1750%	(±)1.5132%
Flowtime values (in arbitrary time units)				
GA	1213553487.5	2344982276.8	4427950665.1	8421751474.6
	(±)0.9532%	(±)0.7980%	(±)0.9792%	(±)0.9917%
StGA	**1205329495.4**	**2293768328.5**	**4401468978.4**	**8399042744.8**
	(±)0.9421%	(±)0.8765%	(±)1.3298%	(±)1.2276%

Table 4: Average Makespan and Flowtime values (± % C.I.) for dynamic instances (C.I.: confidence interval)

Scheduler	**Small**	**Medium**	**Large**	**Very Large**
Makespan values (in arbitrary time units)				
GA	**4148152.90**	**4188204.13**	4415066.05	4441820.13
	(±)0.7560%	(±)0.8501%	(±)1.0724%	(±)1.7805%
StGA	4262331.15	4199261.61	**4381408.54**	**4378104.73**
	(±)0.8109%	(±)1.4350%	(±)1.9363%	(±)1.8390%
Flowtime values (in arbitrary time units)				
GA	1286071183.744	2269852393.768	4536176645.169	8993540827.579
	(±)0.8102%	(±)0.9240%	(±)1.2912%	(±)1.7805%
StGA	**1244873655.6**	**2255039877.2**	**4498453672.8**	**8953201900.1**
	(±)0.8225%	(±)0.8905%	(±)1.3773%	(±)1.9150%

The results show that both GAs are effective methods for keeping the makespan and flowtime on rather low levels, although Struggle GA performed best.

In our future work, we would like to extend our empirical analysis for a wider class of the schedulers and scheduling criteria, and use similar concept for solving the cloud scheduling problems.

REFERENCES

[1] Ali, S., Siegel, H.J., Maheswaran, M., and Hensgen, D.: "Task execution time modeling for heterogeneous computing systems", *Proceedings of Heterogeneous Computing Workshop*, pp. 185–199, 2000

[2] Buyya, R., Murshed, M., Abramson, D., and Venugopal, S.: "Scheduling parameter sweep applications on global Grids: a deadline and budget constrained cost-time optimization algorithm", *Softw. Pract. Exper.*, Vol. 35(5), (2005), pp. 491–512.

[3] Chen D., Wang L., Wu X., Chen J., Khan S.U, Kolodziej J., Tian M., and Huang F.: "Hybrid Modelling and Simulation of Huge Crowd over a Hierarchical Grid Architecture", *Future Generation Computer Systems*, DOI: 10.1016/j.future.2012.03.006, 2013.

[4] Kliazovich, D., Bouvry, P., Audzevich, Y., and Khan, S.U.: "GreenCloud: A Packet-level Simulator of Energy-aware Cloud Computing Data Centers", in *Proc. of the 53rd Globecom*, Miami, FL, USA, December 2010.

[5] Kołodziej J.: *Evolutionary Hierarchical Multi-Criteria Metaheuristics for Scheduling in Large-Scale Grid Systems*, in *Studies in Computational Intelligence* Springer series, Vol. 419, Springer Vlg., Berlin-Heidelberg, 2012.

[6] Kołodziej, J. and Khan, S. U.:"Data Scheduling in Data Grids and Data Centers: A Short Taxonomy of Problems and Intelligent Resolution Techniques", *Transactions on CCI*, Vol X, LNCS 7776, pp. 104–121, 2013.

[7] Kołodziej, J. and Khan, S. U.: "Multilevel Hierarchical Genetic-based Scheduling of Independent Jobs in Dynamic Heterogeneous Grid Environment", *Information Science*, Vol. 214(2012), pp. 1–19, 2012.

[8] Kosar, T. and Balman, M.: "A new paradigm: Data-aware scheduling in grid computing", *Future Gener. Comput. Syst.*, Vol. 25(4), (2009), pp. 406–413.

[9] Michalewicz, Z.: *"Genetic Algorithms + Data Structures = Evolution Program"*, Springer, 1992.

[10] Venugopal, S., and Buyya, R.:"An SCP-based heuristic approach for scheduling distributed data-intensive applications on global grids", *J. Parallel Distrib. Comput.*, vol. 68, pp. 471–487, 2008.

[11] Wang L, and Khan, S.U.: "Review of Performance Metrics for Green Data Centers: A Taxonomy Stud", *Journal of Supercomputing*, pp. 1–18, 2011.

A PERFORMANCE MODELING LANGUAGE FOR BIG DATA ARCHITECTURES

Enrico Barbierato
Dipartimento di Informatica
Università degli Studi di Torino
corso Svizzera 185
10129 Torino, Italy
Email: enrico.barbierato@mfn.unipmn.it

Marco Gribaudo
Dipartimento Di Elettronica,
Informazione E Bioingegneria
Politecnico di Milano
via Ponzio 51
20133, Milano, Italy
Email: gribaudo@elet.polimi.it

Mauro Iacono
Dipartimento di Scienze Politiche
Seconda Università degli Studi di Napoli
viale Ellittico 31
81100, Caserta, Italy
Email: mauro.iacono@unina2.it

KEYWORDS

Big Data; performance modeling; modeling tools; metamodeling

ABSTRACT

Big Data applications represent an emerging field, which have proved to be crucial in business intelligence and in massive data management. Big Data promises to be the next big thing in the development of strategical computer applications, even if it requires considerable investment and an accurate resource planning, as the architectures needed to perform at the requisite speed need to scale easily on to a large number of computing nodes. Appropriate management of such architectures benefits from the availability of performance models, to allow developers and administrators to take informed decisions, saving time and experimental work. This paper presents a dedicated modeling language showing firstly how it is possible to ease the modeling process and secondly how the semantic gap between modeling logic and the domain can be reduced.

INTRODUCTION

Collecting huge quantities of data from the environment, from users' behavior or from massively produced contents have enabled a new perspective in information intensive applications. For instance, most of the core business of companies like Google or Facebook consists of processing data obtained from users to extract valuable information that can be sold to investors, advertisers or other third parties. The ability to create this value depends on the efficiency by which processes are performed, as computing and storage costs per data unit must be reduced (there is no guarantee that processing will produce valuable results, differently from what happens in typical data warehousing applications) and results should be available promptly (as advertisement or recommendations are only significant if provided when needed).

Performance modeling allows developers and administrators to take informed decisions, keeping efficiency high and saving time and experimental work. Designing and evaluating suitable models for these systems is not straightforward, since the number of involved computing nodes is high and can sensibly change during the lifetime of the system. Business can easily require adaptation and data dynamics are very variable. Performance modeling requires specialized expertise, given the complexity of the architectures and the interactions of Big Data oriented environments.

A dedicated language allows domain experts to ignore the methods used by evaluation tools (analytic techniques, simulations, or variants optimized for the peculiar application). It increases also the focus on the analysis process and its results, rather than on the representation of the system by intermediate description languages (e.g. Petri nets, which would require a complete change of perspective, or simulation environment specifications, which would require a deep knowledge of the specific environment and its libraries).

On the one hand, a dedicated language does not enable per se the solution of the models it defines. On the other hand, good language design and the choice of a convenient foundation can definitely solve both the instances of modelers and solver designers. The originality of this approach consists of i) the definition of stochastic models, able to represent the complexity of Big Data applications and architectures, ii) the ability to encompass the problems due to the scalability of a map-reduce pipeline over a high number of nodes and the considerable amount of data involved and iii) the possibility to minimize the semantic gap between the system and the model. Typically, suitable solution methods suffer the state space explosion effect. Firstly, this is caused by the number of configurations of variables of the model, if based on state space oriented analytical techniques. Secondly, the solution may require a long and complex specification of all required elements of the system, if based on generic architectural simulation approaches.

Although the present case study is solved by a simulation engine, this paper focuses on the presentation of the proposed model description language, rather than on the proposal of a solution technique. This does not constitute a limitation, because literature offers appropriate frameworks to support language development and solution process management. A proposal for a solution technique based on the same approach is currently being submitted for publication.

The paper is organized as follows: the first Section presents related works; the next Section is dedicated to the description of the modeling language, this is followed by a case study; the final section provides the conclusions and future work.

RELATED WORK

BIG DATA PERFORMANCE EVALUATION

Big Data is a common expression used to define the application field in which very large, generally unstructured, non relational databases must be analyzed, managed, organized and finally used to support a business. The importance of this theme, whose impetus has been given by the main industrial actors in the field of computing, is widely recognized by analysts and economists (e.g. see Manyika et al. (2011); Eco (2011)), as well as research and academia. Big Data poses important research challenges, with reference to functional and non functional specifications on data and processes.

Proceedings 27th European Conference on Modelling and Simulation ©ECMS Webjørn Rekdalsbakken, Robin T. Bye, Houxiang Zhang (Editors)
ISBN: 978-0-9564944-6-7 / ISBN: 978-0-9564944-7-4 (CD)

Big Data applications sustainability, profitability and exploitation include the following challenges: i) scalability of computing and data storage architecture and algorithms, ii) querying and processing technologies (including data organization and system management), iii) planning techniques and tools and finally iv) fault tolerance. With respect to these themes, a good introduction is given in (Wu et al. (2012); Madden (2012)), and a good presentation of the main themes is given in (Bertino et al. (2011); Fu et al. (2012); Bryant et al. (2008); IBM et al. (2011)). From the architectural point of view Apache Hadoop (Had (2008); White (2009)) appears to be the main reference, even if other approaches are available, such as domain-specific languages (DSL), which play an important role in modeling where a specific representation of a problem is requested. Dryad Isard et al. (2007b) is a general-purpose distributed execution engine working on coarse-grain data-parallel applications. It builds a dataflow graph application using a set of computational vertices and communication channels. The application executes the vertices of the graph on a set of computers, which can exchange data using shared-memory queues and TCP pipes. Oozie (**?**) is a server-based Workflow Engine used to run workflow jobs including control flow nodes and action nodes allowing the execution of Hadoop Map/Reduce jobs. Finally, NoSQL databases such as MongoDB (**?**) and Apache Cassandra (**?**) address the issue raised by relational databases regarding scalability, high availability and performance.

The literature presents some relevant contributions to solve part of the architectural problems. In (Tierney et al. (2012)) a solution for efficient data transfer is presented, based on the RDMA over Converged Ethernet protocol, including a presentation of some of the main issues about the theme. In (Zahavi et al. (2012)) the routing problem is presented together with a comprehensive related work section about adaptive routing and special reference to the needs of the map-reduce paradigm. The problem of protection in Big Data systems by means of cluster de-duplication is examined in (Fu et al. (2012)), to support compliance to QoS parameters. Finally, (Jung et al. (2012)) presents a method to exploit cloud computing infrastructures to optimize Big Data analytics applications. All of these papers provide a good insight on practical approaches to the problem and some reference measures or models, although they require a specific mathematical background beyond the common expertise of practitioners and professionals.

In (Dai et al. (2011)), the authors present a performance analysis approach, based on monitoring tools and on a dataflow-driven technique. It helps designers and administrators in fine-tuning Big Data cloud environments. This approach seems very sound and comprehensive. It implicitly presents some ideas for a description of the system by means of a graphical language although it is meant for a posteriori analysis of the behavior of existing applications, rather than supporting design. A sophisticated synthetic workload generator for map-reduce applications over cloud architectures is described in (Chen et al. (2010)), which is used to evaluate performance trade-offs. It can be a significant support tool for other modeling methods. In (Shi et al. (2010)) a system for benchmarking cloud-based data management systems is presented, giving useful hints on storage performance in the most popular Big Data environments.

FRAMEWORKS FOR THE DESIGN OF MODELING LANGUAGES

The main approach in literature for the definition of custom models and modeling formalisms is based on metamodeling (Bézivin (2005); Van Gigch (1991); Jeusfeld et al. (2009)), a consolidated conceptual tool that has been successfully exploited in several cases (e.g. Model Driven Engineering (Poole (2001)), software engineering (Group (2010)) and multiformalism modeling (Vittorini et al. (2004); Gholizadeh and Azgomi (2010); de Lara and Vangheluwe (2002); Iacono et al. (2012))).

One of the most widespread metamodeling approaches is given by the eCore (Steinberg et al. (2008)) framework, on which the Eclipse Modeling Framework is founded. eCore is a metamodeling stack used to enable the description of user-defined software entities, abstracting them from any detail that is related to the hardware/software platform on which they are meant to be implemented. An eCore model is an abstract definition of an application from an object-oriented approach. This includes the high level detail that describe its business logic, its architecture and the relations between the objects that form the software. Such a model is used to generate automatically the equivalent source code, in a programming language chosen by the user and for the specific execution environment. To obtain this result, the eCore stack bases its models (application descriptions) on a set of modeling primitives (the eCore metamodel) designed to describe a generic object oriented software development language. Finally, it uses different model transformations (one per target environment) to generate code.

A similar metamodeling-based logic is used in literature by two different frameworks, OsMoSys and SIMTHESys. Both support the implementation of multiformalism performance modeling techniques. The OsMoSys framework (Gribaudo et al. (2003); Vittorini et al. (2004); Moscato et al. (2007); Franceschinis et al. (2004); Vittorini et al. (2002); Franceschinis et al. (2002a,b, 2009)) aims to provide a tool built models and reusable model libraries. In OsMoSys, metamodeling offers the description infrastructure to describe different formal languages, with object oriented features for both models and formalisms (modeling languages), extensibility of the set of formalisms and model compositionality. OsMoSys uses a metaformalism (metametamodel) to describe any graph-based formalism, by specifying it in terms of elements (nodes) and arcs that are then specialized by each formalism. Formalisms are used to describe model classes, which describe families of models with a common structure. Elements, arcs and model classes can have properties, which form their data structure and are defined by the formalism developer and the model developer. Model classes are used to obtain reusable model class libraries, and are meant to be instantiated with actual parameters to obtain an evaluable model (model object). The OsMoSys metaformalism allows sophisticated features, including element and formalism inheritance, element hiding, definition of model interfaces, model composition and aggregation. Element, formalism and model class reuse and extension are then possible, following the object oriented general logic. The OsMoSys framework supports the definition of (multiformalism) models evaluation by means of existing external solvers, which are executed according to a business process that is related to the structure of the model and the relations between its parts.

The SIMTHESys framework (Barbierato et al. (2011a,b,c); Iacono and Gribaudo (2010); Iacono et al. (2012); Barbierato et al. (2012a,b)) aims to provide a tool for the rapid development of new formalisms and the automatic generation of related (multiformalism) solvers. Similarly to OsMoSys, it defines a metaformalism used to define formalisms, but it presents many differences. First, the SIMTHESys metaformalism defines formalism elements (indifferently nodes and arcs of a graph) that

have not only properties, but also behaviors describing how elements interact with each other. This allows the specification of the evaluation semantics of formalisms, besides their syntactic structure. Due to this fact, the SIMTHESys metaformalism enables each formalism to implicitly specify how models that use it should be evaluated. This is exploited to generate automatically dedicated solvers for model families using a certain set of formalisms, simply applying the behavioral definitions to a selected set of solving engines (elementary non-specialized solvers implementing common base evaluation techniques). Second, in this case formalisms are directly used to define models. Third, the research effort in SIMTHESys is oriented towards automatic solver generation and formalism integration, rather than in providing sophisticated (e.g. OsMoSys object orientation of formalisms and models) modeling characteristics.

THE MODELING LANGUAGE

Without losing generality in the approach, the reference architecture on which the modeling language has been designed represents the ecosystem based on Apache Hadoop. The modeling language is founded on the SIMTHESys framework, which has been chosen because it offers a flexible choice of the final model solution technique, and because it is more suited to the goals of this research, as it is oriented to the specification of domain-oriented high level formalisms and allows decoupling between modeling abstractions and solution engines.

Hadoop is an implementation of the map-reduce paradigm, previously introduced by Google to manage its applications. The map-reduce paradigm is designed to cope with massively distributed execution of computing tasks with high efficiency, in order to meet the needs of Big Data applications. According to this paradigm, data is organized in a NOSQL structure over data nodes, namely *shards*. Each shard contains table-like structures, each row of which can have a fixed or a variable number of fields, differently from what happens in a relational data base organization. Shards store only a certain number of rows, dimensioned to balance the workload over the system, and each row can be addressed by a key-value based index. To perform a computation, a pipeline consisting of a sequence of stages is set up. Each stage consists of a *map phase* and a *reduce phase*. The former triggers the run of a user-defined code that is sent automatically to all involved shards. The latter efficiently collects and synthesizes the outputs to get to the final result or accounts for the completion of the operations that had to be performed on each shard.

To represent the main elements of the paradigm, the modeling language has been designed to offer the elements shown in Fig. 1.

The available elements are divided into two groups called respectively the *Structural elements* and the *Operational elements*. The former are the elements that form the structure of the architecture, specifically i) *Dataset* representing a logical/physical group of data; ii) *Shards* representing a group of shards, which is put in relation with a Dataset, and on which Dataset data are mapped. The operational elements model the sequence of operations in a map-reduce pipeline and consist of i) *Trigger* representing a data source that generates data towards a Dataset with Poisson arrivals; ii) *Map* representing a map phase in a map-reduce pipeline stage; iii) *Reduce* representing a reduce phase in a map-reduce pipeline stage.

The available arcs are: i) *Share* representing the binding between a logical/physical group of data and the shard on which it is allocated (and related computing is performed); ii) *AddData* representing the binding between a Trigger and the Dataset storing the received data; iii) *ActionArc* representing the binding between two temporally consequent operational elements in a map-reduce pipeline and finally iv) *DataArc*, mapping a Map onto the Dataset on which it is applied.

Element and arc types in a model are identified by the corresponding icons shown in Fig. 1.

Within the SIMTHESys framework, each element and arc is fully specified by its properties and behaviors specifying its structure and its dynamics. In order to keep the description on a modeler the focus will be put on modeling-related properties which must be specified to evaluate an applicative scenario.

A *Dataset* element is characterized by the *TotData* property representing the current amount of contained data, since it influences the performance of the Shards element on which related computing will be performed. A *Shards* element is used to describe the shards over which data are distributed. In particular, each shard is characterized by the *Speed* property, a synthetic nominal performance indicator of a single constituting computing node. Since big-data applications are usually deployed over cloud infrastructures, two types of shards can be defined: *Fixed shards* (denoted by a continuous line) and *Auto-scaling shards* (drawn with dashed lines). The fixed shards are used to model software components distributed over a fixed number of (symmetric) computation nodes. They are characterized by the *NShards* property representing the resources over which data rows are divided. Auto-scaling shards represents computing nodes that exploit the auto-scaling features of cloud computing. In particular, they allow a dynamic deployment of virtual machines, in such a way that each shard has to deal with no more than a fixed amount of data. The property *dataXshards* specifies the maximum number of data rows that a shard can hold. A *Trigger* element is characterized by the *Rate* property, representing the arrival rate of requests. To simplify the computation of performance indices, we consider Poisson arrival processes. A Map element is characterized by the *MapEffort* property that describes the complexity of the map operation. In particular, we imagine that this parameter is composed of two parts: a constant term (*fix*), which is required by every operation, and another term that is proportional to the number of data that must be considered (*Xdata*) . In a similar way, a *Reduce* element is characterized by the *RedTime* property that describes the time required to perform a reduction. This time can be composed by a fixed part (*fix*), a component proportional to the number of shards over which the data were mapped (*Xshard*) and a part that is proportional to the quantity of data that must be considered (*Xdata*). A *Share* arc, connects a *Dataset* to a *Shards* element. It is characterized by the *Weight* property, used to define which fraction of the total amount of data should be put over the considered shards. The optional *Limit* property, represent the maximum number of rows that can be put on each machine of the destination shards. The *AddData* arcs connect *Trigger* to *Dataset* elements. They represent an increase or decrease of data in the destination data set, and they are characterized by the *Qty* property, accounting for the (possibly negative) number of rows that are added (or removed); all other language elements have no significant modeling-related property.

The presented elements and arcs have been described in a SIMTHESys FDL (Formalism Description Language) document, to enable the design of SIMTHESys MDL (Model De-

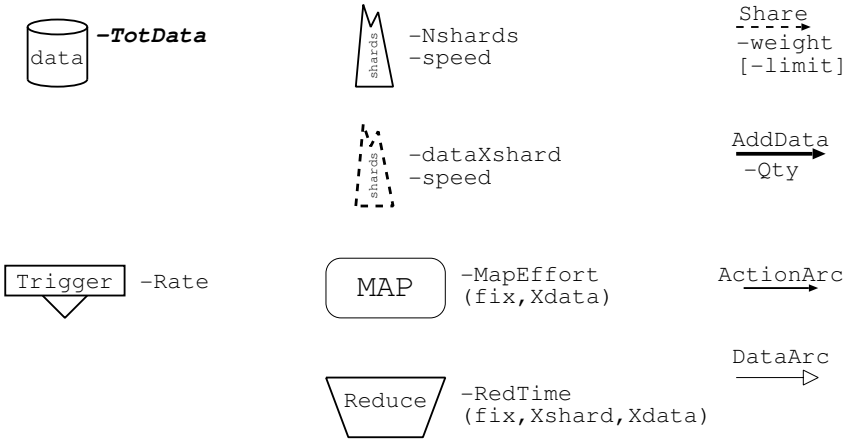

Fig. 1. Elements of the Big Data formalism

scription Language) documents describing models[1].

Before the full integration of the language into the SIMTHESys framework currently in progress, the language has been used to develop an experimental simulator implementing its primitives, supporting and guiding the study of the best solution engine suitable for the field. Although the simulator is fully functional for the goals of this paper, the implemented solution is considered, in the SIMTHESys perspective, a proof of concept because the solver currently does not support the integration of multiple formalisms and the generation of the solver is not completely automated.

A CASE STUDY

The case evaluated in this paper describes a real system, of which performance analysis is needed to evaluate the opportunity of a migration or architectural reconfiguration. The system is used to run an on-line content publishing system, capable of social network functionalities. The application operates by allowing a certain number of journalists to publish articles about different topics. Registered users can publish comments, or other articles as well. Articles are proposed to registered users, according to their user habits and interests, which are profiled by the application. Proposals are generated with a recommendation system. The relevant data set to be stored on the shards consists of: published articles, users' data and users' profiling data.

The recommendation functionality is implemented by a map-reduce pipeline: a first map-reduce stage classifies each new article by a comparison with all existing articles in the system, and returns a synthetic classification, that is compared by a second map-reduce stage to analogous synthetic classifications of the interests of each user, to assign recommendations.

Performance evaluation has been applied to the recommendation functionality. The model is depicted in Fig.2.

The left part of the figure represents the map-reduce pipeline implementing the recommendation system, while the right part represents the architecture and the mapping of datasets and shards. The NewArt *Trigger* element represents the arrival of new articles, that are produced at a rate of $r\ art./min.$, where r is a parameter of the study. An *ActionArc* arc connects it to the MAPcsfy *Map* element, determining when the classification map phase will be performed. Two *AddData* arc connects it to the Art *DataSet* element in opposite direction, and both with the quantity attribute equal to one ($Qty = 1$). This is used to account for the fact that the system tries to maintain constant the number of articles, by replacing an old one (arc going out from the *DataSet* element), with the new arrival (arc going into the *DataSet* element). The number of articles N stored in the dataset is a parameter of the study. The MAPcsfy *Map* element represents the influence in the process of the map phase of the pipeline. It is connected with a *DataArc* arc to the Art *DataSet* element, on which it operates, through which performance of the shards are considered in the phase. The time required to perform this mapping is proportional to the size of the dataset, and does not have a fixed part: each element of the dataset increases the time required to perform the mapping of $0.01\ min.$ The end of the mapping phase triggers the operations of the *Reduce* element, which in turn accounts for the contribution of the reduce phase. The time to perform the reduction requires $2\ min.$ per shard, and $0.001\ min.$ per row in the article dataset, The *Reduce* element is connected by an *ActionArc* to the *Map* element MAPrcmd that performs recommendations (the related *Reduce* phase is negligible in the application and is thus omitted), in turn connected by a *DataArc* arc to the Users *Dataset* element, on which it operates. This operation requires $0.0025\ min.$ per user in the Users dataset. Both the Art and Users *Dataset* elements are connected by *Share* arcs to the Shards *Shard* element. The size of the two datasets is a parameter N of the model. In particular, we imagine that the number of users in the system is ten time greater than the number of articles: this can be clearly seen in Fig.2 by the value assigned to the property *TotData* of the two *DataSet* elements. The number of shards N_s is also a parameter of the model. In this case we imagine all the shards working at the same speed, assigned identically to 1 operation per minute: in this way the effort used to describe the map phases of the model is equal to the time required to perform that operation. Finally, all the data are equally split among the shards: this is represented by the property *weight=1* assigned to the two *Share* arcs.

We begin our study by fixing the number of article $N = 10000$, and varying the number of shards N_s, for different new article arrival rates r. The results are presented in Fig. 3. As it can be seen, the response time has a curved shape with a minimum. For a low number of shards, we have a large response time due to the high work that the few shards have to perform

[1]The FDL document for the language and the MDL document for the case study are omitted for the sake of space, but current versions of both can be freely obtained by sending the authors a request by email

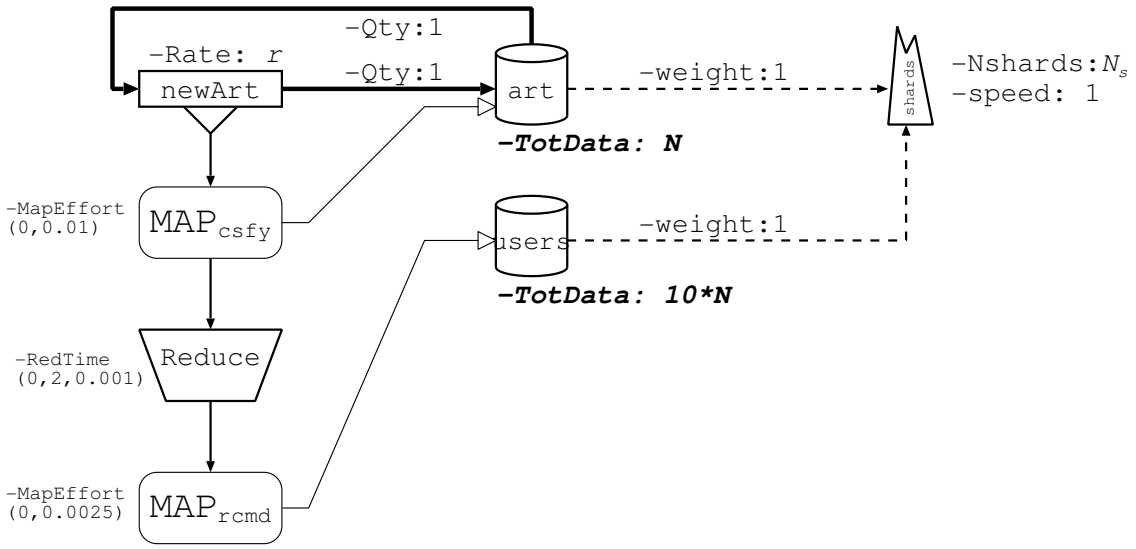

Fig. 2. Model of the case study

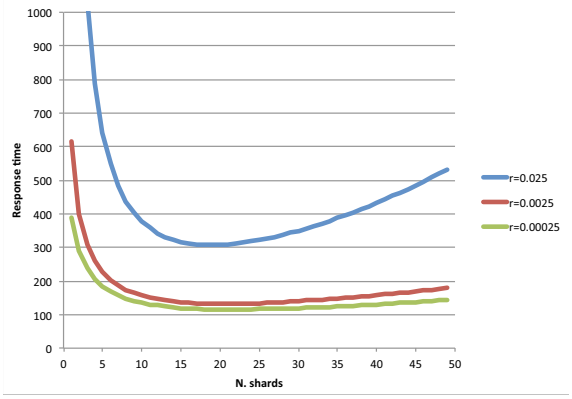

Fig. 3. Response time for a varying number of shards for different article arrival rates r.

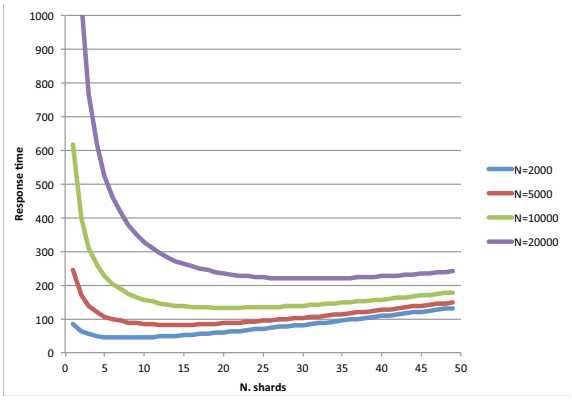

Fig. 4. Response time for a varying number of shards for different number of articles N.

to complete the map operations. When however the number of shards is high, the big latency for waiting all the nodes to finish their task, and the increased complexity of the reduce operations, makes the response time grow again. Thus determining the best number of shards of an application can be a good motivation for using performance evaluation formalisms like the one proposed in this paper. In this case, we can see that the number of shards that gives the minimum response time ($N_s = 22$) is independent on the article arrival rate.

We then study the effect of changing the number of articles N (and thus proportionally the number of users), with a fixed arrival rate of $r = 0.0025\ art/sec$. Resulting response times are plotted in Fig. 4. As it can be seen, also in this case the response time has a minimum for a given number of shards. However, in this case the position of the minimum varies with the size of the dataset. In particular, larger datasets require an higher optimal number of shards. Since simulation was used to compute the presented results, 95% confidence intervals were used. However, only the mean response times were plotted in Fig. 3 and Fig. 4 to simplify the presentation. The obtained intervals were very tight, as can be seen in Table I for some number of shards N_s, considering an arrival rate of new articles $r = 0.0025\ art./min$, and a dataset size of $N = 10000$.

N_s	R^-	R	R^+
5	642.040864	642.822	643.603136
10	377.098435	377.441	377.783565
15	315.831929	316.154	316.476071
20	307.109146	307.475	307.840854

TABLE I: Confidence interval for the response time with different number of shards, for an arrival rate of new articles $r = 0.0025\ art./min$, and a dataset size of $N = 10000$.

CONCLUSIONS AND FUTURE WORK

This paper has presented a novel language for the description of performance models including applications based on the map-reduce paradigm. The main contribution of this work was to allow Big Data application designers and Big Data system administrators to evaluate their choices and experiment with what-if analysis. From the authors' evaluation, the proposed language is suited to the task, as it represents a complex environment such as Big Data applications with a comfortable metaphor. At the same time, it is suitable for the automated generation of solvers without deep expertise, thanks to the fact that it was founded on the SIMTHESys framework.

Work is in progress to allow the language to be used to au-

tomatically generate both analytical and simulation solvers that also enable the designer to incorporate submodels specified in other modeling languages (such as Petri nets variants or Fault Trees). It will also be necessary to extend the simulator to a full version that can be fully integrated in SIMTHESys as a solving engine and can automatically handle a variable number of trigger-generated items and shards, without user intervention on the model.

REFERENCES

(2007). Microsoft Dryad.

(2008). Apache Hadoop.

(2011). Drowning in numbers – digital data will flood the planet—and help us understand it better. *The Economist*.

Barbierato, E., Bobbio, A., Gribaudo, M., and Iacono, M. (2012a). Multiformalism to support software rejuvenation modeling. In *ISSRE Workshops*, pages 271–276. IEEE.

Barbierato, E., Gribaudo, M., and Iacono, M. (2011a). Defining Formalisms for Performance Evaluation With SIMTHESys. *Electr. Notes Theor. Comput. Sci.*, 275:37–51.

Barbierato, E., Gribaudo, M., and Iacono, M. (2011b). Exploiting multiformalism models for testing and performance evaluation in SIMTHESys. In *Proceedings of 5th International ICST Conference on Performance Evaluation Methodologies and Tools - VALUETOOLS 2011*.

Barbierato, E., Gribaudo, M., Iacono, M., and Marrone, S. (2011c). Performability modeling of exceptions-aware systems in multiformalism tools. In Al-Begain, K., Balsamo, S., Fiems, D., and Marin, A., editors, *ASMTA*, volume 6751 of *Lecture Notes in Computer Science*, pages 257–272. Springer.

Barbierato, E., Iacono, M., and Marrone, S. (2012b). PerfBPEL: A graph-based approach for the performance analysis of BPEL SOA applications. In *VALUETOOLS*, pages 64–73. IEEE.

Bertino, E., Bernstein, P., Agrawal, D., Davidson, S., Dayal, U., Franklin, M., Gehrke, J., Haas, L., Halevy, A., Han, J., and Others (2011). Challenges and Opportunities with Big Data.

Bézivin, J. (2005). On the unification power of models. *Software and System Modeling*, 4(2):171–188.

Bryant, R. E., Katz, R. H., and Lazowska, E. D. (2008). Big-data computing: Creating revolutionary breakthroughs in commerce, science, and society. In Computing Research Initiatives for the 21st Century. *Computing Research Association*.

Chen, Y., Ganapathi, A. S., Griffith, R., and Katz, R. H. (2010). Towards Understanding Cloud Performance Tradeoffs Using Statistical Workload Analysis and Replay. Technical Report UCB/EECS-2010-81, EECS Department, University of California, Berkeley.

Dai, J., Huang, J., Huang, S., Huang, B., and Liu, Y. (2011). HiTune: dataflow-based performance analysis for Big Data cloud. In *Proceedings of the 3rd USENIX conference on Hot topics in cloud computing*, HotCloud'11, pages 24–24, Berkeley, CA, USA. USENIX Association.

de Lara, J. and Vangheluwe, H. (2002). Atom3: A tool for multi-formalism and meta-modelling. In Kutsche, R.-D. and Weber, H., editors, *FASE*, volume 2306 of *Lecture Notes in Computer Science*, pages 174–188. Springer.

Franceschinis, F., Gribaudo, M., Iacono, M., Mazzocca, N., and Vittorini, V. (2002a). Towards an Object Based Multi-Formalism Multi-Solution Modeling Approach. In *Proc. of the Second International Workshop on Modelling of Objects, Components, and Agents (MOCA'02), Aarhus, Denmark, August 26-27, 2002 / Daniel Moldt (Ed.)*, pages 47–66. Technical Report DAIMI PB-561.

Franceschinis, G., Gribaudo, M., Iacono, M., Marrone, S., Mazzocca, N., and Vittorini, V. (2004). Compositional modeling of complex systems: Contact center scenarios in OsMoSys. In *ICATPN'04*, pages 177–196.

Franceschinis, G., Gribaudo, M., Iacono, M., Marrone, S., Moscato, F., and Vittorini, V. (2009). Interfaces and binding in component based development of formal models. In *Proceedings of the Fourth International ICST Conference on Performance Evaluation Methodologies and Tools*, VALUETOOLS '09, pages 44:1–44:10, ICST, Brussels, Belgium, Belgium. ICST (Institute for Computer Sciences, Social-Informatics and Telecommunications Engineering).

Franceschinis, G., Gribaudo, M., Iacono, M., Vittorini, V., and Bertoncello, C. (2002b). DrawNet++: a flexible framework for building dependability models. In *In Proc. of the Int. Conf. on Dependable Systems and Networks*, Washington DC, USA.

Fu, Y., Jiang, H., and Xiao, N. (2012). A scalable inline cluster deduplication framework for Big Data protection. In *Proceedings of the 13th International Middleware Conference*, Middleware '12, pages 354–373, New York, NY, USA. Springer-Verlag New York, Inc.

Gholizadeh, H. M. and Azgomi, M. A. (2010). A meta-model based approach for definition of a multi-formalism modeling framework. *International Journal of Computer Theory and Engineering*, 2(1):87–95.

Gribaudo, G., Iacono, M., Mazzocca, M., and Vittorini, V. (2003). The OsMoSys/DrawNET Xe! Languages System: A Novel Infrastructure for Multi-Formalism Object-Oriented Modelling. In *ESS 2003: 15th European Simulation Symposium And Exhibition*.

Group, O. M. (2010). Unified modeling language standards version 2.3.

Iacono, M., Barbierato, E., and Gribaudo, M. (2012). The SIMTHESys multiformalism modeling framework. *Computers and Mathematics with Applications*.

Iacono, M. and Gribaudo, M. (2010). Element based semantics in multi formalism performance models. In *MASCOTS*, pages 413–416. IEEE.

IBM, Zikopoulos, P., and Eaton, C. (2011). *Understanding Big Data: Analytics for Enterprise Class Hadoop and Streaming Data*. McGraw-Hill Osborne Media, 1st edition.

Isard, M., Budiu, M., Yu, Y., Birrell, A., and Fetterly, D. (2007a). Dryad: distributed data-parallel programs from sequential building blocks. *SIGOPS Oper. Syst. Rev.*, 41(3):59–72.

Isard, M., Budiu, M., Yu, Y., Birrell, A., and Fetterly, D. (2007b). Dryad: distributed data-parallel programs from sequential building blocks. In *Proceedings of the 2nd ACM SIGOPS/EuroSys European Conference on Computer Systems 2007*, EuroSys '07, pages 59–72, New York, NY, USA. ACM.

Jeusfeld, M. A., Jarke, M., and Mylopoulos, J., editors (2009). *Metamodeling for Method Engineering*. MIT Press, Cambridge, MA, USA.

Jung, G., Gnanasambandam, N., and Mukherjee, T. (2012). Synchronous parallel processing of big-data analytics services to optimize performance in federated clouds. In *Proceedings of the 2012 IEEE Fifth International Conference on Cloud Computing*, CLOUD '12, pages 811–818, Washington, DC, USA. IEEE Computer Society.

Madden, S. (2012). From databases to Big Data. *IEEE Internet Computing*, 16(3):4–6.

Manyika, J., Chui, M., Brown, B., Bughin, J., Dobbs, R., Roxburgh, C., and Byers, A. H. (2011). Big Data: The next frontier for innovation, competition, and productivity. *Report McKinsey Global Institute*.

Moscato, F., Flammini, F., Lorenzo, G. D., Vittorini, V., Marrone, S., and Iacono, M. (2007). The software architecture of the OsMoSys multisolution framework. In *ValueTools '07: Proceedings of the 2nd international conference on Performance evaluation methodologies and tools*, pages 1–10.

Poole, J. D. (2001). *Model-Driven Architecture: Vision, Standards, And Emerging Technologies. Position Paper Submitted to ECOOP 2001*.

Shi, Y., Meng, X., Zhao, J., Hu, X., Liu, B., and Wang, H. (2010). Benchmarking cloud-based data management systems. In *Proceedings of the second international workshop on Cloud data management*, CloudDB '10, pages 47–54, New York, NY, USA. ACM.

Steinberg, D., Budinsky, F., Paternostro, M., and Merks, E. (2008). *EMF: Eclipse Modeling Framework, 2nd Edition*. Addison-Wesley Professional.

Tierney, B., Kissel, E., Swany, D. M., and Pouyoul, E. (2012). Efficient data transfer protocols for Big Data. In *eScience*, pages 1–9. IEEE Computer Society.

Van Gigch, J. P. (1991). *System design modeling and metamodeling / John P. van Gigch*. Plenum Press, New York :.

Vittorini, V., Franceschinis, G., Gribaudo, M., Iacono, M., and Mazzocca, N. (2002). DrawNet++: Model Objects to Support Performance Analysis and Simulation of Complex Systems. In *Proc. of the 12th Int. Conference on Modelling Tools and Techniques for Computer and Communication System Performance Evaluation (TOOLS 2002)*, London, UK.

Vittorini, V., Iacono, M., Mazzocca, N., and Franceschinis, G. (2004). The OsMoSys approach to multi-formalism modeling of systems. *Software and System Modeling*, 3(1):68–81.

White, T. (2009). *Hadoop: The Definitive Guide*. O'Reilly Media, Inc., 1st edition.

Wu, Y., Li, G., Wang, L., Ma, Y., Koodziej, J., and Khan, S. U. (2012). A review of data intensive computing. In *The 12th IEEE International Conference on Scalable Computing and Communications (ScalCom 2012)*. IEEE.

Zahavi, E., Keslassy, I., and Kolodny, A. (2012). Distributed adaptive routing for big-data applications running on data center networks. In *Proceedings of the eighth ACM/IEEE symposium on Architectures for networking and communications systems*, ANCS '12, pages 99–110, New York, NY, USA. ACM.

AUTHOR BIOGRAPHIES

ENRICO BARBIERATO is a Consultant working for the IT industry. He earned a BSc (Hon) at University of Turin (Italy), an MSc in Advanced Studies in Artificial Intelligence at the Katholieke Universiteit of Leuven (Belgium) and a PhD in Computer Science at the University of Turin (Italy). His research activity concerns performance evaluation of multiformalism models. His email is

enrico.barbierato@mfn.unipmn.it.

MARCO GRIBAUDO is a senior researcher at the Politecnico di Milano - Italy. He works in the performance evaluation group. His current research interests are multi-formalism modeling, queueing networks, mean-field analysis and spatial models. The main applications to which the previous methodologies are applied comes from cloud computing, multi-core architectures and wireless sensor networks.

MAURO IACONO is a tenured Assistant Professor and Senior Researcher in Computing Systems at Dipartimento di Scienze Politiche, Seconda Università degli Studi di Napoli, Caserta, Italy. He received a Laurea in Ingegneria Informatica (MSc) degree cum laude (Hon) in 1999 by Università degli Studi di Napoli "Federico II", Napoli, Italy, and a Dottorato in Ingegneria Elettronica (PhD) degree by Seconda Università degli Studi di Napoli, Aversa, Italy. He published over 35 peer reviewed scientific papers on international journals and conferences and has served as scientific editor, conference scientific committee chairman and member and reviewer for several journals, and is a member of IEEE and other scientific societies. His research activity is mainly centered on the field of performance modeling of complex computer-based systems, with a special attention for multi-formalism modeling techniques. More information is available at http://www.mauroiacono.com.

TOWARDS THE DEPLOYMENT OF FASTFLOW ON DISTRIBUTED VIRTUAL ARCHITECTURES

Sonia Campa
Marco Danelutto
Massimo Torquati

Department of Computer Science
University of Pisa

Horacio González–Vélez
Alina Mădălina Popescu

Cloud Competency Centre
National College of Ireland

KEYWORDS

Parallel Patterns; Algorithmic Skeletons; Language Constructs and Features; Parallel Programming; Distributed Architectures; Performance Analysis; Virtualisation; Cloud Computing

ABSTRACT

In this paper we investigate the deployment of FastFlow applications on multi-core virtual platforms. The overhead introduced by the virtual environment has been measured using a well-known application benchmark both in the sequential and in the FastFlow parallel setting. The overhead introduced for both the sequential and the parallel executions of CPU and memory-intensive applications is in the range of $2-30\%$, while the execution speedup is almost preserved. Additionally, we have ported the FastFlow benchmark to a cloud-based distributed environment in which a task-intensive application has been tested and the performance compared with the corresponding run on a smaller cluster of multi-core machines without virtualisation.

From a parallel programming perspective, we have demonstrated how a unique programming framework based on the structured parallel programming paradigm can cope with very different kind of target architectures without any (or minimal) code intervention.

INTRODUCTION

A declarative description of a parallel activity, a *pattern* focuses on the parallel behaviour of the application rather than on its implementation, expressed in terms of communication channels and hardware/software features of the target architecture.

Patterns can either be:

- 'RISC' type: describe basic and well-assessed patterns of parallelism such as *pipeline, farm, map* and *reduce*; or,
- domain-specific: more significant to the techniques used in a specific domain and express complex parallel computations such as *divide-and-conquer* and *dynamic programming*.

A pattern is implemented via a parallel activity graph (*algorithmic skeleton* or, simply, 'skeleton') which defines a pattern in terms of computational nodes and data and control dependencies among nodes. The overall parallel activity graph of a given application is thus represented by a composition (nesting) of one or more skeletons.

Skeletons can be implemented through higher-order functions, libraries, or syntactic primitives (González-Vélez and Leyton, 2010). In our case, skeletons are implemented through a template library in FastFlow, a C++ parallel programming framework for multi-core platforms (Aldinucci et al., 2013b). Currently, FastFlow supports the execution of skeleton templates on shared memory environments through non-blocking lock-free/fence-free synchronisation mechanisms.

As part of the EU FP7 ParaPhrase project (Hammond et al., 2011), research has been conducted on the distributed (shared-nothing) implementation of skeleton-based applications using FastFlow (Aldinucci et al., 2012a). As FastFlow supports the use of external communication channels from one skeleton graph node to another, FastFlow applications can be executed on different hosts, potentially targeting heterogenous distributed architectures.

Contribution

In this paper, we focus in understanding the behaviour of the FastFlow programming environment with respect to those target architectures for which FastFlow has not been explicitly designed. We have investigated its exploitation on new platforms ranging from single virtual machine to cloud virtual cluster using a base benchmark.

We start with the evaluation of the sequential overhead of the well known matrix multiplication benchmark using different matrix sizes. Then, performance figures have been obtained by executing the parallel version of the application on two different single multi-core machines using the KVM (Kernel Virtual Machine) and Oracle VirtualBox virtual machines respectively. The results have been compared with the ones obtained on the corresponding physical machine without any virtualisation. The overhead measured in a KVM-based virtual environment seems to be predictable and bounded in the range $2-30\%$. The same does not apply, for the considered benchmark and physical platform, to the Oracle VirtualBox environment where we have obtained a much higher overhead.

Since cloud computing elastically exploits resources using location, pay-per-use, and usability constraints, it can potentially represent a very promising deployment platform for FastFlow applications. Employing Amazon EC2, we have run a *farm of farms* (nested farm skeletons) FastFlow application in which the workers of the outer farm are distributed among virtual multi-core nodes of the EC2 cloud. We have then measured scalability and completion time correlated with the number of nodes involved.

Our overall results show that the application performance obtained through the distributed scenarios of FastFlow match similar deployments in the literature, whilst exhibiting substan-

Proceedings 27th European Conference on Modelling and Simulation ©ECMS Webjørn Rekdalsbakken, Robin T. Bye, Houxiang Zhang (Editors)
ISBN: 978-0-9564944-6-7 / ISBN: 978-0-9564944-7-4 (CD)

tially superior portability.

However, the intention of this paper is not to focus on a "yet-another" application that scales, but rather on a programming environment that guarantees the programmer to reach predictable scalability results across platforms. Thus, as a parallel programming environment, FastFlow is able to guarantee the performance boundaries documented in the scientific literature, and, if properly exploited, it can support in this sense not only a single application but a class of them in distributed scenarios.

Moreover, as in the best structured parallel programming tradition, we will demonstrate that an application implemented on top of FastFlow could run on (even extremely) different programming environments without asking for additional efforts to the user programmer: once the distributed/multi-core/virtualized environment has been properly set up, no or minimal adjustments to the code are needed in order to run the application. *To the best of our knowledge,* FastFlow *is the first parallel skeleton programming environment to be efficiently running on clouds and clusters without modification.*

This paper is structured as follows. Firstly, this work critically contrasts the concepts of cloud and virtualisation with those of distributed systems and HPC to substantiate the introduction of a homogenous virtualised environment. Secondly, it provides a background overview of FastFlow, followed by experiments showing the analytical results of our benchmarks. Finally, this paper draws our conclusions and provides future directions to this work.

VIRTUALISATION AND CLOUD COMPUTING

The ICT evolution during years has registered the amalgamation of distinct platforms such as virtualisation, High Performance Computing (HPC), and cloud computing to enable more robust, larger computational environments. Even when a single HPC system contains substantial (physical) computational resources, virtualisation allows the abstraction and efficient utilisation of those physical resources, while cloud computing typically adds flexibility and connectivity to the overall environment (Wang and von Laszewski, 2008; Lonea, 2013).

That is to say, a cloud computing ecosystem is composed of HPC systems or servers, typically virtualised. It provides common, location-independent, online, utility and on-demand services to users. Resource limits, static workload allocation, and on-premise management are the three main differences between traditional virtualisation and cloud computing. Thus, cloud computing extends virtualisation by providing elasticity, dynamic workload allocation using an Application Programming Interface (API), and on-premise and off-premise management (Lonea, 2013).

The on-demand provision of resources in cloud computing increases system reliability and flexibility by delivering more abstract resources and services via a pay-as-you-go formula (Foster et al., 2008; Rings et al., 2009) and, in this way, the delayed allocation of resources is eliminated (Wang and von Laszewski, 2008).

Even if some computational resources are effectively clusters, they are nominally distributed and located in the cloud resource pool, which differentiate cloud from cluster computing (Letaifa et al., 2010; Gong et al., 2010). Another significant distinction between cloud and cluster is the utilisation factor: clusters are mainly used for load balancing and for providing high availability, while cloud computing is used for providing services.

Nevertheless scant research has been conducted to provide seamless structured parallel programming frameworks, which can efficiently scale from tightly-coupled clusters up to clouds, exposing the same programming abstractions (parallel patterns). Typically used for embedding the computational resources within software environments, virtualisation can arguably be used to abstract the instruction sets of parallel software in order to allow—its divided units—to be mapped/re-mapped onto alternative guest virtual machines in different distributed environments.

In this work, we hypothesise that the efficient use of virtualisation can enable the scaling of pattern-based parallel applications mapped into cloud environments. We have empirically tested this mapping process using hosted and hypervisor virtualisation architectures.

A hosted virtualisation architecture consists of an application (e.g. Oracle VirtualBox, VMware Player, ACE) that runs on top of an operating system to enable the virtualisation layer. In a hypervisor-based architecture, the virtualisation layer is installed directly onto the 'bare metal' environment, which seemingly increases the scalability, robustness, and performance (VMware, 2007).

Nonetheless, virtualisation entails a performance overhead. Substantial research has been devoted to investigate the overhead magnitude in multi-tiered systems using Xen and OpenVZ (Padala et al., 2007); for applications that run in virtual based Xen environment (Cherkasova and Gardner, 2005); for HPC benchmark applications (Tikotekar et al., 2008); and, for parallel applications using a private cloud environment based on Xen hypervisor (Ekanayake and Fox, 2010). Xen-based systems have been more intensely analysed as their architecture is geared towards HPC systems. It contains enhanced scheduling policies, faster access to hardware drivers running first a simple device driver (Cherkasova and Gardner, 2005; Tikotekar et al., 2008; Ekanayake and Fox, 2010). Xen adopts the paravirtualisation solution. Besides paravirtualisation, two others types of CPU virtualisation can be realized: full virtualisation and hardware virtualisation. Full virtualisation combines the execution of binary translation and direct execution, without modifying the user level instructions at the running time, compared with the paravirtualisation technique which is a OS assisted virtualisation. Moreover, the third virtualisation technique is the hardware assisted virtualisation, which can be executed within Intel and AMD processors, that have incorporated virtualisation support (i.e. Intel-VT and AMD-V) (VMware, 2007).

THE FastFlow PROGRAMMING FRAMEWORK

A structured parallel programming environment written in C++ on top of POSIX thread library, FastFlow provides programmers with predefined and customisable patterns such as *task-farm*, *pipeline* and recently also *map* patterns working on streams (Aldinucci et al., 2013a). It has been initially designed and implemented to be efficient in the execution of fine grain parallel applications on general purpose multi-core architectures (Aldinucci et al., 2013b).

Parallel patterns in FastFlow implement structured synchronisation among concurrent entities (graph nodes) via shared memory pointers passed in a consumer-producer fashion. The FastFlow run-time support takes care of all the required synchronisation relating to communication among the different nodes resulting from the compilation of the high level FastFlow pattern(s) used in an application. The entire FastFlow graph describing the application is implemented us-

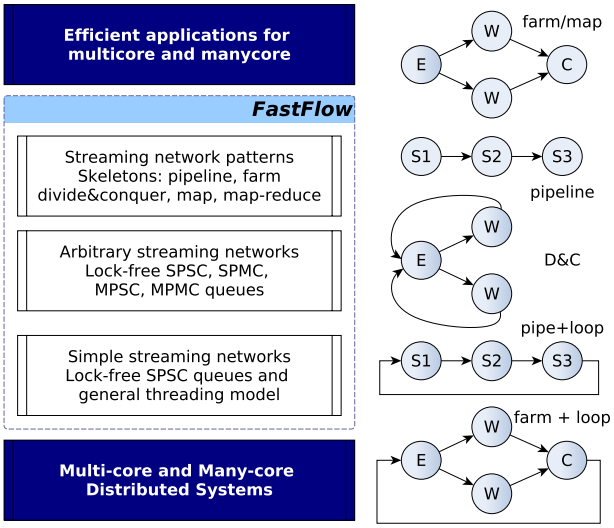

Fig. 1: Layered FastFlow design together with some possible parallel patterns

```
1  class ff_node {
2  protected:
3    virtual bool push(void* data) { return qout->push(data);}
4    virtual bool pop(void** data) { return qin->pop(data);}
5  public:
6    virtual void* svc(void * task) = 0;
7    virtual int   svc_init () { return 0; };
8    virtual void  svc_end()   {}
9    ...
10 private:
11   SPSC* qin;
12   SPSC* qout;
13 };
```

Fig. 2: FastFlow's `ff_node` class schema

ing non-blocking concurrent threads inside a single process abstraction.

The FastFlow framework provides two abstractions of structured parallel computation: i) the *standalone parallel* mode which basically provides the possibility to write full parallel applications as (compositions of) FastFlow parallel design patterns; ii) the *accelerator* mode, supports the self-offloading of parallel computations from within standard C++ sequential code to a software accelerator programmed as a parallel design pattern composition which is running on the "spare" cores of the architecture. FastFlow is being currently extended to offload data parallel computation to many-core GPGPUs (Goli et al., 2012; Goli and González-Vélez, 2013) and to hardware accelerators (Buono et al., 2013).

The FastFlow design is layered (see Fig. 1). The lower layer implements a lock-free and wait-free Single-Producer, Single-Consumer queue (Aldinucci et al., 2012b). On top of this mechanism, the second layer provides Single-Producer Multiple-Consumers and Multiple-Producers Single-Consumer queues using arbiter threads. This abstraction is designed in such a way that arbitrary networks of activities can be expressed while maintaining the high efficiency of the synchronisation. Eventually, the third layer provides, in the form of standard C++ classes, parallel programming patterns. The possibility to efficiently handle both stream parallel and data parallel computations using the same programming model represents an advantage of FastFlow with respect to other frameworks that only (efficiently) support either stream or data parallel computations.

The key concept in the implementation of FastFlow is the `ff_node` class. It is used to encapsulate sequential portions of code implementing functions as well as higher level parallel patterns such as pipelines and farms. The `ff_node` class structure is outlined in Fig. 2.

Predefined FastFlow patterns may be arbitrarily nested, and so we can have pipelines with farm stages and vice versa. Also, the policies used to schedule the input tasks–as well as portions/partitions of the input tasks–to farm workers, and also to gather results from workers onto the farm output queue may be customised via C++ overloading of methods implementing standard policies (round-robin and on-demand). Using the customisation features, different patterns may be implemented in terms of the pipe and farm building blocks.

Recently FastFlow has been extended to target also loosely-coupled distributed systems (Aldinucci et al., 2012a), thus providing the user with a two-tier programming model. At a *lower tier*, a shared-memory implementation of skeletons inside a single multi-core workstation; at an *upper tier*, structured coordination among a set of distributed nodes executing the lower tier computations. More specifically, at the lower tier the user designs a typical FastFlow skeleton graph, employing stream parallelism and the shared memory skeletons offered by the original FastFlow framework. Multiple lower tier FastFlow graphs can be connected together using the mechanisms of the upper tier, that is, using a suitable communication pattern which implements a network channel (i.e. point-to-point, broadcast, scatter, etc.). At this level, the programming model exposed to the programmer can be either SPMD or MPMD.

In order to send and receive tasks from and to other FastFlow graphs, the edge-nodes of the FastFlow application have to be defined as `ff_dnode`. A `ff_dnode` is actually a `ff_node` with an extra communication channel (henceforth *external channel*) which connects the edge-node of the graph with one or more edge nodes of other FastFlow application graphs running on the same or on a different host.

At the second tier no memory is shared among processes and so all iterations have to be implemented using explicit communications, which are the responsibility of the FastFlow runtime support and are completely transparent to the user (see Fig. 3).

External channels are implemented using the ZeroMQ (Aldinucci et al., 2012a) messaging framework. The ease-of-use of ZeroMQ together with the asynchronous communication model offered were the key factors for choosing ZeroMQ for the implementation. The communication patterns currently implemented, are summarised in the following:

unicast	unidirectional point-to-point communication between two peers
broadcast	sends the same input data to all connected peers
scatter	sends different parts of the input data (typically partitions) to all connected peers
onDemand	the input data is sent to one of the connected peers, the choice of which is taken at run-time on the basis of the actual work-load (typically it is implemented using a request-reply protocol)
fromAll	(also known as all-gather) collects different parts of the data from all connected peers combining them in a single data item
fromAny	collects one data item from one of the connected peers

Nonetheless, scant research has been conducted to substantiate the seamless portability of distributed FastFlow applications across platforms, from local clusters and multi-node virtualised environments to fully-virtualised public cloud infrastructures.

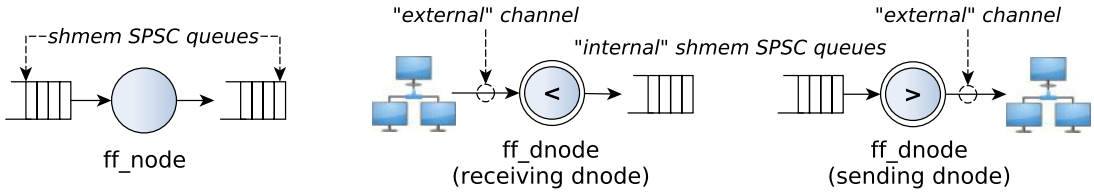

Fig. 3: FastFlow's node vs receiving and sending dnode(s).

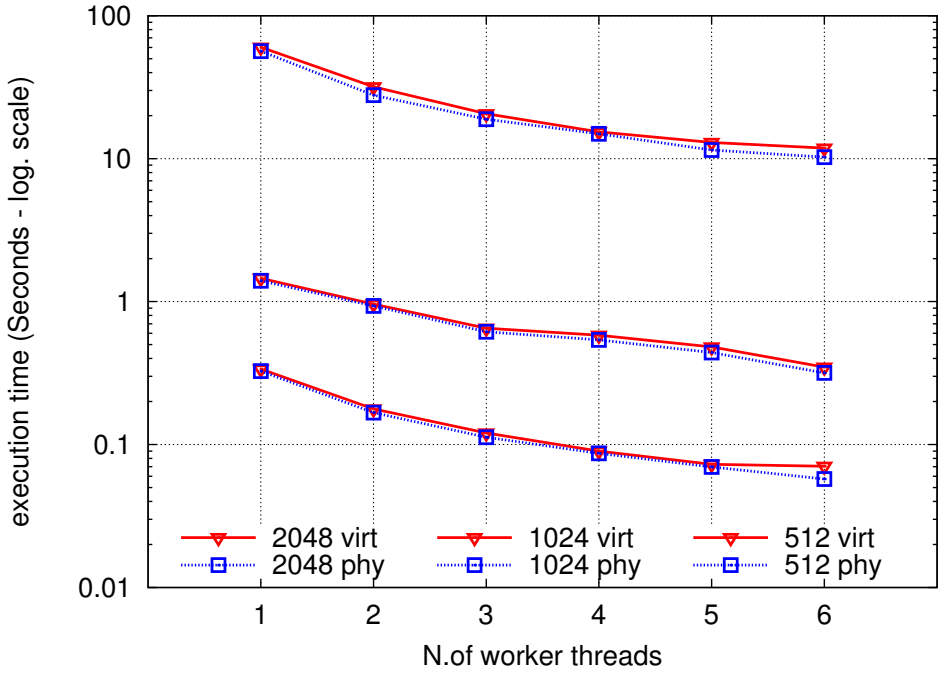

Fig. 4: Virtual vs. Physical execution of the FastFlow MatMul implementation: completion time varying the number of worker threads.

EXPERIMENTS

In this section we have first measured the overhead of running sequential and parallel CPU-intensive applications on virtual multi-core machines, then we extend our tests considering also a cluster of virtual multi-core machines running in a public cloud environment.

The sequential application considered is a simple matrix multiplication algorithm (MatMul). We tested two versions of the sequential algorithm: the standard naive algorithm and a cache oblivious version which computes matrix elements (double precision) in a different order (`for(i) for(j) for(k) C[j][k] += A[j][i]*B[i][k]`.).

First we consider a Linux KVM-based virtualisation environment as part of a Eucalyptus private cloud computing-based architecture (Nurmi et al., 2009; Lonea et al., 2012).

The physical machine used is a Linux CentOS x86_64 and has two 6-core CPUs Intel Xeon E5-2540 2.5 GHz with 8MB L3 cache. We run the sequential algorithm both on the physical and virtual machine varying the matrix size. The virtual machine runs the same OS and has 6 virtual cores. The overhead measured ranges between 6% and 27% for the size tested (see Tab. I). We observed an higher overhead for the cache oblivious version of the algorithm since the absolute time measured are much lower w.r.t. the ones obtained using the standard algorithm thus the overhead as a greater incidence.

Then, we considered the execution of a parallel version of the matrix multiplication algorithm on both physical and virtual machines. The parallel version is designed to use the FastFlow accelerator feature using the task-farm skeleton as described in (Aldinucci et al., 2011). In order to make the results comparable, when the parallel application is executed on the physical machine, the threads of the farm skeleton have been forced to be executed in the same 6 physical cores used by the 6 virtual cores of the virtual machine (We used the *taskset* command to set process's CPU affinity).

The completion time obtained varying the number of worker threads are shown in Fig. 4. Table II reports the maximum over-

TABLE I: Overhead between physical and virtual execution for the sequential MatMul algorithm.

	matrix size		
Seq. MatMul	512	1024	2048
Standard Algorithm	5.96%	6.01%	7.8%
C. Oblivious Algo.	27.43%	11.52%	10.29%

TABLE II: Virtual vs. Physical execution of the FastFlow MatMul implementation: maximum overhead obtained.

	matrix size		
Par. MatMul	512	1024	2048
Max. Overhead	21%	10%	16%

head observed among all runs. As it can be seen, the trend of the execution time is almost the same in all tested cases. We performed other tests (not reported in this paper for the sake of conciseness) for different matrix sizes in the range 384 and 3072. In all cases, the overhead introduced by the KVM virtual environment ranges between 2% and 30% maximum.

The same kind of experiments—both sequential and parallel—have been also run on a different virtual and physical environment. We have considered the Oracle VirtualBox application environment (version 4.0.10) installed on as physical system with 2 CPUs Intel Sandy Bridge Xeon E5-2650 2.0GHz. In this case, the measured overhead for both versions of the algorithms is much higher when compared with the one related to the KVM environment. The parallel speedup trend of the physical and virtual environment is almost the same also in this case. The higher differences are related to the fact that the VirtualBox environment is less integrated with the low-level Linux host system, the VirtualBox environment running as a standard application on the host OS.

As expected, executing CPU and memory intensive application on a virtual environment introduces non-negligible overhead. However, when optimised virtualisation environments are used, such overhead is somehow predictable within a bounded range allowing to know in advance the maximum overhead that will be introduced in the execution.

We wanted to evaluate if the above considerations are still valid when considering distributed application running on cluster of virtual multi-core machines in a public cloud platform. We have therefore considered the Amazon EC2 public cloud, where we deployed 7 Linux Ubuntu 12.04 LTS x86_64 virtual machines: one VM with 8 cores and 6 VMs with 4 cores. The VMs with 4 cores has an Intel CPU E-2670 with 4 virtual core 2.6 GHz with 20MB of L3 cache and 14GB of RAM.

The application taken into account is the one sketched in Fig. 5, which is actually a 3-stage FastFlow distributed pipeline. The first stage generates a stream of square matrices, the second stage computes, on each input, the matrix multiplication with a constant local matrix. The second stage is internally parallel implemented using the FastFlow task-farm pattern so that each worker thread computes an entire matrix multiplication sequentially using the cache-oblivious algorithm.

The last stage collects the results sending them back to the first stage of the distributed pipeline. The communication patterns that link the second stage with the first and with the third are the *onDemand* and the *fromAny* patterns, respectively. They allow replication of the second stage without touching the code for a given number of times, so that its throughput can be increased.

The three involved stages are mapped on the virtual cluster using the following schema: the first and the third stages are mapped in one 8-cores VM whereas the middle stages are mapped each one in a separated 4-cores VM. This mapping is sub-optimal w.r.t. the single node available bandwidth, but allow us to maximise the number of middle stages.

Even in this case we tested three different size of matrices: 512×512, 1024×1024 and 2048×2048 (double elements). In Fig. 7 are shown 3 performance metrics obtained varying the number of middle stages when the 1024×1024 matrix size is considered. The scalability is almost linear up to 7 nodes, whereas the time speedup is more than linear since each node is internally parallel (4 worker threads are used for each middle stage). The maximum time speedup obtained is thus $\sim 8\times$ when compared to the overall sequential time of the application.

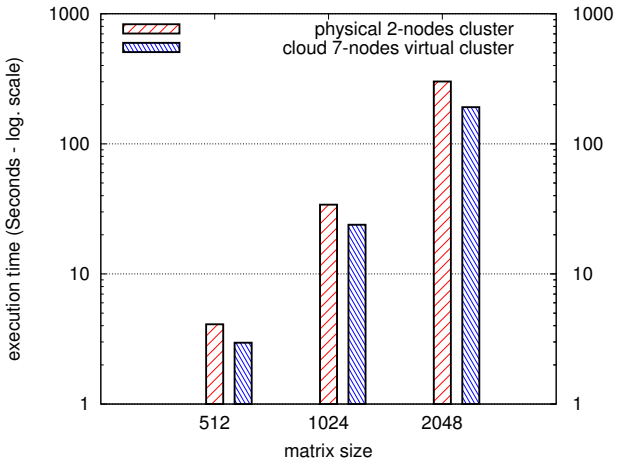

Fig. 6: The minimum completion time obtained running the application in the 32 cores EC2 virtual machines vs. 32 cores physical cluster.

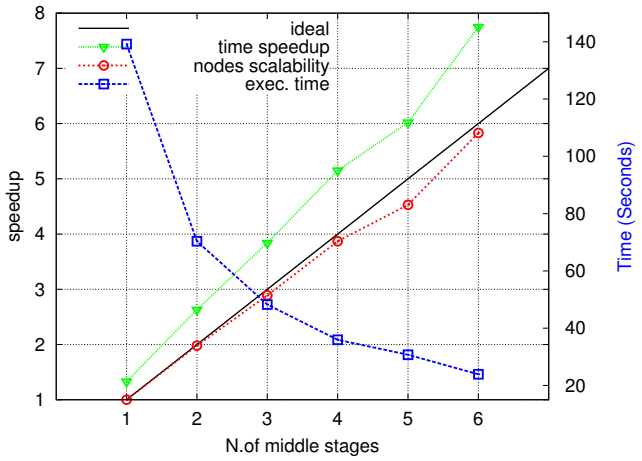

Fig. 7: Completion time, time speedup and node scalability varying the number of middle stages (Number of matrices: 128. Matrix size 1024×1024)

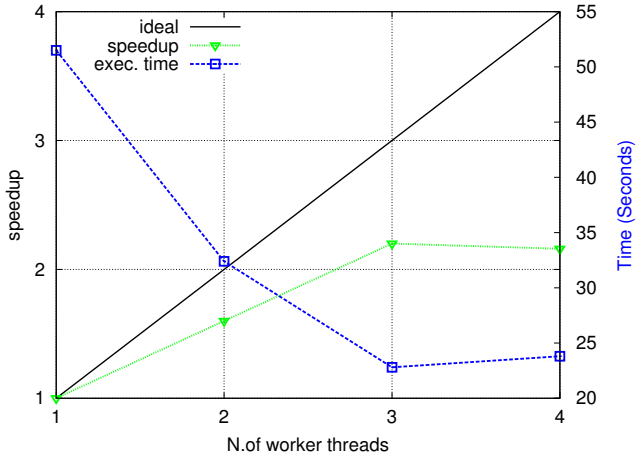

Fig. 8: Completion time and time speedup varying the number of worker threads used inside each middle stage (Number of matrices: 128. Matrix size 1024×1024).

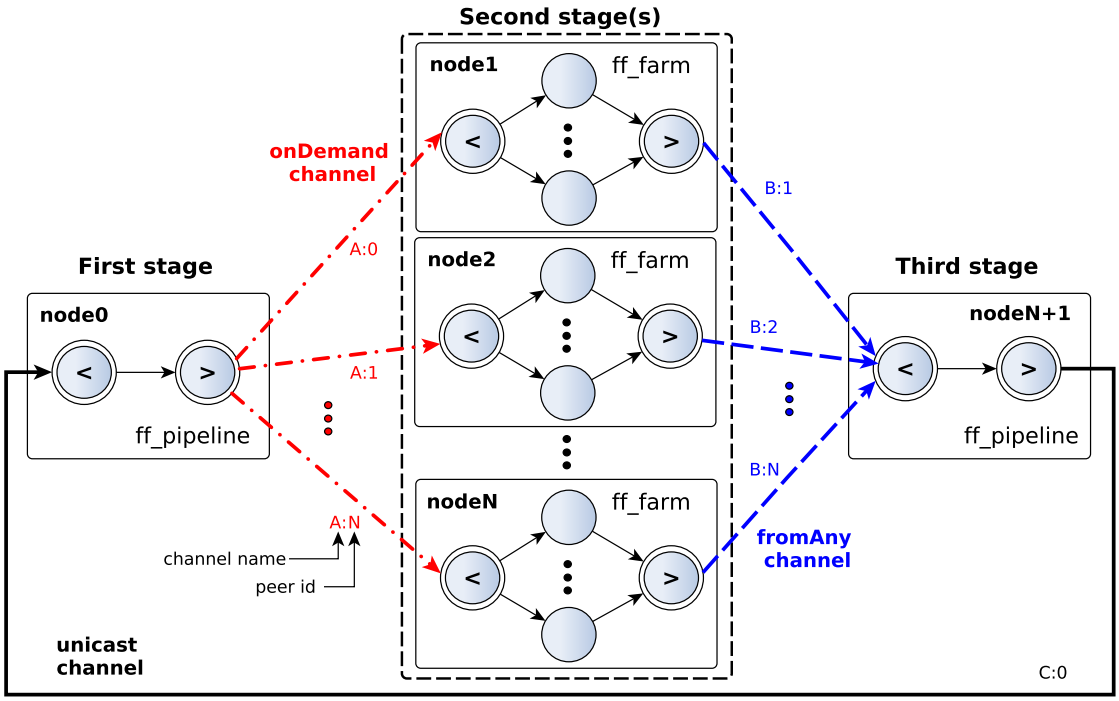

Fig. 5: The schema of the 3-stage pipeline application tested

In Fig. 8 we reported the completion time and the speedup obtained for the case 1024×1024 when 6 middle stages are used and the internal parallelism of each stage is varied between 1 to 4. In this case the performance increase is not particularly good because the first pipeline stage is not able to feed with enough matrices all middle parallel nodes due to the limited available network bandwidth ($\sim$1 Gbit/s bidirectional bandwidth per virtual cluster node).

Finally, in Fig. 6, it is sketched the minimum completion time we obtained running the same 3-stage pipeline in the Amazon EC2 cloud and in a two node physical cluster each one with 2 Intel Sandy Bridge Xeon E5-2650 @2.0GHz with 8 cores each and 20MB L3 shared cache. The physical nodes are connected with an Infiniband Connectx-3 card (40 Gb/s ports). As can be seen using more nodes (and a lower number of cores) we are able to obtain a performance increase from 41% to 57% without additional effort at the application level thanks to the skeleton-based approach used in the implementation.

CONCLUSION

In this paper we have deployed and tested the FastFlow parallel framework on virtual multi-core machines and virtualised public cloud infrastructures. Our experimental evaluation of a distributed application running in the virtual Amazon EC2 public cloud, shows that the FastFlow design is flexible and robust also for such environments. We have demonstrated that applications implemented using FastFlow can run on different parallel and distributed virtualised platforms without additional programming efforts with good performance.

As previously reported in literature, virtualised execution of sequential and parallel applications introduces performance overhead that is affected by many factors. Our tests in a KVM-based virtual environment using a simple micro-benchmark confirm a non-negligible overhead. When measured in both sequential and parallel executions, a performance decrease in the range 2-30% has been observed.

Analogous to the tests performed in Ekanayake and Fox (2010) which use an Eucalyptus Xen-based cloud platform, a part of our tests has been realised in an Eucalyptus KVM-based cloud platform. We have analysed the computational overhead between the local node where the FastFlow-based VM is running and the FastFlow-based VM, using the same hardware and software configuration.

Thus, our tests have dealt with a single FastFlow-based VM in the Eucalyptus private cloud, which was configured to have 6 virtual cores. Unlike our tests, Ekanayake and Fox (2010) have preferred to observe the overhead between the bare-metal and one to multiple VMs, where parallel applications are running as well. They have concluded that increasing the number of VMs per cloud node produces a higher overhead. Likewise, the minimum overhead reported by Ekanayake and Fox (2010) for one VM per hardware node is 8%, while in our results is 6%.

Thus, for both cases the overhead is small and this difference can be explained by the size of the application, by the application itself and by the impact produced by the Xen hypervisor, which interact with the cores of processor using two domains (i.e. Dom 0 and Dom U). Our experimental protocol have extended the performance analysis to include the sequential version of the matrix multiplication application. Both sequential and parallel applications have been tested across different virtual and physical environments.

ACKNOWLEDGEMENTS

This work is based upon research supported as part of ParaPhrase: Parallel Patterns for Adaptive Heterogeneous Multicore Systems `http://paraphrase-ict.eu/`, a research project funded by the European Commission Seventh Framework Programme under contract no.: 288570.

References

Aldinucci, M., Campa, S., Danelutto, M., Kilpatrick, P., Torquati, M., 2012a. Targeting distributed systems in FastFlow, in: Euro-Par 2012 Workshops, Springer-Verlag, Rhodes. pp. 47–56.

Aldinucci, M., Campa, S., Kilpatrick, P., Torquati, M., 2013a. Structured data access annotations for massively parallel computations, in: Euro-Par 2012 Workshops, Springer-Verlag, Rhodes. pp. 381–390.

Aldinucci, M., Danelutto, M., Kilpatrick, P., Meneghin, M., Torquati, M., 2011. Accelerating code on multi-cores with FastFlow, in: Euro-Par 2011, Springer-Verlag, Bordeaux. pp. 170–181.

Aldinucci, M., Danelutto, M., Kilpatrick, P., Meneghin, M., Torquati, M., 2012b. An efficient unbounded lock-free queue for multi-core systems, in: Euro-Par 2012, Springer-Verlag, Rhodes. pp. 662–673.

Aldinucci, M., Danelutto, M., Kilpatrick, P., Torquati, M., 2013b. FastFlow: high-level and efficient streaming on multi-core, in: Programming Multi-core and Many-core Computing Systems. Wiley. Parallel and Distributed Computing. chapter 13, p. 13.

Buono, D., Danelutto, M., Lametti, S., Torquati, M., 2013. Parallel patterns for general purpose many-core, in: Euromicro PDP 2013, IEEE, Belfast. pp. 131–139.

Cherkasova, L., Gardner, R., 2005. Measuring CPU overhead for I/O processing in the Xen virtual machine monitor, in: ATEC '05, USENIX, Anaheim. pp. 24–.

Ekanayake, J., Fox, G., 2010. High performance parallel computing with clouds and cloud technologies, in: Cloud Computing. Springer-Verlag. volume 34 of *LNICST*, pp. 20–38.

Foster, I., Zhao, Y., Raicu, I., Lu, S., 2008. Cloud computing and grid computing 360-degree compared, in: GCE'08/SC'08, ACM/IEEE, Austin. pp. 1–10.

Goli, M., Garba, M.T., González-Vélez, H., 2012. Streaming dynamic coarse-grained CPU/GPU workloads with heterogeneous pipelines in FastFlow, in: HPCC-12, IEEE, Liverpool. pp. 445–452.

Goli, M., González-Vélez, H., 2013. Heterogeneous algorithmic skeletons for FastFlow with seamless coordination over hybrid architectures, in: Euromicro PDP 2013, IEEE, Belfast. pp. 148–156.

Gong, C., Liu, J., Zhang, Q., Chen, H., Gong, Z., 2010. The characteristics of cloud computing, in: ICPPW-2010, San Diego. pp. 275–279.

González-Vélez, H., Leyton, M., 2010. A survey of algorithmic skeleton frameworks: High-level structured parallel programming enablers. Software–Practice & Experience 40, 1135–1160.

Hammond, K., Aldinucci, M., Brown, C., Cesarini, F., Danelutto, M., González-Vélez, H., Kilpatrick, P., Keller, R., Rossbory, M., Shainer, G., 2011. The ParaPhrase project: Parallel patterns for adaptive heterogeneous multicore systems, in: FMCO 2011, Springer-Verlag, Turin. pp. 218–236.

Letaifa, A.B., Haji, A., Jebalia, M., et al., 2010. State of the art and research challenges of new services architecture technologies: Virtualization, soa and cloud computing. International Journal of Grid and Distributed Computing 3, 69–88.

Lonea, A.M., 2013. Private cloud set up using Eucalyptus open source, in: Soft Computing Applications. Springer-Verlag. volume 195 of *Advances in Intelligent Systems and Computing*, pp. 381–389.

Lonea, A.M., Popescu, D.E., Prostean, O., 2012. A survey of management interfaces for Eucalyptus cloud, in: SACI 2012, IEEE, Timisoara. pp. 261–266.

Nurmi, D., Wolski, R., Grzegorczyk, C., Obertelli, G., Soman, S., Youseff, L., Zagorodnov, D., 2009. The Eucalyptus Open-Source Cloud-Computing System, in: CCGRID'09, IEEE, Shanghai. pp. 124–131.

Padala, P., Zhu, X., Wang, Z., Singhal, S., Shin, K., 2007. Performance evaluation of virtualization technologies for server consolidation. Technical Report. HP Laboratories Palo Alto.

Rings, T., Caryer, G., Gallop, J., Grabowski, J., Kovacikova, T., Schulz, S., Stokes-Rees, I., 2009. Grid and Cloud Computing: Opportunities for Integration with the Next Generation Network. Journal of Grid Computing 7, 375–393.

Tikotekar, A., Vallée, G., Naughton, T., Ong, H., Engelmann, C., Scott, S.L., 2008. An analysis of HPC benchmarks in virtual machine environments, in: Euro-Par 2008 Workshops, Springer-Verlag. pp. 63–71.

VMware, 2007. Understanding full virtualization, paravirtualization and hardware assist. white paper.

Wang, L., von Laszewski, G., 2008. Scientific cloud computing: Early definition and experience, in: HPCC-08, IEEE, Dalian. pp. 825–830.

AUTHOR BIOGRAPHIES

Sonia Campa is a Research Fellow of the Department of Computer Science at the University of Pisa. Her main fields of investigation regard models and languages for parallel computation description, with particular emphasis to structured parallel programming environments which she has approached at different levels of abstraction, from formal frameworks to libraries implementations. Email: `campa@di.unipi.it`

Marco Danelutto graduated *cum laudae* from University of Pisa in 1984, where he also got his PhD in Computer Science in 1990. Since 1998, he is an Associate Professor with the Dept. of Computer Science at University of Pisa. His research interests include models and tools for parallel programming, algorithmic skeletons, parallel design patterns, and (parallel) functional programming. Email: `marcod@di.unipi.it`

Massimo Torquati is currently a Research Fellow at the Computer Science Department of the University of Pisa. His main research interests include language, tools and model for parallel and distributed computing. Email: `torquati@di.unipi.it`

Horacio González–Vélez is an Associate Professor and Head of the Cloud Competency Centre at the National College of Ireland. His research interests lie in HPC, cloud computing, and structured parallelism, and their application to the solution of complex computational problems. He earned a PhD in Informatics from the University of Edinburgh. Email: `horacio@ncirl.ie`

Alina Madalina Popescu is a Research Lecturer with the Cloud Competency Centre at the National College of Ireland. She has significant background in Cloud Computing, as a result of her PhD thesis covering the topic of "Security Solutions for Cloud Computing," which was successfully defended at Politehnica University of Timisoara. Dr. Popescu is interested in researching distinct parallel patterns by defining their component states, life-cycle and interfaces to heterogeneous hardware devices from multi-core to cloud computing environment. Email: `Alina-Madalina.Popescu@ncirl.ie`

Efficiency of Memetic and Evolutionary Computing in Combinatorial Optimisation

Magdalena Kolybacz, Michał Kowol, Łukasz Leśniak
Aleksander Byrski, Marek Kisiel-Dorohinicki
AGH University of Science and Technology
Al. Mickiewicza 30, 30-059 Kraków, Poland
magda.kolybacz@gmail.com, michal.kowol@gmail.com, luke.lesniak@gmail.com
olekb@agh.edu.pl, doroh@agh.edu.pl

Abstract— **Difficult search and optimisation problems call for complex techniques for solving them. In particular, in cases when fitness function is costly, applying solutions, such as agent-based computing systems may be fruitful. This approach may yield even better results, in the case of memetic computing, as these algorithms tend to significantly increase the number of fitness function calls, because of their nature. This paper may be treated as a milestone in preparing to tackle combinatorial optimisation problems with memetic approaches in agent-based systems. After discussing the selected problems and details of population-oriented meta-heuristics to solve them, experimental results (with stress put on efficiency) are presented. Then details of applying EMAS-class systems are given and, in the end, preliminary EMAS results obtained for combinatorial optimisation are shown and the work is concluded.**

I. Introduction

Difficult optimization problems (in other words the ones, which domains are very hard or even impossible to be described and explored) cannot be solved using using conventional mathematical apparatuses, like most combinatorial optimization problems [1]. Such problems may be treated as "black-box" problems [2] and may be solved only using general-purpose algorithms, such as meta-heuristics, taking into consideration little, if any information from a problem domain, to devise a solution. As a drawback of such approaches, the one can be mentioned, that the produced results are sub-optimal, and it is impossible to check, whether (and when) they are (if at all) close to the global optimum.

One of the most popular general-purpose meta-heuristics are evolutionary algorithms [3]. Because of their nature, they are very easy to hybridise with other techniques, especially local-search ones constituting so-called memetic systems [4]. Such computing systems have already proven to be effective in solving different difficult combinatorial optimisation problems (see, e.g.,[5], [6]).

A particularly interesting general-purpose approach to optimisation is an evolutionary multi-agent system (EMAS). This technique (along with its variations) has already proven to be an effective tool when dealing with difficult problems in global optimization [7], multi-objective optimization [8], [9], multi-modal optimization [10], and also hybrid methods such as the optimization of neural-network architecture [11], [12]. It was also a subject of theoretical analysis [13] and gained technological support [14]. A valuable feature of EMAS, is a significantly reduced number of fitness function calls needed to obtain similar results, comparing to classical evolutionary algorithms. These results have been obtained for global-optimisation of continuous problems, moreover memetic variations of the tested algorithms have also been researched [7].

However, in the case of combinatorial optimisation, though meta-heuristics applied may be absolutely the same, as in the case of continuous one, the particular configurations, including variation operators applied and their memetic variants pose new challenging problems to the researcher. Therefore, before applying EMAS to solve combinatorial optimisation problems, it might be fruitful for further research to examine evolutionary and memetic solutions of the selected benchmarks. The main aim of this paper is thus to compare experimentally the efficiency of classical evolutionary and memetic algorithms to choose the most promising solutions and reuse them in the preliminary experiments with evolutionary multi-agent systems.

The paper begins with a discussion of three selected combinatorial problems, namely Low Autocorrelation Binary Sequence (LABS), Golomb ruler and Job Shop. After a short review of population-oriented metaheuristics, experimental results (with stress put on efficiency) are presented. In the end, details of applying EMAS-class systems are given together with preliminary results obtained for combinatorial optimisation and the work is concluded.

II. Population-based approaches to combinatorial optimisation

Low Autocorrelation Binary Sequence (LABS) problem was formulated in 1960s by Physics community and has various applications in physics, chemistry and telecommunication. LABS is a very hard optimization problem with simple formulation: find a binary sequences $S = \{s_0, s_1, \ldots, s_{L-1}\}$ with length L where $s_i \in \{-1, 1\}$ which minimizes energy function $E(S)$:

$$C_k(S) = \sum_{i=0}^{L-k-1} s_i s_{i+k} \qquad E(S) = \sum_{i=1}^{n-1} C_k^2(S)$$

The problem has an interesting property: it is symmetric. The energy function $E(S)$ stays the same when sequence is reversed or each element of S is multiplied by -1. The search space for the problem with length L has size 2^L and energy of sequence can be computed in time $O(L^2)$.

LABS problem has no constrains, so S can be represented as a list of binary values, and standard operators for mutation and recombination can be used [15]. In the problem all bits are correlated – there are no blocks of good solutions, so

Proceedings 27th European Conference on Modelling and Simulation ©ECMS Webjørn Rekdalsbakken, Robin T. Bye, Houxiang Zhang (Editors)
ISBN: 978-0-9564944-6-7 / ISBN: 978-0-9564944-7-4 (CD)

uniform crossover is recommended since it provides a new promising start point for the algorithm.

A few local search techniques can be used in memetic algorithms to solve LABS problems: steepest decent local search (SDLS), tabu search [15], [16], and more. The best results are reported to be obtained using some variations of Tabu Search [17].

Job-shop scheduling problem (JSSP) is a well-known, combinatorial optimisation problem that can be defined as follows: given a set of m machines and n jobs (each job is a sequence of m operations), the aim is to find a schedule of operations that minimizes the finishing time of the last operation in the schedule. Each operation of a job has to be processed on specified machine. Operation processing takes time period of a given length and no preemption is allowed. Each machine can process at most one job at a time and each job can be processed on at most one machine at a time. In the paper we focus on the Open-shop scheduling problem (OSSP) which is a variation of JSSP but — unlike in JSSP — the ordering of operations within a job is not defined and may be changed.

To be able to apply memetic or genetic algorithms to OSSP, the solution has to be properly encoded. Various possible representations are widely discussed in literature [18], [19], [20]. In the *permutation with repetitions* representation a chromosome that encodes a solution for n jobs and m machines consists of numbers from 1 to n (each number occurs exactly m times). Each number represents operations from single job—first occurence of a number in chromosome represents an operation on first machine etc. In *permutation* representation (without repetitions) a chromosome consists of numbers from 1 to $n \times m$. Numbers 1 to m represent operations from the first job, numbers $1 \times m + 1$ to $2 \times m$ represent operations from the second job, etc.

The permutational characteristics of the chromosome requires specific mutation and crossing-over operators [20]. For the above-described representation, LOX for crossing-over and SWAP for mutation may be used. As local optimization method, variations of tabu search are commonly used [21].

In Open-shop problem, specific variation of SWAP can be applied to permutation representation (without repetitions). The variation uses domain knowledge — two operations can be interchanged only if they are assigned to the same machine. We use the method as local optimization in one of our memetic algorithms.

The term **Golomb Ruler** is derived from the work by Professor of Mathematics Solomon W. Golomb [22]. Formally Golomb ruler is an ordered sequence of n distinct, nonnegative integers $\langle a_1, a_2, a_3, \ldots, a_n \rangle$ where $a_i < a_{i+1}$ such that all distances $a_j - a_i$ $(1 \leq i < j \leq n)$ are distinct. By convention $a_1 = 0$ and a_n is the length of the ruler. Golomb rulers have applications in many diverse fields such as radio communications, X-ray crystallography, coding theory and radio astronomy.

A construction of valid n-mark ruler is relatively simple, therefore researches are interested in discovering ruler with minimum length. Figure 1 presents an example of valid 4-mark ruler and all discrete lengths, that it measures.

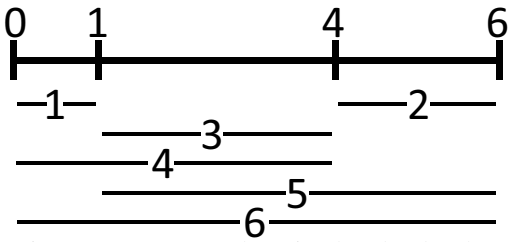

Fig. 1: Known 4-mark optimal Golomb ruler.

Finding optimal Golomb ruler is challenging for optimization methods. The most important issue is how to properly encode Golomb ruler into chromosome, because this will reflect the difficulty of good genetic operators design. Commonly 2 representations are used (the conversion between them is simple and has low cost):

- indirect representation – the distance between adjacent segments is stored as array of integers (e.g. ruler $\langle 0, 1, 4, 6 \rangle$ is encoded into $\langle 1, 3, 2 \rangle$ [23];
- direct representation – is consisted of an array of integers corresponding to the marks of the ruler [24].

Other approaches can be found in the literature e.g. with random keys [25] or binary representation [26], [27].

Second important issue is the decision how to handle constraints and properly design genetic operators. We decided to choose static penalty approach, tournament selection with tourney size of 2 and standard variation operators: segment's length mutation [23] and one-point crossover, both working on indirect representation [28]. Other kinds of genetic operators used include shift mutation [27] or two-point crossover [23], [27].

Population-based algorithms can be enhanced by a local-search method, commonly discussed is the tabu-search in this case [28], [29], [30].

Considering different approaches to find optimal Golomb ruler, best results are obtained in algorithms with binary representation and chromosome repair methods [27]. The algorithms which allow to evolve valid and invalid solutions (without penalty methods) obtain the worst results [23]. However memetic approaches' results are situated in the middle [28].

III. Memetic and evolutionary metaheuristics

Population-based meta-heuristics, particularly evolutionary algorithms [3] may be classified as universal optimisation techniques. Their work is based on the following strategy: instead of directly solving the given problem, the problem undergoes encoding using a predefined way (encoded problem is called a genotype). Group of genotypes create population (that is randomly initialised). Population constructed in this way contains potential sub-optimal solutions of the given problem. Now, using a dedicated evaluation function (so called fitness), selection process is conducted (in this way the mating pool is created) and the subsequent population is created by picking the parents from the mating pool and generating offspring based on their genotypes with use of predefined variation operators (such as crossover and mutation). The process continues until a predefined stopping condition is reached (e.g., maximum number of generations, lack of changes in the best solution found so far). This kind of search has some drawbacks (as possibility of

premature convergence), thus several techniques, as multi-deme approaches [31] are applied.

Evolutionary algorithms may be easily hybridised with local-search methods constituting so called memetic algorithms [4]. In these algorithms, two kinds of search-enhancements can be implemented:

- Baldwinian local search is based on Baldwin theory stating that predispositions may be inherited during reproduction [32]. It is implemented usually as calling of local search in the course of evaluation process. The evaluated genotype receives the fitness function value computed for one of its possible descendants (being an outcome of local-search started from this individual).
- Lamarckian local search is based on Lamarck theory stating that characteristics of individuals acquired in the course of life may be inherited by their descendants [33]. It is implemented usually as specific mutation operator. The search for a mutated individual is based not only on stochastic one-time sampling from the solution space, instead a local-search is started from the genotype and the solution reached becomes the result of this process.

Though both theories turned-out to be false, the meta-heuristics based on them are effective in many problems (see, e.g., [34], [35]).

IV. Experimental results

The experimental results were obtained using extensible distributed computing environment AgE[1] that is being developed as an open-source project by the Intelligent Information Systems Group of AGH-UST. AgE provides a platform for the development and execution of distributed agent-based applications in mainly simulation and computational tasks [14], [36].

For each of the described problems both Lamarckian model of memetic (MA) and evolutionary (EA) algorithms were applied in two configurations: a relatively easy and difficult one. Each experiment was repeated 30 times with the same parameters (tuned for the considered case) and mean values with standard deviations of the best-so-far solution quality obtained in fixed time points of the run (measured in seconds) were calculated. The results were scaled to $[0; 1]$ interval, according to maximal and optimal values for each case (minimisation assumed).

LABS

Configuration:

- common parameters—population size: 50, tournament selection, uniform crossover, bit-flip mutation, $2/L$ elements mutated, total execution time: 300 seconds,
- evolutionary algorithm—mutation probability: 0.75, recombination probability: 0.5,
- memetic algorithm—mutation probability: 0.75, recombination probability: 0.5, local search: RMHC [3] (50 steps) and SDLS.

For MAs, a simple algorithm to recompute efficiently fitness in solution's neighbourhood was used [15].

The results obtained for the easy problem ($L = 30$) are shown in Figure 2 and in Table I. Both algorithms were able to found an optimal solution. MA_{RMHC} and MA_{SDLS} reached it in less than 2 seconds. EA needed 300 seconds to obtain the same result. What is more, EA found the desired result in 40% of tested cases only.

TABLE I: Results obtained for LABS ($L = 30$)

T	EA	MA_{RMHC}	MA_{SDLS}
60	0.20 ± 0.10	0.0	0.0
180	0.13 ± 0.10	0.0	0.0
300	0.10 ± 0.09	0.0	0.0

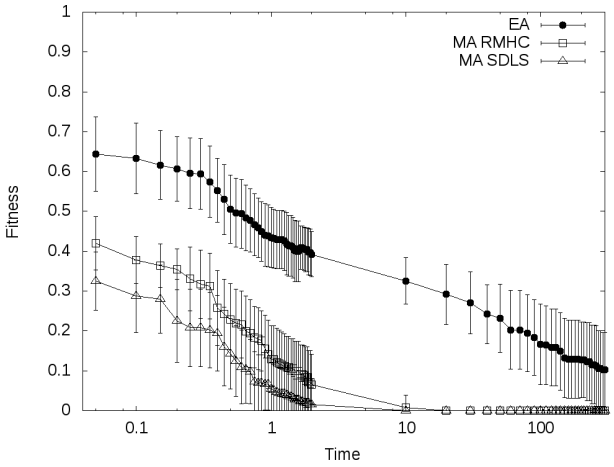

Fig. 2: Simple ($L = 30$) LABS problem in logarithmic scale

The results obtained for harder problem ($L = 50$) are presented in Figure 3 and in Table II. Only MA_{SDLS} was able to reach an optimum after 300 seconds (70% of successful computations took place). Note that EA, MA_{RMHC} and MA_{SDLS}'s error bars in Figure 3 are disjointed—when more sophisticated local search method was used, the results yielded to be significantly better. It is to note that both MAs produced their results in about 10 times less iterations then EA in the same time.

TABLE II: Results obtained for LABS ($L = 50$)

T	EA	MA_{RMHC}	MA_{SDLS}
60	0.52 ± 0.03	0.28 ± 0.05	0.10 ± 0.06
180	0.50 ± 0.02	0.23 ± 0.05	0.04 ± 0.05
300	0.47 ± 0.03	0.21 ± 0.05	0.02 ± 0.04

There has been a try to cache fitness, unfortunately in both EA and MA hit rate of cache was low and there was no improvement in efficiency of algorithms. Hit rate in EA was about 13%, in MA_{RMHC} 26% and in MA_{SDLS} 3%.

There was a Tabu Search implementation, but it turned out to be better than RMHC but worse than SDLS.

Job Shop

Configuration:

- common parameters:
  - population size: 50,
  - tournament selection,
  - swap mutation,
  - LOX recombinantion,
  - first memetic algorithm (MA): local search based on RMHC,

[1] http://age.iisg.agh.edu.pl

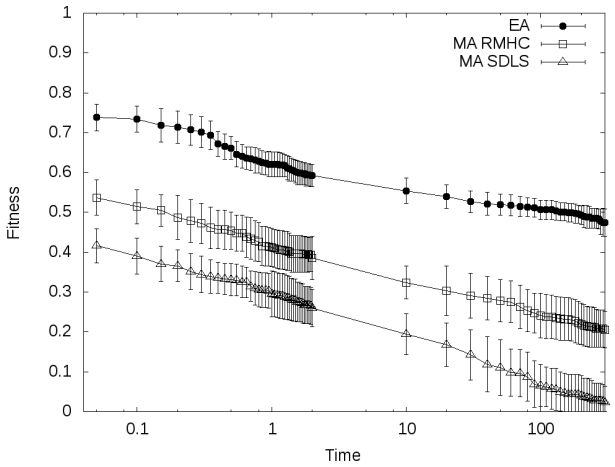

Fig. 3: The hard ($L = 50$) LABS problem in logarithmic scale

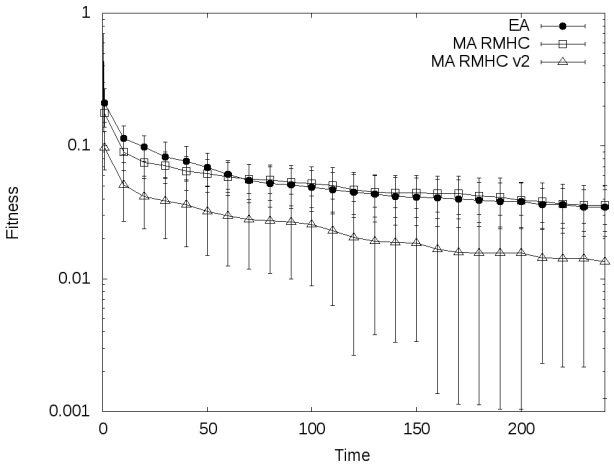

Fig. 4: Comparison of EA and MA for 7x7 OpenShop problem

– second memetic algorithm (MAv2): local search based on RMHC with swaping operations only on single machine mutation

- easy problem (7 jobs and 7 machines):
  – mutation probability: 0.1,
  – recombinantion probability: 0.3 (EA), 0.33 (MA) and 0.35(MAv2)
  – local search: 10 steps,
  – total execution time: 240 seconds,
- difficult problem (15 jobs and 15 machines):
  – mutation probability: 0.03 (EA) and 0.1 (MA and MAv2),
  – recombinantion probability: 0.28 (EA), 0.3 (MA), 0.35 (MAv2)
  – local search: 15 steps,
  – total execution time: 420 seconds.

Both problems were taken from Taillard benchmarks for OSSP [37].

Permutation with repetiton representation was used in evolutionary algorithm and first memetic algorithm. For the second memetic algorithm with single machine swap mutation we used normal permutation representation.

Results for 7×7 problem are presented in Figure 4 and in Table III. As one may notice, evolutionary algorithm and first memetic algorithm gave similar results, however in terms of generations memetic algorithm is much slower—after 60 seconds EA reached ca. 130 000 generation, while MA only 20 000.

Changing mutation in local optimalization for single machine swap (MAv2) gave noticeably better results, even though in terms of generations this algoritm is the slowest—after 60 seconds reached ca. 16 000 generation.

TABLE III: Results for 7×7 problem.

T	EA	MA	MAv2
10	0.114 ± 0.027	0.090 ± 0.025	0.051 ± 0.024
60	0.061 ± 0.016	0.059 ± 0.016	0.030 ± 0.017
240	0.035 ± 0.012	0.036 ± 0.015	0.013 ± 0.012

Results for 15x15 problem are presented in Figure 5 and in Table IV. In this case still the second memetic algorithm (MAv2) gave the best results. However the evolutionary algorithm gave better results than the first memetic algorithm (MA). Admittedly in terms of generations both memetic algorithms gave good results much faster, however one generation in memetic algorithms still takes much more time.

TABLE IV: Results for 15x15 problem.

T	EA	MA	MAv2
10	0.365 ± 0.075	0.322 ± 0.058	0.113 ± 0.029
60	0.218 ± 0.040	0.222 ± 0.053	0.058 ± 0.019
420	0.100 ± 0.030	0.132 ± 0.028	0.021 ± 0.015

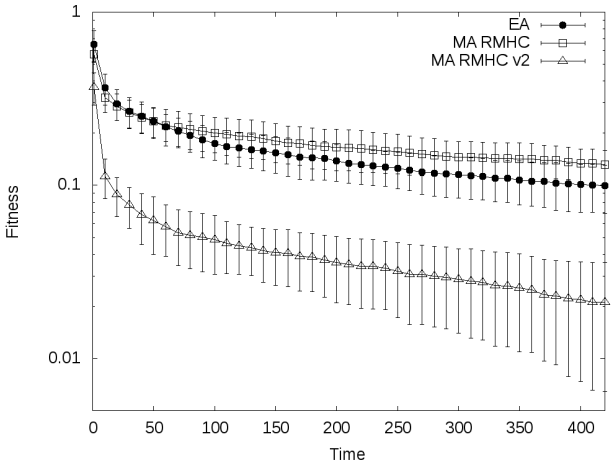

Fig. 5: Comparison of EA and MA for 15x15 OpenShop problem

Golomb Ruler

Configuration:

- common parameters—population size: 100, tournament selection, segment's length mutation with probability of 0.2, one-point crossover with probability of 0.8, total execution time: 300 seconds,
- memetic algorithm—local search based on tabu-search with 10 steps.

The results obtained for simple (7-mark ruler) problem are presented in Figure 6 and in Table V. Both algorithms have found optimal result after approximately the same

range of iterations (10^5), but memetic version completed the computation in less than 10 seconds. Evolutionary algorithm reached optimal result only 46.67% of the all tested cases, not earlier than after 300 seconds.

TABLE V: Results for finding 7-mark OGR.

T	EA result	MA result
60	0.030 ± 0.022	0.000
180	0.024 ± 0.021	0.000
300	0.019 ± 0.020	0.000

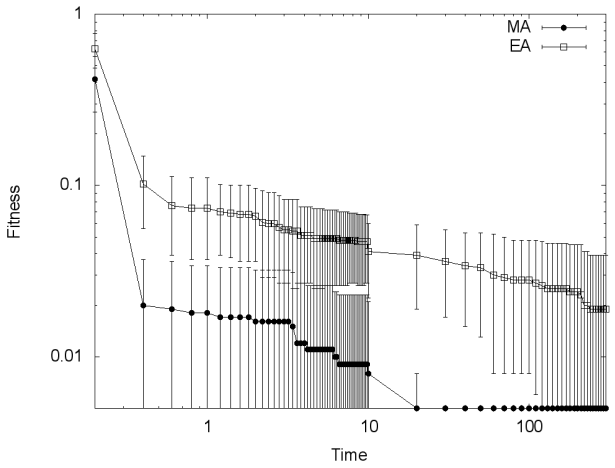

Fig. 6: Comparison of finding 7-mark optimal Golomb ruler by evolutionary (top) and memetic (bottom) algorithm. Both axis are in logarithmic scale.

The results obtained for high difficulty problem (14-mark ruler) are presented in Figure 7 and in Table VI. In this case neither of the algorithms reached optimal result, however both were stable. The memetic algorithm in every case reached better results, but it was much slower. After 300 s., it crossed 10^3 range of iterations, for evolutionary algorithm it was 10^5.

TABLE VI: Results for finding 14-mark OGR.

T	EA result	MA result
60	0.038 ± 0.007	0.022 ± 0.003
180	0.035 ± 0.006	0.020 ± 0.003
300	0.033 ± 0.007	0.018 ± 0.003

V. Preliminary results for memetic and evolutionary agent-based computing

In memetic [7] and evolutionary multi-agent systems (EMAS), agents represent solutions for a given problem, which are inherited from its parent(s) with the use of mutation and recombination. Assuming that no global knowledge is available and autonomy of the agents, selection is based on non-renewable resource, most often called *life energy*. The agents exchange energy meeting one another and comparing the quality of their solutions. At the same time a decisive factor of the agent's activity is the amount of energy it possesses—agents with high energy level are more likely to reproduce, while low energy increases the possibility of death. Each action is attempted randomly with certain probability, and it is performed only some preconditions are met

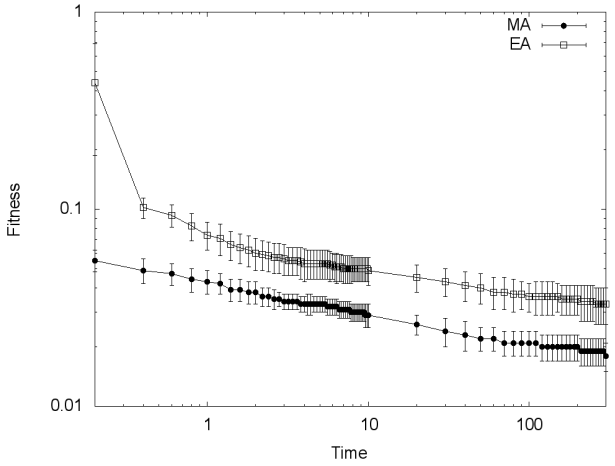

Fig. 7: Comparison of finding 14-mark optimal Golomb ruler by evolutionary (top) and memetic (bottom) algorithm. Both axis are in logarithmic scale.

(e.g. an agent may attempt to perform the action of reproduction, but it will reproduce only if its energy rises above certain level and it meets an appropriate neighbour).

In Fig. 8, preliminary results of optimisation of LABS problem (with lenght 30) were presented. The experiments were repeated 30 times. In both algorithms, the population of 50 individuals was used in the beginning. It is easy to see that in this case EMAS attains significantly worse results than EA. However, consider harder problem, namely

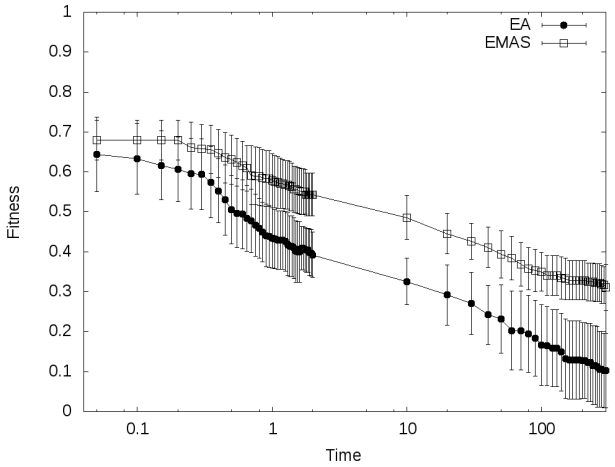

Fig. 8: EMAS and EA fitness for LABS (instance 30)

LABS instance of 50. The results of the solving of this problem with EMAS and EA were presented in Fig. 9. In this case, in the beginning of computation, the results are similar to the ones presented for the easier problem (LABS instance of 30). It is noteworthy, that later EMAS significantly prevails, confirming the well-known statement, that metaheuristics should be used as a *methods of last resort*, only for the complex problems.

Implementation of memetics in EMAS is carried out in a similar way as in classical evolutionary computing. In the case of Baldwinian memetics the evaluation operator is enhanced with local search algorithm. The evaluation of a certain individual starts the local search from this individual and returns the fitness of the solution found instead of the

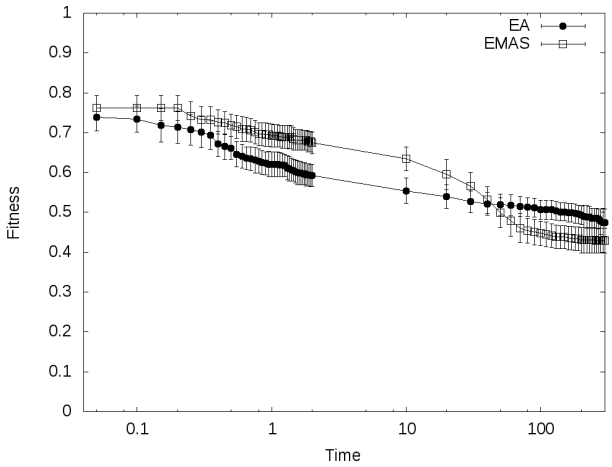

Fig. 9: EMAS and EA fitness for LABS (instance 50)

original fitness value. In Lamarckian model of memetics a dedicated mutation operator is called in the course of agent's life, therefore its genotype may be changed whenever this action is undertaken.

In EMAS, distributed selection mechanism allows for parallel ontogeny, so in one observable moment, certain number of individuals in the population might be about to die, other group could be almost ready for reproduction etc. In EA total synchronisation is maintained, so the whole population of individuals is processed at one time. Therefore, potential possibilities of finding new promising solutions seem to be better in the case of EA, yet the EMAS turns out to be better in this comparison.

To sum up, in Fig. 10, the number of newly produced individuals in each step for EMAS and its modifications is shown. The presented results have been gathered for 30 times repeated experiment consisting in optimisation of popular continuous benchmark function. Note, than in EA, the number of fitness function calls per generation is constant and equals the number of individuals that was 90 per one generation in the conducted experiments. Lamarckian and memetic modification lead to multiplication of this number in the case of the presented experimental results by 100, so the number of fitness computations for memetic EAs equals 900 per generation.

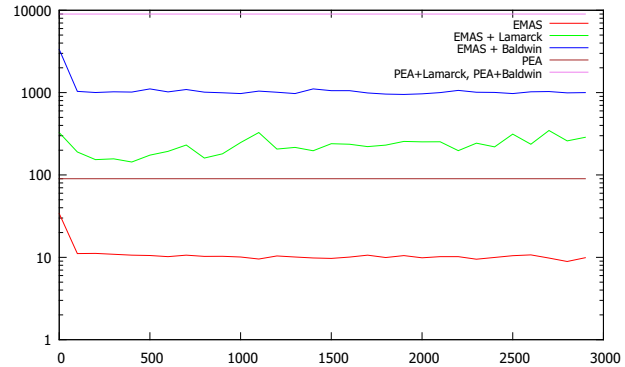

Fig. 10: Number of fitness function calls in EMAS and its memetic variations depending on the step number

However, the number of fitness function calls in the case of EMAS oscillates around 10 is an significant advantage of this computing method, moreover, Lamarckian modification of EMAS leads to obtaining about 200 fitness computations per step (still significantly lower than in the case of EA), while Baldwinian is the most costly one with the 1000 as estimate of the number of fitness computations. It is easy to see that low number of fitness function calls for EMAS makes it an interesting weapon of choice for dealing with problems characterised by a costly fitness function (e.g., inverse problems). In this case, the complexity of the implementation of the whole system, supporting the notion of agency, communication, naming services etc. is overwhelmed by the complexity of fitness function, so looking for a more intelligent search algorithm becomes reasonable, despite the intrinsic complexities imposed by its implementation.

VI. Conclusions

The main aim of the research presented in this paper was to prepare ground for researching agent-based memetic solutions for combinatorial optimisation problems. In order to do this, classical memetic approaches (evolutionary algorithm with Random Mutation Hill Climbing and Steepest Descent Local Search) to solving Low Autocorrelation Binary Sequence, Golomb Ruler and Job Shop were described. Experimental results were also gathered, processed and discussed, with stress on time efficiency.

Almost all the experiments yielded that memetic versions of the researched algorithms are significantly better than classical ones, but one must remember, that the results depend vastly on kind of local search used. However, one of the main problems of memetic algorithms is increased number of fitness function calls, imposed by the nature of this approach.

As a possible answer, moving to agent-based computing is proposed, as the cited results clearly show, that EMAS and its memetic variants significantly reduce the number of fitness function calls. Therefore, this effect merged with the memetic problem pointed out above, may result in fairly effective result, especially in the problems, where the fitness function is complex *per se*. This is preliminary confirmed by the presented experimental results of testing EMAS against EA for LABS problem. The agent-based metaheuristic turned out to be worse than EA for easier instance and significantly better than EA for hard instances of the considered problem.

In the near future the authors plan to further explore the possibilities of dealing with different types of combinatorial optimisation (e.g. more complex benchmarks, dynamic, multi-objective) using agent-based approaches.

Acknowledgment

The research presented here was partially supported by the grant "Biologically inspired mechanisms in planning and management of dynamic environments" funded by the Polish National Science Centre, No. N N516 500039.

References

[1] C. Papadimitriou and K. Steiglitz, *Combinatorial Optimization: Algorithms and Complexity*. Dover Publications, Inc., 1998.

[2] S. Droste, T. Jansen, and I. Wegener, "Upper and lower bounds for randomized search heuristics in black-box optimization," *Theory of*

Computing Systems, vol. 39, pp. 525–544, 2006. [Online]. Available: http://dx.doi.org/10.1007/s00224-004-1177-z

[3] M. Mitchell, *An Introduction to Genetic Algorithms*. Cambridge, MA, USA: MIT Press, 1998.

[4] P. Moscato, "Memetic algorithms: a short introduction," in *New ideas in optimization*. Maidenhead, UK, England: McGraw-Hill Ltd., UK, 1999, pp. 219–234.

[5] P. Moscato and C. Cotta, "A modern introduction to memetic algorithms," in *Handbook of Metaheuristics*, 2nd ed., ser. International Series in Operations Research and Management Science, M. Gendrau and J.-Y. Potvin, Eds. Springer, 2010, vol. 146, pp. 141–183.

[6] W. Hart, N. Krasnogor, and J. Smith, "Memetic evolutionary algorithms," in *Recent advances in memetic algorithms*, ser. Studies in Fuzziness and Soft Computing. Springer-Verlag, 2005, vol. 166, pp. 3–27.

[7] A. Byrski, W. Korczyński, and M. Kisiel-Dorohinicki, "Memetic multi-agent computing in difficult continuous optimisation," in *Proceedings of 6th International KES Conference on Agents and Multi-agent Systems Technologies and Applications, 2013, Hue City, Vietnam, IOS Press (accepted in 2013)*. Springer.

[8] L. Siwik and M. Kisiel-Dorohinicki, "Semi-elitist evolutionary multi-agent system for multiobjective optimization," in *Computational Science - ICCS 2006: Proc. of 6th International Conference*, ser. LNCS, V. N. Alexandrov, G. D. van Albada, P. Sloot, and J. Dongara, Eds., vol. 3993. Springer-Verlag, 2006.

[9] ——, "Improving the quality of the pareto frontier approximation obtained by semi-elitist evolutionary multi-agent system using distributed and decentralized frontier crowding mechanism," in *Adaptive and natural computing algorithms - ICANNGA 2007, Proc. of 8th international conference*, ser. LNCS, vol. 4431. Springer-Verlag, 2007.

[10] R. Dreżewski, "Co-evolutionary multi-agent system with speciation and resource sharing mechanisms," *Computing and Informatics*, vol. 25, no. 4, pp. 305–331, 2006.

[11] M. Kisiel-Dorohinicki, G. Dobrowolski, and E. Nawarecki, "Agent populations as computational intelligence," in *Neural Networks and Soft Computing*, ser. Advances in Soft Computing, L. Rutkowski and J. Kacprzyk, Eds. Physica-Verlag, 2003, pp. 608–613.

[12] A. Byrski and M. Kisiel-Dorohinicki, "Immune-based optimization of predicting neural networks," in *Computational Science - ICCS 2005: Proc. of 5th International Conference*, ser. LNCS, V. S. S. et. al., Ed., vol. 3516. Springer Verlag, 2005, pp. 703–710.

[13] A. Byrski and R. Schaefer, "Formal model for agent-based asynchronous evolutionary computation," in *Proceedings of IEEE Congress on Evolutionary Computation 2009 (IEEE CEC 2009)*, IEEE Computational Intelligence Society. Trondheim, Norway: IEEE Press, 18-21 May 2009.

[14] A. Byrski and M. Kisiel-Dorohinicki, "Agent-based model and computing environment facilitating the development of distributed computational intelligence systems," in *Computational Science - ICCS 2009, Proc. of 9th International Conference*, ser. LNCS, vol. 5545. Springer-Verlag, 2009.

[15] A. J. F. José E. Gallardo, Carlos Cotta, "Finding low autocorrelation binary sequences with memetic algorithms," *Applied Soft Computing*, vol. 9, 2009.

[16] P. V. H. Iván Dotú, "A note on low autocorrelation binary sequences," *Lecture Notes in Computer Science*, vol. 4204, 2006.

[17] F. H. Steven Halim, Roland H. C. Yap, "Engineering stochastic local search for the low autocorrelation binary sequence problem," *Lecture Notes in Computer Science*, vol. 5202, 2008.

[18] R. Cheng, M. Gen, and Y. Tsujimura, "A tutorial survey of job-shop scheduling problems using genetic algorithms, part i: representation," *Comput. Ind. Eng.*, vol. 30, no. 4, pp. 983–997, Sep. 1996. [Online]. Available: http://dx.doi.org/10.1016/0360-8352(96)00047-2

[19] T. F. Abdelmaguid, "Representations in genetic algorithm for the job shop scheduling problem: A computational study," *JSEA*, vol. 3, no. 12, pp. 1155–1162, 2010.

[20] C. Bierwirth, D. C. Mattfeld, and H. Kopfer, "On permutation representations for scheduling problems," in *In 4th PPSN*. Springer-Verlag, 1996, pp. 310–318.

[21] C.-F. Liaw, "A hybrid genetic algorithm for the open shop scheduling problem," *European Journal of Operational Research*, vol. 124, no. 1, pp. 28 – 42, 2000. [Online]. Available: http://www.sciencedirect.com/science/article/pii/S037722179900168X

[22] G. Bloom and S. Golomb, "Applications of numbered undirected graphs," *Proceedings of the IEEE*, vol. 65, no. 4, pp. 562 – 570, april 1977.

[23] A. Soliday, S.W. Homaifar and G. Lebby, "Genetic algorithm approach to the search for golomb rulers," in *6th International Conference on Genetic Algorithms (ICGA'95*. Morgan Kaufmann, 1995, pp. 528 – 535.

[24] B. Feeney, "Determining optimum and near-optimum golomb rulers using genetic algorithms," in *Master thesis, Computer Science, University College Cork*, 2003.

[25] J. Pereira, F.B. Tavares and E. Costa, "Golomb rulers: the advantage of evolution," in *Progress in Artificial Intelligence*. Springer Berlin Heidelberg, 2003, pp. 29 – 42.

[26] F. Tavares, J. Pereira and E. Costa, "Understanding the role of insertion and correction in the evolution of golomb rulers," in *Evolutionary Computation, 2004. CEC2004. Congress on*, vol. 1, june 2004, pp. 69 – 76 Vol.1.

[27] J. Tavares, F. Pereira, and E. Costa, "Evolving golomb rulers," in *Genetic and Evolutionary Computation - GECCO 2004*, ser. Lecture Notes in Computer Science, K. Deb, Ed. Springer Berlin Heidelberg, 2004, vol. 3103, pp. 416–417.

[28] I. Dotu and P. Van Hentenryck, "A simple hybrid evolutionary algorithm for finding golomb rulers," in *Evolutionary Computation, 2005. The 2005 IEEE Congress on*, vol. 3, sept. 2005, pp. 2018 – 2023 Vol. 3.

[29] C. Cotta, I. Dotú, A. Fernández, and P. Hentenryck, "A memetic approach to golomb rulers," in *Parallel Problem Solving from Nature - PPSN IX*, ser. Lecture Notes in Computer Science. Springer Berlin Heidelberg, 2006, vol. 4193, pp. 252–261.

[30] C. Cotta, I. Dotú, A. J. Fernández, and P. Hentenryck, "Local search-based hybrid algorithms for finding golomb rulers," *Constraints*, vol. 12, no. 3, pp. 263–291, Sep. 2007.

[31] E. Cantú-Paz, "A summary of research on parallel genetic algorithms," *IlliGAL Report No. 95007. University of Illinois*, 1995.

[32] J. Baldwin, "A new factor in evolution," *American Naturalist*, vol. 30, pp. 441–451, 1896.

[33] E. N. and G. S.J., "Punctuated equilibria: An alternative to phyletic gradualism," in *Models in Paleobiology*, T. Schopf, Ed. Freeman, Cooper and Co., 1972.

[34] K. Ku and M. Mak, "Exploring the effects of lamarckian and baldwinian learning in evolving recurrent neural networks," in *Proc. of 1997 IEEE Int. Conf. on Evolutionary Computation*. IEEE, 1997.

[35] D. Whitley, V. Scott Gordon, and K. Mathias, "Lamarckian evolution, the baldwin effect and function optimization," in *Proc. of Parallel Problem Solving from Nature III*, Y. Davidor, S. H.-P., and M. R., Eds. Springer, 1994.

[36] K. Pietak, A. Woś, A. Byrski, and M. Kisiel-Dorohinicki, "Functional integrity of multi-agent computational system supported by component-based implementation," in *Proc. of the 4th International Conference on Industrial Applications of Holonic and Multi-agent Systems*, ser. LNAI, vol. 5696. Springer-Verlag, 2009.

[37] E. Taillard, "Benchmarks for basic scheduling problems," *European Journal of Operational Research*, vol. 64, no. 2, pp. 278 – 285, 1993, <ce:title>Project Management anf Scheduling</ce:title>. [Online]. Available: http://www.sciencedirect.com/science/article/pii/037722179390182M

Extensible volunteer computing platform

Grzegorz Jankowski, Roman Dębski, Aleksander Byrski
AGH University of Science and Technology Al. Mickiewicza 30, 30-059 Kraków, Poland
E-mail: jankowskigreg@gmail.com, roman.j.debski@gmail.com, olekb@agh.edu.pl

Abstract—**Existing Volunteer Computing environments are usually dedicated to one project/application and, what is very often unwelcome nowadays, require some software to be installed on each volunteer PC. Moreover, the environments are not completely platform-independent so it is not possible to use a fast growing mobiles computation potential. The idea of utilizing a web browser as an environment for executing a volunteer computational task addresses the last issue. The paper presents an extensible, component oriented volunteer computing platform that may be easily adapted to different problems. After reviewing existing solutions, the architecture and behavior of the platform is discussed, and simulation results are given.**

Keywords—**volunteer computing; distributed computing; computing framework**

INTRODUCTION

There are problems that require great computation power to be solved. However, purchase and maintenance of such devices is costly. On the other hand such problems can be decomposed and distributed to machines of less computation power. Example problems which are computing with this approach are: knapsack problem, traveling salesman problem and others belonging to NPC or NPH classes. In volunteer computing paradigm, computation problem is decomposed and volunteer participants compute the parts on their own computers.

There are existing software solutions that supports volunteer computing. Although popular, they have some drawbacks e.g. they are software or hardware dependent and they can not be used with mobile devices which popularity and computation power grows fast. Moreover, their components needs to be installed on participants' computers. Nowadays computer users, especially those non experienced, are not willing to install anything on their machines. On the other hand almost everyone has an Internet browser installed and know how to use it.

Taking all those aspects into consideration, it was decided to propose and implement a new tool supporting volunteer computing. It is a portable and universal platform which can be used either from an installed application or from an Internet browser. Additional motivation for this paper was to design the architecture of this solution to be extensible and flexible depending on the particular computation problem.

Platform architecture is designed as service oriented architecture (SOA). In order to implement this architecture, services development and hosting technology was needed. Moreover, technology should cooperate with different software and hardware providers because users' computers might be configured variously.

It was decided to implement the platform in the Microsoft. NET technology. It is a popular and robust software development environment that offers interesting opportunities for services development. Windows Communication Foundation technology as a part of the .NET environment, provides runtime environment and ensures communication between them.

In this study, theoretical issues related to the field of computing in distributed systems are presented first. The next chapter describes the platform overview, its architecture and implementation. Lastly, the course of experiments with the platform and the most important conclusions are presented.

PLATFORMS FOR LARGE-SCALE COMPUTATIONS

Many large-scale computations are performed using supercomputers. However, this approach has one big disadvantage – it has always been expensive. That is why computer clusters (as a cost-effective[1] supercomputer substitute) started being used (for example [3]). Yet, sometimes the total cost (and effort) of building a computer cluster can also be too high (e.g. when thousands of computers are needed to perform a computation effectively). In such cases the ideas of *Grid Computing* [9], [14], *Volunteer Computing* [5], [1], *Cloud Computing* [10], [8], [13], [11], [2] or *Augmented Cloud Computing* [7], [4] can be utilized.

The platform presented in this paper utilizes the idea of volunteer computing based on web browsers. The main advantage of this approach is the hardware and software independency. A brief description of this concept is presented in the next two paragraphs.

A. Volunteer Computing.

Volunteer Computing[2] is a type of distributed computing where main computational resources come from the personal or office computers. The resources are shared by volunteers who want to support the specific computation.

Both in the past and at present there are many projects based on the paradigm of volunteer computing.The most famous are *SETI@Home*[3] (started in 1999) and the *Great Internet Mersenne Prime Search*[4] (started in 1996).

The most recognized frameworks for Volunteer Computing projects are Berkeley Open Infrastructure for Network Computing[5] (BOINC) (open source, base of SETI@Home), Xgrid[6] (a proprietary software prepared by and for Apple) or Grid MP[7] (a commercial product).

B. Web Browser Based Volunteer Computing.

Unfortunately, the existing Volunteer Computing environments are usually dedicated to one project/application[8]

[1] mainly because it is based on commodity hardware
[2] or a similar idea – *Sideband Computing* [15]
[3] http://setiathome.berkeley.edu/
[4] http://mersenne.org/
[5] http://boinc.berkeley.edu/
[6] http://www.apple.com/pl/server/macosx/technology/xgrid.html
[7] http://www.univa.com/
[8] And so, it cannot be considered even as a quasi-general purpose platform.

Proceedings 27th European Conference on Modelling and Simulation ©ECMS Webjørn Rekdalsbakken, Robin T. Bye, Houxiang Zhang (Editors)
ISBN: 978-0-9564944-6-7 / ISBN: 978-0-9564944-7-4 (CD)

and, what is very often unwelcome nowadays, require some software to be installed on each volunteer's PC. Moreover, the environments are not completely platform-independent so it is not possible to use a fast growing mobiles computation potential. The idea of utilizing a web browser as an environment for executing a volunteer's computational task addresses the last issue. The idea was already implemented in the past using Java Applets as computational workers (e.g. [12], [6]) but in this paper an approach with JavaScript is utilized.

THE PROPOSED PLATFORM

One of the paper aims was to create a platform supporting distributed computations in volunteer computing paradigm. The platform should provide an infrastructure that can be used by volunteers regardless of their software and hardware configuration.

In the platform surrounding there is an external system that is performing a calculation algorithm. This system delegates such calculations to the platform by sending packages in an well-defined format. A volunteer user who wants to contribute to the calculation connects to the platform by a client program. The client program (e.g. web browser) gets the calculations to perform from the platform and sends the results back to the platform. Finally, the external computing system fetches computation results from the platform.

Simplified conceptual diagram of the platform interaction with surroundings is shown in the diagram 1.

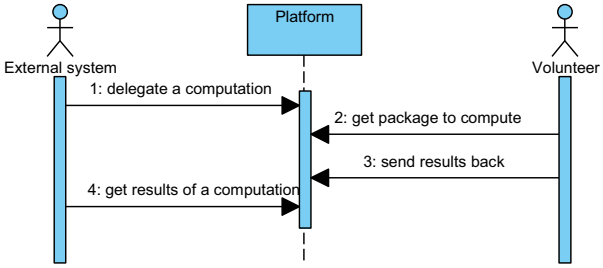

Fig. 1. Platform interaction with surroundings

C. Platform design and architecture

This section describes concepts and architecture assumptions of the platform as well as its implementation. The overall platform architecture is shown in the diagram2.

The external computation system that acts in the platform surrounding communicates with the platform by sending a computation requests or receiving its results in a well-defined package format. The package has a name (identification), data and an algorithm that is used to carry out the calculation. On the other side of the platform there are client programs run by volunteer users that contributes to the calculations. Clients download the packages, perform a calculations and send it back to the platform.

The platform consists of the three kinds of services: persistence services, package services, topology services. All the platform services acts in the pull model (download data from the other services).

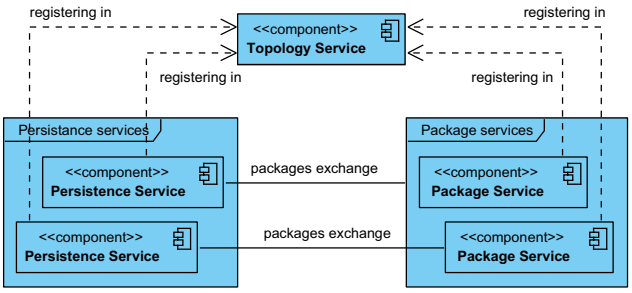

Fig. 2. The platform architecture

C.1 Interaction with surroundings

The platform provides services to its surroundings. The details of this collaboration are shown on the diagram 3.

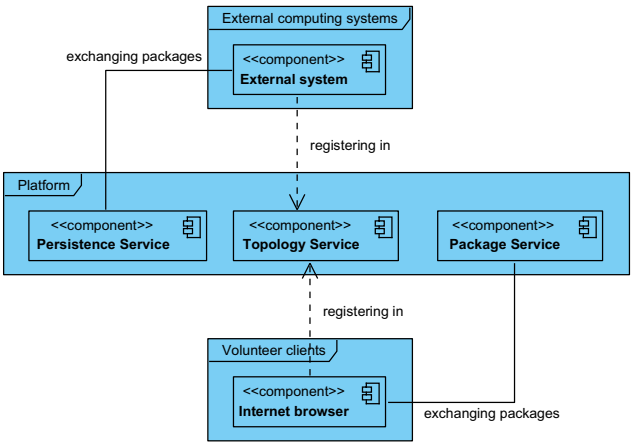

Fig. 3. Platform services interaction

A necessary condition to cooperate with the platform, both for the external computation systems, and volunteer clients is to register in the platform. It is done via topology service contract. Afterwards, an external computing system interacts with a persistence service, and clients with a package service.

C.2 Platform common structures

The section describes the platform common structures that are used by platform services. They are shown on the diagram 4.

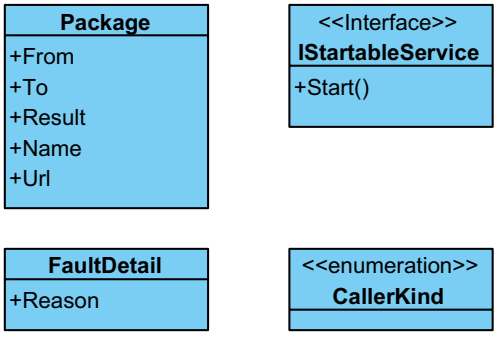

Fig. 4. Classes common for the platform services

Package class defines the data packet. It has a name, the number of the beginning and the end of the data interval, and the url to the library of the algorithm by which to perform the calculation.

FaultDetails class is responsible for providing information about errors.Information about the occurrence and cause of error between the web services platform are sent in the Reason property.

IStartableService interface is implemented by all the platform services. It allows to run the particular service.

CallerKindEnum enumeration indicates the topology service, what kind of service (or client) is registering.

C.3 Persistence service

Persistence service manages calculations delegated to the platform by an external computation system. The service provides the functionality to external systems as well as to the other platform services.

The service has two responsibilities in the interaction with external computation system.

Send a computation to perform to the platform - An external computation system sends the calculation in packages to the platform via the package service. Responsibility of the service is to store the packages for further processing.

Get a result of the computation from the platform - The service is responsible for sending results of the computation back to the external computation system.

The persistence service provides also two responsibilities for the other platform services.

Get a computation to perform - At the request of a package service it provides a package of calculations to perform. Package is shared only for a specific time and marked as shared. After the time expires, it will be marked back as available for download.

Send the result of the computation - Service receives the package with the calculation result and stores it until claimed by the external system. If the packages with the calculation results are sent back after the expiry of the time defined, it will be ignored. This behavior is intended to prevent from waiting for a package that will never be calculated (e.g. due to failure of another service or client).

Class diagram is shown on the diagram 5:

PersistenceService class implements service contract. It has a PackageProvider which responsibility is to provide packages for computations. FileRepository class manages packages serialized as files.

C.4 Package service

The service manages computation packages. It fetches them from a persistence service and provides to the volunteer clients. The package service does not have its own persistence. This implies that clients have just a certain time to perform computation and send the results back to the package service. Then the package service sends it back to the persistence service.

The service has two responsibilities for the volunteer clients.

Get package to compute - Volunteer clients who want to support a computation get packages via the service.

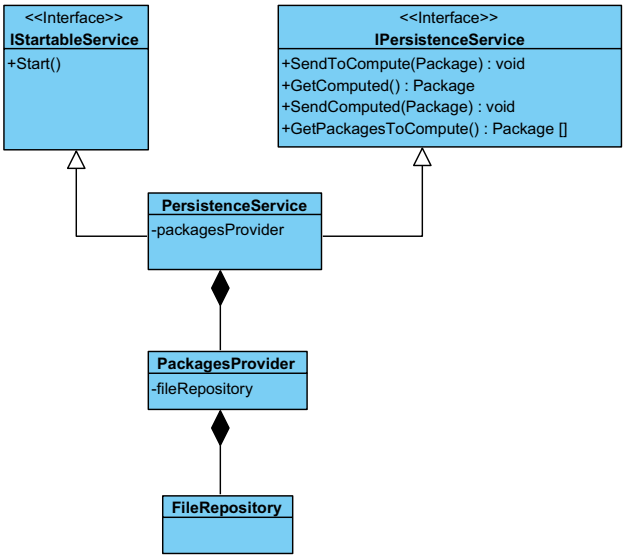

Fig. 5. Persistence service class diagram

Send computed package - After making computations, client sends the package with results back to the platform using the service.

Class diagram is shown on the diagram 6:

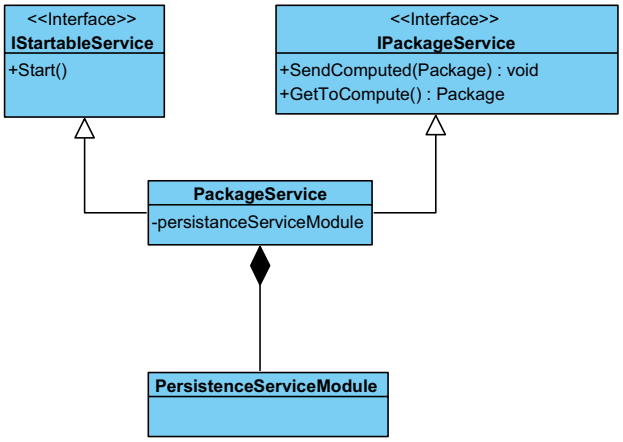

Fig. 6. Package service class diagram

PackageService class implements the service contract. It is so simple that the other classes were unnecessary.

C.5 Topology service

The platform is designed to work in a distributed environment. The topology service is responsible for an intelligent combining platform services with each other as well as clients and external computation systems in order to maximize the platform efficiency.

The service has a single responsibility.

Register - Every other platform service and the platform clients, at the time of its connection to the platform must register via the topology service. As a result the topology service knows about services and clients localization in the network and can manage the platform (e.g. load balancing). When registration is invoked, the topology service returns an address of the service which is the most appropriate for a

caller at the moment:

- For volunteer client: address of appropriate package service,
- For package service: address of appropriate persistence service,
- For persistence service: nothing is returned.

Class diagram is shown on the diagram 7:

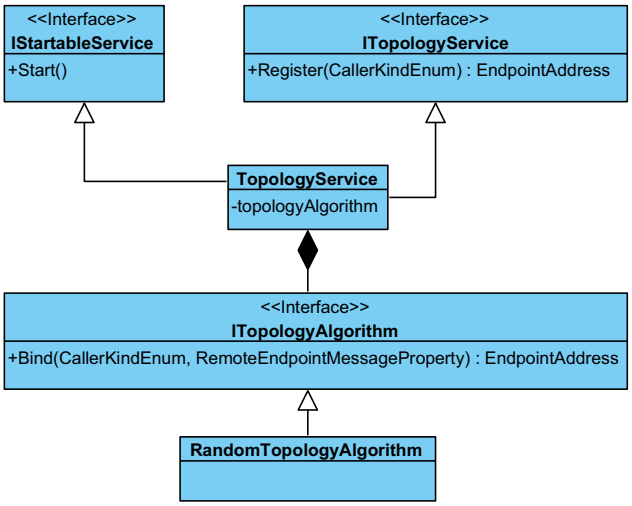

Fig. 7. Topology service class diagram

TopologyService class implements the service contract. Responsibility of the topology service to combine the platform components and the platform with its clients is delegated to a dedicated algorithm. This algorithm has to implement the interface ITopologyAlgorithm. An example algorithm implementation is RandomTopologyAlgorithm, which is combining randomly.

D. Platform deployment

The platform is designed to work in the distributed environment. However, it is also possible to install the platform entirely on one machine. In the further sections, the platform requirements and deployment process will be introduced.

The minimal platform configuration requires one topology service, one package service and one persistence service.

D.1 Requirements

The platform was designed to work on Microsoft Windows. The operating system should have Internet Information Services (IIS) version 6 or later installed. Moreover, .NET Framework 4.0 and Windows Communication Foundation (WCF) 3.5 are needed.

D.2 Installation

Installation of the platform is based on the installation of its services to IIS server through the supplied package (called deployment package).

The installation process should always be started from the topology service installation. It is the most important service from the platform initialization point of view because all the other platform services must register in it. The topology service address should be known within the platform and should be the single platform endpoint visible by the external systems and volunteer users.

EXPERIMENTAL RESULTS

This section will describe the experiments with the platform. The current implementation is only a proof of concept prototype so the empirical results will be provided showing platform potential and limitations.

E. Description and course of the experiment

The experiment consisted of finding prime numbers in a given numerical range.

A simple application imitating external computing system was created for the testing purpose. The application divided a numeric range 1 - 10 million into intervals of the equal count. The intervals boundaries were placed in the packages which were sent to the platform. The algorithm to find prime numbers in Java Script was also implemented. The algorithm was indicated to be executed on the packages data. The algorithm had the computational complexity of $O(n^2)$. The platform was responsible for the packages distribution to client machines. In the experiment participated from 1 to 16 computers. Each of them was running one Google Chrome web browser (version 19). Every computer participating in the experiment was identical to the hardware:

- CPU: Intel Core 2 Duo E6550 2,33 GHz
- RAM: 2GB

The platform which is the subject of research, has been placed, in full, on a single computer with hardware parameters:

- CPU: Dual - Core T2130 1,86 GHz
- RAM: 2GB

The platform was configured to have a single type of every service, which means one topology service, one package service and one persistence service.

F. Experiment results

The platform behavior was studied, depending on the number of compute nodes (computers with web browsers) and the degree of the problem decomposition on the intervals (number of packages to calculate sent to the platform). The time of calculations were measured in minutes started from the first package download from the platform by the client to the last calculated package returned to the platform. For each experiment configuration, three measurements were carried out, and the final result was the average of them. An important observation was, furthermore, that for any particular configuration the three measurements taken were very close to each other, differing at most by 1 minute.

G. Description of results and conclusions

The description of the experimental results, is divided into two parts: the platform support to the calculations in the volunteer computing paradigm and the platform limitations.

G.1 Volunteer computing calculations support

The idea behind the platform is to support the calculations in volunteer computing paradigm. The first observation is taken for the configuration where the proportions in a number of packages and the number of browsers are constant. In these configurations, each browser calculated exactly one data package.

With the increasement in the task decomposition on more packages and web browsers, a decrease in task processing time was observed. This is shown in figure 8. A calculation scenario for 1 package calculated on 1 computer (non-distributed computational task) the processing time was almost 3 hours. Distribution of the task resulted in significant decrease in computation time, up to only 19 minutes for 16 packages and 16 browsers. It was proved that the platform significantly supported the calculation by distributing packages.

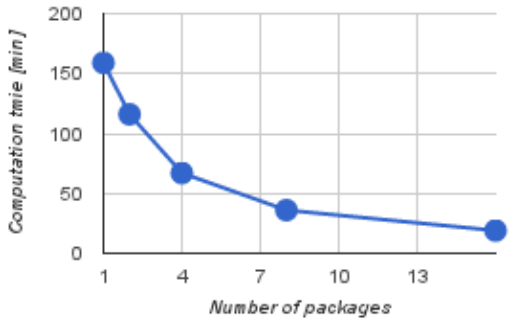

Fig. 8. The processing time for different amounts of web browsers, where each process one packet

The calculation time as an effect of the task decomposition degree was analyzed for a fixed number of 16 web browsers.

With increasement in the number of packages, calculation time initially decreased until it reached its minimum for 256 packages. For more packages, calculation time slightly increased and remained at a constant level. This is shown in figure 9. There are two facts relevant to explain this behavior: first, the computational complexity of the algorithm used was $O(n^2)$, so reducing the data set on which it operated gave significant gains. Second is to consider the overheads associated with communication within the platform and with client machines.

To achieve the minimal computation time - 10 minutes for 256 packages, the profits associated with an increased decomposition of the problem, outweighed losses resulting from the communication overhead. Not only the further increase in the number of packages did not reduce the computation time but even increased it for a one minute, because of the cost of communication. The analyzed results, allow to draw conclusions about the platform communication overhead. The interesting case, showing the platform limitations is described in section -G.2. It turned out that the communication overhead is at some point so significant that the platform can not keep up with it.

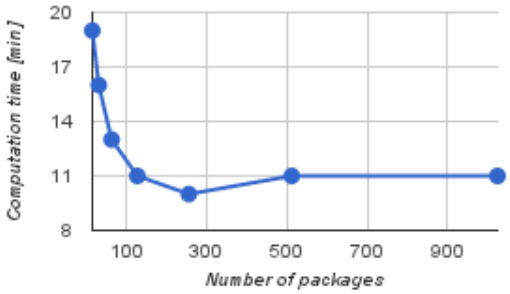

Fig. 9. Processing time for 16 web browsers

G.2 Platform limitations

In the experiment, there was an attempt to show the limit of the packages number when not only the calculation time is not decreasing, but is actually increasing due to communication overheads within the platform.The experiment was performed for 16 web browsers. As described earlier, the optimal number of packages for the investigated problem calculated on 16 compute nodes, was 256. For more packages calculation time slightly increased. However, for 2048 packages, the experiment failed. For this number of packages only 9-10 web browsers succeeded in registering in the platform. The rest have failed to register and start to process, due to the intense platform communication with the other client machines. Such a large number of packages, meant that in a small unit of time, the platform faced too many requests and it was not able to handle them all. This resulted in time limits exceed on requests and their rejection as a result. Prospects for the platform development in the direction of reducing the communication are presented in the summary of the article.

CONCLUSION

The aim of this article was to introduce a platform supporting calculations in volunteer computing paradigm.

The introduced solution met the assumptions. This was confirmed by experiments carried out (see. -E). It was shown that the platform supported the computation task performed in volunteer computing paradigm, by reducing the time of its calculation. The example calculation performed on a single computer lasted 159 minutes. After the calculation distribution by the plaatform to the 16 computers the calculation time decreased to 19 minutes. Therefore more than eight-fold decrease in the calculation time was achieved. The current implementation is most appropriate for coarse granular problems, i.e. in which the computation-to-communication ratio is relatively high.

The platform has a number of possible development direction. Two main trends are the expansion of the experimental research directions on its capabilities and the platform development.

In the experiment the platform consisted of a single topology service, one package service and one persistence service. The platform is designed to allow multiple services of the same type. Thus, another area of research may be different internal platform configurations. For example, with

more package services probably more compute nodes would get connected to the platform (see -G.2).

In the experiment carried out the platform is set up and run in its entirety on a single computer. The platform is a distributed solution itself. The individual components (services) can be placed on different nodes. By distributing the platform implementation the communication impact can be observed not only between the platform and the computational nodes, but also within the platform.

The main experiment to perform in the future, is to examine the platform performance on the Internet. Calculations in volunteer computing paradigm are usually conducted in the global network where many potential users are willing to support the project. In this experiment the impact of Internet communication and possibly other problems, such as firewalls might be examined.

Finally, it is worth to compare the performance of the platform with some existing environments to see advantages and disadvantages of the introduced approach.

The second proposed course of further work is the platform development.

An important component that might be improved is a topology service. Currently, the algorithm that binds platform services to its clients does it in the random way (see -C.5). If experiments are performed according to the scenarios proposed above, in which the configuration of the platform is more complex (there are more services), the algorithm will play a key role in the load balancing. It is therefore necessary to implement a family of algorithms and test their impact on the platform performance.

Limitations of the platform due to the excessive communication (see -G.2) can be tried to resolve in the development matter. In the current version of the platform when a package service receives a request from the client willing to calculate the package, it sends the request to a persistence service. Only after receiving a package from a persistence service, package service sends it to the client. The proposed solution is to introduce a buffer in the package service that will fetch more packages from persistence service than it needs at the moment. As a result, package service would provide packages for clients without the each time additional communication with the persistence service.

ACKNOWLEDGMENT

The research presented here was partially supported by the grant "Biologically inspired mechanisms in planning and management of dynamic environments" funded by the Polish National Science Centre, No. N N516 500039.

REFERENCES

[1] David P. Anderson, Eric Korpela, and Rom Walton. High-performance task distribution for volunteer computing. In *Proceedings of the First International Conference on e-Science and Grid Computing*, 2005.

[2] Michael Armbrust et al. Above the clouds: A Berkeley View of Cloud Computing. Technical report, UC Berkeley, 2009.

[3] David A. Bader and Robert Pennington. Cluster computing: Applications,. *The International Journal of High Performance Computing Applications,*, 15(2):181–185, May 2001.

[4] Aleksander Byrski, Roman Dębski, and Marek Kisiel-Dorohinicki. Agent-based computing in augmented cloud environment. *International Journal of Computer Systems Science and Engineering*, (1):7–18, 2012.

[5] Aleksander Byrski, Michal Felus, Jakub Gawlik, Rafal Jasica, Pawel Kobak, Grzegorz Jankowski, Edward Nawarecki, Michal Wroczynski, Przemyslaw Majewski, Tomasz Krupa, and Jacek Strychalski. Volunteer computing simulation using repast and mason. *Computer Science*, 14(1), 2013.

[6] Bartosz Czerwiński, Roman Dębski, and Kamil Piętak. Distributed agent-based platform for large-scale evolutionary computations. In *Proc. of 5-th Int. Conf. on Complex Intelligent and Software Intensive Systems. IEEE Press*, 2011.

[7] Roman Dębski, Aleksander Byrski, and Marek Kisiel-Dorohinicki. Towards an agent-based augmented cloud. *Journal of Telecommunications and Information Technology*, (1):16–22, 2012.

[8] K.R. Jackson et al. Performance analysis of high performance computing applications on the amazon web services cloud. In *CloudCom'10*, 2010.

[9] Carl Kesselman and Ian Foster. *The Grid: Blueprint for a New Computing Infrastructure*. Morgan Kaufmann Publishers, 1998.

[10] Peter Mell and Timothy Grance. The nist definition of cloud computing (draft). Technical report, National Institute of Standards and Technology, 2011.

[11] Jeffrey Napper and Paolo Bientinesi. Can cloud computing reach the top500. In *UCHPC-MAW'09*, 2009.

[12] Luis F. G. Sarmenta and Satoshi Hirano. Bayanihan: Building and studying web-based volunteer computing systems using java. *Future Generation Computer Systems*, 15:675–686, 1999.

[13] Christian Vecchiola, Suraj Pandey, and Rajkumar Buyya. High-performance cloud computing: A view of scientific applications. In *ISPAN 2009*, pages 4–16. IEEE Computer Society, 2009.

[14] Stephen J. Wright. Solving optimization problems on computational grids, 2000.

[15] Yongyong Xu. Global sideband service distributed computing method. In *Proceedings of the International Conference on Communication Networks and Distributed System Modeling and Simulation (CNDS98)*, 1998.

ABOUT THE AUTHORS

Grzegorz Jankowski obtained his M.Sc. in 2012 at AGH University of Science and Technology in Cracow and right afterwards started Ph.D. studies. He is interested in large-scale computing, in particular in volunteer model.

Roman Dębski is an independent consultant with over 14 years of experience in IT. He holds MSc in Computer Science (AGH University of Science and Technology) and in Mechanical Engineering and a PhD in Computational Mechanics (both obtained at Cracow University of Technology). His current research focuses on the cloud computing.

Aleksander Byrski obtained his Ph.D. in 2007 at AGH University of Science and Technology in Cracow. He works as an assistant professor at the Department of Computer Science of AGH-UST. His research focuses on multi-agent systems, biologically-inspired computing and other soft computing methods.

IN-DEVICE COEXISTENCE SIMULATION FOR SMARTPHONES

Sami Kiminki and Vesa Hirvisalo
Department of Computer Science and Engineering
Aalto University School of Science
P.O.Box 15400, FI-00076 AALTO, Finland
Email: {sami.kiminki,vesa.hirvisalo}@aalto.fi

KEYWORDS

wireless communications, in-device coexistence, smartphones, WiFi, LTE, protocol modeling, discrete event simulation

ABSTRACT

Wireless communication platforms in small enclosures are susceptible to in-device RF interference. Difficult interference cases emerge in the next-generation 4G smartphones using certain LTE bands, and support in MAC and higher protocol layers is required for efficient interference avoidance. Interference and the avoidance mechanisms create coupling between the radios complicating the interaction between the smartphone radios and their respective networks. Therefore, the purely analytical approach for studying radio performance becomes difficult.

In this paper we present RCOEX, an in-device coexistence simulator for the MAC layer. RCOEX simulates simple multi-network setups focusing on various in-device coexistence mechanisms and their performance. The simulation uses the discrete event variable time-delta model. As the protocol models are complex entities with non-trivial interaction, extensive effort has been made to support rich programming environment, including transceiver emulation, threads, and complex event filtering. Within this framework, we study the design of the WiFi model in more detail.

INTRODUCTION

Modern smartphones pack a number of radios in a small enclosure. Due to the current spectrum allocation, cellular (2G/3G/4G) and other radios (*e.g.*, WiFi, Bluetooth) may operate on close frequencies, which makes them susceptible to in-device RF interference. The related study item is known as in-device coexistence (IDC), in which various frequency-domain (FDM) and time-domain (TDM) solutions and mechanisms are studied. As the interference creates coupling between the affected radios, there must be some degree of cooperation between the radios for interference avoidance. (3GPP TR 36.816, 2012; Baghel et al., 2011)

The main interference scenario is the transmitter (TX) to receiver (RX) interference (Fig. 1). Due to non-linearities in RF processing, transmitters inflict noise around the frequencies of the transmitted signal as well as harmonics. Harmonics are easy to filter out but cost, size, and power issues limit reducing noise on the adjacent frequencies. As the TX signal may be more than 100 dB stronger than the RX signal, even small noise leakages may completely overshadow the reception. (Kiminki et al., 2011)

Arguably the most pressing IDC cases are with the LTE bands 7 (uplink 2500–2570 MHz), 40 (2300–2400 MHz), and 41 (2496–2690 MHz). LTE band 7 is one of the main bands allocated for 4G networks around the world, band 40 is common in Asia, and band 41 has been planned for North American region. The ISM band, in which WiFi and Bluetooth commonly operate, is between 2400–2500 MHz, the details varying per region. With unfortunate but not unrealistic network conditions, it may be that, *e.g.*, Bluetooth headset cannot be reliably used for LTE voice calls without specific IDC mechanisms, or the concurrent WiFi connection becomes flaky. (3GPP TR 36.816, 2012)

Our focus is on the IDC TDM mechanisms. Generally, the TDM mechanisms attempt to avoid problematic TX/RX operations by traffic shaping. Due to non-trivial interaction between the smartphone and the networks, and between the different radios in the smartphone, accurate results are difficult to obtain with purely analytical methods.

The nature of RF devices sets multiple requirements for the simulation of their behavior and control. In addi-

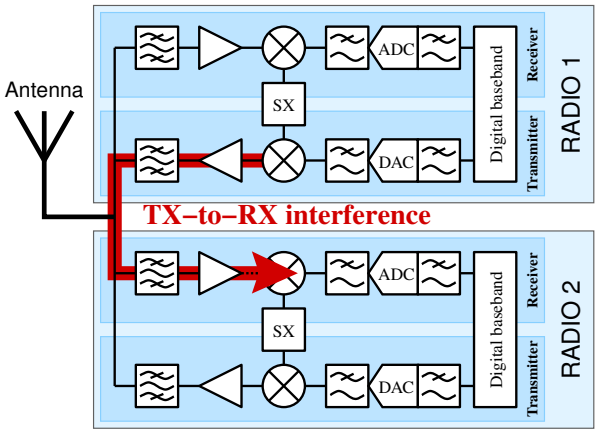

Figure 1: A common in-device interference case is that transmitter noise of one radio leaks to receiver of another

Proceedings 27th European Conference on Modelling and Simulation ©ECMS Webjørn Rekdalsbakken, Robin T. Bye, Houxiang Zhang (Editors)
ISBN: 978-0-9564944-6-7 / ISBN: 978-0-9564944-7-4 (CD)

tion to being real-time systems controlling mixed signal electronics, the related radio systems and in-device radio implementations are complex. Therefore, flexibility for incorporating different aspects and programmability for tackling the complexity of communication protocols are essential in the simulation technology.

There are several simulators available for study of wireless communication, *e.g.*, LTESim (Piro et al., 2011) for LTE, Pamvotis for WiFi (Pamvotis, 2013), and ns-3 (ns-3, 2013) for networks using multiple access protocols. However, we are not aware of simulators implementing in-device coexistence mechanisms for LTE and WiFi with the related protocol extensions.

To study the efficiency and implementation feasibility of the IDC TDM mechanisms, we implemented RCOEX, a MAC-level radio coexistence simulator for LTE (3GPP TS 36.300, 2013) and WiFi (IEEE 802.11, 2012). With RCOEX, we can compare different proposed mechanisms and their effect on bitrates and retransmission rates. RCOEX models the communication between the user device and the network access point, in-device interference propagation, and the required protocol layers from MAC to IP level. To some extent, multi-user network simulations are also possible. At the MAC level and regarding transmission timing, RCOEX follows the standards in detail. We have published some of the research results produced with RCOEX (Kiminki and Hirvisalo, 2012).

Simulating the operation and understanding the properties of IDC TDM mechanisms calls for integrated methods. Hybrid simulators have been extensively studied and applied in practice. For embedded systems, integration to state-based simulators are very common (*e.g.*, Simulink/Statemate). For radios, simulation technology suitable for circuit design can be dominating for methodology, *e.g.*, (Nastov et al., 2007), but sometimes protocols form the dominating part, *e.g.*, (Piro et al., 2011).

Our contribution is in implementing a MAC-level radio coexistence simulator by integrating other mechanisms to a discrete-event variable time-delta simulator. The detailed modeling of the LTE and WiFi operation has been the dominating task for the work. We begin our description by explaining our problem model from the radio IDC point of view. The subsequent section describes our simulator core. The simulator basis is a full-fledged programming language (Java) embedded with an asynchronous simulator kernel by us. We also review how we implemented our WiFi simulation model that uses a bridging layer for incorporating synchronous behaviors. We also discuss our way of modeling related physics. To show the capabilities of the simulator, we explain its application to an LTE-WiFi coexistence scenario, and then, conclude our presentation.

PROBLEM MODEL

We simulate wireless communication of the user device in various IDC scenarios. The user device can be concurrently connected to multiple different networks. During an IDC scenario, there can be in-device interference, which prevents simultaneous operations of different radios such as transmission and reception. The simulation goal is not to study the overall network impact by devices with IDC issues, but instead, the goal is to study the IDC mechanisms in fine-grain manner from the user device perspective. The assumption is that if the mechanism is effective from the user device perspective (*i.e.*, spectrum-efficient and bitrate-efficient), the mechanism is effective also from the network perspective.

Simple network models are therefore sufficient. For LTE, this means modeling the communication between the user equipment (UE) and the base station (eNodeB). For WiFi, the model contains frame exchange between the station and the access point. Detailed temporal behavior models are crucial so that the interfered RX/TX operations affect the communication patterns and network scheduling correctly.

Wireless channels are unreliable by nature. This is modeled by dropping frames with a configurable probability. In-device interference of operations is modeled by projecting RX or TX operations of one radio as interference to RX or TX operations of another. In-device interference is assumed to be hard, *i.e.*, interfered operation always fails. Note that in realistic implementations, RX of more prioritized radio may prevent TX of less, *e.g.*, by forcing power-off of offending RF circuitry, which justifies the RX-to-TX in-device interference modeling.

Detailed temporal behavior at PHY and MAC-level is of importance so that the impact of interfered transmissions and receptions reflects accurately to the changed communication patterns. The TDM-based IDC mechanisms also operate at the PHY/MAC level. The load is IP packets, which allows simulating application-level bitrates.

The general setup in LTE/WiFi IDC scenarios is that the LTE has higher priority. This means that the offending operations of the WiFi radio are averted. For successful IDC, this means that the LTE radio must provide interference-free intervals for the WiFi radio and the WiFi radio must be able to adjust into them.

The IDC mechanisms in a smartphone require internal communication between radios, which is also modeled. For simple mechanisms, the WiFi radio senses the interference in the channel access procedure (CSMA/CA). For more complex mechanisms, the LTE protocol produces conservative predictions on its forthcoming RX and TX gaps. The predictions are maintained in a prediction vector with known RX and TX gaps.

The simulation runs forward in time without clairvoyance. The desired simulation results are usually: application level bitrate, retransmission rate, and power efficiency. This allows comparing different IDC mechanisms. Bitrates and power efficiency measure the impact on user experience. Retransmission rate is a measure of spectrum efficiency, which is important for networks.

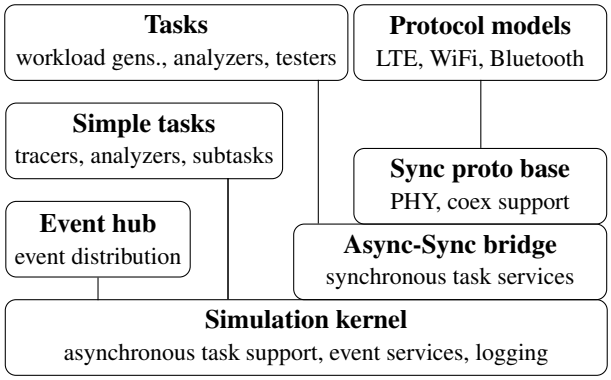

Figure 2: Architecture overview

COEXISTENCE SIMULATION

RCOEX is an event-based simulator with variable time deltas. The simulation consists of different simulation tasks such as protocols, load generators, and tracers. Many of them are further separated into subtasks. Most of the inter-task communication is by events with some of the communication additionally using shared objects such as queues. Simulation of physical transmissions and interference propagation is also implemented with events: start events signaling start of transmission or interference and end events the end of those. An overview of the simulator architecture is presented in Fig. 2.

The tasks are asynchronous at the low level and they are triggered by events and timers. To support synchronous programming model for complex protocol models (*i.e.*, to enable simulated sleeping and event waiting), an asynchronous-to-synchronous bridge layer is implemented. The tracer tasks analyze the event flow, producing bitrate and interfered frame rate measurements, for instance.

RCOEX simulates the timing-wise behavior of protocols in network setups. The ensemble of procedures related to different aspects of communication and protocols is fairly complex with many procedures containing intentionally stochastic behavior. The interaction between the user devices and the network base stations, in-device interaction between the user-device protocols, and interaction with workloads add more to the complexity of the big picture. This requires great flexibility in programming the simulation models and is the reason why considerable effort is paid to make the programming feasible.

The simulator and the simulation models are written in Java with the code base of approximately 20000 lines of code. The main rationale for using Java for the models (instead of dedicated simulation languages) was the existing libraries, debugging, and refactoring tools, which are essential for developing models with thousands of lines of non-trivial code. There is a performance-related trade-off in asynchronous-to-synchronous bridging performance, as synchronous tasks must be run in separate threads. This is because Java does not support continuations or co-operative multitasking, which means that a task that pre-empts cannot simply jump to the next task but has to switch threads. However, as a simulation run finishes usually in a matter of seconds, this trade-off between flexibility and performance is acceptable.

Simulation Kernel

The simulation kernel implements the time-delta simulation loop, event mediation, and provides a framework for implementing various simulation tasks.

The time-delta simulation operates on instances of class `TimeAdvanceAware`, which is the common base class for all tasks including the event hub. For each time-step, the simulation loop (Algorithm 1) polls each `TimeAdvanceAware` for their next wake-up times, possibly advances the simulation time, and invokes the wake up routines. The event hub ties the other tasks together. The tasks may send new events in a broadcast manner and receive events using various filters. The event hub buffers all new events and distributes them when the event hub task is run. The event filters are Boolean functions, which can match event types, event attributes, and they are composable for complex expressions. Custom event filters written in Java are also possible.

Algorithm 1 Simulation loop

```
while true do
    T ← min_{θ∈Tasks}(θ.NEXTWAKEUP())
    if T ≥ T_end then
        return                                  ▷ End of simulation
    end if
    for all θ ∈ Tasks do                        ▷ Inform tasks the new time
        θ.SETTIME(T)
    end for
    for all θ ∈ Tasks do                        ▷ Run tasks
        if θ.NEXTWAKEUP() = T then
            θ.WAKEUP()
        end if
    end for
end while
```

The asynchronous task model is sufficient for simple tasks but becomes cumbersome for many complex tasks such as protocol models. Because of this, RCOEX simulator provides an asynchronous-to synchronous bridge. Synchronous tasks are executed in their own threads and can use higher-level constructs such as DELAY function for sleeping and event queuing mechanisms, *e.g.*, WAITFOREVENT. Essentially, synchronous tasks can be run in a loop.

For simulation purposes, there exists two general event categories shared by all protocol models:

PhyEvent Physical layer event, such as transmission start and end and interference events

L2Event Protocol layer 2 events such as workload frame transmissions and control info events

The PhyEvent category enables modeling the propagation of transmissions between transmitters and receivers of protocol models. The general PhyEvent and L2Event categories can then be traced by analyzer tasks which provide statistics such as bitrates and interfered frame rates. Protocol models use also custom event types for communication between internal tasks.

Protocol Models and Other Tasks

The protocol models are based on synchronous tasks. The base protocol class provides a virtual PHY for transmission and reception, transceiver constraints vectors for IDC purposes, and workload interface.

The virtual PHY communicates with virtual PHYs of other protocol models by PhyEvents. The communication can be beneficial, *e.g.*, exchanging frames between the user device and the network access point, or harmful in case of interference. If interference overlaps with an operation in the virtual PHY, the operation becomes interfered and cannot successfully transmit data.

Transceiver constraint vectors are exchanged between protocols. There are separate constraint vectors for the receiver and the transmitter. The constraint vectors are combined from transmit/receive prediction vectors of higher-priority protocol models in an IDC scenario. The constraint vectors tell when transmissions and receptions are safe. For example, in the LTE/WiFi IDC case where the LTE receiver is interfered by the WiFi transmitter, the WiFi transmitter may be forced to be powered off whenever the LTE receiver is on. The prediction vector for the LTE receiver is then used as the constraint vector for the WiFi transmitter, thus, allowing planned use of the transmitter for interference avoidance.

For complex layered protocols, the protocol models are usually modeled using subtasks. For example, in the LTE protocol model, the uplink and downlink are separate subtasks with shared state. In WiFi protocol model, the frame scheduler, MAC, transmitter and receiver control are separate subtasks. For network simulation, there are separate model variants for protocols running in base stations (LTE eNodeB, WiFi access points) and protocols in user devices (LTE UE, WiFi station).

The protocol models are driven by workloads. For example, a WiFi station can only send or receive data frames if there is data to be sent or there is data in the access point to be received. The workload is IP packets and is provided by workload generators by the workload interface. The mainly used workload generator injects n new IP packets periodically to a protocol model.

Inter-protocol Interaction

In user devices with multiple active radios, in-device signaling between protocols should be simple and generic for practical reasons. Our approach has been to organize radios in priority order, the less flexible and the more important radios with higher priority, and the more flexible with lower priority. The priority order is then used in deciding which radio gets access during conflict. (Kiminki and Hirvisalo, 2012)

In practice, the cellular radios (2G/3G/4G) have highest priority in our scheme. The cellular network organizes scheduling, which usually prevents the user device to autonomously schedule reception or transmission. This is because the cellular spectrum is expensive in a sense that unused slots are away from other users. It is also expensive because many operators have spent considerable amount of money for the licenses.

On the other hand, WiFi and Bluetooth operate on the free bands. By design, the radio access by user devices is flexible in WiFi networks. In power save mode, the only timing-wise fixed operation by user devices is the reception of beacons at regular intervals. The user device can freely decide when it starts to send frames or when it initiates delivery of received frames from access point buffers. In terms of flexibility, Bluetooth is somewhere between WiFi and LTE. Therefore, the WiFi radio is at the lowest priority and the Bluetooth radio is in the middle.

After the prioritization is done, the general idea is that the lower-priority radios adapt to interference-free gaps left by the higher-priority ones. To prevent starvation, the higher-priority radios should be throttled in order to provide the gaps.

Throttling and traffic shaping may be done at higher protocol layers simply by throttling workload. It may also be supported by the MAC layer. In LTE, MAC layer traffic shaping mechanisms include measurement gaps and the DRX mechanism (3GPP TS 36.321, 2012), but the DRX mechanism further requires either workload throttling or extensions.

In the RCOEX simulator, the general model for intermediating the interference-free gap information is prediction vectors. These vectors contain conservative prediction of RX and TX gaps. If a gap is indicated for certain time interval, it is a guaranteed gap. However, a non-gap indicates only uncertainty, which may later change to a gap. Usually as the simulation time advances and the closer the prediction becomes, the more accurate it is. Note that in LTE, accurate gap prediction for the uplink (TX) is possible approximately 2–3 ms in advance by using UL HARQ grant information. During measurement gaps and DRX off-duration, accurate predictions for both uplink and downlink are possible further in advance. In the RCOEX LTE model, the prediction vectors are updated every subframe (1 ms).

The produced prediction vectors can be used for action planning. The WiFi model uses the vectors to decide whether or not to initiate transmission or to trigger delivery of buffered frames. For some delivery mechanisms, the gap prediction information is conveyed to the access point. One such mechanism is the proposed CXA-Poll (Kiminki and Hirvisalo, 2012), which extends the standard U-APSD delivery (Takeuchi et al., 2006) with a delivery deadline. In the RCOEX WiFi model, the prediction vectors are consulted during the CSMA/CA channel

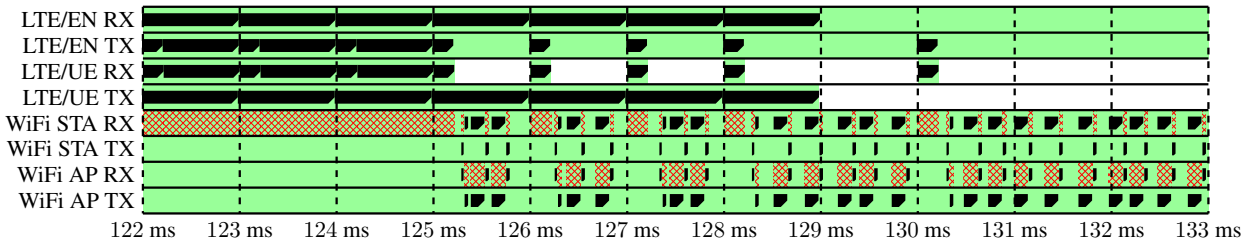

Figure 3: Visualized trace of LTE/WiFi IDC simulation where the use of LTE RX (UE) prevents simultaneous WiFi RX (STA). This setup is used to simulate the use of shared SDR receivers. Note that WiFi TX casts self-interference on WiFi RX. WiFi uses CXA-Poll delivery. Black bars denote transmission or reception, green areas powered-on state, and red crossing interference. UE and STA represent the user device. EN and AP are the LTE and WiFi network access points.

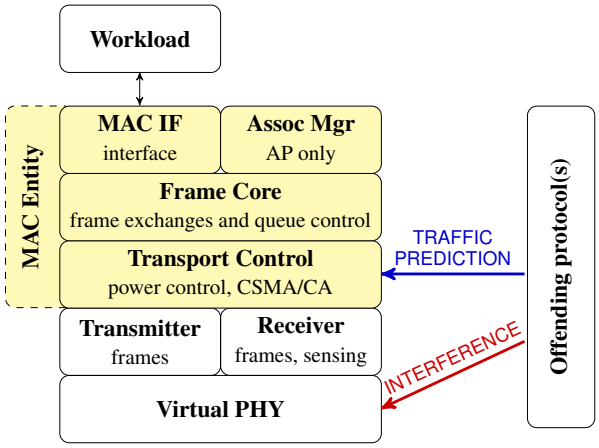

Figure 4: Overview of the WiFi model

access procedure when the CXA-Poll delivery is initiated. For more rudimentary inter-protocol IDC mechanisms, prediction vectors are not used. Instead, virtual sensing of interference may be used to extend the channel access procedure.

Preventing transmitter use because of higher-priority receiver use in RCOEX simulator is modeled by casting interference to the transmitter. This emulates cutting the transmitter power with the identical effect in communication patterns.

CASE: WIFI PROTOCOL MODEL

In this section, we examine the design and implementation of the WiFi simulation model in more detail. The WiFi model is layered with much of the same MAC-level functionality than what a real implementation would have. The WiFi model consists of virtual PHY, separate receiver and transmitter tasks, MAC entity task with multiple subcomponents, and an interface for workload generators. The overview is presented in Fig. 4. Technical details on the WiFi protocol can be found in, *e.g.*, (Gast, 2005), and authoritatively, in (IEEE 802.11, 2012).

The receiver task listens to PHY events from the transmitters of other protocol models. When transmission from an other WiFi node ends and the transmission does not contain interference, an event is sent to the MAC entity. The receiver also performs carrier sensing, which is used in the CSMA/CA procedure. The receiver task is asynchronous.

The MAC entity is also an asynchronous task reacting to events such as received frames and various timeouts (*e.g.*, no ACK frame received for sent data frame). The MAC entity commands transmissions and whether the virtual PHY should be powered or not. The MAC entity is further divided into subcomponents, such as Frame Core handling the lower level frame exchanges (*e.g.*, ACK handling and delivery mechanisms) with segmentation and concatenation of frames, Association Manager for managing associations in access point mode, and Transport Control for low-level frame queuing and CSMA/CA procedure. Transport Control is also responsible for transmission rate control, which uses the Minstrel algorithm in our case.

The transmitter is a synchronous task commanded by the MAC entity. It listens to the MAC entity command events and sends WiFi frames accordingly via the virtual PHY layer.

The main difference between a regular WiFi station and an access point is at the management level. For example, the basic network access for stations and access points uses the same CSMA/CA procedure. The PHY-level access capabilities of devices may be asymmetric, as wireless capabilities of stations are often biased to reception while the bias is on the better transmitter capabilities in the access points. The similarity allows the access point and station models share most of the code in the RCOEX simulator.

The low-level station-side IDC mechanisms are implemented in Transport Control. In WiFi, this means adaptation to interference-free gaps. The most effective mechanisms take advantage of the transceiver prediction vectors of the offending protocol. Frame transmission is postponed in CSMA/CA procedure if there is not enough interference-free time left for transmission and its corresponding acknowledgment. When triggering delivery of buffered frames by proposed CXA-Poll, a relative deadline for the delivery is added. For rudimentary best effort mechanisms, virtual sensing of interference is supported. In the access point and in case of CXA-Poll delivery, the deadline is used as an additional condition for triggering

the end of delivery.

To simplify simulation setups, there is WLAN Configurator, a small start-up time task. It handles setting up the network configuration, and most importantly, the initial associations between the WiFi devices.

The simulation runs produce traces, which can be further processed with tools such as bitrate calculator, spectrum efficiency analyzer, and various correctness analyzers. An example trace is visualized in Fig. 3 using the LaTeX/TikZ-based trace visualizer.

CONCLUSION

We presented the design of RCOEX simulator, an in-device coexistence simulator for smartphones and other space-constrained devices with multiple concurrently active radios. RCOEX is an asynchronous event-based simulator for studying IDC TDM mechanisms and their efficiency. Considerable effort has been made to support the implementation of protocol models focusing on the MAC level. Radio protocols are complex entities with multiple layers and subsystems resulting in non-trivial behavior under different network and workload conditions. Additional complexity comes from inter-protocol interaction due to in-device interference and its avoidance. To exemplify, we discussed the design of the WiFi protocol model.

By using a full-fledged programming language embedded with a simulation kernel we have been able to ensure sufficient programmability for our simulator. This basis also gives us enough flexibility to integrate other behaviors than asynchronous ones to our simulation. Most importantly, we have integrated synchronous behaviors by using a bridging layer. The selected simulation approach is generic, thus, also other radios, *e.g.*, Bluetooth, can be simulated in this way.

The simulators for embedded systems have a long tradition towards hybrid simulators that target control systems. However, embedded systems are becoming more and more software intensive systems. Also, the importance of networking and communication is increasing. This calls for new approaches and methods for simulating such systems. We see this direction the most important considering future research on the area.

REFERENCES

3GPP TR 36.816 (2012). Study on signalling and procedure for interference avoidance for in-device coexistence (V11.2.0).

3GPP TS 36.300 (2013). Overall description, v9.10.0.

3GPP TS 36.321 (2012). Medium access control (MAC) protocol specification, v9.6.0.

Baghel, S. K., Ingale, M. A., and Goyal, G. (2011). Coexistence possibilities of LTE with ISM technologies and GNSS. In *National Conference on Communications*, pages 1–5.

Gast, M. S. (2005). *802.11 Wireless Networks: The Definitive Guide*. O'Reilly, 2nd edition.

IEEE 802.11 (2012). Wireless LAN medium access control (MAC) and physical layer (PHY) specifications.

Kiminki, S. and Hirvisalo, V. (2012). Coexistence-aware scheduling for LTE and WLAN during hard in-device interference. In *ICST Conference on Cognitive Radio Oriented Wireless Networks and Communications*, pages 1–6.

Kiminki, S., Saari, V., Pärssinen, A., Hirvisalo, V., Immonen, A., Ryynänen, J., and Zetterman, T. (2011). Design and performance trade-offs in parallelized RF SDR architecture. In *ICST Conference on Cognitive Radio Oriented Wireless Networks and Communications*, pages 156–160.

Nastov, O., Telichevesky, R., Kundert, K., and White, J. (2007). Fundamentals of fast simulation algorithms for RF circuits. *Proceedings of the IEEE*, 95(3):600–621. Invited paper.

ns-3 (2013). The `ns-3` network simulator. http://www.nsnam.org/ (Accessed Mar 25th 2013).

Pamvotis (2013). Pamvotis — IEEE 802.11 WLAN simulator. http://pamvotis.org/ (Accessed Mar 25th 2013).

Piro, G., Grieco, L. A., Boggia, G., Capozzi, F., and Camarda, P. (2011). Simulating LTE cellular systems: An open-source framework. *IEEE Transactions on Vehicular Technology*, 60(2):498–513.

Takeuchi, S., Sezaki, K., and Yasuda, Y. (2006). Quick data-retrieving for U-APSD in IEEE802.11e WLAN networks. In *IEEE Wireless Communications and Networking Conference*, pages 1421–1427.

AUTHOR BIOGRAPHIES

SAMI KIMINKI received the M.Sc. degree in computer science and engineering from the Helsinki University of Technology (TKK), Finland, in 2007. He is currently working towards the D.Sc. (Tech) degree in Department of Computer Science and Engineering at Aalto University, School of Science, Finland. His primary research interests include various real-time control issues for reconfigurable multi-radio platforms covering hardware resource scheduling algorithms and coexistence mechanisms.

VESA HIRVISALO is senior scientist at the Aalto University Department of Computer Science and Engineering. He received M.Sc., Lic.Sc., and D.Sc. degrees in computer science and engineering from the Helsinki University of Technology, in 1994, 1998, and 2004, respectively. During his career, he has worked on various aspects of embedded systems together with the industry. His expertise area is in compiler technology and simulation mechanisms. His research interests are focused on on parallelism and energy-efficiency in mobile systems.

MAXIMALITY SEMANTIC FOR RECURSIVE PETRI NETS

Djamel-Eddine Saïdouni
Departement of computer science
University of Mentouri
25000, Constantine, Algeria
E-mail: saidouni@misc-umc.org

Messaouda Bouneb
Departement of mathematic and computer science
University of El Arbi ben M'hidi
Oum el boighi, Algeria
E-mail: bounebmessaouda@hotmail.com

Jean-Michel Ilié
Departement of computer science
University of Pierre and Marie Curie
75005, Paris, France
Email: jean-michel.ilie@upmc.fr

KEYWORDS
Formal methods, Dynamic systems, Recursive Petri nets, Maximality semantics.

ABSTRACT

This paper is in the framework of the specification and the verification of concurrent dynamic systems. We are interested by recursive Petri net specification model for which we define a maximality semantics. The underlying semantic model is a maximality-based labeled transition system. For this purpose, we propose a maximality operational semantic for recursive Petri nets. As an illustration, a system of filling medical bottles is specified in terms of recursive Petri net and translated to a maximality-based labeled transition system. This later is used to check the system properties. The properties are expressed using the CTL logic and verified by means of the FOCOVE tool.

INTRODUCTION

A Petri net is both a graphical and mathematical representation, used to formally specify the behaviors of concurrent systems. The marking graph associated with a given Petri net is used for checking the expected properties of the system. Indeed this marking graph is seen as a labeled transition system. However labeled transition systems are based on interleaving semantics. This later represents parallel executions as their interleaved sequential executions. To clarify the idea, we consider the example of two Petri nets (Figures 1.(a) and 1.(b)).

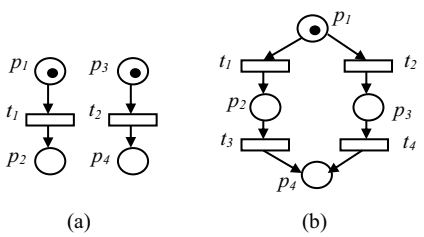

Figure 1: Petri nets.

Figure 1.(a) represents a system which can execute transitions t_1 and t_2 in parallel, whereas Figure 1.(b) represents a system that execute sequentially, either the transitions t_1 and t_3, or the transitions t_2 and t_4.
The marking graphs of the two Petri nets are given respectively by the labeled transition systems (LTS) of Figures 2.(a) and 2.(b). If both transitions t_1 and t_4 are labeled by the action a and t_2 and t_3 by b, then the two marking graphs are isomorphic. Therefore, the concurrent execution of the actions a and b is interpreted as their interleaved execution in time.

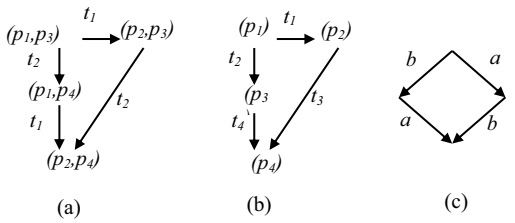

Figure 2: interleaving Semantics

This result is acceptable under the assumption that the firing of each transition corresponds to the execution of an indivisible action with null duration (structural and temporal atomicity of actions). Nevertheless, this assumption is often not realistic in practice.

Taking into account non atomicity of actions in a system has been deeply studied in the literature through the definition of several semantics supporting the concept of action refinement, e.g. L. Aceto and M. Hennessy 1991) (E. Best and al. 1991) (G. Boudol and I. Castellani 1988) (J.P.Courtiat and D.E. Saïdouni 1994) (J.P. Courtiat and D.E. Saïdouni 1995) (P. Darondeau and P. Degano 1989) (P. Darondeau and P. Degano 1991) (P. Darondeau and P. Degano 1993) (P. Degano and R. Gorrieri 1991) (R. Devillers 1992a) (R. Devillers 1992b) (R. Devillers 1993)(E.W. Dijkstra 1971) (W. Janssen and al. 1991) (D.E. Saïdouni 1996) (J.R. van Glabbeek 1990).

As a first advantage, action refinement allows a hierarchical design of systems. A second interest is the ability to semantically characterize concurrent executions of non-instantaneous actions. In this context, the maximality semantic was exploited to specify concurrent systems, through the model of the maximality labeled transition systems. This semantic

Proceedings 27th European Conference on Modelling and Simulation ©ECMS Webjørn Rekdalsbakken, Robin T. Bye, Houxiang Zhang (Editors)
ISBN: 978-0-9564944-6-7 / ISBN: 978-0-9564944-7-4 (CD)

was defined for several models of specifications, including some process algebras and place transition Petri nets (D.E. Saidouni and al. 2008a) (D.E. Saidouni and al. 2008b) (D.E. Saidouni and al. 2009a) (D.E. Saidouni and al. 2009b).

However, the limits of Petri nets have been highlighted when modeling systems with dynamic structures, such as multi agent systems. Therefore, Petri nets were extended to recursive Petri nets and dynamic behaviors are considered through a new kind of transitions, namely an abstract transition. The firing of such a transition represents the execution of a thread. The behavior of any thread is modeled by the recursive Petri net. As abstract transitions can represent non atomic activities, true concurrency semantics appears to be more appropriate than interleaving one. Abstract transitions can be used to design the dynamic system hierarchically.

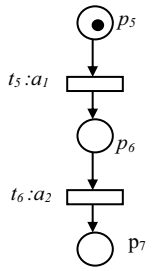

Figure 3: Refinement of abstract transitions.

Consider the two nets of Figure 1 again but assume now that t_1 and t_4 are abstract transitions in order to model the run of complex actions. For sake of simplicity, the behaviors associated with these two transitions accords with the same description, specified by the Petri net of Figure 3, where the transitions t_5 and t_6 are labeled by actions a_1 and a_2 respectively. Any firing of an abstract transition is assumed to create a new thread, whose execution runs from a token in the place p_5 and which can terminate when a token reaches the place p_7. By applying the marking graph generation method from both nets (e.g. in D. Dahmani 2009), we obtain their corresponding labeled systems, highlighted in Figures 4.(a) and 4.(b), respectively.

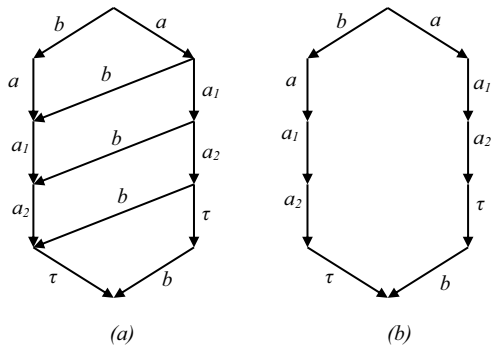

Figure 4: LTS refining the abstract transitions.

At this stage, observe that, the parallelism in the first system is expressed by the interleaved execution of the action *b* and the thread behavioral description related to the action *a*. Due to the differences between the two LTS representations, this example shows clearly that a hierarchical design of systems should be considered under a true concurrency semantic. Actually, two equivalent systems remain equivalent after refining a same action by a same process. Moreover, in the context of recursive Petri net, the interleaving semantic contradicts the fact that abstract transitions model activities (non-atomic actions).

For this purpose we propose a maximality operational semantic for recursive Petri nets. This operational semantic translates any recursive Petri net to a maximality-based labeled transition system. This allows the formal verification of recursive Petri nets. In fact we can use existing approaches and tools which operate on maximality-based labeled transition systems.

RECURSIVE PETRI NETS

Recursive Petri Nets (RPN) has been proposed for the specification and analysis of dynamic systems (S. Haddad and D. Poitrenaud, 2007) (S. Haddad and D. Poitrenaud, 1999) (D. Dahmani and al, 2009) (D. Dahmani and al, 2008).
Formally, recursive Petri nets are defined as follows. The standard definition is extended to associated actions to transitions.

Definition 1 : A recursive Petri net is defined by $R=(P,T,I,W^-,W^+,\Omega,\gamma,K)$ such that:

- P is a finite set of places
- T is a finite set of transitions such that $P \cap T=\emptyset$. It is composed of a disjoin sets of elementary transitions T_{el}, and abstract transitions T_{ab}.
- $I=I_C \cup I_P$ is a finite set of indexes, indicates the cut steps and preemptions.
- $W^-: P\times T\rightarrow \mathbb{N}$ is the precondition matrix.
- W^+: $Px[T_{el} \cup (T_{ab}\times I)\rightarrow \mathbb{N}]$ is the post-condition matrix.
- $\Omega: T_{ab}\rightarrow \mathbb{N}^P$ a function which associates to each abstract transition an ordinary marking (starting marking).
- γ is a family indexed by the set of termination I_C. Each set is specified as an effective representation of semi linear set of final markings.
- $K: T_{el}\times T_{ab}\rightarrow I_P$ a partial function of control which allows the modeling of external preemption.

Definition 2 : A labeled recursive Petri net is a pair $\sum=(R,\lambda)$ where $R=(P,T,I,W^-,W^+,\Omega,\gamma,K)$ is an RPN and $\lambda: T\rightarrow A$ is the action mapping of transitions.

MAXIMALITY BASED TRANSITIONS SYSTEMS

Let Ev be a countable set of event names and A an alphabet of actions.

Definition 3 : A maximality-based labeled transition system defined over Ev is a 5-uplet $(\Omega,\lambda,\mu,\xi,\psi)$ where $\Omega=<S,T,\alpha,\beta,s_0>$ is a system of transitions, such that:

- S is the set of possible states for the system; this set can be finite or infinite.
- T is the set of transitions or changes between states; this set can be finite or infinite.
- α and β are two mappings from T to *S* s.t. for any transition t, we have: α(t) is the source of T and β(t) its destination.
- s_0 is the initial state of the transition system Ω.
- (Ω,λ) is a system of transitions wherein each transition is labeled by an action of A, an occurrence of which must be started ($\lambda:T\rightarrow A$).
- $\psi:S\rightarrow 2^{Ev}$ associates with each state, a finite set of maximal event names, related to the actions
- $\xi:T\rightarrow Ev$ associates with each transition, the event name, identifying a new occurrence of action to be being started.
- $\mu:T\rightarrow 2^{Ev}$ associates with each transition, a finite set of event names corresponding to the actions to terminate in order to process the transition.

We have $\psi(s_0)=\emptyset$ and for each transition *t*, $\mu(t)\subseteq\psi(\alpha(t))$, $\xi(t)\notin\psi(\alpha(t))-\mu(t)$ and $\psi(\beta(t))=(\psi(\alpha(t))-\mu(t))\cup\{\xi(t)\}$.

Notation : Let mlts=$(\Omega,\lambda,\mu,\xi,\psi)$ be a maximality-based labeled transition system such that $\Omega=<S,T,\alpha,\beta,s_0>$. Any transition t is denoted $s \xrightarrow{E^{a}_{x}} s'$, t∈T is a transition such that α(t)=s, β(t)=s′, λ(t)=a, μ(t)=E and ξ(t)=x. For sake of concision, E^{a}_{x} is also noted Ea:x.

MAXIMALITY SEMANTIC FOR PLACE TRANSITIONS PETRI NETS

In this section we recall the maximality semantic of place transition Petri nets, proposed in (D.E. Saidouni and al 2008a). Within the marking graph:

- each place marking in a state is composed of two disjoint parts. The FT part contains free tokens while the BT part contains bound tokens . Therefore each place is marked by a pair (FT, BT).
- each state change (transition) corresponds to the start of execution for an action and is identified by an event name.
- each bound token identifies an action that is eventually being executed (this token corresponds to a maximal event).

Preliminary definitions

Let (P,T,W^-,W^+) be a Petri net and M one of its marking.

- The set of maximal event names in M is the set of all event names that can be used to identify the bound tokens in a marking. Formally, the function ψ is used to compute this set **:**
  $\psi(M)=\cup_{p\in P}\cup_{i=1,\ldots,mp} x_i$,
  assuming that, for all p in P, M(p)=(FT,BT) with $BT=\{(n_1,a_1,x_1),\ldots,(n_{mp},a_{mp},x_{mp})\}$.
- Let E⊂Ev be a non-empty and finite set of event names, the function makefree(E,M) is defined to free the bound tokens of a set E from a marking M, as follows:
  - $makefree(\{x_1,x_2,..,x_n\},M)=makefree(\{x_2,..,x_n\},makefree(\{x_1\},M))$
  - $makefree(\{x\},M)=M'$ such that for all p∈P, considering M(p)=(FT,BT), then:
    - If there is a bound token (n,a,x)∈BT in p then M'(p)= (FT+n, BT-{(n,a,x)})
    - Otherwise, M'(p) = M(p).
- A transition t of T t is enabled in a marking M iff $|M(p)|\geq W^-(p,t)$ for all p∈P. The set of all the transitions enabled in M is denoted *enabled(M)*.
- The marking M is said to be minimal for the firing of the transition t iff $|M(p)|=W^-(p,t)$ for all p∈P.
- Let M_1 and M_2 be two markings of the Petri net (P,T,W^-,W^+) and consider for any p of P that $M_1(p)=(FT_1,BT_1)$ and $M_2(p)=(FT_2,BT_2)$. We have $M_1\leq M_2$ iff $FT_1\leq FT_2$ and $BT_1\leq BT_2$, such that the relation ≤ is extended to sets of bound tokens as follows: $BT_1\leq BT_2$ iff $\forall(n_1,a,x)\in BT_1$, $\exists(n_2,a,x)\in BT_2$ such that $n_1\leq n_2$.
- Let M_1 and M_2 be two markings of the Petri net (P,T,W^-,W^+) such that $M_1\leq M_2$. The difference M_2-M_1 is a marking M_3 (M_2-M_1=M_3) such that for all p∈P, if $M_1(p)=(FT_1,BT_1)$ and $M_2(p)=(FT_2,BT_2)$ then $M_3(p)=(FT_3,BT_3)$ with $FT_3=FT_2-FT_1$ and $\forall(n_1,a,x)\in BT_1$, $(n_2,a,x)\in BT_2$, if $n_1\neq n_2$ then $(n_2-n_1,a,x)\in BT_3$.
- The function *get*:$2^{Ev}-\{\emptyset\}\rightarrow Ev$ is a function which satisfies get(E)∈E for any $E\in 2^{Ev}-\{\emptyset\}$.
- Given a marking M, a transition t and an event name x s.t. $x\notin\psi(M)$, the function occur(t,x,M)=M', assuming M(p)=(FT,BT), and M'(p)=(FT,BT') for all p∈p, is such that $BT' = BT\cup\{W^+(p,t),\lambda(t),x)\}$ if $W^+(p,t)\neq 0$ and BT'=BT otherwise. Hence, M' augments M with new bound tokens w.r.t. t and x.

MAXIMALITY SEMANTIC FOR RECURSIVE PETRI NETS

Let us first explain the proposed approach through simple examples.

A- Start and end of abstract transition firings

Consider the recursive Petri net of Figure 5 where t_2 is an abstract transition, the firing of which represents the execution of the action *b*. The firing of t_2 is a consequence of the end of execution related to the action *a,* attached to the transition t_1. The firing of this abstract transition starts the execution of a "son" thread, in addition to the initial thread. Both act concurrently on recursive Petri net, but with a distinct marking. The ordinary marking attached to the abstract transition is used to initialize the marking of the son Petri net. This is interpreted by the production of a token in the place p_5. The creation of a son Petri net from a thread is

represented by the firing of a virtual transition called *admitted*, here interpreted as the start of the action *b* attached to the abstract transition at the father thread level. The start of execution of the action *admitted(b)* is identified by the event *x*. This firing is similar to the firing of an elementary transition; it is followed by the production of a bound token related to this action in the BT part of the place p_5.

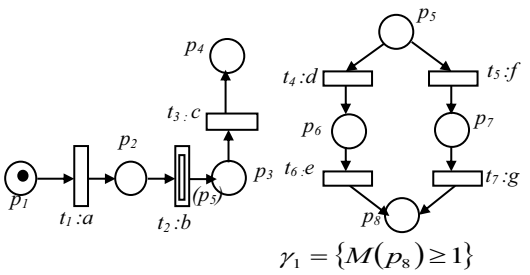

Figure 5: Recursive Petri net

After the generation of a bound token in the place p_5, any transition that can be fired from this thread will be immediately executed. But it is necessary to take into account the satisfaction of the termination predicate $\gamma=\{|M(p_8)|\geq 1\}$. This condition holds when either one of the transition t_6 or t_7 produces a token in the right part of the place p_8. When this predicate becomes true, a transition called *finished* can fire, which makes the return to the father thread, indeed this transition represents the cut step τ of the son thread.

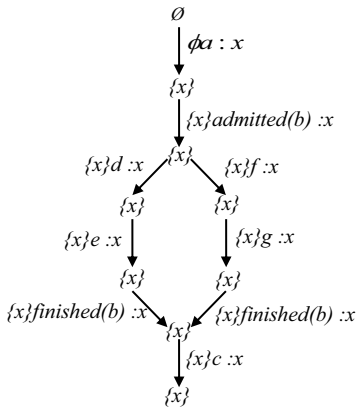

Figure 6: Start and end of an abstract transition

Generally, a transition *finished* is viewed as an elementary transition. Its firing causes the production of tokens in the BT part of all the places which belong to the post set of the abstract transition. Just after the end of the execution of abstract transition, the firing of the transition t_3 may happen. Figure 6 represents, the maximality labeled transitions system generated from this Petri net. Note that the event *x* identifies the action *admitted(b)* as well as the start of execution of the thread itself, thus it can be re-used within this thread. Once the son thread is finished, this event name can be re-used in the father thread.

Semantic of sequencing

Abstract transitions extend the relation of causality to the refinement of threads. Actually, the terminations of a thread can condition the start of another thread. For example in the Petri net of Figure 7, the activities of t_2 causally depends on the end of the activity of t_1.

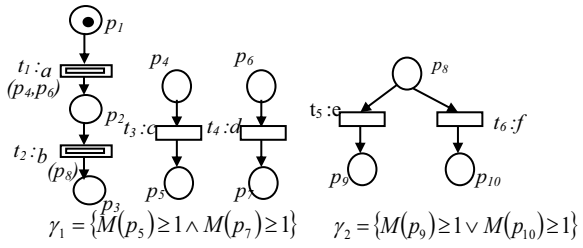

Figure 7: Sequence of activities.

Figure 8 represents the maximality labeled transitions system obtained by applying the maximality approach.

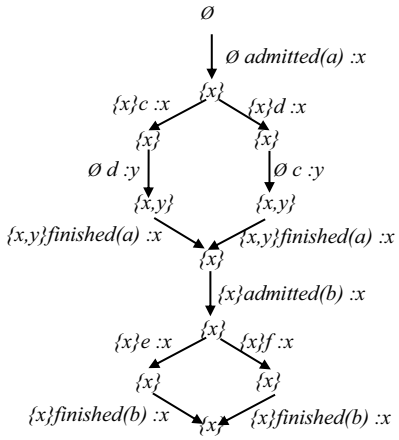

Figure 8: Sequencing and re-use of event names.

Semantic of parallelism

Consider now the recursive Petri net of Figure 9 where t_1 is an abstract transition. The behaviors associated with the two firing occurrences of this transition can be executed concurrently in parallel.

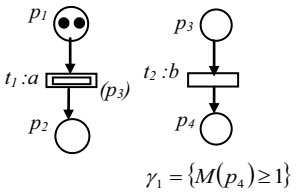

Figure 9: Parallelism of the abstract transitions.

The desired semantic must transform this relation of independence between two firing occurrences of the abstract transition into a parallel execution of two thread activities. The obtained maximality labeled transitions system is represented by Figure 10. The two firing occurrences of the thread, corresponding to the transition t_1, are identified by the event names *x* and *y*.

The set *{x,y}* means that the two corresponding activities implied by t_1 and t_2 may be in parallel execution, unless to be finished.

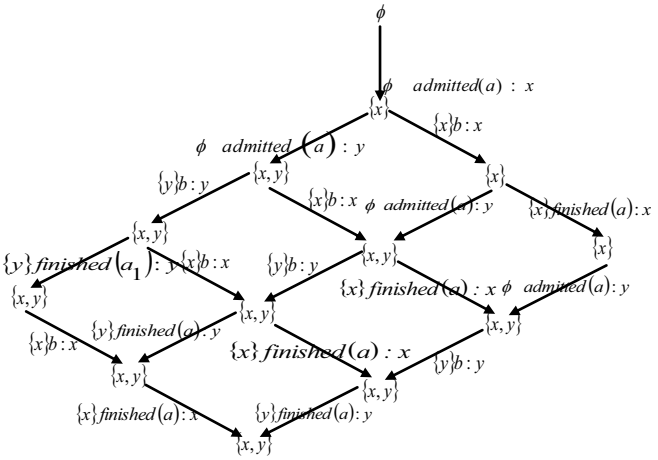

Figure 10 : Semantic of parallelism between threads.

Semantic of preemption

Consider the recursive Petri net of Figure 11. In the initial state of the system, observe that the free token in p_1 enables the firing of the elementary transitions t_1. In the same way the free token in p_2 enables the firing of the abstract transition t_2. The mentioned notation $t_1\{t_2<0>\}$ specifies that each firing of the elementary transition t_1 ends all the thread activities caused by some firings of t_2 (preemption concept).

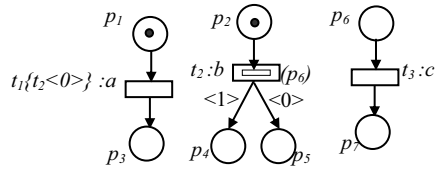

$$\gamma_1 = \{M / M(p_7) \geq 1\}$$

Figure 11 : Modeling of preemption.

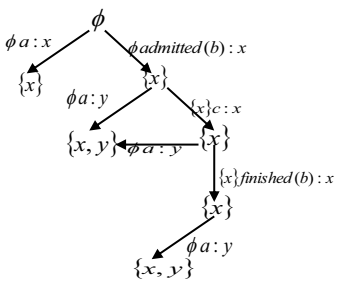

Figure 12 : Semantic scheme of a preemption.

From the initial state, three scenarios are possible, which are summarized in the maximality labeled transitions system of Figure 12. Observe that in all the cases, the firing of t_1 ends the execution of the thread corresponding to the transition t_2. In the first state, labeled by the set *{x,y}*, the event *y* identifies the start of execution of the transition t_1 however the event *x* represents the termination of the abstract transition t_2.

Operational semantic for labeled recursive Petri nets

In this section, we consider a labeled recursive Petri net $R=(S,T,I, W^-, W^+,\Omega,\gamma,K,\lambda)$ and different markings M, M_i, … of R.

Preliminary definitions.

1. We call thread configuration any pair of the form $(TH,(M)^e_{Ta})$ such that :

– M : is a marking of R
– e is an event name
– Ta is an abstract transition
– TH is a set of thread configurations.

Please, note that a thread configuration $(TH,(M)^e_{Ta})$ generally defines a tree of threads linked by a childhood relationship, the root of which is marked by M and is created under *e* by firing *Ta*. Let *THs* be the set of all the possible thread configurations for R.

– The initial thread configuration is built from the initial marking of R, e.g. M_0. It is denoted $(TH,(M_0)^{e_0}_{Ta})$. For sake of homogeneity, an extra event, namely $e_0 \notin$ Ev, is introduced to virtually launch the initial thread.

Moreover, according to any thread configuration $(TH,(M)^e_{Ta})$, let us introduce the following mappings:

- ψ:THs→2^{Ev} is the mapping which yields all the event names referred in a thread configuration and its descents. It is recursively defined by:
  - ✓ $\psi(\emptyset,(M)^e_{Ta})=\psi(M)$
  - ✓ $\psi(TH,(M)^e_{Ta})=\left(\cup_{th\in TH}\psi(th)\right)\cup\psi(M)$
- makefree: 2^{Ev} x THs → THs is used to free bound token within a thread configuration. It is recursively defined by:
  - ✓ $\text{makefree}\left(E,(\emptyset,(M)^e_{Ta})\right)=\left(\emptyset,\left(makefree(E,M)\right)^e_{Ta}\right)$
  - ✓ $\text{makefree}\left(E,(TH,(M)^e)\right)=$
$$\left(\bigcup_{th\in TH} makefree\,(E,th), makefree(E,M)\right)^e_{Ta}$$
- The enabling test of transitions is standard. The set *min(M,t)* denotes the set of all possible minimal markings built from M that enable the transition t. To deal with cut steps, let the mapping *cutstep* be s.t.
  - ✓ $\text{cutstep}\left((TH,(M)^e_{Ta}),\gamma_j\right)$ is true iff
$$\forall p\in P,|M(p)|\geq\gamma_j(p)$$
- The production of tokens specified by the mapping *occur* must be adapted to deal with different cases of firings, elementary and abstract transitions (see below in the semantic rules).

Semantic rules : The following four semantic rules allow one to create the maximality labeled transitions system of any labeled recursive Petri net, automatically.

1. $\dfrac{M,t\in enabled(M)\wedge t\in T_{el}}{(TH,(M)^{e}_{Ta})\xrightarrow{E^{\lambda(t)}x}(TH,(M')^{e}_{Ta})}$ such that:

$$\begin{cases} * \ \forall M'' \in \min(M,t), E=\psi(M''), \\ \qquad M''' = makefree(E, M-M'') \\ * \ M' = occur(t,x,M''') \text{ such that:} \\ \quad \forall p\in P, \text{if } M'''(p)=(FT''',BT''') \text{ and} \\ \qquad M'(p)=(FT',BT') \text{ then} \\ FT' = FT''' \text{ and} \\ BT' = \begin{cases} BT'''\cup\{(W^{+}(p,t),\lambda(t),x)\} \text{if } W^{+}(p,t)\neq 0 \\ \text{and} \\ BT''' \text{ otherwise} \end{cases} \\ * \ x = get\left(M-\left((\psi(M)-E)\cup\psi(TH)\right)\right) \end{cases}$$

2. $\dfrac{M,T_i\in enabled(M)\wedge T_i\in T_{ab}}{(TH,(M)^{e}_{Ta})\xrightarrow{E^{admitted(\lambda(T_i))}x}(TH',(M')^{e}_{Ta})}$ such that

$$\begin{cases} * \ \forall M'' \in \min(M,T), E=\psi(M''), \\ \qquad M''' = makefree(E, M-M'') \\ * \ \forall p\in P, M'(p)=M'''(p) \\ * \ TH' = TH\cup\{(\emptyset,(M_0)^{x}_{T_i})\} \\ \quad \text{such that} \\ \quad \forall p\in P, \ M_0(p)= \\ \begin{cases} (0,\{(\Omega(T_i)(p),admitted(\lambda(T_i)),x)\}) \text{ if } \Omega(T_i)(p)\neq 0 \\ \\ (0,\emptyset) \text{ otherwise} \end{cases} \\ * x = get\left(M-\left((\psi(M)-E)\cup\psi(TH)\right)\right) \end{cases}$$

3. $\dfrac{th_i,\frac{\exists\gamma_j\in\gamma}{cutstep(th_i,\gamma_j)}}{(TH,(M)^{e}_{Ta})\xrightarrow{\{x\}^{finished(\lambda(T_i))}x}(TH',(M')^{e}_{Ta})}$ such that

$$\begin{cases} * \ \forall th_i = \left(TH_i,(M_i)^{e_i}_{T_i}\right)\in TH, \\ \qquad x=e_i, \ TH' = TH-\{th_i\} \\ \\ * \ M' = occur(T_i,x,M) \text{ such that:} \\ \quad \forall p\in P, \text{ if } M'(p)=(FT',BT') \text{ and} \\ \qquad M(p)=(FT,BT) \text{ then} \\ FT' = FT \\ \\ BT' = \begin{cases} BT\cup\{(W^{+}(p,t,j),finished(\lambda(T_i)),x)\} \\ \qquad if \ (W^{+}(p,t,j)\neq 0) \\ \\ BT \text{ otherwise} \end{cases} \end{cases}$$

4. $\dfrac{M,M\in enabled(t),t\in T_{el}\wedge K(t,T_i)\in I_p}{(TH,(M)^{e}_{Ta})\xrightarrow{E^{\lambda(t)}x}(TH',(M')^{e}_{Ta})}$

CASE STUDY

In order to illustrate the interest of the proposed approach, let us consider a fault tolerant system, which consists of a "machine PKB of the society SAIDAL in Algeria". Later, we will use a logical approach of checking. A machine PKB is composed of a turn table which rotates the bottles, a dynamic arm which moves the bottles sequentially in a rectilinear way, a filler which fills the bottles by the medicine, and a stopper closing. The speed of a turn table can cause that some of the bottles can fall. When a bottle falls, a signal crosses the photo cell. This causes the task of shifting bottles to be preempted. The machine enters a state where the problem must be recovered: first raise the bottle, then charge it. The machine PKB is modeled in Figure 13.

The maximality labeled transitions system is brought out by Figure 14. The properties to be checked are expressed in CTL. In a natural way, we can directly reasons about the actions. It should also be noted that all the properties were checked by the tool FOCOVE (Formal Concurrency Verification Environment). For example, we can verify that the execution of the action "signal" directly causes that the thread "treat" responsible for recovering errors, is launched:

AG signal => EX admitted(treat)

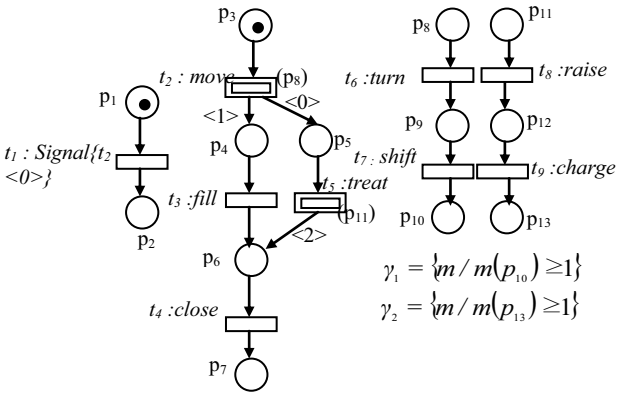

Figure 13: Modeling of a machine PKB

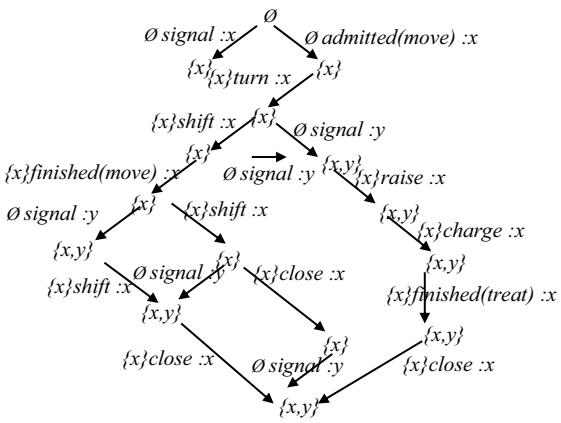

Figure 14: Maximality LTS of the PKB machine.

CONCLUSION

We proposed an operational method for building a maximality labeled transitions system from a labeled recursive Petri nets. This makes possible to take

advantadge of the verification techniques developed for the maximality labeled transitions systems. Here, the properties relating to the good performance of a system specified by a Petri net can be checked on it corresponding maximality labeled transitions system. It worth noting that the structure of the maximality labeled transitions systems represents the parallel execution of actions, as well as the parallel execution of threads.

REFERENCES

Aceto. L and Hennessy. M. 1991. "Adding action refinement to finite process algebra", in J. L. Albert, B. Monien and M. R. Artalejo, eds, ICALP'91, lncs, 510:506-519.

Andrews. D, Groote . J and Middelburg .C, eds, Workshop on Semantics of Specification Languages (SoSL'93), Workshops in Computing, Springer-Verlag, Utrecht, 289-303.

Best E, Devillers R, Kiehn A and Pomello L, 1991, "Concurrent bisimulations in Petri nets", Acta Informatica 28:231-264.

Boudol. G, and Castellani. I. 1988, Concurrency and atomicity, TCS 59:1-60.

Courtiat. J.P and Saïdouni. D.E. 1994, "Action refinement in LOTOS", in A. Danthine, G. Leduc and P. Wolpe, eds, Protocol Specification, Testing and Verification (PSTV'93), North-Holland, 341-354.

Courtiat. J.P and Saïdouni. D.E. 1995, "Relating maximality-based semantics to action refinement in process algebras".

Dahmani D., Ilié J-M., Boukala M. 2009, "Reachability analysis for Recursive Petri Nets with shared places". Abstractions for Petri Nets and Other Models of Concurrency (APNOC'09) - Petri Nets 2009, 65-79.

Dahmani. D. "Extensions of recursive Petri nets for temporal analysis of systems with dynamic structure". Doctoral thesis (2009). University of Sc. Techno. Houari Boumediene algeria.

Dahmani D., Ilié J-M., Boukala M. 2008, "Time Recursive Petri Nets". Transactions on Petri Nets and Other Models of Concurrency I (TopNoc) - Petri nets and system engineering, lncs, vol. 5100-2008, 104-118.

Darondeau. P and Degano. P. 1989, "Causal trees", in ICALP'89, LNCS, Springer-Verlag, 372:234-248.

Darondeau. P and Degano. P. 1991, "About semantic action refinement", Fundamenta Informaticae 14:221-234.

Darondeau. P and Degano. P. 1993, "Refinement of actions in event structures and causal trees", TCS 118:21-48.

Degano. P. and Gorrieri. R. 1991, "Atomic refinement in process description languages", in A. Tarlecki, ed., Mathematical Foundations of Computer Science, LNCS, Springer-Verlag, 520: 121-130.

Devillers. R. 1992a, "Maximality preservation and the ST-idea for action refinement", in G. Rozenberg, ed., Advances in Petri Nets, LNCS Springer-Verlag, 609:108-151.

Devillers. R. 1992b, "Maximality preserving bisimulation", TCS 102:165-183.

Devillers. R. 1993, "Construction of S-invariants and S-components for refined Petri boxes", in M. A. Marsan, ed., ATPN'93, LNCS, Springer-Verlag, 691:242-261.

Dijkstra. E.W 1971, "Hierarchical ordering of sequential processes", Acta Informatica 1(2):115-138.

Hogrefe. D and Leue. S, eds, IFIP TC6/WG6.1, 7th Int. Conf. on Formal Description Techniques (FORTE'94), Chapman & Hall, 293-308.

Janssen. W., Poel. M. and Zwiers. J. 1991, "Action systems and action refinement in the development of parallel systems", CONCUR'91, LNCS, 527:298-316.

Saïdouni D.E. and Courtiat. J.P. 1994, "Syntactic action refinement in presence of multiway synchronization". Semantics of Specification Languages 1993: 289-303

Saïdouni. D.E. 1996, "Maximality semantic: Application to actions refinement in LOTOS", PhD thesis., LAAS-CNRS, 7 av. du Colonel Roche, 31077 Toulouse Cedex France.

Saidouni. D.E., Belala. N and Bouneb. M. "Using maximality- based labeled transitions as model for Petri nets". The International Arab Conference on Information Technology (ACIT'2008).

Saidouni. D. E, Belala. N and Bouneb. M. "Aggregation of transitions in marking graph generation based on maximality semantics for Petri nets". Verification and Evalution of Computer and Communication systems (VECOS'2008).

Saidouni. D. E., Belala. N and Bouneb. M. "Using maximality- based labeled transitions as model for Petri nets". The International Arab Journal of Information Technology (IAJIT'2009a)

Saidouni. D. E, Belala. N and Bouneb. M. "Maximality-Based Structural Operational Semantics for Petri Nets". 2nd Mediterranean Conference on Intelligent Systems and Automation (CISA'2009b).

Van Glabbeek. R. J. 1990, "The refinement theorem for ST-bisimulation semantics", in IFIP Working Conference on Programming Concepts and Methods, North-Holland.

AUTHOR BIOGRAPHIES

Djamel E. Saïdouni was born in Algeria, he obtained his BEng degree from University of Mentouri Constantine, Algeria (1990). He obtained his PhD in theoretical computer science and concurrency from the University of Paul Sabatier, Toulouse, France (1996). Actually he is a professor at the University of Constantine 2 in Algeria and a permanent researcher of MISC laboratory where he is a head of FDCS team. His research domain research concerns formal specification and verification of complex distributed and real time systems.

.

Messaouda Bouneb was born in Algeria, she obtained her BEng degree from University of Mentouri Constantine, Algeria (2005). In February 2009, she obtained her M.Sc. degree in computer science at the University of El Arbi Ben-M'hidi Oum El-Bouaghi, Algeria. Her research domain is formal specification and verification of concurrent systems by the use of Petri nets.

Jean-Michel Ilié was born in France, he obtained several degrees in electronics and informatics among with its PhD thesis from the UPMC University of Paris (1990). Currently, member of the Paris Descartes University in its conference master higher grade (2009), he is also a permanent researcher of the LIP6 laboratory - UPMC. The fields of his research concern the formal validation of complex embedded distributed systems.

AN INTEGRATED MODEL OF PARALLEL PROCESSING AND PSO ALGORITHM FOR SOLVING OPTIMUM HIGHWAY ALIGNMENT PROBLEM

Seyed Farzan Kazemi and Yousef Shafahi
Department of Civil Engineering
Sharif University of Technology
Azadi St., Tehran 11365-9313, Iran
Email: shafahi@sharif.edu

KEYWORDS
Optimum Highway Alignment, Parallel Processing, Synchronous and Asynchronous Parallelization, Particle Swarm Algorithm, Master-Slave Architecture.

ABSTRACT

Optimum highway alignment is among the most substantial, but large and complicated topics in transportation area. Infinite number of feasible solutions, numerous local optima and the constrained feature of the problem, associated with complex and mainly non-linear constraints, has put an extra effort into the problem solving process. This paper focuses on solving highway alignment optimization problem using an integrated model of parallel processing and particle swarm optimization algorithm. To achieve this goal, algorithm parallelization is done in synchronous and asynchronous manner. For assessing parallel performance, corresponding indexes are evaluated. SRTM3 databank is used for solving real-world problems. The penalty function approach is employed for dealing with constraints. The successful application of the model is investigated on two real-world route location problems.

INTRODUCTION

Optimum highway alignment was a cumbersome effort during years. In this respect, many researches have been conducted on automatic route locating and design of highways. In the literature, a considerable number of studies have focused on automatic highway alignment design and many people were active in this area.

Designing optimum highway alignment is the most important part of a highway project, since little changes in alignment design leads to considerable changes in the overall cost of construction and even the maintenance of the project. In highway design, engineers nominate some alternatives as initial routes and try to improve these ones by trial and error, based on design constraints and especial project conditions. Finally, an alternative is picked out and finalized based on engineering justice and economic assessment. Noting that the quality of the selected route is highly dependent on the designer's experience, this method cannot be considered as an exact one. Also, if initial routes were not selected on a right basis, high expenditures will be forced to the project, which cannot be compensated even by using best methods for designing project line.

Choosing the final scheme in a highway project is based mainly on economic considerations. In the problem formulation, all sensitive costs should be taken into account. Cost formulation is a tough process which cannot be done in an exact way. For choosing the final alignment, economical comparison between alternatives may be required. The design is usually done separately for horizontal and vertical alignments. The objective of horizontal alignment design is to find the best route, from the economical point of view, to minimize pavement and user costs. In this respect, curvature and inclination of the route is restricted based on the highway type. In vertical alignment, fitting the project line on the natural ground level is investigated. Earthwork is the most costly component in vertical alignment optimization. There have been lots of studies regarding a model which minimizes cut and fill costs. In sophisticated models, other components of cost, such as pavement cost, right of way cost and user cost are also considered.

Not so much far away, choosing optimum highway alignment was done manually, mainly because of computation constraints and lack of mathematical models. By evolving mathematical models and development of high performance computers, highway engineers attempted to improve the design process by employing exact and practical methods. However, current highway alignment design methods are still manual to a large extent. As a result, finding optimum

Proceedings 27th European Conference on Modelling and Simulation ©ECMS Webjørn Rekdalsbakken, Robin T. Bye, Houxiang Zhang (Editors)
ISBN: 978-0-9564944-6-7 / ISBN: 978-0-9564944-7-4 (CD)

highway alignment using automatic computational methods would have satisfying benefits.

It should be noted that optimum highway alignment problem is a multi-modal problem with continuous search space, which may contain local optimums. Since the problem is typically of a large size, meta-heuristic methods are the only available approach, in order to solve it. To do so, choosing sufficient initial answers is required to reach the global or near-global optimum. Moreover, the computer program compiled on the basis of these algorithms must run adequately to gain satisfying levels of reliability. This process is accompanied by so much difficulty and is time-consuming due to the huge amount of computations and the complexity of the problem, resulting use of parallel processing for decreasing the problem solving time. In solving highway alignment problem, parallel processing may help to decrease the problem solving time and make it feasible.

In this study, the particle swarm method is employed to solve optimum highway alignment problem. Based on the large size of the problem and constraints in the geometric design, which shifts the problem into a constrained one, the idea of using parallel processing is utilized to increase the speed of problem solving and decrease the runtime.

A highway design problem is choosing the economical route between two cities (or two points on the map) which connects them to each other. Even in designing a network, the problem is mitigated into finding the optimum alignment connecting each two successive nodes. In general, the problem of designing a transportation network with more than one route can be converted to decompose the whole network into couple pairs and find the optimum route between each of the two.

LITERATURE REVIEW

There have been lots of studies regarding optimum vertical and horizontal alignments. However, the studies focused more on vertical alignment rather than horizontal alignment due to less cost components in vertical alignment. Furthermore, the problem of recursive routes is not considered for vertical alignment.

One of the first researchers who paid attention to optimizing vertical alignment was Easa (Easa 1988). He proposed a model in which project line should make a balance between cut and fill sections. Easa considered longitudinal gradients and vertical curvature as constraints. In next years, Moreb (Moreb 1996) followed Easa's research by reducing the dimensions of the problem. However, the main difference between the two was that Moreb's model guarantees finding global optimum and is more efficient in terms of computational effort.

Horizontal optimization models were developed gently, due to their complex estimation of cost components. Turners and Miles (Turners and Miles 1971) were among the first ones who proposed a horizontal optimization model based on shortest route, using plaid network. In fact, the optimization problem was converted into the network design problem.

Unlike plenty models which optimize horizontal or vertical alignment separately, development of models optimizing both horizontal and vertical alignments simultaneously has been too slow. It may be because of the complication of dealing with three-dimensional space. However, Chaw et al. (Chew et al. 1988) were among the first researchers who figured out the issue. They employed numerical search in their three-dimensional optimization model. Furthermore, Jong and Schonfeld (Jong and Schonfeld 2003) presented an evolutionary model for highway alignment optimization, in which cost components and design constraints are included comprehensively. Their model is capable of dealing with complex and non-derivative objective functions. Additionally, parabolic curves and simple circular curves are designed for vertical and horizontal alignments, respectively.

As increasing development of evolutionary methods, Shafahi and Bagherian (Shafahi and Bagherian 2012) used a PSO algorithm based model for optimizing both vertical and horizontal alignments, simultaneously. A penalty function approach was employed while facing geometric design constraints.

Searching the literature about the utilization of parallel processing in solving optimum highway alignment problem yielded no results. However, this approach is applied widely in other branches of science like Aerospace, Biomechanics and Computer Science.

PARALLEL PROCESSING

Parallel processing is a method of increasing performance through reducing runtime. This procedure is done by distributing subtasks between processors. In general, the goal of using such an approach might be a reduction in the runtime, achieving more accurate responses and economy by simulating intricate systems where simulation is not feasible without parallel processing (Rauber and Runger 2010).

In this study, *Speed-up factor* and *parallel efficiency* are the two parameters which we will use to assess parallelization performance.

PARTICLE SWARM OPTIMIZATION

Particle Swarm Optimization (PSO) algorithm was first developed by Kennedy and Eberhart (Kennedy and Eberhart 1995). This algorithm is inspired by social behavior of bird flocks and schools of fishes and is based on an iterative process. Each particle is a feasible solution of the problem in the search space and each iteration leads to an update in the position of particles, which is done by the following formula:

$$\boldsymbol{x}_i(t+1) = \boldsymbol{x}_i(t) + \boldsymbol{v}_i(t+1) \quad (1)$$

Where:

$\boldsymbol{x}_i(t+1)$=Position vector for the *i*-th particle at iteration *t+1*;

$\boldsymbol{x}_i(t)$= Position vector for the *i*-th particle at iteration *t*;

$\boldsymbol{v}_i(t+1)$= Velocity vector for the *i*-th particle at iteration t+1

A modified version of this algorithm in which $\boldsymbol{v}_i(t+1)$ is obtained using an inertia factor is proposed by Eberhart and Shi (Eberhart and Shi 1998). In this version, $\boldsymbol{v}_i(t+1)$ is calculated using the following formula:

$$v_{ij}(t+1) = \omega . v_{ij}(t) + c_1 r_1 (p_{ij}(t) - x_{ij}(t)) + c_2 r_2 (p_{gj}(t) - x_{ij}(t)) \quad (2)$$

Where:

$v_{ij}(t+1)$ = The *j*-th dimension of the *i*-th particle's velocity vector at iteration t+1;

ω=Inertia;

$v_{ij}(t)$ = The *j*-th dimension of the *i*-th particle's velocity vector at iteration t;

c_1= Personal cognitive factor;

c_2= Social cognitive factor;

r_1, r_2 = Random numbers lie in the interval [0, 1];

$p_{ij}(t)$ = The *j*-th dimension of the *i*-th particle's best fitness so far at iteration t (Known as *Particle Best*);

$p_{gj}(t)$= The *j*-th dimension of the swarm's best fitness so far at iteration t (Known as *Global Best*)

In this study, inertia (ω) is changing linearly from 0.6 to 0.1 during iterations. Furthermore, personal and social cognitive factors are assumed to be 2.

It worth mentioning that $\boldsymbol{p}_i(t)$ and $\boldsymbol{p}_g(t)$ are updated at the end of iterations.

Algorithm Parallelization

In every iteration of PSO algorithm, each particle moves to its new position, updates its velocity, updates its own new fitness, updates its personal best and finally, the global best of the swarm is updated. All of these tasks, except the latter one, could be done independently for each particle. This is the main idea of parallelizing the PSO algorithm. By assigning particles to processors, all the tasks, other than updating global best, is done independently on each processor. Only evaluating the global best of the swarm should be done using the output of all processors and cannot be done independently for each single one. In other words, $\boldsymbol{p}_{gj}(t)$ in (2) is calculated based on information derived from output of all processors which is determined in the previous iteration. Parallelization in this manner is called *Synchronous Parallelization*.

A practical approach for speeding up parallelization is replacing $\boldsymbol{p}_g(t)$ in velocity update equation with $\boldsymbol{p}_g$, which refers to the best particle found in the swarm *so far*. Parallelization in this manner is called *Asynchronous Parallelization*. In the meantime, each particle attaining a better fitness would update the global best and synchronizing operation which was done at the end of each iteration in synchronous parallelization, is neglected. Despite this little modification, it is likely for both parallelization types to lead to almost same results; although calculation details would be different between the two.

Processors' Architecture

For implementing parallel algorithms, a master-slave architecture based on Message Passing Interface (MPI) is employed. In the defined architecture, the master processor doesn't have any specific computational role and only makes communications between the slave ones. For making use of this architecture, after generating initial particles and assigning them to the processors, fitness is evaluated at the end of any iteration through slave processors and is then transmitted to the master processor. The master processor updates the global best and announces the results to the slave processors.

PROCEDURE OF MODELING THE PROBLEM

For modeling the problem, there are three important issues which should be investigated: generating initial particles (paths), dealing with constraints and evaluating cost components.

Generating Initial Paths

To generate an initial path, a random-based algorithm is developed. The pseudo code for this algorithm is presented in figure 1. The coordinate systems *xoy* and *x'oy'* and are global and local systems, respectively. The results of using this algorithm between cities Tehran and Isfahan (located in Iran) is depicted in figure 2 for the

following parameters in the pseudo-code:

$y'_{max} = -100\text{km},\ -50\text{km},\ +50\text{km},\ +100km;\ n = 300;\ c = 0.05;$

$m_0 = \frac{4y'_{max}}{n \times pd}$.

Pseudo-code for generating initial paths

procedure Generating Initial Paths
  for k=1→ *i* **do**
    input m_0, x_0, y_0
    $pd =$ **sqrt** $((x-x_0)^2+(y-y_0)^2)$
    $d = \frac{2y'_{max}}{pd.\frac{n}{2}(\frac{n}{2}-1)} - \frac{2m_0}{(\frac{n}{2}-1)}$
    for j=1→ *n* **do**
      $x' = (j \times pd) + (0.5 - rand()) \times pd$
      if $j \le \frac{n}{2}$ **then**
        $m = m + d$
        $y' = y' + m \times pd$
      else
        $m = m - d$
        $y' = y' - m \times pd$
      end if
      $y' = y' + c \times (1 - 2rand()) \times y'$
      $\begin{bmatrix} x \\ y \end{bmatrix} = \begin{bmatrix} x' \\ y' \end{bmatrix} \begin{bmatrix} \cos\theta & -\sin\theta \\ \sin\theta & \cos\theta \end{bmatrix}$
      Read *z* from database for each *x*,*y*.
      Save *(x,y,z)* as an intersection point of the route.
    end for
  end for
end procedure

Figure 1: Pseudo-code for generating initial paths

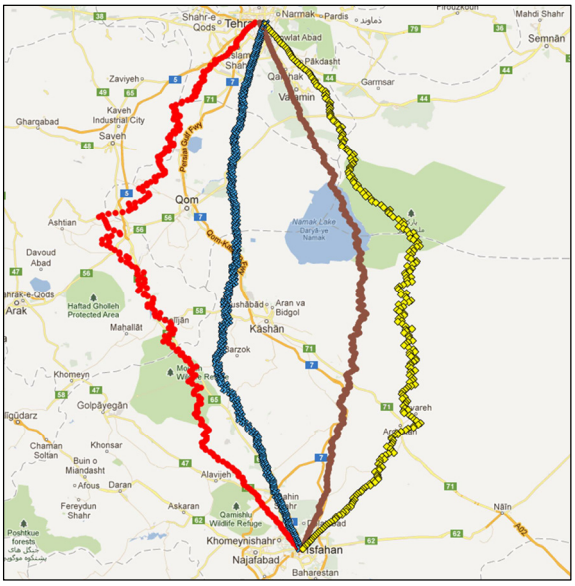

Figure 2: Generating initial paths between cities Tehran and Isfahan (Both cities are located in Iran)

Maximum Curvature of Horizontal Curves

In horizontal alignment, radius of curvature is the most important factor. AASHTO (AASHTO 2004) proposed the minimum permissible radius of horizontal curves as follows:

$$R_{min} = \frac{V^2}{127(0.01e_{\max} + f_{\max})} \tag{3}$$

Where:

$R_{\min}$= Minimum permissible radius, meters;
V= Design speed, km/h;
e_{max}= Maximum allowed superelevation, percent;
$f_{\max}$= Maximum side friction factor

If $L_{i,i+1}$ is the direct distance between intersection points i and i+1 , and Δ_i and Δ_{i+1} are the intersection angles at these points, respectively, one would calculate the minimum radius of curvature between intersection points which prevents the discontinuity of the path, using the following formula:

$$R_{i,i+1} = \frac{L_{i,i+1}}{\tan\frac{\Delta_i}{2} + \tan\frac{\Delta_{i+1}}{2}} \quad \forall i = 1,2,..,\#PI-1 \tag{4}$$

In the latter formula, *#PI* is the number of intersection points. Now we would be able to define a function for calculating penalty function between intersection points i and i+1, which is as follows:

$$C_{H\ i,i+1} = \begin{cases} a.(\frac{1}{\frac{1}{R_{i,i+1}} - \frac{1}{R_{min}}}) & R_{i,i+1} \le R_{min} \\ 0 & R_{i,i+1} \ge R_{min} \end{cases} \quad \forall i = 1,2,..,\#PI-1 \tag{5}$$

In this function, a is a constant which should be tuned based on the nature of the problem in question. The total penalty for route P regarding this constraint can be achieved using the following summation:

$$C_H(P) = \sum_{j=1}^{\#PI-1} C_{H\ j,j+1} \tag{6}$$

Maximum Longitudinal Grade

The longitudinal grade is penalized, as well as horizontal curvature, if it is greater than maximum allowed grade, which is $g_{\max}$. Considering $g_{i,i+1}$ to be the grade between successive intersection points i and i+1, the penalty function proposed by the authors for exceeding maximum allowed gradient is as follows:

$$C_{G\ i,i+1} = \begin{cases} b + c.(|g_{i,i+1}| - g_{max}) & |g_{i,i+1}| \ge g_{max} \\ 0 & |g_{i,i+1}| \le g_{max} \end{cases} \quad \forall i = 0,1,2,..,\#PI \tag{7}$$

In this function, b and c are constants and should be tuned based on the problem type. The penalty cost caused by exceeding maximum grade constraint for path

P would be equal to the following summation:

$$C_G(P) = \sum_{j=0}^{\#PI} C_{G_{j,j+1}} \quad (8)$$

Minimum Length of Vertical Curves

Minimum length of vertical curves is imposed mainly because of satisfying sight distance criteria and is calculated using the following formula, which is proposed by AASHTO (AASHTO 2004):

$$L_{\min} = K.A \quad (9)$$

Where:

$L_{\min}$ = minimum length for vertical curve, meters;

A = Algebraic difference in grades, percent;

K = Rate of vertical curvature, meters

Assuming parabolic symmetric vertical curves for intersection points of the vertical alignment of a highway, the minimum length between intersection points i and i+1 for preventing discontinuity of path is:

$$L_{min\ i,i+1} = \frac{1}{2}(K_i A_i + K_{i+1} A_{i+1}) \quad (10)$$

Again, d is a constant which should be determined empirically. The corresponding penalty function for minimum length of vertical curves is proposed as follows:

$$C_{V\ i,i+1} = \begin{cases} d.(L_{min\ i,i+1} - L_{i,i+1}) & L_{min\ i,i+1} \geq L_{i,i+1} \\ 0 & L_{min\ i,i+1} \leq L_{i,i+1} \end{cases} \quad (11)$$

So, the total penalty function for path P regarding its minimum length of vertical curves may be calculated through the following summation:

$$C_V(P) = \sum_{j=1}^{\#PI-1} C_{V_{j,j+1}} \quad (12)$$

Cost Evaluation

Cost Components are mainly divided into two major types: *construction costs* and *earthwork costs*. In this study, unit costs are derived from the Iranian Price List for Roads and Runways. The intended construction prices comprise paving costs, base and sub-base courses cost, guardrail costs, curbing costs, lining costs and earthwork costs. Earthworks, including both cut and fill, are calculated using one point cross section and the elevation of the ground points is derived from SRTM3 database, which is partially downloaded into MySQL database.

The Procedure of Modeling the Problem

According to presented descriptions in previous sections, the model for solving the problem is demonstrated in figure 3.

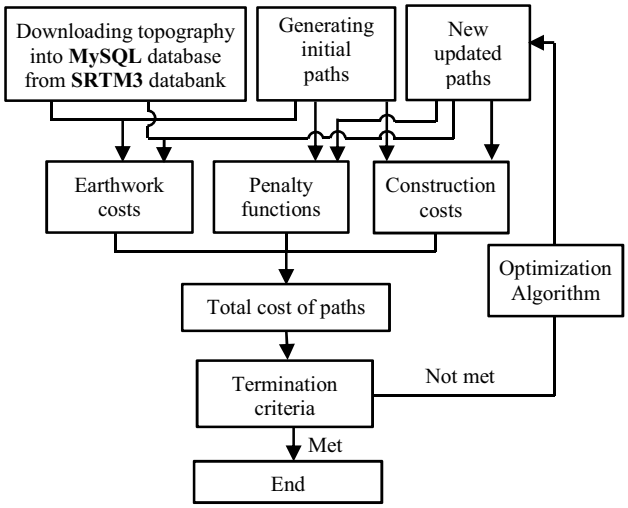

Figure 3: The procedure of modeling the problem

SOLVING REAL WORLD INSTANCES

Two real word route location problem examples are presented and solved based on the proposed model.

First Example: Mashhad-Neyshabur

In the first instance, the optimum highway alignment problem is investigated between the cities Mashhad and Neyshabur, which both are located in Khorasan-e-Razavi province in Iran. Binalood Mountains are located between the two cities and restrict the direct connection of the cities, as can be seen in figure 4. Neyshabur is considered as the origin of the route with coordinates $(36° 12' 48" \text{ N}, 58° 47' 45" \text{ E})$ and Mashhad is considered as destination which is located at $(36° 18' 0" \text{ N}, 59° 36' 0" \text{E})$. The direct distance between the two cities is 72990 kilometers. The earth range spotted as the search space is a rectangular area 110 kilometers in length and 90 kilometers in width. The parallel processing network used is a network with 4 nodes, each node equipped with two quad-core processors. The program is compiled in Java (version 7) and the operation system used was Linux. The program's constraints are as shown in table 1. The final horizontal intersection points are shown in figure 4. Corresponding parallel performance indexes are presented in table 2. This example is parallelized only in synchronous manner. The stopping criterion was considered 100 iterations.

Second Example: Khoramshahr-Abadan

Finding the optimum highway alignment between the cities Khoramshahr and Abadan was selected as the second example. Khoramshahr, as the origin of the path, is located at $(36° 26' 22" \text{N}, 48° 10' 0" \text{E})$ and

Table 1: Design parameters for the first example

	Parameter	Value
Design Parameters	Design speed	110 km/h
	Width of the road	14.6 m
	Slope of cut and fill sections	45°
	Number of intersection points	80
Constraint Parameters	Minimum radius of horizontal curves	450 m
	Maximum allowed longitudinal grade	3%
	Minimum length of crest vertical curves	74A
	Minimum length of sag vertical curves	55A

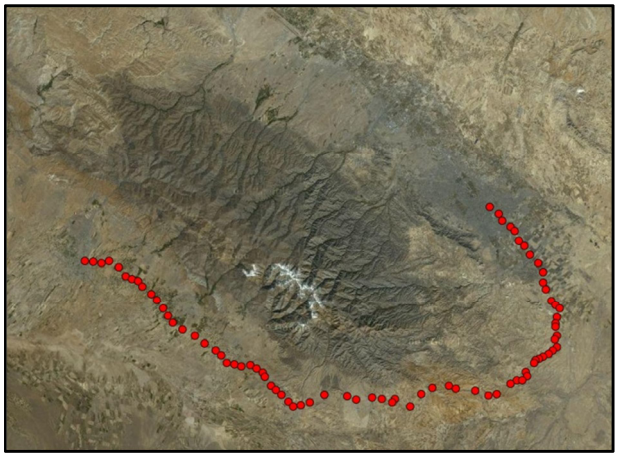

Figure 4: Horizontal alignment of the optimum path for the first example

Table 2: Parallelization indexes for the first example

Number of processors	Runtime (minutes)	Speedup	Parallel efficiency
1	1536	1.00	100.0%
4	403	3.82	95.4%
8	215	7.13	89.1%
16	126	12.19	76.2%
32	84	18.29	57.1%

Abadan, as destination, is located at $(30° 21' 21"N, 48° 18' 15"E)$. The reason for choosing theses cities is that these cities lie in a flat region. This is unlike the first example, where the topography was, to a large extent, mountainous. The rectangular search space for this problem is 20 kilometers in length and 15 kilometers in width, as shown in figure 5. Design parameters are similar to the first example, except road width and number of intersection points, which are 7.3 meters and 30, respectively.

This example uses both synchronous and asynchronous parallelization. The synchronous parallelization was accomplished for 100 iterations. The optimum alignment found is very similar to the path

Figure 5: Search space for the second example

which directly connects the origin and destination points due to the plain topography. The result of synchronous parallelization for the vertical alignment is demonstrated in figure 6. Also, parallelization factors are illustrated in table 3.

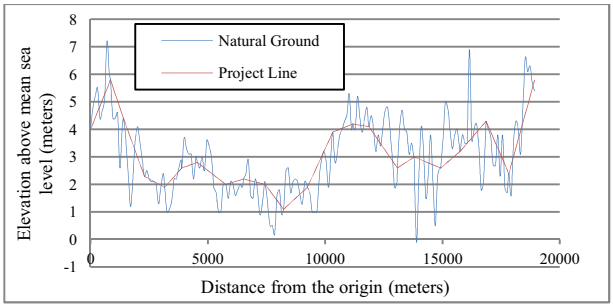

Figure 6: Vertical alignment for the second example (Synchronous parallelization)

Table 3: Synchronous parallelization indexes for the second example

Number of processors	Runtime (seconds)	Speedup	Parallel efficiency
1	5118	1.00	100.0%
4	1344	3.80	95.2%
8	727	7.03	88.0%
16	426	12.01	75.1%
32	291	17.59	55.0%

In asynchronous parallelization, as mentioned before, processors are not necessarily in the same iteration at the same time. In this manner, after completion of an iteration in a processor, the processor enters a new iteration without any delay. Reaching 100 iterations for the first processor was considered as the stopping criterion for this example. It is obvious that the processor with least computational operations will finish its assignments earlier than other processors. It is possible for asynchronous parallelization to have less accurate results, as it is proved by results of this example. The results of applying asynchronous parallelization for reaching the optimum vertical

alignment is reflected in figure 7. Furthermore, parallel indexes are presented in table 4.

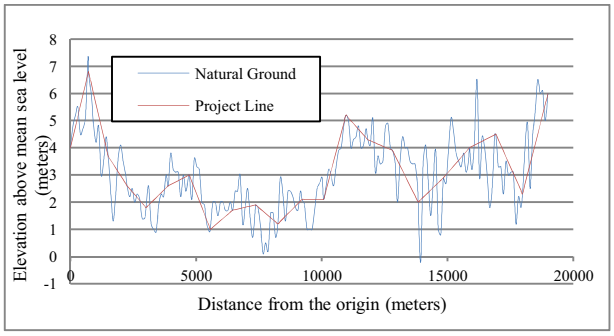

Figure 7: Vertical alignment for the second example (Asynchronous parallelization)

Table 4: Asynchronous parallelization Indexes for the second example

Number of processors	Runtime (seconds)	Speedup	Parallel efficiency
1	3331	1.00	100.0%
4	857	3.82	97.2%
8	416	7.13	95.9%
16	208	12.19	95.1%
32	104	18.29	94.6%

CONCLUSION

In this study, a parallel optimization model was offered to solve optimum highway alignment problem. At the beginning, Particle Swarm Optimization algorithm and two parallel versions of the algorithm were declared. An integrated model of parallel processing and PSO algorithm was then proposed. The application of the offered method on two real world examples was investigated. The first example was a large scale one with mountainous topography. However, the second problem had a flat topography, in order to investigate the efficacy of the model on problems with different types of topography. The second example was solved both synchronously and asynchronously. The results of this example demonstrated that asynchronous parallelization can increase the parallel efficiency considerably, but may have less accurate results. This issue is more likely to occur, especially when the problem in question is large scale. Finally, the results of asynchronous parallelization illustrated that load balancing between processors in solving the problem is of great importance and it is likely to reach less accurate results when applying a poor pattern for distributing particles among processors.

REFRENCES

AASHTO. 2001. *A Policy on Geometric Design of Highways and Streets*. American Association of State Highway and Transportation Officials. Washington, D.C.

Chew, E. P.; C. J. Goh; and T. F. Fwa. 1989. "Simultaneous Optimization of Horizontal and Vertical Alignments for Highways." *Transportation Research Part B*, No.23, 315-329.

Easa, S. M. 1988. "Selection of Roadway Grades that Minimize Earthwork Cost Using Linear Programming." *Transportation Research Part A*, No.22, 121-138.

Eberhart R. C. and Y. Shi. 1998. "A Modified Particle Swarm Optimizer", In *Proceedings of the International Conference on Evolutionary Programming* (Anchorage, AK, May4-9), IEEE, Piscataway, N.J., 69-73.

Jong, J. C. and P. Schonfeld. 2003. "An evolutionary Model for Simultaneously Optimizing Three-Dimensional Highway Alignment." Transportation Research Part B, No.37, 107-128.

Kennedy, J. and R. Eberhart. 1995. "Particle Swarm Optimization." In *Proceedings of IEEE International Conference on Neural Networks* (Perth, WA, Nov.27-Dec.1). IEEE, Piscataway, N.J., 1942-1948.

Moreb A. M. 1996. "Linear Programming Model for Finding Optimal Roadway Grades that Minimize Earthwork Cost" *European Journal of Operational Research*, No.93, 148-154.

Rauber, Th.,and G. Runger. 2010. "Parallel Programming for Multicore and Cluster Systems", Springer, Berlin, Germany.

Shafahi Y. and M. Bagherian. 2012. "A customized Particle Swarm Method to Solve Highway Alignment Optimization Problem." *Computer-Aided Civil and Infrastructure Engineering*, No.28, 52-67.

Turner A. K. and R. D. Miles. 1971. "A Computer-Assisted Method of regional Route Location." *Highway Research Record*, No.348, 1-15.

AUTHOR BIOGRAOHIES

SEYED FARZAN KAZEMI was born in Mashhad, Iran in 1989. He received his Master of Science in Road and Highway Engineering in 2012 from Sharif University of Technology under the supervision of Dr. Shafahi. At this time, he is a doctoral student at University of Tehran. His email address is: s.farzan.kazemi@gmail.com.

YOUSEF SHAFAHI received his Ph.D. in Civil Engineering from University of Maryland, USA in 1997. He joined the Department of Civil Engineering in Sharif University of Technology as an Assistant Professor in 1998 and became an Associated Professor in 2009. His main research interest is operation research in Transportation Planning. His email address is Shafahi@sharif.edu and his web-page can be found at http://sharif.edu/~shafahi.

A DISCRETE-TIME QUEUEING SYSTEM WITH DIFFERENT TYPES OF DISPLACEMENT

Ivan Atencia (speaker)
Inmaculada Fortes
Sixto Sánchez
Department of Applied Mathematics
University of Málaga
29071 - Málaga, Spain
Email: iatencia@ctima.uma.es,
ifortes@uma.es, sixto@uma.es

Alexander V. Pechinkin
Institute of Informatics Problems of RAS
119333 - Vavilova, 44-1,
Moscow, Russia
Email: apechinkin@ipiran.ru

KEYWORDS

Discrete-time system, expulsions, triggered customers, loss probability.

ABSTRACT

The performance prediction in communication, jobs processing in computers, etc, are always influenced by the customers behavior and the provision of this additional information will be useful in upgrading the service. Our paper is concerned under a loss and trigger protocol where each customer has a service requirement which may depend on the arrival of a positive or negative customer. In our study we consider customer expulsions and different types of customers displacements taking into account or not its past time of service.

The main purpose of this work is to spread the discrete-time queueing theory about expulsions and displacement. We provide a unified way to handle the combinations of different conditions such as positive arrival, negative arrival, trigger movements, past time in service, etc.

INTRODUCTION

An investigation of discrete-time queueing system is important due to their application to slotted systems such as communication systems and other related areas and therefore it has been found more appropriate than their continuous-time counterpart.

The study of discrete-time queues was initiated by (Meisling 1958; Birdsall et al. 1962; Powell et al. 1967). Reference works and more detailed applications on discrete-time queueing theory include the monographs (Bruneel and Kim 1993; Takagi 1993). Further, a detailed treatment regarding this subject can be found in a two-volume book on applied probability (Hunter 1983).

A rapid increase in the literature on queueing system with negative arrivals are analyzed extensively in continuous-time models but not so much in discrete-time. The arrival of a negative customer to a queueing system causes one ordinary customer to be removed or killed if any is present. The pioneer work on discrete-time considering negative arrivals without retrials can be found in (Atencia and Moreno 2004; Atencia and Moreno 2005) where the authors considered several killing strategies for the negative customers.

For a survey on this topics the authors refer to (Gelenbe and Label 1998) and (Artalejo 2000), for applications on engineering to (Chao et al. 1999) and for application in communication networks we refer to (Harrison et al. 2000) and (Park et al. 2009).

In many real problems it is also interesting to consider the movement of jobs, customers, etc., from one place to another. This mechanism is called a synchronized or triggered motion, see for example (Artalejo 2000) and (Gelenbe and Label 1998) and concerning with inverse order discipline we refer to (Pechinkin and Svischeva 2004), (Pechinkin and Shorgin 2008) and (Cascone et al. 2011). For service interruptions with expulsions we refer to (Atencia and Pechinkin 2012) and (Atencia et al. 2013).

THE MATHEMATICAL MODEL

We consider a discrete-time queueing system where the time axis is segmented into a sequence of equal time intervals (called slots). It is assumed that all queueing activities (arrivals, departures and retrials) occur at the slot boundaries, and therefore, they may take place at the same time. That is why we must detail the order in which the arrivals and departures occur in case of simultaneity in a discrete-time system. Basically, there are two rules: (i) If an arrival takes precedence over a departure, it is identified with Late Arrival System (LAS) (see Figure 1(a)); (ii) if a departure takes precedence over an arrival, it is recognized by Early Arrival System (EAS) (see Figure 1(b)). The former case is also known as Arrival First (AF) policy and the latter as Departure First (DF) policy. For more details on these and related concepts, see (Gravey and Hébuterne 1992) and (Hunter 1983).

Let us note, that for mathematical convenience, we will follow the second policy, that is the departures occur at the moment immediately before the slot boundaries,

Proceedings 27th European Conference on Modelling and Simulation ©ECMS Webjørn Rekdalsbakken, Robin T. Bye, Houxiang Zhang (Editors)
ISBN: 978-0-9564944-6-7 / ISBN: 978-0-9564944-7-4 (CD)

but arrivals occurs at the moment immediately after the slot boundaries.

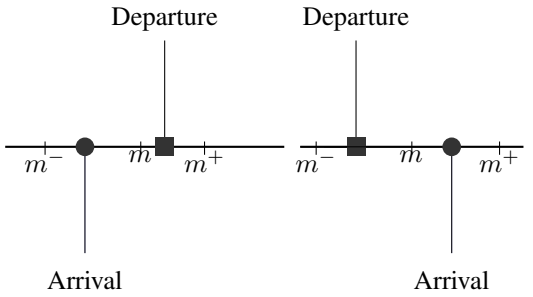

Figure 1: Options of the arrival models

Customers arrive according to a geometrical arrival process with rate a, i.e., a is the probability that an arrival occurs in a slot. Service times are independent and identically distributed with general distribution $\{s_i\}_{i=1}^{\infty}$ and generating function (GF) $S(z) = \sum_{i=1}^{\infty} z^i s_i$. We will denote by $S_k = \sum_{i=k}^{\infty} s_i;\ k \geq 1$, the probability that the service lasts not less than k slots.

If, upon arrival, the server is idle, the service of the arriving customer begins immediately, otherwise, the arriving customer has several options depending on its nature. That is, with probability θ_0 it will join the last place of the queue and with probability θ_1 expels the customer that is currently in the server and starts immediately its service. With probability θ_2 it becomes a triggered customer moving the customer from the server to the first place at the queue but considering for the future its cumulative service and with probability θ_3 it is moved to the last place of the queue without considering its cumulative service. Finally with probability θ_4 it becomes a negative customer expelling out of the system the customer in service. Obviously it verifies that $\sum_{i=0}^{4} \theta_i = 1$. Let us note that the customers arriving from outside has priority on others. In order to avoid trivial cases, we assume $0 < a < 1$.

THE STEADY STATE PROBABILITIES

Let π_0 be the stationary probability that in the moment immediately after a potential arrival the system is empty and $\pi_{i,k};\ i \geq 1,\ k \geq 1$, the stationary probability that there are k customers in the system and that the customer in service has passed exactly i slots of service. Therefore we have

$$\pi_{i,1} = \overline{a}\pi_{i-1,1}\frac{S_{i+1}}{S_i} + a\theta_2\pi_{i-1,1}\frac{S_{i+1}}{S_i};\ i \geq 1, \quad (1)$$

$$\pi_{i,k} = \overline{a}\pi_{i-1,k}\frac{S_{i+1}}{S_i} + a\theta_2\pi_{i-1,k}\frac{S_{i+1}}{S_i} + a\theta_0\pi_{i-1,k-1}\frac{S_{i+1}}{S_i};\ i \geq 1,\ k \geq 2, \quad (2)$$

$$\pi_{0,1} = a(1-\theta_4)\pi_0 + a\sum_{j=1}^{\infty}\theta_0\pi_{j-1,1}\frac{s_j}{S_j} + a\sum_{j=1}^{\infty}\theta_1\pi_{j-1,1} + a\sum_{j=1}^{\infty}\theta_2\pi_{j-1,1}\frac{s_j}{S_j} + a\sum_{j=1}^{\infty}\theta_3\pi_{j-1,1}; \quad (3)$$

$$\pi_{0,k} = a\sum_{j=1}^{\infty}\theta_0\pi_{j-1,k}\frac{s_j}{S_j} + a\sum_{j=1}^{\infty}\theta_1\pi_{j-1,k} + a\sum_{j=1}^{\infty}\theta_2\pi_{j-1,k}\frac{s_j}{S_j} + a\sum_{j=1}^{\infty}\theta_3\pi_{j-1,k} + a\sum_{j=1}^{\infty}\theta_0\pi_{j-1,k-1}\frac{S_{j+1}}{S_j} + a\sum_{j=1}^{\infty}\theta_2\pi_{j-1,k-1}\frac{S_{j+1}}{S_j} + a\sum_{j=1}^{\infty}\theta_3\pi_{j-1,k-1}\frac{S_{j+1}}{S_j};\ k \geq 2. \quad (4)$$

Let us define

$$q_{i,k} = \pi_{i,k}/S_{i+1};\ i \geq 0,\ k \geq 1, \quad (5)$$
$$Q_k = \sum_{i=0}^{\infty} s_{i+1}q_{i,k};\ k \geq 1,$$
$$\pi_k = \sum_{i=0}^{\infty}\pi_{i,k} = \sum_{i=0}^{\infty} S_{i+1}q_{i,k};\ k \geq 1.$$

It is clear, that π_k is the probability that there are k; $k \geq 1$, customers in the system. The system (1)–(4) can be transformed, taking into account the previous definitions, in the following equations:

$$q_{i,1} = (\overline{a} + a\theta_2)q_{i-1,1};\ i \geq 1, \quad (6)$$
$$q_{i,k} = (\overline{a} + a\theta_2)q_{i-1,k} + a\theta_0 q_{i-1,k-1};\ i \geq 1,\ k \geq 2, \quad (7)$$

$$q_{0,1} = a(1-\theta_4)\pi_0 + a\theta_0\sum_{j=1}^{\infty} q_{j-1,1}s_j + a\theta_1\pi_1 + a\theta_2\sum_{j=1}^{\infty} q_{j-1,1}s_j + a\theta_3\pi_1 = a[(1-\theta_4)\pi_0 + (\theta_1+\theta_3)\pi_1 + (\theta_0+\theta_2)Q_1], \quad (8)$$

$$q_{0,k} = a\theta_0\sum_{j=1}^{\infty} q_{j-1,k}s_j + a\theta_1\pi_k + a\theta_2\sum_{j=1}^{\infty} q_{j-1,k}s_j + a\theta_3\pi_k + a\theta_0\pi_{k-1} -$$

$$
\begin{aligned}
&- a\theta_0 \sum_{j=1}^{\infty} q_{j-1,k-1} s_j + a\theta_2 \pi_{k-1} - \\
&- a\theta_2 \sum_{j=1}^{\infty} q_{j-1,k-1} s_j + \\
&+ a\theta_3 \pi_{k-1} - a\theta_3 \sum_{j=1}^{\infty} q_{j-1,k-1} s_j = \\
&= a[(\theta_1+\theta_3)\pi_k + (\theta_0+\theta_2)Q_k + \\
&+ (\theta_0+\theta_2+\theta_3)\pi_{k-1} - \\
&- (\theta_0+\theta_2+\theta_3)Q_{k-1}]; \;\; k \geq 2. \qquad (9)
\end{aligned}
$$

Solving eq. (6) and (7) in k, we obtain

$$
q_{i,k} = \sum_{j=0}^{\min\{i,k-1\}} \binom{i}{j} (a\theta_0)^j (\overline{a} + a\theta_2)^{i-j} q_{0,k-j};
$$
$$
i \geq 1, \;\; k \geq 1. \qquad (10)
$$

Let us determine π_k and Q_k for $k \geq 1$. In order to have a compact formulae, we denote by $\hat{S}(z) = [1 - S(z)]/(1-z)$ and $\tilde{S}(z) = S(z)/z$.

Firstly for $k = 1$, that is from (10), we obtain:

$$
\begin{aligned}
\pi_1 &= q_{0,1} \sum_{i=0}^{\infty} (\overline{a} + a\theta_2)^i \sum_{j=i+1}^{\infty} s_j = \\
&= q_{0,1} \sum_{j=1}^{\infty} s_j \sum_{i=0}^{j-1} (\overline{a} + a\theta_2)^i = \\
&= q_{0,1} \sum_{j=1}^{\infty} s_j \frac{1 - (\overline{a} + a\theta_2)^j}{1 - (\overline{a} + a\theta_2)} = q_{0,1} \hat{S}(\overline{a} + a\theta_2), \qquad (11)
\end{aligned}
$$

$$
Q_1 = q_{0,1} \sum_{i=0}^{\infty} s_{i+1} (\overline{a} + a\theta_2)^i = q_{0,1} \tilde{S}(\overline{a} + a\theta_2), \qquad (12)
$$

where $q_{0,1}$ can be determined by substituting (11) and (12) into (8) and after some algebra we have

$$
q_{0,1} = \frac{a(1-\theta_4)\pi_0}{1 - a(\theta_1+\theta_3)\hat{S}(\overline{a}+a\theta_2) - a(\theta_0+\theta_2)\tilde{S}(\overline{a}+a\theta_2)}. \qquad (13)
$$

With the same procedure but involving equation (9) we have

$$
\pi_k = \sum_{i=0}^{k-1} \frac{(a\theta_0)^i}{i!} q_{0,k-i} \hat{S}^{(i)}(\overline{a} + a\theta_2); \;\; k \geq 2, \qquad (14)
$$

$$
Q_k = \sum_{i=0}^{k-1} \frac{(a\theta_0)^i}{i!} q_{0,k-i} \tilde{S}^{(i)}(\overline{a} + a\theta_2); \;\; k \geq 2, \qquad (15)
$$

where $q_{0,k}$ can be determined by substituting (12), (13) and (10) into (9) and after some algebra we have

$$
\begin{aligned}
q_{0,k} = a\big[&1 - a(\theta_1+\theta_3)\hat{S}(\overline{a}+a\theta_2) - \\
&- a(\theta_0+\theta_2)\tilde{S}(\overline{a}+a\theta_2)\big]^{-1} \times \\
&\times \Bigg[\sum_{i=1}^{k-1} \frac{(a\theta_0)^i}{i!} \big((\theta_1+\theta_3)\hat{S}^{(i)}(\overline{a}+a\theta_2) + \\
&+ (\theta_0+\theta_2)\tilde{S}^{(i)}(\overline{a}+a\theta_2)\big) q_{0,k-i} + \\
&+ (\theta_0+\theta_2+\theta_3)\pi_{k-1} - (\theta_0+\theta_2+\theta_3)Q_{k-1} \Bigg]; \\
&k \geq 2. \qquad (16)
\end{aligned}
$$

We can summarize the above results in the following:

Theorem 1 *The stationary probability π_k; $k \geq 1$, that there are k customers in the system is given in the formula (11) or (14). This formula can be determined by $q_{0,k}$ and Q_k from the formulae (13) and (16) or (12) and (15).*

The stationary probability $\pi_{i,k}$; $k \geq 1$, $i \geq 0$, that there are k customers in the system and the one in the server has already i slots of service is obtained by formula (5) where $q_{i,k}$; $k \geq 1$, $i \geq 1$, can be determined by formula (10).

It should be pointed out that Theorem 1 entails an algorithm that enables us, in a convenient way, to calculate the stationary probabilities π_k and $\pi_{i,k}$.

The probability π_0, included in the obtained formulae, can be calculated under the normalization condition which will be shown in a clear form in the following section. The condition for the existence of the stationary regime will be calculated further on.

GENERATING FUNCTION

In this section we obtain the stationary distribution of the number of customers in terms of its generating functions. For this aim we define the following GF's:

$$
q_0(z) = \sum_{k=1}^{\infty} z^k q_{0,k},
$$
$$
Q(z) = \sum_{k=1}^{\infty} z^k Q_k,
$$
$$
\pi(z) = \sum_{k=1}^{\infty} z^k \pi_k.
$$

Multiplying (13) and (16) by z^k and summing over k we obtain

$$
\begin{aligned}
q_0(z) = a\Big(&[1-\theta_4]z\pi_0 + [(\theta_1+\theta_3) + \\
&+ (\theta_0+\theta_2+\theta_3)z]\pi(z) + \\
&+ [(\theta_0+\theta_2) - (\theta_0+\theta_2+\theta_3)z]Q(z)\Big). \qquad (17)
\end{aligned}
$$

From eqs. (14)–(17) we have

$$
\begin{aligned}
\pi(z) &= \sum_{i=0}^{\infty} \frac{(a\theta_0 z)^i}{i!} q_0(z) \hat{S}^{(i)}(\overline{a} + a\theta_2) = \\
&= \hat{S}(\overline{a} + a\theta_2 + a\theta_0 z) q_0(z), \qquad (18) \\
Q(z) &= \sum_{i=0}^{\infty} \frac{(a\theta_0 z)^i}{i!} q_0(z) \tilde{S}^{(i)}(\overline{a} + a\theta_2) = \\
&= \tilde{S}(\overline{a} + a\theta_2 + a\theta_0 z) q_0(z), \qquad (19)
\end{aligned}
$$

where $q_0(z)$ has the following expression:

$$q_0(z) = \frac{(1-\theta_4)az}{D(z)}\pi_0,$$

and

$$\begin{aligned} D(z) = 1 - a\big([\theta_1+\theta_3+(\theta_0+\theta_2+\theta_3)z]\times \\ \times \hat{S}(\overline{a}+a\theta_2+a\theta_0 z)+ \\ +[\theta_0+\theta_2-(\theta_0+\theta_2+\theta_3)z]\times \\ \times \tilde{S}(\overline{a}+a\theta_2+a\theta_0 z)\big). \end{aligned} \tag{20}$$

In order to find π_0 we use the following normalization condition

$$\sum_{k=0}^{\infty}\pi_k = \pi_0 + \pi(1) = 1, \tag{21}$$

which entails to

$$\begin{aligned} \pi_0 = \big(1 - a\big[(1+\theta_3-\theta_4)\hat{S}(\overline{a}+a\theta_2+a\theta_0) - \\ -\theta_3\tilde{S}(\overline{a}+a\theta_2+a\theta_0)\big]\big)\times \\ \times\big(1-a\theta_3\big[\hat{S}(\overline{a}+a\theta_2+a\theta_0) - \\ -\tilde{S}(\overline{a}+a\theta_2+a\theta_0)\big]\big)^{-1}. \end{aligned} \tag{22}$$

Therefore the necessary condition for the stability of the system is

$$S(\overline{a}+a\theta_2+a\theta_0) > \frac{(\overline{a}+a\theta_2+a\theta_0)(1-\theta_1-2\theta_4)}{(\overline{a}+a\theta_2+a\theta_0)(1-\theta_4)+\theta_3}.$$

It can be proved that the above condition is also sufficient.

Theorem 2 *The following GF's of the number of customers in the system and in the queue are respectively obtained under simple algebraical transformations, that is:*

$$\begin{aligned} \Phi(z) = \pi_0 + \pi(z) = \\ = \Big[1 + \frac{1-S(A(z))}{1-A(z)}(1-\theta_4)z\times \\ \times\Big\{\frac{1}{a} - (1-\theta_4)\frac{S(A(z))}{A(z)} - \\ -[(\theta_1+\theta_3)+(\theta_0+\theta_2+\theta_3)z]\times \\ \times\frac{A(z)-S(A(z))}{A(z)(1-A(z))}\Big\}^{-1}\Big]\pi_0, \end{aligned} \tag{23}$$

$$\Psi(z) = \pi_0 + \frac{\pi(z)}{z}. \tag{24}$$

where $A(z) = \overline{a} + a\theta_2 + a\theta_0 z$.

Differentiating the above GF's in the point $z = 1$, we can obtain the moments for any stationary characteristic of the number of customers in the system and in the queue. Even more, in certain cases, for a determined rational-linear function $S(z)$, Theorem 2 can be used to find directly the stationary distribution of the number of customers in the system and in the queue.

STATIONARY CHARACTERISTICS

In this section we present some performance measures for the system at the stationary regime.

The mean number of customers in the system
In order to find N we differentiate formula (23) in the point $z = 1$, obtaining

$$\begin{aligned} N = \Phi'(1) = \pi'(1) = \\ = \frac{[1-S(A(1))-S'(A(1))(1-A(1))]}{(1-A(1))^2}\times \\ \times\frac{1-A(1)}{1-S(A(1))}a\theta_0(1-\pi_0) + \\ +\frac{1-S(A(1))}{1-A(1)}\cdot\frac{D(1)-D'(1)}{D^2(1)}a(1-\theta_4)\pi_0, \end{aligned} \tag{25}$$

where $D(z)$ it arises from formula (20), that is:

$$\begin{aligned} D(z) = 1 - a\Big((1-\theta_4)\frac{S(A(z))}{A(z)} + [(\theta_1+\theta_3)+ \\ +(\theta_0+\theta_2+\theta_3)z]\frac{A(z)-S(A(z))}{A(z)[1-A(z)]}\Big). \end{aligned}$$

The mean number of customers in the queue
In order to find Q we differentiate formula (24) in the point $z = 1$, obtaining

$$Q = \Psi'(1) = N - (1-\pi_0). \tag{26}$$

Loss probability of customers
Let us define ω as the loss probability of the pure customers, that is, only the customers that have being expelled by a positive customer and not by a negative customer. In order to find this probability we need to give some previous definitions:

Let us define r_i as the stationary probability that the system is not empty on condition that the customer that is currently at service has already spent i slots of service. Therefore:

$$r_i = \sum_{k=1}^{\infty}\pi_{i,k}, \;\; i \geq 0. \tag{27}$$

The stationary loss intensity of customers in the system due to negative or positive customers is given by

$$\mu_{\,\mathrm{loss}} = a(\theta_4+\theta_1)\sum_{i=1}^{\infty} r_{i-1}\frac{S_{i+1}}{S_i}.$$

Therefore we have:

$$\omega = \frac{\mu_{\,\mathrm{loss}}}{l_{\,\mathrm{pos}}}, \tag{28}$$

where $l_{\,\mathrm{pos}} = a(1-\theta_4)$.

The mean sojourn time of a customer in the system
Let T be the mean sojourn time of a positive customer in the system, therefore following Little's formula we have:

$$T = \frac{N}{l_{\,\mathrm{pos}}}. \tag{29}$$

The mean sojourn time of a customer in the queue

Let S be the mean sojourn time of a positive customer in the queue, therefore following Little's formula we have:

$$S = \frac{Q}{l_{\text{pos}}}. \tag{30}$$

NUMERICAL RESULTS

In this section, we present some numerical examples of the performance measures obtained in the previous section in relation with the most specific parameters of our model. For the numerical examples we have considered the values of the following probabilities $\theta_0 = 0.2,\ \theta_1 = 0.15,\ \theta_2 = 0.3,\ \theta_3 = 0.05,\ \theta_4 = 0.3$ and three different probability distributions for the service time, that is, its GF's are of the following type for $0 < p < 1,\ q = 1 - p$ and $0 < \alpha < 1,\ 0 < p_1, p_2 < 1,\ q_1 = 1 - p_1,\ q_2 = 1 - p_2$:

$$S_1(z) = \frac{zp}{1 - qz},$$
$$S_2(z) = \frac{zp^2}{(1 - qz)^2},$$
$$S_3(z) = \frac{\alpha p_1 z}{1 - q_1 z} + \frac{(1 - \alpha) p_2 z}{1 - q_2 z}.$$

Let us note that the position of the three graphics are in concordance to its mean service time which is closely related to the performance measures.

In Figure 1, we show the effect of the probability that the system is empty against the parameter a, for different types of Gf's for the service time distribution.

The effect of these curves is that π_0 decreases as functions of the parameter a. Due to the fact that the parameter has a direct influence on the number of customers in the system, obviously we obtain that the probability that the system is idle decreases. In this case, for each curve the intersections with the abscissas axes correspond to the limiting condition for the stability of our system.

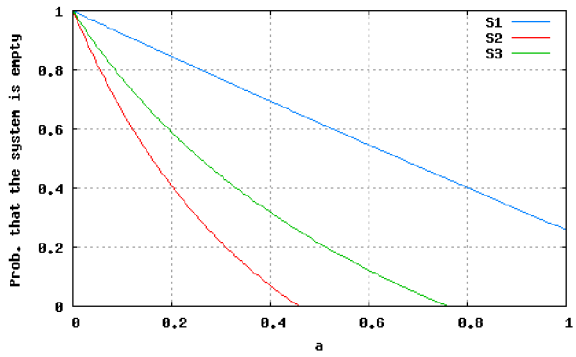

Figure 2: π_0 vs. a

In Figure 2, the mean number of customers in the system, N, is plotted against the parameter a. As it was to be expected, N, is increasing as a function of a which also agrees with the intuitive expectations. As we can observe, all the curves increase asymptotically as they tend to the stability condition of the system.

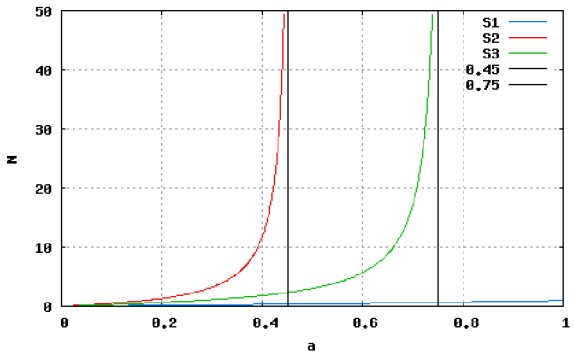

Figure 3: N vs. a

In Figure 3, The mean number of customers in the queue, Q, is plotted against the parameter a. By the expression (26) we can observe that the graphic looks very similar to the previous one. Although we observe that Q increases as a function of a and asymptotically tends to the stability condition of the system.

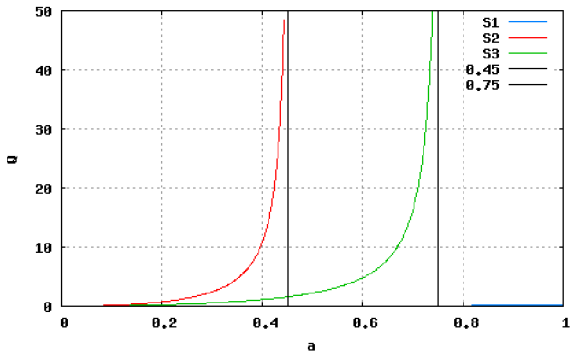

Figure 4: Q vs. a

In Figures 4 and 5, that is, the mean sojourn time of a customer in the system, T, and in the queue S respectively are plotted against the incoming parameter a. We observe that they have the same upward tendency asymptotically to the stability condition of the system.

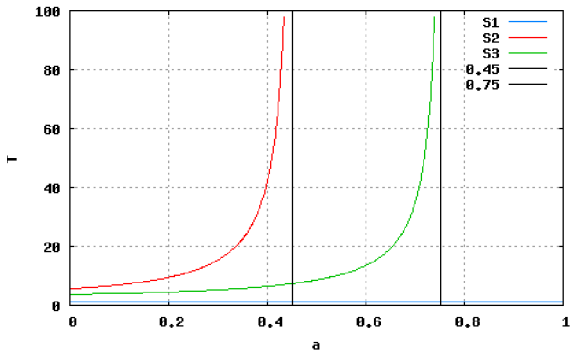

Figure 5: T vs. a

In Figure 6, we represent the distribution function of the number of customers in the system for $a = 0.4$.

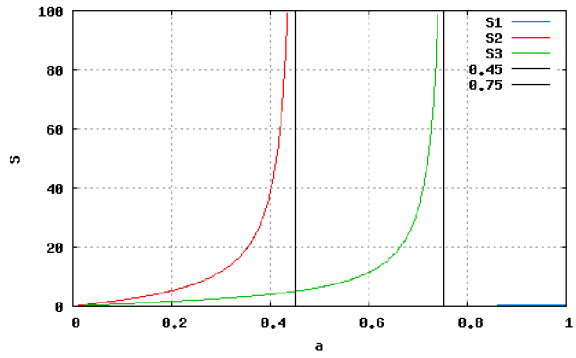

Figure 6: S vs. a

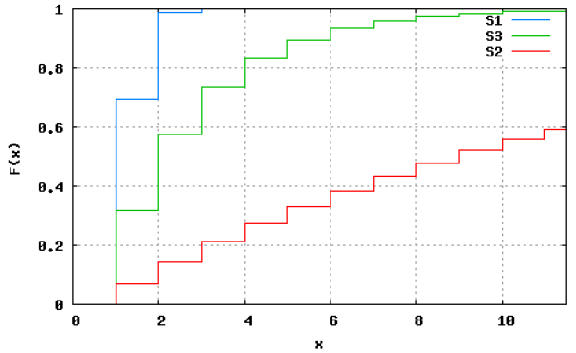

Figure 7: $F(x)$ for $a = 0.4$

SUMMARY

In the foregoing study, a discrete-time queueing system under a loss and trigger protocol has been analyzed to obtain analytical expressions for various performance measures of interest. It is important to select models that can be efficiently solved and for whose tools and solution methodologies are developed and available. Let us note that our system includes many particular cases that can be applied in several practical situations depending on the different types of displacement. To this end, we have managed not a single technique but a combination of different mathematical tools. In this paper, we establish some important results via two theorems in which theorem 1 enables us to calculate the stationary probabilities of the number of customers in the system without considering and considering the passed service slots. Theorem 2 is concerned with the calculation of the generating functions of the number of customers in the system and in the queue obtaining some important stationary characteristics. We also study the loss probability of customers and the mean sojourn time of a customer in the system and in the queue. Several performance characteristics of the model have been calculated and numerical results are given for different distributions.

Notes and Comments. The research of A. Pechinkin was supported in part by the Russian Foundation for Basic Research (grants 11-07-00112, 12-07-00108 and 13-07-00223). The research of I. Fortes and S. Sánchez is partially supported by Junta de Andalucía grant P09-FQM-5233.

REFERENCES

Artalejo, J. R. 2000. "G-networks: A versatile approach for work removal in queueing networks". *European Journal of Operational Research*, 126, Pp. 233–249.

Atencia, I. and Moreno, P. 2004. "The discrete-time Geo/Geo/1 queue with negative customers and disasters". *Computers and Operations Research* 31 (9), Pp. 1537–1548.

Atencia, I. and Moreno, P. 2005. "A single-server G-queue in discrete-time with geometrical arrival and service process." *Performance Evaluation*, 59, Pp. 85–97.

Atencia, I., Fortes, I. and Sánchez, S. 2013. "Discrete-time queueing system with expulsions." *Communications in Computer and Information Science*, 356, Pp. 20–25.

Atencia, I. and Pechinkin, A.V. 2012. "A discrete-time queueing system with optional LCFS discipline". *Annals Operation Research*. 202, Pp. 3–17.

Birdsall, T., Ristenbatt, M. and Weinstein, S. 1962. "Analysis of asynchronous time multiplexing of speech sources". *IRE Transactions on Communication Systems.* 2. vol. 10, Pp. 390–397.

Bruneel, H. and Kim, B.G. 1993. *Discrete-time models for communication systems including ATM. Kluwer Academic Publishers*, Boston.

Chao, X., Miyazawa, M. and Pinedo, M. 1999. *Queueing networks: Customers, signals and product form solutions.* Wiley.

Cascone, A., Manzo, P., Pechinkin, A. and Shorgin, S. 2011. "A $Geom/G/1/n$ system with a LIFO discipline without interruptions in the service and with a limitation for the total capacity for the customers". *Avtomatika i Telemejanika* vol. 1, Pp. 107–120. (In russian).

Gelenbe, E. and Label, A. 1998. "G-networks with multiple classes of signals and positive customers." *European Journal of Operation Research* 108, Pp. 293–305.

Gravey, A. and Hébuterne, G. 1992. "Simultaneity in discrete-time single server queues with bernoulli inputs." *Performance Evaluation* 14, Pp. 123–131.

Harrison, P. G., Patel, N. M. and Pitel, E. 2000. "Reliability modelling using G-queues". *European Journal of Operational Research*, 126, Pp. 273–287.

Hunter, J. 1983. *Mathematical Techniques of Applied Probability.* Operations Research and Industrial Engineering. Academic Press, New York. Vol. 1,2.

Meisling, T. 1958. "Discrete time queueing theory". *Operation Research*, vol. 6, Pp. 96–105.

Park, H. M., Yang, W. S. and Chae, K. C. 2009. "The Geo/G/1 queue with negative customers and disasters". *Stochastic Models*, 25, Pp. 673–688.

Pechinkin, A. and Svischeva, T. 2004. "The stationary state probability in the BMAP/G/1/r queueing system with inverse discipline and probabilistic priority". In *Transactions of XXIV International Seminar on Stability Problems for Stochastic Models* Pp. 141–174, Jurmala, Latvia.

Pechinkin, A. and Shorgin, S. 2008. "A $Geo/G/1/\infty$ system with a one non-standard discipline for the service". *Informatics and it applications*, vol. 2, Pp. 55–62. (In russian).

Pechinkin, A. and Shorgin, S. 2008. "The discrete-time queueing system with inversive service order and probabilistic priority". *Proceedings of the 3rd International Conference on Performance Evaluation Methodologies and Tools*, 20.

Powell, B. and Avi-Itzhak, B. 1967. "Queueing systems with enforced idle times". *Operations Research.* vol. 15(6), Pp. 1145–1156.

Takagi, H. 1993. *Queueing analysis: A foundation of performance evaluation. Discrete-Time Systems.* North-Holland, Amsterdam vol. 3.

AUTHORS BIOGRAPHIES

IVAN ATENCIA graduated in 1997 and obtained his Ph.D. in Mathematics in 2000 from Málaga University, Spain. During this period he collaborated with the Department of Probability Theory and Mathematical Statistics of The Peoples' Friendship University of Russia, Moscow. At present, he is Associate Professor in the Department of Applied Mathematics at Málaga University and actively collaborates with the Institute of Informatics Problems of RAS, Russia (Moscow). His research interests include queueing theory and stochastic modeling of communication systems. His e-mail address is: `iatencia@ctima.uma.es`

INMACULADA FORTES graduated in 1996 and obtained her Ph.D. in Mathematics in 2002 from Málaga University, Spain. She is Associate Professor in the Department of Applied Mathematics at Málaga University. Her research interests are queueing theory, stochastic modelling of communication systems as well as data mining and mathematical logic. Her e-mail address is: `ifortes@uma.es`

ALEXANDER V. PECHINKIN is a Doctor of Sciences in Physics and Mathematics and principal scientist at the Institute of Informatics Problems of the Russian Academy of Sciences, and a professor at the Peoples' Friendship University of Russia. He is the author of more than 150 papers in the field of applied probability theory. His e-mail address is: `apechinkin@ipiran.ru`

SIXTO SÁNCHEZ graduated in 1992 and obtained his Ph.D. in Mathematics in 2002 from Málaga University, Spain. He is Associate Professor in the Department of Applied Mathematics at Málaga University. His research interests are queueing theory, stochastic modelling of communication systems as well as mathematical logic. His e-mail address is: `sixto@uma.es`

COORDINATE-WISE VERSIONS OF THE GRID METHOD FOR THE ANALYSIS OF INTENSITIES OF NON-STATIONARY INFORMATION FLOWS BY MOVING SEPARATION OF MIXTURES OF GAMMA-DISTRIBUTION

Andrey Gorshenin
Institute of Informatics Problems, Russian Academy of Sciences
Vavilova str., 44-2, Moscow, Russia
Email: agorshenin@ipiran.ru

Victor Korolev
Moscow State University, Leninskie Gory, Moscow, Russia
Institute of Informatics Problems, Russian Academy of Sciences
Email: bruce27@yandex.ru

Victor Kuzmin
"Wi2Geo LLC", Russia
Email: shadesilent@gmail.com

Alexander Zeifman
Vologda State Pedagogical University, S.Orlova, 6, Vologda, Russia
Institute of Informatics Problems RAS, ISEDT RAS
Email: a_zeifman@mail.ru

KEYWORDS

Mixture of probability distributions; Gamma-distribution; Information flow; Grid method

ABSTRACT

A coordinate-wise modification of the grid method for separation of mixtures is proposed in the problem of the dynamical monitoring of the stochastic structure of information flows.

INTRODUCTION

Statistical analysis of the traffic in information flows in modern computational and telecommunication systems reveals their noticeable non-stationarity. Within the approach based of representation of the traffic as a stochastic process is very convenient to model this non-stationarity by representing the flow intensity as a non-stationary random process with mixed gamma one-dimensional distributions. As this is so, the evolution of the parameters of these mixtures in time reflects the non-stationarity of the original process and can be used as the estimate of the stochastic structure of the information flow.

GRID METHODS FOR SEPARATION OF MIXTURES OF PROBABILITY DISTRIBUTIONS

EM-type algorithms are traditionally used for the numerical solution of the problem of separation of mixtures of probability distributions when the number of components is comparatively large (Korolev, 2011). If the likelihood function is regular, then these method yields most likely estimates of the parameters of components and weights. But if the likelihood function is irregular and has many local extremes (possibly, infinite), then the EM-algorithm becomes extremely unstable and slow which is absolutely inadmissible for the on-line monitoring of the stochastic structure of information flows, see, e. g., (Korolev, 2011).

To overcome this drawback, recently in the papers (Korolev et al., 2008), (Korolev et al., 2010) the so-called grid algorithms were proposed for the separation of mixtures of probability distributions. The main idea that grid methods rely on is very close to the idea of harmonic analysis.

Consider an identifiable mixture of distribution functions of the form

$$F(x) = \sum_{i=1}^{k} p_i G(x; a_i, \sigma_i), \quad x \in \mathbb{R}, \tag{1}$$

where $k \geq 1$ is an integer. In the classical problem of separation of mixtures, the parameters to be estimated are the triples (p_i, a_i, σ_i), $i = 1, \ldots, k$, with $a_i \in \mathbb{R}$, $\sigma_i \in \mathbb{R}$, $p_i \geq 0$, $p_1 + \ldots + p_k = 1$.

Assume that the numbers $\underline{a}$, $\overline{a}$, $\underline{\sigma}$ and $\overline{\sigma}$ are given so that $\underline{a} \leq a_i \leq \overline{a}$ and $\underline{\sigma} \leq \sigma_i \leq \overline{\sigma}$ for all $i = 1, \ldots, k$. in other words, the finite ranges of the parameters a_i and σ_i are known.

The main idea of the grid methods is in the replacement of the *intervals* $[\underline{a}, \overline{a}]$ and $[\underline{\sigma}, \overline{\sigma}]$ of possible values of the parameters of the components of mixture (1) by *discrete* sets of *known* points. These points may be defined in the following way.

Let ε_a and ε_σ be positive numbers determining the prior requirements to the accuracy of the estimation of the parameters a_i and σ_i:

$$\max_i |a_i - \widehat{a}_i| \leq \varepsilon_a, \quad \max_i |\sigma_i - \widehat{\sigma}_i| \leq \varepsilon_\sigma, \tag{2}$$

Proceedings 27th European Conference on Modelling and Simulation ©ECMS Webjørn Rekdalsbakken, Robin T. Bye, Houxiang Zhang (Editors)
ISBN: 978-0-9564944-6-7 / ISBN: 978-0-9564944-7-4 (CD)

where $\widehat{a}_i$ and $\widehat{\sigma}_i$ are the desired estimates of the parameters. The numbers ε_a and ε_σ also can be interpreted as the thresholds of distinguishability of possible values of the parameters: the values a', a'' and σ', σ'' are, respectively, regarded as undistinguishable, if

$$|a' - a''| \le \varepsilon_a, \quad |\sigma' - \sigma''| \le \varepsilon_\sigma. \tag{3}$$

Let $k_a = [(\overline{a} - \underline{a})/\varepsilon_a] + 1$, $k_\sigma = [(\overline{\sigma} - \underline{\sigma})/\varepsilon_\sigma] + 1$, where the symbol $[z]$ denotes the integer part of a number z. For $r = 1, 2, \ldots, k_a + 1$ set $\widetilde{a}_r = \underline{a} + (r-1)\varepsilon_a$. Similarly, for $l = 1, 2, \ldots, k_\sigma$ let $\widetilde{\sigma}_l = \underline{\sigma} + (l-1)\varepsilon_\sigma$. Then the points with coordinates $(\widetilde{a}_r, \widetilde{\sigma}_l)$ form the nodes of a finite grid covering the rectangle $\{(a, \sigma) : \underline{a} \le a \le \overline{a},\ \underline{\sigma} \le \sigma \le \overline{\sigma}\}$ representing the set of possible values of the parameters of components of mixture (1). The number of nodes of the grid is equal to $K = (k_a + 1)(k_\sigma + 1)$. For convenience, renumber somehow the nodes introducing a *single* index i for the coordinates $(\widetilde{a}_i, \widetilde{\sigma}_i)$ of the node with the number i after renumbering, $i = 1, \ldots, K$.

The basis of the proposed approach is the approximation of mixture (1) by a mixture with a deliberately larger number of *known* components:

$$F(x) = \sum_{i=1}^{k} p_i G(x; a_i, \sigma_i) \approx$$

$$\approx \sum_{i=1}^{K} \widetilde{p}_i G(x; \widetilde{a}_i, \widetilde{\sigma}_i) \equiv \widetilde{F}(x), \quad x \in \mathbb{R}. \tag{4}$$

Such an approximation is practically admissible since, by virtue of (2) and (3), for any pair (a_r, σ_r) of the parameters of a component of mixture (1) there surely exists a pair $(\widetilde{a}_i, \widetilde{\sigma}_i)$ of the parameters of a component of mixture $\widetilde{F}(x)$ which is practically undistinguishable of the original pair. The weights of the rest components of the mixture $\widetilde{F}(x)$, for the parameters of which there is no "close" pair (a_r, σ_r) of the parameters of a component of mixture (1), can be regarded as zero. Indeed, if in relation (4) instead of the *approximate* equality there were the *exact* equality, then due to the identifiability of mixture (1), by the definition of identifiability, the equalities

$$k = K, \quad p_i = \widetilde{p}_i,\ a_i = \widetilde{a}_i,\ \sigma_i = \widetilde{\sigma}_i,\ i = 1, \ldots, k. \tag{5}$$

would hold up to re-indexation. Note that in the mixture $\widetilde{F}(x)$ *only* the weights $\widetilde{p}_1, \ldots, \widetilde{p}_K$ are unknown parameters.

Let $\boldsymbol{x} = (x_1, \ldots, x_n)$ be an independent sample of observations each of which is a realization of a random variable with distribution function $F(x)$ defined by (1).

To find the estimates of the weights $\tilde{p}_i$, $i = 1, \ldots, K$, in the mixture $\tilde{F}(x)$ (see (4)) we will use the maximum likelihood method.

Let $(\tilde{a}_i, \tilde{\sigma}_i)$ be the nodes of the grid covering the set of the values of the parameters of components, $i = 1, \ldots, K$. For convenience by $g(x; a, \sigma)$ denote the density corresponding to the distribution function $G(x; a, \sigma)$,

$$g_{ij} = g(x_j; a_i, \sigma_i), \quad j = 1, \ldots, n;\ i = 1, \ldots, K. \tag{6}$$

To understand whether any numerical algorithm oriented at the maximization of the grid likelihood function will converge or not, we should answer the question whether the grid likelihood function

$$L(\boldsymbol{p}; \boldsymbol{x}) = \log \prod_{j=1}^{n} \sum_{i=1}^{K} \tilde{p}_i g_{ij} = \sum_{j=1}^{n} \log \left(\sum_{i=1}^{K} \tilde{p}_i g_{ij} \right) \tag{7}$$

is convex or concave. The answer to this question is given by the following theorem (Korolev et al., 2010) (also see (Korolev, 2011)).

THEOREM 1. *Any grid likelihood function is concave as a function of the weights.*

In (Korolev et al., 2010) it was demonstrated that the grid maximum likelihood method realized by the algorithm of conditional gradient appeared to be a very efficient tool for the approximate separation of mixtures of one-parameter distributions. However, the efficiency of a grid method strongly depends on the dimensionality of the set of parameters and those grid methods which work very rapidly and efficiently for one-parameter mixtures, become considerably slower when they are applied to multi-parameter mixtures since the volume of computations grows exponentially as the dimensionality of parameter increases. To somehow overcome this drawback (or moderate its effect), in the present communication we propose a modification of the grid method, namely, the coordinate-wise versions of the grid method for separation of mixtures of two-parameter distributions.

COORDINATE-WISE GRID METHOD FOR SEPARATION OF MIXTURES OF GAMMA-DISTRIBUTIONS. THE ALGORITHM

The first step of the algorithm consists in the application of the modified grid algorithm over the whole two-dimensional net. The modifications aim at the noise reduction and rejection of insignificant components with small weights.

By virtue of the inaccuracy of the representation of zero in a computer, it is reasonable to regard a component as insignificant not if $p_i = 0$, but if $p_i < \epsilon$, where $\epsilon > 0$ is a small number. Since the components with zero weights cannot gain a positive probability as the grid algorithm proceeds, the increase of ϵ noticeably speeds up the algorithm. Moreover, the increase of ϵ makes it possible to reject those components whose weights go to zero as

the algorithm proceeds. As a result of empirical experiments it was decided to take $\epsilon = \frac{1}{8(K+1)^2}$.

The second modification consists in rejection of the insignificant components, if the total number of existing components exceeds some preassigned critical number Q (in practice we used $Q = 10$). After every S steps the component with the minimum weight is sifted out if its current weight is less than at the previous steps. After this the weights of the remaining components are normalized.

As a stopping rule we considered the condition

$$\sum_{i=1} (K+1)^2 |p_i^m - p_i^{m-1}| < \delta, \qquad (8)$$

where p_i^m is the weight of the ith component (the weight of the ith node of the grid) on the mth step of the algorithm, $\delta > 0$ is the pre-assigned accuracy. In practice we took $\delta \le 10^{-6}$.

The second step of the algorithm is determined as follows. After the first step is accomplished, we obtain the set of components with non-zero weights $(p_1, r_1, s_1), \ldots, (p_{k_1^r}, r_{k_1^r}, \theta_{k_1^r})$ with some $k_1 \in \mathbb{N}$. Choose all the corresponding different estimates $r_1, \ldots, r_{\widetilde{k}_1^r}$ of the parameter r (clearly, $\widetilde{k}_1^r \le k_1^r$). Construct a new grid based on these fixed values of the parameter r, spreading the grid over the possible values of θ in the way it was done on the first step. So, the obtained grid will have $\widetilde{k}_1^r(K+1) \le (K+1)^2$ nodes.

Again start the grid iterative algorithm on this reduced grid. As the result, we obtain the set of components with non-zero weights $(p_1, r_1, s_1), \ldots, (p_{k_1^\theta}, r_{k_1^\theta}, \theta_{k_1^\theta})$ with some $k_1^\theta \in \mathbb{N}$. Choose all the corresponding different estimates $\theta_1, \ldots, \theta_{\widetilde{k}_1^\theta}$ of the parameter θ (clearly, $\widetilde{k}_1^\theta \le k_1^\theta$). Construct a new grid based on these fixed values of the parameter θ, spreading the grid over the possible values of r in the way it was done on the first step. So, the obtained grid will have $\widetilde{k}_1^\theta(K+1) \le (K+1)^2$ nodes.

And so on. Each next step consists of two applications of the usual grid method on the adaptively reduced grids: on the first step we obtain new estimates for the parameter θ with the fixed values of r obtained on the preceding stage and on the second step we obtain new estimates for the parameter r with the fixed values of θ obtained on the preceding stage.

DISCUSSION

The modified coordinate-wise grid method possesses some advantages as compared to the "classical" grid method.

First, at each mth step the coordinate-wise method works with approximately $(\widetilde{k}_m^r + \widetilde{k}_m^\theta)K$ nodes whereas the classical grid method works with approximately K^2 nodes. Therefore, if $\widetilde{k}_m^r + \widetilde{k}_m^\theta$ is noticeably less than K, then the modified algorithm has noticeably less computational complexity and, hence, is more rapid and more efficient.

Second, since the grid is re-adjusted at each step, the modified algorithm is more sensitive. This circumstance is especially important for processing data obtained from non-stationary processes. For example, the modified grid method processes quite reliably those windows which appear to be problematic for the classical grid algorithm. Unlike the standard grid algorithm with the uniform grid, the modified algorithm shows all the peculiarities of mixtures of gamma-distributions with noticeably stratified (or clustered) values of the parameters of components.

Finally, the use of filters which reject insignificant components makes it possible to obtain more illustrative and sharp pictures of the evolution of the parameters of the mixture in the moving mode.

This research was supported by the Russian Foundation for Basic Research, projects no. 11-07-00112a, 12-07-00115a, 12-07-31267mol_a.

REFERENCES

Korolev, V. Yu. 2011. "Probabilistic and Statistical Methods of Decomposition of Volatility of Chaotic Processes." Moscow: Moscow University Publishing House (in Russian), 31-76.

Korolev, V. Yu., Nepomnyshchiy E. V.; Rybalchenko A. G. and Vinogradova A. V. 2008. "Grid methods for separation of mixtures of probability distributions and their application to the decomposition of volatility of financial indexes." *Informatics and Its Applications.* 2, No. 2, 3-18 (in Russian).

Korolev, V. Yu., Nazarov A. L. 2010. "Separating mixtures of probability distributions with the grid method of moments and the grid maximal likelihood method." *Autom. Remote Control.* 71, 455-472.

AUTHOR BIOGRAPHIES

ANDREY GORSHENIN is Candidate of Science (PhD) in physics and mathematics, senior scientist, Institute of Informatics Problems, Russian Academy of Sciences.

VICTOR KOROLEV is Doctor of Science in physics and mathematics, professor, Department of Mathematical Statistics, Faculty of Computational Mathematics and Cybernetics, M.V. Lomonosov Moscow State University; leading scientist, Institute of Informatics Problems, Russian Academy of Sciences.

VICTOR KUZMIN is researcher, "Wi2Geo LLC", Russia.

ALEXANDER ZEIFMAN is Doctor of Science in physics and mathematics; professor, Dean of the Faculty of Applied Mathematics and Computer Technologies, Vologda State Pedagogical University; senior scientist, Institute of Informatics Problems, Russian Academy of Sciences; leading scientist, Institute of Territories Socio-Economic Development, Russian Academy of Sciences.

MODELLING OF STATISTICAL FLUCTUATIONS OF INFORMATION FLOWS BY MIXTURES OF GAMMA DISTRIBUTIONS

Andrey Gorshenin
Institute of Informatics Problems,
Russian Academy of Sciences
Vavilova str., 44-2, Moscow, Russia
Email: agorshenin@ipiran.ru

Victor Korolev
Moscow State University
Leninskie Gory, Moscow, Russia
Institute of Informatics Problems,
Russian Academy of Sciences
Email: bruce27@yandex.ru

KEYWORDS

Information flows modelling; Stochastic structure; Probability mixtures

ABSTRACT

The paper describes statistical approach to the analysis of traffic of information flows. Stochastic structure of traffic process can be modelled by finite probability mixtures, e.g., mixtures of gamma distributions. The approach is demonstrated on real data from the official website of the Russian Academy of Sciences.

INTRODUCTION

Developing methods of investigating of probabilistic and statistical regularities related to rare events is an important area in the modern theory of probability. In particular, the Poisson theorem is the basis for constructing mathematical models in telecommunication systems. Classical stochastic models of telecommunication systems are based on the hypothesis that the data flows are Poisson. The assumption of the Poisson character of flow entails the fact that the development of a random process in future does not depend on its past and is determined only by its value at the current time. But this model is ideal, because real processes in the telecommunication systems do not satisfy the ideal conditions that imply Poissonity (Gnedenko, Korolev, 1996). So, to describe real complex information systems some generalization is needed.

GAMMA MIXTURE MODEL FOR INFORMATION FLOWS

In general, it may be assumed that the flow of events related to traffic is chaotic. The entropy reasoning leads us to the conclusion that the best model for the distribution of inter-arrival times in a completely chaotic flow is the exponential distribution resulting in that the flow itself is Poisson. The telecommunication systems are not closed systems. Therefore, it may be assumed that the exponential model can be regarded as conditional after conditioning with respect to information flows.

Probably, the best model of homogeneous chaotic stochastic flow is the Poisson process. But because of heterogeneity of chaos in real information systems, compound Cox process (Korolev, 2011) should be used instead of Poisson process. So, we have special reasons to examine finite gamma mixtures for modelling information flows.

For the investigation of the fine structure of information flows we assume the total sample to be locally homogeneous and suggest that within the window (number of elements) the sample is homogeneous. Then the window moves in the direction of the astronomic time making it possible to trace the evolution of the parameters of the gamma distribution in time. This idea is the essence of a method which is called "moving separation of mixtures" (MSM method). Accordingly, the original sample is split into smallers subsamples (windows), and the system is analysed within each window. The MSM method allows to observe time evolution of components. We can reveal dominating components, which form the process, and noise components which appear due to computational inaccuracy.

EM-ALGORITHM FOR MIXTURES OF GAMMA DISTRIBUTIONS

To estimate the parameters of gamma mixtures, the maximum likelihood method is used realized by the EM-algorithm. The formulas for the calculation of the estimates of the parameters on iterative steps have the following form. The shape parameter can be found by a numerical solution of the equation

$$\log r_i^{(m)} - \psi(r_i^{(m)}) = -\frac{\sum\limits_{j=1}^{n} g_{ij}^{(m)} \log \frac{x_j}{A_i^{(m)}}}{\sum\limits_{j=1}^{n} g_{ij}^{(m)}}, \qquad (1)$$

Proceedings 27th European Conference on Modelling and Simulation ©ECMS Webjørn Rekdalsbakken, Robin T. Bye, Houxiang Zhang (Editors)
ISBN: 978-0-9564944-6-7 / ISBN: 978-0-9564944-7-4 (CD)

where $\psi(\cdot)$ is the digamma function, the quantity $A_i^{(m)}$ has the form

$$A_i^{(m)} = \frac{\sum\limits_{j=1}^{n} x_j g_{ij}^{(m)}}{\sum\limits_{j=1}^{n} g_{ij}^{(m)}}, \tag{2}$$

$$g_{ij}^{(m)} = \frac{p_i^{(m)} f_{r_i^{(m)}, \theta_i^{(m)}}(x_j)}{\sum\limits_{l=1}^{k} p_l^{(m)} f_{r_l^{(m)}, \theta_l^{(m)}}(x_j)}, \tag{3}$$

on each step the scale parameter is determined by the relation

$$\theta_i^{(m)} = \frac{A_i^{(m)}}{r_i^{(m)}}, \; i = 1, \ldots, k, \tag{4}$$

and the weights are given by the formula

$$p_i^{(m+1)} = \frac{1}{n} \sum_{j=1}^{n} g_{ij}^{(m)}. \tag{5}$$

APPLICATION FOR REAL DATA

The following section deals with the application of the method for real information data.

Let us consider the average time that the visitors spent on website (see Fig. 1). The quantity equals the difference between time of last and first page browsing during the visit.

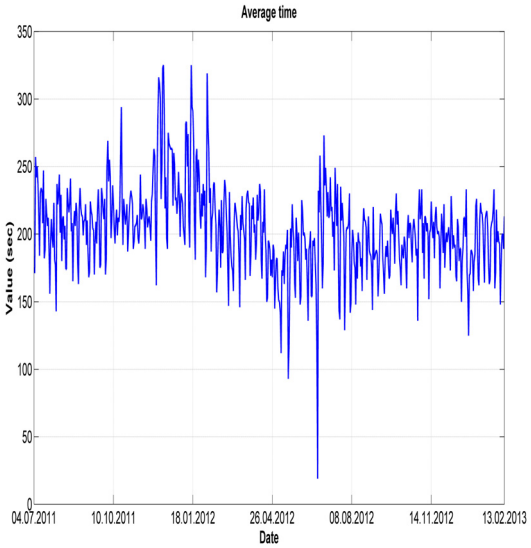

Figure 1: Average time of page browsing

The basic assumption is the existence of 3 components in the mixture. The EM-algorithm is applied in the moving mode, the window width is equal to 200 elements (see Fig. 2).

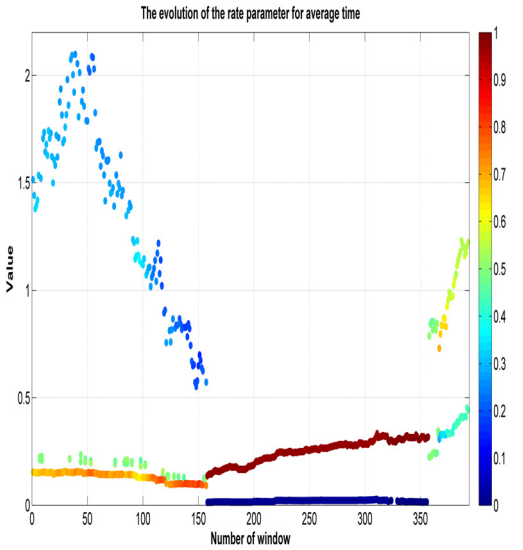

Figure 2: The evolution of rate parameter of gamma distribution in mixture

On the abscissa, the number of the current window in MSM method is plotted. On the ordinate, the values of gamma distributions parameter estimates are located (for the rate parameter of gamma distribution). The colormap corresponds to the weights of components. We can see 2 components during the whole period under review.

Let us consider the number of unique users with at least one visit on website during the period under review (see Fig. 3).

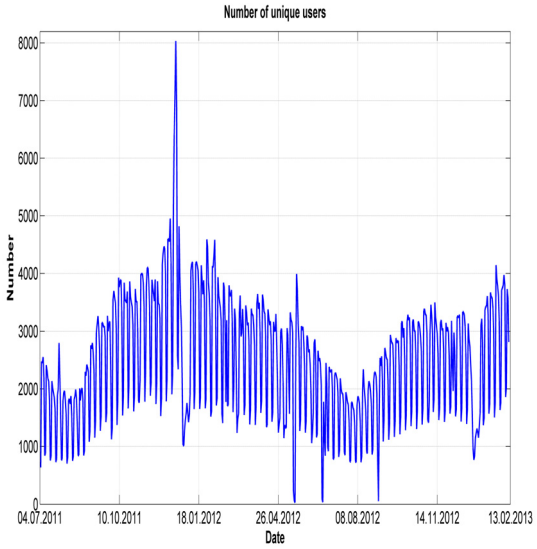

Figure 3: Number of unique users

The basic assumption is the existence of 4 components in the mixture. The EM-algorithm is ap-

plied in the moving mode, the window width is equal to 200 elements (see Fig. 4).

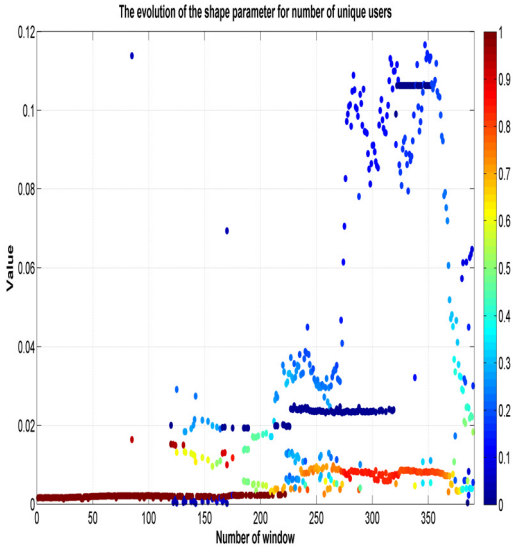

Figure 4: The evolution of the shape parameter of gamma distribution in mixture

On the abscissa, the number of the current window in MSM method is plotted as before. On the ordinate, the values of gamma distributions parameter estimates are located (for the shape parameter of gamma distribution). The colormap corresponds to the weights of components. We can see $2-3$ different components during the period under review. One component exists through the whole time period, but another components arise at some positions and disappear from our view when window is moved.

Naturally, the essence of the components for each considered data type may be different. But the components usually can be interpreted according to knowledge domains. It is one of the possible ways for analyzing and forecasting fine structure of data.

CONCLUSIONS

The representation of the probability distribution of traffic in information flows as a finite mixture of gamma-distributions makes it possible to reveal the stochastic structure of the information flow, that is, separate a finite number of typical sub-structures or classes of more or less similar (within a type) claims (or jobs) being executed at a time, determine the proportion of each substructure and trace the evolution of the stochastic structure in time. As this is so, the number of typical classes and their proportions can change in time also. The parameters of gamma distribution can be interpreted. For example, the ratio of these parameters determines the mean value of each class of jobs or the intensity of the sub-flow of jobs of the specific type. We obtained several different components in each of considered situations which could characterize the behavior of structures forming the information flows. The analysis of the components of flows gives an opportunity to create more detailed models of the functioning of information systems.

The efficiency of the methodology can be applied to various information systems. For example, the results of modeling of information flows in financial markets (the evolution of limit order books) can be found in (Gorshenin et al., 2012).

The new method of automatic data classification is represented in paper. The MSM methodology for traffic research is used for the first time. This approach can be used as basis of investigation in very important modern practical field – big data analysis. The big data in information technologies is combination data with innovation methods of analysis while traditional approaches are not inapplicable. The most important problem of the field is creation of strategies of working with the specific large data. The results mentioned above imply that described approach represents one of the perspective technique for exploring efficiency of software functioning in a changing computing environment. The main advantage of the MSM approach is combination of statistical analysis and data mining methods. Leaving out computational efficiency problem, in the paper we demonstrated reasonableness of approach in the particular example of data with modest size.

The authors express their gratitude to A.V. Bosov and service `http://metrika.yandex.ru/` for the permission to use concrete data.

The research is supported by the Russian Foundation for Basic Research (projects 12-07-00115a, 12-07-31267mol_a and 11-07-00112a).

REFERENCES

Gnedenko B. V., Korolev, V. Yu. 1996. "Random Summation: Limit Theorems and Applications." Boca Raton: CRC Press, 41-152.

Gorshenin A., Doynikov A., Korolev V. and Kuzmin V. 2012. "Statistical Properties of the Dynamics of Order Books: Empirical Results." *VI International Workshop "Applied Problems in Theory of Probabilities and Mathematical Statistics Related to Modeling of Information Systems."* M.: Institute of Informatics Problems, RAS, 2012, 31-51.

Korolev, V. Yu. 2011. "Probabilistic and Statistical Methods of Decomposition of Volatility of Chaotic Processes." Moscow: Moscow University Publishing House (in Russian), 31-76.

AUTHOR BIOGRAPHIES

ANDREY GORSHENIN is Candidate of Science (PhD) in physics and mathematics, senior scientist, Institute of Informatics Problems, Russian Academy of Sciences.

VICTOR KOROLEV is Doctor of Science in physics and mathematics, professor, Department of Mathematical Statistics, Faculty of Computational Mathematics and Cybernetics, M.V. Lomonosov Moscow State University; leading scientist, Institute of Informatics Problems, Russian Academy of Sciences.

APPROACH FOR ANALYSIS OF FINITE $M_2|M_2|1|R$ WITH HYSTERIC POLICY FOR SIP SERVER HOP-BY-HOP OVERLOAD CONTROL

Alexander V. Pechinkin
Rostislav V. Razumchik
Institute of Informatics Problems of RAS
Vavilova, 44-2,
119333, Moscow, Russia
Email: apechinkin@ipiran.ru,
rrazumchik@ieee.org

KEYWORDS

SIP, hop-by-hop overload control, threshold, hysteretic load control, queueing system, matrix-analytic method.

ABSTRACT

Matrix-analytic method for the analysis of finite $M_2|M_2|1|R$ queueing system with bi-level hysteric policy that models signalling hop-by-hop load control mechanism for SIP server is presented. Algorithm for efficient computation of of joint stationary probability distribution and expressions for some performance characteristics are given. Illustrative numerical example is provided to demonstrate some aspects of the proposed method. Results of calculations using proposed method were compared with results obtained from simulation model, developed using GPSS software, and showed good accuracy.

INTRODUCTION

One of the benefits that network operators gained with the beginning of use of packet networks was the opportunity to provide new, additional services for end-users. Since that times number of services increased drastically and the amount of control information, needed to provide those services, that has to be transmitted hither and thither through network, also increased. This naturally led to several problems concerning overload issues in network nodes that handle the control information. It is known that at the moment SIP (Session Initiation Protocol) is the main signalling protocol carrying control information in NGN (Next Generation Network). The SIP protocol has a basic overload control mechanism (503 Service Unavailable response code) but, as stated in RFC 5390 (2008), it cannot be considered as satisfactory because in some cases it may even worsen an overload condition. In RFC 6357 (2011) one can find so called hop-by-hop overload control mechanism which may be considered as a good alternative method for resolution of overload problems in SIP servers' network. Hop-by-hop overload control does not require that all SIP entities in a network support it. It can be used effectively between two adjacent SIP servers if both servers support overload control and does not depend on the support from any other server or user agent. A thorough discussion on this subject one can find, for example, in Abaev et al. (2012a), Abaev et al. (2013a), Yang et al. (2009), Garroppo et al. (2011), Ohta et al. (2009), Shen et al. (2008). In paper Abaev et al. (2012a) there was also developed a method, based on hysteretic policy with thresholds, for realization for hop-by-hop overload control. There was constructed a suitable queuing model with bi-level hysteric policy and algorithm for its performance characteristics was obtained.

Roughly speaking the model of hop-by-hop overload control with bi-level hysteric policy can be described as follows. There are two communicating SIP servers, say sending and receiving. The receiving SIP server (modeled as $M|M|1|R$ queue) may be in three operational states ("normal", "overloaded", "blocking") that are defined with two thresholds. It monitors continuously the current utility of its processor and notifies the sending server when it detects overloading. Then it asks sending SIP server to reduce the number of packets it sends by a certain (desired) factor. If the utility of its processor continues to grow receiving SIP server asks sending SIP server to stop sending packets (i.e. its state changes to "blocking"). When the utilization goes down the state changes back to "overloading" (and sending server starts to send again a certain fraction of packets) and if it continues to go down receiving SIP server switches to "normal" state and sending server starts to send all packets destined to receiving server.

Several generalizations of the queueing model analyzed in Abaev et al. (2012a) were proposed. In Abaev et al. (2012b) consideration was given to $M_2|M|1|R$ with bi-level hysteric policy and and new matrix-method was proposed for calculation of joint stationary distribution and main performance characteristics. In Abaev et al. (2013b) and Abaev et al. (2013c), motivated by the fact that SIP messages may be served for constant time, finite queueing system with deterministic service ($M|D|1|R$) and bi-level hysteric policy was considered. There was developed new approach for calculation of joint stationary distribution, main performance charac-

Proceedings 27th European Conference on Modelling and Simulation ©ECMS Webjørn Rekdalsbakken, Robin T. Bye, Houxiang Zhang (Editors)
ISBN: 978-0-9564944-6-7 / ISBN: 978-0-9564944-7-4 (CD)

teristics, including one of the important characteristics of hysteric mechanism — mean return time of the system back to normal state. Among other recent papers that deal with analysis of queues with hysteric policy one can mention Chydzinski (2004), **?**, Avrachenkov et al. (2011), Bekker (2009), Bekker et al. (2007), Taremi et al. (2012), Choi et al. (2008). The utilized methods (including potential method) allow one to obtain different stationary performance characteristics under different assumptions about service time distribution and incoming flow.

In this paper we analyze queueing system $M_2|M_2|1|R$ with bi-level hysteric policy which is the generalization of model, presented in Abaev et al. (2012b) and develop new effective approach for calculation of its joint stationary distribution which also differs from approaches known from accessible literature, including the one cited above. The consideration of such system is motivated by the fact that SIP messages of different types (INVITE and NON-INVITE) may be served by central processor unit of the SIP server with different speeds, which was not taken into account in models considered earlier. One of the stumble rocks in the steady state analysis of such systems is the fast growth of state space dimension with the growth of threshold values. So though this system may be more adequate for modeling purposes and provide more accurate results, its analysis with classical methods becomes intractable starting from low values of thresholds. Driven by interest in the explicit solution of the considered problem we propose method that allows computation of performance characteristics and of joint stationary distribution of number of INVITE and NON-INVITE messages in the queue and system's state for relatively high values of thresholds.

The rest of the paper is organized as follows. In the next section we give a description of the considered system and introduce several auxiliary variables that constitute the essence of our approach. In the subsequent section using elimination method we derive system of equilibrium equations for stationary joint probabilities and comment on its solution. In the last section some illustrative numerical examples are provided. Conclusion contains short description of the obtained results and remarks on further study.

SYSTEM DESCRIPTION

Consider the queueing system with two poisson incoming flows of customers (say type 1 and type 2) with rate λ_1 and λ_2 respectively, finite queue of size $R < \infty$, and one server. If arriving customer sees R customers in the system, it is considered to be lost. Henceforth we denote by λ the sum of λ_1 and λ_2, i.e. $\lambda = \lambda_1 + \lambda_2$. Type 1 customers have relative priority over customers of type 2 (i.e. no service interruptions are allowed and type 2 customer enters server facility only when it becomes free and there are no type 1 customers in the queue). Customers of type 1 and type 2 are served exponentially with different service rates, say μ_1 and μ_2. The hysteric mechanism operates as follows. Choose arbitrary numbers L, H such that $0 < L < H < R$. When the system starts to work it is empty and as long as the total number of customers in the system remains below $(H-1)$, system is considered to be in "normal" state. When total number of customers exceeds $(H-1)$ for the first time, the system changes its state to "overload" and stays in it as long as the number of customers remains between L and $(R-1)$. Moreover when overloaded, system accepts only type 1 customers. Being in "overload" state, system waits till the number of customers drops down below L after which it changes its state back to "normal", or exceeds $(R-1)$ after which it changes its state to "blocking". In the "blocking" state systems does not accept new arriving customers until the total number of customers drops down below $(H+1)$, after which system's state changes back to "overload".

The operation of the considered queueing system can be completely described by Markov process $\mathbf{X}(t) = \{\xi(t); \eta(t); \nu(t); \theta(t)\}$ with four components: $\xi(t)$ — number of type 1 customers in the queue at time t, $\eta(t)$ — number of type 2 customers the queue at time t, $\nu(t)$ — state of the system at time t, $\theta(t)$ — type of customer being served at time t. Clearly $\mathbf{X}(t)$ is ergodic and thus stationary distribution exists. In the next subsection we introduce auxiliary variables that constitute new method that we propose for the analysis of the system.

Auxiliary variables

The idea of the method is, using the property of ergodic processes (see, for example, Lemma 1.4.1 and Corollary 1.4.1 in Bocharov et al. (2003)), to write out the system of equilibrium equations (SEE) in such a form that it can be solved iteratively with minor manipulations. But before we can write out SEE, several auxiliary variables are needed.

Due to the fact that type 1 and type 2 customers have different priorities and are served with different rates we need to introduce the following notation. Henceforth all matrices that appear are block partitioned matrices which have the structure

$$\mathrm{A}_n = \begin{pmatrix} \mathrm{A}_n^{(11)} & \mathrm{A}_n^{(12)} \\ \mathrm{A}_n^{(21)} & \mathrm{A}_n^{(22)} \end{pmatrix}.$$

Here index $^{(kl)}$, $k = 1, 2$, $l = 1, 2$, means that at some moment of time type k customer is being served and after any event (i.e. arrival or service completion) type l customer is being served.

By E_n henceforth we denote n-by-n identity matrix.

Let at some moment of time there be n, $n = \overline{H+1, R-1}$ customers in the system and i, $i = \overline{0, H-1}$, customers of type 2 in the queue, and the system is in "overload" state. Denote by A_n matrix of size $2H \times 2H$. The $(i,j)^{th}$ entry of A_n is the probability that at the moment of time when the total number

of customers in the system equals $(n-1)$ for the first time, there will be $j,\ j=\overline{0,H-1}$, customers of type 2 in the queue, and until that moment the total number of customers in the system remained below R.

For matrix A_{R-1} it holds

$$\mathrm{A}_{R-1}^{(l1)}=\frac{\mu_l}{\lambda_1+\mu_l}\mathrm{E}_H,\ \ l=1,2;\quad \mathrm{A}_{R-1}^{(12)}=\mathrm{A}_{R-1}^{(22)}=0.$$

Other matrices A_n can be found using the following relations

$$\mathrm{A}_n=\mathrm{U}+\mathrm{V}\mathrm{A}_{n+1}\mathrm{A}_n,\ \ n=\overline{H+1,R-2},$$

where

$$\mathrm{U}^{(l1)}=\tfrac{\mu_l}{\lambda_1+\mu_l}\mathrm{E}_H,\ \ l=1,2;\quad \mathrm{U}^{(l2)}=0,\ \ l=1,2;$$
$$\mathrm{V}^{(ll)}=\tfrac{\lambda_1}{\lambda_1+\mu_l}\mathrm{E}_H,\ \ l=1,2;\quad \mathrm{V}^{(12)}=\mathrm{V}^{(21)}=0.$$

Now let at some moment of time there be $n,\ n=\overline{H+1,R-1}$ customers in the system and $i,\ i=\overline{0,H-1}$, customers of type 2 in the queue, and the system is in "overload" state. Denote by Γ_n matrix of size $2H\times 2H$. The $(i,j)^{th}$ entry of Γ_n is the probability that at the moment of time when the total number of customers in the system equals R for the first time, there will be $j,\ j=\overline{0,H-1}$, customers of type 2 in the queue, and until that moment the total number of customers in the system remained above $(n-1)$.

Matrix Γ_{D-1} is diagonal and its blocks have the form

$$\Gamma_{R-1}^{(ll)}=\frac{\lambda_1}{\lambda_1+\mu_l}\mathrm{E}_H,\ \ l=1,2;\quad \Gamma_{R-1}^{(12)}=\Gamma_{R-1}^{(21)}=0.$$

Other matrices Γ_n can be found from the following relations

$$\Gamma_n=\mathrm{U}\Gamma_{n+1}+\mathrm{U}\mathrm{A}_{n+1}\Gamma_n,\ \ n=\overline{H+1,R-2},$$

where

$$\mathrm{U}^{(ll)}=\frac{\lambda_1}{\lambda_1+\mu_l}\mathrm{E}_H,\ \ l=1,2;\quad \mathrm{U}^{(12)}=\mathrm{U}^{(21)}=0.$$

Now let at some moment of time there be R customers in the system and $i,\ i=\overline{0,H-1}$, customers of type 2 in the queue. Clearly the system is in "blocking" state. Denote by D_n matrix of size $2H\times 2H$. The $(i,j)^{th}$ entry of D_n is the probability that at the moment of time when the total number of customers in the system equals $n,\ n=\overline{H,R-1}$ for the first time, there will be $j,\ j=\overline{0,H-1}$, customers of type 2 in the queue. Because in "blocking" state system does not accept newly arriving customers, for matrices D_n it holds

$$\mathrm{D}_n^{(l1)}=\mathrm{E}_H,\quad \mathrm{D}_n^{(l2)}=0,\ \ l=1,2,\ \ n=\overline{H,R-1}.$$

Further we will use the following notation. Let X_n, Y_n, Z_n and W_n be matrices of size $n\times(n-1)$, $n\times(n-1)$, $n\times(n+1)$ and $n\times(n+1)$ respectively, which have the following structure

$$X_n=\begin{pmatrix}1&0&0&\dots&0&0\\0&1&0&\dots&0&0\\0&0&1&\dots&0&0\\\vdots&\vdots&\vdots&\ddots&\vdots&\vdots\\0&0&0&\dots&1&0\\0&0&0&\dots&0&1\\0&0&0&\dots&0&1\end{pmatrix},$$

$$Y_n=\begin{pmatrix}0&0&0&\dots&0&0\\0&0&0&\dots&0&0\\0&0&0&\dots&0&0\\\vdots&\vdots&\vdots&\ddots&\vdots&\vdots\\0&0&0&\dots&0&0\\0&0&0&\dots&0&0\\0&0&0&\dots&0&1\end{pmatrix},$$

$$Z_n=\begin{pmatrix}1&0&0&\dots&0&0&0\\0&1&0&\dots&0&0&0\\0&0&1&\dots&0&0&0\\\vdots&\vdots&\vdots&\ddots&\vdots&\vdots&\vdots\\0&0&0&\dots&1&0&0\\0&0&0&\dots&0&1&0\end{pmatrix},$$

$$W_n=\begin{pmatrix}0&1&0&0&\dots&0&0\\0&0&1&0&\dots&0&0\\0&0&0&1&\dots&0&0\\\vdots&\vdots&\vdots&\vdots&\ddots&\vdots&\vdots\\0&0&0&0&\dots&1&0\\0&0&0&0&\dots&0&1\end{pmatrix}.$$

Let at some moment of time there be $n,\ n=\overline{L,H-1}$ customers in the system and $i,\ i=\overline{0,n-1}$, customers of type 2 in the queue, and the system is in normal state. Denote by A_n matrix of size $2n\times 2(n-1)$. The $(i,j)^{th}$ entry of A_n is the probability that at the moment of time when the total number of customers in the system equals $(n-1)$ for the first time, there will be $j,\ j=\overline{0,n-2}$, customers of type 2 in the queue, and until that moment the total number of customers in the system remained below H.

For matrix A_{H-1} it holds

$$\mathrm{A}_{H-1}^{(l1)}=\frac{\mu_l}{\lambda+\mu_l}\mathrm{X}_{H-1},\ \ \mathrm{A}_{H-1}^{(l2)}=\frac{\mu_l}{\lambda+\mu_l}\mathrm{Y}_{H-1},\ \ l=1,2.$$

Other matrices A_n can be found using the following relations:

$$\mathrm{A}_n=\mathrm{U}_n+\mathrm{V}_n\mathrm{A}_{n+1}\mathrm{A}_n,$$

where

$$\mathrm{U}_n^{(l1)} = \frac{\mu_l}{\lambda+\mu_l}\mathrm{X}_n, \quad \mathrm{U}_n^{(l2)} = \frac{\mu_l}{\lambda+\mu_l}\mathrm{Y}_n, \ \ l=1,2;$$
$$\mathrm{V}_n^{(ll)} = \frac{\lambda_1}{\lambda+\mu_l}\mathrm{Z}_n + \frac{\lambda_2}{\lambda+\mu_l}\mathrm{W}_n, \ \ l=1,2;$$
$$\mathrm{V}_n^{(12)} = \mathrm{V}_n^{(21)} = 0.$$

Let at some moment of time there be $n,\ n=\overline{L,H-1}$ customers in the system and $i,\ i=\overline{0,n-1}$, customers of type 2 in the queue, and the system is in normal state. Denote by Γ_n matrix of size $2n\times 2H$. The $(i,j)^{th}$ entry of Γ_n is the probability that at the moment of time when the total number of customers in the system equals H for the first time, there will be $j,\ j=\overline{0,H-1}$, customers of type 2 in the queue, and until that moment the total number of customers in the system remained above $(n-1)$.

For blocks of matrix Γ_{H-1} it holds

$$\Gamma_{H-1}^{(ll)} = \frac{\lambda_1}{\lambda+\mu_l}\mathrm{Z}_{H-1} + \frac{\lambda_2}{\lambda+\mu_l}\mathrm{W}_{H-1}, \ \ l=1,2;$$
$$\Gamma_{H-1}^{(12)} = \Gamma_{H-1}^{(21)} = 0.$$

Other matrices Γ_n can be computed from the relations

$$\Gamma_n = \mathrm{U}_n\Gamma_{n+1} + \mathrm{U}_n\mathrm{A}_{n+1}\Gamma_n, \ \ n=\overline{L,H-2},$$

where

$$\mathrm{U}_n^{(ll)} = \frac{\lambda_1}{\lambda+\mu_l}\mathrm{Z}_n + \frac{\lambda_2}{\lambda+\mu_l}\mathrm{W}_n, \ \ l=1,2;$$
$$\mathrm{U}_n^{(12)} = \mathrm{U}_n^{(21)} = 0.$$

Now let at some moment of time there be $n,\ n=\overline{L,H-1}$ customers in the system and $i,\ i=\overline{0,n-1}$, customers of type 2 in the queue, and the system is in "overload" state. Denote B_n — matrix of size $2n\times 2(n+1)$. The $(i,j)^{th}$ entry of B_n is the probability that at the moment of time when the total number of customers in the system equals $(n+1)$ for the first time, there will be $j,\ j=\overline{0,n}$, customers of type 2 in the queue, and until that moment the total number of customers in the system remained above $L-1$.

For matrix B_L is holds

$$\mathrm{B}_L^{(ll)} = \frac{\lambda_1}{\lambda_1+\mu_l}\mathrm{Z}_n, \ \ l=1,2; \quad \mathrm{B}_L^{(12)} = \mathrm{B}_L^{(21)} = 0.$$

Other matrices B_n can be found from relations

$$\mathrm{B}_n = \mathrm{U}_n + \mathrm{V}_n\mathrm{B}_{n-1}\mathrm{B}_n, \ \ n=\overline{L+1,H-1},$$

where

$$\mathrm{U}_n^{(12)} = \mathrm{U}_n^{(21)} = 0; \quad \mathrm{U}_n^{(ll)} = \tfrac{\lambda_1}{\lambda_1+\mu_l}\mathrm{Z}_n, \ \ l=1,2;$$
$$\mathrm{V}_n^{(l1)} = \tfrac{\mu_l}{\lambda_1+\mu_l}\mathrm{X}_n, \quad \mathrm{V}_n^{(l2)} = \tfrac{\mu_l}{\lambda_1+\mu_l}\mathrm{Y}_n, \ \ l=1,2.$$

Now consider the following case. Let at some moment of time there be $n,\ n=\overline{L,H-1}$ customers in the system and $i,\ i=\overline{0,n-1}$, customers of type 2 in the queue, and the system is in "overload" state. Denote by D_n matrix of size $2n\times 2(L-1)$. The $(i,j)^{th}$ entry of D_n is the probability that at the moment of time when the total number of customers in the system equals $(L-1)$ for the first time, there will be $j,\ j=\overline{0,L-2}$, customers of type 2 in the queue, and until that moment the total number of customers in the system remained below n.

Matrix D_L is computed as follows

$$\mathrm{D}_L^{(l1)} = \frac{\mu_l}{\lambda_1+\mu_l}\mathrm{X}_L, \quad \mathrm{D}_L^{(l2)} = \frac{\mu_l}{\lambda_1+\mu_l}\mathrm{Y}_L, \ \ l=1,2.$$

For other matrices D_n it holds

$$\mathrm{D}_n = \mathrm{U}_n\mathrm{D}_{n-1} + \mathrm{U}_n\mathrm{B}_{n-1}\mathrm{D}_n, \ \ n=\overline{L+1,H-1},$$

where

$$\mathrm{U}_n^{(l1)} = \frac{\mu_l}{\lambda_1+\mu_l}\mathrm{X}_n, \quad \mathrm{U}_n^{(l2)} = \frac{\mu_l}{\lambda_1+\mu_l}\mathrm{Y}_n, \ \ l=1,2.$$

Let at some moment of time there be H customers in the system (i.e. the system is in "overload" state) and $i,\ i=\overline{0,H-1}$, customers of type 2 in the queue. Denote D — matrix of size $2H\times 2(L-1)$. The $(i,j)^{th}$ entry of D is the probability that at the moment of time when the total number of customers in the system equals $(L-1)$ for the first time, there will be j, $j=\overline{0,L-2}$, customers of type 2 in the queue.

Matrix D can be determined from the equation

$$\mathrm{D} = \mathrm{U}\mathrm{D}_{H-1} + \mathrm{U}\mathrm{B}_{H-1}\mathrm{D} + \mathrm{V}(\mathrm{A}_{H+1} + \Gamma_{H+1}\mathrm{D}_H)\mathrm{D},$$

where

$$\mathrm{U}^{(l1)} = \tfrac{\mu_l}{\lambda_1+\mu_l}\mathrm{X}_H, \quad \mathrm{U}^{(l2)} = \tfrac{\mu_l}{\lambda_1+\mu_l}\mathrm{Y}_H, \ \ l=1,2;$$
$$\mathrm{V}^{(12)} = \mathrm{V}^{(21)} = 0; \quad \mathrm{V}^{(ll)} = \tfrac{\lambda_1}{\lambda_1+\mu_l}\mathrm{E}_H, \ \ l=1,2.$$

Finally we introduce the last sequence of matrices. Let at some moment of time there be $n,\ n=\overline{1,L-1}$ customers in the system and $i,\ i=\overline{0,n-1}$, customers of type 2 in the queue, and the system is in normal state. Denote by A_n matrix of size $2n\times 2(n-1)$. The $(i,j)^{th}$ entry of A_n is the probability that at the moment of time when the total number of customers in the system equals $(n-1)$ for the first time, there will be $j,\ j=\overline{0,n-2}$, customers of type 2 in the queue. For matrix A_{L-1} it holds

$$\mathrm{A}_{L-1} = \mathrm{U}_{L-1} + \mathrm{V}_{L-1}(\mathrm{A}_L + \Gamma_L\mathrm{D})\mathrm{A}_{L-1},$$

where

$$\mathrm{U}_{L-1}^{(l1)} = \frac{\mu_l}{\lambda+\mu_l}\mathrm{X}_{L-1}, \ \ \mathrm{U}_{L-1}^{(l2)} = \frac{\mu_l}{\lambda+\mu_l}\mathrm{Y}_{L-1}, \ \ l=1,2;$$
$$\mathrm{V}_{L-1}^{(ll)} = \frac{\lambda_1}{\lambda+\mu_l}\mathrm{Z}_{L-1} + \frac{\lambda_2}{\lambda+\mu_l}\mathrm{W}_{L-1}, \ \ l=1,2;$$
$$\mathrm{V}_{L-1}^{(12)} = \mathrm{V}_{L-1}^{(21)} = 0.$$

Other matrices A_n are computed from equations

$$\mathrm{A}_n = \mathrm{U}_n + \mathrm{V}_n\mathrm{A}_{n+1}\mathrm{A}_n, \ \ n=\overline{1,L-2},$$

where

$$\mathrm{U}_n^{(ll)} = \frac{\mu_l}{\lambda+\mu_l}\mathrm{X}_n,\ \ \mathrm{U}_n^{(l2)} = \frac{\mu_l}{\lambda+\mu_l}\mathrm{Y}_n,\ \ l=1,2;$$
$$\mathrm{V}_n^{(ll)} = \frac{\lambda_1}{\lambda+\mu_l}\mathrm{Z}_n + \frac{\lambda_2}{\lambda+\mu_l}\mathrm{W}_n,\ \ l=1,2;$$
$$\mathrm{V}_n^{(12)} = \mathrm{V}_n^{(21)} = 0.$$

STATIONARY JOINT PROBABILITY DISTRIBUTION

Let $\vec{p}_0 = p_0$ be stationary probability of the empty system. Denote by

- $\vec{p}_n,\ n = \overline{1, H-1}$, — row vector of size $2n$, whose first n elements $p_{ni},\ i = \overline{0, n-1}$, are stationary probabilities of the fact that there are total of n customers in the system, including i type 2 customers in the queue, system is in the normal state and type 1 customer is being served; last n elements $p_{ni},\ i = \overline{n, 2n-1}$ are stationary probabilities of the fact that there are n customers in the system, including $(i-n)$ type 2 customers in the queue, system is in the normal state and type 2 customer is being served;
- $\vec{p}'_n,\ n = \overline{L, H-1}$, — row vector of size $2n$, whose first n elements $p'_{ni},\ i = \overline{0, n-1}$, are stationary probabilities of the fact that there are total of n customers in the system, including i type 2 customers in the queue, system is in "overload" state and type 1 customer is being served; last n elements $p'_{ni},\ i = \overline{n, 2n-1}$ are stationary probabilities of the fact that there are n customers in the system, including $(i-n)$ type 2 customers in the queue, system is in "overload" state and type 2 customer is being served;
- $\vec{p}'_n,\ n = \overline{H, R-1}$, — row vector of size $2H$, whose first n elements $p'_{ni},\ i = \overline{0, H-1}$, are stationary probabilities of the fact that there are total of n customers in the system, including i type 2 customers in the queue, system is in "overload" state and type 1 customer is being served; last n elements $p'_{ni},\ i = \overline{H, 2H-1}$ are stationary probabilities of the fact that there are n customers in the system, including $(i-H)$ type 2 customers in the queue, system is in "overload" state and type 2 customer is being served;
- $\vec{p}''_n,\ \ n = \overline{H+1, R}$, — row vector of size $2H$, whose first n elements $p''_{ni},\ i = \overline{0, H-1}$, are stationary probabilities of the fact that there are total of n customers in the system, including i type 2 customers in the queue, system is in "blocking" state and type 1 customer is being served; last n elements $p''_{ni},\ i = \overline{H, 2H-1}$ are stationary probabilities of the fact that there are n customers in the system, including $(i-H)$ type 2 customers in the queue, system is in "blocking" state and type 2 customer is being served.

Finally, introduce the following matrices:

- $\mathrm{U}_n,\ n = \overline{1, H-1}$, of size $2n \times 2n$, where $\mathrm{U}_n^{(ll)} = (\mu_l + \lambda)\mathrm{E}_n,\ \ l = 1,2,\ \ \mathrm{U}_n^{(12)} = \mathrm{U}_n^{(21)} = 0$;
- $\mathrm{U}'_n,\ \ n = \overline{L, H-1}$ of size $2n \times 2n$, where $(\mathrm{U}'_n)^{(ll)} = (\mu_l + \lambda_1)\mathrm{E}_n,\ \ l = 1,2,\ \ (\mathrm{U}'_n)^{(12)} = (\mathrm{U}'_n)^{(21)} = 0$;
- $\mathrm{U}'_n,\ \ n = \overline{H, R-1}$ of size $2H \times 2H$, where $(\mathrm{U}'_n)^{(ll)} = (\mu_l + \lambda_1)\mathrm{E}_H,\ \ l = 1,2,\ \ (\mathrm{U}'_n)^{(12)} = (\mathrm{U}'_n)^{(21)} = 0$;
- $\mathrm{U}''_n,\ \ n = \overline{H+1, R}$ of size $2H \times 2H$, where $(\mathrm{U}''_n)^{(ll)} = \mu_l\mathrm{E}_H,\ \ l = 1,2,\ \ (\mathrm{U}''_n)^{(12)} = (\mathrm{U}''_n)^{(21)} = 0$;
- $\Lambda'_n = \lambda_1\mathrm{E}_{2H},\ \ n = \overline{H, R-1}$, of size $2H \times 2H$;
- $\mathrm{M}_n,\ \ n = \overline{H+2, R}$, of size $2H \times 2H$, where $M_n^{(l1)} = \mu_l\mathrm{E}_H,\ \ l = 1,2,\ \ M_n^{(12)} = M_n^{(22)} = 0$;
- $\Lambda_0 = \lambda_1(1\ \ 0) + \lambda_2(0\ \ 1)$ of size 1×2;
- $\Lambda_n,\ \ n = \overline{1, H-1}$, of size $2n \times 2(n+1)$, where $(\Lambda_n)^{(ll)} = \lambda_1\mathrm{Z}_n + \lambda_2\mathrm{W}_n,\ \ l = 1,2,\ \ (\Lambda_n)^{(12)} = (\Lambda_n)^{(21)} = 0$;
- $\mathrm{M}_n,\ \ n = \overline{L+1, H}$ of size $2n \times 2(n-1)$, where $(\mathrm{M}_n)^{(l1)} = \mu_l\mathrm{X}_n,\ \ (\mathrm{M}_n)^{(l2)} = \mu_l\mathrm{Y}_n,\ \ l = 1,2.$

After making all preliminary remarks we can write out the system of equilibrium equations. It holds

$$\vec{p}_n\mathrm{U}_n = \vec{p}_n\Lambda_n\mathrm{A}_{n+1} + \vec{p}_{n-1}\Lambda_{n-1},\quad n = \overline{1, L-2}, \tag{1}$$
$$\vec{p}_{L-1}\mathrm{U}_{L-1} = \vec{p}_{L-1}\Lambda_{L-1}(\mathrm{A}_L + \Gamma_L\mathrm{D}) + \vec{p}_{L-2}\Lambda_{L-2}, \tag{2}$$
$$\vec{p}_n\mathrm{U}_n = \vec{p}_n\Lambda_n\mathrm{A}_{n+1} + \vec{p}_{n-1}\Lambda_{n-1},\quad n = \overline{L, H-2}, \tag{3}$$
$$\vec{p}_{H-1}\mathrm{U}_{H-1} = \vec{p}_{H-2}\Lambda_{H-2}, \tag{4}$$
$$\vec{p}'_H\mathrm{U}'_H = \vec{p}_{H-1}\Lambda_{H-1} + \vec{p}'_H(\mathrm{M}_H\mathrm{B}_{H-1} + + \Lambda'_H(\mathrm{A}_{H+1} + \Gamma_{H+1}\mathrm{D}_H)), \tag{5}$$
$$\vec{p}'_n\mathrm{U}'_n = \vec{p}'_{n-1}\Lambda'_{n-1} + \vec{p}'_n\Lambda'_n\mathrm{A}_{n+1},\quad n = \overline{H+1, R-2}, \tag{6}$$
$$\vec{p}'_{R-1}\mathrm{U}'_{R-1} = \vec{p}'_{R-2}\Lambda'_{R-2}, \tag{7}$$
$$\vec{p}''_R\mathrm{U}''_R = \vec{p}'_{R-1}\Lambda'_{R-1}, \tag{8}$$
$$\vec{p}''_n\mathrm{U}''_n = \vec{p}''_{n+1}\mathrm{M}_{n+1},\ \ n = \overline{H+1, R-1}, \tag{9}$$
$$\vec{p}'_n\mathrm{U}'_n = \vec{p}'_{n+1}\mathrm{M}_{n+1} + \vec{p}'_n\mathrm{M}_n\mathrm{B}_{n-1},\quad n = \overline{L+1, H-1}, \tag{10}$$
$$\vec{p}'_L U'_L = \vec{p}'_{L+1}\mathrm{M}_{L+1}. \tag{11}$$

The probabilities must satisfy the normalization condition

$$p_0 + \sum_{n=1}^{H-1}\vec{p}_n\vec{1} + \sum_{n=L}^{R-1}\vec{p}'_n\vec{1} + \sum_{n=H+1}^{R}\vec{p}''_n\vec{1} = 1. \tag{12}$$

The main idea behind equations (1)–(11) is the elimination method which can be found in (Bocharov et al., 2003, Chapter 1). Their solution is straightforward. Divide (1)–(11) by p_0 and compute unknown variables consequently from each equation starting from (1). Then

make use of normalization condition (12) to find p_0 and multiply each of the previously obtained variables by p_0.

Let

$$p_n = \sum_{i=0}^{2n-1} p_{ni}, \quad n = \overline{1, H-1},$$

$$p'_n = \sum_{i=0}^{2n-1} p'_{ni}, \quad n = \overline{L, H-1},$$

$$p'_n = \sum_{i=0}^{2H-1} p'_{ni}, \quad n = \overline{H, R-1},$$

$$p''_n = \sum_{i=0}^{2H-1} p''_{ni}, \quad n = \overline{H+1, R},$$

Knowing joint stationary distribution one can calculate a number of performance characteristics. The system utilization is simply $(1 - p_0)$. The probability π_1 (π_2) that the arriving customer of type 1 (type 2) is lost equals

$$\pi_1 = \sum_{n=H+1}^{R} p''_n, \quad \pi_2 = \pi_1 + \sum_{n=L}^{R-1} p'_n.$$

Served load is $\lambda^* = (1-\pi_1)\lambda_1 + (1-\pi_2)\lambda_2$. The mean number Q_1 (Q_2) of customers of type 1 (type 2) in the queue can be calculated as follows:

$$Q_1 = \sum_{n=1}^{H-1}\sum_{i=0}^{n-1}(n-i-1)p_{ni} + \sum_{n=L}^{H-1}\sum_{i=0}^{n-1}(n-1-i)p'_{ni} + \\ + \sum_{n=H}^{R-1}\sum_{i=0}^{H-1}(n-1-i)p'_{ni} + \sum_{n=H+1}^{R}\sum_{i=0}^{H-1}(n-1-i)p''_n,$$

$$Q_2 = \sum_{n=1}^{H-1}\sum_{i=0}^{n-1} i p_{ni} + \sum_{n=L}^{H-1}\sum_{i=0}^{n-1} i p'_{ni} + \\ + \sum_{n=H}^{R-1}\sum_{i=0}^{H-1} i p'_{ni} + \sum_{n=H+1}^{R}\sum_{i=0}^{H-1} i p''_n.$$

Finally, mean time that customer of type 1 (type 2) has to wait in the queue until it receives service can be calculated using Little's law. That is, we have

$$V_1 = \frac{Q_1}{(1-\pi_1)\lambda_1}, \quad V_2 = \frac{Q_2}{(1-\pi_2)\lambda_2}.$$

NUMERICAL RESULTS

In this section we give illustrative numerical examples of application of developed results. In Abaev et al. (2012b) consideration was given to $M_2|M|1|R$ with bi-level hysteric policy for modeling of SIP server with load control. The question of interest is how much one underestimates or overestimates performance characteristics of SIP server if we model it with $M_2|M|1|R$ with bi-level hysteric policy (i.e. if we consider that all incoming messages are served by SIP server with the same rate). The model considered in this paper allows us to do it because it takes into consideration the type (e.g. INVITE or NON-INVITE) of message that arrives at the CPU of SIP server.

For the examples we use the following values of thresholds: $L = 10$, $H = 18$, $R = 25$. Let the mean service time for priority customers (e.g. INVITE messages) be equal 10ms, i.e. $\mu_1 = 0.1$. We assume that the total customers' arrival rate is 200 $(sec)^{-1}$, i.e. $\lambda_1 + \lambda_2 = 0.2\,(ms)^{-1}$. Recall that in "overload" state the system reduces input flow. Let q be the dropping probability of newly arriving customers when system is in "overload" state. Then $\lambda_1 = \lambda(1-q)$ and $\lambda_2 = \lambda q$.

In figure 1 and figure 2 one can see the behaviour of mean queue length (i.e. $Q_1 + Q_2$) and loss probability of type 2 customers (i.e. π_2) as functions of dropping probability q. for different values of mean service time $(\mu_2)^{-1}$ of type 2 customers.

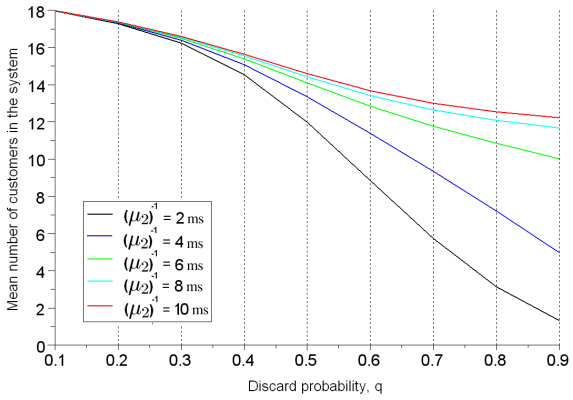

Figure 1: Mean number of customers in the queue

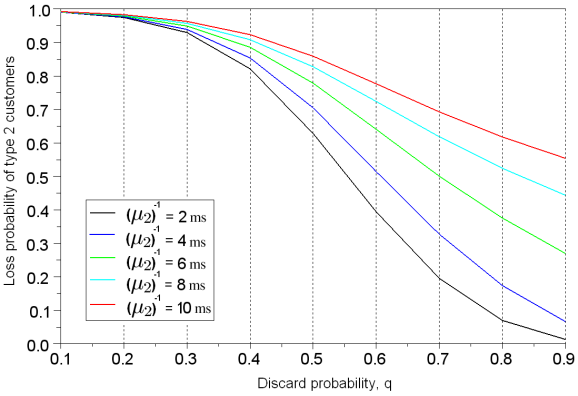

Figure 2: Loss probability of type 2 customers

From figures it is seen that starting from the certain value of q account of different service rates for different types of customers noticeably influences the values of mean queue length and especially of loss probability π_2. In order to check theoretical results there was built a simulation model using GPSS software. The comparisons of numerical and simulation results showed good accuracy.

SUMMARY

In this study matrix-analytic method for the analysis of finite queueing system $M_2|M_2|1|R$ with bi-level hysteric policy that models signalling hop-by-hop load control mechanism for SIP server is presented. Expressions for main performance characteristics are given. Illustrative numerical example is provided. The considered problem is only one of the many other possible formulations. Future work will be connected with the experimental verification of the proposed model using outcomes of real-world experiments. In addition attention will be paid to the analysis of stationary time-related performance characteristics of this system, posing and solution of optimization problems (in order to find appropriate values of thresholds), and the generalization of the proposed approach for cases with more general input flows and service times.

Notes and Comments. This work was supported in part by the Russian Foundation for Basic Research (grants 12-07-00108, 13-07-00223, 13-07-00284).

REFERENCES

Abaev, P., Gaidamaka, Yu., Pechinkin, A., Razumchik, R., Samouylov, K., Shorgin, S. 2012. Hysteretic control technique for overload problem solution in network of SIP servers. Computing and Informatics. (accepted).

Abaev, P., Pechinkin, A., Razumchik, R. 2013. Analysis of queueing system with constant service time for sip server hop-by-hop overload control. Lecture Notes in Communications in Computer and Information Science (LN CCIS). Pp. 1–10.

Abaev, P., Pechinkin, A., Razumchik, R. 2013. On mean return time in queueing system with constant service time and bi-level hysteric policy. Lecture Notes in Communications in Computer and Information Science (LN CCIS). Pp. 11–19.

Abaev, P., Gaidamaka, Yu., Pechinkin, A., Razumchik, R., Shorgin, S. 2012. Simulation of overload control in SIP server networks. Proc. of the 26th European Conference on Modelling and Simulation, ECMS 2012. Pp. 533–539.

Abaev, P., Pechinkin, A., Razumchik, R. 2012. On analytical model for optimal sip server hop-by-hop overload control. Proc. of the 4th International Congress on Ultra Modern Telecommunications and Control Systems ICUMT-2012. Pp. 303–308.

Avrachenkov, K., Dudin, A., Klimenok, V., Nain, P., Semenova, O. 2011. Optimal threshold control by the robots of web search engines with obsolescence of documents. Journal of Computer Networks. Vol. 55. No. 8. Pp. 1880–1893.

Bekker, R. 2009. Queues with Levy input and hysteretic control. Queueing Systems. Vol. 63. Issue 1. Pp. 281–299.

Bekker, R., Boxma, O.J. 2007. An M/G/1 queue with adaptable service speed. Sochastic Models. Vol. 23. Issue 3. Pp. 373–396.

Bocharov, P., D'Apice, C., Pechinkin, A., Salerno, S. 2003. Queueing Theory. Utrecht: VSP Publishing, 450 p.

Choi, D.I., Kim, T.S., Lee, S. 2008. Analysis of an $MMPP|G|1|K$ queue with queue length dependent arrival rates, and its application to preventive congestion control in telecommunication networks. European Journal of Operational Research. Vol. 187. Issue 2. Pp. 652–659.

Chydzinski, A. 2004. The oscillating queue with finite buffer. Performance Evaluation. Vol. 57. No. 3. Pp. 341–355.

Garroppo, R., Giordano, S., Niccolini, S., Spagna, S. 2011. A Prediction-Based Overload Control Algorithm for SIP Servers. IEEE Transactions on Network and Service Management. Vol. 8. No. 1. Pp. 39–51.

Hilt, V., Noel, E., Shen, C., Abdelal, A. 2011. Design Considerations for Session Initiation Protocol (SIP) Overload Control. RFC 6357

Ohta, M. 2009. Overload Control in a SIP Signalling Network. International Journal of Electrical and Electronics Engineering. Pp. 87–92.

Rosenberg, J. 2008. Requirements for Management of Overload in the Session Initiation Protocol. RFC 5390.

Shen, C., Schulzrinne, H., Nahum, E. 2008. Session Initiation Protocol (SIP) Server Overload Control: Design and Evaluation. Lecture Notes in Computer Science. Vol. 5310. Pp. 149–173.

Taremi, M., Reza Salehi Rad, M. 2012. Limit analysis of oscillating batch arrival $M^{[x]}|G|1$ sysmtes with finite capacity: EMC approach. Journal of Economic Theory. Vol. 6. No. 1. Pp. 29–36.

Yang, J., Huang, F., Gou, S. 2009. An Optimized Algorithm for Overload Control of SIP Signaling Network. 5th International Conference on Wireless Communications, Networking and Mobile Computing. Pp. 1–4.

AUTHOR BIOGRAPHIES

ALEXANDER V. PECHINKIN is a Doctor of Sciences in Physics and Mathematics and principal scientist at the Institute of Informatics Problems of the Russian Academy of Sciences, and a professor at the Peoples' Friendship University of Russia. He is the author of more than 150 papers in the field of applied probability theory. His email address is `apechinkin@ipiran.ru`.

ROSTISLAV V. RAZUMCHIK received his Ph.D. in Physics and Mathematics in 2011. Since then, he has worked as a senior researcher at the Institute of Informatics Problems of the Russian Academy of Sciences. His current research activities focus on stochastic processes and queuing theory. His email address is `rrazumchik@ieee.org`

DESIGN AND SOFTWARE ARCHITECTURE OF SIP SERVER FOR OVERLOAD CONTROL SIMULATION

Pavel O. Abaev (speaker)
Yuliya V. Gaidamaka
Konstantin E. Samouylov
Telecommunication Systems Department
Peoples' Friendship University of Russia
Miklukho-Maklaya str., 6,
117198, Moscow, Russia
Email: pabaev@sci.pfu.edu.ru,
ygaidamaka@sci.pfu.edu.ru
ksam@sci.pfu.edu.ru

Sergey Ya. Shorgin
Institute of Informatics Problems of RAS
Vavilova, 44-1,
119333, Moscow, Russia
Email: sshorgin@ipiran.ru

KEYWORDS

Signalling network, SIP, hop-by-hop overload control, hysteretic load control, simulation tool.

ABSTRACT

The rapid development of services provided on SIP networks not only define the necessity of creating new equipment and standards but also requires the development of new methods and programming software tools for modeling and analyzing the effectiveness of the overload control mechanisms in SIP-server networks. The modeling process utilizes mathematical and simulation models as well as simulators. Only simulation tools make it possible to solve problems related to the analysis and optimization of the control parameters. The most appropriate modeler is the simulators reflecting the protocols and functions which are fully or partially built into the original system. Over the last few years, IETF working group SOC (SIP Overload Control) has been actively conducting research aimed at developing an effective mechanism for server overload control in SIP networks. At present, there are no simulators for modeling the work of SIP servers in overload conditions with an application of mechanisms which are currently under development by SOC. A model for a SIP server simulator and approaches to its programming implementation are proposed in the paper.

INTRODUCTION

SIP is an application-layer signaling protocol for creating, modifying, and terminating sessions with one or more participants. In November 2000, SIP was accepted as a 3GPP signaling protocol and main protocol of the IMS architecture. In 2002, recommendation (RFC 3261, 2002) which determines the current protocol form was accepted. The rapid development of the market for services based on the SIP protocol and the growing user needs have revealed a number of shortcomings in the protocol, specifically, in the base overload control mechanism (mechanism 503). In 2009, Rosenberg, one of the protocol designers, demonstrated in (RFC 5390, 2008) the protocols' main shortcomings in regard to overload prevention and formulated the main requirements toward the future overload control mechanism. In mid-2010, the SOC working group was created within the IETF Committee. Its work aims at creating overload prevention mechanisms. The first result of their work was the document (RFC 6357, 2011) which was permanently accepted in August 2011. The document provides a discussion of the available types of overload control mechanisms – local, hop-by-hop, and end-to-end, a classification of SIP networks, and presents the overall architecture of overload-control systems. The SOC group's work focuses on developing two hop-by-hop schemes for overload control as this type of mechanisms has a number of indisputable advantages over the other two types (RFC 6357, 2011; IETF draft SIP Rate Overload Control, 2013). At present, two overload control schemes have been proposed – one with flow sifting on the sender side (LBOC, Loss-based overload control) and one with restricting the flow rate of signaling messages (RBOC, Rate-based overload control). However, only the basic principles were described in SOCs' documents and methods for calculation of the control parameters were not specified. The control parameters can be determined based on analysis of mathematical models or as the results of simulation modeling. As the processes going on in the SIP networks are difficult to describe mathematically and depend on a large number of different factors, the task needs to be solved through the creation of a simulator.

This paper is organised as follows. We analyse IETF experience for SIP-signaling overload control problem solutions. Then we investigate overload control techniques which are implemented on the server and the client side. And finally, we introduce the architecture of the SIP simulation tool for modeling different overload control techniques.

Proceedings 27th European Conference on Modelling and Simulation ©ECMS Webjørn Rekdalsbakken, Robin T. Bye, Houxiang Zhang (Editors)
ISBN: 978-0-9564944-6-7 / ISBN: 978-0-9564944-7-4 (CD)

SIP OVERLOAD CONTROL PROBLEM OVERVIEW

Basic 503 mechanism

The SIP protocol provides a basic overload control mechanism through the 503 (Service Unavailable) response code. SIP servers that are unable to forward a request due to temporary overload can reject the request with a 503 response. The overloaded server can insert a Retry-After header into the 503 response, which defines the number of seconds during which this server is not available for receiving any further requests from the upstream neighbor. A server that receives a 503 response from a downstream neighbor stops forwarding requests to this neighbor for the specified amount of time and starts again after this time is over. Without a Retry-After header, a 503 response only affects the current request and all other requests can still be forwarded to this downstream neighbor. A server that has received a 503 response can try to resend the request to an alternate server, if one is available. A server does not forward 503 responses toward the UA and converts them to 500 Server Internal Error responses instead. The two possible scenarios of the mechanism 503 are shown in Fig. 1. Note that RFC 3261 provides, in the case of overload the recipient to discard incoming messages without notifying the sender.

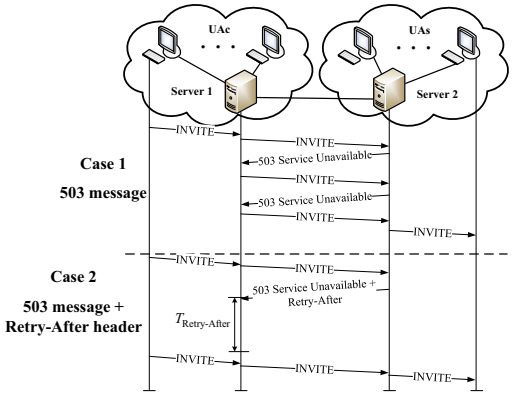

Figure 1: Two scenarios of 503 mechanism

A SIP server overload occurs if a SIP server does not have sufficient resources to process all incoming SIP messages. Several reasons, including Poor Capacity Planning, Component Failures, Avalanche Restart or Flash Crowds and the list of the problems that arise as a result of the 503 mechanism are presented in (RFC 5390, 2008).

Load Amplification. The supplementary result of the 503 mechanism is the tendency to amplify the load during periods of overload significantly, thus causing further aggravation of the problem and bringing the collapse of the network closer.

Underutilization. RFC 3261 does not cover how the 503 message recipient should react. In fact, there are some network configurations where it is not possible to clearly identify the sender of the message if the sender knows only a domain name of the cluster of receivers. So the sender may slow down the load to the entire cluster of servers with no overloaded servers, but not to the actual server in overload.

The Off/On Retry-After Problem. When the sender is balancing requests between a small number of the receivers, the 503 mechanism with Retry-After becomes noneffective because of its all-or-nothing technique. The 503 mechanism with Retry-After tends to cause highly oscillatory behavior under even mild overload.

Ambiguous Usages. The Standards do not clearly determine when the server must send the message with the code 503, and as a result of various implementations the message 503 is used to indicate different states. For example, according to (RFC 3398, 2002) the signaling gateway sends a message 503 in response to reports of inability to handle the request, which does not necessarily mean that the gateway is overloaded.

Rosenberg formulated 23 requirements to overload control mechanisms in (RFC 5390, 2008); mechanisms matching them will be able to predict and to avoid or quickly to cope with an overload on the server.

Explicit Overload Control Scheme

The problem domain of SIP overload control can be split into overload control between a user agent and a SIP server and overload control between SIP servers. The first document (RFC 6357, 2011) developed by SOC, contains the overload control mechanism classification with local, hop-by-hop and end-to-end schemes, and the following network topologies for "server-server" interoperation – load balancer, multiple sources and mesh.

Current work of the group is focused on the development of two hop-by-hop overload control schemes – Loss-based overload control and Rate-based overload control. The choice in favour of hop-by-hop mechanism was made because of the advantages over the other two mechanisms: the solutions implemented hop-by-hop scheme have better scalability and the scheme requires a SIP entity to aggregate overload status values of SIP servers only that each server communicates with.

The basic idea of LBOC scheme is that the sending entity (SE) reduces the number of messages on RE's request which will be send to the receiving entity (RE) by specified in the request amount of the total number of messages. RBOC scheme operates in the following way: RE informs SE about the maximum message rate which RE would like to receive from SE within a specified period of time. RE sends the control information to SE periodically depending on RE load changes.

Both of these schemes based on the idea of feedback control loop shown in Fig. 2 between all neighboring SIP servers that directly exchange traffic. Each loop controls only two entities. The Actuator is located on the sending entity and throttles the traffic if necessary. The receiving entity has the Monitor which measures the current server load.

The four Via header parameters ('oc', 'oc-algo', 'oc-validity' and 'oc-seq') are introduced in (IETF draft SIP

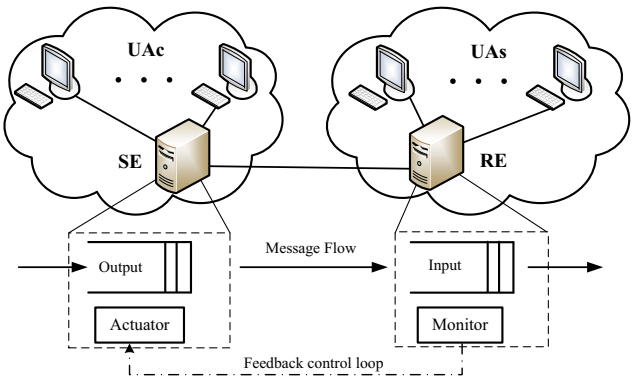

Figure 2: Feedback control loop between receiving and sending entities

Overload Control, 2013) to transfer the control information between two adjacent entities.

The integer parameter 'oc' consisting of 10 digits and its value defines what percentage of the total number of SIP requests are subject to reduction at the SE when the loss-based scheme is used. Analogously, when the rate-based scheme is used it indicates that the client should send SIP requests at a rate of 'oc'-value SIP requests or fewer per second. 'oc-algo' parameter defines the scope of algorithms supported by SE, e.g. oc-algo="loss", "rate". 'oc-validity' parameter contains a value that indicates an interval of time (measured in milliseconds) that the load reduction specified in the value of the 'oc' parameter should be in effect, its default value is 500 ms. 'oc-sequence' is the sequence number associated with the 'oc' parameter, timestamps usually use as its value.

The message format with the control information, the procedures of choice overload control algorithm, and the behavior of client and server using overload control mechanism are described in detail in (IETF draft SIP Overload Control, 2013; IETF draft SIP Rate Overload Control, 2013). However, these documents remains open the following questions that need further research:

– Criteria determining the choice of moments for sending messages with control information from SE to RE;

– Rule for choosing the value of 'oc' parameter;

– Rule for choosing the value of 'oc-validity' parameter.

To address these problems we have developed analytical models which we discuss in the next section.

OVERLOAD CONTROL TECHNIQUES OVERVIEW

Threshold Overload Control on the Server Side

As a criteria determining the choice of moments for sending messages with control information from SE to RE we propose to use hysteretic control technique. The system during operation changes its state depending on the total number of messages n present in it. Choose arbitrary numbers L and H such that $0 < L < H < B$, where B is the buffer capacity. When the system starts to work it is empty, $(n = 0)$, and as long as the total number of messages in the system remains below $H - 1$, system is considered to be in normal state, $(s = 0)$. When total number of messages exceeds $H - 1$ for the first time, the system changes its state to overload, $(s = 1)$, and RE informs SE that traffic load should be reduced: it stays in it as long as the number of messages remains between L and $B - 1$. Being in overload state, RE's system waits till the number of messages drops down below L after which it changes its state back to normal and informs SE about changes, or exceeds $B - 1$ after which it changes its state to blocking, $(s = 2)$, and ask SE for temporary suspension of sending SIP requests. When the total number of messages drops down below $H + 1$, system's state changes back to overload, and RE informs SE that the process of sending of messages can be resumed with the current limitations. Input load function $\lambda(s, n)$ is schematically depicted in Fig. 3.

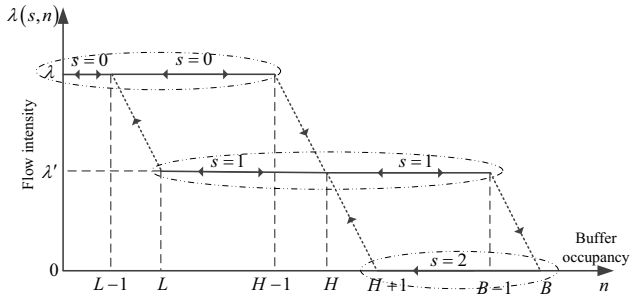

Figure 3: Hysteretic load control with two thresholds

Different analytical models in the form of a queuing system were built to estimate the performance indicators of hysteretic overload control algorithm (Abaev and etc., 2012, 2013). To estimate the optimal value of the thresholds, L and H, two optimization problems were formulated and solved in (Abaev et al., SOC simulation; Queueing System with Constant Service Time, 2012). In addition, such a system has been studied in the nonstationary case. The initial values of the thresholds were taken as a solution of the optimization problem from (Abaev et al., Analytical model for optimal SOC), i.e. $L = 74$ and $H = 85$. The dependency of the buffer occupancy on time t is shown in Fig. 4. The left Y-axis indicates the current buffer occupancy, $n(t)$, and the right Y-axis indicates the overload status of the system, $s(t)$. Server overload status changes are clearly shown in the two subfigures below the main one. Each subfigure depicts the chart to consistently zoom in on the previous figure.

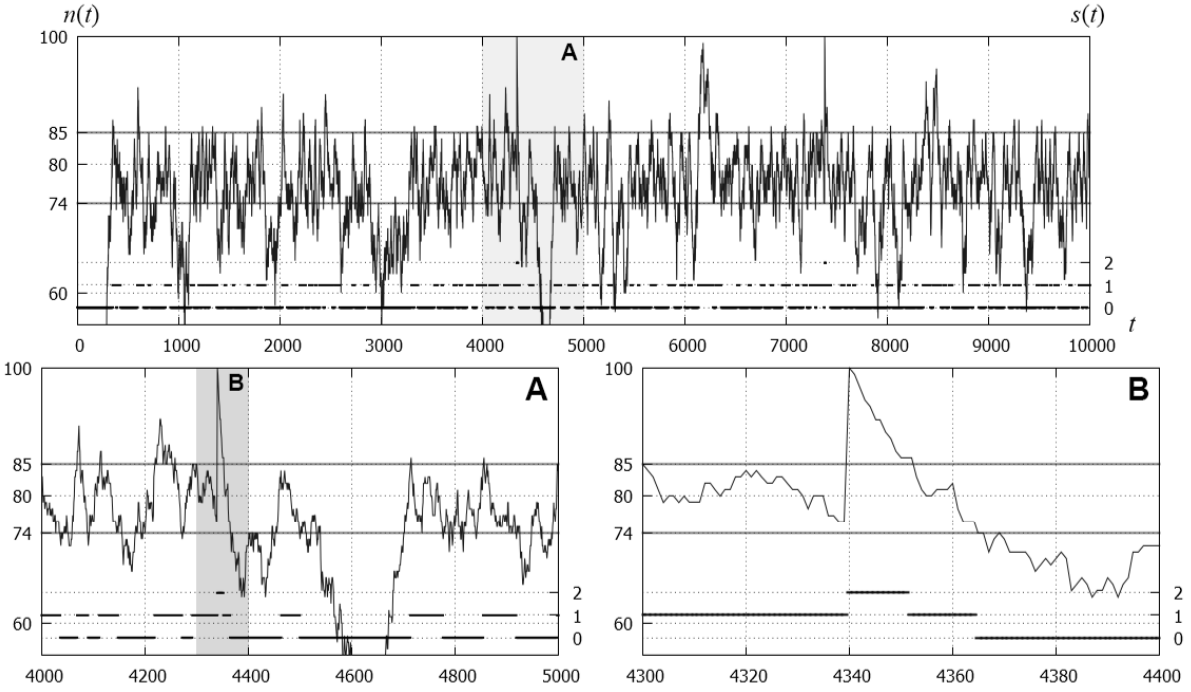

Figure 4: Modeling hysteretic overload control in unsteady condition

Default Algorithm on the Client Side for LBOC case

In the case of LBOC scheme the default algorithm for throttling incoming to the server traffic is used on the client side. The idea of the algorithm presented in (IETF draft SIP Overload Control, 2013) is to sift the client's outgoing flow. Let us consider the example of the implementation of the algorithm.

The client maintains two types of requests – the priority and non-priority. Prioritization of messages is done in accordance with local policies applicable to each SIP-server. In situations where the client has to sift the outgoing flow, it first reduces non-priority messages, and then if the buffer contains only priority messages and further reduction is still needed, the client reduces the priority messages.

Under overload condition, the client converts the value of the 'oc'=q parameter to a value that it applies to non-priority requests. Let N_1 denote the number of priority messages and N_2 denote the number of the non-priority messages in the client's buffer. The client should reduce the non-priority messages with probability $q_2 = \min\left\{1, q\frac{N_1+N_2}{N_2}\right\}$ and the priority messages with probability $q_1 = \frac{q(N_1+N_2)-q_2N_2}{N_1}$ if necessary to get an overall reduction of the 'oc' value.

To affect the reduction rate with probability q_2 from the non-priority messages, the client draws a random number between 1 and 100 for the request picked from the first category. If the random number is less than or equal to converted value of the "oc" parameter, the request is not forwarded; otherwise the request is forwarded. Recalculation of probabilities is performed periodically every 5-10 seconds by getting the value of the counters N_1 and N_2.

Leaky Bucket Algorithm on the Client Side for RBOC case

In the case of RBOC scheme the default Leaky Bucket algorithm (ITU-T I.371, 2004) is proposed to use on the client side to deliver SIP requests at a rate specified in the 'oc' value with tolerance parameter τ (IETF draft SIP Rate Overload Control, 2013). The Leaky Bucket algorithm can be viewed as a finite capacity bucket whose real-valued content drains out at a continuous rate of 1 unit of content per time unit and whose content increases by the increment T for each forwarded SIP request. T is computed as the inverse of the rate specified in the 'oc' value, namely $T = 1/oc$.

It is assumed that the client tries to put some content into the bucket at random times (time of a message arrival).

If at that moment the bucket capacity does not exceed the value τ, the incoming content (incoming message) is added to the bucket and increases the volume of content in the bucket by T. If at that moment the amount of content of the bucket more than τ, the incoming content (message) is not added to the bucket.

The random process of changes of the bucket's content is shown in Fig. 5. Let $X(t) \geq 0$ is the value of the bucket's content at the moment $t \geq 0$, t_k is the moments of arrival of the $k-th$, $k \geq 1$, message, $LCT(t)$ is the last confirmed time before moment t, $n(t)$ is the number of the latest message accepted before the moment t.

These variables satisfy the following relations:

$$n(t) = \sup_{k \geq 1} \{k : \ t_k < t, \ \ X(t_k) \leq \tau\}, \qquad (1)$$

$$LCT(t) = t_{n(t)}, \qquad (2)$$

$$X(t) = X(LCT(t)) - \ [t - LCT(t)]. \qquad (3)$$

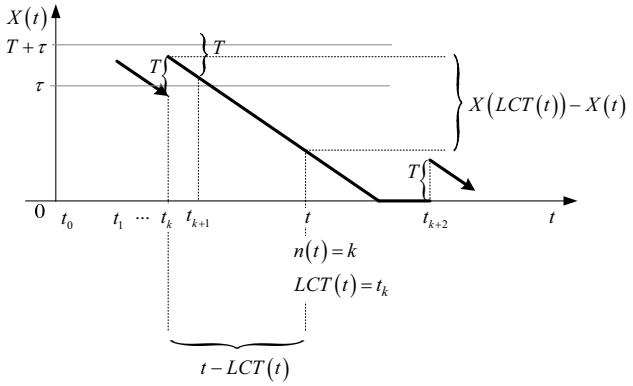

Figure 5: Changes of the value of the bucket's content $X(t)$

Note that the value τ is configured on the client side and chosen depending on the amount of the client's memory and its' processor performance. The problem of finding the optimal values of the parameters 'oc' will not be considered in this article because of space limitations.

OSN FUNCTIONAL REQUIREMENTS

Now we present the capabilities of simulation tool OSN (Open SIP signalling Node) which is under development and supports *nix like OS. Node's software architecture can be logically divided into three levels as shown in Fig. 6: TCP/IP Level, SIP Stack Level and Application Level.

TCP/IP Level corresponds to the first four levels of the ISO/OSI model and is implemented in OS, e.g. Debian or CentOS.

SIP Stack Level can be logically divided into two sublevels: the first one is SIP protocol sublevel which consists of SIP Manager, Message Processing, and Management Entity, the second one is Traffic Load Control sublevel which consists of Actuator, Monitor and Control Function.

The SIP protocol sublevel implements SIP baseline specification (RFC 3261, 2002; RFC 3263, 2002). New modules can be added if necessary. SIP Manager implements the client and server transaction state machines. Message Processing Module provides the complete set of tools for processing SIP messages. Management Entity module is responsible for dumping and aggregation of statistics. The Traffic Load Control sublevel is detailed described in the next subsection.

Application Level contains Presence and Location Modules. The Presence module allows a party to know the ability and willingness of other parties to participate in a call even before an attempt has been made. The module is responsible for handling Presence SUBSCRIBE requests with event package "presence" from Watchers, and enables the application to notify them about the Presence status of the Presentities.

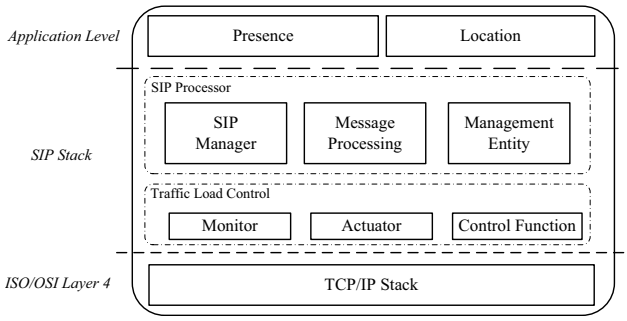

Figure 6: Architecture of the OSN simulation tool

Functional Requirements for Traffic Load Control sublevel

Each module of Traffic Load Control sublevel implements the functionality according to (RFC 6357, 2011). The communication between the modules is shown in Fig. 7. The Monitor measures the current load of the SIP Processor on the receiving entity. It implements the mechanisms needed to determine the current usage of resources relevant for the SIP Processor and reports load samples to the Control Function. The Control Function implements the overload control algorithm. The Control Function uses the load samples and determines if overload has occurred and a throttle needs to be set to adjust the load sent to the SIP Processor on the receiving entity. The Control Function on the receiving entity sends load feedback to the sending entity. The Actuator implements the algorithms needed to act on the throttles and ensures that the amount of traffic forwarded to the receiving entity meets the criteria of the throttle. The Actuator implements the algorithms to achieve this objective, e.g., using message gapping. It also implements algorithms to select the messages that will be affected and determine whether they are rejected or redirected.

In the case of LBOC and RBOC schemes Monitor watches the server's buffer occupancy and Control Function implements hystertic overload control. Module Actuator implements the default algorithm which was described above.

SUMMARY AND FURTHER STUDY

In this paper we give an overview of the problems and requirement analysis for SIP overload control mechanisms. We develop functional requirements for SIP simulation tool which are the result of the authors experience gained from the analytical modeling of overload control techniques performed by the authors in (Abaev and etc, 2012,

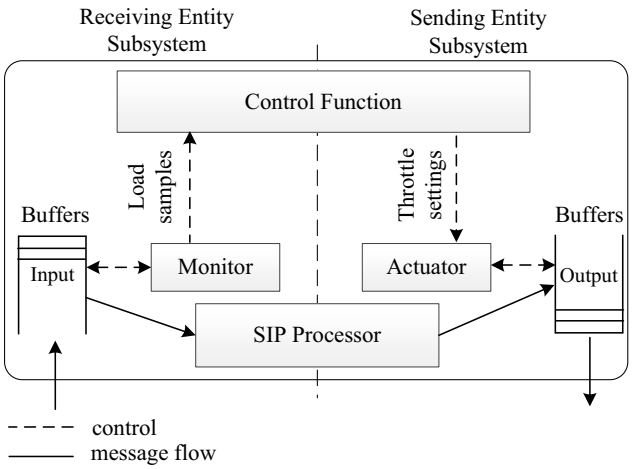

Figure 7: Communications between traffic control modules

2013). Future work will be focused on the development technical requirements of the simulator and mathematical modeling of overload control algorithms to make a proposal for the preliminary values of the control parameters, which will be used as input data for the simulator.

Acknowledgement This work was supported in part by the Russian Foundation for Basic Research (grants 12-07-00108 and 13-07-00665).

The author thank PhD student Andrey Samuylov for modelling hysteretic overload control in unsteady condition and magister Anastasia Khachko for figures design.

REFERENCES

Abaev, P., Gaidamaka, Yu., Samouylov, K. 2012. Modeling of Hysteretic Signaling Load Control in Next Generation Networks. Lecture Notes in Computer Science. Germany, Heidelberg, Springer-Verlag. –Vol. 7469. –P.371–378.

Abaev, P., Gaidamaka, Yu., Samouylov, K. 2012. Queuing Model for Loss-Based Overload Control in a SIP Server Using a Hysteretic Technique. Lecture Notes in Computer Science. Germany, Heidelberg, Springer-Verlag. -Vol. 7469. –P.440–452.

Abaev, P., Gaidamaka, Yu., Pechinkin, V., Razumchik, R., Shorgin, S. 2012. Simulation of overload control in SIP server networks. Proceedings of the 26th European Conference on Modelling and Simulation, ECMS 2012. –Germany, Koblenz. –Pp. 533–539.

Abaev, P., Pechinkin, V., Razumchik, R.. 2012. Analysis of Queueing System with Constant Service Time for SIP Server Hop-by-Hop Overload Control. Proceedings of the 4th International Congress on Ultra Modern Telecommunications and Control Systems, ICUMT 2012. –Saint–Petersburg, Russia. –Pp. 299–304.

Abaev, P., Pechinkin, V., Razumchik, R. 2012. On analytical model for optimal SIP server hop-by-hop overload control. Communications in Computer and Information Science: Modern Probabilistic Methods for Analysis of Telecommunication Networks. Germany, Heidelberg, Springer–Verlag. –Vol. 356. –P.1–10.

Abaev, P., Pechinkin, V., Razumchik, R. 2012. On Mean Return Time in Queueing System with Constant Service Time and Bi-level Hysteric Policy. Communications in Computer and Information Science: Modern Probabilistic Methods for Analysis of Telecommunication Networks. Germany, Heidelberg, Springer–Verlag. –Vol. 356. –P.11–19.

Rosenberg, J., Schulzrinne, H., Camarillo, G. et al. 2002. SIP: Session Initiation Protocol. RFC 3261.

Gurbani, V., Hilt, V., Schulzrinne, H. 2013. Session Initiation Protocol (SIP) Overload Control. draft-ietf-soc-overload-control-12.

Hilt, V., Noel, E., Shen, C., Abdelal, A. 2011. Design Considerations for Session Initiation Protocol (SIP) Overload Control. RFC 6357.

Noel, E., Williams, P. 2012. Session Initiation Protocol (SIP) Rate Control. draft-ietf-soc-overload-rate-control-03.

Rosenberg, J. 2008. Requirements for Management of Overload in the Session Initiation Protocol. RFC 5390.

Traffic control and congestion control in B-ISDN. ITU-T Recommendation I.371. 2004.

Camarillo, G., Roach, A., Peterson, J., Ong, L. 2002. Integrated Services Digital Network (ISDN) User Part (ISUP) to Session Initiation Protocol (SIP) Mapping. RFC 3398.

Rosenberg, J., Schulzrinne, H. 2002. Session Initiation Protocol (SIP): Locating SIP Servers. RFC 3263.

AUTHOR BIOGRAPHIES

PAVEL O. ABAEV received his Ph.D. in Computer Science from the Peoples' Friendship University of Russia in 2012. He has been a senior lecturer in the Telecommunication Systems department of the Peoples' Friendship University of Russia since 2011. His current research focus is on NGN signalling, QoS analysis of SIP, and mathematical modeling of communication networks. His email address is `pabaev@sci.pfu.edu.ru`.

YULIYA V. GAIDAMAKA received the Ph.D. in Mathematics from the Peoples' Friendship University of Russia in 2001. Since then, she has been an associate professor in the university's Telecommunication Systems department. She is the author of more than 50 scientific and conference papers. Her research interests include SIP signalling, multiservice and P2P networks performance analysis, and OFDMA based networks. Her email address is `ygaidamaka@sci.pfu.edu.ru`.

KONSTANTIN E. SAMOUYLOV received his Ph.D. from the Moscow State University and a Doctor of

Sciences degree from the Moscow Technical University of Communications and Informatics. During 1985–1996 he held several positions at the Faculty of Sciences of the Peoples' Friendship University of Russia where he became a head of the Telecommunication Systems Department in 1996. His current research interests are performance analysis of 3G networks, teletraffic of triple play networks, and signaling networks planning. He is the author of more than 100 scientific and technical papers and three books. His email address is ksam@sci.pfu.edu.ru.

SERGEY YA. SHORGIN received a Doctor of Sciences degree in Physics and Mathematics in 1997. Since 1999, he is a Deputy Director of the Institute of Informatics Problems, Russian Academy of Sciences, since 2003 he is a professor. He is the author of more than 100 scientific and conference papers and coauthor of three monographs. His research interests include probability theory, modeling complex systems, actuarial and financial mathematics. His email address is sshorgin@ipiran.ru.

DATA COMPRESSION AND RECOVERY FOR POWER CONSUMPTION AT SPECIFIC TIME INSTANCES AND IN PEAK PERIODS

Tetiana Lutchyn
Department of Electric Power Supply
Institute for Energy Saving and Energy Management
National Technical University of Ukraine "Kyiv Polytechnic Institute"
Borchshagivska 115, 03056,
Kyiv, Ukraine
E-mail:t.lutchyn@mail.ru

Bernt Lie
Faculty of Technology
Telemark University College
Kjoelnes Ring 56, 3901,
Porsgrunn, Norway
E-mail:bernt.lie@hit.no

Anatoliy Voloshko
Department of Electric Power Supply
Institute for Energy Saving and Energy Management
National Technical University of Ukraine "Kyiv Polytechnic Institute"
Borchshagivska 115, 03056,
Kyiv, Ukraine
E-mail:a-voloshko@yandex.ru

ABSTRACT

Compression and recovering of power consumption data through wavelet analysis is described. This technique will reduce the storage needs of such data, enable the reconstruction of data at a sufficient level of accuracy for invoicing, and allow for better energy planning in production facilities.

KEYWORDS

Tariff, peak consumption, data compression, data recovery, wavelet coefficients, level of decomposition.

SECTION 1. INTRODUCTION

Storing large amounts of data in the form of time series has been faced by the process industry for decades. In addition to securely storing the data, it is necessary to be able to efficiently retrieve data for further analysis. In the process industry, it is not uncommon with tens of thousands of sensor signals with a time resolution in the range of 1 s. Typically, 8 bytes may be used to store real numbers. Thus, to store ten thousand real numbered signal values every second leads to some 6.5 Gbyte of data every day.

To handle the resulting large amount of data, a typical data compression strategy is to only store values that fall outside of a defined deadband about the previously stored value, and the respective time stamp. With limited storage capacity, the size of the deadband is meant to give a good compromize between data accuracy and searchability of the data.

Although progress in storage technology has made available low cost disks with capacity in the Tbyte range, secure storage over years and with a need to efficiently search the data still makes it relevant to attempt to compress data in an efficient way.

In the power industry, electricity consumption meters are typically based on counting the number of rotations of a tiny motor driven by the electric current consumption, within a given time period. For households, the normal pricing scheme is a fixed price per consumed energy in the winter season, and another price in the summer season. For large consumers, daily peak and off-peak periods may be defined, with differentiation in price. The length of the periods may vary both with season and with the location of the consumer. Advanced measurement systems (AMS) for homes are planned to be introduced within a few years in Norway, which will make daily price differentiation a possibility also in the household. For these systems, the sampling period will be 1 hour initially, but with more detailed sampling already planned. Although the amount of data is manageable for households with a small population, the more general problem of also including details about consumption in businesses and in larger populations make it relevant to both compress data in an efficient way to reduce the storage needs, and to enable efficient retrieval of data.

Keeping track of electricity consumption is thus of importance both to the electricity producer when producing invoices, and to the consumer in case of disagreements and for making it possible to shift energy-intensive processes to off-peak periods. It is thus necessary to store a large amount of data, and data compression becomes increasingly important; compression must, however be done in such a way that relevant data may be reconstructed at a sufficient level of accuracy. Measured power consumption is typically transmitted from consumer to producer over open communication lines, and it is important to encrypt these data to avoid that outsiders get access to the data. Accurate invoicing of power consumption also requires that it is not possible to tamper with the data. Several methods for data compression and reconstruction exist (Li et. al 2010), (Luo et. al 2009); one promising technique is based on wavelet analysis of the power consumption signal (Cai 2012).

This paper is organized as follows. In section 2, an overview of the electricity tariff system in Norway is given. In section 3, multiresolution analysis for compressing electrical consumption signals is discussed.

Proceedings 27th European Conference on Modelling and Simulation ©ECMS Webjørn Rekdalsbakken, Robin T. Bye, Houxiang Zhang (Editors)
ISBN: 978-0-9564944-6-7 / ISBN: 978-0-9564944-7-4 (CD)

Section 4 discusses the recovery of information from compressed data at specific time instances, while section 5 looks into details of restoring values of consumption in peak periods. In section 6, some conclusions are drawn.

SECTION 2. TARIFF SYSTEM IN POWER ENGINEERING OF NORWAY AND PEAK PERIODS OF ENERGY CONSUMPTION

Electric power consumption varies with the hour and the season, and the power producers need to take this into account when building their production capacity. The power production needs to satisfy demands from society and be economically viable. Various tariffs are developed to both give good economy and to influence the production such as to smooth out peaks in the total consumption from the customers. It follows that it is necessary to keep track of variations in power consumption for the customers, with emphasis on those measures that are of importance in the different tariffs.

The Norwegian power grid consists of more than 200 energy companies of various sizes; these, specify the price depending on the type of consumer (with the presence of the consumption control, voltage class and the distance from the power source), and at the end of the year the predicted and the calculated values are recalculated (Ajodhia 2002).

A single-rate tariff with a transition between the seasons is the simplest tariff in Norway (Sæle and Grande2011); this is divided into two periods: the summer period from 1^{th} of May to 1^{th} of October, and the winter period in the other part of a year. The price for the electricity supply does not change during a period in this tariff system. Basically, this type of calculation is common for the household sector. In recent times,the need for a more detailed tariff regulation of household customers has risen due to peak consumption periods during the morning from $8^{\underline{00}}$ to $10^{\underline{00}}$, and in the evening from $17^{\underline{00}}$ to $19^{\underline{00}}$ (Morch et al. 2007). This fact clearly shows the effect of the household sector to the total value of electrical consumption in the whole power system.

For industrial facilities, the tariff regulation system between the supplier and the consumer has several options. For enterprises with consumption less than 100 MWh, the tariff system is similar to that of household customers. For larger enterprises, an hourly electricity measurement is implemented. These larger enterprises consume about 60% of the total energy in Norway (Morch et al. 2007), (Hansen 2004). As a whole, the transient periods between the peak loads and normal levels of energy consumption have a relatively short duration. Thus, only peak periods and off-peak periods are considered. The prices vary between peak periods and off-peak periods; typically, the price is 30% higher in peak periods (Sæle and Grande 2011). Because of the price variation between peak and off-peak periods, enterprises may be able to re-schedule their production and move some of their productions to off-peak periods, and in this way reduce their power cost.

For the electricity supplying companies, parameters of energy consumption provide useful information during peak load: the increasing of price during that time may stimulate consumers to change their work schedules. Additional control of the data summarizing economic balances is required during the peak period of consumption to hinder consumers from tampering with the information with the result of too low registered power consumption and a loss for the power supplying companies.

For these reasons, the recovery of the measure of energy consumption for enterprises with obligatory control of hourly meter readings is important. One promising method for compressing and recovering information is based on wavelet analysis.

SECTION 3. MULTIRESOLUTION ANALYSIS FOR DAILY SCHEDULE OF ELECTRICAL LOAD

Wavelet-algorithms offer ease of implementation and are connected with high adaptability and effectiveness in comparison with classical statistical methods of data processing. *Multiresolution analysis* (MRA) and the wavelet decompositions of Mallat, Daubechies, Meyer, etc. form elements of a wavelet analysis useful for the study of power measurement signals. Most wavelet transforms are designed to solve one problem and give one answer. If several answers are sought, such as in power signal analysis (consumption in peak periods, consumption at various instances, etc.), it is necessary to either use many existing methods or increase the number of steps in the algorithm.

This paper deals with ways to expand wavelet transforms for multipurpose information processing. For solving a multipurpose task, at first one should consider methods where the wavelet coefficients hold direct information. Existing MRA algorithms (Daubechies 1992) allow obtaining in the last level of the wavelet transform the same quantity of wavelet coefficients as in the original data sample.

This means that for studying a full day of hourly *measurements of electrical load* (MEL), the 24 values of hourly consumption are expanded with 8 additional zeros to get the complete sample of $32 = 2^5$ initial data. In the last level of the wavelet transform,this will give us 32 wavelet coefficients where we know that 8 of these contain redundant information – due to the added 8 zeros. From these last level coefficients, we can recover the original hourly data without loss of accuracy. The decomposition algorithm is indicated by the scheme in Fig. 1.

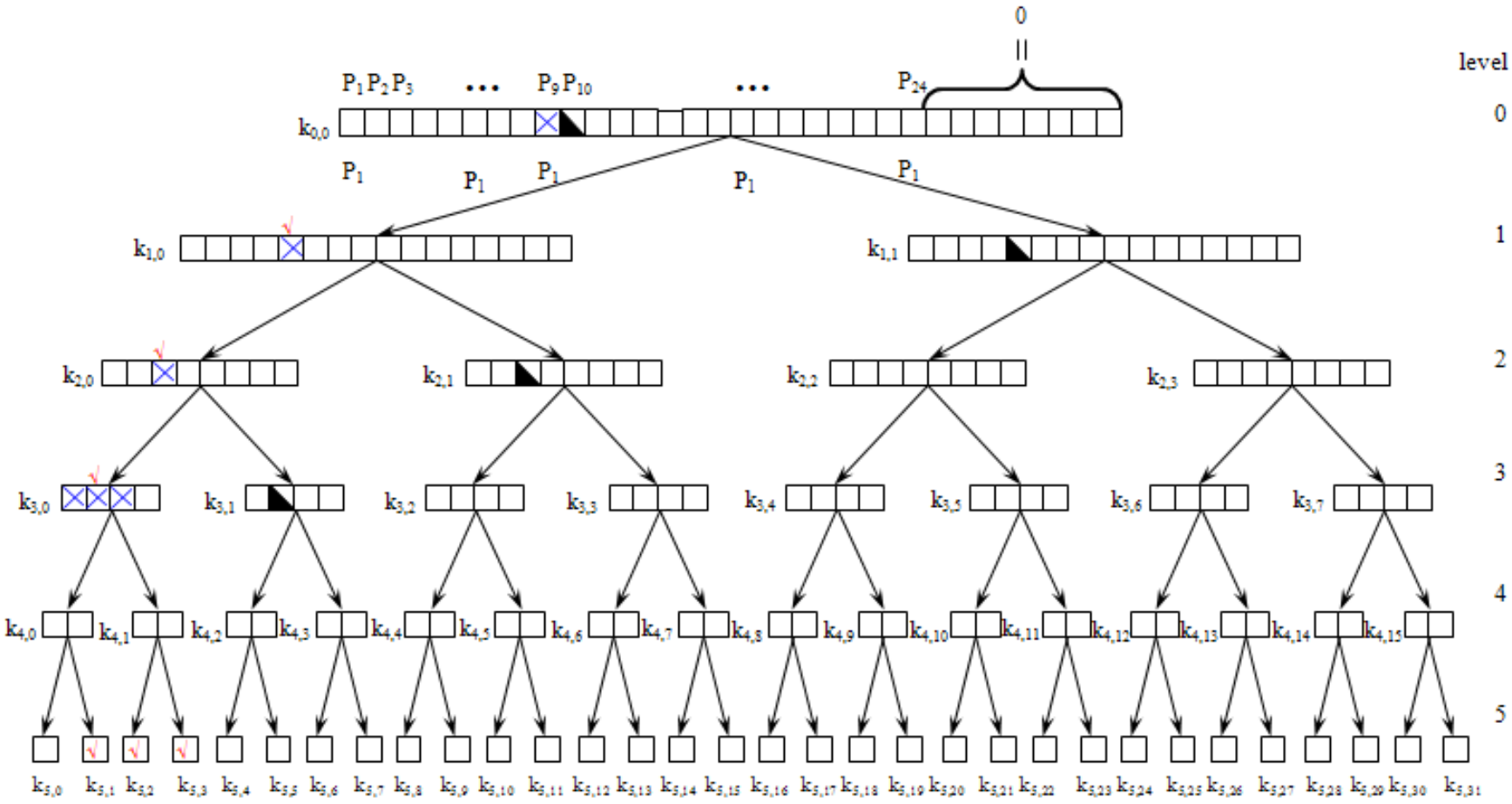

Figure 1: MRA of MEL with Parameter which can be Determined from:

MEL presents a set of discrete values of the power consumption $P_i(t)$, thus MRA leads to a fast calculation scheme for wavelet coefficients of the given power consumption function. The computation of wavelet coefficients is carried out by an iterative formula as follows (Daubechies 1992):

$$\begin{aligned} c_{m,n} &= k_{m,2n} = \frac{k_{m-1,2n} + k_{m-1,2n+1}}{\sqrt{2}}, \\ d_{m,n} &= k_{m,2n+1} = \frac{k_{m-1,2n} - k_{m-1,2n+1}}{\sqrt{2}}, \end{aligned} \tag{1}$$

where c and d are approximation and detail coefficients, respectively; m is the level of the transformation and n is the number of wavelet coefficients.

According to the recovery algorithm of MRA (Daubechies 1992):

$$\begin{aligned} k_{m-1,2n} &= \frac{c_{m,n} + d_{m,n}}{\sqrt{2}} = \frac{k_{m,2n} + k_{m,2n+1}}{\sqrt{2}}, \\ k_{m-1,2n+1} &= \frac{c_{m,n} - d_{m,n}}{\sqrt{2}} = \frac{k_{m,2n} - k_{m,2n+1}}{\sqrt{2}}. \end{aligned} \tag{2}$$

It is of interest to consider the possibility of effective use of MRA to restore MEL with a defined accuracy (Perebin 2002). Structured MRA allows one to conclude that any value that is part of the initial sample can be defined in different ways. The whole tree of MRA (fig. 1) consists of 160 parameters: 5 levels, each of 32 coefficients. For example, the first level is formed by two coefficients (detail and approximation), each of which includes a sample of 16 parameters, i.e., 32 values. The second level contains 4 coefficients with samples of 8 parameters, in result 32 values too, and so on. With this many parameters (coefficients in 5 levels), this opens up the possibility of restoring the original MEL in many different ways – remembering that 32 coefficients should hold the complete information. It also opens up the possibility of compressing the original information by dropping out selected coefficients in away, which gives a good balance between compression level and accuracy.

SECTION 4. LOCAL DATA RECOVERY: RELATIONSHIPS BETWEEN WAVELET COEFFICIENTS

The following example will illustrate how the original sample of power consumption can be transformed into wavelet coefficients at various levels, and how the relevant information for invoicing the customer can be recovered from the wavelet coefficients. In the example, we consider a situation where there is a disagreement between the power supply company and industrial customer within the first peak period (electrical consumption from $9^{\underline{00}}$ to $10^{\underline{00}}$).

The cost of power consumption depends on whether the actual consumption (MEL) exceeds the scheduled consumption, thus it is necessary to recover "estimates" of the actual consumption/the original measurements and compare these with the scheduled consumption. Since there is no need to recover the entire MEL, the quantities in question (consumption between 9 – 10 o'clock) will be realized by 6 parameters.The following algorithm is based on Fig. 1.

There are different ways of modeling the local data recovery. 32 values of the first level contain 24 values of daily energy consumption and 8 auxiliary zeroes (Fig. 1). Obtained wavelet coefficients of the 5th level estimate the magnitude of energy consumption for 8 hours as they are proportional to the level of energy consumption in these areas of schedule: $k_{5,1} \sim \left\{ \sum_{i=1}^{8} P_i \right\}$, $k_{5,2} \sim \left\{ \sum_{i=9}^{16} P_i \right\}$ and $k_{5,3} \sim \left\{ \sum_{i=17}^{24} P_i \right\}$. Because $k_{5,0}$ can be computed from $k_{5,1}$, $k_{5,2}$, $k_{5,3}$ due to redundancy from adding 8 zeros, $k_{5,0} = f(k_{5,1}, k_{5,2}, k_{5,3})$, it is possible to reverse the transformation and perfectly recover the 4 coefficients at the fourth level, and then all connected coefficients at the third level. So the fourth level of coefficients can be skipped. Thus, we have a system of three equations with three unknowns to solve, eq. (3).

$$\begin{cases} k_{5,1} = f(k^1_{3,0}; k^2_{3,0}; k^3_{3,0}) \\ k_{5,2} = f(k^1_{3,0}; k^2_{3,0}; k^3_{3,0}) \\ k_{5,3} = f(k^1_{3,0}; k^2_{3,0}; k^3_{3,0}) \end{cases} \Rightarrow \begin{cases} k^1_{3,0} = g(k_{5,1}; k_{5,2}) \\ k^2_{3,0} = g(k_{5,1}; k_{5,3}) \\ k^3_{3,0} = g(k_{5,2}; k_{5,3}) \end{cases} \tag{3}$$

where f and gareinitial and desired functions, respectively, the upper index of $k_{m,n}$ indicates the number of components of wavelet coefficient.

It should be noted that underlying coefficients $k_{5,1}$, $k_{5,2}$, $k_{5,3}$ should be taken as initial data for recovery for any cases.

As a result, without the fourth level, the algorithm supplies not only the entire solution, but also decreases the total number of wavelet coefficients that are involved in the restoration of the initial value of MEL for within the one-hour peak period (eq. (3)).

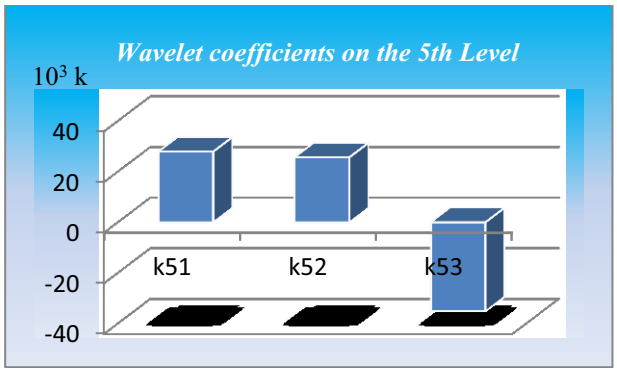

Figure 2: Basic Wavelet coefficients on the 5th Level of Decomposition

The local restoring of actual MEL after transformations given by system 3 is shown in Fig. 2.

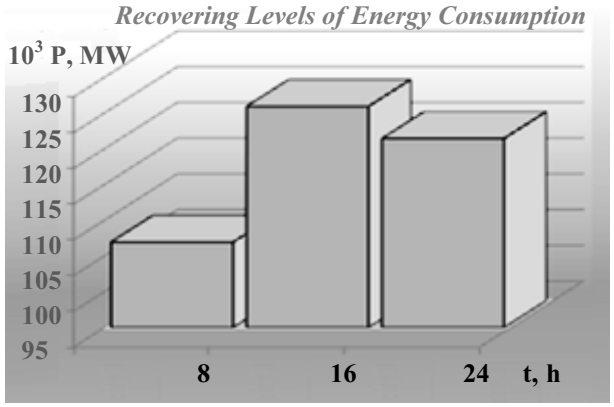

Figure 3: Recovering Levels of Energy Consumption for the 8-Hour Period of Daily MEL

The described algorithm for recovery of values allows for very good data compression if the problem is related to resolving a disagreement about energy consumption. In the MRA, coefficients of the second level have been formed from the third level and equals to the quantity of energy consumption in the period from $8^{\underline{00}}$ to $16^{\underline{00}}$. The value $k^3_{2,0}$ can be recovered in two ways (Fig. 1), either as in eq. (4):

$$k^3_{2,0} = f(k^2_{3,0}; k^2_{2,1}), \quad (4)$$

or as in eq. (5):

$$k^3_{2,0} = f(k^2_{3,0}; k^2_{3,1}). \quad (5)$$

Computing wavelet coefficient $k^3_{2,0}$ according to eq. (4) has the same principles as for the previous calculations; it is the principle of inverse wavelet transform, eq. (2). Using eq. (5) one takes into account the presence of functional dependencies between wavelet coefficients of the entire structure of the decomposition of input data subject to the limitations for avoiding their overlapping.

Note. If one needs to find another arbitrary initial value of MEL no more than three wavelet coefficients from the second, first and zero levels, respectively, need to be used.

$k^2_{2,1}, k^2_{3,0}$ and $k^2_{3,1}$ are formed from the direct relationship of transformed MEL (Fig. 4) with a partitioning step of 4 hours.

A diagram of the solution of eq. 4 is shown in Figure 4.

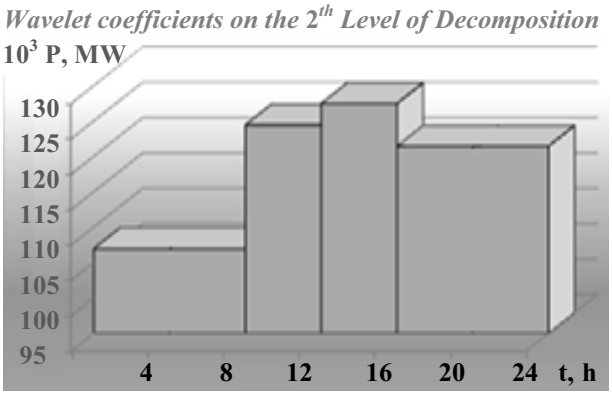

Figures 4: Detailed MEL with Wavelet coefficients on the Second Level of Decomposition

The transition from the second to the first level is identical to the previous principle of transition in eqs. (4) and (5). The result of the calculations is the computation of the coefficient $k^5_{1,0}$.

Thus, using by 5 wavelet coefficients were determined the average energy consumption during 2 hours (Fig. 5), has been determined.

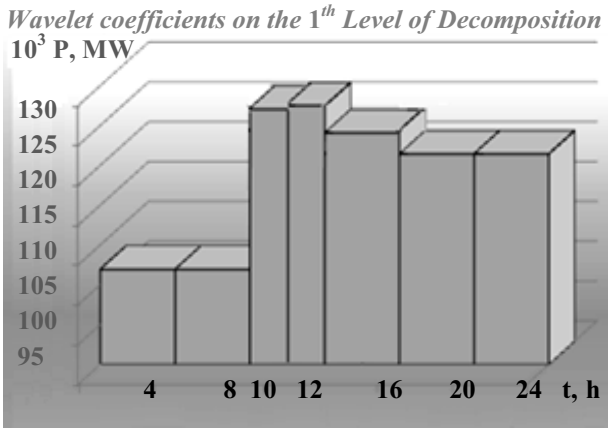

Figures 5:Restoring MEL from Wavelet coefficients on the First Level of Decomposition

From $8^{\underline{00}}$–$10^{\underline{00}}$, the power level is restored with a step equal to 2 hours. The calculated component of the first approximating coefficient $k^5_{1,0}$ is based on the values' $P_9$and P_{10}. Based on functional relationships, one can

find its neighbor value $k^5_{2,0}$, or identify the value of the initial sample P_9 or P_{10}. That is, if one needs to find more accurately the level of energy consumption, one could attempt to restore the graph partially step by step. The approach must beintegrated, by taking into account normalized deviations relative to the prediction of energy consumption.

32 different options for computing the power exist, eq. (6):

$$P_i = f(k_{5,1}, k_{5,2}, k_{5,3}, 3(k_{m,n})), \quad (6)$$

where m and n must not repeat.

Thus, to restore one original value one must have a total of 6 wavelet coefficients. There is 25% of the original sample of 24 values. By considering the full tree decomposition, one needs 3.75% from 160 wavelet coefficients at all levels of the wavelet-transform.

SECTION 5. RESTORATION OF THE VALUES OF POWER CONSUMPTION FOR PEAK PERIODS

According to the previous section with a view to restoring a certain value and presenting possible ways to check the meter readings, let us consider the period from $8^{\underline{00}}$ to $10^{\underline{00}}$, as well as from $17^{\underline{00}}$ to $19^{\underline{00}}$, which corresponds to the maximum consumption in the energy system – the peak periods (Morch et al. 2007).

In the investigation of the daily schedule, we can come to the conclusion that the first demonstration of the peak period is shown in the following coefficients of Fig. 6 a, for the second one according to Fig. 6 b, respectively.

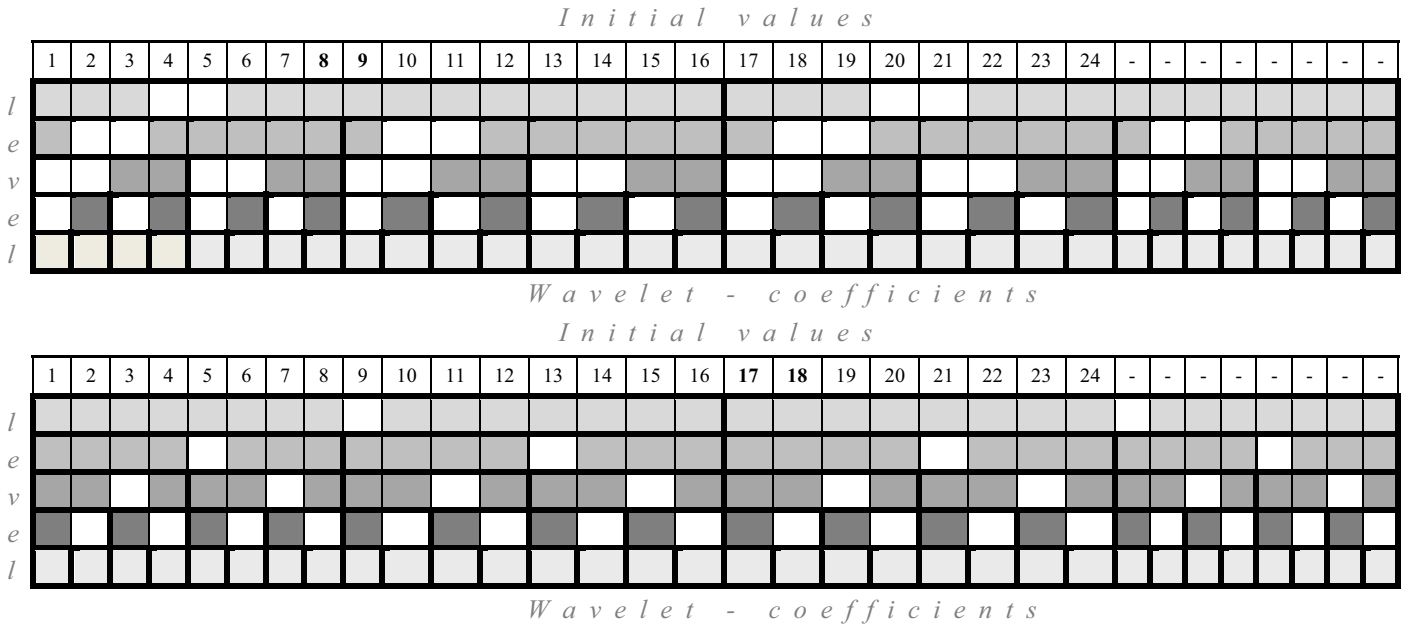

Figure 6: Wavelet coefficients, which Contain the Original Values of Power Consumption a) the First and b) the Second Peak Zones, Respectively

Wavelet coefficients of the fifth level of decomposition are marked by a shade of gray to emphasize the need for correct selection of coefficients without cross-links (within the sample of four values each) due to the initial addition of zeros.

An arbitrary choice of sample values is likely to make the calculation algorithm more complex: in case of controversies (changed data due to transmission errors, or suspicion of tampered data), it is possible to detect accurately the step on which a fault has occurred and correct the transferred data.

Combining the results in Fig. 6 a and 6 b, and taking into account the presence of mutually exclusive relationships between wavelet coefficients in the event of a dispute in peak periods it can be concluded:

1. On the 4th and the 5th levels of decomposition signal, all wavelet coefficients contain information about the initial data, which confirms the possibility of a rapid transition without the 4th level. As shown earlier, at this step the best to use coefficients are $k_{5,1}$, $k_{5,2}$, $k_{5,3}$.

2. For a quick computation, and additional control of values of consumption in the morning peak, in Norway set to from $8^{\underline{00}}$ to $10^{\underline{00}}$, and the evening peak

from $17^{\underline{00}}$ to $19^{\underline{00}}$, it is necessary to apply the following components of wavelet coefficients from:

the 1th level	the 2th level	the 3th level
$k^4_{l,n}, k^5_{l,n}, k^9_{l,n}$	$k^2_{2,n}, k^3_{2,n}, k^5_{2,n}$	$k^1_{3,n}, k^2_{3,n}, k^3_{3,n}$

in the calculations.

SECTION 6. CONCLUSIONS

This paper has considered compression and recovery of power consumption measurements. In an example, a 24 hour time series is analyzed for data compression using a wavelet transform, and it is shown how the original signal can be recovered. To control whether the measured maximum value of energy consumption exceeds the scheduled maximum value, 3.75 % of the total number of 160 wavelet coefficients need to be used, or 25 % from the original sample. It should be noted that knowledge of three basic wavelet coefficients can be used to calculate the amount of energy consumed during 8 hours. Four wavelet coefficients are needed for recovering a 4-hour period of energy consumption and so on. Furthermore, in turn, different possible ways for identifying one value allows one to improve the quality and to control the accuracy of the transmitted data.

The presented approach for analyzing the reliability of power consumption information allows one to realize the possibility of solving disputes in the event of disagreement between power supply companies and the consumers with reduced calculation time and with an opportunity for cross-checking the validity of the recovered value.

REFERENCES

Ajodhia V., 2002 "Integrated price and reliability regulation: the European experience". *.IEEE*, 710–715.

Cai Sh., Ye J., Chen M., Yan J. and Jaggi S., 2012 "Secure Compressed Reading in Smart Grids". *CoRR abs/1202.5202*.

Daubechies I., 1992 "*Ten Lectures on Wavelets*", SIAM.

Hansen P.V.,2004 "Regional electricity spot price responses in Norway".*Statistics Norway, Research Department*, No.13, 20 p.

Li H., Mao R., Lai L., and R. Qiu, 2010 "Compressed meter reading for delay-sensitive and secure load report in smart grid," in *First IEEE International Conference on Smart Grid Communications*.

Luo C., Wu F., Sun J., and C. W. Chen, 2009 "Compressive data gathering for large-scale wireless sensor networks," in *Proceedings of the 15th annual international conference on Mobile computing and networking*, 145–156.

Morch A.Z.; J. Parsons and J.C.P. Kester, 2007 "Smart electricity metering as an energy efficiency instrument: Comparative analyses of regulation and market conditions in Europe".*ECEEE 2007 Summer Study*, 193–202.

Perebin A.V., 2002"About systematization of wavelet-transforms (O sistematizacii vejvlet-preobrazovanij)". *Numerical Methods and Programming*,Vol. 2, 15–40. – (in Russian).

Sæle H. and O. S. Grande, 2011"Demand Response from Household Customers: Experiences from a Pilot Study in Norway".*IEEE Transactions on SMART GRID*, Vol. 2, No.1, 102–109.

TETIANA LUTCHYN is PhD student of Institute for Energy Saving and Energy Management within the National Technical University of Ukraine "Kyiv Polytechnic Institute" in the direction of Energy systems and complexes. In 2010, she received the MSc degree in IESEM within NTUU "KPI". Her e-mail address is: t.lutchyn@mail.ru.

BERNT LIE is professor of informatics at Telemark University College in Porsgrunn, Norway. He received his MSc and PhD degrees in Engineering Cybernetics from NTH (NTNU) in Trondheim in 1982 and 1990, respectively. His research activities have focused on control relevant modeling and advanced control for process systems, and lately also for the energy system. He has taught courses on modeling of dynamic systems and simulation of dynamic systems at NTH and Telemark University College since 1988, as well as courses on advanced control (MPC, etc.) at Telemark University College since 1990. He has visited University of Texas at Austin, University of California at Santa Barbara, Lund University, and Universitat Politècnica de Catalunya during research leaves, and has given intensive courses on modeling and simulation of dynamic systems at University of Moratuwa, Sri Lanka. His e-mail address is:bernt.lie@hit.no.

ANATOLIY VOLOSHKO is associate professor of electrical engineering at the Institute for Energy Saving and Energy Management within the National Technical University of Ukraine "Kyiv Polytechnic Institute". In 1973, he graduated "Kyiv College of electronic devices" with a degree of technologist for the production of semiconductor devices. In 1974, he graduated "Union Institute for Standardization and Metrology" with specialty engineer metrology. In 1983, he graduated "Kyiv Polytechnic Institute" majoring in mining engineer-electrician. In 1986 he received Ph.D. degree with subject of thesis "Methods and means of information control problems of the electricity industry." He is the president of CJSC "Information-saving technologies." His e-mail address is: a-voloshko@yandex.ru.

STATIONARY CHARACTERISTICS OF HOMOGENOUS $GEO|GEO|2$ QUEUE WITH RESEQUENCING IN DISCRETE TIME

Carmine De Nicola
Department of Electronic and Computer Engineer
University of Salerno
84084 - Via Ponte Don Melillo, 1,
Fisciano (SA) Italy
Email: denicola@diima.unisa.it

Alexander V. Pechinkin
Rostislav V. Razumchik
Institute of Informatics Problems of RAS
Vavilova, 44-2,
119333, Moscow, Russia
Email: apechinkin@ipiran.ru,
rrazumchik@ieee.org

KEYWORDS

Resequencing, reordering buffer, discrete time, queueing system.

ABSTRACT

Resequencing problem is a crucial issue in communication systems, databases, production and information networks because correct processing of information by them may often be performed only if original order of packets, queries, jobs is preserved. In this paper consideration is given to one of the queueing systems that may model processes of discrete nature where resequencing phenomenon may arise. Specifically $Geo/Geo/2/\infty$ queueing system with reordering buffer of infinite capacity is being analyzed. Expressions for stationary sojourn time distribution and joint stationary distribution of the number of customers in system and reordering buffer are given in explicit form and in terms of generating functions. Illustrative numerical example is presented.

INTRODUCTION

It is well-known that resequencing problem is a crucial issue in packet switching networks, parallel and distributed systems (see e.g. Baccelli et al. (1981)). The resequencing delay deteriorates the performance of delay-sensitive applications. For example, voice over IP services that gain popularity nowadays suffer from this problem because data packets at receiver's side need to be played out in the same sequence they left the sender's side. Thus the more disordering communication network introduces into the stream of packets the more time it takes for data packets to be resequenced (in de-jitter buffer) and the more difficult it is for network operators to satisfy stringent constraints on end-to-end delay and jitter. Resequencing influences design, performance and optimization of distributed computing systems where subtasks need to be put in sequential order before they can be assembled into one task. Reordering takes place also in modern microprocessors to achieve high application performance at an acceptable level of power dissipation. Here an entity (reordering buffer) is needed for out-of-order instructions to be committed in-order (see e.g. Min Choi et al. (2012)).

In order to analyze impacts of resequencing various analytical methods and models have been proposed. A general survey of queueing theoretic methods and early models for the modeling and analysis of parallel and distributed systems with resequencing can be found in Boxma et al. (1994). The studies that deal with packet disordering in communication networks typically consider communication system, consisting of disordering network and reordering buffer. Disordering network is a prototype of the real network. Data packets, sent from sender's side through real network can be disordered (or even lost) for various well-known reasons and since many applications can only accept packets in the same order they were sent from the sender's side, reordering buffer is needed at receiver's side to reestablish the initial packets' sequence. As reported in Leung et al. (2010), existing papers in the considered field of study can be grouped into two major categories. The first category consists of papers that characterize the disordering network as a queueing system with several servers sharing a single queue (see, e.g. Matyushenko (2010)). In the second category of papers, the disordering network is described as a queueing system with several parallel servers and queues, and each server has its own dedicated queue (see, e.g. Ye Xia et al. (2008)). For a short survey of these two categories see Leung et al. (2010) and Ye Xia et al. (2008). Typically studies are mostly concerned with finding the distribution of number of packets in reordering buffer; distribution and/or mean of the resequencing delay, end-to-end (i.e. sender–receiver) delay; large deviations of the queue size in reordering buffer, asymptotics of the resequencing delay etc.

Among the latest papers on the subject one can cite Leung et al. (2010), Jun Li et al. (2010), Zheng et al. (2010) and Wen-Fen (2011), where authors consider some new problems and improve previous known results. In Leung et al. (2010) authors propose a framework that allows estimation of resequencing delay and reordering buffer occupancy distribution under an orderly dispersion of traffic on multiple disjoint paths in disordering network. The asymptotic properties of the steady-state probability dis-

Proceedings 27th European Conference on Modelling and Simulation ©ECMS Webjørn Rekdalsbakken, Robin T. Bye, Houxiang Zhang (Editors)
ISBN: 978-0-9564944-6-7 / ISBN: 978-0-9564944-7-4 (CD)

tribution of the queue length in reordering buffer are studied in Jun Li et al. (2010). In Zheng et al. (2010) consideration is given to mean resequencing delay for an average packet in a multipath transfer scenario where path delay is assumed to be constant but distinct from path to path. Paper Wen-Fen (2011) is devoted to analysis of the influence of traffic intensity, types and number of paths, that packets traverse, on queue size in reordering buffer. For reordering network that is represented by m parallel $M|M|1$ queues in Gao et al. (2012) a large deviation result is proved for the reordering buffer.

All the systems and papers mentioned above deal with queueing systems that function in continuous time. But for more that a decade it is known that discrete time queueing systems mostly correspond to the discreteness of the real processes in packet networks. Significant number of papers are devoted to the study of the discrete time queueing systems but to our knowledge a little number of them analyze resequencing schemes. Among the latest papers related to resequencing one can mention Li et al. (2010) and De Clercq et al. (2010). In Li et al. (2010) authors propose a novel discrete-time priority queueing network to model selective repeat automatic repeat request protocol and study the performance of the reordering buffer in terms of the mean packet resequencing delay. A discrete-time queueing system with a single server and single queue, in which N types of packets of different priorities enter is being analyzed in De Clercq et al. (2010). Customers that enter the system during the same frame are reordered such that the high-priority customers are served first. The efficiency of this mechanism is under consideration.

In discrete time model time is assumed to be slotted, i.e. consists of concatenation of fixed length intervals (slots). Events are constrained to take place during these slots. A discrete time queue may accept more than one packet during a slot and service more than one packet during a slot. That is multiple event may occur during each slot (which cannot happen in continuous time case). This what makes analysis of discrete time systems more complicated and sometimes intractable, requiring development of special computationally efficient methods and utilization of high performance simulation.

In this paper we build and analyze system with reordering buffer analogous to the one studied in Takine et al. (1994) but functioning in discrete time. The main contributions of this paper are algorithms for obtaining main stationary characteristics of the system. The paper is organized as follows. In the next section we give detailed description of the system under consideration. Then we analyze stationary sojourn time distribution and after that joint stationary distribution. The last section is devoted to illustrative numerical results.

DESCRIPTION OF THE SYSTEM

Without loss of generality we normalize the length of a slot to unit time. Slots are sequentially numbered by non-negative integers so that slot n is located in time interval $[n-1, n),\ n = 1, 2, \ldots$. During one slot events occur in the following sequence (see, e.g. Bruneel et al. (1993)): the customer whose service is completed in slot n leaves the system at instant $(n-0)$; a customer is chosen from the queue at instant n and immediately taken for service; a customer whose generation was completed in the n-th cycle arrives at the system at instant $(n+0)$ (figure 1). Such convention corresponds to Late arrival system rule (LAS).

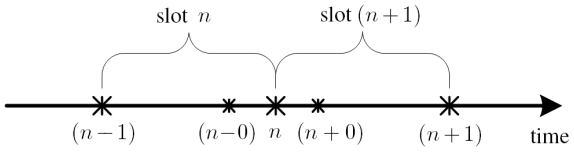

Figure 1: Discrete-time conventions

Consider a discrete-time queueing system with two servers and infinite waiting room (buffer) for customers that wait for service. Customers arrive at the system and obtain sequential number. Without loss of generality we suppose that the sequence starts from 1 and coincides with the row of natural numbers, i.e. the first customer upon entering the (empty) system receives number 1, the second — number 2 and so on and so forth. Customers leave the system strictly in order of their arrival (i.e. in the sequence order). Thus after customer's arrival it remains in the buffer for some time and then receives service. If at the moment of its service completion there are no customers in the system or all other customers present at that moment in the queue and second server have greater sequential number it leaves the system. Otherwise it occupies one place in the reordering buffer which has infinite capacity. Customer from reordering buffer leaves it if and only if its sequential number is less than sequential numbers of all other customers present in the buffer, two servers and reordering buffer. That is customers may leave reordering buffer in groups (figure 2). The departure of customers from reordering buffer (if any) happens immediately after the moment of service completion.

Service of customers can start only at slot boundaries. This means that, when the system is empty at the beginning of a slot, newly arriving customer will enter server but its service will start not in this but in the next time slot. Without loss of generality we assume that if at some time slot j there are no customers in the buffer, one of the servers completes service in slot j and there is an arrival in slot j, then newly arriving customer is put into service.

We also assume that only one customer may arrive at the system during each time slot. Denote the probability of customer's arrival in a slot by a (i.e. the probability of no arrival in a slot is $\overline{a} = 1 - a$) and the probability of service completion in a slot by b (i.e. the probability of no service completion in a slot is $\overline{b} = 1 - b$). Finally, it is assumed that service and arrival processes are mutually

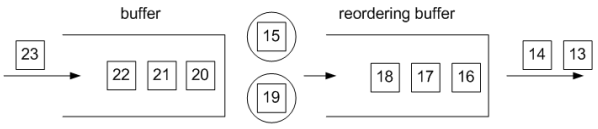

Figure 2: Scheme of the model

independent.

In Kendall's shorthand notation the considered system system is $Geo/Geo/2/\infty$ with reordering buffer of infinite capacity. Let the necessary and sufficient condition of stationarity $\rho/2 < 1$, where $\rho = a/b$ hold for the system.

STATIONARY SOJOURN TIME DISTRIBUTION

Consider two customers that are being served. Henceforth we will call "early customer" one of those two customers which entered the system earlier than the other one. The latter we respectively call "late customer".

Denote by $\{p_i,\ i \geq 0\}$ the stationary distribution of number of customers in the buffer and two servers at slot boundaries (i.e. immediately at the beginning of a random slot) and by $\{p_i^*,\ i \geq 0\}$ the stationary distribution of number of customers in the buffer and two servers as seen by new arrivals (i.e. just before the arrival of a random customer). These distributions coincide with corresponding stationary distributions of number of customers in $Geo/Geo/2/\infty$ queue i.e. are given by (see e.g. Chan et al. (1978), Rubin et al. (1991), Artalejo et al. (2003), Alfa (2010)):

$$
\begin{aligned}
p_0 &= \frac{\overline{a}b^2}{a^2\overline{b}}(1 + \overline{a}\overline{b} + \overline{a}bz_2)p_2, \qquad (1)\\
p_1 &= \frac{b}{a\overline{b}}(b + 2\overline{a}\overline{b} + \overline{a}bz_2)p_2,\\
p`_i &= z_2^{i-2}p_2,\ \ i \geq 3,\\
p_0^* &= p_0 + p_1 b + p_2 b^2,\\
p_1^* &= p_1\overline{b} + p_2 2b\overline{b} + p_3 b^2,\\
p_2^* &= p_2\overline{b}^2 + p_3 2b\overline{b} + p_4 b^2,\\
p_i^* &= z_2^{i-2}p_2^*,\ \ i \geq 3,
\end{aligned}
$$

where z_2 is the maximum root of the equation $\overline{a}b^2z^2 + b(b + 2\overline{a}\overline{b})z - a\overline{b}^2 = 0$, i.e. has the form

$$
z_2 = \frac{-b(b + 2\overline{a}\overline{b}) + \sqrt{b^2(b + 2\overline{a}\overline{b})^2 + 4a\overline{a}b^2\overline{b}^2}}{2\overline{a}b^2}. \qquad (2)
$$

The value of p_2 is determined from normalization condition

$$
\sum_{i=0}^{\infty} p_i = p_0 + p_1 + \frac{1}{1 - z_2}p_2 = 1,
$$

wherefrom after simple computations we obtain

$$
p_2 = \frac{(1 - z_2)\left(a^2\overline{b}\right)}{a^2\overline{b} + (1 - z_2)\left(b^2 + \overline{a}b\left(\overline{a}b + a\right)\left(\overline{b} + bz_2\right) + a\overline{a}b\overline{b}\right)}.
$$

In terms of probability generating functions (PGFs) distributions $\{p_i,\ \ i \geq 0\}$ and $\{p_i^*,\ \ i \geq 0\}$ are expressed as

$$
\begin{aligned}
P(z) &= \sum_{i=0}^{\infty} z^i p_i = p_0 + zp_1 + \frac{z^2}{1 - z_2 z}p_2,\\
P^*(z) &= \sum_{i=0}^{\infty} z^i p_i^* = p_0^* + zp_1^* + \frac{z^2}{1 - z_2 z}p_2^*.
\end{aligned}
$$

Let us compute the distribution of time from the moment when customer enters server until it leaves the system. Note that the customer after service may not leave the system but enter reordering buffer and wait there for some time.

Assume at some time slot both servers are busy. Denote by c the conditional probability of the fact that one of two customers will be served earlier than another provided that at least one of two customers will be served. By $\overline{c} = 1 - c$ denote the conditional probability that both customers will leave servers simultaneously provided that at least one of two customers will be served. The probability that at some time slot at least one of two customers will be served is $1 - \overline{b}^2$.

Meanwhile with probability $2b\overline{b}$ exactly one customer will be served and with probability b^2 both customers will be served simultaneously. Thus we obtain

$$
c = \frac{2b\overline{b}}{1 - \overline{b}^2}, \qquad (3)
$$

$$
\overline{c} = \frac{b^2}{1 - \overline{b}^2}. \qquad (4)
$$

Let us introduce the following notation

- $\omega_0(z)$ — PGF of number of time slots starting from time slot when service commenced till the time slot when the considered customer left the system provided that the considered customer entered empty system or both servers completed service simultaneously and the considered customer was the first in the queue in the buffer;
- $\omega_1(z)$ — PGF of number of time slots starting from time slot when service commenced till the time slot when the considered customer left the system provided that the considered customer entered system when only one of the servers was busy or both servers completed service simultaneously and the considered customer was the second in the queue in the buffer.

For $\omega_0(z)$ and $\omega_1(z)$ it holds

$$
\omega_0(z) = \frac{bz}{1 - \overline{b}z}, \qquad (5)
$$

$$
\omega_1(z) = \frac{(1 - \overline{b}^2)z}{1 - \overline{b}^2 z} \cdot \left(\overline{c} + c\frac{bz}{1 - \overline{b}z}\right). \qquad (6)
$$

Let $w_{i,j,k},\ j \geq 0,\ i \geq 1,\ k = 0, 1$, be the probability that the customer before which j customers reside in the

queue will enter one of the servers in the i-th slot. If $k = 0$ it means that the considered customer arrived at the system earlier than the customer it "saw" in another server when it itself was taken for service; if $k = 1$ it means that the considered customer arrived at the system later than the customer it "saw" in another server when it itself was taken for service. Quantities $w_{i,j,k}$ satisfy the following recurrence relations:

$$w_{i,0,0} = \overline{b}^{2(i-1)} b^2, \;\; i \geq 1, \tag{7}$$

$$w_{i,0,1} = 2\overline{b}^{2(i-1)} b\overline{b}, \;\; i \geq 1, \tag{8}$$

$$w_{i,1,0} = \sum_{m=1}^{i-1} w_{m,0,1} w_{i-m,0,0}, \;\; i \geq 1, \tag{9}$$

$$w_{i,1,1} = w_{i,0,0} + \sum_{m=1}^{i-1} w_{m,0,1} w_{i-m,0,1}, \;\; i \geq 1, \tag{10}$$

$$\begin{aligned} w_{i,j,k} = & \sum_{m=1}^{i-1} (w_{m,0,0} w_{i-m,j-2,k} + \\ & + w_{m,0,1} w_{i-m,j-1,k}), \\ & j \geq 2, \;\; i \geq 1, \;\; k = 0, 1. \end{aligned} \tag{11}$$

Let us introduce the following PGF

$$\omega_{j,k}(z) = \sum_{i=1}^{\infty} z^i w_{i,j,k}, \;\; j \geq 0, \;\; k = 0, 1.$$

From equations (7)–(11), using the standard manipulations, we get

$$\begin{aligned} \omega_{0,0}(z) &= \frac{b^2 z}{1 - \overline{b}^2 z}, \\ \omega_{0,1}(z) &= \frac{2b\overline{b} z}{1 - \overline{b}^2 z}, \\ \omega_{1,0}(z) &= \omega_{0,1}(z) \omega_{0,0}(z), \\ \omega_{1,1}(z) &= \omega_{0,0}(z) + \omega_{0,1}(z) \omega_{0,1}(z), \\ \omega_{j,k}(z) &= \omega_{0,0}(z) \omega_{j-2,k}(z) + \\ & \quad + \omega_{0,1}(z) \omega_{j-1,k}(z), \;\; j \geq 2, \;\; k = 0, 1. \end{aligned}$$

By introducing double PGF

$$\omega_k(z, u) = \sum_{i=1}^{\infty} \sum_{j=0}^{\infty} z^i u^j w_{i,j,k} = \sum_{j=0}^{\infty} u^j \omega_{j,k}(z), \;\; k = 0, 1,$$

from the previous relations we obtain the following equations

$$\begin{aligned} \omega_0(z, u) &= \omega_{0,0}(z) + \omega_{0,1}(z) \sum_{j=1}^{\infty} u^j \omega_{j-1,0}(z) + \\ & \quad + \omega_{0,0}(z) \sum_{j=2}^{\infty} u^j \omega_{j-2,0}(z) = \\ & = \frac{b^2 z}{1 - \overline{b}^2 z} + \frac{zu(2b\overline{b} + ub^2)}{1 - \overline{b}^2 z} \omega_0(z, u), \end{aligned}$$

$$\begin{aligned} \omega_1(z, u) &= \omega_{0,1}(z) + u\omega_{0,0} + \omega_{0,1}(z) \sum_{j=1}^{\infty} u^j \omega_{j-1,1}(z) + \\ & \quad + \omega_{0,0}(z) \sum_{j=2}^{\infty} u^j \omega_{j-2,1}(z) = \\ & = \frac{(2b\overline{b} + ub^2) z}{1 - \overline{b}^2 z} + \frac{zu(2b\overline{b} + ub^2)}{1 - \overline{b}^2 z} \omega_1(z, u), \end{aligned}$$

which have the following solution:

$$\omega_0(z, u) = \frac{b^2 z}{1 - \left(\overline{b} + bu\right)^2 z}, \tag{12}$$

$$\omega_1(z, u) = \frac{(2b\overline{b} + ub^2) z}{1 - \left(\overline{b} + bu\right)^2 z}. \tag{13}$$

The PGF $\omega(z)$ of stationary waiting time, using (1), (12) and (13), can be expressed as

$$\begin{aligned} \omega(z) &= p_0^* + p_1^* + \sum_{j=0}^{\infty} \left[\omega_{j,0}(z) + \omega_{j,1}(z)\right] p_{j+2}^* = \\ & = p_0^* + p_1^* + \frac{(b^2 + 2b\overline{b} + z_2 b^2) z}{1 - \left(\overline{b} + bz_2\right)^2 z} p_2^*. \end{aligned} \tag{14}$$

The PGF $\varphi(z)$ of stationary sojourn time equals

$$\begin{aligned} \varphi(z) = & \, p_0^* \omega_0(z) + p_1^* \omega_1(z) + \\ & + \sum_{j=0}^{\infty} [\omega_{j,0}(z) \omega_0(z) + \omega_{j,1}(z) \omega_1(z)] p_{j+2}^* = \\ = & \, p_0^* \frac{bz}{1 - \overline{b}z} + p_1^* \frac{(1 - \overline{b}^2) z}{1 - \overline{b}^2 z} \left(\overline{c} + c \frac{bz}{1 - \overline{b}z}\right) + \\ & + \frac{b^3 z^2 [1 + \overline{b}(2 + \overline{b}z) + b(1 + \overline{b}z) z_2] p_2^*}{(1 - \overline{b}z)(1 - \overline{b}^2 z)(1 - [\overline{b}^2 + 2b\overline{b}z_2 + b^2 z_2^2] z)}. \end{aligned} \tag{15}$$

Evaluating first-order derivative of $\varphi(z)$ at $z = 1$ yields the following expression for stationary mean sojourn time v:

$$\begin{aligned} v = \varphi'(1) = & \frac{1}{b} p_0^* + \frac{(3 - b)c + \overline{c}}{b(2 - b)} p_1^* + \left(\frac{1}{2b(z_2 - 1)^2} + \right. \\ & \left. + \frac{b - 6}{4b(z_2 - 1)} - \frac{b^2}{4(b - 2)(2 + bz_2 - b)}\right) p_2^*. \end{aligned} \tag{16}$$

Note that $\varphi(z)$ can be represented as a sum of simple fractions and thus the stationary distribution of sojourn time $\{\omega_k, \; k \geq 1\}$ can be written out explicitly. That is we have

$$\begin{aligned} \omega_k = & \left(b p_0^* + \frac{cb(1 + \overline{b})}{\overline{b}} p_1^* + \right. \\ & \left. + \frac{b^2 a_0 \left[1 + 3\overline{b} + 2bz_2\right]}{a_0 \overline{b} - 1} p_2^*\right) \overline{b}^{k-1} + \\ & + \frac{b^3 a_0 \left[1 + \overline{b}\left(2 + \overline{b} a_0\right) + b\left(1 + \overline{b} a_0\right) z_2\right]}{\left(1 - \overline{b} a_0\right)\left(1 - \overline{b}^2 a_0\right) a_0^{k-1}} p_2^*, \;\; k \geq 1, \end{aligned}$$

where $a_0 = \overline{a}/[\overline{b}^2 - b^2 z_2]$.

In the next section we turn out attention to stationary joint probability distribution.

STATIONARY JOINT PROBABILITY DISTRIBUTION

The number $\nu_1(n)$ of customers in buffer and two servers and number $\nu_2(n)$ of customers in reordering buffer at the beginning of a random slot constitute Markov chain. Its set of states $\mathcal{X}$ is

$$\mathcal{X} = (0) \cup \{(i,j),\ i \geq 1,\ j \geq 0\},$$

where pair (i,j) means that there are i customers in the buffer and two servers and j customers in reordering buffer. Clearly, j is not defined for $i = 0$.

Denote by $p_{i,j},\ i \geq 1,\ j \geq 0$, the stationary probability of the fact that the Markov chain is in state (i,j), and by p_0 — stationary probability of the fact that the Markov chain is in state (0). Note that p_0 coincides with probability p_0, defined in the previous section. Moreover probabilities $p_{i,\cdot} = \sum_{j=0}^{\infty} p_{i,j},\ j \geq 1$, are also equal to probabilities p_i defined in (1).

The system of equilibrium equations for $p_{i,j},\ i \geq 1$, $j \geq 0$ can be easily written out using global balance principle. Because of the lack of space we do not state it here but note, that it can be solved recurrently on j and i. Below we give its solution. At first, one should calculate probabilities

$$p_{1,0} = \frac{ap_0 + abp_1 + \left(\overline{a}\overline{b}b + ab^2\right)p_2 + \overline{a}b^2p_3}{1 - \overline{a}\overline{b}}, \quad (17)$$

$$p_{2,0} = \frac{a\overline{b}p_{1,0} + ab\overline{b}p_2 + \left(\overline{a}\overline{b}b + ab^2\right)p_3 + \overline{a}b^2p_4}{1 - \overline{a}\overline{b}^2}, \quad (18)$$

$$p_{i,0} = [1 - \overline{a}\overline{b}^2]^{-1}[a\overline{b}^2 p_{i-1,0} + ab\overline{b}p_i + \\ + (\overline{a}\overline{b}b + ab^2)p_{i+1} + \overline{a}b^2p_{i+2}],\ \ i \geq 3, \quad (19)$$

and then for $j = 1, 2, \ldots$ compute all other probabilities using the following relations:

$$p_{1,j} = \frac{\overline{a}b\overline{b}}{1 - \overline{a}\overline{b}}p_{2,j-1},\ \ j \geq 1, \quad (20)$$

$$p_{2,j} = \frac{\overline{b}\left(ap_{1,j} + abp_{2,j-1} + \overline{a}bp_{3,j-1}\right)}{1 - \overline{a}\overline{b}^2},\ \ j \geq 1, \quad (21)$$

$$p_{i,j} = \frac{\overline{b}\left(a\overline{b}p_{i-1,j} + abp_{i,j-1} + \overline{a}bp_{i+1,j-1}\right)}{1 - \overline{a}\overline{b}^2}, \\ i \geq 3. \quad (22)$$

In order to compute the stationary probabilities $p_{i,j}$ in term of PGFs, let us introduce

$$P_j(z) = \sum_{i=1}^{\infty} z^i p_{i,j},\ \ j \geq 0,$$

$$\tilde{P}(z) = \sum_{i=1}^{\infty} z^i p_i = P(z) - p_0 = zp_1 + \frac{z^2}{1 - zz_2}p_2,$$

$$\hat{P}(z) = \sum_{i=2}^{\infty} z^i p_i = P(z) - p_0 - zp_1 = \frac{z^2}{1 - zz_2}p_2.$$

Using (17)–(19) and making standard manipulations we obtain the following expression for $P_0(z)$:

$$P_0(z) = \Bigg(zap_0 + zabp_1 - \overline{a}b^2p_2 + b\overline{b}z\left(za + \overline{a}\right)p_{1,0} + \\ + \left(\frac{b(za + \overline{a})(z\overline{b} + b)}{z^2}\right)\hat{P}(z)\Bigg) \times \\ \times \left(1 - \overline{b}^2\left(za + \overline{a}\right)\right)^{-1}. \quad (23)$$

Similarly from (20)–(22) for $P_j(z),\ j \geq 1$, we get

$$P_j(z) = \left(1 - \overline{b}^2\left[az + \overline{a}\right]\right)^{-1}\Big(b\overline{b}z\left[az + \overline{a}\right]p_{1,j} + \\ + \frac{b\overline{b}}{z}\left[az + \overline{a}\right]P_{j-1}(z) - b\overline{b}\left[az + \overline{a}\right]p_{1,j-1}\Big). \quad (24)$$

Let introduce the following double PGF

$$\hat{P}(z,u) = \sum_{j=0}^{\infty}\sum_{i=1}^{\infty} u^j z^i p_{i,j} = \sum_{j=0}^{\infty} u^j P_j(z).$$

Using equations (23) and (24), we obtain

$$\hat{P}(z,u) = z\Big(b\overline{b}\left[az + \overline{a}\right](z - u)\breve{P}(u) + azp_0 + abzp_1 - \\ - \overline{a}b^2p_2 + \frac{b(za + \overline{a})(z\overline{b} + b)}{z^2}\hat{P}(z)\Big) \times \\ \times \left[z - \overline{b}\left(az + \overline{a}\right)\left(\overline{b}z + bu\right)\right]^{-1}, \quad (25)$$

where $\breve{P}(u)$ is given by

$$\breve{P}(u) = \sum_{j=0}^{\infty} u^j p_{1,j}.$$

In order to find expression for $\breve{P}(u)$ we have to compute the zeroes of the denominator in right part of (25). Consider the function

$$f(z) = f(z,u) = z - \overline{b}\left(az + \overline{a}\right)\left(\overline{b}z + bu\right),$$

where $0 \leq u \leq 1$. Denote by $z_1 = z_1(u)$ the minimal root of equation the equation $f(z) = 0$, i.e.

$$z_1 = \frac{1 - \overline{a}\overline{b}^2 - a\overline{b}bu - \sqrt{\left(1 - \overline{a}\overline{b}^2 - a\overline{b}bu\right)^2 - 4a\overline{a}\overline{b}^3 bu}}{2a\overline{b}^2}.$$

Since at point $(u, z_1) = (u, z_1(u))$ the numerator of (25) has to be equal to zero, we obtain

$$\breve{P}(u) = \frac{az_1p_0 + abz_1p_1 - \overline{a}b^2p_2 + \frac{b(\overline{a} + az_1)\left(b + \overline{b}z_1\right)}{z_1^2}\hat{P}(z_1)}{b\overline{b}\left(\overline{a} + az_1\right)(u - z_1)}.$$

Finally if we introduce double PGF $P(z,u) = p_0 + \sum_{j=0}^{\infty}\sum_{i=1}^{\infty} u^j z^i p_{i,j}$ one can readily see, that

$$P(z,u) = p_0 + \hat{P}(z,u). \quad (26)$$

Although the expression (26) is difficult to use for computation of joint probabilities $p_{i,j}$, it can be helpful at calculation of the the moments (including mixed moment) of stationary distribution of number of customers in buffer and two server, and reordering buffer.

By putting $z = u$ in (26) one obtains PGF $P_{\text{tot}}(u)$ of stationary distribution of total number of customers in buffer, two servers and reordering buffer:

$$P_{\text{tot}}(u) = P(u,u) = p_0 + \hat{P}(u,u) = p_0 + \\ + \frac{aup_0 + abup_1 - \overline{a}b^2p_2 + \frac{b(\overline{a}+au)(b+\overline{b}u)}{u^2}\hat{P}(u)}{1-\overline{b}\,(\overline{a}+au)}.$$

Evaluating first-order derivative at $u = 1$ yields the expression for total mean number of customers:

$$N_{\text{tot}} = \frac{a(b+a\overline{b})(p_0+bp_1)}{b^2} + \\ + p_2\left(\frac{z_2}{(1-z_2)^2} + \frac{a+b\overline{b}}{b(1-z_2)} - a\overline{a}\overline{b}\right).$$

By putting $z = 1$ in (26) one obtains the PGF $P_{\text{rb}}(u)$ of stationary distribution of number of customers in reordering buffer:

$$P_{\text{rb}}(u) = P(1,u) = p_0 + \hat{P}(1,u) = p_0 + \\ + \frac{b\overline{b}(1-u)\breve{P}(u) + ap_0 + abp_1 - \overline{a}b^2p_2 + \frac{b}{1-z_2}p_2}{1-\overline{b}\,(\overline{b}+bu)}.$$

In the next section we proceed to several illustrative numerical examples.

NUMERICAL EXAMPLES

In this section we present some numerical examples that illustrate the influence of reordering buffer on stationary sojourn time characteristics.

Note that stationary mean sojourn time $v = \varphi'(1)$ is given by (16). In figure 3 one can see the behaviour of v as a function of a for different values of b.

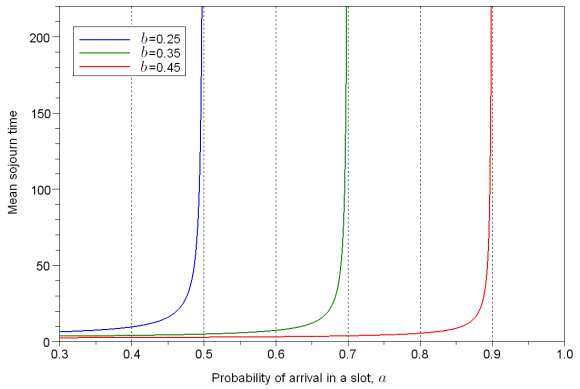

Figure 3: Stationary mean sojourn time as a function of a

Here one can see that v as a function of a has vertical asymptotes (equal to values of a for which system's load is 1) near which v grows without bound.

Let v_{ord} be stationary mean sojourn time in the considered system but without reordering buffer. The expression for v_{ord} simply can be computed by taking derivative of the following expression at point $z = 1$, i.e.

$$v_{\text{ord}} = \left(\frac{bz\omega(z)}{1-\overline{b}z}\right)'_{z=1},$$

where $\omega(z)$ is given by (15). Denote by $k = v/v_{\text{ord}}$. In figure 4 one can see the behaviour of k as a function of a for different values of b.

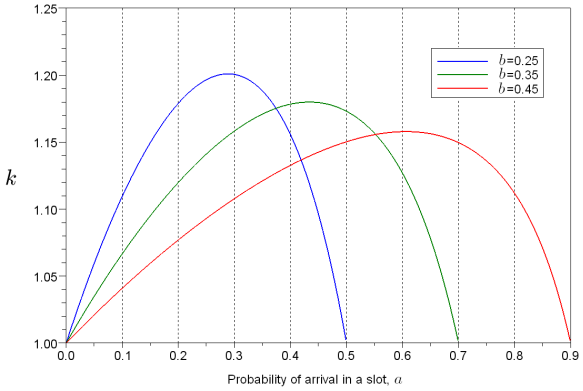

Figure 4: Ratio of v to v_{ord}

As expected the value of k starts to grow as the value of a grows. But after a certain value of a it begins to go back down meaning that values of v and v_{ord} begin to converge as system's load tends to 1.

Finally, in figure 5 one can see cumulative distribution function of the number of slots customer spends in system with and without reordering buffer for different values of a and b.

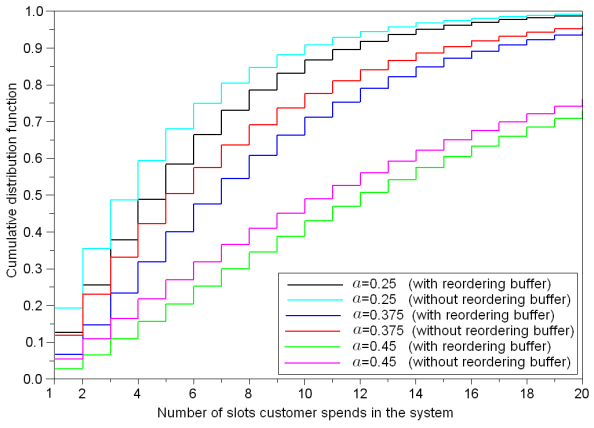

Figure 5: Cumulative distribution function

Here it is seen that the presence of reordering buffer or, almost equivalently, the requirement to preserve the order of arriving customers influences the distribution of the sojourn time.

SUMMARY

In this study, consideration is given to $Geo/Geo/2/\infty$ queueing system with reordering buffer of infinite capacity. Results of the thorough analysis of stationary sojourn time and joint stationary distribution of the number of customers in buffer, two servers and reordering buffer (both explicit and in terms of generating functions) are presented and provided with some illustrative numerical examples. Further study will be devoted to the analysis of more complex discrete-time system with resequencing, specifically with greater number of servers/queues, more general input flows and service time distributions and special queueing disciplines.

Notes and Comments. This work was partially supported in part by the Russian Foundation for Basic Research (grants 11-07-00112, 13-07-00223).

REFERENCES

Attahiru S. Alfa. 2010. Queueing Theory for Telecommunications Discrete Time Modelling of a Single Node System. Springer New York Dordrecht Heidelberg London.

Artalejo, J.R., Hernandez-Lerma, O. 2003. Performance analysis and optimal control of the Geo/Geo/c queue. Performance Evaluation. Vol. 52. No. 1. Pp. 15–39.

Baccelli, F., Gelenbe, E., Plateau, B. 1981. An end-to-end approach to the sequencing problem. Rapports de Recherche, INRIA.

Bocharov, P. P. , DÁpice, C., Pechinkin, A. V., Salerno, S. 2003. Queueing theory. Series "Modern Probability and Statistics". Utrecht: VSP Publishing.

Boxma, O., Koole, G., Liu, Z. 1994. Queueing-theoretic solution methods for models of parallel and distributed systems. Performance Evaluation of Parallel and Distributed Systems Solution Methods. CWI Tract 105 and 106. Pp. 1–24.

Bruneel, H., Kim, B.G. 1993. Discrete-Time Models for Communication Systems Including ATM. The Springer International Series in Engineering and Computer Science.

Chan, W.C., Maa, D.Y. 1978. The GI/Geom/N queue in discrete time. INFOR. Vol. 16. No. 3. Pp. 232–262.

De Clercq, S., De Turck, K., Steyaert, B., Bruneel, H. 2010. A discrete-time queueing system under frame-bound priority. Proceedings of the 5th International Conference on Queueing Theory and Network Applications. Pp. 185–192.

Gao, Y., Zhao,Y. Q. 2012. Large Deviations for Re-Sequencing Buffer Size. IEEE Transactions on Information Theory. Vol. 58. No. 2. Pp. 1003–1009.

Jun Li, Yifeng Zhou, Lamont, L., Minyi Huang, Zhao, Y.Q. 2010. Probabilistic Analysis of Resequencing Queue Length in Multipath Packet Data Networks. IEEE Global Telecommunications Conference (GLOBECOM 2010). Pp. 1–5.

Leung, K., Li, V.O.K. 2010. A resequencing model for high-speed packet-switching networks. Journal Computer Communications. Vol. 33. Issue 4. Pp. 443–453.

Li, J., Zhao, Y.Q. 2010. Modeling and Analysis of Resequencing Delay in Selective Repeat Automatic Repeat Request. Journal of networks. Vol. 5. No. 7. Pp. 792–799.

Matyushenko, S. I. 2010. Stationary characteristics of the two-channel queueing system with reordering customers and distributions of phase type. Informatics and its Applications. Vol. 4. Issue 4. Pp. 67–71. (in Russian).

Min Choi, Jong Hyuk Park, Young-Sik Jeong. 2012. Revisiting reorder buffer architecture for next generation high performance computing. The Journal of Supercomputing. Pp. 1–12.

Rubin, I., Zhang, Z. 1991. Message delay and queue-size analysia for circuit-switched TDMA systems. IEEE Transactions on Communications. Vol. 39. Issue 6. Pp. 905–914.

Takine, T., Ren, J., Hasegawa, T. 1994. Analysis of the Resequencing Buffer in a Homogeneous M/M/2 Queue. Performamce Evaluation. Vol. 19. Issue 4. Pp. 353–366.

Wen-Fen, L. 2011. An Analysis of Resequencing Queue Size at Receiver on Multi-Path Transfers. Proceedings of the International Conference on Internet Technology and Applications (iTAP). Pp. 1–4.

Ye Xia, Tse, D.N.C. 2008. On the large deviations of resequencing queue size: 2-M/M/1 Case. IEEE Transactions on information theory. Vol. 54. No. 9. Pp. 4107–4118.

Zheng, K., Jiao, X., Liu, M., Li, Z. 2010. An Analysis of Resequencing Delay of Reliable Transmission Protocols over Multipath. Proceedings of the IEEE International Conference on Communications (ICC). Pp. 1–5.

AUTHOR BIOGRAPHIES

CARMINE DE NICOLA is an electronics engineer and received his Ph.D. in Mathematics in 2011, at University of Salerno. At the moment he is assistant researcher at University of Salerno. His current research activities focus on queuing theory and operation research. His email address is denicola@diima.unisa.it.

ALEXANDER V. PECHINKIN is a Doctor of Sciences in Physics and Mathematics and principal scientist at the Institute of Informatics Problems of the Russian Academy of Sciences, and a professor at the Peoples' Friendship University of Russia. He is the author of more than 150 papers in the field of applied probability theory. His email address is apechinkin@ipiran.ru.

ROSTISLAV V. RAZUMCHIK received his Ph.D. in Physics and Mathematics in 2011. Since then, he has worked as a senior researcher at the Institute of Informatics Problems of the Russian Academy of Sciences. His current research activities focus on stochastic processes and queuing theory. His email address is rrazumchik@ieee.org

ON CONVERGENCE OF RANDOM WALKS HAVING JUMPS WITH FINITE VARIANCES TO STABLE LÉVY PROCESSES

Victor Korolev
Moscow State University, Leninskie Gory, Moscow, Russia
Institute of Informatics Problems, Russian Academy of Sciences

Vladimir Bening
Moscow State University, Leninskie Gory, Moscow, Russia
Institute of Informatics Problems, Russian Academy of Sciences

Lilya Zaks
Alpha-Bank, Moscow, Russia

Alexander Zeifman
Vologda State Pedagogical University, S.Orlova, 6, Vologda, Russia
Institute of Informatics Problems RAS, ISEDT RAS

KEYWORDS

Stable distribution; Lévy process; α-stable Lévy process; compound doubly stochastic Poisson process (compound Cox process); Skorokhod space; transfer theorem

ABSTRACT

A functional limit theorem is proved establishing weak convergence of random walks generated by compound doubly stochastic Poisson processes to Lévy processes in the Skorokhod space. As corollaries, theorems are proved on convergence of random walks with jumps having finite variances to Lévy processes with mixed normal distributions, in particular, to stable Lévy processes.

Statistical analysis of the traffic in information flows in modern computational and telecommunication systems sometimes shows that this characteristics possesses the property of self-similarity. In applied probability this property is usually modeled by Lévy processes. This communication gives some theoretical grounds to this convention.

In (Kashcheev 2000, 2001) some functional limit theorems were proved for compound Cox processes with square integrable leading random measures. However, the class of limit processes for compound Cox processes having jumps with finite variances and such leading random measures cannot contain any stable Lévy process besides the Wiener process. The aim of the present work is to fill this gap.

Let $D = D[0,1]$ be a space of real-valued right-continuous functions defined on $[0,1]$ and having left-side limits. Let $\mathcal{F}$ be the class of strictly increasing continuous mappings of the interval $[0,1]$ onto itself. Let f be a non-decreasing function on $[0,1]$, $f(0) = 0$, $f(1) = 1$. Let

$$\|f\| = \sup_{s \neq t} \left| \log \frac{f(t) - f(s)}{t - s} \right|.$$

If $\|f\| < \infty$, then the function f is continuous and strictly increasing, hence, it belongs to $\mathcal{F}$.

Define the metric $d_0(x, y)$ in $D[0,1]$ as the greatest upper bound of positive numbers ϵ for which $\mathcal{F}$ contains a function f such that $\|f\| \leq \epsilon$ and

$$\sup_t |x(t) - y(f(t))| \leq \epsilon.$$

It can be shown that $D[0,1]$ is complete with respect to the metric d_0. The metric space $(D[0,1], d_0)$ is referred to as the *Skorokhod space*.

We will consider stochastic processes as random elements in $\mathcal{D} \equiv (D[0,1],\ d_0)$ in the following sense. Let $\mathfrak{D}$ be the class of Borel sets of the space $\mathcal{D}$. The class $\mathfrak{D}$ is the σ-algebra generated by the open sets of $\mathcal{D}$. A mapping X of the basic probability space $(\Omega,\ \mathcal{A},\ \mathsf{P})$ to $\mathcal{D}$ is measurable if $\{\omega : X(\omega) \in B\} \in \mathcal{A}$ for any set $B \in \mathfrak{D}$. By a stochastic process we will mean a measurable mapping X of Ω to $\mathcal{D}$. By the distribution of a stochastic process we will mean the probability measure P^X on the measurable space $(\mathcal{D},\ \mathfrak{D})$ defined for any set $A \in \mathfrak{D}$ by the relation $\mathsf{P}^X(A) = \mathsf{P}\big(\{\omega : X(\omega) \in A\}\big) \equiv \mathsf{P}(X \in A)$. The symbol $\Longrightarrow$ will denote weak convergence: the sequence $\{X_n(t)\}_{n \geq 1}$ of stochastic processes weakly converges to a stochastic process $X(t)$, that is, $X_n(t) \Longrightarrow X(t)$, if

$$\int w(\omega) \mathsf{P}^{X_n}(d\omega) \longrightarrow \int w(\omega) \mathsf{P}^X(d\omega)$$

for any continuous bounded function w.

By a Lévy process, as usual, we will mean a homogeneous stochastically continuous stochastic process $X(t)$, $t \in [0,1]$, with independent increments such that

Proceedings 27th European Conference on Modelling and Simulation ©ECMS Webjørn Rekdalsbakken, Robin T. Bye, Houxiang Zhang (Editors)
ISBN: 978-0-9564944-6-7 / ISBN: 978-0-9564944-7-4 (CD)

$X(0) = 0$ a.s. and the sample paths $X(t) \in D[0,1]$. As is easily seen, for each $t \in [0,1]$ the random variable $X(t)$ has an infinitely divisible distribution.

The strictly stable distribution function with the characteristic exponent $\alpha \in (0,2]$ and parameter θ ($|\theta| \le \theta_\alpha = \min\{1, \frac{2}{\alpha} - 1\}$) determined by the characteristic function

$$\mathfrak{g}_{\alpha,\theta}(s) = \exp\Big\{-|s|^\alpha \exp\Big\{-\frac{i\pi\theta\alpha}{2}\mathrm{sign} s\Big\}\Big\}, \quad s \in \mathbb{R},$$

will be denoted $G_{\alpha,\theta}(x)$. The value $\theta = 0$ corresponds to symmetric strictly stable laws. The values $\theta = 1$ and $0 < \alpha \le 1$ correspond to one-sided strictly stable distributions. As is known, if ξ is a random variable with the distribution function $G_{\alpha,\theta}(x)$, $0 < \alpha < 2$, then $\mathsf{E}|\xi|^\delta < \infty$ for any $\delta \in (0,\alpha)$, but the moments of orders greater or equal to α of the random variable ξ do not exist (see, e.g., (Zolotarev 1986)).

The distribution function of the standard normal law ($\alpha = 2$, $\theta = 0$) will be denoted $\Phi(x)$. It is well known that

$$G_{\alpha,0}(x) = \int_0^\infty \Phi\Big(\frac{x}{\sqrt{u}}\Big) dG_{\alpha/2,1}(u), \quad x \in \mathbb{R} \qquad (1)$$

(see, e.g., (Zolotarev 1986) or (Feller 1971)). To representation (1) there corresponds the representation in terms of characteristic functions:

$$\mathfrak{g}_{\alpha,0}(s) = \int_0^\infty \exp\Big\{-\frac{s^2 u}{2}\Big\} dG_{\alpha/2,1}(u), \quad s \in \mathbb{R}. \quad (2)$$

A Lévy process $X(t)$, $t \in [0,1]0$, is called *α-stable*, if $\mathsf{P}\big(X(1) < x\big) = G_{\alpha,\theta}(x)$, $x \in \mathbb{R}$. It can be shown that if $X(t)$, $t \in [0,1]$, is a Lévy process, then $X(t)$ is α-stable if and only if $X(t) \stackrel{d}{=} t^{1/\alpha} X(1)$, $t \in [0,1]$ (see, e.g., (Embrechts and Maejima 2002)).

Consider a sequence of compound Cox processes

$$Z_n(t) = \sum_{i=1}^{N_1^{(n)}(\Lambda_n(t))} X_{n,i}, \quad t \ge 0, \qquad (3)$$

where $\{N_1^{(n)}(t),\, t \in [0,1]\}_{n\ge1}$ are Poisson processes with unit intensity; for each $n = 1,2,...$ the random variables $X_{n,1}, X_{n,2}, ...$ are identically distributed, moreover, for each $n \ge 1$ the random variables $X_{n,1}, X_{n,2}, ...$ and the process $N_1^{(n)}(t)$, $t \in [0,1]$, are independent; for each $n = 1,2,...$ the random measure $\Lambda_n(t)$, $t \in [0,1]$, is a Lévy process independent of the process

$$X_n(t) = \sum_{i=1}^{N_1^{(n)}(t)} X_{n,i}, \quad t \ge 0,$$

such that $\Lambda_n(0) = 0$, $\Lambda_n(1) \stackrel{d}{=} k_n U_{\alpha,1}^{(n)}$, where $\{k_n\}_{n\ge1}$ is an infinitely increasing sequence of natural numbers and $U_{\alpha,1}^{(1)}, U_{\alpha,1}^{(2)}, ...$ is a sequence of identically distributed a.s. positive random variables having one-sided strictly stable distribution with parameters $\alpha \in (0,1]$ and $\theta = 1$. For definiteness, we assume that $\sum_{i=1}^0 = 0$. From the abovesaid it follows that $\mathsf{E}\Lambda_n^\beta(1) < \infty$ for any $\beta < \alpha$ and

$$\Lambda_n(t) \stackrel{d}{=} t^{1/\alpha}\Lambda_n(1) \stackrel{d}{=} t^{1/\alpha} k_n U_{\alpha,1}^{(n)} \stackrel{d}{=} t^{1/\alpha} k_n U_{\alpha,1}^{(1)}, \quad t \ge 0. \qquad (4)$$

Assume that

$$\mathsf{E}X_{n,1} = 0 \ \text{ and } \ 0 < \sigma_n^2 \equiv \mathsf{E}X_{n,1}^2 < \infty. \qquad (5)$$

Let $t = 1$. Denote $N_n = N_1^{(n)}(\Lambda_n(1))$. Assume that, as $n \to \infty$,

$$\mathsf{P}(X_{n,1} + ... + X_{n,k_n} < x) \longrightarrow \Phi(x), \qquad (6)$$

with the same $\{k_n\}_{n\ge1}$ as in the definition of the random measures $\Lambda_n(t)$. From the classical theory of limit theorems it is known that (6) holds, if, as $n \to \infty$,

$$k_n\sigma_n^2 \longrightarrow 1 \qquad (7)$$

and

$$k_n \mathsf{E}X_{n,1}^2 \mathbb{I}(|X_{n,1}| \ge \epsilon) \longrightarrow 0 \qquad (8)$$

for any $\epsilon > 0$.

Moreover, by virtue of (4) it is obvious that

$$\frac{\Lambda_n(1)}{k_n} \stackrel{d}{=} \frac{k_n U_{\alpha,1}^{(1)}}{k_n} = U_{\alpha,1}^{(1)}.$$

therefore, formally,

$$\frac{\Lambda_n(1)}{k_n} \Longrightarrow U_{\alpha,1}^{(1)}. \qquad (9)$$

But, as it was shown in (Gnedenko and Korolev 1996) (also see, e.g., (Bening and Korolev 2002) or (Korolev et al. 2011)), (9) is equivalent to

$$\frac{N_n}{k_n} \Longrightarrow U_{\alpha,1}^{(1)}. \qquad (10)$$

By the Gnedenko–Fahim transfer theorem (Gnedenko and Fahim 1969) (also see theorem 2.9.1 in (Korolev et al. 2011)) conditions (6) and (10) imply that, as $n \to \infty$,

$$Z_n(1) = X_{n,1} + ... + X_{n,N_n} \Longrightarrow Z, \qquad (11)$$

where Z is the random variable with the characteristic function

$$\mathfrak{f}(s) = \int_0^\infty \exp\Big\{-\frac{s^2 u}{2}\Big\} d\mathsf{P}(U_{\alpha,1}^{(1)} < u), \quad s \in \mathbb{R}.$$

But by virtue of (2)

$$\mathfrak{f}(s) = \int_0^\infty \exp\Big\{-\frac{s^2 u}{2}\Big\} dG_{\alpha,1}(u) = \mathfrak{g}_{2\alpha,0}(s), \quad s \in \mathbb{R},$$

that is, the limit random variable Z in (11) has the symmetric strictly stable distribution with the characteristic exponent $\alpha_0 = 2\alpha$.

Consider an α_0-stable Lévy process $Z(t)$, $t \in [0,1]$, such that $Z(1) \stackrel{d}{=} Z$. Since $Z_n(t)$ and $Z(t)$ are Lévy processes, almost all their sample paths belong to the Skorokhod space $\mathcal{D}$.

Using theorem 15.6 from (Billingsley 1968) we obtain the following result.

THEOREM. *Let $\alpha \in (0,1]$ and a compound Cox process $Z_n(t)$ (see (3)) be controlled by the Lévy process $\Lambda_n(t)$ such that $\Lambda_n(1) \stackrel{d}{=} k_n U^{(n)}_{\alpha,1}$, where $\{k_n\}_{n\geq 1}$ is an infinitely increasing sequence of natural numbers and $U^{(1)}_{\alpha,1}, U^{(2)}_{\alpha,1}, ...$ is a sequence of identically distributed a.s. positive random variables having one-sided strictly stable distribution with parameters α and $\theta = 1$. Assume that the random jumps $\{X_{n,j}\}_{j\geq 1}$, $n = 1, 2, ...$, of the compound Cox process $Z_n(t)$ satisfy conditions (5), (7) and (8) with the same numbers k_n. Then the random walks generated by these compound Cox processes weakly converge in the Skorokhod space $\mathcal{D} = (D[0,1], d_0)$ to a 2α-stable Lévy process $Z(t)$ with $\mathsf{P}\big(Z(1) < x\big) = G_{2\alpha,0}(x)$.*

This research was supported by the Russian Foundation for Basic Research (projects 11-01-00515a, 11-07-00112a, 12-07-00115a), and by the Ministry for Education and Science of Russian Federation (state contract 16.740.11.0133).

REFERENCES

Bening, V. and V. Korolev. 2002. *Generalized Poisson Models and their Applications in Insurance and Finance.* Utrecht: VSP.

Billingsley, P. 1968. *Convergence of Probability Measures.* New York: Wiley.

Embrechts, P. and M. Maejima. 2002. *Selfsimilar Processes.* Princeton: Princeton University Press.

Feller, W. 1971. *An Introduction to Probability Theory and its Applications. Vol. 2.* New York: Wiley.

Gnedenko, B. V. and H. Fahim. 1969 "On a transfer theorem." *Soviet Math. Dokl.* 187. No. 1, 15–17.

Gnedenko, B. V. and V.Yu. Korolev. 1996. *Random Summation: Limit Theorems and Applications.* Boca Raton: CRC Press.

Kashcheev, D.E. 2000. "Functional limit theorems for compound Cox processes." *Surveys in Applied and Industrial mathematics.* 7, 494–495 (in Russian).

Kashcheev, D.E. 2001. *Modelling the Dynamics of Financial Time Series and Pricing Financial Derivatives.* PhD. Thesis. Tver: Tver State University (in Russian).

Korolev, V. Yu.; V.E. Bening and S.Ya. Shorgin. 2011. *Mathematical Foundations of Risk Theory. 2nd Ed.* Moscow: FIZMATLIT (in Russian).

Zolotarev, V. M. 1986. *One-Dimensional Stable Distributions.* Providence: American Mathematical Society.

AUTHOR BIOGRAPHIES

VICTOR KOROLEV is Doctor of Science in physics and mathematics, professor, Department of Mathematical Statistics, Faculty of Computational Mathematics and Cybernetics, M.V. Lomonosov Moscow State University; leading scientist, Institute of Informatics Problems, Russian Academy of Sciences. His email is bruce27@yandex.ru.

VLADIMIR BENING is Doctor of Science in physics and mathematics; professor, Department of Mathematical Statistics, Faculty of Computational Mathematics and Cybernetics, M. V. Lomonosov Moscow State University; senior scientist, Institute of Informatics Problems, Russian Academy of Sciences. His email is bening@yandex.ru.

LYLIA ZAKS is a principal officer, Department of Modeling and Mathematical Statistics, Alpha-Bank, Moscow, Russia. Her email is lily.zaks@gmail.com.

ALEXANDER ZEIFMAN is Doctor of Science in physics and mathematics; professor, Dean of the Faculty of Applied Mathematics and Computer Technologies, Vologda State Pedagogical University; senior scientist, Institute of Informatics Problems, Russian Academy of Sciences; leading scientist, Institute of Territories Socio-Economic Development, Russian Academy of Sciences. His email is a_zeifman@mail.ru.

ON $M_t/M_t/S$ TYPE QUEUE WITH GROUP SERVICES

Alexander Zeifman
Vologda State Pedagogical University, S.Orlova, 6, Vologda, Russia
Institute of Informatics Problems, Russian Academy of Sciences
Institute of Territories Socio-Economic Development, Russian Academy of Sciences

Yakov Satin and Galina Shilova
Vologda State Pedagogical University
S.Orlova, 6, Vologda, Russia

Victor Korolev and Vladimir Bening
Moscow State University, Leninskie Gory, Moscow, Russia
Institute of Informatics Problems, Russian Academy of Sciences

Sergey Shorgin
Institute of Informatics Problems, Russian Academy of Sciences
Vavilova str., 44-2, Moscow, Russia

KEYWORDS

Markovian queueing models; nonstationary Markov processes; group services; rate of convergence

ABSTRACT

We consider $M_t/M_t/S$-type queueing model with group services. Bounds on the rate of convergence for the queue-length process are obtained. Ordinary $M_t/M_t/S$ queue and $M_t/M_t/S$ type queueing model with group services are studied as examples.

INTRODUCTION

First investigations of non-stationary birth-death queueing models were published in 1970-s, see (Gnedenko and Makarov 1971, Gnedenko and Soloviev 1973, D. Gnedenko 1971). Namely, they studied qualitative properties of such models, firstly their ergodic properties. Some related problems were considered from the viewpoint of random summation in (Gnedenko and Korolev 1996, Korolev and Shevtsova 2012). Quantitative approach with estimation on the rate of convergence for non-stationary birth-death processes has been developed in our previous papers, see (Granovsky and Zeifman 2004, Zeifman 1995, Zeifman et al. 2006, Zeifman 2009, Zeifman and Korotysheva 2012).

The problem of construction of the limiting characteristics for the queue-length process for such models via truncations of birth-death processes was considered in (Zeifman et al. 2006).

A new class of Markovian non-stationary queueing models with batch arrivals and group services was introduced and studied in our recent papers, see (Satin et al. 2011, 2012).

The paper (Satin et al. 2011) dealt with finite state space models. First bounds on the rate of convergence and stability under perturbations of intensity matrix were obtained.

The respective countable model was investigated in (Satin et al. 2012). In this work general bounds on the rate of convergence were obtained. Moreover, the first truncation estimates were considered under some additional assumptions.

Erlang-type queueing model with group services was introduced and studied in (Zeifman et al 2013). Namely, in this paper criteria for weak ergodicity and bounds on the rate of convergence have been obtained.

Another popular and one of simplest queuing systems is $M/M/S$ queue. There is a large number of investigations for this model in stationary and non-stationary situations, see for instance, (Granovsky and Zeifman 2004; Zeifman 1995; Zeifman et al. 2006, 2008; Zeifman and Korotysheva 2012).

Here we introduce and study a natural generalization of this model for the queue with possible simultaneous services.

Namely, we suppose that there are S servers and infinitely many waiting rooms in the queueing system, an intensity of arrival of a customer to the queue is $\lambda(t)$, and an intensity of departure (servicing) of a group of k customers is $\mu_k(t) = \frac{\mu(t)}{k}$ for all $1 \le k \le S$.

Let $X = X(t)$, $t \ge 0$ be a queue-length process for the queue.

Let $p_{ij}(s,t) = Pr\{X(t) = j \,|X(s) = i\}$, $i, j \ge 0$, $0 \le s \le t$ be transition probabilities for $X = X(t)$, and $p_i(t) = Pr\{X(t) = i\}$ be its state probabilities.

We suppose that the intensities $\lambda(t)$ and $\mu(t)$ are non-negative functions locally integrable on $[0, \infty)$.

Then the probabilistic dynamics of the process is represented by the forward Kolmogorov system:

$$\frac{d\mathbf{p}}{dt} = A(t)\mathbf{p}(t), \tag{1}$$

Proceedings 27th European Conference on Modelling and Simulation ©ECMS Webjørn Rekdalsbakken, Robin T. Bye, Houxiang Zhang (Editors)
ISBN: 978-0-9564944-6-7 / ISBN: 978-0-9564944-7-4 (CD)

where $A(t)$ is transposed intensity matrix,

$$A(t)=\begin{pmatrix} a_{00}(t) & \mu_1(t) & \mu_2(t) & \mu_3(t) & \cdots & \mu_r(t) & \cdots \\ \lambda(t) & a_{11}(t) & \mu_1(t) & \mu_2(t) & \cdots & \mu_{r-1}(t) & \cdots \\ 0 & \lambda(t) & a_{22}(t) & \mu_1(t) & \cdots & \mu_{r-2}(t) & \cdots \\ \cdots & & & & & & \\ 0 & 0 & \cdots & 0 & \lambda(t) & a_{rr}(t) & \cdots \\ \cdots & & & & & & \end{pmatrix},$$

where $\mu_k(t)=\mu(t)/k$, for $k\le S$, $\mu_k(t)=0,\ k>S$ and $a_{ii}(t)$ are such that all column sums in $A(t)$ equal zero for any $t\ge 0$.

Throughout the paper by $\|\bullet\|$ we denote the l_1-norm, i. e. $\|\mathbf{x}\|=\sum|x_i|$, and $\|B\|=\sup_j\sum_i|b_{ij}|$ for $B=(b_{ij})_{i,j=0}^{\infty}$.

Let Ω be a set of all stochastic vectors, i. e. l_1 vectors with nonnegative coordinates and unit norm.

Then we have $\|A(t)\|=2\left(\lambda(t)+\sum_{k=1}^{S}\mu_k(t)\right)\le 2\left(\lambda(t)+(1+\log S)\,\mu(t)\right)$ for almost all $t\ge 0$. Hence operator function $A(t)$ from l_1 into itself is bounded for almost all $t\ge 0$ and locally integrable on $[0;\infty)$. Therefore we can consider (1) as a differential equation in the space l_1 with bounded operator.

It is well known (Daleckij and Krein 1974) that the Cauchy problem for differential equation (1) has unique solutions for arbitrary initial condition, and $\mathbf{p}(s)\in\Omega$ implies $\mathbf{p}(t)\in\Omega$ for $t\ge s\ge 0$.

Denote by $E(t,k)=E\{X(t)\,|X(0)=k\}$ the mean (the mathematical expectation) of the process at the moment t under initial condition $X(0)=k$.

Recall the basic definitions.

The process $X(t)$ is called weakly ergodic, if $\|\mathbf{p}^*(t)-\mathbf{p}^{**}(t)\|\to 0$ as $t\to\infty$ for any initial conditions $\mathbf{p}^*(0),\mathbf{p}^{**}(0)$.

The process $X(t)$ is called *ergodic (or strongly ergodic)*, if there exists a vector $\pi\in\Omega$ such that $\lim_{t\to\infty}\|\mathbf{p}(t)-\pi\|=0$ for any $\mathbf{p}(0)=\mathbf{p}\in\Omega$. The vector π is called the *stationary distribution* for Markov chain $X(t)$.

The process chain $X(t)$ has the limiting mean $\phi(t)$ if $|E(t,k)-\phi(t)|\to 0$ as $t\to\infty$, for any k.

A detailed discussion of these concepts is given in (Zeifman et al. 2008).

ERGODICITY BOUNDS

Theorem 1. Let there exist $\delta<1$ such that

$$\int_0^{\infty}\alpha^*(t)\,dt=+\infty, \tag{2}$$

where

$$\alpha^*(t)=\sum_{k=1}^{S}\frac{(1-\delta^k)}{k}\mu(t)-\left(\frac{1}{\delta}-1\right)\lambda(t). \tag{3}$$

Then queue-length process $X(t)$ is weakly ergodic.

Proof.

Put $d=\frac{1}{\delta}>1$, and $d_{k+1}=d^k$, $i=0,1,\dots$.

Let D be upper triangular matrix,

$$D=\begin{pmatrix} d_1 & d_1 & d_1 & \cdots \\ 0 & d_2 & d_2 & \cdots \\ 0 & 0 & d_3 & \cdots \\ & \ddots & \ddots & \ddots \end{pmatrix}, \tag{4}$$

and let l_{1D} be the correspondent space of sequences $l_{1D}=\left\{\mathbf{z}=(p_1,p_2,\cdots)^T/\|\mathbf{z}\|_{1D}\equiv\|D\mathbf{z}\|_1<\infty\right\}$.

Define

$$\alpha_i(t)=-a_{ii}(t)-\frac{\lambda(t)}{\delta}-\sum_{k=1}^{i-1}(\mu_{i-k}(t)-\mu_i(t))\delta^{i-k}, \tag{5}$$

and

$$\alpha^*(t)=\inf_{i\ge 1}\alpha_i(t). \tag{6}$$

By introducing $p_0(t)=1-\sum_{i\ge1}p_i(t)$ we obtain from (1) the following equation, see detailed discussion in (Granovsky and Zeifman 2004; Zeifman 1995; Zeifman et al. 2006, 2008):

$$\frac{d\mathbf{z}}{dt}=B(t)\mathbf{z}(t)+\mathbf{f}(t), \tag{7}$$

where $\mathbf{f}(t)=(\lambda(t),0,\cdots)^T$,

$$B=\begin{pmatrix} a_{11}-\lambda & \mu_1-\lambda & \cdots & \mu_{r-1}-\lambda & \cdots \\ \lambda & a_{22} & \cdots & \mu_{r-2} & \cdots \\ 0 & \lambda & \cdots & \mu_{r-3} & \cdots \\ \cdots & & & & \\ 0 & 0 & \cdots & a_{rr} & \cdots \\ \cdots\cdots\cdots & & & & \end{pmatrix}. \tag{8}$$

Consider equation (7) in the space l_{1D}, where $B(t)$ and $\mathbf{f}(t)$ are locally integrable on $[0,+\infty)$.

Then the following bound of logarithmic norm of operator function $B(t)$ holds, see details in (Satin et al. 2012):

$$\gamma(B(t))_{1D}=\gamma(DB(t)D^{-1})=\sup_{i\ge1}\{-\alpha_i(t)\}=-\alpha(t), \tag{9}$$

where

$$DBD^{-1}=\begin{pmatrix} a_{11} & \delta(\mu_1-\mu_2) & \cdots & \delta^{r-1}(\mu_{r-1}-\mu_r) & \cdots & \\ d\lambda & a_{22} & \cdots & \delta^{r-2}(\mu_{r-2}-\mu_r) & \cdots & \\ 0 & d\lambda & \cdots & \delta^{r-3}(\mu_{r-3}-\mu_r) & \cdots & \\ \cdots & & & & & \\ 0 & 0 & d\lambda & a_{rr} & \cdots & \\ \cdots & \cdots & \cdots & \cdots & \cdots & \cdots \end{pmatrix}.$$

We have:

$$\alpha_i(t) = \lambda(t)\left(1-\tfrac{1}{\delta}\right) + \mu(t)\times \left(\sum_{k=1}^{i}\tfrac{1}{k} - \sum_{k=1}^{i-1}\left(\tfrac{1}{i-k}-\tfrac{1}{i}\right)\delta^{i-k}\right) \geq \lambda(t)\left(1-\tfrac{1}{\delta}\right) + \mu(t)\left(\sum_{k=1}^{i}\tfrac{1}{k} - \sum_{k=1}^{i-1}\left(\tfrac{1}{i-k}-\tfrac{1}{i}\right)\right) = \lambda(t)\left(1-\tfrac{1}{\delta}\right) + \mu(t),$$

for $i \leq S$, and

$$\alpha_i(t) = \lambda(t)\left(1-\frac{1}{\delta}\right) + \mu(t)\sum_{k=1}^{S}\frac{1-\delta^k}{k} = \alpha^*(t), \quad (10)$$

for $i > S$. Moreover,

$$\alpha^*(t) = (1-\delta)\left(\mu(t)\left(1+\tfrac{1+\delta}{2}+\cdots+\tfrac{1+\cdots+\delta^{S-1}}{S}\right) - \tfrac{\lambda(t)}{\delta}\right) = (1-\delta)\,\alpha_*(t,\delta),$$

and assumption (2) is equivalent to $\int\limits_0^\infty \alpha_*(t,\delta)\,dt = +\infty$. On the other hand, $\alpha_*(t,\delta)$ is an increasing function of δ. Hence, if assumption (2) holds for some $\delta_0 \in (0;1)$, then it holds for any $\delta_1 \in (0;1)$ such that $\delta_1 > \delta_0$.

Finally, we can choose δ so that $\sum_{k=1}^{S}\frac{1-\delta^k}{k} \leq 1$, and therefore, $\alpha_i(t) \geq \alpha^*(t)$ for $i \leq S$.

Hence,

$$\|V(t,s)\|_{1D} \leq e^{-\int_s^t \alpha^*(u)\,du}, \quad (11)$$

where $V(t,\tau)$ is the Cauchy operator of equation (7), and we obtain the weak ergodicity of $X(t)$ and the following bound:

$$\|\mathbf{p}^*(t)-\mathbf{p}^{**}(t)\|_{1D} \leq e^{-\int_s^t \alpha^*(u)\,du}\|\mathbf{p}^*(s)-\mathbf{p}^{**}(s)\|_{1D}, \quad (12)$$

for any initial conditions $\mathbf{p}^*(s)$, $\mathbf{p}^{**}(s)$ and any s, t, $0 \leq s \leq t$.

Corollary. Under the assumptions of Theorem 1 the following bounds on the rate of convergence hold: (12), and

$$\|\mathbf{p}^*(t)-\mathbf{p}^{**}(t)\|_1 \leq 4\,e^{-\int_s^t \alpha^*(u)\,du}\sum_{i\geq 1} g_i|p_i^*(s)-p_i^{**}(s)| \quad (13)$$

for any initial conditions $\mathbf{p}^*(s)$, $\mathbf{p}^{**}(s)$ and any s, t, $0 \leq s \leq t$, where $g_i = \sum_{n=0}^{i-1}\delta^{-n}$.

Proof. The statement follows from the inequalities:

$$2\|\mathbf{z}\|_{1D} = 2d_1\,|\textstyle\sum_{i=1}^{\infty} p_i| + 2d_2\,|\sum_{i=2}^{\infty} p_i| + 2d_3\,|\sum_{i=3}^{\infty} p_i| + \cdots \geq 2\,(|\textstyle\sum_{i=1}^{\infty} p_i| + |\sum_{i=2}^{\infty} p_i| + |\sum_{i=3}^{\infty} p_i| + \cdots) \geq \textstyle\sum_{i=1}^{\infty}|p_i| = \|\mathbf{z}\|_1,$$

and

$$\|\mathbf{p}^*(t)-\mathbf{p}^{**}(t)\|_1 \leq 2\|\mathbf{z}^*(t)-\mathbf{z}^{**}(t)\|_1 \leq 4\,\|\mathbf{z}^*(t)-\mathbf{z}^{**}(t)\|_{1D} \leq 4\,e^{-\int_s^t \alpha^*(u)\,du}\|\mathbf{z}^*(s)-\mathbf{z}^{**}(s)\|_{1D} \leq 4\,e^{-\int_s^t \alpha^*(u)\,du}\textstyle\sum_{i\geq 1} g_i|p_i^*(s)-p_i^{**}(s)|.$$

Put $W = \inf_{k\geq 1}\frac{1}{k\delta^k} > 0$.

Corollary. Under the assumptions of Theorem 1, the queue-length process $X(t)$ has the limiting mean $\phi(t)$ and, putting $\phi(t) = E(t,0)$, we obtain the following bound on the rate of convergence:

$$|E(t,k)-\phi(t)| \leq \frac{2g_k}{W}\,e^{-\int_0^t \alpha^*(u)\,du}. \quad (14)$$

for any k and any $t \geq 0$.

Proof. Estimate (14) follows from the inequalities

$$\|\mathbf{z}\|_{1D} \geq \frac{W}{2}\,\|\mathbf{z}\|_{1E}$$

where $\|\mathbf{z}\|_{1E} = \sum k|p_k|$, and

$$|E(t,k)-\phi(t)| \leq \|\mathbf{p}^*(t)-\mathbf{p}^{**}(t)\|_{1E} \leq \tfrac{2}{W}\,e^{-\int_0^t \alpha^*(u)\,du}\|\mathbf{e}_k-\mathbf{e}_0\|_{1D} = \tfrac{2g_k}{W}\,e^{-\int_0^t \alpha^*(u)\,du},$$

for respective $\mathbf{p}^*(t)$, $\mathbf{p}^{**}(t)$ and any $k \geq 0$.

Consider now the most important special cases.

1. Let $X(t)$ be a stationary Markov chain (i.e. let intensities λ and μ not depend on t).

Then assumption (2) is equivalent to the inequality

$$S\mu > \lambda. \quad (15)$$

In some cases we can find the best possible value for α^* in the following way.

Consider two functions: $h_1(\delta) = \lambda\left(1-\frac{1}{\delta}\right) + \mu\sum_{k=1}^{S}\frac{1-\delta^k}{k}$, and $h_2(\delta) = \lambda\left(1-\frac{1}{\delta}\right)+\mu$.

Then $h_1'(\delta) = \frac{\lambda}{\delta^2} - \mu\sum_{k=1}^{S}\delta^{k-1}$. We have $h_1'(\delta) > 0$ for $0 < \delta << 1$, and $h_1'(1) = \lambda - S\mu < 0$. On the other hand, $h_1''(\delta) = -\frac{2\lambda}{\delta^3} - \mu\sum_{k=1}^{S}(k-1)\delta^{k-2} < 0$ for any positive δ. Hence $h_1'(\delta)$ is strictly decreasing, and there exists a unique $\delta^* \in (0,1)$ such that $h_1'(\delta^*) = 0$ and $h_1(\delta^*) = \sup_{\delta\in(0,1)} h_1(\delta)$. If

$$h_1(\delta^*) < h_2(\delta^*), \quad (16)$$

then we obtain the respective best possible value of α^*.

Theorem 2. Let $X(t)$ be a stationary Markov chain, and let assumptions (15), (16) be satisfied. Then $X(t)$ is strongly ergodic (with stationary distribution π and the following bounds hold:

$$\|\mathbf{p}^*(t)-\pi\|_{1D} \leq e^{-\alpha^* t}\|\mathbf{p}^*(0)-\pi\|_{1D}, \quad (17)$$

$$\|\mathbf{p}^*(t) - \pi\|_1 \le 4\, e^{-\alpha^* t} \sum_{i\ge 1} g_i |p_i^*(0) - \pi_i|, \quad (18)$$

for any initial condition $\mathbf{p}^*(0)$ and any $t \ge 0$, and

$$|E(t,k) - \phi| \le \frac{2}{W}\, e^{-\alpha^* t} \|\mathbf{p}^*(0) - \pi\|_{1D}. \quad (19)$$

where now the limiting mean $\phi = \sum k\pi_k$, and $\alpha^* = \sum_{k=1}^{S} \frac{\left(1-\delta^{*\,k}\right)}{k}\mu - \left(\frac{1}{\delta^*} - 1\right)\lambda$.

2. Let now the arrival and service rates $\lambda(t)$ and $\mu(t)$ be 1-periodic in t. Then assumption (2) is equivalent to the inequality

$$\int_0^1 \left(S\mu(t) - \lambda(t)\right)\, dt > 0. \quad (20)$$

Theorem 3. Let the arrival and service rates $\lambda(t)$ and $\mu(t)$ be 1-periodic in t, and let (20) be satisfied. Then the process $X(t)$ is weakly ergodic. In addition, the respective limiting regime $\mathbf{p}^{**}(t)$ and limiting mean $\phi(t)$ are also 1-periodic. Moreover, $X(t)$ is **exponentially** weakly ergodic, namely

$$e^{-\int_s^t \alpha^*(u)\, du} \le M e^{-a(t-s)u}, \quad (21)$$

where $M = \exp(\sup_{|t-s|\le 1} \int_s^t \alpha^*(u)\, du)$, and $a = \int_0^1 \alpha^*(t)\, dt$.

EXAMPLES

We consider and compare the following two models: ordinary $M_t/M_t/S$ queue, and its analogue for a queue with group services with the same characteristics. Namely, we suppose that arrival and service intensities are $\lambda(t) = 1 + \sin 2\pi t$ and $\mu(t) = 3 + \cos 2\pi t$ respectively, and let for definiteness, $S = 10^{12}$.

We obtain and compare two limiting characteristics for the both models: the limiting probability of empty queue and the limiting mean.

Put $\delta = 0.5$, then we obtain $W = 1$, $g_k = 2^k - 1$, and $\alpha_k(t) \ge \mu(t) - \lambda(t)$, for any $k \ge 1$, any S, and any $t \ge 0$.

Therefore, we can assume that $\alpha^*(t) \ge 2 + \cos 2\pi t - \sin 2\pi t$, and moreover, inequality (21) holds for $a = 2$ and $M = 2$.

Therefore, we obtain for *both* models the following bounds on the rate of convergence to limiting 1-periodic characteristics $\mathbf{p}^{**}(s)$ and $\phi(t)$ respectively:

$$\|\mathbf{p}^*(t) - \mathbf{p}^{**}(t)\|_1 \le 4\, e^{-2t} \|\mathbf{p}^*(0) - \mathbf{p}^{**}(0)\|_{1D}, \quad (22)$$

for any initial condition $\mathbf{p}^*(0)$, and any $t \ge 0$,

$$|E(t,k) - \phi(t)| \le 4\, e^{-2t} \|\mathbf{e}_k - \mathbf{p}^{**}(0)\|_{1D}, \quad (23)$$

for any k and any $t \ge 0$. Putting $\mathbf{p}^*(0) = \mathbf{0}$, we have from (22) and (23) the inequalities

$$\begin{aligned} \|\mathbf{p}^*(t) - \mathbf{p}^{**}(t)\|_1 &\le 4\, e^{-2t} \|\mathbf{p}^{**}(0)\|_{1D}, \\ |E(t,0) - \phi(t)| &\le 4\, e^{-2t} \|\mathbf{p}^{**}(0)\|_{1D}, \end{aligned} \quad (24)$$

for obtaining the 1-periodic limiting probability of the empty queue and the 1-periodic limiting mean.

In order to be able to use bound (24), we need to estimate the initial condition for 1-periodic limiting regime.

We have $\|\mathbf{f}(t)\|_{1D} \le K = 2$ for any $t \ge 0$, and

$$\|\mathbf{p}^{**}(0)\|_{1D} \le \limsup_{t\to\infty} \|\mathbf{p}^{**}(t)\|_{1D}, \quad (25)$$

on the other hand,

$$\begin{gathered} \|\mathbf{p}^{**}(t)\|_{1D} \le \|V(t)\|_{1D} \|\mathbf{z}^{**}(0)\|_{1D} + \\ \int_0^t \|V(t,\tau)\|_{1D} \|\mathbf{f}(\tau)\|_{1D} d\tau \le \\ \tfrac{KM}{a} + M e^{-at} \|\mathbf{z}^{**}(0)\|_{1D} \le 2 + o(1). \end{gathered}$$

Finally, we obtain for $X(0) = 0$:

$$\|\mathbf{p}^*(t) - \mathbf{p}^{**}(t)\|_1 \le 8\, e^{-2t}, \quad |E(t,0) - \phi(t)| \le 8\, e^{-2t}, \quad (26)$$

for obtaining the 1-periodic limiting probability of the empty queue $p_0^{**}(t)$ and the 1-periodic limiting mean $\phi(t)$.

Now we can use the approach of (Zeifman et al. 2006, Satin et al. 2012) for solving the Cauchy problem of forward Kolmogorov system with initial condition $\mathbf{e}_0$ for truncated processes $X_{N-1}(t)$. Namely, Theorem 2 (Zeifman et al. 2006) and Theorem 6 (Satin et al. 2012) give the following bounds on truncation errors for both models:

$$\begin{aligned} \|\mathbf{p}^*(t) - \mathbf{p}_{N-1}^*(t)\|_1 &\le \tfrac{25Nt}{2^{N-1}-1}, \\ |E(t,0) - E_{N-1}(t,0)| &\le \tfrac{25Nt}{2^{N-1}-1}, \end{aligned}$$

if $X(0) = X_{N-1}(0) = 0$.

Finally, putting $\varepsilon = 10^{-6}$, and $N = 30$, we find the limiting characteristics for both models approximately on interval $[10, 11]$ with error 10^{-3}.

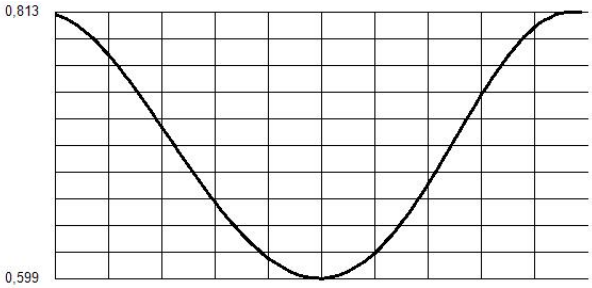

Figure 1: Approximation of the limiting probability of empty queue for ordinary $M_t/M/t/S$ queue on $[10, 11]$ with an error 10^{-3}.

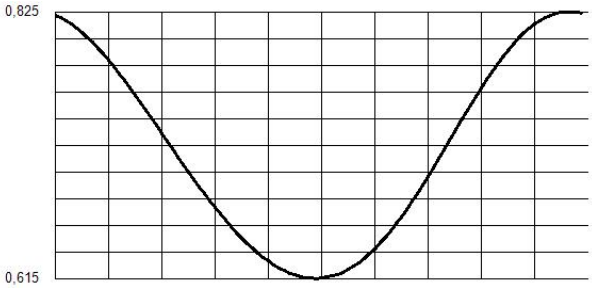

Figure 2: Approximation of the limiting probability of empty queue for analog of $M_t/M/t/S$ queue with group services on $[10, 11]$ with an error 10^{-3}.

Remark. One can see the interesting fact that the limiting mathematical expectations are the same for both examples.

This research was supported by the Russian Foundation for Basic Research, projects no. 11-07-00112a, 12-07-00115a, 12-07-00109a, 13-07-00223a.

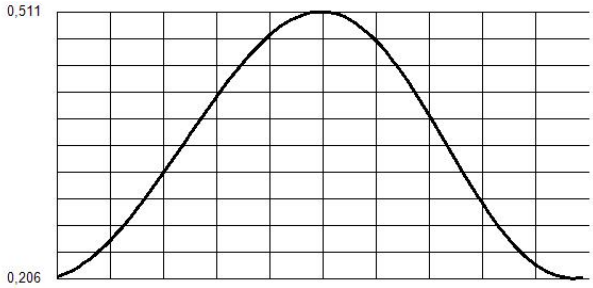

Figure 3: Approximation of the limiting mean for ordinary $M_t/M/t/S$ queue on $[10, 11]$ with an error 10^{-3}.

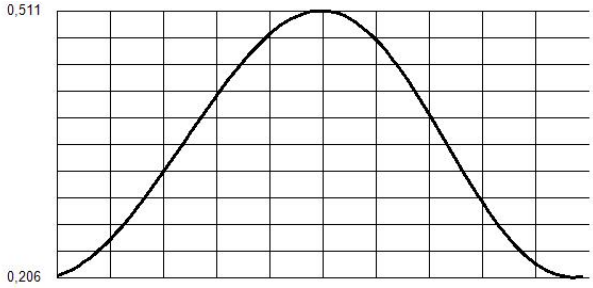

Figure 4: Approximation of the limiting mean for analog of $M_t/M/t/S$ queue with group services on $[10, 11]$ with an error 10^{-3}.

REFERENCES

Daleckij, Ju.L. and M.G. Krein. 1974. *Stability of solutions of differential equations in Banach space.* Amer. Math. Soc. Transl. 43.

Gnedenko, B. V. and V. Yu. Korolev. 1996. *Random Summation: Limit Theorems and Applications.* Boca Raton: CRC Press.

Gnedenko, B.V. and I.P. Makarov. 1971. "Properties of a problem with losses in the case of periodic intensities." *Diff. equations.* 7, 1696–1698 (in Russian).

Gnedenko, B. and A. Soloviev. 1973. "On the conditions of the existence of final probabilities for a Markov process." *Math. Operationsforsh. Stat.* 4, 379–390.

Gnedenko, D.B. 1973. "On a generalization of Erlang formulae." *Zastosow. Mat.* 12, 239–242.

Granovsky, B.L. and A.I. Zeifman. 2004. "Nonstationary Queues: Estimation of the Rate of Convergence." *Queueing Syst.* 46, 363–388.

Korolev V. and I. Shevtsova I. 2012. "An improvement of the Berry–Esseen inequality with applications to Poisson and mixed Poisson random sums." *Scandinavian Actuarial J.* 2, 81–105.

Satin, Ya.A.; A.I. Zeifman; A.V. Korotysheva and S.Ya. Shorgin. 2011. "On a class of Markovian queues." *Informatics and its applications.* 5. No. 4, 6–12 (in Russian).

Satin, Ya. A.; A.I. Zeifman and A.V. Korotysheva. 2012. "On the rate of convergence and truncations for a class of Markovian queueing systems." *Th. Prob. Appl.* 57, 611–621 (in Russian).

Zeifman, A. I. 1995 . "Upper and lower bounds on the rate of convergence for nonhomogeneous birth and death processes." *Stoch. Proc. Appl.* 59, 157–173.

Zeifman, A. I.; V.E. Bening and I.A. Sokolov. 2008. *Continuous-time Markov chains and models.* Elex-KM, Moscow (in Russian).

Zeifman, A.; S. Leorato; E. Orsingher; Ya. Satin and G. Shilova. 2006. "Some universal limits for nonhomogeneous birth and death processes." *Queueing Syst.* 52, 139–151.

Zeifman, A. I. 2009. "On nonstationary Erlang model." *Automation and Remote Control.* 70, 2003–2012.

Zeifman, A. and A. Korotysheva. 2012. "Perturbation bounds

for $M_t/M_t/N$ queue with catastrophes." *Stochastic models.* 28, 49–62.
Zeifman, A.; A. Korotysheva; Ya. Satin; G. Shilova and T. Panfilova. 2013. "On a queueing model with group services," *Lecture Notes in Communications in Computer and Information Science," 356, 198–205.*

AUTHOR BIOGRAPHIES

ALEXANDER ZEIFMAN Doctor of Science in physics and mathematics; professor, Dean of the Faculty of Applied Mathematics and Computer Technologies, Vologda State Pedagogical University; senior scientist, Institute of Informatics Problems, Russian Academy of Sciences; leading scientist, Institute of Territories Socio-Economic Development, Russian Academy of Sciences. His email is a_zeifman@mail.ru and his personal webpage at http://uni-vologda.ac.ru/ zai/eng.html.

YAKOV SATIN is Candidate of Science (PhD) in physics and mathematics, associate professor, Vologda State Pedagogical University. His email is yacovi@email.ru.

GALINA SHILOVA is Candidate of Science (PhD) in physics and mathematics, associate professor, Vologda State Pedagogical University. Her email is shgn@email.ru.

VICTOR KOROLEV is Doctor of Science in physics and mathematics, professor, Department of Mathematical Statistics, Faculty of Computational Mathematics and Cybernetics, M.V. Lomonosov Moscow State University; leading scientist, Institute of Informatics Problems, Russian Academy of Sciences. His email is bruce27@yandex.ru.

VLADIMIR BENING is Doctor of Science in physics and mathematics; professor, Department of Mathematical Statistics, Faculty of Computational Mathematics and Cybernetics, M. V. Lomonosov Moscow State University; senior scientist, Institute of Informatics Problems, Russian Academy of Sciences. His email is bening@yandex.ru.

SERGEY YA. SHORGIN is Doctor of Science in physics and mathematics, professor, Deputy Director, Institute of Informatics Problems, Russian Academy of Sciences. His email is sshorgin@ipiran.ru.

CRITERIA ON STATISTICALLY DEFINED BANS

Alexander A. Grusho, Nick A. Grusho and Elena E. Timonina
Institute of Informatics Problems RAN
Vavilova 44, Moscow, Russia
Email: grusho@yandex.ru

KEYWORDS

Consistent sequences of criteria, bans of probability measures in the discrete spaces, consistency of estimates

ABSTRACT

The method of statistical determination of smallest bans of probability measures on discrete spaces is offered. Consistency of the constructed estimates is shown. The application of the received estimates for testing of statistical hypotheses in the discrete spaces is constructed. It is shown that estimates of bans can generate consistent sequences of criteria in some sense.

INTRODUCTION

Finite probability spaces play an essential role in cases of different simulation problems of network and computer security, cryptography, etc. Information flows analysis is less effective if there is positive probability of false alarms. Besides complexity of statistical analysis sometimes prevents from big data controls in realtime. Bans of finite probability measures can help to solve these problems. We consider the problem of testing of sequence of simple hypotheses $H_{0,n}$ against complex alternatives $H_{1,n}$ in finite spaces. Let $X = \{x_1, ..., x_m\}$ be a finite set, X^n be the Cartesian product of a set X, X^∞ be a set of the infinite sequences with elements from X, $\mathcal{A}$ be the minimum σ-algebra generated by all cylindrical sets (Lehmann, 1997; Neveu, 1964; Bourbaki, 1968). If on X the discrete topology is considered, Tychonof product X^∞ is compact topological space with countable basis (Bourbaki, 1968; Prokhorov and Rozanov, 1993). In this case Borel σ-algebra $\mathcal{B}$ is also σ-algebra $\mathcal{A}$.

Let P_0 - a probability measure on $(X^\infty, \mathcal{A})$. For each n $P_{0,n}$ is a projection of P_0 to the first n coordinates of sequences from X^∞.

Earlier (Grusho and Timonina, 2011a,b) we defined concept of a ban of a finite probability measure. Bans are understood as initial sections of sequences from X^∞ which probabilities are equal to zero. In statistical problems there exist the criteria which critical sets completely are defined by bans. In (Grusho and Timonina, 2011a,b) necessary and sufficient conditions of existence of the consistent sequences of criteria (CSC) which critical sets are completely defined by bans are proved.

The statistical criterions defined by bans, possess the property that in case of a null hypothesis $P_{0,n}(S_n) = 0$, where S_n, $n = 1, 2, ...,$ - critical sets of criteria. In some cases of probability measures it is possible to define bans of these measures quite easily.

Let Λ_n be a finite set of bans of measure $P_{0,n}$. Let's assume that we can independently produce vectors from X^n with probability measures $P_{0,n}$ for any finite n. Then it is possible to construct a consistent estimation of a set Λ_n.

In section 2 estimates of sets Λ_n, $n = 1, 2, ...,$ are constructed, and their consistency are proved. In section 3 we use bans for testing of hypotheses $H_{0,n}$ against $H_{1,n}$ taking into account possibility of inexact determination of sets Λ_n. In conclusion the received results are discussed.

ESTIMATES OF SETS OF SMALLEST BANS

Let on $(X^\infty, \mathcal{A})$ the probability measure P_0 is defined. It is obvious that for any $B_n \in X^n$

$$P_{0,n}(B_n) = P_0(B_n \times X^\infty). \tag{1}$$

Let $D_{0,n}$ be the support of measure $P_{0,n}$:

$$D_{0,n} = \{\overrightarrow{x}_n \in X^n,\ P_{0,n}(\overrightarrow{x}) > 0\}. \tag{2}$$

Denote $\Delta_{0,n} = D_{0,n} \times X^n$. Sequence $\Delta_{0,n}$, $n = 1, 2, ...,$ is nonincreasiing and

$$\Delta_0 = \lim_{n\to\infty} \Delta_{0,n} = \bigcap_{n=1}^{\infty} \Delta_{0,n}. \tag{3}$$

The set Δ_0 is closed and is the support of the measure P_0.

We also consider a set of probability measures $\{P_\theta,\ \theta \in \Theta\}$ on $(X^\infty, \mathcal{A})$ for which $P_{\theta,n}$, $D_{\theta,n}$, $\Delta_{\theta,n}$, Δ_θ are defined.

If $\overline{\omega}_k \in X^k$, then $\widetilde{\omega}_{k-1}$ is received from $\overline{\omega}_k$ discarding of the last coordinate.

Definition 1. In a measure $P_{0,n}$ the vector $\overline{\omega}_k \in X^k$, $k \le n$, such that

$$P_{0,n}(\overline{\omega}_k \times X^{n-k}) = 0 \tag{4}$$

is called the ban.

If $P_{0,k-1}(\widetilde{\omega}_{k-1}) > 0$, then $\overline{\omega}_k$ is called the smallest ban.

If $\overline{\omega}_k$ is the ban of a measure $P_{0,n}$, then for any $k \le s \le n$ and for any vectors $\overline{\omega}_s$ beginning with $\overline{\omega}_k$, we have

$$P_{0,s}(\overline{\omega}_s) = 0. \tag{5}$$

Proceedings 27th European Conference on Modelling and Simulation ©ECMS Webjørn Rekdalsbakken, Robin T. Bye, Houxiang Zhang (Editors)
ISBN: 978-0-9564944-6-7 / ISBN: 978-0-9564944-7-4 (CD)

Further under Λ_n we will understand a set of the smallest bans of $P_{0,n}$.

All bans of a measure $P_{0,n}$ are defined by the smallest bans (Grusho and Timonina, 2011b), i.e. any ban contains at least one element from a set Λ_n. Assume that we don't know what elements enter into a set Λ_n and set capacity. Let's construct a consistent estimate of a set Λ_n in the specified assumptions.

Let $\overline{\omega}_n^{(1)}$, $\overline{\omega}_n^{(2)}$, ..., $\overline{\omega}_n^{(N)}$ be a sample from the distribution $P_{0,n}$. In the received sample we consider frequencies $\nu_n^{(i)}$, $i = 1, 2, ..., m^n$, of occurrence of all vectors. We select vectors from X^n which frequencies are equal to zero. The selected vectors define potential smallest bans of $P_{0,n}$ due to (5).

The constructed set of potential smallest bans Λ'_n as a result of specified algorithm can differ from the true set Λ_n. The set Λ'_n is an estimate of the set Λ_n. The following errors are possible. The s-chain which isn't the smallest ban, randomly never met in the viewed sample and belongs to a set Λ'_n. Then in case of changeover Λ_n by an estimation Λ'_n we receive excess smallest bans. Thus, Λ'_n contains Λ_n.

Let's consider probability of that the n-chain didn't belong to the sample randomly. Let's denote probabilities of appearance of all n-chains through $p_1^{(n)}$, $p_2^{(n)}$, ..., $p_{m^n}^{(n)}$. The probability that the frequency of the chain i is equal to 0, equals to $(1 - p_i^{(n)})^N$. Then mathematical expectation of a number of elements in Λ'_n equals to $\sum_{i=1}^{m^n}(1 - p_i^{(n)})^N$.

Let's denote

$$\epsilon = \min_{1 \le i \le m^n,\, p_i^{(n)} > 0} p_i^{(n)}. \qquad (6)$$

Then mathematical expectation of power of the set Λ'_n equals to $|\Lambda_n| + E\xi$, where ξ - a random variable, equal to number of randomly not met n-chains. It is obvious that

$$E\xi = \sum_{i=1,\, p_i^{(n)} > 0}^{m^n} (1 - p_i^{(n)})^N. \qquad (7)$$

For $E\xi$ the following estimation is fair

$$E\xi \le m^n (1 - \epsilon)^N. \qquad (8)$$

$E\xi$ tends to 0. Let's denote through λ_N probability of that $|\Lambda'_n| > |\Lambda_n|$. Using Markov's inequality, we receive that in case of $N \longrightarrow \infty$ $\lambda_N \longrightarrow 0$.

CONSISTENT SEQUENCES OF CRITERIA WITH USE OF THE SMALLEST BANS

Let's create the criteria depending on bans. Earlier we assumed that there is a family of distributions $\{P_\theta,\, \theta \in \Theta\}$. There is (Grusho and Timonina, 2011a) necessary and sufficient condition of existence of CSC determined by bans. That is the condition $P_\theta(\Delta_0) = 0$ for $\forall \theta \in \Theta\}$.

Let the condition of existence of CSC determined by bans $\bigcup_{n=1}^{\infty} \Lambda_n$ be satisfied. Then the sequence of criteria with the critical sets consisting of all sequences, containing smallest bans, is consistent sequence of criteria for testing of hypotheses $H_{0,n} : P_{0,n}$, $n = 1, 2, ...$, against alternatives $H_{1,n}$.

In (Grusho and Timonina, 2011b) it was proved that the following equations between capacities of supports of $P_{0,n}$, $n = 1, 2, ...$, and numbers of the smallest bans of these measures take place

$$\nu_1 m^{n-1} + \cdots + \nu_{n-1} m + \nu_n + |D_{0,n}| = m^n. \qquad (9)$$

where ν_i - number of the smallest bans of length of i. From this ratio it is clear that if we increase number of the smallest bans the sizes of supports $D_{0,n}$ decrease. It means that instead of the initial measure P_0 with a set of the smallest bans $\bigcup_{n=1}^{\infty} \Lambda_n$ we for determination of the null hypotheses consider some measure P'_0. For this measure the support Δ'_0 can be less, than the support of the initial measure P_0, i.e. $\Delta'_0 \subseteq \Delta_0$. Therefore having checked a condition of existence of CSC depending on bans, for P_0 we guarantee execution of this condition for a measure P'_0 with a set of bans $\bigcup_{n=1}^{\infty} \Lambda'_n$.

It is obvious that $\Delta_0 \backslash \Delta'_0$ is a measurable set. Let's denote $P_0(\Delta_0 \backslash \Delta'_0) = \mu$. Then P'_0 can be defined as follows.

$$P'_0(A) = \frac{1}{1 - \mu} P_0(A \cap \Delta'_0). \qquad (10)$$

Let CSC depending on bans, for testing $H'_{0,n}$ against $H_{1,n}$ (above we proved that such sequence exists) is defined by critical sets S_n, $n = 1, 2, ...$ Then

$$P_{0,n}(S_n) = P_0(S_n \times X^\infty) =$$

$$= P_0((S_n \times X^\infty) \cap (\Delta_0 \backslash \Delta'_0)) +$$

$$+ P_0((S_n \times X^\infty) \cap (\Delta_0 \cap \Delta'_0)). \qquad (11)$$

The second item is equal to zero since a critical set S_n in a measure $P'_{0,n}$ has probability 0.

Using determination of μ, we receive an estimation

$$P_0((S_n \times X^\infty) \cap (\Delta_0 \backslash \Delta'_0)) \le \mu. \qquad (12)$$

From this it follows that the sequence of criteria with critical sets S_n in case of testing $H_{0,n}$ against $H_{1,n}$ has significance value μ. Thus for $\forall \theta \in \Theta$

$$P_{\theta,n}(S_n) \to 1. \qquad (13)$$

Let's recall that μ is a random variable in the probability scheme connected to statistical determination of the smallest bans. We showed that in case of $N \to \infty$ with the probability tends to 1 (in the scheme of an estimation of the smallest bans), $\Lambda'_n = \Lambda_n$. In this case $\mu = 0$ and $P_0 = P'_0$. Thus, we receive that in case of $N \to \infty$ CSC, constructed for testing $H'_{0,n}$ against $H_{1,n}$, will be also consistent for testing $H_{0,n}$ against $H_{1,n}$.

CONCLUSION

Knowledge of a condition $P_\theta(\Delta_0) = 0$ for $\forall\theta \in \Theta$ is enough to define the sequence of criteria depending of bans which asymptotically (in some sense) will be consistent.

Acknowledgements
This work was supported by the Russian Foundation for Basic Research (grant 13-01-00215).

REFERENCES

Bourbaki, N. (1968). *Topologie G'en'erale. Russian translation.* Science. Moscow.

Grusho, A. and Timonina E. (2011). "Prohibitions in discrete probabilistic statistical problems". *Discrete Mathematics and Applications*. 21(3), 275-281.

Grusho, A. and Timonina E. (2011). "Statistical Tests Based on Bans". In *Proceedings of 1st International Symposium and 10th Balkan Conference on Operational Research*, (September 22-24, Thessaloniki, Greece), Vol. 1, 234-241.

Lehmann, E. L. (1997). *Testing Statistical Hypotheses (Springer Texts in Statistics).* 2nd ed. Springer.

Neveu , J. (1997). *Bases mathematiques du calcul des probabilites*. Paris: Masson.

Prokhorov, U. V., and Rozanov, U. A. (1993). *Theory of probabilities*. Moscow: Science.

AUTHOR BIOGRAPHIES

ALEXANDER J. GRUSHO was born 28.08.1946. He is Dr. Sc., Professor, Leading Scientist of IPI RAN. His email is grusho@yandex.ru.

NICK A. GRUSHO was born 15.06.1982. He is PhD., Senior Scientist of IPI RAN. His email is info@itake.ru.

ELENA E. TIMONINA was born 27.02.1952. She is Dr. Sc., Professor, Leading Scientist of IPI RAN. Her email is eltimon@yandex.ru.

Discrete Event Modelling and Simulation in Logistics, Transport and Supply Chain Management

SIMULATION IMPROVES UNIVERSITY CAMPUSES BUS SERVICE

Bai Zou, Xiaofan Hu, Ju Xiong, Mingdi You

Dept. of Industrial and Operations Engineering
1205 Beal Avenue
University of Michigan
Ann Arbor, MI 48109, USA

Edward J. Williams

Decision Sciences, College of Business
University of Michigan - Dearborn
131 B Fairlane Center South
19000 Hubbard Drive
Dearborn, MI 48126, USA

ABSTRACT

Historically, discrete-event process simulation was first and most widely used in manufacturing contexts. As the technology has gradually matured and knowledge of its benefits has become more widely known, simulation usage has spread to warehouse design and operation, health-care delivery, retail customer service, and (as in this paper), the transport of people and/or goods.

This project simulated the Blue Bus system of the University of Michigan. We analyzed the waiting time of passengers at each stop and the utilization of buses under two strategies; one is based on the schedule, the other is adding eight buses of Bursley-Baits during peak time besides the scheduled shifts which is practical Blue Bus running strategy. Under the two strategies, we analyzed the different scenarios that number of passengers increases by some times. We compared these scenarios and found the practical strategy is more robust when there is a sharp increase of passengers.

1 INTRODUCTION

Early in the history of discrete-event process simulation, its use was almost entirely confined to the manufacturing sector of the economy. More recently, and now extensively, its use has expanded to the analysis of entire supply chains. Inevitably, its analytical power to identify and quantify improvements led to use in the design of both local and large-scale transportation networks. For example, locally, (Patlins 2008) greatly improved local delivery times in cities with unstable traffic patterns. The study by (Or, Özbaş, and Yilmaz 2007) greatly improved the efficiency and safety of maritime traffic in the İstanbul strait. Over much wider geographic compass, (Boesel and Bodoh 2004) studied redesign of airspace to use to best advantage the addition of a fourth runway at Detroit Metropolitan Airport.

This study examined and improved the operation of the campus bus system, scheduling, and routes on a large (more than 40,000 students, plus faculty, employees, and guests) metropolitan university campus. As can well be imagined, both the parking and the congestion problems, let alone environmental considerations, require the campus to provide a convenient, efficient bus service as a substitute for privately owned vehicles. The primary aim of the study was to plan for significantly increased capacity demands (expected if car registration fees or outright vehicle bans, both under consideration, are implemented), while identifying current and potential bottlenecks and, preventing current service metrics (waiting time, missed connections) from deteriorating.

Following this introductory section, we describe the current system and its contingencies. In the methods section, we introduce the data collection and sensitivity analysis method. The modeling section provides a basic model description of the Blue Bus system, establishing assumptions to build the model and identifying input based on the real system and data analysis. The results section reports the validation, verification and the direct output of the model, analyzing data from the running of the model. Finally, we provide conclusions drawn from the sensitivity analysis, evaluate measures to improve robustness, and indicate promising direction for follow-up studies.

2 SYSTEM DESCRIPTION

The "Blue Bus" system at the University of Michigan is the campus transportation system connecting three different campuses. The largest transportation demand occurs between north campus and center campus, connected by five bus routes during the day. The major stops are CCLittle at center campus and Pierpont at north campus. Routes connecting the two stops are shown in Figure 1 below

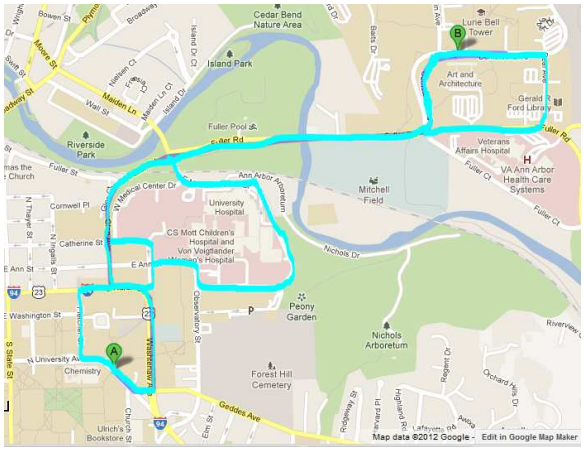

Figure 1: Route between C C Little and Pierpont

Proceedings 27th European Conference on Modelling and Simulation ©ECMS Webjørn Rekdalsbakken, Robin T. Bye, Houxiang Zhang (Editors)
ISBN: 978-0-9564944-6-7 / ISBN: 978-0-9564944-7-4 (CD)

The routes and schedule are fixed for each bus line: Northwood; Northwood Express; Bursley-Baits; Commuter North & South; Diag[onal]-to-Diag[onal] Express; which meet needs of center campus, the medical center and north campus. The schedule of buses on the various routes is fixed and published. Yet in practice, several more buses are added, on an ad-hoc basis, at peak times. The frequency of the bus is every 10 minutes during the day on weekdays. Meanwhile, there is an interactive, real-time Magic Bus system tracing dynamic conditions throughout the system.

3 PROBLEM DESCRIPTION

The current Blue Bus system works reasonably well in terms of meeting basic transportation needs. However, several problems exist when the system is inherently unstable. For example, the current system cannot meet the transportation demand when there is a sharp increase in passengers (e.g., near lunchtime and in between periods scheduled for large classes); also, the passengers' waiting time increases when weather and road conditions reduce bus speed. Hence, sensitivity analysis, undertaken in this study, is a valuable tool to assess system robustness – e.g., how much change in demand can the current system accommodate before the key performance indicators [KPIs] of passenger waiting times and bus utilizations deteriorate severely?

Additionally, disruptions to the system might cause more impact during peak time. For example, the first morning class ends at 10am on center campus, and the second morning class begins at 10:30am on north campus. During that half-hour, the system should fully meet the spike in transportation needs to reduce lateness for classes. Secondly, during peak time a bus might be so overcrowded that it must leave some passengers stranded at starting or intermediate stops waiting for the next bus. Therefore, additional adjustments are required to adapt to the disruptions, high demand variability, and uncertainty exogenous to the system. Therefore, the bus system transportation managers requested that this industrial engineering study develop, evaluate, and compare various alternatives, entailing various investments in capital, labor, and reorganization, to improve system service metrics and the robustness of system service. Predictions were requested for as much as a fivefold (500%) increase in passenger load over the next few years. Campus enrollments are projected to increase only moderately (5% 10% annually), but new regulations under consideration to "*force* people out of their cars" may greatly increase demand.

4 INPUT DATA COLLECTION AND ANALYSIS

4.1 Data Collection

Collection and analysis of model data is a fundamental step in simulation analysis: No model is any better than its data (Seila, Ceric, and Tadikamalla 2003). The data can be divided into two parts, Blue Bus's operational data and passengers' data. Blue Bus's data includes the running schedule (i.e. departure times of buses on different routes), traveling time, and arriving time. Since the schedule of Blue Bus is fixed and published, these data were accessed from the system's Internet web site. For the traveling times and arriving times, we needed to consider the different scenarios and collect the data under a variety of conditions. We collected data of total traveling times of all routes by riding a Blue Bus personally. Meanwhile, we also collected data of arriving time at each stop.

For passengers' data, the main task was to discover the demand at different times and on different routes. So at the bus stops, we collected the total number of passengers during a time period and the interarrival time of passengers. Onboard a bus, we collected the total number of passengers on different routes and the number of students' departures at each stop between Pierpont and C C Little. We also collected the arrival times data at Pierpont and at C C Little. We collected data specifically at these two stops because most passengers take the bus between these two stops and many routes stop at each. These data were collected by: (i) counting number of passengers at Pierpont and CC Little, and (ii) counting number of passengers taking different routes and recording the travelling time of routes between different stops by riding buses.

4.2 Surveys

Distributing surveys was important to improve the efficiency and service quality of Blue Bus. From the survey, we estimated how many students are satisfied with the Blue Bus and collected the feedback of students relative to the punctuality, crowdedness of bus, and suitability of setting each stop and routes. We also asked the passengers how they choose the different buses when different route buses can transport them to the same destination and their expectations when they ride a bus. The same survey was also conducted at different times during a day, to capture the influences of disruption to the satisfaction of passengers. Travel times are calculated from the arrival times and departure times, averaged, as provided by student survey responses.

4.3 Sensitivity Analysis

Sensitivity analysis is a powerful tool for enhancing the power and accuracy of simulation models (Biller and Nelson 2002). The purpose of the sensitivity analyses undertaken was to gain insight into the significance of the factors that influence the efficiency of our Blue Bus routes, especially on the specific routes between CC Little and Pierpont Commons. Although several factors affect the system, this report focuses on the passenger arrival numbers. Therefore, the sensitivity analysis was

conducted based on changing peak time passenger arrivals. Thus, data of average waiting time on major stops and bus utilizations of different lines were analyzed under vastly different arrival levels. Multiple systems, the current one and the proposed one, were compared under the scenarios of drastically increased load.

5 MODEL DEVELOPMENT AND CONSTRUCTION

5.1 Model Description

The Blue Bus model was built using the discrete-event process simulation software ProModel® (Harrell and Price 2003). In the model we established locations, entities, and process logic as follows:

As locations, this model contains most stops of five routes (Bursley-Baits, Northwood, Northwood Express, and Diag to Diag Express, Commuter Southbound, and Commuter Northbound), located mainly between North Campus and Central Campus. We omitted the final stops of Bursley-Baits, Northwood, Commuter Southbound, and Commuter Northbound routes, and focused mainly on the stops between Pierpont and CC Little. There are 54 total locations. Every stop has two locations in ProModel®, distinguished as location A and location B, to represent Blue Buses going through the stop in opposite directions.

Entities are passengers and buses. We have one type of passenger and six routes of buses, as shown in Figure 2. We conceptually attach passengers to a bus by using the logic "load" or "unload" when the passengers get on or off the buses. Since passengers and buses have different identities like arrival time and frequency, and the buses on different routes typically have different arrival points and travel schedules, so treating buses as distinct entities helped us control the identities of both passengers and buses much more efficiently.

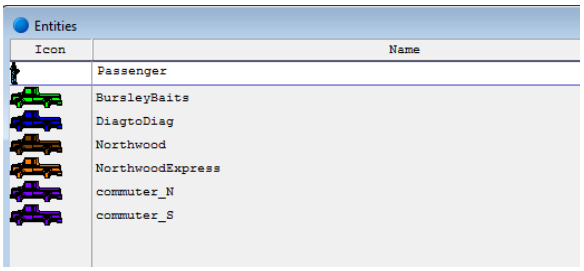

Figure 2. Entities of Simulation Model

The arrivals of entities are subject to the different probability distributions according to the data we collected. For passengers, we used two distributions of frequency, i.e. regular arrival and peak time arrival to represent the fluctuation of number of passengers between regular time and peak time. To construct the scenarios that different passengers may have different destinations, we analyze the data of passengers at different stops, and find the portion of passengers going to various destinations. Then we created user distribution of destination, and assigned the distribution to the passengers when the passengers arrived at various locations. Hence the passengers have a certain probability to get off the bus at any particular location (bus stop).

For the buses, we set frequency of 10 minutes for Bursley-Baits, Diag to Diag Express, Northwood, Northwood Express, and commuter from 8:00 am to 6:30pm, and 20 minutes and 15 minutes respectively for Northwood and Commuter after 6:30pm (18:30).

To implement processing logic in our simulation model, two locations with separation zero represent each bus stop. As illustrated in Figure 3, the basic processing for simulation model is: Once the passenger arrives at one location, the passenger will wait for a load request of a bus. When the bus arrives at a location, we chose to unload all the passengers from the Blue Bus at one location if it already loaded some passengers, and then check the destination of the passenger (in ProModel, we use "stop-re" to indicate, for example, CCLittle-re). We used conditional logic to check the passenger's destination to determine the route that the passenger should follow; if the destination is the current location, then the passenger, having reached his or her desired destination, exists the system. If the destination is not the current location, then the passenger will go to the adjacent location to get on the same bus with higher priority (connecting passenger) than the passenger who just arrived at (walked to) that location. This method successfully avoided the illogical situation that a passenger momentarily unloaded from a bus could not "load" again because of capacity of buses if the destination of the passenger is not the current location.

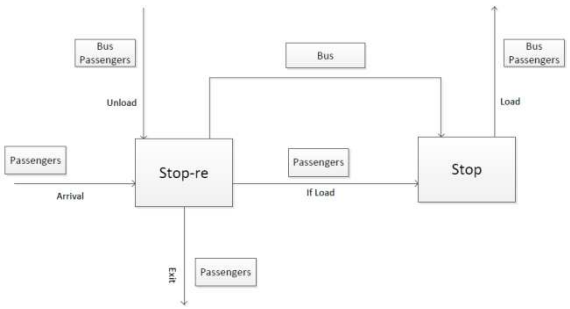

Figure 3: Flow Chart of Processing

5.2 Model Assumptions

In order to simulate the model, we made and documented several assumptions:

1. The passenger arrives at location where he/she is able to take some route to get to the destination. The destination choice of the passenger is modeled probabilistically.
2. If the bus is not full, the passenger boards the bus. If not, the passenger waits for the next available bus, but does not balk or renege.
3. The operation time is scheduled according to the online bus schedule.
4. All buses for different routes have the same capacity, 65 passengers.
5. The time which the bus spends at each stop depends linearly on the number of students who get off and on at that stop.

5.3 Input Modeling

After collecting data, the next step was to incorporate these data into the simulation model. As we verified by using the distribution-fitting software tool Stat::Fit® (Chung 2004), the interarrival times between two consecutive arrivals was exponentially distributed. Then, we needed to estimate the single parameter for exponential random variables based on the data we collected.

Based on our observations, arrivals of passengers at stops other than CC Little, Museum, Cooley and Pierpont are infrequent. Thus, we defined a macro to represent the mean of interarrival times at these stops. For the stops CC Little, Museum, Cooley and Pierpont, the arrivals of passengers are really numerous. Moreover, these arrivals of passengers comprise two types: One type, which we defined as "peak" type, which models the students just dismissed from class and/or just going to class. Arrivals of this passenger type of correspond to the starting and ending time of class in North Campus and Central Campus (for Central Campus, it's 8:30am, 10:00am, etc.; for North Campus, it's 9:00am, 10:30am, etc.). Other passengers are modeled as "regular." From the observations, there are eight peak times at Central Campus and six peak time at North Campus. For each peak time the number of passenger arrivals is modeled as a random number, selected from a uniform distribution with mean and variance again determined by a distribution fitter.

6 VERIFICATION, VALIDATION, AND RESULTS

6.1 Model Verification

Verification is a key step to check the model was correctly built, and that the desired output can be obtained from input parameters. We examined the model output under different input parameters.

To verify the output, we first changed the input parameters of passengers (directional verification). Under the current-situation parameters, the average waiting time was 3.25 minutes. Intuitively, the waiting times should increase when the interarrival time is decreased, because from the real system, the more passengers arrive at one location, the higher the probability that a passenger cannot board a full bus. This directional verification was successful. Second, we increased the frequency of bus arrivals, and waiting times, as expected, decreased. Other verification techniques, such as collaborative structured walkthroughs of the model, and close "stepwise" examination of the animation (for example, to ensure that a passenger is not forced off a bus prior to arrival at intended destination) also proved successful after routine identification and correction of errors.

6.2 Model Validation

This section describes the techniques used to validate that the simulation model represents the real situation. When modeling the arrival number of passengers during different times, we used two parameters of the fitted exponential distribution, i.e. regular rate and peak time rate to represent the fluctuation of arrival passengers through time. From the model, the data shows that the peak time arrival always occurs at the interval time between two classes; for example, 10:00am -- 10:15am, which coincides with a brief heavy demand for transport between north campus and central campus.

To re-validate the simulation inputs (it is perhaps rare to speak of "re-validating" input; in the context of this project, concerns inevitably arose that data values may have "drifted" during the semester as the project progressed), four team members rode various bus routes at different times, and recorded the passengers getting on and off at various stops, plus the travel times between consecutive stops. These observational data matched the inputs to the simulation model under default (current) conditions within 3.5%. Since this effort was concurrent with model development and verification, it did not extend total calendar completion time of the project.

Next, to validate the simulation *outputs* (the typical and indeed vital facet of model validation), we conducted observational and interpersonal surveys to confirm the waiting times of passengers as calculated by the simulation model. We surveyed the waiting time to take a bus among passengers getting off the buses at two main stops, Pierpont and CC Little. The survey found that the average waiting time for the Blue Bus at CCLittle stop is 2.42 minutes, which differs by 5% from our simulation waiting time of 2.31 minutes; the average waiting time for the Blue Bus at Pierpont is 1.44, which has 5% difference of our simulation waiting time of 1.37 (the client deemed agreement within 10% sufficient to support policy decisions). So this key performance metric output of our simulation can be validated. Similarly, bus utilizations and travel times

along entire routes in practice agreed well with predictions of the simulation model.

6.3 Model Outputs

Our outputs of the simulation model are the key performance metrics: Waiting time of passengers and utilizations of the buses. Five waiting time variables were tracked to trace the total waiting time of all stops and waiting time of passengers at Cooly, Pierpont, Museum, and CCLittle. We also tracked six usage variables to trace the usage of buses on each of six routes. For the convenience of model users and decision-makers, these model results were output to a Microsoft Excel® workbook, whence they could conveniently be plotted for easy visualization.

6.4 Output Analysis

In our simulation model, two different Blue Bus running strategies are considered; one based on the current schedule and policy ("Schedule"), the other consists of adding eight buses to the Bursley-Baits routes during peak times ("Practice").

After running the simulation for both scenarios (twenty replications per scenario, each terminating with zero warm-up time, and results compared by Student-*t* tests) we obtain average waiting times of 3.25 minutes for all stops under the current schedule and average waiting time of 3.10 minutes under the proposed addition of eight buses. So the difference of waiting times between two strategies is very small.

Likewise, comparing the utilizations of the buses, we find average utilization of 26.3% for all buses under the current schedule and average utilization of 28.5% under the proposed addition of buses. So the difference of utility between two strategies is also small, and both utilizations are well below 50% (an figure mentioned repeatedly in survey comments and of interesting origin – with this utilization, each student may have "one seat for myself and one seat for my bookbag," and bookbags do not clog the aisle), implying the buses can pick up more passengers and passengers can feel confident and unrushed when taking the buses to classes or appointments.

For individual bus routes, we observe that the utilizations of the Northwood Express and Diag to Diag routes are relatively lower than those of the other routes. Based on these results, those two routes never achieve 100% utilization even during peak times; however, other routes have been 100% used, briefly, at peak times. The average utilization for five routes is shown in Figure 4.

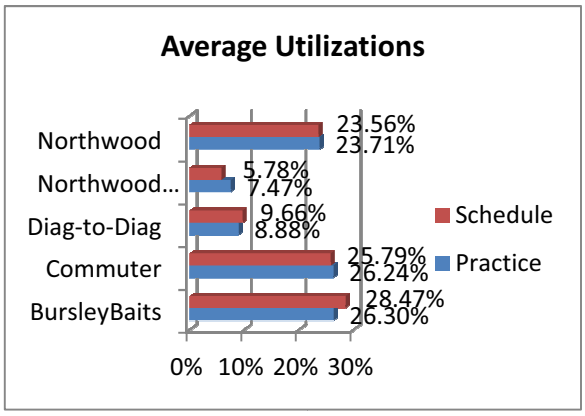

Figure 4. Average Utilization of Five Routes under Two Strategies

scenarios that number of passengers increases by some times. The waiting time under different scenarios are shown in the figure below. The horizontal axis represents the hypothesized percentage of increase in the number of passengers; the vertical axis represents minutes of waiting time on various routes. These comparisons are presented, superimposed in Figure 5.

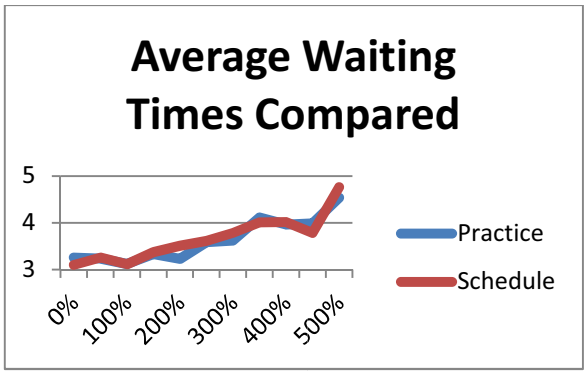

Figure 5. Superposition for Comparison

From Figure 5, we can deduce that the waiting time increases (note *y*-axis does not start at 0) as the number of passengers increases. The difference between the two strategies stays small when passenger numbers increase by 150% or less. However, when the passengers increase by more than 150%, the "Practice" strategy of adding eight buses becomes noticeably more capable of accommodating the increased numbers of passengers.

For each main destination, we have demonstrated that the waiting times at CCLittle stop increase sharply. Therefore, CCLittle is the bottleneck in the Blue Bus route map. Figure 6 shows the average waiting time at CCLittle under each scenario. We observe that the waiting time will be above five minutes, which is a relatively long time to wait for buses in the daytime for students (key "class breaks" are only thirty minutes), when the passengers increased fivefold. Since only two

routes go through the CCLittle stop, the number of passenger transfers there is higher than elsewhere.

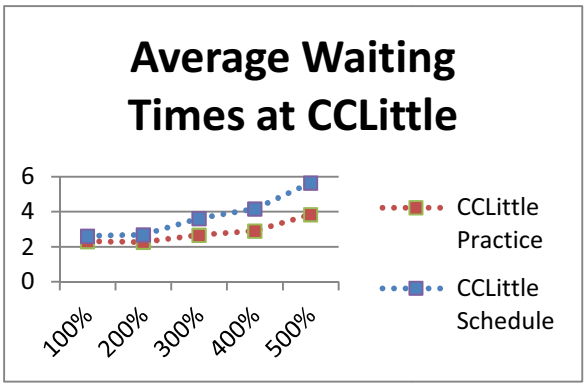

Figure 6. Average Waiting Time at CCLittle

The utilizations for buses on individual routes under different scenarios are shown in Figures 7 through 11. The utilization of buses will increase as arrivals do. For Northwood Express, a sharp increase happens when the passengers increases by 350%. For Bursley Baits, the utilization maintains a higher value compared with other routes. However, after the passengers increased by 350%, the utilization will be above 50%, which means spaces to accommodate more passengers become conspicuously limited.

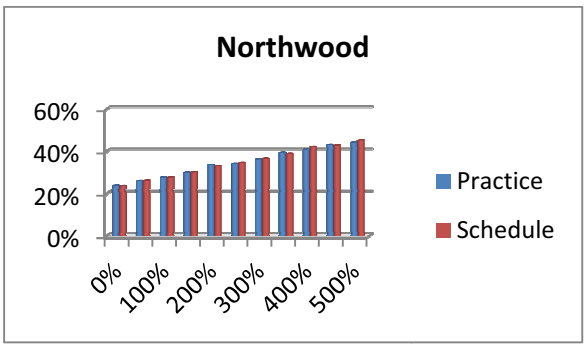

Figure 7 Northwood Route Buses Utilization

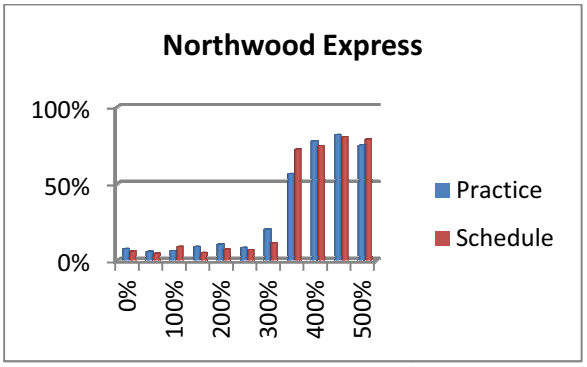

Figure 8 Northwood Express Route Buses Utilization

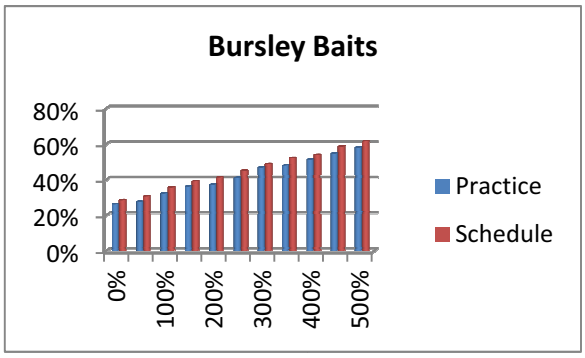

Figure 9 Bursley Baits Route Buses Utilization

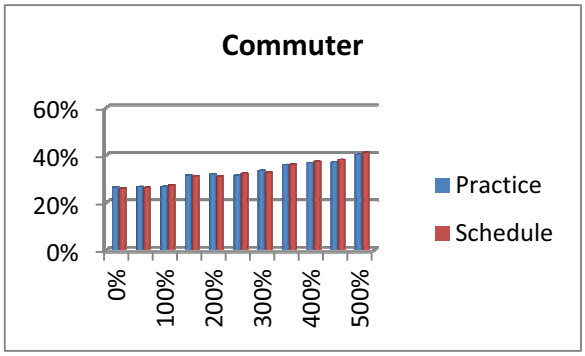

Figure 10 Commuter Route Buses Utilization

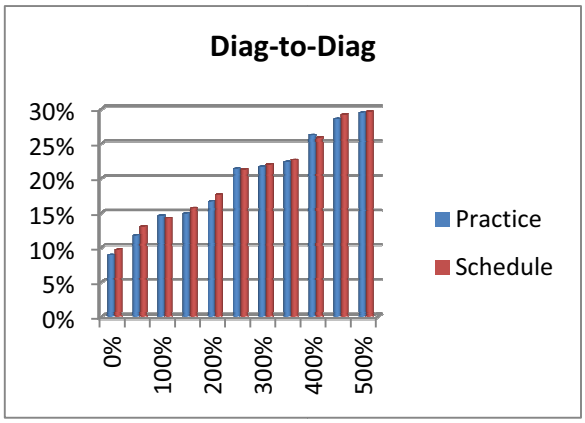

Figure 11 Diag to Diag Route Buses Utilization

7 CONCLUSIONS AND FURTHER WORK

This simulation study has confirmed that the CCLittle station is the bottleneck of the entire Blue Bus system; hence, should the arrivals of passengers increase markedly, the waiting times of the passengers at this station will also increase sharply. Therefore, adding more routes at this station by reconfiguring the route map is an effective short-term expedient to reduce waiting times and improve service. Over a longer planning horizon, the university is considering stringent traffic control measures, already described, to reduce severe congestion on campus. These measures will not only increase demand, but also may affect optimality of bus schedules – more surveys will be required, and

these future surveys must reach people *not* currently using the Blue Bus system. In these scenarios, specified in advance by the client, the sensitivity analyses undertaken to assess service quality under greatly increased passenger load are valuable to enhance capital-expenditure predictions for the additional buses which would be required. Additional aspirations of further analysis include a more stringent examination of correlated delays (e.g., if a snowstorm causes longer travel time on one route, it will surely cause longer travel time on others) and explicit inclusion of the KPI "bus connections missed." From a passenger's perspective, an 11-minute delay and consequent missed connection is far worse than a 9-minute delay (connection successful).

ACKNOWLEDGMENTS

Numerous insightful and perceptive comments from reviewers (and two reviewers in particular) have contributed greatly to the improvement of this paper.

REFERENCES

Biller, Bahar, and Barry L. Nelson. 2002. Answers to the Top Ten Input Modeling Questions. In *Proceedings of the 2002 Winter Simulation Conference*, Volume 1, eds. Enver Yücesan, Chun-Hung Chen, Jane L. Snowdon, and John M. Charnes, 35-40.

Boesel, Justin, and David Bodoh. 2004. Simulating Airspace Redesign for Arrivals to Detroit-Wayne County Airport (DTW). In *Proceedings of the 2004 Winter Simulation Conference*, Volume 2, eds. Ricki G. Ingalls, Manuel D. Rossetti, Jeffrey S. Smith, and Brett A. Peters, 1318-1325.

Chung, Christopher A. 2004. *Simulation Modeling Handbook: A Practical Approach*. Boca Raton, Florida: CRC Press LLC.

Harrell, Charles R. and Rochelle N. Price. 2003. Simulation Modeling Using ProModel Technology. In *Proceedings of the 2003 Winter Simulation Conference*, Volume 1, eds. Stephen E. Chick, Paul J. Sánchez, David Ferrin, and Douglas J. Morrice, 175-181.

Or, İlhan, Birnur Özbaş, and Tuba Yilmaz. 2007. Simulation of Maritime Transit Traffic in the İstanbul Strait – II: Incorporating the Traffic Regime, Arrival Processes, Meteorological Conditions. In *Proceedings of the 21st European Conference on Modelling and Simulation*, eds. Ivan Zelinka, Zuzana Oplatková, and Allesandra Orsoni, 584-553.

Patlins, Pavels. 2008. Local Deliveries Time Optimization for Cities with Unstable Traffic. In *Proceedings of the 22nd European Conference on Modelling and Simulation*, eds. Loucas S. Louca, Yiorgos Chrysanthou, Zuzana Oplatková, and Khalid Al-Begain, 399-402.

Seila, Andrew F., Vlatko Ceric, and Pandu Tadikamalla. 2003. *Applied Simulation Modeling*. Belmont, California: Thomson Learning, Incorporated.

AUTHOR BIOGRAPHIES

BAI ZOU is a graduate student in Industrial and Operations Engineering at University of Michigan, Ann Arbor. She was graduated with a B.S. degree from Southeast University, China. She is interested in supply chain management. Her email address is zoubai@umich.edu.

XIAOFAN HU is a graduate student in Industrial and Operations Engineering at University of Michigan, Ann Arbor. He received his B.S degree from Chongqing University. He is interested in production, logistic and quality areas. His email address is xfhu@umich.edu.

JU XIONG is a graduate student in Industrial and Operations Engineering at University of Michigan, Ann Arbor. He was graduated with a B.S degree from Iowa State University. He is interested in operations research. His email address is juxiong@umich.edu.

MINGDI YOU is a graduate student in Industrial and Operations Engineering at the University of Michigan, Ann Arbor. He graduated with B.S. degree from Southeast University, China. He is interested in mathematical modeling. His email address is mingdyou@umich.edu.

EDWARD J. WILLIAMS holds bachelor's and master's degrees in mathematics (Michigan State University, 1967; University of Wisconsin, 1968). From 1969 to 1971, he did statistical programming and analysis of biomedical data at Walter Reed Army Hospital, Washington, D.C. He joined Ford Motor Company in 1972, where he worked until retirement in December 2001 as a computer software analyst supporting statistical and simulation software. After retirement from Ford, he joined PMC, Dearborn, Michigan, as a senior simulation analyst. Also, since 1980, he has taught classes at the University of Michigan, including both undergraduate and graduate simulation classes using GPSS/H™, SLAM II™, SIMAN™, ProModel®, SIMUL8®, or Arena®. He is a member of the Institute of Industrial Engineers [IIE], the Society for Computer Simulation International [SCS], and the Michigan Simulation Users Group [MSUG]. He serves on the editorial board of the International Journal of Industrial Engineering – Applications and Practice. During the last several years, he has given invited plenary addresses on simulation and statistics at conferences in Monterrey, México; İstanbul, Turkey; Genova, Italy; Rīga, Latvia; and Jyväskylä, Finland. He served as a co-editor of Proceedings of the International Workshop on Harbour, Maritime and Multimodal Logistics Modelling & Simulation 2003, a conference held in Rīga, Latvia. Likewise, he served the Summer Computer Simulation Conferences of 2004, 2005, and 2006 as Proceedings co-editor. He was the Simulation Applications track co-ordinator for the 2011 Winter Simulation Conference. His email address is williame@umd.umich.edu.

SIMULATING DYNAMIC DEPENDENCIES AND BLOCKAGES IN IN-PLANT MILK-RUN TRAFFIC SYSTEMS

Tobias Staab, Eva Klenk and Willibald A. Günthner
Lehrstuhl für Fördertechnik Materialfluss Logistik
Technische Universität München
85748 Garching bei München, Germany
E-mail: staab@fml.mw.tum.de, klenk@fml.mw.tum.de, guenthner@fml.mw.tum.de

KEYWORDS
In-plant milk-run; discrete-event simulation; blockages; in-plant road systems.

ABSTRACT

To provide efficient and flexible material transport, in-plant milk-run systems are used by many companies. However, the large number of influencing factors makes in-plant milk-run systems complex, while dependencies and blockages, e.g. overtaking or stopping, require a dynamic approach to examination. Thus we developed a generic simulation model focusing on traffic situations in in-plant road systems, and defined meaningful performance figures, e.g. capacity efficiency and cycle time. The application to a system of industrial practice enabled us to derive recommendations for planning in-plant milk-run systems. Space for overtaking, the number of trains passing or supplying a stop as well as the directions a stop is approached from were found to be main influencing factors.

MOTIVATION

In-plant milk-runs are a transport concept used for in-plant material supply from a storage zone to production, especially in the automotive industry. Since they are supposed to be efficient, safe, "lean" and flexible, especially for small batch sizes, many companies are working on implementing, re-engineering or standardizing their milk-run systems at present (Dreher et al. 2009).

In-plant milk-run systems supply different points of use with a variety of goods in one run (Takeda 1996). Typically, the milk-run "trains" use fixed routes. In some cases, they are operating on a fixed schedule. The system therefore is comparable to a bus system in public transportation. Depending on the size of the system, several milk-run trains may be operating from the same material source. Most often, milk-runs are tugger trains consisting of a tugger and three to five trailers. A typical milk-run tour consists of loading requested units of material onto trailers at a material source, travelling to the production area, stopping at different points, providing material, picking up empty load units and unloading all empty load units at the end of each tour (cf. Figure 1).

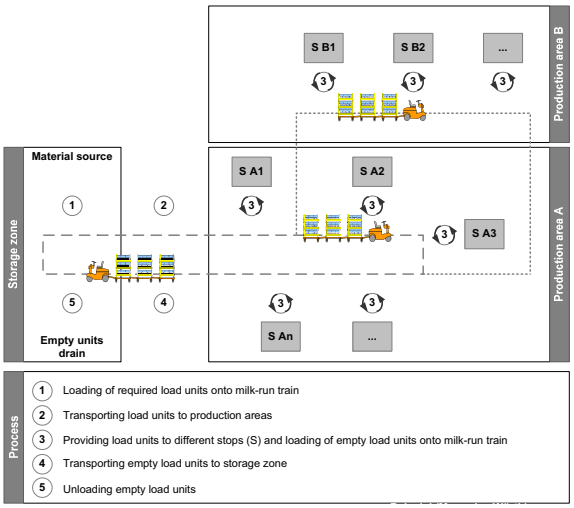

Figure 1: Typical Milk-Run Process

Milk-run systems are complex and dynamic. Several types of materials and types of load units are provided with a number of trains on a number of routes to various points of use. Usually, the number of load units required varies over time and is uncertain or known only a short time in advance. Moreover, in most milk-run systems driveways and resources, e.g. loading stations are used by more than one train. This may result in dependencies and blockages between individual trains, e.g. caused by overtaking or stopping vehicles.

As milk-runs are most often used in just-in-time systems with provision of small lot sizes in high frequency and low buffers of inventory at the points of use, a reliable and stable process is critical for success (Klug 2012). Defects in the process, e.g. late delivery or delivery to the wrong point of use may directly result in a production standstill and therefore high excess cost. Planners are challenged with the task of designing a milk-run system where a defined service level of provision is ensured and high efficiency (high capacity and time utilization) is achieved at the same time.

"Statically" dimensioning a milk-run system, i.e. deciding on which points of use are to be combined into one route and in which order is already a "hard" problem, as the underlying problem is similar to a vehicle routing problem with some added characteristics (Toth and Vigo 2002). The dynamic effects, uncertainties and blockages described above still cannot

Proceedings 27th European Conference on Modelling and Simulation ©ECMS Webjørn Rekdalsbakken, Robin T. Bye, Houxiang Zhang (Editors)
ISBN: 978-0-9564944-6-7 / ISBN: 978-0-9564944-7-4 (CD)

be modelled adequately with such an approach, but may cause significant problems when operating a milk-run system.

Simulation models can be used to examine dynamic systems on a high level of detail (Schenk et al. 2008). Therefore, the paper on hand presents an event-discrete simulation model to model and analyze generic milk-run systems in a planning phase. Comparable models at present sporadically exist in some companies, but are specific to their individual projects and processes and unavailable to the public.

Our model focuses in detail on modelling the physical handling steps performed in typical milk-run systems (e.g. loading, travel, provision) and simulation of the resulting traffic and supply situation for any set of routes and various types of material requisition. The first requirement is a simple and adaptive structure. This enables planners to examine and compare various milk-run systems and to model and analyse different sets of routes quickly and simply. Secondly, all important dependencies between trains are to be modelled. Thus, possible bottlenecks and problems can be identified and solved in advance and better solutions found, e.g. by varying the routes. As a third requirement, requisition notes have to be simulated adequately as the reaction of the system to deviations of material requisition is to be considered. Furthermore, we aim to derive some universal recommendations for designing milk-run systems from our experiments with the model.

METHOD

Based on an analysis of physical handling steps of typical milk-run tours and of the requirements, we will identify relevant elements the reviewed systems consist of and focus on the non-specific elements. Afterwards, we will present the elements, their behaviour and interfaces we designed to establish a modular structure. As a result of the requirements as well as of the system behaviour we will define meaningful performance figures. We will apply the verified and validated simulation model to an example from industrial practice. Finally, we will derive recommendations to improve planning based on experiments using four scenarios.

ELEMENTS AND MODEL STRUCTURE

The increasing use of in-plant milk-run systems for production supply and the lack of established standardized concepts (Günthner et al. 2012) lead as a direct result to the application of various individual systems with their specific structure. Nevertheless, our simulation model shall likewise be applicable as generally as possible and with as few modifications as possible. For this reason, we chose a modular structure for our model. An analysis of existent milk-run systems shows that many elements appear in all milk-run systems and with little variation (Klenk et al. 2012):

- points of use
- stops
- driveways
- turns
- crossroads
- tuggers
- trailers
- load units

Hence, these objects are defined as object classes. These classes are modular and can be adapted with low effort to the respective system by a set of properties. They are sufficient to simulate a generic in-plant road system.

Some elements however, e.g. the loading areas of storages and the removal area for empties are system-specific, since they are influenced by a number of various factors, e.g. the type of trailers used, the size of load units and the space available. These elements must be modelled individually, but can be linked to the system using pre-defined interfaces. To permit an application to various systems, the interfaces between the elements of the road system mentioned above and the individual elements are reduced to a minimum.

Besides, the flow of information is also system-specific, depending on factors such as the available IT-infrastructure and the control system. Thus, the material booking is the only interface between the supply of load units and the stock management which is creating transfer orders.

As in-plant milk-run systems significantly differ from other transport concepts concerning the usage of the road system because of dependencies between trains, we will focus on modelling the traffic and road system. Thus, general applicability of the simulation model is ensured (cf. Figure 2).

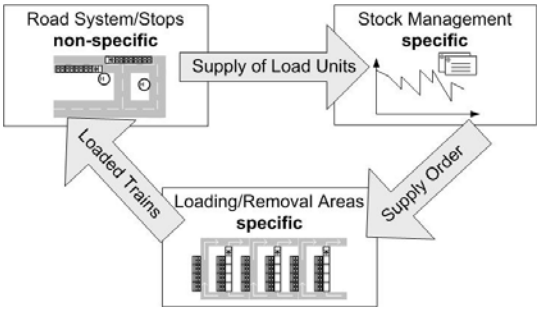

Figure 2: Elements and Interfaces in an In-Plant Milk-Run System

MODELLING INTERDEPENDENCIES AND BLOCKAGES

Compared to production supply with autonomous participants, i.e. forklifts, the milk-run systems reviewed are liable to a fixed routing often combined with a fixed schedule. Each vehicle follows its determined route and never deviates from it, not even as a reaction to events like blockages on driveways. Based on this condition, the system cannot react to critical states, which makes

the dependencies between vehicles an object of central interest.

First of all, a control mechanism has to be installed at crossroads to regulate the right of way as well as the correct turn-off. As a restriction caused by the limited space in crossroads in reality, the maximum amount of simultaneously turning vehicles is set to two. Additionally, in case of more than two vehicles or incompatible turnings (crossing routes), waiting vehicles are given the right of way afterwards following the first-come-first-served rule.

The process of supplying transported material is the most time-consuming physical handling step and therefore liable to cause holdups or blockages. It is thus modelled in detail as any stopping vehicle forces potential successors to either wait or overtake, depending on the available space and whether the successor itself carries along material for the same stop. Steps included are the paths of the driver between tugger, trailer and hand-over places as well as the handling of load units. These steps are repeated for every load unit that is to be supplied. In addition, the simulation model also takes into account the lane the hand-over place is located on and the stopping position of the vehicle. As a result there are three different ways for the driver to reach the hand-over place (cf. Figure 3). The distances that are to be covered per load unit vary between five and eleven times the length of a trailer, not accounting for the breadth of the driveway. This variety of the distance and thus the resulting supplying time make it clear why this process is not simply estimated but calculated in detail: load peaks of the whole system shall not be levelled out by using mean values but shall be measured precisely. To reach this level of detail, all steps are modelled using Methods Time Measurement (MTM).

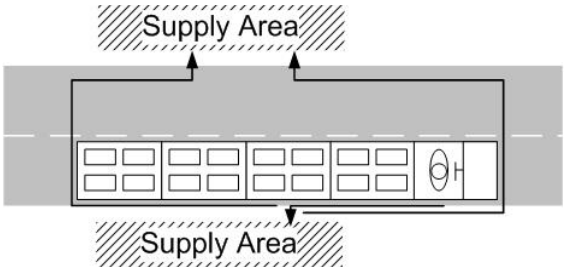

Figure 3: Ways for the driver to reach the Supply Area

In case of two-lane driveways, slow or stopping vehicles will be overtaken by faster successors in reality. Modelling this process with a temporary blockade of the opposite lane is challenging because of the fact that real-life drivers act prospectively and communicate. Thus any failed overtaking can be reacted to by arrangement and adapted behaviour, e.g. slowing down of one of the participants. On the contrary, during the discrete-event simulation there is no possibility of "stepping back" in case of an unexpected situation that leads to a failed overtaking. As a result, at the beginning of a possible overtaking a failure must be excluded by a forecast of the system behaviour in the affected part of the road system. During overtaking the successor changes to the opposite lane and continues until he has overtaken the slower vehicle. When changing the lane again a safe distance both in front and behind is kept. A number of influencing factors are to be considered when forecasting the system behaviour (cf. Figure 4). As a result either another attempt at overtaking may be necessary after a certain time or the process may be aborted completely and lead to waiting. For example, oncoming traffic could continue and allow overtaking after a few seconds, whereas a stop that is to be supplied by the following train forces it to wait. If none of the influencing factors is detected at the beginning, overtaking can happen. Meanwhile any new oncoming traffic is stopped to avoid a collision and failure of the whole process.

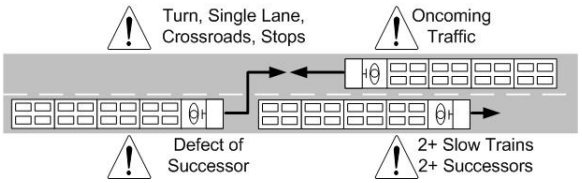

Figure 4: Factors influencing Overtaking

For a better approximation of the real system, the influence of other disturbing factors can also be analysed. At first, some of the driveways are possibly used by other vehicles as well. As a result, the strain of the road system is likely to be increased, which is shown by the number of holdups and queue times, e.g. at crossroads. Additionally, driveways can be blocked by randomly appearing temporary obstacles, e.g. load units on lanes. Similar to stopping vehicles, obstacles also force oncoming traffic to circumnavigate if possible, identically to the overtaking process (cf. Figure 4), including the influencing factors mentioned.

Besides the crossroads control, supplying process, overtaking and disturbances, the loading in the storage zone is another source of dependencies because in general the number of loading points is lower than the number of vehicles. Thus, although the routes are phased in general, delayed tours directly affect successors because of an occupied loading point at the wrong time. On the contrary, vehicles arriving too early have to wait for their next departure in case of a schedule, preferably in a separate parking area to avoid the blockage of driveways. As these dependencies are subject to the system-specific layout and control mode they cannot be described in general terms.

As well as all kinds of dependencies the dynamic reaction of the system to a deviation of material requisition cannot easily be measured by analytic methods because of the large number of influencing factors such as the production program, the amount of pieces per load unit and the stocks in circulation. Hence, two mechanisms to create the material requisitions are provided corresponding to two levels of accuracy of the data available.

If the material requisition is known exactly in terms of time and amount of load units, original data can be used, e.g. a protocol of real Kanban orders. However, this data is seldom available if the system is not already in an advanced state of planning. Hence the second mechanism to simulate material requisitions is based on the average amount of load units per hour and creates periodic single material requisitions. As a result artificial material requisition peaks are generated by the random initial time of material requisitions of every material and the average time between two material requisitions. Both mechanisms can be combined for every combination of material and point of use. This allows widespread application of the simulation model to systems with parts in different states of planning.

PERFORMANCE FIGURES

To examine routing, supply, a possible schedule and the strain of the road system, a set of performance figures is necessary. Based on this standardized data, further examination is allowed to gain insight into the dependencies of the system and to derive recommendations to improve planning. Thus, the following figures are attained per route:

- As the timely supply of material is a central aim of logistics, the service level of a route is measured based on a default replenishment time and defined as the ratio of load units supplied in time and the number of load units transported in total.
- The capacity efficiency per tour measures the share of capacity occupied by load units. As the simulation model does not distinguish between differently sized load units, a larger capacity efficiency directly leads to more supply activities. On the contrary, if the size was considered, the replacement of a small load unit with a larger one would increase the capacity efficiency without changing the number of supply activities.
- Additionally, absolute delays in supply are measured for further clustering and analysis. Both the number and duration are important as a large number of low delays possibly does not affect the stability of production supply in the same way a few high delays could do.
- As soon as the stock at a stop reaches zero, the simulation aborts because of insufficient supply and logs the material and affected stop.
- To monitor the schedule, the effective time of departure is measured and compared to the reference value.
- The cycle time is defined as the time between the start of every tour and the arrival back at the loading area. It contains the constant time (per route) needed for travel as well as a variable part mainly consisting of supplying and waiting.
- As a direct result the temporal efficiency per cycle can be defined as the cycle time in reference to the scheduled cycle time.
- For every milk-run the total times of all activities such as driving, supplying, waiting, removal of empty load units and overtaking are measured separately for further analysis.
- Depending on the characteristics of the system-specific elements (cf. Figure 2) more performance figures can be necessary to rate the system, e.g. a protocol of the activities of a substitute train or the efficiency of a stowing forklift.

The strain of the road system can be rated by the following performance figures attained for every section of driveways:

- As waiting affects the traffic flow by holdups and resulting delays, the total number of waiting vehicles over time is counted on every driveway.
- In addition, overtaking and circumnavigation of obstacles as sources of waiting concerning oncoming traffic are counted over time per section.

APPLICATION TO INDUSTRIAL PRACTICE

After verification and validation of the simulation model, it was applied to an in-plant milk-run system designed for a plant of Brose CZ spol. s r.o. Simultaneous with planning, the current state was modelled. The system includes 3 production lines with a material need of over 300 load units per hour and a road system with more than 1.200 m of driveways and 20 crossroads over an area of 35.000 m².

To enable experiments, system-specific elements had to be added:

- As there are two types of milk-run systems to be analysed simultaneously, resulting from separated storages for small loads carriers (SLC) and large carriers (LC), there are two different loading processes:
  The loading of SLC is based on an automated “drive-through” concept with flow rack trailers (Dewitz et al. 2012). Each train is assigned to a certain route. When a train arrives at the SLC storage, it is assigned to one of four available loading stations, where loading takes place automatically.
  The LC are stowed by a forklift onto E-frame trailers. To reduce the time needed for loading, only the tugger is assigned to a route, while empty trailers are stowed for the next tour on the next route in the meantime and are changed between routes in the storage zone.
- As the loading stations of the SLC trains are filled automatically, trains arriving too early have to wait until their load is prepared. This requires a parking area adjustable to the number of trains to avoid a blockade of driveways and to generate the correct order of trains given by the loading points.
- To compensate for delays, substitute SLC trains can be used, which also requires a parking area for waiting in the meantime.

- Both types of trains use the same empties removal area. As the set of trailers is simply changed to one cleared before, the removal of empties is decoupled from the stopping time of the train.
- The information flow follows the second of the mechanisms given above using mean intervals between two material requisitions.

A simple heuristic was used for route-building: the material requisitions of machines and workplaces were consolidated to blocks bordered by driveways or space not belonging to the reviewed production lines. Each block constitutes the material requirement of an allocated stop. These stops are assigned to routes such that adjacent stops are on the same route and the total material requisition is lower than a defined maximum number of units. Simultaneously, the strain of the road system is considered: we tried for an even strain to avoid bottlenecks by equating the number of passing trains as far as possible for every section. Concerning the given system, 6 routes for SLC and 2 routes for LC are necessary with a constant scheduled cycle time per type.

EXPERIMENTS AND RESULTS

With the elements described above, the road system as well as the system-specific areas and processes could be modelled to an adequate level of accuracy. For the following experiments four scenarios were created to allow the analysis of the system and of influencing factors.

First, the system was parameterized not considering any disturbances to test routing and schedule and to use the resulting level of influences between the vehicles as a base for further experiments. Additionally a substitute SLC train was available to absorb delays. The total times for waiting, driving and supplying revealed the expected high influence of the supplying activities. I.e., the average share of supplying time was at about 75% for SLC. The total time for waiting was volatile over the routes. To examine this, cycle time and efficiency of a route rather unimpaired by waiting were examined (cf. Figure 5). While the capacity efficiency directly follows the material requisition, the cycle time mainly consists of the constant driving time and supplying time depending on the capacity efficiency. Thus the similarity of both graphs reveals the influence of the supplying activities.

On the other hand, a high share of waiting disturbs this similarity by adding waiting as a new relevant time component resulting from dynamic dependencies. To clarify this correlation, the ratio of the capacity efficiency and the temporal efficiency per cycle can be used as a similarity measure (cf. Equation (1)). This ratio can be interpreted as the resulting performance of the system P_{res} relative to the planned performance P_{plan}.

$$\frac{\eta_{cap}}{\eta_{temp}} = \frac{n_{supp}}{N_0}\frac{T_{sched}}{t_{cycle}} = \frac{T_{sched}}{N_0}\frac{n_{supp}}{t_{cycle}} = \frac{P_{res}}{P_{plan}} \quad (1)$$

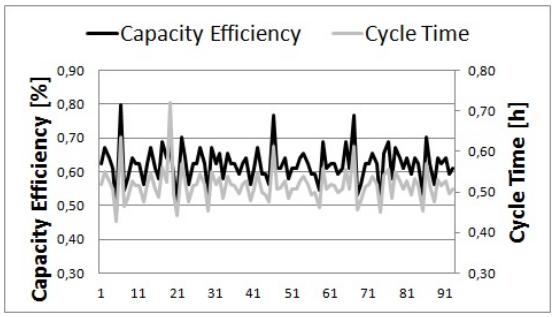

Figure 5: Similarity of Capacity Efficiency and Cycle Time

To estimate the impact of waiting, this ratio is determined for a route unimpaired by waiting (cf. Figure 6) as well as for a second one with a significantly higher share of waiting. A higher waiting time increases the variability of each graph, whereas the conformity of capacity efficiency and cycle time would cause a constant ratio (cf. Figure 6). However, the absolute value of between 0.7 and 0.9 is a matter of the planned performance P_{plan}, influenced by different system-specific parameters such as the total capacity of the trains and the length of each single route. If differently sized load units are considered, Equation (1) must be adapted, as in this case the capacity efficiency is not directly scaling with the number of supply activities.

Over all routes, the cycle time maxima as well as the share of tours with an exceeded planned cycle time reveal that the observance of the schedule varies. As a result, the substitute SLC train is activated to compensate delays on different routes. In this case, the definition of a substitute temporal efficiency as the ratio of active time and total simulation time seems to be useful. Caused by the varying observance of the schedule, the substitute temporal efficiency is between 13% and 20%. When comparing the route the substitute train had to take significantly often with the most strained sections, a clear correlation could be found.

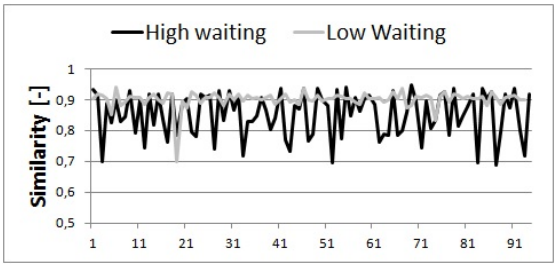

Figure 6: "Similarity" of Capacity Efficiency and Temporal Efficiency

For the second experiment, the substitute SLC train was removed to compare the expected negative effect on the system to the saving of a train and driver held on standby. The results of the first experiment indicated that the lack of a substitute train cannot be compensated if the substitute temporal efficiency is

that high. This indication was confirmed as the supply of production with the required material could not be maintained and the simulation runs aborted because the stock at a point of use reached zero. As a conclusion the substitute train can neither be saved nor is running at a sufficient level of efficiency which makes improvements necessary with focus on the mainly affected route.

The third scenario expanded the first by additional vehicles that both used parts of the road network. It is assumed that the growing number of vehicles in the system increases the strain of the road system and thereby impairs the observance of the schedule. Analogously, obstacles were added for the fourth experiment to analyse the effect of this second type of disturbance. To allow a quantitative evaluation of both experiments, again the cycle time maxima and the share of tours with exceeded planned cycle time were observed. When compared to the results of the first scenario a relation between both the adherence of the schedule and the strain of the road system could be found. Thus, the average share of tours with exceeded planned cycle time was increased significantly (cf. Figure 7).

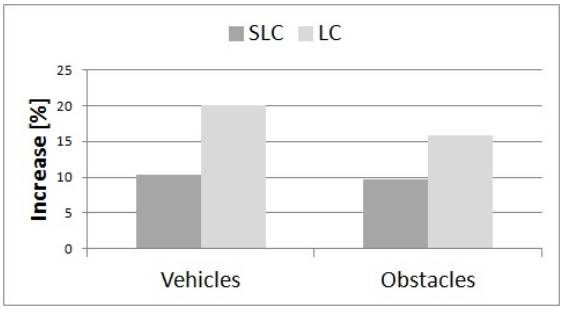

Figure 7: Increase of Exceeded Cycle Times caused by Vehicles and Obstacles

Furthermore, both scenarios confirm the most strained sections of the road system found in the first experiment. The analysis of the number of overtaking processes showed that breakdowns occur at random and do not favour special parts of the road network. At the same time the vehicles' speed diverges too little to be a main influencing factor, as in this case the required space for overtaking grows and is less likely to be available. Thus, routing is assumed to be the main effect: At all sections affected, trains stopped during supplying were overtaken by others passing through.

The driveways most strained by waiting processes could easily be related to stops that are supplied by two or more routes. As the material demand of every stop was allocated to the routes with preferably not splitting it up, the stops per route ratio is low, at the same time increasing the number of load units per stop and tour. In the worst case, if a stop is approached by two trains in the same direction, which is hard to avoid because of the existence of two types of milk-run systems, the follower has to wait for the whole supplying time of his predecessor. One way to reduce this effect would be to establish the supply by a single train, which is impossible in the reviewed system because of the different processes for SLC and LC. Furthermore the allocation of a stopping point to more routes would lower the average supply time per stop and tour and simultaneously the waiting time per follower. If the space available is sufficient for two trains and the drivers who handle load units on each trains' right side, an approach from different directions could be utilized. However, the effect would only be appropriate if there are no further trains passing through because overtaking would be aggravated at the same time. The supplying process is much faster if the driver does not have to circle the train to reach the opposite side of the driveway (cf. Figure 3). Thus, matching both the approaching direction and the side of the hand-over area is another way to lower the strain of the road network.

CONCLUSION AND OUTLOOK

Due to the complexity and size of the system, computer-aided methods such as discrete-event simulation allow the analysis of the material supply of in-plant milk-run systems. As a result of the large variety of these systems the design of certain elements of the model is subject to the specific type of the system.

Thus, the general application was solved by a modular structure of the elements necessary for modelling an in-plant road network. Certain elements, such as areas for loading and removal of empties, cannot be pictured generally. Hence, lean interfaces were designed to allow the simple integration of elements with a system-specific architecture. The information flow contained in the model described above is a Kanban system and allows both the usage of real data as well as the application of mean material requisitions to model material requisition. Like the elements of the material flow, this material requisition mechanism can easily be replaced using the described interfaces. Generic elements of milk-run systems (pathways, crossroads, trains, …) were modelled and focused on picturing all relevant dependencies between the vehicles passing the system, such as behaviour at crossroads, supplying, overtaking and disturbances.

Subsequently a model of milk-run systems that are currently realized at Brose CZ spol. s r.o. was built, containing eight routes for two types of load units with different trailers and loading processes. In a series of experiments, routes as well as the influence of disturbances were tested.

As a result, the influence of the number of load units supplied and of waiting processes could be confirmed. Since they allow the simultaneous analysis of both, capacity efficiency as well as cycle time appear to be important performance figures. Based on this, the ratio of capacity efficiency and temporal efficiency can be used as a quantitative "similarity" measure for the

effect of waiting on a particular route. This ratio can also be interpreted as the ratio of real and planned performance. In addition, the strain of the road system is revealed by the number of overtaking and waiting processes per section. One main influencing factor is trains supplying at stops.

Important recommendations concerning the planning of in-plant milk-run systems were derived from the results. If a stop is approached from both directions, additional trains passing should be avoided. Two-lane driveways and space to overtake are important to lower the number of holdups and improve the traffic flow. In general, the strain of the road network is reduced by a low number of trains passing or supplying the same stop. The number of load units per tour and stop is another main influencing parameter because it determines the supply time the trains needs at a stop.

Some additions still need to be made to the system: Overtaking and turning off at crossroads are not yet combined because of the complexity of new situations related to this, e.g. caused by the incompatibility of the directions the involved vehicles are heading for. In addition, each vehicle can at the same time only be overtaken by one successor, which causes waiting times that do not occur in reality. As the system reviewed in the paper on hand is still subject to planning, the current results are to be compared to recent data based on an advanced status.

Also, we are currently working on developing further modules for other loading concepts, to broaden the application of the model.

Additionally, further experiments will be carried out to examine the effects of one-way traffic and of splitting material requisition onto more and smaller stops.

REFERENCES

Dewitz, M.; S. Galka; W.A. Günthner. 2012. “Drive-Thru Loading Concept for In–Plant Milk Runs”. In: *Proceedings of the XX International Conference on Material Handling, Constructions and Logistics* (Belgrade, Oct.3-5). University of Belgrade Faculty of Mechanical Engineering, 237-242

Dreher, S.; A. Nürnberger; D. Kulus. 2009. “Routenoptimierung in der Produktionslogistik“. *ZWF Zeitschrift für wirtschaftlichen Fabrikbetrieb*. Vol. 104, 131-135.

Günthner, W.A.; S. Galka.; E. Klenk; T. Knössl; M. Dewitz. 2012. *Stand und Entwicklung von Routenzugsystemen für den innerbetrieblichen Materialtransport.* Lehrstuhl fml, Garching bei München.

Klenk, E.; S. Galka; and W.A. Günthner. 2012. “Analysis of parameters influencing in-plant milk-run design for production supply”. In: *Proceedings of the International Material Handling Research Colloquium* (Gardanne, France, Jun. 25-28).

Klug, F. 2010. *Logistikmanagement in der Automobilindustrie*. Springer, Berlin

Schenk, M.; J. Tolujew; T. Reggelin. 2008. “A Mesoscopic Approach to Modeling and Simulation of Logistics Networks”. In: *Logistics and Supply Chain Management: Trends in Germany and Russia* (Moscow, May21-25). Publishing House of the Saint Petersburg State Polytechnical University, 58-67.

Takeda, H. 1996. *Das System der Mixed Production*. Verlag Moderne Industrie. Landsberg

Toth, P. and D. Vigo. 2002. *The Vehicle Routing Problem*. Society for Industrial and Applied Mathematics, Philadelphia, Pa.

AUTHOR BIOGRAPHIES

TOBIAS STAAB studied Automotive and Combustion Engine Technology at the Technische Universität München (TUM). He obtained his degree in 2012 and has worked as a research assistant at the Institute for Materials Handling, Material Flow, Logistics (fml) of TUM since 2013. Focus of his work is the simulation of supply chains.

EVA KLENK studied Industrial Engineering at the Karlsruhe Institute of Technology (KIT). Since 2009 she has worked as a research assistant at the Institute for Materials Handling, Material Flow, Logistics (fml) at the Technische Universität München (TUM). Her main field of research is lean process design for automotive supply chains. Since 2012 she is leading the research group Process Design at the Institute fml.

WILLIBALD A. GUENTHNER is professor and head of the Institute for Materials Handling, Material flow, Logistics (fml) at the Technische Universität München (TUM). He is founder member and treasurer of the Wissenschaftliche Gesellschaft für technische Logistik e.V, deputy chairman of the scientific advisory board of the Bundesvereinigung Logistik (BVL) and member of the board of directors of the Society for Production and Logistics of the Association of German Engineers (VDI-GPL).

WAREHOUSE SIMULATION THROUGH MODEL CONFIGURATION

Jacques Verriet, Roelof Hamberg
TNO-ESI
P.O. Box 513
5600 MB Eindhoven
jacques.verriet@esi.nl
roelof.hamberg@esi.nl

Jurjen Caarls
Dimenco
De Run 4281
5503 LM Veldhoven
jurjen@dimenco.eu

Bruno van Wijngaarden
Vanderlande Industries
Vanderlandelaan 2
5466 RB Veghel
bruno.van.wijngaarden@vanderlande.com

KEYWORDS

Warehouse systems, simulation, configurable models, sensitivity analysis, design-space exploration.

ABSTRACT

The pre-build development of warehouse systems leads from a specific customer request to a specific customer quotation. This involves a process of configuring a warehouse system using a sequence of steps that contain increasingly more details. Simulation is a helpful tool in analyzing warehouse design alternatives, but setting up a detailed simulation is too expensive early in the development process. We show that configurable simulation models can be applied early in the development process with a good cost/benefit ratio. We present a warehouse simulation model that can be configured with customer and topology information and decision algorithms. We show that the simulation results are similar to those of detailed simulations while a warehouse simulation can be configured with little effort and the simulations run fast enough to support sensitivity analysis and design-space exploration.

1 INTRODUCTION

The development of complex systems requires frequent comparisons of different architecture, design, and realization options. Many decisions have to be made, often without having all relevant information at hand. Moreover, the decisions with the highest impact have to be taken at the moment when the degree of uncertainty is also highest.

Warehouses are logistic systems that are characterized by a complex interaction between many different cooperating components. The properties of a warehouse under development are hard to predict from its components. Especially when new components or new methods of operation are involved, assumptions and reasoning are required to make accurate predictions. Moreover, the available effort to estimate any arbitrary system property is very limited.

Simulation is a common way to evaluate a warehouse's performance. Developing a simulation of a warehouse may be very time-consuming. The main reason for this is that the detailed warehouse layout is taken as a starting point for the construction of a simulation model. As an easily configurable alternative we propose the use of highly abstract building blocks to construct a warehouse simulation model, which still takes the transport configuration and main performance parameters into account.

1.1 Related Work

Simulation is commonly used for warehouse performance evaluation. Colored Petri nets have been used to simulate Automated Storage and Retrieval Systems (AS/RS) (Dotoli and Fanti. 2005; Hsieh et al. 1998). Potrč et al. present an AutoMod AS/RS simulation (Potrč et al. 2004). Gibson and Sharp (Gibson and Sharp. 1992) and Petersen (Petersen. 2000) consider simulation of a complete warehouse. They compare different batching and order-picking strategies for specific warehouse topologies. Gagliardi et al. simulate a specific high-volume warehouse (Gagliardi et al. 2007). These simulation results are typically specific for the modeled system although the modeling approach can be reused for other systems.

The simulation by Andriansyah et al. is not limited to a single warehouse (Andriansyah et al. 2011). They present a layered warehouse simulation model built from reusable components. Their approach allows them to vary the number of storage aisles and workstations in a miniload-workstation order-picking system. Although they can handle more than one warehouse, they can only handle one type of warehouse topology.

Brito presents an integrated tool to configure detailed warehouse simulations from CAD drawings and other warehouse information (Brito. 1992). This tool allows a warehouse designer to set up a detailed simulation without any programming, unless the simulation involves specific control rules.

Gu et al. provide an extensive overview of warehouse performance analysis models (Gu et al. 2010). Their overview includes many analytic and simulation models. They claim that simulation models are typically used for evaluating one design alternative, but that they are less suited for design-space exploration.

1.2 Outline

In this paper, we will address the observation made by Gu et al. (Gu et al. 2010) by introducing a warehouse

Proceedings 27th European Conference on Modelling and Simulation ©ECMS Webjørn Rekdalsbakken, Robin T. Bye, Houxiang Zhang (Editors)
ISBN: 978-0-9564944-6-7 / ISBN: 978-0-9564944-7-4 (CD)

simulation concept that can be applied in the early phases of warehouse development. This is achieved by having a highly configurable simulator that can be set up quickly, is sufficiently accurate, and has short simulation times. Our concept is similar to Brito's (Brito. 1992), but requires less information to set up and allows simpler usage of specific control rules. This means our simulation concept can be applied in the early phases of warehouse development.

The paper is organized as follows. Sections 2 and 3 describe the simulation concept with its configuration parameters and the corresponding visualization. Sections 4, 5, and 6 demonstrate the simulator on an existing retail warehouse; they explain how the simulator can be configured for the existing warehouse and compare the configured simulator to a detailed simulation performed by Vanderlande Industries. The paper ends with a reflection on the results.

2 SIMULATOR CONCEPT

A warehouse is a facility that provides temporary storage for many different products (stock keeping units, SKUs) on many physically different locations. The purpose of a warehouse is to fulfill customer orders. Fulfilling an order involves collecting a specific set of stored products and shipping them to the customer. In a typical warehouse many customer orders are handled simultaneously.

One can distinguish two main warehouse principles: man-to-goods and goods-to-man. In a *man-to-goods* warehouse, order pickers travel along a warehouse's storage locations to retrieve the products required for a customer order and putting them in an order bin, called *tote*. After the retrieval of the necessary products, the order picker travels to a consolidation workstation where the tote is dropped off and combined with other totes for the same order. Subsequently, the order picker starts working on the next tote. Note that the order picker can be human, a conveyor system, robots, or a combination of transportation means.

The other main warehouse principle is called *goods-to-man*. In a goods-to-man warehouse, the role of products and orders are interchanged: totes containing products travel towards order pickers in picking workstations where all order collecting is performed.

Our flexible warehouse simulation concept is based on the man-to-goods principle. The simulator mimics the man-to-goods principle using two types of (autonomous) entities: *totes* and *segments*. A warehouse is represented by a collection of segments that form the warehouse's transportation system. Segments are directed arcs along which the totes can travel. Each segment consists of a discrete number of sequential locations, which a tote has to visit to fulfill an order. The tote's movements are synchronized with the segment locations: in each time step, a tote can move exactly one location, i.e. from the current location on its route to the next. This means that the desired travel times are obtained by specifying the appropriate segment lengths.

Totes represent order pickers travelling to storage locations to fulfill customer orders. At several locations in the network, a tote has to stop to perform operations, such as picking a stored item or dropping off picked products at consolidation. These operations are modeled as delays for the totes.

Although our simulation concept is based on the man-to-goods principle, it can also be applied to capture a goods-to-man warehousing process. This is achieved by interchanging the role of storage and picking locations.

Our simulation concept consists of a number of configurable steps divided over two main phases: *configuration* and *simulation*. The phases and the steps are visualized in the state machine in Figure 1: the configuration steps are shown on the left; the simulation steps on the right.

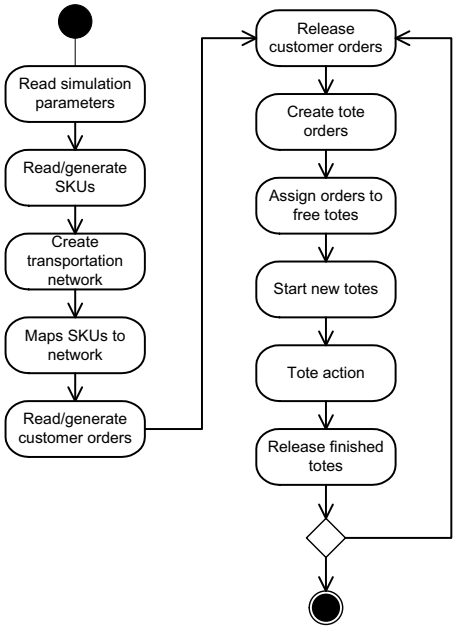

Figure 1: Simulation Concept

2.1 Simulation Configuration

The configuration phase provides the flexibility of our simulation concept. It consists of five steps: (1) reading a parameter file; (2) reading or generating stock keeping units (SKUs); (3) creating a transportation network; (4) allocating SKUs to the network; and (5) reading or generating customer orders. Each of these steps is explained in more detail.

The configuration phase starts by reading a parameter file. This parameter file contains settings for all subsequent steps. For instance, it specifies the files to be read in the following configuration steps. However, it also specifies the number totes in the system and the maximum volume and weight of the totes.

The second configuration step involves either reading a SKU file or generating a collection of SKUs. The SKUs

describe the products stored in the warehouse. This is specified in the parameter file: it specifies either the SKU file to be read or distributions for the dimensions, weights, and expected sales of the SKUs.

The third step involves the creation of a transportation network. There are two ways in which a transportation network can be created. One is a layout file: the parameter file read in the first step includes a layout file to be read. A layout file consists of a list of segments. Each segment is described by a number of parameters. These include the 3D coordinates of its start and end point; its *length*, i.e. the number of locations; its *storage capacity*, i.e. the number of SKUs that can be stored per location; its *width*, i.e. the number of totes that can be at one location at the same time; its *operation type*, i.e. the type of operation performed at the segment (e.g. input, output, picking); and a distribution of the *operation times*, i.e. the time needed for these operations. From the collection of segments, a transportation network is created. If the end location of a segment is adjacent to the start location of another, then they are connected in the transportation network.

The second way to create a transportation network involves a number of pre-defined templates, which facilitates the generation of the transport network. The layout does not have to be created by hand, but rather is generated on the basis of some template-specific parameters, like dimensions and capacities. These parameters are included in the parameter file.

The fourth configuration step takes the collection of SKUs and allocates them to the network segments with a positive storage capacity. This allocation may involve SKUs to be allocated to more than one storage location. By spreading fast-moving products, the picking load can be divided over the warehouse.

The fifth and last configuration step involves reading a customer order file or generating a collection of customer orders depending on what was specified in the parameter file. If an order file is generated, then the expected sales of the SKUs are taken into account as well as an order size distribution.

2.2 Simulation Steps

Our simulator is a time-triggered simulation which repeats the six simulation steps in Figure 1. Each time starts by (1) releasing customer orders and (2) creating tote orders for each of the released customer orders. The creation of tote orders considers the maximum volume and weight of a tote and the SKU storage locations.

The simulation continues by (3) assigning open tote orders to idle totes and computing the corresponding routes for the totes to follow, and (4) introducing the totes into the system.

The most important step of the simulation involves (5) the operation of the totes. If a tote has to perform an operation, then it waits at its current location until the operation's time has passed. Otherwise, it will negotiate with the next location on its route. This involves claiming the network location by a tote. After all totes have made their claims, each network location grants some of the totes' claims. Finally, the totes with granted claims move to the next network location.

The last simulation step involves (6) releasing the totes that have finished their tote order route. These six steps are repeated until all orders have been fulfilled.

2.3 Behavioral Parameters

In the first step of the simulation configuration, a parameter file is read. This parameter file includes two types of parameters: structural and behavioral parameters. The structural parameters include the number of totes and their properties, the SKU and order files, and the distributions for the generation of SKUs and customer orders.

Many of the simulation steps (see Figure 1) involve the assignment of scarce resources. For instance, SKUs are allocated to storage locations, customer orders are assigned to idle totes, and totes compete for network locations on their routes. Decision algorithms handle the assignment of these scarce resources. For each type of decision algorithm, a generic Java interface has been defined. For each of these interfaces, there is a library of Java classes that implement the interface and provide a decision algorithm.

The classes in these libraries can be selected and instantiated at run time. These behavioral parameters are read from the simulator's parameter file. Using Java's introspection, the corresponding classes get instantiated for usage during simulation. A similar approach has been applied by Verriet and van Wijngaarden (Verriet and van Wijngaarden. 2012) for their reference architecture for warehouse control.

The Java interfaces allow easy inclusion of system-specific functionality. If a behavior library does not contain the necessary functionality, then one can create a new Java class that implements the corresponding interface, add it to the library, and specify its usage in the simulation's parameter file.

3 VISUALIZATION

Besides the simulator described in the previous section, we have also developed a 3D visualization that allows the warehouse designer to validate a warehouse design visually, the warehouse behavior in particular. The visualization is a C++ application using OpenSceneGraph. The simulator and the visualization application communicate by sending messages to the visualization over a UDP interface.

Figure 2 shows an example of the simulation's visualization. It shows a Zone Picking System (ZPS). ZPS is a man-to-goods warehouse concept where storage is organized in zones. To fulfill orders, totes visit a number of zones where operators take items from the zones' local storage and put them in the totes.

ZPS is one of the pre-defined templates of our simulator; the system in Figure 2 was created by

specifying the number of aisles, the number of zones per aisle, the zones' buffer lengths, and several other ZPS-specific parameters.

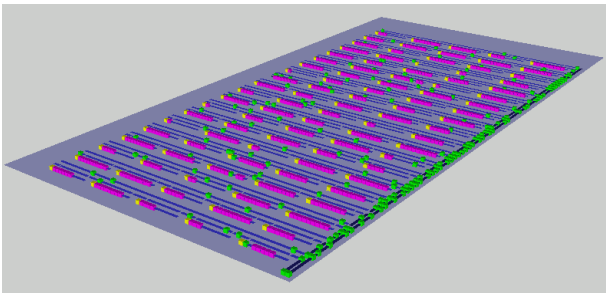

Figure 2: Zone Picking System (ZPS) simulation

4 COMPACT PICKING SYSTEM

In this section, we will demonstrate the application of our simulation concept to an existing retail warehouse. Figure 3 shows a schematic of this warehouse. It is a so-called Compact Picking System (CPS). The system consists of three main components: five *miniload* storage aisles, a main *conveyor loop*, and three picking *workstations*.

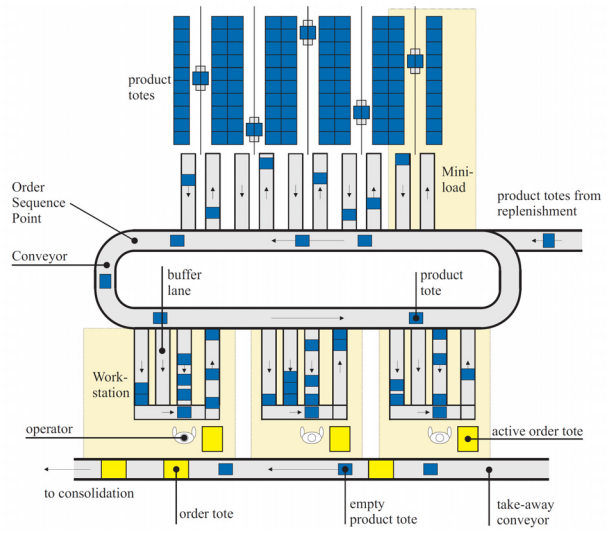

Figure 3: Compact Picking System (CPS)

4.1 Miniloads

The top of Figure 3 shows the five miniloads. Each miniload consists of a storage rack with totes and a crane that can store and retrieve totes. The cranes in Figure 3 can handle up to four totes simultaneously. The outer miniloads have a dual function in the warehouse: they have to supply not only to the CPS workstations, but also to six ZPS workstations (not shown in Figure 3). This effectively means that the retrieval capacity of the outside miniloads is smaller than that of the other three miniloads.

At the start of each retrieval cycle, a miniload determines which totes it will retrieve. This selection is based on the age of the corresponding customer orders and the number of totes underway to the different workstations. The miniload will select the oldest four totes for retrieval, unless the corresponding orders are too young. Each workstation has *pipeline* capacity, i.e. the maximum number of totes underway to the workstation. This pipeline is used to avoid that a workstation runs idle or its input buffers overflow. If a workstation's pipeline is full, then a miniload will not retrieve a tote for that workstation. Moreover, part of a workstation's pipeline is reserved for the oldest order for the workstation. Totes for younger customer orders will not be selected for retrieval if the non-reserved pipeline is full. This means that a miniload may retrieve fewer than four totes per retrieval cycle.

4.2 Central Conveyor

After totes have been retrieved from a miniload, they travel via the central conveyor to a picking workstation. The central conveyor is shown in the middle of Figure 3. This conveyor loop has a sequencing point that is used for releasing customer orders. In the CPS warehouse, totes for at most nine customer orders are retrieved simultaneously. If the last tote of a customer order has passed the sequencing point, then totes of younger customer orders cannot overtake it any more. At that moment, a new customer order is released for retrieval by the miniloads.

4.3 Picking Workstations

Via the central conveyor, totes travel to a picking workstation. There are three such workstations and they are shown at the bottom of Figure 3. At a picking workstation, a human operator takes items from the tote. After this operation, the tote returns to a miniload.

Each workstation is working on one customer order simultaneously; this is the oldest customer order assigned to the workstation. Its three input buffers allow totes of different customer orders to be buffered simultaneously while ensuring that the totes of the oldest customer order are handled consecutively. At any time, totes for three different customer orders can be underway to a workstation. After all totes of one of these three customer orders have passed the central conveyor's sequencing point, then a new order for the workstation can be started.

The CPS warehouse has three picking workstations. Two workstations are operated permanently; the third is an overflow workstation that is operated only if sufficiently many totes have been collected in its input buffer lanes. If X totes have been collected in the overflow workstation's input buffers, then an operator handles exactly X totes and then stops picking until again X totes have been collected.

The distinction between the workstations is also used when retrieving totes from the miniload. Totes for regular workstations have priority over totes for the overflow workstation. This means that a miniload will retrieve a tote for the overflow workstation only if it cannot retrieve a tote for the regular workstations.

5 CPS SIMULATION MODEL

As explained earlier, our simulation concept mimics a man-to-goods principle. The described CPS warehouse does not comply with the man-to-goods principle, but with the goods-to-man principle. To have our simulation model the goods-to-man principle, the role of storage and picking has to be reversed. In other words, in the CPS simulation model, the storage is modeled in the picking workstations and not in the miniloads.

5.1 Transportation Network

Figure 4 shows the transportation network of the simulation model. The picking workstations are shown on the left, the central conveyor loop in the middle, and the miniloads on the right. Since the totes travel over the main conveyor loop in a counter-clockwise direction, the overflow workstation is the one furthest from the miniloads.

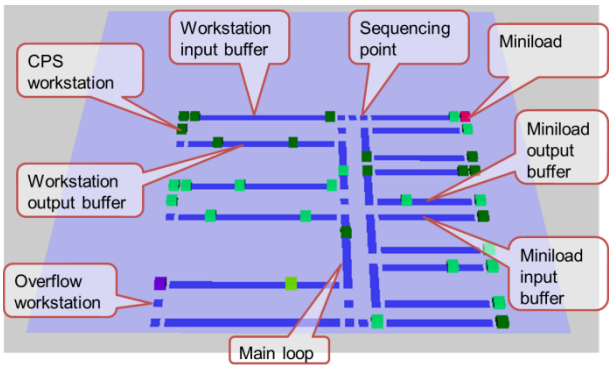

Figure 4: CPS Simulation

If one inspects Figures 3 and 4 carefully, then one can observe a few differences. The miniloads are modeled as two segments, a retrieval segment connected to a miniload output buffer and a storage segment connected to a miniload input buffer. Each tote enters the system via a miniload retrieval segment, visits one workstation (to pick one product), and leaves the system via a miniload storage segment. The miniload storage and retrieval times are modeled as operation times of the input and output segments.

Another difference in the layout involves the picking workstations. The warehouse (in Figure 3) has three input buffers per workstation. The simulation model (in Figure 4) has only one input buffer per workstation. This single input buffer has a width of three, meaning that it can hold three totes in each of its locations.

5.2 CPS-Specific Behaviors

To obtain the warehouse behavior described in the previous section, two CPS-specific behaviors have been implemented. At the end of the workstations' input buffers, there is a segment that holds the totes awaiting picking. In the simulation, these totes claim the picking location and the picking location may select one of them. To ensure that totes of one customer are handled consecutively, a specific behavior has been implemented and added to the simulator's corresponding behavior library. This behavior randomly selects a tote from the active customer order. If the active customer order has not been completed, and no tote for this order is waiting, then it will not allow any tote to go to the workstation's picking location. In other words, the picking location waits for the remaining totes of the active customer order before handling totes of younger orders.

This new behavior also takes care of the behavior of the overflow workstation: the picking location of the overflow workstation will select a tote only if X totes await picking. Then it will select totes in the same manner as the regular workstation, with the difference that it will (sequentially) select exactly X totes and then wait until X totes are waiting again.

Another specific behavior has been implemented for the selection of orders to be started. As explained in the previous section, totes for the regular workstations have priority over those for the overflow workstation. Moreover, a tote for the oldest order will be retrieved only if the corresponding workstation's pipeline is not full and totes for younger customers will be retrieved only if the non-reserved pipeline is not full. These rules have been combined in a Java class implementing the generic tote selection interface.

For the other decision algorithms, a pre-defined behavior from the simulator libraries sufficed. A movie of a running CPS simulation is available on-line (Verriet. 2012).

6 COMPARISON

The simulation model described in the previous section has been validated using real-life SKU and customer order information of the modeled retail warehouse. This information has been the input of a detailed AutoMod simulation model and our simulation model. The AutoMod model was constructed by Vanderlande Industries to validate a warehouse design; in other words, it has not been used during the early phases of warehouse development.

To compare the simulators, we have used twelve scenarios used for design validation using the AutoMod simulation. Several parameter values are varied; these include the size of the workstations' (reserved and non-reserved) pipelines, the workstations' input buffer lengths and the operators' picking times.

We have compared the scenarios using a set of orders for one peak day: 6,856 order lines divided over 156 orders. In the simulation, each order line is handled by one tote and circa 100 totes are active in the CPS system simultaneously (depending on the parameter values).

Figure 5 compares the simulated times for the different scenarios. Figure 6 provides a comparison of other performance criteria. From top to bottom, it compares the number of totes per workstation, the workstations' utilization, and the occupancy rates of the input and output buffers of the workstations and miniloads.

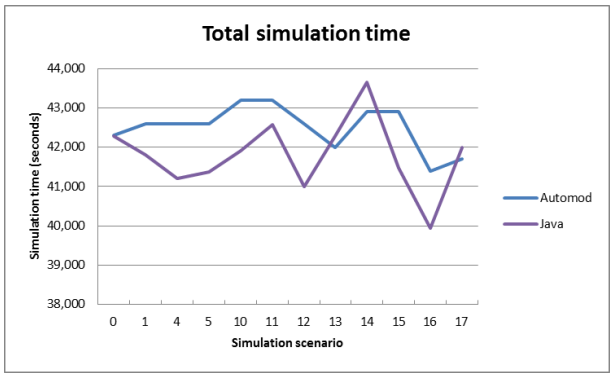

Figure 5: Comparison of Simulation Times

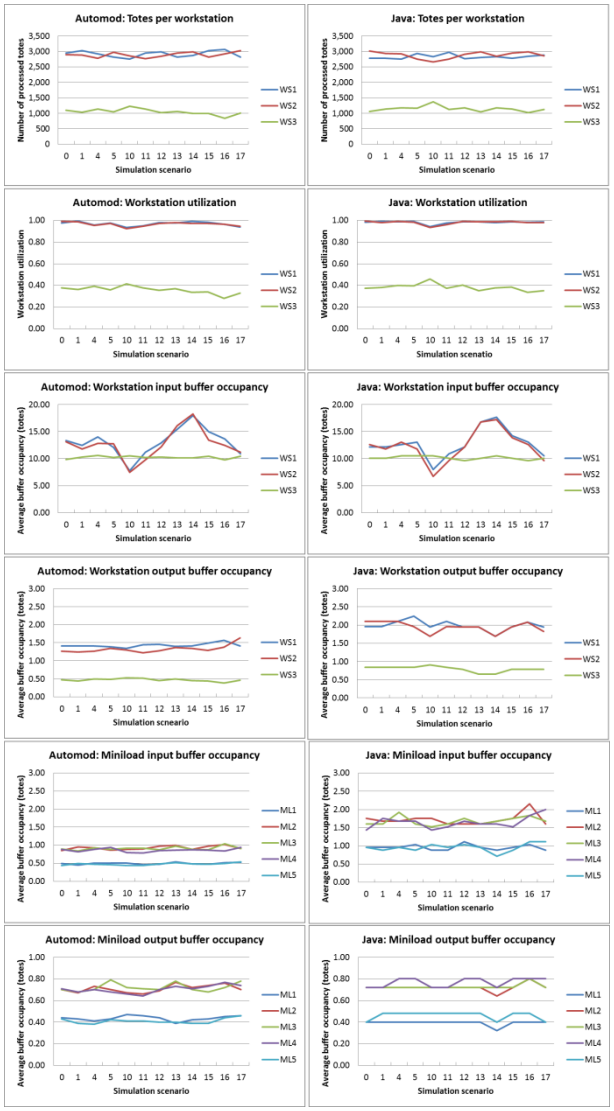

Figure 6: Simulation Comparison

The graphs in Figures 5 and 6 show that most of the performance measures of our simulation are similar to that of the detailed AutoMod simulation; most differ only a few percent. Larger differences can be seen for the occupancy of the input buffers of the miniloads and the output buffers of the workstations, i.e. the segments leading towards the central conveyor loop. These larger differences are (probably) due to the difference in claiming a window on the central conveyor loop; our Java simulator uses a simpler algorithm than the AutoMod simulation. This is due to the fact that our simulator considers the central conveyor as a collection of independent segments instead of a separate entity.

The outcome of the simulations shows a similar performance. However, there is an important difference. Our Java simulation model can be set up much quicker than the detailed AutoMod simulation. Because the transportation network of this CPS warehouse consists of only 56 segments, a first transportation network is set up within an hour. More complex transportation networks may take a few days to construct, but the corresponding visualization supports this by providing visual feedback.

The main effort in setting up the simulation involved the implementation of the warehouse-specific behaviors. Two Java classes had to be implemented in order to obtain the desired strategies for miniload retrieval and tote movement (in particular at the picking workstations). This involved dozens of lines of code, and took several hours to implement and test. Again the visual feedback provided by the visualization is very useful in obtaining the desired system behavior.

Besides the fact that setting up the simulation can be done within a few days, the simulations themselves require little time. Without visualization, the simulation of a peak day takes circa 38 seconds on a Dell Latitude E4300 laptop with an Intel P9600 processor and 4 GB of RAM running 32-bit Windows 7 SP1. This means that the simulation runs more than 1,000 times real-time, because completing the customer orders of the peak day takes about 42,000 seconds (see Figure 5).

The quick simulation setup and the small simulation times allow a warehouse designer to test a warehouse's sensitivity to specific parameter changes. The effect of changing a single (e.g. numerical) parameter can be tested within a few minutes. The fast simulations even support the exploration of a part of the design space. This has been done by Reehuis and Bäck, who have applied an evolutionary algorithm to optimize the performance of a ZPS warehouse modeled with an earlier version of our warehouse simulator (Reehuis and Bäck. 2010). Their (automated) optimization involved more than 20,000 simulation runs using different parameter settings including variations of the system layout and warehouse behaviors.

7 CONCLUSION

In this paper, we have described a warehouse simulator that can be used during the early phases of warehouse development when the most important design decisions are to be made. This is due to the configurability of our simulation concept. Its configuration parameters include SKU and order files, a warehouse network topology, and a variety of structural and behavioral parameters.

A case study of an existing retail warehouse showed that the configurable warehouse simulator provides similar results as a detailed simulation, which is

typically only used in the later stages of warehouse development.

In contrast to detailed simulations, our warehouse simulation can be set up quickly: configuring the simulator takes a few days. The corresponding visualization provides visual feedback to the warehouse designer regarding the correctness of parameter choices. Setting up simulations requires little time and the same goes for the simulations themselves. Since a simulation run typically takes less than one minute, a warehouse designer is able to perform a sensitivity analysis and even perform (automated) design-space exploration.

ACKNOWLEDGEMENTS

This work has been carried out as part of the FALCON project under the responsibility of the Embedded Systems Institute with Vanderlande Industries as the carrying industrial partner. This project is partially supported by the Netherlands Ministry of Economic Affairs under the Embedded Systems Institute (BSIK03021) program.

REFERENCES

Andriansyah, R.; W.W.H. de Koning; R.M.E. Jordan; L.F.P. Etman; J.E. Rooda. 2011. "A process algebra based simulation model of a miniload-workstation order picking system." *Computers in Industry* 62, 292-300.

Brito, A.E.S.C. 1992. "Configuring Simulation Models Using CAD Techniques: A New Approach to Warehouse Design." PhD Thesis, Cranfield Institute of Technology, Cranfield, UK.

Dotoli, M.; M.P. Fanti. 2005. "A coloured Petri net model for automated storage and retrieval systems serviced by rail-guided vehicles: A control perspective." *International Journal of Computer Integrated Manufacturing* 18, 122-136.

Gagliardi, J.P.; J. Renaud; A. Ruiz. 2007. "A simulation model to improve warehouse operations." *Proceedings of the 2007 Winter Simulation Conference* (Washington, DC, Dec. 9-12). IEEE, Piscataway, NJ, 2012-2018.

Gibson, D.R.; G.R. Sharp. 1992. "Order batching strategies." *European Journal of Operational Research* 58, 57-67.

Gu, J.; M. Goetschalckx; L.F. McGinnis. 2010. "Research on warehouse design and performance evaluation: A comprehensive review." *European Journal of Operational Research* 203, 539-549.

Hsieh, S.; J.S. Hwang; H.C. Chou, 1998. "A petri-net-based structure for AS/RS operation modelling." *International Journal of Production Research* 36, 3323-3346.

Petersen II, C.G. 2000. "An evaluation of order picking policies for mail order companies." *Production and Operations Management* 9, 319-335.

Potrč, I.; T. Lerher; J. Kramberger; M. Šraml. 2004. "Simulation model of multi-shuttle automated storage and retrieval systems." *Journal of Materials Processing Technology* 157-158, 236-244.

Reehuis, E.; T. Bäck. 2010. "Mixed-Integer Evolution Strategy Using Multiobjective Selection Applied to Warehouse Design Optimization." In *Proceedings of the 12th Annual Conference on Genetic and Evolutionary Computation* (Portland, OR, Jul. 7-11). ACM, New York, 1187-1193.

Verriet, J. 2012. Falcon Compact Picking System (CPS) simulation. http://www.youtube.com/watch?v=DcJs3ALbDDg.

Verriet, J.; B. van Wijngaarden. 2012. "A Reference Architecture Capturing Structure and Behaviour of Warehouse Control." In *Automation in Warehouse Development*, R. Hamberg and J. Verriet (Eds.). Springer, London, 17-32.

AUTHOR BIOGRAPHIES

JACQUES VERRIET received his MSc and PhD degrees in computer science from Radboud University Nijmegen and Utrecht University, respectively. In 1998 and 1999 he worked as a consultant at the Centre for Quantitative Methods in Eindhoven. He joined Siemens VDO Automotive in 2000 to work as a software engineer/researcher on car navigation. Since 2006 he works as a research fellow at the Embedded Systems Institute, which has become a department of TNO in 2013. His research areas of interest include model-driven system development and system-level control.

ROELOF HAMBERG received his MSc and PhD degrees in Physics from the Universities of Utrecht and Leiden, respectively. He joined Philips Research Laboratories in 1992 to work in the field of perceptual image quality modeling and evaluation methods. In 1998 he joined Océ-Technologies B.V. as a developer of in-product control software and digital system architect later on. Subsequently he became departmental manager, first research, later in product development. Roelof Hamberg joined ESI in 2006 as a research fellow. His research interests are easy specification, exploration, simulation, and yet formal reasoning about system behavior, and systems architecting in general.

JURJEN CAARLS received his MSc degree in Applied Physics from Delft University of Technology. His MSc thesis on 'Fast and Accurate Robot Vision' for the RoboCup robots of the Dutch Soccer Robot team Clockwork Orange won the award of the best MSc thesis of the Applied Sciences faculty in the year 2001. He received his PhD degree in 2009 from Delft University of Technology on camera pose estimation and sensor fusion for Augmented Reality; he worked on robust distributed warehouse control in the FALCON project and is currently Software and Algorithms architect at Dimenco B.V.

BRUNO VAN WIJNGAARDEN received his Master's degree in Electrical Engineering from the Eindhoven University of Technology in 1986. He has 20+ years of experience in logistics and material handling and joined Vanderlande Industries in 2000. In his current position as system architect he is responsible for system design, market analysis and requirements definition for product development.

GROUPING LOGISTICS OBJECTS FOR MESOSCOPIC MODELING AND SIMULATION OF LOGISTICS SYSTEMS

Markus Koch and Juri Tolujew
Institute of Logistics and Material Handling Systems
Otto von Guericke University Magdeburg
Universitätsplatz 2, 39106, Magdeburg, Germany
E-mail: markus.koch@ovgu.de

KEYWORDS
conceptual modeling, logistics systems, complexity, logistics objects, grouping, aggregation, clustering

ABSTRACT

The field of logistics is confronted with an increasing complexity. This mainly results from the immense amount of goods which are part of logistics systems and processes. To address that the description of logistics systems and processes is to be conducted from an object-oriented point of view by including object characteristics and their relations among each other. Therefore, in context of mesoscopic modeling and simulation, this paper presents a procedure which supports the conceptual modeling phase of the mesoscopic simulation approach in grouping and aggregation of logistics objects, i.e. goods and products, in an effective and credible way. This is considered as a method of simplification and will contribute to better model credibility and simulation efficiency as well as reducing model complexity. To demonstrate functionality and effectiveness of the proposed concept the grouping procedure is applied to a modeling and simulation task of a global supply chain.

INTRODUCTION

The field of logistics is confronted with an increasing complexity. Due to globalization production and logistics networks are becoming more international and the number of involved parties is increasing (Simchi-Levi 2008, 312). A rising variant diversity of products, a growing amount of globally sourced goods as well as an increasing availability of information due to new identification technologies contribute to that. Besides rising customer demands, decreasing length of product life cycles or increasing costs pressure, the complexity and heterogeneity of networks and supply chains mainly result from the immense amount of goods which are part of logistics systems and processes (Bretzke 2010, 1–4), (Schenk et al. 2006). This trend has an impact on the sensitivity to disturbances of supply chains, as well. According to this, tools of modeling and simulation provide suitable methods to analyze logistics systems as well as to support a fast adaptation process to changes and disturbances.

Here, the mesoscopic modeling and simulation approach is very promising due to its trade off between simulation time and accuracy as well as providing the opportunity of incorporating logical groups of objects.
To address the rising diversity among the goods, which is a driving factor for complexity, the description of logistics systems and processes is to be conducted from an object-oriented point of view by including object characteristics and their relations among each other. This comprises the application of appropriate concepts for incorporating that aspect and for grouping objects as well as defining standard processes to provide efficient solutions.

In this paper we consider logistics objects to be "physical goods such as raw materials, preliminary products, unfinished and finished goods, packages, parcels and containers or waste and discarded goods. Also, animals and even people can be logistics objects, which need special care and service" (Gudehus and Kotzab 2009, 3). But besides these physical objects also information are to be considered as logistics objects, often referred to abstract objects (Arnold et al. 2008, 3), (Schenk et al. 2007).

The objective of this paper is to present a procedure which supports the conceptual modeling phase of the mesoscopic simulation approach in grouping logistics objects in an effective and credible way. This will contribute to better model credibility and simulation efficiency as well as reducing model complexity. To demonstrate functionality and effectiveness of this grouping procedure an application example related to supply chain modeling and simulation is presented.

MESOSCOPIC MODELING AND SIMULATION OF LOGISTICS FLOW SYSTEMS

Three classes of simulation models exist, namely continuous, mesoscopic and discrete. Continuous models are based on differential equations and are most frequently applied as system dynamics models to reproduce manufacturing and logistics processes (Sterman 2000). Discrete event simulation models provide a high level of detail in modeling logistics systems, but can be very complicated and slow, i.e.

Proceedings 27th European Conference on Modelling and Simulation ©ECMS Webjørn Rekdalsbakken, Robin T. Bye, Houxiang Zhang (Editors)
ISBN: 978-0-9564944-6-7 / ISBN: 978-0-9564944-7-4 (CD)

when it comes to modeling and simulation of complex and diverse system structures or incorporating different scenarios (Banks 2010).

In order to overcome the disadvantages of these traditional simulation approaches Reggelin and Tolujew developed the mesoscopic modeling and simulation approach which will be described in this section shortly. For further reading we recommend (Reggelin 2011), (Schenk, Tolujew and Reggelin 2010), (Schenk, Tolujew and Reggelin 2009). Application examples of mesoscopic models can be found in (Reggelin et al. 2012), (Reggelin and Tolujew 2011), (Schenk, Toluev and Reggelin 2009), (Schenk, Tolujew and Reggelin 2008), (Savrasov and Tolujew 2008), (Tolujew and Alcalá 2004). The developed mesoscopic modeling and simulation approach has the following characteristics:

- Less modeling and simulation effort than in discrete event models,
- Higher level of detail than in continuous simulation models,
- Straightforward development of models.

The mesoscopic modeling and simulation approach is situated between continuous and discrete event approaches in terms of level of modeling detail and required modeling and simulation effort (see Fig. 1). It supports quick and effective execution of analyzing, planning and controlling tasks related to manufacturing and logistics networks.

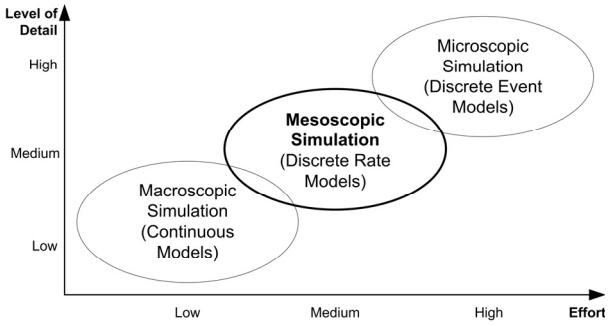

Figure 1: Classification of the Mesoscopic Simulation Approach

This mesoscopic approach is consistent with the principles of the discrete rate simulation paradigm implemented in the simulation software ExtendSim (Krahl Jan. 2009), (Damiron and Nastasi 2008). To ensure a dynamic method the mesoscopic approach monitors quantities that belong to a logical group (e.g. a batch, a delivery, etc.) instead of individual flow objects (e.g. single parts, entities, etc.). Mathematical equations are used to calculate the results as continuous quantities (piecewise constant flow rates) at certain steps of the modeling time which allows for planning events for continuous processes. This contributes to a fast modeling and simulation approach (Schenk, Tolujew and Reggelin 2010).

Even when the term mesoscopic is not explicitly applied, a mesoscopic view often already exists from the start of flow system modeling and simulation. Many practical analysis and planning problems like capacity planning, dimensioning or throughput analysis describe performance requirements, resources and performance results in an aggregated form that corresponds to a mesoscopic view (cp. Schenk, Tolujew and Reggelin 2008).

Mesoscopic models are particularly suited to the analysis of large-scale logistics networks and processes with a homogenous flow of a large number of objects. In most cases, the disproportionate amount of computation required would make item-based discrete event simulation overly complex for these applications.

Due to logistics systems and supply chains often showing a diverse and heterogeneous product or object structure respectively the opportunity to model logical groups is of significant importance to reduce modeling complexity and effort. Nevertheless, as for most descriptive modeling concepts or other simulation approaches, there is no effective support in grouping these objects to logical groups. Therefore, in the following such a procedure is presented to support the straightforward development of these kinds of models.

CONCEPTUAL MODELING PHASE

The conceptual modeling phase of a simulation study is one of the most important parts (Robinson 2008). In context that good conceptual modeling can significantly contribute to a successful outcome of a simulation study, it still is a difficult and hard-to-understand stage in the modeling process (Law 2007). Guidelines for the modeling process can be found in (Law 2007), (Pidd 1999), (Uthmann and Becker 1999).

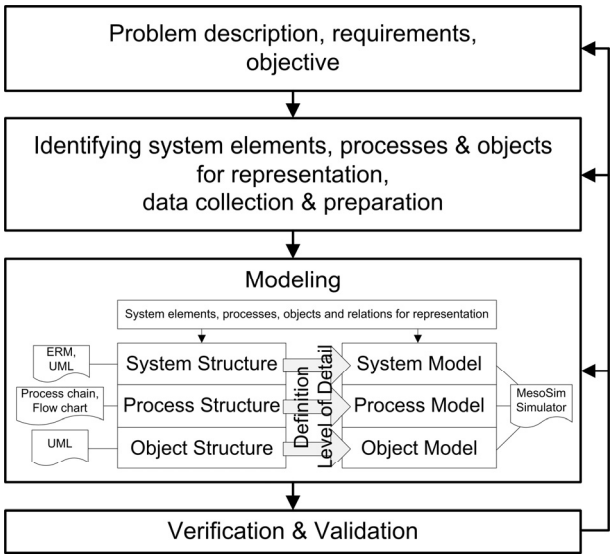

Figure 2: Steps of the Conceptual Modeling Phase for Mesoscopic Simulation

Based on existing frameworks for conceptual modeling (cp. Brooks and Tobias 1996, Pace 2000, Robinson 2004, van der Zee and van der Vorst 2005) four fundamental steps were derived for conducting the conceptual modeling phase for the mesoscopic simulation approach (see Fig. 2).

To support the process of modeling a system, process and object structure, we presented an overview and examination of traditional modeling concepts in (Koch, Tolujew and Schenk 2012) that can be applied appropriately. Another important aspect in the actual modeling step (step 3) is to determine the level of detail of the system, process and product model. As for the product model of the mesoscopic simulation approach an essential and inherent part is the grouping or aggregation of logistics objects.

But there is a lack in supporting this step of the conceptual modeling phase. However, this is of significant importance to approach the increasing complexity of logistics systems and processes efficiently. Zeigler et al. also suggest as one method of simplification for simulation modeling to group components of the model (Zeigler, Praehofer and Kim 2007).

In (Law 2009), (Brooks and Tobias 1996), (Zeigler, Praehofer and Kim 2007) guidelines for determining the level of detail of a simulation model can be found. They are also related to the aspect of simplification by grouping components and elements of the simulation model.

However, these guidelines do not provide a clear procedure in how to approach the grouping of logistics objects, i.e. products or goods.

PROCEDURE FOR GROUPING LOGISTICS OBJECTS

Therefore, to support this step of the conceptual modeling phase a procedure was developed which addresses the effective and credible grouping (aggregation) of logistics objects in context of mesoscopic modeling and simulation (see Fig. 3).

The procedure is based on grouping the considered logistics objects (i.e. products that are processed through logistics systems and processes) according to relevant attributes that are of importance in a specific context of logistics problem tasks and key performance indicators. To address the nesting aspect of logistics objects, grouping is conducted for each nesting level separately. This implies the consideration of the object structure before analyzing the objects according to their attributes.

For conducting the grouping procedure on an attribute basis an attribute catalog and selection matrix will support the process of identifying relevant characteristics of the considered logistics objects. Here, we presented in (Koch and Glistau 2010) a first overview of characteristics related to object analyses in the field of logistics. These relevant attributes are also important in context of validating the grouping results according to homogeneity.

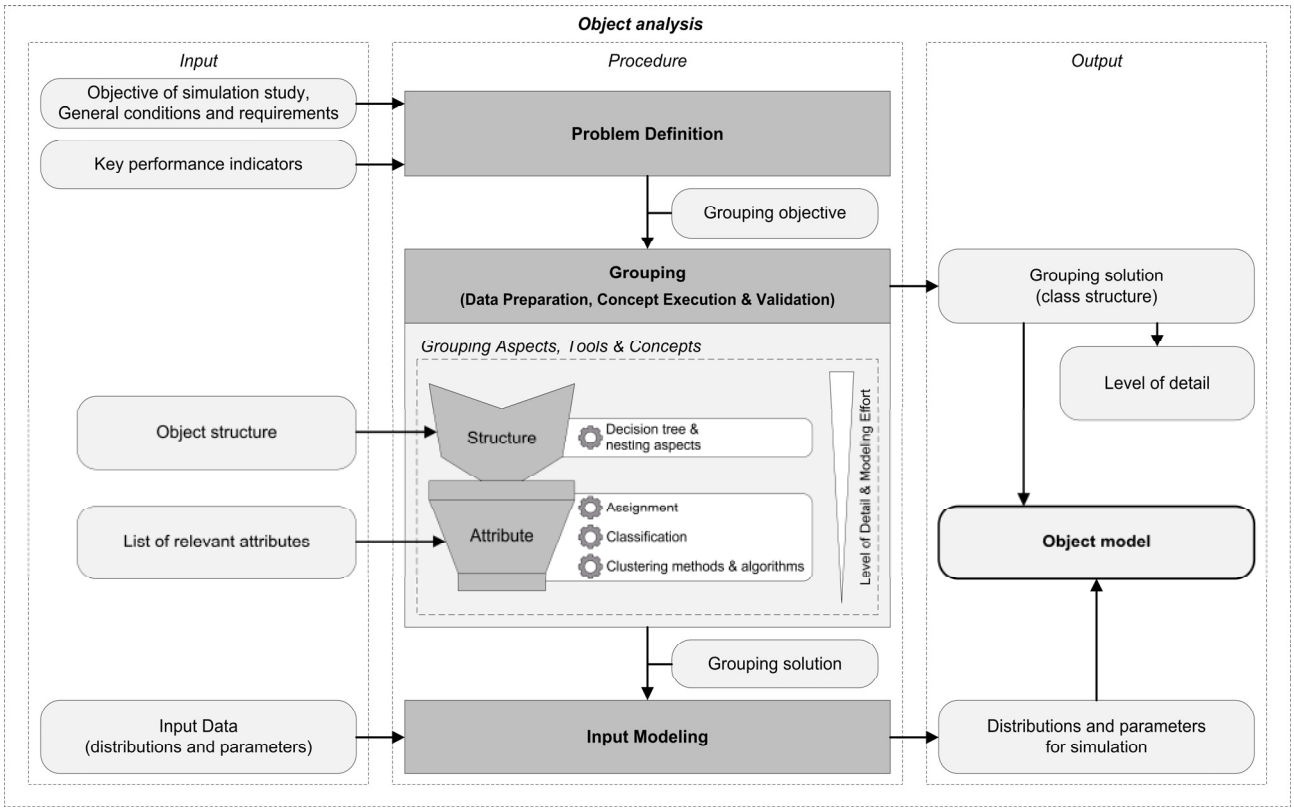

Figure 3: Procedure for Grouping of Logistics Objects

For the grouping procedure different concepts are proposed (see Fig. 3) which allow a credible and supportive grouping in context of modeling and simulation of logistics problem tasks.

The fundamental steps of the procedure are:

- Problem definition
- Grouping
  - Concept selection & data preparation
  - Concept execution & validation
- Input modeling

The problem definition is based on the problem task and objective as well as relevant key performance indicators of the related simulation study. These aspects as well as identified constraints on the level of detail, which are to be defined, have an impact on formulating the objective of the grouping procedure.

The second fundamental step of the procedure is about the actual grouping process. To obtain a representative and sufficient level of detail we propose to consider the grouping for each nesting level (cp. object structure) separately based on the identified relevant attributes.

Three different kinds of grouping concepts are proposed: assignment, classification and clustering methods. Assignment is used for assigning objects to groups that have for example equal process sequences or steps or belong to the same product family. Classification can be applied when objects are classified according to their characteristic values to preexisting categories or groups respectively (e.g. ABC-analysis). Clustering methods belong to structure-discovering concepts grouping objects into clusters which are characterized by a high level of inner-homogeneity and high level of outer-heterogeneity of the formed clusters.

These concepts are not to be considered exclusively and can be used iteratively. In applying these concepts a representative solution and a high quality of the grouping results will be obtained.

In general, the following steps have to be conducted. After identifying and collecting available data an appropriate grouping concept has to be chosen. Here, methods of multivariate data analysis, i.e. clustering methods, are of significant importance due to the multivariate and heterogenic character of the logistics objects. After preparing the data for the chosen concepts, which will contribute to forming an object structure, the grouping method can be applied. In the following the validation and control of the results according to credibility and sufficiency should be conducted.

As a last step there is the process of input modeling for the simulation model which refers to identifying the distributions and parameters of the identified groups out of the raw data of the considered logistics objects. As a consequence the groups or classes respectively can be then implemented in the simulation model.

The complete procedure should be seen as iterative. If the grouping process is not satisfactory and the obtained results, i.e. groups of logistics objects in an appropriate level of detail, are not in line with the grouping objective the procedure should be repeated.

For the mesoscopic simulation approach the identified groups or classes respectively can be implemented as product types in the simulation model. This will reduce model complexity. This effect was already demonstrated in (Koch, Reggelin and Tolujew 2012). Here the proposed approach was successfully applied to an application example in the field of biomass logistics.

APPLICATION

The application example is based on a real-world global supply chain of a company that designs, manufactures, markets and services consumer goods. The consumer goods are transported along several supply chain stages from international suppliers to final customers. For analyzing and planning such complex supply chains the mesoscopic modeling and simulation approach is a proven and effective tool. This was for example demonstrated in (Hennies, Reggelin and Tolujew 2012). Here the advantages of an aggregated level of detail, modeling flexibility and reduced simulation effort as well as time are presented.

In this application example we consider a multi-stage supply chain. The production of the consumer goods was outsourced and is realized by international suppliers. The suppliers are distinguished as main (supplier A) and secondary suppliers (supplier B). Emergency suppliers guarantee deliveries in case of disturbances of regular supplies. The distribution of the consumer goods is conducted by distribution centers which allocate the goods to different regional warehouses. These warehouses realize the sale and delivery to the customers and each faces an individual customer demand pattern. Customers are distinguished as strategic customers (80 percent of total demand) and secondary customers (20 percent of total demand). These elements form the system structure of the model (see Fig. 4).

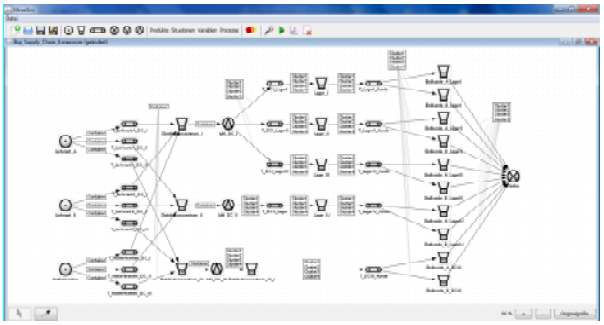

Figure 4: A Mesoscopic Model of a Supply Chain created with the Simulation Software MesoSim

Products are shipped in containers from suppliers via distribution centers to regional warehouses. At the warehouses, material handling is imitated and the

products are distinguished to allow for different demand and appropriate consideration of safety stock levels. The company and the supply chain network are facing a diverse and heterogeneous product structure. In total, there are 207 different consumer goods which are produced and offered for sale. These goods have different characteristic values e.g. related to customer demand or production time.

For grouping the different logistics objects as a significant part of the conceptual modeling phase the proposed grouping procedure on an attribute basis is applied. In the following the key aspects of the presented grouping procedure are explained.

The objective of the company is an inventory level optimization at its warehouses and distribution centers under the condition of realizing as few goods movements as possible. This is to be taken into account when grouping the products.

At first the different objects or products respectively are grouped together according to their belonging to a certain product family (assignment). This reduces the number of objects from 207 to 33 objects or product families respectively. In grouping objects of the same type or kind respectively together a transparent and credible result is attained and presented.

Second, these 33 objects are grouped again on an attribute basis applying a cluster analysis (for further reading on methods of multivariate data analysis we recommend Timm 2002). As a cluster algorithm the Ward's method using a squared Euclidean distance is chosen. The objects are clustered according to two variables: production time and customer demand, which represent the identified relevant attributes. The cluster analysis was conducted with the help of the software tool IBM® SPSS® Statistics Vers. 18.0.

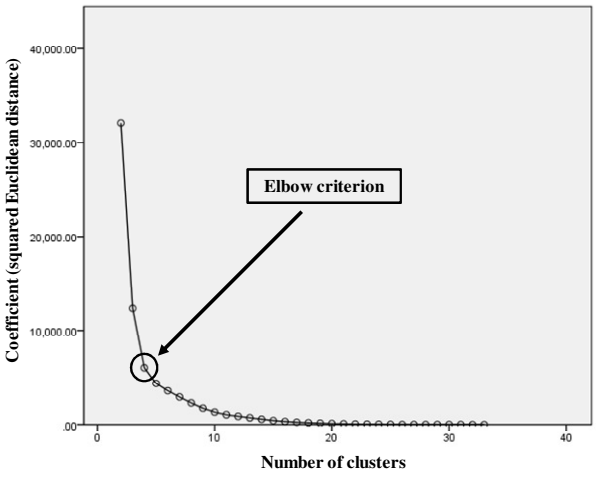

Figure 5: Scree Plot

As a result of the cluster analysis there are several possible cluster solutions. To determine the most appropriate cluster solution a dendogram and a scree plot provide means for decision support. According to the elbow criterion, the scree plot indicates that a cluster solution of four clusters seems to be the most probable solution (see Fig. 5).

But also a cluster solution of two clusters seems to be a reasonable choice. To further validate the homogeneity within the clusters and the heterogeneity among the clusters (which is an important criteria for having an optimal cluster solution) the F-Values of the clusters are considered. The F-Value is a statistical measure of how distinct the cluster groups are. A F-value of less than 1 indicates a homogenous group (Backhaus et al. 2011, 395–455).

Thus, according to the F-Value, Table 1 and Table 2 show that a cluster solution of 4 clusters is deemed as a better and more homogenous solution. Therefore, we choose to group the consumer goods into 4 different groups representing the product types for the simulation model.

Table 1: F-Values for a 2-Cluster Solution

	F-Value	
Cluster	1	2
Production time	**1.39**	0.76
Customer demand	**1.07**	0.09

Table 2: F-Values for a 4-Cluster Solution

	F-Value			
Cluster	1	2	3	4
Production time	0.17	0.92	0.71	**3.49**
Customer demand	0.07	0.01	0.02	0.25

Due to the fact that we also consider the shipment of containers in the model (cp. nesting aspect), we have to add one product type to the model.

In total, it is possible to reduce the number of logistics objects from 208 (including one object type for the containers) to 5. These 5 product types represent the product structure as well as the characteristics of the related products or objects respectively.

Thus, the level of detail is characterized by implementing 4 clusters (plus 1 for the container) as well as their determined distributions and parameters, according to input modeling, into the simulation model. This level of detail is in line with the objective and allows effective simulation in context of the problem statement.

In grouping the logistics objects together with the help of the proposed procedure the amount of entities that need to be considered for computations in the simulation run can be reduced. This has a positive effect on the simulation effort without neglecting aspects of transparency and credibility that impact model accuracy and validity.

Results of simulation runs show that the determined and chosen level of detail contributes to output data that allows for testing scenarios and retrieving statements on how to solve the problem task of the simulation study (see Fig. 6). There was no necessity for further aggregating or decomposing the data to, for example, improve model accuracy or validity.

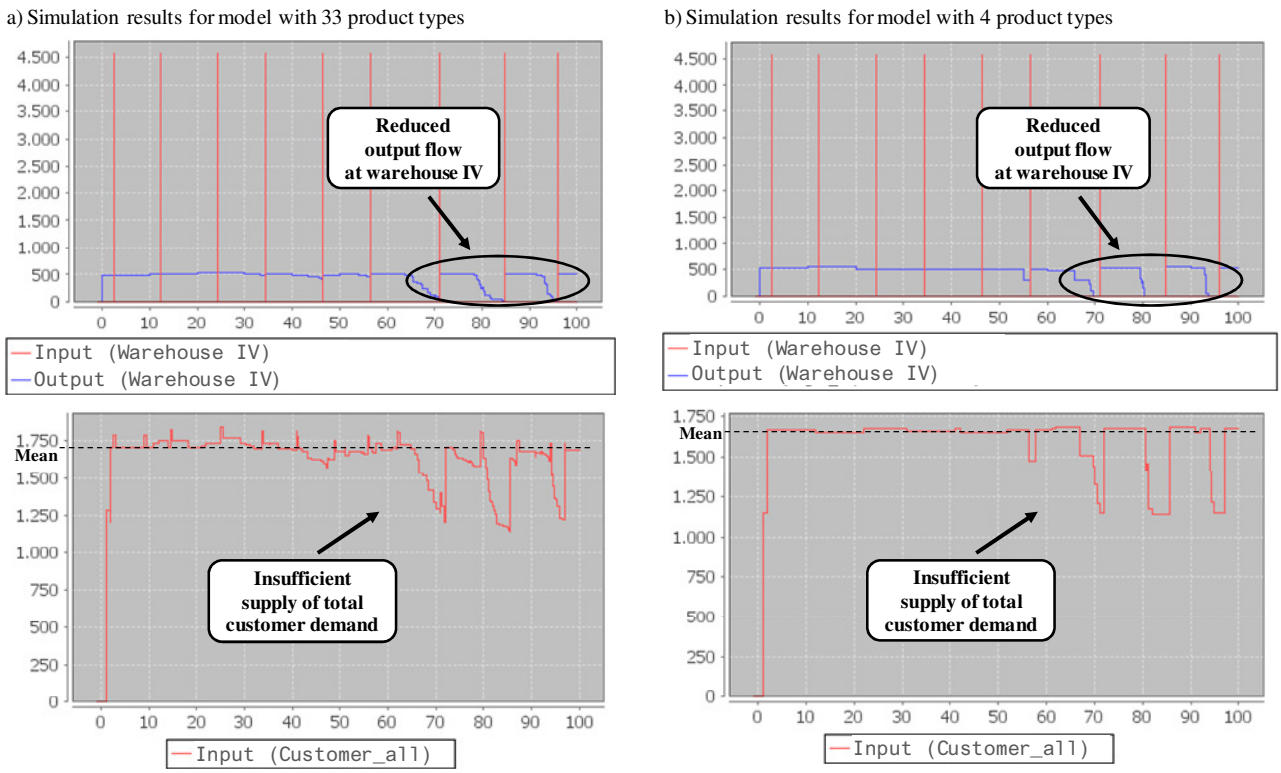

Figure 6: Comparison of exemplary Simulation Results for different Level of Detail

In comparing the simulation results of the model using 4 product types (plus 1 for the container) to a more detailed simulation model implying 33 product types (representing the different product families) it becomes apparent that there is no significant impact on the simulation results (see Fig. 6). There are just minor differences in the occurrence of certain events over the simulation time. Thus, the reduced number of integrated product types does not result in a significant reduced accuracy and validity of the simulation results and conclusions.

CONCLUSION

The paper describes the challenges that are incorporated with the increasing complexity of logistics systems and processes. This complexity is mainly caused by the increasing diversity and heterogeneity of the logistics objects, i.e. the goods processed through the logistics system. Therefore methods for simplification are needed. Zeigler et al. also suggest as one method of simplification for simulation modeling to group components of the model (Zeigler, Praehofer and Kim 2007).

Here, the mesoscopic modeling and simulation approach requires support in grouping logistics objects for simplification purpose in an effective and representative way, because there is a lack in supporting the composition and decomposition of logical groups of logistics objects. However, this is of significant importance to approach the increasing complexity of logistics systems and processes efficiently.

Therefore, the paper presents such a procedure for grouping logistics objects in an efficient way supporting the determination of the right and appropriate level of detail for the simulation model and the considered problem task and logistics system. The benefits and effects of the presented grouping procedure as well as its relevance to the field of logistics were demonstrated by an application example in the field of supply chain modeling. Here the volume of to-be-considered logistics objects was reduced by 97.5 percent resulting in 5 product types to be implemented in the simulation model.

In general, the proposed procedure supports the conceptual modeling phase enhancing the outcome of a simulation study. Model complexity can be reduced while allowing for better model credibility and simulation efficiency. In contributing to less modeling and simulation effort without reducing accuracy and validity of simulation results there is added value to the simulation of logistics systems. This in particular provides benefit to industry applications.

With the described procedure as a part of the conceptual modeling process of the mesoscopic simulation approach there is also support to the modeler in the modeling and decision making process as well as contribution to a transparent, effective and qualitative conceptual modeling phase.

REFERENCES

Arnold, Dieter, Kai Furmans, Heinz Isermann, Axel Kuhn, and Horst Tempelmeier. *Handbuch Logistik*. 3., neu bearb. Aufl. Berlin: Springer, 2008.

Backhaus, Klaus, Bernd Erichson, Wulff Plinke, Rolf Weiber, and Backhaus-Erichson-Plinke-Weiber. *Multivariate Analysemethoden: Eine anwendungsorientierte Einführung.* 13th ed. Springer-Lehrbuch. Berlin: Springer, 2011.

Banks, Jerry. *Discrete-event system simulation*. 5th ed. Upper Saddle River, NJ: Pearson, 2010.

Bretzke, Wolf-Rüdiger. *Logistische Netzwerke*. 2., wesentlich bearb. u. erw. Aufl. Berlin: Springer, 2010.

Brooks, R.J, and A.M Tobias. "Choosing the best model: Level of detail, complexity, and model performance." *Mathematical and Computer Modelling* 24, no. 4 (1996): 1–14.

Damiron, Cecile, and Anthony Nastasi. "Discrete rate simulation using linear programming." In *Proceedings of the 2008 Winter Simulation Conference*. Edited by Scott J. Mason, 740–9. Piscataway, NJ: IEEE Service Center [u.a.], 2008.

Gudehus, Timm, and Herbert Kotzab. *Comprehensive logistics*. Heidelberg: Springer, 2009.

Hennies, Til, Tobias Reggelin, and Juri Tolujew. "Mesoscopic supply chain simulation." In *I3M 2012 : the 9th International Multidisciplinary Modeling & Simulation Multiconference; 19 - 21 September, 2012, Vienna, Austria.* Genova: DIME-DIPTEM University of Genoa.

Koch, Markus, and Elke Glistau. "Lebenszyklusorientierte Logistikplanung." *Forschung vernetzen - Innovationen beschleunigen : 9./10. IFF-Kolloquium, April und November 2010, Magdeburg / Hrsg. Michael Schenk*.

Koch, Markus, Tobias Reggelin, and Juri Tolujew. "Conceptual procedure for grouping logistics objects for mesoscopic modeling and simulation." In *I3M 2012 : the 9th International Multidisciplinary Modeling & Simulation Multiconference; 19 - 21 September, 2012, Vienna, Austria.* Genova: DIME-DIPTEM University of Genoa.

Koch, Markus, Juri Tolujew, and Michael Schenk. "Approaching complexity in modelling and simulation of logistics systems (WIP)." In *Theory of Modeling and Simulation: DEVS Integrative M & S Symposium 2012 : (DEVS 2012); Orlando, Florida, USA, 26 - 30 March 2012*, 25–30. Simulation series 44,4. Red Hook, NY: Curran [u.a.], 2012.

Krahl, David. "ExtendSim advanced techology: discrete rate simulation." In *Proceedings of the 2009 Winter Simulation Conference*, 333–8. Piscataway: IEEE, Jan. 2009.

Law, Averill M. *Simulation modeling and analysis*. 4th ed. McGraw-Hill series in industrial engineering and management science. Boston, Mass: McGraw-Hill, 2007.

Law, Averill, M. "How to build valid and credible simulation models." In *Proceedings of the 2009 Winter Simulation Conference (WSC)*, 24–33. IEEE, 2009.

Pace, Dale K. "Simulation Conceptual Model Development." In *Proceedings of the Spring 2000 Simulation Interoperability Workshop.* 2000. www.sisostds.org (accessed February 26, 2012).

Pidd, M. "Just Modeling Through A Rough Guide to Modeling." *Interfaces* 29, no. 2 (1999): 118–132.

Reggelin, Tobias. *Mesoskopische Modellierung und Simulation logistischer Flusssysteme*. Magdeburg: Universitätsbibl; Univ., Fak. für Maschinenbau, Dissertation - Magdeburg, 2011.

Reggelin, Tobias, and Juri Tolujew. "A mesoscopic approach to modeling and simulation of logistics processes." In *Proceedings of the 2011 Winter Simulation Conference*, 1513–23. Piscataway, NY: IEEE Service Center, 2011.

Reggelin, Tobias, Sebastian Trojahn, Juri Tolujew, and Markus Koch. "Mesoscopic modeling and simulation of biomass logistics networks from harvesting to power generation." In *Flexibility and adaptability of global supply chains : proceedings of 7th German-Russian Logistics Workshop, DR-LOG 2012*, 190–7. 2012.

Robinson, S. "Conceptual modelling for simulation part I: definition and requirements." *Journal of the Operational Research Society* 59, no. 3 (2008): 278–290.

Robinson, Stewart. *Simulation: The practice of model development and use*. Chichester, West Sussex, England, Hoboken, NJ: John Wiley & Sons Ltd, 2004.

Savrasov, M., and J. Tolujew. "Mesoscopic Approach to Modeling a Traffic System." In *International Conference Modelling of Business, Industrial and Transport Systems*, 147–51. Riga: TSI, 2008.

Schenk, Michael, Juri Tolujew, and Tobias Reggelin. "Comparison of three methods of implemention of mesoscopic flow models." *Logistics and supply chain management: modern trends in Germany and Russia* (2009): 36–44.

Schenk, Michael, Juri Tolujew, Katja Barfus, and Tobias Reggelin. "Modellierung und Analyse von räumlichen Relationen zwischen physischen Objekten in logistischen Netzwerken." In *Wissenschaft und Praxis im Dialog: Steuerung von Logistiksystemen - auf dem Weg zur Selbststeuerung : 3. Wissenschaftssymposium Logistik*. Edited by Hans-Christian Pfohl, 26–39. Hamburg: Deutscher Verkehrs-Verlag, 2006.

Schenk, Michael, Juri Tolujew, Katja Barfus, and Tobias Reggelin. "Grundkonzepte zu logistischen Echtzeit-systemen : Monitoring, Event Management und Früh-warnung." In *Jahrbuch Logistik*. Edited by Hanne Wolf-Kluthausen, 222–6. Korschenbroich: free beratung GmbH, 2007.

Schenk, Michael, Juri Tolujew, and Tobias Reggelin. "A Mesoscopic Approach to Modeling and Simulation of Logistics Networks." In *Logistics and Supply Chain Management: Trends in Germany and Russia*. Edited by D. Ivanov et al., 58–67. Saint Petersburg: Publishing House of the Saint Petersburg State Polytechnical Institute, 2008.

Schenk, Michael, Juri Tolujew, and Tobias Reggelin. "Mesoscopic modeling and simulation of logistics networks." *13th IFAC Symposium on Information Control Problems in Manufacturing* (2009): 586–591.

Schenk, Michael, Juri Tolujew, and Tobias Reggelin. "A mesoscopic approach to the simulation of logistics systems." In *Advanced manufacturing and sustainable logistics*. Edited by Wilhelm Dangelmaier, Alexander Blecken and Robin Delius, 15–25. Berlin [u.a.]: Springer, 2010.

Scholz-Reiter, B., H.-D Stahlmann, and A. Nethe, eds. *Process modelling*. Berlin ;, New York: Springer, 1999.

Simchi-Levi, David. *Designing and managing the supply chain: Concepts, strategies, and case studies*. With the assistance of Philip Kaminsky, and Edith Simchi-Levi 3. ed. Boston: McGraw-Hill/Irwin, 2008.

Sterman, John. *Business dynamics: Systems thinking and modeling for a complex world*. Boston: Irwin/McGraw-Hill, 2000.

Timm, Neil H. *Applied multivariate analysis.* Springer texts in statistics. New York: Springer, 2002.

Tolujew, J., and F. Alcalá. "A Mesoscopic Approach to Modeling and Simulation of Pedestrian Traffic Flows." In *Proceedings of the 18th European Simulation Multiconference*, 123–8. Ghent: SCS Publ. House, 2004.

Uthmann, Christoph v., and Jörg Becker. "Guidelines of Modelling (GoM) for Business Process Simulation." In *Process modelling*. Edited by B. Scholz-Reiter, H.-D Stahlmann and A. Nethe, 100–16. Berlin; New York: Springer, 1999.

van der Zee, D. J., and J. G. A. J. van der Vorst. "A Modeling Framework for Supply Chain Simulation: Opportunities for Improved Decision Making." *Decision Sciences* 36, no. 1 (2005): 65–95.

Zeigler, Bernard P., Herbert Praehofer, and Tak-kon Kim. *Theory of modeling and simulation: Integrating discrete event and continuous complex dynamic systems*. 2. ed., [Nachdr.]. Amsterdam: Acad. Press, 2007.

AUTHOR BIOGRAPHIES

Markus Koch is a doctoral student at the Otto von Guericke University Magdeburg. He received his diploma in Industrial Engineering Logistics (2010) from the Otto von Guericke University Magdeburg (Magdeburg, Germany), and his M.Sc. in Engineering Management from the Rose-Hulman Institute of Technology (Terre Haute, IN, USA). His research work under Prof. Michael Schenk focuses on the modeling of logistics systems and the integration of a logistics object perspective.

Dr. **Juri Tolujew** was a lecturer and then assistant professor at the Technical University of Riga from 1976 to 2001. Since 2001, he has been a Research Manager at the Fraunhofer Institute for Factory Operation and Automation IFF in Magdeburg. He earned his Habilitation in Simulation Technology from Otto von Guericke University Magdeburg in 2001. Since 2005, he has also been a member of the faculty of the Institute of Logistics and Material Handling Systems at Otto von Guericke University Magdeburg. His main research and teaching interests are the mathematical modeling and simulation of logistics systems and networks.

E-LEARNING BASED COMPETENCE DEVELOPMENT IN LOGISTICS SOFTWARE APPLICATION FOR SIMULATION AND VISUALIZATION

Gaby Neumann
Faculty of Engineering / Industrial Engineering
Technical University of Applied Sciences Wildau
Bahnhofstr., 15745 Wildau, Germany
E-mail: gaby.neumann@th-wildau.de

KEYWORDS
e-learning, simulation-focused learning, logistics simulation, 3D visualization

ABSTRACT

Logistics is one of the areas where simulation and visualization software is typically applied in practical problem-solving processes. Precondition is sufficient knowledge and understanding on simulation methodology, but also on the syntax, functionality and applicability of professional software packages used. Within this context the paper addresses a learning-while-working scenario presenting the idea and implementation of respective simulation-focused learning resources in a web-based portal. It elaborates simulation competence requirements in logistics, discusses design constraints concerning e-learning material to meet those requirements and gives examples on simulation knowledge representation and interactive knowledge application for logistics simulation and visualization.

INTRODUCTION

In logistics process design and systems engineering the use of discrete event simulation and 3D visualization techniques has become a fundamental methodological approach. There is a wide range of generic or specialized, continuously developing simulation and visualization software tools aiming to support logistics planning. The challenge to the user (i.e. the logistics planning person) consists in both understanding the tool's methodical background and application constraints and keeping track of current functionality according to latest software updates. Especially the latter requires dynamically adjusted training material far beyond a simple README file enlisting changes over the previous version. Instead, e-learning modules are a more promising alternative as they can be provided equally well via the software developer's website or within a dedicated e-learning environment – if designed in a proper way.

From reviewing literature it becomes pretty obvious that simulation competence development closely matches the concept of e-learning. The major reason for this is a quite "natural" one: both fields simulation and e-learning work with the same medium – the computer. This makes their combination particularly convenient; neither change of context nor any additional tool is required. This also contributes to successful learning as subjects tend to be conveyed best in what might be considered their native environment (Rushkoff 2013).

In the early stages of simulation-focused technology-based learning (Neumann et al. 2005) intelligent tutoring systems aimed to present certain aspects of a typical classroom-based simulation course in a computerized way (Taylor and Siemer 1996). With the emergence and wide-scale accessibility of the internet web-based interactive learning environments for teaching simulation facilitated collaborative learning in a heterogeneous environment (Atolagbe, Hlupic and Taylor 2001). Nowadays, simulation education is represented in proprietary, commercial or open virtual learning environments. Topics covered range from theoretical foundations and optimization methods to simulation exercises and cases. Fonseca et al. (2009) compare a variety of those online and blended learning applications and conclude on the use of simulation software, professional-oriented approaches and friendly online environments as being necessary to successfully complete simulation courses. The success in terms of achieving professional simulation competence amongst others depends on the availability of authentic rather than abstract simulation problems and usability of professional rather than academic simulation packages within the e-learning environment. This way simulation learners work already with situations and tools they might get in touch with at their workplaces.

Due to the tools' and their use cases' increasing complexity an e-learning module supporting competence development in logistics software application for simulation and visualization needs to be designed in a way enabling

- easy-updating or extending with regard to the specific software tools explained and applied,
- flexible choice of the way of learning, the mode of knowledge presentation and the method of knowledge application or assessment, and
- personalization in terms of topics and competence level to be achieved.

Especially the latter requires in-depth understanding of what are competence requirements of the individual

Proceedings 27th European Conference on Modelling and Simulation ©ECMS Webjørn Rekdalsbakken, Robin T. Bye, Houxiang Zhang (Editors)
ISBN: 978-0-9564944-6-7 / ISBN: 978-0-9564944-7-4 (CD)

person and even more which competences at what level are required at the labor market. To get an insight into those user needs and market requirements a European project is being run aiming to provide access to attractive training material and to a diagnosis tool for identifying individual competence gaps.

Against this background the paper elaborates requirements for simulation competence in logistics, presents the structural framework for developing professional competence and discusses e-learning design issues for applying simulation and visualization tools within a simulation-focused learning scenario. At the end, concluding remarks summarize findings and identify next steps in the project.

REQUIREMENTS FOR SIMULATION COMPETENCE IN LOGISTICS PRACTICE

The lot4eng.com (Logistics Open Training for Engineering Competence) project has been inspired by the shortage of logistics engineers, which has already been and is yet to be faced by many countries across Europe. Therefore, the objective of the project is to enhance engineering and managerial skills of employees at risk of developing a competence gap in the field of logistics (i.e. employees of logistics, manufacturing or distribution enterprises, and coaches, trainers or vocational trainers in logistics). This is to be achieved by providing access to high quality e-learning materials.

In order to ensure that training materials developed within this framework match current requirements at the labor market, a questionnaire-based survey was run with logistics managers at different management levels and from different types of (logistics) companies. Outcomes of the survey form the basis for developing web-based, interactive training materials that address those needs and enable logistics practitioners (but also newcomers to the field) to develop and improve professional competencies according to their individual requirements.

Table 1: Bloom's Taxonomy

Evaluation	You can pass judgment on something (e.g. assess, conclude, decide, verify)
Synthesis	You can create something new as a result of analysis (e.g. compose, create, design, generate, plan)
Analysis	You can break something down (e.g. compare, detect, order, simplify)
Application	You can take something from one context and use it in another (e.g. choose, collect, complete, develop, use)
Comprehension	You understand what you know (e.g. associate, classify, differentiate, explain, identify, summarize)
Knowledge	You know something (e.g. define, describe, list, match, name, relate)

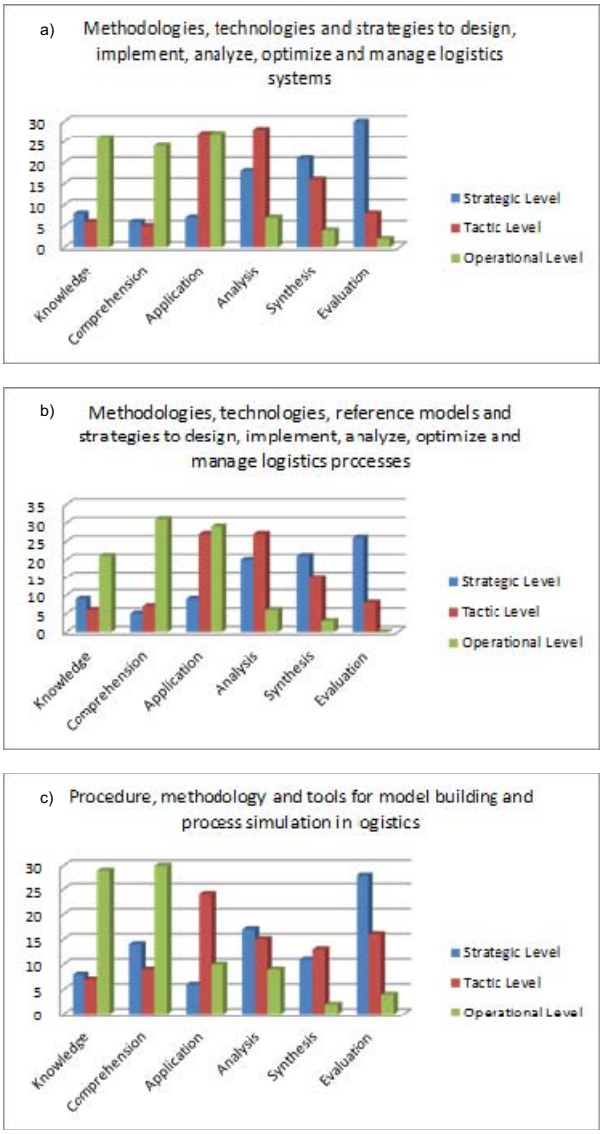

Figure 1: Competence Requirements in Logistics Practice

In the survey participants were asked to indicate the level of thinking (according to Bloom's Taxonomy for educational objectives (Bloom 1956), see Table 1) they would expect to find with a logistician at a certain management level (i.e. strategic, tactical or operational) for a number of managerial and engineering competence areas. Amongst others, questions addressed methodologies, technologies and strategies to design, implement, analyze, optimize and manage logistics processes, systems and networks on one hand and procedure, methodology and tools for model building and process simulation in logistics on the other. Comparing the frequency distribution of responses to those questions (see Figure 1) it becomes visible that the required level of both planning and simulation competences generally increases with the management level the target person is expected to work at:

- *Supervisors in an operational role or first line managers* (i.e. operational level) are expected to

demonstrate a profound understanding on logistics systems and process design, implementation, analysis, optimization and management and eventually apply this understanding within a certain context. With regard to model building and simulation this type of managers should at least understand the procedure, methodologies and tools.

- *Managers or consultants planning, coordinating and controlling different parts of the logistics network* (i.e. tactical level) are expected to apply methods, technologies and strategies for logistics system and process design, analysis and optimization and even further to look for interrelationships and patterns, understand generic structures or make interferences. For this type of managers almost the same average level of competence is required with regard to model building and simulation.
- *Senior managers, senior consultants or directors with considerable experience in logistics management or senior executives who have assumed logistics responsibilities from another business discipline* (i.e. strategic level) are also expected to break down information on logistics system and process design, analysis and optimization into their component parts, but also to demonstrate some ability to create new patterns or structures or propose alternative solutions. For this type of managers almost the same average level of competence is required with regard to model building and simulation.

From this it can be concluded that e-learning material aiming to support model building and simulation competence development in general (i.e. independent of a particular tool) needs to be designed in a way providing introductory knowledge and fundamental understanding, but also allowing to proceed towards a higher competence level if intended. This can only be achieved by modularly structuring the material, providing competence-based and learning-goal oriented access to different parts of the material, and enabling interactive knowledge application through quizzes at different levels of difficulty and analyzing or running case studies at different levels of complexity.

STRUCTURAL FRAMEWORK TO DEVELOP PROFESSIONAL COMPETENCE

Based upon the previously discussed analysis of user needs in terms of competence development and taking into consideration the necessity for applying certain software tools enabling simulation model building and experimentation as well as visualization of the outcomes of a logistics system design process in a three-dimensional virtual reality the e-learning module will be subdivided into independent but interlinked units. Apart from sections explaining basics of simulation methodology and logistics simulation and introducing into logistics simulation projects, the material comprises units introducing to basic functionality of and providing advanced insights into a particular simulation package (DOSIMIS-3) and a tool for creating 3D representation of logistics systems (taraVRbuilder). All units can either be combined within an educational module to be embedded in a learning management system, like e.g. the moodle platform (see Figure 2), or used by providers of those tools as add-on material to their web-sites.

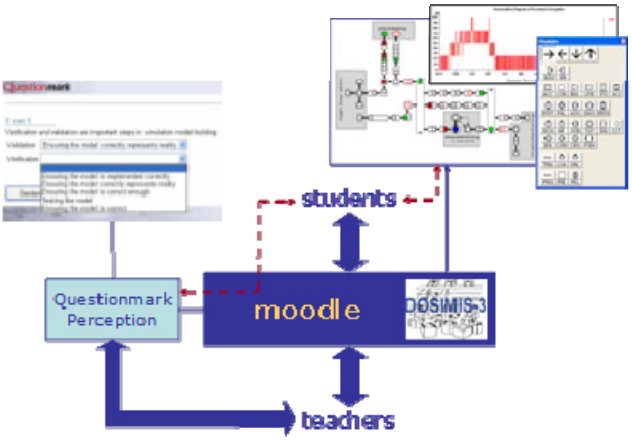

Figure 2: Educational infrastructure

However, within the context of the lot4eng.com project there is a quite different focus: In the first instance e-learning material is not meant to be used in university classes nor as a kind of online tutorials with software providers. Instead the material aims to support logistics managers and engineers in updating and extending their professional competence – amongst others in the field of modeling and simulation. Due to their daily workload time resources for attending classroom training are often limited; therefore learning while working, i.e. workplace learning, is a more promising approach. Although here another challenge is still to face: to help a professional on-the-spot and when dealing with a specific problem in actively creating and successfully passing individual learning processes through guidance-on-demand in a virtual environment.

For this, preconditions are easy real-time access to necessary information resources directly in the workplace (e.g. via an internet portal), almost immediate personalized support in real-life problem-solving (e.g. through a question-based access to specific multimedia instructions), and clear understanding of personal competence deficits and training needs (e.g. based upon individual competence gap analysis). The lot4eng.com platform (see Figure 3) has been designed exactly to fulfill those preconditions. For each of the three target groups addressed, logistics managers, logistics engineers and logistics teachers, there is a specific competence test. Here, user's competences as demonstrated in the test are matched against the target competence level as required from the competence survey. Depending on the results a list of e-learning

units (lessons) is proposed with the help of which missing competences might be developed. All e-learning material contains multimedia elements, is interaction-based, encourages knowledge application and is available in English as well as in the local languages of those countries addressed by the project (Poland, Italy and Germany).

Figure 3: The lot4eng.com portal

In addition to those characteristics, implementation of alternative pedagogical strategies facilitating the acquisition of simulation modeling knowledge is helpful in order to allow learning processes that match with personal preferences. Concerning the latter Atolagbe, Hlupic and Taylor (2001), for example, identified the following concepts as particularly suitable ones for simulation competence development:

- *Learning with scenarios* (i.e. using a real-world scenario as the vehicle for instruction);
- *Learning by doing* (i.e. coaching in step-by-step operations required to perform a particular task);
- *Practicing with contents feedback* (i.e. providing remediation of a problem whenever an error or misconception has been detected); and
- *Free exploration* (i.e. enabling navigation around a case scenario without intervention by the learning environment).

This way informal self-learning is supported rather than formalized educational processes. For the purpose of the lot4eng.com project this exactly meets intentions: support workplace learning with logistics practitioners who want to or need to apply simulation and visualization for logistics problem solving in their daily work. This is achieved best by offering instruction-like and problem-based modules (Neumann 2008) strengthening practical knowledge transfer, whereas description-oriented modules focusing on transferring theoretical knowledge are less suitable here.

E-LEARNING DESIGN FOR APPLYING SIMULATION AND VISUALIZATION TOOLS

Within the lot4eng.com platform simulation and visualization competence development is embedded in an e-learning module on "Application of Logistics Software" (see Figure 4). This module comprises units introducing into software in logistics (overview and general classification), briefly explaining simulation methodology and illustrating how simulations projects are run particularly in the logistics area. This is completed by units on how to use a specific software tool in which a simulation package's syntax is demonstrated, but much more important its problem-oriented application is explained and illustrated.

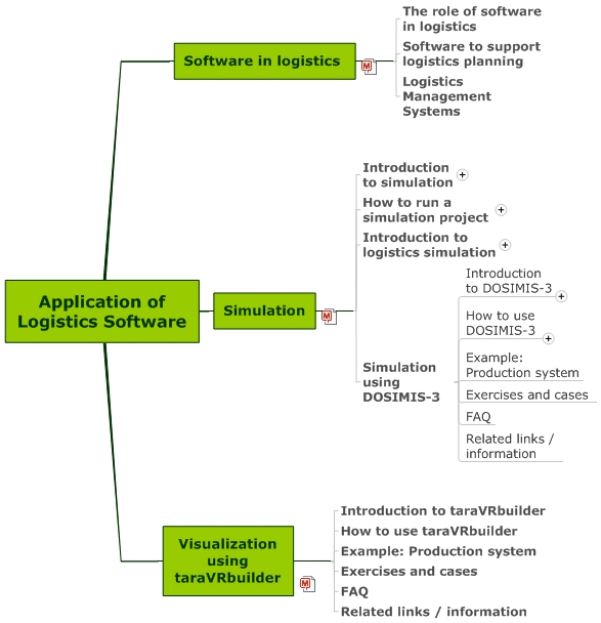

Figure 4: E-learning module structure

For the moment, those tool-specific units cover a simulation package, DOSIMIS-3, on one hand and a 3D dynamic visualization package, taraVRbuilder, on the other. *DOSIMIS-3* (http://www.sdz.de) is a simulation package specialized to answer questions related to functionality and performance measures of logistics systems and processes. It provides an extensive library of components from the material-flow and logistics world, enabling model-building by a few clicks on the basis of a well-structured conceptual model. With this, model building and simulation is brought closer to the experts in the application area – in our case material flows and logistics enabling them to implement and use a simulation model themselves. *taraVRbuilder* (http://www.tarakos.de) is a software tool for 3D configuration and visualization of conveying, material flow and storage/warehouse equipment using virtual reality technology. Models are built from a wide-range library of scalable, animated 3D components eventually even representing specific manufacturer's product catalogue. Possible applications exist in the fields of sales support, planning, engineering and documentation.

It can also be used as a software tool within the context of the "digital factory".

Both software tools were chosen as they are commercial packages well known in logistics practice, but offering demo versions free of charge. They originate from Germany, but they are available at least in English language and used in other countries as well. In terms of the DOSIMIS-3 simulation package the tool has already been translated into several other languages with the two other project languages Polish and Italian amongst them. With this it is possible (and necessary) to prepare and provide instruction media (and not just descriptive texts) in two or even four different languages in order to be as close as possible with the potential users.

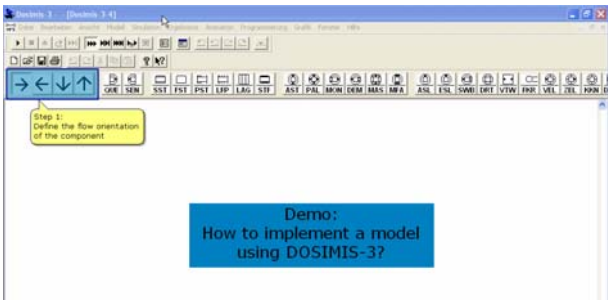

Figure 5: Exemplary demo for DOSIMIS-3

Generally, both units are sub-structured and designed along the same lines. An introduction to the respective software is followed by a kind of interactive tutorial on how this package is being used (see Figure 5). The tutorial first explains in an exploratory way structure and elements of the graphical user interface and presents standard functionality (What is to be found where?). The next section focuses on basic functionality of the software package in order to illustrate how to build a model, how to navigate through a (more complex) model, how to set parameters with model components or how to let the model come to life in simulation, animation or visualization. Additional sections of the tutorial go into detail with specific modeling challenges, presentation of results, and the package's import or export functionality. Working through this material should enable the user to understand what the software package might be used for and how. To deepen knowledge and understanding hopefully acquired from following the tutorial a specific example is given (see Figure 6) which demonstrates the entire application process from introducing the problem and question (including a draft of the system and its parameters) and presenting the complete model to showing and commenting on how the model is being build step-by-step.

After this, exercises and cases request for practical experimenting. Challenges presented to the user include functionality exercises ("Show where you can find…" or "Click on the right button for…"), discovery exercises ("What kind of system/process is represented here?"), model building exercises ("Build a model of the following system/process!"), small case studies and a quiz. A section containing (multimedia) answers to an open set of frequently asked questions and a list of related links or further information sources provide hands-on guidance and direct support to self-directed applications and business projects.

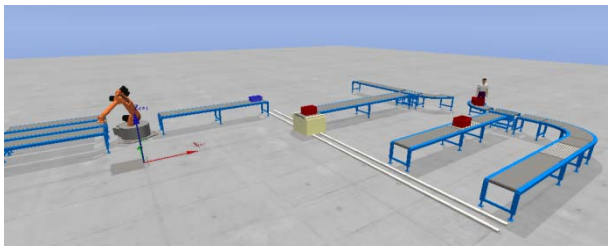

Figure 6: Example from taraVRbuilder

This common structure is applicable to any other kind of software tools too and therefore forms the basis for an open collection of learning units which also can easily be updated with eventually evolving software functionality. In order to enable easy and direct access by the user the units are designed from the user's point of view rather than following the software's structure and functionality. This is achieved by applying a question-based approach. Here, it is assumed that a user does not want or need to get demonstrated full software functionality in a compact sequence, but s/he comes with a particular problem or question concerning software operation. And this problem needs to get solved or this question needs to get answered within the user's specific context. Therefore, each of the demonstrations is related to a "How to …" question. These small-scale learning resources can then be accessed in alternative ways. This includes working through a guided case, following a learning path, scrolling through a listing and navigating through a logical grouping represented by a mindmap.

In contrast to typical e-learning modules learning progress does not need to be assessed inside the module itself, but is to be demonstrated by reusing the competence gap analysis tool of the lot4eng.com portal. Currently, this requires to answer questions only and not to demonstrate any competences or skills in applying simulation software or model building and simulation to solve a problem in logistics planning or operation. Turning this knowledge-focused approach into a competence-oriented one still enabling automatic evaluation and feedback remains an open task.

CONCLUSIONS

The paper presented an approach and environment for e-learning based competence development in logistics software application for simulation and visualization. Due to founding any learning resource development on the results of a survey for competence requirements with logistics managers and engineers, materials

structuring, design and usability can be expected to be close to potential users' needs. However and apart from finalizing implementation, next steps need to focus on giving proof of practicability and functioning in terms of both, technical and learning aspects. For this, final beneficiaries will be involved.

Today, it already can be concluded that e-learning is a promising way to support simulation competence development in a practical environment, i.e. directly at the workplace. Instead of formal training settings keeping human resources away from their daily business, informal and self-learning while working can nicely be integrated in professional problem-solving activities. Precondition is a proper design and structure of the material related to the use of commercial software packages and its availability within an internet platform enabling personal competence gap analysis as well.

ACKNOWLEDGEMENTS

This paper is based upon the outcomes of the lot4eng.com project "Logistics Open Training for Engineering Competence". This project has been funded with support from the European Commission under the Lifelong Learning Programme. This communication reflects the views only of the author, and the Commission cannot be held responsible for any use which may be made of the information contained therein.

REFERENCES

Atolagbe, T.; V. Hlupic; and S.J.E. Taylor. 2001. "Genisa: A Web-Based Interactive Learning Environment for Teaching Simulation Modelling". In *Proceedings of the 2001 Winter Simulation Conference*. eds. B.A. Peters; J.S. Smith; D.J. Medeiros; and M.W. Rohrer. 1605-1612.

Bloom, B.S. 1956. *Taxonomy of educational objectives: the classification of educational goals: handbook I, cognitive domain*. New York: David McKay Co Inc.

Fonceca, P.; A.A. Juan; L.M. Pla; S.V. Rodriguez; and J. Faulin. 2009. "Simulation Education in the Internet Age: Some Experiences on the Use of Pure Online and Blended Learning Models". In *Proceedings of the 2009 Winter Simulation Conference*. eds. M.D. Rossetti; R.R. Hill; B. Johansson; A. Dunkin; and R.G. Ingalls. 299-309.

Hollocks, B. 2005. Assessing Simulation Learning in Higher Education. In *Proceedings of the 2005 Winter Simulation Conference*. eds. M.E. Kuhl; N.M. Steiger; F.B. Armstrong; and J.A. Joines. 2297-2303.

Neumann, G. 2008. "Simulation Education in Logistics: Case Studies in a Virtual Learning Environment". In *Proceedings of the 22nd European Conference on Modeling and Simulation*. eds. L.S. Louca; Y. Crystanthou; Z. Oplatková; and K. Al-Begain. 441-446.

Neumann, G.; B. Page; W. Kreutzer; G. Kiesel; and R. Meyer. 2005. "Simulation and E-Learning". In *The Java Simulation Handbook - Simulating Discrete Event Systems in UML and Java*. B. Page and W. Kreutzer. Shaker, Aachen, 401-433.

Rushkoff, D. 1992. "Online courses need human element to educate". Online at: http://edition.cnn.com/2013/01/15/opinion/rushkoff-moocs/index.html, January 15, 2013.

Taylor, S.J.E. and J. Siemer. 1996. "Enhancing Simulation Education with Intelligent Tutoring Systems". In *Proceedings of the 1996 Winter Simulation Conference*. eds. J.M. Charnes; D.J. Morrice; D.T. Brunner; and J.J. Swain. 675-680.

AUTHOR BIOGRAPHY

GABY NEUMANN holds a professorship in Engineering Logistics at the Technical University of Applied Sciences Wildau. She received a Diploma in Materials Handling Technology from the Otto-von-Guericke-University of Technology in Magdeburg and a PhD in Logistics from the University of Magdeburg for her dissertation on "Knowledge-Based Support for the Planner of Crane-Operated Materials Flow Solutions". Between December 2002 and June 2009 she was Junior Professor in Logistics Knowledge Management at the Faculty of Mechanical Engineering there. Since 1991 she also has been working as part-time consultant in material handling simulation, logistics planning and specification of professional competences in certain fields of logistics. Her current activities and research interests are linked amongst others to fields like problem solving, knowledge management and technology-based competence-building in logistics simulation. She has been or is being involved in a couple of research projects in these fields. Gaby Neumann has widely published and regularly presents related research papers at national and international conferences.

A novel, broadcasting-based algorithm for vehicle speed estimation in Intelligent Transportation Systems using ad-hoc networks

Boyan Petrov[1], Dr Evtim Peytchev[2]
[1]Faculty of Computer Systems and Control, Technical University – Sofia, 8 Kliment Ohridski bulv., Sofia 1000, Bulgaria, email: b_petrov@tu-sofia.bg
[2]School of Science and Technology, Nottingham Trent University, Clifton Lane, Nottingham NG11 8NS, email: evtim.peytchev@ntu.ac.uk

KEYWORDS:
Ad-hoc networks, broadcasting, VANET, MANET, car–to-car communication, mobile networking, wireless communication, intelligent transportation systems (ITS), cooperative traffic condition generation, cooperative driving.

ABSTRACT

There has been a lot of research effort recently dedicated to identifying appropriate communication paradigm based on car-to-car communication for evaluation of traffic conditions. This paper introduces a novel way of evaluation of one such condition - the average speed of all cars in a street in an urban area using simple broadcasting protocol. The paper presents the protocol, describes the simulation model and reports the results that have been achieved using simulation and real wireless devices communications, but in a static mode, i.e. the devices are not moving. It is anticipated that the real-tests will confirm the conclusions drawn in the paper.

INTRODUCTION

With the advance of the wireless devices a number of application area for such devices emerged. Prime candidate for revolutionising the way it works with implementing the wireless technologies as information gathering and distributing tool are ITS. This situation has been recognised by the EU research bodies and a number of projects have been funded. Examples of such projects are DRIVE [3], GST [4] and SAFESPOT [5]. The main aim of all these projects is to help the drivers in enhancing their road safety, effectiveness and comfort. One opportunity that arises from all this research is to develop novel algorithms capable of identifying and distributing the state of the traffic in real-time without using any infrastructure. This requires that relevant information be exchanged on regular intervals between vehicles, effectively creating a cooperative systems for information delivery. Such information identification and delivery must be efficient and quick and depends on how capable the core communications platform is. The main governing factor and concern, though, of the effectiveness and productivity of the applications is the communication technologies used in ITS. Till now, the idea of connecting car-to-car has not been explored and the chief form of communication has been connecting a car to a cell station (infrastructure node) [6], which only makes it more important to build a wireless traffic information systems based on car-to-car communication. This can be done by developing new paradigms for the functioning of wireless mobile computers in Mobile Ad Hoc Networks (MANET) [7].
In this paper a novel such algorithm is described, implemented and tested. The results obtained are showed that algorithm could become essential part of any ITS development.

ALGORITHM FOR COMMUNICATION

The theoretical solution of the problem requires a model for behaviour of moving vehicles which are the target objects of the system. The creation of a full probabilistic behavioural model is a very complicated problem whose development is outside of the purposes of this paper. For the needs for testing the algorithm it is used simplified behavioural model of moving vehicles.

Modelling the behaviour of a moving vehicle

The model should be sufficiently generalized to represent different stages of a vehicle moving cycle – stopped stage, starting stage, uniform movement and stopping stage.

A model of behaviour in [1] is used as a standard for testing fuel consumption for a vehicle in city driving cycle. This model is parameterized for each of the stages shown above.

This model is described as duration in seconds for every stage and it is shown on the figure 1.

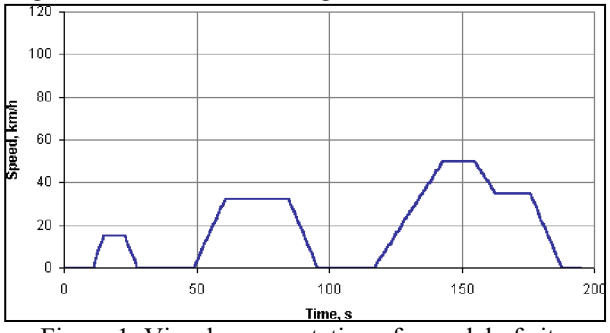

Figure 1: Visual representation of a model of city driving cycle.

This is the model also which is used for calculating the average speed.

Proceedings 27th European Conference on Modelling and Simulation ©ECMS Webjørn Rekdalsbakken, Robin T. Bye, Houxiang Zhang (Editors)
ISBN: 978-0-9564944-6-7 / ISBN: 978-0-9564944-7-4 (CD)

Research for the role of driving lanes in data package transmission

Let it be assumed that the lanes of a given road read section have the same number of vehicles and the distances between them are equal and all of the automobiles have the same radio coverage radius. Therefore, from a statistical point of view, the probability of transmitting data package into middle lane is greater than transmitting it to one of the side lanes.

The purposes of the lanes are that the leftmost is used by faster vehicles and the rightmost – by slower ones (the opposite orientation in the UK). Therefore, the speed in the middle lane is between the other two.

It can be concluded that statistical participation of the lanes is not critical for a given road section.
The communication network should provide the ability of dynamical adding and removing participants. In this case it is necessary to create a protocol which will provide a rule for responding when more than one vehicle receives a data package. There are several different methods for prioritizing the access to the wireless media. One of them is prioritizing it by using a number as a function of distance between the sender and the receiver. In that case the priority for responding is defined as a time delay and the problem with adding and removing vehicles from the network is not critical and the changes in the distances between them is forming the priority dynamically. The priority can be formed in two different ways: "the closest vehicle responds first" and "the farthest vehicle responds first".

A comparison between the algorithms "the closest vehicle responds first" and "the farthest vehicle responds first"

On figure 2 is shown a conditional formation of groups of vehicles on a road section with close speed and small distance between them. Dotted arrows show the movement of data packet which is transmitting using the algorithm "the closest vehicle responds first" (algorithm 1) and in solid lines using "the farthest vehicle responds first" (algorithm 2).

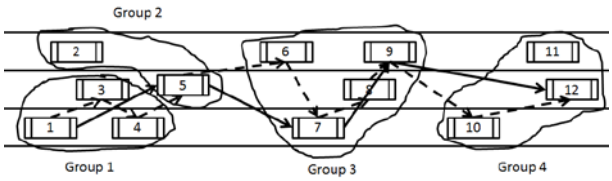

Figure 2: Visual comparison of the two algorithms

In table 1 it is shown the percentage of participation of every group using these two algorithms and the actual percentage of participation.

Group	Actual part.	Algorithm 1	Algorithm 2
Gr. 1	25%	30%	20%
Gr. 2	16.7%	10%	20%
Gr. 3	33.3%	40%	40%
Gr. 4	25%	20%	20%
Number of packages		9	5

Table 1: Participation of every group

As shown on the table the participation of every group using the algorithms is almost the same, so it can be concluded that the average speed using "the farthest vehicle responds first" provides approximately the same result and the time for distribution the data is less because of the smaller amount of responding vehicles. Therefore this algorithm can be used for determining the timeout.

Main parameters for the algorithm for propagating the data

The purpose of the algorithm is to transmit data about the average speed for a road section, so the propagation of the data is in the opposite direction of vehicle movement direction. In this case it is able to warn vehicles which enter the specific road section.

The packets are broadcasted, so the data can be received from every vehicle which is under the coverage of the sending vehicle. For this purpose the package should have fields for the geographic coordinates and the direction of movement. When the package is received every vehicle can determine if it has to process the data.

According to the constraints about propagation the data the only vehicles which should broadcast the package are behind the sender. In order to include the cases when the road bends it is necessary to define a requirement for a vehicle which is behind the sender and it is moving in the same direction as the sender.

1. *Condition for unidirectional movement of two cars* – the difference between the direction of the sender and the receiver should be less than 45^{o}.
2. *Condition for disposition of the receiver behind the sender* – the angle of rotation of the sender according to its current direction should be between 135^{o} and 225^{o}.

When both conditions are true the receiver becomes a candidate for propagating the data.

The choice is among all of the candidates. Because one device does not have an ability to know how many devices are around it, so it is necessary marks be used. The mark is for independent determination of the next sender. This mark is the time. If every candidate waits a different time, the one with the smallest timeout is able to send its modified data. The distance between the sender and the receiver is used to determine the timeout. This distance is different for every candidate, so the

timeout is different. There are two ways for determination of the timeout:

1. The timeout is decreasing with increasing the distance - "the farthest vehicle responds first"
2. The timeout is increasing with increasing the distance "the closest vehicle responds first"

Data structure of transmitting packages

1. Longitude
2. Latitude
3. Average speed in the current road section
4. Number of measurements
5. Moving direction of the sender
6. Fixed array of real numbers which presents the geographic coordinates of the path of measurements.

Calculating average speed for a vehicle

The speed from a GPS receiver is instantaneous. Therefore, the average speed should be calculated using several different in time records. The algorithm which is used is "moving average" [1]. It is low pass filter. It is calculating V_{avgK} from last N speed records using formula 1 where K is the number of current measurement.

$$V_{avgK} = \sum_{n=K-N}^{K} \frac{V_n}{N} \qquad (1)$$

This algorithm needs at least N measurements to be stored which uses memory and every time when there is a new measurement it takes N steps to calculate the new value.

For optimizing the calculation only the last average speed $V_{\text{avg K-1}}$ should be stored. The new average speed has to be calculated using formula 2.

$$V_{avgK} = \frac{(N-1)V_{avg\ K-1} + V_K}{N} \qquad (2)$$

Calculating average speed for a road section

The calculation of the average speed is performed again with the modified "moving average" algorithm. This time every vehicle which is broadcasting the package is adding its data to the received average speed data. The additional data has a specific weight and it depends on the previous number of vehicles which broadcasted the package. The calculation is via formula 3.

$$V_{avg\ street} = \frac{NV_{avg\ street\ prev} + V_{avgK}}{N+1} \qquad (3)$$

When the maximum number of vehicles M is reached the calculation uses formula 4.

$$V_{avg\ street} = \frac{(M-1)V_{avg\ street\ prev} + V_{avgK}}{M} \qquad (4)$$

Describing the goals for the algorithm

The realization of the algorithm aims maximum coverage of vehicles on a specific road section, minimum amount of sent packages – for avoiding overloading the network, maximum speed of propagation the data. The propagation of the data is unidirectional and the direction is opposite the direction of vehicles movement. In this case the cars ahead inform the cars to the rear and the new vehicles for this road section.

The direction of propagation is based on the last vehicle which broadcast the data.

Behaviour of the receiver

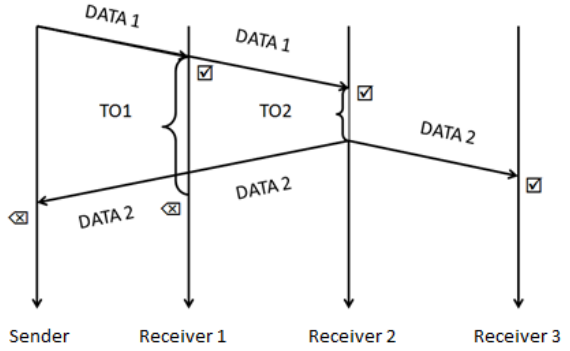

Figure 3: Timing diagram of receiving and broadcasting a package

When a device receives a package, it checks if the direction of movement is the same as its own, it calculates the distance from the sender and the orientation to it. In case the receiver is behind the sender, the receiver stores the data and changes its state to a candidate for broadcasting (☑ on fig. 3). The next sending will be from the farthest candidate**.** The distance from the sender is converted into timeout (TO1 and TO2 on fig. 3), so the longer distance means shorter timeout, so the farthest is able to broadcast its first data when time is up. If a package is received before the timeout and this package is with the same direction of movement but it is received from a source which is behind the current receiver it means that another candidate has broadcasted the data before the current one. Then the timeout is stopped and the current vehicle is no longer a candidate for broadcasting (⌫ on fig. 3).

Behaviour of the sender

A specific vehicle can send a package via the wireless connection in two cases. The first case is when until the timeout event no packages were received which fulfil the conditions from above. Then the device-sender modifies the fields in the package with its own geographic coordinates, direction of movement, calculates new average speed (from the old package and

the average speed at this time), and modifies the number of vehicles.

The second case when a device can broadcast a package is after a specific time when no package was received which fulfils the conditions. This process is called evoking a package.

EXPERIMENTS AND RESULTS

Experiment 1

This experiment is to compare the behaviour of the algorithms in cases where the next sender is fixed N positions away from the current sender and in cases where the next sender is on random positions away in a specific range.

The experimental set is using the described model of movement for a single vehicle.

Let it be assumed that there exists a single lane road, where the distance between vehicles is one second. Every vehicle is using the same model. This will test a behaviour of a motorcade on a road with different obstacles like pedestrians, traffic lights etc.

The comparison between the algorithms is based on the average difference from the absolute average speed and the standard deviation. On figure 4 is shown the simulation set.

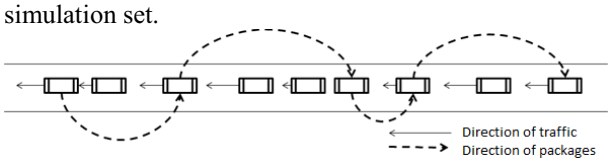

Figure 4: Simulation set for experiment 1

Test configurations of the experiment:

- The distance between the current and the next sender is fixed N positions where N = {1,3,5}
- The distance between the current and the next sender is random positions within the scope. The skipped cars receive the package but they do not broadcast it. The parameter M defines the maximum of a step. This configuration is tested for M = {6, 10}. The values of M are pursuant with the maximum range of IEEE 802.11b transmitters and the number of covered vehicles.
- The distance between the current and the next sender is defined as "the farthest vehicle responds first". The maximum range is 10. There are chosen randomly K cars and the next sender is the one with the greatest value. The test is for values of K = {2, 3}.

Table 2: Set of configurations for experiment 1

Config.	Description	Max leap
1	Each subsequent broadcast	1
2	Every third broadcasts	3
3	Every fifth broadcasts	5
4	A random of next 6 broadcasts	6
5	A random of next 10 broadcasts	10
6	Greater from 2 random broadcasts	10
7	The greatest from 3 random broadcasts	10

The input data for the simulation uses the described model of behaviour of a moving vehicle. The model is defined as speed as function of time in seconds v(t). The position of every vehicle in the motorcade is defined as a delay in seconds from the first car. For example: the car at place k has speed v(t-k). The model is defined for finite number of seconds. In case of t-k < 0 the taken value is (t-k) mod M, where M is the maximum value of seconds where speed is defined.

The output data from the simulation is presented in text files, where every file represents the output data for a certain configuration. The results are real numbers, written on a separate lines and every line is for one tracking of the package from the begin to the end. The count of generated tracings for each configuration is 1 million.

Due to the large number of tracings for the analyses histograms are used. They show the distribution of calculated average speed for each configuration.

The absolute average speed of all cars in the simulation is 17.661 km/h. This speed is used as a reference.

In table 3 are shown the results for each configuration.

Table 3: Results for each configuration

Configurations	Average speed (km/h)	Standard deviation (σ)	Difference with the absolute average speed (km/h)
1	17.5656	7.9549	-0.0951
2	18.1732	3.4089	0.5125
3	18.2307	1.7714	0.5700
4	18.2259	3.3698	0.5652
5	18.2774	1.9673	0.6167
6	18.2473	1.5286	0.5866
7	18.2453	1.4535	0.5846

On figure 4a,b,c,d,e,f,h are shown the histograms of the average speed for each configuration. The horizontal scale for every histogram is the same.

From the results it is clearly shown that the algorithm "the farthest vehicle responds first" causes a "shrinking" in the histograms and the standard deviation decreases. It is shown that the difference between the absolute average speed and the calculated average speed is about 3.3%.

This experiment leads to the following conclusion: applying the algorithm "the farthest vehicle responds first" does not affect the calculated average speed and the distribution of measured average speeds on multiple tests remains the same. Therefore the algorithm is reliable and can be applied.

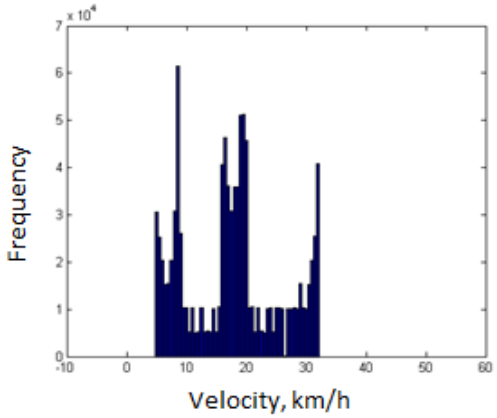

Figure 4a (above): Each subsequent broadcast

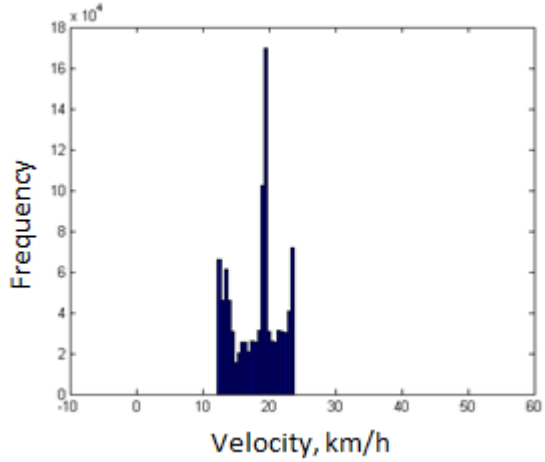

Figure 4b (above): Every third broadcast

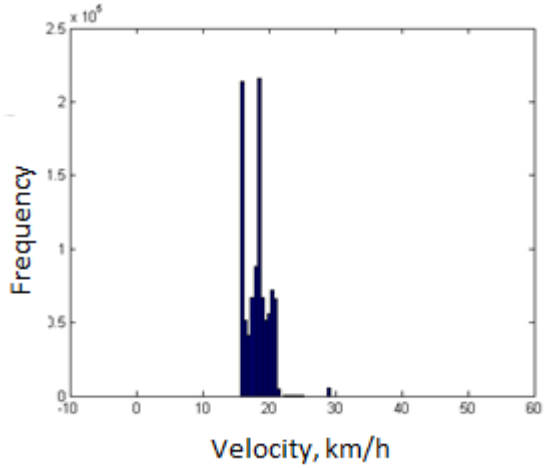

Figure 4c (above): Every fifth broadcast

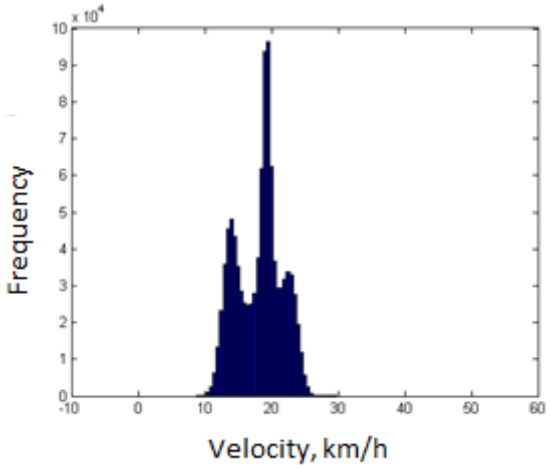

Figure 4d (above): A random sample of next 6 broadcasts

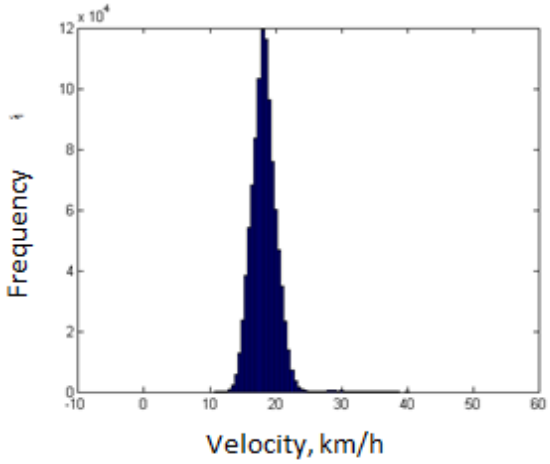

Figure 4e (above): A random sample of next 10 broadcasts

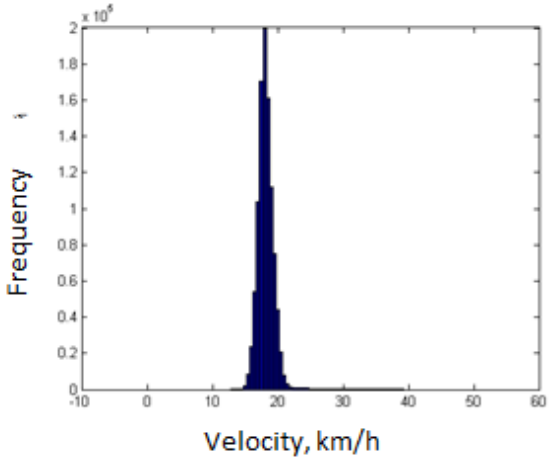

Figure 4f (above): Greater than 2 random broadcasts

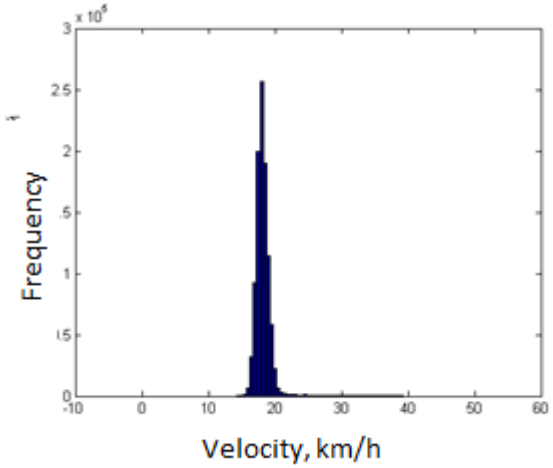

Figure 4g (above): The greatest of 3 random broadcasts

Experiment 2

This experiment is to study the average time for transmitting the package from the beginning of a motorcade to its end and the average time of delay between the intermediate points using the algorithm "the farthest vehicle responds first". For this experiment is used the experimental set, shown on figure 5, like the previous experiment. With t_N are shown the timeout for a specific vehicle before sending the package and T is for the total time from the beginning to the end.

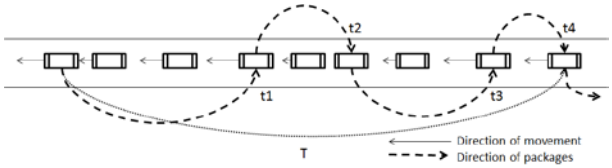

Figure 5: Simulation set for experiment 2

The algorithm "the farthest algorithm responds first" is tested for maximum range 10, where K random numbers are chosen. The greatest of them is the new next sender. Test values for K = {1, 2, 3}. This will show the behaviour of the algorithm on the average time delay as a function of the density of the traffic. Density of the traffic means mans the number of vehicles covered by the sender which have ability to broadcast. The test configurations are shown in the table 4:

Table 4: Configurations for experiment 2

Config.	Description	Density	Max. leap
1	A random sample of next 10 broadcasts	50%	10
2	Greater from 2 random broadcasts	75%	10
3	The greatest of 3 random broadcasts	87.5%	10

The input data for the simulator is a generator of pseudo random. It generates the size of leaps between two positions on the path of the data. The leaps are converted in timeout using a function. The total delay is a sum of every single delay. The average timeout is defined as total delay divided by number of vehicles which broadcast the data.

The output data of the simulation are text files. Every file contains data for one of the test configurations. The results are real numbers written in two columns which are average timeout and total delay. There are 1 million tests for each configuration.

In table 5 are shown the results for every configuration.

Config.	1	2	3
Min t, sec	2.6670	1.7080	1.3480
Average t,sec	4.9665	3.4965	2.7633
Max t, sec	6.6210	5.1950	4.3140
Standard deviation (σ)	0.4124	0.3805	0.3273
Total delay, sec	198.648	108.078	76.667

In figure 6 are shown the visual comparison of the configurations.

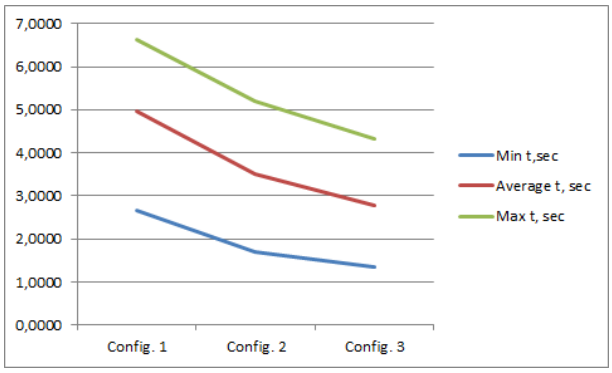

Figure 6: Minimum, Average, Maximum timeouts for every configuration

Figures 7 a, b, c show the histograms of average time delay for different types of density of the traffic – 50%, 75%, 87.5%.

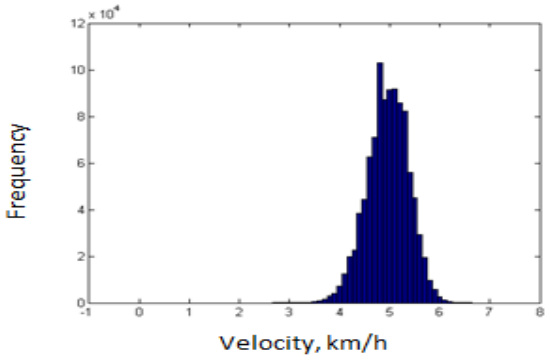

Figure 7a (above): A random sample of next 10 broadcasts

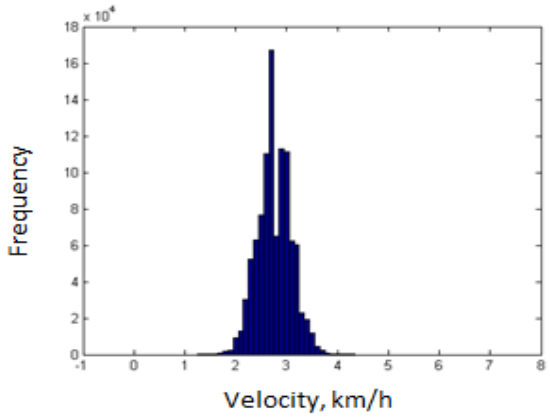

Figure 7b (above): Greater from 2 random broadcasts

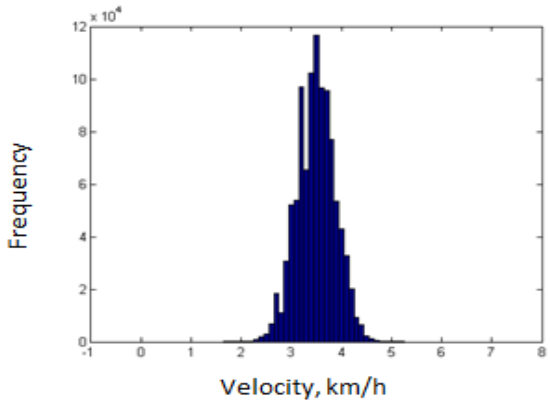

Figure 7c (above): The greatest of 3 random broadcasts

CONCLUSIONS:

Based on the results of the experiment it can be concluded that increasing the density of the average timeout decreases, so in case of situations with higher level of density (e.g. traffic jams) the speed of propagation is faster than without high density.

The algorithm for sending data about the average speed of a road section works successfully and proves the results. The speed of propagation can be increased by using proper hardware realization of device. The amount of data and the packages is low, so the risk of flooding the network is small.

These experiments showed that the distribution of measured average speeds on multiple tests remains the same. Therefore the algorithm is reliable and can be applied for estimating the average speed of the traffic in a given street.

REFERENCES:

[1] Steven W. Smith: The Scientist and Engineer's Guide to Digital Signal Processing, Chapter 15:277-284, California Technical Pub. 1997, ISBN-13: 978-0966017632

[2] EEC Directive 90/C81/01, Emission test cycles for certification of light duty vehicles in Europe, EEC emission cycles (1999)

[3] L. Christodoulides, T. Sammut and R. Tönjes, "DRiVE towards systems beyond 3G," *Proceedings of SCI,* 2001.

[4] GST project, "http://www.gstproject.org"

[5] SAFESPOT, "http://www.safespot-eu.org/pages/page.php"

[6] N. R. Mustary, R. Chander and M. N. Ahmed Baig, "A performance evaluation of VANET for intelligent transportation system," *World Journal of Science and Technology,* vol. 2, 2013.

[7] S. Xu, P. Guo, B. Xu and H. Zhou, "QoS Evaluation of VANET Routing Protocols," *Journal of Networks,* vol. 8, pp. 132-139, 2013.

[8] C. Ma and N. Liu, "Traffic-Aware Data Delivery Scheme for Urban Vehicular Sensor Networks," *International Journal of Distributed Sensor Networks,* vol. 2013, 2013.

[9] L. Uichin, S. Y. OH, M. GERLA, D. S. LUN and W. W. RO, "Delay analysis of car-to-car reliable data delivery strategies based on data mulling with network coding," *IEICE Trans. Inf. Syst.,* vol. 91, pp. 2524-2527, 2008.

[10] V. D. Khairnar and S. N. Pradhan, "Simulation Based Evaluation of Highway Road Scenario between DSRC/802.11 p MAC Protocol and STDMA for Vehicle-to-Vehicle Communication," *Journal of Transportation Technologies,* vol. 3, pp. 88-104, 2013.

AUTHOR BIOGRAPHIES

Boyan B. Petrov was born in Plovdiv, Bulgaria and went to Technical University - Sofia, where he studied "Computer systems and technology" and obtained his bachelor degree in 2012. His e-mail address is: `b_petrov@tu-sofia.bg` and his Web-page can be found at `http://pxpress.net`

Dr Evtim Peytchev is Reader in Wireless, Mobile and Pervasive Computing at School of Science and Technology, Nottingham Trent University, Nottingham, UK. He is research leader of the Intelligent Simulation, Modelling and Networking Group at the school. The group consists of 15 research students, research fellows and lecturers working in the area of Intelligent Transportation Systems (ITS) and it has to its credit numerous journal and conference publications in the area of ad-hoc wireless and mobile networking with traffic information systems as an application domain.

LOGISTIC MODELLING OF ORDER REALIZATION IN THE COMPLEX PARALLEL MANUFACTURING SYSTEM

Bronislav Chramcov
Tomas Bata University in Zlin
Faculty of Applied Informatics
nam. T.G.M 5555, 760 01 Zlin, Czech Republic
Email: chramcov@fai.utb.cz

Robert Bucki
Institute of Management and Information
Technology in Bielsko-Biała
ul. Legionów 81, 43-300 Bielsko-Biała, Poland
Email: rbucki@wsi.edu.pl

KEYWORDS
Heuristic algorithm, discrete event simulation, production system, logistic system, mathematical modelling, optimization criteria, manufacturing strategies

ABSTRACT

The paper highlights the problem of mathematical modeling of the highly complex manufacturing system in which work stations are arranged serially within each production plant. Production plants are located in a parallel way. The specification details and the model resulting from them led to creating the simulator to be employed to solve the problem of realizing customers' orders. Equations of state are given to illustrate the state of the system at each stage. The complex system is controlled by implementing heuristic algorithms. The criteria to be met are defined. The study case is based on randomly generated data and solved by means of the dedicated information tool. The search for the satisfactory solution is carried out either by an increased number of simulation runs or comparing the pairs or combinations of order and plant choosing algorithms. The main goal remains to meet the stated criterion.

INTRODUCTION

The growth of markets towards globalization results in materialization of automated industries with high performance of manufacturing systems. Traditional manufacturing systems are no longer able to satisfy these requirements. In the global market there is an increasing trend toward achieving a higher level of integration between designed and manufacturing functions in industries to make the operations more efficient and productive (Modrak and Pandian 2012).
Effective organization and management of materials, processes and human resources of a company is a prerequisite in today's highly competitive industrial landscape. Key goals are to improve planning and scheduling of processes, increase productivity, minimize inventory level, improve responsiveness to changes in demand, improve quality, and lower operation cost.
These problems are solvable with the use of modelling and simulation of such production systems. One of the most useful tools in the arsenal of an operations research (industrial engineering) management science analyst consists in computer simulation. In this case it is necessary to put attention to the benefits resulting from combining both spheres, the one of formalized algorithms and the other one of the human instinct (Neumann 2011).
The use of simulation, as a support tool to the operational decision making process, allows us to analyze, from a statistical point of view, the behavior of a production or logistic system that is subject generally to either controllable and or not controllable factors. Through computer simulation it is possible to select those operational decisions that maximize an objective function or a system performance parameter, and to evaluate effects of these decisions without controllable factors variability. An approach to implement efficiently and effectively simulation models in manufacturing systems is deployed in (Chramcov et al. 2011). Currently, a wide range of commercial products which use graphic interfaces (e.g. Arena, Witness, MapleSim 4, AutoMod, Quest, PlantSimulation, etc.) offer an extremely wide spectrum of possibilities for modelling and simulation of manufacturing, logistic and other queuing systems (Rizzoli 2009). Nevertheless, the general language C# has been adopted for creation of our production system simulator because the programming logic cannot be easily expressed in GUI-based systems (Babich and Bylev 1991).
The initial specification and consequent modelling of the discussed manufacturing system is described in detail in (Bucki et al. 2012a). This paper is later expanded to the simulation form enabling us to carry out a simple simulation process (Bucki et al. 2012b). The simulation process shows that one of the suggested heuristics minimizes the total order realization time. However, the need to search for the solution to tasks carried out in the complex manufacturing system with buffer stores leads to extending specification details and the subsequent model which finally forms the basics for the simulation process (Bucki 2012). The simulation process is carried out by means of the simulation tool built on the basis of these specification details and the subsequent model (Marusza 2013).

GENERAL SYSTEM FORMULATION

Let us propose the information system imitating the continuous production process carried out in J work

Proceedings 27th European Conference on Modelling and Simulation ©ECMS Webjørn Rekdalsbakken, Robin T. Bye, Houxiang Zhang (Editors)
ISBN: 978-0-9564944-6-7 / ISBN: 978-0-9564944-7-4 (CD)

stations arranged in a series. We assume that there is a machine in each work station which can perform *I* operations. However, we assume that only one tool can be determined to perform the operation on the order unit in each work station. We assume there are buffer stores between the work stations. The capacity of each buffer store is limited. Operations are performed in the work stations in sequence. Further, we assume there are more than one identical production systems available. Let us assume that *A* manufacturing plants are arranged in parallel. This system requires *K* stages to realize the order elements. The matrix of orders at the *k*-th stage is considered in the form (1), where $z_{m,n}^{k}$ is the number of conventional units of the *n*-th order of the *m*-th customer at the *k*-th stage. The stage *k*, *k*=1,…,*K* is the moment of making the production decision.

$$Z^{k} = \left[z_{m,n}^{k} \right] \ ,m=1,...,M;\ n=1,...,N;\ k=1,...,K \tag{1}$$

The order matrix is modified after every decision about production in accordance with the specification (2).

$$z_{m,n}^{k} = \begin{cases} z_{m,n}^{k-1} - x_{m,n}^{k} & \text{if the number of units } x_{m,n}^{k} \\ & \text{is realized at the } k-\text{th stage}, \\ z_{m,n}^{k-1} & \text{otherwise.} \end{cases} \tag{2}$$

Some of the charge materials are used for manufacturing products of the specific order. The assignment matrix of ordered products to charges takes the form (3), where $\omega_{m,n}$ is the number of charge material assigned to the order $z_{m,n}$

$$\Omega = \left[\omega_{m,n} \right] \ , m=1,...,M;\ n=1,...,N \tag{3}$$

Elements of the assignment matrix take values according to (4).

$$\omega_{m,n} = \begin{cases} l & \text{if the order } z_{m,n} \text{ is realized} \\ & \text{from the } l-\text{th charge}, \\ 0 & \text{otherwise.} \end{cases} \tag{4}$$

We also assume that used charge matrix elements are immediately supplemented, which means that we treat them as the constant source of charge material. However, for simplicity reasons, we assume that each *n*-th order of the *m*-th customer is made from the universal charge which enables realization of the given element of the order from any *l*-th charge.

Let *h*, *(h=1,...,H)* be the allowable number of regeneration procedures of the tool. If *h=0*, then the *i*-th tool is subject to replacement. Otherwise, the *i*-th tool can be regenerated *h* times.

General structure of the system

Let us introduce the general structure (assignment matrix) in the form (5) for realizing the order $z_{m,n}$ in each manufacturing plant, where the elements of this structure $e_{m,n}(i,j)$ take values according to (6).

$$E_{m,n} = \left[e_{m,n}(i,j) \right] \tag{5}$$

$$e_{m,n}(i,j) = \begin{cases} 1 & \text{if the } i\text{-th tool is able to be used} \\ & \text{in the } j\text{-th workstation in order} \\ & \text{to realize the order } z_{m,n}\ , \\ 0 & \text{otherwise.} \end{cases} \tag{6}$$

Let us define the route vector of orders in the form (7) where $d_{m,n}(j)$ is the number of the tool in the *j*-th work station to realize the order $z_{m,n}$.

$$D_{m,n} = \left[d_{m,n}(j) \right] \tag{7}$$

If the order $z_{m,n}$ is not realized in the *j*-th work station then $d_{m,n}(j) = 0$.

Life of the tool

The base life vector of the complex system for a new brand set of tools used to manufacture elements of the order matrix takes the form (8), where *g(i)* is the base number of units which can be manufactured by the *i*-th tool before the tool in this station is completely worn out and requires immediate replacement (should there be no active work station, then *g(i)* =-1).

$$G = \left[g(i) \right] \ ;\ i=1,...,I \tag{8}$$

Let $\Psi(i) = \left[\psi_{m,n}(i) \right]$ be the matrix of conversion factors determining how many units of the order $z_{m,n}$ can be realized with the use of the *i*-th tool in each work station, $\psi_{m,n}(i) > 0$. If the order $z_{m,n}$ is not realized by the *i*-th tool at all, then $\psi_{m,n}(i) = -1$.

Let us now define the life matrix for realizing the order $z_{m,n}$ in the form (9), where the life matrix element $g_{m,n}(i)$ is the base number of the order $z_{m,n}$ conventional units which can be realized by means of the *i*-th tool before the tool is completely worn out. This element takes the values according to (10).

$$G(i) = \left[g_{m,n}(i) \right] \tag{9}$$

$$g_{m,n}(i) = \psi_{m,n}(i) \cdot g(i) \tag{10}$$

Buffers

Let $b_{j,\alpha}$ be the buffer store between the *j*-th workstation and the workstation *(j+1)*, *(j=1,...,J-1)* in the α-th manufacturing plant. The capacity of each buffer store is calculated in the number of the ordered semi-products $z_{m,n}$.

Let us introduce now the base capacity matrix of buffer stores in the complex manufacturing system in the form (11), where $gb(j,\alpha)$ is the base capacity of the *j*-th buffer store in the α-th manufacturing plant

$$Gb = [gb(j,\alpha)] \tag{11}$$

STATE OF THE SYSTEM

The state of the complex system consisting of parallel manufacturing plants (state of their tools) changes after every decision about production of the element $z_{m,n}$ in the α-th manufacturing plant. The state of the *i*-th tool in the *j*-th work station in case of the order $z_{m,n}$ manufacturing changes according to (12) where $s^k_{m,n}(i,j,\alpha)$ is the number of conventional units of the order $z_{m,n}$ already realized by the *i*-th tool in the *j*-th work station in the α-th manufacturing plant. This element takes the value according to (13) where $x^k_{m,n}(i,j,\alpha)$ is the number of the order $z_{m,n}$ units realized by the *i*-th tool in the *j*-th work station in the α-th manufacturing plant at the *k*-th stage.

$$s^0_{m,n}(i,j,\alpha) \rightarrow ... \rightarrow s^k_{m,n}(i,j,\alpha) \rightarrow ... \rightarrow s^K_{m,n}(i,j,\alpha) \tag{12}$$

$$s^k_{m,n}(i,j,\alpha) = \begin{cases} s^{k-1}_{m,n}(i,j,\alpha) - \text{if the order } z_{m,n} \\ \text{is not realized by the } i-\text{th tool} \\ \text{in the } j-\text{th workstation of the } \alpha-\text{th} \\ \text{plant at the } k-\text{th stage} \\ \\ s^{k-1}_{m,n}(i,j,\alpha) + x^k_{m,n}(i,j,\alpha) \quad \text{otherwise} \end{cases} \tag{13}$$

The base state of the *i*-th tool in the *j*-th workstation in the α-th manufacturing plant is calculated according to (14).

$$s^k(i,j,\alpha) = \frac{s^k_{m,n}(i,j,\alpha)}{\psi_{m,n}(i)} \tag{14}$$

If in case of another unit of the order $z_{m,n}$ the state of the station is exceeded, it is marked as $s^k_{m,n}(i,j,\alpha) = -1$. It means no unit of any order can be realized in the manufacturing plant and it triggers the need to carry out the replacement process to resume the production in the discussed work station. If the *i*-th tool has to be replaced with a new one, the state of this tool changes to zero after carrying out the replacement procedure.

If the *i*-th tool in the *j*-th work station in the α-th manufacturing plant is not used at the *k*-th stage, then $s^k_{m,n}(i,j,\alpha) = -1$.

Flow capacity of the system

Let $P^k_{m,n}(\alpha) = [p^k_{m,n}(i,j,\alpha)]$ be the matrix of the flow capacity of the α-th manufacturing plant for the order $z_{m,n}$ realization at the *k*-th stage where $p^k_{m,n}(i,j,\alpha)$ is the number of conventional units of the order $z_{m,n}$ which still can be realized with the use of the *i*-th tool in the *j*-th work station of the α-th manufacturing plant. If the flow capacity of the work station does not allow to realize at least one conventional unit of the order $z_{m,n}$ then $p^k_{m,n}(i,j,\alpha) = -1$. If there is remaining flow capacity in the *i*-th tool of the *j*-th work station but the subsequent unit of the order $z_{m,n}$ cannot be realized fully in this station, then the replacement process in this station is carried out automatically.

On the basis of the above assumptions the flow capacity of the *i*-th tool in the *j*-th work station of the α-th manufacturing plant for the order $z_{m,n}$ can be determined in the form (15).

$$p^k_{m,n}(i,j,\alpha) = g_{m,n}(i) - s^k_{m,n}(i,j,\alpha) \tag{15}$$

The base flow capacity of the *i*-th tool in the *j*-th workstation in the α-th manufacturing plant is calculated according to the form (16).

$$p^k(i,j,\alpha) = \frac{p^k_{m,n}(i,j,\alpha)}{\psi_{m,n}(i)} \tag{16}$$

It is then possible to calculate the total base flow capacity of the α-th manufacturing plant at the *k*-th stage according to the formula (17).

$$P^k(\alpha) = \sum_{i=1}^{I}\sum_{j=1}^{J} p^k(i,j,\alpha) \tag{17}$$

PRODUCTION TIME

It is possible to define the matrix of production times in the form (18) where $\tau^{pr}_{m,n}(i,j)$ is the time of realization one conventional unit of the order $z_{m,n}$ with the use of the *i*-th tool in the *j*-th work station.

$$T^{pr}_{m,n} = [\tau^{pr}_{m,n}(i,j)] \tag{18}$$

If the order $z_{m,n}$ is not realized in the *j*-th work station with the use of the *i*-th tool, then $\tau^{pr}_{m,n}(i,j) = -1$.

Throughout the manufacturing process tools get worn out and require replacement. The manufacturing process is brought to a standstill in the work station in which the tool cannot realize any order and, as a consequence, leads to stopping production activities in preceding work stations. For this reason, the replacement is to be carried out as fast as possible.

Let us define the vector of replacement times for the tools in the form (19) where $\tau^{repl}(i)$ represents the replacement time of the *i*-th tool.

$$T^{repl} = \left[\tau^{repl}(i)\right] \tag{19}$$

If the *i*-th tool is not implemented in the production process, then $\tau^{repl}(i) = -1$.

The total manufacturing time of all orders is calculated in accordance with the formula (20) where ΔT is the time during which elements are manufactured simultaneously.

$$T = \sum_{\alpha=1}^{A}\sum_{m=1}^{M}\sum_{n=1}^{N}\sum_{i=1}^{I}\sum_{j=1}^{J} y'(i,j,\alpha)^k \cdot \tau_{m,n}^{pr}(i,j) + \\ + \sum_{\alpha=1}^{A}\sum_{k=0}^{K}\sum_{i=1}^{I}\sum_{j=1}^{J} y''(i,j,\alpha)^k \cdot \tau^{repl}(i) - \Delta T \tag{20}$$

The variable $y'(i,j,\alpha)^k$ represents the value indicating realizing one conventional unit of the product $z_{m,n}$ with the use of the *i*-th tool in the *j*-th work station in the α-th manufacturing plant at the *k*-th stage and $y''(i,j,\alpha)^k$ represents the value indicating replacement of the *i*-th tool in the *j*-th work station in the α-th manufacturing plant at *k*-th stage. Moreover, the variables mentioned above take their values according to the form (21) or (22).

$$y'(i,j,\alpha)^k = \begin{cases} 1 & \text{if realizing the order } z_{m,n} \text{ with the use of the } i\text{-th tool in the } j\text{-th workstation in the } \alpha\text{ - th manufacturing plant at the k - th stage is carried out,} \\ 0 & \text{otherwise.} \end{cases} \tag{21}$$

$$y''(i,j,\alpha)^k = \begin{cases} 1 & \text{if the replacement procedure of the } i\text{-th tool in the } j\text{-th work station in the } \alpha\text{ - th manufacturing plant at the } k\text{-th stage is carried out,} \\ 0 & \text{otherwise.} \end{cases} \tag{22}$$

CONTROL OF THE SYSTEM

The control of the complex of manufacturing systems consists in implementing heuristic algorithms which choose:

- a manufacturing plant from the set of plants to place the order to be realized
- an order from the matrix of orders Z^k for manufacturing.

There are some heuristic algorithms which can be put forward. The control algorithm of either the maximal or minimal orders and the algorithm of either maximal and minimal flow capacity.

The algorithm of the maximal flow capacity of the production plant

This algorithm chooses the α-th manufacturing plant for order realization on condition that it is characterized by the maximal coefficient $\xi^k(\alpha) = \sum_{i=1}^{I}\sum_{j=1}^{J} p_{m,n}^k(i,j,\alpha)$. To determine the λ-th manufacturing plan, where $1 \le \lambda \le \mathrm{A}$, the condition (23) must be met, where $\xi^k(\lambda) = \xi^k(\alpha)$.

$$\left[q_{\max}^k(\alpha) = \xi^k(\lambda)\right] \Leftrightarrow \left[\xi^k(\lambda) = \max_{1\le\alpha\le \mathrm{A}} \xi^k(\alpha)\right] \tag{23}$$

The algorithm of the minimal flow capacity of the production plant

This algorithm chooses the α-th manufacturing plant for order realization on condition that it is characterized by the maximal coefficient $\xi^k(\alpha) = \sum_{i=1}^{I}\sum_{j=1}^{J} p_{m,n}^k(i,j,\alpha)$. To determine the λ-th plant for order realization, where $1 \le \lambda \le \mathrm{A}$, the condition (24) must be met, where $\xi^k(\lambda) = \xi^k(\alpha)$.

$$\left[q_{\min}^k(\alpha) = \xi^k(\lambda)\right] \Leftrightarrow \left[\xi^k(\lambda) = \min_{1\le\alpha\le \mathrm{A}} \xi^k(\alpha)\right] \tag{24}$$

The algorithm of the maximal order

This algorithm chooses the order matrix element characterized by the maximal value $\gamma_{m,n}^k$. To produce the order $z_{\mu,\eta}^k$, $1 \le \mu \le M$, $1 \le \eta \le N$ the condition in the form (25) must be met, where $\gamma_{m,n}^k = z_{m,n}^k$.

$$(q_{z_{\max}}^k = z_{\mu,\eta}^k) \Leftrightarrow \left[\gamma_{\mu,\eta}^k = \max_{\substack{1\le m\le M \\ 1\le n\le N}} \gamma_{m,n}^k\right] \tag{25}$$

The algorithm of the minimal order

This algorithm chooses the order matrix element characterized by the minimal value $\gamma_{m,n}^{k}$. To produce the order $z_{\mu,\eta}^{k}$, $1 \le \mu \le M$, $1 \le \eta \le N$ the condition in the form (26) must be met, where $\gamma_{m,n}^{k} = z_{m,n}^{k}$.

$$(q_{z_{\max}}^{k} = z_{\mu,\eta}^{k}) \Leftrightarrow \left[\gamma_{\mu,\eta}^{k} = \min_{\substack{1 \le m \le M \\ 1 \le n \le N}} \gamma_{m,n}^{k} \right] \tag{26}$$

It is possible to use some manufacturing criteria for evaluation of used control algorithms. In this case, the total order realization time, the lost capacity due to the unavoidable replacement, the remaining capacity at the *K*-th stage and the total tool replacement time criterion are put forward.

CASE STUDY WITH THE USE OF THE SIMULATOR

The simulator of the general manufacturing system was created on the basis of the assumptions described above. The discussed simulator was created with the use of C# environment and it is used for simulating of the dedicated production system.

The simulator is the synthetic representation of the potential real system so the data must be given on condition they match the real ones. During the simulation process operations are analogous to the ones which are carried out in the real system. It is possible due to the fact that special methods were elaborated. These methods are responsible for moving elements between work stations, replacement of tools and carrying out production operations on semi-products. There are also methods responsible for directing orders to manufacturing plants. These methods use either heuristic algorithms or a random choice of orders. The whole process is carried out in a loop as long as all order matrix elements are completely realized and moved to the store of ready products.

Results and a production timescale in a graphic form for all manufacturing plants are presented after completing the simulation process. Simulation results are consequently used for the evaluation of used heuristic control algorithms.

Definition of the specific production system

The case study assumes that the complex production system consists of 3 identical manufacturing plants arranged in parallel. Each plant consists of 5 work stations arranged in a series. There are 5 tools that can perform dedicated operations in each work station. The tools cannot be regenerated. Four customers set orders to be realized by the production system. The number of conventional units of the orders for each specific customer is specified in the matrix (27).

$$Z^{0} = \begin{bmatrix} 240 & 2900 & 0 & 170 \\ 380 & 0 & 150 & 740 \\ 0 & 810 & 0 & 210 \end{bmatrix} \tag{27}$$

We assume that the charge is universal and each buffer store is inactive for this set of data. The orders are realized in accordance with the route vectors presented in the form (28).

$$D = \begin{bmatrix} \{1,2,4,3,5\} & \{2,1,3,5,4\} & \{0,0,0,0,0\} & \{2,4,1,3,5\} \\ \{3,2,1,5,4\} & \{0,0,0,0,0\} & \{4,2,1,3,5\} & \{2,1,4,5,3\} \\ \{0,0,0,0,0\} & \{5,2,1,3,4\} & \{0,0,0,0,0\} & \{2,4,1,5,3\} \end{bmatrix} \tag{28}$$

The base life vector for a new brand set of tools is given in the form (29) and the matrixes of conversion factors for all tools are specified according to (30).

$$G = [120,80,50,40,30] \tag{29}$$

$$\Psi(i) = \begin{bmatrix} 1 & 2 & -1 & 3 \\ 2 & -1 & 1 & 1 \\ -1 & 2 & -1 & 5 \end{bmatrix}, \quad i = 1,...,5 \tag{30}$$

The times of realization of one conventional unit of the order $z_{m,n}$ in each *j*-th workstation with the use of determined tools (according to the route matrix) are defined in the vectors (31).

$$\begin{aligned} &T_{1,1}^{pr} = [23,54,10,15,21], T_{1,2}^{pr} = [23,37,42,26,33], \\ &T_{1,4}^{pr} = [18,23,31,34,42], T_{2,1}^{pr} = [39,41,45,16,49], \\ &T_{2,3}^{pr} = [16,19,21,11,27], T_{2,4}^{pr} = [11,12,20,17,13], \\ &T_{3,2}^{pr} = [10,16,15,22,30], T_{3,4}^{pr} = [14,27,20,35,40], \end{aligned} \tag{31}$$

The vector of replacement times of tools is defined in the form (32).

$$T^{repl} = [15,13,9,5,26] \tag{32}$$

Results of the simulation

The simulation is to be run for some initial values of state of tools and for the discussed control algorithms. Firstly, a random choice of orders and manufacturing plants was used. The random choice was carried out 1000 times. The best results are shown for 10, 100 and 1000 simulations. Consequently, the orders were realized by means of 4 pairs of heuristic control algorithms.

The following control algorithms are implemented:

- the control algorithm of the maximal order [$\hbar$(max)],
- the algorithm of the minimal order [$\hbar$(min)],

- the algorithm of the maximal flow capacity of the production plant [ƛ (max)],
- the algorithm of the minimal flow capacity of the production plant [ƛ (max)].

Some manufacturing criteria are used for evaluation of the implemented control algorithms The results of the simulation for these manufacturing criteria are shown in the following tables. Table 1 presents the results of the total order realization time; the values of the lost capacity due to the unavoidable replacement are shown in Table 2. The values of the left capacity at the *K*-th stage are presented in Table 3. Table 4 shows the values of the total tool replacement time. The minimal or maximal values for each initial value of the state of tools are highlighted.

Table 1: The values of the total order realization time for used control algorithms

Control algorithm		Initial value of tool wear			
		0%	20%	40%	60%
Random choice (number of simuations)	1	137965	139948	134170	148617
	10	122570	122780	122780	122780
	100	122570	122780	122780	122780
	1000	122570	122780	122780	122780
ħ(max) & ƛ (max)		122570	122780	122780	122780
ħ(min) & ƛ (max)		146665	146703	146733	146631
ħ(max) & ƛ (min)		122570	122780	122780	122780
ħ(min) & ƛ (min)		146665	146703	146733	146631

Table 2: The values of the lost capacity due to the unavoidable replacement for used control algorithms

Control algorithm		Initial value of tool wear			
		0%	20%	40%	60%
Random choice (number of simuations)	1	0,00	0,67	1,33	0,67
	10	0,00	0,33	0,33	0,33
	100	0,00	0,00	0,00	0,00
	1000	0,00	0,00	0,00	0,00
ħ(max) & ƛ (max)		0,00	0,00	0,00	0,00
ħ(min) & ƛ (max)		0,33	0,33	0,33	0,33
ħ(max) & ƛ (min)		0,00	0,00	0,00	0,00
ħ(min) & ƛ (min)		0,33	0,33	0,33	0,33

Table 3: The values of the remaining capacity at the *K*-th stage for used control algorithms

Control algorithm		Initial value of tool wear			
		0%	20%	40%	60%
Random choice (number of simuations)	1	1981,67	1829,00	1596,33	1235,00
	10	2141,67	1919,33	1627,33	1205,33
	100	2141,67	2039,67	1677,67	1285,67
	1000	2181,67	2039,67	1677,67	1355,67
ħ(max) & ƛ (max)		2111,67	1919,67	1677,67	1205,67
ħ(min) & ƛ (max)		1981,33	1879,33	1677,33	1205,33
ħ(max) & ƛ (min)		2111,67	1919,67	1677,67	1205,67
ħ(min) & ƛ (min)		1981,33	1879,33	1677,33	1205,33

Table 4: The values of the total tool replacement time for used control algorithms

Control algorithm		Initial value of tool wear			
		0%	20%	40%	60%
Random choice (number of simuations)	1	4698	4886	4996	5042
	10	4796	4952	5028	5017
	100	4793	4969	4844	5030
	1000	4745	4835	4814	4965
ħ(max) & ƛ (max)		4786	4869	4864	4941
ħ(min) & ƛ (max)		4704	4850	4833	4918
ħ(max) & ƛ (min)		4786	4869	4864	4941
ħ(min) & ƛ (min)		4704	4850	4833	4918

The results show that the defined manufacturing system should be controlled by means of the algorithm of the maximal order. If the minimal value of the total tool replacement time is to be prioritized, it is possible to use the algorithm of the minimal order.

On the other hand, the use of the control algorithm of either maximal or minimal flow capacity does not have any impact on the final results. The results also show that to find a good solution, it is advisable to use the method of the random choice of orders and manufacturing plant. Better results were achieved already in 100 simulation runs than in case of implementing pairs of heuristic algorithms.

CONCLUSION

The specification and the subsequent model of the complex manufacturing system were verified by the goals formulated in the case study. In case of the time minimizing criterion as well as the lost capacity due to the unavoidable replacement, the simulation approach (random choice) does not show any improvements. The simulator returns other data for the lost capacity, the remaining capacity at the *K*-th state and the total tool replacement time. However, if there is one big order, in our case $z_{1,2}^{0} = 2900$, then it is very unlikely to obtain a better result in terms of meeting the criterion of time minimizing, so carrying out a bigger number of simulations does not seem reasonable. Generally, as seen in the tables with results, there is a need to carry out simulation runs because in this way it is possible to find better results in accordance with the stated criterion. In our case, better results were achieved for the remaining pass capacity at the *K*-th stage and the total tool replacement time than in case of realizing orders by means of pairs of heuristic algorithms. Nevertheless, if the order matrix is modified, simulation runs should be carried out again in order to seek for the satisfactory solution, better than in case of implementing pairs of heuristic algorithms.

REFERENCES

Babich, V.P and A.S. Bylev. 1991. *An approach to compiler construction for a general-purpose simulation language*. Springer, New York.

Bucki, R. 2012. "Logistic Decision-Making in Modelling and Control of the Complex Production System". In *Antonyová, A. et al. Mathematical Modelling in Logistics – Optimum Control*. Faculty of Management, University of Prešov in Prešov, Grafotlač Prešov, pp. 51-62 ISBN 978-80-555-0602-9.

Bucki, R.; Suchánek, P. and D. Vymětal. 2012. "Information Modelling of the Complex System of the Parallel Manufacturing Process". In *Recent Researches in Automatic Control and Electronics, Proceedings of 14th WSEAS Int. Conf. on Automatic Control, Modelling & Simulation (ACMOS '12)*, WSEAS Press, pp. 43-48, ISBN 978-1-61804-080-0.

Bucki, R.; Suchánek, P. and D. Vymětal. 2012. "Information Control of Allocation Tasks in the Synthetic Manufacturing Environment". *International Journal of Mathematics and Computers in Simulation*. North Atlantic University Union. Issue 3, Volume 6, pp. 324-332, ISSN 1998-0159

Chramcov, B.; Beran, P.; Daníček, L. and R. Jašek. 2011. "A simulation approach to achieving more efficient production systems," *International Journal of Mathematics and Computers in Simulation [online]* , Volume 5, Issue 4, [cit. 2011-06-30]. ISSN 1998-0159.

Marusza, S. 2013. "The Computer Simulator of the Elastic Manufacturing System with the Parallel Structure of Plants and Serial Production Work Stations". Diploma thesis. Institute of Management and Information Technology, Bielsko-Biala, 2013, p. 93.

Modrák, V. and R.S. Pandian. 2012. *Operations Management Research and Cellular Manufacturing Systems: Innovative Methods and Approaches*. IGI Global, p. 439, ISBN 978-1-61350-047-7.

Neumann, G. 2011."Needs and approach for combining formal analysis and human instinct in logistics simulation projects".In *Proceedings - 25th European Conference on Modelling and Simulation*. ECMS 2011, pp. 601-607.

Rizzoli, A.E. 2009. Simulation Tools: A Collection of Modelling and Simulation Resources on the Internet. Available from: http://www.idsia.ch/~andrea/sim/simtools.html, Accessed: 15 September 2010.

BRONISLAV CHRAMCOV studied automatization and control technology at the Faculty of Technology in Zlin at the University of Technology in Brno and he took his degree in 1998. In 2006 he received his doctoral degree from the Faculty of Applied Informatics of Thomas Bata University in Zlin. His doctoral thesis was focused on the utilization of time series prediction for control of technological process. He works as the lecturer at the Faculty of Applied Informatics of Thomas Bata University in Zlin. His research activities are focused on control algorithms for district heating systems, time series forecast in energy and discrete event systems simulation.

ROBERT BUCKI received his Ph.D. in Computer Sciences at The State Scientific and Research Institute of Information Infrastructure in Lviv in 2004. He is the assistant professor at Institute of Management and Information Technology in Bielsko-Biała. Scientific interests: mathematical modeling of logistic processes, computer simulation and modeling in computational linguistics.

SIMULATION MODEL OF CURRENT STOCK OF DIVISIBLE PRODUCTS IN EXTENDSIM ENVIRONMENT

Eugene Kopytov and Aivars Muravjovs
Transport and Telecommunication Institute
1, Lomonosova Street, Riga, LV-1019, Latvia
E-Mail: kopitov@tsi.lv; aivars.muravjovs@gmail.com

KEYWORDS
Current stock, divisible production, simulation, continuous model, optimization, ExtendSim package

ABSTRACT

In the given paper we investigate the problem of constructing a simulation model for the optimization of current stock of divisible productions in the warehouse. Criterion of optimization is minimum of average expenses for goods holding, ordering and losses from deficit and damage to the goods per time of season. The ExtendSim 8 package has been used as the means of simulation. The numerical example of the problem solving is presented.

INTRODUCTION

One of the central problems of the inventory control theory is to find an optimal solution to the task of ordering productions to be supplied, and main result of the task is the answer to two basic questions: how much to order and when to order. Of no less interest it is the task of determining the current stock of certain production (sold by the piece or indivisible production and dry or divisible production) at any given moment of a fixed time period, with any random factors taken into account. By "current stock" we denote the quantity of the production accumulated in the stock, which is used for distribution in the light of the circumstances. Quite a lot of different types of models of varying complexity, purpose and adequacy have been developed in the inventory control theory (Chopra and Meindl 2001, Magableh and Mason 2009). We can classify these models taking in account different their properties: deterministic and stochastic, linear and nonlinear, single- and multi-product, discrete and continuous models, etc. Most of the existing mathematical models in this theory consider indivisible productions (Stewart 2004, Chopra and Meindl 2001, Kopytov et al. 2007, Kopytov and Muravjov 2011).

In the present research we investigate the problem of the inventory control system of divisible productions. In previous works we have investigated the problem of constructing continuous and unsteady mathematical models for determine the volumes of current stock of divisible productions in one or several interconnected warehouses using apparatus of mathematical physics and continuum principle (Kopytov et al. 2010). The simple models are constructed using the theory of ordinary differential equations; for construction of more complex models the theory of partial differential equations are applied (Milstein 1995, Kuznetsov 2007, Tikhonov. and Samarsky 2004).

It should be noted that the practical implementation of this approach and finding a numerical solution is a rather complicated and time-consuming task. For some proposed models we have found an analytical solution in the closed form, and for some of proposed models the discretization is carried out using stable difference schemes (Guseynov et al. 2011). In the given paper we investigate the problem of constructing simulation model for the optimization of current stock of divisible productions. This approach is certainly easier to implement, but it has a lower accuracy of the obtained optimal solutions.

For the considered problem solving the authors have applied ExtendSim package, which is widely used for various systems modelling, but has not been applied for simulation of inventory control system of divisible production. Therefore, the authors set the goal to show the effectiveness of constructing continuous simulation model of current stock of divisible products in ExtendSim environment.

DESCRIPTION OF THE MODEL

We consider a stochastic inventory control model for the stock with homogeneous divisible production. The schema of the current stock of divisible production replenishment and distribution is shown in Figure1.

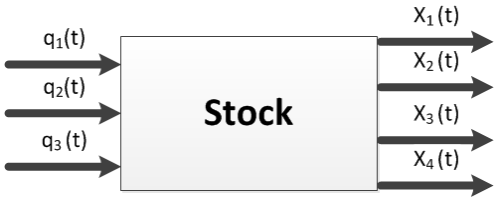

Figure 1: Flows of Production in the Stock

Denote as $z(t)$ the quantity of products in stock in the time moment t. Describing a continuous replenishment and distribution of the current stock we consider the

Proceedings 27th European Conference on Modelling and Simulation ©ECMS Webjørn Rekdalsbakken, Robin T. Bye, Houxiang Zhang (Editors)
ISBN: 978-0-9564944-6-7 / ISBN: 978-0-9564944-7-4 (CD)

change rate of the current stock volume $\frac{dz(t)}{dt}$ at a given time t (Kopytov et al. 2010).

Let us consider the functions which determine the change rate $\frac{dz(t)}{dt}$:

- function $S1(t,z(t))$ determines continuous replenishment of the current stock characterized by input flows of production $q_1(t), q_2(t), q_3(t)$;
- function $S2(t,z(t))$ determines continuous distribution of the current stock characterized by output flows of production $x_1(t), x_2(t), x_3(t), x_4(t)$).

The difference $S1(t,z(t)) - S2(t,z(t))$ is a measure of the change of the current stock volume, i.e.

$$\frac{dz(t)}{dt} = S1(t,z(t)) - S2(t,z(t)).$$

The product replenishment consists of three additive flows (components), namely: from regular replenishment of the stock, which is designated as $q_1(t)$; from irregular replenishment by single orders $q_2(t)$; and from random replenishment $q_3(t)$ (for instance, a random stock replenishment due to an exceptionally high quality of production or an exceptionally low price, or because of an expected sudden deficit of particular products, etc), which can be described mathematically as a random quantity that designating the total volume of production that has been delivered into a particular warehouse from random and/or non-random sources by the time t.

The product distribution consists of four additive flows (components) namely: regular distribution which is denoted as $x_1(t)$; irregular distribution $x_2(t)$; possible losses $x_3(t)$ of divisible productions which take place during holding and distribution processes (for example, for petroleum productions it is evaporation, for grain main reasons of losses are gnawing animals and inundation); and random (rare event) distribution (similar to random replenishment, there can be circumstances due to which random distribution takes place) that can be mathematically presented as a random flow $x_4(t)$ designating the total volume of productions that was taken away from the warehouse by the time t due to random circumstances.

We assume that main parameters of input and output production flows are constant (unchanged) during fixed time span $T = [t_s, t_e]$, where t_s and t_e are day of start and day of the end of the period T, respectively. Usually for petroleum and agricultural divisible productions (wheat, rice, meal, etc.) time period T is the season period occupying 3 months or 90 days. Let us consider the introduced components in detail.

The product replenishment components.
The component $q_1(t)$ can be interpreted as guaranteed replenishment of the current stock of divisible production, that takes place regularly in fixed moments of time $t_0, t_0 + \Delta, t_0+2\Delta, \ldots, t_0 + k \cdot \Delta$ according to a contract during the time period T with the constant volume of products $Q_1 = \text{const}$. The quantity Q_1 is one of control parameters of the optimization model.

The component $q_2(t)$ obviously depends on random demand for products D_τ during time period τ and also on a certain quantity R_0, which designates the minimal volume of stock in a particular warehouse necessary for administering unregulated stock replenishment on condition that such replenishment is guaranteed. In other words, in the moment of time, when the stock level falls till certain level R_0, a new order is placed. The quantity R_0 is called as reorder point. We assume that demand D_τ has a normal distribution with a mean μ_D and a standard deviation σ_D. In considered task the reorder point is calculated by following formula:

$$R_0(t) = [\overline{D}(L) + X_1 \cdot k(L)] \cdot S_0, \qquad (1)$$

where L is lead time (time between placing an order and receiving it); $\overline{D}(L)$ is average demand for products during lead time L (in considered task lead time L is constant); $k(L)$ is number of cases of regulated (according to contracts) distribution X_1 of products during lead time L, (number $k(L)$ depends on the moment of time t, when the order for delivery is placing); S_0 is a safety coefficient which determines certain reserve stock of products, $S_0 \geq 1$.

We suppose that in case of production deficit the last cannot be covered by expected order. In considered optimization model safety coefficient S_0 is the second control parameter.

The flow $q_3(t)$ determines the volume of production Q_3 that is delivered into the warehouse by the time t due to random (rare event) circumstances from random and/or non-random sources. In considered task, we assume that the probability p_3 of occurrence of this event during time unit is known, and it is a quite rare event; for example, for one day we assume that $p_3 = 0.01$.

So, the vector $Q = \{Q_1(T), Q_2(T), Q_3(T)\}$ determines total volume of products replenishment delivered during

time period T, where $Q_1(T), Q_2(T), Q_3(T)$ are regular, irregular and random (rare event) replenishments during period T.

The products distribution components.
The component $x_1(t)$ can be interpreted as "strong" (guaranteed) constant distribution of the current stock of divisible productions, i.e. the volume of the current stock is regularly taken away from the warehouse in fixed moments of time $t_1, t_1+\Delta_1, t_1+2\Delta_1, \ldots, t_1+k\cdot\Delta_1$ according to a contract during the time period T with the constant volume of product X_1.

The component $x_2(t)$ depends on random demand for products D_τ during time unit and regular distribution, which determines the stock volume of divisible productions allowing for its unregulated distribution,

The component $x_3(t)$ describes possible losses of the divisible productions in current stock in the processes of storage and distribution. For instance, if we have the oil productions stock, losses will result from the evaporation and/or from the leakage through the reservoirs; if we have the agricultural productions stock (wheat, rice, meal, etc.), there will be unavoidable losses caused by pests, flood, strong winds, etc. Apparently, the value of these losses is a random one.

The flow $x_4(t)$ determines quantity X_4 designates the total volume of productions (unexpected distribution with a large profit) that has been removed from the warehouse by the time t due to random (rare event) circumstances. In considered task we assume that the probability p_4 of occurrence of this event during time unit is known, and it is a quite rare event; we assume that for one day $p_4 \le 0.01$.

In the considered problem we suppose that the following economic parameters are known:
For *i*-th component of product replenishment ($i = 1,2,3$) the ordering cost of product $C_O^{(i)}(Q_i)$ is a known function of the products quantity Q_i, delivered during time period *T*, and consists of two additive components, namely: constant $c_1^{(i)}$ which includes cost of the order forming and constant part of expenses of products transportation, and variable component $c_2^{(i)}(Q_i)$, which depends on the order quantity Q_i, i.e. $C_O^{(i)}(Q_i) = c_1^{(i)} + c_2^{(i)}(Q_i)$, $i = 1, 2, 3.$

We suppose that in the considered inventory control system for $i = 1, 2, 3$ coefficients $c_1^{(i)}$ and $c_2^{(i)}$ are different: $c_1^{(1)} < c_1^{(2)}$; $c_1^{(3)} = 0$; $c_2^{(2)}(1) < c_2^{(1)}(1) < c_2^{(3)}(1)$, where $c_2^{(i)}(1)$ is determined for one unit of delivered production.

Therefore we can write: $C_0^{(2)}(1) < C_0^{(1)}(1) < C_0^{(3)}(1)$.
The total ordering cost for time period *T* is determined by the following formula:
$E_{OD}(T) = C_O^{(1)}(Q_1(T)) + C_O^{(2)}(Q_2(T)) + C_O^{(3)}(Q_3(T))$.

The holding cost of the product is proportional to its quantity in the stock and the holding time with the coefficient of proportionality C_H.

The losses from the deficit of the product are proportional to the quantity of its deficit with the coefficients of proportionality C_{SH_j} which are different for each type of product distribution. At the same time losses from the deficit of the product for regular distribution are the largest, but for random (unplanned, rare event) distribution these losses (i.e. lost profit) are the lowest, i.e. $C_{SH1} > C_{SH2} > C_{SH3}$. Losses from damage and loss of product are proportional to the cost of product unit C_{CS}.

The total cost $E(T)$ in inventory system during the season period T is calculated by the following formula:

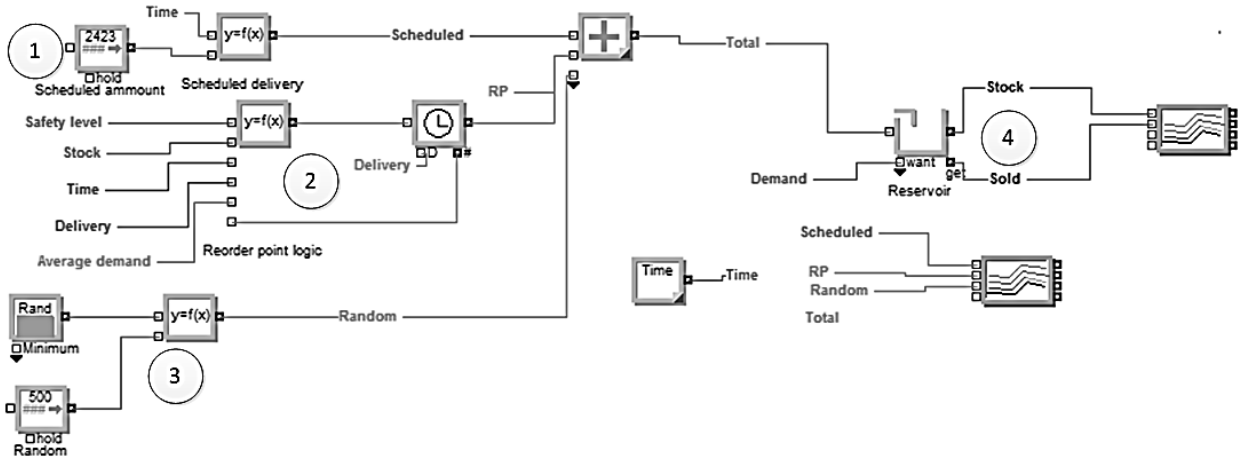

Figure 2: Stock Simulation

$$E(T) = E_{OD}(T) + E_H(T) + E_{SH}(T) + E_{CS}(T), \quad (2)$$

where $E_{OD}(T)$ is ordering cost; $E_H(T)$ is holding cost; $E_{SH}(T)$ is shortage cost; $E_{CS}(T)$ is losses from damage or loses of products during time period T.

Principal aim of the considered task is to define the optimal values of regular order quantity Q_1 and safety coefficient S_0 for irregular replenishment, which are control parameters of the model. Criteria of optimization is minimum of average total cost $\overline{E}(T)$ during time period T, which can be calculated by formula (2) for average costs and loses $\overline{E}_{OD}(T)$, $\overline{E}_H(T)$, $\overline{E}_{SH}(T)$ and $\overline{E}_{CS}(T)$.

SIMULATION MODEL IN EXTENDSIM 8 ENVIRONMENT

For solving the problems considered above we have used simulation method realized in the ExtendSim 8 environment (Strickland 2011). The package ExtendSim can be used to model continuous, discrete event, discrete rate, and agent based systems. ExtendSim's design facilitates every phase of the simulation project, from creating, validating, and verifying the model, to the construction of a user interface that allows others to analyze the system (Kopytov and Muravjov 2011). Simulation tool developers can use ExtendSim's built-in compiled language ModL to create reusable simulation components. All of this is done within a single self-contained software program, which does not require external interfaces, compilers, or code generators.

For this task implementation we have chosen continuous simulation model. The created model consists of four main parts: "Stock", "Demand", "Ordering costs" and "Total costs calculation" that are represented on Figure 2-5. The purposes of blocks shown in Figure 2-5 are given in captions. Let us consider the main sections of the simulation model.

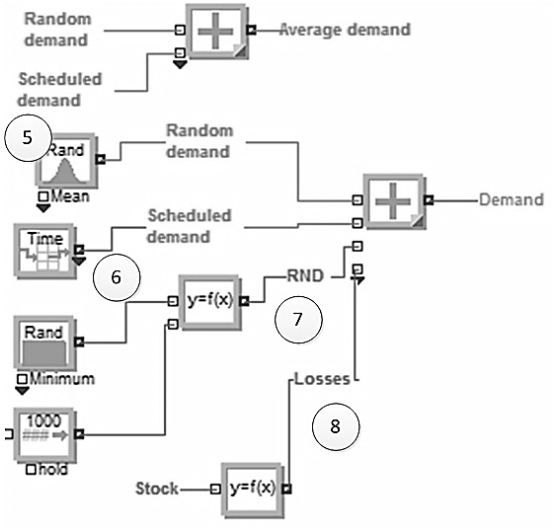

Figure 3: Demand Generation

Section „Stock" (see Figure 2). In area #1 there are placed blocks that are responsible for scheduled delivery simulation. Area #2 is used for generation emergency delivery orders (irregular replenishment) based on current stock level and time between scheduled orders. Next area #3 generates random deliveries cheap that occurs one out of hundred cases ($p_3 = 0.01$).The stock is realized in area #4.

Section "Demand" (see Figure3) is created for product distribution simulation and consists of the blocks responsible for demand generation. There are four demand sources: random demand is realized in area #5, scheduled demand (regular distribution) – in area #6, random demand with different distribution – in area #7, and holding – in area #8.

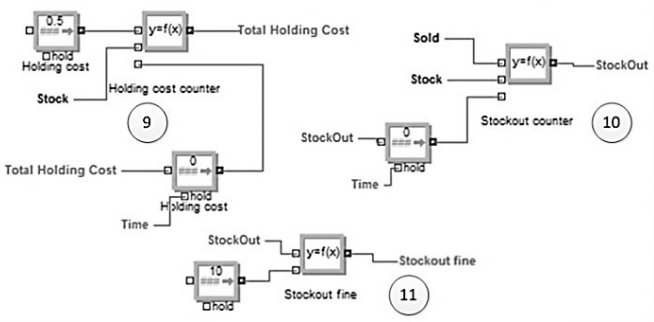

Figure 4: Costs Calculations

Next two sections "Costs" and "Ordering Costs", shown in Figure 4 and Figure 5 accordingly, include costs calculations blocks, namely: holding, ordering and losses costs for all delivery sources described above.

The total holding cost $E_H(T)$ is calculated in the blocks of areas #9 and #11. Current stock is calculated in blocks of area #10.

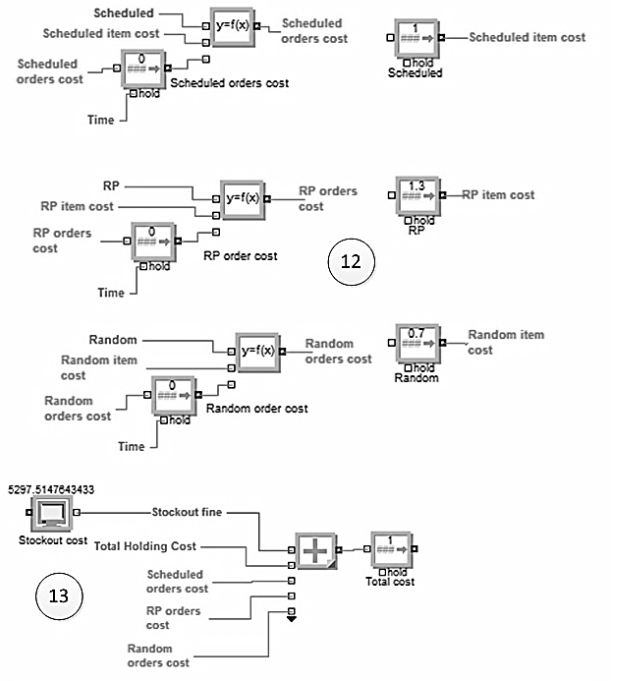

Figure 5: Orderings Costs Calculations

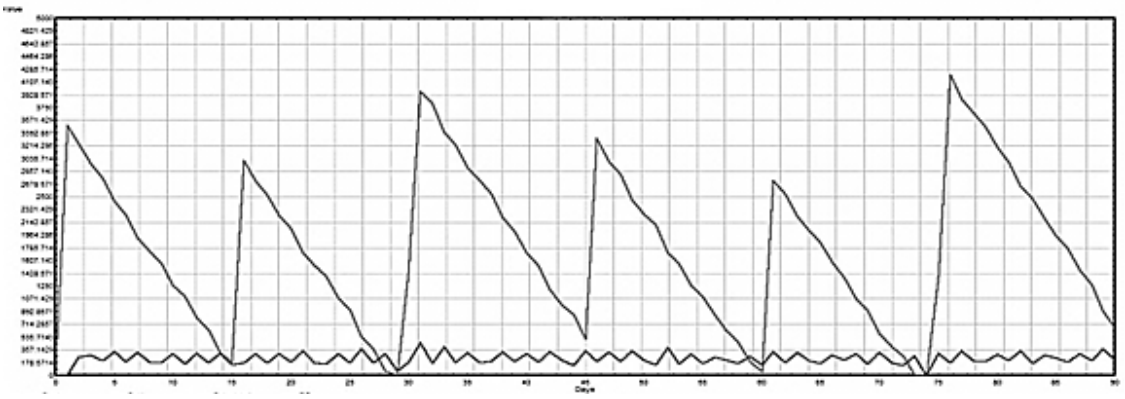

Figure 6: Example of Simulation Process

Blocks in area #12 are used for order costs calculations from each delivery sources. The total cost $E(T)$ in inventory system is calculated in blocks in area #13.
An example of the inventory control process simulation (one realization) is shown in Figure 6. The plot shows the current stock of certain production during period of season T.
Using created simulation model we can find the optimal solution for inventory control of stock of divisible production. One of examples is considered in the next section.

EXAMPLE AND OPTIMIZATION

Let's consider a stochastic inventory control model for the stock with homogeneous divisible production shown in Figure1. Table 1 and Table 2 describe main parameters of the products replenishment and distribution.

Table 1: Initial Data of Product Replenishment

Source	*Amount*	*Schedule*	*Cost / unit, conventional units (C.E.)*
Regular	3000	Bimonthly	1.0
Irregular	According to stock level		1.3
Random	200	Random, p=0.01	0.7

Table 2: Initial Data of Product Distribution

Source	*Amount*	*Schedule*
Irregular	Demand D_τ, normal distribution μ_D=170; σ_D = 30	Daily
Regular	150	Monday, Wednesday, Fryday
Random (rare event)	1000	Random, p=0.01
Holding loses	0.5% of daily stock	Daily

For optimization process we consider that amount of regular replenishment Q_1 can be changed from 1000 to 4000 and safety level S_0 from 1.0 to 1.5. The period of simulation is 3 months (one season period) and the number of realization is 100.

The optimization model was done by ExtendSim optimization tool that gives us flexible solution for optimal result searching. The Figure 7 represents optimization process in ExtendSim environment.

For the given steps of the control parameter Q_1 and S_0 changing, the best result is achieved at point Q_1 = 2435 units and S_0=1.34, where for 100 replications the average total cost of the one season period equals

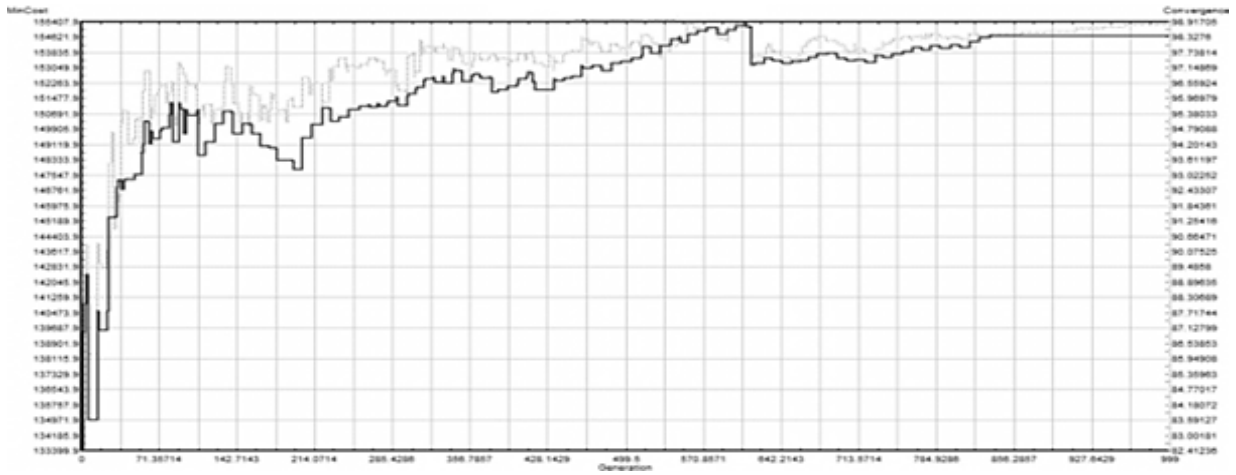

Figure 7: Optimization Process

154695 C.E. It gave us total costs reduction from 163967 C.E. (for initial values of control parameters Q_1 =3000 and S_0 =1.3) to 154695 C.E.

CONCLUSIONS

In the given paper the simulation model for the optimization current stock of divisible productions is created. For the problem solving authors have used a simulation continuous model realized in the package ExtendSim 8, which is the most powerful and flexible simulation tool for analysing, designing, and operating complex systems in the market. The results of simulation indicate the good feasibility of the application of ExtendSim 8 in the tasks of inventory control of divisible productions.

Comparing with analytical approach used in authors' previous works the considered simulation model of inventory control of divisible productions provides the researcher with:

- the clearness of results presentation;
- the possibility of finding optimum solution of an inventory problem in the case when realization of analytical model is rather difficult.

The main problem of the proposed simulation approach is initial values of control parameters and their changing range determination in the searching the best solution.

Further guideline of the current research is to consider the inventory control models for determine the volumes of current stock of divisible productions in several interconnected warehouses.

REFERENCES

Chopra, S. and P. Meindl. 2001. Supply Chain Management. Prentice Hall, London.

Guseynov, Sh.E.; Kopytov, E.A.; Puzinkevich, E. "On continuous models of current stock of divisible productions". Dynamical Systems, Differential Equations and Applications" Vol. I, 2011, Published by the American Institute of Mathematical Sciences (AIMS), 601-613.

Kopytov, E.; Greenglaz, L.; Muravjov, A. and E. Puzinkevich. 2007. "Modeling of Two Strategies in Inventory Control System with Random Lead Time and Demand". Computer Modeling & New Technologies, Vol. 11(1), Riga: Transport and Telecommunication Institute, 21-30.

Kopytov, E., Guseynov, Sh., Puzinkevich, E., Greenglaz, L. 2010. "Continuous Models of Current Stock of Divisible Productions". Computer Modelling and New Technologies, Vol. 14, No 4, p. 19-30.

Kopytov, E. and A. Muravjov. 2011. "Simulation of inventory control system for supply chain "producer – wholesaler – client" in ExtendSim environment". Proceedings of the 25th European conference on modeling simulation (ECMS-2011). (Krakow, June 3-4). Poland, 580-586.

Krahl, D. 2007. "ExtendSim 7". Proceedings of the 39th conference on Winter simulation: 40 years! (Dec. 09-12). S.G. Henderson, B. Biller, M.-H. Hsieh, J. Shortle, J.D. Tew, and R.R. Barton (Eds.). Washington D.C. 226-232.

Kuznetsov, D.F., 2007. Stochastic Differential equations: theory and practice of numerical solutions. St. Petersburg: Polytechnic University (In Russian)..

Magableh, G. M., Mason, S. J. 2009. "An integrated supply chain model with dynamic flow and replenishment requirements". Journal of Simulation, Vol. 3, 84–94.

Milstein, G.N., 1995. Numerical integration of stochastic differential equations. New York-London: Kluwer Academic Publishers.

Stewart, R. 2004. "Simulation – The practice of model development and use". Wiley.

Strickland, J. 2011. "Discrete Event Simulation using ExtendSim 8" Lulu.

Tikhonov, A.N. and A.A. Samarsky. 2004. Equations of Mathematical Physics. Moscow: Lomonosov MSU Press (In Russian).

ACKNOWLEDGEMENTS

The article is written with the financial assistance of European Social Fund. Project Nr. 2009/0159/1DP/1.1.2.1.2/09/IPIA/VIAA/006 (The Support in Realisation of the Doctoral Programme "Telematics and Logistics" of the Transport and Telecommunication Institute).

AUTHOR BIOGRAPHIES

EUGENE A. KOPYTOV was born in Lignica, Poland and went to the Riga Civil Aviation Engineering Institute, where he studied Computer Maintenance and obtained his engineer diploma in 1971. Candidate of Technical science degree (1984), Kiev Civil Aviation Engineering Institute. Dr.sc.ing. (1992) and Dr.habil.sc.ing. (1997), Riga Aviation University. Professor (1999). Present position: Head of Software Engineering Department of Transport and Telecommunication Institute, professor of Computer Science. Member of International Telecommunication Academy. Fields of research: statistical recognition and classification, modeling and simulation, modern database technologies. Publication: 280 scientific papers and teaching books, 1 certificate of inventions.

AIVARS MURAVJOVS was graduated at Transport and Telecommunication Institute where he studied Computer Sciences and obtained Master of Natural Sciences in Computer Science in 2009. Present studying PhD student in Telematics and Logistics. Fields of research: inventory control systems, simulation.

Policy Modelling

DOMAIN-SPECIFIC LANGUAGES FOR AGILE URBAN POLICY MODELLING

Michel Krämer
Fraunhofer Institute for Computer Graphics Research IGD, Competence Center for Spatial Information Management
Fraunhoferstr. 5, 64283 Darmstadt, Germany
Email: michel.kraemer@igd.fraunhofer.de

David Ludlow and Zaheer Khan
University of the West of England (UWE)
Faculty of Environment and Technology
Coldharbour Lane, Bristol BS16 IQY, UK
Email: david.ludlow@uwe.ac.uk
Email: zaheer2.khan@uwe.ac.uk

KEYWORDS

Urban policy modelling, Urban planning, Domain-Specific Languages, Human-computer interaction, Smart cities

ABSTRACT

In this paper we present a new approach of performing urban policy modelling and making with the help of ICT enabled tools. We present a complete policy cycle that includes creating policy plans, securing stakeholders and public engagement, implementation, monitoring, and evaluating a particular policy model. ICT enabled tools can be deployed at various stages in this cycle, but they require an intuitive interface which can be supported by domain-specific languages (DSLs) as the means to express policy modelling aspects such as computational processes and computer-readable policy rules in the words of the domain expert. In order to evaluate the use of such languages, we present a real-world scenario from the urbanAPI project. We describe how DSLs for this scenario would look like. Finally, we discuss strengths and limitations of our approach as well as lessons learnt.

INTRODUCTION

In general, a policy can be referred to as a plan of action adopted by an individual, department, organisation, business or government in a domain-specific problem context. A policy model is a descriptive or graphical representation of the plan of action. The process of developing a policy model can be referred as policy modelling. Ruiz Estrada reviews more than 1,500 scientific articles and discusses the evolution of policy modelling over the past three decades (Ruiz Estrada, 2010). He suggests its classification into 12 categories. According to him, policy modelling can be defined *"as an academic or empirical analytical research work that is supported by the uses of different theories, quantitative or qualitative models and techniques to evaluate the past (cause) and future (effect) of any policy implication(s) on the society anywhere and anytime."* Also his analysis reveals that there is a constant increase of econometric models in policy modelling and a significant lack of non-economic variables such as social, political, technological and natural factors simultaneously, which could increase vulnerability of policy modelling in the policy-making process.

In response to the sustainable development agenda and the rise of partnership-based urban planning, bottom-up policy development approaches, with increasing public participation for collaborative decision-making, are transforming the traditional top-down policy modelling approaches (Lempert, 2002). In particular, sustainable urban development necessitates ICT enabled tools to develop and demonstrate alternative urban models to different stakeholders and public for consultation as well as policy and decision-making. In this regard, the use of modern ICT enabled tools and techniques greatly improves the overall policy-making process. However, these ICT enabled tools require use of innovative technologies such as Web 2.0, 3D visualisation and simulations (Krämer and Kehlenbach, 2013) as well as mechanisms to support automated adoption of local action plans and proposed policy changes.

In addition to the above, techniques from the machine learning domain such as data mining or social mining can be used to refine policy plans based on feedback gathered from public participation or from the experience of actually implementing a particular policy (cf. Hanzl, 2007; Maragoudakis et al., 2011). Therefore, ICT enabled tools often need to perform rigorous analysis of data to take appropriate actions against different events. The tools are driven by operational or computational logic which needs to be defined by domain experts—i.e. urban planners and decision makers—who for that purpose typically have to use a general purpose programming language or scripting language such as Visual Basic.NET, Python, etc.

However, the real challenge can be related to expressiveness of these languages, intuitiveness and flexibility in defining machine-readable rules for domain-specific policies (Saleem et al., 2012). These languages are often hard to understand and to learn for non-IT personnel. In order to avoid requiring the domain experts to have a deep understanding of computer science or programming, a sophisticated, yet easy-to-understand user interface is needed. This interface should not be too generic but instead reflect application-specific and domain-specific issues. In this way, domain experts can focus on the actual problem instead of technical details.

Proceedings 27th European Conference on Modelling and Simulation ©ECMS Webjørn Rekdalsbakken, Robin T. Bye, Houxiang Zhang (Editors)
ISBN: 978-0-9564944-6-7 / ISBN: 978-0-9564944-7-4 (CD)

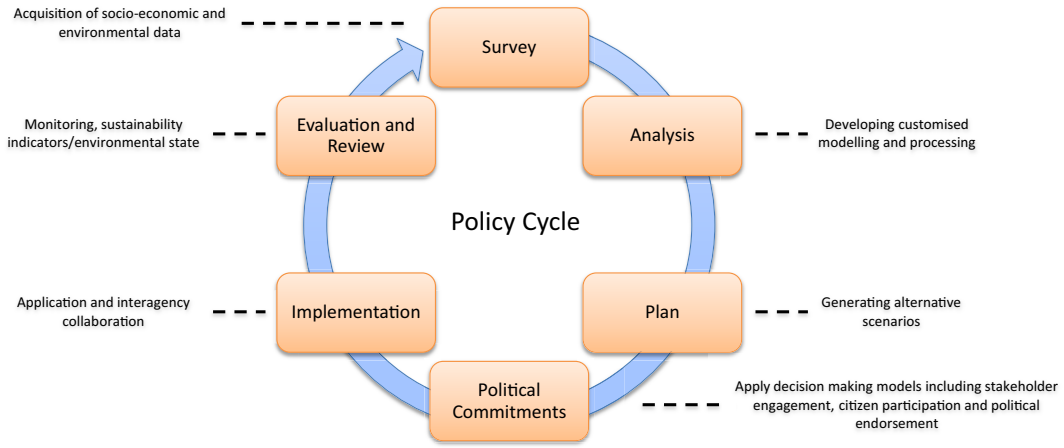

Figure 1: Policy development process

During policy modelling, urban planners often define rules that later provide the basis for policy plans or final policies (Guzy et al., 2008). For example, the municipality's aim to reduce car traffic in the city could be expressed with rules that set upper limits for the number of cars per hour on specific streets (see the real-life example scenario below). ICT enabled tools can automatically check if these rules are met or—semi-automatically—assist domain experts in defining alternatives or new policy rules. Typical ICT tools for that purpose are expert systems or more generally rule-based systems. Expressing machine-readable rules with such systems often requires the user to have a background in computer science. Apart from that, rule-based systems are typically rather generic and flexible and do not focus on domain-specific issues.

Hypothesis

In consequence of the above, in this paper we investigate a new way to express urban policy modelling aspects such as computational processes and machine-readable policy rules with so-called Domain-Specific Languages (DSLs). A DSL is a language that is tailored to a specific application domain. It consists of terms (vocabulary) from that application domain, so it is easily understandable by domain experts. At the same time, the DSL is also machine-readable and—depending on the actual use case—possibly executable. Consequently, a DSL can be used to allow users with non-IT background to communicate with the machine—i.e. to write computer programs or scripts, to declaratively model data, etc.

To summarise, our hypothesis for this research work is as follows:

"Domain-specific languages help urban planners to control ICT tools in the policy cycle and to focus on the actual problem—i.e. policy modelling—without requiring them to have a deep understanding of technical details."

Methodology

In order to evaluate the use of domain-specific languages for urban policy modelling, in this paper we first present the policy cycle which includes deploying policy plans, public participation, implementation and monitoring as well as gathering feedback and including it in future decisions. After that we present the current state of the art in domain-specific language design. In the second part of this paper we describe a real-world scenario from the urbanAPI project which is funded by the European Commission (FP7 RTD). We describe the different stages of the policy cycle that can be automated by ICT tools and where DSLs can assist domain experts in their tasks. We then show two example DSLs that are readable by both policy actors as well as machines. Finally, we discuss strengths, limitations and lessons learnt.

POLICY CYCLE

In order to support policy modelling using ICT, it is necessary to understand the policy-making process. Figure 1 depicts a generic policy process as a cycle representing different stages of the policy-making process (boxes). The process begins with the 'Survey' stage that collects domain specific data—e.g. socio-economic and environmental relevant to the issue of urban development, etc.—either by using surveys, polls, or ICT technologies—e.g. sensor nets, etc.—for problem or issue identification.

The next stage of the policy making process (Analysis stage) utilises data gathered at the survey stage, and provides an assessment of the territorial impacts, in respect of socio-economic and environmental variables, that identify the problem to be resolved by the plan.

The Plan stage is the formulation of a coherent strategy, specified by the technical administration experts (urban planners) in respect of a variety of policy objectives, that address the problems identified in the analysis stage, and which proposes a plan of action over a period of time (five to ten-year period) to resolve these problems.

In the Political commitment stage urban planners provide a proposition for future development of the urban territory typically subject to public and wider stakeholder consultation, following which a political commitment is

made by elected officials of the municipality to the implementation of the plan.

Implementation of the plan (in the Implementation stage) over the plan period of several years involves commitments by a variety of public agencies acting in concert to secure the objectives of the plan in order to respond to the problems identified at the survey/analysis stages and to provide a framework for private investment in the development of the urban area.

The Evaluation and Review stage is focused around the monitoring of the implementation of the plan to identify the extent to which the plan is achieving the objectives identified with the policies of the plan, and where it is failing to fully meet the policy objectives of the plan, to provide a basis for reformulation of the plan in the next stage of the policy cycle.

The process repeats in a cycle in order to assess and improve current policy implementation.

AUTOMATING POLICY MODELLING

From theoretical computer science point of view, policies are defined by rules—i.e. conditions and respective actions—that implement software business and computational logic—e.g. software security policies, etc. These rules can also be used for the policy development process (see the example rules from the real-life scenario presented below). We differentiate between three levels:

i) rules for defining the operational or computational logic for ICT tools used at different stages of the process;

ii) rules for describing policy restrictions and expectations that can be automatically checked by ICT tools or semi-automatically evaluated by domain experts with the help of ICT tools;

iii) rules to integrate process stages in order to automate the flow of information from one stage to the next stage.

The first level necessitates machine-readable domain-specific vocabulary with common semantics and reusable syntax that can be used by ICT enabled tools to collect and rigorously process the data, generate alternative scenarios, perform decision-making and monitor and assess the overall impact of the policy implementation. This information can be reused in the next policy development cycle.

The second level requires a vocabulary that is easy to comprehend for the domain expert and for decision makers or other stakeholders who—in respect to a bottom up policy modelling approach and a participatory process—need to understand the rules for the urban plans. At the same time the language must be machine-readable so it can be used for automatic rule evaluation. It therefore needs a well-defined grammar and syntax.

The third level necessitates defining interoperable interfaces between ICT enabled tools. This enables tools at different stages of the process to interact with each other and to facilitate flow of information from one stage to the next stage.

However, it is difficult to fully automate the policy development process due to necessary engagement of different stakeholders including citizens and policy-makers at different process stages. Nevertheless, ICT enabled tools can provide a semi-automated approach to support socio-technical interactions, data collection, modelling, processing and analysis, and visualisation of alternative domain-specific scenarios for collaborative decision-making (Batty, 2007). In response to the requirements of the three levels described above, we propose to use domain-specific languages as the interface to the user or domain expert. We will present an example use case below where we use DSLs for computational logic and for describing policy restrictions.

DOMAIN-SPECIFIC LANGUAGES

In computer science domain-specific languages are used for a number of purposes. For example, in the UNIX operating system configuration files are typically written in custom languages. In agile software development domain-specific languages are used to quickly adapt to changing user requirements. DSLs are also used for machine-to-machine communication. In the IETF protocol specifications, for example, textual, ASCII-based DSLs avoid platform-dependent details such as encoding issues that would normally arise with binary communication protocols.

In recent times, DSLs have gained a lot of interest, especially in the scientific community. One of the most actively pursued topics is DSL design. Mernik et al. differentiate between five phases of DSL development: decision, analysis, design, implementation and deployment (Mernik et al., 2005). The analysis phase is one of the most important ones since it includes specifying user requirements (Tairas et al., 2009). Mernik et al. identify three common ways to develop a new DSL:

- the DSL will be implemented based on an existing language which will be included completely (so-called internal DSLs are an example for this);
- an existing language will be limited to the means needed for the application domain;
- application-specific vocabulary and language constructs will be added to an existing language.

Apart from that, DSLs can of course be developed from scratch as well. Such languages are typically called external DSLs since they are not embedded into or based on an existing language. In his book "Domain-Specific Languages" Martin Fowler describes a number of methods for developing parsers for such languages (Fowler, 2010). The drawback of external DSLs is that you cannot rely on existing language constructs or compiler components. However, they allow for a much more flexible design

since they are not bound to the syntax and grammar of a host language and the possible restrictions implied by that. Based on this, the DSLs that we describe in the example use case below are external ones.

Since DSLs are used more and more often in modern software systems, there's a growing need for language maintainability. DSLs ought to help reduce maintenance costs in large software systems, but this can only work if maintaining the DSLs itself is not too costly. Therefore some work has already been done in the area of language modularisation. Hudak tries to reuse compiler components such as lexer and parser as well as semantic analysis (Hudak, 1998). Irazabal and Pons present a modularisation technique based on Xtext (Irazabal and Pons, 2010). They import several partial language definitions and merge them into a new single one.

We also identified the problem of maintaining DSLs as well as learnability and commonality as utterly important for our approach. More details on this can be found below in the section on 'building DSLs for urban planning'.

Xtext is a language workbench written in Java and based on the Eclipse Modeling Framework (EMF) and ANTLR as the underlying language recognition tool (http://www.eclipse.org/Xtext). It allows domain-specific languages up to general purpose languages to be defined. In recent times, Xtext has gained prominence and is used for a wide range of applications in the Java community—e.g. the Xtend language that adds useful features to Java, Spray which is a DSL for the Graphiti framework, etc. While Xtext is quite popular its main purpose is to quickly create DSLs for single, separated use cases. As we show later our approach depends on modularity and reusable language constructs. In our experience Xtext currently does not support this enough.

DOMAIN-SPECIFIC LANGUAGES FOR POLICY MODELLING

In this section we will present how domain-specific languages can be applied to the policy-making and implementation process (policy cycle), otherwise characterised as policy modelling. We will first describe an example scenario from the urbanAPI FP7 EU project (http://urbanapi.eu). After that we will discuss at what stages ICT enabled tools and DSLs can be used reasonably. Finally, we will present an example DSL that is both, readable by domain experts and by machines.

Example scenario

In the urbanAPI project, the city of Bologna, Italy is pursuing urban planning and environmental objectives. Khan and Ludlow describe the use case as follows (cf. Khan and Ludlow, 2011, pp. 43–55). The initiatives "Ambiente Vitale" and "Di nuovo in centro" aim for creating new public and green spaces as well as improving the mobility system. In this context, one specific area is of most interest. The San Vitale district is one of the oldest parts of the city with a rather heterogeneous and complex infrastructure. The area has a large population density of 17,464 citizens per km^2 (3,370 citizens in an area of 192,962 m^2). It is very close to the University of Bologna which makes it a popular area for student residence, the urban elite, and—given its location in the heart of the historic city—numerous tourists. In their spare time, citizens of the San Vitale district participate in committees and cultural associations which organise many events during the year. There are many commercial activities centred around the district's core mostly led by immigrants. To summarise, the district is heterogeneous in many ways, in its widespread, ancient infrastructure as well as in its population and cultural life. This has previously led to some oddities and infrastructure problems the municipality would like to avoid.

The urban planners are aware that the initiatives for restructuring this district require to involve all stakeholders. In order to enable public participation, the municipality plans to deploy ICT enabled tools including a 3D virtual reality (VR) application available on the Internet. This application will allow urban planners to present their plans to a wide audience and hence raise the awareness among citizens about future developments.

One central part of improving the mobility system in the San Vitale district is to reduce car traffic and instead extend public transportation by adding new bus routes for example. The city already owns a wide range of data that can be used for the 3D VR application including building footprints and heights, land use, coverage and zoning information. In order to estimate the consequences of changing the mobility system, the municipality plans to exploit GSM data (Global System for Mobile Communications). This data is gathered by mobile devices such as mobile phones, smartphones, tablet PCs or even car sensors. Within the urbanAPI project GSM data will be used to simulate traffic on the streets of Bologna. The simulation results will be included in the 3D VR application.

DSLs in the policy cycle

As described above, rules can be used at various levels: to define operational or computational logic, to describe policy requirements, and to provide platform-independent machine-to-machine communication between the different tools at the various stages in the policy cycle. In this section we will furthermore show at what stages DSLs can be used reasonably. Note that the different stages are rather complex in that they include not only data processing or visualisation but also statistical modelling, monitoring and human interaction. In the following we will only focus on tasks that can be supported by ICT tools and DSLs in particular.

In the scenario depicted above, the municipality of Bologna has already gone through the first stage of the cycle ("Survey"). They have gathered data such as building footprints and heights which can be used to create a simple 3D building block model. They also possess basic socio-economic, transport, utility, vegetation, census data, etc. In stage two ("Analysis") they therefore pre-process

the data. Here they can make use of automated, rule-based processes. A typical DSL that would drive such an automated process could look like this:

```
When there is a building footprint f
and there is a corresponding
    building height h
then extrude f by h.
```

This script would create a simple 3D building block model of the city of Bologna. It could drive a standard geographical information system (GIS) that manages the municipality's cadastre consisting of building footprints (typically 2D polygons) as well as respective building heights attached as metadata or attributes. GISs usually already provide a set of well-known geometrical functions like the polygon extrusion used in this script. Basically, the DSL terms map to GIS functions and parameters (or more precisely function arguments). The term '*there is*' maps to an object query based on its type ('*building footprint*'), '*building height*' maps to an attribute, whereas the term '*corresponding*' links the attribute to the respective building footprint. Finally, the term '*extrude*' maps to the polygon extrusion function whereas '*h*'—i.e. the building height—is the function's first argument.

The DSL used in this script is clearly readable and easily understandable. At the same time it uses a well-defined grammar and can thus be processed by machines. We use the keywords **When** and **then** here—instead of the more commonly used ones **If** and **then**—in order to mimic declarative production rules. Production rule systems are typically event-based, so that *when* something happens *then* the rule-based system will perform some specified action. In our case this means that we can keep the rule system running, so that *when* a new building footprint and a corresponding height is added to the data set *then* the 3D building model will automatically be created.

After preparing the data, the urban planners might want to define rules for their scenario. For example, they want to reduce traffic on street A. At the same time they do not want the traffic on street B—which is an alternative to A—to increase. Therefore they would like to close A for cars and create new bus routes in order to provide an alternative for using the car. In order to evaluate later if the policy has been implemented successfully, the municipality evaluates passively collected GSM (Global System for Mobile) data from active mobile phones for street A and B to measure the number of cars passing by during the day. Such functionality is provided by the Public Motion Explorer application developed in the urbanAPI project. Using a DSL, this task can be performed automatically by ICT tools based on the acceptance criteria defined by the urban planners. A DSL for these criteria could look like as follows:

```
The number of cars on street A per
   day was 3000.
The number of cars on street A per
   day has to be 0.
The number of cars on street B per
   day was 2000.
The number of cars on street B per
   day has to be lower than 2500.
```

The idea of defining acceptance criteria in such manner can also be found in computer science in the area of Behaviour-Driven Development (BDD) where DSLs help developers to create machine-readable, executable code that is also understandable by their clients—i.e. the domain experts (see North, 2009).

These acceptance criteria can now be used in the consecutive stages of the cycle: during stakeholder engagement and for monitoring. The 3D visualisation, for example, can be driven by these rules. The main purpose of this application is to simulate the policy's consequences by visualising the 3D building model in combination with information about traffic density based on GSM data. Whenever one of the rules above do not apply, the user will be notified. For example, we can use the following rule to update the display:

```
When the number of cars on street B
   per day is higher than 2500
then display street B in red.
```

Again, we are using a production rule here. Due to its event-based nature the display will automatically be updated whenever something in the GSM data set has changed or whenever a stakeholder has interacted with the system—e.g. by changing some of the parameters such as number of maximum cars per street.

During the public participation stage, involving engagement with urban stakeholders including citizens, machine learning techniques such as data mining and social mining can be used to analyse how stakeholders react to the policy plan (Hanzl, 2007). For instance, the municipality might use information from the Internet such as page views, comments, likes/dislikes, etc. (Charalabidis et al., 2012, p. 157) to analyse the public opinion and to gain feedback on the policy plan (cf. Maragoudakis et al., 2011). The results from this analysis can be used to improve the acceptance criteria. "Improving" means in this case adding new rules. For example, during stakeholder engagement one might notice that street C is also often used as an alternative to A. Hence, it might be useful to also consider C in the acceptance criteria:

```
The number of cars on street C per
   day was 500.
The number of cars on street C per
   day has to be lower than 600.
```

Furthermore, after the policy has been implemented and its consequences are monitored these rules can be used to automatically assess the policy's success. The results gained from this, which will be identified in the monitoring and plan evaluation stage of the policy process, can then be incorporated into another round of the policy cycle.

Building DSLs for urban planning

As described above, the DSLs presented in this paper are external ones. They are not based on an existing language and they are not embedded into a host language. The main advantage of this approach is that the DSLs can be designed independently and therefore better tailored to the use case and the user requirements. However, this also might necessitate several small DSLs for the different stages of the policy cycle. The example use case above contains at least two of them.

In order to avoid having domain experts to learn a whole lot of different languages, we suggest to use language modularization—as described, for example, by Hudak (1998) or Irazabal and Pons (2010)—and to define a common vocabulary. This makes sure domain experts recognize words, terms and expressions they already know from other languages which makes it a lot easier for them to learn a new one. At the same time, the languages we propose here can be used in different stages of the policy cycle. For example, the rules defined in the plan stage can later be used in the evaluation stage as well. We'd like to point out that the semantics underlying the rules stays the same between the different stages—the meaning of the rules does not change—but the execution might differ. In one case, the rules are used to change the visualization in the political commitment stage, and later exactly the same rules are used to automatically evaluate the policy.

A language's vocabulary is influenced by the domain it is used in as well as user requirements. In order to find a common, reusable vocabulary we propose to make use of techniques known from different areas:

- methods from the semantic web, especially ontology engineering to find domain-specific terms (concepts) and relations;
- object-oriented design, in particular methods to build a domain model;
- techniques from software requirements analysis such as interviewing, contextual inquiry or apprenticing.

An example how a DSL vocabulary can be engineered using these techniques is described by Mauw et al. (2004) and later by Tairas et al. (2009) who suggest to start with creating an ontology (or using an existing one if already available) and then applying additional formal domain analysis methods.

DISCUSSION AND CRITICAL ANALYSIS

The Bologna example, identified above, demonstrates the ways in which the complexities of the policy modelling process can be facilitated by ICT tools. 3D visualisation itself provides a major advance in communication between the policy-making community (urban planners and the political domain) and urban stakeholders, including citizens (Al-Kodmany, 2002). The representation of plan proposals for a particular locality, in this case urban neighbourhood, in a real-life (3D) manner offers a significant advance on previous two-dimensional and plan based communications in which misunderstandings by the urban stakeholders regarding the nature of the policy proposals have been widely reported.

However, ICT enabled policy modelling is a complex process that deals with multiple variables. It consists of socio-technology interactions and often it is difficult for the end-user community to understand the complexity of underlying IT tools and languages. In order to facilitate end-user community engagement, DSLs are identified to define rules for policy development using an intuitive language and interface.

The Bologna example shows that DSLs can indeed be utilised to drive the ICT enabled policy cycle. Scripts and rules written in such a language are easy to understand for domain experts, because they use a domain-specific vocabulary. At the same time, they are machine-readable, since the DSLs have a well-defined grammar and syntax.

DSLs also have some drawbacks (cf. Axelsson et al., 2009). Since they are tailored to a specific application domain and sometimes only to a single use case, they are also rather limited regarding their expressiveness and reusability. A DSL designed for traffic simulation provides means for this specific application only. This means that the same DSL cannot be used for any other use case.

The aim of using DSLs is twofold. On the one hand, they consist of a limited vocabulary which makes them easy to comprehend and to learn. On the other hand, the mere number of different DSLs can overtax users if for each application they have to learn a new language. The key to designing reusable DSLs is to find a good balance between uniqueness of the language—i.e. how much it is targeted to a specific use case—and commonality. In particular, using a common vocabulary for several similar languages will make them easier to learn. Good language design of multiple DSLs therefore starts with defining a basic set of words and expressions from which the more specific languages can then be derived.

From an urban planning perspective, it is frequently argued that the urban planning is highly specific to each locality defined by national and local legislative provisions, structural frameworks and procedural requirements that greatly limit the development of common ICT solutions that enhance the plan making and plan implementation process. This local specificity of urban planning requirements for ICT development in support of urban planning is certainly evident. Nonetheless, the opportunity for the development of generic ICT tools supporting urban planning is evident in the fundamental proposition that cities and towns of Europe, and indeed globally are subject to common drivers of change (economic, social and environmental) that invite and benefit from common solutions.

Common solutions based on generic ICT applied at the local level offer benefits in numerous ways, not least from the perspective of multi-scale governance, in enhancing communication between the levels of government,

whereby upper levels can communicate more effectively with lower-level organisations that have common information requirements and provide common information outputs. Generic and common ICT solutions applied to the cities of Europe also create substantial market opportunity promising procedural efficiencies and cost minimisation.

The generic form of the policy cycle and its stages suggests capturing multiple models/view points—e.g. complex socio-technical interactions between different actors and entities, information model, activity model, etc. Also, each stage itself presents a specific view point suitable for certain type of stakeholders. For instance, the 'evaluation and review' stage should generate necessary information for policy makers to make a decision. Such a multi-model structure heavily relies on a common domain specific vocabulary that not only helps in defining common concepts that can be used across models and stages of policy cycle but also underpins a DSL for communicating across multiple models and stages of the policy cycle. However, in this paper we focused on using DSLs for describing computational logic for ICT tools used at different stages as well as for modelling policy restrictions that can be automatically or semi-automatically checked by domain experts with the help of ICT tools. Communicating across multiple models and stages remains a topic for future research.

CONCLUSION

In this paper we presented a new approach to model urban policies using domain-specific languages (DSLs). These languages can be used to drive ICT tools which assist urban planners during policy making. We presented a complete policy cycle consisting of different stages including plan making, public participation and evaluation. Through a real-life scenario from the urbanAPI project we demonstrated how DSLs can be used reasonably in the various stages of the policy cycle. Scripts written in such DSLs help domain experts to control the ICT tools without requiring them to have a deep understanding in computer science or programming.

Sustainable urban development is transforming the relationship between the urban planning community and urban stakeholders, requiring enhanced engagement and partnership based urban planning. The ICT enabled urban planning applications discussed in this paper provide a major opportunity to deliver the required participatory bottom-up urban planning. Full realisation of this opportunity is critically dependent upon the transition from the current heterogeneity of urban planning systems to one where generic ICT modules can successfully operate. The key to this is twofold. First, the policy-making cycle and model of plan production and implementation is in itself generic. The policy-making cycle utilises different information sources, according to different locally defined procedures, but fundamentally the policy-making cycle is common to all planning agencies.

The second requirement in order to create the opportunity for generic ICT urban planning applications is the recognition that there are many pathways to the desired result of good urban planning. In other words, substitution of certain current working practices by alternative procedures at the local level will permit the adoption of generic ICT solutions and thereby the necessary transformation of urban planning as a stage in the attainment of fully collaborative sustainable development.

In addition, we think the success of generic ICT tools greatly depends on intuitive user interfaces. DSLs as they are presented in this paper can provide such interfaces. They can drive the automated policy cycle and at the same time they are understandable by stakeholders who can therefore clearly see the decisions behind urban policies.

Basically, DSLs have been used quite successfully in computer science already to build intuitive user interfaces that are understandable by non-IT experts. However, until now they have not been applied to the area of urban policy modelling and making. We consider this paper the first step towards supporting the participatory, bottom-up approach to urban planning, and intuitive interfaces (i.e. DSLs) the key factor to its success. However, concrete application of this approach including a practical meta-model and a common vocabulary for urban planning DSLs remains a topic for future research.

ACKNOWLEDGEMENT

Research presented here is partly carried out within the project "urbanAPI" (Interactive Analysis, Simulation and Visualisation Tools for Urban Agile Policy Implementation), funded from the 7th Framework Program of the European Commission, call identifier: FP7-ICT-2011-7, under the grant agreement no: 288577, started in October 2011.

REFERENCES

Al-Kodmany, K. (2002). Visualization tools and methods in community planning: from freehand sketches to virtual reality. *Journal of planning Literature*, 17(2):189–211.

Axelsson, E., Sheeran, M., Stenström, P., Dévai, G., Horváth, Z., and Vajda, A. (2009). Domain Specific Languages: state of the art and future directions. *Ericsson Software Research Day, Stockholm, Sweden*.

Batty, M. (2007). *Cities and complexity: understanding cities with cellular automata, agent-based models, and fractals*. The MIT press.

Charalabidis, Y., Triantafillou, A., Karkaletsis, V., and Loukis, E. (2012). Public policy formulation through non moderated crowdsourcing in social media. In Tambouris, E., Macintosh, A., and Sæbø, Ø., editors, *Electronic Participation*, volume 7444 of *Lecture Notes in Computer Science*, pages 156–169. Springer Berlin Heidelberg.

Fowler, M. (2010). *Domain Specific Languages*. Addison-Wesley Longman.

Guzy, M. R., Smith, C. L., Bolte, J. P., Hulse, D. W., and Gregory, S. V. (2008). Policy research using agent-based modeling to assess future impacts of urban expansion into farmlands and forests. *Ecology and Society*, 13(1):37.

Hanzl, M. (2007). Information technology as a tool for public participation in urban planning: a review of experiments and potentials. *Design Studies*, 28(3):289–307.

Hudak, P. (1998). Modular domain specific languages and tools. *Fifth International Conference on Software Reuse*, pages 134–142.

Irazabal, J. and Pons, C. (2010). Supporting Modularization in Textual DSL Development. *XXIX International Conference of the Chilean Computer Science Society*, pages 124–130.

Khan, Z. and Ludlow, D. (2011). urbanAPI Deliverable D2.1: User Requirements Definition, version 032.

Krämer, M. and Kehlenbach, A. (2013). Interactive, GPU-based urban growth simulation for agile urban policy modelling. In *Proceedings of the 27th European Conference for Modelling and Simulation (ECMS)*.

Lempert, R. (2002). Agent-based modeling as organizational and public policy simulators. *Proceedings of the National Academy of Sciences of the United States of America*, 99(Suppl 3):7195–7196.

Maragoudakis, M., Loukis, E., and Charalabidis, Y. (2011). A review of opinion mining methods for analyzing citizens contributions in public policy debate. In Tambouris, E., Macintosh, A., and Bruijn, H., editors, *Electronic Participation*, volume 6847 of *Lecture Notes in Computer Science*, pages 298–313. Springer Berlin Heidelberg.

Mauw, S., Wiersma, W. T., and Willemse, T. A. C. (2004). Language-driven system design. *International Journal of Software Engineering and Knowledge Engineering*, 14:625–664.

Mernik, M., Heering, J., and Sloane, A. M. (2005). When and how to develop domain-specific languages. *ACM Computing Surveys*, 37(4):316–344.

North, D. (2009). Behaviour-Driven Development. Retrieved February 9, 2013, from `http://behaviour-driven.org/`.

Ruiz Estrada, M. A. (2010). What is Policy Modeling?. *SciTopics*. Retrieved February 8, 2013, from `http://www.scitopics.com/What_is_Policy_Modeling.html`.

Saleem, M., Jaafar, J., and Hassan, M. (2012). A Domain-Specific Language for Modelling Security Objectives in a Business Process Models of SOA Applications. *AISS: Advances in Information Sciences and Service Sciences*, 4(1):353–362.

Tairas, R., Mernik, M., and Gray, J. (2009). Using ontologies in the domain analysis of domain-specific languages. In Chaudron, M. R. V., editor, *Models in Software Engineering*, volume 5421 of *Lecture Notes in Computer Science*, pages 332–342. Springer Berlin Heidelberg.

AUTHOR BIOGRAPHIES

MICHEL KRÄMER is deputy department head of the Spatial Information Management competence center of the Fraunhofer Institute for Computer Graphics Research IGD in Darmstadt, Germany. His research interests are in Compiler Construction, Language Recognition and Artificial Intelligence as well as Big Data and Cloud Computing. He's development lead of the 3D GIS area and has contributed to various open source products. As the Scientific Manager of the urbanAPI project he's responsible for software architecture and the project's scientific progress. Michel Krämer holds a master's degree in computer science from the THM University of Applied Sciences, Gießen, Germany where he's now also a lecturer. His email address is `michel.kraemer@igd.fraunhofer.de`.

DAVID LUDLOW is member of the EU Expert Group on the Urban Environment, and the EU Expert Group contributing to the preparation and definition of the EU Thematic Strategy on Urban Environment (6th Environment Action Programme). He gained detailed knowledge of the subject area of European urban and regional environmental planning and sustainable development as well as the development of information, communication and technology (ICT) applications for sustainable urban management. He is responsible for the development and implementation of more than 40 major EU funded research projects, as well as publications of pan European significance. His email address is `david.ludlow@uwe.ac.uk`.

ZAHEER KHAN is postdoctoral Research Fellow in the Faculty of Environment and Technology of UWE and holds Bachelors, Masters and PhD degrees in computer science. He has over 10 years of experience in academic research and teaching. His research interests are use of ICT technologies for smart cities, urban management and policy modelling. His main expertise lies in the application of the state-of-the-art technologies from distributed computing, grids, clouds, sensor web, software engineering, business process management, data management, software agents, and geospatial information systems in multi-disciplinary application domains. He has been working on the large-scale collaborative SAGE multi-agent system, FP6 Health-e-Child, FP6 HUMBOLDT, FP7 LifeWatch projects, and is leading requirements specifications and evaluation work package in the FP7 UrbanAPI project. His email address is `zaheer2.khan@uwe.ac.uk`.

MULTI-MODEL ECOLOGIES FOR ADDRESSING MULTI-SCALE, MULTI-PERSPECTIVE POLICY PROBLEMS

L.A. Bollinger
Faculty of Technology, Policy and Management
Delft University of Technology
2600 GA Delft, The Netherlands
Email: L.A.Bollinger@tudelft.nl

KEYWORDS

Multi-resolution modeling, Multi-scale modeling, Exploratory modeling, Microworlds, Mental models

ABSTRACT

Many key societal problems share a set of common features – multiple interacting temporal and spatial scales, multiple valid perspectives, changing requirements and unquantifiable uncertainties. These characteristics substantially stress our cognitive and computational resources, limiting our capacity to effectively address these problems. We introduce an approach for dealing with the inherent complexity of such problems. At the core of this approach is the notion of a *multi-model ecology* – an interacting and constantly evolving system of models, datasets, interfaces and humans tasked with enhancing the ability of decision makers to effectively address a complex policy problem. The multi-model ecology approach entails the systematic fragmentation and gradual reconstitution of a problem's multiple components and dimensions in an evolving participatory context. We describe an implementation of this approach currently in progress – focused on electricity infrastructure vulnerability to climate change – and identify several key areas of research for developing this approach further.

INTRODUCTION

There exists a unique class of problems characterized by multiple relevant temporal and spatial scales, multiple valid perspectives, changing requirements and unquantifiable uncertainties (hereafter referred to as MMCU problems). Problems of this class – including climate change adaptation, sustainability, urban poverty, etc. – share aspects of other theoretical notions such as wicked problems (Churchman 1967), deep uncertainty (Lempert et al. 2003) and post-normal science (Funtowicz and Ravetz 1993). MMCU problems are not new and neither is the idea of using quantitative models to address them. Still, they continue to vex scientists and policy makers for several reasons – interactions between different temporal and spatial scales are challenging to conceptualize and formally represent, multiple valid perspectives are difficult to reconcile, and changing requirements and unquantifiable uncertainties mean that no solution is permanent nor optimal.

In an ideal technocratic world, scientists would develop all-encompassing models generating definitive projections upon which policy and strategy decisions could unhesitatingly be based. When it comes to MMCU problems, however, no model can capture more than a minute fraction of the potentially relevant components and relationships – every model is based on tenuous assumptions. Still, the modeling and simulation (M&S) community often treats decision makers as rational agents operating in a tractable environment – expecting that the right scientific input will lead to the right decisions. The reality is that, in dealing with MMCU problems, there are no rational decisions – the available information is too much, too incomplete and too uncertain.

In the wake of Lee's criticisms of the large-scale, monolithic policy models of the 1960s (Lee 1973), the M&S community advanced an array of techniques and approaches to cope with the inherent complexity of policy problems. At the same time, the policy and strategy communities have begun to recognize the limitations of a purely rational and strictly evidence-based approach to decision making (Freiberg and Carson 2010; Nutley et al. 2003). Against the background of these developments, a pertinent question is how the diverse approaches of the modeling and simulation community can be brought together in a coherent manner to more effectively address MMCU problems. The purpose of this paper is to introduce such an approach.

We define a *multi-model ecology* as an interacting

Proceedings 27th European Conference on Modelling and Simulation ©ECMS Webjørn Rekdalsbakken, Robin T. Bye, Houxiang Zhang (Editors)
ISBN: 978-0-9564944-6-7 / ISBN: 978-0-9564944-7-4 (CD)

and constantly evolving system of models, datasets, interfaces and humans tasked with enhancing the ability of decision makers to effectively address a MMCU problem. The notion of multi-model ecologies builds on existing modeling and simulation approaches, including microworlds (Morecroft 1988; Papert 1980), exploratory modeling and analysis (Bankes 1993) and multi-resolution modeling (Davis and Tolk 2007). Its novelty lies in the links drawn between the the M&S process, its components and the realities of complex policy decisions.

The next section of this paper lays the foundation of the multi-model ecologies approach, describing related research from the M&S field as well as psychology and policy. From this starting point, we proceed with a more extensive introduction to the multi-model ecologies approach and highlight its applicability to MMCU problems. Finally, we demonstrate the application of this approach based on a multi-model ecology currently in development, addressing the issue of electricity infrastructure vulnerability to climate change. We conclude with recommendations for future research.

BACKGROUND AND RELATED RESEARCH

The 1960s saw the advent of large-scale, monolithic computer models as prescriptive policy tools. This approach was famously criticized by Lee (1973), who pinpointed a range of shortcomings in the large-scale urban models of that period - hypercomprensiveness, grossness, hungriness, wrongheadedness, complicatedness, mechanicalness and expensiveness. While these criticisms by no means halted the development of large-scale models for addressing complex policy issues, they highlighted the need for alternatives to a monolithic, prescriptive approach.

Insight into possible directions for such alternatives has come from subsequent scientific developments concerning the cognitive processes underlying decision making in complex environments. Multiple studies have highlighted the relevance of "non-rational" decision strategies, particularly intuition, in strategic decision making (Khatri and Ng 2000; Woiceshyn 2009). Subsequent research has elucidated the process behind the use of intuition in decision making. Analogical reasoning, as this process is called, involves the "mapping" of knowledge from a source context of prior experience to a current "target" context – a process which is restricted by the richness of the mental models that map a decision maker's previous experiences (Gary et al. 2012; Gavetti et al. 2005).

This is one reason why MMCU problems pose such an obstacle to decision makers. Effective learning requires specific conditions – in particular, accurate and immediate feedback between the situational conditions and the appropriate response (Tversky and Kahneman 1986). The long timeframes of many MMCU problems and the enormity of variables involved lead to a lack of feedback concerning the effectiveness of previous decisions. This leaves decision makers with limited opportunity to develop their mental models, and subsequently the intuitive mechanisms that would allow them to make effective decisions. Even worse, decision makers may not be aware of this – Kahneman (2011) suggests that when insufficient mental models exist, individuals will gleefully and unwittingly draw from marginally similar experiences that do not serve as adequate guides to the situation at hand.

In line with these findings, research in the policy community has begun to question the assumption that policy should always be based on a rational analysis of available evidence (Freiberg and Carson 2010). Limitations on the rationality of decision makers mean that the links between research, knowledge and policy are "always likely to remain loose, shifting and contingent" (Nutley et al. 2003). Against the background of these limitations, Sanderson (2009) recommends a shift in emphasis from *evidence-based policy making* to *intelligent policy making* – policy making that emphasizes learning and experimentation, and draws from "reserves of experience, intuition, tacit knowledge and all the hidden skills and capacities that technical rationality has relegated to obscurity". It is these hidden skills and capacities on the part of decision makers that the M&S community is well-positioned to develop.

One area of M&S that pushes in this direction is the "microworlds" approach, first proposed by Papert (1980). This approach, originally developed for application in managerial situations, stresses the development of decision makers' mental models – enhancing their contextual understanding and (in theory) enabling them to make better strategic decisions. The key advantage of the microworlds approach lies in its capacity to compress time and space using dynamic simulation, especially system dynamics.

The microworlds approach facilitates learning on the part of decision makers by compressing time and space. But it does not explicitly address the challenges of problem situations that cannot be neatly captured within a single, unified representation of reality – e.g. problems spanning multiple scales of time, space and organization, and problems characterized by multiple valid conceptualizations of reality. Beginning with the work of (Oeren 1991), the modeling and simulation community has begun to

address this topic under the banners of multisimulation and multi-perspective, multi-resolution and multi-aspect modeling (Tekinay et al. 2010; Yilmaz et al. 2007). Such approaches entail the modular representation of systems within a set of interoperable models that capture reality from multiple angles and at multiple levels of fidelity.

Where multisimulation and multi-perspective/-resolution/-aspect modeling enable capturing reality from multiple angles, the technique of exploratory modeling and analysis (EMA) is used to explore the assumptions space of a model. The aim of EMA is to facilitate the identification of *robust* policy options – options which perform well across a range of possible futures – or *hedging* strategies – strategies to prevent the most adverse consequences (Lempert et al. 2004). In theory, the combination of EMA with, for instance, multi-resolution modeling can allow for the exploration of both parametric and structural uncertainties (Davis and Tolk 2007) – helping to provide decision makers with a holistic understanding of the consequences of the uncertainties associated with a problem.

As the paragraphs above have demonstrated, the M&S community has developed a number of techniques – e.g. microworlds, multisimulation and EMA - that address shortcomings of a monolithic, prescriptive approach to using models to address complex policy problems. In the following sections, we discuss how aspects of these techniques can be brought together in the context of a coherent approach to address MMCU problems.

MULTI-MODEL ECOLOGIES

A multi-model ecology is an interacting and constantly evolving system of models, datasets, interfaces and humans tasked with enhancing the ability of decision makers to effectively address a MMCU problem. The multi-model ecology approach entails the systematic fragmentation and gradual reconstitution of a problem's multiple components and dimensions in an evolving participatory context. This approach is particularly suited to addressing MMCU problems for several reasons.

1. Multi-model ecologies facilitate the capture of multiple system levels, multiple timescales and multiple perspectives.

Models in a multi-model ecology are constructed with different scopes, resolutions and perspectives. Independently, each model provides a partial picture of the components and relationships underlying the problem at hand. Together, they provide a multi-dimensionsional representation of the relevant system(s). Drawing hints from the fields of multi-simulation and multi-perspective/resolution/aspect modeling, models in a multi-model ecology are not independent entities, but modules in a larger whole. Each of these models/modules has a clearly defined scope, purpose, resolution and set of inputs/outputs, and rests on a particular set of assumptions.

As illustrated by the schematic in Figure 1, models in a multi-model ecology may interact with one another, with human decision makers, with datasets or with several of the above. Models may dynamically link with one another during runtime, or more statically in sequence. They may also be completely independent of other models in the ecology, receiving input from datasets or interfaces, and generating output to other datasets or interfaces. *Datasets* in a multi-model ecology store both the data inputs to models as well as the data outputs. They may link with models or with interfaces, allowing them to be directly viewed by human decision makers or processed into other forms. *Interfaces* are the links between models or datasets and the mental models of human decision makers. The key aspect of models, datasets and interfaces in multi-model ecologies is their flexible relationship with other entities. Taking a hint from the role of programs in the GNU/Linux operating system (Gancarz 2003), entities in a multi-model ecology can be seen as "filters" for processing and transforming data, and can be linked with other filters in different ways to serve different purposes. The aim in such cases is not "pure composability" (Davis and Tolk 2007) – strict plug-and-play capability – but the cultivation of a set of resources that can be configured and reconfigured to interact with one another in different ways, whether statically, dynamically, directly or indirectly.

The human components of a multi-model ecology include decision makers, domain experts and developers. *Developers* are the programmers and software engineers behind the implementation of models and the maintenance of datasets. *Experts* are the holders of specialized domain knowledge, essential in constructing models and datasets, and evaluating their validity. *Decision makers* are the ultimate users of the ecology. Involved individuals may at times wear different hats, depending on their relevant expertise – e.g. a developer or decision maker knowledgeable in domain aspects may at time play the role of domain expert.

2. Multi-model ecologies support systematic and comprehensive exploration of the assumptions space.

Each of the components in a multi-model ecology rests on a bed of assumptions. The assumptions underlying a model are determined by the concep-

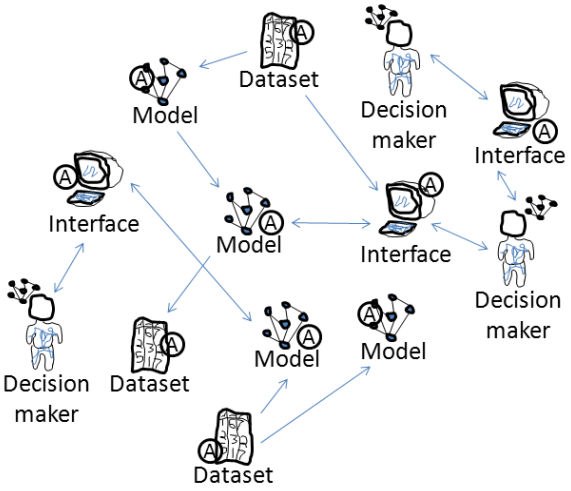

Figure 1: Schematic of a hypothetical multi-model ecology, including models, datasets, interfaces and human decision makers. An encircled "A" refers to the assumptions associated with a component. Domain experts and developers are excluded from the schematic.

tualization of the system being represented, by the scope and fidelity of the model and by the modeling technique being employed. Models based on established theory – such as many physical systems models – may rest on a solid foundation of generally accepted assumptions, whereas models based on less established theory and/or participative processes – e.g. many models of social systems – may sit on an array of tenuous and subjective assumptions. The datasets and interfaces in a multi-model ecology also rest on assumptions. The assumptions underlying a dataset may have to do with the manner in which the data was collected – via questionnaires, direct observation, etc. – or with the assumptions of the model from which the data was generated. The assumptions underlying an interface have to do with the way data is presented to human users and the manner in which users are able to interact with data and models.

Assumptions are an inevitable part of the components of a multi-model ecology, essential remnants of abstraction and simplification processes. Most important in a multi-model ecology approach is that these assumptions are clearly tracked and documented. Drawing from exploratory modeling and analysis, vigilant tracking of assumptions opens up possibilities for deliberate and systematic exploration of the assumptions space underlying a particular configuration of models, datasets and interfaces. Interface tools such as the EMA workbench (Kwakkel 2012) can help to translate the results of this exploration into a form readily understandable to decision makers, helping them to comprehend the consequences of different sets of assumptions, including both parametric and structural uncertainties.

3. Multi-model ecologies foster the development of rich mental models on the part of decision makers.

The ultimate purpose of a multi-model ecology is to facilitate learning on the part of decision makers – to enhance the mental models that serve as a basis for policy decisions. Research has shown that processes of analogical transfer may be enhanced by supporting the ability of decision makers to explore multiple variations of a problem situation, and allowing them the possibility to systematically test hypotheses (Gary et al. 2012). The structure of a multi-model ecology – the presence of multiple, flexibly interlinked models, datasets and interfaces – facilitates this by exposing decision makers to numerous variations of the problem situation. Learning on the part of decision makers may come from systematic interaction with interfaces, but it may also emerge from interactions with domain experts and developers in the context of participatory model development processes, which can help to surface the tacit assumptions of decision makers. These assumptions can then be incorporated into one or more models in the ecology, allowing their consequences to be explored and compared with alternative sets of assumptions.

4. Multi-model ecologies evolve as knowledge of the problem and the needs of decision makers change.

A multi-model ecology is not designed from the top down, but emerges over time as a consequence of interactions between decision makers, experts and developers. Its development is ultimately driven by the changing needs of involved decision makers. At times, it may also be spurred by the exploratory efforts of domain experts and developers seeking to incorporate new knowledge and come to terms with various approaches to capturing the relevant aspects of the problem. Different models, datasets and interfaces within an ecology may develop at different rates and according to different methodologies. Some models may be developed using participatory approaches, allowing decision makers to heavily influence the assumptions underlying the model's structure. Others may be implemented chiefly by experts and developers, with the underlying assumptions based on established theory. Still others may be adopted or adapated from external sources. As a result of the development of new models, datasets

and interfaces, and the maturation and obsolescence of existing ones, the composition of a multi-model ecology changes gradually over time, driven both by the changing requirements of the problem and the availability of new knowledge.

A MULTI-MODEL ECOLOGY IN DEVELOPMENT

This section introduces a multi-model ecology currently in development. The MMCU problem addressed by this ecology is the vulnerability of electricity infrastructures to climate change. Climate change is anticipated to have a variety of impacts on electricity infrastructures (Rothstein et al. 2008). By affecting the range of environmental conditions under which these infrastructures must operate, and the frequency with which extreme conditions may occur, climate change poses multiple threats to these systems, from a gradual degradation of their integrity to sudden and catastrophic blackouts. The problem of electricity infrastructure vulnerability to climate change is characterized by several aspects that categorize it as a MMCU problem: (1) the electricity infrastructure spans multiple organizational and geographic scales; (2) climate change plays out over decades, while weather-induced disturbances may unfold over a period of hours, minutes or even seconds; and (3) Climate change is characterized by unquantifiable uncertainties, and multiple perspectives exist concerning e.g. the dynamics underlying the long-term development of the electricity infrastructure.

Given the decision-makers involved, the current geographic focus of this multi-model ecology is the Netherlands. Amongst these actors, there is a deficit of knowledge concerning the severity of this problem and the necessity of actions to address it. The purpose of the ecology is not to prescribe immediate actions on the part of decision makers, but to enhance their mental models in a manner that can enable them to better incorporate this threat into their decisions.

Composition and evolution of the ecology

Driven by the needs of decision makers, the first task in developing the multi-model ecology was to capture key relationships between weather variables and components of the electricity infrastructure in an initial model of *weather-infrastructure interactions* (item 1 in Figure 2) – based on a combination of known physical relationships (e.g. between power line resistivity and temperature) and statistically identified relationships (e.g. between weather variables and electricity demand (Hekkenberg et al. 2009)). A preliminary version of this model has been implemented in the numerical simulation environment MATLAB.

Given the focus of involved decision makers at the level of the national transmission network, this model was then linked with a preliminary dataset of the components of the Dutch transmission network (item 2). This dataset is housed in a web-based platform called Enipedia (Anonymous 2013; Davis 2012), which uses semantic wiki technology to enable the collabortive cultivation of power industry data. This RDF-based platform allows for the extraction of targeted portions of the dataset using SPARQL queries. By embedding tailored SPARQL queries in the code of our weather-infrastructure interactions model, we establish a runtime link between this model and the web-based dataset.

The aim of the weather-infrastructure interactions model is not only to capture the relationships between weather variables and the performance of infrastructure components, but also the effects of changes in component performance on the network as a whole. Key to enabling this was establishing a runtime link between the weather-infrastructure interactions model and a pre-existing MATLAB-based power flow model (item 3) (Zimmerman et al. 2011). Power flow models are a mature class of models for analyzing power systems in steady state operation, outputting power flows through the lines in a power system under provided supply and demand conditions. Establishing this link required translating the semantic base of the weather-infrastructure interactions model into the language of the power flow model, a process which engendered several important assumptions.

This combination of components (items 1, 2 and 3) provided us with a computational structure for determining the impacts of certain types of extreme weather events on the performance of the infrastructure. We are in the process of linking these components with an R-based interface (item 4), which will allow decision makers to run the model under different parameter conditions and view results in a readily-understandable format. We also plan to link this model with weather datasets (item 5) based on the results of climate models, allowing for the capture of uncertainties associated with the trajectory of climate change. A challenge here will be the different timescales involved – the weather-infrastructure interactions model operates on a timescale of hours, while climate projections are based on models with a timescale of decades.

Further discussions with experts and decision makers revealed the importance of also capturing decade-spanning changes in the topology and technological composition of the electricity network. This incited

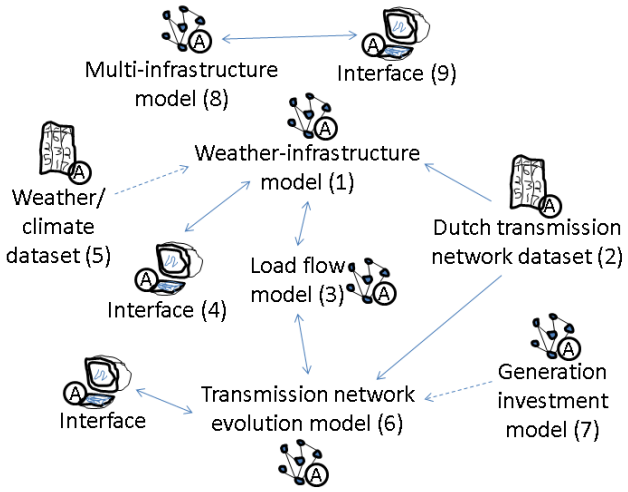

Figure 2: Schematic of the multi-model ecology in development. Solid arrows indicate implemented links between components. Dashed arrows indicate links in planning. Decision makers are excluded from this schematic.

the development of an agent-based *transmission network evolution model* (item 6), in which the growth and evolution of an electricity transmission network is captured as the consequence of repeated decisions and interactions of a transmission system operator and power producers. The initial phase of model development was quite exploratory, driven by the developer and domain experts and based largely on theory. Later phases of model development, however, have been more participatory, involving decision makers in conceptualizing the system and delineating assumptions.

This model is currently implemented in the agent-based modeling platform Netlogo (Wilensky 2012). However, in order to accurately represent the decision making process of the transmission system operator – who needs to calculate projected power flows through his network – it became necessary to establish a runtime link with a power flow model. For this we use the same power flow model employed above (item 3). However, in addition to translating the semantic base, implementation in this case necessitated the development of a software link between Netlogo and GNU Octave (the numerical simulation software used to run the power flow model).

The current version of the transmission network evolution model includes a vastly simplified representation of power producer investment decisions which is unable to capture several of the main drivers of such investments. Based on discussions with decision makers and experts, it was determined that this representation was insufficient. To remedy this, we are planning to implement a static link with an existing Java-based model (item 7) that captures these investment decisions at a higher resolution (Chappin et al. 2012).

Partway through the development of the above models, discussions with experts and decision makers highlighted a new and important sub-problem – the dynamic consequences of links between the electricity infrastructure and other infrastructures such as road, rail and gas. To address this issue, an exploratory model was initiated with the aim of investigating the consequences of random failures in multi-infrastructure networks at an abstract level (item 8). Like the transmission network evolution model introduced above, this model is implemented in Netlogo, and uses the platform's native interface (item 9). The model has not yet been linked to any datasets, nor is it yet clear how or whether the model may link with other models or datasets in the ecology.

Key challenges

The development of this ecology has highlighted several important challenges in realizing multi-model ecologies. Chief amongst these is the semantic gap that exists between models – and between models and databases – developed in different contexts. For instance, a *power substation* in the transmission network evolution model is similar to the notion of a *bus* in the power flow model, but there are also important differences in the use of these concepts that affect the validity of results under certain circumstances. Systematically identifying and tracking these differences is an important challenge with which we are still struggling. In our experience thus far, translation between the ontologies employed by different entities in an ecology is often feasible, but can be time consuming and can engender new assumptions. Moreover, imprecise translations can invalidate results. These challenges can serve as barriers to the use of pre-existing models and datasets, and highlight the importance of systematic documentation with clear delineation of assumptions.

As has been emphasized in the preceding paragraphs, the components of the multi-model ecology described here are not static – new needs may arise in the course of interacting with stakeholders, and insights from one model may lead to new pertinent questions. As such, models, datasets and interfaces need to be developed with an expectation that they will change over time, and that they exist as units in a flexible and ever-changing ecology. We seek as much as possible to use tools that are amenable to this – that are open source, well documented and capable of interaction with other software. An example

of this is Enipedia – the database we have used for cultivating infrastructure data – which enables the extraction and export of targeted data for different uses.

A potential advantage of a multi-model ecology approach lies in enabling the use of models in multiple contexts – a single model can be linked with other models, datasets and interfaces to address multiple research questions. However, it is not always possible to anticipate the future demands that may be placed on a model, which makes it difficult to design them to accommodate this. Our experience with this ecology suggests that the use of a model in multiple contexts within an ecology is sometimes feasible. However, manual modifications are often necessary to enable compatibility, both from a software perspective and an ontological perspective.

CONCLUSIONS AND FUTURE WORK

This paper has introduced and demonstrated the application of a *multi-model ecology* approach to addressing MMCU problems – an approach based around an interacting and constantly evolving system of models, datasets, interfaces and humans. This approach leverages several existing M&S techniques, including microworlds, multi-perspective/resolution/aspect modeling and exploratory modeling and analysis. In the last section, we have described an implementation of this approach currently in progress, focused on the case of electricity infrastructure adaptation to climate change.

This pilot implementation of the multi-model ecology approach has highlighted several important areas for future research. First, the multi-model approach establishes tooling criteria, but does not prescribe specific tools to be used. We believe that these tooling decisions should be context dependent, but see the need for the development or adaptation of additional tools that better match the needs of the multi-model ecology approach. An example here is tools that can aid in the explicit tracking of assumptions across multiple models, datasets and interfaces, and can enhance the ability of decision makers to readily comprehend their consequences.

Additionally, further research is necessary into methods for effectively engendering learning on the part of decision makers dealing with highly complex problems. The microworlds approach offers some hints here, but analyses of its capacity to enhance the mental models of decision makers have demonstrated mixed results (Langley and Morecroft 1996; Stouten et al. 2012). A particular challenge has to do with the capacity of the human mind to comprehend uncertainty – Kahneman (2011) suggests that our subconscious minds are not geared for dealing with multiple incompatible interpretations of the world. How can we train the intuitive mechanisms of decision makers to deal with MMCU problems when their brains may not be wired to comprehend a key aspect of these problems?

From sustainability to climate change adaptation, MMCU problems pose an enormous challenge to a society ill-equipped to deal with them. We believe that M&S can contribute meaningfully to addressing such problems, but only with careful consideration of the limitations of M&S techniques and of the realities of decision making. We offer a small step in this direction.

ACKNOWLEDGEMENTS

This work is supported by the Knowledge for Climate program, project INCAH Infrastructure Networks Climate Adaptation and Hotspots.

REFERENCES

Anonymous. Enipedia. Web site, 2013. URL `http://enipedia.tudelft.nl/wiki/Main_Page`. Accessed February 2013.

S. Bankes. Exploratory modeling for policy analysis. *Operations Research*, 41:435–449, 1993.

E. Chappin, P. Viebahn, J. Richstein, S. Lechtenboehmer, and A. Nebel. Agent-based model of intermittent renewables: Simulating emerging changes in energy markets in transition. In *ESSA 2012 8th Conference of the European Social Simulation Association*, 2012.

C. Churchman. Wicked problems. *Management Science*, 14:141–142, 1967.

C. Davis. *Making Sense of Open Data - From Raw Data to Actionable Insight*. PhD thesis, Delft University of Technology, 2012.

P. Davis and A. Tolk. Observations on new developments in composability and multi-resolution modeling. In S. G. Henderson, B. Biller, M. Hsieh, J. Shortle, J. D. Tew, and R. R. Barton, editors, *Proceedings of the 2007 Winter Simulation Conference*, 2007.

A. Freiberg and W. Carson. The limits to evidence-based policy: Evidence, emotion and criminal justice. *Australian Journal of Public Administration*, 69:152–164, 2010.

S. O. Funtowicz and J. R. Ravetz. Science for the post-normal age. *Futures*, 25:739–755, 1993.

M. Gancarz. *Linux and the Unix Philosophy*. Digital Press, 2003.

M. S. Gary, R. Wood, and T. Pillinger. Enhancing mental models, analogical transfer, and performance in strategic decision making. *Strategic Management Journal*, 33:1229–1246, 2012.

G. Gavetti, D. Levinthal, and J. Rivkin. Strategy making in novel and complex worlds: the power of analogy. *Strategic Management Journal*, 26:691–712, 2005.

M. Hekkenberg, R. Benders, H. Moll, and A. Schoot-

Uiterkamp. Indications for a changing electricity demand pattern: The temperature dependence of electricity demand in the Netherlands. *Energy Policy*, 37: 1542–1551, 2009.

D. Kahneman. *Thinking Fast and Slow*. Farrar, Straus and Giroux, 2011.

N. Khatri and H. Ng. The role of intuition in strategic decision making. *Human Relations*, 53:57–86, 2000.

J. Kwakkel. Exploratory modelling and analysis (EMA) workbench. Web site, 2012. URL `http://simulation.tbm.tudelft.nl/ema-workbench/contents.html`. Accessed February 2013.

P. Langley and J. Morecroft. Learning from microworld environments: a summary of the research issues. In *Proceedings of the 14th international conference of the system dynamics society*, 1996.

D. B. Lee. Requiem for large-scale models. *Journal of the American Institute of Planners*, 39:163–178, 1973.

R. Lempert, S. Popper, and S. Bankes. Shaping the next one hundred years: New methods for quantitative, long-term policy analysis. Technical report, RAND Pardee Center, 2003.

R. Lempert, N. Nakicenovic, D. Sarewitz, and M. Schlesinger. Characterizing climate change uncertainties for decision makers. *Climatic change*, 65:1–9, 2004.

J. Morecroft. System dynamics and microworlds for policymakers. *European Journal of Operational Research*, 35:301–320, 1988.

S. Nutley, H. Davies, and I. Walter. Evidence-based policy and practice: cross-sector lessons from the United Kingdom. *Social Policy Journal of New Zeeland*, 20: 29–48, 2003.

T. Oeren. *Knowledge-based simulation: Methodology and application*, chapter Dynamic templates and semantic rules for simulation advisers and certifiers, pages 53–76. Springer, 1991.

S. Papert. *Mindstorms*. Basic Books, 1980.

B. Rothstein, M. Schroedter-Homscheidt, C. Haefner, S. Bernhardt, and S. Mimler. *Impacts of climate change on the electricity sector and possible adaptation measures*, chapter Impacts of climate change on the electricity sector and possible adaptation measures, pages 231–241. Springer, 2008.

I. Sanderson. Intelligent policy making for a complex world: Pragmatism, evidence and learning. *Political Studies*, 57:699–719, 2009.

H. Stouten, A. Heene, X. Gellynck, and H. Polet. Learning from playing with microworlds in policy making: An experimental evaluation in fisheries management. *Computers in Human Behavior*, 28:757–770, 2012.

C. Tekinay, M. Seck, M. Fumarola, and A. Verbraeck. A context-based multi-perspective modeling and simulation framework. In *Proceedings of the 2010 Winter Simulation Conference*, 2010.

A. Tversky and D. Kahneman. Rational choice and the framing of decisions. *The Journal of Business*, 59:251–278, 1986.

U. Wilensky. Netlogo. Web site, 2012. URL `http://ccl.northwestern.edu/netlogo/`. Accessed February 2013.

J. Woiceshyn. Lessons from good minds: How CEOs use intuition, analysis and guiding principles to make strategic decisions. *Long range planning*, 42:298–319, 2009.

L. Yilmaz, A. Lim, S. Bowen, and T. Oeren. Requirements and design principles for multisimulation with multiresolution, multistage multimodels. In *Proceedings of the 2007 Winter Simulation Conference*, 2007.

R. Zimmerman, C. Murillo-Sanchez, and D. Gan. Matpower: A MATLAB power system simulation package. Web site, 2011. URL `http://www.pserc.cornell.edu/matpower/`. Accessed February 2013.

SIMULATING THE COST OF SOCIAL CARE IN AN AGEING POPULATION

Eric Silverman, Jason Hilton, Jason Noble and Jakub Bijak
The Care Life Cycle Project
University of Southampton
Southampton SO17 1BJ, United Kingdom
Email: e.silverman@soton.ac.uk

KEYWORDS

Policy Modelling, Social Simulation, Agent-Based Modelling, Social Care, Population Change

ABSTRACT

In this paper we present an agent-based model of the ageing UK population. The goal of this model is to integrate statistical demographic projections of the UK population with an agent-based platform that allows us to examine the interaction between population change and the cost of social care in an ageing population. The model captures the basic processes which affect the demand for and supply of social care, including fertility, mortality, health status, and partnership formation and dissolution. The mortality and fertility rates in this population are drawn from statistical demographic projections until 2050 based on UK population data from 1951 - 2011. Results show that, in general, we expect the cost of social care in the UK to rise significantly as the population continues to age. An in-depth sensitivity analysis performed using Gaussian Process Emulators confirms that the level of care need within the population and the age of retirement have the most profound impact on the projected cost of social care.

INTRODUCTION

As the UK population continues to age, the shift in the age structure of the population puts ever-increasing strain on the country's social care infrastructure. The elderly are the primary consumers of social care services, and dropping birthrates combined with lengthening lifespans mean that while the demand for social care continues to increase, we can expect the supply of social care to decrease as the workforce also ages (Coleman 2002).

The Care Life Cycle Project is pursuing an interdisciplinary approach to this critical societal problem (Brailsford et al. 2012). Given the multiple complex life-course transitions that can affect the provision of social care – decisions in partnership formation, changes in health status, internal migration, and many others – understanding the population dynamics underlying this issue requires an approach that can capture the interactions between these factors. While statistical demographic analyses are critical in order to show us the population change we can expect in the coming decades, we must supplement these figures with a more detailed examination of the processes underlying these dynamics in order to make substantive policy recommendations on the distribution and organisation of social care services.

We propose that combining agent-based approaches with empirically-driven statistical demography allows us to better align social simulations with the 'real world'. In addition, such models can benefit the study of population change by harnessing the flexibility of agent-based approaches to allow for exploration of *scenarios* of population change. This allows for a shift in demographic studies toward explaining and understanding the processes underlying population change, rather than focusing entirely on the prediction and description of empirical trends (Silverman et al. 2012).

Our model moves in this direction by presenting an agent-based platform which captures the complex life-course transitions that influence the demand and supply of social care (Noble et al. 2012). Agents are embedded in a 2D space designed to reflect UK geography, and during the course of the simulation they go through processes of fertility, mortality, partnership formation and dissolution, household formation, and internal migration. Combining this approach with empirical projections until 2050 and vital registration data from 1951-2011 has provided us with a platform that combines the explanatory power of agent-based modelling with the macro-level predictive power of statistical demography (Silverman et al. 2011).

THE MODEL

Basics of the model

Space precludes a complete description of the many parameters present within the simulation. We have attempted to provide a comprehensive overview here; for those who wish

Proceedings 27th European Conference on Modelling and Simulation ©ECMS Webjørn Rekdalsbakken, Robin T. Bye, Houxiang Zhang (Editors)
ISBN: 978-0-9564944-6-7 / ISBN: 978-0-9564944-7-4 (CD)

to examine the model more closely, you can find the annotated Python code available at `http://users.ecs.soton.ac.uk/jn2/software.php`. Code for the current version incorporating our demographic modifications will be made available as well.

In order to facilitate the use of UK demographic data, we based the model's spatial environment on a rough representation of UK geography. Agents occupy houses, which are then grouped into towns which consist of clusters of up to 625 houses. The size of these clusters vary according to local population density which varies across the 8×12 grid which represents the UK.

The agent population has a scaling factor of 1:10,000, given that modelling the entire UK population of 62 million individuals would be prohibitively expensive computationally. This is a greater reduction in scale than is used in microsimulation models of populations, given that the spatially-embedded nature of the agents coupled with their complex behaviours requires substantially more computer power.

The model runs on time steps one year in length. The initial population is generated and distributed randomly in simulation year 1860, then the model runs until 2050, at which point the final figures for social care cost are collected. The model starts early in order to ensure that the population dynamics of the agents can settle prior to the integration of empirical data into the model in 1951.

Agents are able to form and dissolve partnerships with one another. We use the term 'partnership' to refer to any possible relationship that may produce children. Every year agents not currently in partnerships will enter the marriage market, which operates on a national level. Agents are paired with available opposite-sex agents if they meet each other's criteria for a mate. Partnership dissolution is driven by an annual age-specific probability that the male partner will leave. The parameters governing partnership behaviour are not, at present, derived from empirical data, but are instead estimates based on observed rates of partnership formation and dissolution.

Health status and care need

Agents in the simulation begin in a normal health state, in which we assume they require no additional care services. There are age- and sex-specific probabilities which may push the agents into a different care need category; these are checked annually amongst all agents in the simulation. Agents can transition into any of several different levels of care need, shown in Table I. Once agents transition into a care-need state, their health status may only degrade further – they do not recover.

The model also investigates the supply side of social care, by linking the provision of informal care to the availability of agents and their household structure. We assume that any agent will provide care to any member of their household who requires it, so long as they have time available. Agents have varying amounts of time available with which to provide care, depending on their current status: dependent children can provide five hours per week; adults still living at home can provide 30 hours; and retired people can provide 60 hours. Agents who require care themselves can provide care as well, but only if their own care-need status is Low, and even then only for half the normal number of hours for their status.

TABLE I: The different care need categories, with the number of hours of care required per week

Care need category	Weekly hours of care required
None	0
Low	8
Moderate	16
Substantial	30
Critical	80

The current model does not explicitly represent formal care institutions, such as care homes or similar. Instead, we assume that all available agents (agents in the same household, or children living in the same town) will provide care to the best of their ability, and any remaining care needs are provided by the formal care system. We assume that the state is able to provide this formal care at a cost of £20 per hour. This figure is a rough estimate, to be supplemented by current data when this becomes available. Inflation is not represented in this model, so all care costs are expressed in 2012 UK pounds.

Agent life-course

Newborn agents are classified as dependent children, transitioning to adulthood at the age of 17. All agents enter the workforce at this time and become tax-payers. Adults are further classified into those who have moved out of the family home and those who have chosen to stay with their parents. Agents who reach the age of 65 retire from the workforce and cease paying tax.

The model allows agents to migrate to a new house on the map under several different conditions. When agents form a partnership, there is a 30% chance that they will choose to form a new household with their partner. Agents who take this option have a 30% probability of moving into their partner's home, which may still be the family home of that partner and thus contain other family members. Agents who choose to move elsewhere will either form a new household in the same town or an adjacent town to the location of one partner. When a partnership dissolves, the male agent will move elsewhere on the map, while any dependent children resulting from that partnership will stay with the mother.

Agents can also migrate to new households independently of an partnership upon reaching adulthood. There is an annual age-specific probability

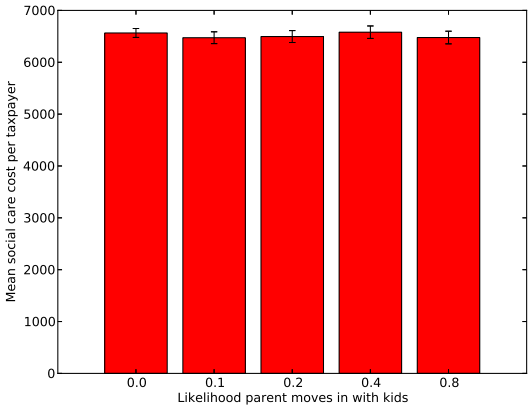

Fig. 1: Results for five different values of the parameter controlling the likelihood of aged parents returning home to live with their children.

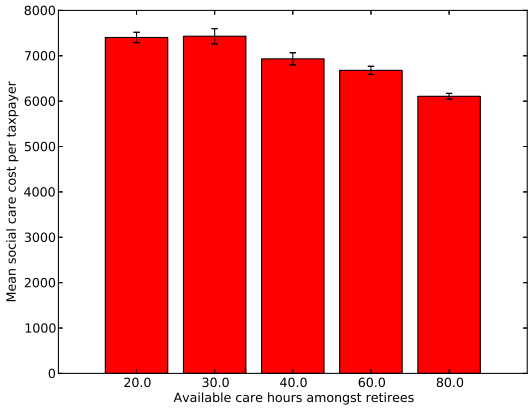

Fig. 2: Results for five different values of the parameter specifying the hours of informal care provided by retired individuals to their family members.

that an agent will make this choice. On occasion, single adults or family groups may make an arbitrary move – representing perhaps a change in career or life circumstances that would require a move. Retired agents who live alone also have a small annual probability of moving in with one of their surviving children, scaling inversely with the distance between their current town of residence and the location of the child.

Finally, on rare occasions dependent children agents will have both parents die prior to them reaching adulthood. In these cases we have the agent adopted by a randomly-chosen couple, and the child will move to join their household.

Demographic Projections

The original version of this model used a simple Gompertz-Makeham mortality model which was tuned to give reasonable mortality rates for a modern industrialised nation (Noble et al. 2012). Fertility rates were represented simply by a flat probability of reproduction for any woman of reproductive age in a partnership. In order to increase the realism of this iteration of the model and to tighten its integration with empirical data, we replaced these simplifications with more robust models of mortality and fertility. The shift toward realistic mortality projections ensures that we capture the complexities of the trend toward longer lifespans, and the incorporation of a realistic and detailed fertility model captures the societal move toward later child-bearing and lower birth-rates. These additions were inspired by previous work combining agent-based models with statistical demography (Silverman et al. 2012).

In the new mortality model, we continue to use the approximations used in the previous iteration until the simulation reaches 1951, at which point we switch to age-specific mortality rates drawn from the Human Mortality database 2011 until simulation year 2009. Similarly, in 1951 the fertility model switches from a single rate to age-specific mortality rates drawn from the Office of National Statistics data 1998 for England and Wales (for simulation years 1951-1972), then the Eurostat database 2011 for UK women of childbearing age (for simulation years 1973–2009).

These rates were projected forward until 2050 using the forecasting method developed by Lee and Carter 1992. The Lee-Carter method uses the leading vectors of a singular value decomposition of the matrix of centred mortality rates to construct a model for mortality with only one time-varying element. This allows easy forecasting using standard times series methods; more details about procedure and estimation are available in Lee and Carter (1992). The forecasts performed through 2050 using this method show life expectancy continually increasing over the period, though the increase slows gradually.

Fertility rates used in this model were also based on empirical data. Age-specific fertility rates from 1973–2009 for UK women of childbearing age were obtained from the Eurostat database (2011), while earlier data for the period 1950–1972 were taken from the Office of National Statistics data for England and Wales (1998).

Once again we used a Lee-Carter model to obtain future fertility rates. In this case two components of the singular value decomposition matrix of fertility rates were used, as two time indices are required to capture the trends in fertility. Projections to 2050 using this method show an initial rise in total fertility rate prior to a convergence at a rate just above replacement fertility. Overall, we see a continuation of the current empirical trend toward later childbearing.

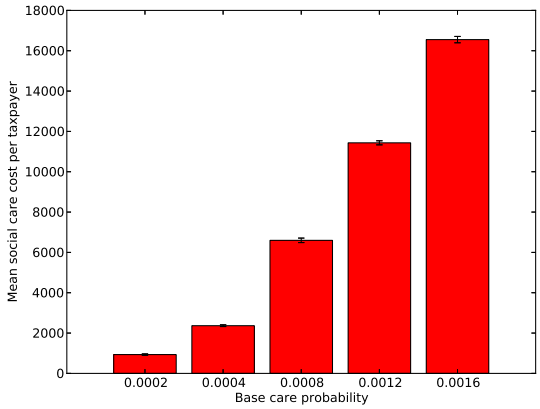

Fig. 3: Results for five different values of the parameter specifying the base probability that an agent transitions to requiring social care.

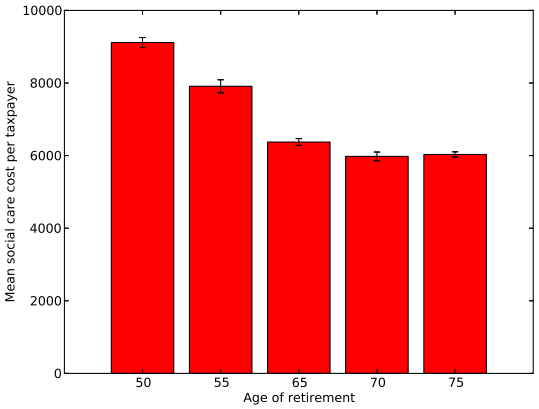

Fig. 4: Results for five different values of the parameter specifying the retirement age for agents within the simulation.

RESULTS

Basic results

Initial investigations of the model were driven by our goal of determining which parameters have the greatest impact upon the cost of social care per taxpayer in 2050. We ran the model under five different variations of four critical parameters for ten runs each, measuring as output the mean social care cost per taxpayer per year at the end of the simulation. In the graphs detailed here, the vertical axis represents care cost, while the horizontal axis displays the mean care cost for ten runs of a given parameter value. The centre bar of each histogram is the default value of that parameter.

The parameters we investigate – the probability of retired parents moving in with children, hours of informal care that can be provided by retirees, base probability for social care need for an individual agent, and retirement age – were chosen because they are areas which policy changes could have some influence (i.e., via changes in formal care provision, institutionalised care provision, tax and welfare changes, etc.). The five variations of each parameter were chosen to give a reasonable range of values from very conservative to very optimistic estimates.

Figure 1 shows the results of a series of runs in which we varied the probability of retired parents returning home to live with their children. We assumed that this may have an impact on the final social care figures, as these retired adults more accessible to informal care from their children. Instead, we found that even significant alterations in this parameter have no perceivable impact on the final figures. This suggests that the share of retired parents moving back in with their children has no significant impact on final care cost figures.

Figure 2 shows the results of varying the number of hours of informal care that can be provided by retired adults. Here we see that high levels of care availability amongst this group do appear to impact the final social care costs, at least at the higher settings. Retirees can provide the largest amount of informal care hours, and as a group are more likely to live in a household with someone who needs care, so a greater availability of informal care in these circumstances appears to take some burden off the costs to the state.

In Figure 3 we see the results of varying the base probability for an agent to transition into a state of care need. This base probability is then modified by the age and sex of each agent; this allows us to represent the increased need for care amongst elderly males as compared to females, for example. Varying this parameter has a dramatic impact on the final care costs; doubling the default value produces social care costs that balloon to far more than double the results we see at the default level.

Finally, in Figure 4 we examine the impact of changing the retirement age within the simulation. The default age is 65, and here we varied that age between 50 and 75 in increments of 5 years of age. Results show a significant reduction in overall care costs when agents retire later in life; this appears to be due to the substantial benefits of having a larger tax base as agents stay in the workforce longer and continue to pay into the system.

Interestingly, this pattern appears to level off at the age of 70, indicating a point of diminishing returns – and at age 75 the cost of social care actually rises slightly. This occurs despite the lack of any modelling of the health or wellbeing impact that may come from working until very late in life. We suspect that this appears in the model due to the reduced availability of care from adults remaining in the workforce; at a certain point, the increased tax payments from elderly workers will be offset by the reduction in available informal care amongst households with elderly members who are more likely to require care.

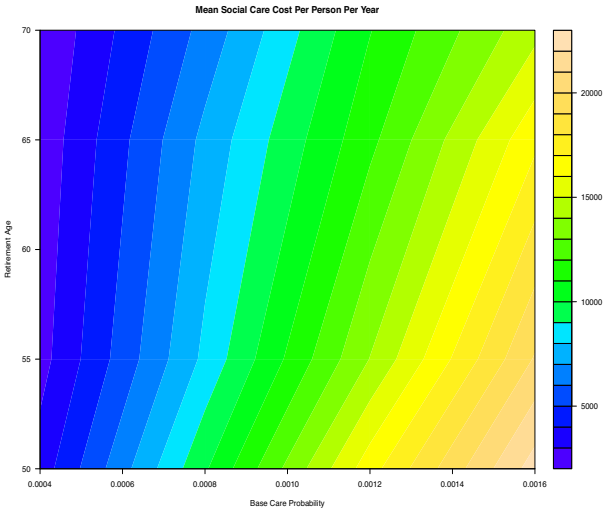

Fig. 5: Filled contour plot showing the model outputs for varying values of the base care probability and retirement age. The plot shows that a low retirement age combined with high care need probability generates the highest social care costs, producing mean costs per taxpayer well above £20,000 per year.

Input name	Variance (%)
Parents Moving In	0.01
Base Care Prob	88.99
Retired Hours	0.88
Retirement Age	8.06
Parents Moving In.Base Care Prob	0.00
Parents Moving In.Retired Hours	0.01
Parents Moving In.Retirement Age	0.01
Base Care Prob.Retired Hours	0.05
Base Care Prob.Retirement Age	1.88
Retired Hours.Retirement Age	0.11
	Total = 99.9876

Fig. 6: Results of a sensitivity analysis performed using GEM-SA software. Results show that probability of care need and retirement age account for the vast majority of variation in the results. Source: GEM-SA software (own calculations).

These results indicate that retirement age and base care-need probability have the strongest impact on model outputs. Figure 5 provides a concise illustration of the impact of these two parameters. High care-need probabilities combined with low retirement age produces some extremely high values for the mean social care cost per taxpayer per year. In contrast a combination of high retirement age and low base care-need probability produce much more manageable figures, as greater numbers of healthy agents are continuing to work and provide care informally well into later life.

Sensitivity Analysis

The results above indicated that some of these parameters are interacting in interesting and perhaps non-obvious ways, in particular the results for altering retirement age and available informal care hours amongst the retired. As part of the Care Life Cycle Project we have been investigating methods for quantifying uncertainty within statistical and computational models, and this model provides an excellent test case for some of these methods, given the complex interactions occurring between the systems represented here.

Here we took inspiration from another project, Managing Uncertainty in Complex Models (`http://www.mucm.ac.uk/`) and used specialised software to build a statistical emulator of the computational model. These emulators are Gaussian processes analysed in a Bayesian framework, allowing us to produce an effective sensitivity analysis which provides insight into the relative importance of various input parameters in the final output variance (O'Hagan 2006). These methods also provide a means of accounting for uncertainty within the program code, using an additional term called a nugget (Kennedy 2004).

Space precludes a detailed description of the statistical methods underlying Gaussian process emulators, so instead we refer the interested reader to Kennedy and O'Hagan (2001). In brief, these emulators function by assuming that the output variable (in this case, mean social care cost per taxpayer per year) can be decomposed into a constant (mean) term, a series of main effects related to particular input parameters, and a series of interaction effects for all possible combinations of input parameters. The final result is a measure of how much of the total output variance is accounted for by each individual input and each possible combination of inputs.

In our case, we used the four parameters investigated above as our input parameters for the emulator, and our output measure was the mean social care cost per taxpayer per year in simulation year 2050. Running multiple sets of runs at all possible combinations of the values shown above for those parameters produced a training set of some 1,300 results, which were then fed into the emulator. The emulator and the resultant analysis were produced by the GEM-SA (Gaussian Emulation Machine for Sensitivity Analysis) software version 1.1 by Kennedy (2004).

The results in Figure 6 show that the vast majority of the output variance is accounted for by our alterations in the base probability of an agent requiring care (88.99%), followed by the retirement age (8.06%). In contrast, the amount of hours available from retired carers and the probability of retired adults moving home had very little impact (accounting for 0.88% and 0.01% of the output variance, re-

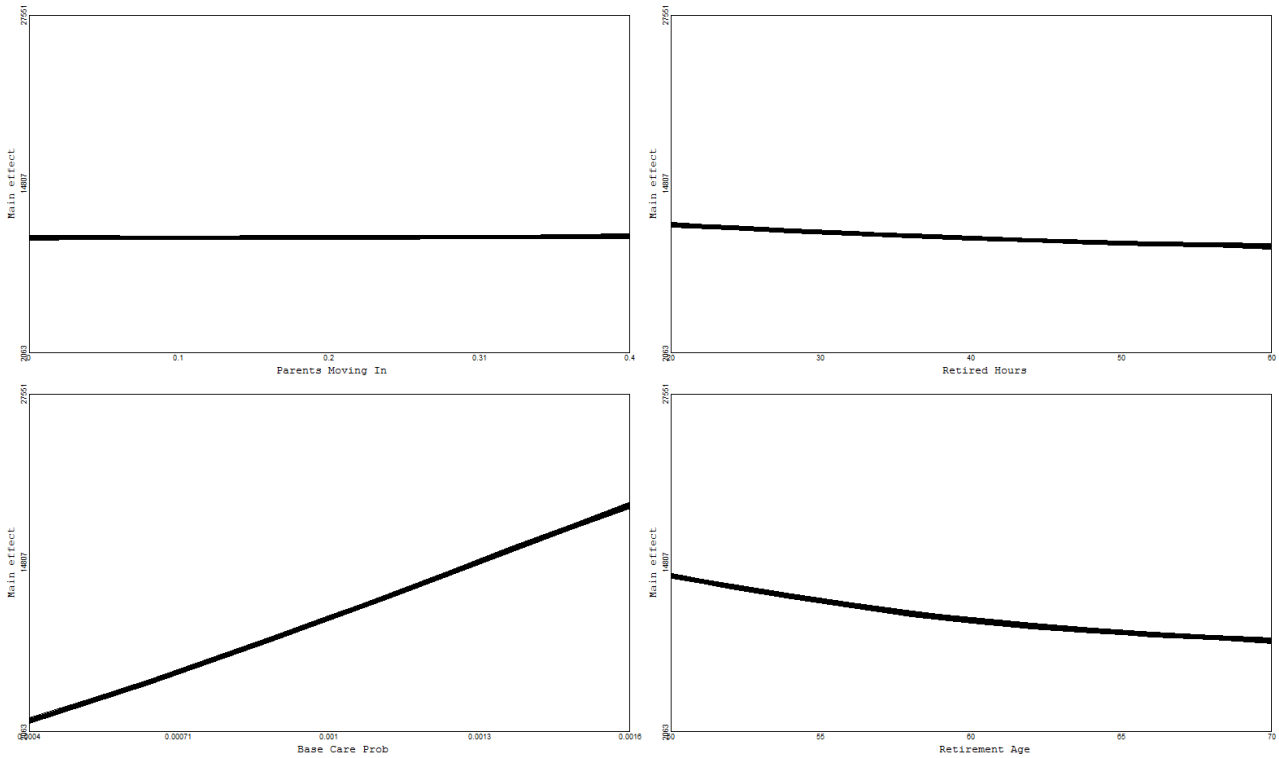

Fig. 7: Results of Gaussian Process Emulator demonstrating the impact of each parameter on final output values. The output value is the mean cost of social care per taxpayer per year at the end of the simulation in year 2050. Source: GEM-SA software (own calculations).

spectively). These results confirm our findings presented in Figure 3 and Figure 4. Figure 7 provides a visual representation of emulator results; each graph shows the main effects of each parameter, with each individual line representing one emulation run.

There was some additional impact from the two-way interactions between these parameters, most noticeably in the interaction between retirement age and the base probability of care need (1.88%). In general however the interaction effects were dwarfed by the impact of the main effects.

CONCLUSIONS

As suggested in our previous work with this modelling framework, we bolstered the realism of our model using significantly more detailed mortality and fertility models derived from statistical demographic data (Noble et al. 2012). The incorporation of Lee-Carter projections (1992) has moved us further toward a useful integration of demographic data and agent-based approaches, and future work will continue to push this forward, as proposed in Silverman et al. (2011).

The results and sensitivity analysis shown here provide a few hints as to the future challenges facing an ageing population. We see dramatic shifts in the results when we alter the retirement age and the probability of agents needing social care. This suggests that two major 'policy levers' which policymakers may examine would be comprehensive programmes for health amongst the elderly population, and a small increase in the retirement age. The former could significantly alter care need levels by providing preventative care, thus reducing long-term social care costs. This could also allow for the provision of more informal care in this age group, as healthier partners would be better able to provide care – and given that most social care in the UK is provided by family members (Vlachantoni et al. 2011), this could have a significant impact. The latter would allow a significant increase in the tax base amongst older citizens, allowing for more funding for social care costs.

However, our results indicate that the benefits of increasing retirement age level off at around 70 years of age. Intriguingly, this occurs even without any explicit representation of the health impact of working until late in life. Future iterations of the model could shed more light on this effect by allowing for more richness in agent decision-making and incorporating the affects of education and socioeconomic status on health in old age.

More generally, future work can refine these predictions by adding more detail to the social care structures in the model, in particular by adding a more detailed representation of formal care provision. We also will add a more robust migration element which allows for international migration, thus representing the impact of young workers entering the UK. Demographic studies have shown that some level of replacement migration in tandem with policies aimed

at increased labour force participation and raising birth rates might ameliorate the challenges of an ageing society (Bijak et al. 2008).

In summary, our model has provided a useful platform for discussion around the issue of social care provision in an ageing UK society, and has shed some light on the interactions between retirement age, informal social care provision and overall social care cost. The combination of these illustrative scenarios and in-depth sensitivity analyses gives us a strong suite of tools with which to examine the potential impact of policy decisions and economic and social shifts on social care provision in an ageing society.

ACKNOWLEDGMENTS

This work was supported by the UK's Engineering and Physical Sciences Research Council, grant EP/H021698/1, funded within the Complexity Science in the Real World theme. We would also like to thank Marc Kennedy and Anthony O'Hagan for making the excellent GEM-SA software freely available.

REFERENCES

Bijak, J., Kupiszewska, D., and Kupiszewska, M. (2008). Replacement migration revisited: Simulations of the effects of selected population and labor market strategies for the aging Europe, 2002–2052. *Population Research and Policy Review*, 27(3):321–342.

Brailsford, S., Silverman, E., Rossiter, S., Bijak, J., Shaw, R., Viana, J., Noble, J., Efstathiou, S., and Vlachantoni, A. (2012). Complex systems modelling for supply and demand in health and social care. In Jain, S., Creasey, R., Himmelspach, J., White, K., and Fu, M., editors, *Proceedings of the 2011 Winter Simulation Conference*. IEEE.

Coleman, D. (2002). Replacement migration, or why everyone is going to have to live in Korea: a fable for our times from the United Nations. *Philosophical Transactions of the Royal Society B*, 357(1420):583–598.

Eurostat (2011). Eurostat statistics database: Domain population and social conditions. `http://epp.eurostat.ec.europa.eu`. Accessed 27/10/2011.

Human Mortality Database (2011). Human mortality database. `http://www.mortality.org/cgi-bin/hmd`. Accessed 26/07/2011.

Kennedy, M. (2004). Description of the Gaussian process model used in GEM-SA. Software manual. `http://ctcd.group.shef.ac.uk/gem.html`. Accessed 23/05/2012.

Kennedy, M. and O'Hagan, T. (2001). Bayesian calibration of computer models. *Journal of the Royal Statistical Society, Series B*, 63(3):425–464.

Lee, R. and Carter, L. (1992). Modeling and forecasting U.S. mortality. *Journal of the American Statistical Association*, 87(419):659–671.

Noble, J., Silverman, E., Bijak, J., Rossiter, S., Evandrou, M., Bullock, S., Vlachantoni, A., and Falkingham, J. (2012). Linked lives: the utility of an agent-based approach to modelling partnership and household formation in the context of social care. In Laroque, C., Himmelspach, J., Pasupathy, R., Rose, O., and Uhrmacher, J., editors, *Proceedings of the 2012 Winter Simulation Conference*. IEEE.

Office for National Statistics (1998). *Birth Statistics, Series FM1 (27)*. Office for National Statistics, London.

O'Hagan, A. (2006). Bayesian analysis of computer code outputs: a tutorial. *Reliability Engineering and System Safety*, 91(10-11):1290–1300.

Silverman, E., Bijak, J., Cao, V., and Hilton, J. (2012). Semi-artificial models of population: Connecting demography with agent-based modelling. In *Proceedings of the 4th World Congress on Social Simulation*.

Silverman, E., Bijak, J., and Noble, J. (2011). Feeding the beast: Can computational demographic models free us from the tyranny of data? In Lenaerts, T., Giacobini, M., Bersini, H., Bourgine, P., Dorigo, M., and Doursat, R., editors, *Advances in Artificial Life, ECAL 2011*, pages 747–754. MIT Press, Cambridge, MA.

Vlachantoni, A., Shaw, R., Willis, R., Evandrou, M., and Luff, J. (2011). Measuring unmet need for social care amongst older people. *Population Trends*, 145:60–76.

AUTHOR BIOGRAPHIES

ERIC SILVERMAN is a Research Fellow on the Care Life Cycle project at the University of Southampton. He received his PhD from the University of Leeds, and previously worked as a JSPS Postdoctoral Research Fellow at the University of Tokyo. His work on the CLC Project focuses on the application of complexity science approaches to the social science domain. His email address is `e.silverman@soton.ac.uk`.

JASON HILTON is a Post-Graduate Researcher at the Institute of Complex Systems Simulation and the Division of Social Statistics and Demography at Southampton. He holds a BA in Politics from the University of York, and an MSc in Demography from the University of Southampton. His PhD work focuses on applications of complex systems simulation in demography. His email address is `jdh4g10@soton.ac.uk`.

JASON NOBLE is a Lecturer in Computer Science at Southampton. He received a DPhil in Cognitive and Computing Sciences from the University of Sussex in 1998. He is the Taught Programme Director for Southampton's Institute for Complex Systems Simulation and has a background spanning AI, philosophy of science, psychology, and statistics. His email address is `jn2@ecs.soton.ac.uk`.

JAKUB BIJAK is a Lecturer in Demography at Southampton. He holds a PhD from the Warsaw School of Economics, obtained for work on Bayesian migration forecasting. His research interests encompass the applications of quantitative methods in demography, with focus on demographic uncertainty, population forecasting, migration and demography of conflict. His email address is `J.Bijak@soton.ac.uk`.

TRACEABILITY IN EVIDENCE-BASED POLICY SIMULATION

Ulf Lotzmann
Maria A. Wimmer
Institute of Information Systems Research
University of Koblenz-Landau
Universitätsstraße 1, Koblenz 56070, Germany
E-mail: {ulf, wimmer}@uni-koblenz.de

KEYWORDS
Model analysis, Model acceptance, Policy-modelling, Agent-based simulation.

ABSTRACT

In the field of policy modelling, a trend to growing complexity of simulation models can be observed. One of the reasons for this development is the fact that for many policy cases of practical interest there are no theories available from which "simple" simulation models could be derived. Instead a sometimes vast amount of information - scenarios describing stakeholders views, documents providing background information - has to be taken into account by the simulation model. Such models are usually referred to as "evidence-based models". In order to foster the use of the simulation method for decision-making, a constructive and structured approach for converting the evidence base into a simulation model is advised.
This paper outlines such a novel approach, which has been developed within the OCOPOMO project. This approach basically consists of a policy development process specification, and a software toolbox supporting this process. Main focus of this paper are simulation related aspects of both the process and the toolbox, with the aim to demonstrate role and benefits of traceability along the process of modelling, simulation and result analysis.

INTRODUCTION

Since the early days of Computational Social Science, actual programming of simulation models for social systems has often been done based on intuition. The way model programmers formalise agent behaviour e.g. by writing rules on the basis of evidence gathered by reading documents or interviewing relevant stakeholders has sometimes the appearance of a "black art" (Edmonds and Wallis 2002).
While for examining emergent (or other) effects in rather small (and sometimes theory-driven) models this approach has regularly proven to be successful (refer e.g. to Epstein and Axtell 1996), in the case of rather complex policy models it can be regarded as questionable (although there is no implication that this approach systematically fails here; examples for successful models can be found e.g. in Barthelemy et al. 2001; Alam et al. 2007). This is primarily due to the following facts:

- typically, no (social) theory exists from which such models could be derived;
- instead, such models are constituted by diverse and possibly very large evidence bases;
- as results from such models are intended to have impact on some application domain, the process of validation may have to be extended to a non-scientific community, e.g. to policy makers and other stakeholders.

In order to find a remedy, research activities have been started with the aim to provide structured approaches for more coherent and, in particular, more provable inclusion of both the evidence base as well as the knowledge and experience of different stakeholders. One of these approaches is investigated in OCOPOMO (Open Collaboration in Policy Modelling), a project co-funded in the 7th Framework Programme of the European Commission (see http://www.ocopomo.eu/). Core of the approach proposed by this project is a process that guides the development and validation of evidence-based models with stakeholder participation, and a toolbox supporting this process (Wimmer et al. 2012).
This paper is directed to the part of the process that deals with the actual simulation models. It basically shows how (and by which technical means) understanding and documentation of models can be enhanced and, finally, how integration into the overall process can be achieved. Two perspectives on simulation models are important in this context:

- the perspective of the model developer, who is interested in traceability in order to understand or to keep track of the structure of the simulation model code,
- the perspective of the stakeholder not directly involved in model development, for whom provenance is essential in order to gain confidence in model results (and the simulation method as such) by unveiling the "black box" simulation model.

The paper is structured in a way that firstly the overall OCOPOMO process is outlined, followed by a description of the trace concept. Subsequently the paper presents some aspects for the realisation of the concept, and finally focuses on a demonstration with the aid of one of the pilot case simulation models.

THE OCOPOMO PROCESS

In OCOPOMO, a novel approach for engaging stakeholders in policy development is conceptualized and implemented (Wimmer et al. 2012). Stakeholders are collaboratively involved in the development of scenario texts relevant in the context of a policy under discussion. In this regard, the term policy is referred to strategic areas of complex

Proceedings 27th European Conference on Modelling and Simulation ©ECMS Webjørn Rekdalsbakken, Robin T. Bye, Houxiang Zhang (Editors)
ISBN: 978-0-9564944-6-7 / ISBN: 978-0-9564944-7-4 (CD)

decision-making with various stakeholders having potentially diverging interests. In OCOPOMO, public policies are investigated and modelled such as renewable energy policy of the Kosice region in Slovakia, housing policy of the city of London or the distribution of structural funds in the Campania region in Italy. The overall OCOPOMO policy development process consists of six phases:

1. An initial scenario describing a policy prospect is developed by policy makers or domain experts.
2. Stakeholders are involved to generate scenarios of potential policy aspects on the basis of the initial scenario, which are complemented with background documents to evidence statements in the scenarios.
3. The policy case is then conceptualized and
4. modelled by experts.
5. Simulations are run to generate outcomes.
6. The results of the simulation are exposed to the stakeholders, who compare their scenarios (of phase 2) and the simulation outcomes in order to either update their scenarios (and start another cycle with phase 3) or accept the insights from the simulation and agree that these are consistent with the inputs the stakeholders provided in phase 2.

The project develops an integrated ICT toolbox to support the policy development process and, in particular, a smooth transformation of policy inputs by stakeholders to inform formal policy models. The ICT toolbox consists of

- a participation platform that enables stakeholders to collaboratively develop their scenarios, to upload and share background documents, and to discuss among themselves about views and issues of a policy (supporting process phases 1 and 2);
- a consistent conceptual description (CCD) tool, which enables policy modellers to develop a conceptual model of a policy domain. The CCD tool supports annotation of scenarios and background documents and therewith keeps track of provenance (supporting process phase 3);
- a simulation tool (DRAMS), which supports policy modellers in programming and running policy simulation models (supporting process phases 4 and 5);
- a CCD2DRAMS transformation tool, which supports the semi-automatic transformation of conceptual policy model constructs into code of formal policy models (link between process phases 3 and 4).

A more detailed description of the OCOPOMO policy development process and the respective tools available in (Wimmer et al. 2012).

A key element in the novel approach of OCOPOMO is to keep track of how policy inputs by stakeholders feed into policy simulation and therewith convey provenance. This way, traceability and transparency in policy development are supported.

TRACES IN SIMULATION MODELS

As pointed out in the previous section, OCOPOMO has developed a policy development process and ICT support toolkit with features to enable keeping track of inputs in form of evidence-based scenarios and background information provided by stakeholders. This way, provenance of arguments by stakeholders is ensured. In the Oxford English Dictionary, provenance is defined as "the origin, or the source of something, or the history of the ownership or location of an object, especially when documented or authenticated" (for a more detailed elaboration of definitions of „provenance", see Munroe et al. 2006). In OCOPOMO, the main purpose of provenance is gather evidence as to the views and background information for the creation of a public policy.

Provenance is thereby ensured through the establishment of traces and links between sources of information (the scenarios and background documents) provided by the stakeholders of a policy domain, and the simulation models developed by policy experts. The links show the evolution of formal elements of a simulation model from the description of the real-world section (the scenarios and background documents, i.e. informal artefacts) which is subject of the model. Usually, not all formal model elements have counterparts in the narrative descriptions/documents. The OCOPOMO process foresees enrichment of models by policy experts to complement and complete the formal simulation model.

To ensure provenance, the links from elements of a simulation model to provenance are stored in the CCD tool. Therewith, traces are enabled, which facilitate navigating from simulation outcomes back to the simulation model back to the conceptual model, and finally back to the provenance documents (i.e. scenarios and background documents). The traces established help stakeholders to better understand simulation models of particular policy perspectives.

Traceability is a key element in ensuring openness and transparency in the OCOPOMO policy development process. Therewith, good governance principles are implemented in policy modelling. Traces and provenance are also important auxiliary means for policy modellers, by helping the experts to better understand complex interrelations of policy aspects and how informal data elements feed into a formal model (provenance). Hence, traces are a basic instrument for model exploration and easier understanding of the structure of a simulation model, for simplification and visualisation.

The next section outlines the concept of a newly developed declarative rule engine as technical basis for maintaining the traces.

A DECLARATIVE RULE ENGINE FOR AGENT-BASED SIMULATION MODELS

As elaborated in (Lotzmann and Meyer 2011), a rule engine is a software system that basically consists of a fact base, a rule base and an inference engine. As part of the OCOPOMO toolbox, DRAMS (a Declarative Rule-based Agent Modelling System) has been developed as a distributed, forward-chaining rule engine. It equips an arbitrary number of agent types with type-specific rule bases and initial fact base configurations.

Heart of the inference engine is the data-driven rule schedule, an algorithm deciding which rules to evaluate and fire at each point of time. In order to decide which rules to evaluate for which agent instances, the schedule relies on a data-rule dependency graph. This is constructed once at the beginning of a simulation from all specified rules and initially available data; the graph does not change unless rule bases are modified. As to detecting fact base

modifications, the schedule keeps track of all fact base operations.
For typical simulation models, DRAMS only takes care of agent deliberation abilities, while the environment is "outsourced" to an external simulation tool. Since DRAMS is implemented in Java, in principle any Java-based simulation tool can be used for this purpose. At the moment, DRAMS provides interface to facilitate the integration with Repast (North et al. 2006).
The data-driven rule scheduling mechanism employed by DRAMS inherently supports the generation of traces. The following chapter will describe the process of creating the traces, together with the necessary prerequisites.

Annotating Model Code

In the path of passing link information from provenance data to simulation results, the segment between model code and raw simulation outcomes can become quite complicated. This is primarily due to the fact that the means for processing initial data configurations within a simulation run can be very complex, and are influenced by manifold factors. When speaking in terms of agent-based declarative simulation models, each "individual" in an agent population of arbitrary size carries up to thousands of facts, which are processed by hundreds of rules. Under such conditions it seems hardly possible to reach the goal of finding adequate ways for extracting useful information in terms of understanding structure and behaviour of the model.
An approach for solving this issue has already been sketched in the first sections of the paper: a conceptual model, the CCD, is developed prior to programming the simulation model. This CCD incorporates and specifies all the crucial elements for the simulation model, but abstracts from technical necessities for making a simulation model "run". With other words, only those simulation model elements are incorporated in the traces which have counterparts in the CCD.
As a starting point, these crucial elements have to be marked in the simulation model code by link annotations. Each element in the CCD is equipped with an unique uniform identifier (UUID), and this link is attached to the related simulation model code element (see Figure 1). In order to comfortably maintain these link annotations, tool support is advisable. For the OCOPOMO toolbox, a model-to-text code generation tool (CCD2DRAMS) is provided for this purpose (Scherer et al. 2012). This code generator adds link annotations to all generated elements, in particular for agent classes and instances, fact templates, facts and rule stubs.
The model programming then consists mainly in creating the code around the generated parts, on the one hand by filling in the complete logic into the rule stubs, on the other hand by providing "glue" code in-between the generated code.
Such development approaches are usually not sequential but rather cyclic; this means that during model programming missing crucial elements are discovered, which then have to be added at the CCD level. The CCD2DRAMS code generator takes care not to overwrite already elaborated rules - situated in a user code section of the source file - when re-transforming a modified CCD.

During parsing of model code by DRAMS, for each element with a link annotation a so called trace tag is generated. This is basically a small data container object, storing the link UUID, and bringing the possibility to define different kinds of neighbour trace tags. These are used as nodes in the generated trace graph, as shown in the next section.

```
/*Object: HouseholdCharacterstics
 *@link _j2N48MdEEeGILbUlSo0ubw
 */
(deftemplate Household::HouseholdCharacterstics
      (uuid:UUID)
      (instName:String)
)

/* Action: calculate the household heat demand
 *@link _KSe8AK8GEeGItqqK0ME1Yw
 */
(defrule Household::"calculate the household heat demand"
(
      // insert LHS clauses here
=>
      // insert RHS clauses here
)
```

Figure 1 Generated DRAMS code with a fact template definition (`deftemplate`) and rule stub (`defrule`) with link UUID annotations (`@link`)

Creating the Traces

In DRAMS, the creation of the trace information is a ancillary procedure of the forward-chaining rule engine process. A simplified description of this algorithm comprises five steps:

1. At the initial state of the rule engine - no rule has fired - a number of fact templates, partly concrete facts for the templates and rules are present. For subsets of each of these elements (for which CCD elements exist), trace tags are attached.
2. When the rule engine is initiated, it firstly checks which rules might fire with the given set of facts. The LHS's (left-hand-sides, specifying the conditions) of these rules are evaluated, and for each successful evaluation, the RHS (right-hand-side, describing the actions) is triggered.
3. The RHS processing starts with checking, whether at least one of the facts evaluated by the LHS (and, hence, determining the data basis for the RHS execution) is attached with a trace tag. If this is the case, a new trace tag for this particular rule firing at the current simulation time is generated, using the information (link UUID) stored in the rule trace tag, if available. All trace tags for the LHS facts are then incorporated as predecessors of the rule firing trace tag.
4. The rule firing trace tag, or the rule trace tag, according to disposability, is then passed to all RHS clauses.
   a. A clause for asserting a new fact to a fact base generates a new trace tag for this fact with the trace tag delivered by the rule as predecessor.
   b. A clause for writing output data (e.g. a log record) passes the trace tag to the output processing facility.
5. When all rules have fired, the newly created facts constitute the new state of the rule engine, and the processing continues with step 2.

If a rule producing a log record or (numerical) outcome data is either equipped with a trace tag, or when any of the elements that lead to firing this rule have had a trace tag attached, then a "connector" trace tag is available as result of the algorithm. This connector trace tag can be seen as root node of a directed acyclic graph, which covers all the important steps for creating this log or outcome.
After finishing a simulation run, a potentially very large graph data structure is available, holding information about traces for all relevant generated facts and simulation outcomes. With this additional data, questions about the cause of a simulation result can be answered with very low additional effort. In order to answer such questions and to perform more sophisticated analyses, the information from the graph must be further processed and/or stored in adequate ways.

Processing Simulation Outcomes

DRAMS brings a plugin interface with which any kind of output processing facilities can be embedded. Such plugins can either write files of a particular format, or can serve as an adapter to an analysis or visualisation tool.
A selection of implemented plugins for DRAMS is described in the following compilation, each representing the trace information in different ways and formats:

- Plain Text / CSV - these two plugins write log records or numerical outcomes in plain text files or CSV tables. In both cases, the trace information can be attached as lists of UUIDs, optionally attached with additional information (e.g. name of the element belonging to the UUID). For these formats, the usage of the UUID is usually restricted to manual handling.
- XML - this plugin creates XML files containing numerical or textual simulation outcomes. These XML files are processed by another component of the OCOPOMO toolbox for creating traceable logs or different types of diagrams. The trace information can be added to the values in different levels of details, e.g. as
  - a simple collection of UUIDs (as for text output above),
  - a diary, showing the involved UUIDs for the different simulation time steps, or
  - a complete XML representation of the evaluation graph.
- Model Explorer Tool - this plugin provides an UI for displaying the simulation log, and by selecting a log entry the related trace information is visualised and can be analysed in various ways. This tool is subject matter of the following section.

ANALYSING SIMULATION OUTCOMES AND USING THE TRACES

One of the simulation models realised as a pilot case in the OCOPOMO project deals with developing a sustainable long-term strategy for use of renewable energy resources in the Kosice Self-governing Region (KSR), Slovakia. "The regional government is interested in a better understanding and identification of potential impacts of policy alternatives in support and exploitation of renewable energy resources, including their impact on employment, environment, financial implications of investments, and a wide range of other related issues" (Scherer et al. 2012).
The version of the model available during the development of the Model Explorer Tool is aimed to explore the effect of rising energy prices and potentially stagnating (and on average rather low) household income. In order to save costs for heating energy, the households can either buy a new (additional) heating technology, insulate the house/flat, or decrease the room temperature. The model comprises 48 Household agents organised in a Household Association, three Heat Producer/Distributor company agents, a Regulatory Office agent and a Government agent. The households are distributed among six buildings of two kinds, namely three one-family houses and three blocks of flats. There are two different heating technologies available, and the houses or flats can be equipped with dozens of combinations of 19 different types of building and insulation materials. Altogether there are around 180 object, actor and relation instances in the CCD. The simulation is expected to shows the change of average room temperatures and the investments in heating technologies and insulation over time.
Particularly important for this model is an evidence-based and, thus, realistic initial set-up of the simulation world, consisting of buildings constructed of meaningful combinations of different building materials, and the distribution of households among the buildings. This initialisation procedure will be used in the following paragraphs for demonstrating traceability to the evidence base.
The part of the conceptual model dealing with these issues is shown in Figure 2. A household agent is situated in a building that is built of several components and that is located in a city. A list of building components describes parameters of these components in regard to heat resistance, a value that can be interpreted as a measure for insulation capability for each component and building. The household association agent is in charge for maintaining this list and for calculating the actual values, in order to enable households to determine their own expenditure for heating energy.

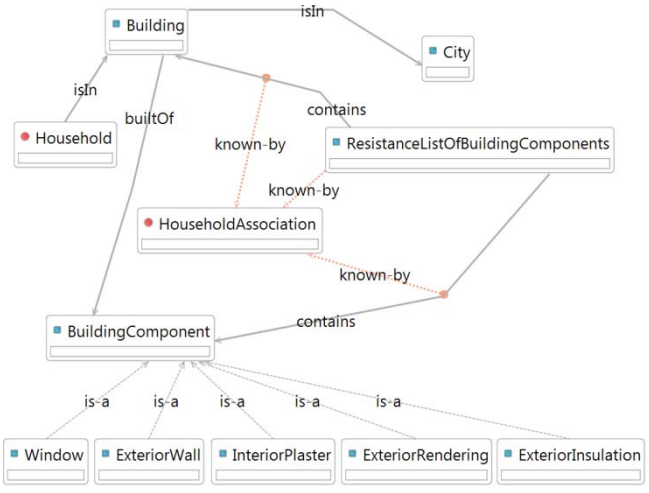

Figure 2 Extract from the Actor Network Diagram of the Kosice model CCD

The initialisation steps are conceptualised in the action diagram in Figure 3. Firstly, the resistance values for both construction material and windows are calculated. This

information is then used to calculate the energy information for buildings. With this information the households are in a position to derive the heating energy demand.

For agents, buildings and all related initial data, link annotations are attached to all CCD elements that are regarded as crucial by the modeller, i.e. to be traced back from (intermediate) simulation results applying the Model Explorer Tool.

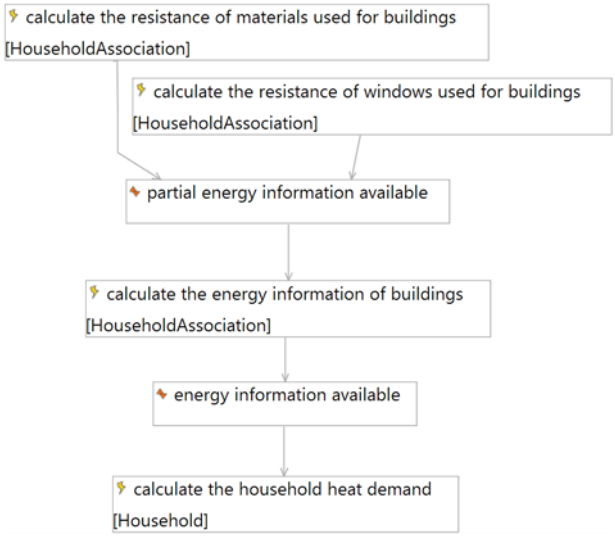

Figure 3 Extract from the Action Diagram of The Kosice model CCD

Model Exploration

The process of exploring a model subsumes different tasks with the aim to gain insights in structure or behaviour of the model. Both aspects usually are interrelated. While it is mainly of interest to understand the behaviour of the model, it becomes necessary to shed light on the structure of the process leading to this behaviour. Furthermore, different users require different levels of abstraction of the presented information. While the model programmer wants any detail of each rule that fired with any data processed by the rule, a decision maker (are other stakeholder) for instance might only want to see an overview of different fact types and how these are related to the actors dealing with facts associated with those types. Hence, a comprehensive Model Explorer Tool has to take all these aspects and perspectives into account. At the current stage, the model programmer perspective has been implemented, while possible designs for further developer and stakeholder perspectives are currently investigated and discussed (and not part of this paper).

Figure 4 shows an overview screenshot of the Model Explore Tool UI. On the right side a list of log records produced by the simulation is shown. The user can select one or an arbitrary set of entries, which then are further processed by the tool.

The first stage of processing is to create an internal data representation of the trace information attached to the selected log entries. As a "natural" approach to present this information, a decent visualisation of the trace graph is displayed left to the log view. The graph shown in the screenshot is the visualisation for a log entry generated in time step 1.0 after calculating the heat demand of a household living in a block of flats, as part of the model configuration described above. The green ovals on the left are all initial facts for building materials, several relations (e.g. in which building this particular household is located) and several other facts (e.g. the current month and year), processed during deriving this particular simulation

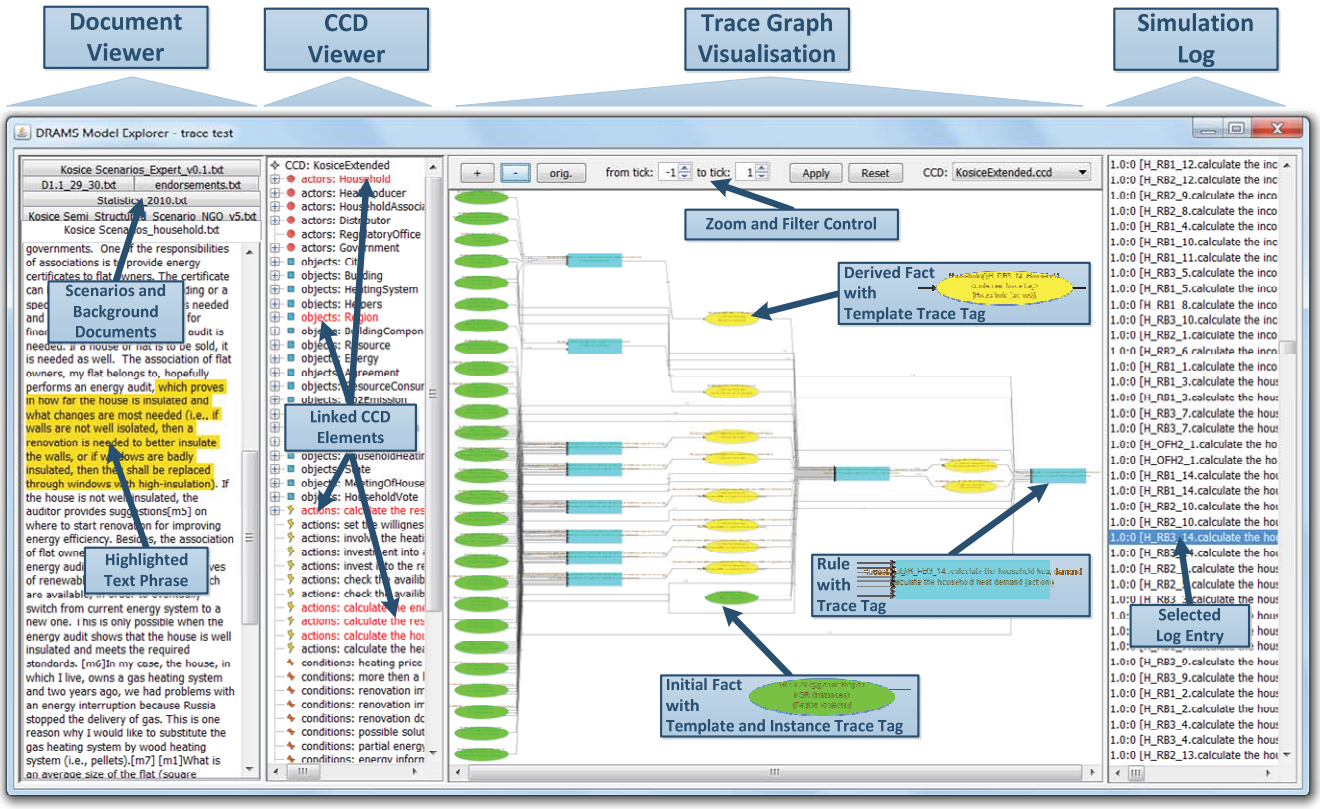

Figure 4: Model Explorer Tool GUI

outcome. The set of blue boxes on the right side to these facts are rules related to calculation of heat resistance, resulting in new facts with "partial energy information" (ovals with colour yellow, since these facts are asserted only during the simulation run). The single box further right represents the rule for calculating the final energy information (pair of yellow ovals), in order to calculate the household heat demand (single box on the right side of the graph visualisation).

All UUIDs from the trace tags contained in the graph are then used to identify the related elements of the conceptual model. These are highlighted in the CCD tree representation left to the graph. Finally, the text phrases attached to the CCD elements are accentuated as coloured text annotations in the editor views on the left-most side of the UI. For each document of the evidence base, an editor tab is present. So, for each simulation result the provenance information is disclosed. Performing these steps in the sequence as described above means following the phases of the OCOPOMO process in reversed order.

An important feature for model programmers is illustrated in Figure 5 (which focuses on the rule producing the final heat demand with two of the pre-condition facts, as a detail of the above-shown graph). Clicking on any element in the graph visualisation opens an info box window, giving details about the selected element. In the figure, an edge from the global fact `BuildingEnergyInformation` to the Household agent rule "`calculate the household heat demand`" is selected. The info box displays (among others) the source code of the rule, with the particular clause highlighted that retrieved the fact at the other end of the edge. Info boxes for facts inform about the concrete content of the fact processed by a succeeding rule, while boxes for fact templates reveal the facts available for the template.

The graph visualisation can also be filtered. Besides restricting the visual elements to any time interval, it is e.g. possible, to pick out a single node and only show

- the direct neighbours of the node,
- the sub-graph of all succeeding nodes, and
- the sub-graph of all preceding nodes.

The UI of the tool can also be employed for visualising the traces on the stakeholder perspective, as information on how the model used the evidence base for generating particular results (i.e. the relevant relations between log entries on the one side, and concepts and phrases on the other side) are already shown. Only the graph view ought to be replaced by a visualisation on a more abstract level

The Model Explorer Tool can be applied for supporting the analysis of simulation results and to feed back to the conceptual model.

Linking Results to the Evidence Base

Simulation outcomes can be either numerical data, showing the change of measurable values over the course of time, or qualitative logs, telling a "story" of the sequence of events. By simulation results, not primarily the raw outcomes of simulation runs are meant. A more important part probably play model-based scenarios. These are narratives written by simulation analysts (i.e. persons who interpret the simulation outcomes, who are in fact often identical with the model developers) on the basis of simulation logs together with appropriately processed representations of numerical outcomes, with the primary goal to condense the

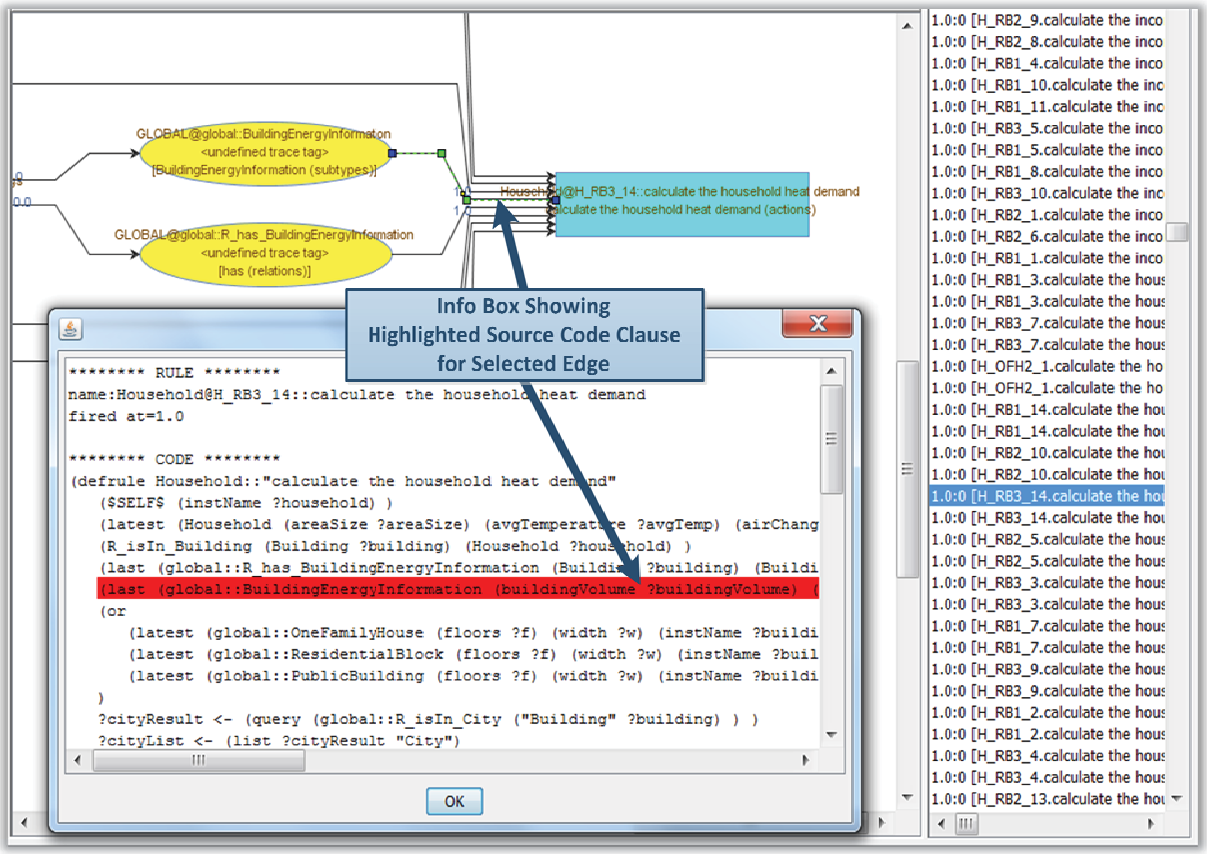

Figure 5 Detail view of the above screenshot with Info Box

sometimes vast amount of generated data into a human readable format. With dedicated tool support (as e.g. another OCOPOMO Toolbox component "Simulation Analysis Tool") it is ensured that the trace information is kept also within model-based scenarios.

As described at the beginning of this paper, one of the basic elements and major added values of the OCOPOMO process is the possibility to support the comparison between simulation results on the one hand, and the evidence provenance base for the simulation model on the other hand. Hence, for both the raw simulation outcomes as well as for model-based scenarios, the trace information can be used to attach simulation results to an enriched CCD.

This enriched CCD can then serve as a basis for a structured approach of comparing initial and stakeholder scenarios with model-based scenarios and other results, and, thus, constitutes a profound information platform for model presentation, discussion and validation. The consolidated CCD that emerges from this examination can in turn be used for developing a more detailed, more precise and with the arguments of stakeholders aligned simulation model. Hence, the modelling cycle proposed by the OCOPOMO process can be closed herewith.

CONCLUSIONS AND FUTURE WORK

The approach presented in this paper shows a way for maintaining traces and provenance during and beyond simulation runs, as parts of a comprehensive development process for evidence-based policy models. Although the example described in the paper shows a part of a model that deals with engineering aspects rather than with social interaction (which one might expect to be more important in a policy model), the traceability concept and implementation should have become clear. It shows furthermore the capability to deal with a considerable level of details in simulation models, of course also with rules for social behaviour.

Mostly positive and promising experiences have been made during implementing and integrating the toolbox components, and applying both toolbox and process to the development of the three pilot case models in OCOPOMO. Firstly, the traces turned out to be extremely helpful for model developers in order to understand model structure and code details for models written by other modellers. Secondly, it is also likely to gain added value in cases where the model developing process is strictly bottom-up, since it allows the modeller to visually perceive the model structure, and, hence, helps to keep track even on large models. The stakeholder perspective is not covered by the Model Explorer yet, but there is another OCOPOMO toolbox component (Simulation Analysis Tool) dedicated to this topic which relies on the techniques described in this paper.

Concluding it can be said that this contribution entails considerable potential for enhancing manageability and maintainability of complex evidence-based simulation models.

In a short-term perspective, the future work will be guided by questions regarding the method for scenario comparison and more enhanced visualisations for policy makers and stakeholders. A long-term perspective will include an exploration of the prospective opportunities and boundaries of this approach, especially related to model verification and validation on a more general level.

ACKNOWLEDGEMENTS

OCOPOMO is co-funded by the European Commission under the 7th Framework Programme. DRAMS, CCD and CCD2DRAMS have been developed in OCOPOMO. This publication reflects the view only of the authors and the project consortium, and the Commission cannot be held responsible for any use, which may be made of the information contained therein.

Parts of this paper have previously been published in (Lotzmann and Wimmer 2012).

REFERENCES

Alam, S.J.; R. Meyer; G. Ziervogel and S. Moss. 2007. “The Impact of HIV/AIDS in the Context of Socioeconomic Stressors: an Evidence-Driven Approach”. *Journal of Artificial Societies and Social Simulation* 10, No. 4, 7.

Barthelemy, O.; S. Moss; T. Downing and J. Rouchier. 2001. “Policy Modelling with ABSS: The Case of Water Demand Management”. CPM Report No. 02-92. Centre for Policy Modelling, Manchester Metropolitan University, Manchester.

Edmonds, B.; and S. Wallis. 2002. Towards an Ideal Social Simulation Language. Technical report. Manchester Metropolitan University.

Epstein, J. M.; and R. Axtell. 1996. "*Growing Artificial Societies – Social Science from the Bottom Up*". MIT Press, Cambridge, MA.

Munroe, S.; P. Groth; S. Jiang; S. Miles; V. Tan; J. Ibbotson; and L. Moreau. 2006. "Overview of the Provenance Specification Effort". University of Southampton Institutional Research Repository ePrints Soton. URL: http://eprints.soton.ac.uk/263055/1/OverviewVision.pdf. Last accessed August 15, 2012.

North, M.J.; N.T. Collier and J.R. Vos. 2006. “Experiences Creating Three Implementations of the Repast Agent Modeling Toolkit”. *ACM Transactions on Modeling and Computer Simulation* 16, No. 1 (Jan.), 1-25.

Lotzmann, U.; and R. Meyer. 2011. "A Declarative Rule-Based Environment for Agent Modelling Systems". The Seventh Conference of the European Social Simulation Association, ESSA 2011. Montpellier, France.

Lotzmann, U.; and M. A. Wimmer. 2012. "Provenance and Traceability in Agent Based Policy Simulation". The 26th European Simulation and Modelling Conference, ESM 2012. Essen, Germany.

Scherer, S.; M.A. Wimmer; and S. Markisic. 2012. "Bridging Narrative Scenario Texts and Formal Policy Modeling through Conceptual Policy Modeling: The Consistent Conceptual Description Tool". Submitted to *AI and Law Journal*.

Wimmer, M.A.; K. Furdik; M. Bicking; M. Mach; T. Sabol; and P. Butka. 2012. Open Collaboration in Policy Development: Concept and Architecture to integrate scenario development and formal policy modelling. In Y. Charalabidis and S. Koussouris, editors, Empowering Open and Collaborative Governance. Springer Berlin / Heidelberg, pp. 199 - 219

Modelling and Simulation in Robotic Applications

DYNAMIC MODELLING OF THE "SEARAZOR" - AN INTERDISCIPLINARY MARINE VEHICLE FOR SHIP HULL INSPECTION AND MAINTENANCE

Cong Liu[1,3], Eilif Pedersen[2], Vilmar Æsøy[1], Hans Petter Hildre[1], Houxiang Zhang[1]

[1]Faculty of Maritime Technology and Operations
Aalesund University College
Postboks 1517, N-6025 Aalesund, Norway

[2]Department of Marine Technology,
[3]Department of Engineering Design and Materials,
Norwegian University of Science and Technology N-7491, Trondheim, Norway

KEYWORDS
Underwater, climbing robot, hull cleaning, bond graph

ABSTRACT

The *Searazor* is a novel underwater vehicle designed for underwater inspection and maintenance of ships and underwater structures. In this paper, the vehicle's dynamic characteristics and control scheme are studied. A series of sub-models, representing the major components of the vehicle, are developed in a bond graph environment. A servo control system that governs the attitude and steering is also implemented. These models are then assembled and operated as a rigid body under the force input from thruster, wheels and environmental factors. The resulting motion of the vehicle under human manoeuvring input is simulated in 20sim software. Analyses and simulations are also implemented for dynamic stabilisation under disturbance from waves and current. The simulation currently provides support for *Searazor* prototype design. The entire model will be the simulation framework for developing and testing control algorithms to maneuvre the vehicle in complex marine environments.

INTRODUCTION

Marine fouling on ship hulls requires constant maintenance in inspection and cleaning. The accumulation of marine fouling increases drag forces and causes extra fuel consumption. Studies have shown that the fuel consumption of various types of ships can increase by up to 40% after six months in temperate waters (Woods Hole Oceanographic Institution 1952). Periodic inspection and removal of marine fouling can significantly reduce both ship operating cost and adverse environmental effects.

In recent years, remote controlled vehicles (ROVs) have gradually replaced traditional manual work done by divers in ship hull inspection and cleaning as shown in Figure 1 (Bohlander et al 1992). These robotic platforms are either manoeuvred in free-water or attach to the surface with supporting wheels.

Figure 1: Manual hull cleaning with hydraulic brush

The *Searazor* prototype aims to transition between these two disciplines, in order to cover complex curvatures, especially at stern, bow or even on the propeller. This design is expected to expand the operation range to inaccessible areas for state-of-the-art underwater vehicles.

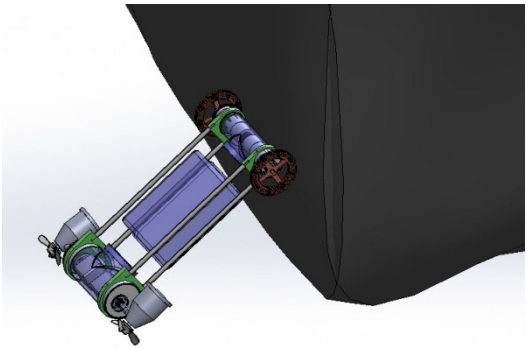

Figure 2: A schematic view of *Searazor's* primary locomotion mode

The *Searazor* is designed as a universal platform to perform inspection and maintenance on various curved surfaces such as ship hulls and other underwater structures (Figure 2). The vehicle is capable of locomotion both in free-water and on ferromagnetic surfaces.

Proceedings 27th European Conference on Modelling and Simulation ©ECMS Webjørn Rekdalsbakken, Robin T. Bye, Houxiang Zhang (Editors)
ISBN: 978-0-9564944-6-7 / ISBN: 978-0-9564944-7-4 (CD)

Its primary locomotion mode, climbing mode, consists of attaching to the ship hull with two magnetic wheels, accompanied by a pair of vectored thrusters to propel and balance the body. The *Searazor*'s secondary locomotion mode, swimming mode, is used when the robot is firstly deployed or detached from the surface, during which the robot can manoeuvre in open water using its thrusters.

The *Searazor* platform is a mechatronic system, which inherits strong dynamic characteristics and demands competent control schemes. Therefore, simulations must be carried out prior to the detailed design. However, due to the fact that the swimming scheme is akin to the movement of an ROV, which has been comprehensively studied in the context of underwater robotics, this paper focuses on the dynamic characteristics during climbing mode. Hence, the thrusters are represented as a single thruster for simplification.

BACKGROUND

The analysis of the dynamics of the *Searazor* shows a combination of wheeled vechicle and marine vehicle dynamics. The bond graph method was adopted as a multi-domain modelling method to represent the system dynamics.

The bond graph method was invented by (Paynter 1961) and extended to many disciplines, especially by Karnopp et al 2006. This method focuses on energy flow, storage and dissipation between elements by surveying effort and flow. By utilising 9 basic elements, these bond graph models can describe the phenomena in mechanical, electrical and hydraulic domains.

Filippini (2004) constructed a nonlinear, four wheel dynamic bond graph model with multiple rigid bodies, including chassis, suspension units, tires and joints. The simulation experiments corresponding to standard vehicle dynamic tests are presented.

Pedersen (2009) suggested using an IC-field in solving rotordynamic problems. Pedersen (2012) then developed general equations of motion for a marine vehicle using a Lagrangian approach (Figure 3). This study investigated the resulting generalised velocity $\vec{v}$ of a rigid body with the inertia matrix $\boldsymbol{M}$, which include the mass m and the skew-symmetric matrix about the position of the centre of gravity $\overrightarrow{r_G}$, under external generalised forces $\vec{\tau}$ with 6 degrees of freedom in a 3-dimensional space, given by equation 1.

$$\boldsymbol{M}(\mathrm{m},\overrightarrow{r_G},\{\boldsymbol{I}\})\dot{\vec{v}} + \boldsymbol{C}(\mathrm{m},\overrightarrow{r_G},\{\boldsymbol{I}\})\vec{v} = \vec{\tau} \qquad (1)$$

The differential equations include the contribution of Coriolis and centripetal forces, which are represented by $\boldsymbol{C}$ matrix and $\{\boldsymbol{I}\}$ is the inertia tensor.

A bond graph framework featuring I-fields for model representation and simulation was derived from these equations as shown in Figure 3. External forces, which vary from different positions and attitudes, are connected to the 1-junction after appropriate transformation by a position and attitude modulated transformer, represented by an MTF element. Damping forces represented by R-fields and restoring forces represented by C-fields can be connected to this 1-junction as well.

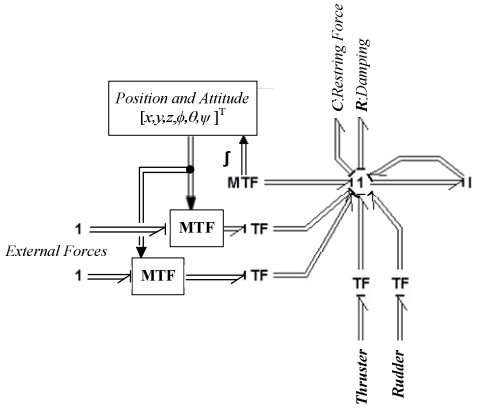

Figure 3: Bond graph model for marine vehicle dynamics

In this paper, analyses of the dynamic characteristics of chassis, actuators and control systems will first be discussed. These mechanisms are further embodied in bond graph models based on Pedersen's framework. The simulation is finally run in the 20sim environment, showing the effectiveness of controllers with animations and graphs.

SEARAZOR DYNAMICS

The analysis and simulation aim to calculate the resulted movement under manoeuvre and environmental forces. These forces and rigid body are analysed and translated into bond graph elements.

Coordinate Frame and Transformation

The inertial reference frame is defined by the X, Y, Z axis and origin O. The vehicle is considered as a rigid body with a total mass and a body fixed coordinate frame with X_b, Y_b, Z_b axes and the origin O_b. The origin o is defined at the centre point between the two wheels, as shown in Figure 4.

The body fixed coordinate is derived from the inertial reference frame with the transitional displacement of D_x, D_y, D_z and Euler angles ψ, θ and φ about the X, Y and Z axes respectively. However, the sequence of the rotation is in the following order: Z, Y and then X (Pedersen 2008).

In addition, in order to illustrate the contact between the wheel and the surface, the trajectory coordinates are introduced with axes X_t, Y_t, Z_t and origin O_t, which

coincides with the origin in body fixed coordinate. In addition, the trajectory coordinate inherit the same Euler angle ψ, whose rotation is firstly made in the derivation of body fixed coordinate, while keeping the Z_t axis perpendicular to the XY plane (Figure 4). The trajectory coordinate can be seen as an intermediate coordinate between the inertial reference frame and body fixed coordinate.

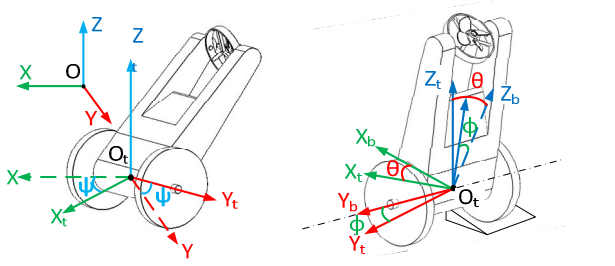

a b

Figure 4: Coordinate transformations

a. Transformation from inertial reference frame to trajectory coordinate made by translating the origin from O to O_t and then rotating ψ about the Z axis.
b. Transformation from trajectory coordinate to body fixed coordinate made by rotating ϕ and θ about Y′ and X′.

In Equation 1, the generalised forces and resulting motion $\vec{v}$ are all defined in the body fixed coordinate. The forces produced by wheels and thrusters are referred to trajectory coordinate. In addition, all the movements are translated to the inertial reference frame for demonstration.

According to [12], the Euler angular velocity transformation $[\dot{\phi}, \dot{\theta}, \dot{\psi}]^T$ are obtained from the angular velocity in body-fixed coordinate system $[\omega_{X_b}, \omega_{Y_b}, \omega_{Z_b}]^T$ using a modulated transformer MTF-element with the following equations.

$$\begin{cases} \dot{\phi} = \omega_{X_b} + \sin(\phi)\cdot\tan(\theta)\cdot\omega_{Y_b} + \cos(\phi)\cdot\tan(\theta)\cdot\omega_{Z_b} \\ \dot{\theta} = \cos(\phi)\cdot\omega_{Y_b} - \sin(\phi)\cdot\omega_{Z_b} \\ \dot{\psi} = \frac{\sin(\phi)}{\cos(\theta)}\cdot\omega_{Y_b} + \frac{\cos(\phi)}{\cos(\theta)}\cdot\omega_{Z_b} \end{cases} \quad (2)$$

By integrating the Euler angular velocity, its corresponding angles $[\phi, \theta, \psi]^T$ can be calculated. The transformation of the linear velocity from body fixed coordinate $[V_{X_b}, V_{Y_b}, V_{Z_b}]^T$ to an inertial reference frame $[V_X, V_Y, V_Z]^T$ and trajectory coordinates $[V_{X_t}, V_{Y_t}, V_{Z_t}]^T$ can be manipulated with the following equations.

$$\begin{bmatrix} V_X \\ V_y \\ V_z \end{bmatrix} = R_{Z,\psi}\cdot R_{y',\theta}\cdot R_{x'',\phi}\cdot\begin{bmatrix} V_{X_b} \\ V_{Y_b} \\ V_{Z_b} \end{bmatrix} \quad (3)$$

$$\begin{bmatrix} V_{X_t} \\ V_{Y_t} \\ V_{Z_t} \end{bmatrix} = R_{y',\theta}\cdot R_{x'',\phi}\cdot\begin{bmatrix} V_{X_b} \\ V_{Y_b} \\ V_{Z_b} \end{bmatrix} \quad (4)$$

$R_{Z,\psi}$, $R_{y',\theta}$ and $R_{x'',\phi}$ matrix about are rotational z, y' and x'' axes. The transformation of the generalised force can be made accordingly with the transposed matrix.

$$\begin{bmatrix} F_{xb} \\ F_{yb} \\ F_{zb} \end{bmatrix} = \left(R_{Z,\psi}\cdot R_{y',\theta}\cdot R_{x'',\phi}\right)^T\cdot\begin{bmatrix} F_x \\ F_y \\ F_z \end{bmatrix} \quad (5)$$

$$\begin{bmatrix} F_{xb} \\ F_{yb} \\ F_{zb} \end{bmatrix} = \left(R_{y',\theta}\cdot R_{x'',\phi}\right)^T\cdot\begin{bmatrix} F_{xt} \\ F_{yt} \\ F_{zt} \end{bmatrix} \quad (6)$$

Chassis

The chassis is regarded as a rigid body, which contributes most to the inertia of the vehicle. The total weight of the vehicle is ballasted equal to the buoyancy. However the distance $\overrightarrow{r_{GB}}$ between the centre of buoyancy C_B and the centre of gravity C_G results in a restoring moment, caused by buoyancy $\vec{B}$ and gravity $\vec{G}$, when the vehicle is not placed vertically as shown in Figure 5.

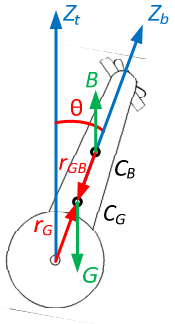

Figure 5: The restoring moment resulting from buoyancy and gravity

As shown in Figure 6, the chassis assembles all the external force inputs through its 1-junction. These forces are superimposed and then apply to the I-field. A resistor element R represents the fluid and mechanical friction applied on the vehicle.

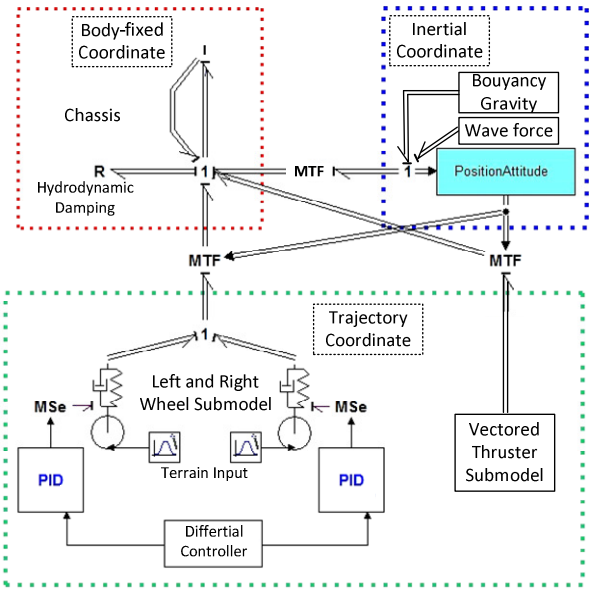

Figure 6: The chassis model acts as a hub, assembling all the force inputs, and generates the resulting movement.

The general modelling structure of the *Searazor* vehicle body is represented by a marine vehicle bond graph

model, as shown in Figure 3. The inertia matrix $\boldsymbol{M}$ is defined by vehicle mass m, the skew-symmetric matrix about the position of centre of gravity $\boldsymbol{r_G}$ and the inertia tensor $\{\boldsymbol{I}\}$,

$$\boldsymbol{M} = \begin{bmatrix} \mathrm{m}I & -\mathrm{m}[\boldsymbol{r_G}] \\ \mathrm{m}[\boldsymbol{r_G}] & \{\boldsymbol{I}\} \end{bmatrix} \quad (7)$$

where I is the identity matrix.

The motion of the vehicle is generated in the form of flow in the body fixed coordinate system. By utilising a modified transformer element MTF, the flow of velocity is then integrated into position and translated into the inertial reference frame for transformation between body fixed coordinate and trajectory coordinate.

Wheels

The two wheels on both sides of the vehicle are driven by two separate servo DC motors. The steering is accomplished by employing differential movement of the wheels.

The design and characteristics of the magnetic wheel refer to Zhang et al 2010. The rubber tire enhances grip between the yoke and the ferromagnetic surface. A magnetic wheel with a 96mm diameter and a 20mm thickness can generate up to 180 N of adhesive force when the tire thickness is 0.6mm. By selecting an optimised tire thickness, it is feasible to tune the magnetic force to yield to the maximum thrust from the thruster, and yet provide sufficient traction for manoeuvre.

Figure 7a shows the forces and torque applied to the wheel. F_{Xt} and F_{Zt} are the tractive force and normal force. The lateral force F_{Yt} is the centripetal force when the vehicle turns. In Figure 7b the forces F_{Xt}, F_{Yt} and F_{Zt} are transformed into the forces with the same magnitude and orientation at the origin O_t, together with induced moments M_{FXt}, $M_{FYt}$and M_{FZt}, where W is the width of the vehicle and r_{wh} is the radius of the wheel. Therefore the forces and torques in Figure 7b show the force input into the chassis from one wheel.

The wheel axis is regarded as the pivot corresponding to angle θ. The wheel applies the force $\overrightarrow{F_{wh}}$ and the induced moment $\overrightarrow{M_{wh}}$ to the chassis.

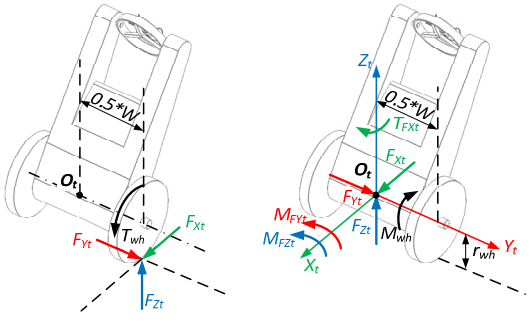

a b

Figure 7: The force input from one wheel

a.The forces and torque applied to one wheel
b.The transformed equivalent forces and moments applied to the chassis

In the bond graph sub-model shown in Figure 8, the wheel is driven by a modulated effort source with a torque input(Figure 6). Besides, the terrain is described as a modulated flow source, determining the lateral movement.

The force F_{Xt} induced by $M_{wh}$is introduced with a zero-junction and a transformer which represents the wheel radius.

The tire is simplified as a classic spring-damper system between the terrain and the chassis. The lateral friction between the tire and surface is manipulated as a coulomb friction model. Therefore, no skid occurs before the lateral force reaches the threshold, which is determined by the force in the Z direction.

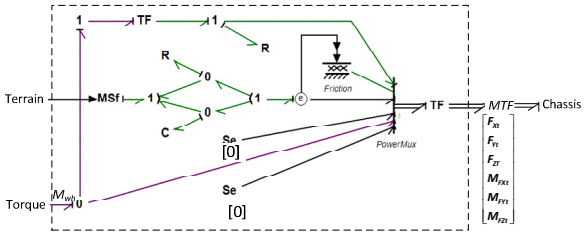

Figure 8: The bond graph model of a single wheel

The output of the wheels model is a multi-bond with 3 forces and 3 moments after being translated by a transformer regarding the origin in trajectory coordinate.

Thruster

The vectored thruster is located on the upper end of the chassis. The thrust orientation is determined by a servo motor, while the thrust value is set to a fixed value that can provide sufficient thrust for manipulating the attitude and propelling against fluid drag (Figure 9a). The thrust of an ROV propeller under variable rotational speed was studied by Healey 1995.

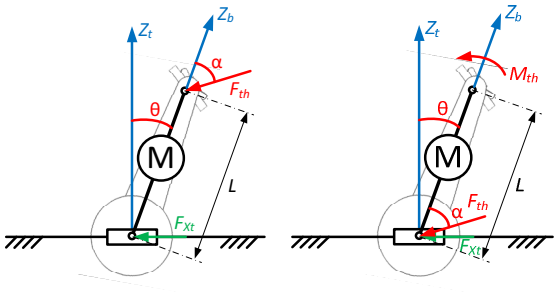

a. b.

Figure 9: The force input from the vectored thruster
a.The force produced by the vectored thruster;
b.The translated equivalent force and moment applied on chassis

However, in this study, the thruster was set at a constant speed while the thruster angle α was assigned as the control parameter. In Figure 9b, the induced thrust force F_{th} is transmitted to the wheel axis in addition to the moment M_{th}.

The balancing moment is then provided by the moment M_{th}, where L is the length of the vehicle, and α is the thrust orientation to the Z_b axis in the body fixed coordinate.

$$M_{th} = F_{th} * L * \sin(\alpha) \quad (8)$$

The PID controller governs the angle θ between chassis and surface by actively adjusting the thruster orientation. The modulated effort source, represented by MSe in Figure10, is modified with an addition signal input of θ and the thrust set-point. The output of non-zero generalised forces is as follows.

$$\begin{cases} F_{Xt} = F_{th} \cdot \cos(\theta + \alpha) \\ F_{Zt} = F_{th} \cdot \sin(\theta + \alpha) \\ M_{Yt} = F_{th} \cdot \sin(\theta) \cdot L \end{cases} \quad (9)$$

The orientation of the vectored thruster is controlled by a position servo motor which has limited rotational speed and a cut-off frequency. Therefore, the output orientation from controller is processed by a rate limiter.

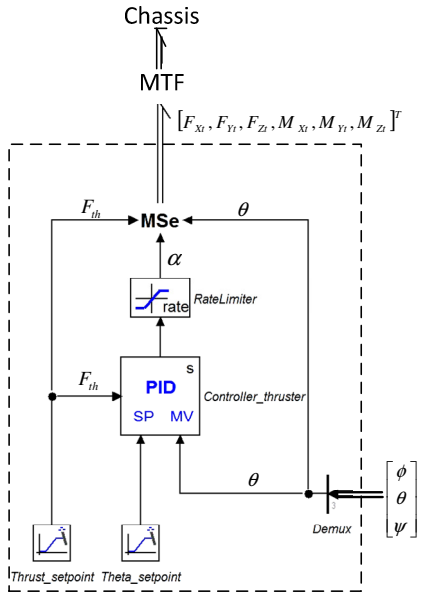

Figure 10: Bond graph sub model of vectored thruster

Hydrodynamic Forces

The effect of hydrodynamic forces is simulated in three major contributions: damping, current disturbance and restoring moment resulted by buoyancy and gravity.

The damping model is simplified as a 6 by 6 R-field, connected to the 1-junction in body fixed coordinate, as shown in Figure 6.

The current disturbance is defined as a time-varying force F_{Dst}, which is applied on the chassis at a distance L_{Dst} to the wheel axis, Figure 11a. In Figure 11b, this force is then transformed into a force at the origin with the induced moment $F_{Dst} \cdot L_{Dst}$.

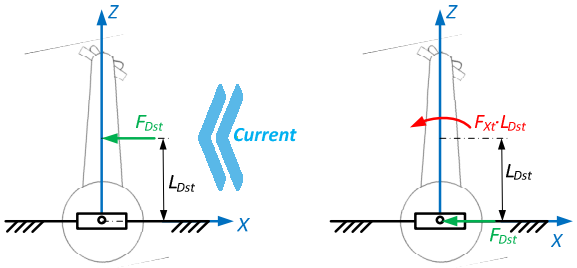

a. b.

Figure 11: Current disturbance on the vehicle
a. The force F_{Dst} is applied on the chassis
b. The transformed equivalent force and moment
c.

The magnitude of the disturbance force and moment is assumed as a superposition of a low-frequency sinusoidal wave and Gaussian Noise, respectively representing the sea wave and random current (Figure 12). Effort source is represented by Se element, where [0] indicate that no effort is input into this chanel.

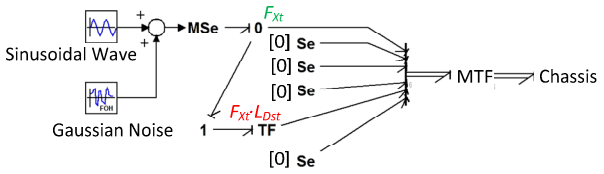

Figure 12: Simplified bond graph model of current disturbance

SIMULATION RESULTS

The simulation was carried out in the 20Sim v4.2 environment. The resulting vehicle movement is reflected by the position and attitude values in the inertial reference frame. Animations and graphs were made correspondingly to depict the reactive motion after receiving manoeuvring signals from a joystick. The thruster was represented with a plate located on top of the chassis, while the tilt of plate indicated thrust orientation. Each wheel was textured with a face in order to show the rotational phase.

Finally, the reaction of the vehicle under wave and current disturbance were also simulated.

Attitude Control

In Figure 13, the vehicle starts from an upright attitude, then adjusts itself to the attitude angle θ by following a predefined ramp profile. This action is accomplished by tilting the thruster to a negative angle in the first 0.9 second. The slight lag between controller output and thruster orientation is due to the delay of servo motor.

When the time reaches 2 seconds, the wheels starts to turn while a moment, which tends to increase θ, is applied to the vehicle. The orientation of the thruster soon switches to a positive value to counteract the

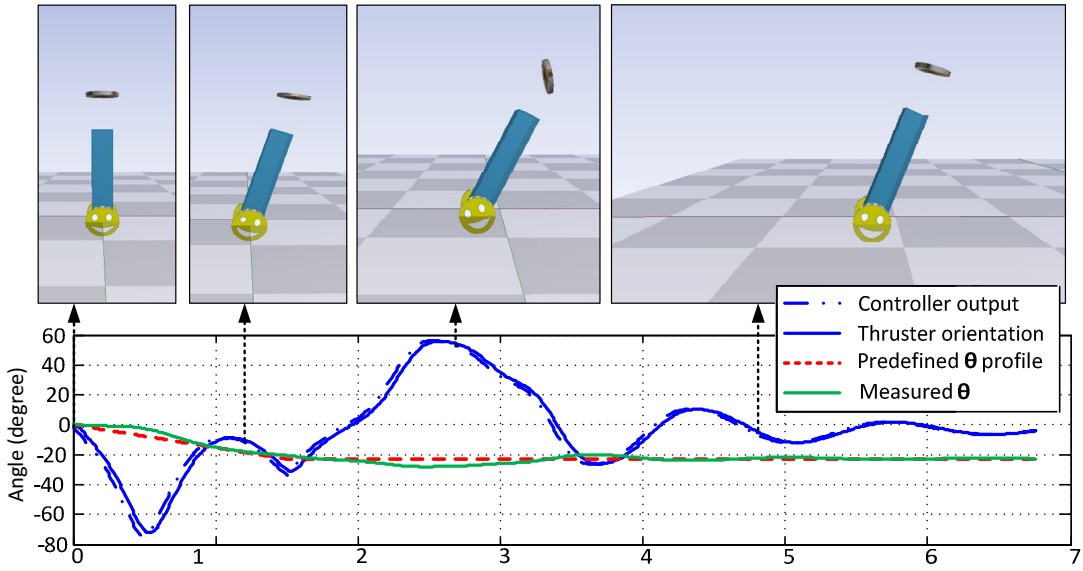

Figure 13: The vehicle's attitude follows the predefined profile by actively adjusting the thruster orientation

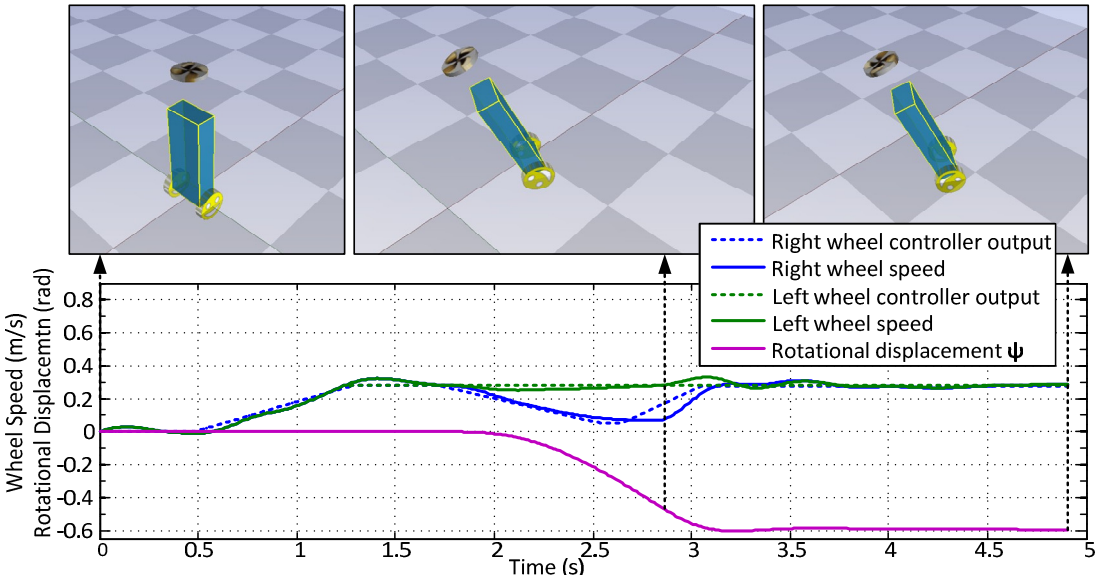

Figure 14: A typical steering movement is accomplished with differential motion on the two wheels governed by separate PID controllers

moment from the wheels. Finally, the vehicle reaches equilibrium at 7 seconds.

Steering

Figure 14 shows the steering movement accomplished with a differential motion on the two wheels. The differential movement starts at 1.7 seconds after the vehicle is released. According to the control scheme, the rotational rate of the inside wheel (the right wheel) decreases. As a result, the vehicle turns by 0.6 rad (34°) before the wheels return to synchronisation.

Dynamic Stabilisation

The focus of stabilisation is to maintain the angle θ at the predefined value when a disturbance force is applied on vehicle.

In this simulation, the wheels are fixed to the original position. Hence the vehicle is considered to be connected to a 1 degree-of-freedom joint. The disturbance force affects angle θ by means of the resulting disturbance moment shown in Figure 15. The thruster orientation shows a manner of actively counteracting the disturbance. As a result of this scheme, the measured angle θ is maintained in the range of [-16˚, -28˚] after θ is steadily set at -23˚.

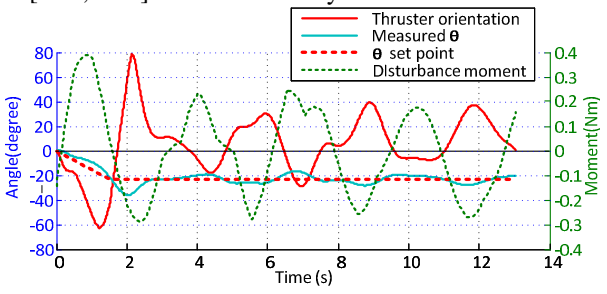

Figure 15: The vehicle attitude under wave disturbance moment

Figure 16 shows the contribution of balance moments form thruster and wheels to counteract the disturbance

moment. The thruster appear to be responsive to the variation of disturbance moment, while the contribution from the wheels shows less fluctuation.

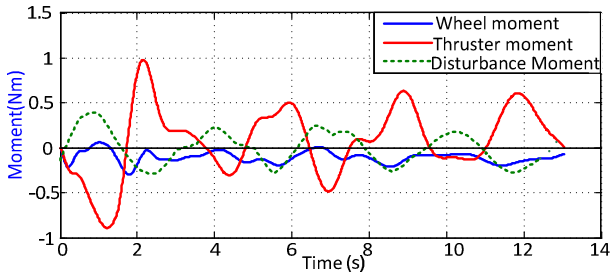

Figure 16: The contribution of balancing moment from thruster and wheels against wave disturbance moment

CONCLUSIONS

In this work, the dynamic characteristics of the *Searazor* underwater vehicle were investigated with bond graph models. The simulation results show the feasibility of attitude control and steering by adopting appropriate control schemes. In the current design session, the simulation result is used to determine actuator specifications.

The simulation model will be the framework for the *Searazor* control scheme in future. However, the current simulation did not take curved surfaces into consideration. Therefore, the control scheme for manoeuvring and navigating on complex surfaces needs to be studied further. Finally, considering the two locomotion modes in free water and on surfaces, the dynamic characteristics in transition also appear to be crucial for the *Searazor*'s potency.

Reference

Bohlander G. S.; Hageman E. G.; Halliwell F. S.; Juers R. H. 1992. Automated Underwater Hull Mainitenance Vehicle. Carderock Division, Naval Surface Warfare Center

Filippini G.; Nigro N; Junco S. "Vehicle dynamics simulation using bond graphs".

Healey, A.J.; Rock, S.M.; Cody, S.; Miles, D.; Brown, J.P..1995. "Toward an improved understanding of thruster dynamics for underwater vehicles". IEEE Journal of Oceanic Engineering 29(4), 354—361.

Karnopp, D. C., Margolis D. L., Rosenberg C. 2006. System Dynamics: Modeling and Simulation of Mechatronic Systems, 4th Ed. John Wiley & Sons.

Paynter H. M. 1961, Analysis and Design of Engineering Systems. MIT Press, Cambridge, Mass.

Pedersen E. 2009. "Rotordynamics and bond graphs: basic models Journal of Mathematical and Computer Modeling of Dynamical Systems", Vol. 15, No. 4, 337-352.

Pedersen E. 2012. "Bond Graph Modeling of Marine Vehicle Dynamics". Bond Graph Modeling: Theory and Practice Symposium at the 7th Vienna International Conference on Mathematical Modeling.

Pedersen E. Engja H.2008. Mathematical Modelling and Simulation of Physical Systems, Lecture Notes in Modelling, Simulation and Analysis of Dynamic Systems, 265-269.

Woods Hole Oceanographic Institution. 1952. Marine fouling and its prevention ; prepared for Bureau of Ships, Navy Dept.

Zhang Y; Dodd, T.; Atallah, K.; Lyne, I.2010. "Design and optimization of magnetic wheel for wall and ceiling climbing robot," Mechatronics and Automation (ICMA), 2010 International Conference on , vol., no., pp.1393-1398.

AUTHOR BIOGRAPHIES

CONG LIU has been working at Aalesund University College as a research assistant since October 2011. He registered as a PhD candidate in Department of Engineering Design and Materials at Norwegian University of Science and Technology in 2012. He received his Master's diploma in Mechanical Electronics Engineering from Beihang University in Beijing.
Email: lico@hials.no.

EILIF PEDERSEN is an associate professor in the Department of Marine Technology at Norwegian University of Science and Technology.
Email: Eilif.Pedersen@ntnu.no.

VILMAR ÆSØY received his PhD in Mechanical Engineering in 1996 at Norwegian University of Science and Technology, department of Marine Technology. From 1997-2002 he worked in the maritime industry as researcher in Aker Maritime and R&D manager in Rolls-Royce Marine. Since 2002 he has been an Assistant Professor in Mechanical and Marine systems engineering at Aalesund University College, Faculty of Maritime Technology and Operations.
Email: ve@hials.no

HOUXIANG ZHANG is a professor on Robotics and Cybernetics at the Department of Technology and Nautical Sciences, Aalesund University College, Norway.
Email: hozh@hials.no.

HANS PETTER HILDRE is a professor on product and system design at the Department of Technology and Nautical Sciences, Aalesund University College, Norway.
Email: hh@hials.no.

Automatic Map Creation for Environment Modelling in Robotic Simulators

Thomas Wiemann, Kai Lingemann and Joachim Hertzberg

Knowledge Based Systems Group
Osnabrück University
Albrechtstr. 28, Osnabrück, Germany
twiemann@uni-osnabrueck.de

DFKI GmbH
Robotics Innovation Center Bremen
Albrechtstr. 28, Osnabrück, Germany
{kai.lingemann|joachim.hertzberg}@dfki.de

KEYWORDS

Environment Modeling, Model Generation, Robot Simulators

ABSTRACT

This paper presents an approach to automatically create polygonal maps for environment modeling in simulators based on 3D point cloud data gathered from 3D sensors like laser scanners or RGB-D cameras. The input point clouds are polygonalized using a modified Marching Cubes algorithm and optimized using a pipeline of mesh reduction and filtering steps. Optionally color information from the point clouds can be used to generate textures for the reconstructed geometry.

INTRODUCTION

Simulators play an important role in the development of algorithms for robotic applications. They allow to test new procedures on synthetically generated data before they are evaluated on the real hardware. In simulators, the emulated data is generated based on physical models and descriptions of the used hardware and the environment the robot is interacting with. Usually polygonal models are used to represent robot and environment. Manual modeling is a time consuming and tedious job, especially for complex geometries.

With the rapid development of 3D scanning technology, real world objects can be scanned faster, more precisely and at higher resolution. State of the art laser scanners are able to acquire in the order of a hundred million points with one single scan. Besides laser scanners, 3D or RGB-D cameras like Microsoft Kinect can be used to digitize complex scenes using specialized SLAM methods like (Henry et al., 2010). Compared to a 3D laser scan, an RGB-D point cloud lacks density and provides a low opening angle; however, as the cameras deliver up to 30 frames per second, the data accumulates to very large registered point clouds as well.

For the use in simulation raw point clouds are clumsy for several reasons. First, large environments would require a huge amount of points to be represented, and, consequently, much memory is needed just to store the raw data. This problem gets worse if search data structures like *kd* trees are used to optimize queries like nearest neighbor searches, needing additional memory. Second, even with optimized search structures, run time is critical. Third and maybe most important: Point clouds, by definition, only contain discrete scan points. Even dense, high resolution point clouds are no substitute for continuous surface representations that are needed to use them as environment models for simulators like Gazebo (Koenig and Howard, 2004).

A common solution to overcome these disadvantages is to compute a polygonal mesh representation that approximates the point cloud data. Being a standard data structure for object modeling in computer graphics, optimal polygonal approximations are memory efficient, and efficient algorithms for rendering and ray tracing are available. In the context of mobile robotics, polygonal environment maps offer great potential for applications ranging from usage in simulators, virtual environment modeling for tele operation to robot localization by generating virtual scans via ray tracing. However, creating polygonal environment maps based on laser scan data *manually* is a tedious job, hence quite a number of automatic surface reconstruction algorithms have been developed over the past years.

The available surface reconstruction algorithms are usually optimized for special use cases and input data, but generally deliver acceptable results. However, when using them in robotic applications, several practical issues arise. Most general surface reconstruction procedures would represent sharp features poorly and produce more triangles than needed to approximate a surface, especially on planes. Other problems occur when the input data is incomplete due to scan shadows that yield holes in the reconstructed meshes. Furthermore, many of reconstruction algorithms like Power Crust (Amenta et al., 2001) and Poisson Reconstruction (Kazhdan et al., 2006) rely on closed geometries, which is generally not the case for arbitrary environments.

In this paper we present a software we call the Las Vegas Surface Reconstruction Toolkit (LVR) (Las Vegas Surface Reconstruction) (Wiemann et al., 2012) to automatically create polygonal environment representations from point cloud data that can be used for the simulation of typical environments in robotic applications. The reconstruction procedure basically consists of three steps: Initial mesh generation using Marching Cubes, mesh optimization and texture generation. All steps are performed automatically without user interaction. The software can use the results of the provided, efficient Marching Cubes implementations as input, or, alternatively, can be used together with other surface reconstruction implementations like the ones in CGAL and PCL (Rusu and Cousins, 2011). We show the practical usability of the software by demonstrating the whole re-

Proceedings 27th European Conference on Modelling and Simulation ©ECMS Webjørn Rekdalsbakken, Robin T. Bye, Houxiang Zhang (Editors)
ISBN: 978-0-9564944-6-7 / ISBN: 978-0-9564944-7-4 (CD)

Fig. 1. Comparison of standard Marching Cubes (left) and Planar Marching Cubes (right). The contours of the marked areas show considerable discretization artifacts when the original Marching Cubes algorithm is used. Planar Marching Cubes on the other side produces smooth contours.

construction process from point cloud to a textured polygon map that is loaded into Gazebo and used to generate simulated laser scan data.

The remainder of this paper is organized as follows: The next section presents the state of the art in polygonal surface reconstruction from point cloud data. The next part presents the implemented mesh generation and optimization techniques followed by an application example. The last section concludes.

RELATED WORK

Automatic construction of meshes from point cloud data has received much interest in computer graphics. The defacto standard method to generate triangle meshes is the Marching Cubes algorithm (Lorensen and Cline, 1987), which comes in a number of variants. (Newman and Yi, 2006) provides a comprehensive review. Marching Cubes is an iso surface extraction algorithm, which means, a continuous mathematical scalar field description of the underlying surface is needed. Typically, the iso value of a surface within this field is 0. The first method to approximate a suitable representation for unorganized point cloud data was developed by Hoppe et al (Hoppe et al., 1992). It uses local approximations of so-called tangent planes to represent a signed distance function that defines a zero surface. A variant of this method together with a GPU implementation of Marching Cubes is used in Kinect Fusion (Izadi et al.) to create meshes of Kinect data in real time, but this method is limited to a predefined maximum reconstruction volume. Other methods to create iso surfaces are variants of Moving Least Squares like APSS (Guennebaud and Gross, 2007) and RIMLS (Öztireli et al., 2009), which are both integrated in Meshlab. While there are reconstruction methods based on Marching Cubes, a number of algorithms exist that directly triangulate point cloud data. One example is the "Growing Cell Structures" (Annuth and Bohn, 2010) that uses a neural network together with unsupervised learning. Other direct methods are based on Delaunay triangulations (Devillers, 2002) (Amenta et al., 2001) or generate greedy triangulations like the one implemented in PCL (Rusu and Cousins, 2011). Another successful approach for closed geometries is Poisson Reconstruction (Kazhdan et al., 2006). The drawback of these approaches is that they are sensitive to the quality of the input data, since every data point is used in the triangulation, resulting in uneven meshes in the presence of noise.

Surface reconstruction algorithms usually produce more triangles than strictly needed to represent a surface. Therefore after creating an initial triangulation of the input data, meshes are usually optimized. Most of the respective algorithms rely on calculating the cost of removing vertices or faces (Garland and Heckbert) (Melax, 1998) and iteratively remove the elements that cause the lowest geometric error. (Hoppe et al., 1992) uses a similar approach, but instead of measuring the local error, a global error sum is used to determine the redundant triangles. These methods work well for curved models, but in meshes with many sharp features, the sharp edges will ultimately blur out. The mesh optimization steps presented in this paper aim at optimizing planar patches bounded by sharp edges, to get an improved triangle mesh.

MAP GENERATION

Our map generation procedure consists of three main parts: Mesh generation, mesh optimization and texturing. The details of the single processing steps are described in the following sections.

Initial Mesh Generation

Many robotic environments are mostly planar. This fact has to be taken into account when choosing the mesh generation method. Our experience has shown, that Marching Cubes based approaches deliver the best results for arbitrary geometries since they do not rely on special properties like convexity, can handle holes in the input data correctly and are very fast and memory efficient. For the task at hand

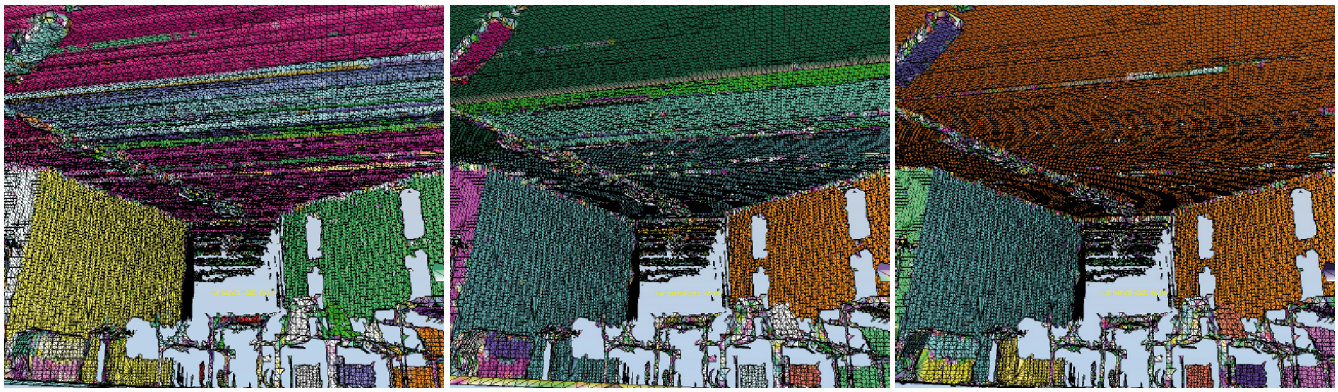

Fig. 2. Region growing based plane detection in the initial reconstructions. Different colors signal different planes. Note that the regions on the ceiling are separated in the first clustering step due to noise (left). Applying the algorithm repeatedly, clusters can be fused (middle) until the whole ceiling plane is finally extracted (right).

we use a modified implementation we call *Planar Marching Cubes*, that is optimized for planar reconstructions. It uses Hoppe's distance function (Hoppe et al., 1992) together with an optimized normal estimation procedure (Wiemann et al., 2012).

The basic idea of Marching Cubes is to calculate the intersection of a surface with a cell within a voxel grid and use precomputed approximation patterns to generate a triangular approximation of the surface's course within the cell. The main problem when approximating planar surfaces is that the classic Marching Cubes approach cannot detect if a surface ends within a cell, due to the fact, that interpolation is only done in one dimension. This results in a noticeable discretization of the reconstruction of planar regions. Our Marching Cubes implementation is optimized to represent the contours of planar objects correctly to create realistic environment models. To model the ending of a surface correctly, we project the created vertices in planar configuration on the nearest data point. This way, we achieve a surface approximation in two dimensions, which results in noticeably better reconstruction, as shown in Fig. 1.

Mesh Optimization

The most noticeable drawback when using Marching Cubes for mesh generation is that the algorithm produces far more triangles than necessary to approximate planar regions, a fact that can also be witnessed in Fig. 1. Since the reconstructions shall be used in simulators, it is mandatory to keep the number of triangles as low as possible to ensure a high update rate of the simulated sensor data. On the other hand, for accurate results, the used polygon map has to be geometrically correct. The Marching Cubes algorithm also is very sensitive to noise, too, resulting in unevenness of the reconstructed planes, which can be seen in the lower left corner of the presented figure. Another problem is the approximation of sharp features. These are usually blurred out due to the used approximation patters. Kobbelt (Kobbelt et al., 2001) describes a technique to reconstruct sharp features, but the used heuristics to identify sharp bends and corners do not work in noisy data. Therefore we implemented several mesh optimization steps to make the reconstruction feasible for the use in simulators.

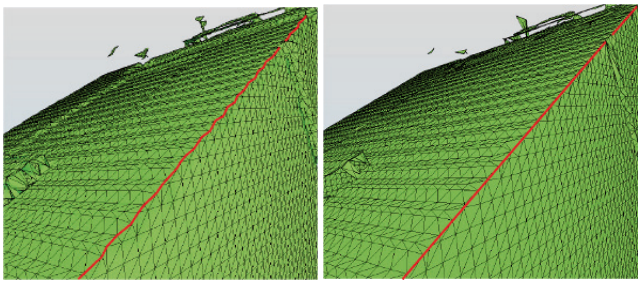

Fig. 3. Optimization of plane intersections. The left image shows the original reconstruction of a bend between two walls (red). The right picture shows the triangle mesh after optimizing the the intersection vertices.

The first step is the optimization of planar regions. To detect planes, we use a region growing based approach. Region-growing is done by checking if the surrounding triangles of an arbitrarily chosen start triangle have a similar surface normal. As long as the normal of a neighbor triangle does not differ more than a user defined threshold from the start triangle, a new search is started recursively from this triangle. This process is carried on, until a bend in the surface is detected. To reduce the noise in the planar regions, we calculate the plane equation using a RANSAC based fit to all vertices and project them into the common plane. Since this process changes the initial geometry, we re-start the region growing afterwards, to fuse regions that may have been separated due to the normal criterion in the first place. This process is repeated until convergence. For the results of this interactive plane detection, see Fig. 2.

After detecting the planes in the mesh, we calculate the exact intersections between them to approximate sharp features between walls, floor and ceiling. To enhance the mesh, we stretch the vertices of triangles near a calculated straight line onto it. The effect on the reconstruction is in Fig. 3.

To reduce the number of triangles in the mesh, we extract and fuse the contour edges of the found planes and re-triangulate them using the OpenGL tesselator. To create an optimal 2D polygon representation of the boundary of a region with a minimal number of vertices we use the Douglas Peucker optimization algorithm (Douglas and Peucker, 1973). Fig. 4 shows an example. The left picture shows the initial mesh. The right picture displays the effect of intersection optimization and mesh reduction via re-triangulation.

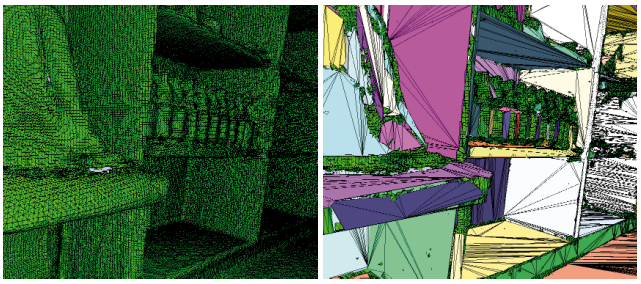

Fig. 4. Mesh reduction via re-triangulation.

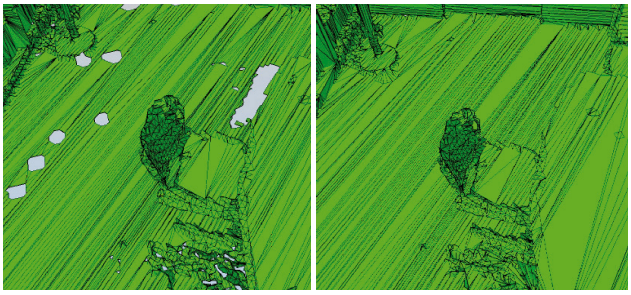

Fig. 5. Exemplary result of the "Hole Filling" function. Before (left) and after (right) application.

The optimized mesh represents sharp features correctly and the number of triangles in the planar regions is significantly reduced, while curved surfaces (bottles) are still represented with the original geometry.

Another optimization feature is hole filling. The hole filling algorithm performs a contour tracking on the mesh and collects all holes up to a certain size which is given by the number of edges in the contour. In a second step the edges of each hole are collapsed using an edge collapse operation until there are only three edges left per hole. The remaining triangle holes are closed by adding new faces to the mesh which close those holes. Fig. 5 displays an application example.

Besides the presented optimization features, we have implemented a number of several other filters to reduce artifacts due to sensor noise and outliers. A full overview of available features can be found on the LVR website (Las Vegas Surface Reconstruction).

Texture Generation

If the input data contains any information that can be mapped to color values, e.g. RGB information, reflectivity values, thermal data etc., LVR can convert these values into textures for the generated polygons. Texture generation is done by putting a rectangular grid of fixed cell size t over each polygon. The voxelsize of the grid determines the resolution of the texture image. For each cell in the grid, a color value is calculated by averaging the colors of the k nearest points in the given point cloud. To keep the textures small, it is necessary to find a grid alignment that maximizes the used area (cf. Fig. 6). In the presented example, an axis aligned pixel grid would contain a large amount of unused pixels (gray) while an image in the green coordinate system would be significantly smaller (only 70% of the axis aligned version). To determine the best alignment we compute the Principle Component Analysis (PCA) of the polygon vertices. The first two eigenvectors of the result deliver a good estimation for the alignment of the polygon in the global coordinate system, thus we define the pixel matrix by determining the bounding box of the polygon in this local system defined by X' and Y'.

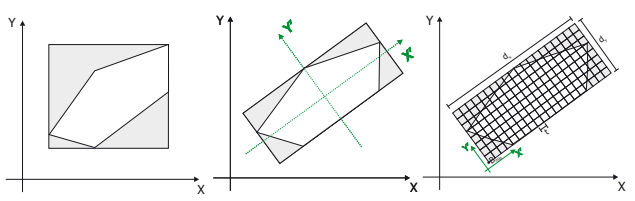

(a)Axis parallel alignment (b)Alignment in local system (c)Calculation of texture pixels

Fig. 6. Finding the right coordinate system for texture generation. In the presented case, an axis aligned pixel grid (a) would result in a lot of unused space (gray). An aligned bounding box would reduce this space (b). The actual pixel map as calculated as shown in (c).

For practical reasons, textures are only calculated for regions above a certain size. Small regions and single triangles are assigned with a single color value to save texture memory and speed up the meshing process. An example of a textured reconstruction is shown in Fig. 7. The left picture shows the input point cloud taken with a Faro laser scanner. The picture in the middle shows the optimized reconstruction. The textured mesh is shown on the right. The large areas on floor, wall and ceiling are textured while the small regions are represented by single colored triangles. It is obvious, that the colored and textured mesh encodes far more information than the pure geometry like the representation of cobblestones on the floor and panels below the ceiling, which are difficult to model geometrically.

The achievable texture quality strongly depends on the quality of the input data. Low point densities will cause blurry textures while dense point cloud data will allow to choose a high resolution for texture generation. For fast rendering the texture resolution shouldn't be too high, since the planar regions can become quite large after reconstruction and the maximum texture size is limited by the graphics hardware.

APPLICATION EXAMPLE

With the methods present above it is possible create high quality textured reconstructions from point cloud data. To prove their usability in simulators we will present an actual application example, where the point cloud data acquired by a 3D laser is automatically processed into a polygonal map that in turn is used in Gazebo to simulate the environment. We will then spawn a robot into the simulation and collect simulated 2D laser scans. The reconstruction will be fully automated without any user interaction or manual editing.

Input Data and Environment Description

As input data we will use a point cloud that was taken at a lecture hall at Osnabrück University called "Reithalle". The data set consists of 6 high resolution laser scans captured with a Leica HDS 6000 laser scanner. The scans were aligned automatically using slam6d (Nüchter et al., 2012) using special markers for initial pose estimation. The laser scanner delivers no color information about the environ-

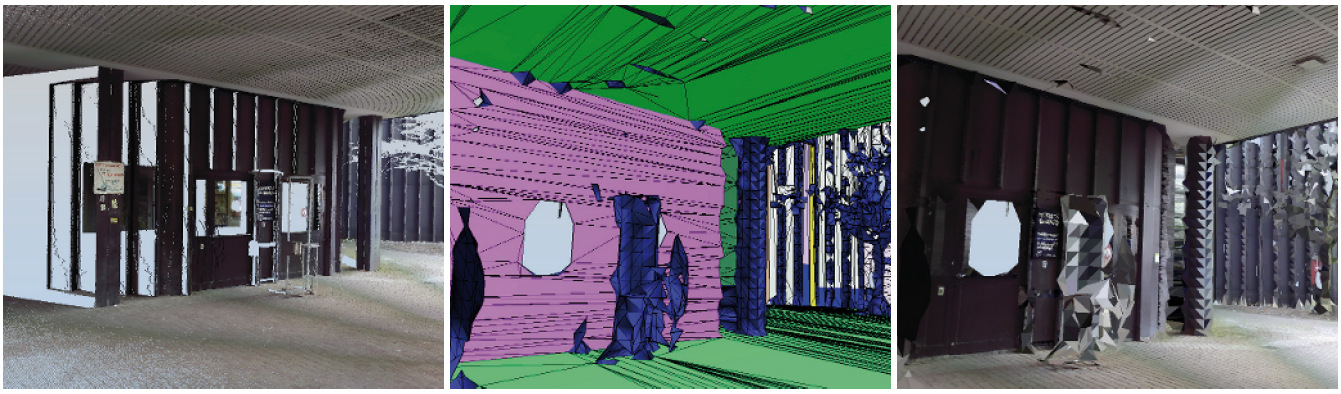

Fig. 7. Textured mesh generation from colored point cloud data: The input point cloud (left), the optimized mesh (middle) and the textured reconstruction (right).

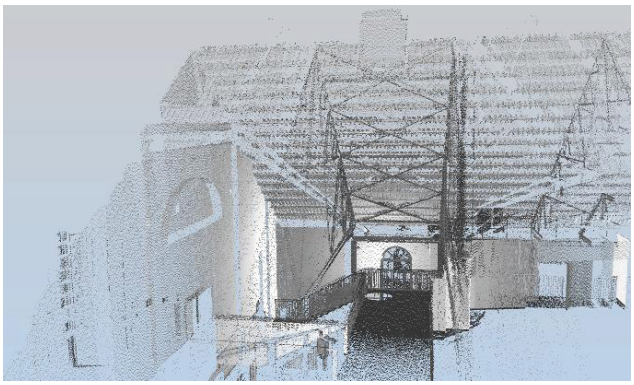

Fig. 8. The input point cloud used in the experiment.

ment, but it returns a reflectance value for each point, that can be used to generate gray scale textures. A rendering of the point cloud is shown in Fig. 8. The environment was chosen to demonstrate the ability to handle large data sets and extensive environments. The geometry of the area is mostly planar and shows drivable surfaces, so that it makes sense to use it in a simulation.

Reconstruction Results

Fig. 9 shows the results of the reconstruction process. The left image shows the initial Marching Cubes reconstruction from the input data. Please note the unevenness on the floor plane due to sensor noise and the smooth transitions between walls and ceilings. The picture in the middle shows the optimized mesh after plane detection, intersection calculation and hole filling. The reconstructed planes show no noise, the intersections are sharp. Due to the plane optimization, some details have been erased from the initial mesh like the door on the right front wall. With texturing this is usually no problem, since these features are represented in the calculated textures, as the picture on the right shows.

The input point cloud contained about 14 million data points. The initial Marching Cubes Reconstruction generated a mesh consisting of 371.640 triangles. This number was reduced down to 98.464 triangles after mesh optimization. The computation time for initial mesh generation was 1:14 minutes on an Intel Core i7 system with 16 GB RAM. Automatic mesh optimization only took 14 s, texture generation another 2:23 minutes. The main bottle neck in the reconstruction is the nearest neighbor search, that has to be performed to estimate the normals for distance function evaluation and to calculate the textures. Currently we are using FLANN (Muja and Lowe, 2009) and OpenMP to parallelize the process. The example demonstrates that our mesh optimization procedure is very efficient and can reduce the number of triangles in the reconstructions significantly. We have tested the optimization with meshes from other mesh generation software (actually the initial mesh in Fig. 4 was created with Kinect Fusion) as well and are currently planning to integrate some algorithms into PCL.

Using the Reconstruction in Gazebo

In our test we have exported the reconstruction into the Collada file format and loaded the mesh into Gazebo. Via the ROS connection of this simulation environment we were able to spawn a model of a Kurt robot (Albrecht et al., 2006) into the reconstructed environment. In our experiments it showed that the rendering front end of Gazebo experienced problems to render the mesh, although the physics simulation was working correctly. The problem here was that the generated environment model was not generated via CSG (Constructive Solid Geometry). Models generated using that technique are always close, i.e. a face is alway pointing towards the spectated. Our meshes on the other hand are single sided, so consequently faces that were not pointing the camera were removed by the renderer ("Back Face Culling"), as can been seen Fig. 10. A quick fix for that problem was to insert each triangle twice with opposite normal directions. We admit that this is merely a hack, but for the time being it solved the rendering problems we experienced.

To check the simulation we navigated the Kurt robot via a ROS node. The model of the robot included the simulation of the robot chassis with differential drive and a Sick LMS200 2D Laserscanner. Visualization of the robot position and the laser scan were done in RVIZ. Our tests proved that the simulation behaved as expected including gravity and collision detection between robot model and environment. Using the double sided reference model, we experienced no performance issues while navigating the robot. An example of an simulated 2D laser scan together with the corresponding geometry is shown in Fig. 12. The left image shows a rendering of the reconstructed model from the

Fig. 9. Reconstruction of the "Reithalle" data set. The images show the initial reconstruction (left), the optimized mesh (middle) and the textured model visualized the reflectance values of the laser scanner.

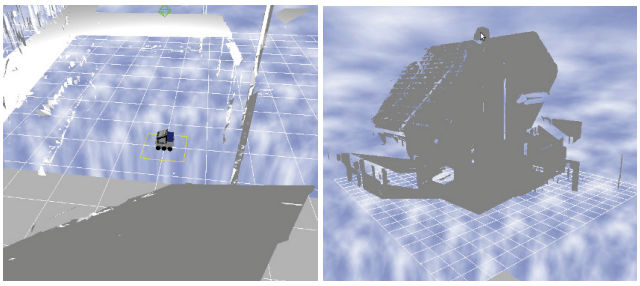

Fig. 10. Rendering of the reconstruction in Gazebo. Without double inserting all triangles the ones that point away from the camera are removed (left). If we double insert the faces with flipped normals the rendering is correct (right).

Fig. 11. Textured reconstruction from a Kinect point cloud. The quality of the reconstructed geometry is acceptable, the quality of the textures is poor due to the relatively sparse point density.

point of view of the robot. The red line indicates the height of the simulated laser scan. The image in the right shows the visualization of the robot's pose and the simulated scan data. From the image it becomes clear that simulated data and loaded geometry match as expected.

DISCUSSION

The presented experiment has shown that LVR reconstructions can be used as environment models in robotic simulation environments. The main problem here is to export the generated polygon models into a data format that can be interpreted by the selected simulator. In case of the Gazebo example we were able to generate a Collada export that was correctly rendered and handled as expected by the simulator. Other simulators like USARSim use proprietary file formats which are not that easy to implement. In principle it may be possible to export the generated meshes to other file formats and re-import them into the proprietary editors, but there is always the risk of loss of information when converting file formats.

In the presented experiment we focused on pure geometry, i.e., we did not evaluate the benefits of the generated textures in the simulator. As shown in Fig. 9, the inclusion of texture information can add more information about the environment then bare geometry, namely the position of the door and signs on the walls. Currently we are not convinced that the quality of textures is high enough to use simulated camera data for vision based robotic applications, so we did not include textures in the simulation. For other purposes like virtual reality or human robot interaction textured models can enhance the human perception of the reconstructed environment significantly.

The presented reconstruction was created using a high resolution laser scanner. Since this kind of sensor is not commonly available on robotic platforms we have also evaluated our reconstruction software on other 3D data like rotating and tilted 2D SICK laser scanners and Kinect data. An example reconstruction for the latter shows Fig. 11. This demonstrates that in principle these sensors can be used as well, but noise and the need of registering a lot of frames make handling uncomfortable. A full evaluation of geometric precision of the generated models from different sensors is beyond the scope of this paper and will be subject of forthcoming publications. For the proof of concept we concentrated on high quality data.

CONCLUSION AND FUTURE WORK

In this paper we have presented an application example where an automatically created polygon model from point cloud data was used as environment model in an robotic simulator. The reconstruction was computed automatically without user interaction. Reconstruction time was less than 4 minutes, which is, especially for complex geometries, quite small compared to the expected effort that is needed to build a model manually.

Future research will concentrate on integration of out-of-core data handling to process even larger data sets. Another interesting field of research is the improvement of texture usage. Currently we generate potentially large textures. By searching for regular patterns it will be possible to reduce the amount of pixel data needed.

REFERENCES

S. Albrecht, J. Hertzberg, K. Lingemann, A. Nüchter, J. Sprickerhof, and S. Stiene. Device level simulation of

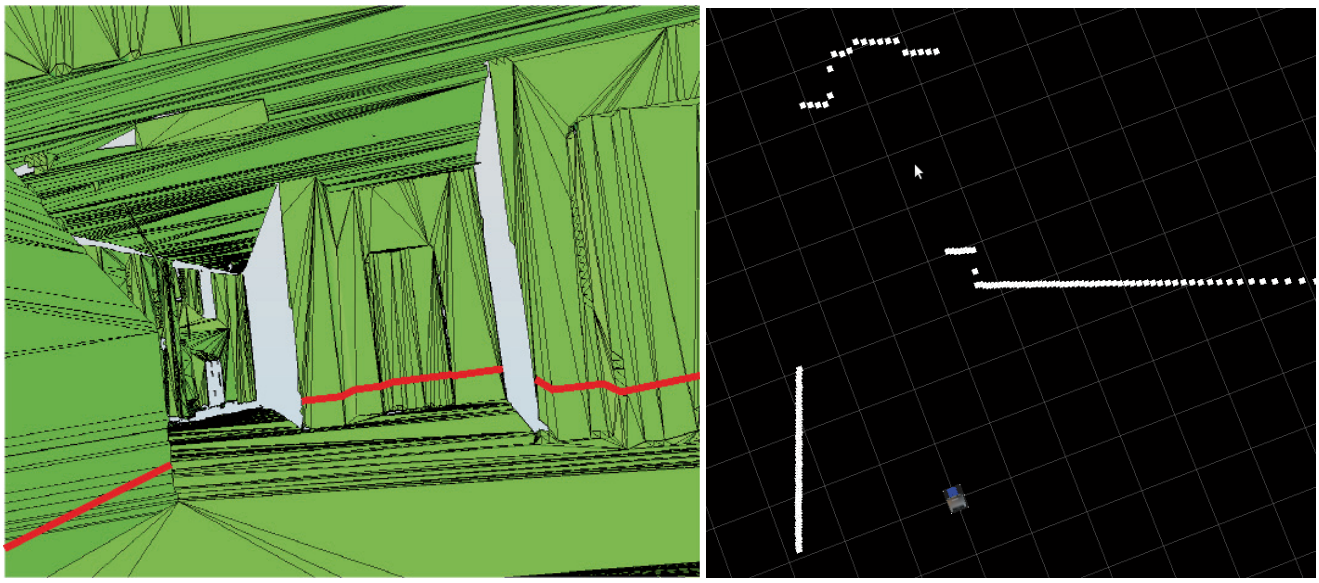

Fig. 12. Simulation of a 2D laser scan in the reconstructed environment. The scanned line in the polygon model is indicated in red (left). The picture on the right shows the robot model at scanning pose and the simulated scan data in RVIZ.

kurt3d rescue robots. In *Proc. SRMED 2006)*, 2006.

N. Amenta, S. Choi, and R. K. Kolluri. The power crust. In *Proceedings of the 6th ACM Symposium on Solid Modeling and Applications (SMA '01)*, pages 249–266, New York, NY, USA, 2001. ACM.

H. Annuth and C.-A. Bohn. Smart growing cells. In Joaquim Filipe and Janusz Kacprzyk, editors, *IJCCI (ICFC-ICNC)*. SciTePress, 2010.

O. Devillers. The Delaunay Hierarchy. *International Journal of Foundations of Computer Science*, 13, 2002.

D. H. Douglas and T. K. Peucker. Algorithms for the reduction of the number of points required to represent a digitized line or its caricature. *The Canadian Cartographer*, (10):112–122, 1973.

M. Garland and P. S. Heckbert. Surface simplification using quadric error metrics. In *Proc. SIGGRAPH '97*. ACM Press.

G. Guennebaud and M. Gross. Algebraic point set surfaces. In *ACM SIGGRAPH 2007 papers*, 2007.

P. Henry, M. Krainin, E. Herbst, X. Ren, and D. Fox. RGBD mapping: Using depth cameras for dense 3d modeling of indoor environments. In *RGB-D: Advanced Reasoning with Depth Cameras Workshop in conjunction with RSS*, 2010.

H. Hoppe, T. DeRose, T. Duchamp, J. McDonald, and W. Stuetzle. Surface reconstruction from unorganized points. *Computer Graphics*, 26(2), 1992.

S. Izadi, R. A. Newcombe, D. Kim, O. Hilliges, and et al. Kinectfusion: real-time dynamic 3d surface reconstruction and interaction. In *ACM SIGGRAPH 2011 Talks*. ACM. ISBN 978-1-4503-0974-5.

M. Kazhdan, M. Bolitho, and H. Hoppe. Poisson surface reconstruction. In *Proc. SGP '06)*, pages 61–70. Eurographics Association, 2006.

L. P. Kobbelt, M. Botsch, U. Schwanecke, and H.-P. Seidel. Feature sensitive surface extraction from volume data. In *Proc. SIGGRAPH '01*, pages 57–66. ACM, 2001.

N. Koenig and A. Howard. Design and use paradigms for gazebo, an open-source multi-robot simulator. In *Proc. IROS '04*, pages 2149–2154, 2004.

Las Vegas Surface Reconstruction. `http://www.las-vegas.uni-osnabrueck.de`.

W. E. Lorensen and H. E. Cline. Marching cubes: A high resolution 3D surface construction algorithm. In *ACM SIGGRAPH*, 1987.

S. Melax. A Simple, Fast, and Effective Polygon Reduction Algorithm. *Game Developer Magazine*, November 1998.

M. Muja and D. G. Lowe. Fast approximate nearest neighbors with automatic algorithm configuration. In *Proc. VISSAPP'09)*, pages 331–340. INSTICC Press, 2009.

T Newman and H Yi. A survey of the marching cubes algorithm. *Computers & Graphics*, 30(5), 2006.

A. Nüchter, K. Lingemann, J. Elseberg, and D. Borrmann. slam6d, 2012. http://slam6d.sourceforge.net.

A. C. Öztireli, G. Guennebaud, and M. Gross. Feature preserving point set surfaces based on non-linear kernel regression. *Computer Graphics Forum*, 28(2), 2009. ISSN 1467-8659.

R. B. Rusu and S. Cousins. 3D is here: Point Cloud Library (PCL). In *Conference on Robotics and Automation*, 2011.

T. Wiemann, K. Lingemann, A. Nüchter, and J. Hertzberg. A toolkit for automatic generation of polygonal maps – las vegas reconstruction. In *Proc. ROBOTIK*, München, 2012.

AUTHOR'S BIOGRAPHIES

Thomas Wiemann is currently finishing his PhD theses on automatic generation of polygonal maps for robotic applications at the Knowledge Based Systems Research group at Osnabrueck University. An important aspect of his research is generating semantic scene interpretations from point cloud data.

Kai Lingemann is a researcher at the Osnabrueck branch of DFKI's Robotics Innovation Center. His research topics include mobile robotics, where he has published over 60 papers and has been involved in a number of research and industrial projects.

Joachim Hertzberg is a full professor for computer science at Osnabrueck University, heading the Knowledge-Based Systems group; he is also head of the Osnabrueck branch of DFKI's Robotocs Innovation Center. His areas of interest, where he has published over 130 papers, are AI and Mobile Robotics, with a focus on plan-based robot control.

THRUST ANALYSIS ON A SINGLE-DRIVE ROBOTIC FISH WITH AN ELASTIC JOINT

Yicun Xu[1]
Dongchen Qin[1]
[1]School of Mechanical Engineering
Zhengzhou University
No. 100, Kexue Road, Zhengzhou,
Henan, P.R. China. 450001

Cong Liu[2,3]
Houxiang Zhang[2]
[2]Faculty of Maritime Technology and Operation
Aalesund University College
Postboks 1517, N-6025 Aalesund,
Norway

[3]Department of Engineering Design and Materials,
Norwegian University of Science and Technology N-7491
Trondheim, Norway

KEYWORDS

Bionics, Robot fish, Thrust, Elastic joint, Simulation

ABSTRACT

This work simplified tuna's swimming mode, then designed a single-drive robotic fish propulsion mechanism which including an elastic joint, and established the dynamics model of the mechanism. The thrust, resistance, resistance power on different peduncle oscillation parameters, and torsional stiffness of the caudal fin joint was simulated. The average thrust, maximum resistance and the average power grow with the increasing of the oscillating amplitude and the frequency. When the torsional stiffness of the caudal fin joint becomes larger, the thrust decreases, the resistance and the average power increase. The simulation results proved that the mechanism can generate thrust in water and it may be used as a robot fish propulsion mechanism.

INTRODUCTION

During millions of years of evolution, fishes have developed optimum body structures and appropriate swimming modes shaped by various environments. Their advantages in efficiency, low noise and maneuverability can potentially compensate the disadvantages of traditional propellers. Therefore, researchers have focused on the fish-mimicking mechanisms, with which the underwater vehicles can be propelled, target at developing a high performance robot fish.

Fishes' swimming modes can basically be categorized into Body and/or Caudal Fin (BCF) locomotion and Median and/ or Paired Fin (MPF) locomotion (Sfakiotakis et al. 1999). Around 85% of fishes adopt BCF locomotion, swim by bending their bodies into a backward-moving wave which extends into its caudal fin (VIDELER, JJ .1993). According to the wavelength and the amplitude enveloped of the wave, the BCF mode is divided into four types: Anguilliform, Subcarangiform, Carangiform and Thunniform (C. C. Lindsey, 1978).

The main difference of the first three types is the characteristics of the body wave which produces the propulsive movement. By thunniform, the front part of the fish body can be basically regarded as rigid, propulsive movement is limited to the 1/3 rear part of the body, especially the caudal peduncle and caudal fin. The caudal fin generates more than 90% propulsion. This mode is suitable for a long-time and high-speed cruise. The fastest marine animals such as yellow-fin tunas represent thunniform. Tunas' swimming speed can be up to 20 knots, and the propulsive efficiency can be as high as 80% or more (Tong Binggang 2000). Therefore, to mimic thunniform swimming is a hot spot in bionic robotic fish researches.

Stix in MIT carried out research on bionic robotic fish. By developing the first complete bionic robotic fish *Robotuna* (Stix, G. 1994). The length of *Robotuna* is about 1.2m. Japan's National Institute of Oceanography developed a thunniform bionic robotic fish, it's length is

Proceedings 27th European Conference on Modelling and Simulation ©ECMS Webjørn Rekdalsbakken, Robin T. Bye, Houxiang Zhang (Editors)
ISBN: 978-0-9564944-6-7 / ISBN: 978-0-9564944-7-4 (CD)

about 1m, and the speed is up to 0.97m/s (www.nmri.go.jp). In China, Beihang University(BUAA) (Liang, J.et al. 2011.), Harbin Engineering University (Cheng Wei et al. 2004), Institute of Automation of Chinese Academy of Sciences(CAS) (Su, Z. et al. 2010) developed different prototypes of thunniform bionic robotic fishes. In order to mimic the oscillation of the caudal peduncle and caudal fin, these prototypes often use 2 or 3 motors as drivers. Both the structure and the control system are relatively complex.

In reality, the fish's flexible bodies can deform under the muscular driving force and the external forces. This makes it possible to generate the desired movements with fewer and simpler drives. Xu (XU et al. 2008, XU et al. 2007) applied this mechanism to the bionic flapping wing aircraft and a robotic fish with MPF swimming mode. Both of these approaches featured a single drive with flexible wings or fins.

In the following chapters, a single-drive bionic propulsive mechanism with an elastic joint was introduced. The propulsive mechanism was analyzed, and a simulation model was built. The relationship between thrust, resistance, power and the peduncle oscillation parameters, the torsional stiffness of the caudal fin joint was obtained by simulation. The simulation results proved the feasibility of such a propulsion mechanism.

MODEL

Model of the robot fish

A typical fish that adopts thunniform swimming mode oscillates the peduncle to lead the caudal fin. At the same time, the attack angle of the caudal fin is changing continuously. The phase of the leading edge is always ahead of the trailing edge (see figure 1). Hence the caudal fin obtained a forward thrust. During this process, the keys to the thrust are the oscillation of the caudal fin and the changing of the attack angle of the caudal fin.

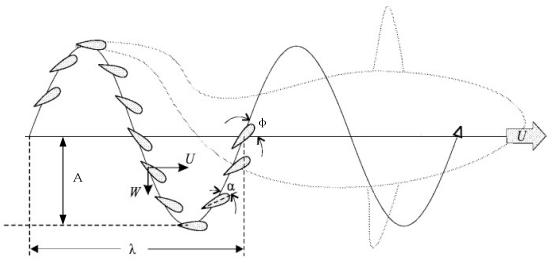

Figure 1 Thunniform swimming mode (adapted from Magnuson 1979)

In Figure 1, A tuna's body is divided into 3 parts for simplification: the body, the caudal peduncle and the caudal fin. The peduncle drives the caudal fin to oscillate, while the caudal fin deflects under the combined effect of hydrodynamic and inertial force. The phase of the leading edge is always ahead of the trailing edge.

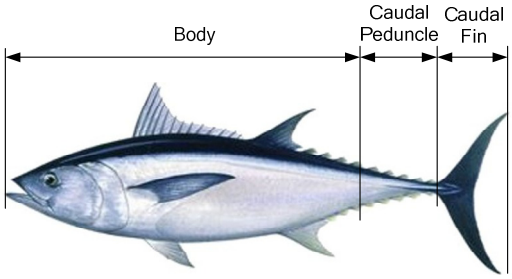

Figure 2 The three parts of a Tuna model

The mechanism in figure 3 is applied on robotic fish, mimicking tuna's swim motion. l stands for the length of peduncle, b indicates the length of the caudal fin, h represents the height of the caudal fin. The propulsion components consist of a body, a caudal peduncle and a caudal fin. The body and caudal peduncle is connected by an active joint, which is driven by a DC servo motor. The connection between caudal peduncle and caudal fin is made with a passive joint, with a tosional stiffness of k. The propulsion mechanism is shown as figure 3 and the simplified diagram is shown as figure 4. θ becomes the oscillation angle of peduncle, ϕ is obtained as the deflection angle, k is expressed as the torsional stiffness of the caudal fin joint. The caudal fin is designed in rectangle shape for simplification, instead of a crescent shape. The peduncle is designed with a length l, while the caudal fin has the length b and width h. The fluid drag and inertia force generated by peduncle is neglected.

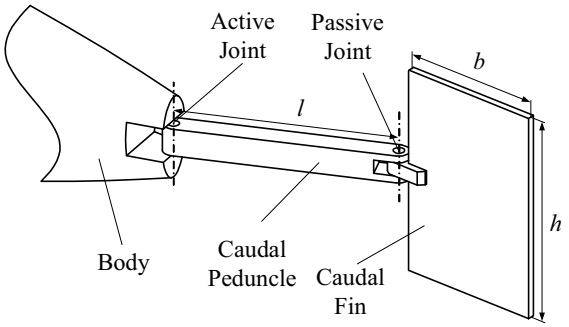

Figure 3 Propulsion mechanism of robot fish

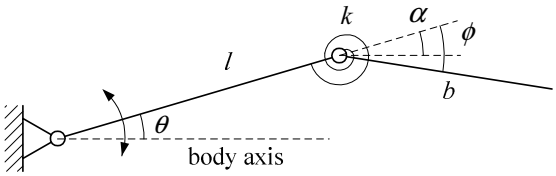

Figure 4 Simplified diagram of the propulsive mechanism

The angle of peduncle relative to the body axis can be written as

$$\theta = \theta_0 + A\sin(2\pi f t) \quad (1)$$

Where θ_0 is the neutral position of the peduncle oscillation, A and f respectively are the amplitude and the frequency.

$\dot{\theta}$ is the angular velocity of oscillation, and $\ddot{\theta}$ is the angular acceleration

Dynamics model of the mechanism

The change of equivalent length resulted by the rotation of caudal fin is neglected. Therefore, the induced velocity yields

$$v = \dot{\theta}\left(l + \frac{b}{2}\right) \quad (2)$$

Caudal fin coincides with peduncle. While the peduncle oscillating, the caudal fin starts to deflect under the hydrodynamic force and inertia force. The deflection angle ϕ, the actual angle of attack of the caudal fin can be derived as

$$\alpha = \theta + \phi \quad (3)$$

The inertia torque applied on caudal fin yields

$$F_{\mathrm{m}} = \ddot{\theta}\left(l + \frac{b}{2}\right)m \quad (4)$$

The resistant force applied on caudal fin yields

$$F_{\mathrm{D}} = \frac{1}{2}C_{\mathrm{D}}\rho S v^2 \cos\phi \quad (5)$$

The orientation of resistance is opposite to the direction of oscillation, where the area $S = bh$, C_{D} is drag coefficient. For a rectangular plate, the drag coefficient is assumed to range between 1.5 and 1.95.

After multiplying the drag and the induced velocity, and integrating in one oscillation period, the average driving power in one cycle is derived as

$$\overline{P_{\mathrm{D}}} = \frac{1}{T}\int_0^T F_{\mathrm{D}} v dt \quad (6)$$

The torque applied on the joint of caudal fin is

$$T_{\mathrm{k}} = F_{\mathrm{m}}\frac{b}{2} + F_{\mathrm{D}}\frac{b}{2}\cos\phi \quad (7)$$

The deflection angle of caudal fin is

$$\phi = \frac{T_{\mathrm{k}}}{k} \quad (8)$$

The thrust generated by caudal fin yields to

$$F_{\mathrm{T}} = \frac{1}{2}C_{\mathrm{D}}\rho S v^2 \sin\alpha \quad (9)$$

Simulation model

According to the equations, a simulation model as shown in figure 5 (Scilab, 2011) is built.

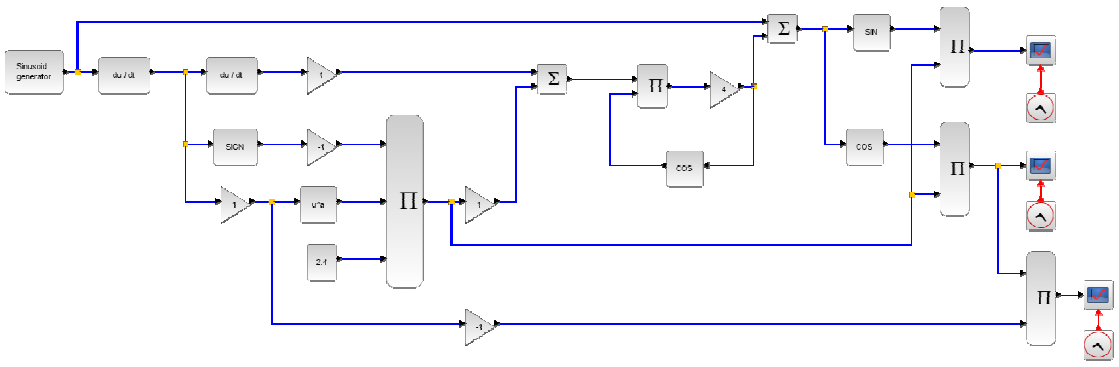

Figure 5 Simulation model

The parameters are listed in table 1.

Table1 Parameters in simulation

Parameter	Symbol	Value	Unit
Amplitude	A	π/18-2π/9	rad
Frequency	f	0.4-2	Hz
Length of caudal peduncle	l	0.1	m
Length of caudal fin	b	0.06	m
Width of caudal fin	h	0.05	m
Mass of caudal fin	m	0.02	kg
Density of water	ρ	1000	kg/m^3
Coefficient of drag	C_d	1.6	1
Torsional stiffness	k	0.2-1	rad /(Nm)

Simulation results

Figure 6, 7 and 8 separately show the thrust, resistance and resistance power versus oscillation angle in two cycles when $A = \pi/9$, $f = 1\text{Hz}$, $k = 0.1\text{rad/(Nm)}$. In Figure 6, the thrust has two peaks during one cycle. Each peak occurs approximately when the maximum velocity of forward and backward exists.

According to equation (5) and (6), the thrust is related to the induced velocity v and the attack angel α. The oscillation velocity and the induced velocity reach their peaks simultaneously. The torque generated by resistance is largest. Hence, there is a peak of thrust.

Instantaneous negative thrust appears in the two oscillation limit positions. This is because of when the caudal fin near the limit positions, the induced velocity reduced. At the same time, the inertial force drives the position of trailing edge beyond the leading edge, a “negative attack angel” appears. Hence, there generated an instantaneous negative thrust.

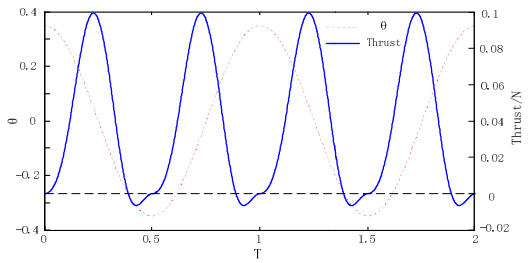

Figure 6 The curves of the oscillation angle and the thrust in two oscillation cycles.

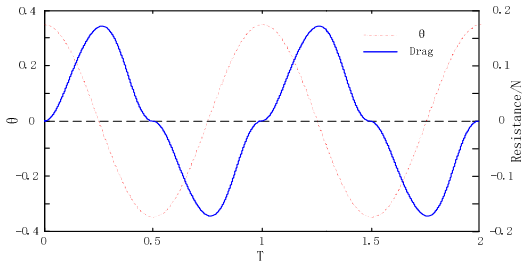

Figure 7 Curves of oscillation angle and resistance in two cycles.

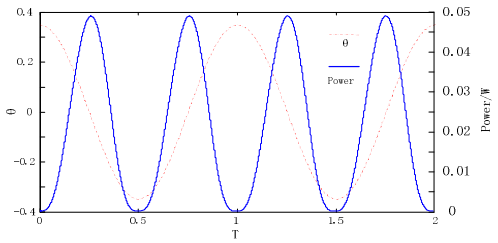

Figure 8 Average powers under different simulation parameters

Figure 9 to figure 11 show the average thrust, maximum resistance and the power in one cycle when oscillating amplitude A, oscillating frequency f and the torsional stiffness of the caudal fin joint k take different values.

With the increasing of oscillating amplitude A, oscillating frequency f, the induced velocity increases, hence the resistance, power and the thrust increase.

When the torsional stiffness k decreases, the same resistance moment leads a bigger deflection angle ϕ, then the resistance and the oscillating power decrease and the thrust increases. This seems like that decrease the torsional stiffness may improve efficiency. However, this model is based on a small deformation assumption, when torsional stiffness decrease to a certain limit, the small deformation assumption will hold no more, and mistakes will occur in simulation.

Analysis from the view point of the physical meaning, when deflection angle becomes larger, the effective area of the fin becomes smaller, there will be a decreasing trend of the resistance. And the decreased resistance limited the deflection angle further increase.

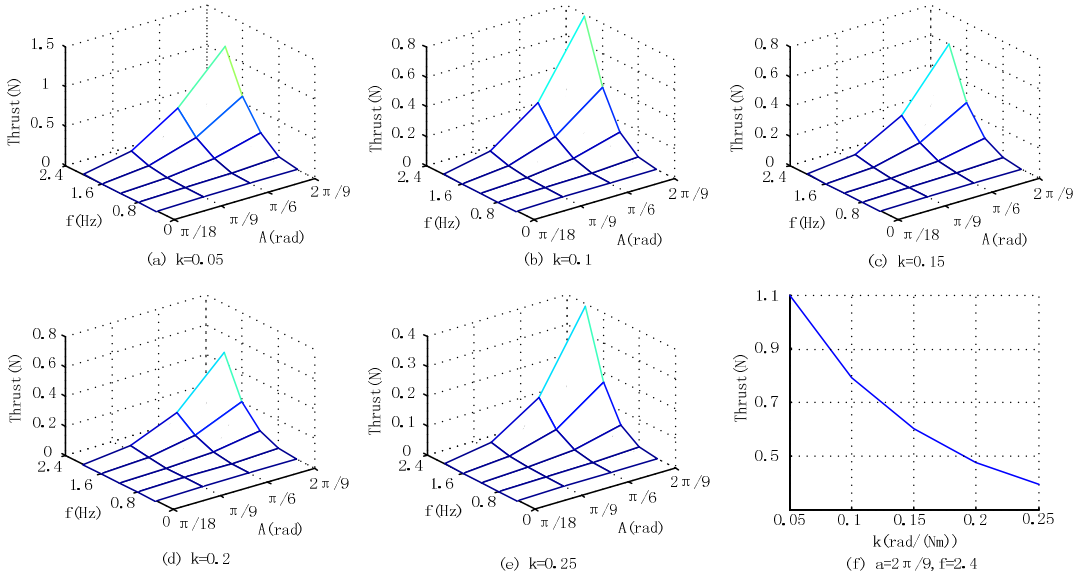

Figure 9 Average thrusts under different simulation parameters

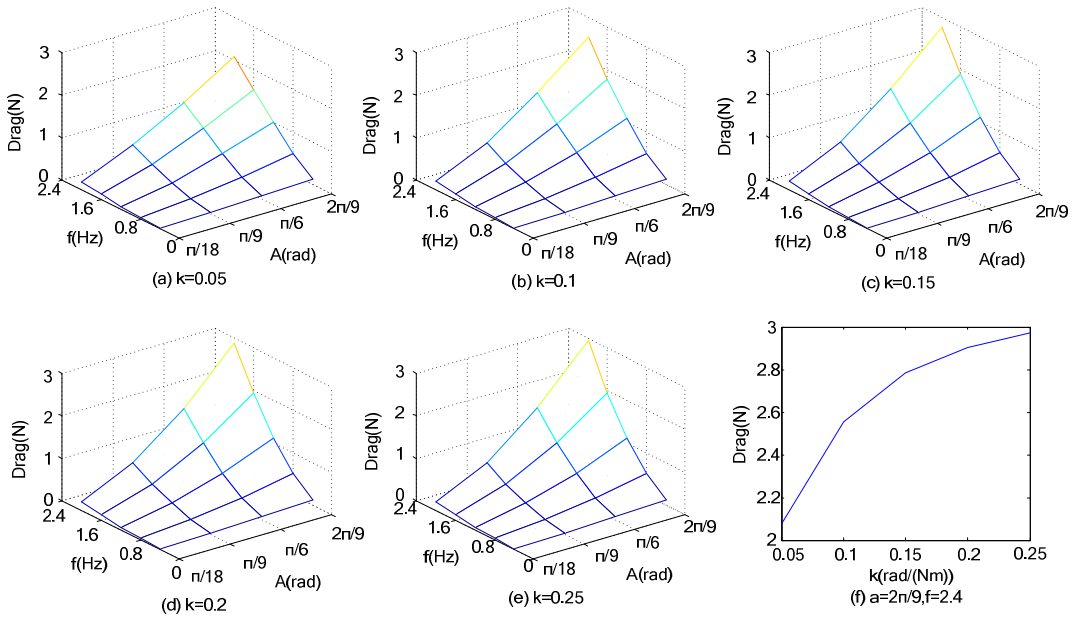

Figure 10 Maximum resistances under different simulation parameters

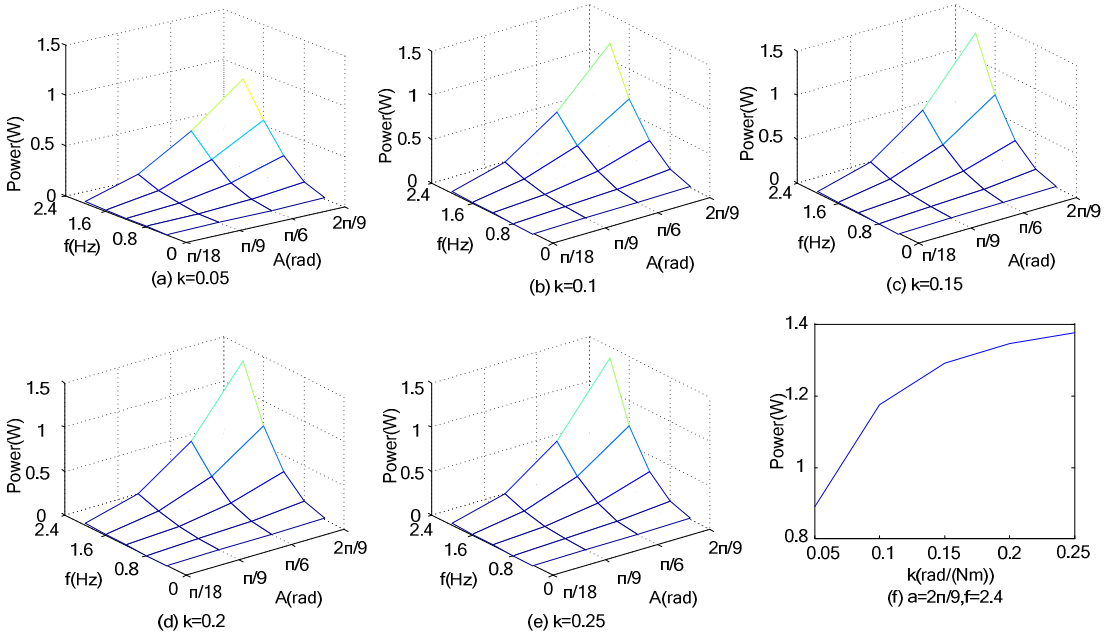

Figure 11 Average powers under different simulation parameters

SUMMARY

This paper aims to analyze Thunniform swimming mode by simplifying the motion of the tuna fish, a typical species of fish that adopts such swimming mode. A propulsion mechanism with a single drive and a flexible joint is then designed.

A dynamic model of the propulsion mechanism was established and simulated. The relationship between thrust, resistance, resistance power and the peduncle oscillation parameters, the torsional stiffness of the caudal fin joint was obtained by simulation. By observing the simulation data in one oscillation cycle, the oscillation resistance and the generated thrust have two peaks in one cycle. Both of the peaks occur when the fin is at neutral position. According to the simulation result under different simulation parameters, with the increasing of the oscillation and frequency, the average thrust, maximum resistance, average resistance power increase. With the increasing of the torsional stiffness of the caudal fin joint, the thrust decreases, the resistance and power increase.

The simulation result proved that such a mechanism may generate thrust in water and it may be used as the propulsive mechanism of a bionic robot fish.

REFERENCES

Sfakiotakis, Michael, David M. Lane, and J. Bruce C. Davies. 1999. "Review of fish swimming modes for aquatic locomotion. " *Oceanic Engineering*, IEEE Journal of 24, no. 2: 237-252
VIDELER, JJ .1993. “Fish Swimming”. London: Chapman and Hall.
C. C. Lindsey, “Form, function and locomotory habits in fish,” in Fish Physiology Vol. VII Locomotion, W. S. Hoar and D. J. Randall, Eds. New York: Academic, 1978, 1–100.
Tong Binggang. 2000. " Fish wavy swimming propulsion mechanism." *Mechanics in Engineering* 22, no. 3: 69-74. (In Chinese)
Stix, G. 1994. “RoboTuna”. *Scientific American*, 270, 142-142
http://www.nmri.go.jp/eng/khirata/fish/experiment/upf2001/index_e.html
Liang, J., Wang, T., & Wen, L. 2011. “Development of a two‐joint robotic fish for real‐world exploration”. *Journal of Field Robotics*, 28(1), 70-79
Cheng Wei, Su yumin, Qin Zaibai and Xu Yuru. 2004. “Development of a bionic underwater vehicle”. *Ship Engineering*, 26(1), 5-8. (In Chinese)
Su, Z., Yu, J., Tan, M., & Zhang, J. (2010, October). Closed-loop precise turning control for a BCF-mode robotic fish. *In Intelligent Robots and Systems (IROS)*, 2010 IEEE/RSJ International Conference on (pp. 946-951). IEEE
XU Yicun, BI Shusheng, ZONG Guanghua. 2008.” Thrust analysis and experimental study of the flexible wings of a flapping-wings aircraft”. *Journal of Aerospace Power*, 23(10), 1892-1895. (In Chinese)
Xu Yicun, Guanghua Zong, Shusheng Bi, and Jun Gao. 2007. "Initial development of a flapping propelled unmanned underwater vehicle (UUV)." *In Robotics and Biomimetics*. ROBIO 2007. IEEE International Conference on, pp. 524-529. IEEE, 2007
Magnuson, J. J. 1979. Locomotion by scombrid fishes: hydromechanics, morphology, and behavior. Fish physiology, 7, 239-313.
Scilab: Free and Open Source software for numerical computation (Windows Edition, Version 5.33) [Software]. Available from: http://www.scilab.org

AUTHOR BIOGRAPHIES

YICUN XU received his PhD in Robotics Institute, Beihang University at 2009. He works in School of Mechanical Engeering, Zhengzhou University since July 2009. Research field includes: biomimetic robotics, mechanical system dynamics.
Email: xuyicun@zzu.edu.cn

CONG LIU works in Aalesund University College as a PhD candidate since October 2011. He received his Master’s diploma in Mechanical Electronics Engineering from Beihang University in Beijing.
Email: lico@hials.no.

HOUXIANG ZHANG worked at the Institute of Technical Aspects of Multimodal Systems (TAMS), University of Hamburg from 2004 to 2011. Prof. Zhang joined Aalesund University College, Norway in 2011, focusing on Robotics and Cybernetics.
Email: hozh@hials.no.

DONGCHEN QIN recivied his PhD in Huazhong University of Scince and Technology at 2007. Work as a professr and deputy dean in School of Mechanical Engeering, Zhengzhou University. The mainly research field includes: Structural Optimization Design, Virtual Prototyping and Simulation, CAD/CAE/CAM System Integration.
Email:dcqin@zzu.edu.cn

PITCHING STABILITY SIMULATION OF A BIONIC COWNOSE RAY

Yueri Cai, Jun Gao and Shusheng Bi
Robotics Institute, Beihang University,
Beijing 100191, P.R. China
E-mail: biss_buaa@163.com

Cong Liu and Houxiang Zhang
Aalesund University College,
Aalesund 6025, Norway
E-mail: hozh@hials.no

KEYWORDS
Bionic fish, Pitching stability, Simulation

ABSTRACT

Swimming stability is essential to a bionic robotic fish which is aiming to be applied to practical application. The stability can be controlled through two kinds of methods, the passive control method and the active control method. The latter one performs more flexibility. Forces of disturbance caused by movements of the bionic pectoral foils and the horizontal tail of a bionic fish imitating cownose ray propelled by oscillating paired pectoral foils are analyzed. Simulation model based on both PID method and fuzzy control method for the stability performance of the bionic fish in condition of compensating work by horizontal tail or not are built. Results show that the stability of the bionic fish can be obviously improved by actively control of the horizontal tail.

INTRODUCTION

Fish propelled by oscillating paired pectoral foils occupies excellent stability and maneuverability (Harris 1938; Rosenberger 2001; Suzuki et al. 2007; Webb 2002). Cownose ray is a typical fish occupying these features (Parson 2011). Some researchers and engineers have been trying to understand the swimming mechanics and to explore the bio-inspired methodology in the design and development of bionic underwater vehicles mimicking this kind of fish (Cai et al. 2010 and 2012; Chen et al. 2011; Elizabeth 2011; IMAE 2012; Wang et al. 2009; Xu et al. 2007; Zhou and Low 2010). As for applications of bionic robotic fish, especially for underwater detection and observation, the ability of stability performs an essential role (Anderson and Chhabra 2002; Hu et al. 2006; Sefati et al. 2012; Wang et al. 2005). Some extent of additional forces will be generated by the oscillating fins when they generate effectual propulsion force by interacting with the coming flow. However, the additional forces have negative effects on swimming stability of bionic robotic fish as they usually pointing to other directions than the useful driving force.

Swimming stability of the robotic fish is essential to the effective propulsion force generation from bionic flapping foils. The swimming speed of a bionic fish propelled by tail fins will be reduced to only 1/3 of the normal, on condition that the yawing motion is not controlled properly, for the movement of flapping fins is weakened and distortion (Wang et al. 2005). The movement mode of fish with paired pectoral foils is different from the ones propelled by tail fins, which can provide better stability. Distance between the gravity center and the propulsion part of the bionic fish utilizing BCF type is large compared with its body length. An obvious yaw motion will be suffered by only small lateral force usually. As for the propulsion parts of bionic fish utilizing MPF type, oscillating paired pectoral foils, are much closer to the gravity center comparatively. Therefore, the additional force generated has limited impact on the stability performance. But, for the same kind of bionic fish mimicking cownose ray, some research have attained the results that the pitching angle must be strictly controlled to within a small range, otherwise the hydrodynamic resistance will increase dramatically and the propulsion efficiency will be reduced (Wang et al. 2005). As a whole, the stability of a bionic fish is essential to its desired performances with high efficiency and high speed as its biomimetic samples in nature. The stability can be improved through optimization of mechanical design and making effective utilization of assisted movement of other functional parts of bionic prototypes developed. Importance of the stability is realized by researchers focusing on studying bionic robotic fish and some research have been carried out either by simulation or experiments (Wilson and Eldredge 2011; Xu et al. 2012; Yu et al. 2012).

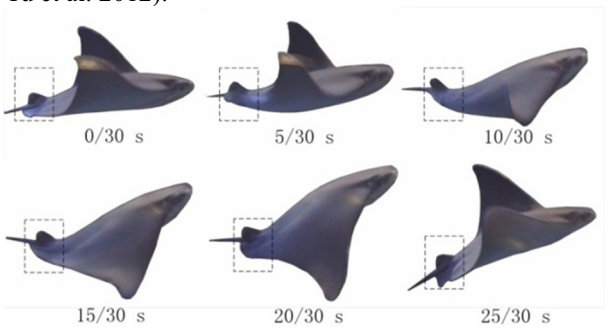

Figures 1: Up-floating Movement of Cownose Ray Assisted by Tail

Based on observations of live cownose ray in aquarium, besides the flexible flapping movement of its pectoral foils, obvious swing motion of the tail part of cownose ray is utilized to support the up-floating and diving movement. Direction of its head during straight forward swimming can be adjusted partly by the supporting movement of its tail. Snapshots of up-floating movement of a sample cownose ray are shown in Fig. 1. During the stable straight forward swimming, the swing

Proceedings 27th European Conference on Modelling and Simulation ©ECMS Webjørn Rekdalsbakken, Robin T. Bye, Houxiang Zhang (Editors)
ISBN: 978-0-9564944-6-7 / ISBN: 978-0-9564944-7-4 (CD)

motions with low-amplitude of its tail are used to keep its body with stability. Effect of the tail part of cownose ray is similar with combined work of rudder and elevator of fix-wing aircraft. Therefore, the simulation and control of the bionic fish propelled by oscillating paired pectoral foils discussed in this paper are realized by a flat elevator mounted on the tail part of the bionic fish.

There are two kinds of methods to control stability of the bionic fish: one is natural stability or static stability, the other is controlled stability (Sun 2011). The underwater vehicle can recover to stable state when suffered by external interference, if it occupies ability of static stability. In condition that the underwater does not occupy this ability or the static stability does not work well, the method of controlled stability should be added to enhance the stability performance. Requirements of design will be reduced by utilizing method of controlled stability.

BASIC SETTINGS

The coordinate system set as shown in Fig. 2 is utilized in calculation and constructing the simulation model. The original point is set at the gravity center of the body of the bionic fish, *x*-axis is coincident with the central body axis and point to the head, *y*-axis is perpendicular to *x*-axis in middle horizontal plane and pointing to right and *z*-axis is decided by the law of Cartesian coordinate system.

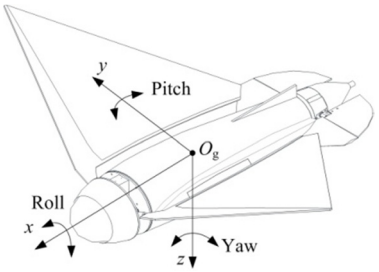

Figures 2: Coordinate System of the Bionic Fish

The settings shown in Fig. 3 are utilized here to analyze the pitching movement caused by the flapping pectoral foils and the horizontal tail of the bionic fish. When the angle generated is minus or the elevator swing downward, the torque generated will make the head of the bionic fish lower or diving; otherwise the angle is positive, the torque generated will make the head of the bionic fish higher or up-floating.

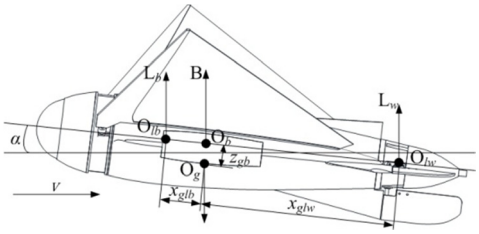

Figures 3: Force Diagram of the Bionic Fish Swimming with a Pitching Angle.

DISTURBANCE BY PECTORAL FOIL

To estimate the disturbance caused by the movement of the flapping foil qualitatively, the calculations of the disturbance force and torque are simplified here. The disturbance torque is mainly caused by the inertial force and fluid force caused by the flapping movement of the pectoral foils. Supposing the pectoral foils flap according to the discipline of:

$$\emptyset(t) = \emptyset_0 \cos \omega t, \tag{1}$$

$$\dot{\emptyset}(t) = -\emptyset_0 \omega \sin \omega t, \tag{2}$$

$$\ddot{\emptyset}(\mathrm{t}) = -\emptyset_0 \omega^2 \cos \omega t. \tag{3}$$

where $\emptyset$ is the flapping angle of the pectoral foil, $\emptyset_0$ is amplitude of the flapping angle and ω is the angle velocity.

Then, the inertial force generated by a finite element on the pectoral foil can be calculated as:

$$dF_{fe} = -\rho_f \ddot{\emptyset} y dx dy. \tag{4}$$

Resolution of the inertial force along *y*-axis and *z*-axis is:

$$dF_{fez} = -\rho_f \ddot{\emptyset} y \cos \emptyset \, dx dy, \tag{5}$$

$$dF_{fey} = -\rho_f \ddot{\emptyset} y \sin \emptyset \, dx dy. \tag{6}$$

As the two pectoral foils are flap symmetrically, components of the force and torque along *y*-axis generated by the two pectoral foils are with equal value but opposite direction. The overall inertial torque generated by one pectoral foil is:

$$M_{fe} = -\iint \rho_f \ddot{\emptyset} \cos \emptyset \, xy dx dy, \tag{7}$$

where $\iint xydxdy$ is product of inertia about *x*-axis and *y*-axis.

The lift generated by the flapping foils is consistent with sinusoidal function as the sinusoidal motion employed by the flapping pectoral foil, as:

$$F_{fl} = F_{\max} \sin \omega t, \tag{8}$$

where $F_{\max}$ is the maximum value of the lift force, and is defined by the frequency, amplitude, velocity of incoming flow and flexibility of the pectoral foil.

Then the pitching moment by a single pectoral foil is:

$$M_{fl} = F_{fl} \cdot x_{fl}, \tag{9}$$

where x_{fl} is the distance between the lift force application point and the *y*-axis. As the two pectoral foils flaps symmetrically, the overall disturbance moment can be calculated by:

$$M_f = \sqrt{k_{f1}^2 + k_{f2}^2} \cdot \sin(\omega t + \varphi), \quad (10)$$

where: $k_{f1} = 2 \iint xydxdy\, \rho_f \emptyset_0 \omega^2 \cos \emptyset,$

$$k_{f2} = 2F_{\max} \cdot x_{fl},$$

$$\varphi = \tan^{-1}(\frac{k_{f1}}{k_{f2}}).$$

Then the differential equation of the pitching disturbance is

$$(J_\mathrm{b} + \Delta J_\mathrm{b})\ddot{\alpha} + k_{w2}\dot{\alpha} + (k_{b1} - k_{b2} + k_{w1})\alpha) = A_0 \cdot \sin(\omega t + \varphi), \quad (11)$$

where $A_0 = \sqrt{k_{f1}^2 + k_{f2}^2}$ is the maximum value of the disturbance moment. Therefore, the pitching disturbance can be taken as vibration of a second-order damping system under harmonic excitation. The steady-state response of the second-order damping system is considered mainly in the simulation here.

The pitching disturbance is mainly affected by two factors: (1) the disturbance moment generated by the flapping pectoral foil. The frequency of the disturbance moment will be consistent with the flapping frequency and the amplitude of the disturbance moment will increase with the flapping frequency and amplitude. (2) the natural characteristics of the pitching system. Based on the analysis presented, the pitching disturbance movement can be controlled by minimized the moment generated by the flapping motion of the pectoral foil.

The method can be obtained by applying the following methods: (1) Utilizing materials featured with less density and more flexibility to lower inertial force and further lower the disturbance (Wilson and Eldredge 2011). (2) Reducing the frequency and amplitude of the flapping motion, which will make the swimming velocity be reduced too. (3) Improving the structure of the bionic fish to reduce the distance between the lift application point and the center of gravity, which is mainly relied on the realization of practical swimming function. (4) Changing the natural characteristics of the pitching movement system of the bionic fish, including the equivalent moment inertia, the equivalent damping and equivalent rigidity. Although these methods can lower the pitching disturbance, realizing these methods in practical development of a real bionic fish is complicated and difficult. Therefore, a better method to improve stable ability is to make use of additional parts, such as horizontal tail mounted on the tail part of the bionic fish, to auxiliary control the pitching disturbance timely.

DISTURBANCE BY HORIZONTAL TAIL

As shown in Fig. 2, supposing the pitching angle is α during straight forward swimming of the bionic fish, torques relative to the gravity center will be generated by the body and the horizontal tail in this condition. Both torques generated by the body and the tail are analyzed through a same method. The flow around the tail will be infected by the body. Under action of viscous effect of the body, the speed of the flow over body will be lower. Generally, the velocity coefficient is set as k, so the flow velocity at the tail part is (Fang 2005):

$$V_w = \sqrt{k}V. \quad (12)$$

Considering the disturbance pitching angle is actually small and swimming velocity of the bionic fish we developed propelled by oscillating paired pectoral fins is much lower than its bionic sample, about 0.7 times of its body length per second, the induction effect on the flow direction is omitted here. The horizontal tail is put on the middle section of the tail part of the body, in condition of zero lift generation the attack angle will be zero too:

$$\alpha_{0w} = 0. \quad (13)$$

The lift generated by the flat tail will be

$$L_\mathrm{w} = 0.5C_\mathrm{w}\rho V_\mathrm{w}^2 S_\mathrm{w}\alpha, \quad (14)$$

where C_w is the lifting line slope of the horizontal tail, S_w is the effective cross-section area of the flat tail. As shown in Fig. 3, supposing the application point of the force generated by the flat tail is O_lw, and the distance between the application point and the gravity center is x_glw, then the pitching torque will be

$$\mathrm{M_{lw}} = -(0.5C_\mathrm{w}\rho k V^2 S_\mathrm{w} x_\mathrm{glw}\cos\alpha)\alpha. \quad (15)$$

During the swing motion, resistance of the horizontal tail can be analyzed as follows. Set $\dot{\alpha}$ as the rotational angle velocity, then the additional velocity at the force application point O_lw is

$$\Delta V = \dot{\alpha} x_\mathrm{glw}. \quad (16)$$

The variation of average attack angle of the horizontal tail is

$$\Delta\alpha = \mathrm{atan}\left(\frac{\Delta V}{V_\mathrm{w}}\right). \quad (17)$$

On condition that the additional velocity raised by disturbance is far less than the flow velocity, $V \ll V_\mathrm{w}$, the equation (17) can be simplified to:

$$\Delta\alpha \approx \frac{\dot{\alpha} x_\mathrm{glw}}{\sqrt{k}V}. \quad (18)$$

The relative increment of the lift is

$$\Delta L_\mathrm{w} = 0.5C_\mathrm{w}\rho\sqrt{k}V S_\mathrm{w}\dot{\alpha} x_\mathrm{glw}. \quad (19)$$

Then, increment of the pitching torque is

$$\Delta M_\mathrm{lw} = -(0.5C_\mathrm{w}\rho\sqrt{k}V S_\mathrm{w} x_\mathrm{glw}^2 \cos\alpha)\dot{\alpha}. \quad (20)$$

This torque generated will prevent the pitching motion of the bionic prototype. A new parameter k_t is

introduced here to give a unified form of the overall damping coefficient of the entire bionic prototype:

$$\Delta M_{\mathrm{t}} = -k_{\mathrm{t}}(0.5C_{\mathrm{w}}\rho\sqrt{k}VS_{\mathrm{w}}x_{\mathrm{glw}}^2\cos\alpha)\dot{\alpha}, \quad (21)$$

where value of k_{t} is usually 1.1~1.25 in this kind of calculation.

Depending on equation (19) to equation (21), the overall torque generated by the horizontal tail can be expressed as:

$$M_{\mathrm{w}} = \Delta M_{\mathrm{lw}} + \Delta M_{\mathrm{t}}. \quad (22)$$

Parameters k_{t1} and k_{t2} are set as:

$$k_{\mathrm{t1}} = 0.5C_{\mathrm{w}}\rho kV^2S_{\mathrm{w}}x_{\mathrm{glw}}, \quad (23)$$

$$k_{\mathrm{t2}} = 0.5k_{\mathrm{t}}C_{\mathrm{w}}\rho\sqrt{k}VS_{\mathrm{w}}x_{\mathrm{glw}}^2. \quad (24)$$

Then the overall torque is

$$M_{\mathrm{w}} = -k_{\mathrm{t1}}\cos\alpha\cdot\alpha - k_{\mathrm{t2}}\cos\alpha\cdot\dot{\alpha} \quad (25)$$

When the bionic fish swims horizontally and the tail elevator is controlled to swing at angle β, the additional lift generated by the tail elevator is

$$\Delta L_{\mathrm{w}} = -0.5C_{\mathrm{w}}\rho kV^2S_{\mathrm{w}}\beta. \quad (26)$$

The additional torque applied to the gravity center:

$$\Delta M_{\mathrm{lw}} = \left(0.5C_{\mathrm{w}}\rho kV^2S_{\mathrm{w}}x_{\mathrm{glw}}\cos\alpha\right)\beta = k_{\mathrm{w1}}\beta. \quad (27)$$

Through kinematic analysis of the propulsion system by oscillating pectoral foils and considering the angle caused by the disturbance is very small, therefore $\sin\alpha \approx \alpha$ and $\cos\alpha \approx 1$ are obtained. Then:

$$(J_{\mathrm{b}} + \Delta J_{\mathrm{b}})\ddot{\alpha} + k_{\mathrm{w2}}\dot{\alpha} + (k_{\mathrm{b1}} - k_{\mathrm{b2}} + k_{\mathrm{w1}})\alpha = M_{\mathrm{f}} + \Delta M_{\mathrm{lw}}, \quad (28)$$

is obtained, where J_{b} is the pitching moment of inertia, ΔJ_{b} is the additional pitching moment of inertia caused by the acceleration of the flow around the bionic robotic fish. Taken the torque generated by the flapping foils as part of disturbance torque, the control equation of pitching movement can be derived as:

$$\left((J_{\mathrm{b}} + \Delta J_{\mathrm{b}})\ddot{\alpha} + k_{\mathrm{w2}}\dot{\alpha} + (k_{\mathrm{b1}} - k_{\mathrm{b2}} + k_{\mathrm{w1}})\alpha\right) = k_{\mathrm{w1}}\beta. \quad (29)$$

As can be seen from the above equation, when the horizontal tail swing an angle of β, it is equal to a step input to a second-order damped pitching system. The system will perform a step response based on this, which is the balance attack angle α relative to the swing angle of horizontal tail when it is in equilibrium state. Therefore, the horizontal tail can be actively controlled to enhance stability of the bionic fish, especially during straight forward swimming. Validity of the control method for enhancing stability through controlling horizontal tail will be verified by simulation in this paper.

SIMULATION MODEL

It can be observed from the former analysis that a compensating torque of $-k_{\mathrm{w1}}\beta$ will be generated, when the horizontal tail is controlled to swing a angle of β. If the torque can be controlled to balance the disturbance torque generated by the flapping pectoral foils, the destabilization affecting swimming performance will be reduced and the stability can be enhanced.

Taking the disturbance torque and the compensating torque by the horizontal tail as an input torque M, then after Laplace transform, the following equation can be derived:

$$(J_{\mathrm{b}} + \Delta J_{\mathrm{b}})S^2\alpha(s) + k_{\mathrm{w2}}S\alpha(s) + (k_{\mathrm{b1}} - k_{\mathrm{b2}} + k_{\mathrm{w1}})\alpha(s) = M(s). \quad (30)$$

Then, the transfer function of pitching movement of the bionic fish is:

$$T(s) = \frac{\alpha(s)}{M(s)} = \frac{1}{J_{\mathrm{eq}}S^2 + c_{\mathrm{eq}}S + k_{\mathrm{eq}}}, \quad (31)$$

where J_{eq} is the equivalent moment of inertia, c_{eq} is the equivalent damping of the system, and k_{eq} is the equivalent stiffness.

Stability of many underwater devices and ships are controlled by classical proportional-integral-derivative (PID) controller for its simple control architecture (Smallwood and Whitcomb 2004; Sun 2011; Tang et al. 2012). The control architecture for enhancing stability of bionic fish propelled by oscillating paired pectoral fins here is shown in Fig. 4, which is simulated in MATLAB to verify the performance of the control method for compensating stability. The characteristics of the servo used is $\frac{20}{S+20}$. The simulation diagram constructed by Simulink is shown in Fig. 5.

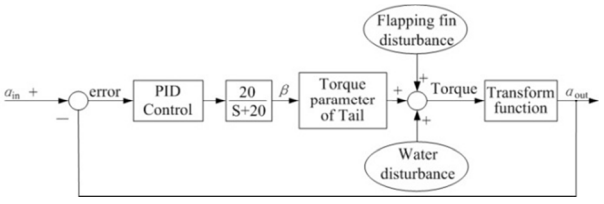

Figures 4: Control Diagram of the Compensating Stability by Horizontal Tail

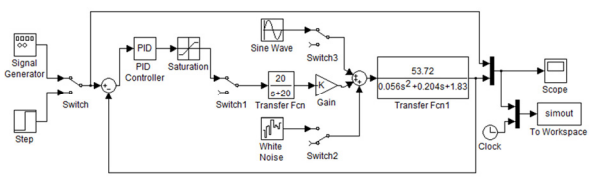

Figures 5: Simulation Diagram of the PID Method of Enhancing Stability

In the simulation, value of coefficient of the servo, k, is 0.98, value of amplification coefficient of the damping torque k_t is 1.15, and other parameters are estimated from the model of the bionic robotic fish. Finally, the coefficients in equation (31) can be derived as:

$$J_{eq} = 0.056, \quad (32)$$

$$c_{eq} = 0.408V, \quad (33)$$

$$k_{eq} = 0.64 + 2.2V^2. \quad (34)$$

Results of underwater experiments carried on the bionic fish prototypes have shown that the vertical disturbance of the bionic fish increases as the frequency and amplitude of the flapping movement of the pectoral foils increased. Therefore, if the disturbance amplitude can be controlled to be in an acceptable range in condition of the maximum disturbance caused by the flapping foils, the control method can be applied to other conditions successfully, for the overall disturbance of the bionic fish will be smaller in other conditions.

The maximum flapping frequency of the bionic pectoral foil is 2 Hz, the maximum flapping amplitude is 30º, and the relative swimming velocity is about 0.5 m/s in this condition. The transfer function can be calculated based on these values. Variation of the transfer function shown in Fig. 5 is caused by the output is based on degree.

The fuzzy logic control method can mimic control by human to some extent, which is more adaptive to the practical control system (Lee et al. 2012; Wen et al. 2012). The two-dimensional fuzzy controller is introduced to the control system aiming to improving the simulated stability of the bionic fish, which is shown in Fig. 6. The fuzzy controller is constructed by:

(1) The input and output variables: the errors between the actual pitching angle and the desired pitching angle ER, variation of the errors EV are set as the input variables; swing angle of the horizontal tail, A, is set as the output variable.

(2) The fuzzy subset of variables ER, RV and A: minus large, minus middle, minus small, zero, positive small, positive middle and positive large, which can be described by {ML, MM, MS, ZE, PS, PM, PL} , the universes of ER, EV and A are {-3, -2, -1, 0, 1, 2, 3}, {-3, -2, -1, 0, 1, 2, 3} and {-4.5, -3, -1.5, 0, 1.5, 3, 4.5} respectively. The quantization factors of EC and EV are K_{EC}=1, K_{EV}=1, and scale factor of the output angle is K_{α}=5.

(3) The fuzzy control rule table is constructed based on the following rules: a) If the error of the pitching angle is ML and the error variation EV is also ML, which means that the pitching angle is large and is still becoming larger, then the swing angle of the servo is controlled to be ML; b) If the error of the pitching angle is ML and the error variation EV is PL, which means that the pitching angle is large but is becoming small, then the swing angle of the servo is controlled to remain unchanged, ZE actually. C) If the pitching angle is PL and the EV is ML, which means that the pitching angle is large but is becoming small, then the swing angle of the servo is controlled to remain unchanged, ZE too. Other control rules are constructed with the similar way. The final fuzzy control rule table is shown in Table 1.

TABLE 1: The Fuzzy Control Rule Table

A / EC / EV	ML	MM	MS	ZE	PS	PM	PL
ML	ML	ML	MM	MM	MS	ZE	ZE
MM	ML	MM	MM	MS	MS	ZE	PS
MS	MM	MM	MS	MS	ZE	PS	PS
ZE	MM	MS	MS	ZE	PS	PS	PM
PS	MS	MS	ZE	PS	PS	PM	PM
PM	MS	ZE	PS	PS	PM	PM	PL
PL	ZE	ZE	PS	PL	PL	PL	PL

Based on the fuzzy control parameters, the simulation model is constructed by MATLAB Simulink, as shown in Figure. 6.

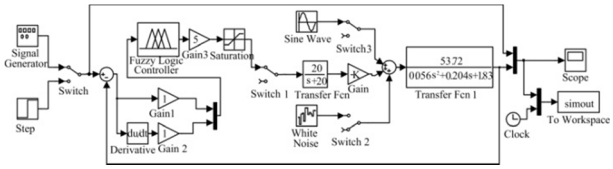

Figures 6: Simulation Diagram of the Fuzzy Logic Method of Enhancing Stability

SIMULATION RESULTS

Without the compensation of the horizontal tail, variation of the pitching angle of the bionic fish is shown in Fig. 7, when it employs the flapping frequency of 2 Hz and flapping amplitude of 30º and there are no effects of incoming flow. As can be observed from the figure, variation frequency of the pitching motion is consistent with the flapping frequency of the pectoral foil, for the variation is mainly caused by the movement of the pectoral foil. The variation amplitude is about 5º after the state is steady.

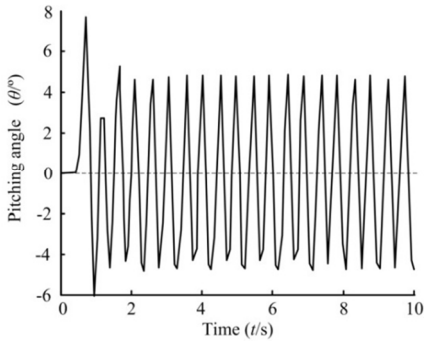

Figures 7: Disturbance without Compensation of the Horizontal Tail

A better condition of disturbance performance is achieved by compensation movement of the horizontal tail being added, which is shown in Fig. 8. The variation amplitude has been lower to 0.9º, which means that the stability of the bionic fish is improved obviously.

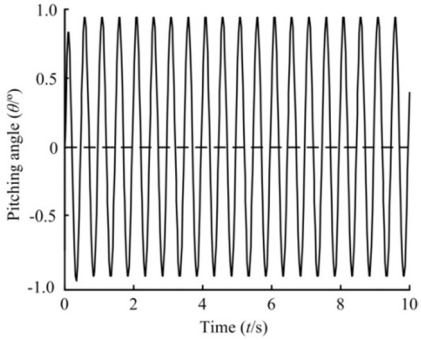

Figures 8: Disturbance with Compensation of the Horizontal Tail

In order to verify the performance of controlling pitching disturbance of the bionic fish by horizontal tail, under condition of flow variation, a random disturbance source is put into the simulation diagram, as shown in Fig. 5. The simulation results are shown in Fig. 9 and Fig. 10. Comparing the results, the compensation effect of the horizontal tail is still working well, as the pitching variation amplitudes are controlled to be approximately within 2º, whereas the simulation results shown in Fig. 9 display a much larger approximate vibration range of 10º without performance of horizontal tail.

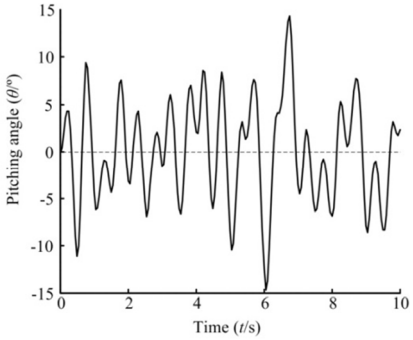

Figures 9: Disturbance without Compensation of the Horizontal Tail under Water Flow

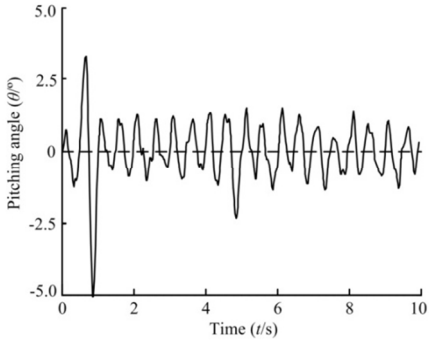

Figures 10. Disturbance with Compensation of the Horizontal Tail under Water Flow

A better stability performance has been obtained by introducing the fuzzy logic control method, as shown in Fig. 11. Same parameters of the structure and movement of the bionic fish are used in simulation of fuzzy logic control method. The disturbance pitching angles are constricted within -0.5º to 0.5º, comparing with the relative larger disturbance angle ranges achieved by the PID method shown in Fig. 10.

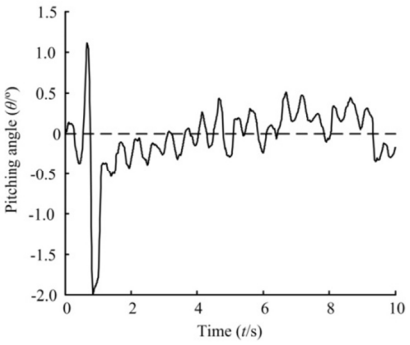

Figures 11. Disturbance with Compensation of the Horizontal Tail Utilizing Fuzzy Control Method

CONCLUSION

Researchers have been focused on developing prototypes of bionic fish propelled by oscillating paired pectoral foils to possess attractive features of their natural samples, such as high speed, high efficiency and low noise. The stability is one of the important factors to realizing these objectives. The main causes of disturbance are raised by variation of the lift force generated by the flapping pectoral foils, which cannot be reduced obviously by optimization of the structures and movement characteristics of the bionic fish, for the object of keeping the bionic fish with desired swimming velocity. Therefore, the method of enhancing stability by auxiliary work of the horizontal tail that is mounted for realizing movements of up-floating and diving. The PID method and fuzzy logic control method are introduced in the simulations of control performances. The simulation models are constructed by Simulink and parameters utilized in the simulations are determined by characteristics of the bionic fish, including characteristics of the servos used. A white noise is added to the simulation models to mimic variation of the incoming flow.

Simulation results show that with auxiliary work of the horizontal tail, an improved performance of pitching disturbance can be obtained. The disturbance pitching angle can be controlled within a range of -1º to 1º without influence of incoming flow with auxiliary work of horizontal tail. The variation of the incoming flow has great effect on stability performance of the bionic fish, for a wide range of pitching angle of -10º to 10º in stable state has been observed in condition of a white noise being introduced even with adjusting compensation of the horizontal tail. Whereas, controlling the swimming motion of the horizontal tail

by fuzzy logic method provides a way to solve this problem. The fuzzy control rules are constructed based on the common two-dimensional controller. The disturbance pitching angles can be restricted within a range of -0.5º to 0.5º even encountered incoming flow, actually a white noise in the simulation model.

The PID control method and the fuzzy logic control method presented in this paper will be further applied to the bionic fish prototype to verify its practicality and improved based on the experimental results.

ACKNOWLEDGEMENT

The work presented in this paper was partly supported by the National Natural Science Foundation of China (No. 51205011), the Chinese Postdoctoral Science Foundation (No. 2012M510304) and the Research Fund for the Doctoral Program of Higher Education of China (No. 20101102110022). Thanks are also due to other members in bionic fish research team graduated or not, for their help and support to the presented work.

REFERENCES

Anderson J M and Chhabra N K. 2002. "Maneuvering and stability performance of a robotic tuna," Integrative and Comparative Biology, vol. 42, pp. 118-126.

Cai Y R, Bi S S and Zheng L C. 2010. "Design and experiments of a robotic fish imitating cow-nosed ray," Journal of Bionic Engineering, vol. 7, pp. 120-126.

Chen Z, Um T I, Zhu J Z and H Bart-Smith. 2011. "Bio-inspired robotic cownose ray propelled by electroactive polymer pectoral fin," *Proceedings of the ASME 2011 International Mechanical Engineering Congress & Exposition* (IMECE 2011), pp. 1-8.

Cai Y R, Bi S S and Zheng L C. 2012. "Design optimization of a bionic fish with multi-joint fin rays," Advanced Robotics, vol. 26, pp. 177-196.

Elizabeth P. 2011. "Bio-inspired engineering: Manta machines Science," vol. 232, pp. 1028-1029.

Fang Z P. 2005. "Aircraft dynamics", Beijing: Beihang University Press.

Harris J E. 1938. "The role of the fins in the equilibrium of the swimming fish II: The role of the pelvic fins," Journal of Experimental Biology, vol. 13, pp. 476-493.

Hu T J, Wang G M, Shen L C and Li F. 2006. "Bionic inspirations of fish-like robots from Rhinecanthus Aculeatus," *Proceedings of the 2006 IEEE International Conference on Mechatronics and Automation*, pp. 639-643, 25-28, June.

IMAE, 2012. Available at: http://www.imae-kagaku.com/mech.htm (in Japanese), accessed in November.

Lee P J, Lee M S and Wang R C. 2012. "A fuzzy control based robotic fish with multiple actuators," International Journal of Fuzzy Systems, vol. 14, pp. 45-53.

Parson J M, Fish F E and Nicastro A J. 2011. "Turning performance of batoids: Limitations of a rigid body," Journal of Experimental Marine Biology and Ecology, vol. 402, pp. 12-18.

Rosenberger L J. 2001. "Pectoral fin locomotion in batoid fishes: Undulation versus occillation," The Journal of Experimental Biology 204, pp. 379-394.

Smallwood D A and Whitcomb L L. 2004. "Model-based dynamic positioning of underwater robotic vehicles: theory and experiment," IEEE Journal of Oceanic Engineering, vol. 29, pp. 169-186.

Suzuki H, Kato N, Suzumori K. 2007. "Load characteristics of mechanical pectoral fin," Experiments in Fluids, vol. 44, pp. 759-771.

Sun Y Q. 2011. "Modern maneuver theory and application of submarine and deep-diving submersible vehicle," Beijing: National Defense Industry Press.

Sefati S, Neveln I, Maciver M A, *et al.* 2012. "Counter-propagating waves enhance maneuverability and stability: A bio-inspired strategy for robotic ribbon-fin propulsion," *The 4th IEEE RAS&EMBS International Conference on Biomedical Robotics and Biomechatronics* (BioRob), pp. 1620-1625, 24-27, June.

Tang Z J, He Q B, Wang S A, *et al.* 2012. "An improved generalized predictive control for AUV yaw," Advanced Materials Research, pp. 1709-1713.

Webb P W. 2002. "Kinematics of plaice, Pleuronectes platessa, and cod, Gadus morhua, swimming near the bottom," Journal of Experimental Biology, vol. 205, pp. 2125-2134

Wang T M, Liang J H, Shen G X, *et al.* 2005. "Stabilization based design and experimental research of a fish robot," *IEEE/RSJ International Conference on Intelligent Robots and Systems*, pp. 954-959, 2-6 August.

Wang Z L, Wang Y W, Li J, *et al.* 2009. "A micro biomimetic manta ray robot fish actuated by SMA," *Proceedings of the 2009 IEEE International Conference on Robotics and Biomimetics*, pp. 1809-1813.

Wilson M M and Eldredge J D. 2011. "Performance improvement through passive mechanics in jellyfish-inspired swimming," International Journal of Non-linear Mechanics, vol. 46, pp. 557-567.

Wen L, Wang T M, Wu G H, *et al.* 2012. "Novel method for the modeling and control investigation of efficient swimming for robotic fish," IEEE Transactions on Industrial Electronics, vol. 59, pp. 3176-3188.

Xu Y C, Zong G H, Bi S S and Gao J. 2007. "Initial development of a flapping propelled unmanned underwater vehicle (UUV)," *Proceedings of 2007 IEEE International Conference on Robotics and Biomimetics*, pp. 524-529.

Xu Y C, Zong G H, Bi S S, *et al.* 2012. "Pitching stability analysis of the pectoral fin propelled robot fish," Robot, vol. 34, pp. 375-379.

Yu J Z, Su Z S, Wang M, *et al.* 2012. "Control of yaw and pitch maneuvers of a multilink dolphin robot," IEEE Transactions on Robotics, vol. 28, pp. 318-329.

Zhou C L and Low K H. 2010. "Better Endurance and Load capacity: An Improved Design of Manta Ray Robot (RoMan-II)," Journal of Bionic Engineering, vol. 7, pp. S137-S144.

JERK BOUNDED TRAJECTORY PLANNING FOR NON-HOLONOMIC MOBILE MANIPULATOR

Atef A. Ata

Department of Engineering Mathematics and Physics
Faculty of Engineering,
Alexandria University
Alexandria 21544, Egypt
atefa@alexu.edu.eg

Amr El Zawawi

Department of Electrical Engineering
Faculty of Engineering,
Alexandria University
Alexandria (21544), Egypt
amr.elzawawi@yahoo.com

Mostafa A.E.Razek

Department of Mechatronics Engineering
Alexandria Institute of Engineering and Technology,
AIET, Alexandria, Egypt
eng.mostafaaa111@yahoo.com

ABSTRACT

Mobile manipulator systems comprising of a mobile platform with one or more manipulators are of great interest in a number of applications. This paper presents a modeling of the system without violating the non-holonomic constraints of the platform. Trajectory planning by soft motion and seventh order polynomial to control jerk acceleration, and velocity, is also presented. The hub torque required to move the manipulator according to a prescribed trajectory and the platform motor torque are also calculated for each trajectory.

INTRODUCTION

Mobile manipulator is nowadays a widespread term referring to robot systems built from a robotic manipulator arm mounted on a mobile platform. Such systems combine the advantages of mobile platforms and robotic manipulator arms and reduce their drawbacks. A mobile manipulation system offers the dual advantages of mobility offered by a mobile platform and dexterity offered by the manipulator. The mobile platform offers unlimited workspace to the manipulator. The extra degrees of freedom of the mobile platform also provide the user with more choices. Papadopoulos and Poulakakis (2000) presented a methodology for computing actuator commands for such systems that allow them to follow desired end-effector and platform trajectories without violating the non-holonomic constraints. They used orthogonal complements and Lagrangian methodology to obtain equations of motion. They applied a third order polynomial trajectory for the joints and a second order polynomial trajectory for the motion of the platform and used a fifth order polynomial trajectory for each link of the manipulator. Mohri et al. (2001) derived the dynamics of the mobile manipulator considering it as the combined system of the manipulator and the mobile platform by Lagrange method. Trajectory planning problem is formulated and optimal control problem with some constraints is solved numerically by using the concept of the order of priority and the gradient function. Chung and Velinsky (1999) developed a dynamic model of a mobile manipulator subject to wheel slip for high load and high speed applications. First, the Newton-Euler method was used to derive the dynamic equations of motion in which Dugoff's tire friction model is utilized. First order polynomial and cyclic motion trajectories are used in this model. Omreen et al. (2003) used the Lagrangian dynamics to express the dynamic model of the complete system. A torque compensation control approach is proposed for the robust motion control of the robot by Chi-wu and Ke-fei (2009). They considered the coupling disturbance between the platform and the manipulator trajectory tracking curve of mobile platform. In all the above mentioned research work, jerk and acceleration problems at start and end of manipulator motion are not considered. On the other hand, (Mostafa et al. 2010) applied fifth order polynomial trajectory which can control the acceleration at start of manipulator motion.

Broqu'ere et al. (2009) applied the soft motion trajectory planner which takes into account both the point to point motion and the transition motion. For each axis, these cubic trajectories share the same time intervals. Due to the direct computation of cubic parameters, the planner is fast enough to be used on-line. The soft motion trajectory planner limits jerk, acceleration and velocity in Cartesian space using quaternion. Tawfik et al. (2011) studied the effect of the trajectory planning method on the dynamic response of six degrees of freedom micro-robot intended for surgery applications. The kinematic equations of motion were obtained using Denavit-Hartemberg representation. The trajectory planning was derived using two different methods: the fifth-order polynomial and the soft motion trajectory planning. A comparison of the dynamic response was carried out to choose the best method that gives the smoother trajectory and better performance of the robot under investigation.

Jerk bounded trajectory for a non-holonomic mobile manipulator is investigated in this paper. The equations of motion of the system are obtained using the Lagrange multipliers technique. Two jerk bounded trajectories are applied and the hub torques of the manipulator are

Proceedings 27th European Conference on Modelling and Simulation ©ECMS Webjørn Rekdalsbakken, Robin T. Bye, Houxiang Zhang (Editors)
ISBN: 978-0-9564944-6-7 / ISBN: 978-0-9564944-7-4 (CD)

calculated for each trajectory for comparison. The paper is organized as follows: Section (1) is introductory in nature, while section (2) focuses on the mobile manipulator kinematics modeling using the Jacobian to calculate the velocity of the end-effector. Section (3) presents the dynamic modeling using Lagrange multipliers taking into account the non-holonomic constraints in the platform wheels. In section (4) trajectory planning by soft motion and 7^{th} order polynomial according to maximum allowed jerk, acceleration and, velocity are presented. Section (5) displays the simulation results for the platform and the links to calculate right and left wheel torques and also hub torque at joint 1 and joint 2 respectively.

KINEMATIC ANALYSIS

There are two configurations of mobile manipulators based on various mobile platform designs. The first design uses differential drive, where The platform moves by driving the two wheels as show in Figure (1). The two driven wheels do not slip sideways and the resulting velocity constraint, for point F, is given by [Papadopoulos and Poulakakis (2000)]:

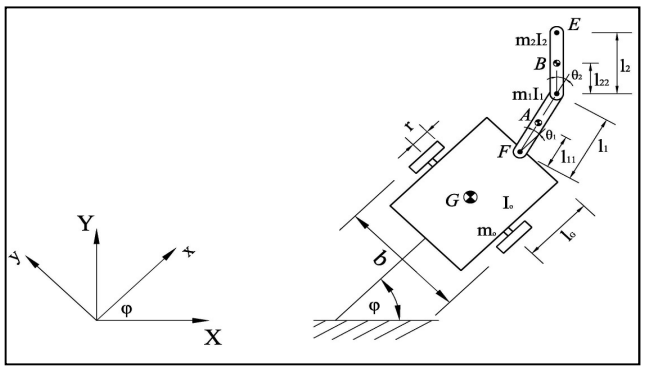

Figure 1: Mobile Manipulator System on a Differentially-Driven Platform

$$\dot{x}_F \sin\varphi - \dot{y}_F \cos\varphi + \dot{\varphi} l_G = 0 \quad (1)$$

Where,

l_G : is the distance between G and F
$\dot{x}_F$: is the velocity component in the x-direction
$\dot{y}_F$: is the velocity component in the y-direction
φ : is the steering angle of platform

Equation (1) represents a non-holonomic constraint which cannot be integrated analytically. The kinematic equations of mobile manipulator are divided into two parts the kinematics of the platform and the robot arm kinematics.

Kinematic Equations of Platform

The differential kinematic equation relating the wheel angular to the linear velocities of point F and the platform rate of rotation, $\dot{\varphi}$ in matrix form, is given by

$$\begin{bmatrix} \dot{X}_F \\ \dot{Y}_F \\ \dot{\varphi} \end{bmatrix} = \begin{bmatrix} \frac{r}{2}c\varphi + \frac{l_G.r}{b}s\varphi & \frac{r}{2}c\varphi - \frac{l_G.r}{b}s\varphi \\ \frac{r}{2}s\varphi - \frac{l_G}{b}c\varphi & \frac{r}{2}s\varphi + \frac{l_G}{b}c\varphi \\ \frac{-r}{b} & \frac{r}{b} \end{bmatrix} \begin{bmatrix} \dot{\theta}_l \\ \dot{\theta}_r \end{bmatrix} \quad (2)$$

Where,
$\dot{\theta}_l$: Angular velocity of the left wheel.
$\dot{\theta}_r$: Angular velocity of the right wheel.
r : Radius of the left and right wheels.
C and S : represent cos and sin of any angle respectively

From Eqn. (2) the base velocity without steering can be given as:

$$\begin{bmatrix} \dot{X}_F \\ \dot{Y}_F \end{bmatrix} = \begin{bmatrix} \frac{r}{2}c\varphi + \frac{l_G.r}{b}s\varphi & \frac{r}{2}c\varphi - \frac{l_G.r}{b}s\varphi \\ \frac{r}{2}s\varphi - \frac{l_G}{b}c\varphi & \frac{r}{2}s\varphi + \frac{l_G}{b}c\varphi \end{bmatrix} \begin{bmatrix} \dot{\theta}_l \\ \dot{\theta}_r \end{bmatrix} \quad (3)$$

It can be seen from Eqn. (3) that if (l_G = 0) the manipulator is mounted on the axis that connects the wheels centers, then the second matrix in Eqn. (3) will be singular. Consequently one degree of freedom will be lost to remove this problem, manipulator must be mount away from the axis connecting wheels centers. To obtain the end-effector velocity we used the Jacobain method as follows:

$$\dot{X}_E = \dot{X}_F + \dot{X}_m \quad (4)$$
$$\dot{Y}_E = \dot{Y}_F + \dot{Y}_m \quad (5)$$
$$\dot{X}_m = -[l_1\dot{\varphi}\cos\theta_1 + l_2\dot{\varphi}\cos(\theta_1 + \theta_2)]\sin\varphi + [l_1\dot{\theta}_1\sin\theta_1 + l_2\dot{\theta}_1\sin(\theta_1+\theta_2) - \dot{\theta}_2\sin(\theta_1+\theta_2)]\cos\varphi \quad (6)$$
$$\dot{Y}_m = [l_1\dot{\varphi}\sin\theta_1 + l_2\dot{\varphi}+\theta_2)]\cos\varphi\,[l_1\dot{\theta}_1\cos\theta_1 + l_2\dot{\theta}_1\cos(\theta_1+\theta_2) + l_2\dot{\theta}_2\cos(\theta_1+\theta_2)]\sin\varphi \quad (7)$$

In which

$\dot{X}_m$: Velocity component in X-axis of the manipulator relative to point F.
$\dot{Y}_m$: Velocity component in Y-axis of the manipulator relative to point F.
l_1 : Length of upper arm.
l_2 : Length of fore arm.
θ_1, and θ_2: joint variables of the manipulator

Substituting from Equations (6) and (7) into (4) and (5) and making use of Eqn. (3) we can write the end-effector velocity in matrix form as:

$$\begin{bmatrix} \dot{X}_E \\ \dot{Y}_E \end{bmatrix} = \begin{bmatrix} \dot{X}_F \\ \dot{Y}_F \end{bmatrix} + \begin{bmatrix} c\varphi & -s\varphi \\ s\varphi & c\varphi \end{bmatrix} \begin{bmatrix} J_{11} & J_{12} \\ J_{21} & J_{22} \end{bmatrix} \begin{bmatrix} \dot{\theta}_1 + \dot{\varphi} \\ \dot{\theta}_2 \end{bmatrix} \quad (8)$$

Where $\dot{X}_E$ and $\dot{Y}_E$, are the x and y velocity components of the end-effector, and the J_{ij} (i, j=1,2) terms are the elements of fixed-base Jacobian of the manipulator and are given by:

$$J_{11} = -l_1\sin\theta_1 - l_2\sin(\theta_1+\theta_2) \quad (9a)$$
$$J_{12} = -l_2\sin(\theta_1+\theta_2) \quad (9b)$$

$J_{21} = l_1 \cos\theta_1 + l_2 \cos(\theta_1 + \theta_2)$ (9c)

$J_{22} = l_2 \cos(\theta_1 + \theta_2)$ (9d)

Combining Eqn. (8) and (2), the forward differential kinematics of the system is obtained as:

$$\begin{bmatrix} \dot{X}_E \\ \dot{Y}_E \\ \dot{X}_F \\ \dot{Y}_F \end{bmatrix} = \begin{bmatrix} c\varphi & -s\varphi & 0 & 0 \\ s\varphi & c\varphi & 0 & 0 \\ 0 & 0 & c\varphi & -s\varphi \\ 0 & 0 & s\varphi & c\varphi \end{bmatrix}$$

$$\begin{bmatrix} r/2 - J_{11}r/b & r/2 + J_{11}r/b & J_{11} & J_{12} \\ -(l_G + J_{21})r/b & (l_G + J_{21})r/b & J_{21} & J_{22} \\ r/2 & r/2 & 0 & 0 \\ -l_G r/b & l_G r/b & 0 & 0 \end{bmatrix} \begin{bmatrix} \dot{\theta}_l \\ \dot{\theta}_r \\ \dot{\theta}_1 \\ \dot{\theta}_2 \end{bmatrix} \quad (10)$$

DYNAMICAL ANALYSIS

Lagrange's equation cannot be applied directly to find the equations of motion for mechanical system due to presence of the non-holonomic constraint. The system under consideration is subject to a single non-holonomic constraint, which is described in matrix form as [Papadopoulos and Poulakakis (2000)]:

$$A(q)\dot{q} = 0 \quad (11)$$

Where,

$A(q) = [\sin\varphi \quad -\cos\varphi \quad l_G \quad 0 \quad 0]$ and
$\dot{q} = [\dot{x}_F \quad \dot{y}_F \quad \dot{\varphi} \quad \dot{\theta}_1 \quad \dot{\theta}_2]^{\mathrm{T}}$

To derive the equations of motion for the mobile manipulator system, an alternative approach which can accommodate the non-holonomic constraint is the Lagrange multipliers. The Lagrangian $\mathbf{L(q, \dot{q})}$ of the system assuming that the mass and the moments of inertia of the casters and the driving wheels are negligible, is given by:

$$L = \frac{1}{2}m_0(\dot{x}_G^2 + \dot{y}_G^2) + \frac{1}{2}J_0\dot{\varphi}^2 + \frac{1}{2}m_1(\dot{x}_A^2 + \dot{y}_A^2) + \frac{1}{2}J_1(\dot{\varphi} + \dot{\theta}_1)^2 + \frac{1}{2}m_2(\dot{x}_B^2 + \dot{y}_B^2) + \frac{1}{2}J_2(\dot{\varphi} + \dot{\theta}_1 + \dot{\theta}_2)^2 \quad (12)$$

Where;
m_0 : mass of platform.
m_1 : mass of first link.
m_2 : mass of second link.
J_0 : moment of inertia of the platform.
J_1 : moment of inertia of the first link.
J_2 : moment of inertia of the second link.
$\dot{x}_G, \dot{y}_G, \dot{x}_A, \dot{y}_A, \dot{x}_B, and\ \dot{y}_B$ are the x, y components of the velocities of the centre of mass of the platform, and the first and the second link respectively

Adding constraint forces as input terms forms the equation of motion of the constrained system. These forces are responsible for not allowing the wheels to slip sideways. The constrained dynamics of the system can be described by [1]:

$$\frac{d}{dt}\frac{\partial L}{\partial \dot{\boldsymbol{q}}} - \frac{\partial L}{\partial \boldsymbol{q}} + A^T(q)\lambda - \xi = \mathbf{0} \quad (13)$$

Where $q = [\,x_F \quad y_F \quad \varphi \quad \theta_1 \quad \theta_2\,]^{\mathrm{T}}$ is the generalized coordinate, λ is the Lagrange multiplier that corresponds to the constraint force, and ξ represents externally applied forces. The columns of $\boldsymbol{A}^T$ from a non-normalized base for these forces.
Expressing Eqn. (12) in terms of the generalized coordinates and substituting the result into Eqn. (13), the system equation of motion are obtained in the form:

$$\mathrm{M(q)\ddot{q} + V(q, \dot{q}) = E(q)\tau - A^T(q)\lambda} \quad (14)$$

Where M(q) is the 5×5 inertia matrix, V(q,$\dot{q}$) is the vector of velocity-dependent forces, $\tau = [\tau_l, \tau_r, \tau_1, \tau_2]^{\mathrm{T}}$ is the 4-dimentional torque vector, E(q) is a 5×4 input transformation matrix, comprised of the left and right wheel torques and the first and second manipulator joint torques, and λ is Lagrange multiplier.

TRAJECTORY PLANNING

Trajectory planning refers to the way that a robot moves from one location to another in a controlled manner. The sequence of movements for a controlled movement between motion segments, in straight-line motion or in sequential motions. Normally the jerk of the desired trajectory has undesired effects on the performance of the tracking control algorithms for robotic manipulators. Controlling the jerk of an industrial manipulator results in improved path tracking and reduced wear on the robot.

Soft Motion Trajectory Planner

We consider the planning of a trajectory defined by a set of points generated by path planning techniques that the end effector must follow in Cartesian space. We propose a soft motion trajectory planner that limits jerk, acceleration and velocity for service robot applications [7]. The trajectory consists of seven cubic polynomials starting by identifying the jerk as follows:

1st, 3rd, 5th and 7th segments

$J(t) = J_{max}$ (15a)
$\alpha(t) = \alpha_0 + J_{max}\, t$ (15b)
$\omega(t) = \omega_0 + \alpha_0\, t + \frac{1}{2}J_{max}\, t^2$ (15c)
$\theta(t) = \theta_0 + \omega_0\, t + \frac{1}{2}\alpha_0\, t^2 + \frac{1}{6}J_{max}\, t^3$ (15d)

2nd and 6th segments

$J(t) = 0$ (16a)
$\alpha(t) = \pm\alpha_{max}$ (16b)
$\omega(t) = \omega_0 + \alpha_{max}\, t$ (16c)
$\theta(t) = \theta_0 + \omega_0\, t + \frac{1}{2}\alpha_{max}\, t^2$ (16d)

4th segment

$J(t) = 0$ (17a)
$\alpha(t) = 0$ (17b)
$\omega(t) = \omega_{max}$ (17c)
$\theta(t) = \theta_0 + \omega_{max}\, t$ (17d)

Where J,α, ω, and θ are the jerk, angular acceleration, angular velocity and joint angle, respectively.

The soft motion trajectory of the mobile manipulator is shown in Fig. 2 where the maximum allowable jerk is 0.5 m/s^3, maximum allowable acceleration is 0.75 m/s^2 and, maximum allowable velocity is 1 m/s. On the other hand Platform trajectory is planned by:

$x_F = 0.1t$, $y_F = 0.1t$ and, $\varphi = \frac{0.3}{2}t^2$

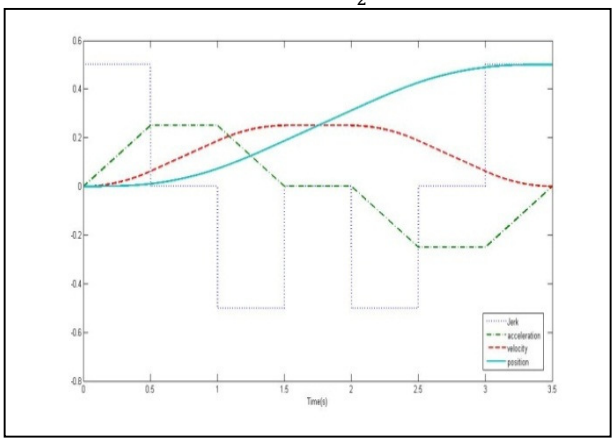

Figure 2: Soft Motion Trajectory for Both Joints

Seventh Order Polynomial Trajectory

By designing the joint trajectory as a third order polynomial, it is only possible to control the initial and final velocities. Increasing the order of the polynomial allows the designer to control the initial and final acceleration as well as the jerk. The seventh order polynomial used to control the initial and final position, velocity, acceleration, and jerk is given by:

$$\theta(t) = c_0 + c_1 t + c_2 t^2 + c_3 t^3 + c_4 t^4 + c_5 t^5 + c_6 t^6 + c_7 t^7 \quad (18)$$

Where $c_0, c_1, c_2, c_3, c_4, c_5, c_6,$ and c_7 are the coefficients to be determined from the initial and final conditions. These coefficients can be determined by solving the following equation:

$$\begin{bmatrix} 1 & t_0 & t_0^2 & t_0^3 & t_0^4 & t_0^5 & t_0^6 & t_0^7 \\ 0 & 1 & 2t_0 & 3t_0^2 & 4t_0^3 & 5t_0^4 & 6t_0^5 & 7t_0^6 \\ 0 & 0 & 2 & 6t_0 & 12t_0^2 & 20t_0^3 & 30t_0^4 & 42t_0^5 \\ 0 & 0 & 0 & 6 & 24t_0 & 60t_0^2 & 120t_0^3 & 210t_0^4 \\ 1 & t_f & t_f^2 & t_f^3 & t_f^4 & t_f^5 & t_f^6 & t_f^7 \\ 0 & 1 & t_f & 3t_f^2 & 4t_f^2 & 5t_f^4 & 6t_f^5 & 7t_f^6 \\ 0 & 0 & 1 & 6t_f & 12t_f^2 & 20t_f^3 & 30t_f^4 & 42t_f^5 \\ 0 & 0 & 0 & 6 & 24t_f & 60t_f^2 & 120t_f^3 & 210t_f^4 \end{bmatrix}$$

$$\begin{bmatrix} c_0 \\ c_1 \\ c_2 \\ c_3 \\ c_4 \\ c_5 \\ c_6 \\ c_7 \end{bmatrix} = \begin{bmatrix} \theta_0 \\ \omega_0 \\ \alpha_0 \\ J_0 \\ \theta_f \\ \omega_f \\ \alpha_f \\ J_f \end{bmatrix} \quad (19)$$

Where t_0 is the initial time and t_f is the final time. Fig. 3 shows seventh order polynomial trajectory planned for the two joints. The initial and final values are:

$\theta_i = 0, \theta_f = 0.5\,rad,\ \omega_i = 0\ , \omega_f = 0\ , \alpha_i = 0\ , \alpha_f = 0\ , J_i = 0.5$, and $J_f = 0.5$.

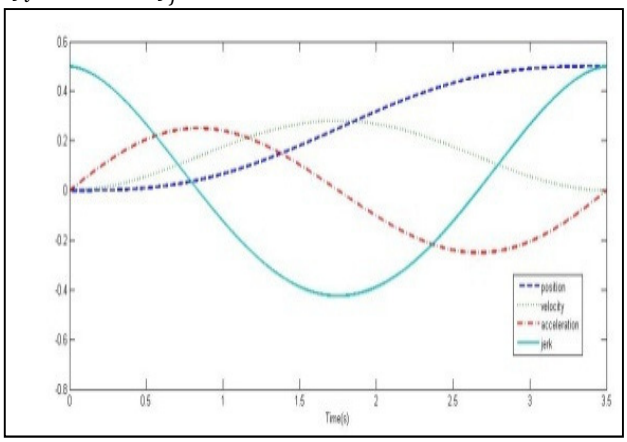

Figure 3: Seventh Order Polynomial Trajectory for Both Joints

NUMERICAL SIMULATION AND DISCUSSION

In order to illustrate the validity of the modeling of mobile manipulator and effectiveness of the motion planning**,** we perform the simulation in MATLAB. The total time was chosen equal to 3.5s.

The kinematic and dynamic parameters of manipulator and platform of simulated robot are given in table 1and 2.

Table 1: Kinematic Parameters of The System

Description	Parameter	Value	Unit
Platform width	b	0.6	m
Platform length	$2l_G$	1	m
Wheel radius	r	0.2	m
Length of link 1	l_1	0.5	m
Length of center link 1	l_{11}	0.25	m
Length of link 2	l_2	0.5	m
Length of center link 2	l_{22}	0.25	m

Table 2: Dynamic Parameters of The System

Description	**Parameter**	**Value**	**Unit**
Platform mass	m_0	50.0	kg
Mass of link 1	m_1	4.0	kg
Mass of link 2	m_2	3.5	kg
Platform Moment	J_0	1.417	kg.m^2
Inertia moment of link 1	J_1	0.030	kg.m^2
Inertia moment of link 2	J_2	0.036	kg.m^2

The simulation procedure is executed as follows:

1. For joint (1) and joint (2) we proposed soft motion trajectory Eqns. (15), (16) and (17) or seventh order polynomial (18) for the platform trajectories, the

following polynomials are proposed: $x_F = 0.1t$, $y_F = 0.1t$ and, $\varphi = \frac{0.3}{2}t^2$.

2. By substituting the trajectory equations in manipulator equations of motion we can compute the first and second joints torque, similarly substitute trajectory equations in platform equations of motion we can compute left and right wheels torque.
The simulated results for the joints torques for the joint 1 and joint 2 for both trajectories are shown on Figures (4) and (5) respectively, while the driving torque for the right and left wheel motors are shown on Figures (6) and (7) respectively.

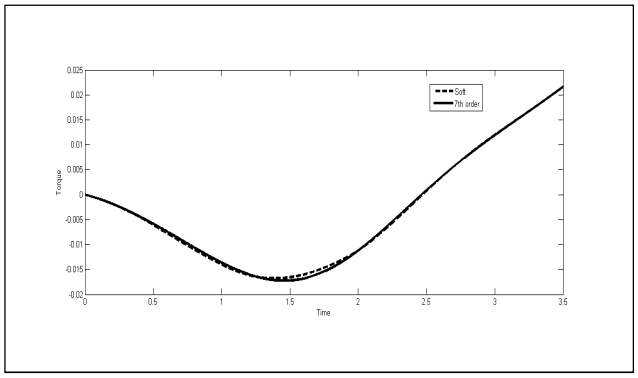

Figure 4: Torque for Joint 1

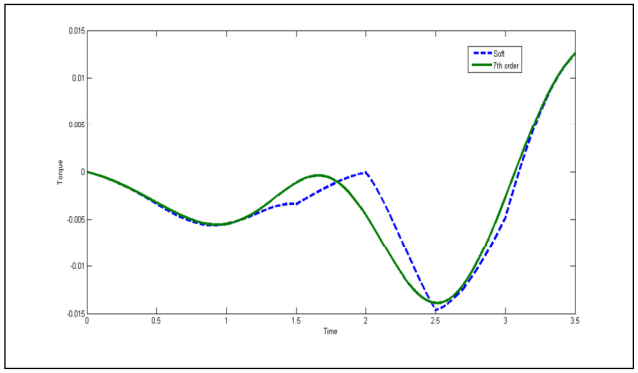

Figure 5: Torque for Joint 2

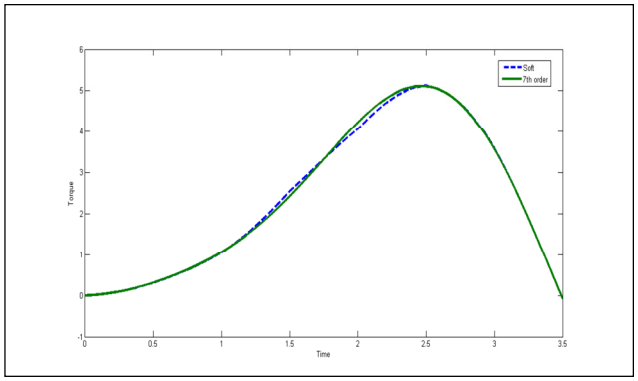

Figure 6: Right Wheel Torque

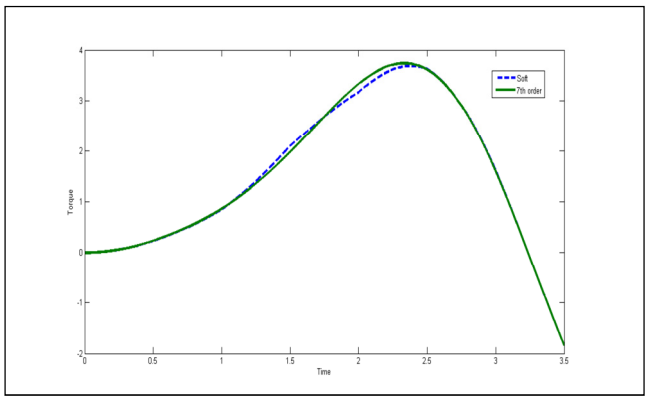

Figure 7: Left Wheel Torque

It can be seen from the simulated results of the driving torques for both joints that there is no considerable change of the torque values using both trajectories and the driving torques have almost the same trend. It should be noticed that the drive torque for joint 2 using the seventh order polynomial is smoother than the torque using the soft motion trajectory. For the right and left wheel motors using either trajectory give the same results. The soft motion trajectory enables the designer to control the jerk throughout the time interval while the seventh order trajectory allow controlling the jerk at the start and end of trajectory only. On the other hand the seventh order trajectory is represented by one polynomial from the start to the end of the time interval.

CONCLUSION

This paper focuses on the mobile manipulator design using kinematic and dynamic modeling using Jacobian method to calculate the velocity of end-effector and dynamics modeling by Lagrange multiplier due to non-holonomic constraint in platform wheels. The equations of motion for platform and links are then calculated to find right and left wheel torque and also joint 1 and joint 2 torques to achieve desired trajectory. A comparison between two jerk bounded trajectories and their effect on the hub torque of each joint is also investigated.

REFERENCES

Broqu'ere, X.; D. Sidobre; and I. Herrera. 2009. "Soft Motion Trajectory Planner for Service Manipulator Robot." *IEEE Trans. on Robotics*, (Apr),281–291.

Chi-Wu, B. and X. Ke-fei. 2009. "Robust Control of Mobile Manipulator Service Robot Using Torque Compensation." *Proc. International Conference on Information Technology and Computer Science, Trondheim*. Norway, (May), 69-72.

Chung, J. and A. Velinsky. 1999. " Robust Control of a Mobile Manipulator - Dynamic Modeling Approach. " Proc. *American Control Conference,* San Diego, California, (June), pp. 2435-2439.

Khaled T. Mohamed; Atef A. Ata; and Bassuny M. El-Souhily. 2011 "Dynamic analysis algorithm for a micro-robot for surgical applications. " *International*

Journal of Mechanics and Materials in Design, Volume 7, (NOV), 17-28.

Mohri, A.; S. Furuno; and M. Yamamoto.2001." Trajectory Planning of Mobile Manipulator with End- Effector's Specified Path." *Intelligent Robots and Systems,* Maui (USA), (Nov), 2264-2269.

Mostafa, S.; G. Mostafa; and M. Masoud. 2010. "Optimal Trajectory Planning of a Mobile Robot with Spatial Manipulator for Obstacle Avoidance. " *International Conference on Control, Automation and Systems,* Gyeonggi-do, Korea, (Oct), 314-318.

Omr'cen, D.; B. Nemec; and L. Zlajpah. 2003 " Torque-Velocity Control Algorithm for On-Line Obstacle Avoidance for Mobile Manipulators." *Proc. Of the ICIT 2003* Maribor, Slovenia, (April), 784-789.

Papadopoulos, E. and J. Poulakakis. 2000. "Planning and Model-Based Control for Mobile Manipulators." *Intelligent Robots and Systems*, IROS 2000 (July), Japan,1810-1815.

Author Biographies

Atef A. Ata was born in Alexandria, Egypt in 1962 and received his B. Sc. Degree with Honor in Mechanical Engineering from Alexandria University in Egypt in 1985. After his graduation he obtained his M. Sc. Degree in Engineering Mathematics (Hydrodynamics) in 1990 from Alexandria university. In 1996 he obtained his Ph. D in Engineering Mathematics (Robotics) as a Joint-Venture between University of Miami, Florida, USA and Alexandria University in Egypt. Currently he is a Professor of engineering mechanics at the Faculty of Engineering, Alexandria University, Egypt. Dr. Atef is a member of IEEE robotics and Automation Society and senior member of IACSIT . His research interest includes Dynamic and Control of Flexible Manipulators, Trajectory Planning, Genetic Algorithms and Modelling and Simulation of Robotic Systems. His E-mail address is atefa@ieee.org

Amr M. O. EL Zawawi was born in Alexandria, Egypt. He obtained his B.Sc. and M.Sc. in Electrical Engineering on 1972 and 1976 respectively. He also obtained a higher studies diploma DEA on 1977 and a Ph.D. in Electrical Engineering from the ENSIEG of the INPG, France on 1980. His main fields of interest are power electronics, artificial intelligence and industrial automation. His e-mail address is amr.elzawawi@yahoo.com.

Mustafa Abdel Razek was born in Alexandria Egypt in 1986. He got his B. Sc. In Mechatronics Engineering from Alexandria Institute of Engineering and Technology (AEIT) in 2009 with Honor. He is now performing his M. Sc. And his area of interest is robot dynamics and Control. His E-mail is eng.mostafaaa111@yahoo.com

Simulation and Optimization

SIMULATION BASED CLEARING FUNCTIONS FOR A MODEL OF ORDER RELEASE PLANNING

Dipl.-Wirt.-Inf. (FH) Frederick Lange, M. Eng.
Professor Dr.-Ing. Frank Herrmann
University of Applied Sciences Regensburg
Innovation Centre for Factory Planning
and Production Logistics
Universitätsstraße 31, 93051 Regensburg, Germany

Professor Dr. Thorsten Claus

Technical University Dresden, IHI Zittau
Professor for Production Economics
and Information Technology
Markt 23, 02763 Zittau, Germany

KEYWORDS
Clearing function, linear programming, order release planning, simulation.

ABSTRACT

In capacitated production systems at high utilization there exists a nonlinear relationship between the orders which are in process and the output. This nonlinear relationship can be described by nonlinear Clearing Functions. We show how a Clearing function will be estimated and integrate it into a model of order releases planning. We compare our model with two inventory management policies under different demand conditions.

INTRODUCTION

Most currently commercially used Enterprise Resource Planning (ERP) and Production Planning and Control (PPC) systems decompose the overall planning problem into subproblems, e.g. the hierarchical production planning proposed by (Hax and Meal 1975). This leads to the master production scheduling, material requirement planning (MRP), with the key components net demand calculation and lot sizing, and the scheduling. In the PPC systems which are used in the industry, there is partly no consideration of limited capacities, such as in the lot sizing policy of Groff. The lead time is crucial for the assessment of exceeding capacities. The widely used MRP procedure (Orlicky 1975; Vollmann et al. 2005) uses fixed lead times to schedule work releases. Also the models of the master production scheduling and aggregate production planning imply linear and partly even fixed relationships between the workload and the lead times. Measurements of the actual lead times indicate a nonlinear relationship between the lead time and the workload in a capacitated production system. Methodologically this nonlinear relationship can be verified by queuing models (Hopp and Spearman 2001). Hence the lead time depends on the systems workload, which in turn is determined by the assignment of work to resources by the planning models.

Different approaches integrate the dependency between lead times and resource utilization in LP models. The first approaches of (Lautenschläger and Stadtler 1998; Spitter et al. 2005) relax the use of lead times and the approaches of (Ettl et al. 2000; Voss and Woodruff 2003) integrate the workload. Finally, the relationship between the workload and lead times is expressed by nonlinear Clearing Functions (CF), e.g. (Asmundsson et al. 2006). This Clearing Function approach is the focus of this paper.

Other authors discussed different iterative approaches, which alternate between a LP model and a simulation model (Hung and Leachman 1996; Byrne and Bakir 1999; Kim and Kim 2001). A LP model determines a production plan based on (initial) estimated lead times. A detailed simulation model of the production facility returns the realized lead times for this production plan. The new lead times are then input into the LP model to determine a new production plan. These procedures iterates until a convergence criterion is satisfied. An analysis of two different iterative approaches is given in (Irdem et al. 2010) and a comprehensive overview of these different approaches and methods can be found in (Pahl et al. 2007; Missbauer and Uzsoy 2010).

In many recent studies the uncertainty, especially of the demand, is focused. The usual approach in the industry is the calculation of safety stocks using methods of the inventory management. The replenishment lead times are approximated by statistical distribution, and the relationship between the workload and the lead times are ignored. The extension to the queuing theory was considered by (Buzacott and Shanthikumar 1993; Rao et al 1998; Hopp and Spearman 2001). The CF approach is quite comparable.

In research, robust planning is also analyzed as stochastic or robust optimization as proposed by (Escudero et al. 1993; Mulvey and Vanderbei 1995; Scholl 2001). One major disadvantage, especially in an industrial environment, is the run time of stochastic optimization models. Most of these models regard demand as uncertain, lead times are usually assumed as being constant.

(Ravindran et al 2011) proposed a production planning model for a single-stage single-product system that integrates release planning and safety stock considerations. Due to the stochastic nature of the demand, chance constraints are used to plan inventories

Proceedings 27th European Conference on Modelling and Simulation ©ECMS Webjørn Rekdalsbakken, Robin T. Bye, Houxiang Zhang (Editors)
ISBN: 978-0-9564944-6-7 / ISBN: 978-0-9564944-7-4 (CD)

to achieve the desired service levels. In our research we extended this model to the consideration of multiple products, as well as for the use in a rolling planning environment. To capture the nonlinear relationship between the resource utilization and the lead times, a nonlinear CF is used to represent the capacity constraint. The next section gives an overview of the Clearing Function concept. Then we introduce our test problem and show how a CF can be estimated. Then the LP-Model as well as the experimental environment will be described. At the end the research results are discussed and future research directions are shown.

PREVIOUS RELATED WORK

Several authors (Karmarkar 1989; Missbauer 2002; Asmundsson et al. 2006, 2009; Ravindran et al. 2011; Kacar et al. 2012) represent the behavior of the relationship between the workload and the output of a capacitated production resources by using nonlinear CFs. Figures 1, based on (Karmarkar 1989), depicts several CFs considered in the literature up to date. The CF "Fixed Capacity" describes a fixed output over the period, regardless of the WIP inventory in the production system or at the resource. The CF "Constant Proportion" by (Graves 1986) characterizes an unlimited linear output at increasing WIP inventories. As a result, it is assumed that the production system, regardless of the workload, have a fix lead time and an infinite amount of output is possible. The CF "Combined" improves the "Constant Proportion", by limiting the maximum amount of output by an upper bound and is described in (Hopp and Spearman 2001). Most LP models avoid a nonlinear capacity constraint by using a linear relation like the CF "Combined". Just the CF "Nonlinear" proposed by (Srinivasan et al. 1988; Karmarkar 1989) takes into account the nonlinear relationship between the workload and the expected output of a capacitated resource or production system.

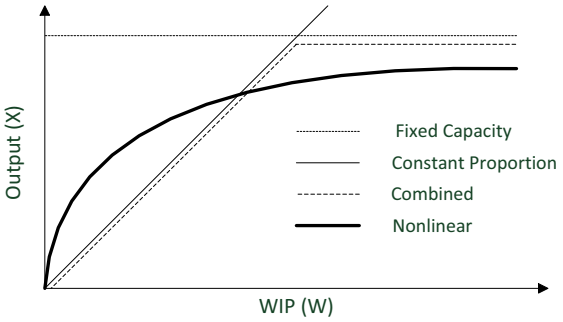

Figures 1: Examples of Clearing Functions (Karmarkar 1989)

To estimate a CF it is a common approach to derive them using steady-state queuing analysis. A CF determines the expected or maximum output of a capacitated resource over a given period of time as a function of some measure of the work in process (WIP) inventory (Missbauer and Uzsoy 2010). In (Asmundsson et al. 2009) the expected WIP for a G|G|1 queuing system in steady state is given as:

$$W = \frac{\left(c_a^2 + c_s^2\right)}{2} \cdot \frac{p^2}{\left(1-p\right)} + p$$

where p denote the utilization of the server and c_a and c_s the coefficients of variation of the service and interarrival times. Solving this equation for p we obtain:

$$p = \frac{\sqrt{\left(W+1\right)^2 + 4W\left(c-1\right)} - \left(W+1\right)}{2\left(c-1\right)}$$

where

$$c = \frac{\left(c_a^2 + c_s^2\right)}{2}$$

(Asmundsson et al. 2009) suggested using the utilization p as a surrogate for the output to obtain the CF which has the desired concave form. For a fixed c value the output increase with a higher WIP inventory (W) at a declining rate. A different approach, suggested by (Missbauer and Uzsoy 2010), derive the CF using a M|G|1 queuing system in steady state. Hence the average throughput E(X) is related to the expected WIP level E(W) as follows:

$$E\left(X\right) = C \cdot \frac{E\left(W\right)}{E\left(W\right)+k} \quad \text{where} \quad k = \frac{\mu\sigma^2}{2} + \frac{1}{2\mu}$$

Here C denotes the maximum capacity per period of the resource and μ, σ the mean and variance of the processing time distribution.

Due to the high complexity and the existing interdependencies, it is not readily possible to build and solve queuing models for real existing production systems. For this reason (Asmundsson et al.2006, 2009; Kacar and Uzsoy 2010; Kacar et al. 2012) suggested an empirical approach to estimate clearing functions. They use in their research a simulation model of a scaled-down semiconductor wafer fabrication facility, studied by their research group (Kayton et al. 1997). The processing time for each workstation is characterized by a statistical distribution and all products are subject to the same processing time distribution at each station. To estimate the CF for this production system, (Asmundsson et al. 2006) generate five randomly demand realizations and develop corresponding release schedules by using the fixed lead-time LP model developed by (Hackman and Leachman 1989) and a planning horizon of 70 periods. For each release schedule and 50 different simulation replications (m=50) the observations of throughput ($x_{t,s}$) and average

WIP ($w_{t,s}$) for Period t and simulation run s were collected. The expected WIP ($E(W_t)$) and the corresponding expected output ($E(X_t)$) for each period t are estimated as follows:

$$E(W_t) = \frac{1}{m}\sum_{s=1}^{m} w_{t,s} \quad \wedge \quad E(X_t) = \frac{1}{m}\sum_{s=1}^{m} x_{t,s}$$

The CF can be estimated by visually fit a CF through the collected data points (Asmundsson 2006).

TEST PROBLEM

We consider a single-level multi-product production system. The demand in each period is independently and normally distributed and the ratio of demand for all products is identical. Our simulation model contains 5 workstation (resources) and 8 products. An overview of our model is given in Table 1.

Table 1: Process chart for the products.

Product	Resource	Setup time [seconds]	Process time [seconds]
Part01	Cutting	20	40
	Turning	50	100
	Milling	50	100
	Grinding	30	50
Part02	Turning	50	150
	Milling	50	100
	Cleaning	30	100
	Grinding	30	80
Part03	Milling	60	90
	Cleaning	30	80
	Grinding	30	100
Part04	Turning	50	30
	Grinding	30	30
Part05	Cutting	20	40
	Turning	50	100
	Milling	50	100
	Grinding	30	50
Part06	Turning	50	150
	Milling	50	100
	Cleaning	30	100
	Grinding	30	80
Part07	Milling	60	90
	Cleaning	30	80
	Grinding	30	100
Part08	Turning	50	30
	Grinding	30	30

In contrast to the approaches of (Asmundsson et al. 2006, 2009; Kacar and Uzsoy 2010; Ravnindran et al. 2011; Kacar et al. 2012) in our research we assume deterministic process times.

DETERMINE CLEARING FUNCTIONS

Per simulation we determine the behavior of the capacitated production system under different workload situations. We assume a constant WIP inventory for all products k over the entire simulation horizon. This desired target WIP inventory is for all products k equal and is set from 1 to 350 pieces. The upper limit was determined as the maximum output of the production system was reached and a higher WIP inventory does not lead to a higher output. To gain statistically significant data the simulation horizon of each run is set to 1000 periods, verified by our tool which analyzes the deviation of the figures.

For each product k we estimate a CF by collecting the output data ($X_{k,t}$) of a product k in a period t over the entire simulation horizon. Due to the mutual interferences of the other products which are released, different WIP constellations can be achieved. At the beginning of a period t the release quantity for each product k is to determine that the desired target WIP inventory is reached. The WIP inventory is represented by the workload which is defined by the quantity released at the beginning of a period t multiplied by the cumulative processing times tb_k. This cumulative processing time is calculated by the sum of all operations o, which must be accomplished for a product k ($o \in O_k$). With $\hat{W}_{k,t}$ denoting the WIP inventory measured in units of time at the end of period t for product k the workload at the end of a period t is defined by the released quantity $R_{k,t}$ multiplied with the cumulative processing times less the units of work which are already processed and defined by $\lambda_{k,t}$.

$$\hat{W}_{k,t} = R_{k,t} \cdot \sum_{o \in O_k} tb_{k,o} - \lambda_{k,t}$$

Hence the release quantity $R_{k,t}$ to achieve the desired target WIP $W_{k,Target}$ is defined by:

$$R_{k,t} = W_{k,\text{Target}} - \frac{\hat{W}_{k,t-1}}{\sum_{o \in O_k} tb_{k,o}}$$

The output values ($X_{k,t}$) of finished goods for each product k and period t are collected and the average output for a product k over all periods t is calculated. In total 350 simulation runs were performed and the target WIP was the same height for all 8 products and was increased simultaneously. For each product k we obtain a CF which defines the expected output for a WIP inventory from 0 to 350 pieces. This leads to an approximation to the average behavior of the capacitated system and the expected output of a product k depending on the WIP inventory of the product k.

MP-DYNIP-B MODEL

We now introduce the production planning model. This model is based on the "dynamic inventory position" (DYNIP) model of (Ravindran et al. 2011). An overview of this model can be found in (Ravindran et al. 2011; Herrmann and Lange 2013). For our research we

extended the model to the consideration of multiple products, as well as for the use in a rolling planning environment. The notation used in the formulation is given below (the expected value of a variable x is described by E(x)).

Parameter:

$\alpha_{k,RLT}$: Service level for product k in the replenishment lead time

$E(D_t)$: Mean of the normally distributed demand of product k in period t.

$G_{k,[t,t+L_t]}$: Distribution Function (CDF) of the cumulative demand from period t to period t + Lt.

h_k : Unit inventory holding cost for product k.

$L_{k,t}$: Lead time for product k in period t.

Decision variables:

$B_{k,t}$: Backorders for product k in period t. Initial backorders at the start of period 1 will be denoted by $B_{k,0}$.

$I_{k,t}$: Inventory at the end of period t for product k. Initial inventory at the start of period 1 will be denoted by $I_{k,0}$.

$R_{k,t}$: Release quantity of product k, released into the system at the beginning of period t.

$X_{k,t}$: Production quantity (output) of product k available at the beginning of period t.

$W_{k,t}$: WIP inventory from product k at the end of period t.

$Y_{k,t}$: Change in planned inventory position of product k in period t.

Objective Function

$$Z = \sum_{k=1}^{K}\sum_{t=1}^{T}\left(h_k \cdot \left(E\left(I_{k,t}\right) + E\left(W_{k,t}\right)\right)\right) \qquad (1)$$
$$\forall 1 \le t \le T \wedge \forall 1 \le k \le K$$

Subject to

$$E\left(I_{k,t}\right) = \left(I_{k,0} - B_{k,0}\right) + \sum_{i=1}^{t} E\left(X_{k,i}\right) - \sum_{i=1}^{t} E\left(D_{k,i}\right) + \sum_{i=1}^{t} E\left(B_{k,i}\right) \quad \forall 1 \le t \le T \wedge \forall 1 \le k \le K \qquad (2)$$

$$E\left(W_{k,t}\right) = W_{k,0} + \sum_{i=1}^{t}\left(Y_{k,i} + E\left(D_{k,i}\right) - E\left(X_{k,i}\right)\right) \qquad (3)$$
$$\forall 1 \le t \le T \wedge \forall 1 \le k \le K$$

$$\left(\left(I_{k,0} - B_{k,0}\right) + W_{k,0}\right) + \sum_{i=1}^{t} Y_{k,i} \ge G^{-1}_{k,[t+1,t+L_t]}\left(\alpha_{k,RLD}\right) \qquad (4)$$
$$\forall 1 \le t \le T \wedge \forall 1 \le k \le K$$

$$E\left(X_{k,t}\right) \le CF_k\left(W_{k,t-1}\right) \quad \forall 1 \le t \le T \wedge \forall 1 \le k \le K \qquad (5)$$

$$Y_{k,t} + D_{k,\min} \ge 0 \quad \forall 1 \le t \le T \wedge \forall 1 \le k \le K \qquad (6)$$

$$E\left(I_{k,t}\right), E\left(W_{k,t}\right), E\left(X_{k,t}\right), E\left(B_{k,t}\right) \ge 0 \quad \forall 1 \le t \le T \wedge \forall 1 \le k \le K \qquad (7)$$

The objective function (1) minimizes the sum of the total costs of finished goods and WIP inventory for all products k and periods t. The inventory balance equation (2) determines the inventory of finished goods at the end of a period t. The right side of this equation must not be negative, since this would wrongly reduce the value of the objective function. Considering a situation where the expected output is lower than the expected demand these quantities have to be produced in previous periods. Hence the output quantity is limited by the capacity constraint (5) this is not always possible. Therefore the backorders $B_{k,t}$ have been integrated into the equation. An integration of the backorders into the objective function is not required as the service level restriction (4) regulate the amount of backorders. Since the model is used in a rolling planning environment backorders can exist at the beginning of a planning run. These backorders at the beginning of a planning run must be taken into account as in equation (2) and (4) done by $B_{k,0}$. Thus the model of (Ravindarn et al. 2011) is in addition to the consideration of multi products, extend by the consideration of backorders to enable the use in a rolling planning environment. The WIP inventory at the end of a period t is determined by the amount of the release quantity and the output of finished goods at the beginning of this period t which is described by the WIP balance constraint (3). We assume a minimum lead time of 1 period to create a consistency to the inventory management. Hence the release quantities, which are released into the production system at the beginning of period t, are at the earliest in the beginning of period t+1 available. To meet the desired service level the demand during the replenishment lead time must be covered by the available stock, determined by the reorder point. This is expressed by the service level constraint (4). The corresponding value of the distribution function for a specific service level is to determine. This can be computed through approximation functions or stochastic tables. Referred to (Herrmann 2011) the service level constraint for a normal distributed demand can be transformed. Hence this leads to the transformed service level constraint given below:

$$\left(\left(I_{k,0} - B_{k,0}\right) + W_{k,0}\right) + \sum_{i=1}^{t} Y_{k,i} \ge L_{k,t} \cdot E\left(D_{k,t}\right) + \sqrt{L_{k,t}} \cdot \sigma_{k,t} \cdot \Phi^{-1}_{N(0,1)}\left(\alpha_{k,RLD}\right) \quad \forall 1 \le t \le T \wedge \forall 1 \le k \le K$$

The capacity constraint (5) is represented by a clearing function for each product which represents the behavior

of the capacitated production system. Depending on the WIP inventory of a product k in the production system, the production quantity (output) is limited. Equation (6) prevent the case, that the release quantity may be negative, where D_{min} is a lower bound on the value of demand in any period. The non-negativity constraints are given by equation (7). It is important to note, that two different lead times are consider within the model. The replenishment lead time in the service level constraint (4) is an exogenous parameter required to approximately achieve the desired service levels. In our experiments the replenishment lead time $L_{k,t}$ is set to 1. The other lead time is the time between work released into the system and becoming available as finished goods, represented by the CF in the capacity constraint (5).

This optimization model determine the required changes of the inventory position represented by $Y_{k,t}$ for each product k and period t. The release quantity $R_{k,t}$ is determined by these auxiliary variable $Y_{k,t}$ and the actual demand $D_{k,t}$, which is described by the equation below.

$$R_{k,t} = Y_{k,t} + D_{k,t} \quad \forall 1 \le t \le T \wedge \forall 1 \le k \le K$$

EXPERIMENTAL DESIGN

In simulation studies we compared the performance of our MP-DYNIP-B model with two base stock inventory policies. For this purpose two performance measures were chosen, the mean value and standard deviation of the stock and the reached service level. In this section we specify the generation of the demand scenarios and introduce the base stock inventory policy used for comparison.

Demand Realization

The uncertainty of the demand is represented by a variation of the mean values and standard deviation of the demand quantities over the time. The coefficient of variation of the demand distribution is assumed to be constant and is set to 0.3. Thus the variances can be different since the means are different in each period. According to (Ravindran et al. 2011) we generate the demand means via two control variables. To specify the number of periods between changes of the mean, the value Δ_n ($1 \le n \le N$) will be introduced. The value N is defined by the required number of mean changes to reach the simulation horizon. This value Δ_n is determined by using a uniform distribution with the lower bound δ_{min} and upper bound δ_{max}. The new mean value μ_n ($1 \le n \le N$) for the next Δ_n periods is also determined using a uniform distribution with a specified lower bound ρ_{min} and upper bound ρ_{max}. By using these control variables we obtain different mean values for the entire simulation horizon. We generated three different demand conditions referred as scenario I (S-I), scenario II (S-II) and scenario III (S-III) by using different parameter for ρ_{min} and ρ_{max}. In S-I we determined the values for the new mean demand by $\mu_n = U(70,80)$, in S-II we used $\mu_n = U(60,90)$ and in S-III the values $\mu_n = U(50,100)$ were chosen. For all three scenarios the number of periods between the changes of the demand means was determined by $\Delta_n = U(3,12)$. These scenarios specify different situations of the demand uncertainties.

Comparison Model

We compare the performance of our MP-DYNIP-B model with two base stock inventory policies. Firstly we consider a dynamic order quantity q, which depends on the actual demand of a period t ($q_t = D_t$). The reorder point s is defined as

$$s_k = L_k \cdot \mu_k + \sqrt{L_k} \cdot \sigma_k \cdot \Phi^{-1}_{N(0,1)}\left(\alpha_{k,RLD}\right)$$

where μ_k and σ_k denotes the average and the standard deviation of the demands over the simulation horizon. This model is referred as Basestock-Policy. Secondly we assume a (s, q)-Policy with a constant order quantity of 120 pieces (q=120). To determine the reorder point s we consider the so-called undershoot (U), which is defined as the difference between the reorder point s and the inventory position at the moment immediately before a replenishment order is released. A detailed description of the determination of the mean E(U) and variance Var(U) of the undershoot for a normal distributed demand can be found in (Herrmann 2011). Hence the mean and variance of the demand during the replenishment lead time is defined by the equation shown below.

$$E\left(Y_k^*\right) = \mu_k + E\left(U\right) \wedge \; Var\left(Y_k^*\right) = \sigma_k^2 + Var\left(U\right)$$

Thus, the reorder point s_k for a product k can be determined by the following equation.

$$s_k = L_k \cdot E\left(Y_k^*\right) + \sqrt{L_k} \cdot Var\left(Y_k^*\right) \cdot \Phi^{-1}_{N(0,1)}\left(\alpha_{k,RLD}\right)$$

The replenishment lead time L_k for product k is for both inventory policies set to 1 period.

EXPERIMENTAL RESULTS

To gain statistical significant figures a simulation horizon of 1000 periods was defined and verified by our tool. As performance measures we compare the average (AVG) and the standard deviation (SD) of the inventory position and the reached service level over all products k and periods t. In table 3 the results for a target service level of 90% are shown.

Table 3: Experimental results of all models and scenarios for a target service level of 90%.

Target Service level = 90%					
Model	Service Level		Inventory Position		Scenario
	AVG	SD	AVG	SD	
Basestock	88.1	2.9	39.7	28.2	S – I
(s, q) – Policy	88.9	1.2	77.7	41.0	S – I
MP-DYNIP-B	90.8	0.8	40.2	28.0	S – I
Basestock	85.5	3.7	42.6	29.5	S – II
(s, q) – Policy	87.3	1.0	81.4	42.2	S – II
MP-DYNIP-B	90.4	1.0	42.9	28.8	S – II
Basestock	85.8	2.3	48.7	30.3	S – III
(s, q) – Policy	84.4	2.1	88.0	45.4	S – III
MP-DYNIP-B	89.6	1.3	45.8	30.3	S – III

For all scenarios the MP-DYNIP-B model nearly reached the desired service level of 90%. In scenario I and II the Basestock-Policy gain lower service levels as the (s, q)-Policy, in scenario III the Basestock-Policy gain a better service level. For all scenarios the average inventory position of the (s, q)-Policy is almost twice as high as in the other models. This is due to the high reorder point, which consider the undershoot, to capture the uncertainty of the demand. The Basestock-Policy performs better, because of the dynamic of the order quantity, depending on the actual demand. The MP-DYNIP-B model determines the capacity better and considers the relationship between the WIP inventory and the output quantity accurate. Table 4 contains the experimental results for a target service level of 95%. These results are similar to the results shown in table 2.

Table 4: Experimental results of all models and scenarios for a target service level of 95%.

Target Service level = 95%					
Model	Service Level		Inventory Position		Scenario
	AVG	SD	AVG	SD	
Basestock	92.8	1.9	42.0	26.3	S – I
(s, q) – Policy	93.8	1.0	87.7	43.3	S – I
MP-DYNIP-B	95.0	0.7	43.7	25.8	S – I
Basestock	91.8	1.6	45.8	27.4	S – II
(s, q) – Policy	92.1	1.4	91.4	44.6	S – II
MP-DYNIP-B	94.9	1.5	46.5	26.9	S – II
Basestock	91.3	1.9	52.1	29.2	S – III
(s, q) – Policy	90.0	1.7	98.7	48.4	S – III
MP-DYNIP-B	93.4	2.2	49.8	28.7	S – III

SUMMARY AND FUTURE DIRECTION

Our research show, how a CF specific to a product k for a capacitated production system, using deterministic process times and multiple products, can be estimated. We extend the model of (Ravindran et al. 2011) to consider multiple products and integrate backorders for the use in a rolling planning environment. The simulation experiments indicate that the MP-DYNIP-B model outperforms the inventory management policies used in this research.

In future studies further insights of the performance of our model may be provided by using different replenishment lead time values and inventory policies. The extension of the model to the consideration of a bill of material as well as the estimation of a CF for such a model is task for further research. Also an extension to the approaches of the stochastic optimization and the consideration of multiple demand scenarios to gain robust planning results should be in the focus of interest.

REFERENCES

Asmundsson, J.M.; R.L. Rardin and R. Uzsoy. 2006. "Tractable nonlinear production planning models for semiconductor wafer fabrication facilities", In *IEEE Transactions on Semiconductor Manufacturing* 19, No. 1, 95-111.

Asmundsson, J.M.; R.L. Rardin; C.H. Turkseven and R. Uzsoy. 2009. "Production planning models with resources subject to congestion", In *Naval Research Logistics* 56, No. 2, 142-157.

Buzacott, J.A. and J.G. Shanthikumar. 1993. *Stochastic Models of Manufacturing Systems*. Prentice-Hall, Englewood Cliffs, NJ.

Byrne, M.D. and M.A. Bakir. 1999. "Production planning using a hybrid simulation-analytical approach", In *International Journal of Production Economics* 59, No. 1, 305-311.

Escudero, L.F.; P.V. Kamesam; A.J. King and R.J. Wets. 1993. "Production Planning via scenario modeling", In *Annals of Operations Research* 43, No. 6, 309-335.

Ettl, M.; G. Feigin; G.Y. Lin and D.D. Yao. 2000. "A supply chain network model with basestock control and service requirements", In *Operations Research* 48, 216-232.

Graves, D.C. 1986. "A tactical planning model for a job shop", In *Operations Research* 34, 552-533.

Hackman, S.T. and R.C. Leachman. 1989. "A general framework for modeling production", In *Management Science* 35, No. 4, 478-495.

Hax A.C. and H.C. Meal. 1975. "Hierarchical integration of production planning and scheduling", In *Studies in Management Science, Volume 1: Logistic*, M.A. Geisler (Eds.), Amsterdam, 53-69.

Herrmann, F. 2011. *Operative Planung in IT-Systemen für die Produktionsplanung und –steuerung. Wirkung, Auswahl und Einstellhinweise*. Vieweg+Teubner, Wiesbaden, Germany.

Herrmann, F. and F. Lange. 2013. „Belastungsorientierte Ansätze in der Produktionsplanung", In *Divergierende Forschungsansätze zur Produktionsplanung und -steuerung*, T. Claus; F. Herrmann; M. Manitz and C. Broduhin (Eds.), in press.

Hung, Y.F. and R.C. Leachman. 1996. "A production planning methodology for semiconductor manufacturing based on iterative simulation and linear programming calculations", In *IEEE Transactions on Semiconductor Manufacturing* 9, No. 2, 257-269.

Hopp, W.J. and M.L. Spearman. 2001. *Factory Physics: Foundations of Manufacturing Management.* Irwin/McGraw-Hill, Boston.

Irdem, D.F.; N.B. Kacar and R. Uzsoy. 2010. “An exploratory analysis of two iterative linear programming-simulation approaches for production planning”, In *IEEE Transactions on Semiconductor Manufacturing* 23, No. 3, 442-455.

Kacar, N.B.; D.F. Irdem and R. Uzsoy. 2012. “An Experimental Comparison of Production Planning Using Clearing Functions and Iterative Linear Programming-Simulation Algorithms”, In *IEEE Transactions on semiconductor manufacturing 25*, No. 1 (Feb), 104-117.

Kacar, N.B. and R. Uzsoy. 2010. “Estimating Clearing Functions from Simulation Data”, In *Proceedings of the 2010 Winter Simulation Conference* (Baltimore, MD, Dec. 5-8). IEEE, Picataway, N.J., 1699-1710.

Karmarkar, U.S. 1989. “Capacity loading and release planning with Work-in-Progress (WIP) and lead-times”, In *Journal of Manufacturing and Operations Management* 2, 105-123.

Kayton, D.; T. Teyner; C. Schwartz and R. Uzsoy. 1997. „Focusing maintenance improvement efforts in a wafer fabrication facility operating under theory of constraints”, In *Production Inventory Management* 38, No. 4, 51-57.

Kim, B. and S. Kim. 2002. “Extended model for a hybrid production planning approach”, In *International Journal of Production Economics* 73, No. 2, 165-173.

Lautenschläger, M. and H. Stadtler. 1998. „Modelling Lead Times Depending on Capacity Utilization“, Research Report, Technical University of Darmstadt, Germany.

Missbauer, H. 2002. “Aggregate order release planning for time-varying demand”, In *International Journal of Production Research* 40, 688-718.

Missbauer, H. and R. Uzsoy. 2010. „Optimization models for production planning“, In *Planning Production and Inventories in the Extended Enterprise*, K.G. Kempf; P. Keskinocak; and R. Uzsoy (Eds.), Springer, New York, 437-508.

Mulvey, J.M. and R.J. Vanderbei. 1995. “Robust Optimizationof large-scale systems”, In *Operations Research* 43, No. 2, 264-281.

Orlicky, J. 1975. *Material Requirments Planning: The New Way of Life in Production and Inventory Management.* McGraw-Hill, New York.

Pahl, J.; S. Voss and D.L. Woodruff. 2007. “Production planning with load dependent lead times: an update of research”, In *Annals of Operations Research* 153, No. 1, 297-345.

Rao, S.S.; A. Gunasekaran; S.K. Goyal and T. Martikainen. 1998. “Waiting line model applications in manufacturing”, In *International Journal of Production Economics* 54, No. 1, 1-28.

Ravindran, A.; K.G. Kempf and R. Uzsoy. 2011. „Production planning with load-dependent lead times and safety stocks for a single product”, In *International Journal of Planning and Scheduling* 1, No. 1/2, 58-89.

Scholl, A. 2001. *Robuste Planung und Optimierung*. Physica-Verlag, Heidelberg, Germany.

Srinivasan, A.; M.Varey and T.E. Morton. 1988. “Resource pricing and aggregate scheduling in manufacturing systems”. *Graduate School of Industrial Administration*, Carnegie-Mellon University, Pittsburgh, PA.

Spitter, J.M.; C.A.J. Hurkens; A.G. de Kok; J.K. Lenstra and E.G. Negenman. 2005. „Linear programming models with planned lead times for supply chain operations planning“, In *European Journal of Operationsal Research* 163, 706-720.

Vollmann, T.E.; W.L. Berry; D.C. Whybark and F.R. Jacobs. 2005. *Manufacturing Planning and Control for Supply Chain Management*. McGraw-Hill, New York.

Voss, S. and D.L. Woodruff. 2003. *Introduction to Computational Optimization Models for Production Planning in a Supply Chain*. Springer, Berlin, Germany.

AUTHOR BIOGRAPHIES

FREDERICK LANGE was born in Regensburg, Germany and went to the University of Applied Sciences Regensburg, where he studied business computer science and logistics. He obtained his master’s degree in March 2011. He is working for the SimPlan AG as consultant and is PhD student at the Technical University Dresden. His e-mail address is: Frederick.Lange@yMail.com

FRANK HERRMANN was born in Münster, Germany and went to the RWTH Aachen, where he studied computer science and obtained his degree in 1989. During his time with the Fraunhofer Institute IITB in Karlsruhe he obtained his PhD in 1996 about scheduling problems. From 1996 until 2003 he worked for SAP AG on various jobs, at the last as director. In 2003 he became Professor for Production Logistics at the University of Applied Sciences in Regensburg. His research topics are planning algorithms and simulation for operative production planning and control. His e-mail address is Frank.Herrmann@HS-Regensburg.de and his Web-page can be found at http://homepages.fh-regensburg.de/~hef39451/dr_herrmann/

THORSTEN CLAUS was born in Papenburg, Germany, and went to the University Osnabrück, where he studied business management and mathematics. 1995 he obtained his PhD about simulation and genetic algorithms. Since his Habilitation in 2004 he works as a Professor for Production Economy and Information Technology at International Institute Zittau (TU Dresden). His research topics are production planning and e-Learning. His e-mail address is Claus@IHI-Zittau.de and his Web-page can be found at http://www.ihi-zittau.de/cms/de/127/Produktionswirtschaft-und-Informationstechnik/

DYNAMIC BEHAVIOR OF SUPPLY CHAINS

Hans-Peter Barbey
University of Applied Sciences Bielefeld
Wilhelm-Bertelsmann-Str. 10, 33602 Bielefeld, Germany
Email: hans-peter.barbey@fh-bielefeld.de

KEYWORDS
Supply chain, bullwhip effect, beer game, simulation, closed-loop control, order strategies.

ABSTRACT

The bullwhip effect has been well known since many years and often takes place in supply chains. It is caused by wrong order policy in real systems. The bullwhip effect can be demonstrated easily through the beer game. It was developed by the MIT in the 60s. All stages of the supply chain operate independently. The only decisions that can be taken in the particular stages of this simulation game are the size of the orders. This beer game was depicted as a simulation with two additional simple control algorithms for the decision of the order quantities. The first algorithm set the time to compensate a difference in the inventory to a specific value, in the second algorithm the quantity of the order is limited. Both algorithms were taken to compensate a sudden and steady increase of the orders. Both control algorithms generated a bullwhip effect. The limited duration strategy for compensation a difference in the inventory led to rising orders in the upstream stages. The limited order strategy led to an increasing time to compensate a difference in the inventories of the upstream stages.
The limited duration strategy was applied to an ordering behavior with a linear trend und to a random ordering behavior. For the linear trend it has been found that the shorter the time for compensation the lower the difference to the nominal stock and the higher the bullwhip effect in the stages upstream. In contrast to that for random orders the time for compensation has to be longer to minimize the bullwhip effect. That is why the setting of the closed-loop control of the stocks in supply chains is an optimization problem. It can only be solved for a real supply chain, if the ordering behavior of the customer is known.

1 INTRODUCTION

Dynamic behavior of the material flow in a supply chain is influenced by the order policy of each particular company of a supply chain. The interaction of all companies creates the bullwhip effect, which has been described first by (Forrester 1958). It is the increasing of a small variation in the requirements of a customer to an enormous oscillation with the manufacturer at the beginning of a supply chain. In many articles, this phenomenon is only described in general terms without a mathematical definition (i.e. Erlach 2010 and Dickmann 2007). Without any mathematical description, the question is if the bullwhip effect can be avoided at all (Bretzke 2008). The main influences of the bullwhip effect are as follows (Gudehus 2005):

- Independent orders of the particular companies in a supply chain
- Synchronic orders (i.e. subsidiaries of one company)
- Wrong order policy in an emergency case
- Speculative order policy or sale actions

To avoid the bullwhip effect, cooperation between all members in a supply chain is necessary. Basically, informations about i.e. orders of customers have to be provided to all subsuppliers in the supply chain. This kind of cooperation is rather difficult in reality. The question is if the bullwhip effect can be avoided without any cooperation and providing of information to all members in a supply chain.

A very nice demonstration of the bullwhip effect gives the beer game. This simulation game was developed by the MIT in the 60s. It simulates a supply chain with 4 stages. The task of this supply chain is to produce and deliver units of beer: the factory produces and the other three stages deliver the beer units until it reaches the customer at the downstream end of the supply chain. The target is to keep the stock at a minimum and to have a 100% service level. The game is designed so simple, that the only decision is to decide about the quantity of the order to compensate a difference in the own inventory. All other influences are eliminated. This decision has been taken each time unit. The time to place an order is 1 time unit. Delivery time is 3 units (fig.1). In total there is a lead time of 4 units for an order. It is obvious that these parameters do not simulate a real supply chain. Normally the lead time is much shorter than the time for the next order. However, this simulation game demonstrates the bullwhip effect

Proceedings 27th European Conference on Modelling and Simulation ©ECMS Webjørn Rekdalsbakken, Robin T. Bye, Houxiang Zhang (Editors)
ISBN: 978-0-9564944-6-7 / ISBN: 978-0-9564944-7-4 (CD)

in an impressive manner. Additionally in a computer simulation the reasons of these effects can be explained.

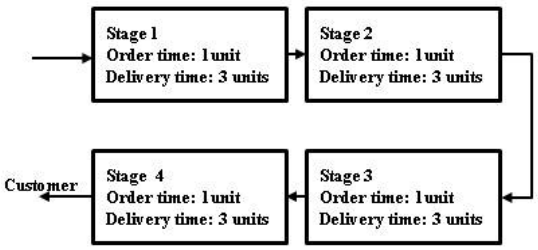

Figure 1: Model of a Supply chain

In principle each particular stage of the supply chain is closed-loop controlled. An Order of a customer reduces the stock. With the delivery of products from a supplier the stock will be filled up to a nominal stock. The closed-loop control of the stock in supply chains has been examined in different articles (Barbey 2011). These examinations demonstrate minimization of the bullwhip effect with a suitable controller. However, the reasons of bullwhip effect are not given there.

For the examination of the bullwhip effect a model of a supply chain according fig. 1 will be used. The behavior of each stage is the same. The time to place an order is 1 time unit. The time for delivery is 3 time units. The lead time to fill up the stock is for one stage 4 time units. If a customer place an order in the supply chain it needs 16 time units to deliver the material. To be able to deliver immediately each stage needs a stock.

2 DYNAMIC BEHAVIOR OF A SUPPLY CHAIN

The question is now, what is the best strategy of one stage in a supply chain to order material with a supplier. Assuming the unrealistic precondition of a zero lead time the best strategy is: “input is output”. Under this precondition there is no need for a stock at all. Now this strategy is applied to a supply chain as described above (fig. 2).

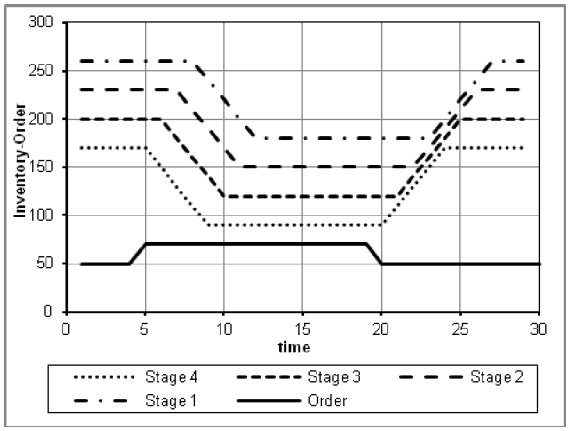

Figure 2: Stock with input=output strategy

If the customer increase his order, here 20 items, the stock of stage 4 decrease in a linear manner. The other stages follow after the order time of 1 unit. After the lead time the stock is constant, because now the output of the stock is equivalent to the input. However there is a difference to the nominal stock. Does the customer reduce his order to the original amount the behavior is vice versa.

Assuming the increase or decrease in the order is permanent, the aim of each particular stage is to equalize the difference to the nominal stock. To get this aim two strategies will be applied. The first strategy is: Each stage equalizes the stock in a definite time.
The result is a stock according fig. 4. The order quantity increases for the upstream stages of the supply chain (fig. 3).

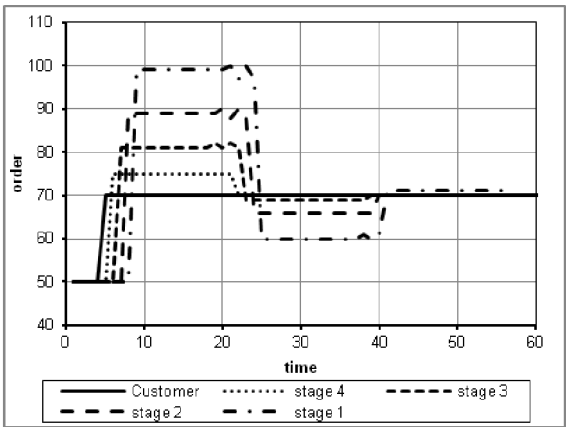

Figure 3: Orders with compensation strategy: four times the lead time

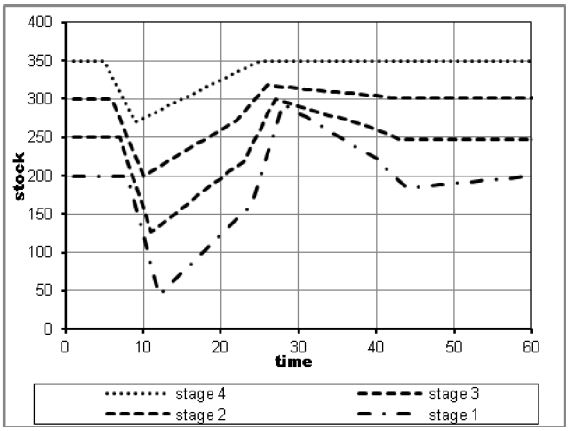

Figure 4: Stock with compensation strategy: four times the lead time

Only the stage at the very end of the supply chain is able to compensate the stock difference within the scheduled time. For all other stages it requires more than double the time. This is quite obvious: The last stage has only to fulfill the customer’s requirement. All other stages have to fulfill the customer’s requirement and have to compensate the stock difference of all

stages downstream. Only when the first stage in the supply chain has balanced the stock difference, the order is reduced to the value of the customer. This is the reason that the bullwhip effect also occurs in the stock (fig.4).

Therefore, the following first thesis can be formulated: If the inventories are compensated in a certain time, then this leads to a bullwhip effect in the amount of order. And the shorter the time, the higher the order!

For this reason, the second strategy is now considered: Each stage may order only a maximum order quantity from the supplier.
The maximum order quantity is limited for all stages to 90 units. Therefore the stages, which are further upstream, need more time to compensate the difference in stock (fig. 5). The result is a stock according fig. 6.

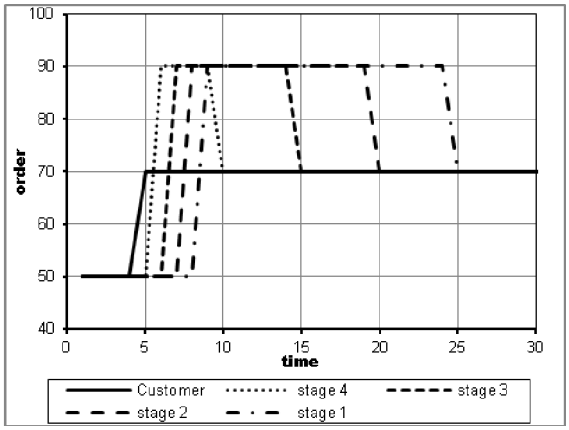

Figure 5: Order with compensation strategy: limited maximum order

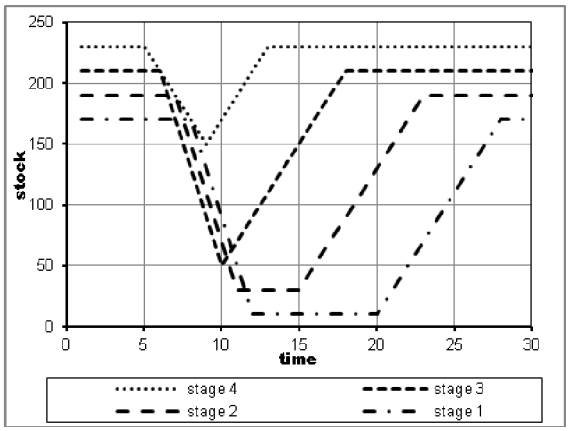

Figure 6: Stock with compensation strategy: limited maximum order

This leads directly to the second thesis: Limiting the orders leads to a bullwhip effect in time to compensate the stock differences.

The conclusion of both theses is: The bullwhip effect is unavoidable in a supply chain. It`s just a matter of optimizing how far and in what way it can be reduced.

3 TREND BEHAVIOR

Seasonal ordering behavior is generally predictable. Therefore it can be included in an order strategy of a supply chain with a predictive controller. This behavior is not included in this simple controlling algorithm. For this study an unexpected trend with a linear increase is assumed. The inventory of each stage is controlled by the algorithm: Compensation in a definite time.
For the stage 4 close to the customer it is clear that a linear increase of the orders create a decrease of the stock (fig.8). After a certain time there is a constant difference to the nominal stock. For the other stages a bullwhip effect is visible. The bullwhip effect occurs in the orders too (fig.7).

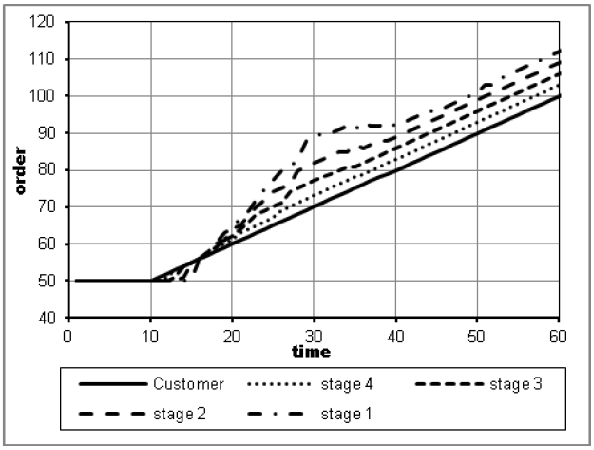

Figure 7: Orders with compensation strategy: four times the lead time

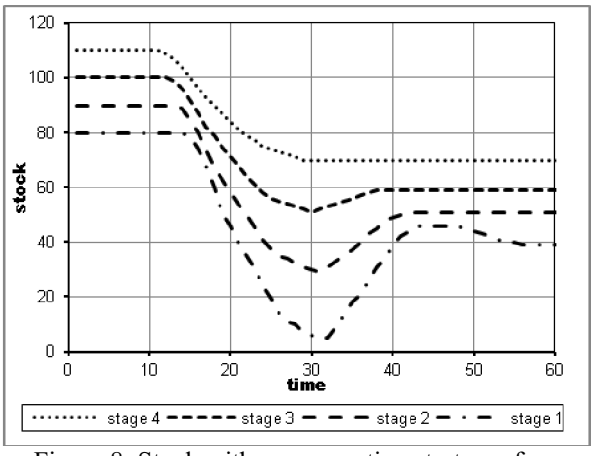

Figure 8: Stock with compensation strategy: four times the lead time

It is possible to reduce the differenc to the nominal stock, by reducing the compensation time. However, this is only an advantage for the stage close to the customer. Due to the occuring bullwhip effect for all other stages the minimum stock is lower than the constant value. However, for a 100% service level the minimum stock is substantial.

4 RANDOM ORDERS

Each order has random fluctuation around a mean value. These fluctuations are so fast that a closed-loop control is not able to compensate the deviation. This is one of the reason to have a stock for compensation of these fluctuations. For all other deviations as trend or a permanent increase a closed-loop control is provided. The question is now how a random fluctuation of the orders affects the closed-loop control. For that the orders of stage 1 has been simulated with three different compensation times (fig.8).

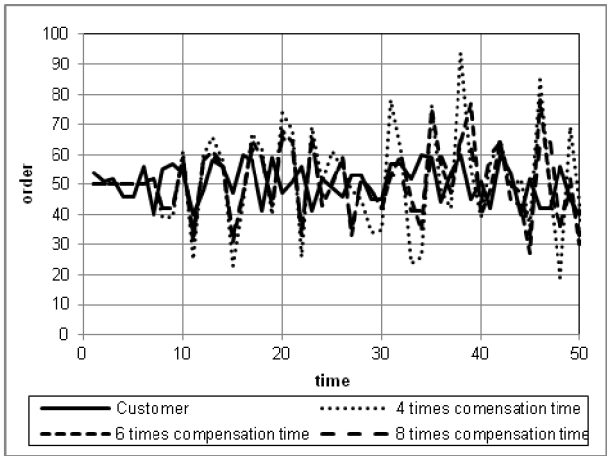

Figure 9: Random orders with different compensation times for stage 1

The customer order has a fluctuation of +/-10% of the average. With the 4 times compensation times the orders of stage 1 has a fluctuation of more than +/-30%. With these parameters a strong bullwhip effect occurs. With the increase to the 8 times compensation time the fluctuation of the orders is nearby to the customer's order.

5 CONCLUSIONS AND FUTURE TASKS

This study is a theoretical view of the bullwhip effect. It based on the beer game created from the MIT. The supply chain model has quite a simple structure. The advantage is to see the main influences of the bullwhip effect. Due to dead times caused by orders and delivery, it is difficult to get a constant stock through a closed-loop control. In this supply chain, the bullwhip effect is manageable if this simple control algorithm is applied, even if the companies handle their stock independently. Different order policies for the customer at the end of the supply chain have been applied. The first policy was a permanent and constant increase of the orders, which could be closed-loop controlled to the nominal stock with a constant time strategy or a maximum order strategy. The second policy of the customer was a linear trend. Here the constant time strategy was applied. A constant deviation from the nominal stock occurred. The third policy was a random order. Here the bullwhip effect was only manageable, if the compensation time increases.

This simulation demonstrates that it possible to handle the bullwhip effect in a supply chain with a quite simple algorithm. The minimizing of the bullwhip effect in a supply chain is an optimization problem. Only with analyzing of the orders it is possible to find an optimum for the compensation time

Not included in this simulation was the examination of the behavior of a supply chain with a seasonal trend. A seasonal trend is comparable with an oscillation. These oscillations are often very difficult to control (Barbey 2011). The impact of a seasonal trend to the bullwhip effect has to be exanimated in a next simulation study. Subsequently, it has to be checked if this theoretical knowledge can be transferred to a real supply chain. A real supply chain has to be simulated then.

REFERENCES

Barbey, H.-P.: A New Method for Validation and Optimisation of Unstable Discrete Event Models", appeared in proceedings of 23. European Modeling & Simulation Symposium (EMSS), Rome, 2011.

Barbey, H.-P.: Simulation des Stabiltätsverhalten von Produktionssystemen am Beispiel einer lagerbestandsgeregelten Produktion, appeared in: Advances in Simulation for Production and Logistics Application, Hrsg.: Rabe, Markus, Stuttgart, Fraunhofer IRB Verlag, 2008, S.357-366.

Barbey, H.-P.: Application of the Fourier Analysis for the Validation and Optimisation of Discrete Event Models appeared in proceedings of ASIM 2011, 21. Symposium Simulationstechnik, 7.9.-9.9.2011, Winterthur.

Bretzke, W.-R.: Logistische Netzwerke, Springer Verlag Berlin Heidelberg, 2008.

Dickmann, P.: Schlanker Materialfluss, Springer Verlag Berlin Heidelberg, 2007.

Erlach, K.: Wertstromdesign, Springer Verlag Berlin Heidelberg, 2010.

Forrester, J.W.: Industrial Dynamics: A major breakthrough for decision makers. In: Harvard business review, 36(4), 1958.

Gudehus, T.: Logistik, Springer Verlag Berlin Heidelberg, 2005.

AUTHOR BIOGRAPHIES

HANS-PETER BARBEY was born in Kiel, Germany, and attended the University of Hannover, where he studied mechanical engineering and graduated in 1981. He earned his doctorate from the same university in 1987. Thereafter, he worked for 10 years for different plastic machinery and plastic processing companies before moving in 1997 to Bielefeld and joining the faculty of the University of Applied Sciences Bielefeld, where he teaches logistic, transportation technology, plant planning, and discrete simulation. His research is focused on the simulation of production processes.

His e-mail address is:
hans-peter.barbey@fh-bielefeld.de
And his Web-page can be found at
http://www.fh-bielefeld.de/fb3/barbey

COMBINING AN EVOLUTIONARY ALGORITHM WITH THE MULTILEVEL PARADIGM FOR THE SIMULATION OF COMPLEX SYSTEMS

Noureddine Bouhmala, Karina Hjelmervik, Kjell Ivar Øvergård
Department of Maritime Technology and Innovation
Vestfold University College
Norway
Email: {noureddine.bouhmala,karina.hjelmervik,koe}@hive.no

KEYWORDS

Maximum satisfiability problem, Multilevel paradigm.

ABSTRACT

Evolutionary Algorithms have become an efficient tool to simulate large and complex systems that require a huge amount of computational resources. Nevertheless, evolutionary algorithms may still suffer from either slow or premature convergence preventing the search to visit more promising areas, and thus leading to solutions of poor quality. In this work, the multilevel paradigm is used in order to enhance the evolutionary algorithm's performance for simulating large industrial instances. The multilevel paradigm refers to the process of dividing large and difficult problems into smaller ones, which are hopefully much easier to solve, and then work backward towards the solution of the original problem, using a solution from a previous level as a starting solution at the next level. Experimental results comparing the multilevel evolutionary algorithm against its single-level variant are presented.

INTRODUCTION

The MAX-SAT problem still deserves much research attention from a wider community of researchers due to its theoretical importance. MAX-SAT is a widely used modeling framework for simulating complex systems that turn out to be of combinatorial nature which can be conveniently formulated to SAT or MAX-SAT in an elegant way (Hoos 2004). Examples include model-checking (Biere et al. 1990) of finite state systems, design debugging (Smith et al. 2005), AI planning (Rintanen et al. 2006) to name just a few. Large and complex systems are hard to solve and require a huge amount of computational resources. Optimization search techniques tend to spend most of the time exploring a restricted area of the search space preventing the search to visit more promising areas, and thus leading to solutions of poor quality. A better approach would be to reduce these complex systems into simplified models so that the optimization algorithms used during the simulation process would be far more efficient. In this paper a multilevel evolutionary algorithm is introduced for MAX-SAT. The key feature of this algorithm involves looking at the simulation as a process that transforms the original problem into a hierarchy of increasingly smaller problems that are much easier to solve. The optimization starts at the coarsest level and works backwards to the finest level where the solution obtained at a child level is fed as an input solution to the parent level.

THE MAXIMUM SATISFIABILITY PROBLEM

Generally, a SAT problem is defined as follows. A propositional formula $\Phi = \bigwedge_{j=1}^{m} C_j$ with m clauses and n Boolean variables is given. Each Boolean variable, $x_i, i \in \{1, \ldots, n\}$, takes one of the two values, True or False. A clause, in turn, is a disjunction of literals and a literal is a variable or its negation. Each clause C_j has the form:

$$C_j = \left(\bigvee_{k \in I_j} x_k \right) \vee \left(\bigvee_{l \in \bar{I}_j} \bar{x}_l \right),$$

where $I_j, \bar{I}_j \subseteq \{1, ...n\}$, $I \cap \bar{I}_j = \emptyset$, and $\bar{x}_i$ denotes the negation of x_i. The task is to determine whether there exists an assignment of values to the variables under which Φ evaluates to True. Such an assignment, if it exists, is called a satisfying assignment for Φ, and Φ is called satisfiable. Otherwise, Φ is said to be unsatisfiable. Most SAT solvers use a Conjunctive Normal Form (CNF) representation of the formula Φ. In CNF, the formula is represented as a conjunction of clauses, with each clause being a disjunction of literals. The maximum satisfiability problem is the optimization variant of SAT. The goal is to minimize the number of unsatisfied clauses. The focus in this work is

Proceedings 27th European Conference on Modelling and Simulation ©ECMS Webjørn Rekdalsbakken, Robin T. Bye, Houxiang Zhang (Editors)
ISBN: 978-0-9564944-6-7 / ISBN: 978-0-9564944-7-4 (CD)

restricted to formulas in which all the weights are equal to 1 (i.e.unweighted MAX-SAT).

THE MULTILEVEL EVOLUTIONARY ALGORITHM (MLVMA)

The proposed multilevel evolutionary goes through four different phases following the general multilevel pattern described in (Bouhmala and Granmo 2011)(Karypis and Kumar 1998)(Walshaw 2001). The algorithm starts creating a hierarchy of increasingly smaller and coarser versions of the original problem (Phase 1). The coarsening phase works by grouping the literals representing the problem into clusters. The coarsening is computed using a randomized algorithm. The literals are visited in a random order. If a literal l_i has not been matched yet, then we randomly select one randomly unmatched literal l_j, and a new literal l_k (a cluster) consisting of the two literals l_i and l_j is created. Unmerged literals are simply copied to the next level. The new formed literals are used to define a new and smaller problem and recursively iterate the coarsening process until the size of the problem reaches some desired threshold. Initialization is then trivial and consists of generating an initial solution for the population located at the coarsest level using a random procedure. The clusters of every individual in the population are assigned the value of true or false in a random manner (Phase 2). The population at the coarsest level P_{m+1} is subject to an improvement phase using an evolutionary memetic algorithm (MA)(Norman and Moscato 1991) (Phase 3). Individuals are combined using the two-points cross-over. The task of the cross-over operator is to reach regions of the search space with better average quality. Combining pairs of individuals can be viewed as a matching process. The individuals are visited in random order. An unmatched individual i_k is matched randomly with an unmatched individual i_l. Thereafter, the two-point crossover operator is applied using a cross-over probability to each matched pair of individuals. The two-point crossover selects two randomly points within a chromosome and then interchanges the two parent chromosomes between these points to generate two new offsprings. The work conducted in (Spears 1995) shows that the two-point crossover is more effective when the problem at hand is difficult to solve. The new individuals resulted from the two-point cross-over are then enhanced with a local search and evaluated. This simple local search seeks for the new variable-value assignment which best decreases the numbers of unsatisfied clauses is identified. Even though the population at P_{m+1} is at a local minimum, the projected population may not be at a local optimum with respect to P_m. The projected population is already a good solution and contains individuals with better fitness value making the evolutionary algorithm to converge quicker within a few generation to a better assignment. During each level, the evolutionary algorithm is assumed to reach convergence when no further improvement of the fittest individual has not been made during 10 consecutive generations. The uncoarsening phase (Phase 4) refers to the inverse process followed during the coarsening phase. Having optimized the assignment on P_{m+1}, the assignment must be extended on its parent level P_m. The extension algorithm is simple; if a cluster $c_i \in P_{m+1}$ is assigned the value of true then the merged pair of clusters that it represents, c_j, $c_k \in P_m$ are also assigned the true value.

EXPERIMENTAL RESULTS

Test Suite & Parameter Settings

The tests were carried out on Unix server with 6 cpu cores, 2.80GHz and 50GB of memory. The code was written in C and compiled with the GNU C compiler version 4.6. All parameters were fixed experimentally using industrial instances that arise in the simulation of faults in model checking and large graph coloring problems from the SAT library benchmark.

instances	VAR	CLS
case1:bmc-ibm-1.cnf	9 658	55 870
case2:bmc-ibm-2.cnf	3 628	14 468
case3:bmc-ibm-3.cnf	14 930	72 106
case4:bmc-ibm-5.cnf	9 396	41 207
case5:bmc-ibm-7.cnf	8 710	39 774
case6:bmc-galileo-8.cnf	58 074	294 821
case7:bmc-galileo-9.cnf	63 624	326 999
case8:bmc-ibm-10.cnf	61 088	334 861
case9:bmc-ibm-11.cnf	32 109	150 027
case10:bmc-ibm-12.cnf	39 598	194 778
case11:bmc-ibm-13.cnf	13 215	65 278
case12:g125.18.cnf	2 250	70 163
case13:g125.17.cnf	2 125	66 272
case14:g250.15.cnf	3 750	233 965
case15:g250.29.cnf	7 250	454 622

TABLE I: Benchmark Instances

The set used in the experiments is taken from [1] and shown at Table I. The second and third column denote the number of variables and clauses respectively. IBM SPSS Statistics version 19 was used for statistical analysis. Due to the randomization nature of the algorithms, each problem instance was run 100 times with a cut–off parameter (max–time) set to 15 minutes. The 100 runs where chosen because pilot runs had shown the size of the difference to be so large that 100 runs where enough for an acceptable statistical power ($power > .95$), this is in accordance with the suggestions given in a recent report on statistical testing of randomized algorithms (Arcuri and Briand 2011) We also performed single runs with MLVMA and MA with a cut–off parameter set to 60 minutes. The intention was to see whether the solutions created by MLVMA and MA converged to identical solutions.

The selected parameters are listed below:

- Crossover probability = 0.85
- Mutation probability = 0.1
- Population size = 50

[1]SATLIB website (http://www.informatik.tu-darmstadt.de/AI/SATLIB)

#Case	Mean (SD)	Range
1	3872.8 (233.7)	3632-4830
2	157.8(8.1)	137-185
3	3320.9 (279.1)	2911-4187
4	1125.8(138.1)	976-1675
5	1475.9 (101.3)	1167-1668
6	12232.9(2464)	9809-23178
7	14412.6(2877.1)	11318-22705
8	2206.1(1117.6)	20621-25275
9	13730.9 (547.5)	13045-15413
10	17477.0 (410.7)	17079-18908
11	3875.7(273.4)	3529-5055
12	37.8 (3,5)	29-48
13	40,7 (3.5)	30-50
14	193.7 (30.9)	173-425
15	214.8(64.3)	177-637

TABLE II: MLVMA mean, standard deviation and range of unsolved clauses.

#Case	Mean (SD)	Range
1	5700.5 (427.6)	5184-7773
2	234.6(16.1)	190-273
3	10049.3 (356.8)	9547-11559
4	3282.5 (276.0)	3024-4651
5	3107.1(152.3)	2870-4044
6	51062.3 (814.1)	49375-53517
7	57301.2(877.1)	55292-59723
8	63720.2 (475.3)	62575-64626
9	26207.8(353.7)	25461-27311
10	35289.7(440.3)	34363-36871
11	8233.4(384.2)	7886-10080
12	323.9 (47.4)	225-481
13	154.2 (20.7)	92-222
14	29565.3 (1068.7)	27587-33040
15	85410.6(1759.2)	80704-89626

TABLE III: MA: mean, standard deviation and range of unsolved clauses.

	BIS: Test^{a,b}	
#Case	MD [99%CI]	Cohen's d
1	1895.2[1827.6, 1962.8]	5,3
2	76.8[71.9,81,3]	6,02
3	6728.4[6610.1,6844.2]	21,01
4	2156.7[2082.4,2238.7]	9,88
5	1631.2[1585.7,1682.1]	12,61
6	38829.4[38119.8, 39450.1]	21,16
7	42888,6[42100.6,43645.6]	20.17
8	41713,8[41396.1, 42020.2]	48,57
9	12476.9[12314.7, 12614.4]	27,07
10	17812,7[17656.6, 17963.]	41,83
11	4446,7[4329.1, 4571.1]	13,33
12	286,1[274.0. 298.4]	8,51
13	113,6[108.3,119.0]	7,66
14	29371.6[29097.1, 29650.6]	38,85
15	85195.8[84753.5, 85638.3	68,44

TABLE IV: MLVMA Vs MA: mean difference and the 99% confidence interval.

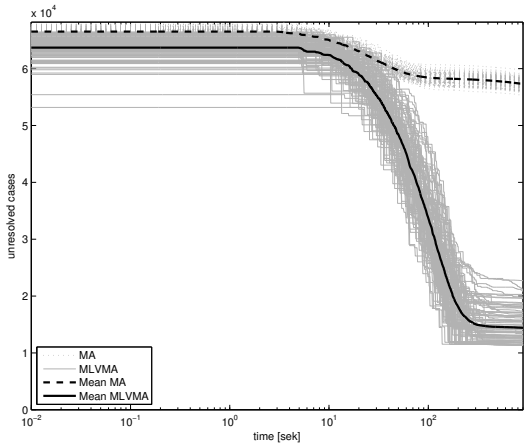

Fig. 1. Log-Log plot: MLVMA Vs MA: bmc-ibm-9.cnf: $|V|$ = 63624 , $|C|$= 326999 - Time development for 100 runs in 15 minutes

• Stopping criteria for the reduction phase: The reduction process stops as soon as the size of the coarsest problem reaches 100 variables (clusters). At this level, MA generates an initial population.
• Convergence during the refinement phase: If there is no observable improvement of the fitness function of the best individual during 10 consecutive generations, MA is assumed to have reached convergence and moves to a higher level.
• Time constraint for each run is 900 seconds and one single run 60 minutes.

Analysis of Results

The comparison of the MA and the MLVMA algorithms for each instance is shown in Tables II-IV. Tables II-III show the mean, standard deviation and the range of unsolved clauses for MLVMA and MA for each instance after a 900 seconds run time. Table IV shows the mean difference and the 99 percent confidence interval for the difference between MA and MLVMA. Bootstrapping was chosen due to the lack of knowledge regarding the statistical distribution of the underlying population. The domination of MLVMA versus MA is strengthened by the fact that none of the confidence intervals for the mean difference between MLVMA and MA contains zero (0)[2]. The standardized effect size measure Cohen's d (Cohen 1988) is very high [3] and in-

[2]we used mean-based statistics to evaluate the difference between the two algorithms because there was no overlap between the compared data sets. This is not in accordance with recent recommendations (Arcuri and Briand 2011) but was found to be necessary because non-parametric rank-based tests of significance such as Mann-Whitney U-test would not entail extra information as non-overlapping data sets would give identical solutions for different instances

[3]The mean-based effects size measure Cohen's delta (Cohen 1988) was used because we used mean-based t-tests to evaluate the difference between the data sets. We also included Cohen's delta because the common language effect size measure $\hat{A}_{12}$ (Vargha and Delaney 2000) would entail no extra information as

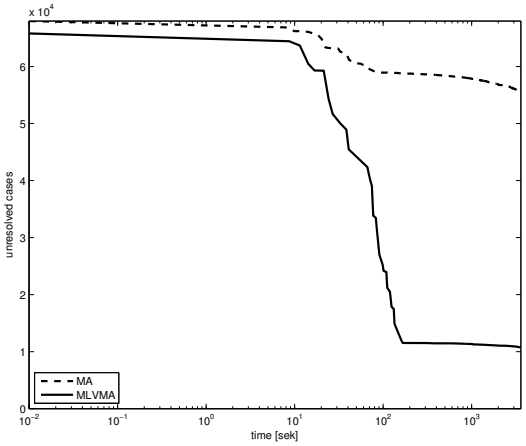

Fig. 2. Log-Log plot: MLVMA Vs MA: bmc-ibm-9.cnf: $|V|$ = 63624 , $|C|$= 326999 - Time development for one run in 60 minutes

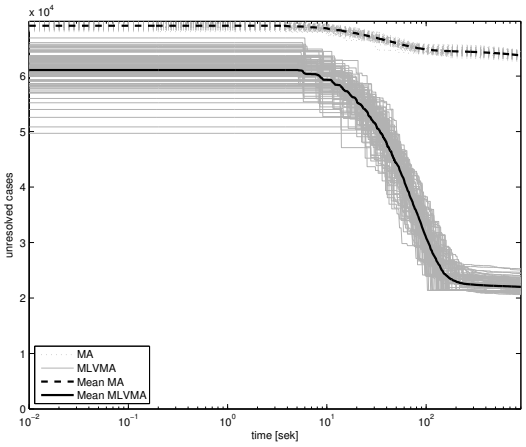

Fig. 3. Log-Log plot: MLVMA Vs MA: bmc-ibm-10.cnf: $|V|$ = 61088 , $|C|$= 334861 - Time development for 100 runs in 15 minutes

dicates that the effect of adding the multilevel paradigm to the memetic algorithm leads to a great improvement of the solutions after a 900 seconds run time.

The plots in Figures 1–4 show the general tendency of the solution quality reached as a function of time for two instances. Single runs with a cut-off parameter of (1 hour) for both algorithms was performed to see whether any cross-over occurred for the two algorithms. Figures 2 and 4 show the 100 runs of MLVMA and MA with a cut-off at 15 min as well as the mean of these runs, while Figures 1and 3 show single runs of the MLVMA and MA with a cut-off parameter of 60 minutes. The plots suggest that problem solving with MLVMA happens in two phases. In the first phase which corresponds to the early part of the search, MLVMA behaves as a hill-climbing method. The best assignment improves rapidly at first, and then flattens off as we mount the plateau, marking the start of the second phase.

The plateau spans a region in the search space where

one model would always be better, e.g. $P_{(MLVMA>MA)} = 1$ for all instances

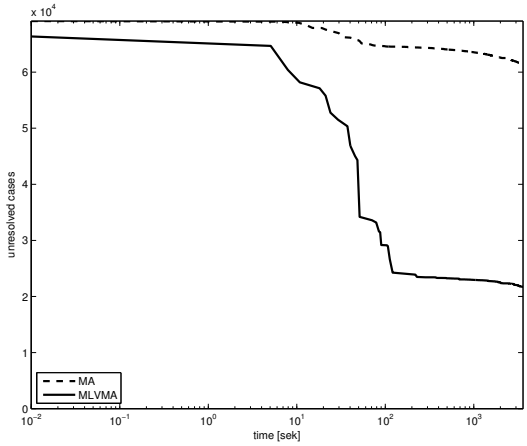

Fig. 4. Log-Log plot: MLVMA Vs MA: bmc-ibm-10.cnf: $|V|$ = 61088 , $|C|$= 334861 - Time development for one run in 60 minutes

flips typically leave the best assignment unchanged, and occurs more specifically once the refinement reaches the finest level. It is clear from the plots that the multilevel variant offers a clear advantage over its single version. We can see from the results that MLVMA have a better asymptotic convergence (to around 89.73%- 99.96% in excess of the optimal solution) as compared to MA which only reach around (80.28%- 99.86%). The instances where both algorithms reach approximately the same solution quality (with MLVMA being marginally better). MLVMA offers a cost effective solution strategy considering the amount of time required.

In our view, the efficiency of MLVMA relies on coupling the refinement process across different levels. This paradigm offers two main advantages which enables MA to become much more powerful in the multilevel context. During the refinement phase MA applies a local transformation (i.e. a move) within the neighborhood (i.e. the set of solutions that can be reached from the current one) of the current solution to generate a new one. The coarsening process offers a better mechanism for performing diversification (i.e. the ability to visit many and different regions of the search space) and intensification (i.e. the ability to obtain high quality solutions within those regions). By allowing MA to view a cluster of variables as a single entity, the search becomes guided and restricted to only those configurations in the solution space in which the variables grouped within a cluster are assigned the same value. As the size of the clusters varies from one level to another, the size of the neighborhood becomes adaptive and allows the possibility of exploring different regions in the search space while intensifying the search by exploiting the solutions from previous levels in order to reach better solutions.

CONCLUSION

A new apperoach has been outlined for solving the satisfiability problem based on a combining a memetic algorithm with the multilevel paradigm. A set of large benchmark instances were used to get a comprehen-

sive picture of the performance of the new approach. The multilevel paradigm greatly improves the MA and always returns a better solution for the equivalent runtime. The tests where MLVMA and MA offer similar asymptotic convergence, MLVMA being slightly better and considerably faster. The broad conclusions that we draw from the presented results is that the multilevel paradigm can enhance the convergence behavior of the memetic algorithm. Our future work aims at investigating other coarsening schemes together with various cross-over operators for the the possible enhancement of the multilevel memetic algorithm.

References

[1] Arcuri, A. and L. Briand. 2011. "A Hitchhiker's Guide to Statistical Tests for Assessing Randomized Algorithms in Software Engineering." Technical report, simula research laboratory, number 13.

[2] Biere, A.; A. Cimatti; E. Clarke, and Y. Zhu. 1999. "Symbolic model cheking without BDDs ". In Tools and Algorithms for the Construction and Analysis of Systems, 193-207.

[3] Bouhmala, N. and O.C. Granmo. 2011. "GSAT Enhanced with Learning Automata and Multilevel Paradigm." International Journal of Computer Science Issues, Vol. 8, Issue 3, 38-54.

[4] Cohen, J. 1988. "Statistical Power Analysis for the Behavioral Sciences." 2nd ed. Lawrence Erlbaum, (1988).

[5] Hoos,T and T. *Stützle*. 2004. "Stochastic Local Search: Foundations and Applications." Morgan Kaufmann.

[6] Karypis, G. and V. Kumar. 1998. "A Fast and High Quality Multilevel Scheme for Partitioning Irregular Graphs.". SIAM J. Sci. Comput., 20(1), 351-392.

[7] Norman, M.G. and P. Moscato. 1989."A competitive and cooperative approach to complex combinatorial search ". Technical Report Caltech Concurrent Com- putation Program, Report. 790, California Institute of Technology, Pasadena, California, USA. expanded version published at the Proceedings of the 20th Informatics and Operations Research Meeting, Buenos Aires (20th JAIIO).

[8] Rintanen, J.; K. Heljanko, and I.Niemelä. 2006. "Planning as Satisfiability: Paralel plans and algorithms for plan search ". Artificial Intelligence, vol. 170, no, 12-13, 1031-1080.

[9] Smith,A.; A.G. Veneris; M.F.Ali, and A. Viglas. 2005."Fault diagnosis and logic debugging using Boolean satisfiability". IEEE Transactions on Computer-Aided Design, Vol. 24, no.10, 1606-1621.

[10] Vargha, A. and H.D. Delaney. 2000."A critique and improvement of the CL Common Language Effect Size statistics of McGraw and Wong". Journal of Educational and Behavioral Statistics, 25(2), 101-132.

[11] Spears, W. 1995."Adapting Crossover in Evolutionary Algorithms". Proc of the Fourth Annual Conference on Evolutionary Programming, MIT Press, 367-384.

[12] Walshaw, C. 2004."Multilevel Refinement for Combinatorial Optimization Problems". Annals of Operations Research 131, 325-372.

A COMPREHENSIVE FORMULATION FOR RAILROAD BLOCKING PROBLEM

Reza Mohammad Hasany
Yousef Shafahi
Seyed Farzan Kazemi
Department of Civil Engineering
Sharif University of Technology
Azadi St., Tehran 11365-9313, Iran

KEYWORDS
Mixed-Integer Non-linear Programming, Railroad Planning, Tactical Level of Managment, Blocking Problem.

ABSTRACT

In rail transportation, there have been several attempts to determine the best routes for shipments (a number of cars with the same origin-destination) through the network. Shipments enter into several intermediate yards on their routes to separate and regroup shipments into new trains. Most of time, every entering into a yard includes excessive delay for shipments; therefore it is an ideal plan that each shipment has been transported by an exclusive train service. Mainly because of restriction on a number of running trains, this plan cannot be adapted in most cases. Finding the optimal route over the rail network with above and other common constraints would be handled by *railroad blocking problem*. From 1980 to the present, many mathematical programs have been proposed in this issue. In literature, however, there has not been any model with all realistic constraints. In this article, we give a brief literature review on railroad blocking problem. Afterwards, we present a comprehensive mixed integer programming formulation for this problem. Finally, we solve a test instance to show our model is in line with our expectation.

INTRODUCTION

A rapid, efficient, and reliable transportation service has been considered as a main factor in development of countries. In most countries, different modes of transport (including road, sea, water, and rail) have been used to provide a better customer service. Due to the intense competition between transportation providers, if customers understand any decline in the quality of delivery service in one mode, it cannot easily survive in such competition for long run. Among different modes of transportation, railway has carried a large amount of domestic freight services. Better environmental compatibility, more fuel efficiency, and more economy often lead to have an endorsement of the governments. Hence, the duty of rail mangers is not only keeping the level of rail delivery system acceptable, but also considering its further development as a part of the national transportation system.

With respect to the investment level, decision making level, and time horizon, railway transportation planning has been divided into three hierarchical levels of planning: *strategic*, *tactical*, and *operational*. In practice, considering the three levels in the form of only one problem is obviously intractable. Thus these levels have been performed individually and sequentially. In this case, we adapt the output of strategic planning as in input of tactical planning, and output of tactical planning as an input of operational planning.

At the strategic level, macro decisions (made by high-rank mangers) require a lot of investment resources, and perform at long-time horizons more than one year. The main issues which arise in the strategic planning include: developing and improving the rail network (Hooghiemstra et al. 1999); determining optimal location of yards and their capacities (Alumur and Kara 2008). Tactical planning focuses on what to do to use efficiently existing railway infrastructures and resources. At this level, most decisions have been taken for interval of one month to one season. In fact, tactical planning plays the role of a bridge between strategic and operational planning. Outline of some issues in this level includes: crew scheduling (Caprara et al. 1997), maintenance management (Shafahi and Hakhamaneshi 2009), and railroad blocking problem (Barnhart et al. 2000). Operational planning explains the short period ways of achieving the goals and detailed daily activities in the rail transportation planning. Timetabling (D'ariano et al. 2007) is discussed in this stage.

In this paper, we only consider the railroad blocking problem which is an important issue in the railroad planning process. This article is organized into six sections. We define the main terms of railroad blocking problem in section 2. Section 3 includes a brief review on relevant studies in blocking problem. In section 4 we present a mathematical formulation that aims at minimizing both user and provider costs over the network, and discuss the scale of the model in a real-size rail network. In section 5 we make use of the proposed model in a test network. We finish the article with some concluding comments and future researches in section 6.

Proceedings 27th European Conference on Modelling and Simulation ©ECMS Webjørn Rekdalsbakken, Robin T. Bye, Houxiang Zhang (Editors)
ISBN: 978-0-9564944-6-7 / ISBN: 978-0-9564944-7-4 (CD)

RAILROAD BLOCKING PROBLEM

Rail (physical) network includes a number of yards linked together by rail tracks to ship a quantity of cargo. In this paper, we only consider the classification yards which have the necessary equipment to separate, sort, and group the incoming cars and finally dispatch them by outgoing trains.

There are two extreme transportation policies for dispatching shipments over the rail network. The first policy is to dispatch the shipments with the first outgoing train from the yard. Reducing shipment lost times, and forming long-length trains are among its advantages. On the contrary, the cars should pass several intermediate yards on their routes and switch their trains to reach the final destination. Jin (1998) reported that using this policy would dramatically increase average delay per car. In the other policy, while one train (transporting only one shipment) is scheduled to depart at the origin, it will bypass any intermediate yard until it reaches to its destination. Although this policy leads to minimization of the time spent at intermediate yards, the train will haul a number of cars less than maximum car which a train can pull.

A common way to decrease the delay is to apply a combination of two above policies. This policy considers the shared arcs in the path of shipments as *blocking arcs*. In the other words, each blocking arc is defined as a virtual arc that represents several successive arcs and yards in the physical network. First and last yards of these consecutive arcs are the beginning and end node of the blocking arc, respectively. While shipments do not reach the end of a blocking arc, no classification operations would be allowed. Set of all blocking arcs a shipment meets from the origin to the destination named a *blocking path*. The *blocking network* is a collection of all blocking arcs and their corresponding start and end nodes. In the blocking network, the weight of each arc is equal to the travel time required to traverse it.

To clarify these definitions, suppose that origin and destination of one shipment are node 1 and node 4, respectively (see figure 1). Also node 2 and node 3 are intermediate classification yards. All candidate paths shipping cars over network have been shown in figure 1. For example, consider blocking path 3. A shipment starts moving from node 1, bypasses node 2, enters into node 3 for classification operations and finally proceeds its route to deliver the shipment at node 4. Obviously all candidate paths traverse the same physical arcs over the physical network, though there are clearly different blocking paths over the blocking network.

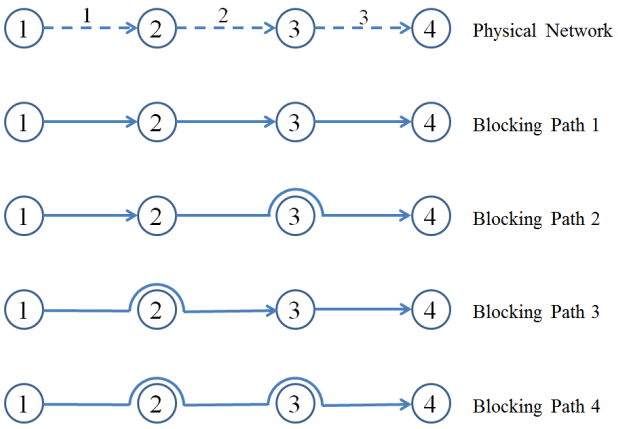

Figure 1: A physical rail network and all candidate blocking paths

LITERATURE REVIEW

Throughout the years, several researchers have proposed a variety of real-world blocking models using mathematics, and some papers also have developed solution techniques for these models. In the following, we briefly review the literature with an emphasis on modeling formulation in this field.

Assad (1980) was one of the first researchers who simplified the representation of blocking problem in the form of quantitative model. Its objective function consists of minimizing the sum of two costs: freight car and locomotive running costs; and classification costs inside yards as a linear function of incoming traffic. Assad (1980) also held the following constraints: conservation of flow which has been widely used in network optimization, and setting upper bound on the total flow moving through each blocking arc. The second constraint guaranteed that no shipment was assigned to the blocking arc not in optimal solution. This article mainly dealt with modeling formulation and just made an offer to adapt the Branch and Bound algorithm as an effective approach for solving the model exactly.

Bodin et al. (1980) proposed a mixed-integer nonlinear programming for railroad blocking problem. There are three differences between Assad (1980) and Bodin et al. (1980). At first, the former did not consider the limitation to total number of cars classifying at each yard, but latter did. Moreover, this model set the maximum on the number of blocking arcs with positive flow formed at every yard. The last difference is in the existence of delay term in objective function. The delay function, associated with incoming cars at each yard, can be presented as linear functions corresponding to the number of outgoing trains at the yard so that an increase in the number of trains dispatched from yards incurs less waiting time. Keaton (1989) proposed a mixed integer program for blocking problem. Unlike earlier efforts, he neglected the delay term and only considered the objective function as a summation of car and locomotive costs. The importance of this research is

mainly due to application of Lagrangian relaxation (a technique for approximating large scale integer programming) to solve the blocking model.

Marín and Salmerón (1996) model was able to obtain the number of trains in blocking arcs in addition to the optimal blocking path of shipments. The objective function involves the investment cost for buying more running locomotives in addition to car and locomotive holding costs. This function is minimized subjected to constraints which are: conservation of car flow, restriction on a number of cars moving on all blocking arcs, and setting a number of blocking arcs formed at every yard. Imposing the number of train variables would significantly increase the computational efficiency in seeking the optimal solution. Therefore, the authors employed three most promising meta-heuristics: taboo search, simulated annealing, and descending methods.

After the Mississippi river flood in 1993, there was a report showing that if there had been a quick method to update planning the active yards on the rail system, the US government would quickly provide relief to whom affected by flood. Accordingly, Newton et al. (1998) represented a model which took into account the common railroad limitations and objective function which have been introduced in earlier efforts. The authors also proposed the algorithm base on Branch and Bound to maintain a relatively small running time of the algorithm in practice. Jin (1998) used Lagrangian relaxation technique to partition Netwon and etal (1998) model into smaller subproblems. For the real data of U.S. railroads, significant improvements have been obtained compare to Newton and etal (1998).

Fugenschuh et al. (2009) proposed the mixed integer programming problem. In addition to constraints commonly used in previous works, the authors obtained more constraints including: the upper bound on travel time for each shipment through network, limitation on the number of outcoming trains from every yard, and the allowable length and weight on each train assembled at yards. This work mainly focused on the modeling formulation and did not discuss on solution approaches.

MODEL FORMULATION

Recent formulations of blocking problem have been along with shortcomings. The main decision tools and realistic constraints that are important to rail mangers would be removed from the models mainly due to CPU-time and memory limitations. Thus primary focus of this paper is on a new formulation here for blocking problem and revising flaws in earlier models. For simplicity, we use the below notations to develop the model:

Parameters:

- φ : The value of travel time ($ per day-car),
- A : Set of all blocking arcs,
- K : Set of all shipments,
- $Q(k)$: Set of all candidate blocking paths for shipment k,
- m : Number of classification yards,
- t_a : Travel time on blocking arc *a* (day),
- PT : Planning time period (day),
- α : Given parameter (usually 2),
- ε : An arbitrarily small positive quantity,
- $\eta(a)$: The yard at starting-point of blocking arc *a*,
- $w_{\eta(a)}$: Time duration required for one car preparation to depart yard $\eta(a)$ (day),
- δ_a^q : 1 if blocking arc *a* is on path *q* and 0 otherwise,
- χ_a : Operating costs for one train running on arc *a* ($ per train),
- d^k : Number of cars belonging to shipment *k* (car),
- ξ_i^a : 1 if *i* is the origin of arc *a* and 0 otherwise,
- $W(i)$: Maximum number of blocking arcs with positive value beginning formed at yard *i*,
- $V(i)$: Maximum number of cars handled in yard *i* (car),
- $N(i)$: Maximum number of trains dispatched from yard *i* (train),
- M_a : Maximum number of trains running on blocking arc *a* (train),
- T^k : Upper bound on the transit time of shipment *k* permitted to spend in the network (day),
- u_a : Maximum number of cars can pull by one train on blocking arc *a* (car per train),
- l_k : Length of one car belonging to shipment *k* (meter per car),
- L_a : Maximum length of one train running on blocking arc *a* (meter),
- w_k : Weight of one car belonging to shipment *k* (ton per car), and
- W_a : Maximum tonnage transported on blocking arc *a* (ton).

Decision Variables:

- n_a : Number of trains running on blocking arc *a* (train),
- f_q^k : The portion of shipment *k* on blocking path *q*,

- Z_a: 1 if blocking arc *a* used and 0 otherwise, and
- X_q^k: 1 if shipment *k* used blocking path $q \in D(k)$ and 0 otherwise.

The proposed model would be formulated as the following mathematical program:

$$Min\ Z$$

$$= \varphi . \sum_{k \in K} \sum_{q \in Q(k)} \left[\sum_{a \in A} (t_a + w_{\eta(a)} + \frac{PT}{\alpha (n_a + \varepsilon)}) . \delta_a^q \right] . f_q^k . d^k + \sum_{a \in A} \chi_a . n_a \quad (1)$$

$$\sum_{q \in Q(k)} \delta_a^q . X_q^k \le \left| Q(k) \right| . Z_a \quad \forall a \in A; k \in K \quad (2)$$

$$\sum_{q \in Q(k)} f_q^k = 1 \quad \forall k \in K \quad (3)$$

$$\sum_{a \in A} \sum_{k \in K} \sum_{q \in Q(k)} \xi_i^a . \delta_a^q . d^k . f_q^k \le V(i) \quad \forall i = 1, ..., m \quad (4)$$

$$\sum_{a \in A} \xi_i^a . Z_a \le W(i) \quad \forall i = 1, ..., m \quad (5)$$

$$f_q^k \le X_q^k \quad \forall k \in K; q \in Q(k) \quad (6)$$

$$\left[\sum_{a \in A} (t_a + w_{\eta(a)} + \frac{PT}{\alpha (n_a + \varepsilon)}) . \delta_a^q \right] . X_q^k \le T^k$$

$$\forall k \in K; q \in Q(k) \quad (7)$$

$$\sum_{k \in K} \sum_{q \in Q(k)} \delta_a^q . d^k . f_q^k \le u_a . n_a \quad \forall a \in A \quad (8)$$

$$n_a \ge Z_a \quad \forall a \in A \quad (9)$$

$$\sum_{a \in A} \xi_i^a . n_a \le N(i) \quad \forall i = 1, ..., m \quad (10)$$

$$\sum_{q \in Q(k)} \delta_a^q . f_q^k . l_k \le L_a . n_a \quad \forall k \in K \quad (11)$$

$$\sum_{q \in Q(k)} \delta_a^q . f_q^k . w_k \le W_a . n_a \quad \forall k \in K \quad (12)$$

$$f_q^k \ge 0; n_a \ge 0 \ and \ Integer;$$

$$Z_a, X_q^k \ binary; \forall k \in K; a \in A; q \in Q(k),$$

Objective function of this program, (1), consists of two parts: *user cost* and *provider cost*. The user cost is equal to monetary value of total travel time which is defined by the travel time in all blocking paths with positive car flow connecting all origins to destinations. In this component, travel time on one blocking path, q, includes three components: time period moving in track rail; time period to handle into classification yards, and waiting time to dispatch trains from yards. The provider cost is equal to the product of unit of train operating cost and number of running trains for all blocking arcs.

Constraint (2) ensures that if one blocking arc, *a*, does not belong to any path for all shipments, then the model will not allow to pass even one car through arc *a*. Constraint (3) makes all cars belonging to shipment *k* moving from origin to destination and not lost in network. Due to geometric design consistency and proper operations into yards, number of cars handled at every yard would be limited. Inequality (4) captures this point. The number of blocking arcs with positive flow from each yard, *i*, is limited to *W(i)* by constraint (5). Constraint (6) represents the logical relationship meaning that if one car is moving on path *q* for shipment *k*, then X_q^k must be one. In other words, while path *q* is an active path for shipment *k*, at least one car must flow on it. Constraint (7) ensures that travel time for shipment *k* does not exceed allowable travel time. Constraint (8) makes number of cars moving in the blocking arc *a* depending on the number of trains running on this arc and also maximum number of cars pulled by one train at that blocking arc. Constraint (9) states that if the flow of a blocking arc is positive, then at least one train should move through the arc. Constraint (10) guarantees the number of trains dispatched from a yard, *i*, must be less than yard capacity, *N(i)*. Due to geometric design restriction or prohibition of railroads and yard-length requirement, standards have been made by managers on the train-length shown in constraint (11). Obviously, passing the heavy weight trains can cause sustaining damages on the railroads in a long-run. Thus providers have stated the restrictions on the weight of train sent from every yard in some countries in the form of constraint (12).

At the end of this section, we estimate the size of proposed model for a real-size network. let the network (Iran railways is in this size) which has about 100 yards (where the trains can be classified), 50 origins, 50 destinations, 5000 shipments moving over network, and consider only ten active paths between each origin-destination. Assume that we can make one blocking arc from any origin to any destination, any origin to any yard, from any yard to any other yard, any yard to any destination. In this case, the total number of candidate blocking arcs is equal to 50×50 + 50×100 + 100×100 + 100×500 = 22500. Thus the proposed model has 22500 non-negative integer variables to determine the number of train for each blocking arc; 22500 binary variables to select or not blocking arcs; 5000×10=50000 binary variables to select or not paths for shipments; 50000 non-negative flow variables; and approximately one hundred million constraints. For this case, optimization problem with this large-scale, exceed the capacity of existing solvers and software tools, especially because of nonlinearity.

AN EXAMPLE OF A SMALL SAMPLE NETWORK

In this section, we use the proposal model on a small instance to test the model. The small physical network consists of origins (node 1 and 2), classification yards (node 1-3), destinations (node 4 and 5), and four physical arcs, shown in figure 2.a. Figure 2.b shows all blocking arcs of the sample network. For example, blocking arc 1 means the car first flows on physical arc 1, bypass the node 3, and terminate at node 4. Our model is a path-based formulation, thus we should list all feasible blocking paths for modeling shown in figure 2.c. In real-scale network, an enumeration of these paths would be nearly impossible. To overcome this problem, Barnhart et al. (2000) suggested using those paths for each OD pair which have the travel time within 150% of length of shortest path.

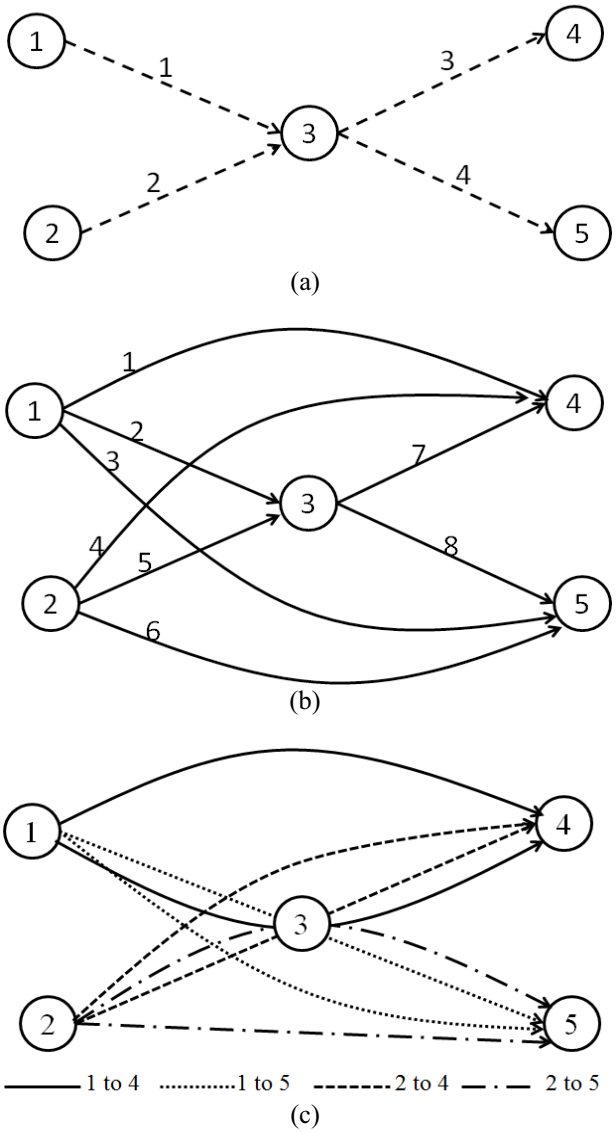

(a)

(b)

(c)

Figure 2: (a) Physical network, (b) blocking arc network, and (c) blocking path network

We now define the example data as follows: the number of cars is 200 cars from node 1 to node 4, 300 cars from node 1 to node 5, 400 cars from node 2 to node 4, and 500 cars from node 2 to node 5. Travel times along physical arcs 1, 2, 3, and 4 are 10, 15, 15 and 10 days, respectively. Maximum numbers of cars classified at all nodes are equal to 2000 cars. Maximum number of blocking arcs with positive flow for all nodes is assumed to be two. Train pulling capacities along arcs 1, 2, 3, and 4 are 34, 40, 40 and 20 cars, respectively. Operating costs on arcs 1, 2, 3, and 4 are 1020, 1680, 2940, and 2010 in unit of cost per car. Length and weight of one car are respectively 20 meters and 40 tons. Maximum of length and weight allowed moving along all arcs are 800 meters and 1600 tons respectively. Duration of planning is assumed to be 100 days.

The example can be solved within a 0.1 second to give the optimal solution (with objective function \$904854) using *GAMS23.4* and optimal value of a number of operating trains is shown in figure 3. Results are obtained on a 2.67 GHz Dual Core computer with 4 GB free RAM.

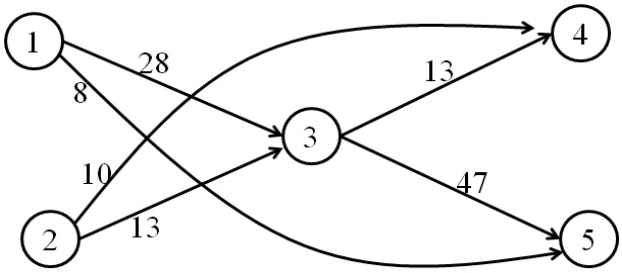

Figure 3: optimal value for n's variables in optimal solution

CONCLUSION

The blocking problem is an important problem in railway planning. By 2013, a variety of studies has been done in Operations Research for modeling this particular issue with realistic constraints. Despite several attempts, additional researches would be necessary to achieve a practical model. This research is an attempt to present the comprehensive optimization model, as a mixed-integer nonlinear program, with the realistic constraints. However the authors have shown that the application of the real networks makes the problem too large to be solved by the exiting commercial softwares. Thus the obvious future research emerging from this article is to introduce an efficient algorithm to solve the model. Effective techniques obtaining quick solutions would help the rail mangers to make their decisions. The authors are currently working on these techniques.

REFERENCES

Alumur, S. and B.Y. Kara. 2008. "Network Hub Location Problems: The State of The Art." *European Journal of Operational Research* 190, No.1 (Oct), 1-21.

Assad, A.A. 1980. "Modeling of Rail Networks: Toward a Routing/Makeup Model." *Transportation Research* 14B, No.1 (Feb), 101-114.

Barnhart, C., Jin, H. and Vance, P.H. 2000. "Railroad Blocking: A Network Design Application." *Operations Research* 48, No.4 (July), 603-614.

Bodin, L.D., Golden, B.L., Schuster, A.D. and William, R.A. 1980. "Model for the Blocking of Trains." *Transportation Research* 14B, No.1 (Mar), 115-150.

Caprara, A., Fischetti, M., Toth, P., Vigo, D. and Guida, P.L. 1997. "Algorithms for Railway Crew Management." *Mathematical Programming* 79, No.1-3, 125-141.

D'ariano, A., Pacciarelli, D. and Pranzo, M. 2007. "A Branch and Bound Algorithm for Scheduling Trains." *European Journal of Operational Research* 183, No.2 (Dec), 643-657.

Fugenschuh, A., Homfeld, H. and Schulldorf, H. 2009. "Single Car Routing in Rail Freight Transport." In *Dagstuhl Seminar 09261 2009*, C. Barnhart, U. Clausen, U. Lauther and R.H. Mohring (Eds.). Schloss Dagstuh, Leibniz-Zentrum.

Hooghiemstra, J.S., Kroon, L.G., Odijk, M.A., Salomon, M. and Zwaneveld, P.J. 1999. "Decision Support Systems Support the Search for Win-Win Solutions in Railway Network Design*." Interfaces* 29, No.2 (Mar), 15-32.

Jin, H. 1998. "Designing Robust Railroad Blocking Plans." Ph.D. Thesis. Department of Civil and Environmental Engineering, Massachusetts Institute of Technology, MA. (June).

Keaton, M.H. 1989. "Designing Optimal Railroad Operating Plans: Lagrangian Relaxation and Heuristic Approaches." *Transportation Research* 23B, No.6 (Feb), 415-431.

Marín, A. and Salmerón, J. 1996. "Tactical Design of Rail Freight Network, Part I: Exact and Heuristic Methods." *European Journal of Operational Research* 90, No.1 (Apr), 26-44.

Newton, H.N., Barnhart, C. and Vance, P.H. 1998. "Constructing Railroad Blocking Plans to Minimize Handling Costs." *Transportation Science* 32, No.4 (Dec), 330-345.

Shafahi, Y. and Hakhamaneshi, R. 2009. "Application of a Maintenance Management Model Based on Markov Chain and Probabilistic Dynamic Programming for the Iranian Railways." *Scientia Iranica* 16, No.1 (June), 87-97.

AUTHOR BIOGRAPHIES

REZA MOHAMMAD HASANY was born in Tehran, Iran in 1984. He is now a doctoral student with an emphasis in Transportation planning working under Dr. Shafahi in Sharif University of Technology, Tehran, Iran. He received his Bachelor of Science degree in Civil Engineering in 2007 and his Master of Science degree in Transportation Planning in 2010 from Sharif University of Technology. His research interests include mathematical programming, large-scale optimization, and optimization under uncertainty. This time, his PhD thesis comprises the application of modeling and optimization in the area of railway planning. His e-mail address is: rmhasany@gmail.com.

YOUSEF SHAFAHI received his PhD in Civil Engineering from University of Maryland, USA in 1997. He joined the Department of Civil Engineering in Sharif University of Technology as an Assistant Professor in 1998 and became an Associate Professor in 2009. His main research interest is Operations Research in Transportation Planning. His e-mail address is: Shafahi@sharif.edu and his Web-page can be found at http://sharif.edu/~shafahi.

SEYED FARZAN KAZEMI was born in Mashhad, Iran in 1989. He received his Master of Science in Road and Highway Engineering in 2012 from Sharif University of Technology under supervision of Dr. Shafahi. At this time, he is a doctoral student at university of Tehran. His email address is: s.farzan.kazemi@gmail.com.

SELECTION OF SYNCHRONOUS REACTIVE FREQUENCY CONVERTER'S SECONDARY WINDINGS PARAMETERS AND OPTIMIZATION OF ROTORS GEOMETRICAL DIMENSIONS TO ENSURE HIGHEST INCREASED FREQUENCY EMF INDUCTION

Aleksandrs Mesņajevs
Andrejs Zviedris
Elena Ketnere
Faculty of Power and Electrical Engineering
Riga Technical University
1 Blvd Kronvalda, 1010 Riga, Latvia
E-mail: kbl@inbox.lv, aaazzz@eef.rtu.lv, ketnere@eef.rtu.lv

KEYWORDS

Finite element method; QuickField; frequency converter.

ABSTRACT

In many spheres of human activities devices that work on increased frequency current are widely applied. 50 Hz current can be converted into increased frequency (100-400 Hz) current using synchronous reactive converters, which are based on exude and usage of higher harmonics.
The goal of this paper is to determine which circumstances must be taken into account to ensure highest increased frequency EMF induction in a secondary winding. To solve this problem the optimization of rotor geometrical shape must be applied. As a result rotor's optimal shape which ensures highest EMF induction is obtained.

INTRODUCTION

While using modern alternative current (AC) network with 50 Hz frequency it is not expedient to apply autonomous power sources with increased frequency. Economically more beneficial is to convert 50 Hz AC into AC with increased frequency.
Increased frequency current usage in hand tools can give significant economical effect. For example, increased frequency hand tools are lighter (in comparison with pneumatic), in addition they have higher technical-economical coefficient, increased frequency tool's actual cost is 8-10 times smaller than pneumatic hand tools, operation costs are 7-8 times smaller (Таращанский 1962).
To fulfil frequency increasing task the synchronous reactive frequency converter (SRFC) can be used.
SRFC is synchronous reactive machine, which uses magnetic field's higher harmonics. In slots of SRFC two windings are placed: primary, which is connected to industrial frequency AC network and secondary, which is used to receive higher frequency. It is possible to note, that synchronous reactive frequency converter is one-machine aggregate, in which the synchronous reactive motor (stator's primary winding – salient pole rotor) and inductor generator (salient pole rotor – secondary winding) are combined.
Primary winding is consuming magnetizing current, which produces rotating magnetic field in the air gap. From induction's distribution curve the necessary higher harmonic is used due to specific form rotor magnetic system and to accordingly selected sir gap's width.
This harmonic induces increased frequency EMF in secondary winding. To achieve this secondary winding's step must be equal to necessary field's higher harmonic pole pitch (or almost equal).
Power with help of magnetic field is transferred from primary winding to secondary winding by means of specific transformation. In this case link between primary and secondary winding isn't provided by mutual induction flux, but by part of it – higher harmonic exuded flux. Power transfer is depending on geometrical shape of a converter. Having one stator (core, stator windings, slot number, etc.), but different rotors a very different EMF value can be received. So it is necessary to determine optimal shape of rotor to receive highest secondary winding's EMF induction.

SELECTION OF SRFC'S CONSTRUCTIVE ELEMENTS AND PARAMETERS

Stator's secondary winding

Salient pole synchronous machines magnetic induction's distribution in air gap is not sinusoidal. Than means, that magnetic induction curve contains not only fundamental harmonic, but also higher harmonics. Higher k harmonic's magnetic field in synchronous machines rotates with synchronous rotation frequency and its pole number $2p_k$ is k-times bigger than fundamental harmonic's pole number $2p$ (Zviedris 1984). So, to use k harmonic's energy in synchronous machines slots secondary winding with pole number

Proceedings 27th European Conference on Modelling and Simulation ©ECMS Webjørn Rekdalsbakken, Robin T. Bye, Houxiang Zhang (Editors)
ISBN: 978-0-9564944-6-7 / ISBN: 978-0-9564944-7-4 (CD)

$$2p_k = 2kp \quad (1)$$

and winding pitch

$$y_k \approx \frac{\tau_z}{k} = \frac{Z_k}{2kp}, \quad (2)$$

where τ_z – fundamental harmonics pole pitch; Z_k – for secondary winding used slots number, must be inserted.

To use k harmonic's energy more efficiently it is important to choose secondary winding shame and parameters correctly. Constructively it is efficient to insert secondary winding in the same slots in which primary winding is placed. If secondary winding is organized as two lair loop winding, it will occupy all Z armature slots. Generally secondary winding can be organized with different phase number m_k (Zviedris 1984).

Possible variants of rotors shapes for different f_2 / f_1 ratio (2:1, 3:1, 4:1)

For SRFC it is important to exude defined magnetic field's higher harmonic so it will have biggest value. To achieve this rotor's magnetic system's shape and air gap must be chosen that in magnetic field necessary harmonic will be exuded, but all other higher harmonics whenever possible are equal to zero.
Rotor's constructive variants for different harmonic exude are presented on table 1.

Table 1: Simplified rotor's constructions

Exuded harmonic $k = f_2/f_1$ / Exude of harmonic	$k = 2$ (even)	$k = 3$ (uneven)
Using direct-ass conductivity	1)	3)
Using quadrature-ass conductivity	2)	4)
Exuded harmonic $k = f_2/f_1$ / Exude of harmonic	$k = 4$ (even)	$k = 5$ (uneven)
Using direct-ass conductivity	5)	7)
Using quadrature-ass conductivity	6)	8)

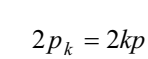 - ferromagnetic part of a rotor,

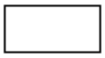 - non-ferromagnetic part of a rotor (aluminum, plastic).

SRFC'S CALCULATION EXAMPLE

Finite element method (FEM) is chosen as magnetic field's research method which is realized in QuickField software (QuickField 2009). For research is chosen commercial asynchronous machine's magnetic system, in which slots primary and secondary windings are placed. To clarify SRFC's magnetic system modeling questions and to asses received characteristics the frequency doubler is selected.
The aim of research is to determine in stator's primary and secondary winding induced EMF fundamental harmonics effective values dependence from SRFC rotor's geometrical parameters, rotor's ferromagnetic parts filling angle β (see Fig. 1.) and from armature current.

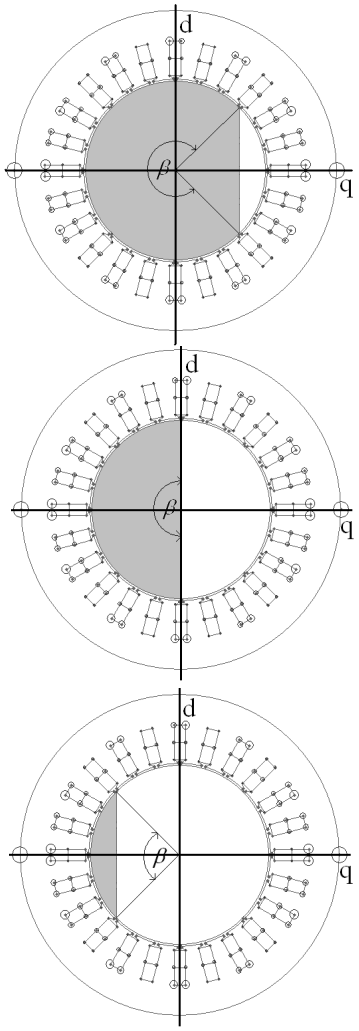

Figures 1. SRFC rotor's designs (with gray the ferromagnetic part is shown)

Calculations are made for idle running, when secondary winding's current $I_2 = 0$.

Conducting magnetic field's mathematical modeling the following magnetic field's picture is received for different rotor's filling angles β.

In primary and secondary winding induced EMF fundamental harmonics values are received (for secondary winding the fundamental harmonic is magnetic field's distribution higher harmonic, in this case 100 Hz) for number of variants:

1. $\beta = 180^\circ$ and $I_a = 16,\ 30,\ 44,\ 58,\ 72$ A;
2. $\beta = 90^\circ,\ 180^\circ,\ 270^\circ$ and $I_a = 16,\ 44,\ 58,\ 72$ A.

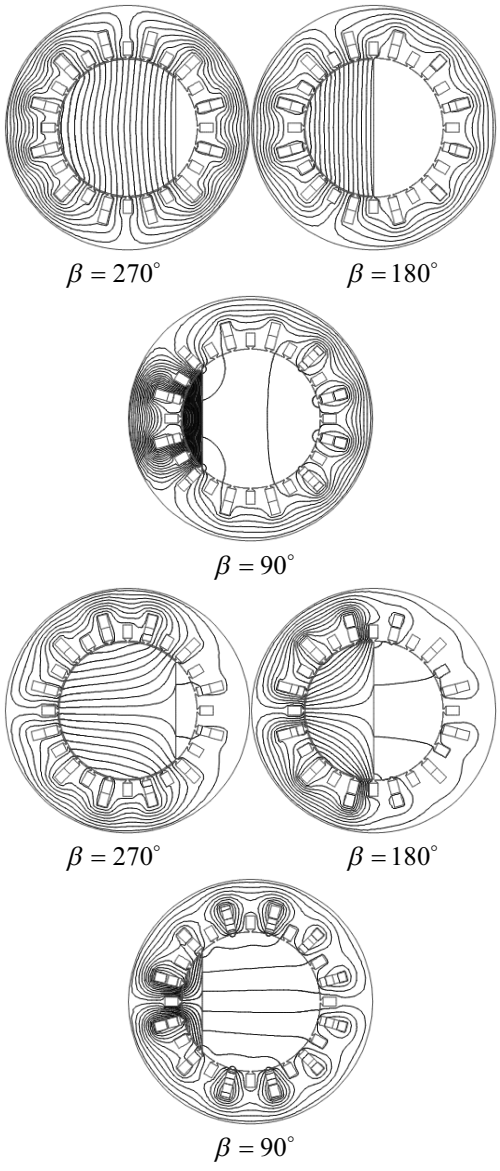

Figures 2. SRFC magnetic field's pictures for $I_a = 44$ A First two rows – direct-axis ($I_a = I_d$ and $I_q = 0$), last two rows – quadrature-axis ($I_a = I_q$ and $I_d = 0$)

Primary and secondary winding induced EMFs are calculated using following formula

$$E = 4{,}44 f\, k_w \frac{2p \cdot q \cdot w_{sp}}{a} 2A_m l, \qquad (3)$$

where f – frequency; k_w – winding coeficient; q – slots number per pole and phase; w_{sp} – coil's turn number; a – parallel turn number; A_m –specific harmonic's vector magnetic potential amplitude value (determined using magnetic field mathematical simulation); l – machine's length in axial direction.

Using first variant data results are presented on figures 3 and 4.

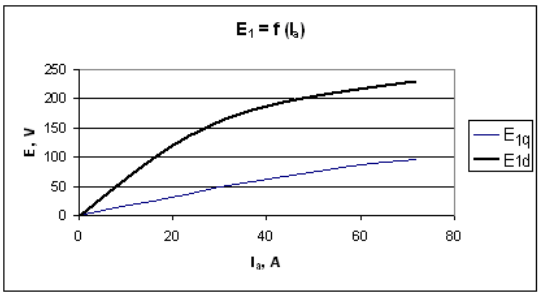

Figures 3. In primary winding induced (direct-axis with index *d*, quadrature-axis with index *q*) EMF effective values dependence form armature current for $\beta = 180^\circ$

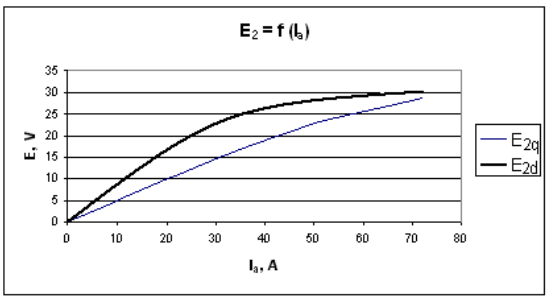

Figures 4. In secondary winding induced (direct-axis with index *d*, quadrature-axis with index *q*) EMF effective values dependence form armature current for $\beta = 180^\circ$

Using second variant data results several similar diagrams are received. On figures 5 - 8 boundary variants are presented

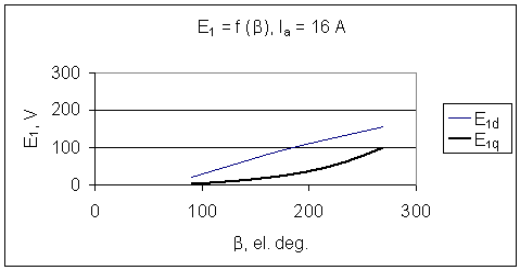

Figures 5. In primary winding induced fundamental harmonic EMF effective values dependence from angle β, if $I_a = 16$ A in direct-axis and quadrature-axis

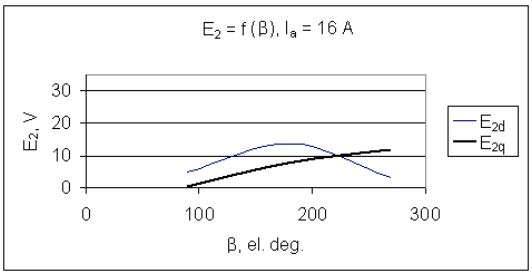

Figures 6. In secondary winding induced fundamental harmonic EMF effective values dependence from angle β, if $I_a = 16$ A in direct-axis and quadrature-axis

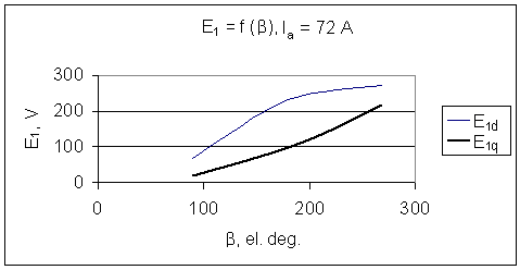

Figures 7. In primary winding induced fundamental harmonic EMF effective values dependence from angle β, if $I_a = 72$ A in direct-axis and quadrature-axis

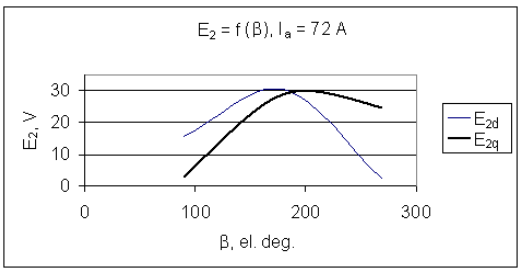

Figures 8. In secondary winding induced fundamental harmonic EMF effective values dependence from angle β, if $I_a = 72$ A in direct-axis and quadrature-axis

OPTIMIZATION OF SRFC'S ROTORS GEOMETRICAL DIMENSIONS

Research task, that is chosen for optimization is as follows.

Optimization systems boundaries are determined with chosen construction (SRFC with asymmetrical rotor and two windings in stator slots). To decrease variable parameter number it is assumed that geometrical dimensions and winding parameters are known.

For optimization quantitative criteria by second harmonics in secondary winding induced EMF E_2 is chosen (idle running).

For systems independence variables following characteristics are chose: SRFC rotor's ferromagnetic parts filling angle β, armature primary windings current I_a.

For base of development system's mathematical model on magnetic field theory supporting equations, which use FEM are chosen.

The aim of research is to determine in stator's secondary winding induced EMF E_2 dependence from angle β and armature current I_a.

Using *QuickField* software SRFC's model is constructed.

In result of research following charts are obtained.

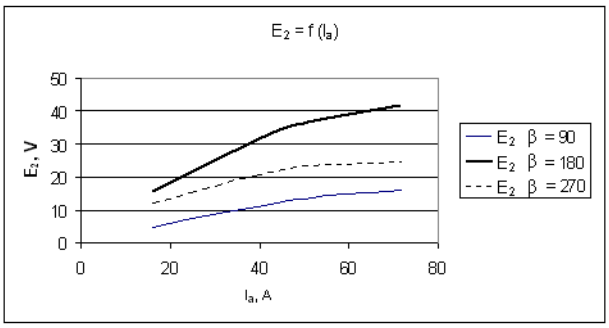

Figures 9. In secondary winding induced EMF dependence from armature current if $\beta = 90^\circ,\ 180^\circ,\ 270$

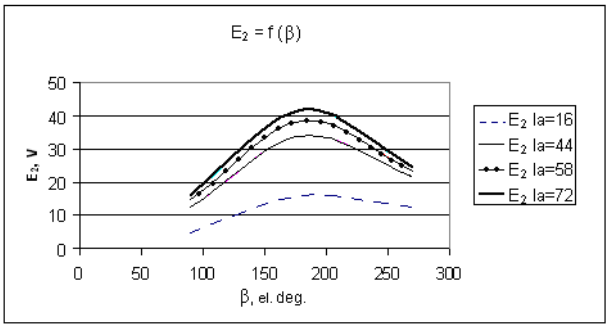

Figures 10. In secondary winding induced EMF dependence from rotor's ferromagnetic parts filling angle β

From figure 9 it is visible, that EMF E_2 curve increases faster when $\beta = 180^\circ$.

From figure 10 it is visible, that highest EMF E_2 value provide β between 180° and 200°.

MAIN RESULT

In order to receive highest in secondary winding induced EMF values frequency doubler's rotor must be made of at least 50% from ferromagnetic material, rotor's ferromagnetic parts filling angle β must be between 180° and 200° and armature current must be as high as possible (in feasible constraint).

REFERENCES

QuickField. 2009. Finite element analysis system. Version 5.7. User's guide. Svendborg. Tera Analysis Ltd. – 1

Mesņajevs, A. Zviedris Salient Pole Synchronous Machine`s Mathematical Simulation Data`s Processing Methods. Slovakia. Elektroenergetika 2011, 142. – 145. p.

Mesņajevs, A. Zviedris, A. Podgornovs Determination of Synchronous Machine's Characteristics Based on the Results of the Mathematical Modelling of the Magnetic Field. Krakow. 25th European Conference on Modelling and Simulation, 175. - 180. p.

Zviedris A. 1984. Elektriskās mašīnas. Rīga. Zvaigzne.

Таращанский М. 1962. Синхронно-реактивные преобразователи частоты. Киев. Государственное издательство технической литературы.

ACKNOWLEDGEMENTS

The travel costs and participation fee to conference was supported by the European Regional Development Fund project «Development of international cooperation projects and capacity in science and technology Riga Technical University», Nr.2DP/2.1.1.2.0/10/APIA/VIAA/003

AUTHOR BIOGRAPHIES

ALEKSANDRS MESŅAJEVS was born 1985 in Latvia. In 2012 he graduated from Riga Technical University, gaining Dr.Sc.ing. degree.

In March 2008 received certificate "Base and advanced simulation using QuickField software".

From 2006 he is working as a laboratory assistant and scientific assistant, from 2012 he is lecturer in Electrical Machines and Apparatus Department of Riga Technical University.

ANDREJS ZVIEDRIS was born 1938 in Latvia. In 1961 he graduated from the Riga Polytechnical Institute (RPI) Faculty of Electrical and Power Engineering, gaining the qualifications of Engineer in the Electrical Machines and Apparatus speciality. In 1970 defended a thesis and obtained a Candidate degree of Technical Sciences. Dr.Sc.ing. degree was conferred to A.Zviedris in 1992.

After graduating the RPI A.Zviedris has worked as an assistant Professor (1968-1973), and Department of Electrical Machines and Apparatus Head (1973-1984). In 2001 he was elected as Associate Professor in the Department of Electrical Machines and Apparatus, where work to date.

Scientific activities of A. Zviedris are related to Mathematical Simulation of magnetic fields in Electrical Machines. The results of his research are aprobated in more than 50 scientific publications and technical reports in International Scientific conferences.

A. Zviedris is an Expert in Standardization Technical Committee of Electrotechnical Terminology of Electrical Engineering, a member of Latvian Union of Scientists.

ELENA KETNERE, Asoc.Prof., Dr.Sc.Ing.

Riga Technical University, Faculty of Power and Electrical Engineering, Electrical Machines and Apparatus cathedra asoc. professor (2006..-), doctor degree (2002.).

Publications themes - Simulation of Gas-Turbine Driven Device. The Research of Stability of Synchronization Process with Unitrol 1000 Application. The Research of Stability of Synchronization Process with Mathematical Model's Application of Synchronous Generators.

BIFURCATION MODEL OF SUCCESSIONS IN ECOSYSTEMS

Serge V. Chernyshenko
Roman V. Ruzich
Department of Applied Mathematics and Social Informatics
Khmelnitsky National University
29000, Khmelnitsky, Ukraine
Email: svc@a-teleport.com; ninasus@gmail.com

KEYWORDS

Succession, biogeocoenose, system of ordinary differential equations, bifurcation.

ABSTRACT

Models of the long-term ecological successions are considered. Succession process is considered as step-by-step changing of dominant association. The model of open Eigen's hypercycle has been used for modeling of the process. Qualitative analysis for three-dimension case has been carried out, and local bifurcations have been investigated. The process of succession can be interpreted as system's choosing a proper level of complexity (or dimension) depending on the capacity of environment (the size of ecological niche). Connections between changing a state of the system and bifurcations in phase space is shown.

INTRODUCTION

Processes, which take place in ecosystems, are extremely complex; their theoretical investigation should be based on abstract concepts, which describe some general properties of the systems on the global level. One of such theoretical simplifications is the concept of succession. The succession is considered as consecutive change of one ecosystem (phitocoenose, biogeocoenoe, etc.) by other in a certain area of environment**.** It is not a simple transformation, but a process of simplification of the structure of the ecosystem. Any state of a system can be characterised by dominate association of species (usually phototrophic), which are "amalgamated" by other satellite species by trophic relations. Such associations appear as the key elements of biogeocoenose.

Stochastic models (Culver 1981; Lippe et al. 1985; Logofet 1997; Lourival 2011) are often used for description of succession processes. The transition probability is basic parameter which determinate the dynamics of the system in such models. Such approach can be useful for simulation the system dynamics of the system, but does not reflect moving forces of the process.

Concerning long-term successions, many researches (Sukachev 1972; Kogan 1977; Tilman 1990; Rabotnov 1992) emphasized essential role of competition for this processes. Use of models of competition of the Volterra type (Lepš and Prach 1981; Chakrabarti et al. 1995; Chernyshenko 1995; Weis et al. 2007) for description of succession process looks as very reasonable.

Additionally to competition, there is evident positive influence of previous stages for next ones. Similar relationships between elements are described by the well-known model of hypercycle (Eigen and Schuster 1979). In the same time, relations between associations during succession have not cyclic character; the hypercycle should be open (Chernyshenko 2005). The model of open hypercycle is similar, but not equivalent to Lotka-Volterra models of the competition or "predator-prey" type. The model reflects a connection between final stage of succession (and corresponding level of complexity of the system) and the size of ecological niche. In the contribution a three-dimension case of the open hypercycle model is considered; change of the ecosystem state is interpreted mathematically as a consequence of bifurcations.

OPEN EIGEN'S HYPERCYCLE

Let's consider dynamics of ecosystem, which is described by the three-dimension open hypercycle model:

$$\begin{cases} \dfrac{dx_1}{dt} = \left(F_1(x) - \dfrac{1}{S_0}\left(x_1F_1(x) + x_2F_2(x) + x_3F_3(x)\right)\right)x_1, \\ \dfrac{dx_2}{dt} = \left(F_2(x) - \dfrac{1}{S_0}\left(x_1F_1(x) + x_2F_2(x) + x_3F_3(x)\right)\right)x_2, \\ \dfrac{dx_3}{dt} = \left(F_3(x) - \dfrac{1}{S_0}\left(x_1F_1(x) + x_2F_2(x) + x_3F_3(x)\right)\right)x_3, \end{cases} \quad (1)$$

here $F_1(x) = N - x_1$, $F_2(x) = a_1x_1 - x_2$, $F_3(x) = a_2x_2 - x_3$ are known as Allen's functions (Allen 1976); $a_1 > 0$, $a_2 > 0$, $N > 0$, $S_0 > 0$, $x_1(t)$, $x_2(t)$, $x_3(t)$ are sizes (biomasses) of the associations, S_0 is capacity of environment, N is a coefficient which determine equilibrium size of the first association, when it develops alone; a_1 is a coefficient which describes a level of dependence of the second association from the first one, a_2 is the same for the third and second associations.

THE EQUILIBRIUM POINTS OF THE SYSTEM (1)

The system equilibrium points can be found as roots of the system of algebraic equations of the third order:

Proceedings 27th European Conference on Modelling and Simulation ©ECMS Webjørn Rekdalsbakken, Robin T. Bye, Houxiang Zhang (Editors)
ISBN: 978-0-9564944-6-7 / ISBN: 978-0-9564944-7-4 (CD)

$$\begin{cases}\left(F_1(x)-\dfrac{1}{S_0}\left(x_1F_1(x)+x_2F_2(x)+x_3F_3(x)\right)\right)x_1=0,\\ \left(F_2(x)-\dfrac{1}{S_0}\left(x_1F_1(x)+x_2F_2(x)+x_3F_3(x)\right)\right)x_2=0,\\ \left(F_3(x)-\dfrac{1}{S_0}\left(x_1F_1(x)+x_2F_2(x)+x_3F_3(x)\right)\right)x_3=0.\end{cases}$$

The solution is trivial; there are 11 equilibrium points:

$P_1:(0,0,0)$; $P_2:(N,0,0)$; $P_3:(N,a_1N,0)$;
$P_4:(N,a_1N,a_1a_2N)$; $P_5:(S_0,0,0)$; $P_6:(0,S_0,0)$;
$P_7:(0,0,S_0)$; $P_8:\left(\dfrac{N+S_0}{a_1+2},\dfrac{S_0(a_1+1)-N}{a_1+2},0\right)$;
$P_9:\left(\dfrac{S_0+N}{2},0,\dfrac{S_0-N}{2}\right)$; $P_{10}:\left(0,\dfrac{S_0}{a_2+2},\dfrac{S_0(a_2+1)}{a_2+2}\right)$;
$P_{11}:\left(\dfrac{S_0+N(a_2+2)}{a_1a_2+a_1+a_2+3},\ \dfrac{(a_1+1)S_0+N(a_1-1)}{a_1a_2+a_1+a_2+3},\right.$
$\left.\dfrac{(a_1a_2+a_2+1)S_0-N(a_1+a_2+1)}{a_1a_2+a_1+a_2+3}\right)$.

One of the signs of system bifurcations is merging of equilibrium points. It is easily possible to find conditions for merging of couples of the points:

P_5 and P_8, if $\dfrac{S_0}{N}=\dfrac{1}{a_1+1}$;

P_8 and P_{11}, if $\dfrac{S_0}{N}=\dfrac{a_1+a_2+1}{a_1a_2+a_2+1}$;

P_9 and P_{11}, if $\begin{cases}\dfrac{S_0}{N}=\dfrac{1-a_1}{a_1+1},\\ a_1\in(0,1);\end{cases}$

P_2, P_5 and P_9, if $\dfrac{S_0}{N}=1$;

P_3 and P_8, if $\dfrac{S_0}{N}=a_1+1$;

P_4 and P_{11}, if $\dfrac{S_0}{N}=a_1a_2+a_1+1$.

Hypothesis 1. In the system (1) the bifurcation values of parameters are following:

$\dfrac{S_0}{N}=\dfrac{1-a_1}{a_1+1}$, when $a_1\in(0,1)$; $\dfrac{S_0}{N}=\dfrac{1}{a_1+1}$;

$\dfrac{S_0}{N}=\dfrac{a_1+a_2+1}{a_1a_2+a_2+1}$; $\dfrac{S_0}{N}=1$; $\dfrac{S_0}{N}=a_1+1$;

$\dfrac{S_0}{N}=a_1a_2+a_1+1$.

ANALYSIS OF THE EQUILIBRIUM POINTS

Let's consider the Jacobi matrix of the system (1):

$$J=\begin{bmatrix}m_{11}&m_{12}&m_{13}\\ m_{21}&m_{22}&m_{23}\\ m_{31}&m_{32}&m_{33}\end{bmatrix}, \qquad (2)$$

$$m_{11}=\frac{3}{S_0}x_1^2-2\frac{N+S_0+a_1x_2}{S_0}x_1+\frac{NS_0+x_2^2}{S_0}+\frac{x_3^2-a_2x_3x_2}{S_0}$$

$$m_{12}=\frac{2x_2-a_2x_3}{S_0}x_1-\frac{a_1}{S_0}x_1^2,\ m_{13}=\frac{2x_3-a_2x_2}{S_0}x_1,$$

$$m_{21}=\frac{a_1S_0-N+2x_1}{S_0}x_2-\frac{a_1}{S_0}x_2^2,$$

$$m_{22}=\frac{a_1S_0-N-2a_1x_2}{S_0}x_1+\frac{1}{S_0}x_1^2-\frac{2S_0+2a_2x_3}{S_0}x_2+\frac{x_3^2+3x_2^2}{S_0}$$

$$m_{23}=\frac{2x_3-a_2x_2}{S_0}x_2,\ m_{31}=\frac{2x_1-a_1x_2-N}{S_0}x_3,$$

$$m_{32}=\frac{2x_2+a_2S_0-a_1x_1}{S_0}x_3-\frac{a_2}{S_0}x_3^2,$$

$$m_{33}=-\frac{N+a_1x_2}{S_0}x_1+\frac{a_2S_0-2a_2x_3}{S_0}x_2+$$
$$+\frac{1}{S_0}x_1^2+\frac{1}{S_0}x_2^2-2x_3+\frac{3}{S_0}x_3^2.$$

Eigenvalues of the matrix (2) in the stationary points:

for P_1 they are $\lambda_1=N$, $\lambda_2=0$, $\lambda_3=0$;

for P_2 they are $\lambda_1=\dfrac{N^2}{S_0}-N$, $\lambda_2=Na_1$, $\lambda_3=0$;

for P_3 they are $\lambda_1=a_1a_2N$ $\lambda_{2,3}=\dfrac{N}{2S_0}\left(N-S_0(a_1+1)\pm\right.$
$\left.\pm\sqrt{N^2+2NS_0(2a_1^2+a_1-1)+S_0^2(a_1-1)^2}\right)$;

for P_4 an analytical form of the eigenvalues was not found. (The Descartes method (Berezin and Zitkov 1959) is used for determination of the stress intervals of the eigenvalues. Three eigenvalues are negative, when $S_0/N\in(1+a_1+a_1a_2;+\infty)$; two negative and one positive when $S_0/N\in(0;1+a_1+a_1a_2)$);

for P_5 they are $\lambda_1,\lambda_3=S_0-N$, $\lambda_2=S_0(1+a_1)-N$;

for P_6 they are $\lambda_1=N+S_0$, $\lambda_2=S_0(a_2+1)$, $\lambda_3=S_0$;

for P_7 they are $\lambda_1=N+S_0$, $\lambda_{2,3}=S_0$;

for P_8 they are

$$\lambda_1=-\frac{N(a_1+1)-S_0}{a_1+2},\ \lambda_2=-\frac{(N+S_0)(S_0(a_1+1)-N)}{S_0(a_1+2)},$$
$$\lambda_3=-\frac{N(1+a_1+a_2)-S_0(1+a_2+a_1a_2)}{a_1+2};$$

for P_9 they are $\lambda_1=\dfrac{N^2-S_0^2}{2S_0}$, $\lambda_2=\dfrac{S_0-N}{2}$,

$$\lambda_3=\frac{S_0(a_1+1)+N(a_1-1)}{2};$$

for P_{10} they are $\lambda_1 = -\frac{S_0(a_2+1)}{a_2+2}$, $\lambda_2 = \frac{S_0}{s_2+2}$, $\lambda_3 = \frac{S_0+N(a_2+2)}{a_2+2}$;

for P_{11} one eigenvalue is $\lambda_1 = \frac{S_0 - N(1+a_1+a_1a_2)}{a_1+a_2+a_1a_2+3}$, the others are roots of a quadratic equation. The analysis of the equation shown that there is a pair of eigenvalues of different sign, if

$$\begin{cases} a_1 \in (0;1), \\ \frac{S_0}{N} \in \left(\frac{1-a_1}{a_1+1}; \frac{a_1+a_2+1}{a_2+a_1a_2+1} \right), \end{cases} \cup \begin{cases} a_1 \in [1;+\infty), \\ \frac{S_0}{N} \in \left(0; \frac{a_1+a_2+1}{a_2+a_1a_2+1} \right), \end{cases}$$

a pair of positive eigenvalues, if

$$\begin{cases} a_1 \in (0;1), \\ \frac{S_0}{N} \in \left(0; \frac{1-a_1}{a_1+1} \right), \end{cases}$$

a pair of negative eigenvalues, if

$$\frac{S_0}{N} \in \left(\frac{a_1+a_2+1}{a_2+a_1a_2+1}; +\infty \right).$$

On the base of these results one can prove that:

P_1 and P_2 are unstable complicated equilibrium points;

P_3 is a saddle with two-dimension unstable subspace, if $S_0/N \in (0,\ a_1+1)$, or two-dimension stable subspace, if $S_0/N \in (a_1+1,\ +\infty)$;

P_4 is a saddle with two-dimension stable subspace, if $S_0/N \in (0, 1+a_1+a_1a_2)$, or stable equilibrium point (node or spiral point) if $S_0/N \in (1+a_1+a_1a_2, +\infty)$;

P_5 is a stable node, if $S_0/N \in \left(0,\ (a_1+1)^{-1}\right)$, a saddle with two-dimension stable subspace, if $S_0/N \in \left((a_1+1)^{-1},\ 1\right)$, and an unstable node, if $S_0/N \in (1,\ +\infty)$;

P_6 and P_7 are unstable nodes;

P_8 is a saddle with two-dimension stable subspace, if $\frac{S_0}{N} \in \left(0,\ \frac{1}{a_1+1}\right) \cup \left(\frac{1+a_1+a_2}{1+a_2+a_1a_2},\ 1+a_1\right)$, a stable node, if $\frac{S_0}{N} \in \left(\frac{1}{a_1+1},\ \frac{1+a_1+a_2}{1+a_2+a_1a_2}\right)$, and a saddle with two-dimension unstable subspace, if $S_0/N \in (1+a_1,\ +\infty)$;

P_9 is a saddle with two-dimension unstable subspace, if

$$\begin{cases} \frac{S_0}{N} \in \left(\frac{1-a_1}{1+a_1}, 1\right) \cup (1, +\infty), \\ a_1 \in (0,1), \end{cases} \cup \begin{cases} \frac{S_0}{N} \in (0,1) \cup (1, +\infty), \\ a_1 \in [1, +\infty), \end{cases}$$

and with two-dimension stable subspace, if

$$S_0/N \in (0,\ (1-a_1)/(1+a_1)), \qquad a_1 \in (0,\ 1),$$

P_{10} is a saddle with two-dimension unstable subspace;

P_{11} is a saddle with two-dimension unstable subspace, if

$$S_0/N \in (0,\ (1-a_1)/(1+a_1)), \qquad a_1 \in (0,\ 1),$$

or a saddle with two-dimension unstable subspace, if

$$\left\{ \frac{S_0}{N} \in \left(\frac{1-a_1}{a_2+1}, \frac{a_1+a_2+1}{a_2+a_1a_2+1} \right);\ a_1 \in (0,1) \right\} \cup$$
$$\cup \begin{cases} a_1 \in [1, +\infty), \\ \frac{S_0}{N} \in \left(0,\ \frac{a_1+a_2+1}{a_2+a_1a_2+1}\right), \end{cases} \cup \frac{S_0}{N} \in (a_1+a_1a_2+1, +\infty)$$

or a stable equilibrium point (node or spiral point) if

$$\frac{S_0}{N} \in \left(\frac{a_1+a_2+1}{1+a_2+a_1a_2}, 1+a_1+a_1a_2 \right).$$

BIFURCATION POINTS

Let's determinate bifurcation values of parameters on the base of analysis of equilibrium points. The bifurcation diagram is presented in Fig.1.

For values of the parameters from the regions I, II, III, IV, there are two complicated equilibrium points, two unstable nodes, three saddles with two-dimension unstable subspace, three saddles with two-dimension stable subspace and one stable node.

For values of the parameters from the regions V, VI, VII, VIII, there are two complicated equilibrium points, three unstable node, three saddles with two-dimension unstable subspace, two saddles with two-dimension stable subspace and one stable node in phase space.

When quotient of the parameters S_0 and N pass through value 1, one saddle disappears and unstable node appears.

Let's consider the phase portrait in the first octant, because of its importance for practical applications. Let's note that there are not equilibrium points, which belongs the first octant for any values of the parameters. Thus, the point P_8 belongs to the first octant, when $\frac{S_0}{N} \geq \frac{1}{1+a_1}$, point P_9 – when $\frac{S_0}{N} \geq 1$, point P_{11} – when $\frac{S_0}{N} \geq \frac{1+a_1+a_2}{1+a_2+a_1a_2}$. One can see that when $\frac{S_0}{N}$ pass through these tree values, topology of the first

octant change. It is possible to summarise the obtained results by a theorem.

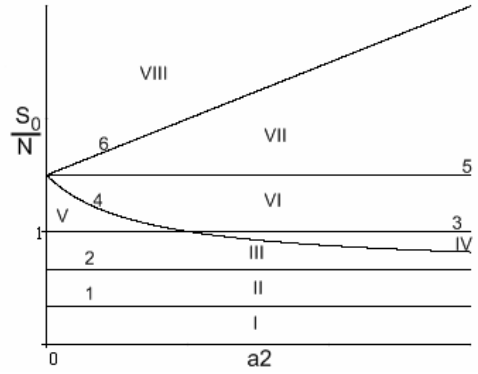

а) $a_1 \in (0,1)$

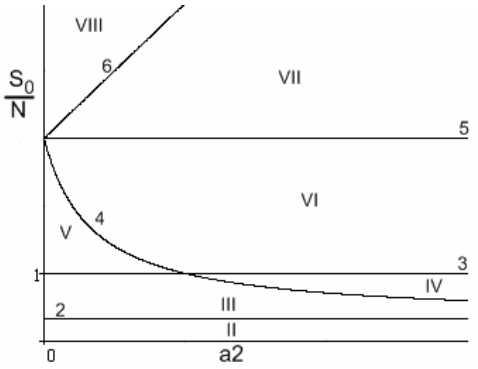

б) $a_1 \in [1,+\infty)$

Figure 1: Sections of the parametric surfaces

$$\left(1.\ \frac{S_0}{N}=\frac{1-a_1}{a_1+1},\quad 2.\ \frac{S_0}{N}=\frac{1}{1+a_1},\quad 3.\ \frac{S_0}{N}=1,\right.$$

$$\left.4.\ \frac{S_0}{N}=\frac{1+a_1+a_2}{1+a_2+a_1a_2},\ 5.\ \frac{S_0}{N}=a_1+1,\ 6.\ \frac{S_0}{N}=1+a_1+a_1a_2\right)$$

Theorem 1. There are following bifurcation values of parameters for the system (1):

1) $S_0 / N = 1$ (for the all phase space);

2) $\frac{S_0}{N}=\frac{1}{1+a_1}$, $\frac{S_0}{N}=1$, $\frac{S_0}{N}=\frac{1+a_1+a_2}{1+a_2+a_1a_2}$ (for the first octant).

Now it is clear, that the Hypothesis 1 is partly wrong. Thus, the equation $\frac{S_0}{N}=\frac{1-a_1}{a_1+1}$ (when $a_1 \in (0,1)$) does not correspond to a bifurcation. When the quotient of the parameters exceeds this value, two-dimension stable subspace of the point P_9 becomes one-dimension and, contra versa, one-dimension stable subspace of the point P_{11} becomes two-dimension.

The similar situation takes place for the equation $S_0 / N = 1 + a_1 + a_1 a_2$: the point P_4 becomes a stable node (spiral point), whereas the point P_{11} changes type from a stable node (spiral point) to a saddle. The topology of the phase space does not change; therefore, there is not a bifurcation for these values of parameters.

A special situation is connected with the equation $S_0 / N = 1$. In this case three equilibrium points (P_2, P_5, P_9) merge into one. When parameters pass through this point, stability (and type) of the equilibrium point P_9 does not change, whereas the point P_5 becomes unstable node and two-dimension unstable subspace of the point P_2 becomes one-dimension. It can be shown that the bifurcation takes place in the first octant.

Let's consider the set of equilibrium points which have two nonzero components: the first and the j-th ($j > 2$). One can find coordinates of such equilibrium points from the system of algebraic equations:

$$\begin{cases}\left(N - x_1 - \left((N - x_1)x_1 - x_j^2\right)/S_0\right)x_1 = 0,\\ \left(-x_j - \left((N - x_1)x_1 - x_j^2\right)/S_0\right)x_j = 0,\\ x_1 \neq 0,\ x_j \neq 0,\ (j > 2).\end{cases}$$

From here $x_1 = (S_0 + N)/2$ and $x_j = (S_0 - N)/2$. Such points form a subset of the set of equilibrium points of the n-dimensional open Eigen's hypercycle model. Every point of this subset appears in nonnegative region of phase space, when $S_0 / N \geq 1$. So, $S_0 / N = 1$ is a bifurcation value. The fact, that at least $n-2$ equilibrium points take part in the above-mentioned bifurcation.

ECOLOGICAL INTERPRETATION

Bifurcations, connected with change of stability of equilibrium points, are especially interesting from practical point of view. Only two bifurcation correspond to this criteria: $\frac{S_0}{N}=\frac{1}{1+a_1}$, $\frac{S_0}{N}=\frac{1+a_1+a_2}{1+a_2+a_1a_2}$.

From the analysis of equilibrium points it was clear that there are four possible stable equilibrium points; during the bifurcations they can change each other, and in any case only one point are an attractor:

1. When $0 < \frac{S_0}{N} < \frac{1}{1+a_1}$, point P_5 is stable. In this case the size of ecological niche is so small, that only one association is able to exist in the ecosystem.

2. When $\frac{1}{1+a_1} < \frac{S_0}{N} < \frac{1+a_1+a_2}{1+a_2+a_1a_2}$, point P_8 is stable. With such values of the parameters (capacity of the environment) there are sufficient resources for the second association, which is in competition with the first one.

3. When $\frac{1+a_1+a_2}{1+a_2+a_1a_2} < \frac{S_0}{N} < 1+a_1+a_1a_2$, point P_{11} is stable. In this case size of ecological niche is so big, that three associations are able to coexist in the biogeocoenose. And that they use all the resources.

4. When $1+a_1+a_1a_2 < S_0/N < +\infty$, point P_4 is stable. This case corresponds to an excess of resources. In the ecosystem there are three associations, which reach their maximal possible sizes.

One of natural questions: why $S_0/N = 1+a_1+a_1a_2$ is not bifurcation value? When capacity of the environment S_0 becomes larger than $(1+a_1+a_1a_2)N$, the topology of the system is not changed, although, formally, the new point becomes to be stable. Such situations are quite usual in mathematical investigations of equilibrium points and bifurcation.

Concerning the bifurcation value $S_0/N = 1$, it is difficult to determine its practical role. One can assume that this critical rate delineates various ways to stabilise the system if it is out of its steady state.

CONCLUSION

In the contribution, the three-dimension open Eigen's hypercycle model (1) was considered. In the case of small (nonzero) size of the ecological niche, only one association is able to exist in the system. When capacity of the environment grows, the second and the third association are included in the ecosystem gradually. It is shown, that the process of origin of next associations is accompanied with bifurcations of system (1). When size of niche is $S_0 > (1+a_1+a_1a_2)N$, there is excess of resources in the biogeocoenose. The situation of appearance of excess of resources is not bifurcation, because topology of the ecosystem does not change and development of the system is continuous.

As it clear from the research, the main parameter, which determines the behaviour of the system is the capacity of the environment S_0. Parameters a_1 and a_2 influence only on relationships between the associations.

Analysis of three-dimension open Eigen's hypercycle model, together with the two-dimension one (Chernyshenko, 1995), allows proposing of the following assumptions for n-dimensional case:

1. In the process of ecosystem successions has n stages. Each of them is characterised by activation of a new association. Number of "activated" associations is determined by size of the environment capacity S_0. If the size of niche is small ($0 < S_0 < N/(1+a_1)$), only one association is able to exist in the ecosystem.

2. Each "activation" of a new association is accompanied with bifurcations of the system. It is interesting, that the first $n-2$ conditions of the activation are the same as for $(n-1)$-dimensional system.

3. There is excess of resources in the ecosystem when size of ecological niche is $S_0 > N\sum_{i=0}^{n}\prod_{j=0}^{n-i} a_j$, $a_0 = 1$. Size of associations in this case is calculated as $x_j = N\prod_{i=0}^{j-1} a_i$, $a_0 = 1$, $j = \overline{1,n}$.

The proof of these assumptions is a matter of future research.

REFERENCES

Allen, P.M. 1976. "Evolution, population dynamics and stability". *Proceedings of the National Academy of Sciences of the USA*, Vol. 73, No. 3, 665-668.

Berezich, I.C. and N.P. Zitkov. 1959. *Computing technique*. Physico-mathematical literature main Press, Moscow.

Chakrabarti, C.G.; Ghosh Sutapa; and Bhadra Syamali. 1995. "Non-equilibrium thermodynamics of Lotka-Volterra ecosystems: Stability and evolution." *Journal of Biological Physics*, Vol. 21, Is. 4, 273-284.

Chernyshenko, S.V. 1995. "Qualitative analysis of two-dimensional modification of the M. Eigen's hypercycle and internal catastrophes" *Problems of applied mathematics and mathematical modelling*. Dniepropetrovsk University Press, 129-134.

Chernyshenko, S.V. 2005. *Nonlinear analysis of forest ecosystems dynamics*. Dnipropetrovsk University Press, Dnipropetrovsk.

Culver, D.C. 1981. "On Using Horn's Markov Succession Model." *The American Naturalist*, Vol. 117, No. 4 (Apr), 572-574.

Eigen M. and P. Schuster. 1979. *The Hypercycle. A principle of natural self-organization*. Springer-Verlag, Berlin, Heidelberg, New York.

Kogan, A.B.; N.P. Naumov; B.G. Rezabek; and O.G. Chorajan. 1977. *Biological cybernetics*. Vysshaja shkola, Moscow.

Lepš Jan and Karel Prach. 1981. "A Simple Mathematical Model of the Secondary Succession of Shrubs." *Folia Geobotanica & Phytotaxonomica*, Vol. 16, No. 1, 61-72.

Lippe E.; J.T. De Smidt; and D.C. Glenn-Lewin. 1975. "Markov Models and Succession: A Test from a Heathland in the Netherlands." *Journal of Ecology*, Vol. 73, No. 3 (Nov), 775-791.

Logofet, D.O. 1997. "Inhomogeneous Markov models for succession of plant communities: New perspectives on an old paradigm." *Izvestiya Akademii Nauk. Seriya Biologicheskaya*, 613-622.

Lourival R.; Martin Drechsler; Matthew E. Watts; Edward T. Game; and Hugh P. Possingham. 2011. "Planning for reserve adequacy in dynamic landscapes; maximizing future representation of vegetation communities under flood disturbance in the Pantanal wetland." *Diversity and Distributions*, Vol. 17, Is. 2 (Mar), 297–310.

Rabotnov, A.T. 1992. *Phytocenology*. MGU Press, Moscow.

Sukachev, V.N. 1972. *Selected transactions: in three volumes. Vol. 1. Bases of forest typology and biogeocenology*. Nauka, Leningrad.

Tilman D. 1990. "Constraints and Tradeoffs: Toward a Predictive Theory of Competition and Succession." *Oikos*, Vol. 58, No. 1 (May), 3-15.

Weis, J.J.; B.J. Cardinale; K.J. Forshay; and A.R. Ives. 2007. "Effects of species diversity on community biomass production change over the course of succession." *Ecology*, Vol. 88, No 4 (Apr), 929-939.

AUTHOR BIOGRAPHY

SERGE V. CHERNYSHENKO was born in Dnipropetrovsk, Ukraine and graduated from the Dnipropetrovsk State University. After obtaining PhD degree on computing in 1986, was, successively, head of Laboratory of Mathematical Modeling in Biology, head of Computer Science Department, dean of Applied Mathematics Faculty at Dnipropetrovsk National University; head of Department of Applied Mathematics and Social Informatics in Khmelnitsky National University. He was a supervisor of several Ukrainian national projects on mathematical modelling. From 2009 he is a visiting professor of Koblenz-Landau University, Faculty of Informatics. His e-mail address is svc@a-teleport.com and his web-site can be found at www.uni-koblenz.de/~svc

ROMAN V. RUZICH was born in Khmelnitsky, Ukraine and graduated from the Khmelnitsky National University. From 2010 he is postgraduate student of Khmelnitsky National University, Department of Applied Mathematics and Social Informatics. His e-mail address is ninasus@gmail.com.

Simulation based priority rules for scheduling of a flow shop with simultaneously loaded stations

Professor Dr.-Ing. Frank Herrmann
Hochschule Regensburg - University of Applied Sciences Regensburg
Innovation and Competence Centre for Production Logistics and Factory Planning (IPF)
PO box 120327, 93025 Regensburg, Germany
E-Mail: Frank.Herrmann@HS-Regensburg.de

KEYWORDS
Simulation of processing time, scheduling, flow-shop, no-buffer (blocking), no-wait, priority rules, real world application.

ABSTRACT
In this study, a real world flow shop with a transportation restriction is regarded. This restriction reduces the set of feasible schedules even more than the no-buffer restrictions discussed in the literature in the case of limited storage. Since this scheduling problem is integrated in the usual hierarchical planning, the tardiness is minimised. This NP-hard problem is solved by priority rules, because of the addressed dynamic environment (and a high number of jobs) at the company site. Due to the technological restrictions the real duration of a job is significantly larger than its net processing time. By a simulation of the processing time many priority rules are improved and some even significantly. With extensive simulations successful priority rules in the literature are analysed.

1. INTRODUCTION

Specific products are produced by special machines which are often grouped in a flow shop. They have to produce small batches with short response times, so scheduling algorithms are needed to ensure that under the constraint of a high average load of the flow shop, the due dates of the production orders are met. Nowadays, such special designed flow shops often have technological restrictions, which complicate the scheduling. For example in cell manufacturing, buffer could be non-existent due to limited space and storage facilities. So, in recent years, a considerable amount of interest has arisen in no-buffer (blocking) scheduling problems and in no-wait scheduling problems, with makespan as objective criteria. Often these production systems deliver products for other systems as well. Due to the hierarchical planning which is implemented in enterprise resource planning systems (ERP system) (see e.g. Jacobs et al. 2010), the local completion times in one production system in many cases determine the earliest possible starting times in another production system. Thus, the delay of the operations in a production system has an impact on the effectivity of this coordination process. Therefore, tardiness is considered as objective criteria.

2. A REAL WORLD APPLICATION

The problem is a modification of a partly automated production line at Fiedler Andritz in Regensburg to produce filter (baskets) with a lot size of 1. All filters have unified constructions. They differ in varying heights of the baskets and there exist different designs.

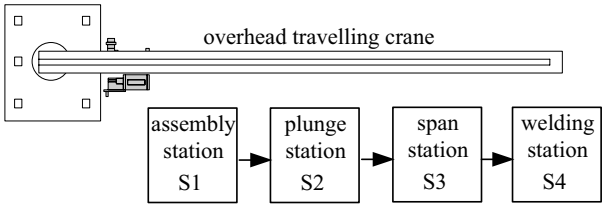

Figure 1: Structure of the production line

The production line consists of 4 stations which are shown in Figure 1. Station 1 assembles 6 single batons (called consoles) on an assembly ground plate to a skeleton of a filter basket. Baton profiles are assembled into the provided slots of the filter basket skeletons. At the plunge station a wire coil is contrived in the device of a lining machine. The lining machine straightens the wire and inserts batons into the slots. To ensure stability, the span station installs span kernels in the case of outflow filter baskets and span belts in the case of inflow filter baskets. Then, the filter basket is lifted from the assembly ground plate and is transported to the welding station, at which the baton profiles are welded on the filter basket skeletons. The accomplished filter basket leaves the production line. Prior to this, the span medium is removed. An overhead travelling crane lifts a filter basket out of a station, transports it to the next station and inserts it directly in this station. This is just possible if this station is free. So, there is no buffer in the production line and each feasible schedule of jobs is a permutation of these jobs. Due to other operational issues the crane can just be moved if all stations are inactive. Since an operation cannot be interrupted, the transport has to be performed after the completion of all operations on the stations in the flow shop. Due to further operational issues this restriction has to be applied also for the first and the last station; note, that the crane loads S1 and unloads S4 as well. In summary, all stations are loaded and unloaded with filters during a common process and this process starts with the last station S4, followed by station S3, S2, until station S1 is reached. It is allowed that a station is empty; then this station is skipped (may be partially) in this process.

There are 10 part types whose processing times are listed in Table 1.

Proceedings 27th European Conference on Modelling and Simulation ©ECMS Webjørn Rekdalsbakken, Robin T. Bye, Houxiang Zhang (Editors)
ISBN: 978-0-9564944-6-7 / ISBN: 978-0-9564944-7-4 (CD)

Table 1: Processing times for all part types in minutes

Part type	Station				Sum of times
	S1	S2	S3	S4	
P1	100,5	50	53,5	9	213
P2	256,5	50	53,5	9	369
P3	122	135	90	75	422
P4	256,5	50	267	9	582,5
P5	182	200	135,5	140	657,5
P6	100,5	300	53,5	300	754
P7	223	250	196	220	889
P8	223	250	206,5	220	899,5
P9	100,5	300	267	300	967,5
P10	256,5	300	267	300	1123,5

At the company's production site, the jobs for filters are generated by an SAP system and produced filters are stored before they are assembled into other products or sold directly to customers. Therefore, all jobs with a release date after the beginning of a period are released at the beginning of this period. One period consists of one day with three 8 hour shifts. For this investigation, sequences of jobs of filter types with lot size 1 are randomly generated for each period t by an generating algorithm which has been designed in accordance with the proceeding in (Russel et al. 1987) and in (Engell et al. 1994): An additional filter type F, released in period t, consumes capacity on each station during the time between t and its due date; the calculation for the capacity just uses the net processing time and does not regard the dependencies between the jobs (released so far). F is accepted as long as this consumed capacity on each station is below a maximal load level, otherwise it will be skipped to the next period. A maximal load level is an (intended) average load $\left(L_0(S)\right)$ plus 0, –30% and +30% of $L_0(S)$. Over the first 5, 10, 15 etc. consecutive periods, the load level variations average to zero.

In reality at the company, there are large numbers of periods with a low number of late jobs and large numbers of periods with a high (or even very high) number of late jobs. To achieve a comparable situation for this investigations, due dates are determined in a way so that scheduling with the FIFO rule (first-in-first-out) causes a specific percentage of late jobs. The company confirmed that job sequences with 30%, 50%, 70% and 85% of late jobs by scheduling with the FIFO rule (called time pressure) are comparable to the ones which occurred in the real operation. As a result of the generating algorithm's calculations the mean difference between the due dates and the release dates are between 2 and 3,5 days with a standard deviation of 0,5 days. Andritz Fiedler has confirmed that such timeframes for processing jobs are representative.

The time needed for loading and unloading a station is negligible compared to the duration of the operation itself. In addition this task is independent from the allocation (or loading) of other stations and the required time is included in the duration of the operation.

The general scheduling problem consists of M stations and a pool of N jobs, which may change at any time, with known earliest possible starting times for release dates $a_i \ (1 \le i \le N)$ and due dates $f_i \ (1 \le i \le N)$ respectively. Also there is the duration $t_{i,j}$ of operation $\left(o_{i,j}\right)$ j $(1 \le j \le M)$ of job i $(1 \le i \le N)$, which is being worked on station j. As performance criteria average tardiness $\left(T_{Mean}\right)$ and standard deviation of the tardiness $\left(T_\sigma\right)$ are primarily analysed.

The time between two consecutive executions of the load process is determined by the maximum of the duration of the operations on the stations in the flow shop. This is called cycle time. This “load”-restriction, the no-buffer condition and the capacity of the stations are the main restrictions. Setup times are relatively small compared to operation times and are included in those.

The no-buffer condition means a relaxation of the scheduling problem with the (above) “load”-restriction. Scheduling problems with the no-buffer are proven to be NP-hard in the strong sense for more than two stations; see e.g. (Hall and Sriskandarajah 1996), which contains a good survey of such problems.

3. LITERATURE REVIEW

As mentioned earlier, the real application is close to the class of no-buffer (blocking) scheduling problems. Solutions for the no-buffer (blocking) scheduling problems are published in various papers. In (McCormick et al. 1989) a schedule is extended by a (unscheduled) job that leads to the minimum sum of blocking times on machines which is called profile fitting (PF). Often the starting point of an algorithm is the NEH algorithm presented in (Nawaz et al. 1983), as it is the best constructive heuristic to minimize the makespan in the flow shop with blocking according to many papers, e.g. (Framinan et al. 2003). Therefore, (Ronconi 2004) substituted the initial solution for the enumeration procedure of the NEH algorithm by a heuristic based on a makespan property proven in (Ronconi and Armentano 2001) as well as by the profile fitting (PF) of (McCormick et al. 1989). (Ronconi 2005) used an elaborated lower bound to realise a branch-and-bound algorithm which becomes a heuristic since the CPU time of a run is limited. Also for minimising makespan, (Grabowski and Pempera 2007) realised and analysed a tabu search algorithm. As an alternative approach, (Wang and Tang 2012) have developed a discrete particle swarm optimisation algorithm. In order to diversify the population, a random velocity perturbation for each particle is integrated according to a probability controlled by the diversity of the current

population. Again, based on the NEH algorithm, (Wang et al. 2011) described a harmony search algorithm. First, the jobs (i.e. a harmony vector) are ordered by their non-increasing position value in the harmony vector, called largest position value, to obtain a job permutation. A new NEH heuristic is developed on the reasonable premise that the jobs with less total processing times should be given higher priorities for the blocking flow shop scheduling with makespan criterion. This leads to an initial solution with higher quality. With special settings as a result of the mechanism of a harmony search algorithm, better results are achieved. Also (Ribas et al. 2011) presented an improved NEH-based heuristic and uses this as the initial solution procedure for their iterated greedy algorithm. A modified simulated annealing algorithm with a local search procedure is proposed by (Wang et al. 2012). For this, an approximate solution is generated using a priority rule specific to the nature of the blocking and a variant of the NEH-insert procedure. Again, based on the profile fitting (PF) approach of (McCormick et al. 1989), (Pan and Wang 2012) addressed two simple constructive heuristics. Then, both heuristics and the profile fitting are combined with the NEH heuristic to three improved constructive heuristics. Their solutions are further improved by an insertion-based local search method. The resulting three composite heuristics are tested on the well-known flow shop benchmark of (Taillard 1993), which is widely used as benchmark in the literature.

To the best of my knowledge, only a few studies investigate algorithms for the total tardiness objective (for flow shops with blocking). (Ronconi and Armentano 2001) have developed a lower bound which reduces the number of nodes in a branch-and-bound algorithm significantly. (Ronconi and Henriques 2009) described several versions of a local search. First, with the NEH algorithm, they explore specific characteristics of the problem. A more comprehensive local search is developed by a GRASP based (greedy randomized adaptive search procedure) search heuristic.

4. HEURISTIC SOLUTION BY PRIORITY RULES

The real application operates in dynamic environments where real time events like station failure, tool breakage, arrival of new jobs with high priority, changes of due dates etc. may turn a feasible schedule into an infeasible one. A feasible assignment of a job is achieved by a priority rule like earliest due date (EDD), because a priority rule orders a queue in front of a station quasi immediately. So, priority rules are still analysed in many studies on scheduling; one example of a recent one is (El-Bouri 2012).

Due to the "load"-restriction the processing time of a job A on the flow shop depends on the other jobs processed on the flow shop at the same time. Therefore, its processing time can be significant larger than the sum of the processing times of its single operations (t_A), called net processing time of job A. A realistic processing time for a job A is achieved, if the processing on the flow shop is simulated with respect to the jobs processed on this flow shop at the same time. After four cycles $(\tau_1,...,\tau_4)$, job A leaves the flow shop. So, these cycle times depend on the three jobs (X1, X2, and X3) on the flow shop as A is assigned to station 1, and the three jobs (B1, B2, and B3) following A in the sequence; this is illustrated in Figure 2. So, $\tau_1+\tau_2+\tau_3+\tau_4$ is the (total) processing time of A (tt_A). This processing time of job A is only correct, if the tail is (structurally) identical with the three jobs which follow job A in the final permutation. Since these are not known a deviation normally occurs between this calculated processing time and the processing time which will really occur if job A is chosen.

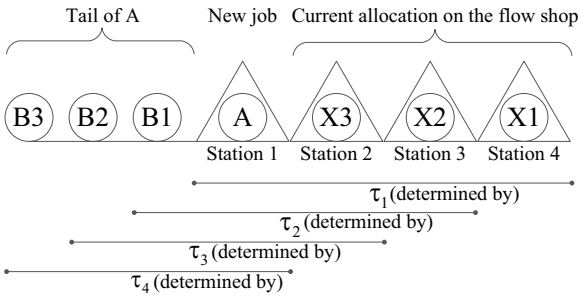

Figure 2: Calculation the processing time of a job A

As known, tardiness is improved by assigning jobs with a small slack; the slack for job i is defined by $f_i - t - tt_i$, where t is the current time and f_i is the due date of job i. Investigations by the author (see also (Engell et al. 1994)) show, that for many job shop problems the rules $\text{CR+SPT} = \begin{cases} \frac{f_i - t}{tt_i}, & f_i - t - tt_i > 0 \\ tt_i, & f_i - t - tt_i \le 0 \end{cases}$ (tt_i is the shortest processing time (SPT), which determines the SPT rule), ODD (which is identical with the EDD-rule for the class of problems regarded here) and $\text{SL/OPN} = \frac{f_i - t - tt_i}{M}$ (note: a low value is always preferred), which is identical with the slack rule (SL) are Pareto optimal to the average, the standard deviation and the maximum tardiness. This explains why SL/OPN and CR+SPT are often used as benchmark; according to (Raghu and Rajendran 1993) other combinations deliver worse results for flow shop problems. As known from several investigations SPT based rules have the tendency to small T_{Mean} at the expense of large T_σ and slack based rules tend to a small T_σ at the expense of a high T_{Mean}; SPT and SL are representatives for this effect.

In addition, more recent rules are adapted to the class of problems regarded here. One is RR, see (Raghu and

Rajendran 1993), which seeks to minimize both mean flow time and mean tardiness of jobs and has originally been defined for job shop problems, see (Raghu and Rajendran 1993). For the adaption the remaining work content is tt_i and the probable waiting time of the successor of this operation (in job i) at the (next) station, which seems to be less effective in flow shops for minimising mean flow time due to (Rajendran and Holthaus 1999), is integrated in the calculation of the cycle times. Thus, the priority index is $(f_i - t - tt_i) \cdot e^{-\eta} + e^{\eta} \cdot tt_i$, with utilisation level η of the entire flow shop defined by $\eta = \frac{b}{b+j}$ with b being the busy time and j being the idle time of the entire flow shop; the job with the lowest priority index will be processed next.

Using the properties of an optimal solution for the single-station weighted tardiness scheduling problem, (Rachamadugu and Morton 1982) developed the weighted slack-based scheduling rule RM. According to the analysis of this rule performed in (Rachamadugu and Morton 1982), it can be assumed that it delivers near optimal results to the one station problem. (Rachamadugu 1987) shows that this rule can be used as an effective pruning device in enumerative methods. Modifications of this rule deliver very good results for flow shop and job shop problems with weighted tardiness criteria (see (Vepsatainen and Morton 1987)). The rule was successfully adapted to resource constrained project scheduling problems (RCPSP) in (Voß and Witt 2007). The priority index for an operation j of a job i is: $\frac{w_{i,j}}{t_{i,j}} \cdot e^{-\frac{k}{\bar{t}} \cdot \max\{sl_{i,j},0\}}$, where $sl_{i,j}$ is the slack, $w_{i,j}$ is a weight, k is an empirically determined "look-ahead" parameter and $\bar{t}$ is the average duration of all jobs processed at the same station; a low value is always preferred. For the real world application jobs get priorities, no weighting is used, so that $w_i = 1$ for each job i, $\bar{t} = \frac{1}{N} \cdot \sum_{i=1}^{N} tt_i$ and the slack is $f_i - t - tt_i$ as usual.

Especially, due to the relatively recent paper of (Voß and Witt 2007) it is motivated to integrate resource costs π_i, so that in total the priority index is: $\frac{1}{\pi_i} \cdot e^{-\frac{k}{\bar{t}} \cdot \max\{f_i - t - tt_i,0\}}$. As local processing time costing $\pi_i^l = tt_i$ is used, called RM local, and as global processing time costing $\pi_i^g = \sum_{i \in U_t} tt_i$, where U_t is the set of unfinished jobs in the pool of orders, excluding job i, is used, called RM global; in (Voß and Witt 2007) job i is included, because a RCPSP is regarded, but here this would mean that for all jobs i waiting in front of the flow shop have the same π_i^g. (Lawrence and Morton 1993) considered additional resource costs which do not fit to our problem or have already been integrated (in other parameters); e.g. a (static) bottleneck resource cost is not applicable because it is assumed that each station is temporary a bottleneck.

5. COMPUTATIONAL RESULTS

The real world application is realised in the simulation tool "Plant Simulation" together with an implementation of the above mentioned hierarchical planning as realised in ERP systems, used in industrial practise. Average tardiness (T_{Mean}) and standard deviation of the tardiness (T_σ) reach a steady state by a simulation horizon of 5000 periods.

A large number of preliminary studies show that the parameter k has a significant impact on the performance of the local and the global RM rule and the best results are achieved with $k = 1$. In (Voß and Witt 2007) k has a negligible influence, but they regard an RCPSP.

The impact of the simulated processing time is analysed first. Due to its implementation, its concrete values depend from the (3) jobs on the flow shop and the (3) jobs following. So, the values should be independent from the priority rules and the time pressure. But, it could be that individual rules prefer permutations of jobs in a cycle. This is observed in experiments with the (above explained) priority rules. In these experiments the mean, the standard deviation, the minimum and the maximum of the simulated processing times are measured. The measured values for all part types and all rules are between those for the SPT rule and the SL rule which are listed in Table 2. These results demonstrate a huge deviation from the net processing time.

Furthermore, the experiments show a significant impact by the tail. The values in Table 2 are representative for many tails. Exceptions occur if each tail only consists of jobs with a small net processing time, as with part type P1, or a high one, as with part type P10. In the first case the simulated processing times have small mean values, e.g. for part type P1 901,1 minutes and for part type P10 1067,6 minutes, and in the second case the mean values are large, e.g. 1248,5 minutes for part type P1 and 1269,2 minutes for part type P10. The standard deviations are in the first case huge e.g. for part type P1 173,1 minutes and for part type P10 187,6 minutes, and the second case low e.g. for part type P1 77,4 minutes and part type P10 61,3 minutes.

As indicated by these results, the performance of a priority rule is influenced by the concrete tail. Instead of regarding all 1000 possible tails, the study is limited on tails whose part types have similar net processing times and those whose part types have significantly different net processing times. The experiments for each priority rule show both significant and minor deviations. These

significant deviations are not exceptions and the reduction is almost one-third (or even more). Results which are close to the best possible results are achieved, if each tail consists of jobs of part type P4 only (i.e. P4, P4, P4); this tail is used in the following. Experiments show that an accidently tail (i.e. the part types for a tail are randomly selected) is a very good alternative.

Table 2: Net processing time (NET) and simulated processing time in minutes for the rules SPT and SL

Part type	SPT				
	Mean	Net	Standard deviation	Mini-mum	Maxi-mum
P1	1116,5	213	151,8	885	1349.5
P2	1159,8	369	100,45	1061	1349.5
P3	1088,6	422	138,1	929	1349.5
P4	1151,7	582,5	96,4	1061	1349.5
P5	1162,9	657,5	88,5	1063,5	1349.5
P6	1233,3	754	95,3	1098,5	1376
P7	1228,1	889	60,1	1164,5	1349.5
P8	1225,5	889,5	57,8	1164,5	1349.5
P9	1237,2	967,5	93,9	1098,5	1376
P10	1322,8	1123,5	27,9	1098,5	1376
	SL				
	Mean	Net	Standard deviation	Mini-mum	Maxi-mum
P1	1179	213	126,5	885	1349.5
P2	1192,6	369	112,3	885	1349.5
P3	1179,3	422	118,1	885	1349.5
P4	1181,7	582,5	111,5	885	1349.5
P5	1184,6	657,5	106,5	885	1349.5
P6	1198,3	754	106,1	885	1376
P7	1203,8	889	101,7	885	1376
P8	1207,9	889,5	98,2	885	1376
P9	1215,9	967,5	98,1	885	1376
P10	1225,9	1123,5	97,5	885	1376

Table 3 contains the percental changes by using simulated processing times instead of net processing times. Due to the characteristic behaviour of the SPT rule and the SL rule to T_{Mean} and T_{σ} (see above), both are analysed first. The SPT rule benefits most from a more realistic processing time. In case of the SL rule there are just small improvements but often significant deteriorations. As long as the CR+SPT rule uses CR – which is some kind of slack – there are deteriorations for T_{Mean}. Since the net processing time is much smaller than the simulated processing time, the CR+SPT rule with simulated processing time decides earlier according to SPT as the CR+SPT rule with net processing time which explains the improvement. Both rules RR and RM are a combination of slack and shortest processing time (SPT). The RR rule benefits from a more precise processing time. A smaller (percental) improvement compared to the SPT rule is caused by already better values if net processing is used and the impact of the slack; The impact of the slack is shown most clearly by a time pressure of 85%. Much better (percental) improvements for T_{Mean} in case of a small time pressure is caused because RR rule prefers critical jobs with positive slack much better than the SPT rule (which does not take due dates into account). The RM rule prefers small jobs if there is no slack and otherwise jobs with small slack. Depending on the degree of influence of the slack on the priority, it can be expected that their changes are between those of the rules SL and CR+SPT. The values in Table 3 confirm this conclusion primarily for the rule RM global. The concrete values depend on the time pressure. In the case of rule RM local the percental improvements for T_{Mean} and for T_{σ} with small time pressure are comparable to the ones of the SPT rule. In the case of T_{σ} a better processing time causes an increase of the (absolute) values for this rule on the level of the values of the SPT rule, except for a low time pressure.

Table 3: Change by using simulated processing time instead of net processing time in percent, compared to the result with net processing time.

Rule	Time pressure			
T_{Mean}	30%	50%	70%	85%
SPT	57.6	10.3	12.3	25.8
SL	-41.2	-2.3	0.23	-17
CR+SPT	-4	-10.3	-7.4	8.9
RR	75.3	4.2	3.9	11.9
RM local	48.9	10.4	11.7	21.5
RM global	3.3	-10.9	-4	-5.8
T_{σ}	30%	50%	70%	85%
SPT	68.65	31.3	27.2	48.11
SL	-20.1	1.2	3.4	-19
CR+SPT	51.4	34.1	37.1	48.6
RR	69.8	14.3	14.4	23.6
RM local	68.3	-21.2	-25.5	-242.8
RM global	50	-10.1	10.4	67.9

The absolute values, listed in Table 4 (just the ones by using simulated processing times), differ partially from the results published in other papers. In order to judge this and the following more detailed results, it should be pointed out that the real world problem in this paper has a very special problem structure, compared to the representative problems usually regarded in the literature. The above mentioned expectation of the SPT and the SL rule – namely small T_{Mean} at the expense of large T_{σ} by the first rule and the opposite by the second one – is fulfilled. For many job shop and flow shop problems the CR+SPT rule outperforms the best results from the SPT and the SL rule. For this real world application CR+SPT delivers always, with one exception, results, which are much worse than the ones of all other rules. Since the rules RR and RM also combine slack and SPT, the worse results of CR+SPT are caused by a too late switch from preferring jobs with small slack to jobs with small SPT. Compared to other job shop problems this is more significant because just a

misguided decision causes long cycles, which reduces the remaining slack for all other jobs much more than in the case of typical job shop problems. In addition, these long cycles could be very ineffective in terms of large times on some stations without any processing.

Table 4: Absolute performance measures for priority rules with simulated processing time in minutes

Rule	Time pressure			
T_{Mean}	30%	50%	70%	85%
SPT	99.1	323.3	326.2	646.9
SL	161.6	321.5	344.7	1149.8
EDD	103.4	300.2	342.2	948.7
CR+SPT	581.97	575.7	574.6	1032.7
RR	40.7	279.5	313.5	823.1
RM local	55.3	267.1	278.6	626.2
RM global	134.9	346.7	359.2	1008.5
T_{σ}	30%	50%	70%	85%
SPT	314.5	449.2	473.4	826.7
SL	353.4	315.3	326.6	787.6
EDD	243.1	293.1	328.9	643.4
CR+SPT	2023.9	916.4	901.2	1464.1
RR	125.1	282.8	305.7	564.6
RM local	235.9	425.8	454.1	1187.4
RM global	395.5	456.2	464.6	890.04

The performance of the RR rule for the real world application is primarily compared with the results in (Rajendran and Holthaus 1999), because in (Raghu and Rajendran 1993) an open shop problem is regarded. In (Rajendran and Holthaus 1999) the RR rule delivers better results than the other rules except for one case. In detail, in most of the cases, the improvements are less significant (partially much less) and the sequences of the regarded rules according to both performance criteria, are different. The results of the priority rules in (Rajendran and Holthaus 1999) and in (Raghu and Rajendran 1993) are significantly impacted by the station utilisation levels, which are primarily 80% and 95%. In addition (Rajendran and Holthaus 1999) uses an allowance factor and (Raghu and Rajendran 1993) uses the due date tightness, which both have a much smaller impact than the station utilisation level. In this investigation the time pressure is only increased by using tighter due dates while the load on the stations remains unchanged. Therefore, it can be expected that the time pressure here has a similar effect as the allowance factor in (Rajendran and Holthaus 1999) or the due date tightness in (Raghu and Rajendran 1993). A much larger impact is caused by a significant fluctuation of the load in the periods, so there are some periods where the load is either much higher than 95% and or much lower than 80% (as in (Rajendran and Holthaus 1999) or in (Raghu and Rajendran 1993)). Thus a tighter due date has a more significant effect in periods with relative very high load than in periods with a relative very small load. In total this seems to cause the different amount of improvement.

The poor results of RM global compared with RM local (with one exception) contradicts the results in (Lawrence et al. 1993). The same happens in the investigation of (Voß and Witt 2007). The local processing time costing prefers more often jobs with short processing times than the global processing time costing. This procedure explains the much better results in the case of those time pressures for which the SPT rule delivers a much better T_{Mean} than to the SL rule. In the other cases this procedure is beneficial if many tardy jobs are waiting in front of the flow job. Finally, in the flow shop in (Voß and Witt 2007) with parallel resources and setup states the differences in the results of the rules are smaller than in this investigation and vice versa for the more general problem structure in(Voß and Witt 2007).

Overall, the simulated processing times should be used in the priority rules. Then, the rules RR and RM local deliver the best mean tardiness. RR is beneficial with low and RM local with (very) high time pressure. The RR rule delivers the best standard deviation of the tardiness (for all time pressures).

6. CONCLUSIONS

This paper presents a real world flow shop scheduling problem with more restrictive restrictions than the ones normally regarded in literature. To ensure online scheduling this investigation is restricted to those priority rules, which are considered in literature as being very effective. The substitution of the net processing time, normally used in priority rules, by a simulated one delivers often significant better results. Some tests with optimisation solutions for a small test problem indicate that priority rules do not recognise when to prefer large variances of cycle times or small ones, respectively, and that the schedules of priority rules have outliers in the cycle times, which are usually avoided by optimal solutions. With this and other characteristics of optimal solutions an efficient metaheuristic like local search or genetic algorithm shall be developed next.

Up to now, the workers for the manual tasks are not scheduled. In addition, limited resources, like the available number of coils or assembly ground plates, occur at some company sites. Such requirements are also left to future investigations.

REFERENCES

El-Bouri, A. 2012. “A cooperative dispatching approach for minimizing mean tardiness in a dynamic flowshop”. *Computers & Operations Research*, Volume 39, Issue 7 (July), 1305 – 1314.

Engell, S.; F. Herrmann; and M. Moser. 1994. “Priority rules and predictive control algorithms for on-line scheduling of FMS”. In *Computer Control of Flexible Manufacturing Systems*, S.B. Joshi and J.S. Smith (Eds.). Chapman & Hall, London, 75 – 107.

Framinan, J.M.; R. Leisten; and C. Rajendran. 2003. “Different initial sequences for the heuristic of

Nawaz, Enscore and Ham to minimize makespan, idletime or flowtime in the static permutation flowshop sequencing problem". *International Journal of Production Research*, 41, 121 – 148.

Grabowski, J. and J. Pempera. 2007. "The permutation flow shop problem with blocking. A tabu search approach.". *Omega*, 35 (3), 302 – 311.

Hall, N.G. and C. Sriskandarajah. 1996. "A survey of machine scheduling problems with blocking and no-wait in process". *Operations Research* 44 (3), 510–525.

Jacobs, F.R.; W. Berry; D. Whybark; T. Vollmann. 2010. "Manufacturing Planning and Control for Supply Chain Management". McGraw-Hill/Irwin (New York), 6 edition.

Lawrence, S. and T. Morton. 1993. "Resource-constrained multi-project scheduling with tardy costs: Comparing myopic, bottleneck, and resource pricing heuristics.". *European Journal of Operational Research* 64, 168 – 187.

McCormick, S.T.; M.L. Pinedo; S. Shenker; and B. Wolf. 1989. "Sequencing in an assembly line with blocking to minimize cycle time". *Operations Research*, 37 (6), 925 – 935.

Nawaz, M.; E.E. Enscore; and I. Ham. 1983. "A heuristic algorithm for the m-machine, n-job flow sequencing problem". *Omega*, 11(1), 91 – 95.

Pan, Q.; and L. Wang. 2012. "Effective heuristics for the blocking flowshop scheduling problem with makespan minimization". *Omega*, 40 (2), 218 – 229.

Rachamadugu, R.M.V. 1987. "Technical Note –A Note on the Weighted Tardiness Problem". *Operations Research*, 35, 450 – 452.

Rachamadugu, R.V. and T.E. Morton. 1982. "Myopic heuristics for the single machine weighted tardiness problem". Working Paper No. 28-81-82, Graduate School of Industrial Administration, Carnegie-Mellon University, Pittsburgh, PA.

Raghu, T.S. and C. Rajendran. 1993. "An efficient dynamic dispatching rule for scheduling in a job shop". *International Journal of Production Economics* 32, 301 – 313.

Rajendran, C and O. Holthaus. 1999. "A comparative study of dispatching rules in dynamic flowshops and job shops". *European Journal of Operational Research*, 116 (1), 156 – 170.

Ribas, I.; R. Companys; and X. Tort-Martorell. 2011. "An iterated greedy algorithm for the flowshop scheduling problem with blocking". *Omega*, 39, 293 – 301.

Ronconi, D.P. and V.A. Armentano. 2001. "Lower Bounding Schemes for Flowshops with Blocking In-Process". *Journal of the Operational Research Society*, 52 (11), 1289 – 1297.

Ronconi, D.P. 2004. "A note on constructive heuristics for the flow-shop problem with blocking". *International Journal of Production Economics*, 39 – 48.

Ronconi, D.P. 2005. "A branch-and-bound algorithm to minimize the makespan in a flowshop with blocking". *Annals of Operations Research*, (138), 53 – 65.

Ronconi, D. and L. Henrique. 2009. "Some heuristic algorithms for total tardiness minimization in a flow shop with blocking". *Omega*, 37 (2), 272 – 281.

Russel, R.S.; E.M. Dar-El; and B.W. Taylor. 1987. "A comparative analysis of the COVERT job sequencing rule using various shop performance measures". *International Journal of Production Research*, 25 (10), 1523 – 1540.

Taillard, E. 1993. "Benchmarks for basic scheduling problems". *European Journal of Operational Research*, 64 (2), 278 – 285.

Vepsatainen, A.P. and T.E. Morton. 1987. "Priority rules for job shops with weighted tardiness costs". *Management Science* 33/8, 95 – 103.

Voß, S. and A. Witt. 2007. "Hybrid Flow Shop Scheduling as a Multi-Mode Multi-Project Scheduling Problem with Batching Requirements: A real-world application.". *International Journal of Production Economics* 105, 445 – 458.

Wang, X. and L. Tang. 2012. "A discrete particle swarm optimization algorithm with self-adaptive diversity control for the permutation flow shop problem with blocking". *Applied Soft Computing*, (12, 2), 652 – 662.

Wang, L.; Q.-K. Pan; and M.F. Tasgetiren. 2011. "A hybrid harmony search algorithm for the blocking permutation flow shop scheduling problem". *Computers & Industrial Engineering*, 61 (1), 76 – 83.

Wang, C.; S. Song, S.; J.N.D. Gupta; and C. Wu. 2012. "A three-phase algorithm for flowshop scheduling with blocking to minimize makespan". *Computers & Operations Research*, 39 (11), 2880 – 2887.

AUTHOR BIOGRAPHY

Frank Herrmann was born in Münster, Germany and went to the RWTH Aachen, where he studied computer science and obtained his degree in 1989. During his time with the Fraunhofer Institute IITB in Karlsruhe he obtained his PhD in 1996 about scheduling problems. From 1996 until 2003 he worked for SAP AG on various jobs, at the last as director. In 2003 he became Professor for Production Logistics at the University of Applied Sciences in Regensburg. His research topics are planning algorithms and simulation for operative production planning and control. His e-mail address is Frank.Herrmann@HS-Regensburg.de and his Web-page can be found at http://www.hs-regensburg.de/index.php?id=2457

ANALYSIS OF BACKTRACKING IN UNIVERSITY EXAMINATION SCHEDULING

Siti Khatijah Nor Abdul Rahim[1,2]
[1]School of Computer Science
University of Nottingham
Jalan Broga, 43500, Semenyih
Selangor, Malaysia
[2]Universiti Teknologi MARA
32610, Bandar Baru Seri Iskandar
Perak, Malaysia

Andrzej Bargiela[3,4]
[3]School of Computer Science
University of Nottingham
Jubilee Campus, Wollaton Road,
Nottingham, NG8 1BB UK,
[4]Institute of Informatics,
Cracow Technical University
Poland

Rong Qu[3]
[3]School of Computer Science
University of Nottingham
Jubilee Campus, Wollaton Road,
Nottingham, NG8 1BB UK

KEYWORDS
Examination Scheduling, Backtracking, Fewer Slots.

ABSTRACT

Simulation modelling of the initial assignments of exams to time-slots provides an alternative approach to the establishment of a set of feasible solutions that are subsequently optimized. In this research, we analyze two backtracking strategies for reassigning exams after the initial allocation of exams to time-slots. We propose two approaches for backtracking, BT1 and BT2. The study indicates that backtracking is an effective approach for improving the quality of the examination schedule where BT2 has outperformed BT1 in a number of cases.

INTRODUCTION

Examination timetabling or scheduling is a process of creating feasible examination schedules with the objective to satisfy all hard constraints and some other soft constraints. There are many approaches proposed in the literature to solve this timetabling problem.

In many examination timetabling problems, satisfying the requirement about the specific number of timeslots in the given examination session is a hard constraint and is frequently quite a challenging task. The methods that generate examinations schedules using an arbitrary number of time-slots are much easier to design and implement but the solutions are clearly unacceptable as the final schedules.

FRAMEWORK OF THE PROPOSED APPROACH

In our previous work (Rahim et. al, 2012), (Rahim et. al, 2013) we have proposed a method to solve the timetabling problems which consists of 1) pre-processing, 2) a two-stage scheduling and 3) timetable optimization.

During scheduling process, the order of processing of exams may sometimes lead to non-optimal assigning of exams to slots which could create an infeasible schedule (i.e.: does not satisfy the minimum number requirement of slots). This situation calls for a reassigning of exams from the initial slot allocation to other slots in order to ensure the number of slots is reduced to the required number and the schedule becomes feasible. Logically, this kind of reassignment will need to relook or backtrack the initial allocation or assignment process, and therefore we will call this a *backtracking* process. In the backtracking process, some assignments already made will be undone in order to schedule these exams in other time-slots. As a result, this simulates a generation of as set of feasible schedules that will be used in the optimization process later.

The objectives of the *backtracking* might include 1) to reduce the number of slots in order to satisfy the minimum number requirement of slots in a given problem; 2) to prepare the non-optimal schedule for further optimization. In this paper, our objective is the latter. Another objective would be to get the lowest number of slots in order to minimize the duration of the examination session.

This is in anticipation that by reducing the number of slots at the early stage, one can minimize the cost of timetables at the later stage during the optimization process. The initial schedule with a few slots (i.e.: less than required number of slots), can always be modified into one with the required slots. We hypothesize that this could provide a useful buffering space during the optimization involving permutations of exams slots.

Proceedings 27th European Conference on Modelling and Simulation ©ECMS Webjørn Rekdalsbakken, Robin T. Bye, Houxiang Zhang (Editors)
ISBN: 978-0-9564944-6-7 / ISBN: 978-0-9564944-7-4 (CD)

Consequently, this has a potential for improving the quality of the schedules (Rahim et. al, 2009), (Rahim et. al, 2012).

It is important to highlight here that the cost of the schedule will be evaluated by the objective function proposed by (Carter et. al, 1996) as follows:

$$\frac{1}{T}\sum_{i=1}^{N-1}\sum_{j=i+1}^{N} s_{ij} w_{|pj - pi|} \qquad (1)$$

where N is the number of exams, S_{ij} is the number of students enrolled in both exam i and j, p_j is the time slot where exam j is scheduled, p_i is the time slot where exam i is scheduled, W is the cost imposed on the timetable for students sitting two exams $| p_j - p_i |$ slots apart, where W_1 =16, W_2=8, W_3=4, W_4=2 and W_5=1 and T is the total number of students. According to this cost function, a student taking two exams that are $| p_j - p_i |$ slots apart, where $| p_j - p_i |$ ={1, 2, 3, 4, 5 }, leads to a cost of 16, 8, 4, 2, and 1, respectively. The objective of this cost function is to minimize the sum of costs per student. The lower the cost obtained, the better is the quality of the schedule, since the gap between two consecutive exams allows students to have additional revision time.

Figure 1 illustrates the backtracking phase in our general framework (Rahim et. al, 2012), (Rahim et. al, 2013) proposed in solving the examination timetabling problem. Note that the backtracking process is proposed to be done right after the initial assignment of exams to slots where both are parts of the scheduling process. The scheduling process is prior to the pre-processing stage and later an optimization stage will follow.

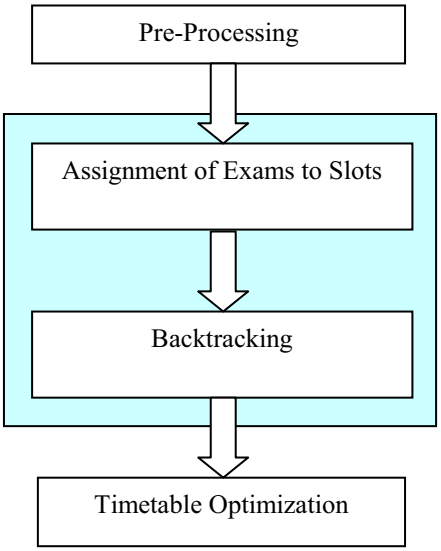

Figure 1: Scheduling Framework With Backtracking

In this study, we use two types of backtracking, as explained in detail in the next section. The pre-processing stage uses the information abstraction ideas as described in detail in (Bargiela et. al. 2002, 2008) and (Pedrycz et. al, 2000).

BACKTRACKING

First Method: Backtracking 1 (BT1)

In the first backtracking method, called here Backtracking 1 (BT1), we attempt to eliminate the last utilized time-slot.

We have implemented the backtracking process by (Carter et. al, 1996) but with some modifications. In contrast to (Carter et. al, 1996) where backtracking was performed during the initial placement of exams, in our approach, the placement of exams to their allocated slots has already been completed therefore we are attempting to convert the infeasible schedule into a feasible one.

After allocations of exams to slots were done, we identified all the exams in the last slot and we assigned them to a waiting list of unscheduled exams. Then, for each exam in this list, we initialized the selection criteria which is known as *Bp* (according to Carter et. al, 1996) for all periods equals to zero (*Bp=0*). Next for each of the exam in the list we proceed by finding the numbers of exams clashing with it in each of the available periods. *Bp* for each period is the number of exams clashing with the exam currently being evaluated in the waiting list. Please note that the exams clashing with the exam in the list are the exams that will be bumped to the waiting list, and thus will be assumed as unscheduled exams. (Note: we process the exams in the list on a First In First Out basis).

By contrast to (Carter et. al, 1996), we have assigned *Bp* equals to *number of exams + 1* (*Bp= nex + 1*) if the exam in the list has bumped any clashing exams encountered in the period we are dealing with. We also assign *Bp = nex+1* for a period, if the exam in the list originated from this period. This is another modification done to Carter's method to avoid cyclic. We continue finding the *Bp* for all periods for each exam in the waiting list.

The purpose of finding the Bp's for all the periods is to determine which period to choose to assign the exams in the waiting list. Bp's that we obtained for all periods can range from the value of *0* to *nex + 1*. So, the best *Bp* would be *0* and the worse *Bp* would be *nex + 1*. This means that, the exam in the waiting list will be assigned to the period with the minimum value of *Bp*.

In the period selection stage, there is always a possibility of having the same Bp's values. If there are a few periods having *Bp = 0*, then our method will choose the

first period with *Bp=0* encountered, or in other words, the first available period with no exams clashing with the exam in the waiting list. In cases, where *Bp* range from the value 1 to nex (*Bp=1* to *Bp=nex*), and there exist multiple periods with the same Bp's, then our method will do a selection based on weighing given to the periods.

The weighing given was based on the total number of students having conflicts in both exams in the periods and the exam in the waiting list. The period with the maximum value of the weighing will be selected, thus the clashing exams in the period with the exam in the waiting list will be bumped to the waiting list. The weighing given is mainly for the purpose of breaking the ties of the same Bp's.

Once the period or the location to assign the exam in the waiting list is determined, the transfer stage follows. Transfer stage is the process of transferring the current exam in the waiting list to the new period selected.

The above process then repeats for other exams in the waiting list. If at the end of the process, some exams fail to be assigned to any periods, then we assume the backtracking process fails, thus the above process will be undone and the previous configurations of allocation of exams to periods will be used.

Second Method: Backtracking 2 (BT2)

In the second backtracking approach (BT2), the objective is to eliminate the slot containing the fewest number of exams after the allocation method. The number of slot that will be eliminated is also 1 (same as BT1).

It is interesting to note here that, in BT2, the slot that will be eliminated could be any slot in the schedule (in BT1 it is always the last slot), therefore it could be the first, in the middle or the last one.

Once the slot with the fewest exams has been determined, all the exams will be put in a waiting list. Each exam in the list will be evaluated for reallocation as per our first approach (BT1).

RESULTS AND DISCUSSIONS

We have evaluated our both approaches of backtracking on the randomly generated benchmark dataset used for the evaluation of examination timetabling algorithms. The dataset can be downloaded from (http://www.cs.nott.ac.uk/~rxq/data.htm).

The benchmark exam timetabling problem dataset consists of 18 different problem instances; 9 small (< 100 exams) and 9 large problems (>= 500 exams). The problems generated have conflict density values from 6% to 47% using 5% intervals. The number of students and their enrolments are variable according to the problem size and conflict density. The problems use the same objective function as in (1).

In the interest of clarity of presentation we used in this research, the 9 small problems. The characteristics of the problems are given in Table 1.

Table 1: Characteristics of the Randomly Generated Problems (Small Problems)

(a) Name of Dataset; (b) No of Exams; (c) No of Students; (d) No of Enrollments; (e) Conflict Density (f) Required No of Slots;

(a)	(b)	(c)	(d)	(e)	(f)
SP5	80	66	194	7%	15
SP10	100	100	359	11%	15
SP15	80	81	314	17%	15
SP20	80	83	344	19%	15
SP25	80	119	503	26%	15
SP30	80	126	577	32%	15
SP35	100	145	811	36%	19
SP40	81	168	798	42%	19
SP45	80	180	901	47%	19

Table 2: Results Obtained by BT1

(a)Name of Dataset; (b) No of Slots (original allocation); (c) No of Slots (after backtracking); (d) Cost (after backtracking); (e) No of Slots (Permutation 1); (f) Cost (after Permutation); (g) No of Slots (after added slots); (h) Cost (after Permutation - after added slots)

(a)	(b)	(c)	(d)	(e)	(f)	(g)	(h)
SP5	7	7	31.85	7	19.59	15	4.12
SP10	10	10	45.06	10	25.19	15	12.18
SP15	9	9	53.07	9	39.78	15	16.68
SP20	10	10	53.75	10	39.96	15	20.3
SP25	13	12	46.39	12	34.87	15	25.48
SP30	13	13	51.03	13	41.83	15	33.62
SP35	19	18	58.63	18	50.94	19	47.5
SP40	17	17	44.59	17	34.18	19	29.01
SP45	18	17	48.78	17	36.82	19	31.76

Table 3: Results Obtained by BT2

(a)Name of Dataset; (b) No of Slots (original allocation); (c) No of Slots (after backtracking); (d) Cost (after backtracking); (e) No of Slots (Permutation 1); (f) Cost (after Permutation); (g) No of Slots (after added slots); (h) Cost (after Permutation - after added slots)

(a)	(b)	(c)	(d)	(e)	(f)	(g)	(h)
SP5	7	7	31.85	7	19.59	15	4.12
SP10	10	10	45.06	10	25.19	15	12.18
SP15	9	9	53.07	9	39.78	15	16.68
SP20	10	10	53.75	10	39.96	15	20.3
SP25	13	12	44.1	12	31.34	15	25.17
SP30	13	13	51.03	13	41.83	15	33.62
SP35	19	18	58.63	18	50.94	19	47.5
SP40	17	17	44.59	17	34.18	19	29.01
SP45	18	17	47.04	17	34.25	19	31.12

Table 4: Comparison of Results by BT1, BT2 and Without Backtracking (W/O) on Dataset SP25, SP35 and SP45.

(a)Type of Experiment; (b) No of Slots (original allocation); (c) No of Slots (after backtracking); (d) Cost (after backtracking); (e) No of Slots (Permutation); (f) Cost (after Permutation); (g) No of Slots (after added slots); (h) Cost (after Permutation - after added slots)

(a)	(b)	(c)	(d)	(e)	(f)	(g)	(h)
SP25							
BT1	13	12	46.39	12	34.87	15	25.48
BT2	13	12	44.1	12	31.34	15	**25.17**
W/O	13	NA	NA	NA	NA	15	25.33
SP35							
BT1	19	18	58.63	18	50.94	19	47.5
BT2	19	18	58.63	18	50.94	19	47.5
W/O	19	NA	NA	NA	NA	19	**46.88**
SP45							
BT1	18	17	48.78	17	36.82	19	31.76
BT2	18	17	47.04	17	34.25	19	**31.12**
W/O	18	NA	NA	NA	NA	18	31.31

BT1 – Backtracking 1
BT2 – Backtracking 2
W/O – Without Backtracking
NA – Not Applicable

For each backtracking approach, we have recorded the number of slots and cost obtained after performing the backtracking (with the reduced number of slots), and later we recorded the results after doing permutations of exams slots (a type of optimization – (Rahim et. al, 2012)). The schedule for each dataset then has been added a number of slots to satisfy the requirement given in the problem (15 slots for the first 6 problems, and 19 slots for the balance). Later, the permutations of exams slots on these schedules (satisfying the requirement number of slots) were repeated to obtain the new cost. All the results by performing the mentioned steps here can be seen in Table 2 and Table 3. Based on these results, it can be seen that 3 datasets SP25, SP35 and SP45 (coincidently the same datasets) managed to reduce the slot after BT1 and BT2. The original number of slots before both backtracking for SP25 is 13 and after is 12, SP35 is 19 and 18; and SP45 is 18 and 17.

In terms of the cost obtained in Table 4, it can be seen that BT2 has outperformed BT1 in 2 datasets SP25 and SP45 (out of the 3 datasets) where lower costs were obtained after the optimization. To evaluate the advantage of the backtracking, we also have presented the results for these 3 datasets if backtracking is not performed. Again, for SP25 and SP45, BT2 has outperformed the ones without backtracking in terms of the costs obtained.

One possible reason why BT2 outperformed BT1 in the cases discussed above, is maybe because BT2 selected the slot with the fewest exams to be eliminated, and therefore only a few exams need to be assigned to other slots which indirectly means that only a few exams will need to be bumped out for further processing. By contrast to this, BT1 always selected the last slot, which does not guarantee that it is the slot containing the fewest exams. If this last slot contains many exams, therefore we can predict that it might involve more exams to be bumped out for further processing (as opposed to BT2).

For SP35, the results for both BT1 and BT2 are the same. This is because, the slot being selected for elimination by both BT1 and BT2 is coincidently the same slot which is the last slot. This is due to the fact that the last slot (selected by BT1) happens to be the same slot selected by BT2 where it has the fewest number of exams.

Figure 2 and Figure 3 (on page 5) illustrate the data structure of slots containing exams before and after backtracking for SP35 respectively. The first column in both Figure 2 and Figure 3 indicates the number of exams in the existing slot (each row). The number(s) in each row (starting from column 2) is the list of the exams allocated to the given slot.

As can be seen, before backtracking, the last slot has been assigned the fewest number of exams (Exam 30 and Exam 49). If we observe carefully, after backtracking, the number of slots has reduced by 1 (only 18 rows exist which represents 18 slots). Another important point to note is that, the ordering of some exams in the slots after backtracking has changed. This is due to the fact that assignment of exams from the waiting list to some slots will bumped out other exams to the waiting list and therefore these affected exams will sometimes be assigned to different slots (other than the initial original slots).

11	19	22	27	47	61	62	76	77	83	98	100
7	4	23	38	45	59	87	91	0	0	0	0
11	9	40	55	56	58	65	68	79	84	89	99
9	18	26	51	52	60	75	80	90	92	0	0
4	16	29	36	67	0	0	0	0	0	0	0
7	37	42	44	73	78	86	95	0	0	0	0
4	1	20	48	50	0	0	0	0	0	0	0
4	2	6	8	72	0	0	0	0	0	0	0
5	11	14	41	66	82	0	0	0	0	0	0
5	13	34	57	74	93	0	0	0	0	0	0
4	7	21	70	85	0	0	0	0	0	0	0
4	35	53	88	96	0	0	0	0	0	0	0
4	3	12	25	32	0	0	0	0	0	0	0
5	5	33	43	46	71	0	0	0	0	0	0
3	10	64	94	0	0	0	0	0	0	0	0
5	15	28	54	81	97	0	0	0	0	0	0
3	17	31	69	0	0	0	0	0	0	0	0
3	24	39	63	0	0	0	0	0	0	0	0
2	30	49	0	0	0	0	0	0	0	0	0

Figure 2: The Data Structure Illustrating the Exams Assignment to Slots Before Backtracking

12	17	24	27	61	62	76	77	79	83	94	98	100
7	20	23	38	45	53	56	87	0	0	0	0	0
9	5	39	48	55	68	84	89	90	99	0	0	0
9	29	33	47	52	60	74	80	91	92	0	0	0
5	18	26	51	75	85	0	0	0	0	0	0	0
8	10	30	40	42	44	65	73	95	0	0	0	0
4	15	43	46	97	0	0	0	0	0	0	0	0
6	1	16	28	49	64	67	0	0	0	0	0	0
6	11	14	41	59	66	82	0	0	0	0	0	0
2	9	37	0	0	0	0	0	0	0	0	0	0
5	13	34	57	72	93	0	0	0	0	0	0	0
6	3	32	35	36	50	96	0	0	0	0	0	0
3	2	8	70	0	0	0	0	0	0	0	0	0
4	31	54	78	86	0	0	0	0	0	0	0	0
3	4	12	88	0	0	0	0	0	0	0	0	0
3	7	71	81	0	0	0	0	0	0	0	0	0
4	19	22	58	69	0	0	0	0	0	0	0	0
4	6	21	25	63	0	0	0	0	0	0	0	0

Figure 3: The Data Structure Illustrating the Exams Assignment to Slots After Backtracking

An interesting point to note based on the results is that for SP35, the scheduling without doing backtracking actually produced better result which is 46.88 compared to BT1/BT2 which is 47.5. This might be due to the elimination of the slots via backtracking has resulted in changing of the initial assignment of exams to slots (through the allocation method) which disturbed the good ordering of exams generated earlier (i.e.. exams spaced out equally).

CONCLUSION

We conclude that the combined scheduling (that does not pay regard to the required number of time-slots) and backtracking (aimed at achieving the required number of time-slots) is an effective approach to examinations timetabling. However, in certain cases, the time-slot-aware scheduling without backtracking could give lower cost schedules because the backtracking can sometimes disturb the original ordering of exams to slots which might already be allocated to slots in an optimal way.

Comparing the two backtracking methods proposed here, we conclude that the second approach (BT2) has outperformed the first approach (BT1) which selected the slot with fewest exams for elimination.

REFERENCES

Abdul-Rahman, S., Burke E.K., Bargiela A., McCollum B., Ozcan E. "A Constructive approach to examination timetabling based on adaptive decomposition and ordering". Annals of Operation Research, 1-19, 2011, doi:10.1007/s10479-011-0999-8.

Abdul-Rahman, S., Bargiela A., Burke E.K., Ozcan E., McCollum B. "Linear combination of heuristic orderings in construction of examination timetable". European Journal of Operational Research , 2011, (published online, Oct. 2011).

Bargiela, A., and Pedrycz, W. 2002. "Granular Computing – An Introduction". Kluwer Academic Publishers. 2002. (doi: 10.1007/978-1-4615-1033-8).

Bargiela, A. and Pedrycz, W. 2008. "Toward a theory of Granular Computing for human-centred information processing". IEEE Trans. On Fuzzy Systems. 16(2): 320-330. (doi:10.1109/TFUZZ.2007.905 912).

Carter M., Laporte G. and Lee S. 1996. "Examination Timetabling: Algorithmic Strategies and Applications". Journal of Operations Research Society, 47 373-383.

Pedrycz W, Smith M.H., Bargiela A. 2000. "Granular signature of data". Proc. 19th Int. (IEEE) Conf.NAFIPS'2000, Atlanta. July 2000; 69-73. (doi: 10.1109/NAFIPS.2000.877387).

Rahim, S. K. N. A., Bargiela, A., & Qu, R. 2009. "Granular Modelling Of Exam To Slot Allocation". ECMS 2009 Proceedings edited by J. Otamendi, A. Bargiela, J. L. Montes, L. M. Doncel Pedrera (pp. 861-866). European Council for Modeling and Simulation. doi:10.7148/2009-0861-0866.

Rahim, SKNA., Bargiela, A., Qu, R. "Domain transformation approach to deterministic optimization of examination timetables". Artificial Intelligence Research, 2(1), 2013, (doi:10.5430/air.v2n1p122).

AUTHOR BIOGRAPHIES

SITI KHATIJAH NOR ABDUL RAHIM received her Bachelor's Degree in Computer Science, majoring in Software Engineering, from Universiti Sains Malaysia (USM), Penang, Malaysia in 2001. She later pursued her Master's Degree at the same university in Computer Science majoring in Computational Intelligence. She started her career as a full time lecturer with Universiti Teknologi Mara, Perak, Malaysia after receiving her Master's Degree in 2003. Currently she is in the final stage of her PhD study at the University of Nottingham Malaysia Campus. Her research interests lie in the area of Computational Intelligence, Granular Computing and Scheduling. Her email address is khyx8skn@nottingham.edu.my or sitik781@perak.uitm.edu.my.

ANDRZEJ BARGIELA is Professor in the School of Computer Science at the University of Nottingham. He served as President of the European Council for Modelling and Simulation (ECMS) during 2002-2006 and 2010-2012. He is Associate Editor of the IEEE Transactions on Systems Man and Cybernetics and Associate Editor of the Information Sciences. His research involves investigation into Granular Computing, human-centred information processing as a methodological approach to solving large-scale data mining. His email address is Andrzej.Bargiela@nottingham.ac.uk.

DR RONG QU is a Lecturer in the School of Computer Science at the University of Nottingham. She gained her PhD in Computer Science from the University of Nottingham in 2002. Her main research areas include meta-heuristics, constraint programming, IP/ILP, case based reasoning methodologies and knowledge discovery techniques on scheduling, especially educational timetabling, healthcare personnel scheduling, network routing problems and graph colouring. In total she has more than 30 papers published or to appear at international journals and peer-reviewed international conferences. Dr Qu is also a guest editor for special issues at the journal of Memetic Computing and the Journal of Scheduling, and the program chair of several workshops and an IEEE symposium. Her email address is rxq@cs.nott.ac.uk.

ARTIFICIAL BEE COLONY ALGORITHM FOR POWER PLANT OPTIMIZATION

Friedrich Biegler-König
Department of Applied Mathematics
University of Applied Sciences
D-33615 Bielefeld
E-Mail: Friedrich.biegler-koenig@fh-bielefeld.de

KEY WORDS

Artificial Bee Colony Algorithm, Evolutionary Methods, Neural Networks, Mixed Integer Optimization, Power Plant Optimization

ABSTRACT

The mathematical model of a fleet of power plants can be optimized with respect to energy production. This involves the solution of a mixed integer problem. Traditionally these problems are solved by linearization of the continuous and non-linear parts and subsequent application of a Simplex-type algorithm. In order to handle nonlinearities, so-called "biomimetic" optimization algorithms can be applied. As an example, we are proposing an approach to first model power plant blocks with fast Neural Networks. Afterwards, we optimize the operation of multi-block power plants over a period of time using an Artificial Bee Colony Algorithm.

1. INTRODUCTION

Increasing prices for fossil fuels and the establishment of CO_2 credits to European markets have intensified the attempts to ensure energy efficient operation of existing power plants.

One of the well-known optimization issues where mathematical modelling has proven to be indispensable is the unit commitment in power generation planning. It deals with the scheduling of start-up/shut-down decisions and operation levels for a fleet of power generation units such that variable costs are minimal, or revenues are maximal. In this optimization, temporal constraints such as time dependency of energy prices at the power exchange, limited availability of certain plants, costs for start-up or shut-down, limits for total emission or fuel consumption within a given period of time should be taken into account. Therefore, the optimization has to be carried out within a certain time window with sufficient time resolution.

Because of the involvement of decision variables (power plant on or off), and the fact that every unit has a non-vanishing lower limit of energy that can be generated, the above-defined problem involves mixed integer programming. The well understood approach to this problem is to use the methods of mixed integer linear programming (Schultz 2003) in this context. It is widely used and allows for optimization with complex temporal constraints with reasonable CPU time consumption.

Recent studies (Biegler-König and Deeskow 2005, Deeskow et. al. 2005, Nolle 2007) have shown that a nonlinear approach has the advantage of easily taking into account the current state of each of the plant components and thus opens additional potential for optimization. It overcomes the generally high CPU time consumption of nonlinear modelling based on closed analytical models by meta-modelling the power plant using neural networks. However, this approach was restricted to a one-point-in-time optimization only.

In this contribution the approach presented in Biegler-König and Deeskow 2005 is extended to consider a model which is discrete in time and covers 24 hours of energy production with complex constraints. The resulting large mixed integer problem is treated by employing biomimetic optimization methods, in this case Simulated Annealing and Artificial Bees Colony algorithm.

2. APPROACHES TO MIXED INTEGER OPTIMIZATION

The common way to optimization in unit commitment uses a linear model of power generation and applies the simplex method of linear programming together with a Branch-and-Bound approach to solve the integer linear problem.

The simplex method is an iterative method to solve linear problems with constraints. Within a finite number of steps, it reaches the solution or proves infeasibility of the problem. The algorithm cannot be applied if some of the variables are restricted to integers. In that case methods are available which apply to a more or less general class of problems.

One of these methods is Branch-and-Bound, which consists of three phases. In the branching phase, the feasible region is partitioned, in the bounding phase linear

Proceedings 27th European Conference on Modelling and Simulation ©ECMS Webjørn Rekdalsbakken, Robin T. Bye, Houxiang Zhang (Editors)
ISBN: 978-0-9564944-6-7 / ISBN: 978-0-9564944-7-4 (CD)

simplex is used to obtain upper and lower bounds of the optimal objective values and in the coordination phase rules are applied for eliminating parts of the feasible region from further consideration.

Unfortunately, the convenience of using the well-known mathematics of mixed integer linear programming comes to the expense of losing details in the modelling. This may have an impact on the potential for optimization.

A different approach is the use of so-called "Biomimetic Methods", i.e. methods which emulate the optimization behaviour of biological or physical systems. Well-known among these are Genetic Algorithms, Simulated Annealing (SA), or Artificial Bee Colony (ABC) algorithms (Pham et. al. 2006).

All these algorithms are iterative, based on heuristics, and have the advantage that they can easily deal with continuous variables as well as with discrete ones.

The number of iterations needed to produce good optimal states of the system is usually high. In most cases, however, it is impossible to prove that a state found is optimal.

The next section gives an introduction to the simulation approach for power plant blocks before SA and ABC algorithms are applied to a problem of the described type in sections 4 and 5.

3. FAST SIMULATION OF POWER PLANTS

We are considering a fleet of power plants with four blocks which are identical in construction (a simple case, but easily expandable). Each block can generate power in the range of 108 MW to 360 MW. A block cannot produce less than 108 MW. If a block is switched off, it can only be started up again at considerable costs.

A detailed model of a power plant block was built using Ebsilon, a programme developed by Sofbid (http://www.sofbid.com/ebsilon/, Brinkmann and Pawellek 2003 and 2004) in Zwingenberg, Germany. Ebsilon is a simulator specialized in power generating facilities. Ebsilon models can be extremely complex. After the model has been constructed, Ebsilon requires about 1 to 10 seconds on a PC to simulate a given situation for one block. This is by far not fast enough since many thousands of model evaluations are usually required for the considered algorithms.

A specific situation of the power plant block is determined by only a few input parameters. The most important parameter is the amount of energy which the block is to produce per time period.

The other parameters describe the external conditions and settings by the operational staff:

- Temperature of cooling water (between 0 and 30 °C).
- Air ratio in combustion chamber (between 1.1 and 1.4).
- Live steam temperature (between 510 and 540 °C).
- Hot reheat temperature (between 510 and 540 °C)
- Flue gas recirculation (between 0 and 50 kg/s).
- 8 more parameters specifying the amount of heat surface fouling.

As main result, Ebsilon supplies is the amount of fuel (in our case coal) required. This in turn determines the main part of the total costs.

As described in Biegler-König and Deeskow 2005, it is possible to replace the simulator Ebsilon by a much faster meta-model based on Neural Networks. The model-error of fitting a Neural Network to the Ebsilon model has the same magnitude as the model-error of an Ebsilon simulation.

The main advantage of the Neural Network model is its response time. It is about 10000 times faster than Ebsilon (response time: less than 0.0001 seconds).

4. SIMULATED ANNEALING

Simulated Annealing is based on the imitation of the cooling process of metals.

Here is a brief mathematical description of the algorithm:

Let $F(x_1, \ldots, x_N)$ be a target function in N variables. These variables can come from different sources: real numbers, binaries, integers, with or without lower and upper bounds. Additionally, these variables are subject to a set of restrictions. We assume that F possesses a global minimum whose position we want to determine.

Simulated Annealing is defined by the following iteration:

- For each component x_i of the vector x = $(x_1, \ldots, x_N)$ define a set of elementary steps C_i whose members change x_i .
- We start with an initial temperature of T_0, and define a final temperature T_E and a cooling factor $\alpha < 1$. We also have a start vector $x^0 = (x_1^0, \ldots, x_N^0)$, which satisfies all constraints. Let, for the beginning, $x^{min} = x^0$ and $F^{min} = F(x^0)$.
- In iteration no. i the following operations will be executed ($i = 1, \ldots$):
  1. Until a new candidate vector x^i is found which satisfies all constraints, choose a random component k of vector x^{i-1} and change it using a randomly chosen elementary step from C_i .
  2. Calculate $F(x^i)$.
  3. If $F(x^i) \leq F(x^{i-1})$, set $F^{min} = F(x^i)$. F^{min} is the new optimal value (so far).
  4. If $F(x^i) > F(x^{i-1})$, we accept x^i as the vector for the next iteration with the probability $p(T_i) =$

$exp((F(x^i)- F(x^{i-1}))/ T_i)$. As the algorithm sometimes accepts a worsening of the values, it is able to leave local minima.

5. If x^i was not accepted, set $x^i = x^{i-1}$.
6. Set $T_i = \alpha T_{i-1}$ and terminate the algorithm if $T_i < T_E$. The system has "cooled down".

The iteration process takes longer with larger T_0 and larger α. The probability of finding the true global minimum increases with the number of performed iteration steps.

Simulated Annealing is not population-based and easy to implement. There are many variations of this standard version of Simulated Annealing (see e.g. Nolle et. al. 2001). Possible changes are:

- A different probability function $p(T)$ can be chosen.
- Instead of a constant α a cooling function $\alpha(T)$ can be used.
- Elementary steps can be defined as being temperature dependent.

5. ARTIFICIAL BEE COLONY ALGORITHM

The Artificial Bee Colony (ABC) algorithm or Bees algorithm is a recent invention (Pham et. al. 2006). It emulates the behavior of a swarm of bees looking for food. A bee hive sends out a certain amount of "scouts" which look for promising food sources (e.g. flower patches). They return to the hive and communicate their findings by performing the "waggle dance". The scouts then go back to their food sources followed by other bees (more followers for better sources). Less favorable sources are abandoned; the corresponding scouts look elsewhere for more promising places.

The observation of the behavior of a bee swarm leads to a population-based swarm intelligence algorithm which can be used to optimize mathematical objective functions as defined above. In pseudo code, the basic form of the ABC algorithm looks like this:

1. Initialize population with random solutions.
2. Evaluate objective function for members of the population.
3. While stopping criteria are not met, build a new population:
4. Select best sites for neighborhood search ("Scouts").
5. Abandon other sites and send their bees to the neighborhood of selected sites.
6. Determine their objective function value.
7. For each neighborhood choose the bee with best objective function value.
8. Distribute all remaining bees randomly over the search space and evaluate their objective function value.
9. End While.

Step 8 will ensure that eventually all regions of the search space are considered. Population size and percentage of scouts are the control parameters of the algorithm. As in Simulated Annealing, elementary steps, i.e. a defined neighborhood of a candidate solution, must be defined.
In step 4, the scouts should all come from different neighborhoods in order to prevent premature convergence.
The distribution of bees to the scouts in step 5 may vary: sometimes all scouts get the same number of bees, sometimes the distribution is done proportionally to the quality of the scout site.

6. POWER PLANT OPTIMIZATION. A CASE STUDY

We will now use SA and ABC algorithms to optimize the performance of our fleet of four power plant blocks for the period of 24 hours.

We assume that every hour a different amount of energy must be produced and that these 24 values are given a day ahead. In reality, these estimates have a high accuracy. They contain information e.g. about the time of the year and weather forecast.

For each time t_i, $i = 1, \ldots, 24$ the production of our power plant with 4 blocks is described by the vector

$$x(t_i) = (E_1, E_2, E_3, E_4, b_1, b_2, b_3, b_4)^T.$$

$b_1, b_2, b_3,$ and b_4 are binary values and indicate whether or not a block is switched off. E_1, E_2, E_3, E_4 are the production rates of the blocks. In every hour of the day, they must add up to the given total production. We also have to consider the restrictions of minimal and maximal production rates: $108MW \leq E_i \leq 360MW$.

The objective function we want to minimize is the cost of energy production accumulated over the day. Since, for every hour in a day, we have a vector of eight variables, the total number of variables in our problem is 24x8 = 192. In our simple model, the total costs consist of the costs for coal and the start-up costs for blocks going on-line. Thus, the aim is not only to minimize the production costs in every single hour, but also to keep the number of switch-on-processes of power plant blocks low.

In order to implement the described algorithms we must still specify the elementary steps. Basically, two kinds of steps can be identified:

1. Change of production rate E_k for block no. k without altering the configuration of the power plant. These steps attempt to optimize a given configuration. This corresponds to solving the continuous part of the problem. In the beginning, a maximal step size S_{max} is

defined. S_{max} is multiplied by a random number between –1 and 1. This yields the current step size. The block number k is also chosen from the set of running blocks.
Afterwards, the restrictions are checked (minimal and maximal production rates, total energy production). If it is not possible to satisfy all boundary conditions, another elementary step must be chosen.
This kind of elementary step is applied with a probability of 90%.

2. Change of power plant configuration. In this case, the binary valued variables are changed. Let n be the number of running blocks. Possible changes of configuration are: Starting up an additional block (4-n alternatives), shutting down a running block (n alternatives), interchanging a running and a pausing block (m alternatives with m=3 if n=1 or n=3, m=4 if n=2, otherwise m=0).
This kind of elementary step is applied with a probability of 10%. Among these, steps are chosen according to the number of alternatives.
After interchanging two blocks, it is not necessary to adjust the production rates since, in our case, all blocks have the same limitations. Starting up or shutting down a block makes it necessary to readjust the production rates in order to assure the restrictions. If this is not possible, another elementary step must be chosen.

In addition to the elementary steps, the following control parameter settings have been used for SA:

- $T_0 = 10{,}000$.
- $T_E = 10^{-6}$.
- $\alpha = 0.99998$.
- Maximal number of iterations: $it_{max} = 1{,}000{,}000$.

The control parameters of ABC algorithm are:

- Population size = 50.
- Percentage of scouts: 10%
- Number of iterations: $it_{max} = 1{,}500$

With this choice of parameters, both algorithms found satisfactory solutions for the total costs over a day, although, of course, it cannot be verified that the solutions found represent global optima.

Example

For our example, we have used the described 4-block power plant of Elbistan (Turkey), a coal price of 30 Euros for a ton and a start-up price of 30,000 Euros for each block. For each hour of the day, a required energy production rate is given. Additionally, the values for heat surface fouling and cooling temperature for block 1 have been changed for the worse; the corresponding values of block 3 have been changed for the better. The parameters of blocks 2 and 4 are in between, the values of block 2 are slightly better than those of block 4.

Starting configuration and initial population have been chosen randomly, but satisfying all constraints. Random starting configurations are usually quite poor, since they contain many start-up processes (see Table 1). Tables 2 and 3 contain the results for SA and ABC algorithms, respectively, with the above settings of parameters.

Table 1: Initial Configuration

Uhrzeit	Vorgabe	Block 1	Block 2	Block 3	Block 4
00:00	530000	360000	170000	0	0
01:00	310000	0	0	0	310000
02:00	200000	200000	0	0	0
03:00	180000	0	0	0	180000
04:00	250000	250000	0	0	0
05:00	320000	0	0	0	320000
06:00	490000	360000	130000	0	0
07:00	650000	0	0	290000	360000
08:00	830000	360000	360000	110000	0
09:00	1030000	0	310000	360000	360000
10:00	1230000	360000	360000	360000	150000
11:00	1130000	282500	282500	282500	282500
12:00	1000000	360000	360000	280000	0
13:00	900000	0	180000	360000	360000
14:00	880000	360000	360000	160000	0
15:00	930000	0	210000	360000	360000
16:00	950000	360000	360000	230000	0
17:00	1000000	0	280000	360000	360000
18:00	1100000	275000	275000	275000	275000
19:00	1240000	160000	360000	360000	360000
20:00	1320000	360000	360000	360000	240000
21:00	1362300	282300	360000	360000	360000
22:00	1223000	360000	360000	360000	143000
23:00	830000	0	110000	360000	360000

Table 2: Solution Computed with SA

Uhrzeit	Vorgabe	Block 1	Block 2	Block 3	Block 4
00:00	530000	0	108565	211437	209998
01:00	310000	0	0	153338	156662
02:00	200000	0	0	199999	0
03:00	180000	0	0	180000	0
04:00	250000	0	126432	123566	0
05:00	320000	0	145880	174120	0
06:00	490000	0	241964	248036	0
07:00	650000	0	265798	272984	111218
08:00	830000	0	115082	359410	355507
09:00	1030000	0	359500	359540	310959
10:00	1230000	153591	359237	357749	359474
11:00	1130000	108104	339363	341302	341231
12:00	1000000	300353	110047	289906	299694
13:00	900000	110631	266104	267436	255828
14:00	880000	267615	111725	241880	258780
15:00	930000	116764	265973	273476	273786
16:00	950000	275284	129582	276409	268724
17:00	1000000	302995	293152	294674	109179
18:00	1100000	108162	329713	330481	331645
19:00	1240000	161862	359837	358664	359637
20:00	1320000	359020	241419	359825	359734
21:00	1362300	357927	359971	359908	284493
22:00	1223000	144060	359202	360000	360000
23:00	830000	0	357988	359923	112090

Table 3: Solution Computed with ABC Algorithm

Uhrzeit	Vorgabe	Block 1	Block 2	Block 3	Block 4
00:00	530000	0	170000	360000	0
01:00	310000	0	0	309999	0
02:00	200000	0	0	199999	0
03:00	180000	0	0	179998	0
04:00	250000	0	0	250000	0
05:00	320000	0	0	320000	0
06:00	490000	0	129999	360000	0
07:00	650000	0	290000	360000	0
08:00	830000	0	342045	359948	128007
09:00	1030000	0	310001	360000	359999
10:00	1230000	150002	359997	360000	360000
11:00	1130000	146206	263796	359999	360000
12:00	1000000	112163	284973	313019	289845
13:00	900000	154280	235359	351367	158995
14:00	880000	137467	222878	281802	237853
15:00	930000	237643	220202	323749	148406
16:00	950000	146816	251191	360000	191991
17:00	1000000	360000	153117	359999	126884
18:00	1100000	157037	273416	360000	309547
19:00	1240000	160001	360000	360000	359999
20:00	1320000	360000	360000	360000	239999
21:00	1362300	360000	282301	360000	359999
22:00	1223000	143001	360000	360000	359999
23:00	830000	0	338076	360000	131924

The first column of the tables contains the time of day, the second the required energy production in kW. Columns 3 to 6 show how the blocks share the production of this energy amount.

The ABC algorithm required about 10 million evaluations of the underlying neural network while SA took about half as many evaluations and, subsequently, about half the computation time. Increasing the number of iterations in SA does not improve the results. The time required for both methods on a normal PC stays well below 30 minutes, thus being always faster than reality.

Both algorithms provide qualitatively similar solutions. They run block 3, which has the highest efficiency, with full capacity. Block 1 is only used if necessary since its efficiency is worst.

SA started with a configuration which costs 1,818,778 euros (configuration of Table 1) for the day and lowered it to 1,297,099 euros (configuration of Table 2). The initial 20 start-up processes where reduced to 3.

ABC algorithm started with a population whose best member costs 1,438,616 euros a day and contains 7 start-up processes. The result configuration of Table 3 costs 1,281,726 euros and also contains 3 start-up processes.

The main weakness of SA is that it may lose good solutions and finally concentrate on less favourable ones. ABC always keeps the so far best solutions and tries to improve on them. This can clearly be seen by comparing the two tables.

The above behaviour of both algorithms was verified with different starting values.

7. CONCLUSION

This paper has discussed a concept for online optimization in power plant technology which combines different numeric state-of-the-art processes to construct a method customized for power-engineering requirements.

Neural Networks can be trained with high accuracy to reproduce the results of the computationally intensive thermodynamic simulation programs on the basis of physical fundamentals. As such, non-linear detailed models of the individual power plant units can be generated, whose response time lies within the range of milliseconds.

Simulated Annealing is a heuristic optimization algorithm, which appears to be suitable for solving the mixed-integer optimization problems arising in power plants and which, together with fast neural network models, allows an online solution for the non-linear optimization problems.

The Artificial Bee Colony algorithm, a population-based heuristic optimization algorithm, yields better results, even though it needs more computation time.

In an earlier study, this concept was successfully applied to a momentary optimization, which already resulted in substantial savings of costs and fuel. The present study demonstrates that a suitable extension of the objective function allows for optimization of a model which is discrete in time and considers constraints linking different time intervals. Thus, it is clearly shown that the described methods allow nonlinear mixed integer optimization of unit commitment in a fleet of power plants.

Because of the non-linear nature of the models, such approaches would be able to solve problems in the future, which so far either cannot be solved at all or only with difficulty using a traditional optimization on the basis of a linear modelling. Examples here are the consideration of the non-linear boundary conditions (temperatures in the steam piping) or a common optimization of the load distribution to multiple units and, at the same time, the mode of operation of the individual units.

REFERENCES

Biegler-König, F. and P. Deeskow. 2005. “Fast Simulation and Optimization with Neural Networks”. *Proc. 19th European Conference on Modelling and Simulation*, Riga.

Brinkmann, K. and R. Pawellek. 2003. “Ebsilon - Examples for the easier design and better operation of power plants”. *Proc. Conf. Energy Forum 2003*, Sv. Konstantin Varna.

Brinkmann, K. and R. Pawellek. 2004. “Optimierte Prozessführung von Kraftwerksblöcken mit Online-Werkzeugen: Betriebserfahrungen“. *Proc. VDI Tagung “Wissensbasiertes Betriebsmanagement senkt Kosten“*, Frimmersdorf.

Deeskow, P.; F. Biegler-König; L. Nolle. 2005. “Schnelle Optimierung von Kraftwerksparks mit Neuronalen Netzen“. *Proc. 6. VDI-Fachtagung Optimierung in der Energiewirtschaft*, Stuttgart.

Nolle, L. ”Non-linear Total Energy Optimisation of a Fleet of Power Plants”. 2007. *Applications and Innovations in Intelligent Systems XIV*.

Pham, D.T.; A. Ghanbarzadeh; E. Koç; S. Otri; S. Rahim; M. Zaidi.2006. “The Bees Algorithm – A Novel Tool for Complex Optimisation Problems”, *Proceedings of IPROMS Conference, pp. 454–461.*

Schultz, R. 2003. Course Material: “Integer Programming Applied to Power Systems' Generation and Operation Planning”. Preprint 557-2003, Institut für Mathematik, Gerhard-Mercator-Universität Duisburg.

L. Nolle, A. Goodyear, A. Hopgood, P. Picton, N. Braithwaite, On Step Width Adaptation in Simulated Annealing for Continuous Parameter Optimisation. *Proc. 7th Fuzzy Days*, Dortmund, 2001, 589-598.

SIMULATION OF ROBUST MASTER PRODUCTION SCHEDULING IN AN INDUSTRIALLY RELEVANT PLANNING ENVIRONMENT

Julian Englberger, M.Eng.
Professor Dr. Frank Herrmann
University of Applied Sciences Regensburg
Innovation Centre for Factory Planning
and Production Logistics
Universitätsstraße 31, 93051 Regensburg, Germany

Professor Dr. Thorsten Claus

Technical University Dresden, IHI Zittau
Professor for Production Economics
and Information Technology
Markt 23, 02763 Zittau, Germany

KEYWORDS
Robust optimisation, production planning, simulation.

ABSTRACT

This paper presents a simulation analysis on the effects of robust master production scheduling. Up to now, relatively highly aggregated planning models for robust master production scheduling were regarded and the realizability of the planning results was not considered. This paper analyses a more detailed model for master production scheduling than in previous works. The evaluation of the planning results is made by providing the planning results to the subsequent planning levels in a hierarchical production planning system and realizing them in a realistic production system. The primary objective of the production system is to minimise tardiness of customer order deliveries. The secondary objective is to minimise inventory of end products. It is shown that robust master production scheduling in such a planning system leads to significant reductions of tardiness of customer order shipment. Compared to an equivalent deterministic approach for master production scheduling, the mean customer order backlog is reduced more than the mean inventory levels are increased.

INTRODUCTION

For a long time, concepts for hierarchical production planning – for example in (Hax and Meal 1975) – have been established in research and industry. In this paper, the planning concept proposed in (Drexl et al. 1994) and (Manitz et al. 2013) is used for production planning. It consists of three planning levels, which are master production scheduling, material requirements planning and scheduling (see Figure 1). Production planning is done over a long horizon – ten weeks in this paper – and bases on demands. As demands are not known deterministically for the whole planning horizon in most applications, production planning is usually done on demand forecasts (see Herrmann 2011). The real demands generally deviate from the forecasts; this leads to both out-of-stock and excessive stock situations. Demand uncertainty has led to intensive research for the last decades. From early on, it was tried to consider uncertainty in the planning concepts, for instance by rolling planning. For an overview over these concepts to consider uncertainty, see (Herrmann and Englberger 2013).

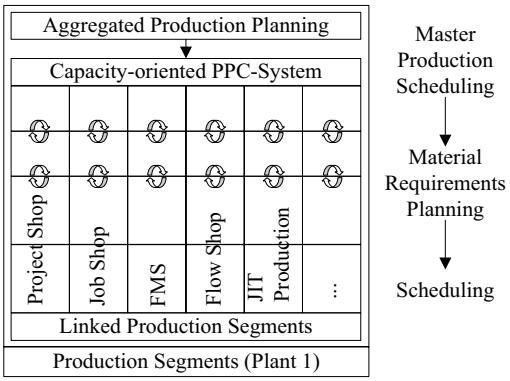

Figure 1: Hierarchical Production Planning (see (Günther and Tempelmeier 2012))

Over the last years, approaches of robust or stochastic optimisation have been in the focus of interest; these approaches are considered in this work. The remainder of this paper is structured as follows: firstly, a review of literature regarding stochastic optimisation for master production scheduling is given. Then, the test problem is described. Afterwards, the considered models for master production scheduling are explained. In the next sections, the simulation experiments and their results are described. At the end, a conclusion and an outlook are given.

LITERATURE REVIEW

(Escudero et al. 1993) propose a multi-stage stochastic production planning approach. Their studies show significant improvements compared to the conventional, deterministic approaches. (Mulvey et al. 1995) characterise the term of robust optimisation as trading off between solution quality and feasibility. To operationalize this trade off the objective function of their two-stage stochastic model is a weighted sum of a conventional cost function and an error variables function. Based on this approach, numerous two-stage stochastic models for aggregate production planning under uncertainty have been developed. (Yu and Li 2000) eliminate several absolute value functions from the error variables function to improve solving speed. Basing on this formulation, (Leung et al. 2007) propose a model for aggregate production planning regarding several production facilities, and costs for production, human labour, keeping inventories and adaption of

Proceedings 27th European Conference on Modelling and Simulation ©ECMS Webjørn Rekdalsbakken, Robin T. Bye, Houxiang Zhang (Editors)
ISBN: 978-0-9564944-6-7 / ISBN: 978-0-9564944-7-4 (CD)

personal capacities. (Al-e-Hashem et al. 2011) expand the model of (Yu and Li 2000) to a multiobjective optimisation model with the primary objective function regarding costs for production, labour including adaption of personal capacities, keeping inventory, transportation and backorders. The second objective function considers the maximum shortages among customer zones in all periods. (Zhang et al. 2011) develop a two-stage stochastic model that minimises annual labour cost, overtime cost, end product inventory cost and raw material inventory cost. (Scholl 2001) develops numerous models for robust production planning using different decision criteria in the objective functions and different modelling approaches. In numerical investigations, (Scholl 2001) concludes that compensation models with relative regret criteria are superior to other approaches in most cases (also see Herrmann and Englberger 2013). Based on his work, (Gebhard 2009) develops a concept for robust hierarchical production planning consisting of two planning levels. In numerical studies, (Gebhard 2009) shows that the robust approach is superior to an equivalent deterministic approach using a simple mathematical model representing basically an objective function and restrictions of a production system for evaluation.

Almost all of these investigations focus on the improvements of the objectives of master production scheduling, which is regularly a cost function. Implicitly, they assume that their master production schedules are realizable. Still, some planning parameters like resource consumptions caused by end products are used for master production scheduling but depend on planning decisions that are yet to be made at the time of master production scheduling. To the knowledge of the authors, robust master production planning never has been analysed in a planning hierarchy that comes close to the planning systems used in industrial applications. In this paper, the effects of robust production planning are evaluated using a planning hierarchy that is common in industrial applications.

TEST PROBLEM

To analyse the benefits of robust production planning, a part of the production of a company building high-voltage electronic devices in Regensburg is considered. This test problem includes five end products. The end products consist of numerous subassemblies and components on four disposition levels (as shown in Figure 2 for end product P1). The total number of products regarded in this case study is 82.

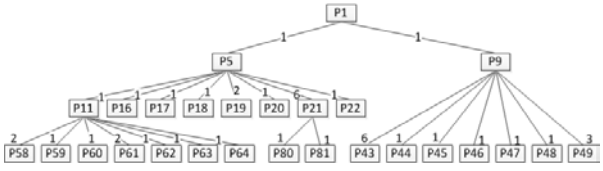

Figure 2: Bill of materials for end product P1

Each product's work plan has between two and six operations that need to be performed. As an example, the work plan for product P19 is displayed in Table 1.

Table 1: Work plan for product P19

Operation Number	Operation	Setup time $\left[\frac{\text{min}}{\text{lot}}\right]$	Operation time $\left[\frac{\text{min}}{\text{piece}}\right]$
1	Cutting	2	4
2	Turning	5	10
3	Milling	5	10
4	Grinding	3	5

These products are built on twelve production segments each consisting of one or several machines. Each production segment has normal capacity that can be used without extra costs, and additional capacity, which is more costly than normal capacity due to shift allowances, et cetera. The capacities of the production segments are listed in Table 2.

Table 2: Production Segments

Production Segment	Normal Capacity $\left[\frac{\text{hours}}{\text{week}}\right]$	Additional Capacity $\left[\frac{\text{hours}}{\text{week}}\right]$	Costs for Additional Capacity $\left[\frac{€}{\text{hour}}\right]$
Punching	336	168	10
Cleaning	224	112	10
Turning	560	280	10
Milling	560	280	10
Hardening	112	56	10
Isolating	112	56	10
Assembly	336	168	10
Testing	224	112	10
Broaching	112	56	10
Cutting	112	56	10
Grinding	448	224	10
Abrasive blasting	112	56	10

MASTER PRODUCTION SCHEDULING

Master production scheduling is performed via a deterministic and alternatively a robust version the model HPPLAN (Hauptproduktionsprogrammplanung) proposed in (Günther and Tempelmeier 2012) and (Manitz et al. 2013). The parameters and variables of the deterministic model HPPLAN are:

Parameters:

$b_{j,t}$ production capacity of production segment j in period t

$d_{k,t}$ demand for product k in period t

$f_{j,k,z}$ resource consumption on production segment j caused by product k in lead period z

h_k inventory costs for product k per unit and period
J number of production segments ($1 \le j \le J$)
K number of end products ($1 \le k \le K$)
T length of the planning horizon in weeks ($1 \le t \le T$)
$U_{j,t}^{max}$ maximum additional capacity for production segment j in period t
u_t costs for one unit of additional capacity in period t
z_k lead time for product k ($1 \le z \le Z_k$)

Variables:

$U_{j,t}$ used additional capacity in production segment j in period t
$x_{k,t}$ production quantity of product k in period t
$I_{k,t}$ inventory for product k at the end of period t

HPPLAN minimises costs for keeping inventory and using additional capacity in its objective function:

$$\text{Minimise } Z = \sum_{k=1}^{K}\sum_{t=1}^{T} h_k \cdot I_{k,t} + \sum_{t=1}^{T}\sum_{j=1}^{J} u_t \cdot U_{j,t}$$

The constraints of HPPLAN are:

- inventory balance constraint

$$x_{k,t} + I_{k,t-1} - I_{k,t} = d_{k,t} \;\forall\; 1 \le k \le K ; \forall\; 1 \le t \le T$$

- restriction of production capacity

$$\sum_{k=1}^{K}\sum_{z=0}^{z_k} f_{j,k,z} \cdot x_{k,t+z} - U_{j,t} \le b_{j,t} \;\forall\; 1 \le j \le J ; \forall\; 1 \le t \le T$$

- restriction of additional capacity

$$U_{j,t} \le U_{j,t}^{max} \;\forall\; 1 \le j \le J ; \forall\; 1 \le t \le T$$

- non-negativity restrictions

$$x_{k,t}, I_{k,t}, U_{j,t} \ge 0 \;\forall\; 1 \le k \le K ; \forall\; 1 \le j \le J ; \forall\; 1 \le t \le T$$

- determination of initial inventory

$$I_{k,0} = \text{given} \;\forall\; 1 \le k \le K$$

The deterministic model HPPLAN is transformed into the two-stage stochastic optimization model TSS-HPPLAN for robust master production planning. Demand uncertainty is represented via a set of demand scenarios Ω, where each scenario consists of the demands $\left(d_{k,t}^{s}\right)_{k=1,t=1}^{K\ T}$ (with $s \in \Omega$). The resulting production plan consists of a basic plan $x_{k,t}^{0}$ that is implemented immediately. After the demands of period $t = 1$ are known, the basic plan is modified with a compensation plan that increases $\left(x_{k,t}^{s+}\right)$ or reduces $\left(x_{k,t}^{s-}\right)$ the basic plan if necessary. The production quantities of period $t > 1$ are then $x_{k,t}^{0} + x_{k,t}^{s+} - x_{k,t}^{s-}$. In addition, $I_{k,t}^{s}$ and $U_{j,t}^{s}$ become scenario dependent. Master production scheduling is realized in a rolling planning environment. The replanning interval for TSS-HPPLAN is one period. Consequently, just the first period of every master production schedule is implemented. As there is no compensation plan for the first period, no compensations are ever realized; instead, a new basic plan is generated and realized every period (also see Alfieri and Brandimarte 2005). The objective function of TSS-HPPLAN minimises the expected costs under the assumption that all scenarios are even likely to occur. It sums up inventory costs, costs for the use of additional capacity and costs for changing production quantities (with cost coefficient c_t) as frequent changes of production quantities usually lead to additional costs (see Kimms 1998). The implementability constraint prevents that compensation plans react on demands that are not yet known at their implementation time (see Rockafellar and Wets 1991, Wets 1989). It says that if two scenarios are identical upon a period, their solutions have to be identical until then as well. The resulting model TSS-HPPLAN has the objective function:

$$\text{Minimise } Z = \frac{1}{|\Omega|}\sum_{s\in\Omega} Z_s$$

$$Z_s = \sum_{k=1}^{K}\sum_{t=1}^{T} h_k \cdot I_{k,t}^{s} + \sum_{t=1}^{T}\sum_{j=1}^{J} u_t \cdot U_{j,t}^{s} + \sum_{k=1}^{K}\sum_{t=1}^{T} c_t \cdot \left(x_{k,t}^{s+} + x_{k,t}^{s-}\right)$$

The constraints of TSS-HPPLAN are:

- inventory balance constraint

$$x_{k,t}^{0} + x_{k,t}^{s+} - x_{k,t}^{s-} + I_{k,t-1}^{s} - I_{k,t}^{s} = d_{k,t}^{s}$$
$$\forall\; s \in \Omega \;\forall\; 1 \le k \le K \;\forall\; 1 \le t \le T$$

- restriction of production capacity

$$\sum_{k=1}^{K}\sum_{z=0}^{z_k} f_{j,k,z} \cdot \left(x_{k,t+z}^{0} + x_{k,t+z}^{s+} - x_{k,t+z}^{s-}\right) - U_{j,t}^{s} \le b_{j,t}$$
$$\forall\; s \in \Omega ; \forall\; 1 \le j \le J ; \forall\; 1 \le t \le T$$

- restriction of additional capacity

$$U_{j,t}^{s} \le U_{j,t}^{max} \;\forall\; s \in \Omega ; \forall\; 1 \le j \le J ; \forall\; 1 \le t \le T$$

- non-negativity restrictions

$$x_{k,t}^{0}, x_{k,t}^{s+}, x_{k,t}^{s-}, \left(x_{k,t}^{0} + x_{k,t}^{s+} - x_{k,t}^{s-}\right), I_{k,t}^{s}, U_{j,t}^{s} \ge 0$$
$$\forall\; 1 \le k \le K ; \forall\; 1 \le j \le J ; \forall\; 1 \le t \le T$$

- determination of initial inventory

$$I_{k,0}^{s} = \text{gegeben} \;\forall\; s \in \Omega \;\forall\; 1 \le k \le K$$

- implementability constraint

$$x_{k,t}^{s+} = x_{k,t}^{s'+}, x_{k,t}^{s-} = x_{k,t}^{s'-} \;\forall\; 1 \le k \le K \;;\forall\; 1 \le t \le T \;;$$
$$\forall\; s,s' \in \left\{\Omega | d_{k,l}^{s} = d_{k,l}^{s'}\right\}$$

SIMULATION

The test problem and the planning system are implemented in a simulation system that is comparable to the production planning systems used in industrial applications.

The primary objective of the production system is to minimise the tardiness of the fulfilment of customer orders. The secondary objective is to minimise the inventory levels of end products. To simulate demand uncertainty, a set Ω^0 of different customer order scenarios is built. Each scenario represents a realistic order situation. Each customer order scenario consists of a set O^s of customer orders. Each customer order o^s with $o^s \in O^s$ regards one product $k\left(o^s\right)$ with $1 \le k\left(o^s\right) \le K$, is due at the beginning of period $t\left(o^s\right)$ within the simulation horizon $1 \le t\left(o^s\right) \le T^{sim}$ and has a demand quantity $d\left(o^s\right)$. One of these scenarios $s^{CO} \in \Omega^0$ is realized in the simulation experiments. The other scenarios $\Omega = \Omega^0 \setminus s^{CO}$ are used for production planning.

Master production scheduling is solved using either the HPPLAN or the TSS-HPPLAN optimisation model. For a simulation horizon of T^{sim} weeks, master production scheduling is performed at the beginning of each week τ for all $1 \le \tau \le T^{sim}$. The master production schedule of the weeks $[\tau, \tau+1]$ is frozen, and with a planning horizon T of ten weeks the actual planning horizon for master production scheduling is $[\tau+2, ..., \tau+11]$.

The demand scenarios are $\left(d_{k,t}^{s}\right)_{k=1,t=1}^{K\;T}$ with $d_{k,t}^{s} = \sum_{o \in \left\{o^s \in O^s : k\left(o^s\right)=k \wedge t\left(o^s\right)=t\right\}} d(o)$. These demand scenarios are used for TSS-HPPLAN. For HPPLAN, a deterministic replacement scenario is built by using the mean values of the scenario specific demands $\left(d_{k,t} = \frac{\sum_{s \in \Omega} d_{k,t}^{s}}{|\Omega|}\right)_{k=1,t=1}^{K\;T}$.

The initial inventories $I_{k,0}$ for HPPLAN and TSS-HPPLAN (which refer to period $\tau+2$) are not known to the planning system at period τ. The expected inventories for period $\tau+2$ base on the current inventory levels $I_{k,\tau}$, all open customer orders from past periods OrderBacklog_k, the expected customer orders ExpectedDemand_k and the production quantities Production_k during the frozen horizon. The initial inventory for master production scheduling is then

$$I_{k,0} = I_{k,\tau} - \text{OrderBacklog}_k - \text{ExpectedDemand}_k + \text{Production}_k .$$

The results of master production scheduling are production quantities $x_{k,t}$, additional capacities per production segment $U_{j,t}$ and inventory levels $I_{k,t}$.

The production quantities as well as the additional capacity are then timely disaggregated as the period size for material requirements planning is days. As inventory levels are already regarded in master production scheduling, the master production schedule represents net requirements. For lot-sizing, the procedures of Groff and Silver-Meal are regarded as superior. As Groff is implemented in commercial planning systems regularly, it has been chosen for this investigations as well as just-in-time lot sizing. Material requirements planning is done at the beginning of each day for the upcoming 21 days. For scheduling, the priority rules first-in-first-out (FIFO) or slack (SL) are used. The produced goods are stored at the end of the day their production was finished in; they are available for customer order shipment or further production at the beginning of the next day.

To get statistically significant results, long-term simulation runs are executed. The warm-up period of the resulting series of tardiness and stock levels is cut off using the MSER-5 heuristic described in (White 1997) and (White, JR. et al. 2000). To evaluate the primary production objective of minimising tardiness, the tardiness $T\left(o^s\right)$ in days of each customer order $o^{s^{CO}}$ is logged. The overall mean customer order tardiness is $T_{mean} = \frac{\sum_{o \in O^{s^{CO}}} T(o)}{\left|O^{s^{CO}}\right|}$. To enable comparisons to inventory management, β service levels are computed additionally as $\beta = 1 - \frac{\sum_{o \in \left\{o^{s^{CO}} \in O^{s^{CO}} : T(o)>0\right\}} d(o)}{\sum_{o \in O^{s^{CO}}} d(o)}$; this is identically to the β service levels used in inventory management. To evaluate the secondary production objective of minimising end product inventory levels, the inventory level $I_{k,t}$ of end products in pieces is logged each period. The overall average inventory level is $I_{mean} = \frac{\sum_{k=1}^{K}\sum_{t=1}^{T^{sim}} I_{k,t}}{K \cdot T^{sim}}$.

Generally, there are two factors that lead to tardiness: firstly, if the master production schedule underestimates future customer demand; secondly, if the production system cannot fulfil the master production schedule. To

differ between those two factors, the degree to which a production system fulfils a master production schedule is measured here as follows: $x_{k,t}$ is the production quantity that should become available in period t according to the master production schedule. $x_{k,t}^{real}$ is the production quantity that actually becomes available. The fulfilment of the master production schedule up to period τ is $x_{k,\tau}^{fulfil} = \sum_{t=1}^{\tau} x_{k,t}^{real} - \sum_{t=1}^{\tau} x_{k,t}$. If $x_{k,\tau}^{fulfil} > 0$, more units of product k have been produced up to period τ then there should; if $x_{k,\tau}^{fulfil} < 0$, the production system has a backlog on the master production schedule. Both cases are in particular due to the use of static lead times for material requirements planning while the real lead times are variable. To analyse the mean fulfilment of the master production schedule, $x_{mean}^{fulfil} = \sum_{k=1}^{K} \sum_{\tau=1}^{T} x_{k,\tau}^{fulfil}$ is computed.

To determine variance and confidence intervals for the mean tardiness and inventory levels, the Overlapping Batch Means heuristic originally proposed by (Meketon and Schmeiser 1984) is used; the optimal batch size is determined using the heuristic of Song proposed in (Song 1996). The resulting confidence intervals with error probability $\alpha = 0,1$ (which is the probability that the averages are not within the confidence intervals) are $\left[CI_{\alpha}^{-}(T_{mean}), CI_{\alpha}^{+}(T_{mean})\right]$ and $\left[CI_{\alpha}^{-}(I_{mean}), CI_{\alpha}^{+}(I_{mean})\right]$. The simulation model is implemented in Tecnomatix Plant Simulation 10.1; the optimization models are implemented and solved with IBM ILOG CPLEX Optimization Studio Version 12.5 on a DELL workstation with two Intel Xeon E5-2643 processors and 64 GB of RAM.

NUMERICAL RESULTS

The simulation parameters for the investigations are shown in Table 3.

Table 3: Simulation parameters

MPS model	{HPPLAN,TSS-HPPLAN}
$\lvert\Omega\rvert$	{5,10,20}
Lot-sizing	{Just-In-Time, Groff}
Scheduling	{FIFO, SL}

Table 4 shows the mean tardiness of the delivery of customer orders when using the master production scheduling models HPPLAN and TSS-HPPLAN with $\lvert\Omega\rvert = 10$, the lot-sizing procedure Just-In-Time and the Scheduling-Rule FIFO. When using HPPLAN, the mean tardiness is $2,65$ days. As the mean daily demand is $7,34$ units, the mean backlog is $19,45$ units. When using TSS-HPPLAN instead of HPPLAN, the mean tardiness is reduced to $0,46$ days, which results in a mean backlog of $3,38$ units. Table 5 shows the mean inventory levels of the analysis. Using TSS-HPPLAN, the mean inventory levels are $14,27$ units, while they are $5,4$ units when using HPPLAN. In consequence, TSS-HPPLAN reduces the mean backlog by $16,07$ units while mean inventory levels increase by just $8,87$ units.

Table 4: Customer order tardiness and service level

MPS model	CI_{α}^{-}	T_{mean}	CI_{α}^{+}	β
HPPLAN	2,49	2,65	2,8	45,34%
TSS-HPPLAN	0,37	0,46	0,55	85,25%

Table 5: Inventory levels

MPS model	CI_{α}^{-}	I_{mean}	CI_{α}^{+}
HPPLAN	5,14	5,4	5,66
TSS-HPPLAN	13,95	14,27	14,6

Table 6: Master production schedule fulfilment

MPS model	CI_{α}^{-}	x_{mean}^{fulfil}	CI_{α}^{+}
HPPLAN	1,38	1,4	1,43
TSS-HPPLAN	1,17	1,22	1,28

These results show that TSS-HPPLAN builds up inventory to cope with uncertain demand. As master production scheduling at week τ determines the production quantities of week τ, but does not yet know the demands in week τ, the only possibility to hedge against demand uncertainty is to build up enough stock to be able to deliver all demand scenarios. If the realized scenario exceeds all demand scenarios or if production cannot fulfil the master production schedule on time, out-of-stock situations can occur. TSS-HPPLAN leads to a significant reduction of tardiness though the master production schedule fulfilment is significantly lower compared to HPPLAN (see Table 6).

When using the slack rule for scheduling instead of FIFO, tardiness decreases while inventory levels increase for both MPS models. When using TSS-HPPLAN, T_{mean} drops $0,26$ days (which is equivalent to a reduction of the mean backlog of $1,91$ units) while I_{mean} increases $4,18$ units compared to the investigation using TSS-HPPLAN and FIFO. When using HPPLAN, T_{mean} drops $0,61$ days ($4,48$ units) while I_{mean} increases $1,2$ units compared to the investigation using HPPLAN and FIFO (see Table 7 and Table 8).

Table 7: Customer order tardiness and service level

MPS model	CI_{α}^{-}	T_{mean}	CI_{α}^{+}	β
HPPLAN	1,9	2,04	2,17	53,59%
TSS-HPPLAN	0,15	0,2	0,25	92,69%

Table 8: Inventory levels

MPS model	CI_{α}^{-}	I_{mean}	CI_{α}^{+}
HPPLAN	6,36	6,6	6,85
TSS-HPPLAN	18,04	18,45	18,87

The reason for the steeper drop of tardiness when using TSS-HPPLAN can be explained when regarding the master production schedule fulfilment shown in Table 9. In contrast to the previous analysis with the FIFO scheduling rule, now the fulfilment of the master production schedule is almost even as shown in Table 9. Under these even conditions regarding the fulfilment, TSS-HPPLAN reduces the mean backlog by $13,51$ units while it increases inventory levels by $11,85$ units.

Table 9: Master production schedule fulfilment

MPS model	CI_{α}^{-}	x_{mean}^{fulfil}	CI_{α}^{+}
HPPLAN	1,4	1,42	1,44
TSS-HPPLAN	1,38	1,41	1,44

When using the Groff procedure for lot-sizing and the slack rule for scheduling, tardiness increases and inventory levels sink (see Table 10 and Table 11) compared to using JIT lot-sizing and the slack rule for scheduling.

Table 10: Customer order tardiness and service level

MPS model	CI_{α}^{-}	T_{mean}	CI_{α}^{+}	β
HPPLAN	2,26	2,4	2,55	51,29%
TSS-HPPLAN	0,24	0,3	0,36	90,13%

Table 11: Inventory levels

MPS model	CI_{α}^{-}	I_{mean}	CI_{α}^{+}
HPPLAN	6,2	6,45	6,7
TSS-HPPLAN	17,23	17,65	18,07

Tardiness increases $0,36$ days for HPPLAN and $0,1$ days for TSS-HPPLAN; inventory levels decrease $0,15$ units for HPPLAN and $0,8$ units for TSS-HPPLAN. The decreases of inventory levels are small due to the inventory levels caused by lot-sizing. The steeper increase for TSS-HPPLAN is due to the lower fulfilment of the master production schedule (see Table 12).

Table 12: Master production schedule fulfilment

MPS model	CI_{α}^{-}	x_{mean}^{fulfil}	CI_{α}^{+}
HPPLAN	0,27	0,41	0,55
TSS-HPPLAN	-0,08	0,07	0,22

The above investigations show that TSS-HPPLAN reduces tardiness significantly compared to HPPLAN. When using TSS-HPPLAN, tardiness and inventory levels largely depend on the number of scenarios $|\Omega|$ used for planning. As shown in Table 13 and Table 14, increasing the number of scenarios from 5 to 20 reduces mean tardiness from $0,86$ days $(6,31$ units$)$ to $0,25$ days $(1,84$ units$)$, while it increases the mean inventory from $11,61$ units to $17,04$ units.

Table 13: Customer order tardiness and service level

$\|\Omega\|$	CI_{α}^{-}	T_{mean}	CI_{α}^{+}	β
5	0,72	0,86	0,99	77,04%
10	0,37	0,46	0,55	85,25%
20	0,19	0,25	0,31	91,03%

Table 14: Inventory levels

$\|\Omega\|$	CI_{α}^{-}	I_{mean}	CI_{α}^{+}
5	11,24	11,61	11,99
10	13,95	14,27	14,6
20	16,43	17,04	17,65

CONCLUSION AND OUTLOOK

In this paper, robust master production scheduling is analysed in an industrially relevant planning environment. A deterministic model for master production scheduling is extended to a stochastic model. Both models are implemented in a simulation model that represents a production planning and control system as it is commonly used in commercial planning systems and a production system basing on a real production system. The analysis shows that tardiness in the delivery of customer orders depends on the master production schedule at one hand and the fulfilment of the master production schedule on the other hand. To determine the effects caused by robust master production scheduling, an indicator is introduced to determine the degree of fulfilment of the master production schedule. The results of the analysis show that tardiness can be reduced significantly by the use of a stochastic model for master production scheduling while end product inventory levels increase significantly.

Future research should address the ability to fulfil master production schedules as well as the run time to solve robust models for master production scheduling.

REFERENCES

Al-e-Hashem, S.M.J.M.; H. Malekly and M.B. Aryanezhad. 2011. "A multi-objective robust optimization model for multi-product multi-site aggregate production planning in a supply chain under uncertainty." *International Journal of Production Economics* 134, 28–42.

Alfieri, A. and P. Brandimarte. 2005. "Stochastic Programming Models for Manufacturing Applications". In *Design of advanced manufacturing systems*, Andrea Matta, Quirico Semeraro (Eds.). Springer, Dordrecht.

Drexl, A.; B. Fleischmann; H.-O. Günther; H. Stadtler and H. Tempelmeier. 1994. "Konzeptionelle Grundlagen kapazitätsorientierter PPS-Systeme." *Zeitschrift für Betriebswirtschaftliche Forschung* 46, 1022–1045.

Escudero, L.; P. Kamesam; A. King and R. Wets. 1993. "Production planning via scenario modelling." *Annals of Operations Research* 43, 311–335.

Gebhard, M. 2009. "Hierarchische Produktionsplanung bei Unsicherheit." Gabler, Wiesbaden.

Günther, H.-O. and H. Tempelmeier. 2012. "Produktion und Logistik." Springer, Berlin.

Hax, A.C. and H.C. Meal. 1975. "Hierarchical Integration of Production Planning and Scheduling". In *Logistics*, Murray A. Geisler (Ed.). North Holland, Amsterdam.

Helber, S.; F. Sahling and K. Schimmelpfeng. 2012. "Dynamic capacitated lot sizing with random demand and dynamic safety stocks." *OR Spectrum*.

Herrmann, F. 2011. "Operative Planung in IT-Systemen für die Produktionsplanung und -steuerung. Wirkung, Auswahl und Einstellhinweise." Vieweg + Teubner, Wiesbaden.

Herrmann, F. and J. Englberger. 2013. "Robuste Optimierung zur Produktionsprogrammplanung". In *Divergierende Forschungsansätze zur Produktionsplanung und -steuerung*, Thorsten Claus, Frank Herrmann, Michael Manitz (Eds.). Springer, Berlin.

Kimms, A. 1998. "Stability Measures for Rolling Schedules with Applications to Capacity Expansion Planning, Master Production Scheduling, and Lot Sizing." *Omega* 26, No. 3, 355–366.

Leung, S.C.; S.O. Tsang; W. Ng and W. Yue. 2007. "A robust optimization model for multi-site production planning problem in an uncertain environment." *European Journal of Operational Research* 181, 224–238.

Manitz, M.; F. Herrmann and J. Englberger. 2013. "Ein hierarchisches Planungskonzept zur operativen Produktionsplanung und -steuerung". In *Divergierende Forschungsansätze zur Produktionsplanung und -steuerung*, Thorsten Claus, Frank Herrmann, Michael Manitz (Eds.). Springer, Berlin.

Meketon, M.S. and B. Schmeiser. 1984. "Overlapping Batch Means: Something for Nothing?". In *Proceedings of the 1984 Winter Simulation Conference*.

Mulvey, J.; R. Vanderbei and S. Zenios. 1995. "Robust Optimization of Large-Scale Systems." *Operations Research* 43, 264–281.

Rockafellar, R. and R. Wets. 1991. "Scenarios and Policy Aggregation in Optimization under Uncertainty." *Mathematics of Operations Research* 16, No. 1, 119–147.

Scholl, A. 2001. "Robuste Planung und Optimierung. Grundlagen - Konzepte und Methoden - experimentelle Untersuchungen". Physica-Verlag, Heidelberg.

Song, W.T. 1996. "On the estimation of optimal batch sizes in the analysis of simulation output." *European Journal of Operational Research, No.* 88, 304–319.

Wets, R. 1989. "The Aggregation Principle in Scenario Analysis and Stochastic Optimization". In *Algorithms and Model Formulations in Mathematical Programming*, S.W Wallace (Ed.). Springer, Berlin.

White, K.P. 1997. "An Effective Truncation Heuristic for Bias Reduction in Simulation Output." *SIMULATION* 69, No. 6, 323–334.

White, K.P., JR.; M.J. Cobb and S.C. Spratt. 2000. "A Comparison of five Steady-State Truncation Heuristics for Simulation". In *Proceedings of the 2000 Winter Simulation Conference*.

Yu, C. and H. Li. 2000. "A robust optimization model for stochastic logistic problems." *International Journal of Production Economics* 64, 385–397.

Zhang, X.; M. Prajapati and E. Peden. 2011. "A stochastic production planning model under uncertain seasonal demand and market growth." *International Journal of Production Research* 49, No. 7, 1957–1975.

AUTHOR BIOGRAPHIES

JULIAN ENGLBERGER was born in Landshut, Germany and went to the University of Applied Sciences Regensburg, where he studied industrial engineering and logistics. He obtained his master's degree in 2011; since he is working at the University of Applied Sciences in Regensburg and is doctoral student at the International Institute Zittau (TU Dresden). His e-mail address is: Julian.Englberger@HS-Regensburg.de.

FRANK HERRMANN was born in Münster, Germany and went to the RWTH Aachen, where he studied computer science and obtained his degree in 1989. During his time with the Fraunhofer Institute IITB in Karlsruhe he obtained his PhD in 1996 about scheduling problems. From 1996 until 2003 he worked for SAP AG on various jobs, at the last as director. In 2003 he became Professor for Production Logistics at the University of Applied Sciences in Regensburg. His research topics are planning algorithms and simulation for operative production planning and control. His e-mail address is Frank.Herrmann@HS-Regensburg.de and his Web-page can be found at http://homepages.fh-regensburg.de/~hef39451/dr_herrmann/

THORSTEN CLAUS was born in Papenburg, Germany, and went to the University Osnabrück, where he studied business management and mathematics. 1995 he obtained his PhD about simulation and genetic algorithms. Since his Habilitation in 2004 he works as a Professor for Production Economy and Information Technology at International Institute Zittau (TU Dresden). His research topics are production planning and e-Learning. His e-mail address is Claus@IHI-Zittau.de and his Web-page can be found at http://www.ihi-zittau.de/cms/de/127/Produktions wirtschaft-und-Informationstechnik/

A SUSTAINABLE MODEL FOR OPTIMAL DYNAMIC ALLOCATION OF PATROL TUGS TO OIL TANKERS

Brice Assimizele*
Faculty of Maritime Technology and Operations
Aalesund University College
P O Box 1517
NO-6025 Ålesund
Norway

Johan Oppen
Planning, Optimization and Decision Support Group
Molde University College
P O Box 2110
NO-6402 Molde
Norway

Robin T. Bye
Faculty of Engineering and Natural Sciences
Aalesund University College
P O Box 1517
NO-6025 Ålesund
Norway

* Corresponding author. Email: bras@hials.no

KEYWORDS
Dynamic Resource Allocation; Mixed Integer Programming; Receding Horizon Control; Maritime Operations.

ABSTRACT

Oil tanker traffic constitutes a vital part of the maritime operations in the High North and is associated with considerable risk to the environment. As a consequence, the Norwegian Coastal Administration (NCA) administers a number of vessel traffic services (VTS) centers along the Norwegian coast, one of which is located in the town of Vardø, in the extreme northeast part of Norway. The task of the operators at the VTS center in Vardø is to command a fleet of tug vessels patrolling the northern Norwegian coastline such that the risk of oil tanker drifting accidents is reduced. Currently, these operators do not use computer algorithms or mathematical models to solve this dynamic resource allocation problem but rely on their own knowledge and experience when faced with constantly changing weather and traffic conditions. We therefore propose a novel sustainable model called the *receding horizon mixed integer programming (RHMIP)* model for optimal dynamic allocation of patrol vessels to oil tankers. The model combines features from model predictive control and linear programming. Simulations run with real-world parameters highlight the performance and quality of our method. The developed *RHMIP* model can be implemented as an operational decision support tool to the NCA.

1. INTRODUCTION

Maritime shipping is an important channel of international trade. More than seven billion tons of goods are carried by ships every year (Acar et al. 2009). In Norway, several hundred oil tankers transit each year along its northern coastline (Bye 2012). This traffic is associated with potential grounding accidents due to oil tankers losing control of steering or propulsion, a problem that is highly underreported and likely occurs almost every day[1]. Such accidents can have severe environmental consequences from oil spill and may even lead to loss of lives.

The VTS center in Vardø, located in the extreme northeast part of Norway, controls a fleet of tugs patrolling the coastline. By means of the automatic identification system (AIS) used by ships and VTS centers all over the world, the VTS center in Vardø obtains static (e.g., identity, dimensions, cargo, destination) and dynamic (e.g., position, speed, course, rate of turn) information about vessels along the coast. In addition to the AIS information, weather forecasts and dynamic models of wind, wave heights, and ocean currents can be used to predict possible drift trajectories and grounding locations of tankers that lose maneuverability. The aim of the patrolling tug vessels is to move along the coastline in a collectively intelligent manner such that potential drift trajectories can be intercepted. The closest tug vessel will then intercept the drifting oil tanker before it runs aground (Eide et al. 2007).

The number of oil tanker transits off the northern coastline of Norway is predicted to increase rapidly in the coming years (Institute of Maritime Research 2010). In addition, the number of patrolling tug vessels may increase as a response to the increase in oil tanker traffic. Consequently, the VTS operators' task of manually commanding the fleet of patrol tugs is becoming unmanageable without the aid of a decision support tool. Addressing this need, Bye (2012) and Bye, van Albada, and Yndestad (2010) used a heuristic and suboptimal *receding horizon genetic algorithm (RHGA)* to dynamically allocate patrolling tug vessels to oil tankers along the northern coastline of Norway. Our aim here is to present a *receding horizon mixed integer programming (RHMIP)* model to *optimally* solve the same fleet optimization problem.

The remainder of this paper is organized as follows: Section 2 explicitly describes the problem whereas Section 3 presents a methodology for the solution. Section 4 reports some computational experiments.

[1] Information provided by the NCA.

Proceedings 27th European Conference on Modelling and Simulation ©ECMS Webjørn Rekdalsbakken, Robin T. Bye, Houxiang Zhang (Editors)
ISBN: 978-0-9564944-6-7 / ISBN: 978-0-9564944-7-4 (CD)

Finally, discussions and propositions for future research are made in Section 5.

2. PROBLEM DESCRIPTION

Oil tankers move, by law, along piecewise-linear corridors well defined in advance and approximately parallel to the coastline. We adopt the problem description used in Bye (2012) and Bye et al. (2010). Accordingly, we assume a set C of oil tankers moving in one dimension along a line of motion z. Moreover, we assume a set P of tug vessels moving along a line of motion y parallel to z and close to shore. An illustration of the problem is presented in Figure 1, where patrol tug vessels are represented as black circles, oil tankers as white circles, predicted oil tanker positions as dashed circles, and circles with a cross represent points where the predicted drift trajectories cross the patrol line y. We refer to these points as *cross points*.

Based on real-time information of oil tankers from the AIS and on a set of forecasting models developed previously by the NCA and partners, we assume that it is possible to predict future oil tankers positions as well as the corresponding potential drift trajectories.

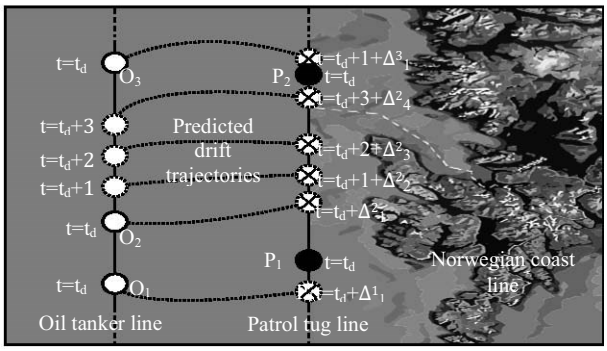

Figure 1: Problem illustration

Specifically, for each current position of a given oil tanker $z(t)$, there is a corresponding predicted drift trajectory which crosses the line y at a cross point $y(t')$ where $t'-t=\Delta$ represents the estimated drift time. Thus, the main goal is to make sure there is always a tug vessel at a position $y'(t')$ close enough to any potential cross point $y(t')$ to rescue the drifting oil tanker. That is, what is the optimal positioning of tug vessels along the coastline for a minimum rescue time of potentially drifting oil tankers?

3. METHODOLOGY

Task allocation in real-time systems in order to meet certain deadlines is known to be an NP-hard problem (Gertphol and Prasanna 2005). In addition, the highly uncertain weather conditions and the dynamic environment add to the complexity of the problem. To overcome these challenges, we propose using a combination of different methods that complement each other. An iterative solution approach for different types of problems that integrate optimization and simulation methodologies have been developed by several researchers in the literature (Acar et al. 2009). Here, we make use of the receding horizon control principle together with a linear optimization approach to develop our novel *RHMIP* model. Whilst this approach can be used to solve the specific problem presented in this paper, our model can likely be extended to solve other problems such as dynamic fleet optimization of platform supply vessels (PSVs) or other resource allocation problems both offshore and on land.

Model predictive control *(MPC)* or receding horizon control *(RHC)* is a class of control algorithms that uses explicit process models to predict the future response of a system and guide a system to a desired output using optimization as an intermediate step (Park et al. 2009). Receding horizon optimization is widely recognized as a highly practical approach with high performance (Zheng et al. 2011). It has become a very successful strategy in real-time control problems (Goodwin et al. 2006). Morari and Lee (1999) showed that many important practical and theoretical problems can be formulated in the RHC framework. The RHC algorithm consists of two main steps: (1) prediction of future system behavior on the basis of current measurements and a system model and (2) solution of an optimization problem for determining future values of the manipulated variables, subject to constraints (Wang et al. 2007). For a given planning time horizon T, with step $k \geq 0$ corresponding to the time instant $t_k = k\lambda$ with λ the sampling time, the future control sequence $\mu(k), \mu(k+1), ..., \mu(k+T-1)$ is computed by solving a discrete-time optimization problem over the period $[t_k, t_{k+T\lambda})$ in a way that a performance index defined over the considered period is optimized subject to some operational constraints. For our problem, tug vessels are constrained to move no faster than their maximal speed, which leads to a limitation on the number of oil tankers allocated to a given tug vessel. Once the optimal control sequence is computed, only the first control sample is implemented, and then the horizon is shifted. Subsequently, the new state of the system is estimated, and a new optimization problem at time t_{k+1} is solved using this new information (Tarău et al. 2011). In effect, the *RHC* principle introduces feedback control, and thus robustness to changes in the environment.

Mixed-integer linear programming (*MIP*) problems are optimization problems with a linear objective function, subject to linear equality and inequality constraints and where some variables are constrained to be integers. The advantage of using this approach is the availability of efficient solvers that can compute the global optimal solution within reasonable time (Tarău et al. 2011).

Despite the high uncertainty related to weather, wave heights and ocean currents, we have decided to develop a deterministic *MIP* model. This decision is justified by the fact that the model is run dynamically and

parameters are updated at every time step, thus implicitly handling the stochasticity of the problem.

3.1 *RHMIP* model

Previous work done by Bye (2012) and Bye et al. (2010) aimed to reduce the distances between all cross points and the nearest patrol points in the planning horizon (which is equivalent to minimizing rescue time if all patrol tugs have the same maximal speed). Indeed, this is a logical choice that tries to maximize the number of oil tankers that can be rescued at any time.

The following cost function was used as a minimization objective: $\sum_{t=t_d}^{t_d+T}\sum_{c=1}^{N_o}\min_{p\in P}\left|y_t^c - y_t^p\right|$

Here, y_t^c represents the cross point of the drift trajectory of oil tanker c at time t, y_t^p is the position of patrol tug p at time t; N_o is the number of oil tankers, P is the set of patrol tugs, and T is the planning horizon. The above cost function can be rewritten as a linear cost function by adding some extra variables and can therefore be solved optimally using linear *MIP*.

In this study, we implement two variants of our model, one using static tug vessels *(Static MIP)* and the other with dynamic tug vessels *(RHMIP)*. The definition of sets, parameters and variables are as follows.

Sets

P set of tug vessels

C set of oil tankers

Parameters

$v_{\max}^p$ maximal speed of tug vessel p

$v_{\max}^c$ maximal speed of oil tanker c

y_t^c cross point of the cth oil tanker's predicted drift trajectory at time t. Note that t represent the time at which the drifting oil tanker crosses the patrol line.

y_0^p initial position of tug vessel p

y_0^c initial position of oil tanker c

$\Delta_{\min}$ drift time of oil tankers

λ length of each time period

T_{RHMIP} number of simulation steps

T length of the planning horizon of the *MIP* optimization model

M a large number[2]

Decision variables

Y_t^p position of tug vessel p in period t

I_t^p, J_t^p direction of tug vessel p in period t. If $I_t^p - J_t^p > 0$ the tug vessel will move forward and backward if $I_t^p - J_t^p < 0$, otherwise it will remain static.

X_t^{cp}, Z_t^{cp} distance between potentially drifting oil tanker c and tug vessel p in period t. One of the variables will contain the distance and the other variable will be equal to zero.

Ψ_t^{cp} distance from potentially drifting oil tanker c to its allocated tug vessel p in period t. Specifically, t represent the time period where the potentially drifting oil tanker c cross the patrol line.

$$W_t^{cp}\begin{cases}1 \text{ if tug vessel } p \text{ is allocated to oil tanker } c\\ \text{in period } t\\ 0 \text{ otherwise}\end{cases}$$

3.2 Algorithm

Below is an algorithm implementing the RHMIP model.

Step 1:

a- *Let* $t := 0$; *let* $y_t^p := \textit{initial value}\ \forall p \in P$;

b- Compute predicted drift trajectories, cross points of oil tankers and the predicted maximal speed of oil tankers and tug vessels.

c- Run *MIP* model to obtain the optimal position and allocation of patrolling tug vessels over the planning horizon $[t, t+1, ..., T]$.

d- Implement the first period of the *MIP* solution

Step 2:

a- *Let t:=t+1;*

Let $y_0^p := y_0^p + v_{\max}^p \cdot t \cdot \left(I_{\Delta_{\min}}^p - J_{\Delta_{\min}}^p\right) \forall \mathrm{p} \in \mathrm{P}$

(Obtain current position of tug vessels)

b- Update the predicted drift trajectories, cross points and the predicted new maximal speed of oil tankers and tug vessels. In addition, update the current number of oil tankers moving along the coastline as well as the available number of tug vessels.

c- Run *MIP* model to obtain the optimal position and allocation of patrolling tug vessels over the planning horizon $[t, t+1, ..., T+t]$.

d- Implement the first period of the new *MIP* solution

Step 3: Go back to Step 2 or stop if *t:=* $T_{RHMIP}+1$

The basic idea in Step 2 is that the maximal speed of oil tankers and tug vessels may vary over time due to changing weather conditions such as ocean currents, wave heights, and wind, or change in cargo weight after loading or unloading. In addition, some tug vessels may be unavailable due to maintenance or change of crew. Finally, an oil tanker leaving the defined protection zone should be removed from the set for the next

[2] See constraints (4) and (8).

planning period, whereas other oil tankers may enter the zone and should be included in the next planning period.

The *MIP* model is used as an optimization phase in the algorithm:

Minimize $\sum_{c\in C, p\in P, t\in\{\Delta_{min}..T\}} \Psi_t^{cp}$

Subject to

$$Y_t^p = Y_{t-1}^p + v_{max}^p \cdot \lambda \cdot \left(I_t^p - J_t^p\right), \quad \forall p \in P, \forall t \in \left\{\left(\Delta_{min}+1\right)..T\right\} \tag{1}$$

$$I_t^p + J_t^p \le 1, \ \forall p \in P, \forall t \in \left\{\Delta_{min}..T\right\} \tag{2}$$

$$X_t^{cp} - Z_t^{cp} = y_t^c - Y_t^p, \ \forall c \in C, \forall p \in P, \forall t \in \left\{\Delta_{min}..T\right\} \tag{3}$$

$$M \cdot \left(1 - W_t^{cp}\right) + \Psi_t^{cp} \ge X_t^{cp} + Z_t^{cp}, \quad \forall c \in C, \forall p \in P, \forall t \in \left\{\Delta_{min}..T\right\} \tag{4}$$

$$\sum_{p\in P} W_t^{cp} = 1, \forall c \in C, \forall t \in \left\{\Delta_{min}..T\right\} \tag{5}$$

$$Y_{\Delta_{min}}^p = y_0^p + v_{max}^p \cdot \Delta_{min} \cdot \left(I_{\Delta_{min}}^p - J_{\Delta_{min}}^p\right), \ \forall p \in P \tag{6}$$

$$Y_t^p \ge 0, \forall p \in P, \forall t \in \left\{\Delta_{min}..T\right\}$$

$$I_t^p, J_t^p \in [0,1], \ \forall p \in P, \forall t \in \left\{\Delta_{min}..T\right\} \tag{7}$$

$$W_t^{cp} \in \{0,1\}, \forall c \in C, \forall p \in P, \forall t \in \left\{\Delta_{min}..T\right\}$$

$$X_t^{cp} \ge 0, Z_t^{cp} \ge 0, \Psi_t^{cp} \ge 0, \forall c \in C, \forall p \in P, \forall t \in \left\{\Delta_{min}..T\right\}$$

$$M \ge \max_{p\in P, c\in C} \left| y_0^p - \left(y_0^c + T \cdot v_{max}^c\right)\right| \tag{8}$$

Constraints (1), (2), and (6) determine the optimal speed and direction of each tug vessel at every time period. Because there are no cross points for $t \in [0, \Delta_{min} - 1]$, the model determines, in constraint (6), the speeds and directions of tug vessels at these time periods for an optimal allocation in period Δ_{min}. Constraints (3) through (5) optimally allocate each oil tanker to one tug vessel, while constraint (7) define bounds on the decision variables.

For each time period of length λ in the planning horizon *T*, there is a predicted drift trajectory for each oil tanker which is expected to cross the patrol line after Δ_{min} periods ahead in time. Thus, there will be cross points at every time period starting from $\Delta_{\min}$. In case an oil tanker starts drifting in period *t*, the model gives direction and speed to its allocated tug vessel at each time period such that their distance, after $t + \Delta_{min}$ time period, is minimized. A tug vessel in period *t* will be allocated to cross point(s) in period $t + \Delta_{min}$ and possibly different cross point(s) at the next time period. The result is that the tug vessels will proactively move to make sure there is enough time to rescue any drifting oil tanker.

3.3 *Static MIP* model

The variant of the model with static tug vessels is obtained by replacing the variable Y_t^p by y_0^p in constraints (3) of the *MIP* model. In addition, only constraints (3), (4), (5) and (8) are kept and the rest are removed. The model is then run once for each time period in the planning horizon. This variant simply gives optimal allocation of static tug vessels to oil tankers and is only used for comparison.

4. COMPUTATIONAL SIMULATION STUDY

In this section, we present the simulation settings and results of the computational experiment used to evaluate the performance of our solution method to the tug vessels allocation problem**.**

4.1 Simulation settings

The mathematical models and algorithms for simulations were coded in AMPL and the *MIP* models were optimally solved with CPLEX 9.0. All the experiments were executed on a personal computer with an Intel Pentium IV 3.0 GHz CPU and 4.0 GB of RAM, with the operating system Microsoft Windows 7.

Notwithstanding the expected increase in oil tanker traffic along the northern coast of Norway, we have decided to use 6 oil tankers and 3 tug vessels for the simulation. These realistic numbers were provided by the NCA in 2010 and are reasonable choices for comparison with previous work done by Bye (2012).

The typical maximum speed of tug vessels in this region is about 28 km/h and the normal operating speed of oil tankers is about 18 to 26 km/h (Bye 2012). Based on this information, we conservatively chose to use a random speed of each oil tanker generated in the interval $\pm[20,30]$ (km/h), whereas a maximum speed of ±30 km/h was used for the tug vessels. In both cases, a positive speed denotes a northbound movement and a negative speed a southbound movement. A drift time of only 10 hours is considered fast drift, while slow drift means most tankers will not run ashore before having drifted for 20 to 30 hours (Eide et al. 2007). For this reason, Bye (2012) used a conservative estimate in the interval $[8,12]$ (hours). Note that this interval represents the possible values of Δ presented in section 2. To be even more risk averse, we decided to use a constant value of $\Delta_{\min} = 8$ hours for each oil tanker in this study.

To introduce nonlinearity of drift trajectories, such as that caused by wave heights, wind, ocean currents, and oil tanker size and shape, we used the same simple formula as Bye (2012), which has no physical relation to real drift trajectories but was merely chosen for its nonlinearity: $y(t') = z(t) + v\sin\left(\frac{2\pi}{T}\Delta_{\min}\right)$. Hence, any oil tanker will follow an eastbound sinusoidal trajectory with period equal to *T* scaled by its velocity *v*. The initial positions of oil tankers on the *z* line were randomly

chosen in the range $[-750, 750](km)$. For simplicity in the implementation, this interval was translated to $[1000, 2500](km)$ to obtain only positive values. In order to compare the dynamic *RHMIP* model with the *static MIP* model, we decided to divide the above interval into 3 equal subintervals and place one tug vessel, at a "tug base", at the center of each segment for the static model.

The *RHMIP* and *static MIP* models were simulated for T_{RHMIP} = 26 hours, a duration picked somewhat randomly, although we emphasize that the models should be simulated for at least a duration long enough to allow the tug vessels to move from initially bad to good positions and thenceforth remain in good positions, where "good" and "bad" positions refer to how well the tugs collectively optimize the cost function presented above.

At every step of λ =1 hour, the associated *MIP* model was run for a planning period of *T*=24 hours, but only the solution for the first hour was implemented. A total number of 30 scenarios were simulated. Details on the simulation settings are presented in Table 1.

Table 1: Simulation settings

Number of oil tankers	6
Random initial position (km)	$[1000, 2500]$
Random velocity (km/h)	$\pm[20, 30]$
Minimal drift time $\Delta_{\min}$ (hours)	8
Number of tug vessels	3
Initial tug positions	$\{1250, 1750, 2250\}$
Maximal velocity (km/h)	±30
Planning horizon T (hours)	24
Simulation step length λ (hours)	1
Simulation steps T_{RHMIP} (hours)	26
Number of scenarios	30

4.2 Results

The static tug vessel policy resulted in an average total distance of 22234, with a high standard deviation of 5880. The best case scenario had a total minimal distance of 12915 while the worst case scenario had a maximal distance of 27325. Unsurprisingly, using the static policy, a considerable number of potentially drifting oil tankers will not be rescued even at a maximal speed of the nearest tug vessel. However, the developed static *MIP* model can at least provide an optimal allocation of tug vessels to oil tankers, which cannot easily be achieved manually or using heuristic methods. The average running time for the *MIP* of this model was 10 sec for each time step.

The average total distance of the *RHMIP* model was 7702 with a standard deviation of 2912. The best case scenario had a minimal total distance of 2989, whereas the worst case scenario had a maximal total distance of 10609. The average performance improvement in terms of mean total distance of the *RHMIP* solution compared to the static policy was 66%. This dynamic variant of the model had a *MIP* average running time of 20 min at each time step, which is in the order of two magnitudes greater than the static *MIP* but is still acceptable for real-time implementation, since the calculation only needs to finish before the beginning of the next hourly receding horizon control step. The results are summarized in Table 2.

The parameters of our simulations were the same as those used in Bye (2012) except for the length of the drift trajectories, where our model was implemented as a worst case analysis with the minimum of 8 hours instead of random drift times in the interval $[8,12]$ (hours). As a consequence, a few of our simulated scenarios will have a slightly higher number of cross points. Nevertheless, the results from the two studies are still comparable, since the scenarios were randomly drawn from the same population but with different random samples. Moreover, the main comparison is based on the performance improvement from the static tug vessel policy. Comparison of RHGA vs. RHMIP simulation results are presented in Table 3.

Table 2: Simulation results

	Static MIP	*RHMIP*	Reduction by *RHMIP*
Mean	22234	7702	66%
STD	5880.7	2911.6	50.5%
Min	12915	2989	-
Max	27325	10609	-
Step time	10 sec	20 min	

The *RHGA* and *RHMIP* approaches used the same planning horizon of 24 hours at the optimization step. Compared with a static policy, the *RHMIP* showed a 66% improvement, whereas the *RHGA* showed 57.5%, thus the *RHMIP* outperformed the *RHGA* by 8.5%.

Table 3: Improvement from static policy

	RHGA	*RHMIP*
Improvement	57.5%	66%

Figure 2 highlights the difference between the *MIP* models. The two models were run once, with the same parameters, for *T=24* hour time periods. The straight lines and piecewise linear functions represent the dynamic allocation of patrolling tug vessels over the planning horizon. The cross points, starting in period eight, are represented by circles in the figure. Compared to the *MIP* for static tug vessels, our dynamic *MIP* model cleverly and optimally allocates and tracks the potential drifting oil tankers for the given fixed planning horizon.

We recall that only the first period of the *MIP* model solution is implemented at each step in the simulation of the *RHMIP* model. At every step, the parameters (current numbers of oil tankers, maximal speeds, cross points and tug vessel positions) are updated. This allows tackling the weather uncertainty at each simulation step and coping with the variation of the parameters.

Another advantage of using the receding horizon approach is that of better tug vessels allocation at each time period. In fact, if we assume a situation where the weather is stable or accurately predicted for *T=24* hours planning horizon, one may be tempted to implement the entire solution planned from a single *MIP* optimization, which will not allow better allocation of tug vessels at each period. The *RHMIP* model, run in the same conditions for T_{RHMIP} = 24 hours, will give better allocation because the planning at each period will not be influenced by that of the previous, which is not the case in the *MIP* model. This is illustrated in Table 4, where the letters A to F represent the oil tankers and columns for distances represent the sum of the distances between a tug vessel and its allocated oil tankers. The total distances demonstrate the advantage of using the *RHMIP* model although the weather is accurately forecasted and the parameters constant.

4.3 Conclusions

The combined features of receding horizon control and mixed integer programming allow our model to optimally control tug vessels and allocate them to oil tankers in a dynamic and highly uncertain environment.

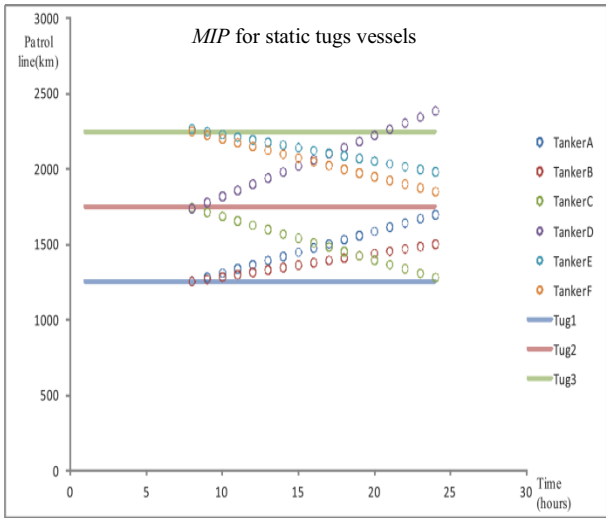

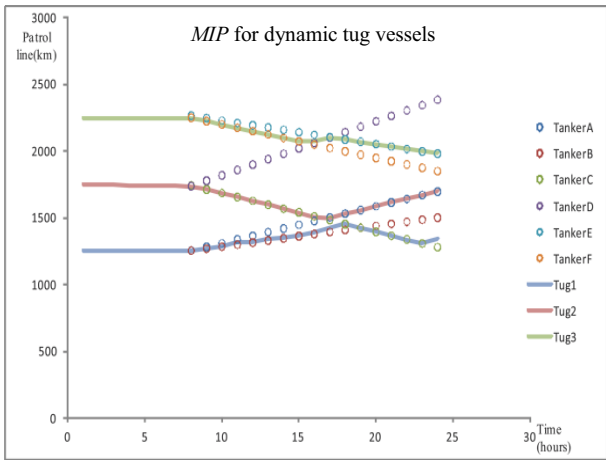

Figure 2: An illustration of employing static (top) and dynamic (bottom) tug vessels for a planning horizon of *T*=24 hours.

Table 4: Tug vessels allocations

		MIP								*RHMIP*						
		A	B	C	D	E	F	Distance		A	B	C	D	E	F	Distance
	Tug1							1								1
t=8	Tug2							7	t=8							7
	Tug3							16								16
	Tug1							13								13
t=9	Tug2							63	t=9							63
	Tug3															23
	Tug1							25								25
t=10	Tug2							132	t=10							132
	Tug3							31								31
...	...	...	...	...	...	...	...		...	...	...	...	...	...	...	
	Tug1							134								305
t=22	Tug2							0	t=22							225
	Tug3							404								0
	Tug1							0								361
t=23	Tug2							387	t=23							14
	Tug3							346								0
	Tug1							223								223
t=24	Tug2							0	t=24							283
	Tug3							536								0
Total distance								5365								4567

5. DISCUSSION AND FUTURE RESEARCH

Combining features from model predictive control and linear programming, this paper presents a novel sustainable model called the *receding horizon mixed integer programming (RHMIP)* model for optimal dynamic allocation of patrol vessels to oil tankers. Compared with previous work (Bye, 2012; Bye et al., 2010) that used a genetic algorithm to suboptimally minimize the proposed cost function, our model provides an exact (optimal) solution at every receding horizon time step. At the expense of slower computational evaluation, our optimal model outperforms the suboptimal heuristic method as well as providing a benchmark for future models.

5.1 Sustainability

International communities and government bodies such as NCA are expressing concern about the environmental impacts from shipping related activities. In fact, international shipping accounts for 2.7% of worldwide CO_2 emissions (Psaraftis and Kontovas 2013). One of the measures used, at a tactical or operational level, to address this issue is the speed reduction of ships. Accordingly, the *RHMIP* is a sustainable model as it explicitly reduces the speed of tugs vessels from the parameters settings and implicitly inside the model as well. Noticeably, the average operational speed of tug vessels was equal to 5 km/h for all scenarios. This is considerable slow-steaming compared to the 30 km/h maximum speed. In addition, a constraint on the maximal daily fuel consumption of tug vessels could be easily included in the model. However, limiting fuel consumption would cause a trade-off to be made between the short term CO_2 emissions reduction plan with long term potential environmental impact caused by drifting oil tankers that could not be rescued on time.

5.2 Robustness

For each time period of one hour in the simulation, the initial speed of each tug vessel is determined by the *MIP* model and a tug vessel is supposed to move with the same speed through the whole time period. However, the wave heights, ocean currents and other factors may also affect the speed of the related tug vessel, thus

causing deviations from the predicted future position of the tugs. This problem is overcome by the receding horizon control strategy, which at every planning interval will take into consideration the very latest current information about tug and tanker positions as well as updated weather forecasts. In addition, some tug vessels may not be available for some time periods due to maintenance or other possible reasons. It will be interesting to run the model with a variable number of tug vessels in the planning horizon.

The consequences of accidents will likely depend on the type and characteristics of oil tankers as well as the place or zone of accident in the coastline. Identifying the high risk zone and weighing the oil tankers will be of great benefit and can be easily included in the model.

Simulations with very large test instance size may highly increase the computational time. But one way of handling this issue is to subdivide the problem into small reasonable sizes. That is, the coastline can be divided into a few numbers of zones and each group of tug vessels will then patrol along its allocated coastline zone.

5.3 Future research

Although oil tankers are required by law to sail along predetermined piecewise linear corridors parallel to the coastline, more research can be done on a 2D dimensions.

This paper aimed to minimize the distance between potential drifting oil tankers and their respective allocated tug vessels. Future research may be focused on other optimizations objective. For instance, one could decide to reduce the probability of an oil tanker running ashore. This can be achieved with probabilistic models or robust optimizations.

The development of oil and gas fields in the Barents Sea will considerably increase the number of oil tankers transits along the coastline in the next 10-15 years (Bye, 2012). Further research could be conducted to determine the optimal number of required tug vessels as well as deciding whether the vessels should be homogeneous or heterogeneous.

ACKNOWLEDGEMENTS

We wish to thank Håkon Bjørlykke, whose research informed the present study, and Trond Ski and Ståle Sveinungsen at the NCA for providing insight into the VTS traffic surveillance and patrolling tug vessels along the Norwegian coast.

REFERENCES

Acar, Yavuz, Sukran N. Kadipasaoglu, and Jamison M. Day. 2009. "Incorporating uncertainty in optimal decision making: Integrating mixed integer programming and simulation to solve combinatorial problems." *Computers & Industrial Engineering* no. 56 (1):106-112.doi:http://dx.doi.org/10.1016/j.cie.2008.04.003.

Bye, Robin, T. 2012. "A receding horizon genetic algorithm for dynamic resource allocation: A case study on optimal positioning of tugs." *Studies in Computational Intelligence* no. 399 (Springer-Verlag: Berlin Heidelberg):131-147.

Bye, R.T., van Albada, S.B., Yndestad, H. "A receding horizon genetic algorithm for dynamic multi-target assignment and tracking: A case study on the optimal positioning of tug vessels along the northern Norwegian coast. *In: Proceedings of the International Conference on Evolutionary Computation. SciTePress* : 114-125.

Eide, Magnus S., Øyvind Endresen, Øyvind Breivik, Odd Willy Brude, Ingrid H. Ellingsen, Kjell Røang, Jarle Hauge, and Per Olaf Brett. 2007. "Prevention of oil spill from shipping by modelling of dynamic risk." *Marine Pollution Bulletin* no. 54 (10):16191633.doi:http://dx.doi.org/10.1016/j.marpolbul.2007.06.0 13.

Gertphol, Sethavidh, and Viktor K. Prasanna. 2005. "MIP formulation for robust resource allocation in dynamic real-time systems." *Journal of Systems and Software* no. 77 (1):55-65. doi: http://dx.doi.org/10.1016/j.jss.2003.12.040.

Goodwin, Graham C., María M. Seron, Richard H. Middleton, Meimei Zhang, Bryan F. Hennessy, Peter M. Stone, and Merab Menabde. 2006. "Receding horizon control applied to optimal mine planning." *Automatica* no. 42 (8):1337-1342. doi: http://dx.doi.org/10.1016/j.automatica.2006.01.016.

Institute of Maritime Research. 2010. "Fisken og havet, særnummer 1a-2010: Det faglige grunnlaget for oppdateringen av forvaltningsplanen for Barentshavet og havområdene utenfor Lofoten. ." *Tech. ep., Institute of Maritime Research (Havforskningsinstituttet)*.

Morari, Manfred, and Jay H. Lee. 1999. "Model predictive control: past, present and future." *Computers & Chemical Engineering* no. 23 (4–5):667-682. doi: http://dx.doi.org/10.1016/S0098-1354(98)00301-9.

Park, Yeonjeong, Jeff S. Shamma, and Thomas C. Harmon. 2009. "A Receding Horizon Control algorithm for adaptive management of soil moisture and chemical levels during irrigation." *Environmental Modelling & Software* no. 24 (9):1112-1121. doi: http://dx.doi.org/10.1016/j.envsoft.2009.02.008.

Psaraftis, Harilaos N., and Christos A. Kontovas. 2013. "Speed models for energy-efficient maritime transportation: A taxonomy and survey." *Transportation Research Part C: Emerging Technologies* no. 26 (0):331-351. doi: http://dx.doi.org/10.1016/j.trc.2012.09.012.

Tarău, A. N., B. De Schutter, and J. Hellendoorn. 2011. "Predictive route control for automated baggage handling systems using mixed-integer linear programming." *Transportation Research Part C: Emerging Technologies* no. 19 (3):424-439. doi: http://dx.doi.org/10.1016/j.trc.2010.06.004.

Wang, Wenlin, Daniel E. Rivera, and Karl G. Kempf. 2007. "Model predictive control strategies for supply chain management in semiconductor manufacturing." *International Journal of Production Economics* no. 107(1):5677.doi:http://dx.doi.org/10.1016/j.ijpe.2006.05.013.

Zheng, Yi, Shaoyuan Li, and Ning Li. 2011. "Distributed model predictive control over network information exchange for large-scale systems." *Control Engineering Practice* no. 19 (7):757-769. doi: http://dx.doi.org/10.1016/j.conengprac.2011.04.003.

An open source software approach to combine simulation and optimization of business processes

Mike Steglich and Christian Müller
Technical University of Applied Sciences Wildau
Bahnhofstraße, D-15745 Wildau, Germany
E-mail: mike.steglich@th-wildau.de, christian.mueller@th-wildau.de

KEYWORDS
Simulation, Optimization, Business Process, Optimization web service, Mathematical Programming Language

ABSTRACT

Business processes of modern companies are characterized by a huge complexity which is caused for example by quickly changing markets, short product life cycles or dynamic interactions between particular subsystems of a company. Business process management is intended to implement efficient and customer orientated processes whereby the simulation of business processes can be used to evaluate the quality of processes and to identify areas of improvements. Since real business processes usually contain decision processes which can be solved by optimization systems, it makes sense to combine the simulation and the optimization of business processes. (März et.al. 2010, p 3ff.)
As an example of a reasonable combined simulation and optimization of business processes, the navigation in a road network is discussed in this paper. Consider vehicles seeking the fastest route from a starting node to a target node using a navigation system. The amount of time spent driving on an arc is influenced by the distance and the amount of the vehicles on this arc and is continuously changing. The structure of the road network and the traffic within the network is described in a simulation model while the fastest path decisions of each vehicle are made by using an optimization system. There is obviously a relationship between the individual decisions made for each of the vehicles and the state of the entire network.
The aim of this paper is to describe how a combined simulation and optimization of business processes can be created through using EPC-Simulator (Müller 2012) as a simulation system and CMPL (Steglich and Schleiff 2010) as an optimization system where the network traffic simulation is used exemplarily.

CREATING SIMULATIONS USING EPC-SIMULATOR

The EPC Simulator is a plugin of the EPC modelling toolbox bflow* (Kern et al. 2010). As shown in Figure 1 the first step to create a simulation model is the specification of a model document and several process documents in bflow*. The model document contains information about the model infrastructure (simulation time, available resources, inter-arrival times of entities, etc.). The process documents contain the process descriptions in EPC notation. Based on these documents, the EPC-Simulator can generate a simulation model. This is a Java Application that uses the DESMO-J Framework, whereby DESMO-J provides the basic functionality of a simulation. (Page and Kreutzer 2005)

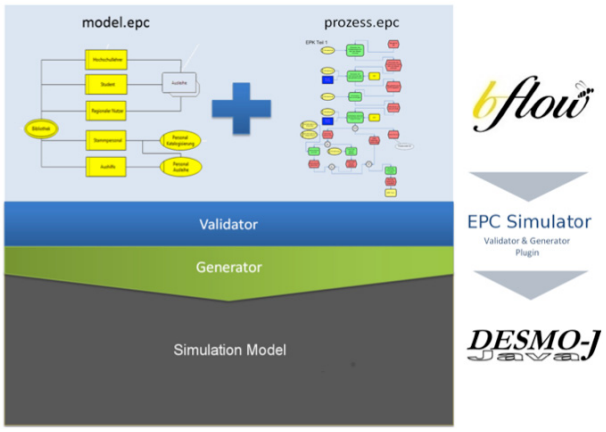

Figure 1: EPC-Simulator and its environment

The Java source code generated by EPC-Simulator contains marked areas where the source code can be extended manually by individual functionalities in functions or decision rules. In this way it is possible to integrate CMPL easily by a code extension through using its Java API.

IMPLEMENTING A ROAD NETWORK SIMULATION IN EPC-SIMULATOR

As described before, to create the road network simulation it is necessary to specify model and process documents. The model document in Figure 2 describes a series of vehicles with the specific inter-arrival times. Each vehicle has to process the vehicle process document. On the basis of this document the EPC-Simulator generates several Java classes on the basis of this model document that can be extended by individual Java code.
A class is `Information_Network_Data` (shown in Listing 1) for that a `NetworkData` object is created automatically by EPC-Simulator. This class is used to specify the road network that can be described as an undirected network $G=(V,A)$ where V is a set of nodes and A is a set of arcs joining pairs of nodes.

Proceedings 27th European Conference on Modelling and Simulation ©ECMS Webjørn Rekdalsbakken, Robin T. Bye, Houxiang Zhang (Editors)
ISBN: 978-0-9564944-6-7 / ISBN: 978-0-9564944-7-4 (CD)

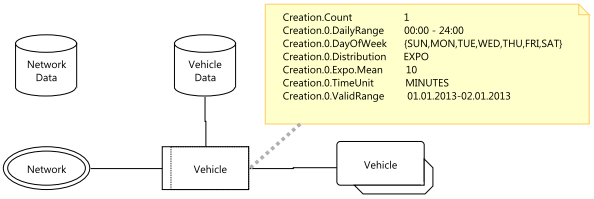

Figure 2: Model document

Considering the simple example in Figure 3, the first individual code after the code marker in line 03 is the definition of the set A of the arcs.

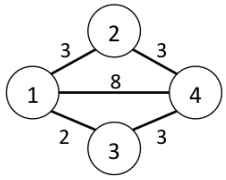

Figure 3: Example of a road network

The time a vehicle needs to drive from a node i to a node j is a function which consists of a fixed term ft_{ij}, which is proportional to the distance between the nodes i and j, and a variable term which is defined by the product of a time factor vt_{ij} and the amount of vehicles q_{ij} on the arc $i \rightarrow j$.

$$c_{ij} = ft_{ij} + vt_{ij} \cdot q_{ij} \; ; \forall (i,j) \in A \qquad (1)$$

Assuming that each arc is only used by one vehicle and the variable time factor is equal to 1, the lines 05 and 06 of Listing 1 describe the fixed and variable factors that are necessary to calculate the needed driving time in line 14. Additional data are the amount of vehicles of the arcs (line 08), the definition of the standard deviation in line 17 and a vector `meanDist` in line 07, which is assigned the current distances of all arcs calculated for each arc by method `getRandomDist`.

Another class is `Information_Vehicle_Data` shown in Listing 2 which is used to generate an individual object for each vehicle. This class is intended to specify vehicle specific data (e.g. the current location and the target node). Because for each vehicle a number of shortest path problems are to be solved it is also necessary to provide a vector of Boolean elements to store the solution of an optimization run (line 05). Additionally, a method for solving the shortest path problem is specified which contains the CMPL language bindings (line 13).

The vehicle process document describes the navigation process of the vehicle. As shown in Figure 4 a vehicle starts at its start position and drives to the next node on the determined shortest path.

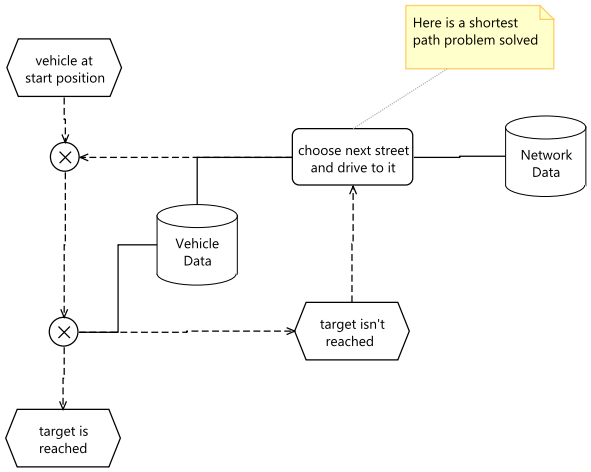

Figure 4: Process document

If the vehicle does not reach the target node a new shortest path depending on the current traffic situation in the network is determined by solving a shortest path problem. Based on the solution the next arc is chosen.

```
01 public class Information_Network_Data {
02
03     //@@_begin of declaration individual code
04     int[][] routes = {{1,2},{1,3},..,{3,4},{4,2},{4,3}};
05     double[] timeFix = { 2.0, 1.0,..., 2.0, 2.0, 2.0 };
06     double[] timeVar = { 1.0, 1.0,..., 1.0, 1.0, 1.0 };
07     double[] meanDist = null;
08     int[] vehicles = null;
09     int nrNodes = 4;
10     …
11     ContDistNormal normDist = null;
12     //@@_end of declaration individual code
13     …
14     //@@_begin of additional individual code
15     public double getRandomDist(int arcIndex){
16         double mean = timeFix[arcIndex]+  timeVar[arcIndex]*vehicles[arcIndex];
17         double stdDev = alpha * mean;
18         return Math.max(0.0, normDist.sample()*stdDev + mean);
19     }
20     …
21     //@@_end of additional individual code
   }
```

Listing 1: Information_Network_Data

```
01 public class Information_Vehicle_Data {
02
03     //@@_begin of declaration individual code
04     int locationNode, targetNode;
05     boolean[] shortestPath = null;
06     …
07     //@@_end of declaration individual code
08     …
09     //@@_begin of additional individual code
10     public boolean solveShortestPath(){
11         boolean ok;
12         …
13         return ok;
14     }
15     //@@_end of additional individual code
16 }
```

Listing 2: Information_Vehicle_Data

CMPL AND CMPLSERVER

Introduction

CMPL (<Coliop|Coin> Mathematical Programming Language) is a mathematical programming language and a system for mathematical programming and optimization of linear optimization problems. CMPL executes CBC, GLPK, Gurobi, SCIP and CPLEX directly to solve the generated model instance. Since it is also possible to transform the mathematical problem into MPS, Free-MPS or OSiL files, alternative solvers can be used. CMPL is an open source project licensed under GPLv3. It is written in C++ and is available for most of the relevant operating systems (Windows, OS X and Linux). CMPL is a COIN-OR project initiated by the Technical University of Applied Sciences Wildau and the Institute for Operations Research and Business Management at the Martin Luther University Halle-Wittenberg. (Steglich and Schleiff 2010)

Formulation of the shortest path problem in CMPL

Consider an undirected network $G=(V,A)$ where V is a set of nodes and A is a set of arcs joining pairs of nodes. The decision is to find the shortest path from a starting node s to a target node t. This problem can be formulated as an LP as follows (Hillier and Liebermann 2010, p. 383f.):

$$\sum_{(i,j)\in A} c_{ij} \cdot x_{ij} \rightarrow \min! \tag{2}$$

s.t.

$$\sum_{(i,j)\in A} x_{ij} - \sum_{(j,i)\in A} x_{ji} = \begin{cases} 1 & , if\ i = s \\ -1 & , if\ i = t \\ 0 & , otherwise \end{cases} ; \forall i \in V \tag{3}$$

$$x_{ij} \geq 0 \ ; \forall (i,j) \in A \tag{4}$$

The decision variables are $x_{ij}\ \forall (i,j) \in A$ with x_{ij}=1 if the arc $i \rightarrow j$ is used. The parameters $c_{ij}\ , \forall (i,j) \in A$ usually define the distance between the nodes i and j, but as formulated in Expression (1) in this work these parameters are interpreted as the time a vehicle takes to drive from node i to node j.

To describe the formulation of the shortest path problem in CMPL the simple example shown in Figure 2 is used. Because parameters, variables, objectives and constraints are to be defined for each optimization model, a CMPL model usually consists of a parameter section, an objective section, a variable section and a constraint section. The set of the arcs A is specified in the lines 02-05 in Listing 3 in the form of a 2-tuple set. The set V of the nodes is a set of single indexing integers (line 07). The parameters s and t are scalar parameters (lines 08 and 09) and c is an array that is defined over the set A (line 11).

```
01 parameters:
02   A := set(  [1,2],[1,3],[1,4],
03              [2,1],[2,4],
04              [3,1],[3,4],
05              [4,2],[4,3]);
06
07   V := 1..4;
08   s := 1;
09   t := 4;
10
11   c[A] := (3,2,8,3,3,2,3,3,3);
12
13   { i in V: {    i=s : b[i]:=1; |
14                  i=t : b[i]:=-1; |
15                  default: b[i]:=0;}  }
16
17 variables:
18   x[A] :real[0..];
19
20 objectives:
21   sum{[i,j] in A: c[i,j]*x[i,j]}->min;
22
23 constraints:
24   node {i in V:
25         sum{ j in (A *> [i,*]):x[i,j]}-
26         sum{ j in (A *> [*,i]):x[j,i]}
27         = b[i];}
```

Listing 3: The shortest path problem in CMPL

The vector of the right hand sides b has been defined in the lines 13-15 by using a loop over the set V and a switch clause depending on the value of a current i and the values of s and t as in Expression (3).
Line 18 contains the definition of the decision vector x over the set A as non-negative continuous variables.
The sum over all valid arcs of the products of the c_{ij} and the x_{ij} is minimized. The formulation of the objective function (2) is done in line 21.
The flow constraints (4) can be formulated as in lines 24-27. The first step is to define a loop over all nodes in V (line 24) where the loop body contains the formulation of the flow constraints. The sums in lines 25 and 26 are defined over a set pattern matching expression. The expression `A *> [i,*]` returns a set consisting of unique elements of A which match the pattern `[i,*]` in order of their first appearance. That means this expression yields all nodes j that can be reached from the node i.

CMPL API and CMPLServer

The CMPL API is intended to integrate CMPL in other software and is available for Python and Java since version 1.9.0.
The main idea of this API is to define sets and parameters within the user application, to start and control the solving process and to read the solution(s) into the application if the problem is feasible. All variables, objective functions and constraints are defined in CMPL. These functionalities can be used with a local CMPL installation or a CMPLServer, but this paper describes only the use of a CMPLServer.
The CMPL API contains three major classes: `CmplSet`, `CmplParameter` and `Cmpl`. The classes `CmplSet` and `CmplParameter` are intended to define sets and parameters that can be used with several `Cmpl` objects. With the `Cmpl` class it is possible to define a CMPL model, to commit sets and parameters to this model, to start and control the solving process and to read the CMPL and solver messages and to have access to the solution(s).
`Cmpl` also provides the functionality to communicate with a CMPLServer that is implemented as an XML-RPC-based web service. XML-RPC provides XML based procedures for Remote Procedure Calls (RPC), which are transmitted between a client and a server via HTTP. (Laurent et al. 2001, p. 1.) Such client-server architecture is reasonable for a combined simulation and optimization of business processes because the capacities of the client can be used for the simulation procedures while the optimization problems can be solved remotely on the CMPLServer.
CMPL provides three XML-based file formats for the communication between a CMPLServer and its clients. A `CmplInstance` file contains an optimization problem formulated in CMPL, the corresponding sets and parameters in `CmplData` file format and all CMPL and solver options that belong to the CMPL model. If the model is feasible and the solution process is finished a `CmplSolutions` file contains the solution(s) and the status of the invoked solver. If the model is not feasible then only the solver's status and the solver messages are given in the solution file. The `CmplMessages` file is intended to provide the CMPL status and (if existing) the CMPL messages.
As shown in figure 5 the first step to communicate with a CMPLServer is the `Cmpl.connect` method that returns (if connected) a `jobId`. After connecting, a problem can be solved synchronously or asynchronously.

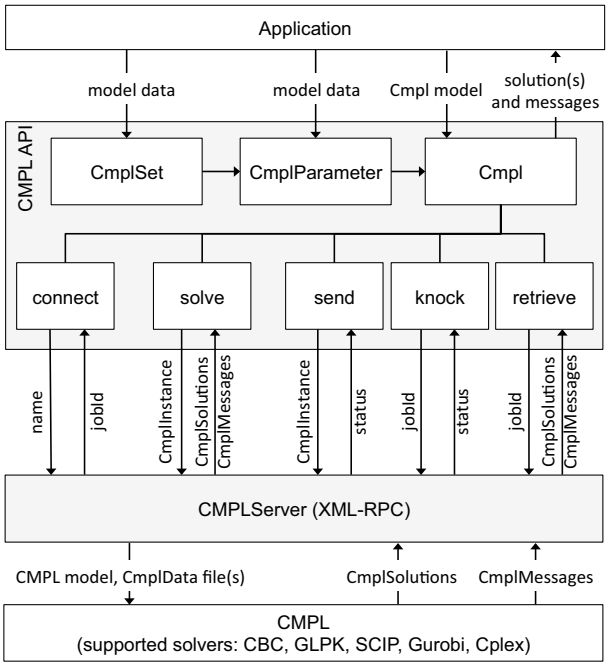

Figure 5: CMPL API and CMPLServer

The `Cmpl.solve` method sends a `CmplInstance` to the connected CMPLServer and waits for the returned `CmplSolutions` and the `CmplMessages`. After this synchronous process a user can access the solution(s) if the problem is feasible or if not one can analyse whether the CMPL formulations or the solver is the cause of the problem. To execute the solving process asynchronously the CMPL methods `Cmpl.send`, `Cmpl.knock` and `Cmpl.retrieve` have to be used. `Cmpl.send` sends a `CmplInstance` to the `CMPLServer` and starts the solving process remotely. `Cmpl.knock` asks for a CMPL model with a given `jobId` whether the solving process is finished or not. If the problem is finished the `CmplSolutions` and the `CmplMessages` can be read into the user application with `Cmpl.retrieve`.

INTEGRATING CMPL INTO THE ROAD NETWORK SIMULATION IN EPC-SIMULATOR

One of the advantages of EPC-Simulator is the opportunity for programmers to develop their own simulation models. Therefore it is possible to integrate optimization routines into simulation models through

using the CMPL Java API. The following steps have to be implemented for all of the simulation nodes.

To optimize the shortest path of each vehicle in the simulation nodes it is necessary to specify the network structure and the current traffic situation. The structure of the undirected network $G=(V,A)$ is given by the set of nodes V and the set A of arcs joining pairs of nodes. The current situation is given by the parameters $c_{ij}\ \forall(i,j)\in A$, which define the time a vehicle takes to drive from node i to node j. The current location of a vehicle describes the starting node s while t is the target node. These sets and parameters are the input of a CMPL model that is similar to the CMPL model in listing 3. But the difference is that this model does not contain static data. The sets and parameters have to be read into the model by using the `%data` entry (Listing 4 - line 1). This CMPL header entry is intended to read data from a `CmplData` file or from an application that uses the CMPL API.

The implementation of a CMPL model in Java is described in Listing 5 which is the completion of `solveShortestPath` in Listing 2. It starts with the definition of a `Cmpl` object (Listing 5 - line 09) with the filename of the model as an argument for the constructor.

```
01 %data : A set[2], V set , c[A], s, t
02
03 parameters:
04   { i in V: {    i=s : b[i]:=1; |
05                  i=t : b[i]:=-1; |
06                  default: b[i]:=0;}  }
07 …
```

Listing 4: sPath.cmpl

To define the sets A and V one has to create `CmplSet` objects (lines 10 and 12). The arguments of the constructor are the name of the set that has to be the same as specified in the CMPL model and the rank of the set if it is greater than one. The set A of the arcs is a set of 2-tuples and has therefore the rank 2 while V is a set of single indexing integers with the rank 1. Both sets are assigned data by using the method `CmplSet.values` where for the enumeration set `arcs` (A) a Java array is used as an argument (line 11)

```
01 import jCmpl;
02
03 public boolean solveShortestPath(){
04     boolean ok = false;
05     Cmpl m;
06     CmplSet arcs, nodes;
07     CmplParameter dist, sNode, tNode;
08     try{
09         m = new Cmpl("sPath.cmpl");
10         arcs = new CmplSet("A",2);
11         arcs.values( networkData.routes );
12         nodes = new CmplSet("V");
13         nodes.values(1,networkData.nrNodes);
14         dist = new CmplParameter("c", arcs);
15         dist.values(networkData.meanDist);
16         sNode = new CmplParameter("s");
17         sNode.values(this.locationNode);
18         tNode = new CmplParameter("t");
19         tNode.values(this.targetNode);
20
21         m.setSets(arcs, nodes);
22         m.setParameters(dist,sNode,tNode);
23         m.connect("http://194.95.45.70:8008");
24         m.solve();
25         if (m.solverStatus()== Cmpl.SOLVER_OK && m.nrOfSolutions()>0) {
26             ok = true;
27             shortestPathStatus = m.solution().status();
28             leftTime = new TimeSpan(m.solution().objValue(), TimeUnit.MINUTES);
29             shortestPath = new boolean[networkData.vehicles.length];
30             for(int i=0; i<m.nrOfVariables(); i++){
31                 shortestPath[i] = (m.solution().variables(i).activity() == 1);
32             }
33             } else {
34                 ok = false; shortestPath = null; shortestPathStatus = "";
35             }
36     } catch(CmplException e){
37         ok = false; shortestPath = null; shortestPathStatus = "";
38     }
39         return ok;
40 }
```

Listing 5: Use of the CMPL Java API

and for the set of ascending integers `nodes` (V) the first and the last element are given (line 13).
For the definition of a CMPL parameter a user has to create a `CmplParameter` object where the first argument of the constructor is the name of the parameter. If the parameter is an array it is also necessary to specify the set or sets trough which the parameter array is defined. Therefore it is necessary to commit the `CmplSet arcs` (beside the name `"c"`) to create the `CmplParameter` array `c` (line 14) while for the definition of the `CmplParameter sNode` and `tNode` only the name of the parameters have been specified (lines 16 and 18).
`CmplSet` objects and `CmplParameter` objects can be used in several CMPL models and have to be committed to a `Cmpl` model by `Cmpl.setSets` and `Cmpl.setParameters` (lines 21 and 22).
Before the solving process is started in line 24 a CMPLServer located at `http://194.95.45.70:8008` is connected (line 23). If `Cmpl.connect` is not executed, a locally installed CMPL is used automatically. After solving the model the status of CMPL and the invoked solver can be analysed through `Cmpl.solverStatus` (line 25) and `Cmpl.cmplStatus`.
If the problem is feasible and a solution is found it is possible to read the names, the types, the activities, the lower and upper bounds and the marginal values of the variables and the constraints into the Java application.
For the combined simulation and optimization of the shortest path problem now it is possible to get in each node s of the simulation the traffic for the next simulation step by analysing the activities of the variables x_{sj}, $\forall (s,j) \in A$ line 31.

SUMMARY

The aim of this paper was to develop an approach to combine a simulation and an optimization of business processes exemplarily described on the basis of the network traffic simulation problem.
It was shown how a network traffic simulation can be created with particular model and process documents in EPC notation, with which the EPC-Simulator (a bflow* plugin) can generate Java source code that uses the DESMO-J Framework. This Java source code contains marked areas for individual extensions which are used in this work to specify the specific data of the road network and the vehicles.
These marked areas for individual extensions were also used to describe how CMPL can be integrated by using the CMPL Java API. This API is indented to define sets and parameters within a Java application, to commit it to a CMPL object, to start and control the solving process and to analyse the solution(s) in Java. The CMPL Java API can be used with a local CMPL installation or a CMPLServer which is an XML-RPC-based web service for CMPL.
Client-server architecture for a combined simulation and optimization business process is reasonable because the capacities of the client can be used for the simulation procedures while the optimization problems can be solved remotely on the CMPLServer.

REFERENCES

Hillier F. S./Lieberman, G. J. 2010. "Introduction to Operations Research." 9th ed., McGraw-Hill Higher Education.

März, L.; Krug, W.; Rose, O. and Weigert, G. 2010. "Simulation und Optimierung in Produktion und Logistik". Springer, Berlin Heidelberg.

Kern, H.; Kühne, S.; Laue, R.; Nüttgens, M.; Rump, F.J. and Storch, A. 2010. "bflow* Toolbox - an Open-Source Business Process Modelling Tool", In: *Proc. of BPM Demonstration Track 2010, Business Process Management Conference 2010* (BPM'10), Hoboken, USA.

Müller, Chr. 2012. "Generation of EPC Based Simulation Models " In: *Proceedings 26th European Conference on Modelling and Simulation 2012*, Koblenz.

Page, B.; Kreutzer, W. 2005. "The Java Simulation Handbook - Simulating discrete Event Systems with UML and Java." Informatics Series, Shaker Publ., Aachen.

St. Laurent, S.; Johnston, J. and Dumbill, E. 2001 "Programming Web Services with XML-RPC." 1st ed., O'Reilly.

Steglich, M. and Schleiff, Th. 2010. "CMPL: Coliop Mathematical Programming Language." In: *Wildauer Schriftenreihe - Entscheidungsunterstützung und Operations Research*, Beitrag 1, Technische Hochschule Wildau [FH].

AUTHOR BIOGRAPHIES

Mike Steglich is a Professor of Business Administration, Quantitative Methods and Management Accounting in the Faculty of Business, Administration and Law of the Technical University of Applied Sciences Wildau in Germany. He is also one of the authors and distributors of the open source project CMPL (<Coliop|Coin> Mathematical Programming Language).

Christian Müller studied mathematics at Free University Berlin. He obtained his PhD in 1989 on network flows with side constraints. From 1990 until 1992 he worked for Schering AG and from 1992 until 1994 for Berlin Public Transport (BVG) in the area of timetable and service schedule optimization. In 1994 he gained his professorship for IT Services at the Technical University of Applied Sciences Wildau, Germany. His research topics are conception of information systems plus mathematical optimization and simulation of business processes.

Modelling and Simulation in Computer Vision for Image Understanding

STEREO VISION AUTO-ALIGNMENT AND THE UNSUPERVISED SEARCH FOR OBJECTS OF INTEREST WITH DEPTH ESTIMATION

Ling-Wei Lee
Neuramatix Sdn Bhd
No. 27-9 Level 9, Signature Office,
Bandar Mid-Valley,
59200 Kuala Lumpur, Malaysia.

Faeznor Diana binti Zainordin
Faculty of Computer Science and
Information Technology,
University of Malaya, Lembah Pantai,
50603 Kuala Lumpur, Malaysia.

KEYWORDS
Stereo vision alignment, objects segmentation, depth mapping, depth estimation.

ABSTRACT

Stereo vision is fast becoming a highly investigated area in the domain of image processing. Depth information may be obtained from stereo or multi-vision images for reconstructing objects in 3D based on 2D information. Robotic applications make use of stereo vision for navigation purposes, locking down targets, as well as simulating human-like behaviour. This paper presents an algorithm for the auto-alignment of stereo images followed by the self-extraction of objects of interest using an unsupervised search. Based on the understanding that different objects or regions are focused at different focal points, alignment between the two images is carried out to determine areas of high overlapping similarities. Objects are then identified in these selected areas with their estimated depth calculated based on the disparities between the stereo images. Results obtained for tests carried out on several experimental image pairs showed good extraction of the objects with close-to-real-world values obtained for the distances of the objects from the cameras.

INTRODUCTION

Human vision is capable of discerning objects from a background and enables a person to easily pick up a targeted object from a group of other entities. The estimation of distance from a person's hand to the target is remarkably accurate and of great precision. This is made possible via a combination of human vision, depth perception as well as input from other sensory organs. Human vision is akin to images captured on a camera – rods and cones in the retina capture scene information which is processed and transmitted to the brain for understanding and analysis. This then leads to questions such as: Are we able to derive useful information from images? Can we extract regions of interest while discarding the rest? Is it possible to execute certain algorithms for gathering further information from the image – information which may not be immediately visible but which requires the application of filtering kernels or functions? Such questions lead to the development of various techniques and algorithms in the domain of image processing.

Early algorithms placed emphasis on obtaining data from single images, and methods have been constantly reviewed and improved over the years thereby producing efficient solutions that are easily implementable. A single image consists of 2-dimensional data in the form of (x, y) spatial coordinates and pixels information. Human vision is able to perceive the 3-dimensional attribute of objects, hence the ability to grasp objects with precision. However, when translated to a 2D image, such characteristics become lost. The question one faces is – are we able to reconstruct 3-dimensional attributes based on captured 2D images? A single image may not provide sufficient information but two or more images may provide ample amount of details for reconstructing the object based on disparity maps. Stereo vision alignment and processing thus becomes a highly researched area applicable to the field of robotics and vision-based navigational systems. However, it is a "computationally expensive process … the accuracy of the disparity (depth) depends strongly on the calibration and rectification" (Sutton and Green, 2010).

Given a set of stereo images, one may notice that different objects in the images get aligned at different offsets when one image is overlaid onto the other. An attempt is made here to determine the regions of maximum overlap followed by procedures for identifying objects of potential interest. These objects are consequently extracted from the stereo images. The second part of this study is to determine if the depth (distance of the object from the cameras) can be estimated to a certain degree of accuracy based on the disparity between the images. A single set of stereo images containing a single object is used for calculation of the reference ratios. Reviews of past studies and implementations are first given in Background, followed by descriptions of the method in The Algorithm. The results of the study are presented in its respective section before the paper concludes with Discussion and Conclusion.

Proceedings 27th European Conference on Modelling and Simulation ©ECMS Webjørn Rekdalsbakken, Robin T. Bye, Houxiang Zhang (Editors)
ISBN: 978-0-9564944-6-7 / ISBN: 978-0-9564944-7-4 (CD)

BACKGROUND

According to Weng et al (1992), "establishing correspondences between different perspective images of the same scene is one of the most challenging and critical steps in motion and scene analysis". One of the main difficulties lies in determining a suitable algorithm for matching attributes of the images involved. Objects may become occluded in one scene with discontinuities detected in the images. There is the challenge of segmenting meaningful regions or objects as well. Early methods employ the use of edge detection and matching for aligning stereo vision (Alwan and Naji, 1996). A method based on the combination of an improved isotropic edge detector and a fast entropic thresholding was developed for obtaining colour edges in input images (Fan et al, 2001). The centroids of all adjacent edge regions act as initial seeds for region growing, thus producing homogenous areas with closed boundaries.

Benera and Prokop (2012) proposed an image segmentation technique based on standard inter-pixel Euclidean distance enhanced by similarities of hues with limits imposed on the size of segments. The method delivered good performance and was shown to be robust. Due to the use of stereo images, algorithms have been designed to carry out stereo matching and object segmentation simultaneously. Bleyer et al (2011) presented an approach wherein a 3D scene consists of visually distinct and spatially coherent objects. Each of the objects may be represented in terms of its associated colour model, a novel 3D connectivity property, and a 3D plane which estimates the disparity distribution. The method is capable of retrieving depths of regions that are fully occluded in one of the stereo views, and is designed as an energy function.

A stereo matching approach based on image segments was proposed by Kamencay et al (2012). The method is a hybrid segmentation algorithm using the Belief Propagation and Mean Shift algorithms for refining disparities and depth maps. Region segmentation is first carried out on the left image followed by a local window-based matching to estimate the disparities for the pixels. The results showed that the final depth map may be generated via application of segment disparities to the input images. In another work by Bleyer et al (2012) the authors combined an unsupervised object extraction method for a single image together with depth estimation from stereo images. 3D scene-consistency is emphasized with a series of "plausible object hypotheses" obtained that can be used as input for object recognition systems.

Depth estimation based on stereo images has been widely investigated. Kytö et al (2011) proposed a method for evaluating the accuracy of the derived depth in human centred applications. A multilevel test target was used and two crucial parameters – the focal length and baseline, were explored using different values. It was reported that the focal length is of larger influence to the accuracy of the estimated depth compared to the baseline. Lin and Setiawan (2008) attempted to identify the orientation of an object in space by using stereo cameras based on the Scale Invariant Feature Transform (SIFT) and Support Vector Machine (SVM). It was found that having an affine transform matrix was shown to outperform features matching in recognizing object orientations. Another method employing the SIFT feature extraction was presented by Lam et al (2009). The authors implemented virtual stereopsis in 3D modeling of human bodies without the use of multiple calibrated cameras. The position of virtual cameras were calculated using SIFT and motion estimation. In a similar study, Kouskouridas and Gasteratos (2011) proposed a novel implementation which used spatial information and a multi-camera system to estimate the location of objects in 3D space. The method was claimed to be simple and computationally efficient.

In the context of mobile robots navigation, studies have been carried out to obtain obstacle information using an omnidirectional stereo vision system (Su et al, 2006). By using triangulation, the 3D coordinates of a point are generated based on the given stereo images. Such systems have become essential features of autonomous mobile robots. Ben-Tzvi and Xu (2010) presented an embedded stereo vision system which catered to flexible baselines for use in compact-sized robots. In an earlier work (Oh and Lee, 2007), a general-purpose system was proposed for tasks associated with industrial robots. Functions like camera calibration, pattern registration and training etc were incorporated into the system.

Depth maps may be generated using just stereo images by applying a series of processes. A novel depth map generation approach using K-means clustering was proposed to classify objects into foreground or background entities (Meng and Jiang, 2012). Tong et al (2010) presented an object-oriented stereo matching algorithm using multi-scale superpixels for the generation of low-resolution depth maps. The approach was able to overcome downsampling-associated disadvantages such as merging of foreground objects to background, edge blurring etc. When tested on the Middlebury test-bed, the method was shown to outperform other low-resolutions approaches. Given sufficient information, 3D versions of the objects could be reconstructed using the stereo images. Ikeda (2005) employed a combination of "photometric stereo with colour segmentation and the binocular stereopsis to reconstruct accurate shapes from two colour images".

Chen et al (2012) employed the use of Markov Random Fields (MRF) to solve labeling problems in the domain of computer vision. In segmenting regions of interest the MRF model has proved to be robust against real scene complexities as well as noise corruption. In view of the many attempts made in aligning stereo vision

(a) Left eye image

(b) Right eye image

Figure 1. (a) The captured image from the left camera. (b) The captured image from the right camera.

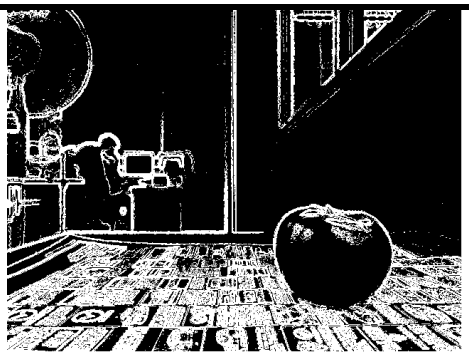

(a) Binarised edges of the left eye

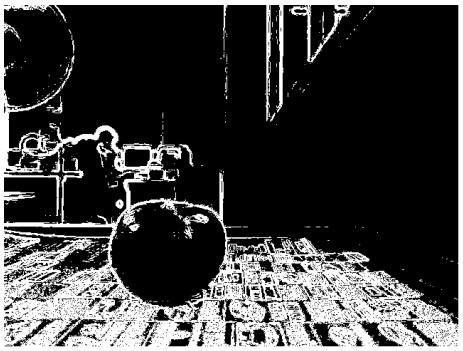

(b) Binarised edges of the right eye

Figure 2. (a) The binarised edges for the left image. (b) The binarised edges for the right image.

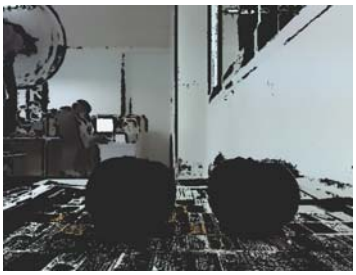

(a)

(b)

(c)

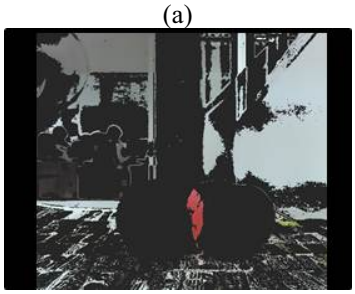

(d)

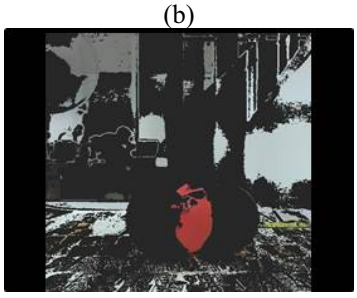

(e)

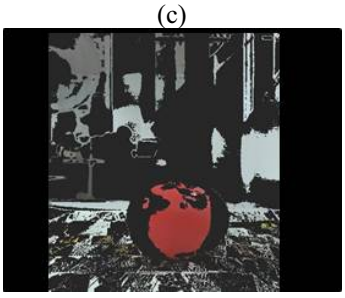

(f)

Figure 3. The alignment process, with the right image overlaid onto the left and shifting the right image to the right. (a) Offset 10. (b) Offset 20. (c) Offset 50. (d) Offset 100. (e) Offset 150. (f) Offset 200. The images show the gradual focusing of the object in the centre.

images and the algorithms developed for extracting objects in recent years, it can be said that stereo vision research is fast gaining interest. This paper proposes a method for the auto-aligning of input images followed by an unsupervised search for objects ofinterest within the regions of different focal points.

THE ALGORITHM

Stereo images for this study are first obtained using two moderately-low resolution cameras arranged in parallel. The images are of dimensions 640x480. A test pair of left and right images is shown in Figure 1.

The images display shadows and regions of lower intensities. In order to increase the contrast, a brightness adjustment was carried out. This was to maximize the results obtained from using an edge detection method which was duly applied. Robert's Edge Detection was selected as the algorithm of choice due to the lower amount of noise produced in the images. A thresholding technique was then used to binarize the images thus segregating the edges and the background into separate groups. The outcome is given in Figure 2.

The next step was to align the stereo images for discovering regions of high correspondences. However, the use of only edges provided insufficient pixel information to determine matches. As such, alignments were carried out based on the brightness-adjusted images. The process is given in Figure 3. Matches were determined by checking the distances of all colour channels for each pixel in the left image to the overlayed pixel in the right image. The RGB values of a pixel were compared to the corresponding pixel values in the other image. A difference of ≤ 30 between the pixels of both images for all Red, Green and Blue channels resulted in the shortlisting of the pixel as a matching point. The right image was overlaid onto the left and shifted to the right pixel-by-pixel, and the total number of matching pixels found at each pixel shift was tabulated. For the above case, the maximum overlaps were found at offsets of 10 pixels and 230 pixels. By using these offset values, the edge-detected images from Figure 2 were then aligned. Figure 4 gives the aligned outputs at these positions.

From Figure 4 the regions of high correspondence were shown as black areas. At offset 10 the background had the highest matches between the left and right images while at offset 230 the object in the foreground was shown to be well correlated. The task now was to determine which region to extract from the alignments at each offset. A simple flood-fill algorithm was used to explore all possible regions, and the three highest-filled regions were automatically selected for the next step of processing. Examples of the flood-fill exploration are given in Figure 5.

By referring to the filled regions, the pixels were consequently replaced with all colour-matching pixels (Figure 6). For example, Figure 5(a) shows a large filled area of the background. By referring to this filled region, pixels of similar colours between both the images were used to replace the region, thereby producing the patches of colours in Figure 6(a). This was due to the fact that not all pixels in the filled region were of similar values. Another check was performed to determine the area consisting of the highest count of colour-matching pixels after replacement, and this region was extracted and reconstructed based on the original images (Figure 7). The final step of the method was to determine the estimated distance of the object

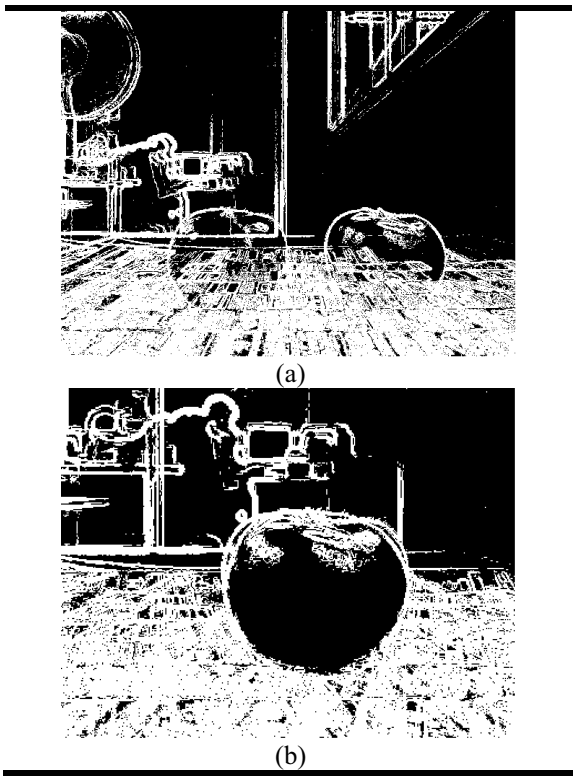

Figure 4. (a) Aligned output at offset 10. (b) Aligned output at offset 230 (image cropped).

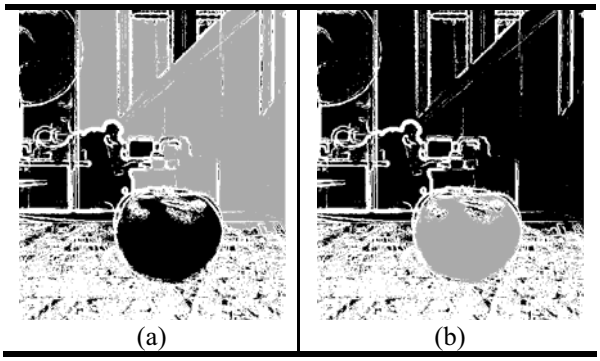

Figure 5. Alignment at offset 230. (a) Flood-fill of the background. (b) Flood-fill of the object.

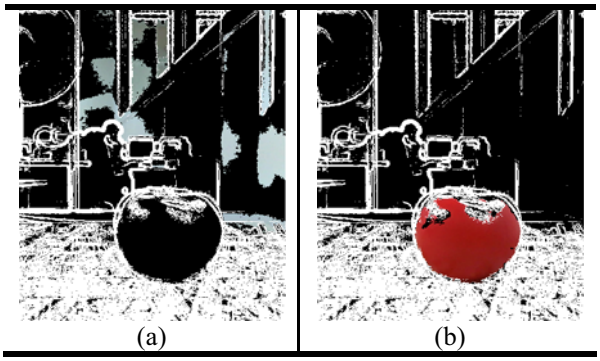

Figure 6. Alignment at offset 230. (a) Replacement of flood-filled region with colour-matching pixels between both the left and right images for the background as depicted in 5(a). (b) Replacement of flood-filled region with colour-matching pixels between both the left and right images for the object as depicted in 5(b). The object is picked over the background due to the high count of colour-matching pixels.

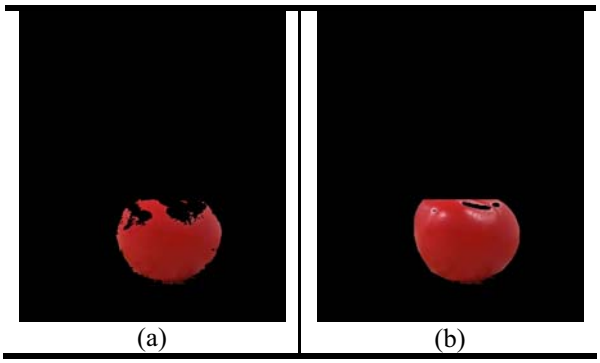

Figure 7. Alignment at offset 230. (a) Extracted object before reconstruction. (b) Extracted object after reconstruction using information from original image.

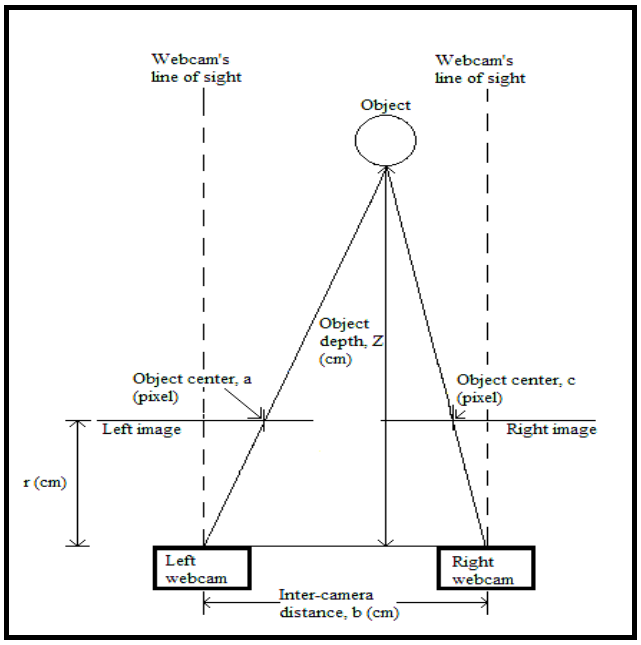

Figure 8. Set-up for obtaining the initial reference ratios for calculating the estimated distance of each identified object.

from the camera. Figure 8 shows the set-up for obtaining the initial measurements and reference ratios for calculation of the estimated distance. The formula is given by Equation (1).

$$Z = \frac{b\,r}{|(a-c)|\,p} \qquad (1)$$

$$p = \text{pixel width (cm)}$$

RESULTS

Experiments were carried out on several sets of images and the results are shown as follows. The left and right images were first shown followed by all extracted objects. The output showed that the objects of interest had been successfully extracted from the original images. The reconstruction process based on information from the input images produced a close-to-original representation of the objects.

Table 1 gives the estimated distances of the objects to the camera based on disparity values obtained from the stereo images. The estimated values are shown to be close to the actual depth, thus indicating the robustness of the algorithm in aligning and selection of objects.

DISCUSSION

The implementation has shown to be capable of auto-extracting objects without prior information from the user. The method takes as input a pair of stereo images and the algorithm proceeds to determine the regions of high matches followed by auto-selection of highly-correlated areas. Objects were shown to be successfully extracted and the reconstruction process produces depictions that are close to the original images.

An analysis of the estimated depth (distances of the objects to the camera) shows promising results. This is useful for robotic applications, especially when the objective of the robot is to identify an object, navigate towards the object and pick up or avoid the object. The method, however, takes approximately 10s to 40s on a Core 2 Duo PC with 2GB RAM to auto-align and identify the regions of interest, depending on the number of alignments obtained. This needs to be substantially improved to achieve real-time processing of stereo vision, and may benefit from using the generalised belief propagation (Chen and Wang, 2012) in which stereo matching was shown to achieve a highly significant speed-up using the reported approach.

The advantage of this method is the fact that it does not require prior knowledge about the objects or the environment to achieve the results. A future work is the application of this method to an actual drone or robot to simulate human-like vision and behaviour. Also included as part of the future work is the use of textured entities as objects of interest, which should pose higher challenges in the identification and extraction process. Research work is currently underway and it is hoped that a robot capable of self-navigating while learning about its environment and new objects can be attained. This work represents the initial studies for such vision-based robotic systems. Factors such as changes in environmental settings as well as the use of complex objects are included into consideration in upcoming experimental studies.

CONCLUSION

An algorithm for the auto-alignment of stereo images followed by the self-extraction of objects of interest using an unsupervised search is presented. The method has shown to be capable of shortlisting regions of high matches between the left and right images and to select regions of high correspondence as output.

Experiment Set I

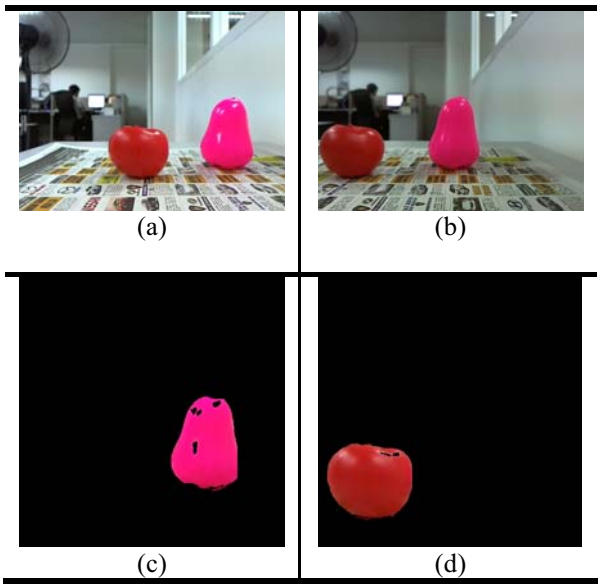

Figure 9. (a) Left image (b) Right image. (c) Extracted object 1. (d) Extracted object 2. Both objects have been reconstructed based on original images.

Experiment Set II

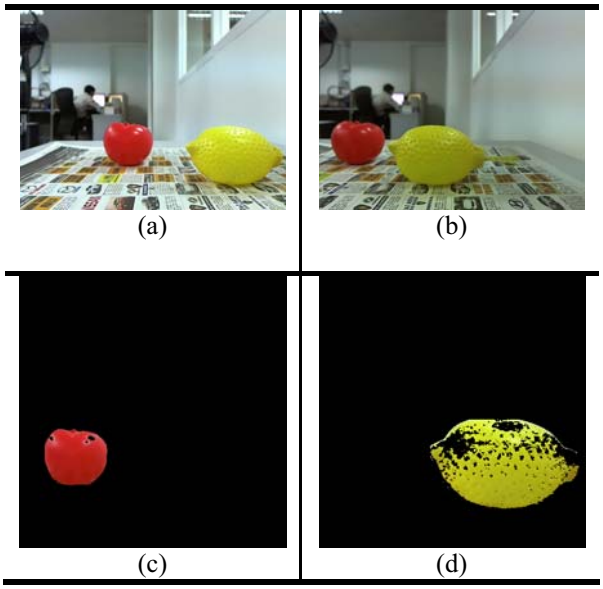

Figure 10. (a) Left image (b) Right image. (c) Extracted object 1. (d) Extracted object 2. Both objects have been reconstructed based on original images.

Experiment Set III

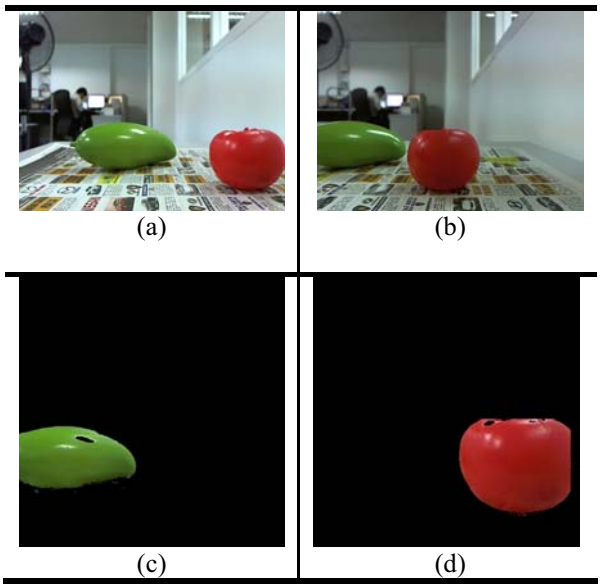

Figure 11. (a) Left image (b) Right image. (c) Extracted object 1. (d) Extracted object 2. Both objects have been reconstructed based on original images.

Experiment Set IV

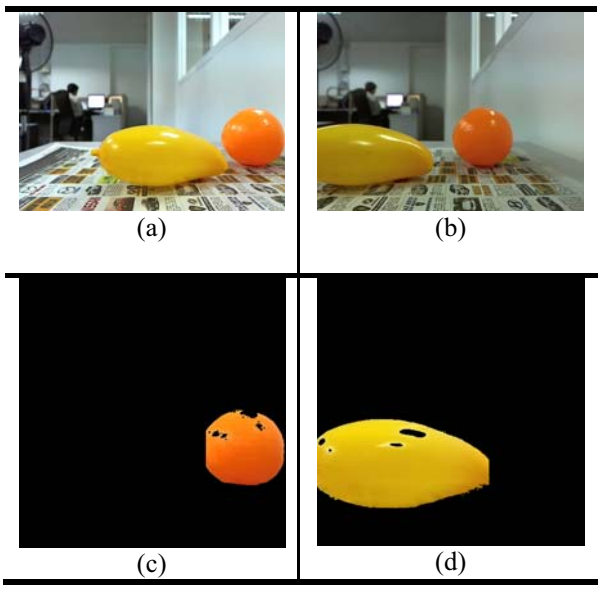

Figure 12. (a) Left image (b) Right image. (c) Extracted object 1. (d) Extracted object 2. Both objects have been reconstructed based on original images.

Table 1. Comparison of actual depth and estimated depth for extracted objects

Experiment	Object	X point at left image (px)	X point at right image (px)	Disparity (px)	Actual Depth (cm)	Estimated Depth (cm)
1	Tomato	286	87	199	18.40	22.64
	Water Apple	496	327	169	25.30	26.66
2	Tomato	261	102	159	26.50	28.34
	Lemon	514	285	229	18.50	19.68
3	Tomato	542	303	239	16.80	18.85
	Mango	272	103	169	26.05	26.66
4	Mango	348	139	209	18.65	21.56
	Orange	567	398	169	25.50	26.66

The extracted objects are free from background interference and retain characteristics from the original images using a reconstruction method. Analysis of the estimated depth proves that the algorithm has successfully aligned the stereo images with the correct depth of the objects. This study will be further extended to applications in real-life drones and robots for the simulation of human-like vision and behaviour.

REFERENCES

Alwan, R.H.; Naji, M.A. 1996. "Automatic Stereo Image Matching using Edge Detection Technique." *International Archives of Photogrammetry and Remote Sensing* XXXI, No. B3, pp. 29-35.

Bleyer, M.; Rother, C.; Kohli, P.; Scharstein, D.; Sinha, S. 2011. "Object Stereo – Joint Stereo Matching and Object Segmentation." In *Proceedings of the 2011 Conference on Computer Vision and Pattern Recognition* (Jun. 21-23) IEEE, Colorado Springs, USA, pp. 3081-3088.

Bleyer, M.; Rhemann, C.; Rother, C. 2012. "Extracting 3D Scene-consistent Object Proposals and Depth from Stereo Images." *Lecture Notes in Computer Science* 7576, pp. 467-481.

Chen, S.Y.; Tong, H; Cattani, C. 2012. "Markov Models for Image Labeling" *Mathematical Problems in Engineering* Vol. 2012, AID 814356, 18 pages., doi: 10.1155/2012/814356.

Chen, S.Y.; Wang, Z.J. 2012. "Acceleration Strategies in Generalized Belief Propogation." *IEEE Transactions on Industrial Informatics* 8, pp. 41-48.

Fan, J.; Yau, D.K.Y.; Elmagarmid, A.K.; Aref, W.G. 2001. "Automatic Image Segmentation by Integrating Color-Edge Extraction and Seeded Region Growing." *IEEE Transactions on Image Processing* 10, No. 10, pp. 1454-1466.

Ikeda, O. 2005. "Shape Reconstruction from Two Colour Images using Photometric Stereo Combined with Segmentation and Stereopsis." In *Proceedings of the 2005 International Conference on Video and Signal Based Surveillance* (Sep. 15-16), IEEE, Como, Italy, pp. 434-438.

Kamencay, P.; Breznan, M.; Jarina, R.; Lukac, P.; Zachariasova, M. 2012. "Improved Depth Map Estimation from Stereo Images Based on Hybrid Method." *Radioengineering* 21, No. 1, April, pp. 70-78.

Kouskouridas, R.; Gasteratos, A. 2011. "Location Assignment of Recognized Objects via a Multi-Camera System." *International Journal of Signal Processing, Image Processing and Pattern Recognition* 4, No. 3 (Sep).

Kytö, M.; Nuutinen, M.; Oittinen, P. 2011. "Method for Measuring Stereo Camera Depth Accuracy based on Stereoscopic Vision." In *Proceedings of SPIE 7864, Three-Dimensional Imaging, Interaction and Measurement Conference*, 786401.

Lam, D.; Hong, R.Z.; DeSouza, G.N. 2009. "3D Human Modeling using Virtual Multi-View Stereopsis and Object-Camera Motion Estimation." In *Proceedings of the 2009 International Conference on Intelligent Robots and Systems* (Oct. 11-15) IEEE/RSJ, St. Louis, USA, pp. 4294-4299.

Lin, C-Y.; Setiawan, E. 2008. "Object Orientation Recognition Based on SIFT and SVM by Using Stereo Camera." In *Proceedings of the 2008 International Conference on Robotics and Biomimetics* (Feb. 21-26) IEEE, Bangkok, Thailand, pp. 1371-1376.

Meng, S.; Jiang, H. 2012. "A Novel Depth Map Generation Method Based on K-means Clustering." In *Proceedings of the Fourth Internation Conference on Digital Home* (Nov. 23-25), Guangzhou, China, pp. 28-32.

Oh, J.; Lee, C. 2007. "Development of a Stereo Vision System for Industrial Robots." In *Proceedings of the 2007 International Conference on Control, Automation and Systems* (Oct. 17-20), Seoul, Korea, pp. 659-663.

Su, L.; Luo, C.; Zhu, F. 2006. "Obtaining Obstacle Information by an Omnidirectional Stereo Vision System." In *Proceedings of the 2006 International Conference on Information Acquisition* (Aug. 20-23) IEEE, Shandong, China, pp. 48-52.

Sutton, D.; Green, R. 2010. "Evaluation of Real Time Stereo Vision System Using Web Cameras. "In *Proceedings of the 25th International Conference of Image and Vision Computing New Zealand* (Nov. 8-9) Queenstown, New Zealand, pp. 1-10.

Tong, H.; Liu, S.; Liu, N.; Barnes, N. 2010. "A Novel Object-Oriented Stereo Matching on Multi-scale Superpixels for Low-Resolution Depth Mapping." In *Proceedings of the 32nd Annual International Conference of the IEEE EMBS* (Aug. 31-Sep. 4) Buenos Aires, Argentina, pp. 5046-5049.

Weng, J.; Ahuja, N.; Huang, T.S. 1992. "Matching Two Perspective Views." *IEEE Transactions on Pattern Analysis and Machine Intelligence* 14, No. 8 (Aug), pp. 806-825.

AUTHOR BIOGRAPHIES

LING-WEI LEE was born in Kuala Lumpur and studied at the University of Nottingham Malaysia Campus where she obtained her honours degree for Computer Science in 2007. She worked for about a year before returning to her alma mater to pursue her PhD with research focus in the field of systems biology. She is now currently working as a computational research scientist with Neuramatix. She can be reached at lingwei@neuramatix.com.

FAEZNOR DIANA BINTI ZAINORDIN was born in Kuala Lumpur, Malaysia and is currently pursuing her undergraduate studies in the field of Computer Science, majoring in Artificial Intelligence. She is attached to the Faculty of Computer Science and Information Technology, University of Malaya. She can be reached at sasuke_eno91@yahoo.com.

ISOGEOMETRIC ANALYSIS FOR DYNAMIC MODEL SIMULATION

Huabin Yin, Qiu Guan, and Shengyong Chen*
College of Computer Science and Technology
Zhejiang University of Technology
310023, Hangzhou, China
E-mail: sy@ieee.org

KEYWORDS
Dynamic model, isogeometric analysis, Non-Uniform Rational B-spline, simulation, control point, error estimation.

ABSTRACT

This paper proposes a method of constructing a dynamic model of a ventricle based on isogeometric simulation so as to diagnose cardiac disease more accurately. Isogeometric simulation is an accurate simulation technology based on NURBS, which has evolved into an essential tool for a semi-analytical representation of geometric entities. Especially, a new method of moving control points is used to achieve a dynamic model of the ventricle. This method promises the model to be very accurate, efficient, and successive, in comparison with traditional models. Furthermore, the paper also puts forward a new error estimation method, which adopts the vector norm to get an overall analysis of the error coefficient in each direction. The error estimation method avoids a complicated estimation for each knot. It can not only be used to evaluate the value of the error accurately, but also reduce the local error by adjusting the control points. Moreover, the proposed NURBS model can especially be useful to analyze the motion and dynamics of the heart, and it is important for doctors to find early cues of cardiac diseases.

INTRODUCTION

With the improvement of people's living standard, more and more people pay much attention to their health. Recently, cardiac disease has become one of the diseases that threaten human health and life safety. According to the report of WHO (World Health Organization), the rate of death lead by cardiovascular disease on average accounts for a third of the total death. There are more than seventeen million people died from cardiac diseases every year. Heart is an extremely complex integrated system. It is integrated with electrophysiology, blood fluid mechanics, dynamics, and biochemical properties. As the Left Ventricle (LV) is the pump of the blood circulation of the whole body, it plays an important role in the cardiac function. The LV is the focus in current researches of heart, and modeling and simulation are two major means to study complex biological problems. With the help of powerful image processing ability and computational ability of the computer, active mechanism of the heart can be carried out thoroughly, a cardiac model can be built too. Moreover, model can not only be used to simulate the heart, but also simulate real movement process of the heart. The simulation of the cardiac valve (Michel 2006), the mechanical properties, and the blood fluid mechanics properties provide information for clinical diagnosis of cardiac disease (Fig. 1).

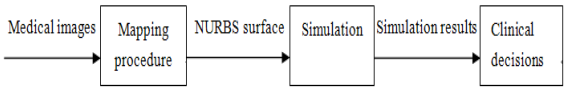

Figures 1: The Process of Computer Aided Diagnosis

At present, imaging techniques, such as computed tomography (CT), magnetic resonance imaging (MRI), positron emission tomography, single photon emission computed tomography, ultrasound, and X-ray, provide noninvasive methods to study internal organs in vivo (Verhaeghe 2007 and Guttman 1997). Medical imaging technology aims to get a surface to represent the accurate geometry of the heart, and of the development of medicinal imaging techniques, much more useful cardiac information has been provided while clinical diagnosis and treatment of cardiac diseases become more complex. It is the first step to obtain many other functional parameters, especially for those related to myocardial kinetics. In the view of geometry, all kinds of cardiac models can be divided into three categories: surface model, solid model and deformable model.

In the early years, scholars and experts did their researches with a simple geometric shape (a bullet without of the top), which represents the LV (Dulce 1993). However, it was rather rough, and it could only offer a few diagnostic parameters. The refinement of the LV surface with a parametric equation method (Such as sine function) was more flexible than other methods. It described more details of the heart at the same time. Mcinerney and Terzopous (1995) had rebuilt the LV surface model by the particularity of the heart's internal material. Furthermore, Young et al. (1995) and Park et al. (2003) used finite-element methods to represent and analyze the cardiac model. Static, comprehensive end-diastolic cardiac surfaces including four cardiac chambers and connected vasculature are presented as a triangular mesh. Mitchell (2002) first proposed a solid model to simulate the dynamic ventricle. The development of a fully three-dimensional active

Proceedings 27th European Conference on Modelling and Simulation ©ECMS Webjørn Rekdalsbakken, Robin T. Bye, Houxiang Zhang (Editors)
ISBN: 978-0-9564944-6-7 / ISBN: 978-0-9564944-7-4 (CD)

appearance model (3-D AAM) requires no additional interactively supplied information. The deformable models had wildly been used in computer vision and graphics, and were adopted by many scholars. This is not only because the deformable model can strongly adapt to the changing nature of the heart, but also because it has more advantages on medical image segmentation, matching, and cardiac motion tracking. Amini proposed a surface deformable model, while Johan Montagnat (2005) extended the deformable model framework to tackle the segmentation of 4D images by introducing temporal regularizing constraints in addition to spatial regularizing constraints.

Nowadays, the traditional finite element method can't make a consecutive mechanical analysis directly with a CAD model (such as B-spline, T-spline), and one mesh is no longer enough. Recent trends taking place in engineering analysis and high-performance computing are demanding greater precision and tighter integration of the overall modeling-analysis process. A finite element mesh is only an approximation of the CAD geometry, which we view as "exact". This approximation (see Fig. 2) can in many situations create errors in analytical results.

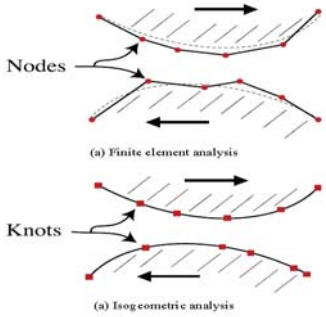

Figures 2: (a) Polynomial Finite Elements (b) Isogeometric Analysis based on NURBS.

It is apparent that the way to break down the barriers between engineering design and analysis is to reconstitute the entire process, but at the same time maintain compatibility with existing practices. A fundamental step is to focus on one, and only one, geometric model, which can be utilized directly as an analysis model, or from which geometrically precise analysis models can be automatically built. This will require a change from classical finite element analysis to an analysis procedure based on CAD representations. This concept is referred to as isogeometric analysis (IGA), and it was introduced in Hughes et al. (2005).

IGA is a new computational method that can provide a consecutive mechanical analysis to the traditional CAD models, and does not need to cater to the FEA with a grid partition. The basic idea of IGA is to analyze and calculate parameters based on the geometric descriptions of entities. Above all, it avoids a classical second modeling compared to the FEA. Later, a NURBS framework was proposed in order to instantiate the concept of IGA. Furthermore, there are two important issues that we have to discuss, but have not appeared in any literatures. One is which model adapts to the changing cardiac shape, where we require the model not only to be dynamic, but also flexible for shape deformation. The other is how to evaluate a model that is accurate for computation of functional parameters. For these emerging problems, this paper proposes the new method of moving the control points to achieve a dynamic model of the LV. From CT cardiac medical images, a manual segmentation is used to find the anatomical boundaries of the cardiac ventricles, and get the coordinates of the point cloud. Then, the coordinates of the control points can be computed, which manipulate the whole heart. Compared to the traditional models, this method has a better accuracy, topology and continuity. What's more, this paper also puts forward a new error estimation method, which avoids a complicated error estimate for each knot.

MODELING

Isogeometric simulation is recently a more accurate simulation technology based on NURBS or T-spline curves. Zhang and Bazilevs (2007) introduced a model for vessel, and it is also based on NURBS isogeometric simulation. Besides, NURBS curve and surface is the most popular approach for modeling. NURBS has the advantages and the convenience for modeling free surface, representing all kinds of conic surface precisely. Furthermore, there are many effective and stable algorithms to develop NURBS entities. Four steps could be concluded through the whole modeling.

The data acquision of LV's CT Images

The data in this paper comes from the patients' CT images. First of all, Anatomical boundaries of the LV can be marked with a manual notation segmentation method (Ru 2012), and many asf files of the data can be created by the MATLAB program. Secondly, the points with the same layer and same number could be obtained by surface fitting method. Resampling helps to solve the problems of integrating the different size at different m-

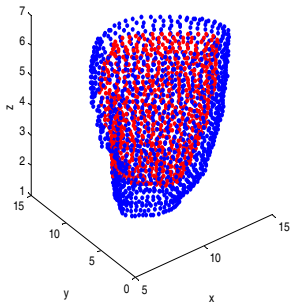

Figures 3: Point Cloud by Manual Notation Method

oments and different layers. Then, the data can be read into MATLAB, which could display the points in the form of 3-D point cloud (see Fig. 3).

NURBS curve and surface

This section gives a brief overview of isogeometric analysis based on NURBS. A more detailed description of the isogeometric approach can be described by T.J.R. Hughes (2005). For an introductory text on NURBS, see Rogers (2001), while a more detailed treatment is given in the book of Piegl and Tiller (1997). Mathematical theory of isogeometric analysis for h-refined meshes may be found in the recent work of Bazilevs et al. (2006).

NURBS is referred to Non-Uniform Rational B-spline curve, which is defined as follows:

$$P(K)=\frac{\sum_{i=0}^{n} N_{i,m}(K)\omega_i P_i}{\sum_{i=0}^{n} N_{i,m}(K)\omega_i} \tag{1}$$

where ***P(K)*** is a position vector of the curve, $N_{i,m}(K)$ is the m-spline basis function. P_i is a control point, ω_i is a weight factor, and ***K*** is a knot vector. The B-spline basis functions are defined recursively starting with piecewise constants:

$$\begin{cases} N_{i,0}(K)=\begin{cases}1 & (K_i \le K \le K_{i+1}) \\ 0 & (other)\end{cases} \\ N_{i,m}(K)=\dfrac{(K-K_i)N_{i,m-1}(K)}{K_{i+m}-K_i}+\dfrac{(K_{i+m+1}-K)N_{i+1,m-1}(K)}{K_{i+m+1}-K_{i+1}} \quad (m\ge 1) \end{cases} \tag{2}$$

The value and space of the knot vector could be unrestricted. So, we can get different mixed-function shape at different intervals, and it provides more freedom for control curve. Any point on the curve impacting the curve has more than a control point (Except of the endpoints of the Bezier), the knot likes a border, when the control point lose influence at this border, another control point will replace it.

Given a control net $\{P_{i,j}\}$, i=1, 2, …, n, j=1, 2, …, m, polynomial order p and q, and knot vectors $\boldsymbol{U}=[u_0, u_1, \ldots, u_{m+p}]$, and $\boldsymbol{V}=[v_0, v_1, \ldots, v_{n+p}]$, a tensor product NURBS surface is defined by:

$$P(u,v)=\frac{\sum_{i=0}^{m}\sum_{j=0}^{n}\omega_{ij}P_{ij}N_{i,p}(u)N_{j,q}(v)}{\sum_{i=0}^{m}\sum_{j=0}^{n}\omega_{ij}N_{i,p}(u)N_{j,q}(v)}, u,v\in[0,1]$$

where $N_{i,p}(u)$ and $N_{j,p}(v)$ are univariate B-spline basis functions of order p and q, corresponding to knot vector ***U*** and ***V***, respectively.

A calculation of control points and weight factor

A tensor product NURBS surface is defined by:

$$P(u,v)=\frac{\sum_{i=0}^{m}\sum_{j=0}^{n}\omega_{ij}P_{ij}N_{i,p}(u)N_{j,q}(v)}{\sum_{i=0}^{m}\sum_{j=0}^{n}\omega_{ij}N_{i,p}(u)N_{j,q}(v)}$$

Assuming constant weights, the matrix equation of each component of the N sampling points (N>m*n) is:

$$P_r^{x,y,z}=\frac{N(i,:)P_w^{x,y,z}N^T(:,j)}{N(i,:)wN^T(:,j)} \tag{3}$$

where m is the number of control points along the u direction, while n is the number of control points along the v direction, i=1, …, m, j=1, …, n, r=i+(j-1) *m. ***N(i, :)*** is the i-th row of the matrix:

$$N=\begin{bmatrix} N_{11} & \cdots & N_{1m} \\ \cdots & \cdots & \cdots \\ N_{i1} & \cdots & N_{im} \\ \cdots & \cdots & \cdots \\ N_{n1} & \cdots & N_{nm} \end{bmatrix}$$

And matrix $\boldsymbol{P^x_w}$ is:

$$P^x_{\omega}=\begin{bmatrix} P^x_{11}\omega_{11} & \cdots & P^x_{1m}\omega_{1n} \\ \cdots & \cdots & \cdots \\ \cdots & \cdots & \cdots \\ P^x_{m1}\omega_{m1} & \cdots & P^x_{mn}\omega_{mn} \end{bmatrix}$$

Matrix ***w*** is:

$$w=\begin{bmatrix} \omega_{11} & \cdots & \omega_{1n} \\ \cdots & \cdots & \cdots \\ \cdots & \cdots & \cdots \\ \omega_{m1} & \cdots & \omega_{mn} \end{bmatrix}$$

Taking advantage of:

$$N(i,:)P_{\omega}N^T(:,j)=[N(i,:)\otimes N^T(:,j)]:P_{\omega}=C(r,:)P_{cv} \tag{4}$$

where $\boldsymbol{P_{cv}}$ is the column vector containing the control points (obtained proceeding row-wise) and ***C(r, :)*** is the row vector containing the elements of $\boldsymbol{N(i, :)\otimes N^T(:, j)}$. We can write the system:

$$P_r^{x,y,z}=C\cdot P_{cv}^{x,y,z} \tag{5}$$

where ***C*** is the matrix whose rows are ***C(r, :)***. Finally, solving the rectangular system for ***B*** in the least square sense we obtain the components of the control points.

Dynamic isogeometric models

A framework of IGA (Bazilevs 2006) consists of five items and features. NURBS is very suitable for representing cardiac shapes because of its advantages of several characteristics. First of all, smooth and continuous; Secondly, flexible to represent both simple and complex shapes by some control points; Last but not the least, easy to be modified locally without

changing the shape in a global way. Usually, there are three methods to modify the shape of NURBS: 1) Move control points; 2) Adjust weight factor; 3) Change the knot vector. In the case of the invariable of LV's knot vector, this paper adopts the first method of moving control points to modify the model, and presents a new dynamic model. The NURBS curve has the homogeneous coordinate representation (Au 1995):

$$C^h(u) = \sum_{i=0}^{n} N_{i,k}(u)\omega_i \begin{bmatrix} C(u) \\ 1 \end{bmatrix}$$

A change in the position of control point P_1 to P_1', moves the curve point $\boldsymbol{C(u)}$ to $\boldsymbol{C'(u)}$, with:

$$C^h(u) = \sum_{i=0}^{n} N_{i,k}(u)\omega_i \begin{bmatrix} P_1 \\ 1 \end{bmatrix}$$

$$C'^h(u) = \sum_{i=0, i\neq j}^{n} N_{i,k}(u)\omega_i \begin{bmatrix} P_1 \\ 1 \end{bmatrix} + N_{j,k}(u)\omega_j \begin{bmatrix} P_1+\Delta P \\ 1 \end{bmatrix}.$$

Let $\triangle \boldsymbol{C^h(u)} = \boldsymbol{C'^h(u)} - \boldsymbol{C^h(u)}$, it follows that:

$$\Delta C^h(u) = N_{i,k}(u)\omega_i \begin{bmatrix} \Delta P \\ 0 \end{bmatrix}$$

So the NURBS curve definition gives:

$$\Delta C^h(u) = \sum_{i=0}^{n} N_{i,k}(u)\omega_i \begin{bmatrix} C'(u) - C(u) \\ 0 \end{bmatrix} \quad (6)$$

Combining these together, the effect of changing a control point can be written as $\triangle \boldsymbol{C^h(u)}$. Similarly, we can conclude that the effect of changing a control point on a NURBS surface is

$$\Delta S(u,v) = \frac{\sum_{i=0}^{m}\sum_{j=0}^{n} \omega_{ij} P_{ij} N_{i,p}(u) N_{j,q}(v)}{\sum_{i=0}^{m}\sum_{j=0}^{n} \omega_{ij} N_{i,p}(u) N_{j,q}(v)} \begin{bmatrix} S'(u,v) - S(u,v) \\ 0 \end{bmatrix} \quad (7)$$

ERROR ESTIMATION

In order to evaluate the LV model developed above, this paper puts forward a new error estimation method. The method will be more precise, it can optimize the model by adjusting the control points. Moreover, it is particularly applicable to estimate a dynamic model because of the characteristic of vector norm. If the model based on isogeometric simulation is called NURBS solid, the equation of the error can be drawn as:

$$\text{Error} = |\text{NURBS solid} - \text{Target solid}| \quad (8)$$

The error from the above formula is just some 3-D coordinate points. However, only through these points can't we find the error intuitively. So, we adopt the vector norm to get an overall analysis of the error coefficient:

$$\varepsilon_x = \frac{\|X' - X\|_2}{\|X\|_2} \quad \varepsilon_y = \frac{\|Y' - Y\|_2}{\|Y\|_2} \quad \varepsilon_z = \frac{\|Z' - Z\|_2}{\|Z\|_2} \quad (9)$$

in each direction. Where ($\boldsymbol{X'}$, $\boldsymbol{Y'}$, $\boldsymbol{Z'}$) are the components of the NURBS solid and ($\boldsymbol{X}$, $\boldsymbol{Y}$, $\boldsymbol{Z}$) are the components of the target solid. When $\varepsilon_x=\varepsilon_y=\varepsilon_z=0$, the error is zero along all three directions (ideal model), while ε_x, ε_y, $\varepsilon_z>0$, the error is proportional to the coefficient, i.s. a bigger coefficient makes a greater error.

DISCUSSION

Experiments and results

Some models based on the method presented above could be built. The method could be not only used to simulate a static object, but also a dynamic one (Fig. 4).

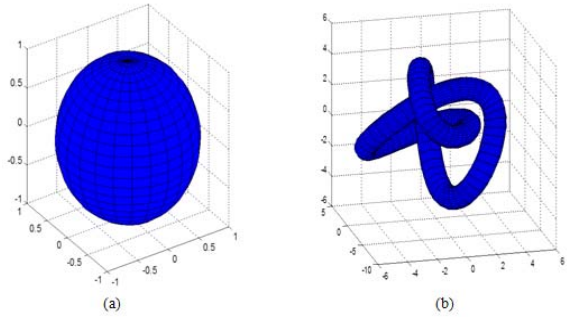

Figures 4: (a) A Static Model-balloon, (b) A Dynamic Model-Deformable Pipeline

So, it is convenient to build a dynamic LV model too. To begin with, the point cloud data can be obtained by manual segmentation. And then, according to the formula (5), we can calculate every 6×10 control points of the internal and external surface of the LV. At last, a three-dimensional control points figure is shown by MATLAB (Fig. 5).

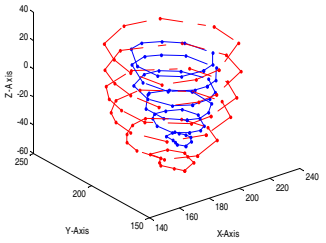

Figures 5: 6×10 Control Points of The Inner And Outer Surface of The LV

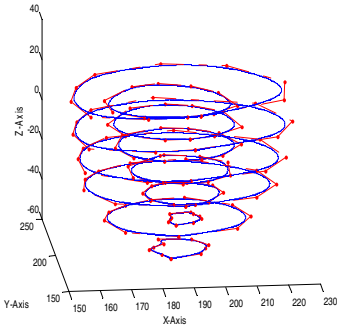

Figures 6: NURBS Curves of The LV

Some curves can be drawn by three order NURBS fitting according to the above control points. These NURBS curves can be used to simulate out the internal and external surface of the LV (see Fig. 6). Fig. 7 is a change of moving one control point, which manipulates the NURBS curve.

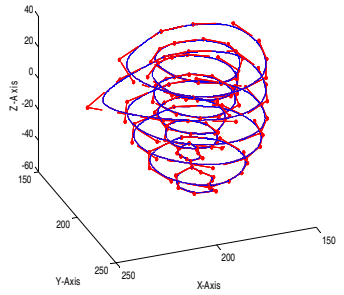

Figures 7: The Change by Moving A Control Point

In summary, a dynamic solid model of the LV based on isogeometric simulation is simulated by NURBS surface fitting (see Fig. 8).

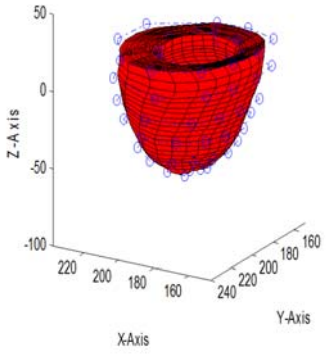

Figures 8: A Solid Model of The LV With Control Points

Traditional finite element model (Jiang 2011), see Fig. 9 (a). The curvature of (a) and (b) (Fig. 10), Compared (a) with (b), (b) line of curvature is smoother than (a) line of curvatu-

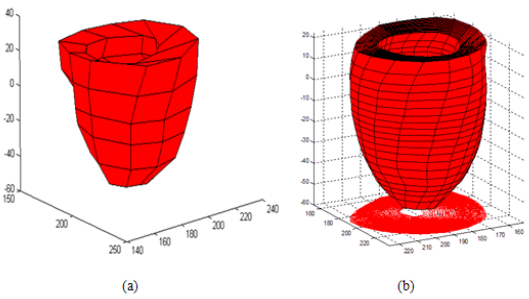

Figures 9: (a) A Traditional Hexahedral Solid Model of The LV Based on The FEA, (b) A Solid Model of The LV Based on The IGA

re expect of the interval [0, 0.1], in which the curvatures are outliers.

The error of the external surface of the LV can be calculated by formula (9), see Fig. 11. From Fig. 11, we can see that when we use the vector norm to test and analyze error, it is easy to decompose the error along

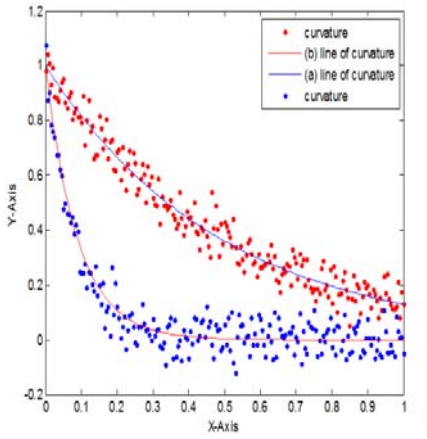

Figures 10: Curvature And Lines of Curvature

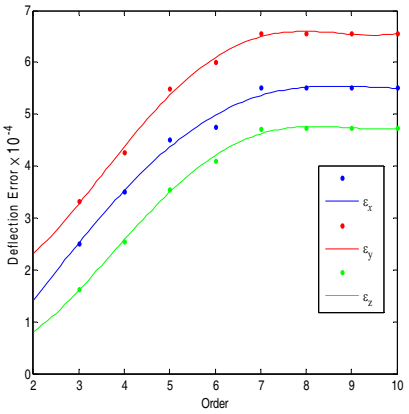

Figures 11: Error Curves of Deflection Error

each direction so that to make a reduction of the error by adjusting the control points conveniently. Moreover, the error will converge to a fixed value, which meets the characteristics of NURBS completely. From the view of fitting, this proves a feasibility of the error estimation.

Efficiency and accuracy

The proposed method is based on a NURBS-based isogeometric model, this methodology, encompassing a very general class of applications, is applied to problems of cardiac left Ventricle modeling and simulation. In addition, a set of procedures enabling the construction of analysis-suitable NURBS geometries directly from patient-specific imaging data is outlined.

The approach is compared with representative benchmark problems, yielding very good results. Here, we further test the efficiency and accuracy of this model. The efficiency is analyzed by both computation complexity and experimental results. However, practical experiments coincide well with the estimations.

For comparison with a few other results, Liu et al. (2000) established a three-dimensional finite element mechanical model of left ventricle. Curvature refers to any of a number of loosely related concepts in different areas of geometry. So, curvature is completely suitable for representing the smoothness of the curve. Compared (a) with (b) (Fig. 10), (a) line of curvature is smoother than (b) line of curvature. The linear change rate of (b) is lower than (a), it indicates that the model of the LV based on the IGA has a better robustness, smoothness, continuity, etc. The new approach is evaluated on two benchmark problems and applied to the cardiac left Ventricle. Very good results are obtained for the benchmark computations and the results for our patient-specific model in qualitative have a higher precision for a patient-specific model. This is because a NURBS curve can exactly represent most of common quadric surfaces or conic curves (Fig. 2). In fact, the error of this model comes from the Data Acquisition of LV's CT Images and the integration of formula (3). To estimate the precision in detail, some previous works on segmentation can be referred to Carneiro G. et al. (2012). From a lot of experiments, we may conclude that higher orders NURBS surfaces do not significantly increase the precision of results, but the computation complexity will increase with the higher order. Therefore, the 7×7 orders are suggested to be enough for practical implementation, it is in qualitative agreement with the results of the error estimation, in which 7×7 orders meet the convergence exactly.

CONCLUSION

Making a mechanical analysis to the traditional CAD models is a dream for the FEA scholars. After the IGA was introduced by Hughes et al., an idea was presented and implemented for generating a dynamic model of the LV based on isogeometric simulation, which was a preliminary work for a mechanical analysis to CAD models. Moving control points was a good method to trims the model in the case of the invariable of LV's weight factor. Owing to the inner advantages of NURBS in modeling, this model has a better accuracy, topology and continuity. Furthermore, a greater precision and efficient error estimation method was put forward in this paper. It adopted vector norm to get an overall analysis of the error coefficient in each direction, and avoided a complicated estimation for each knot. It could be not only used to evaluate the value of the error accurately, but also reduce the local error by adjusting the control points. Moreover, T-spline may be applied to further improve the accuracy of the model. A scheme to use T-spline for modeling will be described later.

REFERENCES

A. Young et al. 1995. "Tracking and finite element analysis of stripe deformation in magnetic resonance tagging." *IEEE Trans. Med. Imaging*, Vol. 14, No. 3, (Sep), 413–421.

C. K. Au and M. F. Yuen. 1995. "Yuen, Unified approach to NURBS curve shape modification, computer-aided design." Vol. 27, No. 2, 85-93.

Chao Jiang. 2011. "Reconstruction of Cardiac Dynamic Model and Stress Strain Analysis." Master, Zhejiang University of Technology.

Carneiro G. et al. 2012. "The Segmentation of the Left Ventricle of the Heart From Ultrasound Data Using Deep Learning Architectures and Derivative-Based Search Methods." *IEEE Transactions on Image Processing*, Volume: 21, Issue: 3, (March), 968 – 982.

Dulce M. C. et al. 1993. "Quantification of the left ventricular volumes and function with cine MR imaging: Comparison of geometric models with three-dimensional data." *Radiology*, 188(2): 371-376.

D. F. Rogers. 2001. "An Introduction to NURBS With Historical Perspective." *Academic Press*, *San Diego*, *CA*.

De Xin Li. et al. 2004. "Research on NURBS Curved Surface Weighted Factor and Its Application." *Journal of Xi'an University of Technology*, Vol. 20, No. 2.

Frangi A F. et a1. 2001. "Three dimensional modeling for functional analysis of cardiac Images: A review." *IEEE Transactions Medical Imaging*, 20 (1), 2-25.

Feng Liu. et a1. 2000. "The use of isoparametric transformation in three dimensional finite element mechanical model of human left ventricle." *BIOPHYSICA SINICA*, Vol.16, No.1 (Mar).

Guttman M A. et a1. 1997. "Analysis and visualization of cardiac function from MR images." *IEEE Computer Graphics and Application*, 17 (1), 30-38.

J.Verhaeghe. et a1. 2007. "Reconstruction for gated dynamic cardiac PET imaging using a tensor product spline basis." *IEEE Trans. Nucl. Sci.*, Vol. 54, No. 1, (Feb), 80–91.

Johan Montagnat and Herve Delingette. 2005. "4D deformable models with temporal constraints: application to 4D cardiac image segmentation [J]." *Medical Image Analysis* , 9(1): 87-100.

J.A. Cottrell. et a1. 2005. "Isogeometric analysis of structural vibrations." *Computer Methods in Applied Mechanics and Engineering*, In press, Available as ICES Report 05-27, UT Austin.

K. Park. et a1. 2003. "A finite element model for functional analysis of 4D cardiac-tagged MR images." *Lect. Notes Comput. Sci.*, vol. 2878, 491–498.

L. Piegl and W. Tiller. 1997. "The NURBS Book (Monographs in Visual Communication)." *2nd ed. Springer-Verlag*, New York.

Michel R. Labrosse. et a1. 2006. "Geometric modeling of functional trileaflet aortic valves: Development and clinical applications." *Journal of Biomechanics*, 2665–2672.

McInerney T. and Terzopoulos D. 1995. "A Dynamic finite element surface model for segmentation and tracking in multidimensional medical images with application to 4D image analysis [J]." *Computerized Medical Imaging and Graphics*, Jan, 19(1): 69–83.

Mitchell S.C. et al. 2009. "3-D active appearance models: segmentation of cardiac MR and Ultrasound images [J]." *IEEE transactions on medical imaging*, 21(9): 1167-1178.

Miao Miao Ru. 2012. "LV Modeling and Statistical Analysis of Parameters based on CT images." Master, Zhejiang University of Technology.

S. Y. Chen and Q. Guan. 2010. "Parametric Shape Representation by a Deformable NURBS Model for Cardiac Functional Measurements [J]." *IEEE Transactions on Biomedical Engineering*, X(Y):1-8.

T.J.R. Hughes. et al. 2005. "Isogeometric analysis Toward Integration of CAD and FEA."

T.J.R. Hughes. et al. 2005. "Isogeometric analysis: CAD, finite elements, NURBS, exact geometry, and mesh refinement." *Computer. Methods Appl. Mech. Engrg*, 194, 4135–4195.

T. J. R. Hughes. 2000. "The Finite Element Method: Linear Static and Dynamic Finite Element Analysis." *Dover Publications, Mineola*, NY.

Xiang Deng and Thomas S. Denney. 2004. "Three-dimensional myocardial strain reconstruction from tagged MRI using a cylindrical b-spline model [J]." *IEEE Transaction on Medical Imaging*, (July), 23(7): 861-867.

Y. Zheng. et al. 2008. "Four-chamber heart modeling and automatic segmentation for 3-D cardiac CT volumes using marginal space learning and steerable features." *IEEE Trans. Med. Imaging*, Vol. 27, No. 11, (Nov), 1668–1681.

Yong Jie Zhang. et al. 2007. "Patient-specific vascular NURBS modeling for isogeometric analysis of blood flow." *Computer methods in applied mechanics and engineering*, 196, 2943-2959.

Y. Bazilevs. et a1. 2006. "Isogeometric analysis: Approximation, stability and error estimates for h-refined meshes." *Mathematical Models and Methods in Applied Sciences*.

Y. Bazilevs. et a1. 2006. "Isogeometric fluid-structure interaction analysis with applications to arterial blood flow." *Mathematical Models and Methods in Applied Sciences*.

AUTHOR BIOGRAPHIES

Huabin Yin was born in Zhejiang, China and went to the Wenzhou University, where he studied mathematics and received his bachelor degree in 2011. He is currently working towards a M.Sc. degree Since 2011. His research interests medical image processing.

Qiu Guan received the M.Sc. degree in control engineering from the Zhejiang University of Technology, Hangzhou, China, in 2004. She is currently an Associate Professor in the Department of Computer Science, Zhejiang University of Technology. Her research interests include computer vision, image processing, and computer aided diagnosis.

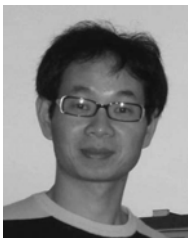

Shengyong Chen received the Ph.D. degree in computer vision from City University of Hong Kong, in 2003. He joined Zhejiang University of Technology, China, in Feb. 2004, where he is currently a Professor in the Department of Computer Science. He received a fellowship from the Alexander von Humboldt Foundation of Germany and worked at University of Hamburg in 2006 - 2007. He worked as a visiting professor at Imperial College, London in 2008 – 2009 and a visiting professor at University of Cambridge, U.K in 2012. His research interests include computer vision, robotics, 3D object modeling, and image analysis. Dr. Chen is a Fellow of IET, a senior member of IEEE, and a committee member of IET Shanghai Branch. He has published over 100 scientific papers in international journals and conferences.

Self-Adaptive Matching in Local Windows for Depth Estimation

Haiqiang Jin, Sheng Liu *, Xuhua Yang and Shengyong Chen
College of Computer Science & Technology
Zhejiang University of Technology
Hangzhou 310023, China
E-mail: edliu@zjut.edu.cn

KEYWORDS
Depth Estimation, Self-Adapting Matching Window, Refining Algorithm.

ABSTRACT

This paper proposes a novel local stereo matching approach based on self-adapting matching window. We improve the accuracy of stereo matching in 3 steps. First, we integrate shape and size information, and construct robust minimum matching windows by applying a self-adapting method. Then, two matching cost optimization strategies are employed for handling both occlusion regions and image borders. Last, we perform a refinement algorithm for obtaining more accurate depth map. Experiment results on the Middlebury stereo image pairs prove that the proposed matching method performs equally well in comparison with other state-of-the-art local approaches.

INTRODUCTION

In machine vision field, depth estimation is a hot research direction all the time. The depth information is able to be applied for auto reversing system, three-dimensional scene reconstruction, obstacle avoidance, and so on. At present, the accuracy of depth results obtained by the local stereo matching methods (Xu et al. 2002; Yoon and Kweon 2006) have been approximated to the one of global approaches (Kohli et al. 2008; Bleyer et al. 2010; Bleyer et al. 2011; Wang and Lim 2010; Li and Chen 2004). And the local methods consume less time than global ones. In the beginning, all kinds of local stereo matching methods (Birchfield and Tomasi 1998; Gerrits and Bekaert 2006; Zhang et al. 2009; Lu et al. 2008; Chen et al. 2012a; Chen et al. 2012b) were proposed for depth estimation. In order to reduce the image ambiguity, early local methods (Zhang et al. 1995; Kwok et al. 2011; Scharstein et al. 2001; Stefano et al. 2004) usually made use of a fixed matching window to aggregate the support from the neighboring pixels within the matching window. Later, because of the known assumption that pixels with similar intensity within a constrained window have similar depth, the matching window was required to adapt its shape and size for the more accurate depth estimation near depth discontinuities (Chen et al. 2011; Chen et al. 2008).

In many fixed matching window based local methods, both SAD (sum of absolute difference) and SSD (sum of square difference) computed the dissimilarity between each pair of matching pixels, while NCC (normalized cross correlation) calculated the similarity. The self-adapting matching window based local approach proposed by (Ke Zhang et al. 2009) was similar with SAD, both of them adopted the absolute difference computation of color information. Nevertheless, this approach had neither considered the shape and size information of self-adapting matching window nor dealt with the situation of smallest matching window properly. In the case of the smallest matching window, the shape and size of self-adapting matching window for pixel will be shrank to the shape and size of pixel, therefore leading to the invalidation of matching window. For avoiding above situation, Ke Zhang et al. performed a minimum matching window of 3x3 for the more robust correspondence matching. Other than familiar global approaches (Wang and Lim 2010; Kolmogorov and Zabih 2001; Zhang et al. 2007) constructing an occlusion term to handle the occlusion regions, we solve the occlusion problem via using a matching cost optimization strategy.

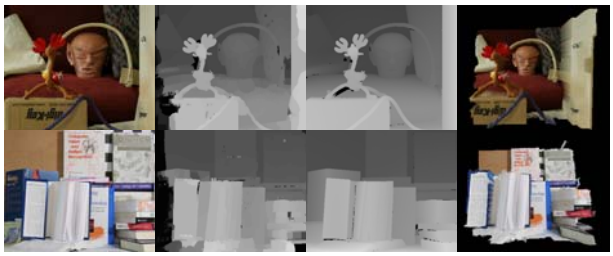

Figure 1: The Reconstructed Three-Dimensional Maps and Dense Depth Maps for the Reindeer and Dolls Stereo Datasets (from top to bottom). From left to right: the input left images, our depth maps, ground truth and reconstructed three-dimensional results. Compared with the ground truth, our depth results obviously acquire most details of the scene with relatively high accuracy.

This paper presented a novel local stereo matching approach for depth estimation. Our method mainly makes the following contributions. Based on original self-adapting local matching method, our approach not only considers the shape and size of matching window, but also improves the method constructing the minimum matching window. And both occlusion regions and border of image problems are solved rely on two matching cost optimization strategies. At last, a new refining method is proposed to calculate the final depth results.

Experimental results on the Middlebury data sets in figure 1 have shown that the proposed local approach is

Proceedings 27th European Conference on Modelling and Simulation ©ECMS Webjørn Rekdalsbakken, Robin T. Bye, Houxiang Zhang (Editors)
ISBN: 978-0-9564944-6-7 / ISBN: 978-0-9564944-7-4 (CD)

able to obtain satisfactory depth maps and is competitive with the state-of-the-art algorithms.

PROPOSED LOCAL STEREO APPROACH

Algorithm overview

The rough procedure of proposed local stereo approach is divided into three steps: First, the raw matching costs are computed relying on the improved local method. Second, we improve the raw matching costs using two matching cost optimization strategies. Third, the final depth map is obtained using a new refining approach. The whole process of our method is illustrated in figure 2.

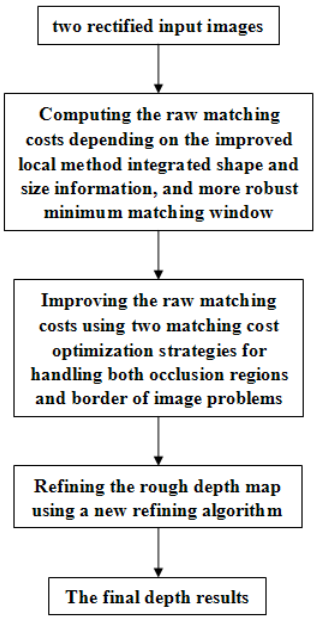

Figure 2: Flow Chart of Our Algorithm.

Improved Local Method based on Self-Adapting Window

In general local stereo matching methods, a fixed matching window is predefined for depth estimation. The matching window for certain pixel is to aggregate the support from neighboring pixels with the same depth within the matching window, but it is not certain that all the pixels in the fixed matching window have the same depth. For example, in the depth result based on NCC with a fixed window, as shown in Fig. 3, there are a mass of noisy depths in weak-textured regions, fuzzy depths in discontinuous boundaries and depths at occlusion areas. Obviously, the proposed approach based on self-adapting window achieves more accurate results shown in figure 3.

Based on the assumption that pixels with similar color within a constrained window have similar depth, it is necessary to produce an appropriate matching window for each pixel adaptively. In this paper, we mainly refer to the local stereo matching method proposed by (Zhang et al. 2009) based on self-adapting matching window. Three improvements are made on the basis of original approach. Firstly, we add the shape and size information of matching window for each pixel, which will further improve the reliability of matching costs. Secondly, a dynamical argument strategy for minimum matching window is presented for more robust correspondence matching. Thirdly, we enforce a replacement strategy for occlusion regions and a suboptimum strategy for border of image.

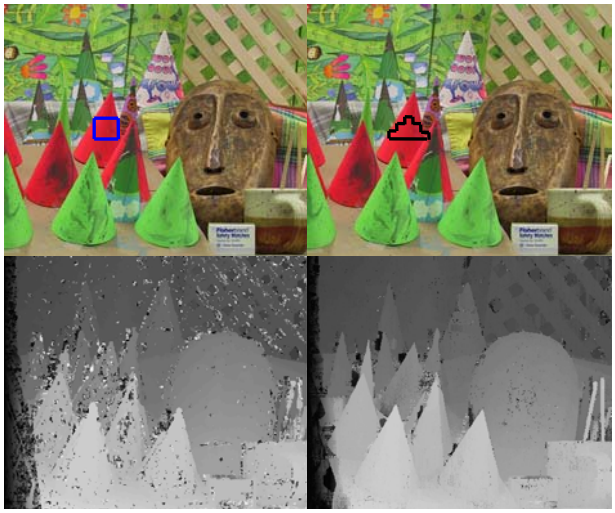

Figure 3: Comparison of Depth Results between Fixed Matching Window and Self-Adapting Matching Window for the Cone (from left to right). Top row: fixed matching window marked by blue, self-adapting matching window marked by black (from left to right). Bottom row: the depth map of NCC with fixed matching window, the depth result of proposed approach with self-adapting matching window (from left to right).

The proposed approach is roughly divided into the following four steps. First, we will determine a self-adapting cross for every pixel in stereo images. Then, the self-adapting window for every pixel is estimated using the cross in stereo images. Thirdly, the matching costs are computed using the self-adapting window. Last, we handle the occlusion regions and border of image.

Step 1. Determining an upright cross for every pixel in stereo images.

$\{h_p^-, h_p^+, v_p^-, v_p^+\}$ are adopted to represent the left, right, up and bottom arm length for the pixel p respectively. A color similarity computation is performed for a consecutive set of pixels which reside on the left horizontal side of the pixel p, L is the preset maximum arm length which controls the size of maximum matching window for the pixel p. I_c denotes the intensity of corresponding color component and τ controls the confidence degree of color similarity. The algorithm for acquiring $\{h_p^-, h_p^+, v_p^-, v_p^+\}$ is as shown in table 1.

In the light of the attained quadruple $\{h_p^-, h_p^+, v_p^-, v_p^+\}$, $H(p)$ and $V(p)$ are attained for each pixel p in stereo

images. *H(p)* stands for the horizontal integral of the pixel *p* as well as the vertical integral of the pixel *p* represented by *V(p)*, and they jointly decide the self-adapting cross for the pixel p shown in figure 4.

Table 1: Estimation of $\{h_p^-, h_p^+, v_p^-, v_p^+\}$.

Algorithm for estimating $\{h_p^-, h_p^+, v_p^-, v_p^+\}$

Input: length L, constant τ, augment τ_{arg}
Initialize $h_p^- \rightarrow h_p^- = 0$, $h_p^+ \rightarrow h_p^+ = 0$,
$v_p^- \rightarrow v_p^- = 0$, $v_p^+ \rightarrow v_p^+ = 0$
Repeat
For i = 1 to L
If $(\max_{c\in\{R,G,B\}}(\lvert I_c(p) - I_c(p_i)\rvert) > \tau)$
Break
end If
end For
$h_p^- \rightarrow h_p^-$ = i-1
For i = 1 to L
If $(\max_{c\in\{R,G,B\}}(\lvert I_c(p) - I_c(p_i)\rvert) > \tau)$
Break
end If
end For
$h_p^+ \rightarrow h_p^+$ = i-1
For i = 1 to L
If $(\max_{c\in\{R,G,B\}}(\lvert I_c(p) - I_c(p_i)\rvert) > \tau)$
Break
end If
end For
$v_p^- \rightarrow v_p^-$ = i-1
For i = 1 to L
If $(\max_{c\in\{R,G,B\}}(\lvert I_c(p) - I_c(p_i)\rvert) > \tau)$
Break
end If
end For
$v_p^+ \rightarrow v_p^+$ = i-1
$\tau \rightarrow \tau = \tau + \tau_{arg}$
Until $(h_p^- + h_p^+) > T_{arms}$ *and* $(v_p^- + v_p^+) > T_{arms}$

$$\begin{cases} H(p) = \left\{(x,y) \middle| x \in \left[x_p - h_p^-, x_p + h_p^+\right], y = y_p\right\} \\ V(p) = \left\{(x,y) \middle| x = x_p, y \in \left[y_p - v_p^-, y_p + v_p^+\right]\right\} \end{cases} \quad (1)$$

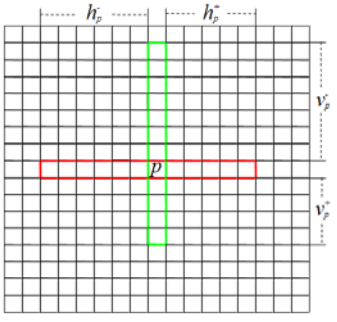

Figure 4: Sketch Map for *H(p)* & *V(p)*. Red frame represents *H(p)*, the length of *H(p)* is $h_p^- + h_p^+ + 1$. And green frame represents *V(p)*, the length of *V(p)* is $v_p^- + v_p^+ + 1$.

Step 2. Estimating the Self-adapting Window for every pixel using the Cross in stereo images.

Given the self-adapting cross for each pixel, we can readily construct a self-adapting matching window *U(p)* for the pixel *p*. The key process is to model the matching window *U(p)* as an area integral of multiple horizontal integrals *H(q)*, sliding along the vertical segment V(p) of the pixel p,

$$U(p) = \bigcup_{q \in V(p)} H(q) \quad (2)$$

where q is a pixel located on the vertical integral V(p).

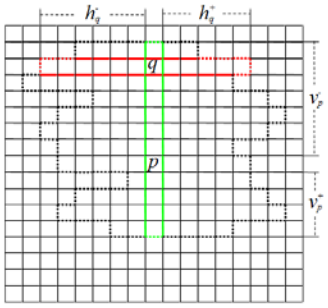

Figure 5: Self-Adapting Matching Window for the Pixel *p*. Green frame represents *V(p)*, and red frame represents *H(q)*. Dotted box stands for the self-adapting region.

Step 3. Computing the Matching Costs using the Self-adapting Window.

We symmetrically consider both self-adapting matching window *U*(p) and *U'*(*p'*) depending on the pixel *p* and *p'* respectively so as to achieve reliable matching cost aggregation. Here, $p' = (x_p - d, y_p)$ is the corresponding pixel in the right image for $p = (x_p, y_p)$ with depth *d* in the left image. The matching cost $C_d(p)$ between the pixel *p* and *p'* is computed as follows:

$$C_d(p) = \frac{1}{\|U_d(p)\|} * \sum_{t \in U_d(p)} e_d(t) * (\log\theta + 1) \quad (3)$$

where $U_d(p) = \left\{(x,y) \middle| (x,y) \in U(p)\right\}$, $(x-d, y) \in U'(p')$, $\theta = \|U(p)\| / \|U_d(p)\|$, $e_d(t)$ denotes the raw matching cost for the pixel *t* with depth *d* and $U_d(p)$ is the combined matching window which only contains these valid pixels. $\|U_d(p)\|$ denotes the number of pixels in $U_d(p)$, used for normalizing the aggregated matching cost $\sum_t \in U_d(p) e_d(t)$. The raw matching cost is computed from a pair of corresponding pixels, for example, the matching cost of *t* in the left image and *t'* in the right image with the depth value *d* is computed as

$$e_d(t) = \min\left(\sum_{c\in\{R,G,B\}} \left| I_c(t) - I'_c(t') \right|, T\right) \quad (4)$$

where T controls the truncation limit of the matching cost.

Step4. Handling the Occlusion Regions and Border of Image.

Being inspired by five major approaches introduced by (Egnal and Wildes 2002), we present a replacement strategy to deal with the occlusion regions. Owing to the common assumption that pixels with similar intensity within a neighboring area have similar depth, the matching costs for occlusion pixels are capable of being replaced with ones for "corresponding" pixels.

For instance, $d(p)$ is the depth for pixel $p = (x_p, y_p)$ in left image, and $d'(p')$ is the depth for pixel $p' = (x_p - d(p), y_p)$ in right image. If $d(p)$, $d'(p')$ and $d(p'')$ satisfy simultaneously the condition that $d(p) > d'(p')$ and $d'(p') \leq d(p'')$ where $p'' = (x_p - d(p) + d'(p'), y_p)$,we would employ a displacement strategy that the matching costs for the pixel p in left image are replaced with ones for the pixel p' in left image are replaced with ones for the pixel p′ in right image.

Neither estimating two depth maps for left-right consistency check (Yoon and Kweon 2006; Tombari et al. 2007) nor applying a simple border extrapolation step, we adopt a suboptimum strategy for border of image. The corresponding pixel p' will locate outside the right image when $(x_p - d(p))<1$, which means that the matching cost can not be achieved by making use of the corresponding pixels.

$$\hat{d} = \arg\min_{d\in[d_{\min},d_{\max}],(x_p-d)>0,\, d\neq d^*} C_d(p) \tag{5}$$

where $\hat{d}$ is the suboptimum label we need, d^* is the optimal label is computed as follows:

$$d^* = \arg\min_{d\in[d_{\min},d_{\max}],(x_p-d)>0} C_d(p) \tag{6}$$

At last, we use $C_d(p)$ as the matching cost for pixel p when $(x_p - d(p)) < 1$. The handling for border of image will work aftering the global optimization process.

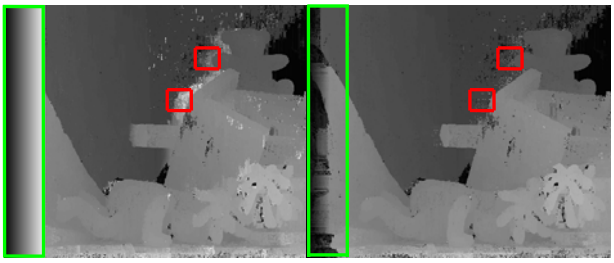

Figure 6: Comparing between the Rough Result without ORBI (Occlusion Regions and Border of Image) Handling and the Rough Result with ORBI Handling for the Teddy (from left to right). Left column: the rough result without ORBI handling. Right column: the rough result with ORBI handling. Occlusion regions are marked by red frames, border of image is marked by green frame.

Refining Algorithm

Although the raw result obtained by proposed approach after the "Winner-Take-All" is of relative good accuracy, there existed many noisy depth areas as shown in figure 7. Therefore we still require further refining the raw result for more accurate result. This paper utilizes a new refining algorithm to achieve this goal. Figure 7 demonstrates that the refining algorithm eliminates a mass of outliers.

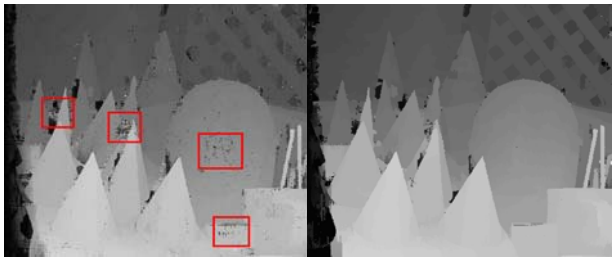

Figure 7: The Comparison between the Depth Maps (before and after refining) for the Cone. It is obvious that the refining method eliminates amounts of noisy depths. Left: the raw result before refining with numerous noisy regions marked by red frame. Right: the result after refining.

Table 2: Refining the Rough Depth Map

Algorithm for refining the rough depth map

Input: Input image P, minimum depth d_{min},
maximum depth d_{max}
Initialize $cost \rightarrow cost = 0$
Do
For $d = d_{min}$ to d_{max}
Do
If $(d'(p)==d)$
$cost \rightarrow cost=cost+1/\bar{C}_{p'}(d)$
end If
While $p' \in U(P)$
$\Phi_p(d) = cost$
$cost \rightarrow cost = 0$
end For
While $p \in P$
Do
For $d = d_{min}$ to d_{max}
If $(\Phi_p(d)>\Phi_p(d\_max))$
$d\_max=d$
end If
end For
$d'(p) = d\_max$
While $p \in P$

In this paper, we mainly refer to the refining approach proposed by (Lu et al. 2008) with a local high-confidence voting scheme. They make a statistic function $\varphi_p(d)$ for the number of pixels with the depth d in the self-adapting neighbourhood $U(p)$ of the pixel p, the maximum of φ_p corresponds to a statistically optimal depth value d^*_p. Accordingly, the depth of the pixel p

Table 3: Quantitative Evaluation Results (bad pixels percentage) of Different Stereo Matching Methods for the Tsukuba, Venus, Teddy, and Cones Stereo Test Pairs.

Algorithm	Tsukuba	Venus	Teddy	Cones	Average percent of bad pixels
VarMSOH(Ben-Ari and Sochen 2010)	3.60	0.49	10.10	8.20	5.60
BioPsyASW(Nalpantidis and Gasteratos 2010)	4.91	3.41	14.10	11.30	8.43
Our Method	5.47	4.05	13.00	11.50	8.51
CSBP(Yang et al. 2010)	3.84	2.52	17.30	14.20	9.47
Regular GC	4.43	6.56	39.80	59.00	27.45

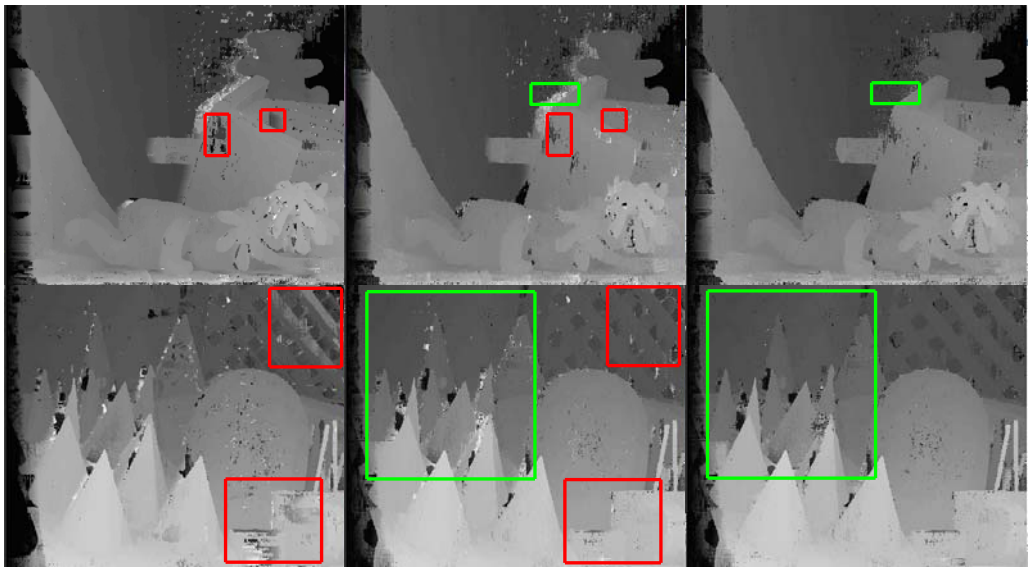

Figure 8: The Evolutive Local Results for the Middlebury Stereo Datasets Teddy and Cones (from top to bottom). First column: the original depth results in (Zhang et al. 2009). Second column: the depth results with integrating size information and improved minimum matching window. Third column: the final local results using the proposed local matching approach. Red frame indicates that the results of second column are more accurate than these of first column. And green frame shows that the results of third column are more competitive in occlusion regions than ones of second column.

after refining, d^*_p, is decided as

$$d^*_p = \arg\max_d \varphi_p(d), \quad d \in [d_{\min}, d_{\max}] \tag{7}$$

After the local matching approach proposed, the matching cost $C_d(p)$ for the pixel p is obtained, and then we can achieve the local depth estimate $d(p)$. Taking advantage of the matching cost $C_d(p)$, we compute a weighted average of matching costs $\bar{C}_p$ for the pixel p in its self-adapting neighbourhood $U(p)$, is followed as

$$\bar{C}_p(d) = \frac{\sum_{p' \in U(p)} C_d(p')}{\|U(p)\|}, \quad d \in [d_{\min}, d_{\max}] \tag{8}$$

where $p' \in U(p)$ is a pixel in the self-adapting neighborhood $U(p)$, $\|U(p)\|$ denotes the total number of pixels in the self-adapting matching window $U(p)$. The algorithm for computing final depth map $d'(p)$ is as shown in table 2.

EXPERIMENTS

In this paper, the performance on weakly textured regions has been mended in some way by integrating shape and size information and improving the minimum matching window. And, a new process has been presented to handle the occlusion pixels. In figure 8, the fence parts of Cones are restored obviously in red frame. And, occlusion areas outside the eave of Teddy are more accurate in green frame after proposed occlusion handling.

All of test sets are from the Middlebury stereo datasets (Scharstein et al. 2001; Scharstein and Szeliski 2003; Scharstein and Pal 2007; Hirschmuller and Scharstein 2007). For the standard Middlebury image pairs with four test pairs, i.e., Tsukuba, Venus, Teddy, and Cones, Table 3 summarizes the quantitative performance of our method and those of other stereo matching methods, roughly in descending order of overall performance. The final depth results prove that our approach is able to competitive with those state-of-the-art approaches.

CONCLUSION

Our local stereo matching approach adopting the shape-size information and the more robust minimum matching window has more excellent performance on weak-textured regions. Meanwhile, the conventional occlusion regions and border of image problems are solved quite successfully depending on two matching cost optimization strategies. And after the handling of new refinement method, the raw local depth result is transformed into the final depth map with high accuracy. In general, our local approach has been proved to be able to obtain good performance on the Middlebury stereo test sets.

REFERENCES

Ben-Ari, R. and N. Sochen. 2010. "Stereo matching with Mumford-Shah regularization and occlusion handling". *IEEE Transactions on Pattern Analysis and Machine Intelligence*, Vol.32, No.11, 2071-2084.

Birchfield, S. and C. Tomasi. 1998. "A Pixel Dissimilarity Measure That Is Insensitive to Image Sampling". *IEEE Transactions on Pattern Analysis and Machine Intelligence*, Vol.20, No.4, 401-406.

Bleyer, M.; C. Rother; and P. Kohli. 2010. "Surface Stereo with Soft Segmentation". In *Proceedings of 2010 IEEE Conference on Computer Vision and Pattern Recognition*. 1570-1577.

Bleyer, M.; C. Rother; P. Kohli; D. Scharstein; and S. Sinha. 2011. "Object Stereo — Joint Stereo Matching and Object Segmentation". In *Proceedings of 2011 IEEE Conference on Computer Vision and Pattern Recognition*. 3081-3088.

Chen, S.; H. Tong; C. Cattani, "Markov models for image labeling", Mathematical Problems in Engineering, Vol. 2012, Article ID 814356, 2012, 18 pages. doi:10.1155/2012/814356.

Chen, S.Y.; Z.J. Wang, "Acceleration Strategies in Generalized Belief Propagation", IEEE Transactions on Industrial Informatics, Vol. 8, No. 1, 2012, pp. 41-48.

Chen, S.Y.; Y.F. Li, "Determination of Stripe Edge Blurring for Depth Sensing", IEEE Sensors Journal, Vol. 11, No. 2, Feb. 2011, pp. 389-390.

Chen, S.Y.; Y.F. Li; J.W. Zhang, "Vision Processing for Realtime 3D Data Acquisition Based on Coded Structured Light", IEEE Transactions on Image Processing, Vol. 17, No. 2, Feb. 2008, pp. 167-176.

Egnal, G. and R.P. Wildes. 2002. "Detecting Binocular Half-Occlusions: Empirical Comparisons of Five Approaches". *IEEE Transactions on Pattern Analysis and Machine Intelligence*, Vol.24, No.8(Aug), 1127-1133.

Gerrits, M. and P. Bekaert. 2006. "Local Stereo Matching with Segmentation-based Outlier Rejection". In *Proceedings of the 3rd Canadian Conference on Computer and Robot Vision*. 66.

Hirschmuller, H. and D. Scharstein. 2007. "Evaluation of cost functions for stereo matching". In *Proceedings of IEEE Conference on Computer Vision and Pattern Recognition*. 1-8.

Kohli, P.; L. Ladicky; and P. Torr. 2008. "Robust Higher Order Potentials for Enforcing Label Consistency". In *Proceedings of IEEE Conference on Computer Vision and Pattern Recognition*. 1-8.

Kolmogorov, V. and R. Zabih. 2001. "Computing Visual Correspondence with Occlusions using Graph Cuts". In *Proceedings of Eighth IEEE International Conference on Computer Vision*. Vol.2, 508-515.

Kwok, N.M.; X. Jia, et al., "Visual impact enhancement via image histogram smoothing and continuous intensity relocation", *Computers & Electrical Engineering*, Vol. 37, No. 5, Sep. 2011, pp. 681-694.

Li, H. and G. Chen. 2004. "Segment-based Stereo Matching Using Graph Cuts". In *Proceedings of the 2004 IEEE Computer Society Conference on Computer Vision and Pattern Recognition*. Vol.1, 74-81.

Lu, J.; G. Lafruit; and F. Catthoor. 2008. "Anisotropic local high-confidence voting for accurate stereo correspondence". In *Proceedings of SPIE-IS&T Electronic Imaging*. Vol.6812.

Nalpantidis, L. and A. Gasteratos. 2010. "Biologically and psychophysically inspired adaptive support weights algorithm for stereo correspondence". *Robotics and Autonomous Systems*.

Scharstein, D.; R. Szeliski; and R. Zabih. 2001. "A taxonomy and evaluation of dense two-frame stereo correspondence algorithms". In *Proceedings of IEEE Workshop on Stereo and Multi-Baseline Vision*. 131-140.

Scharstein, D. and R. Szeliski. 2003. "High-accuracy stereo depth maps using structured light". In *Proceedings of 2003 IEEE Computer Society Conference on Computer Vision and Pattern Recognition*. Vol.1, 195-202.

Scharstein, D. and C. Pal. 2007. "Learning conditional random fields for stereo". In *Proceedings of IEEE Conference on Computer Vision and Pattern Recognition*. 1-8.

Stefano, L.D. ; M. Marchioni et al. 2004. "A fast area-based stereo matching algorithm". *Image and vision computing*, No.22, 983-1005.

Tombari, F.; S. Mattoccia; and L.D. Stefano. 2007. "Segmentation based adaptive support for accurate stereo correspondence" In *Proceedings of Pacific-Rim Symp. Image Video Technol*. 427–438.

Wang, D. and K.B. Lim. 2010. "A New Segment-based Stereo Matching using Graph Cuts". In *Proceedings of 2010 3rd IEEE International Conference on Computer Science and Information Technology*. Vol.5, 410-416.

Xu, Y.; D. Wang; T. Feng; and H.Y. Shum. 2002. "Stereo computation using radial adaptive windows". In *Proceedings of 16th International Conference on Pattern Recognition*. Vol.3, 595-598.

Yang, Q.; L. Wang; and N. Ahuja. 2010. "A constant-space belief propagation algorithm for stereo matching". In *Proceedings of 2010 IEEE Conference on Computer Vision and Pattern Recognition*. 1458-1465.

Yoon, K.J. and I.S. Kweon. 2006. "Adaptive support-weight approach for correspondence search". *IEEE Transactions on Pattern Analysis and Machine Intelligence*, Vol.28, No.4 (Apr), 650-656.

Zhang, K.; J. Lu; and G. Lafruit. 2009. "Cross-Based Local Stereo Matching Using Orthogonal Integral Images". *IEEE Transactions on Circuits and Systems for Video Technology*, Vol.19, No.7, 1073-1079.

Zhang, Z.; R. Deriche et al. 1995. "A robust technique for matching two uncalibrated images fllmugh the recovery of the unknown epipolar geometIy". *Artificial Intelligence*, Vol.78, 87-119.

Zhang, P.; Y. Xu; X. Yang; and L. Traversoni. 2007. "Multi-Scale Gabor Phase-Based Stereo Matchingusing G raph Cuts". In *Proceedings of 2007 IEEE International Conference on Multimedia and Expo*. 1934-1937.

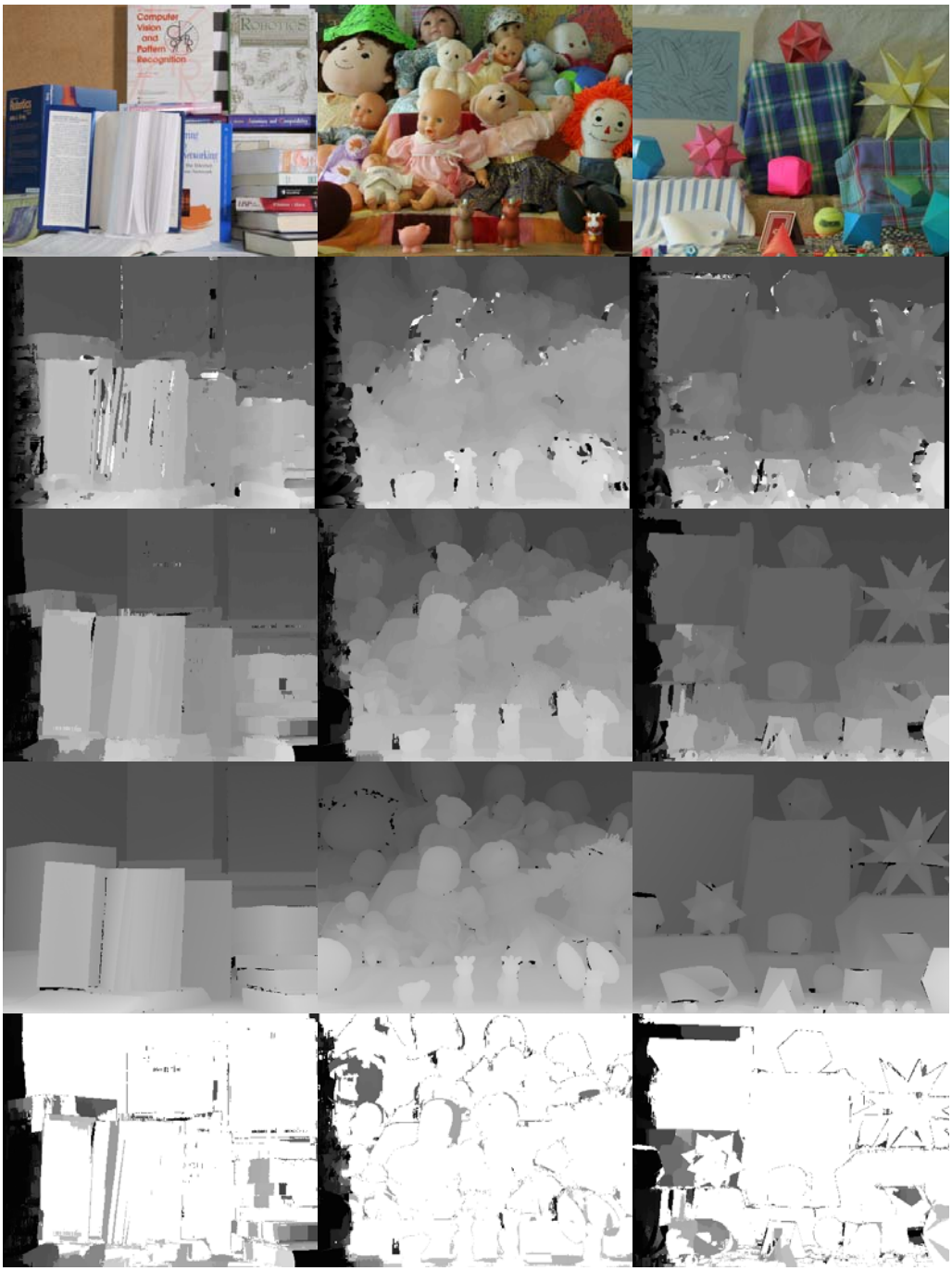

Figure 9: The Comparison of Final Depth Results for the Books, Dolls, and Moebius Stereo Image Pairs (from left to right). Rows from top to bottom: the input left images, results of NCC, final depth results by proposed method, ground truth and “bad pixel” matching results.

IMAGE SUPER-RESOLUTION RECONSTRUCTION USING MAP ESTIMATION

Xin-Long Lu, Sheng-Yong Chen*, Xin Wang, Sheng Liu, Chunyan Yao, Xianping Huang
College of Computer Science and Technology, Zhejiang University of Technology,
Hangzhou 310023, China
Email for correspondence: csy@zjut.edu.cn *
Emails for all authors: luxinlong1988@gmail.com, {csy, xinw, edliu, ycy, hxp}@zjut.edu.cn

KEYWORDS
Super-Resolution, Markov Random Field, Transformed Gradient Field, Maximum A Posteriori, Normalized Convolution.

ABSTRACT

This paper presents a promising super-resolution (SR) approach using maximum a posteriori (MAP) estimation. We consider the high resolution (HR) estimation as a Markov Random Field (MRF), using a transformed gradient field prior to repair the image fuzzy problem caused by MRF. An improved Normalized Convolution method is proposed to obtain a first good estimation. We build a reasonable energy function and minimize the posterior energy by gradient descent algorithm. Experimental results on realistic image sequence and comparisons with several other SR techniques show that our approach gives the best results both qualitative and quantitative.

INTRODUCTION

In the field of electro-optical imaging, the resolution of an image is often the most important technical indicators to evaluate the image quality. The higher the resolution of an image is, the higher pixel density will be. High resolution can provide more information and is conducive to further analysis of image processing (Hardie et al. 1997).

Increasing the density of the sensor is the most direct way to improve the image resolution. However, it's hard to bear the cost of image sensor's high density in general applications. On the other hand, the imaging system is limited by its inherent sensor array arrangement density, which is extremely finite.

An effective way to improve the resolution of the image is using the super-resolution reconstruction.

It generates a high resolution image by extracting additional spatial and temporal information in low resolution (LR) images (Zhang and Shen 2002).

Super-resolution can restore high frequency information in the image which is lost in the imaging process, and effectively remove the noise and blurring without expensive hardware costs. Therefore, it has become a popular research field (Xie 2007).

Because there are many limitations in the existing SR technology, e.g. using simple image prior model; without considering the registration error and noise; using simple interpolation result as initial estimation, etc. Faced with these deficiencies, this paper proposed an overall solution for color image super-resolution reconstruction problem.

PRIOR DISTRIBUTION

The super-resolution reconstruction process can be seen as the inverse process of image acquisition. Its purpose is to obtain a high resolution image by the observation of low resolution images.

As an ill-posed problem in mathematical theory, the estimation of high resolution image z requires the introduction of prior constraints to restrict the solution space and the application of prior knowledge in the reconstruction.

MRF is commonly used in the field of image processing modeling, which is an adaptive smoothness constraint, describing the relationship between points within the image. In this paper, the original high resolution image z is considered as a MRF (Chen et al. 2011; Chen et al. 2012).

Due to the equivalence between Markov Random Field and Gibbs Random Field, we can describe z by a Gibbs distribution, in the following form:

$$P(z) = \exp(-\lambda \sum_{i=1}^{N} \sum_{c \in C} V_c(z_i) / \tau), \quad (1)$$

where λ is a constant, C is a clique and $V_c(x)$ corresponds to a clique potential function. τ is a scale parameter, which controls the shape of the probability distribution. The greater of τ means more flat of the probability distribution.

MRF can effectively describe the spatial continuity within the image. However, the textures and edges in the image do not have the Markov property. Correlation between adjacent pixels within these structures is very weak, even have the opposite characteristics with Markov property. Therefore, using MRF can bring about the problem of image fuzzy, result in the damage of image textures and edges.

The algorithms using MRF as prior is only suitable for the HR scenes composed by homogeneous large plaque, for small patches and linear features (such as roads), and the reconstruction result is poor (Lin et al. 2011). The existing SR techniques often concentrate on modifying the MRF model, those efforts indeed make some improvements to this problem, however,

Proceedings 27th European Conference on Modelling and Simulation ©ECMS Webjørn Rekdalsbakken, Robin T. Bye, Houxiang Zhang (Editors)
ISBN: 978-0-9564944-6-7 / ISBN: 978-0-9564944-7-4 (CD)

most of these methods usually designed only for a special class of scenes and little has been done to fix problems on real natural scenes. In this section, we introduce a prior named Transformed Gradient Field (TGF), which can cooperate well with MRF and significantly improve the reconstruction result.

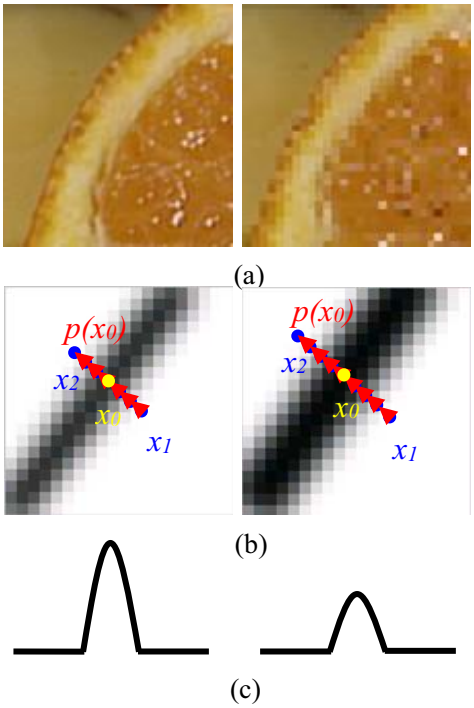

Figures 1: Gradient Profile. (a) two edges with different sharpness. (b) gradient maps (normalized and inverted magnitude) of two rectangular regions in (a). $p(x_0)$ is a gradient profile passing through the edge pixel (zero crossing pixel) x_0, by tracing along gradient directions (two sides) pixel by pixel until the gradient magnitude does not decrease at x_1 and x_2. (c) 1D curves of two gradient profiles.

Jian Sun et al. observed that the relationship of gradient profile sharpness between HR image and LR image follows a statistical dependency (Sun et al. 2008). It means that if we have the (up-sampled) LR gradient profile and the up-sampling factor, then the expected sharpness of the HR gradient profile can be determined. With the statistical dependency, we can compute the ratio between LR gradient profile and HR gradient profile:

$$r = \frac{p(HR)}{p(LR)}, \tag{2}$$

where *p(HR)* is the expected sharpness of the gradient profile in HR image, *p(LR)* is the (up-sampled) LR gradient profile.

Using the LR gradient field ∇I_l^u and the ratio computed in (2), the HR gradient field can be expressed as:

$$\nabla I_h^T = r * \nabla I_l^u \tag{3}$$

In the view of image gradient field, the image fuzzy problem caused by MRF will reduce the sharpness of image gradient field. The use of transformed gradient field can sharp the gradient field and create delicate details and edge information.

MAXIMUM A POSTERIORI

Maximum A Posteriori is a statistical method under the Bayesian framework. Bayesian framework is introduced to the SR reconstruction because of two reasons: First, we have prior knowledge of the original image *z*, which can be applied as an estimated amount. In classic estimation method, it is difficult to apply the prior knowledge. However, under the Bayesian framework, we can easily use the prior and improve the estimation precision. Second, Bayesian estimation is often useful when the minimum variance unbiased estimator of the original image *z* can not be found. By the specified image z, the estimated amount can be designed to obtain. The derived estimation can be considered to be optimal, in the sense of the "average". The estimated amount can be seen as the best estimate in the case of the prior probability density function of the assumed image *z*.

According to estimation theory, we consider $\varepsilon = z - \hat{z}$ as the difference between the estimated amount $\hat{z}$ and the original image *z*, we call $E(\varepsilon^2)$ Bayesian risk, which is used to measure the performance of the estimators. The position which makes the Bayesian risk minimum, also makes the posterior probability density function maximum and is called the maximum a posteriori estimator.

In MAP estimation, we choose *z* to make the probability density function maximum:

$$\hat{z} = \arg\max_z P(z \mid y, \nabla I_h^T), \tag{4}$$

where *z* is the estimation of high resolution images, *y* is the observed low resolution image in the SR reconstruction, ∇I_h^T is the gradient determined by gradient transform method. According to the Bayesian theory:

$$P(z \mid y, \nabla I_h^T) = \frac{P(y, \nabla I_h^T \mid z) P(z)}{P(y, \nabla I_h^T)}. \tag{5}$$

It's maximum is equivalent to the maximum of $P(y, \nabla I_h^T \mid z) P(z)$ because of the non-negative of $P(y, \nabla I_h^T)$, in a simpler form:

$$\hat{z} = \arg\max_z P(y, \nabla I_h^T \mid z) P(z). \tag{6}$$

The formula is equivalent to:

$$\hat{z} = \arg\max_z [\ln P(y, \nabla I_h^T \mid z) + \ln P(z)]. \tag{7}$$

The low quality of the LR frame sets an upper limit to the accuracy of registration, and therefore need to continuously update the SR estimation and registration parameters (Chen and Wang 2012). The purpose of such methods is: based on the observation *y*, construct the maximum posteriori probability of image *z* and

registration parameters *r*. The results $\hat{r}$ and $\hat{z}$ can be estimated using the following form:

$$\begin{aligned}\left(\hat{z},\hat{r}\right) &= \arg\min_{z,r} P(z,r \mid y,\nabla I_h^T) \\ &= \arg\min_{z,r} P(y,\nabla I_h^T \mid z,r)P(z).\end{aligned} \tag{8}$$

This function is equal to minimizing a posteriori energy function $E(z,r \mid y,\nabla I_h^T)$:

$$\begin{aligned}\left(\hat{z},\hat{r}\right) &= \arg\min_{z,r} E(z,r \mid y,\nabla I_h^T) \\ &= \arg\min_{z,r}\{-\log P(y,\nabla I_h^T \mid z,r) - \log P(z)\}.\end{aligned} \tag{9}$$

In this paper, the minimization of the energy function $E(z,r \mid y,\nabla I_h^T)$ is obtained by a gradient descent approach which is called Simultaneous Over Relaxation. During each iteration n, the registration parameters *r* needs to recalibrate:

$$\hat{r}^{n+1} = \arg\min_{r} E(\hat{z}^{n},r \mid y,\nabla I_h^T), \tag{10}$$

$$\hat{z}^{n+1} = \arg\min_{z} E(z,\hat{r}^{n+1} \mid y,\nabla I_h^T). \tag{11}$$

The observed low resolution frames are assumed to be produced by a degradation process which involves warping, blurring, down-sampling performed on the HR frame *z*. Moreover, uncorrelated additive noise is added to each LR frames (Figure 2).

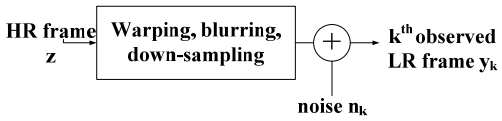

Figure 2: Degradation from HR frame to LR frames

The observation model of the image can be represented as the following formula (Shao and Wei 2007):

$$y_k = \sum_{i=1}^{N} W_i(r_k)z_i + n_k, \forall k = 1,2,...,K. \tag{12}$$

The matrix $W_i(r_k)$ represents the process that HR pixels generate LR pixels by movement, fuzzy and down-sampling, n_k is noise field in frame *k*.

Considering that the noise field is 2D Gaussian sample with variance σ_n^2, then the data likelihood term can be expressed as:

$$\begin{aligned}&P(y \mid z,r) = \prod_{k=1}^{K} P(y_k \mid z,r) = \\ &\prod_{k=1}^{K} \frac{1}{\sqrt{2\pi}\sigma_n} \exp\{-\frac{1}{2\sigma_n^2}(y_k - \sum_{i=1}^{N} W_i(r_k)z_i)^2\}.\end{aligned} \tag{13}$$

MINIMIZATION OF POSTERIOR ENERGY

We use three energy terms to build the energy function. According to the above description, the posterior energy can be expressed as:

$$E(z,r \mid y,\nabla I_h^T) = E_d(y \mid z,r) + E_m(z) + E_g(\nabla I_h \mid \nabla I_h^T) \tag{14}$$

where $E_d(y \mid z,r)$ is the data reconstruction constraints in image domain. $E_m(z)$ is the MRF constraint, characterized by a Gibbs distribution. $E_g(\nabla I_h \mid \nabla I_h^T)$ is a gradient constraint in gradient domain. ∇I_h is the gradient of desired high resolution image, ∇I_h^T is the transformed gradient field.

Gradient constraint requires the gradient of reconstructed high resolution image which should be as similar as the transformed gradient field, expressed as:

$$E_g(\nabla I_h \mid \nabla I_h^T) = \beta \sum_{i=1}^{N} (\nabla I_h - \nabla I_h^T)^2 \tag{15}$$

According to (1) , (13) and(15), the posterior energy can be expressed as:

$$\begin{aligned}E(z,r \mid y,\nabla I_h^T) &= \frac{1}{2\sigma_n^2}\sum_{k=1}^{K}(y_k - \sum_{i=1}^{N} W_i(r_k)z_i)^2 \\ &+ \lambda\sum_{i=1}^{N}\sum_{c\in C} V_c(z_i)/\tau + \beta\sum_{i=1}^{N}(\nabla I_h - \nabla I_h^T)^2,\end{aligned} \tag{16}$$

with derivative:

$$\begin{aligned}\frac{\partial E(z,r \mid y,\nabla I_h^T)}{\partial z_i} &= \frac{1}{\sigma_n^2}\sum_{k=1}^{K}(\sum_{i=1}^{N} W_i(r_k)z_i - y_k)W_i(r_k) \\ &+ \lambda\sum_{i=1}^{N}\sum_{c\in C} V_c'(z_i)/\tau + \beta(\nabla^2 I_h - \nabla^2 I_h^T).\end{aligned} \tag{17}$$

Due to the non-convexity of this function, it will have several local minima. Graduated Non-Convexity (GNC) approach is opted here to minimize the energy function. Initially, we start with a convex approximation of the energy function, denoted by $E^0(z,r \mid y,\nabla I_h^T)$, which contains only one minimum theoretically. The minimum can be obtained using a gradient descent algorithm. Performing the same approach successively to estimate $E^p(z,r \mid y,\nabla I_h^T)$, with $p=\{1,2,...\}$, until the desired form of $E(z,r \mid y,\nabla I_h^T)$ is reached.

The scale parameter τ start from a large value to assure the convexity of $E^0(z,r \mid y,\nabla I_h^T)$. τ is gradually reduced in the iterative process of SOR algorithm. The value of each site *i* at iteration n+1 is updated as the following form:

$$z_i^{n+1} = z_i^n - \omega\frac{1}{T(z_i)}\frac{\partial E(z,r \mid y,\nabla I_h^T)}{\partial z_i}, \tag{18}$$

where $0 < \omega < 2$ is an over-relaxation parameter, $T(z_i)$ is the upper bound of the second derivative of $E(z,r \mid y,\nabla I_h^T)$.

When the following condition is satisfied, the iterative process of *z* is terminated:

$$\frac{\left\|z^n - z^{n-1}\right\|^2}{\left\|z^{n-1}\right\|^2} < 10^{-6}. \tag{19}$$

OBTAINING INITIAL ESTIMATION

Our method described above needs an initial estimate $\hat{z}^0$ of the corresponding HR frame. Existing SR methods usually just choose a simple interpolation of the corresponding LR frame as the initial estimate. Normalized Convolution (NC) is a fast and efficient method to obtain an initial estimation (Katartzis and

Petrou 2007), which can deal with the possible registration errors. A new alternative NC approach is proposed in this article, which considers the existing registration error and wrong pixels in LR frames. We use a non-binary set of certainties, where samples from the reference LR frame get a certainty value of one, whereas samples from other input frames get a positive value p, which reflects the accuracy of the registration method (Figure 4). The value of p is given by:

$$p_i = \beta \frac{m_i}{n}, \tag{20}$$

where n is the frame amount used for registration, m_i is the amount of points obtained from neighboring LR frames via registration, β is a normalization parameter. The sample value at position i is set to the average of all those m_i points (Figure 3).

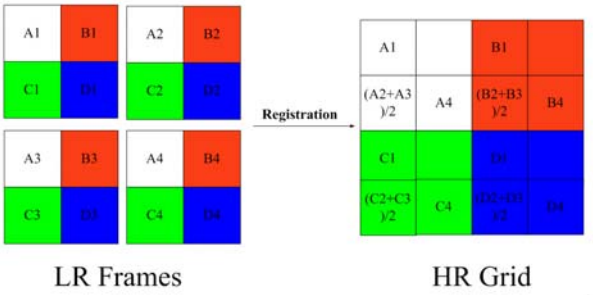

Figure 3: Registration of LR samples in the HR grid

1	0	1	0
1	0.5	1	0.5
1	0	1	0
1	0.5	1	0.5

Figure 4: Certainty matrix of the HR grid in Figure 3

Due to the slowness of applying the higher order NC method , zero-order NC method is used here. Zero-order NC has an feature that can be achieved through simple convolution operations. In the case of zero-order, we can get the following estimation:

$$\hat{z}(x) = \frac{\alpha(x) * (c(x) z(x))}{\alpha(x) * c(x)}, \tag{21}$$

where $0 \le c(x) \le 1$ is the signal certainty matrix, * denoting the convolution operator, $\alpha(x)$ corresponds to an isotropic Gaussian kernel, the size of which equals the support of the considered point spread function.

COMPARATIVE EVALUATIONS

In order to test the effectiveness of the proposed algorithm, we select an image sequence of natural scenes for SR reconstruction experiment. This sequence contains 7 frames in the same scene, with sub-pixel displacement between each other.

We use root mean square error (RMSE) and structural similarity index (SSIM) as quantitative evaluations between the reconstructed image and the corresponding ground truth:

$$RMSE = \sqrt{\frac{\sum_{x=1}^{M}\sum_{y=1}^{N}[f(x,y) - f'(x,y)]^2}{M \times N}} \tag{22}$$

$$SSIM = \frac{(2\mu_x\mu_y + c_1)(2\sigma_{xy} + c_2)}{(\mu_x^2 + \mu_y^2 + c_1)(\sigma_x^2 + \sigma_y^2 + c_2)} \tag{23}$$

The smaller RSME value is the higher similarity of gradation between reconstructed image and corresponding ground truth will be. SSIM value is close to 1 indicating the stronger structural similarity of the two images (Yuan et al. 2010). Good reconstruction results should have low values for RMSE and high values for SSIM.

Super resolution results (upsampling factor is 2) with different methods is showed as below:

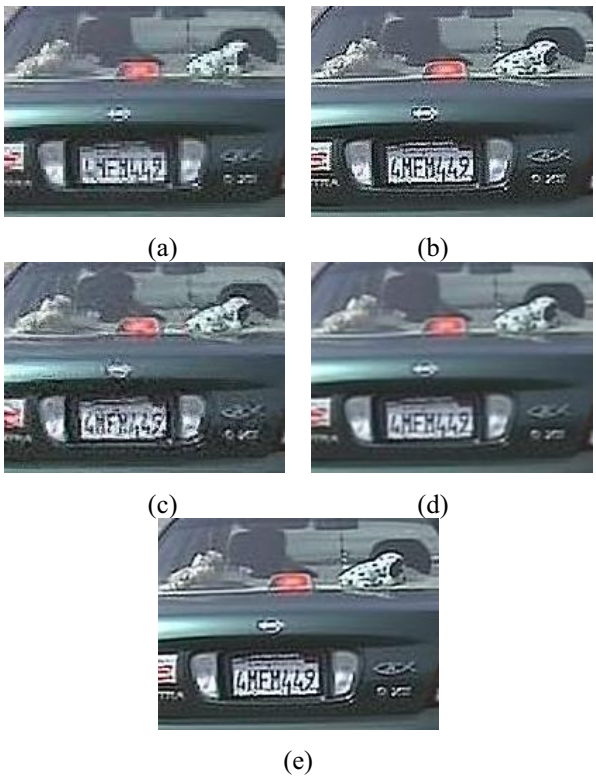

Figure 5: Comparison of super resolution results: (a) neighbor interpolation; (b) POCS method (Blatt and Hero 2006); (c) example based method (Freeman and Liu 2011); (d) MAP method (Zomet and Peleg 2001); (E) proposed method

As can be seen from the experimental results, the results obtained by the proposed method have a better visual effect, the picture becomes clearer, letter recognition becomes easier.

Table 1: Comparison of Reconstructed Image Quantitative Indicators (RMSE/SSIM)

	RMSE	SSIM
Blatt and Hero 2006	25.028	0.741
Freeman and Liu 2011	17.081	0.817
Zomet and Peleg 2001	20.408	0.786
Proposed method	13.994	0.870

Table 1 provides a quantitative assessment of the obtained results. It is evident that the proposed method gives better results, which can be also visually verified by Figure 5.

In short, the proposed method has a better subjective visual result, for quantitative indicators, it has a better gradation similarity and higher structural similarity as well. For video sequences, we can do the similar operation to each frame and get a high resolution video.

CONCLUSION

This paper presents a new Super resolution approach using MAP Estimation, and introduces MRF as prior constraint, using TGF to repair the image fuzzy problem caused by MRF, using a new NC method to obtain a first good approximation, also proposes a reasonable energy function, obtaining the minimum of the posterior energy using gradient descent algorithm. Experimental results on realistic sequence prove that our approach performs well in both qualitative and quantitative aspects. It also shows that the MRF and TGF introduced in this paper can make up their own drawbacks, while mutual interacting, to some extent, will eliminate errors and improve accuracy. The proposed method is a robust MAP approach, can be widely applied to image sequences with translational and rotational motion.

In order to obtain higher quality HR image, the SR reconstruction of the future development need to address the following four aspects: (1) accurate and fast motion estimation algorithm, (2) improving the performance of SR reconstruction algorithm, (3) blind reconstruction problems (Xie et al. 2010), and (4) compressed video SR reconstruction problems. In a word, there still need further study on SR reconstruction methods for its improvement and application.

ACKNOWLEDGMENTS

The work was partially supported by the National Natural Science Foundation of China under Grant 61173096, the Natural Science Foundation of Zhejiang Province, China (Y1110882, Y1110688, R1110679), and the Doctoral Program of Higher Education of China (20113317110001).

REFERENCES

Blatt D, Hero A O. Energy-based sensor network source localization via projection onto convex sets. Signal Processing, IEEE Transactions on, 2006, 54(9): 3614-3619.

Chen S.Y., H. Tong, C. Cattani, "Markov models for image labeling", Mathematical Problems in Engineering, Vol. 2012, Article ID 814356, 2012, 18 pages.

Chen S.Y. and Z.J. Wang, "Acceleration Strategies in Generalized Belief Propagation", IEEE Transactions on Industrial Informatics, Vol. 8, No. 1, 2012, pp. 41-48.

Chen S.Y., J. Zhang, Q. Guan, S. Liu, "Detection and amendment of shape distortions based on moment invariants for active shape models", IET Image Processing, Vol. 5, No.3, April 2011, pp. 273-285.

Freeman W T, Liu C. Markov random fields for super-resolution and texture synthesis. Advances in Markov Random Fields for Vision and Image Processing, 2011.

Hardie R C, Barnad K J, and Amstrong E E. Joint MAP registration and high-resolution image estimation using a sequence of undersampled images. IEEE Transactions on Image Processing, 1997,6 (12):1621-1633.

Jian Sun, Jian Sun, Zongben Xu, Heung-Yeung Shum. Image Super-resolution using Gradient Profile Prior, IEEE Conf. Computer Vision and Pattern Recognition (CVPR), Alaska, USA, 2008.

Kai Xie. Super-resolution Image Restoration Techniques. Beijing Institute of Graphic Communication, 2007,15 (6) :41-44.

Katartzis A, Petrou M. Robust Bayesian Estimation and Normalized Convolution for Super-resolution Image Reconstruction. IEEE Comput. Soc Conf Comput. Vis Pattern Recogn. 2007: 1-7

Lin Haobo, Boyan Chen, Wang J, Song Once Xia. Remote sensing image super-resolution mapping research progress. Journal of Image and Graphics .2011,16 (4) :495-502.

Qiangqiang Yuan, Huanfeng Shen, Pingxiang Li, Liangpei Zhang. Adaptive regularization of multiple images super-resolution reconstruction. Chinese Journal of Image and Graphics, 2010, 15(12): 1720-1727.

Songhua Xie, Li Chen, Hui Nie. Blind super-resolution based on joint interpolation recovery. Computer Applications 2010, 30(2): 0341-0347.

Wenze Shao, Zhihui Wei. Multi-frame image super-resolution reconstruction based on anisotropic MRF modeling. Journal of Software, 2007,18 (10), pp.2434-2444.

Xinming Zhang, Lansun Shen. Super resolution recovery technology development. Measurement and Control Technology, 2002,21 (5) :33-35.

Zomet A, Peleg S. Super-resolution from multiple images having arbitrary mutual motion. Super-Resolution Imaging, 2002: 195-209.

KERNEL-BASED MANIFOLD-ORIENTED STOCHASTIC NEIGHBOR PROJECTION METHOD

Jianwei Zheng, Hong Qiu, Qiongfang Huang, Wanliang Wang and Xinli Xu
School of Computer Science and Technology
Zhejiang University of Technology
310023, Hangzhou, China
E-mail: zjw@zjut.edu.cn

KEYWORDS
Kernel method, Dimensionality reduction, Nonlinear feature extraction, Manifold learning.

ABSTRACT

A new method for performing a nonlinear form of manifold-oriented stochastic neighbor projection method is proposed. By the use of kernel functions, one can operate in the feature space without ever computing the coordinates of the data in that space, but rather by simply computing the inner products between the images of all pairs of data in the feature space. The proposed method is termed as kernel-based manifold-oriented stochastic neighbor projection(KMSNP). By two different strategies, KMSNP is divided into two methods: KMSNP1 and KMSNP2. Experimental results on several databases show that, compared with the relevant methods, the proposed methods obtain higher classification performance and recognition rate.

INTRODUCTION

Kernel-based methods(kernel methods for short) have become a new hot topic in machine learning fields in recent years, their theoretical basis is statistical learning theory. Kernel methods are a class of algorithms for pattern analysis, whose best known element is the support vector machine(SVM) (Dardas and Georganas 2011).The methods skillfully introduce kernel function which not only reduces the curse of dimensionality (Cherchi and Guevara 2012, Xue et al. 2012), but also effectively solves the local minimum and incomplete statistical analysis in traditional pattern recognition methods on the premise of no additional computational capacity. As an availability way to resolve the problem of nonlinear pattern recognition, kernel methods approach the problem by mapping the data into a high-dimensional feature space, where each coordinate corresponds to one feature of the data items, transforming the data into a set of points in a Euclidean space (Chen and Li 2011, Zhang et al. 2008).

The theory of kernel methods can be traced back to 1909, Mercer proposed Mercer's theorem (Mercer 1909) which indicates that any 'reasonable' kernel function corresponds to some feature space. 1964, the use of Mercer's theorem for interpreting kernels as inner products in a feature space was introduced into machine learning by Aizerman et al. (AizermanI et al. 1964), but no sufficient importance has been attached to it. Until 1992, Vapnik et al. (Boser et al. 1992) successfully extended the SVM to the non-linear SVM by using kernel functions, it began to show its potential and advantages. Subsequently, more and more kernel-based methods were presented, such as: kernel principal component analysis(KPCA) (Xiao et al. 2012), kernel fisher discriminator(KFD) (Yang et al. 2005), kernel independent component analysis (KICA) (Zhang et al. 2013), kernel partial least squares(KPLS) (Helander et al. 2012) and so on.

In this paper, we propose to use the kernel idea and present a method called kernel-based manifold-oriented stochastic neighbor projection(KMSNP) method through improving the manifold-oriented stochastic neighbor projection(MSNP) (Wu et al. 2011) technique. MSNP is based on stochastic neighbor embedding(SNE) (Hinton and Roweis 2002) and t-SNE (Maaten and Hinton 2008). The basic principle of SNE is to convert pairwise Euclidean distances into probabilities of selecting neighbors to model pairwise similarities while t-SNE uses student t-distribution to model pairwise dissimilarities in low-dimensional space. Different from SNE and t-SNE, MSNP converts pairwise dissimilarities of inputs to probability distribution related to geodesic distance in high-dimensional space and uses Cauchy distribution to model stochastic distribution of features. Furthermore, it recovers the manifold structure through a linear projection by requiring the two distributions to be similar. Experiments demonstrate MSNP has unique advantages in terms of visualization and recognition task, but there are still two drawbacks in it: firstly, MSNP is an unsupervised method and lack of the idea of class label, so it is not suitable for pattern identification; secondly, since MSNP is a linear feature dimensionality reduction algorithm, it cannot effectively settle the nonlinear feature extraction problem. To overcome the disadvantages of MSNP, we have done some preliminary work. On the first, we introduced the idea of class label and presented a method called discriminative stochastic neighbor embedding analysis(DSNE) (Zheng et al. 2012, Chen

Proceedings 27th European Conference on Modelling and Simulation ©ECMS Webjørn Rekdalsbakken, Robin T. Bye, Houxiang Zhang (Editors)
ISBN: 978-0-9564944-6-7 / ISBN: 978-0-9564944-7-4 (CD)

and Wang 2012). On the second, we think KMSNP can overcome the disadvantage mentioned above well.

The rest of this paper is organized as follows: in Section 2, we provide a brief review of MSNP. Section 3 describes the detailed algorithm derivation of KMSNP. Furthermore, experiments on various databases are presented in Section 4. Finally, we provide some concluding remarks and describe several issues for future works in Section 5.

MSNP

Considering the problem of representing d-dimensional data vectors $\boldsymbol{x}_1, \boldsymbol{x}_2, \ldots, \boldsymbol{x}_N$, by r-dimensional ($r << d$) vectors $\boldsymbol{y}_1, \boldsymbol{y}_2, \ldots, \boldsymbol{y}_N$ such that $\boldsymbol{y}_i$ represents $\boldsymbol{x}_i$. The basic principle of MSNP is to convert pairwise dissimilarity of inputs to probability distribution related to geodesic distance in high-dimensional space, and then using Cauchy distribution to model stochastic distribution of features, finally, MSNP recovers the manifold structure through a linear projection by requiring the two distributions to be similar. Mathematically, the similarity of datapoint $\boldsymbol{x}_i$ to datapoint $\boldsymbol{x}_j$ is depicted as the following joint probability p_{ij} which means $\boldsymbol{x}_i$ how possible to pick $\boldsymbol{x}_j$ as its neighbor:

$$p_{ij} = \frac{\exp(-D_{ij}^{geo} / 2)}{\sum_{k \neq i} \exp(-D_{ik}^{geo} / 2)} \tag{1}$$

where D_{ij}^{geo} is the geodesic distance for $\boldsymbol{x}_i$ and $\boldsymbol{x}_j$. In practice, MSNP calculates geodesic distance by using a two-phase method (Wu et al. 2011). Firstly, an adjacency graph G is constructed by K-nearest neighbor strategy. Secondly, the desired geodesic distance is approximated by the shortest path of graph G. This procedure is proposed in Isomap to estimate geodesic distance and the detail calculation steps can be found in (Tenenbaum et al. 2000).

For low-dimensional representations, MSNP employs Cauchy distribution with γ degree of freedom to construct joint probability q_{ij}. The probability q_{ij} indicates how possible point i and point j can be stochastic neighbors is defined as:

$$q_{ij} = \frac{\left[\pi\gamma(1 + \left\| \frac{\boldsymbol{y}_i - \boldsymbol{y}_j}{\gamma} \right\|) \right]^{-1}}{\sum_{k \neq l} \left[\pi\gamma(1 + \left\| \frac{\boldsymbol{y}_k - \boldsymbol{y}_l}{\gamma} \right\|) \right]^{-1}} \tag{2}$$

where γ is the freedom degree parameter of Cauchy distribution and through a linear projection: $\boldsymbol{y}_i = \mathbf{A}\boldsymbol{x}_i$ ($\mathbf{A} \in \mathbf{R}^{r \times d}$), formula (2) can be formulated as:

$$q_{ij} = \frac{\left[\gamma^2 + d_{ij}^{\,2}(\mathbf{A}) \right]^{-1}}{\sum_{k \neq l} \left[\gamma^2 + d_{ij}^{\,2}(\mathbf{A}) \right]^{-1}} \tag{3}$$

In formula (3), $d_{ij}(\mathbf{A}) = \left\| \boldsymbol{y}_i - \boldsymbol{y}_j \right\| = \left\| \mathbf{A}\boldsymbol{x}_i - \mathbf{A}\boldsymbol{x}_j \right\| = \sqrt{(\boldsymbol{x}_i - \boldsymbol{x}_j)^{\mathrm{T}} \mathbf{A}^{\mathrm{T}} \mathbf{A} (\boldsymbol{x}_i - \boldsymbol{x}_j)}$ is the Euclidian distance between two samples $\boldsymbol{x}_i$ and $\boldsymbol{x}_j$.

MSNP finds the optimal low-dimensional representations for matching p_{ij} and q_{ij} to the greatest extent. This is achieved by minimizing the following penalty function, which is the sum of Kullback–Leibler divergences measuring the difference between two probability distributions:

$$C_i(\mathbf{A}) = KL(P_i \,||\, Q_i) = \sum_{j \neq i} p_{ij} \log \frac{p_{ij}}{q_{ij}} \tag{4}$$

MSNP calculates the optimal low-dimensional representation $\mathbf{A}$ by minimizing $C(\mathbf{A})$ overall datapoints with a gradient descent search, i.e.:

$$\min C(\mathbf{A}) = \sum_{i,j} p_{ij} \log \frac{p_{ij}}{q_{ij}} \tag{5}$$

ALGORITHM DERIVATION OF KMSNP

Obviously, MSNP is a linear feature dimensionality reduction algorithm and has unique advantages in terms of visualization and recognition task, but it cannot effectively settle the nonlinear feature extraction problem. So the remainder of this section is devoted to extend MSNP to a nonlinear scenario using techniques of kernel methods.

Let kernel function κ defines the inner product in an embedding high dimensional space F with the associated nonlinear map $\varphi(\boldsymbol{x})$: $R^d \rightarrow F$:

$$\kappa(\boldsymbol{x}_i, \boldsymbol{x}_j) = \langle \varphi(\boldsymbol{x}_i), \varphi(\boldsymbol{x}_j) \rangle \tag{6}$$

which allows us to compute the value of the inner product in F without having to carry out the map.

It should be noted that we use φ_i to denote $\varphi(\boldsymbol{x}_i)$ for brevity in the following. Next, we express the transformation $\mathbf{A}$ with:

$$\mathbf{A} = \left[\sum_{i=1}^{N} b_i^{(1)} \varphi_i, \ldots, \sum_{i=1}^{N} b_i^{(r)} \varphi_i \right]^{\mathrm{T}} \tag{7}$$

We define $\mathbf{B} = \left[b^{(1)}, \ldots, b^{(r)} \right]^{\mathrm{T}}$ and $\mathbf{\Phi} = \left[\varphi_1, \ldots, \varphi_N \right]^{\mathrm{T}}$, then $\mathbf{A} = \mathbf{B}\mathbf{\Phi}$. Based on above definition, the Euclidian distance between two samples $\boldsymbol{x}_i$ and $\boldsymbol{x}_j$ in the embedding space F can be formulated as:

$$
\begin{aligned}
& d_{ij}^{F}(\mathbf{A}) \\
&= \left\| \mathbf{A}(\varphi_i - \varphi_j) \right\| = \left\| \mathbf{B}\boldsymbol{\Phi}(\varphi_i - \varphi_j) \right\| \\
&= \left\| \mathbf{B}(K_i - K_j) \right\| = \sqrt{(K_i - K_j)^{\mathrm{T}} \mathbf{B}^{\mathrm{T}} \mathbf{B}(K_i - K_j)}
\end{aligned} \tag{8}
$$

where $K_i = \left[\kappa(\boldsymbol{x}_1, \boldsymbol{x}_i), ..., \kappa(\boldsymbol{x}_N, \boldsymbol{x}_i)\right]^{\mathrm{T}}$ is a column vector. It is clear that the distance in the kernel embedding space is related to a kernel function and the matrix **B**.

In this section, we propose two methods to construct the objective function. The first strategy is to parameterize the objective function by the matrix **B**. Firstly, we replace $D_{ij}^{geo\,F}$ with D_{ij}^{geo} in formula (1) and $d_{ij}(\mathbf{A})$ with $d_{ij}^{F}(\mathbf{A})$ in formula (3) so that p_{ij}^{1}, q_{ij}^{1} which are defined to be applied in the embedding high dimensional space F can be written as:

$$
p_{ij}^{1} = \frac{\exp(-D_{ij}^{geo^F} / 2)}{\sum_{k \neq i} \exp(-D_{ik}^{geo^F} / 2)} \tag{9}
$$

$$
q_{ij}^{1} = \frac{\left[\gamma^2 + (d_{ij}^{F}(\mathbf{A}))^2\right]^{-1}}{\sum_{k \neq l} \left[\gamma^2 + (d_{kl}^{F}(\mathbf{A}))^2\right]^{-1}} \tag{10}
$$

By simple algebra formulation, formula (10) can be formulated as:

$$
q_{ij}^{1} = \frac{\left[\gamma^2 + (K_i - K_j)^{\mathrm{T}} \mathbf{B}^{\mathrm{T}} \mathbf{B}(K_i - K_j)\right]^{-1}}{\sum_{k \neq l} \left[\gamma^2 + (K_t - K_l)^{\mathrm{T}} \mathbf{B}^{\mathrm{T}} \mathbf{B}(K_t - K_l)\right]^{-1}} \tag{11}
$$

Then, we denote $C(\mathbf{B})$ by modifying $C(\mathbf{A})$ via substituting **A** with **B** into the regularization term of formula (5). In this work, we use the conjugate gradient method to minimize $C(\mathbf{B})$ as in (Wu et al. 2011). In order to make the derivation less cluttered, we first define two auxiliary variables w_{ij} and u_{ij} as:

$$
w_{ij} = [\gamma^2 + (K_i - K_j)^{\mathrm{T}} \mathbf{B}^{\mathrm{T}} \mathbf{B}(K_i - K_j)]^{-1} \tag{12}
$$

$$
u_{ij} = (p_{ij}^{1} - q_{ij}^{1}) w_{ij} \tag{13}
$$

Afterwards differentiating $C(\mathbf{B})$ with respect to the matrix **B** gives the following gradient, which we adopt for learning:

$$
\begin{aligned}
& \frac{dC(\mathbf{B})}{d(\mathbf{B})} = \sum_{i,j} \frac{p_{ij}^{1}}{q_{ij}^{1}} (q_{ij}^{1})' \\
&= 2\mathbf{B}[\sum_{i,j} p_{ij} \frac{(K_i - K_j)(K_i - K_j)^{\mathrm{T}}}{\gamma^2 + (K_i - K_j)^{\mathrm{T}} \mathbf{B}^{\mathrm{T}} \mathbf{B}(K_i - K_j)}] \\
&-2\mathbf{B}[\sum_{i,j} p_{ij}^{1} \frac{\sum_{k \neq l} (\gamma^2 + (K_k - K_l)^{\mathrm{T}} \mathbf{B}^{\mathrm{T}} \mathbf{B}(K_k - K_l))^{-2}}{\sum_{k \neq l} (\gamma^2 + (K_k - K_l)^{\mathrm{T}} \mathbf{B}^{\mathrm{T}} \mathbf{B}(K_k - K_l))^{-1}} \\
&\quad \frac{(K_k - K_l)(K_k - K_l)^{\mathrm{T}}}{\sum_{k \neq l} (\gamma^2 + (K_k - K_l)^{\mathrm{T}} \mathbf{B}^{\mathrm{T}} \mathbf{B}(K_k - K_l))^{-1}}] \\
&= 2\mathbf{B}[\sum_{i,j} p_{ij}^{1} w_{ij} (\boldsymbol{x}_i - \boldsymbol{x}_j)(\boldsymbol{x}_i - \boldsymbol{x}_j)^{\mathrm{T}} \\
&\quad - \sum_{k \neq l} q_{kl}^{1} w_{kl} (\boldsymbol{x}_k - \boldsymbol{x}_l)(\boldsymbol{x}_k - \boldsymbol{x}_l)^{\mathrm{T}}] \\
&= 2\mathbf{B} \sum_{i,j} u_{ij} (K_i - K_j)(K_i - K_j)^{\mathrm{T}}
\end{aligned} \tag{14}
$$

Let **U** be the N order matrix with element u_{ij}. Note that **U** is a symmetric matrix; therefore, **D** can be defined as a diagonal matrix that each entry is column(or row) sum of **U**, i.e., $\mathbf{D}_{ii} = \sum_j \mathbf{U}_{ij}$. With this definition, the gradient expression (14) can be reduced to:

$$
\begin{aligned}
\frac{dC(\mathbf{B})}{d(\mathbf{B})} &= 2\mathbf{B} \sum_{i,j} u_{ij} (K_i - K_j)(K_i - K_j)^{\mathrm{T}} \\
&= 2\mathbf{B}(\sum_{i,j} u_{ij} K_i K_i^{\mathrm{T}} + \sum_{i,j} u_{ij} K_j K_j^{\mathrm{T}} \\
&\quad - \sum_{i,j} u_{ij} K_i K_j^{\mathrm{T}} - \sum_{i,j} u_{ij} K_j K_i^{\mathrm{T}}) \\
&= 4\mathbf{B}(\mathbf{K}\mathbf{D}\mathbf{K}^{\mathrm{T}} - \mathbf{K}\mathbf{U}\mathbf{K}^{\mathrm{T}})
\end{aligned} \tag{15}
$$

Once the gradient is calculated, our optimal problem can be solved by an iterative procedure based on the conjugate gradient method. For convenience, we name this kernel method as KMSNP1. The description of KMSNP1 algorithm can be given by:

Step1. Make sure the sample matrix **X** and the kernel function, set K-nearest neighborhood parameter k(for geodesic distance), Cauchy distribution parameter γ and the maximum iteration times Mt.

Step2. Compute geodesic distance $D_{ij}^{geo\,F}$ between two samples $\boldsymbol{x}_i$ and $\boldsymbol{x}_j$ on **X**, compute the joint probability p_{ij}^{1} by utilizing formula (9).

Step3. Set t=1 : Mt, we search for the solution in loop: firstly, compute the joint probability q_{ij}^{1} by utilizing formula (11); then, compute gradient $dC(\mathbf{B})/d(\mathbf{B})$ by utilizing formula (15); finally, update $\mathbf{B}^t$ based on $\mathbf{B}^{t-1}$ by conjugate gradient operation.

Step4. Judge whether C^t-C^{t-1}<ε (in this paper, we take ε=1e-7) converges to a stable solution or t reaches the maximum value Mt; If these prerequisites are met, Step5 are performed, otherwise we repeat Step3.

Step5. output $\mathbf{B} = \mathbf{B}^t$.

Another strategy is that we let $C^F(\mathbf{A})$ be the objective function in the embedding space F. Its gradient can be written as:

$$
\begin{aligned}
& \frac{dC^F(\mathbf{A})}{d(\mathbf{A})} = \sum_{i,j} \frac{p_{ij}^{1}}{q_{ij}^{1}} (q_{ij}^{1})' \\
&= -2[\sum_{i,j} p_{ij}^{1} \frac{\mathbf{B}(K_i - K_j)(\boldsymbol{\varphi}_i - \boldsymbol{\varphi}_j)^{\mathrm{T}}}{\gamma^2 + (\mathbf{B}(K_i - K_j))^{\mathrm{T}} \mathbf{B}(K_i - K_j)}]
\end{aligned}
$$

$$
\begin{aligned}
&+2[\sum_{i,j} p_{ij}^{\,1} \frac{\sum_{k\neq l}(\gamma^2+(\mathbf{B}(K_k-K_l))^{\mathrm{T}}\mathbf{B}(K_k-K_l))^{-2}}{\sum_{k\neq l}(\gamma^2+(\mathbf{B}(K_k-K_l))^{\mathrm{T}}\mathbf{B}(K_k-K_l))^{-1}} \\
&\frac{\mathbf{B}(K_k-K_l)(\boldsymbol{\varphi}_k-\boldsymbol{\varphi}_l)^{\mathrm{T}}}{\sum_{k\neq l}(\gamma^2+(\mathbf{B}(K_k-K_l))^{\mathrm{T}}\mathbf{B}(K_k-K_l))^{-1}}] \\
&=-2[\sum_{i,j} p_{ij}^{\,1} \frac{\mathbf{B}Q_{ij}^{(K_i-K_j)}\boldsymbol{\Phi}}{\gamma^2+(\mathbf{B}(K_i-K_j))^{\mathrm{T}}\mathbf{B}(K_i-K_j)}] \\
&+2[\sum_{i,j} p_{ij}^{\,1} \frac{\sum_{k\neq l}(\gamma^2+(\mathbf{B}(K_k-K_l))^{\mathrm{T}}\mathbf{B}(K_k-K_l))^{-2}}{\sum_{k\neq l}(\gamma^2+(\mathbf{B}(K_k-K_l))^{\mathrm{T}}\mathbf{B}(K_k-K_l))^{-1}} \\
&\frac{\mathbf{B}Q_{kl}^{(K_k-K_l)}\boldsymbol{\Phi}}{\sum_{k\neq l}(\gamma^2+(\mathbf{B}(K_k-K_l))^{\mathrm{T}}\mathbf{B}(K_k-K_l))^{-1}}] \\
&=-2\left[\sum_{i,j} p_{ij}^{\,1} w_{ij}\mathbf{B}Q_{ij}^{(K_i-K_j)}-\sum_{i,j} q_{kl}^{\,1} w_{kl}\mathbf{B}Q_{kl}^{(K_k-K_l)}\right]\boldsymbol{\Phi}
\end{aligned}
\qquad (16)
$$

in this form, $Q_{ij}^{(K_i-K_j)}$ can be regard as the $N\times N$ matrix with vector K_i-K_j in the ith column, vector K_j-K_i in the jth column and the other columns are all zeros.

This method is called KMSNP2. Note that $\boldsymbol{\Phi}$ is a constant matrix, furthermore, the observations of formula (16) make us know that updating the matrix $\mathbf{A}$ in the optimization only means updating the matrix $\mathbf{B}$. More important, $\boldsymbol{\Phi}$ does not need to compute since $d_{ij}^{F}(\mathbf{A})$ only depend upon $\mathbf{B}$, K_i and K_j. Therefore, we don't need to explicitly perform the nonlinear map $\varphi(\boldsymbol{x})$ to minimize the objective function $C^{F}(\mathbf{A})$. The description of KMSNP2 algorithm is the same as that of KMSNP1, except for Step3. The Step3 in KMSNP2 should be described as: set t=1 : Mt, we search for the solution in loop: firstly, compute the joint probability $q_{ij}^{\,1}$ by utilizing formula (11); then, compute gradient $d_{ij}^{F}(\mathbf{A})/d(\mathbf{A})$ by utilizing formula (16); finally, update $\mathbf{B}^{t}$ based on $\mathbf{B}^{t-1}$ by conjugate gradient operation. Additionally, the computational complexity of KMSNP1 and KMSNP2 is respectively $O(2rN^2+rNK)$ and $O(2rKN+rN^2)$ in each iteration. Hence, it is obviously that KMSNP2 is faster than KMSNP1 during each iteration.

EXPERIMENTS

In this section, we evaluate the effectiveness of our KMSNP1 and KMSNP2 methods for feature extraction. Several experiments are carried out on U.S. Postal Service (USPS) and ORL face databases to demonstrate their good behavior on classification performance and recognition task. Moreover, the Gaussian RBF kernel $\kappa(\boldsymbol{x}, \boldsymbol{x}') = \exp(-\| \boldsymbol{x} - \boldsymbol{x}' \|^2/2\sigma^2)$ is chosen as the kernel function of KMSNP1 and KMSNP2, where σ is set as the variance of the training sample set of $\mathbf{X}$.

USPS and ORL databases

The databases used in our experiments are summarized as follows:

USPS includes 10 digit characters and 1100 samples in total. The original data format is of 16 x 16 pixels. Figure 1 shows samples of the cropped images from USPS handwritten digits database.

Figure 1: Samples of the cropped images from USPS handwritten digits database.

ORL consists of gray images of faces from 40 distinct subjects, with 10 pictures for each subject. For every subject, the images were taken with varied lighting condition and different facial expressions. The original size of each image is 112 x 92 pixels, with 256 gray levels per pixel. Figure 2 illustrates a sample subject of ORL database.

Figure 2: Sample face images from ORL database.

Visualization using KMSNP1 and KMSNP2

In this subsection, we focus on the classification performance of the proposed methods which are compared with that of the relevant algorithms, including MSNP (Wu et al. 2011), SNE (Hinton and Roweis 2002), t-SNE (Maaten and Hinton 2008) and DSNE (Zheng et al. 2012). The experiments are carried out respectively on USPS and ORL databases. For the sake of computational efficiency as well as noise filtering, we first adjust the size of each image to 32 x 32 pixels on ORL, and then we select fourteen samples from each class on USPS and five samples from each class on ORL.

The experimental procedure is to extract a 20-dimensional feature for each image by SNE, t-SNE, DSNE, MSNP, KMSNP1 and KMSNP2, respectively; then to evaluate the quality of features through visual presentation of the first two-dimensional feature. The parameters are set as: the local neighbor parameter of all the methods is k=15; for MSNP, KMSNP1 and KMSNP2, the degree freedom of Cauchy distribution is γ=4 and the iteration number is Mt =1000; for DSNE, the perplexity parameter is λ=0.1 and the iteration number is 1000 as well; for SNE and t-SNE, the perplexity parameter is $perp$=20 and the iteration number is the same as DSNE.

Figure 3 and Figure 4 show the visual presentation results of the methods mentioned above on USPS and ORL databases. The visual presentation is represented as a scatterplot in which different color determines different class information. The figures reveal that

KMSNP1 and KMSNP2 give considerably better classification result than SNE, t-SNE, DSNE, and MSNP on all databases, for the separation between classes are quite obvious. In particular, it is clearly observed that though DSNE provides much better insight into the manifold structure, the clustering qualities and separation degree of KMSNP1 and KMSNP2 scatterplots are obviously better than the one of DSNE; for MSNP, it has smaller intra-class scatter, but exists overlapping phenomenon among classes; SNE and t-SNE not only get less separation for the inter-class data but also produce larger intra-class scatter, so, it is difficulty to find obvious manifold structure from their results. With regard to KMSNP1 and KMSNP2, we can find from the figures that KMSNP1 shows the best classification performance among all the algorithms on ORL face database, while not on the other database, thereinto, the classification performance of KMSNP1 is inferior to KMSNP2 on USPS.

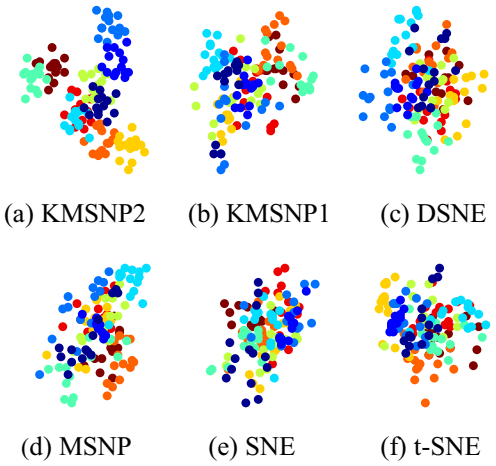

(a) KMSNP2 (b) KMSNP1 (c) DSNE

(d) MSNP (e) SNE (f) t-SNE

Figure 3: Visualization of 140 images from USPS handwritten digits database.

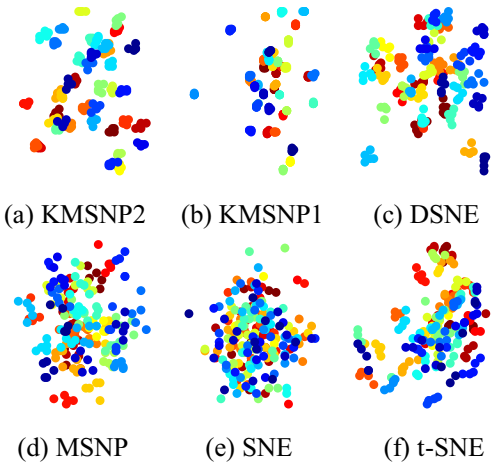

(a) KMSNP2 (b) KMSNP1 (c) DSNE

(d) MSNP (e) SNE (f) t-SNE

Figure 4: Visualization of 200 face images from ORL faces database.

Recognition using KMSNP1 and KMSNP2

In this subsection, we apply KMSNP1 and KMSNP2 to recognition task to verify their feature extraction capability. We compare the performance with MSNP, since it was proved to be better than existing feature extraction algorithms such as SNE, t-SNE and so on in Ref. (Wu et al. 2011). The procedure of recognition is designed as follows: firstly, divide dataset into training sample set $\mathbf{X}_{\text{train}}$ and testing sample set $\mathbf{X}_{\text{test}}$ randomly; secondly, the training process for the optimal matrix $\mathbf{A}$ or $\mathbf{B}$ is taken for MSNP, KMSNP1 and KMSNP2; thirdly, feature extraction is accomplished for all samples using $\mathbf{A}$ or $\mathbf{B}$; finally, a testing image is identified by a nearest neighbor classifier. The freedom degree γ of Cauchy distribution in MSNP is determined by cross validation and the maximum number of iterations is set to be 1000. Let l denotes the number of training samples in each class, we set the K-nearest neighborhood parameter k in MSNP, KMSNP1 and KMSNP2 as $k = l\text{-}1$.

Figure 5 is the results of the experiment in USPS ((a):l=14, (b):l=25), and Figure 6 shows the recognition rate versus subspace dimension on ORL ((a):l=3, (b):l=5). The maximal recognition rate of each method and the corresponding dimension are given in Table 1, where the number in bold stands for the highest recognition rate. From Table 1, we can find that KMSNP1 and KMSNP2 outperform MSNP on USPS and ORL. Obviously, KMSNP2 gives better recognition task than KMSNP1 on USPS while the result is just on the contrary on ORL. That means the performances of KMSNP1 and KMSNP2 vary with databases. Besides, KMSNP1 and KMSNP2 achieve considerable recognition accuracy when feature dimension is 10 on USPS and 20 on ORL. It indicates that KMSNP1 and KMSNP2 grasp the key character of face images relative to identification with a few features. From the nature of dimensional reduction, this result demonstrates that MSNP is inferior to KMSNP1 and KMSNP2.

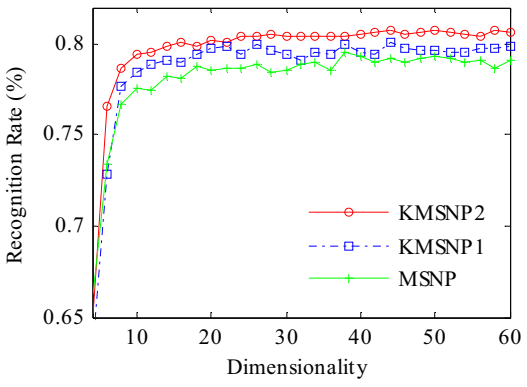

(a) l=14

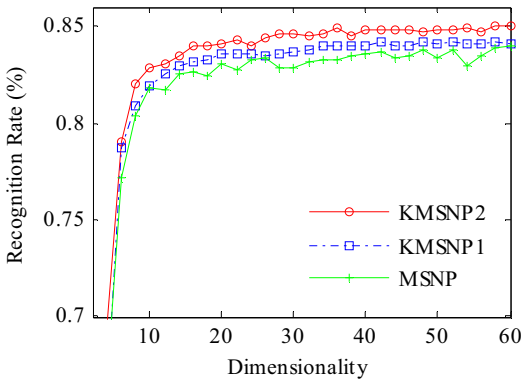

(b) l=25

Figure 5: Recognition rate (%) versus subspace dimension on USPS. (a) l=14. (b) l=25

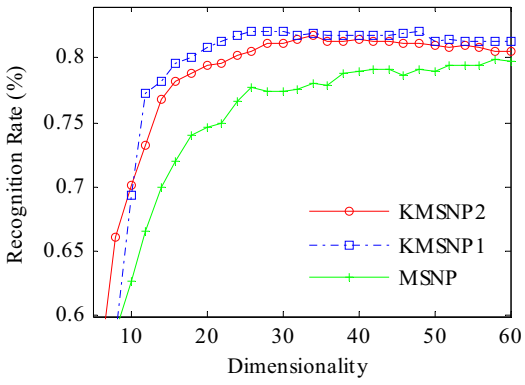

(a) l=3

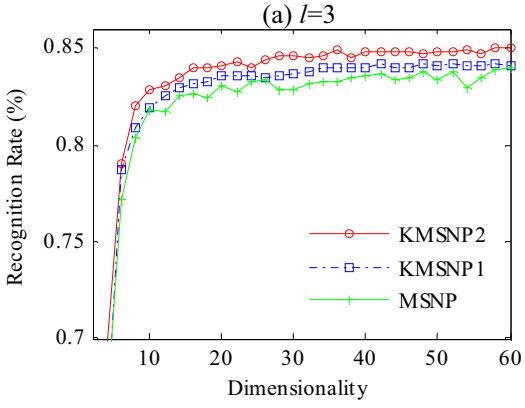

(b) l=5

Figure 6: Recognition rate (%) versus subspace dimension on ORL. (a) l=3. (b) l=5

Table 1: The maximal recognition rates(%) of algorithms versus the dimensions on USPS and ORL

	USPS l =14	USPS l =25	ORL l =3	ORL l =5
MSNP	0.7958 (38)	0.8395 (58)	0.7989 (59)	0.8690 (58)
KMSNP1	0.8007 (44)	0.8422 (42)	**0.8206 (28)**	**0.8825 (34)**
KMSNP2	**0.8077 (58)**	**0.8503 (60)**	0.8170 (34)	0.8780 (40)

CONCLUSION AND FUTURE WORK

On the basis of MSNP, we present a method called kernel-based manifold-oriented stochastic neighbor projection(KMSNP), we extend MSNP to a nonlinear scenario using techniques of kernel methods and present two kernel-based methods by two different strategies: KMSNP1 and KMSNP2. In this paper, it has been shown that the proposed methods may result in performance comparable with the previously used classification methods. Experimental results on USPS and ORL databases demonstrate the superior performance of the proposed methods. Our future work might consider class label information in the feature extraction. We believe that the labeled samples are of great value for classification purpose and recognition task. Therefore, supervised extension of KMSNP may result in more effective features for pattern recognition task. We are currently exploring these problems in theory and practice.

REFERENCES

AizermanI, M.A.; E.M. Braverman; and L.I. Rozonoer. 1964. "Theoretical Foundations of the Potential Function Method in Pattern Recognition Learning." *Automation and Remote Control*, No.6 (Apr), 821-837.

Boser, B.; I. Guyon; and V. Vapnik. 1992. "A Training Algorithm for Optimal Margin Classifiers." *In Proc. Annual Conf. Computational Learning Theory* (D. Haussler, ed.). ACM Press, Pittsburgh, 144-152.

Chen, S.Y. and Y.F. Li, "Determination of Stripe Edge Blurring for Depth Sensing", IEEE Sensors Journal, Vol. 11, No. 2, Feb. 2011, pp. 389-390.

Chen, S.Y. and Z.J. Wang, "Acceleration Strategies in Generalized Belief Propagation", IEEE Transactions on Industrial Informatics, Vol. 8, No. 1, 2012, pp. 41-48.

Cherchi, E. and C.A. Guevara. 2012. "A Monte Carlo experiment to analyze the curse of dimensionality in estimating random coefficients models with a full variance–covariance matrix." *Transportation Research Part B: Methodological*, No.2 (Feb), 321-332.

Dardas, N.H. and N.D. Georganas. 2011. "Real-Time Hand Gesture Detection and Recognition Using Bag-of-Features and Support Vector Machine Techniques." *Instrumentation and Measurement, IEEE Transactions on*, No.11 (Aug), 3592-3607.

Hinton, G.; and S. Roweis. 2002. "Stochastic neighbor embedding." *Advances in neural information processing systems* No.15 (Dec), 833-840.

Helander, E.; T. Virtanen; and M. Gabbouj. 2012. "Voice Conversion Using Dynamic Kernel Partial Least Squares Regression." *Audio, Speech, and Language Processing, IEEE Transactions on*, No.3 (Mar), 806-817.

Mercer, J. 1909. "Functions of Positive and Negative Type, and their Connection with the Theory of Integral Equations." *Philosophical Transactions of the Royal Society of London. Series A. Containing Papers of a Mathematical or Physical Character*, No.209 (Jan), 415-446.

Maaten, L.; and G. Hinton. 2008. "Visualizing data using t-SNE." *Journal of Machine Learning Research*, No.9 (Aug), 2579-2605.

Tenenbaum, J.B.; V. de Silva; and J.C. Langford. 2000. “A global geometric framework for nonlinear dimensionality reduction.” *Science*, No.290 (Aug), 2319-2323.

Wu, S.; Sun, M.; and Yang, J. 2011. “Stochastic neighbor projection on manifold for feature extraction.” *Neurocomputing*, No.17 (Oct), 2780-2789.

Xiao, Y.; H. Wang; W. Xu; and J. Zhou. 2012. “L1 norm based KPCA for novelty detection.” *Pattern Recognition*, NO.1 (Oct), 389-396.

Xue, J., et al., "Bound Maxima as a Traffic Feature under DDOS Flood Attacks", Mathematical Problems in Engineering, Vol. 2012, Article ID 419319, 2012, 20 pages.

Yang, J. et al. 2005. “KPCA plus LDA: a complete kernel fisher discriminant framework for feature extraction and recognition.” *Pattern Analysis and Machine Intelligence, IEEE Transactions on*, No.2 (Mar), 230-244.

Zhang, J., et al., "Normalized weighted shape context and its application in feature-based matching", Optical Engineering, Vol. 47, No. 9, Sep. 2008, 097201.

Zheng, J.; H. Qiu; Y. Jiang; and W. Wang. 2012. “Discriminative Stochastic Neighbor Embedding Analysis Method.” *Computer-Aided Design & Computer Graphics,* No.11 (Nov), 1477-1484.

Zhang, Y.; J. An; and H. Zhang. 2013. “Monitoring of time-varying processes using kernel independent component analysis.” *Chemical Engineering Science*, No.0 (Jan), 23-32.

AUTHOR BIOGRAPHIES

JianWei Zheng was born in Shengzhou, China and went to the Zhejiang University of Technology, where he studied computer science and technology and obtained his doctor degree in 2010. Now he is a lecturer of the Zhejiang University of Technology and his research interest covers machine learning and feature extraction. As a researcher, he has spirit of innovation and yielded some achievements in scientific research. His e-mail address is : zjw@zjut.edu.cn

Hong Qiu was born in Ningbo, China and went to the Zhejiang University of Technology, where she studied computer science and technology and obtained her undergraduate degree in 2012. Now she is a master student at Zhejiang University of Technology. Her research interest covers image processing and machine learning. She has a practical and realistic attitude towards science. Her e-mail address is : qh@stu.zjut.edu.cn

Qiongfang Huang was born in Zunyi, China and went to the Zhejiang University of Technology, where she studied computer science and technology and obtained her undergraduate degree in 2013. Now she is a master student at Zhejiang University of Technology. Her research interest covers image processing and machine learning. She has a great passion towards her major. Her e-mail address is : gdhqf@sina.cn

Wanliang Wang was born in Jiangshu, China and went to the TongJi University, where he studied control theory and control engineering and obtained his doctor degree in 2001. He has devoted nearly 20 years to educational work and now he is the dean of School of Computer Science and Technology at the Zhejiang University of Technology. As a researcher, he is leading a large research group in the field of simulation for small hydropower projects and many valuable achievements have made. His research interest covers intelligent algorithms and network control. His e-mail address is : wwl@zjut.edu.cn

Xinli Xu was born in Yuyao, China and went to the Zhejiang University of Technology, where she studied control theory and control engineering and obtained her doctor degree in 2003. Now she is an associate professor of the Zhejiang University of Technology and her research interest covers scheduling optimization, network science. Her e-mail address is : xxl@zjut.edu.cn

DISCRETE POINT CLOUD FILTERING AND SEARCHING BASED ON VGSO ALGORITHM*

Fengjun Hu
Key Lab of E&M Ministry of
Education & Zhejiang Province
Zhejiang University of Technology
Institute of Information Technology
Zhejiang Shuren University
Hangzhou 310032,China
E-mail: jainism@msn.com

Yanwei Zhao
Wanliang Wang
Xianping Huang
Key Lab of E&M Ministry of
Education & Zhejiang Province
Zhejiang University of Technology
Hangzhou 310032,China
E-mail: zyw@zjut.edu.cn

KEYWORDS
Discrete point cloud, point cloud filtering, KD-Tree, nearest neighbor searching, voxel grid.

ABSTRACT

The massive point cloud data obtained through the computer vision is uneven in density together with a lot of noise and outliers, which will greatly reduce the point cloud search efficiency and affect the surface reconstruction. Based on that, this paper presents a filtering algorithm based on Voxel Grid Statistical Outlier (VGSO): Firstly, 3D voxel grid is created for the massive point cloud data approximating other points inside the voxel with the centroid of all points; then, the neighborhood of discrete points is analyzed statistically, calculating average distance of every point to its neighboring points and filtering the outliers outside the reference ranges of average distance from the data set; finally, the segmentation rules are improved according to the characteristics of KD-Tree. A large amount of experimental results show that this stable and reliable algorithm can compress and filter the point cloud data quickly and effectively. At the same time, it greatly accelerates the search speed.

RELATED WORKS

With the development of high precision laser scanning device and the computer vision technology(Chen et al.2008; Chen and Li.2004), point cloud technology has been widely used in surface reconstruction and three-dimensional simulation etc. But the huge point cloud data collected are very dense, and usually not very uniform because of the interference factors with the superposition of many outliers and noises, which will seriously affect the subsequent work, such as point cloud data search or 3D reconstruction process. Filtering for point cloud data mainly includes the algorithms based on mathematical morphology, the triangulation, wavelet transform etc. Zhang(Zhang et al.2003)proposed a method of morphological filtering method based on incremental window scale which firstly interpolates the point cloud data to be regular grid data, and then uses the assumed initial structure window and threshold for opening operation. Sithole(Sithole.2001)resampled the discrete point cloud to generate regular grid data and then filtered using the method of image processing. This method is superior in terms of processing speed, and can make use of mature image processing theory. The shortcomings are yet the need of interpolation and resampling for the point cloud data, which will lose some accuracy. Jiang(Jiang et al.2007)used Delaunay or KD-tree method to organize the discrete point cloud. It has relatively high accuracy due to the processing of primitive point cloud without resampling and interpolation. But the filtering algorithm in this way is relatively complex with low efficiency.

Domestic and foreign scholars have studied the identification and filtering of outliers of the discrete point cloud. Recognition methods of outlier (Papadimitriou et al.2003) are mainly based on depth, distribution, distance and density (Xu et al.2008). Method based on depth proposed by Johnson (Johnson et al.1998) required to calculate the convex body of point cloud in different levels, with high computational complexity. Knorr(Knorr et al.2000) defined the outliers belonging to none of the point sets. This method cannot calculate the recognition results of optimal outlier.

Breunig (Breunig et al.2000) put forward Local Outlier Factor which can deal with general scattered point cloud data and must first estimate outlier density according to the point cloud density change. These references about filtering algorithm are mostly based on the point cloud data acquired from Lidar. However, domestic and foreign research on he point cloud data based on computer vision is still in its infancy stage domestic and foreign. (Chen et al.2012).

Due to the above question, this paper put forward a filtering algorithm based on VGSO. Firstly, 3D voxel grid is created for the mass point cloud data with the

* Corresponding author. Tel: +86 57188320717; Fax: +86 57188320130.
E-mail address: zyw@zjut.edu.cn

Proceedings 27th European Conference on Modelling and Simulation ©ECMS Webjørn Rekdalsbakken, Robin T. Bye, Houxiang Zhang (Editors)
ISBN: 978-0-9564944-6-7 / ISBN: 978-0-9564944-7-4 (CD)

centroid of all points to approximate other points inside the voxel and sampling can greatly reduce the point cloud density and homogenize the point cloud density; then, statistical analysis is carried out on the discrete points, calculating average distance of all neighboring points to every point, and filtering the outliers outside the reference ranges of average distance from the data set; finally, the segmentation rules are improved according to the characteristics of KD-Tree.

MAJOR ALGORITHM

The basic idea of point cloud data of octree structure is to describe the point cloud space by octree model(Elseberg et al.2013; Bianca et al.2013). The root node of the hierarchical structure represents a cube containing the entire point cloud. If the cube is empty or the number is less than the specified value,then there is no segmentation, otherwise it will be divided into eight small cubes with equal size. For every such small cube, if it is empty or the number is less than the specified number, there is no segmentation, then it will be divided into eight smaller cubes again until it is no need to split or reaches the required level according to this rule.

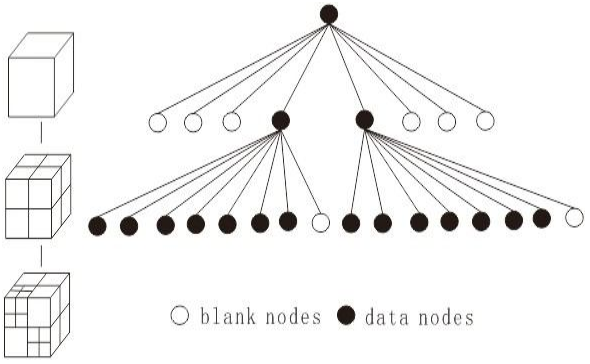

Figures 1: Octree data storage structure

KD-Tree(Schopfer et al.2011) refers to the binary search tree in k dimensions, on which fast nearest neighbor search can be achieved for the given k dimensions data. Each node of KD-Tree represents a point in k dimensional space, and each layer of the tree can make the branch decisions according to the resolution device. The resolution device of i layer is defined as: i mod k. Storage rules are those: if any node of the i layer in the left subtree is not empty, then i mod k dimension values of any node on left subtree are less than the value of node n; if the right subtree is not empty, then i mod k dimension values of any node on right subtree are greater than the value of node n; and its left and right subtrees are KD-Tree respectively.

The point cloud data is three-dimensional, so it can number three axis x,y, z of the point cloud data to 0,1,2, namely split={0,1,2}. We suppose six 3D data points { (2,3,8), (7,5,4), (8,7,2), (3,7,6), (8,3,7), (9,4,5) }, and the processing steps of algorithm are as follows:

1) Determine the value the split field should take: Calculating data variance of x, y, z axis, determining the split threshold and selecting the segmentation direction. In this case:

D(x)=[(2-6.12)^2+(7-6.12)^2+(8-6.12)^2+(3-6.12)^2 + (8-6.12)^2+(9-6.12)^2]=42.49

D(y)=[(3-4.83)^2+(5-4.83)^2+(7-4.83)^2+(7-4.83)^2 + (3-4.83)^2+(4-4.83)^2]=16.83

D(z)=[(8-5.33)^2+(4-5.33)^2+(2-5.33)^2+(6-5.33)^2+ (7-5.33)^2+(5-5.33)^2]=23.33

According to above result, variance in x direction is maximum. Therefore, the split field selects the x direction.

2) Determine the Node-data threshold: according to the axis direction step 1) determines, ranking all the point cloud data in this direction, calculating median value and getting the Node-data=(7,5,4). The split hyperplane of this node is the plane through the point (7,5,4) and perpendicular to the X axis.

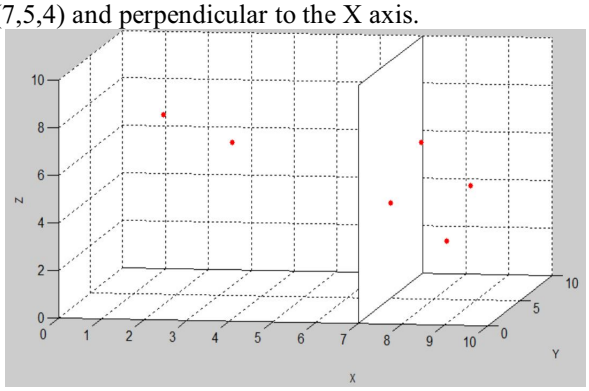

Figures 2: The example of a 3-dimensional KD-Tree

3) Divide the space into two parts through the figure 1: through the recursive call, the split of KD-Tree can be achieved after repeating the operation for the root node to left and right subspace data.

The nearest neighbor search (NNS), also known as "the closest point search ", is an optimization problem to find the nearest points in scale space. Description of the problem is as follows: given a set of points S and a target q∈M in the scale space M, to find the nearest point to q in S. In many cases, M is a multidimensional Euclidean space, and distance is determined by the Euclidean distance or Manhattan distance.

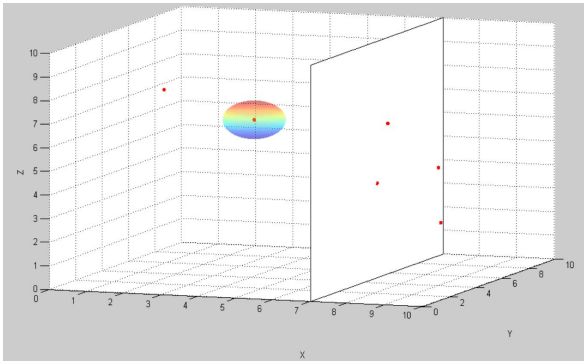

Figures 3: The example of nearest neighbor search

In order to speed up the search speed of neighbor classification, there are two common methods: fast nearest-neighbor samples search algorithm or simple and effective data structure, such as KD-Tree, Partial Distance Search; pretreatment and compression of data, such as Condensed Nearest Neighbor and Reduced Nearest Neighbor Rule.

IMPROVED METHOD

VGSO point cloud filtering algorithm

Voxel, which is a group of cube units distributing in center of the orthogonal grid, can be understood as the extension of two-dimensional pixel in three-dimensional space. The point cloud data generated by computer vision method is usually density-uneven. It samples by the voxel grid method and creates 3D voxel grid for the inputting point cloud data, with centroid of all the points in voxel to approximate the other points, all of which can not only reduce the point cloud data, but also maintain the shape characteristics of point cloud and more accurate approximation of the surface.
All points in the voxel are expressed with a centroid, then:

$$\bar{x} = 1/s \sum_{(x,y,z)\in A} x \tag{1}$$

$$\bar{y} = 1/s \sum_{(x,y,z)\in A} y \tag{2}$$

$$\bar{z} = 1/s \sum_{(x,y,z)\in A} z \tag{3}$$

Among them, S is the total number of discrete points in voxels A. Point cloud data with non-uniform density can be homogenized through the 3D voxel grid filtering, but in measurement computer vision device will produce sparse outliers which is not good for the processing of local point cloud. Statistical analysis is carried out on the discrete points, calculating average distance of every point to all its neighboring points and filtering the outliers outside the reference ranges of average distance from the data set.
The process of SO algorithm is introduced following:
1) Calculate mean value and variance of the global distance

$$\bar{d} = 1/n \sum_{i=1}^{n} dis_i \tag{4}$$

$$D(dis) = \sum_{i=1}^{n} (dis_i - \bar{d})^2 \tag{5}$$

where n is the number of point cloud, dis is the distance between two points.
2) Calculate the global distance threshold

$$d_\theta = \bar{d} + \lambda * \sqrt{D(dis)} \tag{6}$$

λ is standard variance coefficient.
3) Calculate the average distance between a point and its neighborhood point, and determine its relationship with global distance threshold

$$\Pi = \begin{cases} \overline{d_i} > d_\theta, \text{outliers} \\ \overline{d_i} \le d_\theta, inliers \end{cases} \tag{7}$$

It will be easy to remove the outliers from the point cloud data through above algorithm.

Improved KD-tree segmentation rule

Essentially, KD-Tree is a two-fork tree, and each non-leaf node can be divided into two subspaces by split plane. In segmentation, the normal direction of the split plane is selected firstly. Although the direction is optional, it is apparent to be difficult in a direction parallel to the coordinate axes, therefore, we consider only the splitting plane whose normal direction is parallel to the axis. When the direction is selected, it is need to choose the splitting plane position which determines the proportion of two subspaces. According to the different structures of splitting plane, KD-Tree is divided into: midpoint split KD-Tree, proportionate KD-Tree and sliding mid point KD-Tree. The split plane of midpoint KD-Tree lies in the space center, with shared position characteristics of nodes between adjacent layers. The split plane of proportionate KD-Tree uses one of the nodes to make points on both sides of the split plane basically equal. The split plane of sliding midpoint KD-Tree moves the split spane at the center of subspace to the nearest point to segment KD-Tree.
According to traditional idea of binary tree, a full binary tree will be produced after the split of KD-Tree, namely the two nodes in every split should contain the same number of point elements. But it has some problems: Firstly, this method requires to sort the point elements to find a point in the middle; secondly, it must record each split position in the node data, otherwise it cannot determine the space size of current node when accessing the node, and such steps will increase each node space consumption.
We first determine the local coordinate system and the size of bounding box of discrete point cloud $T = \{t_i \in R^3\}$ in space split, and t_o is the average position of T.

$$t_o = \frac{1}{m} \sum_{i=1}^{m} t_i \tag{8}$$

The third order covariance matrix is

$$L = \frac{1}{n} \sum_{i=1}^{m} (t_i - t_o)(t_i - t_o)^T \tag{9}$$

L is a symmetric positive semi-definite matrix with feature vectors orthogonal to each other, then eigenvalue is solved:

$$L - \lambda_i \beta_i = 0, i \in \{1,2,3\} \tag{10}$$

wher λ_i is eigenvalue, β_i is eigenvector, γ_1, γ_2 and γ_3 is eigenvectors of discrete point cloud in three coordinate axis, then

$$\gamma_1 = \frac{1}{2}(\min\{\ t_i\ .\beta_1\} + \max\{\ t_i\ .\beta_1\}) \quad (11)$$

$$\gamma_2 = \frac{1}{2}(\min\{\ t_i\ .\beta_2\} + \max\{\ t_i\ .\beta_2\}) \quad (12)$$

$$\gamma_3 = \frac{1}{2}(\min\{\ t_i\ .\beta_3\} + \max\{\ t_i\ .\beta_3\}) \quad (13)$$

Then the center of bounding box is:

$$\psi_o = \gamma_1\beta_1 + \gamma_2\beta_2 + \gamma_3\beta_3 \quad (14)$$

In this paper, for KD-Tree split, the axis of longest projection length of the node coordinate is chosen as split, namely the direction of the normal vector of split plane.

Suppose node subspace $t_i(x_i, y_i, z_i)$, where x_i is the projection length of nodes in the x axis, y_i is the projection length of nodes in the y axis; z_i is the projection length of nodes in the z axis. If $Max(x_i, y_i, z_i) = z_i$, then plane parallel to z is chosen as split plane. This method only requires to save the space size and position of root node, generates the same split sequence every time, and when the KD-Tree is generated, follows the same split rules to access. The nodes of each KD-Tree level have the same space size and split direction.

ALGORITHM TESTING

Search for unfiltered point cloud data

This algorithm is based on the open Point Cloud Library (PCL) and C++ language, and tested in machine of the CPU I7-3610QM 2.3GHz, memory 8GB, graphics card GTX Geforce 680M. The discrete point cloud data are provided by PCL, such as the table, with a total of 460400 discrete points, very intensive point cloud and a large number of outliers.

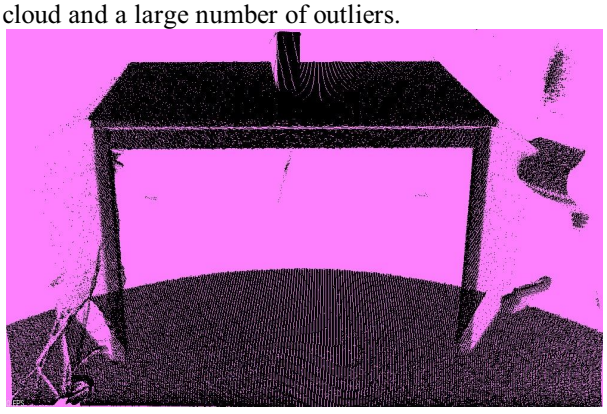

Figures 4: The original point cloud figure of table

This experiment firstly used octree structure to organize the scattered point cloud data, set the k value of neighbor of k as 100, and calculated the time to search a point cloud data, as the following table shows:

K nearest neighbor search at (0.481 0.263 1.197) with K=100.

Table 1: Search result of K neighbor based on octree

coordinate			squared distance
x	y	z	
0.43479	0.042405	-1.0812	5.24099
0.43315	0.042441	-1.0822	5.24569
0.31416	0.051026	-1.0776	5.24657
0.39545	0.055511	-1.0827	5.24740
0.39335	0.055509	-1.0827	5.24777
0.31457	0.055285	-1.0783	5.24783
0.35364	0.056505	-1.0812	5.24906
0.35156	0.056499	-1.0811	5.24914
0.36195	0.055460	-1.0817	5.24972
0.33916	0.055391	-1.0804	5.24977

Here we show only the top ten search results with total time of 1143 milliseconds.

Following, we tested the KD-Tree structure to organize the point cloud data, set the k value of k neighbor is 100, and calculated the time to search a point cloud data, as the following table shows:

K nearest neighbor search at (0.481 0.263 1.197) with K=100

Table 2: K nearest neighbor Based KD-Tree

coordinate			squared distance
x	y	z	
0.43479	0.042405	-1.0812	5.24099
0.43315	0.042441	-1.0822	5.24569
0.31416	0.051026	-1.0776	5.24657
0.39545	0.055511	-1.0827	5.24740
0.39335	0.055509	-1.0827	5.24777
0.31457	0.055285	-1.0783	5.24783
0.35364	0.056505	-1.0812	5.24906
0.35156	0.056499	-1.0811	5.24914
0.36195	0.055460	-1.0817	5.24972
0.33916	0.055391	-1.0804	5.24977

Here we show only the top ten search results, total time of 984 milliseconds. For Octree subdivision, when the point cloud has a large amount of data and local point cloud is dense, it will cause point cloud data unbalanced and redundant data structure, and reduce the search efficiency. KD-Tree is superior in the neighborhood search efficiency, but the record of each splitting node position increase the storage space of nodes.

Filtering effect based on VGSO filtering algorithm

For Figure 4, sampling point cloud density is very big and exist much outliers.Therefore filtering is proposed in this paper based on VGSO algorithm:

Step1.The original point cloud data are filtered using Voxel Grid filter, setting the minimum voxel volume $1cm^3$. Filtering results is in Figure 5.

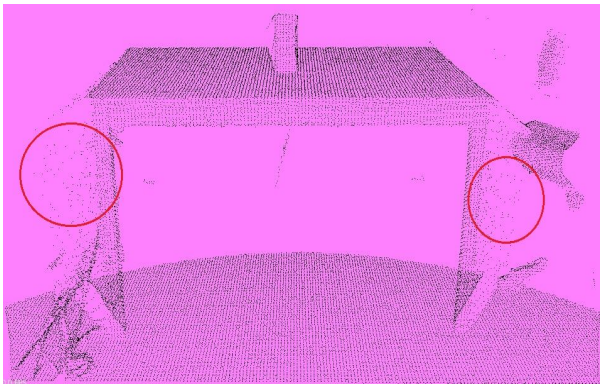

Figures 5: Voxel Grid filtering effect

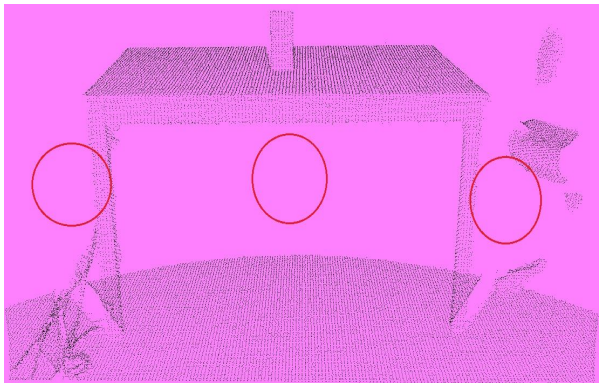

Figures 6: the Statistical Outlier filtering effect

Total Points:41049

Step2. Input point clouds Step1 processed, do Statistical Outlier filtering, set 50 adjacent points for each discrete point . Filtering results is in Figure 6

Step3. Improve KD-Tree split rules, input point cloud data after filtering, and build data structure of KD-Tree. As above, VoxeGrid filtering makes the point cloud data more uniform, and greatly reduces the density of point cloud at the basis of the quality. But in local area, such as the red circle shows, there are still a large number of outliers. The algorithm is not good in processing outlier. Based on this process, we need to carry out the statistical analysis of local information.

As shown in Figure 6, the Statistical Outlier removed a total of 1559 obvious outlier from point cloud in Figure 5 the red circles show, and point cloud data obtained can be better applied to the later. We build KD-Tree using the point cloud data, the search key point (0.481,0.264,1.197), and K to 100 to obtain the following search results, at the consumption of 78 ms search time.

Total Points:39490

K nearest neighbor search at (0.481 0.263 1.197) with K=100

Table 3: K nearest neighbor Based KD-Tree

coordinate			squared distance
x	y	z	
0.324780	0.053260	-1.0793	5.24994
0.313700	0.052554	-1.0787	5.25103
0.291010	0.051576	-1.0777	5.25506
0.302340	0.055333	-1.0793	5.25636
0.286490	0.053208	-1.0787	5.26057
0.274930	0.053222	-1.0777	5.26071
0.445000	0.042583	-1.0858	5.26083
0.424253	0.055322	-1.0875	5.26519
0.285177	0.048134	-1.0791	5.26530
0.354523	0.054573	-1.0849	5.26630

Total Time:78 MS

Table 4: Results with different K value (ms)

k	50	100	300	500	700	1000	1500	2000	2500	3000
Before Filter	980	980	1031	1057	1098	1215	1283	1537	1763	2121
After Filter	78	78	100	120	160	220	340	450	510	630

As shown in Table 4, the search time of point cloud data in figure 4 and Figure 6 are tested based on KD-Tree. From the table we can see search time i is longer than that before data compression, and the better searching efficiency is obtained after filtering.

Chair

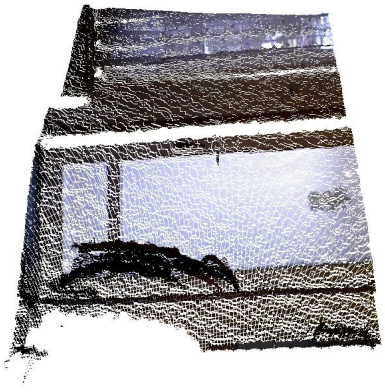

Class

House

Kitchen Shoes Table

Figures 7: point cloud data of different type

In Figure 7, in order to check correctness and effectiveness of this algorithm, 6 groups of point cloud data of different types and scene are tested with large data scale. From table 5, we know in the case of ensuring the point cloud quality, when compression rate reached 67.5%, the highest compression ratio of point cloud can reach to 92.3%. In view of this kind of point cloud data such as Kitchen, with particularly dense and non-uniform point cloud data, the filtering effect is very good, which can be the same with all kinds of data collected from different places..

Table 5: Filtering results of different clouds objects

Object	Chair	Glass	House	Kitchen	Shoes	Table
Number	307200	307200	307200	947003	307200	307200
VG Filter	72264	69214	111376	216808	27170	25196
SO Filter	63760	62664	99837	203181	23602	23504
Compressibility	79.2%	79.6%	67.5%	78.6%	92.3%	92.3%

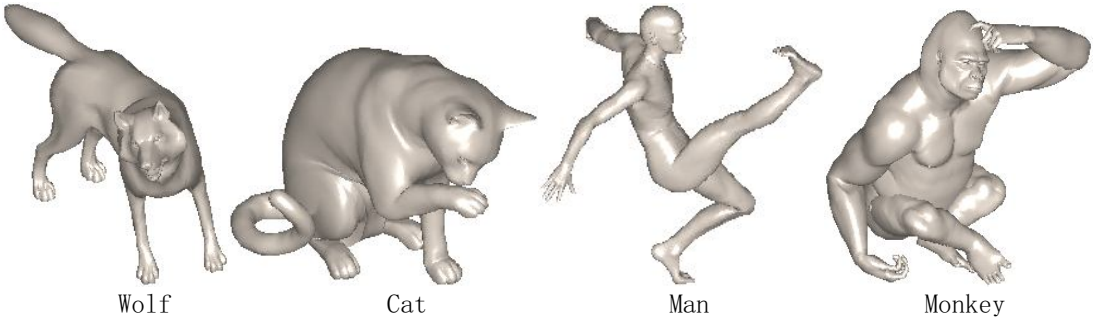

Figures 8: The no data redundancy point cloud

Table 6: No redundant data filtering

	Wolf	Cat	Man	Monkey
Number	4345	27895	52566	41396
VG Filter	4344	27893	52471	41261
SO Filter	3370	22691	43091	34247

As shown in Figure 8 the point cloud model has no outlier, with all point cloud data uniform, smooth. When the VGSO algorithm is applied to the point cloud data model, it can be found by table 6, that VG filtering algorithm is not effective for point cloud model, but after treating by SO filtering algorithm, large number of point cloud data are deleted and mistaken as outliers.

Figures 9: The results of So filter

CONCLUSIONS

This paper put forward a filtering algorithm based on VGSO. Firstly, the VG algorithm can greatly reduce the point cloud density and homogenize the point cloud density; then, the SO algorithm filter the discrete points; finally, the segmentation rules are improved according to the characteristics of KD-Tree. The experimental data showed that the algorithm is effective and feasible, but there are some problems. As shown in Figure 9, part of the body in the Wolf point cloud model was empty. Therefore, future research work will further study curvature judgment of point clouds to reduce the misjudgment of SO filtering algorithm.

ACKNOWLEDGMENTS

This project is supported by National Natural Science Foundation of China (NSFC Grant No. 61070043) and the National Science & Technology Pillar Program during the Twelfth Five-year Plan Period (No.2012BAD10B01).

REFERENCES

Chen S.Y.; Y.F. Li; J.W. Zhang.2008. "Vision Processing for Realtime 3D Data Acquisition Based on Coded Structured Light". *IEEE Transactions on Image Processing*, No.2,167-176.

Chen S.Y.; Y.F. Li.2004. "Automatic sensor placement for model-based robot vision". *IEEE Transactions on Systems, Man, and Cybernetics Part B,*NO.1,393-408.

Zhang K. and S.C. Chen. 2003. "A Progressive Morphological Filter for Revoming No ground Measurements from Airborne LIDAR Data". *IEEE Transactionson Geoscience and Romote Sensing*, No.4,1052-1062.

Sithole G. 2001. "Filtering of Laser Altimetry Data Using a Slope Adaptive Filter." *International Archives of the Photogrammetry, Remote Sensing and Spatial Information Sciences*,No.34,203-210.

Jiang J.Y. ; Z.X Zhang; Y. Ming.2007. "The airborne Lidar points cloud filtering of complex city environment." *Journal of Wuhan University*,No.5,402-405.

Papadimitriou S. ; H. Kitawaga; P.B. Gibbons. et al.2003. "LOCI:fast outlier detection using the local correlation integral". *In Proceedings of the 19th International Conf*erence on Data Engineering(Bangalore, Mar.5-8). IEEE Computer Society,315-326

Xu X.S.; D.M. Song; X Zhang.et al.2008. "Research of detection of outliers based on locally linear weighted value. *Computer Science,* No.5,154-157.

Johnson, t.; I. Kwok; R. Ng.1998. "Fast computation of 2-dimensional depth contours". *In Proceedings of the 4th International Conference on Knowledge Discovery and Data Mining*(New York, Aug.27-31). AAAI Press,224-228.

Knorr E.M.; R.T. Ng; V. Tucakov.2000. "Distance-Based outliers:algorithms and applications". *The VLDB Journal*, No.3,237-253.

Breunig M.M.; H. Kriegel; R.T. NG.2000."Lof: identifying density-based local outliers". *In Proceedings of ACM SIGMOD International Conference on Managernent of Data*(New York, May.16-18). ACM Press, 93-104.

Chen S.Y.; J.H.Zhang; Y.F. Li; J.W. Zhang.2012. "A Hierarchical Model Incorporating Segmented Regions and Pixel Descriptors for Video Background Subtraction". *IEEE Transactions on Industrial Informatics,* No.1,118-127.

Elseberg J.; B. Dorit; N. Andreas.2013. "One billion points in the cloud-An octree for efficient processing of 3D laser scans". *Journal of Photogrammetry and Remote Sensing,*No.76(Feb),76-88.

Bianca S.; A.S.M. Mosa; D.F. Laefer; B. Michela.2013 "Octree-based indexing for 3D pointclouds within an Oracle Spatial DBMS". *Computers and Geosciences,*No.51(Feb),430-438.

Schopfer M.; R. Haschke; H. Ritter.2011. "A Probabilistic Approach to Tactile Shape Reconstruction". *IEEE Transactions on Robotics*, No.3(Jun), 630-635.

IMPROVED PARTICLE SWARM OPTIMIZATION FOR TRAVELING SALESMAN PROBLEM

Xin-Li XU, Xu CHENG, Zhong-Chen YANG, Xu-Hua YANG and Wan-Liang WANG
College of Computer Science and Technology
Zhejiang University of Technology
Hangzhou 310023, China
e-mail: xxl@zjut.edu.cn

KEYWORDS

Particle swarm algorithm, dynamic programming algorithm, scale-free fully informed network, travelling salesman problem.

ABSTRACT

To compensate for the shortcomings of existing methods used in TSP (Traveling Salesman Problem), such as the accuracy of solutions and the scale of problems, this paper proposed an improved particle swarm optimization by using a self-organizing construction mechanism and dynamic programming algorithm. Particles are connected in way of scale-free fully informed network topology map. Then dynamic programming algorithm is applied to realize the evolution and information exchange of particles. Simulation results show that the proposed method with good stability can effectively reduce the error rate and improve the solution precision while maintaining a low computational complexity.

INTRODUCTION

TSP (Traveling Salesman Problem) is a classical combinatorial optimization problem. It is hard to find the optimal solution within polynomial calculation time, as for large-scale problems people are more inclined to seek acceptable approximated optimal solution algorithm in a limited period of time. There are many ways to solve this problem, such as local search strategy, genetic algorithm, ant colony algorithm, particle swarm optimization, immune algorithm, neural network algorithm and dynamic programming algorithm. Traditional dynamic programming algorithm can obtain the optimal solution, but great time complexity and space complexity makes it only available to solve the small scale problem. Other algorithms like genetic algorithms and neural networks can obtain better solutions in a short period of time, but they have disadvantages in terms of the accuracy of solutions and the scale of problems.

To compensate for the shortcomings of existing methods used in TSP, such as the accuracy of solutions and the scale of problems, this paper proposed an improved particle swarm optimization by using a self-organizing construction mechanism and dynamic programming algorithm. Particles were connected in way of scale-free fully informed network topology map. And dynamic programming algorithm was used to realize the position updating of particles. Simulation results show that the proposed method has a good stability and it can effectively reduce the error rate besides it can improve the solution precision while maintaining a low computational complexity.

BASIC PRINCIPLES OF PARTICLE SWARM OPTIMIZATION

Particle swarm optimization (PSO) is a population based stochastic optimization technique developed by Eberhart and Kennedy in 1995, inspired by social behavior of bird flocking or fish schooling. The basic idea of PSO is as follows: assume the population size is N, the current position of the particle can be expressed as $X_i^k = (x_1^k, x_2^k, \dots x_n^k, \dots x_N^k)$, $x_n^k \in [l_n, u_n]$, $1 \le n \le N$, l_n and u_n represent upper and lower bounds in n-th dimensional space, respectively. The current velocity can be expressed as $V_i^k = (v_1^k, v_2^k, \dots, v_N^k)$. V_i^k is between $V_{max}^k = (v_{max,1}^k, \dots v_{max,n}^k, \dots v_{max,N}^k)$ and $V_{min}^k = (v_{min,1}^k, \dots v_{min,n}^k, \dots v_{min,N}^k)$. The updating equation of the velocity and position of the particles are shown as equation (1) and equation (2), respectively.

$$V_i^{k+1} = wV_i^k + c_1 r_1 (P_i^k - X_i^k) + c_2 r_2 (P_g^k - X_i^k) \quad (1)$$

$$X_i^{k+1} = X_i^k + V_i^{k+1} \quad (2)$$

where, c_1 and c_2 are constants called the learning factor used to adjust the relative importance of the individual extremum and the global relative materiality. r_1 and r_2 are uniformly distributed random numbers in (0, 1). P_i^k and P_g^k represent the individual optimal position and the global optimal position of particles in the k-th iteration, respectively.

PARTICLE SWARM OPTIMIZATION ALGORITHM COMBINING WITH DYNAMIC PROGRAMMING METHOD

For traveling salesman problem, the state of particle (X) is represented as N-dimensional vector just like other particle swarm optimization algorithms, and the number of dimensions denotes the total number of cities. We can use the formula (3) to represent the state X.

$$X = (x_1, x_2, \dots x_i, \dots x_N),\ 1 \le i \le N,\ 1 \le x_i \le N \quad (3)$$

In this formula, N represents the number of the cities while x_i represents the corresponding city number. Start

Proceedings 27th European Conference on Modelling and Simulation ©ECMS Webjørn Rekdalsbakken, Robin T. Bye, Houxiang Zhang (Editors)
ISBN: 978-0-9564944-6-7 / ISBN: 978-0-9564944-7-4 (CD)

from the first city x_1, and visit x_{i+1} after x_i, until x_N is visited then revisit x_1. Finally, form the overall access sequence. In the initial phase of the algorithm, M different particles are randomly generated to compose the particle swarm.

Based on the updating equation of velocity and position of the particle are shown as equation (1) and (2), we can see new position of the particle depends on three parts: a) velocity and position of the particle in the previous iteration, that is, the previous state of the particle; b) cognition part, that is, self-learning of the particle; c) social part, that is, the collaboration among particles. In a word, new position of the particle is interdependence of previous state and best self-experience of the particle and best experience the population. So we can define the position updating formula for discrete particle swarm algorithm as follows:

$$X_i^{k+1}=c_2\otimes f(c_1\otimes g(w\otimes h(X_i^k),\ P_i^k),\ P_g^k) \qquad (4)$$

where w is the inertia weight, c_1 is the cognitive coefficient, and c_2 is social coefficient. In generally, w, c_1, $c_2 \in [0,1]$.

The formula (4) consists of three parts:

$$E_i^k=w\otimes h(X_i^k)=\begin{cases} h(X_i^k) & \text{rand}<w \\ X_i^k & \text{otherwise} \end{cases} \qquad (5)$$

The equation (5) represents the influence of previous state of the particle, where rand is the random number in [0, 1]. $h(X_i^k)$ indicates the velocity of the particles and its adjustment is as seen in section velocity updating operator combined with dynamic programming.

$$G_i^k=c_1\otimes g(E_i^k,P_i^k)=\begin{cases} s(E_i^k,P_i^k) & \text{rand}<c_1 \\ E_i^k & \text{otherwise} \end{cases} \qquad (6)$$

$g(E_i^k,P_i^k)$ represents that the particle is adjusted according to its optimal position P_i^k. For $s(E_i^k,P_i^k)$,we can see in the section of crossover operator with interparticle information interaction.

$$X_i^k=c_2\otimes s(G_i^k,P_g^k)=\begin{cases} s(G_i^k,P_g^k) & \text{rand}<c_2 \\ G_i^k & \text{otherwise} \end{cases} \qquad (7)$$

The equation (7) denotes the particle is adjusted based on the global optimal position P_g^k. The operation process of $s(G_i^k,P_g^k)$ is the same to $s(F_i^k,P_i^k)$.

Self-organizing construction mechanism with scale-free network graph

In 1999, Barabási and Albert in the process of research the dynamic evolution of the World Wide Web found that many large-scale complex networks have high ability about self-organization, and the node degrees of most complex network follow a “power law distribution”. The probability of k connections of any node is in proportion to 1/k, namely $p(k) \sim k^{-\gamma}$, where $2 < \gamma < 4$. The network with the characteristic is called scale-free network.

The construction method of scale-free network topology graph is used as a self-organizing construction mechanism in this paper, that is, all particles are combined into a particle swarm in the form of scale-free network topology graph. The topology construction steps can be briefly described as follows. Firstly, we select m most accurate particles from M original particles. Then m particles are connected to form a complete graph, that is, any two particles have an edge connected. Lastly, insert a particle of the M-m remaining particles into the network every time according to a degree preferential attachment scheme. Specifically, for a newly added particle i and an arbitrary existing particle j in the network, there is a probability $P_i=k_j/\Sigma k_i$ to connect the two particles, where k_j denotes the degrees of the particle j.

Based on the above steps, we can adaptively generate the population topology exhibiting scale-free property, that is, the topology will be gradually generated as the construction process and the optimization process progress synchronously.

Velocity updating operator combined with dynamic programming

Velocity updating operator includes TSP sequence splitting and integrating with dynamic programming. TSP often involves hundreds or even tens of thousands of cities. If we carry out dynamic programming to solve TSP in the global situation, the over-scaled problems will consume excessive time, and even the optimal solution will not be found. To solve the above problem, we consider the method from the local situation and split the whole TSP sequence into a number of sub-sequences. In order to ensure more reasonable sub-sequences split, five different strategies of setting truncation places are considered as follow, and thus a TSP sequence including n cities is spitted into $m(1\le m\le n)$ subsequences.

(A) Randomly select m different truncation places in the TSP sequence.
(B) Randomly select a city in TSP sequence, and then set a truncation place after m subsequent cities.
(C) Select a random city in TSP sequence, find its m-1 closest cities, and then set a truncation place after the m cities found.
(D) Select the “oldest” truncation place not to be split, and then set a truncation place in the rear of the m/2 cities after it and the other truncation place in the rear of the m/2 cities before it.
(E) Select a city in front of the “oldest” truncation place not to be split, find its m-1 closest cities, and then

set a truncation place in the rear of the m cities found.

To illustrate the performance of different strategies, rat_783 (TSP case with city size of 783) in TSPLIB is selected to compare with different strategies. The simulation results in table 1 show that the error rate of randomly selecting strategy such as A, B, C, D and E in any one splitting is the smallest, and its CPU times spent is less, which is more than strategy B and D. Hence, randomly selecting strategy such as A, B, C, D and E is used as TSP sequence splitting in this paper.

Table 1: Results based on Different Strategies for Rat_783

Strategies	Error rate(%)	CPU time(s)
A	5.75	133.2
B	24.75	1.89
C	14.73	196.8
D	24.35	1.961
E	13.51	142.7
A, B, C, D, E	3.62	131.3

TSP sequence is divided once, and the problem is simplified how to connect those subsequences into the shortest circuit. At the same time, the sequence direction will be involved in when we integrate those subsequences result from the local splitting. Based on the traditional dynamic programming algorithm for TSP, this paper introduces a new variable c_i indicating the direction of the i-th subsequence. If the direction of the i-th subsequence is positive, then set c_i=1. Otherwise, set c_i=0.

As TSP path is a cyclic path, we can assume that the last access subsequence is the 0-th subsequence whose direction is positive. And thus a new state variable (i,c_i,k) can be obtained, which indicates that the current spot is the i-th subsequence whose direction is c_i. Where k represents several subsequences accessed from the 0-th subsequence to the i-th subsequence in positive direction. In the corresponding binary, if the j-th bit is 1, it means the j-th subsequence has been selected in the access path while 0 means not.

Here, function $f(i, c_i, k)$ is defined as the shortest distance in a certain state (i, c_i, k). Then we can get the function value of initial state, that is, f(0,0,0)=0, and the function value of target state is $f(0,0,2^m-1)$. Hence the transfer equation can be obtained as follow.

$$f(i,c_i,k)=\min_{i\neq j,k/2^j\%2=1}(f(j,c_j,k-2^i)+dist(P(i,c_i),P(j,1-c_j))) \quad (8)$$

In the equation (8), if c_i=0, then $P(i,c_i)$ represents the first city in the i-th subsequence. Otherwise, if c_i=1, then $P(i,c_i)$ represents the last city in the i-th subsequence. $dist(P(i,c_i), P(j,1-c_j))$ represents the distance between the i-th subsequence and the j-th subsequence. $k/2^j\%2=1$ means that the j-th bit of the binary of k is equal to 1, that is, the j-th subsequence has been selected in the previous path walked.

According to the equation (8), the optimal value of $f(0,0,2^m-1)$ can be obtained, and all subsequences can be recombined into a whole TSP sequence including n cities in accordance with the optimal path recorded in the solution.

Crossover operator with interparticle information interaction

We adjust the state of the particles according to their own best position P_i^k and the global best position P_g^k by using crossover operator with interparticle information interaction in the paper, which can be described as follows.

1. We assume that P_i^k or P_g^k is a certain particle Y and E_i^k or G_i^k is a certain particle X.
2. Extract the continuous sub-vector from particle Y, such as $(y_{i+1},y_{i+2},\ldots,y_{i+l})$ called as the vector Z, whose length is l (l is a random positive number less than 10). Each element of the vector Z can be regarded as a breakpoint used to split the vector X, so the vector X can be divided into l segments according to the breakpoints and every segment of the vector X does not contain any element of the vector Z.
   For example, there are two known particles, that is, X is (1,2,3,4,5,6,7,8,9) and Y is (4,3,2,1,4,6,5,7,8,9). We can extract a length-3 sub vector Z from Y, which is (1, 4, 6). And then X can be divided into three sections according to the vector Z, such as (2, 3), (5) and (7, 8, 9).
   Based on the above analysis, we can get l sub-vectors and a sub-vector extracted from the vector Y, so a total number of sub-vectors is l+1.
3. We can use the above dynamic programming method as seen in section B to reassemble into a new particle X'. If X' is superior to the original particle X, X will be replaced with X'.

Procedure of algorithm for TSP

The procedures of improved particle swarm algorithm to solve TSP are as follows:

Step1. Set the population size of particle swarm (M), the max number of iterations (ds), and the parameters (w, $c_1$and c_2). Then randomly generate M different particles, calculate fitness value of each particle X_i, and record the initial local optimal value $P_i=X_i$, $i\in\{1,2,\ldots, M\}$.

Step2. Set t=0, construct an initial scale-free network graph construction with m different particles, and record the global optimal particle $P_g=\min(P_j)$, $j\in\{1,2,\ldots, m\}$.

Step3. Update the position of each particle according to the formula (3), calculate their fitness value, and

then update the local optimal value P_j and global optimal value $P_g=\min(P_j)$, $j \in \{1,2,\ldots, \min(m+t, M)\}$.

Step4. Gradually generate the population topology. At each time step t there is exactly one particle of the remainder M-m-t particles that will be connected with m+t existing particles.

Step5. Add 1 to the time step t. If t > ds, then output the optimal solution and quit. Otherwise, go to Step3.

SIMULATION RESULTS AND ANALYSIS

Effectiveness test of proposed algorithm

In order to validate the performance of the proposed algorithm, numerical simulation experiments of three different-scaled TSP examples are conducted, where the number of cities is 76, 783 and 100000, that is, small scale, medium scale and large scale, respectively. The proposed algorithm has been coded with VC++6.0, runs on a PC with Intel Pentium CPU 2.20GHz processor and 2G of memory and the simulation results are as shown in Figure1.

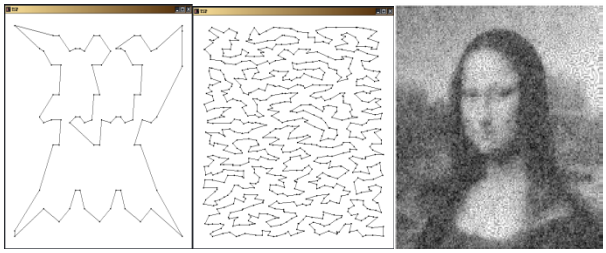

(a) 76 cities (b) 783 cities (c) 100000 cities

Figure 1: TSP with Different Number of Cities

As shown in Figure 1, the improved particle swarm algorithm can obtain good results of any scale TSP, which demonstrates the effective of the proposed algorithm.

In order to illustrate effectiveness of the proposed algorithm, we do further simulation on the rat_783 and extract the results of first 100 iterations and 100 to 300 iterations as shown in Figure 2 and Figure 3.

From Figure 2, we can see that the proposed algorithm has strong convergence at the early stage and an excellent solution can be quickly obtained. Moreover, the proposed algorithm does not lead to "premature" and it is still slowly evolving as shown in Figure 3.

Finally the proposed algorithm is applied to solve 14 different-scale TSP examples from 76 to 85900 in TSPLIB, and simulation results are compared with the optimal path lengths published in TSBLIB. "Error rate" deviating from the optimal solution is used to evaluate quality of the solution, which is the percentage ratio of the deviation between average path length obtained by the proposed algorithm and the optimal path length released in TSPLIB, that is, Error rate=(Average solution – Optimal solution)/Optimal solution×100%. So the smaller the error rate is, the better the quality of the solution will be. Considering path lengths released in TSPLIB are integers while the data aren't rounded in many references, path lengths are not rounded to facilitate comparison with similar methods in this paper, too. The simulation results of 20 independent calculations are shown in the following table 2. If the error rate in table 2 is less than 0, we can know that the solution value is smaller than the optimal solution in TSBLIB, which shows the superiority of the proposed algorithm.

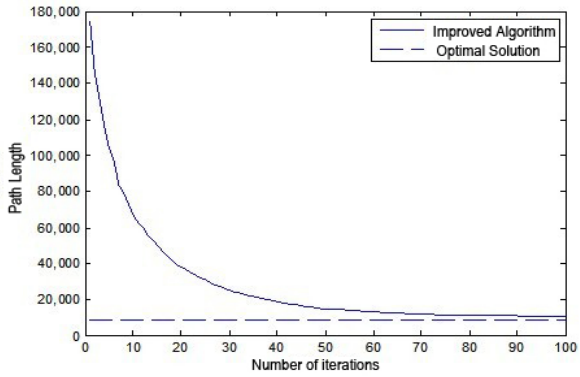

Figure 2: Convergent Graph of the First 100 Iterations

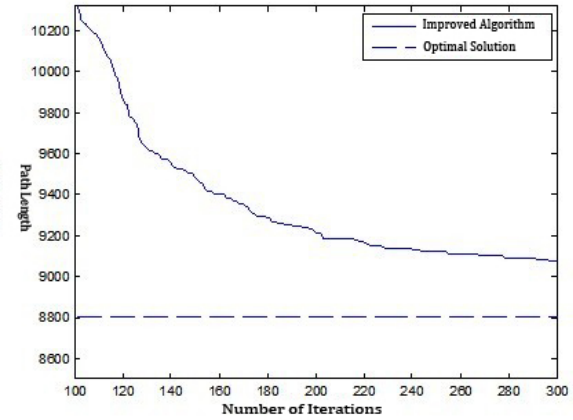

Figure 3: Convergent Graph of from 100 to 300 Iterations

We can find when the scale of problem is small, about 100 or so, the optimal solutions obtained by the improved particle swarm algorithm are extremely approximated to or even smaller than that of TSBLIB, which means the improved algorithm can almost find the optimal solution of the small scaled TSP. Error rate increases as the problem scale increases while remaining in a small scope, which shows good convergence of the algorithm. As is shown in Table 2, the improved algorithm is suitable for good solution of any scale TSP.

Table 2: Results of Different Numbers of Cities

Number	Cases	Number of cities	Optimal solution	Best solution	Average solution	Error rate (%)	Average CPU time (s)
1	pr_76	76	108159	108159.2	108159.4	0.00	1.53
2	kroA_100	100	21282	21282.44	21286.64	0.01	2.97
3	kroB_100	100	22141	22138.26	22139.07	-0.01	1.08
4	pr_107	107	44303	44301.68	44302.88	0.00	2.70
5	pr_144	144	58537	58536.44	58537.87	0.00	5.63
6	lin_318	318	42029	42632.13	42633.17	1.44	24.63
7	pcb_442	442	50778	51526.46	51528.35	1.48	27.29
8	rat_783	783	8806	9124.82	9124.91	3.62	300.55
9	pcb_1173	1173	56892	58335.36	58339.30	2.54	184.63
10	D_1655	1655	62128	64124.65	64126.35	3.22	341.23
11	pcb_3038	3038	137694	142403.53	142404.40	3.42	672.24
12	rl_5934	5934	556045	575345.36	575395.78	3.48	869.11
13	pla_33810	33810	66048945	68208524.23	69408534.49	5.09	2939
14	pla_85900	85900	142382641	154827063.35	154927063.95	8.81	8226

Simulation results Comparison with different algorithms

Simulation results of the improved particle swarm algorithm (IPSO), generalized chromosome genetic algorithm (GCGA), constructive-optimizer neural network algorithm (CONN) and improved elastic net algorithm (Improved-EN) are compared with those of corresponding cases in terms of error rate in Table 3.
An observation of Table 3 demonstrates that the improved algorithm is obviously as good as or better than other algorithms in terms of error rate, namely, the proposed algorithm is more accurate than other algorithms.

Table 3: Comparisons among Error Rate of Different Algorithms

Number	IPSO	GCGA	CONN	Improved-EN
1	0	0.72	4.34	--
2	0.02	1.23	2.57	2.09
3	-0.01	1.81	2.6	3.02
4	0	1.37	2.77	--
5	0	0.04	2.34	--
6	0.73	5.14	--	8.02
7	1.18	8.99	5.72	--
8	1.76	--	7.59	12.73
9	2.13	--	8.9	7.12
10	3.13	--	8.28	--
11	2.04	--	8.04	--
12	2.78	--	13.1	--
13	4.36	--	--	--
14	4.93	--	--	--

CONCLUSION

In this paper, a self-organizing construction mechanism is used to generate the population topology and dynamic programming method is used to update the position of particles in the optimization process progress, which makes the improved particle swarm algorithm with good fusion of the local optimum and the global optimum. Simulation results show that the proposed algorithm surpasses other methods in the accuracy of solution, such as generalized chromosome genetic algorithm (GCGA), constructive-optimizer neural network algorithm (CONN) and improved elasticity network algorithm (improved-EN). Unlike some existing algorithms which can commonly solve TSP with small scale (less than 100), the proposed algorithm can be applied to TSP with various scale. Simulation experiments of 14 TSP with the scale ranging from 76 to 85900 have verified that. In addition, the improved algorithm can be used widely, which can solve TSP in non-planar state, such as 3-dimensional space and spherical space.

ACKNOWLEDGEMENTS

This work was supported by the National Science Foundation of China (61070043, 61105073, and 61203371), and a sub-project of National Science and Technology Support Plan (2012BAD10B0101), and the Open Fund Project of Zhejiang University of Technology (20120814).

REFERENCES

Barabási, A-L. and Albert, R. “Emergence of scaling in random network”, Science, vol .286, pp.509-512, 1999.

Kennedy, J. and Eberhart, R. “Particle swarm optimization”, IEEE Int. Conf. on Neural Networks, Perth, Australia, pp.942-1948,1995.

Chen, S.Y., "Kalman Filter for Robot Vision: a Survey", IEEE Transactions on Industrial Electronics, Vol. 59, No.11, 2012, pp. 4409 - 4420.

Chen, S.Y. and Li, Y.F., "Automatic Sensor Placement for Model-Based Robot Vision", IEEE Transactions on Systems, Man and Cybernetics, Part B, Vol. 34, No. 1, pp. 393-408, Feb 2004.

Eberhart, R. and Kennedy, J. “A new optimizer using particle swarm theory”, Proc of the Sixth International Symposium on Micro Machine and Human Science Conf. Nagoya, Japan, pp.39-43,1995.

Gao, S. Han, B. Wu, X.-J. and Yang, J.-Y. “Solving traveling salesman problem by hybrid particle swarm optimization algorithm”, Control and Decision, vol. 19, no.11, pp.1286-1289, 2004.

Xu, G. Segawa, E. and Tsuji, S. “Robust active contours with insensitive parameters”, Pattern Recognition, vol. 27, No.7, pp.879-884, 1994.

Hall, D. and Gal, L-C. “magicboard:A contribution to an intelligent office environment”, Robotics and Antonomous Systems, pp.211-220, 1999.

Su, J-R. and WANG, J-Z. “Improved particle swarm optimization for traveling salesman problem”, Computer Engineer and Applications, vol.46, no.4, pp.52-75, 2010.

Reinelt, G. “TSPLIB-A traveling salesman problem library”, ORSA Journal on Computing, pp.376-384, 1991.

Wen, S., et al., "Elman Fuzzy Adaptive Control for Obstacle Avoidance of Mobile Robots using Hybrid Force/Position Incorporation", IEEE Transactions on Systems, Man, and Cybernetics, Part C, Vol. 42, No. 4, 2012, pp. 603-608.

Yang, J. Wu, C. Lee, H.P. and Liang, Y. “Solving traveling salesman problem using generalized chromosome genetic algorithm”, Progress in Natural Science Conf. , vol.18, pp.887-892, 2008.

Saadatmand-Tarzjan, M. Khademi, M. Akbarzadeh-T, M. R. and Mghaddam, H. A. “A novel constructive-optimizer neural network for the traveling salesman problem”, IEEE Transactions on Systems, Man, and Cybernetics-Part B: Cybernetics, vol .37 (4), pp.754-770, 2007.

Yi, J. Yang, G. Zhang Z. and Tang,Z. “An improved elastic net method for traveling salesman problem”, Neurocomputing, vol.72, pp. 1329-1335, 2009.

Zhang, C-G. and Yi, Z. “Scale-free fully informed particle swarm optimization algorithm”, Information Sciences, vol.181, pp.4550-4568, 2011.

Zheng, Y., Chen, S., Ling, H., "Agent-based Cooperative Evolutionary Computation for Disaster Rescue Operation Planning", Disaster Advances, Vol. 5, No. 4, 2012, pp. 698-703.

Yao, C-Z. and Yang, J-M. “PSO Algorithm Based on Network Neighborhood Topology”, Computer Engineering, vol.36, no.19, pp.18-23, 2010.

AUTHOR BIOGRAPHIES

Xinli XU received the B.S. degree in automation from China University of Mining and Technology, China, in 2000, the M.Sc. and Ph.D. degrees in control theory and control engineering from Zhejiang University of Technology (ZJUT), China, in 2003 and 2009, respectively. Since 2010, she has been an Associate Professor in the College of Computer science and technology, ZJUT.

Her current research interests include optimization theory and algorithms in production scheduling and hydropower scheduling, and complex networks theory and its applications.

Simulation and Computational Neuroscience

THE DYNAMIC CONNECTOME: A TOOL FOR LARGE-SCALE 3D RECONSTRUCTION OF BRAIN ACTIVITY IN REAL-TIME

Xerxes D. Arsiwalla[1,*], Alberto Betella[1], Enrique Martinez[1], Pedro Omedas[1], Riccardo Zucca[1], Paul F.M.J. Verschure[1,2]
(All authors have contributed equally to this work)

[1]*Synthetic Perceptive Emotive and Cognitive Systems Lab, Universitat Pompeu Fabra, Roc Boronat 138, 08018, Barcelona, Spain*
[2]*Institució Catalana de Recerca i Estudis Avançats (ICREA), Barcelona, Spain*
[*]email: x.d.arsiwalla@gmail.com

KEYWORDS

Human connectome; 3D reconstruction; Virtual reality; Neural dynamics

ABSTRACT

We present a large-scale simulation tool for real-time 3D reconstruction of brain activity in a virtual reality environment. The 3D interactive visualization of the human cortex connectome in virtual reality is achieved by using a gaming engine (Unity 3D). Further, the visualization is bi-directionally interfaced with a real-time neuronal simulator, `iqr`. As a result, by stimulating populations of neurons with external input currents, we are able to reconstruct neural activity propagating in 3D and in real-time. We explicitly demonstrate causal activity propagation in the parietal lobe, indicative of visuo-motor integration. This is a first step to simulating and mapping large-scale brain activity.

INTRODUCTION

Recent interest in whole-brain structural and functional connectivity has given rise to the notion of the human connectome (Hagmann 2005; Sporns et al. 2005). Analogous to the genome, that maps the complete genetic sequence of an organism, the connectome is supposed to map the complete neuronal circuitry of the brain (in the most ambitious interpretation of the term). The organization of these circuits can be physiologically probed at different scales: microscopic, mesoscopic and macroscopic. However, determining the exhaustive array of biophysical mechanisms, that intertwine these scales into one functional architecture, remains a major challenge in neuroscience. Hence, the operational assumption that is often made is that brain organization is hierarchical with respect to scales, such that only ensemble aggregates of lower scales (along with their stochastic fluctuations) are fed as inputs to higher scales (Zhou et al. 2006). For instance, even though the macroscopic scale is dominated by neuronal population dynamics and large-scale structural connectivity, a thorough description of population activity still requires knowledge about synaptic dynamics residing at a microscopic scale. This interplay between population and synaptic dynamics can be described by mean-field models (Wong and Wang 2006). In principle, coupling structural connectivity data with detailed enough population dynamics should be sufficient in predicting functional correlations and large-scale activity patterns. In fact, large-scale interactions across brain regions have recently been touted as the 'fingerprints' of neuronal computations underlying cognitive processes (Siegel et al. 2012).

In this paper, we present a virtual reality based dynamic simulation tool that reproduces activity propagation upon excitation of any chosen brain region. The challenge here is threefold: to implement dynamics pertinent at the macroscopic scale, to construct tools that allow for 3D visualization, and finally perform real-time analysis of neural activity generated from large datasets. The structural connectivity data is obtained from (Hagmann et al. 2008), which is Diffusion Spectrum Imaging (DSI) data. Each node of the connectivity matrix corresponds to a population of neurons. In our simulation, we model the dynamics of this population by a linear-threshold filter, which sums up all the input signals to a population module from various dendrites (within a fixed time window) and fires an output signal to neighboring modules only if the summed inputs cross a designated threshold. Additionally each neuronal population module is stochastic, having Gaussian noise.

In addition to the problem of connecting the different levels of neuronal dynamics, researchers need tools to explore complex data sets such as those deployed in the connectome. For this reason, we adapted our so called, eXperience Induction Machine (XIM), to the immersion and exploration of complex neuroscience data sets

Proceedings 27th European Conference on Modelling and Simulation ©ECMS Webjørn Rekdalsbakken, Robin T. Bye, Houxiang Zhang (Editors)
ISBN: 978-0-9564944-6-7 / ISBN: 978-0-9564944-7-4 (CD)

by human users. The XIM is a virtual/mixed reality environment, which enables user-immersion within the data reconstruction, giving an inside-out perspective of the connections in the brain and allowing the user to 'walk' through pathways in the brain.

In order to understand the relationship between structural connectivity data and neural dynamics and function, we set-up a bi-directional mapping of structural data unto a large-scale real-time neural simulator, `iqr`. Using natural gestures, the user can then inject a current to excite any region of the network and watch real-time neuronal activity propagate through the connectome network. The system allows simultaneous activation as well. This opens out the possibility of analyzing real-time activity propagation due to causal dynamics. Compared to functional correlations, dynamical analysis of causal activity serve as a more powerful tool to unravel mechanisms of large-scale neural circuits. The dynamic connectome tool, that we present in this paper, is a first step in that direction.

METHODS

The connectome we build is based on structural data taken from the human cortex connectivity dataset (Hagmann et al. 2008). This dataset includes DTI recordings of 5 subjects in the resting state (one subject has been scanned twice). The set contains 998 voxels (nodes) and approximately 14000 bi-directional connections for each subject. The 998 Regions Of Interest (ROIs) have an average size of 1.5 cm^2. Each ROI is associated with $\{x, y, z\}$ coordinates as per the Talairach coordinates of ROIs (Talairach et al. 1998). The connection strengths between ROIs is based on white matter fibre tracts from the DTI dataset we used. The network data of interest to us, is stored in the GraphML format, which is based on the XML format and is convenient for representing network data.

The virtual reality environment we create, to visualize the connectome, runs in the eXperience Induction Machine (XIM) (Bernardet et al. 2008; Bernardet et al. 2010). The XIM is a multi-user mixed/virtual reality space with a 5.6x5.4 m^2 surface area and 3.6 m height (Fig. 1). It is equipped with 3 cameras, 3 microphones, 8 steerable theater lights, 4 steerable color cameras, 16 speakers. The space is surrounded by 4 projection screens and 8 video projectors are used to display graphical content. The floor consists of 72 custom-built tiles, each of which is equipped with pressure sensors and can display a color by means of a built-in computer controlled RGB light source (Delbrück et al. 2007). Real-time location of a user can be tracked with the floor sensors, enabling the user to navigate through the mixed/virtual reality environment.

The processing architecture of the XIM integrates external data with the visualization engine (Fig. 2). 3D graphical content is programmed in C# using the Unity

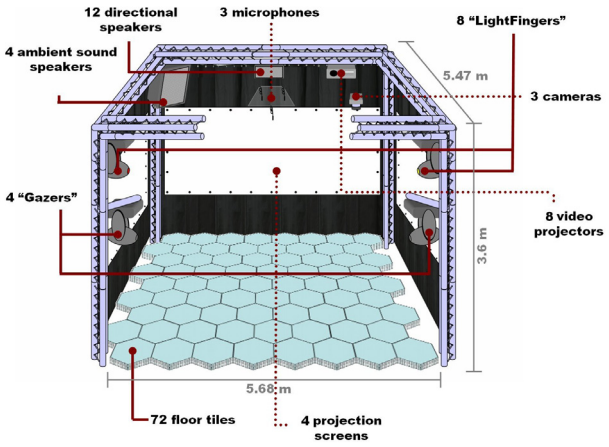

Fig. 1: Schematic illustration of the eXperience Induction Machine (XIM).

3D (http://unity3d.com/) gaming engine. XML data of structural connectivity is read and parsed in Unity and then reconstructed using the Talairach coordinate system of ROIs.

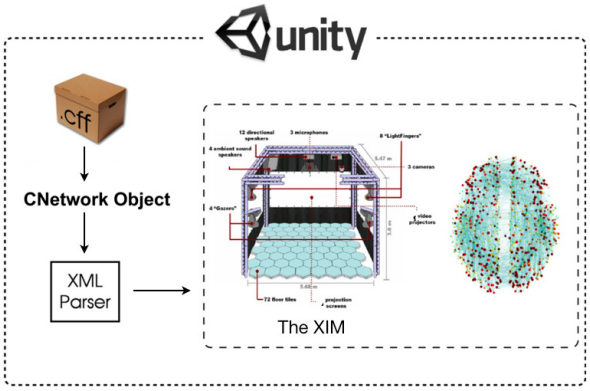

Fig. 2: Processing architecture of the XIM (figure courtesy: Wipawee Kongsantad).

To introduce dynamics into the visualization, the large-scale multi-level neural networks simulator, `iqr` (http://iqr.sourceforge.net/), is bi-directionally interfaced to Unity. (Bernardet and Verschure 2010). `iqr` allows the user to design complex neuronal models through a graphical interface and to visualize, analyze and modify the model's parameters online. The architecture of `iqr` is modular, providing the possibility to define custom neurons and synapses. `iqr` can simulate large neuronal systems up to 500k neurons and connections and can be directly interfaced to external sensors and effectors. In order to enable real-time user interaction with the reconstructed data, user input from Unity is sent to `iqr`. `iqr` computes the processes and broadcasts the output of the simulation back to the Unity engine in the XIM. The simulation runs continuously in real-time, with `iqr` receiving commands through Unity at any time during the simulation. The

simulator transmits activity from each neuronal module back to Unity every 500 ms. The activity has a normalized value between 0 and 1, and is the average activity per group. Gaussian noise of standard deviation 0.1 in introduced in all neuronal modules of the system. Upon receiving input from `iqr`, Unity updates the network reconstruction. Moreover, the user can also stimulate a neuronal group by a natural gesture corresponding to injecting an external excitatory current into the network. Gesture-based signaling within the XIM is supported via the Social Signal Interpretation (SSI) framework (Wagner et al. 2011).

As a proof of principle, the XIM has been previously been tested for visualization and analysis of artificially generated networks (Betella et al. 2012). The system transforms neuronal systems designed with `iqr` into three-dimensional representations of neuronal processes, groups and connections. While exploring the neuronal simulation, users are presented with a visualization of network configurations and associated activity. They can manipulate parameters of the system to perform specific computations. Fig. 3 shows a user exploring a neural network whilst navigating in the XIM. The screen on the left shows output of network activity from `iqr`.

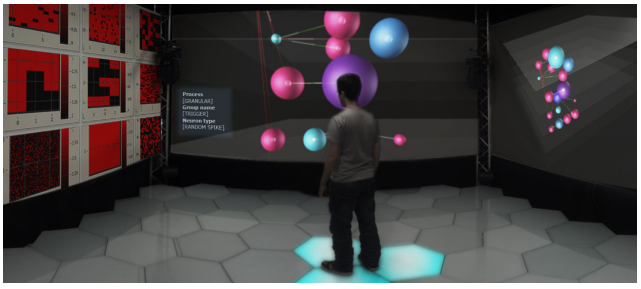

Fig. 3: Neural network 3D reconstruction in the XIM.

With the connectome data, we now push the limits of the XIM for dynamical simulation and analysis of real-world complex networks. This was done by optimizing the Unity engine to improve real-time visualization and interaction with the system. Our results are shown below.

RESULTS

Fig. 4 shows the frontal view of the connectome simulation, when the user is positioned afar from the screen. When the user moves sideways, parallel to the screen, the network will rotate (in the opposite direction to the user's movement) and reveal its side-view. On the other hand, when the user moves directly towards the screen, the visualization becomes immersive Fig. 5, placing the user "within" the 3D network.

Coupling the visualization of the data with `iqr` now allows the user to selectively perturb the system. What

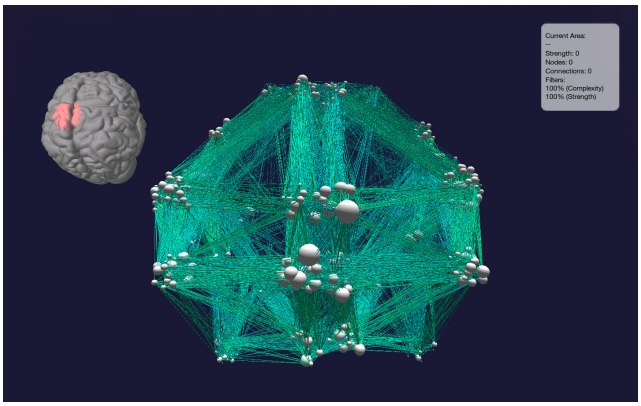

Fig. 4: Frontal view screenshot of the connectome within the XIM dynamical simulation environment.

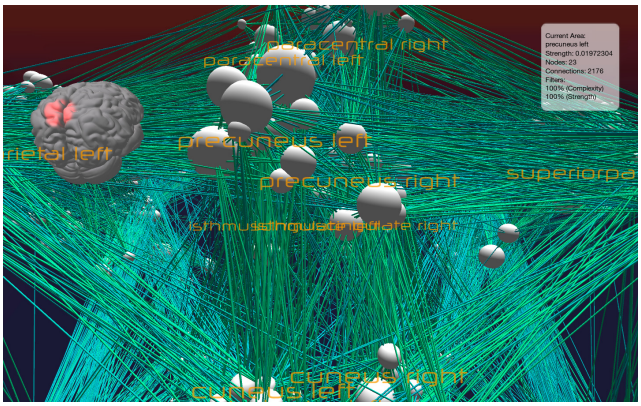

Fig. 5: User-immersed visualization of the connectome within the XIM.

can we learn from these perturbations about causal activity sequences in underlying neural circuits? In the example here, we excite two brain regions (not simultaneously), the left superior parietal (lSP) area and the right superior parietal (rSP) area, by injecting them with an external current. These regions are marked in bold in the cortical atlas provided in Fig. 6. The other regions marked in the atlas are those through which ensuing activity propagates. Causal propagation of activity is shown in Fig. 7. Seven areas are activated in each hemisphere during the sequence following SP stimulation. Column A of Fig. 7 shows stimulation and activity in the left hemisphere, whereas column B shows the same for the right hemisphere. T1 to T6 denote six time-points. T1 is 1 seconds before stimulation. T2 is when stimulation of the two SP areas begin. T3 is 0.5 seconds after stimulation onset. T4 is 5 seconds after onset and this is when stimulation of SP is stopped. T5 shows surviving activity 10.5 seconds after onset and the network returns to its initial state at T6 11.5 seconds after stimulation onset. Persistent activation after stimulation removal is stronger in the right hemisphere. The network shows low levels of default activity even before stimulation, due to Gaussian noise in each module. Specifically regions with more recurrent con-

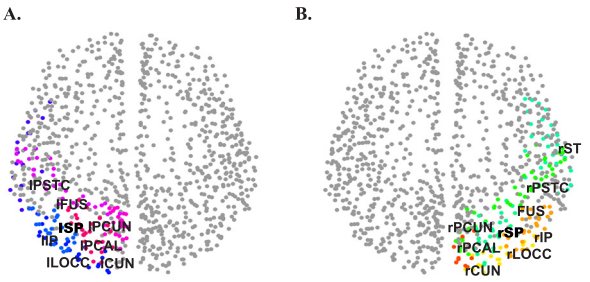

Fig. 6: Atlas of brain areas activated by stimulation of the left (A) and right (B) superior parietal region. Bold labels identify the stimulation site.

nections, show greater default activity and also greater post-stimulation persistent activity.

The superior parietal region is known to primarily control visual guidance of movements of the hands, fingers, limbs, head, and eyes (Wolbers et al. 2003). This region has expanded in humans to include regions controlling not only the actual manipulation of objects but also the mental manipulation of objects. Our simulation predicts that exciting SP leads to persistent activation in regions ST (superior temporal cortex, which is associated to perception of motion), LOCC (lateral occipital complex plays a role in object recognition), pCUN (precuneus is involved in visuo-spatial imagery) and CUN (cuneus is involved in visual processing). All these regions are indeed associated to visuo-motor functions. Hence the causal activation sequence we observe in the parietal lobe is indicative of visuo-motor integration.

DISCUSSION

As techniques of quantitative analysis and measurement devices in neuroscience make improvements, it is becoming more evident that the role of large-scale dynamics and brain-wide quantitative measures cannot be ignored. Local two-point correlations in functional data do not capture these features. Large-scale temporal activity maps across directionally connected brain structures are directly informative of brain-wide neural circuit mechanisms. Moreover, being able to predict these maps by implementing realistic biophysical dynamics brings us a small step closer to identifying the neural correlates of cognitive function.

The dynamic connectome tool, we present in this paper, is a first step in this direction. It opens the possibility of analyzing real-time activity propagation due to causal dynamics. Being immersive, it gives a completely different anatomical perspective, than a standard brain atlas would. As possible applications of this technology, we foresee online user-interaction with simulations as a step toward virtual brain surgery, enabling a surgeon to try out several procedures and assessing their impact by analyzing resulting activity. In our results, we notice a sequence of causal activations in regions that represent cognitively related functions.

As further improvements to this work, we are in the process of implementing more realistic biophysical dynamics, that will enable a finer comparison between empirical data and simulation.

ACKNOWLEDGMENTS

This work was performed within the framework of the "Collective Experience of Empathic Data Systems" (CEEDS) (FP7-ICT-2009-5, project number: 258749).

REFERENCES

[1] Bernardet, U.; Bermudez i Badia, S.; Duff, A.; Inderbitzin, M.; Le Groux, S.; Manzolli, J.; Mathews, Z.; Mura, A.; and Verschure, P.F.M.J. 2010. "The eXperience Induction Machine: A New Paradigm for Mixed-Reality Interaction Design and Psychological Experimentation". In E. Dubois, P. Gray, L. Nigay (Eds.), *The Engineering of Mixed Reality Systems* (pp. 357-379). London: Springer London.

[2] Bernardet, U.; Inderbitzin, M.; Wierenga, S.; Väljamäe, A.; Mura, A.; and Verschure. P.F.M.J. 2008. "Validating Presence by Relying on Recollection: Human Experience and Performance in the Mixed Reality System XIM". In L. G. Anna Spagnolli, editor, 11th Annual International Workshop on Presence, Padova Italy, volume 54.

[3] Bernardet, U.; Verschure, P. 2010. "`iqr`: A Tool for the Construction of Multi-level Simulations of Brain and Behaviour". *Neuroinformatics*, 8(2): 113-134.

[4] Betella, A.; Carvalho, R.; Sanchez-Palencia, J.; Bernardet, U.; Verschure, P.F.M.J. 2012. "Embodied Interaction with Complex Neuronal Data in Mixed-Reality". In proceedings of the 2012 Virtual Reality International Conference, p3, ACM.

[5] Delbrück, T.; Whatley, A.M.; Douglas, R.; Eng, K.; Hepp, K.; Verschure, P.F.M.J. 2007. "A Tactile Luminous Floor for an Interactive Autonomous Space". *Robotics and Autonomous Systems* 55(6): 433-443.

[6] Hagmann, P. 2005. "From Diffusion MRI to Brain Connectomics" [PhD Thesis]. Lausanne: École Polytechnique Fédérale de Lausanne (EPFL).

[7] Hagmann, P.; Cammoun, L.; Gigandet, X.; Meuli, R.; Honey, C.J.; Wadeen, V.J.; Sporns, O. 2008. "Mapping the Structural Core of Human Cerebral Cortex". *PLoS Biol* 6(7): e159.

[8] Siegel, M.; Donner, T.H.; Engel, A.K. 2012. "Spectral Fingerprints of Large-scale Neuronal Interactions". *Nature Reviews Neuroscience* 13: 121-34.

[9] Sporns, O.; Tononi, G.; Kötter, R. 2005. "The Human Connectome: A Structural Description of the Human Brain". *PLoS Comput Biol* 1: 245-251.

[10] Talairach, J.; Tournoux, P. 1998. "Co-planar Stereotaxic Atlas of the Human Brain: 3-Dimensional Proportional System - an Approach to Cerebral Imaging". Thieme Medical Publishers, New York.

[11] Wagner, J.; Lingenfelser, F.; André, E. 2011. "The Social Signal Interpretation Framework (SSI) for Real Time Signal Processing and Recognition". *Proceedings of Interspeech 2011*, Florence, Italy.

[12] Wolbers, T.; Weiller, C.; and Büchel, C. 2003. "Contralateral Coding of Imagined Body Parts in the Superior Parietal Lobe". *Cereb. Cortex*, 13 (4): 392-399.

[13] Wong, K.F.; Wang, X.J. 2006. "A Recurrent Network Mechanism of Time Integration in Perceptual Decisions". *Journal of Neuroscience*, 26(4):1314-1328

[14] Zhou, C.; Zemanova, L. ; Zamora, G.; Hilgetag, C.C.; Kurths, J. 2006. "Hierarchical Organization Unveiled by Functional Connectivity in Complex Brain Networks". *Physical Review Letters*, 97, 238103.

The biographies of the authors are listed on the SPECS webpage: http://specs.upf.edu/people

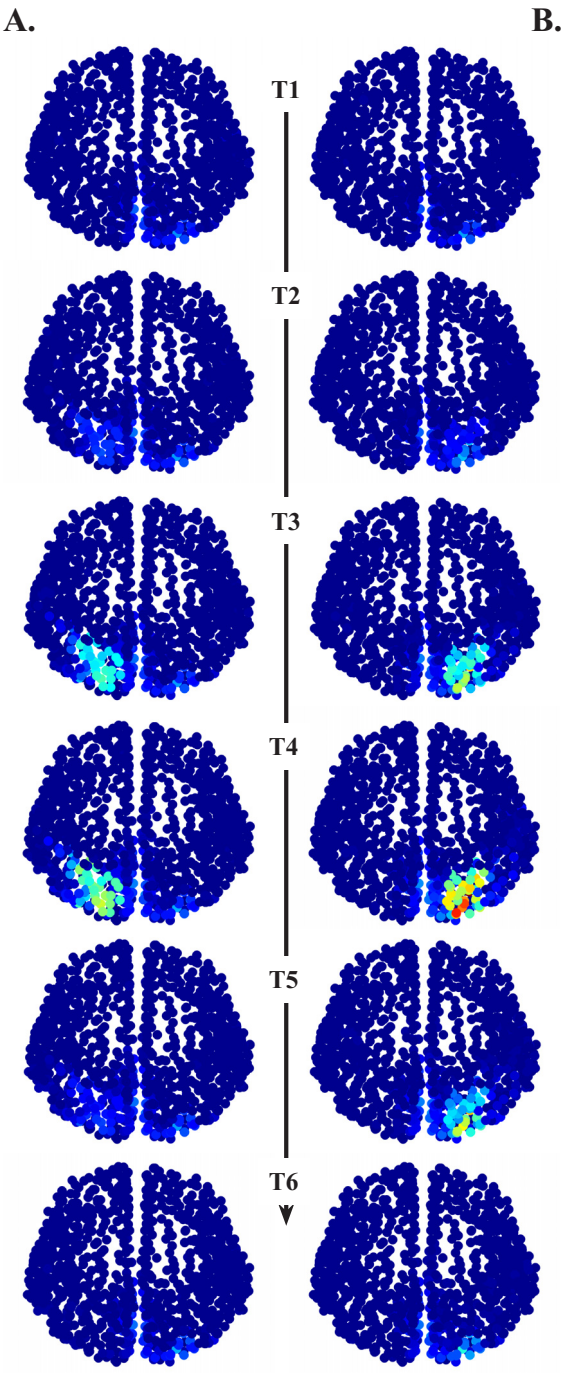

Fig. 7: Activation sequences of the cortical network following stimulation of the left (A) and right (B) superior parietal regions. Stimulation is applied at T2 and released at T4. Warmer colors indicate higher neuronal activity.

ON SPATIO-TEMPORAL PATTERNS IN TWO-LAYER RING TOPOLOGY NEURAL FIELDS

Fayssa Salomon
Evan C Haskell
Division of Math, Science, and Technology
Farquhar College of Arts and Sciences
Nova Southeastern University
Fort Lauderdale, FL 33314 USA
haskell@nova.edu

ABSTRACT

Spatially coherent structures and propagating waves of neural activity are commonly found throughout the central nervous system. These activity profiles are represented in both natural and pathological phenomena. We explore a two-layer neural field model dually constrained by local interactions and a cortical topography described by a ring topology neural network. We examine the conditions for the generation of wave solutions. The constraints on neuronal network computation implied by the dual local constraints may place further constraints on global cortical network architecture to achieve physiologically consistent wave behavior.

INTRODUCTION

Spatially coherent activity states are ubiquitous throughout the central nervous system and in observations from voltage-sensitive dye imaging (VSDI) and multi-electrode arrays (Wu et al., 2008). These patterns including localized activity states, spatially homogeneous oscillations, and wave behavior, may play important roles in neo-cortical processing and nervous system development. These behaviors can arise as an emergent behavior from interacting neural populations (Amari, 1977; Wu et al., 2008). Recurrent network connections have long been proposed as a mechanism for the formation of such patterns observed in many phenomena including feature selectivity in the visual system (Somers et al., 1995; Hansel and Sompolinsky, 1998), working memory (Amit and Brunel, 1997), head direction system (Zhang, 1996), motion perception (Giese, 1998), and in describing EEG rhythms (Nunez, 1995), local field potential spectra (Pinotsis et al., 2012), and wave behavior (Coombes, 2005). Understanding the mechanisms that contribute to the generation of such patterns is important for understanding a host of both natural and pathologic neurobiological behaviors. Propagating waves are observed as sensory evoked waves in cortex, epileptiform waves underlying epileptic seizures, and spontaneous waves of cortical activity, the latter may be of particular import for cortical processing (Wu et al., 2008).

In this report we follow a framework for studying spatially coherent structures and waves of activity in neural fields introduced by Amari (Amari, 1977). Amari demonstrated how the predominantly local interactions in neural populations give rise to localized activity states, oscillations, and stationary traveling waves of activity in a neural field model defined over the real line. Such neural field models are tissue level descriptions of mean membrane potential. In addition to local interactions, topographic maps of sensory features are ubiquitous in cortical sensory systems and some motor systems and may play fundamental roles in sensory processing (Woolsey et al., 1942; Hubel and Wiesel, 1977; Kass, 1997; Silver and Kastner, 2009; Wilimzig et al., 2012). These maps provide a functional network architecture that we explore within the neural field framework presented by Amari. Advances in VSDI have allowed for the in vivo measuring of population responses in superficial cortical layers at high spatial and temporal resolution (Grinvald and Hildesheim, 2004). Taking a cue from the columnar topographic organization of the topographic map for orientation tuning in primate cortex (Blasdel and Salama, 1986) we explore ring topology neural fields.

The interaction of local processing by neural networks and stimulus topography places a strong constraint on cortical processing. Distributions of preferred features may maximize sensitivity throughout the stimulus space (Purushothaman and Bradley, 2004). It has been proposed in primary visual cortical area V1 that the structure of natural stimuli may well serve to shape the network architecture in area V1 (Simoncelli and Olshausen, 2001; Singh et al., 2008). For associative learning tasks, the interaction of local processing and topography may result in a biased distribution of preferred stimulus (Fitzgerald et al., 2013). Indeed, the interaction of local processing and compact topologies implied solely by regular topography of cortical regions for feature selectivity has demonstrated new results for single layer neural fields (Haskell and Bressloff, 2003; Haskell and Paksoy, 2011). We provide a taxonomy of standing wave solutions in two layer neural fields showing that regions of tri-stability observed in single layer fields are also observable in two layer neural fields. We point out that the topology of feature space does not play a factor in homogeneous oscillations but owing to the periodic nature of the ring topology prohibits the formation of traveling front solutions which are observable in single layer neural fields defined over the real line.

Proceedings 27th European Conference on Modelling and Simulation ©ECMS Webjørn Rekdalsbakken, Robin T. Bye, Houxiang Zhang (Editors)
ISBN: 978-0-9564944-6-7 / ISBN: 978-0-9564944-7-4 (CD)

NEURAL FIELD MODEL

Subthreshold level neuronal activity is reflected in recordings from VSDI that represents local mean membrane potential. From the VSDI measurement a prediction of spiking activity by neurons can be made (Chen et al., 2012). The local network processing of this spiking activity results in many emergent behaviors including localized activity states, oscillations, and propagating waves of neural activity (Amari, 1977; Coombes, 2005).

For our model, we consider a continuum of neurons distributed on a ring domain indexed by a stimulus variable $\theta \in [-\pi, \pi)$. Here θ may represent for example the orientation selectivity of a neuron in cortical area V1 which maps directly by the topography of V1 to a continuous position variable. The evolution equation for the mean membrane potential, $u_i(\theta, t)$, for neurons in a m layer network indexed by i receiving a homogenous external input h_i and an inhomogeneous external input $s_i(\theta, t)$ is of the form:

$$\tau_i \frac{\partial u_i(\theta,t)}{\partial t} = -u_i(\theta,t) + h_i + s_i(\theta,t) + \sum_{j=1}^{m} \int_{-\pi}^{\pi} w_{ij}(\theta|\theta^{'}) f[u_j(\theta^{'},t)] \frac{d\theta^{'}}{2\pi} \quad (1)$$

where $w_{ij}(\theta|\theta^{'})$ is a connectivity function representing the mean synaptic efficacy from a neuron at a position $\theta^{'}$ in layer j to a neuron at position θ in layer i, $f[u_i]$ is a transduction function from the mean membrane potential, u_i, to the mean rate of spiking activity or activity level and $\tau_i > 0$ is the time constant for the dynamics of the type of neuron represented in layer i, $f[u]$ should be a non-decreasing saturating function. The simplest choice that exhibits non-trivial dynamics is a Heaviside function where the neuron is fully active when the mean membrane potential is above a firing threshold and inactive otherwise (Amari, 1977; Coombes, 2005; Haskell and Bressloff, 2003; Haskell and Paksoy, 2011). As such, we choose such a function for the analysis presented below:

$$f[u] = \begin{cases} 1 & \text{if } u > 0 \\ 0 & \text{otherwise} \end{cases} \quad (2)$$

Experimental evidence suggests that local circuits operate with neurons connecting to most of their neighbors in a manner that is approximately isotropic and homogeneous (Douglas et al., 1995) as such, we consider a connectivity function $w_{ij}(\theta|\theta^{'})$ that depends only on the relative distance in the case of a position variable or feature dissonance in the case of a feature variable between neurons. In the ring topology this is measured as angular separation, $\theta - \theta^{'}$ (Ben-Yishai et al., 1995; Somers et al., 1995; Haskell and Bressloff, 2003). As well, experimental evidence in orientation preference maps suggests that intracortical excitatory and inhibitory synaptic currents are distributed with differences in preferred orientation (Roerig and Chen, 2002). This homogeneity of the neural field implies a rotational symmetry for the connectivity function that is invariant to the $O(2)$ symmetry group of coordinate rotations and reflections in the ring. Thus $w_{ij}(\theta|\theta^{'})$ with $w_{ij}(\theta)$ a 2π-periodic even function of θ, $w_{ij}(\theta) = w_{ij}(\theta + 2\pi) = w_{ij}(-\theta)$. Any such connectivity function can be written as a cosine series expansion:

$$w_{ij}(\theta) = W_0^{ij} + \sum_{k>0} W_k^{ij} \cos(k\theta)$$

Considering only the first two terms of the expansion,

$$w_{ij}(\theta) = W_0^{ij} + W_1^{ij} \cos(\theta),$$

is sufficient for non-trivial results (Ben-Yishai et al., 1997; Haskell and Bressloff, 2003; Haskell and Paksoy, 2011). Single layer neural fields (m=1) of lateral inhibition type and ring topology with only first two components of the weighting kernel have previously been demonstrated to exhibit stable localized activity states where only a local region of the neural field is active (Haskell and Bressloff, 2003; Haskell and Paksoy, 2011). Lateral inhibition type neural fields correspond to a local connectivity where neurons in close proximity are mutually excitatory while those more distal are mutually inhibitory requiring $W_1^{11} > W_0^{11}$ and $W_0^{11} + W_1^{11} > 0$. When $W_0^{ii} > W_1^{ii} > 0$ for a layer i, the layer is self excitatory.

The discrete layers can be used to represent the heterogeneity of neurons collocated in a cortical tissue. Differences in effective membrane properties and synaptic filtering and latency would be encapsulated respectively in the membrane time constant, τ_i , and time-dependent synaptic efficacy function, $w_{ij}(\theta_i, \theta_j, t)$. Studies of the general properties of cortical networks commonly pool neurons into two layers representing excitatory cells and inhibitory cells respectively (Wilson and Cowan, 1973; Amari, 1977; Haskell and Bressloff, 2003; Haskell and Paksoy, 2011; Ben-Yishai et al., 1997; Pinto and Ermentrout, 2001; Blomquist et al., 2005). To study the formation of spatio-temporal patterns in a topographically constrained network with local interactions, we consider the system (1) with $m = 2$ as a two layer neural field (Amari, 1977; Ben-Yishai et al., 1997; Salomon and Haskell, 2012).

For the two layer neural field we utilize the Amari type connectivity where the excitatory neurons (layer 1) receives input from both layers 1 and 2; while, inhibitory neurons (layer 2) receive only excitatory input from neurons in layer 1 that share the same position variable θ ($W_1^{21} = 0$). Thus the two layer version of system (1) may be written as:

$$\begin{aligned} \tau_1 \frac{\partial u_1}{\partial t} &= -u_1(\theta,t) + \int_{-\pi}^{\pi} w_{11}(\theta - \theta^{'}) f[u_1(\theta^{'},t)] \frac{d\theta^{'}}{2\pi} \\ &\quad - \int_{-\pi}^{\pi} w_{12}(\theta - \theta^{'}) f[u_2(\theta^{'},t)] \frac{d\theta^{'}}{2\pi} + h_1 \\ \tau_2 \frac{\partial u_2}{\partial t} &= -u_2(\theta,t) + W_0^{21} f[u_2(\theta,t)] + h_2 \end{aligned} \quad (3)$$

In order to prevent layer 2 from being persistently fully active (i.e. $u_2(\theta,t) > 0, \forall\theta\ t$) we require $h_2 < 0$; however, for layer 2 to be able to provide feedback to layer 1 we must have $W_0^{21} > -h_2$.

A segregation of the collocated neurons into a layer of excitatory (layer 1) and inhibitory (layer 2) neurons corresponds to $W_0^{11} > W_1^{11}$ and $W_0^{12} > W_1^{12}$. Note that for the description of the connectivity function the excitatory and inhibitory interactions are maximal for neurons with similar feature preference consistent with experimental findings (Roerig and Chen, 2002). In the visual cortex of ferret it has been demonstrated that the overwhelming majority of cortical inputs are local with excitatory inputs being very narrowly tuned to the orientation preference of the cells and inhibitory inputs showing a broader tuning with excitatory post-synaptic currents being dominant from cells with similar orientation preference and inhibitory post-synaptic currents dominant for cells with dissimilar orientation preference (Roerig and Chen, 2002). This is modeled in the two layer neural field (3) by setting $W_0^{11}+W_1^{11} > W_0^{12}+W_1^{12}$ and $W_0^{11}-W_1^{11} < W_0^{12}-W_1^{12}$. Note that in the ferret study the excitatory connections are localized to stimulus feature but not physical location. That is, the connections span across the cortical hypercolumn to the next patch of neurons with similar orientation preference. As such, from a computational perspective, the periodic boundary conditions provide an extension to a periodic media. That is, the traveling wave solutions we find are traveling periodic pulses in sense that $u_i(\theta, t-t_0) = u_i(\theta+vt_0, t)$ where v is an unknown wave velocity and $\theta+vt_0$ is understood to be appropriately shifted by a multiple of 2π (Shigesada and Kawasaki, 1997).

STANDING WAVES

Standing waves manifest as equilibrium solutions, $u_i(\theta,t) = U_i(\theta)$, with continuous regions where the field is active within a given region and inactive outside that region. The active region of the field is characterized by the set function:

$$R[U_i] = \{\theta | U_i(\theta) > 0\}.$$

Two layer Wilson-Cowan equations have been shown to present paired pulse solutions over the real line (Pinto and Ermentrout, 2001; Blomquist et al., 2005) and in ring topologies (Ben-Yishai et al., 1997). For single layer neural field models with compact network topologies and connectivity functions modeled by first order harmonics, a full taxonomy of the localized activity states demonstrates parameter regimes of tri-stability and ability to form localized activity states with homogenous excitatory input (Haskell and Bressloff, 2003; Haskell and Paksoy, 2011). In this section we extend that discussion to the two layer ring topology setting and show regimes of tri-stability and paired pulse solution with homogeneous excitatory input.

Following the Amari analysis for the formation of localized activity states in a single layer, we construct a pair of standing pulse solutions (Amari, 1977; Pinto and Ermentrout, 2001; Blomquist et al., 2005). Without loss of generality we consider the standing pulse in layer 1 to be centered at $\theta = 0$ with an unknown width $2a < 2\pi$,that is, $R[U_1] = (-a, a)$. For $W_0^{21} > -h_2$ we find $R[U_2] = (-a, a)$ otherwise $R[U_2] = \emptyset$. The time independent solution for layer 2 is:

$$U_2(\theta) = \begin{cases} W_0^{21} + h_2 & -a < \theta < a \\ h_2 & \text{otherwise} \end{cases}$$

and layer 1:

$$U_1(\theta) = \frac{1}{\pi}\Big(\big(W_0^{11} - W_0^{12}\big)a + \big(W_1^{11} - W_1^{12}\big)\sin(a)\cos(\theta)\Big) + h_1. \quad (4)$$

The unknown value a is then found by solving the relation $U_1(\pm a) = 0$. As $U_i(\theta)$ is an even function, it is sufficient to consider only $\theta = a$ and seek solutions of

$$W(a) + h_1 = 0$$

where,

$$W(a) = \frac{1}{\pi}\Big(\big(W_0^{11} - W_0^{12}\big)a + \frac{W_1^{11} - W_1^{12}}{2}\sin(2a)\Big). \quad (5)$$

We extend to two layer neural field setting our previous found implications of (5) for single layer neural fields in compact topologies (Haskell and Bressloff, 2003; Haskell and Paksoy, 2011).

Theorem 1: In the absence of inhomogeneous input:
a) There exists a quiescent state if and only if $h_1 < 0$.
b) There exists a fully active state if and only if $W_0^{11} > W_0^{12} - h_1$.
c) There exists a standing wave if and only if $W(a) + h = 0$ for some $a \in (0, \pi)$ and $W_1^{11} > W_1^{12}$.

Proof:

a) The quiescent state corresponds to no activity in layer 1 or 2 so that $R[U_1] = \emptyset, R[U_2] = \emptyset$ implying $U_1(\theta) = h_1$ and $U_2(\theta) = h_2$. This requires $h_1 < 0$. From the model assumptions $h_2 < 0$. If $h_1 < 0$ then $U_1(\theta) = h_1$ yields a quiescent state to the system.

b) A fully active state corresponds to $R[U_1] = [-\pi, \pi)$. This implies that $U_1(\theta) = W_0^{11} - W_0^{12} + h_1$ and $U_2(\theta) = W_0^{21} + h_2$. This requires the mean drive a neuron receives from recurrent connections in layer 1 to be greater than the net mean input the neuron receives from layer 2 and the homogeneous drive, that is, $W_0^{11} > W_0^{12} - h_1$. Note that $W_0^{21} + h_2 > 0$ by model assumption. If $W_0^{11} > W_0^{12} - h_1$ then $U_1(\theta) = W_0^{11} - W_0^{12} + h_1$ is a fully active state.

c) For $R[U_i] = (-a, a), i = 1, 2, U_1(\theta) > 0$ for $-a < \theta < a, U_1(\theta) < 0$ for $a < |\theta| < \pi$, and $U_1(\theta) = 0$ for $\theta = \pm a$. Such a solution with $U_1(\theta) = 0$ for $\theta = \pm a$ occurs if and only if $W(a)+h = 0$. Noting that (4) is a monotonically decreasing (increasing) function for $W_1^{11} > W_1^{12}$ ($W_1^{11} < W_1^{12}$) then $U_1(\theta) < 0$ for $a < |\theta| < \pi$ requires $W_1^{11} > W_1^{12}$.

A taxonomy for the standing wave solutions summarized in figure 1 derives from the existence requirement

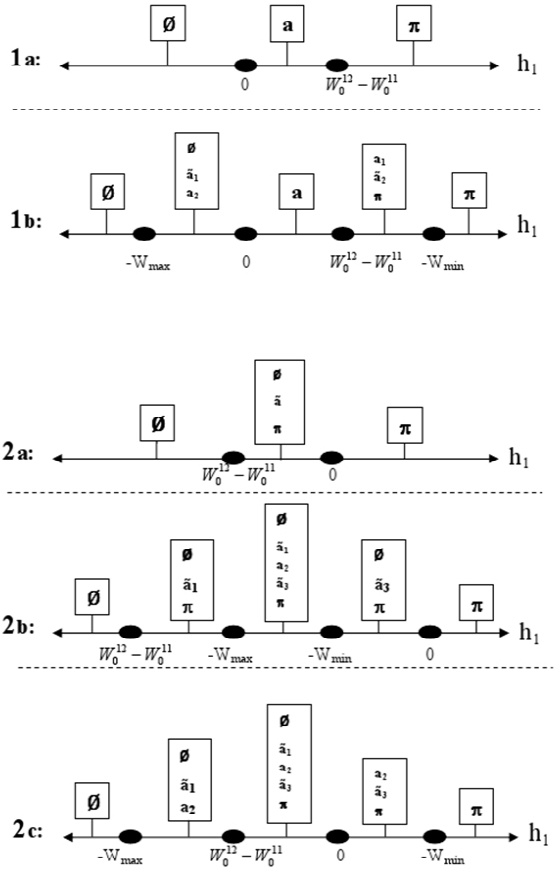

Fig. 1. Equilibrium solutions for various values of h_1. The existence of quiescent ($\emptyset$), fully active (π), and localized activity states ($a_i, a_1 < a_2 < a_3$) are indicated with the corresponding range of h_1 indicated. Unstable localized activity states are indicated with a tilde.

that the modulation of the mean input a layer 1 neuron receives from recurrent connections within layer 1 exceed that received from layer 2 ($W_1^{11} > W_1^{12}$). These solutions can be separated into two distinct cases where the mean input from recurrent connections within layer 1 exceeds or is exceeded by that received from layer 2. Respectively these two cases are represented by case 1 where $W_0^{11} > W_0^{12}$ and case 2 where $W_0^{11} < W_0^{12}$.

Case 1a:$W_0^{11} + W_1^{11} < W_0^{12} + W_1^{12}$: In this case $W(a)$ has no stationary points and is a monotonically decreasing function. There is a standing wave when $0 < h_1 < W_0^{21} - W_0^{11}$.

Case 1b:$W_0^{11} + W_1^{11} > W_0^{12} + W_1^{12}$: $W(a)$ has two stationary points with $W_{max} > 0 > W_{min}$ where W_{max} and W_{min} indicate the maximum and minimum values of $W(a)$ respectively. There are two regions of bi-stability with the standing wave and either the quiescent or fully active state both stable.

Case 2a: $0 < W_1^{11} - W_1^{12} < W_0^{11} - W_0^{12}$: $W(a)$ has no stationary points and is a monotonically increasing function. There is no stable standing wave; however there is a region with an unstable standing wave separating a stable quiescent and all active state.

Case 2b: $W_0^{11} - W_0^{12} < W_1^{11} - W_1^{12} < \gamma\big(W_0^{11} - W_0^{12}\big)$: $W(a)$ has two stationary points with $W_{min} > 0$. We find not just regions of mono- and bi-stability with the quiescent or all active state but also a region of tri-stability when $-W_{max} < h_1 < W_{min}$ where stable quiescent and all active states are found along with a stable standing wave. The value $\gamma \approx 4.6$ separates the region where $W_{min} > 0$ and $W_{min} < 0$ is found numerically (Haskell and Paksoy, 2011).

Case 2c: $\gamma\big(W_0^{11} - W_0^{12}\big) < W_1^{11} - W_1^{12}$: As in 2b $W(a)$ has two stationary points with $W_{max} > 0 > W_{min}$. We again find regions of mono-, bi-, and tri-stability. We note that there is a region of bi-stability between the localized activity state and the fully active state for some positive h_1 values.

In the development of the two-layer field model, we required both $h_2 < 0$ and $W_0^{21} > -h_2 > 0$. Relaxing either of these requirements reduces the question of standing pulses in layer 1 to the case we previously studied for single layer neural fields with compact topology (Haskell and Bressloff, 2003; Haskell and Paksoy, 2011). In the case where $h_2 < 0$ and $W_0^{21} < -h_2$ we find $R[U_2] = \emptyset$ and $W(a) = \frac{1}{\pi}\Big(W_0^{11} a + \frac{W_1^{11}}{2}\sin(2a)\Big)$. In the case where $h_2 > 0$ and $W_0^{21} > 0$ we find $R[U_2] = S^1$ and $W(a) = \frac{1}{\pi}\Big(W_0^{11} a + \frac{W_1^{11}}{2}\sin(2a) - W_0^{12}\Big)$. In this latter special case finding solutions to $W(a)+h_1 = 0$ effectively shifts the values of h_1 that separate different equilibrium behaviors found for a given parameterization previously found by W_0^{12}.

OSCILLATIONS

Oscillations are defined here as spatially homogeneous solutions where every neuron in a given layer is either active ($u_i > 0$) or inactive ($u_i \leq 0$) independent of the feature or position variable, i.e. $u_i(\theta, t) = u_i(t)$.

For the ring topology, the connectivity function, $w(\theta)$, was expressed as a cosine series. More generally, any integrable function $f(\vec{x})$ can be expressed in an infinite series expansion using a set of orthonormal basis functions, $B_{i_1,i_2,\ldots,i_n}(\vec{x})$, for the function space:

$$f(\vec{x}) = \sum_{i_1,i_2,\ldots,i_n} a_{i_1,i_2,\ldots,i_n} B_{i_1,i_2,\ldots,i_n}(\vec{x})$$

where $B_{i_1,i_2,\ldots,i_n}(\vec{x})$ satisfies the orthogonality relations

$$\int B_{i_1,i_2,\ldots,i_n}(\vec{x}) B_{j_1,j_2,\ldots,j_n}(\vec{x}) \mathfrak{D}(\vec{x}) = \begin{cases} 0 & \text{if} \quad i_k \neq j_k \quad \text{for some k} \\ 1 & \text{if} \quad i_k = j_k \quad \text{for each k} \end{cases}$$

and $\mathfrak{D}(\vec{x})$ is the integration measure on the space. Given the orthogonality of the basis functions we have $\int f(\vec{x})\mathfrak{D}(\vec{x}) = a_{0,0,\ldots,0}$. As such the oscillations are not influenced by the topology of the feature space.

Integrating over θ, the system (3) reduces to the system of ordinary differential equations:

$$\tau_1 \frac{du_1}{dt} = -u_1(t) + W_0^{11} f[u_1(t)] - W_0^{12} f[u_2(t)] + h_1$$
$$\tau_2 \frac{du_2}{dt} = -u_2(t) + W_0^{21} f[u_1(t)] + h_2 \qquad (6)$$

We summarize the conditions for monostable, bistable, and oscillatory behavior in a spatially homogeneous network given in Amari (Amari, 1977). Depending on the sign of u_1 and u_2 the system will seek to move to a corresponding equilibrium point in the (u_1, u_2) phase plane which is shifted between the quadrants by the value of h_1 and h_2. Thus depending on the value of h_1 and h_2 when $W_0^{11} \geq W_0^{12}$ the system (6) exhibits either monostable or bistable behavior. When $W_0^{11} < W_0^{12}$, the system (6) can exhibit monostable, bistable, or oscillatory behavior depending on the values h_1 and h_2.

TRAVELING WAVE SOLUTIONS

Pairs of propagating pulses in the Wilson-Cowan equations with ring topology are obtained for networks where the excitatory layer receive isotropic excitatory external input (Ben-Yishai et al., 1997). We demonstrate the existence of pulse pairs when the excitatory layer receives isotropic inhibitory external input. Single layer neural fields over the real line may demonstrate traveling front solutions (Coombes, 2005). However, in the ring topology such traveling front solutions can not occur.

When the two layer neural field (3) exhibits a pair of propagating pulse solutions, we can express the solution in terms of the stationary waveforms:

$$u_i(\theta, t) = g_i(\theta - vt), i = 1, 2$$

Where g_1 and g_2 are the wave forms in layers 1 and 2 and v is the unknown wave velocity. Introducing the new variable $y = \theta - vt$ we rewrite the system (3):

$$\begin{aligned} -v\tau_1 g_1^{'} =& -g_1(y) + \int w_{11}(y - y^{'}) f[g_1(y^{'})] \frac{dy^{'}}{2\pi} \\ & - \int w_{12}(y - y^{'}) f[g_2(y^{'})] \frac{dy^{'}}{2\pi} + h_1 \end{aligned} \quad (7)$$

$$-v\tau_2 g_2^{'} = -g_2(y) + W_0^{21} f[g_1(y)] + h_2 \quad (8)$$

Where $g_i^{'}(y) = \frac{dg_i}{dy}$. Without loss of generality we assume that the wave form in layer 1 is centered at $y = 0$ and the unknown width of the excited region is $2a$. The excited regions of the field for layer 1 and 2 are:

$$R[g_1] = (-a, a), \; R[g_2] = (y_1, y_2)$$

where $y_1 < y_2$ denote the unknown boundaries of the excited region of layer 2. Under the boundary condition $g_2(-\pi) = g_2(\pi)$ reflecting the periodic nature of the ring topology we find explicit solution to (8):

$$g_2(y) = \begin{cases} W_0^{21} \frac{\sinh\left(\frac{a}{v\tau_2}\right)}{\sinh\left(\frac{\pi}{v\tau_2}\right)} e^{\frac{y+\pi}{v\tau_2}} + h_2 & -\pi \leq y < -a \\ W_0^{21} \frac{\sinh\left(\frac{a-\pi}{v\tau_2}\right)}{\sinh\left(\frac{\pi}{v\tau_2}\right)} e^{\frac{y}{v\tau_2}} + W_0^{21} + h_2 & -a \leq y < a \\ W_0^{21} \frac{\sinh\left(\frac{a}{v\tau_2}\right)}{\sinh\left(\frac{\pi}{v\tau_2}\right)} e^{\frac{y-\pi}{v\tau_2}} + h_2 & a \leq y < \pi \end{cases}$$

As the waveform in layer 2 trails layer 1, $0 < y_2 \leq a$. From $g_2(y_2) = 0$, y_2 is found:

$$y_2 = v\tau_2 \ln \frac{-W_0^{21} - h_2}{W_0^{21}\left(\frac{\sinh\left(\frac{a-\pi}{v\tau_2}\right)}{\sinh\left(\frac{\pi}{v\tau_2}\right)}\right)} \quad (9)$$

However, given the periodic nature of the ring topology y_1 could lie in either the region $-\pi \leq y_1 \leq -a$ or $a \leq y_1 < \pi$ depending on the layer 2 membrane properties (τ_2), strength of the drive from layer 1 to layer 2 (W_0^{21}), the width and velocity of the wave in layer 1 $(2a, v)$, and the level of homogeneous input to level 2 (h_2). When $-\pi \leq y_1 \leq -a$ then $y_1 = y_a$ where:

$$y_a = v\tau_2 \ln \frac{-h_2}{W_0^{21}\left(\frac{\sinh\left(\frac{a}{v\tau_2}\right)}{\sinh\left(\frac{\pi}{v\tau_2}\right)}\right)} - \pi \quad (10)$$

Otherwise, $y_1 = y_a + 2\pi$ admissible regions.

The expressions for y_1 and y_2 imply two necessary conditions for the existence of traveling wave solutions with non-zero wave velocity for the two layer neural field model. These conditions are $h_2 < 0$ from (10) and $W_0^{21} > -h_2$ from (9). Violation of either of these necessary conditions could potentially lead to a standing wave solution in layer 1 previously described. Note that the values for y_1 and y_2 depend upon the unknown values a and v.

Given $R[g_2]$ we solve for $g_1(y)$. Rewriting (7) as:

$$-v\tau_1 g_1^{'} = -g_1(y) + K(y) + h_1$$

where

$$\begin{aligned} K(y) =& \int_{-a}^{a} w_{11}(y - y^{'}) \frac{dy^{'}}{2\pi} - \int_{R[g_2]} w_{12}(y - y^{'}) \frac{dy^{'}}{2\pi} \\ =& \frac{1}{2\pi}\Big(2aW_0^{11} - W_0 12\Delta y + 2W_1^{11} \sin(a)\cos(y) \\ & - 2W_1^{12} \sin\big(\frac{\Delta y}{2}\big)\cos(y - \bar{y})\Big) \end{aligned}$$

and Δy and $\bar{y}$ are the width and center respectively of the layer 2 waveform. When $v > 0$ and $-\pi \leq y_1 \leq -a$, $\Delta y = y_2 - y_1$ and $\bar{y} = \frac{y_2 + y_1}{2}$.

With boundary condition $g_1(-\pi) = g_1(\pi)$, an explicit solution to (7) is found:

$$\begin{aligned} g_1(y) =& \frac{a}{\pi} W_0^{11} - \frac{\Delta y}{2\pi} W_0^{12} + h_1 \\ & + \frac{1}{1 + (\tau_1 v)^2} \frac{\sin(a)}{\pi} W_1^{11}\big(\cos(y) - \tau_1 v \sin(y)\big) \\ & - \frac{1}{1 + (\tau_1 v)^2} \frac{\sin\left(\frac{\Delta y}{2}\right)}{\pi} W_1^{12} \\ & \big(\cos(y - \bar{y}) - \tau_1 v \sin(y - \bar{y})\big) \end{aligned}$$

From the relations $g_1(\pm a) = 0$ we numerically find the width of the active region in layer 1, $2a \approx 0.72\pi rad$, and wave velocity, $v \approx 0.19\pi rad/\tau$ for the parameter set:

$$W_0^{11} = 3, W_1^{11} = 2, W_0^{12} = 2, W_1^{12} = 1, W_0^{21} = 1,$$

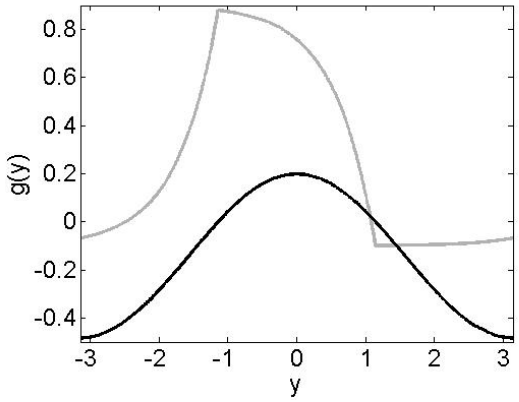

Fig. 2. Waveforms for traveling wave solution with positive wave velocity. Shown are $g_1(y)$ (black line) centered at $y = 0$ and corresponding $g_2(y)$ (grey line).

$$h_1 = h_2 = -0.1, \tau_1 = \tau_2 = 1.$$

The corresponding stationary waveforms are shown in figure 2. For layer two, the boundaries for the pulse are $y_2 \approx 0.34\pi rad$ and $y_1 \approx -0.79\pi rad$ resulting in a width of the waveform in layer 2 of $\Delta y \approx 0.88\pi rad$.

The symmetry of the connectivity function allows for pulses to propagate with either a positive or negative velocity. For the analysis of propagating pulses, it was sufficient to study just the waves with positive velocity as the symmetry of the problem will yield a "mirror" result for the waves with negative velocity. That is,whenever a pair (a, v) is found that permits a traveling wave solution, the pair $(a, -v)$ will also permit a traveling wave solution.

Traveling front solutions

In both the single layer and two layer neural field models (1) under certain parameter regimes the field has two stable stationary homogeneous states. However, the boundary condition of the ring topology, $u(-\pi, t) = u(\pi, t)$, prohibits the formation of a traveling front solution. For example, a disturbance $g(\theta - vt)$ of the quiescent state with non-zero velocity v, whose width is not such that the field enters the fully active state would necessarily have a homoclinic orbit in the $\Big(g(y), g^{'}(y)\Big)$ phase-plane where $y = \theta - vt$. That is, owing to the periodic nature of the boundary condition $u(\theta, t) = u\big(\theta, t + \frac{2\pi}{v}\big)$, any point where $u(\theta, t) \leq 0$ will return to this state within a time period of $\frac{2\pi}{v}$ from the disturbance. Situations where a quiescent state could be carried to a stable all active state may be highly undesirable as in a stable all active state it is very difficult to return network to a quiescent state where neurons could be responsive to new input.

DISCUSSION

Cortical neurons receive most of their input locally through synaptic interactions with other neurons that are in close physical proximity. Amari utilized this idea to develop a model for neural tissue that exhibited both spatial and dynamic pattern formation (Amari, 1977). However, VSDI and other experiments have demonstrated that cortical neurons also organize topographically on the cortical surface properties of stimulus features (Blasdel and Salama, 1986; Grinvald and Hildesheim, 2004; Hubel and Wiesel, 1977; Woolsey et al., 1942). The dual constraints of local processing and topographic representation of stimulus features have strong influence on neural computation and cortical processing. Utilizing compact topologies implied by topographic maps in cortex have shown new results in spatial pattern formation in single layer neural fields of lateral inhibition type (Haskell and Bressloff, 2003; Haskell and Paksoy, 2011). In this study a mechanism through the network interactions that generates and sustains standing and traveling waves in a two layer ring topology neural field has been explored. To what respect the ring topology is an appropriate network topology depends on the cortical area of study. However, given the dual constraints of local connectivity and network topology it is important to understand the influence that topology may have in generating the dynamic behaviors that are observed in a host of natural and pathological cortical conditions.

While the model presented takes into account both the nature of local processing and topography in cortex, the symmetry of the connectivity functions places no constraint on whether the wave velocity will be positive or negative. Traveling waves of spontaneous activity are ubiquitous in developing nervous systems, default mode fMRI studies, and evoked cortical responses. The direction of these waves may indicate an order to information flow through the nervous system that may be important in development and maintenance of normal brain function. Using the orientation tuning example, an experiment where a researcher measures the response in primary visual cortex area V1 to a rotating bar would result in a directed wave of excitation through the hypercolumn following the direction of the orientation. This is a locking of the response to the stimulus that is known to occur in populations of neurons from both experiments (Sirovich, 2012) and from theoretical considerations (Ben-Yishai et al., 1995; Knight, 1972; Sirovich, 2012). While stimulus locking can provide directionality in evoked responses, spontaneous responses may require an alternate mechanism. In area V1 it has been observed experimentally that long-range lateral connections can serve to modulate neural activity (Hirsch and Gilbert, 1991). This modulation of the local drive of the neural population could serve to provide an imbalance to the local activity that gives the wave a specific direction. The ability of the local network to support waves in any direction provides a strong constraint to the global network structure.

ACKNOWLEDGEMENTS

This work has been supported by a Nova Southeastern University Presidents Faculty Research and Devel-

opment Grant award to ECH.

REFERENCES

Amari, S. (1977). Dynamics of pattern formation in lateral-inhibition type neural fields. *Biol. Cybern.*, 27:77–87.

Amit, D. and Brunel, N. (1997). Model of global spontaneous activity and local structured activity during delay periods in the cerebral cortex. *Cerebral Cortex*, 7(3):237–252.

Ben-Yishai, R., Bar-Or, R. L., and Sompolinsky, H. (1995). Theory of Orientation Tuning in Visual Cortex. *Proceedings of the National Academy of Sciences*, 92:3844.

Ben-Yishai, R., Hansel, D., and Sompolinsky, H. (1997). Traveling Waves and the Processing of Weakly Tuned Inputs in a Cortical Network Module. *Journal of Computational Neuroscience*, 4(1):57–77.

Blasdel, G. G. and Salama, G. (1986). Voltage-Sensitive Dyes Reveal a Modular Organization in Monkey Striate Cortex. *Nature*, 321:579–585.

Blomquist, P., Wyller, J., and Einevoll, G. (2005). Localized activity patterns in two-population neuronal networks. *Physica D: Nonlinear Phenomena*, 206(3):180–212.

Chen, Y., Palmer, C., and Seidemann, E. (2012). The relationship between voltage-sensitive dye imaging signals and spiking activity of neural populations in primate V1. *Journal of Neurophysiology*, 107(12):3281–3295.

Coombes, S. (2005). Waves, bumps, and patterns in neural field theories. *Biological Cybernetics*, 93(2):91–108.

Douglas, R. J., Koch, C., Mahowald, M., Martin, K. A. C., and Suarez, H. H. (1995). Recurrent Excitation in Neocortical Circuits. *Science*, 269:981–985.

Fitzgerald, J. K., Freedman, D. J., Fanini, A., Bennur, S., Gold, J. I., and Assad, J. A. (2013). Biased associative representations in parietal cortex. *Neuron*, 77(1):180–191.

Giese, M. (1998). *Dynamic neural field theory for motion perception*. Kluwer Academic Publishers.

Grinvald, A. and Hildesheim, R. (2004). VSDI: a new era in functional imaging of cortical dynamics. *Nature Reviews Neuroscience*, 5(11):874–885.

Hansel, D. and Sompolinsky, H. (1998). Modeling feature selectivity in local cortical circuits. In Koch, C. and Segev, I., editors, *Methods in neuronal modeling*, pages 499–567. MIT Press, Cambridge, MA.

Haskell, E. C. and Bressloff, P. (2003). On the formation of persistent states in neuronal network models of feature selectivity. *Journal of Integrative Neuroscience*, 2(01):103–123.

Haskell, E. C. and Paksoy, V. (2011). Localized Activity States for Neuronal Field Equations of Feature Selectivity in a Stimulus Space with Toroidal Topology. In Machado, J. A. T., Baleanu, D., and Luo, A. C., editors, *Nonlinear and Complex Dynamics: Applications in Physical, Biological, and Financial Systems*, pages 207–216. Springer, New York.

Hirsch, J. A. and Gilbert, C. D. (1991). Synaptic Physiology of Horizontal Connections in the Cat's Visual Cortex. *Journal of Neuroscience*, 11:1800–1809.

Hubel, D. and Wiesel, T. (1977). Ferrier lecture: Functional architecture of macaque monkey visual cortex. *Proceedings of the Royal Society of London. Series B, Biological Sciences*, pages 1–59.

Kass, J. H. (1997). Topographic Maps Are Fundamental to Sensory Processing. *Brain Research Bulletin*, 44:107.

Knight, B. (1972). Dynamics of encoding in a population of neurons. *Journal of General Physiology*, 59:734–766.

Nunez, P. (1995). *Neocortical dynamics and human EEG rhythms*. Oxford University Press, USA.

Pinotsis, D. A., Moran, R. J., and Firston, K. J. (2012). Dynamic causal modeling with neural fields. *NeuroImage*, 59:1261–1274.

Pinto, D. and Ermentrout, G. (2001). Spatially structured activity in synaptically coupled neuronal networks: II. Lateral inhibition and standing pulses. *SIAM Journal on Applied Mathematics*, 62(1):226–243.

Purushothaman, G. and Bradley, D. (2004). Neural population code for fine perceptual decisions in area mt. *Nature Neuroscience*, 8(1):99–106.

Roerig, B. and Chen, B. (2002). Relationships of Local Inhibitory and Excitatory Circuits to Orientation Preference Maps in Ferret Visual Cortex. *Cerebral Cortex*, 12:187–198.

Salomon, F. and Haskell, E. C. (2012). Travelling wave solutions for ring topology neural fields. In Vigo-Aguiar, J., editor, *12th International Conference Computational and Mathematical Methods in Science and Engineering (CMMSE 12)*, pages 1523–1531.

Shigesada, N. and Kawasaki, K. (1997). *Biological invasions: theory and practice*. Oxford University Press, USA.

Silver, M. and Kastner, S. (2009). Topographic maps in human frontal and parietal cortex. *Trends in cognitive sciences*, 13(11):488–495.

Simoncelli, E. P. and Olshausen, B. A. (2001). Natural Image Statistics and Neural Representation. *Annual Review of Neuroscience*, 24:1193–1216.

Singh, G., Memoli, F., Ishkhanov, T., Sapiro, G., Carlsson, G., and Ringach, D. (2008). Topological analysis of population activity in visual cortex. *Journal of vision*, 8(8).

Sirovich, L. (2012). The faithful copy neuron. *Journal of Computational Neuroscience*, 32(3):377–385.

Somers, D., Nelson, S. B., and Sur, M. (1995). An Emergent Model of Orientation Selectivity in Cat Visual Cortical Simple Cells. *Journal of Neuroscience*, 15:5448–5465.

Wilimzig, C., Ragert, P., and Dinse, H. (2012). Cortical topography of intracortical inhibition influences the speed of decision making. *Proceedings of the National Academy of Sciences*, 109(8):3107–3112.

Wilson, H. and Cowan, J. (1973). A mathematical theory of the functional dynamics of cortical and thalamic nervous tissue. *Biological Cybernetics*, 13(2):55–80.

Woolsey, C., Marshall, W., and Bard, P. (1942). Representation of cutaneous tactile sensibility in the cerebral cortex of the monkey as indicated by evoked potentials. *Bull Johns Hopkins Hosp*, 70:399–441.

Wu, J., Huang, X., and Zhang, C. (2008). Propagating waves of activity in the neocortex: what they are, what they do. *The Neuroscientist*, 14(5):487–502.

Zhang, K. (1996). Representation of spatial orientation by the intrinsic dynamics of the head-direction cell ensemble: a theory. *The journal of neuroscience*, 16(6):2112–2126.

FAYSSA SALOMON holds a BS degree in Biology from Nova Southeastern University. Currently Ms. Salomon is pursuing the MS in Medical Sciences at the University of South Florida.

EVAN HASKELL is an Associate Professor of Mathematics at Nova Southeastern University. Dr. Haskell holds a Ph.D. in Mathematics from the Courant Institute of Mathematical Sciences, New York University. Previously Dr. Haskell was a visiting member of Cognitive Neuroscience sector at the International School for Advanced Study (SISSA) in Trieste, Italy, Scott Assistant Professor of Mathematics at University of Utah, and Visiting Assistant Professor of Mathematics at College of William and Mary.

Orally presented in the track:

Simulation and Computational Neuroscience

Modeling What You Can Measure In The Brain With Modern Multielectrodes

Gaute Einevoll

Stable Grid Cells Are Generated From Inhibitory Networks

Aree Witoelar

A Model For The Development Of Grid Cells

Yasser Roudi

Mean Field Theory For Network Inference With Stochastic Hidden Units

John Hertz, Yasser Roudi, Joanna Tyrcha, Benjamin Dunn

Learning In Restricted Boltzmann Machine

Bjorn Juel

Statistical Modeling Of Multi-Neuronal Recordings From The Entorhinal Cortex

Marie Morreaunet

Proceedings 27th European Conference on Modelling and Simulation ©ECMS Webjørn Rekdalsbakken, Robin T. Bye, Houxiang Zhang (Editors)
ISBN: 978-0-9564944-6-7 / ISBN: 978-0-9564944-7-4 (CD)

Simulation of Social Interaction

WHEN COMPETITION IS PUSHED TOO HARD. AN AGENT-BASED MODEL OF STRATEGIC BEHAVIOUR OF REFEREES IN PEER REVIEW

Juan Bautista Cabotà
Departament d'Informàtica
Universitat de València
Avinguda de la Universitat, s/n
46100 Burjassot-València
Email: juan.cabota@uv.es

Francisco Grimaldo
Departament d'Informàtica
Universitat de València
Avinguda de la Universitat, s/n
46100 Burjassot-València
Email: francisco.grimaldo@uv.es

Flaminio Squazzoni
Department of Economics and Management
University of Brescia, Via San Faustino 74/B 25122 Brescia
E-mail: squazzon@eco.unibs.it

KEYWORDS
Peer review; referees; competition; rational cheating; fairness; agent-based model.

ABSTRACT

This paper examines the impact of strategic behaviour of referees on the quality and efficiency of peer review. We modelled peer review as a process based on knowledge asymmetry and subject to evaluation bias. We built two simulation scenarios to investigate large-scale implications of referee behaviour and judgment bias. The first one was inspired by "the luck of the reviewer draw" idea. In this case, we assumed that referees randomly fell into Type I and Type II errors, i.e., recommending submissions of low quality to be published or recommending against the publishing of submissions which should have been published. In the second scenario, we assumed that certain referees tried intentionally to outperform potential competitors by underrating the value of their submissions. We found that when publication selection increased, the presence of a minority of cheaters may dramatically undermine the quality and efficiency of peer review even compared with a scenario purely dominated by "the luck of the reviewer draw". We also found that peer review outcomes are significantly influenced by differences in the way scientists identify potential competitors in the system.

INTRODUCTION

Pressures towards competition have recently increased in science, with scientists harshly competing for funds and reputation at a national and international level (e.g., Fanelli 2010). The digitalization of scientific publications and the development of scientometrics now permit to measure the scientist's performance through a variety of indicators, such as the impact factor, the "*h* index" and so on. By objectively ranking everyone, these measures allow us to compare our respective achievements and better identify potential competitors. Although specificities of standards exist even between sister disciplines, the strength of quantitative rankings is especially strong in the realm of the so-called "hard sciences", whereas it is certainly less true for the humanities, where objective measures are hardly systematically applicable.

The increasing importance of performance indicators requires to understand whether competitive spirits of scientists could influence the peer review process. For instance, referees could be tempted to exploit strategically their important gatekeepers' position to outperform potential competitors (Thurner and Hanel 2011; Grimaldo and Paolucci 2013; Callahan 2004). Indeed, while the debate on misbehaviour followed by submission authors has gained momentum, even in the media, less is known about the possible effect of referee behaviour (e.g., Bornmann 2011). On the one hand, as shown by the recent Stapel scandal, unfair scientists might profit from information asymmetry of referees and editors by manipulating experimental data and overselling their results. In doing so, they gain competitive advantages against fair colleagues (Crocker and Crooper 2011). On the other hand, referees could be induced to deliberately underrate potential competitors by providing unfair judgment, especially when possible publication of work by these colleagues does not have positive effects on their own reputation (e.g., in terms of citations), includes results that challenge referees' work or increases reputation of competing research groups for funding.

Our paper aims to examine these problems by proposing a modeling approach that looks at scientist behaviour in the peer review process to understand complex macro implications (e.g., Edmonds *et al*. 2011; Roebber and Schultz 2011; Thurner and Hanel 2011; Allesina 2012; Payette 2012; Squazzoni and Gandelli 2012). We modelled a population of agents interacting as authors and referees in a selective science system. Following Thurner and Hanel (2011) and Grimaldo and Paolucci (2013), we tested macro implications of unfair referee behaviour for the quality of peer review. Unlike these studies, we also considered efficiency problems and focused on aggregate consequences in terms of system's resource allocation and growth inequality.

Proceedings 27th European Conference on Modelling and Simulation ©ECMS Webjørn Rekdalsbakken, Robin T. Bye, Houxiang Zhang (Editors)
ISBN: 978-0-9564944-6-7 / ISBN: 978-0-9564944-7-4 (CD)

The rest of the paper is as follows. In the second section, we introduce the model and the simulation parameters, while in the third we present our simulation scenarios. In the fourth one, results are illustrated, while, in the concluding section, we present a summary of results and draw some implications for the current debate on peer review.

THE MODEL

Following Squazzoni and Gandelli (2012; 2013), we assumed a population of N scientists (N = 200) randomly selected each to playfill one of two roles: author or referee. The task of an author was to submit an article with the goal of having it accepted to be published. The task of a referee was to evaluate the quality of author submissions. As informed by the referees' opinion, only the best submissions were published (i.e., those exceeding the publication rate).

We gave each agent a set of resources which were initially homogeneous (R_a=1). Resources were a proxy of academic status, position, experience, and scientific achievement. The guiding principle was that the more scientists published, the more resources they had access to, and thus the higher their academic status and position.

We assumed that resources were needed both to submit and review an article. With each simulation step, agents were endowed with a fixed amount of resources f, equal for all (e.g., common access to research infrastructure and internal funds, availability of PhD. students, etc.). They then accumulated resources according to their publication score.

We assumed that the quality of submissions varied and was dependent on agent resources. Each agent had resources $R_a \in \mathbb{R}$, from which we derived an expected submission quality μ as follows:

$$\mu = \frac{v * R_a}{v * R_a + 1} \qquad (1)$$

where v indicated the velocity at which the quality of the submission increased with the increase of author resources. For instance, this means that for v = 0.1 each agent needed R_a = 10 to reach a medium-sized expected quality submission (μ = 0.5).

We assumed that authors varied in terms of the quality of their output depending on their resources. More specifically, the quality of submissions by authors followed a standard deviation σ which proportionally varied according to agent resources and followed a normal distribution $N(\mu, \sigma)$. This means that, with some probability, top scientists could write average or low quality submissions, and average scientists had some chance to write good submissions.

We assumed that successful publication multiplied author resources by a value m, which varied between 1.5 for less productive published authors and 1 for more productive published authors. We assigned a heterogeneous value of m after various explorations of the parameter space. This was seen as mimicking reality, where publication is crucial in explaining differences in scientists' performance, but is more important for scientists at the initial stages of their academic careers and cannot infinitely increase for top scientists. Thus, the resources of published authors grew accordingly, leading to subsequent submissions of presumably higher quality. If not published, following the "winner takes all" rule characterizing science, we assumed that authors lost all resources invested prior to submitting.

The chance of being published was determined by evaluation scores assigned by referees. The value of author submissions was therefore not objectively determined (i.e., it did not perfectly mirror the real quality of submissions), but was instead dependent on the referees' opinion. We assumed that reviewing was a resource-intensive activity and that agent resources determined both the agent's reviewing quality and the cost to the reviewer (i.e., time lost for publishing their own work). The total expense S for any referee was calculated as follows:

$$S = \frac{1}{2} R_r[1 + (Q_a - \mu_r)] \qquad (2)$$

where R_r was the referee's resources, Q_a was the real quality of the author's submission and μ_r was the referee's expected quality. This last was calculated as in equation (1). It is worth noting that, when selected as referees, agents not only needed to allocate resources toward reviewing but also potentially lost additional resources as a result of not being able to publish their own work in the meantime.

We assumed that authors and referees were randomly matched one to one so that multiple submissions and reviews were not possible and the reviewing effort was equally distributed among the population. We assumed that reviewing expenses grew linearly with the quality of authors' submissions. We assumed that, if referees were matched with a submission of a quality close to a potential submission of their own, they allocated 50% of their available resources toward reviewing. They spent fewer resources when matched with lower quality submissions, more when matched with higher quality submissions. Reviewing expenses, however, were proportionally dependent on agent resources, meaning that top scientists would be expected to spend less time reviewing in general, as they have more experience and are better able to evaluate sound science than average scientists are. They will lose more resources than average scientists, however, because their time is more valuable than the latter.

SIMULATION SCENARIOS

We first built various simulation scenarios to test the impact of referee behaviour on the quality and efficiency of the peer review process. By quality, we meant the ability of peer review to ensure that only the

best submissions were eventually published (e.g., Casati *et al*. 2009). By efficiency, we meant the ability of peer review to achieve quality by minimizing the resources lost by authors and the expenses incurred by referees.

In the first scenario, called "*random behaviour*", we assumed that referees had a constant probability of being biased in their judgment. When fair, referees had the ability to provide a consistent and unequivocal opinion which truly reflected the quality of the submission. In this case, they did their best to provide an accurate evaluation and spent all needed resources for reviewing. We assumed that referees estimated the authors' resources following a normal distribution of the actual authors' resources and a narrow standard deviation ($\sigma = R_a/10$). Then, they estimated the author submissions' quality as in (1). This meant that the evaluation scores by fair referees were likely to approximate the real value of author submissions, but we assumed that there was a chance for some bias in order to mimic typical knowledge and information asymmetries between authors and referees which characterize peer review.

In the case of unfairness, referees fell into type I and type II errors: recommending submissions of low quality to be published or recommending against the publishing of submissions which should have been published (e.g., Laband and Piette 1994; Bornmann and Daniel 2007). More specifically, when unfair, referees spent half of the resources spent by fair referees, and under- or over- estimated author submissions. To avoid the possibility that referees assigned the real value to submissions by chance we assumed that, when they underrated a submission, they estimated the authors' resources as described for fair referees, but applying an underrating factor to the actual authors' resources (u = 0.1). An opposite factor was applied in the case of overrating (i.e. o = 1.9).

In the second scenario, called "*cheating*", we assumed that referees intentionally outperformed potential competitors by systematically underrating their submission, even at their own expenses (e.g., resources spent for reviewing). More specifically, we assumed that referees were capable to estimate submission authors' resources (R_a) and identify each author with an expected R_a similar or higher than his/her R_r as a competitor.

To measure the quality of peer review, we considered the percentage of errors made by referees by calculating the optimal situation, in which submissions were published according to their real value, and by measuring the discrepancy with the actual situation in each simulation step (e.g., see evaluation bias in Tab. 1).

RESULTS

Tab. 1 shows the impact of referee behaviour on the quality and efficiency of peer review under various conditions of the publication rate (25%, 50%, and 75% of published submissions). Data were averaged across 10 simulation runs on 200 simulation steps. Results indicated that cheating increased evaluation bias particularly when the selection rate of publication was stronger. This also caused higher productivity loss, in terms of resources wasted by unpublished authors who deserved publication and more considerable reviewing expenses. We measured *productivity loss* as the percentage of resources wasted by unpublished authors who deserved to be published, while *reviewing expenses* were the percentage of resources spent by referees compared with the resources invested by submitting authors. Obviously, less competitive publication rates decreased the negative impact of cheating.

Tab. 2 shows the number of cheaters in the population in situations of more or less selective publication rate. Results indicated that, in case of stronger selection for publication, a percentage of 27% of cheaters was sufficient to generate 70.86% of low quality published authors who should not deserve publication (see also Tab. 1). In case of less selective publication rates, even higher probability of cheating caused less biased allocation of publications (e.g, 35% of cheaters produce 20.07% of evaluation bias under the weak selection environment).

Table 1: The impact of referee behaviour on the quality and efficiency of peer review in various selective environments (values in percentage).

Scenario	Evaluation bias	Productivity loss	Reviewing expenses
Weak selection (75% published submissions)			
Random behaviour	16.51	7.68	25.98
Cheating	20.07	4,91	21.34
Medium-level selection (50% published submissions)			
Random behaviour	25.27	14.98	30.77
Cheating	56.63	28.02	32.21
Strong selection (25% published submissions)			
Random behaviour	29.42	15.00	29.42
Cheating	70.86	34.72	35.24

Table 2: Percentage of cheaters among the referees in the "cheating scenario" in various selection rate environments (values of cheaters in percentage on the total number of referees).

Selection rage	Cheaters
Strong selection	0.27
Medium selection	0.28
Weak selection	0.35

We next calculated the resources of all agents at the end of the simulation run in each scenario. Figures 1 and 2 compare system productivity accumulation in weakly and strongly publication selection rate. Results showed that, in case of stronger competition for publication, cheating implied less concentration of resources.

We also considered inequality of resource distribution by calculating a Gini index, which typically

measures the inequality among values of a frequency distribution. In our case, inequality meant an unequal allocation of resources, such as ideal academic status, reputation, and career (see Tab. 3). Results showed that, in case of stronger competition for publication, cheating caused less inequality of resource allocation in the system. The situation was different in case of less competition for publication.

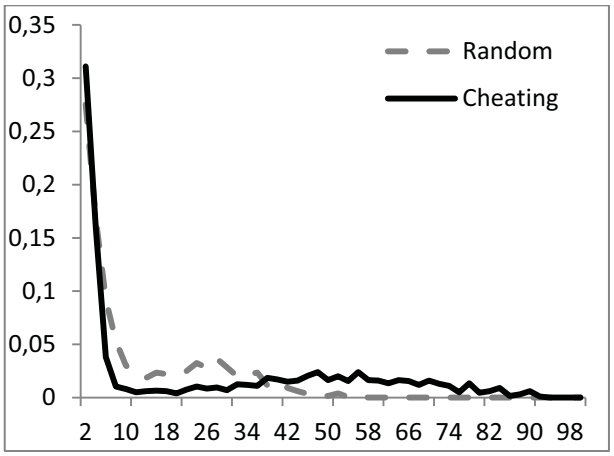

Figure 1: The impact of agent behaviour on system resource accumulation when competition for publication was weak. The "random behaviour" scenario is in dotted grey, the "cheating" scenario is in solid black. In the x-axis, the resources. In the y-axis, the percentage of agents.

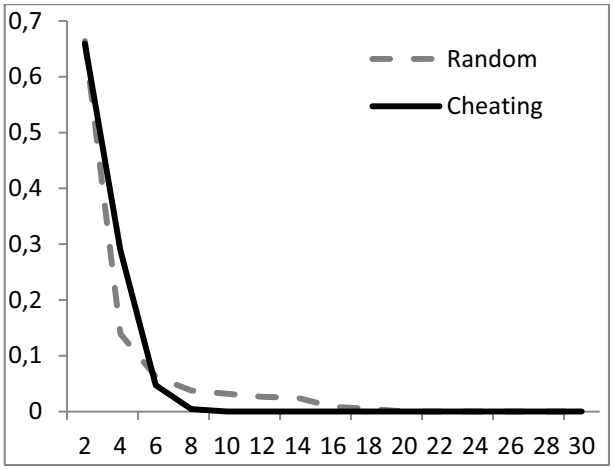

Figure 2: The impact of agent behaviour on system resource accumulation when competition for publication was strong. The "random behaviour" scenario is in dotted grey, the "cheating" scenario is in solid black. In the x-axis, the resources. In the y-axis, the percentage of agents.

Table 3: The Gini index in weak and strong competition for publication (values calculated at the end of the simulation). The index takes 0 when there was complete equality in resource distribution among agents and 1 when a single agent had everything.

Weak competition for publication	Gini index
Random behaviour	0.54
Cheating	0.57
Strong competition for publication	Gini index
Random behaviour	0.47
Cheating	0.28

This is coherent with previous findings (e.g., Squazzoni and Gandelli 2012): in a competitive, "winner takes all" system such as academic science, a better functioning peer review process determines an unequal resource distribution as advantages accrue to the best scientists. This can be attributed to the fact that the best published authors gain access to more resources and more chances to be re-published by taking advantage of the fairness of certain referees. It is worth noting that this kind of "Saint Matthew effect" (i.e., "the rich get richer, the poor get poorer") has been widely acknolwedged in science, from the classical contribution by Merton (1973) to recent findings (e.g., Barabási, Song and Wang 2012; Tol 2013).

The next step was to consider that competitive behaviour of scientists could be influenced by different possible ways of identifying potential competitors. For instance, in certain scientific communities, especially among the so-called "hard sciences", widely shared objective measures exist that help everyone to precisely commensurate his/her respective performance with that of others. This means that competitors might be precisely identified across the whole population. This does not hold in other scientific communities, especially those revolving around the humanities, where these standards do not exist and are even widely contested. In these cases, the definition of potential competitors depends on the stratification of scientists in local groups, with the prevalence of disciplinary or group specificities of standards (e.g., Laudel and Gläeser 2006; Lamont 2009).

We created two supplementary scenarios where we modified the way in which cheaters identified their competitors. Unlike the previous *"cheating"* scenario, which followed a threshold function to detect possible competitors, we tested a "*local competition*" scenario, where this function followed a Gaussian shape and a "*glass ceiling*" scenario, where competitors' detection function followed a logistic shape.

In the first case ("*local competition*"), we assumed that scientists detected possible competitors only in their own performance neighbourhood. This was to mimic certain fragmented scientific communities where scientists tend to compete locally. More specifically, we assumed that competitor's detection followed a normal distribution $N(R_r, \sigma_2)$ where R_r was the referee's resources and σ_2 was the standard deviation calculated as a proportion of R_r.

In the second case ("*glass ceiling*"), we assumed that scientists tried to similarly outperform the less and the more productive colleagues. This was to protect against upstart and outperform superior scientists. The shape of the logistic function is shown in Fig. 3.

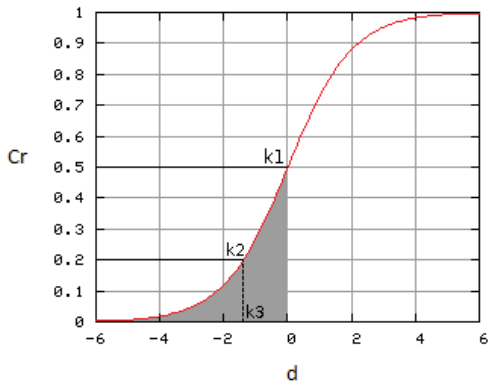

Figure 3: The logistic function for competitor detection in the"*glass ceiling*" scenario.

More specifically, the probability C_r of a referee to cheat a submission author followed equation (3), where d indicated the respective distance of author's and referee's resources (i.e., $d = R_a - R_r$).

$$C_r = \frac{1}{(e^{-(b_1 * d + b_0)} + 1)} \qquad (3)$$

The constants b_0 and b_1 determined the shape of the curve shown in Fig. 3 and were calculated as in the equations (4) and (5). These equations were related to the following three parameters (also shown in Fig. 3): k_1 indicated the probability of cheating (C_r) when both referees and authors had the same amount of resources (i.e. *d=0*), and k_2 indicated the probability of cheating when the distance between the author's and the referee's resources was equal to k_3.

$$b_0 = -\ln\left(\frac{1 - k_1}{k_1}\right) \qquad (4)$$

$$b_1 = \frac{ln\left(\frac{1 - k_2}{k_2}\right) + b_0}{k_3} \qquad (5)$$

Compared with the baseline scenario (i.e., threshold function), results showed that "*local competition*" scenario ensured less bias independently of the publication selection rates. In case of higher selection rate for publication, this scenario also guaranteed higher efficiency in terms of minimization of wasted resources for authors and reviewing expenses.

On the other hand, the "*glass ceiling*" scenario determined levels of bias and unefficiency similar to the baseline scenario. This means that the logistic function for competitor's detection performed similarly to the threshold one.

Table 4: The impact of different competition detection scenarios on the quality and efficiency of peer review in various selective environments (values in percentage).

Scenario	Evaluation bias	Productivity loss	Reviewing expenses
Weak selection (75% published submissions)			
Cheating	20.07	4.91	21.34
Local competition	14.65	4.21	22.56
Glass ceiling	16.67	3.68	21.66
Medium-level selection (50% published submissions)			
Cheating	56.63	28.02	32.21
Local competition	33.86	18.39	30.97
Glass ceiling	43.06	15.30	23.16
Strong selection (25% published submissions)			
Cheating	70.86	34.72	35.24
Local competition	31.04	15.63	30.13
Glass ceiling	70.35	34.70	34.56

Tab. 5 shows the number of cheaters in the population. For shortage of space, we reported only the case of strong competition for publication. Results showed, first, that the "*glass ceiling*" scenario determined higher number of cheaters. Secondly, they showed that although "*local competition*" scenario included a considerable percentage of cheaters (i.e., 20%), this did not have a negative effect on the quality of peer review. In case of strong competition for publication, 20% of cheaters caused only 31% of biased judgment.

Table 5: Percentage of cheaters among the referees in various competitor detecting scenarios with strong competition for publication (values of cheaters in percentage on the total number of referees).

Scenario	Cheaters
Cheating	0.27
Local competition	0.20
Glass ceiling	0.34

Figure 4 and Tab. 6 show the impact of various cheating mechanisms on the growth and distribution of resources in the case of strong competition for publication. Results showed that "cheating" and "*glass ceiling*" scenarios generated similar outcomes, whereas "*local competition*" implied higher inequality of resource distribution.

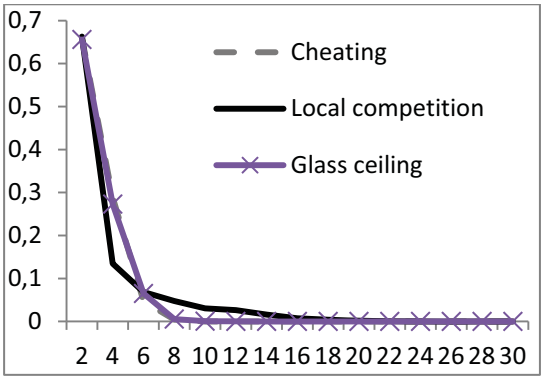

Figure 4: The impact of cheating on system resource accumulation in strongly selective environments. The "cheating behaviour" scenario is in dotted grey, the "local competition" scenario is in solid black and the "glass ceiling" scenario is in solid gray. In the x-axis, the resources. In the y-axis, the percentage of agents.

Table 6: The Gini index in the "local competition" and the "glass ceiling" scenarios in strongly selective environments (values calculated at the end of the simulation). The index takes 0 when there was complete equality in resource distribution among agents and 1 when a single agent had everything.

Scenario with strong selection	Gini index
Cheating	0.28
Local competition	0.46
Glass ceiling	0.29

CONCLUSIONS

Previous computational studies have indicated that even a small proportion of referee cheating may dramatically distort the publication quality (Thurner and Hanel 2011). Our results confirmed these findings but also permitted us to consider implications of cheating for the system's resource allocation in terms of growth dynamics and distribution inequality. Furthermore, we found that peer review outcomes are sensitive to differences in the way scientists identify their competitors. Certain mechanisms, such as the stratification of scientists in local competing groups and the presence of niches of competition, might reduce the negative effect of cheating on the quality of the peer review process as scientists can develop more competent judgment.

It is important to outline that making any strong generalisation on peer review from these simulation studies is inappropriate. Developments that integrate theoretical models and empirical data are fundamental both to test aggregate findings and realistically calibrate important model parameters. However, it must be also said that computational models of peer review allow us to pinpoint the importance of considering micro-behavioural and interaction aspects, which are unfortunately difficult to look at empirically (Squazzoni and Takács 2011).

ACKNOWLEDGEMENTS

This work has been jointly supported by the Spanish MICINN and the European Commission FEDER funds, under grant TIN2009-14475-C04. Usual disclaimers apply.

REFERENCES

Allesina, S. 2012 "Modeling Peer Review: An Agent-Based Approach". *Ideas in Ecology and Evolution* , 5, 2, 27-35.

Barabási, A.-L., Song, C. and Wang, D. 2012. "Handful of Papers Dominates Citation". *Nature* 491, 40.

Bornmann, L. 2011 "Scientific Peer Review". *Annual Review of Information Science and Technology*, 45, 199-245.

Bornmann, L., Daniel, H.-D. 2007. Convergent Validation of Peer Review Decisions Using the *H* Index: Extent of and Reasons for Type I and Type II errors. *Journal of Informetrics*, 1(3), 204-213.

Callahan, D. 2004. "Rational cheating: Everyone's doing it". *Journal of Forensic Accounting*, 5, 577-580.

Casati, F., M. Marchese, A. Ragone and M. Turrini. 2009. "Is Peer Review Any Good? A Quantitative Analysis of Peer Review". DISI University of Trento, Technical Report # DISI-09-045, accessible at: <http://eprints.biblio.unitn.it/archive/00001654/>.

Crocker, J., M. L. Cooper. 2011. "Addressing Scientific Fraud". *Science,* 334 (6060), 1182.

Edmonds, B., Gilbert, N., Ahrweiler, P., Scharnhorst, A. 2011. Simulating the Social Processes of Science. Journal of Artificial Societies and Social Simulation 14(4) 14: http://jasss.soc.surrey.ac.uk/14/4/14.html.

Fanelli, D. 2010. "Do Pressures to Publish Increase Scientists' Bias? An Empirical Support from US States Data". *PLoS ONE* 5(4): e10271.

Grimaldo, F. and Paolucci, M. 2013. "A Simulation of Disagreement for Control of Rational Cheating in Peer Review. *Advances in Complex Systems*, forthcoming.

Laband, D. N. and J. M. Piette. 1994. "Favoritism Versus Search of Good Papers. Empirical Evidence Regarding the Behavior of Journal Editors". *Journal of Political Economy*, 102, 194-203.

Lamont, M. 2009. *How Professors Think. Inside the Curious Worlds of Academic Judgment*. Cambridge, MA: Harvard University Press.

Laudel, G. and J. Gläeser. 2006. Tensions between Evaluations and Communication Practices. *Journal of Higher Education Policy and Management*, 28: 289-295.

Merton, R. K. 1973. *The Sociology of Science. Theoretical and Empirical Investigations*. Chicago: University of Chicago Press.

Payette, N. 2012. "Agent-Based Models of Science". In A. Scharnhorst, K. Börner & P. van den Besselaar (Eds.), *Models of Science Dynamics*, Complexity Series. Springer.

Roebber, P. J. and D. M. Schultz, 2011. "Peer Review, Program Officers and Science Funding". *Plos One*, 6, 4, e18680, accessible at: http://www.plosone.org/article/info:doi%2F10.1371%2Fjournal.pone.0018680.

Squazzoni, F. and C. Gandelli. 2012. "Saint Matthews Strikes Again. An Agent-Based Model of Peer Review and the Scientific Community Structures". *Journal of Informetrics*, 6: 265-275.

Squazzoni, F. and C. Gandelli. 2013. "Opening the Black Box of Peer Review. An Agent-Based Model of Scientist Behaviour. *Journal of Artificial Societies and Social Simulation*, 16(2) 3: http://jasss.soc.surrey.ac.uk/16/2/3.html.

Squazzoni, F. and K. Takács. 2011. "Social Simulation that 'Peers into Peer Review'". *Journal of Artificial Societies and Social Simulation*, 14(4) 3: http://jasss.soc.surrey.ac.uk/14/4/3.html.

Thurner, S. and R. Hanel. 2011. "Peer Review in a World with Rational Scientists: Toward Selection of the Average". *The European Physical Journal B*, 84, 707-711.

Tol, R. S. J. 2013. The Matthew Effect for Cohorts of Economists. *Journal of Informetrics*, 7(2), 522-527.

AUTHOR BIOGRAPHIES

JUAN BAUTISTA CABOTÀ is PhD. Student at the Universitat de València in the Networks and Virtual Environments Group (GREV, http://grev.uv.es). His research interests include agent-based modelling and simulation and intelligent decision-making support systems. His email address is: juan.cabota@uv.es.

FRANCISCO GRIMALDO is lecturer at the Universitat de València and member of the Networks and Virtual Environments Group (GREV). His research is focused on applied artificial intelligence, agent-based modelling/simulation and computational social choice. He is member of the HiPEAC network of excellence and the IEEE Systems, Man & Cybernetics Society. His email is francisco.grimaldo@uv.es and his webpage can be found at: http://www.uv.es/grimo/.

FLAMINIO SQUAZZONI is assistant professor of economic sociology at the University of Brescia, where he leads the GECS-Research Group on Experimental and Computational Sociology. He is President of *ESSA* The European Social Simulation Association. His e-mail is: squazzon@eco.unibs.it and his web-page can be found at: http:www.eco.unibs.it/gecs/Squazzoni.html

IMPACT OF HOMOPHILY ON DIFFUSION DYNAMICS OVER SOCIAL NETWORKS

Mustafa Yavaş
Gönenç Yücel
Socio-Economic System Dynamics Research Group
Bogazici University Industrial Engineering Department
34342 Bebek Istanbul Turkey
mustafa.yavas@boun.edu.tr, gonenc.yucel@boun.edu.tr

KEYWORDS

Homophily, diffusion, threshold models, social networks, formal models, simulation, segregation.

ABSTRACT

The purpose of this study is to find out under what conditions homophily reinforce the diffusions over social networks or undermines them. To realize this aim, formal modeling approach is utilized and an Agent-Based Model is constructed. Afterwards, diffusion of a non-sticky innovation is investigated with the experiments having varying homophily levels in a social network with two distinct kinds of agents as the primary control variable. The results show that (i) homophily reinforces itself (ii) looking at the macro-behavior of the diffusion, initial increases in the level of homophily has a positive effect on adopted fraction of the population whereas further increases have a negative impact, and (iii) looking at the micro-behavior of the diffusion, increasing homophily can result in local maxima even the macro trend is decreasing. Connectedness and average degrees interacting with social persuasion are the two explanatory remarks in the course of investigating the impact of homophily. As a by-product, the model is also capable of capturing the segregation dynamics over social networks. Future research involves allowing the adopted innovation to lead to value homophily, exploration of the different diffusion initiation types and adoption heuristics.

INTRODUCTION

People tend to form social links more with people who are similar to them and this refers to the principle called *homophily*: "Birds of a feather flock together" (McPherson, Smith-Lovin, and Cook 2001). Homophily is ubiquitous, it can be observed in almost all kind of social network ties such as marriage, friendship, membership in an organization, information exchange, trade and business transactions, and the like. People consider the other party's race, gender, age, religion, culture, education level, and many other personal properties when it comes to social interactions. Being that much pervasive, it is one of the key explanations why some characteristics are localized in social space. In addition to having an inclination to bond more, people meet more frequently and more intensely with friends alike. Furthermore, close friends, who are usually friends alike in some certain qualities, have more influence on us than dissimilar ones (McPherson et al. 2001). Taking all into account, localization of a social aspect is realized via homophily principal in every kind of social networks.

Homophily determines the network of a person. Hence, along with localization, it is also significant in access to information (Choudhury, Sundaram, and John 2010), spread of behaviors, innovations, ideas, and even states of health such as obesity (Christakis and Fowler 2007), opinion and norm formation (Centola, Willer, and Macy 2005), intergroup inequalities (Paul DiMaggio and Filiz Garip 2012; F Garip and P DiMaggio 2011), and so forth. Among these, the interplay between homophily and diffusion covers the most of the recent debate (Jackson and Lopez-Pintado 2011). In this paper, we will only focus on the effect of homophily on diffusion dynamics.

Homophily has a significant impact on the diffusion patterns over a social network via two distinct processes. First, homophily has an impact on the development of a network, hence on its topology. Second, people are more effective in exerting social influence on people alike. However, it is unclear whether homophily is in favor of diffusion or works against the spread. On the one hand, it can promote the diffusion via attaining the critical mass faster than otherwise (Centola 2010; Rogers 2003). On the other hand, homophily can lead the innovation, the norm or the behavior that is supposed to diffuse to become localized in some clusters within the network (Centola 2011; Rogers 2003). Hence, it is not straightforward to see the overall impact of homophily on the diffusion patterns.

The ultimate purpose of this study is to find out under what conditions homophily promotes or prevents the diffusion of an innovation which can be an idea, an attitude, a behavior, a product, and so on.. To do so, a dynamic simulation model will be used to address how the diffusion patterns change when homophily level in a

Proceedings 27th European Conference on Modelling and Simulation ©ECMS Webjørn Rekdalsbakken, Robin T. Bye, Houxiang Zhang (Editors)
ISBN: 978-0-9564944-6-7 / ISBN: 978-0-9564944-7-4 (CD)

social network varies. As a by-product, we will also have the chance to show how homophily changes the network topology.

This article is structured as follows; the following section will elaborate on the problem. In Section 3, the simulation model will be explained. Afterwards, Section 4 presents the outcomes of the simulation experiments conducted to reveal the impact of homophily. In Section 5, interesting results and the factors that give rise to them are discussed. Lastly, Section 6 is devoted to key findings of this study and its limitations, and future research directions.

PROBLEM DEFINITION

Diffusion dynamics is a hot topic in various academic research environments and the problems are ubiquitous. Depending on the nature of the innovation as well as the context within which it is expected to diffuse, the diffusion problems can come in very different forms. However, there are three significant aspects that define diffusion problems in which homophily has a strong potential to influence dynamics. These three aspects, which will be discussed below, define the type of diffusion problems considered in the scope of this study.

Firstly, we will consider an innovation that is quite social in the sense that an individual's adoption is very sensitive to the adoption behavior of the others around. In other words, we will only consider cases of diffusion where social influence, rather than pure personal preference, is the key determinant of a person's adoption decision.

Secondly, it is assumed that the influence of the people alike is significantly stronger than other social contacts in adoption decisions of individuals. Simply put, homophily is active in adoption-related social influence. As we talk about "people alike", it is important to mention a relevant distinction in similarity and related types of homophily: *status homophily* is based on similarities in ascribed status such as race, ethnicity, age or gender and acquired status religion, education, occupation etc., whereas *value homophily* is based on values, innovations, and beliefs (Lazarsfeld and Merton 1954). Status homophily seems like one of the most effective factors leading to strongest divides in sociodemographic space (McPherson et al. 2001). With that motivation, we will focus on status homophily in this study.

Thirdly, the nature of the innovation is also an important aspect. In these types of studies, it is important to distinguish two distinct kinds of innovations: Innovations that can accumulate inertia can be called as sticky innovations, which once adopted, cannot be changed for a long time. On the other hand, innovations with negligible or no inertia can be called as non-sticky innovations, which can be changed frequently. Studying sticky innovations as the diffusing phenomenon decrease the explanatory power of a model that aims to study the impact of homophily due to the fact that inertia has as a confounding effect. Instead, non-sticky innovations would maximize the potential to investigate the impact of homophily. Thus, we will focus on the dynamics of the diffusion of a non-sticky innovation.

To summarize, we will focus only on status homophily and its impact on the diffusion of a non-sticky innovation. For the sake of simplicity and not lose explanatory power, the social network that we will focus on will have two kinds of people with respect to a hypothetical status which leads them to form homophilious ties: green and red. We will assume that this status is a permanent one such as race, or gender. We will further assume that this status is essential to adopting the innovation that is supposed to diffuse. Only the individuals of the same status will have an influence on each others' adoption and quitting decisions.

Taking such a problem into account, it can be stated that there are no global but local interactions and the micro rules of them are well-known; individuals form ties more with people alike and they are influenced only by them. Furthermore, each individual has heterogeneous attributes that are closely related to diffusion process such as having adopted the innovation or not, qualities relating the network such as number of friends, her exact position in the topology, fraction of similar friends around her, etc. Additionally, due to aforementioned conflicting effects of homophily, it is not straightforward to deduce the macro pattern in a diffusion study with homophily being included both in evolution of network and affecting the adoption process and a computational model would be helpful. Taking all those into account, Agent-Based Modeling (ABM) is evaluated as a promising approach for our study (Epstein and Axtell 1996; Gilbert and Troitzsch 2005; Railsback and Grimm 2011). An agent-based model that depicts the diffusion environment that is defined by our main assumptions will be developed and it will be used to conduct experiments to analyze the overall effect of homophily on diffusion dynamics.

MODEL DESCRIPTION

To address the impact of homophily, two distinct phases should be completed. First, a network which has already some measurable level of homophily is needed to be built. After such a given network, initiation of the diffusion by choosing early adopters should take place and we will let the diffusion begin. In this regard, the model will be described in two parts, i.e. network evolution and diffusion.

Homophilious Network Evolution

The evolution process of the homophilious network is inspired by the famous "Segregation Model" (Schelling 1971). The process starts with a *small world* network (Wilensky 2005). On this network, each agent has a

threshold value for her "happiness level", as in Schelling's model, related to the fraction of the similar friends in the agent's network neighborhood. "Unhappy" agents will make ties with agents alike, and break ties with others.

%-similar-wanted is the model parameter that represents this personal threshold. After setting a value for *%-similar-wanted*, the following rules will be applied:

Homophilious network evolution routine:

Create a "small world" network

WHILE average "happiness level" is less than %-similar-wanted

{Ask each agent:

IF her "happiness level" is less than %-similar-wanted

THEN form a new tie with a similar person from your friends' friendship networks

AND dissolve a tie with a dissimilar friend of yours

ELSE do nothing

Calculate average "happiness level"}

IF the network is connected THEN do nothing ELSE return to the beginning and create a new network

In the above routine, "happiness level" refers to the fraction of similar friends in an agent's friendship network. Note that all agents have the same threshold value for "happiness level" and that is equal to *%-similar-wanted*. The above heuristic ensures that the average degree of the social network stays the same. Nevertheless, in the end, agents are still heterogeneous in terms of "happiness level", average degree (i.e. number of friends), network statistics values of each agent's friendship network such as clustering coefficient, and centrality values such as betweenness-centrality, closeness-centrality, and so forth.

As the network evolves according to the set *%-similar-wanted* value, the homophily level of the network is measured with the average of fractions of similar friends in agents' friendship networks (*%-similar-total*). Although, to the best of our knowledge, there is no well-known and widely accepted measure for homophily, there are examples of the one that is used here (Jackson 2008). Note that in the beginning, due to random assignments of agents, on average, *%-similar-total* is 50% and it changes as the network evolves homophiliously with respect to value of *%-similar-wanted.*

In *Figure 1*, we see a similar result as in Schelling's Segregation Model: as *%-similar-wanted* increases, network tends to become more segregated.

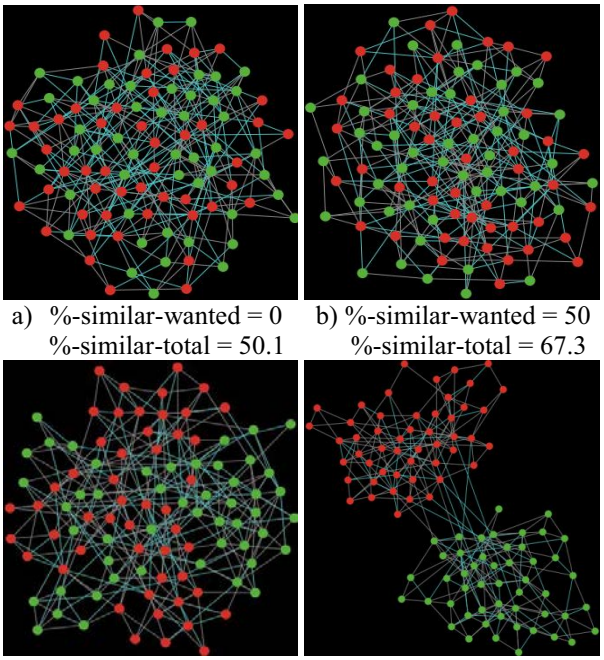

a) %-similar-wanted = 0 %-similar-total = 50.1
b) %-similar-wanted = 50 %-similar-total = 67.3
c) %-similar-wanted = 75 %-similar-total = 86.9
d) %-similar-wanted = 85 %-similar-total = 97.7

Figure 1: Instances of social networks with 50 nodes per status and average degree of 6.

Diffusion

Besides its role in network evolution, homophily is also influential during the diffusion. However, the network structure will stay the same since homophily will be present only in the adoption decisions. In other words, we assume that the adopted behavior does not create homophilious tie formation or dissolution.

Diffusion starts with the initiation of the early adopters and takes off as people make decisions whether to adopt the innovation or not via social influence. The adoption mechanism in this study is an example of *threshold models* (Granovetter 1978). The most important ingredient of adoption decision is "adoption threshold". As its name implies, it is the threshold fraction of similar friends who already adopted the innovation. After the initiation step, in each round, the following heuristic will begin to run until the adoption dynamics reach equilibrium:

Adoption routine:

Ask each agent:

IF (#-of-similar-friends-adopted / #-of-similar-friends) is greater than adoption threshold THEN

IF he has not adopted THEN make her adopt it ELSE do nothing

ELSE

IF he has not adopted THEN do nothing ELSE make her drop it

EXPERIMENTS & RESULTS

Initiation & Experimental Setup

In all of the experiments, diffusion starts with initiation of it via making certain fraction of agents from each status adopt the innovation. There are many different ways to select these early adopters. However, in this study we will only report the results of the experiments with the selection of most sociable agents -the ones with maximum number of friends- as early adopters. Note that this choice is in favor of adoption. Furthermore, optimistically–after having many trials-, it is decided that 10% of the population will adopt the innovation at time zero with an equal number of agents from both statuses. Moreover, it is seen that the meaningful cases mostly occur when adoption threshold is around 30%. If it is lower this value, than the diffusion is too easy that having a differentiating observation is impossible. If it is higher, then the diffusion turns out to be too hard that again, drawing conclusions is impossible.

There are two important points about the results reported in this paper. Firstly, they are the most interesting ones among many others that are obtained via extensive experimentation. A range of values are tried out for parameters such as average degree, number of nodes, and many other network parameters. Secondly, the experiments are replicated on significantly many different networks and averages of the results are reported.

Experimental Design

In order to reveal the impact of homophily, we will try different "happiness thresholds", i.e. *%-similar-wanted,* to obtain different levels of homophily across the network. We will keep track of *%-similar-total,* as the network-wide (overall) homophily level. As we increase *%-similar-wanted*, we will get a more homophilious network and it is visible in *Figure 2*. Note that the homophily level always turns out to be more than what is wanted. It is clear when the three lines are compared with the reference line. This observation suggests us that when agents interact according to their individual preferences, the global level of homophily becomes more than agents' intended levels. In other words, even a small homophily tendency can reinforce itself and lead to more homophily than desired.

Results

The diffusion dynamics for different levels of homophily can be seen in *Figure 3* and *Figure 4*. In these plots y-axis refers to the fraction of population that is adopted at the final equilibrium level. Note that, to decrease the confounding effect of randomness, all the values in all plots are averages of results of 500 simulation runs per case (e.g. in *Figure 4* 100 nodes network, *%-adopted* is 26.5%, that is the average of 500 simulation runs where *%-similar-wanted* is 85% and average degree is 8 in each of these). After investigation of these plots, four important observations become noteworthy:

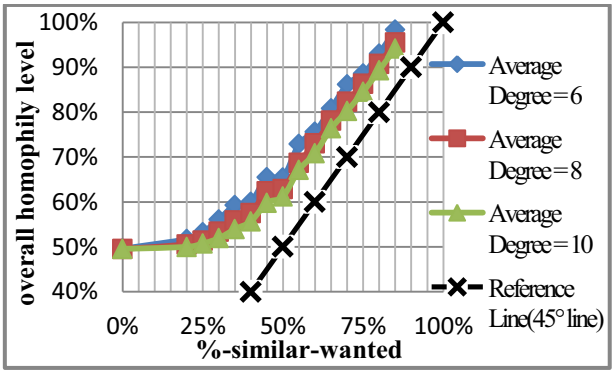

Figure 2: The homophily level changes proportional to parameter %-similar-wanted.

Firstly, both in *Figure 3* and *Figure 4,* it is seen that for low values of homophily, the adoption fractions are higher. However, after some point, as homophily level increases the adoption decreases. This macro-behavior is valid for all networks considered, 100 or 200 nodes networks and 6, 8, or 10 average degrees networks. With a low resolution view of these plots, it can be said relatively small degrees of homophily is in favor of homophily. Nevertheless, after a certain amount, it leads to decrease in the adoption.

Secondly, comparing 100 nodes network and 200 nodes network, it is obvious that the adoption is higher in 200 nodes network. This makes sense since the initial number of adopted agents is higher than 100 nodes network, allowing a higher adoption rate initially.

Thirdly, comparing the different average degree networks, it is clearly observed that as average degree increases, the adoption decreases. In other words, as agents becomes more sociable and have more friends, the overall adoption decreases. This might seem counterintuitive due to the fact that having more friends, the probability of having a friend similar to you and who adopted the innovation is higher. On the other hand, the social persuasion becomes harder since the threshold of adopting the innovation becomes higher for an agent with more friends. It turns out that the latter mechanism is more dominant.

Fourthly, although macro-behavior is understandable, micro-behavior is confusing and in some cases is in contradiction with the macro-behavior. Specifically, after the adoption makes a peak –the trend changes from "as homophily increases, adoption also increases" to "as homophily increases, adoption also decreases"- there are some local minima and maxima along the plots. Apparently, the behavior –local minima and maxima along the plot- is persistent, it is independent of number of nodes (the persistancy of the patterns can be discerned more easily in *Figure 4* since the data points lay on the same x-coordinates on the plots).

Furthermore, almost the same kind of behavior repeats itself in different average degree networks.

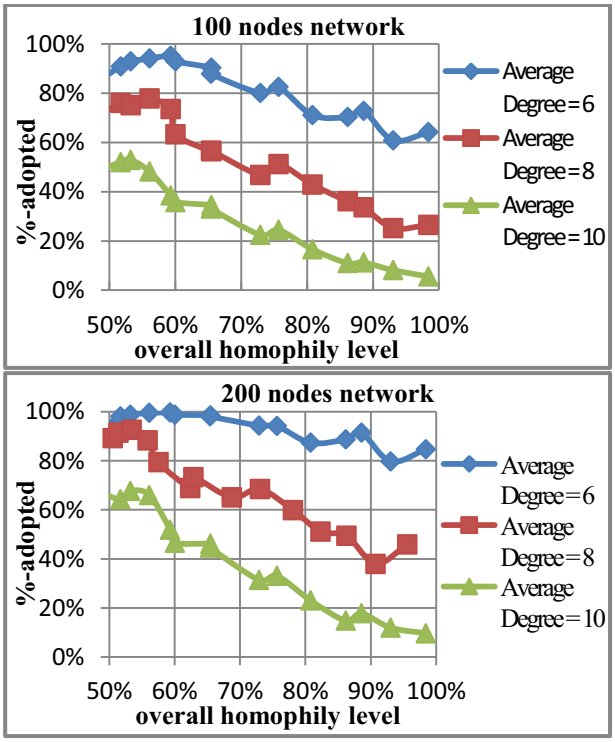

Figure 3: The plots of adoption percentages versus homophily level in the social network

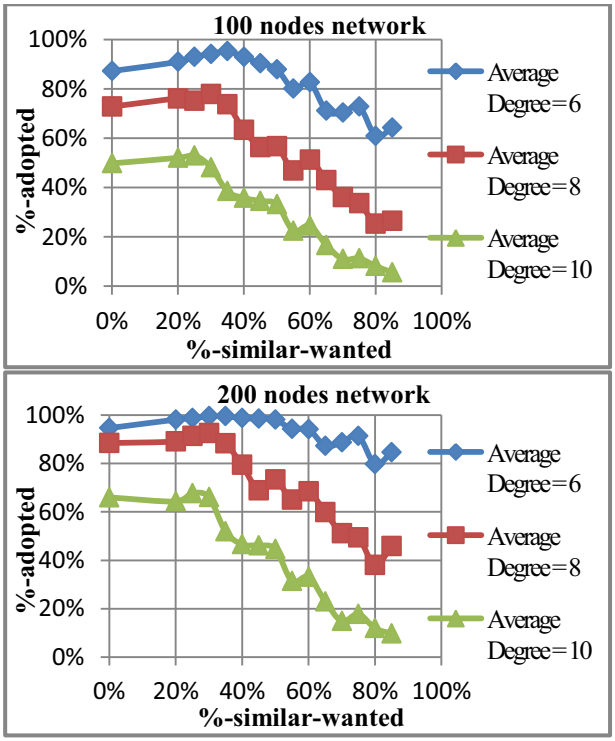

Figure 4: The plots of adoption percentages versus "happiness" thresholds

DISCUSSIONS

In this section, we will try to elaborate on the key remarks from the previous section. First, why initial increases in homophily reinforce the diffusion will be elucidated. Secondly, the negative impact of homophily will be analyzed.

The social networks studied in this paper are actually the amalgamation of two networks: the networks of the green agents and the networks of the red agents. Putting one on the top of the other gives us the same network if we were to divide it into two since diffusion takes place solely over homophilious ties. Hence, we will focus on one of the networks in isolation. For instance, *Figure 5* has two examples of the networks of the green agents. It is seen that the network with no homophily at all -the network on the left- has three disconnected groups whereas the mixed network is connected (in the homophilous network evolution routine we make sure that the emerging network is connected). Having disconnected groups, it may be impossible to reach full adoption if the initial adopters are not present in some disconnected groups. However, a slight increase in the level of homophily, the networks of green agents usually turns out to be connected and in a connected network full adoption is much more likely.

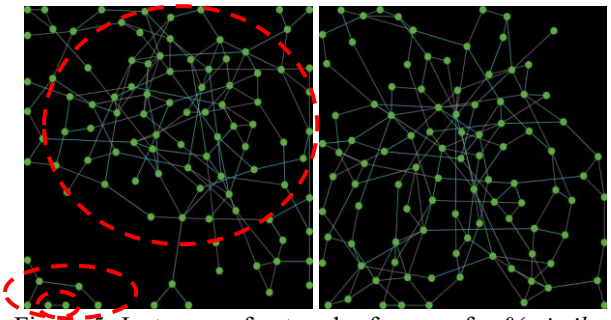

Figure 5: Instances of network of greens for *%-similar-wanted* values of 0% and 30%, respectively.

Another supporting argument to the above explanation can be found in *Figure 6* where we see the plot of average number of "weak components". A weakly connected component is simply a group of nodes where there is a path from each node to every other node. It is seen that a slight increase in the homophily level is followed by the number of weak components decreasing to one, saying that the network is connected.

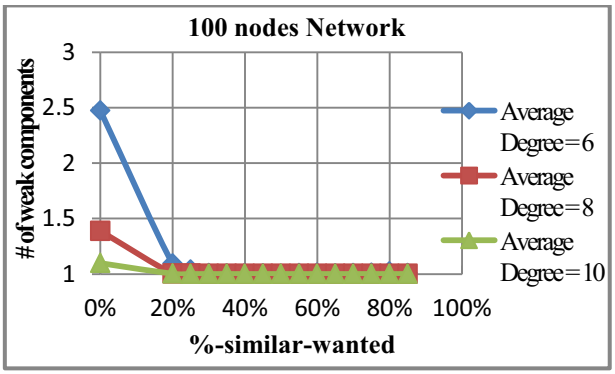

Figure 6: The plots of average number of weak components in the networks of green agents.

To explain the negative effect of homophily, we are inspired from the explanation of the impact of average degrees on the adoption. In *Figure 7*, we see that as the homophily increases in the network of the green agents, the average degree increases as well, leading to decrease in adoptions via making social persuasion to adopt harder.

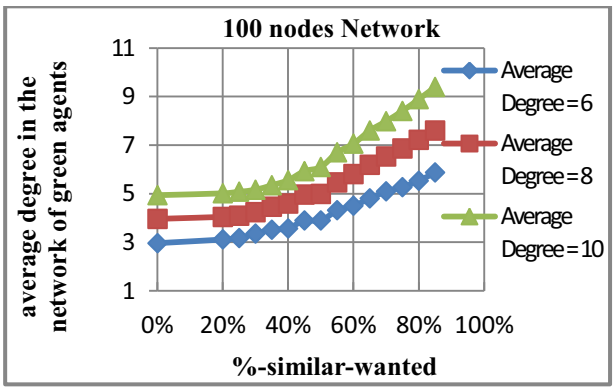

Figure 7: The plots of average degrees in the networks of green agents.

These explanations are still incomplete to explain the macro behavior of the diffusion with respect to homophily. When the network evolves homophiliously, the topology and all statistics of the network actually changes. *Figure 8* has the most important network statistics, average path length and clustering coefficients. The values are the averages of the results of 500 simulation runs. As it is clear, the trends in all are consistent.

These changes in average path length and clustering coefficient also have impacts on diffusion. However, their effect cannot be understood easily since they are distorted with the impact of homophily. To see the impact of the changes in average path length and clustering coefficient, randomly changing the statuses (i.e. colors) of agents after the network evolve homophiliously can help. An instance of such a trial can be found in *Figure 9*. First, the network evolves with respect to each *%-similar-wanted* parameter. After the network reaching the equilibrium, half of the agents' colors are swapped and the homophily levels (i.e. *%-similar-total*) are stabilized to 50%. Nevertheless, the topology of the network has already changed in the same way as in previous cases. Hence, the clustering coefficient and average path length values follow the same trends as in *Figure 8*.

From *Figure 9*, it is seen that the impact of the changes in clustering coefficient and average path length is illegible. Because, in the network where average degree is 6, the adoption decreases as *%-similar-wanted* increases whereas in the network where average degree is 10, the adoption increases and then decreases.

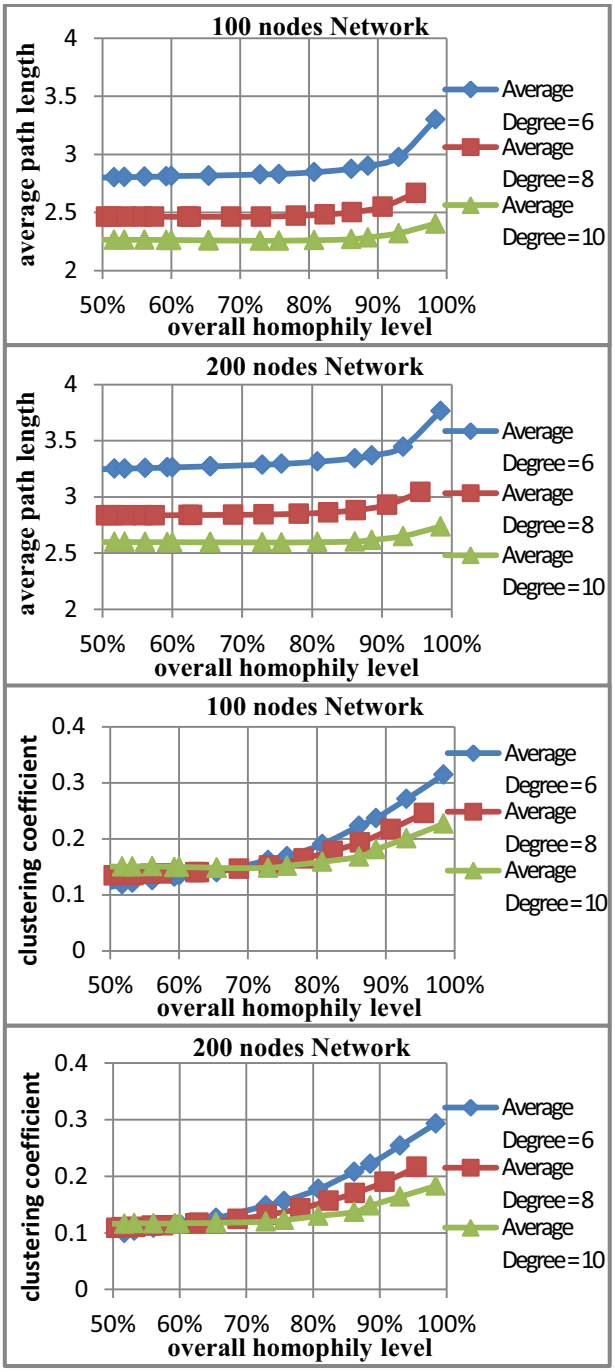

Figure 8: The plots of average path length and clustering coefficients in the homophilious networks.

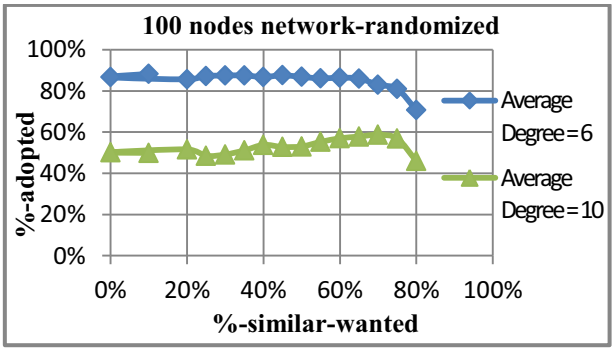

Figure 9: The plots of %-adopted in the randomized networks where %-similar-total is 50%.

CONCLUSION & FUTURE RESEARCH

In this study, it is seen that homophily reinforces itself and always leads to higher values than desired. The model presented here is capable of capturing segregation dynamics over social networks. Moreover, it is shown that small increases in homophily are in favor of diffusion whereas large increases affect negatively. It is also shown that increasing average degree of a network does not necessarily reinforce the diffusion. On the contrary, making social persuasion harder, it negatively affects the overall diffusion patterns.

The shortfall of this study, which is a future research topic, is to explain the persistent micro-level behaviors that are the local minima and maxima in the adoption plots. Although many network statistics such as clustering coefficient, average path length, average closeness-centrality, average betweenness centrality, variance of degree distributions, number of weak component, number of maximal cliques and biggest maximal cliques, and number of bi-components are tried to explain the trend, we could not come up with an explanation that elucidates the ups and downs in the decreasing part of adoption curves.

Many other future research directions can proliferate from this study and some of the promising ones are as follows: The co-evolution of the individual behavior and the network is an exciting direction. For instance, the adopted innovation can create a value homophily and during the diffusion process and accordingly, the network structure can change via new tie formations and dissolutions. However, this seems challenging since allowing the network to change during the diffusion process makes it very hard to come up with causal explanation to the observed outcome. Furthermore, having unequal number of agents in greens and reds can be interesting, addressing different societies. Lastly, different selection strategies for early adopters can yield significantly different dynamics of diffusion and hence, should be explored.

REFERENCES

Centola, Damon. 2010. "The spread of behavior in an online social network experiment." *Science (New York, N.Y.)* 329(5996):1194–97.

Centola, Damon. 2011. "An experimental study of homophily in the adoption of health behavior." *Science (New York, N.Y.)* 334(6060):1269–72.

Centola, Damon, Robb Willer, and Michael Macy. 2005. "The Emperor's Dilemma: A Computational Model of Self-Enforcing Norms." *American Journal of Sociology* 110(4):1009–40.

Choudhury, Munmun De, H. Sundaram, and A. John. 2010. "birds of a feather": Does user homophily impact information diffusion in social media." *Arxiv preprint* 1.

Christakis, Nicholas a, and James H. Fowler. 2007. "The spread of obesity in a large social network over 32 years." *The New England journal of medicine* 357(4):370–79.

DiMaggio, Paul, and Filiz Garip. 2012. "Network Effects and Social Inequality." *Annual Review of Sociology* 38(1):93.

Epstein, Joshua M., and Robert L. Axtell. 1996. *Growing Artificial Societies: Social Science From the Bottom Up*. Washington DC: Brookings Institution Press.

Garip, F., and P. DiMaggio. 2011. "How Network Externalities Can Exacerbate Intergroup Inequality." *American Journal of Sociology* 116(6).

Gilbert, Nigel, and Klaus G. Troitzsch. 2005. *Simulation for the Social Scientist*. 2nd ed. New York: Open University.

Granovetter, Mark. 1978. "Threshold models of collective behavior." *American journal of sociology* 83(6):1420–43.

Jackson, MO. 2008. *Social and economic networks*. Princeton University Press P. 19.

Jackson, MO, and D. Lopez-Pintado. 2011. "Diffusion and contagion in networks with heterogeneous agents and homophily." *Available at SSRN 1950476* (2001):1–18.

Lazarsfeld, PF, and RK Merton. 1954. "Friendship as a social process: a substantive and methodological analysis." Pp. 18–66 in *Freedom and Control in Modern Society*, edited by M Berger. New York.

Marsden, Peter. 1987. "Core discussions networks of Americans." *American Journal of Sociology* (52):122.

McPherson, M., L. Smith-Lovin, and JM Cook. 2001. "Birds of a feather: Homophily in social networks." *Annual review of sociology* 27(2001):415–44.

Railsback, Steven F., and Volker Grimm. 2011. *Agent-based and Individual-based Modeling: A Practical Introduction*. Princeton University Press.

Rogers, EM. 2003. *Diffusion of innovations*. 5th ed. New York: Free Press Pp. 305–8.

Schelling, TC. 1971. "Dynamic models of segregation†." *Journal of mathematical sociology* 1(2):143–86.

Wilensky, U. 2005. "Net Logo Small Worlds model."

AUTHOR BIOGRAPHIES

MUSTAFA YAVAS received his B.S. in Industrial Engineering from Boğaziçi University. He is now pursuing M.S. in Industrial Engineering from Boğaziçi University where he is also a research assistant at Socio-Economic System Dynamics Research Group (SESDYN). His research interests are system dynamics and agent-based modeling methods, and diffusions over social networks, economic inequality, and economics of population aging.

GÖNENÇ YÜCEL received his B.S. and M.S. degrees in Industrial Engineering from Boğaziçi University in 2000 and 2004. After earning his PhD degree in Policy Analysis from Delft University of Technology, he joined Boğaziçi University Industrial Engineering Department as an assistant professor. In general, Gönenç has been focusing on simulation methodology, and simulation-supported policy analysis in his research, utilizing agent-based, as well as system dynamics models. For more information; http://www.gyucel.net/Personal/Academic.html

HOW MANY PARAMETERS TO MODEL STATES OF MIND?

Krzysztof Kułakowski, Piotr Gronek, Antoni Dydejczyk

Faculty of Physics and Applied Computer Science,
AGH University of Science and Technology,
al. Mickiewicza 30, 30-059 Cracow, Poland
E-mail: kulakowski@fis.agh.edu.pl

KEYWORDS

Social modeling, parameterization, fitting

ABSTRACT

A series of examples of computational models is provided, where the model aim is to interpret numerical results in terms of internal states of agents' minds. Two opposite strategies or research can be distinguished in the literature. First is to reproduce the richness and complexity of real world as faithfully as possible, second is to apply simple assumptions and check the results in depth. As a rule, the results of the latter method agree only qualitatively with some stylized facts. The price we pay for more detailed predictions within the former method is that consequences of the rich set of underlying assumptions remain unchecked. Here we argue that for computational reasons, complex models with many parameters are less suitable.

INTRODUCTION

Since the times of Max Weber, social scientists agree that mere external observations do not provide sufficient information to understand human actions. Beliefs, expectations, emotions and norms play a major role there and should enter to theories and models. On the other hand, these internal properties cannot be measured directly; information on these variables can be collected by interviews, and the relation between the interview results and the internal properties remains at best subtle.

The aim of this text is to highlight the connection between emotional and behavioral aspects in selected computational models of states of mind. As a rule, these models are postulated with the aim to interpret some observed effects; a successful model should also suggest the way to refine methods of research. If a model does not offer any contact with reality, it deserves to be described with the Pauli's famous statement "not even wrong".

It is obvious that a model with more parameters allows to reproduce observed data with more details. In our view, this option is a dangerous temptation; we argue that, paradoxically, models with more internal parameters are less suitable to infer about internal variables. Our argumentation is directed against models, which intend to capture reality by fitting parameters. This procedure is well established in physics; also in mathematics we sometimes determine unknown parameters from the condition of existence of a nontrivial solution. On the contrary, in social sciences parameters can be fixed only rarely. Even if so, their values fluctuate from one society to another, from one time instant to another. It is not sufficient, therefore, to demonstrate that this or that social effect can be reproduced within a given model. We should check how our model works for the parameter values taken from some ranges, justified by the model context; only then we keep control of the model outcome. The procedure, known as the sensitivity analysis, is hard to be applied for purely computational reasons if the number K of parameters is large; the number of program runs increases exponentially with K. Consequently, the analysis of the results is more likely to remain superficial.

MESSAGE RECEIPT

The first story to bring up here is a method proposed to unify two earlier approaches of public opinion (Zaller 1992; Deffuant et al. 2000; Kulakowski 2009). Actually, both models (Zaller 1992; Deffuant et al. 2000) readily apply to the more general problem of social communication. The Zaller book provides an extended frame of analysis of social receipt of messages, as dependent on their content and on individual characteristics of recipients. At the core of this frame, a multidimensional parameterization was developed, with separate parameters related to the credibility of the message, the awareness on resistance to persuasion, the predisposition on resistance to persuasion, the message intensity, the strength of a relationship between awareness and reception and some others. This kind of modeling aims to refer to individual emotional predispositions of the message recipient, related to particular messages. As the outcome of the mathematical formulas, we get the probabilities that the recipient receives and accepts a given message or simply ignores it. Then, these probabilities allow to infer on the recipient's behavior: a reaction triggered by the message or lack of it.

A general problem encountered with multidimensional

Proceedings 27th European Conference on Modelling and Simulation ©ECMS Webjørn Rekdalsbakken, Robin T. Bye, Houxiang Zhang (Editors)
ISBN: 978-0-9564944-6-7 / ISBN: 978-0-9564944-7-4 (CD)

parameterizations is that the sensitivity analysis cannot be performed. With ten parameters and only three trial values of each (large, small, medium) there is already almost 60 thousands model results to be analyzed. What is even more important here, the number of parameters should be smaller than the number of calculated outcomes; otherwise the model is reduced to a parameterization, which allows to encode potentially each expected/demanded result in the input. More about principles of social modeling can be found in (Edmonds 2000; Edmonds 2005; Helbing and Balietti 2011).

The Deffuant model and its later extension seem to be a remedy to the problem of many parameters. The model (Deffuant et al. 2000) explores the concept termed 'bounded confidence', what – in a broad sense - means that people ignore opinions, messages and other persons which and who are more distant, than some prescribed threshold. In this way, the idea of distance is introduced to psychological and social considerations. This idea, although it can seem trivial for a physically oriented mind, brings two specific properties: first, it is expressed in numbers, and second, it fulfills the so-called triangle inequality. The latter means that the distance between two objects, say A and B, is not greater than the distance between A and C plus the distance between B and C; this should be true for any object C. This inequality, basic for Euclidean geometry, has never been proved in relations to social sciences; on the contrary, it is possible to break it, what is known as intransitive preference (Noteboom 1984). It appears that the introduction of distance is a strong condition which allows to reduce the number of parameters to one or two. Although as arbitrary as the Zaller parameterization, it makes the model of social communication much simpler.

In the unified version (Kulakowski 2009) of the Zaller-Deffuant model, points in a planar area represented messages on two basic issues, say safety and welfare. Agents' knowledge and experience with respect to these issues were growing, as the agents were able to receive messages which were not too far from messages received previously. The threshold distance from a previously received message to a newly accepted, although far, one, represented the mental ability of an agent in the unified model. The basic result of (Kulakowski 2009; Malarz et al. 2011; Malarz and Kulakowski, 2012) is that agents with smaller abilities are more prone to extreme opinions. Apparently, this result does not depend on the choice of the threshold value. In this way, the difficulty of the multidimensional parameterization is evaded.

Above we noted that the Zaller model allows to infer about the behavior of the message recipients; they react or ignore the message, depending on the relation between the message and their ability and experience. The same is true with respect of the Zaller-Deffuant model. A trivial example is when the warning about an emergency is announced in an unknown language; this warning will be ignored till the moment when unquiet behavior of local groups will be imitated by strangers. Less trivial is the conduct of children when alarm is heard in a school building; this signal will be probably interpreted by them with less attention than by teachers, who are responsible for their evacuation.

WHOM WE LIKE, WHOM WE FIGHT

Another approach to be mentioned here deals with the problem of (Kulakowski and Gawronski 2009). It is motivated by the Prisoner's Dilemma, but is free from the parameters which describe payoffs. In this model, the probability that X cooperates with Y depends on the reputation of Y and the overall propensity (altruism) of X to cooperate. In various model variants, reputations and altruisms of agents vary or remain constant. Recently we could demonstrate, that an exclusion of agents with bad reputation does not undermine the social rate of cooperation (Jarynowski et al. 2012). Here again, an interpretation that cooperation is often limited to people with similar social status, seems natural (Weber 1978, p.932). We can make this conclusion more firm, using the concept of reciprocity (Fehr and Gachter 2000) ; people who do much better will not reciprocate my cooperation, because they are not afraid of my punishment; I will not reciprocate the cooperation of a poor for the same reason. Also, the numerical outcome can in principle be verified by a careful experiment.

In this model, the connection between behavior and emotions is assured by the link between a cooperative behavior, a hope for reciprocity and the fear of punishment. The results reported in (Jarynowski et al. 2012) indicate, that once these emotions are absent, cooperation fails. A historical example is provided by the evacuation of American diplomats from Saigon in 1975 (McNamara 1997), when the evacuees could not gain anything by cooperation with their Vietnamese allies.

The description of the next model should be started from a reference to experiment. In 70's, Wayne Zachary investigated social relationships among 34 members of a karate club at an American university (Zachary 1977). Zachary wrote down these relationships as a 34x34 connectivity matrix, indicating who had contacts with whom. During this research, a conflict appeared between the administrator and the teacher, and the club happened to divide into two groups. The matrix and the actual division (who with whom) entered to a data base, useful for social analysts. In particular, a simple set of nonlinear differential equations has been proposed to describe the time evolution of relations between agents (Kulakowski et al. 2005). The calculations – with the connectivity matrix as an input – exactly reproduced the division of the club.

The driving mechanism was the attitude to remove the cognitive dissonance (Festinger 1957); an emotional discomfort which we feel when some parts of our environment are mutually incoherent. In the case of the Zachary measurement, the discomfort experienced by the club members was related to their colleagues; some seemed to be more sympathetic, some less. These classifications were not mutually independent: the karatekas ordered their views according to the principle "friend of my enemy is my enemy" and the like. As a behavioral consequence, the club split appeared to be in accordance with their internal feelings.

The examples given above provide an evidence that the inference from/to emotions and behavior is possible at the model level. In all these examples some kind of behavior (reaction for a message, cooperation, solidarity) was one of two options, and the adherence to this behavior was motivated by a definite mental state which also could appear or not appear. We note that in some social situations, a given emotion can be believed to appear without alternatives. In this case, the aim of modeling is just to investigate consequences. A good example is the text (Malarz et al. 2006) on the Bonabeau model (Bonabeau et al. 1995); the latter was formulated with a reference to animal rather than human societies. Most briefly, the problem can be presented as follows. A group of agents wanders a given area, and those who met have to fight. The fight outcome is that the winner gets some goods from the loser. Also, the probability that an agent wins depends on his amount of goods before the fight. On the other hand, the differences between wealth of agents decrease between fights. The problem is, if the variance of wealth will be large or moderate? A phase transition between those two options was previously identified in the literature, and our text (Malarz et al. 2006) is devoted to an analysis of this phase transition. Perhaps the model could be an illustration of increasing differences in power between local rulers in medieval Europe. A beautiful and deep description of this process was given by Norbert Elias in his monumental book „The Civilization Process" (Elias 1939). However, we do not learn anything on human beings from the numerical results. The driving emotions, supposedly fear and hate between rivals, is built into the model without alternatives.

FEELINGS IN CROWD

When looking from this perspective, there is some analogy between the Bonabeau model and the modeling of crowd dynamics, as in the so-called Social Force Model (Helbing et al. 2000). There, pedestrians are represented as particles in a two-dimensional space, with appropriately chosen masses, radii, elastic and friction coefficients. We note that this careful design allowed to reach numerous interesting properties of the crowd, with undoubted accordance with reality (Johansson et al. 2007). The human nature of the simulated pedestrians manifests in that they prefer to keep mutual distance (hence „Social Force") and in their ability to select direction and velocity of their motion. This characteristics can be enriched by an individual modification of their parameters or even by some manipulation of their purposes (Gawronski and Kulakowski 2011; Gawronski et al. 2012), but all that is to be done by hand.

This list of our social modeling is to be compared with the research strategy applied in large scale by Treur and Sharpanskykh and their cooperators (Sharpanskykh 2010; Bosse et al. 2011). The declared aim of the paper (Sharpanskykh 2010) is to define relations between different cognitive processes of an agent in a socio-technical system. The list of these processes is derived from the literature. These are: belief revision, trust dynamics, generation and development of feelings and emotions, and decision making. Reading the text, we learn that the essence of work is to introduce the desired dependences of related variables by properly placed instructions of a specially designed computer language. In a section „Experiments", three runs of the simulation of an evacuation are reported. As numerical results, three different curves are presented on the time dependence of the number of persons in the room.

The paper (Bosse et al. 2011) reports a more direct connection to experimental data. Namely, the aim here is to reproduce the motion of people, filmed during the panic outbreak in Amsterdam, May 4, 2010. To achieve this, a total difference between filmed and calculated trajectories was minimized, tuning two global parameters and individual time dependences of the maximal speeds of people involved. This difference – a measure of the simulation error – was compared for three different cases: people did exchange emotions, people did not exchange emotions, people did not move at all. The exchange of emotions was built in to the general simulation frame, the same as in the previous paper (Sharpanskykh 2010). The first option gave the smallest error. In their conclusions, the authors underline this result as an argument that people do exchange emotions.

We are tempted to suspect that it is the general, multidimensional frame used here what makes the contact with experimental data superficial. The conclusion that panicking people do exchange emotions is certainly reasonable. However, one can ask if this conclusion could not be obtained within a simpler model? Similarly to the Zaller approach, the general modeling frame used by Sharpanskykh and Treur does contain so many internal parameters of the simulated agents, that the abundance of these parameters disables any systematic analysis of their role.

DISCUSSION

Still, the issue becomes more complex when we realize that the multidimensional modeling could be defended as follows: if we fix all parameters but one, the obtained model should be formally equivalent to a model with one parameter. What is wrong with adding new parameters if we keep them constant? Perhaps a subtle but simple answer can be found in the prescription of modeling, given in (Edmonds and Paolucci 2012) in a book review. The authors write: „To assess the usefulness of a modeling technique one has to look at the strength of three stages in the use of a model (...): (encoding) the map from the known or hypothesized facts and processes into the model set-up, (inference) the deduction of results from the set-up to the outcomes, and finally (decoding) the mapping of the results back to the phenomena of concern. Roughly, the usefulness of a model is the reliability of the whole modeling chain: encoding + inference + decoding." The answer could be that in multidimensional models, this reliability is particularly difficult to be controlled.

The models brought up here as examples are different. The Zaller model of public opinion does not provide more insight, than the data it uses as an input; this is just a translation from the data to a set of coefficients, which can be measured only through these data. The bounded confidence model brings instead the concept of distance and one control parameter. One can wonder, if messages can be distributed in a geometrical space or rather on a network. Basically, we should be able to verify the Deffuant model by checking if the small world effect applies to the set of opinions; we imagine that this could be done by carefully designed interviews. Also, if the triangle inequality is broken in a given system, the whole concept of distance cannot be maintained. Taking this into account, we admit that the model assumptions are susceptible to a falsification; in terms of Wolfgang Pauli, this model can be right or wrong.

In a reformulation of the Prisoner's Dilemma multi-agent game (Kulakowski and Gawronski 2009) a distribution of reputations of N agents about N others has been used. The essence of the model was to propose the rule of evolution of these reputations. We note that the reputations can be measured by interviews. Moreover, the aim of (Kulakowski and Gawronski 2009) has not been to compare the results with a given set of data, but rather to check if cooperation without payoffs is possible. No fitting has been done there. Similarly, the differential equations used to simulate the removal of cognitive dissonance in (Kulakowski et al. 2005) have been designed to illustrate the mechanism, and the accordance with experimental data of (Zachary 1977) should be treated as to some extent fortuitous. No parameters have been fitted there. Advantages of simple models are commonly known (Edmonds 2000; Edmonds 2005). Yet, as is also known, their flaw is that the condition of simplicity drives these models far from reality. We perceive their role to be similar to the one of verbal syllogisms in ancient philosophy: they should improve the clarity of our thinking of social systems.

The list of approaches presented above is limited to computational models, embedded in literature. It is worthwhile to mention also direct measurements of physiological variables which reflect emotional states of the subjects (Riener et al. 2009; Kashif et al. 2010). In some sense, however, the situation in these experiments mirrors the one in modeling. We expect that emotions are present in some situations, as when driving during the rush hours, we can even infer that a particularly risky strategy of driving, when observed, could be due to some specific mental state, but – more than often – the connection between behavior and emotions remains unverified. It is precisely the internal character of emotional states what makes the research of social systems so complex. We suspect that these states influence the system behavior and almost always we are right. But more insight into this internal world cannot be attained without a dedicated research. The next step – what determines these emotions? – is related with past experience of our subjects, and therefore it is even more far.

To summarize, either we can measure or at least evaluate our parameters, or the sensitivity analysis is necessary. In the case of internal parameters which can be measured only indirectly, the latter analysis seems unavoidable. Once stated, this rule seems trivial; yet sometimes the practice is different. In the social world of fluctuating parameters, an accordance of model predictions with a set of experimental data is often fortuitous. Therefore, on the contrary to natural sciences, it cannot be treated as the final proof of truth. The famous irony of John von Neumann "with four parameters I can fit an elephant, and with five I can make him wiggle his trunk" finds its target again.

ACKNOWLEDGEMENTS

It is good occasion for one of authors (K.K.) to express his gratitude to Cristina Beltran-Ruiz, Vanessa Camilleri, Vikas Chandra, Maggie Ellis, Alois Ferscha, Matthew Fullerton, Przemek Gawronski, Jan Kantelhardt, Mirko Kampf, Ruediger Korff, Gosia Krawczyk, Paul Lukowicz, Krzysztof Malarz, Janusz Malinowski, Hermann de Meer, Matthew Montebello, Lev Muchnik, Eve Mitleton, Gevisa La Rocca, Khalid Saeed, Alexei Sharpanskykh, Wiesia Sikora, Jarek Wąs and Martin Wirz for kind discussions and cooperation. We are also grateful to our Referees for their criticism and tolerance.

REFERENCES

Bonabeau, E., G. Theraulaz, J.L. Deneubourg. 1995. "Phase diagram of a model of self-organizing hierarchies." *Physica A*, 217, 373-392.

Bosse, T., M. Hoogendoorn, M.C.A. Klein, J. Treur, and C.N. van der Wal CN, 2011. "Agent-based analysis of patterns in crowd behaviour involving contagion of mental states." *LNAI* 6704, 566-577.

Deffuant, G., D. Neau, F. Amblard, and G. Weisbuch, 2000. "Mixing beliefs among interacting agents", *Adv. Complex Syst.,* 3, 87-98.

Edmonds, B. 2000. "The Use of Models - making MABS more informative." In Moss, S. and Davidson, P. (eds.) Multi Agent Based Simulation 2000, *LNAI*, 1979:15-32.

Edmonds, B. 2005. "Simulation and Complexity - how they can relate." In Feldmann, V. and Mühlfeld, K. (eds.) Virtual Worlds of Precision - computer-based simulations in the sciences and social sciences. Lit Verlag, 5-32.

Edmonds, B., and M. Paolucci. 2012. JASSS 15, Issue 2.

Elias, N. 1939. *Über den Prozess der Zivilisation*. Verlag Haus zum Falken, Basel.

Fehr, E. and S. Gächter. 2000."Fairness and retaliation: A theory of reciprocity. *Journal of Economic Perspectives,* 14, 159-181.

Festinger L. 1957. *A theory of cognitive dissonance*, Stanford UP, Stanford.

Gawronski, P. and K. Kulakowski. 2011. "Crowd dynamics – being stuck." *Comp. Phys. Commun.* 182, 1924-1927.

Gawronski, P., K. Kulakowski, M. Kampf, J.W. Kantelhardt. 2012. "Evacuation in the Social Force Model is not stationary." *Acta Phys. Pol. A*, 121, B77-B81.

Helbing, D., I. Farkas and T. Vicsek. 2000. "Simulating dynamical features of escape panic", *Nature* 407, 487-490.

Helbing, D. and S. Balietti. 2011. *How to do agent-based simulations in the future: from modeling social mechanisms to emergent phenomena and interactive systems design*, Santa Fe Institute working paper, 2011

Jarynowski, A., P. Gawronski, and K. Kulakowski. 2012. How the competitive altruism leads to bistable homogeneous states of cooperation or defection. *LNCS,* 7204, 543-550.

Johansson, A., D. Helbing and P.S. Shukla. 2007. "Specification of the social force pedestrian model by evolutionary adjustment to video tracking data." *Adv. Complex Syst.* 2007;10:271-288.

Kashif, Z., A. Riener and A. Ferscha. 2010. "Reduction of driver stress using AmI technology while driving in motorway merging sections." *LNCS* 6439, 127–137.

Kulakowski, K., P. Gawronski and P. Gronek. 2005. "The Heider balance: a continuous approach", *Int. J. Modern Phys. C* 16, 707-716.

Kulakowski K. 2009. "Opinion polarization in the Receipt-Accept-Sample model", *Physica A,* 388, 469-476.

Kulakowski, K., and P. Gawronski. 2009. "To cooperate or to defect? Altruism and reputation." *Physica A* 388, 3581-3584.

Malarz, K., D. Stauffer and K. Kulakowski.2006. "Bonabeau model on a fully connected graph", *Eur. Phys. J. B* 50, 195-198.

Malarz, K., P. Gronek, K. Kulakowski. 2011. "Zaller-Deffuant model of mass opinion." *JASSS*, 14, Issue 1.

Malarz, K., and K. Kulakowski. 2012. "Bounded confidence model: addressed information maintain diversity of opinions." *Acta Phys. Pol. A*, 121, B86-B88.

McNamara, F.T., *Escape with honor: my last hours in Vietnam*. Dulles; Brassey's; 1997.

Nooteboom, B. 1984. "Intransitive preferences in retailing." *Service Industries Journal* 4, 82-92.

Riener A, M. Aly and A. Ferscha. 2009. "Heart on the road: HRV analysis for monitoring a driver's affective state", 1st International Conference on Automotive User Interfaces and Interactive Vehicular Applications, Essen, Germany, page 8.

Sharpanskykh, A. 2010. "Integrated modeling of cognitive agents in socio-technical systems." *LNCS,* 6071, 262-271.

Weber M, *Economy and Society. An Outline of Interpretive Sociology*, Berkeley: Univ. of California Press; 1978.

Zachary, W.W. 1977. "An information flow model for conflict and fission in small groups." *J Anthropological Research* 33, 452-473.

Zaller, J. R. 1992. *The Nature and Origins of Mass Opinion*. Cambridge UP, Cambridge.

KRZYSZTOF KUŁAKOWSKI was born in Zakopane, Poland. He studied theoretical physics at the Jagiellonian University in Cracow, and obtained MSc diploma in 1975. Since then he has been a member of staff of various faculties at the AGH University of Science and Technology in Cracow. He received PhD degree in solid state physics in 1984. He is a coauthor of 180 refereed papers. Since 2000 he is involved in applications of statistical physics to social phenomena. His e-mail address is: kulakowski@fis.agh.edu.pl and his Web-page can be found at: http://www.ftj.agh.edu.pl/~kulakowski/.

PIOTR GRONEK was born in Kielce, Poland. He studied technical physics at AGH University of Science and Technology (AGH-UST) in Cracow, and obtained MSc diploma in 1990. There, he received PhD degree in technical nuclear physics in 1997. Since then he has been a member of the teaching staff at Faculty of Physics and Applied Computer Science, AGH-UST. His e-mail address is: Piotr.Gronek@fis.agh.edu.pl and his Web-page can be found at: http://www.fis.agh.edu.pl/~gronek.

ANTONI DYDEJCZYK was born in Zabrze, Poland. He studied technical physics at AGH University of Science and Technology (AGH-UST) in Cracow, and obtained MSc diploma in 1981. Since then he has been a member of the staff at Faculty of Physics and Applied Computer Science, AGH-UST. He received PhD degree in technical nuclear physics in 2006. His e-mail address is: Antoni.Dydejczyk@fis.agh.edu.pl and his Web-page can be found at: http://www.fis.agh.edu.pl/~antek.

MULTI-PATCH COOPERATIVE SPECIALISTS WITH TAGS CAN RESIST STRONG CHEATERS

Bruce Edmonds
Centre for Policy Modelling
Manchester Metropolitan University
All Saints Campus, Oxford Road, Manchester, M15 6BH, UK.
E-mail: bruce@edmonds.name

KEYWORDS
Symbiosis, meta-population, multi-patch, cooperation, agent-based simulation, tags, defection.

ABSTRACT.

The paper looks at tag-based cooperation within abstract simulation models. Previous models of this kind have been shown to either have 'programmed in' cooperation or to be vulnerable to "strong cheaters". Previous work by the author included a model of social specialisation and cooperation, but where only a single dominant tag-group arose at any one time and where cooperation eventually collapsed. Here a multi-patch version of this model is explored and show to not to collapse but seed itself indefinitely. Furthermore, the model seems to be resistant to significant levels of strong cheaters.

INTRODUCTION

There is a large and growing body of work exploring the necessary and sufficient conditions for cooperation to arise, in particular in terms of the kind of mechanism that might bring this about. The tag approach is one of these. It is a lightweight mechanism that does not require kin selection, memory, or explicit enforcement (by, say, punishment). The idea was introduced by Holland 0, and has since been explored in a number of variants, including: (Hales 2000; Riolo, Choen and Axelrod 2001; Shutters and Hales 2013).

The idea of a 'tag' is that it is an externally observable trait that does not have any 'hard-wired' connection with behaviour, but which can be used as a fallible indicator of group membership and hence allow cooperation to develop where otherwise it would not. The basic rule is to cooperate with those with similar tags to one's own. A key feature of such models is that there is no a priori reason why someone similar is more likely to be trustworthy than anyone else. An obvious social interpretation is the accent and appearance of people – one can (almost always) tell whether someone belongs to your area/type or not. As Hales (2000) pointed out, this mechanism works through the rising and falling of groups with similar tags – although each group is eventually invaded by non-cooperators, destroying the cooperation, an overall high level of cooperation is maintained globally by the constant formation of new cooperative groups (and the dying off of non-cooperative groups).

There are several ways of implementing tag-based mechanisms; each needs a method for representing the tags and a similarity criterion. Hales (2000) uses a simple integer for the tag and the similarity criteria that only agents with identical integers are similar. In the later models of (Hales and Edmonds 2005) tags are only implicitly indicated by network links and agents are similar if they are connected by a link. Here, I follow (Riolo, Choen and Axelrod 2001) and give each agent two floating-point numbers from the interval [0, 1]: one for the tag and one for its tolerance. The similarity criterion is that the difference between another's tag value and one's own has to be strictly less than my tolerance value[1]. Thus donation is not necessarily reciprocal – one agent might be within the tolerance of another's (and hence get donated to) but have a smaller tolerance and not donate back. Agents with a zero tolerance will not donate to any other agent – the possibility of agents adapting zero tolerances is important as it means agents are not 'forced by design' to donate to others with exactly the same tag value, as occurs in (Riolo, Choen and Axelrod 2001). This is shown in Figure 1.

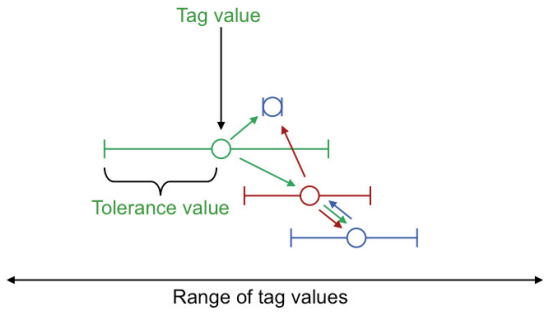

Figure 1. An Illustration Of Tags With Floating-Point Values And Tolerances

[1] Notoriously (Riolo, Choen and Axelrod 2001) used the similarity criterion of the difference ≤ tolerance which meant that agents with identical tags were forced to be altruistic0.

Proceedings 27th European Conference on Modelling and Simulation ©ECMS Webjørn Rekdalsbakken, Robin T. Bye, Houxiang Zhang (Editors)
ISBN: 978-0-9564944-6-7 / ISBN: 978-0-9564944-7-4 (CD)

In this illustration for each agent the value of the tag is shown as a circle and the tolerance as a range either side of this. The arrows show directions of potential donation. Donation can occur indirectly via a third party. Individuals with zero tolerance only receive donations they do not give.

This method has the advantage that groups are 'fuzzy' in definition but can clearly emerge.

THE SINGLE PATCH MODEL OF SPECIALISTS WITH TAGS

In this model (Edmonds 2006), there are a small fixed number of types of nutrient, which all agents need in order to live. The basic premise of the model is that agents are all specialists and can each only produce one of these types. However if they have more than a specified amount they will distribute the excess to others, but only to those who are sufficiently similar to them. Thus in this model (and the multi-patch version) agents have to receive donations of the kinds of nutrient they do not produce in order to survive (and reproduce).

Each agent has the following attributes: its specialist type of nutrition, its tag, its tolerance and the amount of food (of each kind) that it has. Key to understanding this model is its 'economy' in terms of food. Food is distributed within the patch divided between the different kinds of nutrition. Each agent gets its share of the kind of nutrition it specialises in. Agents are randomly paired with others within the patch and if (a) it has an excess of a kind of food and (b) a paired agent is sufficiently similar to itself (as described above). During donation the amount of the donation is subtracted from the donor but only a proportion is added to the done (i.e. some is lost)[2]. Each time click a 'life tax' of each kind of food is subtracted from each agent and those who have zero of any type die. Those who achieve above a certain level in all kinds reproduce, with a set amount of all of the food kinds being passed to the offspring. Thus individuals continually: appear (arrive or are born), donate, consume resources, (possibly) reproduce, and die (of starvation or old age). The population level is thus variable — determined by the available resources and the efficiency of the sharing structures between them. When agents reproduce, the offspring inherits the characteristics of the parent, but with some chance of mutation occurring to both tag and tolerance values. To get the process started random new agents are introduced to the patch[3]. A more complete description can be found in the appendix of (Edmonds 2006).

This is enough for cooperative tag groups to arise and a short-term burst of cooperation to be established. The whole process can be seen as a life cycle of the tag groups, which although not precisely defined, are obvious when you see them. The cycle goes like this: (1) after a while it happens by chance that a set of individuals with specialisms covering all the nutrient types and whose tag + tolerance values allow them to mutually donate so that all get the nutrient types that they need to thrive, (2) this tag group grows quickly in terms of numbers, (3) a sub-population of these evolves with a smaller tolerance value so these essentially parasitize on the group, receiving donations but not giving them – this causes a kind of predator-prey kind of dynamic (4) finally the parasites dominate and 'kill off' the group and the model enters an unviable period. The persistence of stage (3) is important as it allows the group to tolerate the presence of non-cooperators for a while.

This process is illustrated in Figure 2 below. In this figure each line shows the population of individuals specialising in each of the kinds of nutrients. Different phases are evident: UV an un-viable phase where individuals enter the simulation but quickly 'die off', CE a phase of cooperative existence where a group of mutually donating individuals forms and thrives, and PP where predator-prey type dynamics arise and eventually destroy the group.

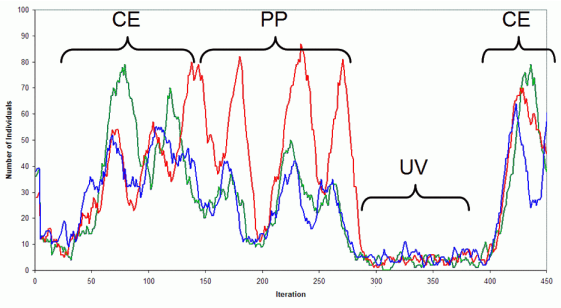

Figure 2. Typical Intra-Population Dynamics Within The Single Patch Model

In earlier versions of this model it was found that some individuals built up huge stores and lived indefinitely, reproducing many times. It was felt that this was unrealistic and so maximum store sizes (for each nutrition kind) and maximum ages (after which agents die and their stores are lost) were introduced to make the task of establishing cooperation more challenging. Not that in this

[2] One way to 'engineer in' cooperation is to allow donation to 'create' new value with the donee receiving more than the donor lost, in this example the efficiency of donation was set at 90%.

[3] In the original model (Edmonds 2006) the introduction of new agents was continual, but in these versions it only occurs until a viable population is established.

model, without a constant 're-seeding' of new agents the population collapses to unviability, even without any strong cheaters.

DIFFERENT KINDS OF CHEATER

Simulation models that explore cooperation have, at least since sought to show how cooperation can persist when non-cooperators can arise or invade and where individual can adapt. The problem is that in the short term it is in the interest of individuals to adapt and stop cooperating and gain the benefit of the cooperators aroun d and not suffer the cost of cooperation themselves, even though they could gain more in the longer term by cooperating if others do the same. The engineering problem is to design a system such that cooperation is not built in, but can arise and 'mend' itself flexibly, but that it is as resistant as possible to uncooperative agents.

Of course, what counts as not "building in" cooperation and what counts as a "cheater" to test the system is a matter of definition. Shutters and Hales (2013) look at different 'strengths' of "cheaters" and examine a range of models to see which are resistant to which kinds. They define "weak cheaters" as

…agents that may evolve a tolerance so low that they do not donate to any other agent but will likely receive donations. However, these agents still have a trait for tolerance and the mechanism for altruistically donating. If mutation drives the tolerance of a weak cheater back to a positive value, it may resume altruistic behavior. (para. 4.2)

Several of the model versions they explored were resistant to weak cheaters. However they also defined "strong cheaters" as

… agents that have no ability to donate and thus no tolerance trait. They simply display a tag and reap the rewards of displaying that tag to altruistic donors. There is no possibility of a mutation in tolerance causing a return to altruistic behavior because they have no capacity for such behavior and thus – they effectively have no tolerance trait. (para. 4.3)

These are implemented by adding an extra property that indicates being a strong cheater, which when activated stops all cooperation in them or their offspring[4]. None of the models investigated in0 were able to maintain high levels of cooperation when there such agents could arise. The single patch version of the model described above did not 'need' strong cheaters to destroy cooperation, since cooperation collapses after a while with only its own internal "weak cheaters", which naturally evolve within it. Adding strong cheaters into the single patch version of the model does not radically change this, but does somewhat complicate the internal population dynamics – sometimes their introduction acts to kill the group quicker but sometimes it extends its lifetime by predating on otherwise parasitical sub-populations.

THE MULTI-PATCH MODEL OF SPECIALISTS WITH TAGS

This version of the model is composed of a 2D grid of connected patches, with the same dynamics of the single patch model *within* each of these patches, but with three changes:

(1) a (low) probability of migration between neighbouring patches (those that share an edge), so that each individual in each time click has a given probability of being relocated to an adjacent patch;

(2) a probability that in any creation of new individuals (via random introduction or reproduction) they are set as strong cheaters (this requires the introduction of an extra Boolean "strong-cheater" attribute to agents that is passed down to offspring);

(3) the introduction of random new individuals is restricted to the start of the simulation and stops after a viable population (defined by the total population reaching a given threshold) is reached.

The first of these changes (1) is the essential move to a multi-patch version of the model, otherwise the model would be simply a collection of independent single-patch simulations. The introduction of (2) allows us to test the multi-patch model with strong cheaters. (3) is simply the removal of a 'cludge' in the single-patch model that is no longer needed in the multi-patch version (since re-seeding is now endogenised via migration between patches).

[4] (Shutters and Hales 2013) also includes "medium" cheaters under this definition – those with some possibility of this extra property being switched back, but we do not bother with that variety here, preferring only the strong stuff.

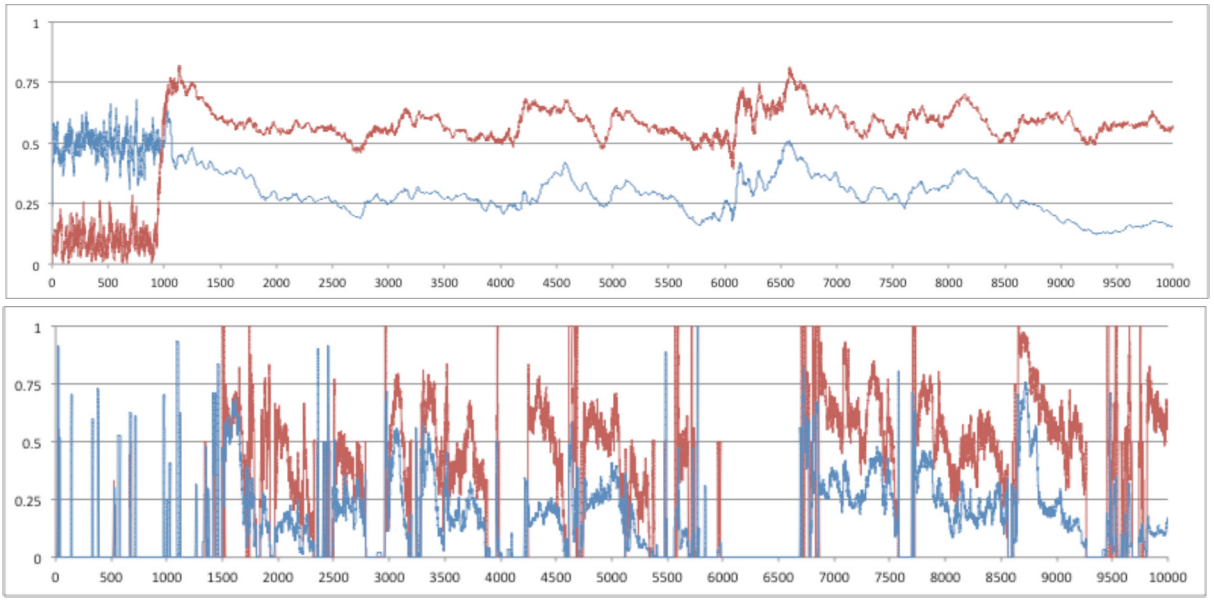

Figure 3. Donation Rates (top line) and Average Tolerance (bottom), both as a proportion of their maximum value, for 10,000 time steps: (above) for the whole 10x10 grid of patches (below) for one specific patch.

With these changes each patch can seed its neighbours with individuals allowing cooperative groups to start afresh in their arms race with both weak and strong cheaters and thus a high level of global cooperation is maintained even though the cooperation always eventually collapses in any one patch, resulting in the demise of individuals there (both co-operators and cheaters).

Figure 3 above shows the donation rate and average tolerance level for a run of 10,000 time steps, the top showing global statistics and the bottom the statistics for a particular patch. Figure 4 below is for the same run but for numbers of individuals: the top graph for total number and number of cheaters, the bottom for number of cheaters and each skill type in the same particular patch as graphed in Figure 3.

I hypothesise that the robustness of the set-up to strong cheaters is due to: (a) when a new cooperative group starts on a patch it is likely to be composed of only co-operators, thus they have a chance to get established before cheaters arrive, (b) as was shown in the single patch model patches have some resistance to cheaters (both weak and strong) due to the internal predator-prey dynamics that occurs and (c) the multi-patch setup allows group-level selection to occur, with cheaters eventually killing themselves due to destroying the efficacy of the group they rely on. However the relative importance of these is yet to be established.

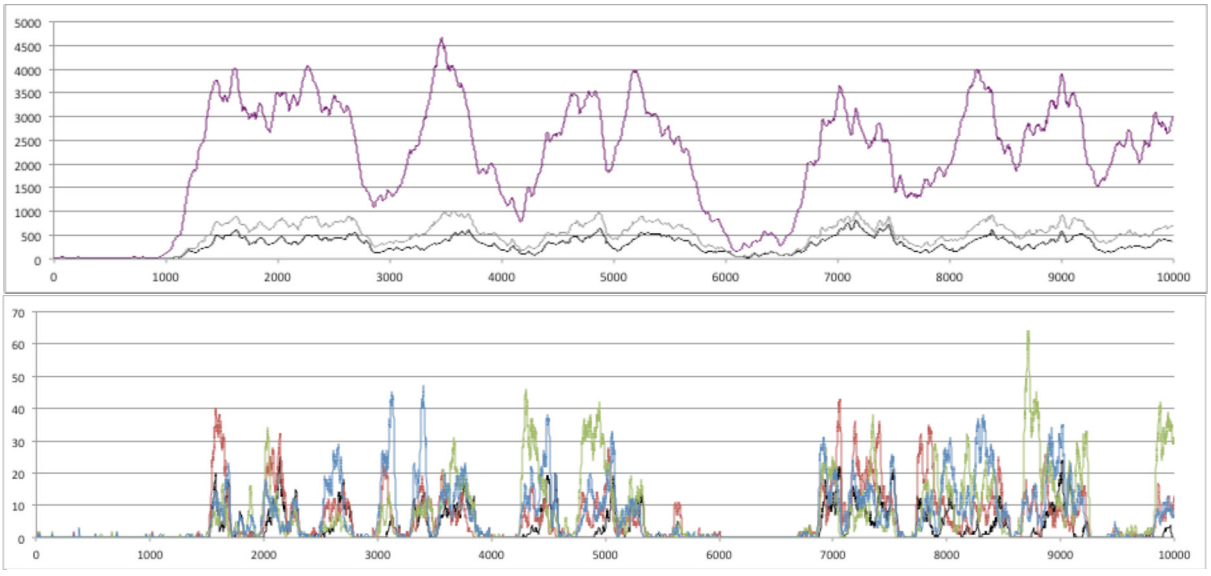

Figure 4. Number of Individuals over 10,000 time steps (above) for the whole 10x10 grid: purple=total population, grey=weak+strong cheaters, **black**=strong cheaters (below) for a particular patch: top line=individuals with skill 1, bottom= those with skill 2, blue=with skill 3, **black**=strong cheaters.

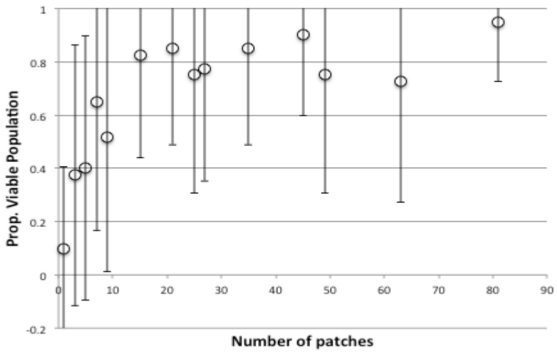

Figure 5. Proportion Of Times There Is A Viable Population After 4000 Time Clicks With Sizes Of Grid, Without Strong Cheaters (0% Probability)

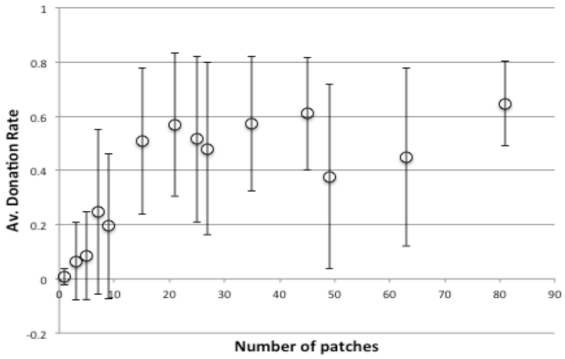

Figure 6. Average Donation Rate After 4000 Time Clicks With Sizes Of Grid, Without Strong Cheaters (0% Probability, Bars Indicate 1SD)

Figure and 6 above shows statistics over the last 1000 time steps (out of 5000) over 20 runs for the multi-patch model, with different sized grids: Figure 53 shows the proportion of runs in which the simulation is viable with different numbers of patches, with Figure 6 showing the average donation rates (both as a proportion of the maximum possible). As the number of patches increase, so does the donation rate and viability, with little increase after a size of 16 patches.

When we introduce a 1% rate of cheater entry into the model (out of new individuals born) the picture is similar, with a delayed plateau starting at 45 patches and slightly depressed levels of viability and donation (Figure & 8). Thus strong cheaters do take their toll, draining the system of some resources and making the whole system less efficient but this is often not a critical one.

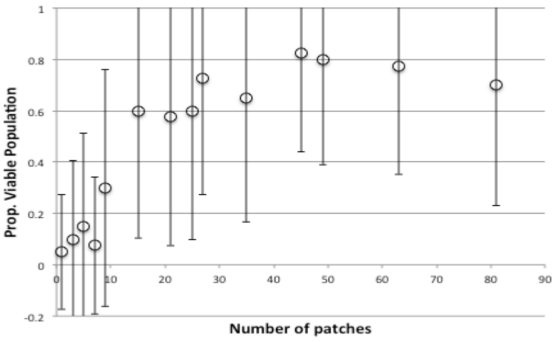

Figure 7. Proportion Of Times There Is A Viable Population After 4000 Time Clicks With Sizes Of Grid, With Strong Cheaters (1% Probability)

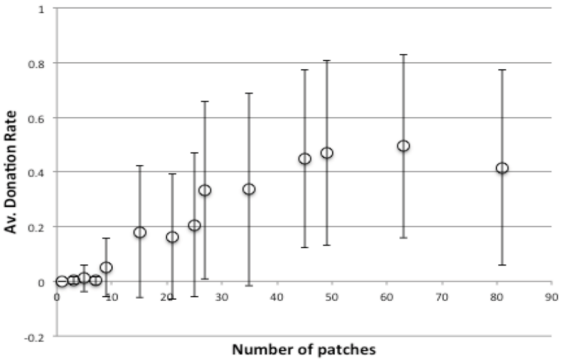

Figure 8. Average Donation Rate After 4000 Time Clicks With Sizes Of Grid, With Strong Cheaters (1% Probability)

On investigation, the response of a multi-patch version of the model to the cheater rate seems to be graceful. The impact of different levels of cheater introduction rate on population size (Figure 9) and donation rates (Figure 10) are shown.

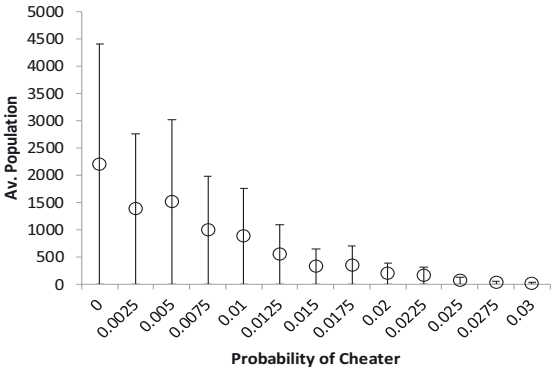

Figure 9. Varying The Rate Of Strong Cheater Introduction On Donation Rate

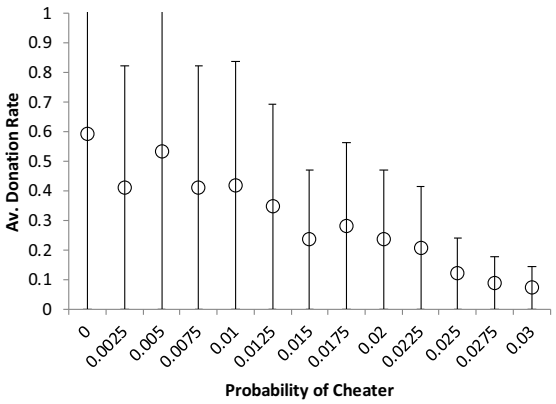

Figure 10. Varying The Rate Strong Cheater Introduction On Average Population Size

Since this is reported in many papers on tag-based cooperation, Figure 11 shows the effect of varying the number of random pairings (opportunities for donation) and the efficiency of donation on the donation rate for runs with a 1% rate of strong cheater introduction (bottom) and without them (top). As with varying the number of patches the presence of strong cheaters means a slightly higher threshold of pairings and donation efficiency occurs and a slightly overall depression of donations rates (which is unsurprising as strong cheaters will not donate).

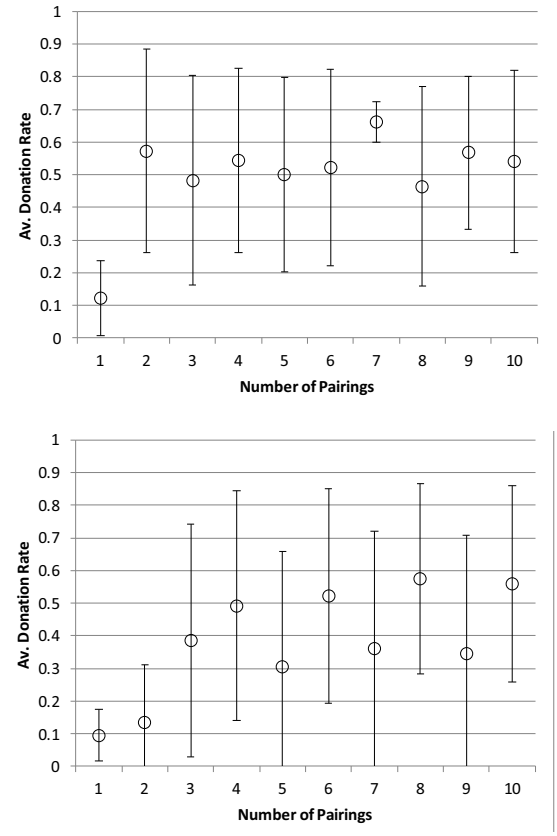

Figure 11. Effect of number of pairings on Donations rate (top) with no strong cheaters, (bottom) with 1% strong cheater rate

Finally, for the record we examine the effects of donation efficiency on donation rates without strong cheaters (top) and with a 1% rate of strong cheaters (bottom). As for varying the number of pairings the effect of having a continual presence of strong cheaters seems to merely require slightly higher numbers of pairings each tick (from 2 to 3) or donation efficiency (from 0.7 to 0.8).

Thus we see that the presence of strong cheaters does degrade the level of cooperation and their presence does require slightly higher levels of parameters that promote the onset of cooperation, but the effect is (a) gradual (Figure 10) and (b) for small but pervasive levels (i.e. a 1% rate) marginal (as in Figures 11 and 12).

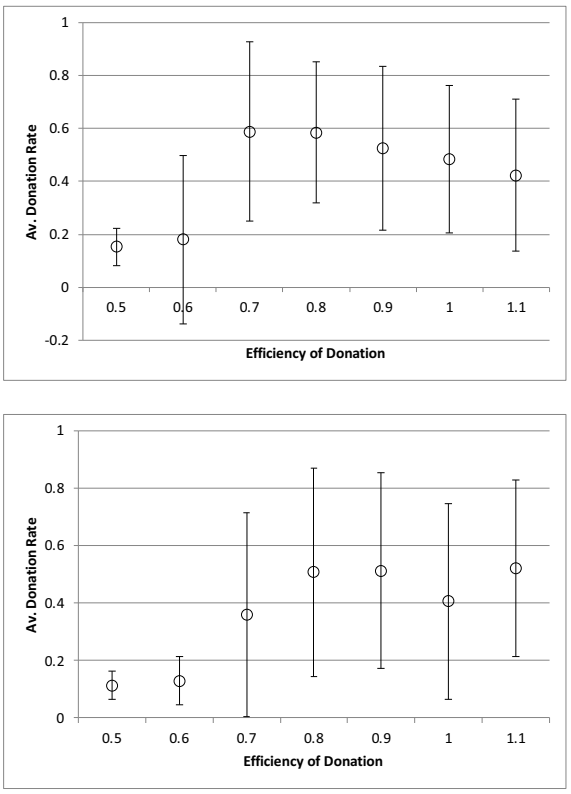

Figure 12. Efficiency of donation against donation rate (top) with no strong cheaters, (bottom) with 1% strong cheater rate

CONCLUDING DISCUSSION

Shutters and Hales (2013) discuss ways that might defeat strong cheaters. The second of which was

… through multi-level selection, in which populations of agents compete against other populations for survival… Those populations that can internally regulate or eliminate non-donors typically displace populations that cannot… enabling tag-mediated altruism to persist dynamically with cheaters in a larger metapopulation. (para. 7.6)

The multi-patch model described here is of this kind. Each patch can host a population and the whole model is a meta-population model. However, there is no displacement of one population by another here, simply the parallel coexistence of populations. Here each population can somewhat resist strong cheaters, but is eventually overwhelmed. When that happens most of the agents in that population die, including the cheaters there – all but the few that happened to migrate. Thus when a population explosion of strong cheaters occurs most of them then die. This is like a parasite that can easily kill its host and hence itself.

Of course, given enough understanding of this (or any model) we could invent a "super-strong cheater" that would defeat this model. There is no ultimate escape from an "arms race" for survival given a sufficiently inventive foe. However, these might not be realistic in the sense that they might not meaningfully correspond to anything observed or potentially existent.

What this does show is that enforcing specialisation along with partial division into sub-populations might help "harden" systems against malicious invasion. The more individuals have to rely on a set of other kinds of skills the more difficult it is to dominate – it is much easier to dominate a monoculture – and the smaller the group in which individuals act, the more the consequences reflect back on that group. Thus the results of this paper and others might follow (Hales and Edmonds 2005) and (Pitt, Schaumeier and Artikis 2012) in applying such biological and socially inspired mechanisms to the design of more robust computational systems, but this will only be a route to reliability if we manage to fully understand the social interaction that underlies these mechanisms.

ACKNOWLEDGEMENTS

This research was partially supported by the Engineering and Physical Sciences Research Council, grant number EP/H02171X/1.

REFERENCES

Edmonds, B. (2006) The Emergence of Symbiotic Groups Resulting From Skill-Differentiation and Tags. *Journal of Artificial Societies and Social Simulation*, **9**(1), 10. http://jasss.soc.surrey.ac.uk/9/1/10.html

Edmonds, B., & Hales, D. (2003). Replication, Replication and Replication: Some Hard Lessons from Model Alignment. *Journal of Artificial Societies and Social Simulation,* **6**(4), 11 http://jasss.soc.surrey.ac.uk/6/4/11.html.

Hales, D. (2000). Cooperation without memory or space: Tags, groups and the prisoner's dilemma. In S. Moss & P. Davidsson (Eds.), *Multi-Agent-Based Simulation*, **1979**, 157-166.

Hales, D., & Edmonds, B. (2005). Applying a socially inspired technique (tags) to improve cooperation in P2P networks. *IEEE Transactions on Systems Man and Cybernetics Part a-Systems and Humans,* **35**(3), 385-395.

Holland, J. (1993). The Effect of Labels (Tags) on Social Interactions. Working Paper 93-10-064. Santa Fe Institute. Sante Fe, New Mexico.

Pitt, J., Schaumeier, J. & Artikis, A. (2012) Axiomatization of Socio-Economic Principles for Self-Organizing Institutions: Concepts, Experiments and Challenges. *ACM Transactions on Autonomous and Adaptive Systems* **7**(4):39.

Riolo, R. L., Cohen, M. D., & Axelrod, R. (2001). Evolution of cooperation without reciprocity. *Nature,* **414**(6862), 441-443.

Roberts, G., & Sherratt, T. N. (2002). Does similarity breed cooperation? *Nature,* **418**(6897), 499-500.

Shutters, S. T. & Hales, D. (2013) Tag-Mediated Altruism is Contingent on How Cheaters Are Defined. *Journal of Artificial Societies and Social Simulation*, **16**(1), 4 http://jasss.soc.surrey.ac.uk/16/1/4.html.

APPENDIX

There was not space for a full ODD description of the model in this paper. However more details, a working version of the model and its code is at:
http://cfpm.org/models/meta-population%20model.html

BRUCE EDMONDS: is Director of the Centre for Policy Modelling and a Senior Research Fellow at the Manchester Metropolitan University. His first degree was in pure mathematics, his PhD in the philosophy of science. He now does a mixture of computer science and sociology. More about him can be discovered via his web page at: `http://bruce.edmonds.name`

ON THE BASIC BINDING STRUCTURE OF A BASIC INTERACTION SCHEME

Antônio Carlos da Rocha Costa
Centro de Ciências Computacionais/PPGComp
Universidade Federal do Rio Grande – FURG
96.203-900 – Rio Grande – RS – Brasil
Email: ac.rocha.costa@gmail.com

ABSTRACT

This paper introduces and analyses the idea of the *binding structure* of a *social interaction scheme*. Binding structures are proposed as means to model the binding power that an interaction scheme imposes on agents interacting according to the scheme, in a social context. The paper considers the case of a *basic interaction scheme*, namely, the basic *Producer-Consumer* scheme, to explain the way the binding structure builds on the operational structure of that scheme, in particular how the binding structure is constructed in terms of *binding relations*. In addition, the non-reducibility of binding structures to their component binding relations is established. The importance of a detailed analysis of the *derivation scheme* of binding structures from operational structures of interaction schemes, including the role that *legal and moral norms* may play in such derivation, is briefly indicated. The relevance of the ideas introduced in the paper for the concrete representation of macro-level social structures as macro-level artifacts in social simulation is also indicated.

INTRODUCTION

In this paper, we introduce the idea of the *binding structure* of a *social interaction scheme*.

The binding structure of a social interaction scheme models the positive, observational components of the interaction scheme that contribute to socially bind the agents that interact according to the scheme, namely, the following set of *binding relations*: objective dependence relations, elementary social functions, exchange value-based dependence relations, and functional rights and duties.

The paper shows how binding structures derive from the *operational structures* that organize the temporal dependence of the behaviors involved in interaction schemes. This allows for a systematic organization of binding structures in terms of the binding relations that constitute them.

For simplicity, the paper restricts itself to the analysis of the so-called *basic binding structure* of the *basic Producer-Consumer interaction scheme*, a sequential and synchronic version of the well-known *Producer-Consumer* form of social interaction.

The paper is structured as follows. Initially, the paper introduces the concept of binding structures of interaction schemes, and their relation to the operational structures of such schemes. Then, the paper characterizes the basic Producer-Consumer interaction scheme in terms of its operational and basic binding structures.

Next, various sections respectively characterize, both in general and in the particular case of the basic *Producer-Consumer* interaction scheme, the four main binding relations that constitute a basic binding structure: objective dependence relations, elementary social functions, exchange value-based dependence relations, and functional rights and duties.

Then, the paper analyses the inter-relations between the four types of binding relations, showing that, in general, they are not reducible to each other, because each brings a specific contribution to the binding power of the basic binding structure of the basic *Producer-Consumer* interaction scheme.

Following, related work – additional to the ones discussed during the development of the paper – are briefly analyzed.

Finally, the Conclusion discusses the possible relevance of the ideas introduced in the paper for the work on simulation of agent societies, in general, and social interactions, in particular.

INTERACTION SCHEMES, AND THEIR OPERATIONAL AND BINDING STRUCTURES

By *interaction scheme* we understand a way through which two or more agents exchange matter, energy, or information among them[1].

Interaction schemes comprise both an *operational* and a *binding* structure:

- By *exchange behavior* we understand a behavior that an agent performs, through which it exchanges matter, energy, or information, with another agent.
- By *operational structure* of an interaction scheme we understand the specification of the temporal organization of the exchange behaviors that the agents perform,

[1]So that interaction schemes do not concern only the exchange of messages among the agents, but also the exchange of products and behaviors.

Proceedings 27th European Conference on Modelling and Simulation ©ECMS Webjørn Rekdalsbakken, Robin T. Bye, Houxiang Zhang (Editors)
ISBN: 978-0-9564944-6-7 / ISBN: 978-0-9564944-7-4 (CD)

while operating according to the interaction scheme[2].

- By *binding relationship* we understand any relationship that two or more agents take into account when interacting, and that motivates them to keep interacting with each other, without discontinuing the interaction or changing partners.
- By *binding structure* of an interaction scheme we understand the interconnected set of *binding relationships* that bind together the agents involved in the interaction scheme.

The scheme illustrated in Fig. 1, is here proposed for the *derivation* of the basic binding structure of an interaction scheme, from the operational structure of that scheme.

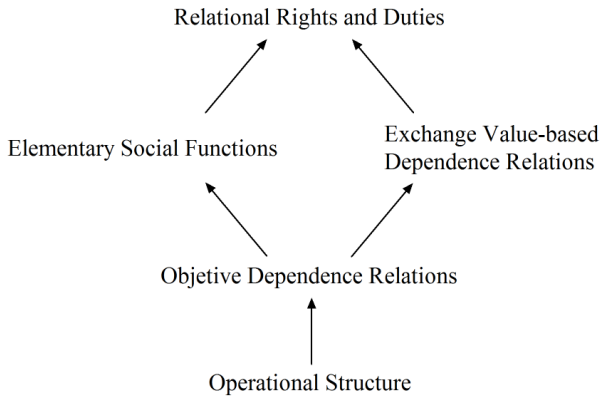

Fig. 1. Derivation of the basic biding structure from the operational structure of an interaction scheme.

BASIC PRODUCER-CONSUMER INTERACTION SCHEME

A. Operational Structure of the Basic Producer-Consumer Interaction Scheme

Figure 2 illustrates the operational structure of the basic `Producer-Consumer` interaction scheme.

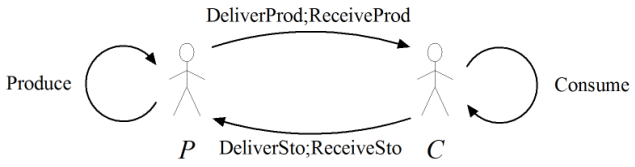

Fig. 2. The basic *Producer-Consumer* scheme.

The scheme defines a way for interaction between two agents, the *Producer* (P) and the *Consumer* (C): the *Producer* periodically produces some *product* (object or service) and the *Consumer* periodically consumes that *product*, as it is produced.

The following procedure clarifies the operational structure shown in Fig. 2:

1. The *Producer* delivers the *product* to the *Consumer* by storing the *product* in a *storage* (not explicitly represented in the scheme), after producing the it;
2. The *Consumer* consumes the *product* only after receiving it from the *storage*;
3. After consuming the *product*, the *Consumer* frees the *storage* to the *Producer* store the next *product* it will produce;
4. The *Producer* only produces a new *product* after receiving a free *storage* to store it;
5. This *production-consumption* cycle is repeated permanently[3].

[2]The kernel of an operational structure is, thus, a temporal relation, partially ordering in time the actions of the exchange behaviors involved in the interaction scheme.

B. Basic Binding Structure of the Basic Producer-Consumer Interaction Scheme

We define the *basic binding structure* of the basic Producer-Consumer interaction scheme as constituted by the following four *binding relations*:

- Objective Dependence Relations
- Elementary Social Functions
- Exchange Value-based Dependence Relations
- Functional Rights and Duties

The rest of this paper analyses these four binding relations, and the way they relate to each other, and to the operational structure of the basic Producer-Consumer interaction scheme, as suggested by the derivation scheme shown in Fig. 1.

OBJECTIVE DEPENDENCE RELATIONS

C. Social Dependence Relations in General

The theory of social dependence relations [3] states that social organization arises from social phenomena (power, influence, etc.) that emerge from *social dependence relations* that are objectively established between agents when agents operate in a shared environment.

As such, social dependence relations – and the social dependence networks that aggregate the set of social dependence relations that exist in a society – are seen as a foundation for social organization and for society itself.

An essential feature of the notion of social dependence relation is the part that cognition plays in its definition: dependence relations that are established between agents derive from both cognitive notions such as agent goals and plans, and non-cognitive notions such as environmental resources and the agents' capabilities of action performance.

Formally, we express social dependence relations as follows. Let ag_1 and ag_2 be two agents of an agent society S that respectively have tasks θ_1 and θ_2 to perform, the tasks being respectively determined by $\theta_1 = (g_1, \varepsilon_1)$ and $\theta_2 = (g_2, \varepsilon_2)$, that is, the task of agent ag_1 is to achieve goal g_1 by using some element (resource, action, behavior, etc.) ε_1 and the task of agent ag_2 is to achieve goal g_2 by using some element ε_2.

We say that the agent ag_1 *depends on* agent ag_2, with respect to goal g_1 and element ε_1 if, at the time t at

[3]Note the features that make the interaction scheme shown in Fig. 2 a basic one: the actions performed by the agents are organized in a sequential way, so that their behaviors are constrained to occur in a synchronic way. The general *Producer-Consumer* interaction scheme is not subject to such constraints, so that the behaviors of the agents may proceed concurrently, in an asynchronous way.

which ag_1 tries to achieve g_1, agent ag_1 does not have access to element ε_1 and if, at that time, agent ag_2 can provide the access to element ε_1 to agent ag_1.

The dependence of ag_1 on ag_2, with respect to the goal g_1 may be denoted either by $Dep_S(ag_1, ag_2, \varepsilon_1, g_1)$ or else as:

- $(ag_1 \prec ag_2 : \varepsilon_1 \prec g_1)_S$

The social dependence relations so defined are considered to be *objective* [3], in the sense that their existence is not a consequence of the beliefs of the agents about their respective situations.

D. Objective Dependence Relations in the Basic Producer-Consumer Interaction Scheme

The following are the objective dependence relations of the basic Producer-Consumer interaction scheme:

- the *Producer* alternates between three main goals: *ReceiveSto*, *Produce*, and *DeliverProd*;
- the *Consumer* alternates between three main goals: *ReceiveProd*, *Consume*, and *DeliverSto*;
- the *Producer* depends on the *Consumer* performing the *DeliverSto* action, to be able to achieve the goal *ReceiveSto*; having achieved the goal *ReceiveSto* the *Producer* is free to perform by itself the action *Produce* and achieve the goal *Produce*;
- the *Consumer* depends on the *Producer* performing the *DeliverProd* action, to be able to achieve the goal *ReceiveProd*; having achieved the goal *ReceiveProd* the *Consumer* is free to perform by itself the action *Consume* and achieve the goal *Consume*.

Formally, we express the objective dependencies between the two agents as:

- $(Producer \prec Consumer : DeliverSto \prec ReceiveSto)$
- $(Consumer \prec Producer : DeliverProd \prec ReceiveProd)$

Note how an objective dependence relation refers basically to a dependence between an agent's goal and an action of another agent, which is able to immediately enable the achievement of that goal.

As such, objective dependence relations operate as motivators for the realization of social interactions, thus, also as binding relations in interaction schemes.

ELEMENTARY SOCIAL FUNCTIONS

E. Social Functions in General

Functionalism has a large tradition in Social Sciences, having received since its beginning both wide acceptance and strong criticisms [6]. Its central idea is that of *social function* – the satisfaction of a social need (either a need of a component of a social system or a need of the social systems as a whole) through the performance of an activity (either by a system component or by the social system as a whole).

By the term *elementary social function* we mean a social function where:

- the notion of *need* is interpreted as an *operational requirement*, namely, that the performance of an activity by an agent ag_2 requires, for its accomplishment, that ag_2 interacts in a certain way with some other agent ag_1, so that ag_1 provides ag_2 with some element e that is indispensable for the correct execution of ag_2's activity;
- the notion of *satisfaction of a need* is interpreted as the providing of the element e by ag_1 to ag_2;
- as proposed in [9], the performance of a *function* by ag_1 for ag_2 occurs when a renewable need of ag_2 is repeatedly satisfied by a *persistent interaction* between ag_1 and ag_2 (not, as is often considered, cf. e.g. [4], when a single occurrence of a need of ag_2 is satisfied by a single occurrence of a behavior of ag_1).

We formalize the notion of elementary systemic function as follows. Let ag_1 and ag_2 be two agents of a social system S. Let ag_2 operate in S according to a *behavior requirement* BR_2, which also imposes an additional *interaction requirement* $IR_{1,2}$ between ag_1 and a ag_2, so that the realization of BR_2 by ag_2 is viable only if ag_1 interacts with ag_2 in a way that meets $IR_{1,2}$.

We denote the fact that ag_2 behaves according to the behavior requirement BR_2 by $(ag_2 : BR_2)$. Similarly, we denote the fact that ag_1 interacts with ag_2 in such a way that their interaction meets the interaction requirement $IR_{1,2}$ by $(ag_1 : IR_{1,2} : ag_2)$.

Additionally, we denote the fact that the behavior requirement BR_2 imposed upon ag_2 requires the presence in S of an agent ag_1 capable of an interaction with ag_2 that satisfies the interaction requirement $IR_{1,2}$ by $BR_2 \rightarrowtail IR_{1,2}$.

Thus, we say that ag_1 performs an elementary function for ag_2 in S if and only if:

- $(ag_2 : BR_2)$, that is, ag_2 operates in S according to a behavior requirement BR_2;
- $BR_2 \rightarrowtail IR_{1,2}$, that is, BR_2 requires the presence of another agent ag_1 in S, which interacts with ag_2 in a way that satisfies the interaction requirement $IR_{1,2}$;
- $(ag_1 : IR_{1,2} : ag_2)$, that is, ag_1 interacts with ag_2 in a way that meets the interactional requirement $IR_{1,2}$.

We denote the fact that ag_1 performs an elementary function for ag_2 in S by interacting with ag_2 in a way that meets the interaction requirement $IR_{1,2}$ imposed by the behavior requirement BR_2 of ag_2 by

- $(ag_1 : IR_{1,2} : ag_2) \triangleright_S (ag_2 : BR_2)$

We say that ag_1 is the *performer* of the function, and that ag_2 is its *beneficiary*.

F. Elementary Social Functions in the Basic Producer-Consumer Interaction Scheme

Figure 2 shows that two elementary social functions are being performed in the *Producer-Consumer* scheme, namely:

$$PC = (P : DeliverProd; ReceiveProd : C) \triangleright (C : Consume)$$

$$CP = (C : DeliverSto; ReceiveSto : P) \triangleright (P : Produce)$$

that is:

- a function PC such that the *Producer* delivers *products* to the *Consumer*, so that the *Consumer* can realize its *Consume* behavior;

• and a function CP such that the *Consumer* delivers *storage*s to the *Producer*, so that the *Producer* can realize its *Produce* behavior.

Note how an elementary social function concerns basically the performance of an interaction process between two agents that enables the achievement of a goal that is of *central importance* for the beneficiary agent.

As such, social functions operate as motivators for the realization of social interactions, thus, also as binding relations in interaction schemes.

EXCHANGE VALUE-BASED DEPENDENCE RELATIONS

G. Exchange Value-based Dependence Relations, in General

Social exchange theory [15] conceives social relations as exchanges of elements (matter, energy, or information) among agents.

The agents, by attaching some set of subjective, qualitative values to the behaviors or the elements involved in the exchanges, can subjectively assess the exchanges with regard to their quality, utility, etc. [12], and on the basis of such assessments take several decisions: wether to continue or discontinue the interactions, which partners to select for interactions, etc.

In our work, we adopt Piaget's model of social exchanges [19] to support the conceptual model of agent interactions that we have been developing (cf. [8] and the references cited there).

Figure 3 illustrates the set of exchange values that the agents may attach to their exchanges, and the two types of interactions with which they may perform exchanges.

The two types of values that are involved in the assessment of social exchanges are:

• *actual values* – i.e., $r_{\mathrm{I}}, s_{\mathrm{I}} v_{\mathrm{II}}, s_{\mathrm{II}}$ – meaning values concerned with elements that actually occurred in the interaction, like investments and satisfactions;

• and *virtual* (or, better, *potential*) *values* – i.e., $t_{\mathrm{I}}, v_{\mathrm{I}}, v_{\mathrm{II}}, t_{\mathrm{II}}$ – meaning values representing debts and credits arisen in the interaction, thus concerning values that are to be realized in future interactions.

The two types of interactions are:

• Type I, where ag_1 acts on behalf of ag_2, resulting in ag_2 acquiring a debt t_{I} regarding ag_1, and ag_1 acquiring a credit v_{I} regarding ag_2;

• Type II, where ag_1 charges ag_2 a return behavior with value proportional to the credit v_{II} that it has regarding ag_2, and ag_2 performs a return behavior proportional only to the debt t_{II} that it acknowledges to ag_1.

Whenever needed, agents may change the roles they play in the interaction, with either ag_2 acting on behalf of ag_1, or ag_2 charging ag_1 for a credit previously accumulated.

In addition, Piaget's model makes use of qualitative comparisons between exchange values, to define so-called *equilibrium conditions*, which may be used to support the continuation/discontinuation decisions of the agents about their interaction with each other:

• Equilibrium condition:

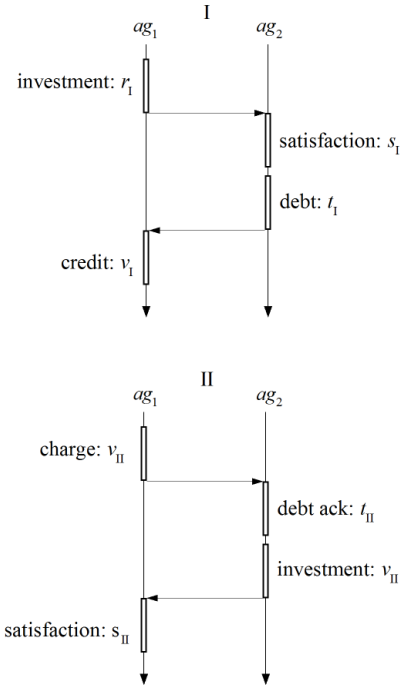

Fig. 3. Operational structure of a social exchange, and associated exchange values.

– $r_{\mathrm{I}} \simeq s_{\mathrm{I}}$ and $s_{\mathrm{I}} \simeq t_{\mathrm{I}}$ and $t_{\mathrm{I}} \simeq v_{\mathrm{I}}$, so that $r_{\mathrm{I}} \simeq v_{\mathrm{I}}$

– $r_{\mathrm{II}} \simeq s_{\mathrm{II}}$ and $s_{\mathrm{II}} \simeq t_{\mathrm{II}}$ and $t_{\mathrm{II}} \simeq v_{\mathrm{II}}$, so that $r_{\mathrm{II}} \simeq v_{\mathrm{II}}$

– $v_{\mathrm{II}} \simeq v_{\mathrm{I}}$

so that $s_{\mathrm{II}} \simeq r_{\mathrm{I}}$

• Among the various types of disequilibrium condition, the following examples:

– $r_{\mathrm{I}} > s_{\mathrm{II}}$: ag_1 is not being properly compensated for his action on behalf of ag_2

– $s_{\mathrm{I}} > t_{\mathrm{I}}$: ag_1's action on behalf of ag_2 is being depreciated by ag_2

Piaget makes use of such mechanism of social exchange values, and the equilibrium/disequilibrium conditions which it gives rise to, to characterize the behavioral rules that impose themselves to the agents, when deciding about the continuation/discontinuation of their interactions, or when choosing partners for social exchanges [19]. Examples of such rules are:

• If the exchange is in equilibrium, agents tend to continue interacting with each other.

• If an agent is in advantage with respect to the other, it may initiate an interaction that will benefit the other, in order to restore the equilibrium condition.

• If the two agents consider, in common agreement, that one of them has a higher social status than the other, then it may become acceptable to both that their interaction continuously benefits the former much more than the latter.

From the point of view of a dependence relation between the agents, in the *equilibrium* condition, one may say that the two agents are *mutually dependent* on each other, for each depend on the proper behavior of the other for the maintenance of such beneficial situation.

In the disequilibrium condition, on the other hand, when one agent is being benefited more than the other, one may say that the former is *dependent* on the latter,

for it depends on the latter continuing to accept such disadvantageous situation, in order for the former to continue benefiting of the situation in such large extent.

Formally, we may express the two dependence situations by:

- $ag_1\langle b_2|b_1\rangle ag_2$

meaning: ag_1 and ag_2 mutually depend on each other, for there is an equilibrium in values exchanged between them, with ag_1 performing behavior b_1 on behalf of ag_2, and ag_2 performing behavior b_2 on behalf of ag_1;

- $ag_1[b_1\rangle ag_2$

meaning: ag_2 is dependent on ag_1 performing behavior $b_!$, for there is a disequilibrium favoring ag_2 with respect to ag_1, when the latter perform that behavior on behalf of the former.

As such, exchange value-based dependence relations operate as motivators for the realization of social interactions, thus, also as binding relations in interaction schemes.

H. Exchange Value-based Dependence Relations in the Basic Producer-Consumer Interaction Scheme

In the basic *Producer-Consumer* interaction scheme, one may identify two different, coordinated flows of elements among the two agents, namely:

- a flow of *full storage places*, filled with products, flowing from the *Producer* to the *Consumer*, allowing the *Consumer* to consume products;
- a flow of *empty storage places*, flowing from the *Consumer* to the *Producer*, allowing the *Producer* to deliver products that it has produced.

Assuming that each of the two agents is interested in the continued realization of the flow that respectively allows it to achieve its behavioral goal (production, for the *Producer*; consumption, for the *Consumer*), we may determine the following possible *dependence conditions* in their interaction:

- $Producer\langle DeliverSto|DeliverProd\rangle Consumer$

meaning that the agents are in equilibrium and thus are mutually dependent on each other;

- $Producer[DeliverProd\rangle Consumer$

meaning that the *Consumer* is in advantage with respect to the *Producer*, benefiting from the interaction more than the latter (for example, because the cost of the delivery of the product is much higher than the cost of the delivery of the empty storage);

- $Consumer[DeliverSto\rangle Producer$

meaning that the *Producer* is in advantage with respect to the Consumer, benefiting from the interaction more than the latter (for example, because of the poor quality of the product, that keeps low the cost of its production).

FUNCTIONAL RIGHTS AND DUTIES

I. Functional Rights and Duties, in General

We have proposed [7] (cf. also [9]) the term *functional rights* and *functional duties* to denote the moral and juridical concepts that correlate to each other in social interactions, and that have been identified, analysed, and given importance in several social contexts [18], [17], [19]:

- a *right* is an authorization given to an agent, to exact a behavior from its partner;
- a *duty* is an obligation assigned to an agent, to behave in a certain way, directed toward its partner.

As such, functional rights and duties operate as *normative motivators* for social interactions, thus, also as binding relations in interaction schemes.

The strong correlation of rights and duties makes them occur together in any situation. Thus, we formally represent them by the following basic RD operator [7]:

- $RD(ag_2, ag_1)[b]$

meaning: ag_2 is allowed to exact ag_1 to perform behavior b and ag_1 has the functional duty to perform behavior b for ag_2.

More generally, however, the functional right and the functional duty involved in a social interaction do not concern one single behavior, that an agent has to perform for the other: often, the functional duty involved in the interaction is a behavior b_1 that ag_1 has to perform in order to *enable* a behavior b_2 that ag_2 has the functional right to perform.

So, we get formally [7]:

- $RD(ag_2, ag_1)[b_1 \rightsquigarrow b_2]$

meaning: ag_2 is allowed to exact ag_1 to perform behavior b_1 and ag_1 has the functional duty to perform behavior b_1 for ag_2, so that ag_2 is enabled to perform behavior b_2, which it has the functional right to perform.

J. Functional Rights and Duties in the Basic Producer-Consumer Interaction Scheme

In the basic *Producer-Consumer* interaction scheme, we may identify the following functional rights and duties:

- $RD(Consumer, Producer)$
  $[DeliverProd \rightsquigarrow ReceiveProd]$

meaning: the *Producer* has the functional duty to perform $DeliverProd$ to enable the *Consumer* to perform its functional right to $ReceiveProd$; and:

- $RD(Producer, Consumer)$
  $[DeliverSto \rightsquigarrow ReceiveSto]$

meaning: the *Consumer* has the functional duty to perform $DeliverSto$ to enable the *Producer* to perform its functional right to $ReceiveSto$.

INTER-RELATION OF THE BASIC BINDING RELATIONS OF THE BASIC PRODUCER-CONSUMER INTERACTION SCHEME

We collect in Table I the set of *basic binding relations* that we have identified in the basic *Producer-Consumer* interaction scheme.

Such set of basic binding relations constitute the *basic binding structure* of that interaction scheme.

Clearly, there is no equivalence among the various binding relations, meaning that each type of binding

TABLE I: The binding structure of the basic *Producer-Consumer* interaction scheme

1) Binding relations based on **objective dependence relations**:

$(Producer \prec Consumer : DeliverSto \prec ReceiveSto)$
$(Consumer \prec Producer : DeliverProd \prec ReceiveProd)$

2) Binding relations based on **elementary social functions**:

$(Producer : DeliverProd; ReceiveProd : Consumer) \rhd (Consumer : Consume)$
$(Consumer : DeliverSto; ReceiveSto : Producer) \rhd (Producer : Produce)$

3) Binding relations based on **exchange value-based dependence relations**:

$Producer\ \langle DeliverSto | DeliverProd \rangle\ Consumer$ - if the exchange is equilibrated
$Producer\ [DeliverProd \rangle\ Consumer$ - if the exchange favors the *Consumer*
$Consumer\ [DeliverSto \rangle\ Producer$ - if the exchange favors the *Producer*

4) Binding relations based on **functional rights and duties**:

$RD(Consumer, Producer)[DeliverProd \rightsquigarrow ReceiveProd]$
$RD(Producer, Consumer)[DeliverSto \rightsquigarrow ReceiveSto]$

relation has a contribution of its own to the binding structure:

- the *objective dependence relations* extract, from the operational structure of the interaction scheme, the operational dependencies between the behaviors involved in the interaction;
- the *elementary social functions* add information about the functions performed by the agents, for each other, in the interaction scheme;
- the *exchange value-based dependence relations* add information about the state of equilibrium or disequilibrium of the interaction;
- the *functional rights and duties relations* express in a normative way the binding conditions in the scheme.

In other words, there is no possibility of reducing the basic binding structure of an interaction scheme to one of its constitutive binding relations, and the basic binding structure has always to be consider in its various *dimensions*: objective dependence relations, elementary social functions, exchange value-based dependence relations, functional rights and duties.

SOME ADDITIONAL RELATED WORKS

The idea that interaction schemes build binding structures on the basis of their operational structures comes from three sources. Firstly, from Durkheim's explanation of the importance of the division of social labor for the integration of societies [18]. Secondly, from Kelsen's explanation of the coercive nature of the legal orders. Thirdly, from Elias' [11] idea of the *integration level* of a social context.

In all three cases, emphasis is put both on the persistent and relational nature of the operational structure of the social interactions that are relevant for the organization of societies, and on the binding nature of the various social relations that accompany such social interactions.

What the paper does, in this respect, is to organize such binding relations in a systematic way, with the concept of binding structure.

Of particular importance, here, is to notice the difference between the extensional, observational approach adopted here – in the vein of Durkheim and Kelsen –, and the intensional, subjectivist approach adopted in may other works on socially binding relations developed in the area of multiagent systems, in particular the works about commitments (e.g., [2], [20]), teamwork [5], and responsibility in the joint performance of tasks (e.g., [16]).

The approach adopted here allows for the exploration of the part that positive norms (both moral and legal) play in the construction of binding structures, as explained in the Conclusion.

DISCUSSION

The *Producer-Consumer* interaction scheme is a general one, capable of modeling a large number of interaction situations.

The well-known *Client-Server* interaction scheme, for instance, is a particular application of the *Producer-Consumer* scheme, with the *Client* taking the place of *Consumer*, *Server* taking the place of *Producer*, the flow of *client requests* taking the place of the flow of empty slots, and the flow of storage places filled with products going from the *Server* to *Client*.

The basic *Producer-Consumer* interaction scheme that we considered in the paper is a restricted, sequential and synchronized version, of the general *Producer-Consumer* scheme. It served, however, the purpose of simplifying the study of the binding structure that builds on its operational structure, when it is put into operation in a social system. In this respect, the paper restricted itself to the basic binding structure associated with the basic Producer-Consumer scheme.

However, in the basic Producer-Consumer scheme it is a central feature that the interaction that it organizes is assumed to be *persistent* in time, a necessary feature of all social relations that structure agent societies (cf., e.g., [1], where economic exchanges are treated just as one-shot events, thus not leading to their view as supports for binding structures).

Some other features of the binding structure should be contemplated in future work, in particular, the separation of functional rights and duties into legal and moral rights and duties, allowing for a the distinction between legal and moral systems in agent societies.

The clarification of the role of norms in the derivation of binding structures is also a future work that merits immediate research effort, to allow a better understanding of the derivation scheme.

Finally, we should mention the importance of the adoption of the two place operator *RD*, for the denotation of functional rights and duties, that makes explicit the co-occurrence of those two notions in functional interactions.

The *RD* operator should be contrasted with the one place operator *Obl* that usually denotes obligations in normative systems. The contrast between them makes clear that functional rights and duties are not respectively reducible, in a simple minded way, to obligations and permissions, which may occur in isolation of each other.

CONCLUSION

There seems to be two main kinds of macro-level social structures, studied in social sciences: one seems to appear as unintended effects of social interactions that occur between individuals, at the micro-level. In the context of social simulation, this type of structures have been studied for a long time, e.g., [13].

A second type of macro-level structures, however, seem to appear as deliberately constructed and imposed (possibly by force) by intentional processes carried on by certain individuals or groups of individuals. Law, as explained by Kelsen [17], is one important example of those intentionally constructed and deliberately imposed macro-level structures.

It seems to us that the right way to deal with such deliberately constructed macro-level structures in simulation model is to have them explicitly represented in data objects generally made accessible for the agents that constitute the population of the simulated social systems. This should be essentially not different from the explicit representation of positive law in legal documents, as it occurs in the legal systems of modern human societies.

One purpose of identifying binding structures of interaction schemes, a problem that this paper tackled at a basic level, is to identify their components and, so, allow for the identification of data objects suitable for their explicit representation in simulation models, thus allowing simulated agents to access and take into account those deliberately constructed binding structures in their simulated interactions.

We notice a special concept developed for dealing with explicit representations of macro-level structures, namely, the so-called "organizational artifacts" [14], that seem adequate for our purpose (cf. an application of this idea of macro-level artifacts to the modeling of public policy processes in [10]).

ACKNOWLEDGEMENTS

Work partially supported by CNPq and FAPERGS.

REFERENCES

[1] Varol Akman and Murat Ersan. Commonsense aspects of buying and selling. *Cybernetics & Systems*, 27:327–352, 1996.

[2] Cristiano Castelfranchi. Commitments: From individual intentions to groups and organizations. In Victor Lesser and Les Gasser, editors, *Proceedings of the First International Conference on Multiagent Systems - ICMAS 95*, pages 41–48, Cambridge, 1995. MIT Press.

[3] Cristiano Castelfranchi, Amedeo Cesta, and Maria Miceli. Dependence relations among autonomous agents. In Erich Werner and Yves Demazeau, editors, *Decentralized A.I.-3*, pages 215–227, Amsterdam, 1992. Elsevier.

[4] B. Chandrasekaran. Representing function: Relating functional representation and functional modeling research streams. *Artificial Intelligence for Engineering Design, Analysis and Manufacturing*, 19:65–74, 2005.

[5] Philip R. Cohen and Hector Levesque. Teamwork. *Noûs*, 25(4):487–512, 1991.

[6] Randall Collins. *Four Sociological Traditions*. Oxford University Press, London, 1991.

[7] Antônio Carlos Rocha Costa. Functional rights and duties at the micro and macro social levels. Invited Talk at RDA2 - Workshop on Rights and Duties of Autonomous Agentes, co-located with ECAI 2012 - 20th European Conference on Artificial Intelligence, Montpellier, France, 2012.

[8] Antônio Carlos Rocha Costa and Graçaliz Pereira Dimuro. A minimal dynamical organization model. In V. Dignum, editor, *Multi-Agent Systems: Semantics and Dynamics of Organizational Models*, pages 419–445. IGI Global, Hershey, 2009.

[9] Antônio Carlos Rocha Costa and Graçaliz Pereira Dimuro. On the interactional account of the social functions of agent societies. In *BWSS 2010, Second Brazilian Workshop on Social Simulation*, pages 74–81, New York, 2010. IEEE. (Available at IEEE Xplore - `http://ieeexplore.ieee.org`).

[10] Antônio Carlos Rocha Costa and Iverton Adão Silva dos Santos. Toward a framework for simulating agent-based models of public policy processes on the jason-cartago platform. In *AMPLE@ECAI 2012 - 2nd International Workshop on Agent-based Modeling for Policy Engineering*, Montpellier, 2012. ECAI.

[11] Norbert Elias. *The Society of Individuals*. Univ. College of Dublin Press, Dublin, 2011.

[12] R. Emerson. Social exchange theory. In A. Inkeles, J. Colemen, and N. Smelser, editors, *Annual Review of Sociology*. Annual Reviews, Palo Alto, 1976.

[13] Joshua M. Epstein and Robert L. Axtell. *Growing Artificial Societies: Social Science from the Bottom Up*. MIT Press, Cambridge, 1996.

[14] Jomi F. Hübner, Olivier Boissier, R. Kitio, and Alessandro Ricci. Instrumenting multi-agent organisations with organisational artifacts and agents: Giving the organisational power back to the agents. *Journal of Autonomous Agents and Multi-Agent Systems*, 20(3):369–400, May 2010.

[15] G. Homans. *Social Behavior – Its Elementary Forms*. Harcourt, Brace & World, New York, 1961.

[16] Nick Jennings. On being responsible. In *3rd European Workshop on Modelling Autonomous Agents in a Multi-Agent World (MAAMAW-91)*, pages 93–102, Amsterdam, 1992. North Holland.

[17] Hans Kelsen. *Pure Theory of Law*. The Law Book Exchange, New Jersey, 2009.

[18] Émil Durkheim. *The Division of Labor in Society*. Free Press, New York, 1997.

[19] Jean Piaget. *Sociological Studies*. Routlege, London, 1995.

[20] Munindar P. Singh. Commitments among autonomous agents in information rich environments. In M. Bonam and W. van de Velde, editors, *8th European Workshop on Modelling Autonomous Agents in a Multi-Agent World*, number 1237 in LNAI, pages 141–155. Springer, Berlin, 1997.

AUTHOR INDEX